Cave and Karst Systems of the World

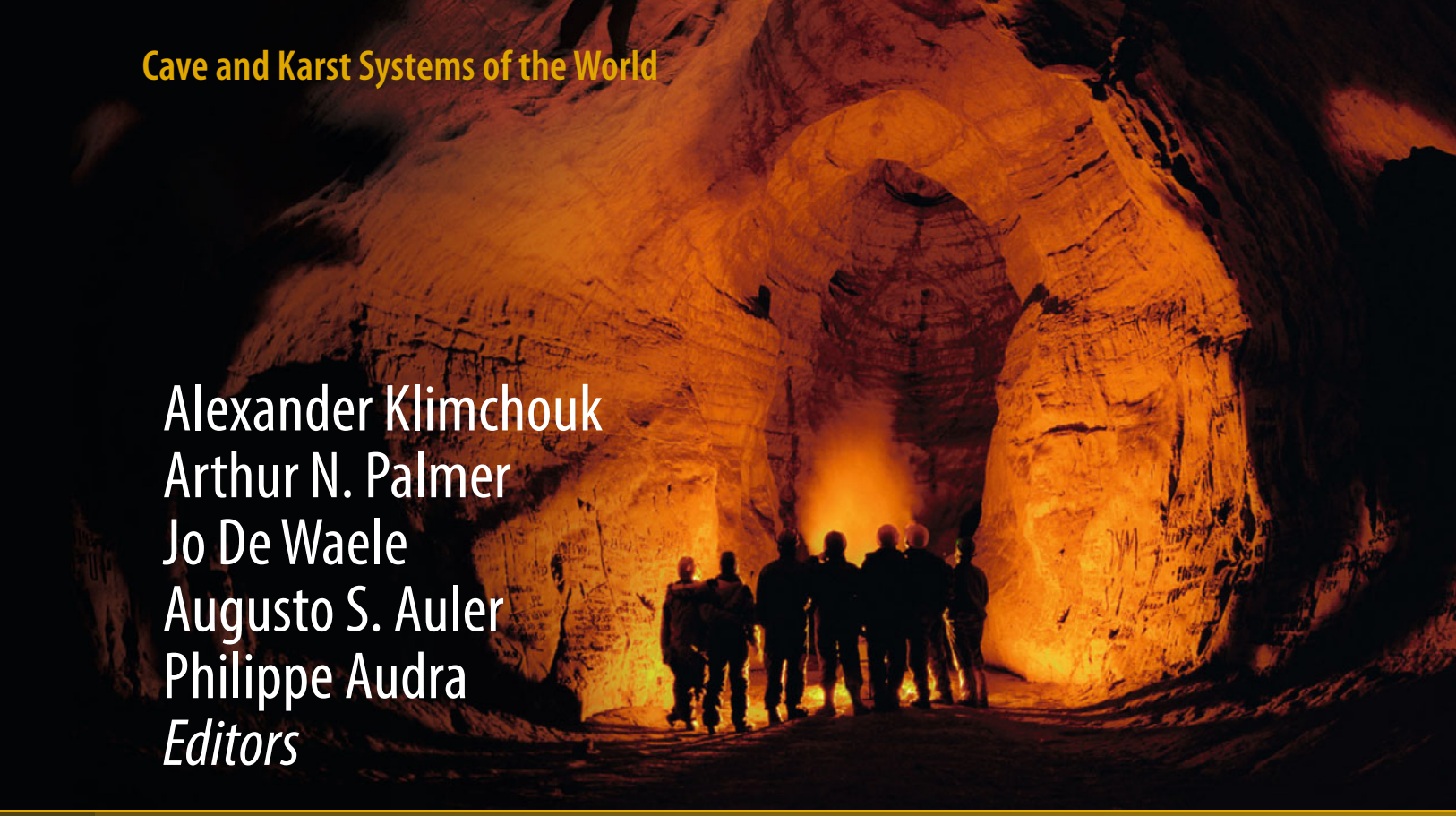

Alexander Klimchouk
Arthur N. Palmer
Jo De Waele
Augusto S. Auler
Philippe Audra
Editors

Hypogene Karst Regions and Caves of the World

Springer

Cave and Karst Systems of the World

Series editor

James W. LaMoreaux, Tuscaloosa, USA

More information about this series at http://www.springer.com/series/11987

Alexander Klimchouk
Arthur N. Palmer · Jo De Waele
Augusto S. Auler · Philippe Audra
Editors

Hypogene Karst Regions and Caves of the World

Springer

Editors
Alexander Klimchouk
Department of Hydrogeological Problems
Institute of Geological Sciences
Kiev
Ukraine

Arthur N. Palmer
Department of Earth and Atmospheric Sciences
State University of New York
Oneonta, NY
USA

Jo De Waele
Department of Biological, Geological, and Environmental Sciences
Universita di Bologna
Bologna
Italy

Augusto S. Auler
Instituto do Carste
Belo Horizonte, Minas Gerais
Brazil

Philippe Audra
University of Nice Sophia Antipolis
Sophia Antipolis Cedex
France

ISSN 2364-4591 ISSN 2364-4605 (electronic)
Cave and Karst Systems of the World
ISBN 978-3-319-53347-6 ISBN 978-3-319-53348-3 (eBook)
DOI 10.1007/978-3-319-53348-3

Library of Congress Control Number: 2017937725

© Springer International Publishing AG 2017
This work is subject to copyright. All rights are reserved by the Publisher, whether the whole or part of the material is concerned, specifically the rights of translation, reprinting, reuse of illustrations, recitation, broadcasting, reproduction on microfilms or in any other physical way, and transmission or information storage and retrieval, electronic adaptation, computer software, or by similar or dissimilar methodology now known or hereafter developed.
The use of general descriptive names, registered names, trademarks, service marks, etc. in this publication does not imply, even in the absence of a specific statement, that such names are exempt from the relevant protective laws and regulations and therefore free for general use.
The publisher, the authors and the editors are safe to assume that the advice and information in this book are believed to be true and accurate at the date of publication. Neither the publisher nor the authors or the editors give a warranty, express or implied, with respect to the material contained herein or for any errors or omissions that may have been made. The publisher remains neutral with regard to jurisdictional claims in published maps and institutional affiliations.

Printed on acid-free paper

This Springer imprint is published by Springer Nature
The registered company is Springer International Publishing AG
The registered company address is: Gewerbestrasse 11, 6330 Cham, Switzerland

Preface

Ideas that karst can develop at depth without direct genetic relationship to the surface have a long history, but remained on the periphery of karstological thinking, not influencing the traditional paradigm of karst until the last 25 years. More attention to hypogene karst since 1990, and particularly the dramatic burst of studies in this field during the last decade, has changed our notion of hypogene karst from a curiosity to one of the fundamental categories of karst, at least of compatible importance with more familiar epigene karst.

Hypogene karst develops where the ascending flow of reactive fluids migrates across lithologies that are soluble in those particular fluids. Ascending fluid flow is ubiquitous in most of the upper crust in which deep-seated flow takes place. It is also a significant component of the circulation pattern in the uppermost zones of meteoric groundwater flow. A wide range of pressure–temperature conditions and the variety of compositions of fluids within the upper crust offer the potential for diverse dissolutional mechanisms to operate in a variety of lithologies. The depth limit for the development of dissolutional macro-porosity is difficult to establish, but available data suggest that it can form within depths of at least several kilometers. The time during which hypogene karstification may take place in deep-seated rocks is much greater than the common lifetimes for epigene karst systems in exposed formations. Hence, the potential for the development of hypogene karst is immense, not only in the continental domain but also in the oceanic domain.

The association of hypogene speleogenesis with ascending flow (leakage and discharge in confined fluid systems) was the major development that caused the recent burst in hypogene karst studies. It allowed (1) identifying the common genetic background and explaining the similarity of a large array of caves previously considered unrelated, which formed in different rock types by a variety of dissolutional mechanisms; and (2) interpreting hypogene karst in the context of regional hydrogeology and geodynamics. This triggered a dramatic expansion of regional and cave-specific studies and reinterpretation of many cases in light of the new conceptual framework.

Progress in regional studies has been reviewed in a series of conferences and their subsequent publications, such as "*Advances in Hypogene Karst Studies*" (edited by K. Stafford, L. Land, and G. Veni, 2009), "*Hypogene Speleogenesis and Karst Hydrogeology of Artesian Basins*" (edited by A. Klimchouk and D. Ford, 2009), "*Hypogene Cave Morphologies*" (edited by A. Klimchouk, I. Sasowsky, J. Mylroie, S.A. Engel, and A.S. Engel, 2014), and "*Origins, resources, and management of hypogene karst*" (edited by T. Chaves and P. Reehling, 2016).

This book was proposed as a next step in consolidating the growing wealth of regional data about hypogene karst. It is neither an inventory, nor a comprehensive coverage of all hypogene karst regions and caves of the world, but is rather a selection of regional and cave-specific case studies that represent a remarkable variability of relevant patterns and settings (geological, hydrogeological, tectonic, and geodynamic). In this way, it provides a solid reference for further generalizing and modeling studies of the topic, which may be the focus of a future collaborative volume on hypogene karst.

The book contains 61 chapters authored by 131 scholars from 25 nations and all continents. It starts with a chapter that reviews basic concepts about hypogene karst, speleogenesis, fluid dynamics, and hydrodynamic zoning of the upper crust, and outlines a pattern for classifying hypogene karst and its settings. Specific case studies are organized into four large geographic regions or continents. Although coverage is truly global, it is not uniform. Whereas 25 chapters are concerned with regions in Europe and 24 chapters deal with the North American regions, only 11 concern other parts of the world. This reflects the uneven distribution of research rather than scarcity of hypogene karst in underrepresented regions. On the basis of geological characteristics and fragmented reports of features scattered throughout petroleum and mining publications, it is evident that hypogene karst is widespread in many regions of Africa, Asia, Australia, and South America, although there are few focused studies. Moreover, even in Europe and North America, many areas have been recognized only recently to host hypogene karst, and its study is still ongoing. This means that next editions of volumes under this title will be needed.

Most contributions in this book deal with karst systems accessible to direct examination, which presently occur in the shallow subsurface. Most are relict systems, decoupled from their original genetic environments and brought into the shallow subsurface from considerable, sometimes large, depth. The advantages of direct observations and sampling, and of using methods developed in karst and cave science, make it possible to obtain unique information about patterns, processes, conditions, and controls of the origin of void-conduit systems at depth and about their hydraulic function. Many parameters of cave-forming environments can be reconstructed from mineralogical and geochemical footprints or inferred from other considerations, such as paleo-hydrogeological analysis. Studies of features that are analogues of deep-seated void-conduit systems are indispensable for interpreting data from drilling and geophysical surveys and for the development of conceptual models. Unfortunately, a wealth of information about the topic in mining areas and petroleum fields is difficult to obtain by karst scholars. Bridging the gap between karst science and industrial geology is a promising opportunity for further developments in hypogene karst studies.

Recognition of hypogene karst and the scale of its phenomena dramatically expand both the boundaries of karst and the significance of karst science far beyond the traditional, dominantly epigenic, karst paradigm. This has numerous scientific and practical implications. Hypogene karst studies hold a promise to help solve many problems in prospecting and exploration of deep petroleum, ore, and geothermal resources in soluble rocks. Proper reservoir characterization and modeling requires a skillful genetic interpretation of void-conduit systems and understanding of their hydraulic function. The role of hypogene karstification lies not only in enhancing reservoir properties but also in facilitating vertical fluid migration across heterogeneous strata. Therefore, it plays a dual role: It not only creates pathways for migration of hydrocarbons and metalliferous fluids to sites of deposition, but also contributes to the loss of the deposits by compromising the integrity of their seals. The latter aspect of hypogene karst also has important implications for the exploration of unconventional oil and gas resources and the sequestering of CO_2 and other troublesome fluids. The recognition of specific characteristics and functioning of hypogene karst is crucial for assessment and mitigation of environmental/engineering hazards, including sinkhole formation and groundwater flooding of mines.

The preparation of this book was initiated and coordinated by the Commission on Karst Hydrogeology and Speleogenesis of the International Union of Speleology, as a part of its ongoing HypoKarst project ("*Hypogene Karst & Speleogenesis: Nature, Processes, Mechanisms, Manifestations and Applications*"). The conference "DeepKarst 2016" held in Carlsbad, NM, organized and hosted by the National Cave and Karst Research Institute (NCKRI) has played an important role in the preparation of this book. Our special thanks to Margaret V. Palmer for her help in editing the chapters on North America.

The editors thank all contributing authors for their productive collaboration, as well as the many researchers and cave explorers who have documented caves and karst features in various parts of the world.

We hope that this book will stimulate further research into hypogene karst and caves around the globe, as well as interaction between karst scientists and industrial geologists.

Kiev, Ukraine — Alexander Klimchouk
Oneonta, USA — Arthur N. Palmer
Bologna, Italy — Jo De Waele
Belo Horizonte, Brazil — Augusto S. Auler
Sophia Antipolis Cedex, France — Philippe Audra

Contents

1 Types and Settings of Hypogene Karst 1
Alexander Klimchouk

Part I Europe

2 Hypogenic Caves in the UK 43
Andrew R. Farrant and Tony Harrison

3 Hypogene Caves in France 61
Philippe Audra

4 Evidence for Regional Hypogene Speleogenesis in Murcia (SE Spain) 85
Fernando Gázquez, José María Calaforra, Tomás Rodríguez-Estrella, Andrés Ros, José L. Llamusí, and Juan Sánchez

5 Hypogene Imprints in Coastal Karst Caves from Mallorca Island (Western Mediterranean): Morphological Features and Speleogenetic Approach 99
Joaquín Ginés, Joan J. Fornós, Francesc Gràcia, Antoni Merino, Bogdan P. Onac, and Angel Ginés

6 Hypogene Karst in Austria 113
Christoph Spötl, Lukas Plan, and Yuri Dublyansky

7 Hypogenic Caves in the Apennine Mountains (Italy) 127
Sandro Galdenzi and Marco Menichetti

8 The Frasassi Caves: A "Classical" Active Hypogenic Cave 143
Sandro Galdenzi and Daniel S. Jones

9 The Coastal Sulfuric Acid Cave System of Santa Cesarea Terme (Southern Italy) 161
Ilenia M. D'Angeli, Marco Vattano, Mario Parise, and Jo De Waele

10 The Thermal Hypogenic Caves of Acquasanta Terme (Central Italy) 169
Sandro Galdenzi

11 Inactive Hydrothermal Hypogenic Karst in SW Sardinia (Italy) 183
Jo De Waele, Fernando Gázquez, Paolo Forti, and Angelo Naseddu

12 An Overview of the Hypogene Caves of Sicily 199
Marco Vattano, Giuliana Madonia, Philippe Audra, Ilenia M. D'Angeli, Ermanno Galli, Jean-Yves Bigot, Jean-Claude Nobécourt, and Jo De Waele

13 Hypogene Gypsum Caves in Piedmont (N-Italy) 211
Cinzia Banzato, Bartolomeo Vigna, Adriano Fiorucci, and Jo De Waele

14 Hypogene Speleogenesis in Greece. 225
Georgios Lazaridis

15 Hypogene Karst in Macedonia 241
Marjan Temovski

16 Hypogene Caves of Romania 257
Bogdan P. Onac and Virgil Drăguşin

17 Fluid Flow Systems and Hypogene Karst of the Transdanubian Range, Hungary—With Special Emphasis on Buda Thermal Karst 267
Judit Mádl-Szőnyi, Anita Erőss, and Ádám Tóth

18 Caves of the Buda Thermal Karst. 279
Szabolcs Leél-Őssy

19 Hypogene Caves in Slovakia. 299
Pavel Bella and Ľudovít Gaál

20 Hypogene Features in Sandstones: An Example from Carboniferous Basins of Central and Western Bohemia, Czech Republic 313
Václav Suchý, Ivana Sýkorová, Jiří Zachariáš, Jiří Filip, Vladimír Machovič, and Ladislav Lapčák

21 Hypogene Caves in Germany, Geological and Geochemical Background. . . . 329
Stephan Kempe, Ingo Bauer, and Stefan Glaser

22 Hypogene Speleogenesis in the Karst of Poland—Regional Review 349
Michał Gradziński and Andrzej Tyc

23 Gypsum Karst in the Southwest Outskirts of the Eastern European Platform (Western Ukraine): A Type Region of Artesian Transverse Speleogenesis. 363
Alexander Klimchouk and Viacheslav Andreychouk

24 Zoloushka Cave (Ukraine–Moldova)—A Prime Example of Hypogene Artesian Speleogenesis in Gypsum. 387
Viacheslav Andreychouk and Alexander Klimchouk

25 Hypogene Speleogenesis in the Crimean Piedmont, the Crimea Peninsula . . . 407
Alexander Klimchouk, Gennadiy Amelichev, Elizaveta Tymokhina, and Yuri Dublyansky

26 The Role of Hypogene Speleogenesis in the Formation of the Ordinskaya Cave, Fore-Urals, Russia 431
O.I. Kadebskaya and N.G. Maksimovich

Part II The Middle East and Central Asia

27 Geodynamic Control of Hypogene Karst Development in Central Anatolia, Turkey 449
C. Serdar Bayarı, N. Nur Özyurt, A. Koray Törk, Pınar Avcı, İ. Noyan Güner, and Emrah Pekkan

28 The Judean Desert—The Major Hypogene Cave Region of the Southern Levant 463
Amos Frumkin, Boaz Langford, and Roi Porat

29 An Introduction to Hypogene Karst Regions and Caves of Iran 479
Hossein Karimi Vardanjani, Shirin Bahadorinia, and Derek C. Ford

30 Hypogene Karst in the Tyuya-Muyun and the Kara-Tash Massifs (Kyrgyzstan) 495
Yuri Dublyansky, Wasili Michajljow, Katalin Bolner-Takács, Jaroslav Hromas, Kinga Székely, Attila Hevesi, and Sandor Kraus

Part III North America

31 Hypogene Speleogenesis in the Guadalupe Mountains, New Mexico and Texas, USA 511
Harvey R. DuChene, Arthur N. Palmer, Margaret V. Palmer, J. Michael Queen, Victor J. Polyak, David D. Decker, Carol A. Hill, Michael Spilde, Paul A. Burger, Douglas W. Kirkland, and Penelope Boston

32 Hypogene Evaporite Karst of the Greater Delaware Basin 531
Kevin W. Stafford

33 Geology of Quartz-Lined Hypogene Caves of Southeastern Arizona 543
Nicole K. Davis and Brian A. McMillan

34 A Conceptual Model for Hypogene Speleogenesis in Grand Canyon, Arizona 555
Victor J. Polyak, Carol A. Hill, Yemane Asmerom, and David D. Decker

35 Condensation Corrosion Speleogenesis in the Amargosa Desert and the Tecopa Basin 565
Yuri Dublyansky, John Klenke, and Christoph Spötl

36 Structural Settings and Hypogenic Flow Paths for Three Colorado Caves 575
R. Mark Maslyn, Harvey R. DuChene, and Frederick G. Luiszer

37 Sulfuric Acid Caves of the Bighorn Basin, Wyoming 591
Margaret V. Palmer, Arthur N. Palmer, and Donald G. Davis

38 Hypogenic Versus Epigenic Aspects of the Black Hills Caves, South Dakota 601
Arthur N. Palmer

39 Hypogene Karst Collapse of the Devonian Prairie Evaporite Basin in Western Canada 617
Paul L. Broughton

40 Orogeny and Hydrothermal Karst: Stratabound Pb–Zn Sulphide Deposition at Pine Point, Northern Canada 633
Paul L. Broughton

41 Hypogene Processes in the Balcones Fault Zone Segment of the Edwards Aquifer of South-Central Texas 647
Geary M. Schindel and Marcus Gary

42 Hypogenic Caves and Paleokarst of the Arbuckle Mountains, Oklahoma . . . 653
Kevin William Blackwood

43 Hypogene Speleogenesis in the Southern Ozark Uplands, Mid-Continental United States 663
Rodney Tennyson, Van Brahana, Victor J. Polyak, Adriana Potra, Matt Covington, Yemane Asmerom, Jim Terry, Erik Pollock, and David D. Decker

44 Sulfides in the Mammoth Cave Area, Kentucky 677
Rickard A. Olson

45 Sulfur-Based Speleogenesis in the Cumberland Plateau, USA 683
Lee J. Florea

46 Hypogene Caves of the Central Appalachian Shenandoah Valley in Virginia 691
Daniel H. Doctor and Wil Orndorff

47 Hypogene Karst Springs Along the Northeastern Border of the Appalachian Plateau, New York State 709
Arthur N. Palmer, Penny M. Taylor, and Levia A. Terrell

48 Carbonate-Hosted Massive Sulfide Deposits and Hypogene Speleogenesis: A Case Study from Nanisivik Zinc/Lead Mine Baffin Island, Canada 721
Derek C. Ford

49 Hypogene Speleogenesis on the Florida Platform 735
Sam B. Upchurch

50 Hypogene Karst Influences in the Upper Floridan Aquifer 745
Jason D. Gulley and Jason S. Polk

51 Bahamian Flank Margin Caves as Hypogene Caves 757
John Mylroie and Joan Mylroie

52 Sistema Zacatón: Volcanically Controlled Hypogenic Karst, Tamaulipas, Mexico 769
Marcus Gary

53 The Naica Caves, Chihuahua, Mexico 783
Paolo Forti

54 Sulfur-Rich Caves of Southern Tabasco, Mexico 803
Louise D. Hose and Laura Rosales-Lagarde

Part IV South America, Africa, and Australia

55 Hypogene Caves and Karst of South America 817
Augusto S. Auler

56 Origin and Evolution of Toca da Boa Vista and Toca da Barriguda Cave System in North-eastern Brazil 827
Augusto S. Auler, Alexander Klimchouk, Francisco Hilário R. Bezerra, Caroline L. Cazarin, Renata Ennes-Silva, and Fabrizio Balsamo

57 Hypogene Speleogenesis in the Vazante Group, Minas Gerais, Brazil 841
Augusto S. Auler and Tatiana A.R. Souza

58 Hypogene Caves in North Africa (Morocco, Algeria, Tunisia, Libya, and Egypt) 853
Philippe Audra

59 Hypogene Karst in Southern Africa 865
J. Martini

60 A Review of the Geomorphological Context and Stratigraphy of the Sterkfontein Caves, South Africa 879
Dominic Stratford

61 Hypogene Caves of the Tasmanic Karsts of Eastern Mainland Australia 893
R.A.L. Osborne

Contributors

Gennadiy Amelichev Crimean Federal University, Simferopol, Russia; Ukrainian Institute of Speleology and Karstology, Simferopol, Ukraine

Viacheslav Andreychouk Pope John Paul II State School of Higher Education, Biala Podlaska, Poland

Yemane Asmerom Department of Earth and Planetary Sciences, University of New Mexico, Albuquerque, NM, USA

Philippe Audra University of Nice Sophia Antipolis, Sophia Antipolis Cedex, France

Augusto S. Auler Instituto do Carste, Belo Horizonte, MG, Brazil

Pınar Avcı Department of Geological Engineering, Hydrogeological Engineering Section, Hacettepe University, Ankara, Turkey

Shirin Bahadorinia Karst Research Institute ZRC SAZU, Postojna, Slovenia

Fabrizio Balsamo NEXT—Natural and Experimental Tectonic Research Group, Department of Physics and Earth Sciences, University of Parma, Parma, Italy

Cinzia Banzato Department of Environment, Land and Infrastructure Engineering, Politecnico di Torino, Turin, Italy

Ingo Bauer Institut für Angewandte Geowissenschaften, TU-Darmstadt, Darmstadt, Germany

C. Serdar Bayarı Department of Geological Engineering, Hacettepe University, Ankara, Turkey

Pavel Bella State Nature Conservancy of the Slovak Republic, Slovak Caves Administration, Liptovský Mikuláš, Slovakia; Pedagogical Faculty, Department of Geography, Catholic University in Ružomberok, Ružomberok, Slovakia

Francisco Hilário R. Bezerra Geodynamics and Geophysics, Federal University of Rio Grande do Norte, Natal, Brazil

Jean-Yves Bigot Association Française de Karstologie (AFK), Montpellier, France

Kevin William Blackwood East Central University, Ada, OK, USA

Katalin Bolner-Takács Hungarian Speleological Society, Budapest, Hungary

Penelope Boston NASA Astrobiology Institute, Ames Research Ctr., Moffett Field, Mountain View, CA, USA

Van Brahana Department of Earth and Planetary Sciences, University of Arkansas, Fayetteville, AR, USA

Paul L. Broughton Calgary, AB, Canada

Paul A. Burger National Park Service, Anchorage, AK, USA

José María Calaforra Department of Biology and Geology, University of Almeria, Almería, Spain

Caroline L. Cazarin Centro de Pesquisa e Desenvolvimento Leopoldo Américo Miguez de Mello (Cenpes), Petrobras, Rio de Janeiro, Brazil

Matt Covington University of Arkansas, Fayetteville, AR, USA

Ilenia M. D'Angeli Italian Institute of Speleology, Department of Biological, Geological and Environmental Sciences, University of Bologna, Bologna, Italy

Donald G. Davis Denver, CO, USA

Nicole K. Davis Tucson, AZ, USA

Jo De Waele Italian Institute of Speleology, Department of Biological, Geological and Environmental Sciences, University of Bologna, Bologna, Italy

David D. Decker Department of Earth and Planetary Sciences, University of New Mexico, Albuquerque, NM, USA

Daniel H. Doctor U.S. Geological Survey, Reston, VA, USA

Virgil Drăgușin Emil Racoviță Institute of Speleology, Romanian Academy, Bucharest, Romania

Yuri Dublyansky Institute of Geology, University of Innsbruck, Innsbruck, Austria; Ukrainian Institute of Speleology and Karstology, Simferopol, Ukraine

Harvey R. DuChene Lake City, CO, USA

Renata Ennes-Silva Geodynamics and Geophysics, Federal University of Rio Grande do Norte, Natal, Brazil

Anita Erőss Department of Physical and Applied Geology, Eötvös Loránd University, Budapest, Hungary

Andrew R. Farrant British Geological Survey, Keyworth, Nottingham, UK

Jiří Filip Institute of Geology of the CAS v. v. i., Academy of Sciences of the Czech Republic, Prague, Czech Republic

Adriano Fiorucci Department of Environment, Land and Infrastructure Engineering, Politecnico di Torino, Turin, Italy

Lee J. Florea Indiana Geological Survey, Indiana University, Bloomington, IN, USA

Derek C. Ford Geography and Earth Sciences, McMaster University, Hamilton, ON, Canada

Joan J. Fornós Grup de Ciències de la Terra (Geologia i Paleontologia "Guillem Colom"), Universitat de les Illes Balears, Palma de Mallorca, Spain

Paolo Forti Italian Institute of Speleology, Department of Biological, Geological and Environmental Sciences, University of Bologna, Bologna, Italy

Amos Frumkin Cave Research Center, Institute of Earth Sciences, The Hebrew University of Jerusalem, Jerusalem, Israel

Ľudovít Gaál State Nature Conservancy of the Slovak Republic, Slovak Caves Administration, Liptovský Mikuláš, Slovakia

Sandro Galdenzi Jesi, Italy

Ermanno Galli Dipartimento di Scienze della Terra, University of Modena and Reggio Emilia, Modena, Italy

Marcus Gary Edwards Aquifer Authority, San Antonio, TX, USA

Fernando Gázquez Godwin Laboratory for Palaeoclimate Research, Department of Earth Sciences, University of Cambridge, Cambridge, UK; School of Earth and Environmental Sciences, University of St. Andrews, Fife, Scotland, UK

Angel Ginés Grup de Ciències de la Terra (Geologia i Paleontologia "Guillem Colom"), Universitat de les Illes Balears, Palma de Mallorca, Spain

Joaquín Ginés Grup de Ciències de la Terra (Geologia i Paleontologia "Guillem Colom"), Universitat de les Illes Balears, Palma de Mallorca, Spain

Stefan Glaser Krailling, Germany

Francesc Gràcia Grup de Ciències de la Terra (Geologia i Paleontologia "Guillem Colom"), Universitat de les Illes Balears, Palma de Mallorca, Spain

Michał Gradziński Institute of Geological Sciences, Jagiellonian University, Kraków, Poland

Jason D. Gulley School of Geosciences, University of South Florida, Tampa, FL, USA

İ. Noyan Güner Hydrogeological Research Unit, General Directorate of Mineral Research and Exploration, Ankara, Turkey

Tony Harrison Ivy Dene, Burtersett, Hawes, North Yorkshire, UK

Attila Hevesi Institute of Geography and Geoinformatics, University of Miskolc, Miskolc-Egyetemváros, Hungary

Carol A. Hill Department of Earth and Planetary Sciences, University of New Mexico, Albuquerque, NM, USA

Louise D. Hose Department of Geological Sciences and Engineering, University of Nevada, Reno, NV, USA

Jaroslav Hromas Cave Administration of the Czech Republic, Průhonice, Czech Republic

Daniel S. Jones BioTechnology Institute & Department of Earth Sciences, University of Minnesota, Minneapolis, MN, USA

O.I. Kadebskaya Mining Institute of the Ural Branch of the RAS, Perm, Russia

Stephan Kempe Institut für Angewandte Geowissenschaften, TU-Darmstadt, Darmstadt, Germany

Douglas W. Kirkland Carrollton, TX, USA

John Klenke Nye County Nuclear Waste Repository Project Office, Pahrump, NV, USA

Alexander Klimchouk Institute of Geological Sciences, National Academy of Sciences of Ukraine, Kiev, Ukraine; Ukrainian Institute of Speleology and Karstology, Simferopol, Ukraine

Sandor Kraus Hungarian Speleological Society, Budapest, Hungary

Boaz Langford Cave Research Center, Institute of Earth Sciences, The Hebrew University of Jerusalem, Jerusalem, Israel

Ladislav Lapčák University of Chemistry and Technology Prague, Prague 6, Czech Republic

Georgios Lazaridis Laboratory of Geology and Palaeontology, Department of Geology, Aristotle University of Thessaloniki, Thessaloniki, Greece

Szabolcs Leél-Őssy Department of Physical and Applied Geology, Eötvös Loránd University, Budapest, Hungary

José L. Llamusí Centre for Natural and Marine Environmental Studies, CENM-Naturaleza, Cartagena, Murcia, Spain

Frederick G. Luiszer Department of Geological Sciences, University of Colorado, Boulder, CO, USA

Vladimír Machovič University of Chemistry and Technology Prague, Prague 6, Czech Republic

Judit Mádl-Szőnyi Department of Physical and Applied Geology, Eötvös Loránd University, Budapest, Hungary

Giuliana Madonia Dipartimento di Scienze della Terra e del Mare, University of Palermo, Palermo, Italy

N.G. Maksimovich Institute of Natural Science of Perm State University, Perm, Russia

J. Martini Rue du Perbet, Saint Remèze, France

R. Mark Maslyn Littleton, CO, USA

Brian A. McMillan Tucson, AZ, USA

Marco Menichetti Department of Pure and Applied Sciences, University of Urbino, Urbino, Italy

Antoni Merino Grup de Ciències de la Terra (Geologia i Paleontologia "Guillem Colom"), Universitat de les Illes Balears, Palma de Mallorca, Spain

J. Michael Queen Carlsbad, NM, USA

Wasili Michajljow Foundation for Preservation and Studies of Caves, Bishkek, Kyrgyzstan

Joan Mylroie Department of Geosciences, Mississippi State University, Mississippi State, MS, USA

John Mylroie Department of Geosciences, Mississippi State University, Mississippi State, MS, USA

Angelo Naseddu Speleo Club Domusnovas, Domusnovas, Italy

Jean-Claude Nobécourt CRESPE, Vence, France

Rickard A. Olson Cave City, KY, USA

Bogdan P. Onac Karst Research Group, School of Geosciences, University of South Florida, Tampa, USA; Emil Racoviță Institute of Speleology, Romanian Academy, Cluj-Napoca, Romania

Wil Orndorff Virginia Natural Heritage Program, Christiansburg, VA, USA

R.A.L. Osborne Sydney School of Education and Social Work, The University of Sydney, Sydney, NSW, Australia

N. Nur Özyurt Department of Geological Engineering, Hydrogeological Engineering Section, Hacettepe University, Ankara, Turkey

Arthur N. Palmer Department of Earth and Atmospheric Sciences, State University of New York, Oneonta, NY, USA

Margaret V. Palmer Department of Earth and Atmospheric Sciences, State University of New York, Oneonta, NY, USA

Mario Parise Department of Earth and Geo-Environmental Sciences, University of Bari Aldo Moro, Bari, Italy

Emrah Pekkan Research Institute of Satellite and Space Sciences, Anadolu University, Eskisehir, Turkey

Lukas Plan Karst- und Höhlen-Arbeitsgruppe, Naturhistorisches Museum Wien, Vienna, Austria

Jason S. Polk Department of Geography and Geology, Western Kentucky University, Bowling Green, KY, USA

Erik Pollock Stable Isotope Lab, University of Arkansas, Fayetteville, AR, USA

Victor J. Polyak Department of Earth and Planetary Sciences, University of New Mexico, Albuquerque, NM, USA

Roi Porat Cave Research Center, Institute of Earth Sciences, The Hebrew University of Jerusalem, Jerusalem, Israel

Adriana Potra University of Arkansas, Fayetteville, AR, USA

Tomás Rodríguez-Estrella Department of Mining Engineering, Geology and Mapping, University of Cartagena, Cartagena, Spain

Andrés Ros Centre for Natural and Marine Environmental Studies, CENM-Naturaleza, Cartagena, Murcia, Spain

Laura Rosales-Lagarde Department of Physical and Life Sciences, Nevada State College, Henderson, NV, USA

Juan Sánchez Centre for Natural and Marine Environmental Studies, CENM-Naturaleza, Cartagena, Murcia, Spain

Geary M. Schindel Edwards Aquifer Authority, San Antonio, TX, USA

Tatiana A.R. Souza Instituto do Carste, Belo Horizonte, MG, Brazil

Michael Spilde Department of Earth and Planetary Sciences, University of New Mexico, Albuquerque, NM, USA

Christoph Spötl Institute of Geology, University of Innsbruck, Innsbruck, Austria

Kevin W. Stafford Department of Geology, Stephen F. Austin State University, Nacogdoches, TX, USA

Dominic Stratford Department of Archaeology, School of Geography, Archaeology and Environmental Studies, University of the Witwatersrand, Johannesburg, South Africa

Václav Suchý Praha 6, Czech Republic

Ivana Sýkorová Institute of Rock Structure and Mechanics v. v. i., Academy of Sciences of the Czech Republic, Prague 8, Czech Republic

Kinga Székely Institute for Nature Conservation, Budapest, Hungary

Penny M. Taylor Department of Geology, Mt. Holyoke College, South Hadley, MA, USA

Marjan Temovski Hertelendi Laboratory of Environmental Studies, Institute for Nuclear Research, Hungarian Academy of Sciences, Debrecen, Hungary

Rodney Tennyson Alpena, AR, USA

Levia A. Terrell Arcadis Engineering, East Syracuse, NY, USA

Jim Terry Toronto, AR, Canada

A. Koray Törk Cave and Karst Research Unit, General Directorate of Mineral Research and Exploration, Ankara, Turkey

Ádám Tóth Department of Physical and Applied Geology, Eötvös Loránd University, Budapest, Hungary

Andrzej Tyc Department of Geomorphology, University of Silesia, Sosnowiec, Poland

Elizaveta Tymokhina Crimean Federal University, Simferopol, Russia; Ukrainian Institute of Speleology and Karstology, Simferopol, Ukraine

Sam B. Upchurch SDII Global Corporation, Tampa, FL, USA

Hossein Karimi Vardanjani AbAtiPazhouh Consulting Engineers, Ahwaz, Iran

Marco Vattano Department of Earth and Marine Sciences, University of Palermo, Palermo, Italy

Bartolomeo Vigna Department of Environment, Land and Infrastructure Engineering, Politecnico di Torino, Turin, Italy

Jiří Zachariáš Faculty of Science, Charles University, Praha 2, Czech Republic

Types and Settings of Hypogene Karst

1

Alexander Klimchouk

Abstract

This chapter discusses the notion of hypogene karst, reviews its diversity and further develops the hydrogeological approach to classifying hypogene karst and its settings. Since an understanding of hypogene karst requires much deeper and broader hydrogeological and geodynamic context as compared to more familiar epigene karst, this chapter provides an overview of basic concepts about fluid dynamics and hydrodynamic zoning of the upper crust and about the influence of the mantle processes on crustal fluids. The relationships of hypogene karstification with metasomatism and other processes of fluid-induced transformations of rocks are examined. It is argued that the phenomena of the so-called ghost-rock karstification (commonly attributed to epigene settings) and cavernous decay (commonly attributed to external weathering) are manifestations of hypogene karstification and related alteration of rocks around conduits. Genetic categorization and discrimination of characteristic settings of hypogene karst are based on consideration of driving forces and conditions for fluid circulation and ascending flow in the upper crust in the context of tectonic/geodynamic positions and history of regions. Development and distribution of hypogene karst of the artesian type in gravitational flow systems of cratons are governed by the basin's configuration, topography and hydrostratigraphy. Hypogene karst of the endogenous type is governed by the geodynamic regimes and intimately related to cross-formational fluid-conducting systems. Hypogene karst is a significant component of fluid-induced lithogenesis and plays an important role in the porosity and permeability development in many sedimentary rocks and some metamorphic rocks.

Keywords

Hypogene karst • Deep hydrogeology • Geofluids • Karst and metasomatism • Hypogene karst types • Hypogene karst settings

1 Introduction

This chapter is aimed to clarify the notions of hypogene karst and speleogenesis, to review their diversity and outline approaches to reasonable classification of hypogene karst and settings of its development. The author believes that the problem of the origin of hypogene karst and of its further genetic subdivision should be approached from the hydrogeological perspective. Understanding of hypogene karst requires much deeper and broader hydrogeological and geodynamic context and commonly in much far-reaching retrospective than studies of more familiar epigene karst. Since hypogene karstification often occurs in greater depths than those commonly tackled in karst research and conventional hydrogeology, this chapter provides an overview of basic concepts about fluid dynamics and hydrodynamic

A. Klimchouk (✉)
Institute of Geological Sciences, National Academy of Sciences of Ukraine, Kiev, Ukraine
e-mail: klim@speleogenesis.info

© Springer International Publishing AG 2017

A. Klimchouk et al. (eds.), *Hypogene Karst Regions and Caves of the World*,
Cave and Karst Systems of the World, DOI 10.1007/978-3-319-53348-3_1

zoning of the upper crust and about the influence of the mantle processes on crustal fluids.

The dissolution-dominated formation of macroscopic void-conduit systems at large depth is intimately related to other processes of fluid-induced transformations of rocks, particularly to metasomatism, which requires examining their relationships. This chapter will also demonstrate a genetic affinity of the phenomena of the so-called ghost-rock karstification and cavernous decay (commonly attributed to external weathering) and argue that both are manifestations of hypogene karstification.

Genetic categorization and distinguishing of characteristic settings of hypogene karst are derived from consideration of driving forces and conditions for fluid circulation and ascending flow in the upper crust in the context of tectonic/geodynamic positions and history of regions.

1.1 Genetic Types of Karst

The karst paradigm was changing during last decades, and the notion of karst has been defined from different perspectives (Klimchouk 2015). Karst was viewed as the totality of macroscopic dissolution phenomena in water-soluble rocks (a tradition traced back from E.-A. Martel), as terrain with distinctive hydrology and landforms (Ford and Williams 1989), as a geological environment (Huntoon 1995) or as a groundwater (fluid) flow system with specific properties (Worthington and Ford 2009; Klimchouk 2015). Some definitions equate karst to the process of dissolution, but reduction of a geological (hydrogeological) process to a chemical one is methodologically inappropriate and misleading. At the same time, karstification can be viewed as a complex process: of water–rock interaction (Zverev 1999), of metasomatic alteration of rocks (Ezhov et al. 1992), of hydrogeological mass transfer/mass transport (Klimchouk 2015), of destruction and obliteration of permeable soluble rocks (Sokolov 1962) or, more broadly, as a geological process (an interconnected set of processes) of transformation of soluble rocks by moving fluids with the dominant role of flow-dissolution feedback and respective self-organization of the groundwater flow system (Klimchouk 2015).

Regardless the approach, it was realized that most of the specific properties attributed to karst owe their origin to the development of organized dissolution porosity/permeability structures in soluble rocks (Ford and Williams 1989; Palmer 1991), i.e., karst is a function of speleogenesis (Klimchouk et al. 2000). Since speleogenesis is the primary mechanism of the formation of karst, genetic types of karst are to be distinguished based on types of speleogenesis (Klimchouk 2013b, 2015). Two fundamental types of speleogenesis, hypogene and epigene, are determined mainly by distinct hydrodynamic characteristics of the parent groundwater flow systems: (1) confined stratiform aquifer systems, or cross-formational fracture-vein systems, of varying depths and degrees of confinement, and (2) hydraulically open (unconfined), near-surface systems. They differentiate due to differences in hydraulic boundary conditions, geochemical and physical conditions of respective speleogenetic domains, hydrodynamic regimes of groundwater (fluid) flow and speleogenesis, and evolutionary trajectories of corresponding karst systems (Klimchouk 2015). Accordingly, two major genetic types of karst are distinguished within the upper part of the Earth's crust: hypogene and epigene. The respective karst systems differ in spatial distribution, the hydrogeological functioning, geomorphic expression, characteristics of void-conduit systems (their patterns, morphology, sediments, mineralogy, inhabitant biota, etc.) and related resources and hazards.

In contrast to epigene karst systems that develop in intimate interaction with the landscape and have both surface and underground components, hypogene karst evolves without direct genetic linkage with the surface, being originally represented exclusively by void-conduit systems at depth. When a hypogenically karstified rock formation is brought to the shallow subsurface by uplift and denudation, hypogene void-conduit systems are commonly relict (i.e., already decoupled from the original cave-forming environment). Although they can be intercepted by the denudation surface and become expressed in the landscape, the resultant geomorphic features are commonly destructive with respect to the hypogene karst system, i.e., they are not the inherent functional components of the latter (e.g., collapse features). In some cases, parts of hypogene karst systems can be overprinted by epigene karst systems, but the degree of their integration into the latter commonly remains limited due to the difference in driving forces, organization and functioning of respective parent flow systems. Since hypogene karst systems are initially comprised only of voids and conduits, the terms "hypogene karst (karstification)" and "hypogene speleogenesis" are frequently used interchangeably.

1.2 Definitions of Hypogene Speleogenesis

There are two different approaches on how to define hypogene speleogenesis. Palmer (2000) defined hypogenic caves as "*those formed by water in which the aggressiveness has been produced at depth beneath the surface, independent of surface or soil CO_2 or other near-surface acid sources.*" This approach, often termed "geochemical," emphasizes the place of the origin of the aggressiveness with respect to the surface. Another approach, known as "hydrogeological," is based on the acknowledgment that in any given geological environment the potential for dissolution and distribution of

its effects, and hence localization, patterns, and morphology of the forming void-conduit systems, is determined largely by the regime, pattern and intensity of fluid flow, i.e., by hydrogeologic factors (Klimchouk 2007, 2015). With this approach, hypogene speleogenesis was defined as *"the formation of solution-enlarged permeability structures (void-conduit systems) by fluids that recharge the cavernous zone from below, driven by hydrostatic pressure or other sources of energy, independent of direct recharge from the overlying or immediately adjacent surface"* (Klimchouk 2007).

The above two approaches are not contradictory, but they determine slightly differing sets of caves and speleogenetic environments to be considered as hypogenic. The hydrogeological approach, though not specifying this directly, tacitly implies that the aggressiveness is produced at a depth below the cave-forming zone, whereas the rising flow is not necessarily implied by the geochemical definition. Based on the geochemical approach, Palmer (2007) places the artesian transverse cave development in evaporites into the realm of epigene speleogenesis, whereas cave development due to mixing at hydrochemical interfaces in unconfined aquifers, such as at the freshwater/saline water interface in coastal settings (Mylroye and Carew 1995), or the vadose/phreatic interface (Dreybrodt et al. 2009), is placed into the hypogenic category. Within the hydrogeological approach, the classifying of speleogenesis in these respective environments is the opposite.

The above-cited "hydrogeological" definition has been recently refined (Klimchouk 2015) by eliminating the non-specific and hence unnecessary requirement for upwelling fluids to be "*driven by hydrostatic pressure or other sources of energy*," and by adding more distinctness with regard to flow pattern and source of fluids. The primary criterion for distinguishing hypogene speleogenesis is that the cave-forming fluid comes from a hydrostratigraphically lower unit, although this unit is not necessarily the source aquifer. Cave development by flow uprising in the discharge segment of a phreatic conduit system (i.e., coming from below, relative to this segment), where flow is confined only by the conduit wall rock but recharge, through-flow and discharge occur within the same largely unconfined aquifer, should not be regarded as hypogene. With these reasons in mind, hypogene speleogenesis is redefined as *the formation of solution-enlarged permeability structures (void-conduit systems) by upwelling fluids that recharge the cavernous zone from hydrostratigraphically lower units, whereas fluids originate from distant, estranged (by low-permeability strata) or deep sources, independent of recharge from the overlying or immediately adjacent surface.*

The hydrogeological approach provides a theoretically and methodologically sound basis not only for defining and identifying hypogene speleogenesis but also for its further categorization and spatial and temporal prognosis in the context of global and regional hydrogeology and geodynamics.

1.3 Diversity of Hypogene Speleogenesis

Case studies included to this book demonstrate that hypogene speleogenesis operates in various geodynamic settings and geological/hydrogeological conditions, at varying depths (ranging from the shallow subsurface to several kilometers), and in rocks of different compositions (all kinds of carbonate rocks, evaporites, conglomerates, sandstones, quartzites, and even in igneous rocks) and ages (from Proterozoic to Pleistocene). Its distribution is not limited to continents—with the advent of new sensing technologies and expansion of offshore petroleum prospecting, evidence grow rapidly that hypogene karstification also occurs in the seafloor, especially in regions of active plate boundaries and hot spots (e.g., Betzler et al. 2011; Chen et al. 2015), although its proper identification is often hindered due to constraints of the traditional paradigm of karst (Michaud et al. 2005). Rising fluid flow migrates across lithologically diverse strata and aquifers, and upwelling is accompanied with changes in pressure and temperature. This causes disequilibrium conditions at different levels and supports diverse mineral reactions, including those resulting in the creation of macro-porosity. Hypogene karstification involves diverse dissolution mechanisms (Klimchouk 2012), operating either in combination or sequentially in time and space. The depth limit for hypogene speleogenesis is difficult to establish, but available data suggest that it operates within at least several kilometers.

In view of the broad variability of processes and conditions of hypogene speleogenesis and resultant void-conduit patterns, further subdivision into genetic types within this broad genetic category is needed, as well as a typification of settings of its development.

2 Hydrogeologic Context of Hypogene Speleogenesis

Whereas epigene karstification is associated mainly with meteoric flow systems in shallow hydraulically open unconfined settings, hypogene karst development commonly occurs at greater depths and is linked with ascending (discharge) components of flow systems of different nature and varying degrees of confinement. Thus, studying hypogene karst requires an understanding of much deeper and broader hydrogeological and geodynamic context, and commonly in much far-reaching retrospective.

The subject of "deep hydrogeology" (i.e., hydrogeology of those parts of basins and the metamorphic/crystalline

basement that are below the uppermost interval routinely investigated for groundwater supply and geological engineering purposes—commonly below several hundred meters) is still controversial and ill-understood. Fundamental modern reviews performed from the essentially hydrogeological perspective are rare (e.g., Djunin 2000; Ague 2003; Djunin and Korzun 2005), although there are excellent reviews of geochemistry of deep aqueous fluids in sedimentary basins (e.g., Kharaka and Hanor 2004) and basement rocks (Frape et al. 2004; Bucher and Stober 2010). Deep fluid systems receive in-depth treatment in studies on the role of groundwater in geologic processes (e.g., Ingebritsen et al. 2006). Important progress has been made during last decades due to the intense quest for deep petroleum reserves and developments in the reservoir analysis (e.g., Kirkinskaya and Smekhov 1981; Cubitt et al. 2004; Shepherd 2009; Chilingar et al. 2005; Agar and Geiger 2014; Cathles and Adams 2005). Much of our understanding of deep basinal and crustal fluids has come from studies in sedimentology (diagenesis, basin's evolution; e.g., Kyser and Hiatt 2003; Galloway and Hobday 1996; Bjørlykke 1993; Warren 2006), petrology (metamorphism and metasomatism; e.g., Fyfe et al. 1978; Shmulovich et al. 1994; Ague 2003; Kissin 2009; Harlov and Austrheim 2013; Yardley 2013) and ore geology (e.g., Cathles and Adams 2005; Ingerbitsen and Appold 2012), particularly from geochemical/thermodynamic modeling and fluid inclusions. These studies, however, are more concerned with pervasive fluid fluxes. Channelized (focused) fluid flow remains much less studied, although researches of ore-forming systems provide some important insights on it (Ingerbitsen and Appold 2012). Evidence of massive fluid flow in the deep portions of the upper crust come from studies of metamorphic and metasomatic processes (e.g., Harlov and Austrheim 2013), particularly of fluid-dominated infilling of secondary porosity (including ore formation) and alteration of the original rock. High time-integrated fluid fluxes are inferred in many thermal aureoles and regional metamorphic belts (Rubenach 2013) and subduction zones (Bebout 2013; Schmidt and Poli 2014). Inhomogeneities in fluid distribution in both the lithospheric mantle and deep to middle crust are recorded by geophysical techniques (Kissin 2009; Unsworth and Rondenay 2013).

2.1 Origin of Aqueous Fluids

Free (i.e., mobile and available to flow) aqueous fluids in the crust are ultimately derived from atmospheric water, seawater, water that is physically and chemically bound in sediments and from devolatilization of the middle-lower crust and the mantle. In hydrogeology, the origin of aqueous fluids is commonly distinguished according to ways by which they penetrate into the lithosphere, or to processes by which they are released or generated within it (Fig. 1).

Meteoric water is the water derived from atmospheric precipitation and infiltrated from the surface. *Connate water* is the water (commonly seawater) trapped in the pores of a rock at the time of their formation. Waters of these two origins dominate in the uppermost portion of the crust.

Metamorphic (thermogenic) fluids originate as the result of devolatilisation reactions in sedimentary or magmatic rocks in course of metamorphism, which occurs around magma chambers or at large depth. *Magmatic (juvenile) fluids* are released during crystallization or solidification of magma within the crust (also called *volcanic fluids*) or originate from the mantle and core degassing (called by some *trans-magmatic fluids*; Pinneker 1983).

Meteoric and connate waters are considered exogenic (meteoric waters have also been termed epigenetic; Crossey et al. 2006), whereas metamorphic and magmatic origins of fluids can be treated as endogenic (e.g., Pinneker 1983; Crossey et al. 2006). Where rising to and across the sedimentary cover, metamorphic and trans-magmatic (mantle input) fluids are inevitably mixed in proportions which are often difficult to determine, so that referring to them as to endogenic fluids is convenient (Crossey et al. 2006). The term "basinal waters (fluids)" is often used for deep fluids that have originated in a basin, i.e., expelled connate water and metamorphic water.

Aqueous fluids in varying physical states constantly circulate in the crust, either directly or via the processes of the geologic cycle (Fig. 1), and may retain in the subsurface continuously during several successive hydrogeological cycles (i.e., periods starting with subsidence and marine sedimentation, continuing through uplift, denudation and exposure and closing with the new marine transgression; Kartsev et al. 1969). This leads to ubiquitous mixing of fluids of different origins. Meteoric waters can be found in the relatively pure (unmixed) form in uppermost parts of the crust, well flushed by the meteoric regime (particularly in recharge segments of groundwater flow systems), and connate waters may overwhelmingly dominate in young subsiding basins. Upon their generation, metamorphic fluids immediately mix with preexisting pore fluids, as well as with magmatic fluids, if any. Endogenic fluids (metamorphic and magmatic) mix with formation waters during upflow across sedimentary successions. The term "formation waters (fluids)" is commonly used to underscore genetic uncertainty of waters in deep parts of basins, especially mature ones, which are almost universally of mixed origins (Kharaka and Hanor 2004).

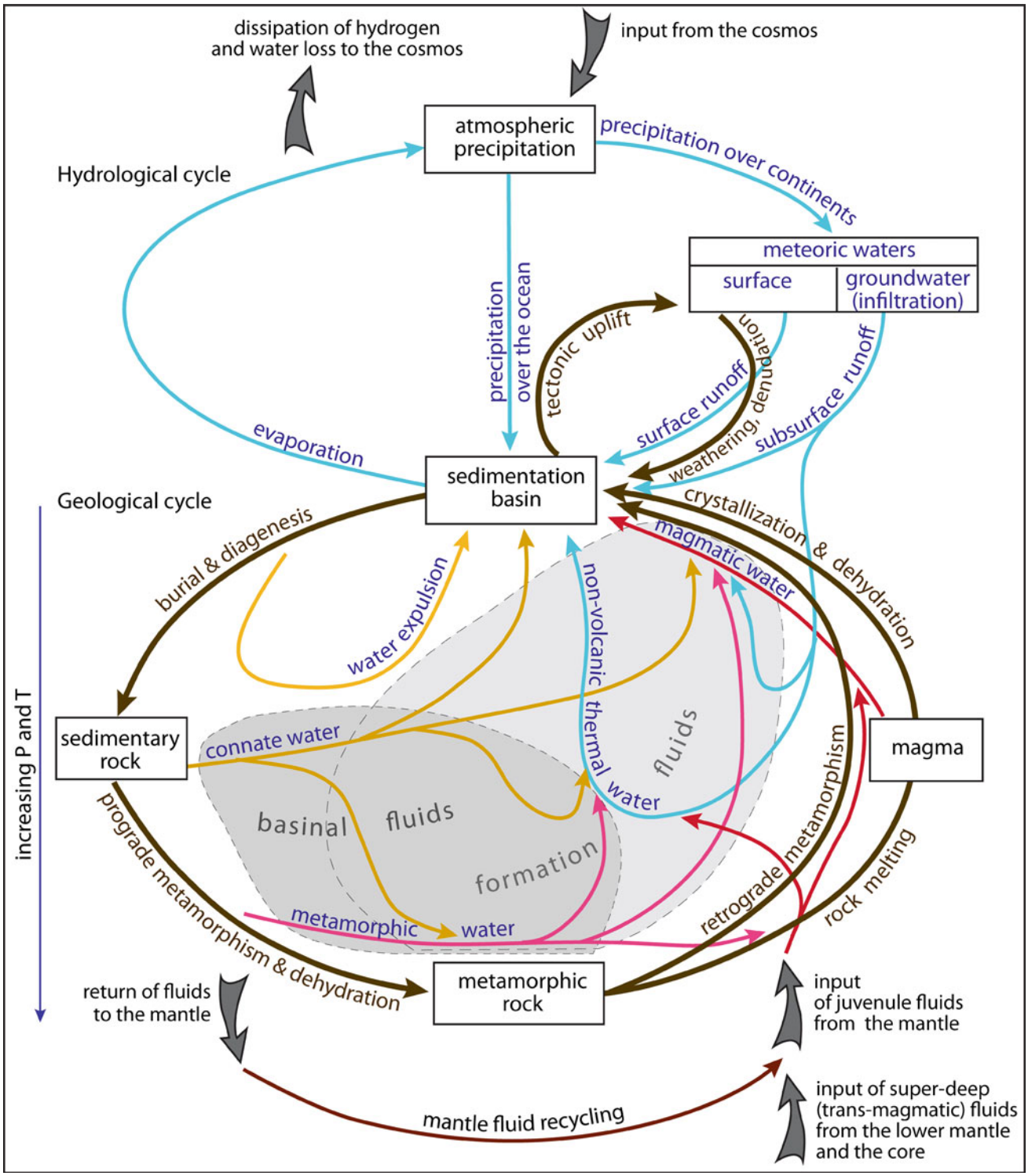

Fig. 1 Relations between the hydrologic and geological water cycles and genetic paths of fluids in the crust. *Thicker dark brown arrows* denote the petrological cycle. *Thinner arrows* of various colors denote genetic and mixing paths of fluids in the crust. The overall configuration of the cycles and their compartments follow Pinneker (1980), but the nomenclature and relationships of fluids are severely modified

2.2 Flow Regimes

Different fluid flow regimes occur in the upper crust, determined by variations in the nature and magnitude of pressure and the degree of hydrodynamic confinement (Kissin 1985; Bjørlykke 1993; Galloway and Hobday 1996; Shvartzev 1996; Deming 2001; Hiscock and Bense 2014). Importantly, the notion of a flow regime (the source and realization of fluid motion) should not be confused with the origin of the fluid itself.

2.2.1 Compactional Regime

In young subsiding basins, the dominant flow drive in progressively buried strata is the pressure head generated by compaction due to increasing lithostatic loading, which requires an expulsion of pore fluids (connate and meteoric) from the sediments. The compactional regime is also termed expulsion, elision and exfiltration regime. Flow is directed generally upward and outward, on the regional scale—from areas of greatest subsidence to basin margins. Varying susceptibility of sediments to compaction and pressure solution, as well as to chemical water–rock interactions, leads to increasing heterogeneity in porosity and permeability. Where low-permeability confining formations are present above compacting sediments, significant overpressure can develop. When tectonism is imposed, the compactional regime can be also generated by tectonic compression in the vicinity of collision and uplift areas. Compaction-driven fluid flow is complex because it is inseparable from rock deformation and because the hydraulic properties that limit fluid flow through the rock matrix, such as permeability and porosity, are dynamic (Connolly and Podladchikov 2013).

The compactional regime in mature sedimentary basins is unlikely to drive considerable fluid fluxes due to its transitional nature (Deming 1994; Djunin 2000; Djunin and Korzun 2005) and the loss of most of the connate water during earlier stages of the basin development. It is considered of limited importance for hypogene speleogenesis (Klimchouk 2013b). However, it can be important during the early stages of burial (during eogenesis and the transition to meso-genesis, during and immediately after progressive burial), especially in sequences containing alternating sediments with contrasting susceptibility to compaction, from which water is expelled at drastically different rates. It can be particularly important in creating cross-formational permeability structures in upper, still poorly indurated successions due to the focused expulsion of overpressured fluids from the underlying strata. The fluid-focusing role of such early structures can be retained or renewed during the later stages of diagenesis. The abundance of such structures, well expressed as seafloor pockmarks and expulsion chimneys beneath them, is shown by numerous studies during the last decades (e.g., Hovland et al. 2002; Hovland 2003; Cartwright and Santamarina 2015).

2.2.2 Thermobaric Regime

With still deeper burial and further rise of temperature and lithostatic loading, the thermobaric regime develops, in which the fluid pressures are caused mainly by the thermal expansion of water and/or by the release of water by mineral dehydration in a low-permeability environment. This regime underlies the compactional regime and commonly mingles with it. Thermobaric flow is commonly highly overpressured and directed generally upward. The thermobaric regime can be initiated by the deep endogenous regime, with which it mingles at greater depth.

2.2.3 Deep Endogenous Regime

Aqueous fluids originating from metamorphism and devolatilization in the lower crust, as well as magmatic/juvenile fluids released from the mantle and the core (superdeep fluids; Letnikov 1992, 2001; Lukin 2014, 2015), can intrude up into the upper crust and sedimentary cover, introducing anomalously high energy. These intrusions contribute to the thermobaric regime in the deepest portions of sedimentary basins and cause strong anomalies in parameters of thermal, baric, hydrochemical, geochemical and permeability fields.

Upwelling of endogenous fluids through the upper crust is a manifestation of the global Earth degassing process. Letnikov (1992) emphasized the distinction between two branches of the Earth degassing:

1. Monotonously diminishing in time, whole-planet degassing of the upper part of the lithosphere, resulted in its depletion in fluids, and in lowering of the fluid front to depth. The energy potential of the deep lithospheric fluid systems declined since the Archean through the Cenozoic. The character of the distribution of these systems changed in time from continuous in the Archean, through clustered in the Proterozoic and linear in the Phanerozoic, to discrete in the Cenozoic.
2. On the background of the general lithospheric degassing—a pulsed degassing of the Earth liquid core via mantle plumes. The plume-related degassing occurs periodically and impacts certain areas varying in size, during varying periods of time.

Deep-rooted mantle plumes (superplumes) have been the subjects of numerous studies (e.g., Larson 1991; Letnikov, 1992; Condie 2001; Ernst and Buchan 2001; Maruyama et al. 2007; Yuen et al. 2007) and vigorous debates. Recent work of French and Romanowicz (2015) provided robust evidence, based on an advanced seismic tomography

technique and a global whole-mantle shear-wave velocity model, for large, vertically continuous, low-velocity columns in the lower mantle beneath many prominent hot spots. The imaged trans-mantle conduits, rooted at the mantle-core boundary, are broader (typically 600–800 km) than commonly invoked thermal plume tails, which suggests that they are long-lived and have a thermochemical origin (French and Romanowicz 2015).

Superplumes are thought to be composed mainly of reduced gasses, primarily by hydrogen, and they possess tremendous energy potential when departing from the mantle-core boundary (pressure >1300 kbar, temperature >4000 °C, hydrogen enthalpy 1200–1000 kJ g^{-1}; Letnikov and Dorogokupets 2001). In the course of upwelling through the mantle, their thermal energy is renewed by exothermic reactions of hydrogen and reduced gasses with oxygen-bearing mantle minerals, so that superplumes are capable of reaching the crust without major loss of thermal energy (Letnikov 1992). Additionally, superplumes may assimilate water from the top lower mantle, where its large reserves are now inferred from petrologic modeling, laboratory experiments and seismic data processing (Murakami et al. 2002; Schmandt et al. 2014). When reaching the core, superplumes give rise to its tectonic activation, magmatism, metamorphism and the origin of various fluid systems, among other geologic consequences (Larson 1991; Condie 2001). The area of invasion of superplumes into the lithosphere can be as large as of many thousands of km^2. The evolution of superplumes is accompanied by their structural differentiation into derivative plumes varying in sizes, thermobaric regimes, geodynamic and fluid-dynamic activity, that determines variations in their lithogeodynamic impact on particular basins (Lukin 2014, 2015). Breaking through the brittle/ductile transition zone, plume-derived fluid systems determine the deep endogenous regime in the upper crust, with fluids propagating to and across the sedimentary cover via magmatic columns or deep-rooted faults. Invasion of deep endogenous fluids gives rise to various transformations of sedimentary rocks, including diffuse and infiltration (focused) metasomatism (Korzhinskiy 1957; Zharikov et al. 2007), and fracture and dissolutional porosity creation and infilling (Ezhov et al. 1992; Klimchouk 2012).

Kropotkin (1986) introduced a useful notion of "degassing tubes" (chimneys)—sub-vertical contours across the sedimentary succession that embrace manifestations of deeply derived gasses, zones of abnormally high pressures and geochemical and thermal anomalies related to invasion of deep gas–vapor fluids (including hydrocarbons) and their vertical migration. Lukin (2015) expanded the concept of degassing tubes to include multifarious alterations of rocks due to endogenous metasomatism induced by rising fluids of the deep origin. Kropotkin (1986) distinguished two branches of degassing: *"hot degassing,"* where fluids migrate through the crust along with magma, or across high-temperature zones in the vicinity of intrusions, and "*cold degassing*," where rising reduced fluids do not encounter magmatic bodies and other strongly heated rock masses.

The deep endogenous regime has great potential to support endogenous hypogene speleogenesis in various rocks, including siliciclastic, in deep parts of basins affected by endogenic fluids.

2.2.4 Meteoric Regime

The meteoric regime (syn. gravitational, infiltration, topography-driven regime) evolves with the beginning of a continental exposure and occupies the uppermost parts of the crust. Infiltrated meteoric waters, driven by gravitational head imposed by differences in the topography of the water table (and ultimately of the land surface), increasingly flush out the formation waters from basins. The meteoric groundwater circulation can penetrate to depths of over 3 km affecting deeply buried strata in geologically and topographically favorable conditions, especially in tilted and faulted basins adjacent to mountainous areas, and in intermountain basins. Localized freshwater discharges at depths of several hundred meters below the sea level are documented in many coastal regions, and meteoric groundwater flow was found by ocean drilling far offshore. During prolonged exposure periods, the meteoric regime progressively substitutes the compactional regime in the uppermost crust, although the compactional and other endogenous regimes may still predominate in deep environments. Patterns and dynamics of groundwater flow driven by this regime are discussed in the context of the upper hydrogeologic story in Sect. 2.4.1.

2.2.5 Other Flow Drives

Other significant drivers for flow in the deep parts of basins include convection induced by thermal or salinity gradients (variable density flow) and seismic pumping driven by dilation and contraction in seismically active areas. The convection regime is favored where pronounced density inversion with depth (due to heating and sometimes decreasing salinity) is combined with high vertical permeability across large thicknesses (permeable relatively homogenous successions, steeply dipping aquifers, or extensively faulted or fractured sections), allowing large-scale vertical fluid movement due to density differences (Galloway and Hobday 1996). Convection circulation can be pronounced in the vicinity of magmatic intrusions, in thick sequences containing evaporites, and in coastal regions. The potential of density-driven convection within the compactional or thermobaric regimes is controversial (Bjorlykke et al. 1988; Hanor 1987; Phillips 1991). Seismic pumping is defined as fluid flow driven by repeated episodes

of dilation and contraction in seismically active areas, particularly near and within faults zones (Sibson et al. 1975). Fluids are driven toward newly opened fractures and dilated pore space.

2.2.6 The Nature, Evolution and Interaction of the Regimes

Since waters involved in the meteoric regime are mainly of the meteoric origin, and since the meteoric regime is intimately controlled by the surface topography and other external factors such as climate, it can be considered as exogenous. Other forced flow regimes are characterized by abnormally high pressures and generally upward flow. Since the drives for flow in these regimes are created by internal processes, these regimes can be termed endogenous.

The fluid flow regimes are transitional in geological timescales, and their domains, boundaries and relative importance, as well as properties of fluids, change during basinal and post-basinal evolution. Changing relationships between the regimes reflects stages (geostatic, transitional, hydrostatic and endogenous; Pinneker 1977) in the hydrogeologic evolution of basins. The compactional regime dominates young actively subsiding basins, and still deeper burial leads to the increasing development of the thermobaric regime in the deepest portions (the geostatic stage). Respectively, the fluid flux under these regimes attains the maximum. With the termination of subsidence and progression of uplift and continental exposure, these regimes dissipate and respective fluxes cease, being increasingly displaced by the expanding meteoric regime (the transitional stage). Invasion of meteoric waters starts from the basin's margins, but with the growth of the topographic relief, the meteoric regime embraces the upper story in the internal regions. It further expands in depth and becomes dominating in mature basins (the hydrostatic stage). In collision belts, the compactional regime can be reactivated and affect adjacent basins due to the loading imposed by thrust sheet stacking. The thermobaric regime can be maintained at depth, and the deep endogenous regime can expand upward in geodynamically active areas, where mantle plumes and asthenosphere upwellings contribute to abnormal P-T conditions and fluid flow. The expansion of the endogenous regime (the endogenous stage) may occur at any stage of the basin evolution.

Since mixing of fluids contrasting in physicochemical properties often results in bursts of the aggressiveness, zones of interaction between different regimes are potentially favorable for hypogene speleogenesis. Hypogene speleogenesis is commonly a part of mixed flow systems, where rising flows of the endogenous regimes interact with the meteoric waters. The geometry of interaction zones is controlled by respective fluid potentials and geological heterogeneities and is time-dependent. The boundaries can be blurred, but they are often more distinct where they coincide with low-permeability strata of a regional extent. Importantly, the domain of the meteoric flow, perched on ubiquitously ascending fluids of the endogenous regimes, is often pierced by rising cross-formational injections and plumes of deep fluids driven by the endogenous regimes, guided by major sub-vertical tectonic disruptions (Klimchouk 2012). Thermobaric and geochemical anomalies induced by such intrusions are often traced vertically across several aquifers in stratified shallower aquifer/aquitard systems.

2.3 Endogenic Fluids in the Deep Crustal Settings and Their Connection to the Upper Crust

Fluids in the middle/deep crust originate from in situ chemical reactions driven by the heating of rock masses (see Sects. 2.1 and 2.2.3) and come from degassing of the asthenosphere and the core. Fluid flux from crustal devolatilization is a major contributor to planetary volatile cycling and principal geologic processes (Ague 2003).

Within the huge range of P–T conditions in the middle/deep crust and mantle, aqueous fluids are highly variable in composition (generally represented by H_2O, different nonpolar gasses like CO_2 and CH_4, and different dissolved metal halides like NaCl or $CaCl_2$) and exhibit specific physicochemical properties (Liebscher 2010). The cited work is an excellent recent review of phase relations in one- and multi-component fluid systems at high pressure and temperature. The supercritical fluids, combining comparably low viscosity with high solute contents, are very effective metasomatising agents (Liebscher 2010; Yardley 2013). Although solubilities of many rock-forming minerals in brines vary in a complex manner with changes in P-T conditions, pH and fluid composition, they are commonly much higher in the middle/deep crustal settings than at ambient conditions (Newton and Manning 2002, 2005; Caciagli and Manning 2003; Dolejs and Manning 2010), suggesting a possibility of enhanced dissolution of various rocks. Evaluation of dissolution potential and processes (including metasomatic ones) in high P-T conditions from the perspective of karstification is still an open research area. When a multi-component endogenous gas–vapor fluid rises through permeable zones, down along the pressure and temperature gradients, complex processes of phase transformations and geochemical evolution occur, with the formation at different levels of alkaline solutions and strong acids, such as HCL and H_2SO_4 (Malyshev 2011), which causes the vertical zoning of specific environments aggressive to different lithologies (Klimchouk 2013b).

The origin and behavior of fluids in the deep crustal settings are a matter of much controversy. Metamorphic

fluid fluxes are likely controlled by dewatering rates of metamorphic piles undergoing devolatilization (Yardley and Bodnar 2014). Estimates of fluxes of metamorphic fluids by different methods for different regions vary in six orders of magnitude (Ague 2003). The highest fluxes are inferred to occur in subduction zones where dehydration of subducting oceanic lithosphere occurs (Breeding and Ague 2002; Schmidt and Poli 2014) and in the continental collision and mid-crustal shear zones. Aque (2003) estimated that regional devolatilization fluxes for zones of continental collision with the dominant pervasive flow are less than $\approx 10^4$ m^2 m^{-2}, averaging around 500 m^3 m^{-2}, but focusing of flow by structural features such as ductile shear zones may provide fluxes in excess of 10^5 m^3 m^{-2}. The total flux from the deep crust in active mountainous belts is estimated to be in excess of $\approx 10^{17}$ kg Myr^{-1} (Ague 2003). Fluxes of volcanic fluids can be high around and above magma bodies crystallizing in the crust (Oppenheimer et al. 2014), especially those intruded into shallow crustal settings (Yardley and Bodnar 2014). The input of external H_2O-bearing fluids, such as those derived from dilatancy pumping (Sibson et al. 1975), dehydrating schists (Aque 2003; Schmidt and Poli 2014) or mantle and core sources (see Sect. 2.2.3), can contribute significantly to the total flux.

Highly overpressured fluids inevitably escape upward to the upper crust where they invade hydrothermal systems and mix with formation fluids. The "single pass" flow model is widely accepted for fluid dynamics in the middle/lower crust (Fig. 2; Ague 2003; Yardley and Bodnar 2014). Single pass fluid flow can be pervasive or channelized into fractures and faults or along more permeable layers. A possibility of the "multi-pass flow" recirculating by convection is commonly questioned due to generally low-permeability environment and problematic passing of the brittle/ductile transition (BDT), although studies in some active mountain belts (e.g., in Pakistan and New Zealand) suggest that shallow fluids can penetrate close to this boundary (Templeton et al. 1998; Poage et al. 2000). In the upper crust, multi-pass systems driven by convection are common in the vicinity of thermal anomalies (geothermal circulation). A study by Wing and Ferry (2002) suggests that the metamorphic fluid flow can locally be very complex and include upward, downward, up-temperature and down-temperature components, illustrating that the common current notions of fluid dynamics in the middle/deep crust are highly generalized and incomplete.

From the perspective of hypogene karstification, one of the key issues is assessing the potential for upflow of deep fluids to the upper crust where they may contribute to the endogenous regime and cause anomalous conditions in the sedimentary cover (Kissin 1967; Ezhov et al. 1992; Klimchouk 2012). Of particular importance here is the permeability distribution.

Ingerbitzen and Manning (2010) and Ingerbitzen and Appold (2012) pointed out that metamorphic petrologists have long recognized that permeability of the middle/deep crust is a dynamic parameter responding to tectonic stress, dewatering and fluid production, and other geochemical reactions. The above-cited works comment that this view is in stark contrast to the traditional hydrogeologic concept of permeability as a relatively static material property that exerts control on fluid flow. It is worth noting, however, that this view is certainly compatible with the understanding of permeability in karst science, where its dynamic self-adjustment is seen as one of the defining attribute of karst (Worthington and Ford 2009; Klimchouk 2015).

A large-scale crustal permeability estimate based on geochemical data and heat and mass transport models for rocks that underwent substantial fluid flow (Manning and Ingerbitzen 1999) yielded a permeability-depth curve log $k \approx -14$–3.2 log z (where permeability k is in m^2 and depth z is in km; Fig. 3a), but the data below about 12.5 km are actually fitted just as well by a constant permeability of $10^{-18.3}$ m^2 (Fig. 3b; Ingebritsen and Manning 2003). In other publication (Ingebritsen and Manning 2010), data have been compiled that represent local-to-regional-scale, transient, permeability-generation events that entail permeabilities much higher than these mean k–z relations would suggest. These data yield a curve log k ≈ -11.5–3.2 log z. Both data sets suggest a high variance and strong depth dependence of permeability at crustal depths of less than 10–15 km, with less variance and essentially no depth dependence below this level, which supports a general distinction between the hydrodynamics of a brittle upper crust and a ductile lower crust that is dominated by devolatilization reactions and internally derived fluids (Ingebritsen and Manning 2010). Ingebritsen and Manning (2010) noted that even the disturbed-crust values may underestimate the maximum transient permeabilities.

The change in the curves in Fig. 3b to vertical at depth of about 12 km corresponds to the brittle/ductile transition. It is broadly accepted that this transition occurs, depending on the density of the rock column and the geodynamic regime, at depths varying from 7 to 15 km (even at lesser depths in some cases), and that the maximum compaction of rocks and vanishing of open porosity in the base of the brittle domain causes steep decrease in permeability in this interval, thus creating a global hydrologic seal (Mukhin 1965; Ivanov 1966, 1970; Ezhov and Vdovin 1970; Etheridge et al. 1983; Ezhov and Lysenin 1986, 1988; Bailey 1990; Fournier 1991; Ivanov and Ivanov 1993). This interval (the "buffer" sub-zone of the meso-zone in Fig. 4c and d, according to Ezhov and Lysenin 1986, 1990) separates the upper domain of predominantly hydrostatic fluid pressures from the underlying domain of irregular very high and (still deeper) nearly lithostatic pressures. At deeper levels, where the ductile regime predominates, rocks are weak and the near-lithostatic fluid pressures encountered during

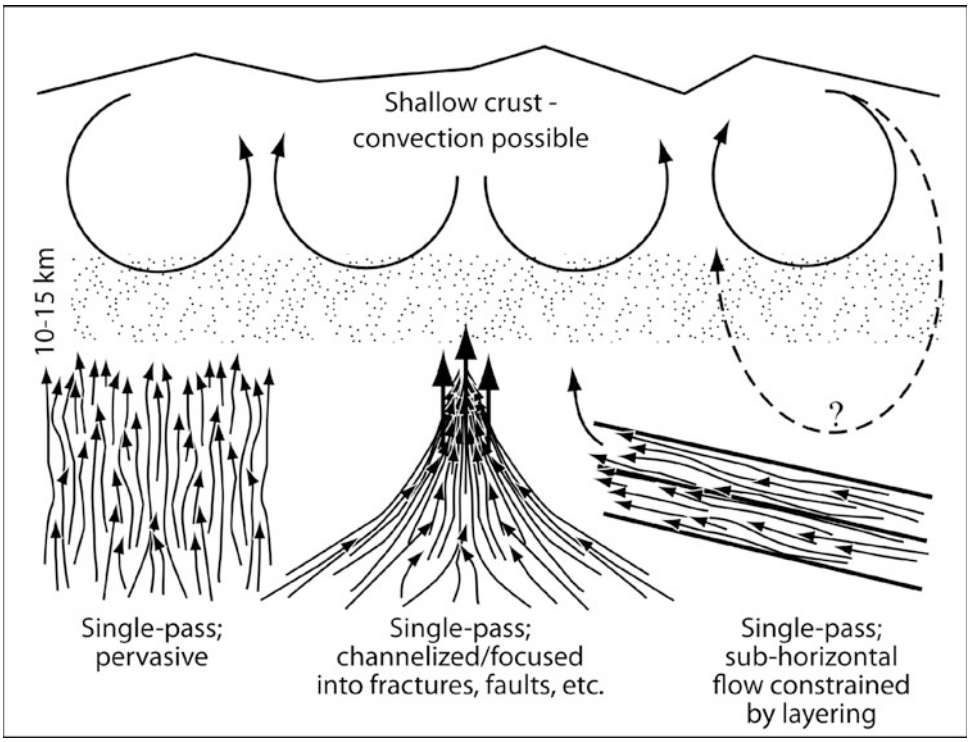

Fig. 2 Schematic cross section through the crust illustrating some possible modes of metamorphic fluid flow (reprinted from Treatise on Geochemistry, vol. 3, Ague JJ, Fluid Flow in the Deep Crust, pp. 203–247, 2003, with permission from Elsevier)

metamorphism result in relatively high permeabilities. The BDT (the "buffer" sub-zone) serves as a planetary-scale regulator of devolatilization of the deep crust and the mantle degassing, restricting the transfer of deep fluids to the upper crust and the hydrosphere (Ezhov and Lysenin 1986, 1988; Ivanov and Ivanov 1993). It is generally thought that large deep faults originate above the BDT but not cross through it, and many researchers believe that fluid transfer through this boundary occurs mainly by magmatic intrusions or diffusion.

Ezhov and Lysenin (1988) inferred that breakthroughs of deep fluids through the buffer sub-zone occur in a localized and pulsed manner, where and when the fluid pressures below build up high enough to exceed tensile strength and cause hydrofracturing. In this way, highly overpressured fluids periodically invade into the brittle upper crust and propagate upward, creating zones of baric, thermal and geochemical anomalies in the above-lying zone of hydrostatic pressures. Similar views were developed by Connolly (1997, 2010) and Connolly and Podladchikov (2013) into an elaborate and elegant model suggesting that metamorphic devolatilization reactions generate deformation-propagated fluid flow in form of pulses of fluid that travel upward as porosity waves, leaving trails of interconnected pore space in their wake. These trails act as preferential pathways for subsequent fluid flow. The models of periodic breakthroughs of deep endogenous fluids into the upper crust are corroborated by mounting evidence (from studies in many geological disciplines, particularly in petroleum geology, ore geology, geochemistry, sedimentology and non-volcanic hydrothermalism) of episodically high fluid pressures, fluid flow occurring in pulses or in multiple phases, and often at extraordinary rates, and of multifarious anomalies of fluid properties and composition in deep parts of the upper crust.

That deep fluids can traverse the BDT, and upflow to the upper crust in an advective regime without magma melts is strongly supported by numerous unambiguous identifications of mantle-derived volatiles, such as noble gasses and CO_2, in shallow aquifers in various regions devoid of recent volcanic activity. Kulongoski et al. (2005) showed a strong correlation between deep crust (^{4}He) and mantle-derived (^{3}He) helium isotopes in the eastern Morongo Basin, California, and association of sources for these components with faults. They dismiss a basin-wide diffusive flux of the mantle helium as the dominant process to transfer mantle volatiles to the shallow crust. They suggest that an advective flow regime drives He transport through the crust and that episodic fracturing in the Eastern California Shear Zone regulates mantle- and deep crust-derived fluxes of helium. Kennedy and van Soest (2007) show that mantle volatiles (He) leak over a wide area in the Basin and Range Province, southwestern USA, with ^{3}He/^{4}He ratios much higher than expected for regions with little magmatic activity. This indicates the enhanced flow of mantle fluids through the lower/middle crust and the BDT. These authors suggest that the shear force twisting the regional strain generates vertical faults that link the brittle upper crust with the ductile lower crust. Strain localization induced by an increasing dextral shear component superimposed on the extensional stress

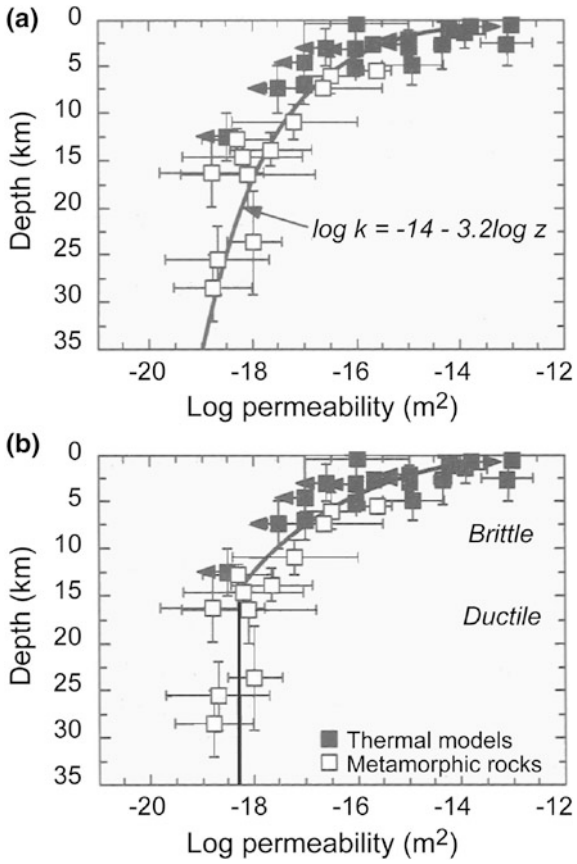

Fig. 3 Estimates of permeability based on hydrothermal modeling and the progress of metamorphic reactions showing **a** log fit to data and **b** data below 12.5-km depth fitted with a constant value of $10^{-18.3}$ m^2 (reprinted from Journal of Geochemical Exploration, issue 78–79, Ingebritsen SE and Manning CE, Implications of crustal permeability for fluid movement between terrestrial fluid reservoirs, pp. 1–6, 2003, with permission from Elsevier)

field must mechanically couple the brittle and ductile crustal zones, generating vertically oriented downward fault splays that extend through the ductile crust and into the mantle. These splays would act as conduits for fluid flow (Kennedy and van Soest 2007).

Newell et al. (2005) and Crossey et al. (2009, 2016) also provide ample evidence of heterogeneous mantle degassing and inputs from deep crustal sources throughout the western USA. Mantle-derived volatiles, including noble gasses and CO_2, are contained in travertine-depositing thermal and nonthermal springs in a variety of locations and tectonic settings throughout the entire region, such that many aquifer systems are influenced by mixing of deeply sourced and circulated waters. Karlstrom et al. (2013) determined that 27% of helium in springs in the Colorado Rocky Mountains is mantle derived, and 76 ± 20% of CO_2 come from deep (endogenic) sources. The endogenic CO_2 component in springs yields an integrated annual flux of deeply derived CO_2 to the groundwater system of $\sim 1.4 \times 10^9$ mol/yr (Crossey et al. 2009). Newell et al. (2005), Karlstrom et al. (2013) and Crossey et al. (2016) show that variations in mantle helium signals correlate best with low seismic-velocity (fluid-rich) domains in the mantle and lateral contrasts in mantle velocity.

Karlstrom et al. (2013) and Crossey et al. (2016) summarized features of the distribution of mantle helium signals in the western USA. The maximum $^3He/^4He$ values are associated with the active volcanic center in Yellowstone, reinforcing the models for its plume origin and emphasizing the role of magmatic intrusions in transferring mantle fluids to the crust. Very high values (approaching the values characteristic of mid-ocean ridges) are also found above the Cascadia subduction zone and San Andreas transform, indicating that plate boundaries provide zones for flux of asthenosphere-derived volatiles. High but heterogeneously distributed $^3He/^4He$ values elsewhere in the western USA, even in areas away from active volcanic regions and plate margins, unambiguously indicate that in regions of extending continental lithosphere mantle-derived volatiles can indeed transit through the brittle/ductile transition and rise to mix with aquifers in the shallow crust along deeply penetrating extensional fault networks (Crossey et al. 2016). There is a growing body of evidence for asthenosphere-derived volatiles, particularly CO_2, in the upper crust from many other regions of Cenozoic lithospheric extension, based on the integration of $\delta^{13}C$ data with noble gas isotopic tracers. Such regions include (just to name a few) many regions of China (Xu et al. 1995), the Pannonian and the Vienna basins (Sherwood-Lollar et al. 1997), the Bohemian massif (Weinlich et al. 1998), the Great Artesian Basin of Australia (Crossey et al. 2011; Italiano et al. 2013) and the Central Anatolia of Turkey (Bayari et al. Chap. 27). It is not surprising that those regions host remarkable examples of hypogene karst.

2.4 Hydrodynamic Zoning of the Upper Crust in Continents

Fluid properties and regularities of fluid flow dynamics systematically change with depth. There are several approaches to generalizing these changes within various schemes of vertical hydrodynamic zoning. Zones are distinguished based on (Fig. 4c) generalized hydrostratigraphy (hydrogeologic stories; Vsevolozhskiy 1983), hierarchy of gravitational flow systems (Tóth 1963, 2009), circulation intensity (Ignatovich 1950), dominating flow regimes (Shestopalov 2014; Vsevolozhskiy and Kireeva 2014) and distribution of fluid pressures (Mukhin 1965; Ezhov and Lysenin 1990). Although categories and terminology of these schemes are sometimes difficult to reconcile (Fig. 4),

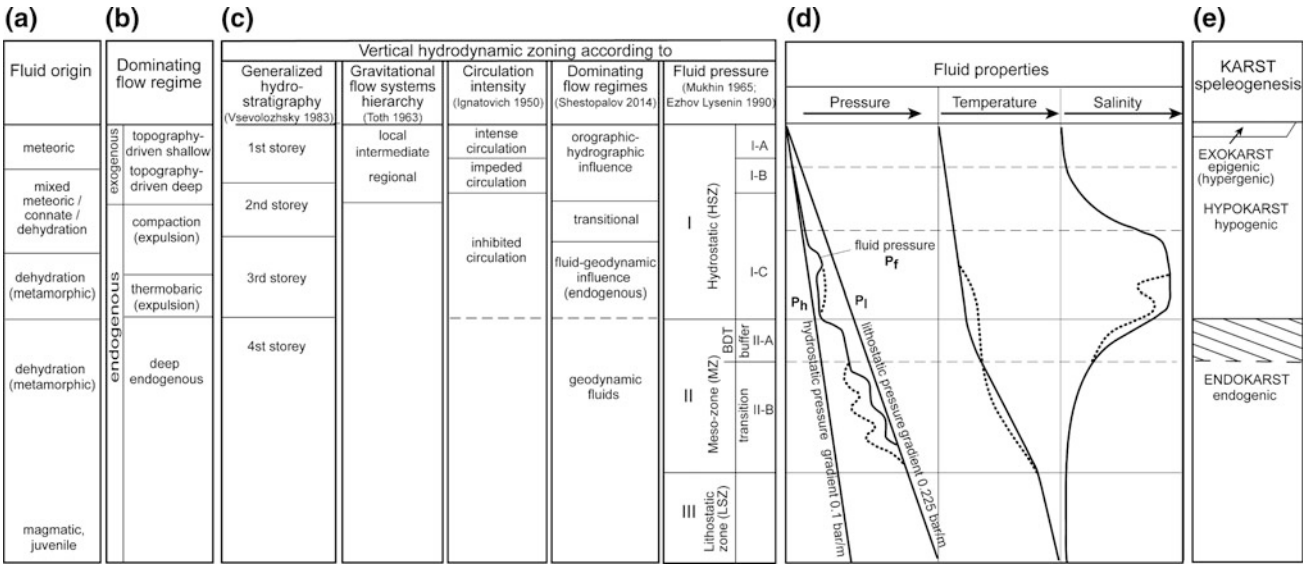

Fig. 4 Summary and approximate reconciliation of views on fluid origin (**a**), flow regimes (**b**), vertical hydrodynamic zoning (**c**), fluid properties (**d**) and vertical karst zoning (**e**) in the upper crust in continents. This illustration is a revised and extended version of a figure published in Klimchouk (2012). Pressure/depth relation curves on D are from Ezhov et al. (1992)

they form a conceptual framework to reveal major features and singularities of fluid dynamics at different depths. In looking for a basis for a sensible genetic classification of hypogene karstification, this section attempts to summarize and correlate views on hydrodynamic zoning and fluid dynamics in the upper crust.

2.4.1 Hydrogeologic Stories

A convenient framework to specify hydrodynamics in large sedimentary (artesian) basins is their division into hydrogeologic stories—a generalized extension of the hydrostratigraphy approach. This division, widely used in the Russian language literature, is based on the character and degree of communication of groundwaters with the modern surface (the upper hydraulic boundary), which depends on the distribution of regionally extensive low-permeability sequences (Vsevolozhskiyi 1983; Djunin 2000; Fig. 5). The stories are viewed not only as hydrostratigraphic units (the largest) but also as hydrodynamic domains holding a definite position in the basin's cross section (Vsevolozhskiy 2007).

The first hydrogeologic story encompasses the uppermost portion of the basin cross section, entirely occupied (in hydrogeologically mature basins) by the topography-driven flow regime, where aquifers and aquifer systems have substantial hydraulic communication with the surface throughout the entire basin area. The first story often includes several confined aquifers and aquifer systems and is limited at the base by the first thick aquitard of a basin-wide extension. The unsaturated (vadose) zone and the upper unconfined aquifer are the domain of epigene karstification, while hypogene karst develops mainly in confined conditions.

The views on the hydrodynamics of confined aquifers within the meteoric regime had been significantly changing during the second half of the twentieth century. The traditional artesian paradigm was based on the views of lateral through-flow in largely isolated aquifers, from elevated marginal recharge areas toward distant discharge areas. It was gradually replaced by the paradigm of the basin-wide hydraulic continuity, which implies significant vertical groundwater exchange (leakage) between aquifers in a system across separating aquitards throughout the entire area of a basin (Mjatiev 1947; Girinsky 1947; Hantush and Jacob 1955; Tóth 1963, 1995, 2009; Freeze and Witherspoon 1966; Llamas and Cruces de Abia 1978; Castany 1981; Shestopalov 1981, 1988, 1989; Bredehoeft et al. 1982; Vsevolozhskiy 1983, 2007; Fig. 6b).

The amount and direction of cross-formational hydraulic communication (leakage) across poorly permeable beds between vertically adjacent aquifers in a multiple aquifer system, and between aquifer systems, or segments of vertically extensive fracture-vein structures, depends on the vertical pressure gradients controlled mainly by the topography of the water table in the major unconfined aquifer above, and eventually by the surface topography. For a given aquifer in the confined multi-story aquifer system, recharge and discharge across aquitards can take place simultaneously and occur throughout the whole area of its lateral extent. Beneath topographic highs (zones of piezometric highs; recharge areas), hydraulic heads in aquifers decrease with depth, and leakages across aquitards are directed downward.

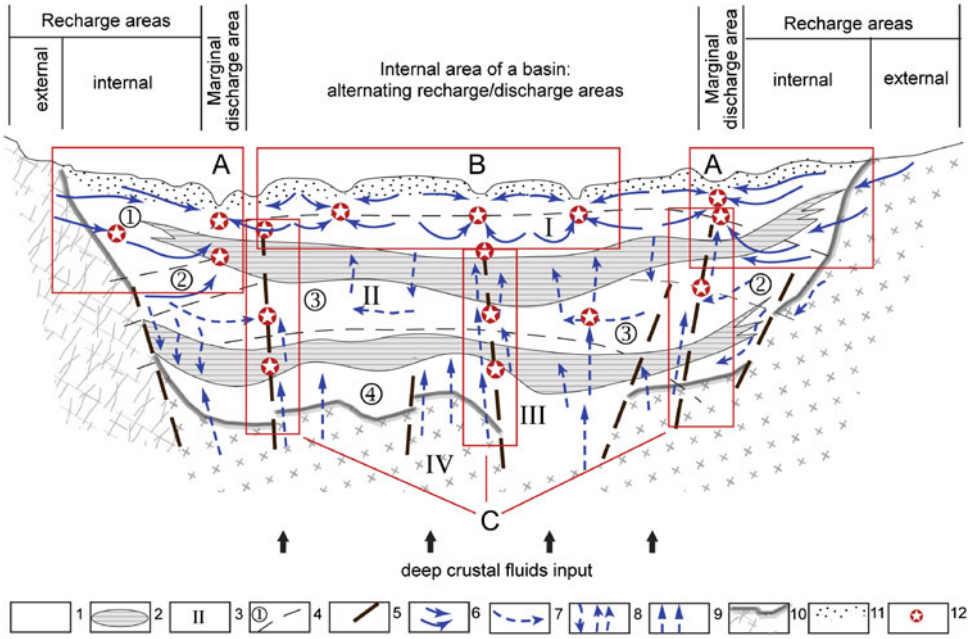

Fig. 5 Diagram illustrating generalized groundwater (fluid) flow pattern in an artesian basin of the platform type (from Klimchouk 2013b, modified from Vsevolozhskiy 2007). Legend: *1* multi-story aquifer systems within hydrogeological stories; *2* regionally extensive low-permeability strata (aquitards); *3* numbers of the hydrogeological stories; *4* boundaries and numbers of hydrodynamic zones; *5* zones of tectonic discontinuities; *6* flow pattern generated by the meteoric regime; *7* flow pattern in the intermediate zone, generated by various regimes; *8* sub-vertical leakages across aquitards; *9* flow pattern generated by the endogenous regime; *10* basement rocks with a weathering zone; *11* domain of epigene karst; *12* inferred localizations of hypogene karstification. *Red rectangles* (A, B and C) denote some characteristic settings of hypogene karstification (see Fig. 6 and Sect. 5)

Topographic lows (zones of piezometric lows; discharge areas) are characterized by upward head gradients and respective directions of leakages. Generally, recharge areas are more extensive than discharge areas, and ascending discharge is commonly further channelized by cross-formational discontinuities (Shestopalov 1989). Throughout the area, the alternation of areas of downward and upward leakage, along with lateral flows between them within aquifers, creates the pattern of local to subregional multi-level hydrodynamic cells (Fig. 6b) that may vertically encompass several aquifers. Such circulation pattern in a multi-story confined aquifer system is referred to as the Mjatiev's scheme in the Russian-speaking school, after a hydrogeologist who first provided its mathematical substantiation (Mjatiev 1947). Regional hydrogeological data and modeling studies suggest that the groundwater exchange in the confined systems of the first story is dominated by vertical leakages according to the Mjatiev's scheme rather than by regional lateral flows from marginal recharge areas (e.g., Llamas and Cruces de Abia 1978; Castany 1981; Shestopalov 1981, 1989; Bredehoeft et al. 1982; Vsevolozhskiy 1983).

The second story comprises aquifer systems that have substantial communication with the surface only on the periphery of the basin (Fig. 6a), and in crests of local uplifts (anticlines) (Fig. 6d) but are separated from the first story and the upper hydraulic boundary by a regionally extensive poorly permeable sequence throughout most of the basin area. Regional hydrodynamics of this story is determined by a configuration and structure of the peripheral areas, internal uplifts and large depressions and most notably by the location of contemporaneous discharge areas. Three characteristic areas distinguished for large basins (Vsevolozhskiy 1983; Fig. 5) are best expressed with respect to the second story: (1) *the marginal recharge area*, where both local recharge and recharge from adjacent regions reach aquifers of this story due to elevated head and overall enhanced permeability of sedimentary sequences along the basin's periphery, (2) *the marginal discharge area*, in which abrupt decrease of flow in confined stratal aquifers occurs due to increasing resistance to lateral flow and enhanced upward leakage to the first story, and (3) *the basin's internal area* with severely diminished inflow from the marginal recharge areas. In the internal area, the vertical interaction of aquifers and the exchange with the first story through leakages induced by the topography-controlled distribution of heads (the Mjatiev's scheme) may also occur, although in a weakened mode. A number of regional studies have demonstrated that the topographic influence over the hydrodynamics may reach up to depths of 1000–1500 m and

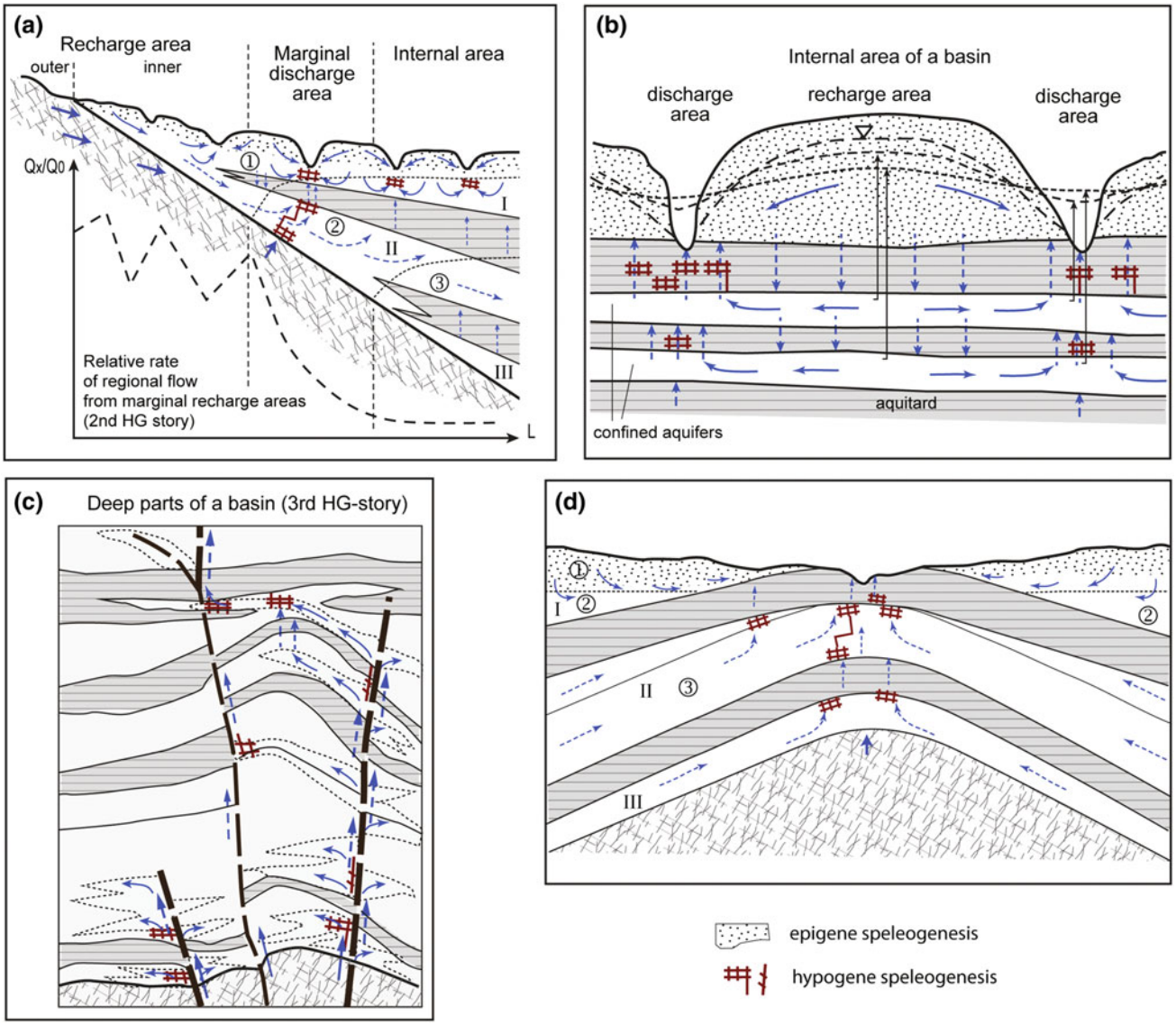

Fig. 6 Flow pattern in characteristic settings of hypogene karstification in large basins (see Sect. 5 for further discussion). **a** Basin's marginal discharge area; **b** upper hydrogeologic story in the basin's internal area; **c** deep-rooted faults and fractures in the basin's deep zones (3rd hydrogeologic story); **d** crests of anticlinal folds in the basin's internal area. Hydrostratigraphy and flow patterns adopted and modified from: a—Vsevolozhskiy (2007); b—Shestopalov (1981) and Vsevolozhskiy (2007); c—Djunin (2000)

more (Hitchon 1969; Shestopalov 1981, 1989), extending into the second hydrogeologic story. Upward cross-formational leakages induced by topographic lows, especially large river valleys, are commonly more focused and intense and are manifested to greater depths, than the downward leakages in topographic highs (Shestopalov 1989). Complications in the flow pattern of the second story can be introduced by the influence of residual domains of the compactional regime and by ascending recharge from the lower stories via cross-formational permeability structures. Although regional flows can form in the second story, particularly in its lower sections, and in younger basins, views about their ubiquity and hundred km-scale propagation (e.g., Garven 1985) appear to be exaggerated.

The third story encompasses the deepest parts of basins and comprises aquifer systems that have very limited hydraulic communication with the surface due to separation by several poorly permeable sequences throughout the whole basin. Generally low permeability and the presence of sub-vertical cross-formational hydrodynamic boundaries of varied nature determine domination of a "block-stratal" structure of the hydrodynamics in this story, characterized by lateral fragmentation of stratal aquifer systems (Vsevolozhskiy 1983; Djunin 2000; Djunin and Korzun 2005; Shestopalov 2014). High energy saturation of aquifers

and the increase in pressure with depth determine domination of upward fluid flow along sub-vertical discontinuities. The main conditions for fluid flow here are the impeded communication with the upper-lying stories and internal recharge/pressure sources. Within relatively isolated blocks, dynamics is determined by compaction and dehydration processes, geodynamic strains, the inflow of fluids from the basement, outflow (discharge) conditions, and the drawdown of elastic reserves (Djunin and Korzun 2005). Direct water sampling and measurements are limited, and data from few isolated localities are often generalized and extrapolated across large areas, leading to dubious notions about long-distance regional flows in deep aquifers. However, data from various regions that have been studied in more details suggest that hydrogeology of this story is characterized by non-systematic distribution of formation pressures and temperatures, local flows with varying directions, gradients and velocities, and variable chemical composition of fluids, often manifested across short distances even within same hydrostratigraphic/lithologic units (Vsevologhskiy and Dyunin 1996; Uma and Mosto Onuoha 1997; Djunin 2000; Bagdasarova 2001; McCartney et al. 2004; Djunin and Korzun 2005; Shestopalov 2014; Vsevolozhskiy and Kireeva 2014). These characteristics are incompatible with still widely accepted views of the prevalence of long-distance regional flows in deep aquifers. Hydrochemical inversions (decreasing salinity with depth), as well as occurrences of brines of anomalous composition, in a number of regions are accompanied with values of chemical indices (B/Br, Cl/Br, rNa/rCl, etc.) which exclude the origin of these fluids by metamorphism of connate waters or (in case of inversions) by generation of low-salinity fluids from thermal destruction of organic matter and dehydration of clays, but invoke sub-vertical migration from the basement of gas–vapor fluids enriched in CO_2 and H_3BO_3 (Ezhov 1978; Vsevolozhskiy and Kireeva 2009). In general schemes of hydrodynamics of a mature basin, the internal region is considered as an area of impeded discharge of fluids of the third story, although focused upward discharge along crosscutting tectonic discontinuities may occur elsewhere (Fig. 5).

The fourth story in deep basins embraces the metamorphic/crystalline basement. Due to the very low permeability of most crystalline basement rocks at the hand specimen scale, the fluid movement mainly occurs in fractures and faults. At large depth, fluid presence and transport strongly depend on the tectonic/geodynamic regime (Frost and Bucher 1994; Kissin 2009; Yardley and Bodnar 2014). At the onset of cooling of the basement rocks, retrograde hydration reactions consume water at significant rates, so that the basement may absorb overpressured fluids from the sedimentary cover (Stober and Bucher 2004; Yardley and Bodnar 2014). In tectonically active regions undergoing prograde metamorphism (the heating stage), fluid generation in this process develops strong overpressure and upflow into the sedimentary cover. Invasions of fluids originated from deeper parts of the crust and degassing of the upper mantle and the core may also occur (see Sect. 2.2.3). Further with depth, fluid pressures generally approach nearly lithostatic values, so that vertical fluid flow is driven by the difference between the hydrostatic (typically 10 MPa km^{-1}) and lithostatic (typically 23 MPa km^{-1}) pressure gradients.

The lower limit of the fourth hydrogeologic story is not explicitly specified, but it can be arbitrary drawn at the brittle/ductile transition (BDT), typically occurring within the interval of 10–15 km under geothermal gradients common for regional metamorphism, where interconnected porosity is believed to vanish (Ivanov and Ivanov 1993; Bucher and Stober 2010). The BDT is normally at temperatures below the critical point of H_2O.

2.4.2 Hierarchy of Gravitational Flow Systems

The basin-scale model of gravity-driven groundwater flow (Tóth 1963, 2009) describes the flow pattern that embraces several upper aquifers—within the first and (in mature basins with pronounced topography) second hydrogeological stories (Fig. 4c). Because the flow pattern is controlled by topographic elements of different scales, it includes hierarchically nested components commonly termed local, intermediate and regional flow systems. In a local system, recharge and discharge areas are adjacent to each other. In an intermediate system, recharge and discharge areas are separated by one or more topographic highs and lows. In a regional system, recharge areas are major topographic highs, and discharge areas lie at major lows (depressions, valleys). In basins with pronounced layered heterogeneity, the flow pattern includes sub-vertical leakages across low-permeability beds (aquitards) and lateral components in high-permeability beds (the Mjatiev's scheme), as described in Sect. 2.4.1. Lateral components of intermediate and regional systems commonly correspond to different aquifers in a multi-story system.

The Tóthian hierarchy of flow systems has the obvious meaning of hydrodynamic zoning, with the circulation intensity and total flux diminishing, and depth, residence time, dissolved solids content and temperature—increasing from local systems to regional. Epigene karst development is largely linked with local and intermediate flow systems, often encompassing entirely upper unconfined aquifers, whereas hypogene karstification within the gravitational

flow regime is associated with discharge segments of regional flow systems (Klimchouk 2007).

2.4.3 Hydrodynamic Zoning According to Circulation Intensity

The hydrodynamic zoning of the uppermost part of the crust according to the intensity of groundwater circulation was introduced by Ignatovich (1950) and was widely used in the East European schools. This scheme included three zones: (1) intense circulation, (2) impeded circulation and (3) stagnant regime. Criteria for drawing boundaries between the zones were continuously discussed and not unequivocally defined. Most researchers placed the lower boundary of the first zone at the top of the first aquitard not breached by the contemporary erosional network (commonly within 100–300 m). In the second zone, circulation was believed to be impeded due to the absence of direct communication with the surface, but slow regional flows at diminished rates were assumed to operate at this regime. According to modern views, recharge and discharge of aquifers in this hydrostratigraphic position in mature basins with substantial relief occur mainly through vertical leakages (the Mjatiev's scheme), and the circulation is more intense than it was previously thought. Both these zones are within the first hydrogeologic story, with possible exempt of the marginal basin's areas where the zone of the intense groundwater circulation may extend into the second story up to a depth of 1000 m (Fig. 6). The zone of a stagnant regime was believed to embrace the second hydrogeologic story within the internal area of a basin, as well as the entire third story. Later modifications of this scheme proposed to distinguish the zone of the strongly impeded circulation (corresponding to the second story in the basin's internal area) and move the zone of a stagnant regime into the third hydrogeologic story.

This scheme was based on the old artesian paradigm that implied the formation (recharge) of groundwaters in confined aquifers largely in the marginal surface outcrops, without recognizing the role of cross-formational communication in multi-story aquifer systems, internal sources and endogenous flow drives (regimes). It underestimates dynamics of deep parts of basins and is overall obsolete (Shestopalov 2014).

2.4.4 Hydrodynamic Zoning According to Distribution of Fluid Pressure

It is widely held that according to the distribution of fluid pressures, continental crust is divided into two main domains, the upper crust with dominating near-hydrostatic pressures and the lower crust with near-lithostatic pressures, with the transitional zone in between. These views were elaborated and codified by Russian researchers into a planetary-scale scheme of hydrodynamic zoning (Ivanov 1966, 1970; Ezhov and Vdovin 1970; Ezhov and Lysenin 1986, 1988; Ivanov and Ivanov 1993; Ezhov et al. 1992; Fig. 4c–d).

The zone of hydrostatic pressures (zone I) contains waters at a pressure that is hydrostatic or does not exceed it by more that 10–15% in aquifers or by 15–20% in dense low-permeability beds. The thickness of this zone ranges from 0.5–0.6 km up to 6–7 km and more. Three sub-zones within this zone, distinguished by Ezhov and Lysenin (1986), generally correspond to the Ignatovich's zones by the circulation intensity (see Sect. 2.4.3).

The meso-zone (zone II) is transitional between the domains (zones) of hydrostatic pressures above and lithostatic pressures below. The pressures in the meso-zone increase with depth non-linearly, often abruptly. Two sub-zones are distinguished in the meso-zone: a "buffer" sub-zone (II-A) of the maximum compaction, which serves as an imperfect hydrologic seal and regulates devolatilization of the deep crust and the mantle, and a transition sub-zone (II-B) of variable supra-hydrostatic pressures, in which porosity increases irregularly due to hydrofracturing and dissolution by high-pressure aggressive fluids ascending from below. When the pressure of fluids beneath the buffer sub-zone exceeds the tensile strength of rocks in the latter, fluids break through the buffer into the overlying hydrostatic zone causing thermal, baric, geochemical and other anomalies in shallower aquifers (Ezhov and Lysenin 1988). The thickness of the meso-zone varies between one and several kilometers, depending on lithologies, geodynamic regime and the fluid properties. Its upper boundary lays closer to the sea floor under seas and oceans than to the land surface on the continents, due to additional pressure from the water column.

The zone of lithostatic pressures (zone III) is characterized by the decreased rock density in fluid-rich areas due to permanent hydrofracturing. Fluid dynamics is dominated by ascending fluxes of metamorphic (locally derived) and juvenile (passing from below) fluids, although geophysical data suggest the presence of lateral fluid-rich intervals as well (Kissin 2009).

Although recent studies, based on petrological, geochemical and geophysical data and modeling, have significantly improved and detailed understanding of fluids distribution, properties and behavior in the Earth's crust (e.g., Ague 2003; Kissin 2009; Ingebritsen and Manning 2010; Connolly and Podladchikov 2013; Yardley and Bodnar 2014), they are broadly in agreement with this general scheme.

2.4.5 Hydrodynamic Zoning According to Dominating Flow Regimes

Shestopalov (2014) suggested an approach to hydrodynamic zoning based on consideration of leading factors and regularities of groundwater dynamics in the upper part of the

Earth crust, determined by major flow regimes. He distinguishes three main hydrodynamic zones: (1) the zone of oro-hydrographic/climatic influence, (2) the intermediate (transitional) zone and (3) the zone of fluid-geodynamic (endogenous, AK) influence (Fig. 4c).

In the first zone, groundwater dynamics is governed by gravitational head imposed by differences in the topography of the water table (and ultimately of the land surface) and variations in meteoric recharge (the meteoric regime; see Sect. 2.2.4). It corresponds to the gravitational flow systems of Tóth (2009) and extends to depths ranging from a few hundred to 1000–1500 m. The lower boundary of this zone is determined by the draining influence of major rivers. Shestopalov (2014) divided this zone into four sub-zones: (1a) aeration zone (vadose); (1b) of unconfined/confined aquifers, partly or completely incised by the erosional network; (1c) of confined multi-story aquifers with substantial circulation, not disrupted by erosional incision; (1d) of confined aquifers with subdued circulation, in which the draining influence of only major rivers, coinciding with active faults, is manifested.

The third zone embraces the lower part of the sedimentary cover in deep basins (the third hydrogeologic story; see Sect. 2.4.1) and the part of the crystalline basement where hydrodynamics is influenced by geodynamic processes in the lower crust and the mantle and is largely determined by the sub-vertical migration of high-temperature gas–vapor fluids (see Sects. 2.2.3 and 2.3). It starts from depths varying from several hundred meters to 2–3 km and extends to 10–15 km in regions of Cenozoic tectonic activation, to ca. 25 km in regions of Paleozoic and Mesozoic orogens and to ca. 80 km in regions of Precambrian folding. Shestopalov (2014) stresses that the basement and deep parts of the sedimentary cover should be treated as a single hydrodynamic domain, since the influence of ascending deep fluids causes substantial epigenetic transformations of the percolation environment in both segments, wearing off differences in their permeability structure, enhancing their vertical communication and leading to the formation of the vertically stretched cellular structure. Vsevolozhskiy and Kireeva (2014) provided strong evidence from several large regions for the influence of fluids rising from the basement on hydrodynamics and geochemistry of deep sections in cratonic basins, which results in the block-stratal differentiation and mosaic distribution of hydrodynamic, baric, thermal and geochemical parameters. Based on this, they dismiss still popular views of the presence of the zone of strongly impeded circulations (stagnant) in deep parts of basins and distinguish the zone of the endogenous regime instead. Shestopalov (2014) distinguishes in the lower zone a sub-zone (3a) of isolated focused (channelized) ascending fluid flow and dilatancy, grading to the depth into a sub-zone (3b) of lateral occurrence of deep fluids linked with regional granitization processes.

The intermediate (transitional) zone (2) between the upper and lower zones is determined by the weakened influence on hydrodynamics of both, oro-hydrographic and endogenous factors. Aquifers in this zone may receive weak descending or ascending recharge from adjacent zones, and its hydrodynamics is characterized by low lateral and vertical pressure gradients. This zone can be pierced, however, by focused cross-formational and trans-zonal ascending flows, transmitted by active deep faults, causing strong thermobaric and hydrochemical anomalies. This zone is subdivided (Shestopalov 2014) into (2a) a sub-zone of dominant influence of external factors, (2b) a sub-zone of regional minimums of lateral gradients and (2c) a sub-zone of the weakened influence of endogenous factors.

This scheme, based on a synthesis of modern data on the hydrodynamics of the upper crust, provides the most suitable framework for the analysis of hypogene karstification.

3 Genetic Divisions of Hypogene Karst

In view of the high variability of processes and conditions of hypogene karstification and resultant void-conduit patterns, a further division into genetic types within this broad genetic category is needed. Genetic types of hypogene speleogenesis are often distinguished according to dissolution chemistry involved: sulfuric acid speleogenesis (SAS), hydrothermal speleogenesis, "mixing corrosion" speleogenesis, evaporite-dissolution speleogenesis, etc. Several dissolution mechanisms may operate simultaneously or sequentially, which makes recognition of their respective roles in many cases difficult to impossible. Moreover, major attributes of hypogene void-conduit systems, such as their patterns and morphologies, do not generally exhibit systematic singularities specific to the dissolutional mechanisms. To the contrary, hypogene caves formed by different dissolutional mechanisms in different lithologies often demonstrate remarkable multifaceted similarity in patterns and morphology determined mainly by the hydrodynamic factors (such as the overall ascending vector of flow, the hydrostratigraphic control, the specific speleogenetic mechanism due to the suppression of the flow/conduit growth feedback and the role of natural convection circulation).

3.1 Genetic Types According to Hydrodynamic Environments

Since the main genetic types of karst are discerned on the hydrogeologic basis, and since hypogene karstification is associated with rising flow components of confined

groundwater systems, further genetic categorization of hypogene karst can be derived from consideration of driving forces and conditions for circulation and ascending flow. These are appropriately generalized by the modern views on hydrodynamic zoning and distribution of the flow regimes (Vsevolozhskiy and Kireeva 2014; Shestopalov 2014; see Sect. 2.4.5).

Klimchouk (2012, 2013b) distinguished three types of hypogene speleogenesis, presented here as genetic types of hypogene karstification and redefined in the light of the above discussion:

(1) *Artesian hypogene karstification*, related to the upward inter-stratal and inter-formational hydraulic communication in confined multi-story aquifer systems, in the hydrodynamic zone of oro-hydrographic/climatic influence (Fig. 6b). Speleogenesis in this type is supported by the meteoric (gravity-driven) regime of groundwater exchange and is governed by upward leakages between aquifers. It is particularly common (although not exclusive) for the upper parts of mature cratonic sedimentary (artesian) basins and post-orogenic regions marked by notable layered heterogeneity in permeability, the presence of stratal aquifers, massive and deep penetration of meteoric waters and pronounced influence of the topography on the groundwater flow.

(2) *Endogenous hypogene karstification*, related to the upwelling inter-formational flow in, and from, the zone of fluid-geodynamic influence (Figs. 6c, 7). It is commonly localized along cross-formational fluid-conducting faults and fracture zones (fracture-vein fluid systems). Karstification of this type occurs in substantial depths (likely up to several km), but may also occur within the upper hydrodynamic zone when the latter is pierced by focused structurally controlled rising flows of deep basinal or basement fluids and associated anomalies. However, in the case of endogenous hypogene speleogenesis driven by carbonic acid dissolution by rising geothermal fluids, its continuation in shallow settings is hindered by a switch to the onset of precipitation due to a drastic drop in fluid pressure and CO_2 degassing (Dublyansky 2013). Hypogene karstification of the endogenous type occurs in varied geodynamic settings. It is common for regions of the extensional tectonic regime, especially for intracontinental rift basins, as well as for active margins and collision fold-thrust regions. Two groups can be distinguished in the type of endogenous karstification: (1) related to volcanogenic degassing (volcanogenic karst) and (2) related to other endogenous volatiles ("cold" degassing of Kropotkin 1986; see Sect. 2.2.3).

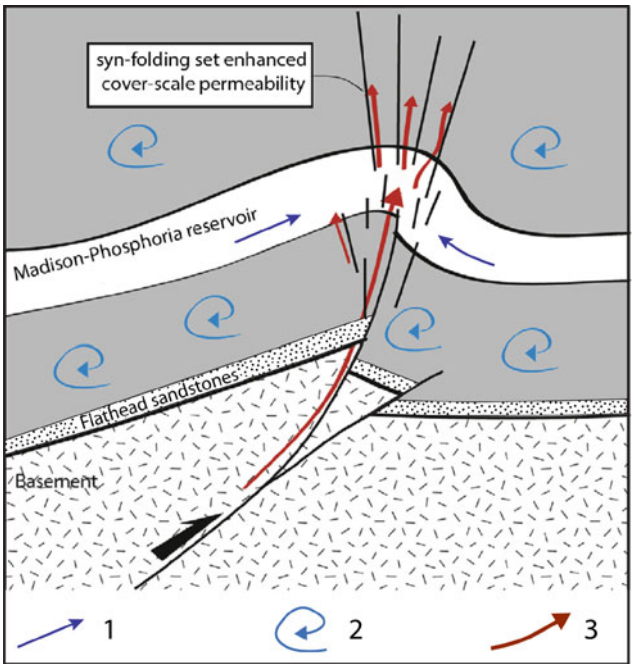

Fig. 7 A conceptual model of fluid system at Sheep Mountain Anticline, illustrating a setting for endogenous hypogene speleogenesis. The inferred fluid system is composed of a mix of fluids that rise from the basement and formation fluids in the Flathead sandstones and Madison limestones (Beadoin et al. 2011, 2015). Upward fluid migration is channelized along the thrust in the sedimentary cover through shale formations until fluids reach the fractured limestone formations and then diffused through the whole fracture pattern at fold scale thanks to synfolding set III fractures that enhanced overall fracture connectivity. Post-compaction basement-cored folding and related fracturing occurred at depth > 2 km and developed enough vertical permeability to allow fluid from depth to invade the strata (Beadoin et al. 2015). Legend: *1* formation fluids in aquifers; *2* formation fluids in low-permeability shales; *3* basement fluids (Reprinted from Journal of Structural Geology, vol. 70, Beaudoin N. et al., Fluid systems and fracture development during syn-depositional fold growth: An example from the Pico del Aguila anticline, Sierras Exteriores, southern Pyrenees, Spain, Implications of crustal permeability for fluid movement between terrestrial fluid reservoirs, pp. 23–38, 2015, with permission from Elsevier)

3) *Combined, artesian/endogenous hypogene karstification*, where deep basinal and/or basement fluids ascending along cross-formational discontinuities significantly interact with overlying stratiform aquifers in the hydrodynamic zone of oro-hydrographic/climatic influence. Karstification of this type is particularly common for active intramountain and intermountain basins and geodynamically active cratonic basins. Speleogenesis tends to concentrate along major deep-rooted faults and fracture zones, interfaces between different flow regimes, and along basin margins.

4) *Hypogene karstification in unconfined/confined aquifers, partly incised by the erosional network, or side-open to*

the sea. This type corresponds to the sub-zone 1b of the Shestopalov's scheme (Shestopalov 2014). Two varieties of speleogenesis can be further distinguished here.

One is *sulfuric acid speleogenesis, where deep H_2S-bearing fluids rise to an unconfined carbonate aquifer and the water table*. The boost in the aggressiveness due to H_2S oxidation and H_2SO_4 formation is most expressed along the water table, which determines an intense cave enlargement at this level, as well as above it via the condensation-corrosion process (Palmer 2013; De Waele et al. 2016; Audra Chap. 3; Galdenzi Chap. 8; Palmer et al. Chap. 37). Although the cave development by the sulfuric acid attack at and above the water table may radically transform the cave pattern by adding a pronounced sub-horizontal component to it, this mode of speleogenesis still relies on rising channeled confined flow from depth via a cross-formational conduit system, though these input elements are often masked by sediments. The cave development in the water table-controlled acidic environments commonly represents a late phase of hypogene speleogenesis of type 3 in a given aquifer already devoid of the confinement.

Another variety is c*oastal hypogene speleogenesis*, where fresh groundwater in carbonate aquifers interacts with saline marine water along aquifer margins (Fig. 8). The standard flank-margin speleogenetic model originally developed for isolated islands on carbonate platforms (Mylroie and Carew 1990) was based on an assumption that the rock sequence is homogenous, and the freshwater lens was considered as a perfectly unconfined aquifer. Development of dissolutional voids in the margins of a freshwater lens, under the flank of the enclosing land mass, is favored by three conditions that exist there: mixing dissolution; organic decay horizons; and the increase in freshwater flow rate (Mylroie and Mylroie Chap. 51). As these caves result from slow diffuse flow decoupled from surface hydrology and acidity sources, and the aggressiveness has been produced at depth beneath the surface, they fit the geochemical definition of hypogene speleogenesis (see Sect. 1.2). Recent discussions reveal that flank-margin speleogenesis may also fit the hydrogeological definition (ascending flow from the underlying hydrostratigraphic unit). Klimchouk (2014) pointed out that considerable layered heterogeneity in permeability (up to three orders of magnitude; e.g., Budd and Vacher 2004) and hence the leaky confinement can be present even in young carbonates. Along with the hierarchy of flow lines in the freshwater aquifer due to the island geometry, surface topography and uneven distribution of recharge, this should lead to situations when deeper flows of freshwater from central and/or higher-elevation areas are forced to extend seaward below the saline water at the lens margins and rise across less permeable beds there to mix with the saline water and develop macro-porosity (Fig. 8b). This is corroborated by observations by the present author of the wide presence of feeder-like speleogenesis in and just above the lithified and less permeable paleosol horizons in many caves in the Bahamas, which were previously interpreted as sink points (John Mylroie, personal communication, 2014), Alternatively, Mylroie and Mylroie (Chap. 51) suggest that the flow from the interior to the coast in the freshwater lens creates a drag on the underlying marine water, such that marine flow is dragged seaward and upward to the lens margin.

Hypogene karstification of all types localizes where ascending fluid flow and dissolution-inducing disequilibrium conditions were supported, continuously or intermittently, during a sufficiently long time, mainly in zones of discharge and/or interaction of fluid flow systems and regimes of different nature, depth and scales. The localization is influenced by structural features and particularities of regional flow pattern and geodynamic and geomorphological evolution. Peculiar features of pre-speleogenetic permeability distribution and fluid dynamics and composition in different hydrodynamic zones, as described in previous sections, cause distinctions in cave-forming flow patterns, flow rates and chemical mechanisms of hypogene speleogenesis of the above-defined types, resulting in different characteristics of caves. In the cross-sectional view, the variety of patterns of hypogene void-conduit systems (Palmer 1991; Klimchouk 2007, 2012, 2013a; Audra et al. 2009; Audra and Palmer 2015) can be broadly grouped into four types: (1) *stratiform*, with diffused inputs from below, (2) *cross-formational*, aligned to prominent discontinuities conducting focused flow, (3) *water table- or sea level controlled* and (4) *composite*. Stratiform patterns are common for artesian hypogene speleogenesis, cross-formational patterns are common for endogenous hypogene speleogenesis (although they may form also by focused leakage from deeper aquifers in artesian speleogenesis), and water table- or sea level-controlled patterns are common for hypogene speleogenesis in unconfined/confined aquifers. Composite patterns most commonly form by a combination of types 1 and 2, or 2 and 3, but sometimes of all three original types.

3.2 Endokarst

The term "endokarst" (endogenous karst) is widely but misleadingly used in the literature to denote the entirety of subsurface karst features including those of the epigene origin. In geosciences, the adjective "endogenous" refers to phenomena caused by forces originating from within the Earth, but epigene karst features clearly do not fit this category.

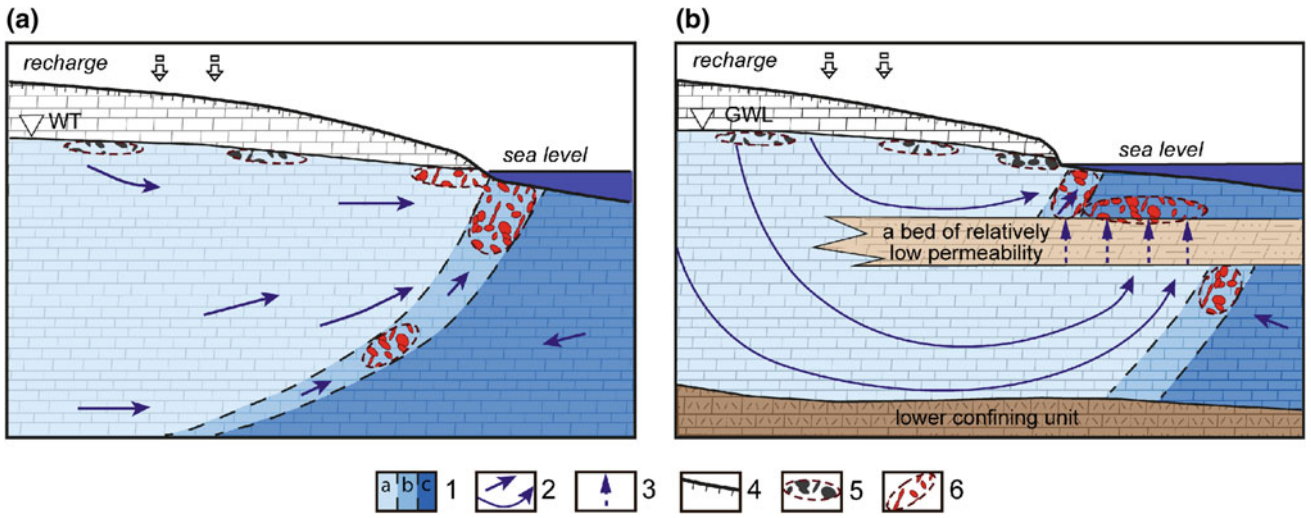

Fig. 8 Speleogenesis in coastal areas: **a** the standard flank-margin model for homogenous rocks (redrawn after Mylroie and Carew 1995); **b** an expanded model with elements of layered heterogeneity (the hydrogeological setting is borrowed from Barlow 2003). Legend: *1*—groundwaters: **a**—fresh, **b**—brackish, **c**—saline (seawater); *2* inferred flow directions and flow lines; *3* ascending leakage across the aquitard; *4* epikarst; *5* cavities formed of by mixing of vadose and phreatic freshwaters along the water table; *6* cavities formed by mixing of freshwater and seawater. *WT* water table. The images are vertically exaggerated

An original concept of endokarst has been suggested by Ezhov and Lysenin (1990) and further developed in Ezhov et al. (1992). According to these views, the realm of endokarst (the endokarst story) encompasses the domain of variable supra-hydrostatic and nearly lithostatic pressures beneath the "buffer" sub-zone—an imperfect hydrologic seal that regulates devolatilization of the deep crust and the mantle (see Sect. 2.4.4 and Fig. 5). In extremely high P-T conditions of the middle/deep crust, the fluids are highly aggressive with respect to many sedimentary, metamorphic and igneous rocks. Fluid-filled porosity may exist in the endokarst story because fluids are under close-to-lithostatic pressures so that the effective stress is close to zero. However, voids can be preserved while passing through the buffer sub-zone and the BDT only if filled with some secondary mineral such as calcite or anhydrite.

Although dissolution processes certainly operate in the zone of lithostatic pressures, little is known about conditions in the middle/deep crust (geological heterogeneities, dynamics of fluid and their physicochemical parameters, etc.) which may control focusing of fluid flow and dissolution processes, i.e., formation of void-conduit systems. It is likely that the mechanisms of speleogenesis known to operate in the upper crust are not applicable to the deeper zone. It is, therefore, not clear whether the phenomena hypothesized by Ezhov and co-workers can be classified as karst. It is much more certain, however, that pulsed breakthroughs of deep fluids into the hydrostatic zone, that propagate upward along deep-rooted faults and other heterogeneities, transecting this zone to various heights and up to the surface, play an important role in generating endogenous hypogene karstification as defined in the previous section. For more details and discussions of the endokarst concept of Ezhov and Lysenin, see Andreychouk et al. (2009) and Klimchouk (2012).

4 Hypogene Karstification, Metasomatism and Weathering

4.1 Metasomatism

Metasomatism, a fluid-induced mass transfer process of re-equilibration of a rock involving a change in the chemical composition (mineral replacement), is widely recognized to play a major role in the formation of the Earth's continental and oceanic crust and the lithospheric mantle (e.g., Korzhinskii 1953; Pospelov 1973; Zharikov et al. 1998, 2007; Harlov and Austrheim 2013; Yardley and Bodnar 2014). In ore deposit geology, this process is commonly called alteration. Metasomatism may coexist with metamorphism, or even considered as its variety, but also includes a range of fluid-induced processes which are not metamorphic (e.g., sediment diagenesis, fluid-aided ore mineralization, alteration of rock by hydrothermal or meteoric fluids). Metasomatic modification of rocks by moving fluids (infiltration metasomatism) is most spread in the upper crust, where fluid fluxes are largest (Yardley 2013). Zharikov et al. (2007) note that the term "metasomatism" is conventionally limited by hydrothermal conditions related to endogenous processes, although they admit that hypergenic metasomatism also occurs. Yardley and Bodnar (2014) point

out that any fluid that moves across boundaries between contrasting lithologies, or between regions with different temperature and pressure, may cause metasomatism in the wall rocks, although the process is especially liable to occur under elevated temperature and pressure. Pospelov (1973) considered metasomatism as a through process that is a component in other major processes of rock transformation including karstification, as shown in Fig. 9.

Rock transformations in metasomatic zones and the resultant metasomatites (or alterites) vary greatly, depending on physicochemical conditions (the compositions of parent rocks and metasomatising fluids, and the temperature and pressure conditions). The products of metasomatism are systemized in a hierarchical classification of metasomatic facies and families (Korzhinskii 1953; Zharikov et al. 2007). Among metasomatic families that occur in carbonate rocks, the most common are *scarns* and *argillisites*. Scarns are metasomatites formed at the contact between a carbonate rock and a silicate rock or magmatic melt, or around veins and fractures, or fractured zones, crossing carbonate rocks (Zharikov et al. 2007). Dolomitic scarns (Warren 2000) as well as structurally controlled hydrothermal dolomite bodies (e.g., Davies and Smith 2006) widely occur, being formed over a wide range of temperatures. Replacement by iron ores and silicification (replacement by chalcedony, chert or quartz) are other common metasomatic processes in carbonates. Argillisites are metasomatites consisting of clay mineral assemblages, formed by low-temperature hydrothermal fluids around veins and fractures. They commonly accompany carbonate-hosted uranium, strata-bound massive sulfide Pb-Cu-Zn and a wide range of epithermal deposits (Zharikov et al. 2007).

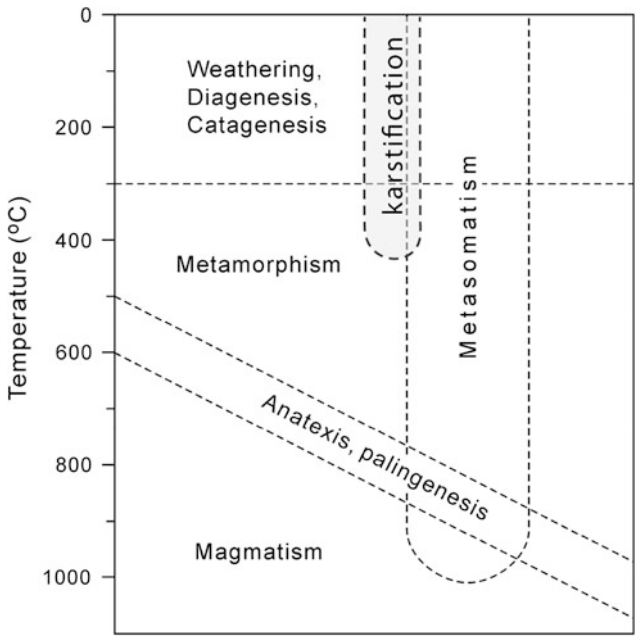

Fig. 9 Fields of major processes of rock transformation in the crust and the upper mantle. Compiled by Ezhov et al. (1992) from various sources and modified by adding the "karstification" field

4.2 Metasomatism and Karstification

Both, metasomatism and karstification, occur through a fluid-aided dissolution–transport–precipitation process, which underpins their likely intimate relationship. However, the mechanism, particularly the transport component, is considered operating on different space and timescales for these phenomena (Ezhov et al. 1992). The conventional concept of metasomatism implies that precipitation occurs in situ and synchronously with dissolution, thus conforming to Lindgren's (1925) rule of constant volume during metasomatism. Korzhinskii (1953) and Zharikov et al. (2007) explicitly state that metasomatism is separated from processes that include the development of cavities and their subsequent infilling. Such views were shown to be ambiguous by Pospelov (1973), why introduced the concept of *extended metasomatism* in which operation of zones of dissolution, transport and precipitation is stretched in time or space or both. According to Pospelov, dissolution in extended metasomatism may lead to the development of macropores, cavities or even chambers. He considered that the volume-disequilibrium development may locally occur, resulting in the formation of cavities (intersomatism). Further developing the Pospelov's ideas, Ezhov et al. (1992) asserted that karst is a component of a more general process of metasomatism. They defined karst as "*a 'through' process of metasomatic alteration of rocks, which consists of the creation and subsequent filling of cavities and proceeds along a general scheme: dissolution-transport-precipitation of the matter*" (translated from Ezhov et al. 1992).

Regardless of admitting this radical view or not, it is clear that in reactive rocks such as carbonates (and other lithologies under appropriate conditions) the processes of "normal" (micropore-scale) metasomatism and hypogene karstification are intimately related. Mechanisms of metasomatism and speleogenesis depend on spatial and temporal variations in the compositions of rocks and metasomatising fluids and P-T conditions, and these variations can lead to a breach of a balance between dissolution and precipitation causing a local prevalence of dissolution, i.e., speleogenesis (the Pospelov's extended metasomatism). The metasomatic increase in porosity may serve to focus fluid flow and speleogenesis, and in turn, speleogenesis may facilitate "normal" metasomatism by increasing fluid flow and changing the conditions of water–rock interaction; the degree of individualization of these mechanisms and their relative role depend on the above-mentioned variations of the conditions in space and time. Since rising endogenous fluids are characterized by

variable flow rates and composition, the relationships between alteration and proper speleogenesis are complex.

Metasomatites and other alterites formed from carbonates commonly have macroscopic vugs and often metric-sized cavities, and hypogene caves often have zones of metasomatic or isochemical alteration in the wall rock, or such zones are found in the vicinity of hypogene conduits. The development of hypogene caves is often guided by distinct zones of strong alteration along fractures, suggesting that a phase of fluid flow with the domination of isovolumetric alteration was followed by a phase with the dominant creation of open cavities. Remarkable examples of this kind of relationship have been observed by the author in the Buda Thermal Karst (Hungary) where large rift-like passages in some caves (e.g., Pál-völgy Cave System) were formed along fractures that have up to meter-thick zones of the friable, often silicified, alterite, still preserved in distal parts. In other regions, such as the Piedmont Crimea in south Ukraine (Klimchouk et al. Chap. 25), fractures with argillisites and strongly altered wall rocks are found side-by-side with open hypogene conduits guided by fractures of the same set, suggesting that fluids of the later phase selectively excavated cavities in the set of fractures affected by metasomatism (Klimchouk et al. 2013). A metasomatic or isochemical alteration that accompanied or followed major speleogenetic phases is typical for many hypogene caves, which is evidenced by the common occurrence in them of boxwork and so-called corrosion residue (Northup et al. 2000) or speleosols (Spilde et al. 2009; DuChene et al. Chap. 31). It is suggested here that boxwork is the result of later selective dissolution in the altered zone of the cave wall rock, with the partial exhumation of a 3D lattice of denser material (veins) precipitated in fractures and microfractures within this zone during the alteration phase. The formation of the corrosion residue, an oxide-rich Fe–Mn layer that develops on the walls of many hypogene caves, is strongly influenced by microbiological activity (Northup et al. 2000; Spilde et al. 2003). It is suggested here that this enhanced activity is favored by the presence of the porous and chemically enriched zone of alteration in the cave wall rocks rather than is the primary cause for the formation of this zone.

The most remarkable manifestations of the link between metasomatism (rock alteration) and karstification (or between the two aspects of the same general process of extended metasomatism) are the "ghost-rock karstification" (Sect. 4.3) and the development of tafoni and honeycomb structures (Sect. 4.4). The lack of understanding of the genetic affinity of these phenomena (and of their common fluid-aided nature) gave rise to ambiguous and muddling terminology, numerous conflicting conceptions and long-lasting interpretive problems.

4.3 Ghost-Rock Karstification

The term "*ghost-rock karstification*" is increasingly used in the karst literature during the last two decades to describe a two-stage process of cave formation by (1) chemical weathering of wall rocks by groundwater flow, focused in permeable paths (such as joints and bedding planes), in a low-hydrodynamic energy environment, and (2) subsequent removal of the porous and weakened altered rock (ghost-rock) by fast-flowing groundwater after a base level drop, mainly in the vadose zone (Dubois et al. 2014). This phenomenon was recognized by Schmidt (1974) in the USA, but it was intensely studied and internationally publicized by Belgium researchers since the end of the last century (e.g., Vergari and Quinif 1997; Vergari 1998; Quinif and Bruxelles 2011; Dubois et al. 2014, and references therein), and also described in France, Italy and UK. The first stage of the process is also termed rock phantomization. The formation of open cavities by removal of the alterite may only selectively use the joint-controlled lattice of the ghost-rock, but in places results in substantial caves, often in maze systems of passages, commonly displaying typical phreatic morphology. The published accounts present a number of well-documented and convincing examples including those in Belgium, France, Italy and UK, showing that this phenomenon is, indeed, rather widespread. The increasing awareness of the phenomena of ghost-rock karstification is certainly an important advance in karst science. However, its existing interpretation (in the works cited above) needs in some clarifications and adjustment of the terminology, which somewhat changes the perspective and implications. A detailed discussion is beyond the scope of this chapter, but two aspects should be touched, though in brief.

First, it is important to recognize that isovolumetric alteration of the fracture wall rock by moving fluids, when accompanied also by substantial chemical changes (reported in the above-cited works on the ghost-rock karstification), is nothing else but infiltration metasomatism—the process which is well known in petrology, ore geology and sedimentology (see Sect. 4.1). Strange enough, but none of the already numerous publications on the ghost-rock karstification acknowledged this, and the relevant knowledge of metasomatic processes was not applied, which hampered understanding of the phenomenon. The ghost-rock karstification could be more appropriately termed as metasomatic karstification, i.e., karstification through metasomatism. In the petrologic and ore geology literature, the term "ghost-rock" is often used to denote the alteration product, particularly if some elements of texture and structure of the parent are retained in it. Therefore, the term "ghost-rock karstification" has a strict meaning of "karstification of the alterite," which is awkward.

Second, the ghost-rock karstification has been attributed to epigene processes, the phenomenon was considered in the context of landscape evolution, and in terms of weathering that propagates from the surface with the downward infiltration. Although chemical weathering (hypergene metasomatism) can indeed propagate to substantial depths in the subsurface, in highly reactive rocks such as limestones the water–rock interaction is commonly dominated by congruent dissolution, with little residue. In typical situations of diffused (authigenic) infiltration from the surface, this results in the formation of the epikarst and underlying conduit systems. Substantial isovolumetric wall rock alteration of carbonates (either isochemical or metasomatic), which requires low-hydrodynamic energy environment and specific conditions of water–rock interaction, although not excluded in epigene settings, is more liable to occur in the deep subsurface due to the action of hypogene fluids. Most of illustrations and descriptions of site-specific settings for field examples presented in the above-cited works are suggestive of the hypogene origin of the phenomena. Audra (Chap. 3) favors the hypogene origin of the ghost-rock karstification, noting that most of the regions in France where its manifestations have been documented are now known to be affected by hypogene karstification. See also Temovski (Chap. 15) for an example of hypogene ghost-rock karstification.

The removal of the alterite and creation/increase of a cavity-type open space can occur in different environments and through different processes. It may occur in the hypogene conditions through dissolution induced by changes in pressure and temperature or in the composition of fluids. Still in the hypogene conditions, it may occur through mechanical removal (erosion) when flow rates increase dramatically following a breach of the major upper confining unit. Publications on the ghost-rock karstification emphasize the mechanical removal of the alterite in the water table and vadose conditions, which is certainly an efficient mechanism. Finally, when still alterite-filled conduits are exposed to the surface, especially in sub-vertical faces in structurally controlled cliffs, they can be quickly cleaned out by the external weathering agencies and display typical hypogene morphology, as shown by Klimchouk et al. (2013b) for the Crimean Piedmont (see also Klimchouk et al. Chap. 25).

4.4 Cavernous Decay Features: Tafoni and Honeycomb Structures

Tafoni and honeycomb structures, often collectively termed as "*cavernous weathering*" or "*cavernous rock decay*" features, are variously shaped and arranged cavities and hollows in rock surfaces ranging in size from a few millimeters to several meters. There are many other descriptive terms used for these features, but the terminology is highly inconsistent and entangled (see Groom et al. 2015 for a recent review). There is a tendency of using "*tafoni*" (singular: "*tafone*") for larger (meter-sized) features, and "*honeycomb*" for smaller, millimeter- to decimeter-sized forms, although the latter is often considered a subclass of the former. Larger tafoni are also called "rock shelters," "rock overhangs," "alcoves" or "abri." Whereas tafoni may occur separately and isolated, individual cells in honeycomb structures are closely spaced and arranged into characteristic patterns. "Honeycomb" and "honeycomb weathering" are often interchanged with "alveoli" and "alveolar weathering." Other terms used for honeycomb-like structures include stonelace, lacework, boxwork, fretwork, fretting and pitting. Tafoni and honeycomb structures are most commonly found on sub-vertical outcrop surfaces (side-wall tafoni) and on boulders but much less frequently occur at sub-horizontal outcrops. Despite variability in size, morphology and patterns, honeycomb features have quite a characteristic appearance, maintained across a wide range of lithologies and environmental conditions.

Studies of features and processes of the cavernous decay are a prominent part of geomorphology for more than 100 years, particularly in such branches as weathering research and sandstone landscapes, with a large body of the literature on the subject. Notable works and recent reviews include Mustoe (1983), Martini (1978), Young and Young (1992), Goudie and Viles (1997), McBride and Picard (2004), Turkingston (2004), Turkington and Phillips (2004), Turkington and Paradise (2005), Viles (2005), Brandmeier et al. (2011), Paradise 2013, Groom et al. (2015). However, despite more than a century of scientific research, tafoni and honeycomb structures remain one of the most enigmatic and puzzling geomorphologic phenomenon. *"While it is largely accepted that lithology, the presence of salts, climate and exposition form a complex system of weathering conditions, the major processes controlling tafoni-type-weathering are poorly understood"* (Brandmeier et al. 2011). Turkingston (2004, p. 128) note: "*Considerable literature has accumulated on the nature of both tafoni and alveoli, but as more information has been presented, their possible origins, rather than being clarified, seem to have become more confused.*" Groom et al. (2015, p. 10) write: "*Notwithstanding substantial academic attention, scientific understanding of the principal driving mechanisms for cavernous decay remains yet to be discovered.*" Similar confessions can be found in other recent reviews in the subject.

Tafoni and honeycomb structures occur in a wide range of rocks including sandstone, limestone, quartzite, granite, graywacke, dolerite, rhyolite, conglomerate and tuff. They have been described from regions in various climatic zones and environments of all continents, from deserts to humid areas, from coasts and lowlands to high mountains, and even

Fig. 10 Examples of tafoni and honeycomb structures in different rocks and environmental conditions. **a** and **b**—nested tafoni in a larger cavity: **a** in the Cretaceous arkose sandstone, Bohemia, Czech Republic; **b** in the Eocene limestone, Piedmont Crimea, Ukraine; **c** and **d**—honeycomb structures: **c** in the Eocene limestone, Piedmont Crimea, Ukraine; **d** the Cretaceous arkose sandstone, Western Caucasus, Russia. **e** and **f**—tafoni-like cavities: **e** in the Cretaceous limestone, Owl Mountains, Texas, USA; **f** in the Eocene limestone, Piedmont Crimea, Ukraine. **g** and **h**—"fresh" (**g**) and degrading (**h**) tafoni and stratiform notches in two cliff outcrops of the same exposition, located ca. 10 km apart, in the same unit of the Eocene limestone, Piedmont Crimea, Ukraine. Both cliffs have been formed by toppling of block detached along vertical fracture conduits: **g** about 10 ka (estimated based on the geomorphologic situation), **h** within 130–150 ka (estimated based on the geomorphologic situation and speleothem dating). Note that no new features form on denuded surfaces, as well as on the freshly exposed (ca. a few thousand years ago) fracture wall surface in the left of the cliff in **h**, which was not affected by the alteration. Photograph **a** by V. Suchy, photograph **d** by A. Ostapenko; photograph **e** by K. Stafford, other photographs by the author ►

on Mars (Rodriguez-Navarro 1998). Assorted processes have been invoked to explain the formation of tafoni and honeycomb, including eolian deflation, weathering through insolation, frost action, wetting and drying, chemical and salt weathering and biological decay. Case hardening and/or core softening were thought by some to play a major role. Salt weathering is most commonly invoked. Although all these processes can certainly contribute to granular disintegration and flaking, none of them alone, or in combination with other processes, has been shown to satisfactory explain selective localization, development and distribution of tafoni and honeycomb structures and their characteristic morphologies. In searching a way out of the obvious explanatory crisis, recent works invoke the polygenetic nature of the cavernous decay phenomenon, which is thought to be "… *the result of multiple, if not simultaneous, decay processes varying case to case*" (Groom et al. 2015). Others invoke self-organization characterized by positive feedback as a response to dynamic instability within the weathering system, independent of the particular decay processes (Turkington and Phillips 2004). These approaches bring no clarity to the problem and do not offer answers to simple questions —why patches of honeycombing with the same appearance can develop across different lithologies within the same outcrop? Why quite different patterns can develop in seemingly homogenous rock, in the same lithostratigraphic unit and in the same cliff face? Why same patterns can develop on different rocks (Fig. 10; compare A and B), exposed in drastically different local environmental conditions (Fig. 10; compare C and D)? Why same features can develop on rocks, although of generally same lithology but of different age and diagenetic maturity, outcropping in regions with contrasting climatic conditions (Fig. 10; compare E and F)? Why tafoni in the region, in cliffs of the rock and the same exposition, displays a fresh appearance in one outcrop and clear signs of degradation in another (Fig. 10; compare G and H)?

The major problem in studies of the cavernous decay features is that they have always been constrained by the weathering paradigm, i.e., the action of external agencies (the weathering system) onto exposed rock surfaces was a priori considered as the principal factor in the formation of these features. However, the occurrence of cavernous decay features across such wide ranges of lithologies and environmental conditions, either regional or local or both, strongly suggests that their formation is determined by a factor which role overarches variations in these conditions and weathering processes. It is proposed here that this factor is the pre-exposure isovolumetric alteration in the walls of fluid-conducting discontinuities such as fractures due to the fluid–rock interaction, which occurs mainly in deep-seated settings.

The alteration zone in the wall rock is characterized by more or less distinct boundary at the rear (the alteration front), which has the complex but generally smooth geometry, with deeper embayments and intervening salients, developed due to initial permeability variations in the rock matrix and hence variations in the interaction between the pore fluids and the flow in the major fracture conduit. The geometry of the alteration front determines the future morphology of larger cavernous features such as tafoni (Fig. 10 **a** and **b**), very much like in the case of cavities created by the ghost-rock karstification, as described in Sect. 4.3.

Within the porous and weakened bulk mass of the alteration zone, a 3D pattern of more dense material is often created by precipitation in larger pores and microfractures. According to Putnis (2002), the dissolution-reprecipitation mechanism allows fluids supersaturated with respect to certain phases to be transported through the microporous matrix without crystallizing until a larger pore volume or fracture is encountered. Preferential precipitation in larger pores and fractures leads to the formation of the latent structured heterogeneity in the bulk porous alterite, predetermining diverse and intricate patterns of the future honeycomb structures (Figs. 10b, c and 11).

The tafoni and honeycomb morphologies manifest themselves after partial or complete removal of the bulk mass of the porous and weakened alterite in the wall rock. As noted while discussing the ghost-rock karstification, the removal of the alterite can occur in different environments and through different processes. It may occur due to speleogenesis and groundwater flow (either ascending or descending) along the same fracture or nearby fractures, or through subaerial weathering in the cave environment so that

(a)
(b)
0.5 m
(c)
(d)
(e)
(f)
(g)
(h)
degrading tafoni
degrading notch
fresh fracture surface
inclined rock shelters

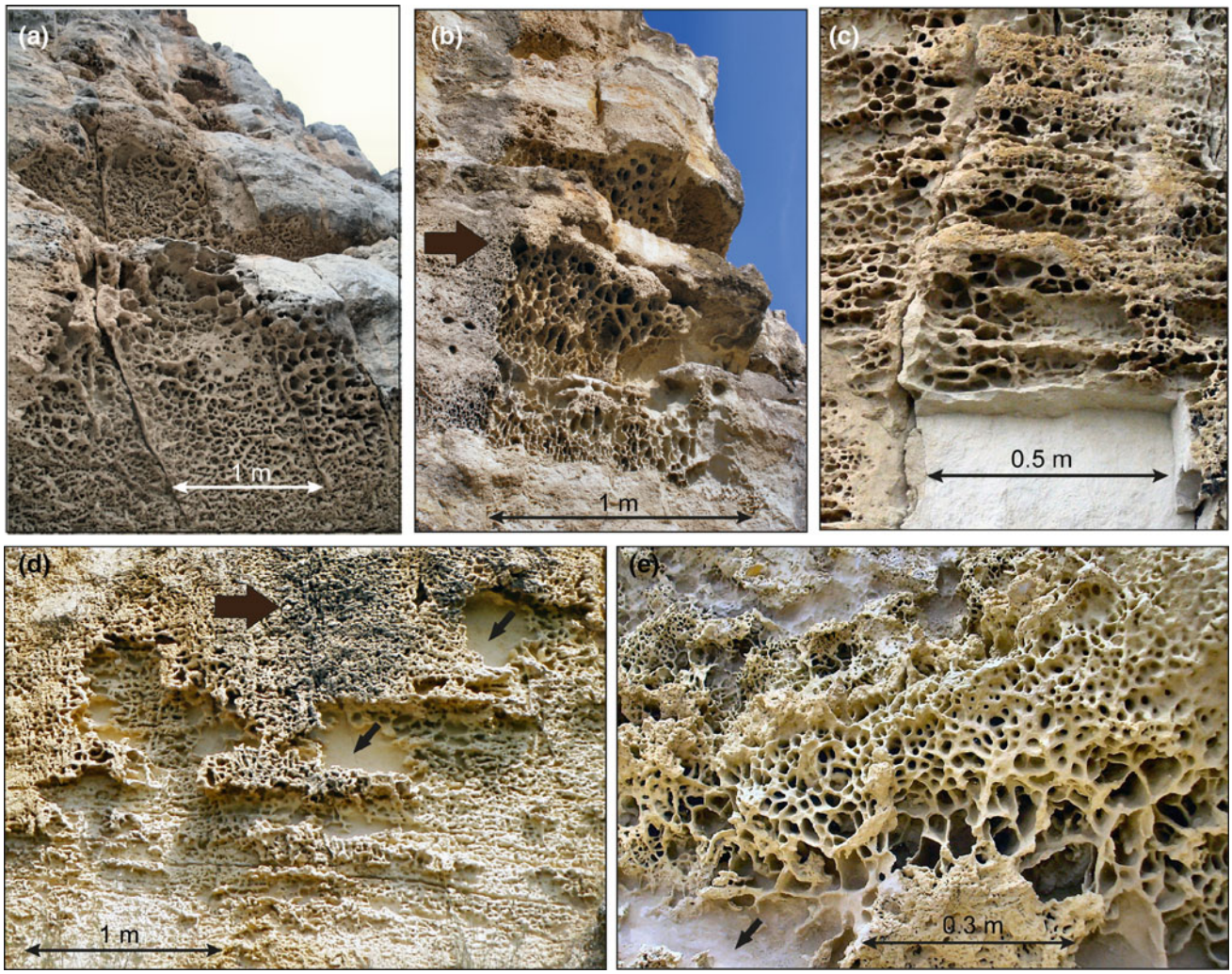

Fig. 11 Varied morphology of honeycomb structures in the Crimean Piedmont, south Ukraine. **a**, **c** and **d**—in the Paleogene limestones, **b** and **e**—in the Eocene limestones. *Large arrows* in **b** and **d** indicate the well-preserved remnants of the original fracture wall. *Small arrows* in **d** and **e** point to the surfaces where the alterite and honeycombs have been totally destroyed—new features do not form on them. The *white area* in **c** is the surface where the rock unaffected by the alteration is exposed—new features do not form on it

honeycomb structures will become a part of the cave morphology (see photograph **d** in Fig. 10). Boxwork surfaces in the walls and ceilings are common in many hypogene caves. Photograph **e** in Fig. 10 shows tafoni-like cavities in a cliff face; most of which represents the fracture wall that was partially exposed only recently by a block failure. This fracture extends to the right in the original closed state (the exposure limit is outlined by the dotted line and pointed to by the arrow), but it can be clearly seen that tafoni are already present there. More often, however, the weakened alterite is removed by weathering after the fracture wall is exposed to the surface in cliffs or steep slopes. Which particular weathering processes are involved is not critical for the formation of the cavernous features, and their exposure and appearance are only slightly controlled by local environmental conditions.

This model allows to soundly discriminating between two types of the cavernous decay features: (1) those whose morphology is controlled by the geometry of the alteration front (commonly larger, tafoni-like cavities; Fig. 10a and b) and (2) those whose morphology is determined by the 3D pattern of hardened structures within the alteration zone (honeycomb-like features; Fig. 11). These types can be combined where the 3D pattern of hardened structures is formed at the rear of the alteration zone, along its front so that after the removal of the alterite honeycomb features will be displayed on the walls of a tafoni-like cavity (Fig. 11a and b).

The proposed model explains well other characteristic traits of the cavernous decay features such as (to name a few):

- preferential development on sub-vertical outcrops such as cliffs (which are commonly structurally controlled, i.e., formed by block retreat along fractures affected by karstification and alteration);
- preferential occurrence in coastal areas (due to the wide occurrence of structurally controlled cliffs) and desert areas (due to better preservation of exposed wall rock morphologies);
- the occurrence of honeycomb/boxwork features on the walls of larger tafoni-like and "normal" hypogene cavities (Fig. 10a, b and d; Fig. 11a and b);
- the common occurrence of honeycomb/boxwork features within a well-defined zone in the wall, beneath which they do not develop (see white patches in photographs **d** and **e** in Fig. 11);
- degradation of the cavernous decay features in exposed conditions (Fig. 10h).

Degradation of the cavernous decay features is barely considered in the literature, although degrading features are often found proximal to outcrops displaying articulate features. Why tafoni and honeycomb develop in one outcrop and degrade in another one nearby is another hard question for the weathering school which tacitly implies the primary control of local environmental conditions. According to the proposed model, the evolution of cavernous features under the action of weathering after their exposure has two stages: (1) prograde development, when the features are being progressively cleaned from the bulk mass of the alterite on the recently exposed fracture wall (Fig. 10g), and (2) retrograde development, when the exposed features are being destroyed by weathering and denudation (Fig. 10h). The cavernous decay features are relatively short-lived, being ultimately wiped out by weathering. New features are generated only through the exposure of new fractures that have the altered wall rocks, but they do not form on the rock surfaces where the alteration zone was totally denuded (Fig. 11d and e) or never present (the left portion of the outcrop in Fig. 10h; Fig. 11c).

Recent detailed studies in regions rich in tafoni and honeycomb structures, such as the Crimean Piedmont (Crimea, south Ukraine; Klimchouk et al. 2013; see also Klimchouk et al. Chap. 25) and central-western Bohemia (Czech Republic; see Suchy et al. Chap. 20), as well as field observations by the author in various regions around the world, strongly suggest that the formation of these features is predetermined by alteration of the fracture conduit wall rocks by ascending hypogene flow, as described above. The ghost-rock karstification, which is closely related to, or is a part of, hypogene karstification (see Sect. 4.3; Audra Chap. 3; Temovski Chap. 15), is basically the same phenomenon. This points to a possibility of redefining hypogene karstification in order to accommodate the fluid-aided alteration of wall rocks as a legitimate part of the formation of hypogene dissolution-dominated void-conduit systems, as discussed in the entire Sect. 4. In any case, it is suggested here that tafoni, honeycomb structures and ghost-rock karst forms can be regarded as features strongly indicative, if not diagnostic, for past rising flow and hypogene karstification.

The recognition of the role of the hypogene fluid-induced wall rock alteration and karstification in the origin of large cavernous features, such as rock shelters, tafoni and similar cavities, suggests that their conventional ascription to the pseudokarst category is misleading and should be revisited.

5 Settings of Hypogene Karst

The hydrogeological approach to defining hypogene karstification (speleogenesis), particularly its association with ascending fluid flow, suggests the possibility of distinguishing characteristic settings and predicting localization of hypogene karst at the large scale (Klimchouk 2013b, c). Hypogene karstification localizes where ascending flow and disequilibrium conditions causing dissolution were supported, continuously or intermittently, during a sufficiently long time—mainly in zones of discharge and/or interaction of groundwater (fluid) flow systems and regimes of different nature, depth and scales. The localization is controlled mainly by the particularities of the regional geodynamic (tectonic), geomorphological and hydrogeological evolution and structure. Therefore, characteristic settings of hypogene karstification can be distinguished based on consideration of patterns and evolution of flow regimes and systems, particularly of discharge conditions at regional (basin-wide) scale, in the context of a tectonic/geodynamic position and history of a region.

This possibility is especially feasible for hypogene karstification of the artesian type related to meteoric (gravitational) flow systems, in which the pattern of groundwater circulation in the zone of oro-hydrographic influence in large sedimentary/artesian basins in cratonic settings is largely systematic, determined mainly by the basin's configuration, topography and hydrostratigraphy (Shestopalov 1981, 1988, 1989; Tóth 1995, 2009; Vsevolozhskiy 1983, 2007). It is less regular in the deep parts of basins and in orogenic regions where the areas of upward flow are strongly controlled by cross-formational fluid-conducting structures and internal fluid sources. These settings are characterized by the dominance of hypogene karstification of the endogenous type.

The following systematics is not comprehensive, but it includes some most common and important settings of hypogene karstification. In the upper hydrogeologic stories (1st and 2nd) of mature artesian basins of the cratonic type, the upward flow and hypogene karstification tend to localize in (1) marginal discharge areas and (2) prominent topographic lows within the internal basin area. Upward flow from deeper parts of basins (leakage to aquifers of the upper hydrodynamic zone, and ultimate discharge) preferentially occurs in (3) large anticlinal folds or uplifted tectonic blocks within the internal basin area where the upper regionally extensive aquitard is thinned or partially breached, and (4) along linear-local zones of deep-rooted cross-formational faults conducting upward flow of the endogenous regimes across the upper hydrodynamic zone. Hypogene karstification is favored in (5) young disrupted intermontane basins, in which the endogenous regimes often dominate. Peculiar conditions for hypogene karstification are found in (6) large carbonate platforms side-open to the ocean. Orogenic regions, including foreland basins, offer diverse tectonic and hydrogeological settings, and their systematics from the perspective of hypogene karstification is still to be developed. The predictability of distribution of areas of the upward flow in tectonically deformed and mountainous regions is significantly lesser than in large basins and platforms because of the complexity and variability of geological and structural conditions, relief and a geodynamic history in such regions. Massifs in orogenic regions are characterized by the dominance of cross-formational fracture-zone-controlled groundwater systems, although sequences of the upper structural story often host stratiform aquifer systems. Upward flow and hypogene speleogenesis are strongly controlled by faults, especially at junctions between large tectonic structures and boundaries between structural stories, and by the geodynamic evolution. A remarkably distinct setting, characterized by a specific kind of endogenous hypogene speleogenesis, is represented by (7) areas of young volcanism.

5.1 Basin's Marginal Discharge Areas

Recharge from often elevated areas at basin's margins, where aquiferous rocks commonly outcrop at the surface, may penetrate to a considerable depth into the second hydrogeologic story (Fig. 6a). Groundwaters moving from the margins in dipping confined aquifers soon reach the condition that resistance to lateral flow becomes greater than resistance to vertical transverse flow, as the aquifer permeability diminishes in the direction toward the basin's interior. In this area, massive upward leakage and discharge to the surface can occur through the overlying low-permeability formations, commonly facilitated by the enhanced vertical permeability of aquitards at the basin's marginal areas due to irregularities in the basement topography, differential compaction, and tectonic disturbances. Pronounced hypogene karstification related to marginal discharge areas is found in many basins around the world, and instructive examples include areas stretched along the eastern flank of the Roswell Artesian Basin in New Mexico, USA (Land 2003; Land and Huff 2010; Fig. 12); the northwest flank of the Western Canadian Sedimentary Basin, Alberta, Canada (Broughton Chap. 39), the southern flank of the Prichernomorskiy Artesian Basin in the Piedmont Crimea, south Ukraine (Klimchouk et al. Chap. 25), and flanks of several basins in the Western Europe (Audra Chap. 3; Kempe et al. Chap. 21). Hypogene karst in this setting is often characterized by the development of large and deep collapse features (Fig. 12), especially if evaporites are present in cross section.

5.2 Basin's Internal Areas

Localization of hypogene karstification in the upper hydrogeological stories in the basin's internal areas is mainly controlled by topographic lows, such as river valleys, which induce upward cross-formational communication according to the Mjatiev's scheme (Fig. 6b; see Sect. 2.4.1 and characterization of the upper story therein). This is the favorable setting for hypogene speleogenesis of the artesian type, characterized by the development of stratiform, often multi-story, maze caves. Remarkable examples include the giant gypsum mazes in the western Ukraine (Klimchouk and Andreychouk Chap. 23, Andreychouk and Klimchouk Chap. 22), maze caves in gypsum in the Paris Basin (Bigot 2010; see also Audra Chap. 3) and isolated single-passage and maze caves in the Neogene limestones in the Prichernomorskiy Artesian Basin in the south Ukraine (Klimchouk 2013b; Klimchouk et al. 2010).

Hypogene karstification in the deep parts of basins in the internal areas is localized at large anticlinal folds and at uplifted tectonic blocks, and along cross-formational permeable structures such as faults and fracture corridors, as described in Sects. 5.3 and 5.4.

5.3 Anticlinal Folds and Uplifted Blocks

In large anticlinal folds and in uplifted tectonic blocks within the internal basin area, the upper regional aquitard is often thinned or partially breached by erosion (Fig. 6d; Fig. 13). Also, such structures are commonly characterized by enhanced vertical permeability across thick sedimentary successions due to fracturing and faulting and are often

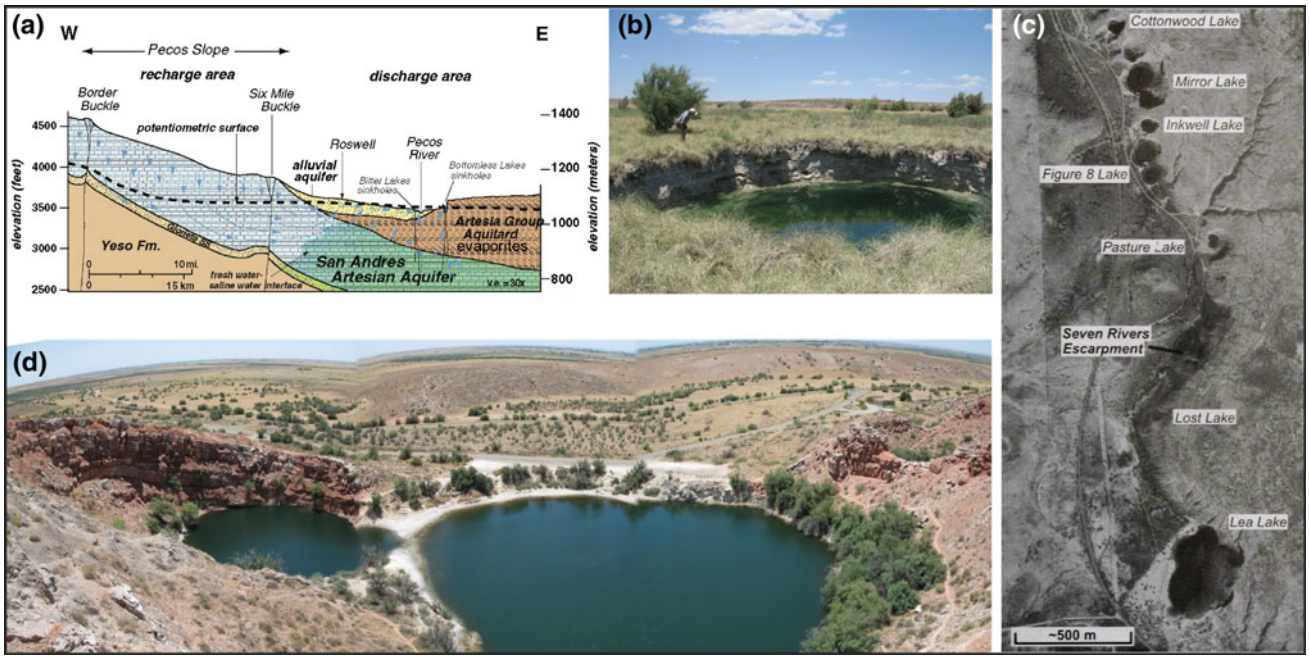

Fig. 12 An example of hypogene karstification in the basin's marginal discharge area, characterized by intense sinkhole development (Roswell Artesian Basin, New Mexico, USA). **a** hydrogeologic profile across the Roswell Basin showing localization of the Bottomless Lakes sinkholes; **b** recently formed sinkhole in the Pecos River floodplain; **c** orthophoto image of the Bottomless Lakes sinkholes, the Seven Rivers Escarpment, and the adjacent floodplain of the Pecos River (note the compound morphology of Lea Lake; **d** panoramic photograph of two sinkholes in the Bottomless Lakes series. **a** is from Journal of Hydrogeology vol. 18, 2010, p. 457, Land L and Huff GF (copyright Springer-Verlag 2009), with permission of Springer; **c** is from Land (2003), photographs **b** and **d** by the author

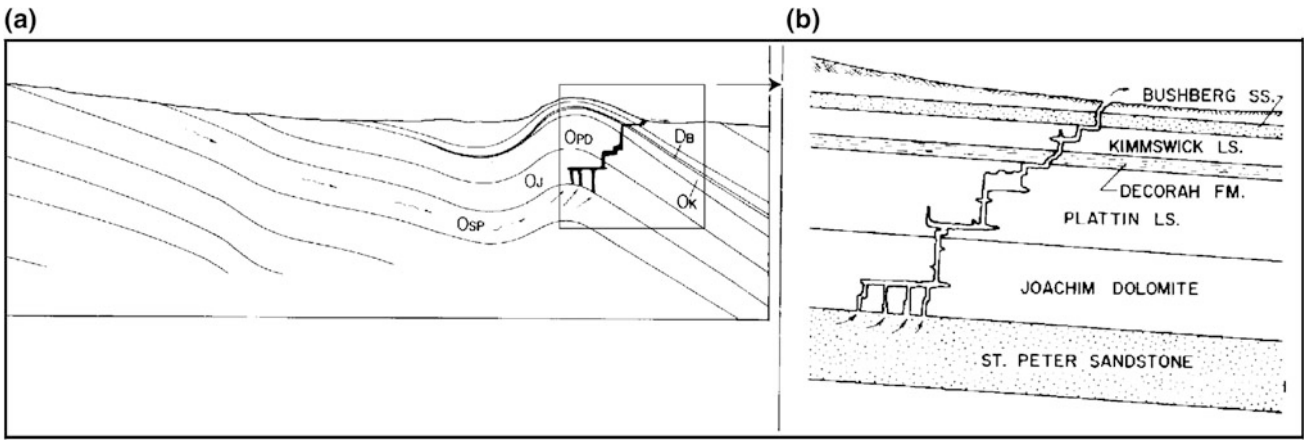

Fig. 13 Development of fracture-controlled caves and ascending shafts by flow rising along an anticlinal structure in eastern Missouri (from Brod 1964)

related to large basement-cored faults (Fig. 7) which could provide focused upflow of deep fluids to the cover. These factors favor cross-formational upward flow and hypogene karstification, mainly of the endogenous type, in such structures. Instances are numerous in many cratonic and foreland basins; see Brod (1964; Fig. 13) and Palmer et al. (Chap. 37) for notable examples, respectively, from Missouri State and the Bighorn Basin (Wyoming) in the USA.

5.4 Zones of Deep-Rooted Faults

Fluid flow in the lower hydrogeological stories of basins is strongly controlled by deep-rooted cross-formational faults and associated fracture zones, and the hydrodynamics largely depends on internal recharge/pressure sources (including those in the basement) and a degree of hydraulic communication with the upper-lying stories along such zones (see

Sect. 2.4.1; Figs. 6c and 7). These zones are, therefore, the most favorable loci for endogenous karstification in deep basin's sections, and the upward leakage of deep fluids along them often determines combined artesian/endogenous hypogene karstification in aquifers of the upper stories.

5.5 Young Disrupted Basins

In young intramountain basins with dominating geostatic regime, hypogene karstification is favored at marginal discharge areas where circulation systems of different origins and regimes may interact, such as meteoric water flows from adjacent margins or uplifted blocks, basinal fluids expelled from the basin's interiors, and deep endogenous fluids rising along deep-rooted faults from the basement (in tectonically active, extensional basins).

A remarkable example is the Buda Thermal Karst in Hungary, where groundwater systems of different regimes interact in the zone of the junction of the Transdanubian Range and the Tisza Basin, along the Danube valley (Mádl-Szőnyi et al. Chap. 17). It is important to note that speleogenesis of the outstanding caves in the Buda Hills, now uplifted to and above the drainage level of the Danube River, has likely occurred at depths greater than ca. 800 m, according to the fluid inclusion data (Dubljansky 2000), which is in agreement with the fact that large cavities at depth about 1000 m have been encountered by boreholes in the adjacent Pest plane.

5.6 Large Carbonate Platforms, Side-Open to the Ocean

Large carbonate platforms, side-open to the ocean, represent a peculiar setting where ascending flow across stratified sequences, driven by both topography-induced head gradients and density gradients, may involve mixing with seawater. Florida in the North America is a type example, though hypogene karst was only recently recognized in this region (Klimchouk 2007, 2013b; Cunningham and Walker 2009; Upchurch Chap. 49). Modern carbonate platforms with continuing sedimentation and their ancient buried counterparts are numerous around the globe. In the coastal areas, deeper flows of freshwater from inland higher-elevation areas can be forced to extend seaward below saline aquifers and rise across less permeable beds there to mix with saline water and develop macro-porosity, as shown in Figs. 8b and 14b.

In Florida, fresh groundwaters of the upper Floridan aquifer extend seaward for tens of km from the shore and rise from the shelf in many high-discharge submarine springs. At greater depth, in the lower Floridan aquifer, cool seawater intrudes along the coast and moves toward the platform interior, driven by the geothermal gradient and convective circulation within the Floridan aquifer system, as suggested by Kohout et al. (1977). The saline water can then rise in the coastal and inland areas through cross-formational discontinuities due to the geothermal heating (according to the Kohout's scheme; Krause and Randolph 1989; Spechler

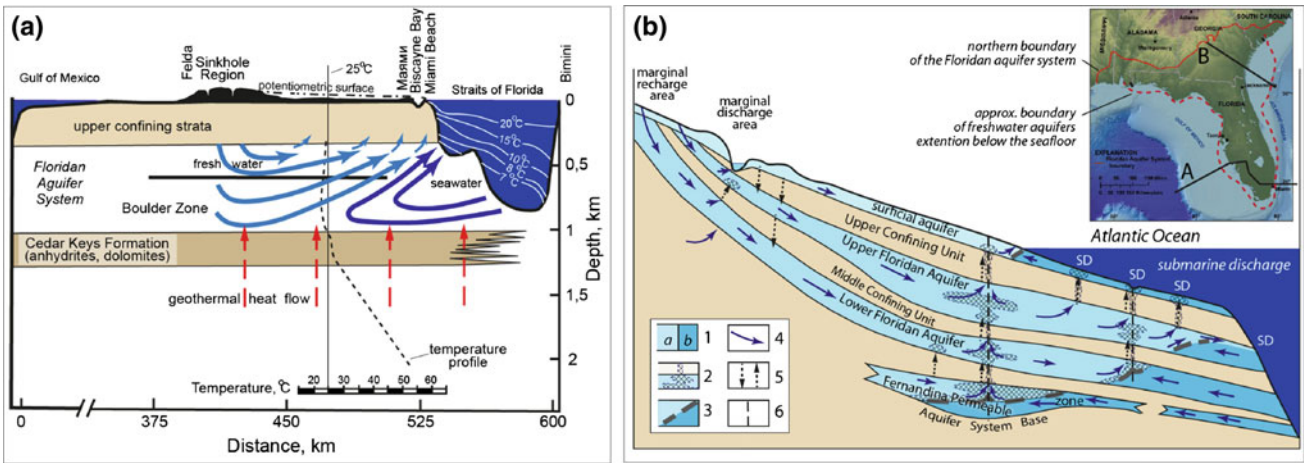

Fig. 14 Diagrams illustrating groundwater circulation in a confined aquifer system in coastal regions of large carbonate platforms side-open to the ocean (the example of the Florida Peninsula; from Klimchouk 2013b). **a** conceptual model of convective circulation driven by the geothermal gradient, with lateral inflow of seawater (redrawn after Kohout et al. 1977); the profile corresponds to A-line in the map inset. **b** possible localization of hypogene karstification in the Floridan aquifer system, using the example of a conceptual hydrogeological profile for the northeast part of Florida (B-line in the map inset). The profile is synthesized from drawings in Krause and Randolph (1989) and Spechler (1994). Legend: *1* groundwaters: a—fresh, b—saline; *2* zones of freshwater/saline water mixing and hypogene karstification; *3* zones of halocline speleogenesis; *4* directions of groundwater flow in aquifers; *5* directions of vertical leakages; *6* cross-formational permeable zones

1994), interacting with upper freshwater aquifers and inducing hypogene speleogenesis (Fig. 14; Klimchouk 2013b). This possibility is further discussed by Upchurch (Chap. 49). Flow simulation by Hughes et al. (2007) confirmed the Kohout's model and shown that the inflow of seawater from the Straits of Florida would be similar even without the heat flow, but the flow pattern would be more asymmetric in the platform cross section. Modeling by Jones and Xiao (2006) for a buried carbonate platform that hosts the supergiant Tengiz oil field in the northeastern Caspian (Kazakhstan) demonstrated that such circulation scheme could be an efficient engine for the development of dissolutional porosity during a pre-burial stage.

5.7 Areas of Young Volcanism

Specific and very favorable settings for hypogene speleogenesis are found in regions of young volcanism and related hydrothermal activity. They are characterized by the anomalous geothermal regime and commonly low-mineralized groundwaters (but sometimes brines) of specific chemical and gas composition, with high CO_2 and often substantial H_2S content. Geochemical indications for a contribution of magmatic fluids are found in many such regions. The presence of highly conductive disruptions provides good conditions for both, penetration of meteoric fluids to considerable depths, with their heating near shallow-lying magma chambers, and the focused raise of overpressured and hot gas–vapor fluids. Mixing of raising fluids with lateral flows in shallower stratal aquifers causes intense hypogene speleogenesis at the base or across carbonate and other rocks. Due to the focused character and high aggressiveness of raising fluid flows, voluminous cavities can form at depth, which is attested by large and deep collapse shafts (sinkholes) commonly found in these regions. Outstanding examples of volcanogenous hypogene speleogenesis, related to Miocene-Pleistocene or Pleistocene-Holocene volcanism, are the Zacaton System in the northeastern Mexico (Gary and Sharp 2006; Gary Chap. 52), the Konya Basin in Central Anatolia, Turkey (Bayari et al. 2009; Bayari et al. Chap. 27), the Mt Gambier area in southeastern Australia (Webb et al. 2010) and the Kavminvody and Kabardino-Balkaria regions in the North Caucasus in Russia (Vakhrushev 2009; Klimchouk 2013b). The latter region is located in a homocline artesian basin at the slope of the Great Caucasus orogen, in which the stratified Malm-Eocene cover is disrupted by numerous magmatic intrusions, injection uplifts and linear and concentric faults (Fig. 15a). Focused inflows of deep endogenous fluids, rich in CO_2, mix with lateral flows in stratal aquifers causing intense hypogene karstification. According to estimates by Vartanyan (1977), discharges of thermal waters in the Kavminvody region removed about 1400 km^3 of carbonate rocks from the subsurface during last 1.5 million years. To the southeast of Kavminvody, in the Kabardino-Balkaria region, a linear group of over 30 large collapse sinkholes is located, five of which host deep lakes (Fig. 15b). The deepest lake is Cerik-Kel measured to a depth of 368 m, followed by the Kel-Ketchkhen Lake, 177 m deep.

6 Lithogeodynamic Perspective of Endogenous Hypogene Karstification

Endogenous hypogene karst depends on the raising flow of hypogene fluids, and the potential for deep basement fluids to rise into the sedimentary cover is largely determined by the geodynamic regime. Therefore, the potential for global distribution of hypogene speleogenesis of the endogenous type can be accessed based on studies that summarize the geodynamic regimes and various signatures of deep fluid discharges around the globe. Such valuable study has been performed by Belenitskaya (2011) who compiled global data on modern discharges of raising fluids in sedimentary basins and their influence on sedimentary processes (Fig. 16). Only the "cold" branch of discharge (in the sense of Kropotkin 1986) has been analyzed, i.e., discharges which do not show obvious signs of links with magmatism, regulated mainly by seismo-tectonic activity (although they may have temperatures elevated up to 100–150 °C and more).

The "cold" discharges into sedimentary basins are understood as gas–liquid injections of mineralized waters and brines, oils, gasses (CH, H_2S, CO_2, H_2, N_2 and others), as well as their combinations with plastic-flowable (salt, clayey, etc.) and fluidized rock masses, that rise from basements composed of older sedimentary and metamorphic complexes (Belenitskaya 2011). The map in Fig. 16 shows the distribution of such discharges (diffused and focused fluid discharges, fields of mud volcanoes, areas of salt diapirism, etc.) on the background of the neo-geodynamic regimes.

Belenitskaya (2011) note that, as the map clearly demonstrates, discharges of different types are conjugated into large-scale associations, such as nodes, extensive zones and belts, the global distribution of which depends on the neo-geodynamic regimes. Discharges localize predominantly within modern active belts (including their peripheral areas)—riftogenic, activated passive margins, active margins and collision belts. Belenitskaya stresses the huge scale of the cold discharge phenomena, huge amounts of discharging masses and an importance of the fluid-induced lithogenesis. Although this map shows only modern discharges, similar relationships exist between past manifestations and paleo-geodynamic regionalization and phases of fluid paleo-activity.

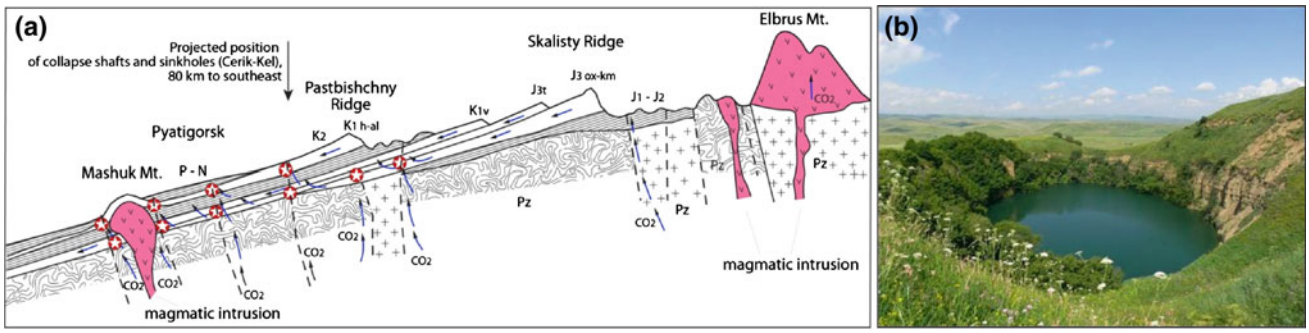

Fig. 15 Volcanogenic karst in the Caucasus Mineral Water Region (Russia): **a** geologic profile showing localization of hypogene karstification and some prominent features; **b** photograph of one of 40 deep sinkholes known in the area. Legend: *1* effusives and crypto-intrusives: predominantly freshwaters of the weathering crust; *2* Paleozoic granites: fresh and mineral waters containing CO_2 along tectonic faults; *3* Paleozoic crystalline schists: fracture fresh and mineral waters; *4* non-soluble rocks of the sedimentary cover: $K_{1\ h\text{-}al}$—sandstones, clays and argillites; P-N—marls with interbeds of sandstones and clays; *5* soluble rocks: $J_{3ox\text{-}km}$—medium- and thick-bedded limestones; J_{3t}—variegated sandy-clay succession with interbeds of limestones and lenses of gypsum; K_{1V}—dolomitic limestones; K_2—limestones and marls; *6* large tectonic faults; *7* directions of groundwater flow; *8* zones of intense intake of deep-seated CO_2 into limestones. Modified from Vakhrushev (2009)

Belenitskaya (2011) outlines a fluid-induced (fluidogenic) system of lithogenesis—the system composed of fluids themselves, the geofluid system of the crust, the plumbing system of the ascending fluid transfer, discharge modes and centers, areoles of their influence, fluid-induced biotopes, biocenoses and tafocenoses and the final segment—fluid-induced sediments and fluid-induced rock and ore associations. Hypogene karst (the process of karstification and its manifestations—void-conduits systems and associated altered rocks and mineral formations) are clearly an important component of the fluid-induced system of lithogenesis. Therefore, the regularities of the global distribution of the "cold" discharges are applicable to hypogene karstification, and the map in Fig. 16 can serve as a useful background for a future analysis, which is to be performed, of the global distribution of the phenomena in question. A comprehensive approach should include paleogeodynamic analysis and analysis of past fluid phases.

7 Outlook

Ascending fluid flow is ubiquitous in the upper crust. It overwhelmingly dominates in the domain of the endogenous regimes (in most of the upper crust) and is a significant component of flow patterns in the meteoric regime (in the uppermost part of the crust). Hypogene karstification occurs where the ascending flow of reactive fluids is structurally and/or stratigraphically focused and where dissolution-inducing disequilibrium conditions are supported for a sufficiently long time—mainly in zones of discharge and/or interaction of fluid flow systems and regimes of different nature, depth and scales. A wide range of P–T conditions and the variety of compositions of fluids within the upper crust offer a potential for diverse dissolution mechanisms to operate in a number of rocks including those (such as sandstones and quartzites) which were not commonly considered as karst-supporting within the traditional, dominantly epigenetic, karst paradigm. The time during which hypogene karstification may commence and develop in deep-seated rocks is much greater than common lifetimes for epigene karst systems in exposed formations. Geodynamic and hydrogeological evolution during long geological times causes the conditions prone to generate hypogene karst to migrate through the rock media, offering a potential for respective void-conduit structures to form at some depths in many regions. These reasons, along with a possibility of hypogene karst to develop not only in the continental crust but also in the oceanic, suggest that this phenomenon can be globally even more widespread than epigene karst.

Hypogene speleogenesis plays a very important role in the development of the cross-formational plumbing system in the upper crust, further focusing the flow and thus facilitating fluid migration, fluid-induced transformations of rocks and the formation of various anomalies in the geological media. It also plays an important role in the reservoir formation in reactive rocks, especially beneath hydrostratigraphic barriers. When formations hosting hypogene void-conduit structures are brought into the shallow subsurface and the weathering/denudation domain, such structures can greatly influence the geomorphic development and give rise to the formation of specific landscapes—a research field still to be appreciated by geomorphology.

An understanding of these roles of hypogene karstification dramatically expands both the realm of karst and the significance of karst science in the Earth sciences family, as compared to the traditional, dominantly epigenetic, karst paradigm. This has numerous scientific and practical

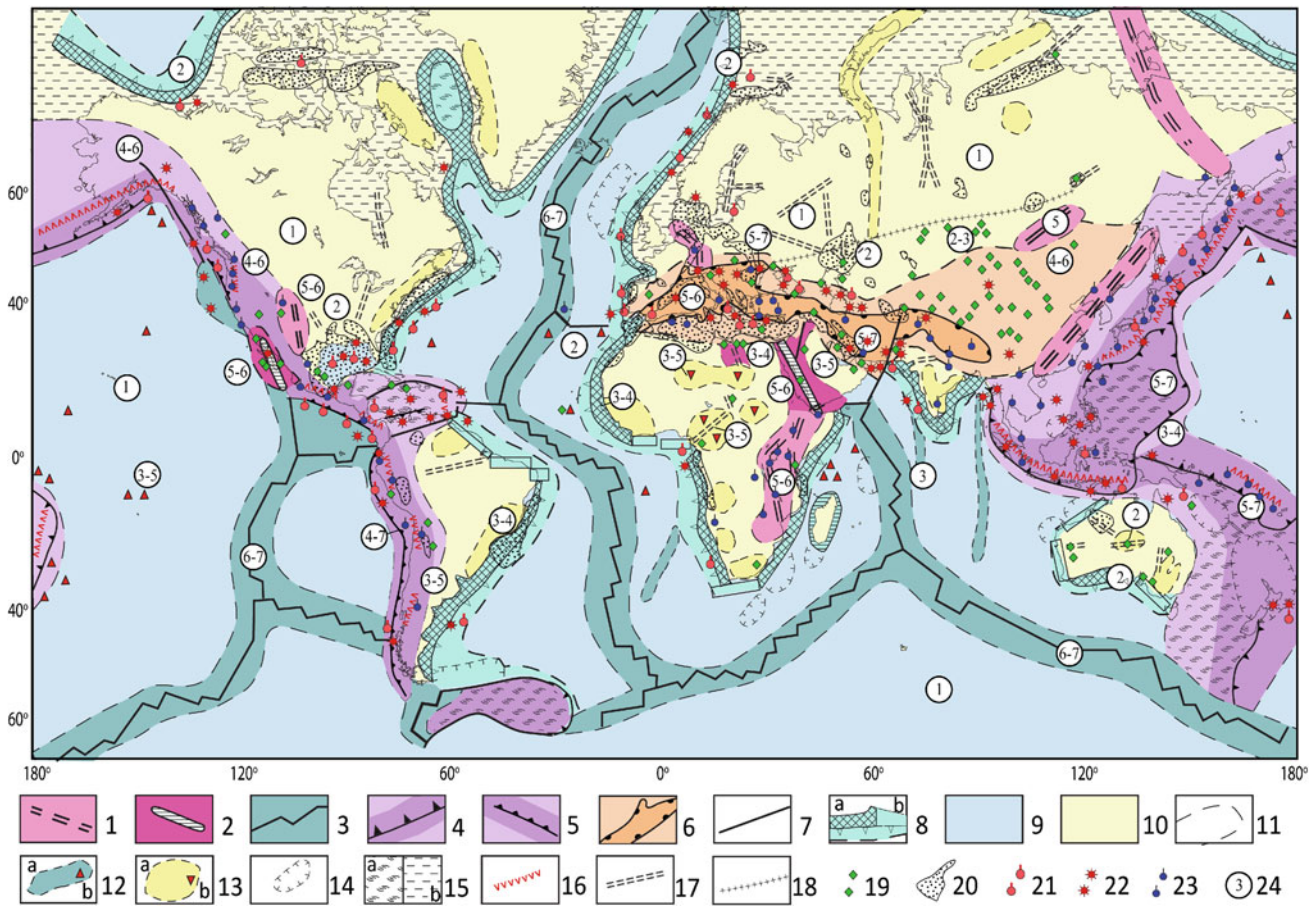

Fig. 16 Modern geodynamic and deep fluid activity in the world (redrawn from Belenitskaya 2011). Legend: 1–6—active geodynamic belts (pale coloring indicates peripheral zones): 1–3—rifting zones (*1* intracontinental, *2* intracontinental, *3* oceanic); *4* subduction zones related to island arcs; *5* subduction zones along continental margins; *6* collision zones; *7* transform plate boundaries; *8* passive margins of continents and large microcontinents: a—riftogenic, b—transform; 9–10 intraplate stable areas: *9* oceanic; *10* continental; *11* boundaries between areas of the different geodynamic regimes; *12–13* areas of intraplate activation, without (**a**) or with (**b**) manifestations of volcanism: *12* oceanic; *13* intracontinental; *14* submerged blocks with the continental crust in oceans (microcontinents, undersea plateaus); *15* water areas of marginal and inner seas: a—deepwater with the oceanic crust; b—wide shallow and shelf areas; *15* volcanic arcs; *16* buried rift fragments that control supra-rift depressions; *17* the northern boundary of the peri-orogenic region in Eurasia; *18* manifestations of modern discharge of brines and associated halogenesis; *19* areas of salt diapirism; *20* zones of intense discharge of hydrocarbon fluids in deepwater areas; *21* mud volcanoes; *22* hot springs; *23* hot springs; *24* rough estimate of the geodynamic and fluid activity (in arbitrary units: 1—minimal, 2—maximal)

implications. Hypogene karst studies hold a promise to crucially contribute to solving many problems in prospecting and exploration of deep petroleum, ore and geothermal resources associated with soluble formations. A proper reservoir characterization and modeling requires adequate genetic interpretation of void-conduit systems and understanding of their hydraulic functioning. As the role of hypogene karstification lays not only in enhancing reservoir properties but also in facilitating the vertical fluid migration across heterogeneous strata, it plays a dual role—it not only creates pathways for migration of hydrocarbons and metalliferous fluids to places of their subsequent accumulation but also contributes to the loss of the deposits by compromising the seal integrity. The latter aspect of hypogene karst has important implications also for environmental assessments related to exploration of unconventional oil and gas resources and geological sequestration of CO_2. The recognition of specific characteristics and functioning of hypogene karst is crucial for assessment and mitigation of environmental/engineering hazards, including sinkhole formation, groundwater inrushes to mines.

As shown in this chapter, potential localizations of hypogene karst are rather predictable at large to medium scales, based on the analysis of geological structure, hydrostratigraphy, regional hydrogeology, geodynamic and geomorphological evolution. However, this theoretical

possibility has to be fully realized through further synthesis and generalization of detailed regional and local studies that document field relationships.

Most of hypogene karst systems accessible for direct examination are relict, decoupled from their genetic environments and brought into the shallow subsurface from considerable, sometimes large, depth. Their studies, richly represented in this book, provide unique information about processes, conditions and controls of the formation of void-conduit systems at depth and about hydraulic functioning of these systems, which is indispensable for an adequate interpretation of data acquired from drilling and geophysical surveys.

References

Agar SM, Geiger S (eds) (2014) Fundamental controls on fluid flow in carbonates: current workflow to emerging technologies. The Geological Society of London, Special Publications, p 406

Ague JJ (2003) Fluid flow in the deep crust. In: Holland HD, Turrekian KK (eds) Treatise on geochemistry, vol 3. Elsevier, Amsterdam, pp 203–247

Andreychouk V, Dublyansky Y, Ezhov Y, Lysenin G (2009) Karst in the Earth's crust: its distribution and principal types. University of Silesia and Ukrainian Institute of Speleology and Karstology, Sosnowiec-Simferopol

Audra P, Mocochain L, Bigot J, Nobecourt JC (2009) Hypogene cave patterns. In: Klimchouk AB, Ford DC (eds) Hypogene speleogenesis and karst hydrogeology of artesian basins. Ukrainian Institute of Speleology and Karstology, Simferopol, pp 23–32

Audra P, Palmer AN (2015) Research frontiers in speleogenesis. Dominant processes, hydrogeological conditions and resulting cave patterns. Acta Carsologica 44(3):315–348

Bagdasarova MV (2001) Features of fluid systems of oil and gas accumulation zones and geodynamic types of oil and gas fields. Geol Nefti i Gaza (Russia) 3:50–56 (in Russian)

Bailey RC (1990) Trapping of aqueous fluids in the deep crust. Geophys Res Lett 17:1129–1132

Barlow PM (2003) Ground water in freshwater-saltwater environments of the Atlantic Coast. US Geological Survey, Reston, Virginia

Bayari CS, Özyurt N, Pekkan E (2009) Giant collapse structures formed by hypogenic karstification: the obruks of the Central Anatolia, Turkey. In: Klimchouk AB, Ford DC (eds) Hypogene speleogenesis and karst hydrogeology of Artesian Basins, Ukrainian Institute of Speleology and Karstology, Special Paper n. 1, Simferopol, pp 83–90

Beaudoin N, Bellahsen N, Lacombe O, Emmanuel L (2011) Fracture-controlled paleohydrogeology in a basement-cored, fault-related fold: Sheep Mountain Anticline, Wyoming, United States. Geochem Geophys Geosyst 12:Q06011

Beaudoin N, Huyghe D, Bellahsen N et al (2015) Fluid systems and fracture development during syn-depositional fold growth: an example from the Pico del Aguila anticline, Sierras Exteriores, southern Pyrenees, Spain. J Struct Geol 70:3–38

Bebout GE (2013) Metasomatism in subduction zones of subducted oceanic slabs, mantle wedges, and the slab-mantle interface. In: Harlov DE, Austrheim H (eds) Metasomatism and the chemical transformation of rock. Springer-Verlag, Berlin Heidelberg, pp 289–349

Belenitskaya GA (2011) "Fluid" branch of lithology: state of the art, objects, and challenges. Uchenyye Zap Kazanskogo Universiteta (Russia) 153(4):97–113 (in Russian)

Betzler C, Lindhorst S, Hübscher C, Lüdmann T (2011) Giant pockmarks in a carbonate platform (Maldives, Indian Ocean). Mar Geol 289:1–16. doi:10.1016/j.margeo.2011.09.004

Bigot JY (2010) Le karst du gypse. In: Audra P (ed) Grottes et karsts de France. Karstologia Mémoires, Association française de karstologie 19:86–87

Bjørlykke K (1993) Fluid flow in sedimentary basins. Sediment Geol 86(1):137–158

Bjørlykke K, Mo A, Palm E (1988) Modelling of thermal convection in sedimentary basins and its relevance to diagenetic reactions. Mar Pet Geol 5(4):338–351

Brandmeier M, Kuhlemann J, Krumrei I et al (2011) New challenges for tafoni research. A new approach to understand processes and weathering rates. Earth Surf Process Land 36(6):839–852

Bredehoeft JD, Back W, Hanshaw BB (1982) Regional ground-water flow concepts in the United States: historical perspective. GSA Spec Pap 189:295–316

Breeding CM, Ague JJ (2002) Slab-derived fluids and quartz-vein formation in an accretionary prism, Otago Schist, New Zealand. Geology 30:499–502

Brod LG (1964) Artesian origin of fissure caves in Missouri. National Speleol Soc Bull 26(3):83–112

Bucher K, Stober I (2010) Fluids in the upper crust. Geofluids 10:241–253

Budd DA, Vacher HL (2004) Matrix permeability of the confined Floridan Aquifer, Florida, USA. Hydrogeol J 12:531–554

Caciagli NC, Manning CE (2003) The solubility of calcite in water at 6–16 kbar and 500–800 °C. Contrib Mineral Petrol 146:275–285

Cartwright J, Santamarina C (2015) Seismic characteristics of fluid escape pipes in sedimentary basins: implications for pipe genesis. Mar Petrol Geol 65:126–140

Castany G (1981) Hydrogeology of deep aquifers. The hydrogeological basin as the basis of groundwater management. Episodes 3:18–22

Cathles III LM, Adams JJ (2005) Fluid flow and petroleum and mineral resources in the upper (< 20-km) continental crust. In: Hedenquist JW, Thompson JFH, Goldfarb RJ, RJP (eds) Economic geology; one hundredth anniversary volume, 1905–2005, Society of Economic Geologists, Littleton, CO, United States, pp 77–110

Chen D, Wu S, Völker D, Dong D et al (2015) Tectonically induced, deep-burial paleocollapses in the Zhujiang Miocene carbonate platform in the northern South China Sea. Mar Geol 364:43–52. doi:10.1016/j.margeo.2015.03.007

Chilingar GV, Buryakovsky LA, Eremenko NA et al (2005) Oil and gas bearing rocks. Dev Pet Sci 52:19–38

Condie KC (2001) mantle plumes and their record in Earth history. Cambridge University Press, Cambridge

Connolly JAD (1997) Devolatilization-generated fluid pressure and deformation-propagated fluid flow during prograde regional metamorphism. J Geophys Res 102:18149–18173

Connolly JAD (2010) The mechanics of metamorphic fluid expulsion. Elements 6:165–172

Connolly JAD, Podladchikov YY (2013) A hydromechanical model for lower crustal fluid flow. In: Harlov DE, Austrheim H (eds) Metasomatism and the chemical transformation of rock. Springer-Verlag, Berlin Heidelberg, pp 599–658

Crossey LJ, Fischer TP, Patchett PJ et al (2006) Dissected hydrologic system at the Grand Canyon: interaction between deeply derived fluids and plateau aquifer waters in modern springs and travertine. Geology 34(1):25–28

Crossey LJ, Karlstrom KE, Schmandt B et al (2016) Continental smokers couple mantle degassing and distinctive microbiology within continents. Earth Planet Sci Lett 435(2016):22–30

Crossey LJ, Karlstrom KE, Springer A et al (2009) Degassing of mantle-derived CO_2 and ^3He from springs in the southern Colorado Plateau region-flux rates, neotectonics connections, and implications for understanding the groundwater system. Geol Soc Am Bull 121:1034–1053

Crossey LJ, Shand P, Karlstrom KE et al (2011) The mound springs of the Great Artesian Basin, Australia: origin of a long-lived linked system of CO_2-rich springs and travertines. In: Abstracts of the 11th Australasian environmental isotope conference & 4th Australasian Research Conference, Cairns, 12–14 July 2011, James Cook University, p 72

Cubitt JM, England WA, Larter S (eds) (2004) Understanding petroleum reservoirs: Towards an integrated reservoir engineering and geochemical approach. Geological Society, London, Special Publications vol 237

Cunningham KJ, Walker C (2009) Seismic-sag structural systems in Tertiary carbonate rocks beneath southeastern Florida, USA: evidence for hypogenic speleogenesis? In: Klimchouk A, Ford D (eds) Hypogene speleogenesis and karst hydrogeology of artesian basins. Ukrainian Institute of Speleology and Karstology Special Paper 1, Simferopol, pp 151–158

Davies GR, Smith LB Jr (2006) Structurally controlled hydrothermal dolomite reservoir facies: an overview. AAPG Bulletin 90 (11):1641–1690

De Waele J, Audra P, Madonia G et al (2016) Sulphuric acid speleogenesis (SAS) close to the water table: examples from southern France, Austria, and Sicily. Geomorphology 253:452–467

Deming D (1994) Fluid flow and heat transport in the upper continental crust. Geol Soc Lond Spec Publ 78:27–42

Deming DC (2001) Introduction to hydrogeology. McGraw-Hill ISBN, Dubuque, Iowa

Djunin VI (2000) Hydrogeodynamics of deep horizons of oil-gas basins. Nauchnyy Mir, Moscow (in Russian)

Djunin VI, Korzun VI (2005) Hydrogeodynamics of oil-gas basins. Nauchnyy Mir, Moscow (in Russian)

Dolejs D, Manning CE (2010) Thermodynamic model for mineral solubility in aqueous fluids: theory, calibration and application to model fluid-flow systems. Geofluids 10:20–40

Dreybrodt W, Romanov D, Kaufmann G (2009) Evolution of isolated caves in porous limestone by mixing of phreatic water and surface water at the water table of unconfined aquifers: a model approach. J Hydrol 376:200–2008

Dubljansky YV (2000) Hydrothermal speleogenesis in the Hungarian Karst. In: Klimchouk A, Ford DC, Palmer AN, Dreybrodt W (eds) Speleogenesis: evolution of karst aquifers. National Speleological Society, Huntsville, pp 298–303

Dublyansky YV (2013) Karstification by geothermal waters. In: Shroder J (Editor in Chief), Frumkin A (ed) Treatise on geomorphology, vol 6 karst geomorphology. Academic Press, San Diego, pp 57–71

Dubois C, Quinif Y, Baele JM et al (2014) The process of ghost-rock karstification and its role in the formation of cave systems. Earth-Sci Rev 131:116–148

Ernst RE and Buchan KL (eds) (2001) Mantle plumes: their identification through time. Geological Society of America Special Papers 352, Boulder, Colorado

Etheridge MA, Wall VJ, Vernon RH (1983) The role of the fluid phase during regional metamorphism and deformation. J Metamorph Geol 1:205–226

Ezhov YA (1978) On chemical inversion in the subterranean hydrosphere. Sovetskaja Geologiia (Soviet Geol) 12:132–136 (in Russian)

Ezhov YA, Lysenin GA (1986) Vertical hydrodynamic zoning of the Earth's crust. Sovetskaja Geologiia (Sov Geol) 8:111–120 (In Russian)

Ezhov YA, Lysenin GA (1988) The significance of the zone of transitional pressures in the subterranean hydrosphere. Sovetskaja Geologiia (Sov Geol) 8:107–114 (In Russian)

Ezhov YA, Lysenin GP (1990) Vertical zonation of karst development. Izvestija AN SSSR serija geologii 4:108–116 (in Russian)

Ezhov YA, Vdovin YP (1970) On the hydrodynamic zoning of the Earth's crust. Sovetskaja Geologiia (Sov Geol) 8:66–76 (In Russian)

Ezhov YA, Lysenin GP, Andreychouk VN, Dublyansky VN (1992) Karst in the Earth's crust. Sibirskoye otdeleniye Instituta geologii, Novosibirsk

Ford DC, Williams PW (1989) Karst geomorphology and hydrology. Unwin Hyman, London

Fournier RO (1991) The transition from hydrostatic to greater than hydrostatic fluid pressures in presently active continental hydrothermal systems in crystalline rock. Geophys Res Lett 18:955–958

Frape SK, Blyth A, Blomqvist R et al (2004) Deep fluids in the continents: II. Crystalline rocks. In: Drever JI, Holland HD, Turekian KK (eds) Treatise on geochemistry vol 5, Surface and ground water, weathering, and soils. Elsevier, Amsterdam, pp 541–580

Freeze RA, Witherspoon PA (1966) Theoretical analysis of regional groundwater flow. 2. Effect of water-table configuration and subsurface permeability variations. Water Resour Res 3(2):623–635

French SW, Romanowicz B (2015) Broad plumes rooted at the base of the Earth's mantle beneath major hotspots. Nature 525:95–99

Frost R, Bucher K (1994) Is water responsible for geophysical anomalies in the deep continental crust? A petrological perspective. Tectonophysics 231:293–309

Fyfe WS, Price NJ, Thompson AB (1978) Fluids in the Earth's crust. Elsevier, Amsterdam

Galloway WE, Hobday DK (1996) Depositional systems and basin hydrology. In: Galloway WE, Hobday DK (eds) Terrigenous clastic depositional systems, pp 297–326

Garven G (1985) The role of regional fluid-flow in the genesis of the Pine Point deposit, western Canada sedimentary basin. Econ Geol 80:307–324

Gary MO, Sharp JM (2006) Volcanogenic karstification of Sistema Zacatón, Mexico. In: Harmon RS, Wicks CW (eds) Perspectives on karst geomorphology, hydrology and geochemistry, GSA Special Paper 404. Boulder, Colorado, pp 79–89

Girinsky NK (1947) Some questions of groundwater dynamics. Gidrogeologija i inzhenernaja geologija (USSR) 9:27–32 (in Russian)

Goudie AS, Viles HA (1997) Tafoni, alveoles, honeycombs, and overhangs, in salt weathering hazards. Wiley, New York

Groom KM, Allen CD, Mol L et al (2015) Defining tafoni: re-examining terminological ambiguity for cavernous rock decay phenomena. Prog Phys Geogr 39(6):775–793

Hanor JS (1987) Origin and migration of subsurface sedimentary brines. SEPM short course lecture notes 21, Society of Economic Paleontologists and Mineralogis, Tulsa

Hantush MS, Jacob CE (1954) Plane potential flow of ground water with linear leakage. EOS Trans AGU 35(6):917–936. doi:10.1029/TR035i006p00917

Hantush MS, Jacob CE (1955) Nonsteady radial flow in an infinite leaky aquifer. Trans Am Geophys Union 36:95–100

Harlov DE, Austrheim H (eds) (2013) Metasomatism and the chemical transformation of rock. Springer, Berlin-Heidelberg

Hiscock KM, Bense VF (2014) Hydrogeology: principles and practice, 2nd edn. Wiley, New York

Hitchon B (1969) Fluid flow in western Canada sedimentary basin 1. Effect of topography. Water Resour Res 5:186–195

Hovland M (2003) Geomorphological, geophysical, and geochemical evidence of fluid flow through the seabed. J Geochem Explor 78:287–291

Hovland M, Gardner JV, Judd AG (2002) The significance of pockmarks to understanding fluid flow processes and geohazards. Geofluids 2(2):127–136

Hughes JD, Vacher HL, Sanford WE (2007) Three-dimensional flow in the Florida platform: theoretical analysis of Kohout convection at its type locality. Geology 35(7):663–666

Huntoon PW (1995) Is it appropriate to apply porous media groundwater circulation models to karstic aquifers? In: El-Kadi A (ed) Groundwater models for resources analysis and management. Lewis Publishers, Boca Raton, pp 339–358

Ignatovich NK (1950) Zoning, formation and activity of groundwater in relation with geostructures development. In: Voprosy gidrogeologii I inzhenernoy geologii [Questioins of hydrogeology and engineering geology] vol 13, Izdatelstvo MGU, Moscow, pp 6–22 (in Russian)

Ingebritsen SE, Appold MS (2012) The physical hydrogeology of ore deposits. Econ Geol 107(4):559–584

Ingebritsen SE, Manning CE (2003) Implications of crustal permeability for fluid movement between terrestrial fluid reservoirs. J Geochem Explor 78–79:1–6

Ingebritsen SE, Manning CE (2010) Permeability of the continental crust: dynamic variations inferred from seismicity and metamorphism. Geofluids 10(1–2):193–205

Ingebritsen SE, Sanford WE, Neuzil CE (2006) Groundwater in geologic processes, 2nd edn. Cambridge University Press, Cambridge

Italiano F, Yuce G, Uysal IT, Gasparon M, Morelli G (2013) Insights into mantle-type volatiles contribution from dissolved gases in artesian waters of the Great Artesian Basin, Australia. Chem Geol 378–379:75–88. doi:10.1016/j.chemgeo.2014.04.013

Ivanov SN (1966) Singularities of hydrothermal ore formation beneath the continental surface and sea. Doklady AN SSSR 169(1):177–180 (in Russian)

Ivanov SN (1970) Maximum depth of open fractures and hydrodynamic zoning of the Earth's crust. In: Exhegodnik Instituta geol. geochim. Uralskogo filiala AN SSSR, Sverdlovsk, pp 212–233 (in Russian)

Ivanov SN, Ivanov KS (1993) Hydrodynamic zoning of the Earth's crust and its significance. J Geodyn 17(4):155–180

Jones GD, Xiao Y (2006) Geothermal convection in the Tengiz carbonate platform, Kazakhstan: reactive transport models of diagenesis and reservoir quality. AAPG Bull 90(8):1251–1272

Karlstrom KE, Crossey LJ, Hilton DR, Barry PH (2013) Mantle ^{3}He and CO_2 degassing in carbonic and geothermal springs of Colorado and implications for neotectonics of the Rocky Mountains. Geology 41(4):495–498

Kartsev AA, Vagin SB, Baskov EA (1969) Paleohydrogeology. Nedra, Moscow (in Russian)

Kennedy BM, Van Soest MC (2007) Flow of mantle fluids through the ductile lower crust: Helium isotope trends. Science 318 (5855):1433–1436

Kharaka YK, Hanor JS (2004) Deep fluids in the continents: I. sedimentary basins. In: Drever JI, Holland HD, Turekian KK (eds) Treatise on geochemistry vol 5, Surface and ground water, weathering, and soils. Elsevier, Amsterdam, pp 499–540

Kirkinskaya VN, Smekhov EM (1981) Carbonate rocks—reservoirs of oil and gas. Nedra, Leningrad (in Russian)

Kissin IG (1967) Hydrodynamic anomalies in the underground hydrosphere. Nauka, Moscow

Kissin IG (1985) Hydrodynamic regime and geological cycle of water in the Earth's crust. In: Underground waters and evolution of the lithosphere vol. 2, Nauka, Moscow, pp 31–35 (in Russian)

Kissin IG (2009) Fluids in the Earth's crust: geophysical and tectonic aspects. Nauka, Moscow (in Russian)

Klimchouk AB (2007) Hypogene Speleogenesis: Hydrogeological and Morphogenetic Perspective. National Cave and Karst Research Institute, Special Paper No. 1, Carlsbad, New Mexico. 106 pp

Klimchouk A (2012) Speleogenesis, hypogenic. In: Culver DC, White BW (eds) Encyclopedia of caves, 2nd edn. Elsevier, Chennai, pp 748–765

Klimchouk AB (2013a) Hypogene speleogenesis. In: Shroder J (Editor in Chief), Frumkin A (ed) Treatise on geomorphology, vol 6 karst geomorphology. Academic Press, San Diego, pp 220–240

Klimchouk AB (2013b) Hypogene speleogenesis, its hydrogeological significance and the role in evolution of karst. DIP, Simferopol (in Russian)

Klimchouk AB (2013c) Hydrogeological approach to distinguishing hypogene speleogenesis settings. In: International symposium on hierarchical flow systems in Karst Regions, Book of Abstracts, Sep. 2013, Budapest, Hungary, pp 94

Klimchouk A (2014) The methodological strength of the hydrological approach to distinguishing hypogene speleogenesis. In: Klimchouk A, Sasowsky ID, Mylroie JE et al (eds) Hypogene karst morphologies, Karst Waters Institute Special Publication 18, pp 4–12

Klimchouk A (2015) The karst paradigm: changes, trends and perspectives. Acta Carsologica 44(3):289–313

Klimchouk AB, Ford DC, Palmer AN, Dreybrodt W (eds) (2000) Speleogenesis: evolution of karst aquifers. National Speleological Society, Huntsville (AL), p 527

Klimchouk AB, Pronin KK, Timokhina EI (2010) Speleogenesis in the Pontian limestones of Odessa. Speleol Karstology (Ukraine) 5:76–93 (in Russian)

Klimchouk AB, Tymokhina EI, Amelichev GN et al (2013) Hypogene karst of the Crimean Piedmont and its geomorphological role. DIP, Simferopol (in Russian)

Kohout FA, Henry HR, Banks JE (1977) Hydrology related to geothermal conditions of the Floridan Plateau. In: Smith KL, Griffin GM (eds) The geothermal nature of the Floridan Plateau, Florida Department of Natural Resources Bureau of Geology Special Publication 21, pp 1–34

Korzhinskii DS (1953) Infiltration metasomatism at the presence of temperature gradient and contact metasomatic leaching. Zapiski Vses Mineral Obshch (Russia) 282:161–172 (in Russian)

Korzhinskiy DS (1957) Physico-chemical basement of the mineral parageneses analysis. Nauka, Moscow (In Russian)

Krause RE, Randolph RB (1989) Hydrology of the Floridan aquifer system in southeast Georgia and adjacent parts of Florida and South Carolina. U.S. Geological Survey Professional Paper 1403-D, USGS, Reston, VA (US)

Kropotkin PN (1986) Degassing of Earth and the origin of hydrocarbons. Zjurnal Vsesojuznogo Khimicheskogo Obshchestva (USSR) 31(5):481–587 (in Russian)

Kulongoski JT, Hilton DR, Izbicki JA (2005) Source and movement of helium in the eastern Morongo groundwater Basin: the influence of regional tectonics on crustal and mantle helium fluxes. Geochim Cosmochim Acta 69(15):3857–3872

Kyser K, Hiatt EE (2003) Fluids in sedimentary basins: an introduction. J Geochem Explor 80:139–149

Land L, Huff GF (2010) Multi-tracer investigation of groundwater residence time in a karstic aquifer: Bitter Lakes National Wildlife Refuge, New Mexico, USA. Hydrogeol J 18:455–472

Land LA (2003) Evaporite karst and regional ground water circulation in the lower Pecos Valley. In: Johnson KS, Neal JT (eds) Evaporite Karst and engineering/environmental problems in the United States, Oklahoma Geological Survey Circular 109. Norman, Oklahoma Geological Survey, pp 227–232

Larson RL (1991) Geological consequences of superplumes. Geology 19(10):963–966

Letnikov FA (1992) Super-deep fluid systems of Earth. Nauka, Novosibirsk (in Russian)

Letnikov FA (2001) Super-deep fluid systems of Earth and problems of ore formation. Geologiya rudnych mestorozhdeniy 43(4):291–307 (in Russian)

Letnikov FA, Dorogokupets PI (2001) To the question of the role of super-deep fluid systems of the Earth's core in endogenous geological processes. Doklady NAN 378(4):535–537 (in Russian)

Liebscher A (2010) Aqueous fluids at elevated pressure and temperature. Geofluids 10(1–2):3–19

Lindgren W (1925) Metasomatism. GSA Bulletin 36(1):247–262

Llamas MR, Cruces de Abia J (1978) Conceptual and digital models of the ground water flow in the Tertiary basin of the Tagus River (Spain). In: Proceedings of the international hydrogeological conference, Budapest, pp 186–202

Lukin AE (2014) Fluid-induced lithogenesis—the most important direction of lithological research in XXI century. Geologichnyy Zhurnal (Ukraine) 4:27–42 (in Russian)

Lukin AE (2015) The system "superplume—deep-seated segments of petroliferous basins"—an inexhaustible source of hydrocarbons. Geologichnyy Zhurnal (Ukraine) 2:7–20 (in Russian)

Malyshev AE (2011) Gas factor in endogenous processes. Ekaterinburg (in Russian)

Manning CE, Ingebritsen SE (1999) Permeability of the continental crust: implications of geothermal data and metamorphic systems. Rev Geophys 37:127–150

Martini IP (1978) Tafoni weathering, with examples from Tuscany, Italy. Zeitschrift fur Geomorphol 22(1):44–67

Maruyama S, Yuen DA, Windley BF (2007) Dynamics of plumes and superplumes through time. In: Yuen A, Naruyama S, Karato S-I et al (eds) Superplumes: beyond plate tectonics. Springer, New York

McBride EF, Picard MD (2004) Origin of honeycombs and related weathering forms in Oligocene Macigno sandstone, Tuscan coast near Livorno, Italy. Earth Surf Process Land 29:713–735. doi:10.1002/esp.1065

McCartney RA, Winefield P, Webb P, Kuhn O (2004) Spatial variations in the composition of formation waters from the central North Sea: implications for fluid flow in the deep high-pressure high-temperature hydrocarbon play. In: Cubitt JM, England WA and Larter S (eds) Understanding petroleum reservoirs: towards an integrated reservoir engineering and geochemical approach. Geological Society, London, Special Publications 237, pp 283–303

Michaud F, Chabert A, Collot J-Y et al (2005) Fields of multi-kilometer scale sub-circular depressions in the Carnegie Ridge sedimentary blanket. Mar Geol 216(4):205–219. doi:10.1016/j.margeo.2005.01.003

Mjatiev AN (1947) Confined complex of underground waters and wells. Izvestija AN SSSR otd. tekhnich. nauk 9:33–47 (in Russian)

Mukhin YV (1965) Processes of compaction of clay sediments. Nedra, Moscow (in Russian)

Murakami M, Hirose K, Yurimoto H et al (2002) Water in Earth's lower mantle. Science 295:1885–1887

Mustoe GE (1983) Origin of honeycomb weathering. GSA Bulletin 93:108–115

Mylroie JE, Carew JL (1990) The flank margin model for dissolution cave development in carbonate platforms. Earth Surf Process Land 15:413–424

Mylroie JE, Carew JL (1995) Karst development on carbonate islands. In: Budd DA, Harris PM, Saller A (eds) Unconformities and porosity in carbonate strata. AAPG Memoir 63:55 − 76

Newell DL, Crossey LJ, Karlstrom KE et al (2005) Continental-scale links between the mantle and groundwater systems of the western United States: evidence from travertine springs and regional He data. GSA Today 15(12):4–10

Newton RC, Manning CE (2002) Experimental determination of calcite solubility in H_2O-NaCl solutions at deep crust/upper mantle pressures and temperatures: implications for metasomatic processes in shear zones. Am Mineral 87:1401–1409

Newton RC, Manning CE (2005) Solubility of anhydrite, $CaSO_4$, in NaCl–H_2O solutions at high pressures and temperatures: applications to fluid–rock interaction. J Petrology 46(4):701–716

Northup DE, Dahm CN, Melim LA et al (2000) Evidence for geomicrobiological interactions in Guadalupe caves. J Cave Karst Studies 62(2):80–90

Oppenheimer C, Fischer TP, Scaillet B (2014) Volcanic degassing: process and impact. In: Turekian KK, Holland HD (eds) Treatise on geochemistry, vol 4, 2nd edn., The CrustElsevier-Pergamon, Oxford, pp 111–179

Palmer AN (1991) Origin and morphology of limestone caves. GSA Bulletin 103:1–21

Palmer AN (2000) Hydrogeologic control of cave patterns. In: Ford D, Palmer A, Dreybrodt W (eds) Klimchouk A. Evolution of Karst Aquifers, National Speleological Society, Huntsville (AL), Speleogenesis, pp 77–90

Palmer AN (2007) Cave geology. Cave Books, Dayton

Palmer AN (2013) Sulfuric acid caves: morphology and evolution. In: Shroder J (Editor in Chief), Frumkin A (ed) Treatise on geomorphology, vol 6 karst geomorphology. Academic Press, San Diego, pp 241–257

Paradise TR (2013) Tafoni and other rock basins. In: Shroder J (ed) Treatise on geomorphology. Academic Press, San Diego, pp 111–126

Phillips OM (1991) Flow and Reactions in permeable rocks. Cambridge University Press, Cambridge

Pinneker EV (1977) Problems of regional hydrogeology: regularities of distribution and formation of groundwaters. Nauka, Novosibirsk

Pinekker EV (ed) (1980) Principles of hydrogeology. General Hydrogeology, Nauka Siberian Branch, Novosibirsk, p 231

Pinneker EV (1983) General hydrogeology. Cambridge University Press, Cambridge

Poage MC, Chamberlain CP, Craw D (2000) Massif-wide metamorphism and fluid evolution at Nanga Parbat, northern Pakistan. Am J Sci 300:463–482

Pospelov GL (1973) Paradoxes, physicochemical nature and mechanisms of metasomatism. Nauka, Novosibirsk (in Russian)

Putnis A (2002) Mineral replacement reactions: from macroscopic observations to microscopic mechanisms. Mineral Mag 66:689–708

Quinif Y, Bruxelles L (2011) L'altération de type "fantôme de roche": processus, évolution et implications pour la karstification. Géomorphologie 4:349–358

Rodriguez-Navarro C (1998) Evidence of honeycomb weathering on Mars. Geophys Res Lett 25(17):3249–3252

Rubenach M (2013) Structural controls of metasomatism on a regional scale. In: Harlov DE, Austrheim H (eds) Metasomatism and the chemical transformation of rock. Springer-Verlag, Berlin Heidelberg, pp 93–140

Schmandt B, Jacobsen SD, Becker TW et al (2014) Dehydration melting at the top of the lower mantle. Science 344(6189):1265–1268

Schmidt MW, Poli S (2014) Devolatilization during subduction. In: Turekian KK, Holland HD (eds) Treatise on geochemistry, vol 4, 2nd edn., The CrustElsevier-Pergamon, Oxford, pp 669–701

Schmidt VA (1974) The paleohydrology of Laurel Caverns, Pennsylvania. In: Proceedings of the 4th conference on karst geology and hydrology, Morgantown, W.Va, West Virginia Geological and Economic Survey, pp 123–128

Shepherd M (2009) Oil field production geology. AAPG Memoir 91

Sherwood-Lollar B, Ballentine CJ, O'Nions RK (1997) The fate of mantle-derived carbon in a continental sedimentary basin: integration of C/He relationships and stable isotopic signatures. Geochim Cosmochim Acta 61(11):2295–2307

Shestopalov VM (1981) Natural resources of underground water of platform artesian basins of Ukraine. Naukova Dumka, Kiev (In Russian)

Shestopalov VM (1988) Methods of study of underground water natural resources. Nedra, Moscow (in Russian)

Shestopalov VM (2014) On hydrodynamic zoning and water exchange in hydrogeologic structures. Geologichesky Zhurnal 4(349):9–26 (In Russian)

Shestopalov VM (ed) (1989) Water exchange in hydrogeological structures of Ukraine. Water exchange under natural conditions, Naukova Dumka, Kiev (in Russian)

Shmulovich KI, Yardley BWD, Gontchar GG (1994) Fluids in the crust. Chapman & Hall, London

Shvartzev SL (1996) General hydrogeology. Nedra, Moscow (in Russian)

Sibson RH, Moore JMM, Rankin AH (1975) Seismic pumping—a hydrothermal fluid transport mechanism. J Geol Soc 131(6):653–659

Sokolov DS (1962) Principal conditions of karst development. Gosgeoltehizdat, Moscow (in Russian)

Spechler RM (1994) Saltwater Intrusion and quality of water in the Floridan aquifer system, northeastern Florida. U.S. Geological survey Water-Resources Investigations Report 92-4174, USGS, Tallahassee, Florida

Spilde MN, Boston PJ, Northup DE (2003) Subterranean soil development. J Cave Karst Stud 65(3):188

Spilde MN, Kooser A, Boston PJ at al (2009) Speleosol: a subterranean soil. In: Proceedings of the 15th international congress of speleology, Kerrville, Texas, pp 338–344

Stober I, Bucher L (2004) Fluid sinks within the Earth's crust. Geofluids 4:143–151

Templeton AS, Chamberlain CP, Koons PO et al (1998) Stable isotopic evidence for mixing between metamorphic fluids and surface-derived waters during recent uplift of the southern Alps, New Zealand. Earth Planet Sci Lett 154:73–92

Tóth J (1963) A theoretical analysis of groundwater flow in small drainage basins. J Geophys Res 68:4795–4812

Tóth J (1995) Hydraulic continuity in large sedimentary basins. Hydrogeol J 3(4):4–15

Tóth J (2009) Gravitational systems of groundwater flow: theory, evaluation, utilization. Cambridge University Press, Cambridge

Turkington AV (2004) Cavernous weathering. In: Goudie AS (ed) Encyclopedia of geomorphology, vol 1. Routledge, London, pp 128–130

Turkington AV, Phillips JD (2004) Cavernous weathering, dynamical instability and self-organization. Earth Surf Process Land 29:665–675

Turkington AV, Paradise TR (2005) Sandstone weathering: a century of research and innovation. Geomorphology 67(1):229–253

Uma KO, Mosto Onuoha K (1997) Hydrodynamic flow and formation pressures in the Anambra basin, southern Nigeria. Hydrol Sci J 42 (2):141–154

Unsworth M, Rondenay S (2013) Mapping the distribution of fluids in the crust and lithospheric mantle utilizing geophysical methods. In: Harlov DE, Austrheim H (eds) Metasomatism and the chemical transformation of rock. Springer-Verlag, Berlin Heidelberg, pp 535–598

Vakhrushev BA (2009) Singularities of hypogene speleogenesis of the mountain-folded region of Western Caucasus. In: Klimchouk AB, Ford DC (eds) Hypogene speleogenesis and karst hydrogeology of Artesian Basins Special Paper 1. Ukrainian Institute of Speleology and Karstology, Simferopol, pp 271–276 (in Russian)

Vartanyan GS (1977) Deposits of carbonated waters of mountain folded regions. Nedra, Moscow (in Russian)

Vergari A (1998) Nouveau regard sur la spéléogénèse: le "pseudo-endokarst" du Tournaisis (Hainaut, Belgique). Karstologia 31:12–18

Vergari A, Quinif Y (1997) Les paléokarsts du Hainaut (Belgique). Geodin Acta 10(4):175–187

Viles H (2005) Self-organized or disorganized? Towards a general explanation of cavernous weathering. Earth Surf Process Land 30:1471–1473

Vsevolozhskiy VA (1983) Groundwater flow and water balance of platform structures. Nedra, Moscow (in Russian)

Vsevolozhskiy VA (2007) Principles of hydrogeology. Moscow University Publ, Moscow (in Russian)

Vsevologhskiy VA, Dyunin VI (1996) Analysis of hydrodynamics regularities of deep stratal aquifer systems. Vestnik MGU Serija geol. 3:61–72 (in Russian)

Vsevolozhskiy VA, Kireeva TA (2009) On the problem of the formation of inversions in hydrochemical zoning. Vestnik MGU seriya Geologiya (Russia) 5:19–25 (in Russian)

Vsevolozhskiy VA, Kireeva TA (2014) The role of endogenous fluids in the formation of vertical hydrogeological zoning of oil-gas-bearing basins of the platform type. Glubinnaja Neft (Deep Oil) 1, [http://journal.deepoil.ru/index] (in Russian)

Warren J (2000) Dolomite: occurrence, evolution and economically important associations. Earth-Sci Rev 52(1):1–81

Warren JK (2006) Evaporites: sediments, resources and hydrocarbons. Springer-Verlag, Berlin Heidelberg

Webb JA, Grimes KG, Lewis ID (2010) Volcanogenic origin of cenotes near Mt Gambier, southeastern Australia. Geomorphology 119 (1):23–35

Weinlich FN, Tesar J, Weise SM et al (1998) Gas flux distribution in mineral springs and tectonic structures in the western Eger Rift. J Czech Geol Soc 43(1–2):91–110

Wing BA, Ferry JM (2002) Three-dimensional geometry of metamorphic fluid flow during Barrovian regional metamorphism from an inversion of combined petrologic and stable isotopic data. Geology 30:639–643

Worthington SRH, Ford DC (2009) Self-organized permeability in carbonate aquifers. Ground Water 47(3):326–336

Xu S, Nakai SI, Wakita H et al (1995) Helium isotope compositions in sedimentary basins in China. Appl Geochem 10(6):643–656

Yardley BWD (2013) The chemical composition of metasomatic fluids in the crust. In: Harlow DE, Austrheim H (eds) metasomatism and the chemical transformation of rock the role of fluids in terrestrial and extraterrestrial processes. Springer-Verlag, Berlin Heidelberg, pp 17–52

Yardley BW, Bodnar RJ (2014) Fluids in the continental crust. Geochem Perspect 3(1):1–2

Young R, Young A (1992) Sandstone landforms, 11. Springer series in physical environment. Springer, Heidelberg-Berlin

Yuen A, Naruyama S, Karato S-I et al (eds) (2007) Superplumes: beyond plate tectonics. Springer, New York
Zharikov V, Pertsev N, Rusinov V et al (2007) Metasomatism and metasomatic rocks. In: Fettes D, Desmons J (eds) Metamorphic rocks: a classification and glossary of terms. Cambridge University Press, Cambridge, pp 58–68
Zharikov VA, Rusinov VL, Marakushev AA et al (1998) Metasomatism and metasomatic rocks. Nauchnyy Mir, Moscow (in Russian)
Zverev VP (1999) Mass flows of the underground hydrosphere. Nauka, Moscow, pp 96 (in Russian)

Part I
Europe

Hypogenic Caves in the UK

2

Andrew R. Farrant and Tony Harrison

Abstract

The UK has a wide variety of hypogenic caves, including transverse maze caves, relict hydrothermal caves, gypsum mazes and hypogenic karst associated with water rising up deep thrust faults. While few of these are particularly extensive, they offer insights into the mechanisms of speleogenesis and mineralisation. The best developed hypogenic caves in the UK are in the Carboniferous limestones of northern England where at least nine network maze caves with plan lengths exceeding 1 km are known, almost all of which are accessible only via disused mine workings. In South Wales, relict hypogenic cave networks have been documented from cave systems surrounding the South Wales Coalfield. Hydrothermal cave systems are also known in the Bristol region in southern England, the Derbyshire Peak District and North Wales where they are associated with Pb–Zn mineralisation. In all three of these areas, active deep phreatic groundwater circulation is ongoing. Elsewhere in the UK, transverse artesian groundwater flow through Permo-Triassic gypsum in the Ripon area has led to the development of hypogenic cave systems and numerous sinkholes. This chapter documents for the first time all the known hypogenic cave systems found in the UK, discusses their modes of formation and outlines the potential for future discoveries.

Keywords

UK • Hypogene karst • Northern England • Maze caves

1 Introduction

The UK has many distinct karst regions, predominantly developed within limestones of Early Carboniferous age (Fig. 1), although significant karst also occurs in Devonian limestones in southwest England, Cambrian limestones in Scotland, and within Permian and Triassic evaporites in Northern England and the Midlands. Each has a distinctive character and style of cave development. The vast majority of UK caves are epigenic, but significant hypogenic karst does occur, particularly associated with Pb–Zn mineralisation hosted in the Carboniferous limestones. Two main types of hypogenic caves occur in the UK: isolated phreatic vein cavities associated with deep phreatic dissolution along mineral veins; and maze caves associated with transverse rising artesian flow (Klimchouk 2000). The latter occurs in both limestones and Permian gypsum aquifers.

A.R. Farrant (✉)
British Geological Survey, Keyworth, Nottingham, NG12 5GG, UK
e-mail: arf@bgs.ac.uk

T. Harrison
Ivy Dene, Burtersett, Hawes, North Yorkshire, DL8 3PA, UK
e-mail: ac.tonyharrison@btinternet.com

2 Northern England

Northern England includes several significant karst areas, including the Yorkshire Dales and the Northern Pennines. The majority of cave systems occur in the Lower

© Springer International Publishing AG 2017

A. Klimchouk et al. (eds.), *Hypogene Karst Regions and Caves of the World*,
Cave and Karst Systems of the World, DOI 10.1007/978-3-319-53348-3_2

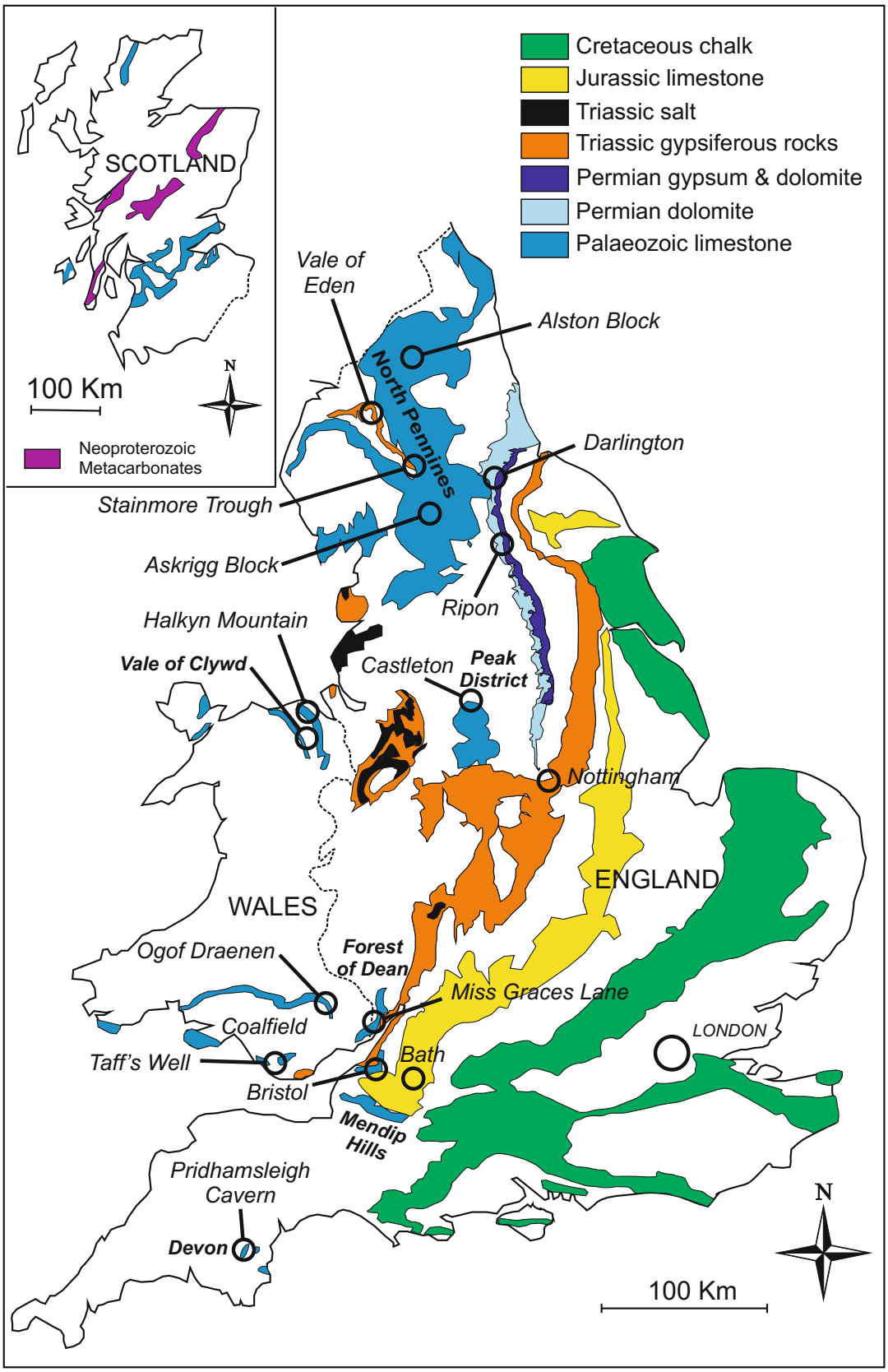

Fig. 1 Karst areas of the UK. The labelled *black circles* indicate features and areas of relevance mentioned in the text

Carboniferous Great Scar Limestone Group, but significant karstic development also occurs in the overlying Yoredale Group. Carbonate deposition was influenced by the development of structural highs and troughs including the Northumberland and Stainmore troughs, the Askrigg Block and the Alston Block (Fig. 2). Consequently, there are marked facies and thickness variations across the region (Aitkenhead et al. 2002). The principal carbonate unit, the Great Scar Limestone Group, is up to 800 m thick in the Stainmore Trough, thinning to 400 m on the Askrigg Block and 100 m thick on the Alston Block. Above, the 1200-m-thick Yoredale Group comprises a series of upward-coarsening cycles of marine limestone, shale and thin sandstone beds, commonly topped with coal. Of the many limestone units, the Great Limestone Formation is commonly the thickest (usually 20–25 m), but others including the Melmerby Scar Limestone and Middle Limestone formations can be significant.

The northern part of the Askrigg Block and the whole of the Alston Block are extensively mineralised, forming the Northern Pennine Orefield. Numerous mineral veins, primarily of galena, criss-cross the region and have been mined for centuries (Ryder and Harrison 2016). These veins are often several kilometres long, but mostly no more than a few metres wide and of limited vertical extent.

It is within the thin limestones of the Yoredale Group in the Northern Pennines that the UK's most significant hypogenic cave systems are found (Fig. 2). They are all maze caves, with evidence for transverse hypogenic speleogenesis (Klimchouk 2007, 2009) including a characteristic suite of dissolution features diagnostic of rising flows during development—'the morphological suite of rising flow'. These include floor slots (feeders for incoming water), wall channels, cupolas and ceiling slots (flow outlets).

Maze caves have been known about in the Northern Pennines for many years, nearly all having been originally discovered by nineteenth-century lead miners (Sopwith 1833; Bramall 1921; Gill 1993). Nine maze caves with a plan length of >1 km are presently known. Only one opens directly to the surface, eight being accessed from old mine workings, two of which are currently inaccessible. All are located in the limestones of the Yoredale Group, three in the Alston Block (the Silverband Mine Caves, Knock Fell Caverns and Hudgill Burn Mine Caverns) and six in the Askrigg Block (Grassington Moor Cavern, Windegg Mine Caverns and two separate mazes in each of Devis Hole Mine and Faggergill Mine). Most of these caves have many features in common not only with each other but also with hypogenic mine caves in Sardinia (De Waele et al. 2013). All are unrelated to the modern landscape. All are now dry, with no known links to existing watercourses. All are located in the top or middle of broadly horizontal sections of a Yoredale Group limestone; eight are in the Great Limestone Formation, and one (Grassington Moor Cavern) is in the Middle Limestone Formation. All cave floors are covered with sediment, generally preventing observation of the bedrock base of the cave passages. All of the limestone locations are sandwiched between layers of sandstone and shale, typically with the sandstone as a base to the limestone and shale as a cap (except where erosion has removed the younger overlying strata). The predominant passage profiles in all the caves are tall vertical rifts and circular tubes. All mazes display network (rectilinear) passage outlines with high passage densities although these parameters differ dramatically from maze to maze. Most of the cave passages are dominated by NNW–SSE or N–S orientations, with WSW–ENE also an important direction. All of the caves are intersected by or adjacent to mineral veins, which mostly contain galena and in some cases sphalerite (Harrison 2016).

2.1 The Alston Block

The longest and most northerly of the Pennine maze caves is Hudgill Burn Mine Caverns (Fig. 3) near Alston in Cumbria (Dale et al. 2015). Discovered by nineteenth-century lead miners, it was not fully explored until 2014. It comprises a horizontal phreatic network developed within the Great Limestone Formation, here sandwiched between beds of sandstone and shale, with a surveyed plan length of 13.24 km enclosed within an area of 34,000 m^2. In plan view, the cave has a reticulate geometry with most passages aligned on and parallel to four major joint sets, within an area about 500 m long and 220 m wide at the northern end, decreasing to 70 m in the middle of the system and widening slightly to about 90 m wide to the south-east. The system shows many of the characteristics of transverse hypogenic speleogenesis, having no apparent relationship to the present landscape and a high passage density. It is two-dimensional comprising only one storey, lies on an essentially planar surface and displays rising flow features. Passage dimensions are locally up to 5 m high and 2–3 m wide with rift, V-shaped (triangular), circular and arched morphologies present, although a thick layer of sediment in the lower parts of the passages commonly obscures the true passage morphology and dimensions (Fig. 4).

Many of the passages have a distinctive 'sooty' black and brown deposit on all passage walls and ceilings; this is a zinc-rich birnessite-type phyllomanganate. The source of the zinc is probably sphalerite, originally present as a primary mineral and has undergone subsequent oxidation to smithsonite, convertible to soluble cations capable of sorption into birnessite-type minerals.

Most hypogene maze caves in the Northern Pennines are thought to have developed through sulphuric acid speleogenesis, the acid being derived from the alteration of primary

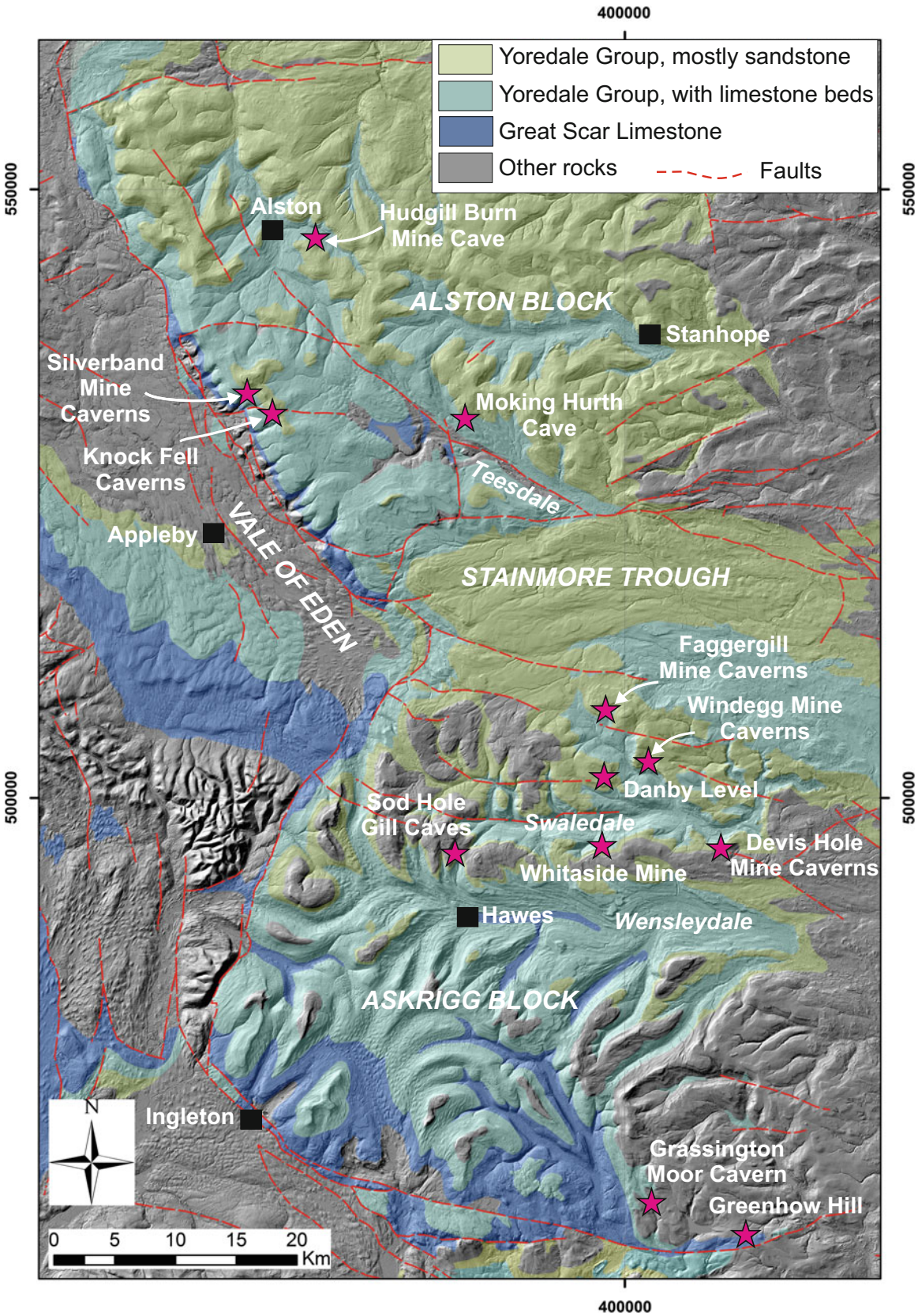

Fig. 2 Location of maze caves in the Northern Pennines (after Harrison 2016). Geology is based on the British Geological Survey 1:625,000 scale digital geological map. Topography is ©NEXTMap Britain DTM

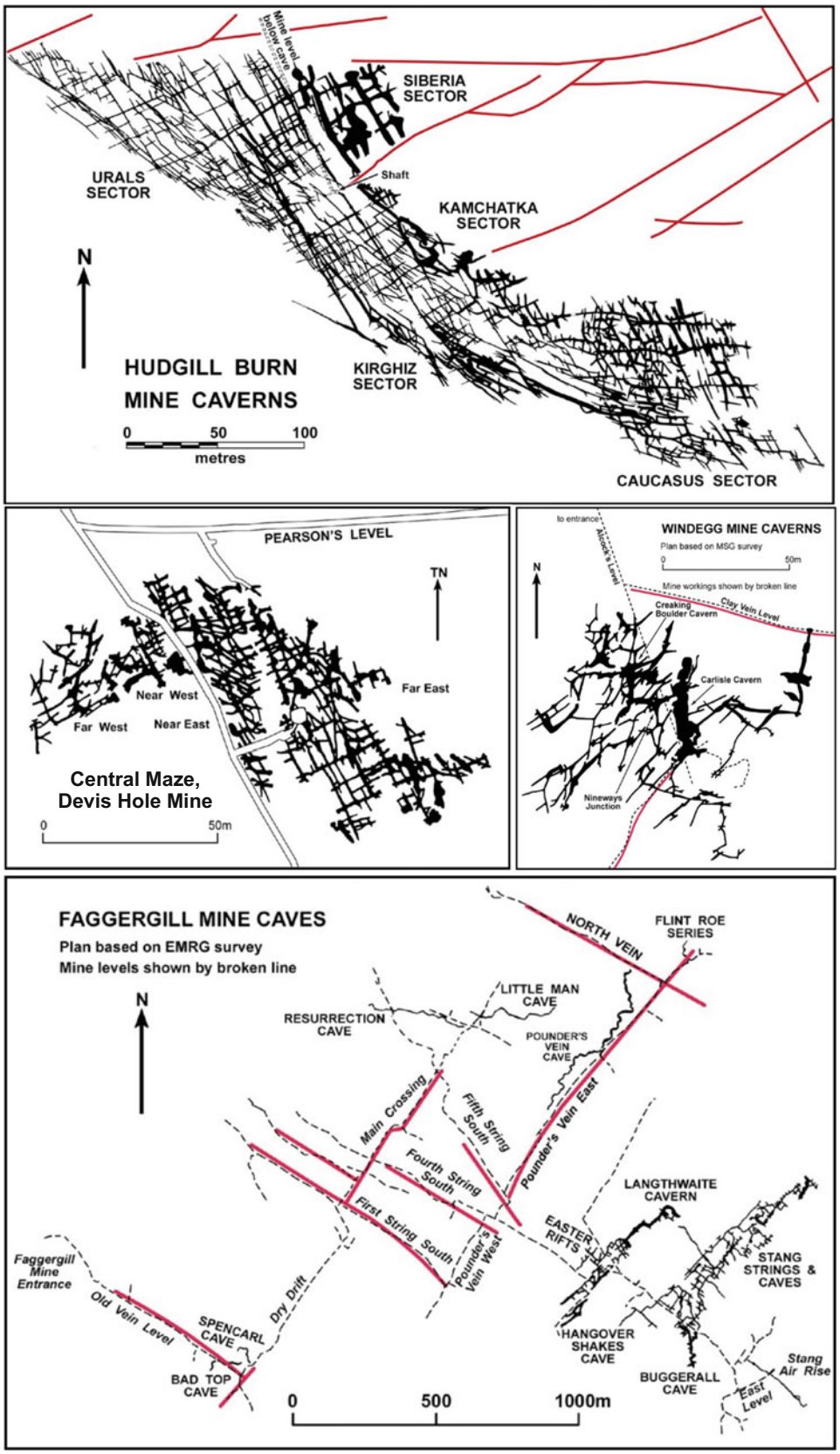

Fig. 3 Outline plans of some Pennine maze caves including Hudgill Burn Mine Cave, the central maze in Devis Hole Mine, Windegg Mine Cavern and Faggergill (from Harrison 2016). *Red lines* indicate mineral veins

Fig. 4 A complex junction of passages in Hudgill Burn Mine Caverns (*Photograph* J Dale)

sulphide minerals to carbonates, releasing hydrogen sulphide which then reacted with oxygenated groundwater to form sulphuric acid (Dale et al. 2015). Hudgill Burn Mine Caverns lies within a complex zone of epigenetic mineral veins that were originally rich in galena (lead sulphide, PbS) although much of the ore extracted from the mine was in the form of cerussite (lead carbonate, $PbCO_3$). Disseminated stratiform Pb–Zn mineralisation also occurs at multiple elevations within the Great Limestone a few kilometres east of Hudgill Burn Mine. The alteration of sphalerite to birnessite-type phyllomanganate would have also generated acidic metabolic by-products, again assisting further dissolution (Dale et al. 2015). Speleogenesis occurred after mineralisation which commenced in the late Carboniferous and continued into the Permian. The caves were drained during Pliocene–Early Quaternary uplift of Northern England.

The second large maze cave in the Alston Block is Knock Fell Caverns. This cave, at 760 m above sea level, is one of the highest caves in England and is situated about 15 km south of Hudgill Burn Mine Caverns. It was discovered in 1979 at the bottom of a sinkhole in a bench of the Great Limestone. Exploration uncovered a highly rectilinear system totalling 4.5 km in an area about 320 m long and 120 m broad with a high areal extent and passage density. The cave is the only maze in the Northern Pennines not reached through a mine level and was entered at its eastern edge where overlying sandstone and shale had been eroded. The cave is characterised by many narrow rifts and triangular passages, some with narrow outlet channels in the roof. Speleogenetic features associated with the morphologic suite of rising flow (Klimchouk 2007) are easily recognisable including cupolas, inlet feeders and outlet tubes despite a substantial overprint of water table and vadose features. About 3 m below some passages at the northern end of the system, a discrete lower series has been entered, which, although much smaller, has a much higher passage density. The cave is very close to the Knock Ore Gill Vein (Sutcliffe 1985; Smith and Murphy 2011). A similar speleogenetic mechanism to Hudgill Burn Mine Caverns is proposed.

A third maze cave is known from the Silverband Mines, about 2 km north of Knock Fell Caverns, again within the Great Limestone Formation. This cave, presently inaccessible, is much modified by mining (Myers 1967). Most of the cave is in two sections, separated by a small fault such that the two cave sections have a difference in level of some 3–4 m. The evidence suggests the Silverband Mine Caverns is a typical transverse hypogenic maze with a total length >1 km, but with a much lower passage density and areal extent than Hudgill Burn Mine Caverns.

Three other smaller hypogenic caves, all isolated from any present surface water features, are known in the Alston Block. Two are close to Silverband Mine Caverns on Great Dun Fell: Silverband Pot is a phreatic cross-rift system, subsequently modified by vadose infiltration, and Silver Jubilee Pot is another short phreatic system with several blind shafts in the floor. Both of these pots are capped by shale. Another system with rectilinear characteristics, again isolated from any existing significant water course, is Moking Hurth and the connected Moking Pot in Upper Teesdale, with a total length of 550 m. All three of these smaller caves are in limestone interbedded with sandstone and shale.

2.2 The Askrigg Block

The Askrigg Block is noted for several maze caves, all originally discovered and in places modified by lead miners. Faggergill Old Level in Arkengarthdale intersected several areas of natural cave in the Great Limestone Formation (Fig. 3). All of these natural passages were probably originally phreatic, and two sections show maze or network characteristics: the Easter Rifts Maze and the Stang Strings Maze, respectively, about 2.4 and 6.3 km long (Harrison and Ryder 2016).

The Stang Strings maze, with characteristic mud-covered floors, has a low passage density and areal extent, but nevertheless displays many of the features expected for hypogenic mazes including passage profiles with rising flow characteristics. It comprises essentially a reticular maze of passages, commonly widening into small largely linear caverns. The maze is separated from the nearby Easter Rifts Maze, some 150 m farther west by a small fault. The Easter Rifts maze also has a low areal coverage and passage density but differs from the Stang Strings Maze in comprising two large caverns that are joined by a network of tight rift passages. The phreatic Langthwaite Cavern in the north-east of the system is 300 m long and up to 15 m high and is one of the largest chambers yet discovered in a Northern Pennine maze cave. To the south of the system is Hangover Shakes Cave, another large cavern about 110 m long.

A few kilometres to the south-east of the Faggergill Mine Caves, an extensive series of natural caverns occurs in the Great Limestone Formation in Windegg Old Level (Fig. 3). Rediscovered in the early 1970s (Ryder 1975), the cave system comprises about 1100 m of reticular passages. Many of the passages have been enlarged by collapse, resulting in some quite sizeable chambers, and several intersect or are aligned with mineral veins. Like the maze caves described above, the system shows all the hallmarks of having resulted from a transverse hypogenic speleogenetic process. Four kilometres further south is Danby Level, another nineteenth-century lead mine which intersects a complex network of tall, narrow rifts commonly 3–4 m high and 0.3–0.4 m wide, over 200 m in plan length and clearly showing hypogenic morphologies.

At the foot of Arkengarthdale is Devis Hole Mine, which contains three maze cave networks (Harrison 2006). Near the mine entrance is the Central Maze which consists of 1.62 km of passages, crammed into an area of about 120 by 45 m (Fig. 3). The passages, all floored with thick mud deposits, are generally small and narrow. Passage cross sections are commonly rift-shaped or tubular (Fig. 5), narrowing downwards, typical of hypogenic speleogenesis (Ryder 1975). Some 80 m further south, Wellington Vein, a natural passage much modified by mining activity, intersects a small natural network cave system, the Occidental Series, 490 m of primarily rift-shaped passages. About 300 m beyond Wellington Vein is the Southern Maze, essentially a single phreatic system totalling about 3.6 km in length. In part modified by miners, this mud-floored system has a relatively low passage density and areal coverage, but has many characteristic rising flow features, including high rift passages with narrow ceiling slots (Harrison 2006, 2012a, b).

A few kilometres to the west of the Devis Hole Mine Caves and also in the Great Limestone Formation, two more phreatic caves have been discovered, accessed only from mine levels. These are the caves in the Smithy Level of Whitaside Mine, 6.5 km west of Devis Hole Mine, and Summer Lodge East Level, 2 km farther west. The caves, probably segments of larger systems, are, respectively, 200 and 140 m in length and have typical tube-shaped passage profiles (Harrison 2012a).

Further south in Wensleydale, a group of eight caves including Sod Hole Gill Caves and Shivery Gill Pot may be isolated remnants of a single large phreatic network system (Ryder 1975). The caves may have developed as closely grouped clusters, a common characteristic of transverse hypogenic speleogenesis (Klimchouk 2013). The caves are entered by short vertical or sloping shafts in a line of shakeholes on an outcrop of the Great Limestone Formation. The joint-guided passages exhibit a rectilinear network structure and commonly have tubular or rift-shaped profiles with large

Fig. 5 A rift passage in the Southern Maze of Devis Hole Mine, a typical profile for maze cave passages in the region (*Photograph* J Dale)

amounts of clay infill blocking many of the passages. The overlying sandstone has been eroded away, and the cave system is undergoing breakdown and fragmentation.

Another possible hypogenic maze cave, now inaccessible, is documented in old mining records below Grassington Moor in Upper Wharfedale. Miners discovered and surveyed a cave 412 m long in the Middle Limestone Formation, with numerous small side passages that were not explored or surveyed (Brook and Murphy 2016). The cave is now inaccessible following collapse of the mine shafts and was known as Grassington Moor Cavern or the Lost Cavern of Grassington Moor. Further east, sediment-filled karstic cavities known locally as 'gulfs' or 'gulphs' were encountered by miners between Nidderdale and Wharfedale around Greenhow Hill. These are thought to have formed as deep phreatic hypogenic cavities along mineral veins (Murphy and Everett 2013).

More as yet undiscovered hypogenic caves are likely to exist in the Northern Pennines. The presence of interbedded limestone, shale and sandstone adjacent to or intersecting mineral veins containing sulphide minerals are conducive to hypogenic cave formation. These will almost certainly be

remote from present surface features and in most cases probably only accessible from mine workings unless the covering rocks have been eroded away (as at Knock Fell Caverns), or where a modern valley happens to intersect them.

3 The Peak District

The Peak District, situated at the southern end of the Pennines, comprises a broad anticlinal structure cored by 1500 m of Lower Carboniferous limestones, locally interbedded with basaltic lava and ash deposits. It is flanked by Upper Carboniferous mudstones, fluvial and coal-bearing siliciclastics. The Peak Limestone Group is extensively mineralised, especially in the northern part of the outcrop where galena, fluorite, barite and calcite have been mined. The region is host to many cave systems including the 18-km-long Peak–Speedwell Cave system near Castleton (Waltham et al. 1997).

Evidence for active deep groundwater flow comes from the presence of several thermal springs, although none has yet been associated with known caves. Ten thermal springs grouped in seven centres are recognised in the area (Fig. 6), the best known being the Buxton and Matlock Bath springs with water temperatures of 27.5 and 20 °C, respectively, compared with ambient groundwater temperatures of about 9 °C. Isotope studies suggest these thermal waters were more than 15 years old and originate from local meteoric waters that have circulated to considerable depths. Radiocarbon dating showed that at least some of the thermal waters had bulk ages of up to several thousand years, although locally some of the springs, such as those at Buxton, also have a minor modern recharge component (Gunn et al. 2006; Abesser and Smedley 2008). There are significant differences between the water chemistry at the different thermal centres, but separate springs within each centre are of the same chemical type. This supports the idea that each centre originates from a separate flow cell with chemical differences reflecting variations in flow characteristics (Abesser and Smedley 2008). While most thermal waters are believed to originate within the Carboniferous Limestone sequence, isotope evidence suggests some of the springs, notably those at Buxton, have interacted with non-limestone lithologies (Gunn et al. 2006; Brassington 2007).

Evidence for deep hypogenic speleogenesis occurs in the northern part of the limestone outcrop around Castleton. Here a number of large, commonly isolated, phreatic dissolution cavities on mineral veins ('rakes'), faults and fractures have been identified (Fig. 7). These tall phreatic caverns are known from many of the ore fields, but are especially common in the Peak District. They occur either as vertical open shafts where intersected by surface lowering, or are accessed via cave systems or old mine workings. More than 50 such vein cavities have been described (Ford 2000), including several entered from the Peak–Speedwell Cave system including the 160-m-deep Titan, the UK's deepest known shaft. The upstream limit of the Speedwell Cavern streamway, Main Rising, is a vein cavity where divers have descended to a depth of 74 m. Surface shafts include the 70-m-deep Eldon Hole and Bull Pit.

The development of the vein cavities was initiated in late Carboniferous times as mineralising fluids rising from adjacent sedimentary basins at temperatures between 70 and 120 °C emplaced a network of mineral veins in the limestone (Ford 2000). Following uplift and unroofing of the limestone in mid- to late Cenozoic times, circulation of groundwater was initiated. The relatively open vein and fracture network provided laterally extensive vertically oriented inception routes for deep phreatic groundwater flow (Ford 1995). With no effective base to the limestone, the slow circulation could have gone to virtually any depth, only to rise again at the resurgence points. Evidence from Peak Cavern suggests these vein cavities have a vertical range of several hundred metres. Slow dissolution would pick out any weakness in veins and slowly enlarge them so that an undulating phreatic drainage system could be developed (Ford 2000). These early cavities provided inception routes for subsequent groundwater movement through the limestone massif, thereby stimulating later phreatic and vadose development of the Peak–Speedwell cave system. The modern conduits still locally utilise these early cavities.

4 Wales and the Forest of Dean

The Carboniferous limestones of South Wales and the Forest of Dean host some of Britain's longest cave systems, two of which, Ogof Draenen and Miss Grace's Lane Cave, contain significant hypogene maze networks. Ogof Draenen is located on the northern margin of the South Wales coal basin (Fig. 1) where gently dipping Lower Carboniferous limestones are overlain by a thick sequence of Upper Carboniferous siliciclastics. Some deep artesian groundwater flow occurs beneath the coalfield emerging on the southern flank at Taff's Well near Cardiff with an average temperature of 21.6 ± 0.5 °C (Farr and Bottrell 2013).

In Ogof Draenen, two major maze networks occur within a larger branch-work cave system: the Squirrel Rifts maze and the Snowball-Hexamine Highways maze (Farrant and Simms 2011). They are typified by high narrow phreatic rift passages, with numerous junctions and blind passages, developed on several levels and generally do not display any clear dissolutional flow markings or scalloping. They occur at different stratigraphical levels, sandwiched between other

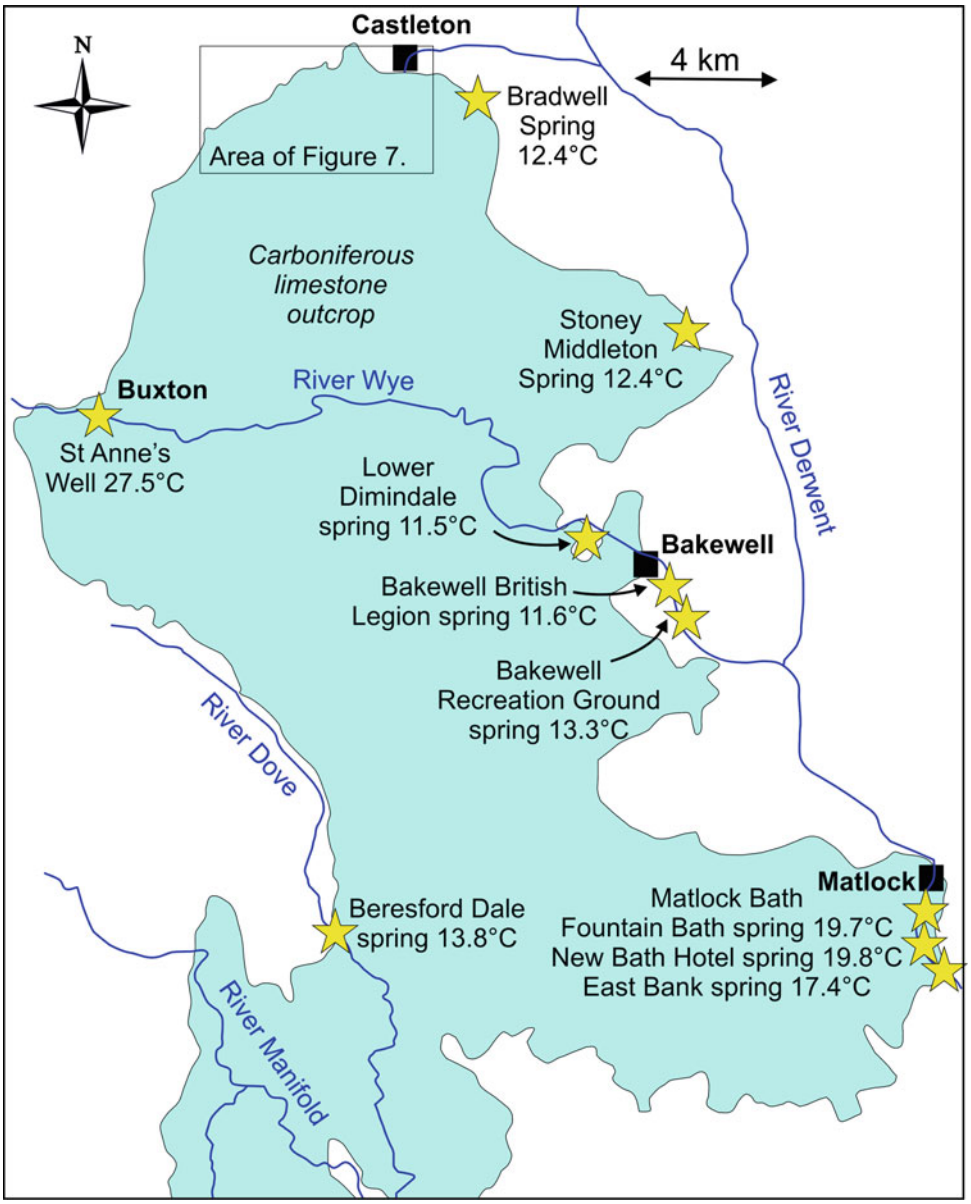

Fig. 6 Thermal springs in the Derbyshire Peak District

non-porous, but permeable, cavernous carbonate lithologies. These maze networks appear to have developed through hypogenic speleogenesis driven by the oxidation of metallic sulphides within the limestone and the overlying coal-bearing strata (Ball and Jones 1990). Locally abundant gypsum flowers, needles and anthodites are present.

In the Forest of Dean, Miss Grace's Lane Cave near Chepstow is a 4-km-long phreatic joint-guided rectilinear maze developed within Lower Carboniferous limestones. Little is known about its speleogenesis, but its interstratal setting beneath the Drybrook Sandstone may be significant. Perched over 150 m above the River Wye, it is now totally relict. No other hypogenic cave systems are known, but several mineralised palaeokarstic cave systems of possible Triassic age have been discovered by miners extracting iron ore including Clearwell Caverns and Wigpool Iron-ore Mine (Bowen 2009).

In North Wales, limestone outcrops surrounding the Vale of Clwyd host many cave systems (Appleton 1989; Ebbs 2000). This area is extensively mineralised, and many of the caves were discovered by miners searching for lead. By the late 1600s, the driving of adits became necessary to drain the mine workings. In 1818, the 8-km-long Halkyn or Deep Level Tunnel was driven, followed by the Milwr Tunnel in 1897 (Fig. 8). This extended 16 km from the coast at Bagillt to Cadole near Mold (Ebbs 2008).

These tunnels and mines intersected several natural caves at depth, all phreatic and most now thought to be the result of hypogenic speleogenesis. Thirteen natural caves or groups of caves have been intersected in 42 km of mine passages.

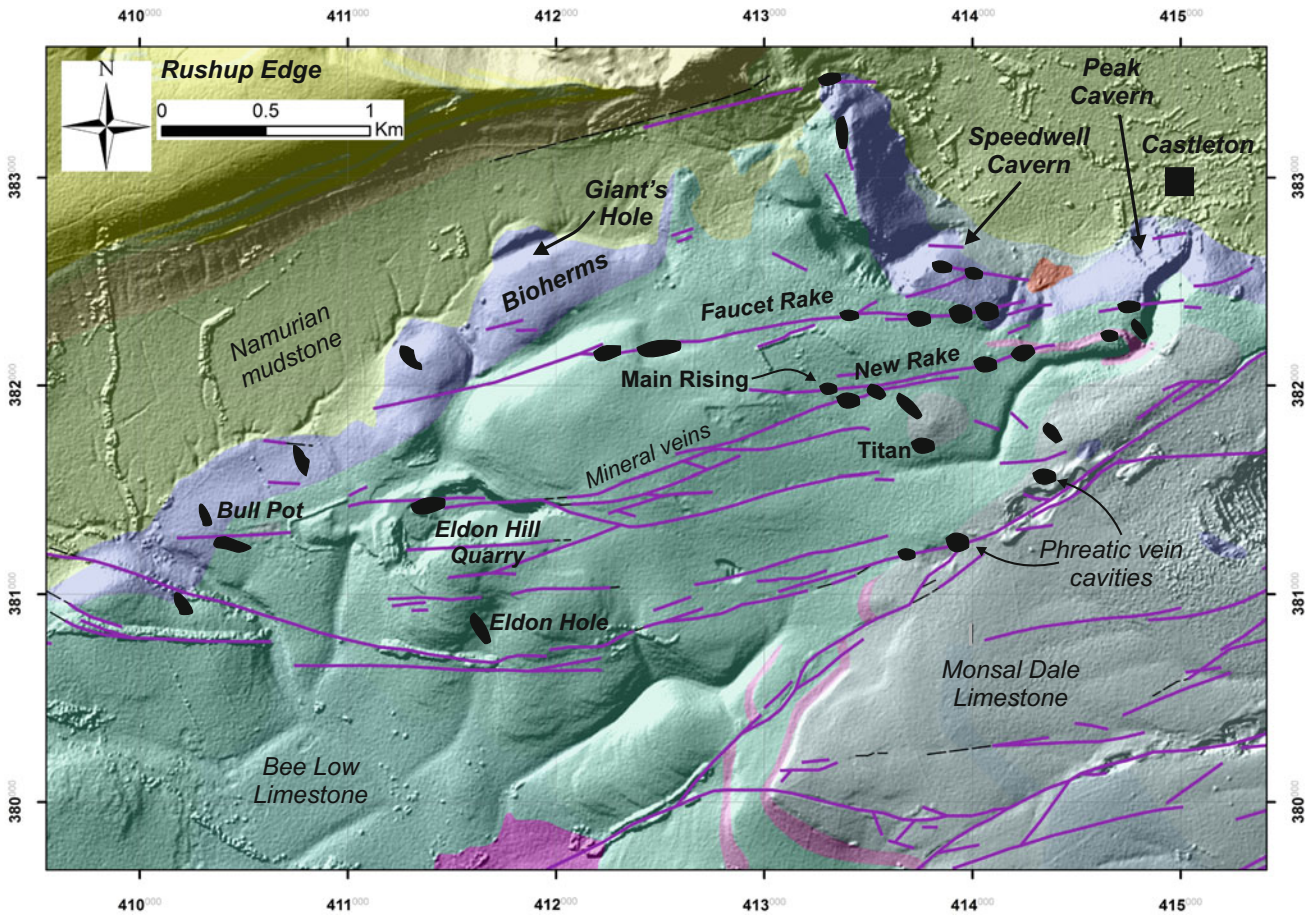

Fig. 7 Map of the known and probable vein cavities (*black ellipses*) in relation to the mineral veins near Castleton, Derbyshire (after Ford 2000). Geology is based on the British Geological Survey 1:50,000 scale digital geological map. Topography is ©NEXTMap Britain DTM

The largest is the Powell's Lode Cavern, first entered in 1931. The cavern is 70 m long, 20 m wide and about 20 m high (Fig. 9) and with a 20-m-diameter lake at its southern end which has been dived to a depth of 42 m (Fig. 10). A second lake was plumbed to a depth of around 60 m (c. 40 m below sea level) but was infilled with mining spoil. Mine plans show the cavern rising a further 50 m, giving an overall vertical extent of at least 110 m. Water resurges here at a rate of about 380 l/s, fed by a large conduit at a depth of at least 60 m below sea level. The water used to emerge at St. Winefride's Well at Holywell, over 8 km to the north, prior to the lowering of the water table by mining (Ebbs 2000). A passage was driven north from the lake on Barclays Lode through further natural chambers which extend continuously for 320 m until dipping below water level. A similar water-filled vein cavity was intersected on the Pant Lode during the construction of the Milwr Tunnel in 1917. The resulting flood disrupted work for many weeks and caused St Winefride's Well to dry up 11 h later. The water temperature emerging from the east side of the vein was about 9 °C, while that on the west was 13 °C. Other chambers intersected by the miners include the Halkyn Lode Chamber, a large cave near the junction of the Halkyn Tunnel with Halkyn Lode, about 30 m long, 10 m wide and 38 m in height, now partially filled, and the nearby Cornel-y-Cae Chamber, 20 m in diameter and 20 m high. Lode 621 Chamber, another large natural chamber about 10 m in diameter and 20 m high, has good wall scalloping indicating a strong upward flow of water. These isolated phreatic caverns suggest there is an active deep-seated hypogenic cave system extending under Halkyn Mountain now partially intersected by mine workings.

5 The Bristol District

Hypogene caves and thermal springs are known in the Bristol–Bath area of southern England (Fig. 11). The area is geologically complex, dominated by thrusted and folded Devonian sandstones and Lower Carboniferous limestones. These Palaeozoic rocks were uplifted and exposed during the Triassic, subsequently buried by a thick Jurassic to

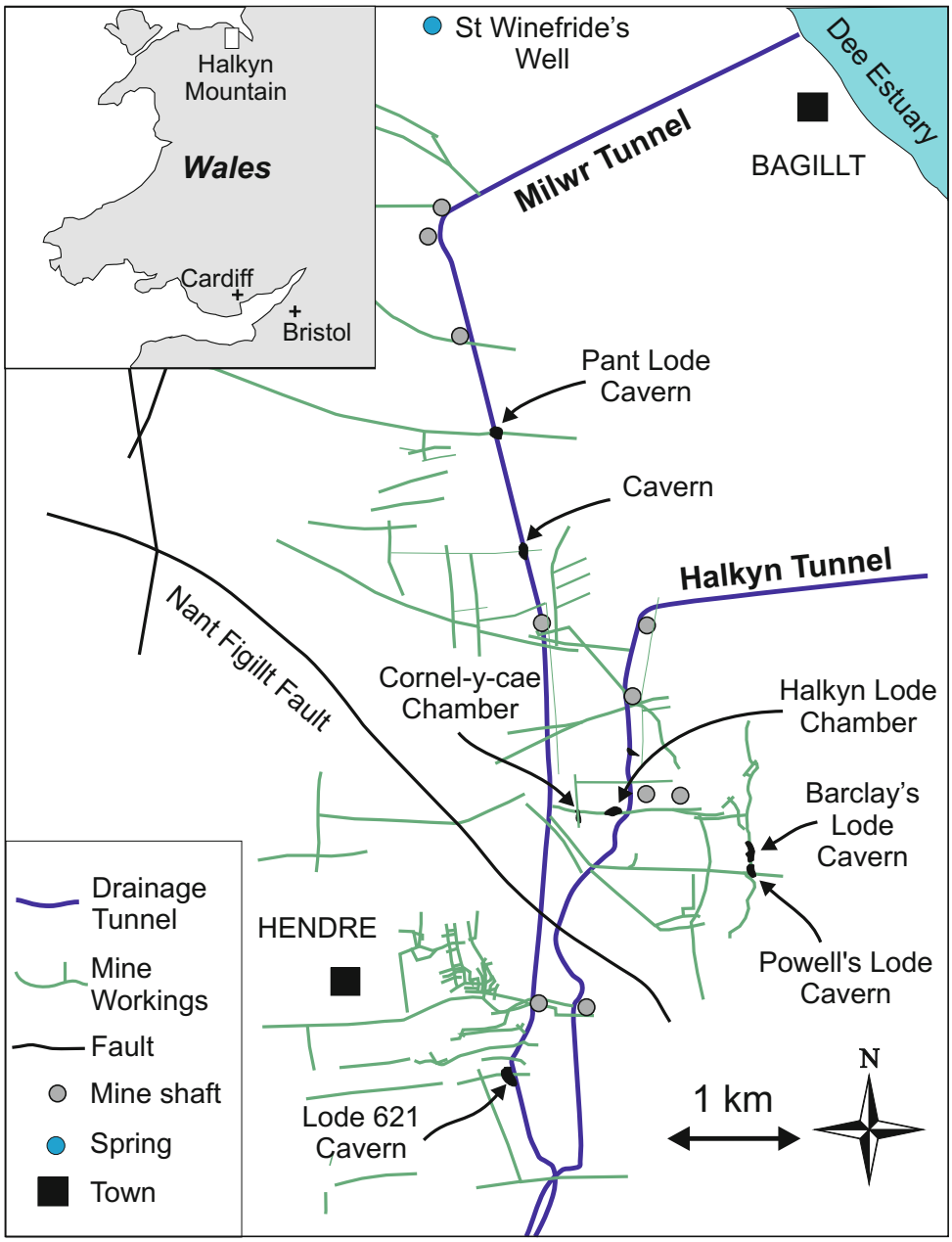

Fig. 8 Location of hypogenic cavities (*in black*) intersected by mine workings beneath Halkyn Mountain, North Wales

Palaeogene cover, and now partially exhumed by Quaternary uplift and erosion. Active thermal springs provide evidence for hypogenic cave development and deep groundwater circulation. Those at Bath are well known, but several other thermal springs occur at or close to the present level of the River Avon which flows east–west through the region. The thermal waters at Bath emerge under artesian head at 39–46 °C from three springs in the centre of the town with a combined flow of 16.7 l/s. They rise up from Carboniferous limestones at depth, emerging through a thin Triassic cover. The springs are thought to form the outlet of a regional thermal aquifer within Lower Carboniferous limestones that descend to depths >2.7 km within the North Somerset coal basin (Atkinson and Davison 2002). Isotopic evidence (Edmunds et al. 2014) suggests the water has been heated to a maximum temperature in the range 64–96 °C, indicating a most probable maximum circulation depth of 3 km, and a residence time of between 1 and 12 ka. Thermal waters were also encountered in a borehole at Batheaston, a few kilometres east of Bath. In Bristol, thermal springs occur at Hotwells; at Jacobs Well in Clifton; and at several points in the intertidal zone along the Avon Gorge.

Fig. 9 Powell's Lode Cavern looking north, showing abandoned mid-twentieth-century mining equipment (*Photograph* J Dale)

The only known relict hypogene cave system is Pen Park Hole (Fig. 11) in north Bristol (Mullan 1993). This short cave, with a surveyed length of 112 m and a depth of 61 m, was discovered during quarrying around 1669. It consists of a short, fault-guided entrance series which opens out into a large chamber occupied by a lake whose surface fluctuates by up to 27 m. The cave is confined to a narrow zone of steeply dipping limestone no more than 20 m thick. The first recorded descent was on the 2nd July 1669. The cave was surveyed in September 1682 and published in January 1683 (Southwell 1683), making it one of the earliest published cave surveys in the world (Shaw 1979). It is perhaps noteworthy that it was the cave's hypogenic origin that led to the cave being surveyed at such an early date!

Evidence of hypogene speleogenesis includes the dendritic, upward-branching passage morphology aligned along the fault planes; deep, rounded cupolas; and highly corroded bedrock where steam has condensed above hot pools. Several phases of mineralisation are evident. The first phase was the deposition of minor amounts of galena, followed by a 2- to 3-cm-thick crust of coarsely crystalline calcite up to 15 cm thick covering most of the floor, walls and roof of the cave (Fig. 12). A second phase of dissolution led to the etching of the calcite, followed by the deposition of a thin layer of limonite over the calcite throughout most of the cave. The cave appears to have been formed by hydrothermal waters rising up to emerge as thermal springs, similar to those seen in the region today, possibly during the early Pleistocene prior to the incision of the nearby Avon Gorge, although a Jurassic age cannot be ruled out. A similar, hot spring origin has recently been suggested for the main fissure at Cromhall Quarry, some 17 km to the north-east (Simms 1990).

No definitive hypogene caves are known from the Mendip Hills, although some of the lead and zinc mineralisation was undoubtedly accompanied by karstic development.

Fig. 10 The Lake, Powell's Lode Cavern (*Photograph* J Dale)

However, some isolated phreatic chambers and caves in the western Mendips may have a hypogenic origin. These include Axbridge Hill Cavern, Loxton Cavern and other nearby caves. These are associated with ochre (iron) workings and may be associated with hypogene karstic development at or just below the Triassic unconformity. Similarly, Pridhamsleigh Cave in Devon may be associated with deep groundwater flow in Devonian limestones rising up thrust planes.

6 Transverse Hypogenic Gypsum Karst of Northern England and the East Midlands

Traverse hypogenic karst associated with groundwater flow through interbedded dolomite and gypsum occurs within Permian and Triassic strata in parts of Northern England and the Midlands. The main areas of gypsum karst are in the Permian outcrop east of the Pennines, particularly around Ripon and Darlington, where two gypsum- and anhydrite-rich mudstone units (the Edlington and Roxby formations) are sandwiched between dolomite aquifers (the Cadeby and Brotherton formations) (Fig. 13). This heavily karstified gypsum and dolomite succession crops out in a narrow belt approximately 140 km long and 3 km wide from Darlington through Ripon to Doncaster. It is characterised by active subsidence and abundant sinkholes, particularly around Ripon. The topography and easterly dip of the strata enables artesian water to flow up through the dolomite into the overlying gypsum sequences, emerging as sulphate-rich springs with temperatures between 9 and 12 °C (Cooper et al. 2013). It seems likely that there are extensive active transverse hypogene cave systems developing within the gypsum and anhydrite, especially in the Ripon area (Cooper et al. 2013). Although many sinkholes are present in the

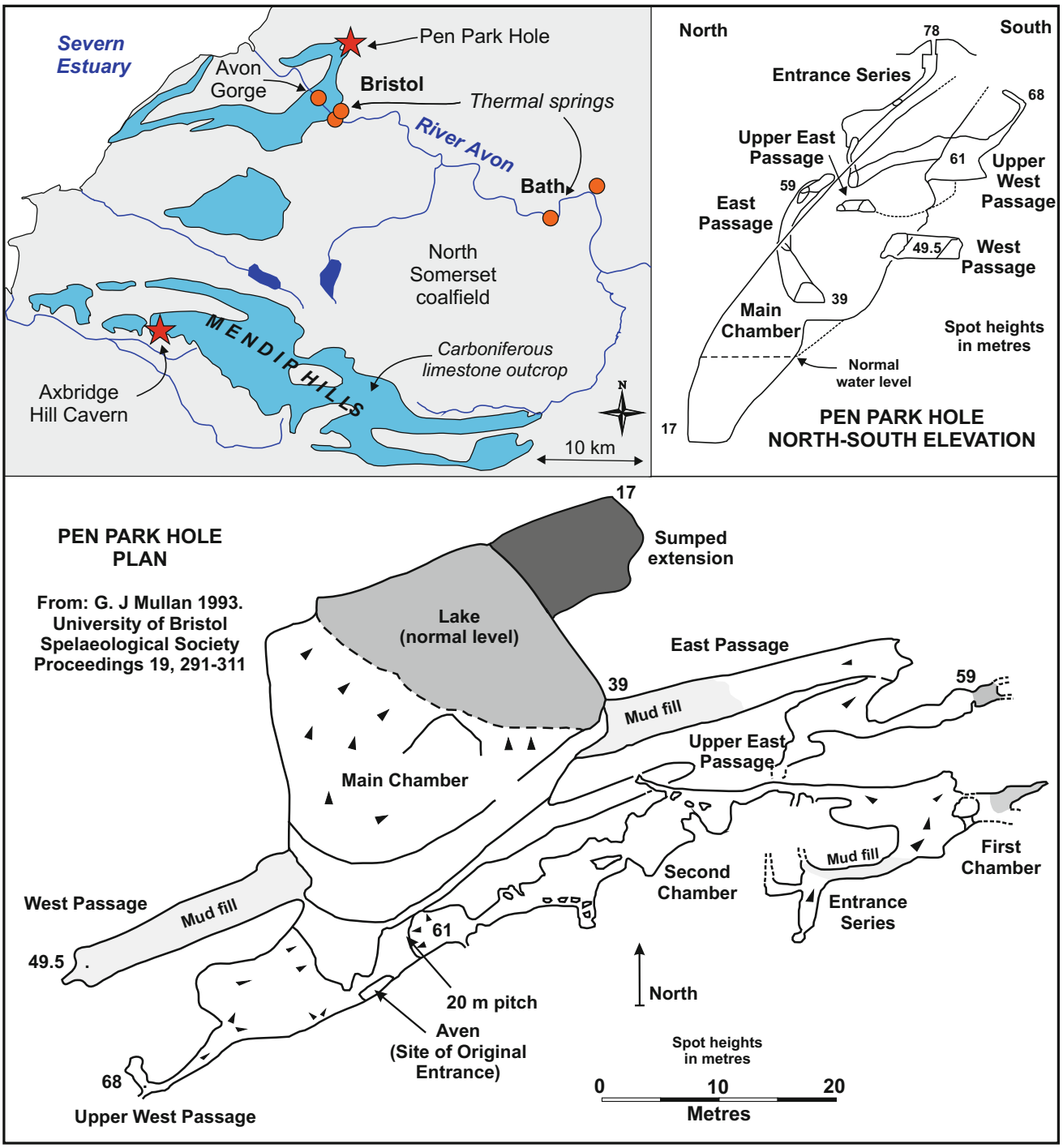

Fig. 11 Plan survey and section of Pen Park Hole, Bristol. *Inset map* Location of hypogenic caves and thermal springs in the Bristol–Bath area, including the Mendip Hills

Fig. 12 Hydrothermal calcite crust in the entrance series of Pen Park Hole. Crystals are 2–3 cm across (*Photograph* A Farrant)

region, some up to 20 m deep, no accessible hypogenic caves have yet been found. However, numerous karstic cavities including clay-filled cavities up to 20 m high have been discovered in boreholes (Waltham and Cooper 1998; Cooper and Waltham 1999).

Further south, fragments of caves have been observed within gypsum mines in the Triassic Mercia Mudstone Group south of Nottingham and Derby, but these are poorly recorded. It is possible that some of these may have a transverse hypogenic origin, fed by artesian water rising up sequence through dipping strata.

A smaller area of gypsum karst occurs in Permian strata in the Vale of Eden. Thin beds of gypsum are present in the Eden Shales Formation. Four distinct evaporite beds exist, labelled A to D (Stone et al. 2010). In 1988, the Houtsay Quarry Cave was discovered in the 'B' Bed in a gypsum quarry at Kirkby Thore near Penrith (Ryder and Cooper 1993). The cave, which has now been quarried away, was a relict horizontal phreatic system with passage diameters between 1 and 4 m and averaging about 2 m and a total length of about 140 m. Scalloping suggested upward water movement, implying that the cave resulted from hypogenic transverse flow up through the system similar to that now occurring in the Ripon area. Similar features may be widespread in the gypsum belt of the Vale of Eden.

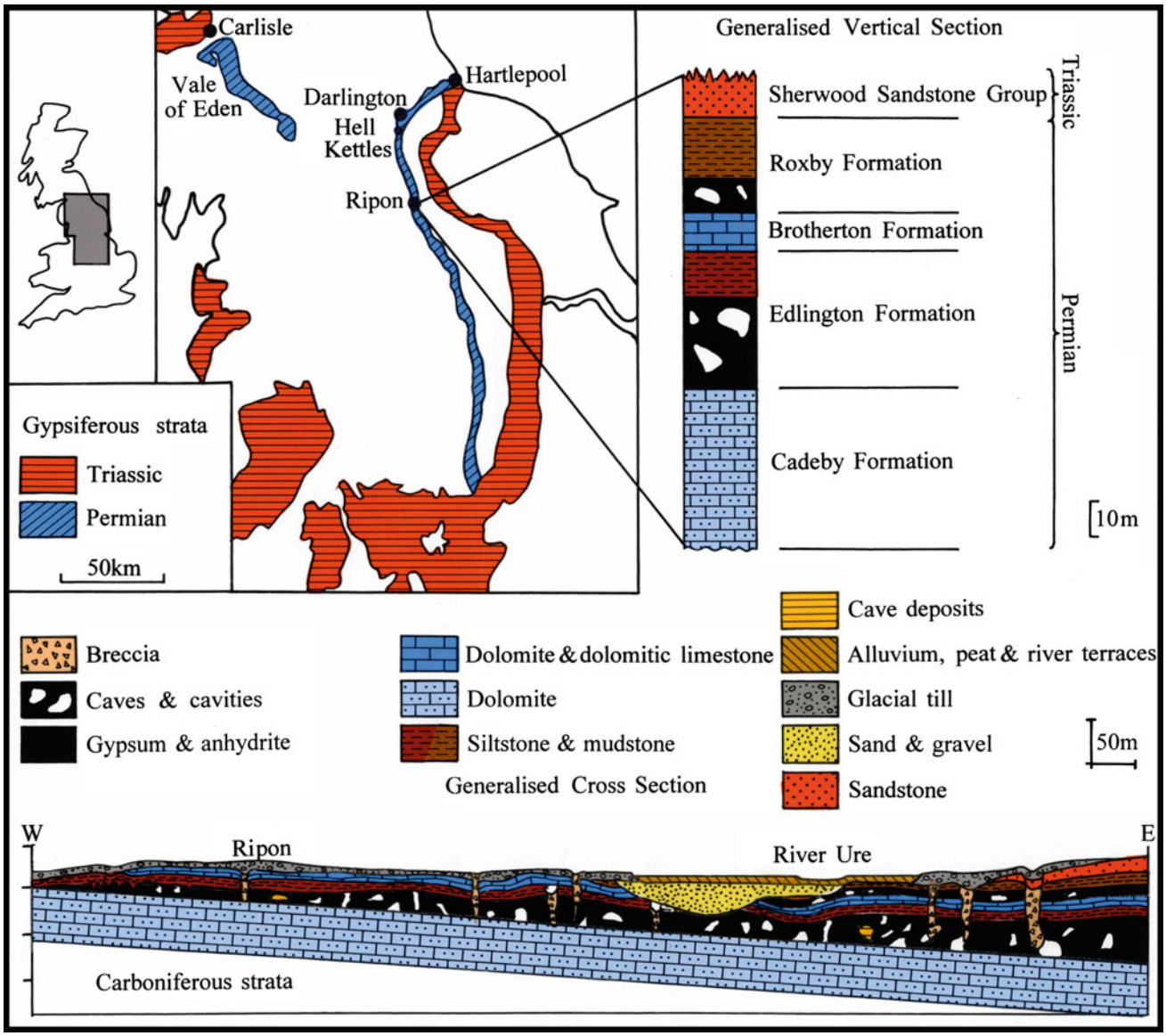

Fig. 13 Map of Northern England showing the outcrop of and generalised section through the Permian gypsiferous strata. *Inset* Cross section through the Permian sequence in the Ripon area, showing the development of gypsum karst (from Cooper 1998)

References

Abesser C, Smedley PL (2008) Baseline groundwater chemistry of aquifers in England and Wales: the Carboniferous Limestone aquifer of the Derbyshire Dome. OR/08/028. British Geological Survey, Keyworth

Aitkenhead N, Barclay WJ, Brandon A, Chadwick RA, Chisholm JI, Cooper AH, Johnson EW (2002) British regional geology: the Pennines and adjacent areas, 4th edn. British Geological Survey, Keyworth

Appleton P (1989) Limestones and Caves of North Wales. In: Ford TD (ed) Limestones and caves of Wales. Cambridge University Press, pp 217–254

Atkinson TC, Davison RM (2002) Is the water still hot? Sustainability and the thermal springs at Bath, England, vol 193. Geological Society, London, Special Publications

Ball TK, Jones JC (1990) Speleogenesis in the limestone outcrop north of the South Wales Coalfield: the role of micro-organisms in the oxidation of sulphides and hydrocarbons. Cave Sci 17:3–8

Bowen C (2009) An interim report on Wigpool Cave: a syncline-guided, palaeo drainage cave in the Forest of Dean limestone basin, UK. Cave Karst Sci 36(2):59–62

Bramall V (1921) The mining, manufacture and uses of barytes in the neighbourhood of Appleby, Westmorland. Trans Inst Min Eng 61:42

Brassington FC (2007) A proposed conceptual model for the genesis of the Derbyshire thermal springs. Q J Eng Geol Hydrogeol 40:35–46

Brook D, Murphy P (2016) Caves of Grassington Moor. In: Waltham AC, Lowe DJ (eds) Caves and Karst of the Yorkshire Dales vol 2. British Cave Research Association, Buxton. Online at http://bcra.org.uk/pub/dales/

Cooper AH (1998) Subsidence hazards caused by the dissolution of Permian gypsum in England: geology, investigation and remediation. Geol Soc Lond, Eng Geol Spec Publ 15:265–275

Cooper AH, Waltham AC (1999) Subsidence caused by gypsum dissolution at Ripon, North Yorkshire. Q J Eng Geol 32:305–310

Cooper AH, Odling NE, Murphy PJ, Miller C, Greenwood CJ, Brown DS (2013) The role of sulfate-rich springs and groundwater in the formation of sinkholes over gypsum in eastern England. In: Land L, Doctor DH, Stephenson JB (eds) Sinkholes and the engineering and environmental impacts of karst: Proceedings of the thirteenth multidisciplinary conference, Carlsbad, New Mexico, 2013. National Cave and Karst Research Institute, pp 141–150

Dale J, Harrison T, Roe P, Ryder PF (2015) Britain's longest maze cave: Hudgill Burn Mine Caverns, Cumbria, UK. Cave Karst Sci 42:20–41

De Waele J, Forti P, Naseddu A (2013) Speleogenesis of an exhumed hydrothermal sulphuric acid karst in Cambrian carbonates (Mount San Giovanni, Sardinia). Earth Surf Proc Land 38(12):1369–1379

Ebbs C (2000) An introduction to the caves of north-east Wales. Cris Ebbs, Llanarmon-yn-ial

Ebbs C (2008) The Milwr Tunnel: Bagillt to Loggerheads. Cris Ebbs, Llanarmon-yn-ial

Edmunds WM, Darling WG, Purtschert R, Alvarado JAC (2014) Noble gas, CFC and other geochemical evidence for the age and origin of the Bath thermal waters, UK. Appl Geochem 40:155–163

Farr G, Bottrell S (2013) The hydrogeology and hydrochemistry of the thermal waters at Taffs Well, South Wales, UK. Cave Karst Sci 40 (1):5–12

Farrant AR, Simms MJ (2011) Ogof Draenen: speleogenesis of a hydrological see-saw from the karst of South Wales. Cave Karst Sci 38(1):31–52

Ford TD (1995) Some thoughts on hydrothermal karst. Cave Karst Sci 22(3):107–118

Ford TD (2000) Vein cavities: an early stage in the evolution of the Castleton Caves, Derbyshire, UK. Cave Karst Sci 27:5–14

Gill MC (1993) The Grassington mines, vol 46. Br Min (Northern Mines Research Society), Keighley

Gunn J, Bottrell SH, Lowe DJ, Worthington SRH (2006) Deep groundwater flow and geochemical processes in limestone aquifers: evidence from thermal waters in Derbyshire, England, UK. Hydrogeol J 14(6):868–881

Harrison T (2006) Further phreatic cave systems in Swaledale, North Yorkshire, UK. Cave Karst Sci 33(2):65–72

Harrison T (2012a) Further phreatic cave systems under the Swaledale-Wensleydale surface watershed in the Yorkshire Dales, UK. Cave Karst Sci 39(1):23–33

Harrison T (2012b) Phreatic maze caves, Grinton Moor, Swaledale, UK: survey of Devis Hole Mine Caves. Cave Karst Sci 39(2):59–62

Harrison T (2016) Maze caves of the Northern Pennines, UK. Cave Karst Sci 43(1):21–36

Harrison T, Ryder PF (2016) Caves of Swaledale. In: Waltham AC, Lowe DJ (eds) Caves and Karst of the Yorkshire Dales, vol 2. British Cave Research Association, Buxton. Online at http://bcra.org.uk/pub/dales/

Klimchouk AB (2000) Speleogenesis under deep-seated and confined settings. In: Klimchouk AB, Ford DC, Palmer AN, Dreybrodt W (eds) Speleogenesis: evolution of karst aquifers. National Speleological Society, Huntsville, AL, pp 244–260

Klimchouk AB (2007) Hypogene speleogenesis: hydrogeological and morphogenetic perspective. Special paper no. 1. National Cave and Karst Research Institute, Carlsbad, p 106

Klimchouk A (2009) Morphogenesis of hypogenic caves. Geomorphology 106(1):100–117

Klimchouk AB (2013) Hypogene Speleogenesis. In: Shroder J, Frumkin A (eds) Treatise on geomorphology. Academic Press, San Diego, pp 220–240

Mullan GJ (1993) Pen Park Hole, Bristol: a re-assessment. Proc Univ Bristol Spelaeological Soc 19:291–311

Murphy PJ, Everett S (2013) The "gulfs" of Greenhow Hill, North Yorkshire, UK. Cave Karst Sci 40:87–91

Myers JO (1967) The Caverns of Silverband. Northern Pennine Club Journal 3(1):34–40

Ryder PF (1975) Phreatic network caves in the Swaledale Area, Yorkshire. Trans Br Cave Res Assoc 24:177–192

Ryder PF, Cooper AH (1993) A cave system in Permian gypsum at Houtsay Quarry, Newbiggin, Cumbria, England. Cave Sci 20 (1):23–28

Ryder PF, Harrison T (2016) Caves of the Northern Pennines. In: Waltham AC, Lowe DJ (eds) Caves and Karst of the Yorkshire Dales, vol 2. British Cave Research Association, Buxton. Online at http://bcra.org.uk/pub/dales/

Shaw TR (1979) History of cave science: the scientific investigation of limestone caves, to 1900, vol 2. Anne Oldham, Crymych, Dyfed

Smith R, Murphy S (2011) Mines of the West Pennines, vol 91. British mining. Northern Mine Research Society, Nelson

Simms MJ (1990) Triassic palaeokarst in Britain. Cave Sci 17:93–101

Sopwith T (1833) An account of the mining districts of Alston Moor, Weardale and Teesdale in Cumberland and Durham; comprising descriptive sketches of the scenery, antiquities, geology, and mining operations in the upper dales of the rivers Tyne, Wear and Tees. W Davison, Alnwick

Southwell R (1683) A description of pen-park-hole in Glocestershire. Philos Transac Royal Soc 13(143):2–6

Stone P, Millward D, Young B, Merriott JW, Clarke SM, McCormac M, Lawrence DJD (2010) British regional geology: Northern England. British Geological Survey, Keyworth

Sutcliffe R (1985) Knock fell caverns. Gritstone Club J 6:70–74

Waltham AC, Cooper AH (1998) Features of gypsum caves and karst at Pinega (Russia) and Ripon (England). Cave Karst Sci 25:131–140

Waltham AC, Simms MJ, Farrant AR, Goldie HS (1997) Karst and caves of Great Britain, geological conservation review series, vol 12. Chapman and Hall, London

Hypogene Caves in France

3

Philippe Audra

Abstract

Hypogene speleogenesis (HS) describes cave development by rising fluids independent of recharge from the overlying or adjacent areas. Dissolution includes deep-seated acidic sources (CO_2/H_2S), "hydrothermal" cooling, mixing corrosion, and Sulfuric Acid Speleogenesis (SAS) at and above the water table. HS localizes in basin at sites of upward flows and convergences, in deformed strata at structural highs and major faults. In disrupted basins, geothermal gradient "pumps" downward meteoric water. Volcanism and magmatism produce "hyperkarst" combining CO_2, H_2S, thermalism, and microbial activity. Hypogene caves in France are presented according to a conceptual model. Isolated geodes are lined by calcite spar. 3D multistory caves (Pigette, Adaouste) show CO_2 degassing morphologies (bubble trails, folia, tower cones, coral towers) and "hydrothermal" minerals (Fe–Mn oxi-hydroxides, barite, celadonite), with condensation–corrosion cupolas above the water Table. 2D maze caves develop below less permeable strata. Giant ascending shafts (Salins shaft), collapse shafts, and breccia pipes (called "organs" in the N.-French coal basin) correspond to "hyperkarst" phenomena. Caves with ore deposits are associated with sulfurs (Fe, Pb, Zn) or oxidized Fe. They often record past positions of base level and harbor unique features (black tubes, ghost-rock) or rare minerals. Along the water table, thermal gradient and CO_2/H_2S degassing make condensation–corrosion and HS above the water table. Chevalley Aven shows upward dendritic pattern. Eventually, cupolas expand to large isolated chamber. Water table sulfuric caves develop headward with typical morphologies (corrosion tables, condensation domes, sulfuric karrens). Vapor shafts form by warm air convections and condensation–corrosion.

Keywords

Cave pattern • Sulfuric Acid Speleogenesis (SAS) • Condensation–corrosion • Hypogene caves in France • Speleogenesis

1 Introduction

The infiltration of meteoric water owing its aggressivity from biogenic CO_2 is responsible for the genesis of the so-called epigene caves. Besides epigene caves, a minority of caves owes its origin to upward flow, the so-called hypogene caves. Hypogene caves result from the combination of complex dissolution processes often involving deep-seated acidic sources, sometimes originating from the mantle or from volcanic activity, but also from "normal" rising meteoric water. The importance of regional flow was recently stressed to explain the distribution and characteristics of rising flows at the basin scale. Flow convergence, upward flow, and outflow loci are responsible for focusing

P. Audra (✉)
University of Nice Sophia Antipolis,
Sophia Antipolis Cedex, France
e-mail: audra@unice.fr

© Springer International Publishing AG 2017

A. Klimchouk et al. (eds.), *Hypogene Karst Regions and Caves of the World*,
Cave and Karst Systems of the World, DOI 10.1007/978-3-319-53348-3_3

hypogene speleogenesis, allowing the development of cave systems in specific settings, which are controlled by both topography and hydrogeology (Klimchouk 2013b, c). They generally contain features and patterns that show evidence for upward flowing of deep water, often with high CO_2–H_2S concentration and with a thermal component. The pattern of hypogene caves shows a development in phreatic conditions, sometimes at great depth, and also close to the water table. Recent investigations stressed the role of thermal air convections causing condensation–corrosion, which can produce caves in short time spans due to extreme acidic conditions, especially in the presence of sulfuric acid.

A constantly increasing number of caves are being classified as hypogene caves since their clear distinction occurred only a few years ago (Klimchouk 2007). In France, more than 100 caves are hypogene (Audra et al. 2010). Generally of very small size, some may develop over several kilometers or can reach a depth of almost 200 m. They display various patterns developed both at depth in the phreatic zone or above the water table. Some of them harbor unique morphological features and mineralizations.

In this paper, we present the hypogene speleogenetic characteristics and the hydrogeological settings, and the resulting patterns of cave systems with specific morphologies and mineralizations known to date in France.

2 Hypogene Speleogenesis: Definition and Characteristics

Hypogene speleogenesis is defined as *the formation of solutionally enlarged permeability structures by the upwelling groundwater flow, independent of recharge from the overlying or immediately adjacent surface* (Klimchouk 2015). The upwelling is often focused along main regional fault lines allowing cross-formational flow, but it can be pervasive (leakage) beneath topographic lows in multistory aquifer systems.

Discussion about this definition and the details of hypogene speleogenesis are found in several papers (e.g., Dublyansky 2014; Palmer 1991, 2000; Klimchouk 2013a, 2014, 2015). The following characteristics are generally observed for hypogene speleogenesis (Audra and Palmer 2015, and references therein):

- The aggressiveness involves deep-seated sources of CO_2, of sulfides, and/or thermal processes (Palmer 2000). Water chemistry often shows significant higher concentrations in sulfides, sulfates, or dissolved carbon dioxide, together with metals and trace elements. Deep upwelling waters are generally depleted in oxygen, i.e., reducing, allowing transport of metallic species. Incidentally, this is the genesis of "hydrothermal" ores, which in the karst environment represent some of the largest concentrations such as Mississippi Valley Type (MVT) deposits. However, some variants involve cold meteoric freshwater, such as *artesian waters rising across evaporites where aggressiveness is not produced at depth and does not rely on any acids* (Klimchouk 1992, 2013a).
- Water that rises rapidly from depth can remain relatively warm compared to the local shallow groundwater, within a range of a few degrees up to almost 100 °C. Although thermalism is frequent or at least observable with slight temperature anomalies, some typical hypogene cases involve "normal" cold temperature, such as Frasassi Caves (Galdenzi and Menichetti 1995).
- Due to the considerable distance between recharge and discharge areas, groundwater flow is driven by regional hydraulic gradients. Outflows are generally not, or only weakly, influenced by rain events or seasonal climatic cycles, displaying regular flow rates with low velocity. Water mineralization is much more stable, and no solid load is observed. Pure deep water origin is rare, and generally hypogene flow mixes several components from deep and shallow origin. The outflow may be influenced by rain events, with decreases in temperature and mineralization, discharge, and turbidity, whereas long recessions allow the return of low discharge of less influenced deep water.
- Traditionally, hypogene caves are considered to have no relation to karst features formed by surficial processes. However, in the topography-driven flow systems of the unconfined and "artesian" aquifers, their relationship with the surface is strongly dependent of topography, since discharge areas tend to be located in topographic lows (e.g., valleys) where groundwater flow converges and wells up (Klimchouk 2007). Consequently, hypogene caves often represent excellent proxies for base-level records.
- Hypogene speleogenesis must not be confused with meteoric deep phreatic loops, such as vauclusian systems that may sometimes reach several hundreds of meters in depth. In such "vauclusian" epigene systems, water is simply flowing along deep loops before outflowing with a large range of discharges and unstable mineralization.

2.1 Hypogene Solutional Processes

Many solutional processes from upwelling hypogene flow may combine, with generally one being dominant for a given case (Klimchouk 2007, 2013a; Palmer 2000, 2013; Audra and Palmer 2015):

- Dissociation of evaporites by meteoric undersaturated water entering from below, such as for the giant gypsum mazes in Ukraine (Klimchouk 1992, 2000a), and probably also in Paris (Bigot 2010) and Piedmont basins (Vigna et al. 2010).
- Carbonic acid solution due to deep-seated sources of CO_2 such as volcanism, mantle, and metamorphism (Gary and Sharp 2009). Such contribution is effective for springs located along the Corbières area and the Cévennes fault (Bakalowicz 1988). Close to Montpellier, the Madeleine Cave (Villeneuve-lès-Maguelone) is an underground river degassing CO_2, and the Grotte de la Baume (Balaruc-les-Bains) is a cave associated with a breccia pipe originating in Miocene from carbonic degassing. However, deep source of CO_2 is probably more frequent for any spring located along deep-rooted faults.
- Increasing solubility of calcite along ascending flowpaths due to water cooling, which is frequently called "hydrothermal speleogenesis."
- "Mixing corrosion" of waters of different chemistry. Such a process may occur along upwelling flowpaths when a given water mixes with another water body, including shallow meteoric waters. Mixing corrosion is probably the most active process at depth, when different solutions are converging.
- Common-ion effect with mixing of sulfates and carbonates producing dedolomitization.
- Sulfuric acid solution. Deep sulfate beds are first converted to H_2S in the presence of hydrocarbons or organic carbon from marls. Deep H_2S-rich upwelling water mixes with shallow meteoric oxygenated water, producing sulfuric acid. This process commonly called "sulfuric acid speleogenesis" (SAS), accounts for some of the largest hypogene caves in the world, such as Lechuguilla Cave and Carlsbad Cavern in New-Mexico (Hill 1987; Polyak et al. 1998; Palmer and Palmer 2000; Calaforra and De Waele 2011; De Waele et al. 2016). SAS occurs at shallow depth in the phreatic zone but especially above the water table due to H_2S degassing in the cave atmosphere. Sulfuric acid that reacts instantaneously with the carbonate host rock produces replacement gypsum and carbon dioxide (Galdenzi and Maruoka 2003). CO_2 can dissolve in water again and increase its aggressiveness even more. Enlargement of the voids mainly happens by condensation–corrosion processes in a highly acidic environment (Audra et al. 2007; De Waele et al. 2016). Condensation is greatly enhanced in the presence of thermal differences between the upwelling waters and the cave walls and atmosphere, even in low thermal environments where the temperature contrast reaches only a few degrees (Sarbu and Lascu 1997; Gàzquez et al. 2015). Dissolution of carbonate rock in these conditions is extremely fast compared to normal epigene caves and can cause the formation of sizeable cavities in probably only a few thousands of years. Also, the local oxidation of sulfides, such as pyrite, often present in carbonate sequences, can generate sulfuric acid, boosting rock dissolution (Auler and Smart 2003; Tisato et al. 2012; Audra et al. 2015; De Waele et al. 2016).

2.2 The Ghost-Rock Karstification

Ghost-rock karstification is a process that was first studied in detail in Belgium (Vergari 1997; Dubois et al. 2014, and references herein). The first stage of ghost-rock karstification is chemical dissolution and removal of the most soluble crystals of a grain-heterogeneous rock, i.e., the calcite grains in impure limestone, or the smallest micritic crystals vs. sparite in pure limestone. It requires low hydrodynamic energy and creates a ghost-rock feature, mimicking the fracture pattern, filled with the residual weathering products, the ghost. The ghost has a highly porous texture, where initial rock features are preserved, such as calcite dikes and fossils. The ghost-rock karstification can develop at considerable depth below base level, providing some fresh flow is able to maintain the aggressivity and to transport the solutes during a long-lasting time, several orders of magnitude longer than in the classical epigene speleogenesis. The second stage is characterized by mechanical erosion of the remaining undissolved particles of the ghost. It requires high hydrodynamic energy, i.e., a base-level drop after uplifting and/or valley incision, and it is only then that open galleries are created, mostly by mechanical erosion and transport of the fine grains. It results in cave systems adjusted to the fracture pattern, such as mazes. However, branching patterns are also present after ghost-rock karstification, since flow driven by gravity may select only some of the ghost directions corresponding to the flow lines. Passage morphologies are very similar to those of phreatic passages, with round profiles, bridges, dead ends, etc.

The ghost-rock karstification process has been poorly recognized up to now. Firstly, because the second phase of mechanical removal of the ghost cancels the initial evidence, which may remain only in dead ends and in areas protected from turbulent flow (Fig. 1), and secondly, because the resulting morphologies (maze pattern with phreatic-like passages) were often misinterpreted as phreatic in origin.

Originally, the ghost-rock karstification has been attributed to epigene processes, i.e., a kind of weathering slowly developing downward from the surface (Quinif 2010, and references therein). Such an origin is evident in many places; however, it now appears that entire regions of ghost-rock karstification have been clearly affected by hypogene flows (Bruxelles and Wienin 2009). In France, most of the

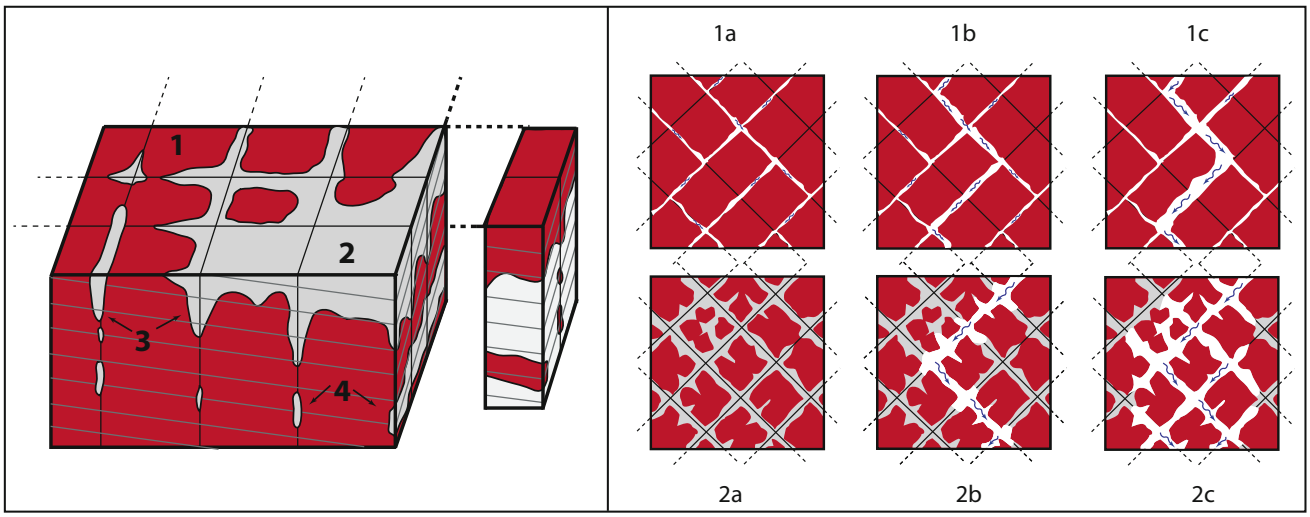

Fig. 1 *Left* different types of ghost rock. The unweathered rock (1) is cut by numerous discontinuities (joints and bedding planes), which are partly used by the ghost-rock karstification. The ghost rock occurs as weathered masses (2), as pockets and corridors (3), and as pseudo-endokarst with a hard rock ceiling, which prefigures the future cave passages (4). *Upper right* (*1a*, *b*, *c*): "normal" karst evolution by complete removal of rock and branching pattern development. *Lower right* (*2a*, *b*, *c*): ghost-rock karstification. In the early stage of low gradient, slow flow produces the residual matrix but cannot remove the weathering products (**a**). After a base-level drop resulting in a steep hydraulic head, turbulent flow is installed and transports the fine particles by headward erosion (**b**). Gradually, the fracture frame is revealed and a maze appears in the place of the initial ghost (**c**). The remote parts, away from the turbulent flow, remain filled with the ghost rock (Bruxelles et al. 2009)

marginal areas of basins at the contact of cratons were subject to hypogene processes by deep upward flow expelled from the basin's central deep zones (peripheries of Central Massif, Vosges Mountain, etc.). Such low regions are now characterized by the association of mineralized sulfide ores and caves of predominantly maze pattern. These caves result from the removal of the ghost rock following the rearrangement of the karst drainage after the recent uplifts. If the process is now well understood at the scale of the ghost (Quinif 2010), a more general conceptual model at the regional scale will probably soon integrate the ghost-rock karstification model with both epigene and hypogene processes.

3 Hydrogeological Setting

The principle of hypogene speleogenesis relies on recharge at distance (or from internal sources), slow transfer at depth, and focused discharge in topographic lows or tectonically predisposed locations, typically along faults allowing fast and easier cross-formational upwelling. Flow transfer in the upper portion of basins is described by the "Regional Gravity Flow" concept (Tóth 1970, 2009), adapted to hypogene speleogenesis by Klimchouk (2007, 2013b, c). Topographic highs act as recharge areas, whereas topographic lows act as discharge areas (see Klimchouk Chap. 1, and particularly Figs. 6 and 7). At shallow depth, local loops of meteoric water are dominant. For deep aquifers within gravity-driven meteoric flow, most of the marginal recharge is discharged in marginal areas, whereas the internal area of the basin displays mainly vertical flow, with very low contribution of lateral flow from basin margins (Klimchouk Chap. 1). In confined aquifer systems, lateral flow is dominant in more pervious units, whereas vertical flow is dominant in less pervious units. Klimchouk (2013b, c) distinguished several hydrogeological settings with different regularities of localization of upwelling flows and hypogene speleogenesis. These include large cratonic artesian basins (divided in marginal areas, internal areas, and deep zones), coastal aquifer systems in large carbonate platforms, fold/thrust regions, young disrupted intramountain basins, and areas of young volcanism. We follow his hydrogeological subdivision in the next paragraphs.

3.1 Marginal Basin Areas

In marginal areas of sedimentary basins, meteoric water descending from recharge areas mixes with deep basinal water and wells up along topographic lows (typically river valleys), forming a belt of hypogene speleogenesis with large sinkholes corresponding to deep breccia pipes and sagging zones (see Klimchouk Chap. 1, and particularly Fig. 13). In the NW European coal basin stretching between Northern France and Belgian Hainault, such breccia pipes were first

described in the XIXth century and called geological "orgues" (organs), "Dièves shafts" (Renault 1970) or "crans" (Quinif 1994). They are now buried under Upper Cretaceous strata, some reaching a depth of 1200 m, and contain dinosaur remains. Such conceptual approach has to be taken into consideration for maze caves located in the periphery of the French cratons, i.e., the Massif Central, the Vosges, where ghost-rock weathering is widespread (see below).

3.2 Internal Basin Areas

In the upper hydrogeological stories of internal areas of the basins, the layered aquifer/aquitard system displays a topography-controlled flow pattern (Klimchouk 2013c). In aquitards, vertical flow is predominant with downward cross-formation communication below topographic highs and upward communication below valleys (Klimchouk Chap. 1). Large valleys can induce upward flow with vertical relief up to 1.5 km. In aquifers, lateral flow is directed from topographic highs to lows. The maze caves in gypsum of the Paris Basin (such as Réseau Denis Parisis) are related to such hydrogeological conditions (Klimchouk 2000b; Bigot 2010), so are the Ukrainian gypsum mazes, which are the largest in the world (Klimchouk and Andreychouk Chap. 22).

3.3 Basin Deep Zone

In deep basinal zones, flow is predominantly vertical along blocks and faults where deep fluids from the basement and upper mantle are rising and mix with upper stratiform aquifers (Klimchouk 2013b). Flow and pressure are highly irregular. Physical–chemical parameters evolve along upwelling flowpaths causing selective solution and precipitation. Thermal and geochemical anomalies thus develop in the upper stories (Klimchouk Chap. 1). Such conditions are poorly studied in France, since in happens at depth. However, several karst ore deposits, which are now at shallower depth after long surficial erosion, might be related to such conditions.

3.4 Coastal Basins

Coastal basins represent a variant where sea water plays the part of the confined basin internal area. Upward flow in the coastal and submarine discharge zone can be driven by both topography-induced head and density gradients where freshwater aquifers extend below saline water aquifers and the seawater, plus geothermal heating of seawater entering the platform at deep levels (Klimchouk Chap. 1; Upchurch Chap. 49). Florida and Yucatan peninsulas match with this model (Cunningham and Walker 2009; Thomas 2010; Klimchouk 2013c). Such speleogenetic conditions should be taken into consideration for sedimentary basins opened to the sea, such as Aquitanian and Paris basins.

3.5 Deformed Strata

In deformed strata, as in marginal areas of the sedimentary basins, meteoric water descending from recharge areas mixes with deep basin water and wells up along faults or structural highs (anticlines, horsts), allowing groundwater to discharge at topographic lows. These topographic lows are valleys cutting through the geological structures, where valleys act as windows in the aquifer. Many valleys are incised by the influx of deep aquifer water, which has risen along brecciated zones (Camus and Bruxelles 2013). Upward flow uses anticlines, faults intersecting anticlines that provide more efficient routes for upward flow, such as French Northern Alps (Fig. 2) or along overthrusts in French Provence (Fig. 3).

3.6 Disrupted Basins

In young disrupted basins in tectonically active regions, there is a strong gradient (topographic, hydraulic, and thermal) between displaced blocks. Upper blocks act as recharge areas for meteoric flow systems. The cold meteoric water feeds shallow and deeper loops toward the basin depths. The high geothermal gradient warms up the deep water that rises quickly along extensional faults at the edge of confining sediments of the basin. In addition, compaction-driven flow of formation fluids may still be significant in depth of young basins, contributing to ascending discharge. This model, best expressed in the Budapest thermal karst (Madl-Szonyi et al. Chap. 16), matches with the western edge of the Rhône valley from Gard to Ardèche and along Alès Basin. In these areas, geode caves filled with calcite spar and iron ores are found close to Alès, Viviers, Donzère (Audra 2007), Saint-Péray (Rochers de Crussol), and Châteaubourg (Audra and Cailhol 2014).

3.7 Volcanic and Magmatic Intrusions

Volcanic and magmatic intrusions are a source of deep acids and heat. The geothermal gradient acts as a driving force for deep upward flows that can rise quickly to the surface using tectonic disruptions and attracts complementary downward recharge from remote areas. The presence of concentrated acids (from CO_2, H_2S) boosts the dissolution. Microbial activity using sulfo-oxidant pathways strongly participates in

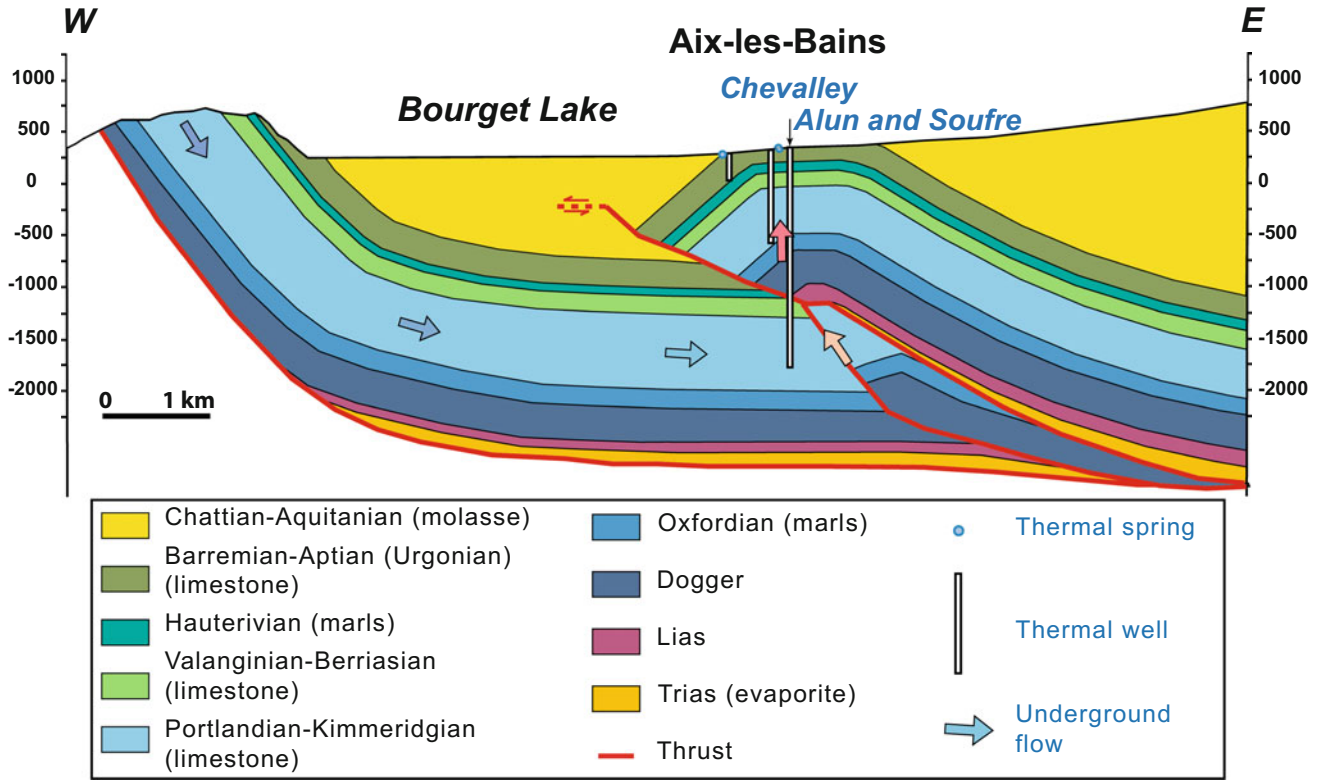

Fig. 2 The Aix-les-Bains thermal springs and caves discharge water from a deep Jurassic syncline upwelling along the overthrusted anticline where it acquires its sulfuric component at the contact with Triassic evaporites before mixing with shallow cold meteoric water (geology after Gallino 2007, in Hobléa et al. 2010)

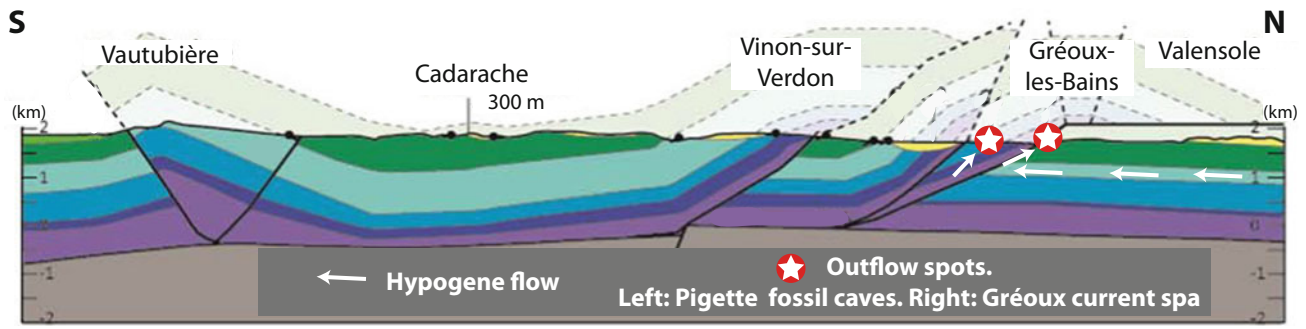

Fig. 3 Hypogene speleogenesis in Pigette Caves (*left star*) focused above the overthrust allowing deep upward flow, mainly from the Jurassic aquifer. Current thermal springs are located at Gréoux-les-Bains (*right star*), where also Saint-Sebastien Cave is located (geology after Guyonnet-Benaize 2011; hydrogeology after Toro 1988)

the rock solution. This combination of geothermal gradient, deep-seated acids, major fractures, and chemoautotrophic microbial activity is so intense that it can be considered "hyperkarst" (Audra et al. 2009a, b). Elsewhere, it explains some giant phreatic shafts, such as Pozzo del Merro in Italy (Caramanna 2002), Zacaton in Mexico (Gary 2010), or huge collapse dolines called "Obruks" in Turkey (Bayari et al. 2009; see also Bayari et al. Chap. 26). In France, volcanic and magmatic bodies are not frequent in karst areas; however, such occurrences may be considered around Massif Central in Ardèche and Grands Causses, where large collapse dolines were identified as maar craters (Bruxelles 2001 and references therein).

4 Types of Hypogene Caves in France

A synthesis based on field experience and literature takes into account geological structure, hydrology, morphology of caves at different scales (wall features, passage morphology,

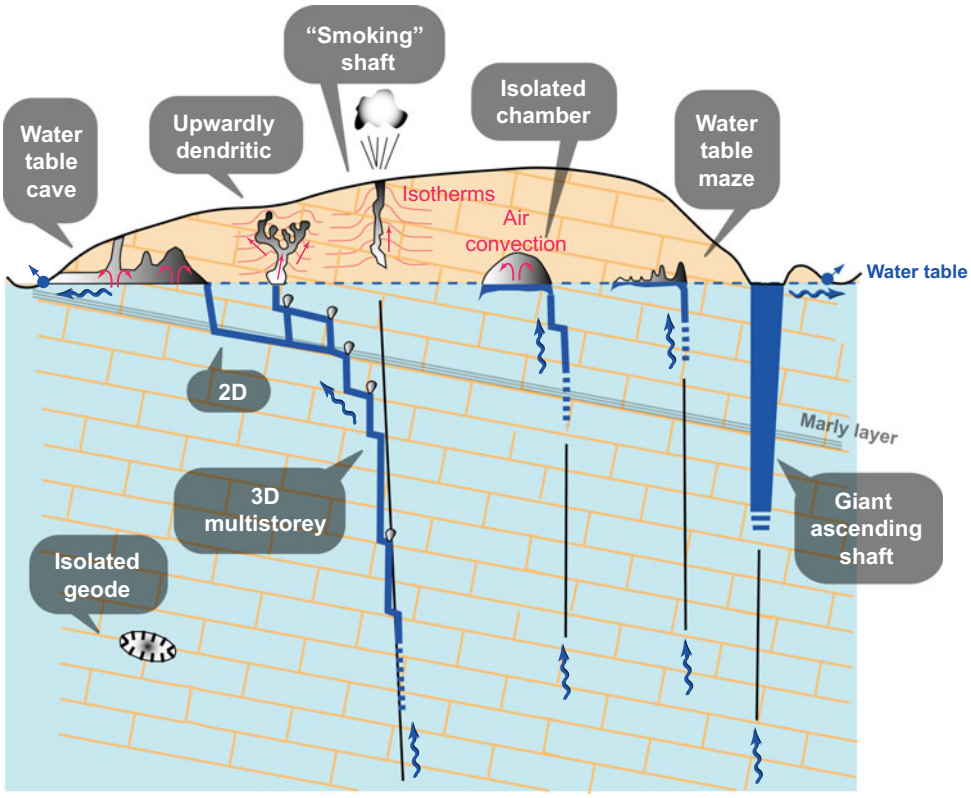

Fig. 4 Conceptual model of most typical hypogene cave types, according to geological structure and type of flow (Audra 2007, Audra et al. 2009a, b)

and cave pattern), mineralogy, deposits, etc. The geological framework and speleogenetic processes can be combined into a conceptual model of cave pattern, integrating most typical hypogene caves (Fig. 4) (Audra 2007; Audra et al. 2009a, b). Patterns are subdivided into two main types: deep phreatic systems generally developed in confined aquifers by transverse speleogenesis (sensu Klimchouk 2000b), and cave systems developed above the water table, where condensation–corrosion plays a paramount role. Currently, more than 50 hypogene caves are identified in France, from which about 15 have been studied (Fig. 20; Table 1). Their extension range is wide, from a few meters to several kilometers of passages and vertical extension overpassing 250 m. Some pristine examples display some of the best expressed or even unique hypogene morphologies, like in Baume Galinière, aven du Chat, grotte de l'Adaouste, grotte du Chat, grotte des Champignons, grotte des Iboussières, etc.

4.1 Hypogene Cave Pattern in Phreatic Conditions

4.1.1 Isolated Geodes

In deep zones, vertical upward flow and mixing of deep fluids of different types of water allows complex dissolution and deposition processes. Dissolution voids are poorly integrated and some are huge. Large crystals (calcite, gypsum, etc.) are deposited in slightly saturated water, together with diverse minerals such as metallic sulfides, such as in the famous Naica Cave, Mexico (Forti and Sanna 2010; see also Forti et al. Chap. 52) and in the Santa Barbara Cave, Sardinia, with its barite crystals (Pagliara et al. 2010; De Waele et al. 2013). In France, geode-like caves are known in the departments of Ardèche (Fig. 5), in Gard close to Uzès (phosphatières de Saint-Maximin), in Vaucluse plateau at Oppedette (Chaire à Prêcher). Their walls are entirely covered with large calcite spar, generally associated with iron oxi-hydroxides, giving the aspect of geode. Since they were formed at great depth and later exposed by surface erosion, relationships with their conditions of development are still obscure. However, it appears they are clearly connected with main regional deep-rooted fault lines where easy upward flow was possible.

4.1.2 3D Multistory Maze Caves

The rising hypogene flow alternately follows joints and bedding planes, producing a 3D maze cave, in a staircase pattern. Generally, the cave displays a main trunk where hypogene flow was rising, surrounded by 3D mazes, smaller in size. In Pigette Caves (Audra 2007; Fig. 6), the lower part displays strong corrosion of the host rock associated with mineralization (Fe–Mn oxi-hydroxides, barite; celadonite occurrence in cave was first found here) associated with the sulfuric hydrothermal flow which is still active at the nearby

Table 1 Overview of the current hypogene caves recognized in France, with main diagnostic features

Name	Commune	Department	Area	Speleometry (length/depth)	Observation	Hypogene cave
Carrière (aven de la)	Banon	Alpes-de-Hte-Prov.	Albion	some m.	Calcite spar lining	x
Chaire à Prêcher	Oppedette	Alpes-de-Hte-Prov.	Albion	≈15 m	Calcite spar geode along fault	x
Galinière (baume)	Simiane-la-Rotonde	Alpes-de-Hte-Prov.	Albion	191 m/ ±11 m (−6/+5)	Sulfuric Cave. Unique (6 jarosites minerals)	xx
Pont (gr. du)	Oppedette	Alpes-de-Hte-Prov.	Albion	4 m	Cupolas	?
Chat (aven du)	Lagnes	Vaucluse	Albion	−60	Unique 60 m-high iron trunk, made of coalescent iron pool fingers. Mined for iron	xx
Espérelles (gr. des)	Lagnes	Vaucluse	Albion	50/−12	Mined for iron	x
Or (baume de l')	St-Léger-du-Ventoux	Vaucluse	Albion	≈50 m	Mined for iron	?
Piei (grotte du)	Lagnes	Vaucluse	Albion	328/ ± 39	Mined for iron	xx
Pin (aven du)	Fontaine-de-Vaucluse	Vaucluse	Albion	15/−5	Mined for iron	x
Sénanque (aven-mine et gr.-mine de)	Gordes	Vaucluse	Albion	−26	Mined for iron	?
Vache d'or (gr. de la)	Fontaine-de-Vaucluse	Vaucluse	Albion	<25 m	Mined for iron	?
Vache (ou Cabre) d'Or (gr.-mine de la)	Fontaine-de-Vaucluse	Vaucluse	Albion	33/−8	Mined for iron	x
Valette (aven de la)	Fontaine-de-Vaucluse	Vaucluse	Albion	31/−7	Mined for iron	x
Salaou (sce de la)	Castellane	Alpes-de-Hte-Prov.	Arc de Castellane	?	Thermal spring (14 °C, 1 m^3/s), in gypsum	?
Thermes (gr. des)	Digne-les-Bains	Alpes-de-Hte-Prov.	Arc de Castellane	8 m/0	Close to the spa, rising channels	x
Mescla (gr. de la)	Malaucène	Alpes-Maritimes	Arc de Castellane	≈3.5 km/ ± 339 m (−267/+ 72)	Thermal-salted spring 23 °C	x
Chat (gr. du)	Daluis	Vaucluse	Arc de Castellane	1 km/12 m (−2/+10)	Sulfuric cave. Unique corrosion tables	xx
Ermite (gr. de l')	Ornolac-Ussat-les-Bains	Ariège	Ariège valley	−70	Folia, thermal groundwater (21°C)	x
Vapeur (gfre. de la)	Ornolac-Ussat-les-Bains	Ariège	Ariège valley	−50	Smoking shaft, thermal groundwater (18 °C)	x
Savonnières (viailles de)	Savonnières-en-Perthois	Meuse	Paris Basin	<100 m	Enlarged fractures intersected by recent epigene caves and quarry	x
Denis Parisis (réseau)	Béthemont-la-Forêt	Val d'Oise	Paris Basin	≈3 km	Maze cave in gypsum, similar to Ukrainian	xx

(continued)

Table 1 (continued)

Name	Commune	Department	Area	Speleometry (length/depth)	Observation	Hypogene cave
Serpents (gr. des)–Chevalley (gfre.)	Aix-les-Bains	Savoie	Bauges	±11 (−3/+ 8) −27	Sulfuric caves. Spheres, corrosion tables. Groundwater 43 °C	xx
Antre (gourg de l')-Doux (las)	Soulatgé	Aude	Corbières	800 m/+ 25 m	Thermal water (19 °C)	?
Mas d'en Caraman	Paziols	Aude	Corbières	77 m/−47	Thermal spring (22 °C)	?
Font-Estramar (sce de)	Salses-le-Château	Pyrénées-orientales	Corbières	2.9 km/−262 m	Thermal branch (21 °C) with Mn deposits	Partly
Sorine (sce de)	Saint-Geniez	Alpes-de-Hte-Prov.	Durance	10 m?	Sulfuric-thermal spring (22 °C) in gypsum	?
Adaouste (gr. de l')	Jouques	B.-du-Rhône	Durance	1.1 km/−191	Folia, tower cones, coral towers, bubble trails, dripping holes…	xx
Malacoste quarry	Mirabeau	Vaucluse	Durance	0	Fe–Mn hypogene deposits in a pre-burdigalian paleokarst	xx
Baume (gr. de la)	Balaruc-les-Bains	Hérault	Gardiole	600 m/−35	3D maze in a breccia pipe; miocene thermal outflow; folia	xx
Madeleine (gr. de la)	Villeneuve-lès-Maguelonne	Hérault	Gardiole	339 m/−30	CO_2 degassing cave,thermal spring (16 °C)	x
Grande Vernissière (mine de la)	Durfort-et-St-Martin-de-Sossenac	Gard	Garrigues	<50 m	F-Zn ore, ghost weathering	x
St-Maximin (phosphatières de)	St-Maximin	Gard	Garrigues	−70	Phosphate ores in caves lined with large calcite spar	x
Baravon (gr. du)	Gras et Lagorce	Ardèche	Ibie valley	4 caves <20 m	Calcite spar lining, fluid incl. TH > 70 °C	x
Consolation (gfre de la)	Accous	Pyrénées-Atl.	Iseye	−700	Chamber covered by large pyrite crystals at about 70 m depth	Locally
Fosse Mobile and other caves of the area	La Rochette and neighboring municipalities	Charente	Karst de La Rochefoucault	Several systems >15 km	Maze caves, ghost-rock; Touvre spring-180	Probably
Douze (sce de la)-Bize (gr. de)	Bize	Aude	Minervois	Several caves (max. ≈ 100 m)	Thermal spring (21 °C); cluster of caves with many feeders	x
Fortinière (géodes de La)	La Bazouge-de-Chéméré	Mayenne	Carboniferous Laval synclinorium	5 m	Old cave (Eocene) lined by calcite spar	x
Oilloki (gr. d')	Arette	Pyrénées-Atl.	Pierre St-Martin	50 m/−10	Mineralized cave (PbS), with the presence of Bi; outflow along overthrust	xx
Carrière St-Robert (gr. de la)	Viviers	Ardèche	Rhône valley	Several caves < 20 m	Calcite spar lining	x
Champlang (gr. de)	Viviers	Ardèche	Rhône valley	≈150 m	Calcite spar lining and Fe	x
	Saint-Péray, Châteaubourg	Ardèche	Rhône valley	Several < 20 m	Miocene mazes, Sulfides	x

(continued)

Table 1 (continued)

Name	Commune	Department	Area	Speleometry (length/depth)	Observation	Hypogene cave
Crussol-Châteaubourg karst						
Pont de la Caille (géodes du)	Cruseilles	Savoie	Salève	<5 m	Calcite roses geodes, filled with (fluvio) glacial material, old spa below	x
Leicasse (aven de la)	Saint-Maurice-Navacelles	Hérault	Séranne		1 geode intersected by epigene cave	x
Champignons (gr. des)	Puyloubier	B.-du-Rhône	Ste-Victoire	±48 (−26/+22)	Isolated chamber	xx
Saint-Ser (ermitage de)	Puyloubier	B.-du-Rhône	Ste-Victoire	<15 m	Next to Champignons Cave	x
Orgière (grotte d')	Bourg-St-Maurice	Savoie	Tarentaise	40 m	Thermal-sulfuric old spa below (Bonneval-les-bains)	?
Salins (gfre de)	Salins-les-Thermes	Savoie	Tarentaise	−70	Giant shaft, thermal (33 °C), sulfuric	x
BR 13 160	Malataverne	Drôme	Vallée Rhône	−47	Next to Iboussières	x
Iboussières (gr. des)	Malataverne	Drôme	Vallée Rhône	−49	Black tubes	xx
Crêche des Santons (gr. de la)	Gréoux-les-Bains	Alpes-de-Hte-Prov.	Verdon	−7	2D network	x
Pierres (Baume des)	Quinson	Alpes-de-Hte-Prov.	Verdon	117 m/−22	Evidence of rising flow	x
Pigette (gr. de)	Gréoux-les-Bains	Alpes-de-Hte-Prov.	Verdon	−43/−48	3D network; Fe, barite, celadonite	xx
Saint-Sébastien (gr. de)	Gréoux-les-Bains	Alpes-de-Hte-Prov.	Verdon	319 m/−8	2D network	x
Vallon du Salut (sce thermale du)	Bagnères-de-Bigorre	Htes-Pyrénées	Zone N-pyrénéenne	56 m/−16	Thermal spring (17 °C) in the spa park	?

Keys gr. = grotte (cave); gfre = gouffre (shaft); sce = source (spring) xx = major or studied; x = ascertain; ? = possible

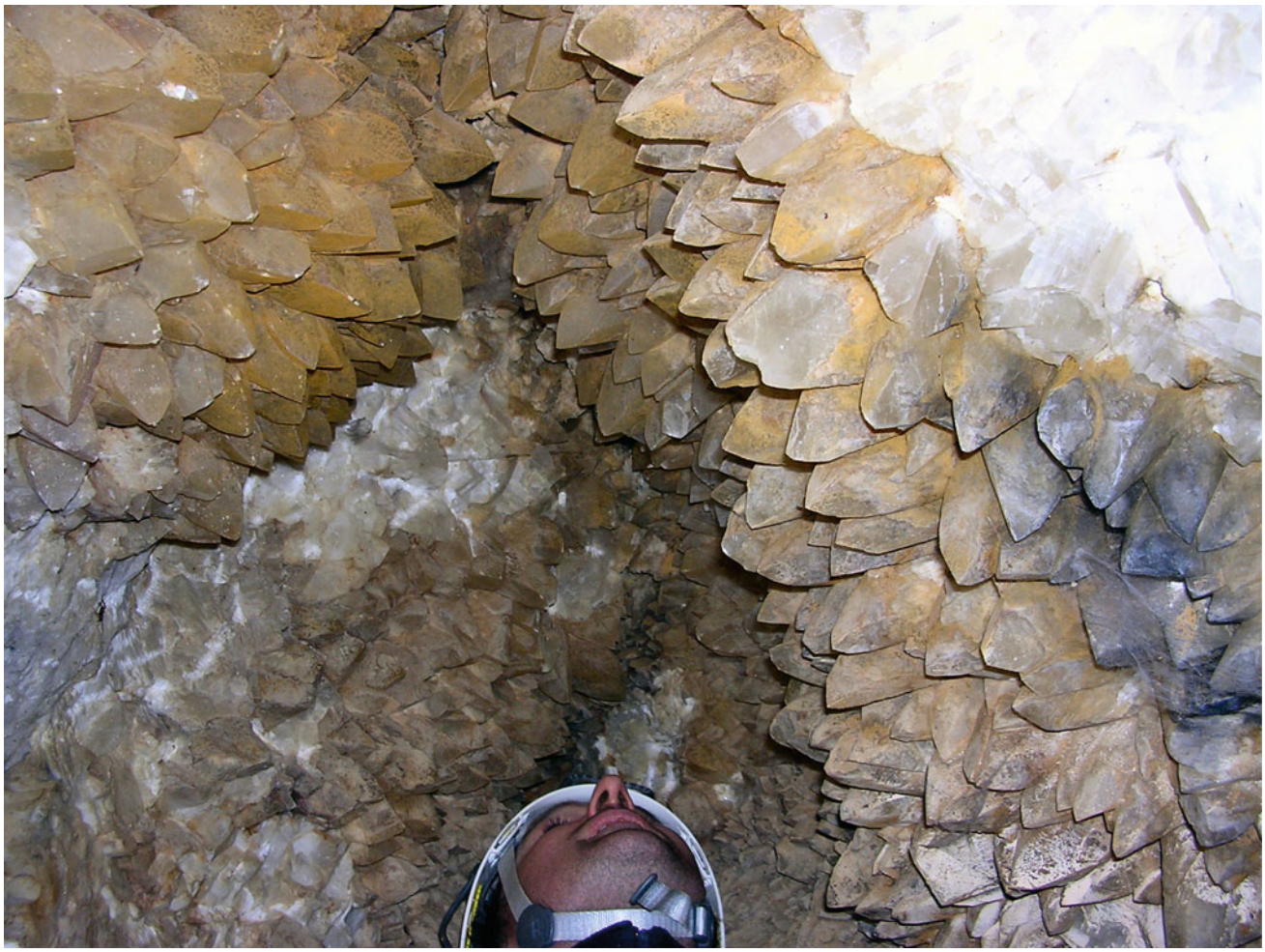

Fig. 5 Geode lined with calcite spar. Cave in Ardèche, France (*Photo* P. Deconinck). This small cave, together with similar occurrences in Ardèche, is located along one branch of the transcurrent deep-rooted Cévennes fault, which allowed uprising of deep flow. Slightly oversaturated and warm water, probably mixing with colder meteoric component, allow depositing of large calcite spars lining the walls, together with iron oxi-hydroxides

thermal spring of Gréoux-les-Bains (Fig. 3). The upper part displays a high density of spherical cupolas, evidencing degassing processes at shallow depth. Consequently, the entrances record past base-level positions where the caves discharged while active.

The Adaouste Cave (Jouques, Bouches-du-Rhône) was active in the Late Miocene. Located along the Durance Valley and its deep-rooted fault, it was discharging thermal-carbonic water (Audra et al. 2002, 2009c). At shallow depth below the water table, CO_2 degassing produced bubble trails and supersaturated water with strong underwater calcite deposition (folia, tower cones, tower corals), whereas deep pockets trapped CO_2 causing the highly corrosive atmosphere to create boxwork and deep acid drip holes (Fig. 7). Above the water table, active air convections produced strong condensation–corrosion, carving cupolas and condensation channels cutting through older flowstones.

Both cases display an evolution in shallow phreatic zone, with at least in a late stage of base-level lowering an evolution of the upper part of the cave above water table where condensation–corrosion played a major morphological role. They are also clearly located along main regional faults or overthrusts, at places where structural highs (overthrust front and anticline, respectively) allowed discharge at the topographic lows.

Such pattern also corresponds to some of the largest hypogene cave systems in the world: Monte Cucco Cave, Italy, is the hypogene cave with the greatest vertical amplitude in the world (Galdenzi and Menichetti 1995). In the Black Hills, South Dakota, USA, Jewel and Wind Caves rank among the largest maze caves of the world (Palmer and Palmer 2000, 2009; Palmer et al. 2015). Toca da Boa Vista, Brazil, has also been demonstrated to be a similar deep-seated system (Klimchouk et al. 2016; Auler et al. Chap. 55).

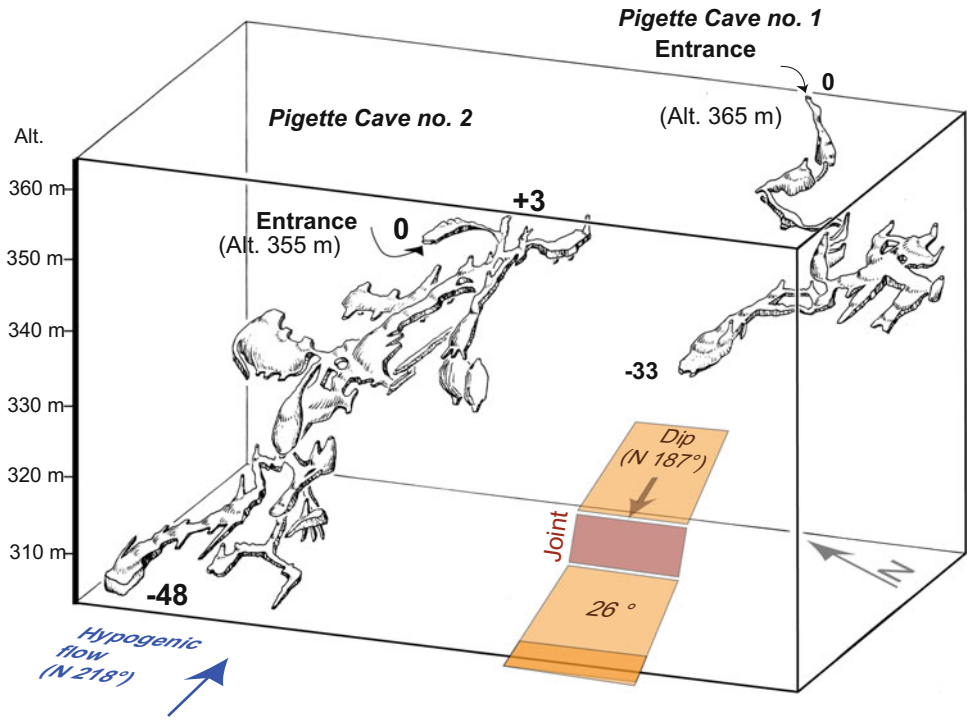

Fig. 6 Pigette Cave, Gréoux-les-Bains, France, is a 3D maze developed in the shallow phreatic zone. Rising flow enlarged alternatively bedding planes and vertical joints, producing a *staircase-like* pattern (survey J.Y. Bigot)

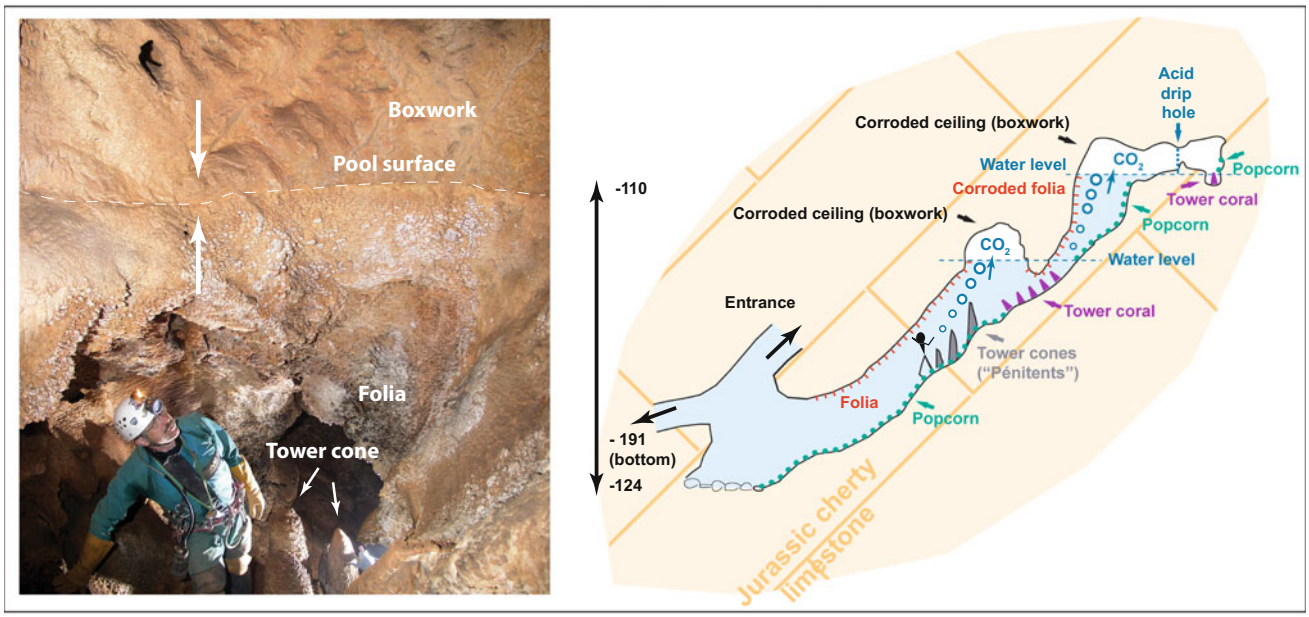

Fig. 7 A blind chimney at depth in Adaouste Cave. CO_2 degassing produces supersaturation and underwater calcite deposition (folia, tower coral). Sinking calcite rafts build *tower cones* (*Photo* J.Y. Bigot). In cupolas, trapped CO_2 produces highly corrosive atmosphere, causing the formation of boxwork and acid drip holes. After dewatering, a later stage allowed the formation of aerial popcorn (Audra et al. 2002)

4.1.3 2D Maze Caves

If a significant permeability difference exists between two strata, and if no significant fracture allowing transverse flow is present, a 2D maze cave can develop in the more permeable bed and below the less impermeable ceiling. The 2D maze cave is a subtype of 3D maze cave; some parts of 3D mazes locally develop as 2D mazes, when a less permeable stratum is present on the ceiling. The passages are

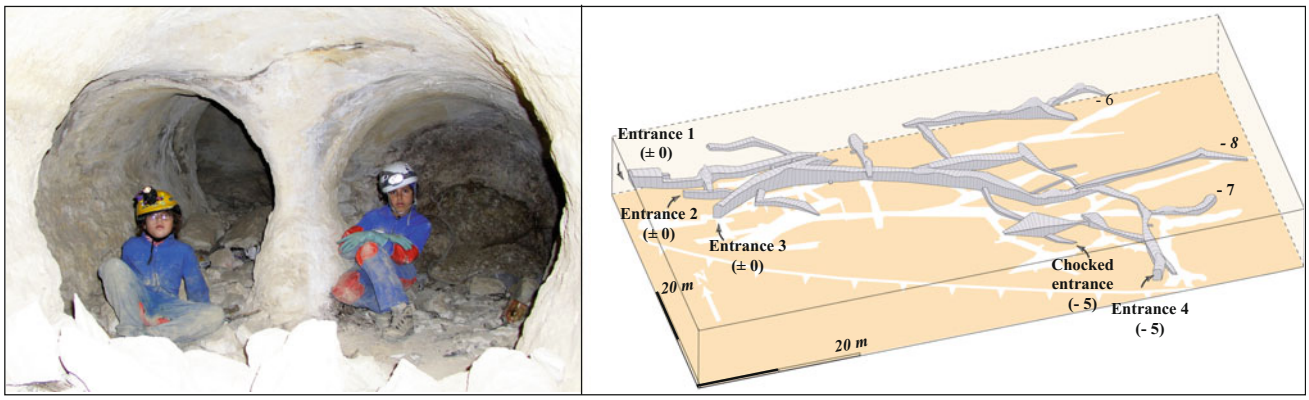

Fig. 8 The cave of Saint-Sébastien (Gréoux-les-Bains, Alpes-de-Haute-Provence) is a 2D maze. It is an inclined planar maze confined below a marly ceiling. Dip is oriented toward the SE, the thermal water rose toward the NW (toward the *left* in the sketch) (*Photo* J.Y. Bigot)

horizontal or inclined, according to the dip. The Saint-Sébastien Cave (Figs. 3 and 8) develops below the inclined marly cover, enlarging the fracture network according to the preferential flow direction as typical round phreatic conduits (Fig. 8; Viseur et al. 2014). The Denis Parisis System, in the central part of the Paris Basin, develops horizontally into a gypsum layer sandwiched between marls (Bigot 2010, Fig. 9). The mazes of Charente

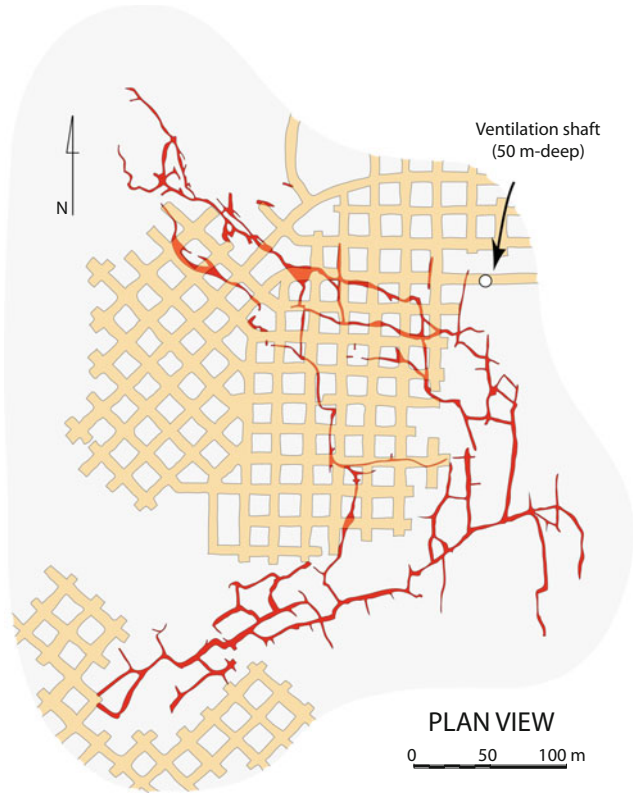

Fig. 9 The Denis Parisis System is located in the center of Paris Basin. It is a 2D maze developed in a horizontal layer of gypsum sandwiched in between impermeable layers. It originated from hypogene transverse flow similar to the giant mazes in Ukraine (after Bigot 2010)

(Fig. 20), which are the largest in France (up to 15 km), are partly related to ghost-rock processes (Dandurand 2012) and are possibly of hypogene origin.

4.1.4 Giant Ascending and Collapse Shafts

In active tectonic areas, the combination of rising warm water, CO_2 and H_2S outgassing, and microbial activity causes "hyperkarst" phenomena to develop along active deep-rooted faults or around magmatic bodies, producing the largest ascending and collapse shafts of the world (Klimchouk 2007; Audra and Palmer 2015). Fractures are initially enlarged, eventually leading to collapse shafts. In France, the most demonstrative example is the Salins shaft, in Savoy (Fig. 10). Warm water (33 °C) rose from a vertical fracture in gypsum rock, previously explored to 70 m deep. Now, it is plugged at 14 m deep and no significant discharge occurs. In addition to high temperature, the water had a typical pattern of such a type of ascending shaft, with H_2S and CO_2 degassing, together with a high salinity (chlorides, sulfurs), and also noble gases and radioactivity showing a deep component. This matches with the location of the shaft in the vicinity of one of the main alpine thrust, between the inner and outer domains. In Italy, Pozzo del Merro is more than 450 m deep including the collapse doline (Caramanna 2002). It is associated with the Tivoli travertines and to the recent volcanic activity of the Latium. A similar origin can be attributed to Hranica propast in Czech Rep., which is now 473 m deep (including 70 m of entrance collapse). It is located along an active deep-rooted fault of the European plate releasing deep CO_2 (Geršl et al. 2011). And the 319 m-deep Zacaton collapse shaft in Mexico, which displays as a cylindrical collapse shaft (Gary 2010), is also located close to a recent magmatic body.

4.1.5 Caves Associated with Ore Deposits

Ore deposits in karstic caves are frequently referred to as "hydrothermal mineralizations." Some epigene caves may

trap minerals brought in by surficial erosion (bauxite, iron, etc.). However, most of mineral concentrations are deposited by deep upward fluid flow. Metallic ions are transported as solutes from depth by reduced water and eventually deposited after mixing with shallow oxygenated meteoric water, where pH/Eh conditions are changing. The caves correspond to the outflow points, generally located at the boundary between the karst aquifer and its impervious cover, especially where intersected by regional deep-rooted faults. According to these conditions, limestone rock solution occurs together with ore deposition that gradually fills the voids. Such speleogenesis and mineralization generally occur at shallow depth in the phreatic zone, creating caves composed of maze patterns, breccia zones, or subhorizontal passages along the water table, connected to narrow fractures acting as deep feeders. Mineral deposition may occur either as oxides or as reduced sulfides (galena, pyrite, sphalerite, etc.), forming Mississippi Valley Type (MVT) ore deposits. The oxidation of sulfides, during or after deposition, is associated with an intense microbial activity, clearly visible on the spongy and filamentous texture of the ferruginous deposits. Later evolution may produce a large variety of sulfate minerals, some of rare occurrence in caves.

The Piei Cave (Lagnes, Vaucluse) was mined around 1830 for its ferruginous deposits (Audra et al. 2013). They are displayed as massive strata or spongy texture where microbial remnants are preserved (Fig. 11). The cave is made of a horizontal main drain which was connected to the base level, and several feeders and breccia pipes along a

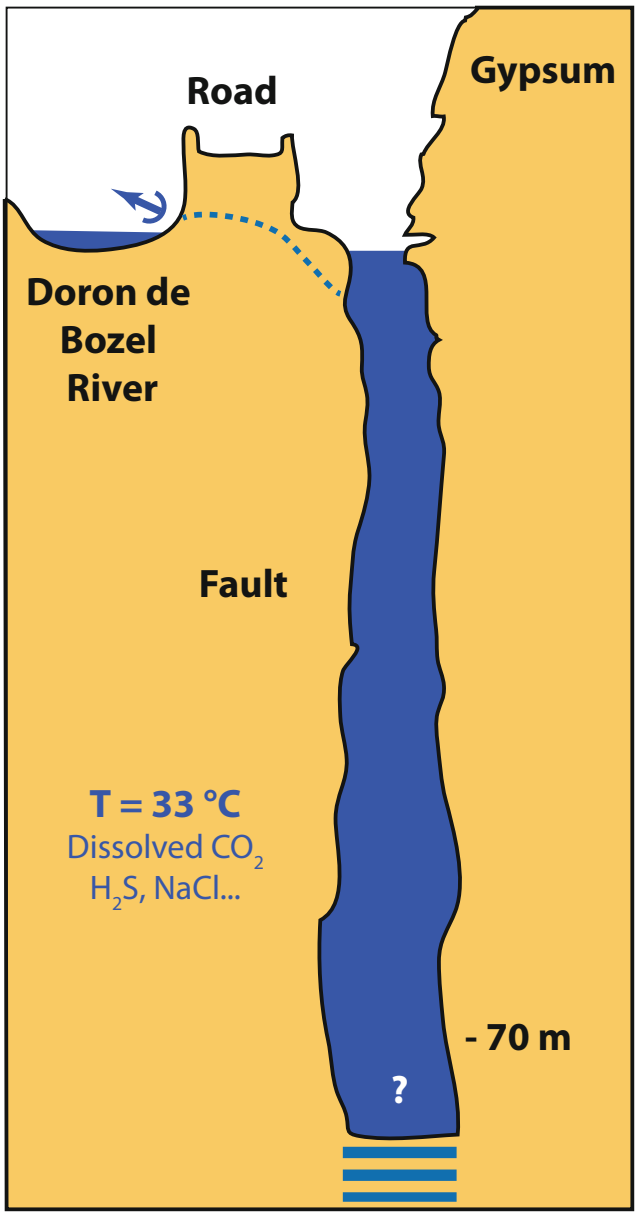

Fig. 10 The giant ascending shaft of Salins (Savoy) is developing in a Triassic gypsum stripe of highly deformed alpine structures. It discharges warm water (33 °C) and degasses CO_2, H_2S, nitrogen, and noble gases. NaCl concentration reaches 12 g/L, associated with KCl, sulfates, carbonates, arsenates, and traces of bromine and iodine. It also contains dissolved iron and radioactive substances (Moret 1950; Hobléa 1999)

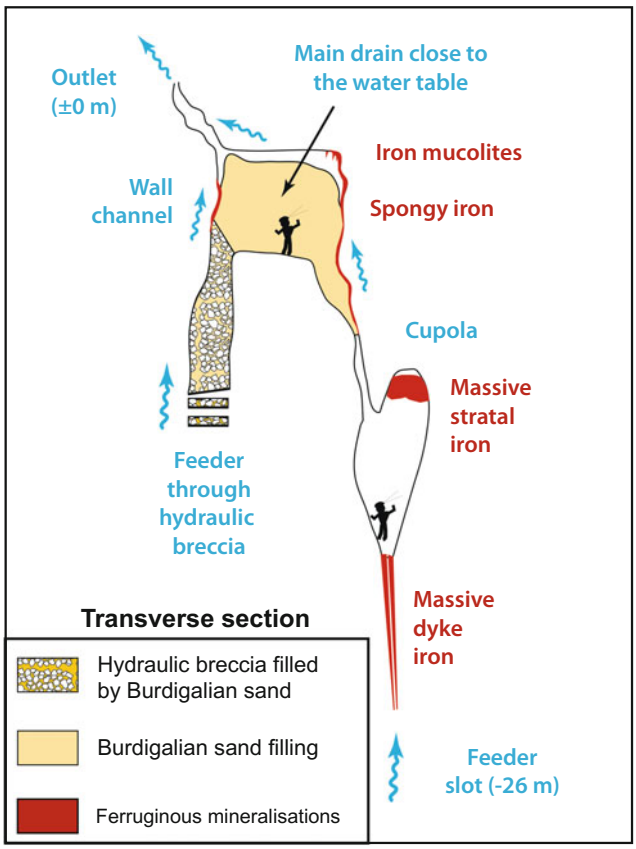

Fig. 11 Piei Mine-Cave. Diagrammatic distribution of the ferruginous mineralization facies according to depth: dyke in fractures at depth, massive deposits in the first voids, spongiform and mucoliform masses in the draining voids and between wall and sediment

fracture where upflow was rising. This cave records a Late Miocene uplifting stage of the Vaucluse plateau.

The Oilloki Cave (Arette, Pyrénées-Atlantiques) is located at the foot of the Pierre Saint-Martin massif, above the Kakouetta canyon. It was entirely opened by miners for its galena (PbS) filling. Associated minerals are cerussite ($PbCO_3$), which derives from oxidation of the lead sulfide, and ferruginous masses with microbial evidences. Bismuth was also found here, as first cave mineral occurrence (Audra 2009). The upward flow was rising from depth along a main overthrust at the contact of Triassic evaporites, depositing the ore at shallow depth after mixing with meteoric water, and outflowing at the contemporaneous base level.

The Iboussières Cave (Malataverne, Drôme) is located along the Rhône valley rift. Large chambers are connected to deep narrow feeders. Ferruginous deposits are concentrated at the top of the cave, above clay filling and in cupolas. The facies of the ferruginous deposits are typically microbial with spongy texture (Audra and Hofmann 2004). Along walls, the "black tubes" are wall channels filled with spongy ferruginous deposits (Fig. 12). These are exceptional features only known in two other sites in Utah (Herron 1997) and Romania (Onac, pers. comm.).

The Cévennes massif is famous for its lead-zinc ores mined since the Bronze Age. The Grande Vernissière Cave (Durfort, Gard) originated from ghost-rock weathering associated with galena, sphalerite (ZnS), and fluorite (CaF_2) (Bruxelles and Wienin 2009; Fig. 13). The mineralizing hydrothermal fluids migrated from the basin by gravity at the regional scale during the Pyrenean orogenesis during the Eocene (Jost et al. 2004). Such a model probably accounts for many ores in the periphery of the Central Massif, and probably might also explain the high density of ghost-rock features in this area.

The Baume Galinière (Alpes-de-Haute-Provence) locates at the foot of the Vaucluse plateau. It is an original case where a large part of the sulfuric corrosion originates from the oxidation of a small pyrite ore, still ongoing through

Fig. 12 The "*black tubes*" in Iboussières Cave. They correspond to the mold of wall channels filled with spongy microbial ferruginous material, exhumed after erosion of the clay filling (*Photo* J.-Y. Bigot)

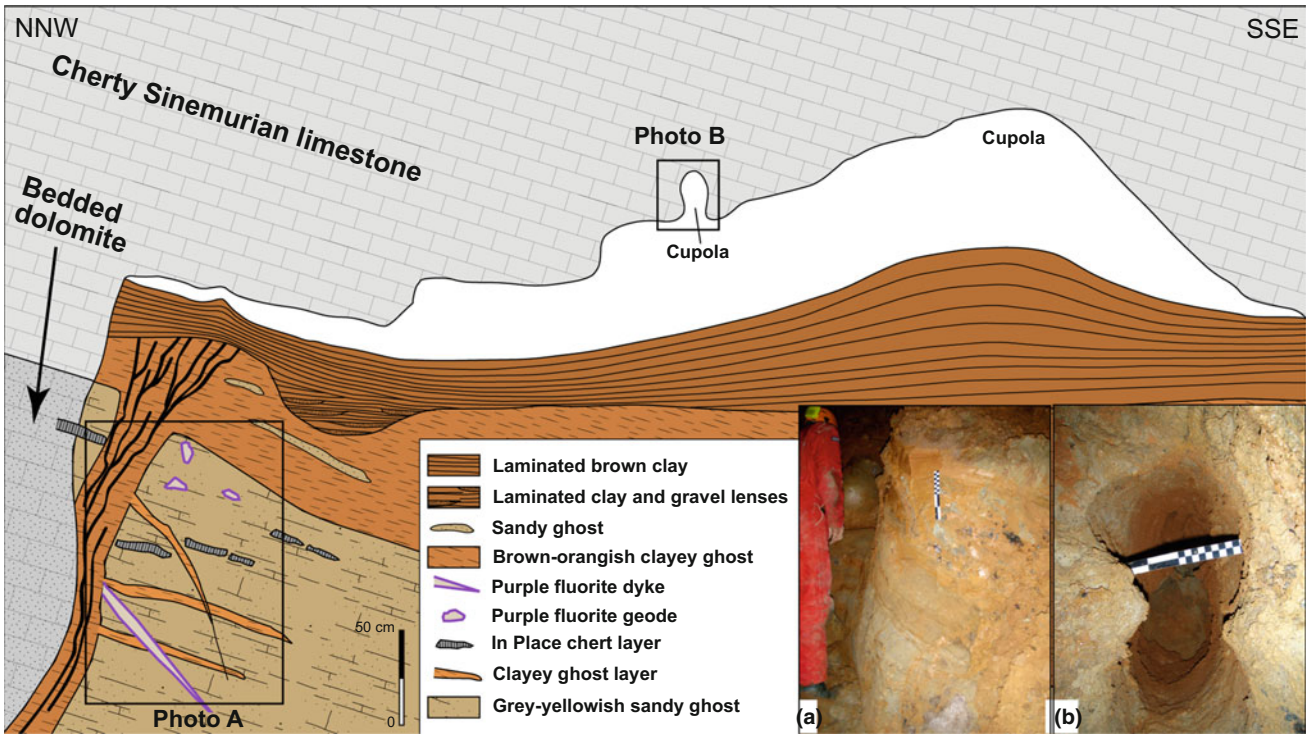

Fig. 13 Section of a gallery in the Grande Vernissière Cave showing the relationship between the mineralized hydrothermal ghost rock and the late classical karstification. A: Detail of the ghost rock with unweathered fluorite dykes and cherty layers in the ghost rock showing the original structure. B. Detail of the ceiling cupola (Bruxelles and Wienin 2009)

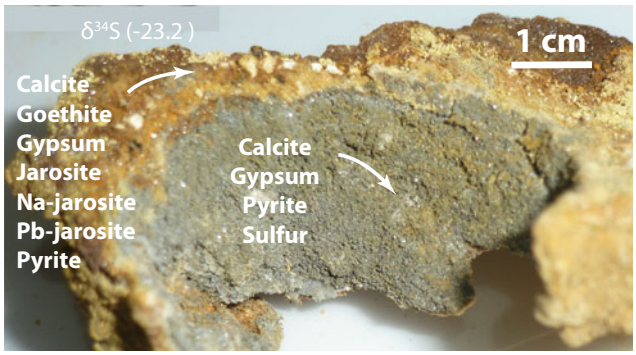

Fig. 14 Detail of the crust developing through oxidation onto the pyrite masses of the Baume Galinière Cave. Sulfur is released through microbial activity, low mobile iron oxi-hydroxides concentrate, and sulfates deposit as a *light brown* crust. In this sample, three minerals of the jarosite subgroup are present (jarosite, natrojarosite, plumbojarosite)

condensation water from air moisture. Together with ferruginous deposits witnessing microbial activity, this oxidation is responsible for the occurrence of rare sulfates, especially fibroferrite and the six members of the jarosite subgroup, of which argentojarosite is the first occurrence reported in a cave (Audra et al. 2015; Fig. 14). Finally, the Baume Galinière also records the position and retreat of the impervious cover in relation to valley incision caused by uplift and tilting of the Vaucluse block during the Neogene.

4.2 Hypogene Cave Pattern Along or Above the Water Table

At shallow depth along the water table, degassing, sulfide oxidation and mixing with oxygenated meteoric water produces strong dissolution. This corrosive process also propagates through the cave atmosphere above the water table by thermal air convection carrying aggressive droplets.

4.2.1 Upward Developing Dendritic Caves

CO_2 and H_2S degassing enhance aggressivity. By condensation–corrosion, cupolas develop upward as a dendritic pattern of stacked spheres (Fig. 15; Audra et al. 2007). The development of two neighboring spheres will be divergent, toward the greatest potential heat transfer, because the rock in between the two spheres has less transfer potential and remains warm (Szunyogh 1990), giving the bush-like structure, as found in the Sátorkö-puszta Cave, Hungary, which is the model for such type of cave. Above thermal water, condensation occurs at the ceiling which is cooler.

In Chevalley Aven and Serpents Caves (Aix-les-Bains, Savoy, Fig. 2), the thermal aquifer is intersected close to the spring. CO_2 and H_2S degassing occurs and water temperature may reach 41 °C, causing condensation enhanced by carbonic-sulfuric corrosion and microbial activity (Audra et al. 2007; Hobléa et al. 2010). Serpents extends

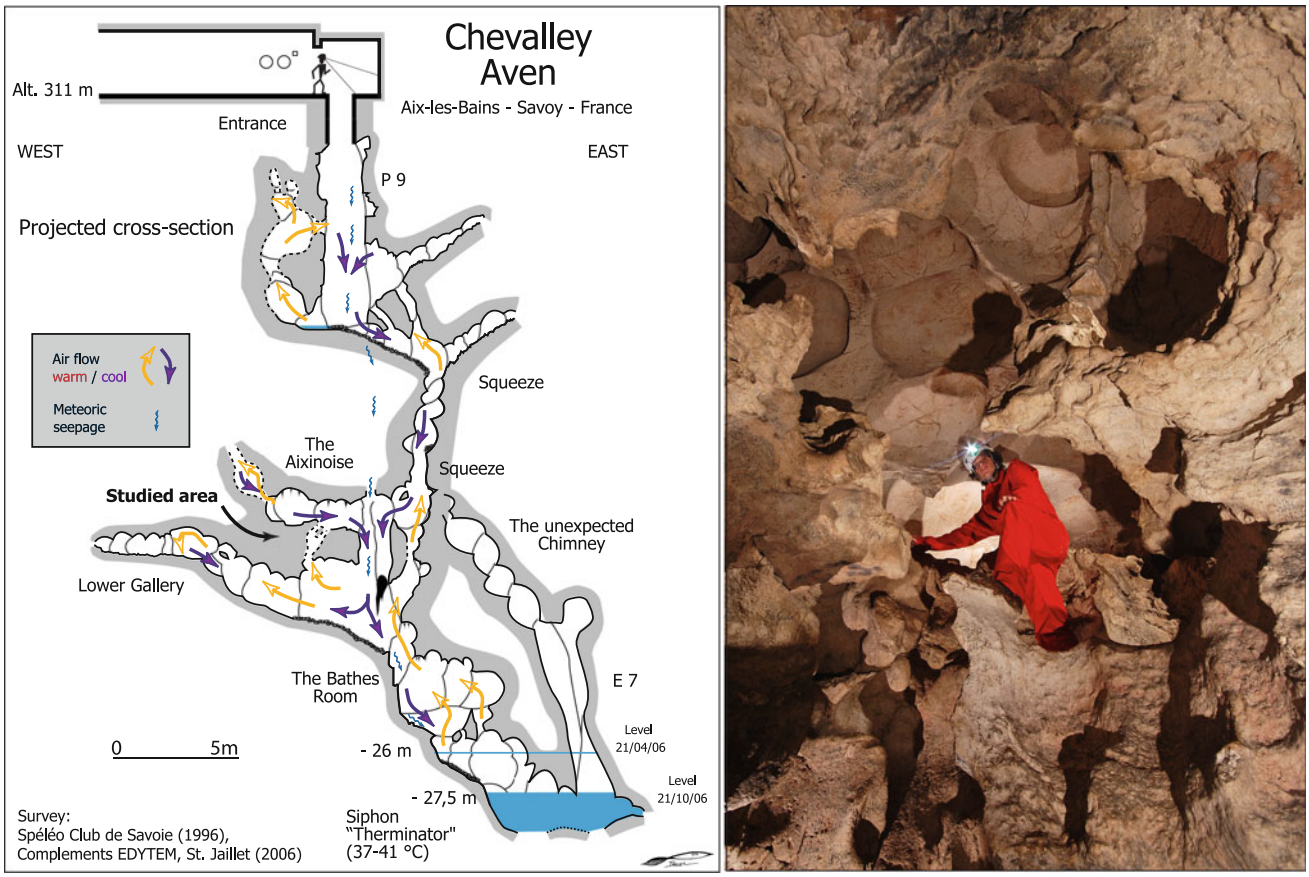

Fig. 15 *Left* the Chevalley Aven (Aix-les-Bains, Savoy) is an upward developing dendritic cave, formed by aggressive convections of warm air above the thermal water table. Air loops are cooling while rising, producing condensation–corrosion and allowing the development of biofilms on wet walls (Audra et al. 2007; Hobléa et al. 2010). *Right* condensation–corrosion stacked spheres in the ceiling of Serpents Cave (*Photo* S. Jaillet)

horizontally as a sulfuric water table cave (see below), whereas Chevalley Aven is made of vertically stacked spheres developing upward and laterally. Microbial biofilms are present on wet smooth walls where the hot rising air cools and produces condensation. Gypsum develops in places where cooler sinking air is warming and drying.

4.2.2 Isolated Chambers

When strong degassing occurs, upward developing dendritic spheres enlarge and merge, eventually producing large isolated chambers (Fig. 16; Audra et al. 2002). Taking into account the moderate thermal gradient and pCO_2, modeling has shown that such volume can develop in a rather short time span, in about 10,000 years (Lismonde 2003). From examples in Israel, Frumkin and Fischhendler (2005) assign the origin of isolated chambers to phreatic convection.

4.2.3 Sulfuric Water Table Caves

Above the water table, sulfuric vapors and thermal convections produce strong condensation–corrosion, replacement gypsum crusts, corrosion tables, and sulfuric karrens (Egemeier 1981; De Waele et al. 2016 and references herein). The main drain develops headward from the springs (Fig. 17). Due to the sulfuric corrosion, the long profile displays a very low gradient (Fig. 18). These caves precisely record the base-level position and minor changes in base-level cause the flow to migrate vertically or laterally forming incipient mazes (Audra 2007; Audra et al. 2009a, b; Piccini et al. 2015). Condensation domes develop upward and may breach the surface (Fig. 17). The most demonstrative water table sulfuric caves in France are Chat Cave, Alpes-Maritimes (De Waele et al. 2016; Fig. 18) and Serpents Cave (Audra and Hobléa 2007; Figs. 2 and 15). Abroad, water table sulfuric caves are represented by Kane Caves, Wyoming, USA (Egemeier 1981; Engel et al. 2004), Acqua Fitusa, Italy (De Waele et al. 2016; see Vattano et al. Chap. 12, and particularly Fig. 4), Kraushöhle and Bad Deutsch Altenburg Caves in Austria (Plan et al. 2012; De Waele et al. 2016; see Spötl et al. Chap. 6). In case of major base-level lowering, distinct horizontal cave flevels develop: Frasassi Cave, Italy (Galdenzi and Menichetti 1995; Galdenzi and Maruoka 2003), Montecchio Cave, Italy (Piccini et al. 2015).

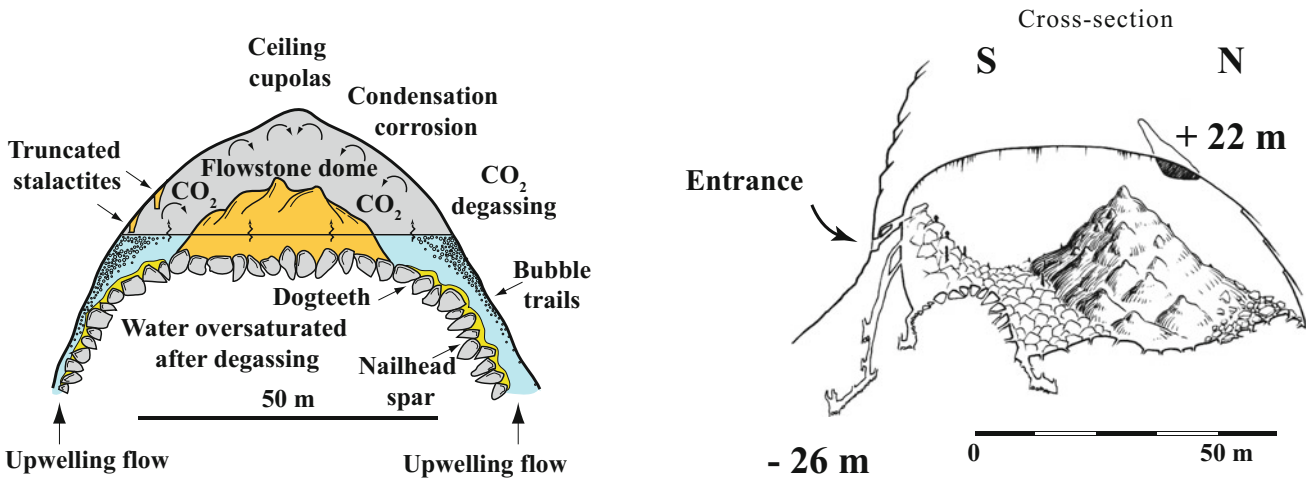

Fig. 16 The Champignons Cave, Provence, France, is an isolated chamber. Thermal hypogene flow degassed CO_2 at shallow depth. Thermal convection enhanced condensation–corrosion to develop a large isolated chamber more than 50 m wide, which tends toward a hemispherical shape. Simultaneously, massive calcite deposits occurred in the lake, which was supersaturated with calcite because of CO_2 degassing (Audra et al. 2002)

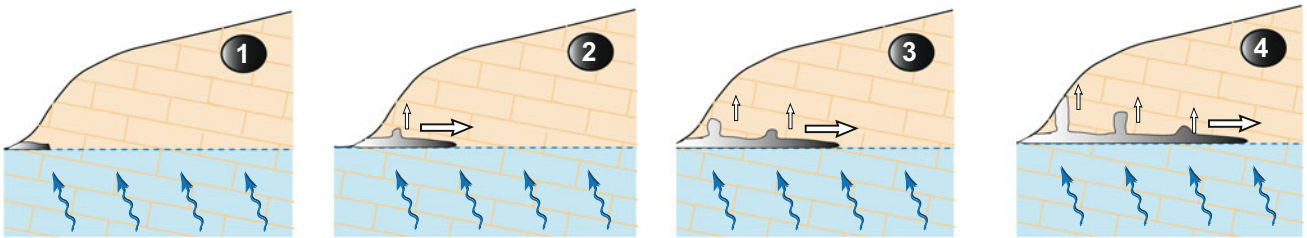

Fig. 17 Conceptual model of the development of water table sulfuric acid cave. Headward evolution by condensation–corrosion along the water table, supplied by major sulfuric upwelling along a fracture. Simultaneously, hydrothermal conditions lift the hot air so that condensation–corrosion occurs, cupolas and chimneys develop, and some finally break through to the surface. The *white arrows* indicate the direction of cave development; inspired by Villa Luz Cave, Mexico (Hose and Pisarowicz 1999; Hose et al. 2000; Audra et al. 2009a, b)

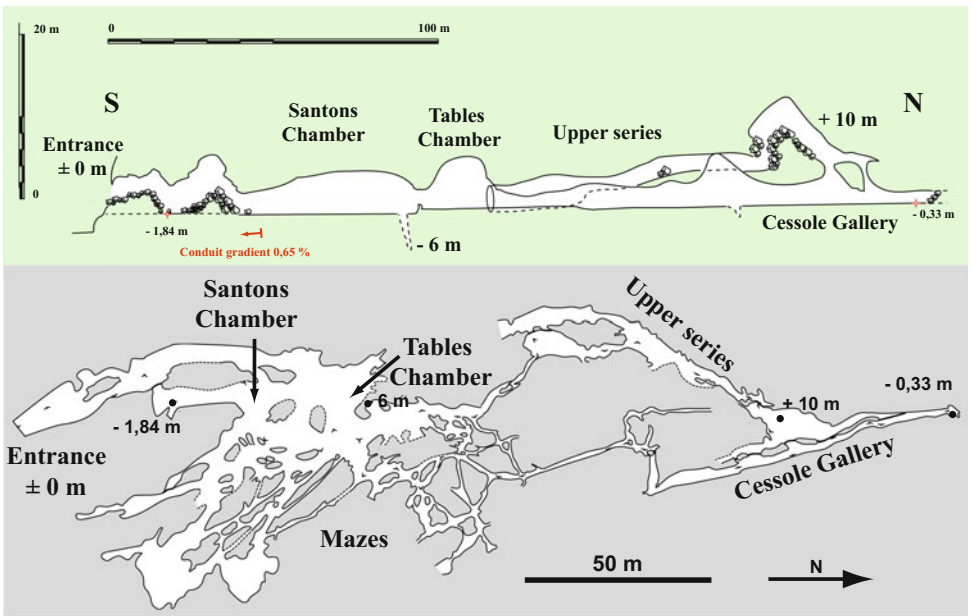

Fig. 18 Chat Cave, France. The longitudinal profile (*top*) shows a very low gradient (<0.65%) made by sulfuric flow along the water table. A dead-end closes the passage upstream to the last sulfuric slot. The plan view (*below*) shows mazes, developed successively after lateral migration of the flow toward the west, following very small base-level drops. The largest chambers in the center developed by integration of the neighboring mazes around the main sulfuric slots (Audra et al. 2009a, b; De Waele et al. 2016)

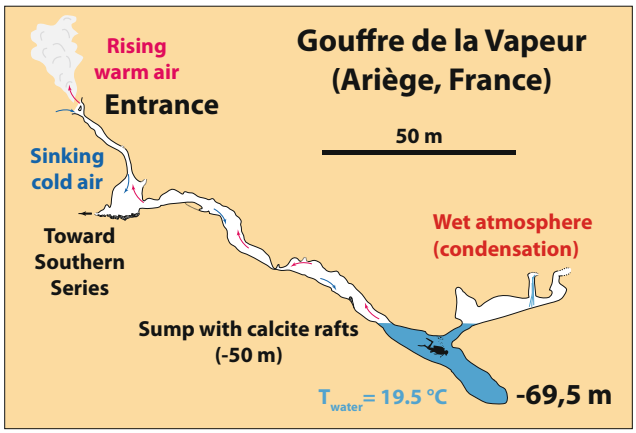

Fig. 19 Vapeur Shaft (Ornolac-Ussat-les-Bains, Ariège) is a « smoking » shaft. In winter the inner hot air is expelled outside producing fog and condensation–corrosion along its ascending path that makes condensation channels and cupolas resembling phreatic features (Survey after P. Sorriaux, M. Guinot, M. Buttard 1973 and www.plongeesout.com for the sump)

4.2.4 "Smoking" Shafts in the Vadose Zone

Above thermal aquifers, the rock is significantly heated by the geothermal gradient. In winter, the atmosphere of open shafts is unstable: The cold air sinks inside the shaft and expels the warm air of the shaft outside making it condense, giving the impression that the shaft is smoking. The rising warm air flow follows ceiling channels where condensation–corrosion focuses while cooling. Eventually, it produces condensation ceiling cupolas and channels, which could lead to their misinterpretation as phreatic in origin. These shafts are generally guided by mechanical fractures; the hypogene role through thermal gradient and air convection is indirect and limited to the etching of the wall features. Beside Vapeur Shaft in France (Fig. 19), similar caves outside of France are Nasser Schacht, Austria (Plan et al. 2006), Fumarollas and Vapor Shafts, Spain (Audra 2007).

5 Conclusions

The understanding of hypogene speleogenesis has increased considerably in the past decade, and this has helped to explain the pattern of caves in hypogene context. The diversity of hypogene caves is now placed in a global model, explaining main types of patterns, depending on the geological structure, the groundwater recharge, and the speleogenetic processes.

The concept of Regional Gravity Flow, which applies to the topography-driven meteoric flow, i.e., to the large majority of situations, offers a framework explaining the location and the conditions of upwelling flows that produce discrete caves in discharge areas. Cave patterns display 3D networks developed in the phreatic zone. The giant ascending shafts, which result from "hyperkarst" processes combining deep-seated acids (CO_2 + H_2S), thermalism and microbial activity, are generally formed in active regions of volcanism or deep-rooted faults. In addition to hypogene caves developed at depth by mixing corrosion and rising flow, some caves are developing in the atmosphere at the water table or above the water table. The development along the water table points toward processes involving Sulfuric Acid Speleogenesis (SAS), where thermal air convection and condensation–corrosion play a key role, a process that has often been underestimated up to now. Most of these caves related to the position of the water table can be considered as precise indicators of past base-level positions and thus represent precious tools for the geomorphic reconstructions, providing insights of the evolution of karst areas, of valley incision, and of uplift rates. Ghost-rock karstification must be investigated more thoroughly, since it is probably a widespread process producing maze patterns, especially in low relief areas such as plains and plateaus. The origin of ghost weathering is still under debate. Originally considered epigene, it now appears to be more frequently hypogene. Ore deposits in caves, especially sulfides, display a wide variety of secondary minerals, mainly sulfates, some of rare occurrence.

France harbors an increasing number of hypogene caves (Fig. 20; Table 1). Among them some display unique features. The Chevalley-Serpents Caves is the most important active cave, where thermal, SAS, condensation–corrosion and microbial activity are clearly visible. Champignons Cave displays a huge cupola chamber. Adaouste Cave is a deep rising chimney with carbonic degassing, displaying unique folia and cone towers. Baume Galinière is a unique site of rare sulfates. And Chat Cave, even if inactive, is one of the most didactic caves in Europe for SAS features. Many other caves, some already identified as hypogene, others not yet, would require detailed studies for their hydrogeologic origin, their morphology, and their mineralogy.

Acknowledgements For courtesy of illustrations we are grateful to the following persons: Stéphane Jaillet, Jean-Yves Bigot, Patrick Sorriaux, Laurent Bruxelles, Stéphanie Gallino-Josnin, P. Deconinck, and Fabien Hobléa.

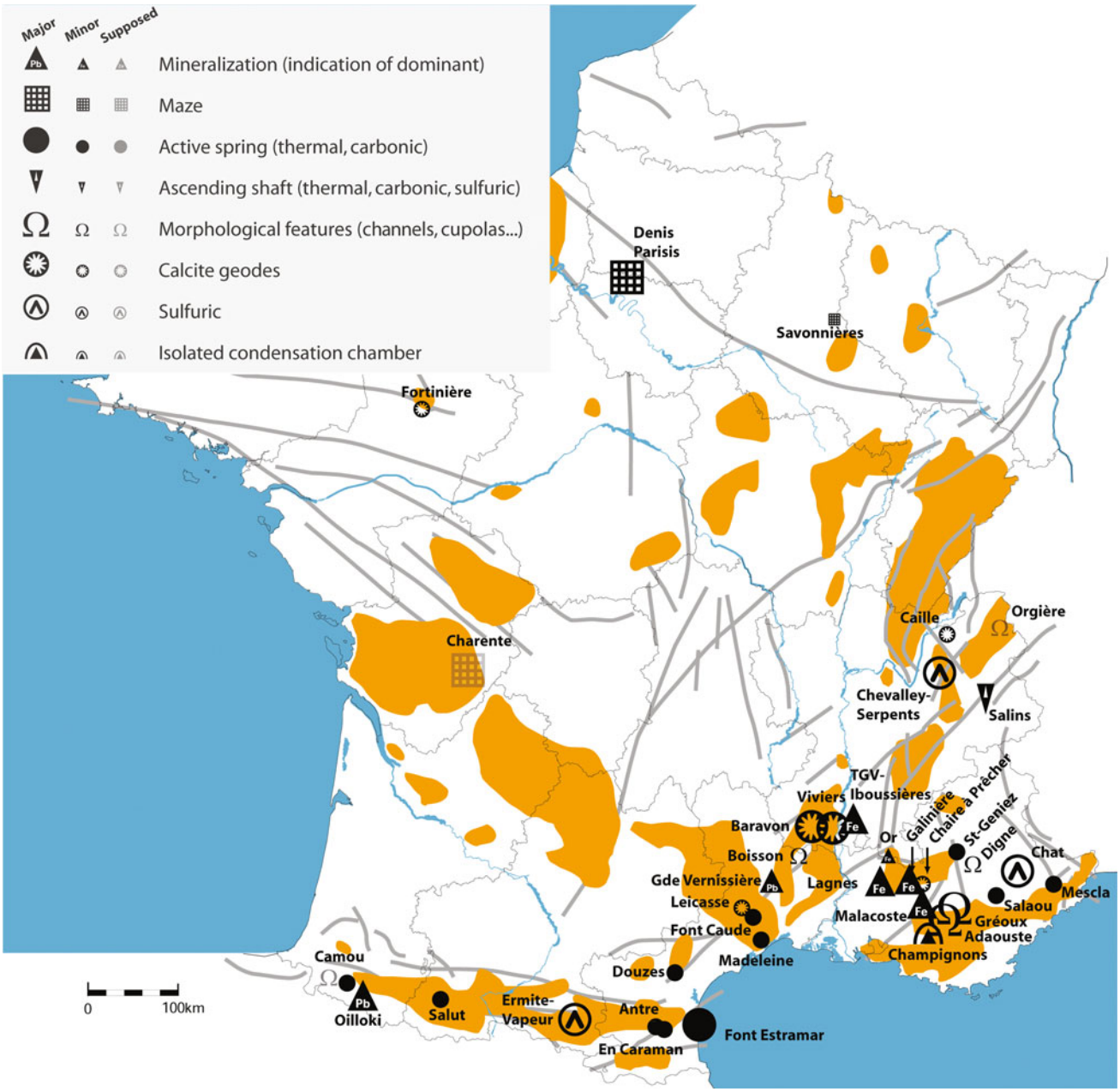

Fig. 20 Distribution of hypogene caves in France, with their dominant characteristics. Maze caves due to transverse cross-formational upflow are present in sedimentary basins. Ghost-rock caves with mineralizations are present around cratons in Causses. Thermal, sulfuric, carbonic caves are located in the periphery of plateaus at the intersection with deep-rooted faults and impervious covers, or in the deformed strata of the Alpine and Pyrenean ranges

References

Audra P (2007) Karst et spéléogenèse épigènes, hypogènes, recherches appliquées et valorisation. Habilitation Thesis, University of Nice Sophia-Antipolis

Audra P (2009) Une cavité à minéralisation hypogène dans le massif de la Pierre Saint-Martin: la grotte-mine d'Oilloki (Sainte-Engrâce, Pyrénées-Atlantiques). Recherches préliminaires (A mineralized hypogenic cave in Pierre Saint-Martin massif: the Oilloki Cave (Sainte-Engrâce, Pyrénées-Atlantiques). Preliminary investigations). In: International Congress, The karst, an efficient indicator of past and present environment, Arette 2007. Association française de karstologie, Karstologia Mémoires, vo 17, pp 176–182

Audra P, Cailhol D (2014) Contexte géomorphologique des grottes de Soyons, Ardèche. 23e Rencontre d'Octobre, Le Châtelard 2013. Spéléo-club de Paris

Audra P, Hobléa F (2007) The first occurrence of jurbanite [Al(OH SO_4) $5H_20$], associated with alunogen [Al_2 $(SO_4)_3$ $17H_20$] and tschermigite [$NH_4Al(SO_4)_2$ $12H_20$]: thermal-sulfidic Serpents Cave, France. J Cave Karst Stud 69(2):243–249

Audra P, Hofmann BA (2004) Les cavités hypogènes associées aux dépôts de sulfures métalliques (MVT). Le Grotte d'Italia 5:35–56

Audra P, Palmer AN (2015) Research frontiers in speleogenesis. Dominant processes, hydrogeologic conditions and resulting cave pattern. Acta Carsologica 44(3):315–348. doi:10.3986/ac.v44i3.1960

Audra P, Bigot JY, Mocochain L (2002) Hypogenic caves in Provence (France). Specific features and sediments. Acta Carsologica 31: 33–50

Audra P, Hobléa F, Bigot JY, Nobécourt JC (2007) The role of condensation-corrosion in thermal speleogenesis. Study of a hypogenic sulfidic cave in Aix-les-Bains. Acta Carsologica 36:185–194

Audra P, Mocochain L, Bigot JY, Nobécourt JC (2009a) The pattern of hypogenic caves. In: White WB (ed), Proceedings of 15th international congress of speleology, Kerrville Texas, vol 2, pp 795–800

Audra P, Mocochain L, Bigot JY, Nobécourt JC (2009b) Hypogene cave patterns. In: Klimchouk AB, Ford DC (eds) Hypogene speleogenesis and karst hydrogeology of Artesian basins. Special Paper, Ukrainian Institute of Speleology and Karstology, Kiev, vol 1, pp 17–22

Audra P, Mocochain L, Bigot JY, Nobecourt JC (2009c) The association between bubble trails and folia: a morphological and sedimentary indicator of hypogenic speleogenesis by degassing, example from Adaouste Cave (Provence, France). Int J Speleol 38(2):93–102

Audra P, Bigot JY, Nobécourt JC (2010) Hypogenic caves in France. Speleogenesis and morphology of the cave systems. Bulletin de la Société géologique de France 181(4):327–335

Audra P, Bigot JY, Camus H, Gauchon C, Wienin M (2013) Hypogenic speleogenesis with ferruginous ore. The Piei mine-cave (Lagnes, Vaucluse, France). 2nd International-symposium on mine caves, Iglesias, Italy, Memorie dell'Istituto Italiano di Speleologia II(28):41–70

Audra P, Gázquez F, Rull F, Bigot JY, Camus H (2015) Hypogene Sulfuric Acid Speleogenesis and rare sulfate minerals in Baume Galinière Cave (Alpes-de-Haute-Provence, France). Record of uplift correlative cover retreat and valley dissection. Geomorphology 247:25–34. doi:10.1016/j.geomorph.2015.03.031

Auler AS, Smart PL (2003) The influence of bedrock-derived acidity in the development of surface and underground karst: evidence from the Precambrian carbonates of semi-arid northeastern Brazil. Earth Surf Proc Land 28(2):157–168

Bakalowicz M (1988) La formation des travertins: aspects géochimiques. Essai de synthèse et discussion. In: Vaudour J (ed) Les édifices travertineux et l'histoire de l'environnement dans le Midi de la France. Travaux de l'URA 903 XVII:261–268

Bayari CS, Pekka E, Ozyurt NN (2009) Obruks, as giant collapse dolines caused by hypogene karstification in central Anatolia, Turkey: analysis of likely formation processes. Hydrogeol J 17:327–345

Bigot JY (2010) Le karst du gypse. In: Audra P (ed.) Grottes et karsts de France. Karstologia Mémoires, Association française de karstologie, vol 19, pp 86–87

Bruxelles L (2001) Reconstitution morphologique du Causse du Larzac: Rôle des formations superficielles dans la morphogenèse karstique. Karstologia 38:25–40

Bruxelles L, Wienin M (2009) Les fantômes de roche de la mine de la Grande Vernissière (Fressac, Gard). Premières observations sur l'origine de certains karsts de la bordure cévenole (The ghost rocks of the mine of La Grande Vernissière (Fressac, Gard). First observations about the origin of some karsts of the bordure cévenole). International congress, the karst, an efficient indicator of past and present environment, Arette, 2007. Karstologia Mémoires, Association française de karstologie 17:192–200

Bruxelles L, Quinif Y, Wienin M (2009) How can ghost rocks help in karst development? In: 15th International congress of speleology, Kerrville, vol 2, pp 814–818. http://www.karstportal.org

Calaforra JM, De Waele J (2011) New peculiar cave ceiling forms from Carlsbad Caverns (New Mexico, USA): the zenithal ceiling tube-holes. Geomorphology 134(1):43–48

Camus H, Bruxelles L (2013) Formes et couvertures karstiques des Avants-Causses du St-Affricain et du Causse du Guilhaumard. In: Étude hydrogéologique des Avants-Causses du St-Affricain et du Causse Guilhaumard, Rapport PROTEE PRO-R-2011-12, GEOTER GTR-PNR-1212-1016

Caramanna G (2002) Exploring one of the world's deepest sinkholes: The Pozzo del Merro (Italy). Underwater Speleology February: 4–8

Cunningham KJ, Walker C (2009) Seismic-sag structures in Tertiary carbonate rocks beneath south-eastern Florida, USA: evidence for hypogene speleogenesis? In: Klimchouk AB, Ford DC (eds) Hypogene speleogenesis and karst hydrogeology of Artesian basins. Ukrainian Institute of Speleology and Karstology, Special Paper, Simferopol, Ukraine, vol 1, pp 151–158

Dandurand G (2012) Cavités et remplissages de la nappe karstique de Charente (bassin de la Touvre, La Rochefoucauld). Spéléogenèse par fantômisation, archives pléistocène et holocène, rôle de l'effet de site. Karstologia 60:61–62

De Waele J, Forti P, Naseddu A (2013) Speleogenesis of an exhumed hydrothermal sulphuric acid karst in Cambrian carbonates (Mount San Giovanni, Sardinia). Earth Surf Proc Land 38 (12):1369–1379

De Waele J, Audra P, Madonia G, Vattano M, Plan L, D'Angeli IM, Bigot JY, Nobécourt JC (2016) Sulphuric acid speleogenesis (SAS) close to the water table: examples from southern France, Austria, and Sicily. Geomorphology 253:452–467

Dublyansky YV (2014) Hypogene speleogenesis—discussion of definitions. In: Klimchouk AB, Sasowsky I, Mylroie J, Engel SA, Engel AS (eds) Hypogene cave morphologies. Karst Waters Institute Special Publication, vol 18, Leesburg, Virginia, pp 1–3

Dubois C, Quinif Y, Baele JM, Barriquand L, Bini A, Bruxelles L, Dandurand G, Havron C, Kaufmann O, Lans B, Maire R, Martin J, Rodet J, Rowberry MD, Tognini P, Vergari A (2014) The process of ghost-rock karstification and its role in the formation of cave systems. Earth-Sci Rev 131:116–148

Egemeier SJ (1981) Cavern development by thermal waters. NSS Bulletin 43(2):31–51

Engel AS, Stern LA, Bennet PC (2004) Microbial contributions to cave formation: new insights into sulfuric acid speleogenesis. Geology 32:369–372

Forti P, Sanna L (2010) The Naica project. A multidisciplinary study of the largest gypsum crystals of the world. Episodes 33(1):23–32. http://episodes.org/index.php/epi/article/viewFile/62140/48441. Accessed 19 July 2016

Frumkin A, Fischhendler I (2005) Morphometry and distribution of isolated caves as a guide for phreatic and confined paleohydrological conditions. Geomorphology 67(3–4):457–471

Galdenzi S, Maruoka T (2003) Gypsum deposits in the Frasassi caves, Central Italy. J Cave Karst Stud 65:111–125

Galdenzi S, Menichetti M (1995) Occurrence of hypogene caves in a karst region: examples from central Italy. Environ Geol 26:39–47

Gallino S (2007) Hydrogéologie, géochimie et modélisation hydrodynamique-thermique d'un système thermo-minéral associé à un contact structural alpin (Aix-les-Bains, Savoie). Ph.D. thesis, University of Savoie

Gary MO (2010) Karst hydrogeology and speleogenesis of Sistema Zacatón, Tamaulipas, Mexico. Ph.D. Thesis, University of Texas, Austin. AMCS Bulletin, Association for Mexican Cave Studies, Austin 21, pp 114

Gary MO, Sharp JM (2009) Volcanogenic karstification: implications of this hypogene process. In: Stafford KW, Land L, Veni G (eds) Advances in hypogene karst studies, NCKRI Symposium, National Cave and Karst Research Institute, Carlsbad, NM 1:27–39

Gàzquez F, Calaforra JM, Forti P, De Waele J, Sanna L (2015) The role of condensation in the evolution of dissolutional forms in gypsum caves: Study case in the karst of Sorbas (SE Spain). Geomorphology 229:100–111

Geršl M, Geršlová E, Hypr D, Kolejka V (2011) Sub-crustal CO_2 Flux Measurement in the Hranice Hy-drothermal Karst.- In: 21th Goldschmidt Conference "Earth evolution", Prague, 2011. European Asso-ciation of Geochemistry, [Online] Available from: http://goldschmidt.info/2011/abstracts/G.pdf. Accessed 24 Apr 2015

Guyonnet-Benaize C (2011) Modélisation numérique 3D haute résolution des structures géologiques de la Moyenne Durance, Provence, SE France (Multi-scale 3D modeling of geological structures of Middle Durance fault region SE France). Ph.D. thesis, Aix-Marseille University

Herron DA (1997) Origin and geologic history of the Timpanogos cave national monument Utah County. Thesis, Brigham Young University, Utah. MSc

Hill CA (1987) Geology of Carlsbad cavern and other caves in the Guadalupe Mountains, New Mexico and Texas. New Mex Bur Mines Min Resour 117:1–150

Hobléa F (1999) Contribution à la connaissance et à la gestion environnementale des géosystèmes karstiques montagnards: études savoyardes. University of Lyon, Thesis

Hobléa F, Gallino-Josnin S, Audra P (2010) Genesis and functioning of the Aix-les-Bains hydrothermal karst (Savoie, France): past research and recent advances. Bull de la Soc Géol de France 181:315–326

Hose LD, Pisarowicz JA (1999) Cueva de Villa Luz, Tabasco, Mexico: reconnaissance study of an active sulfur spring cave and ecosystem. J Cave Karst Stud 61:13–21

Hose LD, Palmer AN, Palmer MV, Northup DE, Boston PJ, Duchene HR (2000) Microbiology and geochemistry in a hydrogen-sulphide-rich karst environment. Chem Geol 169:399–423

Jost A, Violette S, Macquar JC, Dromart G (2004) Rôle potentiel des paléo-circulations de fluides engendrés par l'orogenèse pyrénéenne dans la genèse des minéralisations plomb-zinc péri-cévenoles: essai de modélisation. Bull de la Soc géologique de France 175(4):317–329

Klimchouk AB (1992) Large gypsum caves in the Western Ukraine and their genesis. Cave Sci 19(1):3–11

Klimchouk AB (2000a) Speleogenesis of great gypsum mazes in the Western Ukraine. In: Klimchouk AB, Ford DC, Palmer AN, Dreybrodt W (eds) Speleogenesis: evolution of karst aquifers. National Speleological Society, Huntsville, AL, pp 261–273

Klimchouk AB (2000b) Speleogenesis under deep-seated and confined settings. In: Klimchouk AB, Ford DC, Palmer AN, Dreybrodt W (eds) Speleogenesis: evolution of karst aquifers. National Speleological Society, Huntsville, AL, pp 244–260

Klimchouk AB (2007) Hypogene speleogenesis. Hydrogeological and morphogenetic perspective. NCKRI Special Paper Series, 1, National Cave and Karst Research Institute, Carlsbad, p 77

Klimchouk AB (2013a) Hypogene speleogenesis. In: Shroder J. (ed. in chief), Frumkin A. (ed) Treatise on geomorphology, vol. 6 (Karst geomorphology). Academic Press, San Diego, pp 220–240

Klimchouk AB (2013b) Hydrogeological approach to distinguishing hypogene speleogenesis settings. In: International symposium on hierarchical flow systems in karst regions, Budapest, Hungary, book of Abstracts, pp 94. http://www.karstflow2013.org/?nic=boo. Accessed 24 Apr 2015

Klimchouk AB (2013c) Hypogene Speleogenesis, its hydrogeological significance and role in karst evolution (in Russian). Simferopol, 180 pp. http://www.institute.speleoukraine.net/uisk_pages/download.php?id=12680. Accessed 24 Apr 2015

Klimchouk AB (2014) The methodological strength of the hydrogeological approach to distinguishing hypogene speleogenesis. In: Klimchouk A et al. (eds.) Hypogene cave morphologies. Karst Waters Institute, Leesburg, Virginia, pp 4–12

Klimchouk AB (2015) The karst paradigm: changes, trends and perspectives. Acta Carsologica 44(3):289–313

Klimchouk AB, Auler AS, Bezerra FHR, Cazarin CL, Balsamo F, Dublyansky Y (2016) Hypogenic origin, geologic controls and functional organization of a giant cave system in Precambrian carbonates, Brazil. Geomorphology 253:385–405. doi:10.1016/j.geomorph.2015.11.00

Lismonde B (2003) Limestone wall retreat in a ceiling cupola controlled by hydrothermal degassing with wall condensation. Speleogenesis Evolution Karst Aquifers 1(4):3. http://www.karstportal.org/FileStorage/Speleogenesis/seka_pdf4478.pdf. Accessed 25 July 2016

Moret L (1950) Sources thermales alpines et grands travaux de barrages. Géologie alpine 28:79–96. http://geologie-alpine.ujf-grenoble.fr/articles/GA_1950_28_79_0.pdf. Accessed 25 July 2016

Pagliara A, de Waele J, Forti P, Galli E, Rossi A (2010) Speleothems and speleogenesis of the hypogenic santa barbara cave system (south-west sardinia, italy). Acta Carsologica 3(552):39

Palmer AN (1991) Origin and morphology of limestone caves. Geol Soc Am Bull 103:1–21

Palmer AN (2000) Hydrogeologic control of cave patterns. In: Klimchouk AB, Ford DC, Palmer AN, Dreybrodt W (eds) Speleogenesis: evolution of karst aquifers. National Speleological Society, Huntsville, AL, pp 77–90

Palmer AN (2013) Sulfuric acid caves. In: Shroder J. (ed. in chief), Frumkin A (ed) Treatise on geomorphology, vol. 6 (Karst Geomorphology). Academic Press, San Diego, pp 241–257

Palmer AN, Palmer MV (2000) Hydrochemical interpretation of cave patterns in the Guadalupe Mountains, New Mexico. J Cave Karst Stud 62:91–108

Palmer AN, Palmer MV (2009) Caves and karst of the USA. National Speleological Society, Huntsville AL

Palmer AN, Palmer MV, Paces JB (2015) Geologic history of the Black Hills caves, South Dakota. In: Feinberg J, Gao Y, Alexander EC Jr (eds) Caves and karst across time. Geological Society of America Special Paper 516:87–101. doi:10.1130/2015.2516(07)

Piccini L, De Waele J, Galli E, Polyak VJ, Bernasconi SM, Asmerom Y (2015) Sulphuric acid speleogenesis and landscape evolution: Montecchio cave, Albegna river valley (Southern Tuscany, Italy). Geomorphology 229:134–143

Plan L, Pavuza R, Seemann R (2006) Der Nasse Schacht bei Mannersdorf am Leithagebirge, NÖ (2911/21) - eine thermal beeinflusste Höhle am Ostrand des Wiener Beckens. Die Höhle 57:30–46

Plan L, Tschegg C, De Waele J, Spötl C (2012) Corrosion morphology and cave wall alteration in an Alpine sulfuric acid cave (Kraushöhle, Austria). Geomorphology 169(170):45–54

Polyak VJ, McIntosh WC, Provencio P, Güven N (1998) Age and origin of Carlsbad Caverns and related caves from 40Ar/39Ar of alunite. Science 279:1919–1922

Quinif Y (1994) Le puits de Flenu: la plus grande structure endokarstique du monde (1200 m) et la problématique des puits du Houiller (Belgique). Karstologia 24:29–36

Quinif Y (2010) Fantômes de roche et fantômisation. Essai sur un nouveau paradigme en karstogenèse. Karstologia Mémoires 18, pp 196

Renault P (1970) La Formation des cavernes. Presses Universitaires de France, Paris

Sarbu SM, Lascu C (1997) Condensation corrosion in Movile cave, Romania. J Cave Karst Stud 59(3):99–102

Szunyogh G (1990) Theoretical investigation of the development of spheroidal niches of thermal water origin. Second approximation. In: Proceedings of the 10th international congress of speleology, Budapest 1989, Hungarian Speleological Society, Budapest. III: 766–768

Thomas C (2010) Le karst du Yucatàn: rôle du flux géothermique, des failles, de l'eau de mer et des évaporites dans sa genèse. Karstologia 55:1–18

Tisato N, Sauro F, Bernasconi SM, Bruijn R, De Waele J (2012) Hypogenic contribution to speleogenesis in a predominant epigenic karst system: a case study from the Venetian Alps, Italy. Geomorphology 151(152):156–163

Toro G. (1988) Les eaux thermales et minérales dans les Alpes de Haute-Provence (Sud-Est de la France); relations avec le cadre structural. Thesis, Univ. of Marseille

Tóth J (1970) A conceptual model of the ground water regime and the hydrogeologic environment. J Hydrol 10(2):164–176

Tóth J (2009) Gravitational system of groundwater flow: theory, evaluation. Cambridge University Press, Utilization

Vergari A (1997) Contraintes paléokarstiques dans l'exploitation du calcaire carbonifère sur le bord nord du synclinorium de Namur en Hainaut occidental. Ph.D. thesis, Faculté polytechnique de Mons

Vigna B, Fiorucci A, Banzato C, Forti P, De Waele J (2010) Hypogene gypsum karst and sinkhole formation at Moncalvo (Asti, Italy). Zeitschrift für Geomorphologie, Suppl. Issues 54(2):285–306

Viseur S, Jouves J, Fournillon A, Arfib B, Guglielmi Y (2014) 3D stochastic simulation of caves: application to Saint-Sébastien case study (SE, France). Karstologia 64:17–24

Evidence for Regional Hypogene Speleogenesis in Murcia (SE Spain)

4

Fernando Gázquez, José María Calaforra, Tomás Rodríguez-Estrella, Andrés Ros, José L. Llamusí, and Juan Sánchez

Abstract

Signs of hypogenic speleogenesis have been detected in a number of caves of the Murcia Region (SE Spain), in some cases revealing active speleogenetic mechanisms rarely observed in hypogene cavities elsewhere in the world. Here, we investigate the hypogenic morphologies and speleothems of four caves in this region, namely Sima de la Higuera, Sima Destapada, Cueva del Agua and Cueva del Puerto. Also, other ten caves showing evidence for hypogenic speleogenesis has been preliminary described. Processes related to ancient and current hydrothermal activity, the discordance of permeability structures in the adjacent beds and the spatial arrangement of the regional hydrogeology have given rise to maze patterns and typical subaqueous hypogenic morphologies. These include spongework mazes, rising wall channels and shafts, feeders, bubble trails, solution pockets, megascallops and rising of chains cupolas, among others. Carbonic acid speleogenesis is responsible for the formation of most of these cave features; however, evidence of sulfuric acid speleogenesis (SAS) has been observed in Cueva del Puerto and Sima del Pulpo, which host massive secondary gypsum deposits. Speleothems typically linked to hydrothermal water upwelling and CO_2 degassing close to the water table are present in most of these cavities, including folia, calcite spar crystals, cave clouds, calcite rafts deposits and several types of cave raft cones. The wide variety of hypogenic speleogenesis indicators and speleothems whose genesis is unconnected to meteoric water seepage reveals that the hydrothermal field of the Murcia Region hosts one of the densest active hypogenic subterranean networks in the world.

Keywords

Hypogenic caves • Hydrothermal speleogenesis • Hydrothermal speleothems

F. Gázquez (✉)
School of Earth and Environmental Sciences, University of St. Andrews, Irvine Building, St. Andrews, KY16 9AL Fife, Scotland, UK
e-mail: f.gazquez@ual.es

J.M. Calaforra
Department of Biology and Geology, Carretera de Sacramente s.n, University of Almeria, La Cañada de San Urbano, 04720 Almería, Spain

T. Rodríguez-Estrella
Department of Mining Engineering, Geology and Mapping, University of Cartagena, Paseo Alfonso XIII, 52, Cartagena, 30203, Spain

A. Ros · J.L. Llamusí · J. Sánchez
Centre for Natural and Marine Environmental Studies, CENM-Naturaleza, Alcántara, 5, 30394 Cartagena, Murcia, Spain

1 Introduction

The Murcia Region is located in the southeastern margin of the Iberian Peninsula, being the most hydrothermally active regions of Spain. Despite limited surface water resources (less than 400 mm of annual precipitation) this region hosts extensive karstic aquifers that have been historically exploited for agricultural purposes. Indeed, many aquifers in this region are hydrothermal, with temperature exceeding 40 °C (Fig. 1), so some of their waters have been traditionally used to supply thermal baths (Pinuaga-Espejel et al. 2000). Groundwater overexploitation over the past 50 years has produced dramatic lowering of the water table on a regional

© Springer International Publishing AG 2017

A. Klimchouk et al. (eds.), *Hypogene Karst Regions and Caves of the World*, Cave and Karst Systems of the World, DOI 10.1007/978-3-319-53348-3_4

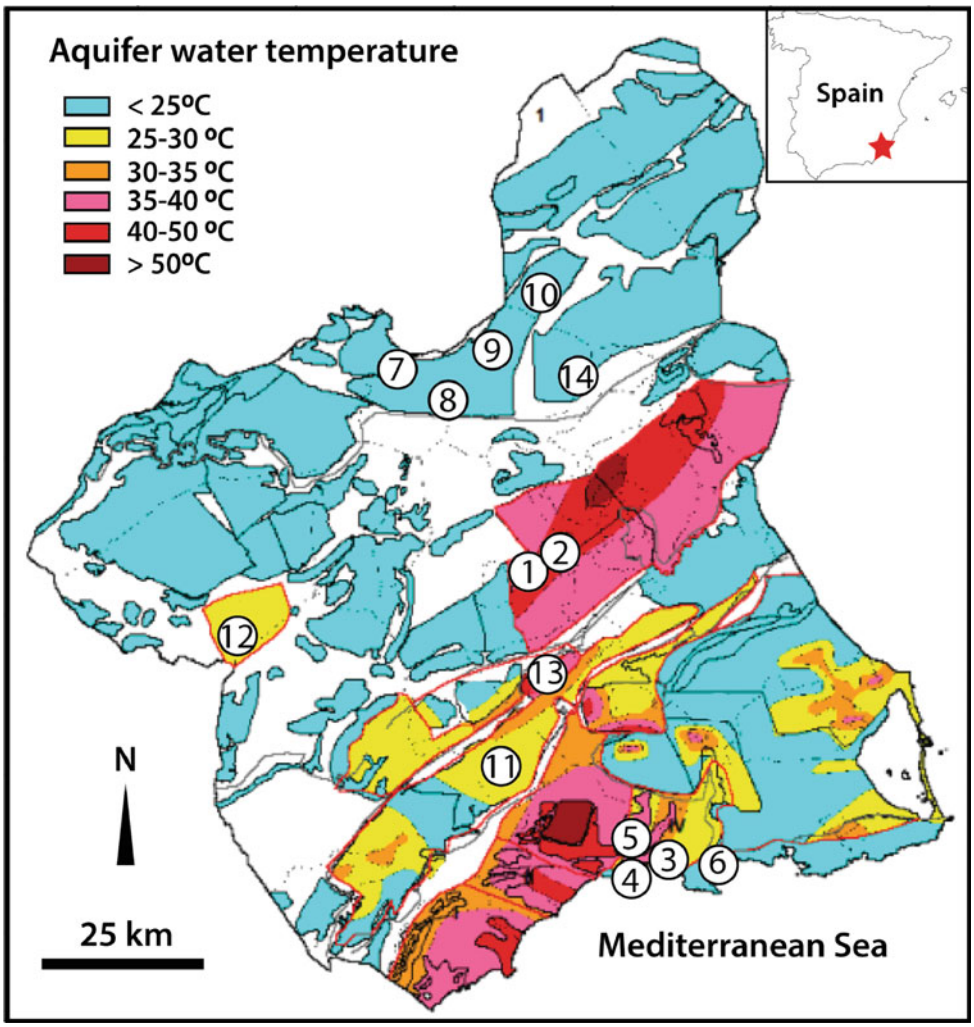

Fig. 1 Location of Sima de la Higuera (*1*), Sima del Almez (*2*), the Sima Destapada (*3*), Cueva del Agua (*4*), Cueva de la Plata (*5*), Cueva del Gigante (*6*), Cueva del Puerto (*7*), Sima del Pulpo (*8*), Sima de Benis (*9*), Cueva del Pozo (*10*), Cueva del Agua-Lorca (*11*), Cueva de Luchena (*12*), Sima del Vapor (*13*) and Cueva de la Almagra (*14*). The temperature of the modern aquifer waters is given (after Rodríguez-Estrella 2005)

scale, which has allowed access to several phreatic caves that were previously flooded (Ros et al. 2011, 2014a, b).

The lack of relationship between subterranean morphologies and seepage water from the surface can serve as a criterion for identifying hypogenic caves. However, relict or fossil hypogenic features can be easily masked by sediment accumulation or overprinted epigenic elements, especially in humid climates. These traits have motivated the search for recognizable signatures of hypogenic speleogenesis that allow clear identification of this kind of caves.

Recent studies have proposed a series of indicators to flag hypogenic caves, including morphological features and characteristic speleothems (Audra et al. 2009; Klimchouk 2009; Palmer 2011; among others). This includes the model of morphologic suite of rising flow (MSRF) proposed by Klimchouk (2007) that has been widely applied to characterize hypogenic caves. It is based on the identification of a set of so-called hypogenic patterns that result from water upwelling, usually thermal fluids. These features can be split into three categories: (1) inlets of ascending flow into the system (feeders), usually located at the bottom of chambers and master passages; (2) transition wall and ceiling features that connect the cave levels with upper passages (usually ceiling domes, channels and solution pockets); and (3) upward leakage structures (outputs), typically located on the ceilings of upper cave levels.

In addition, the presence of speleothems formed under subaqueous conditions from a solution that was highly saturated in calcium carbonate can provide evidence of the hypogenic origin of caves. Nevertheless, it is worth mentioning that the occurrence of these types of speleothem is not restricted to hydrothermal caves but has also been described in non-thermal, epigenic caves (D'Angeli et al. 2015), where high saturation in calcite is reached due to elevated production from plants, as well as intense CO_2-degassing and evaporation in the cave.

In the Murcia Region, these distinctive patterns are widespread in many caverns that have recently been suggested as having a hypogenic/hydrothermal origin (Ros et al.

2011, 2014a, b; Gázquez et al. 2016a, b). These caves accommodate a wide variety of speleothems usually related to hydrothermal flows. In the present study, we sum up the investigations conducted over the past 5 years in Sima de la Higuera, the most renewed hypogenic cave in the Murcia Region because of its outstanding hypogenic morphologies and speleothems (Gázquez et al. 2012; Gázquez and Calaforra 2013a, b). In addition, we selected two of the most important karstic complex in this region, the Sima Destapada-Cueva del Agua System and Cueva del Puerto, for preliminary description and morphological analysis. Moreover, other smaller caves, also hypogenic in origin, have been investigated. This includes Cueva del Gigante, Sima del Almez, Sima de Benis, Cueva del Pozo, Sima del Vapor, Sima de la Plata, Cueva de la Almagra, Cueva del Agua-Lorca, Cueva de Luchena and Sima del Pulpo. It is worth mentioning that most of these caves still show positive thermal anomalies with respect to the mean external temperature ($\sim$18 °C) (Table 1). This provides further evidence of the hypogenic/hydrothermal processes in these caves, which are still active in some cases.

2 Regional Geological and Hydrogeological Setting

The geology of the Murcia Region comprises materials of the Betic Mountain range that run from the Gibraltar strait to the Balearic archipelago. This mountain chain represents the westernmost edge of the Alpine Orogeny. In the Murcia Region, the three main domains of the Betic mountain range (Prebetic, Subbetic and Betic) are present. The Prebetic domain crops out in the NW part of the region, mainly comprising Cretaceous limestone and dolostone, and dolostone and marls of Paleocene and Eocene Ages. The Subbetic domain contains Jurasiss limestone and dolostone, clays and Triassic gypsum deposits. The Betic comprises phyllites, schists and micaschists of the Maláguide, Nevado-Filábride and Alpujárride. These metamorphic materials serve as impervious basement to the aquifers most parts of this area. In general terms, Triassic limestones and dolostone with different degrees of metamorphisms and subsequent karstification constitute the aquifer units that, in some cases, are topped by impervious/aquitards materials (e.g., Tortonian or Liassic marls and calcoschists). These acted as the confining upper layer for the hypogenic aquifers in some cases.

The geothermal fluxes in the Murcia Region are intrinsically linked to neotectonic events, the presence of deep faults and distensive tectonic movements, all controlled by the relative movements of the Euroasian and African plates (Rodríguez-Estrella 2005). Indeed, this is the most seismically active region of Spain and the epicenters are aligned along the main regional faults, which include the Alhama, Baños, and Murcia-Cartagena Faults, among others, most located in the SE sector of the region. Volcanic events during the Upper Pliocene-Pleistocene (2.8–1 Ma) are responsible for part of the hydrothermal anomalies observed in this area. In some cases, volcanic phenomena were associated with post-orogenic basin sedimentation and the relative thinning of the earth's crust (Pinuaga-Espejel et al. 2000). Modern hydrothermalism is especially active in the SE and central parts of the region, with groundwater temperatures that exceed 50 °C in some cases (Fig. 1).

3 Hypogenic Caves in the Murcia Region

3.1 Caves of Sierra Espuña Mountain Range

Sima de la Higuera (Fig Tree Cave) is located in the Sierra de Espuña mountain range, in the municipal district of Pliego. Its entrance lies at 485 m a.s.l. Speleological exploration of the cave began in 1997, although there is evidence that it was discovered earlier than this date (Cuatro Pico Club and Pliego Espuña Club 2001). Its surveyed length is 5500 m and its deepest part is 156 m below the cave entrance (82 m below the base of the entrance shaft) (Fig. 2a). The cave is located in the Malaguide complex of the Betic domains and has formed, in ascending order, within calcarenites and dedolomitized calcarenites, calcareous microconglomerates and slightly dolomitized limestones of Oligo-Miocene Age. The carbonate sequence is quite fractured due to NW-SE pressure that caused a series of joints and faults, which subsequently determined the cave's morphology, particularly in its deeper levels. Significant hydrothermal springs currently arise in the vicinity of the cave, with temperatures of around 32 °C (Rodríguez-Estrella 2015).

Typical features of phreatic speleogenesis such as scallops and megascallops, appear in this cave, especially in the upper levels above the −85 m level. Furthermore, dissolution forms like bubble trails and alteration calcite crusts (Fig. 3b) are seen above the −85 m level. A 10-m-long diaclase along the floor of Paradise Chamber (−98 m) seems to have acted in the past as a feeder of deeper thermal water into this cave level. The hydrothermal dissolution of the bedrock occurred preferentially along fractures, giving rise to labyrinthine passages (a three-dimensional "maze cave") that are typical of hypogenic caves and which are especially well-developed in Sima de la Higuera (Fig. 2a) (Gázquez and Calaforra 2013a, b; Gázquez et al. 2016a, b).

Sima de la Higuera accommodates most of the typical speleothems described for hypogenic caves, including calcite spars (which fill fractures in the bedrock), cave clouds, folia and calcite raft cones (Fig. 3) (Gázquez and Calaforra

Table 1 Hypogenic features in caves in the Murcia Region

	Higuera	Almez	Destapada	Agua-Cartagena	Plata	Gigante	Puerto	Benis	Pulpo	Pozo	Luchena	Agua-Lorca	Vapor	Almagra
Location	Pliego	Pliego	Cartagena	Cartagena	Cartagena	Cartagena	Calasparra	Cieza	Cieza	Jumilla	Lorca	Lorca	Alhama	Fortuna
Length (m)	5500	220	3400	3062	378	610	4389	350	4780	1023	561	546	85	755
Maximum air temperature (°C)	21	n.m	29	30	n.m	21	20	25	21	n.m	n.m	21	43	29
Hypogenic morphologies														
Maze caves	X		X				X				X	X		X
Chimneys	X		X			X	X			X	X	X		
Bubble trails	X	X		X					X			X		
Megascallops	X	X	X	X			X	X	X	X	X	X		
Ceiling pockets	X	X	X			X	X	X		X	X	X		
Cupola and domes	X	X	X	X	X	X	X	X	X	X	X	X		X
Feeders	X	X	X	X		X	X	X?	X	X	X	X	X?	
Pendants	X		X	X		X	X		X			X		
Blind ascending passages	X		X	X		X	X		X	X	X	X		
Partitions	X		X				X							X
Boxwork	X		X	X?		X	X					X		
Micritic crusts	X													
Hydrothermal speleothems														
Cave raft cones	X				X				X?			X		
Cave clouds	X				X			X	X					
Calcite spars	X		X				X		X			X		
Folia	X				X?			X	X					
Calcite rafts	X		X				X		X			X		
Ferromanganese crusts	X		X	X		X	X		X			X		
Gypsum speleothems							X	X	X					

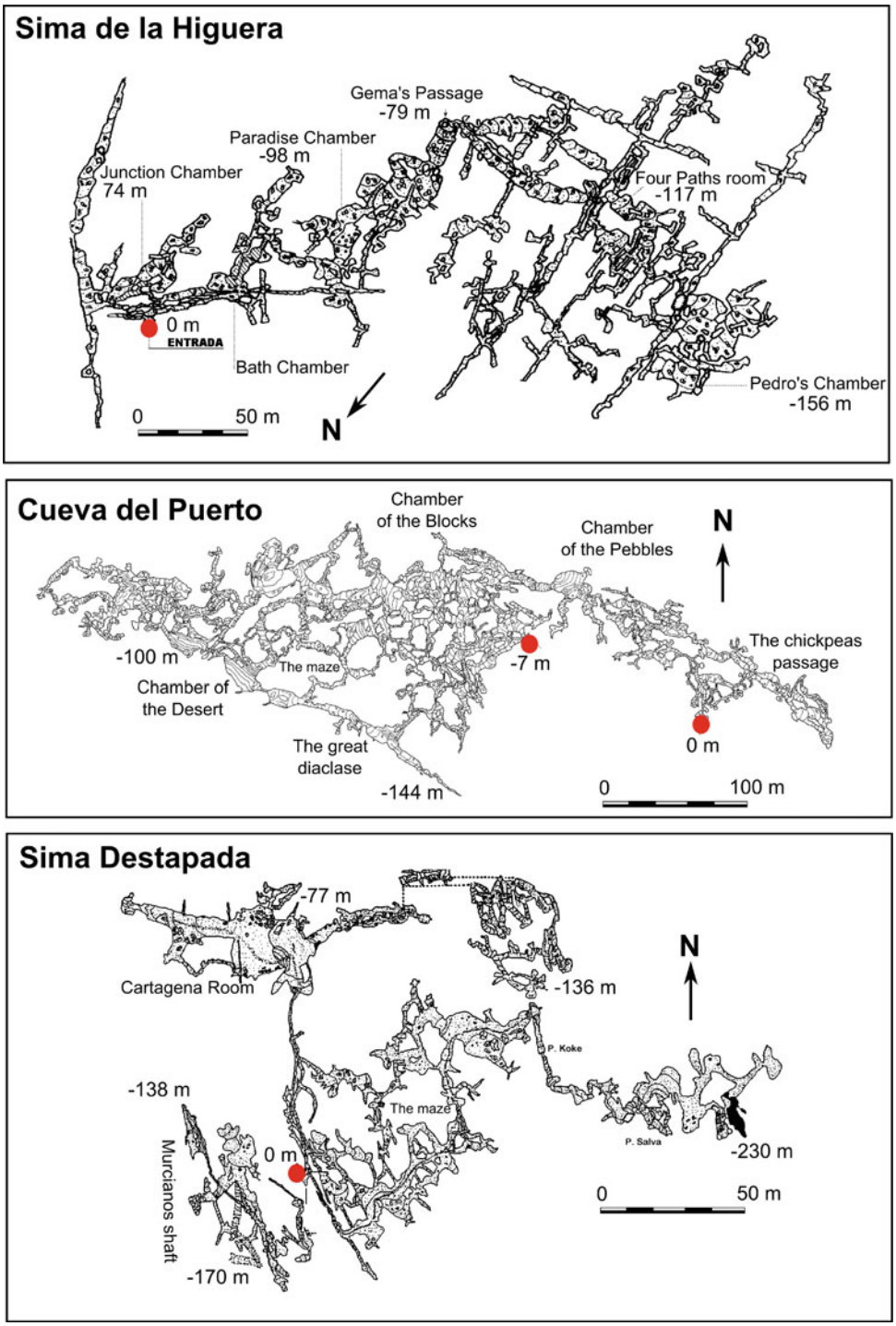

Fig. 2 Topography of the three longest hypogenic caves in the Murcia Region: Sima de la Higuera (Cuatro Pico Club and Pliego Espuña Club 2001); Sima del Puerto (Cuatro Picos Club 1996); Sima Destapada (Ros et al. 1988). The *red circles* indicate the cave entrances

2013a, b). All these speleothems are usually precipitated under phreatic or epiphreatic conditions from water that is highly saturated in calcium carbonate, typical of hydrothermal environment. This cave also exhibits outstanding examples of *boxwork* coated with ferromanganese crusts, whose origin was linked to subaqueous precipitation of hydrothermal calcite in cracks of the hostrock and subsequent mechanisms of corrosion under subaerial conditions (Fig. 3) (Gázquez et al. 2012).

Interestingly, in Paradise Chamber, ninety-two raft cones have been inventoried, displaying two different morphologies: roughly 40% can be considered as tower cones (or simple-tower raft cones), while the remaining 60% have a notch in the middle and look like two cones, one

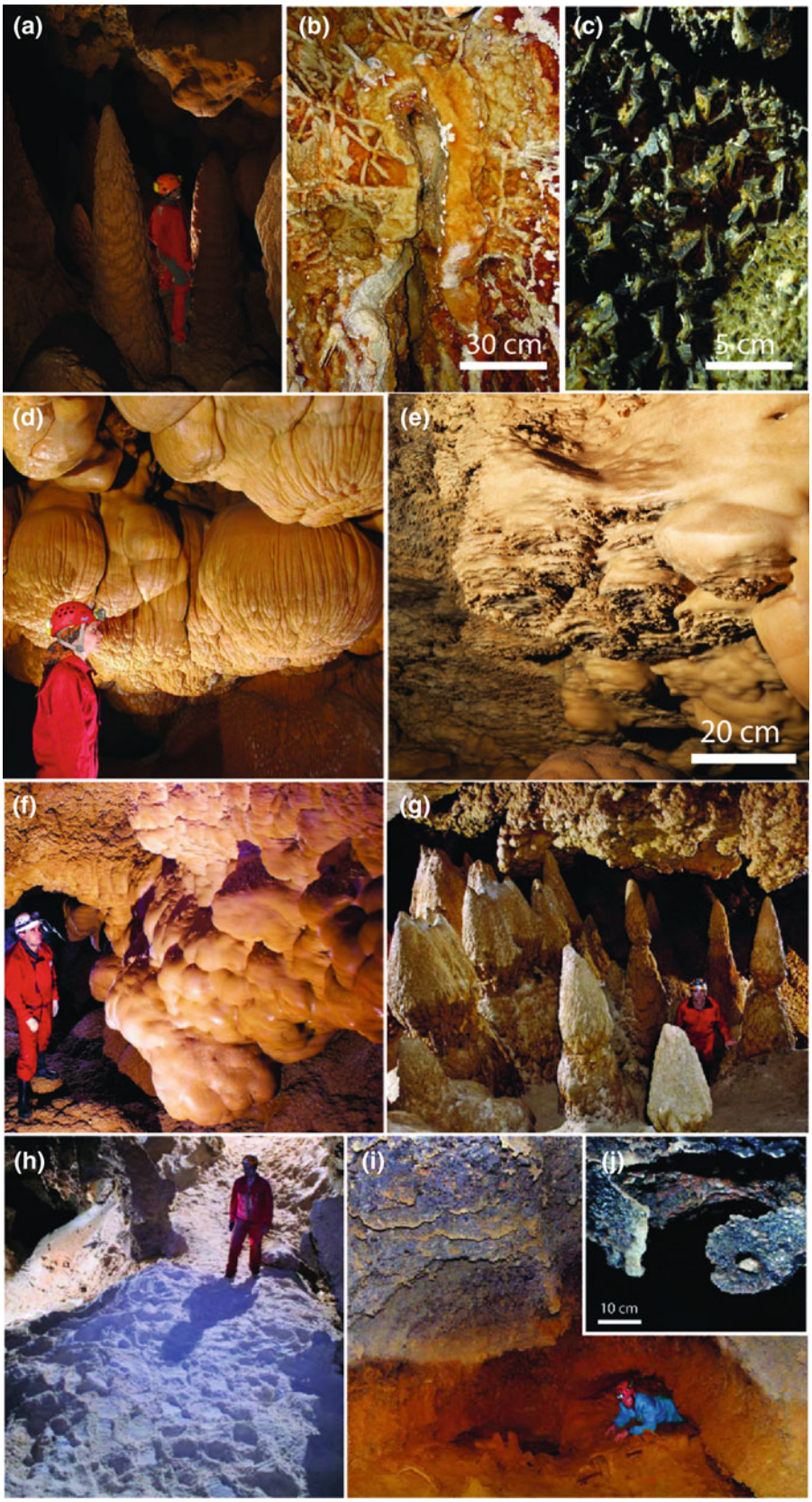

Fig. 3 Speleothems linked to the hypogenic origin of Sima de la Higuera Cave: **a** tower raft cones; **b** bubble trails and boxwork; **c** calcite 'spar' crystals coated with ferromanganese oxihydroxides; **d** cave clouds; **e** folia; **f** cave clouds; **g** double-tower raft cones; **h** piles of calcite rafts; **i** and **j** boxwork and ferromanganese coatings in Manganese Gallery (*Photographs* Víctor Ferrer)

superimposed over the other (Fig. 3). These cones formed in a hydrothermal and epiphreatic environment where dripwater, dripping repeatedly over the same spot, sinks calcite rafts that were floating on the water surface of a cave pool. In particular, the genetic mechanism that gave rise to the double-tower cones also included an intermediate stage of rapid calcite raft precipitation, caused by a drop in the water table and by changes in cave ventilation leading to greater CO_2 degassing and evaporation over the surface of the thermal lake where these speleothems formed. Calcite rafts were deposited in Paradise Chamber, completely covering many of the cones. Later, conditions for slower calcite raft precipitation were restored and some of the cones continued to grow at the same points. When the water table finally fell below the level of Paradise Chamber, the tower cones became exposed, as the incongruent deposits of calcite rafts were dissolved and mobilized to lower cave levels (Gázquez and Calaforra 2013b). Today, calcite raft deposits are scarce in this shallower level (above −82 m) but they do appear at the depth of the Paradise Chamber in Sima de la Higuera, and are especially abundant in deeper passages, such as the Four Paths Chamber (−117 m) (Fig. 3), where numerous calcite raft piles are found (Gázquez and Calaforra 2013a, b).

It is worth mentioning that in the Sierra Espuña mountain range there is another smaller cave (220 m long and 33 m deep), named Sima del Almez. This cave exhibits morphological signs of rising water flow, including linear half-tube structures with smooth surfaces (ceiling half-tubes), solution pockets and ascending chains of scallops that are vestiges of water flows that dissolved the carbonate bedrock (Ros et al. 2015) (Fig. 7).

3.2 The Caves of the Hydrothermal Field of Cartagena

Sima Destapada and Cueva del Agua are located in the Mazarrón Gulf, on the southeastern coast of the Murcia Region, near the town of Isla Plana. The entrance to Sima Destapada is at the top of the Cabezo de Hornos Mountain (285 m a.s.l). It was discovered in 1975 and speleologically surveyed in the 1980s. This exploration produced a precise topographic map, with more than 3300 m of the cave surveyed, extending to a maximum depth of −221 m (Ros et al. 1988). In regard to Cueva del Agua, its natural entrance lies barely 300 m from the shoreline (1 m a.s.l) although no man-size passage connecting the cave with the sea has been found to date. Here, surveys started in the early 1970s and are still in progress. Exploration of this cave has been particularly complex because more than 95% of the cave profile lies below sea level (Ros et al. 2011). Both caves are developed in Triassic marbles, dolostone and limestone. In places, phyllites, quartzite, shales and reddish sandstones of Permo-Triassic age can be found.

Despite being less than 1600 m apart, no connection between the two caves has been found yet (Fig. 4). The deepest emerged level of Sima Destapada lies 221 m below the cave entrance. Beneath that, the cave passages are submerged in thermal water (31 °C) and remain in part unexplored. To date, 400 m of the submerged karstic network has been surveyed. In Cueva del Agua, a freshwater body (7–8 mS/cm) occupies shallower strata (0–6 m deep), overlying a brackish thermal water body (42–43 mS/cm and 30 °C) that has a maximum depth of 20 m. The cave follows the main SE-NW axis, with a surveyed length to date of 3620 m (May-2016).

In Sima Destapada, in addition to the 50 m-deep pits that connect the intermediate emergent cave levels with the hydrothermal aquifer, several blind shafts (without man-sized access to the lower level) are found along the floor of the upper passages. These are distributed in various parts of the cave, and probably acted as feeders in the past (Fig. 5a). In places, dissolution of this wall left pillars where some of the passages have partly disappeared and been incorporated into larger chambers. Pendant-like features, related to the same phreatic dissolution-corrosion

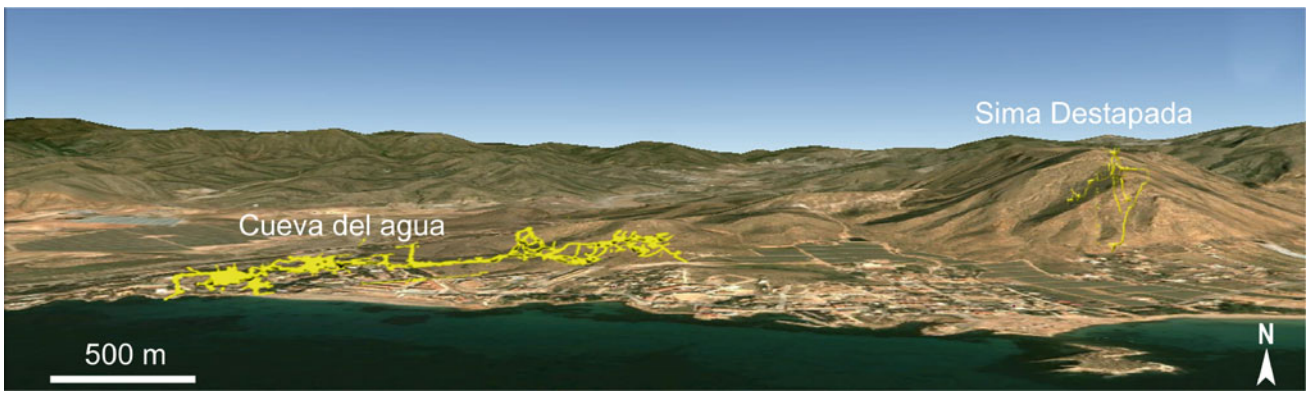

Fig. 4 Topographies of Cueva del Agua and Sima Destapada, located near the village of Isla Plana (Murcia Region)

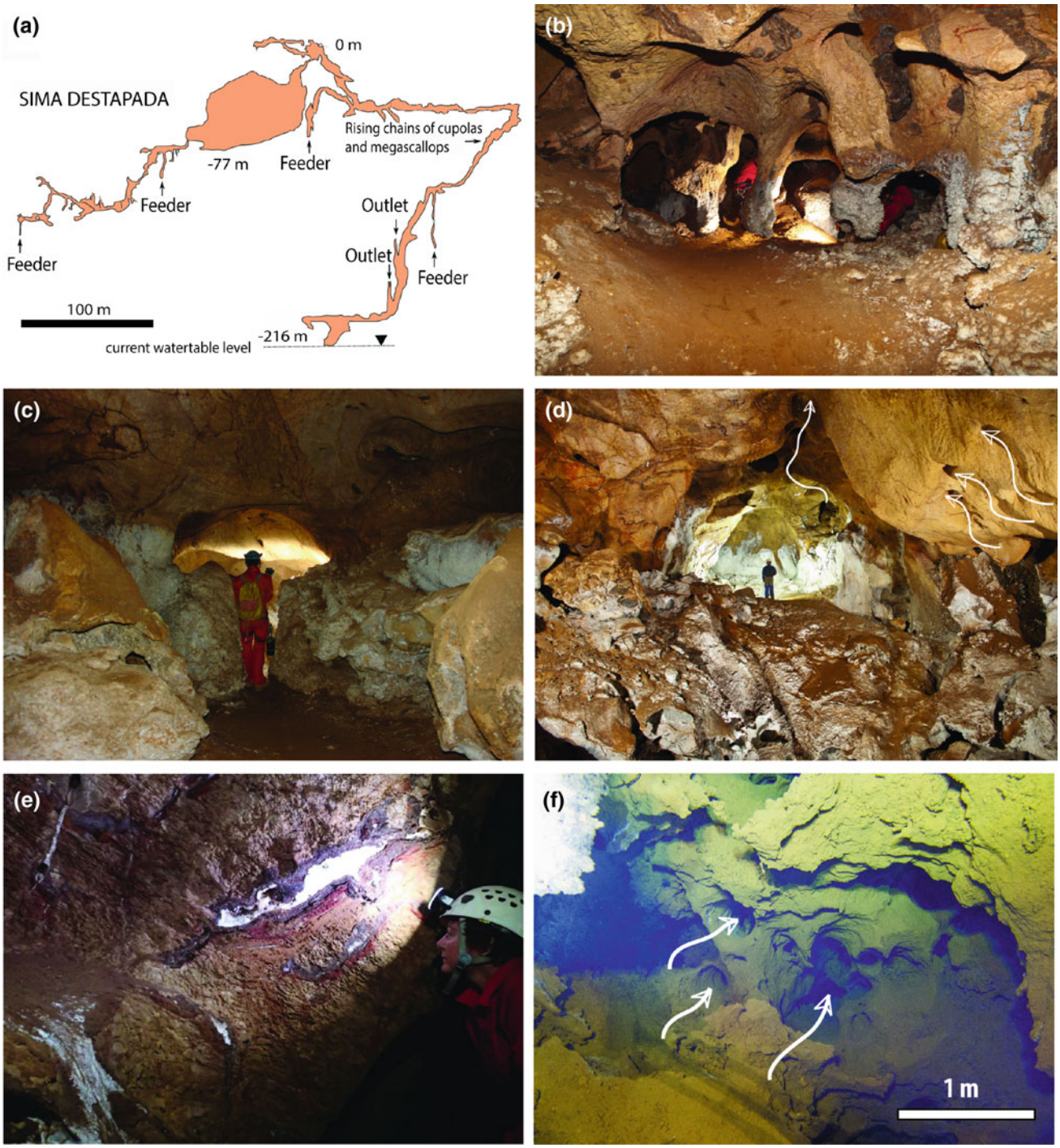

Fig. 5 Evidence for hypogenic speleogenesis in Sima Destapada and Cueva del Agua (Cartagena): **a** topographic profile of Sima Destapada showing feeders and outlets (José Luis Llamusí and others); **b** pendants and partition walls in Sima Destapada; **c** typical passage morphology in Sima Destapada; **d** bubble trails in Sima Destapada; **e** calcite infills in Sima Destapada; **f** subaquatic, probably active, spongework morphologies in the ceiling of Cueva del Agua (Cartagena) (*Photographs* Andrés Ros, José Luis Llamusí and Juan Sánchez)

mechanism, have also been identified in this cavity (Fig. 5b, c), as well as linear half-tube structures with smooth surfaces (ceiling half-tubes) that are evidence of the water flows that dissolved the carbonate bedrock (Fig. 5d). Sometimes, the CO_2 bubbles followed an ascending path, producing bubble's trails (Fig. 5d).

In places, solution pockets and cracks in the carbonate bedrock appear to be filled with calcite spars as a kind of

geode. Interestingly, two generations of calcite crystals have been identified: a first rim, usually 10 cm-thick, made of reddish calcite, and a core of whitish calcite (Fig. 5e). These features are a vestige of phreatic, hydrothermal stages, when thermal water dissolved the limestone along planes of weakness in the bedrock. Later, a fall in water temperature favoured calcite precipitation, which occurred in two stages. The oxygen isotopic composition of the reddish calcite ($\delta^{18}O = -10.5‰$, with respect to the V-PDV standard) is 2.3 lower than that of the whitish calcite ($\delta^{18}O = -8.2‰$). Assuming isotopic equilibrium and that the isotopic composition of solution did not change with time, the water temperature may have be decreased by ~15 °C between the first and the second calcite precipitation stage (Gázquez et al. 2016b). Furthermore, the presence of vast deposits of calcite rafts suggests intense CO_2-degassing close to the water table to have occurred in this cavity. In connection with this, other speleothems formed by the sinking of calcite rafts in shallow (~20 cm) pools, such as tower corals, have been observed.

Sima Destapada also accommodates outstanding examples of subaerial aragonite crystallizations in the form of frostwork, which are especially well-exhibited in the Flowers passage. Remarkably, these speleothems cover only one of the passage walls, while the facing wall is coated with calcite crusts and is completely lacking aragonite crystallizations. In the absence of further information, the interpretation might be due to differences in the geochemical composition of the substrate of the two walls (probably higher Mg/Ca favouring the crystallization of aragonite over calcite) or microclimatic differences related to the temperature of the rock and the cave air.

Cueva del Agua runs NW, from the shoreline to Cabezo de Hornos Mountain. Its passages are irregular and the walls show evidence of intense corrosion. This weathering mechanism has produced in situ accumulation of clayey sediments from decalcification of the rock. These muddy layers, tens of centimeters thick, coat the passage walls and ceilings; they detach only due to the turbulence produced by cave divers during surveys. This makes surveying in this cave especially complicated due to resultant loss of visibility. Under natural conditions, there is practically no turbulent water flow and the decalcified detrital materials remain attached to the cave walls in a sort of equilibrium. Evidence for a morphologic suite of rising flow can be found on the cave ceiling, where "swish-cheese" morphologies, bell-shape features and small hemispherical ceiling pockets (some 20 cm in diameter) can be found between the bedrock and the hydrothermal water at the depth of −14 m (Fig. 5f).

In recent times, other smaller caves with signs of hypogenic/hydrothermal processes have been found in this area, including Cueva de la Plata and Cueva del Gigante. The former is located barely 1100 m from the entrance of Sima Destapada; it exhibits splendid examples of cave clouds and cave cones (Fig. 7). Cueva del Gigante is 10 km east of Sima Destapada-Cueva del Agua System. Its ceilings display examples of boxwork, ferromanganese coatings and condensation cupolas.

3.3 Caves of the North-Western Sector

Cueva del Puerto is located in the NW of the Murcia Region in the Sierra del Puerto Mountain Range, near the town of Calasparra. The cave is developed in limestones and dolostones of the Upper Cretaceous, belonging to the external Prebetic domain; these materials are overlain by marls of Miocene age that served as the impervious confining cap to the aquifer.

Cueva del Puerto was discovered in the early 1970s by the GECA-OJE speleological team; its two entrances lie at 503 and 495 m a.s.l. and its karstic network extends over 4300 m, forming the second largest known cave in the Murcia Region, after Sima de la Higuera (Cuatro Pico Club and Pliego Espuña Club 2001). The cave morphology is determined by two faults running NW-SE that are 250 m apart (Fig. 2). It exhibits clear spongework and maze morphologies. The hydrothermal flow into the system occurred through a 100-m-long fault, which served as water feeder to the system in the past. Transitional features connect passages and chambers at different depths. Several 100 m-deep subvertical fractures connect the Gran Diaclasa Chamber (~−80 m) with the shallower Bloques Chamber (~−40 m) (Fig. 2). This master passage runs W-E and its walls and ceiling exhibit examples of hypogene morphologies including rising chains of cupolas, partition walls and bubble trails (Fig. 6). Frequently, the accumulation of air bubbles on the cave ceiling under phreatic conditions generated solution pockets and corrosion cupola, usually attributed to a condensation-corrosion mechanism resulting from the high content of CO_2 from water degassing (Cigna and Forti, 1986; Plan et al. 2012). On occasions, boxwork formations have been identified on the surface of cupolas (Fig. 6b).

Cueva del Puerto shows several examples of speleothems related to hydrothermal waters. This includes calcite spars in cracks in the bedrock and deposits of calcite rafts. These two types of speleothems represent two different stages of the cave's development. The calcite spars formed under subaqueous conditions. In contrast, calcite rafts precipitated on the water surface, which indicates that the water table intercepted the cave level at some point. The absence of other speleothems usually formed close to the water surface (e.g., cave clouds, raft cones and folia) indicate that the fall in water level was probably relatively abrupt. In addition to carbonate speleothems, gypsum is present in Cueva del Puerto, which

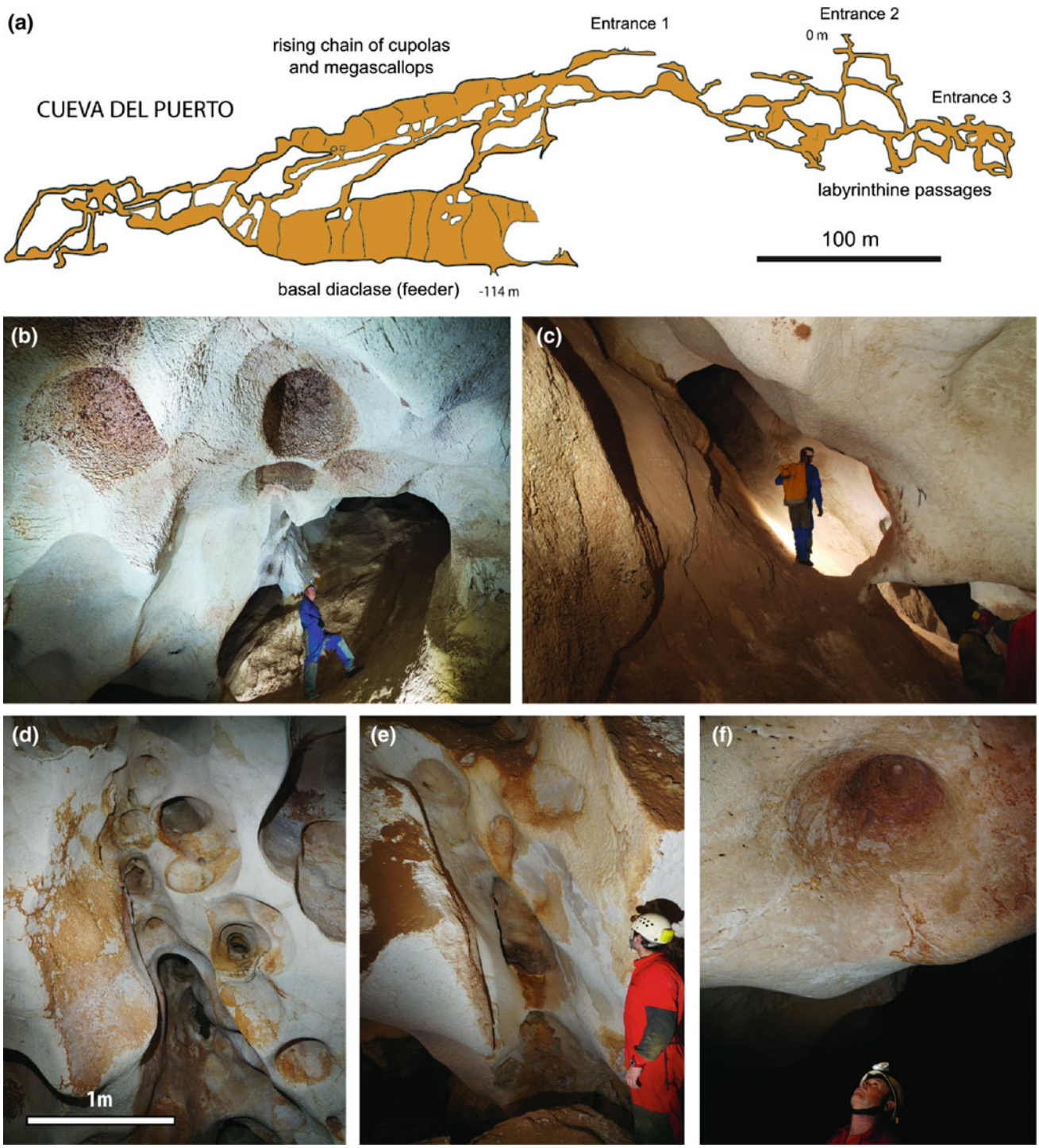

Fig. 6 Evidence for hypogenic speleogenesis in Cueva del Puerto (Calasparra): **a** topographic profile showing the maze cave network (Cuatro Picos Speleoclub); **b** cupolas and boxwork; **c** partitions; **d** cupolas; **e** rising channels; **f** cupola (*Photographs* Andrés Ros and José Luis Llamusí)

Fig. 7 Evidence for hypogenic speleogenesis in other caves of the Murcia Region. **a** Ceiling half-tubes in Sima del Almez (*Photograph* Andrés Ros and José Luis Llamusí); **b** slow phreatic dissolution features in Cueva de Luchena (*Photograph* A. González-Ramón); **c** cupolas and partition walls in Sima de la Almagra (*Photograph* Andrés Ros and José Luis Llamusí); **d** pile of calcite rafts in Sima del Pulpo (*Photograph* Andrés Ros and José Luis Llamusí); **e** rising chains of cupolas in Cueva de Luchena. (*Photograph* A. González-Ramón); ▶ **f** phreatic dissolutional forms in Cueva del Agua-Lorca (*Photograph* Andrés Ros and José Luis Llamusí); **g** cave cones in Cueva de la Plata (*Photograph* Andrés Ros and José Luis Llamusí); **h** solutional pockets and megascallops in Sima del Almez; **i** tower coral in Cueva de la Plata (note that this are note exclusive of hypogenic caves) (*Photograph* Andrés Ros and José Luis Llamusí)

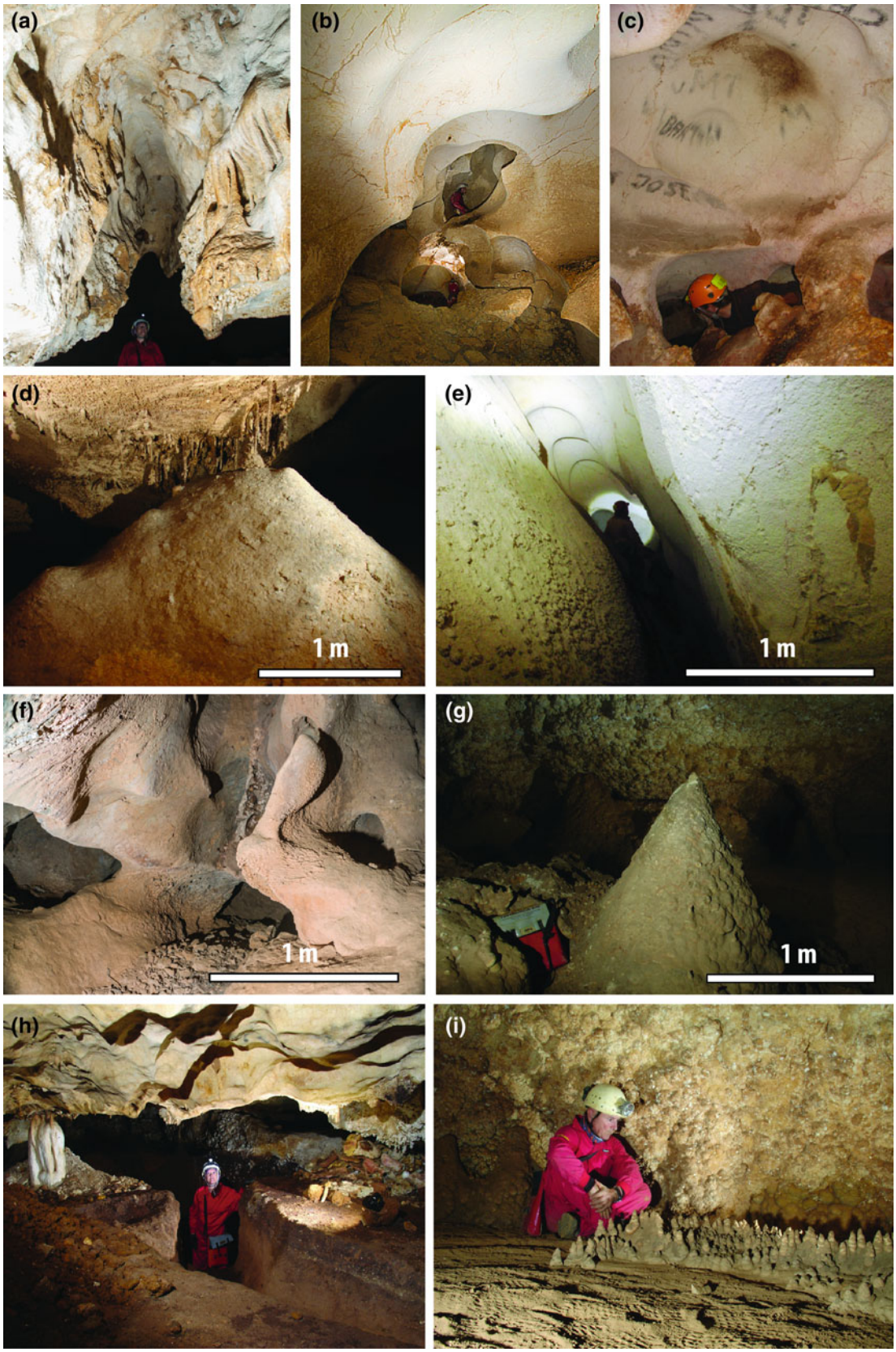
(a)
(b)
(c)
(d)
1 m
(e)
1 m
(f)
1 m
(g)
1 m
(h)
(i)

appears in the form of crusts and gypsum flowers. The origin of sulfates in this cave is unknown to date, but is probably linked to sulfuric acid speleogenesis (SAS) as described for many other caves worldwide (e.g., Palmer and Palmer 2012; Audra et al. 2015; De Waele et al. 2016).

In the setting of Cueva del Puerto, there are other smaller caves where evidence for hypogenic processes has been observed. For instance, Sima del Pulpo (Cieza) also accommodates examples of gypsum speleothems, such as the one named 'the white octopus' (Grupo Atalaya 1997). This indicates that its origin was probably also related to the same events of SAS that generated Cueva del Puerto. Indeed, examples of folia, cupolas and ceiling dissolution pockets can be found in this cavity, suggesting their hypogenic origin. Also, Sima de Benis (Cieza) (Pérez-López et al. 2009) hosts splendid examples of folia, cave clouds and phreatic dissolution forms (Fig. 7), as well as some gypsum speleothems. Finally, in Cueva del Pozo (Jumilla) there is evidence of a morphologic suite of rising flow (Federacion Espeleologica de la Region de Murcia 1995).

3.4 Other Hypogenic Caves in the Murcia Region

In addition to the caves in the three areas described above, there are other karstic systems in the Murcia Region that show clear evidence of hypogenic processes. For example, in Cueva del Agua of Lorca, in the Talayón mountain range (Lorca), the recent lowering of the water table has allowed access to several vertical shafts that acted as feeders in the past. The air temperature in this cave oscillates around 21 °C. It accommodates spectacular examples of euhedral calcite spars and boxwork, bubble trails, rising chains of cupolas and partitions, among other hypogenic feature (Gázquez et al. 2016a).

Cueva de Luchena, in the Pericay mountain range, exhibits rising chains of cupolas, feeders and outlets, partitions and cupolas (Fig. 7). However, speleothems typically related to hydrothermal waters have not been found in this cavity. This has been interpreted to mean that the water table did not lie close to the cave level for a long time and that the water level fall that emerged the cave was relatively rapid (González-Ramón et al. 2014).

Sima del Vapor (Alhama de Murcia) is a 85 m-deep vertical cave located on the hill of Castillo, near the town of Alhama de Murcia. Air temperatures vary and increase with depth, ranging from 27 to 43 °C. The carbon dioxide concentration in the cave atmosphere is relatively high (1.8%), whereas the oxygen content is around 18.5% (Asencio and Aboal 2011). Given such extreme environmental conditions, topographic surveys and research have been extremely complex. Nevertheless, this cavern has been a site for the study of the role of cyanobacteria on acetylene reduction and nitrogen fixation in extreme environments (Asencio and Aboal 2011).

Finally, Cueva de la Almagra is located near the thermal baths of the town of Fortuna. This cave displays clear evidence of a hypogenic origin, including labyrinthine passages (maze cave pattern), examples of cupolas and partitions (Fig. 7). The current cave air temperature is around 28 °C, suggesting relatively recent hydrothermal processes.

4 Conclusions

Signs of hypogenic mechanisms have been detected in fourteen caves in the Murcia Region so far. CO_2-based hydrothermal processes are proposed for the formation of Sima de la Higuera, Sima Destapada, Cueva del Agua-Cartagena, Cueva de la Plata, Cueva del Gigante, Sima de Benis, Cueva de Luchena, Cueva del Pozo, Sima del Alméz, Cueva del Agua-Lorca, Sima del Vapor and Cueva de la Almagra. In contrast, Cueva del Puerto and Sima del Pulpo, where massive deposits of gypsum have been identified, were probably generated by SAS mechanisms. The wide range of hypogenic speleogenesis indicators and hydrothermal speleothems reveal that the hydrothermal field of the Murcia Region hosts one of the densest active hypogenic subterranean networks in the world. Surveys of this karstic network are still in progress, and so important discoveries in the Murcia Region caves are possible in the coming years.

Acknowledgements This work was supported by the Federación de Espeleología de la Región de Murcia and RODCLE®. The authors are grateful to Carlos Munuera, Juan Francisco Plazas, Alba Sánchez, Andrés Hurtado, Roberto Trives, Juan Antonio García, Ana Belén Cáceres, Antonio David Granados, Rita Martínez, Belén López, José L. Carcelén, Antonio Latorre, José Soto, Andrés Marín, José David Lisón, José Florencio, Jesús López and David Bayón. Víctor Ferrer and Antonio González-Ramón are warmly acknowledged for kind permission to use their photographs of Sima de la Higuera and Cueva de Luchena. Sarah Steines is also thanked for revising the English. The authors are grateful to Professor Alexander Klimchouck and Jo de Waele for their thoughtful comments on the early version of the manuscript.

References

Asencio AD, Aboal M (2011) In situ acetylene reduction activity of Scytonema julianum in Vapor cave (Spain). Int J Speleol 40:17–21

Atalaya G (1997) El Karst de Cieza (Region de Murcia). Subterranea 7:20–25

Audra P, Bigot JY, Mocachain L et al (2009) The association between bubble trails and folia: a morphological and sedimentary indicator of hypogenic speleogenesis by degassing, example from Adaouste Cave (Provence, France). Int J Speleol 38:93–102

Audra P, Gázquez F, Rull F et al (2015) Hypogene sulfuric acid speleogenesis and rare sulfate minerals in baume galinière cave (Alpes-de-Haute-Provence, France). Record of uplift, correlative cover retreat and valley dissection. Geomorphol 247:25–34

Cigna AA, Forti P (1986) The speleogenetic role of air flow caused by convection. 1st contribution. Int J Speleol 15:41–52

Cuatro Pico Club and Pliego Espuña Club (2001) Sima de la Higuera. El mayor complejo subterráneo topografiado de la Región de Murcia. Subterránea 16:35–41

Cuatro Picos Club (1996) La Cueva del Puerto (Calasparra, Murcia). Subterranea 5:46–53

D'Angeli IM, De Waele J, Ceballo-Melendres O et al (2015) Genesis of folia in a non-thermal epigenic cave (Matanzas, Cuba). Geomorphol 228:526–535

De Waele J, Audra P, Madonia G et al (2016) Sulfuric acid speleogenesis (SAS) close to the water table: examples from southern France, Austria, and Sicily. Geomorphol 253:52–467

Federacion Espeleologica de la Region de Murcia (1995) Avance al Catalogo Regional de Cavidades. No. 3. http://cuevasdemurcia.com/bibliografia/bibliografia/30-avance-al-catalogo-regional-de-cavidades-vol-3

Gázquez F, Calaforra JM (2013a) Hypogenic speleogenesis and speleothems of Sima de la Higuera (Murcia, Southeast Spain). 16th International Congress of Speleology, Brno, Vol III, pp 78–83

Gázquez F, Calaforra JM (2013b) Origin of double-tower raft cones in hypogenic caves. Earth Surf Land Proces 38:1655–1661

Gázquez F, Calaforra JM, Rull F (2012) Boxwork and ferromanganese coatings in hypogenic caves: an example from Sima de la Higuera Cave (Murcia, SE Spain). Geomorphol 117–118:158–166

Gázquez F, Calaforra JM, Ros A et al (2016a) Hypogenic morphologies and speleothems in caves of the Murcia Region, south-eastern Spain. In: Proceeding of the 3rd international DeepKarst conference, Carlsbad, pp 53–60

Gázquez F, Calaforra JM, Rodriguez-Estrella et al (2016b). Evidencias geoquímicas preliminares del origen hidrotermal de Sima de la Higuera y Sima Destapada (Región de Murcia). In: Asociación Española de Cuevas Turísticas (eds) El karst y el hombre: las cuevas como Patrimonio Mundial, pp 283–294

González-Ramón A, Segura-Herrera A, Sánchez-Díaz TJ et al (2014) La cueva de Luchena, un ejemplo de cavidad hipogénica relacionada con descargas de aguas subterráneas en el acuífero Pericay-Luchena (Lorca, Murcia). In: Calaforra JM, Durán JJ (eds) Iberoamérica Subterránea. Asociación Española de Cuevas Turística, pp 321–331

Klimchouk AB (2007) Hypogene speleogenesis: hydrogeological and morphogenetic perspective. National Cave and Karst Research Institute Special Paper #1, Carlsbad

Klimchouk AB (2009) Morphogenesis of hypogenic caves. Geomorphol 106:100–117

Palmer AN (2011) Distinction between epigenic and hypogenic caves. Geomorphol 134:9–22

Palmer MV, Palmer AN (2012) Petrographic and isotopic evidence for late-stage processes in sulfuric acid caves of the Guadalupe Mountains, New Mexico, USA. Int J Speleol 41(2):231–250

Pérez-López R, Rodríguez-Pascua MA, Ginés-Robles JL et al (2009) Speleoseismology and palaeoseismicity of Benis Cave (Murcia, SE Spain): coseismic effects of the 1999 Mula earthquake (mb 4.8). J Geol Soc Lond 316:207–216 (Special Publications)

Pinuaga-Espejel JI, Martínez Parra M, González Casal I (2000) Potencial hidromineral de la Región de Murcia. En: Panorama actual de las aguas minerales y Mineromedicinales en España. Madrid, pp 361–373

Plan L, Tschegg C, De Waele J et al (2012) Corrosion morphology and cave wall alteration in an Alpine sulfuric acid cave (Kraushöhle, Austria). Geomorphol 169:45–54

Rodríguez-Estrella T (2005) Consideraciones sobre la explotación de los recursos geotérmicos en las Cuencas Neógenas de la Región de Murcia. In: López Geta JA, Pulido Bosch A, Baquero Úbeda JC (eds) Capítulo del libro: Agua, Minería y Medio Ambiente. Libro Homenaje al profesor Rafael Fernández Rubio. Edita IGME, pp 515–532

Rodríguez-Estrella T (2015) Capítulo de Hidrogeología en el libro: "Sima de la Higuera. Monumento Nacional". Edita Ayuntamiento de Pliego. pp 35–49. ISBN: 978-84-608-2585-2

Ros A, Llamusí J, Inglés S (1988) Sima Destapada, Hornos, Isla Plana (Cartagena). Caliza 4–12

Ros A, Llamusí JL, Sánchez J (2011) Exploración en Sima Destapada y Cueva del Agua, dos cavidades de origen hidrotermal (Murcia). VIII Simposio Europeo de Espeleología, Marbella, pp 481–517

Ros A, Llamusí JL, Sánchez J (2014a) Cuevas hipogénicas en la Región de Murcia (España). En: Iberoamérica Subterránea. In: Calaforra JM, Durán JJ (eds) Asociación Española de Cuevas Turística, pp 405–416

Ros A, Llamusí JL, Sánchez J (2014b) Cuevas hipogénicas en la Región de Murcia (España). Ed: CENM-naturaleza, Murcia, vol I, 25 pp

Ros A, Llamusí JL, Sánchez J et al (2015) La Sima del Almez. Pliego, Murcia. Apuntes sobre su morfología hipogénica. Centro de Estudios de la Naturaleza y el Mar CENM-naturaleza. Publicaciones digitales http://www.cuevashipogenicasdemurcia.es/CATASTRO/sima%20Almez/SIMA%20DEL%20ALMEZ-15.df.pdf

Hypogene Imprints in Coastal Karst Caves from Mallorca Island (Western Mediterranean): Morphological Features and Speleogenetic Approach

5

Joaquín Ginés, Joan J. Fornós, Francesc Gràcia, Antoni Merino, Bogdan P. Onac, and Angel Ginés

Abstract

The southern and eastern coasts of Mallorca Island (western Mediterranean) host abundant karst caves, some of them containing solutional features and deposits presumably related to hypogene basal recharge. The caves were formed in calcarenites whose ages range from Upper Miocene (reef deposits) to Middle Pleistocene (eolianites), which form a fringing postorogenic belt deposited over Mesozoic folded and thrusted carbonate deposits. The hydrogeological setting corresponds to an unconfined coastal aquifer in very porous eogenetic rocks, but showing important lateral and vertical permeability variations related to different sedimentary facies. Six caves containing hypogene features are distributed in three main coastal areas: the Llucmajor Upper Miocene platform, the Campos Plio-Pleistocene basin, and the Portocristo Upper Miocene littoral fringe. The first two areas are spatially coincident with low-grade geothermal anomalies reported in southern Mallorca, which are associated to important SW–NE faults. The observed cave features include a suite of solutional rising forms embracing, among others, subvertical feeder-like conduits and small ascending wall channels of variegated morphologies and dimensions. Sediments and black crusts enriched in Fe and Mn oxides are frequent along with some uncommon minerals, documenting a deep recharge rising into the unconfined littoral groundwater. Regarding their speleogenesis, the studied sites must be considered as complex littoral caves in which the imprints of hypogene processes are evident, but intermingled with other morphogenetic vectors like coastal mixing processes and a substantial meteoric recharge. The lithofacies variability of the carbonate rocks introduces additional complexity, affecting the hydrological behavior of the coastal aquifers as well as the pattern and morphology of the resulting caves.

J. Ginés (✉) · J.J. Fornós · F. Gràcia · A. Merino · A. Ginés
Grup de Ciències de la Terra (Geologia i Paleontologia "Guillem Colom"), Universitat de les Illes Balears, Palma de Mallorca, Spain
e-mail: jginesgracia@yahoo.es

J.J. Fornós
e-mail: joan.fornos@uib.es

F. Gràcia
e-mail: xescgracia@yahoo.es

A. Merino
e-mail: tonymerinoj@gmail.com

A. Ginés
e-mail: agines.gracia@yahoo.es

B.P. Onac
Karst Research Group, School of Geosciences, University of South Florida, 4202 E. Fowler Ave., NES 107, Tampa, FL 33620, USA
e-mail: bonac@usf.edu

© Springer International Publishing AG 2017
A. Klimchouk et al. (eds.), *Hypogene Karst Regions and Caves of the World*, Cave and Karst Systems of the World, DOI 10.1007/978-3-319-53348-3_5

Keywords
Coastal caves • Mallorca Island • Hypogene speleogenesis • Geothermal activity • Lithofacies variability

1 Introduction

In recent years, hypogene speleogenesis has arisen as a new paradigm that explains the formation of a substantial amount of karst caves, developed by upwelling waters coming from depth (Klimchouk 2007, 2009) in a diversity of geological settings. A growing interest on this topic has led to abundant contributions on the matter, presented in several specific conferences on hypogene speleogenesis (Klimchouk and Ford 2009; Stafford et al. 2009; Otoničar et al. 2013; Klimchouk et al. 2014; Chavez and Reehling 2016). The wideness of this research field is really important, embracing different lithologies (limestone, gypsum) and well-differentiated geochemical processes, namely sulfuric acid speleogenesis, cooling of thermal waters, or mixing processes (Klimchouk 2009; Dublyansky 2013; Audra and Palmer 2015). The complexity of this topic includes terminological issues on the exact meaning of the term "hypogenic", as previously discussed by Palmer (2007) and Mylroie and Mylroie (2009). Nowadays, according to Dublyansky (2014) and Klimchouk (2014), a wide consensus exists about hypogene speleogenesis considered as an assemblage of porosity creation processes that are decoupled from the meteoric domain, both with respect to hydrogeology (rising deep-seated recharge) and geochemistry (aggressiveness of waters not linked to atmospheric or edaphic CO_2).

Cave development in islands and coastal settings, as explained in many references (e.g., Mylroie and Carew 1990; Mylroie and Mylroie 2009), shares several common issues with hypogene speleogenesis. In this respect, mixing between fresh and marine waters is usually considered to be the dominant source of aggressiveness in coastal limestone areas, and consequently the availability of biogenic CO_2 and/or the amount of meteoric recharge are far from being the main drivers of cave forming processes. Recent alternative research from Gulley et al. (2015) emphasizes the role of heterogeneously distributed vadose CO_2 in the complex geochemical processes occurring in littoral karst settings. Therefore, the resulting solutional morphologies are slow-flow or convection-controlled speleogens (Mylroie 2013), rather similar to many hypogene confined-flow features (Audra et al. 2009; Klimchouk 2009). For these reasons, some authors (i.e., Palmer 2007) have argued, in the past, that coastal speleogenesis falls in some way in the category of hypogene cave forming mechanisms.

Within this broad scenario, the references to hypogenic processes in coastal karst areas are really scarce (Klimchouk 2014; Audra and Palmer 2015) and, because of this, Mallorca Island (western Mediterranean) is a convenient place to evaluate and discuss the contribution of deep-seated processes in littoral speleogenesis. Eogenetic karst caves are abundant all along the island, mainly in its eastern and southern coasts. The vast majority of these caves show morphological features compatible with a coastal mixing origin (e.g., spongework and ramiform caves extensively affected by collapse), documented for example in Ginés and Ginés (2007) and Ginés et al. (2013). A few of these caves display some features pointing toward the involvement of hypogenic processes in their formation, as earlier suggested in the case of the extensive cave system of Cova des Pas de Vallgornera (Ginés et al. 2008, 2009, 2014; Onac et al. 2014). The present chapter reviews the role of hypogene speleogenesis in the coastal karstification of the island, employing up-to-date knowledge on specific morphogenetic features documented in some Mallorcan caves.

2 Geographical and Geological Setting

Located in the middle of the western Mediterranean basin, Mallorca is the largest island (3667 km^2) of the Balearic Archipelago (Spain). Climate is typically Mediterranean, characterized by hot and dry summers and mild, relatively wet winters. Mean annual temperature is around 17 °C (mean winter and summer values are 10 and 25 °C, respectively), and precipitations are mostly concentrated in autumn showing average annual values of 580 mm/a for the whole island, but reaching only 300–400 mm/a in the southern and eastern littoral regions (Guijarro 1995).

In general terms, Mallorca is built up by folded Mesozoic to Middle Miocene rocks that are discordantly covered and flanked by slightly deformed Upper Miocene to Pleistocene sediments. Carbonate rocks are represented almost continuously since the Middle Triassic and were affected by a compressive and thrusting tectonic phase lasting from the Paleogene to the Middle Miocene (Fornós and Gelabert 1995; Fornós et al. 2002). Therefore, Mallorcan mountains are the NE continuation of the Alpine Betic thrust and fold belt that configures the southern part of the Iberian peninsula.

From a physiographical point of view, the island is composed of two more or less parallel mountain ranges (Serra de Tramuntana and Serres de Llevant), along with some small hills in its central part. Graben-like depressed

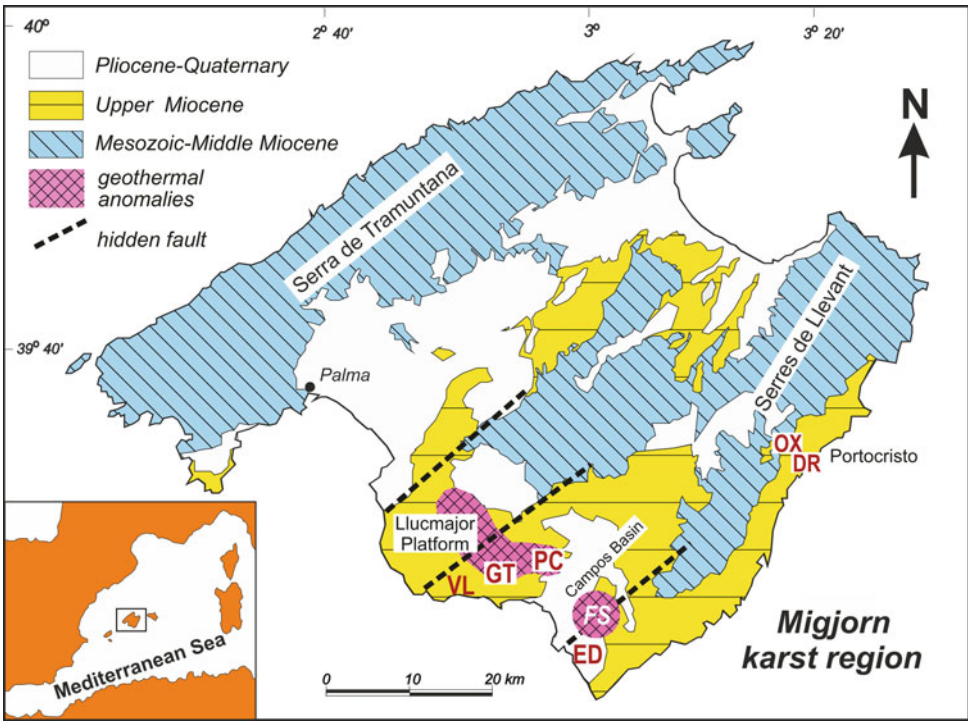

Fig. 1 Simplified geological map of Mallorca Island with the location of the caves and geographical sites referred in the text. *VL* Cova des Pas de Vallgornera, *GT* Cova de sa Guitarreta, *PC* Pou de Can Carro, *FS* Font Santa de Sant Joan, *ED* Es Dolç, *OX* Cova de s'Ònix, *DR* Coves del Drac

areas are developed on the foreland of these folded ranges, being filled with sediments of Upper Miocene to Quaternary ages. Additionally, these post-tectonic deposits are disposed around the folded areas, forming a continuous littoral platform located in the southern half of the island, the so-called Migjorn karst region (Fig. 1). The lithostratigraphy of this region is mainly constituted by an Upper Miocene Reef Complex (Fornós et al. 2002), but locally, relatively thick Plio-Quaternary rocks (shallow marine to littoral Pliocene sediments and Pleistocene eolianites) are also present, which are filling preferentially some areas, like the Campos Basin in the southernmost end of the island.

As a general trend, the Upper Miocene carbonates outcropping along the sea cliffs of the Migjorn region comprise two main sedimentary units: the Reef Complex *stricto sensu*, which is Upper Tortonian–Early Messinian in age, and the upper unit or Terminal Complex assigned to the Messinian that includes mangrove swamp deposits and oolitic sand shoals with stromatolites (Pomar and Ward 1994; Ginés et al. 2014). The Reef Complex consists in a series of progradational reef-rimmed platforms that present diverse facies associations, characterized in this region by well-differentiated reef front and back reef deposits (Fornós et al. 2002; Ginés et al. 2008). Most of the caves considered in this paper are housed in the Upper Tortonian–Early Messinian Reef Complex, although others (Es Dolç, Pou de Can Carro) developed in Plio-Quaternary shallow marine deposits and eolianites.

Worth mentioning is the existence of a geothermal activity in southern Mallorca, particularly associated with the Neogene extensional faults that are responsible for the geometry of the above-mentioned Campos Basin. The faults delimitating these graben-type structures enable the hydraulic connection between Mesozoic deep reservoirs and the unconfined aquifers existing in the Upper Miocene and Plio-Quaternary rocks (López and Mateos 2006; López 2007). The principal geothermal anomalies occur in the Llucmajor Platform (exploitation wells with groundwater temperature near 50 °C) and the Campos Basin (Fig. 1), where the thermal baths called Font Santa de Sant Joan are located, exploiting hot waters (37 °C) since the fifteenth century.

3 Caves Containing Hypogene Features

The Migjorn karst region stretches along more than 100 km of the southern and eastern shorelines of Mallorca, being limited by rather continuous sea cliffs that are interrupted by some beach extensions as well as by striking narrow coastal embayments corresponding to a network of dry valleys incised over the carbonate plateau. This karst region is undoubtedly the richest cave area in Mallorca with over a hundred of significant coastal caves, formed mainly in Upper Miocene reefal carbonates by coastal mixing processes (Ginés et al. 2013). From a morphological and topographical point of view, they are not strictly "flank margin caves" as described by Mylroie and Carew (1990); in this respect, subsurface phenomena in the Migjorn include complex and long caves, in which breakdown mechanisms have largely destroyed and masked the initial speleogenetic phases (Ginés and Ginés 2007). Historical caves like the world-wide

famous Coves del Drac, explored in 1896 by Edouard A. Martel, are located in this region and have greatly contributed to the touristic attraction of the island.

Only six caves in this part of the island show evidences pointing toward the involvement of hypogene speleogenesis in their formation; none, however, display proofs of sulfuric acid speleogenesis. Four of the considered caves are located in the vicinity of geothermal anomalies reported in the southern half of Mallorca (López 2007). Basically, the caves can be assigned to three geographical subunits: the Llucmajor Platform, the Campos Basin, and the eastern coastal fringe near the town of Portocristo (Fig. 1).

3.1 Llucmajor Upper Miocene Platform

This rather monotonous and flat section of the Migjorn karst region, exceeding 200 km^2, has very few known caves. Nevertheless, the most important cave in the Balearic Islands, both in terms of size and unique natural value, is located close to the southern coast of this area. From the geological point of view, the architecture of the Upper Miocene Reef Complex is very well-represented along the sea cliffs of the platform, where some internationally renowned outcrops are located (Pomar and Ward 1994; Fornós et al. 2002); on the other hand, it is worth noting the large geothermal anomaly documented in the vicinity of Llucmajor town (Fig. 1).

3.1.1 Cova des Pas de Vallgornera

Currently this cave exceeds 78 km in length (Merino et al. 2014), including over 18 km of underwater passages drowned by brackish phreatic waters. It is a quite complex coastal cave whose pattern and morphology is strongly controlled by the textural characteristics of the Upper Miocene reefal carbonates, which show sharp facies variations both laterally and vertically. Generally speaking, in the seaward part of the cave, spongework passages and mazes are the dominant features, along with important breakdown phenomena, both corresponding to the highly permeable reef front facies (Fig. 2). In contrast, owing to the presence of more calcisiltitic or even marly deposits, joint-guided galleries and conduits are common in the less permeable carbonate rocks of the back reef facies (Ginés et al. 2014).

Particularly in the inner passages forming the landward part of Cova des Pas de Vallgornera, and in its upper maze, features of a possible hypogene origin were previously described by Ginés et al. (2008), and subsequently documented with more detail in several papers (Ginés et al. 2009, 2014; Gràcia et al. 2009; Merino and Fornós 2010; Fornós et al. 2011). These features consist of solutional morphologies of ascending flow that include—as the most diagnostic forms—feeder-like vertical or lateral conduits in the floor of the passages (Fig. 3a), and very abundant and variegated solutional ascending channels carved in wall and ceilings (Fig. 3b, c). The width of these rising flow runnels ranges from a few millimeters to a few decimeters; the narrow and

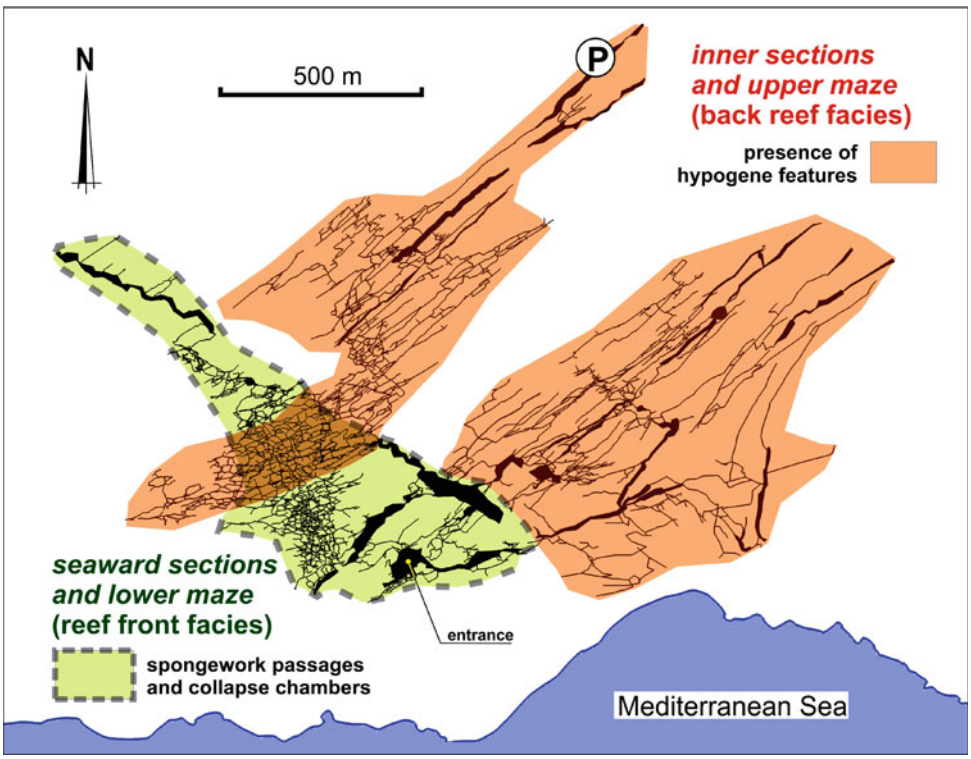

Fig. 2 Lithofacies control over the pattern of Cova des Pas de Vallgornera. *P* Paleontological deposit corresponding to the allochthonous infilling associated to a collapsed ancient cave entrance

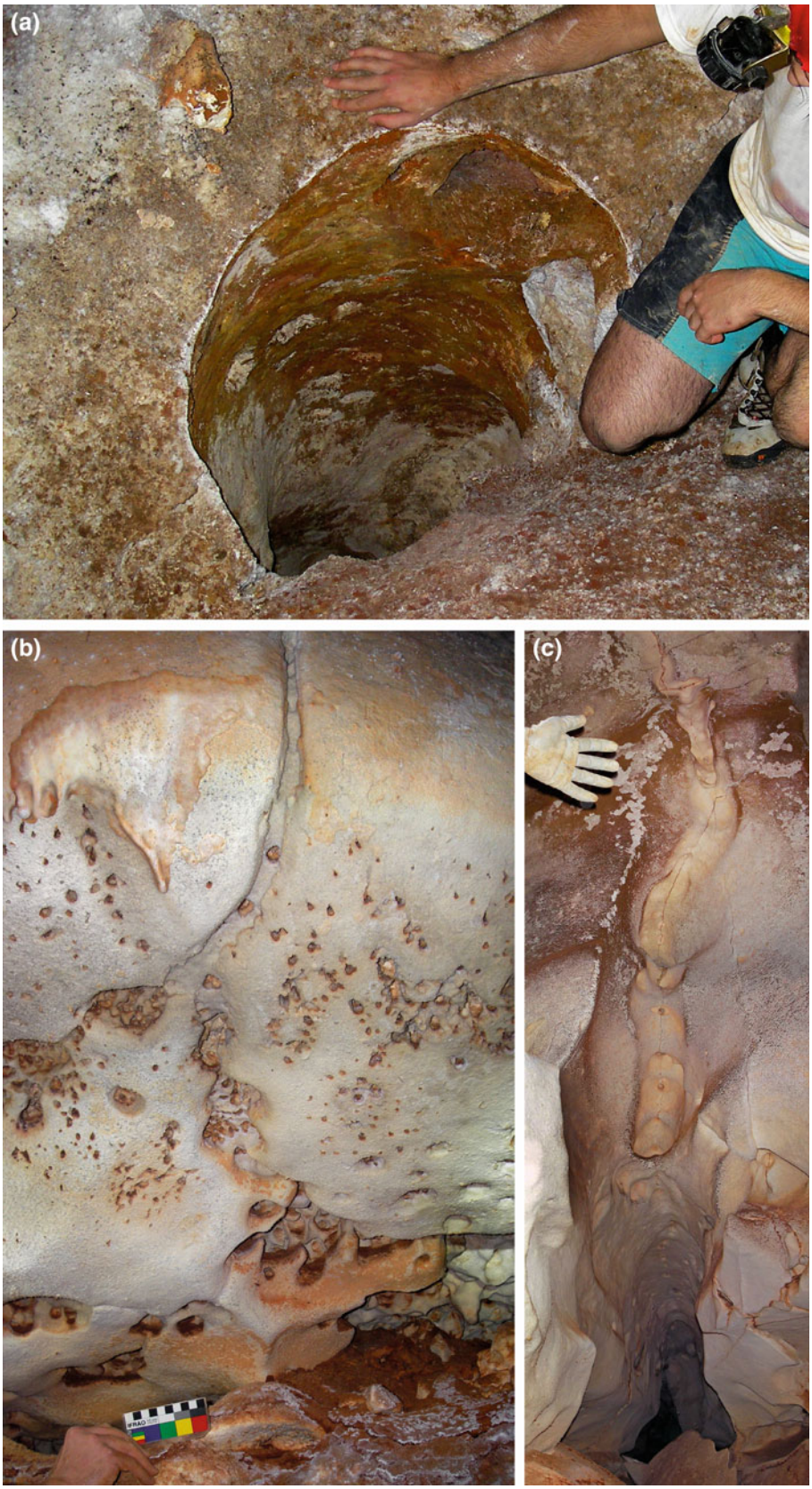

Fig. 3 Hypogene speleogens in Cova des Pas de Vallgornera. **a** Feeder-like vertical conduit. **b** Anastomosing rising channels and solutional alveoli. **c** Ascending channel developed from a lateral feeding point (*Photos* A. Merino)

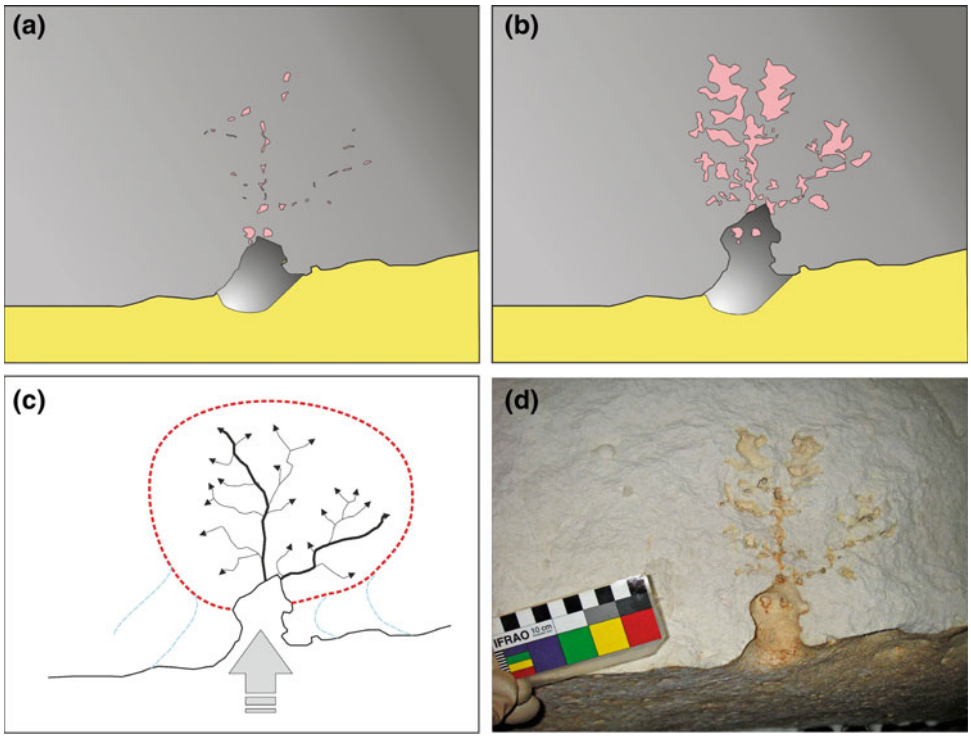

Fig. 4 Evolutionary diagram of a solutional alveolus in Cova des Pas de Vallgornera. **a–b** Enlargement of an initial hollow in the ceiling of the cave or its overhanging walls, due to aggressive flows exploiting the high porosity of the rock. **c** Sketch of the flow directions through the rising alveolus. **d** Cross-sectional image of a solutional alveolus, observable on the face of a rock block fallen from the ceiling (modified from Merino and Fornós 2010)

singularly sharp ascending grooves (less than 1–2 cm in width) are particularly abundant and very similar to the "bubble trails" described by Audra et al. (2009). Their formation by ascending aggressive solutions can be envisaged due to the lack of carbonate precipitates associated with CO_2 degassing at the water table (folia, calcite rafts, etc.). Frequently, the feeder-like features are present as narrow slots in the floor of some maze areas and galleries. Conspicuous solution alveoli cover extensive areas of the ceilings and overhanging walls, having been developed by aggressive rising flows exploiting the high porosity of the calcarenitic rock (Figs. 3b and 4).

Crusts and sediments rich in Fe and Mn oxides and hydroxides (goethite, hematite, romanèchite, todorokite) are present in the landward inner sections of the cave, along with some uncommon mineral deposits (barite, celestine, strontianite, chamosite, gibbsite, jacobsite, nordstrandite, etc.; Fig. 5), presumably linked to a deep hypogene recharge (Merino et al. 2009; Onac et al. 2014). These mineral assemblages are located close to the feeder-like features or vents that appear distributed along the floor of some passages. Thus, they support the involvement of deep-seated groundwaters in their deposition, either from dissolved species transported by warm solutions or by weathering of the bedrock by warm and humid air condensed onto the cave walls.

Regarding the genesis of the whole cave system, three speleogenetic vectors have been invoked: (1) coastal mixing dissolution in an unconfined coastal aquifer, affecting particularly the seaward reef front facies; (2) a hypogenic basal recharge affecting the less permeable back reef carbonates; and (3) a substantial meteoric recharge evidenced by the important sandy and clayey detritic sedimentation (up to 2.5 m thick) linked to an ancient entrance to the cave system (Fornós et al. 2014; Ginés et al. 2009, 2014). The concurrence of a strongly contrasting geochemistry between the three invoked speleogenetic vectors could explain the development of this extensive maze cave in phreatic conditions (Palmer 2011; Audra and Palmer 2015).

Chronologically, the main phases in the formation of Cova des Pas de Vallgornera probably correspond to the Middle Pliocene or even earlier, considering the vertebrate remains recovered inside the cave (Fig. 2). These include up to 5 mammal species, at least 14 bird species, 1 reptile and 1 amphibian (Bover et al. 2014). From this outstanding paleontological deposit—associated to an ancient, now collapsed entrance—were recovered bones of *Myotragus* aff. *kopperi* (with an age around 2.4–2.6 Ma), a species that belongs to a genus of bovidae that colonized the Balearics during the Messinian salinity crisis and subsequently evolved, isolated from the mainland, during the Pliocene and Pleistocene. These paleontological remains suggest that the ancient cave entrance collapsed very sudden causing its total sealing from the surface in the very early Pleistocene times. In view of this fact, obviously, the formation of the cave system must date back to the Pliocene.

The hypogene deep recharge, postulated above, can be related to the geothermal phenomena documented in the area (López and Mateos 2006), with groundwater at temperatures

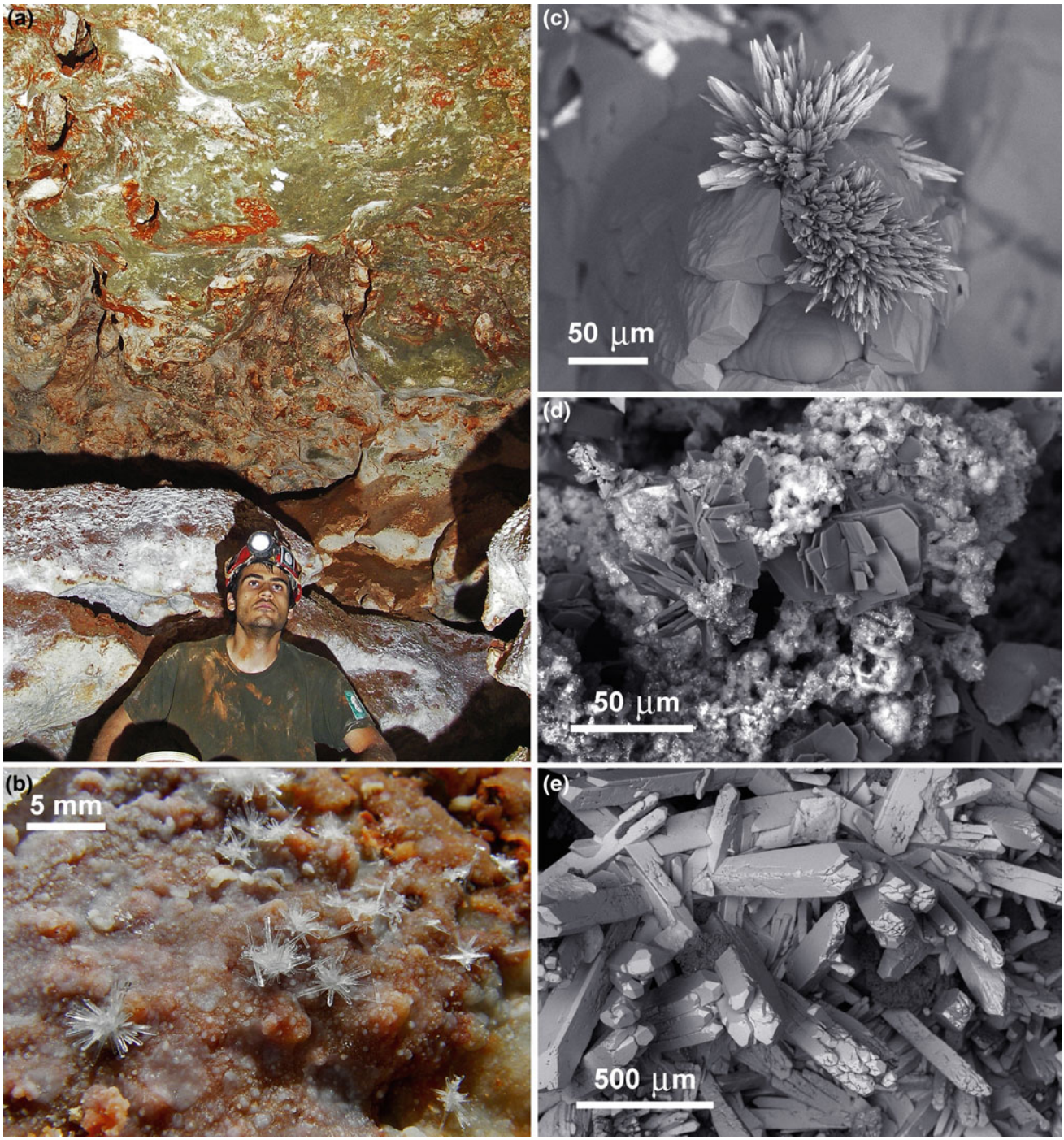

Fig. 5 Mineral deposits in Cova des Pas de Vallgornera. **a** Multicolored fluffy coatings mainly consisting of Fe and/or Mn oxides and hydroxides. **b** Bouquets of celestine crystals over dolomite or gypsum crusts (*Photos* A. Merino). SEM images of minerals collected around hypogene-related features: clusters of prismatic strontianite crystals over dolomite aggregates **(c)**; radiating clusters of tabular nordstrandite crystals **(d)**; crystals of celestine displaying subhedral and pyramidal morphologies **(e)**

exceeding 50 °C near the Llucmajor town. Currently the abundant phreatic pools in Cova des Pas de Vallgornera do not show temperature anomalies (mean water temperature is 20 °C). However, Cova de sa Guitarreta located in the vicinity (Fig. 1) intersects in its lower part the aquifer whose groundwater temperature is 27.1 °C (Merino et al. 2011). This cavern does not show hypogene diagnostic features and consists of a major collapse chamber, probably generated by the dissolution in depth associated to a basal geothermal recharge to the unconfined coastal aquifer.

3.2 Campos Plio-Pleistocene Basin

Toward the southeast, the Llucmajor Platform connects with the Campos Basin, a graben-like depressed area filled up with Plio-Quaternary sediments (Fig. 1) that are bounded by hidden faults trending SW–NE. This southern part of the Migjorn karst region hosts only a few penetrable caves, likely due to the fact that the Upper Miocene reefal carbonates are located below the current sea-level in this slightly subsiding area. The most significant caves are developed, at least partially, in rocks corresponding to the Plio-Pleistocene sequence, only a few kilometers away of the sole thermal baths existing in Mallorca.

3.2.1 Pou de Can Carro

In the western flank of the basin there is an interesting cavity, artificially opened when drilling a hole to plant a tree. It is a rather vertical cave, 45 m in depth, that reaches the water table of the unconfined coastal aquifer (Merino et al. 2011); the temperature of the brackish phreatic waters shows a weak thermal anomaly, with values around 23.6 °C. The lower part consists of a breakdown chamber developed in Upper Miocene reefal calcarenites, but the upper 10–15 m of the cave was formed in reddish Pliocene eolianites (Fig. 6).

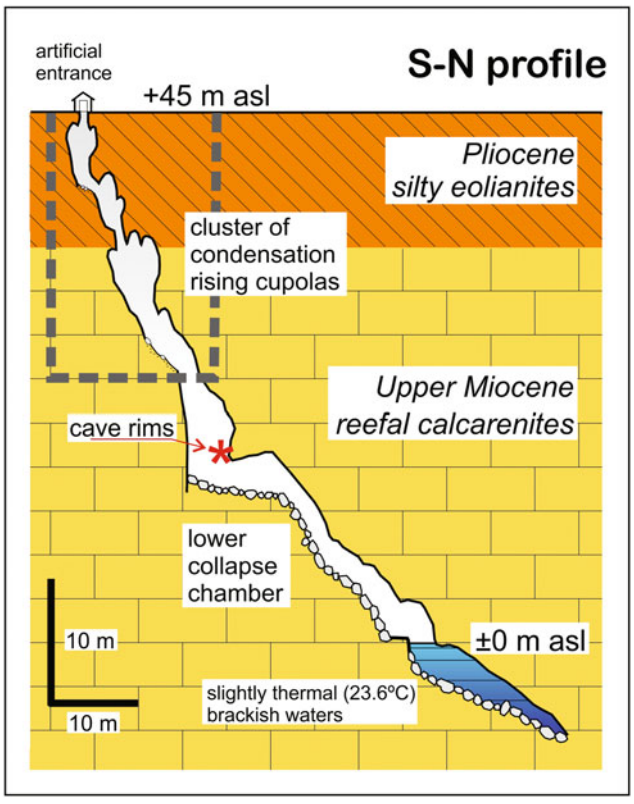

Fig. 6 Schematic morphological and lithostratigraphical profile of Pou de Can Carro (vertical scale approx. ×1.5)

This upper section is composed of a nice succession of spherical voids and cupolas, 1–2 m wide, which are connected one to each other vertically all the way to the surface. In the upper part of the main chamber, several conspicuous cave rims were formed owing to the convective air cells established between the low-grade thermal pool and the chain of ascending cupolas leading to the surface. The cave was excavated along an important fracture by condensation-corrosion processes leading to the granular disaggregation of the Upper Tortonian calcarenites and, particularly, the Pliocene eolianites.

3.2.2 Es Dolç

The commercial thermal baths known as Font Santa de Sant Joan are located in the eastern flank of the Campos Basin; they exploit waters at a temperature of 37 °C. To the south of this locality a recently explored underwater cave called Es Dolç is situated (Fig. 1). It has a development of more than 4 km (Gràcia et al. 2014) and a rather linear but wandering planimetric pattern, with short extensions scattered along the main passage (Fig. 7). The cave discharges brackish waters directly to the sea and has two more collapse entrances located inland in a coastal flat landscape with an elevation less than 15 m a.s.l.

One of the most interesting aspects of Es Dolç is related to the fact that the cave develops mainly in Plio-Pleistocene eolianites, with its lower passages reaching the underlying Pliocene shallow marine deposits (Gràcia et al. 2014). Breakdown processes are extensive in the thin-bedded eolianites, producing wide passages with relatively low ceilings and scarce solutional features.

Regarding the hypogene speleogens, there are solutional rising features like tiny and sharp ascending dissolution channels (Gràcia and Fornós 2014), but the most striking morphologies are several ascending passages that begin from the underlying Pliocene rocks and continue up until they connect with the main conduit in the Plio-Pleistocene eolianites (Fig. 7a). Some of these features are quite spectacular, as the so-called Crater, which is a collapse phenomenon affecting a couple of vertical conduits rising from beneath (Fig. 8). In general terms, feeder-like features are the most abundant hypogene speleogens, embracing from more than one meter wide funnels, opened in the floor of the galleries, to narrower vertical pipes (only a few centimeters wide) hollowing the pavements as well as the walls and ceilings of some passages (Fig. 9).

Apart from the described hypogene imprints, Es Dolç has noticeable drainage functionality within the littoral brackish aquifer. In spite of being relatively close to the Font Santa baths, no thermal anomalies were detected nowadays in its phreatic waters.

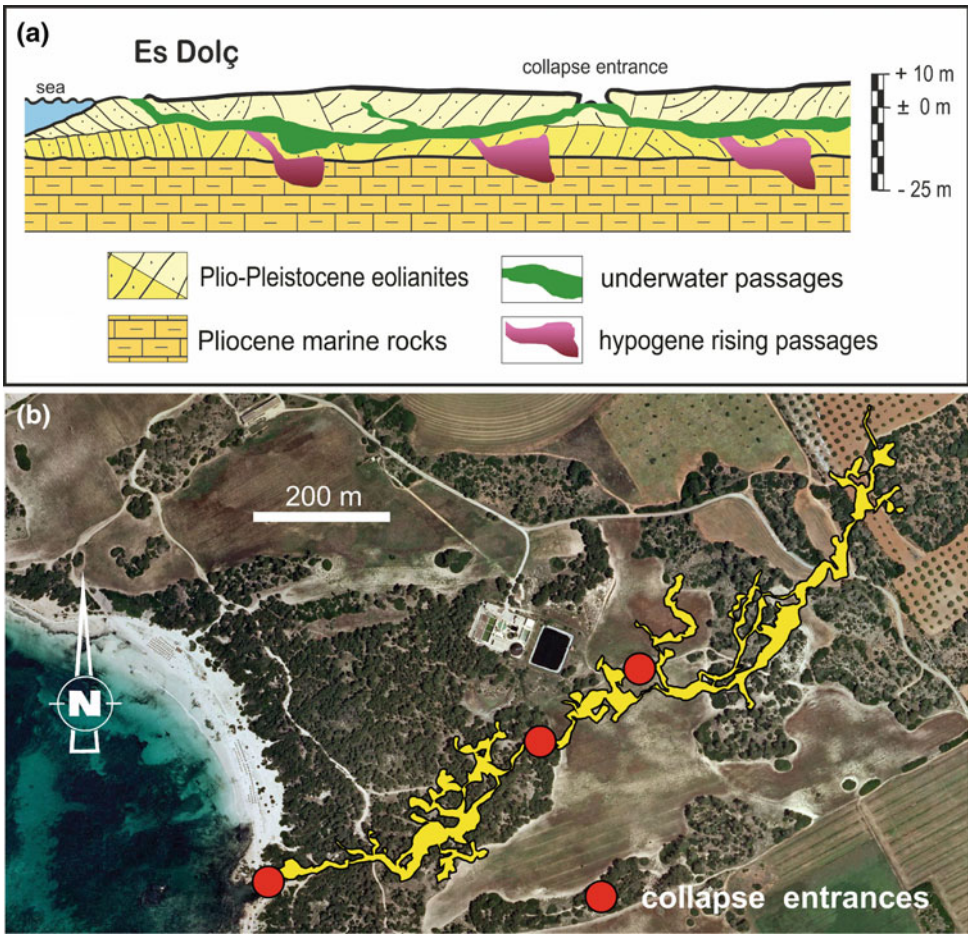

Fig. 7 Es Dolç cave system. **a** Schematic profile showing the lithostratigraphical context of the underwater passages (vertical scale approx. ×2; modified from Gràcia et al. 2014). **b** Superposition of the cave survey over an orthophotography of the area

3.3 Portocristo Upper Miocene Littoral Fringe

The eastern coastal belt of Migjorn karst region stretches as a narrow fringe of Upper Miocene calcarenites (max. width of 3 km) that are discordantly disposed over the structured low relief mountains of Serres de Llevant (Fig. 1). This section is one of the richest cave areas in the island, with up to seven coastal caves exceeding 1 km in development (Ginés et al. 2013); among them, two are the most important touristic caves in Mallorca.

3.3.1 Cova de s'Ònix

This cavity opens relatively inland (2 km from the coastline), with its lowermost chambers reaching the Jurassic folded basement, where some sea-level controlled pools occur. The cave shows some hypogene-related imprints that are worth mentioning (Merino et al. 2011), as a few narrow dissolution ascending channels present in its overhanging walls.

Furthermore, this site is the only place in Mallorca where folia occur in a narrow band of phreatic crystallizations, located at +2.9 m a.s.l. and related to the last interglacial sea-level (Tuccimei et al. 2006). In some coastal settings, the genesis of this kind of speleothem seems to be controlled by the tidally fluctuating water table (D'Angeli et al. 2015), although a possible hypogenic origin for the folia occurring in this cave cannot be ruled out.

3.3.2 Coves del Drac

In the outskirts of Portocristo town, close to the coastline, the renowned Coves del Drac opens (Fig. 1). This internationally acclaimed show cave has been previously interpreted as fully representative—from the morphogenetic point of view—of the coastal caves existing along the eastern littoral of Mallorca (Ginés and Ginés 2007). The underwater explorations recently performed have extended the development of the cave to more than 6.5 km (Gràcia 2015), with over 4 km of subaqueous passages (Fig. 10). The diving and surveying tasks are currently in progress at this site and have allowed to recognize numerous hypogene features chiefly distributed in the submerged sections of the cave. On the other hand, the air-filled chambers are the result of extensive breakdown processes, having their lower parts extensively occupied by sea-level controlled brackish pools.

The hypogene speleogens documented in Coves del Drac are mainly solutional rising channels, from a few millimeters to some centimeters in width, carved in the overhanging

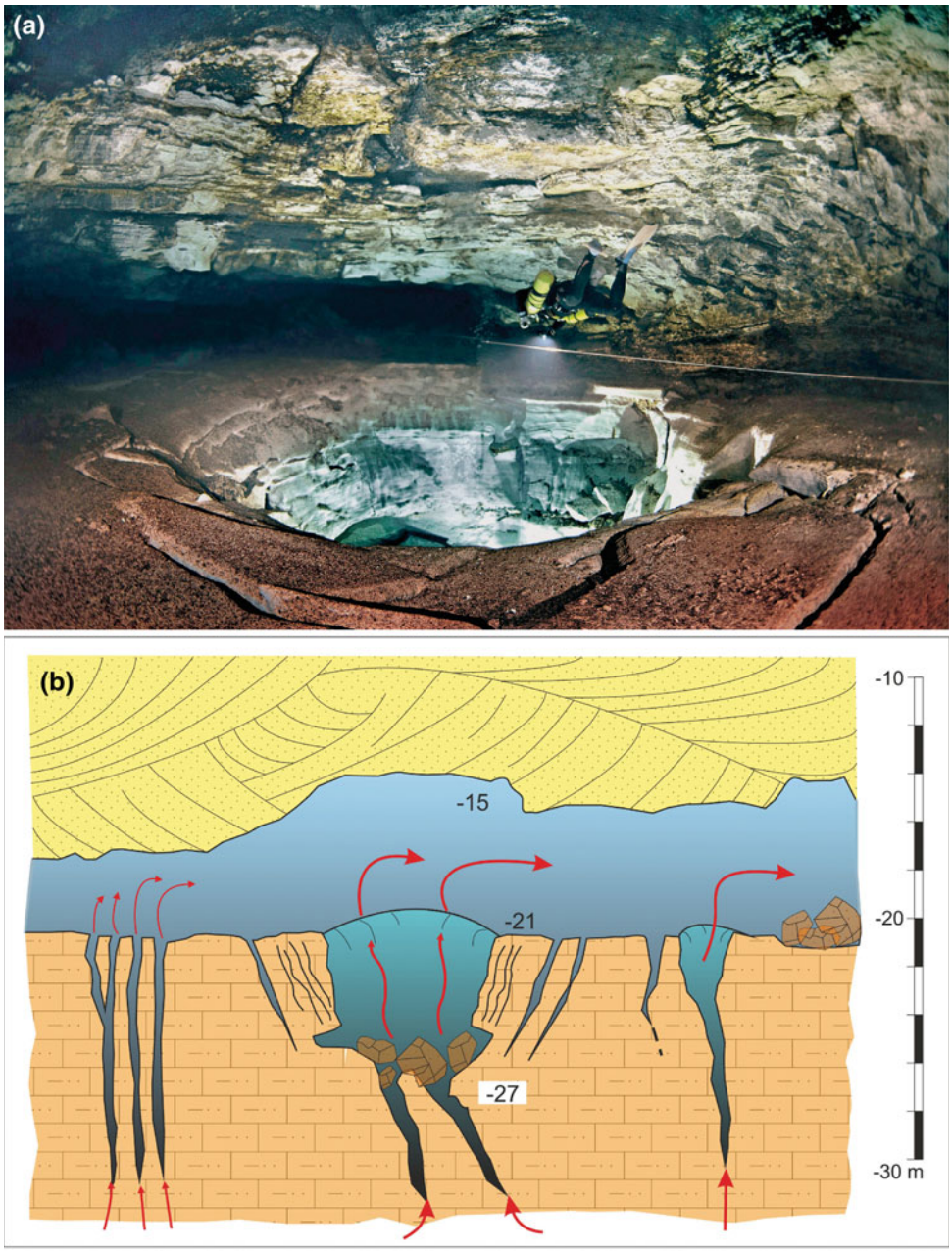

Fig. 8 **a** The "Crater" in the underwater passages of Es Dolç. It is a collapse feature leading to subvertical feeder-like conduits in the Pliocene rocks at its bottom. The ceiling of the gallery corresponds to Plio-Pleistocene eolianites. (*Photo* Grup Nord de Mallorca). **b** Morphogenetic sketch of this hypogene feature

walls or ceilings of the underwater passages and chambers (Fig. 11). Many of these channels display winding trajectories along the relatively flat ceilings, having lengths that usually exceed a few meters. Many of these rising features are really striking because of the contrast between the whitish trajectory of the ascending dissolution runnels and the wall rocks that are black-coated by Fe- and Mn-rich crusts (Fig. 11b). Some feeder-like features are also present in the underwater passages.

This part of the eastern coastal fringe of Mallorca is not associated to current geothermal activity and, moreover, the cave pattern of Coves del Drac (Fig. 10) is clearly from spongiform to ramiform (Palmer 2007) and without any evident drainage functionality. Regarding its speleogenesis, the hypogene imprints in this cave—although abundant—are not especially significant in terms of the generated volume of voids; it seems that these imprints are limited to slightly reshaping the walls and ceilings of the passages.

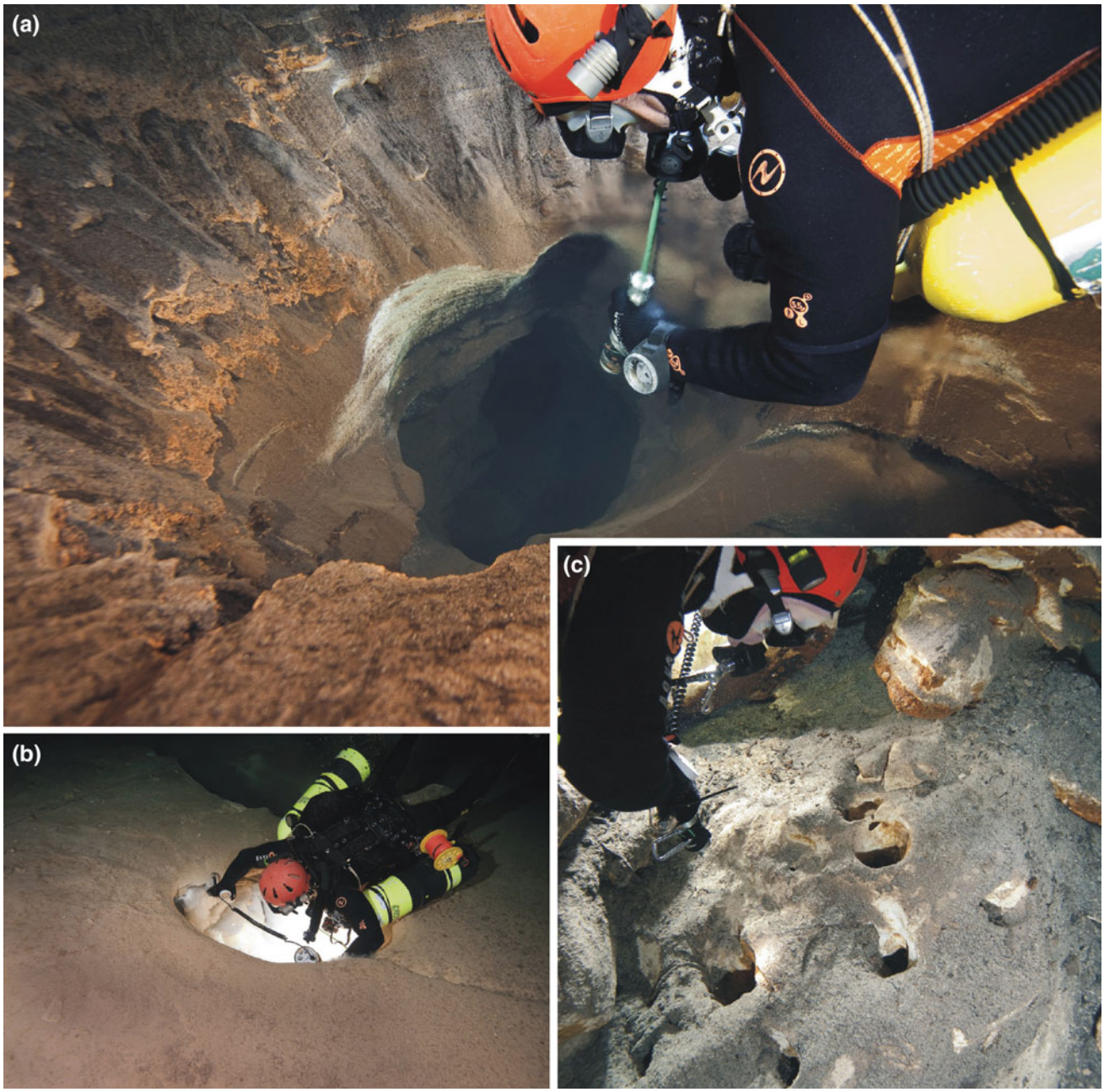

Fig. 9 Hypogene solutional morphologies from Es Dolç. **a**–**b** Feeder-like features, both funnel-shaped or circular, are common along the underwater passages. **c** Abundant uprising solutional pipes are present in the floor of some galleries, being also carved in its walls and ceilings (*Photos* Grup Nord de Mallorca)

4 Final Discussion

Nowadays we reckon that, undoubtedly, there are evidences of hypogene processes involved in the morphogenesis of some coastal caves from southern and eastern Mallorca. The majority of caves referred in this contribution are closely related to the geothermal activity documented in the southern half of the island (López and Mateos 2006; López 2007), though there are no definite clues of hypogenic processes currently active in the investigated caves; nevertheless, weak thermal anomalies (24–27 °C) have been reported in some of its subterranean phreatic pools. At the current state of knowledge, there are no evidences of sulfuric acid speleogenesis.

Exclusively in the case of Pou de Can Carro, the present-day morphology of this cave is mostly conditioned by the presence of hypogene speleogens, namely the

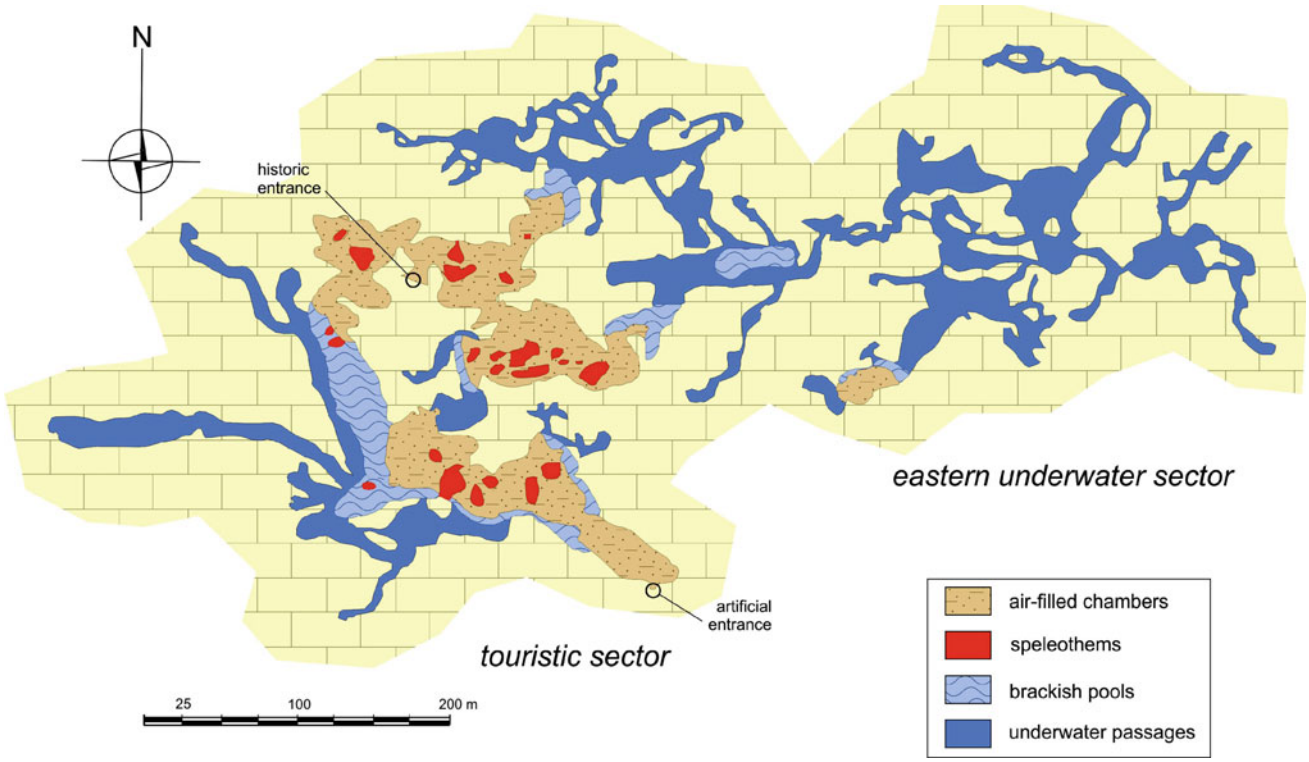

Fig. 10 Simplified survey of Coves del Drac (compiled by the Grup Nord de Mallorca divers team, 2010–2015). The hypogene features are almost restricted to the underwater passages, which are disposed according to a ramiform pattern; the air-filled chambers with their extensive pools are the result of generalized breakdown processes

spectacular array of condensation-corrosion spherical voids and cupolas that form the upper part of the cave, as a result of the weak thermal character of the unconfined aquifer intersected in its lower part (Merino et al. 2011). In other localities, like Es Dolç and Cova des Pas de Vallgornera, the morphological suite of rising flow (Klimchouk 2009) is well-represented, being the ascending channels of diverse dimensions the most diagnostic features (Ginés et al. 2014; Gràcia and Fornós 2014). Feeder-like vertical to subvertical conduits and/or slots are abundant in the floor of the passages in both caves.

Specifically in Cova des Pas de Vallgornera, uncommon minerals (barite, celestine, chamosite, strontianite, nordstrandite, etc.) have been reported supporting the contribution of a deep hypogene recharge in the genesis of this extensive speleological system (Merino et al. 2009; Onac et al. 2014). Additionally, Fe- and Mn-rich black crusts or coatings are quite frequent, although similar deposits are also present in other underwater coastal caves of the island in which hypogene features have not been observed.

The speleogenetic mechanisms probably include at least three different but complementary pathways: coastal mixing, deep hypogene circulation, and a substantial meteoric recharge evidenced at least in some specific cases (Cova des Pas de Vallgornera and Es Dolç). In the eastern littoral fringe close to Portocristo, the hypogene imprints are evident in two caves, Coves del Drac and Cova de s'Ònix. However, it is not clear whether this particular speleogenetic vector can be generalized to all the coastal caves of the area, or it has just a limited relevance by contributing to minor and local morphological retouches. In this specific geographical unit, the association to geothermal phenomena does not exist today, but the recharge from the underlying Jurassic folded basement is a fact.

It is necessary to remark the morphological convergence existing between the features generated by littoral speleogenesis and those strictly related to hypogenic processes (Mylroie and Mylroie 2009). This situation becomes more complex as a result of the mélange of very well-differentiated geochemical endmembers, including coastal mixing waters, very variable CO_2-rich meteoric inputs and, finally, a thermal deep-seated contribution. As a consequence, in the case of Mallorca it seems more convenient to speak about coastal karstification with certain relevant hypogene imprints, rather than refer to strictly hypogenic phenomena.

Regarding chronological issues, these hypogene speleogenetic phases have occurred from the Middle Pliocene, as documented by the paleontological remains in Cova des Pas

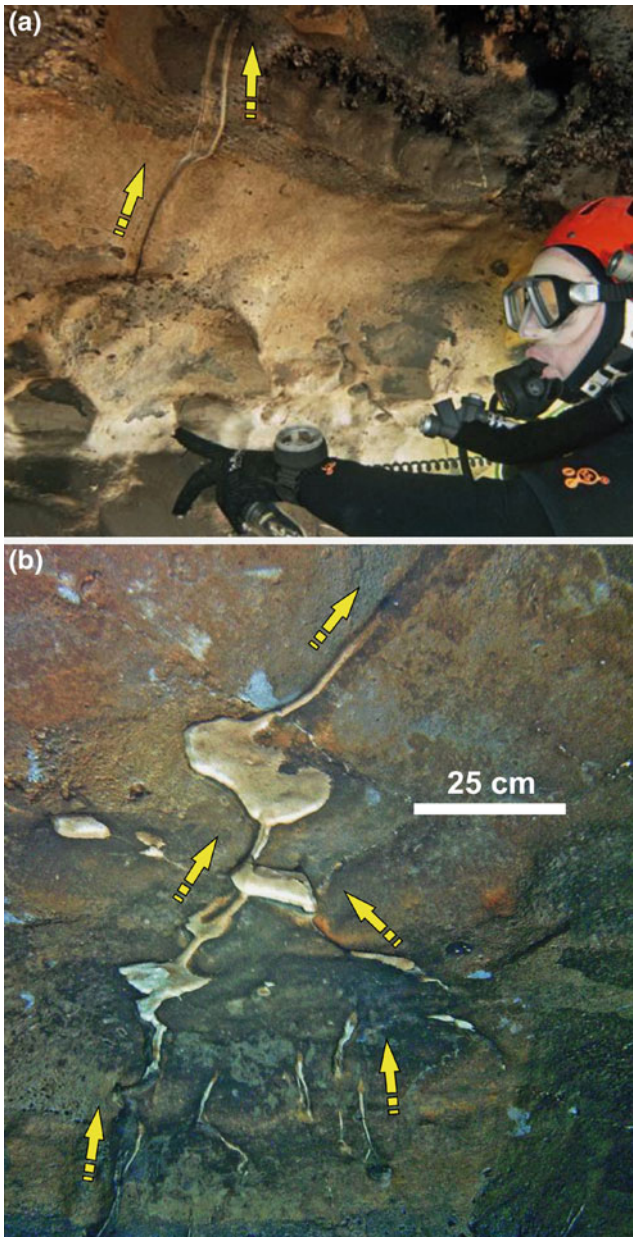

Fig. 11 Solutional ascending channels in the underwater passages of Coves del Drac. **a** Narrow channel developed from a subdued wall pocket (*Photo* A. Cirer). **b** Rising channels carved on the walls and ceiling are contrasting with the Mn- and Fe-rich black coatings (*Photo* F. Gràcia)

de Vallgornera (Bover et al. 2014), to Quaternary, documented in Es Dolç whose passages are mainly developed in Pleistocene eolianites (Gràcia et al. 2014).

Finally, the influence of the lithofacies variability of the involved eogenetic rocks is highly remarkable, which introduces additional complexity to the coastal karstification affecting both the hydrological behavior of the littoral aquifers and the planimetric pattern of the caves formed in this particular setting.

Acknowledgements The results reported were generated within the investigation projects CGL2013-48441-P of the MINECO (Spanish Government) and CGL2016-79246-P (AEI-FEDER, UE). The exploration of the underwater extensions of the caves has benefited from the unconditional involvement of the cave-divers team from Grup Nord de Mallorca. The "Conselleria de Medi Ambient, Agricultura i Pesca" (the regional environmental authority) has approved and supported the present investigations. We acknowledge the managers of Coves del Drac for the facilities and support kindly supplied while exploring and investigating this show cave.

References

Audra P, Palmer AN (2015) Research frontiers in speleogenesis. Dominant processes, hydrogeological conditions and resulting cave patterns. Acta Carsologica 44(3):315–348

Audra P, Mocochain L, Bigot JY, Nobécourt JC (2009) Morphological indicators of speleogenesis: hypogenic speleogens. In: Klimchouk AB, Ford DC (eds) Hypogene speleogenesis and karst hydrogeology of artesian basins. Special paper 1. Ukrainian Institute of Speleology and Karstology, Simferopol, Ukraine, pp 23–32

Bover P, Valenzuela A, Guerra C, Rofes J, Alcover JA, Ginés J, Fornós JJ, Cuenca-Bescós G, Merino A (2014) The Cova des Pas de Vallgornera (Llucmajor, Mallorca): a singular deposit bearing an exceptional well preserved Early Pleistocene vertebrate fauna. Int J Speleol 43(2):175–192

Chavez T, Reehling P (eds) (2016) Proceedings of DeepKarst 2016: origins, resources, and management of hypogene karst. Symposium 6. National Cave and Karst Research Institute, Carlsbad, New Mexico, p 203

D'Angeli IM, De Waele J, Ceballo O, Tisato N, Sauro F, Grau González ER, Bernasconi SM, Torriani S, Bontognali T (2015) Genesis of folia in a non-thermal epigenic cave (Matanzas, Cuba). Geomorphol 228:526–535

Dublyansky YV (2013) Karstification by geothermal waters. In: Frumkin A, Shroder J (eds) Treatise of geomorphology, vol 6. Academic Press, San Diego, pp 57–71

Dublyansky YV (2014) Hypogene speleogenesis—discussion of definitions. In: Klimchouk AB, Sasowsky I, Mylroie JE, Engel SA, Engel AS (eds) Hypogene cave morphologies. Special publication 18. Karst Waters Institute, Leesburg, Virginia, pp 1–3

Fornós JJ, Gelabert B (1995) Lithology and tectonics of the Majorcan karst. In: Ginés A, Ginés J (eds) Karst and caves in Mallorca. Endins 20, Monografies de la Societat d'Història Natural de les Balears 3, Palma de Mallorca, Spain, pp 27–43

Fornós JJ, Pomar L, Ramos-Guerrero E (2002) Balearic Islands. In: Gibbons W, Moreno T (eds) The geology of Spain. The Geological Society, London, pp 327–334

Fornós JJ, Merino A, Ginés J, Ginés A, Gràcia F (2011) Solutional features and cave deposits related to hypogene speleogenetic processes in a littoral cave of Mallorca Island (Western Mediterranean). Carbonates Evaporites 26(1):69–81

Fornós JJ, Ginés J, Gràcia F, Merino A, Gómez-Pujol L, Bover P (2014) Cave deposits and sedimentary processes in Cova des Pas de Vallgornera (Western Mediterranean). Int J Speleol 43(2):159–174

Ginés A, Ginés J (2007) Eogenetic karst, glacioeustatic cave pools and anchialine environments on Mallorca Island: a discussion of coastal speleogenesis. Int J Speleol 36(2):57–67

Ginés J, Ginés A, Fornós JJ, Gràcia F, Merino A (2008) Noves observacions sobre l'espeleogènesi en el Migjorn de Mallorca: els condicionants litològics en alguns grans sistemes subterranis litorals. Endins 32:49–79

Ginés J, Ginés A, Fornós JJ, Merino A, Gràcia F (2009) On the role of hypogene speleogenesis in shaping the coastal endokarst of southern Mallorca (Western Mediterranean). In: Klimchouk AB, Ford DC (eds) Hypogene speleogenesis and karst hydrogeology of artesian basins. Special paper 1, Ukrainian Ins Speleol Karstology, Simferopol, Ukraine, pp 91–99

Ginés A, Ginés J, Gràcia F (2013) Cave development and patterns of caves and cave systems in the eogenetic coastal karst of southern Mallorca (Balearic Islands, Spain). In: Lace MJ, Mylroie JE (eds) Coastal karst landforms. Coast Res Libr, Springer, Dordrecht, vol 5, pp 245–260

Ginés J, Fornós JJ, Ginés A, Merino A, Gràcia F (2014) Geologic constraints and speleogenesis of Cova des Pas de Vallgornera, a complex coastal cave from Mallorca Island (Western Mediterranean). Int J Speleol 43(2):105–124

Gràcia F (2015) Les cavitats subaquàtiques de les zones costaneres del llevant i migjorn de Mallorca. PhD dissertation, Programa de Doctorat de Geografia, Universitat de les Illes Balears, Palma de Mallorca, Spain, p 984

Gràcia F, Fornós JJ (2014) Les morfologies de dissolució hipogèniques i de la zona de mescla litoral a Es Dolç (Colònia de Sant Jordi, Ses Salines, Mallorca). Endins 36:97–112

Gràcia F, Fornós JJ, Gamundí P, Clamor B, Pocoví J (2009) Morfologies de corrosió a la part submergida de la Cova des Pas de Vallgornera. Sector Antic, sector de Gregal i sector de les Grans Sales. Endins 33:73–98

Gràcia F, Clamor B, Gamundí P, Cirer A, Fernández JF, Fornós JJ, Ginés A, Ginés J, Uriz MJ, Munar S, Vicens D, Ginard A, Betton N, Vives MA, Jaume D, Mas G, Perelló MA, Cardona F, Timar-Gabor A (2014) Es Dolç (Colònia de Sant Jordi, Ses Salines, Mallorca). Cavitat litoral amb influències hipogèniques excavada a les eolianites quaternàries i als materials del Pliocè. Endins 36:69–96

Guijarro JA (1995) Bioclimatic aspects of karst in Mallorca. In: Ginés A, Ginés J (eds) Karst and caves in Mallorca. Endins 20, Monografies de la Societat d'Història Natural de les Balears 3, Palma de Mallorca, Spain, pp 17–26

Gulley JD, Martin JB, Moore PJ, Brown A, Spellman PD, Ezell J (2015) Heterogeneous distributions of CO_2 may be more important for dissolution and karstification in coastal eogenetic limestone than mixing dissolution. Earth Surf Proc Land 40(8):1057–1071

Klimchouk AB (2007) Hypogene speleogenesis: hydrogeological and morphogenetic perspectives. Special paper 1. National Cave and Karst Research Institute, Carlsbad, New Mexico

Klimchouk AB (2009) Morphogenesis of hypogenic caves. Geomorphol 106:100–117

Klimchouk AB (2014) The methodological strength of the hydrogeological approach to distinguishing hypogene speleogenesis. In: Klimchouk AB, Sasowsky I, Mylroie JE, Engel SA, Engel AS (eds) Hypogene cave morphologies. Special publication 18. Karst Waters Institute, Leesburg, Virginia, pp 4–12

Klimchouk AB, Ford DC (eds) (2009) Hypogene speleogenesis and karst hydrogeology of artesian basins. In: Conference proceedings, Chernivtsi. Special paper 1. Ukrainian Institute of Speleology and Karstology, Simferopol, Ukraine, p 292

Klimchouk AB, Sasowsky I, Mylroie JE, Engel SA, Engel AS (eds) (2014) Hypogene cave morphologies. In: Conference proceedings. Karst Waters Institute, Special Publication 18, San Salvador Island, Bahamas, p 103

López JM (2007) Las manifestaciones hidrotermales del sur de Llucmajor, Mallorca. Research report, Departament de Ciències de la Terra, Universitat de les Illes Balears, Palma de Mallorca, Spain, p 132

López JM, Mateos RM (2006) Control estructural de las anomalías geotérmicas y la intrusión marina en la plataforma de Llucmajor y la cubeta de Campos (Mallorca). In: Las aguas subterráneas en los países mediterráneos. Instituto Geológico y Minero de España, Serie Hidrogeología y Aguas Subterráneas 17, Madrid, pp 607–613

Merino A, Fornós JJ (2010) Los conjuntos morfológicos de flujo ascendente (morphologic suite of rising flow) en la Cova des Pas de Vallgornera (Llucmajor, Mallorca). Endins 34:85–100

Merino A, Fornós JJ, Onac BP (2009) Preliminary data on mineralogical aspects of cave rims and vents in Cova des Pas de Vallgornera, Mallorca. In: White WB (ed). Proceedings 15th International Congress of Speleology. National Speleological Society, Kerrville, Texas, vol 1, pp 307–311

Merino A, Ginés J, Fornós JJ (2011) Evidències morfològiques de processos hipogènics a cavitats de Mallorca. In: Gràcia F, Ginés J, Pons GX, Ginard A, Vicens D (eds) El carst: patrimoni natural de les Illes Balears. Endins 35, Monografies de la Societat d'Història Natural de les Balears 17, Palma de Mallorca, Spain, pp 165–182

Merino A, Mulet A, Mulet G, Croix A, Kristofersson A, Gràcia F, Perelló MA (2014) Cova des Pas de Vallgornera, (Mallorca, Spain): history of exploration and cave description. Int J Speleol 43(2):95–104

Mylroie JE (2013) Coastal karst development in carbonate rocks. In: Lace MJ, Mylroie JE (eds) Coastal karst landforms. Coast Res Libr, Springer, Dordrecht, vol 5, pp 77–109

Mylroie JE, Carew JL (1990) The flank margin model for dissolution cave development in carbonate platforms. Earth Surf Proc Land 15:413–424

Mylroie JE, Mylroie JR (2009) Diagnostic features of hypogenic karst: is confined flow necessary? In: Stafford KW, Land L, Veni G (eds) Advances in hypogene karst studies. Symposium 1. National Cave and Karst Research Institute, Carlsbad, New Mexico, pp 12–26

Onac BP, Fornós JJ, Merino A, Ginés J, Diehl J (2014) Linking mineral deposits to speleogenetic processes in Cova des Pas de Vallgornera (Mallorca, Spain). Int J Speleol 43(2):143–157

Otoničar B, Gostinčar P, Gabrovšek F (eds) (2013) Hypogene speleogenesis (between theory and reality…). 21st International Karstological School Classical Karst, Guide Book and Abstracts. Karst Research Institut ZRC SAZU, Postojna, Slovenia, p 98

Palmer AN (2007) Cave geology. Cave Books, Dayton, Ohio

Palmer AN (2011) Distinction between epigenic and hypogenic maze caves. Geomorphol 134(1):9–22

Pomar L, Ward WC (1994) Response of late Miocene Mediterranean reef platform to high-frequency eustasy. Geology 22:131–134

Stafford KW, Land L, Veni G (eds) (2009) Advances in hypogene karst studies. Symposium 1, National Cave and Karst Research Institute, Carlsbad, New Mexico, p 182

Tuccimei P, Ginés J, Delitala C, Ginés A, Gràcia F, Fornós JJ, Taddeucci A (2006) Last interglacial sea level changes in Mallorca island (Western Mediterranean). High precision U-series data from phreatic overgrowths on speleothems. Z Geomorphol 50(1):1–21

Hypogene Karst in Austria

6

Christoph Spötl, Lukas Plan, and Yuri Dublyansky

Abstract

Despite its small size Austria is home to about 16,000 caves. The vast majority is epigene in origin and occurs in uplifted karst plateaus. Only about hundred caves of hypogene origin are known, whose features and modes of origin are reviewed in this article. Most currently known hypogene caves cluster along the rim of the southern Vienna Basin. Some of these caves, including Eisensteinhöhle, are characterized by a slight thermal anomaly associated with warm springs. A second province with hypogene karst features is also structurally controlled and occurs south of the Salzach fault in the Central Alps, where caves show morphologies, mineralization and geochemical patterns diagnostic of hypogene origin. In the same area lukewarm springs emerge at lower elevations. A third region where hypogene processes resulted in cave development is the area of the Periadriatic Lineament in Carinthia. Caves such as Kozakhöhle show Laughöhle morphologies and are perched above the valleys, but the presence of CO_2-rich springs suggests that speleogenesis may still be ongoing in the subsurface. Only very few hypogene caves are currently known from the Northern Calcareous Alps (NCA). Most of those seem again to be related to upwelling of aggressive waters enriched in CO_2, while only one cave in this part of the Eastern Alps shows evidence of sulfuric acid speleogenesis (Kraushöhle). Radiometric dates constrain the final stage of the process to between about 160 and 86 ka before present, while the presence of a lukewarm H_2S-bearing spring in a gorge below the cave provides evidence of minor water–rock interactions involving dissolved sulfur species still operating today at this site.

Keywords

Austria • Karst • Hypogene speleogenesis • Review

C. Spötl (✉) · Y. Dublyansky
Institut für Geologie, Universität Innsbruck, Innrain 52, 6020 Innsbruck, Austria
e-mail: christoph.spoetl@uibk.ac.at

Y. Dublyansky
e-mail: juri.dublyansky@uibk.ac.at

L. Plan
Karst- und Höhlen-Arbeitsgruppe, Naturhistorisches Museum Wien, Museumsplatz 1/10, 1070 Vienna, Austria
e-mail: lukas.plan@nhm-wien.ac.at

1 Introduction

Austria is a mountainous country that occupies close to one third of the European Alps as well as adjacent forelands and basins in the north, east and southeast. Formed during the alpine orogeny (Cretaceous to Neogene) the Alps constitute a complexly structured belt of basement and sedimentary cover rocks (Pfiffner 2014). A zone of metamorphic rocks in the

© Springer International Publishing AG 2017

A. Klimchouk et al. (eds.), *Hypogene Karst Regions and Caves of the World*,
Cave and Karst Systems of the World, DOI 10.1007/978-3-319-53348-3_6

core of what is known as the Central Alps of Austria forms the main alpine ridge reaching up to 3798 m a.s.l. In addition to low- to high-grade metamorphic silicate rocks Paleozoic marbles are also present, which constitute an important karst host rock, e.g., in the southeastern part of Austria. North of the metamorphic zone of these Central Alps a band of Mesozoic sedimentary rocks stretches from the Swiss–Austrian border in the west to the Vienna Basin (and underneath it) in the east. Referred to as Northern Calcareous Alps (NCA), this thin-skinned thrust belt escaped the alpine metamorphism (except for its southernmost rim). The lower part of the Permomesozoic stratigraphy of the NCA is dominated by thick carbonate platform sediments of Triassic age, which form major karst rocks and host the longest and deepest caves in Austria. Jurassic and Cretaceous sediments are generally thinner and dominated by marls.

Parallel to the NCA a smaller and less continuous band of Mesozoic sedimentary rocks straddles along the southern rim of the Central Alps. These so-called Southern Calcareous Alps are split into two units by the Periadriatic Lineament, the largest strike-slip fault in the Alps. Although karst phenomena occur in both of these carbonate-dominated units (e.g., in the northern Karawanken Mountains and the Carnic Alps), they are conspicuously less abundant than in the NCA, despite similar host rocks. A zone of Mesozoic and Tertiary sedimentary rocks is present north as well us underneath the NCA. Cretaceous limestones form a major stratigraphic unit in this Helvetic zone and host many caves in the westernmost part of Austria.

Some 16,000 caves are currently registered in Austria (Spötl et al. 2016a), and the majority developed in the alpine part of Austria including its margins. Maxima in cave abundance and length are concentrated in the central and eastern parts of the NCA, where high-lying and tectonically less disturbed plateaus of Middle and Upper Triassic limestones form the dominant geological and topographic element, as well as in low-grade metamorphic Devonian limestones north of the city of Graz. The vast majority of these caves, which includes the longest cave in the European Union (Schönberg-Höhlensystem, 146 km long) and the deepest through-trip cave in the world (Lamprechtsofen, 1632 m vertical extent)—both part of the NCA—are epigene in origin. Many studies, some dating back to the early twentieth century, provide evidence that these karst systems started to form in the Oligocene and Miocene and today many of them are uplifted fossil phreatic passages, dissected by vadose shafts and canyons (Frisch et al. 2008) and exhumed by erosion. Hydrologically active (epi)phreatic systems are present close to the modern valley floors. The second most abundant group of caves in Austria formed by processes other than karst dissolution, i.e., by weathering, erosion and gravitational mass movements (Oberender and Plan 2015; Plan and Oberender 2016). The third and by far smallest group of caves shows features diagnostic of hypogene speleogenesis, and they are the topic of this overview chapter.

2 Hypogene Karst in Austria

Austria has a long tradition of karst research going back to the first half of the nineteenth century. Until the late twentieth century, however, hypogene karst phenomena went largely unrecognized, although the first studies were already carried out more than one hundred years earlier. Starting point of research on hypogene karst in Austria was Kraushöhle, a limestone cave in northern Styria hosting gypsum deposits. Kraushöhle was discovered and explored by Franz Kraus, an eminent speleologist and author of the first textbook on cave science written in German (1894, facsimile edition 2009). Kraus scrutinized the cave which was later named after him and developed it into a show cave (1882), the oldest one in Europe using electric power to illuminate its interior (1883). Kraus (1891) and before him Hauer (1885) studied Kraushöhle and suggested a link between its gypsum deposits and the presence of a lukewarm H_2S-bearing spring in the gorge below the cave. The prevalent view at that time was that Kraushöhle was formed as a "normal," i.e., epigene cave, which was later overprinted by waters carrying sulfuric acid. With the exception of a single study involving sulfur isotopes to assess the origin of gypsum in Kraushöhle (Puchelt and Blum 1989) no research was performed on this and any other hypogene cave in this country for more than a century. Fueled by new insights into hypogene processes (e.g., Klimchouk et al. 2000; Klimchouk 2009; Palmer 2007) research on hypogene caves in Austria took off during the last decade, and these results are reviewed here.

Currently, close to 100 caves of hypogene origin are known in Austria, but it is likely that this number will increase given that research on this topic has only commenced. Figure 1 provides an overview of the locations of these caves in relation to the overall structural and geological setting. Most hypogene caves are associated with major fault systems, such as the boundary faults of the southern Vienna Basin, the Salzach fault and the Periadriatic Lineament.

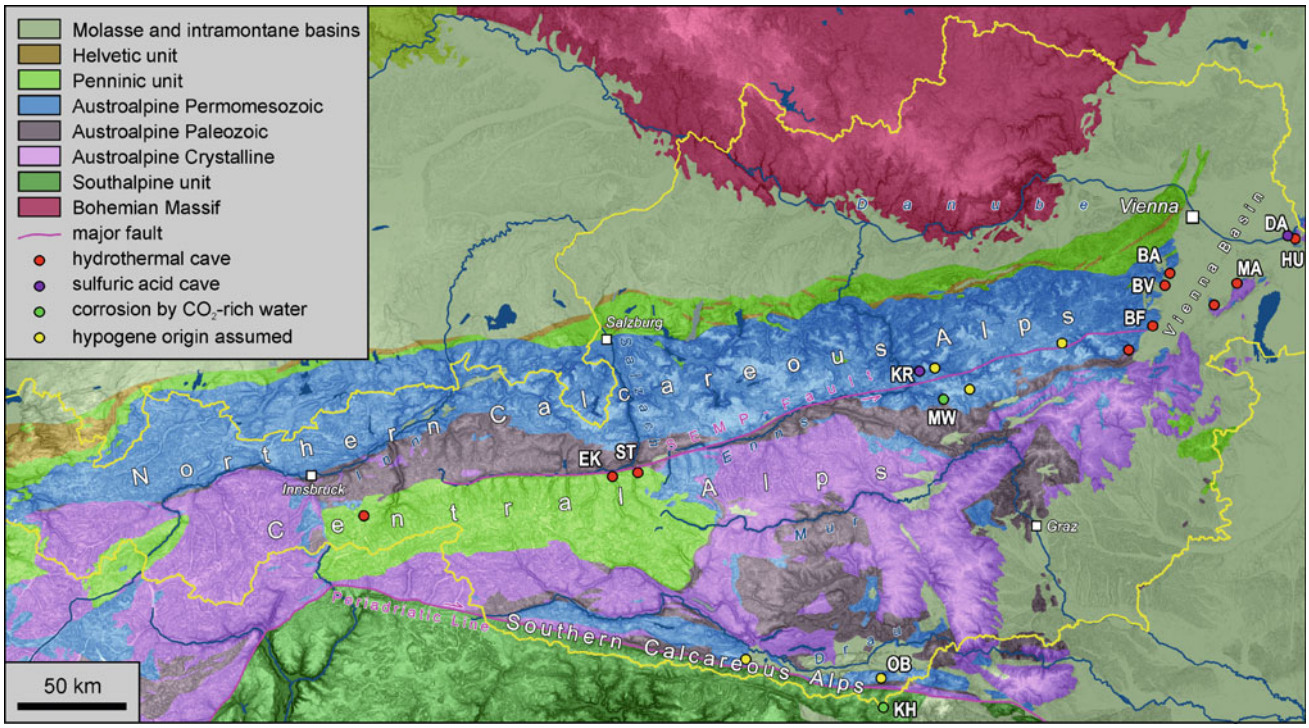

Fig. 1 Simplified geological map of Austria showing the location of currently known hypogene caves. Those mentioned in the text are labeled (from west to east; note that at some of these locations several hypogene caves exist): *EK* Entrische Kirche and tunnel at Lend, *ST* Stegbachgraben, *OB* Obir Caves, *KH* Kozakhöhle, *KR* Kraushöhle, *MW* Märchenhöhle and Wasserhöhle, *BF* Bad Fischau (including Eisensteinhöhle and Fraisloch), *BV* Bad Vöslau, *BA* Baden, *MA* Mannersdorf (including Nasser Schacht), *DA* Bad Deutsch-Altenburg (including Stephanshöhle), *HU* Hundsheim (including Güntherhöhle and Zwerglloch). *SEMP* Salzach-Ennstal-Mariazell-Puchberg Fault

Noteworthy is the widespread absence of such caves in the NCA, apart from a few exceptions near its southern margin. No hypogene caves are currently known from the Helvetic unit.

Some of these systems appear to be still active, in particular caves along the western and eastern margin of the southern Vienna Basin, which show slight thermal anomalies and evidence of ongoing condensation corrosion. Thermal springs spatially associated with hypogene cavities (at higher elevations) occur south of the Salzach Valley (Liechtensteinklamm, Lend tunnel) and at Kraushöhle (Nothklamm). Several more thermal springs are known in Austria (see recent compilation by Elster et al. 2016), but no hypogene caves appear to be associated with them. Springs rich in CO_2 and rare mofettes are known from the area south of Bad Eisenkappel indicating a partially active deep-seated source and the potential for ongoing hypogene speleogenesis.

3 Examples of Hypogene Karst in Austria

3.1 Margin of the Vienna Basin

This large pull-apart basin formed some 20 Ma ago and hosts up to 6-km-thick sediments of marine and freshwater origin. Some of the faults are still active. Warm springs (up to 31 °C) emerge along these faults in the southern part of the basin, both on the western and the eastern margin. The former are more abundant and are aligned along a set of straight lines striking NNE-SSW and include the spas of Baden and Bad Vöslau, both known since Roman times. These thermal springs are linked to a regional deep groundwater circulation (Wessely 1983), whereby karst water from the adjacent NCA in the southwest infiltrates along karstified and fractured Triassic carbonate rocks, reaches depths of up to a few kilometers, acquires heat and

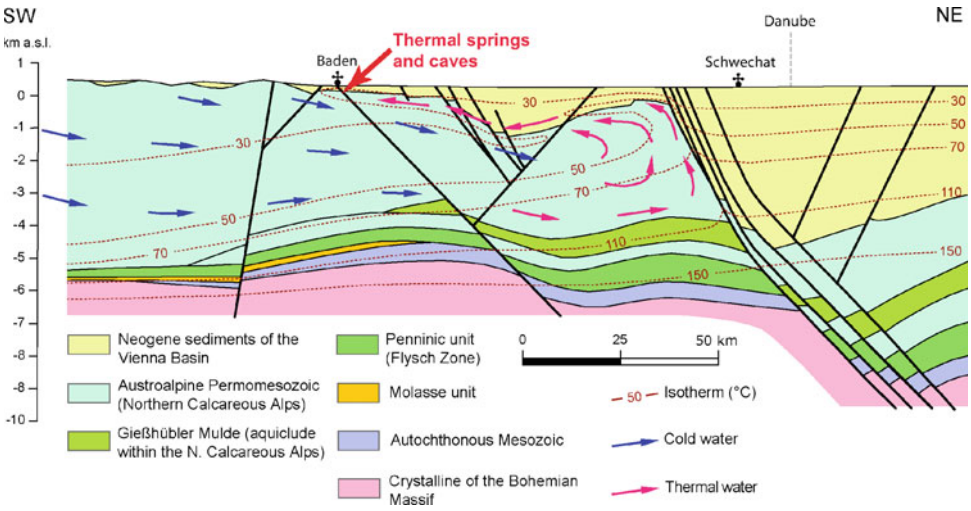

Fig. 2 Section across the western margin of the Vienna Basin illustrating the general groundwater flow pattern, the location of major faults and the occurrence of thermal springs and hypogene caves (modified after Schubert 2006, based on Wessely 1983)

solutes and ascends along major faults in the center of the basin (Fig. 2). As these faults get less permeable closer to the surface, the thermal water migrates back to the margin, giving rise to hypogene karstification and warm springs. Thermal springs also occur along the eastern margin of the basin (e.g., Bad Deutsch-Altenburg), and their waters generally show a higher degree of mineralization (Küpper 1977). Low stable oxygen and hydrogen isotopes show that the thermal waters of the southern Vienna Basin contain a significant old water component of glacial age. This is consistent with high radiocarbon model ages (Elster et al. 2016), testifying for a long residence time in the basin.

Some 70 caves of hypogene origin and/or with hypogene overprint have been identified in this region, rendering it the most important hypogene karst province of Austria.

Eisensteinhöhle is the best-known cave in this region and developed as a show cave. It has no natural entrance and was encountered during quarrying. The cave developed along a fissure, which was overprinted by hypogene karstification. A spring emerges 73 m below the entrance of this subvertical cave whose air temperature is about 15 °C in the lower parts, some 6 °C above the mean annual air temperature. High Rn contents (up to 6500 Bq/m^3) and pCO_2 values (up to 2%) characterize the cave atmosphere. While many parts of the cave show crevice morphologies, i.e., fissures divided into several levels by boulders, in some parts typical hypogene morphologies (cupolas, blind chimneys and pendants —Fig. 3a) prevail. Examples of condensation corrosion ceiling channels are seen in the first chamber. Coralloids as well as frostwork (calcite and aragonite) are common, while hydromagnesite and huntite are rare in this cave. The nearby 333 m-long and 39 m-deep Fraisloch is an inactive hypogene cave showing a complex 3D maze pattern and well-developed cupolas (Fig. 3d).

At the eastern margin of the Vienna Basin there are two main regions with thermal springs and hypogene karst: Mannersdorf am Leithagebirge and Bad Deutsch-Altenburg. Large quarries near Mannersdorf intersected some 25 caves, whereby Nasser Schacht is the biggest one with a length of 260 m and 40 m depth. The upper parts developed in a Miocene limestone (Leithakalk) that rests discordantly on weakly metamorphic Triassic dolomite. Strikingly, the passage dimensions and morphologies—again cupolas and condensation corrosion ceiling channels—do not differ significantly between these two contrasting lithologies (Plan et al. 2006). The water in a pond at the deepest point of the cave has a temperature of 15.5 °C, but its hydrochemistry is different from the thermal spring in Mannersdorf (22 °C). Similar speleothems as in Eisensteinhöhle are present, and coralloids form mushroom-like features up to 4 cm in diameter and epsomite and dolomite crusts are present.

The thermal spring of Bad Deutsch-Altenburg shows a temperature of 25 °C and the highest concentration of hydrogen sulfide of any spring in Austria (up to 37 mg/l—Zötl 1997). In its vicinity, eight caves were intersected during quarrying for Triassic dolomite showing gypsum replacement pockets and morphologies typical of sulfuric acid water table caves (Fig. 3b; De Waele et al. 2016). The up to 133 m-long caves (Stephanshöhle being the largest) show maze patterns and are aligned along a rectangular set of fissures. These caves developed only few meters above the present level of the nearby Danube River. Therefore, the lack of gypsum and other speleothems typical of sulfuric acid speleogenesis (SAS) can be explained by later flooding by Danube-derived groundwater. In a large quarry in the nearby Pfaffenberg several partly connected caves with a cumulative length of more than 500 m were encountered and destroyed. Many sections were filled with sediments rich in mammal bones of Early Pleistocene age (2.59–0.78 Ma; Mais and Rabeder 1984). The presently accessible caves in this quarry are much smaller and show cupolas and abundant coralloids as well as calcite rafts but no signs of SAS.

Fig. 3 Examples of morphologies of hypogene caves on the margin of the Vienna Basin. **a** Ceiling pendant in Eisensteinhöhle, **b** typical gallery in Stephanshöhle with a vertical feeder fissure and ragged cave walls covered by replacement pockets above the prominent notch, **c** bubble trails on overhanging cave wall in Güntherhöhle (knife for scale), **d** nearly spherical cupola in Fraisloch cave, **e** cupolas in Güntherhöhle

Historical quarries near Hundsheim located 3 km SE of Bad Deutsch-Altenburg also intersected some caves in metamorphic Triassic limestone and dolomite. The 209 m-long Güntherhöhle shows cupolas up to 4 m in diameter and bubble trails in its lower part (Figs. 3c, e). Some galleries are rich in popcorn, and dating of a calcitic flowstone indicates that the cave is more than 400 ka old (Spötl et al. 2007). Nearby Zwerglloch is the only cave in the area with a natural entrance, but abundant cupolas also suggest hypogene influence during speleogenesis.

3.2 Salzach Fault System

The W-E-trending Salzach Valley between Krimml and St. Johann im Pongau follows the sinistral Salzach fault (Wang and Neubauer 1998), which is part of one of the major strike-slip faults in the Eastern Alps, known as Salzach-Ennstal-Mariazell-Puchberg-(SEPM) line (Fig. 1). Formed during the lateral extrusion and the subsequent exhumation of the Tauern Window, this almost 400-km-long fault zone has accommodated 60 km of left-lateral

displacement in Oligocene–Miocene times (Linzer et al. 2002). Steeply dipping, mylonitic calcite marbles of Upper Jurassic age (Klammkalk) are present south of the fault hosting both caves and thermal water. A series of small karst conduits were intersected during the construction of a valley parallel headrace tunnel between Taxenbach and Schwarzach, near Lend. They followed N-S-striking fractures and contained 23–31 °C water, in one case with an initial discharge of 600 l/s. Despite the high rock overburden of up to 700 m the spring discharge reacted to snowmelt and heavy rainfall events within 1–2 days (Horninger 1957, 1959). In addition to these small karst conduits two larger caves were encountered. The first one was 15–20 m high and up to 3 m wide, and the marble showed a marked alteration zone up to 0.5 m wide. The second cavern east of the Gastein Gorge was 30 m wide, and its walls were also bleached down to a depth of a few tens of centimeters. In contrast to the first cave which contained warm water, the second cave was dry and its walls were lined with up to 0.5 m thick secondary calcite, consisting of scalenohedral and rhombohedral crystals, reaching up to 15 cm in length (Horninger 1958, 1959; Spötl et al. 2009). The cave was filled by yellowish brown, laminated loam. Smaller cavities intersected by the tunnel also showed strongly corroded marble (Fig. 4).

A deep drilling was completed in 2007 about 1.5 km south of the tunnel and encountered fractured marble between 575 and 737 m below the surface including fractures up to 0.5 m wide. The groundwater had a temperature of 33.6 °C at the well head, and tritium data indicate a significant contribution of a young water component (Elster et al. 2016).

Another small cave was encountered during construction of the railway tunnel in the Gastein gorge. Scalenohedral calcite crystals 6–10 cm in length lined the walls of the cave, and gray clay-rich loam filled part of the cavity (Becke 1902). Karst pipes and fractures lined by euhedral calcite crystals reaching 20 cm in length were also reported from surface outcrops west of the Gastein gorge (Kristallgraben; Heissel 1955; Exner 1979; Cudrigh 2002).

A 1.6 km-long cave, known as Entrische Kirche, opens in the steep eastern flank some 250 m above the gorge, attesting to its origin prior to the incision of the deep Gastein Valley draining toward the Salzach Valley. Entrische Kirche shows no thermal anomalies and consists of a subhorizontal passage and a series of shafts. Although the macro-, meso- and micromorphology of Entrische Kirche lacks elements diagnostic of a hypogene origin, clear hints of an early hypogene origin, later overprinted by epigene processes were identified in drill cores which penetrated a cave wall that was later overgrown by flowstone. The top 4–5 cm of the marble underneath the calcitic flowstone was conspicuously bleached. Stable isotope analyses show a drastic decrease in $\delta^{18}O$ from values of about −3‰ down to −14‰ VPDB and a somewhat smaller decrease in $\delta^{13}C$ in a several cm-thick zone near the cave wall surface (Spötl et al. 2009). These compositions differ strongly from those measured in Pleistocene and Holocene stalagmites and flowstone from the same cave and fall on an alteration trend whose lowest

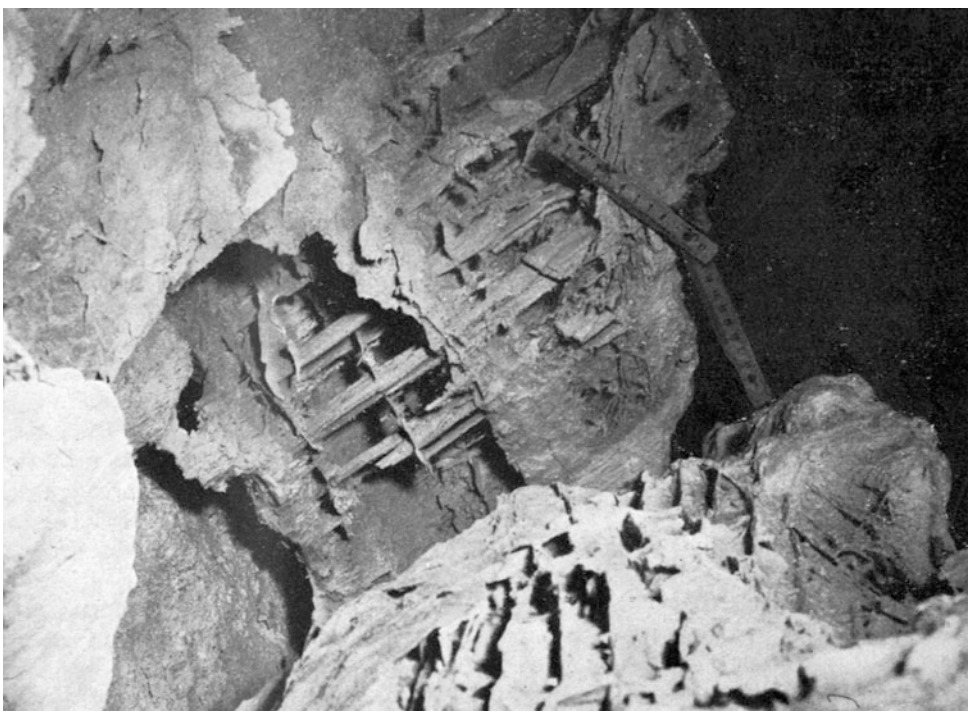

Fig. 4 Corrosion by thermal water gave rise to the skeletal appearance of the Klammkalk marble resembling boxwork. Historical photograph taken during construction of the headrace tunnel near Lend, Salzburg (from Horninger 1959). Ruler with cm grading for scale. Width of image about 0.6 m

Fig. 5 Hypogene cavities at Stegbachgraben filled by coarse crystalline spar. **a** Partly mined, 3–4 m-wide subvertical fracture filled by spar (*arrow*), surface outcrop. **b** Rhombohedral crystal tips in open calcite-lined cavity. **c** Banded calcite alternating with brown limonitic clay layers lining wall of cavity. *Note* Corrosive boundary of calcite toward the underlying marble. Width of image 1.5 m. **d** Brecciated marble with blocks floating in white calcite matrix

$\delta^{18}O$ values approach those of coarse crystalline, euhedral calcite from cavities in the Lend area (see above), in which two-phase fluid inclusions indicate homogenization temperatures of 75–80 °C (Spötl et al. 2009). These are higher than today's water temperature, e.g., in the Lend tunnel and the drilling nearby, and suggest a hotter deep water circulation system in the past. The age of the base of the overlying flowstone (about 240 ka) provides a minimum age for the bleaching and isotopic alteration of the cave wall in Entrische Kirche.

Additional support for a more active hydrothermal system in the past comes from Großarl Valley, some 10 km east of Gastein Valley. At Stegbachgraben near Alte Wacht, a system of caverns is exposed in steeply dipping Klammkalk marble some 200 m above the gorge of Großarlbach. These chambers are up to 30 m wide and show conspicuous round morphologies, and the walls are covered by coarse crystalline banded calcite, reaching up to 1 m in thickness (Fig. 5a–d). Calcite crystals, which reportedly were up to 30 cm long, were mined between 1945 and 1950. The latest generation of calcite forms rhombohedral crystal tips several centimeters in size (Fig. 5b). Only all-liquid fluid inclusions are present in these crystals attesting to their formation at temperatures less than ca. 50 °C (Spötl et al. 2009; Dublyansky et al. 2009). This is consistent with $\delta^{18}O$ values between −13.0 and −15.5‰, i.e., higher than those of

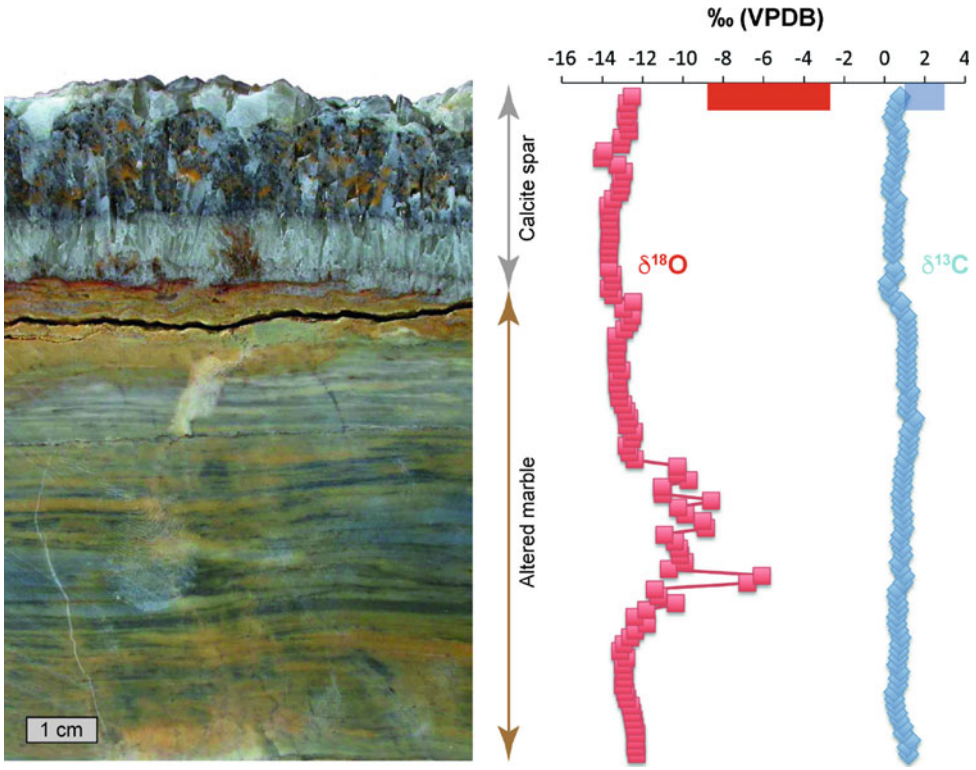

Fig. 6 Geochemical alteration of cave wall rock exemplified by a polished slab of the top of Klammkalk marble overgrown by spar (Stegbachgraben). The stable isotope composition of this marble is significantly lower than that of unaltered samples (indicated by the red and blue rectangles; from Spötl et al. 2009). The isotopically least altered parts are those which (partly) preserve the initial gray rock color, while the remaining marble has been stained light brown due to interaction with thermal water. Note that there was no change in the stable isotopic composition between the time when hypogene karstification and wall–rock alteration occurred and the subsequent episode of calcite crystallization

scalenohedral calcite in cavities near Lend (see above). Bright Mn^{2+}-activated cathodoluminescence and extremely low uranium concentrations suggest low Eh-conditions during calcite crystallization interrupted by episodes of more oxidizing conditions manifested by brown iron-oxide-rich layers separating calcite generations (Fig. 5 c). Drill cores and hand specimens of cave wall rock show clear evidence of bleaching, whereby strongly oxidized (i.e., light brown) zones show the highest degree of isotopic alteration, with $\delta^{18}O$ values as low as −14‰ (Fig. 6). Lukewarm springs emerge in the deeply incised gorge of the Großarlbach some 300 m below the calcite deposits. They reach a temperature of up to 15–17 °C (Cudrigh 2002), and their chemical composition is similar to the thermal waters encountered in tunnel near Lend (Spötl et al. 2009). Tritium analyses suggest a mean residence time of about 12 years (Hilberg and Strick 2016).

Taking together, the zone south of the Salzach Valley shows evidence of deep groundwater circulation facilitated by the near-vertical dip of the highly deformed and fractured Klammkalk. Although modern groundwater does not exceed 31 °C, there is compelling evidence from the presence of coarse crystalline spar and geochemical as well as fluid inclusion data that higher temperatures prevailed in the past. The close association between caves (several lacking natural entrances) either lined by spar and/or showing evidence of wall–rock alteration strongly suggests that thermal water circulation in the past gave rise to hypogene speleogenesis. When the waters became slightly supersaturated, several generations of calcite formed at still elevated temperatures (from water of the same stable isotope composition—Fig. 6), followed by erosional unroofing.

3.3 Periadriatic Lineament

This 700-km-long strike-slip fault system is the largest tectonic structure in the Alps (Fig. 1). Its western branch has accommodated some 100 km of dextral displacement in Oligocene–Miocene times (Schmid et al. 2004), while its eastern segment, which runs in W–E direction close to the southern border of Austria, experienced 30–40 km displacement during the Miocene eastward extrusion of the Central Alps (Polinski and Eisbacher 1992). In southeastern Carinthia, the Periadriatic Lineament separates the Northern from the Southern Karawanken Mountains. The former consist of

Fig. 7 Kozakhöhle contains chambers with inclined walls and nearly flat ceilings, characteristic of hypogene Laughöhle-type morphologies. *Note* A series of water table marks on the right image documenting the progressive lowering of the karst water table

Permo-Triassic sedimentary rocks dominated by Middle Triassic limestone. The latter are comprised of very low-grade metamorphic sedimentary rocks of Paleozoic age. During the Oligocene tonalitic magma intruded along the fault system and transpression continued until the Neogene and possibly up to the present day giving rise to a prominent flower structure (Pfiffner 2014). These deep-seated fractures provided pathways for CO_2 derived from an igneous source or the mantle as shown by $\delta^{13}C$ values of about −7‰ (Neubauer 2008). No thermal anomalies, however, are associated with these faults. This deep-seated CO_2 gives rise to springs rich in CO_2, which occur between Bad Eisenkappel and Bad Vellach. Locally, near Seeberg, CO_2 exhales as mofettes (Kahler 1978; Zötl and Goldbrunner 1993).

Some 50 caves, most of them less than a few tens of meters in length, are known around Bad Vellach, and a few of them show distinct morphologies suggesting a hypogene origin. The best-studied example is Kozakhöhle, which is 309 m long and consists of a main subhorizontal passage with conspicuous rounded chambers, and a few very narrow shafts at the end, possibly representing former feeder shafts. The cave shows cupolas, cusps and V-triangular-shaped chambers of the Laughöhle-type (cf. Kempe 1972), as well as notches (Fig. 7). Vadose speleothems, mostly aragonite, formed after the hypogene speleogenesis was terminated, and the surrounding Devonian carbonate rock was exhumed due to uplift and erosion of the nearby Vellach river. Radiometric dating indicates that the phreatic phase ended more than 0.5 Ma ago (Spötl et al. 2016b). Drill cores show no evidence of carbon or oxygen isotope alteration of the wall rock; calcite spar is absent in this and other caves in this region. The origin of these caves is attributed to upwelling of aggressive, CO_2-rich groundwater, whose temperature is unknown but unlikely to have been high.

A second province of CO_2-rich springs emerges at the Periadriatic Lineament in the area south and southwest of Bad Eisenkappel, adjacent to a tonalite body (Zötl and Goldbrunner 1993). A few kilometers to the north, on the eastern flank of Hochobir (2139 m a.s.l.), a 2-km-long network of caves formed in Middle Triassic limestone of the Wetterstein Fm. Collectively known as Obir-Tropfsteinhöhlen (Obir Caves for short), these caverns lack natural entrances and were only discovered during mining for Pb–Zn ores between 1862 and 1879. This cave system, part of which was opened as a show cave in 1991, consists of large chambers—locally hosting blind chimneys—connected by narrow passages with maze character. Features characteristic of epigene phreatic or vadose speleogenesis such as phreatic tubes or meanders and canyons, respectively, are conspicuously absent. Instead, pendants, cusps and small Laughöhle-type chambers can be seen. Locally, small rounded chambers are aligned giving rise to a bush-like pattern, reminding of Sátorkö-puszta Cave in Hungary (Dublyansky 2012). Research on Obir Caves has just commenced and is partly hampered by the abundance of speleothems—these caves are among the most decorated dripstone caves in the Alps—and the occurrence of breakdown. The oldest dated speleothems date back some 400 ka providing a minimum age for the presumed hypogene origin of these caves. This timing is consistent with the elevation difference between the caves and the level of the Vellach river (ca. 500 m a.s.l., which is some 600 m below the Obir Caves) suggesting a Neogene age of cave formation.

While the Obir Caves are a fossil, uplifted system, an active hydrological regime exists below the Vellach Valley to the east, where springs with a cumulative discharge of 350 l/s emerge near the riverbed. The temperature of these springs is slightly higher than expected from this setting

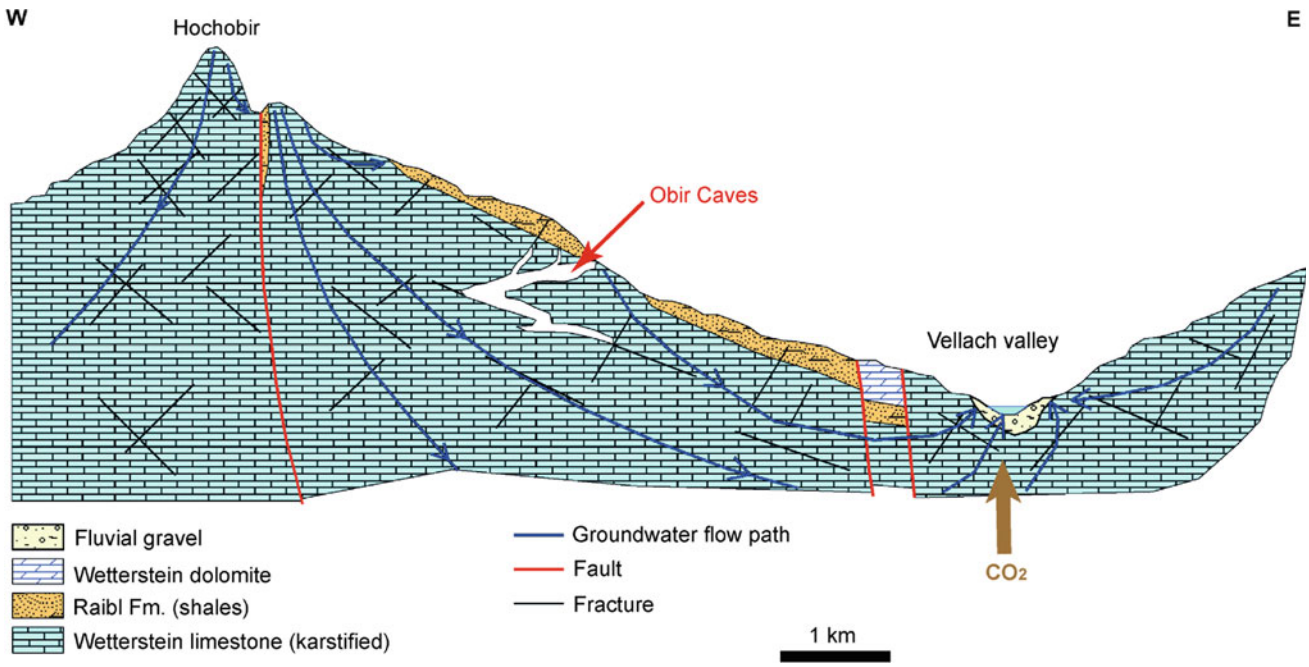

Fig. 8 Sketch showing the location of the modern groundwater circulation system north of Bad Eisenkappel and the location of the uplifted Obir Caves, whose hypogene origin was likely linked to a precursor hydrological system in Neogene times. Modified after Brenčič and Poltnig (2008)

suggesting a moderately deep convection system (Fig. 8). Some of these springs are characterized by significantly enriched alkalinity values, whose stable carbon isotopic composition suggests admixture of deep-seated CO_2 (Poltnig and Strobl 1996; Herzog 1999). No direct evidence of hypogene speleogenesis is currently available in the valley due to the absence of drilling or geophysical observations, but similar to the Vellach region south of the Periadriatic Lineament these springs appear to be related to a system of upwelling aggressive waters creating cavities in carbonate formations which later became overprinted by epigene processes and are now close to the surface as a result of uplift and erosional exhumation.

3.4 Northern Calcareous Alps

This fold-and-thrust belt is one of the speleologically best explored karst provinces in Europe, in particular the prominent karst plateaus composed of Middle and Upper Triassic carbonate formations, including Tennengebirge, Dachstein, Totes Gebirge and Hochschwab. Several levels of paleophreatic and epiphreatic caves, later overprinted by vadose karst processes and collapse, are known and can be attributed to uplift concomitant with fluvial and glacial lowering of the valleys and basins between the karst plateaus. Only a handful of caves in the NCA shows unequivocal evidence of a different, i.e., hypogene origin (Fig. 1), and they fall into two groups: caves formed presumably by the interaction with CO_2-rich, but sulfate-poor upwelling waters and one cave, Kraushöhle, which was already introduced above as an example of SAS.

Only two caves of the first group are currently known (plus a few more awaiting detailed studies), and they occur next to each other at the southern margin of the NCA in northern Styria. Märchenhöhle and Wasserhöhle open at 1560 and 1551 m a.s.l., respectively, near the crest of a mountain ridge, 700–800 m above the adjacent valleys. Despite their presumably old age these caves show well-preserved chambers, showing Laughöhle-type triangular cross sections (Fig. 9a) and remains of a former feeder channel, now filled by thick dark red and yellowish clay-rich residue containing unusual biscuit-like speleothems. Märchenhöhle was surveyed using laser scan techniques, documenting among others two different types of notches, sharp, wedge-shaped ones and others with rounded profiles.

Interestingly, there is an angular unconformity of ca. 20° between these notches (Dublyansky et al. 2016), suggesting tectonic tilting. While Wasserhöhle contains only few speleothems, the walls of Märchenhöhle below prominent notches are covered by cave clouds typically 10 cm thick (Fig. 9b). U–Th dating of these calcite speleothems suggests an old age but also a partially open system. Coring of the cave wall revealed clear indications of wall–rock alteration prior to mammillary calcite deposition: the few centimeters of the light gray Triassic limestone show a fabric consisting of a dense network of thin fractures which are stained light brown and show halos extending into the intervening

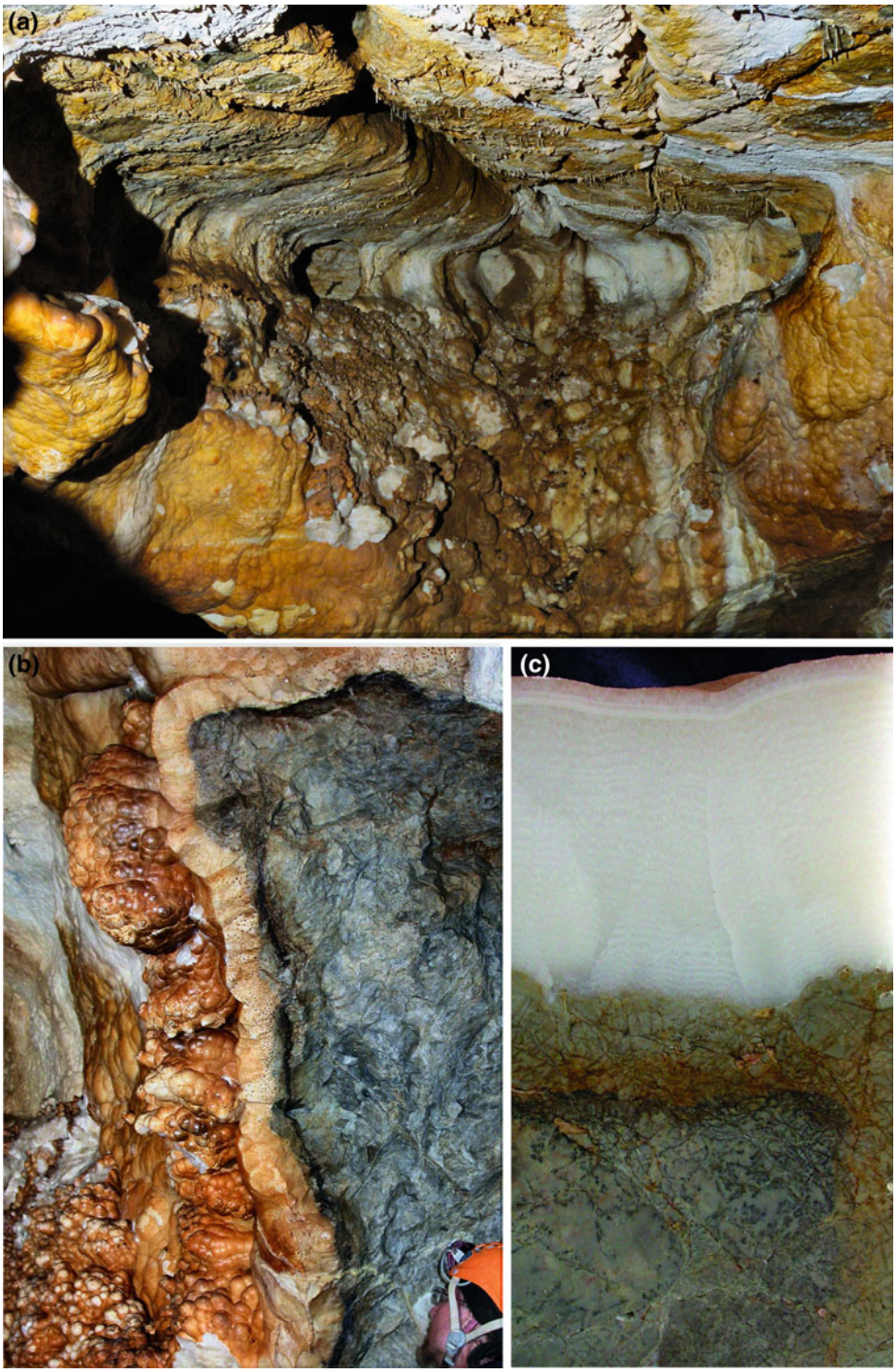

Fig. 9 **a** Laughöhle chamber in Märchenhöhle, about 10 m wide in the foreground. *Note* The presence of cave clouds below the prominent notch. **b** Cave clouds exposed due to breakdown showing a distinctly dark colored alteration zone near the top of the limestone. **c** Altered Triassic wall rock of Märchenhöhle overgrown by white, banded calcite forming cave clouds. Height of image 16 cm

unfractured limestone (Fig. 9c). Also the limestone underneath this bleached zone shows abundant microfractures, commonly stained dark gray. The stable O and C isotopic composition is highly variable across these cores, reflecting the dense fracture network. $\delta^{18}O$ and $\delta^{13}C$ values are depleted by 1–3‰ at these microfractures, but the host rock lacks a pervasive resetting as observed at Entrische Kirche or Stegbachgraben (see above). The cave clouds yielded isotope values distinctly lower than the most depleted host rock samples: $\delta^{18}O$ fluctuated mostly between −8.9 and −7.4‰, while $\delta^{13}C$ exhibits larger swings ranging from −8.7 to −4.2‰ which co-vary with $\delta^{18}O$. Interestingly, the biscuit-like speleothems found interbedded with fine-clastic sediments in the feeder channel yielded the same carbon and

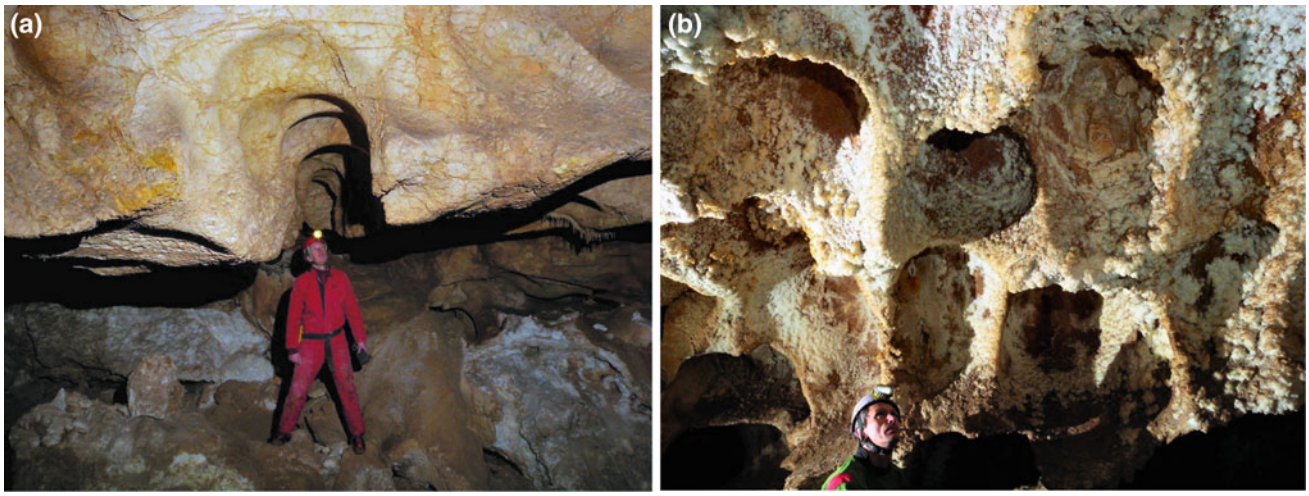

Fig. 10 Examples of morphologies in Kraushöhle: **a** ceiling channel and **b** cupolas coated by white gypsum

oxygen isotope values and the same type of rhythmic oscillations possibly pointing toward a synchronous formation with the mammillary calcite.

No paleotemperature data are currently available from these sites, because no primary fluid inclusions were found and attempts to extract microsamples of fluid inclusion water for stable isotope analyses failed for the same reason (Fig. 10).

Only one cave in the NCA is currently known whose origin is related to sulfuric acid interacting with limestone. Kraushöhle, already mentioned in the historical introduction, owes its existence to a lukewarm (9–20 °C) sulfidic spring at the end of Nothklamm, a narrow gorge near Gams bei Hieflau (De Waele et al. 2009; Plan et al. 2012). The artificial visitor entrance of Kraushöhle opens 93 m above this spring in reddish limestones of the Jurassic Hirlatz Formation. The 793 m-long cave consists of two chambers (the largest, Haupthalle is 50 × 15 m wide) from where several partly connected and slightly inclined galleries branch off forming a 3D-maze. Many galleries and some chimneys terminate blindly including Kristallschlot, which reaches 30 m above the floor of Haupthalle. Parts of the cave unaffected by younger vadose drip waters and runnels host massive gypsum deposits with strongly depleted $\delta^{34}S$ values (Puchelt and Blum 1989), and in some parts gypsum crystals reach up to 25 cm in length. Also other sulfate minerals including alunite, jarosite, and meta-alunogen, the hydroxide gibbsite, the silicate halloysite, and opal indicate highly acidic conditions and point toward SAS. Micro- and meso-scale morphologic features comprise gypsum replacement pockets, partly still containing gypsum, cupolas, very deeply incised and narrow-slot-shaped corrosion notches, convection niches, sulfuric karren, and mega-scallops formed by ascending aggressive air. A feature described from Kraushöhle for the first time are ceiling pendant drip holes (Plan et al. 2012). These cup-shaped hollows on the cave floor measure a few tens of centimeters in diameter and are surrounded by up to 15-cm-high walls. These depressions are located below triple junctions of cupolas that form pendants or lowest points along the ceiling where water is forced to drip down. Their formation is attributed to corrosion by drip water. As the ceiling neither shows signs of calcite corrosion nor precipitation the water was apparently saturated with respect to calcite but took up H_2S directly from the cave atmosphere or from bacterial strands (snottites or mucolites).

Geochemical and petrographical data highlight the interaction between the sulfuric acid and the limestone leading to the replacement by gypsum (Plan et al. 2012). A distinctive but only mm-thin alteration layer of highly increased porosity formed at the interface between the host limestone and the secondary gypsum. The lack of carbon and oxygen isotope alteration halos strongly suggests that the rate of dissolution outpaced the rate of geochemical alteration. Structural and petrographic studies revealed that the gypsum preserved the original calcite fabric confirming the early report by Hauer (1885) showing individual crinoid stalk fragments in the host limestone being pseudomorphosed by gypsum. These observations clearly hint toward a nearly constant volume process.

$^{40}Ar/^{39}Ar$ dating of an alunite sample yielded an age of 80 ± 80 ka (i.e., younger than 160 ka; De Waele et al. 2009). This surprisingly young age is in agreement with U–Th-dated calcite samples from the base of stalagmites, which yielded ages between 6.8 and 86.0 ka (Spötl et al. 2014).

4 Summary and Outlook

Despite a long history of speleological studies, research on hypogene karst phenomena in Austria is still in its infancy. It is expected that the percentage of currently documented and

assumed hypogene caves (less than 1% of all caves in this country) will increase in the future. The small number of well-studied caves of hypogene origin already reveals a spectrum of mechanisms ranging from thermal water circulation, aggressive waters charged by carbon dioxide at greater depth to sulfuric acid reactions. In most cases these caves are located near major fault systems highlighting their role in providing high-permeability pathways for deep groundwater circulation and supply of deep-seated CO_2 responsible for carbonate aggressiveness of karst-forming waters.

Most hypogene systems in Austria are inactive, uplifted and overprinted by epigene processes, but it is highly likely that active speleogenesis is still ongoing in the deeper subsurface, including the margins of the Vienna Basin and the area near the Periadriatic Lineament.

Key to identify past hypogene processes and caves formed thereby is a combination of cave morphological investigations (ideally aided by semi-automated laser scanning techniques) and studies of hypogene minerals (if present). As epigene karstification commonly overprints and locally even obliterates preexisting hypogene cave morphologies, the study of wall–rock alteration is an important way forward to unambiguously identify hypogene water–rock interaction, in particular in limestones and calcite marbles.

References

Becke F (1902) Calcit vom oberen Klammtunnel an der Strecke Schwarzach-St. Veit–Gastein der Tauernbahn. Tschermaks Min Petrogr Mitt 21: 460

Brenčič M, Poltnig W (2008) Grundwasser der Karawanken. Versteckter Schatz, Vehling, Ljubljana

Cudrigh SF (2002) Die Wasserwegigkeit des Gasteiner Thermalwassersystems unter Berücksichtigung der Strukturgeologie und im Vergleich zum Thermalsystem Lend. Unpubl. Master thesis, Univ. Salzburg

De Waele J, Audra P, Madonia G, Vattano M, Plan L, D'Angeli IM, Bigot J-Y, Nobécourt J-C (2016) Sulfuric acid speleogenesis (SAS) close to the water table: examples from southern France, Austria, and Sicily. Geomorphology 253:452–467

De Waele J, Plan L, Audra P, Rossi A, Spötl C, Polyak V, McIntosh B (2009) Kraushöhle (Austria): Morphology and mineralogy of an alpine sulfuric acid cave. In: White WB (ed) Proceedings of the 15th International Congress of Speleology, Kerrville Part vol 2, pp 31–37

Dublyansky Y (2012) Hydrothermal caves. In: White WB, Culver DC (eds) Encyclopedia of caves, 2nd edn. Academic Press, Chennai, pp 391–397

Dublyansky Y, Roncat A, Spötl C, Dorninher P (2016) Hypogene cave morphology at high resolution: full 3-D survey of Märchenhöhle (Austria). In: Chavez T, Reehling P (eds) Proceedings of DEEPKARST 2016: origins, resources, and management of hypogene karst. National Cave and Karst Research Institute, Carlsbad, New Mexico, pp 183–187

Dublyansky Y, Spötl C, Steinbauer C (2009) Stegbachgraben, a mineralized hypogene cave in the Grossarl valley, Austria. In: Klimchouk A, Ford D (eds) Hypogene speleogenesis and karst hydrogeology of artesian basins. Ukrainian Institute of Speleology and Karstology, special paper 1, pp 117–120

Elster D, Goldbrunner J, Wessely G, Niederbacher P, Schubert G, Berka R, Philippitsch R, Hörhan T (2016) Erläuterungen zur geologischen Themenkarte Thermalwässer in Österreich 1:500000. Geol. Survey Austria, Vienna

Exner C (1979) Geologie des Salzachtales zwischen Taxenbach und Lend. Jahrb Geol Bundesanstalt 122:1–73

Frisch W, Kuhlemann J, Dunkl I, Székely B (2008) Die geomorphologische Entwicklung der Ostalpen. Mitt Österr Geogr Ges 150: 123–162

Hauer F (1885) Die Gypsbildung in der Krausgrotte bei Gams. Verh Geol Reichsanstalt 1885:21–24

Heissel W (1955) Aufnahmsbericht 1954 Kartenblätter 124-Saalfelden und 125-Bischofshofen. Verh Geol Bundesanstalt 1955:36–37

Herzog U (1999) Zur Karsthydrogeologie des Obirmassivs. In: Golob B (ed) Der Hochobir. Naturwiss, Verein Kärnten, Klagenfurt, pp 127–134

Hilberg S, Strick D (2016) Thermalwasserregime Klammkalk zwischen Taxenbach und der Liechtensteinklamm. GeoTirol 2016, annual meeting DGGV, 25–28 Sep 2016, Innsbruck, Austria, abstract volume, p 115

Horninger G (1957) Geologische Ergebnisse bei einigen Kraftwerksbauten. Verh Geol Bundesanstalt 1957:99–103

Horninger G (1958) Geologische Ergebnisse bei einigen Kraftwerksbauten. Verh Geol Bundesanstalt 1958:282–286

Horninger G (1959) Auslaugungen an Karbonatgesteinen. Geologie und Bauwesen 24:159–164

Kahler F (1978) Die natürlichen Heilvorkommen Kärntens. Raumordnung in Kärnten 10:1–134

Kempe S (1972) Cave genesis in gypsum with particular reference to underwater conditions. Cave Sci 49:1–6

Klimchouk AB (2009) Morphogenesis of hypogenic caves. Geomorphology 106:100–117

Klimchouk AB, Ford DC, Palmer AN, Dreybrodt W (2000) Speleogenesis. Evolution of Karst Aquifers. National Speleol. Soc, Huntsville

Kraus F (1891) Höhlenbildung durch Metamorphismus. Die Natur 40:197–199

Kraus F (1894) Höhlenkunde. Facsimile reprint 2009. Wiss. Beiheft zur Zeitschrift Die Höhle 56

Küpper H (1977) Über Thermen, Karst-, Formations- und Grundwässer im südlichen Wiener Becken. Verh Geol Bundesanst 1977: 105–120

Linzer H-G, Decker K, Peresson H, Dell'Mour R, Frisch W (2002) Balancing lateral orogenic float of the Eastern Alps. Tectonophysics 354:211–237

Mais K, Rabeder G (1984) Das große Höhlensystem im Pfaffenberg bei Bad Deutsch Altenburg (Niederösterreich) und seine fossilen Faunen. Die Höhle 35:213–230

Neubauer E (2008) Chemische und isotopengeochemische Entwicklung von Kohlensäuerlingen—Geländearbeit und Experimente. Unpublished master thesis Technology University Graz

Oberender P, Plan L (2015) Cave development by frost weathering. Geomorphology 229:73–84

Palmer AN (2007) Cave geology. Cave Books, Dayton

Pfiffner AO (2014) Geology of the Alps, 2nd edn. Wiley Blackwell, Chichester

Plan L, Oberender P (2016) Nicht-Karsthöhlen. In: Spötl C, Plan L, Christian E (eds) Höhlen und Karst in Österreich. Oberösterreichisches Landesmuseum, Linz, pp 61–72

Plan L, Tschegg C, De Waele J, Spötl C (2012) Corrosion morphology and cave wall alteration in an Alpine sulfuric acid cave (Kraushöhle, Austria). Geomorphology 169–170:45–54

Plan L, Pavuza R, Seemann R (2006) Der Nasse Schacht bei Mannersdorf am Leithagebirge, NÖ (2911/21)—eine thermal beeinflusste Höhle am Ostrand des Wiener Beckens. Die Höhle 57:30–46

Polinski RK, Eisbacher GH (1992) Deformation partitioning during polyphase oblique convergence in the Karawanken Mountains, southeastern Alps. J Struct Geol 14:1203–1213

Poltnig W, Strobl E (1996) Einflüsse von CO_2-Exhalationen en aus dem Bereich der Periadriatischen Naht auf Karstwässer des Hochobirmassivs (Karawanken, Kärnten). Beitr Hydrogeol 47:145–158

Puchelt H, Blum N (1989) Geochemische Aspekte der Bildung des Gipsvorkommens der Kraushöhle/Steiermark. Oberrhein geol Abh 35:87–99

Schmid SM, Fügenschuh B, Kissling E, Schuster R (2004) Tectonic map and overall architecture of the Alpine orogen. Eclogae Geol Helv 97:93–117

Schubert G (2006) Erläuterungen zur Hydrogeologischen Karte von Österreich 1:500.000. Geological Survey of Austria, Vienna

Spötl C, Offenbecher KH, Boch R, Meyer M, Mangini A, Kramers J, Pavuza R (2007) Tropfstein-Forschung in österreichischen Höhlen —ein Überblick. Jahrb Geol Bundesanst 147:117–167

Spötl C, Dublyansky Y, Meyer M, Mangini A (2009) Identifying low-temperature hydrothermal karst and palaeo waters using stable isotopes: a case study from an alpine cave, Entrische Kirche, Austria. Intern J Earth Sci 98:665–676

Spötl C, Boch R, Moseley G, Brandstätter S, Edwards RL, Cheng H, Mangini A, Plan L (2014) Wann entstanden die Tropfsteine in der Kraushöhle bei Gams (Steiermark)? Die Höhle 65:18–24

Spötl C, Desch A, Dublyansky Y, Plan L, Mangini A (2016a) Hypogene speleogenesis in dolomite host rock by CO_2-rich fluids, Kozak Cave (southern Austria). Geomorphology 255:39–48

Spötl C, Plan L, Christian E (2016b) Höhlen und Karst in Österreich. Oberösterreichisches Landesmuseum, Linz

Wang X, Neubauer F (1998) Orogen-parallel strike-slip faults bordering metamorphic core complexes: the Salzach-Enns fault zone in the Eastern Alps, Austria. J Struct Geol 20:799–818

Wessely G (1983) Zur Geologie und Hydrodynamik im südlichen Wiener Becken und seiner Randzone. Mitt Österr Geol Ges 76:22–68

Zötl JG (1997) The spa Deutsch-Altenburg and the hydrogeology of the Vienna basin (Austria). Environ Geol 29:176–187

Zötl J, Goldbrunner JE (1993) Die Mineral- und Heilwässer Österreichs. Geologische Grundlagen und Spurenelemente, Springer, Vienna

Hypogenic Caves in the Apennine Mountains (Italy)

7

Sandro Galdenzi and Marco Menichetti

Abstract

Hypogene speleogenesis is important for karstification in the Apennines because of widespread, aggressive groundwaters containing endogenic H_2S and CO_2. Evidence for karst processes can be found throughout the region, from solutional limestone caves to deposition of carbonate travertine. The caves are up to few tens of kilometers long and show different patterns, ranging from phreatic to almost ideal water table caves. The caves often have a maze pattern and contain large rooms, cupola roofs, blind pits, and anastomotic zones. Solutional processes prevailed in the phreatic zone, also in deep-seated conditions, but subaerial corrosion is developed as well and can play an important morphogenetic role. The main cave-forming processes are related to the H_2S oxidation to sulfuric acid, a process that involves chemotrophic microbial activity, and are responsible for the diffuse deposition of replacement gypsum in subaerial conditions. The great variety of geological settings makes the Apennines a good place to study hypogene karst, and the existence of active branches in several caves also permits a direct study of the cave-forming processes and the comparison with the resultant morphologies.

Keywords

Hypogene caves • Apennines • Italy • Sulfuric acid speleogenesis • Endogenic CO_2

1 Introduction

The Apennine Mountain chain constitutes the peninsular part of Italy, with the highest general elevations in the central part (Gran Sasso, 2912 m asl). An articolate water-divide between Adriatic and Tyrrhenian Sea runs over large limestone outcrops along the whole chain (Fig. 1). The peninsula offers important and diverse examples of both epigenic and hypogenic caves. Epigene speleogenesis is a process that normally propagates downward from the surface to depth through the subsurface drainage network. The main corrosive chemical agent for epigenic carbonate caves is soil-derived CO_2. On the other hand, hypogene speleogenesis is related to the upward flow of deep-seated fluids (water or gas) coming from depth, and the development of limestone caves can be related to diverse chemical and physical processes (such as the enrichment of CO_2, the presence of H_2S, or the cooling or mixing of rising waters).

The Apennine region is probably the world's best location to observe both active and fossil hypogenic caves in different geological contexts (Galdenzi and Menichetti 1995; Galdenzi 2009; Menichetti 2011) (Fig. 1). All the end members of the karst processes can be found in the area, from epigenic limestone caves to hypogenic mazes to deposition of carbonate travertine.

Many of the hypogene caves in the area can be related to sulfuric acid speleogenesis (SAS). The importance of SAS was understood by Principi (1931), who described a small cave intercepted in an artificial tunnel near the sulfidic

S. Galdenzi (✉)
Jesi, Italy
e-mail: galdenzi.sandro@tiscali.it

M. Menichetti
Department of Pure and Applied Sciences, University of Urbino, Campus Scientifico Urbino, 61029 Urbino, Italy
e-mail: marco.menichetti@uniurb.it

© Springer International Publishing AG 2017

A. Klimchouk et al. (eds.), *Hypogene Karst Regions and Caves of the World*,
Cave and Karst Systems of the World, DOI 10.1007/978-3-319-53348-3_7

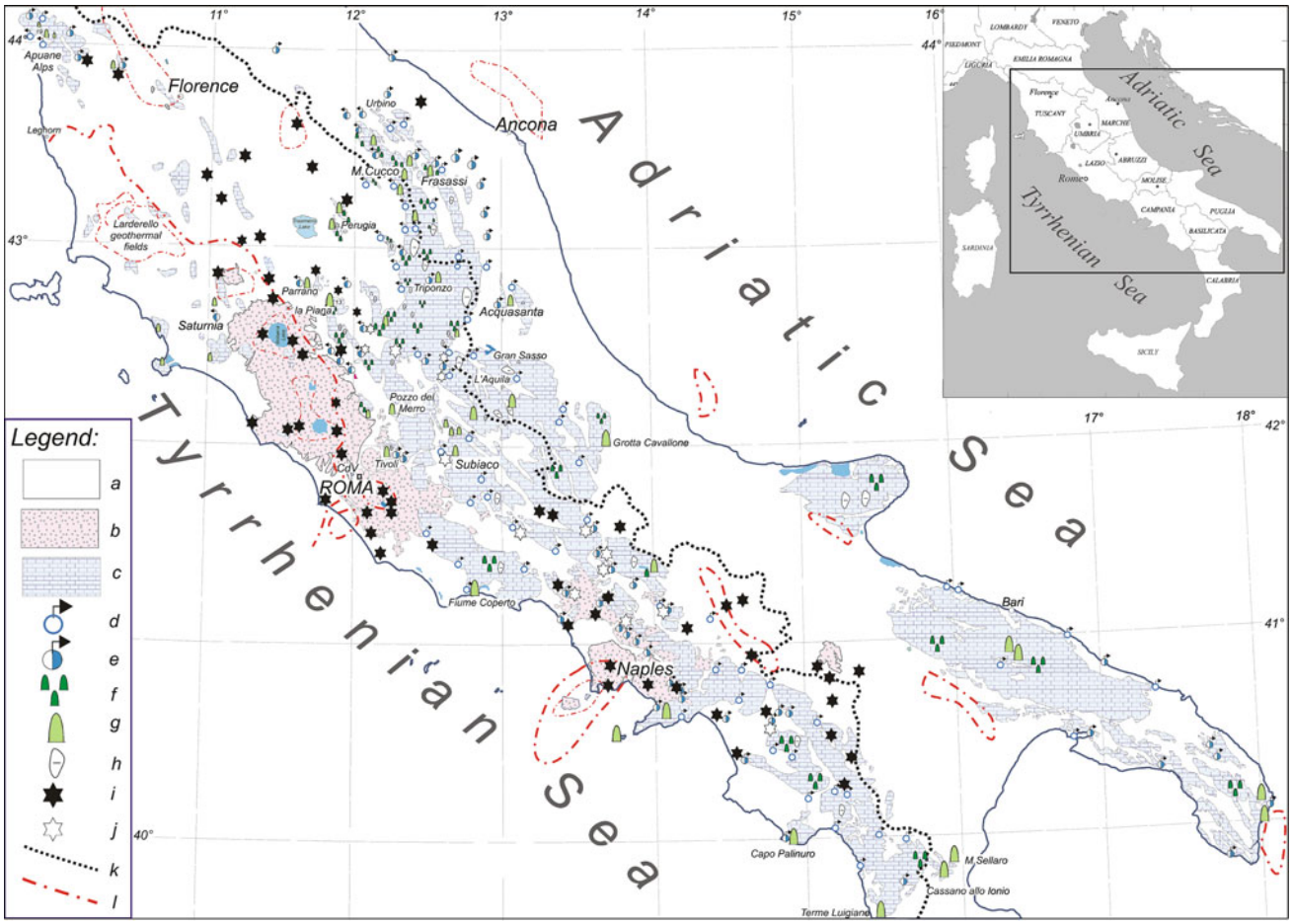

Fig. 1 Map of the main karst features in Central Italy. Legend: *a* Cenozoic succession; *b* Quaternary volcanic rocks; *c* Mainly carbonatic Mesozoic succession; *d* larger karst spring; *e* main mineralized spring; *f* important cave; *g* confirmed or probable hypogene cave; *h* closed valley with karstic drainage; *i* CO_2–rich vent; *j* CO_2–rich spring; *k* Apennines water divide; *l* geothermal anomaly—*thick dotted line* represents 100 mW/m

thermal Triponzo spring. Principi wrote (in Italian): "the cave was not formed by normal karst dissolution, but developed as a consequence of sulfidic water action, which replaced limestone with gypsum, easily removed by flowing water." Principi's early ideas, however, did not influence later authors, who ignored or underestimated the role of H_2S as a speleogenetic agent or only considered it for secondary mineralogical effects (Bertolani et al. 1975).

The possibility that the sulfidic water itself could form caves was not reconsidered in Italy until the end of 1980s, due to research on the active Frasassi caves and the fossil system of Mt. Cucco (Forti et al. 1989; Galdenzi and Menichetti 1990; Galdenzi 1989, 1990). In particular, Galdenzi (1990) proposed a genetic model for the Frasassi caves entirely based on the mixing of rising sulfidic water with descending oxygen-rich seepage water.

In the following years, the difficulty associated with recognizing the role of H_2S in fossil caves that no longer retain gypsum deposits caused authors to refer to caves as simply "hypogenic in origin", rather than identifying a specific chemical agent (Galdenzi and Menichetti 1995, 1997). A hypogenic origin is, in fact, also recognizable from the geologic setting, the water flow path, the cave pattern and the meso-morphologies (Palmer 1991; Klimchouk 2007).

In the early 1990s, models for the origin of Apennine caves were revised; Galdenzi differentiated the large hypogene caves from various types of smaller epigenic caves in the Umbria–Marche Apennines (Galdenzi 1996) and analyzed some examples of hypogene caves in the Calabria region, South Italy (Galdenzi 1997). Galdenzi and Menichetti (1995) described a set of hypogene caves in different locations in Central Italy, and suggested a possible hypogenic origin for many Italian caves, due to favorable geologic conditions that induce the enrichment of rising water with CO_2 or H_2S (Galdenzi and Menichetti 1997).

In the following years, research on the hypogenic caves extended to new localities in western Umbria (Menichetti

2011), Tuscany (Montecchio cave, Menichetti 2009; Piccini et al. 2015), Latium (Galdenzi 2003), Campania (Capo Palinuro, Forti and Mocchiuti 2004), and outside the Apennines in Sicily (Vattano et al. 2013; De Waele et al. 2016) and Sardinia (De Waele et al. 2013). New research also re-examined evidence for speleogenesis in the previously studied Monte Cucco system (Galdenzi 2004; Menichetti et al. 2008), Acquasanta Terme caves (Menichetti 2008; Galdenzi et al. 2010), and the Frasassi Caves (Galdenzi et al. 1997, 2008; Galdenzi 2012; Galdenzi and Campagnoli 2015). New work also focused on other aspects of the cave environment, including the sulfidic cave ecosystem (Southward et al. 1996; Mattison et al. 1998; Sarbu et al. 2000; Forti et al. 2002), cave microbiology (Vlasceanu et al. 2000; Macalady et al. 2006, 2007; Jones et al. 2008, 2010), the depositional setting and geochemistry of gypsum deposits (Galdenzi and Maruoka 2003), quantitative measurements of corrosion rates (Galdenzi et al.1997; Mariani et al. 2007; Galdenzi 2012), and measurements of biological oxidation and degassing in the consumption of the H_2S in the water (Jones et al. 2015).

2 Geological Setting

2.1 Geological Structures of the Apennines

The Apennine chain is a part of the circum-Mediterranean Alpine system, constituted by a fold and thrust belt, with vergence that gradually changes from NE in the Northern to E in Central and Southern Apennines (Fig. 1). The orogen results from the continental collision processes between the Corsica/Sardinia and the subducted Adriatic plates during the Cenozoic.

On the Tyrrhenian side of the Apennine belt, the results of the Neogene–Quaternary backarc extensional process are a reduced thickness of the lithosphere, a system of NW–SE-striking normal faults and related basins, and a high heat flow. A rich K-undersaturated volcanism activated during mid-Pleistocene time (i.e., since about 700 ka) and remained intermittently active until recent times, with some carbonatite magmas extruded in several spot in the Apenninic chain (Cavazza and Wezel 2003). At present, the geological and geophysical data highlight two main sectors within the region: a western Tyrrhenian side where there is a Neogene–Quaternary active backarc extensional tectonic and an eastern Adriatic side with an active compressional stress field (Crescenti et al. 2004 and references therein).

In the Apennines marine sedimentation ceased in the Late Miocene and Early Pliocene, when the chain emerged completely from the sea, while the isostatic uplift reached its climax during the Pleistocene (Mayer et al. 2003).

Karst-bearing rocks are located in a transitional area between these two domains (Fig. 1) and pertain to sedimentary successions deposited in the Tethyan Meso-Cenozoic basins and comprising different lithological units.

A Norian continental siliciclastic accumulation (red beds) covers the Paleozoic phyllitic basement with variable thickness. The overlying marine sediments consist of dolomitic or evaporitic sequences about 1000 m thick. In particular, the evaporite rocks (alternating dolostone and anhydrite) represent the base of the overlying Jurassic carbonates in a large part of the northern Apennines and in the Apulia region.

The central part of the succession is mostly carbonate, with a total thickness ranging between 2500 and more than 3000 m. A Lower Jurassic carbonate platform extends over almost the entire area. The platform survived until the Miocene only in the Central and Southern Apennines, while in the remaining areas hemi-pelagic cherty limestones with minor marl units were deposited. These platforms, bordered by basins with hemi-pelagic and detritic sedimentation, constitute the limestone massifs of central–southern Italy (Fig. 1). In western Tuscany and particularly in the Apuane Alps, the carbonates are metamorphosed to the greenschist facies and represent the deep roots of the collisional orogen.

A few thousand meters of Neogene marl and turbidite foredeep sediments complete the succession. These Neogene deposits contain only minor karst-bearing levels, mainly represented by Messinian evaporites. Epigenic gypsum caves, not considered in this paper, are quite common in the hilly zones mainly on the eastern side of the chain.

2.2 Hydrogeology and Geochemistry

The limestone succession hosts important aquifers, fed by abundant precipitation that dominates over the Apennine chain (over 1000 mm a^{-1}). Bicarbonate waters derived from the infiltration and seepage of the surface meteoric waters contain 200–400 mg L^{-1} of total dissolved solids, but in many localities the groundwater is enriched in dissolved salts, generally with a significant sodium, chloride and sulfate content. These mineralized waters can be cold or thermal, with temperature ranging from 14 to over 40 °C and a TDS than sometimes largely exceeds 2000 mg L^{-1} (Fig. 2). The dissolved ions often can be related to deep routes involving Triassic anhydrite in a complex regional flow path, with residence times up to some decades.

Along the peninsula, gas emissions are quite common, often close to important karst systems. On the Tyrrhenian side, the Neogene–Quaternary backarc extensional processes are associated with hydrothermal vents rich in H_2S and CO_2

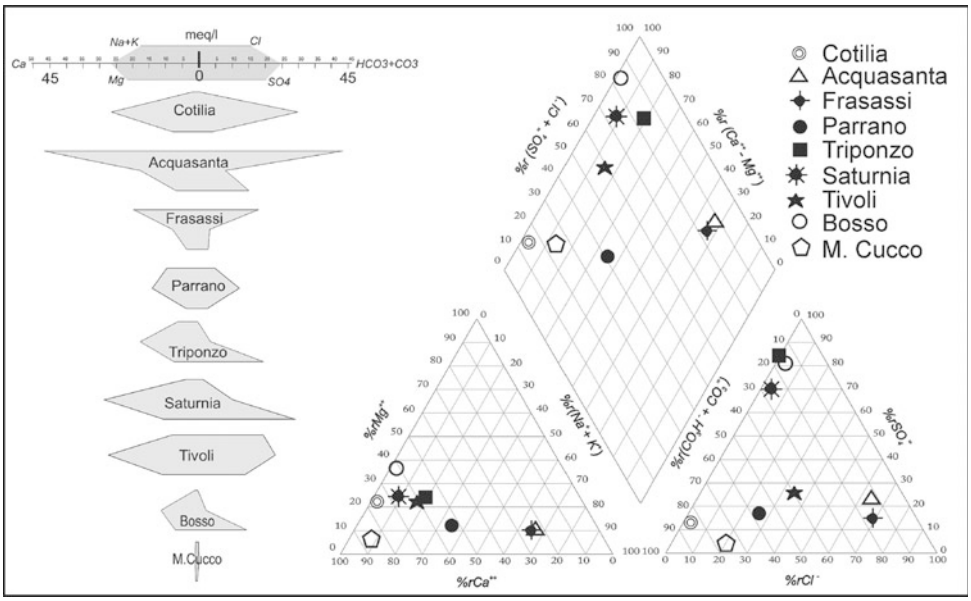

Fig. 2 Geochemistry of spring waters in the karstic area of Central Italy. Stiff diagram in the *left* and Piper diagram in the *right* (after Menichetti 2009)

(Minissale 2004). On the Adriatic side mud volcanoes, salt springs, CH_4 emission are well documented due to extensive hydrocarbon exploration (Conti et al. 2000).

The rise of gases can be associated to the high heat flow, especially on the Tyrrhenian side. The H_2S can reach concentrations up to 0.5 mmol L^{-1} and the endogenic CO_2 in the water reaches values close to 100 mg L^{-1}. The volume of fluid flow through the carbonate rocks is very large, especially for CO_2, which was estimated in 10^{11} mol a^{-1} (Rogie et al. 2000).

The origin of the gases is still a matter of debate both for H_2S and CO_2. The dissolved gases are often associated with CH_4 and He (Minissale et al. 2000; Minissale 2004). The CO_2 derives from volcanism and related thermo-metamorphic processes, but an additional non-volcanic source seems related to mantle degassing. The H_2S can originate from volcanic hydrothermal fluids, especially on the Tyrrhenian side of the Apennines, or derive from the reduction in buried sulfate deposits, present in two distinct stratigraphic levels. The Miocene evaporitic succession, with gypsum and associated shales, is common in the eastern sides, where it is overthrust by the limestone anticlines. The very thick (up to 2000 m) Triassic evaporites underlie the Jurassic carbonate platform over a large part of the peninsula.

This gas enrichment can play an important role in hypogene karst. The acidity of H_2S itself can partially contribute to limestone dissolution, but it becomes more important if it oxidizes to sulfuric acid after the mixing with oxygen-rich groundwater. A further contribution to solutional processes is also due to a positive feedback between the H_2S oxidation and the subsequent release of new CO_2 from limestone dissolution. Cave morphologies show that the oxidation processes are not restricted to the shallow phreatic zone, but can occur also in deeper sections of the aquifers due to input of freshwater via the complex regional hydrogeological flow paths.

The high content of endogenic CO_2 in the groundwater, with a pCO_2 range from 0.03 to 0.1 atm, increases the solubility of $CaCO_3$ by an order of magnitude compared to the soil pCO_2 of karstic waters. The importance of this endogenic CO_2 in cave formation, especially if it operates at low temperature, is not easy to detect in old cave systems, and cave morphology alone may not provide conclusive evidence for this mechanism of cave formation (Menichetti 2011). Travertine and tufa deposits represent an end member of the process of gas rise from these deep-seated fluids. Several important deposits are common at the edge of the mountain ridges, mostly but not exclusively on the Tyrrhenian side, and many of them formed as a result of degassing of surfacing CO_2-rich groundwater containing >2 mmol L^{-1} calcium (Fig. 3).

Finally, geothermal anomalies can also favor solution processes, as the cooling of thermal water during its ascent along conduits increases solutional aggressiveness and causes a corrosive effect that acts almost uniformly along the conduit surfaces, producing a dramatic increase in the hydrologic flow and karst void development (Andre and Rajaram 2005).

3 Karst

Karst landforms and caves are not homogeneously distributed in the large limestone outcrops of the Apennines, and both epigenic and hypogenic caves frequently coexist, often within the same structure (Galdenzi 1996, 1997).

Fig. 3 Active travertine deposition in the thermal sulfidic stream fed by Saturnia springs

The geological structure of the Apennines, being typical of a complex orogenic area, is very different from that of other less tectonized regions known for hypogene caves, such as the Guadalupe Mountains in the USA. In the Apennines, many of the carbonate massifs are divided from each other by low-permeability units, but large faults favor cross-formational communication at depth and provide routes for the rise of mineralized fluids to the surface, creating favorable conditions for hypogene speleogenesis.

Active and fossil hypogenic caves are known throughout the whole Apennine chain, with a wide variety of patterns and morphologies including three-dimensional maze systems and deep shafts (Fig. 4). In many cases, the caves are developed at multiple levels, related to the evolution of the external hydrographic network.

The geological structure influences the cave patterns and groundwater drainages and allows us to define zones with different characteristics. In the Northern Apennines and western Latium, the main aquifers are located in the anticlines, formed by the hemi-pelagic limestone and bordered by non-karstic, low-permeability Miocene deposits in the main synclines. The Early Jurassic carbonate platform at the core guides the groundwater flow paths. Minor aquifers perched above the main base level occur because of low-permeability marl levels interbedded with the limestone. Minor-confined carbonate structures (up to a few km^2 wide) are common and often karstified in hypogenic conditions.

In the Central–Southern Apennines, the carbonate platforms host larger aquifers (many tens of km^2 wide), mainly with authigenic recharge. These structures are bordered by narrow valleys developed in the overthrust deposits of the Jurassic basins (pelagic limestones, marls, and cherts).

The Calabria zone has a very complex geological structure, due to a complicated tectonic history. Large outcrops of Meso-Cenozoic carbonate platforms are present, but some minor outcrops buried by non-karst-bearing rocks are known as well.

Minor limestone outcrops, often karstified, also occur in Apennine regions where non-karst-bearing units predominate. In the Alpi Apuane, Jurassic metamorphic limestones are well karstified, and these regions host some of the most important and deepest Italian caves (Piccini 2011).

3.1 Northern Apennines

Hypogene caves in the Northern Apennine region are well known, in particular in the Umbria–Marche area (Galdenzi and Menichetti 1995) that can be considered the "cradle" of hypogene cave studies in Italy. Multiple hypogenic cave systems that consist of tens of kilometers of solutional passages are known in the region, generally at the core of anticlines underlying low-permeability units.

Across the region, all the developmental stages of these hypogene caves can be observed. Caves directly related to active sulfidic water flow are in the Frasassi Gorge, Acquasanta Terme, Saturnia area, and Pozzo del Merro. Active, non-sulfidic hydrothermal caves are well known in the Monsummano area, near Pistoia (Piccini 2000). Elsewhere, hypogenic fossil caves developed above active sulfidic springs (Parrano Gorge, Mt. Rotondo, Buco del Pretaro) or in completely fossil systems, such as the Mt. Cucco cave systems, Cittareale Cave, Pozzi della Piana (Galdenzi and Menichetti 1995), and Mount Soratte area

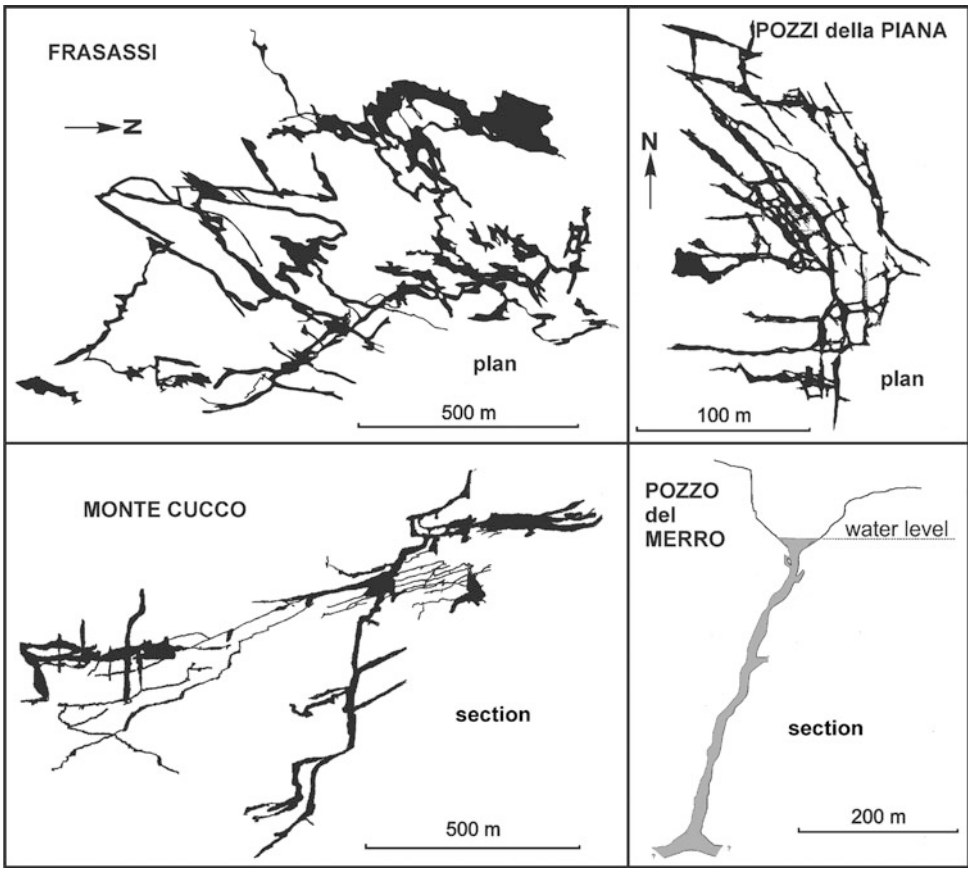

Fig. 4 General patterns of some hypogene caves in the Apennines

(Mecchia et al. 2003), where the caves have no relationship with existing surface drainage networks.

The caves open at different stratigraphic levels, more commonly the Jurassic carbonate platform (Monte Cucco, Frasassi) but also in Paleogene limestone (Acquasanta) up to Pleistocene travertine (Pozzi della Piana). These caves often have a ramified pattern, typical of hypogene caves (Palmer 1991), with large rooms abruptly closed in narrow passages or fissures. Labyrinthic networks are known as well, such as in the Pozzi della Piana, and, in part, the Frasassi caves (Fig. 4). Large rooms may develop in the caves: many passages in Monte Cucco and Frasassi caves reach a volume largely $>10^4$ m^3, while the Abisso Ancona hall in the Frasassi caves reaches almost 10^6 m^3 in volume. Meso-structures as cupolas, blind pits, anastomotic passages, and spongework zones are common.

Many caves have a mainly sub-horizontal development, including almost perfect water table caves such as Pozzi della Piana. The horizontal passages are often fed by inclined or vertical feeders, or directly from narrow slots in the floor. Some isolated domes developed by the same mechanism, above a main feeder or a system of fissures and crevasses (Fig. 5).

Solutional processes occurred also below the shallow phreatic zone, and most caves have significant vertical development. Very deep pits show similar corkscrew solutional patterns both in the fossil cave of Mt. Cucco and in the active Pozzo del Merro close to Rome (Fig. 4) that reaches —332 m below the sea level (Mecchia et al. 2003, with references).

The development of the cave systems is influenced by the surface geomorphic evolution and in particular by the downcutting in the river valleys and the consequent lowering of the local base level. This is evident in the sub-horizontal caves located in the gorges, where caves commonly occur in a series of discreet sub-horizontal levels, such as in Frasassi and Pozzi della Piana (Galdenzi and Menichetti 1995) (Fig. 6). In caves where the solutional processes occurred under deep-seated conditions below the local base level, the surface stream can be perched above the groundwater and encounters preexisting phreatic passages during the deepening of valleys, as in the Acquasanta caves (Galdenzi et al. 2010) and in the Parrano Gorge (Menichetti 2011) (Fig. 7).

Anti-gravitational channels, grooves, and bubble trails are common in both active and fossil karst systems, indicating the importance of rising aggressive fluids (gas or water). Areas where sulfidic groundwaters are exposed to the cave atmosphere facilitate the release of H_2S and CO_2 gas that cause subaerial limestone corrosion. Subaerial corrosion is important in the horizontal caves, where water-filled

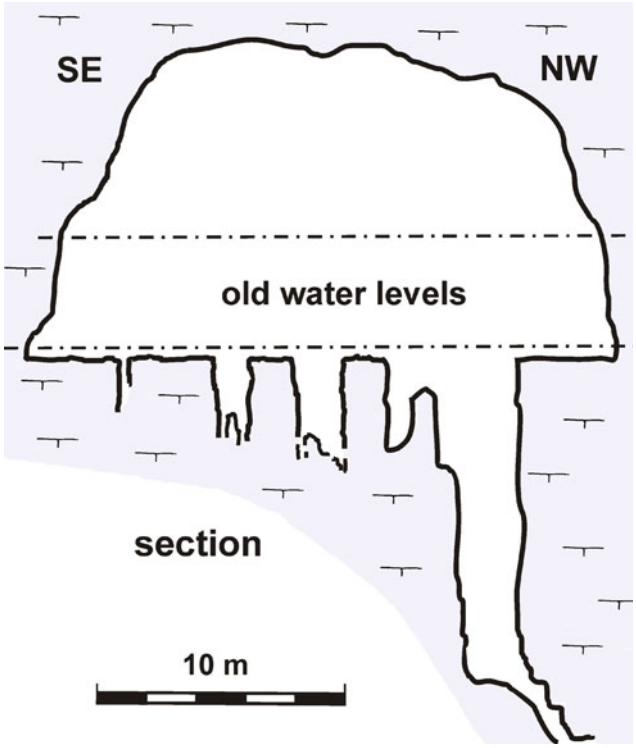

Fig. 5 An isolated chamber, with several feeder crevasses and pits for sulfidic water from the floor. (Sala del Limone, Frasassi caves). Survey by GS.Al.Va.P. (2011)

passages alternate with free surface zones, but it can also occur when the deep-seated karst passages emptied after the lowering of the water table. Active subaerial corrosion generally impacts the walls in close proximity to degassing streams, but air convection can extend the influence of subaerial dissolution processes in the thermal caves.

Above the water table, the oxidation of H_2S causes limestone replacement with gypsum. If the degassing rate is high, the process can begin with small white gypsum spots less than a few cm in diameter, which can expand into a continuous wall-covering rim of microcrystalline gypsum. Sulfur-oxidizing bacteria play an important role in this process, and acidic biofilms with pH < 1 form web-like structures and thin "stalactites" on cave walls (Sarbu et al. 2000; Macalady et al. 2007). The gypsum often has a squashy, toothpaste-like texture and it can easily fall on the floor, where it is dissolved and removed by flowing cave waters.

Wall crusts and large gypsum floor deposits in relict passages are known from many caves, including Mt. Cucco, Frasassi, Pozzi della Piana, and Acquasanta. Floor deposits often occur as "gypsum glaciers", produced by post-depositional flow and accumulation (Fig. 8). A similar subaerial origin is consistent with their depositional setting and stable isotope content. All these deposits have negative values of $\delta^{34}S$ ratio, which can only be explained by their formation from H_2S gas released by groundwater. In the sulfidic groundwater, sulfide and dissolved sulfate have significantly different $\delta^{34}S$ values, the former always negative and the latter always highly positive (Galdenzi and Maruoka 2003; Menichetti et al. 2008).

Other sulfate minerals (barite and celestite) and products of acid weathering of clays (alunite, jarosite, halloysite,

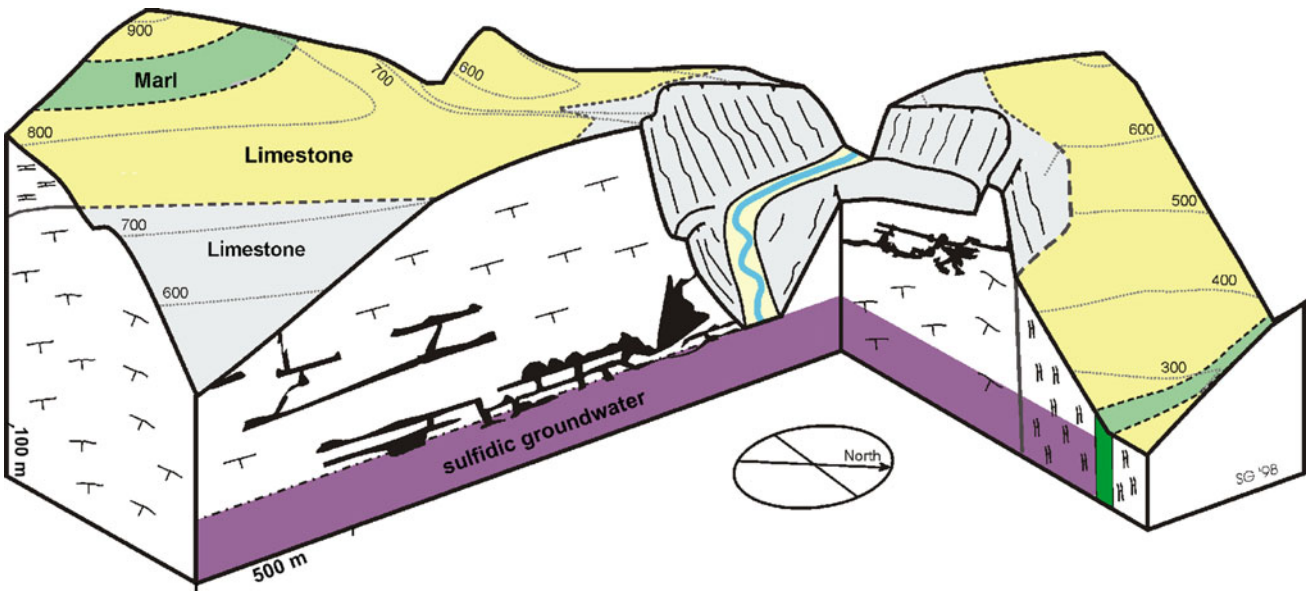

Fig. 6 Schematic section of Frasassi caves. The groundwater level and the development of cave levels were influenced by the downcutting in the river valley (after Galdenzi and Maruoka 2003 modified)

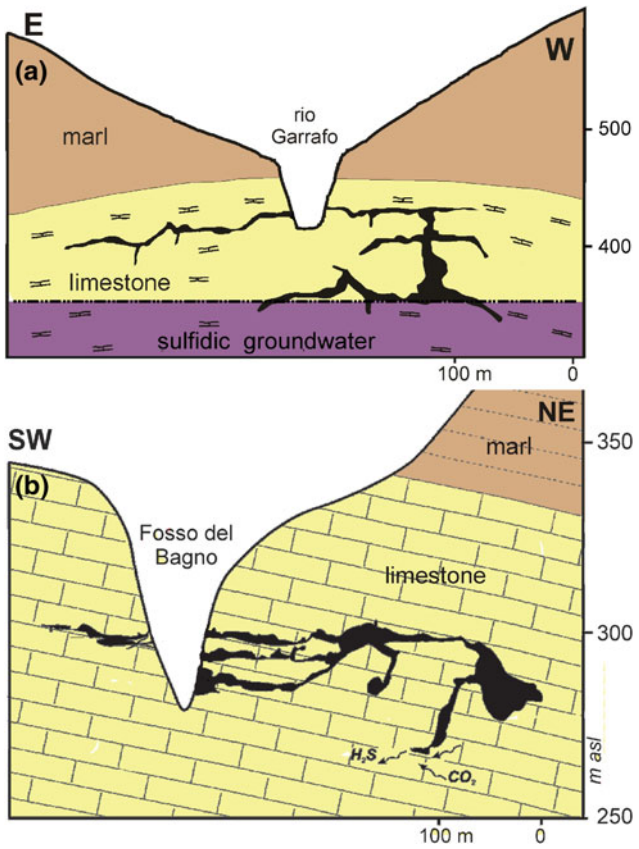

Fig. 7 Caves formed in a phreatic setting into buried limestone and cut by the surface streams. **a** Rio Garrafo caves, Acquasanta Terme; **b** Parrano caves

kaolinite) were described in the Frasassi caves (Bertolani et al. 1975), Faggeto Tondo cave at Mt. Cucco (Forti et al. 1989), and Montecchio (Piccini et al. 2015).

Corrosion rates in sulfidic water were measured in the Frasassi cave system using limestone tablets. The corrosion rate was approximately 0.05 mm a^{-1}, both in the air and water, and gypsum developed on the subaerial tablet (Galdenzi et al. 1997). A subsequent dissolution experiment in the groundwater showed that corrosion rate is influenced by flow dynamics and can increase up to 1 mm a^{-1} in weakly turbulent flow. A comparison between measured corrosion rate and cave wall retreat has shown that active corrosion processes have acted at the same intensity throughout the caves' history (Galdenzi 2012).

In Frasassi, white sulfur-oxidizing microbial communities are conspicuous in sulfidic cave waters (Macalady et al. 2006). The sulfur-oxidizing bacterial communities, which use H_2S as energy source, support invertebrate life in a wholly chemoautotrophic aphotic ecosystem in the Frasassi sulfidic cave sections (Sarbu et al. 2000). The role played by these microbial communities in the limestone corrosion is complicated, and data from the Frasassi caves indicate that oxidizing bacteria living in the cave streams are important for sulfide oxidation but may not play an active role in the production of acidity (Jones et al. 2015).

Some well-known cave systems in the region are important for their characteristics and structure. Among them, Mt. Cucco and the western Umbria caves will be described in detail below. The active sulfidic systems of Frasassi and Acquasanta Terme are described in specific chapters of this book (Galdenzi and Jones, Chap. 8; Galdenzi, Chap. 10).

3.2 Mt. Cucco Caves

The Mt. Cucco caves are among the best known hypogene caves of Italy and develop for over 20 km in pure Jurassic limestone in the upper part of Mt. Cucco (1566 m asl), at the core of an anticline. The fold is asymmetric, east verging, and its eastern limb is cut by an important N–S strike-slip fault that borders the most karstified zone of the limestone massif to the east (Fig. 9). The main cave, La Grotta, is ~900 m deep. The upper levels consist of large, relict passages of phreatic origin, developed toward the SSW in zones with high syngenetic porosity along bedding planes, inclined at 20°–25° (Menichetti 1989). Transverse sub-horizontal regions exist in the entrance zone and in the southern sector. Some blind shafts extend more than 100 m below the phreatic passages, and a sequence of wide, deep pits reaches the cave bottom and the groundwater level at ~560 m asl. Inside the cave, there are also active zones of seepage water flow that follow a network of small meanders and pits, which fortuitously intersect the large fossil passages.

Other important caves, a few km long (Buca di Faggeto Tondo and Buca Futura), occur at the top of the Lower Jurassic limestone, below a thin and poorly permeable Middle and Upper Jurassic limestone. These caves tend to have an inclined development parallel to the stratigraphic boundary and develop close to the mountain surface. The poorly permeable cover protects large parts of these caves from seepage of meteoric water, and their original morphologies and deposits are well preserved.

Most phreatic passages are located at elevations between 1050 and 1400 m. The present water table is at ~500 m, with a main spring (Sorgente Scirca) located at the foot of the mountain, where surface erosion has removed the sedimentary cover and exposed the Jurassic limestone at the lowest elevations. The spring has a discharge of ~200 L s^{-1}, and a direct relationship between the cave water and the spring was verified with tracers (Menichetti et al. 1997).

Large gypsum deposits are widely preserved in the fossil zones of the caves, especially where overlying low-permeable units shield them from dissolution by seepage water. The gypsum deposits consist of fine-grained white

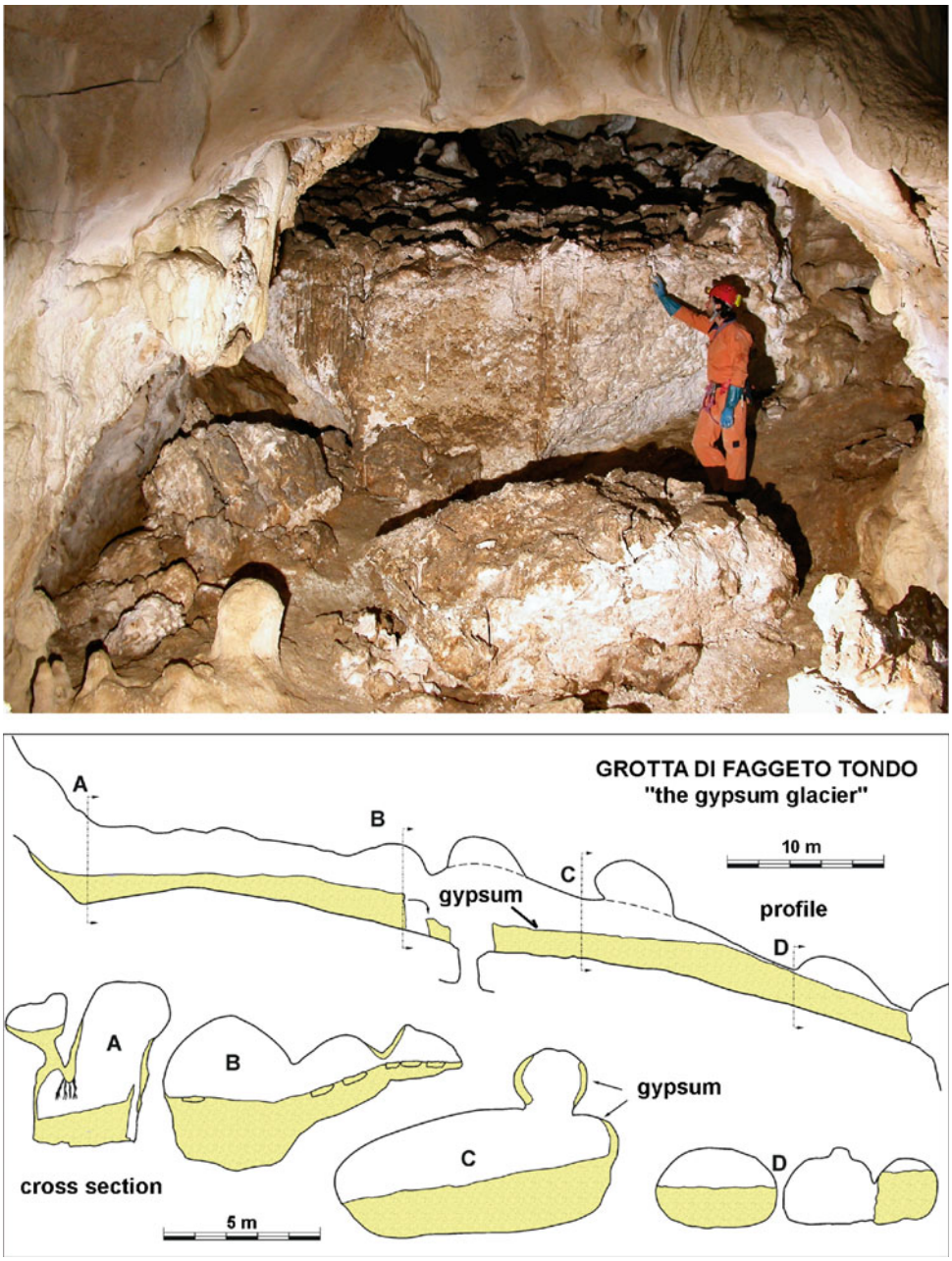

Fig. 8 The "gypsum glacier" of Faggeto Tondo cave (profile and section after Galdenzi 2004)

material that occurs as wall crusts and floor deposits and are often recrystallized at the surface. Relict gypsum and other cave minerals testify to the presence of sulfidic water during cave development (Forti et al. 1989). The replacement gypsum crusts grew on limestone walls and resulted in deep and irregular corrosion pockets, gravitationally shaped, which indicate deposition in a subaerial environment (Fig. 10). The negative values of $\delta^{34}S$ of the gypsum replacement crust and massive floor deposits confirm its derivation from H_2S oxidation above the water table (Galdenzi 2004; Menichetti et al. 2008).

A subaerial source is also consistent with the large volume of a gypsum glacier ($\sim$700 m^3) that almost entirely fills a cave passage in the Faggeto Tondo Cave (Fig. 8). In fact, the replacement of calcite with gypsum caused a volume increase of $\sim$240%. Replacement of approximately 20 cm of wall limestone, over the whole passage crosssection would have been sufficient to produce the massive gypsum glacier (Galdenzi 2004).

Cave development, therefore, can be divided into two main phases: an earlier phase related to the past flow of sulfidic water, and the present phase related to descending

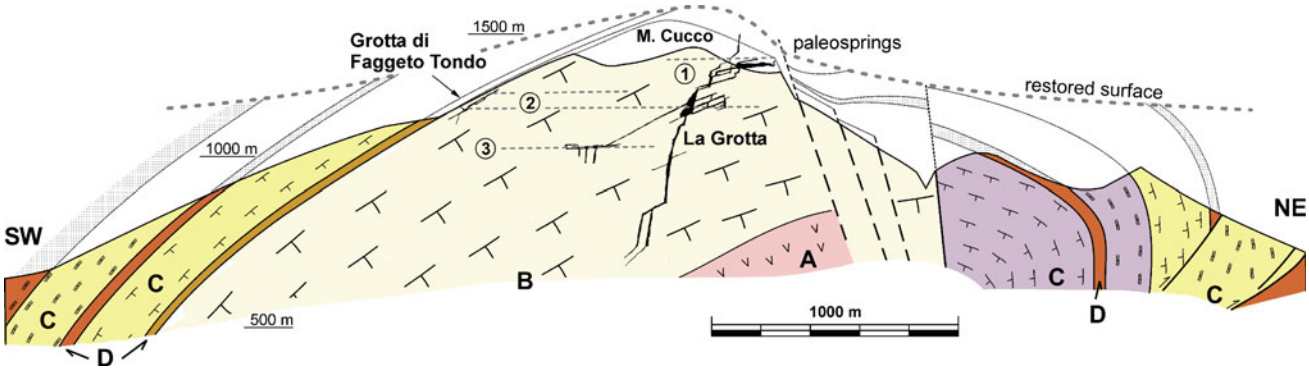

Fig. 9 Crosssection of Mt. Cucco and restored profile at the beginning of cave evolution (the cave section is projected on the geologic section). The erosion removed the marls cover and exposed larger karst surface. *A* Triassic evaporites; *B* carbonate platform limestone; *C* hemi-pelagic cherty limestone; *D* main low-permeable levels; *1*, *2*, *3* supposed old water table levels (after Galdenzi 2004, modified)

Fig. 10 Gravitational shape of limestone pockets evidenced by the removal of the replacement gypsum (Faggeto Tondo cave)

meteoric water. The earlier phase has no evident relationship with present surface topography and stream patterns and can be related to a wholly different geomorphic and hydrogeologic setting from the present.

It was previously proposed that a hanging paleostream on the east side of the mountain sunk through the mountain and emerged at lower altitude on the western side (Menichetti 1989). The interaction between the stream water and rising sulfidic water could have promoted the solutional processes. Alternatively, the cave could have formed under deep-seated conditions in the Upper Pliocene and the Lower Pleistocene, during the evolution of the paleo-erosional surfaces that are partly preserved near the top of the mountain. In that period, sulfidic water could have risen through the most permeable levels of the Lower Jurassic limestone, almost completely covered by the overlying, poorly permeable units (Galdenzi 2004) (Fig. 9).

In either scenario, the cave evolved as a consequence of progressive, discontinuous surface erosion. The lowering of the poorly permeable covers and the consequent drop of the water table emptied sections of the old phreatic passages, producing widespread air–water interfaces. This allowed for the release of H_2S, which promoted subaerial corrosion processes and the deposition of replacement gypsum above the water level.

The rise of sulfidic water in the limestone ceased when regional isostatic uplift produced the entrenchment of the river valleys into the old erosional surface probably at the end of the Lower Pleistocene (Mayer et al. 2003). The consequent drop of the water table caused the alteration of groundwater drainage patterns and, since this event, the caves have evolved only by the flow of descending meteoric water from the karst surface.

3.3 Western Umbria

Western Umbria has a hilly landscape of marls and turbidite sandstones, with minor outcrops of Cretaceous and Tertiary limestone and marl that contain hypogene caves (Galdenzi and Menichetti 1995; Menichetti 2011). Active gas vents

and mineralized springs are known in the region (Chiodini et al. 1999) and Quaternary travertine outcrops of different sizes and thickness are also present. The area was directly influenced by Plio-Quaternary volcanism, and there are small volcanic centers and dykes associated with carbonate-rich (about 10 wt%) pyroclastic rocks. These events have $^{40}Ar/^{39}Ar$ ages of 265 and 390 ka (Laurenzi et al. 1994).

The Abisso Monticelli cave is a vertical shaft that opened north of Perugia after a strong rain event in 1961 (Passeri 1968). The cave consists mainly of a subvertical and circular-shaped shaft 10 m in diameter and 78 m in depth, connected at its base with a parallel blind chimney and a narrow inclined passage. A seasonal stream flows in this passage with a discharge of several L s^{-1}, and below the shaft CO_2 concentrations close to 10% have been detected (Passeri 1968). The cave morphology and the development in poorly karstified lithologies suggest an origin related to the high concentration of endogenic CO_2 (Menichetti 2011)

The Pozzi della Piana caves, on the north side of the Tiber valley, developed in a massive travertine formation. The travertine has low organic content and high Sr content, suggesting it was deposited from thermal water rising through the Triassic anhydrites (Fig. 11). The caves consist of a network of horizontal passages (Fig. 4) developed on two main levels that extend over 2.5 km and contain microcrystalline gypsum deposits that provide evidence for a direct role of sulfidic water in speleogenesis. The cave only reaches the base of the travertine deposits in its western branch, in the widest cave room (Sala dei Vortici) (Menichetti 2011). Evidence for sulfidic waters includes metric cupolas on the roof as well as a few small blind pits that could represent the original ascending hydrothermal conduits. Both the cave development and travertine deposition are related to the rise of sulfidic water, but the temporal relationship between the two processes is undefined, and it is possible that speleogenetic processes coexisted with the growth of the travertine body.

The Parrano caves include at least eight different caves, for a total development that exceeds 1 km. The caves occur at different elevations on both sides of a small, deep gorge with an intermittent stream. These caves open inside a small limestone body at the core of an anticline that is almost completely overlain by poorly permeable rocks (Fig. 7b). A thermal sulfidic spring with an average discharge of 15 L s^{-1} and a temperature of 26 °C rises along the main fault that borders the limestone body.

The caves are mainly sub-horizontal, with irregular profiles, and some shafts descend to a maximum depth of 50 m. Gypsum rims and goethite coatings testify to the past circulation of mineralized water. In the deepest zones, thermal influx increases the air temperature by over 10 °C (up to 25 °C) and the CO_2 concentration to 0.02% (Menichetti 2011), even though thermal water does not presently occur anywhere.

3.4 Carbonate Platforms of the Central–Southern Apennines

Hypogene caves are also known in the carbonate massifs of the Central–Southern Apennines (Galdenzi 2009). In these areas, recharge at the massif surface feeds karst circulation through prevailing surficial circuits, and important karst springs and some caves occur near the base of the massifs. Epigenic caves are common in some of the massifs, with a prevalence of inflow caves in the vadose zone, generally with vertical and inclined patterns. The rise of mineralized water, however, favors hypogene speleogenesis, which is well documented in some caves of the Lessini Mountains and at Capo Palinuro.

3.4.1 Capo Palinuro

Capo Palinuro is a limestone cape (203 m elevation) with more than 30 known caves along a cliff, located between 0 and −33.5 m below sea level, and some sulfidic springs. The caves were partially or totally submerged by the Holocene sea level rise and are accessible only by diving (Alvisi et al. 1994b; Ferranti and Antonioli 1997). Warm sulfidic water actively flows in 13 explored caves.

Cave development occurred near the water table at different elevations, related to changes in sea level. The corrosion processes can be attributed to the rise and oxidation of sulfidic water (Alvisi et al. 1994b), although an epigenic origin due to a past connection with the main carbonate structures inland was also hypothesized to explain the wide dimensions of the lowest cave levels (Ferranti and Antonioli 1997).

The present speleogenetic conditions are well documented. The sulfidic water is less dense than the saltly seawater, even in the summer when saltwater temperatures exceed those of the sulfidic water. Because of these density differences, the sulfidic waters rise to the surface of the cave rooms and form a layer that floats on the marine water. In some caves, sulfidic lakes originate in partly flooded rooms. Detailed measurements of the depths of the sulfidic water–saltwater interface show that it varies between 7 and 11 m in different caves (Alvisi et al. 1994b). The less dense sulfidic water is trapped against the ceilings of the enclosed cave rooms, but it may flow near the chemocline, between the ceiling of submerged passage but above the layer of dense marine water (Fig. 12).

Chemoautotrophic bacteria are abundant in the sulfidic water, permitting the development of an unusually rich benthonic marine fauna inside the cave (Southward et al. 1996; Mattison et al. 1998). In the subaerial zones, the

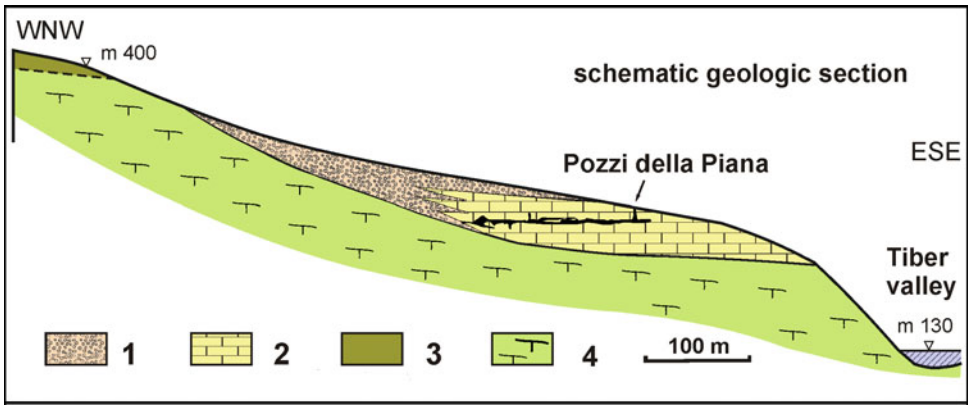

Fig. 11 Schematic crosssection through the Pozzi della Piana cave. *1* Pleistocene slope deposits; *2* Pleistocene travertine; *3* Paleogene marl; *4* Paleogene limestone

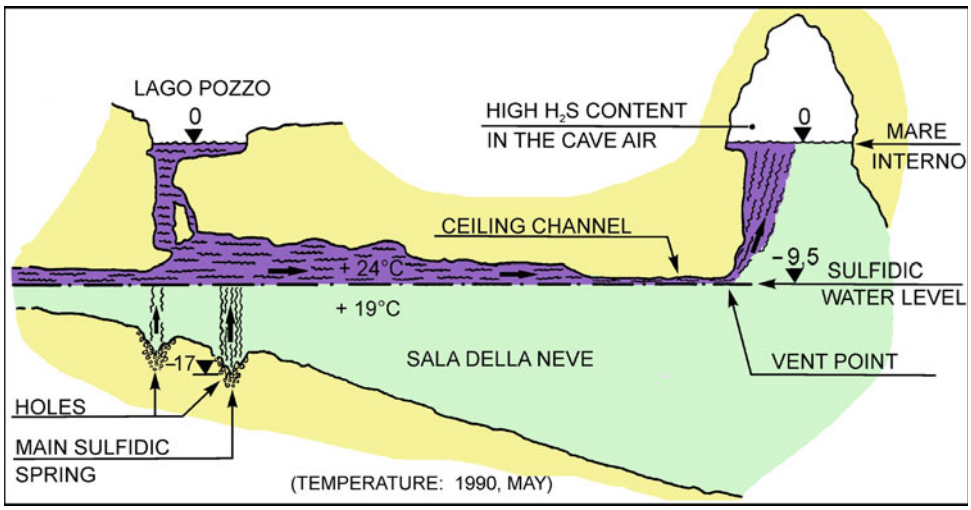

Fig. 12 Crosssection of Grotta Azzurra, Capo Palinuro, showing the stratification of sulfidic water above the sea water in a cave room (after Alvisi et al. 1994a, modified)

oxidation of the released H_2S produces replacement gypsum and elemental sulfur (Forti and Mocchiuti 2004).

3.4.2 Latium Mountains

In southern Latium, large springs (discharge up to few m^3) rise from the limestone massif, at the base of the mountain slope in the Pontina Plain. Some springs have elevated salinity and H_2S, due to mixing between freshwater from shallow flow routes and water rising from a deeper flow path. The sulfidic springs originate travertine deposits, interbedded with marine and continental Pleistocene deposits, and are often karstified (Bono 1995). Sulfidic lakes can fill karst depressions in the travertine.

Small caves in the Lepini Mountains show features and deposits that result from the flow of H_2S-rich groundwater. The Fiume Coperto cave is an active cave (~170 m long) at the base of the mountains, near a large sulfidic spring. A gypsum rim derived from subaerial H_2S oxidation covers large parts of the limestone wall, and rillenkarren formed by seepage of acidic water can be observed above the water table. The evolution of the cave was influenced by the changes of base level, related to Pleistocene sea level variations. At present, intense pumping for irrigation in the Pontina Plain caused a water table decline of ~1 m and the consequent reduction in the flow of sulfidic water and sulfuric acid corrosion (Galdenzi 2003). Many small stagnant sulfidic pools occur throughout the cave and are covered by a thin organic layer containing bacteria and fungi (Latella et al. 1999). Other small caves with gypsum deposits are reported in surrounding areas (Mecchia et al. 2003).

3.5 North Calabria

In North Calabria, widespread outcrops of limestone and dolostone host several epigenic caves, but caves also occur in small limestone outcrops, surrounded by low-permeable units, where thermal sulfidic springs emerge (Fig. 1). Research on hypogene processes in the region is in its infancy, but preliminary results are encouraging. Hypogene caves were described in the northern part of Calabria, near thermal sulfidic springs around the Sibari Plain, on the Ionian Sea (Galdenzi 1997). Other caves are on the

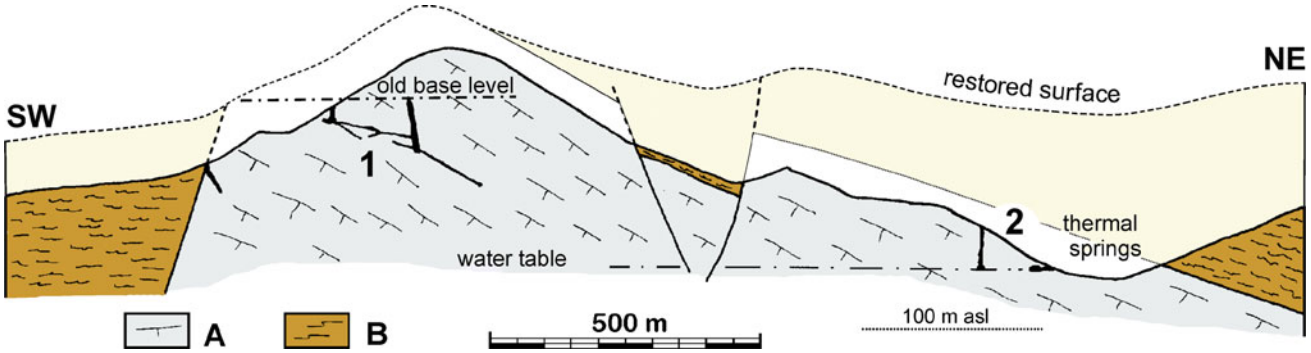

Fig. 13 Crosssection through the southeastern side of Mt. Sellaro, with the restored profile at the beginning of cave evolution. Note the denudation of the limestone surface and the migration of springs in the NE side of the mountain. *A* Cretaceous and Paleocene limestone; *B* low-permeable cover; *1* Grotta di Serra del Gufo; *2* active caves (after Galdenzi 1997, modified)

Fig. 14 Wall notches produced by sulfidic thermal water (maximum passage width ~2.5 m) (Grotte di Sant'Angelo, Cassano allo Jonio)

Tyrrhenian side of the region, near the Terme Luigiane thermal baths.

One hypogenic system occurs in the Monte Sellaro structure, the only structure in which active sulfidic zones are directly accessible. The main cave (Grotta di Serra del Gufo, ~2 km long) is a relict cave on the eastern side of a monocline in Cretaceous and Paleogene limestone, surrounded by the overthrust low-permeability units. The cave is mainly developed along inclined passages that rise toward the surface. It probably originated under phreatic conditions before the erosion caused the denudation of the karst surface, the lowering of the water level and the migration of the spring to the opposite side of the mountain (Fig. 13). The sulfidic water has temperatures that vary from 28 to 40 °C and presently flows inside small caves at the spring and in the bottom of a 100-m-deep shaft. H_2S oxidation is actively producing gypsum replacement crusts on the limestone walls, and gypsum deposits are known in the older, non-sulfidic cave levels.

The most important cave system is located in a steep isolated dolostone hill (Mount San Marco) surrounded by low-permeable units near Cassano allo Jonio. Several caves are known, some only recently explored, for a total length exceeding 4000 m. The main caves are developed on multiple levels at similar elevations, about 100 m above the thermal (~25 °C) sulfidic springs. Zones with active SAS

are not known. The separate caves have similar features and consist of several sub-parallel relict passages, generally developed along faults and often overlapping. Some major rooms derive from breakdown of passages from different levels. Widespread interfaces between sulfidic water and cave atmosphere produced characteristic morphologies. Flat solutional floors and walls notches are common (Fig. 14), as is replacement gypsum, which was even quarried in the past. In addition to gypsum and detrital minerals, mineralogical studies found deposits of thin globular concretions and crystals of barite on corrosional pockets, and thin films of halite or rare sylvite crystals coating the gypsum (Catalano et al. 2014).

The Terme Luigiane caves open in a gorge cut through a small carbonate outcrop, representing a tectonic window below low-permeable metamorphic rocks. Due to the tectonic setting, an important sulfidic thermal spring rises in different emergences at the gorge outlet, with temperatures that vary between 22 and 47 °C. Some small relict caves related to past flows of thermal water are known in the upper part of the structure, with evidence of a complex multiphase history. The caves show typical phreatic sections and contain some deposits of barite, fluorite, and gypsum.

4 Conclusions

Hypogenic caves are common in the Apennines, and it is likely that they are even more widespread than presently known. The best conditions for hypogene cave development typically occur in limestone outcrops bounded by low-permeability units, where the fluids rising from depth flow toward the surface. However, some hypogenic caves also occur in open hydrogeologic massifs where epigenic caves prevail, due to the high intensity of the corrosional processes involved in the hypogene speleogenesis. The oxidation of H_2S is the driving corrosive process, enhanced where rising sulfidic waters reach an oxidizing environment or mix with descending freshwater.

Hypogenic caves generally evolve over multiple stages, related to the progressive downcutting of surface streams and the lowering of the related base level. However, the specific geological, hydrogeological, and geochemical conditions need to be documented for each individual system. A dynamic view of cave pattern development and evolution in space and time should take into account variations in the elevation of the regional water table, and possible changes in the rising waters flow path.

Some active caves provide excellent opportunities to study the biological and geological aspects of active corrosional processes. Most caves, however, are relict, and the hypogenic origin is recorded by characteristic passage morphologies and gypsum deposits, or from the general geological setting.

Cave patterns can be very different, ranging from phreatic caves, typically developed when karst evolves under partly confined conditions, up to almost ideal water table caves. This great variety of examples in different geological settings makes the Apennines an exceptional place to study the influence of geologic and geomorphic factors on hypogene speleogenesis.

References

Alvisi M, Barbieri F, Bruni R, Cinelli F, Colantoni P, Grandi GF, Maltoni P (1994a) La Grotta Azzurra di Capo Palinuro. Mem Ist It Speleol s II 6:51–56

Alvisi M, Barbieri F, Colantoni P (1994b) Le grotte marine di Capo Palinuro. Mem Ist It Speleol s II 6:143–182

Andre BJ, Rajaram H (2005) Dissolution of limestone fractures by cooling waters: early development of hypogene karst systems. Water Resour Res 41:w01015. doi:10.1029/2004WR03331

Bertolani M, Rossi A, Garuti G (1975) The speleological complex "Grotta Grande del Vento—Grotta del Fiume" in the Frasassi Canyon (Ancona-Italy). A petrological and mineralogical study. In: Proceedings of the 6th international congress of speleology, Olomouc, 1973, vol 1, pp 357–366

Bono P (1995) The sinkhole of Doganella (Pontina Plain, central Italy). Environ Geol 26:48–52

Catalano M, Bloise A, Miriello D, Apollaro C, Critelli T, Muto F, Cazzanelli E, Barrese E (2014) The mineralogical study of the Grotta Inferiore di Sant'Angelo (southern Italy). J Cave Karst Studies 76(1):51–61. doi:10.4311/2012ES0284

Cavazza W, Wezel FC (2003) The Mediterranean region—a geological primer. Episodes 26:160–168

Chiodini G, Frondini F, Kerrick DM, Rogie J, Parel-lo F, Peruzzi L, Zanzari AR (1999) Quantification of deep CO_2 fluxes from Central Italy. Examples of carbon balance for regional aquifer and of soil diffuse degassing. Chem Geol 159:205–222

Conti A, Sacchi E, Chiarle M, Martinelli G, Zuppi GM (2000) Geochemistry of the formation waters in the Po plain (Northern Italy): on overview. Appl Geochem 15:51–65

Crescenti U, D'Offizzi S, Merlino S, Sacchi L (eds) (2004) Geology of Italy. Special volume of Italian geologic society for the 32nd international geologic congress, Florence

De Waele J, Audra P, Madonia G, Vattano M, Plan L, D´Angeli IM, Bigot J-Y, Nobécourt J-C (2016) Sulfuric acid speleogenesis (SAS) close to the water table: examples from southern France, Austria, and Sicily. Geomorphology 253:452–467

De Waele J, Forti P, Naseddu A (2013) Speleogenesis of an exhumed hydrothermal sulphuric acid karst in Cambrian carbonates (Mount San Giovanni, Sardinia). Earth Surf Proc Land 38:1369–1379

Ferranti L, Antonioli A (1997) Le grotte sottomarine di Capo Palinuro (Campania, Italia). Aspetti geomorfologici e implicazioni speleogenetiche. In: Pensabene G. (ed) Atti 17th Congresso Nazionale di Speleologia, Castelnuovo Garfagnana, 1994, vol 1, pp 189–203

Forti P, Mocchiutti A (2004) Le condizioni ambientali che permettono l'evoluzione di speleotemi di zolfo in cavità ipogeniche: nuovi dati dalle grotte di Capo Palinuro (Salerno, Italia). Le Grotte d'Italia, s V 4:39–48

Forti P, Galdenzi S, Sarbu SM (2002) The hypogenic caves: a powerful tool for the study of seeps and their environmental effects. Cont Shelf Res 22:2373–2386

Forti P, Menichetti M, Rossi A (1989) Speleothems and speleogenesis of the Faggeto Tondo Cave (Umbria, Italy). In: Gadoros M (ed) Proceedings of the 10th international congress of speleology, Budapest, 1989, vol 1, pp 74–76

Galdenzi S (1989) I depositi gessosi nelle grotte calcaree di Frasassi: giacitura ed origine. In: Atti 15th Congresso Nazionale di Speleologia, Castellana Grotte, 1987, pp 251–258

Galdenzi S (1990) Un modello genetico per la Grotta Grande del Vento. In: Galdenzi S, Menichetti M (eds) Il carsismo della Gola di Frasassi. Atti del Convegno Nazionale, San Vittore di Genga, September 1988. Mem Ist It Speleol, s II, vol 4, pp 123–142

Galdenzi S (1996) Il carsismo profondo nell'Appennino Umbro Marchigiano (Italia). In: Proceedings international congress "Alpine Caves: alpine karst systems and their environmental context", Asiago, pp 229–242

Galdenzi S (1997) Initial geologic observations in caves bordering the Sibari Plain (southern Italy). J Cave Karst Stud 59(2):81–86

Galdenzi S (2003) L'azione morfogenetica delle acque sulfuree nella Grotta di Fiume Coperto (Latina). Le Grotte d'Italia, s V 4:17–27

Galdenzi S (2004) I depositi di gesso nella Grotta di Faggeto Tondo: nuovi dati sull'evoluzione geomorfologia dell'area di Monte Cucco (Italia centrale). Studi Geologici Camerti, ns 2:71–83

Galdenzi S. (2009) Hypogene caves in the Apennines (Italy). In: Klimchouk AB, Ford DC (eds) Hypogene speleogenesis and karst hydrogeology of artesian basins. Ukrainian Institute of Speleology and Karstology, SP 1, pp 101–115

Galdenzi S (2012) Corrosion of limestone tablets in sulfidic groundwater: measurements and speleogenetic implications. Intern J Speleol 41(3):149–159

Galdenzi S, Campagnoli A (2015) Piano quotato dell'acquifero carsico di Frasassi. In: De Nitto L et al (eds) Atti 22nd Congresso Nazionale di Speleologia, Pertosa-Auletta (SA). Mem Ist It Speleol, s II, vol 29, pp 375–380

Galdenzi S, Maruoka T (2003) Gypsum deposits in the Frasassi caves, Central Italy. J Cave Karst Stud 65(2):111–125

Galdenzi S, Menichetti M (1990) Evolution of underground kasrt systems in the Umbria-Marche Appennines in Central Italy. In: Hazslinszky T, Takacs Bolner K (eds) Proceedings of the 10th international congress of speleology, Budapest, 1989, vol 3, pp 745–747

Galdenzi S, Menichetti M (1995) Occurrence of hypogenic caves in a karst region: examples from central Italy. Environ Geol 26:39–47

Galdenzi S, Menichetti M (1997) Le grotte ipogeniche in Italia. In: Pensabene G (ed) Atti 17th Congresso Nazionale di Speleologia, Castelnuovo Garfagnana, 1994, vol 1, pp 135–138

Galdenzi S, Cocchioni M, Morichetti L, Amici V, Scuri S (2008) Sulfidic ground-water chemistry in the Frasassi caves, Italy. J Cave Karst Stud 70(2):94–107

Galdenzi S, Cocchioni F, Filipponi G, Selvaggio R, Scuri S, Morichetti L, Cocchioni M (2010) The sulfidic thermal caves of Acquasanta Terme (central Italy). J Cave Karst Stud 72(1):43–58

Galdenzi S, Menichetti M, Forti P (1997) La corrosione di placchette calcaree ad opera di acque sulfuree: dati sperimentali in ambiente ipogeo. In: Jeannin PY (ed) Proceedings of the12th international congress of speleology, La Chaux-de-Fonds, vol 1, pp 187–190

Jones DS, Lyon EH, Macalady JL (2008) Geomicrobiology of biovermiculations from the Frasassi cave system, Italy. J Cave Karst Stud 70(2):78–93

Jones DS, Polerecky L, Galdenzi S, Dempsey BA, Macalady JL (2015) Fate of sulfide in the Frasassi cave system and implications for sulfuric acid speleogenesis. Chem Geol 410:21–27

Jones DS, Tobler DJ, Schaperdoth I, Mainiero M, Macalady JL (2010) Community structure of subsurface biofilms in the thermal sulfidic caves of Acquasanta Terme, Italy. Appl Env Microb 76(17):5902–5910. doi:10.1128/AEM.00647-10

Klimchouk A (2007) Hypogene speleogenesis: hydrogeological and morphogenetic perspective. Nat Cave and Karst Research Institute, Carlsbad

Latella L, Di Russo C, De Pasquale L, Dell'Anna L, Nardi G, Rampini M (1999) Preliminary investigations on a new sulfurous cave in central Italy. Memories Biospeleologie 26:131–135

Laurenzi MA, Villa I, Stoppa F (1994) Eventi ignei monogenici e depositi piroclastici nel Distretto Ultra-alcalino Umbro-laziale (ULUD): revisione, aggiornamento e comparazione dei dati cronologici. Plinius 12:61–65

Macalady JL, Jones DS, Lyon EH (2007) Extremely acidic, pendulous microbial biofilms from the Frasassi cave system, Italy. Environ Microbiol 9:1402–1414

Macalady JL, Lyon EH, Koffman B, Albertson LK, Meyer K, Galdenzi S, Mariani S (2006) Dominant microbial populations in limestone-corroding stream biofilms, Frasassi cave system, Italy. Appl Environ Microbiol 72:5596–5609

Mariani S, Mainiero M, Barchi M, van der Borg K, Vonhof H, Montanari A (2007) Use of speleologic data to evaluate Holocene uplifting and tilting: an example from the Frasassi anticline (northeastern Apennines, Italy). Earth Planet Sci Lett 257:313–328

Mattison RG, Abbiati M, Dando PR, Fitsimons MF, Pratt SM, Southward AJ, Southward EC (1998) Chemoautotrophic microbial mats in submarine caves with hydrothermal sulphidic springs at Capo Palinuro, Italy. Microb Ecol 35:58–71

Mayer L, Menichetti M, Nesci O, Savelli D (2003) Morphotectonic approach to the drainage analysis in the North Marche region, central Italy. Quat Intern 101–102:157–167

Mecchia G, Mecchia M, Piro M, Barbati M (2003) Le grotte del Lazio. Collana Verde dei Parchi, Serie Tecnica n 3, A.R.P. Lazio, Roma

Menichetti M (1989) Analisi spazio-temporale del sistema carsico del M. Cucco. In: Atti 15th Congresso Nazionale di Speleologia, Castellana Grotte,1987, pp 731–762

Menichetti M (2008) Assetto strutturale del sistema geotermico di Acquasanta Terme (Ascoli Piceno). Rend Online Soc Geol It 1:118–122

Menichetti M (2009) Speleogenesis of the hypogenic caves in Central Italy. In: White BW (ed) Proceedings 15th international congress of speleology, Kerrville, vol 2, pp 909–915

Menichetti M (2011) Hypogenic cave in Western Umbria (Central Italy). Acta Carsologica 40(1):129–145

Menichetti M, Chirenco MI, Onac BP, Bottrell S (2008) Depositi di gesso nelle grotte del M.Cucco e della Gola di Frasassi, Considerazioni sulla speleogenesi. In: Atti 20th Congresso Nazionale di Speleologia, Iglesias, 2007. Mem Ist It Speleol, s II, vol 21, pp 308–325

Menichetti M, Tosti S, Salvatori F (1997) Idrodinamica del sistema carsico del Monte Cucco (Umbria, Italia) (Appennino Umbro-Marchigiano). In: Pensabene G. (ed) Atti 17th Congresso Nazionale di Speleologia, Castelnuovo Garfagnana, 1994, vol 1, pp 237–256

Minissale A (2004) Origin, transport and discharge of CO_2 in Central Italy. Earth Sci Rev 66:89–141

Minissale A, Magro G, Martinelli G, Vaselli O, Tassi F (2000) Fluid geochemical transect in the Northern Apennines (Central-Northern Italy): fluid genesis and migration and tectonic implications. Tectonophysics 319:199–222

Palmer AM (1991) Origin and morphology of limestone caves. Geol Soc Am Bull 103:1–25

Passeri L (1968) L'abisso II di Monticelli, 126 U/PG. In: Atti 9th Congresso Nazionale di Speleologia, Trieste, 1963, pp 77–85

Piccini L (2000) Il carsismo di origine idrotermale del Colle di Monsummano (Pistoia–Toscana). Le Grotte d'Italia, s V 1:33–43

Piccini L (2011) Speleogenesis in highly geodynamic contexts: the Quaternary evolution of Monte Corchia multi-level karst system (Alpi Apuane, Italy). Geomorphology 134(1):49–61

Piccini L, De Waele J, Galli E, Polyak VJ, Bernasconi SM, Asmerom Y (2015) Sulphuric acid speleogenesis and landscape evolution: Montecchio cave, Albegna river valley (Southern Tuscany, Italy). Geomorphology 229:134–143

Principi P (1931) Fenomeni di idrologia sotterranea nei dintorni di Triponzo (Umbria). Le Grotte d'Italia 5:1–4

Rogie JD, Kerrick DM, Chiodini G, Frondini F (2000) Flux measurements of non-volcanic CO_2 emission from some vents in central Italy. J Geophys Res 105:8435–8445

Sarbu SM, Galdenzi S, Menichetti M, Gentile G (2000) Geology and Biology of the Frasassi Caves in Central Italy, an ecological multi-disciplinary study of a hypogenic underground ecosystem. In: Wilkens H et al (eds) Ecosystems of the world. Elsevier, New York, pp 359–378

Southward AJ, Kennicutt MC II, Alcalà Herrera J, Abbiati M, Airoldi L, Cinelli F, Bianchi CN, Morri C, Southward EC (1996) On the biology of submarine caves with sulfur springs: appraisal of $^{13}C/^{12}C$ ratios as a guide to trophic relations. J Marine Biol Ass UK 76:265–285

Vattano M, Audra P, Benvenuto F, Bigot JY, De Waele J, Galli E, Madonia G, Nobécourt JC (2013) Hypogenic caves of Sicily (southern Italy). In: Filippi M, Bosak P (eds) Proceedings of the 16th international congress of speleology, Brno, vol 3, pp 144–149

Vlasceanu L, Sarbu SM, Engel AS, Kinkle BK (2000) Acidic cave-wall biofilms located in the Frasassi Gorge, Italy. Geomicrobiol J 17:125–139

The Frasassi Caves: A "Classical" Active Hypogenic Cave

8

Sandro Galdenzi and Daniel S. Jones

Abstract

The Frasassi caves present a unique opportunity to study sulfuric acid speleogenesis in a large karst system that contains active sulfidic processes as well as relict features produced by past speleogenetic episodes. The caves consist of a network of ramifying, mainly subhorizontal passages that reach more than 30 km in total length, and are organized in superimposed and interconnected levels. Sulfidic groundwaters are accessible in the lowermost levels. The water chemistry in the shallow phreatic zone is influenced by mixing phenomena between the sulfidic groundwaters and descending oxygenated water and, to some extent, gas exchange with the cave atmosphere. The sulfidic waters are corrosive with respect to limestone, with average limestone dissolution rates around 100 mm 10^{-3} $year^{-1}$ for submerged tablets. The release of gases to the air also causes wall corrosion (linear corrosion rate up to 85 mm 10^{-3} $year^{-1}$), which produces gypsum replacement crusts above the water table. Morphological and isotopic analyses show that large relict gypsum deposits in the upper dry levels were created by the same mechanism. Sulfide-oxidizing chemosynthetic bacteria living in the cave produce organic matter and support a rich and diverse ecosystem in the sulfidic branches, and these microorganisms contribute to sulfur cycling and cave formation processes. The evolution of the older cave levels during the Pleistocene was a complex result of changing regional geomorphological and hydrogeological regimes as well as local factors that affect water movement and gas exchange in the shallow phreatic zone within the cave.

Keywords

Frasassi caves • Hypogenic caves • Sulfidic water • Apennine • Italy

1 Introduction

The Frasassi caves are one of the most famous Italian cave systems because of their importance as a show cave. They are also the best studied hypogenic caves in Italy and present a unique opportunity to study active processes in the lower branches and relict features and deposits in the upper levels within the same large cave system.

The active growth of replacement gypsum near the cave entrance was long considered to be a secondary mineralogical process, without realizing the importance of sulfuric acid speleogenesis (SAS) for cave development. A relationship between the sulfidic water and cave development was hypothesized by local speleologists only after the exploration of new important branches since 1971, although a coherent genetic model was not initially produced. A speleogenetic model based on SAS (Galdenzi 1990) was first discussed in 1988, during a national meeting on the Frasassi caves. In the following years, the caves were

S. Galdenzi (✉)
60035 Jesi, Italy
e-mail: galdenzi.sandro@tiscali.it

D.S. Jones
BioTechnology Institute & Department of Earth Sciences, University of Minnesota, Minneapolis, MN, USA
e-mail: dsjones@umn.edu

© Springer International Publishing AG 2017

A. Klimchouk et al. (eds.), *Hypogene Karst Regions and Caves of the World*,
Cave and Karst Systems of the World, DOI 10.1007/978-3-319-53348-3_8

considered in a regional study on hypogene caves in central Italy (Galdenzi and Menichetti 1995), and a chemoautotrophic ecosystem was documented in Frasassi (Sarbu et al. 2000). Isotope measurements of sulfur deposits demonstrated that the gypsum was sourced from H_2S oxidation (Galdenzi and Maruoka 2003), supporting the previously proposed model. In the following years, new research on cave biology and geology further expanded knowledge of the cave and its environment.

2 Geological Setting

The cave system (Fig. 1) is located in the Frasassi Gorge (12° 57′E, 43° 24′N), a 500-m deep and 2-km long canyon where the Sentino River cuts through a small anticline ridge in the Northeastern Apennines, Italy, 40 km from the Adriatic Sea.

The area has a mountainous landscape, with elevation ranging between 200 m at the bottom of the valleys to about 1000 m in the surrounding mountains. The climate is subcontinental, with an annual average temperature of about 13 °C and an average annual rainfall of about 1000 mm/year. Precipitation generally reaches a maximum in autumn and spring, whereas evaporation exceeds precipitation in summer.

The steep cliffs of the Frasassi Gorge clearly show the geological structure (Fig. 2). The anticline is asymmetric, with a main NNE vergence, and was formed in the Late Miocene during a tectonic compressive phase that also caused the Apennine uplift and emersion. The eastern limb is cut by a system of N–S faults. The caves develop mainly in the Calcare Massiccio Fm. (Early Jurassic), which constitutes the core of the anticline and outcrops across the whole gorge and in the hinge zone. The Calcare Massiccio is a very pure limestone, massively bedded, and consisting mainly of wackestone and packstone facies without any significant clay or silica minerals. The formation is very permeable, due to high syngenetic porosity, a well-developed network of fractures, and high rates of karstification.

This Jurassic limestone overlies a buried 1800-m-thick upper Triassic (210 Ma) evaporitic formation, consisting mainly of anhydrite and dolomite, which represents a possible source for the ions in the mineralized Frasassi aquifer water. The upper section of the carbonate succession (Jurassic-Eocene) comprises thin-layered cherty limestones containing a thin level of Jurassic marl and a 50-m-thick middle Cretaceous marl formation (Fig. 2).

The marine sedimentation in the area terminated at the end of Miocene, and during the Pliocene the landscape evolved as a low energy relief, which is partially preserved as gently sloping surfaces at the tops of ridges. Large paleovalleys developed during the Late Pliocene and Early Pleistocene (Ciccacci et al. 1985), while rapid tectonic uplift at the end of Early Pleistocene elevated the whole region, favoring linear erosion in the river valleys and their entrenchment into the old erosional surfaces (Ambrosetti et al. 1982; Bartolini et al. 2003; D'Agostino et al. 2001). During the Pleistocene, climatic changes also heavily influenced geomorphic evolution. In the mountain areas, the valleys were filled with alluvial gravel deposits during glaciations (Coltorti and Dramis 1988), while during interglacials the alluvial deposits and the bedrock were eroded by the rivers.

Surface karst is poorly developed, but over 100 caves are known in the area. Most of the caves are small, with lengths that range from a few meters to ~ 500 m. The major cave (i.e., Grotta del Fiume—Grotta Grande del Vento System) consists of over 30 km of cave passages located at elevations between 200 (at the riverbed) and 360 m. Two important caves (Buco Cattivo, over 5000 m long, and the Grotta del Mezzogiorno-Grotta di Frasassi System, 3500 m long) occur at higher elevations, between 360 and 500 m.

The caves developed primarily in the core and eastern limb of the anticline, and consist of a network of ramifying, mainly subhorizontal passages and are organized in superimposed and interconnected levels, the genesis of which is related to stepwise lowering of the base level.

3 The Groundwater

The Cretaceous marls represent the local aquiclude and define a recharge area of about 5 km^2, which feeds the main aquifer hosted in the Calcare Massiccio and, partly, in the Cretaceous limestone. These two units are in hydraulic continuity due to the faults in the eastern limb of the anticline (Fig. 2).

In the recharge area, diffuse infiltration prevails, and the drainage network is limited, with only temporary flows in a few channels after major rainstorms. A few low discharge springs originate from small aquifers perched on the Jurassic or Cretaceous marls. The thin Jurassic marls do not impede the recharge of the main aquifer, although they concentrate infiltration along faults that cut through the marls and isolate some lower sectors of the cave and surrounding limestone from seepage waters. In the limb, the Cretaceous marls facilitate drainage toward the springs, located in the eastern side of the gorge, where the down-cutting of the river valley lowered the marl cover (Fig. 3).

The water table is close to the river level and can be accessed at many locations in the lower sections of the

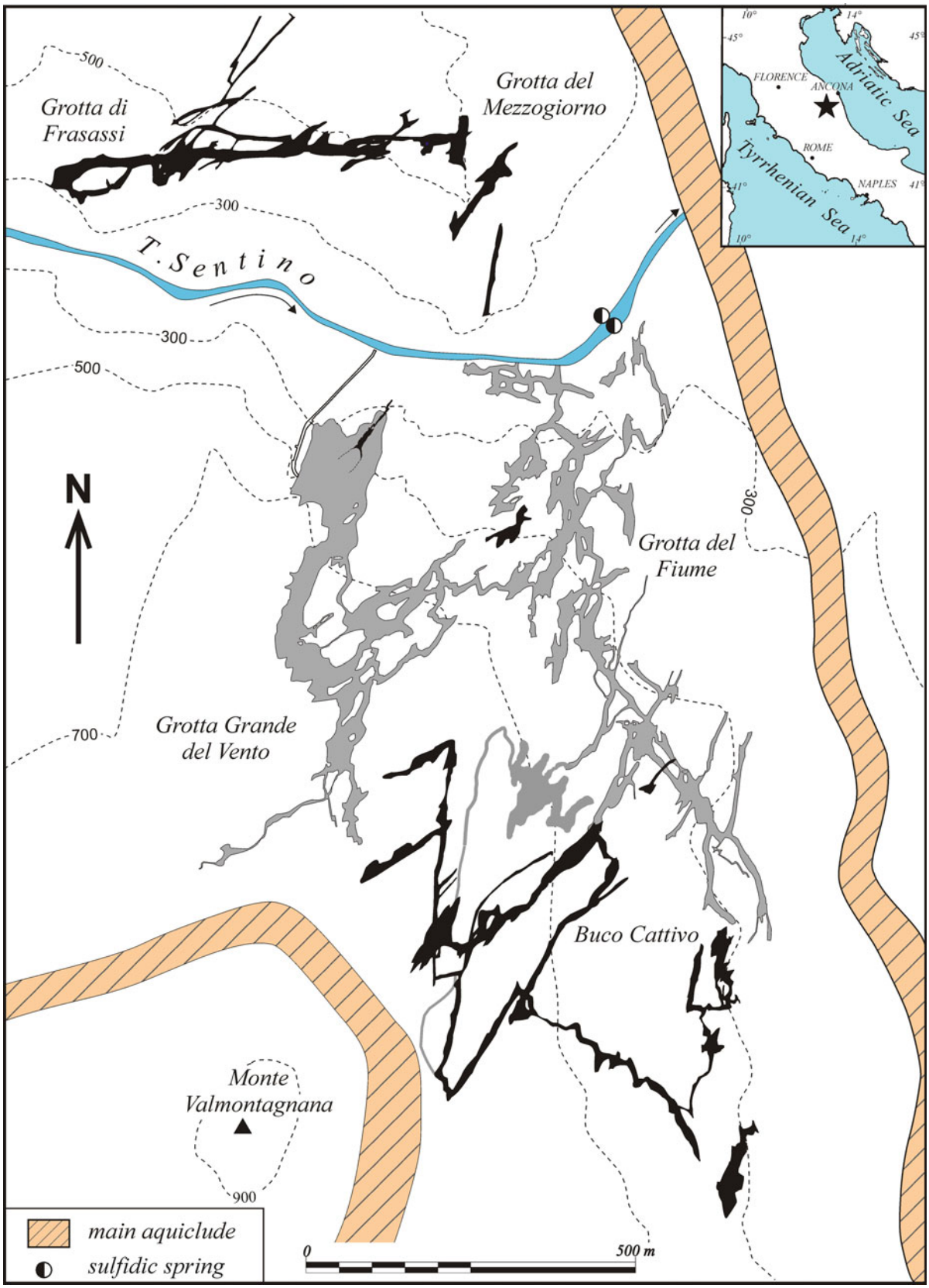

Fig. 1 Schematic plan of the Frasassi area. Cave maps are from surveys by Federazione Speleologica Marchigiana (FSM) speleological groups

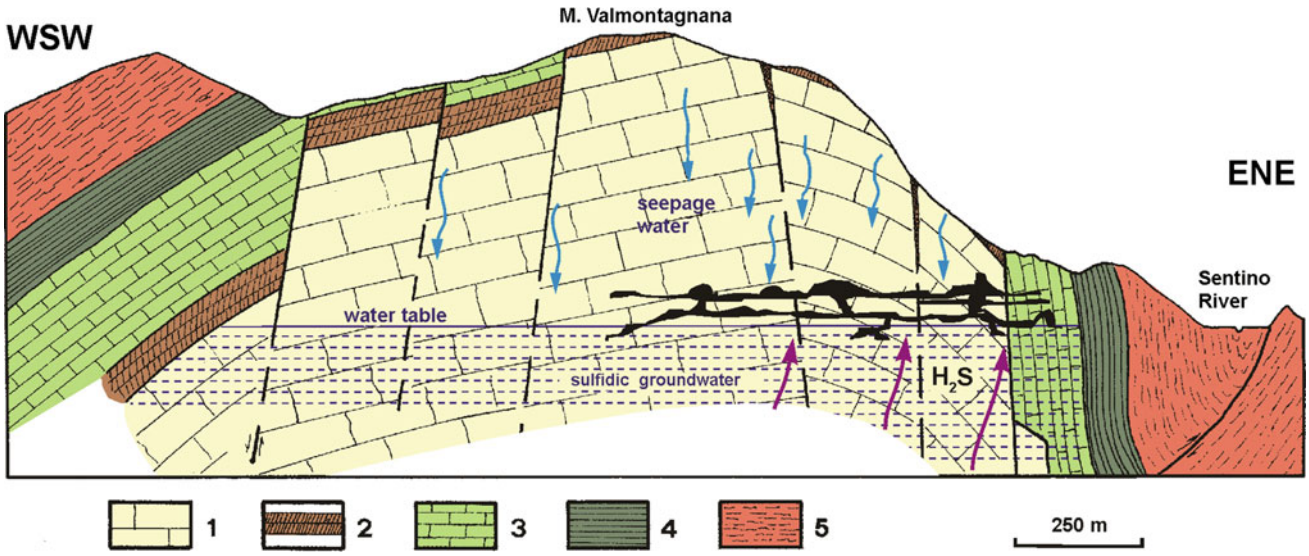

Fig. 2 Geological cross section of the Frasassi anticline, with the main groundwater flowpaths outlined. *1* Pure Jurassic limestone; *2* poorly permeable Jurassic limestones; *3* Cretaceous cherty limestone; *4* Cretaceous marls; *5* Cretaceous and Paleogene cherty and marly limestone

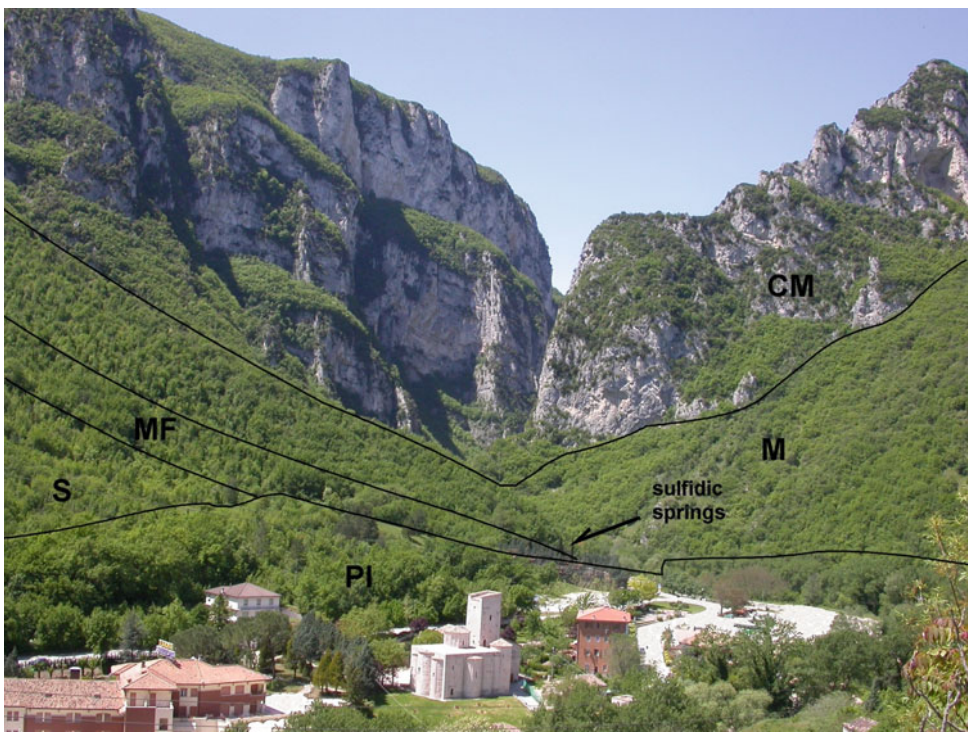

Fig. 3 View of the Frasassi Gorge. *CM* Jurassic Calcare Massiccio limestone; *M* Cretaceous limestone; *MF* Cretaceous marls; *S* Cretaceous and Paleogene limestone; *Pl* continental Pleistocene deposits (after Galdenzi et al. 2008)

caves. Wide free interfaces between sulfidic groundwater and the cave atmosphere exist in the northeast region of the cave, where flowing sulfidic streams form. In the other cave regions, water flow is less evident, and a stagnant groundwater surface can be accessed at the bottom of shafts or in narrow passages, 25 m below the lowermost of the main cave levels.

3.1 Chemistry

General characteristics of the hydrology and geochemistry of the cave system were described by Galdenzi et al. (2008), Galdenzi (2012), and references therein. Groundwater consists of two main types: bicarbonate and sulfidic, which differ in their chemical composition and origin. The

bicarbonate water derives from direct infiltration of surface meteoric water through the limestone and is found in the vadose zone and in small aquifers perched on interbedded marls. This water has a low salinity (about 200–400 mg L^{-1}), low sulfate, and high dissolved oxygen (about 0.32 mM).

The sulfidic water characterizes the main aquifer and feeds the main springs in the gorge. It is cold (about 13 °C) and saline, up to 2 g L^{-1}, with sodium and chloride as the major ions. The waters contain H_2S (up to 0.5 mM) and sulfate (up to 2.5 mM), and are undersaturated with respect to gypsum. These ions are generally believed to originate during flow through the underlying anhydrite formation, before the groundwaters rise into the limestones. The dissolved sulfide is likely derived from bacterial sulfate reduction in the underlying anhydrites. Isotopic data on $\delta^{18}O$, $\delta^{2}H$, and tritium discussed by Tazioli et al. (1990) suggested a meteoric origin for the sulfidic groundwater. These authors estimated a recharge area located at elevations of 600–1000 m, with a brief residence time in the aquifer.

Mixing phenomena between descending bicarbonate and rising mineralized water determine the composition of the groundwater in the shallow phreatic zone (Galdenzi et al. 2008). During the study year (2001), freshwaters diluted the mineralized sulfidic water by 30% in the "dry period" (summer and autumn) and 60% in the "wet period" (roughly corresponding to winter and spring). (Figure 4). These periods are not strongly related to seasonal precipitation, which have two maxima, a main one in the autumn and a secondary one in the spring. Only winter and spring precipitation directly influence the groundwater, because evapotranspiration in the summer and soil storage in the autumn reduce the amount of recharge. Some authors have hypothesized that the river may also play a role in groundwater dilution (Tazioli et al. 1990; Ciancetti and Pennacchioni 1993; Caprari et al. 2001).

Despite high permeability, the shallow phreatic zone is characterized by significant differences in water chemistry. Some pools, like Lago Verde, are fed more directly from deep aquifer zones and have higher salinity. In Lago Verde, the dilution due to freshwater is relatively low (20% maximum) and is more directly related to freshwater infiltration from the surface during the rainy periods.

In many isolated stagnant pools, water composition is affected by local factors and groundwater stratification occurs. Depending on the location, surface layers with lower salinity can vary in thickness from a few cm up to 5 m (Galdenzi et al. 2008; Mariani et al. 2007). The chemistry of the surface layer can be purely bicarbonate, or intermediate between seepage and mineralized water, typically with dissolved O_2 and without any measurable H_2S content.

3.2 Hydrodynamics

Water levels and conductivity were discussed by Galdenzi et al. (2008) and Galdenzi (2012). Galdenzi and Campagnoli (2015) also produced a map of groundwater levels in the cave, based on a survey with a digital level. These measurements revealed that the aquifer has a flat free surface with a low hydraulic gradient ($\sim$3‰) from the inner pools toward the emergence, located in the riverbed slightly above the mean river level (Fig. 5). The locally turbulent flow of the water in the NE cave sector is not due to a difference in gradient, but probably derives from a cave morphology that favors a free flow between the different pools. The inner pools, in contrast, are isolated and stagnant at the surface, but may be fed from the bottom; moving sulfidic water over 9 m below their surface was encountered during diving expeditions.

The thalweg slope of the Sentino River is about 1%. Near the entrance to Grotta del Fiume, the groundwater level is equivalent to that of the riverbed. Further upstream, the elevation of the river exceeds that of the cave water table, and the gradient between river and groundwater can reach up to 30‰ under normal conditions. These highly variable gradients in the groundwater are evidence for the importance of karst channels in increasing the permeability of the rock in different directions.

The water table level varies less than 50 cm during the year, except during major flooding events in the Sentino River when the water can rise quickly over 1.5 m for short periods (Fig. 4). Water level changes occur at the same time throughout the cave due to the high permeability of the karst aquifer, probably via submerged conduits that connect the pools.

The influence of the river and infiltrating meteoric water on the sulfidic groundwater dilution is based on evidence from temperature and conductivity changes during flooding events (Galdenzi et al. 2008), as well as from absolute measurements of water levels (Galdenzi and Campagnoli 2015). However, similarities between the chemistry of cave drip waters and the river make it difficult to use chemical parameters.

Increases in the level of the water table correspond to lower temperatures and higher dilution, and are related to the increased recharge of cold seepage water in the few days following rainfall events (Galdenzi et al. 2008). Groundwater dilution from river water can be inferred from the measured gradients and was documented during an important and isolated flooding event (Galdenzi and Campagnoli 2015). The influence of the river was perceptible only in the external zone of the cave and decreased toward the interior (Fig. 6), where variable recharge of seepage water from the karst surface is the primary cause of sulfidic groundwater

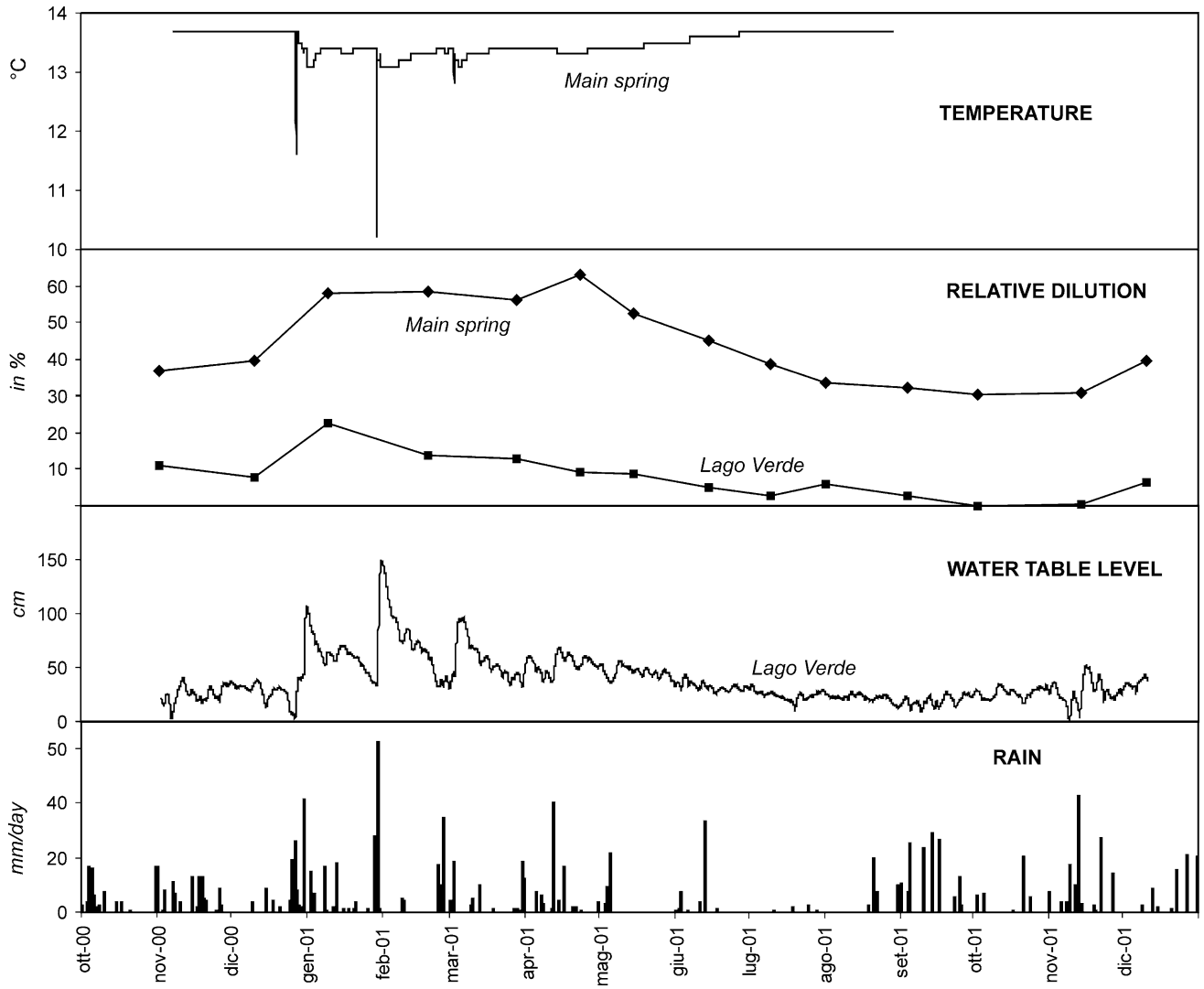

Fig. 4 Correlation between rainfall, groundwater level, groundwater temperature, and the dilution ratio between rising sulfidic water and descending seepage water (after Galdenzi et al. 2008)

dilution in the shallow phreatic zone. This observation does not exclude the possibility that the river could participate in more general recharge and dilution of the groundwater, as proposed by some authors (Tazioli et al. 1990; Ciancetti and Pennacchioni 1993; Caprari et al. 2001).

4 Cave Morphology

The Frasassi caves are organized in several superimposed horizontal levels, the genesis of which is related to stepwise deepening of the river valley and related base level. The lower parts of the cave system are developed near the present local base level, at 200 m elevation, and include two main levels at 225 and 250 m, with some minor levels. These cave levels formed in the middle and upper Pleistocene, as confirmed by correlation with the gravel terraces in the river valleys (Bocchini and Coltorti 1990) and by uranium series dating of speleothems, with ages of up to 200,000 years (Taddeucci et al. 1992).

The lower levels developed under geomorphological and hydrogeological conditions similar to the present, and for this reason the cave-forming processes that are active in the lowermost zones can be compared with the morphologies and deposits of the older inactive zones (Galdenzi 1990; Galdenzi and Maruoka 2003).

Each cave level consists of a network of ramifying horizontal passages, where wide rooms alternate with smaller tubes and spongework zones. The major room, Abisso Ancona, has a volume of about 10^6 m^3. Some vertical and

Fig. 5 Almost stagnant sulfidic water in a cave lake

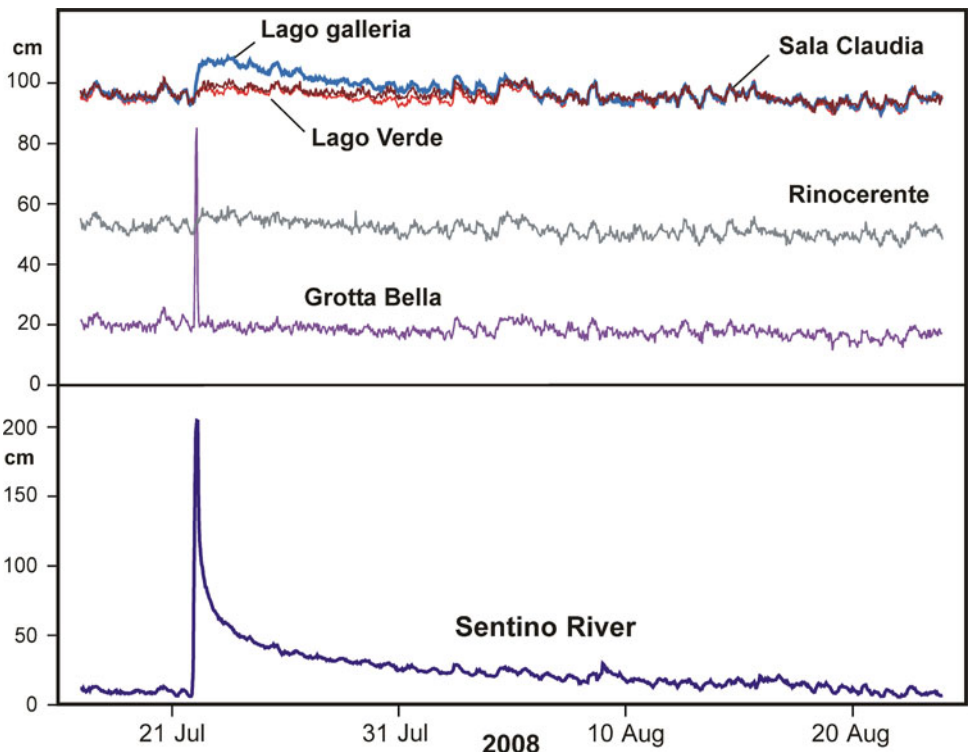

Fig. 6 The effects of an isolated flooding event on the groundwater level in the cave pools close to the river (Grotta Bella and Lago Galleria) and toward the interior (after Galdenzi and Campagnoli 2015)

inclined passages were produced by the ascending flow of deep-seated sulfidic water, but in general, solutional processes prevailed in the shallow phreatic zone.

Extensive zones show purely phreatic morphologies (Fig. 7), with rounded pendant and knife shapes that can be dominant at some locations. Roofs and walls are often incised by rising grooves and channels coming from the tops of cupolas or directly from rock fissures (Fig. 8). These rising features were produced by aggressive fluids that, upon entering in the nearly stagnant water of the main passage, flowed along the walls toward the surface due to the lower density of the fluids.

Fig. 7 One of the characteristic morphologies of the phreatic passages (image width ~1.5 m)

Wide horizontal passages and rooms were formed by sulfidic water rising through subaqueous feeder conduits or directly from narrow slots in the floor (Fig. 9). Downstream, additional sulfidic water recharge occurred through minor infeeder conduits, slots, and crevasses. Corrosional features due to subaerial and subaqueous processes often coexist in the same passage. Above the water table, subaerial corrosion due to H_2S oxidation and high CO_2 levels acted to enlarge walls and ceilings, producing the final passage section. Some isolated domes developed by the same mechanism, either above a main feeder or a system of fissures and crevasses.

The caves at the highest elevations, between 360 and 500 m (i.e., the Buco Cattivo and Mezzogiorno-Frasassi cave systems), probably formed in a different geomorphological setting, prior to a rapid entrenchment of the surface drainage network at the end of the Early Pleistocene (Ambrosetti et al. 1982). Fluvial deposits preserved at the lower entrance of the Mezzogiorno-Frasassi system (360 m elevation) yielded a cosmogenic burial age of 0.75 ± 0.26 Ma (Cyr and Granger 2008). The features of the Buco Cattivo and Mezzogiorno-Frasassi cave systems are also slightly different from those in the Fiume-Vento System, likely due to a different hydrogeological setting. Some important branches evidently developed in the deep phreatic zone, while morphologies due to subaerial SAS are rare.

Fig. 8 Corrosional channel carved by rising fluids in the shallow phreatic zone (after Galdenzi 1990)

A few gypsum deposits related to an old water table level and some replacement pockets in limited areas of the caves indicate that SAS was active, and that some free interfaces between sulfidic water and the cave atmosphere existed during the development of these older passages.

5 Cave Deposits

The caves contain abundant clastic sediments, mainly breakdown in the fault zones and thin floor deposits. The abundant fine-grained sediments were initially thought to be mainly a residuum of limestone dissolution (Bertolani et al. 1977), but they could also be derived from river and seepage water, based on the presence of pollen and allochthonous microfossils. Some gravels entered the cave near the river, or from the surface due to descending freshwater in periglacial conditions.

Chemical deposits are mainly carbonate and sulfate minerals. Large amounts of white pure calcite are deposited by dripping waters, probably enhanced by a common ion

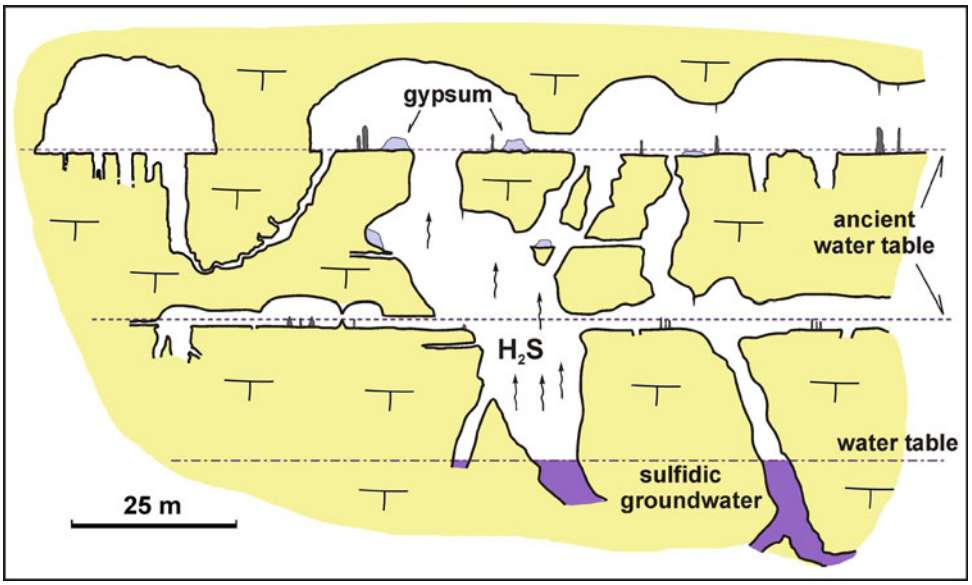

Fig. 9 Schematic section of the cave, showing multiple levels produced after successive lowering of the sulfidic groundwater. Main passages and domes were fed from below, and subaerial and subaqueous corrosional processes could coexist in the same environment

effect as waters descended through overlying gypsum deposits. Some minerals (halloysite, barite and jarosite) related to the sulfidic water have been detected (Bertolani et al. 1977), but the most significant deposit is surely the gypsum. It predominantly occurs as a white microcrystalline replacement crust over the limestone walls or thick deposits over the floor. Large prismatic crystals of gypsum are rather common due to the diagenesis of the microcrystalline deposits and to the seepage of supersaturated waters inside mud deposits.

The most important deposits of massive gypsum occur on the floor of the main rooms, which form mounds several meters thick in places, commonly below wide cupolas. Gypsum also occurs as small "glaciers" (Fig. 10) with a maximum thickness of 5 m and a volume up to over 1000 m^3 (Galdenzi 1990). Based on sedimentary structures and depositional setting, these floor deposits were interpreted to have formed by the detachment and flow of slushy gypsum from the limestone walls, which was initially produced as replacement crusts in zones exposed to intense H_2S vapors (Galdenzi 1990). Isotopic analyses on sulfur confirmed this proposed mechanism (Galdenzi and Maruoka 2003; Menichetti et al. 2008). The $\delta^{34}S$ values of the gypsum are highly negative (range from −6.4 to −19.6‰), compared to the positive values of sulfate in the sulfidic groundwater (from +20 to +22‰). As it is impossible to produce such large isotopic fractionations during precipitation from water, the gypsum cannot have been produced by precipitation from gypsum-saturated groundwater. Instead, the low $\delta^{34}S$ values of gypsum are similar to that of the H_2S ($\delta^{34}S$ from −13 to −15‰), confirming their origin from sulfide oxidation in the cave atmosphere (Galdenzi and Maruoka 2003).

The distribution and thickness of gypsum forming today in the Frasassi caves is much more limited than it was in the past. This may be due to the present hydrological setting, because a free interface between groundwater and cave air nowadays exists only at the bottom of shafts or descending passages, where gypsum is forming in restricted areas. Moreover, most of these pools are stratified, and the oxygenated water that overlies the sulfidic groundwater prevents H_2S degassing and subaerial corrosion. In some past periods, the cave was an almost ideal water table cave, with many partly flooded rooms and passages (Galdenzi 1990). The extensive distribution of old replacement gypsum crust is a testament to the importance of subaerial corrosion for cave enlargement during those times.

6 Active Speleogenetic Processes

In Frasassi, access to the groundwater free surface provides an opportunity to study active cave development in a range of situations. Active speleogenetic processes are most evident in the northeastern region of Grotta del Fiume, which has flowing sulfidic waters. The submerged walls of the stream passages are clean, corroded, and covered by an evident biofilm. Flowing sulfidic water produces notches along the cave walls at the water–air surface that can indicate old water levels.

In most stagnant lakes, the stratified bicarbonate surface water prevents any significant active corrosional processes near the water–air interface, and floating calcite rafts sometimes occur where waters are supersaturated at the surface.

Fig. 10 A thick gypsum deposit

Clear evidence for speleogenesis is associated with H_2S degassing. H_2S released by the groundwater oxidizes on wall surfaces, producing sulfuric acid that corrodes the limestone (Fig. 11) and causes its replacement by gypsum. Where H_2S degassing is slow, only a thin crystalline rim covers the limestone surface. Higher degassing rates cause highly corroded walls that are partially or completely covered by white, fine crystalline gypsum. Some large crystals grow on the gypsum crusts or directly on the limestone. Small amounts of elemental sulfur can occur where the process is even more intense. The gypsum forms as lumps that expand from the limestone surface (Fig. 12) forming a continuous crust up to many centimeters thick. The limestone surface under the gypsum crust is severely corroded, with hemispheric replacement pockets several centimeters deep. (Figure 12) Active gypsum production occurs in small areas strongly influenced by the flowpaths of the rising gas, and the process decreases rapidly with distance. In the surrounding areas, however, the high CO_2 concentration hampers the growth of calcite deposits, and well-developed mud vermiculations or "biovermiculations" (discussed below) cover the walls (Fig. 13).

Air monitoring showed that rapid gas exchange with the upper, non-sulfidic levels maintains normal oxygen concentration. Gases that originate from the groundwater varied seasonally from 1 to 8 ppm for H_2S, and from 1500 to

Fig. 11 Drip holes in the limestone floor, ~50 cm deep, produced by dripping acidic waters

Fig. 12 Replacement gypsum on the cave walls, occurring as a thin rim of dark crystals and white finely grained lumps (*left*). Wall pockets resulting from removal of the gypsum lumps (*right*). *Panel A* shows the detail of a replacement gypsum lump

Fig. 13 Wall vermiculations ("biovermiculations") are extensive in the sulfidic sections of the cave (image width ~20 cm)

5600 ppm for CO_2 (Galdenzi et al. 2008). H_2S can be detected only at short distances from the sulfidic sections, before it is quickly oxidized. In contrast, carbon dioxide maintains higher values in the surrounding rooms. Thus, the concentration of H_2S in the air is directly correlated with its concentration in the water, while cave air CO_2 does not exhibit a clear relationship with the bicarbonate content of the water, although it was observed to increase with groundwater dilution (Galdenzi et al. 2008).

6.1 H_2S Degassing

Studies by Jones et al. (2015) quantified the importance of three different processes involved in the removal of H_2S from the cave streams: (i) H_2S degassing from streams to the cave atmosphere, where it is oxidized in condensation droplets on the walls and ceiling; (ii) microbially mediated H_2S oxidation in benthic stream biofilms; and (iii) abiotic sulfide oxidation in the bulk stream water.

Field measurements and transport modeling showed that H_2S degassing accounted for the majority of sulfide removal from the streams, highlighting the potential importance of subaerial sulfide oxidation for speleogenesis. Model results showed that 60–98% of the sulfide lost from streams was due to degassing, and that microbial oxidation below the water table was responsible for the remainder. Abiotic oxidation was largely insignificant.

These results pertain to areas where sulfidic groundwaters are in direct contact with cave air, wherever groundwaters with high sulfide concentrations emerge as flowing streams and pools. Degassing is predicted to be most important in sulfidic cave streams with turbulent flow and high dissolved sulfide concentrations. The rapid H_2S degassing near streams is broadly consistent with subaerial corrosion features, the distribution of microbial life above the water table, and the distribution of gypsum deposits in the old cave levels.

Biological oxidation accounts for significant sulfide disappearance from Frasassi streams (2–25%), but pH microsensor profiles inside the biofilms do not show evidence for significant amounts of acidity (Jones et al. 2015). The majority of the sulfide is likely oxidized to intermediate sulfur species such as zero-valent sulfur ($2H_2S + O_2 \rightarrow 2SO + 2H_2O$), which is abundant in Frasassi biofilms and sediments (Macalady et al. 2008). Sulfuric acid does not appear to be a major end product of microbial sulfide oxidation in the cave streams. Interestingly, pH decreases in the anoxic sediments below the biofilms, suggesting that acid production associated with anaerobic microbial processes may be an important but yet unexplored mechanism for limestone corrosion in the streams.

6.2 Limestone Dissolution Measurements

Limestone tablets were applied to measure corrosion rates in the cave environment by Galdenzi et al. (1997). Tablets of uniform, pure micritic Cretaceous limestone were placed in both the sulfidic water and in the atmosphere for five years. The measured mass loss was then converted to a linear dissolution rate for the limestone surfaces.

The tablets exposed to acidic vapors in the cave atmosphere were covered by a layer of replacement gypsum, and the limestone surface after the gypsum removal was severely corroded, with incipient dissolutional pockets (Fig. 14). The linear corrosion rate reached values up to 85 mm ka^{-1}. The average rate was ~50 mm ka^{-1}, and increased from 42 to 69 mm ka^{-1} after 2.5 and 5 years of exposure. The site conditions strongly influenced the results, and significant differences occurred among tablets located only a few centimeters apart, depending on the rising gas flow path. Similar values (58 mm ka^{-1}) were obtained in the sulfidic groundwater, without differences due to the length of exposure and site conditions. The limestone had a slightly rough surface with calcite veins protruding in relief (Fig. 14).

Fig. 14 Photographs of limestone tablets that were exposed to the sulfidic water. A tablet that was placed in the groundwater, coated by a biofilm with worms (**a**), compared with one that was placed in the cave atmosphere (**b**). The white material in B is replacement gypsum. Tablets photographed after gypsum and biofilm removal: underwater (**c**) and in the atmosphere (**d**). Tablets after six months in flowing sulfidic water (**e** and **f**)

Similar measurements made in another non-circulating stratified body of water in Frasassi (Mariani et al. 2007) resulted in lower corrosion values, likely because a different material, Carrara marble, was used. The maximum weight loss occurred in the upper part of the sulfidic layer, near the chemocline (average value $\sim$0.09% a^{-1}, corresponding to $\sim$1.7 mm ka^{-1}), and decreased in both the deep part of the sulfidic layer ($\sim$1.3 mm ka^{-1}) as well as in the weakly mineralized non-sulfidic water above the chemocline.

Detailed measurements of dissolution in the sulfidic water were repeated in different flow conditions and depths (Galdenzi 2012). A linear average corrosion rate of 24 mm ka^{-1} was measured in the stagnant pools, fed by less diluted sulfidic water coming from deep zones of the aquifer. Dissolution rates were higher (68–106 mm ka^{-1}) in slowly flowing waters, and very evident changes in the tablets shape (up to over 1 cm) were observed after only a few months in weakly turbulent waters (Fig. 14).

The variation in corrosion in the shallow phreatic zone mainly depends on the availability of the oxygen, which is influenced by several factors: the existence of large surface interfaces between groundwater and cave atmosphere; the flow of water and its turbulence; and the slow seepage or the direct, fast recharge of O_2-rich meteoric water from the vadose zone.

7 Life

The Frasassi caves are a thriving oasis for subterranean life. The dissolved sulfide that enters the system in anoxic groundwaters represents a plentiful fuel source for microbial

chemosynthesis. Microbial life is especially robust near the water table, where oxygenation of the sulfidic groundwaters provides energy for aerobic sulfide-oxidizing microorganisms that form the base of the cave food web. Diverse invertebrate life occurs in the sulfidic groundwaters and in adjoining chambers. Most of these species are troglobitic and several are endemic to Frasassi. Organic carbon and nitrogen stable isotopes show that fauna in the sulfidic zones are supported by in situ chemosynthesis, while animals in the non-sulfidic regions of Frasassi are dependent on organic inputs from surface sources (Sarbu et al. 2000).

In cave streams, sulfide-oxidizing microorganisms form white biofilms that cling to submerged rocks and coat sediments (Fig. 15). Most of these biofilms are produced by filamentous microorganisms in the Gamma- and Epsilonproteobacteria classes. These filamentous bacteria are important primary producers that create the biofilm matrix, although the communities also support diverse populations including sulfate reducers and other sulfide oxidizers. Sulfur oxidizers and reducers often occur in close associations that may facilitate sulfur cycling over micron spatial scales (Macalady et al. 2006). Extensive sampling and molecular analysis of the white stream communities revealed that different biofilm-forming populations occur in distinct geochemical and hydrodynamic niches defined by differences in dissolved sulfide, oxygen, and water flow velocity (Macalady et al. 2008).

Hydrogen sulfide degassing from streams provides energy for life above the water table. Sulfide gas flux is highest near the fastest flowing and most turbulent reaches of the streams (Jones et al. 2015). In these areas, small viscous biofilms commonly known as “snottites” or “mucoliti” hang over the stream from gypsum wall crusts (Fig. 16). The biofilms have pH values between 0 and 2, and represent the most acidic microenvironments in the cave. The biofilms are formed by sulfide-oxidizing bacteria that rely on sulfide gas from the cave atmosphere, and contain simple communities of acid-tolerant bacteria and archaea (Vlasceanu et al. 2000; Macalady et al. 2007; Jones et al. 2012). The numerically abundant organism in Frasassi snottites is *Acidithiobacillus thiooxidans*, which is a chemosynthetic sulfide oxidizer that represents an important primary producer in the subaerial cave environment (Jones et al. 2014). It is likely that *Acidithiobacillus* are responsible for creating the biofilms.

Further from the streams, gypsum crusts diminish and patterned wall deposits known as biovermiculations occur on exposed limestone surfaces (Fig. 13). Biovermiculations are films of organic-rich sediment that stand up to 1 cm in relief from the limestone surface, and range in morphology from discreet dots to spectacular dendritic and meandering designs. In some places, biovermiculations become so robust that the sediment patterns merge and form entire wall-covering mats. Biovermiculations support diverse microbial communities that likely play a role in generating the organic-rich material in the sediments, although their

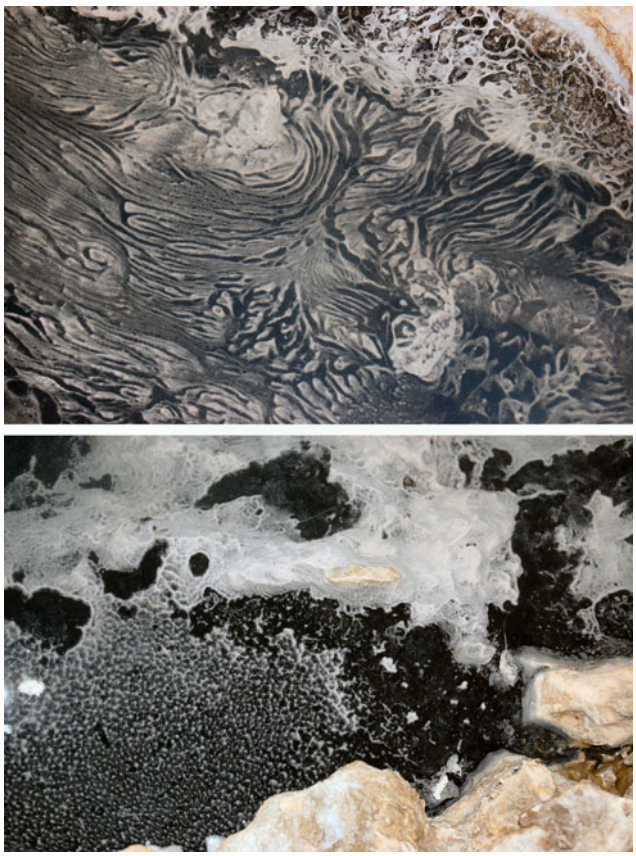

Fig. 15 Biofilm coating the dark, organic-rich mud in the sulfidic water (images width ~80 cm)

Fig. 16 Hanging organic wall biofilms, 1–2 cm long, growing in a spider web. The pH of the droplets is <1

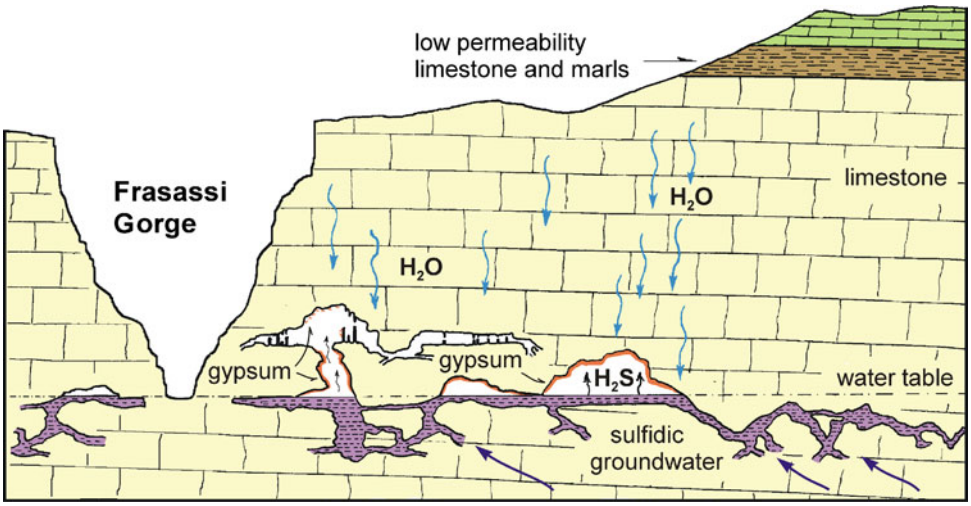

Fig. 17 Surface geology and cave development. The increase in O_2-rich seepage at the boundary between the limestone and marl units favored solutional processes, causing the widening of the passage section and the increase in free interfaces between sulfidic water and the atmosphere. Only small phreatic tubes, tapering inward, developed under the poorly permeable cover (modified after Galdenzi 1990)

contribution to the patterns themselves remains unknown (Jones et al. 2008; Boston et al. 2009).

There is still much to learn about life in the Frasassi caves. Little is known about the microbial communities in the black sediments that occur below the white stream biofilms, or in the gypsum wall crusts themselves (Lyon et al. 2004). Relict gypsum crusts and vermiculations in older cave levels may preserve information on the microbial processes that were active during earlier episodes of cave formation. Other mysteries remain, such as enigmatic microbial "ropes" that occur in the stratified sulfidic lakes (McCauley et al. 2010). Frasassi has also proven valuable as a natural laboratory for probing fundamental microbial ecology concepts, such as resource ratio theory (Macalady et al. 2013) and microbial biogeography (Jones et al. 2016). The Frasassi caves are truly a treasure trove for microbial ecologists.

8 Speleogenesis

The general structure and the morphology of the caves and the presence of gypsum deposits in the upper passages show that sulfide oxidation has played an important role during the development of the Frasassi caves. Solutional processes prevailed in the shallow phreatic zone, where the supply of oxygen enhances redox processes, although vertical and inclined passages produced by the ascending flow of sulfidic water developed up to some tens of meters below the water table (Fig. 9).

The freshwater responsible for oxidation processes is mainly derived from surface infiltration, with possible limited contributions from river water. Differently than first hypothesized (Galdenzi et al. 1999), sulfide-oxidizing bacteria living in the biofilms that cover rock and sediment near the surface of the water bodies are responsible for a significant biomass production in the cave, but may not have an important direct role in the production of the acidity (Jones et al. 2015).

The non-uniform recharge of meteoric water influenced speleogenesis, and the surface geology affects the cave structure. A general enlargement of the passage section and a strong increase in the subaerial corrosional processes occur below the stratigraphic boundary between the limestone and the overlying thin marls (Fig. 17). Many rooms and passages in the different cave levels are located along the same fault systems, where both the rise of sulfidic water and the recharge of freshwater can occur.

Phreatic and subaerial corrosional processes commonly coexisted in the same passages, and they are often overprinted because the height of the water table level in the cave is controlled by the Sentino River in the Gorge. Consequently, a passage may be submerged or exposed following changes in the local base level due to alternating cycles of erosion and sedimentation in the river.

The progressive, long-term, deepening of the river valley also caused a lowering of the water table in the cave. The corrosion processes due to sulfidic waters moved to deeper regions, forming new cave levels. Old feeder conduits remained above the water table, joining the different cave levels and providing a pathway for H_2S gas transfer to upper levels. Old feeder conduits therefore may have facilitated periodic corrosion and gypsum deposition in the upper dry levels, alternating with the calcite deposition by seepage water.

The importance of subaerial versus subaqueous speleogenesis in the cave varied during past episodes of cavern development, and overprinting can make it challenging to evaluate their true importance. In the ancient caves (Buco Cattivo and Mezzogiorno-Frasassi caves), features and deposits due to subaerial corrosion are less common. In contrast, widespread relict structures in the Fiume-Vento

cave show that subaerial corrosion was of greater importance overall during some periods of the cave history than in the present. This is also confirmed by the size and depositional setting of massive gypsum glaciers in the old levels of the same cave, indicating a level of gypsum production that far exceeds that of the modern sulfidic zones.

Differences in the magnitude of degassing throughout the cave history likely resulted from changing hydrodynamic conditions, which can reduce or favor extensive H_2S release to the cave atmosphere. It should also be noted that the presence of extensive air–water interfaces would increase the supply of dissolved oxygen to shallow cave waters, which would favor the oxidation processes in the water itself.

The development of each cave level is influenced by two main factors: (1) the length of time the water table remains at the same elevation, which is directly influenced by the general geomorphic evolution of the area; and (2) the intensity of corrosion, which varies both in the different zones of the cave and with time. The linear corrosion rates measured in the cave show that the size of the main rooms and passages are compatible with the high corrosion rate measured with the limestone tablets, considering the presumable lifetime of each level (Galdenzi 2012). On the contrary, the values measured in the area with stagnant water are too low to account for the development of the main cave levels.

The development of the main cave levels therefore cannot be simply related to the stages of valley deepening. The water table must remain stable for a long period, but favorable conditions are also required to promote a high corrosion rate. The amount of sulfidic water rising from depth and the input of descending freshwater from the surface, the possibility of widespread gas exchanges with the cave atmosphere, and flow conditions in the aquifer can all influence the shape and size of each cave level.

References

Ambrosetti P, Carraro F, Deiana G, Dramis F (1982) Il sollevamento dell'Italia Centrale tra il Pleistocene inferiore e il Pleistocene medio. CNR, Progetto Finalizzato "Geodinamica", Publ 513 II:219–223

Bartolini C, D'Agostino N, Dramis F (2003) Topography, exhumation, and drainage network evolution of the Apennines. Episodes 23 (3):212–217

Bertolani M, Garuti G, Rossi A, Bertolani Marchetti M (1977) Motivi di interesse mineralogico e petrografico nel complesso carsico Grotta Grande del Vento-Grotta del Fiume. Le Grotte d'Italia s IV 6:109–144

Bocchini A, Coltorti M (1990) Il complesso carsico Grotta del Fiume Grotta Grande del Vento e l'evoluzione geomorfologica della Gola di Frasassi. In: Galdenzi S, Menichetti M (eds) Il carsismo della Gola di Frasassi. Atti del Convegno Nazionale, San Vittore Genga, September 1988. Mem Ist It Speleol, s II, vol 4, pp 155–180

Boston P, Curnutt J, Gomez E, Schubert K, Strader B (2009) Patterned growth in extreme environments. In: Proceedings of the third IEEE international conference on space mission challenges for information technology, 2009, Citeseer, pp 221–226

Caprari M, Galdenzi S, Nanni T, Ramazzotti S, Vivalda P (2001) La sorgente di Gorgovivo: analisi idrogeologica finalizzata all'individuazione delle zone di tutela, rispetto e protezione. Mem Soc Geol It 56:157–169

Ciancetti GF, Pennacchioni E (1993) Idrologia superficiale ed alimentazione della falda dell'area carsica di Frasassi. Geologia applicata ed idrogeologia 28:285–293

Ciccacci S, D'Alessandro L, Dramis F, Fredi P, Pambianchi G (1985) Geomorphological and neotectonic evolution of the Umbria-Marche Ridge, Northern Sector. Stud Geol Camerti 10:7–15

Coltorti M, Dramis F (1988) The significance of stratified slope waste deposits in the Quaternary of Umbria-Marche Apennines (Central Italy). Zeitschrift für Geomorphologie, Suppl Bd 71:59–70

Cyr AJ, Granger DE (2008) Dynamic equilibrium among erosion, river incision, and coastal uplift in the northern and central Apennines, Italy. Geology 36(2):103–106

D'Agostino N, Dramis F, Funiciello R, Jackson JA (2001) Interactions between mantle upwelling, drainage evolution and active normal faulting: an example from the central Apennines (Italy). Geophysical J Intern 147:475–497

Galdenzi S (1990) Un modello genetico per la Grotta Grande del Vento. In: Galdenzi S, Menichetti M (eds) Il carsismo della Gola di Frasassi. Atti del Convegno Nazionale, San Vittore di Genga, September 1988. Mem Ist It Speleol, s II, vol 4, pp 123–142

Galdenzi S (2012) Corrosion of limestone tablets in sulfidic ground-water: measurements and speleogenetic implications. Intern J Speleol 41(3):149–159

Galdenzi S, Campagnoli A (2015) Piano quotato dell'acquifero carsico di Frasassi. In: De Nitto L et al (eds) Atti 22nd Cogresso Nazionale di Speleologia, Pertosa-Auletta (SA), 2015. Mem Ist It Speleol, s II, vol 29, pp 375–380

Galdenzi S, Maruoka T (2003) Gypsum deposits in the Frasassi caves, Central Italy. J Cave Karst Studies 65:111–125

Galdenzi S, Menichetti M (1995) Occurrence of hypogenic caves in a karst region: examples from central Italy. Environ Geol 26:39–47

Galdenzi S, Cocchioni M, Morichetti L, Amici V, Scuri S (2008) Sulfidic ground-water chemistry in the Frasassi caves, Italy. J Cave Karst Stud 70:94–107

Galdenzi S, Menichetti M, Forti P (1997) La corrosione di placchette calcaree ad opera di acque sulfuree: dati sperimentali in ambiente ipogeo. In: Jeannin PY (ed) Proceedings of the 12nd international congress of speleology, La Chaux-de-Fonds, vol 1, pp 187–190

Galdenzi S, Menichetti M, Sarbu S, Rossi A (1999) Frasassi caves: a biogenic hypogean karst system? In: Audra P (ed) Proceedings European Conference Karst 99. Université de Provence, Etudes de Géographie physique, suppl 28, pp 101–106

Jones DS, Albrecht HL, Dawson KS, Schaperdoth I, Freeman KH, Pi Y, Pearson A, Macalady JL (2012) Community genomic analysis of an extremely acidophilic sulfur-oxidizing biofilm. ISME J 6:158–170

Jones DS, Lyon EH, Macalady JL (2008) Geomicrobiology of biovermiculations from the Frasassi cave system, Italy. J Cave Karst Stud 70:78–93

Jones DS, Polerecky L, Galdenzi S, Dempsey BA, Macalady JL (2015) Fate of sulfide in the Frasassi cave system and implications for sulfuric acid speleogenesis. Chem Geol 410:21–27

Jones DS, Schaperdoth I, Macalady JL (2014) Metagenomic evidence for sulfide oxidation in extremely acidic cave biofilms. Geomicrobiol J 31:194–204

Jones DS, Schaperdoth I, and Macalady JL (2016). Biogeography of sulfur-oxidizing *Acidithiobacillus* populations in extremely acidic cave biofilms. ISME J. doi:10.1038/ismej.2016.74

Lyon E, Koffman B, Meyer K, Cleaveland L, Mariani S, Galdenzi S, Macalady J (2004) Geomicrobiology of the Frasassi Caves. In: Galdenzi S (ed) Frasassi 1989–2004: Gli sviluppi nella ricerca, Consorzio Frasassi, pp 152–157

Macalady JL, Dattagupta S, Schaperdoth I, Jones DS, Druschel GK, Eastman D (2008) Niche differentiation among sulfur-oxidizing bacterial populations in cave waters. ISME J 2:590–601

Macalady JL, Hamilton TL, Grettenberger CL, Jones DS, Tsao LE, Burgos WD (2013) Energy, ecology and the distribution of microbial life. Phil Trans R Soc B 368:20120383

Macalady JL, Jones DS, Lyon EH (2007) Extremely acidic, pendulous microbial biofilms from the Frasassi cave system, Italy. Environ Microbiol 9:1402–1414

Macalady JL, Lyon EH, Koffman B, Albertson LK, Meyer K, Galdenzi S, Mariani S (2006) Dominant microbial populations in limestone-corroding stream biofilms, Frasassi cave system, Italy. Appl Environ Microbiol 72:5596–5609

Mariani S, Mainiero M, Barchi M, van der Borg K, Vonhof H, Montanari A (2007) Use of speleologic data to evaluate Holocene uplifting and tilting: an example from the Frasassi anticline (northeastern Apennines, Italy). Earth Planet Sci Lett 257:313–328

McCauley R, Jones D, Schaperdoth I, Steinberg L, Macalady J (2010) Metabolic Strategies in energy-limited microbial communities in the anoxic subsurface (Frasassi Cave System, Italy). In: AGU fall meeting abstracts, 2010, p 0317

Menichetti M, Chirenco MI, Onac B, Bottrell S (2008) Depositi di gesso nelle grotte del M.Cucco e della Gola di Frasassi, Considerazioni sulla speleogenesi. In: Atti 20th Cogresso Nazionale di Speleologia, Iglesias 2007. Mem Ist It Speleol, s II, vol 21, pp 308–325

Sarbu SM, Galdenzi S, Menichetti M, Gentile G (2000) Geology and biology of the Frasassi caves in Central Italy, an ecological multi-disciplinary study of a hypogenic underground ecosystem. In: Wilkens H et al (eds) Ecosystems of the world. Elsevier, New York, pp 359–378

Taddeucci A, Tuccimei P, Voltaggio M (1992) Studio geocronologico del complesso carsico "Grotta del Fiume–Grotta Grande del Vento" (Gola di Frasassi, AN) e indicazioni paleoambientali. Il Quaternario 5:213–222

Tazioli GS, Cocchioni M, Coltorti M, Dramis F, Mariani M (1990) Circolazione idrica e chimismo delle acque sotterranee dell'area carsica di Frasassi nelle Marche. In: Galdenzi S, Menichetti M (eds) Il carsismo della Gola di Frasassi. Atti del Convegno Nazionale, San Vittore di Genga, September 1988. Mem Ist It Speleol, s II, vol 4, pp 93-108

Vlasceanu L, Sarbu SM, Engel AS, Kinkle BK (2000) Acidic cave-wall biofilms located in the Frasassi Gorge, Italy. Geomicrobiol J 17:125–139

The Coastal Sulfuric Acid Cave System of Santa Cesarea Terme (Southern Italy)

9

Ilenia M. D'Angeli, Marco Vattano, Mario Parise, and Jo De Waele

Abstract

Santa Cesarea Terme in Salento is the only area in which hypogenic caves have been recognized in the Apulia region. In this spa area, the rising of sulfidic thermal waters that mix with both recent fresh infiltration waters and coastal salt water has formed four active sulfuric acid speleogenesis (SAS) caves. These caves are characterized by the typical set of sulfuric acid meso- and micromorphologies, and also by the presence of both gypsum and native sulfur. In all caves, biofilms are visible in the sulfidic thermal waters and on the cave walls.

Keywords

Thermal water • Spa • Speleogenesis • Hypogenic cave

1 Introduction

Apulia (southeastern Italy) is one of the Italian sectors most affected by karst processes, due to the widespread presence of carbonate rocks. The configuration of the region as an elongated peninsula makes the Apulian coastlines extensively carved by karst caves and coastal karst landforms (Palmentola 2002; Inguscio et al. 2007; Parise 2008; De Waele et al. 2011; Parise et al. 2013), including sinkhole features both along the low-lying coasts (Bruno et al. 2008; Margiotta et al. 2012; Basso et al. 2013) and offshore (Taviani et al. 2012). Salento, the southernmost part of the peninsula, is particularly rich in remarkable karst caves along the coast, with sites of great paleontological and archeological importance (Grotta Romanelli, Porto Badisco) (Margiotta and Sansò 2014), together with sites opened to public (Zinzulusa show cave; Parise 2011; D'Agostino et al. 2015) and the many caves visited during the summer season by tourists.

In such scenario, Santa Cesarea Terme stands as an important spa area, known since the nineteenth century, with many sites of emergence of thermal waters. In this paper, after describing the main geological and morphological features of the area, we summarize the hydrogeology of the Santa Cesarea Terme aquifer and the morphological and mineralogical characteristics of the caves.

I.M. D'Angeli · J. De Waele (✉)
Italian Institute of Speleology, Department of Biological, Geological and Environmental Sciences, University of Bologna, Via Zamboni, 67, 40126 Bologna, Italy
e-mail: jo.dewaele@unibo.it

I.M. D'Angeli
e-mail: dangeli.ilenia89@gmail.com

M. Vattano
Department of Earth and Marine Sciences, University of Palermo, Via Archirafi 22, 90123 Palermo, Italy
e-mail: marco.vattano@unipa.it

M. Parise
Department of Earth and Geo-Environmental Sciences, University of Bari Aldo Moro, Via E. Orabona 4, 70125 Bari, Italy
e-mail: mario.parise@uniba.it

2 Geology and Karst Geomorphology

The sulfur springs of Santa Cesarea Terme (Fig. 1) flow out along a coastal sector of the Salento peninsula, part of the Apulian carbonate platform (Ricchetti et al. 1988; Bosellini et al. 1999; Bossio et al. 2005). The carbonate succession, consisting of over 5-km-thick Jurassic and Cretaceous limestone and dolostone, rests above Late Triassic evaporites

© Springer International Publishing AG 2017

A. Klimchouk et al. (eds.), *Hypogene Karst Regions and Caves of the World*, Cave and Karst Systems of the World, DOI 10.1007/978-3-319-53348-3_9

Fig. 1 A view of the Santa Cesarea Terme spa area: The *milky color* in the sea (*yellow arrows*) is due to plumes of sulfur-rich waters coming out of the thermal sulfuric acid speleogenesis (SAS) caves. Photograph Mario Parise

and is unconformably overlain by Cenozoic calcareous successions.

Starting from the Early Triassic, the area was part of the Apulian carbonate platform, characterized by shallow-water carbonate sedimentation (Mostardini and Merlini 1986). Since Cretaceous times, it experienced a number of transgression–regression phases, giving rise to a succession constituted by multiple unconformities. Eventually, during the Middle Pleistocene, the area underwent a severe regional uplift (Doglioni et al. 1994).

As concerns the main geological structures, the Santa Cesarea Terme area shows extensional and trans-tensional structures, with related pull-apart features. The NW–SE faults are the most diffuse, with subordinate presence of NE–SW, E–W and N–S fault systems. In particular, the NW–SE transtensional faults appear to be the youngest (Zuffianò et al. 2013), also controlling the development of the main karst landforms in the area. The thermal springs are located, as the village of Santa Cesarea Terme, on a structural high, with the caves distributed along the NW–SE fault zones.

The study area hosts a variety of karst surface landforms, mostly represented by dolines and by typical karst valleys, locally termed *lame* (Parise et al. 2003). Apart from a number of inland caves (mostly with development limited to a few tens of meters, and maximum depth around 40 m), the most relevant karst features are distributed along the coast (Fig. 2) and correspond to the three caves within the spa area (PU105 Grotta Gattulla, PU102 Grotta Fetida and PU103 Grotta Sulfurea) and an additional one further south (PU914 Grotta Solfatara).

3 The Santa Cesarea Terme Caves

Known and described by several scholars since 1800 (Mauget 1875; De Giorgi 1882), and used starting from the 1930s as spa (Corti 1992), the set of caves at Santa Cesarea Terme represents a significant tourist attraction in this coastline stretch of southern Apulia. Apart from the touristic and therapeutic interests (Dell'Oca 1962), the caves are of great scientific importance, being, nowadays in Apulia, the only caves of hypogenic origin sensu Klimchouk (2007) and De Waele et al. (2014).

All caves are clearly developed along N30°E fractures running perpendicular to the coast and developing up to a little over 100 m landward. In their innermost parts, sulfur-rich thermal waters enter the caves from below. The cave passages are up to ten meters wide, but generally rather low (on average 3–4 m, never exceeding 10 m) and show no signs of former water levels. The walls and roofs are intensely corroded, with dissolution enlarging every possible fracture, forming a network of enlarged joints and less corroded pendants (Fig. 3a). At a centimeter scale, replacement pockets can be seen in many places (Fig. 3b), with gypsum crusts covering the walls of the fractures and the inner parts of the pockets. All caves have their floor flooded by the sea on which the thermal milk-colored sulfuric water flows (Fig. 3c, d).

Gypsum occurs as solid crusts, but covers the walls also with fine and delicate crystals from which biofilms hang (Fig. 3e). The microbial mats are also present in the form of very nicely drawn patterns of biovermiculations of

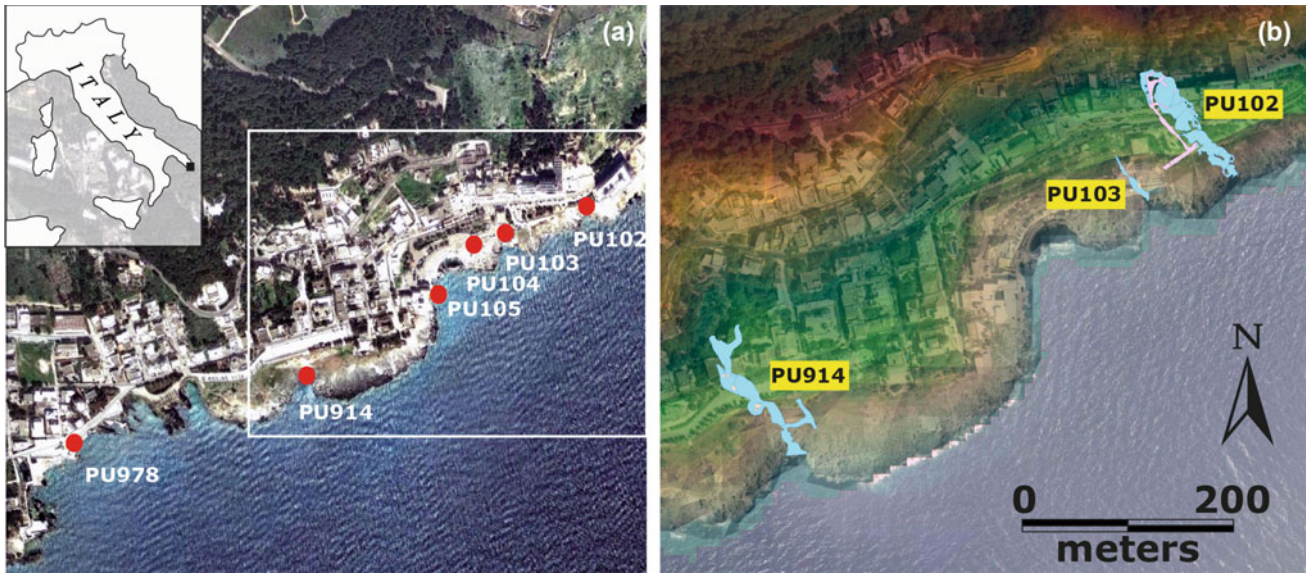

Fig. 2 **a** Google Earth image showing the distribution of caves along the Santa Cesarea Terme coastline. PU 102 = Grotta Fetida; PU 103 = Grotta Sulfurea; PU 104 = Grotta Bagno Marino; PU 105 = Grotta Gattulla; PU914 = Grotta Solfatara; PU 978 = Riparo Gli Archi. **b** Sketch showing the map of Grotta Fetida, Grotta Sulfurea and Grotta Solfatara. Surveys Apulian Speleological Federation (FSP)

brownish–yellowish color (Fig. 3f) and white moonmilk materials with low pH close to 0–1.

The replacement gypsum occurs in different forms: as toothpaste-like, not yet consolidated, material, as prismatic crystals (Fig. 4b) or as hard crusts (Fig. 4c) or powder crusts inside the replacement pockets (Fig. 4d). As observed in an Austrian sulfuric acid cave (Plan et al. 2012), gypsum is pseudomorphic, replacing the mineralogy of original fine sedimentary structures of the replaced limestone, including fossils (Fig. 4a). In one of the caves, Grotta Gattulla, the walls are covered with an over 1-cm-thick coating of vivid yellow native sulfur (Fig. 4c, e) that formed above the present water level. In Grotta Fetida, fine crystalline gypsum crusts covering the limestone walls occur alongside the biovermiculations (Fig. 4f).

In Grotta Sulfurea, some common calcite speleothems (stalactites, flowstones and stalagmites) decorate the cave. Stalagmites and columns are now submerged by the sea and occur up to 2 m below sea level (Fig. 5). These appear to be slightly corroded and have developed when sea level was at least several meters lower than today. The rather fresh appearance of these speleothems seems to demonstrate that dissolution in these sulfidic waters is not very active, or has started rather recently, or that dissolution/corrosion processes occur mainly on the surficial water layer (i.e., at the water–air interface) where H_2S can oxidize becoming H_2SO_4.

It is obvious that cave enlargement occurred downstream of the sulfur springs, where the oxidation of hydrogen sulfide produces sulfuric acid that immediately reacts with the host rock replacing calcite with gypsum. This process appears to be active essentially above the water level, on the wet walls and ceiling. Dissolution rates are being monitored since October 2015 following the method by Galdenzi (2012), in order to understand which is the dominant phenomenon/process (H_2S degassing vs. water mixing) in submerged environments and cave atmosphere. Limestone and gypsum tablets have been located in three environments: water, interface and air in several cave sections moving from a site dominated by sea water to the deep part of the cave, dominated by rising H_2S-rich fluids. We observed that dissolution at the water–air interface is faster in the median cave sector (where mixing between sea and deep water occurs), while dissolution in air is higher in the deeper part of the cave, where H_2S degassing is more abundant.

Different hypotheses about the springs have been presented in the literature, but there is no accordance so far on their origin (Zezza 1980; Calò et al. 1983; Calò and Tinelli 1995), and several uncertainties still exist.

The caves are distributed along a 500-m-long coastline stretch at sea level, at the base of the carbonate coastal cliff. As concerns water types, the overall system seems to be due to three components, in all creating a mixing solution undersaturated with respect to calcite: (i) the fresh water deriving from meteoric infiltration in the carbonate rocks, (ii) the brackish water due to seawater intrusion and (iii) a sulfur-rich thermal saline fluid.

The thermal waters coming from the caves are distributed in the Na–Cl–SO_4 quadrant of the *Ludwig–Langelier* diagram, and their pH ranges from 6.9 to 7.3 from the ones dominated by deep water to those mainly influenced by water mixing (seawater–deep water). As pointed out by previous studies, their spring waters show variable

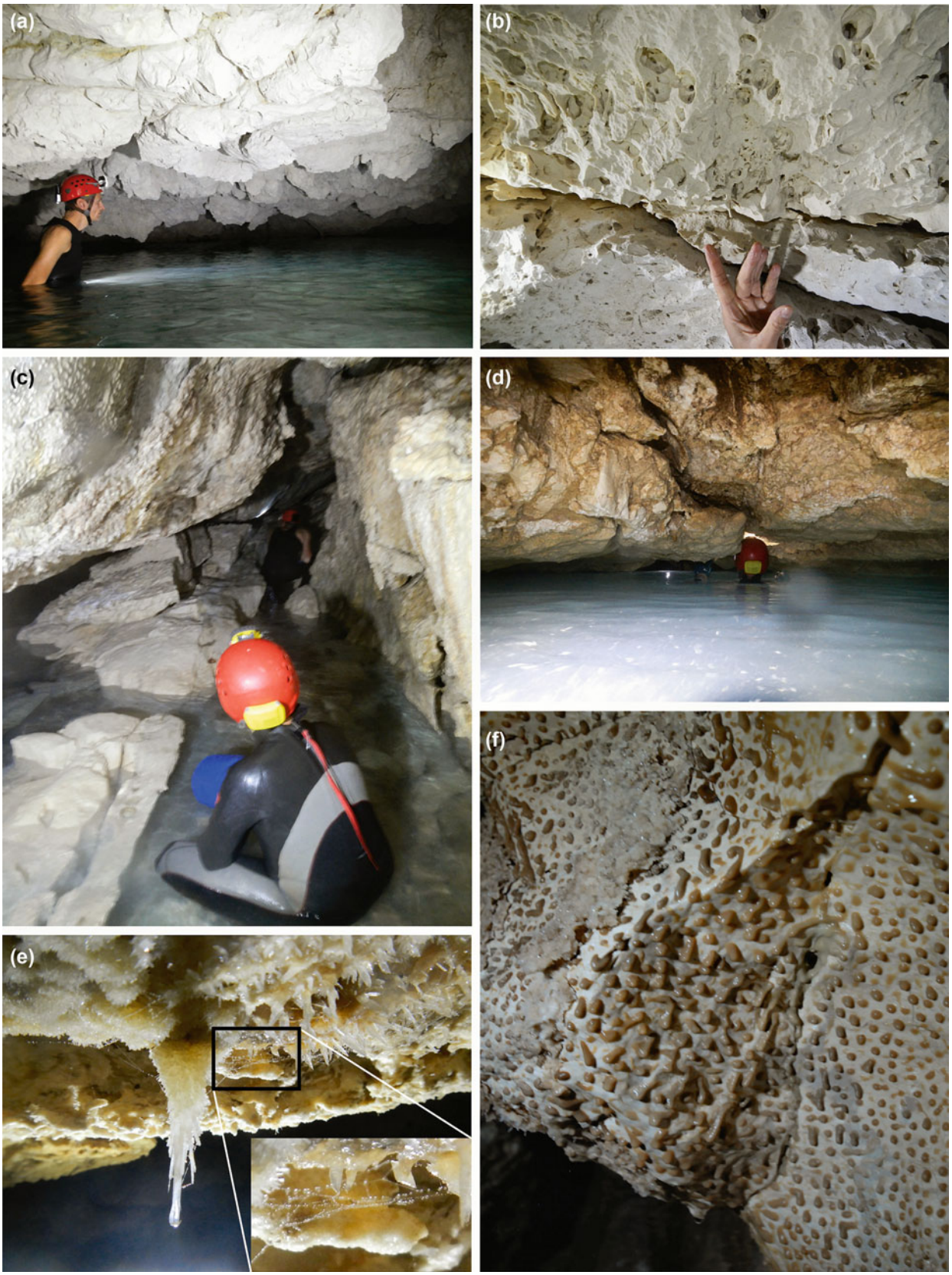

Fig. 3 Morphologies of the sulfuric acid caves: **a** corroded cave roof in fossiliferous limestones, Grotta Sulfurea; **b** replacement pockets, Grotta Sulfurea; **c** the main fracture from which sulfuric waters rise (note the *milky color* of the water), Grotta Solfatara; **d** swimming in the milky sulfuric water, Grotta Solfatara; **e** gypsum crystals with biofilms, mainly visible on the roof: the crystals are 2 cm long (Grotta Solfatara); **f** biovermiculations in Grotta Fetida, field of view is half a meter wide. Photographs Marco Vattano

Fig. 4 **a** Pseudomorphic replacement gypsum still showing the fossils of the original limestone, Grotta Fetida; **b** needle crystals of gypsum, Grotta Gattulla; **c** gypsum and sulfur crusts in Grotta Gattulla; **d** sugar-like gypsum still present in replacement pockets, Grotta Gattulla; **e** *thick* native sulfur crusts, Grotta Gattulla; **f** gypsum crust and biovermiculations in Grotta Fetida. Photographs Jo De Waele

chemical–physical properties, essentially as a function of the tides. For example, changes in the content of ion chloride, hydrogen and temperature have been observed between low and high tide (Visintin 1945; Polemio et al. 2012).

The cave development is certainly controlled by the main geological–structural elements in the area. This can be deduced from the cave entrances, from their N30°E development, as well as at many sites within the cave systems.

Fig. 5 Vadose speleothems in Grotta Sulfurea occur below present sea level. *Photographs* Marco Vattano

The spring waters are well recognizable due to milky white plumes of warm floating sulfur-rich waters flowing out of the caves, visible only in particularly calm sea and wind conditions (Fig. 1).

The Santa Cesarea Terme caves, thanks to their interesting location, show very typical inner morphologies and a mineralogy associated with sulfuric acid speleogenesis. These evidences, together with the geochemical analysis, can shed some new insights on the mixing of thermal sulfur-enriched water with salt and freshwater and their interaction with carbonate rocks and elucidate the velocity and the main processes of cave formation in this unique geochemical and geological setting.

From the hydrogeological point of view, meteoric waters can penetrate at depth through the high porosity and permeability of the calcareous rocks, or flow directly into the sea due to the presence of Quaternary impermeable deposits (Zuffianò et al. 2013). Saltwater strongly interacts with the freshwater not only along the halocline, but also inland, thus creating salt water intrusion problems due to intense water withdrawal for agriculture and human settlements (Tadolini and Bruno 1993).

Shallow waters can occasionally interfere with deepwater bodies flowing in calcareous and calcareous–dolomitic Cretaceous rocks of the Salento peninsula (Tadolini and Bruno 1993). The deep water presents a very high salt concentration (58 g/L) and temperature of 22–33 °C (several degrees higher than the waters coming from shallow sources, showing temperatures of 18–19 °C; Zuffianò et al. 2013). Such values are probably due to the exothermic reaction of sulfate contained in the seawater interacting with organic matter in the Miocene calcarenite layers (Zezza 1980; Calò et al. 1983).

Geochemical studies (Santaloia et al. 2016) revealed that these waters are undersaturated with respect to calcite, dolomite and seem to be undersaturated with respect to gypsum, too. The high lithium content (Zuffianò et al. 2013) and the tritium concentration, ranging from 0.46 to 0.33 TU, lower than the present seawater (2.2 TU) (Santaloia et al. 2016) are clear indicators of very long residence time of groundwater in the aquifer (Edmunds and Smedley 2000). This evidence, together with stable isotope analyses of $\delta^{18}O$ (between −3.5 and +2‰) and δ D (between −23 and +5‰), suggests that the thermal springs appear to be at least partially fed by groundwater with a residence time greater than 55 years and connected to a deep circulation system (Zuffianò et al. 2013). Radiocarbon analysis (Santaloia et al. 2016) on thermal water suggests the recharge to be occurred in a period varying from 19849 to 21050 BP (late Pleistocene times).

4 Conclusions

The Santa Cesarea Terme caves represent the only hypogenic system in Apulia, which has never been studied from a speleogenetical point of view. The research described in this paper brought us to identify a number of peculiar morphologies (replacements pockets, cupola-like morphologies) and of minerals such as huge amounts of gypsum deposits, native sulfur coatings and jarosite, which characterize the caves and allow to define them as a SAS system. From the geochemical standpoint, the waters are enriched with Na–Cl–SO_4 and colonized by white soft floating microbial filaments. On the ceiling and roof, brown and yellowish biovermiculations and white gypsum toothpaste materials (moonmilk) can be observed, especially at those sites where H_2S degassing is important. In submerged environments, mixing between sulfidic rising fluids and seawater seems to have an important role on dissolution processes. Experiments with limestone tablets placed in air, in the air-water interface, and under water in several spots of the cave (from the most inner parts to the outside) have shown

that dissolution at the water–air interface is faster in the middle section (where mixing between sea and deep water occurs), while dissolution in air is higher in the deep section, where H_2S degassing is more abundant.

At the same time, a further issue under investigation is the role of microbial substances on the speleogenesis of Santa Cesarea Terme caves, in particular the role of sulfo-oxidizing and sulfo-reducing bacteria (Jones et al. 2011) involved in secondary mineral precipitation and rock dissolution.

Acknowledgements We thank the staff at the Santa Cesarea Terme spa for their availability. The Apulian Speleological Federation is kindly acknowledged for the work carried out during the cave surveys. We thank all the collaborators that helped us during the monitoring and sampling stage and the reviewers who gave us several interesting suggestions to improve this chapter.

References

Basso A, Bruno E, Parise M, Pepe M (2013) Morphometric analysis of sinkholes in a karst coastal area of southern Apulia (Italy). Environ Earth Sci 70(6):2545–2559

Bosellini A, Bosellini FR, Colalongo ML, Parente M, Russo A, Vescogni A (1999) Stratigraphic architecture of the Salento coast from Capo d'Otranto to Santa Maria di Leuca (Apulia, southern Italy). Riv Ital Paleont Strat 105(3):397–416

Bossio A, Mazzei R, Monteforti B, Salvatorini G (2005) Stratigrafia del Neogene e Quaternario del Salento sud-orientale (con rilevamento geologico alla scala 1:25.000). Geol Romana 38:31–60

Bruno E, Calcaterra D, Parise M (2008) Development and morphometry of sinkholes in coastal plains of Apulia, southern Italy. Preliminary sinkhole susceptibility assessment. Eng Geol 99:198–209

Calò GC, Tinelli R (1995) Systematic hydrogeological study of a hypothermal spring (S. Cesarea Terme, Apulia), Italy. J Hydrol 165:185–205

Calò GC, Spizzico M, Tinelli R, Zezza F (1983) Hydrogeological investigations on the area surrounding Santa Cesarea Terme springs (southern Apulia). Geol Appl e Idrogeol 18(2):129–144

Corti E (1992) Relazione sul Convegno Nazionale di Speleologia di Castro, 14-15-16 settembre 1936. Itinerari Speleol 6:89–97

D'Agostino D, Beccarisi L, Camassa M, Febbroriello P (2015) Microclimate and microbial characterization in the Zinzulusa show cave (South Italy) after switching to led lighting. J Cave Karst Stud 77(3):133–144

De Giorgi C (1882) I bagni solfurei di Santa Cesarea in Terra d'Otranto. Riv Idrol e Clim Med 4:8

Dell'Oca S (1962) Note di speleologia economica. Rassegna Speleol Ital 1:76–109

De Waele J, Lauritzen SE, Parise M (2011) On the formation of dissolution pipes in quaternary coastal calcareous arenites in Mediterranean settings. Earth Surf Proc Land 36(2):143–157

De Waele J, Galdenzi S, Madonia G, Menichetti M, Parise M, Piccini L, Sanna L, Sauro F, Tognini P, Vattano M, Vigna B (2014) A review on hypogene caves in Italy. In: Klimchouk A, Sasowski ID, Mylroie J, Engel SA, Summers Engel A (eds), Hypogene cave morphologies, vol 18. Karst Water Institute, special publication, pp 28–30

Doglioni C, Mongelli F, Pieri P (1994) The Puglia uplift (SE-Italy): an anomaly in the foreland of the Apenninic subduction due to buckling of a thick continental lithosphere. Tectonics 13(5):1309–1321

Edmunds WM, Smedley PL (2000) Residence time indicators in groundwater: the East Midlands Triassic sandstone aquifer. Appl Geochem 15:737–752

Galdenzi S (2012) Corrosion of limestone tablets in sulfidic ground-water: measurements and speleogenetic implications. Int J Speleol 41(2):149–159

Inguscio S, Lorusso D, Pascali V, Ragone G, Savino G (eds) (2007) Grotte e carsismo in Puglia. Regione Puglia, p 200

Jones AA (2011) Microbe-mineral affinity in sulfuric acid karst systems. University of Austin, Thesis

Jones DS, Polerecky L, Galdenzi S, Dempsey BA, Macalady JL (2015) Fate of sulfide in the Frasassi cave system and implications for sulfuric acid speleogenesis. Chem Geol 410:21–27

Klimchouk AB (2007) Hypogene speleogenesis: hydrogeological and morphogenetic perspective. Natl. Cave Karst Res. Inst, Carlsbad

Margiotta S, Sansò P (2014) The geological heritage of Otranto-Leuca Coast (Salento, Italy). Geoheritage 6(4):305–316

Margiotta S, Negri S, Parise M, Valloni R (2012) Mapping the susceptibility to sinkholes in coastal areas, based on stratigraphy, geomorphology and geophysics. Nat Hazards 62(2):657–676

Mauget A (1875) Note geologiche sulla Provincia di Lecce. Lecce

Mostardini F, Merlini S (1986) Appennino centro meridionale. Sezioni geologiche e proposta di modello strutturale. Mem della Soc Geol Ital 35:177–202

Palmentola G (2002) Il paesaggio carsico della Puglia. Grotte e dintorni 4:203–220

Parise M (2008) Elementi di geomorfologia carsica della Puglia. In: Parise M, Inguscio S, Marangella A (eds), Atti del 45° Corso CNSS-SSI di III livello di Geomorfologia Carsica, Grottaglie, 2–3 febbraio 2008, p 93–118

Parise M (2011) Some considerations on show cave management issues in Southern Italy. In: Van Beynen PE (ed) Karst management. Springer, Dordrecht, pp 159–167

Parise M, Federico A, Delle Rose M, Sammarco M (2003) Karst terminology in Apulia (southern Italy). Acta Carsol 32(2):65–82

Parise M, De Pasquale P, Martimucci V, Meuli V, Pentimone N, Pepe P (2013) Grotta della Rondinella a Polignano a Mare: un progetto di ricerca della Federazione Speleologica Pugliese. In: Cucchi F, Guidi P (eds) Proceedings of the XXI National Congress Speleologia "Diffusione delle conoscenze", Trieste, 2–5 giugno 2011, Ed. Università di Trieste, pp 437–448

Plan L, Tschegg C, De Waele J, Spötl C (2012) Corrosion morphology and cave wall alteration in an Alpine sulfuric acid cave (Kraushöhle, Austria). Geomorphology 169:45–54

Polemio M, Limoni PP, Zuffianò LE, Santaloia F (2012) Santa Cesarea thermal springs (Southern Italy). In: Thangarajan M, Mayilswami C, Kulkarni PS, Singh VP (eds) 5th international groundwater conference (IGWC) assessment and management of groundwater resources in hard rock systems with special reference to basaltic terrain vol 15, 737–752

Ricchetti G, Ciaranfi N, Luperto Sinni E, Mongelli F, Pieri P (1988) Geodinamica ed evoluzione sedimentaria e tettonica dell'Avampaese Apulo. Mem della Soc Geol Ital 41:57–82

Santaloia F, Zuffianò LE, Palladino G, Limoni PP, Liotta D, Minissale A (2016) Coastal thermal springs in a foreland setting: the Santa Cesarea Terme system (Italy). Geothermics 64:344–361

Tadolini T, Bruno G (1993) The influence of geostructural setting upon water thermo-mineralization in certain areas of Apulia (Southern Italy). In: Proceedings of the Antalya symposium and field seminar, vol 207, Oct 1990, IAHS, pp 75–83

Taviani M, Angeletti L, Campiani E, Ceregato A, Foglini F, Maselli V, Morsilli M, Parise M, Trincardi F (2012) Drowned karst landscapes offshore the Apulian Margin (Southern Adriatic Sea, Italy). J Cave Karst Stud 74(2):197–212

Visintin B (1945) Studio sull'acqua della Grotta Gattulla delle Terme demaniali di S. Cesarea Ann Chim Appl 35(6–7):97–111

Zezza F (1980) Le sorgenti ipotermali solfuree di Santa Cesarea Terme. Azienda di cura e soggiorno e turismo Santa Cesarea Terme. Salentum, pp 1–2

Zuffianò LE, Palladino G, Santaloia F, Polemio M, Liotta D, Limoni PP, Parise M, Pepe M, Casarano D, Rizzo E, Minissale A, De Franco R (2013) Geothermal resource in a foreland environment: the Santa Cesarea Terme thermal springs (Southern Italy). European Geothermal Congress 2013, Pisa, 3–7 June 2013, p 6

The Thermal Hypogenic Caves of Acquasanta Terme (Central Italy)

10

Sandro Galdenzi

Abstract

The karst area of Acquasanta Terme is located in the eastern side of central Apennine. The thermal sulfidic springs reach the surface in the core of the anticline where the river valley reaches the top of a Meso-Cenozoic limestone succession, capped by less permeable rocks. An important terraced travertine deposit was produced by the thermal water throughout the Pleistocene. The most interesting caves are in the valley of the Rio Garrafo, a tributary of the Tronto River. These caves developed mainly below the valley bottom, and a part of the stream water sinks through preexisting karst passages mixing with the thermal groundwater ~50 m below. Water temperature in the caves reaches 42 °C, and the water has high salinity (up to > 6 g L^{-1}) with elevated levels of chloride, sulfates and carbonates. Sinking water from the caves and the travertine plate is responsible for the significant dilution of thermal water at the main spring, located 2 km downstream, in the Tronto Valley. The speleogenetic process is mainly related to H_2S oxidation, which is enhanced by the recharge of oxygenated fresh water from the surface. Cave development occurred in different phases. Early passages formed mainly in the phreatic zone, due to the rising thermal water. Deepening of the main surface stream (Tronto River) caused lowering of the water table. As a result, the Rio Garrafo caves were partly dried and invaded by sinking water, while rising gases activated condensation corrosion and the growth of replacement gypsum crusts.

Keywords

Acquasanta Terme • Hypogene caves • Thermal caves • Apennine • Italy

1 Introduction

The thermal hypogenic caves of Acquasanta Terme represent a window into active sulfuric acid speleogenesis. Some caves in the area have been known since ancient times due to their large entrances and easy accessibility, and the Acquasanta cave has been partly adapted for thermal baths for a long time. Modern exploration, however, only began after World War II. It was not until the 1970s and 1980s that new important caves were explored, which also reach active thermal zones below the valley of the Rio Garrafo. At present, the total extent of cave passages exceeds 3000 m in length.

In early studies of the Acquasanta caves, the role of the thermal sulfidic water was misunderstood and considered responsible for only minor chemical alteration of the walls of a preexisting cave (Maucci 1954). After the Italian XVII National Congress of Speleology (1994), cave development was linked to the mixing of the rising sulfidic waters with descending freshwaters from the Garrafo stream (Galdenzi 1997), and the caves were reported as hypogenic (Galdenzi and Menichetti 1995). More recently, new research analyzed the microbiota of the thermal zone of the cave (Jones et al. 2010, 2014), while Galdenzi et al. (2010) analyzed the

S. Galdenzi (✉)
60035 Jesi, Italy
e-mail: galdenzi.sandro@tiscali.it

© Springer International Publishing AG 2017

A. Klimchouk et al. (eds.), *Hypogene Karst Regions and Caves of the World*,
Cave and Karst Systems of the World, DOI 10.1007/978-3-319-53348-3_10

general structure and morphology of the caves, the atmosphere and water characteristics, and discussed the present and past conditions for the cave development.

2 Geological Setting

2.1 Location and Climate

Acquasanta Terme is a village on the eastern side of the Apennine Mountains, 40 km from the Adriatic Sea, in central Italy. It is located in the deep transverse valley that the Tronto River cuts into the northern termination of the Laga Mountains, a chain that reaches altitudes up to 2000 m. A mountainous landscape prevails, with altitudes ranging between 300 m at the bottom of the valley to about 1100 m in the surrounding mountains (Fig. 1).

The climate is semicontinental, with an annual average temperature of about 12 °C and an average rainfall of about 950 mm a^{-1} in the valley (Nanni 1991). Precipitation generally reaches maxima in autumn and spring, and thunderstorms are frequent at the end of summer. In the winter, snowfall is common in the mountains, and thawing occurs at the beginning of the spring.

2.2 Geology

The karst area is located in the Laga Basin, at the periclinal termination of the Acquasanta Anticline, an asymmetric, east-verging structure, trending N 170°. Gently dipping bedding prevails in the core of the structure, with some detachment levels (Marsili and Tozzi 1995). In the eastern limb, the bedding inclination increases rapidly, and the Acquasanta Anticline overthrusts the Miocene sandstone of the Laga Fm (Fig. 1), with a throw that does not exceed 2 km (Scisciani and Montefalcone 2005). The Acquasanta Anticline, 10 km to the west, lies in the footwall of the Sibillini Mountain Thrust, a regional structure that carries the Mesozoic limestone above the Miocene succession.

The Miocene deposits comprise prevailing marl units and a thick Messinian (Upper Miocene) foredeep turbiditic siliciclastic succession (Laga Fm, over 3000 m thick), where thick beds of sandstone alternate with thinner mudstone and a few gypsum-arenitic turbidites that record the evaporitic conditions in the source area due the Mediterranean salinity crisis. The pre-Miocene rocks include Oligocene marls, Paleogene, Cretaceous and Jurassic mainly carbonatic deposits and 2000 m thick Upper Triassic evaporites.

The thick Oligocene and Miocene succession outcrops everywhere, and the top of the limestone succession is only exposed in the valley of the Rio Garrafo, at the core of the anticline. The outcropping carbonates comprise reddish cherty limestone and marly limestone (Scaglia Rossa and Scaglia Variegata, Upper Cretaceous—Eocene), well stratified in layers of ~20 cm, with marl content increasing upwards. These karst-bearing units are overlain by gray Oligocene marls (Scaglia Cinerea, ~200 m thick) and by Miocene marl units (Fig. 1), which together constitute the most important regional aquiclude, over 500 m thick, and cap the thermal aquifer.

The marine formations were exposed during Pliocene uplift, and deep fluvial valleys cut into the old surface. Some terraced sand and gravel deposits document the last phases of this evolution, influenced by climate changes between glacial and interglacial periods that caused alternating depositional and erosional periods in the valleys. The most significant terrestrial unit, however, is the large plate of travertine that extends for several kilometer square at three different elevations along the right bank of the Tronto River, whose deposition was related to the rise of sulfidic water from a confined aquifer (Boni and Colacicchi 1966). Carbonate precipitation produced homogeneous, low porosity travertine where inorganic chemical precipitation dominated. Less compact or mixed deposits formed where the thermal water rise interacted with the development of vegetation or with river flow and sedimentation (Madonna et al. 2005).

2.3 Hydrogeology

The Tronto River and its tributaries have irregular discharge patterns, due to the low permeability of their basins and seasonal contributions from snowmelt. The groundwater in the area consists mainly of the thermal sulfidic water that rises from the capped aquifer hosted in the carbonate succession. The most important spring in the area is in the village of Acquasanta Terme, at the outflow of the Acquasanta Cave (Fig. 2). This spring has a discharge that seasonally varies between 60 and 220 L s^{-1} (Perrone 1911) and is located in the right bank of the Tronto River, near the core of the anticline in the Oligocene marl.

Some additional minor thermal springs are located downstream near the river bed and also at higher altitude in the right side of the valley (Fig. 1). One spring is located at the bottom of a large shaft in the terraced travertine deposits, ~100 m above the river bed. The thermal groundwater can also be accessed in the lower sections of the caves in the tributary valley of the Rio Garrafo.

The groundwater flow path in the area is heavily influenced by the geologic setting. The prevailing low-permeability formations that cap the thermal aquifer reduce the local recharge of the aquifer. Only in the Rio Garrafo gorge does sinking stream water directly mix with the thermal water inside caves.

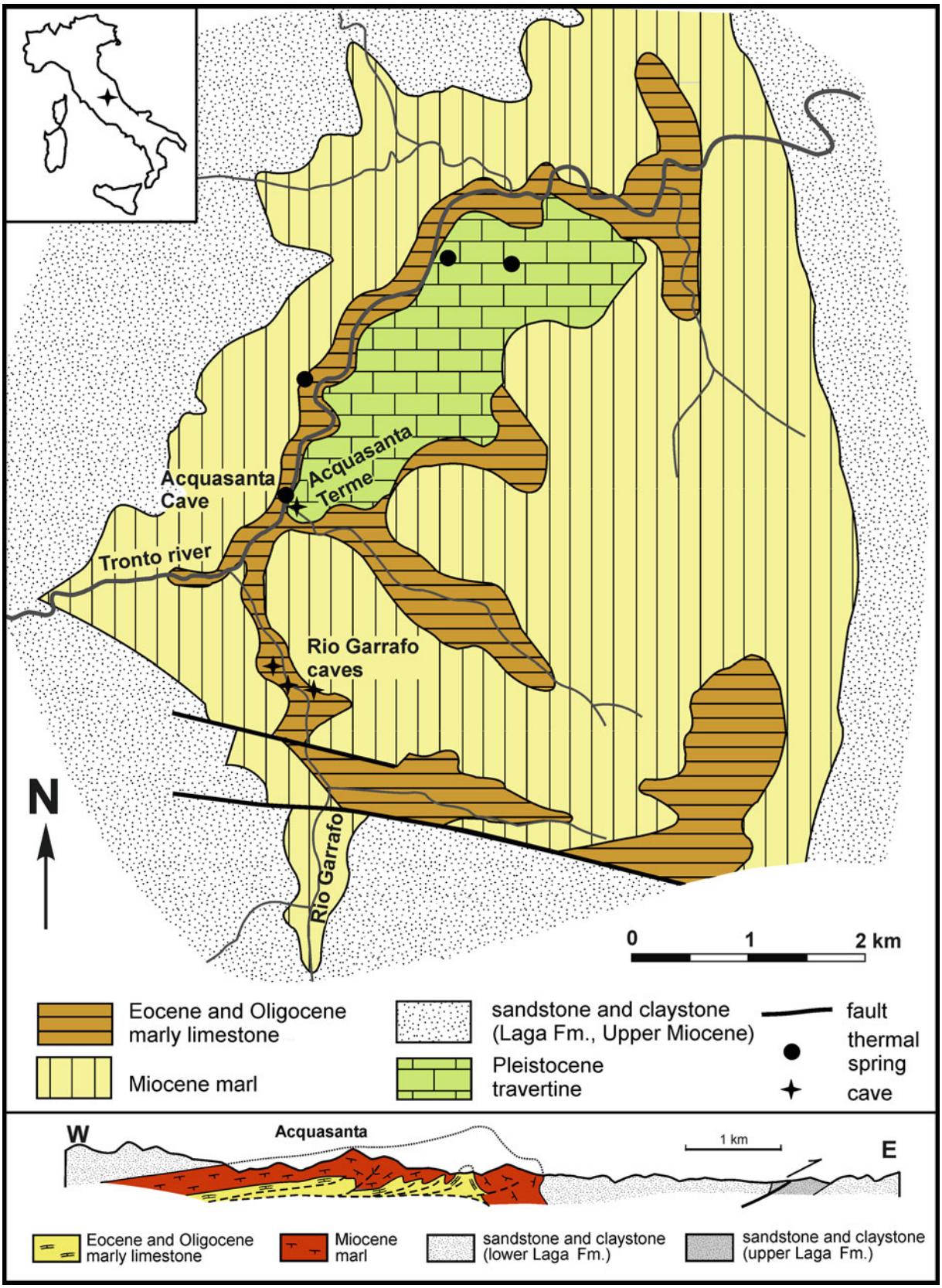

Fig. 1 Schematic geologic map of the study area. Geologic section after Scisciani and Montefalcone (2005), simplified

Fig. 2 Thermal spring of Acquasanta Terme

Elevated Cl^- and Na^+ in the spring water, along with isotopic data (Zuppi et al. 1974), indicate the coexistence of a deep circuit involving thermal sulfidic water with a probable meteoric origin that rises and dilutes with a variable amount of cold water coming from fast surface circuits. The recharge area for the thermal water was thought to be in the Sibillini Mountains to the west (Menichetti 2008), but might also be in the Laga Mts. to the south.

The high salt content could be acquired from the underlying Triassic evaporites at the core of the anticline, or through Messinian gypsum in the footwall of the Acquasanta thrust (Nanni and Vivalda 2005). Madonna et al. (2005) hypothesized that volcanic fluids from a magmatic intrusion at the core of the anticline contribute to the water chemistry and the high temperature of the geothermal field of Acquasanta. This intrusion, however, is not reported by most authors that have analyzed the deep structure of the anticline (see Scisciani and Montefalcone 2005 and references therein).

3 The Karst Area of Acquasanta Terme

Surface karst phenomena are not well developed in the area, where siliciclastic or marly formations prevail. The largest limestone outcrop, the large travertine plate, is generally covered by colluvial deposits or soils, and only small-scale corrosion features develop in narrow zones where the limestone surface is directly exposed to meteoric water. Deep karst, however, is more extensively developed in a hypogenic setting. Thirteen caves are known, with a total length that exceeds 3 km. Only a few caves are related to the large travertine deposits, and the major caves develop in the small outcrop of marine limestone in the Rio Garrafo Valley.

3.1 Grotta di Acquasanta

The Grotta di Acquasanta (length: ~300 m) represents the main emergence of sulfidic water in the area. It is a wide chamber, flooded by sulfidic water that directly feeds an abandoned piscine and reaches the Tronto River through a lateral active passage (Fig. 3a). This passage might have been artificially created to facilitate the water outflow, although no historical documentation exists. The Grotta di Acquasanta opens at the base of the travertine body, where it overlies the Oligocene marl formation of Scaglia Cinerea. This cave cannot be considered a karst cave in a strictest sense because passages are developed inside the marl itself and in overlying fluvial deposits, formed by sandstone boulders, carbonate and sandstone gravels and sands. The thermal water rises by artesian flow to the final pool (Fig. 3b) through a highly inclined passage, explored up to 12 m depth (Maucci 1954). Gas release causes

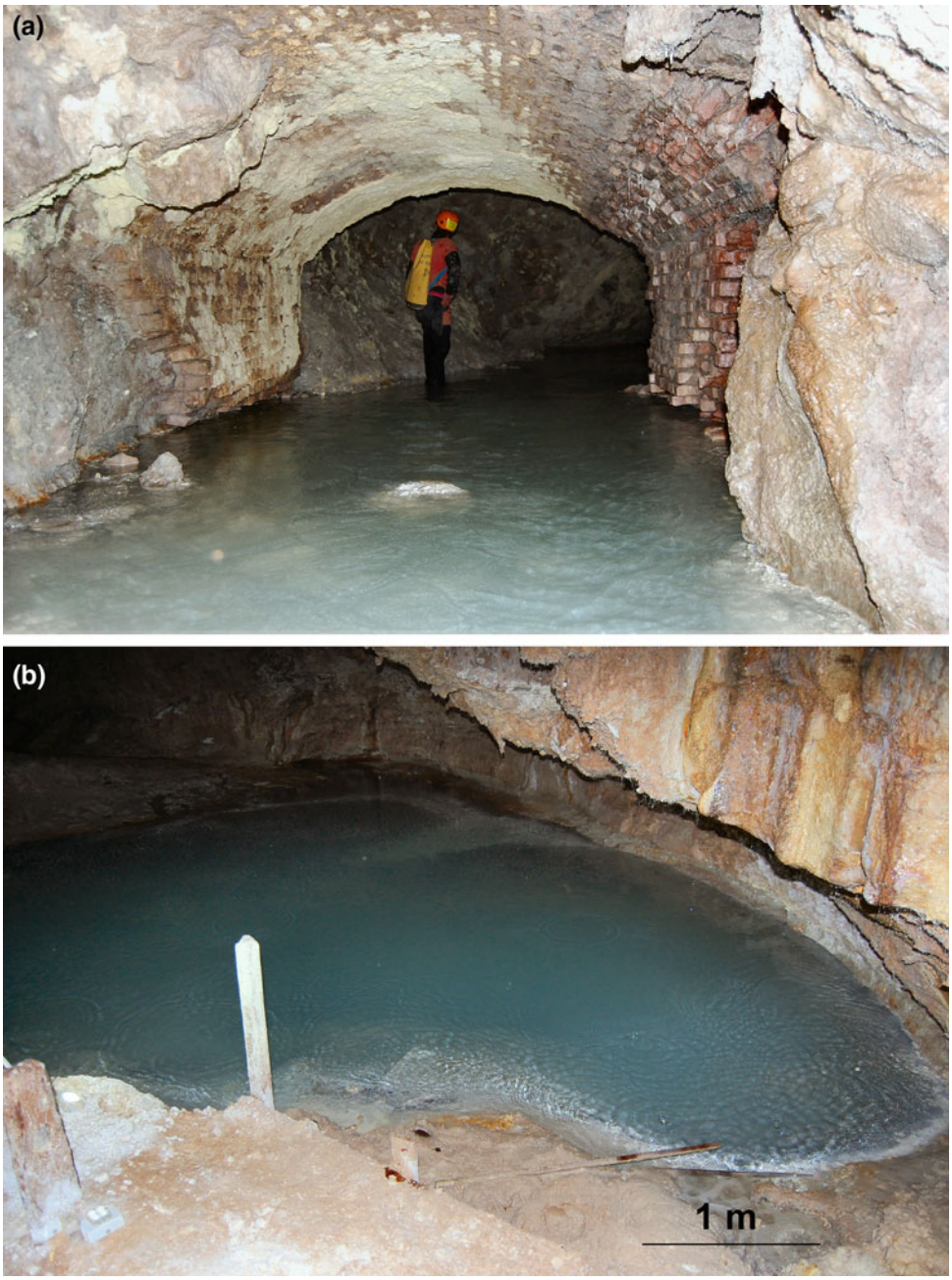

Fig. 3 Grotta di Acquasanta. **a** Retaining walls in the outflow passage. **b** The thermal spring in the cave termination

the corrosion of walls and ceilings in the entire cave system, interacting with the carbonate component of the bedrock and leaving an abundant insoluble residue. The thermal stream water is causing carbonate deposition at the spring.

At present, the cave is not directly utilized for thermal baths, and water in the nearby commercial bath is derived from a drilled well. An artificial entrance tunnel to the thermal baths provides access to some additional cave passages in the marls that are not directly exposed to thermal water and have typical phreatic sections, high air temperatures, and walls adorned by calcite dripstones.

3.2 The Rio Garrafo Caves

The most important caves are in a small area in the lower part of the Rio Garrafo valley, almost entirely carved in the Miocene turbidites at altitudes ranging from 300 to 2000 m, where the stream entrenches in a narrow canyon inside the top of the limestone succession (Fig. 4).

Small travertine deposits overlying coarse fluvial gravel are located in the canyon walls, about 100 m downstream from the main cave entrances. Their presence demonstrates that in the past the thermal water fed springs directly in the canyon. The caves open in the vertical sides of the canyon

Fig. 4 Rio Garrafo gorge, at the entrance to Grotta Fredda

and can be referred to two different morphological types, developing along bedding planes or faults.

3.2.1 Sub-Horizontal Caves

Sub-horizontal caves were formed by water movement along bedding planes toward the Rio Garrafo valley. Embryonic forms are still present in the gorge walls (Fig. 5). Grotta Fredda, ~1500 m long, is one the most important caves and opens on the right side of the valley, a few meters above the stream. It has a ramified pattern consisting mainly of sub-horizontal bedding-plane passages that extend mostly beneath the marly cover, which outcrops above the canyon (Fig. 6). The main passage has an ascending profile, from the east toward the canyon, clearly following the limestone bedding. Fractures and faults influence cave development, causing local changes in the direction of the main passages and originating small lateral branches. Some fracture passages developed below the main passage, originating as crevasses that sometimes descend into warm dry zones. The low permeability of the overlying formation reduces the

Fig. 5 Embryonic passages along the bedding planes in the Rio Garrafo gorge

recharge of seepage water; therefore, flowstones develop mainly below the main fractures. Phreatic features prevail in the main passages, with some wide cupolas in the ceilings (Fig. 7). On the floor, widespread deposits of sand, locally encrusted by calcite flowstone, were probably carried in the cave during Rio Garrafo flooding events. More recent flooding events deposited wood and shells on the walls of some internal rooms.

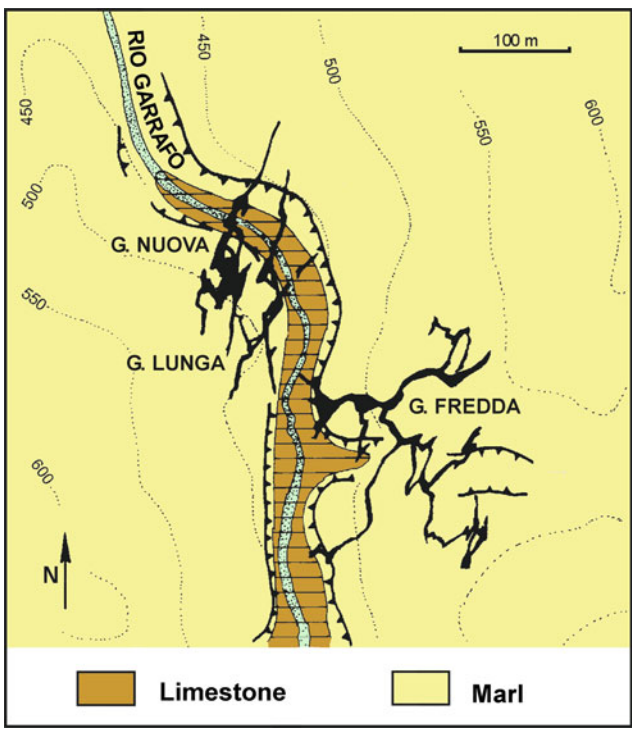

Fig. 6 Plan view of the caves in the Rio Garrafo gorge. Note that caves develop below the marly cover. Cave maps based on survey by Gruppo Speleologico Marchigiano

White microcrystalline gypsum occurs mainly as replacement crusts on the walls, and generally, it is recrystallized at the surface. The most important floor deposits can be 1–2 m thick and are clearly associated with replacement crusts and wide cupolas on the ceilings (Fig. 7). These deposits often overlie siliceous silt that contains chert or limestone clasts. Together the gypsum and the silt can constitute pebbly mud due to flow and re-deposition.

3.2.2 Fault Caves

Other caves formed along faults, with a mainly vertical structure, often below the river bed. These caves can develop in the same karstified fracture on both the sides of the canyon, and the open fissures in the river bed were artificially sealed in a crude attempt to prevent loss of water from the stream. In fact, in the past, the water sinking from the stream was identified as the cause of the cooling of the thermal spring at the Acquasanta village.

The most important caves (Grotta Lunga and Grotta Nuova) represent a single cave system that extends ~1200 m with a mainly vertical development, with some horizontal or inclined passages at different elevations. The cave entrances occur near the top of the canyon, but the caves are mostly developed below the stream. Thermal

Fig. 7 A cupola in the Grotta Fredda. The floor and the *right* wall are covered by replacement gypsum

groundwater can be accessed approximately 50 m below Rio Garrafo river bed (Figs. 6 and 8).

An upper sub-horizontal zone occurs at the same elevation of Grotta Fredda and contains sand deposits similar to those in Grotta Fredda. In the inclined and vertical passages, ceiling features show the original ascending flow of thermal water in the phreatic zone (Fig. 9). Some of these passages are now conduits for water descending from the Rio Garrafo stream to the thermal aquifer.

Flowing thermal waters are accessible at four different areas in the lower regions of the cave. In these areas, freshwater dilution and air flow influences the local environmental conditions (Fig. 8). Thermal water first emerges as a stagnant pool in an enclosed room, with high temperatures and an oxygen-depleted atmosphere. Then, flowing water emerges as interconnected pools and streams, with some free surfaces. Clouds of warm vapor rise from the stream to the upper cave sections, and air exchange permits speleologists to enter these rooms for a short time.

Gypsum deposits in the caves occur as replacement crusts on the cave walls. Gypsum can encrust entire passage sections, forming a continuous rim a few centimeters thick. Large floor deposits are rare, but one is actively forming in the thermal zone and filling the downstream passage. Dripping water from the karst surface produces abundant calcite deposits in the zone not affected by the thermal waters.

4 The Cave Environment

Detailed measurements of water and atmosphere characteristics confirmed the influence of descending freshwater from the surface stream on the thermal waters. The measured parameters were also influenced by the seasonal changes and location of sampling sites (Galdenzi et al. 2010).

4.1 The Cave Water

Bicarbonate water in the caves derives from the infiltration of meteoric water in the travertine bodies or through fissures in the low-permeability marl. In the Rio Garrrafo caves, the most significant amount of surface water sinks directly from the Rio Garrafo stream.

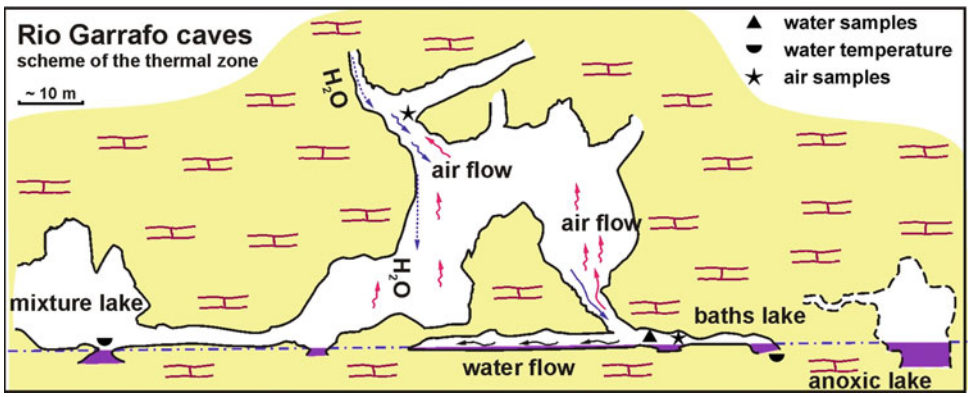

Fig. 8 Schematic view of the thermal section of the cave (after Galdenzi et al. 2010, modified)

Fig. 9 Grotta Nuova. A bedding controlled structure in the ceiling created by rising water

The stream water has low salinity (TDS: 250–300 mg L^{-1}) and a prevailing bicarbonate composition, with only minor seasonal changes. Once the stream water enters the cave, it flows in wide, inclined karst channels, and quickly joins the thermal water.

The sulfidic, thermal water has a high content of chloride, sodium, calcium, bicarbonate, sulfate, and contains hydrogen sulfide. In the period sampled by Galdenzi et al. (2010), 2003–2004, TDS and water temperatures in the Rio Garrafo caves ranged from 7.2 g L^{-1} and 42.2 °C to 4.4 g L^{-1} and 33.1 °C. The dissolved components are acquired before the water rises upward. The sulfidic water at the outflow of the Acquasanta Cave is more diluted than in the Grotta Nuova (TDS from 4.6 to 1.9 g L^{-1} and temperatures from 31.4 to 21.9 °C). The seasonal trend between the two localities was similar, but the two sites had different pH and H_2S content. The pH was consistently lower in the Rio Garrafo caves than in Acquasanta spring, where the deposition of small amounts of carbonate is occurring. During flooding events, pH values decreased in both locations. Dissolved H_2S concentrations were higher in Grotta Nuova (up to 0.66 mmol L^{-1}) compared to Acquasanta spring, where the maximum value was as high as 0.31 mmol L^{-1}. The sulfide, however, represents a small percentage (not exceeding 6%) of the total dissolved sulfur species, and its concentration decreased during the floods.

Thermographs confirm the importance of freshwater dilution, both locally and in the overall dilution of the thermal water. In the Rio Garrafo caves, water temperatures in the two sampling points (baths and mixture lakes) were influenced by the placement of the main freshwater input from the surface stream (Fig. 8).

Thermographs from the Rio Garrafo caves and the Acquasanta Caves have the same general trend, and changes in temperature have similar timing and duration (Fig. 10). A quick drop in temperature occurs in both caves after large floods, but the changes persist for longer in the Acquasanta Cave. The Acquasanta Cave represents the main emergence and is probably influenced by additional sources of water infiltration, including from the large overlying travertine plate.

Recharge of cold water from the Rio Garrafo was strongly reduced in the summer, but the temperature of thermal water stabilized to values lower than the average annual temperature, probably due to slow water flow, and heat exchange with the rock. The temperature then increased following a rainy period, which restored the “normal” conditions at the end of the dry season. These data suggest that the infiltration of surface water causes thermal water dilution, and maintains a hydraulic gradient that favors the upwelling of thermal water.

4.2 Cave Atmosphere Composition

The cave atmosphere is influenced by the gas released from the thermal water, with differences due to the ease of air exchange between the thermal zones and the surface. Extremely dangerous conditions for humans are present in isolated rooms, where small water-filled entrances reduce air exchange with fresh air from the upper cave levels.

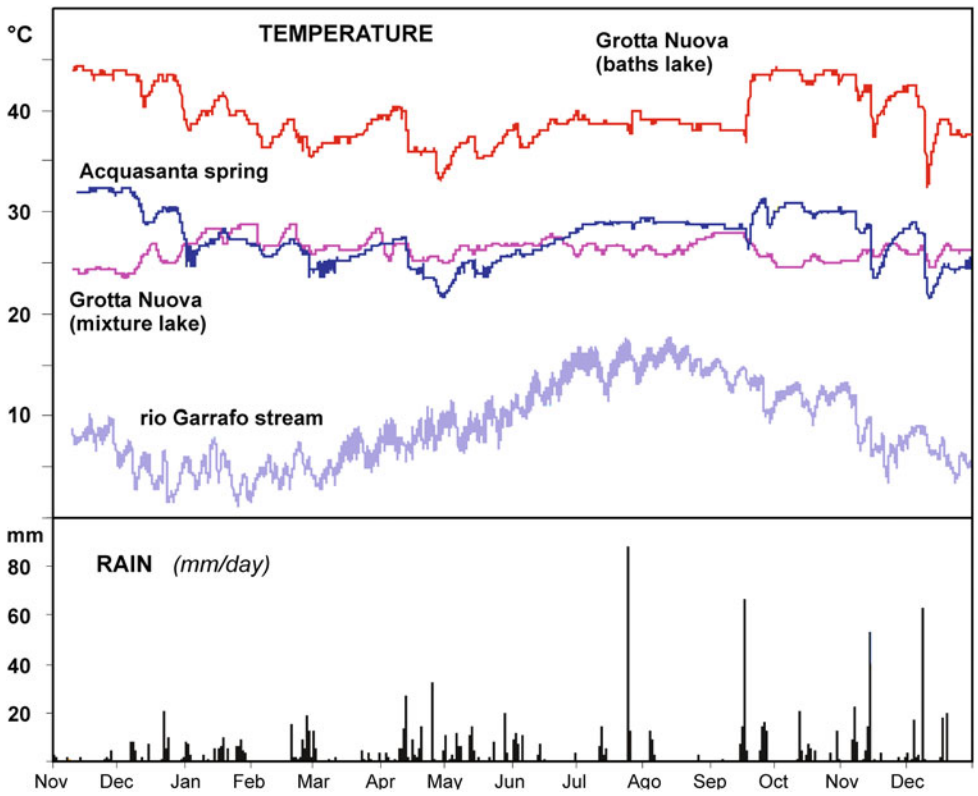

Fig. 10 Temperature in groundwater and its relationship to precipitation events during the monitoring period. Sampling sites in the Rio Garrafo caves are shown in Fig. 8 (after Galdenzi et al. 2010)

The high temperature gradient favors air flow, and sulfur gases are detectable far from the thermal zones. Descending cold oxygenated air can also enter the thermal sections, which can maintain a high oxygen concentration (~20%).

In the thermal zones, measurements with gas pump recorded values of CO_2 between 0.44 and 2.7%, H_2S between 4 and over 240 ppm, and SO_2 between 1.1 and 9.2 ppm (Galdenzi et al. 2010). Changes in gas concentrations are clearly related to the hydrologic cycle. The highest values occurred during the floods, when the thermal water dilution is at a maximum, and could be related to lower pH values and to changes in the hydrodynamics.

4.3 Active Cave Processes

The general features of the caves developed mainly during phreatic conditions, but each zone in the cave system has been influenced by different processes that occurred after it was drained of thermal water. Thermal water flow continues down into the lowest sections of the caves.

Above the water table, processes related to descending seepage water have minor importance due to the thick marl cover that prevents infiltration. Furthermore, the sinking water from the Rio Garrafo does not play a significant morphogenetic role and only causes minor changes in the old phreatic passages through which the water descends.

Condensation corrosion is currently the dominant cave forming process above the water table, due to the release of gases (CO_2 and H_2S) from the thermal water. Steep air temperature gradients favor air convection, and gases released from the groundwater consequently rise toward the upper levels.

H_2S oxidation leads to an active widespread replacement of the limestone with gypsum, even where the walls are not directly exposed to the thermal water flow. The gypsum can be white or weakly colored due to impurities in the marly limestone and generally occurs as thin crusts that are recrystallized at the surface (Fig. 11). The intensity of the corrosion strongly increases in the thermal regions where the walls are more directly exposed to corrosive gases. In these regions, a continuous crust of gypsum covers the walls and ceilings (Fig. 11a). The crust can be dry, and it can often be seen detaching from the limestone (Fig. 11b). In the places most directly exposed to degassing, elemental sulfur deposits are found on the walls.

Unlike other sulfidic caves in the region, the characteristic replacement pockets produced after gypsum removal are absent from the walls, and the replacement gypsum grades into the underlying limestone without a well-defined

Fig. 11 Grotta Nuova. **a** Crystalline gypsum crust on the cave wall; **b** dry gypsum crusts detaching from the marly limestone

boundary. This is probably due to the higher clay content of the limestone (Galdenzi et al. 2010).

Microbial mats colonize flowing sulfidic waters in the thermal regions, but evidence of life above the water table was found only where the temperature is not too high. Compared to other caves known to have active gypsum formation, such as Frasassi (Sarbu et al. 2000) and Cueva de Villa Luz (Hose et al. 2000), the growth of gypsum replacement crusts at Acquasanta occurs without obvious biofilms. Thin, extremely acidic (pH 0–1) organic formations are present at the entrance to the thermal zone of the Rio Garrafo and Acquasanta caves (Fig. 12). These thin, weak structures form "curtains," "stalactites" and balloons and their development is likely related to sulfide oxidizing bacteria or archaea (Jones et al. 2010, 2014).

5 Origin and Evolution of the Caves

The development of the Acquasanta caves is related to rising thermal waters at the core of the anticline, and the oxidation of H_2S, enhanced by the recharge of oxygenated freshwater, is probably the main cave forming process (Galdenzi 1997). The characteristics of each cave are influenced by individual hydrologic and geomorphologic settings, and also by their evolution through time.

The Acquasanta Cave is a young cave, formed after the deposition of the lowest travertine plate in the Tronto Valley. The explored part of the cave represents the outflow of sulfidic water rising from the thermal aquifer and flowing in the marls and alluvial deposits at the bottom of the travertine plate. The cave has evolved near the water table, and easy

Fig. 12 Grotta di Acquasanta, thermal zone. Organic "stalactites" on actively forming gypsum, with acidic droplets and remains of spider web

gas exchanges with the atmosphere produce condensation corrosion on the walls throughout the cave.

The Rio Garrafo caves have had a more complex history and represent a useful example of the evolution of speleogenetic conditions in hypogenic caves as a consequence of the increase in direct connections with the surface. The cave development began because of the rise of thermal water to the surface through the bedding planes and vertical fissures. These first phases, which were partly concealed by the subsequent evolution, probably occurred in the capped aquifer under purely phreatic conditions before the stream valley had cut down to the top of the limestone succession.

After the stream reached the limestone, cutting through the gorge, some of the preexisting small passages remained perched above the water table, while the thermal water flow continued into the upper part of the limestone succession. The main caves evolved in this phase, and thermal springs in the gorge produced the small travertine deposits located downstream from the cave entrances (Fig. 13a). Because the stream bed was close to the water table, small changes in the river elevation could have emptied the cave passages or caused a return to phreatic conditions, causing sand deposition in the caves.

An important change in the evolution of these upper cave levels was due to the deepening of the main valley of Tronto River, which also caused the deepening of its tributaries and the generalized lowering of the regional base level. The most important consequence of this event was the lowering of the water table in the Rio Garrafo Valley, where it became significantly lower than the canyon bottom (Fig. 13b). After this event, a direct outflow of thermal water in the canyon was no longer possible, and the cave water emerged at the main spring farther downstream in the Tronto Valley. Moreover, the stream remained perched above the already karstified limestone, and rapid recharge of surface water to the aquifer through the preexisting phreatic karst passages became very easy.

The descending oxygen-rich freshwater had only minor influences on cave features in the vadose zone, but it enhanced H_2S oxidation and limestone corrosion when it mixed with the thermal groundwater. The deepening of the canyon bottom also prevented direct flooding of stream water into wide sectors of the caves.

The changes in the geomorphic and hydrologic setting significantly modified the speleogenetic process over time. At first, recharge of freshwater from the surface was probably low, and the cave evolved mainly under phreatic conditions, even if the progressive deepening of the Rio Garrafo Valley facilitated exchanges between thermal and surface stream water in the caves (Fig. 13a). After the deepening of the main surface stream (Tronto River) and resulting lowering of the water table, the amount of water descending from the Rio Garrafo strongly increased (Fig. 13b), and rapid air exchange between the thermal water and the cave atmosphere also favored condensation corrosion and gypsum formation inside the preexisting cave passages.

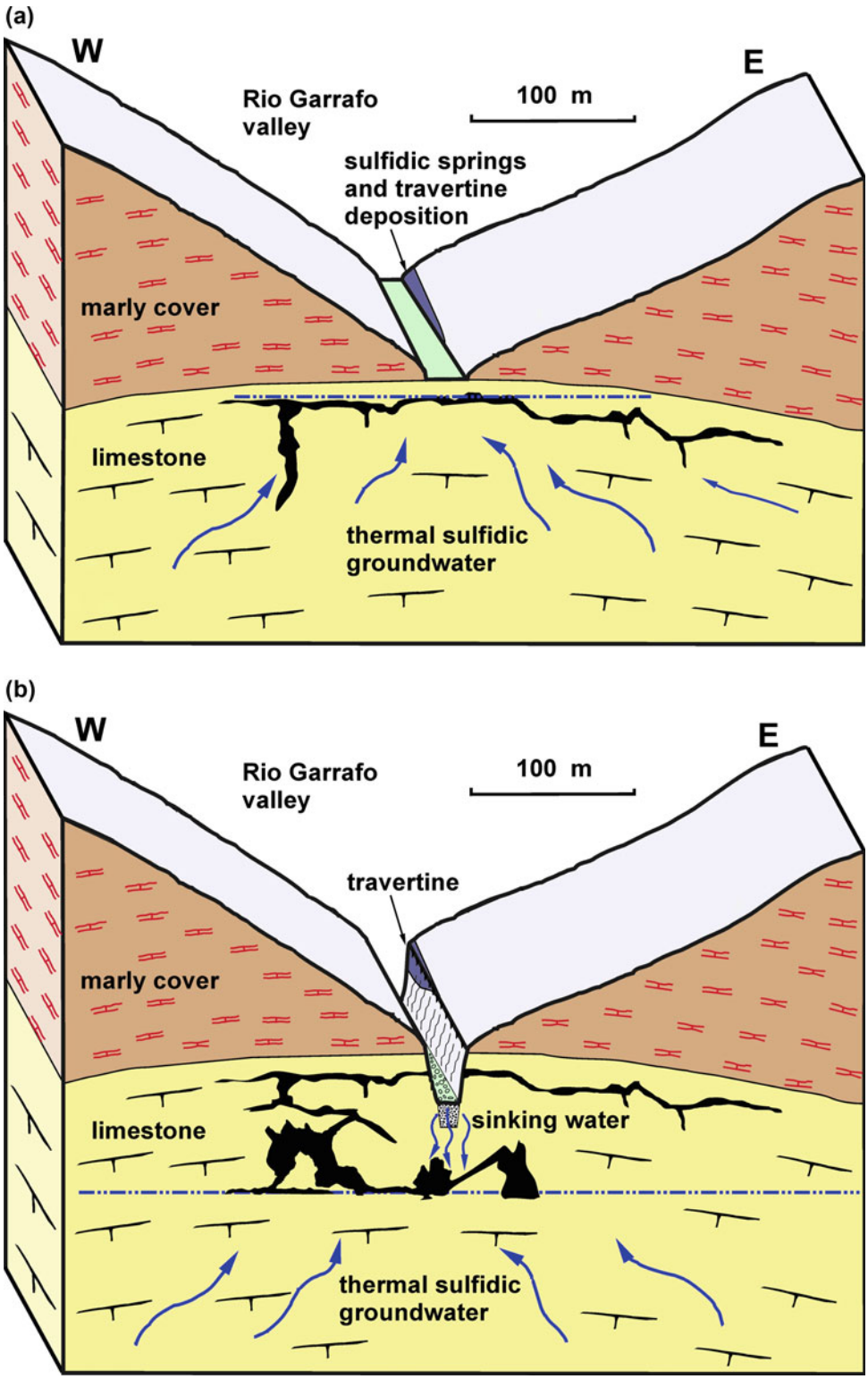

Fig. 13 Sketch of the Rio Garrafo karst area. **a** The gorge in the past, with sulfidic spring located in the valley. **b** The gorge at present, after the lowering of the water table. Descending stream waters can easily reach the thermal groundwater (after Galdenzi et al. 2010)

References

Boni C, Colacicchi R (1966) I travertini della valle del Tronto. Mem Soc Geol It 5:315–339

Galdenzi S (1997) Le grotte termali di rio Garrafo (Marche). In: Pensabene G. (ed) Atti 17th Congresso Nazionale di Speleologia, Castelnuovo Garfagnana, 1994, vol 1, pp 235–238

Galdenzi S, Menichetti M (1995) Occurrence of hypogenic caves in a karst region: examples from central Italy. Environ Geol 26:39–47

Galdenzi S, Cocchioni F, Filipponi G, Selvaggio R, Scuri S, Morichetti L, Cocchioni M (2010) The sulfidic thermal caves of Acquasanta Terme (central Italy). J Cave Karst Stud 72(1):43–58

Hose LD, Palmer AN, Palmer MV, Northup DE, Boston PJ, DuChene HR (2000) Microbiology and geochemistry in a hydrogen-sulphide-rich karst environment. Chem Geol 169:399–423

Jones DS, Schaperdoth I, Macalady JL (2014) Metagenomic evidence for sulfide oxidation in extremely acidic cave biofilms. Geomicrobiol J 31:194–204

Jones DS, Tobler DJ, Schaperdoth I, Mainiero M, Macalady JL (2010) Community structure of subsurface biofilms in the thermal sulfidic caves of Acquasanta Terme, Italy. Appl Env Microb 76(17):5902–5910. doi:10.1128/AEM.00647-10

Madonna R, Signanini P, Crema G, Di Sabatino B, Rainone ML, Di Nunzio A (2005) The geothermal area of Acquasanta Terme (Central Italy): main characteristics and an attempt of field evaluation. In: Proceedings World Geothermal Congress, Antalya, Turkey, 2005, pp 1–8

Marsili P, Tozzi M (1995) Un livello di scollamento nella dorsale di Acquasanta (AP). Boll Soc Geol It 114:177–194

Maucci W (1954) La Grotta termale di Acquasanta. In: Atti 6th Congresso Nazionale di Speleologia, Trieste, 1954, pp 1–12

Menichetti M (2008) Assetto strutturale del sistema geotermico di Acquasanta Terme (Ascoli Piceno). Rend Online Soc Geol It 1:118–122

Nanni T (1991) Caratteri idrogeologici delle Marche. In: Minetti A et al (eds) L'ambiente Fisico delle Marche. Regione Marche, SELCA, Firenze, pp 115–209

Nanni T, Vivalda P (2005) The aquifers of the Umbria-Marche Adriatic region: relationships between structural setting and groundwater chemistry. Boll Soc Geol It 124:523–542

Perrone E (1911) Carta idrografica d'Italia. Ministero Industria e Commercio, Roma

Sarbu SM, Galdenzi S, Menichetti M, Gentile G (2000) Geology and biology of the Frasassi Caves in Central Italy, an ecological multi-disciplinary study of a hypogenic underground ecosystem. In: Wilkens H et al (eds) Ecosystems of the world. Elsevier, New York, pp 359–378

Scisciani V, Montefalcone R (2005) Evoluzione neogenico-quaternaria del fronte della catena centro-appenninica: vincoli del bilanciamento sequenziale di una sezione geologica regionale. Boll Soc Geol It 124:579–599

Zuppi GM, Fontes JCh, Letolle R (1974) Isotopes du milieu et circulation d'eaux sulfurées dans le Latium. In: Proceedings Isotope techniques in ground water hydrology. International Atomic Energy Agency, Vienna, vol 1, pp 341–361

Inactive Hydrothermal Hypogenic Karst in SW Sardinia (Italy)

11

Jo De Waele, Fernando Gázquez, Paolo Forti, and Angelo Naseddu

Abstract

In Sardinia, no active hypogenic caves have yet been discovered or described. Although there are a few thermal springs, mostly correlated to Quaternary volcanic activity, none of these thermal waters have interacted with carbonate rocks. Nevertheless, in the SW of the Island many metal ore deposits hosted in Cambrian limestones have been exploited over the last two centuries, allowing the discovery of so-called mine caves, some of which are clearly of hypogenic origin. These caves formed by thermal waters in a phreatic setting and are now located far above the water table and are no longer active, apart from some recent dripstone formation. The mine tunnels in Mount San Giovanni, near Iglesias and Gonnesa towns, have cut most of these caves: among them the well-known Santa Barbara cave, covered with barite crystals, Santa Barbara 2 cave, with its unique oxidation vents, and Crovassa Ricchi in Argento. Other hypogenic caves have been discovered in the mines of Campo Pisano and Monteponi (Iglesias), Mount Onixeddu (Gonnesa), and especially Masua (Iglesias). A very special case of hypogenic cave is the Corona 'e Sa Craba quartzite system, known for its barite crystals and rich in many mineral species. This chapter summarizes these known inactive hydrothermal and sulfuric acid caves.

Keywords

Hypogenic caves • Sardinia • Mine caves • Cave minerals • Quartzite cave

1 Introduction

Despite the fact that less than 10% of its surface is characterized by the outcropping of carbonate rocks, Sardinia is one of Italy's most popular caving areas, hosting some of the most beautiful and extensive cave systems of the entire country. None of these caves, however, appear to be of hypogenic origin, and all most important systems are epigenetic ones in which surface runoff collects and flows downstream to the karst springs.

The only exception to this general rule appears to be the so-called mine caves, natural often bell-shaped voids inter-

J. De Waele (✉) · P. Forti
Italian Institute of Speleology, Department of Biological, Geological and Environmental Sciences, University of Bologna, Via Zamboni, 67, 40126 Bologna, Italy
e-mail: jo.dewaele@unibo.it

P. Forti
e-mail: paolo.forti@unibo.it

F. Gázquez
Godwin Laboratory for Palaeoclimate Research, Department of Earth Sciences, University of Cambridge, Downing Street, CB2 3EQ Cambridge, UK
e-mail: fg331@cam.ac.uk

A. Naseddu
Speleo Club Domusnovas, Via Roma 809015 Domusnovas, Italy
e-mail: angelonaseddu@alice.it

© Springer International Publishing AG 2017

A. Klimchouk et al. (eds.), *Hypogene Karst Regions and Caves of the World*,
Cave and Karst Systems of the World, DOI 10.1007/978-3-319-53348-3_11

cepted by industrial mining activities in the SW of the Island. Mine tunneling occurred at various altitudes and extended deep below the surface, and even below the present sea level, thanks to an ingenious system of artificial lowering of the water table. This allowed discovering also natural voids deep below the natural water table level. These caves never extend for more than a couple of hundred meters and are characterized by a set of typical hydrothermal morphologies (cupolas, megascallops, etc.) and a wide variety of cave minerals. One of the richest mineralogical sites is the Corona 'e Sa Craba cave, near Barbusi, a unique hydrothermal cave carved in quartzite.

Here we summarize the present knowledge on this inactive hypogenic karst and its caves, with details on their speleogenesis, their morphology, and their secondary cave deposits.

2 Geographical and Geological Outline

All inactive hypogenic caves in Sardinia are located in the Iglesiente-Sulcis mining district, in the SW of the Island (Fig. 1). This area is characterized by almost hundred abandoned mines that mainly exploited ore deposits of lead, zinc, silver, and barium (Bechstadt and Boni 1996). Mine activities started around 600 B.C. with Sardinian (Nuragic) people followed by Phoenicians and Romans. These exploitations went on discontinuously in the Medieval age and developed industrially in the second half of the nineteenth century. The most important of these mines have been closed down in the period 1960–1990. The main Mississippi Valley-type Pb–Zn ores are hosted in the carbonate lithologies of the Cambrian sequence, constituting the oldest outcropping rocks of Italy. This poorly metamorphosed sedimentary succession starts

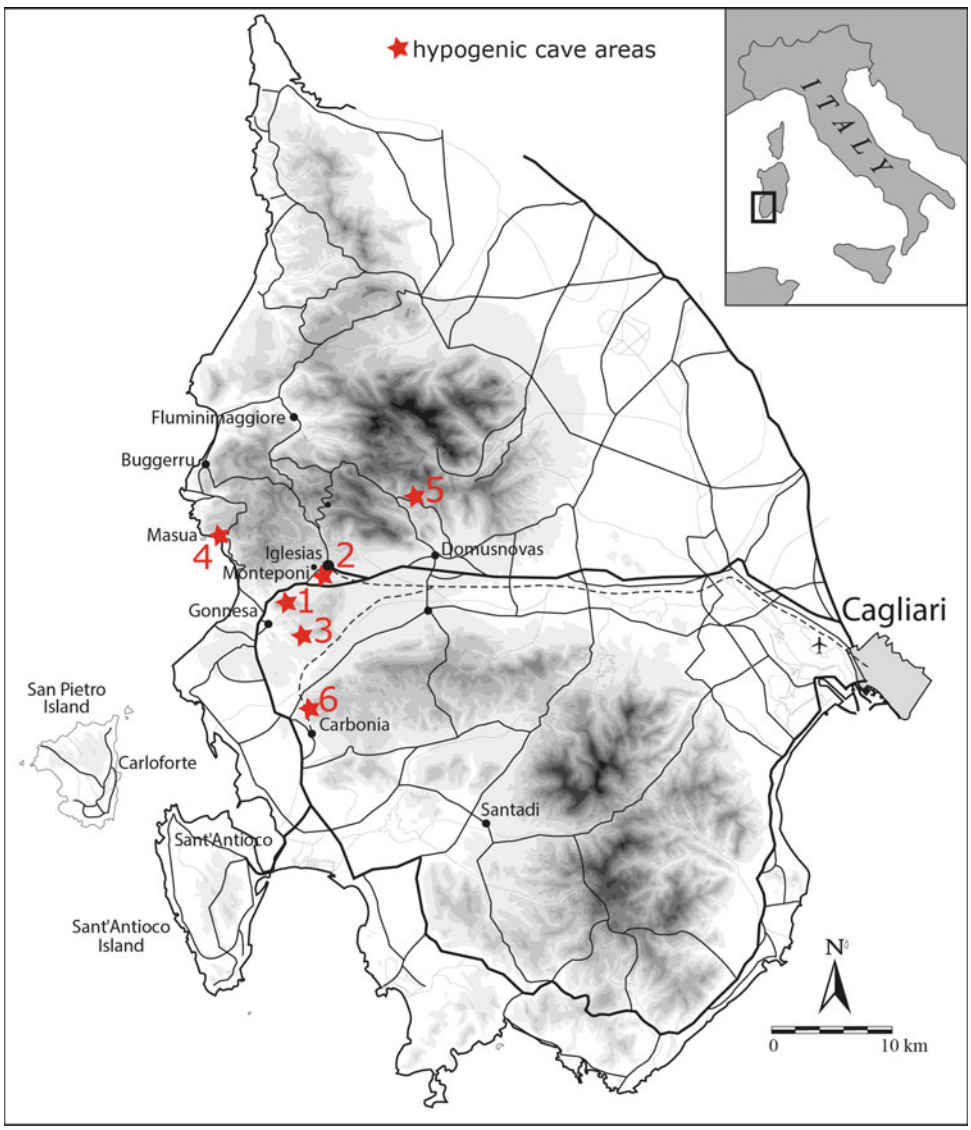

Fig. 1 Iglesiente-Sulcis area (SW Sardinia) and the main mine areas in which hypogenic caves have been encountered: *1* Monte San Giovanni; *2* Monteponi–Campo Pisano; *3* Monte Onixeddu–Monte Barega; *4* Masua; *5* Monte Guisi; *6* Corona 'e Sa Craba

with sandstones of the Nebida Group, followed by the dolomites and limestones of the Gonnesa Group and ending with the Nodular limestones and slates of the Iglesias Group. An angular unconformity separates these rocks from the overlying Ordovician and Silurian clastic sediments (Bechstadt and Boni 1996; Pillola 1989). This part of Sardinia was submerged again from Middle Ordovician to Middle Carboniferous, undergoing surface and subsurface erosion and corrosion during Late Carboniferous–Lower Triassic. Many of the hypogenic caves have probably formed during this continental period under thermal phreatic conditions (De Waele et al. 2013). A new transgression during Middle–Late Triassic submerged the area again, and most of the caves have been below the water table ever since. An intense tectonic and volcanic activity related to the opening of the Balearic and Tyrrhenian basins in the Oligocene–Miocene caused a renewal of circulation of thermal waters, probably remobilizing ore deposits and causing the deposition of many of the calcite spars and barite crystals found in the hypogenic caves. During the Quaternary, most of the higher located caves moved out of the phreatic zone and vadose speleothems could start developing, other caves were located in the epiphreatic or shallow phreatic zone with deposition of mammillary calcite (cave clouds), while others were located deep in the aquifer until very recently, when the mine exploitation required pumping the water level far below sea level (Cidu et al. 2011).

3 The Main Hypogenic Caves

Mines have occasionally intercepted caves since a long time, and some of these are mentioned in reports of the mine engineers. In an E–W striking longitudinal profile of Mount San Giovanni along the ore bodies of the "Ricchi in Argento" sector of the mine, many karst bodies and voids are clearly visible, some of which correspond to caves explored and surveyed almost a century later (Fig. 2). One of the most famous mine caves is the Santa Barbara cave, discovered in 1952 and, with reason, protected by the mine company itself because of its exceptional beauty. This cave has been surveyed by cavers from Bologna almost 30 years later (Fabbri and Forti 1981) and is now a show cave with limited visitors (Pagliara et al. 2010). A student in mine engineering and caver from Turin, who spent some time working in the mine in the late 1950s, also reports on some caves in San Giovanni mine (Fusina 1959), accurately describing some of the large caverns encountered by the mine tunnels. Well-organized exploration of the caves in the mines started when the exploitation of ores came to an end, in the late 1970s to early 1980s. Speleological exploration in the abandoned mines is still ongoing, and from time to time new caverns are discovered and surveyed.

Table 1 reports some of the most important hypogenic mine caves of SW Sardinia. Some mine caves of hypogene origin but of smaller dimensions are not reported in this table [e.g., Grotta Eraldo (Barega), Grotta di Monte Guisi (Domusnovas), Grotta del Gas and Grotta delle Budella (Masua)].

3.1 Mount San Giovanni

The most important and best-studied area for what concerns the hypogenic mine caves is the Mount San Giovanni, near Iglesias (De Waele et al. 2013). This mine has exploited the southern limb of the Iglesias syncline, composed of Cambrian limestones and dolostones sandwiched between the lower lying sandstones and overlying phyllites of the same age (Brusca and Dessau 1968). The over 100 km of mine galleries and shafts have allowed to discover more than 50 karst voids without any natural entrance at the surface, for a total development of around 4 km of cave passages. Most of these caves are of hypogenic origin and are now inactive except for some recent dripstone formation.

3.1.1 Santa Barbara Cave System

Surely the best-known hypogenic cave of Sardinia is the Santa Barbara system, composed of two caves developed along the contact between the "*Calcari Ceroidi*" of the San Giovanni and the "*Dolomia Rigata*" of Santa Barbara formations and separated vertically by only a few tens of meters (Fig. 3). Santa Barbara 1 develops between 180 and 227 m a.s.l. and was the first discovered during mining activities in 1952 (Fabbri and Forti 1981). It is famous because its walls and ceiling are entirely covered with brownish barite crystals (Rossetti and Zucchini 1956) and the main room is filled with large carbonate flowstones (Pagliara et al. 2010). The lower Santa Barbara II cave (between 52 to 145 m a.s.l.) (Fabbri and Forti 1986; Badino and Messina 2005) is instead poor in speleothems (except for the widespread presence of mammillary calcite coating the walls which formed in shallow phreatic conditions) and filled with a thick sedimentary sequence (Bini et al. 1988). This cave has a series of very spectacular corrosion morphologies, including megascallops, cupolas, and the extremely rare oxidation vents (De Waele and Forti 2006) clearly showing its hypogenic origin.

3.1.2 Crovassa Ricchi in Argento–Grotta Pisani–Grotta Quarziti

In the same mountain, but more to the west, a series of hypogenic caves has been unveiled along the Idina mine tunnel, at around 220 m a.s.l (Messina et al. 2005). Those are named Grotta Quarziti, in which a unique large hemimorphite flowstone has been found (Forti et al. 1999;

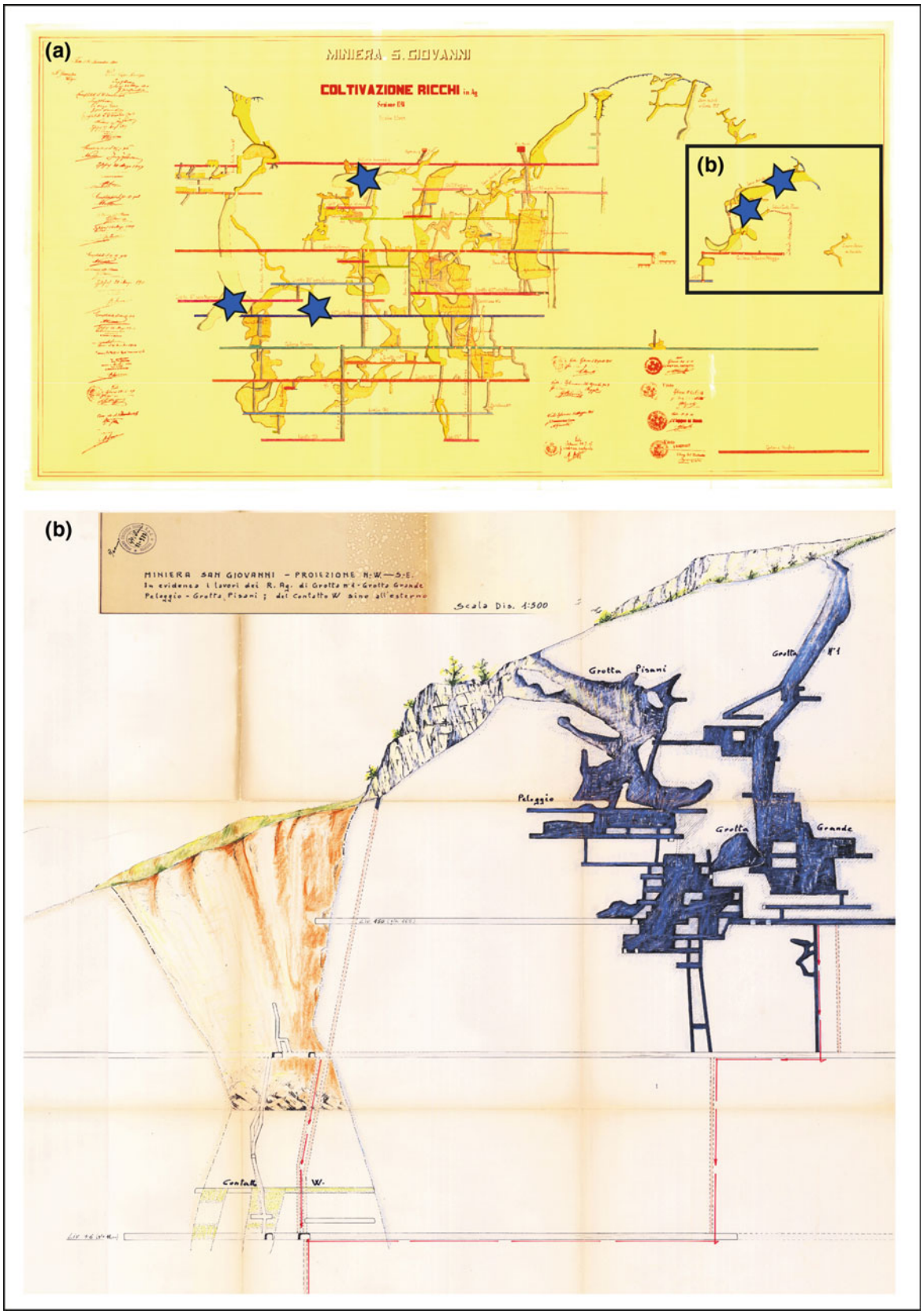

Fig. 2 E–W cross section through the "Ricchi in Argento" sector of San Giovanni Mine. **a** The *stars* indicate the caves signed on the map (they are mentioned with the word "Crevasse"); **b** detail of the western sector (inset **b** in **a**) with the Grotta Pisani and Grotta Grande mentioned. Both maps are from the first decade in the twentieth century

Table 1 List of the main hypogene mine caves of Sardinia and their specific volume

N°	Name of cave		Length (L) (in m)	Volume (V) (in m^3)	Specific volume (V/L) (in m^3/m)
210	Grotta S. Barbara	S. Giovanni	55	6000	110
639	Grotta della Colonna Egiziana	S. Giovanni	40	12,000	300
1122	Grotta Grande M. Onixeddu	Onixeddu	40	10,000	250
1381	Grotta delle Cinque Colonne	Onixeddu	25	1000	40
1527	Grotta Barega	Barega	60	70,000	120
1695	Grotta Phaff 1	Masua	35	18,000	510
1696	Grotta Phaff 2	Masua	35	17,000	480
1838	Crovassa de S'Azzurra	S. Giovanni	15	1500	100
1842	Grotta Eraldo	Barega	40	1500	40
1843	Grotta Cantiere S. Barbara	Monteponi	32	10,000	310
1872	Grotta delle Cupole	Masua	20	7000	350
2320	Grotta di S. Barbara 2	S. Giovanni	40	10,000	250
2405	Sa Crovassa de Trexentusu	S. Giovanni	75	30,000	400
2469	Crovassa Quarziti	S. Giovanni	40	20,000	500
2470	Grotta Pisani	S. Giovanni	60	24,000	400
2534	Crovassa "Ricchi in Argento"	S. Giovanni	100	90,000	900
2785	Grotta Grande di Pelloggio	S. Giovanni	30	3000	100
2789	Grotta di Albert n° 7	S. Giovanni	30	4500	150

Gázquez et al. 2015) (Fig. 4), and Grotta Ricchi in Argento, with thermal calcite spars covered with orange indurated crusts (Gázquez et al. 2013). At a higher level (around 275 m a.s.l), the Grotta Pisani cave still hosts the signs of ancient mining works.

3.1.3 Crovassa Azzurra

Close to the Idina Gallery, another mine adit (Peloggio level) allows to reach the well-known Crovassa Azzurra, at 218 m a.s.l. This cave is a small isolated room that was originally filled with exceptional blue aragonite flowstones. The morphology of the cave is typical of a hypogenic origin. Recently the mineralogy and geochemistry of these blue aragonite flowstones have been studied in great detail (Caddeo et al. 2011).

3.1.4 Massa Riccardo–Albert

Almost at the same altitude (226 m a.s.l), another mine gallery has cut several caves, some of which are vadose shafts, but others are of clear hypogenic origin. The two caves at Massa Riccardo are bell-shaped caves with nice cupola morphologies and speleothems (stalactites and stalagmites) composed of hydrozincite.

3.2 Campo Pisano–Monteponi

On the other flank of the Iglesias syncline two other mines have excavated over 100 km of underground galleries, encountering several mine caves, some of which are of clear hypogenic origin. These caves are typically bell-shaped isolated rooms of deep phreatic origin (Naseddu 1993). One of these is the Gran Sorgente that discharged over 1 m^3/sec into the mine and obliged the mine companies to carve an 8-km-long drainage gallery to allow the water to be drained from 8 m a.s.l directly to the sea at Funtanamare (Forti and Perna 1982; Civita et al. 1983).

3.3 Mount Onixeddu–Mount Barega

Another Cambrian limestone ridge outcrops a couple of kilometers south of the Iglesias syncline and contains a series of mines. Several mine caves have been discovered in Mount Onixeddu and are similar to the other mine caves of hypogenic origin (Sanna et al. 1999).

At the nearby Barega mine, a few mine caves have been discovered, in one of which (Grotta Eraldo) large

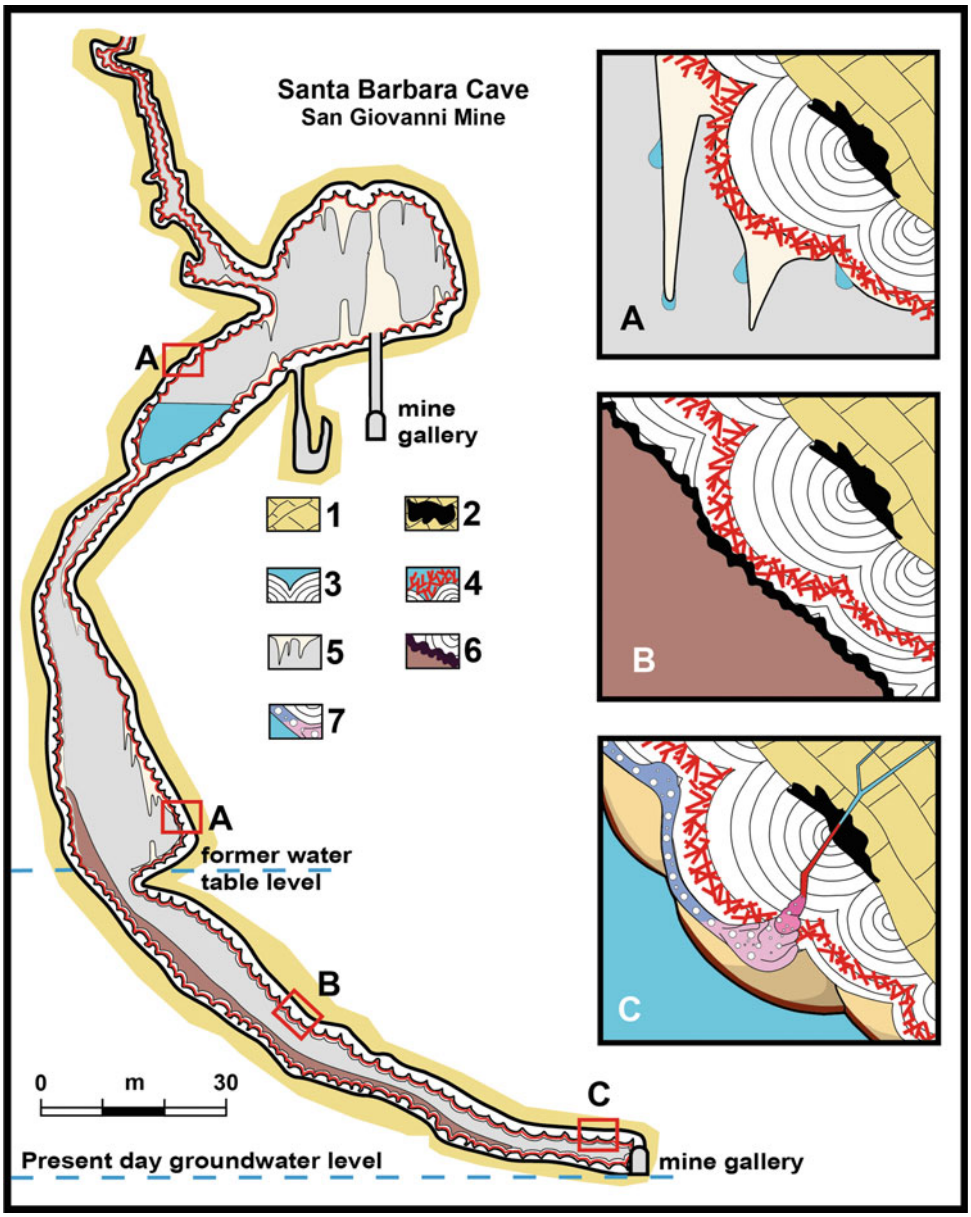

Fig. 3 Santa Barbara cave system: *1* Cambrian carbonate rocks; *2* MVT ore deposits (mainly galena and sphalerite); *3* mammillary calcite (cave clouds); *4* barite crystals; *5* vadose speleothems (stalactites, stalagmites, columns, etc.); *6* corrosion of cave clouds (and deposition of oxides–hydroxides, *black*) under clayey deposits (*brown*); *7* creation of bubble trails and oxidation vents. The evolution of the whole system was the same until the lowering of the groundwater level (not later than 250 ka) caused the differentiation of the processes above and below. In the upper part of Grotta Santa Barbara *1* and *2* vadose speleothems developed (*A*), while in the flooded parts oxidation processes induced the strong corrosion of the cave clouds below the thick clay deposits (*B*), while oxidation vents developed over the cave clouds not in contact with the mud (*C*)

sedimentary deposits of a sulfuric acid derived mineral halloysite were discovered (De Waele et al. 2008), together with nice barite crystals tapering the walls of the cave and filling a fracture (Naseddu 1993). A typical bell-shaped room covered with calcite crystals and also containing aragonite helictites has also been surveyed in this mine (De Waele and Messina 2004).

3.4 Masua

Another mine in which many hypogenic caves have been discovered is Masua, along the coast in front of the Pan di Zucchero islet (Forti et al. 1981). Several bell-shaped rooms are known (Phaff caves), some of which are entirely covered with calcite dogtooth spar, with crystals reaching several decimeters in length (Forti and Perna 1982) (Fig. 5). Fluid inclusions in these crystals and in barite and quartz have clearly demonstrated their thermal origin (De Vivo et al. 1987).

Two other caves have been discovered in this mine, both of which have clear signs of being formed under thermal conditions (Chiesi and Forti 1987). They are located in the mine level −42 m below sea level and became accessible when the mine pumped the water. The walls of both caves are covered with mammillary calcite (cave clouds), which in Grotta delle Budella cover corroded calcite crystals grown in thermal waters.

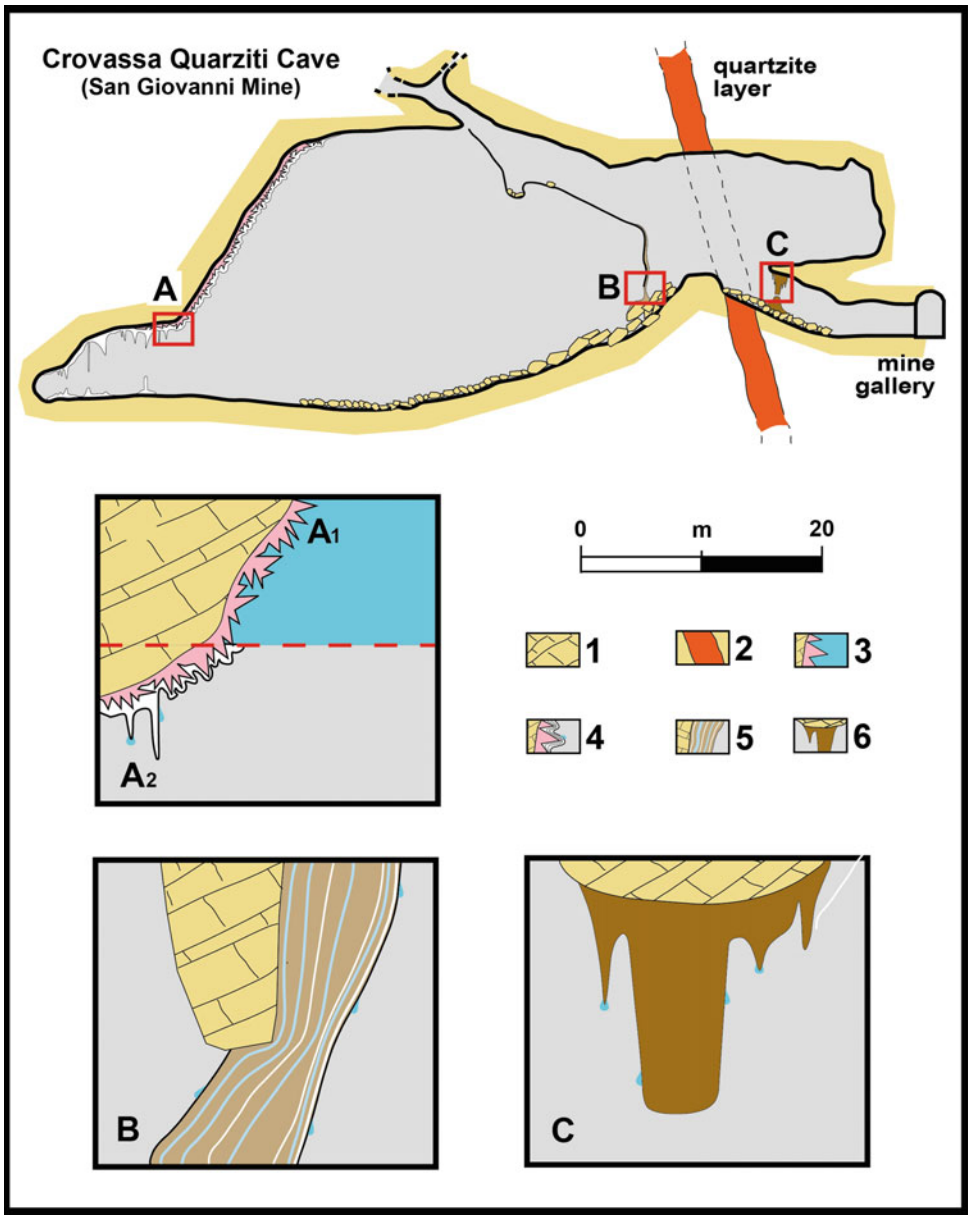

Fig. 4 Grotta Quarziti: *1* Cambrian carbonate rocks; *2* quartzite vein; *3* calcite dogtooth spar; *4* vadose calcite speleothems; *5* opal–hemimorphite–calcite flowstone; *6* hemimorphite dripstones. The thermal calcite macrocrystals (*A1*) represented the first stage in the chemical deposition. These calcites were later covered by cave clouds and after the lowering of the groundwater (ca. 250 ka) by gravitational speleothem formations (*A2*); during the latest vadose stage, an opal–hemimorphite–calcite flowstone (*B*) and a large hemimorphite dripstone (*C*) developed both being related to the quartzite layer and sulfide orebodies

3.5 Monte Guisi Cave

Monte Guisi is located 8 km north of Domusnovas, at the contact between Cambrian limestones and the granitic Variscan basement rocks. The intrusion of these granites has caused the limestones to be metamorphosed, also resulting in the emplacement of a calcic skarn deposit containing Pb, Zn, Fe, and Cu. The cave is carved in these skarns probably in several episodes, some of which are clearly of thermal hypogenic nature. The cave is a small labyrinth accessible by an accidental shaft and shows some clear hypogenic dissolution morphologies (cupolas, swiss cheese morphologies). It is only 70 m long, but it is of a great mineralogical interest (Moldovan et al. 2013).

3.6 Corona ‘e Sa Craba Quartzite Cave

Close to Carbonia, near the small village of Barbusi, a 100 m thick quartzite vein scars the landscape forming a prominent N–S-oriented ridge. Within this quartzite, a 250-m-long cave has been carved (Sauro et al. 2014). The Corona ‘e Sa Craba cave is renowned for its beautiful bluish barite crystals covering parts of its roof. The cave also hosts

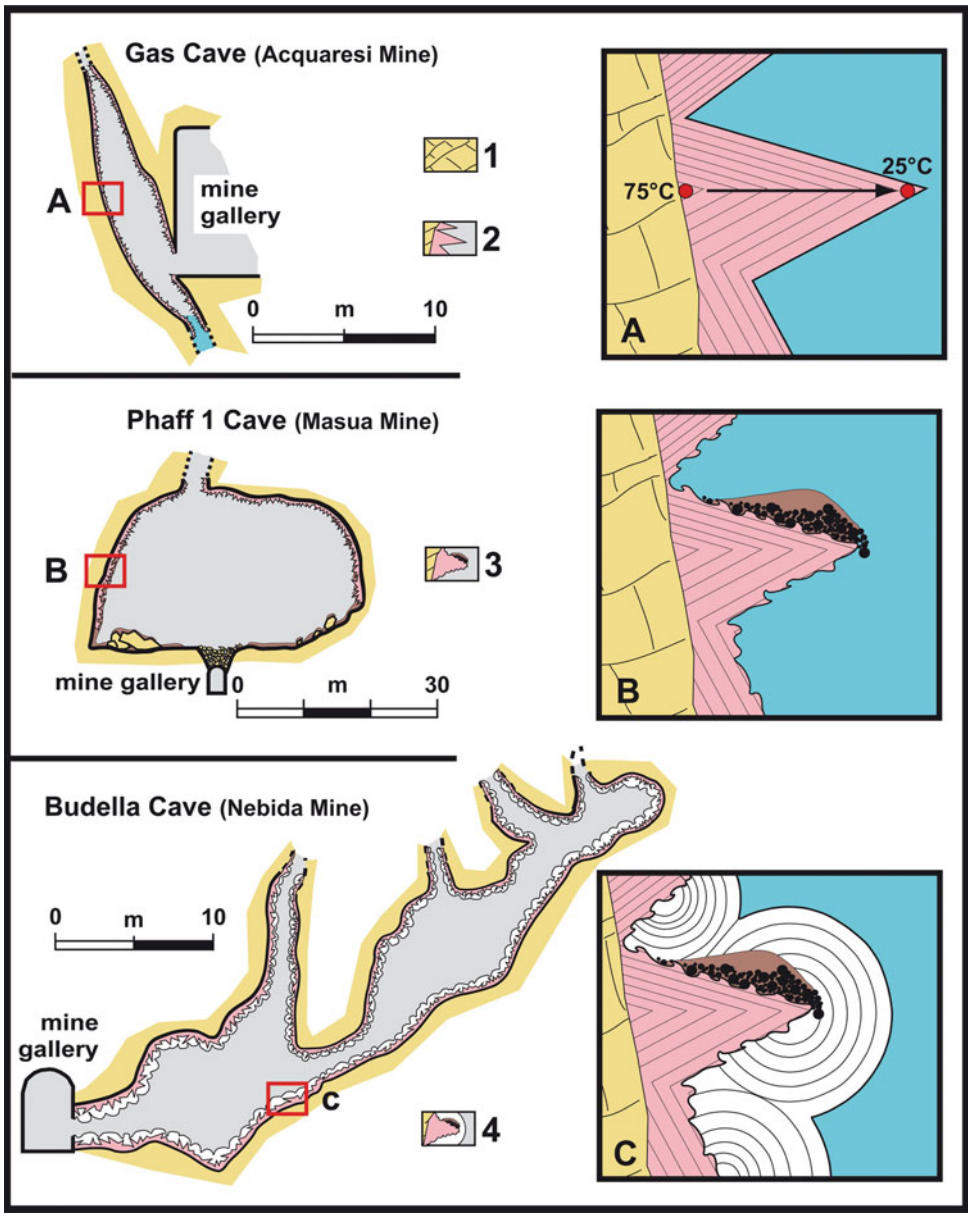

Fig. 5 Hypogene mine cave in the Masua area. *1* Cambrian carbonate rocks; *2* calcite dogtooth spar; *3* corroded calcite spars with oxidation residues; *4* mammillary calcite (cave clouds). The entire cave evolution occurred under phreatic conditions, and the first depositional stage was common to all caves and led to the evolution of thermal calcite dogtooth spar (*A*). Gas cave stopped its development at this stage. In the other two cavities, calcite macrocrystals underwent strong corrosion due to oxidation of the orebodies with deposition of oxides–hydroxides on the *upper* crystal faces (*B*); during a final stage, which took place only in the Budella cave, mammillary calcite (cave clouds) covered the corroded thermal calcite crystals (*C*)

other sulfates, besides many phosphates related to the presence of a large bat colony. Clear signs of intense corrosion in a thermal aquifer have allowed this quartzite cave to be defined as a hydrothermal hypogenic cave.

4 Morphological, Mineralogical and Geochemical Evidence for Hypogene Processes

Until recently, the speleological and scientific community did not regard the Iglesiente mine caves as being of hypogenic origin, despite the fact that several indices (i.e., fluid inclusion in calcite spars) were rather evident. This is mainly because many of these caves were not easily accessible (at least until the mines were closed), and abundant vadose speleothems cover and hide their typical hypogene characteristics. However, the shear size and shape of some of the voids clearly points to their origin in a thermal water body. The specific volume (the volume of the room divided by its major axis) of many of the mine caves clearly matches the typical values of those obtained in thermal caves (Frumkin and Fischhendler 2005) (Table 1).

Alongside this general morphology there are also several smaller subterranean parietal forms that indicate an origin in a setting of rising (thermal) fluids. Bubble trails, cupolas, and megascallops are widely present in many caves. Also local oxidation of the sulfide ores has enhanced the

formation of sulfuric acid producing typical morphologies and replacement minerals (sulfates) (Audra et al. 2015). These processes probably occurred a long time ago, explaining the fact that gypsum, the most typical replacement mineral of sulfuric acid speleogenesis (SAS), is no longer present (De Waele et al. 2013). The unique oxidation vents in Santa Barbara 2 cave are clear evidence of these SAS episodes (De Waele and Forti 2006).

In addition to the morphological indicators that connect the genesis of the caves of the Sulcis-Iglesiente mining district to hypogene agents, there are a number of characteristic speleothems, whose presence indicates the ascent of deep-seated thermal waters and oxidation of Pb-Zn sulfides in the past. Typical secondary minerals found in the hypogenic caves are reported in Table 2. Note that many of these minerals are not associated with the active hypogene speleogenetic phases, but some (dogtooth calcite spars, and mainly oxides, hydroxides, silicates and sulfates) can be related to the cave-forming processes (Figs. 6a and 7b). The first vestige of high-temperature speleogenetic processes dates back to the Cambrian, as yellow speleothemic dolomite crystals (known as "dolomia gialla") filled small pockets of the carbonate bedrock. These primitive infillings are still visible in Santa Barbara Cave (Pagliara et al. 2010) and other locations in the Monte San Giovanni mine. In subsequent stages (Middle Ordovician–Middle Carboniferous), active oxidation of polymetallic sulfide orebodies took place as a consequence of the enhanced circulation of warmer meteoric water inside the system; this oxygen-rich water generated an intense alteration of sulfides and a partial re-mobilization of the ore bodies (De Vivo et al. 1987; Cortecci et al. 1989) and probably was responsible for deposition of massive metallic oxy-hydroxide deposits (Figs. 6b, 7b, d). Stable isotopes ($\delta^{18}O$ and $\delta^{34}S$) and micro-thermometry of fluid inclusions in barite from this period provide further support for this scenario of seawater–meteoric water mixing (Cortecci et al. 1989).

During this stage of sulfuric acid speleogenesis (SAS), precipitation of polymetallic oxy-hydroxides occurred in the upper, more oxygenated part of ore deposits, usually called *gossan* or iron cap. This intensely oxidized, weathered bedrock hosts iron–manganese oxides and quartz, often in the form of *boxwork* and pseudomorphs replacing the pyrite and primary ore minerals. This primitive stage of subaqueous speleogenesis and polymetallic oxy-hydroxides precipitation is clearly exposed in several caves of the Mount San Giovanni mine, including Massa Riccardo, Santa Barbara Cave, Crovassa Ricchi in Argento, and Grotta Quarziti (Figs. 3, 4, 6c, 7b, and 7d).

Massa Riccardo Cave shows massive goethite (α-FeO(OH)) and haematite (Fe_2O_3) deposits, which genesis preceded the precipitation of hydrozincite ($Zn_5(CO_3)_2(OH)_6$) (Fig. 6e), usually observed as white crusts, a few millimeters thick. The occurrence of hydrozincite could indicate a change in the pH of the solution, from acidic to more basic conditions, which enabled this mineral to precipitate. Likewise, Santa Barbara Cave hosts deposits of polymetallic oxy-hydroxides, including goethite, haeterolite ($ZnMn_2O_4$), hydrohaeterolite ($Zn_2Mn_4O_8 \cdot H_2O$), cesarolite ($PbMn_3O_7$ H_2O) and calcofanite ($ZnMn_3O_7 \cdot 3H_2O$), along with barite ($BaSO_4$), galena (PbS), sphalerite (ZnS), and cerussite ($PbCO_3$) (Pagliara et al. 2010). Phreatic and vadose conditions alternated from the Oligocene to the Pliocene, with periods of seawater ingression in the karst.

Subsequent stages were marked by the lowering of water temperature, as the solution reached the supersaturation in quartz (SiO_2) and calcite. First, quartz precipitated from highly saline solutions (13.3–23.3% NaCl eq.) at high temperature (70–112 °C). Later, water temperature decreased to 50–90 °C; then, rhombohedral and scalenohedral spars of calcite precipitated in voids of the bedrock from low-saline meteoric solutions (0.5–2.7% NaCl eq.) (De Vivo et al. 1987). This stage of relatively high-temperature and calcite precipitation is evidenced by the many widespread examples of calcite spars (sometimes tens of centimeters in size), covering the walls of most mine caves in the Sulcis-Iglesiente area, including Crovassa Azzurra (Caddeo et al. 2011), Crovassa Ricchi in Argento (Gázquez et al. 2013) (Fig. 7b), Grotta Quarziti (Fig. 7d), Grotta Barega (Fig. 7c), and the caves of the Masua mine (Figs. 5 and 6a) (De Vivo et al. 1987) among others (De Waele et al. 2013). Moreover, an additional phreatic stage of barite precipitation at around 50 °C has been suggested to occur in the setting of Corona 'e Sa Craba Cave (Sauro et al. 2014).

Further subaqueous freshwater conditions alternated with vadose stages during the Quaternary. During certain phase, the aquifer water level was relatively close to the level of the caves and subaqueous calcite speleothems precipitated, including mammillary calcite (cave clouds) and calcite crusts observed in the Capstan room of Masua mine (Fig. 5) and in the deeper levels of Santa Barbara Cave (Figs. 3 and 6d). These last calcite deposits formed at around 247 ± 17 ka (De Waele and Forti 2006) in epiphreatic conditions, by a slow mechanism of CO_2 degassing close to the water table; this appears to have occurred at temperature similar to the modern cave temperature (15–20 °C) or slightly higher, as suggested by $\delta^{18}O$ analyses of speleothemic carbonate (De Vivo et al. 1987). Interesting examples of low-temperature epiphreatic calcite speleothems have been described in Crovassa Azzurra, where cave clouds are exposed in the cave roof, whereas conical dogtooth calcite crystals, 5 to 10 cm in length, cover the walls to the height of roughly 3 m from the cave bottom. These calcite crystals probably formed during the Quaternary and indicate the position of the water level (~210 m a.s.l) at the time of formation. Cave clouds are also widely present in Santa Barbara 2 cave,

Table 2 Minerals of hypogenic mine caves in Sardinia

Mineral	Chemical formula	Mining area	Caves
Sulfides			
Galena	PbS	All	Many localities
Sphalerite	ZnS	All	Many localities
Cinnabar	HgS	Barbusi	Corona 'e Sa Craba
Oxides/Hydroxides			
Cuprite	Cu_2O	Monte Guisi	Monte Guisi
Monteponite	CdO	Monteponi–Campo Pisano	Monteponi
Haematite	Fe_2O_3	M. S. Giovanni, Barbusi, M. Guisi	M. Riccardo, CSC, M. Guisi
Pyrolusite	MnO_2	Monte Guisi	Monte Guisi
Goethite	α-FeO(OH)	M. S. Giovanni, Barbusi, M Guisi	M. Riccardo, S. Barbara, CSC, M. Guisi
Lepidocrocite	FeO(OH)	Monte Guisi	Monte Guisi
Hetaerolite	$ZnMn_2O_4$	Mt San Giovanni	S. Barbara
Hydrohetaerolite	$Zn_2Mn_4O_8 \cdot H_2O$	Mt San Giovanni	S. Barbara
Cesarolite	$PbMn_3O_7 \cdot H_2O$	Mt San Giovanni	S. Barbara
Chalcophanite	$ZnMn_3O_7 \cdot 3H_2O$	Mt San Giovanni	S. Barbara
Coronadite (?)	$PbMn_8O_{16}$	Mt San Giovanni	S. Barbara
Carbonates			
Calcite	$CaCO_3$	All	Almost all locations
Siderite	$FeCO_3$	Monteponi–Campo Pisano	Monteponi
Smithsonite	$ZnCO_3$	Masua	Several caves
Aragonite	$CaCO_3$	All	Almost all locations
Cerussite	$PbCO_3$	Almost all	Many localities
Dolomite	$CaMg(CO_3)_2$	All	Almost all locations
Azurite	$Cu_3(CO_3)_2(OH)_2$	Monte Guisi	Monte Guisi
Rosasite	$(Cu, Zn)_2(CO_3)(OH)_2$	Monte Guisi	Monte Guisi
Malachite	$Cu_2(CO_3)(OH)_2$	Monte Guisi	Monte Guisi
Phosgenite	$Pb_2(CO_3)Cl_2$	Monteponi–Campo Pisano	Monteponi
Hydrozincite	$Zn_5(CO_3)_2(OH)_6$	Mt San Giovanni	Albert 7
Aurichalcite	$(Zn, Cu)_5(CO_3)_2(OH)_6$	Mt San Giovanni	Crovassa Azzurra
Dundasite	$PbAl_2(CO_3)_2(OH)_4 \cdot H_2O)$	Monte Guisi	Monte Guisi
Arsenates			
Ediphane	$Ca_2Pb_3(AsO_4)_3Cl$	Mt San Giovanni	S. Barbara
Sulfates			
Barite	$BaSO_4$	All	Corona 'e Sa Craba, Barega, S. Barbara
Anglesite	$PbSO_4$	M. S. Giovanni, Monteponi–Campo Pisano, M. Guisi	San Giovanni, Monteponi, M. Guisi
Bianchite	$Zn_2Fe(SO_4)_3 \cdot 18H_2O$	Monteponi–Campo Pisano	Campo Pisano
Epsomite	$MgSO_4.7H_2O$	Mt San Giovanni	San Giovanni
Brochantite	$Cu_4SO_4(OH)_6$	Monte Guisi	Monte Guisi
Alunite	$KAl_3(SO_4)_2(OH)_6$	Barbusi	Corona 'e Sa Craba
Basaluminite (= Felsőbányaite)	$Al_4(SO_4)(OH)_{10} \cdot 4H_2O$	Barbusi	Corona 'e Sa Craba

(continued)

Table 2 (continued)

Mineral	Chemical formula	Mining area	Caves
Phosphates			
Tanarakite	$H_6K_3Al_5(PO_4)_8 \cdot 18H_2O$	Barbusi	Corona 'e Sa Craba
Strengite Al rich	$(Fe, Al)(PO_4) \cdot 2H_2O$	Barbusi	Corona 'e Sa Craba
Robertsite	$Ca_2Mn_3(PO_4)_3O_2 \cdot 3H_2O$	Barbusi	Corona 'e Sa Craba
Spheniscidite	$(NH_4, K)(Fe, Al)_2(PO_4)_2(OH) \cdot 2H_2O$	Barbusi	Corona 'e Sa Craba
Silicates			
Hemimorphite	$Zn_4Si_2O_7(OH_2 \cdot H_2O)$	Mt San Giovanni, M. Guisi	San Giovanni, M. Guisi
Shattuckite	$Cu_5(SiO_3)_4(OH)_2$	Monte Guisi	Monte Guisi
Plancheite	$Cu_8(Si_4O_{11})_2(OH)_4 \cdot H_2O$	Monte Guisi	Monte Guisi
Kaolinite	$Al_2Si_2O_5(OH)_4$	Mt San Giovanni	S. Barbara
Halloysite	$Al_2Si_2O_5(OH)_4$	Barbusi, Barega	Corona 'e Sa Craba, Grotta Eraldo
Lizardite	$Mg_3Si_2O_5(OH)_4$	Barbusi	Corona 'e Sa Craba
Chrysocolla	$(Cu, Al)_2H_2Si_2O_5(OH)_4 \cdot nH_2O)$	Monte Guisi	Monte Guisi
Quartz	SiO_2	Barbusi	Corona 'e Sa Craba
Opal	SiO_2	Mt San Giovanni	San Giovanni

where they are intensely corroded (Fig. 6d), and in some caves in the Masua mine (e.g., Grotta delle Budella and Grotta delle Cupole) (Chiesi and Forti 1987). Although this kind of speleothem is typical of hypogenic/hydrothermal caves (e.g., Audra et al. 2009; Gázquez and Calaforra 2013, among others), some examples of cave clouds and other epiphreatic formations related to waters highly saturated in calcite have been described in non-thermal epigenic caves (e.g., D'Angeli et al. 2015).

During some periods, the karstic network was partially filled with detrital clayey sediments with significant amounts of Fe (8.4 wt%), Ba (3.8 wt%), K (2.9 wt%), and Zn (1.1 wt %), in addition to a great array of trace elements (Mn, Pb, Cu, etc.) below 0.5 wt% (Gázquez et al. 2013). Such high content of metals suggests that fine detrital materials interbedded in the carbonate sequence (mainly clay and silt) were decalcified and the insoluble residues incorporated into the subterranean flow. These red mud deposits are especially well preserved in Crovassa Ricchi in Argento (Fig. 7b) and Santa Barbara Cave (Fig. 7a). Oxidation of metallic ions in subaerial conditions in the wet clayey matrix lowered the pH and occasionally caused the corrosion of calcite spars and formation of orange indurated crusts (Gázquez et al. 2013). This is particularly well visible in the Phaff caves at Masua (Forti et al. 1981).

In Grotta Quarziti, goethite and haematite have been detected as a few centimeters thick layer on quartz substrate (Gázquez et al. 2015). Quartzite in this region formed during silicification events of tectonic breccia of dolomite clast (calcitic skarn), probably by fluids derived from deep-seated leucogranites during the Permian (Boni et al. 1992) or volcanic fluids in the Lower Oligocene (Sauro et al. 2014). Unlike in other caves of the Mount San Giovanni mine, in Grotta Quarziti the deposition of iron oxides probably occurred in subaerial conditions from a water film that flowed on the surface of the quartzitic substrate. During the Late Quaternary, high metal content in water supplied by mineralization in the host rock favored quartz dissolution and gave rise to relatively high concentration of H_4SiO_4 (aq) under neutral or slightly basic conditions. This produced subaerial hemimorphite ($Zn_4Si_2O_7(OH)_2 \cdot H_2O$) speleothem precipitation during the Late Quaternary in this and other caves (Fig. 7f) (i.e., Mount Guisi Cave; Moldovan et al. 2013; Gázquez et al. 2015) (Fig. 4).

Similar subaerial weathering processes have generated a wide variety of uncommon cave minerals, probably in "recent" times, such as anhydrous and hydrous sulfates and phosphates. In total, over 50 cave minerals have been described in these mine caves, enlarging the list originally published by De Waele and Forti (2005) (Table 1). This includes the recent discovery of the new cave minerals dundasite ($PbAl_2(CO_3)_2(OH)_4 \cdot H_2O$) and plancheite ($Cu_8(Si_4O_{11})_2(OH)_4 \cdot H_2O$) in Mount Guisi Cave (Moldovan et al. 2013) and several rare phosphates and sulfates in Corona 'e Sa Craba Cave (Sauro et al. 2014). Also, during the Late Quaternary "conventional" carbonate speleothems formed in some of these caves, including stalagmites,

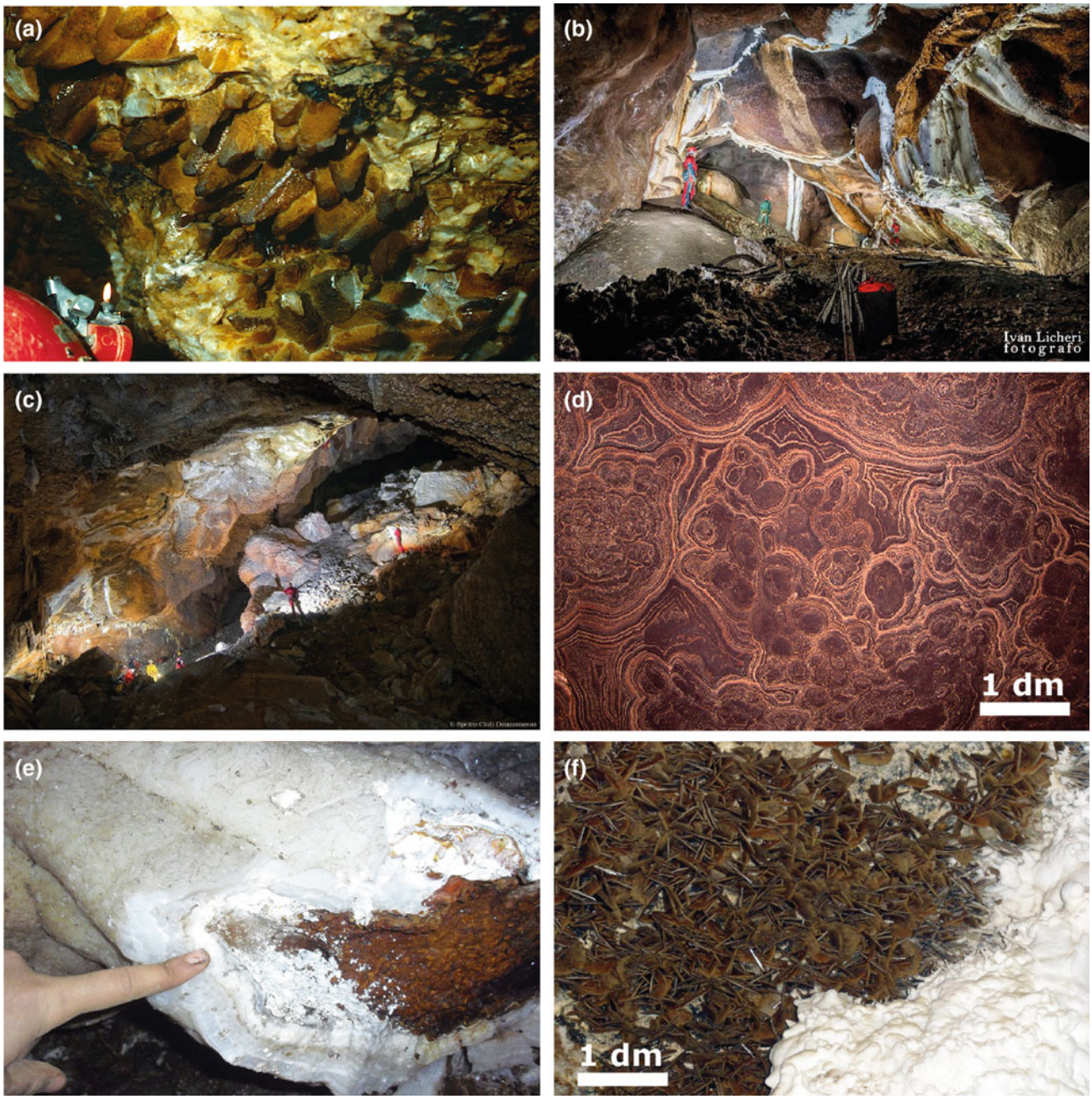

Fig. 6 Hypogene mine caves of Sardinia. **a** Big calcite dogtooth spar in one of the Phaff caves (Masua) (photograph Paolo Forti); **b** overview on the big phreatic chamber in Crovassa Ricchi in Argento cave. Note the rounded cave clouds and the dark oxide–hydroxide coating on the roof (photograph Ivan Licheri); **c** Grotta Pisani and the typical bell-shaped room with mammillary calcite covering the roof (photograph Michele Pili); **d** mammillary calcite (cave clouds) in Santa Barbara 2 cave, completely corroded and showing internal layering (photograph Paolo Forti); **e** 1-cm-thick white layer of hydrozincite coating the red-brownish oxides in the core of the sample and covered by white layered aragonite–calcite layers, Massa Riccardo Cave (photograph Fernando Gázquez); **f** brown centimeter-sized barite crystals covering the walls of Santa Barbara 2 cave (photograph Fernando Gázquez)

stalactites, and flowstones. Among them, the blue aragonite flowstone of Crovassa Azzurra deserves special mention (Fig. 7e). In this cave, subaerial aragonite precipitation was favored over calcite because of inhibition of calcite by relatively high Zn^{2+} concentrations (Caddeo et al. 2011).

5 Conclusions

Many caves discovered during mine tunneling in SW Sardinia have the typical characteristics of thermal hypogene caves. These wide, often bell-shaped voids have also been

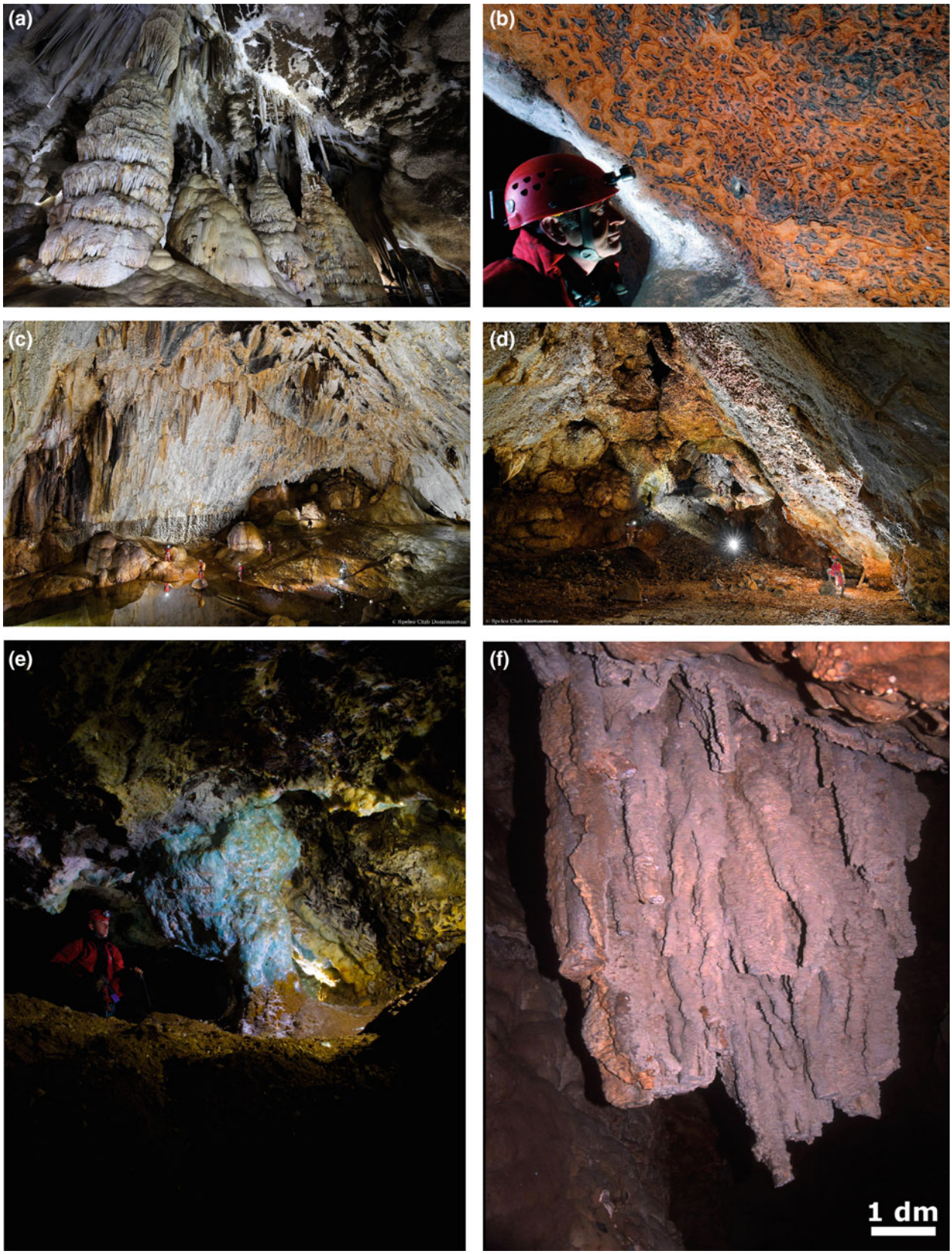

Fig. 7 **a** Santa Barbara 1 cave. Note barite-covered cave clouds (*dark*) on the roof and the giant vadose calcite flowstones (photograph Angelo Naseddu); **b** calcite ghosts with oxides in Crovassa Ricchi in Argento (photograph Victor Ferrer Rico); **c** the large room of Grotta Barega: the high water level can be seen as a dark horizontal line on the white cave walls (photograph Michele Pili); **d** the *bell-shaped* room in Crovassa Quarziti: the right wall is completely covered with calcite dogtooth spar (photograph Michele Pili); **e** *blue* aragonite pillar in the Crovassa Azzurra cave (photograph Angelo Naseddu); **f** the big hemimorphite flowstone in Crovassa Quarziti (photograph Angelo Naseddu)

encountered more than hundred meters below the present sea level, thanks to the fact that the water table was artificially lowered to allow Pb–Zn and barite exploitation. Although the typical hypogene features are often covered with vadose speleothems, or have been masked by the subsequent stages of cave formation and aquifer evolution, there is enough evidence that unmistakably shows these caves to have formed in thermal conditions. Also oxidation of the widespread sulfide ore bodies has caused the local creation of sulfuric acid speleogenesis conditions. One of the hypogene caves is unique for being developed in quartzite (Corona 'e Sa Craba cave) (Sauro et al. 2014). Others are well known for the presence of barite (Fig. 6f) covering the entire cave walls (i.e., Santa Barbara cave, Pagliara et al. 2010), or of thermal calcite dogtooth spars (Quarziti cave, Crovassa Ricchi in Argento (Gázquez et al. 2013), Phaff caves (Forti et al. 1981). Because of their unique setting, their morphological importance and their richness in secondary minerals, these caves deserve to be adequately protected.

Acknowledgements All geomorphological surveys and sampling campaigns have been possible thanks to the help of many cavers, without whom most of the scientific work in these mine caves would have been impossible. A special thanks to the cave photographers Victor Ferrer Rico, Ivan Licheri, Michele Pili, and many others for having shared their nice pictures.

References

Audra Ph, Bigot JY, Mocochain L, Bigot JY, Nobecourt JC (2009) The association between bubble trails and folia: a morphological and sedimentary indicator of hypogenic speleogenesis by degassing, example from Adaouste Cave (Provence, France). Int J Speleol 38:93–102

Audra P, Gázquez F, Rull F, Bigot JY, Camus H (2015) Hypogene sulfuric acid speleogenesis and rare sulfate minerals in Baume Galinière Cave (Alpes-de-Haute-Provence, France). Record of uplift, correlative cover retreat and valley dissection. Geomorphology 247:25–34

Badino G, Messina M (2005) L'esplorazione della grotta di Santa Barbara 2. Mem dell'Istituto Ital di Speleol 17:93–98

Bechstadt T, Boni M (eds) (1996) Sedimentological, stratigraphical and ore deposits field guide of the autochtonous Cambro-Ordovician of Southwestern Sardinia. In: Memorie descrittive della Carta Geologica d'Italia, vol 48. Servizio Geologico Italiano, Roma, p 390

Bini A, Cremaschi M, Forti P, Perna G (1988) Paleokarstic fills in Iglesiente (Sardinia, Italy): sedimentary processes and age. Ann Soc Géol Bel 111:149–161

Boni M, Iannace A, Köppel V, Früh-Green G, Hansmann W (1992) Late to Post-Hercynian hydrothermal activity and mineralization in Southwest Sardinia (Italy). Econ Geol 87:2113–2137

Brusca C, Dessau G (1968) I giacimenti piombo-zinciferi di S. Giovanni (Iglesias) nel quadro della geologia del Cambrico sardo. L'Ind Mineraria 19:1–53

Caddeo GA, De Waele J, Frau F, Railsback LB (2011) Trace element and stable isotope data from a flowstone in a natural cave of the mining district of SW Sardinia (Italy): evidence for Zn^{2+}-induced aragonite precipitation in comparatively wet climatic conditions. Int J Speleol 40(2):181–190

Chiesi M and Forti P (1987) Studio morfologico di due nuove cavità carsiche dell'Iglesiente (Sardegna Sud occidentale). Ipoantropo 4:40–45

Cidu R, Frau F, Da Pelo S (2011) Drainage at abandoned mine sites: natural attenuation of contaminants in different seasons. Mine Water Environ 30(2):113–126

Civita M, Cocozza T, Forti P, Perna G, Turi B (1983) Idrogeologia del bacino minerario dell'Iglesiente (Sardegna sud-occidentale). Mem dell'Istituto Ital di Speleol 2(2):1–139

Cortecci G, Fontes JC, Maiorani A, Perna G, Pintus E, Turi B (1989) Oxygen, sulfur, and strontium isotope and fluid inclusion studies of barite deposits from the Iglesiente-Sulcis mining district, Southwestern Sardinia, Italy. Miner Deposita 24:34–42

D'Angeli IM, De Waele J, Ceballo Melendres O, Tisato N, Sauro F, Grau-Gonzalez E, Bernasconi SM, Torriani S, Bontognali TRR (2015) Genesis of folia in a non-thermal epigenic cave (Matanzas, Cuba). Geomorphology 228:526–535

De Vivo B, Maiorani A, Perna G, Turi B (1987) Fluid inclusion and stable isotope studies of calcite, quartz and barite from karstic caves in the Masua mine, Southwestern Sardinia, Italy. Chemische Erde 46:259–273

De Waele J, Forti P (2005) Mineralogy of mine caves in Sardinia (Italy). Proceeding of the 14th International Congress of Speleology:306–311

De Waele J, Forti P (2006) A new hypogean karst form: the oxidation vent. Zeitschrift fur Geomorphol N.F. Supplementband 147: 107–127

De Waele J, Messina M (2004) Barega, una grotta rivisitata. Anthèo 8:26–29

De Waele J, Frau F, Muntoni A, Cannas C (2008) Ritrovamento di Halloysite nella Grotta Eraldo (Barega, Iglesias, Sardegna sud-occidentale). Atti del XX Congresso Nazionale di Speleologia, Iglesias 27–30 aprile 2007, pp 245–254

De Waele J, Forti P, Naseddu A (2013) Speleogenesis of an exhumed hydrothermal sulphuric acid karst in Cambrian carbonates (Mount San Giovanni, Sardinia). Earth Surf Proc Landf 38(12):1369–1379

Fabbri M, Forti P (1981) Esplorazioni nell'Iglesiente. Sottoterra 59: 31–35

Fabbri M, Forti P (1986) Recenti esplorazioni nelle miniere dell'Iglesiente (Sardegna Sud Occidentale). Sottoterra 74:1–9

Forti P, Perna G (1982) Le cavità naturali dell'Iglesiente. Mem dell'Istituto Ital di Speleol 2(1):1–229

Forti P, Perna G, Turi B (1981) Genetical observations on some natural cavities of the Masua Mines. In: Sardinia SW (eds) Proceedings of the 8th international congress speleologia. Bowling Green, USA, pp 779–781

Forti P, Messina M, Naseddu A, Papinuto S, Sanna F, Sotgia S (1999) Emimorfite in una "grotta di miniera" Gonnesa-Sardegna. Speleologia 41:61–68

Frumkin A, Fischhendler I (2005) Morphometry and distribution of isolated caves as a guide for phreatic and confined paleohydrological conditions. Geomorphology 67(3):457–471

Fusina P (1959) Grotte nella miniera di San Giovanni. Grotte 10:1–23

Gázquez F, Calaforra JM (2013) Origin of double-tower raft cones in hypogenic caves. Earth Surf Proc Landf 38:1655–1661

Gázquez F, Calaforra JM, Forti P, De Waele J, Sanna L, Rull F, Sanz A (2013) Corrosion of calcite crystals by metal-rich mud in caves: Study case in Crovassa Ricchi in Argento Cave (SW Sardinia, Italy). Geomorphology 198:138–146

Gázquez F, Calaforra JM, Rull F, Medina J, Sanz-Arranz A, Forti P, De Waele J (2015) Microprobe and micro-raman determination of hemimorphite speleothems in mine caves of SW Sardinia (Italy). Macla 20:65–66

Messina M, Naseddu A, Papinuto S, Sanna F, Sotgia S, Forti P, De Waele J (2005) Le esplorazioni speleologiche della miniera di San Giovanni: prime sintesi. In: De Waele J, Naseddu A (eds), Le Grotte di Miniera: Tra economia mineraria ed economia turistica, vol 17. Memorie dell'Istituto Italiano di Speleologia, pp 69–86

Moldovan C, Calugar MI, Onac B, De Waele J, Naseddu A, Fornos JJ (2013) A contribution to the mineralogy of Monte Guisi cave (SW Sardinia, Italy). In: Filippi M, Bosak P (eds) Proceedings of the 16th international congress of speleology vol 3, pp 486–489

Naseddu A (1993) Grotte in miniera. Sardegna Speleol 3:8–14

Pagliara A, De Waele J, Forti P, Galli E, Rossi A (2010) Speleothems and speleogenesis of the hypogenic Santa Barbara cave system (South-West Sardinia, Italy). Acta Carsol 39(3):551–564

Pillola GL (1989) Trilobites du Cambrien inférieur du SW de la Sardaigne, Italie. Paleontogr Ital 78:1–174

Rossetti V, Zucchini A (1956) Baritina della Grotta di Santa Barbara. Rend del Seminario della Facoltà di Sci Univ di Cagliari 26(3–4):240–255

Sanna F, Sotgia S, Messina M, Naseddu A, Papinuto S (1999) Prime conoscenze sui fenomeni carsici di Monte Onixeddu. Sardegna Speleol 15:2–10

Sauro F, De Waele J, Onac BP, Galli E, Dublyansky Y, Baldoni E, Sanna L (2014) Hypogenic speleogenesis in quartzite: the case of Corona'e Sa Craba Cave (SW Sardinia, Italy). Geomorphology 211:77–88

An Overview of the Hypogene Caves of Sicily

12

Marco Vattano, Giuliana Madonia, Philippe Audra, Ilenia M. D'Angeli, Ermanno Galli, Jean-Yves Bigot, Jean-Claude Nobécourt, and Jo De Waele

Abstract

Karst in Sicily develops in both Messinian gypsum and Mesozoic or Tertiary limestone rocks. Caves are also found in the basalts of Mount Etna. Except for some rare cases, until recently most caves developed in limestone were considered to be of epigenetic origin. The discovery of gypsum in some of these caves, and especially detailed morphological studies, have allowed defining a hypogenic origin for a dozen of caves up to now. In some of these, the hypogenic evidences are very clear, while others remain in doubt because of the widespread presence of well-developed condensation-corrosion morphologies not necessarily related to hydrothermal fluids. This paper reports the present knowledge of hypogenic caves in the Island of Sicily.

Keywords

Hypogenic caves • Sicily • Sulfuric acid speleogenesis • Condensation-corrosion • Wall sculpturing

1 Introduction

In recent years, knowledge on hypogene karst increased significantly in many aspects. Studies on hypogenic caves in Sicily are quite recent. Except for some investigations carried out at Monte Inici and Monte Kronio (Messana 1994; Perotti 1994 and references therein), systematic research only began in 2010. These investigations have allowed identifying several hypogenic karst systems, previously thought to be epigenetic caves fed by meteoric water. The analysis of pattern, large- and mid-scale morphologies,

M. Vattano · G. Madonia
Dipartimento di Scienze della Terra e del Mare, University of Palermo, Via Archirafi 22, 90123 Palermo, Italy
e-mail: marco.vattano@unipa.it

G. Madonia
e-mail: giuliana.madonia@unipa.it

P. Audra
University of Nice Sophia Antipolis, Sophia Antipolis Cedex, France
e-mail: audra@unice.fr

I.M. D'Angeli · J. De Waele (✉)
Italian Institute of Speleology, Department of Biological, Geological and Environmental Sciences, University of Bologna, Via Zamboni, 67, 40126 Bologna, Italy
e-mail: jo.dewaele@unibo.it

I.M. D'Angeli
e-mail: dangeli.ilenia89@gmail.com

E. Galli
Dipartimento di Scienze della Terra, University of Modena and Reggio Emilia, Largo S. Eufemia 19, 41121 Modena, Italy
e-mail: ermanno.galli@unimore.it

J.-Y. Bigot
Association Française de Karstologie (AFK), 21 rue des Hospices, 34090 Montpellier, France
e-mail: jeanbigot536@gmail.com

J.-C. Nobécourt
CRESPE, Avenue des Poilus, 06140 Vence, France
e-mail: jcnobecourt@free.fr

© Springer International Publishing AG 2017
A. Klimchouk et al. (eds.), *Hypogene Karst Regions and Caves of the World*, Cave and Karst Systems of the World, DOI 10.1007/978-3-319-53348-3_12

Table 1 List of the Sicilian hypogene cave systems

Cave system	Studied	Under investigation	Length (m)	Depth (m)
1 Abisso dei Cocci—Grotta dell'Eremita	X		2000 2900	+61/−300; −306
2 Grotta dei Personaggi	X		1700	+15/−32
3 Grotta dei Personaggini		X	110	−16
4 Grotta Barone		X	85	−14
5 Monte Kronio	X		not available	not available
6 Grotta dell'Acqua Fitusa	X		700	+10/−16
7 Abisso del Vento		X	2,000	−210
8 Grotta dell'Acqua Mintina		X	not available	not available
9 Grotta Palombara		X	800	−80
10 Grotta Scrivilleri		X	2,000	not available
11 Grotta Monello		X	200	−32
12 Grotta Chiusazza		X	190	0

mineral deposits and the presence of warm springs in areas close to the cavities in fact suggest that the genesis of these caves is linked to hypogenic processes (Vattano et al. 2012, 2013, 2015; De Waele et al. 2016).

New explorations allowed inferring the hypogenic origin of other caves based on the presence of peculiar morphologies and deposits. In most cases, speleogenetic, geomorphological, mineralogical and biological studies are still in progress (Table 1).

In this paper, we illustrate the main morphological, mineralogical and speleogenetic features of the hypogenic caves investigated up to now.

2 Geology

Sicily is a segment of the Alpine collisional belt that develops along the Africa–Europe plate boundary and links the southern Apennine and the Calabrian Arc to the Tellian and Atlas systems of northeastern Africa. The Sicilian collisional complex consists of several stratigraphic and tectonic elements (Catalano et al. 2013b and references therein; Avellone et al. 2010; Gasparo Morticelli et al. 2015, Fig. 1): (a) the Hyblean foreland (Hyblean Plateau) outcropping in southeastern Sicily, made up of Triassic–Liassic platform and scarp-basin carbonates overlain by Jurassic–Eocene pelagic carbonates and Oligocene–Quaternary open shelf carbonates; (b) a NW-dipping foredeep located north of the foreland, consisting of Plio-Pleistocene pelagic marly limestones, silty mudstones and sandy clays overlying Messinian evaporites; (c) a complex composed of an E- to SE-vergent fold and thrust belt consisting of: a "European" element (Peloritani–Calabrian Units), exposed in NE Sicily, composed of allochthonous Paleozoic igneous and metamorphic rocks overlain by remnants of a mostly carbonate Mesozoic–Cenozoic sedimentary cover; a "Tethian" element, characterized by repeated imbricated units deriving from the deformation of Sicilidi Units, made of uppermost Jurassic–Oligocene deepwater carbonates and sandy mudstones and covered by Upper Oligocene–Lower Miocene flysch deposit nappes; an "African" element (Sicilian Units) composed of several thrust systems involving the deformation of Permian–Miocene deepwater carbonates and bedded cherts (Imerese and Sicanian basins), and Mesozoic–Cenozoic shelf-to-pelagic carbonates (Panormide, Trapanese, Saccense and Iblean–Pelagian carbonate platform or seamount facies domain); a thrust wedge (Gela Thrust System) consisting of Miocene–Pleistocene coeval foreland, wedge-top and foredeep basin sediments (terrigenous, evaporitic and clastic carbonate rocks).

The fold and thrust belt of Sicily resulted from a progressive accretion of thrust sheets and duplex formation combined with the clockwise rotation of allochthonous blocks started in the Middle Miocene and continued up to Middle–Late Pleistocene (Gasparo Morticelli et al. 2015). Plio-Pleistocene high-angle extensional faults affect the northern coastal sectors of Sicily and the foreland area (Catalano et al. 2013a).

3 Hypogene Caves

In Sicily hypogene caves developed in carbonate rocks and are located in different sectors of the Sicilian collisional complex; hypogenic caves also occur in the foreland area in southeastern corner (Hyblean Plateau) (Fig. 1).

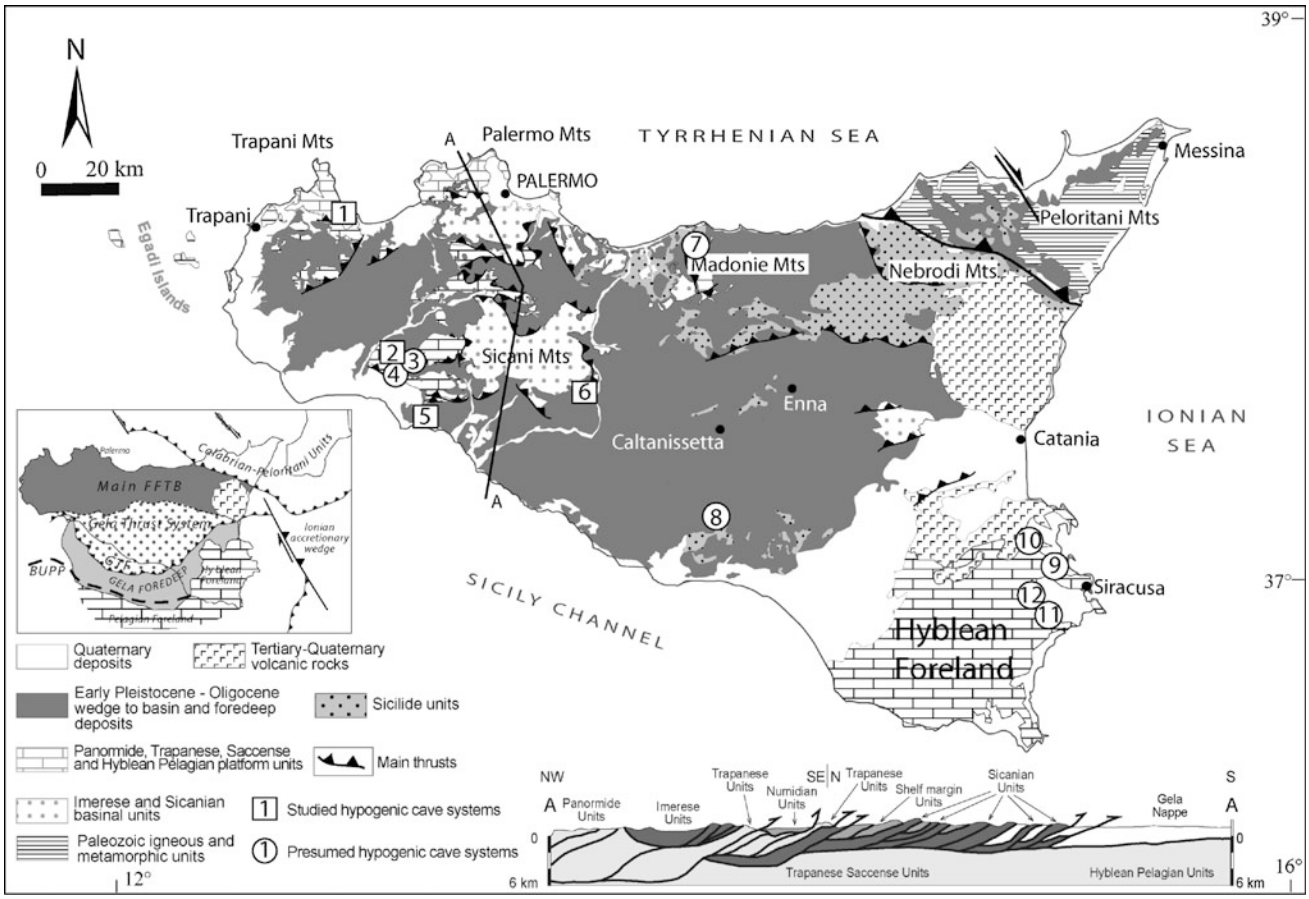

Fig. 1 Geological map of Sicily (from Catalano et al. 2000, 2013b) and location of hypogenic cave systems. *1* Monte Inici caves; *2* Grotta dei Personaggi; *3* Grotta dei Personaggini; *4* Grotta Barone; *5* Monte Kronio caves; *6* Grotta dell'Acqua Fitusa; *7* Abisso del Vento; *8* Grotta dell'Acqua Mintina; *9* Grotta Palombara; *10* Grotta Scrivilleri; *11* Grotta Monello; *12* Grotta Chiusazza. *Inset* map shows the main elements of the collisional complex of Sicily (FFTB, fold and thrust belt; BUPP, boundary of undeformed hyblean-pelagian carbonate platform)

Most of these are inactive sulfuric acid speleogenesis (SAS) caves mainly formed by corrosion processes of carbonate rock by H_2S-rich thermal water rising along important faults. Thermal waters, some of which used for therapeutic and recreational purposes, often spring out close to the caves (Grassa et al. 2006 and references therein).

These active and inactive SAS caves are among the most developed systems of the Island, reaching lengths of almost 3 km and depth of 300 m. A clear example of inactive SAS water-table cave is represented by the "Grotta dell'Acqua Fitusa," which despite its small dimensions shows many diagnostic features of this type of caves (Vattano et al. 2012; Plan et al. 2012; De Waele et al. 2016).

Hypogenic caves with dendritic pattern of stacked spheres seem to be linked mainly to condensation-corrosion processes by airflow rich in CO_2 (i.e., Grotta dei Personaggi).

All the caves have developed along structures such as bedding, fracture or fault planes; an important role in enlarging voids is played by processes of condensation-corrosion caused by thermal convective airflow in the cave atmosphere.

3.1 The Monte Inici Cave System

The Monte Inici cave system is located in NW Sicily (Fig. 1), along the SE side of Mt. Inici, a gently westward—dipping monoclinal relief affected by NW–SE, NE–SW and NNW–SSE high-angle faults. It is composed of two caves, Grotta dell'Eremita and Abisso dei Cocci, formed in Lower Jurassic platform limestones and dolomitic limestones (Inici Fm.), and Upper-Middle Jurassic pelagic reddish-gray limestones with ammonites (Buccheri Fm.) of the Trapanese Domain. Thermal springs with temperature between 44.2 and 49.6 °C and chloride-sulfate alkaline-earth waters (Grassa et al. 2006) are located eastward and at lower altitude with respect to the cave system (Fig. 2a).

Grotta dell'Eremita and Abisso dei Cocci are 3D inactive phreatic maze caves characterized by large subhorizontal

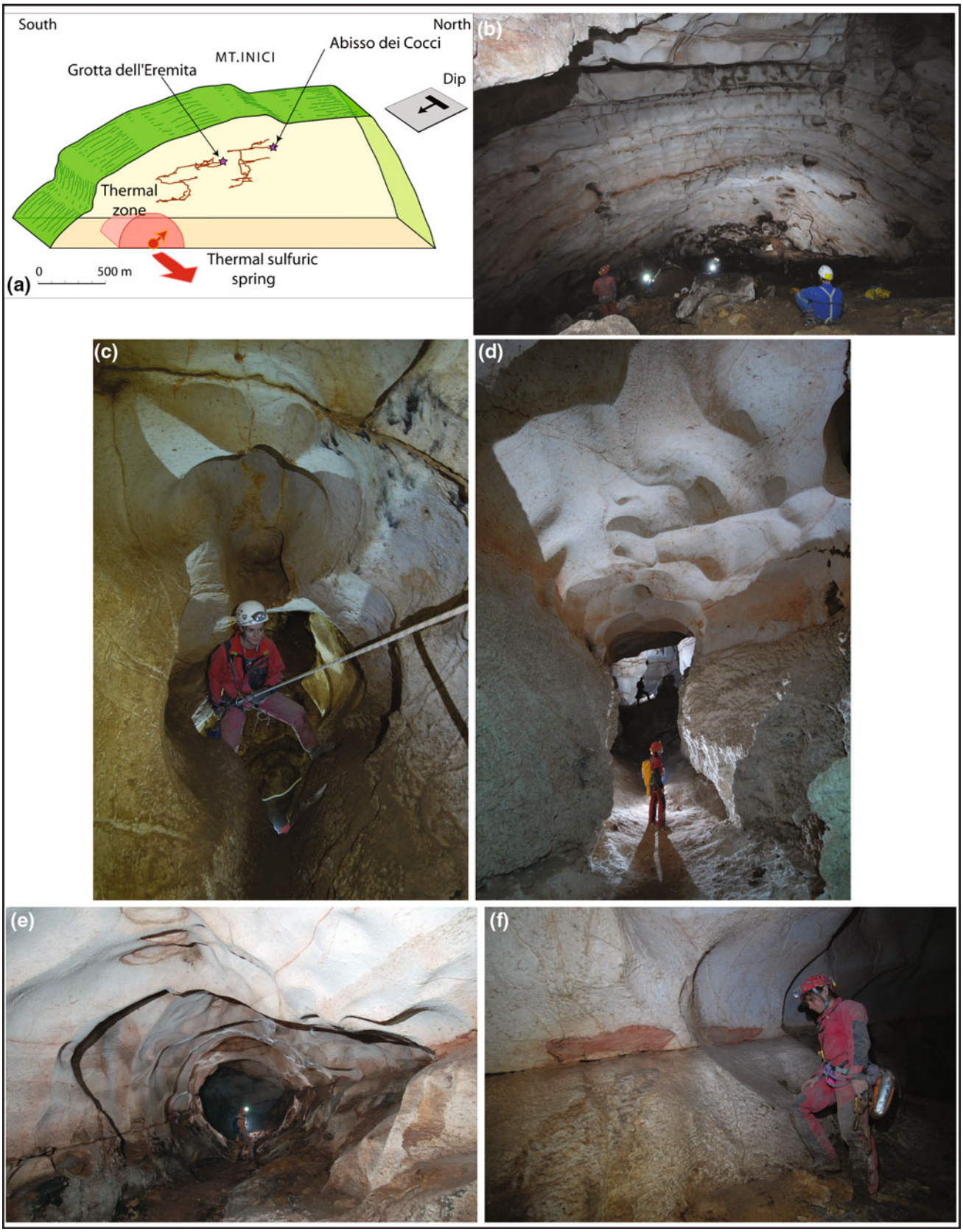

Fig. 2 Monte Inici cave system. **a** Sketch of Monte Inici and its caves and location of the thermal zone (from Vattano et al. 2013); **b** big chamber enlarged by condensation-corrosion processes caused by huge guano deposits (Grotta dell'Eremita); **c** vertical passage with rounded walls and cupolas on the roof (Abisso dei Cocci); **d** entrenched phreatic passage characterized by cupolas, and calcite/aragonite and gypsum deposits in the lower parts (Abisso dei Cocci); **e** inclined passage along a bedding plane with large convection wall niches and ceiling cupolas (Grotta dell'Eremita); **f** close view of protoconduits filled by continental silt along the gallery shown in Fig. 2e

galleries and chambers connected by deep shafts, which reach, respectively, a total length of more than 2 km and a depth of about 300 m (Fig. 2b, c). Some galleries are inclined and follow the dip of bedding planes, whereas the shafts correspond to vertical fissures or fault planes. Passages display subcircular cross sections, or vadose entrenchments (Fig. 2d, e). In some galleries of the Grotta dell'Eremita several small conduits filled by well-cemented fine reddish sediment of continental nature occur at the bedding plane along which the passage develops (Fig. 2f).

Morphologies due to condensation-corrosion processes are widespread in both caves. The walls and ceiling of several passages are tapered by convection wall niches, megascallops, ceiling cupolas (Fig. 2d) and spheres, spongework-like forms, while in some cases passages are divided by partitions.

Both caves lack alluvial sediments. Chemical deposits consist mainly of calcite occurring in powder, thin crusts, frostwork, popcorn or reddish laminae (Grotta dell'Eremita) and gypsum in the form of crusts, and small acicular, fibrous or tabular crystals along the lower parts of the walls of several passages. The caves are rich in phosphate minerals (i.e., hydroxylapatite, taranakite, crandallite, carbonate-apatite, montgomeryite) derived from the transformation of large fossil bat guano deposits. Beside powders or crusts, apatite often occurs as small stalactites and stalagmites (Messana 1994; Vattano et al. 2013).

Patterns and cross sections of the main passages of the Abisso dei Cocci and Grotta dell'Eremita suggest that the early speleogenetic phases took place under phreatic conditions by rising thermal water. In the Grotta dell'Eremita, phreatic conditions are recorded also by the several sediment-filled anastomosed protoconduits visible at the bedding plane, along which the passages develop. After switching from phreatic to vadose conditions, as a consequence of the uplift phases of this sector of the Sicilian chain, entrenchment of passages and development of 3D maze caves occurred. In addition, widening of subterranean voids was connected to significant condensation-corrosion processes by airflow rich in H_2S that also favored the deposition of gypsum deposits in the lower parts of the passages.

In the Abisso dei Cocci, a more recent epigenetic phase is recorded by important calcite speleothems (i.e., flowstones, stalactites, stalagmites) fed by dripping meteoric water.

3.2 The Monte Kronio Cave System

The active hypogenic Monte Kronio cave system is unique in Sicily and probably in the world. It is characterized by the rising of hot moist air linked to a deep thermal aquifer, lying below the explored caves. Although this system was visited by man since the end of the Mesolithic for shelter, place of worship, necropolis and from the I century BC for thermal purposes, yet little is known about its real development and speleogenetic mechanisms due to the harsh environmental conditions with temperatures of about 38 °C and humidity of 100%, which make exploration extremely difficult. The first attempts to explore the caves date back to the end of the seventeenth century; since the 1940s several exploration campaigns organized by the Commission Grotte "E. Boegan" of Trieste identified and surveyed the cave system discovering an extended maze of passages up to 200 m deep (Perotti 1994).

The cave system opens NE of Sciacca town (South Sicily), in the southern scarp of Mt. Kronio or Mt. San Calogero. Mt. Kronio consists of a complex structure linked to ENE-striking, closely spaced imbricate thrust sheets, involving Triassic to Miocene platform and pelagic platform carbonate deposits (Monaco et al. 1996). It is made up of a series of caves, whose origin is probably linked to Na–Cl waters some of which rich in H_2S (Dongarrà and Hauser 1982), with temperature ranging between 32 and 55 °C (Grassa et al. 2006 and references therein) emerging along the southern slope of Mt. Kronio at lower altitude with respect to the cave entrances.

The caves are located at different altitudes and consist of subhorizontal passages (Fig. 3a) connected by deep shafts or steep passages. The passages linking the different branches of this cave system are not always big enough to allow a person to pass (Fig. 3b). Some galleries breach the southern scarp of Mt. Kronio through small openings, some of which emit hot air, while other ones let cold air in from outside. Walls and ceiling of the caves are weathered, characterized by condensation-corrosion forms and powdery and/or crusty gypsum deposits are present (Fig. 3c, d; Vattano et al. 2013). Multidisciplinary studies are currently in progress to improve our knowledge on the extent, speleogenesis and the evolution of this important cave system.

3.3 Grotta dell'Acqua Fitusa

The Grotta dell'Acqua Fitusa represents a good example of inactive water-table sulfuric acid cave (De Waele et al. 2016). The cave is located in central Sicily (Fig. 1), along northeastern fault scarp of a N–S-oriented westward-vergent anticline forming the Mt. La Montagnola. This relief consists of rocks belonging to the basinal Imerese Domain, overthrusting the succession of the Sicanian Domain and the clastic Oligo-Miocene covers (Catalano et al. 2013a). Triassic interbedded calcilutites and marls with abundant pyrite and bitumen may occur at the base of the basinal Imerese and Sicanian Domain. The cave formed in the Upper Cretaceous rudist breccias member of the Crisanti Fm. (Imerese

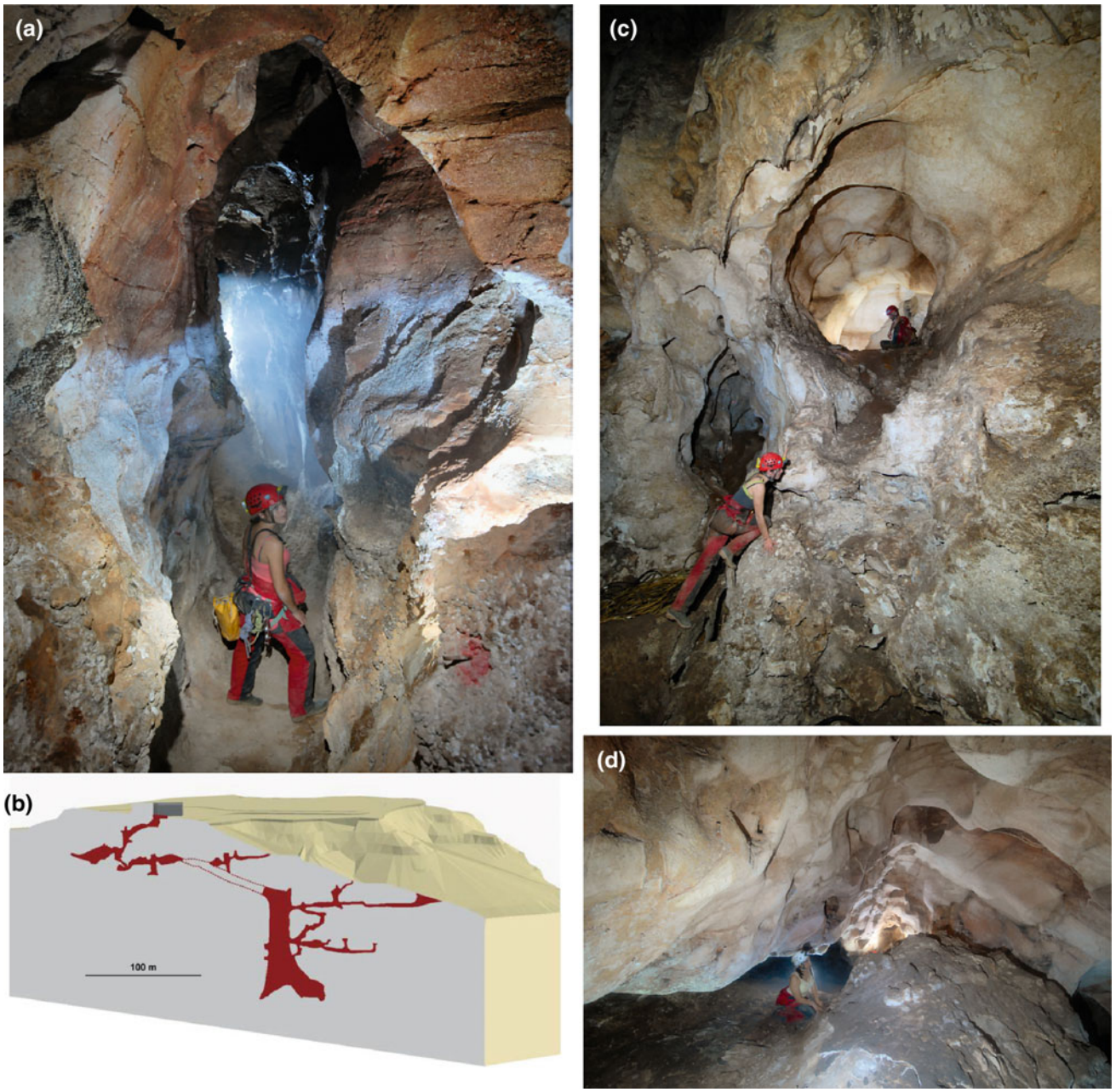

Fig. 3 Monte Kronio cave system. **a** Gallery where the condensation level of the airflow is visible on the walls. Above the caver it is possible to see fog linked to different air temperature: hot in the *upper* part, cold at the *bottom*; **b** 3D sketch of the karst system (after www.boegan.it); **c** passages with forms due to condensation-corrosion processes, separated by partitions; **d** gypsum deposits in the form of crusts, below cupolas in the hot part of the cave system

Domain), composed of conglomerates and reworked calcarenites with rudist fragments and benthic foraminifera. Chloride-sulfate alkaline-earth waters with temperature of 25.2 °C (Grassa et al. 2006) still emerge 300 m north and at a lower altitude than the cave.

The cave consists of at least three stories of subhorizontal conduits (Fig. 4a), arranged in a maze pattern following sets of joints oriented in ENE–WSW, E–W and N–S directions, forming large rooms on their intersections. The cave reaches a total length of 700 m and a vertical range of 25 m.

The passages are developed at the former level of the piezometric surface and are characterized by a very low gradient from the upstream discharging points to the spring. They all show a flat floor breached by discharging feeders up to 10 m deep along their path and notches with flat roof along the walls indicate lateral corrosion processes by the

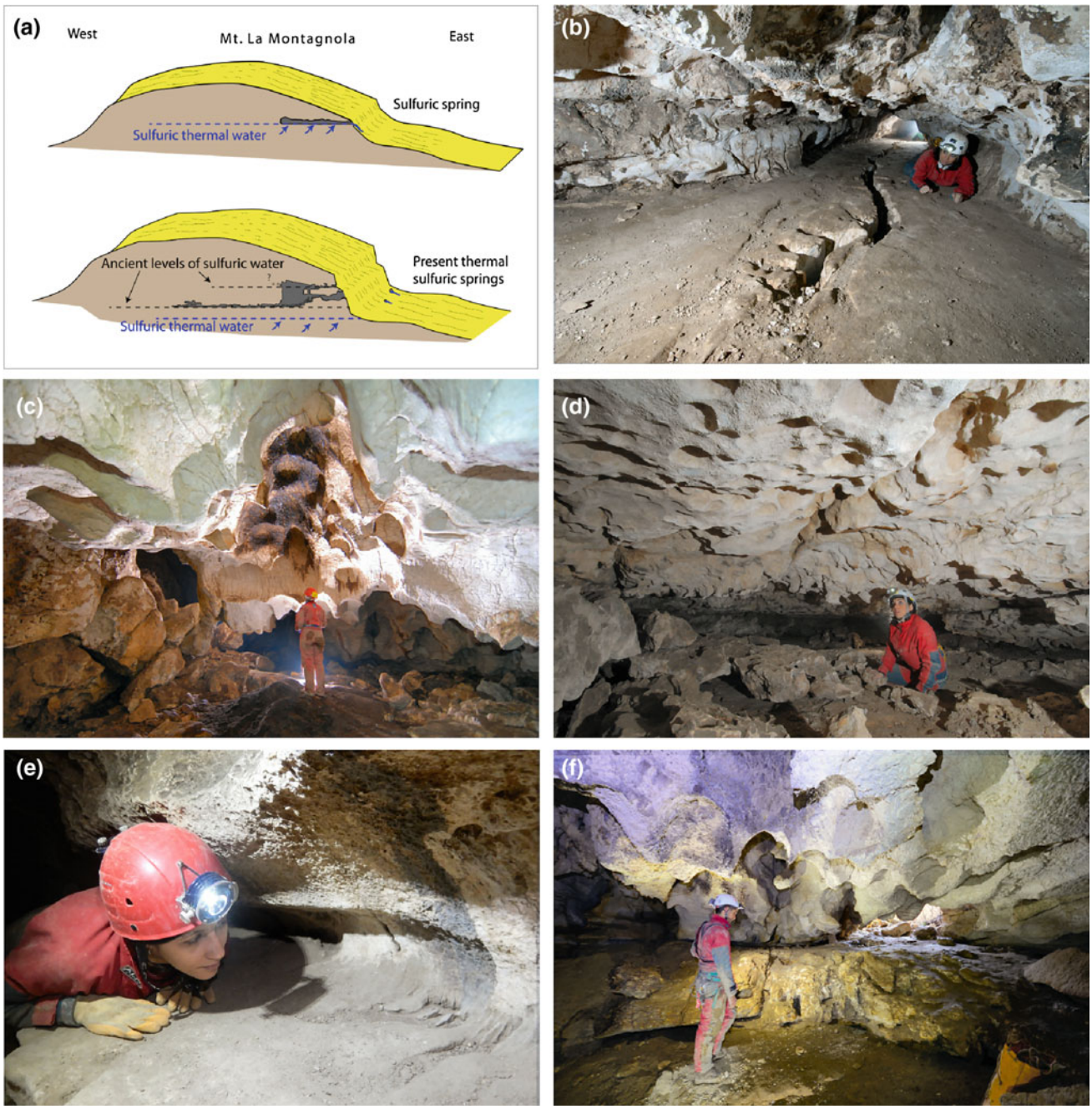

Fig. 4 Grotta dell'Acqua Fitusa. **a** Sketch of the cave and its evolution due to different stages of base-level lowering; **b** passage with discharge feeder at the floor and different levels of wall convection niches; **c** convection ceiling cupolas in the largest chamber of the cave; **d** room characterized by replacement pockets on the roof; **e** sulfuric karren formed by condensation water film; **f** massive gypsum deposit below cupolas

sulfuric thermal water (Fig. 4b). Blind-ending passages develop upstream of the discharge points.

The cave is rich in different small and large morphological features generated by condensation-corrosion processes above the water table, due to H_2S degassing in the cave atmosphere, oxidation of sulfides and thermal convection of the acid air flows (Audra et al. 2010 and references therein). Ceiling cupolas and large wall convection niches occur in the largest rooms of the cave (Fig. 4c); deep wall convection niches, in places forming notches, incise cave walls at different heights (Fig. 4b); condensation-corrosion channels similar to ceiling-half tubes carve the roof of some passages; boxworks, and replacement pockets due to condensation-corrosion processes are widespread (Fig. 4d). In some places, the

condensation waters with a high degree of acidity have produced sulfuric karren, such as rills and solution pans (Fig. 4e).

Beside calcite speleothems due to recent dripping water, gypsum is the most abundant mineral in the cave. Replacement gypsum crusts fill large vertical fissures along the walls, cover wall convection notches or replacement pockets and totally coat narrow blind passages. A deposit of about 50 cm of thickness occurs on the floor of the biggest room in correspondence of which on the roof small ceiling cupolas and pendants are associated (Fig. 4f). Finally centimeter-sized euhedral gypsum crystals grew inside mud sediments.

Since the genesis of the cave is closely related to the piezometric surface position, the different stories of passages record past stages of stability of the water table, in relation to changes of the base-level (Fig. 4a; Audra et al. 2010 and references therein).

Further research on dissolution rates, according to Galdenzi (2012), is being performed.

3.4 Grotta dei Personaggi

The Grotta dei Personaggi is located in SW Sicily, south of the Montevago village. The cave is known since the early 1900s and is famous for the archeological findings inside, but it was never surveyed and studied in detail from a geological point of view. The cave opens along a fault scarp in the NW sector of the Magaggiaro Mount and developed in well-bedded white platform limestones (Inici Fm., Lower Jurassic) and in nodular or massive reddish to brown pelagic limestones with ammonites (Buccheri Fm., Upper-Lower Jurassic) of the Saccense Domain (Di Stefano et al. 2013). Thermal springs, characterized by chloride-sulfate alkaline-earth waters with an average temperature of 39.2 °C (Grassa et al. 2006), are located about 3 km NW of the cavity.

The cave consists of subhorizontal passages that follow bedding and fault planes oriented in the NNE–SSW, NE–SW and NW–SE directions forming a maze pattern. In many sectors of the cave cupolas develop upward in a dendritic pattern of stacked spheres. The cave reaches a total length of roughly 1.7 km, a highest point at +15 m and a depth of −32 m. It is characterized by morphologies linked mainly to condensation-corrosion processes by convective airflow. Deep feeders guided by the main joints and fault planes (Fig. 5a), and vents connecting levels of galleries occur in several sectors of the cave. Megascallops and cupolas (Fig. 5b) are found in all the passages; big cupolas develop mainly on the pelagic limestone where they sometimes stack upward forming vertical passages. Condensation-corrosion channels often associated with cupolas are widespread. Pillars, blades and thin partitions preserved from condensation-corrosion separate different passages located at different levels or along the same level (Fig. 5b, c). Limestone on the walls and roof is weathered, whereas boxwork occurs in the upper portions of the walls.

In many cases, calcite rims and popcorn due to evaporation of condensation waters are located in the lower sides of the corrosion forms such as cupolas, channels and vents (Figure 5c).

The Grotta dei Personaggi hosts a large bat colony (Vattano et al. 2015) responsible for an extensive amount of guano, which influences the cave morphology in several places through condensation-corrosion processes or by chemical corrosion at the guano–rock contact.

The cavity lacks alluvial deposits; on the other hand, mineral deposits rich in phosphates, iron, manganese and silica are present (Fig. 5d). The speleogenetic evolution of the cave after a first phase under phreatic conditions seems to be linked mainly to intensive convective thermal condensation-corrosion processes by acid airflow. Calcite speleothems linked to seepage water are related to a more recent epigenic evolution of the cave.

3.5 Grotta dell'Acqua Mintina

The Grotta dell'Acqua Mintina is located in south-central Sicily and was described by Lugli et al. (2014). It opens in the Messinian Calcare di Base of the Gruppo Gessoso-Solfifero in the brecciated and laminated clastic limestone facies (Fig. 6a; cf. Manzi et al. 2011), along a valley slope cut by a small stream fed by a sulfur spring.

It is a small horizontal cave in which carbonate walls and ceilings are extensively covered by native sulfur and gypsum. Sulfur occurs as centimeter-thick laminated and microcrystalline speleothems, crystals up to 1 cm long, clouds and popcorn-like speleothems (Fig. 6b) and dusty crusts covering acicular gypsum crystals. Fibrous and prismatic crystals of gypsum have been recognized (Fig. 6c; Lugli et al. 2014); they formed both in small pools on the floor of the room close to the entrance and near clay deposits.

Some morphologies such as wall convection niches due to condensation-corrosion and the large amount of gypsum and native sulfur deposits suggest that the cave is linked to sulfuric acid dissolution of limestone in an oxidizing environment.

Fig. 5 Grotta dei Personaggi. **a** Deep feeder along a fault plane enlarged by condensation-corrosion processes; **b** passage with cupolas interpenetrating upward and partitions in the lower parts; **c** cupolas due to condensation-corrosion and calcite popcorns in their lower part linked to evaporation processes; **d** passage characterized by megascallop-like forms partially covered by phosphate crusts

Fig. 6 Grotta dell'Acqua Mintina. **a** Entrance of the cave in laminated limestone. **b** Native sulfur covering almost completely roof and walls; **b** prismatic gypsum crystals

4 Conclusions

The new surveys carried out in several karst systems highlighted that hypogenic caves are very common in Sicily and that several caves previously considered to be of epigenic origin are instead connected to the rising of deep thermal water. All the hypogenic caves are developed in carbonate rocks. Most of them are SAS caves, and their speleogenetic evolution is strongly influenced by the structural features of the rocks, changes of the water-table position and by significant thermal convective condensation-corrosion processes in aerated environment.

Recently detailed studies started to better understand their morphologies, deposits, environmental features and their evolution in relation also to the geomorphological evolution of the area in which they develop. New studies are planned to improve knowledge about the origin and characteristics of rising deep fluids and the residence time of deep water in the caves.

Multidisciplinary researches are in progress in the newly presumed hypogenic caves to establish their origin and speleogenetic evolution.

Acknowledgements The authors wish to thank cavers from ANS Le Taddarite of Palermo, for the support in the field activities. We also wish to thank Augusto Auler and Alexander Klimchouk for their constructive comments that have significantly contributed to the improvement of this paper. The access to Grotta dell'Acqua Mintina was possible thanks to Mr. Giovanni Stuppia and Dr. Rosario Ruggieri.

References

Audra P, D'Antoni-Nobécourt JC, Bigot JY (2010) Hypogenic caves in France. Speleogenesis and morphology of the cave systems. Bull Soc Géol Fr 181(4):327–335

Avellone G, Barchi MR, Catalano R et al (2010) Interference between shallow and deep-seated structures in the Sicilian fold and thrust belt, Italy. J Geol Soc 167(1):109–126

Catalano R, Franchino A, Merlini S et al (2000) Central Western Sicily structural setting interpreted from seismic reflection profiles. Mem Soc Geol It 55:5–16

Catalano R, Agate M, Albanese C, et al (2013a) Walking along a crustal profile across the Sicily Fold and Thrust Belt. AAPG international conference and exhibition. post conference field trip guide. Geol F Trips 5(2.3):213

Catalano R, Valenti V, Albanese C et al (2013b) Sicily's fold-thrust belt and slab rollback: the SI.RI.PRO. seismic crustal transect. J Geol Soc 170(3):451–464

De Waele J, Audra P, Madonia G et al (2016) Sulfuric acid speleogenesis (SAS) close to the water table: examples from southern France, Austria, and Sicily. Geomorph 253:452–467

Di Stefano P, Renda P, Zarcone G et al (2013) Carta geologica d'Italia alla scala 1:50.000 e note illustrative del Foglio 619, Santa Margherita di Belice. ISPRA, Servizio Geologico d'Italia, Roma

Dongarrà G, Hauser S (1982) Isotopic composition of dissolved sulphate and hydrogen sulphide from some thermal springs of Sicily. Geotherm 11(3):193–200

Galdenzi S (2012) Corrosion of limestone tablets in sulfidic ground-water: measurements and speleogenetic implications. Int J Spel 41(2):149–159

Gasparo Morticelli M, Valenti V, Catalano R et al (2015) Deep controls on foreland basin system evolution along the Sicilian fold and thrust belt. Bull Soc Géol Fr 186:273–290

Grassa F, Capasso G, Favara R et al (2006) Chemical and isotopic composition of waters and dissolved gases in some thermal springs of Sicily and adjacent volcanic islands, Italy. Pure Appl Geoph 163:781–807

Lugli S, Ruggieri R, Orsini R et al (2014) The Acqua Mintina cave: a rare geosite with a sulfur smell. In: 4th international symposium on karst in the South Mediterranea area "Karst Geosites. Conservation Protection Fruition", Favignana Italy, 30 May–2 June 2014, pp 38–39

Manzi V, Lugli S, Roveri M et al (2011) The Messinian "Calcare di Base" (Sicily, Italy) revisited. Geol Soc Am Bull 123(1–2):347–370

Messana E (1994) Il sistema carsico del gruppo montuoso di M. Inici (Castellammare del Golfo, TP). Boll Acc Gioenia Sc Nat 27 (348):547–562

Monaco C, Mazzoli S, Tortorici L (1996) Active thrust tectonics in western Sicily (southern Italy): the 1968 Belice earthquake sequence. Terra Nova 8:372–381

Perotti G (1994) Kronio—Le stufe di San Calogero e il loro flusso vaporoso. Boll Acc Gioenia Sc Nat 27(348):435–475

Plan L, Tschegg C, De Waele J et al (2012) Corrosion morphology and cave wall alteration in an Alpine sulfuric acid cave (Kraushöhle, Austria). Geomorph 169:45–54

Vattano M, Audra P, Bigot JY et al (2012) Acqua fitusa cave: an example of inactive water-table sulphuric acid cave in Central Sicily. Rend Online Soc Geol It 21:637–639

Vattano M, Audra P, Benvenuto F et al (2013) Hypogenic Caves of Sicily (Southern Italy). In: Filippi M, Bosak P (eds) Proceedings of the 16th international congress of speleology, vol 3, Brno 19–27 Jul 2013, pp 144–149

Vattano M, Scopelliti G, Fulco A et al (2015) La Grotta dei Personaggi di Montevago (AG), una nuova segnalazione di cavità ipogenica in Sicilia. In: De Nitto L, Maurano F, Parise M (eds) Atti del XXII Congresso Nazionale di Speleologia, Pertosa-Auletta (SA), 30 May–02 June 2015. Mem Ist It Spel 2(29):295–300

Hypogene Gypsum Caves in Piedmont (N-Italy)

13

Cinzia Banzato, Bartolomeo Vigna, Adriano Fiorucci, and Jo De Waele

Abstract

Piedmont (N-Italy) is one of Italy's regions where Messinian gypsum outcrops most extensively. Some gypsum caves have been explored in the past, but no detailed speleogenetic studies have been carried out. The discovery of unexpected large underground voids in a gypsum quarry near Moncalvo has demonstrated the presence of intrastratal karst systems with an origin at least partly linked to rising groundwater flow. A detailed look at one of the gypsum caves near Alba (Monticello cave) has revealed this labyrinth to be another classical example of intrastratal gypsum karst, clearly formed by the rising of undersaturated groundwater through a confined Messinian gypsum bed. This chapter deals with the typical hypogene morphologies in these caves and also reports some new results on the geochemistry of the waters of the Moncalvo area.

Keywords

Messinian gypsum • Intrastratal karst systems • Maze caves • Karst geomorphology • Hydrogeochemistry

1 Introduction

Italy is among the world's richest countries in regard to hypogenic cave systems and karst areas (Galdenzi and Menichetti 1995; Klimchouk 2007; De Waele et al. 2014). Most of these caves are hosted in limestone, and many are of sulfuric acid speleogenesis type (D'Angeli et al. 2016; De Waele et al. 2016; see also Galdenzi and Menichetti in this volume). Also gypsum caves are very common in Italy, with hundreds of caves in several regions such as Emilia Romagna, Calabria, and Sicily (Forti and Sauro 1996; Di Maggio et al. 2012). These caves are normally epigenic through-flow systems (Columbu et al. 2015).

Gypsum outcrops in several areas in Piedmont (N-Italy), but especially in the area of Moncalvo (North of Asti) and Alba, in the central southern part of this region (Fig. 1). These caves, unlike most gypsum caves in Italy, show typical rounded (phreatic) morphologies and are developed in rather thin gypsum beds (max. 40 m thickness) sandwiched in between less permeable clayey and marly sediments. Some of these caves (Moncalvo) have been subject to recent studies (Bonetto et al. 2008; Vigna et al. 2010a, b) and are of clear hypogenic origin. Another labyrinthic cave east of Alba (Monticello cave) is a typical example of intrastratal karst system. The morphologies observed in these caves show many of the characteristic features typical of hypogene speleogenesis sensu Klimchouk (2007).

This paper aims at describing in detail the geological, structural, and stratigraphical conditions allowing the

C. Banzato · B. Vigna · A. Fiorucci
Department of Environment, Land and Infrastructure Engineering, Politecnico di Torino, Turin, Italy
e-mail: bartolomeo.vigna@polito.it

J. De Waele (✉)
Italian Institute of Speleology, Department of Biological, Geological and Environmental Sciences, University of Bologna, Via Zamboni, 67, 40126 Bologna, Italy
e-mail: jo.dewaele@unibo.it

© Springer International Publishing AG 2017

A. Klimchouk et al. (eds.), *Hypogene Karst Regions and Caves of the World*, Cave and Karst Systems of the World, DOI 10.1007/978-3-319-53348-3_13

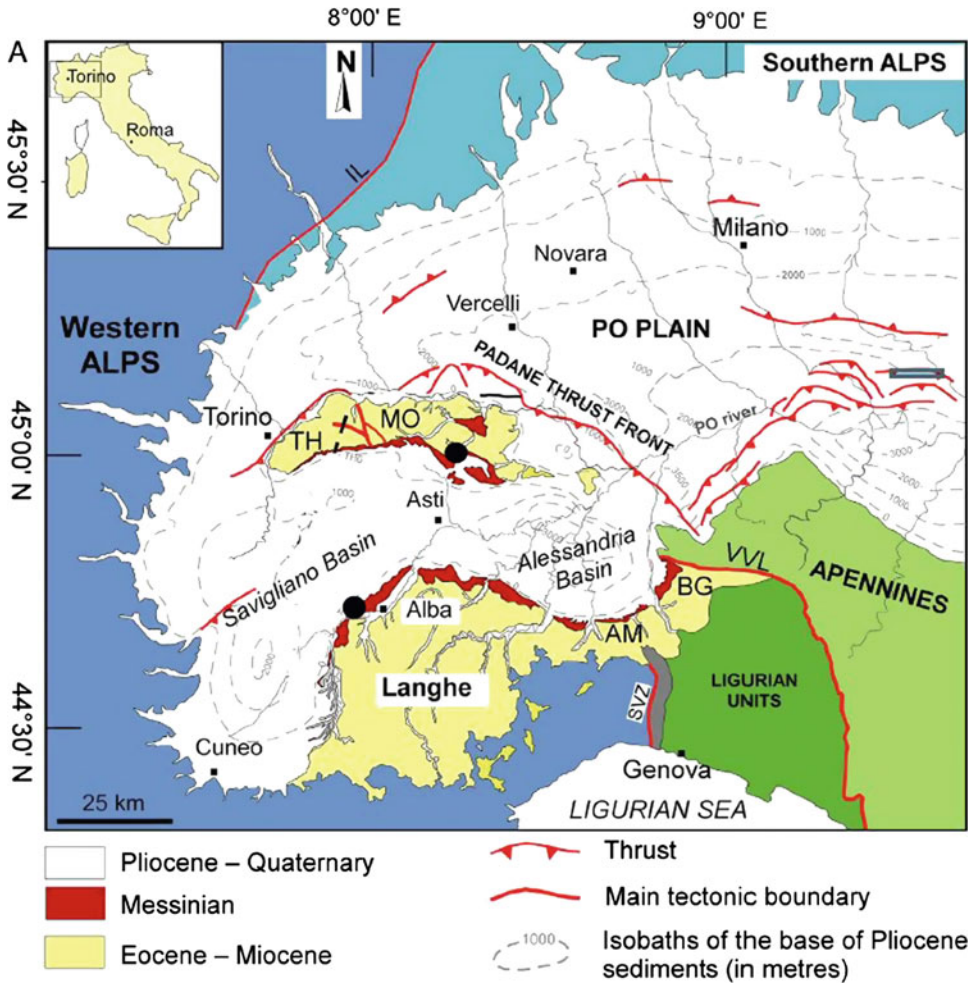

Fig. 1 Geological sketch map of the Tertiary Piedmont Basin

formation of these hypogenic caves and also brings some new data on the morphological characteristics of these caves and the geochemistry of the waters in the Moncalvo area.

2 Geological and Structural Setting of the Gypsum Areas

The Tertiary Piedmont Basin (TPB) outcrops in the hills south of the Alpine Arc occupying a large part of central-south Piedmont (Fig. 1). The stratigraphic succession is composed of a very thick (around 5 km) terrigenous sedimentary sequence ranging in age between the Upper Eocene and the Quaternary. The Tertiary deposits outcrop north in Lower Monferrato and in the Torino Hills and south in Upper Monferrato and in the Langhe. The Messinian sequence, surfacing in the hills around Monferrato and in the Langhe, has been subdivided in three main successive intervals (Fig. 2): a lower clayey level (pre-evaporitic phase) deposited in a normal to moderately hypersaline environment; an evaporitic facies with levels of gypsum and marls deposited in a hypersaline lagoon environment (evaporitic and syn-evaporitic phase); and finally an upper sequence of salty lagoon, delta, and lake sediments (post-evaporitic phase) (Mayer-Eymar 1867; Selli 1960).

2.1 Pre-evaporitic Messinian Deposits

The Messinian pre-evaporitic succession is characterized by the Sant'Agata Fossili marls (Tortonian–Messinian), composed of cyclic alternations of laminated fine sediments and homogeneous marls. In the hills of the Langhe area (around Alba), the succession is characterized by a slumping level around 80 m thick covering the Tortonian deposits and the Sant'Agata Fossili Marls (Clari et al. 2008) and by clays with infrequent levels of sands (Sturani 1973, 1978; Dela Pierre et al. 2014). In the area around Monferrato, the succession is mainly made out of gray and gray-greenish, clayey to silty, locally relatively fractured marls.

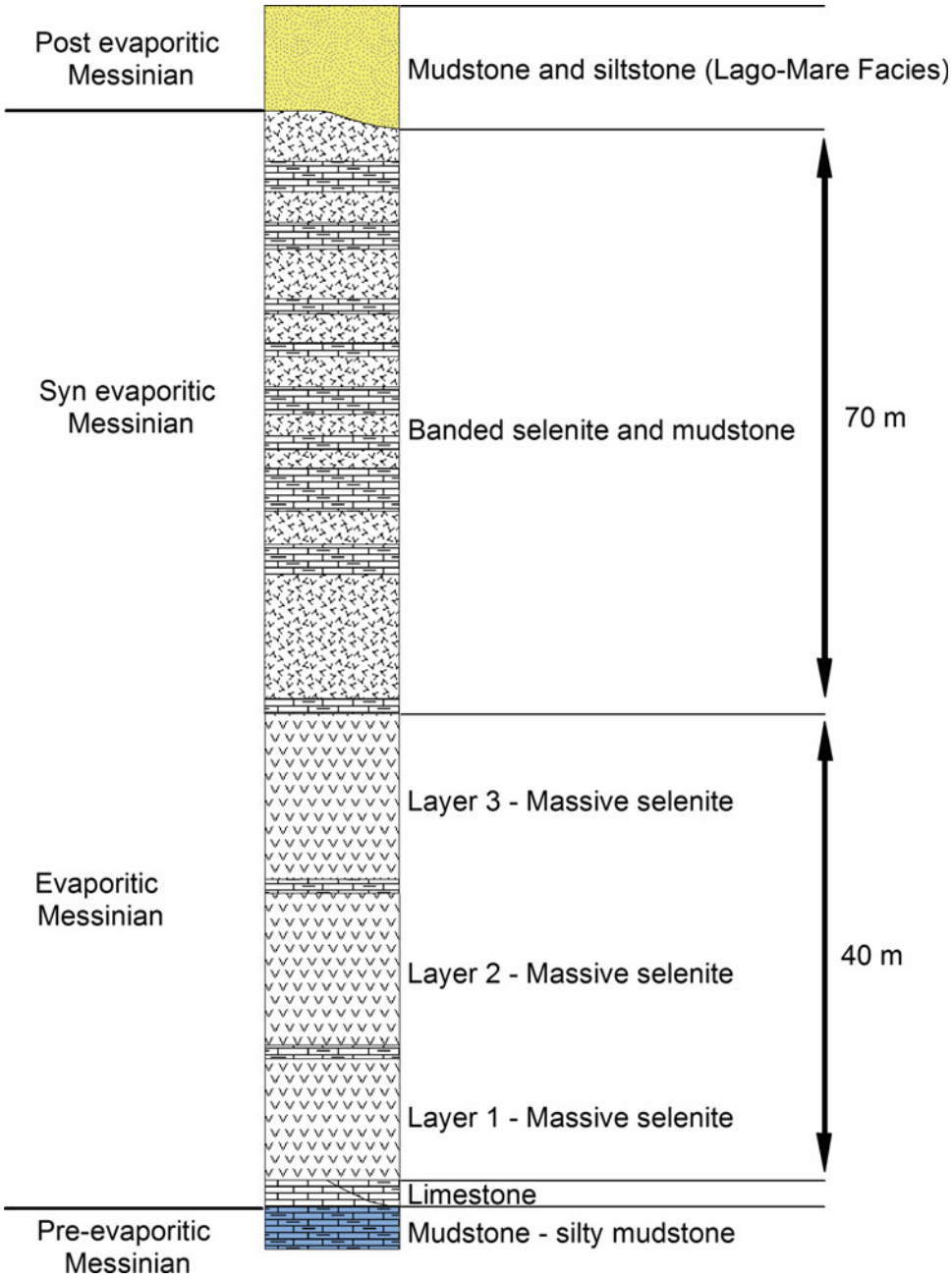

Fig. 2 Lithostratigraphy of the Messinian sedimentary sequence

2.2 Messinian Evaporitic and Syn-Evaporitic Deposits

While the lower marine succession (pre-evaporitic sequence) is rather homogeneous, the upper deposits, composed of primary evaporites of the Vena del Gesso Formation and of fine-grained basin sediments of the same age (syn-evaporitic), are very heterogeneous at both local and regional scale. It must be stressed that in Piedmont the large number of outcropping gypsum levels are partially resedimented bodies and thus do not belong to a well-defined stratigraphic interval.

In the area of Moncalvo and Calliano, North of Asti, along the northern margin of Lower Monferrato, some primary evaporite beds are present both in outcrop and in the subsurface (Vigna et al. 2008). In these locations, the evaporite sequence is locally underlain by a thin bed of limestone and calcareous marls (Calcare di Base) less than a meter thick. The evaporite sequence comprises three beds of macrocrystalline (selenitic) gypsum of a regular thickness (10–12 m) (Fig. 3), occurring over a large area as evidenced by many exploration boreholes. These gypsum beds are separated by dark metric marly–clayey interbeds with fine lamination and abundant fossil plant remains. The overall

Fig. 3 Three main macrocrystalline gypsum beds in the open-pit quarry near Moncalvo

thickness of this first part of the succession is around 40 m. The considerable lateral extension, the constant thickness of the beds, and the large selenitic gypsum crystals in original vertical growth position show the formation of these evaporites to have occurred in a hypersaline environment (evaporitic lagoon) characterized by a very low slope and very low energy.

These three gypsum beds are overlain first by a microcrystalline gypsum bed 10–15 m thick, of a significant lateral continuity and constant thickness, composed of amalgamated levels of tabular to lenticular shape. Thick coarse-grained massive gypsum-arenites with rip-up clasts composed of marly clays or microcrystalline gypsum blocks can be found at various levels.

The evaporitic sequence is completed by the deposition of ten additional gypsum levels of decreasing upward thickness in the sequence, ranging from some meters to only a few decimeters. These gypsum levels are separated by finely laminated gray marly–clayey intercalations of variable thickness (between some decimeters to several meters) becoming thicker upwards in the sequence (syn-evaporitic deposits). The total stratigraphic thickness of this microcrystalline gypsum interval, including the first decametric bed, is around 65–70 m. The upper erosive surface of the succession is responsible of its irregular erosion and consequently of the great lateral variations in thickness ranging between 20 and 70 m.

Primary evaporites outcrop also on the hilly slopes of the Langhe and Roero, along the western margin of the TPB, close to the city of Alba. The entire Messinian succession, outcropping between the villages of Magliano Alfieri and Narzole, has been described by Sturani (1973, 1978) and later by Clari et al. (2008) and Dela Pierre et al. (2011). On the basis of the different evaporitic facies, these authors divide the evaporitic interval in three distinct members. The lower member, of a total thickness ranging between 15 and 30 m, is composed of selenitic gypsum beds of very limited areal extent, interbedded with black laminated clays. The intermediate member is composed of a microcrystalline laminated gypsum bed of some tens of meters in thickness and with a lateral continuity of over 30 km. The upper member is mainly made of densely laminated grayish-blackish fine sediments alternated with micro- and macrocrystalline gypsum in irregular levels of 1 m in thickness for a total thickness that can reach 30 m.

2.3 Deposits of the Post-Evaporitic Messinian

The Messinian post-evaporitic succession is limited downward by an important unconformity of tectonic nature, as testified by the evident angular contact observed in seismic profiles (Ghielmi et al. 2002). Related to this lower limit an important uplift is registered in the sectors of the Hills of Turin, Lower Monferrato, the area of the Langhe and the southern Alpine sector. The resedimentation of large volumes of chaotic deposits (comprising large blocks and olistoliths of primary evaporites), gypsum-rudites and

gypsum-arenites, visible both in outcrops and underground, at the base of the sequence, is ascribed to this important tectonic mobility, correlated to the Intra-Messinian Phase (Dela Pierre et al. 2002, 2003; Rossi et al. 2009; Mosca et al. 2010). The importance of the angular unconformities recognized in subsurface, and the extension and the volumes of these chaotic complexes show this Intra-Messinian Phase to be the most important tectonic phase registered in the TBP in the interval Messinian–Pleistocene. During the post-evaporitic Messinian, a final important regressive phase, known in the literature as "Lago-Mare," is registered (Hsu et al. 1972; Ryan and Cita 1978). The exceptional sea level drop associated with this phase caused the emersion of the marginal areas of the TBP, with the contemporary deposition, at least in certain areas, of continental deposits or the formation of a subaerial erosional surface and a hiatus that can involve most or even the entire evaporite sequence. This regressive phase is followed in the Langhe and Upper Monferrato by the deposition of gravel, sands, and thick intervals of greenish clays of delta, lagoon, or lake environment, known as "Lago-Mare" or "Congerie" facies of Sturani (1973), included in the "Conglomerates of Cassano Spinola Formation" (Boni and Casnedi 1970). Along the northern border of Lower Monferrato, the sequence is characterized by fine clayey–marly sediments of brown color, typical of a lake–sea or continental environment as shown in different geognostic drillholes carried out in the areas of Moncalvo and Calliano (Vigna et al. 2008). A thick Plio-Pleistocene marine sedimentary succession has been deposited after the Messinian evaporitic-continental episode in the TBP.

3 Relationship Between the Geological and Structural Framework and Deep Karstification

The geology and structure of the Messinian succession, controlled by intense Appennine compressional and transpressional tectonics, have greatly conditioned karst development in the evaporite beds. The erosional surface found at the top of the sequence, caused by the Intra-Messinian tectonic event that has uplifted and tilted the entire sedimentary succession in the TBP, with consequent local erosion phenomena and/or partial or even total remobilization of the evaporite sequences, is very well exposed in the area of Moncalvo and Calliano. Stratigraphic profiles based on a series of boreholes allowed ascertaining that this erosional surface has involved the entire evaporitic succession, eroding tens of meters of gypsum deposits and locally even reaching the lowermost levels. The uplift event has certainly influenced the karstification of the gypsum rocks during the several thousands of years in which these rocks were exposed, before they were covered with terrigenous deposits. Surface waters, derived from direct infiltration from rainfall and/or from allogenic recharge, have interacted with the evaporites during this period. With the following deposition of hundreds of meters of mainly clayey deposits during the Upper Messinian and Lower Pliocene, these karst systems have been completely isolated from the surface infiltration, thus slowing down deep karst processes.

Two important compressional deformation phases involved the sedimentary succession during the Plio-Pleistocene: the first occurred during the final stages of the Lower Pliocene, a second one at the onset of the Gelasian (Ghielmi et al. 1998, 2010; Minervini et al. 2008).

These three deformational phases (Intra-Messinian tectonic event and two Plio-Pleistocene compressional deformation phases) are responsible for the formation of a dense fracture network in the bedrock. In the hills of the Langhe, the entire Miocene succession is characterized by fractures that are almost parallel to the bedding planes and show intense microfractures and evident sigmoid structures and reddish oxidation crusts, indicative of water circulation (Vigna 2014). This demonstrates that even in the clayey–marly horizons, that were believed to be impermeable, deep water circulation can take place.

Following Quaternary erosion phases, the gypsum rocks have been exhumed, with renewed development of karst phenomena in the areas where the evaporites came in contact with surface and infiltration waters. It has to be pointed out that in almost all the areas of the TBP the evaporite sequence is mostly still completely overlain by terrigenous deposits, and only in local areas where fluvial networks have entrenched the landscape some small gypsum bodies outcrop.

4 The Caves of Moncalvo d'Asti

Surface expression of gypsum bodies is rare in the Monferrato hills, access being provided by both underground and open-pit mines. Close to the town of Moncalvo, two closely spaced quarries have allowed the investigation of gypsum caves. In the first open-pit quarry, the excavation of the gypsum beds has intersected small cavities and a series of steep-walled sinkholes up to 10 m deep, most of which entirely plugged by silty–clayey deposits. The second (underground) quarry extends for over 20 km of galleries. In 2005, during the development of galleries aimed at reaching the second macrocrystalline gypsum bed, a cave completely filled with water was intercepted at the excavation front (Fig. 4). This has caused an inrush of water and mud with a flow rate of several m^3/s that flooded the lower level of the quarry (Vigna et al. 2008, 2010a, b). Subsequent speleological explorations have allowed the investigation of two

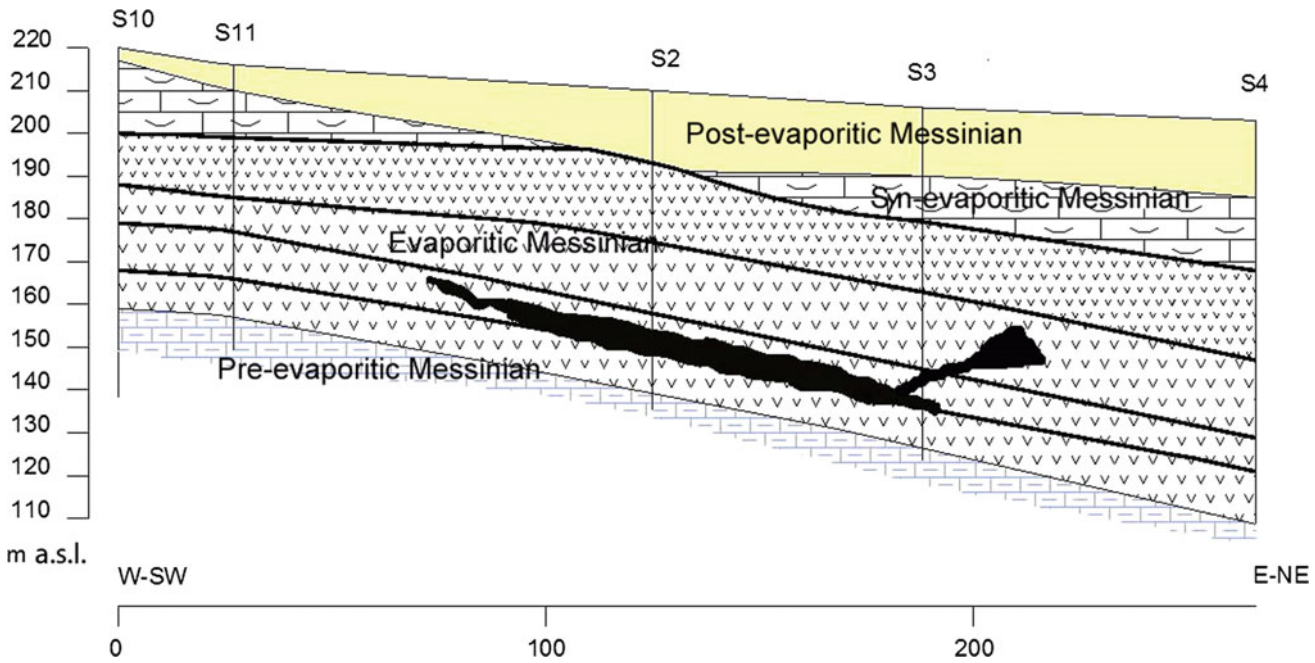

Fig. 4 Sketch profile showing the Moncalvo cave system developed between the first and the second gypsum beds

sectors of a cave, Moncalvo 1 and 2, separated by a sediment-filled section of passage only a few meters long. The first sector (Moncalvo 1) has a total development of 370 m and a positive altitude difference of 30 m, while the second one (Moncalvo 2) is 480 m long and 30 m deep. Both sectors are part of a single system (Fig. 5) of phreatic conduits developed along a layer of 1 m of finely laminated clayey–marly sediments that separate the first and the second macrocrystalline gypsum bed. A secondary branch of the Moncalvo 1 sector (Fig. 6), developing for around 100 m, crosses all three gypsum beds and ends in a wide collapse room with a roof made out of marls, in association with a sinkhole that formed at the surface immediately after the water inrush. The main cave branch develops in a NW direction and is characterized by a more or less cylindrical passage 4–6 m wide. Big pendants that sometimes divide the passage are widespread (Fig. 7), and the floor, covered with debris and marly blocks, is entrenched with a channel formed when the passages were rapidly drained immediately after the interception of the cave by the mining works. Sediments that prevent exploration of other sectors of the cave system block the farthest parts of the cave. Also a secondary 20 m long branch, directed toward the second sector of the cave (Moncalvo 2), is clogged by sediments in the same way. A small 10 m long descending conduit was visible on the left of the entrance of the cave. It ended in a small sump from where the water flow came from. In February 2010, a further artificial lowering of the water level has been carried out to allow the safe extraction of gypsum from the lower levels. Some boreholes drilled in the lowermost areas of the quarry have intercepted the thin carbonate layer present at the base of the evaporite sequence. This limestone bed is intensely karstified and has drained most of the water from the quarry.

The access to the second sector of the cave (Moncalvo 2) is through a small opening at the excavation front of the second level of the underground quarry. This entrance gives access to a small passage 1.5–2 m high. The phreatic morphologies are immediately evident, with a series of cupolas created by upward flow (Fig. 8). After 30 m, a main bifurcation is found: upward a small passage (0.7 × 0.8 m) allows to access a wide passage (Branch of the Flat Ceiling) that will be described later, while downward the conduit of variable size continues with an alternation of narrowings and wider parts and some rising shafts perforating the above lying marly layer that separates the different gypsum beds. The entire downstream branch is carved in the uppermost part of the gypsum bed and often reaches the marly layer above. There are a large number of secondary inlets to the main conduit, all displaying narrow phreatic tubes that become unpassable after a few meters. In the final parts of Moncalvo 2, there are many narrow passages, partly clogged with sediments, interconnecting small rooms in which large gypsum crystals up to 1 m long occur. These crystals have formed in the fractures of the marly interbed, precipitated from oversaturated waters. The rapid dewatering of the cave passage triggered collapse in this section, resulting in broken gypsum crystals on the floor. At 200 m from the entrance,

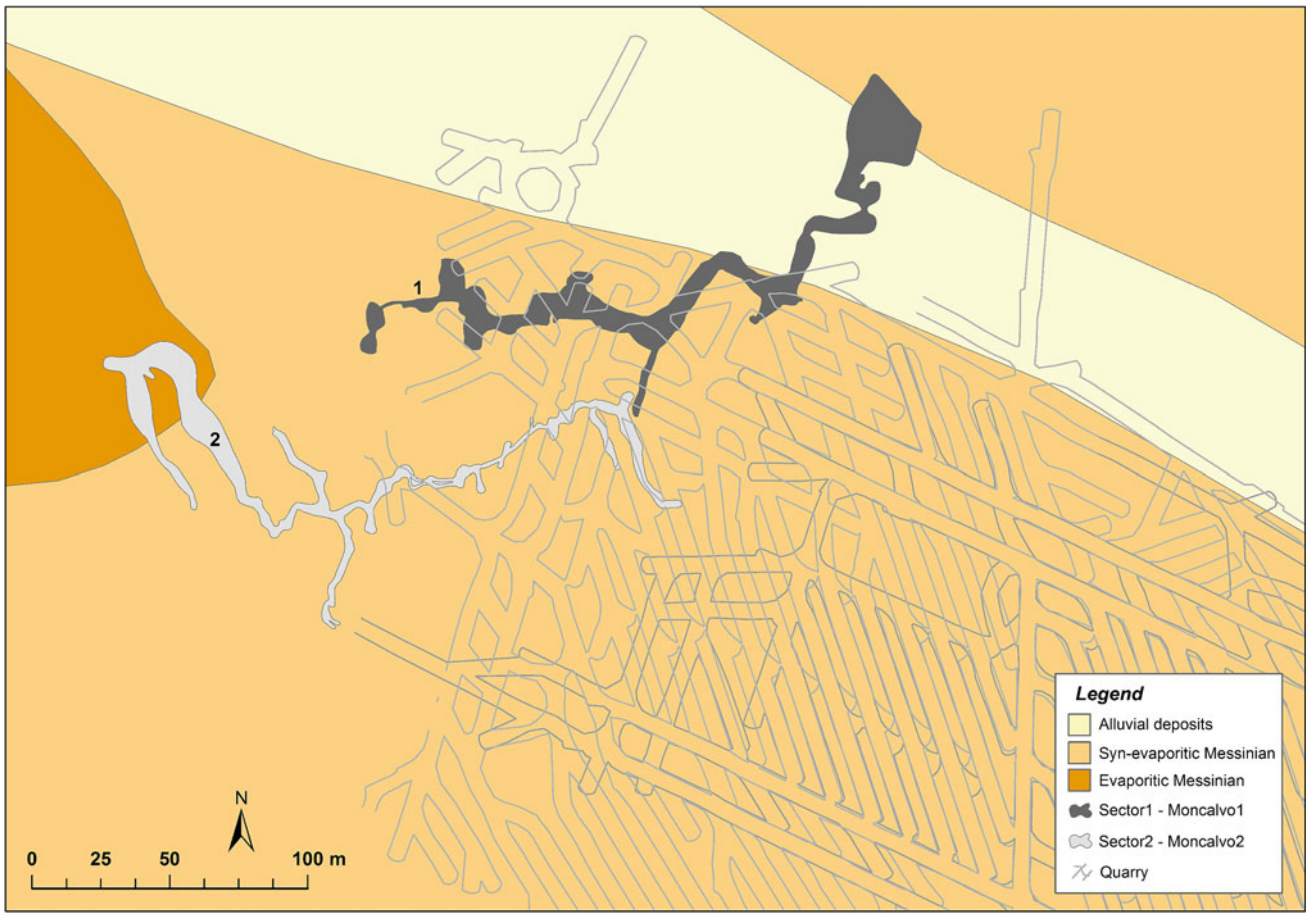

Fig. 5 Moncalvo cave system

Fig. 6 Typical phreatic morphology of the Moncalvo cave passages

Fig. 7 Moncalvo: gypsum pendants on the roof divide the cave passage

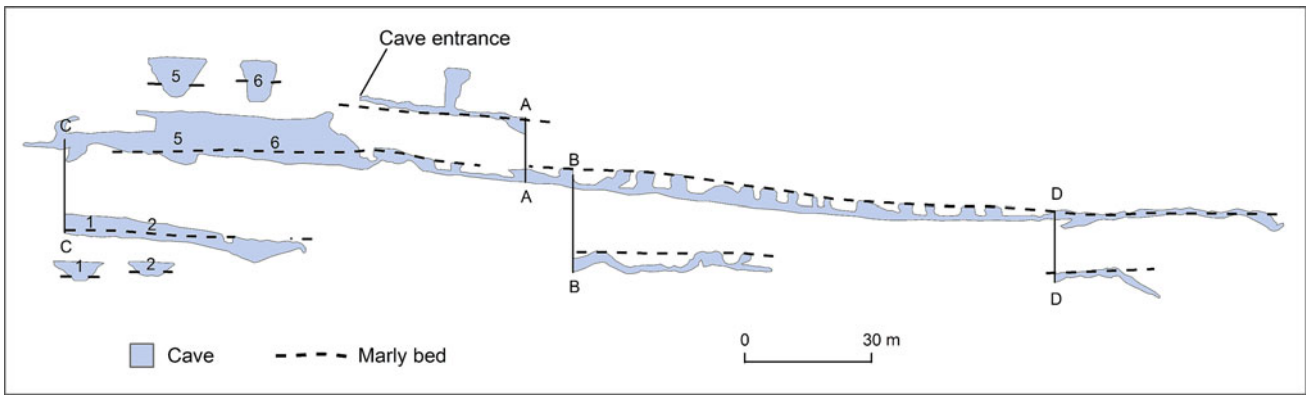

Fig. 8 Longitudinal profile of Moncalvo cave 2: the cave develops on the upper boundary of the first gypsum bed and has a series of ceiling cupolas partially carved in the marly bed

the passage becomes blocked by marly debris. There is strong airflow in this passage, being only 4 m away from Moncalvo 1 sector.

The Branch of the Flat Ceiling is 150 m long and is characterized by a very large passage with a height between 5 and 10 m and width between 5 and 10 m. In the distal end of the upstream part, the ceiling is perfectly flat and carved with small vertical fractures enlarged by descending infiltration water (Fig. 9). This flat ceiling seems to define the highest level reached by the water table before the caves were intercepted by the underground quarry. The elevation of this ceiling matches exactly the water level measured in two piezometers of the quarry, before the occurrence of the water inrush. The entire cave system develops around 20–60 m below the ground surface.

4.1 Groundwater Chemistry

Following the 2005 water inrush, a geochemical study of the groundwater in the Moncalvo area was implemented. Chemical analysis of different waters in this karst system

Fig. 9 Moncalvo: the flat ceiling with a small ceiling channel results from a stationary water table level prior to the interception by the underground quarry

(from caves, fractures in the quarry galleries, boreholes) was carried out, multiparametric sensors were installed, and flow rates were monitored.

From a geochemical point of view, all the waters circulating in the gypsum aquifer are of the calcium-sulfate facies, but there are some differences between the waters depending on flow routes through the aquifer and their provenance. Redox potential (Eh) and the nitrate content (NO_3^-) have allowed the chemical differentiation of these waters. The waters coming from the surface above ("local infiltration water"—LIW samples in Fig. 10) are characterized by very positive redox potential and high concentrations in nitrates (often exceeding 20 mg/L). These waters come in contact with the gypsum rocks after having filtered through the above lying silty–clayey deposits and are slightly undersaturated with respect to gypsum. These waters often create vertical shafts between the overlying sediments and the gypsum rocks. Other waters sampled from fractures in the evaporite rocks have negative redox potential ("deep circulation water"—DCW samples in Fig. 10), low nitrate content, often below detection limit (0.01 mg/L) and are supersaturated in gypsum. These waters circulate below the described evaporitic sequence, whose temperature is similar to that flowing in the karst systems (slightly higher), flowing in the underlying fractured marly rocks (Marls of S. Agata Fossili), and should be strongly undersaturated with respect to gypsum. Waters of similar characteristics have also been found in some springs flowing out of the Pre-Messinian successions close to Moncalvo (negative redox potentials, absence of nitrates and strongly undersaturated in gypsum). When these fluids come in contact with the evaporite rocks, they have a very strong dissolving capacity. Water corresponding to a mixture of the two earlier mentioned ones have also been found in the underground quarries and in a series of boreholes that have intercepted the basal limestone bed at the onset of the evaporite sequence ("mixed water"—MW samples in Fig. 10).

4.2 Speleogenetic Hypothesis

On the basis of the available data, a first hypothesis on the genesis of the Moncalvo gypsum caves can be advanced (Vigna et al. 2010a, b). The karst network was in complete phreatic environment until its interception by the underground quarry in 2005. The hydrogeological behavior of the system, monitored over the last 10 years, shows flow rates of 8–10 l/s, in part conditioned by the infiltration of surface waters (waters rich in nitrates and with a positive redox potential), and in part by the input of deep waters (characterized by low nitrate contents and negative redox potential).

The carbonate horizon at the base of the evaporite sequence is of fundamental importance in the karstification of the entire gypsum body. On the basis of the large number of boreholes drilled in the underground gypsum quarry and its surroundings, this horizon appears to present a very intensely karstified network of small conduits that are able to transmit a significant amount of water flow to the above lying gypsum beds. In this carbonate level surface infiltrating waters and deep waters flowing in the fractured marly

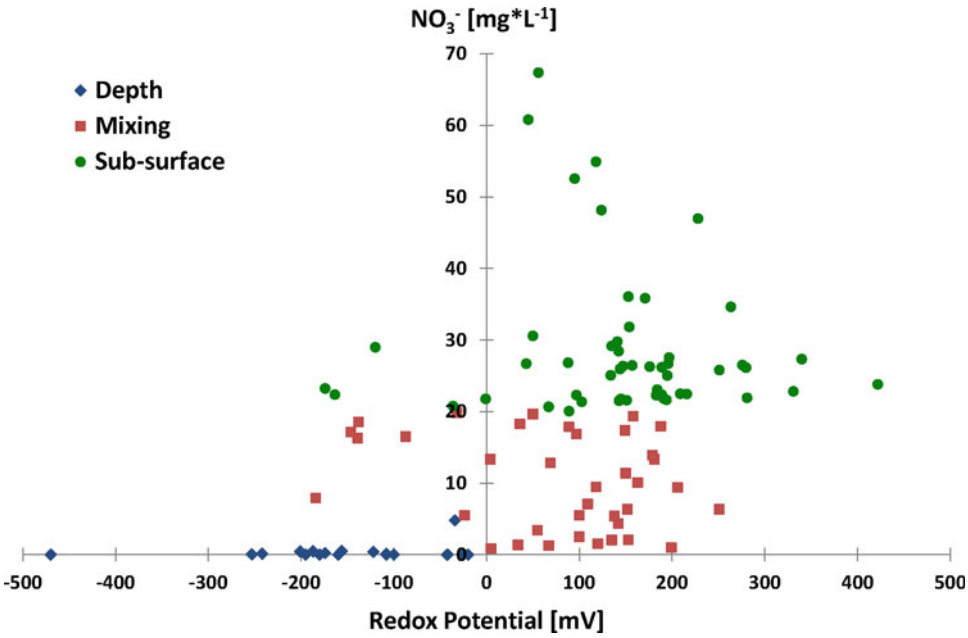

Fig. 10 Chemistry of the three different waters types in the Moncalvo cave area

Fig. 11 Moncalvo: small close-to-vertical conduit is visible on the floor of the cave

rocks and the thin sand levels of the Marls of S. Agata Fossili mix. The waters then rise from this level flowing through a series of small close-to-vertical conduits (these are clearly visible on the floor of the cave, Fig. 11). These waters are still undersaturated in respect to sulfates, and dissolution takes place when these come in contact with the gypsum rocks flowing upward to reach the marly horizon that forms one of the major discontinuities of the sequence. Once this marly horizon is reached, water flows along the gypsum–marl contact dissolving the underlying gypsum. In this way, a karst system develops at the upper contact of the first gypsum layer and the start of the second one. This karst system was entirely flooded (phreatic), and the water pressure was close to 3 bar before the inrush event, based on water levels measured in nearby boreholes before the lowering of the water level.

5 The Cave of Monticello d'Alba

A series of small gypsum outcrops occur on the hilly slopes of the Langhe and of Reoro, along both sides of the Tanaro River. Some of these gypsum bodies were exploited by open-pit quarries in the past. Close to the village of Monticello d'Alba, there is a subterranean excavation some hundreds of meters long that has intercepted in several parts a karst network of approximately 650 m length, now completely dry. This network (Fig. 12), that follows the three main directions N–S, E–W, and NE–SW, is perfectly horizontal and with a labyrinthine plan and shows no vadose morphologies. The cave is developed in the intermediate member of the evaporitic sequence, locally composed of a series of laminated microcrystalline gypsum beds, of less than a meter in thickness, interbedded with marly horizons with a NW strike and a dip of around 10°. This alternation of gypsum and marly horizons causes an evaporite sequence of around 10 m thickness (sandwiched between underlying and above lying clayey deposits), that extends for over 20 km. Under this sequence, there are some fine sandy levels (Sturani 1973; Dela Pierre et al. 2014) that may have played a role in the feeding of the waters that have carved the karst system.

The karst system is composed of a series of small-sized passages with a height of around 2–3 m, filled with silty–sandy deposits up to a meter thick. These sediments do not appear to originate from the surface, but instead seem to derive from the local deposition of the insoluble fraction of the gypsum sequence (Fig. 13). The passages typically follow joints in the ceiling, being wider (about 2 m) at the base and narrowing upwards (Fig. 14). Having developed along thin gypsum beds separated by clayey–marly horizons, these passages often have irregular cross sections due to the differential dissolution and sedimentation on their pavements.

5.1 Speleogenetic Hypothesis

The cave is certainly of the phreatic type, developed in an area in which all the fractures in the evaporite rocks were exploited by speleogenesis. Despite the fact that the gypsum beds dip by 10°, the cave is perfectly level along a horizontal plane that appears to be related to the former elevation of the local water table. The recharge of this aquifer may have two possible sources: a surface infiltration water and a deeper circulating water. The area is located close to the River Tanaro that flows around 30 m below the cave floor. During the entrenchment of the fluvial network, this river might have intercepted the gypsum bed creating a local base level and thus a karstification phase. We believe this cave is a typical example of intrastratal karst where waters rising from below have carved all available discontinuities forming the maze system. In fact, the Messinian stratigraphic sequence of this area contains thin beds of rather permeable sediments (sands) at the base of the evaporite rocks that have acted as feeding lower aquifer. The morphologies of the conduits clearly indicate that part of the waters came from below, with a higher dissolution in the lower part of the cave passages with respect to the ceiling. The maze pattern does not appear to have formed by floodwater, since alluvial sediments are completely lacking. Unfortunately the thick sediment deposits completely shield the original floor from view, thus hiding possible feeder tubes.

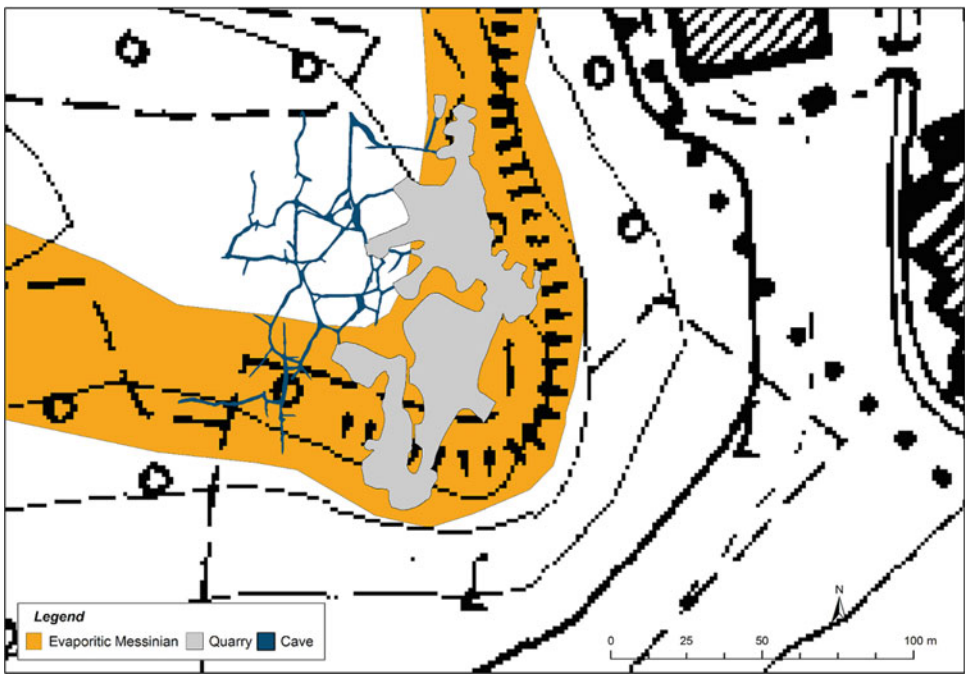

Fig. 12 Monticello d'Alba: detail of the gypsum quarry and the intercepted cave labyrinth

Fig. 13 Monticello d'Alba: cave sediments cover the entire floor of the maze passages

Fig. 14 Monticello d'Alba: the triangular cross section with the wider part down

6 Conclusions

The geological and structural framework of the Messinian gypsum rocks of the TBP surely played a major role in the speleogenesis of the caves described in this chapter. In all other Italian gypsum karst areas, epigenic surface streams sink underground forming through caves composed of a swallow hole, many inlets (dolines), a main drain, and a karst spring (Forti and Sauro 1996; Vigna and Banzato 2015). These karst systems are characterized by rapid

drainage from sink to spring mostly developed in the vadose zone. In Piedmont, on the contrary, the gypsum bodies are sandwiched in between beds of low permeability. In these situations, underground drainage is poorly developed and is focused in the more permeable lithologies (i.e., the limestone bed at the base of the evaporite sequence) or in the sandy horizons of the clayey–marly interbeds. The water circulating in these horizons is undersaturated with respect to gypsum and feed the gypsum beds through the few narrow fissures and discontinuity planes. This leads to the development of phreatic two- to three-dimensional karst networks inside the gypsum beds, with typical phreatic morphology and evidence of very slowly moving water. This explains the fact that extremely fragile and differentially corroded cave walls and precarious pendants have survived in the Moncalvo caves. The chemistry of these feeding waters indicates a mixed origin, partially deriving from the surface, but also from a hypogenic source. The hypogenic waters do not appear to come from great depths given their low temperatures, but have flowed slowly along the permeable horizons that underlie the gypsum.

References

Bonetto S, Fiorucci A, Fornaro M, Vigna B (2008) Subsidence hazards connected to quarrying activities in a karst area: the case of the Moncalvo sinkhole event (Piedmont, NW Italy). Est J Earth Sci 57 (3):125–134

Boni A, Casnedi R (1970) Note illustrative della Carta Geologica d'Italia. Sheets 69 (Asti) and 70 (Alessandria). Serv Geol It, p 64

Clari P, Bernardi E, Cavagna S, Dela Pierre F, Irace A, Lozar F, Martinetto E, Trenkwalder S, Violanti D (2008) Alba e tramonto della Crisi Messiniana. Alba, 10–11 ottobre 2008, Excursion Guidebook, p 43

Columbu A, De Waele J, Forti P et al (2015) Gypsum caves as indicators of climate-driven river incision and aggradation in a rapidly uplifting region. Geology 43(6):539–542

D'Angeli IM, De Waele J, Galdenzi S et al (2016) Sulfuric acid caves of Italy: an overview. Deepkarst, Carlsbad 11–14 Apr 2016, pp 85–88

Dela Pierre F, Clari P, Cavagna S et al (2002) The Parona chaotic complex: a puzzling record of the Messinian (Late Miocene) events in Monferrato (NW Italy). Sedim Geol 152:289–311

Dela Pierre F, Piana F, Fioraso G et al (2003) Note illustrative della Carta Geologica d'Italia alla scala 1:50.000, Sheet 157 (Trino). APAT and Dipart Dif Suolo, p 147

Dela Pierre F, Bernardi E, Cavagna S et al (2011) The record of the Messinian salinity crisis in the Tertiary Piedmont Basin (NW Italy): The Alba section revisited. Palaeogeogr Palaeoclim Palaeoecol 310:238–255

Dela Pierre F, Clari P, Natalicchio M, Ferrando S, Giustetto R, Lozar F, Lugli S, Manzi V, Roveri M, Violanti D (2014) Flocculent layers and bacterial mats in the mudstone interbeds of the Primary Lower Gypsum unit (Tertiary Piedmont basin, NW Italy): Archives of palaeoenvironmental changes during the Messinian salinity crisis. Mar Geol 355:71–87

De Waele J, Galdenzi S, Madonia G, Menichetti M, Parise M, Piccini L, Sanna L, Sauro F, Tognini P, Vattano M, Vigna B (2014) A review on hypogene caves in Italy. In: Klimchouk A, Sasowski ID, Mylroie J, Engel SA, Summers Engel A (eds) Hypogene cave morphologies. Karst Water Institute, Special Publication 18:28–30

De Waele J, Audra P, Madonia G et al (2016) Sulfuric acid speleogenesis (SAS) close to the water table: examples from southern France, Austria, and Sicily. Geomorph 253:452–467

Di Maggio C, Madonia G, Parise M, Vattano M (2012) Karst of Sicily and its conservation. J Cave Karst Stud 74(2):157–172

Forti P, Sauro U (1996) The gypsum karst of Italy. Int J Spel 25 (3):239–250

Galdenzi S, Menichetti M (1995) Occurrence of hypogenic caves in a karst region: examples from central Italy. Env Geol 26:39–47

Ghielmi M, Rogledi S, Rossi M (1998) Studio stratigrafico-sedimentologico dell'area padana. Rapporto Interno Agip, San Donato Milanese, Italia, p 72

Ghielmi M, Vigna B, Violanti D et al (2002) Evoluzione tettono-sedimentaria della successione plio-pleistocenica nel settore del Piemonte centro-meridionale. Atti 81[a] Riunione estiva della Società Geologica Italiana, Torino, 10–12 settembre 2002, pp 181–182

Ghielmi M, Minervini M, Nini C et al (2010) Sedimentary and Tectonic Evolution in the Eastern Po-Plain and Northern Adriatic Sea Area from Messinian to Middle Pleistocene (Italy). In: Sassi FP (ed) Nature and geodynamics of the Lithostere in Northern Adriatic. Rend Fis Acc Lincei 21(Suppl. 1):131–166

Hsu KJ, Ryan WBF, Cita MB (1972) Late Miocene desiccation of the Mediterranean. Nature 242:240–244

Klimchouk AB (2007) Hypogene speleogenesis: hydrogeological and morphogenetic perspective. Natl. Cave Karst Res. Inst., Carlsbad, USA, p 106

Mayer-Eymar K (1867) Catalogue systématique et descriptif des fossiles des terraines tertiaires qui se trouvent au Musée Fedéral de Zürich. Mayer, Zürich

Minervini M, Ghielmi M, Rogledi S et al (2008) Tectono-stratigraphic framework of the Messinian-to-Pleistocene Succession in the Western Po-Plain Foredeep (Italy). 84° Congresso Nazionale della Società Geologica Italiana—Sessione 26, Sassari (Italy), 15–17 Settembre 2008, pp 562–563

Mosca P, Polino R, Rogledi S et al (2010) New data for the kinematic interpretation of the Alps-Apennines junction (Northwestern Italy). Int J Earth Sci Geol Rundsch 99:833–849

Rossi M, Mosca P, Polino R et al (2009) New outcrop and subsurface data in the Tertiary Piedmont Basin (NW Italy): unconformity-bounded units and their relationships with basin modification phases. Riv Ital Paleontol Stratigr 115(3):305–335

Ryan WB, Cita MB (1978) The nature and distribution of Messinian erosional surfaces—indicators of a several-kilometer-deep Mediterranean in the Miocene. Mar Geol 27(3):193–230

Selli R (1960) Il Messiniano Mayer-Elmar 1867. Proposta di un neostratotipo. Giorn Geol Ser. 2(28):1–33

Sturani C (1973) A fossil eel (Anguilla sp.) from the Messinian of Alba (Tertiary piedmontese basin). Palaeoenvironmental and palaeogeographic implications. "Messinian events in the Mediterranean". Koninklijke Nederlandse Akademie van Wetenschappen, Amsterdam, pp 243–255

Sturani C (1978) Messinian facies in the Piedmont Basin. Mem Soc Geol Ital 16(1976):11–25

Vigna B (2014) L'attività del Politecnico di Torino per lo studio dei fenomeni di scivolamento planare delle Langhe. Parte I: assetto geologico-strutturale ed idrogeologico. Atti Convegno L'alluvione del 5–6 Novembre 1994 in Piemonte. Venti anni di Attività nella previsione e prevenzione in ambito geo-idrologico. Torino, 28–29 ottobre 2014, pp 269–274

Vigna B, Banzato C (2015) The hydrogeology of high-mountain carbonate areas: an example of some Alpine systems in Southern Piedmont (Italy). Env Earth Sci 74(1):267–280

Vigna B, Accattino G, Amalberto S et al (2008) La successione messiniana nel settore di Moncalvo—Calliano (Basso Monferrato): un tipico bacino cannibalistico? In: Alba e tramonto della crisi messiniana, Alba 10–11 ottobre 2008

Vigna B, Fioraso G, Banzato C, De Waele J (2010a) Evolution of karst in messinian gypsum (Monferrato, Northern Italy). Geod Acta 23 (1–3):29–40

Vigna B, Fiorucci A, Banzato C, Forti P, De Waele J (2010b) Hypogene gypsum karst and sinkhole formation at Moncalvo (Asti, Italy). Z Geom Suppl 54(2):285–306

Hypogene Speleogenesis in Greece

14

Georgios Lazaridis

Abstract

Many hypogene caves have been recognized in several locations in Greece in the last decade. Their identification is mostly based on morphological criteria and in some cases on geochemical evidence, including mineral and water chemistry. Several patterns of cave development have been recorded along with various small-scale morphological features. In this chapter, hypogene caves are presented per region in terms of different geotectonic units. These caves cover the whole Greek mainland and some islands of the Aegean archipelago. Their altitudinal distribution ranges from the sea level up to about 2000 m elevation. Nowadays, most caves are uplifted relicts of hydrothermal systems. The dissolution was caused mainly due to CO_2-rich water, and in a few cases speleogenesis was driven by H_2S. Speleogenesis in most cases took place below the water table in a deep phreatic setting, by slowly convecting waters. However, there are water-table caves, commonly related to H_2S speleogenesis. It is demonstrated that hypogene speleogenesis in Greece is strongly related to the hydrothermal regime. Cave morphology, stratigraphy, hydrogeology, volcanism, tectonics, mineralogy and geochemistry are briefly discussed with respect to the structure of the Hellenic alpine orogene and its evolution.

Keywords

Hypogene • Hydrothermal • Cave • Hellenic orogene

1 Introduction

Hypogene caves are defined by hydrogeological and geochemical criteria opposed to those found related to the typical processes of epigene speleogenesis. Definition and terminology have undergone extensive discussion by various authors (e.g., Palmer 2000, 2007; Klimchouk 2007, 2009, 2016; Dublyansky 2013, 2014). Identification of hypogene caves is based on morphological, mineralogical and geochemical criteria that have been discussed in a series of overview papers and case studies (e.g., Klimchouk 2000, 2007; Audra et al. 2009a, b; Dublyansky 2013; Klimchouk et al. 2014; De Waele et al. 2016).

Systematic study of hypogene speleogenesis in Greece initiated in 2005, in the caves of the "Almopia Speleopark" (northern Greece) by the author advised by Prof. Stephan Kempe (Lazaridis 2005, 2006a, b). At the same time, this research was also expanded to other areas of northern Greece such as the Aghia Paraskevi caves (Lazaridis et al. 2011) and the Petralona cave (Lazaridis 2009; Veni et al. 2009) and finally covered a great part of the Greek mainland and some islands of the Aegean archipelago (Lazaridis 2014a, b, c). Based on recent research, more than fifteen regions and more than 90 caves and cavernous forms of hypogene origin have been recognized in Greece.

In this paper, hypogene caves are described per geological zone and units of the Hellenic orogene (Fig. 1). Greece is structurally complex with three main parts from east to

G. Lazaridis (✉)
Laboratory of Geology and Palaeontology, Department of Geology, Aristotle University of Thessaloniki, 54124 Thessaloniki, Greece
e-mail: geolaz@geo.auth.gr

© Springer International Publishing AG 2017

A. Klimchouk et al. (eds.), *Hypogene Karst Regions and Caves of the World*, Cave and Karst Systems of the World, DOI 10.1007/978-3-319-53348-3_14

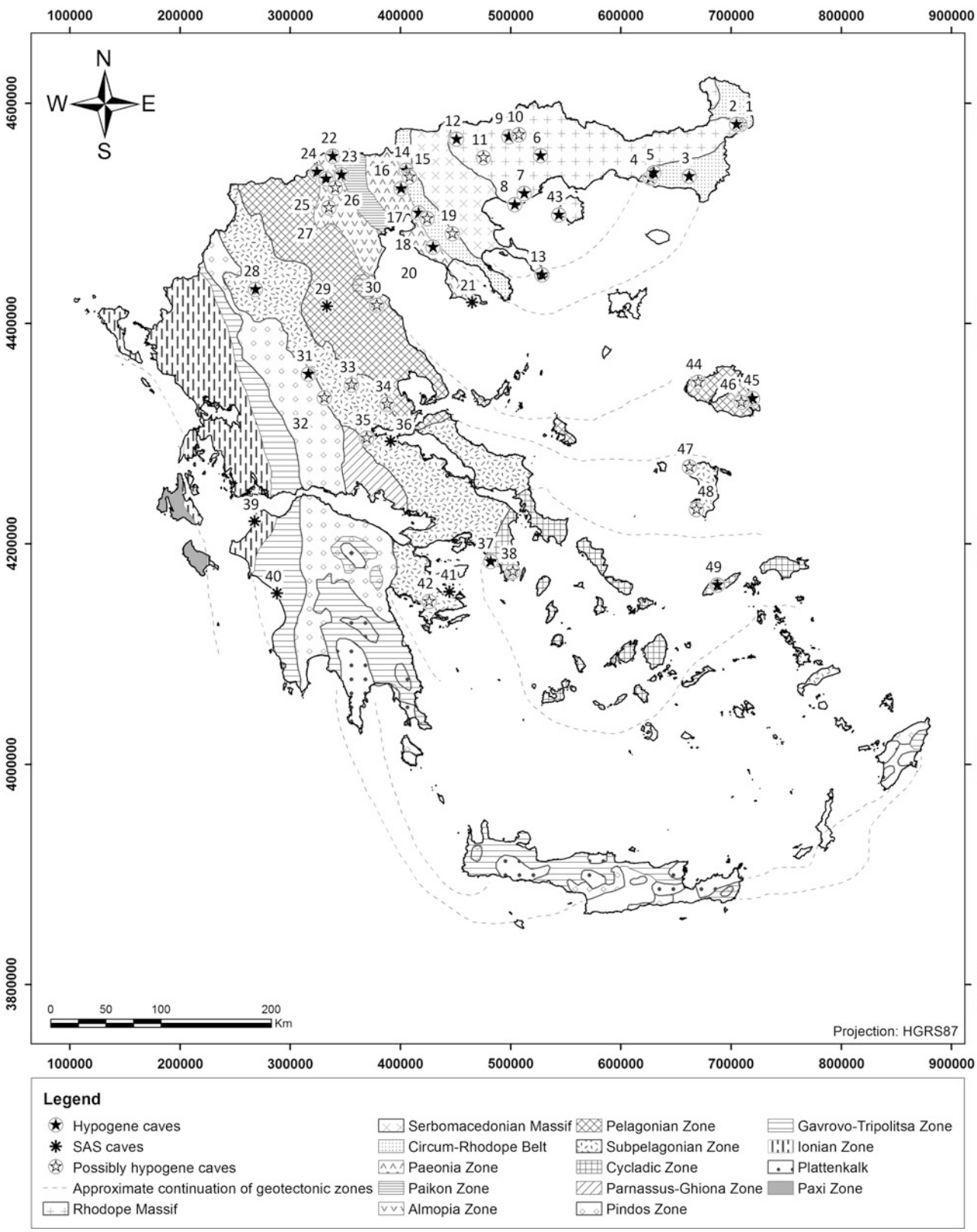
100000
200000
300000
400000
500000
600000
700000
800000
900000
4600000
4400000
4200000
4000000
3800000
N
W
E
S
0 50 100 200
Km
Projection: HGRS87
Legend
Hypogene caves
SAS caves
Possibly hypogene caves
Approximate continuation of geotectonic zones
Rhodope Massif
Serbomacedonian Massif
Circum-Rhodope Belt
Paeonia Zone
Paikon Zone
Almopia Zone
Pelagonian Zone
Subpelagonian Zone
Cycladic Zone
Parnassus-Ghiona Zone
Pindos Zone
Gavrovo-Tripolitsa Zone
Ionian Zone
Plattenkalk
Paxi Zone

◀ **Fig. 1** Map of Greece (adopted from http://geodata.gov.gr/) with hypogene cave locations and geotectonic units (according to Mountrakis 2010). *1* Didymoteicho, *2* Koufovouno Quarry cave, *3* Avas cave, *4* Maroneia cave, *5* Strimni caves, *6* Peristeronas Pothole, *7* Pholia pothole, *8* LE 1, *9* Falakro spar cavities, *10* Chionotrypa, *11* Theohari trypa, *12* MVQ cave, *13* Panagia cave, Athos cave, Pachoumios Kelli, Small cave, Cavernous forms, *14* Kilkis cave, *15* Zoodochos Pigi 1–3, Kampanis cave, Kampanis, shelter cave, *16* Pikrolimni pothole, *17* Retziki cave, *18* Arkoudotrypa, *19* Smentsa, Aghios Prodromos, *20* Petralona, Nycteridon, Katsika1, Varathron, Anonymo 1 and 2, *21* Aghia Paraskevi WTG1-3, BRCG1-2, QG1-3, *22* Petroti 1-2, Kleisoura, *23* Theodorakion 1-3, *24* Varathron, Antarton, Bearcave, Kx, Pyromaxikon, Zita cave, Plotsa, Gremos, Keramikon, Grammaton, Anonymo, Avra, *25* Polykarpi pothole, Polikarpi Quarry, *26* Nea Zoe 1-4, *27* Rodochori cave, *28* Orliakas pothole, *29* Melissotrypa, *30* Rapsani, *31* Krya Vrysi cave, *32* Koudounotrypes, *33* Vasilotrypa, *34* Titanospilia, *35* Psoroneria caves, *36* Kammena Vourla, *37* Vouliagmeni-1, *38* Chaos sinkhole, *39* Kounoupeli, *40* Anigridon Nymfon, *41* Peristeri, *42* Didyma cave, *43* Skala Marion, *44* Antisa cave, *45* Fissure-1, CR-1, Quarry cavities, Kourtzi cave, Latomeio 1, Qz1, *46* Mihou, *47* Aghio Galas, *48* Sykia Olympos, *49* Kalogerospilia

west (e.g., Mountrakis 2010 and references therein): the hinterland, the external Hellenides and internal Hellenides consisting of a number of zones and units divided according to their paleogeography. Internal Hellenides and hinterland are comprised of pre-Alpine and Alpine rocks. Sedimentation has been interrupted during Upper Jurassic–Lower Cretaceous when ophiolites were emplaced. Furthermore, plutonic intrusions, volcanic manifestations and magmatic-hydrothermal ore mineralization were formed since the Late Eocene. On the contrary, the external Hellenides include thick carbonate formations and are characterized by continuous sedimentation. Pre-Alpine rocks and magmatism have not been observed in the external Hellenides.

More than 90 hypogene caves have been found in Greece. Their dimensions range from few meters up to several hundreds of meters and the largest caves cover areas of more than 10,000 m^2. Apart from some exceptions, accounts on most of these caves remain unpublished at least from the perspective of speleogenesis. This chapter is an overview of hypogene caves that attempts to provide new data about their speleogenesis at a regional scale.

2 Hypogene Caves of Greece

2.1 Hinterland

The hinterland of the Hellenic orogene includes the Rhodope and the Serbomacedonian Massifs. The Rhodope Massif is divided in the Sidironero and Pangaeon Units. Many hypogene caves have been found in the carbonates of the Pangaeon Unit. A hypogene cave of high interest has been found in Mavros Vrachos quarry at Sidirokastro (Fig. 2). This cave is a 56-m-deep pothole with two branches and a chamber. Its entrance is artificially opened, and the morphology of the cave includes ascending passages and cupolas. The cave is partially lined with goethite (Fig. 3) deposited by microorganisms (P. Boston pers. com.). Speleothems that are formed by dripping water are rare. This cave is an uplifted part of an active hydrothermal system that recharges a few hundred meters away.

A possibly hypogene cave, located close to the top of Falakro Mountain in Drama region, is the Chionotrypa cave. A great part of the cave is covered by an ice plug that obscures the observation of wall and floor morphology. Its entrance forms a large sinkhole due to ceiling collapse, and its deepest accessible part is located at 108 m below surface. At the lower parts of the mountain, some small cavities lined with hydrothermal calcite have been found. These cavities prove that the essential conditions for hypogene speleogenesis existed in the area. Similar findings occur at the Elephtheres area, where there is a hydrothermal field and thermal springs.

Apart from the mentioned cavities with hydrothermal calcite, no other caves of that type are known in the area. In Thasos Island, barite has been found in a cave close to Skala Marion that has been identified as hypogene (Vaxevanopoulos 2009).

The Pholia pothole (Fig. 2) in Kavala region is one of the deepest potholes in northern Greece, and it is opened along the contact of schists and marbles (Lazaridis and Pipera 2008). This cave has two entrances at the same level, and a large chamber is formed just below them. Its total depth is about 150 m. At the bottom, there are blocks due to breakdown and a smaller pothole as well. A study of fluid inclusion in calcite from the Pholia pothole and from the Peristeronas pothole, also located in Kavala region, indicated hydrothermal speleogenesis (Toumanidou 2014).

Finally, some possible hypogene caves, such as the Trypa tou Theochari, are located at the foothills of Menikion Mountain. Some other caves at a higher altitude could also be re-examined under the perspective of hypogene speleogenesis. This assumption is based on morphological evidence observed in these caves that could be confirmed by future geochemical studies.

2.2 Internal Hellenides

2.2.1 Circum-Rhodope Belt

This belt surrounds the hinterland of the Hellenic orogene and consists of three units from east to west (Kauffmann et al. 1976; Kockel et al. 1977; Georgiadis et al. 2007):

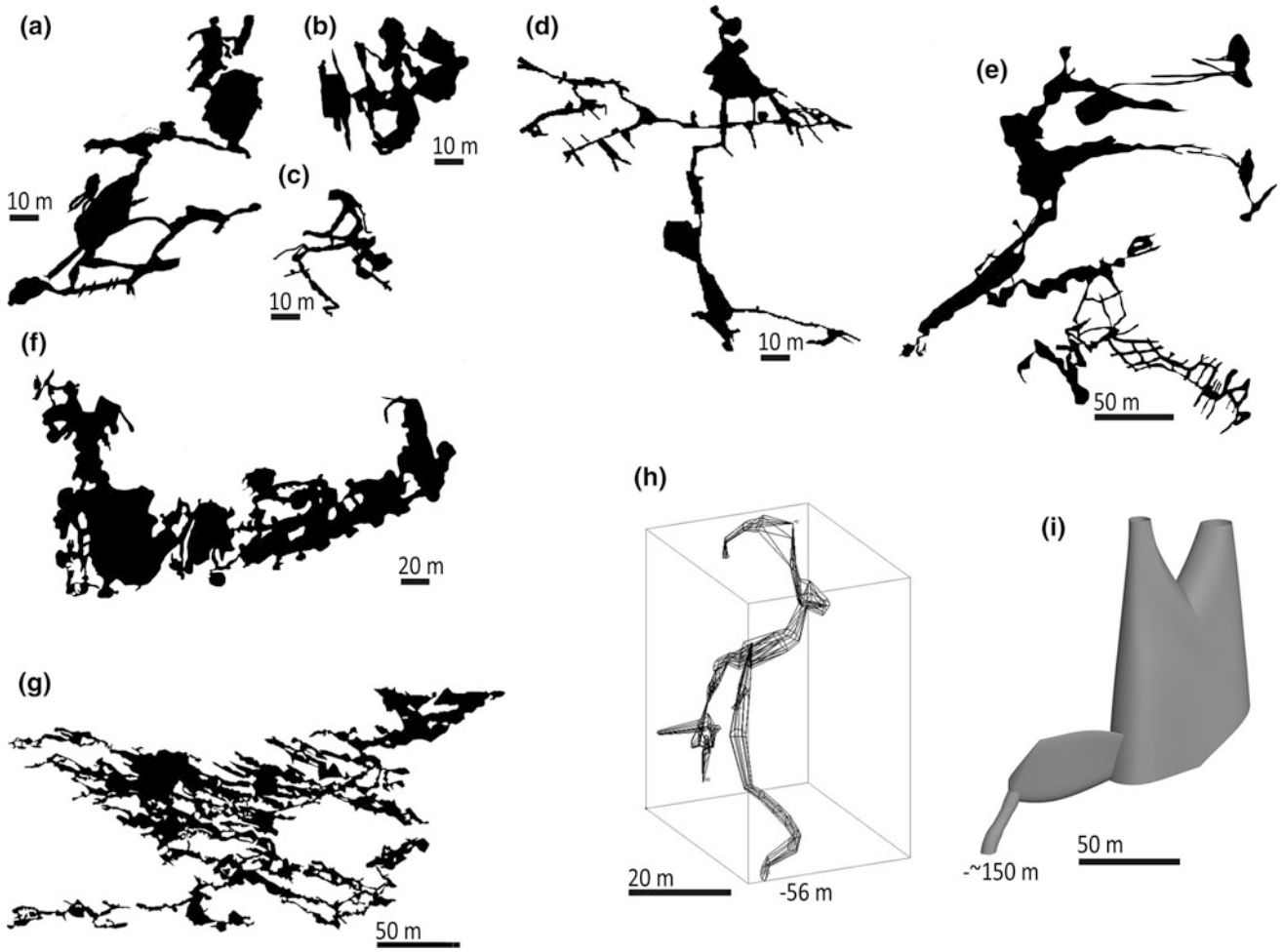

Fig. 2 Ground plans and stereograms of selected Greek hypogene caves. **a** Varathron, Almopia zone (modified from Lazaridis 2005), **b** Antarton cave, Almopia zone (modified from Lazaridis 2005), **c** Keramikon cave, Almopia zone (modified from Lazaridis, 2005), **d** Kilkis cave, Circum-Rhodope Belt, **e** Melissotrypa cave, Gavrovo zone (modified from Vaxevanopoulos, 2006), **f** Maronia cave, Circum-Rhodope Belt (modified from Petrocheilou 1984), **g** Petralona cave, Paeonia Zone (modified from Poulianos 2007), **h** Mavros Vrachos quarry cave, Pangaeon unit, **i** Pholia Pothole, Pangaeon unit

(1) Deve Koran-Doubia Unit with volcanosedimentary (Upper Paleozoic) and neritic carbonate (Triassic) rocks, (2) Melissochori-Cholomon Unit with pelagic carbonate rocks and phyllites (Triassic) and flysch metasediments (Jurassic) and (3) Aspri Vrisi-Chortiatis Unit, with metaclastic rocks, and neritic carbonate rocks (Permian-Triassic) and deep-sea sediments at the upper part of the unit that include ophiolites. Hypogene caves have been found in all these three units.

Hypogene caves in Deve Koran Unit develop in Triassic limestone. The Kilkis cave is the largest one, and it is located in the hill of Kilkis town, being developed as a show cave. It is a two-dimensional maze cave (Fig. 2) with narrow and high fracture-guided passages that commonly terminate abruptly. Some chambers have been formed due to breakdown, while some entrances are presently blocked with sediment. Nowadays, the cave is accessible due to an artificial entrance. The total length of the cave passages reaches almost 500 m, and the cave area is about 800 m^2. Meso-scale morphology includes several cupolas and sidewall pockets, rock bridges and pendants. However, in many places it is clearly noticed that these features also develop over speleothems, revealing the importance of condensation corrosion and dating their formation as post-speleogenetic. Measurements of condensed water's pH were around 4.

A group of small caves is found close to Kolchis village. These caves show evidence of a phreatic origin. Nowadays, one of them is used as a church, named Zoodochos Pigi. Close to Kampanis village, there is a small sediment-chocked horizontal corridor with ceiling half-tube, cupolas, sidewall feeders and pendants. Its termination resembles a rising chain of cupolas.

In Retziki area close to Thessaloniki, there is a cave (Retziki cave or Trypa tou Fournari), partially destroyed by

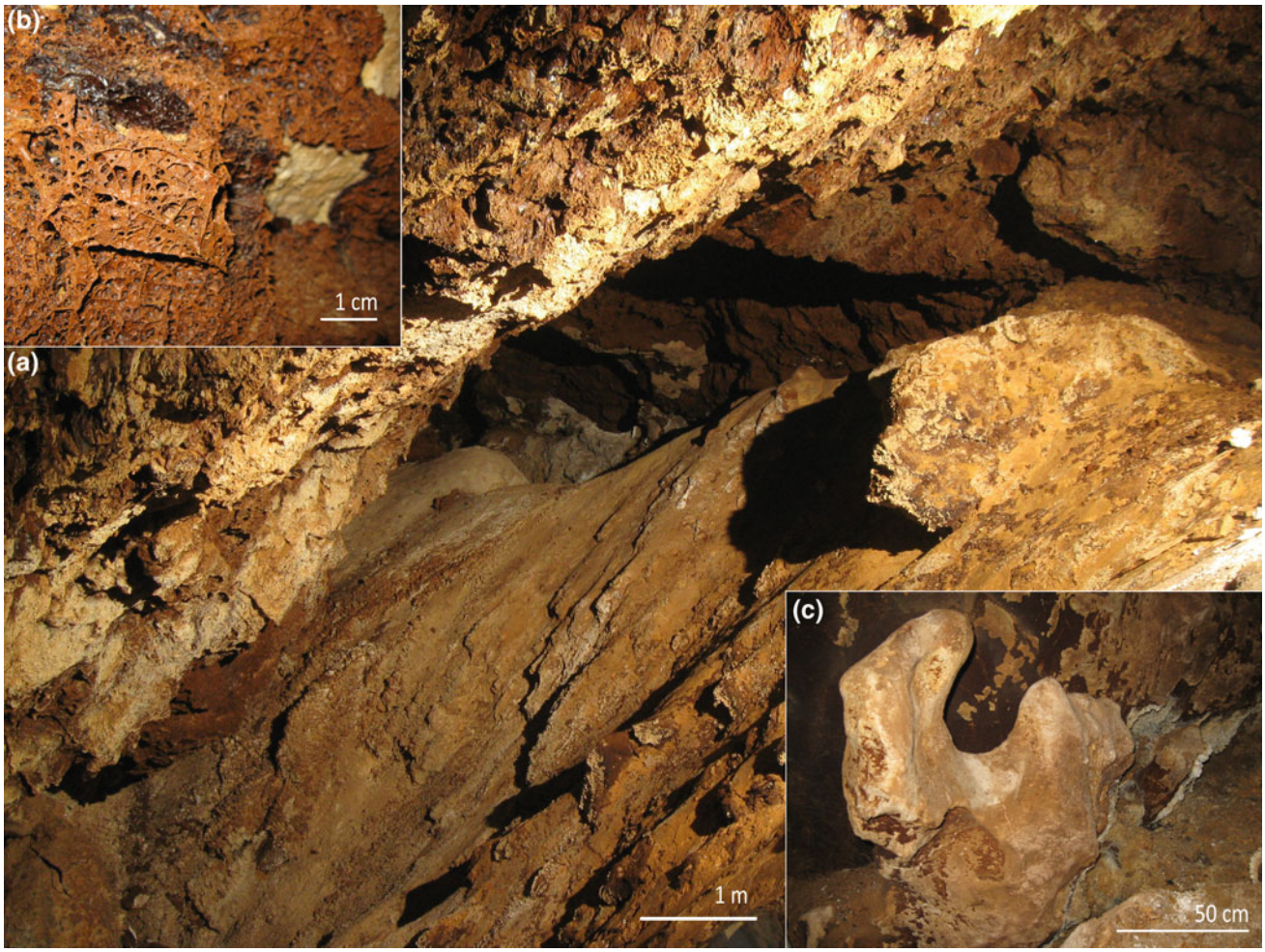

Fig. 3 Mavros Vrachos quarry cave, Pangaeon unit, **a** view of the largest chamber with sidewalls covered with goethite layer. In the central part, a ridge of calcite crusts is formed. **b** detail of goethite, **c** characteristic corrosion form on the floor of a sub-vertical passage

marble-quarrying works. It is a single fracture-guided passage that resembles those of Kilkis maze cave. Its speleogenesis has been misinterpreted as of vadose origin (Pennos et al. 2015). However, vadose features are absent, and at its mined part to the west there are remains of well-developed cupolas. Moreover, the cave contains hydrothermal calcite. Some other caves in the same limestone include the Arkoudotrypa of Chortiatis Mountain and some small (not accessible by man) passages that have been found in quarries of Galatista village in Chalkidiki.

In the central part of Chalkidiki and close to Aghios Prodromos village, there are two known caves: the Smentsa cave and an unexplored pothole. Both caves have a low-oxygen atmosphere (below 10% oxygen), preventing safe exploration of the pothole. The entrance of Smentsa cave is formed due to a breakdown. The cave consists of some interconnected large chambers and few abruptly terminating passages. The whole explored area covers a rectangle of dimensions 75 × 35 m. Both caves are opened along thin-bedded recrystallized limestone and quartz–sericite marble intercalated with phyllites of the Melissochori-Cholomon Unit. The limestone is overlaid by phyllites and quartzites that show discrete evidence of folding. The cave entrances are located approximately parallel to the b-axis of the folding. However, the Smentsa cave passages are developed roughly perpendicular to the b-axis of the fold. Apart from mammilaries that cover sections of Smentsa cave, speleothems originating from dripping water are relatively limited. This indicates a low karstification of the infiltration zone. At present, the reason for the low-oxygen atmosphere in these caves is not clear. It could be related to geogenic CO_2 emissions that occur in the broader area of Chalkidiki or due to accumulation of biogenic gases combined with the natural poor ventilation of the caves.

The peninsula of Agion Oros (Chalkidiki, N. Greece) comprises a large number of caves in varied lithology and setting. In the southern part of the peninsula, the Athos Mt.

is the largest occurrence in the entire area of carbonate rocks (limestone and marble) that are included in the Aspri Vrisi-Chortiatis Unit. A group of at least five hypogene caves of considerable volume and several other small cavernous forms have been found (Lazaridis et al. 2014a, b, c) at the southern part of the mountain at about 1000–1500 m of altitude above sea level (a.s.l.). Two of these caves (the Pachoumios Kelli and a cave close to Panagia church) are partially lined with calcite spar of hydrothermal origin. Similar crystals have also been found close to the mountain's top (2033 m a.s.l.) in small cavities. All these caves share similar morphology. There are cupolas, small wall pockets with flat ceiling, partitions and phreatic shafts. Their entrances are mainly opened at their lower parts, and the caves are developed mainly upward with diminishing dimensions at their highest parts. This intriguing observation seems to be related to normal faults [e.g., at the southern part of the mountain (Georgiadis et al. 2007)] rather than to typical denudation processes that intersects the highest parts of the caves forming potholes.

Another cave opened in rocks of Aspri Vrisi-Chortiatis Unit is located at a small limestone outcrop in Pikrolimni lake of Kilkis region. In the surroundings, the area is covered by Neogene and Quaternary sediments. According to Dotsika et al. (2009), water at the lake appears to be of meteoric origin mixed with salt water of deep and probably warm horizons related to the geothermal field of the area. During summer evaporite (trona, burkeite, thenardite and halite) is deposited in this lake. The cave is a sediment-chocked pothole. However, the accessible part of the cave includes a small cupola-shaped chamber. In general, it lacks morphological features related to vadose conditions and resembles hypogene morphology.

In Thrace, at the northeastern part of Greece, Circum-Rhodope Belt crops out with Makri and Drimos-Melia Units. The Maroneia cave (Fig. 2) is the largest hypogene cave of Thrace, the hypogene character being identified due to its morphological features, fluid inclusion study and morphometry (Vaxevanopoulos and Melfos 2010; Lazaridis et al. 2014a). It has been developed in nummulitic limestone (M. Eocene) of Makri Unit. Other hypogene caves have been described from the areas of Avas, Koufovouno, Didymoteicho and Strimni villages (Lazaridis et al. 2014a). In particular, caves of Didymoteicho and Koufovouno show typical hypogene morphology with feeders, cupolas, phreatic shafts with mega-scallops, fracture-guided blind passages, etc.

2.2.2 Paeonia Zone

The caves of this zone are opened in Jurassic limestone in Kalavros Mt. at Petralona village and in Aghia Paraskevi of Kassandra Peninsula. Their hypogene origin has already been recognized (Lazaridis 2009; Veni et al. 2009; Lazaridis et al. 2011). In Petralona's caves, the geochemistry of mammilaries' calcite revealed a correlation with the waters of the local geothermal field (Lazaridis and Melfos in prep.), which circulates deep in the underlying granodiorite and ascents rapidly through the limestone (Dotsika et al. 2010). Speleogenesis is probably driven by carbonic acid. On the other hand, the Aghia Paraskevi caves are the only known case of active sulfuric acid speleogenesis in northern Greece. Some caves are developed close to the sea level as well as uplifted containing gypsum deposits (Fig. 4).

2.2.3 Paiko Zone

A number of hypogene caves have been identified in the eastern mountainous area of Almopia at Pinovo in Upper Cretaceous limestones and dolomites. The morphology of Petroti and Kleisoura caves is given by Lazaridis et al. (2014c). Two other caves have been found in the same rocks close to Theodorakion village. Although they have been partially destroyed by denudation and breakdown, they display a ramiform cave pattern and hypogene passage morphology.

2.2.4 Almopia Zone

At the northern part of Almopia Zone, there is a group of more than ten caves with varying size located at the valley of the Thermopotamos stream (Nikolaou valley), close to the Loutraki village. This group of caves is known as "Almopia Speleopark." The caves are opened in Maastrichtian limestone. Their morphology (Figs. 2 and 5) includes rock bridges and ridges, pendants, cupolas, flat ceiling and inwardly inclined walls (facets; Kempe et al. 1975), feeders, windows between chambers, partitions (Lazaridis 2005, 2006a). Furthermore, fluid inclusion study of hydrothermal calcite in Varathron cave shows mean homogenization temperature at about 150 °C (Lazaridis and Melfos in press). Southward of Almopia Speleopark, at Polikarpi village, there is a pothole in Upper Cretaceous limestone. It is a single linear fracture-guided passage that terminates in a small non-accessible passage, with strong air current. Although its morphology does not show any diagnostic features, the cave is located close to an old quarry, where, at the quarry face, there is a cross section of a similar pothole lined with hydrothermal calcite. A number of small eroded, possibly hypogene cave passages are located close to Nea Zoe village. Finally, further south close to Rodochori village, there is another group of caves opened in Upper Cretaceous limestone, which are possibly hypogene according to their morphology.

2.2.5 Pelagonian Zone

Hypogene caves in this zone have been found in its mainland part as well as in its continuation at Aegean in Mytilene Island.

Fig. 4 Gypsum crust in the deepest dry part of the QG1 cave in Aghia Paraskevi, Paeonia zone

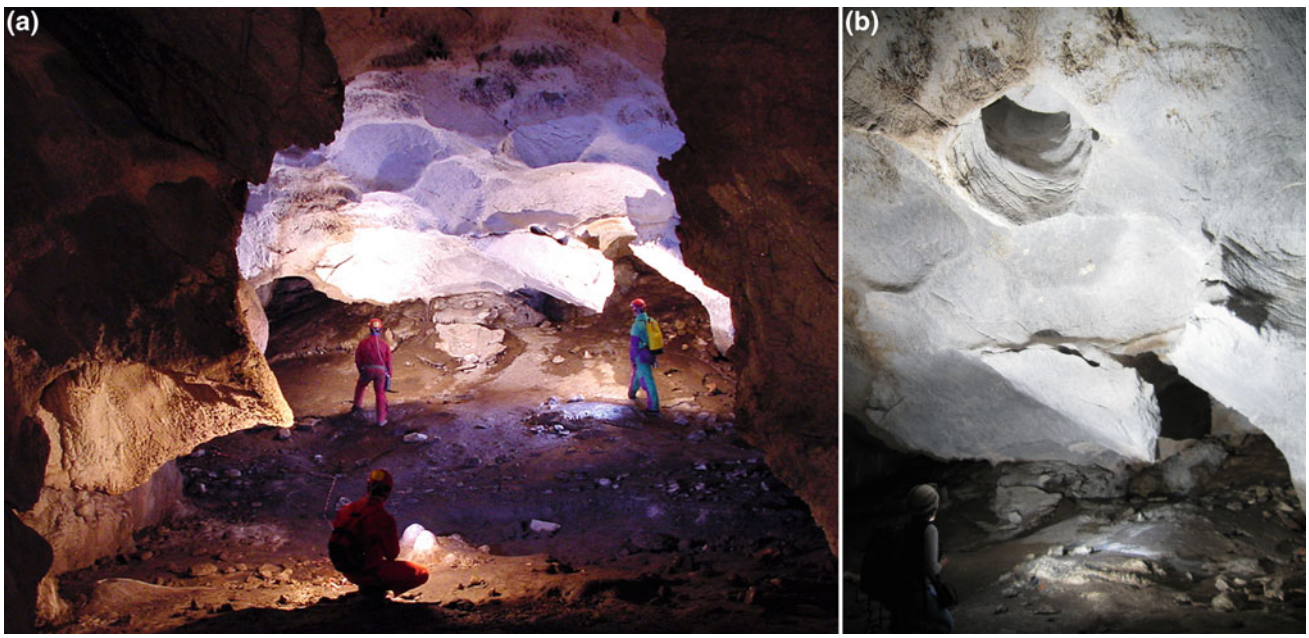

Fig. 5 **a** Characteristic chamber in Almopia Speleopark (Antarton cave) and **b** detail of lateral small cupola-shaped chamber and chain of cupolas

Routsi cave close to Rapsani village at the broader region of Olympos Mt. has two entrances, one of which is formed due to ceiling collapse and the other due to denudation. It is opened in recrystallized limestone of Ossa Unit (possible Jurassic-Middle Eocene) that underlain flysch (Eocene). Phreatic conditions can be inferred during speleogenesis. Morphology includes ceiling half-tubes, isolated cupolas and series of fracture-guided cupolas. The sidewalls are partially

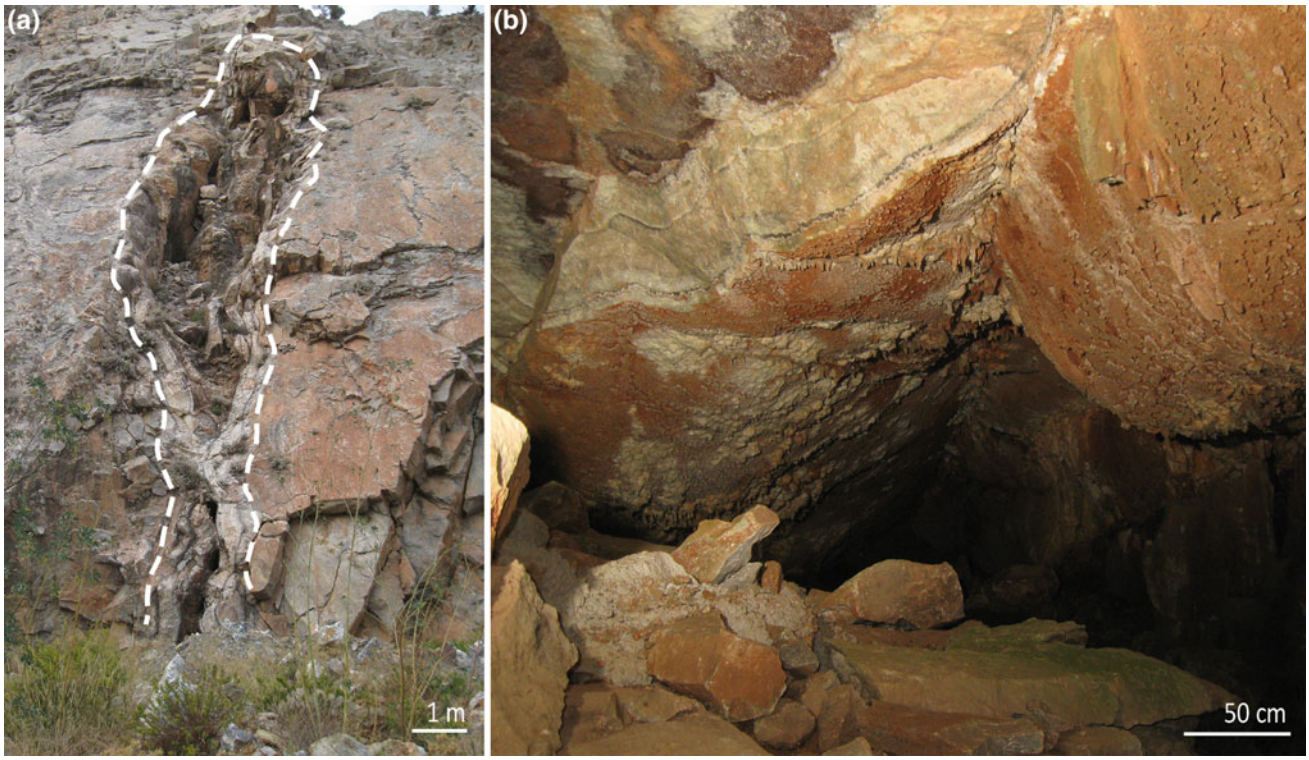

Fig. 6 A cave in Mytilene Island, Pelagonian zone, **a** mined vertical passage (*dashed line*) lined with hydrothermal calcite layers and **b** chamber formed at the bottom of the vertical passage appears to be covered with mammilaries

covered with calcite crusts that resemble corroded mammilaries. Photoluminescence of the calcite (Shopov 1997) indicates cold-forming water. Although it is a possible hypogene cave, its speleogenesis remains unclear.

In Mytilene Island, there are numerous caves and almost all visited by the author are definitely hypogene. However, there are still a great number of potholes that remain unexplored. Horizontal caves sometimes are connected with large phreatic vertical shafts lined with hydrothermal calcite. Mammilaries cover passages in many cases (Fig. 6). The most typical hypogene caves have been found in the eastern part of the Mytilene. In other cases, some possible hypogene caves, such as the Antissa cave in the NW part of the island, comprise just isolated chambers.

Another important cave of this zone located in Methana Peninsula (Peloponnesus), the westernmost part of the south Aegean volcanic arc, is the Peristeri cave. This cave is one of the few active sulfuric acid caves of Greece and has an entrance formed by ceiling collapse.

In Argolida region (Peloponnesus), there is a group of large sinkholes located between Didyma and Pelei villages. Their diameter ranges from 110 to 210 m, and they have been formed due to cave-ceiling collapses. These forms are favored by the generally low dip of the limestones and are related to large possibly hypogene chambers.

2.2.6 Subpelagonian Zone

A small hypogene pothole is located in Orliakas Mt. of Grevena (N. Greece). It is opened in Cretaceous limestone with rudists. The lower part of the cave, about ten meters below the entrance, forms a cupola-shaped chamber, blocked with rocks. The entrance consists of two rounded openings, and the entire cave is a chain of rising cupolas intersected by erosion. The lower part is partially covered by ~30-cm-thick hydrothermal "island spar" covered by a few millimeters thin calcite crust.

Titanospilia pothole consists of a 25-m-deep phreatic shaft (outlet) connected at the roof of a large chamber at 50 m below the surface. A linear feeder located at the chamber's edge goes down to 90 m. The cave is formed in Upper Cretaceous limestones that underlain flysch. Vasilotrypa cave is also formed in the same limestone and consists of linear feeders and chambers.

Some small caves associated with the sulfuric thermal spring of Psoroneria are possibly hypogene.

In the region of Thermopyles, there are many cavernous forms related to hypogene speleogenesis. In particular to Kammena Vourla, there is a partially explored hypogene cave and sulfuric water spring. The explored part of that cave consists of a partially water-filled corridor that is more than ten meters long. At the eastern part of the Aegean Sea

some caves that exist in Chios Island (e.g., Aghio Galas cave) are possibly hypogene, but a detailed study is pending.

2.2.7 Cycladic Zone

An important cave system of this zone is located in Vouliagmeni region in Attica. This cave system is intruded by the sea. A pothole at the sea bottom, well known as Pigadi and the Germaniko pothole, are possibly parts of this cave system (Giannopoulos 2000). Germaniko pothole contains a 60-m-deep lake at 95 m depth and shows typical morphology for hypogene speleogenesis such as cupolas, juts (Slabe 1995; Dublyansky 2013), pendants, blades that form a characteristic morphology called by Greek cavers as "cheese" (Fig. 7). Vouliagmeni's main entrance is located in a huge sinkhole formed due to ceiling collapse. The cave includes a water-filled chamber about 1.2 million m^3 and a spring of thermal water mixed with sea water (Giannopoulos 2000). In the broader surroundings of the cave, there are potholes and small caverns. In the latter, hydrothermal calcite, indicative of hypogene process, has been noticed by the author. Thus, Vouliagmeni cave should be reinterpreted as hypogene. Some other caves in the broader area, such as

Fig. 7 Germaniko Pothole, Attiki, Cycladic zone. The so-called cheese part of the cave is very characteristic for its spongework dissolution pattern due to the formation of various shapes of partitions, e.g., cupolas, juts, pendants and blades. Photograph: George Portokaloglou

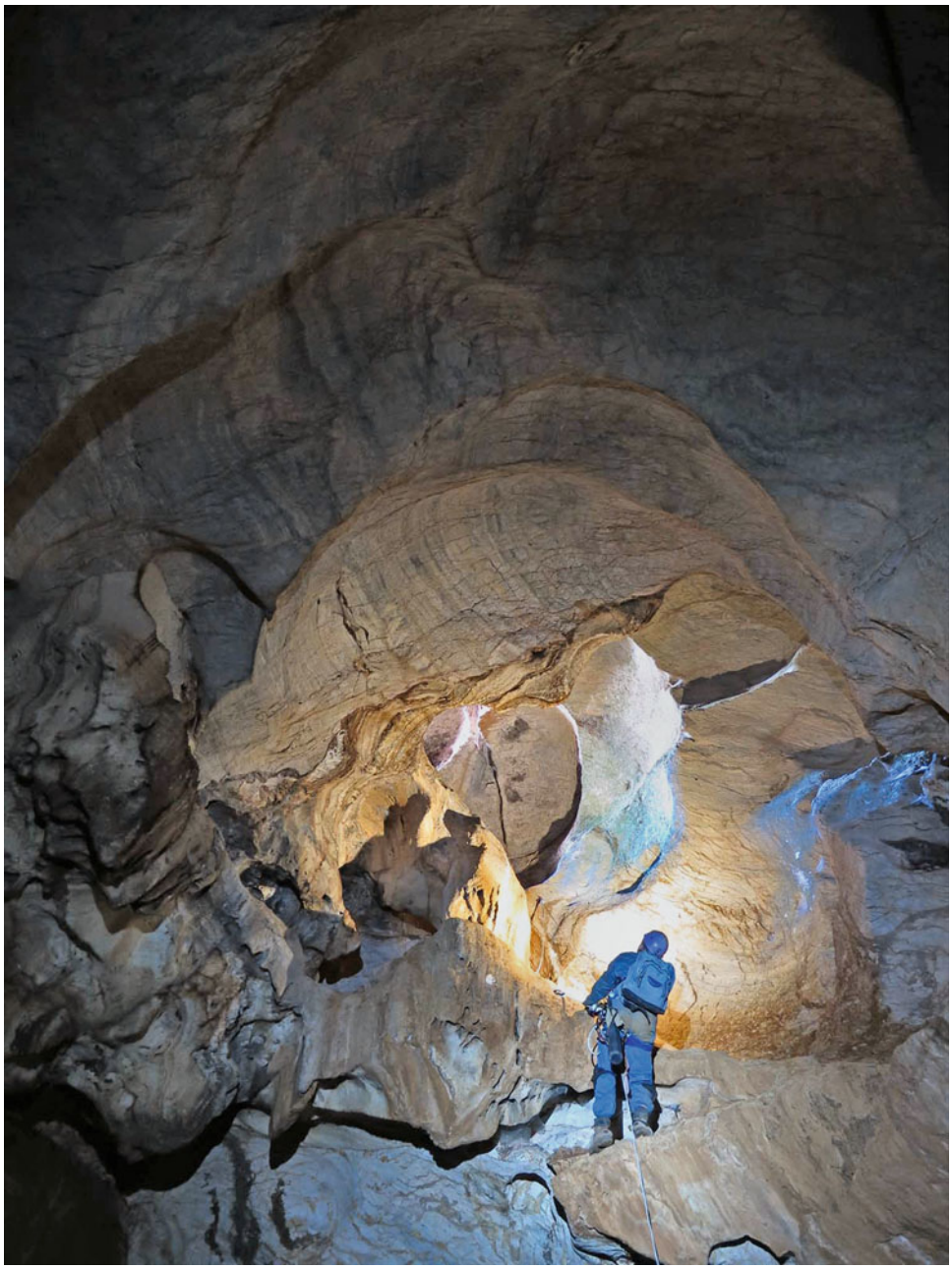

Fig. 8 Aghia Marina cave, Attiki, cycladic zone. An assemblage of cupolas in the main vertical passage of the cave. *Photograph* Vasilis Athanasopoulos

Aghia Marina, display also large and well-developed cupolas (Fig. 8). This cave has a vertical entrance and a large chamber formed at the bottom. The formation of cupolas is probably related to condensation corrosion, since flowstones appear sometimes corroded as well as parts of the cupolas.

Additionally, Chaos sinkhole with diameter of about 160 and 50 m depth has been formed due to cave collapse and could be related to hypogene speleogenesis. It is located close to Aghios Konstantinos and Lavrion villages; an area dominated by hydrothermal ore deposits exploited since ancient times.

Finally, there are some hydrothermal caves in Ikaria Island at the Aegean Sea where hydrothermal calcite has been found (Kalogerospilia) and some other possible ones (e.g., Raos Choutra cave, Tu Atsacha).

2.3 External Hellenides

2.3.1 Pindos Zone

A number of caves in the surroundings of Karditsa town show a pattern commonly found in hypogene caves that

Fig. 9 Krya Vrysi cave, Pindos zone: hydrothermal calcite spar and crust that cover the cave walls

includes large chambers interconnected to fracture-guided passages and linear feeder-like potholes. Among them, the Krya Vrysi cave, located southern of the homonymous village is the most characteristic hypogene cave presently found in the Pindos zone, containing hydrothermal calcite crystals (Fig. 9). It is opened in Jurassic limestone of the Koziakas series.

2.3.2 Gavrovo Zone

Melissotrypa cave in Ellasona is opened in Mesozoic marble of Krania Unit. Its entrance is vertically developed, and its overall pattern forms a two-dimensional maze cave. There are numerous cupolas, pendants, rock bridges and ridges (Fig. 10). Gypsum has been found in some speleothems at one cave passage, and hydrogen sulfide has been reported in a small cave lake (Vaxevanopoulos 2006). The strongest evidence that supports a possible sulfuric acid speleogenesis is the presence of replacement pockets and sulfuric karren (Fig. 11).

The Anigridon Nymfon cave (or Kaiafas Loutra) is located in the western part of Peloponnesus, and it is an active sulfuric acid cave. Thermal water ascends along a

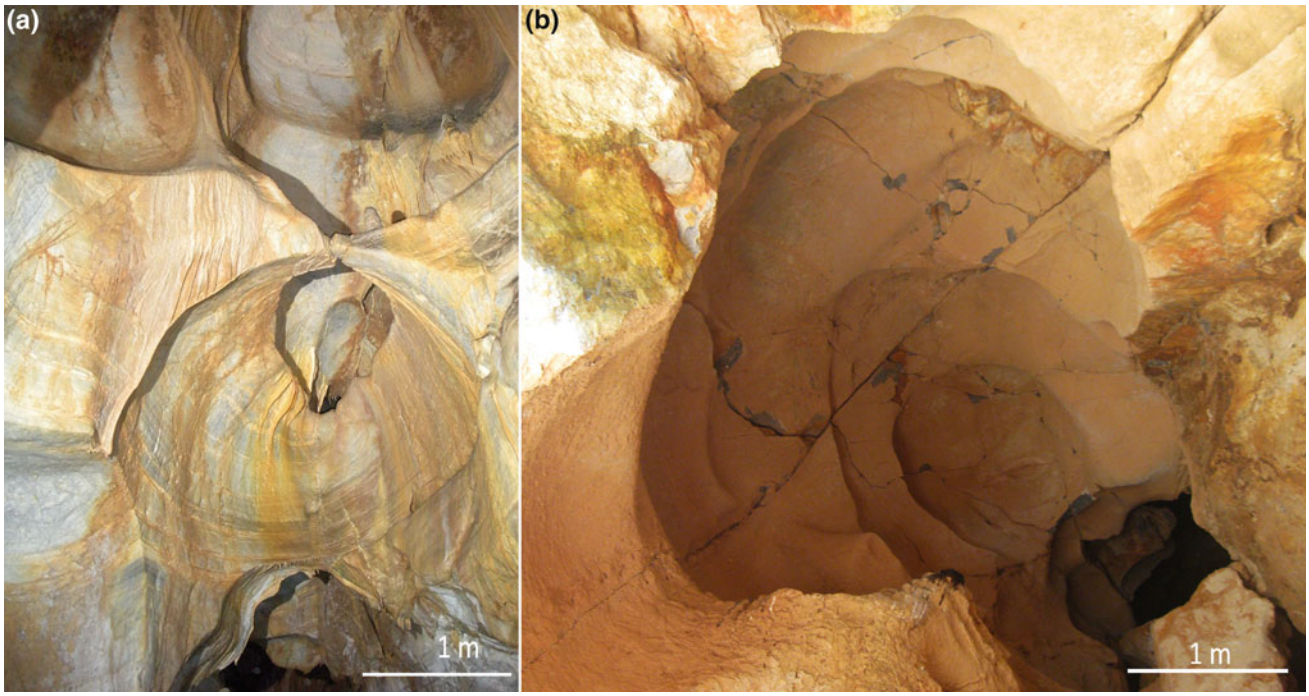

Fig. 10 Cupola morphology in **a** Melissotrypa cave, Gavrovo zone, and **b** QG1 cave in Aghia Paraskevi, Paeonia zone

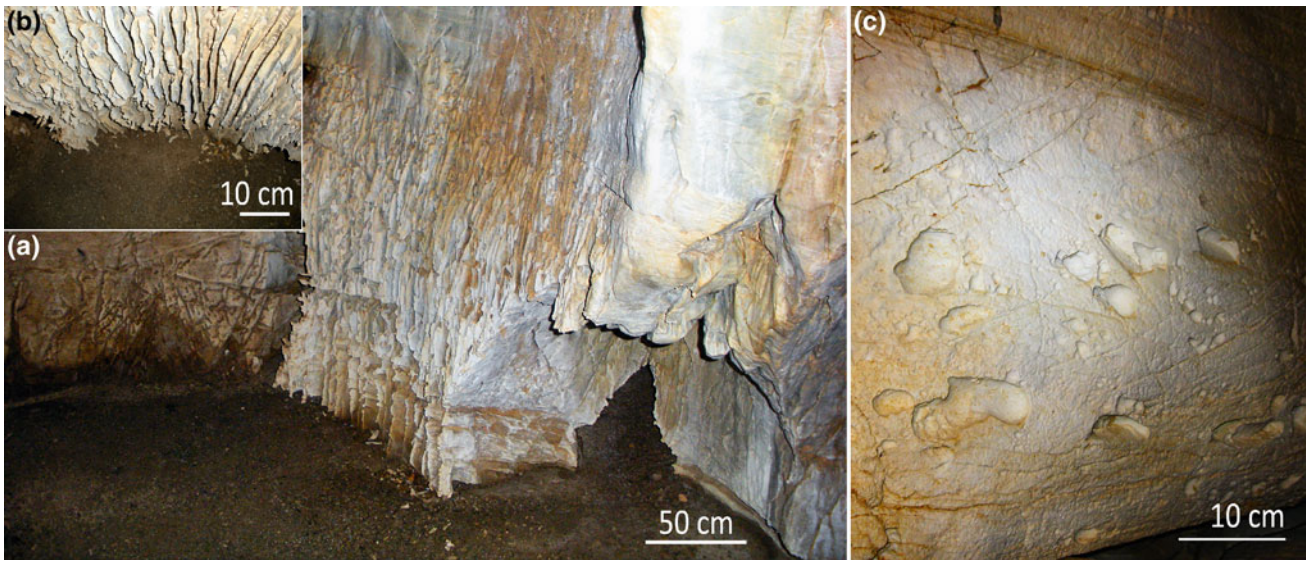

Fig. 11 Melissotrypa cave, Gavrovo zone, **a** sulfuric karren on the cave wall, **b** detailed view from above of sulfuric karren, where sharp limestone ridges are seen, **c** replacement pockets on the walls

fault zone, and it is rich in methane and sulfur compounds that are produced by petroleum generation processes (Etiope et al. 2006).

2.3.3 Ionian Zone

This zone consists of Triassic evaporites, Late Triassic to Eocene carbonates and the Oligocene flysch that are deformed to mega-synclines and anticlines. Kounoupeli cave in western Peloponnesus is developed at the sea level. Thermal water ascends along faults. It is an active sulfuric acid cave and consists of a fracture-guided corridor of triangular shape with flat bottom and a medial discharge slot. Its length is about 50 m, and its segments are of N–S and E–W orientation. Laterally, there are water-table notches. These morphological features are typically found in sulfuric acid caves (De Waele et al. 2014, 2016).

3 Speleogenetic Remarks

Hypogene caves in the Hellenic orogene have been recognized either due to their morphological features or by the presence of active thermal springs and/or mineral deposits at their interior. The latter are the main evidence for the recognition of hydrothermal caves (Dublyansky 2013), and this is commonly the case in Greece. Most cases appear to be related to hydrothermal activity along the various geotectonic units. Faults appear to be important for the movement of thermal water. Regarding their morphology, the simplest forms are potholes and mainly vertically developed caves, whereas the most complex ones are mazes, ramiform and spongework caves. Cave entrances are opened due to ceiling collapse, intersection by erosion or artificially. In some cases fault activity assisted by slope erosion might be of importance in the formation of entrances.

The caves are developed in folded, faulted and dipping karstifiable rocks, commonly capped by impermeable rocks such as schists, flysch, Neogene clastic sediments. Structural unconformities have played an important role in the speleogenesis, and the majority of cave passages are fracture guided. However, there are also passages or caves that follow bedding planes. In some cases caves follow contacts between karstifiable and non-pervious rocks, e.g., the Pholia pothole along marble–schist contact. They are commonly closely related to large tectonic faults where upwelling of thermal water is favored.

Speleogenesis is mainly driven by carbonic acid. However, in some cases sulfuric acid speleogenesis (SAS) occurs. This process has been mainly observed in the active hydrothermal caves of Greece. In the internal Hellenides, SAS occurs in the Aghia Paraskevi region (Paeonia Zone) where there are both water-table caves with thermal water and dry uplifted ones. Additionally, the Peristeri cave of Methana Peninsula in Pelagonian Zone is also a cave with active sulfuric acid thermal water. Other known SAS caves are located in the western part of Peloponnesus (Anigridon Nymfon and Kounoupeli caves) and are developed at the water level. Hydrogen sulfide may derive from volcanic activity, reduction of sulfates or hydrocarbons (Onac et al. 2011). In Aghia Paraskevi caves may be related to pyrite oxidation; Peristeri cave is located in the Methana Peninsula where volcanism may have contributed, whereas the caves of western Peloponnesus have been formed by thermal waters enriched in H_2S due to sulfate reduction (Lambrakis and Kallergis 2005). Another cave where sulfuric acid may have been contributed to speleogenesis is the Melissotrypa cave.

In most examples given in this work, there are mineral deposits related to hydrothermal activity. Calcite is by far the main mineral formed in these caves followed by gypsum, Fe-oxides and other sulfates such as alunite, pickeringite, tamarugite and orpiment and sulfides such as barite. Investigation of calcite by photoluminescence suggests formation temperatures above 60 °C (Dubljansky 2000). Fluid inclusions in these calcites have demonstrated a hydrothermal origin (V. Melfos pers.com). From a mineralogical perspective, Aghia Paraskevi water-table caves are the most interesting examples. In that area there are uplifted cave passages lined with hydrothermal calcite and others filled with clastic sediments and alunite or overhanging gypsum crusts. Aghia Paraskevi seems to be an example of carbonic acid speleogenesis at depth followed by uplifting and sulfuric acid speleogenesis close to the water table. Similarly, in Provalata cave, located at the continuation of Pelagonian zone in Former Yugoslavian Republic of Macedonia (FYROM), carbonic acid speleogenesis has been followed by sulfuric acid dissolution (Temovski et al. 2013). Another remarkable cave is the Mavros Vrachos quarry cave, which is lined with goethite deposited by microbial activity. The speleogenetic process in that cave may have similarities with the formation of the hypogene karstic iron ore deposit in Jordan, studied by Al-Malabeh et al. (2008), where methane may have played an important role.

The majority of the hypogene caves in Greece are located in the internal part of the orogene, and only few cases have been identified in the external Hellenides. Many carbonate outcrops with hypogene caves show absence of significant epigene forms, e.g., Petralona area, Almopia Speleopark, limestones of Circum-Rhodope zone. However, between these regions there are areas with epigene caves, e.g., at the southern part of Serbomacedonian massif between the Circum-Rhodope Belt and Rhodope Massif. In general, hypogene caves are rare toward southwestern Greece. Nevertheless, this observation may be biased due to differences in the exploration efforts and field work dedicated at each area by the author. On the other hand, these areas of the external Hellenides show a great number of caves and the major concentration of epigene caves in Greece (e.g., Crete Island has more than 35% of Greek caves including a great number of vadose potholes and epigene caves). In this area, carbonates exceed two thousand meters of exposed thickness and commonly the deepest caves of Greece appear in these geotectonic units, along with a number of large deep gorges. Volcanic manifestations, magmatism and hydrothermal ore deposits are absent in the southwestern Greece. Furthermore, in Epirus region (northwestern Greece) there are considerable epigene karst systems fed by meteoric water, according to Nikolaou et al. (2011). However, the same authors found that 20% of the water resources are enriched in SO_4^{2-} in groundwater systems that are in contact with evaporites of the Ionian zone. Similarly, hydrogen sulfide in western Peloponnesus thermal springs originates from reduction of sulfates in Triassic evaporites (Kallergis and Lambrakis 1992). These waters are responsible for hypogene speleogenesis in the coastal basins of southwestern Greece

(Kounoupeli and Anigridon Nymfon caves). Thus, hypogene karstification potentially occurs in the external Hellenides mainly where water circulates deep in contact with the evaporites and upwells through faults.

4 Conclusions

When hypogene caves were first identified in Greece, they were considered as exceptions among "typical karstification" (= epigene). Their increased recognition demonstrates that they are an important karstification process in great part of Greece and predominant in some regions or geotectonic units (e.g., Circum-Rhodope Belt). Almost exclusively these are related to hydrothermal fields as indicated by hydrothermal calcite. Carbonic acid is the main speleogenetic agent although considerable sulfuric acid caves exist mainly in coastal basins. All available data presently indicate speleogenesis by deeply circulating groundwater originally infiltrated as meteoric water. Their geographical distribution shows a concentration in the internal Hellenides and hinterland emphasizing the importance of magmatism and volcanism at their formation. Active sulfuric acid caves occur mainly in coastal areas close to the sea level.

5 Acknowledgements

This work is based on more than 15 years of field work in Greek caves accomplished with the assistance of numerous collaborators and friends to whom I am grateful. I would like to thank Assistant Professor Vasilios Melfos for our fruitful discussions on geochemistry and mineralogy, Georgia Karadimou for her assistance in the preparation of the GIS-based map of hypogene caves in Greece and Iraklis Kalogeropoulos for illustration editing. Dr. Augusto Auler and Dr. Alexander Klimchouk are thanked for their comments and suggestions that improved this paper.

References

Al-Malabeh A, Kempe S, Henschel HV, Hofmann H, Tobschall HJ (2008) The possibly hypogene karstic iron ore deposit of Warda near Ajloun (Northern Jordan), its mineralogy, geochemistry and historic mine. Acta Carsol 37(2–3):241–253

Audra P, Mocochain L, Bigot J-Y, Nobécourt J-C (2009a) Morphological indicators of speleogenesis: hypogenic speleogenesis. In: Klimchouk A, Ford D (eds) Hypogene speleogenesis and karst hydrogeology of artesian basins. Institute of Speleology and Karstology, Simferopol, Ukrainian, pp 17–22

Audra P, Mocochain L, Bigot JY, Nobecourt JC (2009b) Hypogene cave patterns. In: Klimchouk A, Ford D (eds) Hypogene speleogenesis and karst hydrogeology of Artesian basins. Institute of Speleology and Karstology, Simferopol, Ukrainian, pp 23–32

De Waele J, Plan L, Audra P, Vattano M, Madonia G (2014) Sulfuric acid water table caves (Grotte du Chat/Acqua Fitusa/Bad Deutsch Altenburg + Kraushöhle). In: Klimchouk A, Sasowsky I, Mylroie J, Engel SA, Engel AS, (eds) Hypogene cave morphologies. Karst Waters Institute, Special Publication 18, Leesburg, Virginia, pp 31–35

De Waele J, Audra P, Madonia G, Vattano M, Plan L, D'Angeli IM, Bigot JY, Nobécourt JC (2016) Sulfuric acid speleogenesis (SAS) close to the water table: examples from southern France, Austria, and Sicily. Geomorphology 253:452–467

Dotsika E, Poutoukis D, Tzavidopoulos I, Maniatis Y, Ignatiadou D, Raco B (2009) A natron source at Pikrolimni lake in Greece? Geochemical evidence. J Geochem Explor 103(2):133–143

Dotsika E, Poutoukis D, Kloppmann W, Guerrot C, Voutsa D, Kouimtzis TH (2010) The use of O, H, B, Sr and S isotopes for tracing the origin of dissolved boron in groundwater in Central Macedonia, Greece. Appl Geochem 25(11):1783–1796

Dubljansky YV (2000) Hydrothermal speleogenesis in the Hungarian karst. In: Klimchouk A, Ford DC, Palmer AN, Dreybrodt W (eds) Speleogenesis: evolution of karst aquifers. National Speleological Society, Huntsville, pp 298–303

Dublyansky YV (2013) Karstification by geothermal waters. In Shroder J, Frumkin A, (eds) Treatise on geomorphology. Academic Press, San Diego, vol 6, pp 57–71

Dublyansky YV (2014) Hypogene speleogenesis—discussion of definitions. In: Klimchouk A, Sasowsky I, Mylroie J, Engel SA, Engel AS (eds) Hypogene cave morphologies. Karst Waters Institute, Special Publication 18, Leesburg, pp 1–3

Etiope G, Papatheodorou G, Christodoulou DP, Ferentinos G, Sokos E, Favali P (2006) Methane and hydrogen sulfide seepage in the northwest Peloponnesus petroliferous basin (Greece): origin and geohazard. AAPG Bull 90(5):701–713

Georgiadis G, Tranos M, Mountrakis DM (2007) Late-and post-alpine tectonic evolution of the Southern part of the Athos Peninsula, Northern Greece. In: Proceedings of the 11th international congress, Bull. Soc. Geol. Greece, vol 40, Athens, pp 309–320

Giannopoulos V (2000) A contribution to the study of contemporary and paleo-environments of the most significant caves of Greek peninsula. Dissertation, National and Kapodistrian University of Athens

Kallergis G, Lambrakis N (1992) Contribution a l' etude des sources thermominarales de Grce: les sources thermominerales de Kaiafa. Hydrogeologie 3:127–136

Kauffmann G, Kockel F, Mollat H (1976) Notes on the stratigraphic and paleogeographic position of the Svoula Formation in the Innermost Zone of the Hellenides (Northern Greece). Bull Soc Geol France 18(2):225–230

Kempe S, Brandt A, Seeger M, Vladi F (1975) "Facetten" and "Laugdecken", the typical morphological elements of caves developing in standing water. Ann Spéléol 30(4):705–708

Klimchouk AB (2000) Speleogenesis under deep-seated and confined settings. In: Klimchouk A, Ford DC, Palmer AN, Dreybrodt W (eds) Speleogenesis: evolution of karst aquifers. National Speleological Society, Huntsville, pp 244–260

Klimchouk AB (2007) Hypogene speleogenesis: hydrogeological and morphogenetic perspective. Special Paper no. 1, National Cave and Karst Research Institute, Carlsbad, pp 1–106

Klimchouk AB (2009) Morphogenesis of hypogenic caves. Geomorphology 106:100–117

Klimchouk AB (2016) Advances in understanding of hypogene karst. In Stafford K (ed) Hypogene Karst in Texas

Klimchouk AB, Sasowsky ID, Mylroie J, Engel SA, Engel AS (eds) (2014) Hypogene cave morphologies. Karst Waters Institute, Special Publication 18, p 103

Kockel F, Mollat H, Walther HW (1977) Erlauterungen zm geologischen Karte der Chalkidhiki und angrenzender Gebietel: I00.000 (Nord-Griechenland). Bundesanstalt fur Geowisseschaften und Rohstoffe, Hannover, p 119

Lambrakis N, Kallergis G (2005) Contribution to the study of Greek thermal springs: hydrogeological and hydrochemical characteristics and origin of thermal waters. Hydrogeol J 13(3):506–521

Lazaridis G (2005) Speleological research in the Loutra Arideas area (Macedonia, Greece). Neue Forschungen zum Höhlenbären in Europa—Naturhistorische Gesellschaft Nürnberg 45:57–64

Lazaridis G (2006a) Almopia Speleopark (Pella, Macedonia, Greece): Morphology-speleogenesis of the caves. Scientific annals, School of geology, Aristotle University of Thessaloniki, Special volume 98, pp 33–40

Lazaridis G (2006b) Speleology-speleogenesis. In Tsoukala E (ed) A guide to Speleopark of Almopia. Geology-Paleontology-Speleology. Aridea, Greece, pp 42–60

Lazaridis G (2009) Petralona cave: morphological analysis and a new perspective on its speleogenesis. In: Klimchouk A, Ford D (eds) Hypogene speleogenesis and karst hydrogeology of Artesian basins. Institute of Speleology and Karstology, Simferopol, Ukrainian, pp 233–239

Lazaridis G, Melfos V (in press) Morphological features and conditions of formation of the Almopia Speleopark caves (Kato Loutraki, N. Greece). In: E. Tsoukala & G. Rabeder (eds) Paleontology of Loutra Arideas cave (N. Greece)

Lazaridis G, Pipera K (2008) Preliminary report on granite caves in Greece. Cad Lab Xeol Laxe 33:101–113

Lazaridis G, Melfos V, Papadopoulou L (2011) The first cave occurrence of orpiment (As_2O_3) from the sulphuric acid caves of Aghia Paraskevi. Int J Speleol 40(2):133–139

Lazaridis G, Kalogeropoulos I, Gkeme A (2014a) Hypogene morphology of caves in Evros, Greece (Didimoteicho, Koufovouno, Strimni, Avantas and Samothraki Island). In: Proceedings of the Balkan speleological conference "Sofia 2014", pp 41–46

Lazaridis G, Zhalov A, Makrostergios L, Genkov A, Gyorev V, Stoichkov K, Radulescu A, Agapov I, Kaminskiy S (2014b) Hydrothermal caves in Athos Mt. (Agion Oros). In: Proceedings of the Balkan speleological conference "Sofia 2014", pp 36–40

Lazaridis G, Kalogeropoulos I, Dimitraki D (2014c) Caves in eastern Almopia (N. Greece) and hypogene speleogenesis. In: Proceedings of the V international scientific correspondence conference. Speleology and spelestology. To the centenary of A.V. Ryumin's birth, Nabereznye Chelny, pp 101–106

Mountrakis D (2010) Geology and geotectonic evolution of Greece. University Studio Press, Greece, p 374 (in Greek)

Nikolaou E, Pavlidou S, Katsanou K (2011) Aquifer systems of Epirus, Greece: an overview. In: N Lambrakis et al (eds) Advances in the research of aquatic environment, vol 1, Springer, Berlin, Heidelberg, pp 425–433

Onac BP, Wynn JG, Sumrall JB (2011) Tracing the sources of cave sulfates: a unique case from Cerna Valley, Romania. Chem Geol 288(3):105–114

Palmer AN (2000) Hydrogeologic control of cave patterns. In: Klimchouk A, Ford DC, Palmer AN, Dreybrodt W (eds) Speleogenesis: evolution of karst aquifers. National Speleological Society, Huntsville, pp 77–90

Palmer AN (2007) Cave geology. Cave Books, Dayton, p 454

Pennos C, Lauritzen S-E, Gkarlaouni C, Sotiriadis Y (2015) Speleotectonic constrains from the 'Tripa tou Fournari' cave, Thessaloniki, Greece (a preliminary report). Advances in Active Tectonics and Speleotectonics. Natural History Museum Vienna & University of Vienna (www.researchgate.net. Accessed May 2016)

Petrohilou A (1984) The caves of Greece. Ekdotiki Athinon Ltd., Athens, p 160

Poulianos NA (2007) The cave of the petralonian archanthropinae, 8th edn, p 97. ISBN 960-86804-3-3

Shopov YY (1997) Luminescence of cave minerals. In: Hill C, Forti P (eds) Cave minerals of the world, 2nd edn. NSS, Huntsville, pp 244–248

Slabe T (1995) Cave rocky relief and its speleological significance. Zbirka ZRC Ljubljana

Temovski M, Audra P, Mihevc A, Spangenberg J, Polyak V, McIntosh W, Bigot J (2013) Hypogenic origin of Provalata cave, Republic of Macedonia: a distinct case of successive thermal carbonic and sulfuric acid speleogenesis. Int J Speleol 42(3): 235–246

Toumanidou O (2014) Formation conditions of hypogene caves in N. Greece through the study of fluid inclusions. Diploma Thesis, School of Geology, Aristotle University of Thessaloniki, p 48 (in Greek)

Vaxevanopoulos M (2006) Tectonic conditions in the speleogenetic process of Melissotrypa cave in Kefalovriso of Elassona (Central Greece). M.Sc. thesis. Aristotle University of Thessaloniki, p 106 (in Greek)

Vaxevanopoulos M (2009) Identifying hypogenic features in Greek caves. In Proceedings of 15th international congress of speleology, Kerrville, Texas, USA, vol 3, pp 1713–1716

Vaxevanopoulos M, Melfos V (2010) Hypogenic features in Maronia cave, Thrace, Greece. Evidence from morphologies and fluid inclusions. Bul Geol Soc Greece, 43(2):948–957

Veni G, Poulianos NA, Golubovic-Deligianni M, Poulianos AN (2009) Preliminary hydrogeologic survey of Petralona cave, Chalkidiki, Greece. In: Proceedings of 15th international congress of speleology, Kerrville, Texas, USA, vol 1, pp 717–1,722

Hypogene Karst in Macedonia

15

Marjan Temovski

Abstract

Research on hypogene karst in Macedonia is quite a recent topic, with systematic study of some areas starting only few years ago, although certain caves with genetic characteristics attributable to hypogene speleogenesis have been described before. Hypogene karst is presently known from three areas: Mariovo, Katlanovo and Krčin. All of the registered examples are connected to hydrothermal karstification in pre-Cenozoic rocks, along the boundaries of Neogene basins formed within the South Balkan extensional system (northern part of the Aegean extensional regime). Deep circulating meteoric waters were heated due to the increased geothermal gradient, discharging mostly along faults at basin boundaries, with subsequent evolution of the hypogene karst systems governed by the lowering of the base level due to valley incision, thus controlling spring positions. Best studied is the hypogene karst in Mariovo, where hydrothermal karstification is locally combined with ghost-rock weathering (in dolomitic marble and dolomite, e.g., Karši Podot Cave and Allchar ore deposit), and sulfuric acid speleogenesis (e.g., Provalata Cave, likely connected to the nearby coal basin; or due to oxidation of metal sulfides, i.e., Allchar ore deposit/Kožuf thermal springs). At Katlanovo Spa, where hypogene karst is developed in marble, thermal springs are found at the bottom of the valley discharging water from deep faults, with thick travertine deposits found also at higher elevation. A similar situation is found in the southern parts of Krčin Mountain, with thermal springs discharging from both limestone (Banjište Spa) and evaporites (Kosovrasti Spa), and a number of caves with hot air circulation located above the Banjište Spa.

Keywords

Hypogene karst • Hydrothermal karst • Sulfuric acid speleogenesis • Ghost-rock weathering • Macedonia

1 Introduction

Karst areas in Macedonia cover 12% of the country's surface, based on the extension of karst rock outcrops (Temovski 2012). Karst systems are developed in different types of rocks, mostly marble (dolomitic and calcitic) and limestone, with travertine, dolomite and especially evaporite rocks (gypsum and anhydrite) less represented. Karst rocks range from Precambrian to recent in age, but mostly are pre-Cenozoic. While in some areas the outcrop extension is more or less representative of the karst rocks at depth, in other parts karst rocks are covered due to overthrusting or by a wide extension of Cenozoic basin deposits. This is especially important when considering possible hypogene karstification. Most of the karst systems are epigene in origin, located in mid- to high-mountain areas, with an extensive

M. Temovski (✉)
Hertelendi Laboratory of Environmental Studies,
Institute for Nuclear Research, Hungarian Academy of Sciences,
Bem tér 18/C, 4026 Debrecen, Hungary
e-mail: temovski.marjan@atomki.mta.hu

© Springer International Publishing AG 2017

A. Klimchouk et al. (eds.), *Hypogene Karst Regions and Caves of the World*,
Cave and Karst Systems of the World, DOI 10.1007/978-3-319-53348-3_15

vadose zone, but in many areas they also have a deep phreatic zone. The deepest cave system, Slovačka Jama on Karadžica Mt., is 610 m deep (Holúbek et al. 2013), with total vertical potential of more than 1500 m, and the deepest phreatic cave, Matka Vrelo, is explored to the depth of 212 m below the spring (Vandermeulen 2015). The longest cave is Slatinski Izvor with 4 km in length (Carlin et al. 2011). In total, not more than 500 caves are known, although there is no official cave register.

Hypogene karst in Macedonia, as in many parts of the world, has become the focus of karst research only recently, although some hypogene occurrences have been noticed before. The main focus of recent studies was in Mariovo area, where hypogene karstification was one of the central research topics. In other areas, hypogene karst and caves were not studied primarily, but were documented as part of various different research works, mainly general hydrogeological and hydrochemical studies connected to thermal waters in carbonate rocks, as well as some descriptions of caves with hot water/air.

Hypogene karstification has been documented in three areas: Mariovo, Katlanovo and Krčin, with some preliminary indication also from Dojran, Banjiče (Šar Planina), Proevci (Kumanovo) and Kočani (Fig. 1). Most of the results are based on studies made in caves and thermal springs with only few data coming from deeper parts (boreholes). Nevertheless, recent results point to certain common characteristics of hypogene karst systems in Macedonia, such as hydrothermal dissolution, with the hydrogeological control and the increased geothermal gradient being connected to the extensional tectonic evolution in Macedonia during the Cenozoic. Therefore, a short review of the geotectonic framework in Macedonia will be provided, with main focus on the Cenozoic tectonic evolution.

2 Geological and Geomorphological Context

2.1 Pre-Cenozoic Structure

Five major tectonic units are found in the Macedonian pre-Cenozoic crust, from west to east: Cukali-Krasta, Western Macedonian zone, Pelagonian massif, Vardar zone and Serbo-Macedonian massif (Fig. 1; Arsovski 1997; Dumurdžanov et al. 2005). The Cukali-Krasta zone contains Late Cretaceous and early Tertiary sedimentary rocks, and in Macedonia they can only be found as a small window in the western part of the country. They are overthrusted by low- to medium-grade metamorphosed Paleozoic sedimentary and igneous rocks and Mesozoic (mostly Triassic, but also some Jurassic) sedimentary rocks of the Western Macedonian zone, deformed during Paleozoic, Mesozoic and Cenozoic time. The Pelagonian massif is a high-grade metamorphic core of a NW-trending and plunging anticlinorium, mostly composed of Precambrian gneiss and schist with a thick marble section in the upper part, and abundant granitic plutons. To the east of the Pelagonian massif lies the Vardar zone, a Triassic to Early Cretaceous ocean with a complex history of subduction, composed of Paleozoic and Mesozoic metasedimentary rocks and numerous belts of ophiolitic rocks, that were strongly deformed in latest Cretaceous to Paleocene time (Laramide phase). The Serbo-Macedonian massif is the easternmost pre-Cenozoic tectonic zone in Macedonia, composed of Precambrian to early Paleozoic mafic rocks, schists and phyllites, intruded by large bodies of Paleozoic granites.

2.2 Cenozoic Evolution as Part of the South Balkan Extensional System

The Cenozoic tectonic evolution in Macedonia is related to a geodynamic system of E-directed subduction that migrated westward from the Vardar zone in latest Mesozoic–early Cenozoic time to northern Greece, Albania and Montenegro (Fig. 2; Dumurdžanov et al. 2005; see also Burchfiel et al. 2008 for wider context). The evolution is presented by two phases of basin development in late Eocene to recent time, reflecting two major periods of extensional deformation, separated by a short period of shortening (Dumurdžanov et al. 2004, 2005).

The Vardar zone ocean closed during latest Cretaceous or earliest Paleogene, followed by deformation (Laramide phase) due to continued eastward underthrusting of lithosphere containing crustal fragments of Western Macedonian and Pelagonian tectonic units beneath the Serbo-Macedonian tectonic unit. After the suturing along the Vardar zone, subduction was shifted westward in the Cukali-Krasta and Pindus zones in Albania and northwestern Greece. In late Eocene–Oligocene time, connected to this subduction, NW-trending extensional structures were formed in eastern Macedonia, with (Paleogene) basins, filled with lacustrine-to-marine deposits, lying to the west (Tikveš-Ovchepole basin) and east (Kriva Palanka, Delchevo and Stojakovo basins) of the coeval magmatic arc, that stretched also northward to eastern Serbia, eastward to western Bulgaria and southward to northern Greece (Dumurdžanov et al. 2005; Burchfiel et al. 2008).

This was followed by a short period of shortening in late Oligocene–early Miocene time, as a result of the arrival of the Kruja continental crust in the Cukali-Krasta subduction zone, resulting in folding of the Paleogene strata (Dumurdžanov et al. 2005).

Extension continued from Middle Miocene in eastern and central Macedonia, with formation of NW-trending, E-tilted grabens (Skopje, Probištip), followed by westward shifting

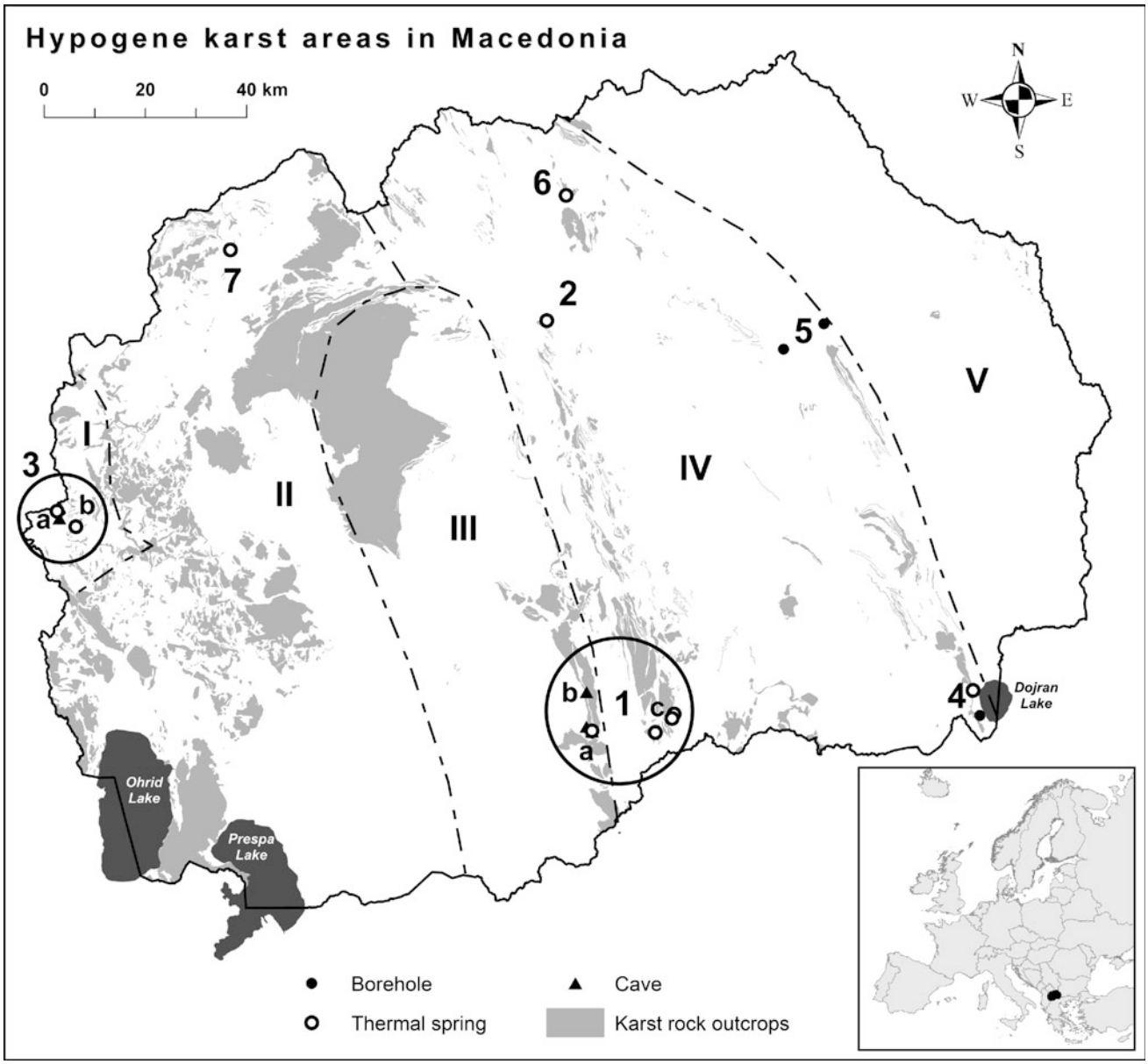

Fig. 1 Hypogene karst features in Macedonia (modified from Temovski 2013b): *1* Mariovo (*a* Melnica, *b* Podot, *c* Kožuf), *2* Katlanovo, *3* Krčin (*a* Banjište, *b* Kosovrasti), *4* Dojran, *5* Kočani Basin, *6* Proevci (Kumanovo), *7* Banjiče (Šar Planina). Pre-Cenozoic tectonic zones: *I* Cukali-Krasta zone, *II* Western Macedonian zone, *III* Pelagonian massif, *IV* Vardar zone, *V* Serbo-Macedonian massif

of younger basin development in Late Miocene (Berovo-Delčevo, Kumanovo, Strumica, Veles, Tikveš, Mariovo, Pelagonian, Polog, Kichevo, Prespa), connected to westward migration of the subduction zone in Albania, with continuation of the magmatic arc development, but with rock types showing different characteristics (Dumurdžanov et al. 2005). In latest Miocene and Pliocene, there is a further basin development (Ohrid, Debarca, Debar, Poreče, Dojran) and westward migration of the general E–W extension, with change of orientation in the eastern part of Macedonia to an N–S extension (Slaviški, Kočani, Valandovo S-tilted half grabens and continued subsidence of the Strumica half graben), connected to the southward movement of the Aegean Sea lithosphere separated by the North Anatolian fault zone, with both patterns overlapping in the central parts (Dumurdžanov et al. 2005; Burchfiel et al. 2008).

2.2.1 Possible Impact of the Messinian Salinity Crisis

A Gilbert-type fan delta, the resulting signature of the Messinian Salinity Crisis (MSC), has been documented in the Pliocene sediments southward of Skopje at Dračevo

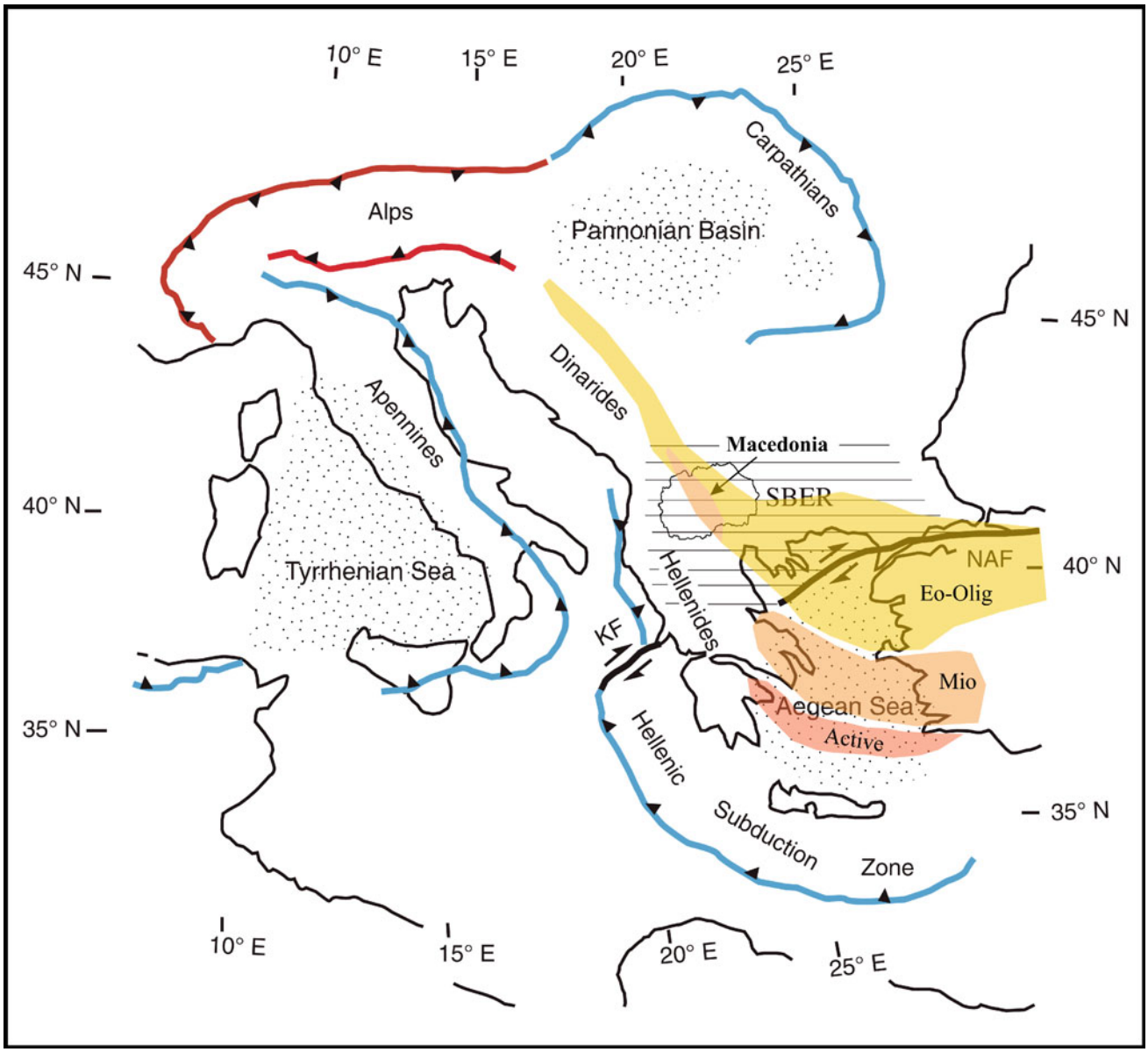

Fig. 2 Position of Macedonia within the South Balkan extensional system (SBER; *horizontal line pattern*) and wider regional setting (adapted from Burchfiel et al. 2008). Retreating subduction zones are given in *blue*, and related backarc extensional regions are shown by *dotted pattern*, with advancing subduction zones and related areas of backarc shortening given in *red*. NAF—North Anatolian Fault. KF—Kefalonia fault zone

(Clauzon et al. 2008). It follows a previous phase of incision of deep valleys due to the lowering of base level as a result of almost complete drying out of the Mediterranean Sea at the end of the Miocene. Continuing research on this topic proposes a marine gateway through central Macedonia, connecting the Mediterranean and Paratethys prior and after the MSC event (Suc et al. 2015).

The deep MSC incision followed by Pliocene aggradation likely impacted the development of the karst systems (epigene or hypogene). Per-ascensum development of passages in several caves in the lower part of the Crna Reka basin has been attributed to the Pliocene aggradation (Temovski 2016), with several vauclusian springs as well as thermal springs located on basin boundaries near Pliocene deposits in different areas in Macedonia.

Considering the fact that there is a hiatus of deposition at the end of the Miocene in most of the Neogene basin deposits in Macedonia (Dumurdžanov et al. 2004), especially in the Vardar zone, the extent of the impact of the MSC in Macedonia should be studied in further detail, and its possible impact should be considered when studying karst systems, both epigene and hypogene.

2.2.2 Quaternary Uplift, Draining of Lakes and Fluvial Evolution

Quaternary evolution is connected to general uplift, draining of the extensive lake systems and fluvial network development. The draining of the lakes started as early as Early Pleistocene (i.e., Mariovo Lake; Temovski et al. 2013) and as late as Middle Pleistocene (i.e., Central Macedonian Lake; Dumurdžanov et al. 2005). Valley incision, with temporary climate-induced aggradations (i.e., Temovski et al. 2016), was controlling the general evolution of the landscape. This has influenced also the evolution of the karst systems, lowering spring positions and exposing underground karst features.

3 Hypogene Karst Systems in Macedonia

The most detailed study on hypogene karst in Macedonia has been done recently in Mariovo area, with characteristics and evolution of hypogene karstification being the main focus of the research. Consequently, the main results presented here are focused on the Mariovo hypogene karst. Examples from other areas are based on literature review and interpretation of data obtained from different research works, where hypogene karst, or even karst, was not the central part of the research, with the focus being mostly on exploitation of hydrothermal resources or hydrogeological investigations in a wider context. Preliminary findings indicate a much wider occurrence of hypogene karst systems, which is rather expected, considering the tectonic setting and geological evolution of Macedonia.

3.1 Mariovo

Mariovo is a region in the southern part of Macedonia, with mostly hilly to mountainous landscape, dissected by the deep valleys of Crna Reka and its tributaries (Manakovik and Andonovski 1984; Temovski 2016). It belongs mostly to the Pelagonian massif, with the Vardar Zone present only in the eastern parts. Cenozoic tectonics is expressed by the Mariovo basin and the westernmost parts of the Tikveš basin, and the Kožuf-Kozjak volcanic centers on the southeastern mountainous border. Karst areas are found only in the eastern parts, in both the Pelagonian massif and the Vardar Zone, developed in Precambrian and Cambrian marbles, Triassic limestones and dolomites, Upper Cretaceous limestones as well as Pliocene-Quaternary tufaceous limestones, travertines and tufas.

Hypogene karstification has been registered in three localities: Melnica, Podot and Kožuf (Fig. 3). In Melnica area, hypogene karstification can be identified by the presence of three fossil caves (Provalata Cave, Melnička Peštera 1 and 2), the Melnica thermal spring, and some remnants of hypogene karstification exposed at the surface at several locations. Karši Podot Cave, an active thermal cave, is found in Podot locality, while in Kožuf area hypogene karstification is interpreted based on the presence of karstic thermal springs and rock alteration processes connected to the Allchar ore deposit.

Provalata Cave is the most remarkable and best studied example of hypogene speleogenesis in Mariovo and Macedonia (Temovski et al. 2013; Temovski 2016). It is a rather small cave with ~230-m-long ramifying passages, developed in Cambrian calcitic marbles on the northeastern edge of the Mariovo basin, near the valley of Buturica River. Its evolution is connected to two geochemically different speleogenetic phases (Fig. 4). In the first phase, phreatic morphologies (passages, cupola) were formed along sets of parallel NW-SE oriented fractures due to cooling of rising carbonated thermal waters, later covered with thick calcite crust (Fig. 5) due to the shift to a shallower phreatic environment. Fluid inclusion analyses indicate deposition of the calcite minerals at moderate depths from low-temperature (<50 °C) thermal waters, of meteoric origin (Dublyansky 2013 pers. comm.; Temovski 2016). These passages were then filled with clay deposits (Fig. 5), originating from weathering of pyroclastic sediments from Mariovo Lake (Late Pliocene–Early Pleistocene). The system was completely, or at least partly, closed after continuing sediment deposition in the Mariovo basin. Between 1.8 and 1.6 Ma Mariovo Lake drained (at least in the upstream parts) and Buturica River cut its superimposed valley in the pre-Cenozoic rocks, thus lowering the water table. This started the second speleogenetic phase (Fig. 4), where condensation–corrosion by sulfuric vapors created vadose morphologies (replacement pockets, second generation cupola and pockets, vents, half-tube wall and ceiling channels), partly or completely imprinted onto the first-phase morphologies. On the contact with the calcite crust and underlying marble, the sulfuric vapors created gypsum replacement crusts, while on the contact of sulfuric acid with clay sediments minerals such as alunite, natroalunite and jarosite were produced (Fig. 5), which were $^{40}Ar/^{39}Ar$ dated to 1.6–1.46 Ma, thus placing the second speleogenetic phase in the Early Pleistocene, as well as constraining the timing of the onset of fluvial drainage in the Mariovo basin. The source of sulfur in the sulfuric speleogenesis of the second phase was likely the Mariovo basin Upper Miocene coal deposits, with the cave situated next to the coal seam (Fig. 6). Currently below the cave, there is a small, low-temperature (23 °C) thermal spring, the Melnica spring, located in the riverbed of Buturica River, with position controlled by a lens of schist in the marble formation, which acted as a local hydrogeological barrier in the evolution of the cave.

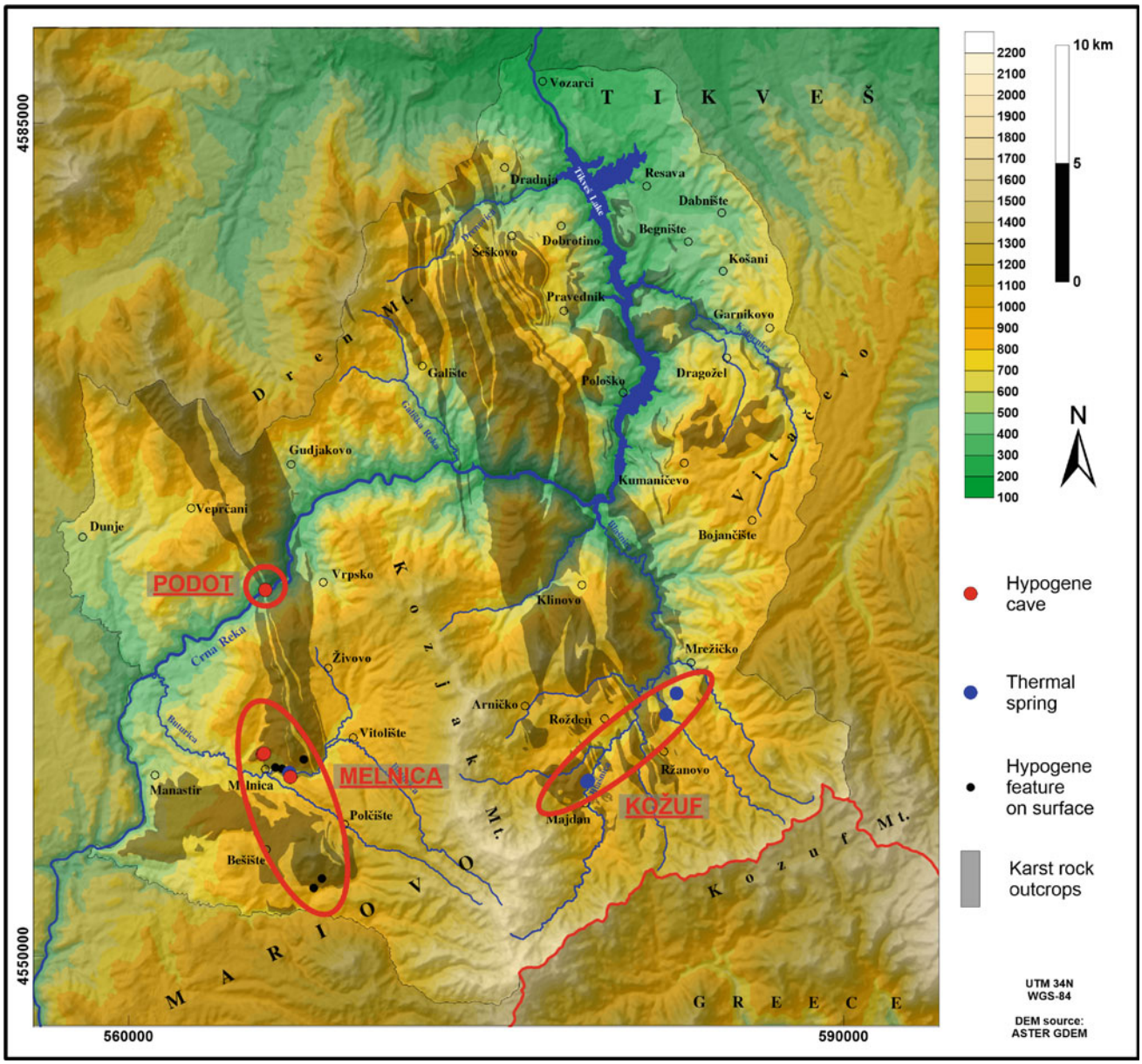

Fig. 3 Hypogene karst localities in Mariovo (after Temovski 2016)

Melnička Peštera 1 and 2 are located on the opposite side of Buturica Valley, at a slightly higher elevation with respect to Provalata Cave (Fig. 6). They are developed in carbonate breccias and conglomerates, close to the contact with underlying Precambrian dolomitic marbles. Melnička Peštera 1 is the largest one with ~700 m of explored passages, while Melnička Peštera 2 is smaller and most likely part of the same cave system. These are horizontal caves with mostly branching to spongework maze plan pattern of passages, carved by numerous cupola and pockets, which result in a lot of collapses, partly masking the primary morphology. At several places these passages and cupola are covered with mammillary calcite coatings in which secondary pockets and cups are developed. There is a lack of typical vadose speleothems (except near the entrances where there is vadose percolation along gravitational fractures connected to slope retreat) and lack of fluvial deposits, with floors partly covered by authigenic clays and carbonate gravel/pebbles originating from weathering of the breccia–conglomerate host rocks. To the north and northeast, the passages end in the dolomitic marbles. The speleogenesis is attributed to hydrothermal dissolution, followed by calcite deposition and later condensation–corrosion, similar to the first speleogenetic phase of Provalata Cave (Temovski 2016).

Karši Podot Cave is located 8 km to the north of Provalata Cave, in Podot locality, just above Crna Reka River

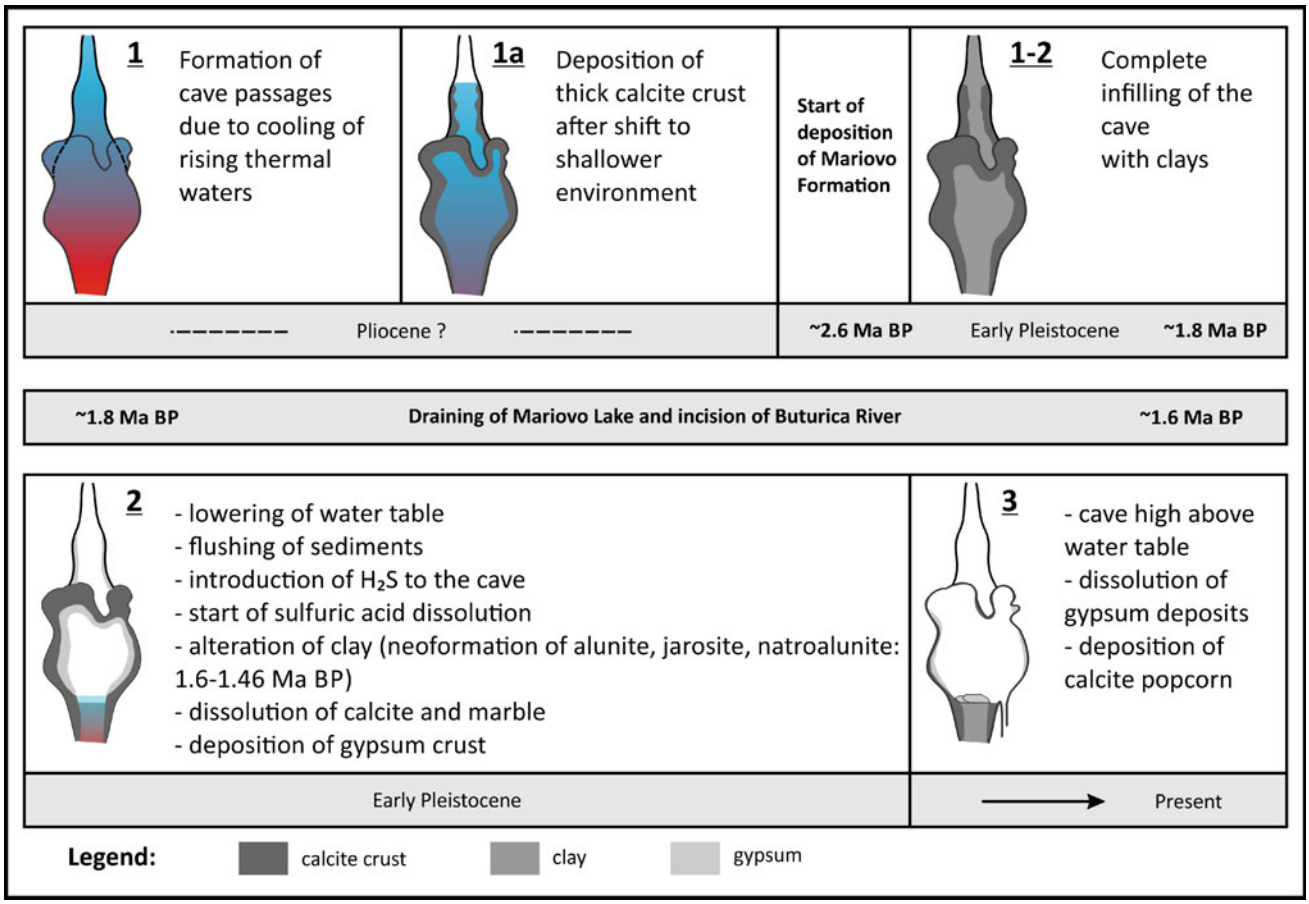

Fig. 4 Schematic illustration of the evolution of Provalata Cave (after Temovski et al. 2013)

(Fig. 3). It is developed in Precambrian dolomitic marbles and partly in terrace deposits (alluvial sediments and palustral tufaceous limestone). The inner part, which is developed in dolomitic marbles, has one large room from which a blind passage continues to the south, at the end of which a profile of dolomitic sand is found with a bedding structure that continues in the marble host rock. Pendant-like and spongework morphology can be seen along the walls and ceiling of the main room and the southern passage, leading to collapses of unstable rock which in the end created the large room. Two thermal springs are emerging from the western wall of the main room, with temperature of 23 °C. The primary porosity was created by ghost-rock weathering in the dolomitic marbles (Fig. 7), where due to cooling of thermal waters, calcite minerals were preferably dissolved, leaving in situ dolomitic sand residue (alterite), with the slowly moving thermal waters lacking sufficient energy to carry the remaining dolomite sand away (Temovski 2013a). The alteration was controlled by fractures and foliation, creating a weathered halo. Later back-flooding of Crna Reka removed the dolomitic sand, creating the cave voids and partly redepositing the material as cross-bedded sediments of dolomitic sand and non-carbonate silt and clay, originating from Crna Reka floodwaters or local terrace deposits.

Remnants of features of the hypogene karstification registered in Provalata and Karši Podot caves can be found also on the surface in Melnica locality. Two thermal vents are found on the southern slopes of Gola Skrka and Pantelejmon, with the last one (Uškova Koliba vent) having active flow of warm air (21.2 °C in winter time). Near to the active vent, in an erosional cliff (Čavkarnik), remnants of cave features with convective morphology (cupola, pockets) are exposed, covered by calcite crust and also partly by stratified clay deposits, similar to what happened in Provalata Cave (first phase). Between Provalata Cave and Melnička Peštera 1 and 2, in the same dolomitic marble formation as in Karši Podot Cave, in several locations alterations of the dolomitic marbles can be seen, with patches of dolomitic sand residue (result of ghost-rock weathering). This dolomitic sand is easily removed by surface erosion, leaving protruding remnant features of unaltered (or less altered) dolomitic marble. At places this weathering is followed by some iron mineralization (goethite).

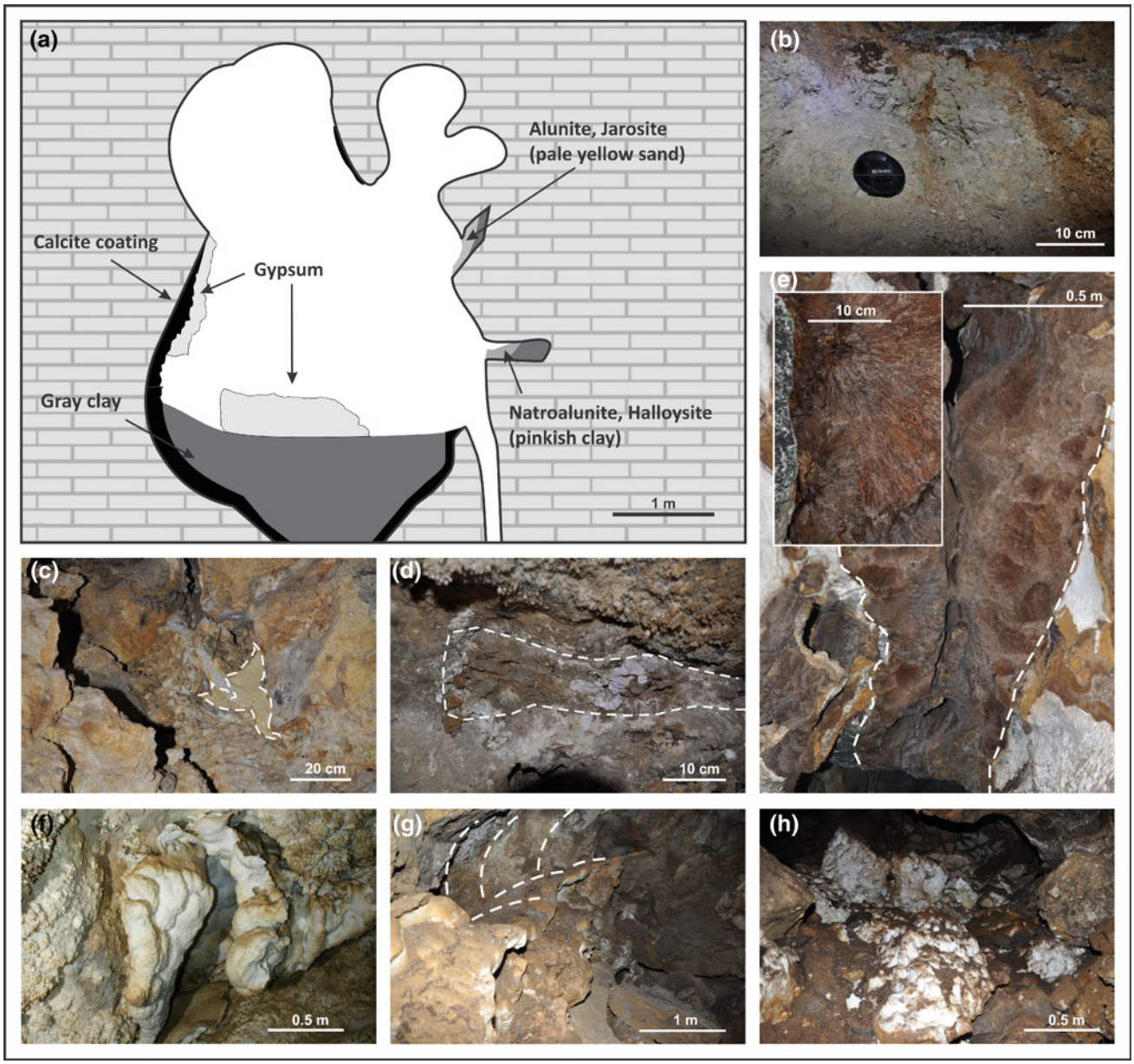

Fig. 5 Characteristic deposits in Provalata Cave (Temovski et al. 2013; Temovski 2016). **a** Schematic cross section of sediments, showing stratigraphic relationships. **b** *Gray clay* (montmorillonite, kaolinite, sanidine, albite, muscovite and quartz). **c** *Pale yellow sand* (alunite, jarosite, muscovite and quartz). **d** *Pink clay* (halloysite-7Ä, natroalunite, muscovite and quartz). **e** Corroded calcite crust. **f** Replacement gypsum crust. **g** Gypsum crust, detached from the wall. **h** Detached gypsum crust piled as gypsum blocks

Allchar (Alšar) is a complex, polychrono-polygenetic volcano-hydrothermal Sb–As–Tl–Au deposit, located between the eastern foothill of Kozjak Mt. and the western foothill of Kožuf Mt. (Fig. 8). It is situated in the Kožuf volcanic complex at the cross section between the transversal Kožuf–Kilikis structure (E–W) and the Vardar zone (NW–SE to N–S) structures (Boev et al. 2012). The local geology is represented by Upper Triassic bedded and massive carbonate rocks (dolomite, marble) underlain by Middle Triassic sandstone and claystone, unconformably, overlain by Pliocene dolomites and tufaceous dolomites grading to ash, crystal tuffs, tuff breccia and lacustrine tufaceous sediments, also partly covered by Quaternary glacial till (Percival and Radtke 1994; Boev and Serafimovski 1996; Boev et al. 2012). The ore deposits are hosted in both Triassic and Tertiary rocks and closely connected to the Kožuf volcanism, with two principal volcano-intrusive phases identified (Boev et al. 2012; Boev and Jelenković 2012): the Miocene phase (14.3–8.2 Ma), and the most significant Pliocene phase (5.1–3.9 Ma).

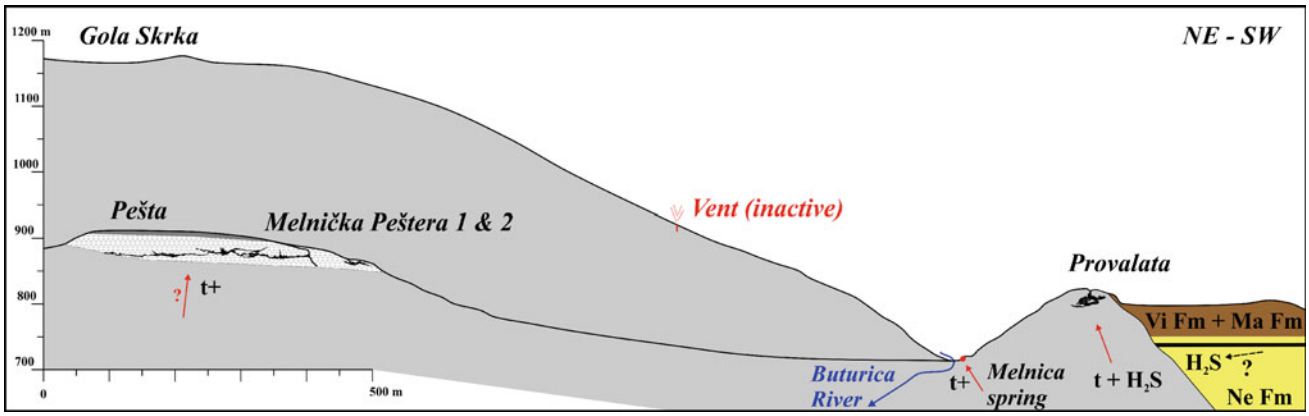

Fig. 6 Cross section of Buturica Valley (Melnica) with hypogene karst features and relationship to Mariovo basin deposits (after Temovski 2016). Ma Fm—Mariovo Formation (Early Pleistocene), Vi Fm—Vitačevo Formation (Pliocene), Ne Fm—Nerezi Formation (Upper Miocene), *black layer* in Ne Fm represents a coal seam

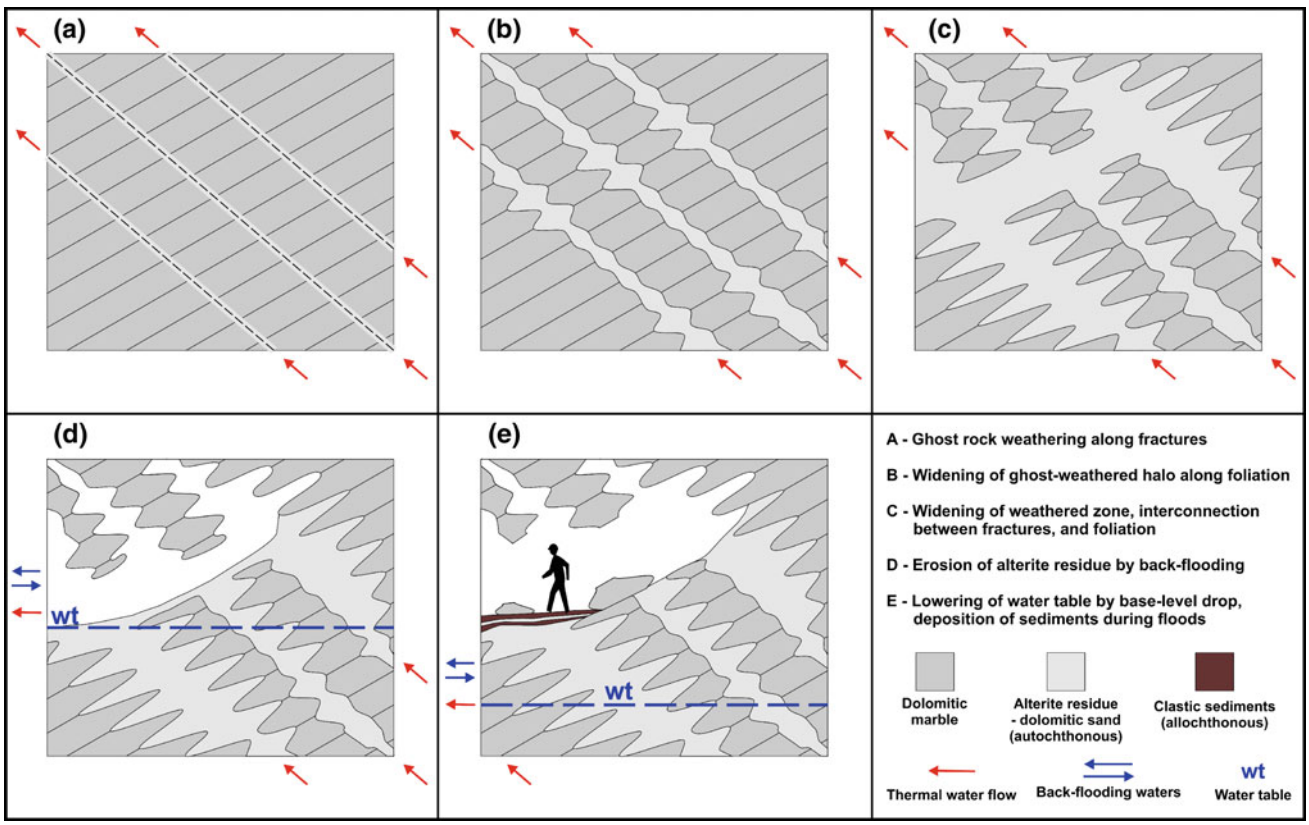

Fig. 7 Schematic model of ghost-rock weathering and phantom cave development in Karši Podot Cave (adapted from Temovski 2016)

Percival and Radtke (1994) described six types of hydrothermal alteration (decalcification, silicification, argillization, veining, dolomitization and supergene alteration) in different rocks throughout the ore deposits, of which decalcification and dolomitization are the two types that contributed to the increase in porosity in the carbonate rocks at greater depths, therefore interpreted as hypogene speleogenetic processes (Temovski 2016). Later supergene alteration due to oxidation likely had an impact on the speleogenetic evolution at shallow depths, or close to the surface. Decalcification (removal of calcite and dolomite from the carbonate rocks, i.e., dissolution, corrosion) at places is followed by deposition of replacement silica (silicification) and later argillic alteration. A second style of

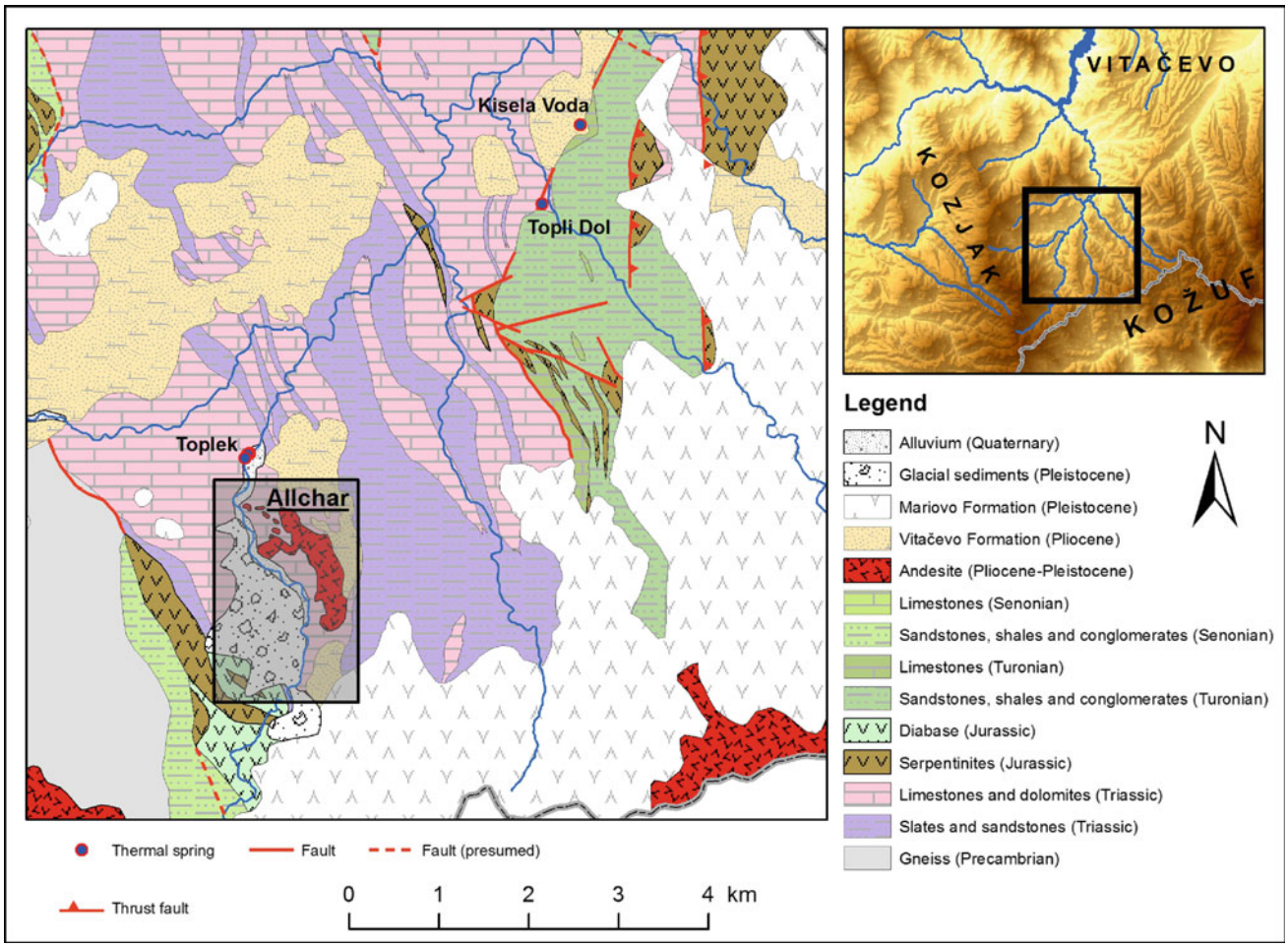

Fig. 8 Geological setting of the Kožuf hypogene karst (after Temovski 2016). Allchar ore deposit is outlined with the *shaded rectangle*

decalcification, "sanding" was described by Percival and Radtke (1994) as common for the Tertiary dolomite, where the intergranular corrosion by hydrothermal fluids removed the fine-grained matrix, leaving predominantly granular dolomite sand, commonly preserving primary textural features (i.e., ghost-rock weathering, like the one described in dolomitic marbles in Melnica and Podot localities) and lacking later silicification. The process of dolomitization, described in the Triassic marbles, produced typically lighter colored, locally mottled, fine-grained, non-layered, highly jointed dolomitized rocks, containing manganese and iron oxides and grading into undolomitized marble. Percival and Radtke (1994), suggest that the dolomitization is the result of removal of calcium carbonate from dolomitic rocks by low-pH hydrothermal fluids.

The evolution of this hydrothermal ore body started with hydrothermal karstification at depth by ore mineral-bearing fluids. Water was flowing along high-angle faults and favorable bedding planes, dissolving carbonate rocks (decalcification after Percival and Radtke 1994) and also producing alteration such as silicification (replacement of carbonate with silica), as well as the so-called sanding decalcification (ghost-rock weathering) of dolomite rocks (Percival and Radtke 1994). This process increased porosity in the carbonate rocks, which served as a host for ore mineral formation in several phases of deposition due to lowering of temperature and pressure (Boev and Serafimovski 1996). Oxidation processes close to the surface or due to mixing with shallow oxygen-rich waters influenced supergene alteration of the ore bodies, with oxidation of iron sulfides producing iron oxides and sulfuric acid, which then produced various sulfate minerals (Percival and Radtke 1994). The ore deposition occurred before 4.31 ± 0.02 Ma, at depths of 200–430 m and temperatures of 280 to $\sim$120 °C (Jelenković and Boev 2011). Water in this hydrothermal system is most likely of meteoric origin (Volkov et al. 2006), heated by a high geothermal gradient due to the proximity of the shallow-seated intrusive rocks of the Kožuf volcanism, with most of the ore elements originating from the intrusive igneous rocks with smaller contribution from the

surrounding sedimentary rocks (Percival and Radtke 1994; Boev and Serafimovski 1996). Pleistocene uplift and erosion have exposed the ore mineral deposits, with present-day low-temperature thermal springs (Toplek Spring) found near the northern part, at the riverbed of Majdanska Reka.

Thermal springs in Kožuf area include also Topli Dol and Kisela Voda springs (Fig. 8), and together with Toplek Spring they all have relatively low temperatures (28, 21 and 22°C, respectively) and mean discharge (2, 0.7 and 15 l/s), with also high dissolved content (total dissolved solids of 884, 900 and 396 mg/l) and similar chemical composition (Boev and Lepitkova 2003). Only Toplek Spring has lower values and is located close to a nearby cold spring, indicating mixing with cold epigene waters, which are draining the upper parts of the Triassic carbonate formation. Toplek has also the highest SiO_2 content (Boev and Lepitkova 2003), which is in good agreement with the spring being located near the Allchar ore deposit (current discharge zone of the hydrothermal system). Sulfate ions present in all of the springs indicate oxidation of iron sulfides in the shallower parts of the systems and sulfuric acid speleogenesis.

The current results from the ***hypogene karst in Mariovo*** suggest hydrothermal karstification in various carbonate rocks, by deeply circulating meteoric waters heated due to the increased geothermal gradient connected to the Kožuf-Kozjak volcanism which was active from the Upper Miocene to Pleistocene. Water was flowing upward along fractures and faults at basin boundaries with spring positions mostly controlled by the incision of the valleys of Crna Reka and its tributaries, Buturica and Blašnica River. The current position of the springs is between 620 and 730 m (Melnica and Kožuf localities) and 320 m (Podot locality). Temperatures of thermal waters in Kožuf locality, located next to/near the volcanic centers, were much higher than in Melnica and Podot, which are located at 7–15 km from Kožuf-Kozjak volcanic centers. The main speleogenetic process is dissolution due to cooling of thermal waters. Locally, due to geological and/or lithological control, hydrothermal dissolution converged with ghost-rock weathering in dolomitic rocks, and also sulfuric acid speleogenesis in the output parts of the karst systems, with the Mariovo coal deposits considered as a source of sulfur in the Provalata Cave, and oxidation of iron sulfides previously deposited in the same hydrothermal system, at Kožuf thermal springs (Temovski 2016).

3.2 Katlanovo

Numerous thermal springs discharge from Katlanovski Rid (Katlanovo Hill) on the southeastern edge of Skopje basin, several of which are captured for the Katlanovo Thermal Spa (Fig. 1). The main springs are located along the intersection of the prominent NW-SE fault, Turska Puknatina (Turkish Fissure) and the valley of Pčinja River, having discharge of 0.1–4 l/s and temperatures of 22–55 °C, also rich in CO_2 and locally with presence of H_2S. The main reservoir is the Paleozoic marbles, with waters from meteoric origin being heated by granitic intrusions, and in the output area (Pčinja River) discharging also through Eocene conglomerates and travertine deposits (Gjuzelkovski 1999).

Thermal karstification has been previously discussed on the occurrence of thermal springs in Katlanovo Spa (Jovanović 1929; Manakovik and Andonovski 1976). On the western parts of Katlanovski Rid, Manakovik and Andonovski (1976), describe the Turska Puknatina Cave (Fig. 9), a 29-m-long fault-controlled fissure cave, developed in tufa deposits by ascending thermal (24–26 °C) waters with increased concentration of CO_2, and possible presence of other gases. In Katlanovo Spa, the morphology of the main feeding channel, as shown in Fig. 9, displays convection features like wall niches and ceiling channel.

3.3 Krčin (Banjište-Krasta and Kosovrasti)

On the southern and southeastern foothills of Krčin Mt. near the western border of Macedonia, there are two thermal springs in the Cretaceous formation belonging to the Cukali-Krasta tectonic unit. Banjište thermal spring is discharging from limestones, and Kosovrasti thermal spring is discharging from gypsum and anhydrite deposits (Fig. 10). Both springs have similar chemical compositions with SO_4^{2-} being the major anion, followed by HCO_3^- and Cl^- ions, and Mg^{2+} as the major cation, followed by Ca^{2+} and Na^+ (Gjuzelkovski 1999). Banjište and Kosovrasti springs have, respectively, discharges of 100 and 60 l/s with temperatures of 4 and 48 °C (Popovska-Vasilevska and Armenski 2016).

Sulfate rocks in this area were first considered as a metasomatic product of limestone rocks and sulfur-bearing thermal waters (Petkovski and Ivanovski 1980), but sulfur and oxygen stable isotope studies confirmed their sedimentary, evaporitic origin, precipitating in a lagoonal marine environment, with $\delta^{34}S$ ranging between 16.6 and 20.6‰ and $\delta^{18}O$ between 11.9 and 15‰ (Jančev et al. 1999).

Nevertheless, the chemical composition of the thermal waters from both springs suggests water circulation through both carbonate and evaporite rocks, with discharge zones located in limestone (Banjište) and gypsum (Kosovrasti).

In the limestone outcrops above the Banjište thermal spring, 14 caves, vents and fissures with warm air circulation (20–34 °C) were registered (Fig. 10), located above 1100 m elevation (>200 m above the thermal spring). They are formed along fractures and are mostly vertically developed, with the deepest cave, Krasta 11 (Brezno št.11 na Krasti) being explored to the depth of 50 m (DZRJ Ljubljana 1982). Continuous measurements in vents above the thermal spring

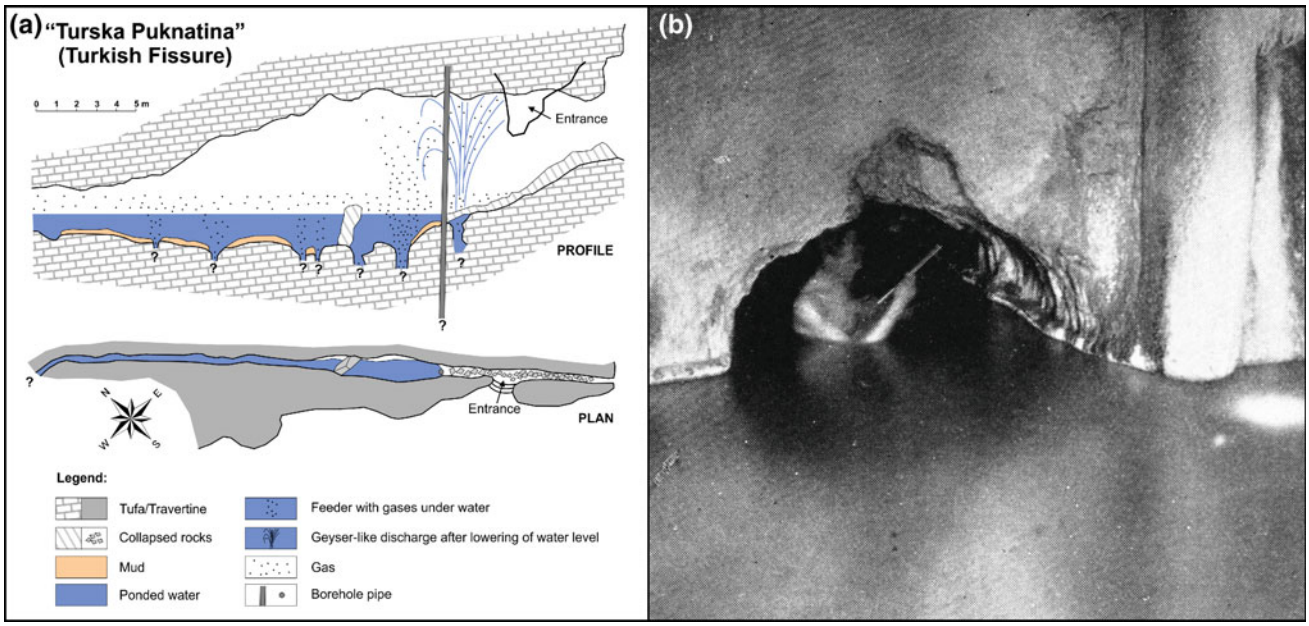

Fig. 9 Some hypogene features from Katlanovo area. **a** Cave map of Turska Puknatina (redrawn from Manakovik and Andonovski 1976). **b** Photograph from the main feeding channel in Katlanovo Spa (Vajić 1928)

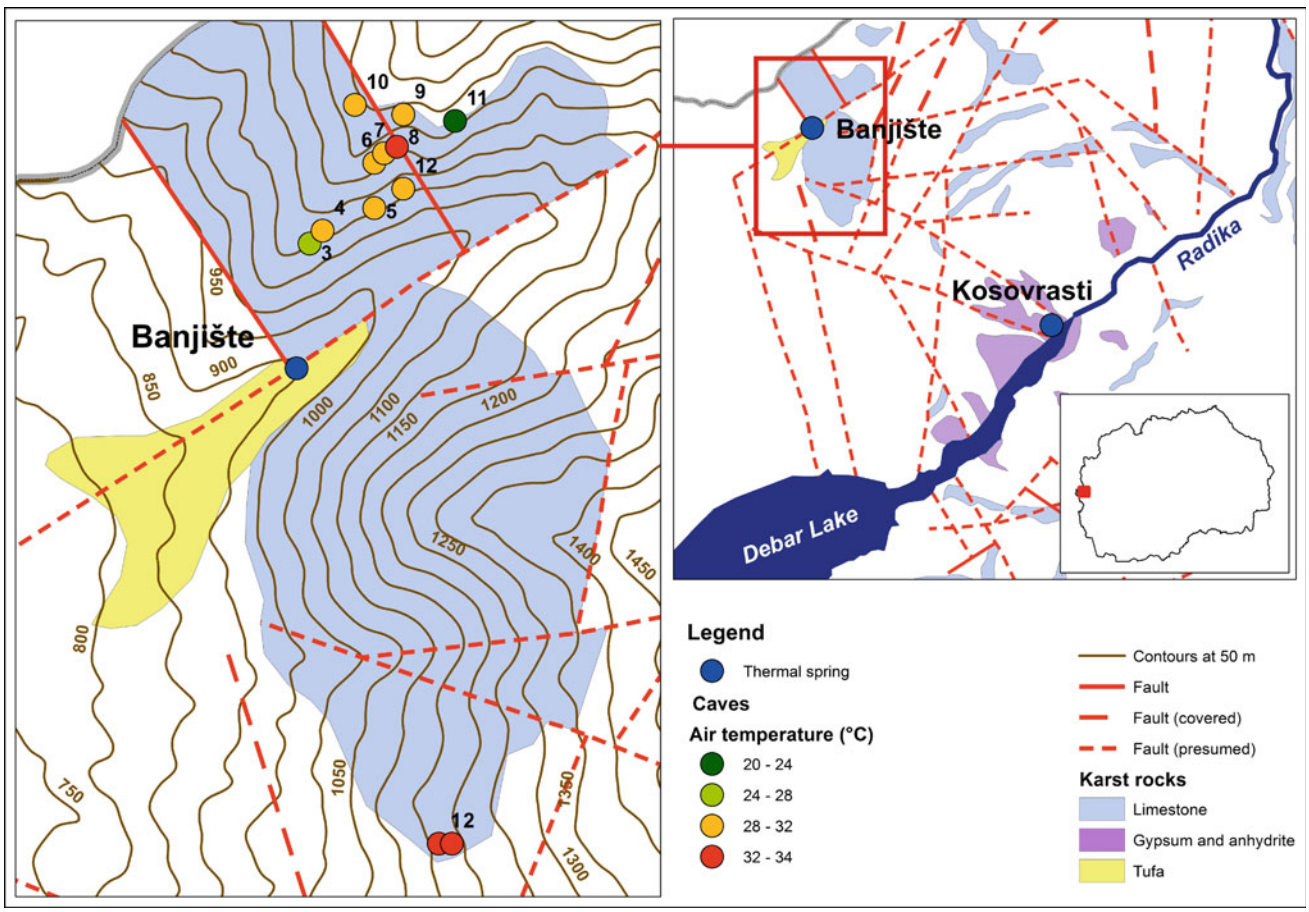

Fig. 10 Hypogene caves and thermal springs in Krčin area (adapted from Temovski 2013a). Cave data after DZRJ Ljubljana (1982)

showed air temperature changes between 25.4 and 33.2 °C, humidity of 100%, and air current speed up to 13 m/s. Based on the dynamics of the meteorological changes and the calculated energy released from the caves, it was estimated that they are situated above a hydrothermal karst system with temperatures above 60 °C (Urbančič 1985). Based on their position in the hypogene system, as well as their morphological characteristics, the caves above Banjište thermal spring can be considered as smoking shafts (Temovski 2013b), developed by condensation–corrosion above a thermal water body (sensu Audra et al. 2009).

3.4 Other Examples

Other localities where hypogene karstification can be described are the thermal springs near Dojran Lake, Proevci (Kumanovo), Banjiče (Šar Planina) and the lower part of the Kočani artesian basin (Fig. 1). In all of these localities, hypogene karstification is expected based on the presence of thermal waters in carbonate rocks, mostly Paleozoic marbles (Gjuzelkovski 1999). At Dojran, Kumanovo and Banjiče springs, thermal waters are discharging along faults, with spring position controlled by local topography and stratigraphy (i.e., valleys of rivers Kumanovska Reka and Pena), and in Kočani basin, thermal waters are feeding the artesian aquifer in the pyroclastic deposits from the underlying Paleozoic marbles.

4 General Conclusions on Hypogene Karst in Macedonia

4.1 Speleogenetic Mechanisms

All of the registered cases of hypogene karst in Macedonia are connected to circulation of thermal waters in carbonate (and partly evaporite) rocks, with hypogene speleogenesis being the result of hydrothermal dissolution (sensu Dublyansky 2000). Waters feeding the hypogene karst systems are of meteoric origin, being heated due to deep circulation in areas with increased geothermal gradient.

Local lithological control is manifested in dolomitic rocks, where hydrothermal speleogenesis is coupled with ghost-rock weathering, dissolving calcite minerals and leaving a dolomitic sand residue. The slow upward water flow of the hypogene systems seems to be favorable for ghost-rock weathering in lithologically suitable rocks, with the thermal waters lacking the energy to physically remove the residue.

Sulfuric acid speleogenesis is another hypogene mechanism identified/possible in three areas: Mariovo, Katlanovo and Krčin. Except in Krčin area, where gypsum rocks are part of the aquifer, in Katlanovo and Mariovo no sulfate rocks are found in the stratigraphy. In Kožuf locality (Mariovo), sulfuric acid speleogenesis is probably connected to oxidation of iron sulfides, previously deposited in the deeper parts of the karst system. In the case of Provalata Cave (Melnica, Mariovo) where sulfuric acid speleogenesis is clearly demonstrated (Temovski et al. 2013), nearby Upper Miocene coal deposits are likely to be the source of sulfur. This might also be the case at the Katlanovo karst system, with the thermal springs located near the Upper Miocene coal field of Skopje basin.

In unconfined settings the upper parts of the hydrothermal hypogene karst systems were exposed to condensation–corrosion, which could also be by sulfuric vapors (cf. De Waele et al. 2016), as in the case of Provalata Cave (Temovski et al. 2013) and probably also in the caves above Banjište thermal spring.

4.2 Geodynamic Control on the Development of Hypogene Karst Systems

Although there is lack of data on the temporal (and spatial) evolution of most of the hypogene karst systems, based on the insight from the evolution of the Mariovo karst systems (Fig. 11) we can derive a general model of hypogene karst evolution in Macedonia.

Neogene extensional tectonics, as part of the South Balkan extensional system, created a twofold control on the development and evolution of the hypogene hydrothermal karst systems in Macedonia: firstly, by creating the favorable structural settings (grabens) for deep circulation of water in intermediate to regional hydrogeological systems, mostly toward basin boundaries; and secondly, through the accompanying magmatic activity, increasing the geothermal gradient, which allowed heating of the deeply penetrating waters and hydrothermal speleogenesis in the output areas of the hypogene karst system (confined and unconfined).

4.2.1 Hypogene Karst Development and the South Balkan Extensional System in Macedonia

All of the registered hypogene karst systems are located along Neogene basin boundaries, and most of them are currently discharging from thermal springs located at the bottom of Quaternary valleys (Fig. 12). Upward flow of thermal waters is directed along fractured and faulted zones controlling basin development.

Among them, the oldest basins are the Skopje, Kumanovo and Kočani basins, with deposits of late Badenian to middle Sarmatian age (Middle Miocene to early Late Miocene) up to Quaternary age (Cycle I–V in the Neogene–Quaternary tectonic evolution of Macedonia, after

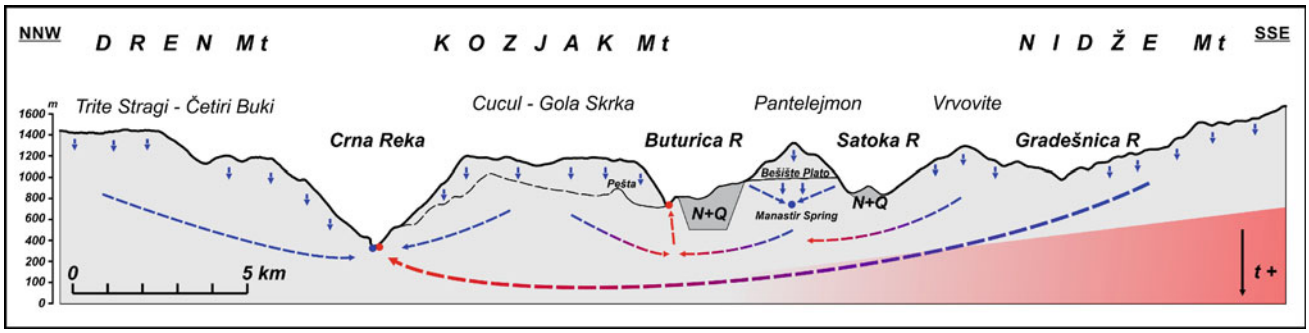

Fig. 11 Cross section through Podot (Crna Reka) and Melnica (Buturica R.) hypogene karst localities in Mariovo with schematic representation of the possible hydrogeological relationships (after Temovski 2016). N + Q indicates Neogene and Quaternary Mariovo Basin deposits and *fading red shade* indicates the geothermal gradient

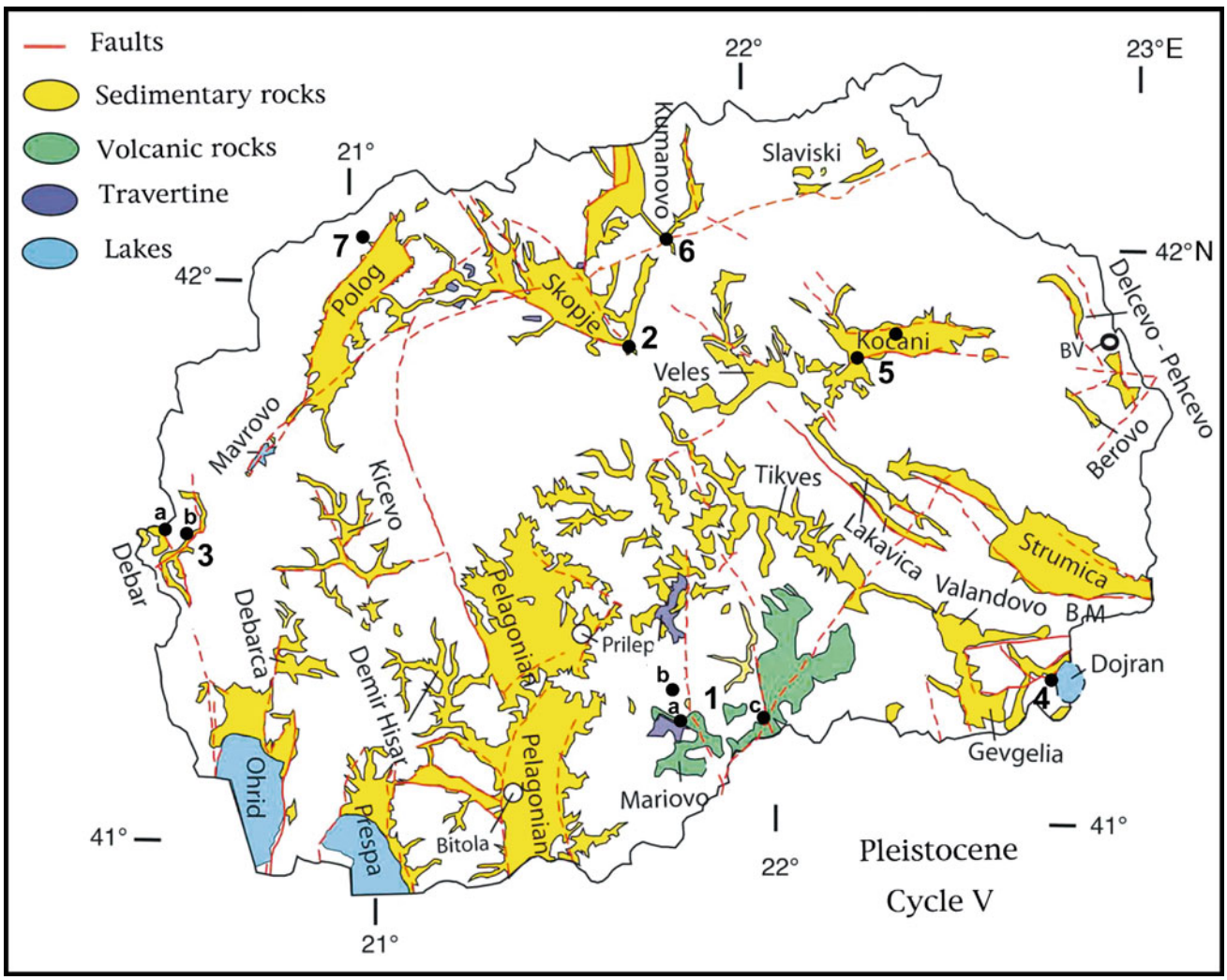

Fig. 12 Locations of hypogene karst features (*black points*) in Macedonia shown on the situation map during Cycle V (Pleistocene) of the Neogene-Quaternary tectonic evolution in Macedonia (modified from Dumurdžanov et al. 2005). Numerations of hypogene karst areas are the same as in Fig. 1

Dumurdžanov et al. 2005). Their development is controlled by W–E, NW–SE, N–S and NE–SW faults. The Katlanovo hypogene karst system is discharging from thermal springs located along a NW–SE fault on the southeastern edge of Skopje basin, with thick Pliocene–Quaternary travertine sediments deposited in the surroundings, indicating functioning of the karst system at least since Pliocene. Travertine deposits were subsequently also affected by hydrothermal speleogenesis, with subsidence of the basin and later also Quaternary incision of Pčinja River lowering the position of the springs. Proevci thermal springs in Kumanovo are likely controlled by the regional ENE-trending fault zone, with the hypogene karst system being opened after the erosion of the overlying Neogene deposits, previously likely developing under confined conditions, similar to the Kočani basin. In Kočani basin the hypogene karst system represents the lower part of an artesian aquifer, feeding the overlying Neogene formation composed of mostly pyroclastic deposits. Skopje and Kumanovo basins were situated in a forearc position with respect to the coeval magmatic arc, with Kočani basin likely situated within, and the magmatic intrusions providing the heat to the hydrothermal systems.

With the extensional system migrating westward, newer basins developed in middle Late Miocene (Cycle II after Dumurdžanov et al. 2005), among which were the Tikveš and Mariovo basins, as well as the Kožuf-Kozjak volcanic complex, located to the south of them. The Mariovo hypogene karst systems are located in the eastern part of the Mariovo basin and southwestern edge of Tikveš basin, controlled by older (reactivated) NW-SE faults and younger NE-SW faults and currently discharging low-temperature thermal waters at the bottom of Quaternary valleys. Deeply circulating meteoric waters were heated due to the increased geothermal gradient connected to the volcanic centers, with higher temperatures in areas closer to the volcanic centers (>120 °C in Allchar) and lower temperatures further away (<50 °C in Melnica). Mariovo hypogene karst systems were active at least since Early Pliocene (e.g., Allchar) and were at least partly closed (confined) after continued deposition in the basins, contributing also to the deposition of sedimentary carbonates in both basins. Locally hydrothermal speleogenesis was coupled with ghost-rock weathering in dolomitic rocks, with also sulfuric acid speleogenesis active after Quaternary incision of valleys (at least since 1.6 Ma in Provalata Cave) (Temovski et al. 2013).

Dojran basin is located in the southeastern part of the country, but it is considered to have formed during Cycle III, Late Miocene (Dumurdžanov et al. 2005), with Dojran Lake being one of the three remaining Neogene lakes in Macedonia (together with Ohrid and Prespa Lakes). It is bounded by faults on all sides, with a NNW-trending fault controlling the western boundary, along which the Toplek thermal spring is situated (with also a number of sublacustrine springs), representing the discharging point of a hypogene karst system developed in Paleozoic marbles. Northern and southern boundaries are controlled by ENE-trending faults, which follow a major tectonic change in eastern and central Macedonia due to the arrival of the North Anatolian fault in the northern Aegean Sea (ca. 6 Ma; Dumurdžanov et al. 2005; Burchfiel et al. 2008).

The westernmost basin is Debar basin, lying to the west of a regional NW-trending fault, with the oldest deposits of Late Miocene age (Cycle III, Dumurdžanov et al. 2005). The thermal springs of Banjište and Kosovrasti are located on the northern edge of the basin, developed in Cretaceous limestones and evaporites, fault guided and with the spring position controlled by the base-level changes due to Quaternary valley incision. Considering that the whole extensional system in Macedonia migrated to the west, with basins being progressively younger to the west (Dumurdžanov et al. 2005), Debar basin and thus the hydrothermal karst systems located on its northern boundary (Banjište and Kosovrasti) are likely one of the youngest developed hypogene karst systems in Macedonia. The evolution of Banjiče thermal springs (Pena River, Šar Planina) is presently difficult to interpret due to lack of information, but considering its location, the Paleozoic marbles from which they are discharging were likely exposed relatively recently (Late Pleistocene), after erosion of the overlying Paleozoic schist rocks due to the incision of Pena River.

4.2.2 Geomorphological Control on Hypogene Karst Evolution

Most of the hypogene systems are currently discharging from springs located along bottoms of river valleys, with spring position controlled by the incision or aggradation of the valley, controlling also the exposure of local geological contacts. Some are feeding overlying formations and have no direct surface expression (e.g., Kočani artesian basin). A similar situation might have existed in most of the hypogene systems during the lacustrine phase, prior to the Pleistocene draining, when they were either feeding permeable Pliocene–Pleistocene formations, or directly contributing to the lakes by subaqueous springs. Their contribution to the lake deposition is indicated by various lacustrine-to-palustral carbonate deposits (travertine, tufa, tufaceous limestone), although epigene karst systems also contributed.

Pleistocene uplift and subsequent fluvial incision greatly influenced their development, with lowering of spring positions and changing geochemical settings by shifting them into shallower conditions, forcing deposition of various mineral assemblages, with condensation–corrosion acting in the upper parts of the system (above the water table) and also erosion/corrosion exposing hypogene features at the surface.

Acknowledgement Part of the preparation of the chapter was supported by MTA Postdoctoral Fellowship Programme, No. PP-030/2015 (2015–2017).

References

Arsovski M (1997) Tektonika na Makedonija (Tectonics of Macedonia). Rudarsko-geološki fakultet, Štip

Audra P, Mocochain L, Bigot J-Y, Nobecourt J-C (2009) Morphological indicators of speleogenesis: hypogenic speleogens. In: Klimchouk A, Ford DC (eds) Hypogene speleogenesis and karst hydrogeology of Artesian Basins, special paper 1. Ukrainian Institute of Speleology and Karstology, Simferopol, pp 23–32

Boev B, Jelenković R (2012) Allchar deposit in Republic of Macedonia-petrology and age determination. In: Al-Juboury A (ed) Petrology—new perspectives and applications. InTech, Croatia, pp 131–168

Boev B, Lepitkova S (2003) Geohemiski karakteristiki na termomineralnite vodi na planinata Kožuf (Geochemical characteristics of the thermomineral waters on Kožuf Mt.). In: Zbornik na trudovi od vtoroto sovetuvanje za geotermalna energija vo Republika Makedonija, Bansko, 3–5 Oct 2003, pp 61–64

Boev B, Serafimovski T (1996) General genetic model of the Alshar deposit. In: Popov P (ed) Plate tectonic aspects of the alpine metallogeny in the Carpatho-Balkan region. UNESCO IGCP project 356. Proceedings of the annual meeting, vol 1. Sofia, pp 75–84

Boev B, Jovanovski G, Makreski P (2012) Geology and mineralogy of Allchar Sb–As–Tl–Au deposit. In: Jovanovski M, Boev B (eds) 2nd congress of geologists of Republic of Macedonia, Special publication 3. Geologica Macedonica, Kruševo, pp 215–232

Burchfiel BC, Nakov R, Dumurdžanov N, Papanikolaou D, Tzankov T, Serafimovski T, King RW, Kotzev V, Todosov A, Nurce B (2008) Evolution and dynamics of the Cenozoic tectonics of the South Balkan extensional system. Geosphere 4:919–938

Carlin R, Angelov N, Oktavian M, Grozdanovski H, Žežovska D, Žežovski I (2011) Unknown natural rarities in Macedonia. Speleological Society "Peoni", Skopje, pp 1–63

Clauzon G, Suc J-P, Dumurdžanov N, Melinte-Dobrinescu M, Zagorchev I (2008) The Pliocene Gilbert-type fan delta of Dračevo (Skopje area, Republic of Macedonia). Geol Maced 2:21–28

De Waele J, Audra P, Madonia G, Vattano M, Plan L, D'Angeli IM, Bigot J-Y, Nobécourt J-C (2016) Sulphuric acid speleogenesis (SAS) close to the water table: examples from southern France, Austria, and Sicily. Geomorphology 253:452–467

Dublyansky YV (2000) Dissolution of carbonates by geothermal waters. In: Klimchouk A, Ford DC, Palmer AN, Dreybrodt W (eds) Speleogenesis: evolution of karst aquifers. National Speleological Society, Huntsville, pp 158–159

Dumurdžanov N, Serafimovski T, Burchfiel BC (2004) Evolution of the Neogene-Pleistocene basins of Macedonia. Geol Soc Am Digit Map Chart Ser 1:1–20

Dumurdžanov N, Serafimovski T, Burchfiel BC (2005) Cenozoic tectonics of Macedonia and its relation to the South Balkan extensional regime. Geosphere 1:1–22

DZRJ Ljubljana (1982) Report from the cave exploration in the vicinity of Banjšte Thermal Spa, Debar (unpublished)

Gjuzelkovski D (1999) Podzemni vodi (izdan) za rešavanjeto na vodosnabduvanjeto vo R. Makedonija i nivna zaštita (Groundwater [aquifer] for solving the water supply in R. Macedonia and its protection). Geohidroproekt, Skopje

Holúbek P, Pokrievka P, Sluka M, Šmoll J, Votoupalet S (2013) Balkánske speleologické výpravy v roku 2012. Spravodaj SSS 2:36–46

Jančev S, Pezdič J, Szaran J, Halas S (1999) Characteristics of sulphate occurrences near Kosovrasti, Macedonia. RMZ 46(3):501–508

Jelenković R, Boev B (2011) Vertical mineralization interval and forecast of the position of an ore-body in the Alšar Sb–As–Tl deposit, Macedonia. Ann Geol Penins Balk 72:119–129

Jovanović PS (1929) Katlanovska Banja (Katlanovo Spa). *Glasnik Skopskog Naučnog Društva, 6*, pp 41–67

Manakovik D, Andonovski T (1976) Hidro-speleološki ispituvanja na del od Katlanovskiot Rid (Hydro-speleological research on part of the Katalanovski Rid). Geogr Rev 14:5–16

Manakovik D, Andonovski T (1984) Geomorfologija (Geomorphology). In: Stojmilov A, Panov M, Manakovik D, Gaševski M, Sinadinovski J (eds) Mariovo—kopleksni geografski proučuvanja. Geografski fakultet, Skopje, pp 41–81

Percival JC, Radtke AS (1994) Sedimentary-rock-hosted disseminated gold mineralization in the Alšar District, Macedonia. Can Mineral 32:649–665

Petkovski P, Ivanovski T (1980) Explanatory notes for the general geological map of Kičevo (1:100 000). Federal Geological Survey, Beograd, pp 1–58

Popovska-Vasilevska S, Armenski S (2016) Geothermal potential of Macedonia and its utilization. In: Papić P (ed) Mineral and thermal waters of Southeastern Europe. Springer International Publishing, pp 131–146

Suc J-P, Popescu S-M, Do Couto D, Clauzon G, Rubino J-L, Melinte-Dobrinescu MC, Quillévéré F, Brun J-P, Dumurdžanov N, Zagorchev I, Lesić V, Tomić D, Sokoutis D, Meyer B, Macaleţ R, Jelen B, Rifelj H (2015) Marine gateway vs. fluvial stream within the Balkans from 6 to 5 Ma. Mar Petrol Geol 66:231–245

Temovski M (2012) Površinska rasprostranetost na karstnite karpi vo Republika Makedonija (Extension of karst rock outcrops in Republic of Macedonia). Geogr Rev 46:21–35

Temovski M (2013a) Phantom speleogenesis in a thermal environment. In: Otoničar B, Gostinčar P, Gabrovšek F (eds) Guidebook and abstracts of the 21st international Karstological school "Hypogene speleogenesis", Postojna, Slovenia, 10–14 June 2013

Temovski M (2013b) Karakteristiki na hipogenata karstifikacija i pojava na hipogen karst vo Republika Makedonija (Characteristics of hypogenic karstification and occurrence of hypogenic karst in Republic of Macedonia). Geogr Rev 47:11–29

Temovski M (2016) Evolution of karst in the lower part of Crna Reka river basin. Springer International Publishing, Heildelberg, Springer Theses

Temovski M, Audra P, Mihevc A, Spangenberg J, Polyak V, McIntosh W, Bigot J-Y (2013) Hypogenic origin of Provalata Cave, Republic of Macedonia: a distinct case of successive thermal carbonic and sulfuric acid speleogenesis. Int J Speleol 42(3):235–264

Temovski M, Pruner P, Hercman H, Bosák P (2016) A cave response to environmental changes in Late Pleistocene: study of Budimirica Cave sediments, Macedonia. Geol Croat 69(3):307–316

Urbančič J (1985) Debarske atmoterme. Glas Podzemlja 17:45–47

Vajić B (1928) Mineralne i lekovite vode u južnoj Srbiji (hemiske analize) (Mineral and healing waters in south Serbia [chemical analyses]), Glasnik Skopskog Naučnog Društva 4:144–168

Vandermeulen M (2015) 12 ans d'exploration de Matka Vrelo en République de Macédoine. Regards 80:16–33

Volkov AV, Serafimovski T, Kochneva NT, Tomson IN, Tasev G (2006) The Alshar epithermal Au–As–Sb–Tl deposit, southern Macedonia. Geol Ore Deposits 48:175–192

Hypogene Caves of Romania

16

Bogdan P. Onac and Virgil Drăguşin

Abstract

Few caves exist in Romania that have provided clear evidences of their hypogene origin; these were described mainly in connection with investigations conducted on ore deposits or thermal water resources used in spas. Genetically, they are grouped in three categories: (1) caves related to upwelling of H_2S-rich thermal waters along Cerna Valley (SW Romania) and around the town of Mangalia (SE Romania), (2) voids created in skarns and limestones during ascending flow of hot metasomatic and hydrothermal ore fluids (caves located mainly in the northern and western part of the country), and (3) mixing of salt and fresh water near the present Black Sea shore (e.g., Piatra Cave). Among all caves in these categories, Movile, a world-renowned biospeleological hot spot, the skarn-hosted caves from Băiţa, and Valea Rea, an underground mineralogical treasure, are the most representative.

Keywords

Speleogenesis • Ore deposits • Hypogene caves • Romania

1 Introduction

Karst studies (mainly mineralogical) carried out in Romania have revealed the existence of limited, but outstanding examples of hypogene caves (see Onac 2013 for a review). However, in terms of research topic, with one exception (Movile Cave, a world renown biospeleological hot spot), hypogene speleogenesis has never been the main focus of any particular publication. Maybe for this reason, from over 12,000-catalogued caves in the country (Vlaicu, personal communication), only a handful are recognized as having clear hypogene origin.

A survey of the existing literature indicates that documented hypogene caves are concentrated in several karst areas of Romania (Fig. 1). In Cerna Valley (Fig. 1a) and Dobrogea (Fig. 1f–h), the genetic mechanisms are related to ascending hydrogen sulfide-rich thermo-mineral waters (Horoi 1994; Sarbu and Lascu 1997; Onac et al. 2009), as well as to a presumed mixing of freshwater and saltwater. Apart for these two regions, scattered across the country there are a number of ore-related cavities (Fig. 1b–e), whose origin was ascribed to metasomatic alteration (Mârza and Silvestru 1988) or rising of post-magmatic acidic hydrothermal solutions (Nedopaca and Grama 1987; Mârza et al. 1995; Onac 2002; Vişan and Tămaş 2011).

This study captures representative examples of caves from each hypogene speleogenetic pathway. For every case, we first provide the general geological and hydrogeological settings, and then, we illustrate those features

B.P. Onac (✉)
Karst Research Group, School of Geosciences,
University of South Florida, 4202 E. Fowler Ave.,
NES 107, Tampa, FL 33620, USA
e-mail: bonac@usf.edu

B.P. Onac
Emil Racoviţă Institute of Speleology, Romanian Academy,
Clinicilor 5, 400006 Cluj-Napoca, Romania

V. Drăguşin
Emil Racoviţă Institute of Speleology, Romanian Academy,
Frumoasă 31, 010986 Bucharest, Romania
e-mail: virgil.dragusin@iser.ro

© Springer International Publishing AG 2017

A. Klimchouk et al. (eds.), *Hypogene Karst Regions and Caves of the World*,
Cave and Karst Systems of the World, DOI 10.1007/978-3-319-53348-3_16

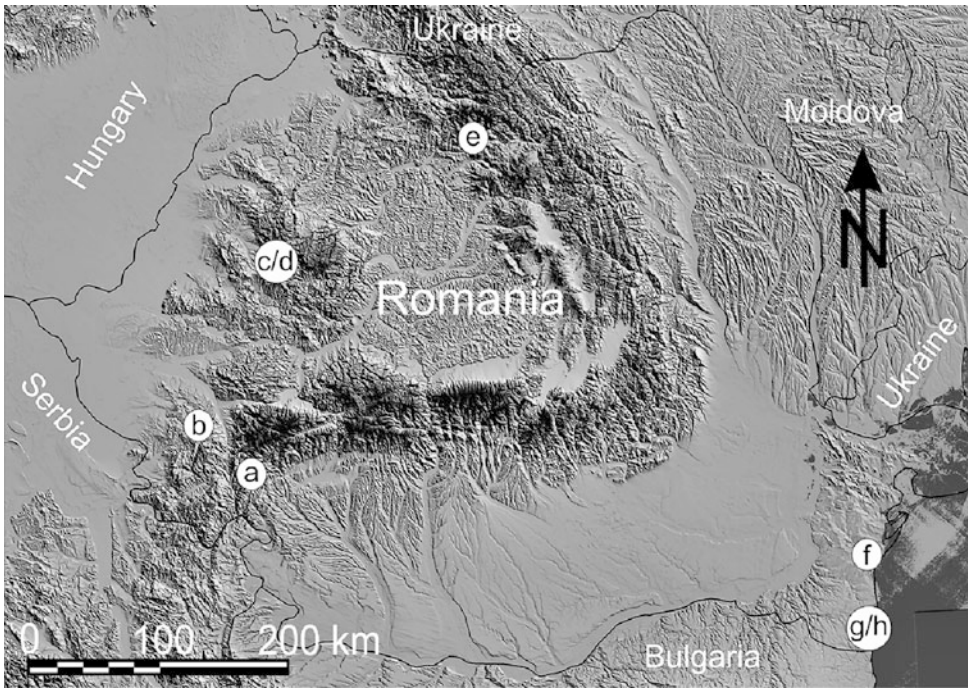

Fig. 1 Location of the sites discussed in this chapter. *a* Cerna Valley, *b* Dognecea, *c*, *d* Băița Bihor mining area and Valea Rea Cave, *e* Rodna Veche ore district, *f* Piatra Cave, *g*, *h* Movile and Limanu caves

(morphological and mineralogical) that are diagnostic for caves with hypogene origin.

2 Cerna Valley

Cerna Valley is situated on an asymmetric graben whose western side follows a master fault with dextral strike-slip motion (Conovici et al. 2013). The graben is crossed by transversal faults and at their intersections with the master fault, H_2S-rich thermo-mineral waters (up to 53 °C) rise and emerge in caves at lower altitudes (e.g., Diana, Despicătura, Hercules), whereas in those at higher altitudes (e.g., Grota cu Aburi, Adam Cave) hot vapors emerge (Povară et al. 1972). The reason of this thermo-mineral activity is a local geothermal anomaly produced by the convection of heat via transcrustal faults that delimitate the Cerna Graben (Veliciu et al. 1983). For a more detailed account on the geology and hydrogeology of the Cerna Valley, readers are directed to Povară et al. (2008).

Caves formed along the valley are typically short, except the Great Șălitrari Cave (~1500 m), and are all formed in limestone of Jurassic–Lower Cretaceous age. They were mainly studied in the context of thermo-mineral waters that are used in Herculane Spa since the antiquity. More recently, mineralogical and stable isotope analyses performed on minerals precipitated from thermal waters emerging in caves provided several lines of evidence indicating that imprints characteristic for hypogene origin exist in the vast majority of the Cerna Valley caves.

Diana Cave is by far the richest and more diverse in terms of minerals (Onac et al. 2009). Abundant steam and H_2S rises from the thermal water to condensate on the walls and ceiling of the cave. The sulfuric acid produced by H_2S oxidation/hydrolysis causes a strong acid–sulfate weathering of the bedrock, generating in combination with Al^{3+} and Na^{+} from the marls and thermal water, a paragenesis that includes native sulfur, bassanite, epsomite, halotrichite group minerals, alunite, anhydrite, tamarugite, and rapidcreekite. The last three sulfates have their type locality in this carbonate cave environment (Diaconu 1974; Onac et al. 2013; Puşcaş et al. 2013).

Morphologically, features that may provide evidences for at least a hypogene stage in the origin of many of the Cerna Valley caves include ascending narrow passages, blind galleries, floor feeders, and subspherical voids.

A study of the S isotopic composition of the thermo-mineral waters showed that relatively variable concentrations of methane in these waters coupled with increasing concentrations of total dissolved S drives differences in the extent of sulfate reduction, allowing for the progression of sulfate reduction to be seen in the waters of the wells and springs of the Cerna region (Wynn et al. 2010). The $\delta^{34}S$ versus $\delta^{18}O$ values of sulfates and sulfides from the investigated caves plot in three different fields (Fig. 2), each characterized by homogeneous composition, but having clearly distinct values from one to another (Onac et al. 2011). $\delta^{34}S$ values (−19.4 to −27.9‰) of group 1 correspond to gypsum crusts from Sălitrari and Bîrzoni caves (northern part of the Cerna Valley) and are consistent with

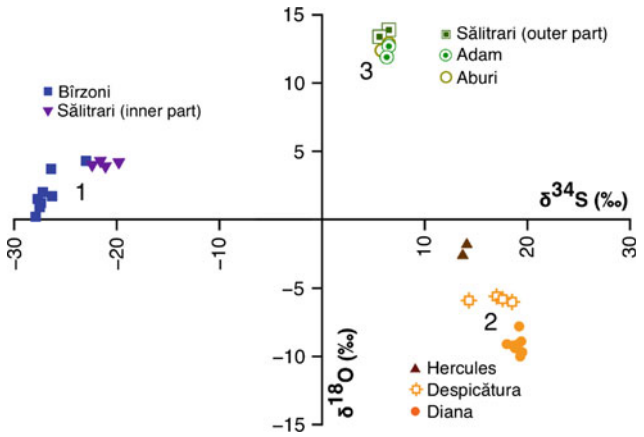

Fig. 2 Isotopic data of cave sulfates from selected caves along Cerna Valley. See text for more information on the three cave groups labeled 1–3

oxidation of dissolved sulfide produced during methane-limited thermochemical sulfate reduction (TSR, low H_2S:SO_4^{2-}) that characterizes the chemistry of springs in this area (Wynn et al. 2010). Group 2 includes sulfates from caves downstream Cerna Valley (southern part) for which the S isotopic composition (14.3–19.4‰) is compatible with oxidation of dissolved sulfide in springs of which $\delta^{34}S$ values characterize sulfate-limited TSR (high H_2S:SO_4^{2-}) environments. The gypsum crusts in caves of the third group has intermediate $\delta^{34}S$ values (5.8–6.5‰), suggesting an origin related to either oxidation of pyrite present in limestone bedrock or oxidation of dissolved sulfide formed during methane-limited TSR, but with incomplete oxidation during sulfuric acid speleogenesis (SAS).

It has been shown in other karst regions of the world that SAS produces ^{34}S-depleted cave sulfates (Hill 1987; Galdenzi and Maruoka 2003). In contrast, the sulfate $\delta^{34}S$ values in caves along the Cerna Valley (ranging between −27 and +19.2‰), show that even in a single hydrological system, the sulfate isotope values in different SAS caves depend not only on the source of the S, but also on the completeness of subsequent S species reactions. Thus, ^{34}S-depleted isotopic composition of the minerals alone does not provide enough information to clearly distinguish SAS from other more complex speleogenetic processes (Onac et al. 2011).

3 Dobrogea

The karst region around the town of Mangalia (SE Romania; Fig. 1g, h) is developed on Sarmatian oolithic and fossiliferous limestone, and covers an area of ~20 km^2 on land (Constantinescu 2002), whereas a far larger surface is now submerged under the Black Sea. The limestone outcrops along valleys while on the interfluves it is mostly covered by thick Quaternary loess deposits. It is underlain by an Jurassic-Cretaceous-Eocene carbonate sequence with a thickness of around 500 m. An important characteristic of this area is the presence of H_2S- and CH_4-rich thermal groundwater that rises along a system of local faults of which Kara Oban and Mangalia are the most important (Marin and Nicolescu 1989; Povară 1994). Along the Kara Oban fault, 21 thermal springs were identified, having a total discharge of 210–250 L/s (Feru and Capotă 1991; Feru 1993). In this region (Fig. 1g, h), two caves stand out: Movile, a rich chemosynthesis-based ecosystem (Sarbu et al. 1996) and Limanu with its labyrinth of passages totaling more than 3 km (Dumitrescu et al. 1965).

Movile Cave was discovered in 1986 during prospection work for an industrial project on the western outskirts of the town of Mangalia. Here, a group of large collapse dolines and their outer rims make a special type of karst known as "Movile type karst" (Constantinescu 1989, 2002), which resembles on a small scale the tropical cockpit karst features (Fig. 3). We could speculate that such a morphology, unique to Romania, might be the remnants of former labyrinth systems, as unroofed caves.

While the water table in Movile Cave has the same elevation as the Black Sea level and hints toward the latter controlling the genesis of the lower cave level, we can further speculate that these former labyrinth caves were formed during periods when the past water table was close to the sea level.

Movile Cave is situated below the rim of the Obanul Mare and the access is made through a 18-m-deep artificial shaft. The cave has a dry level consisting of 200 m of passages and a submerged one, adding an extra 40 m to the total length (Fig. 4). The water in the lower level has a temperature of 21 °C and a concentration of 0.3 mM/L of H_2S, 0.3 mM/L ammonium, and 0.2 mM/L methane (Sarbu and Lascu 1997). Around the water surface, gypsum crusts associated with acicular aragonite are common. Their occurrence is less significant as distance increases from the water. Corrosion niches coated with gypsum crusts are also present near the water surface, where the pH could be as low as 3.

At present, the cave morphology above the water surface (in both the lower and upper passages) is modeled by the H_2S degassing from the upwelling waters. Lascu et al. (1995) and Sarbu and Lascu (1997) showed that inside Movile Cave the corrosion process has two components. Around the water surface, H_2SO_4 resulting from the oxidation of the degassing H_2S corrodes the walls, forming wall niches and cupolas (Fig. 5). This reaction produces CO_2 that enriches the atmosphere of the upper dry level, to values of up to 1.5%. The carbonic acid resulting from the mixing of CO_2 with condensing water corrodes the walls of the upper passage causing the present-day modeling of the dry

Fig. 3 Aerial view of the area surrounding Movile Cave (*arrow* indicates its entrance), with the Movile type karst visible around the Obanul Mare large collapse doline (photograph courtesy of M. Baciu)

passages. Horoi (1994) showed that the corrosion of the upper passage walls results in a clear layering: the first layer is made of 2 cm of insoluble clay particles and is followed by 10 cm of ooliths whose cement was dissolved. These two layers are followed by a transition toward unaltered limestone.

A few kilometers south of Movile lies Limanu Cave, a maze of more than 3 km of passages (Fig. 6). It is located on the southern shore of the Limanu Lake and has a single main level with a total relief of only 5 m and an average underground temperature of 13 °C. Archeologists first studied the cave in the 1920s and, while assuming a fluvial origin of the passages, they also mentioned that limestone slabs were mined in many passages. The human use of this cave is traced back to the antiquity, when it was documented to have been used as a shelter during wars. Subsequently, the cave was mainly studied by biospeleologists (Dumitrescu et al. 1965; Sarbu et al. 1996) and more recently, investigated from a mineralogical standpoint by Diaconu et al. (2008). Although none of these studies dealt with the origin of Limanu Cave, judging on its network pattern, regional hydrochemical context (H_2S-rich water), and abundant gypsum deposits, the cave is a good candidate for further study that could document a hypogene origin.

Piatra Cave (Fig. 1f), also known as the Water Cave from Taşaul Lake, was formed in Oxfordian age limestones pertaining to the Casimcea Syncline (Drăgănescu et al. 1979; Lascu et al. 2000). It is located ~10 km from the Black Sea coast on the shore of Taşaul Lake, which formed when the Holocene sea level rise led to the formation of a sandy bar that blocked Casimcea Valley. At present, the cave is flooded and the water level stands ~1 m above present sea level

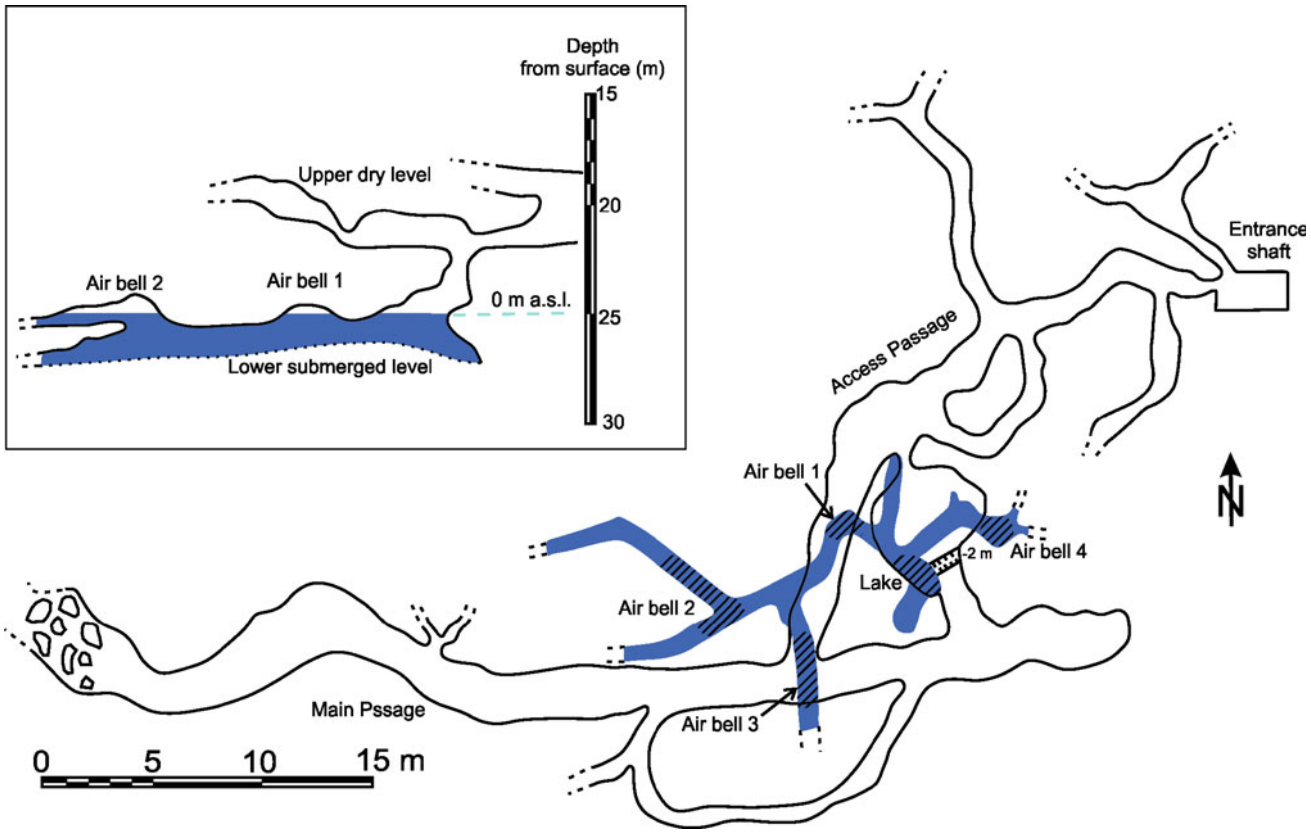

Fig. 4 Map and profile of the Movile Cave (after Sarbu 2000, with permission)

(Fig. 7). The cave has one main gallery of ~100 m in length with frequent cupolas and floor feeders (Lascu and Sârbu 1988). There are also rich calcite speleothems, proof that the cave evolved subaerially at times and meteoric water reached the cave. Its close proximity to the Black Sea, along with evidences of weathered (corroded) speleothems may be indicative of periods when the cave was evolving at the fringe of the mixing zone. Also, considering the feeders present in cave, we argue that part of its passages might have been formed due to hypogene processes.

4 Mine Caves

The particular hypogene speleogenesis of selected mine caves from Romania was recently reviewed by Onac (2013). Mârza and Silvestru (1988) discuss in detail the hypothesis that the karst voids discovered during mining operations in the Rodna Veche ore district (northern Romania; Fig. 1e) were formed during the early post-magmatic period through the corrosion of the carbonate host rock by hydrothermal acid solutions upwelling along tectonic fractures. The paper describes speleothem-like hydrothermal deposits (draperies, stalactites, crusts, etc.) composed of marmatite (ferroan variety of sphalerite; ZnS), marcasite, and pyrite. Calcite, quartz, and barite crystals often cover these sulfide speleothems. It is worth noting that the authors concluded their paper with a proposal for a genetic classification of karst, i.e., using *endogenous* for all karst features generated by hypogenous agents (e.g., post-magmatic fluids) and *exogenous* when subaerial agents shape karst landscapes above and below ground.

Another example of hydrothermal karst was document by Mârza et al. (1995) from the Ocna de Fier–Dognecea mining area (Fig. 1b). In this area, the authors describe coatings, draperies, and stalactites made of magnetite that decorates the walls of a small cavity (<1 m across) formed within the Zn–Pb (Cu)-mineralized skarn. Karst voids of this type are interpreted to be the product of hydrothermal dissolution of the carbonate support during the post-skarn stage. As hydrothermal solutions cooled down, speleothem-like formations were deposited.

At Băița Bihor metallogenic district (western Romania; Fig. 1c, d), the hypothesis of caves linked to the presence of hydrothermal solutions in relation to the ore deposit was first mentioned by Stoici (1983). In this metallogeny-based

Fig. 5 Condensation-corrosion cupola in Movile Cave showing abundant weathering residue (*photograph* B.P. Onac)

study, he briefly touches on a series of karst voids intercepted by mine adits and shafts, suggesting their possible endogene origin.

Onac (2002) directly investigated 8 of the 12 cavities known in this area where bodies of skarn hosting economic concentrations of Mo, W, Bi, B, Cu, Pb, and Zn were mined for decades (Stoici 1983). The caves consist of predominantly ascending, single or branched passageways (length varies from 8 to over 550 m) along which chambers sometimes occur. They develop within the skarn bodies (Fig. 8a) and along fault lines or at the contact between dykes and mineralized skarns (Fig. 8b). Genetically, they appear to be the result of contact metamorphism when limestone suffers decarbonation, a process that liberates CO_2, which increases the acidity of the hydrothermal fluids, thus enhancing their dissolution capacity.

Most of these caves display cupolas and corrosion notches at the ceiling level. Geode-type single rooms are also common and were intercepted well within skarn bodies. They are interpreted to reflect voids generated by the flow of hot metasomatic fluids moving upwards along bedding planes, faults, or lithologic boundaries (Onac 2002).

Regardless of the cave type, their walls are covered with thick calcite crusts (dominantly) and mineral assemblages that never occur in low-temperature, near-surface ordinary caves. Three groups of minerals were recognized: (1) precipitated directly from hydrothermal solutions (wittichenite, Cu_3BiS_3; Sb-rich luzonite, $Cu_3(As_{0.64}Sb_{0.36})S_4$; quartz), (2) secondary products (malachite, azurite, glaukosphaerite, rosasite, aurichalcite, goethite, chalcanthite) formed by weathering of minerals in group 1, and (3) deposited from low-temperature vadose solutions (calcite, aragonite, hydromagnesite, and norsethite). Although only the minerals in category 2 and 3 are satisfying the definition of true cave minerals (Hill and Forti 1997), those belonging to group 1 are diagnostic for hypogene (hydrothermal-related) speleogenesis.

The most studied cave that shows evidences of past hypogene processes is Valea Rea, a system of over 16 km in length that reaches a depth of 384 m below the entrance (Damm 2000; Zih-Perényi et al. 2017). The Valea Rea Cave is situated in the Bihor Mountains at an elevation of 1300 m (Fig. 1c, d). It is mostly developed in middle Triassic dolostone and limestone, as part of the Finiș-Ferice Nappe

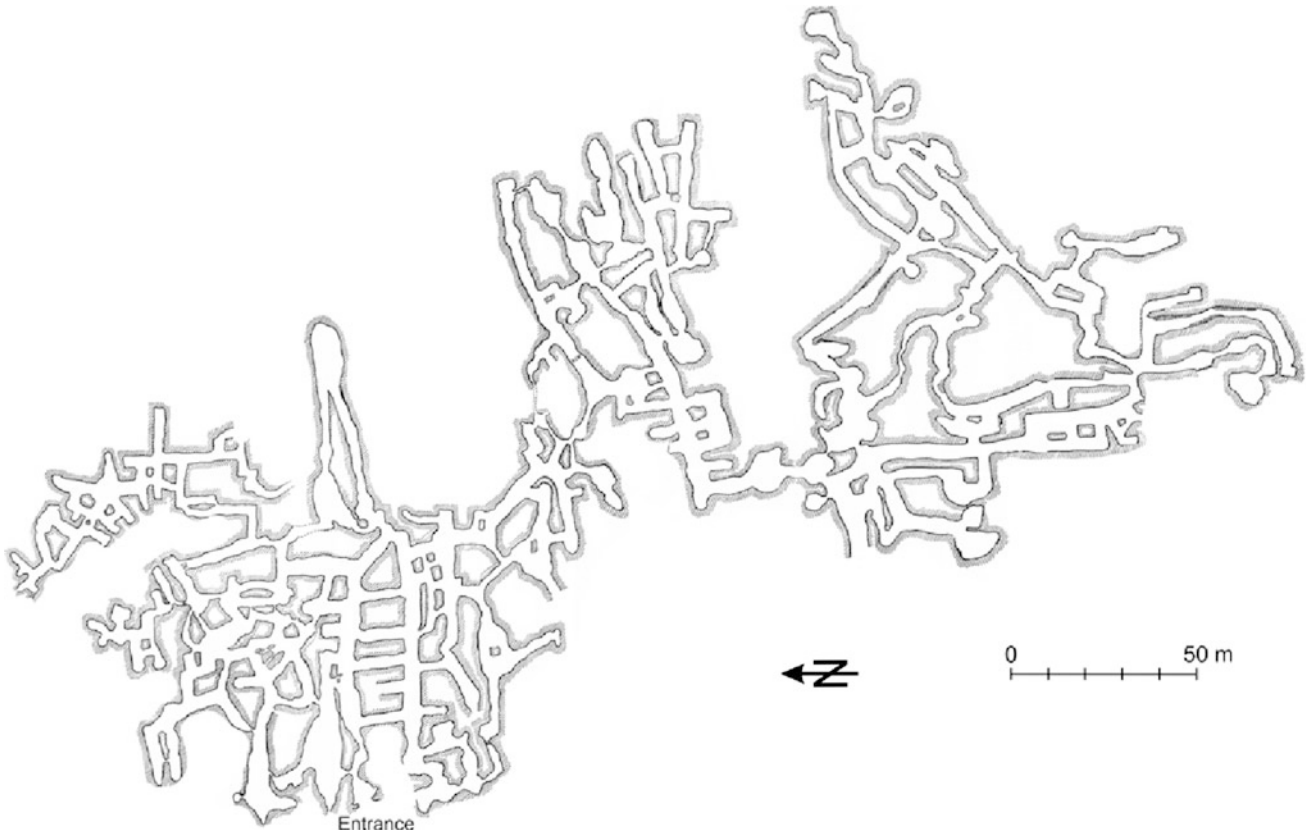

Fig. 6 Map of Limanu Cave (simplified, after Dumitrescu et al. 1965)

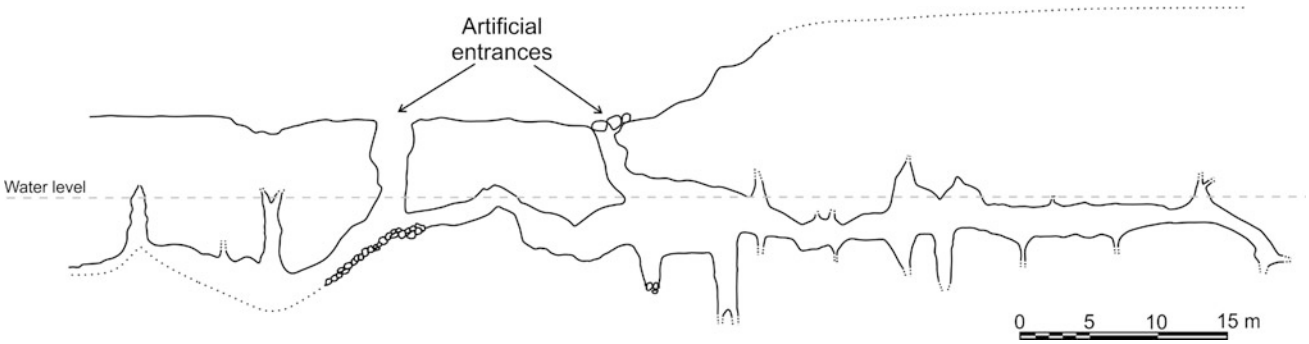

Fig. 7 Longitudinal profile of Piatra Cave (S. Sârbu, with permission). The scale is similar for both horizontal and vertical axes

(Balintoni 1997), a unit with very diverse petrography that includes quartzitic sandstones, conglomerates, slates, siltites, quartzitic conglomerates, gray limestones, black limestones with cherts, marly slates, and limestone breccias. The closeness of igneous rocks nearby the cave likely promoted the ascending flow of mineralized, hot solutions along fault lines and fractures. These are possibly responsible for opening/shaping some of the early passages or filling (mineralized veins) preexisting ones. Clearly, they contributed to the deposition of certain unusual cave minerals, namely metatyuyamunite [$Ca(UO_2)_2(VO_4)_2 \cdot 3H_2O$], epidote [$Ca_2(Al_2Fe^{3+})[Si_2O_7][SiO_4]O(OH)$], periclase (MgO), and quartz among the most representative (Onac et al. 1995, 2000; Feier 2003). Weathering of the silicates resulted in the accumulation of kaolinite, dickite, and nacrite. They all complete a long list of other more or less common cave minerals that comprises aragonite, calcite, dolomite, hydromagnesite, malachite, rhodochrosite, anhydrite, celestine, gypsum, brushite, strengite, bobierrite, vivianite, and wavellite.

Later, Ghergari et al. (1997) investigated two hydrothermal veins of oval shape and diameters of 30–50 cm, mostly

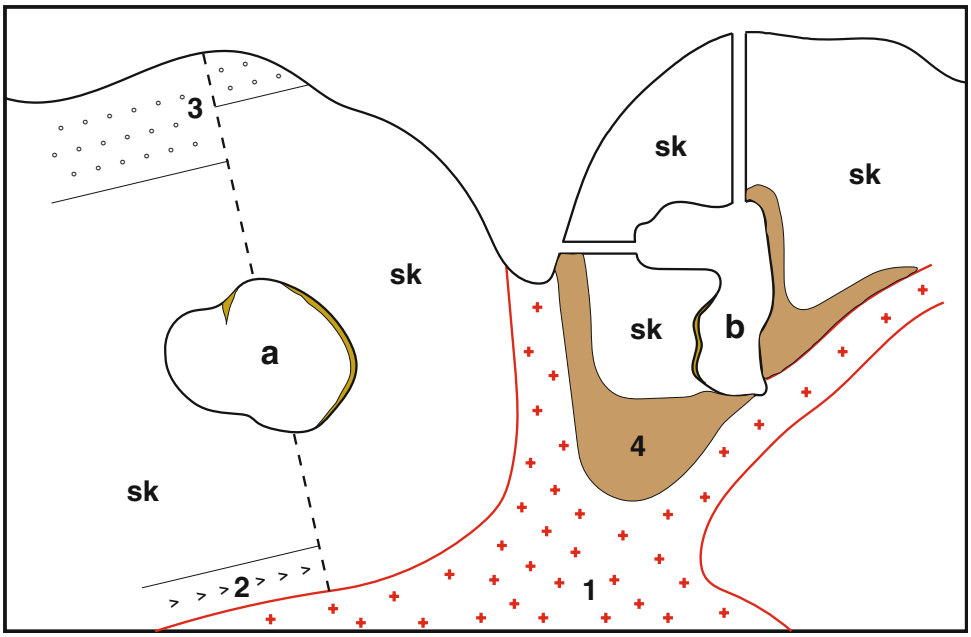

Fig. 8 Idealized sketch showing the location of caves (*a* deep seated, *b* shallow) in relation to skarn and mineralized bodies in Băița Bihor mining area. *1* Upper Cretaceous pluton and dykes, *2* hornfels, *3* Permian–Triassic detrital rocks, *4* mineralized skarn

filled with quartz. Other minerals identified in these veins are calcite, Fe-rich dolomite, gold, barite, and pyrite. Clay mineral associations are represented by dickite, smectite/dioctahedral chlorite, illite/montmorillonite, and montmorillonite.

The multi-story maze morphology, upward branching chimneys, highly corroded wall crusts, presence of hydrothermal veins, and the occurrence of many exotic minerals all point toward at least two hypogene stages in the formation of the Valea Rea Cave.

5 Conclusions

Although not intended as a comprehensive study, this chapter assembles to most significant examples of hypogene caves from six different areas of Romania. Their mineral assemblages and cave morphologies may serve as good examples in detecting hypogene speleogenesis in other karst regions worldwide. Our review summarizes three categories of caves genetically related to: (1) sulfuric acid dissolution (resulted from oxidation of H_2S-rich thermal waters) affecting many caves along the Cerna Valley and in Southern Dobrogea, (2) *per-ascendum* flow of metasomatic and hydrothermal fluids associated with volcanic bodies, and (3) corrosion of limestone due to possible mixing of fresh and salt water on the shore of the Black Sea. Each of these genetic mechanisms acting either alone or in combination left clear cave morphologies imprints, which are of many kinds. The most common are wall and ceiling corrosion pockets, cupolas, blind ascending passages, and floor feeders. Taking into account the particular network pattern of Limanu Cave, this is the only clear example of a relationship between the type of groundwater recharge (sulfuric acid or/and coastal mixing) and structural character of the bedrock, suggesting a possible hypogene origin.

The mineralogy of caves attributed to the first two categories is by far the richest, with over 40 species encompassing the groups of native element, sulfides, oxides, sulfates, and carbonates. Of these, 12 have their type locality in Diana (anhydrite, rapidcreekite, and tamarugite) and in Valea Rea caves (gold, lansfordite, meta-aluminite, periclase, and wavellite), and in the skarn-hosted caves of Băița Bihor area (wittichenite, norsethite, glaukosphaerite, and natrolite).

References

Balintoni I (1997) Geotectonica terenurilor metamorfice din România. Carpatica, Cluj-Napoca

Conovici M, Povară I, Orașeanu I, Marin C (2013) Geological and hydrogeological features of Cerna Valley (Arșasca-Iuta area, SW Romania). Carpath J Earth Environ Sci 8(3):219–230

Constantinescu T (1989) Considerations sur la zone karstique de "La Movile" (Mangalia, Dobrogea du Sud, Roumanie). Misc Speol Rom 1:7–12

Constantinescu T (2002) Le karst de la zone Mangalia et la Grotte de Monde (Dobrogea de Sud-Roumanie). Ann Valahia Univ Târgoviște Geogr Ser 2(1):147–156

Damm P (2000) Evolution of karst in the Valea Rea-Cornu Munților area (Bihor Mountains, NW Romania). In: Onac BP, Tămaș T (eds) Proceedings of the joint meeting "Friends of Karst" and "Theoretical and Applied Karstology". Presa Universitară Clujeană, Cluj-Napoca, pp 22–25

Diaconu G (1974) Quelques considérations sur la présence de l'anhydrite dans la grotte "Pestera Diana" (Băile Herculane-Roumanie). Trav Inst Spéol "Emile Racovitza" 13:191–194
Diaconu G, Marincea Ş, Dumitraş D (2008) Data on the Limanu Cave mineralogy, South Dobrogea. Trav Inst Spéol "Emile Racovitza" 47:65–77
Drăgănescu A, Ghenea A, Ghenea C, Mirăuţă E (1979) Geological map of Romania scale 1:50000 Gura Dobrogei sheet. Geology and Geophysics Institute, Bucharest
Dumitrescu M, Orghidan T, Tanasachi J, Georgescu M (1965) Contribuţii la studiul monographic al Peşterii de la Limanu. Trav Inst Spéol "Emile Racovitza" 4:21–58
Feier N (2003) New data on the mineralogy of Valea Rea Cave, Bihor Mountains. Ecocarst 4:22–24 (in Romanian)
Feru MU (1993) Considérations sur la génèse et la circulation des eaux thermominérales karstiques de la zone de Mangalia (Roumanie). Theor Appl Karstol 6:189–198
Feru MU, Capotă A (1991) Les eaux thermominérales karstiques de la zone de Mangalia (Roumanie). Theor Appl Karstol 4:143–157
Galdenzi S, Maruoka T (2003) Gypsum deposits in the Frasassi caves, central Italy. J Cave Karst Stud 65(2):111–125
Ghergari L, Tămaş T, Damm P, Forray F (1997) Hydrothermal paleokarst in Peştera din Valea Rea (Bihor Mountains, Romania). Theor Appl Karstol 10:115–125
Hill CA (1987) Geology of Carlsbad Cavern and other caves in the Guadalupe Mountains, New Mexico and Texas. New Mexico Bur Mines Min Res Bull 117:150
Hill CA, Forti P (1997) Cave minerals of the world, 2nd edn. National Speleological Society, Huntsville
Horoi V (1994) The corrosion process in "Peştera de la Movile" Cave (Southern Dobrudja – Romania). Theor Appl Karstol 7:189–194
Lascu C, Sârbu S (1988) La grotte de Taşaul et l'histoire géologique de la région Taşaul – vallée de la Casimcea. Bul Spéléo Club Paris XIV(2):21–24
Lascu C, Popa R, Sârbu S (1995) Le karst de Movile (Dobrogea de Sud) (II). Rev Roum Geogr 30:31–40
Lascu C, Constantin S, Lauritzen S-E (2000) Black Sea level oscillations based on preliminary U-series datings of submerged speleothems from Peştera Piatra (Central Dobrogea, Romania). In: Onac BP, Tămaş T (eds) Proceedings of the joint meeting "Friends of Karst" and "Theoretical and Applied Karstology". Presa Universitară Clujeană, Cluj-Napoca, pp 72–76
Marin C, Nicolescu T (1989) The geochemistry of groundwater from southeastern Dodrogea, Romania. Trav Inst Spéol "Emile Racovitza" 32:229–247
Mârza I, Silvestru E (1988) First mention of the hydrothermal karst phenomenon in Romania, associated to the Neogene metasomatic sulphide ore deposits from Rodna Veche. Studia UBB Geologia XXXIII(1):77–81
Mârza I, Nicolescu S, Gruescu C (1995) La magnétite – draperie stalactitique (formation de karst hydrothermal) du gisement de Ocna de Fier (Banat). Rom J Mineral 76:101–103
Nedopaca M, Grama C (1987) Mineralizaţiile hidrotermale cu cuarţ din peşterile de la Trestia-Baiţa (jud. Hunedoara). Bul Speol FRTA-CCSS 11:9–14
Onac BP (2002) Caves formed within Upper Cretaceous skarns at Băiţa Bihor County, Romania: mineral deposition and speleogenesis. Can Mineral 40:1693–1703
Onac BP (2013) The scientific relevance of mine, quarry, and mine caves of Romania: a review. Mem Ist It Speol II 28:135–154
Onac BP, Bengeanu M, Botez M, Zih J (1995) Preliminary report on the mineralogy of Peştera din Valea Rea (Bihor Mountains, Romania). Theor Appl Karstol 8:75–79
Onac BP, Kearns JB, Damm P, White WB, Matyasi S (2000) The first reported occurrence of metatyuyamunite—$Ca(UO_2)_2VO_4)_2$. 3-5H_2O in Romania. Rom J Mineral 80:5–10
Onac BP, Sumrall JB, Tămaş T, Povară I, Kearns JB, Dârmiceanu V, Vereş D, Lascu C (2009) The relationship between cave minerals and H_2S-rich thermal waters along the Cerna Valley (SW Romania). Acta Carsologica 38:27–39
Onac BP, Wynn JG, Sumrall JB (2011) Tracing the sources of cave sulfates: a unique case from Cerna Valley, Romania. Chem Geol 288(3–4):105–114
Onac BP, Effenberger HS, Wynn JG, Povară I (2013) Rapidcreekite in the sulfuric acid weathering environment of Diana Cave, Romania. Am Mineral 98:1302–1309. doi:10.2138/am.2013.4452
Povară I (1994) Characteristics of the water table topography in the southern part of the Romanian Black Sea Coast. Theor Appl Karstol 7:127–132
Povară I, Diaconu G, Goran C (1972) Observations préliminaires sur les grottes influencées par les eaux thermo-minérales de la zone Baile-Herculane. Trav Inst Spéol "Emile Racovitza" XI:355–365
Povară I, Simion G, Marin C (2008) Thermo-mineral waters from the Cerna Valley Basin (Romania). Studia UBB Geologia 53(2):41–54. doi:10.5038/1937-8602.53.2.4
Puşcaş CM, Onac BP, Effenberger HS, Povară I (2013) Tamarugite-bearing paragenesis formed by sulphate acid alteration in Diana Cave, Romania. Eur J Min 25(3):479–486. doi:10.1127/0935-1221/2013/0025-2294
Sarbu SM (2000) Movile Cave: a chemoautotrophically based groundwater ecosystem. In: Wilkens H, Culver DC, Humphreys WF (eds) Ecosystems of the world (Subterranean Ecosystems). Elsevier, Amsterdam, pp 319–343
Sarbu SM, Lascu C (1997) Condensation corrosion in Movile Cave, Romania. J Cave Karst Stud 59(3):99–102
Sarbu SM, Kane TC, Kinkle BK (1996) A chemoautotrophically based cave ecosystem. Science 272:1953–1955
Stoici S (1983) The Băiţa Bihor metallogenic district. Ed Academiei RSR, Bucureşti (in Romanian with extended English abstract)
Veliciu S, Năstăseanu S, Zamfir A (1983) Geothermal researches in the Cerna graben (Northern Segment). Geological report, IGG Archive, Bucharest
Vişan I, Tămaş T (2011) Mineralogy of caves from Dealul Popii (Rodnei Mountains, N. Romania). In: Proceedings of the 7th symposium on karst protection, Bela Palanka, Serbia, pp 7–8
Wynn JG, Sumrall JB, Onac BP (2010) Sulfur isotopic composition and the source of dissolved sulfur species in thermo-mineral springs of the Cerna Valley, Romania. Chem Geol 271(1):31–43. doi:10.1016/j.chemgeo.2009.12.009
Zih-Perényi K, Zih J, Damm PE, Szűcs Sz, Onac BP (2017) Valea Rea Cave. In: Ponta G, Onac BP (eds) Cave and karst systems of Romania. Springer, Berlin (accepted)

Fluid Flow Systems and Hypogene Karst of the Transdanubian Range, Hungary—With Special Emphasis on Buda Thermal Karst

17

Judit Mádl-Szőnyi, Anita Erőss, and Ádám Tóth

Abstract

Carbonate regions have great economic importance for water supply, oil and gas reservoirs, geothermal fluids and also Mississippi Valley-type ore deposits. Therefore, the understanding and consequences of flow pattern in carbonates require special interest. The hypogene and epigene karst areas of carbonate sequences were distinguished and associated with different orders of groundwater flow. However, the effect of confinement on flow pattern of carbonate aquifers was not fully considered in previous studies. We demonstrated the most important prerequisites and consequences of the application of the gravity-driven regional groundwater flow concept for carbonate sequences at different degrees of confinement. The results put into a frame the distribution of different springs and caves (epigene and hypogene) of the carbonate system of the Transdanubian Range, Hungary, and provide insights for better understanding of the hydrogeology of areas with similar unconfined and confined settings. Relationship among different flow regimes, distribution and character of springs and hypogene karstification processes, in addition to natural discharge-related phenomena, such as mineral and microbial precipitates, were recognized in the area of Buda Thermal Karst. This area is a natural laboratory where the connection between groundwater flow and karstification processes can be studied.

Keywords

Spring • Groundwater flow • Mineral and microbial precipitate • Confined and unconfined carbonate aquifers • Basinal fluid

1 Introduction

Deep and thick carbonate systems with different degrees of confinement constitute the most important thermal water resources in terrestrial areas outside of volcanic ranges (Goldscheider et al. 2010; Mádl-Szőnyi 2015; Mádl-Szőnyi and Tóth 2015). These deep and confined carbonate sequences are exposed to porosity enlargement processes, summarized under the term hypogene speleogenesis, involving various dissolution mechanisms, which was reviewed by Palmer (1991, 1995), Klimchouk (2000, 2012) and Goldscheider et al. (2010). Thermal and mineral waters of carbonate sequences are used by spas for recreation purposes all over the world. In addition, geothermal installations use these resources for electricity production and district heating (Mádl-Szőnyi 2015). Geothermal installations apply thermal water often with CH_4 combustion or with CO_2 sequestration (Han and McPherson 2009; Zhang et al. 2011).

Based on these considerations, it is a scientific and practical question to better understand why thermal water resources and hypogene karstification processes are so closely connected to terrestrial carbonate systems. The review paper of Goldscheider et al. (2010) dealt with this issue in a

J. Mádl-Szőnyi (✉) · A. Erőss · Á. Tóth
József and Erzsébet Tóth Endowed Hydrogeology Chair, Department of Physical and Applied Geology, Eötvös Loránd University, Pázmány P. stny. 1/C, Budapest, 1117, Hungary
e-mail: szjudit@ludens.elte.hu

© Springer International Publishing AG 2017

A. Klimchouk et al. (eds.), *Hypogene Karst Regions and Caves of the World*, Cave and Karst Systems of the World, DOI 10.1007/978-3-319-53348-3_17

comprehensive way. The authors pointed out the significance of the understanding of thermal water resources and hypogene karstification processes in the framework of hierarchical flow systems. In their Fig. 2 (Goldscheider et al. 2010), the hypogene and epigene karst areas are distinguished and complemented with supposed flow paths (cold, lukewarm and thermal) and different geochemical processes influencing hypogene karstification. The source of basinal fluids was supposed to lie in the basement, and the significance of terrestrial heat flow was also indicated. This figure is purely conceptual and is not based on any physically proven flow pattern.

Klimchouk (2007) was the first who put the potential dissolution processes in carbonates into the framework of the so-called Tóthian-type flow systems (Tóth 1999). The title of his Fig. 1 (Klimchouk 2007) was "Epigenic and hypogenic karst in the context of basinal groundwater flow." He also mentioned the constraints that "the figure shows mainly gravity-driven flow in an idealized homogeneous basin. In reality, most sedimentary sequences are highly heterogeneous, and gravity-driven flow interacts with other flow mechanisms." He recognized that epigene karstification corresponds to local flow systems while hypogene to regional or intermediate ones. However, based only on the two unconfined sub-basins of Tóth, the location and characteristics (chemical and temperature distribution) of thermal and lukewarm springs and the near-surface and underground locations of hypogene karstification cannot be properly explained.

This discrepancy was resolved by the conceptualization of Tóthian-type flow pattern for idealized connected confined and unconfined sub-basins based on the joint interpretation of numerical flow and heat transport simulation and spring analysis (Mádl-Szőnyi and Tóth 2015). Based on this adapted flow model in carbonate sequences, we can distinguish between those parts of the system where carbonates are partially covered with siliciclastic sediments (unconfined or semiconfined sub-basin) and those where carbonates are fully confined with dominantly siliciclastic sediments (with low hydraulic conductivity). In this system, the sub-basin where the carbonates can be found under thick siliciclastic sediments is, in fact, confined. The significance of the boundary between these two sub-basins was revealed explicitly based on flow and heat transport simulations in Mádl-Szőnyi and Tóth (2015). These two sub-basins and consequent heat and flow pattern can be handled as a new adaptation of Tóthian flow concept for carbonate sequences. With these settings, the numerically derived asymmetric flow pattern can explain the distribution of springs, the heat pattern and the mixing of basinal and fresh waters (of local, intermediate and regional flow systems) and the potential location of epigene and hypogene speleogenesis.

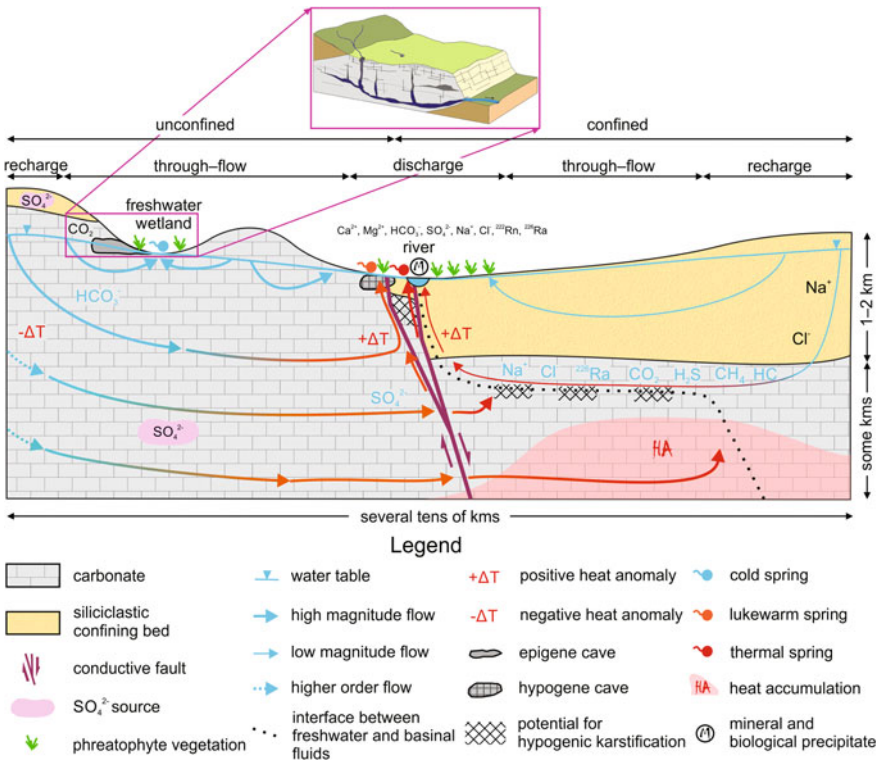

Fig. 1 Conceptual Tóthian-type GDRGF pattern for the boundary of unconfined and confined sub-basins. The consequences on flow-related manifestations imply that the shallow karst aquifer (*inset*; modified after Goldscheider and Drew 2007) is embedded into the regional flow pattern as a local system (after Mádl-Szőnyi and Tóth 2015)

The detailed explanation of Fig. 1 can be found in Mádl-Szőnyi and Tóth (2015).

The first part of this chapter demonstrates the most important prerequisites and consequences of the application of gravity-driven regional groundwater flow concept for carbonate sequences. The results are used to explain the distribution of different springs and caves (epigene and hypogene) of the carbonate system of the Transdanubian Range, Hungary, and provide insights for better understanding the hydrogeology of areas worldwide with similar unconfined and confined settings. The second part summarizes the relationship between flow regimes, springs and hypogene karstification processes for the Buda Thermal Karst. This area is a natural laboratory where the connection of groundwater flow and karstification processes can be studied.

2 Fluid Flow Systems and Hypogene Karstification in Confined and Unconfined Carbonate Ranges—Theoretical Considerations

2.1 Cross-Formational Flow and Confinement of Carbonates

Regarding the potential for the evolution of epigene and hypogene caves, the most decisive geological factor in carbonate sequences is the confinement of carbonate aquifers, in agreement with the findings of Klimchouk (2007). However, confinement usually refers only to the existence of thick siliciclastic cover above carbonate sequence, but does not reveal its influence on flow pattern and consequent fluid distribution in the system. Therefore, we have to understand the evolution of flow pattern in such regions to learn more about its effect on both epigene and hypogene karstification.

Especially, the cross-formational flow (ascending or descending vertical flow component) has great significance on hypogene karstification processes as it was highlighted by Klimchouk (2007). The direction and intensity of flow are determined by not only the hydraulic conductivity (aquifer or aquitard units) but also the driving forces determined by fluid potential (Hubbert 1940) differences.

We can assume a given basin with two (confined and unconfined) sub-basins and cross-formational flow driven by topographic differences operating in both parts. Until now, however, the physically based flow patterns were not derived for such situations because first, there were not enough measured data to reveal it and second, basin-scale numerical simulations were not available due to conceptual limitations since the applicability of equivalent porous medium (EPM) approach was formerly debated for carbonate sequences.

2.2 Heterogeneity of Permeability on Basin Scale

Owing to the heterogeneity of a karst aquifer in recharge and permeability pattern (matrix, fissured and enhanced permeability due to dissolution), difficulties arise in the adaptation of the gravity-driven regional groundwater flow (GDRGF) concept (LaMoreaux et al. 1975; Scanlon et al. 2003; Wellman and Poeter 2006). However, this issue can be overcome by focusing not on an individual aquifer and its detailed permeability distribution but on a carbonate system or basin with its enhanced permeability (see in details in Mádl-Szőnyi and Tóth 2017). In addition, heterogeneities of a basin need to be interpreted based on the consequences of artificial or natural changes of flow pattern (Tóth 1995). This requires a different basin-scale approach and methods compared to usual catchment or aquifer-scale consideration (Mádl-Szőnyi and Tóth 2015).

2.3 Hydraulic Continuity in Carbonates

Thick carbonate systems should be considered as hydraulically connected components of a carbonate basin with unconfined and confined subregions where water-table differences induce gravity-driven flow. The hydraulic continuity can be interpreted on a given timescale for a basin, if a change in hydraulic head at any point of the flow domain causes a head change at any other point, within the time interval of the observation (Tóth 1995). It was derived by Mádl-Szőnyi and Tóth (2015) that hydraulic continuity is more effective in carbonates as compared to siliciclastics due to the higher hydraulic diffusivity of carbonates. Consequently, artificial and natural changes in hydraulic head (and pressure) propagate at higher speed and over greater distances and depths in carbonate rocks than in clastic sediments.

2.4 Significance of Springs

Since springs are natural discharge features (Tóth 1971; Engelen and Kloosterman 1996; Ford and Williams 2007; Kresič and Stevanovič 2009; Tóth 2009b), they represent the termination of the underground flow paths. Consequently, their areal distribution and basic characteristics can help to understand the basinal hydraulic pattern of gravity-driven groundwater flow (which could be influenced by additional driving forces) in carbonate regions. If springs are considered in the context of flow systems, their regularities become clear. The most specific basic parameters are: elevation of spring discharge point, water temperature, total dissolved solids (TDS) and chloride content and volume discharge (Mádl-Szőnyi and Tóth 2015).

The elevation of discharge points of springs represents the hierarchy of the gravity-driven flow. Their exact location and topographic position can be used to delineate terminal zones of flow systems and to indirectly differentiate between flow systems of different orders. Cold karst springs theoretically have to discharge at the elevated parts of a basin, while lukewarm and thermal springs occur near the boundary of confined and unconfined carbonates (Mádl-Szőnyi and Tóth 2015). These springs are often related to marginal conductive structural elements.

In carbonate sequences, advective heat transport facilitated by flowing groundwater also affects the flow pattern (Domenico and Palciauskas 1973; Sass 2007). It can be simply supposed that the water temperature of springs is indicative of the order of flow, connected to local, intermediate and regional systems. Different driving forces, such as gravity, buoyancy (i.e., thermal convection or thermal density effect) can contribute to this, but their effects cannot be simply separated (Havril et al. 2016).

The water in unconfined karst systems has basically meteoric origin; therefore, the hydrogeochemical character of water in short (local) flow systems and in recharge areas of longer (intermediate or regional) flow systems has basically calcium–magnesium bicarbonate facies. The TDS for all gravity-driven flow systems generally increases along the flow paths. The ratio of SO_4^{2-}/HCO_3^- increases due to the decrease in the CO_2 of soil origin (Back 1966; Tóth 1999, 2009a). The sulfate can be of biotic or abiotic origin, from oxidation of sulfide minerals and hydrogen sulfide related to organic matter maturation, dissolution of gypsum and anhydrite, etc., and can appear in lukewarm and thermal waters (Langmuir 1971; Bretz 1949; Egemeier 1981; Hill 1987; Worthington and Ford 1995; Gunn et al. 2006). Toward the discharge areas (i.e., the springs), the chemical composition can change from calcium–magnesium and sodium bicarbonate–sulfate to sodium chloride in the confined karst. Thermal springs are characterized by elevated chloride content, and the deep origin of CO_2 and H_2S may also be characteristic for them (Goldscheider et al. 2010). Regarding the findings for the Transdanubian Range, the source of NaCl-type water in the systems was the thick, dominantly low-permeability siliciclastic confining layer. Its contribution to the underlying karst water is responsible for the appearance of additional basinal flow component. This "basinal fluid" can be represented by its chloride content as a conservative component of flow systems (Mádl-Szőnyi and Tóth 2015).

The magnitude, intensity and variability of spring discharge are topography dependent. Spring discharge is affected by geological conditions and climate as well. Therefore, the variability of spring discharge is also characteristic because springs fed by local flow systems supposedly display higher variability than those with a higher order of flow systems (Mádl-Szőnyi and Tóth 2015; Bodor et al. 2014). The variability of discharge of thermal springs, in general, is low, i.e., steady due to the buffering effect of the large storage capacity of the rock framework of the regional flow system (Klimchouk 2007; Tóth 2009a; Bodor et al. 2014).

2.5 Conceptual Flow Model and Connected Manifestations for an Unconfined and Confined Carbonate Basin

The flow is basically lateral in an unconfined carbonate system, with limited vertical flow components compared to siliciclastic basins, and the hierarchy of flow systems is not well developed (Fig. 1). In unconfined carbonates, the water has basically meteoric origin and the temperature of springs systematically increases toward the lowest elevation discharge point. The flow pattern at the margin of unconfined and confined carbonates is more complex due to the asymmetric recharge rates at the two sides. The "fresh" karst water, which originated from meteoric recharge through unconfined carbonates, is shifted toward the confined carbonates due to limited recharge across the confining strata. The limited meteoric recharge may flush some Cl^--rich basinal fluids from the low-permeability siliciclastic cover into the underlying carbonates, therefore creating an interface between "freshwater" and "basinal fluids" under the confined sub-basin. Along this interface the upwelling basinal fluids contribute to the chemical composition of thermal and partially lukewarm springs with dominantly meteoric origin. The interface of fresh and basinal fluids governed by gravity-driven flow and modified by other driving forces can be economically important due to potential for porosity enlargement and hydrocarbon and heat accumulation. The ^{226}Ra, ^{222}Rn and dissolved gas content (CO_2, H_2S and CH_4) of thermal springs originates from the "basinal fluid component." The hypogene karstification (connected porosity enlargement) can be related to those biogeochemical processes which appear along the interface between fresh and meteoric fluids. A basin-scale conceptual model was derived to summarize and generalize these findings. This model can explain the position of cold, lukewarm and thermal springs in a basin as well as their chemical facies. In addition to the hypogene and epigene karstification, mineral precipitates can be directly connected to this generalized flow pattern (Mádl-Szőnyi and Tóth 2015).

3 Fluid Flow Systems and Hypogene and Epigene Karst of the Transdanubian Range

The hydrogeologically complex thick carbonate system of the Transdanubian Range (TR) is located in the Central Pannonian Basin, Hungary, and bounded by tectonic lines and built up by thick Paleozoic metamorphic and Permian–Cretaceous sedimentary sequences; however, the Triassic–Early Jurassic carbonates form the main karst system of the area, which is dissected by major faults and influenced by folding. The carbonate range has 300 km × 100 km in extent (Csepregi 2007) and is partially confined by thick Neogene sediments mainly at the edges (Fig. 2).

The hydraulic continuity of the TR was inferred by long-term (1950–1990) mine dewatering (Alföldi and Kapolyi 2007) which has resulted in drying up of springs at the highest elevations and caused changes in chemical composition, temperature and spring discharge at lower elevations. In addition, the hydraulic head decrease could be followed on a regional scale for the whole reservoir (Csepregi 2007).

Cluster and discriminant analyses were carried out based on a database containing geodetical, volume discharge and chemical data of 800 springs before artificial intervention took place based on Hungarian Spring Register. Spring elevation, water temperature, chloride content and discharge data were used during the evaluation (Bodor et al. 2014). The derived groups were compared with the results of numerical simulations. Finally, springs were grouped into different flow systems (Mádl-Szőnyi and Tóth 2015) (Fig. 3).

The character and pattern of springs show a systematic distribution in the Transdanubian Range. The local flow-related spring groups can be found at the highest elevation (above 175 m asl); their temperature is lower than 12.2 °C; and there is no difference between their chloride content (<6 mg/l) based on medians of the different parameters of the groups. However, their discharge volume shows marked variations (1×10^{-4} to 6×10^{-4} m^3 s^{-1}). The springs of the second group are separated from local flow systems. Their discharge elevation is higher than 120 m asl, and their temperature is elevated, around 19 °C based on medians. These springs can be connected to intermediate flow systems. Finally, the springs with highest temperature (42.3 °C) and chloride content (154 mg/l) and lowest discharge elevation (104 m asl) can be connected to regional flow systems. The discharge volume cannot be interpreted directly in terms of flow systems (Mádl-Szőnyi and Tóth 2015).

Thermal springs related to deep regional flow systems can be found only in the NE margin of the system, along the River Danube. Lukewarm springs of intermediate flow systems discharge at or close to the boundary of the confined and unconfined parts of the system, whereas local flow relates to cold springs and discharges in the unconfined part of the system (Fig. 3) (Tóth and Mádl-Szőnyi 2016).

Taking into consideration the basin-scale distribution of epigene caves, it can be concluded that they are associated with the subsurface drainage of the unconfined system. Hypogene caves were developed or are developing at the boundary of confined carbonates. Inactive or dry hypogene caves occur at higher elevation in unconfined carbonates. This indicates a considerable erosion of siliciclastic cover and downward shift of the discharge zones related to the Late Miocene uplift (Haas 2001; Dombrádi et al. 2010).

4 Buda Thermal Karst: The Regional and Intermediate Discharge Area and Hypogene Karst Region of the Transdanubian Range

The northeastern regional and intermediate discharge zone of the TR is located close to the River Danube (Figs. 2 and 3). This particular part of the system, the Buda Thermal

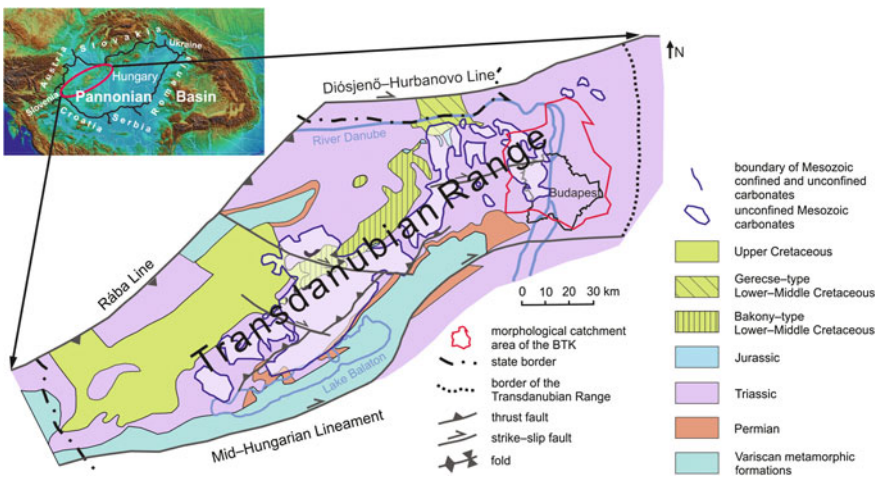

Fig. 2 Transdanubian Range Unit: boundaries of the range and the Paleozoic and Mesozoic formations with the indication of main structural features and the area of unconfined carbonates (modified after Fülöp in Haas 2001 and Fodor 2010) and also the morphologically delineated catchment area of Buda Thermal Karst (BTK) (after Mádl-Szőnyi et al. 1999)

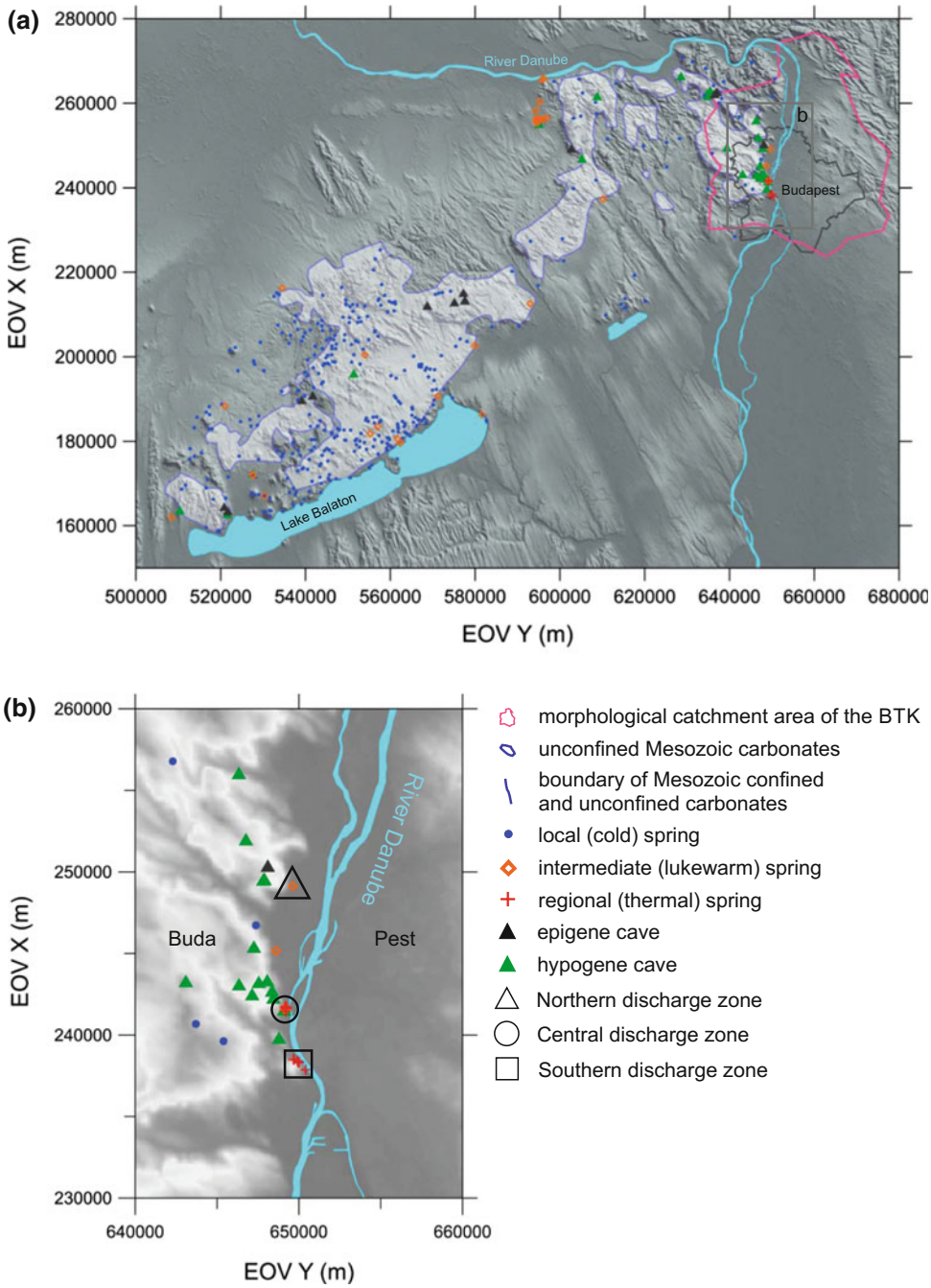

Fig. 3 **a** Surface manifestation of GDRGF for the TR. Springs are related to local (cold), intermediate (lukewarm) and regional (thermal) flow systems based on the classification of Mádl-Szőnyi and Tóth (2015). Location of epigene and hypogene caves is based on the data from the Hungarian Ministry of Agriculture and Rural Developments, Hungary (A. Gazda 2014, personal communication). The figure is complemented by the morphologically delineated catchment area of Buda Thermal Karst (BTK) (after Mádl-Szőnyi et al. 1999). **b** Spring groups and epigene and hypogene caves of Budapest and surroundings (EOV is the Hungarian National Grid which is a transverse Mercator projection—positive X is pointed to north and positive Y is pointed to east. Coordinates refer to meters)

Karst (BTK), is situated within and in the surroundings of Budapest. The area is strongly controlled by Cretaceous, Paleogene–Miocene, Miocene–Pliocene and Pleistocene structural elements, mainly normal and reversed faults trending in NW–SE, NE–SW and N–S directions (Fodor et al. 1994). These tectonic elements act as conduits or barriers and have strongly affected the paleo and recent fluid migration (Poros et al. 2012; Erőss et al. 2008; Havril et al. 2016). The tectonic boundary of unconfined and confined carbonates can be seen inside the morphologically delineated catchment area of BTK (Figs. 2 and 3a). This hydrogeological situation established the famous bath culture of Budapest and is responsible for the development of hypogene caves as well.

4.1 Gravity-Driven Flow Pattern and Fluid Components of BTK

The BTK area receives fluid from several sources (meteoric and basinal), in agreement with the conceptual model (Fig. 1). In addition to meteoric fluids, the contribution of

basinal fluids at the discharge area of the BTK was first suspected based on water chemical analyses of Alföldi (1979) and was proved based on recent fluid analyses by Erőss (2010), Erőss et al. (2012a) and on mineralogical and fluid inclusion studies by Poros et al. (2012). The origin of the basinal fluid was determined to be related to the confining layers of the carbonates. The mechanisms of its contribution to spring discharge were also revealed in the form of vertical downward leakage from the confining layer to carbonates and upward flow to the springs (Mádl-Szőnyi et al. 2015; Mádl-Szőnyi and Tóth 2015).

The discharging fluids from different origins (meteoric and basinal) with different flow systems (intermediate and regional) result in a wide range of discharge features including springs, caves and also mineral precipitates. Extensive hypogene cave systems have been developed (e.g., Takács-Bolner and Kraus 1989; Leél-Őssy 1995; Leél-Őssy and Surányi 2003; Leél-Őssy 2017, in this volume) and are actively forming at present due to the interaction between fluids and the carbonate rocks (Erőss 2010; Erőss et al. 2011b). Therefore, the BTK system can be considered as a prime example of an active hypogene karst (Erőss 2010).

The natural discharge of the system is manifested mainly in the form of springs along and in the riverbed of the River Danube (Fig. 3a) forming three distinct discharge areas and are strongly influenced by tectonic pattern (Alföldi et al. 1968; Ötvös et al. 2013; Erhardt et al. 2017). The Northern discharge zone of the BTK is characterized by lukewarm springs (18–24 °C, TDS < 1000 mg/l); in the Central zone both lukewarm (21–27 °C, TDS < 1000 mg/l) and thermal springs (53–63 °C, TDS > 1000 mg/l) occur, while in the Southern discharge area of the system temporally and spatially uniform thermal water discharge (33–45 °C, TDS 1500–1700 mg/l) is characteristic (Papp 1942; Alföldi et al. 1968; Erőss et al. 2008). The lukewarm springs were evaluated as belonging to intermediate flow systems and the thermal springs as the discharge of regional flow systems based on cluster analysis (Bodor et al. 2014) and numerical simulations (Mádl-Szőnyi and Tóth 2015).

Since the second part of the nineteenth century, deep wells were increasingly used in addition to natural springs. Déri-Takács et al. (2015) evaluated the waters in Budapest by multivariate exploratory techniques, and the influence of the temperature and chloride content was the strongest in grouping springs according to their characteristics. Besides the previously distinguished three temperature-based groups, which are reflecting the natural discharge conditions, an extra group of the deep wells was determined in the confined part of the system.

A comprehensive hydrogeological study was carried out for the characterization of processes acting presently and their resulting parameters at the discharge zone of the BTK (Erőss 2010; Erőss et al. 2011b, 2012a, b). Studying the attributes of springs and wells, caves, mineral precipitates, that is, the entire range of phenomena related to discharge (Tóth 1971), information can be obtained related to the parent flow system, its hydrogeological environment and the processes taking place throughout the entire length of the flow system and in the close vicinity of the discharge zone. Moreover, the identification and understanding of recently active processes and their manifestations in this hypogene karst area will help to identify and understand paleo-phenomena both in the BTK and in other hypogene karst areas with similar settings.

The relationships between flow systems and hypogene karstification were examined for the Central and Southern discharge zone, with further input from the deep wells for the characterization of the confined part of the system in Pest (Fig. 3b). Two distinct conceptual flow (Fig. 4a, b) and cave development models were developed for the Central and Southern discharge areas.

4.2 Flow Models and Fluid Components for Central and Southern Discharge Areas

According to hydraulic and hydrogeochemical studies and analyses of radionuclides, considerable differences were identified between the flow systems and discharging waters for Southern and Central systems (Erhardt et al. 2017; Erőss et al. 2012a, b).

Radionuclides (^{226}Ra and $^{234+238}$U) as natural tracers were used to characterize the different flow systems based on their different geochemical behavior: radium is mobile in reducing, and uranium in oxidizing conditions. Discharging waters of regional flow systems are characterized by reducing conditions and therefore with negligible uranium content, whereas local flow systems represent oxidizing environments and consequent low radium content. The radium content of waters in the Southern discharge area is in the range of 221–870 mBq/l, while in the Central discharge zone it is between 53 and 591 mBq/l. The uranium values in the Southern zone vary between 11 and 33 mBq/l, while in the Central discharge zone are in the range of 10–83 mBq/l (Erőss et al. 2012b). With the aid of radionuclides (^{226}Ra and $^{234+238}$U), the mixing end-members for the discharging waters of the Central system were identified: a meteoric end-member with an average temperature of 12 °C and 775 mg/l TDS, and a thermal end-member with a temperature of 76.5 °C and 1440 mg/l TDS, respectively (Fig. 4a). The thermal end-member has also dominantly meteoric origin (regional flow component) with additional basinal fluid component based on the numerically proved conceptual model (Fig. 1). The cold meteoric end-member could be identified due to a local flow component (Mádl-Szőnyi and Tóth 2015). Taking into consideration the derived flow systems, the cold meteoric end-member and the

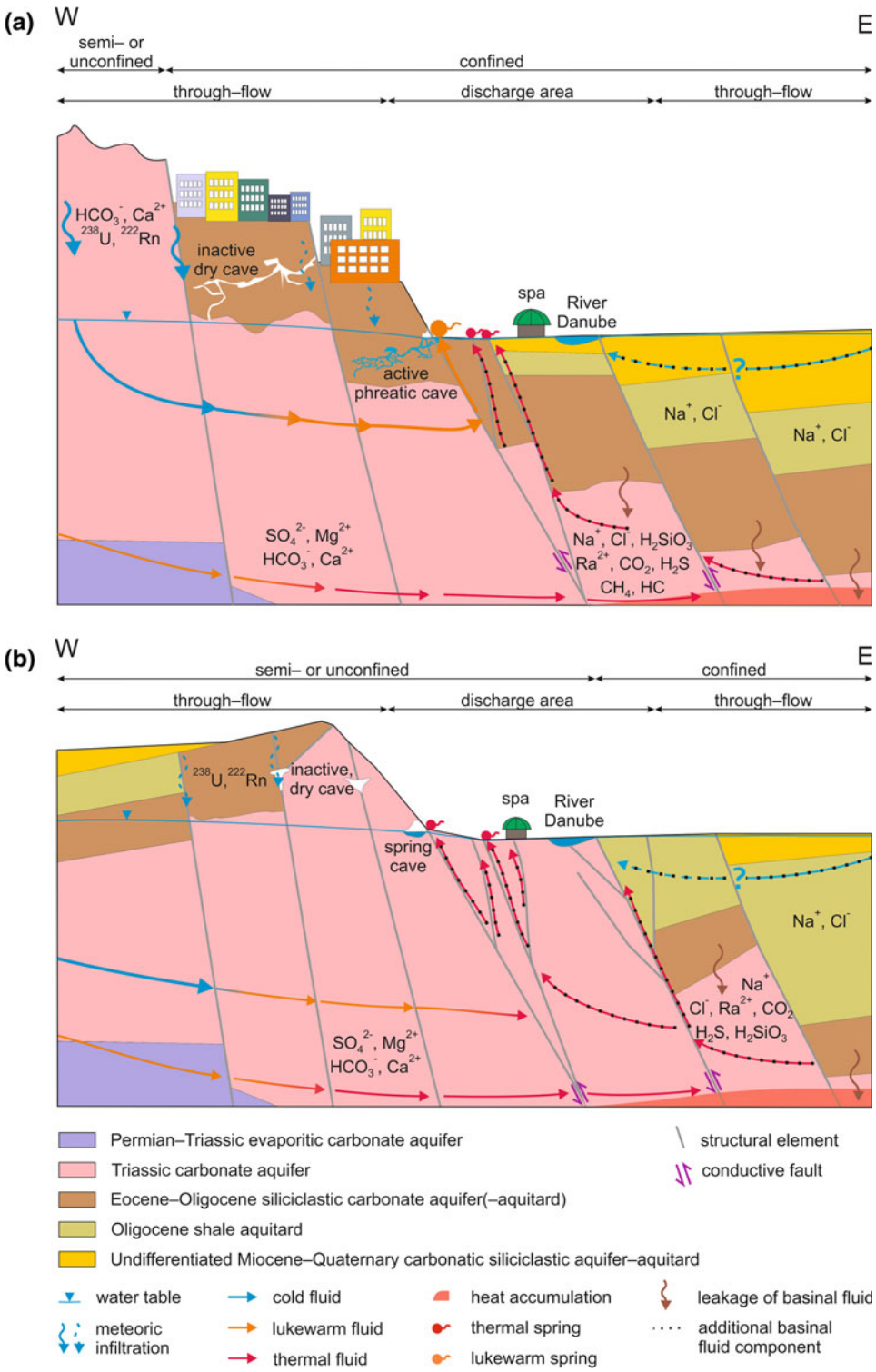

Fig. 4 Conceptual flow models: **a** Central system; **b** Southern system (modified after Erőss 2010 based on the generalized model of Mádl-Szőnyi and Tóth 2015)

thermal end-member represent different flow systems (local and regional) resulting different end-member composition.

For the Southern system, the thermal waters range from 35 to 47 °C temperature and 1400 to 1800 mg/l TDS, and only one component could be inferred with the help of the radionuclides (Erőss et al. 2012b) (Fig. 4b). Comparing the two systems, the Southern zone is characterized by elevated Ca^{2+}, Mg^{2+}, HCO_3^-, SO_4^{2-} and TDS content. These higher values correspond to lower temperatures within a narrower range (35–47 °C). The aforementioned differences

highlighted between the two areas are also apparent on the distribution of parameters in relation to depth. However, with regard to Na^+ and Cl^- (i.e., the basinal fluid component) there are no differences between the two systems.

The contribution of basinal fluids to the discharging waters of BTK was identified in the form of Na^+, K^+, Cl^-, H_2SiO_3, CO_2, H_2S, CH_4 and liquid hydrocarbons (Erőss 2010; Erőss et al. 2012a; Mádl-Szőnyi and Tóth 2015). The similar Na^+, Cl^- and CO_2 content of the waters in both systems also highlights the common basinal origin. However, slight differences were also identified between the two systems regarding the basinal components, e.g., no hydrocarbon was found in the Southern system (Erőss 2010).

The geochemical and temperature difference between the sub-systems is due to the slightly different hydrogeological environment. The recharge area of Central system is composed of large exposed carbonate surfaces facilitating the recharge and resulting in a larger volume (>10,000 m^3/day) of discharge of meteoric origin (Papp 1942; Alföldi et al. 1968). As opposed to the unconfined recharge area, the discharge area can be characterized by confined conditions; therefore, the discharge of the cold meteoric karst water and the upwelling thermal fluids is structurally controlled having an important effect on the mixing of these waters. Mixing can only occur through structures. Since the recharge area of the Southern system can be characterized by a limited surface of exposed carbonates, the meteoric contribution is also limited in the discharge area. Furthermore, a significant strike-slip fault and some hydrostratigraphical changes also impede water flow from the western recharge areas toward the discharge area (Erhardt et al. 2017). The natural discharge rate of the Southern system (3200 m^3/day; Papp 1942; Alföldi et al. 1968) is thus lower when compared to the Central system, reflecting differences in the recharge conditions.

4.3 Hypogene Karstification Processes for the Central and Southern Discharge Areas

In the Southern discharge area, due to the lack of mixing members, different processes are proposed to be responsible for the formation of the caves compared to the Central area. Based on hydrogeological considerations and recent microbiological investigations (Borsodi et al. 2012; Anda et al. 2014), microbially mediated sulfuric acid speleogenesis is proposed as the dominant cave-forming process for the Southern area (Erőss et al. 2011a, 2012a). This process is further supported by actively forming gypsum crusts on the cave walls above the water table.

Based on the radionuclide study, it can be confirmed that the dominant cave-forming process in the Central area is, indeed, mixing corrosion. According to the observed discharge characteristics at the Central discharge zone, where the discharge of lukewarm and hot springs were clearly separated and tectonically controlled, mixing could only exist either by dispersion or along faults. Therefore, the dissolutional porosity also has a strong structural control, as can be seen on the cave maps, the distribution of the passages following the main structural directions. This study highlights the importance of hydrogeological investigations in the understanding of cave formation.

4.4 Mineral and Microbiological Precipitates

Besides hypogene karstification processes, mineral precipitates can also be characteristic in discharge zones. Beside travertines, calcite-rich mud and rafts, gypsum crust and iron–manganese–hydroxides seem to be the most characteristic active geochemical byproduct at the Buda Thermal Karst. Iron–hydroxides are composed by poorly crystallized ferrihydrite and goethite, based on Mössbauer spectroscopy measurements (Erőss 2010; Kuzmann et al. 2014). The occurrence of iron–manganese–hydroxide precipitates may denote the mixing of anoxic deep waters and oxygen-rich meteoric waters in case of the Central zone as these precipitates were found in deep phreatic conditions. In the southern caves, they may be indicative of the presence of an oxidation zone, as they are found at the spring outlets.

The ^{226}Ra activity of the recent iron–hydroxide precipitate is 1460–3680 (±10%) Bq/kg (dolomite background: 45 Bq/kg). It was also proved that this iron–hydroxide is the source of the ^{222}Rn content of the discharging waters (Erőss 2010; Erőss et al. 2012b). Besides radium, accumulation of iron, manganese, arsenic and other trace elements (Pb, Cr, Cu, Ni, Zn, Mo, U) as biominerals on the surface of precipitate are observed in the discharge zones (Erőss 2010; Dobosy et al. 2016). According to Tazaki (2009), microbial mats can accumulate heavy metals and radionuclides through precipitation and complexation on and within the bacterial cell surface containing carboxyl and hydroxyl groups.

Iron–hydroxide precipitates were also found associated with calcite rafts in the dry paleo-caves of the BTK. It can therefore be deduced that the same principle may apply to ancient precipitates. The mineralogical composition of these old iron–hydroxide precipitates is dominantly goethite and can also be characterized by similar trace element content as the recent ones (Erőss 2010). Accordingly, their common

occurrence with calcite rafts in paleo-systems can be used as evidence of cave formation. This association thus can serve as a cave level marker and can be used to identify former hypogene cave discharge areas.

5 Summary and Conclusion

The evaluation of hypogene karstification in a flow system context can help to improve the understanding of associated processes in a comprehensive way. The numerical and conceptual adaptation of unconfined Tóthian-type flow for thick carbonate regions with unconfined and confined basinal settings (Mádl-Szőnyi and Tóth 2015) led to the identification of a very special asymmetric flow pattern with different (local, intermediate and regional) flow systems. These fluids have dominantly meteoric origin. Additionally, as a new factor, the contribution (via leakage) of basinal fluids from the confining cover in hypogene karstification was also proved and recognized. It could be also concluded that the underground interface between basinal and meteoric fluids is of special interest, because along this interface very different fluids with different origin (meteoric and basinal) can contribute to hypogene karstification (Mádl-Szőnyi and Tóth 2015). The physically based conceptual model can help to interpret the hypogene karstification as the manifestation of groundwater flow (Fig. 1).

The model is illustrated by the example of the Transdanubian Range, Hungary. The distribution of natural springs in the region can indicate the terminal zones of natural flow systems. Therefore, these discharge features have special significance in the understanding of flow patterns. Numerical simulations based on EPM approach can reveal the pattern of springs for the region (Mádl-Szőnyi and Tóth 2015). The comparison of clustering of springs and the derived flow systems for the TR led to good correlation between groups and flow systems. It was found that springs related to local flow systems appear at the elevated part of the range and are characterized by low chloride content and low, but increasing temperature toward the lower surface elevations. It was also shown that lukewarm and thermal springs appear close to and at the boundary of the confined and unconfined settings. The thermal springs appear at the lowest elevations, and they have the highest chloride content originated from basinal fluid contribution. The correlation between springs and epigene and hypogene caves as discharge features of groundwater flow was also demonstrated. The epigene caves can be found at the elevated part of the system; however, inactive hypogene caves can be found not only in the surroundings of thermal and lukewarm springs but also in a higher position than the recent boundary of unconfined and confined settings. This can be explained by the uplifting and erosion of the confining layers since the Late Miocene.

The correlation between flow systems and hypogene karstification was demonstrated on the example of Buda Thermal Karst. Hydraulic, hydrogeochemical and radionuclide studies revealed the flow pattern and fluid components for the BTK (Erhardt et al. 2017; Erőss et al. 2012a, b). Based on these data, distinct flow models were derived for the Central and Southern discharge areas (Erőss 2010; Erőss et al. 2012a). We can interpret the first model as characterized by intermediate and regional flow, while the latter as due to only regional flow. The origin of fluids is mostly meteoric, but additional basinal fluids from the confined basin also contribute. The differences in the chemical composition of discharging water can be explained by the differences in the hydrogeological environment of the BTK.

The distinct flow models could be connected to different dominant hypogene karstification processes. In the case of the Central discharge area, this is represented by mixing corrosion, while for the Southern discharge area microbially mediated sulfuric acid speleogenesis was found to be the dominant process. It was also recognized that not only karstification but also precipitation (in the form of calcite rafts and iron–hydroxide precipitate) can be correlated with the cave-forming process.

The example of Buda Thermal Karst in the frame of the Transdanubian Range demonstrates the importance of the flow system concept in hypogene speleogenesis. The flow model for confined and unconfined settings can be used to understand the connected subsurface and discharge-related processes in similar hypogene karst regions of the world. Furthermore, this knowledge can be used for planning thermal water utilization (Mádl-Szőnyi 2015).

Acknowledgements The research was supported by the Hungarian OTKA Research Fund (NK 101356).

References

Alföldi L (1979) Budapesti Hévizek. Thermal waters of Budapest. VITUKI Közl 20:1–102

Alföldi L, Kapolyi L (eds) (2007) Bányászati karsztvízszintsüllyesztés a Dunántúli-középhegységben [Mining-dewatering in the Transdanubian Range]. Geography Institute of Hungarian Academy of Sciences, Budapest

Alföldi L, Bélteky L, Böcker T, Horváth J, Korim K, Rémi R (eds) (1968) Budapest hévizei [Thermal waters of Budapest]. Hungarian Institute for Water Resources Research Budapest, Budapest

Anda D, Büki G, Krett G, Makk J, Márialigeti K, Erőss A, Mádl-Szőnyi J, Borsodi A (2014) Diversity and morphological

structure of bacterial communities inhabiting the Diana-Hygieia thermal spring (Budapest, Hungary). Acta Microbiol Immunol Hung 61(3):329–346

Andre BJ, Rajaram H (2005) Dissolution of limestone fractures by cooling waters: early development of hypogene karst systems. Water Resour Res 41:W01015

Back WB (1966) Hydrochemical facies and ground-water flow patterns in northern part of the Atlantic Coastal Plain. US Geol Survey Prof Pap 498A:42

Bodor P, Tóth Á, Kovács J, Mádl-Szőnyi J (2014) Multidimensional data analysis of natural springs in a carbonate region. Extended Abstract, EAGE/TNO workshop: basin hydrodynamic systems in relations to their contained resources, Utrecht, The Netherlands, 6–8 May 2015

Borsodi A, Knáb M, Krett G, Makk J, Márialigeti K, Erőss A, Mádl-Szőnyi J (2012) Biofilm bacterial communities inhabiting the cave walls of the Buda Thermal Karst System, Hungary. Geomicrobiol J 29(7):611–627

Bögli A (1964) Mischungskorrosion, ein Beitrag zur Verkarstungsproblem. Erdkunde 18:83–92

Bretz JH (1949) Carlsbad Caverns and other caves of the Guadalupe block, New Mexico. J Geol 57:447–463

Csepregi A (2007) A karsztvíztermelés hatása a Dunántúli–középhegység vízháztartására [The effect of water withdrawal on the water balance of the Transdanubian Range]. In: Alföldi L, Kapolyi L (eds) Bányászati karsztvízszintsüllyesztés a Dunántúli-középhegységben [Mining-dewatering in the Transdanubian Range]. Geography Institute of Hungarian Academy of Sciences, Budapest, pp 77–112

Déri-Takács J, Erőss A, Kovács J (2015) The chemical characterization of the thermal waters in Budapest, Hungary by using multivariate exploratory techniques. Environ Earth Sci 74(12):7475–7486. doi:10.1007/s12665-014-3904-3

Dobosy P, Sávoly Z, Óvári M, Mádl-Szonyi J, Záray G (2016) Microchemical characterization of biogeochemical samples collected from the Buda Thermal Karst System, Hungary. Microchem J 124:116–120

Dombrádi E, Sokoutis D, Bada G, Cloetingh S, Horváth F (2010) Modelling recent deformation of the Pannonian lithosphere: lithospheric folding and tectonic topography. Tectonophysics 484:103–118

Domenico PA, Palciauskas VV (1973) Theoretical analysis of forced convective heat transfer in regional ground-water flow. Geol Soc Am Bull 84:3803–3814

Dreybrodt W (1988) Processes in karst systems. Springer, Berlin

Egemeier SJ (1981) Cavern development by thermal waters. Nat Speleol Soc Bull 43:31–51

Engelen GB, Kloosterman FH (1996) Hydrological systems analysis: methods and applications. Kluwer, Dordrecht

Erhardt I, Ötvös V, Erőss A, Czauner B, Simon Sz, Mádl-Szőnyi J (2017) Hydraulic evaluation of the hypogenic karst area in Budapest (Hungary). Hydrol J doi:10.1007/s10040-017-1591-3

Erőss A (2010) Characterization of fluids and evaluation of their effects on karst development at the Rózsadomb and Gellért Hill, Buda Thermal Karst, Hungary. PhD thesis, Eötvös Loránd University

Erőss A, Mádl-Szőnyi J, Csoma ÉA (2008) Characteristics of discharge at Rose and Gellért Hills, Budapest, Hungary. Cent Eur Geol 51:267–281

Erőss A, Mádl-Szőnyi J, Csoma ÉA (2011a) New conceptual flow and cave development models of the Buda Thermal Karst (Hungary). In: Bertrand C, Carry N, Mudry J, Pronk M, Zwahlen F (eds) Proceedings H2Karst, 9th conference on limestone hydrogeology, Besancon (France). UMR 6249 Chrono-Environnement, pp 165–168

Erőss A, Mádl-Szőnyi J, Borsodi AK, Knáb M, Csoma ÉA, Mindszenty A (2011b) Results of in situ dissolution experiment to understand hypogenic karstification processes, Buda Thermal Karst, Hungary. In: Bertrand C, Carry N, Mudry J, Pronk M, Zwahlen F (eds) Proceedings H2Karst, 9th conference on limestone hydrogeology, Besancon (France). UMR 6249 Chrono-Environnement, pp 161–164

Erőss A, Mádl-Szőnyi J, Csoma ÉA (2012a) Hypogenic karst development in a hydrogeological context, Buda Thermal Karst, Budapest, Hungary. In: Maloszewski P, Witczak S, Malina G (eds) Groundwater quality sustainability. IAH selected papers on hydrogeology 17. Taylor and Francis, London, pp 119–133

Erőss A, Mádl-Szőnyi J, Surbeck H, Horváth Á, Goldscheider N, Csoma AÉ (2012b) Radionuclides as natural tracers for the characterization of fluids in regional discharge areas, Buda Thermal Karst, Hungary. J Hydrol 426–427:124–137

Fodor L (2010) Mezozoos-kainozoos feszültségmezők és törésrendszerek a Pannon-medence ÉNy-i részén: módszertan és szerkezeti elemzés [Stress-fields and structural settings in the NW Pannonian Basin: Methods and structural analysis]. PhD thesis, Magyar Tudományos Akadémia

Fodor L, Magyari Á, Fogarasi A, Palotás K (1994) Tercier szerkezetfejlődés és késő paleogén üledékképződés a Budai-hegységben. A Budai-vonal új értelmezése (Tertiary tectonics and Late Paleogene sedimentation in the Buda Hills, Hungary. A new interpretation of the Buda line) [in Hungarian]. Földtani Közlöny 124(2):130–305

Ford DC, Williams PDW (2007) Karst hydrogeology and geomorphology. Wiley, Chichester

Goldscheider N, Drew D (2007) Methods in Karst hydrogeology. IAH international contributions to hydrogeology. Taylor & Francis, London

Goldscheider N, Mádl-Szőnyi J, Erőss A, Schill E (2010) Review: thermal water resources in carbonate rock aquifers. Hydrogeol J 18 (6):1303–1318

Gunn J, Bottrell SH, Lowe DJ, Worthington SRH (2006) Deep groundwater flow and geochemical processes in limestone aquifers: evidence from thermal waters in Derbyshire, England, UK. Hydrogeol J 14:868–881

Haas J (ed) (2001) Geology of Hungary. Eötvös University Press, Budapest

Han WS, McPherson BJ (2009) Optimizing geologic CO_2 sequestration by injection in deep saline formations below oil reservoirs. Energ Conv Manag 50(10):2570–2582

Havril T, Molson J, Mádl-Szőnyi J (2016) Evolution of fluid flow and heat distribution over geological time scales at the margin of unconfined and confined carbonate sequences. Mar Pet Geol 78:738–749. doi:10.1016/j.marpetgeo.2016.10.001

Hill CA (1987) Geology of Carlsbad Cavern and other caves in the Guadalupe Mountains, New Mexico and Texas. NM Bureau Mines Min Resour Bull 117:150

Hubbert MK (1940) The theory of ground-water motion. J Geol 48 (8):785–944

Klimchouk AB (2000) Speleogenesis under deep-seated and confined settings. In: Klimchouk A et al (eds) Speleogenesis: evolution of Karst Aquifers. National Speleological Society, Huntsville, pp 244–260

Klimchouk AB (2007) Hypogene speleogenesis: hydrogeological and morphogenetic perspective. Special paper no. 1, National Cave and Karst Research Institute, Carlsbad, NM

Klimchouk AB (2012) Speleogenesis, hypogenic. In: Culver DC and White WB (eds.), Encyclopedia of caves, 2nd edn. Elsevier, Academic Press, Chennai, pp 748–765

Kresič N, Stevanovič Z (2009) Groundwater hydrology of springs: engineering, theory, management, and sustainability. Elsevier, Amsterdam

Kuzmann E, Homonnay Z, Kovács K, Zsabka P, Erőss A, Mádl-Szőnyi J (2014) Mössbauer study of biofilms formed at spring caves of Buda Karst, Hungary. Hyperfine Interact 226(1–3):571–577

LaMoreaux PE, LeGrand HE, Stringfield VT, Tolson JS (1975) Progress of knowledge about hydrology of carbonate terranes. Alabama Geol Surv Bull 94, part E

Langmuir D (1971) The geochemistry of carbonate ground waters in central Pennsylvania. Geochim Cosmochim Acta 35:1023–1045

Leél-Őssy Sz (1995) A Rózsadomb és környékének különleges barlangjai (Particular caves of the Rózsadomb Area) [in Hungarian]. Földtani Közlöny 125(3–4):363–432

Leél-Őssy Sz, Surányi G (2003) Peculiar hydrothermal caves in Budapest, Hungary. Acta Geol Hung 46(4):407–436

Leél-Őssy Sz (2017) Caves of the Buda Thermal karst. In: Klimchouk AB, Palmer AN, De Waele J, Auler AS, Audra P (eds) Hypogene Karst Regions and Caves of the World. Springer International Publishing

Mádl-Szőnyi J (2015) Genesis and utilization of thermal flow in deep carbonate systems. In: Stevanovic Z (ed) Karst aquifers—Characterization and engineering. Springer International Publishing, Cham, pp 654–667

Mádl-Szőnyi J, Tóth Á (2015) Basin-scale conceptual groundwater flow model for an unconfined and confined thick carbonate region. Hydrogeol J 23(7):1359–1380. doi:10.1007/s10040-015-1274-x

Mádl-Szőnyi J, Tóth Á (2017) Topographically driven fluid flow at the boundary of confined and unconfined sub-basins of carbonates: basic pattern and evaluation approach. In: Renard P, Bertrand C (eds) EuroKarst 2016, Neuchâtel, advances in the hydrogeology of karst and carbonate reservoirs. Springer, Switzerland

Mádl-Szőnyi J, Király L, Müller I, Pethő S, Baross G, Faragó É, Halupka G, Nyúl K in Mindszenty A (ed) (1999) A Rózsadombi termálkarszt monitoring működtetése (Operation of the monitoring system in the Rózsadomb area). Unpublished report, 2nd part (in Hungarian). ELTE TTK Alkalmazott és Környezetföldtani Tanszék, Budapest

Mádl-Szőnyi J, Pulay E, Tóth Á, Bodor P (2015) Regional underpressure: a factor of uncertainty in the geothermal exploration of deep carbonates, Gödöllő Region, Hungary. Environ Earth Sci 74 (12):7523–7538

Ötvös V, Erhardt I, Czauner B, Erőss A, Sz Simon, Mádl-Szőnyi J (2013) Hydraulic evaluation of the flow system of Buda Thermal karst, Budapest, Hungary. In: Szőcs T, Fórizs I (eds) Proceedings of the IAH Central European groundwater conference 2013. Szeged University Press, Szeged, pp 135–136

Palmer AN (1991) Origin and morphology of limestone caves. Geol Soc Am Bull 103:1–21

Palmer AN (1995) Geochemical models for the origin of macroscopic solution porosity in carbonate rocks. AAPG Special Volume 77-101

Papp F (1942) Budapest meleg gyógyforrásai [Thermal medicinal springs of Budapest]. A Budapesti Központi Gyógy- és Üdülőhelyi Bizottság Rheuma és Fürdőkutató Intézet Kiadványa [Book of the Central Resort Spa and Rheumatology Research Institute], Budapest

Plummer LN, Wigley TML, Parkhurst DL (1978) Kinetics of calcite dissolution in CO_2-water systems at 5 °C to 85,560 °C and 0.0 to 1.0 atm CO_2. Am J Sci 278(2):179–216

Poros Z, Mindszenty A, Molnár F, Pironon J, Győri O, Ronchi P, Szekeres Z (2012) Imprints of hydrocarbon bearing basinal fluids on a karst system: mineralogical and fluid inclusion studies from the Buda Hills, Hungary. Int J Earth Sci 10:429–452

Sass I (2007) Geothermie und Grundwasser [Geothermics and groundwater]. Grundwasser 12(2):93

Scanlon BR, Mace RE, Barrett ME, Smith B (2003) Can we simulate regional groundwater flow in a karst system using equivalent porous media models? Case study, Barton Springs Edwards aquifer, USA. J Hydrol 276(1):137–158

Takács-Bolner K, Kraus S (1989) A melegvizes eredetű barlangok kutatásának eredményei (Results of research into caves with thermal water origins) [in Hungarian]. Karszt és Barlang 1–2:61–66

Tazaki K (2009) Observation of microbial mats in radioactive hot springs. Sci Rep Kanazawa Univ 53:25–37

Tóth J (1971) Groundwater discharge: a common generator of diverse geologic and morphologic phenomena. IASH Bull 16(1–3):7–24

Tóth J (1995) Hydraulic continuity in large sedimentary basins. Hydrogeol J 3(4):4–16

Tóth J (1999) Groundwater as a geologic agent: an overview of the causes, processes, and manifestations. Hydrogeol J 7:1–14

Tóth J (2009a) Gravitational systems of groundwater flow theory, evaluation, utilization. Cambridge University Press, Cambridge

Tóth J (2009b) Springs seen and interpreted in the context of groundwater flow-systems. GSA annual meeting 2009, Portland, 18–21 Oct 2009. Geol Soc Am Abst Prog 41(7):173

Tóth Á, Mádl-Szőnyi J (2016) Scale-dependent evaluation of an unconfined carbonate system—Practical application, consequences and significance. In: Stevanovic Z, Kresic N, Kukuric N (eds) Karst without boundaries, IAH—Selected papers on hydrogeology 23. CRC Press, Taylor and Francis, London, pp 199–214

Wellman TP, Poeter EP (2006) Evaluating uncertainty in predicting spatially variable representative elementary scales in fractured aquifers, with application to Turkey Creek Basin, Colorado. Water Resour Res 42(8):W08410

Worthington SRH, Ford DC (1995) High sulfate concentrations in limestone springs: an important factor in conduit initiation? Environ Geol 25:9–15

Zhang G, Taberner C, Cartwright L, Xu T (2011) Injection of supercritical CO_2 into deep saline carbonate formations: predictions from geochemical modeling. SPE J 16(4):959–967. doi:10.2118/121272-PA

Caves of the Buda Thermal Karst

18

Szabolcs Leél-Őssy

Abstract

The Buda thermal karst is one of the most characteristic hypogene karst systems of the world developed in Triassic and Eocene limestone and marl in Budapest, on the right side of the Danube, under 300–400 m high hills. Due to the mixing corrosion enhanced by CO_2 and perhaps sulfuric acid, the water circulation formed multi-storey cave systems with different morphologies and complicated layout along the tectonic fissures. The arrangement of caves is independent of surface topography. The world-famous medicinal waters of Budapest come to the surface through cave passages. Due to the incision of the Danube and the uplift of the area in the Pleistocene, most passages are presently dry; now they lie 100 m above the Danube, though there are still passages below the water-table. The length of the five largest known caves and about 100 smaller ones reaches 55 km, and it is reasonable to estimate the length of unknown underground passages to be comparable. Caves are characterized by complex morphology, suggesting the formation by rising flow, and by rich carbonate-sulfuric mineral precipitations. Some of them (e.g. barite and calcite veins) are associated with bedrock formation and thus predate the cave forming process. There are minerals that precipitated from the warm water that dissolved the cave (Fe- and Mn-containing minerals formed by bacterial colonies, or cave rafts and folia). Evaporitic precipitations (e.g. popcorns, and frostworks) are remarkable. There are frequent precipitations of gypsum (chandeliers, gypsum flowers, etc.) due to the pyrite content of the marl above the passages. Discovering the concealed and hidden caves since the early twentieth-century was helped by quarries and earthworks followed by systematic and deliberate exploration.

Keywords

Budapest • Tectonic preformation • Mixing corrosion: solution forms • Carbonate-sulfate minerals

1 Introduction

The first cave known in the area of present Budapest was Sziklatemplom ("rock church") on Gellért Hill (Adamkó et al. 1992). Its 10-m high open mouth could be seen from a great distance. The cave was inhabited through centuries, and there was even a building inside.

All the other caves were concealed, entranceless caverns, which were later opened artificially and then explored deliberately and systematically. János Molnár discovered the first hypogene cave in 1857. He only explored the dry 20 m upper storey of the vertical cave, the bottom of which reaches the active part of the 7 km long cave. This cave was named after him.

S. Leél-Őssy (✉)
Department of Physical and Applied Geology, Eötvös Loránd University, Budapest, Hungary
e-mail: losz@geology.elte.hu

© Springer International Publishing AG 2017
A. Klimchouk et al. (eds.), *Hypogene Karst Regions and Caves of the World*,
Cave and Karst Systems of the World, DOI 10.1007/978-3-319-53348-3_18

The expanding city demanded a large amount of stones and cement at the turn of the nineteenth and twentieth-century. Numerous quarries were opened in the Rózsadomb, in the Pál Valley. The stone quarries sometimes excavated 40–50 m long galleries into the hills opening up several cavities that were created by the dissolving action of warm water. Later, hikers and cavers came to explore these cavities, which resulted in discovering increasingly larger caves. First a few 100 m long passage of Harcsaszájú ("catfish mouth") Cave was discovered in 1902. After 1904, 1 km of passages was explored in Pál-völgy Cave, then the 2 km Szemlő-hegy Cave in 1930. Several kilometers of passages in Mátyás-hegy Cave were found by the end of the 1930s. In the meantime, in 1933, Ferenc-hegy Cave was discovered during canalization. After World War II, the groundworks led to new discoveries, the most valuable of which was József-hegy Cave found in 1984. The technical advance of scuba diving equipment made it possible to explore the underwater parts of Molnár János Cave after 1972. The development of geophysical methods and the improvement of cave exploration equipment fostered the research of known cavities at the turn of the millennium.

Today, after exploring the connections between several separate caves, the area of the Buda Thermal Karst (BTK) includes five larger systems (Pál-völgy Cave System, Molnár János Cave, József-hegy Cave, Ferenc-hegy Cave and Szemlő-hegy Cave) and about one hundred smaller and larger caves with a total length of around 55 km (Leél-Őssy 2015). The Vár Cave on Castle Hill merits a special mention: this 3 km system was artificially created by connecting small caverns, which singularly extended only over a few tens of meters.

2 The Study Area

On the eastern slopes of the Buda Hills, three groups of active lukewarm-warm springs are known along the right bank of the Danube (see Mádl-Szőnyi et al. Chap. 17). These are from north to south: Csillaghegy springs (Northern system), József-hegy springs (Central system) and Gellérthegy springs (Southern system). The group of inactive springs of Vár Hill, that deposited a layer of 6–10 m thick travertine between 350 and 190 ka BP (Krolopp et al. 1976), is located between the latter two groups of springs. Towards the end of the period during which these springs were active, when the water could not rise up to the surface anymore due to hydrodynamic reasons, the waters dissolved small and isolated, merely 0.5–1 m high cavities in the travertines, in the lower part of this freshwater limestone, above the underlying Buda Marl.

No cave passages are known in the northern group of springs, but several fossil spring channels were identified in the József-hegy group of springs, which includes all the known larger caves of the area (Fig. 1a).

The springs of the thermal baths at the foot of Gellért Hill (Gellért Bath, Rudas Bath, and Rác Bath) dissolved only smaller caves (between a few meters and a few tens of meters) due to the disadvantageous lithological setting (lack of limestone) and the different main cave forming processes (Erőss 2010) (Fig. 1b).

It is mainly in the József-hegy group of springs that the water dissolved larger cavities in an area of five to six square kilometers. There are substantial caves up to 2 km away from the present riverbed of the Danube.

Due to continuous rising of the area since the Pliocene and the lowering of the karst water table associated with the incision of the Danube, a few of these caves are located up to 60–100 m above the Danube (approximately, the present karst water table). The vertical extension of the largest explored caves exceeds 100 m.

3 Geological Setting of the Caves

The oldest rocks of the area, which are also visible on the surface, were formed in the Upper Triassic more than 200 million years ago at the northern side of the Tethys Ocean, mostly in the neritic zone. These older rocks include the compact textured whitish Dachstein Limestone, poor in microfossils, and the Main Dolomite, which consist of the accumulation of the skeletons of marine organisms. The Dachstein Limestone outcrops at the surface a few kilometers west of the caves of Rózsadomb, and only contains small caves (Fig. 2).

The fractured, whitish-greyish Main Dolomite is poor in macroscopic fossils (small ammonites can be found at some places). This rock also appears in the immediate neighbourhood of Rózsadomb, but no cavities are known there. Minor spring caves (e.g. the cavity of Török Spring) were formed in this rock only in the area of Gellért Hill.

The layers of the Mátyáshegy Formation are built up of limestone, dolomite and marl, which all deposited in deeper water. They are visibly folded and contain a significant amount of chert originated from siliceous sponges (Haas 2004; Esteban et al. 2009). The chert can be as big as a fist and occurs in nodules that are found parallel to the layers. No macroscopic fossils were found in it. On the surface of Triassic carbonates, there is a distinct discordancy.

The following known rocks are 150–160 million years younger. It is not clear when the area became subaerial or what amount of sediments was removed by erosion. In any case, there are no sediments found from the Jurassic or Cretaceous. At the end of the Eocene, about 40 million years ago, significant transgression followed. At the foot of the cliffed shores, several-meter thick abrasion

Fig. 1 **a** Caves and cave passages (cave-polygons) longer than 1 km of Rózsadomb (data from the National Cave Register map: satellite image by Google Earth IKONOS), compiled by Magdolna Virág; **b** caves and cave passages (cave-polygons) longer than 1 km of Gellért Hill (data from the National Cave Register map: satellite image by Google Earth IKONOS), compiled by Magdolna Virág

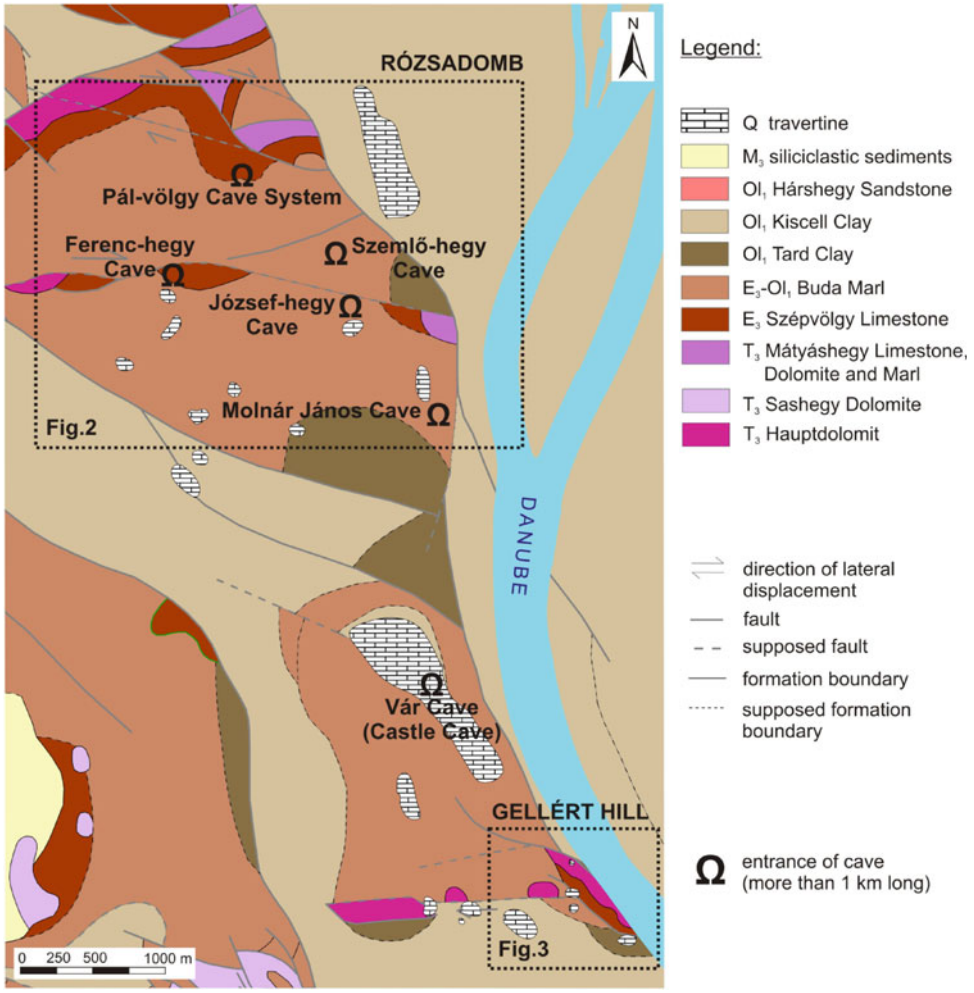

Fig. 2 Geological map of the Buda Thermal Karst (modified after Fodor in Mindszenty et al. 2000) without quaternary deposits with the exception of travertines (Wein 1977; Kele et al. 2009, 2011). The studied and discussed areas are indicated. Compiled by Magdolna Virág

breccia (mainly from the chips of chert) and abrasion conglomerate (mainly from the carbonate debris) accumulated in lacustrine distribution (Wein 1977).

With the deepening of the sea, somewhat clayey layers of the sublittoral Szépvölgy Limestone of platform facies deposited generally in 40–60 m, maximum up to 100-m in thickness. This rock contains a significant amount of macrofossils: the larger foraminifers (mainly Nummulites and Discocyclina) are the most characteristic ones—the original name of this rock was Nummulitic limestone. The layers appear in meter thick beds. The majority of cave passages in the Rózsadomb area have formed in this rock. The further deepening of the sea facilitated the settling of clay grains in larger quantities, and the Szépvölgy Limestone was covered by the Buda Marl. This formation was up to several hundred meters thick, and its basal layers are rich in carbonates (calcareous marl). The base of the Buda Marl still contains cave passages (the majority of the passages in Molnár János Cave developed in this rock) and forms a transition between the Szépvölgy Limestone and the more clayey, typical Buda Marl. It occurs also on Gellért Hill; Citadella Crystal Cave develops entirely in this rock. It covers the dolomite in the southern side of the hill in 10–20 m thick layers; chips of chert can also be found in it.

The proportion of clay grains in the sediment increased as the sea gradually deepened. The typical Buda Marl can already be qualified as clayey marl; there are no cave passages in it. This rock frequently contains limestone interbeddings, derived from re-sedimented calcareous mud transported from shallow waters to the deeper sea by submarine slides.

After settling, Tard Clay deposited in the area of Rózsadomb, Castle Hill and Gellért Hill. A short, few million-year old subaerial period (Telegdi-Roth 1914) was followed by transgression, which left behind the Hárshegy Sandstone (silica sand and silica pebbles), which is several 100 m thick and serves as the base of the Kiscell Clay, which was formed in a deeper sea. The cave passages developed after the Kiscell Clay was denuded (Kovács and Müller 1980). This rock can be found on the surface outside

of the two NW–SE faults bordering the uplifted karst of Rózsadomb, and commonly occurs on the left side of the Danube, under the Pest Plain. The Kiscell Clay can also be found on Gellért Hill and Castle Hill.

The younger sediments (from the late Oligocene and early Miocene) are clayey sandy layers formed in brackish water and normal saline water (Báldi 1986). The carbonate layers were formed in normal saline water in the mid Miocene and in brackish water in the late Miocene. These rocks are absent from the Rózsadomb area, though the Törökbálint Sandstone from the late Oligocene can be found on Gellért Hill.

The youngest rock in the study area is the freshwater limestone (travertine), which is quite common in small occurrences (Kele et al. 2009, 2011). This rock precipitated from spring-waters, sometimes from smaller lakes; it has a porous structure with whitish and sometimes yellowish color due to its clay content. It occurs at dozens of sites in Rózsadomb, but always locally, and the size of occurrences is just a few tens of meters. Travertine occurs also on the top of Gellért Hill in similar extension, but the plateau of Castle Hill is completely built up of this 6–8 m thick rock. There are caves found below some of its surface occurrences.

4 Tectonics Features in the Caves

The main directions of passages in the caves of Buda are usually NE–SW and NW–SE: e.g., Ferenc-hegy Cave, Pál-völgy Cave System (Fig. 3a). However, numerous passages run E–W (e.g. József-hegy Cave). In fact, the caves indicate the major tectonic directions since the upwelling and descending branches of water circulation systems preferentially migrated along the fracture systems related to former stress fields, dissolving their walls.

The caves of the Rózsadomb area, which belong to the József-hegy Spring Group, the area richest in caves in the BTK, are marked by two roughly NW–SE-trending faults, which meet at an angle of 20°–25° (Wein 1977). Kiscell Clay covers the surface in an area several-hundred meters to the NE and SW of the faults. This area of 5–6 km^2 is bordered by the Danube in the east and a NE–SW-trending fault in the NW on Látó Hill. There are also numerous N–S faults in the area. Inside József-hegy Cave, there are even 30 m differences in the level of the Triassic–Eocene boundary (Fig. 4a). The main fissures in the caves (particularly in Szemlő-hegy Cave and József-hegy Cave) are en-echelon fractures (Fodor et al. 1991, Fig. 3b): every subsequent parallel fissure is somewhat shifted to the east. The main fissures in József-hegy Cave have directions of 82° and 92°; they developed in the right-lateral shear zone of ENE–SSW strike produced by the NW–SE compressions and NE–SW extensions during the Oligocene—early Miocene (Fodor et al. 1991). The thermal water could come up to the surface along the E–W right-lateral displacements (which can be explained as secondary Riedel shears) and the NW–SE-trending tension faults; thus, with the help of mixing corrosion, the water was able to dissolve the passages. The main fractures of the caves follow these secondary Riedel shears and they also preserve their en-echelon pattern. In the openings of the primary NW–SE fissures, barite veins precipitated either in the early Oligocene some 34–30 million years ago (Báldi 1986) or were associated with andesitic volcanism in the Badenian about 15–14 million years ago (Müller 1989; Fodor et al. 1991; Molnár and Gatter 1994).

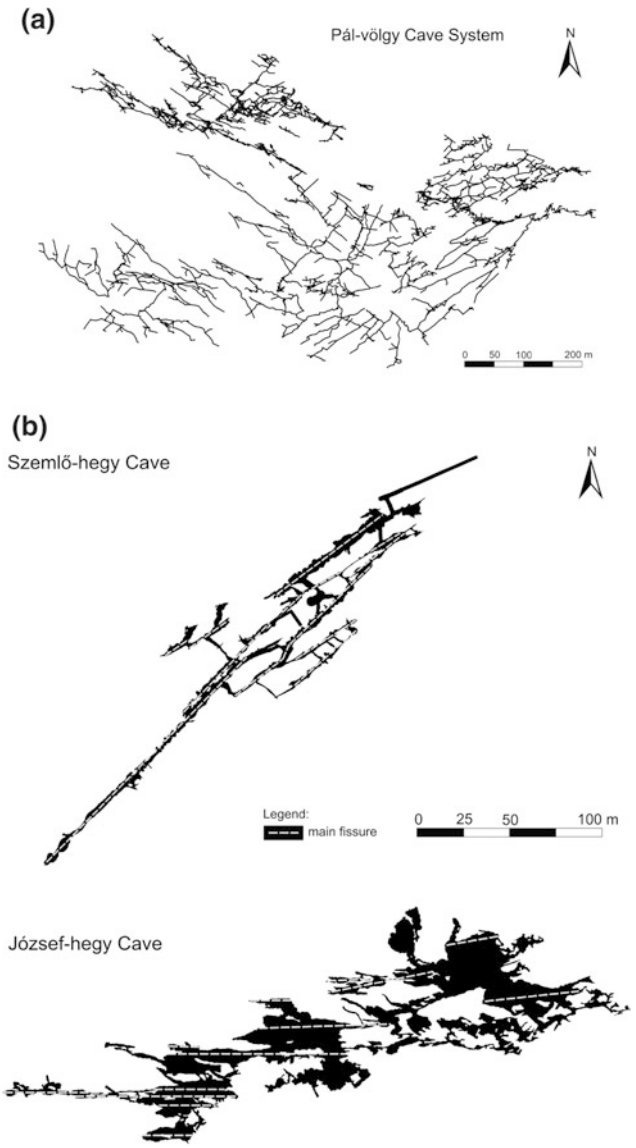

Fig. 3 **a** Survey lines (cave-polygon) of the Pál-völgy cave system (speleological data from the National Cave Register map). Compiled by Magdolna Virág; **b** survey lines (cave-polygon) of Szemlő-hegy Cave and József-hegy Cave (speleological data from the National Cave Register map). Compiled by Magdolna Virág

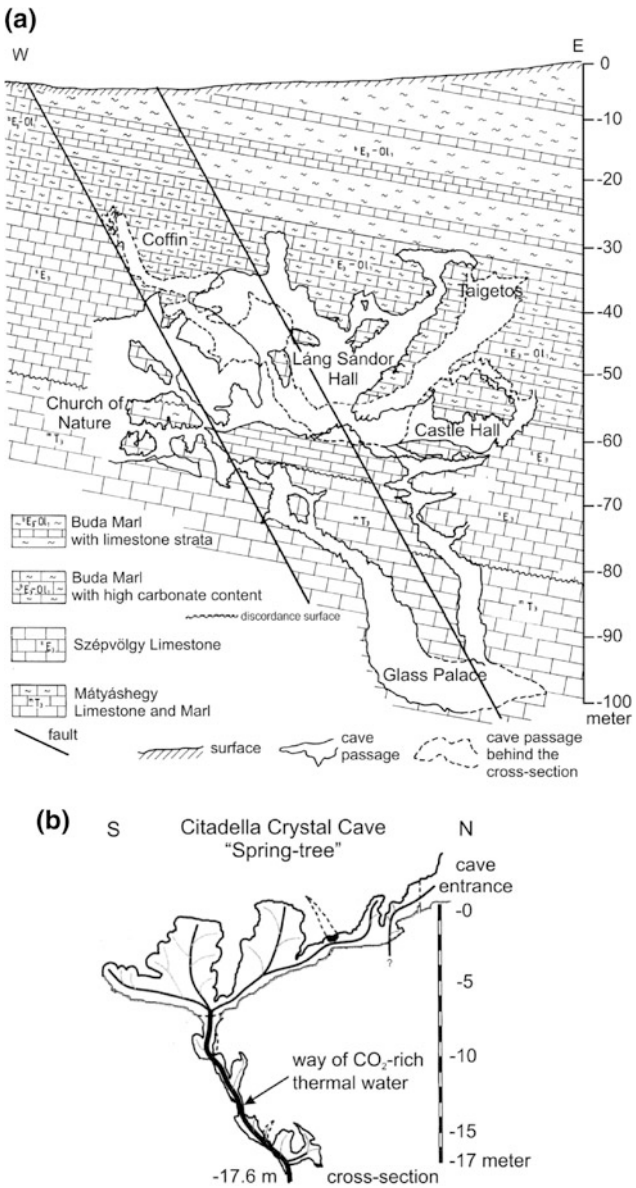

Fig. 4 **a** Spring tree of Citadella Crystal cave (after Leél-Őssy Cs et al. 2007); **b** cross-section of the central part of József-hegy Cave (after Leél-Őssy Sz 1997)

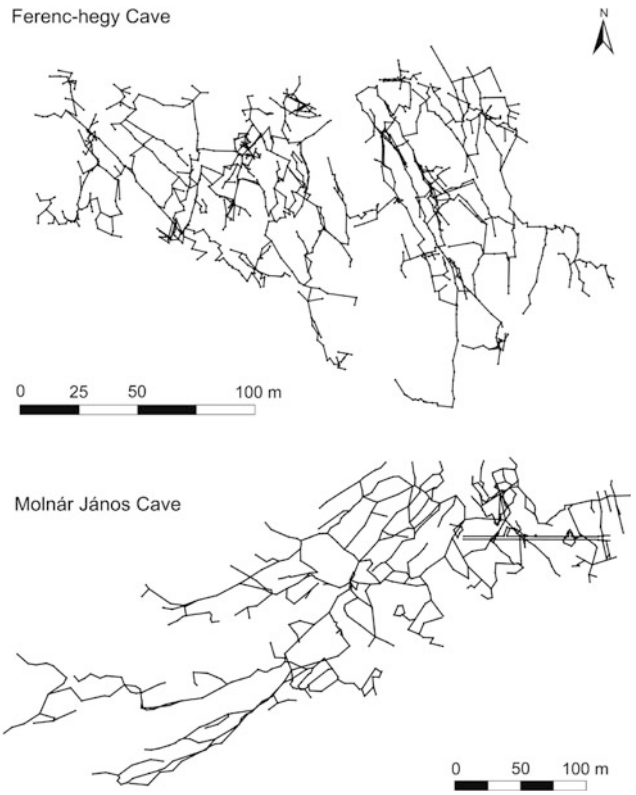

Fig. 5 Outline maps of Ferenc-hegy Cave and Molnár János Cave (speleological data from the National Cave Register map). Compiled by Magdolna Virág

On the basis of equilibrium graphs of calcite crystals below the barite veins, the age of some of the barite veins may be only about 1 million years old. Wein (1977) assigns the uplifting of the area to the Pleistocene. This tectonic uplift reactivated and widened the former fractures, which were often filled by barite veins, opening the way to the evolution of large and contiguous systems of passages, controlled by parallel main fissures and (subordinate) cross-fissures.

The fissures run parallel to each other in certain regions of the larger caves, although the direction of fissures may differ between the regions: e.g., the fissures in the western and eastern regions of Ferenc-hegy Cave run at an angle of about 25° (see Fig. 5). The main fissures in the western and eastern parts of József-hegy Cave exactly run at the same angle (see Fig. 3b).

The directions of the main fissures correspond to the Riedels (see above), the "twisted" direction of lines matches the direction of the main shear zone, which developed later and connected the Riedels. This would be in accordance with the general development of displacement zones, where the connecting master fault forms only in a later phase of evolution, after the development of Riedel faults (Sylvester 1988). In the case of Ferenc-hegy Cave and Pál-völgy Cave, the passages between the main fissures are almost as significant as the main ones (see Figs. 5 and 3a), but they are much less significant in Szemlő-hegy Cave and József-hegy Cave (see Fig. 3b).

The structural elements can rarely be measured on the walls (particularly on the level of the main passage) of Ferenc-hegy Cave, Szemlő-hegy Cave and József-hegy Cave, because the walls are covered by abundant mineral precipitations everywhere; only the youngest, N–S faults can be measured because they often have bare walls. Where there is no mineral precipitation, striae as well as spectacular microtectonic features can be seen on the walls. The length of the observable individual striae is 10–100 cm, and the

overlap between the striae is 5–15 cm. The small faults enclose at an angle of 10°–30° with the shear zone in which they appear. The faults shifting to the left can be interpreted as Riedel faults in a dextral shear zone (Fodor et al. 1991). These structures indicate the early evolution stage of faults (Tcalenko 1970). These small occurrences properly illustrate that the main fault had not yet been formed, so the foreseeable ENE–WSW displacement zone had not yet developed (Gamond 1987; Sylvester 1988).

The passages of Mátyás-hegy Cave follow the dip of strata: they become deeper towards SE. This pattern cannot be observed in the other caves, but an arrangement of three storeys is noticeable in Pál-völgy, Ferenc-hegy and József-hegy caves. The lower storey was dissolved in the well-bedded and noticeably folded cherty limestone of the Triassic Mátyáshegy Formation. The various solution forms are less prominent here. The middle storey lies in the Eocene Szépvölgy Limestone with its upper part often protruding into the more calcareous section of the Buda Marl characterized by bryozoan fossils. Spectacular solution forms (mainly corrosion pockets) decorate this part which belongs to the main storey (Virág et al. 2013a; Albert et al. 2015). The upper storey lies in the increasingly clayey Buda Marl, but the most beautiful solution forms, regular spherical niches, can often be found in this storey. This storey is characterized by passages filled by detrital-clay, because the marl leaves its insoluble high clay content. The passages of the lower storey can be either completely bare or richly decorated with mineral concretions; the middle storey is generally marked by abundant concretions (with the exception of Pál-völgy Cave and Molnár János Cave), while the upper story is mostly devoid of chemical deposits.

The main fissures in the caves are generally perpendicular or less frequently very steep with 60°–80° dip angles. The Eocene Szépvölgy Limestone and Buda Marl (the formation of which continued into the Oligocene) inclines at 20°–25° towards SSE in the area.

5 Genesis of the Caves

Pávai-Vajna (1930) was the first in Hungary who recognized the role of warm water springs and warm vapors-gases in the formation of caves. The explanation of the process of dissolution received a decisive support from the theory of mixing corrosion (Laptyev 1939) and from the realization of its role in the formation of caves (Bögli 1963, 1965). The importance of mixing corrosion in the formation of hypogene caves is now generally accepted (Runnels 1969; Plummer 1975; Müller and Sárváry 1977; Bakalowicz et al. 1987; Ford and Williams 2007; Jakucs 1994; Dublyansky 1995; Klimchouk et al. 2000, 2016; Palmer 2007; Virág et al. 2013b and references therein). This theory became widely acknowledged also in Hungary (Takács-Bolner and Kraus 1989; Leél-Őssy et al. 2011; etc.). Nádor (1991), Palmer (2007), Erőss (2010) and Leél-Őssy (2014) hold the opinion that the increase of the solutional capacity of the gradually cooling ascendant solutions is also an effective factor.

The BTK is one of the most significant and best studied hypogene cave areas of the world (Virág et al. 2013b). All comprehensive studies published in the last decades have mentioned the BTK and they uniformly hold mixing corrosion as responsible for the evolution of the caves (Ford and Williams 2007; Dublyansky 1995, 2000; Klimchouk 2007; Palmer 2007, etc.). Ford and Williams (2007) raise the possibility of sulfuric acid cave formation—the latest studies increasingly justify the rightfulness of this proposal. Poros et al. (2012) render it likely that these processes are associated with the organic material content originating in the basin sediments that turned into hydrocarbon on the left bank of the Danube. The geological conditions in the study area resemble the setting of the caves in the Carlsbad Caverns National Park in New Mexico, the formation of which by sulfuric acid is generally accepted (Hill 1987, 1990, 1995; Palmer et al. 1991).

Conceptual models of water circulation that resulted in the formation of the BTK caves were set up by many authors (Schafarzik 1921; Kovács and Müller 1980; Alföldi 1981; Tóth 1999, Erőss et al. 2011). This was supported and further developed by numerical flow and heat transport simulations for the margin of unconfined and confined carbonates based on the hydrogeological setting of the BTK not only from the Buda side but also from the confined karst of Pest as far as the Gödöllő Hills (Mádl-Szőnyi and Tóth 2015; Mádl-Szőnyi et al. 2015; see also Mádl-Szőnyi et al. Chap. 17). These authors found that the waters of the siliciclastic cover (basinal fluids) get into the confined carbonates via leakage and contribute to the discharge of thermal waters. The solutions originating in the surface rainwater penetrate deeper than 1000 m; they not only warm up at depth, but also become acidic due to taking up of dissolved CO_2 and H_2S produced under reducing conditions. H_2S probably originated in Permian evaporites (Szabó et al. 2009). In the ascending branch of this water circulation, the waters follow the tectonic lines along the river and meet near Rózsadomb, at the junction of the tectonically uplifted carbonate Buda Mountains (on the right-side bank of the Danube) and the sediment-covered Pest Plain (on the left-side bank of the Danube). This is the place where the mixing corrosion takes place. The caves discussed in this chapter were formed in this way during the past one million years. The mixing of waters along certain circulation paths were detected based on radionuclide analysis by Erőss (2010) and Erőss et al. (2012). The hydrological research by Bodor (2014) and Bodor et al. (2014) studied the interaction of groundwater by the river Danube and the relationship with

direct precipitation. The evolution of cavities is most intensive near the drainage level, but cavities with large volume are known at depths of 100 m in Molnár János Cave. Furthermore, there are data from deep drillings indicating that cavities of considerable size exist even at greater depths.

No mixing was detected in the area of Gellért Hill (Erőss 2010; Erőss et al. 2008, 2010, 2012). Probably, the role of sulfuric acid dissolution facilitated by the microbes is significant there (Borsodi et al. 2012; Anda et al. 2014, 2015). The unfavorable petrographic circumstances (dolomite environment) together with the weaker mixing corrosion may have caused these caves, which are active even today, to be only just of a few meters long and 0.5–1 m wide.

The migration of various solutions and their mixing as well as the evolution of caves took and still takes place along tectonic discontinuities in the case of Molnár János Cave see (Fig. 4), where local studies and dissolution measurements (Erőss et al. 2011) indicated active dissolution (and precipitation in certain cases).

Most caves in fact functioned as reservoirs, and the water of the fossil springs came to surface through them. These cave passages gradually transfer from the phreatic zone to the vadose zone due to the lowering of the water table, which is related to the uplifting of the Buda Hills (Poros et al. 2012). The hypogene processes come to an end, and epigene processes become dominant (Virág 2016). The hypogene caves become blocked and they reach their final evolutive phase (Leél-Őssyy 1957).

6 Morphology of the Caves

Anyone visiting the thermal karst caves of Buda will easily recognize the general features of hypogene caves described by Takács-Bolner (1989), Ford (1995), Ford and Williams (2007) and Klimchouk (2007). They are summarized here as follows:

(a) The larger cave passages are from 1 to 4 m wide, generally from 5 to 15 m high, and they run roughly parallel to each other: cave passages follow tectonic directions, as can clearly be observed on maps (Fig. 5).
(b) The floor of the passages is mostly buried by several-meter thick deposits of debris and clays derived from the insoluble residues of rocks and destruction of the overlying marls. Alluvial sediments of underground streams are almost missing. Presently there are no active water flows in these caves; periodically, some dripping or trickling water collects only in the lowest passage of Mátyás-hegy Cave, which is now part of the Pál-völgy Cave System.
(c) Spherical niches (Fig. 6a) and corrosion pockets (Fig. 6b) frequently occur in the caves, even in the smallest ones. The highest parts of the caves were often discovered when their cupola were intercepted by surface excavations (Ferenc-hegy Cave, József-hegy Cave, Pusztaszer Cave, Buda Cave, etc.). Intensive excavation was often required to reach the open cave passages, which are often 10 or 20 m below, from these small artificial entrances.
(d) It is a common characteristic of these caves that the larger, often 10–30 m wide halls and spacious corridors are connected by very narrow passages, hardly accessible to explorers. This sudden and large-scale change in size can be observed also in caves whose extent is just a few tens of meters. The spherical niches developing next to each other sometimes form strings like a cluster of grapes: the direction of the upwelling thermal water that dissolved the cave is well traceable. The profile showing the flow of the water is named "spring tree" (Fig. 4b).
(e) The rock surfaces, often even in the smallest caves, are richly decorated with carbonate-sulfuric mineral precipitations. These are mostly calcite, especially various popcorns. As for the sulfates, barite and gypsum are most widespread.
(f) Passages climb up and down repeatedly in the larger caves, and because they are located at various elevations they often run over or below each other. This multi-storey, complicated network of passages is characteristic of all the larger caves.
(g) Examination of the topographical map of the caves convincingly demonstrates that the evolution of cave passages was independent of the surface morphology; there is no evidence on the undisturbed surface terrain that there are caves below, and no systematic relationships with larger landscape features.

It is interesting to note that the caves of the BTK often expose some isolated paleokarstic solution forms.

7 Mineralogy

The physical-chemical conditions of the caves changed continuously over time, from the onset of hydrothermal dissolution to complete drying. These conditions determined the generation of chemical deposits and infillings in the passages. A good recent summary about speleothems can be found in Hill and Forti (1997) and Fairchild and Baker (2012). The types of chemical deposits in BTK are presented below according to their history of formation.

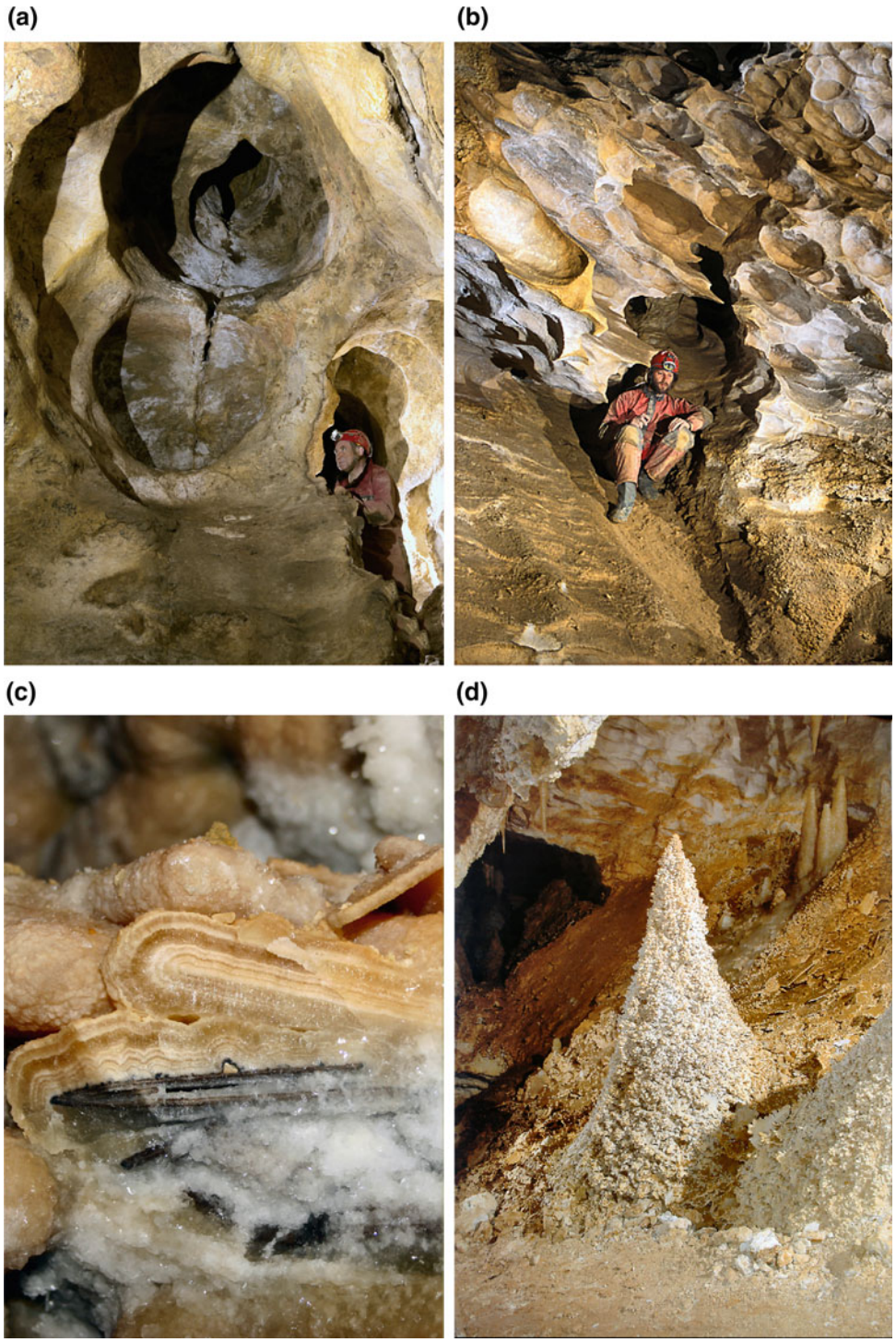

Fig. 6 **a** Spherical niches in József-hegy Cave. *Photo* Csaba Egri; **b** corrosion pockets in the Pál-völgy Cave System. *Photo* Csaba Egri; **c** thick cave raft (roso) in József-hegy Cave. *Photo* István Czajlik; **d** cave cone in the Pál-völgy Cave System. *Photo* Attila Kiss

7.1 Vein Minerals Older than the Caves

It is possible to observe and study minerals in the caves of the BTK that are older than the age of caves, so these mineral elements of the rocks are not speleothems; the passages only expose them and make them accessible.

7.1.1 Calcite Veins

Calcite veins densely penetrate the bedrock in which the cave is carved. The veins and veinlets run parallel to the major tectonic directions, having a width of 0.2–1.0 cm.

Grown-up calcite scalenohedrons up to 4 cm developed in some wide diaclases. They tend to form double or triple twin crystals such as in Mátyás-hegy Cave. Their color is generally whitish or yellowish. According to the fluid inclusion measurements performed by Dublyansky (1995), they might have precipitated at 55–91 °C. Most frequent are the 1–4 cm long dogtooth spars on the sidewalls of fissures and in geodes.

7.1.2 Barite

The somewhat elongated, tabular and diamond shaped crystals of barite (001) can be found not only in the caves but also in the outcrops and exposed faces of quarries in the nearby hills.

Small size barite crystals (the edges are shorter than 1 cm) are best observable in Ferenc-hegy Cave, where they can be seen on the plane of faults. The barite precipitated on the tip of calcite scalenohedrons frequently, and the negatives of crystals can be observed on the underside of the barite in several places. The study of fluid inclusions by Gatter (1984) and Molnár and Gatter (1994) indicated that they originated at temperatures of 150–300 °C, while similar analyses by Dublyansky (1992) suggested a much lower temperature of precipitation.

The barite crystals usually have a shade of yellowish color, at some places covered by thin, white calcite or gypsum coating. In Molnár János Cave and József-hegy Cave, however, a black, manganese-oxide or hydroxide coating covers the 2–3 cm edge long crystals.

7.1.3 Pyrite

Pyrite occurs in the form of small, mm-sized cubes in calcite veins. However, the pyrite may have a significant effect on the dissolution of passages and on the formation of siliceous zones (see below).

7.1.4 Silica or Geyserite

It is particularly characteristic of the Pál-völgy Cave System that the ceiling or a part of the ceiling of the upper lying passages is composed of a 1–3 m wide siliceous and friable rock mass. Formerly, they were erroneously explained as siliceous vein-fillings (Jaskó 1948). Takács-Bolner and Kraus (1989) observed that larger foraminifers and even Chlamys bivalves appear in the "siliceous zones". They were transformed into siliceous matter later. Calcite veins can often be found in the siliceous zones that apparently contain pyrite (e.g. in Molnár János Cave). It is probable that sulfuric acid developed because of the oxidation of pyrite (Tisato et al. 2012; Vörös et al. 2013) and dissolved the carbonate content of the Eocene rocks. The strongly acidic agent transformed the clayey minerals and produced significant silica content. This whitish and light reddish clay consists of 65% quartz and 35% of various clay minerals such as kaolinite and montmorillonite (Sásdi 1993; Leél-Őssy et al. 2011). It has not yet been proven what caused the transformation: solutions seeping in along the faults made aggressive by sulfuric acid (Sásdi 1993), or the upwelling solutions that dissolve the cave passages and incidentally also carry hydrogen sulfide (Leél-Őssy 2014). A recent study (Virág 2016) supports the latter explanation.

7.1.5 Alunite and Jarosite

Győri et al. (2011) used scanning electron microscopes to study the siliceous zones, and they found grown-up alunite crystals in the pores. Virág and Bendő (in Vörös et al. 2013) used microanalysis, and they identified tiny, tabular and rhombohedral jarosite grains in the calcite veins, which were similar to alunite (Audra et al. 2015).

7.1.6 Fluorite, Cinnabar, Metacinnabar

Nádor (1991, 1992), Sásdi (1993) and Nagy (2008) demonstrated the presence of cinnabar and metacinnabar in Ferenc-hegy Cave when they studied the calcite and barite veins. In 2000, at the opening of Pusztaszer Cave, the author found a few mm-sized fluorite crystals in the calcite veins at the entrance to the cave.

7.2 Pool Deposits Precipitated from Warm Water

When the area was uplifted and the erosional base level lowered, the level of the lukewarm-warm water began to sink accordingly. As a result, drained (air-filled) sections developed above the ponds in the cave. This process did not take place at the same time in the caves of the BTK. In those passages that were uplifted higher (e.g. Ferenc-hegy Cave), it occurred earlier, while in the passages that were (and still are) closer to the base level the process took place later (e.g. in Aragonit Cave of Gellért Hill). About 98% of the passages of Molnár János Cave still contain thermal water.

The development of drained passages in the caves presented the opportunity for CO_2 degassing (Dublyansky

1995; Palmer 2007, etc.). This naturally led to the precipitation of carbonates from the waters, which passed through carbonate rocks at deeper levels and thus became saturated in calcium carbonate. The calcite precipitated from the water in diverse forms at various places.

7.2.1 Subaqueous Coating

The structure of the subaqueous calcite is similar to that of flowstones; however, this coating appears not only on the sloping wall surfaces, but also on vertical sidewalls. Their surface is uneven and rough ("warty", sometimes like cauliflower, with roundish though often almost flat surface); they precipitated under the water level on the side and bottom of the pond basin. The coating usually consists of 3–6 layers that together make up a thickness of 1–5 cm. The age of the samples collected in the BTK area is set between 100 and 400 ka (Leél-Őssy et al. 2011).

7.2.2 Cave Rafts

Calcite also precipitates from the pond simultaneously with degassing, but not on the wall of the basin only. The cave rafts develop through degassing from the surface of the water (Viehmann 1992; Hill and Forti 1997; Palmer et al. 1991; Palmer 2007; D'Angeli et al. 2015 and references therein). Their occurrences at various elevations were useful for U/Th dating and for determining the lowering of the paleo-water table (Szanyi et al. 2012). Age of the cave rafts at higher elevations exceeds the limit of alpha spectrometry uranium series dating, but they are commonly from 200 to 300 ka old. Plates of the cave rafts commonly have a thickness from 1 to 3 mm, although it may be 1 cm as in Szemlő-hegy Cave and Pál-völgy Cave, or even 3 cm as in József-hegy Cave (Fig. 6c). This is explained in the following way: water drops or water moves due to earthquake (Réthly 1952) it breaks the layer, then it sinks onto the bottom of the pond, where it is thickened further until it gets in contact with water, and is finally buried by other rafts (Kraus 1993; Takács-Bolner and Kiss 2004). The total thickness of the accumulation may be as high as 1 m. The thick precipitations developed in this way are named *roso* (that is sunken objects of raft origin; Leél-Őssy et al. 2011). They have a whitish-yellowish colour, but they are pinkish when illuminated. It is possible to collect samples of calcite rafts developed on the surface of the 35–40 °C water in the small cavity of Ősforrás Spring at the foot Gellért Hill.

7.2.3 Cave Cones

If the water is permanently dripping, the cave rafts always break at the same place and the laminae descend to the bottom of the pond; these laminae accumulate and form cones (Palmer et al. 1991; Hill and Forti 1997; Palmer 2007; Gázquez and Calaforra 2013). The continuous precipitation of calcite in the pond cements the laminae together, creating steep-walled cone-shaped raft accumulations (Kraus 1991; Takács-Bolner 1993; Piccini 2000). They are often covered by coralloids. The tallest cones are over 2 m tall (Fig. 6d).

7.2.4 Pool Fingers

The pool fingers are 1–2 cm thick and 3–5 cm long tubes (Fig. 7a). They surely precipitated below the water level of the pond that once filled the cave (Davis 1996; Hill and Forti 1997). They can be found on overhanging walls. Where they are corroded, 2–3 mm empty pipes can be observed in their center. They usually appear in large clusters; their color is whitish-yellowish.

7.2.5 Angular Botryoids

The angular botryoids in Pál-völgy Cave and József-hegy Cave (Kiss and Takács-Bolner 1987; Kraus 1993; Leél-Őssy and Surányi 2003) are bordered by 0.5 cm sized curved laminae; their form looks globular from a distance (Fig. 7b). They are snow white.

7.2.6 Folia

From the vertical or overhanging sidewalls stand out 1–2 cm thick parallel rims. There may be even 50 rims below each other. Since they always precipitate at the current water level, the ribs superposed to each other. They can be good indicators of the recessing water level. The vertical thickness of calcite-based precipitations can be more than 1 cm (Hill and Forti 1997; Audra et al. 2009; Davis 2012; D'Angeli et al. 2015). These precipitations are attributed to the quick release of carbon dioxide at or close to (below) a fluctuating standing body of water (Palmer 2007; Davis 2012; D'Angeli et al. 2015).

7.2.7 Romanechite and Hollandite Coating

The pitch-coal-black coatings that are hair thin cover certain wall sections. X-ray diffraction, electro microscopic microanalysis and spectroscopy showed that these coatings are composed of two relatively rare manganiferous minerals, romanechite and hollandite (Nagy 2008). According to Ehrlich (1996), microbial processes accelerated the precipitation. In a project led by J. Mádl-Szőnyi this year, the diver Zsolt Szilágyi managed to collect several such bacterium cultures from the warm water springs in the area of the BTK (Molnár János Cave, cave of Török Spring, Ősforrás, Rác Bath), which have an important role in the precipitation of certain minerals.

7.2.8 Calcite Coating on Mud Cracks (Septaria)

When the cave pond desiccated due to the lowering of the water table, the surface of the mud that accumulated on the floor of the main passage split into cracks, and this produced 1–2 cm gaps between the 20–50 cm polygons. Later, the water table rose and flooded this passage storey again and

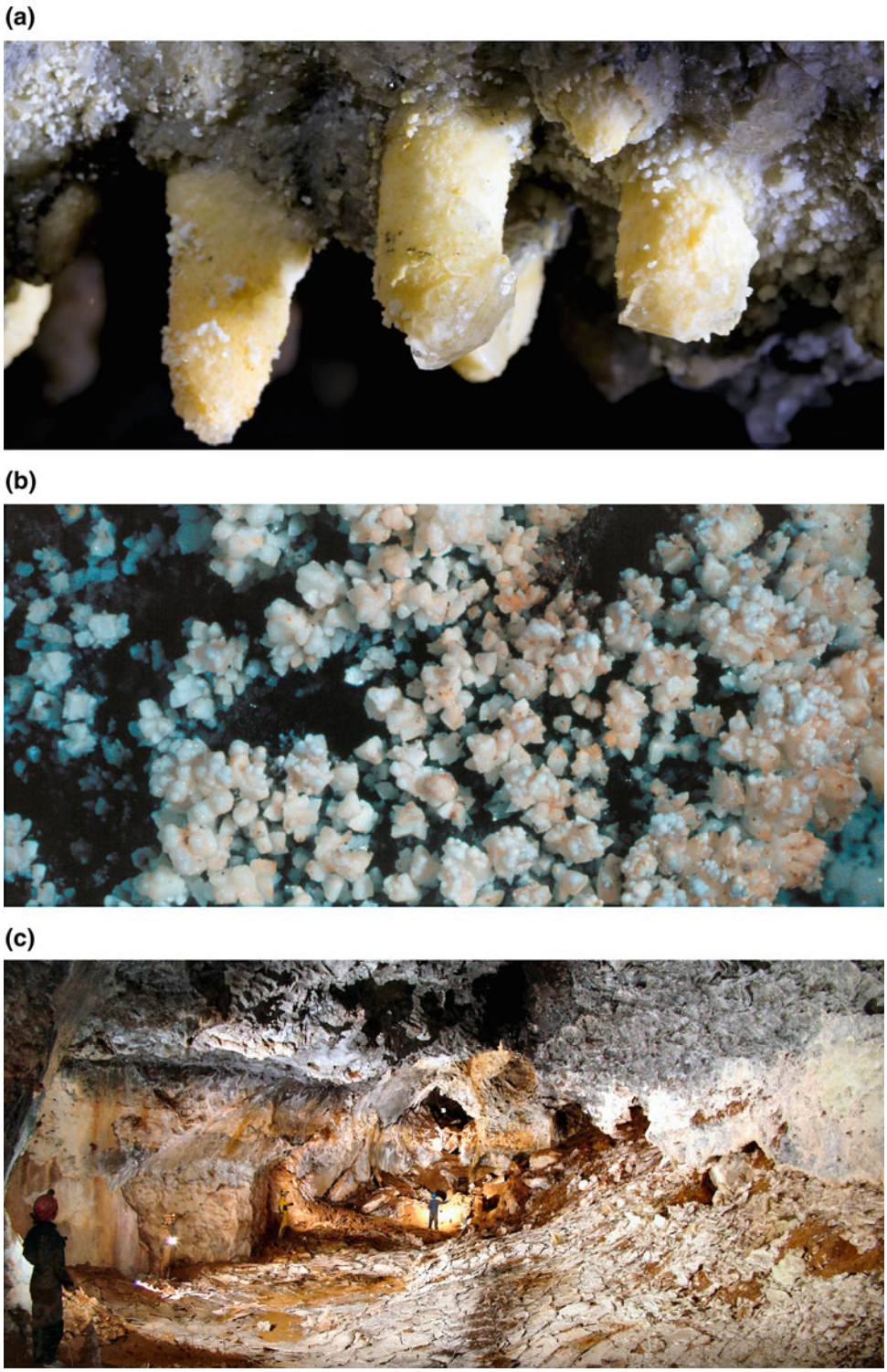

Fig. 7 **a** Pool fingers in József-hegy Cave. *Photo* Richárd Kovács; **b** angular botryoids in József-hegy Cave. *Photo* István Czajlik; **c** calcite coating on mud cracks (septarias) in József-hegy Cave. *Photo* András Hegedűs

calcite coating settled in 0.5–2.0 cm thickness on the clay polygons (Fig. 7c). The uranium series dating of the calcite coating indicated that all this happened around 200,000 years ago (Leél-Őssy et al. 2011). The precipitated calcite coating often buried and preserved the gaps between the polygons, thus forming pseudomorphs. The gypsum precipitating from the seeping waters thinly cover this calcite coating, which then looks like peculiar snow-covered ice sheets.

7.3 Speleothems Precipitated by Evaporation

The most spectacular speleothems in the area of the BTK include the group of coralloids (popcorn) and frostwork.

7.3.1 Coralloids (Popcorn)

Clearing up the genetics of this type of speleothems is not easy, because seemingly similar speleothems can develop in various ways: due to the evaporation of lukewarm/warm pond or small discharge of cold-water infiltrations, or even due to humid cave air, however evaporation is always involved. Nevertheless, somewhat similar forms may develop underwater too: the surface of the subaqueous coating is sometimes so rough either in cold or lukewarm water that they look like botryoids (e.g. in Szemlő-hegy Cave).

The "common" popcorn as named by Leél-Őssy (1995) is the most characteristic speleothem in the caves of the BTK. There are systems of passages where they almost uninterruptedly cover the walls of the main passage story (Szemlő-hegy Cave, Ferenc-hegy Cave). They are generally yellowish, though they are white in József-hegy Cave. The layered structure with very thin spheroidal shells can be well observed on re-dissolved samples. Size of individual cave popcorns is about 1 cm. Their genesis by evaporation is now widely accepted (Hill and Forti 1997; Palmer 2007; Kraus 2010; Caddeo et al. 2015). Aragonite frostwork often grows on the popcorn of calcite material (Fig. 8a).

Through U-series dating it is clear that they are much younger speleothems than the subaqueous coatings and cave rafts collected from the same level and that unquestionably precipitated as pool deposits: they are about 100 ka younger, and this also proves their vadose origin. Their age is generally within 100–200 ka, but some in Ferenc-hegy Cave, which is at a topographically higher position, were dated as 350 ka old (Ford and Takács-Bolner 1992).

7.3.2 Christmas Tree Stalagmite

Altogether, only a few samples (in the forms of candles and cones), which remind us of dripstone stalagmites or cave cone, can be found in Szemlő-hegy Cave and József-hegy Cave. For the origin of the term *Christmas tree stalagmite* see Hill and Forti (1997).

7.3.3 Frostwork

This speleothem occurs in the caves of Rózsadomb, in József-hegy Cave and Szemlő-hegy Cave as well as in Citadella Crystal Cave and Aragonit Cave on Gellért Hill. They are always snow-white crystals, in which the individual crystal needles bordered by plane faces are 1–2 mm thick and 1–3 cm long (Fig. 8b). Since there are multiple branches in the strings, these remarkable crystal clusters are called crystal Christmas tree (Hill and Forti 1997). They usually hang from the ceiling or stick out from the sidewall. Rarely, they can be found on the floor.

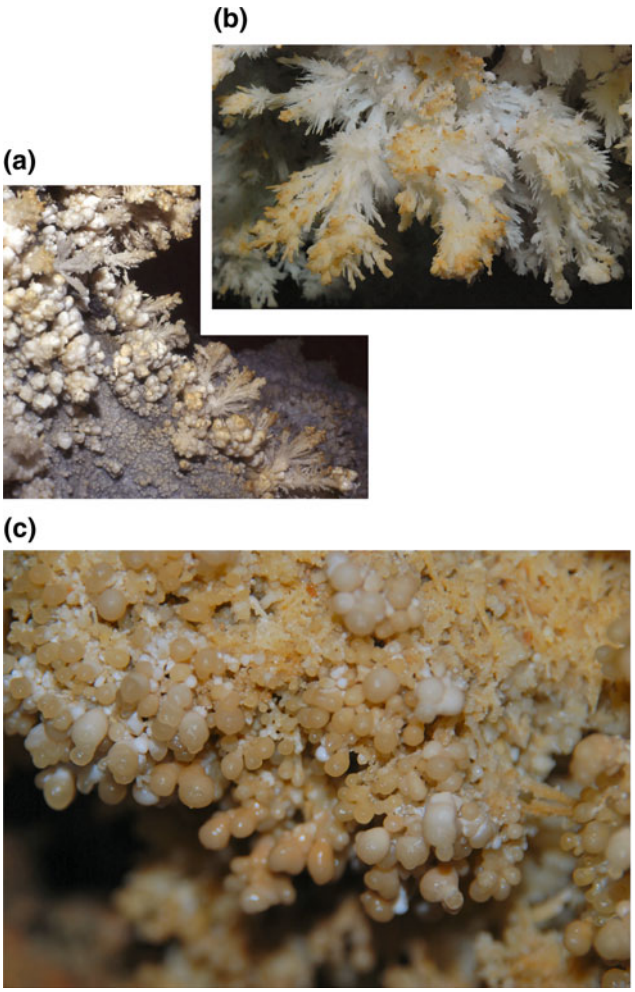

Fig. 8 **a** Aragonite needles on popcorns in József-hegy cave. *Photo* Szabolcs Leél-Őssy; **b** aragonite frostwork in József-hegy Cave. *Photo* Szabolcs Leél-Őssy; **c** glass-ball botryoids in József-hegy Cave. *Photo* Szabolcs Leél-Őssy

Frostwork aggregates easily re-dissolve in the percolating water, which often has a pH value of 6.4–6.8. This process is observable in many places. Their composition is mostly aragonite (the Sr content of the seeping waters is about 0.8–1.3 ppm even today), but sometimes the proportion of dolomite is more than 50% (oral communication by László Bognár 1986).

7.4 Speleothems Formed in Drained Cave Passages by Infiltration from the Surface

7.4.1 Dripstone

Dripstones (stalactites, stalagmites, columns, flowstones and draperies) occur only subordinately in the area of the BTK. The reason is that the Szépvölgy Limestone where most of the cave passages are formed contains some clay. The water seeping through the calcareous marl of the several tens of meter thick Buda Marl Formation (which often covers the limestone), and through its clayey marl close to the surface cannot collect enough bicarbonate content to produce dripstones in the cave. Nevertheless, beautiful, clean and colorful, but usually small-sized dripstones can be found mainly in the new passages of the Pál-völgy Cave System discovered in the past decades, and in some sections of József-hegy Cave: flowstones, stalactites and smaller stalagmites, and sometimes draperies have been reported. Among the few centimeter-long stalactites (at some places there are soda-straws in groups).

7.4.2 Glass-Ball Botryoid

Waters, sometimes of pH 6.5, seeping into the cave often re-dissolve the frostworks (see Sect. 7.3.3) and the common popcorn speleothems. The degassing of CO_2 from the water film and the evaporation cause further loss of CO_2; this process leads to the growing of fairly regular, roundish botryoids, which usually consist of spherical concretions of a few millimeters in diameter (Fig. 8c). This rare speleothem has been named glass-ball botryoid (Leél-Őssy 1997; Leél-Őssy et al. 2011.) Due to their regular shape, they can be easily discerned from the common popcorns. Uranium series dating suggests that their age is just a few thousand years in every case. Around these forms, the age of the original coralloids (which were re-dissolved) are 150–200 ka old.

7.4.3 Draught Botryoid

It frequently happens that a special form of coralloids, tiny, globular, calcite speleothems develop from condensation-evaporation processes in caves. They occur as snow-white, 1–3 mm balls in the BTK area. They are young and fragile formations (Gádoros and Cser 1986).

7.4.4 Pool Deposit

This speleothem is notably prominent in Pál-völgy Cave and the cave of Török Spring on Gellért Hill, though it can be found also in József-hegy Cave. The trickling cold water periodically collects in small, less than 1-m diameter pools, and 0.1–1.0 cm calcite rhombohedra precipitate on the bottom of the pool.

7.4.5 Moonmilk: Calcite, Hydromagnesite and Huntite

Moonmilk can be found in various phases of formation in the caves of BTK. Generally, it is white and beige; if dried, it becomes hard and breakable; István Dódony used SEM to examine the samples gathered near to the entrance of Ferenc-hegy Cave, and they turned out to be microcrystalline calcite (Horányi and Leél-Őssy 1980). The X-ray powder diffraction measurement of the samples collected in Szemlő-hegy Cave, József-hegy Cave and Citadella Crystal Cave showed that they are composed of huntite and hydromagnesite.

7.4.6 Gypsum Crust

The 0.5–6.0 cm thick glittering gypsum crusts covering the walls in Szemlő-hegy Cave have been known since its discovery in 1930. They usually appear in large clusters consisting of 1–2 mm snow-white crystals. They are widely distributed also in József-hegy Cave and Citadella Crystal Cave on Gellért Hill (Leél-Őssy et al. 2007). Gypsum needles often protrude from the surface of the crusts. These needles are 1–2 cm long and bordered by 1–3 mm wide plane faces. Larger parallel intergrowths of skeletal crystals (frequently of several cm^2) also formed on the lower part of the crust. The gypsum crusts often fall down from the rocks.

The gypsum crust, being younger, usually appears on coralloids, on the tip of aragonite crystals, and sometimes on older dripstones. This material can be originated from the pyrite content of the marl layers that cover the cave (Leél-Őssy et al. 2011). The sulfate content of the dripping water was found to be 200 mg/l.

7.4.7 Gypsum Chandeliers

They can be found in József-hegy Cave only, where the largest crystal clusters are almost 1 m long (Fig. 9a). Their surface is not covered by tiny crystals but by crystal faces of several cm^2. They always appear on the ceiling or on overhanging sidewalls. Generally, they have 3–4 arms and look like spread fingers.

7.4.8 Gypsum Flowers

The gypsum flowers have a fibrous structure; in the caves of Buda they are generally as thick as a pencil, not longer than 15 cm, and they have a flower-like morphology (Fig. 9b). The crystal bundles are often curved and sometimes even spirally twisted due to the deformation along the translation planes parallel to the c-axis. They can be found on the ceiling and on the floor, but sometimes also on the sidewall.

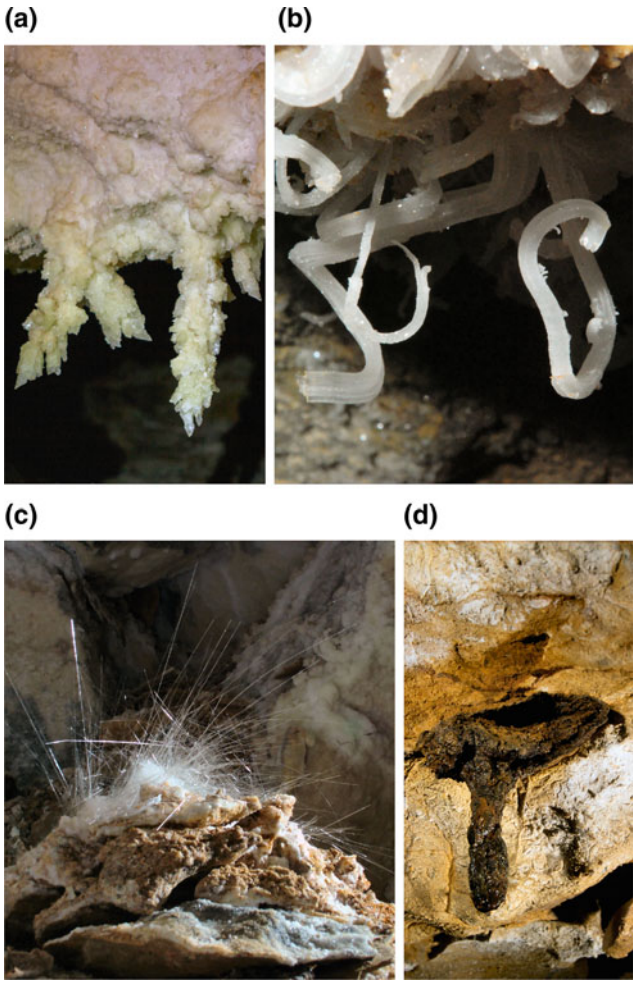

Fig. 9 **a** Gypsum chandeliers in József-hegy Cave. *Photo* Szabolcs Leél-Őssy; **b** gypsum flowers in József-hegy Cave. *Photo* Szabolcs Leél-Őssy; **c** gypsum hair. *Photo* András Hegedűs; **d** "limonite" dripstone. *Photo* Richárd Kovács

7.4.9 Gypsum Hair

In the BTK area, Gadó (1965) described this speleothem from Szemlő-hegy Cave, though its occurrence there is only occasional. They appear in larger quantities in József-hegy Cave and in Citadella Crystal Cave, which was discovered in 2007 (Fig. 9c).

The threads are as thin as a single hair, 0.1–1.0 m long. They usually hang from the ceiling or overhanging sidewalls, but they can be found also on the floor, where they often form wadding-like brushes.

7.4.10 Selenite Needles

In some places, 1–4 mm thick and generally 5–20 cm long, translucent crystal needles (bordered by plane faces) can be found on the clayey floor (József-hegy Cave, Citadella Crystal Cave, Pál-völgy Cave System).

7.5 Cave Fills and In Situ Minerals Produced by the Weathering of Rocks

7.5.1 Clay Minerals (Kaolinite, Montmorillonite)

The insoluble residues of the Szépvölgy Limestone, where the cave passages develop, contain clay that accumulates on the floor of cave passages. In the upper passages, these materials are mixed with the insoluble residues of the Buda Marl, which contains more than 20% clay. The color of the clayey infillings is generally red-brown due to the small amount of iron. XRD and DTA measurements indicated that their mineral composition is kaolinite and montmorillonite.

The clayey infillings are mixed with breakdown material that often forms several-meter thick accumulations of collapsed blocks.

7.5.2 "Limonite"

The accumulations of goethite and lepidocrocite in the caves basically originate from the pyrite content of the marl. There are 3–10 cm diameter "nodules" in the smaller "pockets" of the rock in the passages formed in marl. They were probably dissolved by sulfuric acid that developed during the oxidization of pyrite. They can be found in the upper storey of every cave that reaches the marl. In József-hegy Cave, the water infiltrated through a larger limonite knob and "rebuilt" the nodule: a regular, 10 cm long stalactite was formed here (Fig. 9d). The accumulations of clayey debris that cover the floor of passages are also colored by the limonite.

7.5.3 Quartz, Zircon, Pyroxene and Garnet

The XRD and thermoanalytical measurements performed by Petho (1996) detected quartz in the accumulations on the floor of passages. András Szarka (oral communication, 1993) studied the heavy minerals and he detected garnet, zircon and augite in the samples of these infillings.

7.5.4 Cave Collapse

It is probable that significant collapses already occurred in the course of the dissolution in these caves and that clayey material accumulated on the floor of passages. The collapses probably already (partly) occurred after the temporary lowering of the water level and that the breakdown material was, probably at the time of the rising water table in the interglacial between Riss and Würm, covered again by the thermal water. This debris is cemented by calcite coating precipitating from the warm water in many places. During the exploration of József-hegy Cave in 1984, cavers penetrated for 40 m into one of these collapses, but there was no need to support the breakdown due to the cementation of the blocks (Adamkó and Leél-Őssy 1986). The passages in the lower storey, where the solution occurred in Triassic limestone, are quite free of fallen rocks and clay; however, the

floor of the main passage storey, carved in mostly Eocene clayey limestone, is often covered by a 3–4 m thick accumulation of rocks and clay. The passages that developed in the younger above lying marl are of smaller volume, but the accumulation of rock debris and clay is more conspicuous.

8 Conclusions

In the capital of Hungary, Budapest, there are medicinal baths known all over the world. The lukewarm-warm water of springs dissolved more than 100 caves (including five large caves, which are longer than 2 km) by the mixing corrosion in the phreatic zone in the second half of the Pleistocene. The total length of the known caves is around 55 km. The caves had no natural entrance and were discovered by quarry and ground works in the last hundred years.

The host rock of the caves is mainly Eocene Szépvölgy Limestone, but the upper levels are in the Eocene–Oligocene Buda Marl, and the lower levels are in the Upper Triassic cherty limestone or dolomite (this belongs to the Mátyáshegy Formation and the Main Dolomite).

The largest caves are in the Rózsadomb area, at 5–6 km^2. There is a 20–30 m difference in the level of the Triassic–Eocene discordant border, and there is a small difference (about 25°) between the direction of the passages in two parts of the same cave. It is possible to observe remarkable microtectronic features on the walls in places with no mineral precipitation.

Sometimes the cave passages follow the limits of the Eocene limestone—Eocene–Oligocene marl, which inclines at 20°–25° towards SSE.

The Gellért Hill caves are smaller, because there was no water mixing, and the host rock is dolomite.

The water of the springs which dissolved the cave passages (e.g. in Molnár János Cave) along the tectonic lines by mixing corrosion has a meteoric origin, and flows through long subsurface routes. Not only CO_2 but also sulfuric acid may have played a role in the genesis of the cave passages.

During the past hundred thousand years the Danube has incised its channel, and the karst water table has fallen, leaving many caves passages in the vadose zone. The main cave levels are at 160 m above sea level (the water level of the Danube is about at 100 m asl).

Speleogenesis is most intensive near to the drainage level, but cave passages filled with water are also known in Molnár János Cave, 100 m under the karst water table. Based on the recent experiments, the speleogenesis there is still active. In other dry caves, which moved from the phreatic zone into the vadose zone, there are no hypogene but epigenetic processes which result in cave.

The main peculiarities of the dry cave passages are as follows:

(a) The large cave passages are parallel to the main tectonic lines (their directions are SW–NE, NW–SE or E–W).
(b) No water flows in the caves. The few-meter thick deposit of debris and clay originated from the host rock.
(c) Spherical niches and corrosion pockets adorn the caves of the BTK.
(d) The variation in the size of the passages is very characteristic. Large rooms are followed by very narrow passages.
(e) These caves have a multi-storey, complex ground-plan system.
(f) The position of the caves is unrelated of the morphology of the surface.
(g) The caves are well decorated with carbonate-sulfuric mineral precipitations. Based on their genesis we can classify the minerals into five groups, with many sub-divisions. The most frequent minerals are the calcite, gypsum, aragonite and barite.

Acknowledgements Many thanks to Prof. Stein-Erik Lauritzen for his advice and for the opportunity to work in his U-series laboratory; to Magdolna Virág and to Tamás Garamhegyi geologists (presently Ph.D. students) for compiling my figures; and to Gábor Gercsák for his assistance in writing my chapter in English.

References

Adamkó P, Leél-Őssy Sz (1986) Budapest új csodája: a József-hegyi--barlang (New wonder of Budapest: the József-hegyi Cave). Karszt és Barl 1984:1–8 (in Hungarian with English abstract)

Adamkó P, Dénes Gy, Leél-Őssy Sz (1992) Caves of Buda, Issue of the council of Budapest

Albert G, Virág M, Erőss A (2015) Karst porosity estimations from archive cave surveys—studies in the Buda Thermal Karst System (Hungary). Int J Speleol 44(2):151–165. doi:10.5038/1827-806X.44.2.5

Alföldi L (1981) A budapesti geotermikus áramlási rendszer modellje (the model of geothermal flow system of Budapest). Hidrológiai Közlöny 1981(9):397–403

Anda D, Büki G, Krett G, Makk J, Márialigeti K, Erőss A, Mádl-Szőnyi J, Borsodi A (2014) Diversity and morphological structure of bacterial communities inhabiting the Diana-Hygieia Thermal Spring (Budapest, Hungary). Acta Microbiol Immunol Hung 61(3):329–346. doi:10.1556/AMicr.61.2014.3.7

Anda D, Makk J, Krett G, Jurecska L, Márialigeti K, Mádl-Szőnyi J, Borsodi A (2015) Thermophilic prokaryotic communities inhabiting the biofilm and well water of a thermal karst system located in Budapest (Hungary). Extremophiles 19:787–797. doi:10.1007/s00792-015-0754-1

Audra P, Mocochain L, Bigot JY, Nobécourt JC (2009) The association between bubble trails and folia: a morphological and sedimentary

indicator of hypogenic speleogenesis by degassing, example from Adaouste Cave (Provence, France). Int J Speleol 38(2):93–102
Audra P, Gázquez F, Rull F, Bigot J, Camus H (2015) Hypogene sulfuric acid speleogenesis and rare sulfate minerals in Baume Galinière Cave (Alpes-de-Haute-Provence, France). Record of uplift, correlative cover retreat and valley dissection. Geomorphology 247:25–34
Bakalowicz MJ, Ford DC, Miller TE, Palmer AN (1987) Thermal genesis of solution caves in the Black Hills, South Dakota. Bull Geol Soc Am 99:729–738
Báldi T (1986) Mid-tertiary stratigraphy and paleographic evolution of Hungary. Akadémiai Kiadó, Budapest
Bodor P (2014) A rózsadombi megcsapolódási terület felszín alatti vizeiben bekövetkező időbeli változások vizsgálata (assessment of the temporal changes in groundwater in the discharge area of Rózsadomb). Manuscript, MSc Thesis, ELTE TTK Department of Physical and Applied Geology, Budapest
Bodor P, Erőss A, Mádl-Szőnyi J, Czuppon G (2014) A Duna és a felszín alatti vizek kapcsolata a rózsadombi megcsapolódási területen (the connection between the Danube and the groundwater system in the discharge area of Rózsadomb). Karsztfejlődés XIX:63–75
Borsodi A, Knáb M, Krett G, Makk J, Márialigeti K, Erőss A, Mádl-Szőnyi J (2012) Biofilm bacterial communities inhabiting the cave walls of the Buda Thermal Karst System, Hungary. Geomicrobiol J 29(7):611–627
Bögli A (1963) Beitrag zur Enstehung von Karsthöhlen. Die Höhle 63–68
Bögli A (1965) The role of corrosion by mixed water in cave forming. In: Stekl O (ed) Problems of the speleological research, Czechoslovakia. Academy of Science, Prague, pp 125–131
Caddeo GA, Railsback LB, De Waele J, Frau F (2015) Stable isotope data as constraints on models for the origin of coralloid and massive speleothems: the interplay of substrate, water supply, degassing, and evaporation. Sed Geol 318:130–141
D'Angeli IM, De Waele J, Melendres O, Tisato N, Sauro F, Gonzales ERG, Bontognali TR (2015) Genesis of folia in a non-thermal epigenic cave (Matanzas, Cuba). Geomorphology 228:526–535
Davis DG (1996) Extraordinary features of Lechuguilla Cave. Natl. Speleo. Soc, Conv. Progr. Salida, Aug. 5–9, pp 48–49
Davis DG (2012) In defense of a fluctuating-interface, particle-accretion origin of folia. Int J Speleol 41(2):189–198
Dublyansky YV (1992) A Budai-hegység hidrotermás paleokarsztja—a folyadékzárvány vizsgálatok első eredményei (the hydrothermal paleokarst of Buda Mountains—the first results of the examinations of fluid inclusions). Karszt és Barlang 1991(1–2):19–24
Dublyansky YV (1995) Speleogenetic history of the Hungarian hydrothermal karst. Environ Geol 25:24–35
Dublyansky JV (2000) Hydrothermal speleogenesis in the Hungarian Karst. In: Klimchouk A, Ford DC, Palmer AN, Dreybodt W (eds) Speleogenesis. Evolution of karst aquifers. National Speleological Society, Huntsville, Alabama, USA, pp 298–303
Ehrlich HL (ed) (1996) Geomicrobiology, 3rd edn. Marcel Dekker, New York
Erőss A (2010) Characterization of fluids and evaluation of their effects on karst development at the Rózsadomb and Gellért Hill, Buda Thermal Karst, Hungary. PhD Dissertation, Eötvös L. University, Budapest
Erőss A, Mádl-Szőnyi J, Csoma AÉ (2008) Characteristics of discharge at Rose and Gellért Hills, Budapest, Hungary. Cent Eur Geol 51(3):267–281
Erőss A, Mádl-Szőnyi J, Csoma AÉ (2010) The effects of mixed hydrothermal and meteoric fluids on karst reservoir development, Buda Thermal Karst. Hungary, EMR Final Report SIEP Rijswijk
Erőss A, Mádl-Szőnyi J, Borsodi A, Knáb M, Csoma ÉA, Mindszenty A (2011) Results of in situ dissolution experiment to understand hypogenic karstification processes, Buda Thermal Karst, Hungary. In: Bertrand C, Carry N, Mudry J, Pronk M, Zwahlen F (eds) Proc. H2Karst, 9th conference on limestone hydrogeology, Besançon (France), pp 161–164
Erőss A, Mádl-Szőnyi J, Surbeck H, Horváth Á, Goldscheider N, Csoma AÉ (2012) Radionuclides as natural tracers for the characterization of fluids in regional discharge areas, Buda Thermal Karst, Hungary. J Hydrol 426–427:124–137
Esteban M, Budai T, Juhász E, Lapointe O (2009) Alteration of Triassic carbonates in the Buda Mountains—a hydrothermal model. Cent Eur Geol 52(1):1–29
Fairchild IJ, Baker A (2012) Speleothem science. Wiley-Blackwell, Oxford
Fodor L, Leél-Őssy Sz, Tari G (1991) En-echelon fractures in a dextral shear zone—tectonic heritage for a hydrothermal cave (Budapest, Hungary). Terra Nova 4:165–170
Ford DC (1995) Some thoughts on hydrothermal caves. Cave Karst Sci 22(3):107–118
Ford DC, Williams PW (2007) Karst geomorphology and hydrology. Wiley, Chichester
Ford DC, Takács-Bolner K (1992) Abszolút kormeghatározás és stabil izotóp vizsgálatok budai barlangi kalcitmintákon (absolute age determination and stable isotope measurements on cave-calcite samples of Buda Mountains). Karszt és Barl 1991(I–II):11–18
Gadó P (1965) A Szemlő-hegyi-barlangban talált kristályszálról készült röntgenvizsgálat eredménye (The result of X-ray examination of crystal needle from Szemlő-hegy Cave). Karszt és Barl 1965(I): 19–20
Gádoros M, Cser F (1986) Aerosol in caves. Critical considerations in proceedings of the 9th international congress of speleology, Barcelona I:90–92
Gamond (1987) Bridge structures as sense of displacement criteria in brittle fault zones. J Struct Geol 9:609–620
Gatter I (1984) A karbonátos kőzetek érkitöltéseinek és a barlangok hévizes kiválásainak folyadékzárvány-vizsgálata (the fluid inclusion measurement of vein-fillings of calcareous rocks and on hydrothermal precipitations of the caves). Karszt és Barl 1980(II):9–18
Gázquez F, Calaforra JM (2013) Origin of double-tower raft cones in hypogenic caves. Earth Surf Proc Land 38(14):1655–1661
Győri O, Poros Z, Mindszenty A, Molnár F, Fodor L, Szabó R (2011) Budai-hegységi paleogén karbonátos kőzetek diagenezistörténete (diagenetic history of the Paleogene carbonates, Buda Hills, Hungary). Földtani Közlöny 141(4):341–361 (in Hungarian with English abstract)
Haas J (2004) Triász (Triassic). ELTE, Eötvös Kiadó
Hill CA (1987) Geology of Carlsbad cavern and other caves in the Guadalupe Mountains. New Mexico and Texas, New Mexico Bureau of Mines and Mineral Resources, Bulletin, p 117
Hill CA (1990) Sulfuric acid speleogenesis of Carlsbad Cavern. Am Ass Petrol Geol Bull 74(1):1685–1694
Hill CA (1995) Sulfur redox reactions, native sulfur, Mississippi Valley-type deposits and sulfuric acid karst. Environ Geol 25:16–23
Hill CA, Forti P (1997) Cave minerals of the World. National Speleological Society, Huntsville
Horányi G, Leél-Őssy Sz (1980) A hegyitej ásványtani vizsgálata magyarországi előfordulásokon (Mineralogical examination of Hungarian Moonmilch). Manuscript, ELTE, Department of Physical and Historical Geology
Jakucs L (1994) A Budai-hegység hidrotermális karsztja (the hydrothermal karst of Buda Mountains). Földrajzi Értesítő 43(3–4):235–246
Jaskó S (1948) A Mátyás-hegyi-barlang (the Mátyás-hegy Cave). MÁFI Évi Jelentés 10:133–147

Kele S, Scheuer G, Demény A, Shen CC, Chiang HW (2009) U-series dating and isotope geochemical study of the Gellért Hill (Budapest) travertine. Cent Eur Geol 52:199–224

Kele S, Scheuer G, Demény A, Shen C-C, Chiang HW (2011) A Rózsadomb (Budapest) édesvízi mészköveinek U/Th sorozatos kormeghatározása és stabilizotóp-geokémiai vizsgálata (Uranium-series dating and geochemical analysis of the travertines located on the Rózsadomb, Budapest). Földtani Közlöny 141:293–312 (in Hungarian with English abstract)

Kiss A, Takács-Bolner K (1987) Újabb jelentős feltárások a Pál-völgyi-barlangban (new important discoveries in Pál-vögyi Cave) Karszt és Barl 38

Klimchouk A (2007) Hypogene Speleogenesis: Hydrogeological and Morphogenetic Perspective. Special Paper No. 1, National Cave and Karst Research Institute, Carlsbad

Klimchouk AB, Ford DC, Palmer A, Dreybodt W (2000) Speleogenesis. Evolution of Karst aquifers. National Speleological Society, Huntsville

Klimchouk A, Auler AS, Bezerra FHR, Cazarin CI, Balsamo F, Dublyansky Y (2016) Hypogenics origin, geologic controls and functional organization of a giant cave system in Precambrian carbonate, Brazil. Geomorphology 253:385–405

Kovács J, Müller P (1980) A Budai-hegyek hévizes tevékenységének kialakulása és nyomai (Evolution and traces of hydrothermal activity in the Buda Mountains). Karszt és Barlang 1980(II):93–98

Kraus S (1991) A budai barlangok hévizes karbonátkiválásai (Carbonate precipitations of thermal water origin of Buda). Karszt és Barlang 1990(2):91–97

Kraus S (1993) A Szemlő-hegyi-barlang vízszintváltozásai (Water level changing of Szemlő-hegy Cave). Karszt és Barlang 1993(I–II):47–53

Kraus S (2010) Borsókövek és cseppkövek váltakozása (Alternating of botryoids and dripstones). Karszt és Barlang 2009(I–II):41–42

Krolopp E, Schweitzer F, Scheuer G, Dénes G, Kordos L, Skoflek I, Jánossy D (1976) A budai Várhegy negyedkori képződményei (quaternary forms of Várhegy in Buda). Földtani Közlöny 106: 193–228

Laptyev FF (1939) Agresszivnoje dejstvije vody na karbonatnyje porody, gipsy i betony. Moscow–Leningrad (in Russian)

Leél-Őssy Cs, Leél-Őssy Sz, Adamkó P (2007) A Citadella-kristálybarlang (The Citadella Crystal Cave). Karszt és Barlang 2007(I–II): 67–78

Leél-Őssy S (1957) A Budai-hegység barlangjai (The caves of Buda Mountains). Földrajzi Értesítő VI(2):155–169

Leél-Őssy Sz (1995) A budai Rózsadomb és környékének különleges barlangjai (Special caves of Rózsadomb on Buda and its environs). Földtani Közlöny 125(3–4):363–432 (in Hungarian with English abstract)

Leél-Őssy Sz (1997) A József-hegyi-barlang (Budapest) termálkarsztos keletkezése és fejlődése (Thermal karstic genesis and development of József-hegy Cave, Budapest). PhD thesis, Hungarian Academy of Sciences

Leél-Őssy Sz (2014) Kristálybarlang a nagyváros alatt. A budapesti József-hegyi-barlang (Crystal cave under the big city. The József-hegy Cave in Budapest). GeoLitera, SZTE TTIK Geographical and Geological Dept, Szeged

Leél-Őssy Sz (2015) Caves in the Buda Mountains. In: Lóczy D (ed) Landscapes and landforms of Hungary. Springer, Heidelberg, pp 121–128

Leél-Őssy Sz, Surányi G (2003) The peculiar hydrothermal caves in Budapest (Hungary). Acta Geol Hung 46(4):407–436

Leél-Őssy Sz, Szanyi G, Surányi G (2011) Minerals and speleothems of the József-hegy Cave (Budapest, Hungary). International Journal of Speleology 40(2):191–203

Mádl-Szőnyi J, Pulay E, Tóth Á, Bodor P (2015) Regional underpressure: a factor of uncertainty in the geothermal exploration of deep carbonates, Gödöllő Region. Hung Environ Earth Sci 74(12):7523–7538. doi:10.1007/s12665-015-4608-z

Mádl-Szőnyi J, Tóth Á (2015) Basin-scale conceptual groundwater flow model for an unconfined thick carbonate region. Hydrogeol J 23(7):1359–1380. doi:10.1007/s10040-015-1274-x

Mindszenty A, Mádl-Szőnyi J, Pethő SL, Kovács J, Müller I, Fodor L, Kádár M, Angelus B, Erőss A, Nyúl K, Poyanmehr Z, Varga R (2000) A Rózsadombi termálkarszt monitoring optimalizálása. Zárójelentés a 2000. évben végzett munkáról (Optimizing of rózsadomb thermal karst monitoring. Final report of the work in 2000) manuscript. ELTE Department of Applied and Environmental Geology, p 111

Molnár F, Gatter I (1994) Magyarországi üledékes és hidrotermás baritkristályok összehasonlító ásványtani-genetikai vizsgálata (comparative mineralogical-genetical examinations of Hungarian sedimentological and hydrothermal barite crystals). Földtani Közlöny 124(1):43–57

Müller P (1989) Hydrothermal paleokarst of Hungary. In: Bosák P, Ford DC, Glazek J, Horácek J (eds) Paleokarst—a systematic and regional Review. Academia, Praha, Elsevier, Amsterdam, pp 155–163

Müller P, Sárváry I (1977) Some aspects of development in Hungarian speleology theories during the last 10 years. Karszt és Barlang (Special Issue):53–59

Nádor A (1991) A Budai-hegység paleokarszt jelenségei és fejlődéstörténetük (The paleokarst phenomenas and its evolutionary on Buda Hills). PhD Dissertation, ELTE Department of Physical and Historical Geology

Nádor A (1992) Mineralogy and stable isotope geochemistry of spelean carbonates from hydrothermal caves. Proc Conf Karst Cave Res, Jósvafő 1991:23–29

Nagy S (2008) A Budai-hegység hidrotermás folyamatainak szerepe a Bátori-barlang és a Ferenc-hegyi-barlang kialakulásában (The role of the hydrothermal activity in the genesis of Bátori Cave and Ferenc-hegy Cave in Buda Hills). Manuscript, MSc Thesis, ELTE TTK, Department of Mineralogy

Palmer AN (2007) Cave geology. Cave books, Dayton

Palmer AN, Palmer M, Davis D (1991) Geology and origin of Lechuguilla Cave. In: Widmer U (ed) Lechuguilla jewel of the underground. Speleoprojects, Basel

Pávai-Vajna F (1930) A forró oldatok, gőzök és gázok szerepe a barlangképződésnél (the role of the hot solutions and vapours and gases in the speleogenesis). Hidrológiai Közlöny 10:115–122

Pethő S (1996) A budapesti József-hegyi-barlang egyes képződményeinek vizsgálata, különös tekintettel a borsókövekre (examination of formations of József-hegyi cave in Budapest, considering of botryoids) Manuscript ELTE TTK, Department of Physical and Historical Geology

Piccini L (2000) Il carsismo di origine idrotermale del Colle di Monsummano (Pistoia–Toscana)[The hydrothermal-origin karst from the Monsummano Hills (Pistoia–Tuscany]. Le Grotte d'Italia 1:33–43

Plummer LN (1975) Mixing of seawater with calcium carbonate groundwater. Geol Soc Am Memoirs 142:219–236

Poros Z, Mindszenty A, Molnár F, Pironon J, Győri O, Ronchi P, Szekeres Z (2012) Imprints of hydrocarbon-bearing basinal fluids on a karst system: mineralogical and fluid inclusion studies from the Buda Hills, Hungary. Int J Earth Sci (Geol. Rundsch.) 101:429–452

Réthly A (1952) A Kárpát-medence földrengései 455–1918 (the earthquake of Carpathian Basin 455–1918). Akadémiai Kiadó, Budapest

Runnels DD (1969) Diagenesis, chemical sediments and the mixing of natural waters. Jour of Sed Petr 39:1188–1201

Sásdi L (1993) A Budai-hegység paleokarsztjai és fejlődéstörténetük. II. Termális hatást tükröző paleokarsztok (The palaeokarsts of Buda Mountains and their developing. II. The thermal effect reflecting palaeokarsts). Karszt és Barlang 1993(I–II):39–46

Schafarzik F (1921) Visszapillantás a budai hévforrások fejlődéstörténetére (Back-glance for developing of Buda thermal springs) Hidrológiai Közlöny I914

Sylvester AG (1988) Strike-slip faults. Geol Soc Am Bull 100: 1666–1703

Szabó V, Fórizs I, Hałas S, Pelc A, Deák J (2009) A budapesti hévizek szulfátjának eredete stabilizotópos mérések alapján (the origin of sulphate-content of thermal water of Budapest, based on stable isotope measurings). A Miskolci Egyetem Közleményei, A sorozat, Bányászat 77:73–81

Szanyi G, Surányi G, Leél-Őssy Sz (2012) Cave development and Quaternary uplift history in the Central Pannonian Basin derived from speleothem ages. Quat Geochronol 14:18–25

Takács-Bolner K (1989) Regional and special genetic marks of the Pál-völgy Cave, the largest cave of thermal water origin in Hungary. Proceedings of the 10th International Congress of Speleology, Budapest, III, pp 819–822

Takács-Bolner K (1993) Ritka karbonátkiválás típusok (rare carbonate precipitation types). Karszt és Barlang 1993(1–2):29–38

Takács-Bolner K, Kraus S (1989) The results of research into caves of thermal water origin. Karszt és Barlang (Special Issue):31–38

Takács-Bolner K, Kiss A (2004) Pál-völgyi-barlang—egy felfedezés 100 éve (The Pál-völgy Cave—100 years of a discovery). Danube-Ipoly National Park, Budapest

Tcalenko JS (1970) Similarities between shear zones of different magnitudes. Geol Soc Am Bull 81(6):1625–1640

Telegdi-Roth K (1914) A Magyar Középhegység északi részének felső oligocén rétegeiről, különös tekintettel az egervidéki felső oligocénre (about the upper Oligocene layers of the northern part of Hungarian Middle-mountains, considering of upper Oligocene of Eger). Koch Emlékkönyv, pp 111–126

Tisato N, Saur F, Bernasconi SM, Bruijn RH, De Waele J (2012) Hypogenic contribution to speleogenesis in a predominant epigenic karst system: a case study from the Venetian Alps, Italy. Geomorphology 151:156–163

Tóth J (1999) Groundwater as a geologic agent: an overview of the cases, processes and manifestations. Hydrogeol J 7(1):1–14

Viehmann I (1992) Experimental methods in studying the cave rafts. Theor Appl Karstology 5:213–215

Virág M, Kálmánfi-Ast H, Mindszenty A (2013a) Barlangszintek, barlangi kiválások és travertínók térbeli jellemzése (Spatial characterization of cave levels, cave minerals and travertines). In: (Mindszenty A (ed.): Budapest: földtani értékek és az ember. Városgeológiai tanulmányok (Budapest: geoheritage and humans—urban geological studies) („In urbe et pro urbe"). ELTE Eötvös Kiadó, Budapest, pp 259–263

Virág M, Leél-Őssy Sz, Mindszenty A (2013b) Szpeleológiai adottságok. A felszín alatti víz oldóhatásának tanúi: a budai barlangok (Speleological fundamentals. Speleogenesis in the Buda Thermal Karst). In: Mindszenty A (ed) Budapest: földtani értékek és az ember. Városgeológiai tanulmányok (Budapest: geoheritage and humans—urban geological studies) („In urbe et pro urbe"). ELTE Eötvös Kiadó, Budapest, pp 104–111

Virág M (2016) Történeti áttekintés a budai barlangok keletkezéséről—a klasszikus karsztfejlődéstől a hipogén barlangképződésig (speleogenesis in the Buda Thermal Karst—a historical review from the "classical" epigenic to hypogenic theories). Karszt és Barl 2012–14:24–46 (in Hungarian with English abstract)

Vörös P, Virág M, Mindszenty A, Bendő Z, Németh T, Leél-Őssy Sz (2013) Eocén kőzeteket átszelő repedéskitöltésekhez kapcsolódó elváltozott zónák a budai barlangokban (Altered zones along the vein-filling mineral paragenesis in Eocene host rocks in the caves of Buda Thermal Karst). In: Mindszenty A (ed) Budapest: földtani értékek és az ember. Városgeológiai tanulmányok (Budapest: geoheritage and humans—urban geological studies) ("In urbe et pro urbe"). ELTE Eötvös Kiadó, Budapest, pp 34–39

Wein Gy (1977) A Budai-hegység tektonikája (tectonics of Buda Mountains). MÁFI, Budapest

Hypogene Caves in Slovakia

19

Pavel Bella and Ľudovít Gaál

Abstract

During the Alpine orogeny of the Western Carpathians, hypogene caves have originated in different settings and epochs. Several caves of hydrothermal origin in crystalline limestones and metasomatic secondary quartzites (metasomatic silicites) are known in the central zone of the Štiavnica stratovolcano, Štiavnické vrchy Mountains. The early phases of speleogenesis in the crystalline limestone near Sklené Teplice Spa were caused by post-magmatic dissolution linked either to the emplacement of subvolcanic granodiorite intrusions during Late Badenian time or to the spatially associated Late Sarmatian epithermal system. Speleogenesis in metasomatic secondary quartzites in the Šobov quarry is related to deep-seated hydrothermal processes associated with a diorite intrusion in the northern part of the central zone of the Štiavnica stratovolcano during its pre-caldera evolution phase in Upper Badenian. Unusual caves in metasomatic magnesite, with mineralogical evidences of their hydrothermal origin, were investigated in the Revúcka vrchovina Mountains. Paleokarst geoda-like cavities and small hydrothermal caves occur in nappe structures of Triassic carbonates that were uplifted within the Tatra-Fatra belt of core mountains (many of these cavities are integrated into younger and larger non-hypogene caves). Cavities with thermal water in underlying and faulted Mesozoic carbonates (covered by Neogene or Paleogene sedimentary rocks) were identified by boreholes in some intermontane basins (Rimavská kotlina Basin, Liptovská kotlina Basin). A phreatic shaft formed by progradational collapse of non-carbonate beds disrupted by artesian karstification of underlying carbonates occurs at Tornaľa Town in the Rimavská kotlina Basin. Several caves with hypogene morphologies have originated along marginal faults of horst structures or fault edges of horst–graben structures (speleogenesis by thermal or slightly heated ascending waters, but mineralogical evidences of hydrothermal karstification were not found).

Keywords

Artesian karstification • Hydrothermal cave • Post-magmatic dissolution • Magnesite karst • Cavernous metasomatic secondary quartzites • Western Carpathians

P. Bella (✉) · Ľ. Gaál
State Nature Conservancy of the Slovak Republic, Slovak Caves Administration, Hodžova 11, 031 01 Liptovský Mikuláš, Slovakia
e-mail: pavel.bella@ssj.sk; Pavel.Bella@ku.sk

Ľ. Gaál
e-mail: ludovit.gaal@ssj.sk

P. Bella
Pedagogical Faculty, Department of Geography, Catholic University in Ružomberok, Hrabovská cesta 1, 034 01 Ružomberok, Slovakia

1 Introduction

More than 7100 caves are known in Slovakia (Central Europe), which are mainly formed in carbonate rocks (limestones, dolomitic limestones, dolomites, magnesite, and travertine). Karst areas, orographically belonging to the Western Carpathians, cover more than 2700 km^2. More than

© Springer International Publishing AG 2017

A. Klimchouk et al. (eds.), *Hypogene Karst Regions and Caves of the World*,
Cave and Karst Systems of the World, DOI 10.1007/978-3-319-53348-3_19

250 caves are formed in andesite, basalt and their volcanoclastics, sandstone, granite, metasomatic secondary quartzites, or some other unsoluble rocks. Epigene caves (vadose solution caves sculptured by seeping meteoric waters, fluvially modeled vadose and epiphreatic caves, phreatic solution caves, crevice caves, frost weathering caves, etc.) are much more numerous. Although hypogene caves are less common, several of them represent remarkable and rare natural phenomena. This chapter reports the various types of hypogene caves that increase the diversity of genetic types of caves in Slovakia. Whereas some hypogene caves are not sufficiently investigated, also supposed localities of hypogene speleogenesis and related problems for further research are outlined and partially analyzed.

2 Geological Background

The Western Carpathians represent the folded-nappe mountain arc with a complicated geological structure, which has been formed since Paleozoic. The Alpine orogeny affected the area in several stages from Jurassic to Neogene (the Carpathian Mountains are part of the northern branch of the Alpine-Himalayan system). Parts of Tethys Ocean were subducted under the African plate, and Western Carpathian blocks were thrusted over the margin of the Eurasian plate. Tectonic units of the Western Carpathians are arranged in a belt-like order, with the Outer Western Carpathians in the north (Carpathian Foredeep and flysch belt), Central Western Carpathians (klippen belt, Tatra-Fatra zone of core mountains, Vepor and Gemer zones), and Inner Western Carpathians in the south (Meliata, Bükk, Bakon and Zemplín zones). The Jurassic–Cretaceous tectonic structure was later changed by post-nappe complexes—Paleogene and Neogene intermontane basins and the Tertiary and Quaternary neovolcanites (see Andrusov 1958; Mišík et al. 1985; Maheľ 1986; Plašienka et al. 1997; Plašienka 1999; Hók et al. 2001, 2014 and others). The major part of the Western Carpathians arc lies in Slovakia, it extends also to the territory of northeastern Austria, eastern and northeastern Moravia (Czech Republic), southern Poland, and northern Hungary.

Carbonate rocks mostly occur in the Central Western Carpathians (Tatry Mountains, Nízke Tatry Mountains, Chočské vrchy Mountains, Veľká Fatra Mountains, Malá Fatra Mountains, Strážovské vrchy Mountains, Malé Karpaty Mountains, Muránska planina Plateau, Slovenský raj, Slovenský kras, etc.). Surface and subsurface karst landforms preferentially formed in pure Middle Triassic Gutenstein, Steinalm, and Wetterstein limestones, also in Upper Triassic Waxenec and Dachstein limestones, originated on the lagoon carbonate platforms of extensive continental shelfs.

From a geomorphological and morphostructural viewpoint, karst areas in Slovakia occur in middle mountain (plateau karst, dissected karst of massive ridges, horsts, and combined fold-fault structures, dissected karst of monoclinal crests and ridges, karst of klippen structures, karst of travertine cascades), high mountain (karst on fold-fault and inclined structures), and intermontane basin positions (karst of isolated blocks and monadnocks, karst of foothill plains and terraces, karst of travertine mounds and cascades) (Jakál 1993). Cryptokarst in lenses of Devonian crystalline limestones (marble) and Carboniferous magnesite within impervious rocks (mostly schists and phyllites) sporadically occur in the Slovenské rudohorie (Slovak Ore) Mountains (Gaál and Ženiš 1986; Ženiš and Gaál 1986a, b).

In Slovakia, hypogene caves have originated in diverse settings (in limestones, magnesite, and metasomatic secondary quartzites by several processes) and epochs (from the Cretaceous to the present). They are known from underlying carbonate structures of intermontane basins (Rimavská kotlina Basin), nappe structures of carbonates in uplifting fold-fault and horst mountains or at fault edges of mountains (Nízke Tatry Mountains), and fractured carbonates hydrothermally altered along epithermal veins and stockworks (Štiavnické vrchy Mountains), as well as from lenses of magnesite (Revúcka vrchovina Mountains) and bodies of metasomatic secondary quartzites (Štiavnické vrchy Mountains). Some limestone caves are entirely hypogene, and in several cases, hypogene cavities were integrated into younger and larger epigene caves (Fig. 1). Hypogene speleogenesis is linked to the complicated geological structure and development of the Western Carpathians, especially during the Alpine orogeny.

3 Hypogene Speleogenesis in Diverse Settings

During the early stages of the Alpine orogeny, the hydrothermal karst in the Central Western Carpathians originated along the tectonically predisposed thrust planes of cover nappes in the Lower Cretaceous. Cellular dolomite (Rauwacke) and associated breccias occurring at these thrust planes are considered as a product of this hydrothermal system (Činčura and Milovský 2000). Considering the complicated geological evolution of the Western Carpathians (folded-nappe structures, horst and graben structures, volcanism), hydrothermal caves (and cavities) in Slovakia have been originated in several, mutually different geological or hydrogeological conditions and during several geological epochs to the present (Bella et al. 2009; Bella and Gaál 2012, 2014a).

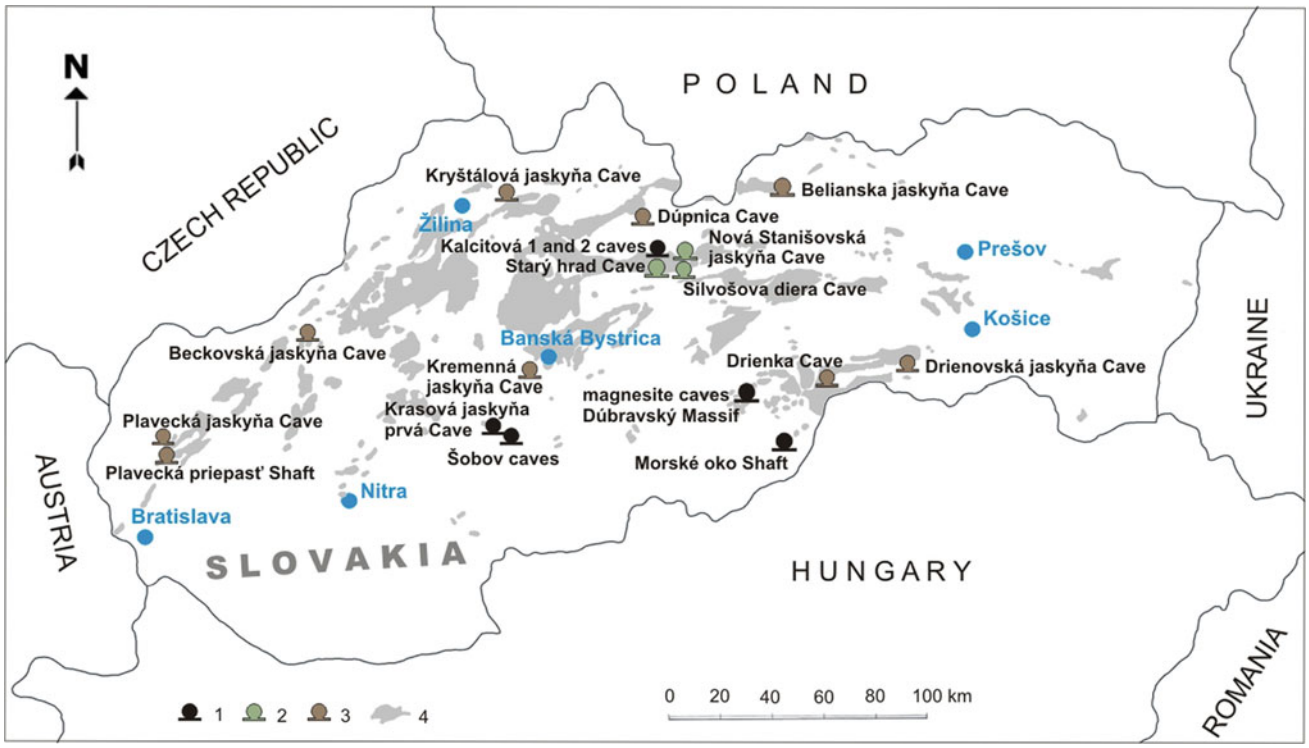

Fig. 1 Map of Slovakia with location of described caves (*1* caves of hypogene origin, *2* caves with exposed hypogene cavities, *3* caves originated by water ascending along faults with some features of hypogene origin, *4* karst areas)

3.1 Faulted and Intrastratal Structures of Mesozoic Carbonates in Intermontane Basins

The occurrence of thermal waters in intermontane basins (grabens) is associated with deep fault structures of karstified Mesozoic carbonates covered by Paleogene and Neogene sedimentary rocks. The flooded shaft named Morské oko (Sea Eye), with a depth of 38 m, is located at Tornaľa Town in the eastern part of the Rimavská kotlina Basin (Fig. 2). It is formed in the Oligocene–Miocene strata of calcareous siltstone. This vertical pit is an outflow of mineralized and slightly heated artesian waters (29–35 L/s, average temperature 16.2 °C, calcium bicarbonate type, mineralization 769 mg/L including sulfates) from underlying Mesozoic carbonates, which are replenished by infiltrating meteoric water from the southwestern fault edge of the Silická planina Plateau (Orvan 1960, 1973; Gaál 1987, 2008; Zakovič et al. 1994; Gaál et al. 2007). The average annual air temperature in the area is 9 °C. The Morské oko Shaft represents a collapse pit originated due to intensive karstification of underlying carbonates in artesian conditions (Bella and Gaál 2012, 2014a). By morphology, it resembles deep collapse depressions (sinkholes) named *obruks* in Turkey that originated in consequence of hypogene karstification (see Bayari et al. 2009; Bayari et al. Chap. 27). The water from the Morské oko Shaft belongs to low heated waters (called *teplica* in Slovak) with their temperature from 15 to 20 °C (they do not freeze in winter). According to Spötl et al. (2009), caves originated by water heated less than 50 °C are assigned to low-temperature hydrothermal karst.

Some solution cavities in Steinalm limestone of the Silicicum Unit, several meters long and with hot waters of 38–49 °C, were found by boreholes at depths of 1930–2515 m below ground surface in the Rimavská kotlina Basin (Straka 1986; Gaál 1987). They originated by corrosion of hydrothermal water circulating along deep tectonic discontinuities in conditions of intrastratal karst (Bella et al. 2009; Bella and Gaál 2012, 2014a). Indications of intrastratal hydrothermal karst development are known also in some other intermontane basins. In the Chočské podhorie Foothills on the northwest edge of the Liptovská kotlina Basin, a karst cavity with an inflow about 100 L/s of water at 32 °C was found by borehole BJ-101 at the depth of 77.6–87.0 m in the middle part of the spring area of Lúčky Spa (Klago 1984).

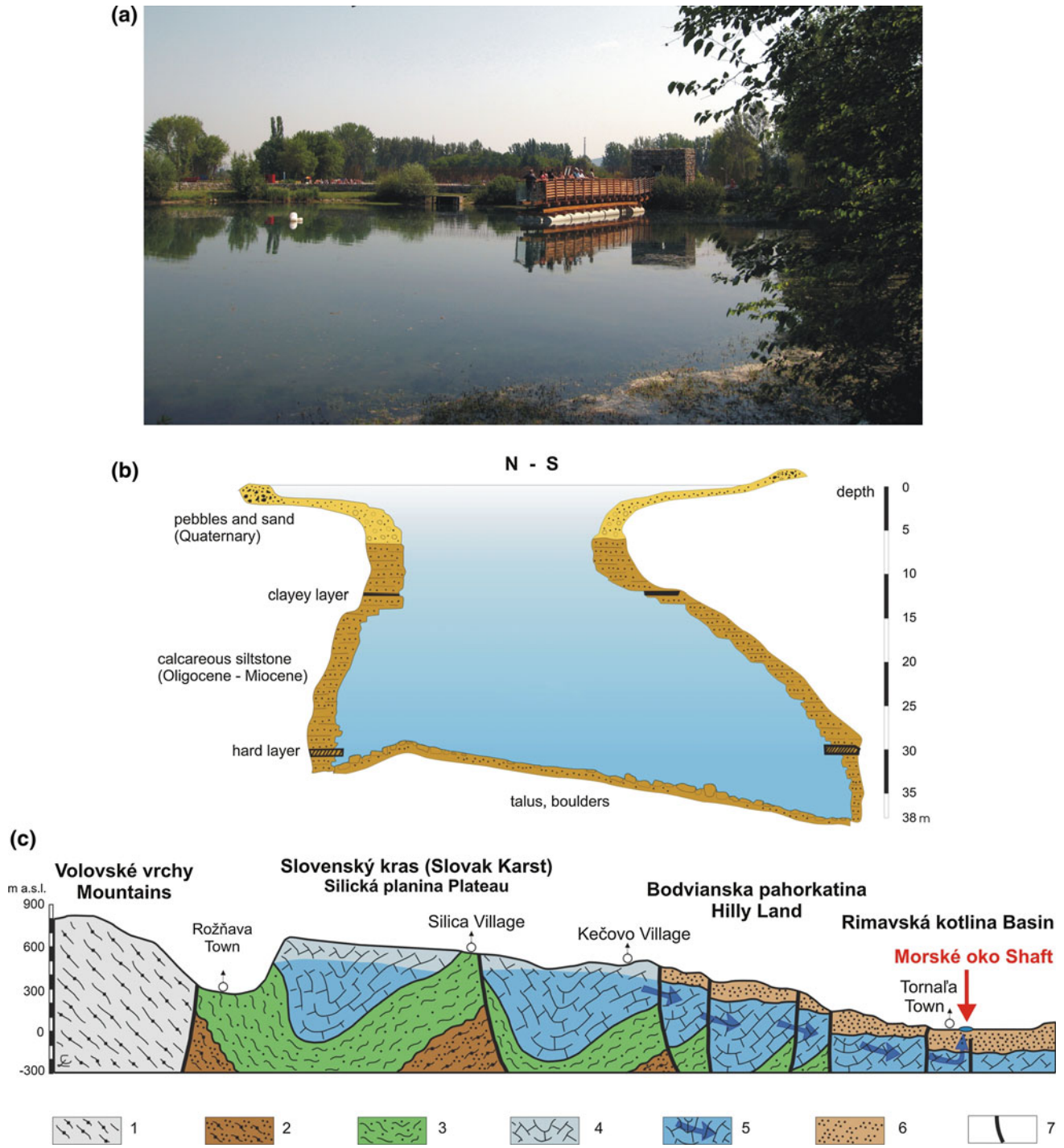

Fig. 2 Morské oko Shaft, Rimavská kotlina Basin: **a** flooded collapsed shaft with an outflow of mineralized and slightly heated artesian waters (photograph taken by P. Bella), **b** geological section through the shaft (topography after J. Hovorka, modified by Ľ. Gaál), **c** hydrogeological section through the western part of the Slovenský kras (Slovak Karst) and eastern part of the Rimavská kotlina Basin showing the circulation of underground karst water to the Morské Oko Shaft: *1* graphite-sericite schists, phyllites (Gemericum), *2* limestones, shales (Meliaticum), *3* shales (Silicicum), *4* limestones (Silicum), *5* water flow, *6* calcareous siltstones, and *7* faults (after Gaál 2008)

3.2 Significant Faults in Tectonically Fractured Nappe Structures of Mesozoic Carbonates Within Uplifting Mountains

Ascending thermal or slightly heated water flowed especially along the more significant faults disrupting the nappe structures of Mesozoic carbonates. Under such conditions, small hydrothermal caves were originated. However, hydrothermal cavities integrated into caves of multiprocess genesis are more numerous. During a later stage of their development, hydrothermal cavities became part of younger passages or other underground voids created by waters of meteoric origin. Mostly, they are visible as spherical hollows at the edges of the younger parts of the caves.

In several caves on the northern part of the Nízke Tatry Mountains, e.g., Silvošova diera Cave, Nová Stanišovská jaskyňa Cave, and Starý hrad (Old Castle) Cave, large calcite crystals of hydrothermal origin were found in geode-like cavities cut by younger passages of fluvial origin. The Kalcitová (Calcite) 1 and 2 caves in the upper part of the Mt. Poludnica (1548 m asl) are 7 and 12 m long. These hydrothermal cavities were probably formed before the Pliocene. They originated in the Miocene or even during orogenic phases in the Paleogene (Orvošová et al. 2004; Orvošová 2005; Orvošová and Hurai 2008).

Many calcite crystals were formed in the 57-m-long Kryštálová jaskyňa Cave (Crystal Cave) at Mt. Malý Rozsutec (1343 m asl) in the northern part of the Malá Fatra Mountains. Renčko et al. (2013) noted its hydrothermal origin, but only based on measuring quanta of radioisotopes in calcite and its comparison with relevant data from carbonate rocks formed in the surrounding mountains. This assumption about the hydrothermal origin of the Kryštálová jaskyňa Cave must be verified by analyses of fluid inclusions in calcite crystals as well as stable isotope composition of calcite crystals and host rock.

3.3 Mesozoic Carbonates Below or Close to Miocene Stratovolcanoes

The origin of hydrothermal caves in the Štiavnické vrchy Mountains near Sklené Teplice Spa is linked with the complex development and metallogeny of ore deposits of the Miocene Štiavnica stratovolcano, which was formed in several stages from Badenian to Sarmatian (see Lexa et al. 1999; Konečný and Lexa 2001; Chernyshev et al. 2013).

The Krasová jaskyňa prvá Cave (First Karst Cave) originated by multiple dissolution of Middle Triassic, mostly metamorphosed Gutenstein dolomites and limestones, and Steinalm limestones of the Hronicum Unit by hydrothermal solutions (Bella et al. 2011b, c, 2016; Bella and Gaál 2012, 2014a). Hydrothermal alteration occurred in each of these carbonate types, mainly along veins and stockworks. Steinalm limestones have been recrystallized to marble. The entrance artificial shaft leading to the cave, 10 m deep, was dug by miners 200–300 years ago. A natural cave opening to the surface is unknown. Original cave passages and several smaller geode-like cavities were encountered at the base of the shaft. Two blind mine tunnels, 20 and 16 m long, were dug along ore veins that intersect the cave. The length of the cave and mine tunnels is approximately 100 m with a vertical range of 21 m. The total depth with the entrance artificial shaft is 31 m (Ivan 1991). The cave is a downsloping passage with several stair steps controlled by faults of E–W and N–S directions (Fig. 3).

The hydrothermal origin of this cave is evidenced by irregular spherical morphologies sculptured by rising thermal water, fluid inclusions in calcite crystals, hydrothermal alteration of host rocks, and clays of hydrothermal origin composed variably of smectite-kaolinite and goethite. Stable isotopes and fluid inclusions indicate two hydrothermal phases of cave development. Geode-like cavities with calcite crystals and druses originated during the first hydrothermal phase (115–170 °C, mostly heated meteoric water). The main passage with spherical hollows originated during the second hydrothermal phase (112–180 °C, heated meteoric waters mixed with hydrothermal fluid containing some amounts of magmatic origin). The smectite-kaolinite and goethite mineral associations are related to both phases. Smaller spherical hollows uncovered during the excavation of the northern mine tunnel resemble the geode-like ones (sensu Audra et al. 2009). Other geodes and geode-like cavities, visible in some cave walls, were intersected and integrated into the main cave passage during the most important development phase of the cave. Also, a fault zone with illite and quartz crystals was uncovered on the cave wall. The origin of the quartz crystals and illite has been connected to the hydrothermal origin of adjacent large epithermal vein systems (before the formation of the cave). Numerous small cupolas, ceiling pockets and holes, upward-convex arches, rising wall channels, and oval chimneys occur in the main cave passage (Fig. 3). The chain of coalesced cupola-like forms and upward-convex arches that extends from the lower to upper part of the cave indicates that water circulated upward in the past (Bella et al. 2016). The vertical conduit in the lowest part of the cave resembles a feeder (sensu Klimchouk 2007, 2009) through which fluids were rising into the cave. Probably, this cave is the fragment of a larger three-dimensional cave system.

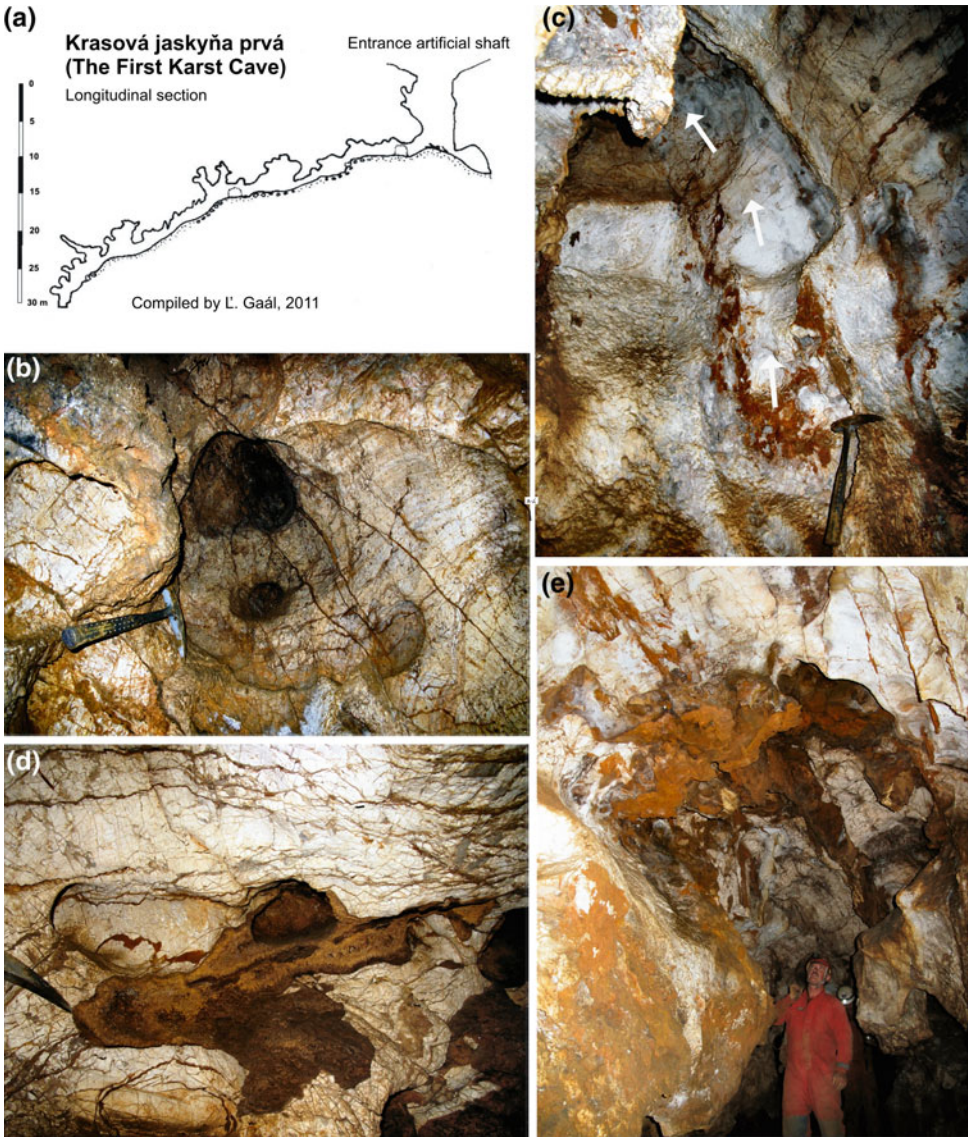

Fig. 3 Krasová jaskyňa prvá Cave, Štiavnické vrchy Mountains: **a** simplified longitudinal section through the cave and entrance artificial shaft, **b** ceiling blind spherical hollows, **c** rising wall channel with asymmetrical dissolution depressions on a steep wall originated by ascending water flow, **d** mineral fills of primary cavities exposed on the wall of younger main passage, and **e** morphology of main passage in the *upper part* of the cave (all photographs taken by P. Bella)

Hydrothermal processes responsible for the origin of Krasová jaskyňa prvá Cave were most likely part of a complex extensive system forming hydrothermal ore deposits 3 km from the cave. The hydrothermal deposits evolved during various stages of the development of the Štiavnica stratovolcano. The deposits include pre-caldera stage skarn–porphyry systems (Sklené Teplice Spa—Vydričná dolina Valley and Kozí vrch Hill) and post-caldera stage Ag–Au epithermal vein systems (Windischleuten vein). The Sklené Teplice system is believed to have caused silicification of carbonates north of the cave at Mt. Bukovec (707 m asl), while the Windischleuten vein system south of the cave is related to the horst uplift in the center of the caldera. The northwest part of the Windischleuten vein cuts into Triassic limestones, dolomites, and siliceous sediments of the Veľký bok Group, in which the First Karst Cave is developed (Bella et al. 2011b, c, 2016).

3.4 Lenses of Fractured Metamorphosed Rocks of Hydrothermal or Metasomatic Origin

Hydrothermal caves in magnesite and metasomatic secondary quartzites have a character of spherical, geode-like cavities or elongated fissures controlled by faults along which thermal fluids flowed. They represent isolated cavities at a depth of several tens to hundreds of meters below the surface and were discovered during the excavation of mine tunnels.

3.4.1 Caves in Magnesite

Magnesite lenses in Slovakia occur in the Slovenské rudohorie (Slovak Ore) Mountains, in the 120-km-long Carboniferous rock belt between Lučenec and Košice towns, located along the boundary zone between the Gemeric and Veporic tectonic units of the Western Carpathians (in the

close vicinity of the Lubeník-Margecany thrust plane separating both units). Until now, altogether 16 caves in magnesite deposits were speleologically investigated and mapped in Slovakia. Except for one, all of them are accessible only in underground mines. Generally, their lengths are between 10 and 20 m, but the longest cave reaches up to 73 m. These caves occur in Carboniferous magnesite–dolomite lenses surrounded by graphite-sericite schists or phyllites of the Gemeric Unit. Klír (1962, 1968) assumes that many karst phenomena in magnesite were formed in the Miocene.

Several investigated caves in magnesite in the Revúcka vrchovina Highlands have morphological and mineralogical evidences of hydrothermal origin including boxwork structures. These caves are featured by irregular morphology with angular protrusions of host rock or mineralizations (Ostrohovitá jaskyňa Cave and Kryštálová puklina Cave in the Dúbravský Massif; Bella et al. 2013, Fig. 4), with oval shapes (DM-7 Cave, Kryštálová jaskyňa Cave in the Dúbravský Massif without ochers; Gaál and Ženiš 1984) or round, respectively, geode-like cavities (LK-1 Cave in the Lubeník deposit; Gaál and Ženiš 1986). In addition to the dissolution of magnesite in a hydrothermal environment, probably the oxidation of Fe impurities was also active (goethite is the product of the oxidation of Fe minerals also in a hydrothermal environment). Mineral fills of hydrothermal origin (mainly crystals of calcite and dolomite), in some places also ocher, occur in these caves. Dolomite and calcite crystals have been formed during cooling of thermal fluids. They mostly grew on a brown-black mass formed by oxides of Mg (hollandite) and Fe (goethite, magnetite, hematite), which are probably residues from the decomposition of magnesite during the formation of cavities. Microthermometry of primary gaseous-liquid fluid inclusions in dolomite crystals from the Kryštálová jaskyňa Cave indicates a homogenization temperature of about 200–300 °C (Bella et al. 2013). Coincidentally, this is a temperature range similar to that of hydrothermal solutions that have formed metasomatic magnesite deposits in the Gemeric Unit (180–310 °C; Hurai et al. 2011), which host the caves.

The caves in magnesite originated due to the post-Upper Cretaceous shearing of the Alpine deformation phase, which caused the origin of the penetrative NE–SW-trending regional shear faults in the western segment of the magnesite bearing Carboniferous belt, encompassing the caves in the Podrečany, Burda, Lubeník, and Dúbrava Massif magnesite bodies. In the eastern segment of the belt with the Bankov deposit, the NW–SE-trending faults of this phase are dominant. In particular cases, the faults may represent the reactivated discontinuities of earlier Alpine phases from the Lower and Upper Cretaceous (Németh et al. 2004; Sasvári and Kondela 2007). Faults crossing the whole magnesite bodies allowed penetration of high-temperature hydrothermal solutions throughout them. The fissures were widened by a hydrothermal karstic process, accelerated by oxidation of Fe in the oxidation zone.

Low-temperature hydrothermal activity was active also in younger epochs, especially in parts of the massif below the local erosion base (Bella and Gaál 2014b). Slightly heated water of deep circulation actually rises from the Dubravský Massif to the surface through Teplá voda Spring with a constant temperature of 14.5 °C (Halečka 1983, the average annual air temperature in the area is 8 °C). Since 1986, groundwater is drained into the dewatering mine tunnel (Bajtoš 2004).

At the present, many karst cavities are already dry (hydrologically inactive or closed). They were mostly created in several developmental stages. Sasvári and Kondela (2010) classified them as fossilized karstic structures.

3.4.2 Caves in Metasomatic Secondary Quartzites

The caves in the Šobov quarry near Banská Štiavnica Town in the Štiavnické vrchy Mountains are cavernous cavities in metasomatic secondary quartzites. These metamorphic rocks originated by acid leaching and silicification of andesite porphyries by magmatic fluids associated with the emplacement of a subvolcanic diorite intrusion in the footwall of the altered andesite during the pre-caldera stage of development of the Štiavnica stratovolcano in Early to Upper Badenian (Štohl et al. 1994; Lexa et al. 1999; Konečný and Lexa 2001; Lexa 2001).

The Šobovská jaskyňa Cave is a steeply inclined oval cavity 3.5 m long with several ceiling blind hollows, developed along zones of weakness. It is a fragment of a larger cave which upper part has been cut in the upper level of the quarry. Its lower part has been exposed during excavation of the exploration mine tunnel.

The Šobovský komín Chimney is a vertical fissure cavity 6.3 m high originated along a steep to near-vertical fault (Fig. 5). Blind cupola-like hollows occur in its upper part, and small quartz crystals were found in the fissure exposed by this cavity (Bella et al. 2010, 2011b, 2016). The spherical morphology sculptured by ascending fluids, hydrothermal alteration of host rocks, and the occurrence of quartz crystals are distinct indicators of hydrothermal origin of these caves, related to a paleohydrothermal system associated with high-temperature (>200 °C), magmatic fluids of high oxidation state ("high sulfidation" or "acid sulfate" systems), which formed in two stages (see Sillitoe 1989; Hedenquist and Arribas 1999). The first (major) stage is related to rising

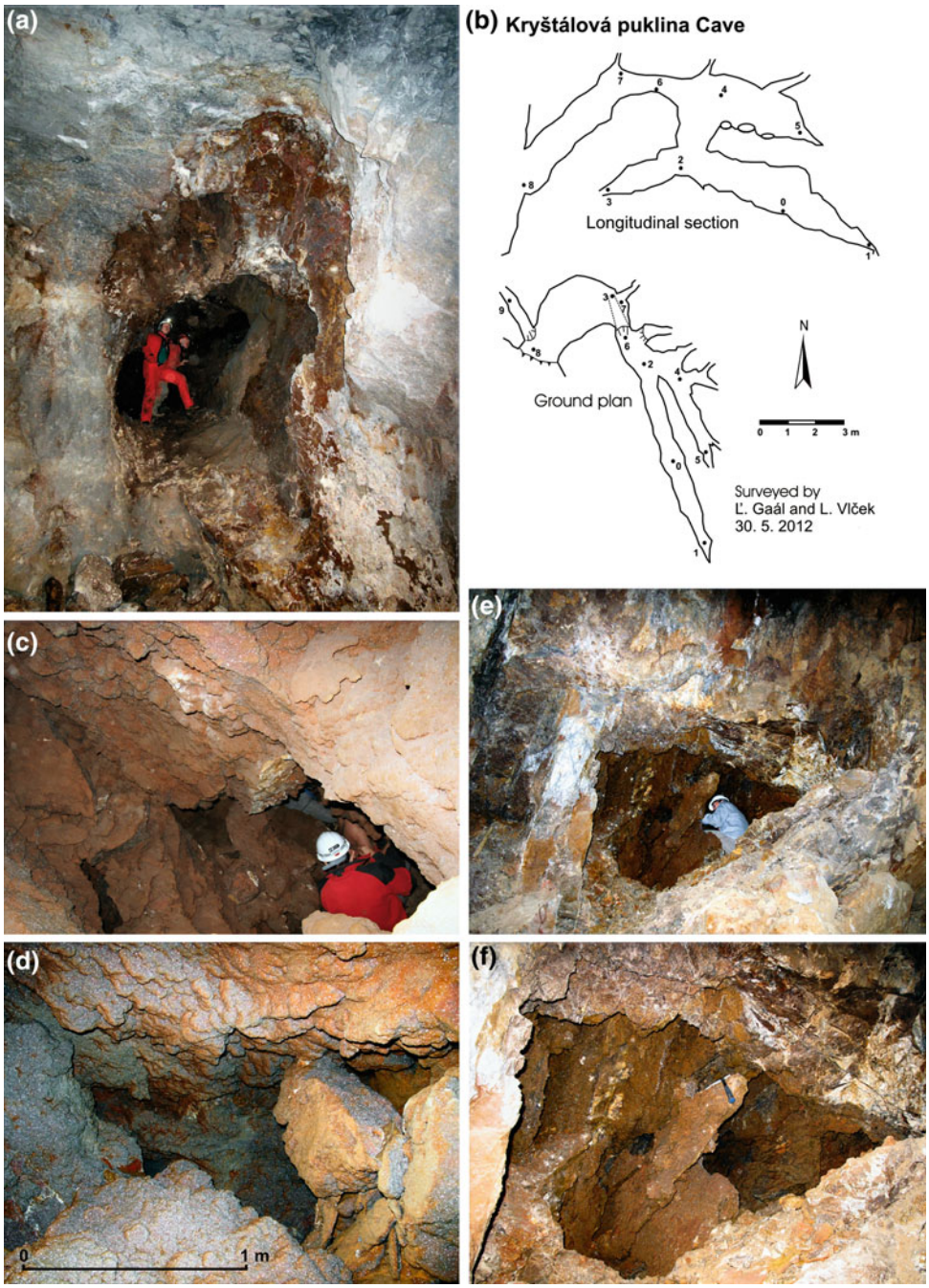

Fig. 4 Caves in magnesite of the Dúbravský Massif, Revúcka vrchovina Mountains: **a** opening of the Kryštálová puklina Cave cut by a mine tunnel, **b** plan of the Kryštálová puklina Cave, **c** sharp-edged morphology of passage controlled by fault in the Kryštálová puklina Cave, **d** *lower part* of the Kryštálová puklina Cave with walls covered by calcite and magnesite crystals, and **e** opening of the Ostrohovitá jaskyňa Cave cut by a mine tunnel, **e** sharp-edged morphology of the Ostrohovitá jaskyňa Cave (all photographs taken by P. Bella)

magmatic fluids containing HCl, SO_2, and HF that within the central upflow column condense into the hydrothermal system, forming H_2S and H_2SO_4 and a very acidic (pH 1–3) solution (Rye et al. 1992). This acidic fluid is capable of leaching most of the major elements from the host rock, resulting in vuggy textures. Cavernous and metasomatic secondary quartzites occur in the center of the system, surrounded by argillized rocks affected by advanced argillic style of alteration (including alunite, pyrophyllite, dickite, and quartz). The origin of cavities and caves in the Šobov area is probably related to this early stage of leaching (Bella et al. 2011b, 2016). Acids reacted with andesite, altering it to metasomatic secondary quartzites that are locally cavernous, especially in their upper part. The mushroom-shaped body of metasomatic secondary quartzites is surrounded by a zone rich in illite, pyrophyllite, and pyrite (Uhlík and Šucha 1997; Uhlík et al. 2001). The presence of pyrophyllite indicates a temperature in excess of 270 °C, while the amount of pyrophyllite and pyrite decreases with the increasing distance from the siliceous body.

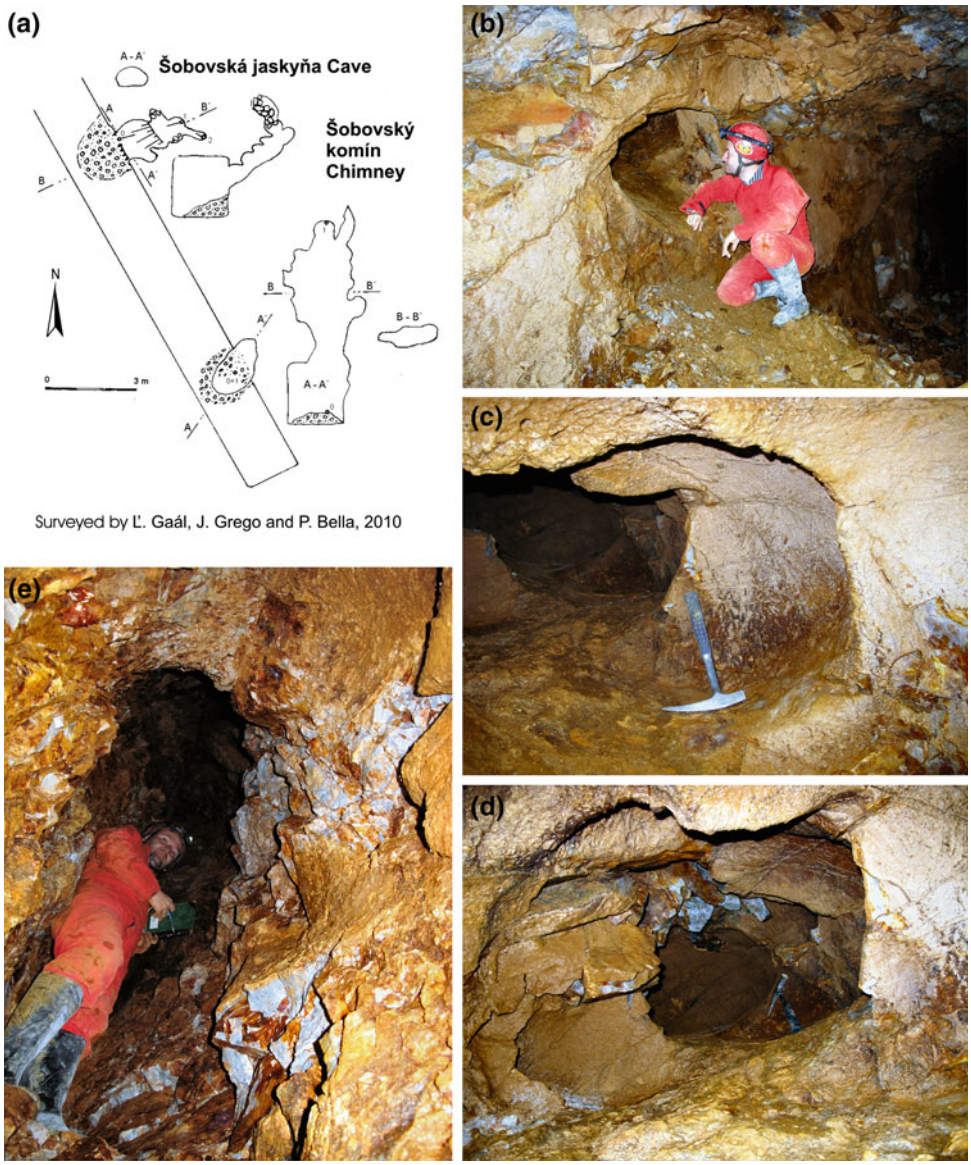

Fig. 5 Caves in the Šobov quartzite quarry, Štiavnické vrchy Mountains: **a** plan of the Šobovská jaskyňa Cave and Šobovský komín Chimney, **b** access to the Šobovská jaskyňa Cave cut by an exploration mine tunnel, **c** wall niche in the lower part of the Šobovská jaskyňa Cave, **d** rising chain of cupola-like forms in the upper part of the Šobovská jaskyňa Cave, and **e** artificial access of the Šobovský komín Chimney (all photographs taken by P. Bella)

The second stage is caused by penetration of more neutral fluids, possibly with a meteoric component. In the Šobov hydrothermal system, these flowing and cooling fluids were responsible for precipitation of quartz crystals in cavities and local opal/chalcedony veins in the upper part of the system (Bella et al. 2011b, 2016). Microthermometry of fluid inclusions in quartz crystals indicates high temperatures and low salinity during the origin of metasomatic secondary quartzites (homogenization temperatures from 200 to 300 °C; salinities lower than 2.7 wt% NaCl eq., with major components NaCl and KCl) at a minimum depth of origin 660 m beneath the surface (Oružinský and Hurai 1985). Post-hydrothermal waters have washed out these mineral fills in a later stage.

4 Supposed Localities of Hypogene Speleogenesis: Problems for Further Research

Several other caves may have a hypogene origin (Fig. 1), e.g., Beckovská jaskyňa Cave on the western edge of the Považský Inovec Mountains, Dúpnica Cave on the western edge of the Západné Tatry Mountains, and some caves on the fault zones of uplifted horst mountains and the dropped edges of lowlands or intermontane basins (Pospíšil 2004; Sluka 2014; Bella et al. 2015). The morphology of several other caves (e.g., Belianska jaskyňa Cave with numerous cupolas, Plavecká jaskyňa Cave, and Plavecká priepasť Shaft) indicates former ascending water flow during their

formation (morphological indicator of hypogene speleogenesis), but no mineral fills of hydrothermal origin were found in them. However, they have not been studied in much detail (Bella 2010; Bella et al. 2011c; Bella and Bosák 2012 and others). Osborne (2009) refers to outstanding examples of cupolas and other hypogene speleogens in the Belianska jaskyňa Cave. The hypogene origin of these caves needs to be confirmed by studying the origin of calcite crystals (analysis of fluid inclusions and stable isotopes) which are found in some of them, e.g., Dúpnica Cave, Kryštálová jaskyňa Cave in the Malá Fatra Mountains, or in the upper part of the Drienovská jaskyňa Cave in the Slovenský kras (Slovak Karst) (see Zacharov 2013). During the last years, other caves with large calcite crystals were discovered in the Veľká Fatra Mountains and Belianske Tatry Mountains.

Spherical shapes as well as the occurrence of hydrothermal minerals in the Kremenná jaskyňa Cave (Quartz Cave), Chalcedónová jaskyňa Cave (Chalcedony Cave), and Opálová jaskyňa Cave (Opal Cave) on the eastern edge of the Kremnické vrchy Mountains at Horné Pršany Village may indicate the primary hydrothermal origin of at least some parts of those small caves (Bella and Gaál 2012). They are formed in the silicified brecciated dolomite, and their lengths are 3.1–9.5 m. After the denudation of the volcanic overburden, these caves formed by selective chemical and mechanical weathering of different sized dolomite bodies; moreover, they could also have been anthropogenically modified (Vítek 1987, 1989; Mitter 1990; Beaudouin et al. 2001 and others).

In addition, conditions for hydrothermal speleogenesis due to Miocene volcanism and accompanying metallogeny of carbonates, similar to the Štiavnica stratovolcano, are also found in the Mesozoic limestones near Poniky Village in Bystrická vrchovina Highland (Starý Drienok Cave), near Tisovec Town on the Muránska planina Plateau, in the vicinity of Veľké Pole and Píla villages in the Tribeč Mountains or at Ardovo Village on the southwestern edge of the Silická planina Plateau in the Slovenský kras (Polák 1955; Bacsó 1964; Slavkay 1971; Burian et al. 1985; Slavkay and Beňka 1995). However, in these areas, detailed speleogenetic researches have not yet been performed. In the Hrádok Massif in the Ponický kras (Ponický Karst), Slavkay (1963, 1970) refers to a number of irregular cavities in size from 0.5 to 13 m (identified by boreholes), as well as several caves discovered during the excavation of the exploratory adit (including the cave at the contact of limestone and dolomite with small galena mineralization). Based on the presence of calcite crystals, Gaál (2008) postulates the hydrothermal development of the Drienka Cave on the Silická planina Plateau, as being due to the Sarmatian or Pannonian postvolcanic activity that occurred in the vicinity of the Slovenský kras.

On the basis of the morphology of underground spaces with numerous, irregularly arranged larger and smaller spherical depressions, Nicod (1976) and Choppy (1994) suggested a hydrothermal origin of the Ochtiná Aragonite Cave in the Revúcka vrchovina Mountains. It is formed in the Lower Devonian crystalline limestones, which were partly metasomatically altered into ankerite and siderite during hydrothermal ore mineralization of the Hrádok Massif by magnesium-ferrous thermal solutions in the Late Cretaceous (Gaál 2004 and others). No minerals of hydrothermal origin are found in its underground spaces (Cílek et al. 1998; Bosák et al. 2002). According to Rajman et al. (1993), ore mineralization of surrounding rocks (mainly pyrite) significantly affected the chemistry of seeping meteoric waters and increased their aggressiveness (the "pyrite-effect" responsible to speleogenetic processes has been later recognized and in more detail described in some other caves, e.g., Auler and Smart 2003; Tisato et al. 2012). Allophane was found in the cave, which probably originated by chemical weathering conditioned by the presence of pyrite (Cílek et al. 1998). Corrosion was growing also due to sulfidic weathering of mineral deposits and release of CO_2 in the decomposition of siderite and ankerite (with production of goethite) caused by meteoric water seeping along faults (Bosák et al. 2002). Kempe (2009) describes CO_2 generated by siderite weathering as a reaction causing hypogene speleogenesis around the ore bodies (the siderite started to weather when the groundwater level dropped far enough to allow oxygen-bearing seepage water to penetrate into the ore body).

5 Conclusions

In the Western Carpathians, hypogene caves were originated in different ways:

(1) as sections of deep groundwater circulation paths controlled mostly by faults disrupting karst hydrogeological structures and enabling CO_2 to rise from depths (faulted and intrastratal structures of carbonates covered with strata of Paleogene and Neogene sedimentary rocks in intermontane basins),
(2) as sections of ascending groundwater circulation paths in fractured nappe structures of carbonates in uplifting fold-fault and horst mountains or at fault edges of mountains,
(3) as sections of paleohydrothermal systems (with epithermal veins and stockworks) caused by magmatic intrusions into the fractured limestone basement of Miocene stratovolcanoes,
(4) as sections of paleohydrothermal systems in lenses or bodies of fractured metamorphic rocks of hydrothermal or metasomatic origin: (i) caves in

magnesite, containing FeO, originated by hydrothermal fluids causing the dissolution of magnesite and the oxidation of Fe minerals with the origin of Fe-hydroxides and (ii) cavernous cavities in metasomatic secondary quartzites originated within the paleohydrothermal high sulfidation system by acid leaching and silicification of andesite porphyries by magmatic fluids associated with the emplacement of a subvolcanic diorite intrusion in the footwall of the altered andesite).

The origin of hypogene caves is linked to the diverse and complicated geological and hydrogeological conditions and processes during the evolution of the Western Carpathians. From a lithological and genetic point of view, the hydrothermal caves originated in the Šobov metasomatic secondary quartzites (Štiavnické vrchy Mountains) and in the magnesite of the Dúbravský Massif (Revúcka vrchovina Highlands) are rare and exceptional caves of a kind not found in Central Europe and also in the world.

The research of hypogene caves in Slovakia must continue because some other caves may share such origin. It can be assumed that the diverse geological structure of the territory of Slovakia predetermined hypogene speleogenesis to a greater extent than is presently documented.

References

Andrusov D (1958) Geology of Czechoslovak Carpathians, vol. 1. Publishing house of the Slovak Academy of Sciences, Bratislava, p 304 (in Slovak)

Audra P, Mocochain L, Bigot JY, Nobécourt JC (2009) Hypogene cave patterns. In: Klimchouk AB, Ford DC (eds) Hypogene speleogenesis and karst hydrogeology of artesian basins. Ukrainian Institute of Speleology and Karstology, Simferopol, Special Paper 1, pp 17–22

Auler AS, Smart PL (2003) The influence of bedrock-derived acidity in the development of surface and underground karst: evidence from the precambrian carbonates of semi-arid northeastern Brazil. Earth Surf Proc Land 28(2):157–168. doi:10.1002/esp.443

Bacsó Z (1964) Post-Triassic skarn deposits at Tisovec Town (in Slovak). Geologické práce, Správy 31:13–45

Bajtoš P (2004) Groundwater chemical composition changes in the Dúbravský Massif hydrogeological structure, induced by magnesite exploitation. Acta Petrol Sin 20(4):887–898

Bayari CS, Ozyurt NN, Pekkan E (2009) Giant collapse structures formed by hypogenic karstification: the obruks of the central Anatolia, Turkey. In: Klimchouk AB, Ford DC (eds) Hypogene speleogenesis and karst hydrogeology of artesian basins. Ukrainian Institute of Speleology and Karstology, Simferopol, Special Paper 1, pp 83–90

Beaudouin H, Gaál Ľ, Galvánek J (2001) Values of inorganic nature of the Kremenia natural monument and human impact on them. Ochrana prírody 19:5–24 (in Slovak)

Bella P (2010) Formation of caves by waters ascending along a marginal fault of Malé Karpaty Mts. near Plavecké Podhradie, Western Slovakia—hydrogeological conditions and morphological features. Aragonit 15(2):65–70 (in Slovak)

Bella P, Bosák P (2012) Speleogenesis along deep regional faults by ascending waters: case studies from Slovakia and Czech Republic. Acta Carsol 41(2–3):169–192

Bella P, Gaál Ľ (2012) Hypogenic caves in Slovakia: current knowledge and research objectives (in Slovak). Geomorphologia Slovaca et Bohemica 12(1):38–50

Bella P, Gaál Ľ (2014a) The origin and morphology of hydrothermal caves in the Western Carpathians and their foreland. Geomorphologia Slovaca et Bohemica 14(2):15–30 (in Slovak)

Bella P, Gaál Ľ (2014b) Caves in magnesite: morphogenetic differences and basic typology. Aragonit 19(1–2):3–10 (in Slovak)

Bella P, Gaál Ľ, Bosák P (2009) Conditions and indications of evolution of hypogenic caves in Slovakia. Aragonit 14(2):159–161 (in Slovak)

Bella P, Gaál Ľ, Grego J (2010) Hydrothermal quartzite caves in the Šobov quarry near Banská Štiavnica. Slovenský kras 48(1):19–30 (in Slovak)

Bella P, Bosák P, Pruner P, Głazek J, Hercman H (2011a) The development of the Biela River valley in relation to the genesis of the Belianska jaskyňa Cave. Geografický časopis 63(4):369–387 (in Slovak)

Bella P, Gaál Ľ, Šucha V, Koděra P, Grego J (2011b) Hydrothermal caves in the Štiavnické vrchy Mountains. Aragonit 16(1–2):59–60 (in Slovak)

Bella P, Šucha V, Gaál Ľ, Koděra P (2011c) The First Karst Cave in the Štiavnické vrchy Mountains, Central Slovakia—hydrothermal speleogenesis in basement carbonates of miocene stratovolcano. Slovenský kras 49(1):5–21 (in Slovak)

Bella P, Gaál Ľ, Milovská S, Milovský R, Koděra P (2013) Caves in magnesite—another example of hydrothermal speleogenesis in Slovakia. Aragonit 18(1):42–44 (in Slovak)

Bella P, Littva J, Pukanská K, Gašinec J, Bartoš K (2015) Use of terrestrial laser scanning for the investigation of structural geological discontinuities and morphology of caves: the example of the Dúpnica Cave, Západné Tatry Mts., Slovakia (in Slovak). Acta Geol Slovaca 7(2):93–102

Bella P, Gaál Ľ, Šucha V, Koděra P, Milovský R (2016) Hydrothermal speleogenesis in carbonates and metasomatic silicites induced by subvolcanic intrusions: a case study from the Štiavnické vrchy Mountains, Slovakia. Int J Speleol 45(1):11–25. doi:10.5038/1827-806X.45.1.1879

Bosák P, Bella P, Cílek V, Ford DC, Hercman H, Kadlec J, Osborne A, Pruner P (2002) Ochtiná Aragonite Cave (Western Carpathians, Slovakia): morphology, mineralogy of the fill and genesis. Geol Carpath 53(6):399–410

Burian J, Slavkay M, Štohl J, Tözser J (1985) Metallogeny of neovolcanites in Slovakia. Mineralia Slovaca—monography, Alfa, Bratislava, p 269 (in Slovak)

Chernyshev IV, Konečný V, Lexa J, Kovalenker VA, Jeleň S, Lebedev VA, Goltsman YV (2013) K–Ar and Rb–Sr geochronology and evolution of the Štiavnica Stratovolcano (Central Slovakia). Geol Carpath 64(4):327–351. doi:10.2478/geoca-2013-0023

Choppy J (1994) La première karstification. Synthèse spéléologique et karstique, Les facteurs géographiques, 3, Spéléo-Club de Paris, Club Alpin Français, Paris, p 69

Cílek V, Bosák P, Melka K, Žák K, Langrová A, Osborne RAL (1998) Mineralogical researches in the Ochtiná Aragonite Cave. Aragonit 3:7–12 (in Czech)

Činčura J, Milovský R (2000) Hydrothermal karst of the cover nappe systems of the Central Western Carpathians. Slovenský kras 38:33–38 (in Slovak)

Gaál Ľ (1987) Karst of the Rimavská kotlina Basin. Slovenský kras 25:5–27 (in Slovak)
Gaál Ľ (2004) Geology of the Ochtiná Aragonite Cave. Slovenský kras 42:37–56 (in Slovak)
Gaál Ľ (2008) Geodynamics and evolution of caves of the Slovak Karst. State Nature Conservancy of the Slovak Republic, Slovak Caves Administration, Liptovský Mikuláš, p 168 (in Slovak)
Gaál Ľ, Ženiš P (1984) Caves in magnesite of the Dúbravský Massif (in Slovak). Spravodaj Slovenskej speleologickej spoločnosti 15(4):3–11
Gaál Ľ, Ženiš P (1986) Karst of the Revúcka vrchovina Mountains. Slovenský kras 24:27–60 (in Slovak)
Gaál Ľ, Balciar I, Belanová E, Megela M, Papáč V, Vaněková H (2007) The flooded chasm Morské oko in Rimava basin. Aragonit 12:4–9 (in Slovak)
Halečka J (1983) Final report Dúbravský Massif—PP, hydrogeological evaluation of magnesite deposit. Manuscript. Geofond, Bratislava, p 128 (in Slovak)
Hedenquist JW, Arribas A Jr (1999) The tops and bottoms of high sulphidation epithermal ore deposits. In: Stanley CJ et al (eds) Mineral deposits: processes to processing. Balkema, Rotterdam, Brookfield, pp 515–518
Hók J, Kahan Š, Aubrecht R (2001) Geology of Slovakia. Comenius University, Bratislava, p 43 (in Slovak)
Hók J, Šujan M, Šipka F (2014) Tectonic division of the Western Carpathians: an overview and a new approach. Acta Geol Slovaca 6(2):135–143 (in Slovak)
Hurai V, Huraiová M, Koděra P, Prochaska W, Vozárová A, Dianiška I (2011) Fluid inclusion and stable C–O isotope constraints on the origin of metasomatic magnesite deposits of the Western Carpathians, Slovakia. Russ Geol Geophy 52(11):1474–1490. doi:10.1016/j.rgg.2011.10.015
Ivan K (1991) Operational area of the regional speleological group B. Štiavnica (in Slovak). Spravodajca Slovenskej speleologickej spoločnosti 21(1):24–28
Jakál J (1993) Karst geomorphology of Slovakia. Map 1: 500,000. Slovenský kras 31:13–28 (in Slovak)
Kempe S (2009) Siderite weathering as a reaction causing hypogene speleogenesis: the example of the Iberg/Harz/Germany. In: Klimchouk AB, Ford DC (eds) Hypogene speleogenesis and karst hydrogeology of artesian basins. Ukrainian Institute of Speleology and Karstology, Simferopol, Special Paper 1, pp 59–60
Klago M (1984) Lúčky—sources of termomineral waters (in Slovak). In: Dovina V (ed) Fresh and mineral underground waters of the Liptovská kotlina Basin and surrounding mountains. Hydrogeological guide of the 8th national hydrogeological conference (Račkova dolina Valley—Západné Tatry Mountains, 6–8 June 1984). Geological Institute of Dionýz Štúr, Bratislava, pp 67–70 (in Slovak)
Klimchouk A (2007) Hypogene speleogenesis: hydrological and morphogenetic perspective. National Cave and Karst Research Institute, Carlsbad, Special Paper 1, p 106
Klimchouk A (2009) Morphogenesis of hypogenic caves. Geomorphology 106(1):100–117. doi:10.1016/j.geomorph.2008.09.013
Klír S (1962) Hydrogeology of Slovak magnesite deposits in Carboniferous of the Gemerides. Geologické práce, Zprávy 24:97–122 (in Czech)
Klír S (1968) Subsurface waters of the magnesite karst in Czechoslovakia. Steirische Beitraege zur Hydrogeologie 20:5–22
Konečný V, Lexa J (2001) Structure and evolution of the Štiavnica stratovolcano. Mineralia Slovaca 33(3):179–196 (in Slovak)
Lexa J (2001) Metallogeny of the Štiavnica stratovolcano. Mineralia Slovaca 33(3):203–214
Lexa J, Štohl J, Konečný V (1999) The Banská Štiavnica ore district: relationship between metallogenetic processes and the geological evolution of a stratovulcano. Miner Deposita 34(5–6):639–654
Maheľ M (1986) Geological structure of Czechoslovak Carpathians/Paleoalpine units 1. Veda, Bratislava, p 503 (in Slovak)
Mišík M, Chlupáč I, Cicha I (1985) Stratigraphical and historical geology. SPN, Bratislava, p 541 (in Slovak)
Mitter P (1990) Cave in quartz. Spravodajca Slovenskej speleologickej spoločnosti 21(1):39–40 (in Slovak)
Németh Z, Prochaska W, Radvanec M, Kováčik M, Madaras J, Koděra P, Hraško L (2004) Magnesite and talc origin in the sequence of geodynamic events in Veporicum, Inner Western Carpathians, Slovakia. Acta Petrol Sin 30:837–854
Nicod J (1976) Les régions karstiques de Slovaquie et de Hongrie septentrionale. Bulletin de la Société géographique de Marseille 82, nouvelle série 12:11–25
Oružinský V, Hurai V (1985) Fluid inclusions in secondary quartzites of the Štiavnica stratovolcano. Mineralia Slovaca 17(5):415–424 (in Slovak)
Orvan J (1960) About the origin of mineral waters in Šafárikovo. Geologické práce, Správy 17:203–213 (in Slovak)
Orvan J (1973) Hydrogeological situation of the Rimavská kotlina Basin. Mineralia slovaca 5(3):271–278 (in Slovak)
Orvošová M (2005) Calcite crystals in relicts of fossil hydrothermal karst in the Nízke Tatry Mountains. Slovenský kras 43:53–66 (in Slovak)
Orvošová M, Hurai V (2008) Calcite crystals in Kalcitová 1 and 2 caves in Mt. Poludnica, Nízke Tatry Mountains. Slovenský kras 46(1):87–97 (in Slovak)
Orvošová M, Hurai V, Simon K, Wiegerová V (2004) Fluid inclusion and stable isotopic evidence for early hydrothermal karstification in vadose caves of the Nízke Tatry mountains (Western Carpathians). Geol Carpath 55(5):421–429
Osborne RAL (2009) Hypogene caves in deformed (fold belt) strata: observations from Eastern Australia and Central Europe. In: Klimchouk AB, Ford DC (eds) Hypogene speleogenesis and karst hydrogeology of artesian basins. Ukrainian Institute of Speleology and Karstology, Simferopol, Special Paper 1, pp 33–43
Plašienka D (1999) Tectochronology and paleotectonic model of the Jurassic-Cretaceous evolution of the Central Western Carpathians. Veda, Bratislava, p 125 (in Slovak)
Plašienka D, Grecula P, Putiš M, Kováč M, Hovorka D (1997) Evolution and structure of the Western Carpathians: an overview. In: Grecula P, Hovorka D, Putiš M (eds) Geological evolution of the Western Carpathians. Mineralia Slovaca–Monograph, Košice, pp 1–24
Polák S (1955) Metasomatic occurrences of galena in the Middle Triassic limestones at Píla village, Nová Baňa district. Geologické práce, Správy 2:53–60 (in Slovak)
Pospíšil P (2004) 30-year survey of the Landrovská jaskyňa Cave. Spravodaj Slovenskej speleologickej spoločnosti 35(2):57–61 (in Slovak)
Rajman L, Roda Š Jr, Roda Š Sr, Ščuka J (1993) Unterchungen über die Genese der Aragonit-höhle von Ochtiná (Slowakei) Die Höhle 44(1): 1–8
Renčko A, Čipáková A, Toporila M (2013) Slovakian Mexico or Kryštálová jaskyňa Cave. Spravodaj Slovenskej speleologickej spoločnosti 44(4):16–24 (in Slovak)
Rye RO, Bethke PM, Wasserman MD (1992) The stable isotope geochemistry of acid sulfate alteration. Econ Geol 87(2):225–238
Sasvári T, Kondela J (2007) Demonstration of alpine structural phenomena at the structure of magnesite deposit Jelšava—Dúbrava Massif. Metalurgija 46(2):117–122
Sasvári T, Kondela J (2010) Structural and tectonic composition and origins of the magnesite deposit within Dúbravský Massif near Jelšava, based on studies at the 220 m elev. Level (Western Carpathians). Acta Montanistica Slovaca 15(3):256–260

Sillitoe RH (1989) Gold deposits in Western Pacific island arcs: the magmatic connection. In: Keays RR, Ramsay WRH, Groves DI (eds) The geology of gold deposits: the perspective in 1988. Econ Geol Monogr 6:274–291

Slavkay M (1963) Ponický Karst. Slovenský kras 4:57–69 (in Slovak)

Slavkay M (1970) Aragonite cave in the Ponický Karst. Slovenský kras 8:95–99 (in Slovak)

Slavkay M (1971) Deposits of polymetallic ores at Poniky Village. Mineralia Slovaca 11(3):181–213 (in Slovak)

Slavkay M, Beňka J (1995) Geology, mineralogy and metallogeny of lead and zinc ores at Ardovo village. Mineralia Slovaca 27(2): 79–88 (in Slovak)

Sluka M (2014) Else about the Beckovská jaskyňa cave. Spravodaj Slovenskej speleologickej spoločnosti 45(4):38

Spötl C, Dublyansky Y, Meyer M, Mangini A (2009) Identifying low-temperature hydrothermal karst and palaeowaters using stable isotopes: a case study from an alpine cave, Entrische Kirche. Austria Int J Earth Sci Geol Rundschau 98(3):665–676. doi:10.1007/s00531-007-0263-2

Štohl J, Lexa J, Kaličiak M, Bacsó Z (1994) Genesis of stockwork base metal mineralizations in the Neogene volcanics of West Carpathians. Mineralia Slovaca 26(2):75–117 (in Slovak)

Straka P (1986) Deep structural borehole MEL-1 Meliata. Regionálna geológia Západných Karpát 21:89–92 (in Slovak)

Tisato N, Sauro F, Bernasconi SM, Bruijn RH, De Waele J (2012) Hypogenic contribution to speleogenesis in a predominant epigenic karst system: a case study from the Venetian Alps, Italy. Geomorphology 151:156–163. doi:10.1016/j.geomorph.2012.01.025

Uhlík P, Šucha V (1997) Distribution of pyrophyllite in the Šobov deposit and comparison with pyrophyllite from Vígľašská Huta deposit (Central Slovakia). Mineralia Slovaca 29(1):73–79 (in Slovak)

Uhlík P, Šucha V, Madejová J, Puškelová Ľ, Šamajová E (2001) Clay minerals in the area of the Štiavnica stratovolcano. Mineralia Slovaca 33(3):287–288 (in Slovak)

Vítek J (1987) Kremenia—unique natural site of the central Slovakia. Krásy Slovenska 64(12):34–36 (in Czech)

Vítek J (1989) Caves and microforms in neovolcanites of the Kremnické vrchy Mountains. Československý kras 40:129–131 (in Czech)

Zacharov M (2013) New knowledge from the research of Drienovská jaskyňa Cave. Slovenský kras 51(2):111–120 (in Slovak)

Zakovič M, Bodiš D, Orvan J, Lopašovský K (1994) Hydrogeology of the Rimavská kotlina Basin and the eastern part of Cerová vrchovina Mountains. Západné Karpaty 123:119–142

Ženiš P, Gaál Ľ (1986a) New caves in magnesites of the Slovenské rudohorie Mountains. Spravodaj Slovenskej speleologickej spoločnosti 15(4):3–11

Ženiš P, Gaál Ľ (1986b) Magnesite karst in the Slovenské rudohorie Mts. (Czechoslovakia). Communications, vol. 2, 9th International Congress of Speleology, Barcelona, pp 36–39

Hypogene Features in Sandstones: An Example from Carboniferous Basins of Central and Western Bohemia, Czech Republic

20

Václav Suchý, Ivana Sýkorová, Jiří Zachariáš, Jiří Filip, Vladimír Machovič, and Ladislav Lapčák

Abstract

Concave and cavernous forms including rising wall channels, rising sets of coalesced copula, ceiling half-tube channels, separate ceiling copula, ceiling chimneys, and half-spherical upward-convex arches locally occur in surface outcrops of Carboniferous arkose sandstones in central and western Bohemia. Many of these negative forms conventionally described as tafoni and/or honeycombs have been traditionally interpreted as products of various exogenous weathering processes. Based on the line of indirect evidence, we propose an alternative interpretation in which these features represent transitional and outlet members of the morphologic suite of rising flow (MSRF), indicative of their subsurface hypogene origin. The negative forms are commonly associated with bedding planes and subvertical fractures mineralized with goethite and jarosite. The reflectance of coal particles embedded in sandstone along mineralized bedding planes (0.91–1.03% R_r) is appreciably higher with respect to those of adjacent unaltered arkose host rocks (0.61–0.85% R_r), pointing to the thermal overprint by hot fluids. Moreover, the walls of many cavities are covered by sandy-disintegrated alterite locally mineralized with gypsum, dickite, goethite, authigenic quartz, pickeringite, and bischofite. We suggest that these phenomena, including the origin of characteristic concave forms and mineralogical alterations of arkose host rocks, may have been due to warm, CO_2-saturated and possibly H_2S-rich brines that ascended from the deepest stratigraphic units of the Carboniferous succession via the network of subvertical tectonic fractures and migrated laterally outward along permeable bedding planes. As indicated by the apatite fission track analysis and wider geological observations, the alteration of arkose sandstones probably occurred at relatively shallow depth of burial, during the Tertiary uplift of the Bohemian Massif 15–20 Ma ago. In this environment, the alteration may have been accelerated by the effects of mixing corrosion where heated deep basinal fluids interacted with shallower interstratal

V. Suchý (✉)
Jiránkova 1136/4, 163 00 Praha 6, Czech Republic
e-mail: suchy@tc.cz

I. Sýkorová · V. Machovič
Institute of Rock Structure and Mechanics v. v. i.,
Academy of Sciences of the Czech Republic,
V Holešovičkách 41, 182 09 Prague 8, Czech Republic
e-mail: sykorova@irsm.cas.cz

J. Zachariáš
Faculty of Science, Charles University, Albertov 6,
128 43 Praha 2, Czech Republic
e-mail: zachar@natur.cuni.cz

J. Filip
Institute of Geology of the CAS v. v. i.,
Academy of Sciences of the Czech Republic, Rozvojová 269, 165 00 Praha 6-Lysolaje, Czech Republic
e-mail: filip@gli.cas.cz

V. Machovič · L. Lapčák
University of Chemistry and Technology Prague,
Technická 5, 166 28 Prague 6, Czech Republic
e-mail: Vladimir.Machovic@vscht.cz

L. Lapčák
e-mail: Ladislav.Lapcak@vscht.cz

© Springer International Publishing AG 2017

A. Klimchouk et al. (eds.), *Hypogene Karst Regions and Caves of the World*,
Cave and Karst Systems of the World, DOI 10.1007/978-3-319-53348-3_20

waters. When the uplifted sandstone sequences eventually reached the surface, the hypogene cavities and altered cliff walls were subjected to subaerial weathering and fluvial erosion processes the effects of which were superimposed on older hypogene features.

Keywords
Speleogenesis • Sandstone • Vitrinite reflectance • Fission tracks • Diagenesis • Weathering

1 Introduction

During the last two decades, an increasing number of caves traditionally viewed to be of epigenic origin have been re-evaluated as being caused by hypogene waters, the aggressiveness of which has been produced at depth beneath the surface, independent of surface or soil CO_2 or other near-surface acid sources (Dublyansky 1990; Palmer 2000; Klimchouk 2007, see also Klimchouk 2015; Audra and Palmer 2015 and the references therein). Beside caves sensu stricto, some other less obvious dissolution phenomena like the development of spongework zones and cavernous porosity along ancient fracture-controlled conduits have been also reinterpreted as products of hypogene speleogenesis (Klimchouk et al. 2012). Most of these features believed to represent the results of hypogene processes have been recognized in soluble carbonate rocks, particularly in limestone sequences. So far, however, only a few examples of hypogene speleogenesis have been described from siliciclastic sediments (Plózer 1977; De Waele et al. 2014; Sauro et al. 2014).

In this paper, we describe yet another example of probable hypogene features that developed in Carboniferous coal-bearing sandstones in central and western Bohemia. We combine field observations with several modern analytical tools in an attempt to constrain paleothermal and geochemical conditions of hypogene processes and its timing. Our data suggest that the hypogene speleogenesis occurred under the influence of hot upward-migrating basinal brines, the movement of which was associated with the general uplift of the Bohemian Massif since the Neogene period.

2 Geological Setting

A series of dismembered continental basins filled with Upper Carboniferous to Lower Permian clastic sediments is present in central and western Bohemia (Fig. 1). According to paleogeographic reconstructions (Ziegler 1990), these basins once developed in the interior of Variscan Europe, approximately 300–400 km from the North Variscan Foredeep dominated by shallow marine deposition. The tectonic nature of the basins was variously interpreted. Havlena (1982) preferred a model of a simple asymmetric mega-graben which developed on the Neoproterozoic basement, but more

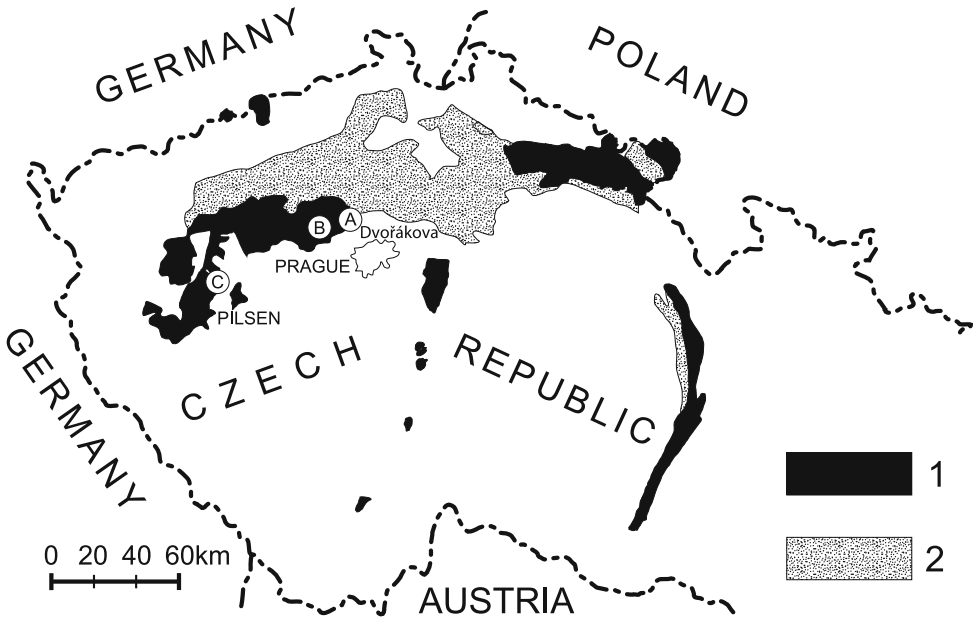

Fig. 1 Schematic map showing the occurrence of limnic Carboniferous deposits of the Czech Republic (Mísař et al. 1983) *1* surface outcrops of Carboniferous deposits and *2* Carboniferous deposits under the cover of younger sedimentary formations. The positions of three distinct localities mentioned in the text are also shown *A* Dvořákova stezka escarpment; *B* Podlešínská jehla Rock; and *C* Plzeň–Radčice

recent studies emphasized the role of NW–SE-trending wrench fault tectonics related to the oblique collision between Gondwana and Baltica (Pašek and Urban 1990).

Carboniferous rocks forming the basinal fill can be directly observed in natural outcrops along the southern erosive margins of the basins, while further to the north a substantial volume of the Carboniferous deposits is hidden under the cover of younger Cretaceous and Tertiary deposits. Rich data on these subsurface coal-bearing formations have been accumulated during intensive coal exploration and mining in the area during the last two centuries (Pešek 1996; Holub et al. 2001).

The sedimentary fill of the basins, the thickness of which locally exceeds 1600 m, is traditionally divided into four lithostratigraphic formations characterized by the alternation of red coal-barren and gray coal-bearing deposits (Fig. 2). The oldest Carboniferous sediments cover the eroded crystalline basement of slightly metamorphosed Neoproterozoic to Ordovician rocks. Cyclic deposition, interrupted by numerous hiatuses, then lasted until the end of the Carboniferous, or possibly till the early Permian. The lithology of the Carboniferous succession is generally dominated by variable clastic sediments, notably sandstones, arkoses, and conglomerates that often intercalate with siltstones, altered volcanic tuffs, and coal seams. These sediments accumulated in a range of continental environments including extensive alluvial floodplains, incised river valleys, swamps, and ephemeral lakes (Pešek 1996; Opluštil 2005). The oldest stratigraphic units (Kladno and Týnec formations) deposited predominantly in fluvial environments that gradually evolved into the lacustrine facies in younger units (Slaný and Líně formations; Holub et al. 2001). The main sediment input came from exposed Variscan granitic intrusions located south of the basins (Kukal 1983). The Carboniferous

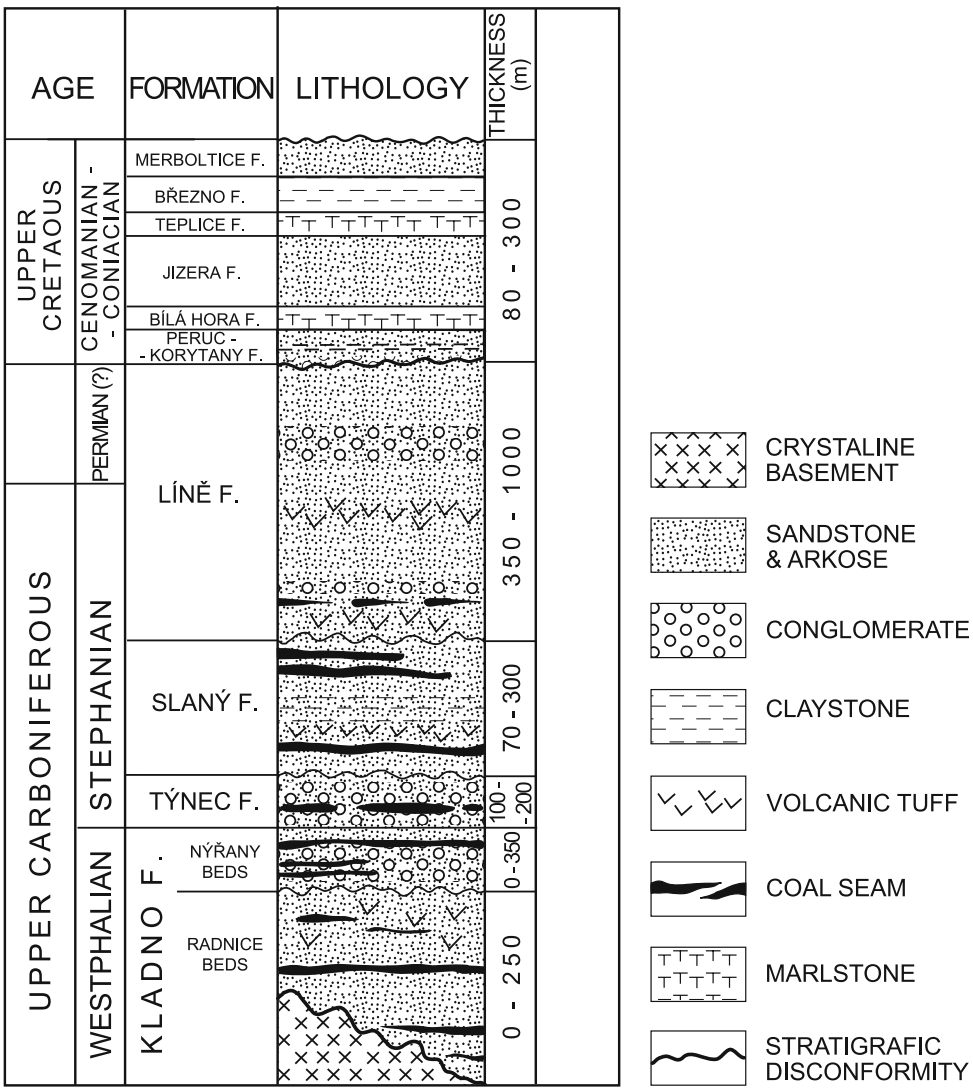

Fig. 2 Schematic lithostratigraphy of Carboniferous and Cretaceous deposits for the central part of the Czech Republic (Čech et al. 1980; Holub 1982). See the text for details

strata experienced maximum heating (~100 °C) and burial to the depth of about 2000 m during the Permian, followed by erosion of a part of the succession (Holub et al. 1997).

The Carboniferous deposits are locally overlain by an Upper Cretaceous sedimentary cover, which overlaps with a slight discordant unconformity (Fig. 2). The Cretaceous sediments are dominated by shallow marine sandstones, marlstones, and claystones. These deposits, up to 900 m thick, accumulated in an extensive epicontinental sea that propagated into the territory of Bohemia during the Cenomanian time (Čech et al. 1980).

3 Samples and Methods

We examined concave forms developed in Carboniferous clastic sediments at three distinct natural outcrops, notably at spectacular rock cliffs above the Dvořákova stezka path near Kralupy nad Vltavou, at the Podlešínská jehla Rock near Slaný, and at Čertova kazatelna Rock near Plzeň–Radčice (Fig. 1). The host rocks here are massive coarse-grained arkoses and sandstones that locally intercalate with conglomerates and thin coal seams which all belong to various stratigraphic members forming the lower part of the Carboniferous succession (e.g., Kladno, Týnec, and Slaný formations).

Optical and scanning electron microscopy using Technival 2 (Carl Zeiss Jena) stereomicroscope, UMSP 30 Petro Opton-Zeiss petrographic microscope, and JEOL JSM-6380LV and TESCAN Vega scanning electron microscopes was applied to a series of petrographic thin sections and natural rock chips collected from the surface of solution forms and adjacent unaltered clastic sediments.

In order to evaluate the maximum thermal exposure and to discriminate potential influence of hot fluids on the sediments, samples of thin dark coaly claystone partings were separated from unaltered arkose host rocks and from its contacts with Fe-mineralized bedding planes and examined for its **vitrinite light reflectance**. The polished rock sections were studied using an Olympus BX51 microscope equipped with Zeiss Photomultiplier MK3 under both reflected light and fluorescence regime using a lens with 40× magnification. The Pelcon point counter was used for maceral analysis. Random and actual reflectance values of organic particles were determined using the Spectra Vision software calibrated with sapphire (R = 0.596%), yttrium aluminum garnet (R = 0.894%), and gadolinium gallium garnet (R = 1.717%) reflectance standards.

Micro-Raman spectroscopy was performed on hand-picked natural chips of altered arkoses and its mineralized bedding planes. A Raman Thermo-Scientific Model DXR microscope linked to the confocal Olympus microscope was used for the analysis. Excitation was with a 10 mW 532.2 nm laser with power limited to 0.5 mW to avoid thermal destruction of the samples. The acquisition time of 10 s was used; 10 accumulations were co-added to form a spectrum. Spectra were obtained using a 50× objective, a 900 lines/mm grating, and an thermoelectric cooled charge-coupled charge-coupled device (CCD) multi-channel detector. The spectra of jarosite subgroup minerals were compared with those reported by Frost et al. (2006), Audra et al. (2016), and Ling et al. (2016). The composition of K–Na jarosite was calculated from equation K-number = $-11.876 \times$ Band v_1 $-4.207 \times$ Band v_3 + 16678 published by Ling et al. (2016).

In addition, **apatite fission track analysis** was applied to the sample of arkose sandstone from Dvořákova stezka outcrops in order to reveal the low-temperature evolution of the rock. Apatite grain concentrate was obtained from approximately 7 kg rock sample by using the standard heavy mineral liquid separation technique. The external detector method (Wagner and Van den Haute 1992) was applied for fission track analysis. The grains were mounted in Epofix®, polished and etched in 2.5% HNO_3 for 70 s to reveal the fission tracks. Low-uranium muscovite detector (Jahre GmbH Wilhelmshaven, Germany) was fasted on polished surfaces and stacked in irradiation cassette with CN5 glass neutron dosimeters. The cassette was irradiated by thermal neutrons in TRIGA Mk. II Research Reactor, The Oregon University. A nominal fluence of thermal neutrons 8.14×10^{15} cm^{-2} was reached. Densities and lengths of spontaneous and induced tracks were measured by an Axioplan 2 (Zeiss) microscope equipped with AUTOSCAN™ stage. Mean chloride contents of apatite grains were determined by CAMECA SX-100 Electron Probe Micro Analyser. Fission track ages were calculated using zeta calibration method after Hurford and Green (1982, 1983). As age standard apatites from Fish Canon volcanic tuff, Durango and Mount Dromedary intrusive complexes were used. The ages were determined using the TRACKKEY program (Dunkl 2002). The thermal history of the rocks (T-t path) was computed by applying the AFTSolve program (Donelick and Ketcham 1998; Ketcham et al. 2000) with multi-kinetic annealing model (Carlson et al. 1999; Donelick et al. 1999, Ketcham et al. 1999).

4 Results

4.1 Field Observations

At three spectacular outcrops of Carboniferous arkoses, we identified ample evidence of specific concave forms. Of these, the most abundant features are spherical and half-spherical cavities, pockets, and niches on the walls with typical sizes of 0.5–1.5 m that often tend to aggregate

together to form a grapelike patterns (Fig. 3a, i, j). Subspherical cavities on the walls are often associated with vertical half-tube channels that are either straight or bush-like branching (Fig. 3a, i). Some half-spherical cavities and rock galleries, however, are not interrelated with any wall channels but seem to be linked to prominent bedding planes, instead (Fig. 3b, c). Vertically stacked chains of successive half-spherical cavities are another common type of concave forms that can be seen on the walls (Fig. 3a).

Except these small-scale concave features, more extensive true cave-like cavities also occur (Fig. 3c, i). Most of these caves display lenticular or circular shapes with limited interconnections, but some larger cavities consisting of several coalescing spherical cupolas up to 2 m in diameter were also observed (Fig. 3h, j). The floor of the caves is typically flat, almost completely devoid of internal sediments and slightly ascending from the entrance to the blind ends of the caves, thus crosscutting obliquely the subhorizontal

Fig. 3 Characteristic concave forms in Carboniferous sandstones interpreted as elements of the morphological suite of rising flow (MSFR; Klimchouk 2007); **a** Dobrovského ulice street, Kralupy nad Vltavou; **b–h**: Dvořákova stezka escarpment, Kralupy nad Vltavou; **i** Podlešínská jehla Rock; **j** Plzeň–Radčice. **a** rising chains of half-spherical cavities (to the *right*, just *behind the person*) and grapelike aggregates of cupola-like cavities (in the *upper middle* and to the *left*). The *arrow* shows the eroded remains of a vertical tube channel which is partially blanketed by ivy leafs. **b** Precisely eroded half-spherical upward-convex arches. *Note* the development of the arches above the prominent bedding plane. **c** Larger cave-like cavities and rock galleries developed along the bedding planes. Upward-convex arches and half-spherical cavities can also be seen in the *upper part* of the outcrop. **d** Vertical blind-ended chimneylike "kettles" on the ceiling of a cave. **e** A prominent horizontal ceiling half-channel (to the *left of the person*) and a number of half-spherical and chimneylike cavities on the ceiling of a cave. **f** Complex interferences of copula-like cavities that protrude in the cave ceiling. *Note* also the steeply inclined cave floor, which is devoid of sediments. **g** View straight upward into a chimney-shaped solutional "kettle" in the ceiling that blindly terminates to form a precisely eroded cupola. **h** A complex interplay of spherical cavities of various diameters. The *upward*-progressing growth of spherical cavities apparently resulted in a partial destruction of the cave ceiling. **i** The eroded remains of subvertical feeder channels (*arrowed*) leading into a system of blind spherical niches. **j** Small cave-like cavities and half-spherical grapelike forms on the walls (*upper right*). *Arrows* point to the equidistant set of vertical N-S striking, goethite-mineralized fractures through which the aggressive fluids probably ascended

bedding of the host sandstone (Fig. 3f). The ceiling features of the caves commonly exhibit a plethora of coalescing half-spherical cavities (Fig. 3f) and less commonly, sub-horizontal ceiling half-tube canals (Fig. 3e). The cylindrical chimneylike ceiling "kettles" that blindly terminate with cupolas are also present (Fig. 3d, g).

Cave walls and ceilings are generally barren and lacking any speleothems. The walls of many concave forms are, however, commonly covered by an up to 1- to 2-cm-thick compact mineral crust of gray, black, or reddish color. Below the crust, there is often a layer of soft, powdery material, extending into the wall up to 2–10 cm in which the host rock has been converted into whitish, loose, fine-grained chalk-like substance. This alteration zone eventually grades into hard, massive, unaltered arkose (Fig. 4).

The arkose outcrops that host concave forms commonly display a ferruginous mineralization along some prominent bedding planes (Fig. 5a). A similar type of hardened, up to 1–2-cm-thick rusty brown-red ferruginous coatings can also be seen on some subvertical fractures that cut through the sequence (Fig. 5a, b) as well as on the surface of some concave forms themselves (Fig. 5c). In addition, hollow Fe-mineralized tubes or "rolls," 1–2 cm in diameter, also occur within some arkose beds (Fig. 4).

4.2 Microscopic Observations

4.2.1 Petrography and Mineralogy

Fresh arkose sandstones consist of dominant quartz and feldspar grains cemented with illite and kaolinite-group minerals (Fig. 6). The rock is moderately compacted, tightly cemented, and apparently has very low, if any, effective porosity. Most of its quartz grains are anhedral, poorly sorted, and rectangular in shape, but some well-rounded quartz particles and euhedral bipyramidal ß-quartz crystals probably derived from volcanic rocks also occur, suggesting several detrital sources of a variable proximity (Fig. 7).

In contrast, altered arkose collected from the surface layers of concave cavities is of a soft chalky consistence that easily disintegrates into fine sandy sediment consisting of individual quartz grains, intensely corroded feldspar crystals, mica chips, and a minute clay mineral fraction. Petrographic observations suggest that the arkose alteration is primarily due to an intense leaching of feldspars and clay mineral cements, leading to the liberation of individual quartz grains. Many large quartz grains as well as quartz and metamorphic rock pebbles that protrude from altered arkose outcrops appear to be also partially etched and exhibit numerous pores and fractures.

The mineral composition of the hardened crust that locally covers the altered arkose walls appears to be of two different types. At some localities (e.g., Plzeň–Radčice), it consists of massive reddish to black ferruginous coatings composed primarily of goethite with subordinate gypsum and jarosite subgroup sulfate minerals. The very mineral composition is also characteristic for the ferruginous impregnation that occurs along bedding planes and subvertical fractures. Two different

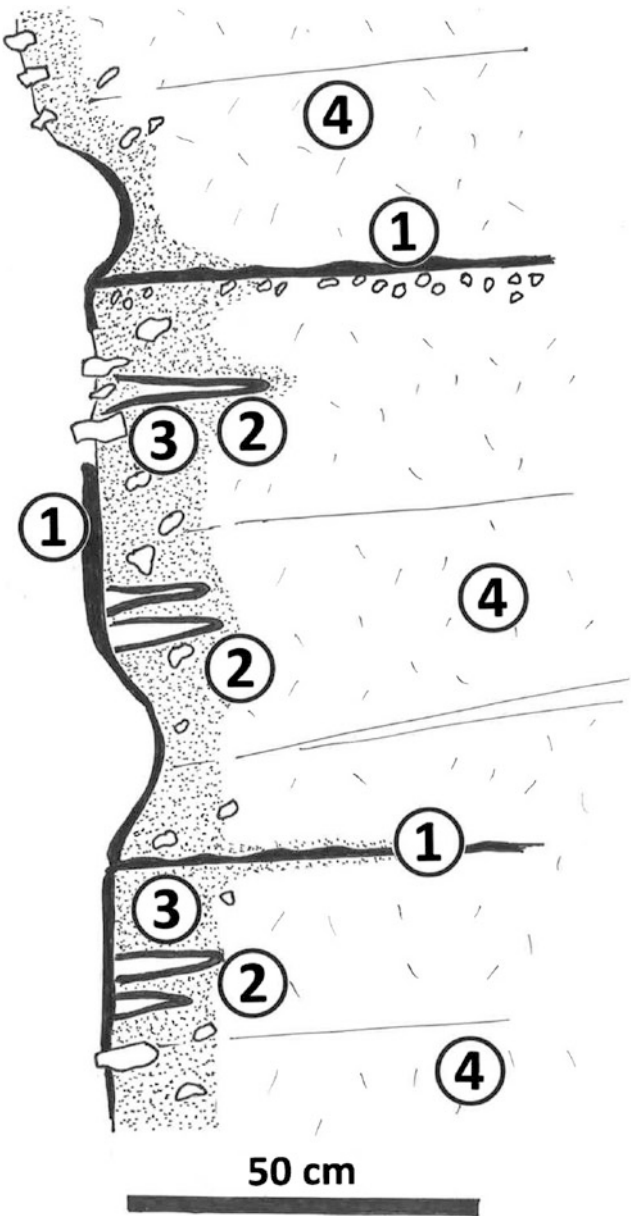

Fig. 4 Sketch showing the typical zoning observed on altered arkose outcrops. The ferruginous crust covers the *vertical* walls of the outcrops and its concave features *1*, and some bedding planes *1*, the ferruginous "rolls" *2*, and altered sandy zone *3* are developed underneath the Fe-crust. The altered zone of sandy disintegration grades into fresh unaltered arkose *4*. The sandy deterioration of the arkoses appears to be similar to the sandy decomposition of carbonate rocks known as so-called alterite from some hydrothermal caves (e.g., Jakucs 1977; Dublyansky 1995; Klimchouk et al. 2012)

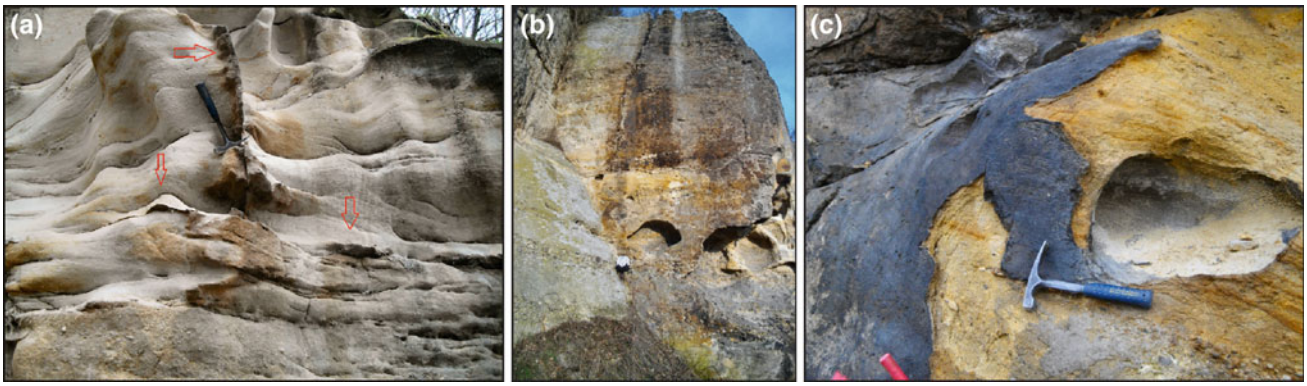

Fig. 5 Field aspects of mineralization of arkose sandstones and its concave forms (**a** Dvořákova stezka escarpment; **b** and **c** Plzeň–Radčice). **a** subvertical fracture and horizontal bedding plane (*arrowed*) mineralized with goethite and jarosite. The ferruginous impregnations which are more weathering-resistant than the arkose host rock protrude from the wall. Some other thin bedding planes are *black-colored* due to finely disseminated coaly fragments. **b** Goethite-mineralized plane of a subvertical fracture. *Note* the intimate link with the cavities that have developed along the fracture plane. The rucksack for scale is about 50 cm high. **c** *Dark*, about 0.5–1.0-cm-*thick* partially eroded ferruginous crust developed over the surface of an altered arkose. *Note* that the crust covers also a concave form (to the *right* of the hammer) that is now partly filled with light sandy sediment derived from the altered arkose below the crust

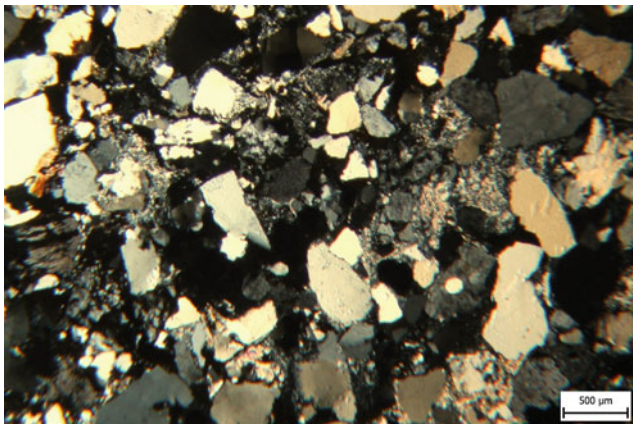

Fig. 6 Photomicrograph showing aspects of an unaltered arkose from the Dvořákova stezka escarpment, the Nýřany Beds. Angular and subrounded quartz and feldspar grains are the main rock components that are cemented by kaolinite and illite. Many of the feldspar grains show incipient replacement by sericite (minute bright crystals). Partly crossed polars

jarosite subgroup minerals were identified in these samples by means of the micro-Raman spectroscopy—hydronium jarosite $\left[(H_3O)Fe^{3+}{}_3(SO_4)_2(OH)_6\right]$ and K–Na jarosite $\left[K_{0.83}Na_{0.17}Fe^{3+}{}_3(SO_4)_2(OH)_6\right]$ (Fig. 8 and Table 1).

The second type of alteration crust is a light gray to black thin coating over the altered arkose and has been recognized at outcrops above the Dvořákova stezka pathway. It consists chiefly of neomorphic gypsum and dickite (Fig. 9). Minor tiny crystals and up to 10 µm thick overgrowths of authigenic α-quartz over clastic quartz grains were also observed in some samples (Fig. 9f).

4.2.2 Organic Petrology

In examined claystone samples, common types of coaly organic fragments ranging in size up to 100–200 µm have been identified, including vitrinite-group macerals derived from cellular plants, inertinite-group particles which resulted from an incomplete combustion of wood tissues during wild fires, and liptinite macerals derived from hydrogen-rich plant materials such as resins, waxes, fats, and oils, as well as from bacterial degradation of carbohydrates (e.g., Taylor et al. 1998; Fig. 10). A similar assemblage of individual dispersed organic remains has been reported previously from other Upper Carboniferous coal-bearing and lacustrine sedimentary formations of central and western Bohemia (Libertín et al. 2009; Lojka et al. 2010).

The random reflectance of vitrinite particles from unaltered samples outside the contacts with mineralized bedding planes typically ranges from about 0.61 to 0.85% R_r (Table 2). These values which are directly comparable to those known to represent general coalification grade of Carboniferous coals in a given area (R_r from ~0.40 to ~0.80%; Holub et al. 2001; Pešek and Sýkorová 2006) would correspond to maximum burial temperatures in the range of 96–112 °C, based on the empirical equation of Barker and Pawlewicz (1994).

In contrast, vitrinite reflectance values markedly higher than these background values (R_r from 0.91 to 1.03%) were found in several centimeter-wide contact zones immediately adjacent to ferruginous bedding planes. In rapidly heated, liquid-dominated geothermal systems, these vitrinite reflectance values are characteristic of maximum temperatures between 140 and 156 °C (Barker and Pawlewicz 1994).

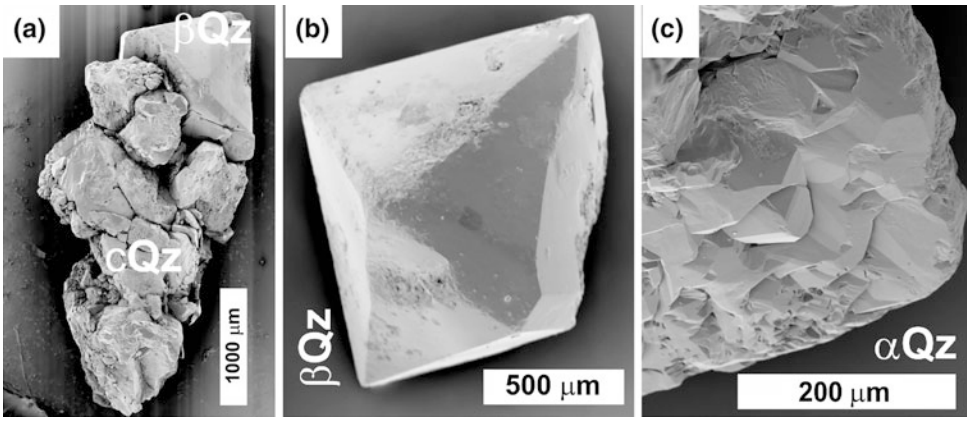

Fig. 7 Scanning electron microphotographs showing aspects of detrital grains of the arkose. Dvořákova stezka escarpment, the Nýřany Beds. **a** An aggregate of clastic quartz (cQz) and feldspar grains. The quartz (βQz) of euhedral bipyramidal habit was probably derived from nearby magmatic rocks. **b** A close-up of a bipyramidal detrital grain of magmatic quartz. **c** Detrital quartz grain overgrown by finely crystalline authigenic euhedral quartz (αQz)

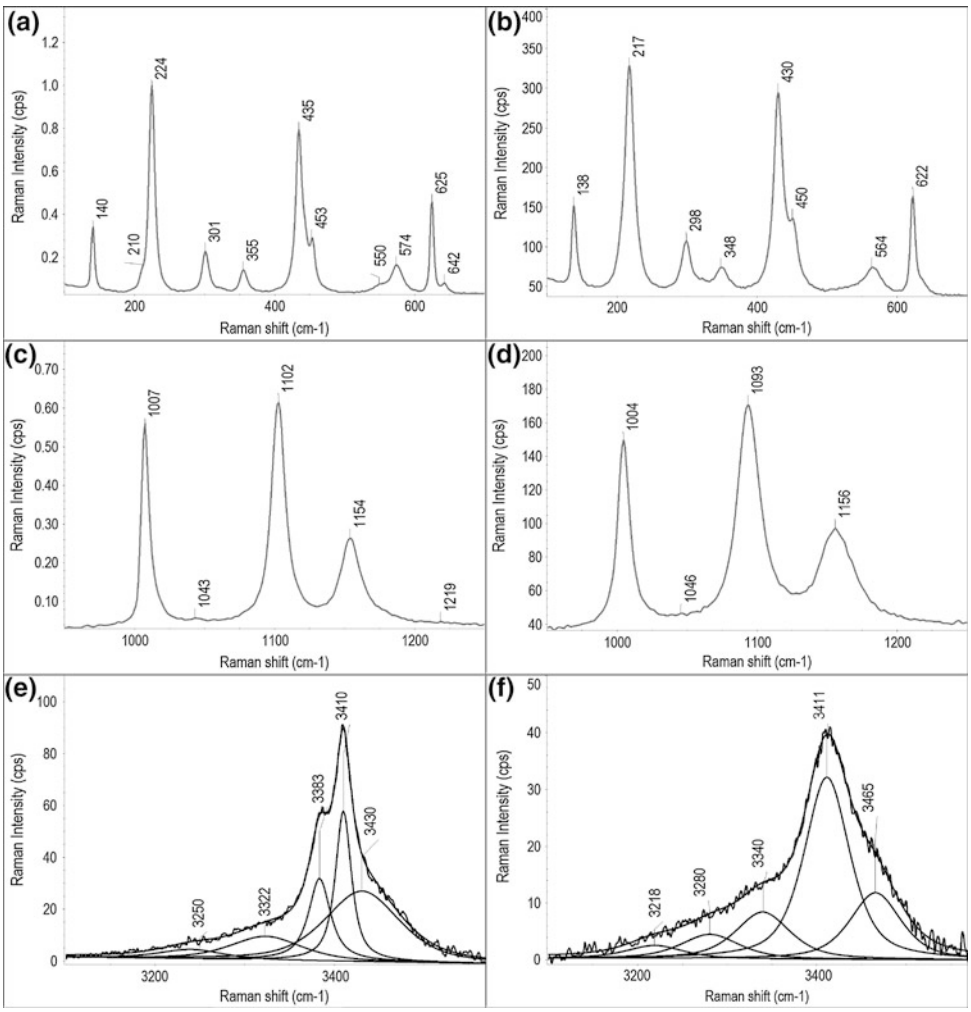

Fig. 8 Raman spectra of K–Na jarosite in the regions of 100–700 cm^{-1} (**a**), 950–1250 cm^{-1} (**c**), 3100–3570 cm^{-1} (**e**) and hydronium jarosite in the regions of 100–700 cm^{-1} (**b**) 950–1250 cm^{-1} (**d**) and 3100–3570 cm^{-1} (**f**)

Table 1 Raman wave numbers and assignments of Na–K jarosite and hydronium jarosite samples

Dvořákova stezka sample 7	Dvořákova stezka sample 8	
$K_{0.83}Na_{0.17}Fe_3^{3+}(SO_4)_2(OH)_6$	$(H_3O)Fe^{3+}{}_3(SO_4)_2(OH)_6$	Assignment
3430	3465	ν(OH) stretch.
3410	3411	ν(OH) stretch.
3383	3340	ν(OH) stretch.
3322	3280	ν(OH) stretch.
3250	3218	ν(OH) stretch.
1154	1156	$\nu_3(SO_4)$ asym. stretch.
1102	1093	$\nu_3(SO_4)$ asym. stretch.
1007	1004	$\nu_1(SO_4)$ sym. stretch.
642		$\nu_4(SO_4)$ asym. bend
625	622	$\nu_4(SO_4)$ asym. bend
574	564	γ(OH)
550		γ(OH)
453	450	$\nu_2(SO_4)$ sym. bend
435	430	$\nu_2(SO_4)$ sym. bend
355	348	Fe–O
301	298	Fe–O
224	217	Fe–O
140	138	Fe–O

Another evidence of fast pyrolytic heating observable in the vitrinite grains includes the development of numerous tiny pores and contraction fissures inside the macerals and possibly also reaction rims in the outer zones of some particles (Fig. 10c, e). In a way similar to vitrinite, some liptinite macerals from Fe-mineralized bedding planes also exhibit slightly higher reflectance values (up to 0.42% R_r) and fluorescence colors that changed from yellow to orange and brown. In addition, dark, non-fluorescent finely porous organic matter was also found in altered sediments which is believed to represent bitumen drops derived from terrestrial organic matter or coal exposed to a fast pyrolytic heating (e.g., Littke 1993; Taylor et al. 1998; Fig. 10f).

4.3 Apatite Fission Track Analysis

Apatite fission track analysis (AFTA) of a sample of unaltered arkose from Dvořákova stezka escarpment revealed that confined tracks were significantly shortened from their initial length of 16.3 µm to about 11.6 µm. This indicates that the apatite grains were gradually annealed while its host rock was slowly uplifted from the zone of total apatite annealing.

The time–temperature inverse modeling of the tracks shows that the total annealing of apatite grains, which is commonly completed at temperatures in excess of about 120 °C, occurred before ~200 Ma (Triassic–Jurassic transition). Unfortunately, due to a complete annealing of the tracks, the AFTA method alone does not allow to reconstruct the earlier pre-Jurassic thermal history of the sample, nor the maximum temperatures to which the sample was exposed in the past. The reliably reconstructed post-Jurassic *T-t* path of the sample, however, clearly shows that after its ascend from the zone of total annealing, during a substantial part of the Mesozoic and Tertiary eras, the sample resided in a zone of stable, relatively low temperatures of about 80 °C. This thermal pattern is consistent with a long period of non-deposition and/or moderate erosion that prevailed in the central part of the Bohemian Massif during this time (e.g., Malkovský 1979). Eventually, about 15–20 Ma ago, the rock experienced an accelerated cooling from ~80 °C to the recent surface temperature (Fig. 11). This late-stage thermal event is consistent with an episode of general fast uplift due to the tectonic pressures transmitted from the Alpine region that affected the Bohemian Massif since the Neogene period (e.g., Filip and Suchý 2004).

5 Interpretation and Discussion

Cavities, hollows, and small caves developed in the Carboniferous arkose sandstones in central and western Bohemia including those described in this study have been previously interpreted in the framework of a classical epigenic scenario as pseudokarst (tafoni and honeycomb)

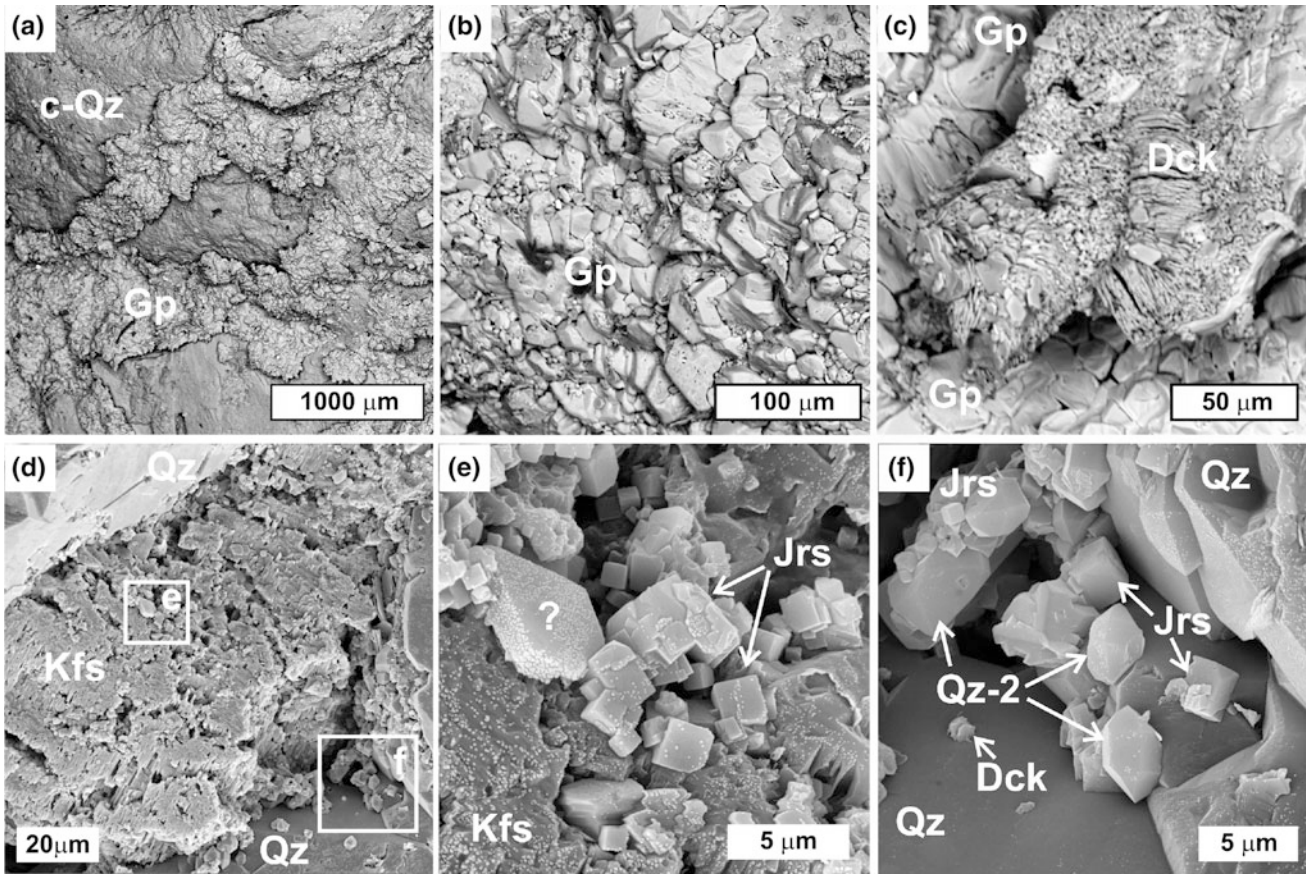

Fig. 9 Scanning electron microphotographs showing aspects of altered arkose samples. Dvořákova stezka escarpment, the Nýřany Beds. **a** Finely crystalline gypsum (Gp) overgrowing rounded clastic quartz (c-Qz); **b** a close-up of crystalline gypsum (Gp) coating from the same sample as in photograph (**a**); **c** stacked platy crystals of an authigenic Al–Si–O-composed clay mineral which is believed to be dickite (Dck), overgrown by late-stage gypsum (Gp); **d** intensely leached porous grain of K-feldspar (Kfs); **e** a close-up of a framed area in photograph (**d**) showing tiny pseudocubic crystals of jarosite (Jrs) and an unidentified Al–Si–O–S mineral (?) on the surface of an altered feldspar grain; and **f** a close-up of tiny crystals of α-quartz (Qz-2) of supposed authigenic origin which locally overgrows clastic quartz. *Note* also small jarosite crystals (Jrs) that, in turn, postdate Qz-2 type neomorphic quartz

phenomena and explained in terms of selective weathering combined with fluvial and/or salt erosion (Vítek 1987; Cílek 1993; Fediuk 1999). Cílek (1993) analyzed composition of surface alteration crust developed over Carboniferous arkoses from Dvořákova stezka cliffs and identified, beside predominant gypsum, the exotic sulfate and chloride minerals, pickeringite [$MgAl_2(SO_4)_4{\cdot}22H_2O$] and bischofite ($MgCl_2{\cdot}6H_2O$), which he attributed to the anthropogenic contaminants, particularly to industrial fertilizers and deicing salts.

We are aware that individual concave features similar to those observed in Carboniferous sandstones including cupola-form cavities, ceiling channels, or ceiling chimneys can be found elsewhere in surface outcrops and epigenic caves where they often form in phreatic or subaerial conditions (e.g., Bruthans et al. 2009; Groom et al. 2015). However, the spatial associations of these forms in the outcrops we studied provide a strong indication that these features originated through the mechanisms of hypogene speleogenesis. In fact, the concave forms we describe (e.g., vertical half-cylindrical channels, half-spherical cavities and chains of upward-rising cupolas on the walls, coalescing spherical cavities, caves with flat upward ascending floors and partly eroded ceilings, blind ceiling "kettles," etc.) essentially correspond to the transitional wall, ceiling, and outlet features of the so-called morphologic suite of rising flow (MSRF; Klimchouk 2007, 2009) which is now recognized as a diagnostic evidence for hypogene speleogenesis (Fig. 12). Typical rising inlet conduits ("feeders" or "risers") forming the lowermost members of this morphologic suite have not been observed in the field yet, but in view of a limited extent and a poor exposure of the outcrops available for direct observations, it is likely that these features may still been hidden below the present-day surface.

Associations of similar concave forms in limestone cliffs of the Crimean Piedmont have been recently reinterpreted as

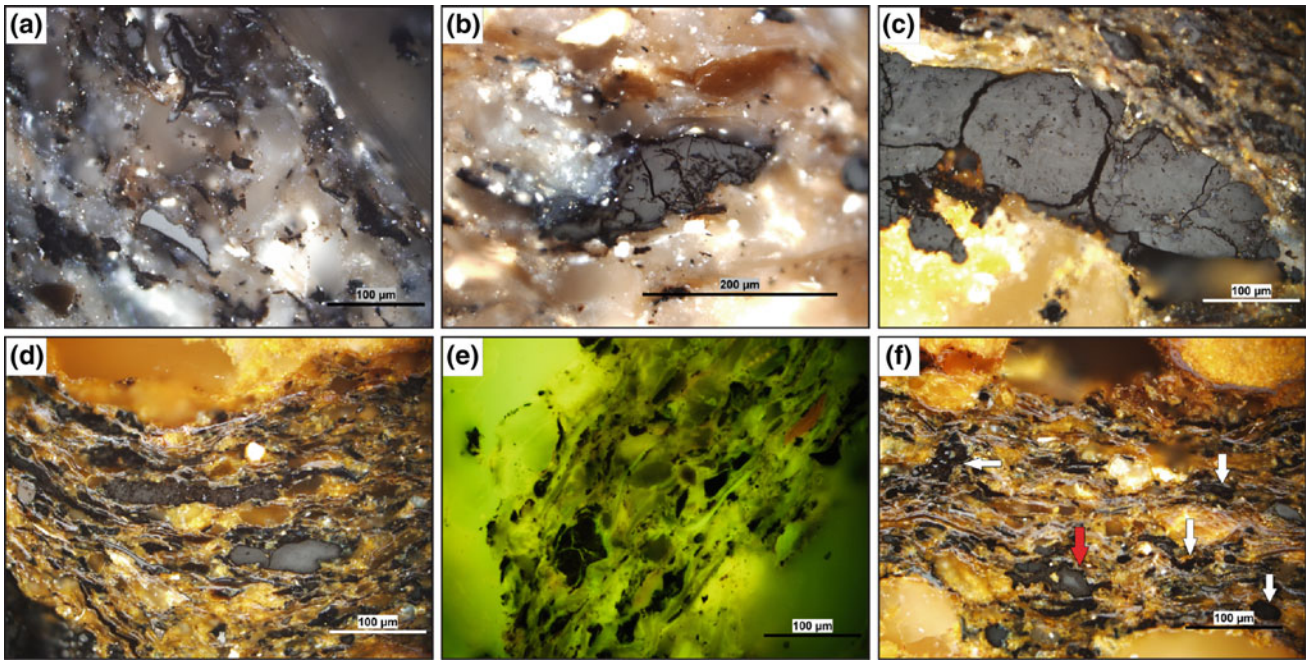

Fig. 10 Photomicrographs of coaly particles showing various macerals from unaltered (**a**, **b**) and altered claystone samples (**c**–**f**). All photographs were taken under reflected light, except photograph (**e**) that shows the sample in the fluorescence mode. Dvořákova stezka escarpment, the Nýřany Beds. See the text for details. **a** *light gray* inertinite particles (*lower* and *upper center*) and darker fine-grained liptinite particles; **b** large vitrinite particle (Rr = 0.65%) with well-visible internal cellular structure. *Brown* residues above the vitrinite fragment are probably sporinites; the brightly reflecting grains disseminated within the clay matrix are sulfide minerals; **c** thermally altered vitrinite particle showing the development of contraction and oxidative fissures, numerous tiny internal pores, and a variable optical reflectance. The enclosing *reddish* rock matrix has been impregnated by ferruginous minerals; **d** altered arkose with intensely Fe-impregnated matrix that hosts an association of various organic macerals. *Medium gray* vitrinite (*centre*) associates with *light gray* inertinite (*left*) and *dark brown* porous bitumen particles (*upper centre* and *left*); **e** association of variable organic remains in an altered arkose under the fluorescence excitation. Dark non-fluorescent particles are vitrinites, intertinites, and bitumens, while *yellowish* to *dull brown* fluorescing fragments are liptodetrinites, bituminites, and sporinites; **f** association of intertinite fragments (thin *light gray* particles stretched parallel to the bedding), altered vitrinite grains with dark reaction rims (*red* arrow) and *dark brown,* finely porous bitumen particles (*white arrows*) embedded within an arkose matrix. Note an intense staining of the host sediment by ferruginous minerals that affected also individual quartz grains

the result of dissolution and metasomatic alteration of walls of fracture conduits by rising deep flow, and subsequent removal of the alterite by superimposed speleogenic and/or weathering processes (Klimchouk et al. 2013a, b; see also Klimchouk Chap. 1). We presently think that the concave forms recognized in Carboniferous sandstones in central and western Bohemia may have originated in a similar way.

Besides the morphology and spatial associations of concave forms, additional arguments supporting their hypogene origin include the links of many cavities to mineralized fractures and bedding planes. A significant difference in vitrinite reflectance values ascertained between the samples collected from mineralized bedding planes and those of unaltered host rock clearly shows that the bedding planes were exposed to temperatures that were about 30–60 °C higher than the adjacent thermal diagenetic background. This, in turn, suggests that some bedding planes and vertical fractures once served as migration pathways for heated mineralized solutions responsible for ferruginous deposits, local silicification, and most probably, the erosion of nearby cavities. Similar fracture-controlled migration of hot fluids heated substantially above ambient burial temperatures has been recently described from the Carboniferous strata elsewhere in the area, based on fluid inclusion analysis of fracture-filling minerals (Zachariáš and Pešek 2011).

The nature of inferred hypogene fluids and the timing of their migration can be partly deduced from wider geological knowledge. Highly mineralized (up to 86.6 g/L), warm (up to 78 °C), highly CO_2-saturated Na–Cl brines have been encountered in the area by a number of coal exploration boreholes that penetrated into the oldest stratigraphic members of the Carboniferous succession to depths greater than 600–1000 m (Jetel 1970, 1982). These deeply buried basinal fluids, the origin of which is still poorly understood, are locally sulfate-rich (1.2–7.4 g/L) and contain substantial concentrations of trace elements (Li, B, I, Br, Sr, Ba, F; Malkovský et al. 1974; Jetel and Rybářová 1985). Due to its high CO_2 content and aggressive chemical composition,

Table 2 Organic–petrological characteristics of coal fragments from Dvořákova stezka a Radčice

Sample No.	Locality	Host rock lithology	Vitrinite R_r (%)	σ	n	Vitrinite (vol. %)	Liptinite (vol. %)	Inertinite (vol. %)	Minerals (vol. %)
14/001	Kralupy	Non-altered arkose	0.77	0.09	55	9.3	6.0	13.8	69.5
14/001B	Kralupy	Non-altered arkose	0.85	0.09	68	10.4	4.9	15.1	65.8
14/002	Kralupy	Non-altered arkose	0.73	0.08	15	1.0	1.6	1.3	93.4
15/221	Kralupy	Non-altered arkose	0.63	0.09	100	26.8	6.5	9.2	57.5
15/222	Kralupy	Non-altered arkose	0.63	0.09	75	24.4	2.1	10.4	63.1
15/223	Kralupy	Non-altered arkose	0.61	0.07	150	43.4	26.4	20.9	9.3
16/110	Radčice	Altered arkose	0.91	0.19	15	5.3	0	2.0	92.7
16/111	Kralupy	Altered arkose	0.95	0.16	55	17.6	3.4	4.5	74.5
16/112	Kralupy	Altered arkose	1.03	0.17	150	43.4	4.6	23.1	27.7
16/113	Kralupy	Altered arkose	1.02	0.12	12	5.0	0	1.1	93.9

See the text for details

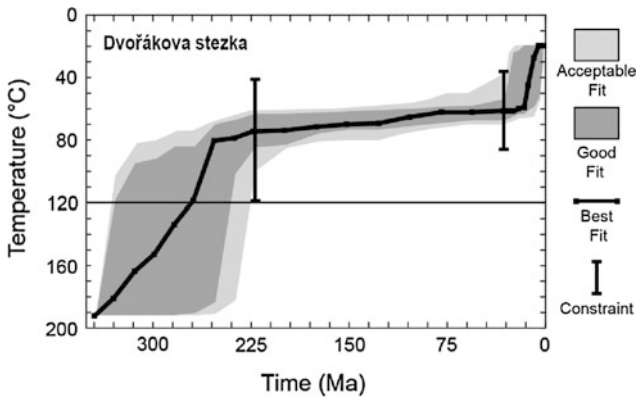

Fig. 11 Time–temperature evolution of apatite grains from Dvořákova stezka escarpment (the Nýřany Beds). See the text for details

the brines caused severe technological complications including repeated catastrophic events, which essentially terminated the deep coal mining operations in the area in 1989–1990.

Although direct evidence from fluid inclusions embedded in vein minerals is lacking, we presume that these hot, saline, sulfate, and CO_2-rich fluids may have been involved in the formation of hypogene forms in the Carboniferous arkoses. If so, it appears that any of three chemical processes presently known as driving mechanisms of hypogene speleogenesis may have contributed to the formation of the cavities, including alteration by hot waters, alteration by waters rich in carbonic acid, and alteration by waters containing H_2S/diluted sulfuric acid (e.g., Klimchouk 2007). In this context, the characteristic mineral assemblage identified on the walls and along the bedding planes and fractures cutting through the arkose sequence (e.g., goethite, jarosite, gypsum, quartz, pickeringite, and bischofite) can represent specific by-products of late stages of hypogene speleogenesis, rather than products of subaerial weathering or anthropogenic contaminations (e.g., Marszalek et al. 2014). All these minerals have been recently recognized in various hypogene caves around the world, often in caves that are believed to have originated through H_2S–H_2SO_4-dominated speleogenesis (Lueth et al. 2016; Lazaridis et al. 2011; Plan et al. 2012; Puşcaş et al. 2013; Temovski et al. 2013; Polyak et al. 2014; Kempe 2014; Audra et al. 2016). Moreover, the K–Na jarosite which was also identified in ferruginous impregnations along fractures and bedding planes appears to crystallize exclusively in hydrothermal conditions (e.g., Desborough et al. 2010; Ling et al. 2016).

Sulfide minerals, as an obvious source of acidity, are almost absent in the Bohemian arkose sequences. However, abundant sulfate ions able to produce sulfate minerals may have been supplied by ascending brines themselves which are known to be locally sulfate-rich (e.g., Krásný et al. 2012). Another source of acidity may have been thermal degradation of coal seams that occurs in abundance throughout the Carboniferous succession. Alternatively, selective feldspar leaching and clay mineral dissolution observed in altered arkoses may have been also caused by its reaction with CO_2-saturated brines, as described by Brophy et al. (2010) and Kaszuba et al. (2013), or with weak organic carboxylic acids which are commonly contained in deep basinal fluids interacting with hydrocarbons (e.g., Surdam 1984). The iron necessary for goethite formation may have been mobilized by the very aggressive brines upon their

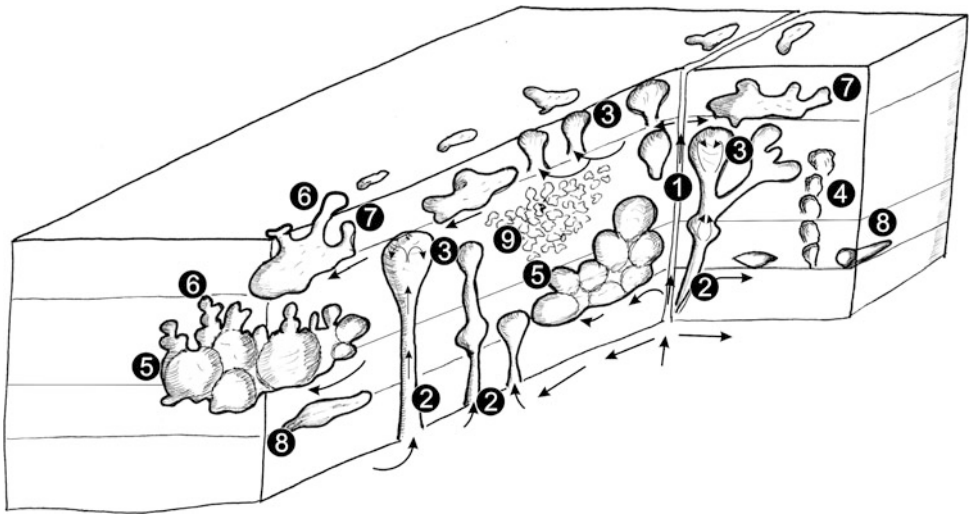

Fig. 12 Schematic representation of hypogene karst morphostructural elements for the Carboniferous sandstone rocks of central and western Bohemia. Not to scale. *Arrows* show inferred migration routes of hypogene fluids. Explanation: *1* subvertical fracture conduit, *2* rising feeder channels, *3* half-spherical and spherical niches with blind upward terminations, *4* vertical chains of half-spherical niches, *5* large cave-like hollows made by the interplay of spherical niches, *6* blind ceiling potholes, *7* niches and galleries developed along bedding planes, *8* small sheath-like and bottle-like cavities parallel to the bedding, and *9* complex small-scale alveolar (honeycomb) forms on the walls

Fig. 13 Typical field aspects of ferruginous mineralization of Cretaceous sandstones (Jizera Formation), the Kokořín area, central Bohemia. **a** Eroded remains of an about 80-cm-thick intensely Fe-impregnated bed of a coarse-grained conglomerate forming characteristic erosion-resistant "hats." Močidla Gorge. **b** Massive, partially mined-out bulbous goethite crust covering the plane of a subvertical fracture. Note spectacular three-dimensional complex honeycomb pattern in the underlying sandstone that apparently predates the deposition of a ferruginous crust. Abandoned ironstone quarry near Tupadly

upward migration through iron-rich red-colored sedimentary formations of the Carboniferous succession.

The migration of brines through the Carboniferous succession may have likely occurred during the Paleogene–Neogene time when the Carboniferous rocks experienced a substantial uplift and reactivation of regional fracture systems (e.g., Zeman et al. 2000). This scenario is indirectly supported by the presence of morphologically and mineralogically similar ferruginous mineralization that can be observed in immediately overlying well-permeable Cretaceous sandstones (Fig. 13).

Combining this field evidence with the known time–temperature evolution of Carboniferous rocks as revealed by the AFTA method, it follows that the inferred hypogene events affected the arkose sequence at relatively shallow depth of burial, most probably during its uplift toward the erosive surface. In these conditions, fracture-confined, upward-migrating deep basinal brines may have interacted with shallower formation waters where fracture conduits intersected with permeable beds or bedding planes. Such interaction of the two waters of contrasting chemistry, differing in H_2S and CO_2 contents, may have invoked the effects of mixing corrosion which, in turn, enhanced speleogenetic effects in affected sediments, as described by Klimchouk et al. (2012).

Following the exposure of Carboniferous strata, the sandstone cliffs were subjected to the processes of

exogenous weathering (e.g., fluvial, frost, wind, and biogenic erosion), the effects of which were partly superimposed on older hypogene features.

6 Conclusions

The main conclusions resulting from this study can be summarized as follows:

(1) The Upper Carboniferous arkose sandstones exposed in central and western Bohemia locally display a variety of concave forms which are reinterpreted as the members of the morphologic suite of rising flow (MSFR Klimchouk 2007), indicative of hypogene speleogenesis.
(2) The concave forms are intimately associated with goethite and jarosite mineralized bedding planes and subvertical fractures, while the altered arkose forming the walls of concave forms is commonly mineralized with neomorphic gypsum, quartz, jarosite, pickeringite, and bischofite.
(3) The vitrinite reflectance-based thermometry indicates that the sediments immediately adjacent to mineralized fractures and bedding planes were exposed to paleotemperatures substantially exceeding the adjacent burial-diagenetic background.
(4) Combined evidence from apatite fission track analysis and wider geological observations suggests that the major alterations occurred below the surface, during the Paleogene–Neogene period when the sandstone sequences were subjected to uplift and tectonic fracturing. The fluids responsible for the alterations were probably warm CO_2- and sulfate-rich brines which migrated upward from the deepest parts of Carboniferous basinal fill and mixed with shallower formation waters.
(5) When the uplifted sandstone sequences reached the surface, the hypogene cavities and altered cliff walls were subjected to the subaerial weathering and fluvial erosion processes, the effects of which were superimposed on older hypogene features.

Acknowledgements We wish to acknowledge the support provided by the Operational Program Prague—Competitiveness, project "Centre for Texture Analysis" (No. CZ.2.16/3.1.00/21538) and the program of a long-term conceptual development of the research organization RVO: 67985891. Our gratitude also goes to Dr Antonín Zeman (formerly the Institute of Theoretical and Applied Mechanics CAS) for his assistance with optical microscopic research. Ms Lenka Borecká (Institute of Rock Structure and Mechanics ASCR) has been helpful with the preparation of the diagrams. The paper has substantially benefited from constructive reviews and editorial effort of the editors Alexander Klimchouk and Jo De Waele.

References

Audra P, Palmer AN (2015) Research frontiers in spelogenesis. Dominant processes, hydrogeological conditions and resulting cave patterns. Acta Carsol 44:315–348

Audra P, Gázquez F, Rull F, Bigot JY, Camus H (2016) Hypogenic sulfuric acid speleogenesis and rare sulfate minerals in Baume Galinière cave (Alpes-de-Haute-Provence, France). Record of uplift, correlative cover retreat and valley dissection. Geomorphology (in press)

Barker CE, Pawlewicz MJ (1994) Calculation of vitrinite reflectance from thermal histories and peak temperatures. A comparison of methods. In: Mukhopadhyay PK, Dow WG (eds) Vitrinite reflectance as a maturity parameter. Applications and limitations, ACS symposium series, vol 570. American Chemical Society, Washington, DC, pp 216–229

Brophy JG, Lahann RW, Rupp JA (2010) Selective feldspar dissolution in response to elevated CO_2 pressure. AAPG search and discovery article #90116. AAPG eastern section meeting, Kalamazoo, Michigan, Sept 25–29 2010

Bruthans J, Jenč P, Churáčková I, Schweigstillová J (2009) Vykroužené dutiny Českého ráje: jak a kdy vznikaly? [Rounded cavities in Bohemian Paradise: how and when they developed?] Speleofórum 28:101–105 (in Czech)

Carlson WD, Donelick RA, Ketcham RA (1999) Variability of apatite fission track annealing kinetics I: experimental results. Am Miner 84:1213–1223

Čech S, Klein V, Kříž J, Valečka J (1980) Revision of the Upper Cretaceous Stratigraphy of the Bohemian Cretaceous Basin. Věstn Ústředního ústavu geologického 55(5):277–296

Cílek V (1993) Solné výkvěty v pseudokrasových jeskyních výklencích na Dvořákově stezce u Nelahozevsi [Salt efflorescations in pseudokarst caves close to Nelahozeves, Prague region]. Speleo 11(18): 12 (in Czech)

De Waele J, Galdenzi S, Madonia G, Menichetti M, Parise M, Piccini L, Sanna ., Sauro F, Tognini P, Vattano M, Vigna B (2014) A review of Hypogene Caves in Italy. In: Klimchouk A, Sasowsky ID, Mylroie J, Engel SA, Engel AS (eds) Hypogene Cave morphologies, selected papers and abstracts of the symposium held February 2 through 7, 2014, San Salvador Island, Bahams. Karst Water Institute Special Publication 18, Karst Water Institute, Leesburg, Virginia, pp 28–30

Desborough GA, Smith KS, Lowers HA, Swayze GA, Hammarstrom JM, Diehl SF, Leinz RW, Driscoll RL (2010) Mineralogical and chemical characteristics of some natural jarosite minerals. Geochim Cosmochim Acta 74:1041–1056

Donelick RA, Ketcham RA (1998) AFTSolve. Apatite fission track modelling software. Donelick analytical Inc., Katy

Donelick RA, Ketcham RA, Carlson WD (1999) Variability of apatite fission track annealing kinetics II: crystallographic orientation effects. Am Miner 84:1224–1234

Dublyansky YV (1990) Zakonomernosti formirovania i modelirovania gidrotermokarsta [Principles of development and modelling of hydrothermal karstfication]. Trudy Instituta geologii i geofiziki imeni 60-letia Soyuza SSR 756, Nauka, Sibirskoe otdelenie, Novosibirsk (in Russian)

Dublyansky YV (1995) Speleogenetic history of the Hungarian hydrothermal karst. Environ Geol 25:24–35

Dunkl I (2002) TRACKKEY: a Windows program for calculation and graphical presentation of fission track data. Comput Geosci 28:3–12

Fediuk F (1999) Geologický a vlastivědný výlet do levobřežního dolního Povltaví [Geological excursion to the lower left-bank area of the Vltava River]. Sprint Foto Servis, Liberec (in Czech)

Filip J, Suchý V (2004) Thermal and tectonic history of the Barrandian Lower Paleozoic, Czech Republic: is there a fission-track evidence

for Carboniferous-Permian overburden and pre-Westphalian alpinotype thrusting? Bull Geosci 79(2):107–112

Frost RL, Wills RA, Weier ML, Martens W, Mills S (2006) A Raman spectroscopic study of selected natural jarosites. Spectrochim Acta A 63:1–8

Groom KM, Allen CD, Mol L, Hall K (2015) Defining tafoni: re-examining terminological ambiguity for cavernous rock decay phenomena. Prog Phys Geogr 39(6):775–793

Havlena V (1982) Limnické pánve permokarbonu Českého masivu—geneze, třídění, vyplňování a zlomová tektonika [Permo-Carboniferous limnic sedimentary basins of the Bohemian Massif: its origin, classification, depositional evolution and thrust tectonics]. In: Sborník IV. uhelně geologické konference Přírodovědecké fakulty Univerzity Karlovy, Univerzita Karlova, Praha, pp 37–44

Holub V (1982) Explanatory notes to the lithotectonic profile of the Permo-Carboniferous basins of the Central Bohemian region (ČSSR). In: Tectonic regime of molasse epochs. Zentralinstitut für Physics der Erde, Potsdam, p 66

Holub V, Eliáš M, Hrazdíra P, Franců J (1997) Geological research into gas sorbed in the coal seams of the Carboniferous in the Mšeno-Roudnice Basin, Czech Republic. In: Gayer R, Pešek J (eds) European coal geology and technology, vol 25, pp 409–423 (Geological Society special publication)

Holub V, Jaroš J, Malý P, Martínek K, Pešek J, Prouza V, Spudil J, Tásler R (2001) Geologie a ložiska svrchnopaleozoických limnických pánví České republiky [Geology and deposits of upper palaeozoic limnic sedimentary basins of the Czech Republic]. Český geologický ústav, Praha (in Czech)

Hurford AJ, Green PF (1982) A user's guide to fission-track dating calibration. Earth Planet Sci Lett 59:343–354

Hurford AJ, Green PF (1983) The Zeta calibration of fission-track dating. Chem Geol 31:285–317

Jakucs L (1977) Genetic types of the Hungarian karst. Karszt és Barl Special Issue:3–18

Jetel J (1970) Hydrogeologie permokarbonu a křídy na opěrném profile Mělník—Ještěd [Hydrogeology of the Permo-Carboniferous and Cretaceous in the profile line Mělník–Ještěd]. Sborník geologických věd, řada HIG 7:1–42 (in Czech, with English summary)

Jetel J (1982) Hydrogeologie mšenské pánve a černouhelných ložisek mezi Mělníkem a Benátkami nad Jizerou [Hydrogeology of the black-coal deposits in the Mšeno Basin]. Sborník geologických věd, řada HIG 16:33–86 (in Czech, with English summary)

Jetel J, Rybářová L (1985) Nové poznatky o hydrogeologii permokarbonu roudnické a mnichovohradišťské pánve [New data on hydrogeology of the Roudnice and Mšeno basins]. Zprávy o geologických výzkumech v roce 1985:80–82 (in Czech)

Kaszuba J, Yardley B, Andreani M (2013) Experimental perspectives of mineral dissolution and precipitation due to carbon dioxide–water–rock interactions. Rev Miner Geochem 77(1):153–188

Kempe S (2014) Hypogene limestone caves in Germany: geochemical background and regionality. In: Klimchouk A, Sasowsky ID, Mylroie J, Engel S, Engel AS (eds) Hypogene cave morphologies, vol 18, pp 48–56 (Karst Water Institute special publication)

Ketcham RA, Donelick RA, Carlson WD (1999) Variability of apatite fission track annealing kinetics III: extrapolation to geological time scales. Am Miner 84:1235–1255

Ketcham RA, Donelick RA, Donelick MB (2000) AFTSolve: a program for multi-kinetic modelling of apatite fission-track data. Geol Mater Res 2:1–32

Klimchouk AB (2007) Hypogene speleogenesis: hydrogeological and morphogenetic perspective (Special paper No. 1), 2nd edn. National Cave and Karst Research Institute, Carlsbad, pp 1–106

Klimchouk A (2009) Morphogenesis of hypogenic caves. Geomorphology 106:100–117

Klimchouk A (2015) The Karst paradigm: changes, trends perspectives. Acta Carsol 44(3):289–313

Klimchouk A, Tymokhina E, Amelichev G (2012) Speleogenetic effects of interaction between deeply derived fracture-conduit flow and intrastratal matrix flow in hypogene karst settings. Int J Speleol 41(2):161–179

Klimchouk AB, Amelichev GN, Tymokhina EI, Tokarev SV (2013a) Hypogenic speleogenesis in the Crimean fore-mountains (the Black sea region, south Ukraine) and its role in the regional geomorphology. In: Filippi M, Bosák P (eds) Proceedings of the 16th international congress of speleology, vol 3. Czech Speleological Society, Praha, pp 364–366 (Brno, July 2013)

Klimchouk AB, Tymokhina EI, Amelichev GN, Dublyansky YV, Spötl C (2013b) The Hypogene Karst of the Crimean piedmont and its geomorphological role. DIP, Simferopol (in Russian)

Krásný J, Čurda S, Datel JV, Dvořák J, Grmela A, Hrkal Z, Kříž H, Marszalek H, Šantrůček J, Šilar J (2012) Podzemní vody České republiky. Regionální hydrogeologie prostých a minerálních vod [Underground waters of the Czech Republic. Regional hydrogeology of surface and mineral waters]. Česká geologická služba, Praha

Kukal Z (1983) Granitoidové plutony byly hlavním zdrojem živců permokarbonských sedimentů [Granitoid plutons were the main source of feldspars of the Permo-Carboniferous sediments]. Čas mineral geol 28(4):423–428

Lazaridis G, Melfos P, Papadopoulou L (2011) The first cave occurrence of orpiment (As_2S_3) from the sulfuric acid caves of Aghia Paraskevi (Kassandra Peninsula, N. Greece). Int J Speleol 40(2):133–139

Libertín M, Opluštil S, Pšenička J, Bek J, Sýkorová I, Dašková J (2009) Middle Pensylvanian pioneer plant assemblage buried in situ by volcanic ash-fall, central Bohemia, Czech Republic. Rev Palaeobot Palynol 155:204–233

Ling Z, Cao F, Ni Y, Wu Z, Zhang J, Li B (2016) Correlated analysis of chemical variations with spectroscopic features of the K–Na jarosite solid solutions relevant to Mars. Icarus 271:19–29

Littke R (1993) Deposition, diagenesis and weathering of organic matter-rich sediments. Lect Notes Earth Sci 47:1–216

Lojka R, Sýkorová I, Laurin J, Matysová P, Matys Grygar T (2010) Lacustrine couplet-lamination: evidence for late Pennsylvanian seasonality in central equatorial Pangaea (Stephanian B, Mšec Member, Central and Western Bohemian basins). Bull Geosci 85:709–734

Lueth VW, Rye RO, Peters L (2016) "Sour gas" hydrothermal jarosite: ancient to modern acid-sulfate mineralization in the southern Rio Grande Rift. Chem Geol (in press)

Malkovský M (1979) Tektogeneze platformího pokryvu Českého masívu [The tectogenesis of the platform cover of the Bohemian Massif]. Knih Ústředního ústavu geologického 53:1–179

Malkovský M, Benešová Z, Čadek J, Holub V, Chaloupský J, Jetel J, Müller V, Mašín J, Tásler R (1974) Geologie české křídové pánve a jejího podloží [Geology of the Bohemian Cretaceous Basin and its basement]. Ústřední ústav geol Acad, Praha (in Czech)

Marszalek M, Alexandrowicz Z, Rzepa G (2014) Composition of weathering crust on sandstones from natural outcrops and architectural elements in an urban environment. Environ Sci Pollut Res Int 21:14023–14036

Mísař Z, Dudek A, Havlena, Weiss J (1983) Geologie ČSSR I. Český masív [Geology of the ČSSR I. The Bohemian Massif]. Státní pedagogické nakladatelství, Praha (in Czech)

Opluštil S (2005) Evolution of the Middle Westphalian river valley drainage system in central Bohemia (Czech Republic) and its palaeogeographic implication. Palaeogeogr Palaeoclimatol Palaeoecol 222:223–258

Palmer AN (2000) Hydrogeologic control of cave patterns. In: Klimchouk A, Ford D, Palmer A, Dreybrodt W (eds) Speleogenesis: evolution of karst aquifers. National Speleological Society, Huntsville, pp 77–90

Pašek J, Urban M (1990) The tectonic evolution of the Plzeň basin (Upper Carboniferous, West Bohemia): a review and reinterpretation. Folia Musei Rerum Nat Bohem Occidentalis. Geologica 32:1–56

Pešek J (1996) Geologie pánví středočeské svrchopaleozoické oblasti [Geology of central Bohemian Upper Paleozoic sedimentary basins]. Český geologický ústav, Praha

Pešek J, Sýkorová I (2006) A review of the timing of coalification in the light of coal seam erosion, clastic dykes and coal clasts. Int J Coal Geol 66:13–34

Plan L, Tschegg C, De Waele J, Spötl C (2012) Corrosion morphology and cave wall alteration in an Alpine sulfuric acid cave (Kraushöhle, Austria). Geomorphology 169:45–54

Plózer I (1977) Situation of Hungarian cave diving in 1976. Karszt és Barlang, Special Issue, pp 67–69

Polyak VJ, Asmerom Y, Hill C, Palmer AN, Provencio PP, Palmer MV, McIntosh WC, Decker DD, Onac BP (2014) Isotopic studies of byproducts of hypogene speleogenesis and their contribution to the geologic evolution of the western United States. In: Klimchouk A, Sasowsky ID, Mylroie J, Engel S, Engel AS (eds) Hypogene cave morphologies, vol 18. Karst Water Institute special publication, pp 88–96

Puşcaş CM, Onac BP, Effenberger HS, Povară I (2013) Tamarugite-bearing paragenesis formed by suphate acid alteration in Diana cave, Romania. Eur J Miner 25(3):479–485

Sauro F, De Waele J, Onac BP, Galli E, Dublyansky Y, Baldoni E, Sanna L (2014) Hypogenic speleogenesis in quartzite: the case of Corona´e Sa Craba Cave (SW Sardinia, Italy). Geomorphology 211:77–88

Surdam RC (1984) The chemistry of secondary porosity. In: McDonald DA, Surdam RC (eds) Clastic diagenesis. The American Association of Petroleum Geologists, Tulsa, pp 127–149

Taylor GH, Teichmüller M, Davis A, Diessel CFK, Littke R, Robert P (1998) Organic Petrology. Gebrüder Borntraeger, Berlin

Temovski M, Audra P, Mihevc A, Spangenberg JE, Polyak V, McIntosh W, Bigot JY (2013) Hypogenic origin of Provalata cave, Republic of Macedonia: a distinct case of successive thermal carbonic and sulfuric acid speleogenesis. Int J Speleol 42:235–246

Vítek J (1987) Pseudokrasové tvary v karbonských sedimentech severozápadně od Plzně [Pseudokarst features in Carboniferous sediments NW of Pilsen]. Československý kras 38:125–127 (in Czech)

Wagner GA, Van den Haute P (1992) Fission-track dating. Ferdinand Encke Verlag, Stuttgart

Zachariáš J, Pešek J (2011) Fluid inclusion study of carbonate-dominated veinlets from coal seams and rocks of the central and west Bohemian basins, Czech Republic. Acta Geodynamica et Geomater 8(2):133–143

Zeman A, Suchy V, Stejskal M, Janku J, Cermak J, Turek K (2000) Migration of fluids controlled by equidistant fracture systems: an example from Central Europe (Czech Republic, Slovakia and Austria). J Geochem Explor 69(70):499–504

Ziegler PA (1990) Geological atlas of western and central Europe. Shell, The Hague

Hypogene Caves in Germany, Geological and Geochemical Background

21

Stephan Kempe, Ingo Bauer, and Stefan Glaser

Abstract

Germany exhibits a very diverse geological history. Thus, a large number of stratigraphically, petrographically and tectonically different carbonate and sulfate rock deposits exist that have been subject to karstification. First, we discuss the possible "*agents*" (sensu Klimchouk) of hypogene karstification. Three principally different processes are identified: water rising because of buoyancy (either thermally or concentration induced), *in situ* oxidation of siderite or rising gases (CO_2, CH_4 or H_2S). Next, German caves and karst are discussed in order of stratigraphy. Applying the most pertinent epigene versus hypogene morphological characteristics, it becomes evident that hypogene caves occur in many different areas, often side by side with clearly epigene caves. For many areas, the agents of hypogene speleogenesis still remain unclear. This applies for most caves in the Paleozoic limestones of the Rhenish Schist Massif. The largest of these caves is the >700 × 200 20 m measuring cavity at the bottom of the Wülfrath quarry, filled with Lower Cretaceous sand. Only the Iberg/Harz caves seem to be a clear case; here, the worldwide highest concentrations of siderite weathering-induced caves occur. In the South Harz, large cavities were discovered in anhydrite below the water level by mining for the underlying upper Permian Copper Shale. Apparently these were formed by water rising from underlying carbonate aquifers. The large cavities discovered recently in the Blauhöhlen System and some of the deep pit-caves in Upper Jurassic limestone of the Swabian Alb may have their explanation in volcanic CO_2, having emanated from some of the 355 pipes of the Swabian volcanic field. Most striking is the high concentration of hypogene caves in the central Franconian Alb that occur in a small area while the surrounding areas are almost devoid of larger caves. In the geological past, this region formed the center of a continental basin where artesian water was able to ascend along major fractures. This could explain the strange geographic cave distribution as well as suggest that the ascending waters carried sulfide or methane from below.

Keywords

Germany • Hypogene caves • Speleogenesis • Regional speleology • Siderite weathering

This paper is a composite of already published papers, namely Kempe (2014a, b), Glaser (2013), and Kempe et al. (2016).

S. Kempe (✉) · I. Bauer
Institut für Angewandte Geowissenschaften, TU-Darmstadt, Schnittspahnstr. 9, 64287 Darmstadt, Germany
e-mail: kempe@geo.tu-darmstadt.de

S. Glaser
Albrecht-Dürer-Straße 29, 82152 Krailling, Germany
e-mail: sglasers@gmx.de

1 Introduction

Hypogene karstification is a more common and geochemically more complicated process than anticipated decades ago. It is defined as caused by the upward movement "*of the cave-forming agent*" (sensu Klimchouk 2012). This "*agent*" may be either the water itself rising or a compound available

© Springer International Publishing AG 2017

A. Klimchouk et al. (eds.), *Hypogene Karst Regions and Caves of the World*, Cave and Karst Systems of the World, DOI 10.1007/978-3-319-53348-3_21

in situ at depth or rising from the depth of the crust. Water can rise due to buoyancy created either by warming (thermal convection) or by the additional dissolution of some compound causing the increase in density and hence the sinking of water (natural convection). This latter case is the cause of some of the large sulfate caves in the South Harz (see below). On the other hand, a number of chemical reactions are discussed that give rise to hypogene karstification by in situ processes or advection of certain compounds.

In 1971, Kempe showed that siderite weathering can produce appreciable caves far below the water level (Kempe 1971, 1975, 1998a, 2008, 2009; Svensson and Kempe 1989).

According to:

$$4FeCO_3 + O_2 + 6H_2O \rightarrow 4FeO(OH) + 4HCO_3^- + 4H^+. \quad (1)$$

The ferrous carbonate, the mineral siderite, is oxidized to the ferric oxy-hydroxide, the mineral goethite, thereby liberating free protons and CO_2 following the dissociation of the ensuing carbonic acid. These can in turn attack surrounding carbonate rocks, forming hypogene cavities around and near the oxidizing iron ore.

The simplest case involving a rising gaseous agent would be CO_2 derived from either volcanic vents or dikes or from other sources at depth. In such a scenario, the caves should be largest very near to the base of the karstified limestone stratum.

Another process was identified producing hypogene cavities, i.e., oxidation of rising H_2S (e.g., Morehouse 1968; Palmer and Hill 2012; Plan et al. 2012):

$$H_2S + 2O_2 \rightarrow 2H^+ + SO_4^{2-} \leftrightarrow H^+ + HSO_4^-. \quad (2)$$

This process appears to be capable of corroding very large cavities in the periphery of oilfields, such as in the Capitan Reef complex at the Permian Basin, New Mexico and Texas (e.g., Hill 1987). There, some of the largest rooms and the largest caves of the world are found such as Lechuguilla and Carlsbad Cavern (e.g., Kambesis 2012). The process has been identified as operative because during limestone dissolution, gypsum is forced out of solution (e.g., Galdenzi and Maruoka 2003). In spite of the high solubility of gypsum, it has survived attack by later seepage water in drier corners of the caves, thus forming "the smoking gun" of this important cave-forming process.

However, there may yet be a third process, i.e., methane oxidation (Kempe 2008):

$$CH_4 + O_2 \rightarrow 4H^+ + CO_2. \quad (3)$$

Since methane is much more common than H_2S in the subsurface, it may play a much larger role than the former in corroding large subterranean cavities. There is one problem with methane: Its oxidation does not leave a "smoking gun." Thus, it may be difficult to finally prove its importance. One possibility does, however, exist: If the carbonates dissolved by methane-generated CO_2 precipitate where degassing of CO_2 is possible, then these speleogenetic carbonates should have a very low $\delta^{13}C$ signature, lower than the $\delta^{13}C$ of normal speleothems. This is because crustal methane has a very low $\delta^{13}C$, i.e., up to 70‰ lower than the organic matter it has been derived from (Rosenfeld and Silverman 1959). We all should look out for such cases. A first trace of speleogenetic methane is documented in low $\delta^{13}C$ (−32 to −65‰) calcite in Zoloushka Cave (Western Ukraine) (Klimchouk 1997).

2 Hypogene Caves of Germany

Germany has a complex geology featuring large tracts of Devonian, Carboniferous, Permian, Triassic, Jurassic, Cretaceous and Tertiary carbonates and sulfates. The Devonian and Carboniferous rocks have been subject to the Upper Carboniferous Variscan orogeny with intensive folding and thrusting. Thereafter Central Europe was sinking almost continuously, allowing marine and continental basins to fill with thick strata beginning in the Upper Carboniferous and the Permian and ending in the Upper Cretaceous. Since then, these rocks were subject to gradual uplift and fracturing by "inversion tectonism" (e.g., Kley 2013), i.e., phases of extension and compression (formerly termed "Saxonische Tektonik") and, in the south of Germany, to alpine orogenic thrusting (Fig. 1). Thus, there is ample opportunity for karstification under various stratigraphic, tectonic, petrographic, morphologic, and altitudinal setting. Moreover, these caves have been under severe permafrost conditions during glacials. Accordingly, there are numerous different conditions under which caves are forming and have formed in Germany in the past.

In spite of its extensive limestone areas, Germany has only 15 caves longer than 5 km (Müller and Wolf 2013; VdHK 2016). When looking at cave densities, we find large differences: Some of the Devonian rocks appear to be Swiss cheese with numerous caves in small areas while some of the Triassic, Jurassic and Cretaceous rocks appear to be devoid of significant cavities over large regions. Even if this impression may be skewed because we yet have to find caves in those seemingly cave-less areas, it already suggests that cave formation is not a statistical process, such as one

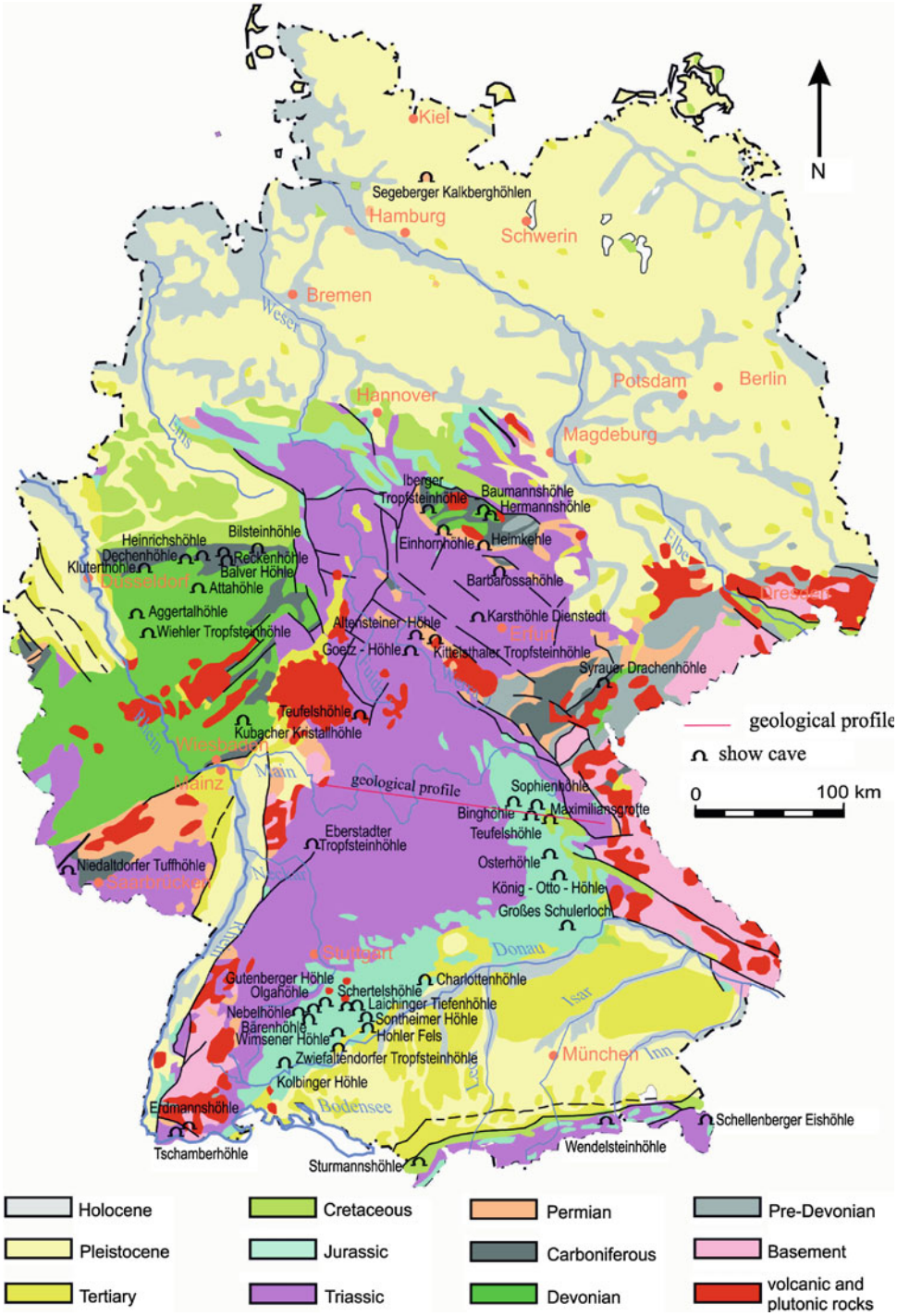

Fig. 1 Geological map and show caves of Germany that also mark the most important cave sites. The geological profile line refers to Fig. 14

would expect if caves would form exclusively according to "Dreybrodt-type-epigene-cave-models" (e.g., Dreybrodt 2008).

It is not entirely clear how to separate fossil epigene caves from those of hypogene origin, but Table 1 gives a rough matrix of criteria that may serve for the majority of cases.

According to these criteria, and in some cases without actually having visited the caves, one can try to differentiate German caves (Kempe and Rosendahl 2008) into the two classes (obviously with leaving room for discussion).

The Rhenish Schist Massif is the largest area with Paleozoic rocks folded during the Variscan orogeny. It contains many small limestone outcrops of Middle to Upper Devonian age that show high degrees of karstification. Many of the caves are well-known show caves. Nevertheless, no overview exists about their genesis in general. Some of the

Table 1 Criteria to differentiate between hypogene and epigene limestone caves according to own experience

Evidence for	Epigene	Hypogene
General layout of cave	Linear, dendritic tributary cave of substantial longitudinal extent, following the hydraulic gradient	Maze, isolated cavities, extensive cave passages limited to small areas, preexisting inhomogeneities of the host rock are enhanced
Entrances	Former ponors or springs	No natural entrance or cave opened accidentally by erosion
Shape of rooms	Canyons, waterfall pits, seepage shafts, or phreatic round or oval passages with relatively constant cross sections	Large chambers interconnected (if at all) by narrow passages, shafts, passages of rough cross section, blind ends
General wall morphology	Meandering passages, erosion pots, scallops	Ceiling cupolas, solutional ceilings, solution cusps, sloping side walls
Wall roughness	Smoothed and polished walls, silicified fossils sometimes exposed	Walls irregular with pockets, harder veins protruding, sparitic fossils often exposed
Sediments	Allochthonous or autochthonous gravel, sandy and fluvially sorted material	Fine-grained, autochthonous sediments

caves are (mostly?) epigene, like the newly discovered and still active >10-km-long Herbstlabyrinth near Herborn (Dorsten et al. 2016). Others, specifically those that are fossil are difficult to judge. For example, the Kluterthöhle is a 5.7-km-long joint-controlled maze cave (e.g., Koch 1992), suggesting hypogene origin. However, it has later also been invaded by epigene waters connecting a sink and a spring. This could be a secondary stream capture, thus complicating the interpretation. Other maze caves include the Aggertalhöhle and 6.7-km-long Attahöhle, while the Dechenhöhle and the Heinrichshöhle show linear development. At least one cave is clearly of hypogene origin, the Kubacher Kristallhöhle near Weilburg. It features a nearly 200-m-long, up to 23-m-wide and 30-m-high cavity created by deep phreatic corrosion (picture see Kempe 2014a). Since iron ores have been mined in the vicinity and siderite is a common ore in the Lahn-Dill district, the Kubacher Cave may also have been formed by siderite weathering even though there are no immediate remains of an ore vein in the cave.

Also the largest—and most likely hypogene—cave room yet discovered in Germany is situated in the Rhenish Massif: the at least 700-m-long, 200-m-wide and 20-m-high cavity at the bottom of the limestone quarry Rohdenhaus-Süd near Wülfrath (Buchas 2000; Drozdzewski et al. 1998). The cave is entirely filled with quartz sand that contains layers of charred plant remains dating into the Lower Cretaceous. Thus, the cave is at least 100 million years old. Even more, at its center an impressive limonitic ore deposit at least 50 m wide and 10 m thick was unearthed. This suggests that the ascending "*cave-forming agent*" was anaerobic, carrying ferrous iron into the cave and creating a speleogene iron ore deposit possibly similar to what is found in Jordan at Warda (Al-Malabeh et al. 2008) and, to a much smaller extent, in the Bismarckgrotte (see below).

The second-largest Variscan block containing karstified limestones are the Harz Mountains. Here two Upper Devonian reef limestone complexes, the Iberg–Winterberg near Bad Grund and the Elbingerode Massif are exposed. The Iberg/Winterberg, roughly 2 km^2 in size, is a prime example of high density of caves of both groups, hypogene and epigene. The Winterberg, a large limestone quarry, exposed a number of epigene caves: large, steep canyons (now destroyed except for the Neue Winterberghöhle). In contrast to this, the neighboring Iberg is the worldwide most important example for hypogene cavities caused by siderite weathering. Within an area of 250 m × 250 m, at least 8 km of passages are recorded (Fig. 2). Iron ore mining has connected these originally isolated caves (Fig. 3) into one large 3D-maze, composed of large irregular halls and passages following former siderite veins (Reimer and Kempe 1989; Reimer 1990). In some ponds in the former mine, siderite weathering is still going on, forming small analogs of this sort of hypogene karstification (Svensson 1988; Svensson and Kempe 1989).

The fact that siderite weathering is truly hypogene may be questioned because the oxygen needed to trigger the process comes from above with seepage water. Palmer (2000) gives a broader interpretation: "*hypogenetic caves are formed by water in which the aggressiveness has been produced at depth beneath the surface, independent of surface or soil* CO_2 *or other near surface acid sources*." Referring to Palmer's definition, the Iberger caves are clearly examples of hypogene speleogenesis because the acid source is autochthonous caused by siderite weathering. Palmer does not consider oxygen in his definition but it is understood that the caves of the Guadalupe Mountains, such as Carlsbad Cavern, Lechuguilla and others are made possible only by atmospheric oxygen infiltrating the deep-seated reservoirs of

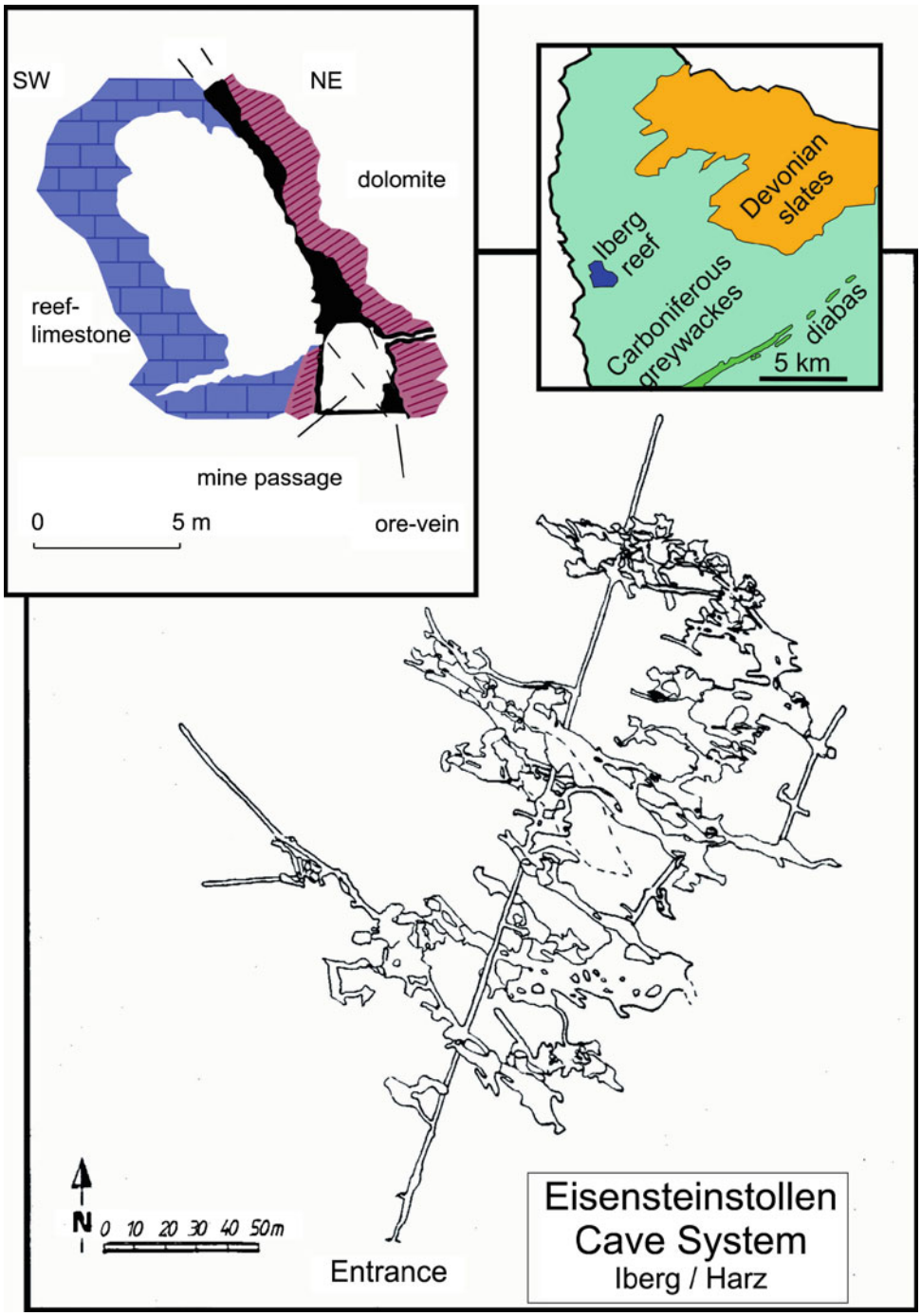

Fig. 2 Map of the 5-km-long Eisensteinstollen-System, the largest (but not the only) hypogene cavity caused by siderite weathering at the eastern flank of the Iberg, Harz. It consists of natural large halls connected by mine passages (plan after Reimer and Kempe 1989, based on survey of Fricke and co-worker). Numbers refer to water samples (T = pools, S = seepage water). *Inset right* Location of the Iberg/Winterberg in the northern Harz. *Inset left* Cross section through a cavity in the Eisensteinstollen-System formed along a former siderite vein and accompanying cave (after Reimer and Kempe 1989)

H_2S from the surface. Thus, the source of the oxygen that in itself is not cave-forming does not play a role in the definition of what is considered to be a hypogene cave formation or not.

The Iberger Tropfsteinhöhle, the only show cave on the Iberg/Winterberg, is situated above the Eisensteinstollen-System (Kempe et al. 1985, 2016). Miners searching for iron ore several centuries ago originally discovered two of its four independent cavities. Today all cavities are connected by artificial galleries. The largest cavity is listed with a length of 123 m and an altitude difference of 27 m. It forms a loop due to a short artificial connection. It contains some flowstone unlike most of the other caves in the quadrant. The foot of the largest stalagmite has recently been dated to 399.5 +79/−50 ka, showing that the cave must have been above the water table at least since that time (Kempe et al. 2016). In order to document morphology, we scanned the Iberger Tropfsteinhöhle on June 11, 2014, with a

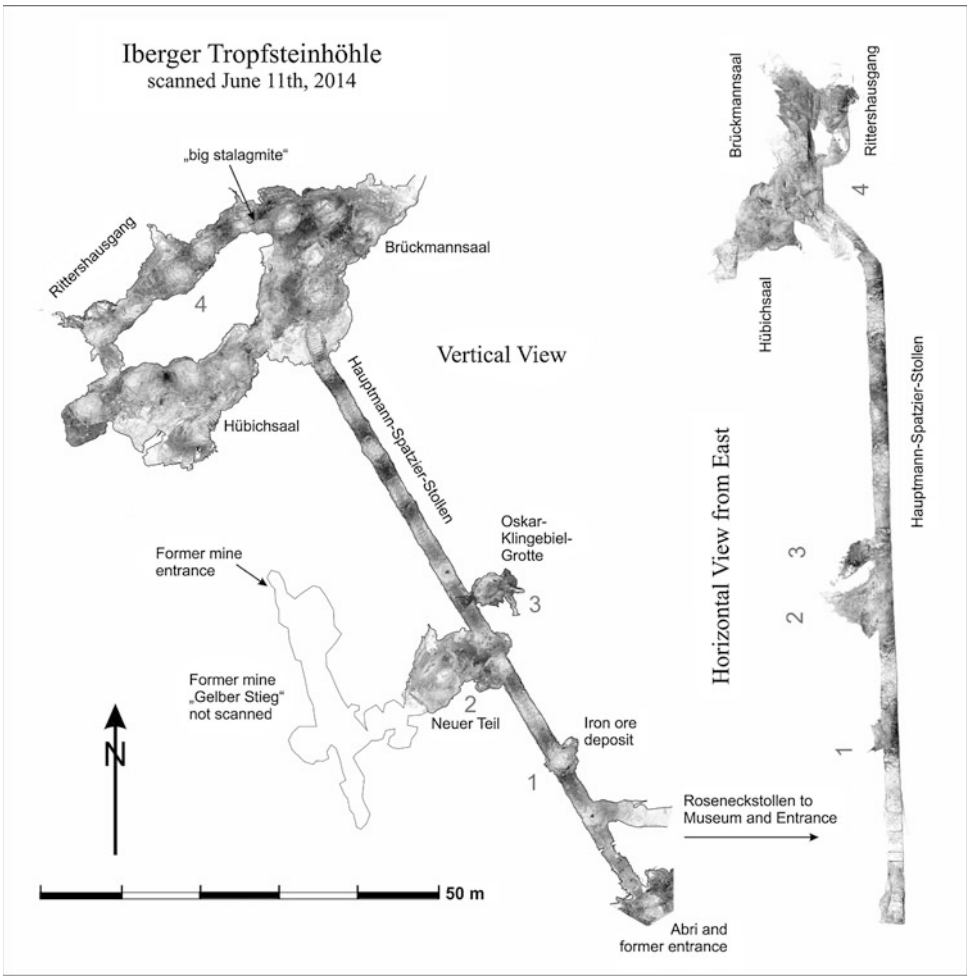

Fig. 3 3D Scan of the show cave Iberger Tropfsteinhöhle, viewed vertically from above (*left*) and viewed horizontally from the east (*right*). Note the four different parts that were connected by the "Hauptmann Spatzier Stollen," the access passage dug in 1911

Focus3D-S120 laser scanner by FARO (Fig. 3a, b). Each of the 32 scans covers an area of 360° horizontally and 90° to −60° vertically. The resolution amounts to 10.240 points/360°, which adds up to 44 million points per station. Each point is defined by its polar coordinates and a value measuring the intensity of the reflected laser beam. This value yields a graphic representation of gray shades similar to a black and white picture. Integrated compass and inclinometer are used to give direction and horizontality to the point cloud. Reference spheres of 14 cm diameter assure the linkage of the individual scans in a geometric precise way by triangulation. Linkage of point clouds and graphic representation was carried out with the SCENE program package provided by FARO EuropeGmbH.

The morphology of the cave, as well as all of the natural cavities in the vicinity, is indicative of phreatic origin shaped by slow natural, i.e., density-driven, convection: The walls show sloping side walls ("facets"; Fig. 4a) and sets of ceiling, blind-ending concave cupolas and wall-cusps (Fig. 4c) (e.g., Klimchouk 2007; Kempe 2008). The Oskar-Klingebiel-Grotto (Figs. 3 and 4c, d) is an isolated small cave, not immediately noticed when the Hauptmann Spatzier Passage was dug. The Grotto was filled halfway with goethite loam and only excavated in 1941. A NE–SW striking fracture (Fig. 4c bottom left) provided both for the ascend of iron-rich solution when the small siderite deposit was formed and for the O_2-bearing water when the siderite decomposed to goethite, causing the stacked cupolas to form (Fig. 4d).

The oxidation of the siderite was still active when the valleys started to cut down. This is evident from two negative (i.e., undercutting) water level marks found in the main cave: one in the Hübich Hall (Fig. 4b) and one in the Brückmann Hall about 5 m lower in altitude.

The Elbingerode reef complex was also mined, but no large cave appears to have been discovered. Rather, the caves in Elbingerode concentrate on both flanks of the Bode valley: The Baumannshöhle (1.95 km long), the earliest regularly managed show cave, is located on the west and the longer Hermannshöhle (3.36 km long) on the east. The Baumannshöhle appears to be deep phreatic; none of the epigene characteristics are present. What sort of agent was

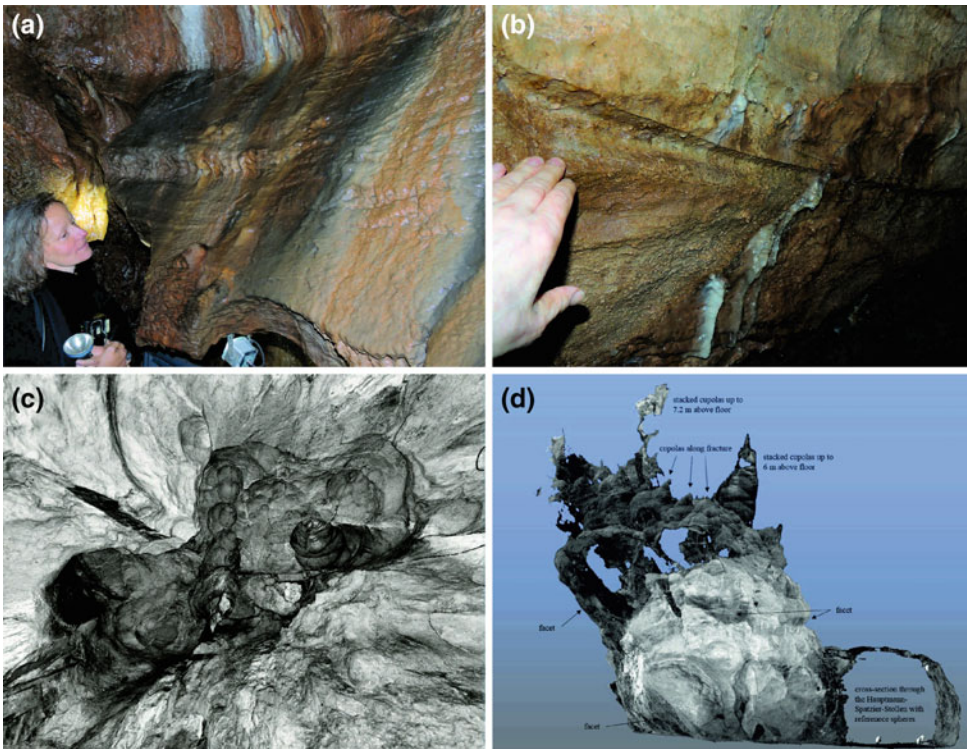

Fig. 4 **a** "Facet" (sloping side wall) in the Rittershaus Passage, a typical feature of slow phreatic convection. Note also the cupola on its lower edge. **b** Hübich Hall, E-wall: the most prominent of several water level undercuttings. **c** 3D Scan picture of sets of symmetrical cupolas aligned along fractures in the ceiling of the Oskar-Klingebiel-Grotto, an originally isolated chamber of the cave (width of picture about 3 m). **d** 3D Scan of the Oskar-Klingebiel-Grotto seen from the NW; picture revealing actual dimension of the cupolas above the former siderite deposit in the lower part of the cavity. The transparent sections are shadows on both sides of the cave not visible for the scanner (size 7 × 7 m)

responsible for its formation remains everybody's guess. The Hermannshöhle, on the other hand, is a largely epigene cave, linear in shape and with an active creek at its lower level. Other caves in the vicinity show solution ceilings and are also phreatic. They are not, however, associated with known siderite veins.

The Harz and its smaller sister to its south, the Kyffhäuser, are unconformably overlain by Upper Permian strata. The outcrops include the Werra, Stassfurt and Leine evaporite cycles of the Zechstein (today a lithostratigraphic group roughly equivalent to the Upper Permian and the Lopoginium Formation, 260–252 Ma ago), ideally forming a set of escarpments (Fig. 5a). These strata surround nearly continuous and with varying outcrop width both Harz and Kyffhäuser. Along the southern rims the strata dip with about 15° S or SE. The only cave in dolomite in these strata to speak of is the Einhornhöhle (Unicorn Cave), a show cave famous for its cave bear bones (Paul and Vladi 2001). Only part of the cavity is visible, most of its volume is buried by sediments, including thick layers of loam and gravel. In spite of this and its general linear development, it is not clear at all what the exact origin of the cave is.

Locally the Werra sulfate—gypsum along the surface and anhydrite below—can reach more than 250 m in thickness. Most sulfate caves are developed in either the Werra or in the Leine sulfate. Apart from a very few epigene caves with active creeks flowing through them (e.g., Trogstein-Fitzmühlen System [435 + 545 m long], Himmelreich Cave [550 m long]), these sulfate caves developed either in shallow phreatic settings (show caves Barbarossa Cave [670 m long] and Heimkehle [1.78 km long], Numburg Cave [1.75 km], and caves of the Hainholz area [Jettenhöhle, 750 m long, and Marthahöhle, 450 m long]), or in deep phreatic settings (e.g., Biese 1931; Kempe 1996). The deep phreatic cavities, locally called "Schlotten" (e.g., Kupetz and Knolle 2015), were discovered by mining for the metalliferous Copper Shale (Cu concentration up to 5%), underlying the Werra anhydrite and carbonate (Zechsteinkalk) (Table 2). The caves proved to be a bonus for the miners who could use them to dump mine refuse and to drain water into them. Accordingly, their ownership was worthwhile to fight for in court, thereby leaving documentation. By building deeper and deeper water solving mine passages, more and more of these caves appeared. Some are still accessible through mine shafts and with special permits, such

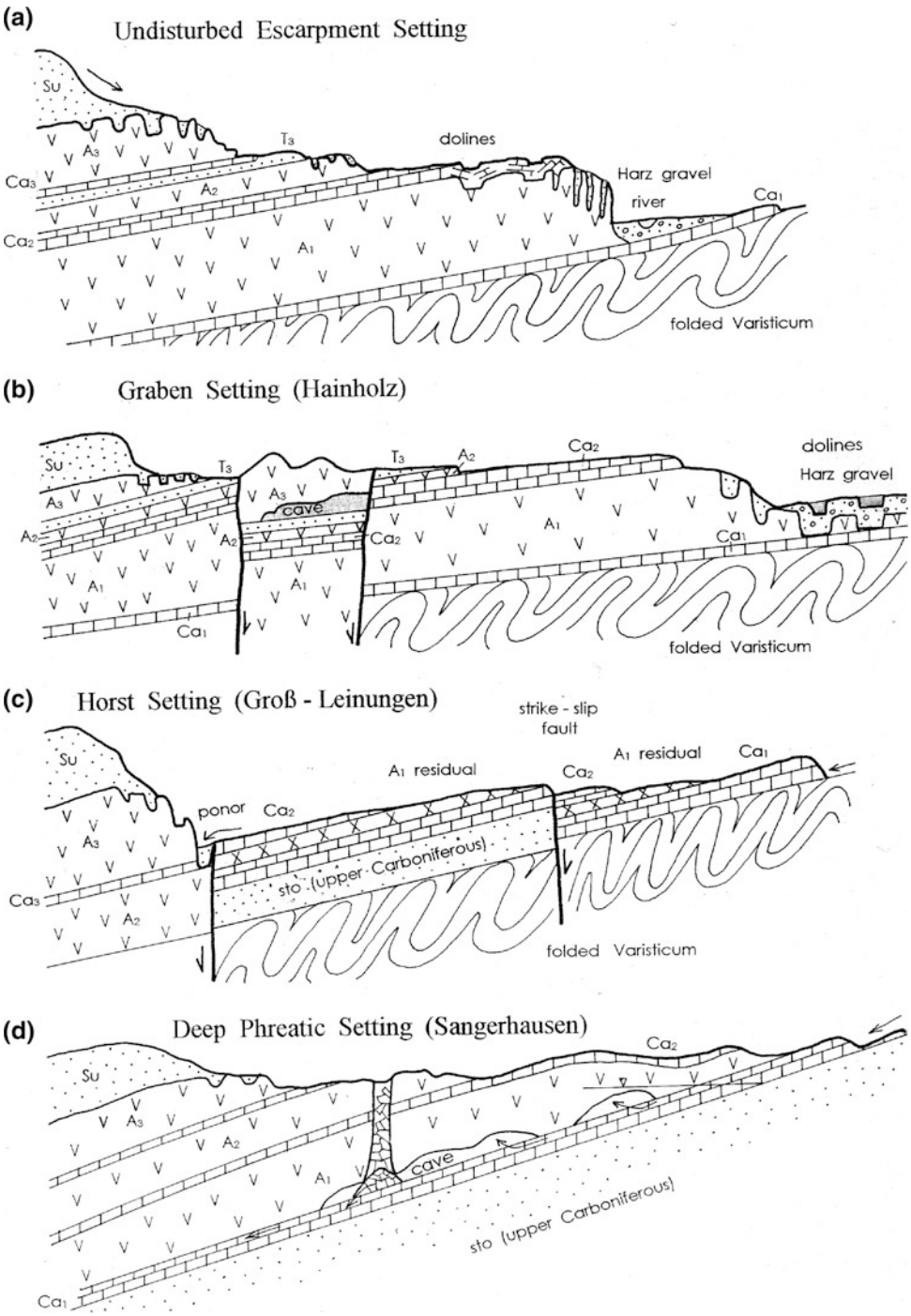

Fig. 5 Various tectonic situations of the South Harz Zechstein series, fostering different speleogenetic settings (Kempe 1996). Stratigraphy: *Ca* limestone, dolomite, *A* anhydrite, gypsum, *T* clay stones; *1* Werra Series, *2* Stassfurt Series, *3* Leine Series; *Su* Lower Buntsandstein (Lower Triassic); *sto* Upper Stefanium (Upper Carboniferous)

as the Wimmelburger Schlotten (Fig. 6), here listed with 2.8 km of passage. This is the length to which the cavities were mapped, but much more was apparently accessibly prior to the shut-down of the Copper Shale extraction in the Mansfelder Mulde in the 1980s (pers. com. R. and C. Völker).

Already Freiesleben (1809) understood that the Schlotten formed convectively below the water table. He was thus one of the earliest geologists describing "hypogene" speleogenesis. Morphologically, the Wimmelburger Schlotten displays large cupolas, textured by small-scale "Laugnäpfe" (solution cusps) and facetted walls (Fig. 7). The general tectonic situation of the Schlotten is given in Fig. 5d, showing that the "*dissolving agent*," i.e., calcium sulfate undersaturated water, derives from water sinking in the underlying Zechsteinkalk-aquifer, a 6–10-m-thick package of well-jointed, micritic limestone beds. Because of its lower buoyancy, the carbonate-saturated water rises into the hanging Werra anhydrite, dissolving it and thereby

Table 2 List of deep phreatic, hypogene anhydrite caves in the Zechstein along the southern (Sangerhäuser Mulde) and eastern (Mansfelder Mulde) rim of the Harz Mountains

No.	Name			Length (m)	Area (m^2)
1	Wimmelburger Schlotten	Wimmelburg, E-Harz, Sachsen-Anhalt		2838	28,866
	Large, deep phreatic and hypogene cave system 1931, Stolberg (1943), Völker and Völker (1986)				
2	Helbraer Schlotten	Helbra, E-Harz, Sachsen-Anhalt		2505	20,675
	(a) Ottiliaeschacht	1701 m ca.	15,000 m^2		
	(b) Schlotte am Schacht E	725 m	5525 m^2		
	(c) Connecting passages	70 m	150 m^2		
	Large, deep phreatic and hypogene cave system (Stolberg 1943; M. Brust, personal communication, 6/16)				
11	Brandschächter Schlotte	Sangerhausen, S-Harz, Sachsen-Anhalt		530	13,267
	Deep phreatic and hypogene cave system (Stolberg 1943; Völker 1983)				
15	Schlotte am Eduardschacht	Mansfeld, E-Harz, Sachsen-Anhalt		ca.400	n.d.
	Deep phreatic and hypogene cavity (Kupetz and Brust 1996)				
16	Elisabethschächter Schlotte	Sangerhausen, S-Harz, Sachsen-Anhalt		357	2082
	Deep phreatic and hypogene cavity (Stolberg 1943; Völker and Völker 1982a)				
18	Segen Gottes Schlotte	Sangerhausen, S-Harz, Sachsen-Anhalt		240	1279
	Deep phreatic and hypogene cavity (Stolberg 1943; Völker and Völker 1982b)				

These cavities were discovered by mining for the underlying copper shale. Many more were encountered but only those in the list were documented by maps. The numbering follows the list of longest sulfate caves in Germany (data and citations after Kempe and Helbing 2000; Kempe 1998b; M. Brust, personal communication)

becoming denser, consequently returning into the limestone layer driving up additional, less sulfate-saturated water. Thus, over time large convective cavities can be formed at the base of the Werra anhydrite. The sediments consist of fine-grained carbonates, including dolomite (Kupetz and Knolle 2015).

Apart from the Schlotten, many sulfate caves are formed in a shallow phreatic setting. This is aided (Fig. 5) by the specific tectonic setting of the South Harz where multiple NW–SE and W–E striking faults cause (southern blocks thrusted up) repeated outcrops of the same strata, thereby broadening the gypsum karst area considerably to several kilometers. In addition, graben and horst blocks occur, all allowing for a wide variety of hydrological settings for karstification. In the Beierstein-Hainholz Natural Preserve a graben (Fig. 5c) is instrumental: Here water rises from Stassfurt carbonate (Stinkschiefer) and dissolves the gypsified Leine anhydrite from below (Brandt et al. 1976; Kempe 1982). This is specifically evident for the pools in the Jettenhöhle (Fig. 8), which are not gypsum-saturated and able to dissolve gypsum in large quantities. By destabilization of the walls, breakdown is generated, forming vaulted ceilings reaching far above the water table. Breakdown blocks are consecutively dissolved, continuing the cave genesis. Even though these pools have open surfaces, the "*cave-forming agent*," i.e., water undersaturated in calcium sulfate, rises from below. By definition, these caves are therefore also hypogene (Kempe 2014b).

The northernmost cave in Germany and its northernmost show cave is the Segeberger Kalkberghöhle (Fig. 1), a typical, 2-km-long maze cave developed in the Leine anhydrite capping the Segeberg salt dome. Most of the Table 1 criteria would put the cave into the hypogene category, i.e., the morphology is lacking epigene characteristics. The cave shows only elements of slow, convective dissolution (sloping side walls, solution ceiling, solution cusps, etc.) (Fig. 9). Nevertheless, it is not clear whether the water came from below, as is the case in the Jettenhöhle; it seems rather to have infiltrated from the glacial sediments adjacent to the anhydrite and the altitude of this water exchange was not only near the groundwater level but was also restricted to a thickness of less than 2–3 m. Fresh water must have come in

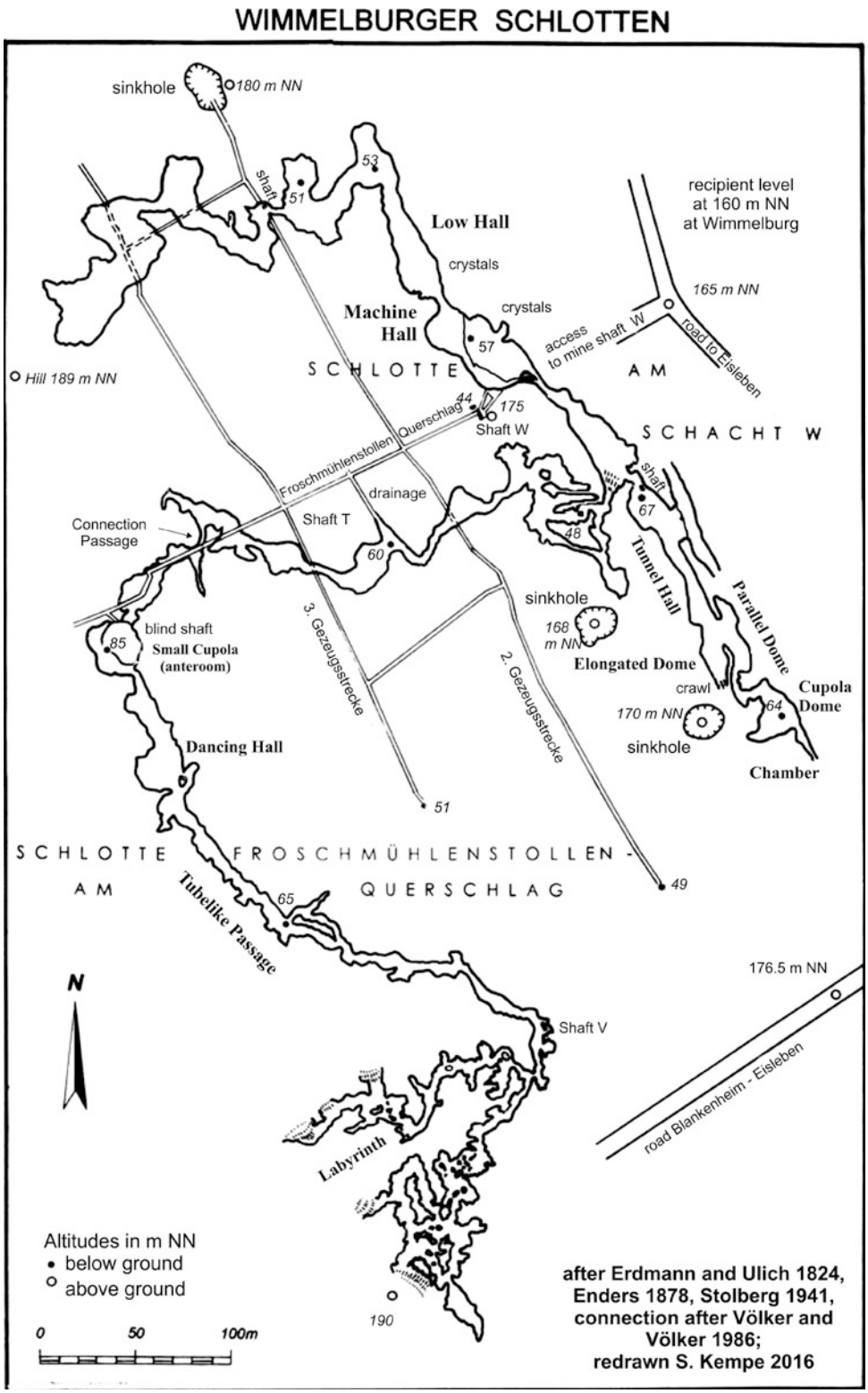

Fig. 6 Map of the Wimmelburger Schlotten, the largest deep phreatic Zechstein cave system, situated in the Mansfelder Syncline. It was originally discovered and drained by mining for the underlying Copper Shale and is partly still accessible by (rarely granted) permit (Kempe 1996). The cave system is composed of two sections ("Schlotte am Schacht W" in the NE and "Schlotte am Froschmühlenstollen-Querschlag" in the SE). The 2nd and 3rd "Gezeugstrecke" follow the NW–SE dip of the ore strata, while the NE–SW "Querschläge" run along the strike of the strata. The "Dancing Hall" was the site of a historic mining gathering. The water is drained by the Froschmühlenstollen at an altitude of about 40 m NN (above sea level), toward the Saale River, thus ensuring that part of the Schlotten stay above the ground water level

along the ceiling of the passages (where they are widened fastest) and left, after being saturated with gypsum, either through floor cracks or laterally back to the glacial sand or till body surrounding the mountain.

By area, the Middle Triassic Muschelkalk formation (lithostratigraphic unit of the "Germanic Trias": Higher Anisium and begin of Ladinium; 243–235 Ma ago) is one of the largest limestone areas in Germany, occupying much of

Fig. 7 View into a room of the Wimmelburger Schlotten. Note sloping wall facets and convective cupola with solution cusps (*photo* Kempe)

Fig. 8 Cave pool (Pfeilersee) in the Jettenhöhle where water upwells from the carbonate aquifers below (Leine sulfate, Hainholz, Osterode, South Harz; *photo* Kempe)

the center of the country. Nevertheless, it is the limestone formation with the lowermost number of caves. The Eberstadter Tropfsteinhöhle, one of the few Muschelkalk show caves, and the parallel, over 3-km-long Hohler Stein Cave are clearly epigene, however, also of strange character: These caves appear to have been formed by erosion of back-cutting waterfalls and not so much by turbulent dissolution. Other caves in the (Upper) Muschelkalk are large maze caves such as the Fuchslabyrinth (9.4 km in length) and the associated Schandtauberhöhle (3.7 km), both today

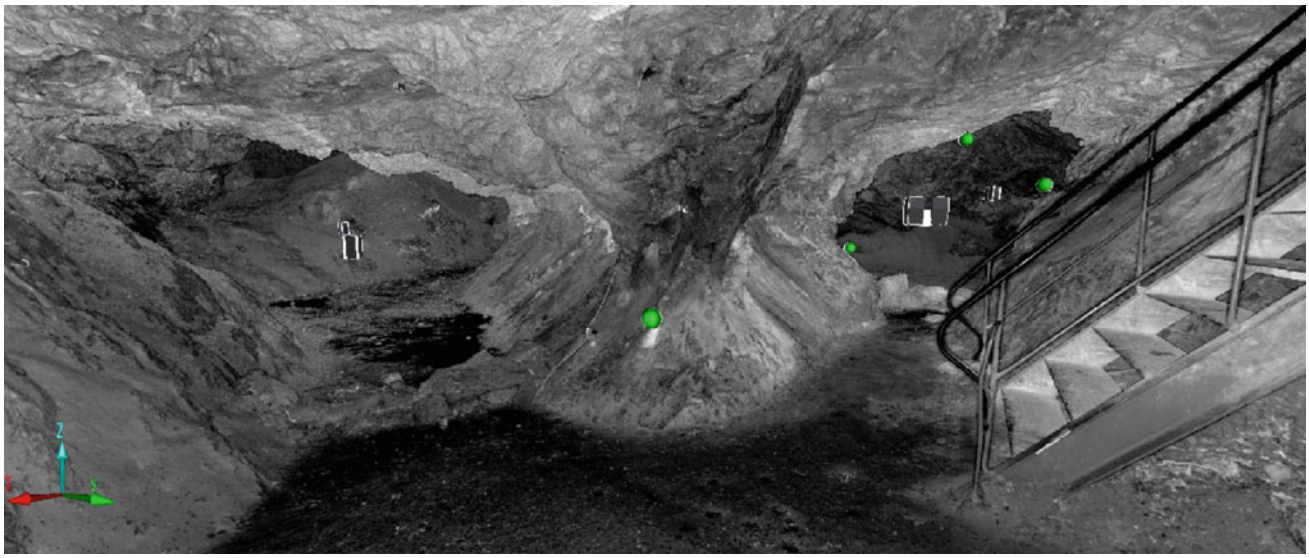

Fig. 9 3D scan of a solutional passage of the Segeberger Kalkberghöhle in anhydrite with typical sloping sidewalls and horizontal ceilings characteristic of a cave created by natural convection. Note stairs for scale. *Green* reference balls are 14 cm in diameter

with an epigene hydrology but the maze parts of the Fuchslabyrinth are possibly also of hypogene origin (compare Klimchouk 2007).

The Upper Jurassic (Malm, Oxfordium to Tithonium, 163.5–145 Ma ago) limestone is the next important stratigraphic unit hosting karst and caves. In the Weserbergland, in Northern Germany, we find a group of caves (Schillathöhle, Riesenbergsystem situated in the "Korallenoolith") that are linear in ground plan but lack other epigene morphological characteristics. Thus, Table 1 does not allow a clear grouping of these caves that at best are shallow phreatic caves with no real signs of an "*agent coming from below*."

The largest continuous karst area in Germany is the "Alb," a limestone and dolomite plateau stretching from the Frankonian Alb in the east and southeast to the Swabian Alb in the west, divided by the Nördlinger and Steinheimer impact craters in the center (Fig. 1). The south-dipping strata are terminated in the North by an imposing escarpment. Several thousand caves are known in the Malm; however, kilometer-long caves are rare.

In the Swabian Alb recent exploration by diving and digging down more than 100 m in sinkholes discovered a large cave system, the 11.5-km-long Blauhöhle (Hinderer and Kücha 2012) and the Hessenhauhöhle with over 4 km (Arbeitsgemeinschaft Blaukarst 2014). It discharges its water through the Blautopf, one of largest karst springs in Germany. In spite of the fact that the system is largely linear and active, the tremendously large halls do not fit the small tributary area of the present cave nor its missing aggressivity (Kempe et al. 2002). Therefore, doubt remains about what "*agent*" was responsible in forming this voluminous system. One of the possibilities is that volcanic CO_2 was involved because some of the 355 vents of the Swabian Volcanism dissected the strata 16–17 Ma years ago. Their slow degassing could have provided the necessary "*agent*." There are also reports of methane emanating in the Swabian Alb (even killing a miner in the past; Schwäbisches Tagblatt 2012). If this were true, then hypogene agents would have caused an epigene-looking cave system. In this context the presence of deep vertical caves such as the 86 m deep Laichinger Tiefenhöhle (1.35 km long) and the 127-m-deep Laierhöhle (2.43 km long) may be of interest as well. These are not former sinks of surface waters but may also represent hypogene features. The Swabian Alb holds many more epigene caves, including the Wulfbachquellhöhle (6.5 km), the Mordloch (4.4 km long) and the Wimsener Höhle, not to mention the large cave system that currently diverts the water of the upper Danube toward the Achtopf and the Rhine. There are also many fossil epigene caves, like the Nebelhöhle and the Charlottenhöhle. Thus, overall the character of the larger caves in the Swabian Alb is seemingly more epigene than hypogene.

In much of the Frankonian Alb, exposed dolomitized stromatolite and sponge reefs form a hummocky landscape. Depressions in between represent areas with bedded, micritic limestone, some of them forming banks famous for their reptilian fossils and their even quality used in lithography. It appears that the reefs attracted the cave-forming processes while caves in the bedded strata are rare. In contrast to the Swabian Alb, in the Frankonian Alb clearly hypogene caves dominate. Until the Mühlbachquellhöhle (7.9 km) was discovered, not many sizeable, epigene caves were known in

the area, among them the fossil, linear show cave Bing Höhle, situated in the lower, bedded section of the Malm and the Fellner Doline, an active, vertical sinkhole.

Most of the other, larger caves (Kaulich and Schaaf 1980) seem to be hypogene, featuring irregular halls like in the Geisloch (50 × 30 m and up to 15 m high) (Fig. 10a, b), connected by small passages or pits like in the historically famous Zoolithenhöhle (e.g., Heller 1972) to which William Buckland paid a visit in search for proof of the "deluge." Clearly hypogene are also the labyrinthic caves Schönstein-Brunnstein (Fig. 10c) and Stein am Wasser, the show caves Maximiliansgrotte (Fig. 10e) (Abteilung für Karst- und Höhlenkunde der NHG Nürnberg 1994), Sophienhöhle and Teufelshöhle, as well as the Bismarckgrotte (1.2 km long) (Fig. 10d). Some of the caves consist of one large cavity only, such as the Riesenburg and the

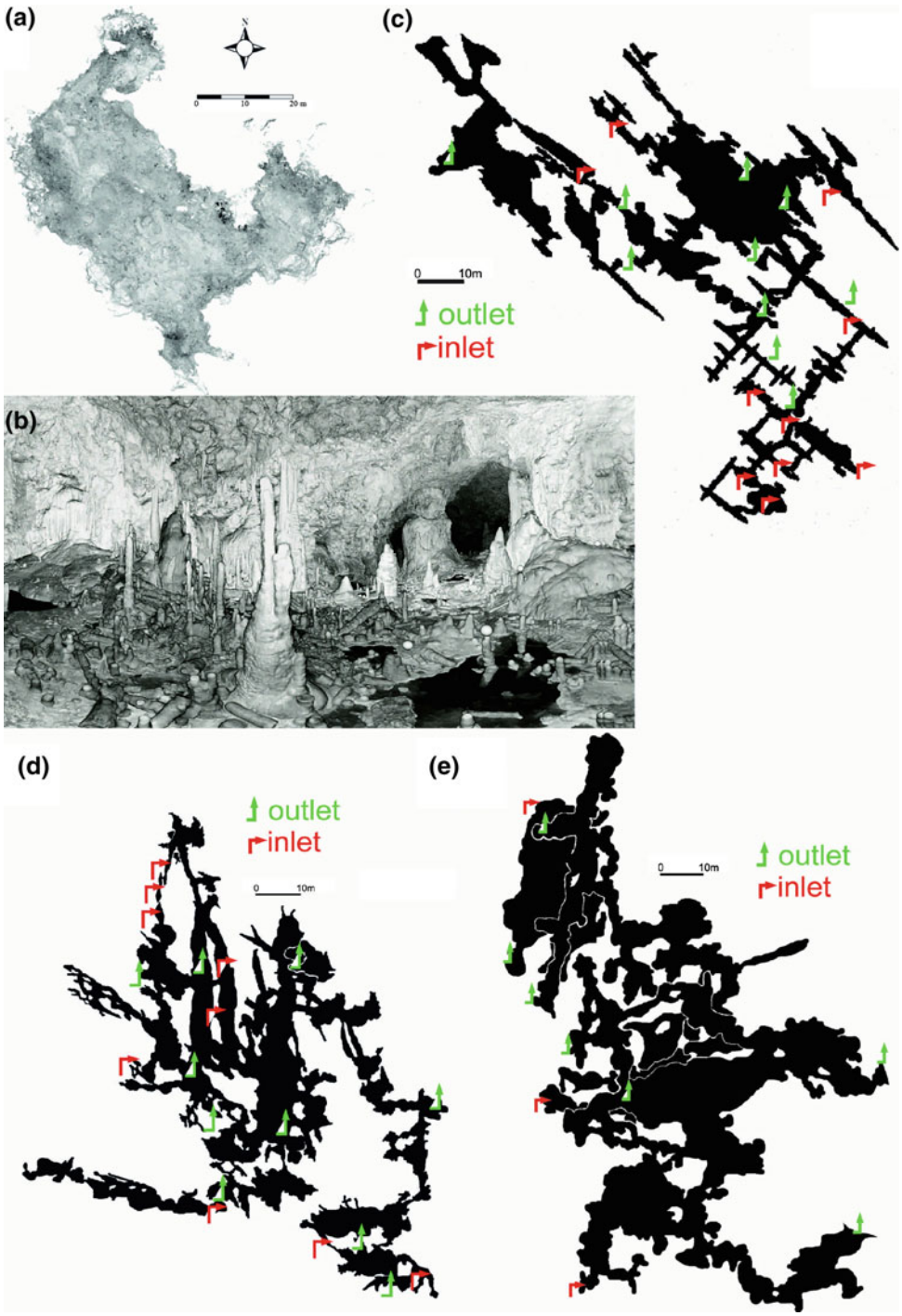

Fig. 10 **a** Top view of the 3D-scan of the main hall of the Geisloch. **b** Showing solution cupolas on the ceiling and copious speleothems, many of them damaged and deposited on the floor by glacial cave ice (Fenzlein 2015). **c** Map of the joint-oriented labyrinthic Schönstein-Brunnstein Höhle (map after Cramer and Oedel 1933). **d** Map of the highly irregular and labyrinthic Bismarckgrotte (after Leja 1985). **e** Map of the highly irregular and labyrinthic Maximiliansgrotte (after Leja 1989). Sites where water presumably entered and left the system are marked by *arrows* (Glaser 2013)

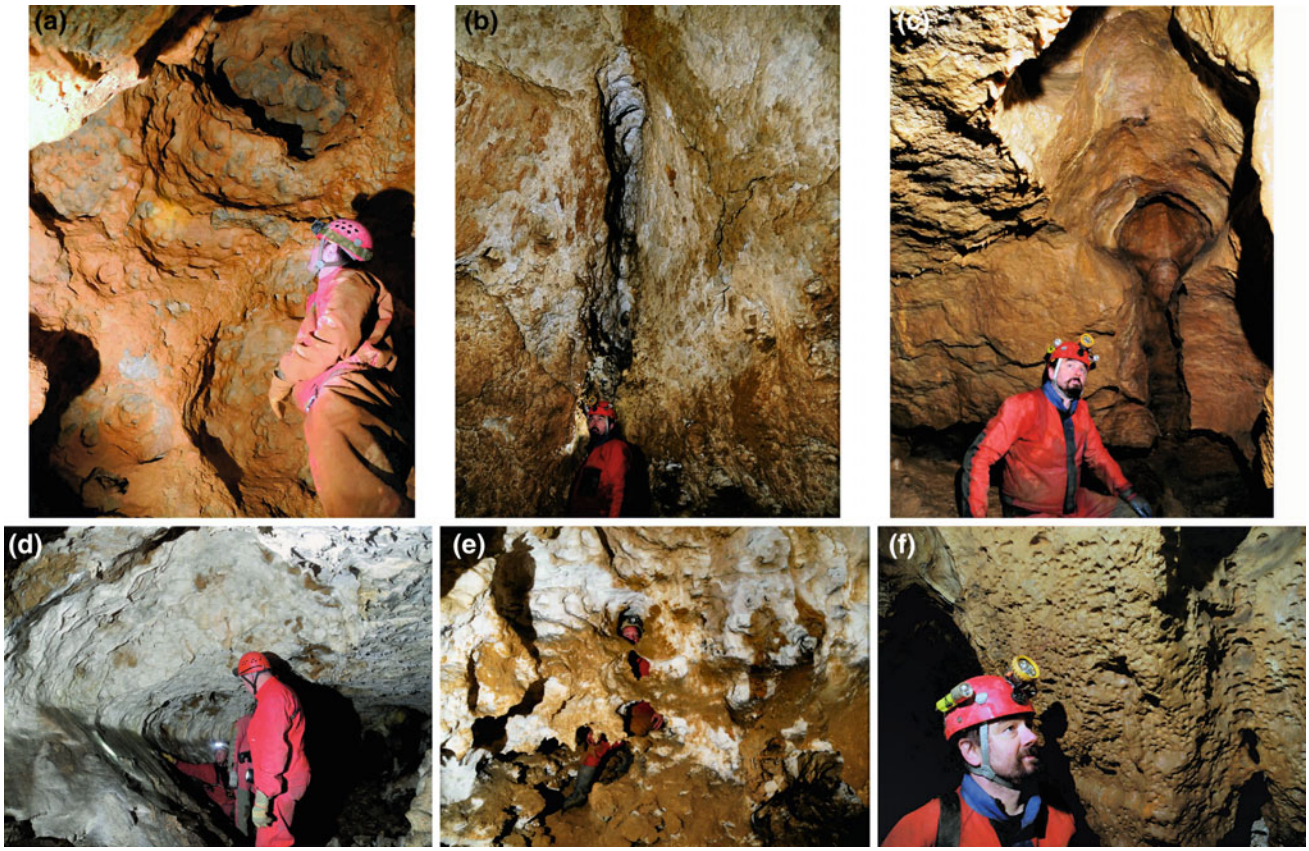

Fig. 11 **a** Concave ceiling cupolas in the "Guckloch," a cave in the Frankonian Alb. **b** View of the "Marthakeller" in the Schönsteinhöhle featuring an ascending wall channel leading up into a ceiling half-pipe that leads up into the main story of the cave. **c** An ascending wall channel leading up into a narrow chimney in the "Labyrinth" of the Schönsteinhöhle. **d** Flat solution ceiling (behind caver on the *right*), low vaulted ceiling cupola (to *left* of caves) and sloping wall facet (*left*) in the Maximiliansgrotte. **e** "Hacheln," irregular wall cusps that structure the walls in many of the Frankonian caves (Bismarckgrotte). **f** Small-scale solution cusps near one of the places where apparently undersaturated water ascended in the Schönsteinhöhle

Rosenmüllerhöhle, named after the scientist who established the cave bear as the first extinct mammal species (*Ursus spelaeus*) in 1794. Many other caves, mostly known locally, fall also in this class like the Windloch at Kürmreuth, the Breitensteiner Bäuerin, the Alfelder Windloch, the Windloch near Sackdillig, the Ludwigshöhle, the Großmeinfelder Windloch, the Guckloch and the Lupberghöhle (Glaser 2013). Many one-room-caves and grottos open up along the valley flanks providing shade to the weary wanderer such as the Oswald, Witzen, the Esper caves and many other smaller ones, often impacted in their morphology by frost shattering.

All these caves have very similar morphological features. They do not only feature large halls connected by narrow passages or pits, but also display ceiling cupolas (Fig. 11a) or flat solution ceilings (Fig. 11d), small, concave wall cusps, called locally "Hacheln" (Fig. 11e), or sloping wall facets (Fig. 11d), but also ascending ceiling channels (Figs. 11b, c), and small-scale solution cusps (Fig. 11f). Mapping possible pathways of ascending water in some of these caves (Figs. 10c–e) confirms the hypothesis that these caves were formed by hypogene processes (Glaser 2013).

Two further clues exist as to the origin of these caves: Most of their locations seem to fall into a narrow NW–SE striking corridor (Fig. 12) and fragments of goethite crusts were found in the Bismarckgrotte (Fig. 13). All this must be seen in terms of the paleohydrological situation of the Frankonian Alb (Fig. 14).

Figure 12 shows that most of the caves are grouped in the center of the Alb at around Muggendorf on the flanks of the Wiesent valley. The valleys in the northern Frankonian Alb are striking mostly NW–SE, a direction called "hercynian" in Central Europe. Other directions are NNE–SSW ("rhenish") and NE–SW ("erzgebirgisch" or "variscan"). The tectonic domination of the Alb valleys has long been noticed (for an overview see Baier 2008). Thus, it appears that the site of the hypogene caves is controlled by tectonic fractures. The Frankonian Alb has been subject to compression, resulting in a shallow bowl-shaped basin (Streit 1974, 1977),

Fig. 12 Google Earth view with some of the larger hypogene caves in the Frankonian Alb pinned. *Blue* outline of the Malm escarpment; *yellow* Hercynian lineaments; *green* other lineaments. Note the same directions in the map of the Schönstein-Brunnstein Cave (Fig. 10c)

visible in the direction of the river network that focuses toward the center of the bowl. Thus, it is conceivable that deep-reaching fractures formed that opened migration paths for crustal fluids and gases. Below the Malm, we find a thick package of Middle and Lower Jurassic pyrite-rich clays. Thus, sulfide-rich fluids could have been mobilized from below promoting the observed hypogene karstification. Further down, a thick suite of Triassic rocks occurs, including the Middle Muschelkalk evaporites that could have functioned as methane trap that were tapped by the fractures. The methane could have evolved from the Lower Muschelkalk, a marine, marly limestone. Thus, several options exist, to obtain reducing gases. Furthermore, the upwelling of artesian water could have caused thermal convection. Figure 14 reconstructs the tectonic situation and land surface elevation prior to the uplift to the present altitude. Along the Keuper sandstone, water could have migrated to below the lower Jurassic, pyrite-rich clay layers, forcing artesian-like sulfide-rich water up into the Malm. Similarly, the Middle Jurassic "Eisensandstein" could have served as an aquifer conveying water to below the Malm. This would have been specifically easy in the competent, dolomitized reefs. Oxidation of sulfide or methane could have occurred at depths where oxygen-bearing seepage water would have been encountered.

Rising CO_2 on the other hand does not seem to be an option. This must be concluded from the fact that the discussed caves are not found at the base of the Malm but in its upper layers. Also they are more horizontal than vertical in shape suggesting control by the oxygen front in the former groundwater body. This scenario is substantiated by the finding of goethite crusts in the Bismarckgrotte (Fig. 13). These may even have had the form of chimneys, such as if they represented "black smokers." Unfortunately, these crusts have been much destroyed by the traffic through the cave. If such crusts are present at the bottom of other caves cannot be ascertained. This is because German caves are generally filled by glacial solifluction loams close to the surface. In case of the Bismarckgrotte, the site where these crusts occur is away from the entrance pits, so that it was not covered by later sediments.

The cave at Stein am Wasser (actually called "Höhle ohne Namen"), a large maze cave, may be a different case. Here we measured a CO_2 concentration of up to 1% in the passages furthest away from the entrance, a value much higher than normally found in our caves (Kempe et al. 1998). Since

Fig. 13 Piece of goethite/limonite with a vertical texture from the bottom of the Bismarckgrotte. It could suggest that anaerobic waters (high in ferrous iron solutions) entered the cave to be oxygenated, thereby producing acidic byproducts that corroded the cave and precipitated the goethite in situ

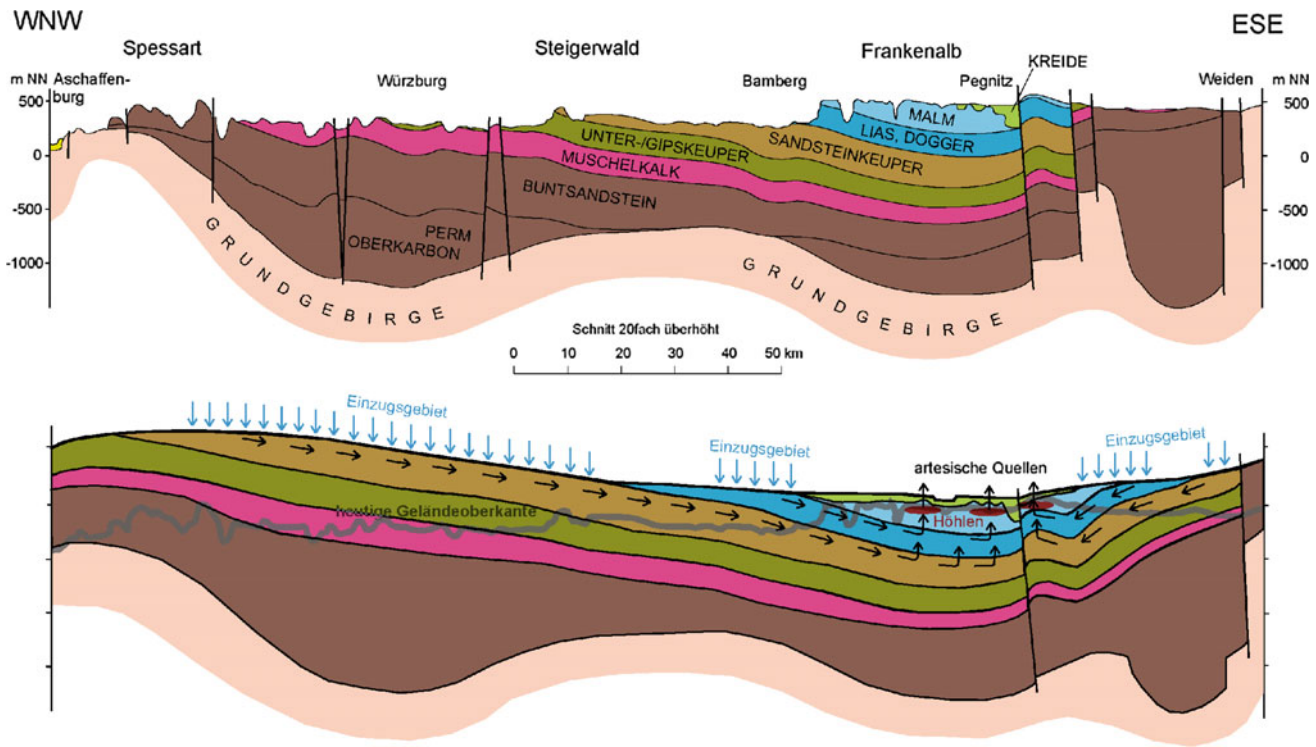

Fig. 14 Geological NW–SE profile through the Frankonian Alb and its former tributary area prior to the general uplift after the Upper Cretaceous (*bottom*) in comparison to the present situation (*top*) (altered after Bayerisches Geologisches Landesamt 2004; Glaser 2013)

the water table is intersecting the cave, it appears as if it is the source of this high CO_2-value. This cave is situated in the northeast of the Franconian Alb close to the Eger Rift. Its volcanic activity began in the Oligocene and is still active with CO_2 springs and earthquakes. Juvenile CO_2 from to the Eger Rift is also supposed to be responsible for the formation of deep-seated phreatic maze caves discovered during marble mining close to Marktredwitz in the "Wunsiedler Marmor" (Glaser 2013).

The southernmost karst areas of Germany are represented by the few Alpine carbonate mountain massifs along the border with Austria. These areas seem to have a rather high cave density. Here the longest and deepest caves in Germany (Riesending, 19.3 km long, 1.148 m deep; Hölloch 11.3 km

long, 452 m deep; VdHK 2016) have recently been explored. Most caves are series of vadose shafts connected by epigene canyons and leading to long phreatic horizontal passages. The Alps also feature the only show cave in Cretaceous rocks in Germany, the Sturmannshöhle. It is the upward directed branch of a former phreatic spring. Some extended maze caves in the Untersberg in the easternmost part of the Bavarian Alps seem to form an exemption from the generally epigenetic character of the alpine caves. In contrast to other karst plateaus in the Bavarian Alps the Untersberg region was lifted above the sea level already during the Cretaceous and possibly again during the Eocene. Both erosive phases were followed by transgression and sedimentation. Within the preexisting karstic voids a slow thermal convection may have taken place forming the mazes before the current epigenetic karstification started (Glaser 2013).

Even though much of northern Germany is also underlain by thick Cretaceous sediments, no larger caves are known. However, large springs (Pader spring, Lippe spring) show that karstification is present and hydrologically active.

3 Conclusions

This overview of German caves is intended to trigger discussion about their classification. Most of them have been known for a long time but have hardly been viewed in context. Here we attempt to show that (i) hypogene caves are very common in Germany and (ii) that some of them form well-defined clusters, such as at the Iberg/Harz, the Schlotten in the South Harz and those in the Frankonian Alb. Other cave areas seem to show mixed evidence with epigene caves formed side by side with caves of tentative hypogene origin, such as in Elbingerode/Harz, in the Rhenish Schist Massif and in the Swabian Alb. Except for the Iberg, where siderite seems to provide the cave-forming agent, and the Schlotten where ascending water is the cave-forming agent, the causes of hypogene cave formation mostly remain undecided. It could be anything from rising volcanic CO_2 (as in the Swabian Alb) or any of the other gases, methane or hydrogen sulfide. When looking at the petrography of underlying strata and paleohydrology, all of these agents seem reasonable. In some cases, the location within a continental basin favoring artesian upwelling across the formations and mixing corrosion during the contact with locally recharged groundwater may also be an option (Klimchouk 2007). We yet have to wait for some lucky find (such as gypsum preserved in some dry, obscure corner of a cave) or a method to extract information from initial autochthonous sediments in order to judge leaching conditions that formed the caves millions of years ago.

Acknowledgements Over the decades, many friends, colleagues and students have accompanied the authors during caving trips in Germany. Thanks to all of you.

References

Abteilung für Karst- und Höhlenkunde der NHG Nürnberg (1994) Die Maximiliansgrotte bei Krottensee, 4th ed., Nürnberg

Al-Malabeh A, Kempe S, Henschel H-V, Hofmann H, Tobschall HJ (2008) The Warda iron ore deposit and historic mine near Ajloun, (Northern Jordan): Mineralogy and geochemistry of a potential speleogene iron ore deposit. Acta Carsologica 37(2–3):241–253

Arbeitsgemeinschaft Blaukarst (2014) Expedition Hessenhau. Berghülen

Baier A (2008) Karstphänomene und Karsttektonik im Oberen Leinleitertal nördlich Markt Heiligenstadt/Lkr. Bamberger Land (Nördliche Frankenalb). Geologische Blätter NO-Bayern 58(1–4): 117–183

Bayerisches Geologisches Landesamt (ed) (2004) GeoBavaria—600 Millionen Jahre Bayern, München

Biese W (1931) Über Höhlenbildung, 1. Teil, Entstehung der Gipshöhlen am südlichen Harzrand und am Kyffhäuser. Abh. Preuß. Geol. Landesanst., Neue Folge 137: 71 pp

Brandt A, Kempe S, Seeger M, Vladi F (1976) Geochemie, Hydrographie und Morphogenese des Gipskarstgebietes von Düna/Südharz. Geologisches Jahrbuch C 15:3–55

Buchas H (2000) Analyse einer unterkretazischen Höhlenfüllung im devonischen Massenkalk von Wülfrath, Nordrhein-Westfalen. Diploma thesis, Inst. for Applied Geosciences, TU-Darmstadt

Cramer H, Oedl R (1933) Das Schönstein-Höhlengebiet (Fränkische Schweiz). Speläol Jb 14(14):29–47

Dorsten A, Dorsten I, Finke M, Meyer S, Mischel S, Zaenker S (2016) Das Herbstlabyrinth und der Karst in Breitscheid im Westerwald. Speläologische Arge Hessen e.V., Herborn

Dreybrodt W (2008) Von der Kluft zum Urkanal, Chemie und Physik der Höhlenentstehung. In: Kempe S, Rosendahl W (eds) Höhlen: verborgene Welten. Wissenschaftliche Buchgesellschaft Darmstadt, Darmstadt, pp 39–53

Drozdzewski G, Hartkopf-Fröder C, Lange F-G, Oestreicher B, Ribbert K-H, Voigt S, Vrede V (1998) Vorläufige Mitteilung über unterkretazischen Tiefenkarst im Wülfrather Massenkalk (Rheinisches Schiefergebirge). Mitteilungen des Verbandes der deutschen Höhlen- und Karstforscher 44(2):53–66

Freiesleben JC (1809) Geognostischer Beytrag zur Kenntniß des Kupferschiefergebirges, 2nd Vol. Craz und Gerlach, Freiberg, 169–205

Fenzlein R (2015) Statistische Auswertung der Sinterschäden im Geisloch bei Oberfellendorf (Oberfranken, Bayern). Bachelorarbeit, Institut für Angewandte Geowissenschaften, TU-Darmstadt, 55 pp + Appendix (unpublished)

Galdenzi S, Maruoka T (2003) Gypsum deposits in the Frasassi caves, Central Italy. J Cave Karst Stud 65:111–125

Glaser S (2013) Hypogene Höhlengenese: Aufsteigendes Grundwasser und Erdwärme als Antrieb der Entstehung labyrinthischer Höhlen in der nördlichen Frankenalb und in anderen Teilen Bayerns. Laichinger Höhlenfreund 48:39–68

Heller F (ed) (1972) Die Zoolithenhöhle bei Burggaillenreuth/Ofr., 200 Jahre wissenschaftliche Forschung 1771–1971. Erlanger Forschungen B/5

Hill CA (1987) Geology of Carlsbad cavern and other caves in the Guadalupe Mountains, New Mexico and Texas. New Mex Bur Min Mineral Resour Mem 117:1–150

Hinderer E, Kücha A (2012) Forschungsaktivitäten der Arge Blautopf in der Blauhöhle 2011/2012. Mitteilungen des Verbandes der deutschen Höhlen- und Karstforscher 58(3):79–81
Kambesis P (2012) Lechuguilla Cave, New Mexico, U.S.A. In: White WB, Culver DC (eds) Encyclopedia of caves, 2nd edn. Academic Press/Elsevier, Amsterdam, pp 456–465
Kaulich B, Schaaf H (1980) Kleiner Führer zu Höhlen um Muggendorf. Naturhistorische Gesellschaft Nürnberg e.V., Nürnberg
Kempe S (1971) Speläogenetisch wirksames CO_2 durch Verwitterung von Siderit? Mitteilungen des Verbandes der deutschen Höhlen- und Karstforscher 18:38
Kempe S (1975) Siderite weathering, a non-biogenetic source of CO_2 (illustrated by the Iberg/Harz/Fed. Rep. of Germany). Annales de Spéléologie 30/4:703–704
Kempe S (1982) Long-term records of CO_2 pressure fluctuations in fresh waters. Habilitation thesis. In: Degens ET (ed.). Transport of Carbon and minerals in major world rivers, Pt. 1, Mitteilungen aus dem Geologisch-Paläontologischen Institut der Universität Hamburg, SCOPE/UNEP Sonderband 52:91–332
Kempe S (1996) Gypsum karst of Germany. In: Klimchouk AB, Lowe D, Cooper A, Sauro U (eds) Gypsum karst of the world. Int J Speleol 25(3–4):209–224
Kempe S (1998a) Siderite weathering, a rare source of CO_2 for cave genesis: the Eisensteinstollen System and adjacent caves in the Iberg, Harz Mountains, Germany. Proc Nat Speleol Soc Conv, Sewanee, TN, p 78
Kempe S (1998b) Gipskarst und Gipshöhlen in Deutschland. In: Gipskarstlandschaft Südharz - aktuelle Forschungsergebnisse und Perspektiven. A. Töpfer Akademie f. Naturschutz (NNA), Schneverdingen, 11(2):25–35
Kempe S (2008) Vom Urkanal zur unterirdischen Kathedrale, Höhlenformen und ihre Entstehung. In: Kempe S, Rosendahl W (eds) Höhlen: verborgene Welten; Wissenschaftliche Buchgesellschaft Darmstadt, Darmstadt, pp 54–64
Kempe S (2009) Siderite weathering as a reaction causing hypogene speleogenesis: the example of the Iberg/Harz/Germany. In: Klimchouk AB, Ford D (eds) Hypogene speleogenesis and karst hydrogeology of Artesian Basins. Ukrainian Institute of Speleology and Karstology, Special Paper 1, Simferopol, pp 59–60
Kempe S (2014a) Hypogene limestone caves in Germany: geochemical background and regionality. In: Klimchouk A, Sasowsky ID, Mylroie J, Engel SA, Engel AS (eds) Hypogene cave morphologies, Proceedings San Salvador, vol 18, Bahamas, 2–7 Feb 2014. Karst Waters Institute Special Publication, pp 48–56
Kempe S (2014b) How deep is hypogene? Gypsum caves in the South Harz. In: Klimchouk A, Sasowsky ID, Mylroie J, Engel SA, Engel AS (eds) Hypogene cave morphologies, Proceedings San Salvador, vol 18, Bahamas, 2–7 Feb 2014. Karst Waters Institute Special Publication, pp 57–64
Kempe S, Helbing A (2000) Die „Größe“ deutscher Gipshöhlen. Die Höhle 51(1):13–20
Kempe S, Rosendahl W (eds) (2008) Höhlen: Verborgene Welten. Wissenschaftliche Buchgesellschaft Darmstadt, Darmstadt
Kempe S, Reinboth F, Knolle F (eds) (1985) Die Iberger Tropfsteinhöhle bei Bad Grund (Harz). Bad Grund
Kempe S, Neander F, Hartmann J, Klughardt W (1998) CO_2-Druck der Luft in der “Höhle ohne Namen”, Steinamwasser (Nördliche Frankenalb). Mitteilungen des Verbandes der Deutschen Höhlen- und Karstforscher 44(2):39–44
Kempe S, Ebert M, Morlock W (2002) ESEM Untersuchungen des dunklen Belages aus dem Blautopf und Schlussfolgerungen für die Interpretation von Lösungsexperimenten mit Rocktablets. Mitteilungen des Verbandes der Deutschen Höhlen- und Karstforscher 48 (3):67–71
Kempe S, Bauer I, Krause O (2016) Iberger Tropfsteinhöhle, Iberg, Harz Mountains, Germany: hypogene morphology and origin by Siderite Weathering. In: Chavez T, Reehling P (eds) Proceedings of DeepKarst 2016: origins, resources, and management of hypogene Karst. Carlsbad, New Mexico, April 2016, NCKRI Symposium 6, pp 35–44
Kley J (2013) Saxonische Tektonik im 21. Jahrhundert. Z. Dt. Ges. Geowiss. (German J Geosci) 164(2):295–311
Klimchouk A (1997) The role of karst in the genesis of sulphur deposits, Pre-Carpathian region, Ukraine. Environ Geol 31(1/2): 1–20
Klimchouk AB (2007) Hypogene speleogenesis: hydrogeological and morphogenetic perspective. Special Paper no.1. National Cave and Karst Research Institute. Carlsbad. New Mexico, p 106
Klimchouk AB (2012) Speleogenesis, hypogenic. In: White W, Culver DC (eds) Encyclopedia of caves, 2nd edn. Academic Press/Elsevier, Amsterdam, pp 748–765
Koch L (1992) (ed) Das Klutert-Buch. Linnepe Verlag, Hagen
Kupetz M, Brust M (1996) Historisches zum Begriff der „Mansfeldischen Kalkschlotten“ sowie ein Beitrag zur nomenklatorischen Bestimmung dieses Höhlentyps. Karst und Höhle 1994/95:91–105
Kupetz M, Knolle F (2015) Die Mansfelder Schlotten – Verbreitung und Genese der größten mitteleuropäischen Anhydrit-Schichtgrenzhöhlen. Z. Dt. Ges. Geowiss. (German J Geol) 166 (4):327–339
Leja F (1985) Die Bismarckgrotte im Landkreis Amberg-Sulzbach, Oberpfalz (Frankenalb). Mitt. Abt. Karst- u. Höhlenk. Naturhis. Ges. Nürnberg 28:1–72
Leja F (1989) Zur Tektonik der Maximiliansgrotte A27 (Frankenalb). Mitt. Abt. Karst- u. Höhlenk. Naturhis. Ges. Nürnberg 33:5–19
Morehouse D (1968) Cave development via the sulfuric acid reaction. Nat Speleol Soc Bull 30:1–10
Müller T, Wolf A (2013) Liste der längsten und tiefsten Höhlen Deutschlands: Es gibt jetzt drei 10-Kilometer-Höhlen in Deutschland. http://www.arge-grabenstetten.de/www2/forschung/liste-der-langsten-und-tiefsten-hohlen-deutschlands/. Accessed Nov 2013
Palmer AN (2000) Hydrogeologic control of cave patterns. In: Klimchouk AB, Ford DC, Palmer A, Dreybrodt W (eds) Speleogenesis: evolution of karst aquifers. National Speleological Society, Huntsville, pp 77–90
Palmer AN, Hill CA (2012) Sulfuric acid caves. In: White WB, Culver DC (eds) Encyclopedia of caves, 2nd edn. Academic Press/Elsevier, Amsterdam, pp 810–819
Plan L, Tschegg C, De Waele J, Spötl C (2012) Corrosion morphology and cave wall alteration in an Alpine sulfuric acid cave (Kraushöhle, Austria). Geomorphology 169(170):45–54
Paul J, Vladi F (2001) Zur Geologie der Einhornhöhle bei Scharzfeld am südwestlichen Harzrand. Berichte der Naturhistorischen Gesellschaft, Hannover 143:109–131
Reimer A (1990) Untersuchungen zur Geologie, Lagerstättenkunde und Speläogenese des Eisensteinstollensystems im Iberg/Harz. Diploma Thesis FB Geologie, Univ. Hamburg
Reimer A, Kempe S (1989) Recent and paleokarst systems and their relation to ore mineralization in the Iberg-reef-complex, Harz Mountains. In: Proceedings 10th international congress of speleology, Budapest, August 1989, pp 1–2
Rosenfeld WD, Silverman SR (1959) Carbon isotope fractionation in bacterial production of methane. Science 130:1658–1659
Schwäbisches Tagblatt (2012) Gasaustritt am Scheibengipfeltunnel. 30.10.2012 (http://www.tagblatt.de/Nachrichten/Gasaustritt-am-Scheibengipfeltunnel–186105.html, accessed 07/16)
Stolberg F (1943) Die Mansfelder Schlotten. Z. f. Karst- u. Höhlenkunde 1942(43):11–35

Streit R (1974) Das Bruchschollenmosaik zwischen Fichtelgebirge und der Fränkischen Alb nach einer Luftbildauswertung. Geologische Blätter NO-Bayern 24(3):211–219

Streit R (1977) Das Bruchschollenland der Nördlichen Frankenalb und ihrer Umgebung etc. Geologisches Jahrbuch A 37:3–32

Svensson U (1988) Hydrochemische Untersuchungen an dolomitischen Karstwässern einer bergbaulich überprägten Großhöhle im Iberg/Harz. Diploma Thesis FB Geologie, Univ. Hamburg

Svensson U, Kempe S (1989) Hydrochemistry of karst waters in the Iberg-reef-complex, Harz Mountains. In: Proceedings of the 10th international congress of speleology, Budapest, August 1989, pp 3–5

VdHK (Verband deutscher Höhlen- und Karstforscher) (2016) Größte Höhlen Deutschlands: http://www.vdhk.de/die-groessten-hoehlen.html (accessed July 10th, 2016)

Völker R (1983) Die Brandschächter Schlotte bei Pölsfeld. Mitt. Karstmuseum Heimkehle, Uftrungen, Heft 6–7:21–32

Völker R, Völker C (1982a) Die Elisabethschächter Schlotte. Mitt. Karstmuseum Heimkehle, Uftrungen, Heft 2, 24 pp

Völker R, Völker C (1982b) Die Segen Gottes Schlotte. Mitt. Karstmuseum Heimkehle, Uftrungen, Heft 3, 15 pp

Völker C, Völker R (1986) Die Wimmelburger Schlotte. Mitt. Karstmuseum Heimkehle, Uftrungen, Heft 13, 60 pp

Hypogene Speleogenesis in the Karst of Poland—Regional Review

22

Michał Gradziński and Andrzej Tyc

Abstract

Karstified rocks are widely distributed in Poland; most of them are covered by unconsolidated Cenozoic deposits. Paleozoic and Mesozoic carbonates and Neogene evaporites host numerous paleokarstic features and solution caves, being of polygenetic and multi-stage origin. Works on hydrothermal karst and sulfide ores emplaced in caves of the Silesian-Kraków region, the large paleokarst caves filled with Permian internal sediment or thermal convection model for caves in the Polish Jura date back to the 1970s. Quite well-documented hydrothermal karst is preserved as paleokarstic features in several localities in the Silesian-Kraków region, Holly Cross Mts. and Sudetes. Characteristic cave sediments including crystalline calcite spar, sulfide ores emplaced within hydrothermal cave sediments and solution-collapse breccias are associated with these features. Travertines, which are surface manifestation of hypogene karst, dated through their paleontological assemblage, support their post-Variscan—Permian and Late Triassic age. Their hydrothermal origin was also determined by detailed studies of sediments and fluid inclusions. Less certain, based mainly on studies of relict cave morphology and limited calcite spar, are the Cenozoic—Paleogene and Neogene hypogene events in the Carpathians (Tatra Mts.) and their foreland (Polish Jura). Review of published references and concepts related to hypogene origin of caves and karst in Poland is presented in this contribution.

Keywords

Hypogene speleogenesis • Hydrothermal karst • Ascending caves • South Poland

1 Introduction

Among more than 5000 caves in Poland there are some which owe their origin to hypogene speleogenesis. They are distributed in various karst regions of Poland. None of them is active. The majority represents only small remnants of formerly more extensive karst systems; others are completely filled with sediments. The former can be classified as a relict cave (sensu Bosák et al. 1989), whereas the latter as true paleokarst forms. Only a few caves, predominantly paleokarst ones, contain deposits which shed some light on the chemistry and temperature of parent fluids. Thus, deciphering the origin of many caves is based predominantly, or only, on the analysis of their solutional forms and their geological setting. Consequently, origin of some caves, for example those in the Polish Jura, is related to 'artesian flow' because nothing is known about the factors controlling the aggressiveness and temperature of parent water (e.g., Gradziński et al. 2009a, 2011; Tyc 2009a, b). However, some scenarios

M. Gradziński
Institute of Geological Sciences, Jagiellonian University,
ul. Oleandry 2a, 30-063 Kraków, Poland
e-mail: michal.gradzinski@uj.edu.pl

A. Tyc (✉)
Department of Geomorphology, University of Silesia,
ul. Będzińska 60, 41-200 Sosnowiec, Poland
e-mail: andrzej.tyc@us.edu.pl

© Springer International Publishing AG 2017

A. Klimchouk et al. (eds.), *Hypogene Karst Regions and Caves of the World*,
Cave and Karst Systems of the World, DOI 10.1007/978-3-319-53348-3_22

of their origin which take into account possible geological and hydrologic situation were put forward.

The concept of possible hypogene origin of some Polish caves and paleokarst caves dates back to the 1970s. Interestingly, at the beginning this idea touched upon paleokarst rather than accessible caves. Bogacz et al. (1970) postulated the association of karstification and emplacement of lead–zinc ores in the Middle Triassic (Muschelkalk) carbonates in the Silesian-Kraków region to hydrothermal karst. The idea was subsequently evolved by Dżułyński (1976), Dżułyński and Sass-Gustkiewicz (1982, 1989 and their other papers). In the late 1970s, Paszkowski found large paleokarst caves filled with specific Permian sediment (Paszkowski and Wieczorek 1982).

As for accessible caves, ceiling cupolas were noticed in many caves of the Polish Jura (Kraków-Wieluń Upland or Kraków-Częstochowa Upland are also used in the literature), which were explained as being associated with phreatic flow (Gradziński 1962). The temperature and origin of water were not discussed in detail. It was not until late 1970s that Rudnicki (1978) associated the cupolas with dissolution driven by thermal convection processes. His conclusions were based on observations done in Hungarian caves and theoretical considerations on fluid dynamics. As a result of this, he put forward the concept of hydrothermal origin of some caves in the Polish Jura region.

The concept of hypogene origin of some Polish caves started outgrowing in mid-1990s. The subject was discussed during several conferences, including international ones. Some sites were presented during scientific field sessions. Nonetheless, only a few papers have been published so far. Thus, the present contribution is based also on conference abstracts and some personal observations and ideas of the authors and their collaborators. The term ‘hypogene’ is used here in its broad meaning, that is it embraces the processes related to deep circulation of water whose aggressiveness should be associated with deep-seated agents (see Dublyansky 2013). Such circulation most often demands specific hydrologic conditions with a confining bed over the karst aquifer. The karst features which owe their origin to ascending flow (vauclusian) of meteoric water are excluded from this category.

2 Geological Setting of Karst and Caves Distribution in Poland

The geological structure of Poland has a long-lasting and complex history. Rocks older than Quaternary crop out exclusively in central and southern part of the country. Northern part of Poland is covered almost completely with thick Pleistocene glacial deposits and Holocene alluvia. The karst rocks are widely distributed (Fig. 1), but their outcrops are rather small and occupy only about 2.5% of the country area, that is about 8000 km^2 (Głazek et al. 1972, 1982; Głazek 1989). These rocks host roughly 5000 caves (Gradziński and Kicińska 2013).

Southern part of Poland is occupied by the Carpathians which are a part of the Alpine orogenic belt. The Polish Carpathians are subdivided into two parts—the Outer and Inner Carpathians (the latter are also called Central Carpathians by the Slovak geologists). The Outer Carpathians are composed of several nappes which were thrusted to the north. They are built of siliciclastic rocks, mainly of flysch type. Only pseudokarst caves are registered there. The Pieniny Klippen Belt, a narrow zone stretching from Vienna (Austria) to Maramureş (Romania), is traditionally regarded as the boundary between the Inner and Outer Carpathians. The Tatra Mts. are the only one mountain range of the Inner Carpathians which belongs to Poland. Both Pieniny Klippen Belt and the Tatras are partly composed of Mesozoic carbonate rocks (Fig. 1). There are more than 800 caves in the Polish part of the Tatras (Gradziński and Kicińska 2013). The Pieniny Klippen Belt hosts mainly pseudokarst caves; nonetheless, many of them are developed in limestone.

The zone of uplands, called the Central Polish Uplands, occurs in the Carpathian foreland. The uplift of the upland zone in Miocene time resulted from formation and development of fore-deep basin in the front of the Carpathian nappes and from thrusting of these nappes to the north. The Carpathian foreland is built of various upper Paleozoic, through Mesozoic, to Cenozoic rocks. Karst phenomena are developed predominantly within Upper Jurassic limestone which composes the Polish Jura. It occupies the central parts of the upland zone and stretches from NNW to SSE forming a belt of more than 100 km in length and more than 20 km in width (Fig. 1). More than 2100 caves are accessible there (Gradziński and Kicińska 2013). Paleokarst of pre-Miocene age occurs in this area as well (Głazek 1989). The caves, more than 150, and paleokarst features are also hosted by Middle Triassic carbonates which crop out in the Silesian-Kraków region in the western part of the Carpathian foreland (Fig. 1). Some caves (more than 100) are formed in Miocene gypsum; they are known from the Nida River Basin (Fig. 1). The Holy Cross Mountains occupy a specific position within the Carpathian foreland. Their core composed of Paleozoic rocks folded in Variscan orogenesis, and their post-orogenic cover of the Permian age is mantled by Mesozoic strata. Several caves (more than 130) and many paleokarst forms have been recognized in this area (Gradziński and Kicińska 2013). They are formed predominantly in the thick sequence of Devonian carbonates which occur within the core of the Holy Cross Mountains and in the rocks of their Mesozoic cover (Fig. 1).

The Sudetes, located in the southwestern part of Poland, are composed mainly of metamorphic rocks. Some patches

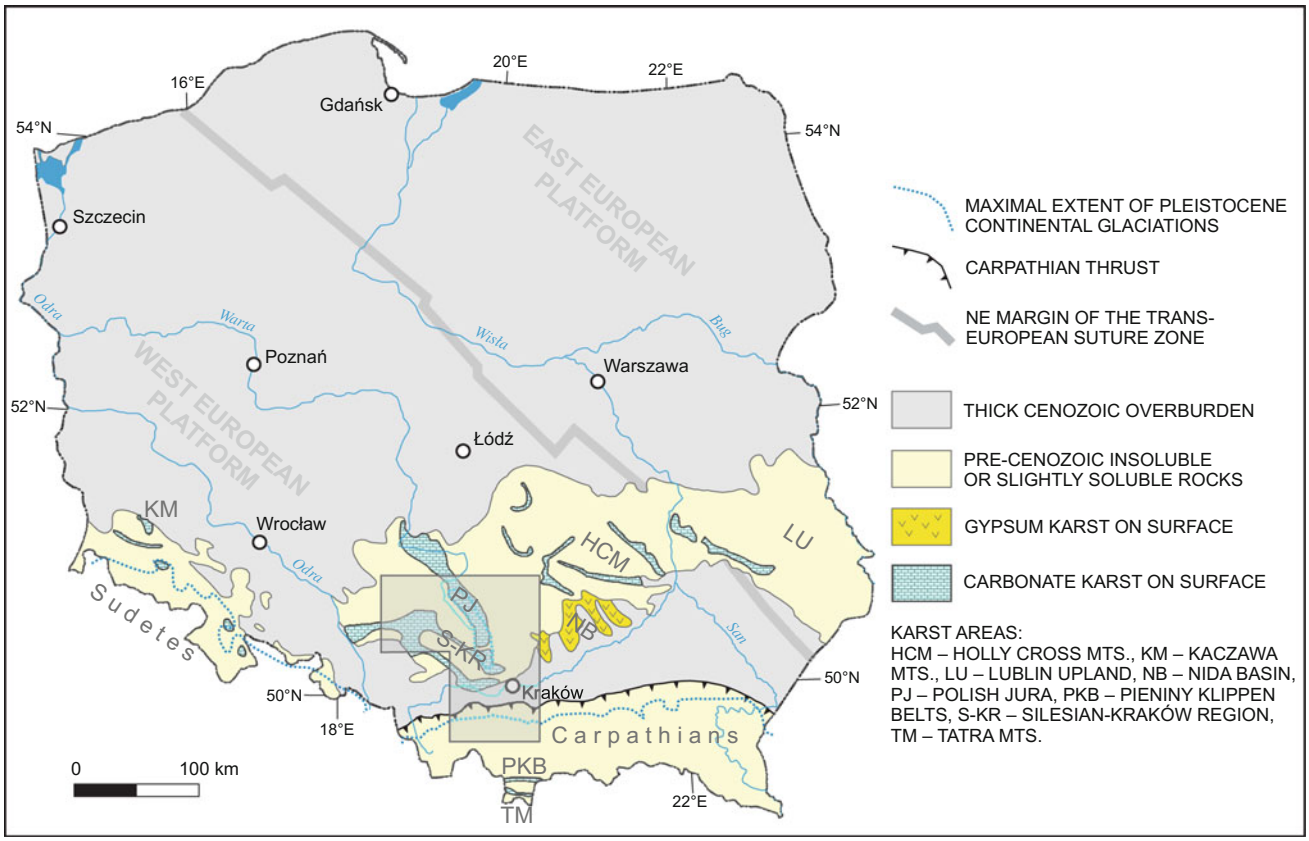

Fig. 1 Geological settings of karst in Poland (after Głazek et al. 1982; Głazek 1989 modified), polygon marks the area shown in Fig. 4. *HCM* Holly Cross Mts., *KM* Kaczawa Mts., *LU* Lublin Upland, *NB* Nida Basin, *PJ* Polish Jura, *PKB* Pieniny Klippen Belt, *S-KR* Silesian-Kraków region, *TM* Tatra Mts.

of sedimentary rocks and magmatic rocks are preserved locally. More than 180 caves are known in the Sudetes (Gradziński and Kicińska 2013). Most of karst caves in the Sudetes are developed in Precambrian and Paleozoic marbles (Fig. 1).

3 Post-Variscan and Pre-Cenozoic Hydrothermal Karst and Its Sediments

3.1 Permian Karst

Karst forms completely filled with internal sediment were encountered in Mississippian limestones around 30 km northwest of Kraków. The limestones crop out from beneath the Mesozoic cover rocks. Paleozoic rocks were folded and faulted at the transition between the Carboniferous and Permian (Bogacz 1980), whereas the Permian and Mesozoic rocks are almost horizontal in this area. In this region, the Permian tectonic activity was connected with the major transcontinental strike-slip Hamburg-Kraków-Dobruja fault zone (its segment in the Silesian-Kraków region is referred to as the Kraków-Lubliniec fault zone—KLFZ) which induced a series of minor, *en echelon*, extensional faults (Żaba 1999).

The karst forms are especially well exposed in a large, still active Czatkowice quarry, where the whole sequence of Mississippian limestone is exposed. A giant cavity with a minimum diameter of 100 m and minimum depth of 50 m was found in the southern part of the quarry in the late 1970s (Paszkowski and Wieczorek 1982). The cavity was almost completely quarried out in 1980s. Only some relicts of its basal part survived (Paszkowski 2000). Later on, some small cavities were discovered during the exploitation. All these cavities were completely filled with sediment of a bizarre type. Totally, five forms of such a type have been registered

in the Czatkowice quarry so far. They were subsequently quarried out or covered with heaps; hence, they are inaccessible now.

Four sedimentary facies of internal sediment have been distinguished (Paszkowski and Wieczorek 1982; Gradziński et al. 2014): (i) massive, subaqueous, coarse crystalline calcite spar, (ii) crystalloclastic, bedded limestones, (iii) jasper lenses and (iv) kaolinitized tuffs. The sediment is characterized by red color caused by iron compounds and the complete lack of fauna fossils. Such facies are unknown from any younger paleokarst forms recognized within Mississippian limestone of this area. Laminated, coarse crystalline calcite spar forms beds up to several dozen centimeters in thickness (Fig. 2). They line the walls of the cavities and interbed with crystalloclastic limestone (Gradziński et al. 2014). Crystalloclastic limestone is composed of detrital calcite crystals, from silt size to a few millimeters across. Some of the crystals are of skeletal type. This limestone displays normal grading (Gradziński et al. 2014). Kaolinitized tuff with lenses of decorative jasper underlain the carbonates and fill the bottom parts of karst forms (Paszkowski 2000). Tuff is graded and cross-laminated in places (Paszkowski and Wieczorek 1982).

The internal sediment underwent deformations of various types. Some layers of calcite spar and crystalloclastic limestone experienced brittle deformations; they were broken and subsequently cemented again forming breccias (Fig. 2). Tuff displays plastic deformations and hosts dykes filled with crystalloclastic limestone (Paszkowski 2000). The ceiling or wall of the giant cavity described by Paszkowski and Wieczorek (1982) must have collapsed since angular blocks of Mississippian limestone were found in the uppermost part of its filling.

Veins filled with onyx-type carbonates of milky-white and pinkish color traditionally called ‘różanka’ (which in Polish means pinkish carbonate material) are spatially connected with the cavities described above. The vein carbonates have been intensively quarried since the sixteenth century and used as highly decorative elements in many buildings in Kraków, especially those of monumental character, for instance in several churches (Rajchel 2004).

The age of karst system and its internal sediment cannot be directly dated; however, it can be estimated. The internal sediment is horizontally layered, which testifies that it is younger than tectonic deformation of the host Paleozoic carbonates. On the other hand, clasts composed of this sediment were found within younger paleokarst which is precisely dated to Early Triassic by a unique assemblage of vertebrates (Paszkowski 2009). This, in turn, proves the pre-Triassic age of the deposit and karst forms which are filled by it.

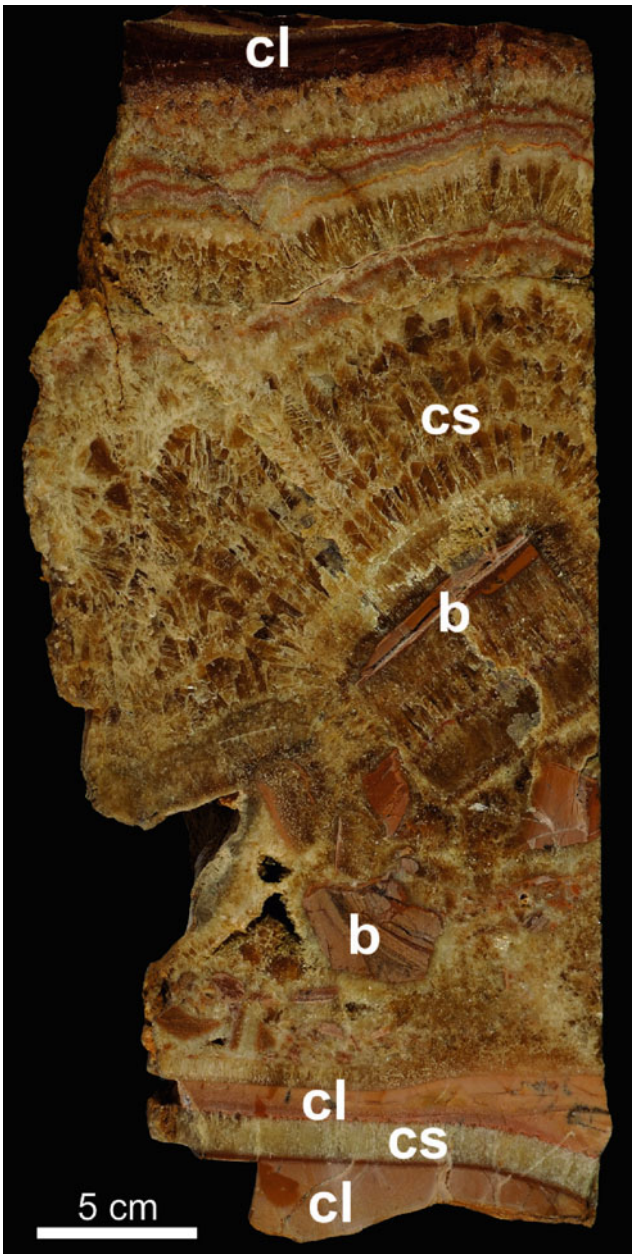

Fig. 2 Massive, subaqueous, coarse crystalline calcite spar (cs) interlayered with crystalloclastic, bedded limestones (cl); synsedimentary brecciation (b) of both facies is visible in the center of photograph; sample collected in Czatkowice quarry by Michał Gardziński, Anna Lewandowska and Mariusz Paszkowski (photograph by Waldemar Obcowski)

The extensive karst system is interpreted as fed by waters of elevated temperature rich in endogenic CO_2 which is suggested by analyses of inclusions and stable carbon isotope ratios (Gradziński et al. 2014). The roots of the system are represented by fissures filled with onyx-type carbonate. This system is hypothesized to be genetically related to

post-Variscan volcanic activity in the Kraków area (Paszkowski 2000; Gradziński et al. 2014), which is dated to the transition between the Carboniferous and Permian (Nawrocki et al. 2008). Modern analogues of such systems are known, for instance, from Mexico (Zacatón—Gary and Sharp 2009), Turkey (they are called 'obruks'—Bayari et al. 2009; Bayari et al. Chap. 27) and Italy (Pozzo del Merro—Audra and Palmer 2015), whereas inactive caves of similar origin occur, for instance, caves from Madagascar (Gilli 2014) and Slovakia (Bella et al. 2016).

Karst system was originally connected with the surface, which enabled introduction of pyroclastic material. The system was unroofed during post-Permian erosion (Paszkowski and Wieczorek 1982; Paszkowski 2009). It cannot be excluded that some voids filled with bone-bearing deposits during early Triassic were formerly also part of this system (Paszkowski 2009). Water issuing from this system on the surface resulted in precipitation of spring-fed carbonates. Red travertine, which is a facies proximal to water outflow points, is preserved only as clasts in the Lower Permian conglomerates deposited in the local tectonic depressions (Gradziński et al. 2014). The more distal facies is presumably represented by calcareous tufa, known as Karniowice tufa, famous for an assemblage of fossil flora (Szulc and Cwizewicz 1989).

Karst cavities and veins with similar internal sediment are also known from the Holy Cross Mountains (Rubinowski 1971; Migaszewski et al. 1996; Urban 2007). They are hosted predominantly by Devonian carbonates. Calcite filling these forms crystallized in temperatures between 25 and 122 °C. The internal sediment is postulated to be Late Permian or Permian/Triassic in age (Urban 2007 and Migaszewski et al. 1996, respectively).

Another example of post-Variscan paleokarst cave filled with clastics, which are cemented by palisadic calcite, is mentioned by Głazek and Kozłowski (2003) from the Kaczawa Mts. (Sudetes). The cave is hosted by Paleozoic marbles. Temperature of crystallization was estimated at 66–107 °C. The age of the cave and its filling is not precisely known. Głazek and Kozłowski (2003) postulated Permian or younger age.

3.2 Upper Triassic Karst

One of the most spectacular and well-documented (e.g., Bogacz et al. 1970; Sass-Gustkiewicz 1974; Dżułyński 1976; Dżułyński and Sass-Gustkiewicz 1982, 1989; Sass-Gustkiewicz and Dżułyński 1998) examples of hypogene karst in Poland are the Silesian-Kraków hydrothermal ore-bearing deposits emplaced in karst cavities. There are many similarities between these hydrothermal ores and the Mississippi Valley-type lead and zinc deposits occurring in many localities in the world (see Dżułyński and Sass-Gustkiewicz 1985, 1989).

Lead–zinc and iron sulfide ores of the Silesian-Kraków region consist of sphalerite, galena, marcasite and pyrite predominantly and occur within nearly flat-lying Middle Triassic (Muschelkalk) carbonates. The host rocks of these hydrothermal deposits are the ore-bearing dolomites, produced by recrystallization of early-diagenetic dolostones and dolomitization of limestones (e.g., Bogacz et al. 1975). These dolomites occur in the form of laterally extensive, irregular bodies within marine facies of Middle Triassic carbonates. According to works of authors mentioned above, dolomitizing solutions predated the ore-bearing ones. Hydrothermal karst and sulfide ores emplaced in its features are located along the metasomatic contact between the ore-bearing dolomite and the Middle Triassic carbonates. This patchy boundary constitutes the lower limit of occurrence of both—karst features and mineralization.

Solution-collapse breccias are among the most prominent features of the hydrothermal karst of the Silesian-Kraków region. According to works of Sass-Gustkiewicz (1974) and later Sass-Gustkiewicz and Dżułyński (1998 and other papers) the breccias resulted from sequence of overlapping brecciation and sulfide precipitation stages. Significant simultaneity of both processes is the key evidence for hydrothermal origin of this karst. Hydrothermal caves contain residues and products of solutional disintegration of the host rocks. They form internal clastic sediments, consisting of solutionally disaggregated ore-bearing dolomites ('dolomitic sands'), clasts of the enclosing rocks, ore fragments and crystals of precipitated sulfides (Dżułyński 1976; Dżułyński and Sass-Gustkiewicz 1989). Both phenomena—solution-collapse breccias and internal clastic sediments—were recognized during Zn–Pb sulfide ores exploitation in the Olkusz and Chrzanów mining districts.

The temperature range for sulfide ores precipitation established on the basis of gas–fluid inclusions is 80–158 °C (Kozłowski 1995). Lead–zinc and iron sulfides of the Silesian-Kraków region occur commonly in cryptocrystalline, colloform or fibrous habits, indicating rapid discharge of ore-forming solutions. They commonly comprise sulfide crusts on the blocks of ore-bearing dolomites (Fig. 3). The galena forms also large, centimeters-sized crystals, recognized mostly in the southern part of the region (Kozłowski 1995). Sobczyński and Szuwarzyński (1975), Motyka and Szuwarzyński (1989) described sulfide, mainly sphalerite speleothems occurring in interfragmental voids within the solution-collapse breccias. Sulfide stalactites and coralloid or popcorn speleothems are regarded to be the product of the same ore-forming processes as these are responsible for the hydrothermal karst and mineralization (Dżułyński and Sass-Gustkiewicz 1989).

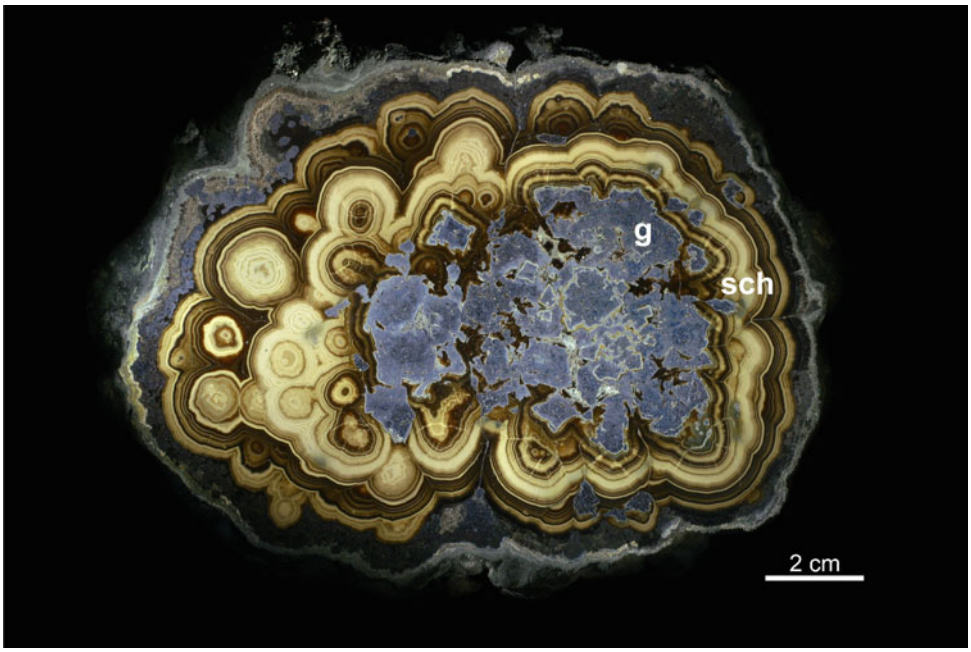

Fig. 3 Schalenblende (sphalerite and wurtzite mixture) (sch) on galena (g); 'Pomorzany' mine, Olkusz Zn–Pb ores district (collection and photograph by Eligiusz Szełęg)

As the age of hydrothermal karst and ores is still disputable, authors are following the concept of Sass-Gustkiewicz and Dżułyński (1998) on two separate events of hot ascending solution action in the regional scale —Late Triassic and Paleogene. The first one was the most important for hypogene speleogenesis in the Middle Triassic carbonates. Sulfide ores were precipitated in karst features. The primary ore-bearing solutions were originally related to the Variscan magmatic activity, associated with igneous intrusions and polymetallic ores in the Paleozoic rocks of the region. Heavy metal compounds from these rocks become remobilized by deep groundwater circulation during the Late Triassic plate-tectonic movements and redeposited within the confined aquifer of the Middle Triassic carbonates (Sass-Gustkiewicz and Dżułyński 1998). Głazek (1989) explained the hydraulic head responsible for deep circulation, its pressure and elevated temperature as being due to infiltration of meteoric waters from the northern slopes of the Vindelician Arch into Paleozoic carbonates and sandstones.

Another phenomena, related to the Upper Triassic hydrothermal event, is a belt of freshwater carbonates, called Woźniki Limestone, which occurs in the northwestern part of the Silesian–Kraków region. These carbonates were deposited within shallow swampy environments, fed by springs of deep-circulating groundwater (Szulc et al. 2006). Part of the Woźniki Limestone facies are travertines precipitated directly near these springs. It has been postulated (Głazek 1989; Sass-Gustkiewicz and Dżułyński 1998) that these freshwater carbonates can be related to the late (final) stage of hydrothermal activity in the region.

There is a regularity of a regional distribution of the Upper Triassic hypogene phenomena in the Silesian–Kraków area, as well as associated mineralization and travertines. All these phenomena are localized along the KLFZ and subparallel major faults (Fig. 4). Presumably faults were the main route of deeply circulating solutions to reach the near-surface or even surface environments, as will be described later.

During the Paleogene, the second postulated ore-bearing event in the region, ascending flow of hydrothermal solutions was reactivated and fault-hosted (not karst hosted as the previous one) sulfide ore veins were deposited (Sass-Gustkiewicz and Dżułyński 1998). This event was presumably related to faulting and folding of the Carpathians. However, this was less important for hydrothermal karst and mineralization within the Middle Triassic carbonates, although it was probably prominent for hypogene speleogenesis within the Upper Jurassic limestones of Polish Jura, as will be described later.

4 Cenozoic Karst

4.1 Carpathian Foreland

The hypogene origin of accessible caves in the Carpathian foreland, namely in the area of Polish Jura, is discussed since the late 1970s, when Rudnicki (1978) published his paper on the role of convection in shaping of specific solutional features in caves. Based on his model of hydrothermal cave

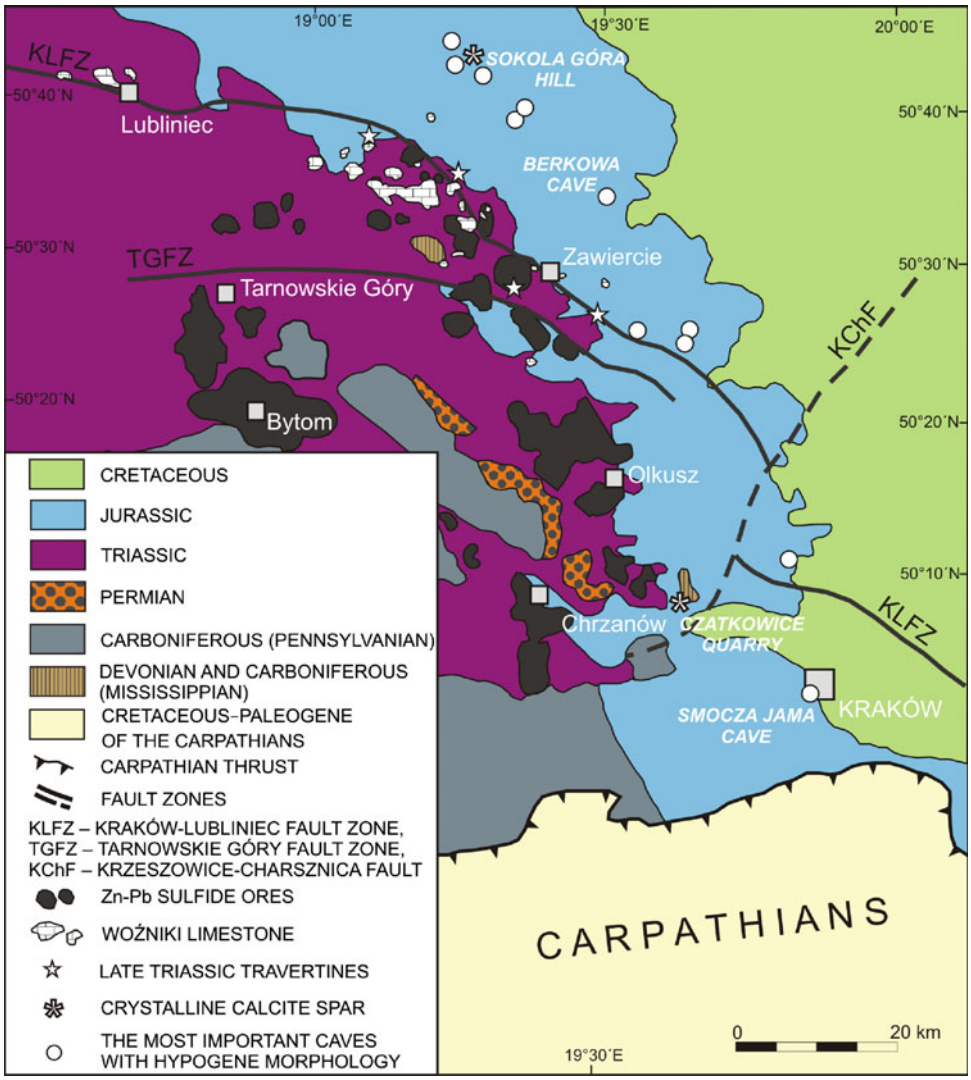

Fig. 4 Hypogene phenomena recorded in the Carpathian foreland (based on Sass-Gustkiewicz and Dżułyński 1998; Szulc et al. 2006; Tyc 2009a; Gradziński et al. 2009a, 2011, 2014; Matyszkiewicz et al. 2015); geological settings without Cenozoic cover; main fault zones underneath the Mesozoic cover. *KLFZ* Kraków-Lubliniec fault zone, *TGFZ* Tarnowskie Góry fault zone, *KChF* Krzeszowice-Charsznica fault; sites mentioned in the text: *BC* Berkowa Cave, *SGH* Sokola Góra Hill, *SJC* Smocza Jama Cave, *CzQ* Czatkowice quarry

morphology in Bátori and Sátorköpuszta caves (Hungary), he presented a concept of the origin of hemispherical niches, forming complex, grape-like structures in Berkowa Cave in Podlesice (Fig. 5). The process of thermal convection is, in Rudnicki's (1978) opinion, responsible for their origin. Following his concept Głazek and Szynkiewicz (1980) indicated a possible explanation for the origin of other small relict caves in the Polish Jura applying the same thermal convection model. Numerous remnants of phreatic cave morphology, being assumed as a result of ascending water circulation in confined conditions, presumably of elevated temperature, were recorded there (e.g., Pulina et al. 2005; Gradziński et al. 2009a, 2011; Osborne 2009; Tyc 2009a, b). Geomorphological evidences can indicate the ascending stage in cave origin (see Osborne 2004; Klimchouk 2009), but these are not sufficient for confirming a hypogene speleogenesis. There is still lack of certain geochemical evidences of this speleogenesis in the Polish Jura. Some data are coming from calcite spar occurrence in caves of the northern part of this region, but the most of the calcite was mined in the past (Tyc 2009b; Gradziński et al. 2011). The calcite spar lines the walls of caves, filling completely some of them. Calcite rhombohedra, with crystals perpendicularly oriented to the cave wall and length over 10 cm, found in caves of Sokola Hill, were studied by Gradziński et al. (2011). According to them, the calcite spar was crystallized underwater in phreatic conditions, presumably from water of slightly elevated temperature, but simultaneousness of calcite crystallization and cave-forming processes was not confirmed.

The ghost-rock weathering (rock phantomization) mentioned by Osborne and Tyc (2013) or so-called micro-disintegration changes in the Upper Jurassic limestone discussed by Wrzak and Manecki (2013) can be regarded as a possible processes of rock disaggregation by thermal solutions. The role of chemical weathering and

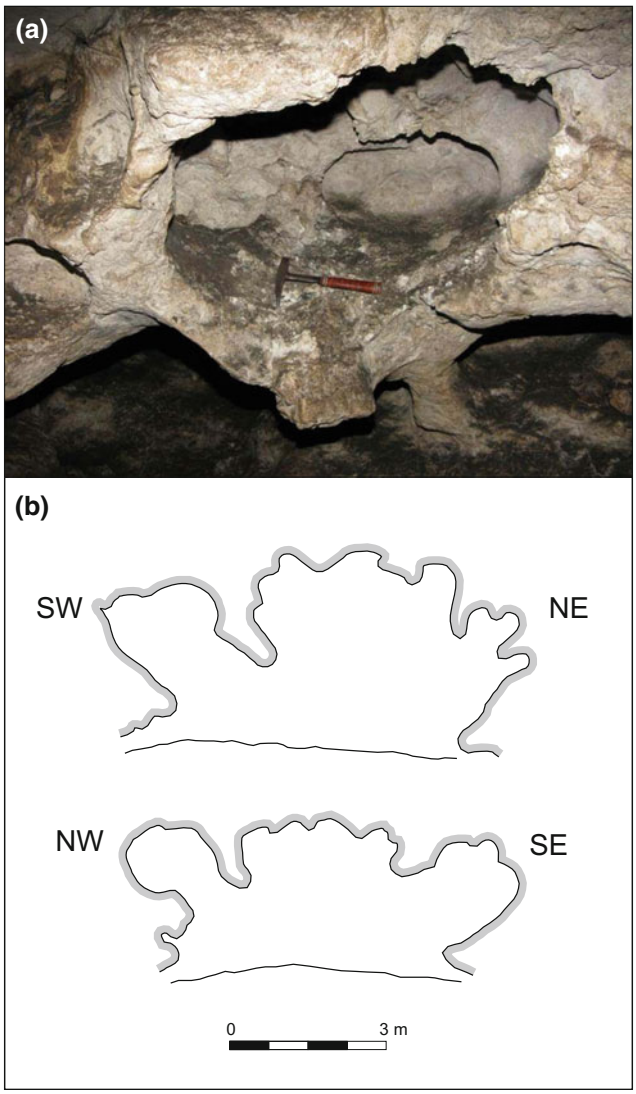

Fig. 5 Complex hemispherical niches in the main chamber of Berkowa Cave: **a** detailed view of the most characteristic feature; length of hammer handle is 30 cm (photograph by Andrzej Tyc) and **b** chamber cross sections (based on Rudnicki 1978)

carbonate rock disaggregation by hydrothermal processes has been recently emphasized in the karst literature (e.g., Dubois et al. 2014; Temovski 2016; see also Klimchouk Chap. 1). Ghost-rock weathering can be regarded as responsible for the occurrence of specific internal sediments in caves, containing rock fragments or pebbles of non-gravitational or non-fluvial origin, respectively.

The age of hypogene speleogenesis in the Polish Jura is still disputable. Since no dating is available, the discussion is centered on the assumption of possible occurrence of confining conditions (the occurrence of impermeable cover over the Upper Jurassic carbonates) and ascending flow conditions driven by tectonics or relief.

The most probable time of a hypogene event in the Polish Jura is Paleogene (Głazek and Szynkiewicz 1980; Gradziński et al. 2011); however, some authors pointed to possible hydrothermal circulation between Late Jurassic and Late Cretaceous time (Bednarek et al. 1985). The processes were active prior to the removal of the confining Upper Cretaceous marls. It is worth mentioning that traces of hydrothermal silicification were also noted below the Cretaceous marls in the southern part of the Polish Jura (Matyszkiewicz 1987). All recorded evidences—cave morphology, remnants of calcite spar lining and structural conditions controlling speleogenesis, allow to assume that a significant hypogene event imprinted in the phreatic stage of caves in the Polish Jura took place during the Paleogene (up to Eocene). Possible paleohydrological conditions for this speleogenetic event are presented as the first scenario in Fig. 6 (see Gradziński et al. 2011). Suitable structural conditions for the ascending flow and presumably low-temperature hydrothermal processes were especially present on the northeastern margin of the KLFZ (Fig. 4; see also Żaba 1999; Pulina et al. 2002; Żaba and Tyc 2007; Tyc 2009a; Matyszkiewicz et al. 2015). Basement movements influenced deformations of Paleozoic sedimentary cover and created positive flower structure, reactivated later and propagated also in Permo-Mesozoic cover (Żaba 1999). Changeable in time transpressional movements of basement and following stress system, resulted in diverse tectonically derived processes, hypogene among them (Żaba and Tyc unpublished data). Deep-seated fault zones and related faults of flower structures are prone for hydrothermal speleogenesis (Palmer 2007).

The possible conditions leading to hypogene speleogenesis in the Carpathian foreland may have been associated with expulsion of water by the tectonic loading of the Carpathian nappes (second scenario in Fig. 6; Gradziński et al. 2011). The water may have migrated to the north under confined conditions within the Upper Jurassic limestones below the impermeable Miocene clastics. This concept is based on the idea that impermeable clastics of Middle Miocene age covered the Polish Jura in Late Miocene time (Głazek and Szynkiewicz 1987; Głazek 1989). Accepting this scenario, the hypogene event must postdate deposition of the mentioned clastics and must be related to thrusting of

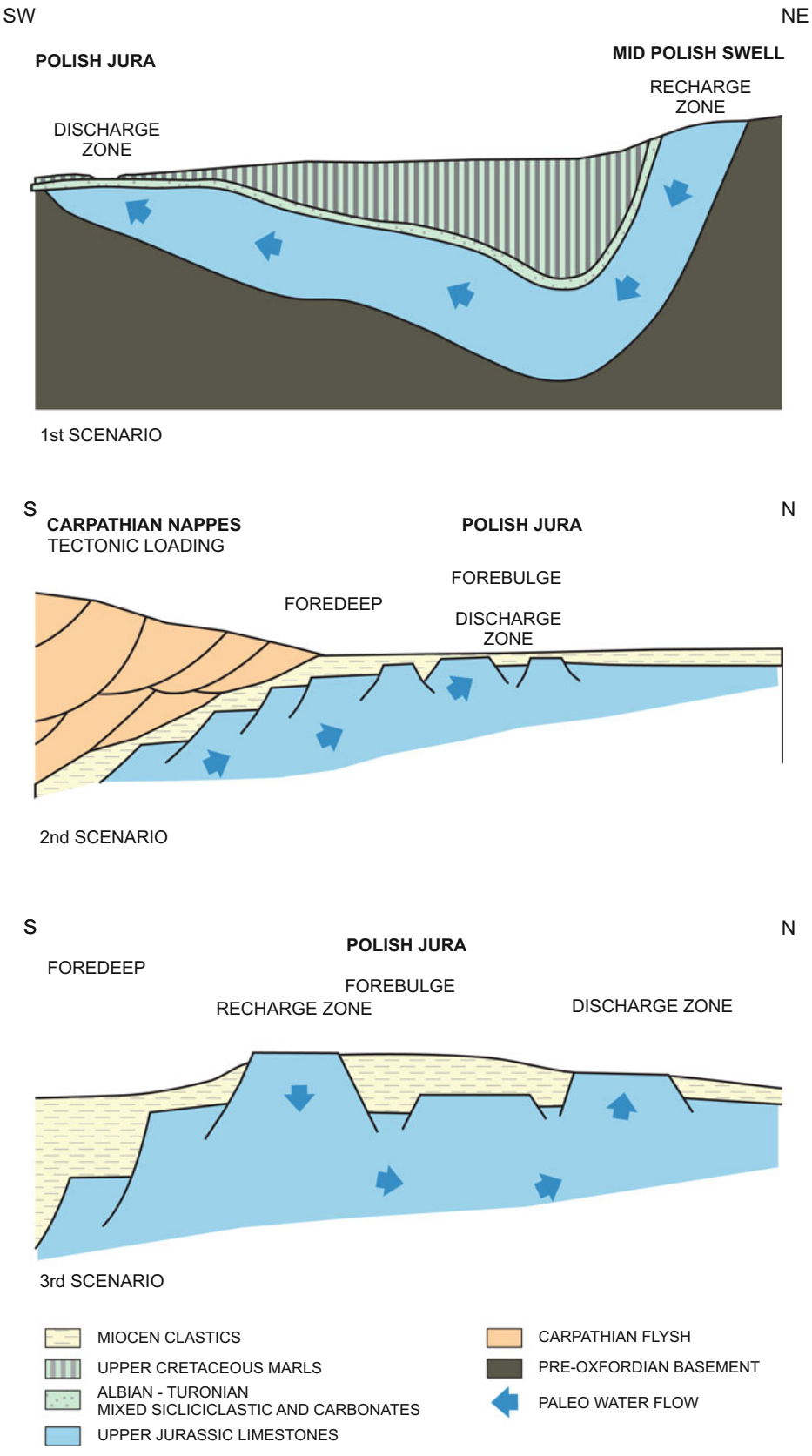

Fig. 6 Scenarios of possible paleohydrological conditions favorable for Cenozoic ascending circulation and hypogene speleogenesis in the Polish Jura (after Gradziński et al. 2011, modified; with permission)

the Carpathian nappes. Thus, the event can be dated to Badenian, Sarmatian or Pannonian age (see Oszczypko et al. 2005).

Postulated recently, the Late Neogene (Miocene/Pliocene) artesian stage of speleogenesis in the Carpathian foreland, as the second Cenozoic hypogene event in the region, manifests itself in the abundance of phreatic-rising morphology of caves. Possible mechanism of ascension and speleogenesis in confined conditions of this age explains the presence of numerous ceiling solution cavities (high cupolas and niches) in Smocza Jama in Kraków (Gradziński et al. 2009a). The cave was developed in the isolated limestone (Upper Jurassic) horst, located within a foreland basin and covered by fine-grained Miocene sediments. The artesian flow and hydraulic head were results of the height difference (up to 200 m) in the paleotopographic scheme of the southern Polish Jura. Paleohydrological and structural conditions controlling the origin of this cave were suitable to create deep circulation and presumably slight elevation of water temperature (see third scenario in Fig. 6).

As most of the caves and karst in Neogene gypsum of the Nida River Basin are epigene, few caves with phreatic-ascending morphology were noticed by Urban et al. (2009, 2015). They assumed hypogene origin of these caves and postulated a Late Neogene age of the artesian episode in speleogenesis, when evaporites were still covered by Miocene siliciclastics. Thus, postulated conditions were analogous to those controlling the development of well-known giant caves in Neogene evaporites of Ukraine (see Klimchouk and Andreychouk Chap. 23).

Although several caves in the Polish Jura display features of ascending flow due to relatively warm water, all factors controlling their origin and development have not yet been recognized and require further studies. The lack of internal deposits and remodeling of caves during further stages of their developments are the most important impediments. It cannot be ruled out that some caves are related to ascending flow of meteoric water and thus they cannot be regarded as true hypogene features.

4.2 Carpathians

The Tatra Mts. are the only karst region in Poland where relatively large and deep caves occur (see Gradziński et al. 2009c for details). The northern slopes of the Tatras are composed of several nappes comprising Mesozoic rocks, predominantly carbonates, whereas their main ridge and, especially, its southern slopes are composed chiefly of various crystalline rocks. The majority of Tatra caves is genetically associated with the geomorphic evolution of this karst region in Neogene and Pleistocene time. Pleistocene glaciations exerted a substantial influence on cave morphology. However, some caves formed by fluids of deep circulation have also been recognized.

Fig. 7 High cupolas dissected by erosion over the entrance to Dziura cave (photograph by Michał Gradziński)

Bac-Moszaszwili and Rudnicki (1978) put forward a concept of a possible hydrothermal origin of Dziura cave. The cave is located in the short Ku Dziurze Valley, which is entrenched into the northern slopes of the Tatras. Dziura cave, with a length of about 175 m, is guided by almost vertical bedding planes and fissures. There are spherical forms, up to 5 m across, in the cave ceiling. Similar forms but dissected by erosion are visible on the rock-cliff face near the cave entrance (Fig. 7). Another cave is located ca. 30 m higher (Bac-Moszaszwili and Rudnicki 1991). Large crystals

of calcite spar, mainly scalenohedral, were found in these caves. Some crystals, collected by local boys before the Second World War, are stored in a local museum.

Analyses of the stable isotope composition of the crystals prove that successive growth zones crystallized in different conditions (Gradziński et al. 2009b). The values of $\delta^{13}C$ increase systematically upward, starting from values as low as –28.8‰ (vs. VPDB). Such a low value strongly suggests the influence of CO_2 generated by oxidation of hydrocarbons. This trend is accompanied by the decrease of temperature which was demonstrated by fluid inclusion analyses. Thus, Gradziński et al. (2009b) hypothesized that these caves were formed under the influence of two components: ascending deep-circulation water which mixes with shallow circulation water. The above-mentioned trends of the stable isotope ratio coupled with the record of temperature changes mutually indicate the decreasing influence of the former component, which included hydrocarbons, during the crystal growth. This is interpreted as a record of karstification during a systematic uplift and associated erosion. The Tatra Mts. were uplifted along a prominent boundary fault on the south and southeast in Miocene time. Impermeable Paleogene rocks, which originally covered the Tatra Mts., started being eroded at this time. At the beginning, their thickness originally exceeded 3 km. They acted as confining beds and the formation of the mentioned caves proceeded below their cover. These caves were formed in Neogene time during the erosion of the impermeable flysch-type Paleogene rock cover.

It is worth mentioning that Belianska Cave—another cave which is interpreted as genetically connected with deep circulation—is located in the Slovak part of the Tatra Mts. (Bella et al. 2011; Bella and Gaál Chap. 19). Its position is analogous to the position of the caves in the Ku Dziurze Valley. Moreover, at present impermeable Paleogene rocks seal the confined basin, called 'the Podhale artesian basin' located to the north of the Tatras. Outflows of highly mineralized water of elevated temperature are located in so-called hydrologic windows. The most spectacular outflow is situated in the village of Vyšné Ružbachy (Slovakia), where Mesozoic carbonates crop out from beneath the impermeable rock cover. Therefore, the area of Vyšné Ružbachy, traditionally called a 'Mesozoic island,' resembles to some extent the Tatra Mts. in Neogene time, when the Paleogene cover only started to be eroded and Mesozoic rocks of the Tatras cropped out only locally (Gradziński et al. 2015). The water in Vyšné Ružbachy has been precipitating copious amounts of travertine, which is an indirect evidence of karstification which constantly proceeds in the deeper subsurface. Some small caves in the Pieniny Klippen Belt, which are located north to the Tatra Mts., and which bordered the 'Podhale artesian basin' from the north, can be of hypogene origin as well (Gradziński—unpublished data).

5 Final Remarks

Despite significant transformation of caves and karst of Poland by subsequent epigenetic processes, including strong effects of frost wedging during Pleistocene glaciations, features of hypogene speleogenesis are still widely observed in the southern part of the country. However, although there are no active hypogene caves in Poland, and most of these are of polygenetic and multi-stage origin, features that could be attributed to hypogene speleogenesis can be recognized, which are indicated in Fig. 8.

Quite well-documented hydrothermal karst is preserved as paleokarstic features in several localities in the Silesian-Kraków region, Holly Cross Mts. and Sudetes. Specific internal cave sediments and crystalline calcite spar, sulfide ores emplaced within hydrothermal cave sediments and solution-collapse breccias as well as travertines are related to the post-Variscan—Permian and Upper Triassic hypogene events. Their hydrothermal origin was determined by detailed studies of sediments and fluid inclusions. Less certain, based mainly on studies of relict cave morphology and sparse calcite spar, are the Cenozoic—Paleogene and Neogene hypogene events in the Carpathians (Tatra Mts.) and their foreland (Polish Jura predominantly). Tectonic structure played an important role in all hypogene events recorded in the broadly defined Silesian-Kraków region.

Although studies of hypogene speleogenesis and especially hydrothermal karst of economic importance have a long tradition in Poland, dating back to 1970s, several aspects of postulated hypogene origin of caves require more detailed research.

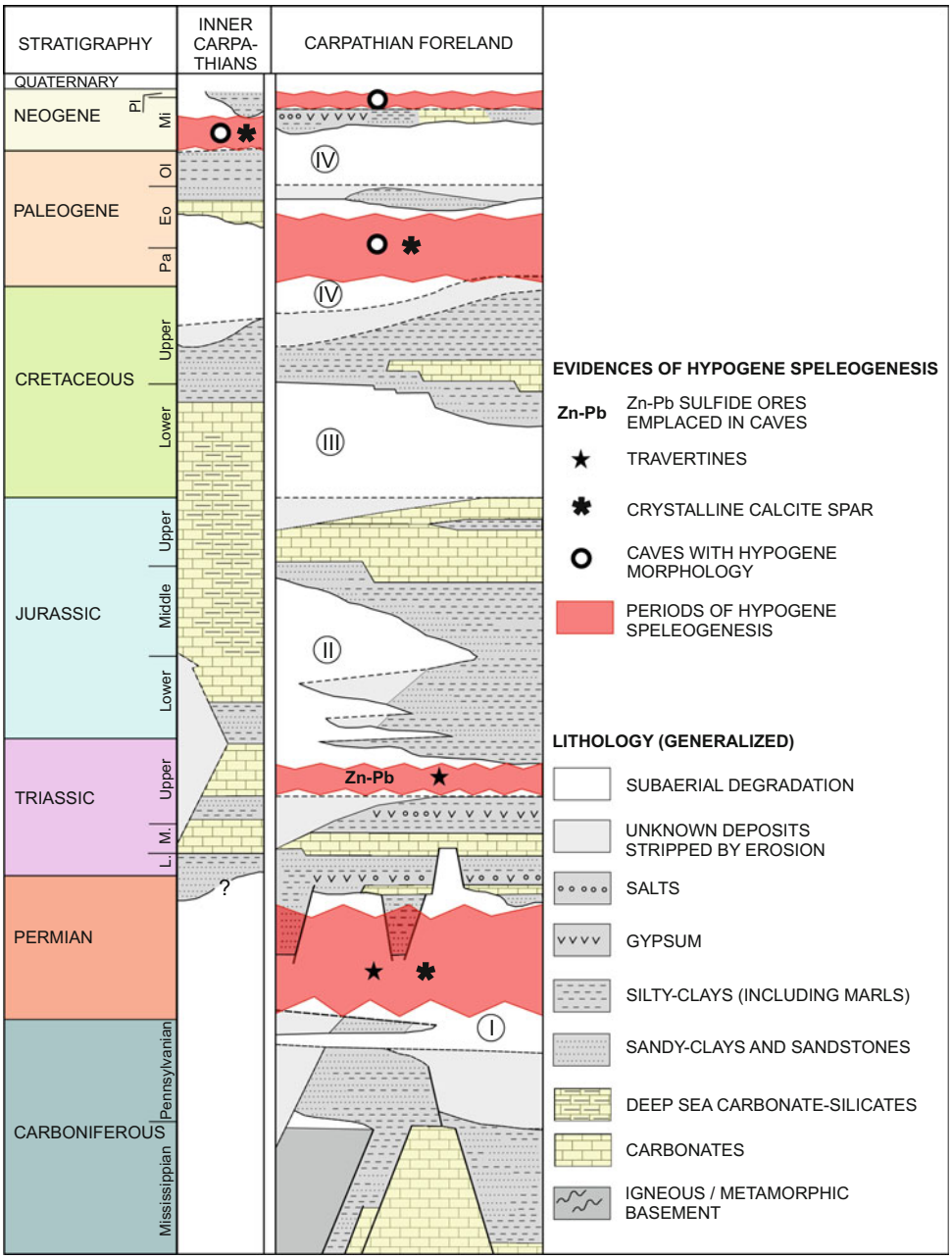

Fig. 8 Time distribution of evidences and periods of hypogene speleogenesis in southern Poland (lithology and periods of karstification/I–IV/after Głazek 1989, modified)

Acknowledgements The authors wish to thanks anonymous reviewers for constructive comments and Augusto S. Aurel for editorial handling.

References

Audra P, Palmer AN (2015) Research frontiers in speleogenesis. Dominant processes, hydrogeological conditions and resulting cave patterns. Acta Carsol 44:315–348

Bac-Moszaszwili M, Rudnicki J (1978) O możliwości hydrotermalnej genezy jaskini Dziura w Tatrach. Kras Speleol 2:84–89

Bac-Moszaszwili M, Rudnicki J (1991) Jaskinia Dziura przykład krasu hydrotermalnego w Tatrach. Tatry 1:10–12

Bayari CS, Pekkan E, Ozyurt NN (2009) Obruks, as giant collapse dolines caused by hypogenic karstification in central Anatolia, Turkey: analysis of likely formation processes. Hydrogeol J 17:327–345

Bednarek J, Górecka E, Zapaśnik T (1985) Tectonically controlled development of ore mineralization in Jurassic sequence of the Silesian-Cracovian Monocline. Ann Soc Geol Pol 53:43–62 (in Polish, English summ)

Bella P, Bosák P, Pruner P, Głazek J, Hercman H (2011) The development of the River Biela Valley in relation to the genesis of the Belianska Cave. Geografický Časopis 63:369–387 (in Slovak, English summ)

Bella P, Gaál Ľ, Šucha V, Koděra P, Milovský R (2016) Hydrothermal speleogenesis in carbonates and metasomatic silicites induced by

subvolcanic intrusions: a case study from the Štiavnické vrchy Mountains, Slovakia. Int J Speleol 45:11–25
Bogacz K (1980) Tectonics of the Palaeozoic rocks of the Dębnik region. Rocz Pol Tow Geol 50:183–208 (in Polish, English summ)
Bogacz K, Dżułyński S, Harańczyk C (1970) Ore-filled hydrothermal karst features in the Triassic rocks of the Cracow-Silesian region. Acta Geol Pol 20:247–267
Bogacz K, Dżułyński S, Harańczyk C, Sobczyński P (1975) Origin of the ore-bearing dolomite in the Triassic of the Cracow-Silesian Pb-Zn ore district. Rocz Pol Tow Geol 45:139–155
Bosák P, Ford DC, Głazek J (1989) Terminology. In: Bosák P, Ford DC, Głazek J, Horáček I (eds) Paleokarst, a systematic and regional review. Akademia, Prague, pp 25–32
Dublyansky YV (2013) Karstification by geothermal waters. In: Shroder J, Frumkin A (eds) Treatise on geomorphology, vol 6. Academic Press, San Diego, pp 57–71
Dubois C, Quinif Y, Baele J-M, Barriquand L, Bini A, Bruxelles L, Dandurand G, Havron C, Kaufmann O, Lans B, Maire R, Martin J, Rodet J, Rowberry MD, Tognini P, Vergari A (2014) The process of ghost-rock karstification and its role in the formation of cave systems. Earth-Sci Rev 131:116–148
Dżułyński S (1976) Hydrothermal karst and Zn-Pb sulfide ores. Rocz Pol Tow Geol 46:217–230
Dżułyński S, Sass-Gustkiewicz M (1982) The role of hydrothermal karst processes in the emplacement of sulfide ores. Kras Speleol 4:21–32
Dżułyński S, Sass-Gustkiewicz M (1985) Hydrothermal karst phenomena as a factor in the formation of Mississippi Valley-type deposits. In: Wolf K (ed) Handbook of strata-bound and stratiform ore deposits, 13. Elsevier, Amsterdam, pp 391–439
Dżułyński S, Sass-Gustkiewicz M (1989) Pb-Zn ores. In: Bosák P, Ford DC, Głazek J, Horáček I (eds) Paleokarst, a systematic and regional review. Akademia, Prague, pp 377–397
Gary M, Sharp JM Jr (2009) Volcanogenic kartification: implications of this hypogene process. In: Stafford K, Land L, Veni G (eds) Advances in hypogene karst studies. National Cave and Karst Research Institute, Carlsbad, pp 27–39
Gilli E (2014) Volcanism-induced karst landforms and speleogenesis in the Ankarana Plateau (Madagascar). Hypothesis and preliminary research. Int J Speleol 43:283–293
Głazek J (1989) Paleokarst of Poland. In: Bosák P, Ford DC, Głazek J, Horáček I (eds) Paleokarst, a systematic and regional review. Akademia, Prague, pp 77–105
Głazek J, Kozłowski A (2003) Kras hydrotermalny w Górach Kaczawskich. In: Gradziński M, Szelerewicz M (eds) Materiały 37. Sympozjum Speleologicznego, Wojcieszów, 24–26 Oct 2003. Sekcja Speleologiczna PTP, Kraków, p 44
Głazek J, Szynkiewicz A (1980) Kras między Pilicą a Wartą i jego praktyczne znaczenie. Przewodnik 52 Zjazdu Pol Tow Geol, Bełchatów, Inst Geol, Warszawa, pp 84–99
Głazek J, Szynkiewicz A (1987) Stratigraphy of the Late Tertiary and Early Quaternary karst deposits in Poland and their paleogeographic implications. In: Jahn A, Dyjor S (eds) Problemy młodszego neogenu I eoplejstocenu w Polsce. Zakład Narodowy im. Ossolińskich, Wyd. PAN, Wrocław, Warszawa, Kraków, Gdańsk, Łódź, pp 113–130 (in Polish, English summ)
Głazek J, Dąbrowski T, Gradziński R (1972) Karst of Poland. In: Herak M, Stringfield VY (eds) Karst. Important karst regions of the northern hemisphere. Elsevier, Amsterdam, pp 327–340
Głazek J, Gradziński R, Pulina M (1982) Preface—karst and caves of Poland. Kras Speleol 4:9–18
Gradziński M, Kicińska D (2013) Caves in Poland. In: Kicińska D (ed) Polish caving. Caving Committee of Polish Mountaineering Association, Warsaw, pp 4–7
Gradziński M, Duliński M, Hercman H, Żywiecki M, Baryła J (2009b) Cave development influenced by hydrocarbon oxidation: An example from the Polish Tatra Mts. In: White WB (ed) 15th International Congress of Speleology, Proceedings. International Union of Speleology, Kerville, Texas, USA, p 1511, 19–26 July 2009
Gradziński M, Hercman H, Kicińska D, Barczyk G, Bella P, Holúbek P (2009a) Kras tatrzański – rozwój wiedzy w ostatnich trzydziestu latach. Przegl Geol 57:674–684
Gradziński M, Hercman H, Kicińska D, Pura D, Urban J (2011) Ascending speleogenesis of Sokola Hill: a step towards a speleogenetic model of the Polish Jura. Acta Geol Pol 61:341–365
Gradziński M, Lewandowska A, Paszkowski M, Duliński M, Nawrocki J, Żywiecki M (2014) Bizarre freshwater carbonates associated with Permian hydrothermal karst; Kraków region, Poland. In: 19th International Sedimentological Congress, Sedimentology at the Crossroads of New Frontiers. Abstracts Book. Université de Genevè, Geneva, p 258
Gradziński M, Motyka J, Górny A (2009b) Artesian origin of a cave developed in an isolated horst: a case study of Smocza Jama (Kraków Upland, Poland). Ann Soc Geol Pol 79:159–168
Gradziński M, Wróblewski W, Bella P (2015) Cenozoic freshwater carbonates of the Central Carpathians (Slovakia): facies, environments, hydrological control and depositional history. In: Haczewski G (ed) Guidebook for field trips accompanying 31st IAS meeting of sedimentology held in Kraków on 22nd–25th of June 2015. Polish Geological Society, Kraków, pp 217–245
Gradziński R (1962) Origin and development of subterranean karst in the southern part of the Cracow Upland. Rocz Pol Tow Geol 32:429–492 (in Polish, English summ)
Klimchouk A (2009) Morphogenesis of hypogenic caves. Geomorphology 106:100–117
Kozłowski A (1995) Origin of Zn-Pb ores in the Olkusz and Chrzanów districts: A model based on fluid inclusions. Acta Geol Pol 45:83–141
Matyszkiewicz J (1987) Epigenetic silification of the Upper Oxfordian limestones in the vicinity of Kraków. Ann Soc Geol Pol 59:201–232
Matyszkiewicz J, Kochman A, Rzepa G, Gołębiowska B, Krajewski M, Gaidzik K, Żaba J (2015) Epigenetic silicification of the Upper Oxfordian limestones in the Sokole Hills (Kraków-Częstochowa Upland): relationship to facies development and tectonics. Acta Geol Pol 65:181–203
Migaszewski ZM, Hałas S, Durakiewicz T (1996) The age and origin of the calcite mineralization in the Holy Cross Mts based on lithologic-petrographic and isotopic evidence (Central Poland). Przegl Geol 44:275–281. (in Polish, English summ)
Motyka J, Szuwarzyński M (1989) Growth of speleothems below the karst-water table: considerations on the genesis of sulphide stalactites from the Upper Silesian Zn-Pb ore bodies. Ann Soc Geol Pol 59:417–433
Nawrocki J, Fanning M, Lewandowska A, Polechońska O, Werner T (2008) Palaeomagnetism and the age of the Cracow volcanic rocks (S Poland). Geophys J Int 174:475–488
Osborne RAL (2004) The troubles with cupolas. Acta Carsologica 33:9–36
Osborne RAL (2009) Hypogene caves in deformed (fold belt) strata: observations from Eastern Australia and Central Europe. In: Klimchouk A, Ford D (eds) Hypogenic speleogenesis and karst hydrology of artesian basin. Ukrainian Institute of Speleology and Karstology, Special Paper 1:33–43
Osborne RAL, Tyc A (2013) Caves of the Rockhampton (Queensland, Australia) and their significance for understanding of the Częstochowa Upland speleogenesis. In: Tyc A, Gradziński M (eds),

Materiały 47. Sympozjum Speleologicznego, Olsztyn, 17–20 Oct 2013. Sekcja Speleologiczna PTP, Kraków, p 65 (in Polish)

Oszczypko N, Krzywiec P, Popadyuk I, Peryt T (2005) Carpathian Foredeep basin (Poland and ukraine): its sedimentary, structural, and geodynamic evolution. In: Golonka J, Picha FJ (eds), The Carpathians and their foreland: geology and hydrocarbon resources. American Association of Petroleum Geology Memoir 84, pp 293–350

Palmer AN (2007) Cave geology. Cave Books, Dayton

Paszkowski M (2000) Pre-callovian multiple karstification of carboniferous limestone: In: Gradziński M (ed), Climate change—the karst record II, guidebook & abstracts. Institute of Geological Sciences, Polish Academy of Sciences, Institute of Geological Sciences, Jagiellonian University, Kraków, pp 16–21

Paszkowski M (2009) The Early Triassic karst of Czatkowice I, Southern Poland. Palaeont Pol 65:7–16

Paszkowski M, Wieczorek J (1982) Fossil karst with Mesozoic bone breccia in Czatkowice (Cracow Upland, Poland). Kras Speleol 4:32–42

Pulina M, Tyc A, Żaba J (2002) The role of endogenic processes in evolution of karst in Central European Platform (example of South Polish Uplands). In: Gabrovsek F (ed) Evolution of Karst: From Prekarst to Cessation. Zbirka Carsologica, Ljubljana-Postojna, pp 425–432

Pulina M, Żaba J, Polonius A (2005) Relation between karst forms of Smoleń-Niegowonice Range and tectonic activity of Cracow-Wieluń Upland base. Kras Speleol 11:39–85 (in Polish, English summ)

Rajchel J (2004) Kamienny Kraków. Uczelniane Wydawnictwo Naukowo-Dydaktyczne AGH, Kraków

Rubinowski Z (1971) The non-ferrous metals ores of the Świętokrzyskie Mountains and their metallogenic position. Biul Inst Geol 247:3–166 (in Polish, English summ)

Rudnicki J (1978) Role of convection in shaping subterranean karst forms. Kras i Speleol 2:92–101

Sass-Gustkiewicz M (1974) Collapse breccias in the ore-bearing dolomite of the Olkusz Mine (Cracow-Silesian Region, Poland). Rocz Pol Tow Geol 44:217–226

Sass-Gustkiewicz M, Dżułyński S (1998) The origin of strata-bound Zn-Pb ores in the Upper Silesia, Poland. Ann Soc Geol Pol 68:267–278

Sobczyński P, Szuwarzyński M (1975) Sphalerite dripstones from the Trzebionka mine (Cracow-Silesian Region). Rocz Pol Tow Geol 45:171–175

Szulc J, Cwizewicz M (1989) The Lower Permian freshwater carbonates of the Slawkow Graben, southern Poland: sedimentary facies context and stable isotope study. Palaeogeogr, Palaeoclim, Palaeoecol 70:107–120

Szulc J, Gradziński M, Lewandowska A, Heunisch C (2006) The Upper Triassic crenogenic limestones in Upper Silesia (southern Poland) and their paleoenvironmental context. Geol Soc Amer 416:133–151

Temovski M (2016) Evolution of karst in the lower part of Crna Reka River Basin. Springer Theses, Dordrecht

Tyc A (2009a) Hypogenic ascending speleogenesis in the Kraków-Częstochowa Upland (Poland)—evidence in cave morphology and surface relief. In: Klimchouk A, Ford D (eds) Hypogenic speleogenesis and karst hydrology of Artesian Basin. Ukrainian Institute of Speleology and Karstology, Special Paper 1, pp 201–208

Tyc A (2009b) Karst and caves of the Częstochowa Upland—morphology and the outline of speleogenesis. In: Stefaniak K, Tyc A, Socha P (eds) Karst of the Częstochowa Upland and of the Eastern Sudetes. Palaeoenvironments and Protection. Faculty of Earth Science University of Silesia, Zoological Institute, University of Wrocław; Sosnowiec-Wrocław, pp 11–36

Urban J (2007) Permian to Triassic paleokarst of the Swiętokrzyskie Mts, central Poland. Geologia 33:5–50

Urban J, Andreychouk V, Kasza A (2009) Epigene and hypogene caves in the Neogene gypsum of the Ponidzie area (Niecka Nidziańska region), Poland. In: Klimchouk A, Ford D (eds) Hypogenic speleogenesis and karst hydrology of Artesian Basin. Ukrainian Institute of Speleology and Karstology, Special Paper 1, pp 223–232

Urban J, Chwalik-Borowiec A, Kasza A (2015) The development and age of the karst in gypsum deposits of the Niecka Solecka (Solec Basin) area. Biul Państw Inst Geol 462:125–152 (in Polish, English summ)

Wrzak J, Manecki A (2013) A role of mineralogy in identifying the ascension genesis of karst hollows at the example of Nietoperzowa and Ciemna caves. In: Tyc A, Gradziński M (eds), Materiały 47. Sympozjum Speleologicznego, Olsztyn, 17–20 Oct 2013. Sekcja Speleologiczna PTP, Kraków, pp 85–86 (in Polish)

Żaba J (1999) The structural evolution of Lower Palaeozoic succession in the Upper Silesia Block and Małopolska Block border zone (Southern Poland). Prace Państw Inst Geol 166:1–162 (in Polish, English summ)

Żaba J, Tyc A (2007) Tectonic and karst phenomena of the Ogrodzieniec area. In: Socha P, Stefaniak K, Tyc A (eds), Karst and cryokarst – guidebook and abstracts, Sosnowiec-Wrocław, Poland, pp 120–121, 19–26 Mar 2007

Gypsum Karst in the Southwest Outskirts of the Eastern European Platform (Western Ukraine): A Type Region of Artesian Transverse Speleogenesis

23

Alexander Klimchouk and Viacheslav Andreychouk

Abstract

The gypsum karst in the Western Ukraine occurs in the southwestern outskirt of the Eastern European Craton and is a model example of evolution of intrastratal karst and of artesian transverse speleogenesis in this lithology. Speleogenesis commenced in the regionally extensive confined Miocene aquifer system, in which the Middle Miocene (Badenian) gypsum bed is sandwiched between two "normal" aquifers with diffused permeability. Speleogenesis developed due to ascending leakage across the gypsum induced by valleys incising into the upper confining sequence. Large gypsum caves in the region (including the five longest gypsum caves in the world) are generally stratiform multi-story mazes of passages developed along vertical and steeply inclined fissures. Cave patterns in plan and the cross section are variable depending on fracture stratigraphy, patterns and connectivity, areal distribution of recharge (at the lower contact) and discharge (at the upper contact) points, and local hydrodynamic conditions and history. Patterns and meso-morphology of the caves clearly demonstrate functional organization that evolved in response to ascending hydraulic communication between the aquifers in the Miocene aquifer system, reflecting the complex pattern of transverse flow across the gypsum. This study demonstrates that artesian transverse speleogenesis is of fundamental importance to groundwater circulation in the region-wide Miocene aquifer system. It has important implications for regional and site-specific hydrogeology, the origin of large bioepigenetic sulfur deposits, and assessment of collapse/subsidence hazard. The style and principal characteristics of the large maze caves in the gypsum karst in the Western Ukraine are not specific to dissolution of sulfate rocks but exemplify general regularities of artesian transverse speleogenesis that are applicable to other lithologies including carbonates.

Keywords

Hypogene speleogenesis • Artesian speleogenesis • Maze caves • Gypsum karst • Western Ukraine

A. Klimchouk (✉)
Institute of Geological Sciences, National Academy of Sciences of Ukraine, 55-b Gonchara Str., 01054 Kiev, Ukraine
e-mail: klim@speleogenesis.info

V. Andreychouk
Pope John Paul II State School of Higher Education, Biala Podlaska, Poland
e-mail: czeslaw.andrejczuk@gmail.com

1 Introduction

The area underlain by the Middle Miocene (Badenian) gypsum in the southwest outskirts of the Eastern European Craton in the Western Ukraine extends over 20.000 km^2, which makes the area one of the largest gypsum karst regions in the world. This region is renowned for its giant

© Springer International Publishing AG 2017

A. Klimchouk et al. (eds.), *Hypogene Karst Regions and Caves of the World*,
Cave and Karst Systems of the World, DOI 10.1007/978-3-319-53348-3_23

maze caves in gypsum. It hosts the five longest gypsum caves in the world, accounting for well over half of the total known length of gypsum caves on Earth.

Origin of these caves remained enigmatic and controversial for a long time, being originally interpreted from the perspective of the epigenic karst paradigm (Dublyansky and Smol'nikov 1969; Dublyansky and Lomaev 1980; Jakucs and Mezosi 1976, 1991). In late 1980s–1990s the concept of artesian transverse speleogenesis has been suggested for the region (Klimchouk 1990, 1992, 1996b, 2000b). This theory has explained well major features of cave distribution, patterns and morphology, resolved many controversies in regional geology and hydrogeology (e.g., hydrogeology and hydrochemistry of the Miocene aquifer system in the confined zone, origin of sulfur deposits, etc., Klimchouk 1997a), and was subsequently expanded to represent the type of artesian transverse speleogenesis (Klimchouk 2000a, 2003), one of the two main types of hypogene speleogenesis (Klimchouk 2016).

The gypsum karst and caves in the Western Ukraine are well documented and serve as a model example of artesian transverse speleogenesis, an outstanding illustration of its main regularities. Main factors which favored unambiguous interpretation of the regional speleogenesis and determined its typological significance include:

- speleogenesis developed in young rocks and relatively simple geological settings;
- it evolved in a regionally extensive and uniform confined aquifer system in which the gypsum bed is sandwiched between two "normal" aquifers with diffused permeability;
- preservation of the clay cover over most of the gypsum area during post-artesian (unconfined) stages protected hypogene karst systems from significant modification and destruction by infiltrating groundwaters;
- since dissolution of gypsum is very sensitive to hydrodynamic and hydrochemical conditions, meso-morphology of caves distinctly reflects groundwater circulation patterns;
- cave patterns in plan and profile excellently demonstrate major controls over cave development: initial permeability structure in different stratigraphic units (lithostratigraphy/fracture stratigraphy control) and flow pattern (hydrodynamic control);
- a possibility of unambiguous reconstruction of groundwater circulation patterns and identification of stratigraphic and structural controls allowed clear understanding of functional organization of complex multi-story hypogene conduit systems;
- regional geomorphological development in response to differential neotectonic movements caused respective evolution of hydrogeological conditions and differentiation of distinct evolutionary types of karst, which allowed examining evolution of karst systems and overprint of epigene karstification over preformed hypogene artesian systems.

Building on published data and new findings, this chapter aims to synthesize an overall picture of speleogenesis in this important region and highlight the role of the above-mentioned factors in karst development. We emphasize that the style and peculiarities of speleogenesis, which are exemplified by the gypsum karst of the Western Ukraine, are not specific to dissolution of sulfate rocks as proposed in some works (i.e., Bella and Bosák 2012), but are an expression of general regularities of hypogene artesian speleogenesis that are applicable to other lithologies including carbonates.

2 Geological and Geomorphological Settings

Gypsum in the Western Ukraine deposited during the Badenian (the Middle Miocene) salinity crisis in the Central Paratethys area, in an evaporite basin that occupied the Carpathian Foredeep and the outskirt of the West and East European Platforms adjacent to north and northeast (Polkunov 1990; Oszczypko et al. 2006; Babel and Bogucki 2007). In the southwestern outskirt of the East European Platform, gypsum occurs as a single bed with thickness varying from a few to 40 m. It stretches in a belt ranging from several kilometers to 40–80 km wide along the edge of the platform for a distance of over 300 km, from the Polish border in the northwest to the Romanian and Moldovian borders in the southeast (Fig. 1).

The Miocene strata across the platform margin comprise sediments of Badenian and Sarmatian age resting on the eroded surface of the Cretaceous terrigenous and carbonate succession. The gypsum is underlain by the Lower Badenian unit, which is composed mainly by carbonaceous, argillaceous and sandy beds (10–90 m thick) in the area adjacent to the foredeep, and grades into a calcareous biohermal and sandy facies (10–30 m thick) toward the platform interior (area to the north of the Dniester).

Overlying the gypsum is a bed of evaporitic and bioepigenetic limestone, locally called Ratynsky, ranging in thickness from half a meter to more than 25 m. The bioepigenetic variety of the Ratynsky limestone formed by replacement of gypsum in course of sulfate reduction, which is evidenced by pronounced $\delta^{13}C$ depletion (−32 to −65‰; Mamchur 1972; Lein et al. 1977). The gypsum and the Ratynsky limestone together comprise the Tyrassky

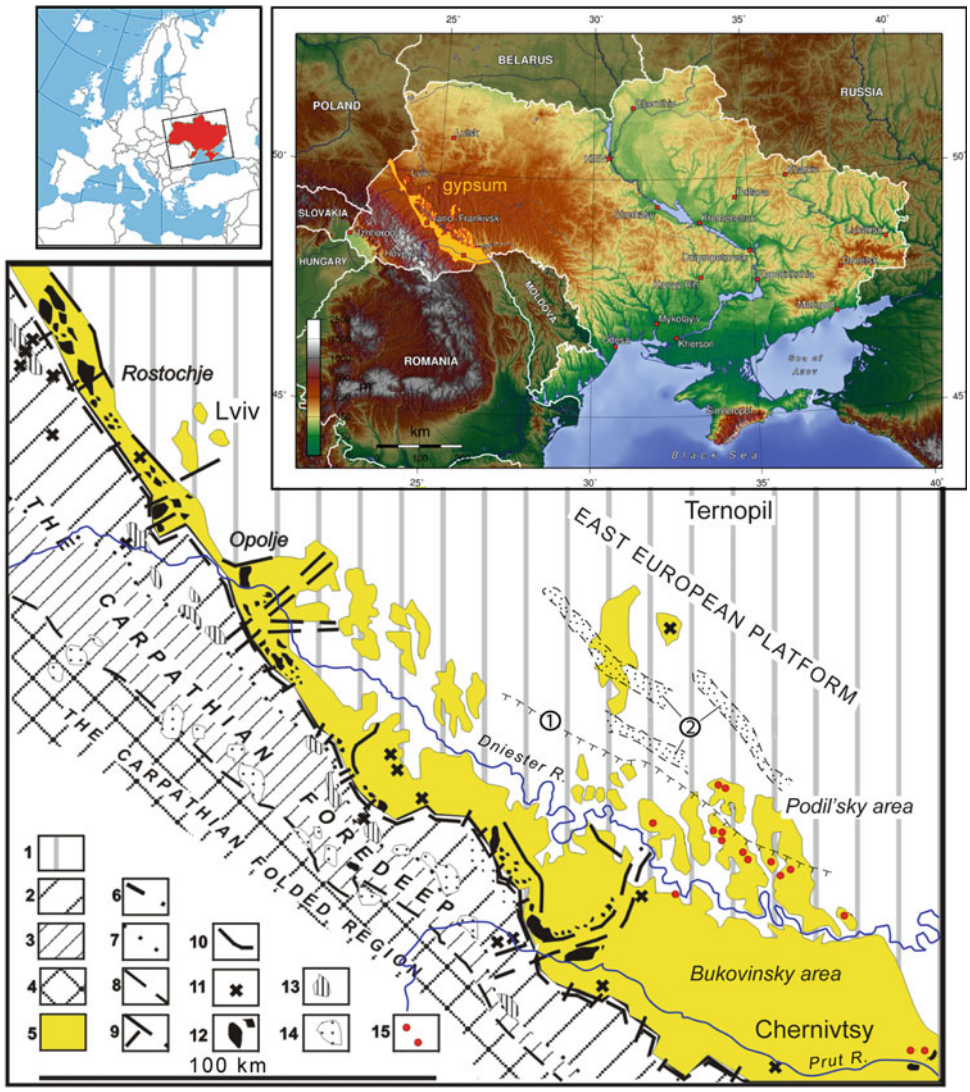

Fig. 1 Location and geological settings of gypsum karst in Western Ukraine. Tectonic settings and locations of deposits are taken from Polkunov (1990). Legend: *1* the SW outskirt of the Eastern European Craton; *2–3* the Carpathian Foredeep: *2* outer zone, *3* inner zone; *4* the Carpathian folded region; *5* gypsum rocks on the craton outskirt (not shown in the foredeep). Tectonic boundaries: *6* craton/foredeep; *7* outer zone/inner zone of the foredeep; *8* foredeep/folded region; *9* other major faults; *10* flexures; *11* sulfur mineralization; *12* sulfur deposits; *13* gas deposits; *14* oil deposits; *15* large maze caves in gypsum. Circled numbers: *1* approximate northern border of ancient terrace (7-6) sediments of Dniester; *2* reconstructed Late Pliocene buried valleys (from Svynko 1979)

Formation, which is overlain by the Upper Badenian sequence, comprised by argillaceous and marly limestones and sandstone in the platform interior and by marls and clays of the Kosovsky Formation in the area adjacent to the foredeep. Thickness of capping marls and clays reaches 80–100 m there. In the platform interior parts of the gypsum belt the clay cover is constituted by the Lower Sarmatian sequence, up to 40–50 m thick.

The Miocene succession is overlain by Late Pliocene and Pleistocene glacio-fluvial sands and loams in the northwest section of the gypsum belt, and by sand and gravel alluvial terrace sediments left by the Dniester and Prut Rivers (Late Pliocene—Pleistocene) across the present-day interfluves in the Podil'sky and Bukovinsky areas.

The gypsum lays almost horizontally in the platform interior (north of the Dniester), where it is broken into blocks by faults with no or minor vertical displacement (up to 5–7 m). To the south and southwest of the Dniester, toward the foredeep, large tectonic blocks plunge in a series of stairs, resulting in increase in depth of the gypsum occurrence and thickness of the clay cover. Along the line of regional faults separating the platform from the foredeep, the gypsum drops down to depth of many hundred meters, compensated by the respective increase in thickness of the Kosovsky clays. Toward the inner zone of the foredeep, sulfate facies are replaced by Na and K salts and evaporites are submerged to depths of over 1 km (Babel and Bogucki 2007).

The geomorphological development of the region since the regression of the Sarmatian sea was closely guided by the differential uplifts and the evolution of the Dniester valley. During the Late Pliocene and Early Pleistocene the pre-Dniester has migrated across a wide and shallow fluvial valley, which northeastern border is traced up to 30 km from the present river course (Fig. 1). Buried valleys of Late Pliocene to Middle Pleistocene age, entrenched up to 30–50 m into the clay cover and, locally, into the

supra-gypsum limestones, are documented in the Rostochje area in the northwestern section of the gypsum belt and to the north of the wide paleo-Dniester valley in the Podil'sky area (Fig. 1). By the end of the Early Pleistocene, the Dniester valley had fixed along its present course and his left north–south trending tributaries began to incise into the clay cover and extend to the north. Since the Middle Pleistocene, the Dniester started incising into the Miocene succession forming its present canyon-like valley (Fig. 2a). This was followed by progressive incision of its left tributaries resulting in dissection of the Miocene succession and isolation of sub-parallel plateau-like interfluves (Fig. 2b). To the southwest of the Dniester, in the Bukovinsky area (especially in Prut R. basin), the uplifts were less intense during the Pleistocene, further decreasing in tectonic blocks adjacent to the foredeep (including those in the northwest section of the gypsum belt). In these areas fluvial valleys are shallow, remaining within the clay cover, except of a few places where isolated tectonic blocks were uplifted to cause valley incision into the Miocene succession (Zoloushka Cave; see Andreychouk and Klimchouk Chap. 24).

3 Hydrogeological Settings, Their Evolution, and Types of Karst

The region belongs to the Volyno-Podil'sky artesian basin of the platform type (Shestopalov 1981), occupying its southwestern portion. Meteoric circulation commenced in the Late Miocene, after the retreat of the Sarmatian sea. The present-day regional diversity of hydrogeological settings of the Miocene aquifer system (MAS) evolved from initially universal confined (artesian) conditions, in result of differential neotectonic movements, geomorphological development and geological particularities.

The poorly permeable sequence of Sarmatian and Kosovsky clays and marls, with hydraulic conductivity values normally less than 10^{-6} cm/s, serves as the upper confining unit. It is underlain by the Upper Badenian carbonates with diffused pore-dominated permeability, and the Ratynsky limestone bed with diffused fracture-dominated permeability. These units constitute the upper (supra-gypsum) aquifer in the system. Hydraulic conductivities of this aquifer are commonly within 10^{-2} cm/s.

The Lower Badenian sandy-carbonate sequence constitutes the lower aquifer dominated by diffused pore and granular permeability. Hydraulic conductivities are normally in the order of 10^{-3} to 10^{-2} cm/s but can locally reach 7×10^{-1} cm/s. Underlying this aquifer is the 5- to 20-m-thick Cretaceous succession comprised mainly by marls and sandstones with generally poor permeability, which serves as the lower confining unit for the MAS. In places, this unit contains groundwaters and is hydraulically connected with the MAS.

Hydraulic properties of the gypsum bed, intervening between the two aquifers in the MAS, changed with time, and vary through the area. Matrix permeability of gypsum is negligible, so that non-fractured and non-karstified gypsum could be an effective aquiclude. Fracturing in the gypsum bed, which evolved in result of diagenetic transformations, far-reach response to tectonism in the adjacent Carpathian region and local uplifts, created complex permeability paths allowing some leakage between the aquifers—a critical precondition for artesian transverse speleogenesis (see the next section). The development of conduit systems in the gypsum eventually resulted in good hydraulic connection

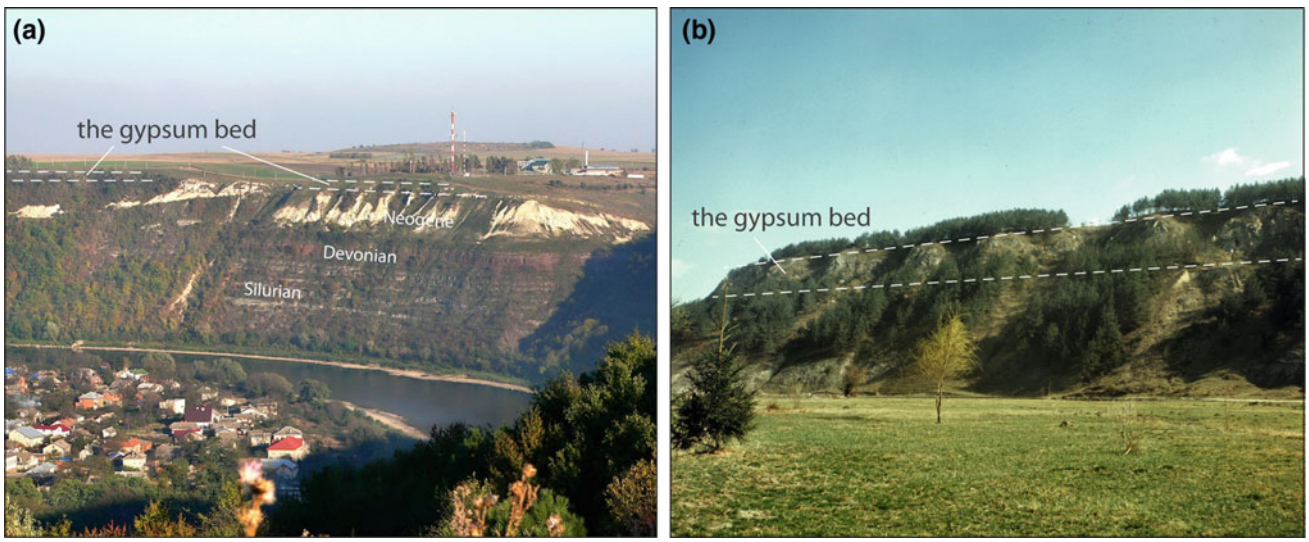

Fig. 2 Views of the Dniester valley (**a**) and of one of its left tributary valleys (**b**). Photograph **b** shows gypsum outcrops near Kristal'na Cave

between the sub-gypsum and supra-gypsum aquifers within karstified areas, although distribution of the latter through the area is clustered.

Prior to the Middle Pleistocene, when erosional valleys were shallow and not incised below the bottom of the capping clays, the confined (artesian) conditions in the MAS dominated across the entire region. Although recharge from more elevated areas adjacent to the north and northeast and devoid of the clay cover and the gypsum, contributed to the MAS, the groundwater circulation in the wide southeast section of the gypsum belt was mainly governed by topography-controlled vertical leakages across the confining units—downward in topographic highs (recharge) and upward in topographic lows (discharge). During most of the Pliocene, the groundwater circulation in the MAS was sluggish due to low topographic relief. The circulation intensity increased in the Late Pliocene–Early Pleistocene in result of the uplifts in the Podil'sky area, more substantial incision of erosional valleys and decrease in thickness of the confining clays at their bottoms, causing initial transverse speleogenesis in the gypsum by upward flow.

Breaching by the Dniester and its left tributaries into the upper aquifer in the beginning of the Middle Pleistocene has greatly accelerated groundwater circulation in the MAS and speleogenesis in gypsum. Further incision into the gypsum caused the establishment of subjacent karst settings and water table conditions, with subsequent expansion of the respective zone to the north of the Dniester along the left tributaries. In the Podil'sky area, yet another phase of uplift and incision of the Dniester and its left tributaries caused transition to entrenched karst settings by the beginning of the Late Pleistocene.

In contrast, in the area to the south, southeast of the Dniester (the Bukovinsky area), deep-seated karst settings (confined) lasted until the Late Pleistocene, and they still dominate presently in areas along the foredeep (Fig. 3). This is due to much slower rates of uplift (and even subsidence in some tectonic blocks), shallower incision depth even of major rivers (e.g., Prut) and greater depth of the gypsum occurrence.

The present-day distribution of zones with different karst types is shown in Fig. 3a. The Zone I, where gypsum was completely removed by denudation, lies in the north of the region. In the northwestern section of the gypsum belt, this zone is almost immediately adjacent to Zone IV (deep-seated karst), serving as a recharge area for the confined MAS. In the wider central and southeastern section, the Zone II (entrenched karst) occupies the entire Podil'sky region in the left side of the Dniester, and a narrow strip in the right side. The valleys incised well below the lower aquifer and effectively drain the MAS, but the clay cover remains largely intact across interfluves, only locally cut by gullies and punctured by isolated sinkholes with swallow holes. Water table rises into the gypsum for a few meters only in some relatively submerged tectonic blocks in internal parts of the interfluves. The Zone III (subjacent karst), where gypsum is universally inundated at least for a part of its thickness, stretches in internal parts of the Dniester–Prut interfluve massive, grading into the Zone IV (deep-seated karst) with further increase in the thickness of the confining clays and depth of the gypsum occurrence toward the foredeep (Fig. 3b). Within the Zone IV, the MAS is confined and artesian transverse speleogenesis in the gypsum still operates. In places where the Prut valley cuts across more uplifted tectonic blocks, subjacent karst settings with unconfined conditions of MAS occur within this zone, such as in areas of Zoloushka and Bukovinka Caves (Andreychouk 1988).

The Zone IV represents hydrogeological conditions under which speleogenesis initially evolved in the whole region. In this zone, several large open-pit quarries were operating

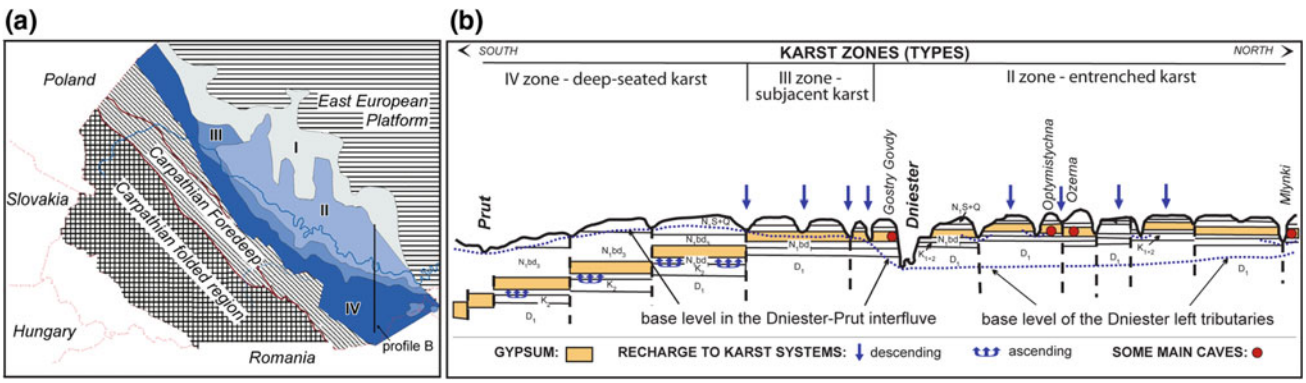

Fig. 3 Distribution of zones with different evolutionary types of gypsum karst in Western Ukraine (**a**). **b** Profile showing systematic changes in depth of the gypsum, thickness of the clay cover, and depth of erosional incision, in the direction from the platform interiors toward the Dniester and the foredeep. **a** From Klimchouk (2000b), **b** from Klimchouk (2004)

during the 1970s–1990s for mining sulfur from the Ratynsky limestone (the upper aquifer). To open quarries, the confining caprock has been removed, inducing intense upwelling discharge from the MAS, which roughly mimicked situations where rivers incised to the upper aquifer in other parts of the region in the past, breaching the original confinement. A comparison of hydrochemical data for MAS during the pre-quarrying and the quarrying stages is therefore particularly instructive for understanding conditions of artesian transverse speleogenesis (Klimchouk 1997a; Klimchouk and Aksem 2005).

During the pre-quarrying stage, groundwaters in the lower aquifer, the major one in the MAS, had HCO_3–Ca composition with TDS commonly below 1.0 g/L and SO_4 content within 0.15–0.30 g/L. These waters were highly undersaturated in gypsum (average saturation index Sig = −1.6). Locally the composition changed to HCO_3–SO_4–Ca or SO_4–Ca, with sulfate contents above 1.0 g/L (up to 1.7 g/L), which indicates the effect of backward density-driven circulation loops from cavities in the gypsum. In places, Cl–Na methane-bearing waters with TDS up to 7.5 g/L were identified, rising along faults adjacent to the foredeep.

During the quarrying stage, TDS and SO_4 contents in the lower aquifer decreased considerably (average 0.72 and 0.16 g/L, respectively), with respective increase in the dissolving capability (average SIg = −1.8) and solution rates (in the order of 1–10 mm/year). This is explained by breaking of backward circulation loops in the gypsum due to steepening of vertical head gradients, and by increase in lateral inflow from the adjacent marginal recharge zone.

When circulating through the gypsum bed, groundwaters gain SO_4–Ca composition. With the decrease in oxygen and Eh, the reducing environment promotes sulfate reduction and H_2S generation. The SO_4 content and dissolution rates vary substantially depending upon sampling locations in the void–conduit system relative to the structure of internal currents. Currents directly rising from feeding conduits may have rather low SO_4 content and keep substantial undersaturation even in the middle part of the gypsum, while the bulk water is more saturated with SO_4. Under the quarrying conditions, SO_4 content in the middle of the gypsum ranged from 0.98 to 1.54 g/L (average 1.21 g/L) and SIg ranged from −0.2 to 0.05 (average −0.03). Solution rates measured in boreholes in the gypsum varied in a range of 3.54–0.42 mm/year (1.07 mm/year in average).

In the upper aquifer, the waters that ascend across the underlying gypsum mix with the lateral flow component. TDS averaged 2.75 g/L and SO_4 1.2 g/L during the pre-quarrying stage, although in some areas these values were higher (3.0–5.0 and 1.5–2.0 g/L, respectively). High H_2S (34–200 mg/L) and CO_2 (120–170 mg/L) were commonly observed in the upper aquifer. During the quarrying stage, the average values for TDS and SO_4 dropped to 1.32 and 0.3 g/L, respectively, mainly because of inflow of water from the lower aquifer through well-developed cave systems, in which water–rock interaction was minimal.

In the present-day unconfined settings (Zones II and III), in areas where the water table in the MAS stays within the gypsum, cave systems are inundated to some levels. Flow in hydraulically connected pools is very sluggish, and distinct chemical stratification develops. Average SO_4 contents change from 0.8 g/L in the uppermost (<5 cm) layer of water through 1.0 g/L at depth between 5 and 15 cm to 1.3 g/L at depths below 20 cm. Correspondingly, average SIg decreases between these levels from −0.26 through −0.11 to 0.03, and solution rates in the uppermost layer are roughly ten times greater than in the bulk water body at depth. This has a pronounced speleogenetic effect.

4 Textural and Structural Variations of Gypsum and Their Influence on Fracture Stratigraphy and Flow Pattern

Gypsum rock across the bed is variable in structure and texture (Klimchouk 2000b; Klimchouk et al. 2009; Peryt 2001; Babel and Bogucki 2007). Lithostratigraphic variations have been shown to play an important role in vertical distribution of fractures (fracture stratigraphy) and hence in speleogenesis in gypsum (Klimchouk and Andreychouk 1988; Klimchouk 1996b, 2000b; Klimchouk et al. 2009; Fig. 4).

Through the most of the Podil'sky region, the gypsum typically displays a three-unit composition: fine-grained massive gray gypsum in the lower part (2c), variably grained laminated gray gypsum with inclusions of large (3–5 cm) brown crystals and dome-like structures in the middle (2b) and dominantly brown macrocrystalline gypsum with large dome-like structures and characteristic saber-like crystals (selenite) in the upper part (2a). The middle unit 2b is characterized by upward-increasing undulations in lamination and the presence of concentric-zoned dome-like structures of 0.5–3 m in diameter in the top. Unit 2b is separated from the above-lying unit 2a by a 5- to 10-cm-thick layer of the bluish-gray bentonitic clay, which is almost universally present in the Podil'sky area and is important as a marker for stratigraphic correlation and speleogenetic analysis. The most distinctive feature of unit 2a is an occurrence of giant dome-like structures, which can attain 8–10 m across a polyhedral figure formed by bounding fractures in the plan view, but typically are 4–6 m across. They are not regular half-spheres but are elongated vertically, have pillar-shaped microcrystalline cores, concentric layering around them, and radial-beam pattern in the peripheral parts. Fractures that commonly bound the dome-like structures have polygonal pattern in plan (Fig. 4, left). The dome-like structures in

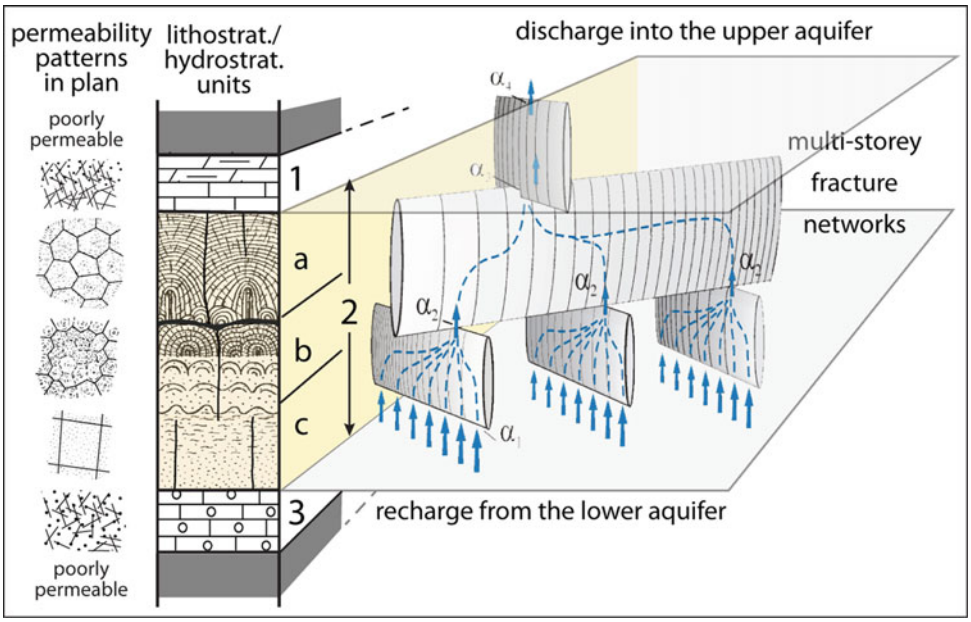

Fig. 4 Lithostratigraphy and hydrostratigraphy of the MAS, fracture stratigraphy of the gypsum and pattern of transverse flow across the soluble unit (modified from Klimchouk 2003)

units 2b and 2a are probably the result of synsedimentary and diagenetic re-crystallization of large domical stromatolites (Klimchouk et al. 2009).

In some areas along the northeastern border of the region, almost the entire thickness of the bed is comprised of fine-grained varieties of light-gray and light-brown gypsum of massive alabastrine and flat-layered stromatolitic structure, with inclusions of larger brown crystals. The bed is divided in the middle by a thin gypsarenitic layer, correlative to the bentonitic clay layer in other areas. Locally, deep pockets up to several meters across, filled with brecciated gypsum and/or gypsum-carbonate rhythmite, occur in the upper unit. In the southwestern part of the region, along the Prut River (Zoloushka Cave), the gypsum bed is composed of massive light-gray and gray aphanitic gypsum at the bottom section, layered (wavy) gray gypsum in the middle and variously grained grayish-beige gypsum with inclusions of large crystals in the upper section.

These lithostratigraphic variations in the gypsum bed determined distinct fracture stratigraphy, with largely independent fracture networks in different units (Fig. 4). Distinctions in fracture patterns and frequency in different units and variations of vertical connectivity of their fracture networks imposed strong control on transverse flow across the gypsum and hence on speleogenesis (Klimchouk 1996a, 2000b; Klimchouk et al. 2009). Rising flow has complex pattern determined by distribution of fractures in the lower unit (input features), distribution and hydraulic efficiency of points of vertical connection between fractures in different levels, lateral continuity in the fracture networks, and distribution of fractures at the upper story connected to the supra-gypsum aquifer (output features). Imperfect vertical connection between fracture networks at different stories creates leaky "barriers" to vertical flow and causes lateral flow to occur locally (Fig. 4). These peculiarities in the initial permeability structure and flow are well reflected in patterns and morphology of caves, as discussed below.

5 Caves

5.1 General Characteristics, Regional Distribution and the Relationship with Landscape

The gypsum karst of Western Ukraine is renowned for its large to gigantic maze caves that are well documented in the international literature (Klimchouk 2000b, c; Klimchouk et al. 2009). These caves and regional speleogenesis are comprehensively described in numerous articles in Ukrainian and Russian. In addition, several well-illustrated books in these languages have been published in the last decade about some major caves (Andreychouk 2007; Zimels 2008, 2009; Zimels and Snigur 2012). Recent explorations have considerably extended limits and parameters of some caves, and revealed many features that strongly corroborate the established model of transverse artesian hypogene speleogenesis.

Fifteen large caves over 1 km in length are known in the region, including five caves that are the longest gypsum caves in the world. Their locations are shown in Fig. 1, and main parameters are summarized in Table 1. Most of these caves are presently relict, being located north of the Dniester, within the Zone II (entrenched karst). Two other large

caves, Zoloushka and Bukovinka, are in the Bukovinsky area, generally in the area of artesian flow (Zone IV) but within individual relatively uplifted tectonic blocks where incision by the Prut into the upper part of the gypsum caused unconfined (subjacent karst) conditions to establish during the Holocene.

Regional distribution of major caves points to their relationship to paleo-valleys (Fig. 1), where thickness of the upper confining sequence was reduced promoting upward leakage from the MAS. In the Podil'sky area, most of the caves are situated within a belt stretching sub-parallel to the trend of the present Dniester valley on the left side, within the limits of the 25- to 30-km-wide ancient (Late Pliocene) Dniester fluvial plane (the 7th and 6th terraces). Two caves that are shifted to the north of the limits of ancient terraces are located on the continuation of a separate buried valley that has been traced in that area (Fig. 1). Within the zone of artesian flow (Zone IV) in the northwestern section of the gypsum belt, areas with anomalously high hydraulic conductivities in the confined MAS and cavities in the gypsum detected by boreholes often coincide with buried valleys that cut to the upper aquifer and are filled by the Early to Middle Pleistocene fluvioglacial sediments (Klimchouk 1997a).

The large gypsum caves in the region are mazes arranged into laterally extensive multi-story networks, which have developed along vertical and steeply inclined fissures. Interconnecting passages form lateral two- to four-story systems that extend over areas of up to two km^2. Most of the mazes have only one entrance, either through swallow holes at the interfluves or at gypsum outcrops in slopes of the major valleys. Entrances to five caves were opened by gypsum quarries (Atlantida, Dzhurinska, Gostry Govdy, Zoloushka and Bukovinka).

Despite the fact that some caves have entrances via sinkholes on the plateaus or in ravine bottoms, there is no genetic relationship of caves with sinkholes (point recharge). Most of sinkholes in the region are cover-collapse sinkholes, which formation was induced by preexisting cave systems. A detailed study of mechanisms of sinkhole formation through mapping of breakdown bodies in caves (Klimchouk and Andreychouk 2002) revealed that in most cases the breakdown process initiates in localities where high solution cupolas opened to the bottom of the overlying layer, and that only some breakdown bodies propagated to the surface across the caprock to form sinkholes, while others ceased the upward growth due to bulking. In the caves, breakdown bodies commonly overlay thick clay fill in passages, that points to their formation (and hence, the formation of sinkholes at the surface) late in the speleogenetic history.

Location of the maze caves does not show regular relationships with modern river valleys. Some caves are located near slopes of the Dniester, its sub-parallel left tributaries or

Table 1 Morphometric parameters of large gypsum caves in the Western Ukraine

No	Cave names[a]	Length, km	Volume-to-length ratio, m^3/m	Density of passages, km/km^2	Areal coverage, %	Cave porosity, %
1	Optymistychna	250.0	2.8	147	17.6	2.0
2	Ozerna	140.0	6.0	150	44.6	5.0
3	Zoloushka[b]	92.0	8.5	179	47.1	6.5
4	Mlynki	42.0	3.3	141	37.6	3.4
5	Kristal'na	22.6	5.0	169	29.2	6.0
6	Slavka	9.1	3.7	139	27.6	3.4
7	Verteba	8.5	6.0	118	34.7	12.0
8	Mushkarova Yama	5.2	n.d.[c]	n.d.	n.d.	n.d.
9	Atlantida	6.7	4.5	168	30.0	4.0
10	Bukovinka[b]	2.4	2.5	120	21.5	4.4
11	Ugryn	2.12	3.8	177	33.3	5.7
12	Gostry Govdy[b]	3.58	1.7	270	17.5	4.0
13	Jubilejna	1.5	2.3	278	37.0	4.0
14	Komsomol'ska	1.24	2.1	177	24.3	3.0
15	Dzhurinska	1.13	2.4	126	17.8	2.0

[a]The names are given here according to the Ukrainian spelling. In many other publications, Russian spelling was used, where most names end with "-skaya" or "-aya"

[b]Caves located in the Bukovinsky area, in the Dniester–Prut interfluve. Other caves are located in the Podil'sky area, on the left side of the Dniester valley (see Fig. 1)

[c]*n.d.* not determined

lower-order tributaries, while others lay beneath internal parts of interfluve massifs (Fig. 5, 1–3). Mazes occurring in valley sides do not show any systematic changes in patterns and passage morphology in the direction from the internal parts toward the valley. This suggests that valleys cut through already existing cave systems, that downcutting of the gypsum layer occurred rather fast, and that speleogenetic effects of direct recharge from the surface streams during downcutting were localized in the immediate vicinity, not extending into the massif interior. Those parts of cave systems which have been substantially modified during downcutting were removed by the subsequent slope retreat.

All known maze caves are located in the eastern section of the gypsum belt (Fig. 1), where direct exploration is possible due to complete or partial draining of the gypsum. In the deep-seated karst zone (Zone IV; Fig. 3a) that stretches along the foredeep, large cavities are frequently intercepted by boreholes. Detailed analysis of data from nearly 100 boreholes from some areas where their density is high (Jazovsky sulfur deposit in the northwestern section of the gypsum belt and Nikolaevsky clay deposit in the central section) revealed that up to 35% of them cut across meter-scale sediment-open cavities that demonstrate two-story distribution in the gypsum cross section (Klimchouk 1997a). This is comparable to the "areal coverage" parameter of explored cave systems in the Podil'sky and Bukovinsky areas (average 29.5%; see Table 1 for variations), which represents the probability that a randomly placed borehole intercepts a passage. Heights of intercepted cavities of 3–6 m are common, whereas maximum documented heights are 9.7 m at the Nemirovsky sulfur deposit and 12 m at the Jazovsky sulfur deposit. These data suggest that caves in the deep-seated karst zone are likely to have patterns and dimensions similar to those of explored caves in the Podil'sky and Bukovinsky areas.

Besides maze caves, which have no or only indirect relationship with the modern landscape, there is a number of evidently epigenic caves in the region, strongly linked with surface landforms. These caves are linear, commonly consisting of a single passage, rarely with small tributaries, and have predominantly vadose morphology. They were formed by intermittent streams captured underground in ravines that directly connect to major rivers (Fig. 6a), or are low-order tributaries in internal parts of the interfluves. In the Podil'sky area (entrenched karst zone), swallowing caves in sinkholes on plateaus are small, commonly encountering a preexisting maze network maximum in a few tens of meters from the entrance, where the concentrated flow dissipates and infiltrates to the lower aquifer. In the Bukovinsky area, several vadose caves that start from sinkholes on the plateau open to the Dniester canyon (Polyakova Ducha, 587 m long; Balamutivska, 263 m; Ruhotynska, 147 m). Their stream passages develop along the contact with underlying carbonates. In the internal part of the Dniester–Prut interfluves, within the subjacent karst zone, a number of caves developed where shallow valleys cut through the gypsum (Chornopototska—1031 m, Pionerka—642 m, Kadubivska—270 m, Fushteyka—208 m). They capture streams by ponors in the valley heads and convey them underground to resurgences in the downstream, or across the massif to a neighboring deeper valley (Fig. 6b-1). Some of the caves have two to three stories formed due to successive downcutting (Fig. 6b-2).

5.2 Views on the Origin of the Caves and the Model of Transverse Artesian Hypogene Speleogenesis

Prior to 1990s, two models existed to explain the origin of the maze caves in the region, and both are essentially epigenic.

According to the most popular model by V. Dublyansky (Dublyansky 1966; Dublyansky and Smol'nikov 1969; Dublyansky and Lomaev 1980), the caves formed in phreatic conditions due to groundwater through-flow in the gypsum between the sub-parallel left tributaries of the Dniester in the course of their incision in this layer (Fig. 5a). This model had many flaws and discrepancies. First, enlargement of fractures along extensive lateral flow pathways (3–10 km across the interfluve massifs) would be impossible due to fast gypsum dissolution kinetics. Groundwaters would reach saturation over short distances of flow in gypsum and loose the capability for further conduit enlargement. Second, capturing of river flow is a highly focused recharge, which cannot lead to the formation of maze patterns. Third, differences in incision rates and depth between any pair of the sub-parallel Dniester tributaries were too small to cause substantial hydraulic gradients to drive lateral through-flow in the gypsum across the interfluve massifs. When river beds reached the top of the gypsum layer, fast downcutting took place, given high dissolution rates of the mineral in surface streams and small thickness of the layer (10–20 m in the Podil'sky area). Fourth, conduit networks at different stories are clustered, and not laterally continuous for long distances. There are no systematic changes in passage size and morphology that could be related to flow between the valleys. Therefore, patterns and morphology of maze caves do not fit into this model.

The model suggested by Jakucs and Mezosi (1976, 1991) implied that maze caves developed by point recharge via swallow holes on the plateau and lateral flow in the gypsum toward adjacent valleys (Fig. 7b). This model also lacks any agreement with actual characteristics of the caves and their distribution, and contradicts to basic principles of speleogenesis. As shown in the preceding section, the caves have no genetic relationship to sinkholes, and formation of

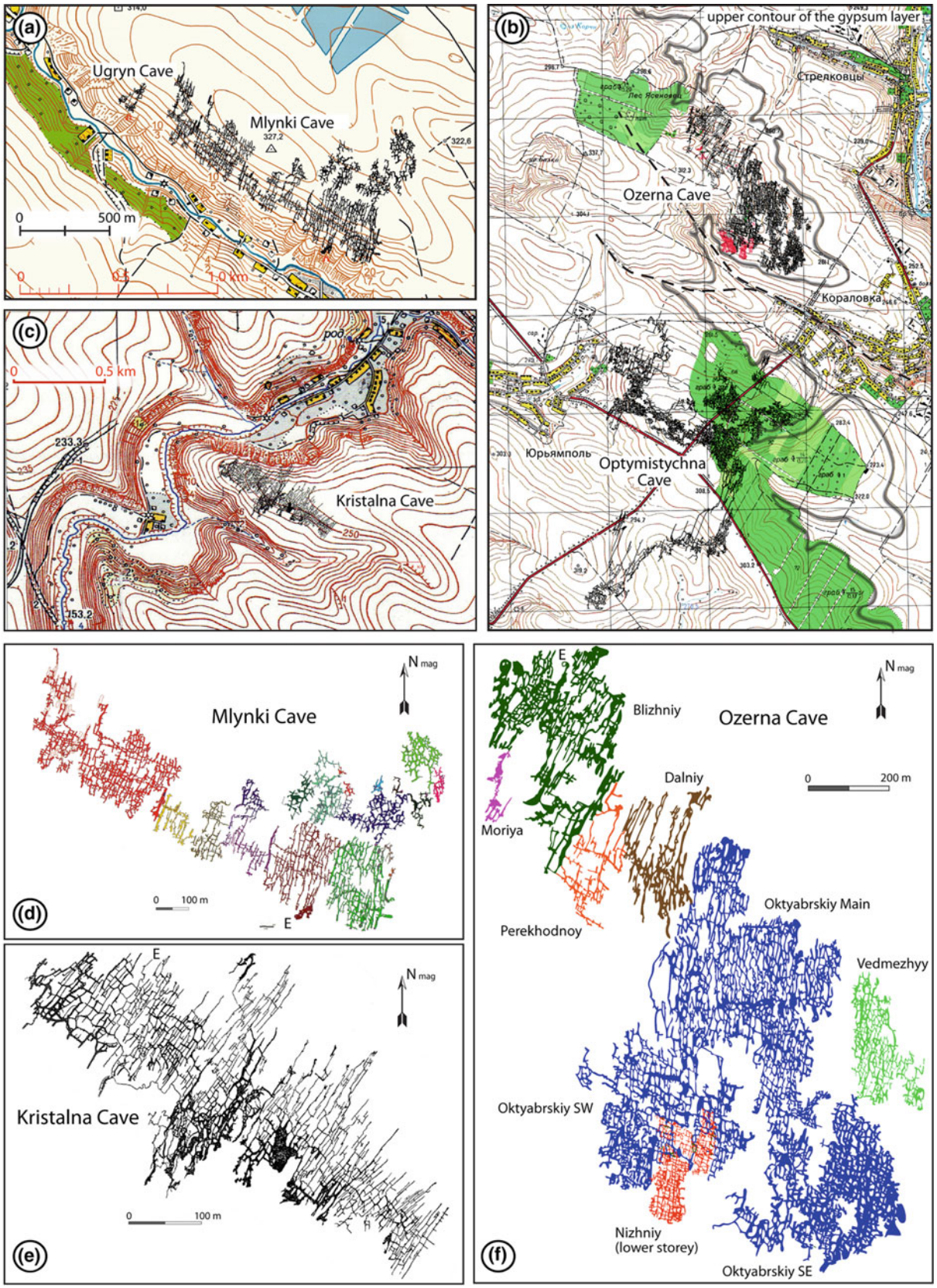

Fig. 5 Occurrence in the modern landscape (**a**–**c**) and plan patterns (**d**–**f**) of some large gypsum maze caves. Figures **a**–**c** by B. Maksimov (Ternopil Speleo-Club "Podillia," by permission). Cave maps **d** and **f**—courtesy of speleological clubs "Kristal" (Chortkiv) and "Podillia" (Ternopil), by permission; **e** from Dublyansky (1966). *Colors* in **d** and **f** indicate "cave regions"—clusters of passages of similar morphological characteristics (see Sect. 5.3)

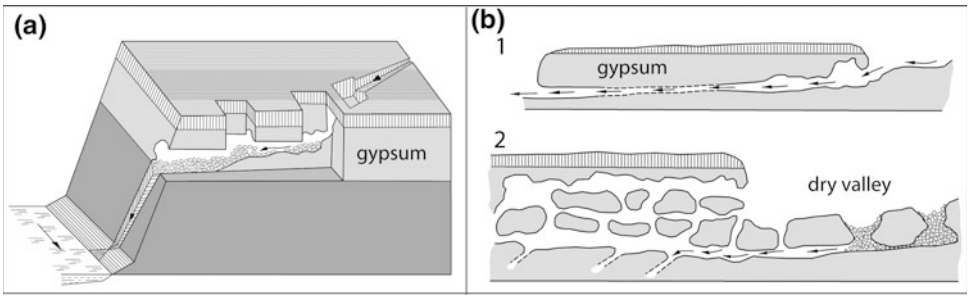

Fig. 6 Epigene caves formed by point recharge: **a** in ravines that directly connect to major rivers; **b** in low-order valleys in internal parts of interfluve massifs

sinkholes postdates the caves. Patterns and morphology of the maze caves do not fit into the model. It has long been recognized (e.g., Lukin 1966; Ford 1971; Ford and Ewers 1978; Ford and Williams 1989) and subsequently confirmed by many numerical modeling works (e.g., Palmer 1991; Dreybrodt et al. 2005) that in settings like those depicted in Fig. 7b the principles of flow–dissolution feedback and speleogenetic competition inevitably lead to the formation of branching cave patterns. This regularity is further reinforced in case of speleogenesis in gypsum due to fast kinetics and high rates of dissolution of this mineral, which leads to suppressed branching and prevalence of linear caves to form in such settings (Klimchouk 2000c, 2012a). The above-described epigenic, single-passage or crudely branching caves in the region, developed in settings as depicted in Fig. 7b, excellently illustrate this argument.

One of the major flaws of both models is that they did not address the formation of maze patterns, the most distinctive characteristic of large caves in the region, and were not capable of adequately explaining them in the particular regional context of Western Ukraine. The origin of maze caves presented a challenging problem in general (Palmer 1975), and even more so—in gypsum. Fast kinetics and high rates of dissolution of gypsum impose even more severe limitations on the formation of uniform maze patterns in this rock than in carbonates. Any of three speleogenetic mechanisms for maze caves proposed in the above-cited work (diffuse recharge from the overlying permeable bed, high gradient zone due to a local obstruction to focused flow, and backflooding from a river) could not be applied to this region. Lateral flow in confined settings (a "classical" artesian paradigm) was shown to be not able to produce maze patterns (Palmer 1975, 1991).

In the late 1980s–1990s, a new conceptual model has been suggested for regional speleogenesis (Klimchouk 1990, 1992, 1996b, 2000b, 2012c). According to this model (Fig. 7c), the maze caves were formed in a multi-story confined (artesian) aquifer system due to upward leakage between the aquifers across the gypsum. Cross-formational upward flow in such systems and overall discharge from them occur in areas of piezometric lows that correspond to topographic lows. Downcutting of the ancient valleys into the confining clays (Late Pliocene–Early Pleistocene) established initial zones of upward leakage in the MAS, prone to transverse speleogenesis in the gypsum. Within such zones, fracture stratigraphy and varying degree of the vertical connectivity between fracture networks in different units determined complex pattern of transverse flow across the gypsum (Fig. 4) and the formation of multi-story caves. Numerous individual segments of transverse flow interacted laterally via connected fracture networks in some stories to form integrated passage clusters and large cave systems.

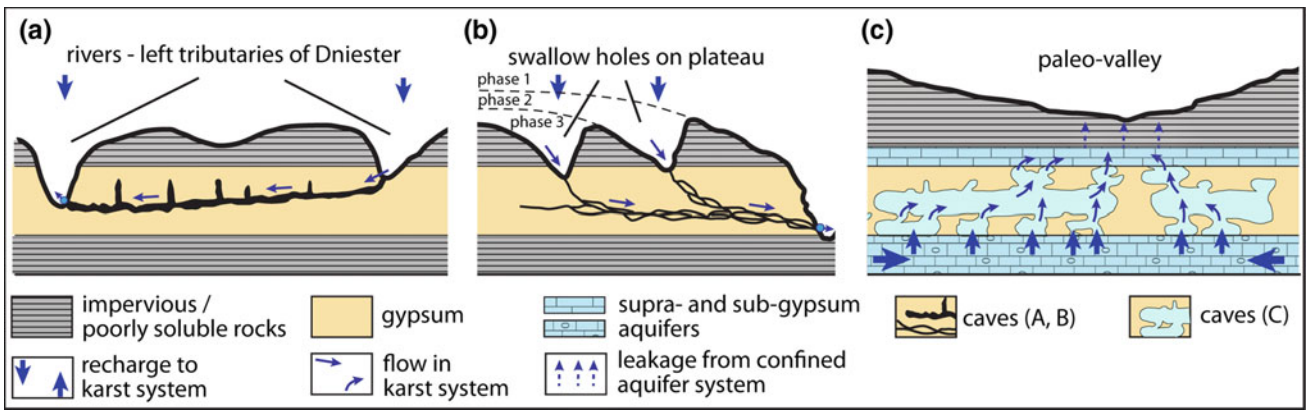

Fig. 7 Conceptual models of speleogenesis of large maze caves in Western Ukraine: **a** and **b** epigene models: **a** by V. Dublyansky, **b** by L. Jakucs and G. Mezosi; **c** the artesian transverse (hypogene) model by A. Klimchouk. See text for explanations

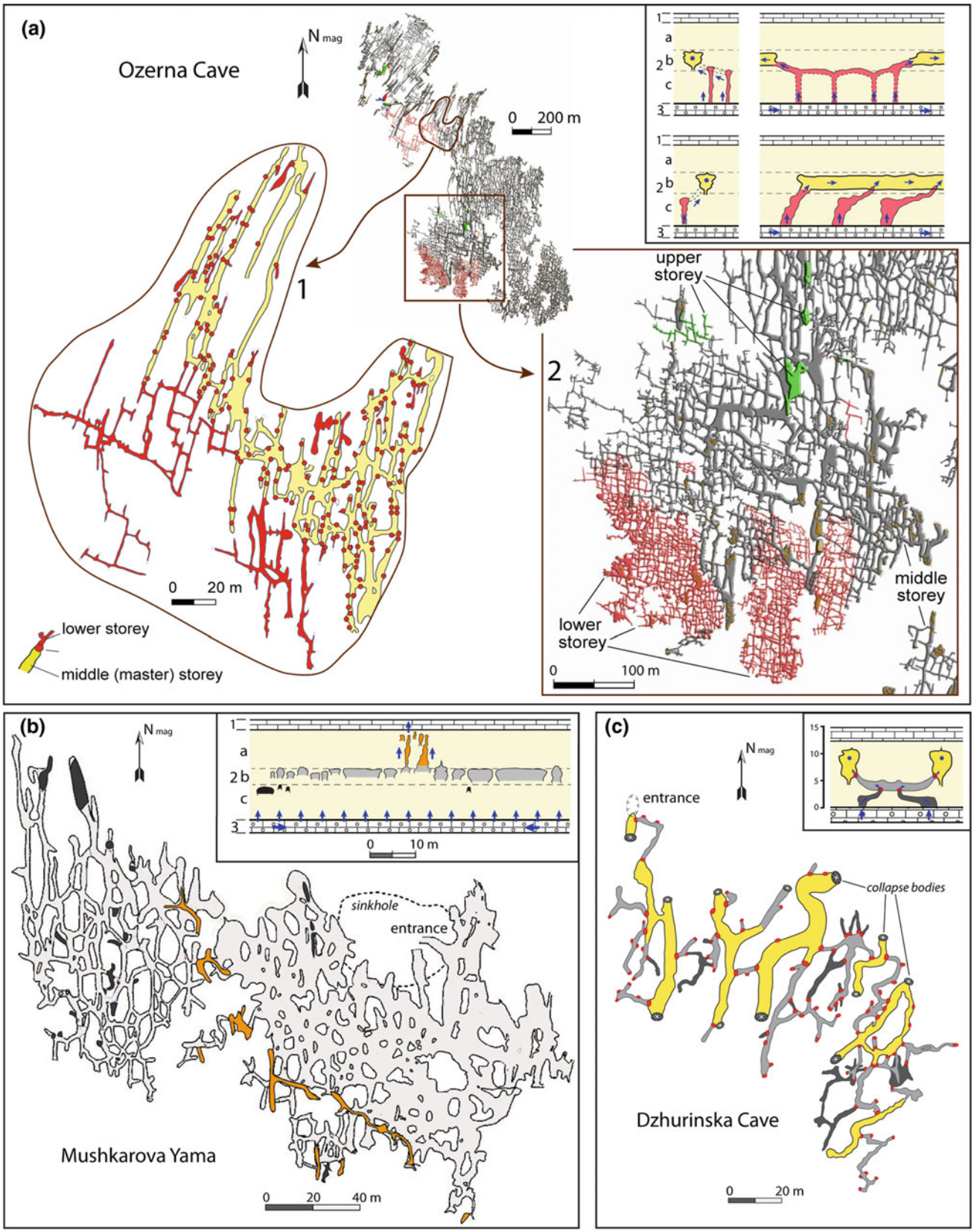
(a)
Ozerna Cave
N mag
0 200 m
1
2
0 20 m
lower storey
middle (master) storey
upper storey
middle storey
lower storey
0 100 m
1
a
2 b
c
3
(b)
N mag
a
2 b
c
3
0 10 m
sinkhole
entrance
Mushkarova Yama
0 20 40 m
(c)
N mag
entrance
collapse bodies
Dzhurinska Cave
0 20 m
15
10
5
0

◀ **Fig. 8** Variations in patterns of maze caves. **a** Ozerna Cave (see also Fig. 5f), with enlarged map fragments, showing patterns and relationships between cavities in different stories. In fragment 1, points where individual conduits of the lower-story join master passages of the middle story are indicated by red circles (not shown in fragment 2). In the southeast of the fragment, passages in the lower story form substantial networks. In fragment 2, more extensive networks in the lower story are seen in the southeast but individual feeders are not shown. Also shown in green in this fragment are several "outlet" cavities in the upper story. Fragment 2 is an extract from the large-scale map of the cave by the Ternopil Speleo-Club "Podillia" (by permission). **b** Mushkarova Yama (modified from Pokalyuk et al. 2010). **c** Dzhurinska Cave. In *insets* are profiles showing the relationships between the stories. *Numbers* and *letters* to the left of profiles in **a** and **b** refer to lithostratigraphic units as in Fig. 4

This mode of speleogenesis was supported by high aggressiveness with respect to gypsum of groundwater that entered the layer from below, the dispersed mode of such recharge, short distances of transverse flow through gypsum in individual flow segments, and natural convection effects (i.e., upward-pointed dissolution by buoyant freshwater currents that tend to penetrate high in the cave space). Artesian transverse speleogenesis involves a specific mechanism (Klimchouk 2000a, 2003, 2012b, 2015). When transverse proto-conduits reach the breakthrough condition, their further growth does not accelerate dramatically because at some point the control over discharge switches to the hydraulic conductivity of the least permeable unit in the system (the external conservative control over discharge). This switch subdues the positive feedback loop and the speleogenetic competitiveness and allows alternative conduits to continue their growth, favoring formation of pervasive, maze-like patterns.

This model explains well major features of cave distribution, patterns and morphology, as shown in the following sections. It has been successfully generalized to describe artesian transverse speleogenesis that occurs in multi-story artesian systems containing soluble formations (Klimchouk 2000a, 2003)—one of the types of hypogene speleogenesis recognized nowadays (Klimchouk 2016; Klimchouk Chap. 1). This model was also confirmed by numerical modeling (Birk 2002; Rehrl et al. 2008).

5.3 Cave Patterns

The large gypsum caves in the region are generally stratiform multi-story mazes of passages developed along vertical and steeply inclined fissures. Cave patterns in plan and cross section are variable (Figs. 5, 8 and 9), depending on fracture stratigraphy, patterns of fracture networks in different stories and degree of their vertical connectivity (Fig. 4, left), areal distribution of recharge (at the lower contact) and discharge (at the upper contact) points, and local hydrodynamic conditions and history (Klimchouk et al. 2009).

Most of the caves exhibit reticular plan patterns, with linear elementary passages organized in systematic or polygonal networks. Networks are characterized by very high passage density (measured by the ratio of mapped length to the area of a cave field), which varies between 118 and 270 km/km^2 (Table 1). Values of areal coverage and cave porosity (fractions of, respectively, the total area and volume of the rock within a cave field, occupied by passages) vary for individual caves from 17.5 to 48.4% (average 29.5%) and from 2 to 12% (average 4.5%), being roughly an order of magnitude greater than these characteristics for typical epigenic caves (Klimchouk 2003; 2012c).

The fields of large caves are commonly comprised of numerous clusters of well integrated passages, called "regions" in the caver's slang. Cave regions may differ within a single-cave system in a number of stories, in network patterns, and in passage morphology. Regions are usually connected only by a single passage or a few passages. In some cases, cave regions occur in individual tectonic blocks separated by faults (commonly without, or with only small vertical displacement), but in other cases the presence of tectonic boundaries is not apparent. The clustered structure of large caves is illustrated here by maps of Mlynki and Ozerna caves with clusters shown by different colors (Fig. 5d, f).

The caves have two to four stories. Passage networks in certain stories can be laterally continuous and well interconnected across considerable areas, or fragmented. Laterally continuous passage networks form the principal story in a given cave region ("master story"), which collects recharge from numerous scattered recharge points (feeders) or separate passage clusters in the lower story and redistributes flow laterally to points where discharge to the upper aquifer occurs (outlets). Most commonly, the master story is the middle one. In Ozerna Cave, passages in the middle story form most of the maze. Several substantial lower-story passage clusters occur along the southeast contour of the cave, occasional small clusters occur elsewhere and thousands of individual conduits in this story diffusely scatter through the cave, representing characteristic "feeders" in points of junction with master passages (Fig. 8a). Cavities in the upper story, opened to the upper aquifer, are much less frequent. In Ozerna Cave, outlet features are represented by isolated cavities, sometimes arranged in line, that likely reflects the control by tectonic disruptions and respective zones of enhanced permeability in the upper aquifer and the confining clays (see fragment 2 in Fig. 8a).

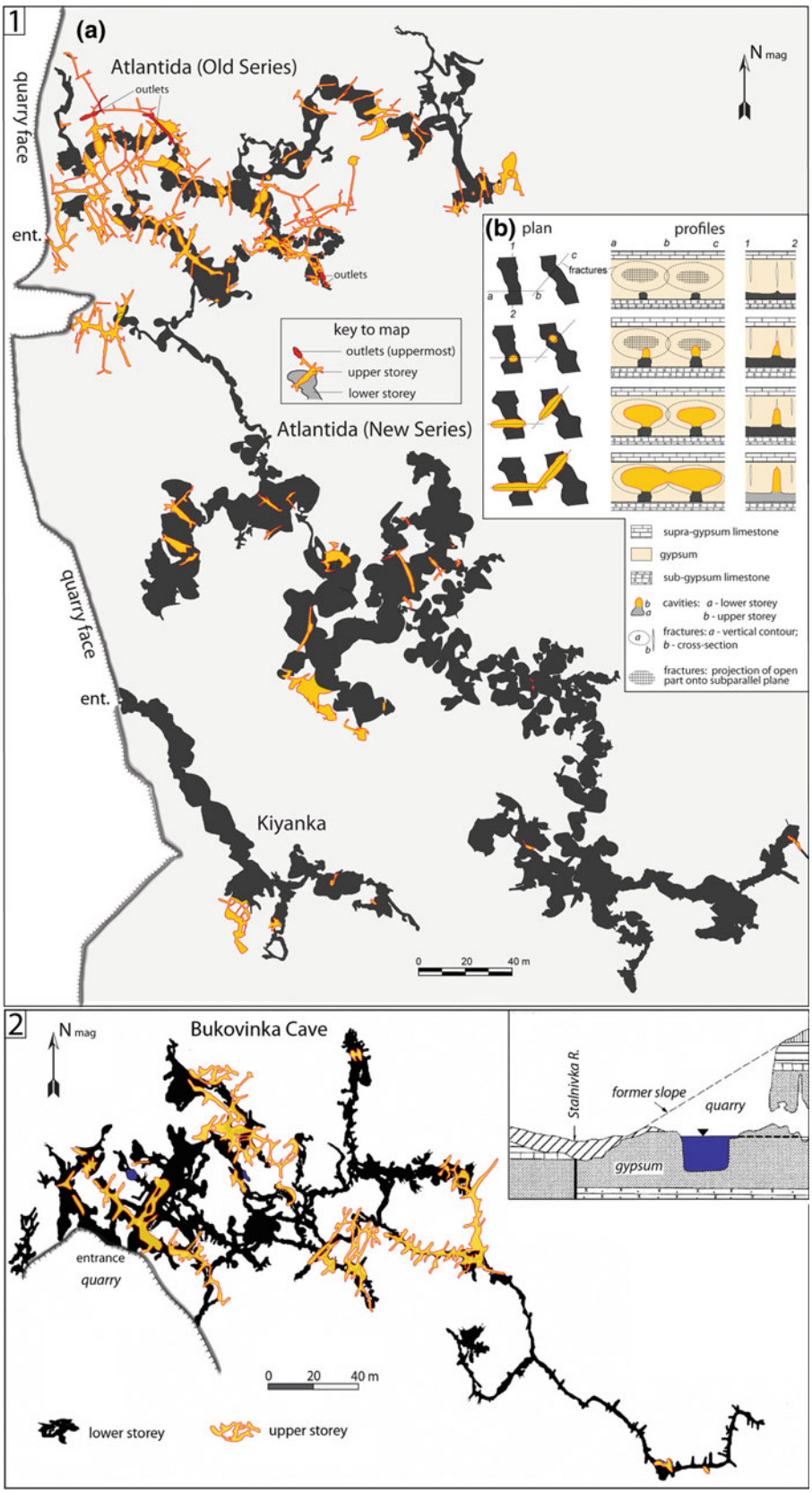

Fig. 9 Variations in patterns of maze caves. *1* Atlantida and Kiyanka Caves (**a** plan, **b** *inset* showing a conceptual model of speleogenesis). *2* Bukovinka Cave (map by speleological club "Troglodit"). The map in **a** is simplified from a map provided by S. Kriven (speleological club "Kristal") and P. Kuprich (speleological club "Troglodit"); *inset* modified from Klimchouk and Rogozhnikov (1982)

A similar three-story vertical pattern is exemplified by Mushkarova Yama (Fig. 8b). Most of the maze occurs in the middle story. The plan pattern differs between the eastern and western parts of the cave. In the west, a joint-controlled network with well-individualized passages and isolated scattered lower-story conduits (feeders) dominates, whereas in the east, passages of the original network are enlarged so that they laterally merged into a vast space with pillars. Only a few feeders are documented in this part because they are obscured due to a high level of sediments arriving through an adjacent sinkhole. A NE–SW-trending chain of separate upper-story passages stretches between the western and eastern parts of the maze, indicating a discharge zone. The western and the eastern maze clusters are highly individualized, connected only in one point. The morphological difference between them is determined by variations in hydrodynamic conditions. Both clusters discharged via the same zone, but the eastern cluster received more prolific recharge from the lower aquifer due to its enhanced hydraulic conductivity in this area.

Fracture networks, and hence passage networks in the lower and middle stories commonly have rectilinear systematic patterns, with two dominating sets (Figs. 5d–f and 8a). A somewhat special case is exemplified by Dzhurinska Cave, where larger master passages in the middle story fan out to the north through northeast (Fig. 8c). They are fragmented by collapse bodies at each end and connect via feeding sub-systems of lower conduits arranged in two sub-stories. The cave pattern, consisting of subordinated elements, is clearly organized to collect recharge from below to the master passages (see profile in inset in Fig. 8c). No outlet (discharge) features are documented in the cave, likely because they triggered collapses and were utilized by breakdown piles that now block master passages.

Another specific case is represented by Atlantida and Bukovinka Caves (Fig. 9). The gypsum in these areas has two units in the cross section, so the caves have two stories. The master story is the laterally extensive lower one, formed by large passages or chains of connected chambers. The plan pattern of this story is spongework, with some linear elements. Cavities of this story occur at the contact with the lower aquifer, carve upward 2–6 m into the gypsum and have numerous convection cupolas in the ceiling. Where high cupolas intercept fractures of the upper level, the latter facilitate further upward propagation of buoyancy dissolution, with the formation of strongly elongated passage-like cavities at the top (see inset in Fig. 9). In places where fracture networks in the upper unit are laterally continuous, such upper-story passages originating from adjacent master cavities may connect laterally, forming a maze. In the Old Series of Atlantida, there are three separate maze clusters in the upper story, besides numerous isolated passages. It should be noticed that most of the cavities in the upper story remain blind also upward, i.e., their ceilings do not open to the bottom of the upper aquifer. Only two passages in the northwestern part of the cave open to the upper aquifer, providing hydraulic outlets from the system.

The case of Atlantida Cave attests an important role of natural convection in speleogenesis in deep-seated settings, particularly in evaporites. Here not only the lower-story cavities at the base of the gypsum, but also high cupolas and most of the upper-story passages developed by buoyant dissolution in freshwater rising from the lower aquifer, with return of dissolved sulfates to the same aquifer and their removal with the regional flow. Most of the cave was formed without forced transverse flow across the gypsum, which established only in the late stages of artesian development. The same mechanism was shown earlier to be responsible for the formation of numerous giant Schlotten-type caves in the Zechstein (the Upper Permian) gypsum in the South Harz region of Germany at depths up to 400 m (Kempe 1996).

5.4 Meso-Morphology of Caves

Sizes and cross-sectional shapes of passages vary considerably between the caves, cave regions and cave stories. The volume-to-length ratio (calculated by dividing total volume by total length, m^3/m) represents the average cross-sectional area of cave passages. It varies between 1.7 and 8.5 m^2, which gives an idea of the range of typical passage sizes. Sizes and morphology of passages tend to be similar within the same story in the same cave region, although some more voluminous passages may occur on the background of the uniform network (Fig. 8a-2). They stand out due to locally enhanced recharge from below, or because they were in favorable positions to conduct more vigorous flow between recharge and discharge points in a given cluster.

Typical passage shapes are shown in Fig. 10. Slot-like and rift-like passages (photographs a–d) are the most common, particularly for networks in the middle and upper stories. These basic shapes are usually modified in two ways:

1 during the confined stage, more aggressive water rises from feeders and flows laterally in the uppermost available space of rift-like conduits, developing a tubular "swell" there (photographs c and d);
2 during the water table stage, the density stratification causes the aggressive freshwater to occupy the uppermost 5–10 cm layer of the water body in inundated conduits (Klimchouk and Aksem 2005), which leads to the formation of laterally extensive horizontal notches in the walls (photographs f, g, h and j in Fig. 10; Fig. 11a). The decrease in the aggressiveness in downward

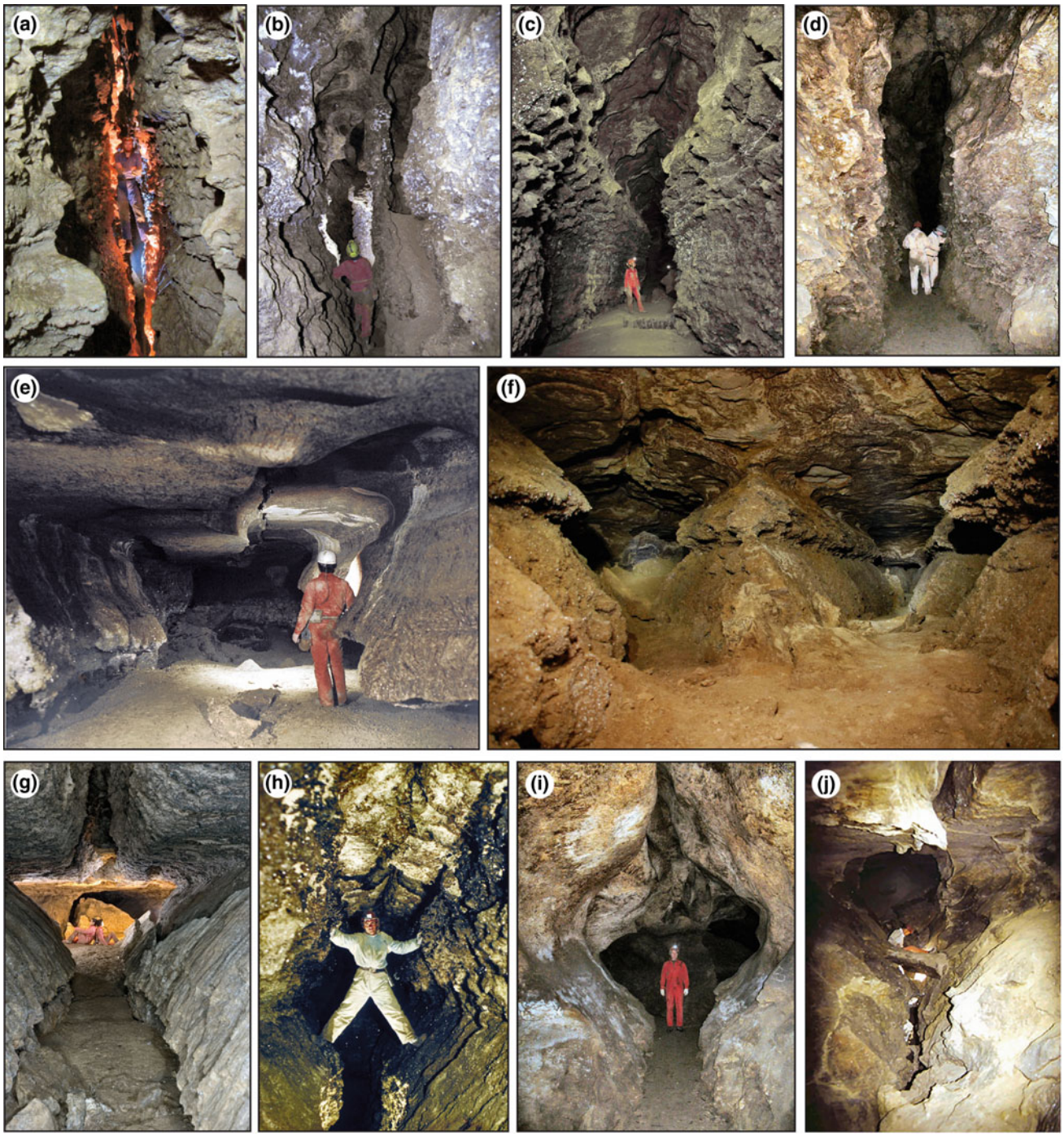

Fig. 10 Common morphotypes of passages in the gypsum mazes: **a**, **c** and **j** Mlynki Cave; **b** Slavka Cave; **d** and **i** Jubilejna Cave; **e** Dzhurinska Cave; **f**, **g** and **h** Ozerna Cave. Photograph **a** by E. Naumenko, **c** by Yu. Zarembovsky, **f** by V. Apostolyuk; other photographs by A. Klimchouk

convection currents causes the formation of inclined facets in the passage cross section.

The resultant cross sections usually have the widened parts at the top, and canyon-like (fissure-like) parts in the middle and lower parts. The latter are commonly filled with sediments (photographs e, g and i in Fig. 10) but remain open in some cave regions (photographs h and j).

The large gypsum caves in Western Ukraine abundantly demonstrate morphological features indicating a confined hydrogeological environment with sluggish dynamics and generally ascending flow pattern. Such features occur in

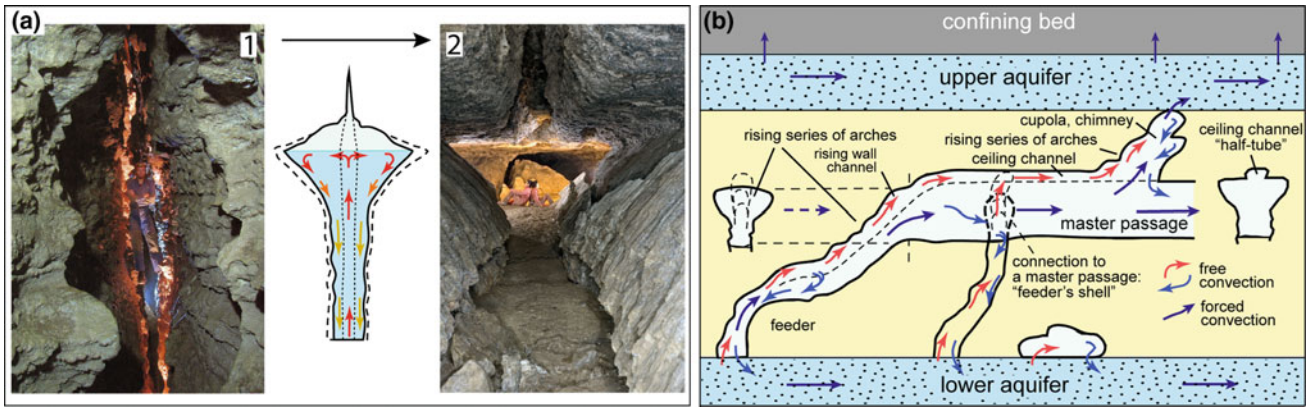

Fig. 11 Meso-morphology features in the gypsum caves: **a** transformation of a basic rift-type passage *1* into a passage with horizontal notches and inclined facets *2* in the water table conditions; **b** conceptual representation of the morphologic suite of rising flow (MSRF). The cartoon was originally developed to illustrate typical meso-morphology features, the role of natural convection in their formation and the relationships of different cave stories in gypsum maze caves in Western Ukraine (Klimchouk 1997b). It was subsequently generalized to conceptually represent the morphologic suite of rising flow (MSRF; Klimchouk 2007)

spatially and functionally related groups (Fig. 11b) where ascending flow currents, including buoyant convection components, can be unambiguously recognized from solutional sculptures. These features include (in order of their involvement in transmitting rising flow):

- rising inlet conduits in the lower story and their characteristic orifices at points where they connect to passages of the next upper story (feeders; Fig. 12h–k);
- transitional wall and ceiling forms (rising wall channels and ceiling channels; Fig. 12e–g);
- spherical ceiling pockets (cupolas) and rising chimneys that broke through to the upper aquifer (outlets; Fig. 12 a–d).

This set of functionally related meso-forms was documented in its integrity for the first time in the caves of Western Ukraine (Klimchouk 1997a, b, 2000b). It reflects the "per ascensum" mode of the cave-forming flow in a soluble formation, and thus is generic for hypogene caves. It has been later generalized as the "morphologic suite of rising flow" (MSRF; Klimchouk 2007, 2009), which diagnostic efficiency for identification of the hypogene origin of caves has been subsequently confirmed in numerous publications by different authors, for many different regions and settings.

Other common features of meso-morphology are thin partitions between adjacent passages (an example is shown in Fig. 10b) that often have sharp-edged through windows. Also common are rock pendants, left in between adjacent ceiling channels cut by floating freshwater currents. Partitions indicate sluggish rising flow in independently recharged closely spaced cavities, and the formation of rock pendants illustrates upward-pointed dissolution by buoyant convection (Klimchouk 2007, 2009).

A characteristic feature of plan patterns of the maze caves in the region (and hypogene maze caves in general) is the presence of numerous blind terminations of passages (dead ends) and deep alcoves in passage walls. These features are difficult to explain when lateral cave-forming flow is implied, but they are perfectly natural for hypogene speleogenesis. Passage terminations are not "blind" in terms of rising transverse flow, but are points where feeders connect to a given cave story. Although the presence of feeders at "dead ends" is often obscured by sediments, many of them are clean of any fill, unambiguously proving this functioning (Fig. 12h, j, k).

5.5 Cave Sediments

Clays and silts are by far the predominant sediments in the maze caves in the region, filling passages to a variable extent. The greatest thickness of the fill is observed in master stories. Two types of facies can be distinguished (Fig. 13): 1—phreatic/impounding facies and 2—fluvial deltaic facies.

Sediments of the phreatic/impounding facies are the most abundant. They commonly have a few meters in thickness in master passages, up to 5–7 m as documented in the deepest sampling trenches. Typical sequences comprise rather monotonous fine (80–99% of particles < 0.01 mm) laminated clay in the lower and middle parts, grading upward into more silty material with distinct layers of silt. In the upper part, lamination is disturbed in some intervals, or the structure becomes lumpy, and cm-thick powdery layers of Fe–Mn hydroxides occur, indicating repeated events of desiccation and flooding, and transitions from reducing to oxidizing conditions. In Zoloushka Cave, where a rapid dewatering caused by groundwater abstraction during the

Fig. 12 Meso-morphology features in the gypsum caves (in order of their involvement in transmitting rising flow; *bottom* to *top*): **h**–**k** feeders, sometimes with alcoves in hanging walls; **e**–**g** rising wall channels and ceiling channels; **a**–**d** outlets (rising chimneys and broken cupolas). Functional relationships between these forms are shown in Fig. 11b. Photographs **a**, **b** and **h** Ozerna Cave; **c** and **e** Atlantida Cave; **d** and **k** Zoloushka Cave; **g** Jubilejna Cave; **i** and **j** Optymistychna Cave. Photographs **a** and **b** by V. Apostolyuk; other photographs by A. Klimchouk

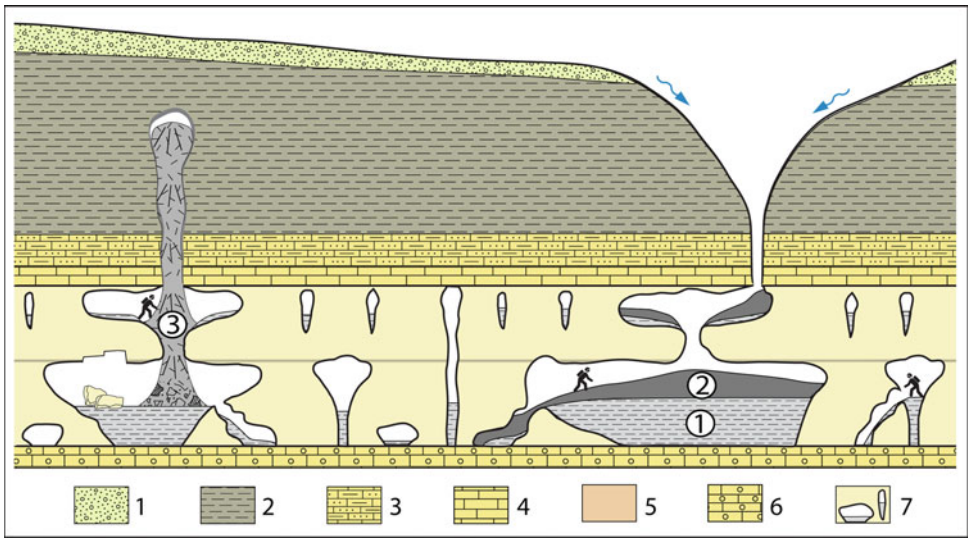

Fig. 13 Distribution of principal types of clastic sediments in the maze caves (*number in circles*): *1* phreatic/impounding facies; *2* fluvial deltaic facies; *3* breakdown deposits. Legend: *1* ancient terrace sediments (Plio-Pleistocene); *2* caprock clays; *3* argillaceous limestone; *4* bioepigenetic limestone (Ratynsky); *5* gypsum; *6* biohermal limestone; *7* cavities

past 60 years gave rise to a number of transitional geochemical processes with microbial involvement, massive deposition of Fe–Mn compounds in the form of powdery layers at the top of the clay fill (up to 50 cm thick), coatings, stalactites and stalagmites has occurred (Andreychouk and Klimchouk 2001; Andreychouk et al. 2009; Andreychouk and Klimchouk Chap. 24). The content of montmorillonite in the cave clays (60–73%) is 15–25% greater than in the source clay formation, indicating that re-sedimentation was accompanied with montmorillonitization, which points to reducing conditions. The composition of heavy minerals in the cave clays largely correspond to that of the overlying clays.

The phreatic/impounding facies accumulated during the late phase of confined stage and the transition to the water table stage, in sluggish hydrodynamics environment, by re-distribution in suspension of the material of the overlying clays introduced with early collapses (Klimchouk 1984). Importantly, the distribution of these sediments strongly corroborates that the caves have received recharge from the underlying aquifer. A peculiar feature of the distribution is that cavities at the lower story, including most of the feeders, remain empty, completely or largely devoid of the clay fill, whereas adjacent master passages have thick successions with much higher levels of the fill. This is because upwelling recharge from the underlying aquifer, which operated during the confined stage and continued through the water table stage, prevented sedimentation in feeders and lower-story clusters, whereas sediments have accumulated mainly in master passages where flow was more sluggish. In case of the overall descending cave-forming flow, the lowermost cavities would be the first to be filled with sediments.

The fluvial deltaic facies (2 in Fig. 13) are represented by sediment complexes forming where swallowed surface streams enter a sub-horizontal maze cave and eventually a body of groundwater. Entering the relict maze, streams stay focused only for a few tens of meters from a swallow hole even at the high flow, and then dissipate and infiltrate to the lower aquifer. The carried load of different materials, which may include eroded sands and gravels from the ancient alluvial terraces on the plateaus, clays from the capping formation, and various clasts from the Upper Badenian beds, is sorted and deposited in the vicinity of a swallow hole as a fining outward facies. The underground deltaic complexes overlie the phreatic/impounding facies and never occur in the lower and middle parts of the latter. This further confirms the absence of mass flux from the surface during most of the cave history.

Breakdown masses are the third common type of clastic sediments. They can be represented by fallen blocks of gypsum, collapsed gypsum-carbonate rhythmite bodies (when the latter are intercepted by passages from below), and breakdowns that penetrate into the overburden. In the cave space, they form breakdown cones comprised at the base of blocks of the Ratynsky limestone and the Upper Badenian argillo-carbonaceous and sandstone rocks, whereas the main breakdown columns consist of displaced overlying clays (3 in Fig. 13). According to the detailed survey of breakdowns in several caves (Klimchouk and Andreychouk 2002), extrapolated density of collapse bodies varies from a few hundred to over 5000 features per km^2 in different cave regions.

5.6 Functional Organization of Cave Systems

Structure and meso-morphology of the large gypsum maze caves in the region clearly demonstrate functional organization that evolved in response to ascending hydraulic communication between the aquifers in the MAS across the

gypsum (Figs. 4 and 7c). Reflecting the pattern of ascending transverse flow in the given framework of preferential permeability elements (e.g., fractures), the cave systems are comprised of a number of relatively independent compartments (passage clusters, or cave regions; Fig. 5d, f), which include more tightly integrated numerous individual cells—conduits and channelized meso-forms that evolved to connect individual input points at the bottom of the gypsum (feeders) with output points at the top of the bed (outlets) (Fig. 11). The number of outputs is much less than the number of inputs; hence, lateral transmission occurs using those multi-story fracture networks which are well connected laterally. In this way, the master story stands out in the cave system, providing integration of numerous cells within the compartment. Lateral integration of passage clusters occurs due to hydrodynamic interaction between the flow compartments in the course of speleogenetic evolution and change of boundary conditions.

6 The Role of Speleogenesis in the Formation of Sulfur Deposits

The fore-Carpathian region is a sulfur-bearing basin, one of the largest in Eurasia, where native sulfur deposits are spatially and genetically related to the Miocene gypsum (Aleksenko 1967; Polkunov 1990; Fig. 1). Most of large deposits and occurrences of sulfur are found along the boundary with the foredeep, mainly in the northwestern portion of the gypsum belt, within the Zone IV dominated by confined hydrogeological conditions in the MAS. Sulfur mineralization is associated with the Ratynsky bioepigenetic limestone (Mamchur 1972; Lein et al. 1977) that overlies, and locally entirely replaces, the gypsum.

It is well established that sulfur deposits in the region are of the bioepigenetic origin, i.e., the result of anaerobic microbially mediated reduction of gypsum to H_2S in hydrocarbon-bearing groundwaters rising from the lower aquifer (with the formation of the replacement calcite as a by-product), and concomitant and subsequent oxidation of the H_2S. However, a region-specific genetic model for the formation of the sulfur deposits was a matter of controversies for a long time. Problems and discrepancies were mainly caused by attempts to fit the above-mentioned generic model of the bioepigenetic origin of the native sulfur to inadequate notions of groundwater circulation in the MAS which dominated at the time, lacking in understanding of the origin and role of karst. The gypsum bed was commonly considered as an aquiclude separating the lower and upper aquifers in the MAS and preventing water exchange between them, hindering the interpretation of mechanisms of sulfur formation. The communication between the aquifers was thought to occur only through faults and stratigraphic windows where the gypsum is absent. Though the presence of karst cavities in the gypsum was documented and recognized, their origin, patterns and hydrogeological functioning were not understood.

An application of the model of artesian transverse speleogenesis has allowed resolving major controversies about the MAS hydrogeology in the confined zone and developing a new model for the origin of the sulfur deposits in the region (Klimchouk 1997a). This type of speleogenesis has played a fundamental role in the latter by creating extensive clusters of high vertical permeability in the gypsum, providing large quantities of dissolved sulfates for reduction and by creating the necessary pattern of migration of reactants and reaction products in the MAS. Aerobic conditions in the lower aquifer favored microbially mediated transformation of hydrocarbons to simple organic compounds that could be readily utilized by sulfate-reducing bacteria. Waters from the lower aquifer ascended through the gypsum, forming areally pervasive, although clustered, void–conduit systems, as described in the preceding sections. Intense sulfate reduction took place in the upper part of the gypsum under anaerobic conditions to form bioepigenetic calcite (the Ratynsky limestone) at the top, which became a part of the upper aquifer. In the upper aquifer, the ascending H_2S oxidized by moderate lateral inflow of O_2-bearing waters. During the mature stage of speleogenesis, oxygenated water was also supplied vertically from below in places where upwelling plumes of water from the lower aquifer established through the well-developed cave systems ("punctures" of oxygenated waters through an otherwise reducing media). Regional paleohydrogeological analysis suggests that the most favorable conditions for sulfur ore formation were from the Early to Middle Pleistocene, although in some areas the process is operative even today.

The above-mentioned inadequate notions of the "impermeability" and the separating role of the gypsum in the MAS caused severe mistakes in planning large open-pit mining operations for sulfur. It was assumed that after opening quarries to the level of the sulfur-bearing limestones major groundwater inflow would be a function only of the specific storage in the upper aquifer (Tsjurupa 1960). However, during the quarry development, considerable and progressively increasing inflow occurred from the lower aquifer across the gypsum, which necessitated much greater groundwater withdrawal than predicted and made it difficult to achieve the projected level of lowering. To maintain the operation, groundwaters were pumped out with rates reaching 3.3 m^3/s in individual quarries. This caused the formation of wide drawdown cones in the piezometric surface around the quarries (up to 10–12 km in diameter), the reversal of the circulation pattern in the MAS, dramatic increase in groundwater flow velocities, aggressiveness and gypsum solution rates (Klimchouk and Aksem 2005), and

eventually massive occurrence of collapses in the vicinity of quarries. Most of quarries were halted during the 1990s due to unacceptable environmental damage.

7 Breakdown and Sinkhole Formation

The accessibility of numerous laterally extensive maze cave systems in the region provided an excellent opportunity for direct mapping of breakdown structures on the level of their origin to examine morphogenetic and geological controls of their initiation and reveal mechanisms of their development (Andreychouk 1999; Klimchouk and Andreychouk 2002). It was found that, contrary to common views, distribution of breakdown structures propagating into the overburden does not appreciably correlate with the size of passages and rooms. Breakdowns are initiated mainly at specific speleogenetically or geologically "weakened" localities, which classify into a few distinct types. Most of them originate at the outlet cupolas/chimneys that opened to the bottom of the overlying limestone bed. By virtue of their hydrogeological function in the hypogene transverse system (discharge), these features exploited the points of compromised integrity in the main bridging unit of the upper aquifer, or in the entire overburden. Most of breakdowns have originated during transition from confined to unconfined stages, due to the loss of buoyant support. The breakdown development (upward stoping) proceeds in several stages. Several distinct mechanisms of breakdown development were revealed, depending on the structure and hydrogeological conditions in the overburden. The ability of a breakdown structure to reach the surface and form a collapse/subsidence sinkhole depends on: (1) cross-size of an outlet feature at the contact between the gypsum and Ratynsky bed, and the receptacle capacity (size) of a master cavity beneath, (2) the coefficient of loosening (bulking) of the overburden material, (3) the thickness of the overburden and (4) involvement of the processes of hydrodynamic destruction (Klimchouk and Andreychouk 2002).

8 Summary

The gypsum karst in Western Ukraine is a model example of evolution of intrastratal karst and of artesian transverse speleogenesis in this lithology. Regional geomorphological development in response to differential neotectonic movements caused respective evolution of hydrogeological conditions and differentiation of zones with distinct evolutionary types of karst. The succession of intrastratal karst types in the region (from deep-seated, through subjacent, to entrenched) provides an excellent illustration of the evolutionary typology of karst (Klimchouk 1996a; Klimchouk and Ford 2000) and allows examining evolution of karst systems and overprint of epigene speleogenesis over preformed hypogene artesian caves.

Speleogenesis in the region commenced in a regionally extensive confined aquifer system, in which the gypsum bed is sandwiched between two "normal" aquifers with diffused permeability. It developed due to ascending leakage across the gypsum induced by valleys incising into the upper confining sequence. Lithostratigraphic variations in the gypsum bed determined distinct fracture stratigraphy, with largely independent fracture networks in different units. Distinctions in fracture patterns and frequency in different units and variations of vertical connectivity of their fracture networks imposed strong control on transverse flow across the gypsum and hence on speleogenesis.

The large gypsum caves in Western Ukraine are generally stratiform multi-story mazes of passages developed along vertical and steeply inclined fractures. Cave patterns in plan and cross section are variable depending on fracture stratigraphy, patterns and connectivity, areal distribution of recharge (at the lower contact) and discharge (at the upper contact) points, and local hydrodynamic conditions and history. Patterns and meso-morphology of the caves clearly demonstrate functional organization that evolved in response to ascending hydraulic communication between the aquifers in the Miocene aquifer system, reflecting the complex pattern of transverse flow across the gypsum. The cave systems are comprised of a number of relatively independent compartments (passage clusters or cave regions), which include more tightly integrated numerous individual cells, conduits and channelized meso-forms that evolved to connect individual input points at the bottom of the gypsum (feeders) with output points at the top of the bed (outlets).

This study demonstrates that artesian transverse speleogenesis is of fundamental importance to groundwater circulation in the region-wide Miocene aquifer system. It has important implications for regional and site-specific hydrogeology, the origin of large bioepigenetic sulfur deposits, and assessment of collapse/subsidence hazard.

The outstanding typological significance of the large maze caves in the region is in part determined by singularities of gypsum dissolution. Since dissolution of gypsum is very sensitive to hydrodynamic and hydrochemical conditions, meso-morphology of the caves distinctly reflects groundwater circulation patterns and allows unambiguous interpretation. However, the style and principal characteristics of the large maze caves in the gypsum karst of Western Ukraine are not specific to dissolution of sulfate rocks but exemplify general regularities of artesian transverse speleogenesis that are applicable to other lithologies including carbonates.

Acknowledgements The authors are indebted to cavers from many speleological clubs of Ukraine for their support of our field studies through many years. We thank speleological clubs "Kristal" (Chortkiv), "Podillia" (Ternopil) and "Troglodit" (Chernivtsy), and particularly B. Maksimov, S. Kriven, and P. Kuprich for cave maps they provided. E. Naumenko, Yu. Zarembovsky, and V. Apostolyuk are thanked for providing some photographs.

References

Aleksenko II (1967) Sulphur of the pre-Carpathian. Nedra, Moscow (in Russian)

Andreychouk VN (1988) The tectonic factor and peculiarities of the sulfate karst of Bukovina: geology, geomorphology and hydrogeology of karst. Institute of Geology and Geochemistry, Sverdlovsk (in Russian)

Andreychouk VN (1999) Collapses above gypsum labyrinthic caves and stability assessment of karstified terraines. Prut, Chernivtsy (in Russian)

Andreychouk VN (2007) Zoloushka Cave. Silesian University and Ukrainian Institute of Speleology and Karstology, Sosnowiec-Simferopol (in Russian)

Andreychouk VN, Klimchouk AB (2001) Geomicrobiology and redox geochemistry of the karstified Miocene gypsum aquifer, Western Ukraine: the study from Zoloushka Cave. Geomicrobiol J 18:275–295

Andreychouk VN, Klimchouk AB, Boston P, Galuskin EI (2009) Unique iron-manganese colonies of microorganisms in Zoloushka Cave (Ukraine-Moldova). In: Speleology and Karstology 3:5–25. Available at: http://scholarcommons.usf.edu/ijs/vol34/iss1/4 (in Russian)

Babel M, Bogucki A (2007). The Badenian evaporite basin of the northern Carpathian Foredeep as a model of a meromictic selenite basin. In: Schreiber B, Lugli S, Babel M (eds) Evaporites through space and time. Geological Society, Special Publications, London 285, pp 219–246

Bella P, Bosák P (2012) Speleogenesis along deep regional faults by ascending waters: case studies from Slovakia and Czech Republic. Acta carsologica 41(2–3):169–192

Birk S (2002) Characterisation of karst systems by simulating aquifer genesis and spring responses: model development and application to gypsum karst. Tübingen Geowissenschaftliche Arbeiten, Reine

Dreybrodt W, Gabrovsek F, Romanov D (2005) Processes of speleogenesis: a modeling approach. Karst Research Institute at ZRC SAZU, Ljubljana

Dublyansky VN (1966) Karst caves of the Middle Dniester region. In: Voprosy izucheniya karsta Russkoy Rabniny. MOIP, Moscow, pp 99–109 (in Russian)

Dublyansky VN, Lomaev AA (1980) Karst caves of Ukraine. Naukova dumka, Kiev (in Russian)

Dublyansky VN, Smol'nikov BN (1969) Karstological and geophysical investigations of karst cavities of the Pridnestrovskaya Podoliya I Pokutye. Naukova dumka, Kiev (in Russian)

Ford (1971) Geologic structure and a new explanation of limestone cavern genesis. Trans Cave Res Group Great Br 13(2):81–94

Ford D, Ewers R (1978) The development of limestone cave systems in the dimensions of length and depth. Can J Earth Sci 15(11):1783–1798

Ford D, Williams PW (1989) Karst geomorphology and hydrology. Unwin Hyman, London

Jakucs L, Mezosi G (1976) Genetic problems of the huge gypsum caves of the Ukraine. Acta Geographica XXVI:15–38

Jakucs L, Mezosi G (1991) Podoliai gypszbarlangok genetikajarol. Karst es Barlang (I–II):45–52

Kempe S (1996) Gypsum karst of Germany. In: Klimchouk A, Lowe D, Cooper A, Sauro U (eds) Gypsum karst of the world. Int J Speleology 25(3–4):209–224

Klimchouk AB (1984) Detailed study of water-mechanical sediments of a large cave system. In: Peschery (Caves), Permskiy Universitet, Perm, pp 70–88 (in Russian)

Klimchouk AB (1990) The artesian genesis of the large maze caves in the Miocene gypsum of Western Ukraine. Doklady Akademii Nauk Ukrainskoj SSR ser. B (Kiev) 7:28–32 (in Russian)

Klimchouk AB (1992) Large Gypsum Caves in the Western Ukraine and their genesis. Cave Sci 19(1):3–11

Klimchouk AB (1996a) The typology of gypsum karst according to its geological and geomorphological evolution. In: Klimchouk A, Lowe D, Cooper A, Sauro U (eds) Gypsum karst of the world. Int J Speleology 25(3–4):49–60

Klimchouk AB (1996b) Gypsum karst in the western Ukraine. In: Klimchouk A, Lowe D, Cooper A, Sauro U (eds) Gypsum karst of the world. Int J Speleology 25(3–4):263–278

Klimchouk AB (1997a) The role of karst in the genesis of sulphur deposits, Pre-Carpathian region, Ukraine. Environ Geol 31(1/2):1–20

Klimchouk AB (1997b) Speleogenetic effects of water density differences. In: Proceedings of the 12th International Congress of Speleology, vol 1, La Chaux-de-Fonds, Switzerland

Klimchouk AB (2000a) Speleogenesis under deep-seated and confined settings. In: Klimchouk AB, Ford DC, Palmer AN, Dreybrodt W (eds) Speleogenesis: evolution of karst aquifers. National Speleological Society, Huntsville, pp 244–260

Klimchouk AB (2000b) Speleogenesis of great gypsum mazes in the Western Ukraine. In: Klimchouk AB, Ford DC, Palmer AN, Dreybrodt W (eds) Speleogenesis: evolution of karst aquifers. National Speleological Society, Huntsville, pp 261–273

Klimchouk AB (2000c) Speleogenesis in gypsum. In: Klimchouk AB, Ford DC, Palmer AN, Dreybrodt W (eds) Speleogenesis: evolution of karst aquifers. National Speleological Society, Huntsville, pp 431–442

Klimchouk AB (2003) Conceptualisation of speleogenesis in multistory artesian systems: a model of transverse speleogenesis. Speleogenesis Evol Karst Aquifers 1(2). http://speleogenesis.info/journal/publication.php?id=4475. Accessed 15 Sept 2016

Klimchouk AB (2004) Gypsum caves and karst in the Western Ukraine: speleogenetic and typological significance. In: Gypsum karst areas in the world: their protection and tourist development. Istituto Italiano di Speleologia, Memoria XVI, s.II, pp 35–50

Klimchouk AB (2007) Hypogene Speleogenesis: hydrogeological and morphogenetic perspective. National Cave and Karst Research Institute, Carlsbad

Klimchouk AB (2012a) Gypsum Caves. In: Culver DC, White WB (eds) Encyclopedia of caves, 2nd edn. Elsevier, Academic Press, pp 364–373

Klimchouk AB (2012b) Speleogenesis, hypogenic. In: Culver DC, White WB (eds) Encyclopedia of caves, 2nd edn. Elsevier, Academic Press, Chennai, pp 748–765

Klimchouk AB (2012c) Ukraine Giant Gypsum Caves. In: Culver DC, White WB (eds) Encyclopedia of caves, 2nd edn. Elsevier, Academic Press, Chennai, pp 827–833

Klimchouk AB (2015) The karst paradigm: changes, trends and perspectives. Acta Carsologica 44(3):289–313

Klimchouk AB (2016) Types of hypogene speleogenesis. In: Chavez T, Reehling P (eds) Proceedings of deep karst: origins, resources, and management of hypogene karst, NCKRI Symposium 6, National Cave and Karst Research Institute, Carlsbad, New Mexico, 11–14 April 2016

Klimchouk AB, Aksem SD (2005) Hydrochemistry and solution rates in gypsum karst: case study from the Western Ukraine. Environ Geol 48:307–319

Klimchouk AB, Andreychouk VN (1988) Geologic and hydrogeologic conditions of development of large gypsum caves in the Western Ukraine and their genesis. In: Peshchery (Caves). Gypsum and anhydrite caves. Permskiy Universitet, Perm, pp 12–25 (in Russian)

Klimchouk AB, Andreychouk VN (2002) Karst breakdown mechanisms from observations in the gypsum caves of the Western Ukraine: implications for subsidence hazard assessment. Int J Speleology 31(1/4):55–88

Klimchouk AB, Ford DC (2000) Types of karst and evolution of hydrogeologic settings. In: Klimchouk AB, Ford DC, Palmer AN, Dreybrodt W (eds) Speleogenesis: evolution of karst aquifers. National Speleological Society, Huntsville, pp 45–53

Klimchouk AB, Rogozhnikov VY (1982) Conjugate analysis of the formation history of a large cave system (on example of Atlantida Cave). Institute of Geological Sciences of NASU, Kiev (in Russian)

Klimchouk AB, Andreychouk VN, Turchinov II (2009) The structural prerequisites of speleogenesis in gypsum in the Western Ukraine. Silesian University and Ukrainian Institute of Speleology and Karstology, Sosnowiec-Simferopol

Lein AJ, Ivanov MV, Rivkina EM, Bondar VA (1977) Differences in isotope composition of carbon of pelitomorphic and crystalline limestones of sulphur deposits in the Pre-Carpathians. Geokhimija 4:578–588 (in Russian)

Lukin VS (1966) About focusing of karst. In: Voprosy isucheniya karsta Russkoi ravniny. Moscow University, Moscow, pp 92–94 (in Russian)

Mamchur GP (1972) Peculiarities of carbon isotopes distribution in carbonates of exogenous sulphur deposits and the possibility of their application for practical purposes. In: Geokhimia i mineralogia sery. Nauka, Moscow, pp 240–252 (in Russian)

Oszczypko N, Krzywiec P, Popadyuk I, Peryt T (2006) Carpathian Foredeep Basin (Poland and Ukraine): its sedimentary, structural, and geodynamic evolution. In: Golonka J. Picha FJ (eds) The Carpathians and their foreland: geology and hydrocarbon resources. AAPG, Memoir 84, pp 293–350

Palmer AN (1975) The origin of maze caves. NSS Bull 37:57–76

Palmer AN (1991) Origin and morphology of limestone caves. Geol Soc Am Bull 103(1):1–21

Peryt TM (2001) Gypsum facies transitions in basin–marginal evaporites: middle Miocene (Badenian) of west Ukraine. Sedimentology 48:1103–1119

Pokalyuk VV, Prokhorenko VP, Grachev AP et al (2010) Integrated morphostructural leveling of horizontal multilevel cave in gypsums (Dnister Podillia region). In: Speleologiya I spelestologia: razvitie i vzaimodeystviye nauk. Naberezhnyye Chelny (Russia), pp 89–93 (in Russian)

Polkunov VF (1990) Mineral concentrations of native sulphur. In: Geotektonika Volyno-Podolii. Naukova dumka, Kiev, pp 229–232 (in Russian)

Rehrl C, Birk S, Klimchouk AB (2008) Conduit evolution in deep-seated settings: conceptual and numerical models based on field observations. Water Resour Res 44:W11425. doi:10.1029/2008WR006905

Shestopalov VM (1981) Natural resources of underground water of platform artesian basins of the Ukraine. Naukova Dumka, Kiev (in Russian)

Svynko IM (1979) Geomorphology and neotectonics. In: Gerenchuk K, I (ed) Nature of the Ternopil'sky region. Vyshcha Shkola, Lviv, pp 48–54 (in Ukrainian)

Tsjurupa PV (1960) Hydrogeological conditions of the Pre-Carpathian sulphur-bearing basin and of its major deposits. Trudy GIGHS 6:112–133 (in Russian)

Zimels YL (2008) Kristal'naya Cave. Ternopil'sky Speleo-Club "Podillia", Ternopil (in Ukrainian)

Zimels YL (2009) Ozernaya Cave. Aston, Ternopil (in Russian)

Zimels YL, Snigur VA (2012) Mlynki Cave, Ugryn Cave. Ternopil'sky Speleo-Club "Podillia", Ternopil (in Ukrainian)

Zoloushka Cave (Ukraine–Moldova)—A Prime Example of Hypogene Artesian Speleogenesis in Gypsum

24

Viacheslav Andreychouk and Alexander Klimchouk

Abstract

Zoloushka Cave, the third longest gypsum cave in the world (92 km) and the world's largest gypsum cave by volume (>0.7 million cubic meter), is an outstanding example of a large maze cave formed in a multi-story artesian aquifer system due to the upward leakage between the aquifers across a soluble unit. Although local settings and evolution caused some peculiar features in speleogenesis, as compared to other large maze caves in Western Ukraine, these singularities provide further insights on variants and mechanisms of both regional and general models of hypogene artesian speleogenesis. The cave is located in the area where the host aquifer system is generally confined until present, but in one of the more uplifted tectonic blocks where the gypsum was partially incised by the nearby valley of the Prut River during the Holocene and rapidly drained due to the quarry operations since 1946. The cave experienced considerable modifications and transformations in the course of the recent transition to unconfined conditions and subsequent artificial dewatering. The geomorphological breaching of the confined aquifer system in the cave area occurred in the Holocene, i.e., later than in the area where most other large maze caves in the region are located. A relatively stable position of the water table in the upper part of the gypsum during most of the Holocene caused pronounced widening of passages, which determined the anomalously large size of passages and high indices of areal karstification in some regions of the cave. The most intense development of conduits occurred in areas where the input of freshwater from the lower aquifer was more abundant. Quarry operation and accompanying groundwater withdrawal during the last 70 years caused drastic and rapid transformations in the cave environment.

Keywords

Hypogene speleogenesis • Artesian speleogenesis • Gypsum karst • Western Ukraine • Zoloushka Cave

V. Andreychouk
Pope John Paul II State School of Higher Education,
Biala Podlaska, Poland
e-mail: czeslaw.andrejczuk@gmail.com

A. Klimchouk (✉)
Institute of Geological Sciences, National Academy of Sciences
of Ukraine, 55-b Gonchara Str., 01054 Kiev, Ukraine
e-mail: klim@speleogenesis.info

© Springer International Publishing AG 2017

A. Klimchouk et al. (eds.), *Hypogene Karst Regions and Caves of the World*,
Cave and Karst Systems of the World, DOI 10.1007/978-3-319-53348-3_24

1 Introduction

Zoloushka Cave is the third longest gypsum cave in the world (92 km), after Optymistychna (250 km) and Ozerna (131.4 km) caves located in the same region, but it is the world's largest gypsum cave by volume (>0.7 million cubic meter). The cave has been explored since 1976 when few entrances were opened in the face of an active gypsum quarry. It has been thoroughly studied in various aspects and documented in numerous publications in Russian and Ukrainian languages (e.g., Andreychouk 1984, 1986, 1994, 1988, 1999, 2007; Andreychouk and Korzhik 1984), but only cursory described in the international literature in contexts of specific topics (Andreychouk and Klimchouk, 2001; Klimchouk and Andreychouk 2002).

Unlike most of other large maze caves in Western Ukraine, Zoloushka Cave is located in the area where the host Miocene aquifer system is generally confined until present, but in one of the more uplifted tectonic blocks where the gypsum was partially incised during the Holocene by the nearby valley of Prut River and further drained by the quarry since 1946. It is, therefore, an instructive example of a large cave system, which was unequivocally formed under confined conditions but has experienced considerable transformations due to recent transition to unconfined conditions in the Holocene and further artificial lowering of the water table during last 70 years. Being a strong case in support of the regional speleogenetic model for Western Ukraine (see Klimchouk and Andreychouk Chap. 23), the cave has some singularities of patterns, morphology and sediments, in comparison with other large maze caves of the region, determined by local geology, specific speleogenetic history of the cave, and the above-mentioned rapid transformations. This makes the case of Zoloushka Cave especially important for understanding speleogenesis in the region and further development of the general model of artesian transverse speleogenesis.

2 Location and Settings

An overview of regional settings for gypsum karst development in Western Ukraine is given in Klimchouk and Andreychouk (Chap. 23) so that this section is focused on local settings.

The cave is located in the very southeast of the Ukrainian sector of the gypsum belt, in the area of the junction of borders of three countries: Ukraine, Moldova and Romania (Fig. 1). The cave was opened by a gypsum quarry in 1946, although its exploration and mapping only started in 1977. A considerable part of the mapped cave was destroyed by mining since then. The maze extends from Moldova to Ukraine across the border, nearly reaching the southern outskirts of the Podvirne village. The documented cave is part of a larger karst system, which is evidenced by collapse and subsidence sinkholes in the surrounding area and cavities encountered by wells in Podvirne and Kriva villages. Since the 1990s, a mining front in the quarry has been advancing to the east, systematically opening cavities there.

2.1 Geology

The area to the southwest of the Dniester River is the zone of the junction of the East European Platform with the Carpathian Foredeep, where the sedimentary cover is broken into numerous tectonic blocks plunging in a stair-like manner toward the foredeep. Within each step, arrays of individual tectonic blocks are distinguished as macro-blocks, based on their relative uplift or subsidence with respect to adjacent structures (Andreychouk 1984, 1988). Individual tectonic blocks have the area of 10–50 km^2 and can be displaced up to 20 m relative to adjacent blocks in the macro-block, whereas an amplitude of displacement between macro-blocks can reach a few dozens of meters. Zoloushka Cave is located in the relatively uplifted Khotyn–Mamalyga macro-block, in which erosional incision during Holocene has reached or nearly reached the top of the gypsum (Fig. 2).

The geological section exposed in the Kryva quarry is shown in Fig. 3a. The Middle Badenian gypsum bed in the cave area is 23–25 m thick, resting on marls and sands of the Lower Badenian unit (2–4 m in thickness). The latter in turn overlies eroded Upper Cretaceous (Senomanian) limestones and sandstones (12–18 m in thickness).

The gypsum is overlain by up to 1.5-m-thick layer of the beige-gray Ratynsky limestone. It is represented by both marine evaporitic and bioepigenetic varieties, with the latter commonly comprising the lower part of the layer at the contact with the gypsum. Overlying the Ratynsky limestone is the Upper Badenian Kosivsky Formation. It is 5 to 60 m thick (depending on the local relief) and is comprised mainly of clays and argillaceous sediments. Clays consist of montmorillonite (up to 38%) and hydroillite (25–30%). The basal part of the Kosivsky Formation is lithologically variegated, with sandstone and limestone beds of the variable thickness, and is enriched in dispersed sulfates and iron–manganese concretions with cores composed of crumbly manganese oxides. The eroded surface of the Kosivsky Formation is overlain by the sandy–gravel Quaternary alluvium of the upper (III–IV) Prut terraces and loam sediments (Fig. 3b).

The gypsum in the quarry area is chemically quite pure (97.4% $CaSO_4x2H_2O$ in average), containing 1.04% of insoluble residue, but it is variable in structural and textural characteristics. The upper (7–8 m) part of the bed is the most

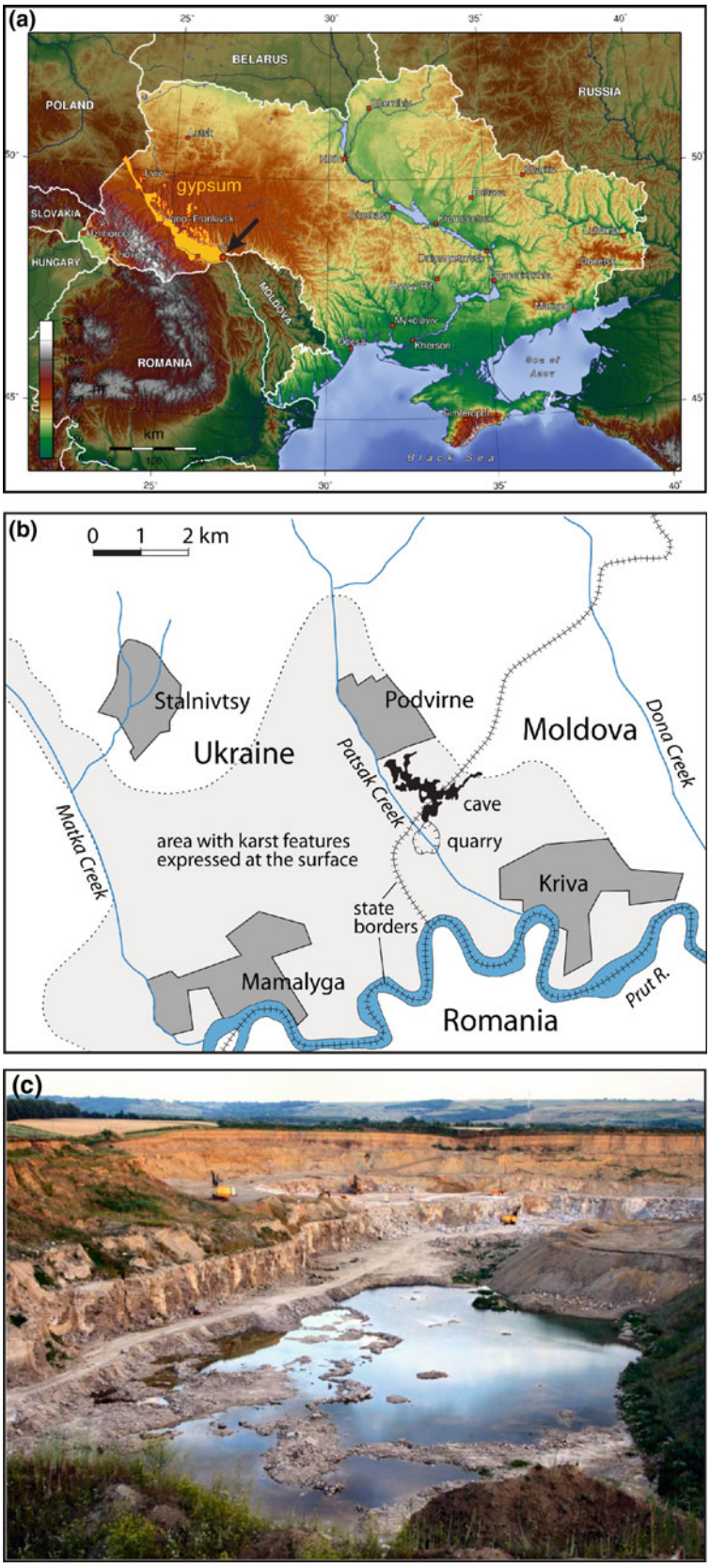

Fig. 1 Location of Zoloushka Cave (**a** and **b**) and a view of the quarry from north to south (**c**). The plateau in the far view is the territory of Romania behind the Prut River. Photograph by V.Andreychouk

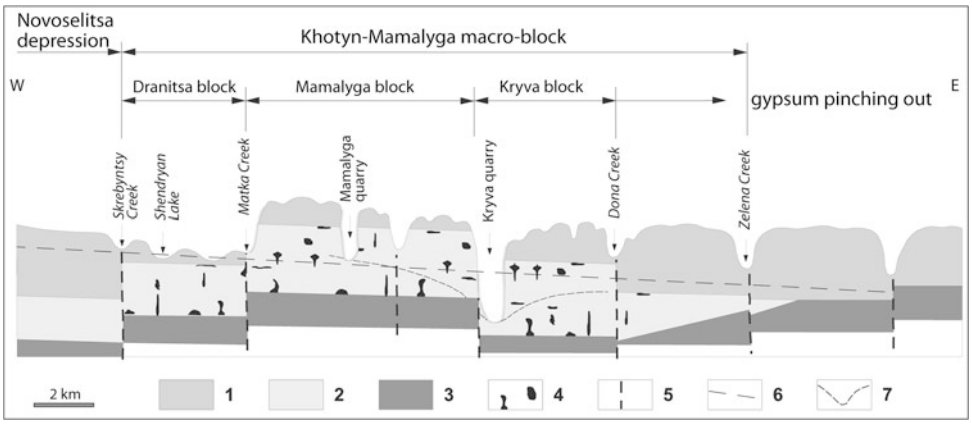

Fig. 2 Section across the southern part of the Khotyn–Mamalyga tectonic macro-block showing its internal block structure, the position of quarries, erosional valleys of Prut tributaries and of the base level of the Prut River (an inclined line across the section) (from Andreychouk 2007). Legend: *1* overburden (Upper Badenian), *2* the gypsum bed (Middle Badenian), *3* underlying rocks (Lower Badenian), *4* cavities, *5* faults, *6* base level of the Prut River, *7* drawdown cone in the piezometric surface of the Miocene aquifer due to pumping from the Kryva quarry

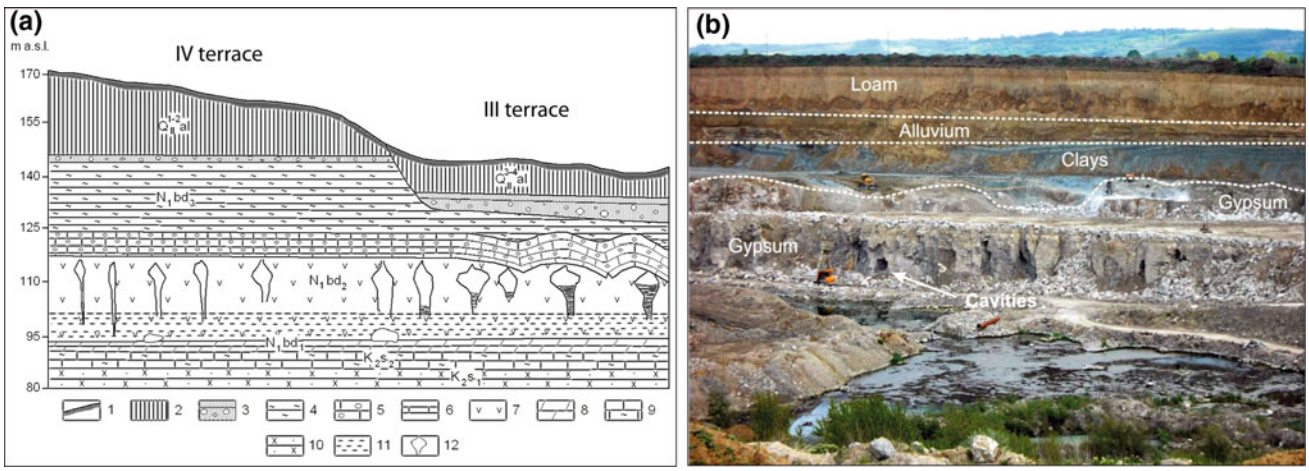

Fig. 3 Geological cross section along the lines 1–2 in Fig. 4 (**a**) and a view of the quarry showing numerous cavities opened by the quarry faces (**b**). Legend to **a**: *1* Holocene, dark-gray soil; *2–3* deposits of the third and fourth terraces of the Prut valley (*2* loess, *3* gravel); *4* silty clay; *5* limestone and sandstone; *6* Ratynsky limestone; *7* gypsum; *8* marl; *9* clayey limestone; *10* quartz–glauconite sandstone; *11* water-saturated part of the gypsum; *12* karst cavities. *Q* Pleistocene; N_1bd Badenian; K_2S_2 Senomanian. Photograph by V. Andreychouk

diverse, represented by a mosaic mix of medium- and large-crystalline varieties comprising patterned meso-structures. Sizes of large crystals vary from 1–2 to 8–10 cm, although larger crystals of selenite up to 1 m in cross-size occur. The middle part of the gypsum bed shows distinct layering formed by alternating medium-grained beige and fine-grained gray layers, 5–15 cm in thickness. Locally, limestone interbeds up to 1 m in thickness occur in this part. The lower part of the bed (starting from 13 to 14 m from the top) is comprised by fine- and cryptocrystalline light-gray gypsum with tiny layering, and massive dark-gray gypsum at the base.

Throughout the entire cross section, bodies of rhythmites occur of 0.3–1.0 m in cross-size, comprised of alternating gypsum, calcite and dolomite layers, with admixtures of celestite (up to 5–6%), clay minerals (smectite, illite and kaolinite; up to 5%) and quartz (up to 3%). These bodies are likely the syngenetic features, formed by sulfate–carbonate material filling holes and pockets at the periodically dried surface of an evaporite basin.

Characteristics of fractures and their networks in the gypsum, as well as their distribution across an area and the vertical section (fracture stratigraphy), have been shown to play an important role in determining the pattern of transverse flow across the bed and the pattern and morphology of maze caves in the region (Klimchouk and Rogozhnikov 1982; Klimchouk et al. 2009). These works demonstrated that fractures in the gypsum are of different ages and origins. Singularities of fracture distribution in the study area

determine many peculiar features of the pattern and morphology of Zoloushka Cave (Andreychouk 1984, 2007).

The earliest generation of fractures is represented by syngenetic fractures developed in the upper part of the gypsum where they form discontinuous polygonal networks with 3-beam nodes. These fractures formed due to contraction of the fresh sulfate sediment in a drying basin and were filled with carbonate material. When the host gypsum rock was dissolved out in the cave, these fills form characteristic thin partitions in passages. Fractures formed early during burial (diagenetic, or lithogenetic, fractures) constitute the next generation, also forming polygonal networks in the upper part of the gypsum. Diagenetic fractures remained open and thus were utilized by speleogenesis. Both these types of fractures were formed due to contraction and belong to the endokinetic group (i.e., formed in the course of petrogenetic processes by strains generated by the energy accumulated in a rock; Chernyshev 1983). Tectonic fractures are also heterochronous, evolved during the Late Miocene–Pleistocene in response to tectonic events in the adjacent Carpathian region. They partly utilized the contractional fractures of suitable orientations, reactivating (opening) them. Large vertical fractures that dissect the whole or most of the gypsum thickness form continuous systematic rectilinear networks with dominating orientations NE–SW and NW–SE and typical spacing at 5–8 m. The 3D array of open fractures of different origins, which existed and were available for transverse flow during the main phase of speleogenesis, determined most of the essential peculiarities of the Zoloushka Cave pattern and morphology (the other important factors being the mode of flow and the dissolution kinetics).

2.2 Geomorphology

The cave is located in the hilly Dniester–Prut interfluve massif, 1.5 km north of the Prut River. The cave area lies in the southern part of the Khotyn–Mamalyga uplift and the corresponding tectonic macro-block. The terraces of the Prut valley are quite distinct in the cave area. The fifth terrace with absolute elevations at 210–240 m was formed in the Early Pleistocene. The fourth (160–190 m) and third (130–140 m) terraces were formed during the Middle Pleistocene and the second (118–120 m) and first terraces—during the Late Pleistocene—beginning of the Holocene. The explored part of the cave lies beneath the fourth terrace (Figs. 3 and 4). To the west, the cave is bounded by the valley of Patsak Creek, the bottom of which corresponds to the second terrace.

Prut River in the cave area flows at elevations of 109–110 m, 8–9 m below the top of the gypsum within the floodplain and 13–14 m below the top of the bed in the quarry (123 m a.s.l.). The gypsum bed beneath the flood plain and the first terrace is heavily destroyed, remaining in residual blocks separated by clay masses. Sinkholes occur in clusters on the second terrace but are most abundant on the third terrace (up to 20–30 features per km). Some sinkholes occur along the slope of the fourth terrace, but they completely disappear further toward the interfluve with the increase in the caprock thickness.

2.3 Hydrogeology

The Miocene aquifer system (MAS; see Klimchouk and Andreychouk (Chap. 23) for regional characterization) is hydraulically connected with the underlying Upper Cretaceous rocks in the cave area. It was originally comprised of two confined aquifers separated by the gypsum bed—the upper aquifer in the Ratynsky limestone and the base of the Kosovsky Formation and the lower aquifer in the Lower Badenian and Upper Cretaceous (Senomanian) sandy–carbonate beds. When transverse speleogenesis in the gypsum commenced, these aquifers merged hydraulically. Geomorphologic data suggest that during the Pleistocene the bed of the Prut River was 50 to 2–3 m above the bottom of the clay sequence, which implies confined conditions in the MAS. Since the beginning of the Holocene, with the incision of the Prut valley into the upper aquifer and then below the gypsum top, the MAS became unconfined in the uplifted Mamalyga and Kryva blocks (Fig. 2), whereas outside of these blocks the Miocene–Senomanian aquifer system remained confined. The piezometric surface in the Mamalyga and Kryva blocks has been further depressed by pumping during the quarrying operation (Fig. 5).

Above the confining clays of the Kosovsky Formation lays the aquifer in the alluvial sediments of the upper Pleistocene terraces (III–IV), feeding many small springs in the valley slopes and leaking vertically downwards along breakdown chimneys at isolated points where the chimneys have intercepted this aquifer from below. The alluvium of the first and the second terraces also host aquifers. The groundwaters have low TDS contents (0.4–0.6 g/L) and HCO_3–Mg–Ca composition. The abundance of water in these aquifers decreases from the lower terraces to the upper ones.

Prior to the start of the quarrying operations (before 1946), the water table in the Badenian–Senomanian aquifer was positioned 2–3 m below the top of the gypsum, 1–2 m below the ceiling of the Zoloushka's upper story passages. Groundwater flow toward the Prut River occurred mainly via the fractured and porous sub-gypsum sequence. The lateral through-flow in the gypsum itself was slow because

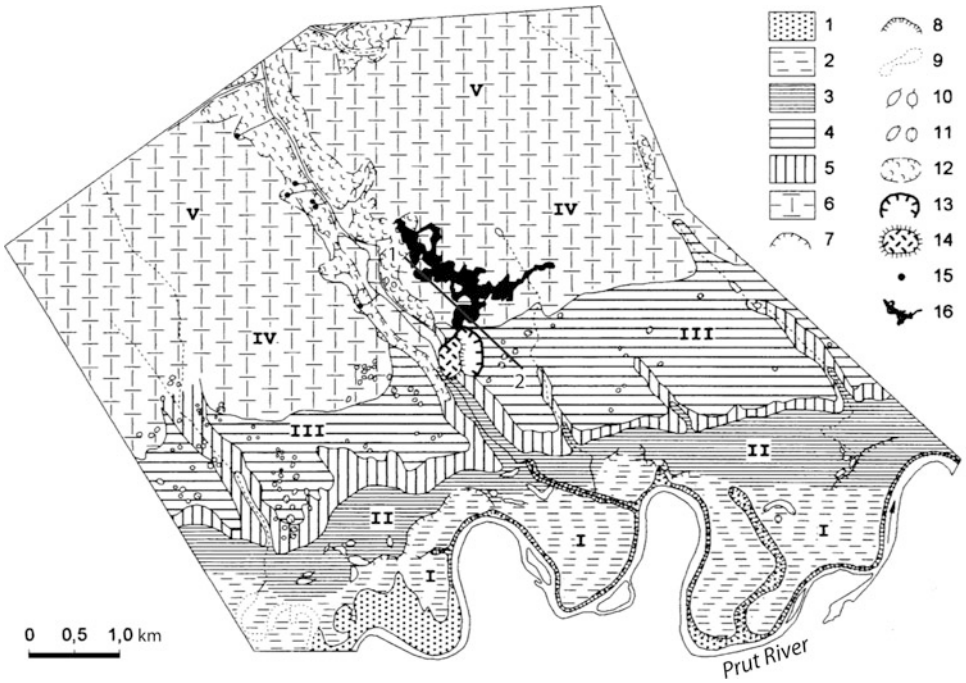

Fig. 4 Geomorphological map of the Zoloushka Cave area (Andreychouk 2007). Legend: *1* floodplain of Prut River; *2* first terrace; *3* second terrace; *4* third terrace; *5* slope of the third terrace; *6* fourth and fifth terraces; *7* slope of the second terrace; *8* slope of the first terrace; *9* oxbows; *10* residual hills on terrace surfaces; *11* karst sinkholes; *12* landslides; *13* the Kryva quarry; *14* dump; *15* springs; *16* Zoloushka Cave

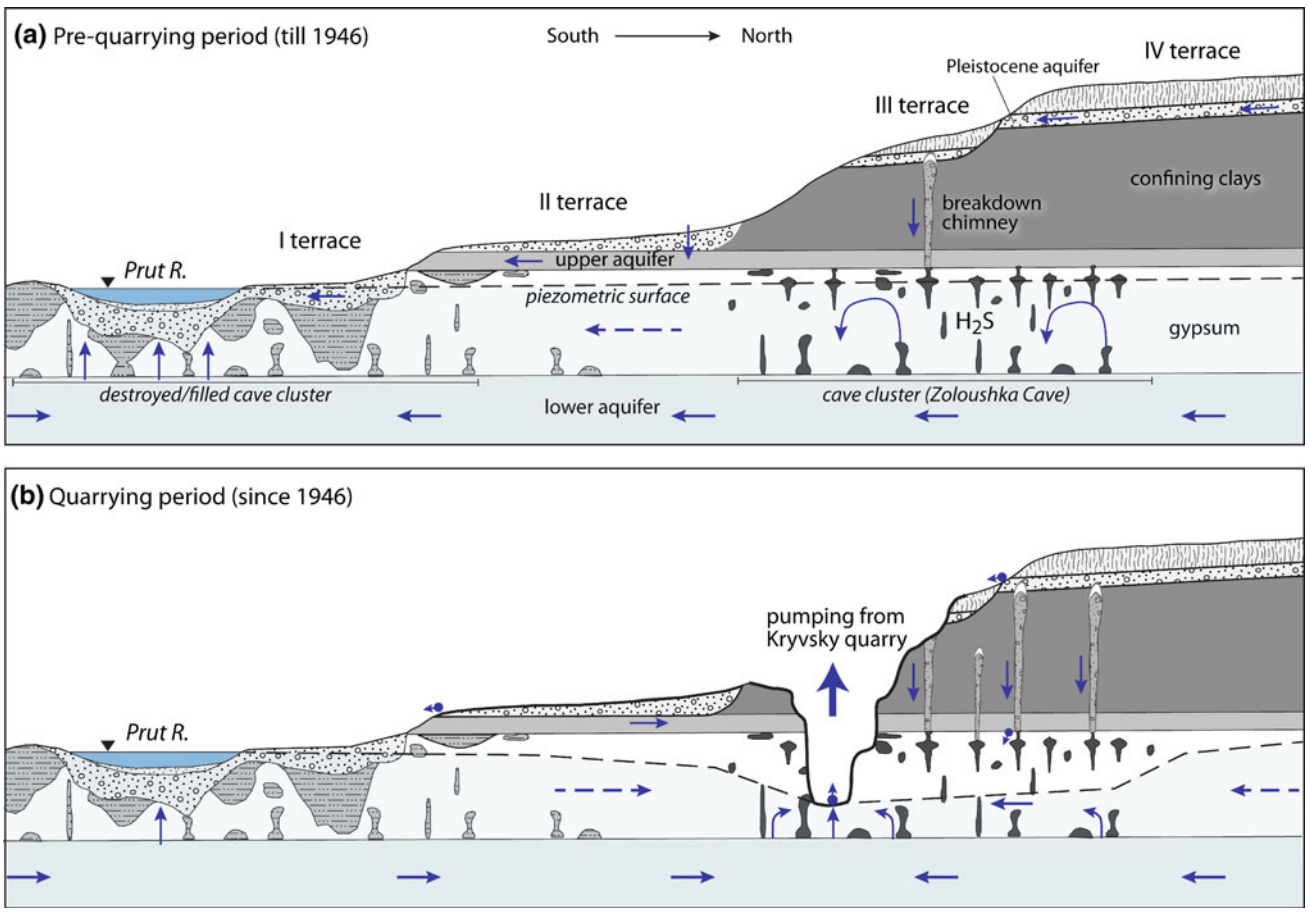

Fig. 5 Hydrogeological settings in the Zoloushka Cave area in the pre-quarrying period (**a**) and their changes due to quarrying (**b**). *Arrows* denote direction of groundwater flow, *dotted-line arrows* sluggish forced flow, *curved arrows* natural convection

Zoloushka Cave represented a separate conduit cluster, not connected to the river via conduits. In the gypsum, convection circulation occurred within the cave cluster (Fig. 5). The waters in the gypsum had high contents of H_2S (> 100 mg/L) and dissolved solids (3.0–4.5 g/L).

With the start of the quarrying, the quarry became the drainage focus. During the first years, when the quarry entrenched in the gypsum for 2–3 m, the inflow of groundwaters to the bottom was at 6–14 L/s. With the entrenchment to 8–9 m, pumping rates increased to 28–140 L/s. Since the mid of the 1960s, with the quarry deepening up to 18 m below the gypsum top, pumping rates have reached 200–230 L/s, remaining at this level till now. The water table in the quarry has been lowered by 15 m as compared to the pre-quarrying period. The lowering was most rapid during the 1960s. Most of the cave was drained since that, and the drawdown cone expanded up to several kilometers in diameter.

Due to continuous withdrawal, groundwater circulation in the cave area has dramatically intensified. TDS content of groundwater in the gypsum decreased up to 1.9–2.6 g/L, attesting increasing inflow from the lower aquifer and decreasing residence time in the gypsum. Degassing of groundwaters occurred: H_2S dropped to 2–6 mg/L by the beginning of the 1980s, to 0–1.3 mg/L by 1986, and completely disappeared by the end of the 1980s.

The lowering of the water table and ventilation of the cave caused desiccation and substantial shrinkage of water-logged clay sediments. During 25–30 years since the start of the cave exploration, the clay-filled bottom of most passages has subsided by 1–2 m, and the volume of air-filled cavities increased by 25–35%. This led to activation of preexisting breakdown chimneys in the caprock in the cave area. Many breakdown chimneys have breached upward across the whole thickness of the confining clays and reached the alluvium aquifer, increasing drainage of the latter. Perennial springs along certain breakdown chimneys with discharge of up to 0.1 L/s, some of which flowed during 10 years, were observed in the cave. This led to the separation of the alluvium aquifer into isolated lenses and its subsequent depletion.

The analysis of the hydrogeological settings and their evolution in the Zoloushka Cave area unambiguously attests that the cave development took place under confined settings till the beginning of the Holocene and that rapid transformation of these conditions occurred during the last 70 years. This makes the Zoloushka case particularly important for validation of the regional speleogenetic model.

3 The Cave

3.1 Cave Pattern

Zoloushka Cave is an extensive multi-story maze with plan patterns varying through the area from dominantly systematic (i.e., with a few orientations of passages being strongly expressed) to pronouncedly polygonal. Most of the cave passages develop in the upper part of the gypsum (the upper story), although many rift-like passages cut across most of the gypsum thickness. There are discontinuous passage networks (clusters) in the lower part (the lower story) and some passages in different levels that do not form distinct stories.

The cave network extends along two wings, the eastern (smaller), trending southwest to northeast, and the western (larger), stretching southeast to northwest (Fig. 6). It has a very irregular outer contour and is uneven across the area with regard to passage patterns and density. Clusters of well-integrated passage networks are surrounded or separated by poorly karstified or non-karstified areas. Such clusters, called "cave regions," are commonly connected by only a few passages or a single passage and commonly differ in morphology. Within such regions, however, patterns and morphology of passages are rather uniform, which is caused by relative uniformity of structural prerequisites (fracture distribution) and hydrodynamic conditions. Cave regions, therefore, represent the largest speleomorphogenetic units in the maze cave. Based on structural and morphologic considerations, 18 cave regions are distinguished in Zoloushka Cave (Fig. 6; Table 1).

In Table 1, the cave regions are compared by their main morphometric characteristics, some of which are average values while others are sums. Passage heights vary from 2.2 to 7.0 m, with the whole-cave average height of 3.2 m. The greatest heights are observed in the Kamikadze region (10 in Fig. 6; Table 1) that consists of rift-type passages with a low level of clay fill. As this parameter characterizes the height of the upper part of passages that is free of sediments, but not their true height, it mainly reflects variations in the sedimentation level between regions, as illustrated in Fig. 7. Passage widths vary from 1.0 to 3.7 m, with an average passage width of 2.65 m. Regions with widest passages are located in the central part of the cave (regions 3, 4, 13 and 14) and in the near part of the eastern wing (15 and 16). The widths decrease to 2.0–2.5 m toward peripheral parts of the maze and even to 1–2 m in the northwest (regions 9 and 10).

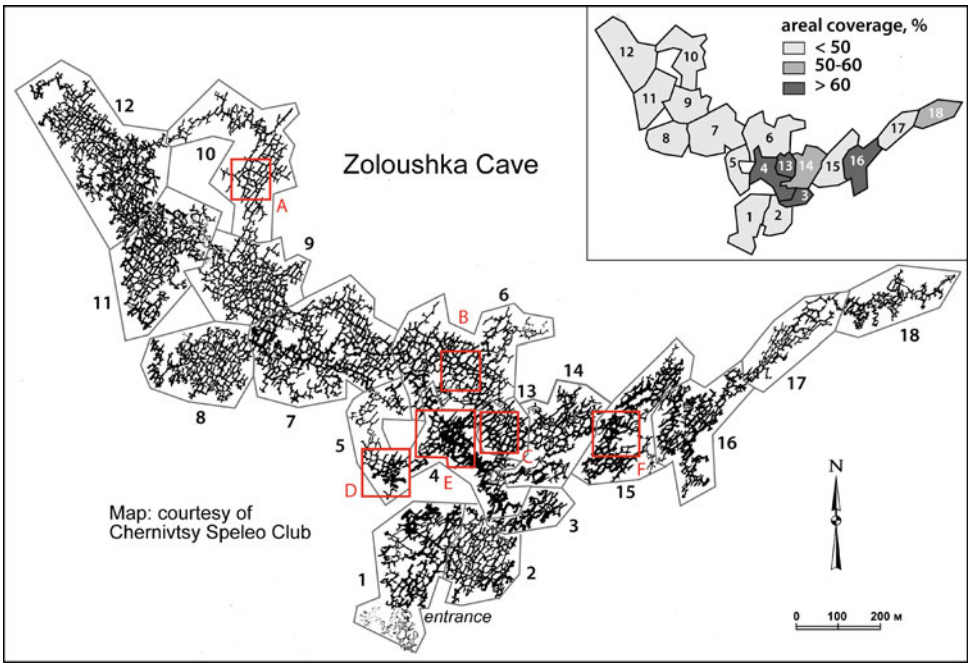

Fig. 6 The map of Zoloushka Cave showing structural–morphological regions (**a**) and variations of the areal coverage parameter between the cave regions (**b**). Numbers label cave regions as in Table 1. *Rectangles* (*red* in the color version) indicate map fragments shown in detail in Fig. 8

The areal coverage (the fraction of the area occupied by cavities; it represents a probability that a randomly placed borehole would intercept a cavity) correlates well with passage width and varies between the regions from 13.7 to 72.6%. Values are greatest in the center and the near east of the cave (see inset in Fig. 6), decreasing toward peripheral areas. The whole-cave average coverage is 47.2%—the highest among the gypsum caves in Western Ukraine.

The cave porosity (the fraction of the rock volume occupied by cavities) varies from 3.1 to 13.7%, displaying the same regularity in distribution through the area. The whole-cave average porosity is 6.6%. We note that this indicator is calculated using volumes of the cave spaces that are free of sediments, and hence, it is substantially underestimated. Based on the accepted speleogenetic model and a conservative estimate of the sediment thickness, we estimate true solutional porosity values to be nearly two times greater, e.g., the true whole-cave average will be at 10–12%.

The passage density (measured as the ratio of the mapped length to the area of a cave field) varies between the cave regions from 135 to 218 km/km^2, and the whole-cave value is 177.4 km/km^2. These values are typical for the region (Klimchouk and Andreychouk Chap. 23). There is no clear regularity in the distribution of this parameter across the cave; regions with high passage density are adjacent to those with considerably lower values.

The volume-to-length ratio (specific volume; calculated by dividing total volume by total length, m^3/m = m^2; Klimchouk 2004) represents the average cross-section area of cave passages and gives a good idea of typical passage sizes. It varies between the cave regions from 4.8 to 16.1 m^3/m, and the whole-cave average is 8.5 m^3/m. These values are also underestimated at least by one-third because of the sediment fill factor (Fig. 7). In any case, they indicate that Zoloushka Cave has the most voluminous passages among the caves in Western Ukraine. Largest passages are concentrated in the center and the near east of the maze, and their sizes diminish toward peripheral regions in two to three times.

The primordial plan pattern is comprised by rectilinear passages organized in a predominantly systematic network with two dominant orientations and four-beam junctions. In places, the network has a polygonal arrangement with three-beam junctions and varied orientations. Cross-dimensions of rock blocks between adjacent passages vary from 3–4 to 30–50 m depending on the density of guiding fracture networks. Values of the areal coverage index for such patterns are less than 50%. Further widening of passages, which occurred mainly during the water table stage (as discussed in Sect. 4.2), led to increase in the areal coverage and coalescence of adjacent passages, as illustrated by a succession of map fragments (left to right) in the upper row in Fig. 8. The result is the formation of large chambers with

Table 1 Main morphometric characteristics of regions in Zoloushka Cave

Region		Average passage height, m	Average passage width, m	Length[a], m	Area[a], m^2	Volume[a], m^3	Density of passages, km/km^2	Area-to-length ratio, m^2/m	Volume-to-length ratio, m^3/m	Areal coverage, %	Cave porosity, %
1	Privhodovuy	2.2	2.7	5600	15,195	33,773	160	2.71	43.2	4.2	6.03
2	Zabludshih	2.7	2.4	4331	10,484	28,671	198	2.42	47.1	5.9	6.62
3	Perspectiv	3.0	3.5	1238	4362	13,261	180	3.50	63.3	8.4	10.70
4	Chamber of Chernivtsy cavers	3.2	3.7	3919	14,439	45,663	165	3.70	61.1	8	11.65
5	Mayskiy	2.7	2.1	1424	2958	8101	135	2.10	26.3	3.1	5.68
6	Centralnyi	2.9	2.6	7879	20,301	59,700	168	2.58	43.2	5.6	7.58
7	Zapadny-Anakonda	2.8	2.8	8906	24,049	68,332	161	2.70	43.4	5	7.67
8	Veselyi	2.3	2.2	5317	11,833	27,040	218	2.23	48.4	4.8	5.08
9	Gollandskyi Syr	2.4	2.0	3000	6000	14,400	208	2.00	41.5	4.3	4.80
10	Kamikadze	7.0	1.0	2500	2500	17,500	136	1.00	13.7	4.2	7.00
11	Geokhimicheskyi	2.5	2.6	5000	16,000	30,000	210	3.20	44	3.6	6.00
12	Dikiy Zapad	n.d.	n.d.	n.d.	n.d.	n.d.	n.d.	n.d.	n.d.	n.d.	n.d.
13	Metropolitan	3.7	3.7	2337	8636	37,557	195	3.70	72.6	13.7	16.10
14	Ozernyi	3.8	3.1	4129	12,922	49,110	169	3.13	54	8.8	11.89
15	Goticheskyi	4.5	3.0	4092	12,416	56,239	153	3.03	45.9	9.8	13.75
16	Vostochnyi	3.6	3.1	4769	14,678	53,100	210	3.10	60.7	9.6	11.10
17	Dalnevostochnyi	3.4	2.3	2414	5616	19,039	168	2.33	39.1	5.8	7.89
18	Kamchatka	2.4	2.4	1084	2638	6251	215	2.43	52.8	5.2	5.76
Whole-cave averages/ **totals**		3.24	2.65	67,938	185,027	567,737	179.4	2.70	8.53	47.1	6.5

n.d. not determined; [a]the data for the time of calculations, not including exploration and survey progress in recent years

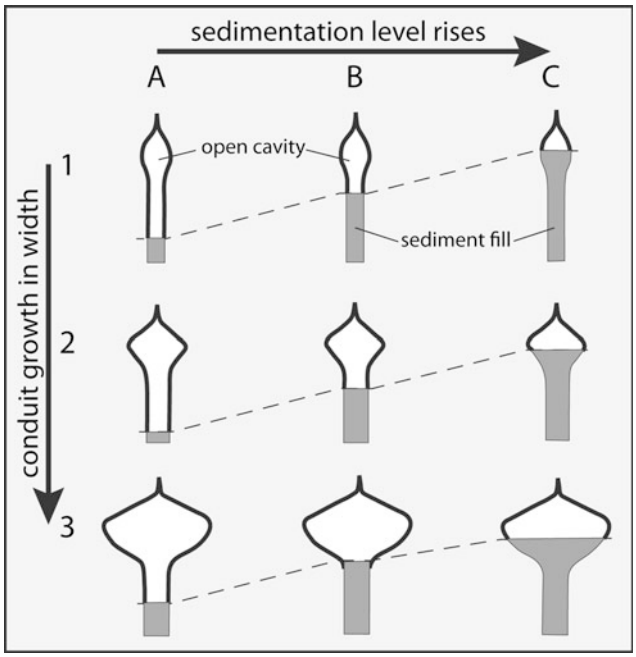

Fig. 7 Typical cross-section shapes of passages and their variations depending on solutional development (*top* to *bottom*) and sedimentation level (*left* to *right*)

numerous small pillars. The configuration of such chambers in plan would classify as a ramifying pattern rather than network (the lower row in Fig. 8). The areal coverage index for such patterns is above 60%, reaching 72.6 in one cave region).

3.2 Cave Meso-Morphology

3.2.1 Passages

The most common type of passages cross sections is a keyhole: relatively high and narrow base part with more or less expressed widened part at the top (Fig. 7). This is not always apparent, however, due to variations in the sediment fill level. Where the sediment level is high, the fill conceals the middle/lower rift-like part of the cross section so that its visible part assumes an oval or a rhomb-like shape, stretched either vertically or horizontally (Fig. 9a–f). With still higher level of the fill, the open passage assumes a triangular shape (Fig. 7c). Another reason for the variability of the apparent morphology is the degree of development in width of the basic rift-type passages and their top swells, as illustrated in Fig. 7 (compare rows 1–3) and in Fig. 9 (compare photographs a, b and c).

The rift part of the keyhole cross sections can be 0.5–3.0 m wide and up to 10–15 m high (deep, if observed from the top swell, as in photograph H in Fig. 9). Areas with a low level of the fill, where most of the passage cross section can be observed, occur in the central and the near eastern parts of the cave. Some large chambers formed by

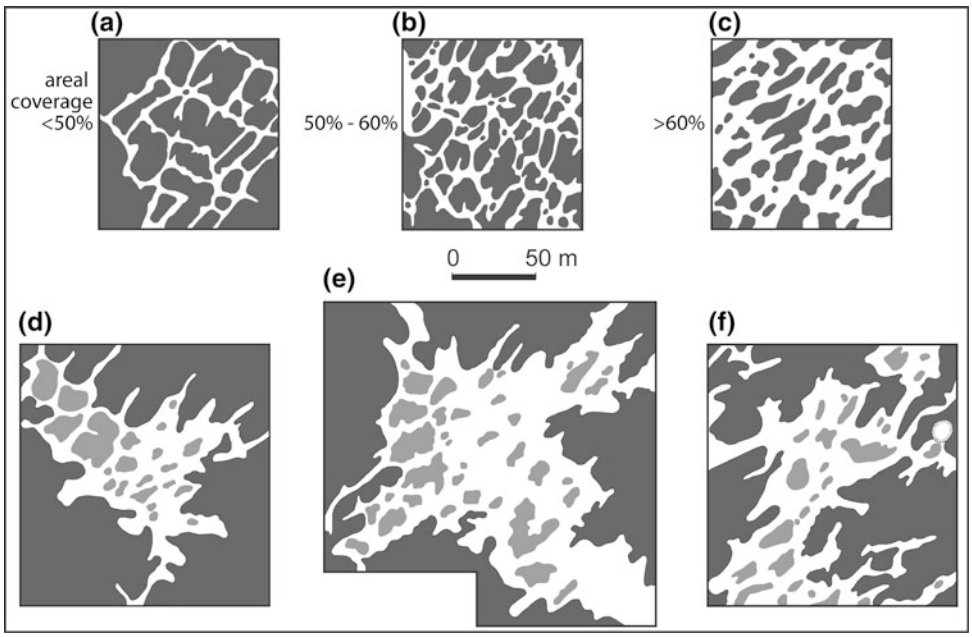

Fig. 8 Plan patterns in Zoloushka Cave: *upper row* (**a**, **b** and **c**) variations of patterns according to the areal coverage: **a** network pattern (Kamikadze region), **b** transitional pattern (Centralnyi region), **c** "chamber-with-pillar" pattern (Metropolitan region); *lower row* examples of chambers with pillars: **d** Mayskyi region, **e** chamber of Chernivtsy cavers, **f** Vostochyi region. See Fig. 6 for locations of the areas

Fig. 9 Typical passage morphologies in Zoloushka Cave. **a** through **f** apparent oval shapes represent the top swells of entire cross sections, whereas rift canyons in the bottoms are concealed by the sediment fill. In photograph **g**, the middle rift-like part of the passage cross section is visible. Photographs H and I show open rift canyons in the bottoms of ▶ large passages (**h** from above; **i** inside). Photographs **b** through **f** by V. Kisselev, other photographs by V. Andreychouk

(a)
2 m
(b)
(c)
(d)
(e)
(f)
(g)
10 m
(h)
2 m
(i)

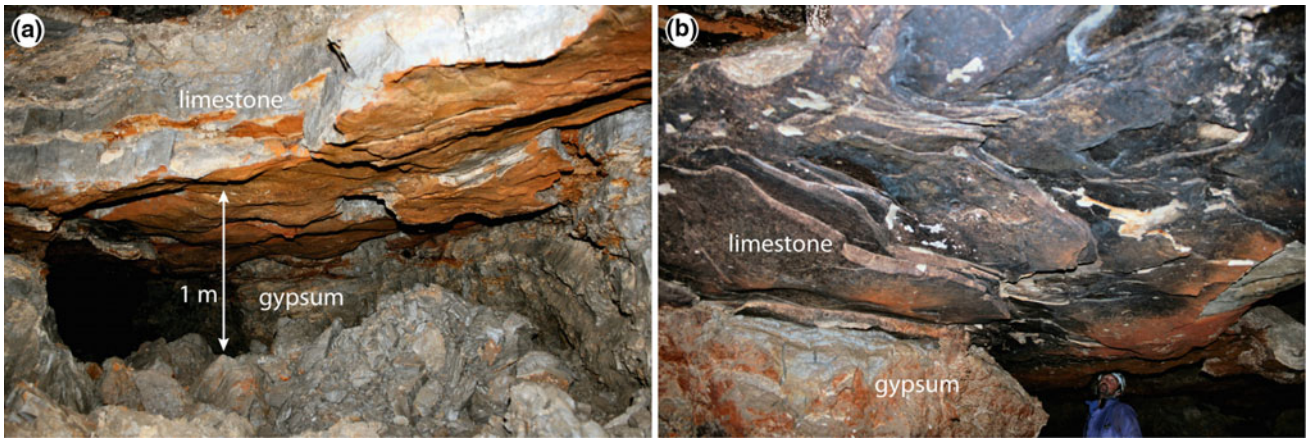

Fig. 10 Passages and chambers beneath carbonate interbeds in the middle part of the gypsum. Photograph by V. Andreychouk

merging of top swells in adjacent passages have numerous rifts in the bottom, which indicates the initial (before merging) network pattern.

Apart from the keyhole passages that cut across most of the gypsum, there are variously shaped passages at different levels that are constrained to certain parts of the bed. In the upper story (the level of the top swell), such passages connect adjacent master passages. In the middle part of the gypsum, low passages develop beneath local carbonate interbeds, forming small network clusters and sometimes merging into low flat-topped chambers (Fig. 10). Small passage clusters locally occur in the lower part of the gypsum, below the present water table.

3.2.2 Horizontal Notches and Inwardly Inclined Facets

In the central and the near eastern regions of the cave, passages in the upper story commonly have expressed horizontal notches in the walls. The main notch corresponds to the level of the maximum width (lateral apex) of the top swells in the keyhole passages (Fig. 9a through g) and passages connecting them. In places, the main notch has two closely spaced apexes (Fig. 9c). This level, continuous across large areas, lays 2–3 m below the gypsum top, marking the water table position during the Holocene. Locally, there are notches at about 3 m below the main notch, presumably cut during some stage of the quarrying period.

The top swells in the passage cross sections commonly have facets in the lower parts of their walls, just above the bottom rift, inwardly inclined at 45–50° (Fig. 7, rows 2 and 3; Fig. 9b through h). They form due to the diminishing aggressiveness in a film of the denser water sliding downward along the wall in convection cells (Kempe et al. 1976).

3.2.3 Rock Partitions, Windows and Cut Pillars

The formation of large chambers due to coalescence of adjacent passages in the level of the maximum development of horizontal notches at the former water table gives rise to characteristic morphological features, such as rock partitions (thinned pillars; Fig. 11a and b), windows (a, b and c) and cut pillars (d). They are most abundant in the central and the near eastern regions of the cave and do not occur in the peripheral regions. Lateral edges of rock partitions at the level of maximum thinning and windows in the partitions are typically sharp, which attests sluggish hydrodynamic environment and absence of noticeable lateral flow across these features.

3.2.4 Fracture Fill Partitions

Partitions (including prominent projections) comprised of indurated carbonate material filling preexisting fractures, exposed into the cave space by subsequent dissolution of the host rock, are very common in Zoloushka Cave (Fig. 12). In other words, such partitions are casts of pre-speleogenetic fractures exhumed by dissolution. Their linear dimensions (measured from the wall/ceiling surface at the base to the edges) vary from several tens of centimeters to a few meters, and the thickness varies from 1–2 cm to 10–30 cm. These features represent contraction fractures formed and filled in periods of desiccation of the evaporite basin. Such filled fractures are most abundant in the upper part of the gypsum. Their casts often thicken upward (Fig. 12f) and can be traced up to the overlying Ratynsky limestone bed (c).

Some filled fractures apparently conducted rising flow during the main speleogenetic phase, which is suggested by the development of cave elements along them (Fig. 12c).

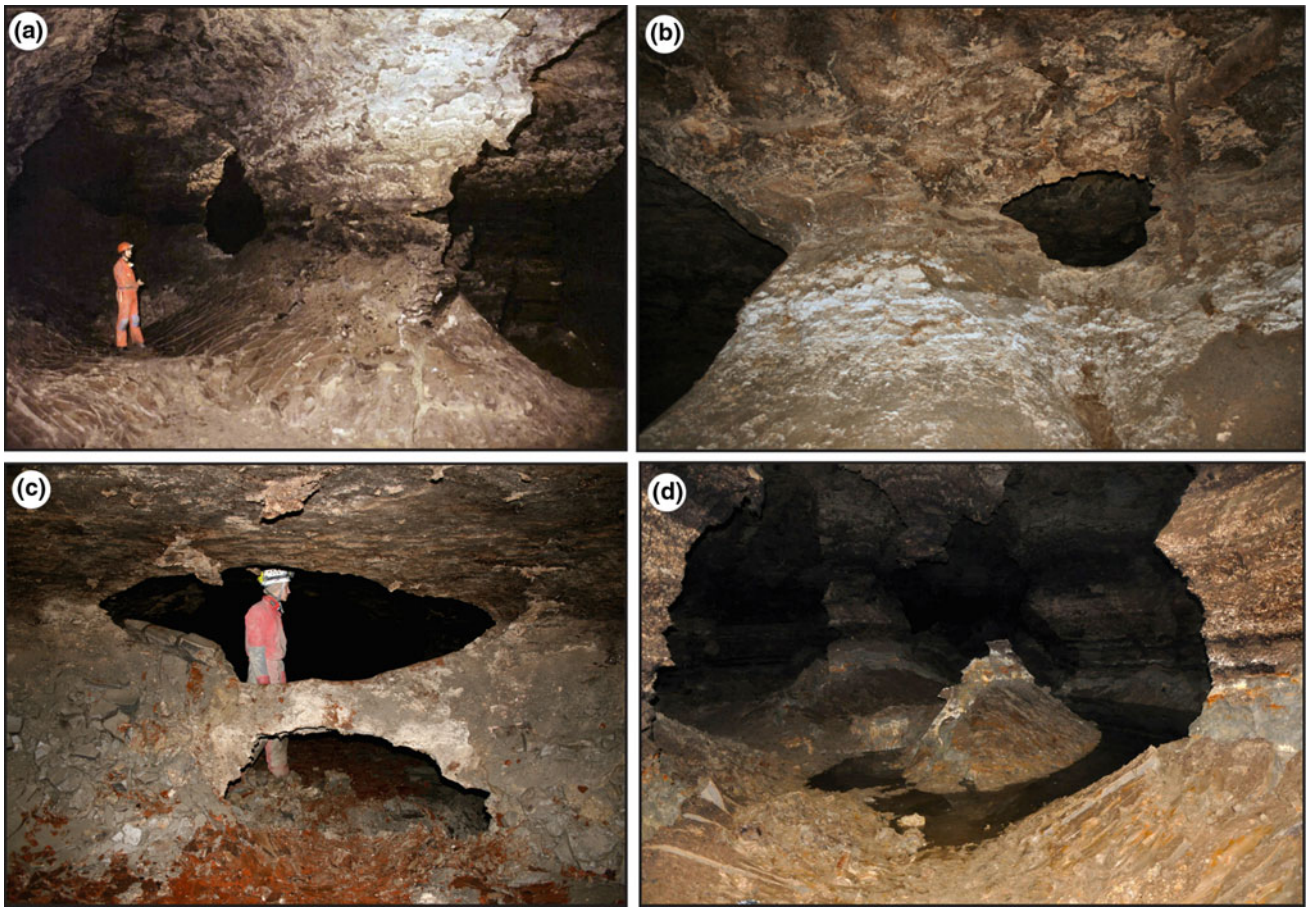

Fig. 11 Examples of rock partitions (**a** and **b**), windows (**a**, **b** and **c**) and cut pillars (**d**). Photographs by V. Andreychouk

Others were not hydrogeologically active and were exposed by dissolution along open fractures of a later generation that crossed the pre-speleogenetic fractures at various angles. Large fracture fill partitions can close in a large part (Fig. 12e) or completely (f) passages that stretch normal to them, whereas the passage morphology remains the same on both sides of the partition. This presents strong evidence that the passages were developed by sluggish vertical transverse flow but not by lateral flow. Thin partitions of this type are fragile, and many of them collapsed when they lost buoyant support during dewatering of the cave.

3.2.5 Feeders

Point-wise feeders (orifices of rising conduits through which water input occurred to a given cavity; Fig. 13) are common in passages of the upper story, although not that numerous as feeders typically occur in other maze caves in the region. This is because most of the upper story passages in Zoloushka cave have rifts in the bottom (either concealed by sediments, or open), which functioned to convey water from the lower aquifer. Typical feeders open in the lower parts of the walls, connecting to the system small clusters of cavities that were isolated in lower levels from deep-rooted (rift-like) main passages. Feeders located under the hanging walls commonly have side alcoves above them (Fig. 13c), formed by rising flows of aggressive water.

3.2.6 Rising Shafts with Spherical Heads

Particular to Zoloushka Cave (not found in other maze caves of Western Ukraine) are large rising shafts with domed ceilings (Fig. 14a, b). They are 15–18 m high, cylindrical in the middle part with diameters of 4–6 m and almost spherical in the top where diameters reach 8 m. Morphology of the shafts and their junctions with the master passages suggests that the shafts did not function as feeders to the system but were blind during their upward growth until the late stage of speleogenesis when they were intercepted by the passages of the upper story. In the water-filled bottom area of one shaft, cave divers have explored a small cluster of underwater passages at the lower level. In another shaft, a side access to the elongated bottom area is provided via a feeder in the lower wall of an adjacent master passage, but the shaft itself opens upward to a large spherical cavity which remains blind (Fig. 14c).

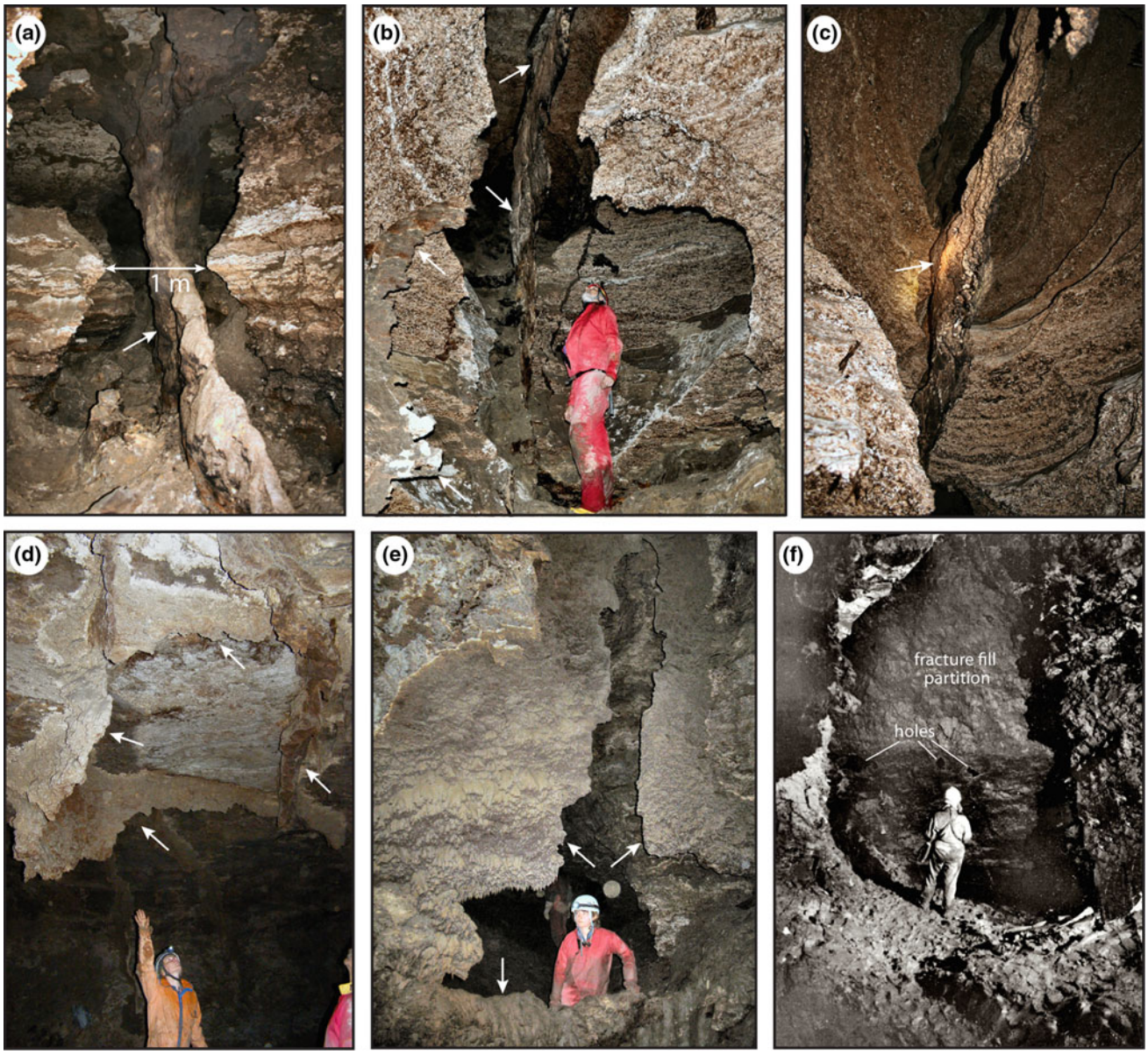

Fig. 12 Fracture fill partitions in Zoloushka Cave (pointed to by *arrows*). Photograph **c** shows the partition that guided the development of a rising chimney (outlet) opened to the bottom of the overlying Ratynsky limestone. Other photographs show the partitions transected and exhumed by the upper story passages. Photographs **e** and **f** by A. Klimchouk, other photographs by V. Andreychouk and B. Ridush

Fig. 13 Typical point-wise feeders in the upper story passages of Zoloushka Cave. Photograph **a** by V. Andreychouk, **b** and **c** by A. Klimchouk

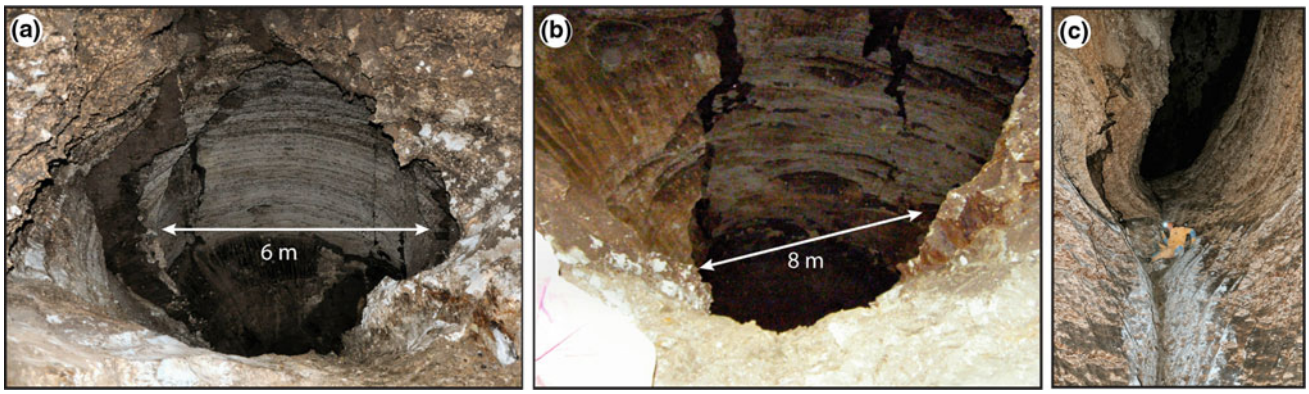

Fig. 14 Large rising shafts with spherical heads: **a** and **b** looking down from the intercepted heads, **c** looking up from the bottom to the blind spherical cavity at the top. Photograph **a** by V. Andreychouk, photograph **b** by A. Klimchouk, photograph **c** by B. Ridush

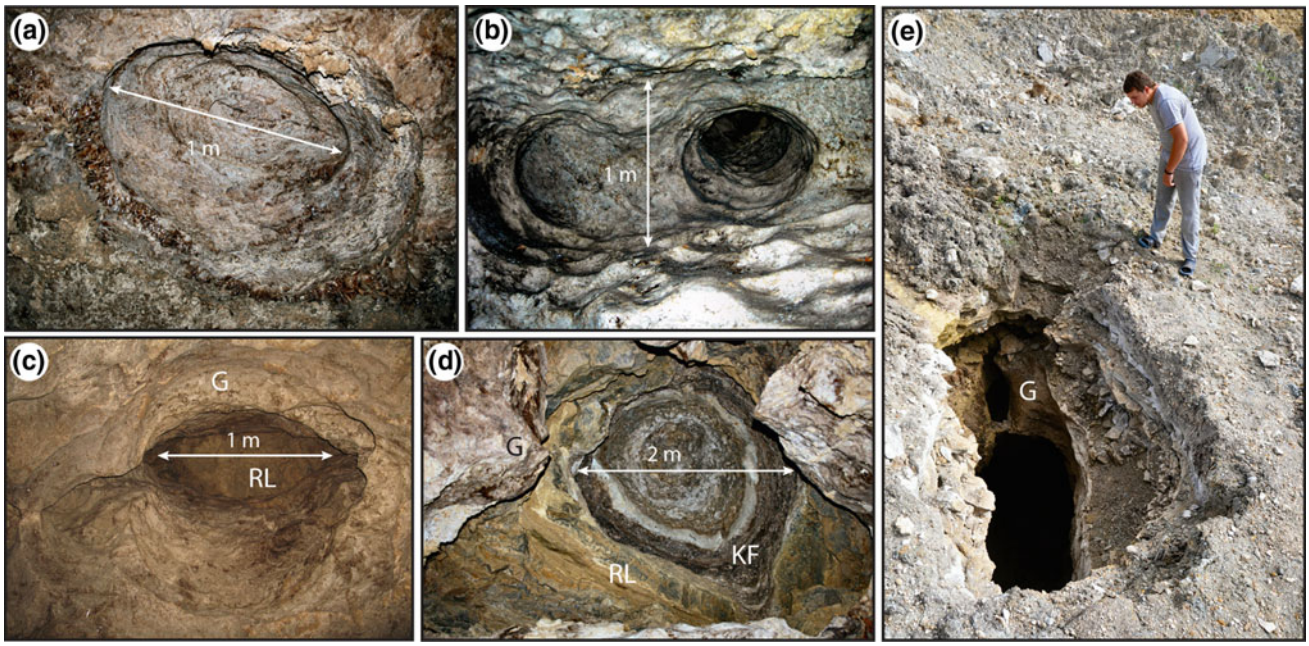

Fig. 15 Ceiling cupolas and rising chimneys in Zoloushka Cave: **a** a blind cupola; **b** a doubled feature, the blind cupola and the chimney; **c** a chimney open to the overlying limestone bed (outlet); **d** a chimney that broke through the Ratynsky limestone bed into the base of the Kosovsky Formation; **e** a chimney opened from above in the quarry when clearing the gypsum from the overburden. Photographs **a**–**c** by V. Andreychouk, photograph **e** by B. Ridush

3.2.7 Ceiling Cupolas and Rising Chimneys

Cupolas (domed hollows in the ceiling that have comparable lateral and vertical dimensions) and solution chimneys (hollows in the ceiling which height is substantially greater than their diameter) in passages of the upper story are omnipresent in Zoloushka Cave (Fig. 15a through d). These features are rarely greater than 2 m in lateral dimensions. Most of the chimneys that rise from the upper story passages are not more than 3 m in height (the maximum distance to the overlying limestone bed). Cupolas and chimneys occur both separate and in groups; laterally coalesced features (couple/triplet) are common. Some features are controlled by vertical fractures but many do not have any structural control, which points to the leading role of ascending convection currents in their location and formation.

Most of cupolas are blind (Fig. 15a), but many chimneys open to the contact with the overlying Ratynsky limestone (b and c) or penetrate still higher, into the base of the Kosovsky Formation (d). Such features are outlets in terms of the functioning of the transverse flow system as they provided the hydraulic connection with the upper aquifer. Propagation of chimneys above the gypsum top occurred not through dissolution but through the failure of blocks of the Ratynsky limestone (commonly densely fractured and brecciated) and

spalling of the overlying argilo–carbonate material (visible in the chimney vault in Fig. 15d). This stage is indicated by the formation of breakdown cones beneath chimneys. Further upward stoping across the caprock involves some other processes as well (Klimchouk and Andreychouk 2002). Cupolas and chimneys that broke into the caprock are frequently found in the quarry when clearing the gypsum from the overburden (Fig. 15e). Klimchouk and Andreychouk (2002) have demonstrated that most of breakdown chimneys in the caprock and resultant collapse sinkholes at the surface are related to the outlets, i.e., they are speleogenetically predetermined.

There are many cupolas and chimneys in flat-topped passages and chambers that form clusters beneath carbonate interbeds in the middle part of the gypsum. They develop in places where the carbonate bed in the ceiling is broken and rise up to 3–4 m above the ceiling. Most of such features are blind, but some connect to the upper story passages to form typical feeders.

3.3 Rapid Transformations During the Quarrying Stage

Before the quarrying, the water table was positioned in the upper part of the gypsum, circulation was sluggish, and waters in the cave and fractures were reduced and contained high SO_4 and H_2S (see Sect. 2.3 for more details). The air space above the water table had low oxygen and high CO_2 content. Prospecting drilling and the start of the quarry in 1946 opened an inflow of oxygen to the cave system, and groundwater withdrawal intensified circulation and caused the decline of the water table. This led to drastic and rapid hydrogeochemical transformations and other changes in the cave environment, including a burst in microbiological activity, massive deposition of Fe–Mn hydroxides, formation of microbialites, redistribution and early diagenesis of clays, and intensification of the breakdown processes (Andreychouk and Korzhik 1984; Volkov et al. 1987; Volkov 1990; Andreychouk 1988, 2007; Andreychouk and Klimchouk 2001; Klimchouk and Andreychouk 2002; Andreychouk et al. 2009).

4 Discussion

4.1 Speleogenetic Model and Singularities in the Evolution of Zoloushka Cave

Local geological settings, geomorphological and hydrogeological evolution of the area and characteristics of patterns and morphology of Zoloushka Cave perfectly correspond to the regional model of hypogene artesian speleogenesis developed by Klimchouk (Klimchouk 1990, 2000, 2012; see also Klimchouk and Andreychouk Chap. 23). Although local settings and evolution caused some peculiar features in the Zoloushka Cave development and resultant patterns and morphology, as compared to other large maze caves in the region, these peculiarities further illustrate variants and mechanisms of the general model.

According to the regional model (see Fig. 7c in Klimchouk and Andreychouk Chap. 23), the maze caves were formed in the multi-story confined Miocene aquifer system due to an upward leakage between the aquifers across the gypsum. Cross-formational upward flow in such systems occurs in areas of piezometric lows that correspond to topographic lows (valleys). In the Podil'sky region, where most of other large maze caves are located, significant downcutting of the ancient valleys into the confining clays, which established initial zones of slow upward discharge from the MAS and initiated transverse speleogenesis in the gypsum, occurred during the Late Pliocene—Early Pleistocene. Most of the cave development occurred there during the first half of the Middle Pleistocene when the Dniester River and its left tributaries incised close to the MAS and started opening the upper aquifer (Klimchouk 2000, 2012).

In the Zoloushka Cave area (the Khotyn–Mamalyga macro-block; see Fig. 2), such conditions were met later than in the Podil'sky region. The activation of upward transverse flow and initiation of the cave system can be related to the beginning of the Middle Pleistocene when the downcutting for about 40 m of the fifth terrace occurred. The main phase of the cave development occurred in the confined MAS in the course of the formation of the fourth and third terraces during the Middle Pleistocene. By the end of this age, the Prut River shifted to the south of the cave area, and the downcutting of the third terrace marked the start of hydraulic opening of the upper aquifer. Improved discharge conditions caused more intense groundwater circulation and dissolution. With the incision of the river into the second terrace in the beginning of the Holocene, the water table conditions established in the cave system—again, this transition had occurred in Zoloushka Cave later than in the caves of the Podil'sky region. Zoloushka Cave is therefore significantly younger than its counterparts there. Another peculiarity in the evolution of Zoloushka Cave is a stable position of the water table in the upper part of the gypsum during most of the Holocene, which resulted in the formation of horizontal notching and widening of passages at the upper story. In the Podil'sky area, rivers incised through the gypsum faster due to higher uplift rates there, so that modifications related to the water table were generally much less pronounced.

4.2 Main Controls Over the Cave Development

Before speleogenesis commenced, the permeability of the gypsum was determined by fractures and was generally very low. Within an area where a potential for upward flow across the gypsum exists, overall configuration of an evolving cave system in a soluble bed, sandwiched between two aquifers with diffuse permeability, will depend on (Klimchouk 2007, 2013):

(1) distribution of areas of enhanced hydraulic conductivity in the lower aquifer, particularly in its upper part (along the contact with the soluble bed),
(2) distribution of fractures that are connected across the bed (or can be potentially connected through the upward growth of conduits from the lower contact due to natural convection circulation) to provide vertical hydraulic communication between the lower (feeding) and the upper (receiving) aquifers,
(3) distribution of areas of enhanced hydraulic conductivity in the upper aquifer and of leakage paths across the confining cover.

The overall plan configuration of Zoloushka Cave marks the area where these conditions have favorably combined. It is safe to assume that the area that underlies the passage networks is characterized by enhanced hydraulic conductivity in the lower aquifer, as compared to surrounding areas (Fig. 16). Within the limits of the already evolved and integrated cave system, differences in the degree of the solutional development of conduits (expressed in their morphology and morphometric parameters) reflect differences in the availability of recharge from the lower aquifer, which depends on further lateral variations of hydraulic conductivity in this aquifer. Hence, based on the distribution of large passages and chambers in the system, it is possible to delineate the zone of high hydraulic conductivity, which encompasses the central and the near eastern parts of the cave system (Fig. 16). Within this zone, the lower aquifer supplied more abundant recharge to the gypsum not only during the stage of confined development but also during the water table stage, which is evidenced by respective modifications of passage morphology and by the distribution of cave sediments.

Fracture stratigraphy (i.e., vertical distribution of fractures in the gypsum) does not play such important role in determining the pattern of Zoloushka Cave as in other maze caves in the region. Most of passages in Zoloushka developed along tectonic fractures that dissect the whole or most of the gypsum thickness, although there are clusters of passages that developed along fractures confined to the lower and the middle parts of the gypsum, forming discontinuous cave stories in these levels (Fig. 17). The presence of carbonate interbeds in the middle part of the gypsum in some areas (particularly in the western wing of the cave) contributed to fracture stratigraphy and served to constrain vertical flow, favoring the formation of the passage story beneath them (Fig. 17c). In the upper part of the gypsum, the development of swells in the top of rift-like conduits (further enlarged laterally by dissolution at the water table) and lateral connections between them along lithogenetic fractures determined the formation of the well integrated and continuous upper story.

All morphotypes of rift-based passages depicted in Fig. 7 and shown in Fig. 9 developed from initial rifts fed from the lower aquifer. Larger (wider) rifts developed in the central

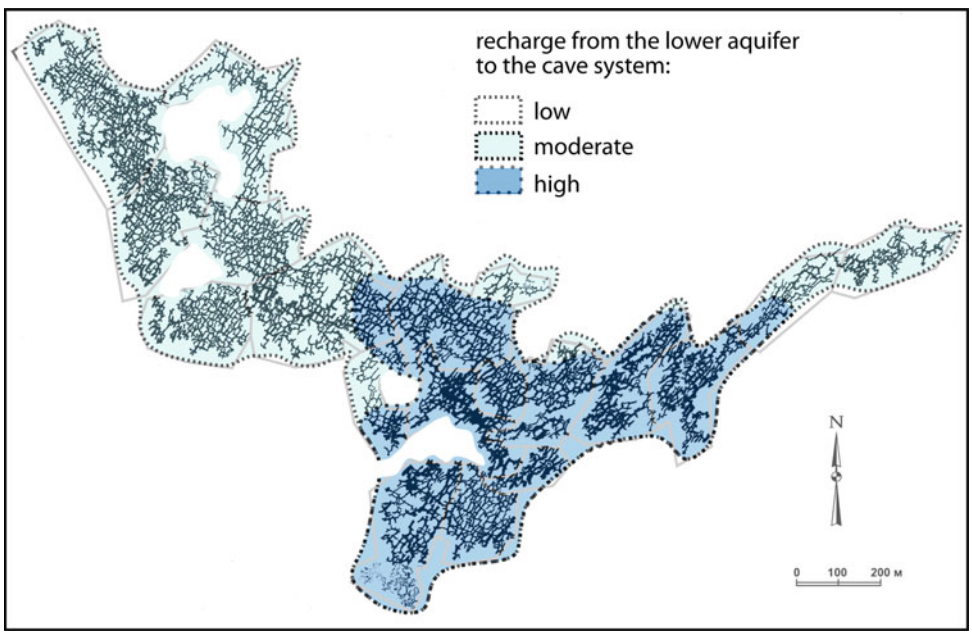

Fig. 16 Distribution of areas of relatively high hydraulic conductivity in the lower aquifer which provided enhanced recharge to the cave system

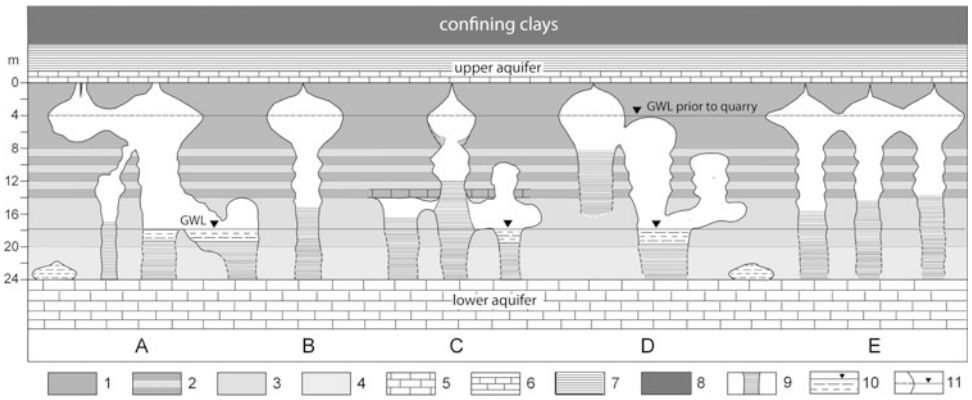

Fig. 17 Distribution of cavities in the cross section and typical conjunctions of main morphological elements of Zoloushka Cave. *1* coarse- and medium-crystalline gypsum; *2* layered medium- and fine-crystalline gypsum; *3* fine-crystalline and finely stratified gypsum; *4* aphanitic gypsum; *5* underlying carbonates (marl, limestone) and calcareous sandstones; *6* overlying Ratynsky limestone; *7* argilo–carbonate sediments in the base of the Kosovsky Formation; *8* clays of the Kosovsky Formation; *9* cave sediments (clays); *10* groundwater level; *11* groundwater level before quarrying

and the near eastern regions of the cave, where recharge from below and transverse flow during the confined stage was higher than in other areas. The swells in the top of the rifts began to form in confined conditions because natural convection due to differences in the solute content drives the fresh aggressive water to rise and flow laterally beneath the upper contour of evolving transverse conduits. However, most of the development in width in the top swells occurred during the latest phase of speleogenesis in the Holocene, when the free aquifer surface established in the upper part of the gypsum. Aggressive buoyant water that had been rising through rifts from the lower aquifer then floated at the top of the water body, attacking the walls. Hydrochemical and experimental studies have revealed that dissolution rates of gypsum in the uppermost 5-cm layer below the water table are roughly one order of magnitude greater than in the bulk water at a depth below 20 cm (Klimchouk and Aksem 2005), which causes pronounced horizontal notching in the walls and widening of cave passages.

The aggressiveness of the top water layer and respective modifications of passage morphology during the unconfined stage were not uniform throughout the cave. Again, they were greater where the input of freshwater from the lower aquifer was most abundant, i.e., in areas of greater conductivity in the lower aquifer and better hydraulic connection between permeability structures there with conduits in gypsum. Intense horizontal notching by dissolution along the water table led to the formation of chambers with pillars (Fig. 8 lower row; Fig. 11d) and chambers with bottom rifts where pillars were completely cut (Fig. 17e). As the result, the areal coverage parameter increased to >60% in some cave regions, particularly in the central and the near eastern parts of the maze (see inset in Fig. 6).

In addition to morphological evidence, comparatively high recharge to the gypsum from below during the unconfined stage in the zone delineated in Fig. 16 is also attested by the topography of the cave fill level. In this zone, the level of the clay fill is generally low, though uneven. In many localities (around some rifts, and in rising shafts and feeding conduits), it is even lower. In the eastern wing of the cave, a steep gradient is observed at the boundary between the Vostochnyi (Eastern) and the Dalnevostochnyi (Far-Eastern) regions (numbers 17 and 18 in Fig. 6, respectively), with altitudes of the passage bottom in the latter being 3–8 m higher than in the former. In the western wing, the bottom altitudes increase more gradually but with the same magnitude, starting from the Zapadnyi region (number 7 in Fig. 6) toward the western and northwestern periphery. The clay material was introduced into the karst system as a result of intense collapses triggered by the lowering of the piezometric surface below the gypsum top (Andreychouk 1999; Klimchouk and Andreychouk 2002). Distribution and settling of suspended particles were governed by hydrodynamic conditions: sedimentation was minimal in points and areas of vigorous upwelling inflow from the lower aquifer, and the suspended material was pushed into the peripheral areas of the cave where recharge from below and circulation were sluggish.

The presence of large rising shafts with domed ceilings (Figs. 14 and 17d) demonstrates the potential for large cavities to develop upward solely through dissolution by buoyant currents. Such cavities were not integrated into the trans-stratal forced flow system until recent interception of passages at the upper story, although many smaller cavities of the same type that intercepted the integrated system earlier (such as the left conduit in the cluster A in Fig. 17)

functioned as feeders to the system during the confined stage. They formed by upward-pointed dissolution in a closed-loop convection pattern, above places in which aggressive water of the lower aquifer was abundantly supplied to the bottom of the gypsum. Dissolved calcium sulfate returned to the lower aquifer with descending currents of convection cells and was removed by the lateral flow there. Representing a self-standing speleogenetic mechanism, known to operate at a large scale in other regions, e.g., in the South Harz, Germany (Kempe 1996), such convection cavities play an important role in transverse speleogenesis as they create hydraulic connections of the source aquifer with the permeability structures in the soluble unit that were not originally integrated into the transverse flow pattern, e.g., with fracture networks confined within some upper horizon (Klimchouk 2000, 2007).

5 Conclusions

Zoloushka is an outstanding example of a large maze cave formed in a multi-story artesian aquifer system due to the upward leakage between the aquifers across a soluble unit. The cave is an extensive multi-story maze with plan patterns varying through the area from dominantly systematic to pronouncedly polygonal. Most of cave passages develop in the upper part of the gypsum (the upper story), although many rift-like passages cut across the most of the gypsum thickness. There are also clusters of passages that developed along fractures confined to the lower and the middle parts of the gypsum, forming discontinuous cave stories in these levels. Although it perfectly illustrates the established regional model of speleogenesis, the cave has some singularities in patterns, morphology and sediments, in comparison with other large maze caves of Western Ukraine, determined by the peculiarities of local geology and the speleogenetic history.

Unlike most of other large maze caves in Western Ukraine, Zoloushka Cave is located in the area where the host Miocene aquifer system is generally confined until present, but in one of the more uplifted tectonic blocks where the gypsum was partially incised by the nearby valley of the Prut River only during the Holocene and further rapidly drained by the quarry during the last 70 years. It, therefore, represents a large cave system, which was doubtlessly formed under confined conditions but has experienced considerable modifications and transformations in the course of the recent transition to unconfined conditions and modern dewatering. The cave is significantly younger than its counterparts elsewhere in Western Ukraine. Another peculiarity in the evolution of Zoloushka Cave is a stable position of the water table in the upper part of the gypsum during most of the Holocene. This caused pronounced widening of passages along the water table—in some regions of the cave to a degree that adjacent passages amalgamated into large chambers.

During both confined and unconfined stages, the most intense development of conduits occurred in areas where the input of water from the lower aquifer was abundant, i.e., in areas of greater conductivity in the lower aquifer and better hydraulic connection between permeability structures there with conduits in gypsum. Hence, patterns and morphology of stratiform artesian transverse cave systems reflect heterogeneity in the distribution of hydraulic conductivity in the underlying aquifer. In Zoloushka Cave, the zone of enhanced recharge from the lower aquifer encompasses the central and the near eastern regions of the cave system, where the most voluminous passages and chambers have developed.

Due to the quarry operation and accompanying groundwater withdrawal during the last 70 years, drastic and rapid hydrogeochemical transformations and other changes occurred in the cave environment, including an intensification of microbiological activity, massive deposition of Fe–Mn hydroxides, formation of microbialites, redistribution and early diagenesis of clays, and an increase in breakdown processes. This makes Zoloushka Cave, in addition to its speleogenetic significance, a unique playground for in-depth studies of geomicrobiological processes and mechanisms of cover-collapse formation.

References

Andreychouk VN (1984) Regularities of karst development in the south-east part of the zone of junction of Russian craton and Pre-Carpathian Foredeep. Abstract of PhD thesis, Perm (in Russian)

Andreychouk VN (1986) Some regularities of speleogenesis in the south part of Podolian-Bukovinian karst region. In: Caves. Methods of study, Perm (in Russian)

Andreychouk VN (1988) The tectonic factor and peculiarities of the sulfate karst of Bukovina: geology, geomorphology and hydrogeology of karst. Institute of Geology and Geochemistry, Sverdlovsk (in Russian)

Andreychouk VN (1994) Zoloushka Cave. In: The questions of physical speleology, Moscow (in Russian)

Andreychouk VN (1999) Collapses above gypsum labyrinthic caves and stability assessment of karstified terraines. Prut, Chernovtsy. p 51 (in Russian)

Andreychouk VN (2007) Zoloushka Cave. Silesian University and Ukrainian Institute of Speleology and Karstology, Sosnowiec-Simferopol (in Russian)

Andreychouk VN, Klimchouk AB (2001) Geomicrobiology and redox geochemistry of the karstified Miocene gypsum aquifer, Western Ukraine: the study from Zoloushka Cave. Geomicrobiol J 18: 275–295

Andreychouk VN, Klimchouk AB, Boston P, Galuskin EI (2009) Unique iron-manganese colonies of microorganisms in Zoloushka

Cave (Ukraine-Moldova). In: Speleology Karstology 3:5–25. Available at: http://scholarcommons.usf.edu/ijs/vol34/iss1/4 (in Russian)

Andreychouk VN, Korzhyk VP (1984) Zoloushka cave system. Caves, Types and methods of study, Perm (in Russian)

Chernyshev SN (1983) Fractures of rocks. Moscow, Nauka, 240 pp (in Russian)

Kempe S (1996) Gypsum karst of Germany. In: Klimchouk A, Lowe D, Cooper A, Sauro U (eds) Gypsum karst of the world. Int J Speleology 25(3–4):209–224

Kempe S, Brandt A, Seeger M, Vladi F (1976) "Facetten" and "Laugdecken", the typical morphological element of caves developing in standing water. Ann De Speleologie 30(4):705–708

Klimchouk AB (1990) The artesian genesis of the large maze caves in the Miocene gypsum of the Western Ukraine. Doklady Akademii Nauk Ukrainskoj SSR ser. B, 7:28–32 (in Russian)

Klimchouk AB (2000) Speleogenesis of great gypsum mazes in the Western Ukraine. In: Klimchouk AB, Ford DC, Palmer AN, Dreybrodt W (eds) Speleogenesis: evolution of karst aquifers. National Speleological Society, Huntsville, pp 261–273

Klimchouk AB (2004) Morphometry of caves. In: Gunn J (ed) Encyclopedia of caves and karst science. Taylor & Francis, pp 524–526

Klimchouk AB (2007) Hypogene speleogenesis: hydrogeological and morphogenetic perspective. National Cave and Karst Research Institute, Carlsbad

Klimchouk AB (2012) Ukraine Giant Gypsum Caves. In: Culver DC, White WB (eds) Encyclopedia of caves, 2nd edn. Elsevier, Academic Press, Chennai, pp 827–833

Klimchouk AB (2013) Hypogene speleogenesis, its hydrogeological significance and the role in evolution of karst. DIP, Simferopol (in Russian)

Klimchouk AB, Aksem SD (2005) Hydrochemistry and solution rates in gypsum karst: case study from the Western Ukraine. Environ Geol 48:307–319

Klimchouk AB, Andreychouk VN (2002) Karst breakdown mechanisms from observations in the gypsum caves of the Western Ukraine: implications for subsidence hazard assessment. Int J Speleology 31(1/4):55–88

Klimchouk AB, Andreychouk VN, Turchinov II (2009) The structural prerequisites of speleogenesis in gypsum in the Western Ukraine. Silesian University and Ukrainian Institute of Speleology and Karstology, Sosnowiec-Simferopol

Klimchouk AB, Rogozhnikov VY (1982) Conjugate analysis of the formation history of a large cave system (on example of Atlantida Cave). Institute of Geological Sciences of NASU, Kiev (in Russian)

Volkov SN (1990) Geochemical transformations of the environment under technogenic impact on the karst cave Zoloushka. Geochimiia (Moscow) 5:741–751 (in Russian)

Volkov SN, Andreychouk VN, Yanchuk EA, Smirnov BI (1987) Modern iron-manganese formations of Zoloushka Cave. Mineralogichesky sbornik (Lviv) 41(1):79–83 (in Russian)

Hypogene Speleogenesis in the Crimean Piedmont, the Crimea Peninsula

25

Alexander Klimchouk, Gennadiy Amelichev, Elizaveta Tymokhina, and Yuri Dublyansky

Abstract

The chapter demonstrates, based on multiple lines of evidence, that hypogene speleogenesis was responsible for the origin of caves and conspicuous landform features in the Crimean Piedmont, a part of the Crimean Mountains located in the south of Crimea, a large peninsula in the North Black Sea. The region is located at the margin of the Prichernomorsky artesian basin, along a geodynamically active regional suture zone which separates the fold-thrust structure of the Crimea Mountains from the Scythian plate. Speleogenesis occurred in confined conditions by flow that rose across the Upper Cretaceous–Paleogene–Neogene clay–carbonate succession along cross-formational tectonic discontinuities and interacted with lateral flow in stratabound aquifers. A conceptual model of hypogene speleogenesis in the region links different types of cavities occurring in different lithostratigraphic units into integral, complexly structured, but functionally united void-conduit systems. These systems are shown to play an important role in the formation of cuesta escarpments in the Inner Range of the Crimean Mountains. The Crimean Piedmont is an outstanding example of a region where the recognition of hypogene speleogenesis entails a fundamentally new interpretation of the regional geomorphological evolution and the origin of remarkable landscape features, previously attributed to weathering processes.

Keywords

Hypogene speleogenesis • Crimea • Crimean mountains • Crimean piedmont • Cuesta landscape

A. Klimchouk (✉)
Institute of Geological Sciences, National Academy of Sciences of Ukraine, 55-B Gonchara Str., Kiev 01054, Ukraine
e-mail: klim@speleogenesis.info

G. Amelichev · E. Tymokhina
Crimean Federal University, 4 Vernadsky Ave., Simferopol, Russia

Y. Dublyansky
Institute of Geology, University of Innsbruck, Innrain 52, 6020 Innsbruck, Austria

A. Klimchouk · G. Amelichev · E. Tymokhina · Y. Dublyansky
Ukrainian Institute of Speleology and Karstology, Simferopol, Ukraine

1 Introduction

The Crimean Piedmont is a part of the Crimean Mountains located in the south of Crimea, a large peninsula in the North Black Sea. The region embraces two ranges (the Inner Range and the Outer Range) arching to the northwest and north of the Main Range along the suture zone that separates the fold-thrust region in the south of the peninsula from the Scythian Plate that extends to the north. The most prominent Inner Range is comprised of the homocline Paleocene and Eocene sequences of alternating carbonate and marly–clayey

© Springer International Publishing AG 2017

A. Klimchouk et al. (eds.), *Hypogene Karst Regions and Caves of the World*, Cave and Karst Systems of the World, DOI 10.1007/978-3-319-53348-3_25

sediments, in which carbonate units are expressed in the landscape as distinct cuesta ridges. The Outer Range is comprised by the Neogene carbonates and is less expressed in relief.

Until recently, karst was considered as being only scarcely developed in the Crimean Piedmont, which was explained by unfavorable geological and climatic conditions. Rare surficial karstic forms described in the Inner Range include subdued karren features and a few small sinkholes on the cuesta dip slopes. Contrasting to this is the occurrence of caves with well-developed phreatic morphology. Although all the caves display no functional relationships with the landscape, they were interpreted as epigenic caves (Dublyansky and Lomaev 1980; Dushevsky 1987). A possibility of the hypogene origin of karst was never considered for the region until recently.

The Inner Range is characterized by an abundance of various unusual geomorphological features such as rock amphitheaters, protruding rocks ("bastions") and pinnacles ("rock idols") along the cuesta ledges, rock shelters, stratiform notches, niches, half-conduits and various forms of "cavernous weathering" (e.g., tafoni and honeycomb structures) in cliffs. Although no focused studies have been done with regard to these features, they were all loosely attributed to weathering and differential erosion on exposed surfaces, following conventional geomorphological views.

Systematic studies carried by the Ukrainian Institute of Speleology and Karstology since 2006 have revealed the hypogene origin of caves in the region, based on multiple lines of evidence (Amelichev et al. 2011; Klimchouk et al. 2009, 2011, 2013; Klimchouk and Timokhina 2011; Timokhina et al. 2011, 2012). It was also shown that the above-mentioned unusual geomorphological features are the result of the destruction and exposure of structurally controlled hypogene void-conduit systems. This chapter provides a synthesis of recent studies of hypogene speleogenesis in the region and presents a speleogenetic model, which has important implications for the regional geomorphology.

2 Background

The Crimean Mountains in the south of the Crimean Peninsula are a part of the Alpine fold-thrust belt. The Main Range of the mountains is a chain of plateau-like massifs (locally called "yaylas") composed mainly of Jurassic limestones, an arena of an intense epigene karst development superimposed on relict hypogene karst structures. Adjacent to the northwest and north lays the Piedmont, separated from the Main Range by longitudinal erosional depressions (Fig. 1a, b). The Crimean Piedmont includes the Inner (the Second) and the Outer (the Third) ranges of the Crimean Mountains, as well as the inter-range lowlands. It stretches for some 130 km as an arched belt of 5–15 km in width, from the hills of the Mekenzievy Mountains near the city of Sevastopol in the west to the Agarmysh massif near the town of Stariy Crym in the east. The flatland of the North Crimean Plain and the Kerch Peninsula are located to the north and east, respectively.

Structurally, the Crimean Piedmont is located at the junction between the fold-thrust structure of the Mountainous Crimea and the Scythian Plate (Fig. 1a). The first-order element of this zone is the Mesozoic Predgornaya Suture, formed as a result of the collision of the paleo-terrain of the Mountainous Crimea with Eurasia in Jurassic to Early Cretaceous times (Yudin 2011). The upper tectonostratigraphic story of the Piedmont comprises alternating marly–clayey and carbonate rocks of the Upper Cretaceous, Paleogene and Neogene, which form a homocline dipping at 5°–15° to the northwest and north (Fig. 1b, c). Further in these directions, under the North Crimean Plain, the Cretaceous–Paleogene strata plunge steeply to a depth of 600–1000 m. The distinct limestone beds of Paleocene (Upper Danian) and Eocene (Ypresian and Lutetian) comprise the dip slope of the Inner Range, while the south- and southeast-facing frontslopes are typically steep, resulting in a prominent cuesta relief with limestone cliffs. The Inner Range is dismembered along its stretch into a series of cuesta massifs by transverse valleys of rivers that originate in the Main Range.

Lithostratigraphic composition and geomorphic character of the Inner Range vary along its stretch (Fig. 1b). *In the southwestern sector* (from Sevastopol to the Bodrak River), outcropped in the cuesta front cliffs are Paleocene limestones and marls and Eocene limestones. In this sector, the Paleocene and Eocene limestone beds, separated by a marly–clayey sequence, constitute two cuesta ridges of which the Paleocene one is the most prominent, with elevations at the crest typically ranging from 500 to 580 m and relative relief from 200 to 250 m.

In the central sector (from the Bodrak River to the Kuchuk–Karasu River), the Paleocene carbonates are missing in the cross section. The Inner Range is comprised by the Eocene limestones which directly overlay the Maastrichtian marls or (within the Simferopol' uplift) Lower Cretaceous and older sediments. To the northeast of Simferopol and till the Biyuk–Karasu River, the Inner Range has a relatively low prominence in the landscape, with the 5–20 m high cliffs of the Eocene limestone present only in fragments.

In the eastern sector, the Paleocene carbonates appear again beneath the Eocene limestones, represented by bedded marls and marly limestones. This sector begins with the prominent Ak-Kaya massif, in which impressive vertical cliffs of Danian marls and Eocene limestones reach 100 m in height. The Inner Range is well expressed in the landscape in this sector, with elevation reaching over 700 m and the

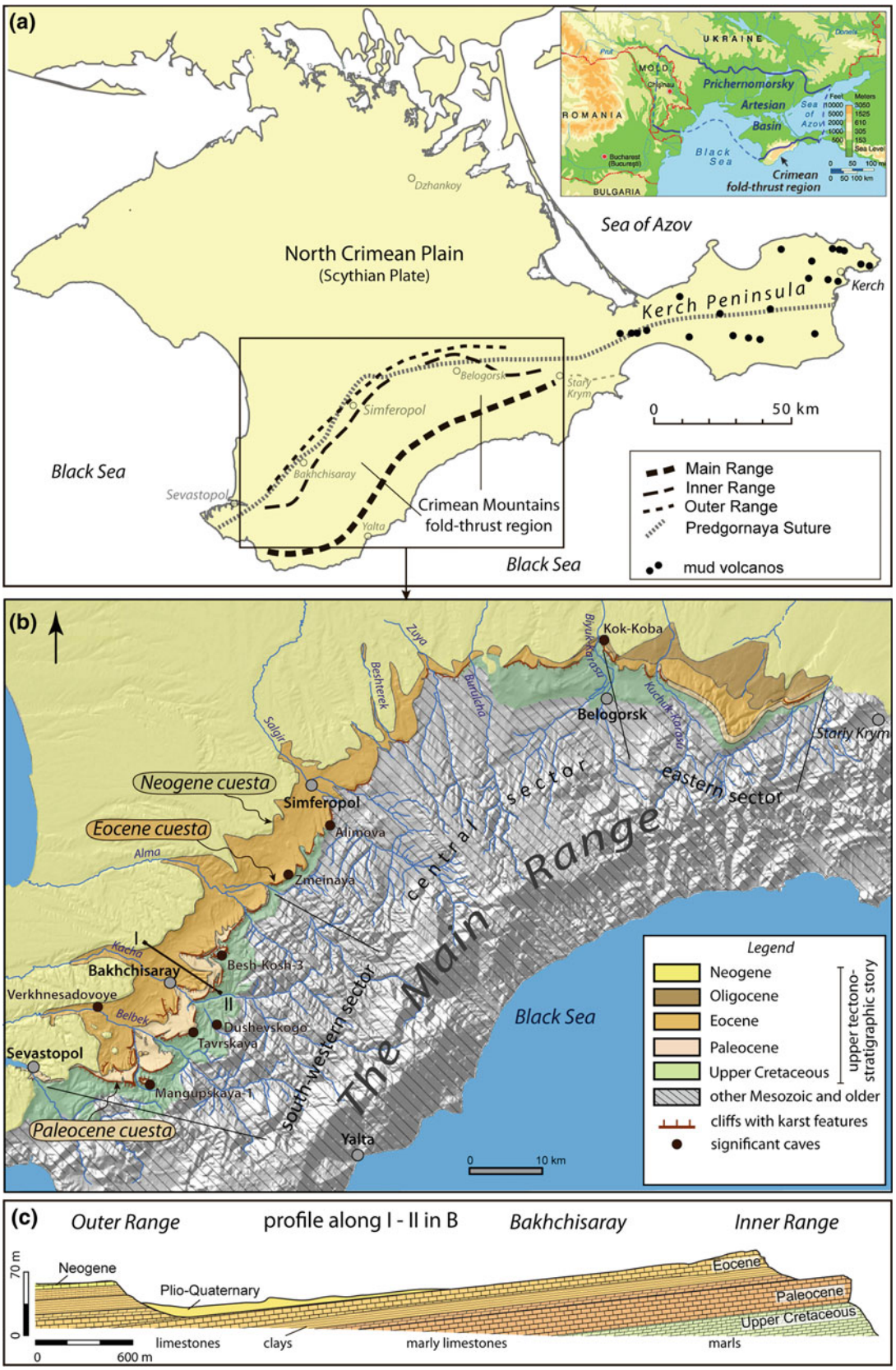

Fig. 1 Location and main orographic and geologic features of the Crimean Piedmont. **a** Outline of the Crimean Peninsula showing the relations of major tectonic structures and location of the ridges of the Crimean Mountains. **b** Shaded relief map of the Crimean Mountains with the overlay showing formations of the upper tectonostratigraphic story (contours of geological units from Yudin 2011). **c** Geological section along the line *I–II* in **b**

relative relief about 200 m, but further to the east it declines and disappears orographically.

The homocline sequence of the upper tectonostratigraphic story is relatively weakly dislocated. Individual karst conduits and linear segments of cliffs are controlled by large sub-vertical fractures with N–S, W–E, and oblique orientations. Fracture traces of 30–50 to 200–300 m in length are easily recognizable on satellite images in the crest areas of cuesta massifs. In cross section, fractures normally extend vertically for 10–40 m across several lithostratigraphic units but often terminate upward at certain stratigraphic boundaries. Also common in the Inner Range, particularly within the upper part of the Eocene limestones, are pinnate fractures inclined at 25°–40°, associated with major sub-vertical cross-formational and bed-encased disruptions. Fractures are unevenly distributed. Whereas fracturing is rather intense in cliffs and the crest areas of cuesta massifs, it is getting very low in short distances away from cliffs, as evidenced by observations in numerous quarries located on the dip slopes. This suggests that the valley entrenchment followed linear 100–400 m-wide zones of densely spaced karstified fractures, beyond which rocks remain largely intact. Such distribution corresponds to a concept of fracture corridors (swells or clusters), structural features recognized in many regions (Bush 2010; Singh et al. 2008; Questiaux et al. 2010; Ogata et al. 2014). In the Crimean Piedmont, faults with substantial displacement in Paleocene strata are identified only in a few places, although they can be present in deeper parts of the geological section. Fracture corridors observed in the Inner Range fit best to a type of "fault tip process zone corridors" in a classification suggested by Ogata et al. (2014), although some of the linear zones which had been exploited by major longitudinal valleys at the front of cuesta massifs may also fall into the type of "fold-related crestal fracture corridors."

According to the hydrogeological regionalization (Shestopalov et al. 2010), the Crimean Piedmont is situated on the south edge of the North Crimean artesian basin, a part of the larger Prichernomorsky (translated as "Near-Black Sea") artesian basin that extends through the continental Ukraine in the North Black Sea region (see inset in Fig. 1a). In the present geomorphological situation, the Inner and the Outer ranges constitute a marginal recharge area of the basin. The Eocene and Paleocene limestones are characterized by high matrix porosity, but it varies significantly between particular layers. Lygina (2010) gives layer-specific porosity values at 5–10%, 15–17% and 25–30% for the Eocene limestones. Matrix porosity of the Paleocene limestones commonly varies within 5–20% but is sometimes as high as 40% (Gorbach 1972). Both limestones contain aquifers separated by a marly–clayey series. These aquifers are now completely drained in the crest of the Inner Range, but they contain groundwater and become confined with a plunge of the strata to the northwest and north. In the dip direction, chemical types of groundwater change from Ca–HCO_3 and Na–Mg–HCO_3 to Na–Ca–Cl, Na–Cl, Na–HCO_3 and Ca–SO_4–Cl, TDS changes from 0.3–0.7 to 18 g/dm^3 (locally to 55 g/dm^3) and temperature rises to 38 °C (Lushchik et al. 1981, 1988). There are numerous flowing artesian wells from the Paleocene and Eocene aquifers in the lower dip slope, the inter-range lowland and the Outer Range. Some wells and rising springs are characterized by elevated contents of dissolved gasses and degassing of N, CO_2, CH and H_2S. In places, groundwaters have elevated contents of helium, radon and Hg vapor (Lushchik et al. 1981, 1988). The presence of cross-formational faults and fracture corridors, as well as pressure relationships, allows for the vertical hydraulic communication between confined aquifers in the upper tectonostratigraphic story and localized upwelling inflow to shallower aquifers from deeper groundwater systems. The contribution of deep components is indicated by locally anomalous hydrochemical and gas composition.

In the southwestern sector, the continuity to the northwest of the lower Cretaceous and Jurassic formations comprising the Main Range is disrupted by longitudinal erosional depressions, so that the Inner Range is completely separated hydrogeologically from the Main Range. In the northeastern part of the central sector and in the eastern sector, these formations are laterally continuous through most of the northern slope of the Main Range. This provides conditions for recharge within the Main Range and groundwater flow in aquiferous beds in the dip direction. This flow partly discharges upward in the Piedmont, leaking across the Upper Cretaceous, Paleocene and Eocene carbonates along fracture zones and partly contributes to groundwater resources in the North Crimean artesian Basin.

3 Patterns and Morphology of Caves

Cavities and conduits in the Upper Cretaceous, Paleocene and Eocene carbonates in the Piedmont vary in morphology, sizes and patterns. Almost all of them occur in the cuesta cliffs of the Inner Range. Following conventional notions about these features, and for the purpose of basic description, we group them into the following categories: (1) karst rifts, (2) "common" caves, (3) rock shelters and tafoni and (4) isolated chambers. An additional group of cavities is represented by conduits in clayey marls (5).

3.1 Karst Rifts

In cave and karst science, the term "rift" is used to denote "*a cave passage that is relatively high, narrow and generally straight, reflecting that it is commonly guided by, and*

developed along vertical or sub-vertical fissures, joints, and faults" (Monroe 1970). Here we extend the meaning of the term to encompass any generally straight sub-vertical fissure, solutionally enlarged to a width of more than 10 cm and having over few meters in height and length.

Rifts are common in the Inner Range, occurring in cliffs and adjacent crest areas of cuesta massifs and extending vertically across multiple beds. Height dimensions of individual rifts vary from several meters to 40–60 m, and their length varies from a few tens to a few hundred of meters. Widths of rifts are also highly variable. Wider portions that attain human-penetrable dimensions are often aligned to individual beds at different heights. Rifts have lateral terminations more or less gradually pinching out into narrow, almost unchanged fractures. In some cases, wider areas of rifts pinch out abruptly in the lateral directions (Fig. 2h) but extend vertically through most of the rift height, resulting in a vertical conduit of a lenticular shape in the plan view.

Figure 2 shows conditions of occurrence and morphology of typical rifts. Large rifts can be accessible either vertically from the top, through crevice-like entrances in the upper parts of the dip slopes of cuesta massifs (Fig. 2a), or laterally from cliffs (c and d). Although some rifts are oriented oblique or normal to the cliff faces, most of them are parallel to cliffs. It is quite common that a cliff with abundant solution features continues laterally as a rift sharing the same wall, which retains the same morphology (Fig. 2b). Rifts that occur parallel to the cliff face and next to it, being separated from the cliff by thin (3–10 m) partitions, are often accessible via "windows" formed by partial breach of partitions to the valley side (Fig. 2g, h). These situations, as well as the presence on the footslopes of large fallen rock boulders that retain fragments of solutionally sculptured walls of the original rifts, unambiguously indicate that the cliffs form mainly through the unwalling of karst rifts by block toppling and that their peculiar morphology is caused mainly by speleogenetic processes rather than by weathering.

Rifts are generally slot-like and fissure-like in the cross section, but in many rifts, there are symmetrically or asymmetrically widened intervals corresponding to sub-horizontal niches developed in particular beds or along bedding planes. As such intervals are stratigraphically controlled, the widened space (sometimes the only human-passable part of a rift) may look like a horizontal or slightly inclined passage with narrower vertical slots extending down and up. The meso-morphology of rift walls is characterized by diverse sculptured features.

For rifts in the Eocene limestones, corrugated surfaces are common, with sub-horizontal ridges and notches controlled by lithostratigraphy variations (Fig. 2b, g). The morphologies of the opposed walls clearly mismatch each other, which rules out the possibility that rifts were formed as mode-one stress release fractures further opened due to gravitational mass movement toward the valley slope. Notches are often complicated by various hollows such as pockets, niches, tafoni and small side conduits. Smooth sculpturing of the walls and the character of forms suggest that dissolutional widening of original fractures took place under phreatic conditions. Niches in bed-controlled notches are sometimes arranged in vertically stacked series, with smoothly lowered crests of dividing horizontal ridges, which makes such series looking as vertical solution half-tubes. Upward terminations of rifts, when observable, are often widened, with smooth ceilings, cupolas and upward-extending chimneys. Rifts in the Upper Danian sequence of the Paleocene cuesta, which form most of vertical cliffs in the southwestern sector, display less bedding control over solutional morphology. Rifts in the Lower–Middle Danian marly limestones and marls, which form the feet of the cuesta frontslope in the southwestern and eastern sectors, also display corrugated surfaces with numerous pockets (Fig. 3a).

Features associated with free downward percolation or flows of meteoric waters (vertical flutes and grooves, rillenkarren, vadose shaft-like conduits, etc.) are exceptionally rare. When present, they are clearly superimposed on and erasing, the original phreatic morphology. Laterally isolated occurrence of many rifts rules out a possibility of their development by lateral flows.

Dushevskogo Cave, located some 2 km to the southeast of the Paleocene cuesta in the southwestern sector (see Fig. 1b for the location), is a remarkable example of a large rift in the Maastrichtian succession comprised of silicified marly limestones. The entrance is located at the top of an elongated hill, opening down into a large NE–SW-trending rift (Figs. 2f and 3c). The 1–2-m-wide rift, explored to the depth of 50 m, is blocked by breakdown plugs at various levels. Wedged boulders and slabs also block the rift continuations along the strike. Based on the presence of small blowing holes at the surface along the line of the rift, its length is estimated to be at least 200 m.

The described characteristics of karst rifts strongly suggest that they were formed through the widening of large cross-formational fractures by upwelling groundwaters, which dissolution capacity was locally enhanced due to mixing with lateral matrix flows conducted by more permeable beds and bedding planes. This interaction was responsible for the formation of specific morphological features in the rift walls such as stratiform notches and convection pockets (Klimchouk et al. 2012).

3.2 "Common" Caves

Karst rifts described above have only limited portions with human-penetrable widths and thus were not regarded as

(a)
(b)
(c)
(d)
(e)
(f)
(g)
(h)

◀ **Fig. 2** Karst rifts in the cuesta cliffs of the Inner Range. **a** Rift normal to the cliff face as seen on the cuesta crests and dip slopes; **b** rift co-planar to the cliff face; **c**, **d** and **e** internal morphology of rifts (**e** is a rift shown in **a**, at about 15 m below the surface); **f** entrance of the Dushevskogo rift cave viewed from below; **g** and **h** rifts that occur parallel and next to the cliff faces, accessed via side openings formed due the breach of partitions separating the rifts from the cliffs. All photographs are from the southwestern sector of the Piedmont. **b**, **c**, **d**, **g** and **h** rifts in the Eocene cuesta; **a** and **e** rifts in the Paleocene cuesta; **f** rift (Dushevskogo Cave) in the Maastrichtian marls to the southeast of the Paleocene cuesta (see Fig. 1 for the location)

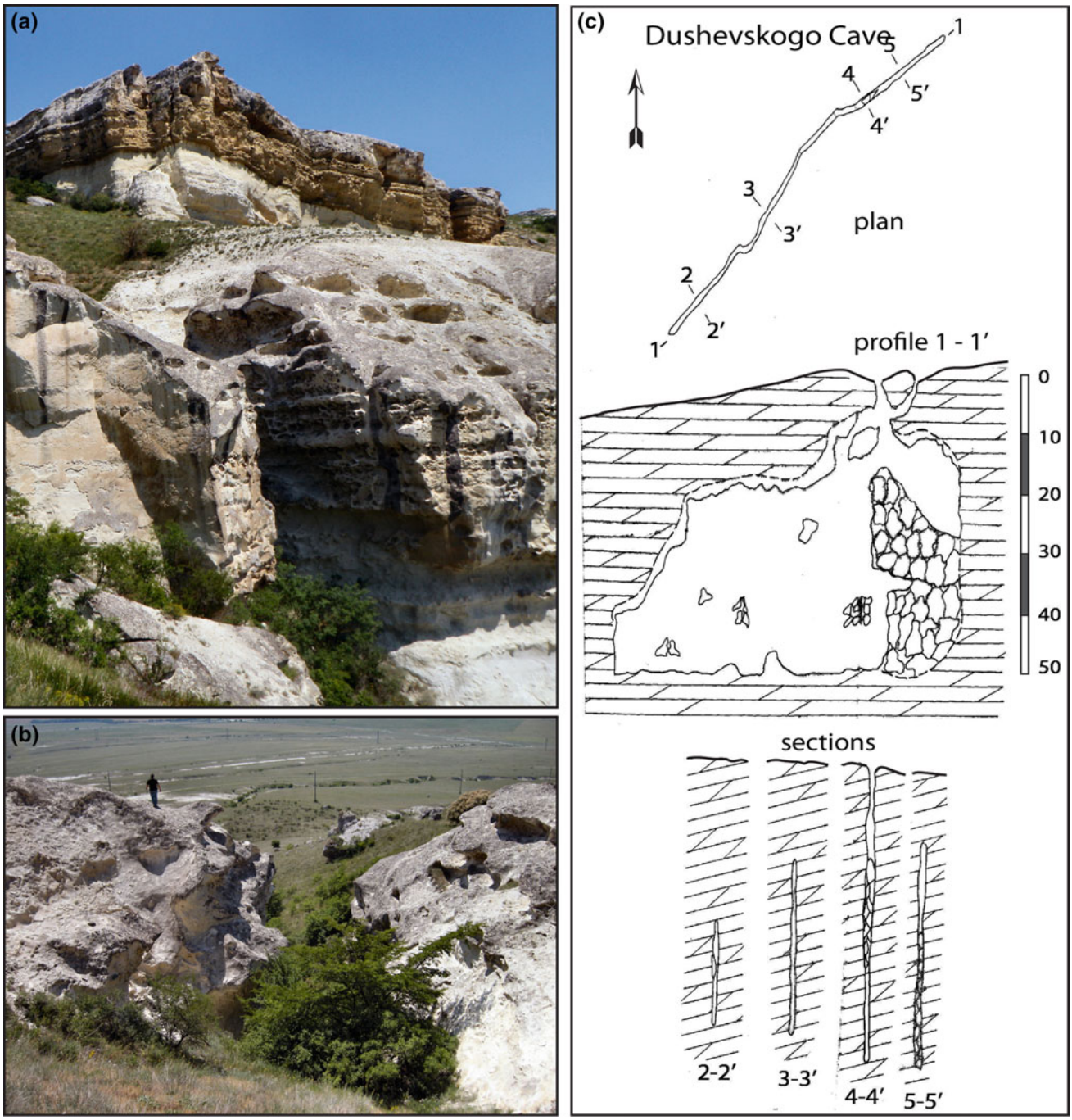

Fig. 3 **a** and **b** Rift in the Lower–Middle Danian marly limestones in the eastern sector (**a** view from the *side*, **b** view from *above*); **c** Dushevskogo Cave—large rift in the Maastrichtian marly limestones in the foot of the Paleocene cuesta in the southwestern sector

caves in the regional cave inventory (with an exception of the Dushevskogo Cave). Further uncertainty about caves in the Crimean Piedmont arises from the lack of clear distinction between them and much more abundant rock shelters (see Sect. 3.4). Those chamber-like cavities in the cuesta cliffs that extend into the massif deeper than the width dimension of the entrance may classify as caves, but this criterion is formal and has no speleogenetic sense. In the group of "common" caves, we include 35 caves in the Inner Range that have evidently elongated human-penetrable elements (passages) and a length of more than 20 m. Six of these caves are longer than 100 m, and one is more than 500 m in length.

All caves in this group are located in the southwestern sector and the adjacent part of the central sector of the Inner Range and have entrances in the cuesta cliffs. Almost all caves are characterized by linear patterns comprised of short fracture-controlled segments, laterally connected to form a continuous zigzagging passage that follows a certain trend (Fig. 4). Main passages are stratigraphically controlled and are slightly inclined from the entrances toward the ends according to an orientation of the trends relative to the dip of the rocks.

The longest in the region is Tavrskaya Cave (507 m) developed in the Paleocene limestone. The longest in the Eocene limestone is Zmeinaya Cave (310 m). The maps and profiles of these caves are given in Fig. 5. All smaller caves of this group are structurally and morphologically similar to these largest caves or conform to their certain components. It is, therefore, instructive to give descriptions of these caves in some details.

3.2.1 Zmeinaya Cave

Zmeinaya Cave is located in the central sector and developed in the nummulitic Eocene Limestones. The cave opens to the cliff as a large unroofed rift, which crosses vertically almost the entire limestone sequence except for the upper 5–7 m (Fig. 5a)

The main passage is represented by a widened to 1.5–3 m upper part of the rift (Fig. 6d). There is a "false" floor 2–3 m from the ceiling through the large part of the cave, comprised of clasts wedged in and blocking the narrower lower sections of the rift. In parts of the main passage where the bottom slot is gapping one can descent 2–5 m down through the rift, till the next level of blockage. The map and observations in the cave show that this rift, generally trending N70W (normal to the front cliff and roughly parallel to the nearest cliffs in transverse valleys; see Fig. 4), is composed of a series of laterally connected individual fissures of S80W, N45E, N78W and N45W orientations. The main passage is wider near the entrance and gets progressively narrower toward the end of the cave, eventually pinching out to an impassable conduit. There are no indications in the far reaches of the cave that either inflow or outflow could occur laterally or from the surface.

The ceiling of the main passage is solutionally sculptured, smooth and concave through most of the cave, suggesting that guiding vertical fractures did not extend above the ceiling level and were completely reworked by dissolution. There are numerous cupolas in the ceiling rising 2–5 m above the normal ceiling level (Fig. 6h, i). Many cupolas are complex features, in which smaller cupolas are nested in a larger cupola. The morphology of ceiling channels indicates local lateral flow toward nearest cupolas. The tops of highest cupolas terminate at the same level, reaching a specific densely fractured bed in the upper part of the sequence. Near the entrance, there are several small side conduits, constrained to a particular bed, pinching out in 2–4 m away from the main passage. The same bed controls shallow side notches present in several sectors of the main passage. Throughout the entire cave, there are no morphological indications of descending flow or seepage from the surface.

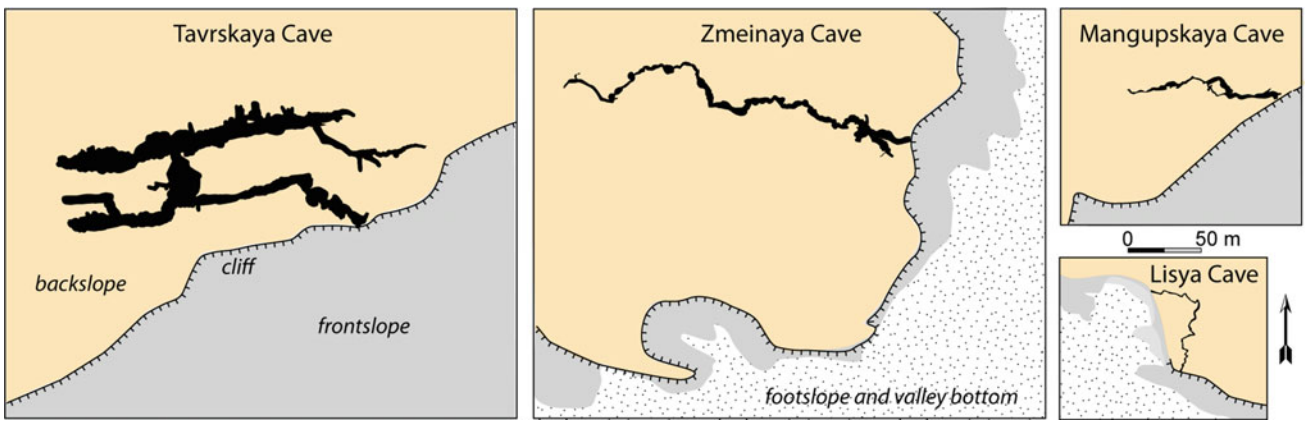

Fig. 4 Plan patterns of some significant "common" caves in the Inner Range and their occurrence in the cuesta massifs

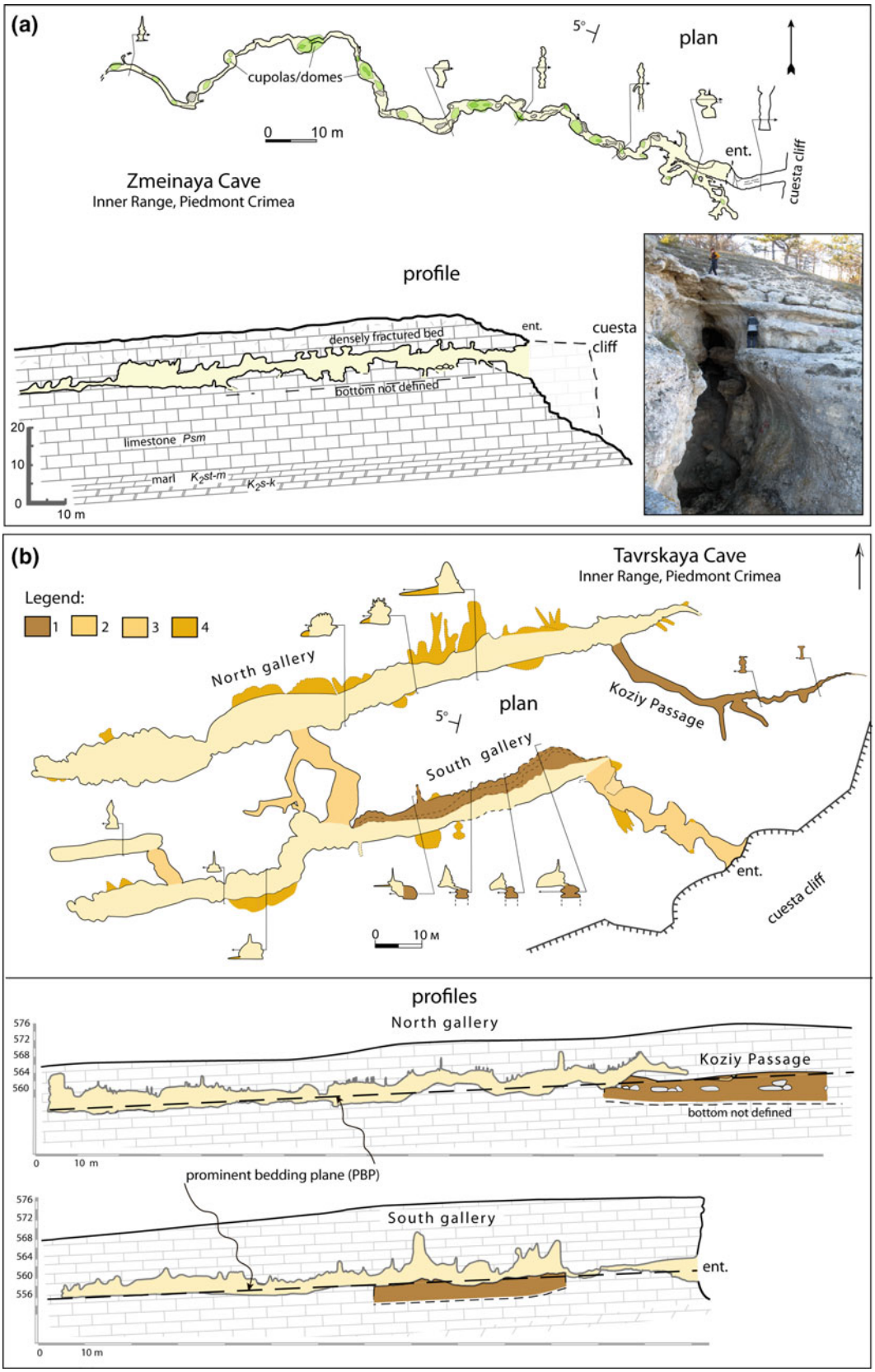

Fig. 5 Maps and profiles of the longest caves in the Crimean Piedmont: **a** Zmeinaya Cave in the Eocene limestones; **b** Tavrskaya Cave in the Paleocene limestones. Legend for **b** *1* rift passages; *2* main galleries; *3* bedding-plane passages; *4* side conduits

(a)
0.5 m
(b)
(c)
2 m
(d)
(e)
1 m
(f)
1 m
(g)
1.3 m
(h)
1 m
(i)
(j)
(k)
1 m
(l)
(m)
(n)

◀ **Fig. 6** Morphological features of caves in the Inner Range. **a**–**g** typical passage cross sections, showing rift-like base with widened portions that can be either controlled by a particular bed (**a**–**c**) or develop at the top of rifts (**d**–**g**); **h** and **i** ceiling channels and cupolas; **j** and **k** rising wall channels; **l**–**n** feeders. Caves in the Paleocene limestones: Mangupskaya Cave (**a** and **b**), Besh-Kosh-3 (**j**) and Tavrskaya Cave (**k** and **n**). Caves in the Eocene limestones: unnamed cave fragment in the group of "rock idols" near Bakhchisaray (**c**), Sary-Kaya Cave (**d**), Lisya Cave (**e**), Alimova Cave (**l** and **m**), Zmeinaya Cave (**g**, **h** and **i**). See Fig. 1b for cave locations

The cave completely lacks speleothems (except of localized thin calcite crust) and sediments of fluvial origin.

The morphological analysis allows unambiguously reconstructing the functioning of the conduit system during speleogenesis. The cave was formed under confined conditions by waters rising along a series of laterally interconnected fractures, which terminated upward at the same stratigraphic level. The upper termination of fractures caused the rising water to flow laterally toward nearest structural weaknesses breaching this hydrostratigraphic barrier. These weaknesses were exploited by cupolas that ultimately reached the densely fractured, diffusely permeable bed at the top of the Eocene limestone sequence to provide discharge from the conduit system. Local lateral flow components at the level of the upper terminations of fractures caused the upper parts of the forming rifts to grow in width more efficiently, resulting in a top swell in their cross section. The widening of the top part of rifts was also facilitated by the presence of a bed in this level with elevated pore permeability, which supplied the matrix aquifer water to mix with the conduit (rift) water and enhance dissolution. Based on the size of cavities, it is apparent that the rising water flow was greater in the part of the cave adjacent to the present cliff than in the distant part of the cave.

As the limestone sequence was overlain by confining marls and clays of the Novopavlovskaya Suite, a part of the Middle Eocene succession that separated it from the stratigraphically higher Miocene carbonates (now removed in the Inner Range), the densely fractured and diffusely permeable bed at the top of the limestone distributed the flow toward places where the confinement was structurally compromised, allowing for further upward leakage and eventual discharge. It is apparent that such places were associated with major fracture/fault systems that controlled the formation of the Inner Range escarpment.

3.2.2 Tavrskaya Cave

Tavrskaya Cave entrance opens in the 23 m high cliff of the Paleocene cuesta, 8 m above the base of the vertical cliff face exposing the Upper Danian limestone (see Fig. 1 for the location). The detailed morphogenetic mapping of the cave revealed four different morphotypes of cavities (Klimchouk and Timokhina 2011), as shown by different colors in Fig. 5b. They are (1) main galleries, (2) side conduits to main galleries, (3) rift passages and (4) bedding plane passages. The entrance passage is controlled by a bedding plane (referred to below as PBP) that is morphologically prominent in almost all Paleocene cuesta cliffs in the southwestern sector.

Main galleries (the North and South galleries) are wide (3–10 m) and high (up to 8 m) major elements of the cave, oriented at N75E, which occur almost parallel to the cliff face in the entrance sector, 30–60 m from it (Figs. 4 and 5b). Both galleries occur at the same stratigraphic level and are gently inclined to ESE. The ceiling of the South gallery lays 9–12 m beneath the cuesta dip slope, of the North gallery −7–8 m, but some cupolas come as close as 2–4 m from the surface.

Each main gallery was formed by merging of two closely spaced narrower fracture-controlled passages due to breakdown of partitions that once divided them, as shown in Fig. 7a, b. This is evidenced by the presence of two sub-parallel fracture-controlled lines of half-conduits and cupolas at the ceiling of each gallery, separated by a breakout surface at the center (clearly visible in the South gallery but masked by a band of stalactites in the North gallery; see photographs a and b in Fig. 7), and of solutionally sculptured fragments of the fallen partitions piled along the axis of the galleries (see also photograph h in Fig. 7). Meso-morphological features of the main galleries include feeders in the bottom (Fig. 7f, g) and abundant phreatic speleogens in the walls (rising wall channels and solution pockets; Fig. 6k; Fig. 7a, b, c, f, h) and the ceiling (ceiling channels, cupolas and bell-holes), which together constitute a suite indicative of rising flow and an important role of natural convection circulation (Klimchouk 2007, 2009). The highest cupolas rise at least 3–4 m above the average ceiling level. There is a 30-m-long passage with similar morphology between the major galleries in the eastern part of the cave, connected to the South gallery through a low bedding plane passage. The main galleries terminate abruptly at their level to the east, although the North gallery has a distinct point feeder at the termination (Fig. 7g), blocked by sediments at 1.5 m depth.

Side conduits and notches (indicated by yellow color in the cave map; Fig. 5b) are low cavities adjacent to the main galleries, which pinch out a few meters away from them. They occur in the same bed that lies immediately above the PBP and apparently has higher matrix permeability. The simplified morphogenetic map in Fig. 5b shows that these features occur asymmetrically relative to the galleries, mainly along the outer sides of the main galleries. As

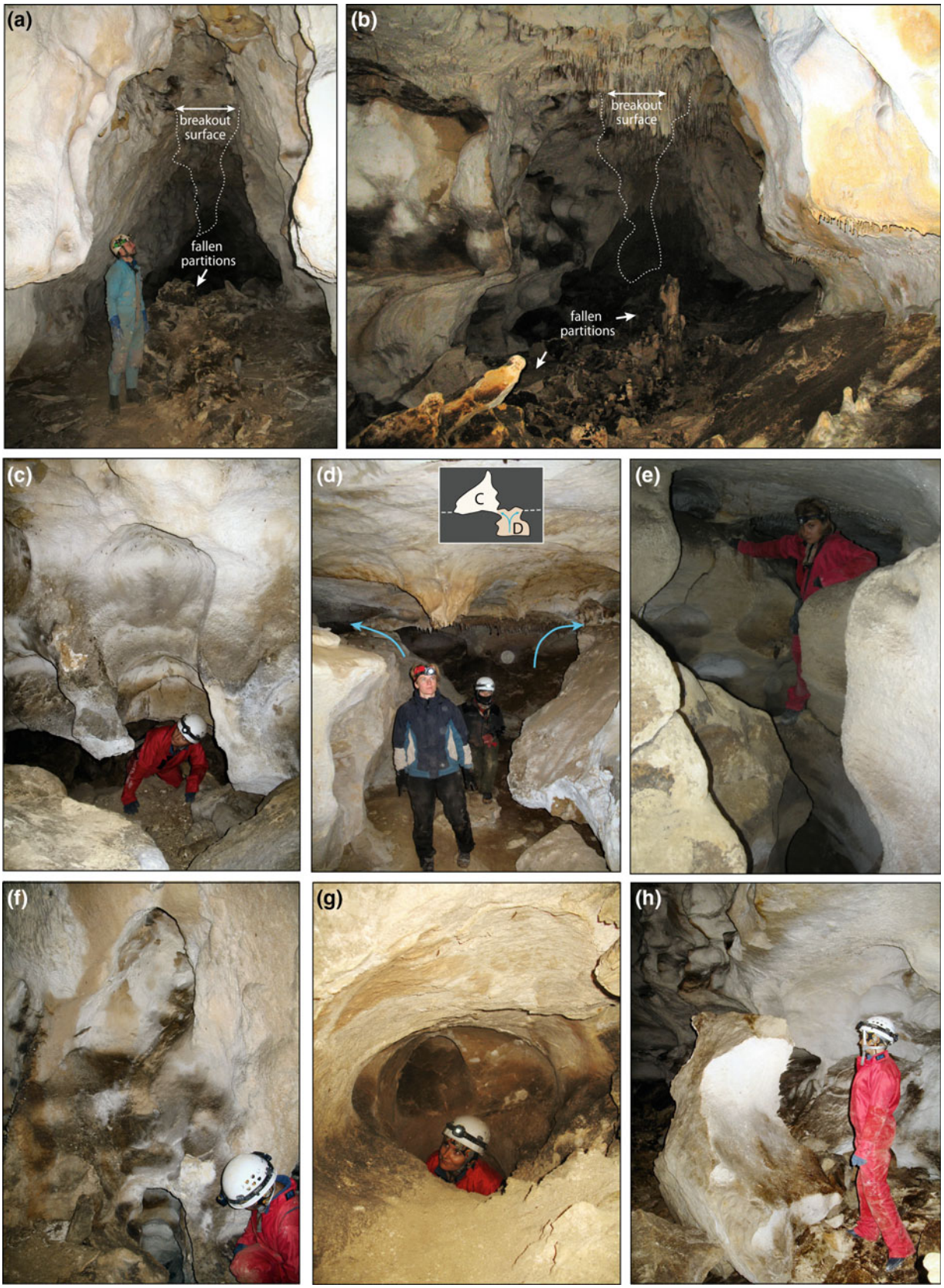
(a)
breakout surface
fallen partitions
(b)
breakout surface
fallen partitions
(c)
(d)
C
D
(e)
(f)
(g)
(h)

◀ **Fig. 7** Morphological features of Tavrskaya Cave: **a** the South gallery; **b** the North gallery (both passages were formed by merging of two closely spaced rift-like passages separated by partitions, as shown by a *dotted line*); **c** rising channel in the hanging wall in the South gallery above the adjacent rift-like passage shown in **d** (*inset* in **d** shows the relative positions of these elements, and *arrows* indicate inferred directions of the cave-forming flow); **e** rift-like passage in the western part of the cave (Koziy Passage; see also Fig. 6f); **f** and **g** point feeders; **h** fragment of a fallen rock partition

demonstrated by Klimchouk et al. (2012), such side conduits and notches form due to mixing corrosion where groundwater in a more permeable bed in a stratified aquifer is drained to major cross-formational conduits that conduct rising flow.

Rift passages occur below the floor level of the main galleries and below the PBP (see profiles in Fig. 5b). There are two rifts passages accessible in the Tavrskaya Cave (marked by dark brown color in the map and profiles): one is well individualized and joins the Northern gallery from the east (Koziy Passage), and another rift extends along the northern edge of the South gallery and connects to it through the widened PBP (see photograph d in Fig. 7 and insert there). The connection contour is marked by a series of rising channels in the hanging wall of the South gallery (Fig. 7c), unambiguously indicating that the rift functioned as a linear feeder to the South gallery. The rift along the South gallery is wider (up to 2 m) and shallower, plugged by sediments at the bottom (Fig. 7d), whereas the Koziy Passage rift is narrow and deep (Figs. 6f and 7e). Both rifts extend down probably to the bottom of the limestone unit, which is suggested by the presence of fragments of upward-extending passages with similar morphology in the cliff near its base. Both rifts terminate upward at the PBP, with the smooth concave ceiling developed at the base of the next upper bed (Figs. 6f and 7d, e).

Bedding plane passages are low (0.5–1.0 m) and wide (2–5 m) passages developed along the PBP. One leads from the entrance at the cliff to the South gallery, and the others connect the main galleries.

The structure of the cave system is determined by sub-vertical tectonic fractures of three sets, oriented at N70-80E (the North and South galleries, the far reach of the Koziy passage, and the cliff face near the South gallery), N60-70W (the middle part of the Koziy passage, the northern part of the passage that connects the main galleries, and the entrance passage), and N30W (the northern segment of the Koziy passage and the bedding plane passage that connects the western part of the South gallery and an isolated conduit to the north). These directions are well expressed in the cuesta faces and in local tectonics. Fractures that control the rift passages terminate upward at the PBP, and fractures that control the main galleries in the upper part of the limestone sequence probably do not extend down below the PBP. Passages developed along the PBP laterally interconnect the sub-vertical elements occurring in different parts of the sequence.

The functional organization of the conduit system during speleogenesis can be unambiguously inferred from the morphogenetic analysis of the cave. There are no indications in the pattern and morphology that the cave was developed by lateral flow in the limestone sequence or that it has ever received any recharge from the overlying surface. In contrast, evidence suggesting that the cave was developed by rising flow is obvious and overwhelming. The main inputs of rising waters were through the Koziy passage and the rift adjacent to the South gallery. The flow that rose through fractures located below the PBP reached the upper-level fractures either via direct intersections (such as in the junction of the Koziy passage and the North gallery) or followed the PBP locally to connect the near upper-level fractures (the case of the rift adjacent the South gallery; see the cave map in Fig. 5b and photographs c and d in Fig. 7). Conduits developed along the PBP also provided the connection between the parallel rift series at the upper level, such as those which gave rise to the North and South passages. The entrance passage was a bedding-plane connection between the South gallery and the inferred next series of rifts further to the south, along which the cliff was formed later on. Discharge from the cave occurred via several high rising solution chimneys in the main galleries, which conveyed flow to conductive features in the once overlying succession, now removed by denudation.

The PBP and the highly permeable bed above it also provided lateral inflow of the aquifer waters to mix with the rising conduit waters, which caused enhanced dissolution at the intersection level and determined the complex pattern of convection circulation in the cave space above the PBP. The role of the lateral inflow from this particular horizon is reflected in the abundance of respective convection morphs in the main galleries (solution pockets and niches, rising wall channels, cupolas, bell-holes, etc.), whereas these are less common in the rift passages below the PBP. The merging of closely spaced rift-like passages above the PBP due to the breakdown of thin partitions, which created the wider present-day galleries, probably occurred during the transition from phreatic conditions to vadose due to the loss of the buoyant support—a common case in hypogenic caves.

3.2.3 Morphological Features of Other "Common" Caves

Most of other caves of this group in both Eocene and Paleocene limestones are morphologically similar to Zmeinaya Cave and rift-like passages in Tavrskaya Cave. They

are all linear caves developed along a series of laterally interconnected fractures, rarely having small side passages (Fig. 4). It can be generalized that principal human-accessible passages in these caves are widened intervals of sub-vertical karst rifts. The widened intervals develop either along the line of intersection of a sub-vertical fracture with certain beds and bedding planes of relatively high permeability, where stratiform notches form in the walls (Fig. 6a, b, c), or/and at the very top of the guiding fractures, along their upper termination (Fig. 6d, e, f, g). Widened up to a few meters intervals (actually mapped cave passages) have much narrower rift-like extensions downward, commonly inaccessible because of their smaller cross-size and blockage by sediments but locally penetrable or traceable for several meters down. There is a remarkable similarity in the morphology of passages between caves occurring in the Eocene and Paleocene limestones (compare e and f in Fig. 6). There are no indications in the pattern and morphology of the caves (as well as in sediments; see Sect. 5) that they ever received recharge from the overlying surface and conducted focused lateral flow. All the caves are characterized by meso-morphological features indicative of rising flow and of an important role of natural convection circulation.

3.3 Isolated Chambers

Another distinct type of caves is represented by isolated flattened chambers that occur at the contact between the Eocene limestones and underlying Maastrichtian and Paleocene marls in the central and eastern sectors of the Inner Range. Such chambers can be isometric or elongated along a sub-vertical fracture, are 1–3 m in height and up to 50 m in width, and open to the surface either from above through collapsing of the roof (Fig. 8a–c) or from a cliff (Fig. 8d–f). Some chambers have smooth cupolas and channels in the ceiling. Seemingly isolated chambers have been repeatedly opened by excavations during construction works in cities of Sevastopol (in the Neogene limestones) and Simferopol (in the Eocene limestones). Depending of dimensions and geomorphological position of entranced and dimensions of voids, such features can be formally classified as caves or rock shelters.

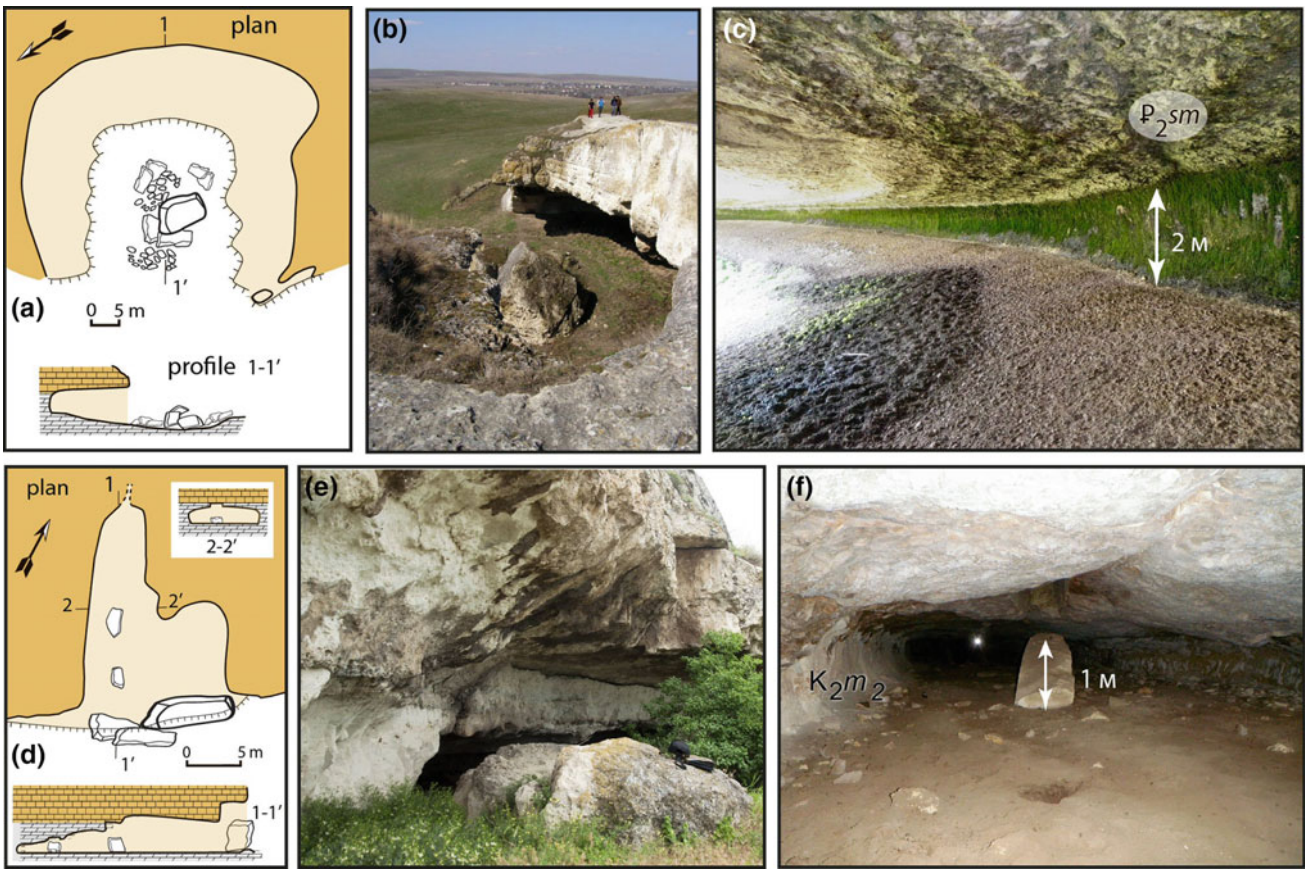

Fig. 8 Isolated chambers in the Inner Range: **a–c** in the Ak-Kaya massif in the eastern sector (**a** plan and profile; **b** and **c** views from *outside* and *inside*); **d–f** in the Sary-Kaya massif in the central sector (**d** plan and profiles; **e** and **f** views from *outside* and *inside*)

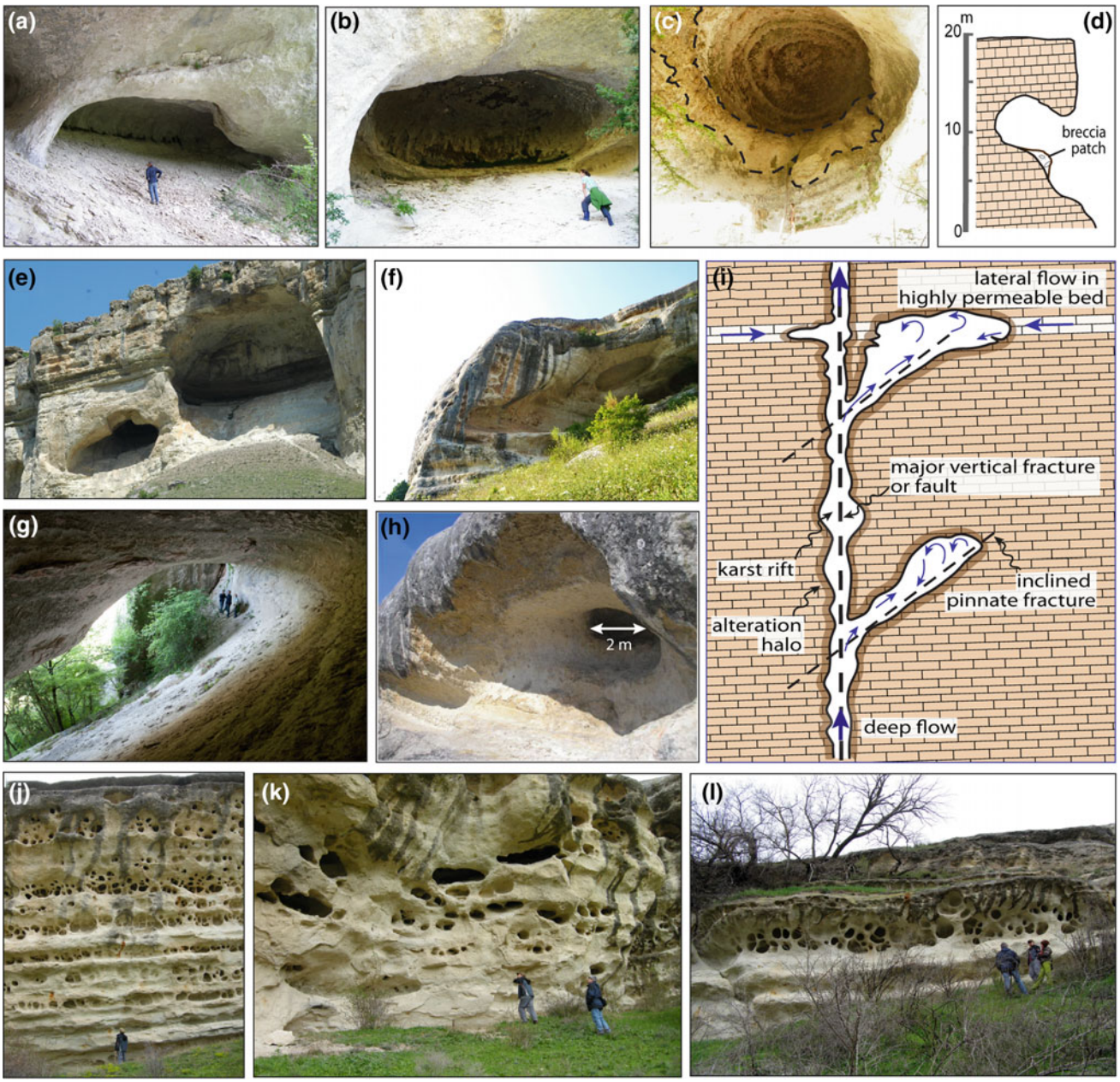

Fig. 9 Rock shelters and tafoni in the Inner Range of the Crimean Piedmont. **a**, **b**, **g**, **j**, **k** and **l** in the Eocene limestones; **c** and **h** in the Paleocene limestones; **e** near the contact between the Paleocene and Eocene limestones in the eastern sector. The *black dashed line* in **c** outlines patches of breccia (shown in the profile view in **d**) accumulated during the rift stage; **i** conceptual model of the formation of side cavities (future rock shelters) and the alteration halo (future zones of tafoni and honeycomb development) along karst rifts. **j**, **k** and **l** show tafoni in the Eocene limestones

3.4 Rock Shelters and Tafoni

Rock shelters are wide but shallow cavities in vertical and steeply inclined cliffs, in which the width dimension is greater than their normal-to-cliff extension into the rock. There are thousands of rock shelters in the cliffs of the Paleocene and Eocene cuestas in the Inner Range (Fig. 9a–h). They also occur in outcrops of the Neogene limestones in the Outer Range but have generally smaller dimensions and lesser variability in morphology and conditions of occurrence there.

Rock shelters are found in cliffs that have varied exposition and heights (ranging from 5–10 to 80–100 m) and occur in different geomorphological and environmental situations: in the main front of the cuesta massifs, in large transverse valleys, in narrow gorges and ravines dissecting

the massifs in different directions, in open and forested escarpments. They occur in all textural and structural varieties of Paleocene and Eocene limestones and marls exposed in the cuesta cliffs, at different heights above the cliff base.

Despite the variability of these conditions, rock shelters display some persistent characteristics allowing classifying them into several types. The most common are features that have the floor inclined outward at 25°–40° and the concave vault (Fig. 9a, b, e, f, g). Such rock shelters often have a gentler slope or a sub-horizontal bench at the rear (Fig. 9b, e). They are commonly 10–30 m wide (although sometimes are up to 60–80 m wide) and 3–10 m high, extending into the massif for 10–30 m relative to the cliff face. Many rock shelters have nested alcoves at the rear (Fig. 9a, b) and oval or spherical cupolas in the vaulted ceiling (Fig. 9c, f, h). Some rock shelters have ceiling half-channels in the overhanging visors. In the cliffs of the Eocene cuesta in the southwest sector of the Piedmont, inclined rock shelters of remarkably similar morphology often occur in series along straight cliff segments, at a regular distance of 80–100 m between individual features, and at the same height above the base.

Less common, although not infrequent, are rock shelters with horizontal floors, associated with contacts between different rock units. They typically have lateral dimensions up to 10 m and heights up to 2–3 m and are similar in morphology to isolated chambers described in Sect. 3.3. Also common are rock shelters that have more or less isometric shapes (roughly half-spherical), and features that are low and elongated along the cliff, grading to what can be described as notches. In rock shelters of all types, nested morphological features closely resembling convection-related speleogens found in hypogene caves are frequently observed.

The term "tafoni" refers to a certain category of cavernous decay features found in rock surfaces, although it is vaguely and contradictory defined in the literature (see Klimchouk Chap. 1 for further discussion). The term is used here to denote decimeter- to meter-sized cavities in cliffs, i.e., features that are larger than honeycomb cells but smaller than rock shelters (Fig. 9j, k, l). They occur extensively in cliffs of the Eocene cuesta in the southwest sector of the Inner Range and occasionally in other sectors. Individual cavities are closely spaced and arranged in stratiform series corresponding to certain beds and notches developed along them (Fig. 9j, l), although in places the stratigraphic control over tafoni distribution in cliffs is blurred (Fig. 9k). Tafoni are characterized by smooth concave inner surfaces, with smaller features often nested in larger ones. Typical dimensions are within several decimeters. Occasionally 1–2 m-sized features occur and rarely features of several meters in dimensions (although the later formally fall in the category of rock shelters). Geomorphological observations suggest that cliffs with the best-expressed tafoni were formed relatively recently (at time scales of hundred to thousand years) by detachment and toppling of large blocks toward the valleys. Cliffs with greater time of exposition show the presence of tafoni degrading under the action of weathering (see Fig. 11h in Klimchouk Chap. 1).

Honeycomb structures—smaller forms of cavernous weathering characterized by closely spaced hollows arranged into characteristic patterns—widely occur in cliffs of all rocks in the Piedmont cuestas. They often occur in rock shelters or are closely associated with them. General discussion of honeycomb structures is given in Klimchouk (Chap. 1), and photographs of typical examples from the Inner Range are shown in Fig. 12 therein.

The origin of rock shelters, tafoni and honeycomb structures in the Crimean Piedmont was loosely attributed, following a deeply rooted geomorphological tradition, to various weathering processes including aeolian deflation, desquamation through frost action, wetting and drying, salt weathering and stress release (e.g., Dushevsky 1987; Dushevsky and Kuznetsov 1991; Blaga and Popov 2009). None of these processes, however, can adequately explain conspicuous morphology of rock shelters and cavernous weathering features and their occurrence in a wide range of geomorphological, lithological and environmental conditions.

The detailed study of these features in the Crimean Piedmont demonstrated their genetic affinity to hypogene speleogenesis (Klimchouk et al. 2013). It is proposed that the formation of inclined rock shelters was guided by inclined pinnate fractures associated with major sub-vertical fractures and faults, which control the formation of karst rifts by rising deep flow (Fig. 9i). Such inclined fractures are widely observed in cliffs, controlling the characteristic facets in the ledges of cuesta massifs. Traces of these fractures are often visible in the rear and side parts of rock shelters (Fig. 9a, g). As shown in Fig. 9i, pinnate fractures were cul-de-sacs for rising flow, in which circulation was dominated by convection. Where the upper parts of pinnate fractures intercepted high-permeability beds in the limestone aquifer, dissolution could be enhanced due to mixing. Other types of rock shelters correspond to various widened areas of karst rifts or to isolated chambers formed at bedding contacts. These features of hypogene morphology became rock shelters when cliffs have formed along karst rifts in the course of the cuesta frontslope retreat by block toppling. This conceptual model explains well all major features of morphology and distribution of rock shelters. It is also supported by frequent occurrences of patches of cemented breccia, attached to inclined or even vertical surfaces of rock shelters at their mouth (as shown in Fig. 9c, d), comprised of unsorted angular rock shatter. Such accumulations of breccia have apparently formed before the formation of the cliffs, in karst rifts opened at the top to the cuesta dip slope (see Fig. 2a for an example).

Tafoni and honeycomb structures are interpreted as the result of fluid-induced isovolumetric alteration of the host rocks in the walls of hypogene karst conduits and voids (the process also termed as "phantomization" in the ore geology and karst literature; e.g., Dubois et al. 2014) and the subsequent removal of the alterite by groundwater flow or by weathering after the exposure of the rift wall in a cliff (see Klimchouk Chap. 1 for further discussion of this model). Cleaning of internal hardened structures, formed within the alteration halo, produces honeycomb features, whereas an exhumation of the alteration front produces tafoni.

3.5 Conduits in Clayey Marls

In the southwestern sector of the Crimean Piedmont, near the Verkhnesadovoye town in the foot of the Outer Range, a road cut exposed a vertical fracture plane in clayey marls of the Novopavlovskaya Suite of the Middle Eocene (see Fig. 1 for the site location). This plane exhibits several vertical half-channels and has an opening to a small cave (Fig. 10). The morphology of the fracture wall, half-channels in it, and the cave show smooth concave surfaces and clear indications of rising flow, such as cupolas and (in the cave) rising chimneys in the ceiling. Up-slope above the cliff, there are several small sinkholes apparently formed by recent collapsing of similar cavities, fragments of which are visible at the sinkhole bottoms and sides. Accessible fragments also display smoothed cupola-like features.

The clayey marls of the Novopavlovskaya Suite, exposed in the bottom of the valley between the Inner and Outer Ranges, are a part of the marly–clayey succession that separates the underlying nummulitic limestones from the Miocene carbonate sequence that lays stratigraphically higher and outcrops in the cuesta of the Outer Range to the north of the study site. In this location, the Eocene nummulitic limestones occur at depth exceeding 100 m, and the Paleocene limestones lay at depth of several hundred meters, both hosting confined aquifers. A flowing well located 400 m to the west, pours thermal (25.7 °C) H_2S-laden water from depth of about 540 m. The documented features represent a conduit cluster formed by upward leakage from the Paleogene aquifer system across the marly–clayey succession (see Sect. 8 and Fig. 15 for a conceptual model).

4 Speleogenetic Morphologies in Cuesta Cliffs

Limestone cliffs of the Eocene and Paleocene cuestas of the Inner Range abundantly display conspicuous sculptured features of diverse morphology. Most typical are cliffs morphologically identical to walls of karst rifts, as described in Sect. 3.1 and shown in Fig. 2. Most of cliffs are rich in rock shelters, tafoni and honeycomb structures as described in Sect. 3.3 and shown in Fig. 9. Besides, there are numerous concave features that can be best described as half-conduits (Fig. 11). Most common are vertical and sub-vertical half-conduits (Fig. 11c, d) and vertically stacked niches that together form vertical conduits (Fig. 11b). Some features are laterally extended as notches (Fig. 11e, f, g). Some cliffs demonstrate complex arrays of concave forms constituting interconnected pattern of half-conduits (Fig. 11a). Many larger features have nested smaller concave forms such as cupolas, ceiling channels, alcoves and pockets, as well as honeycomb patches. Some have elements

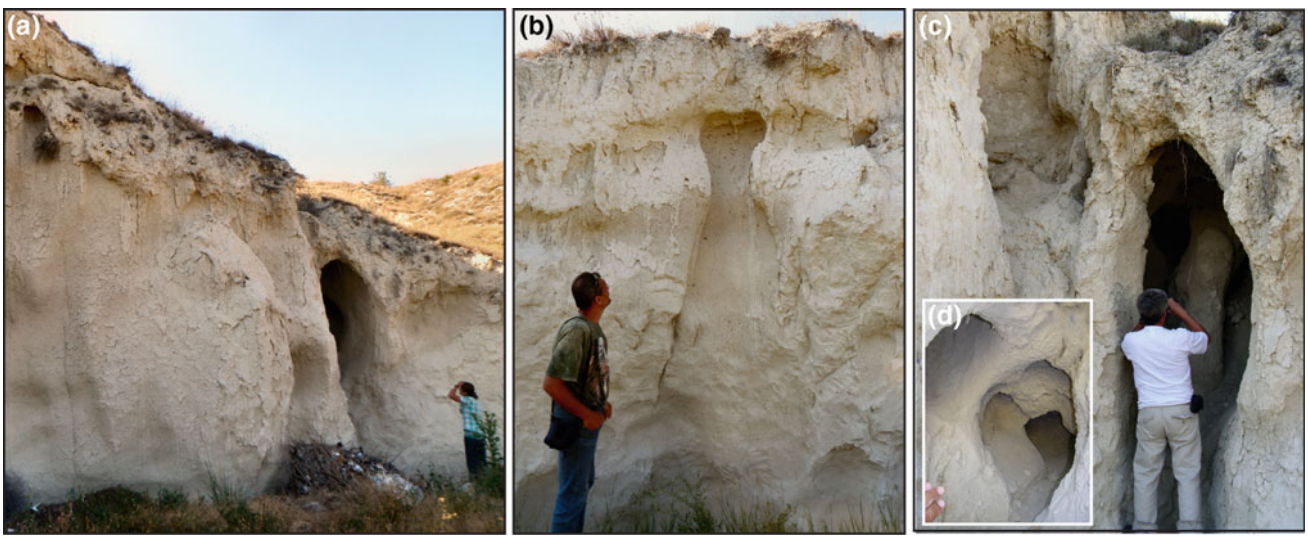

Fig. 10 Conduits with phreatic morphology and indications of rising flow in the Middle Eocene clayey marls that separate the Eocene and Neogene limestone sequences

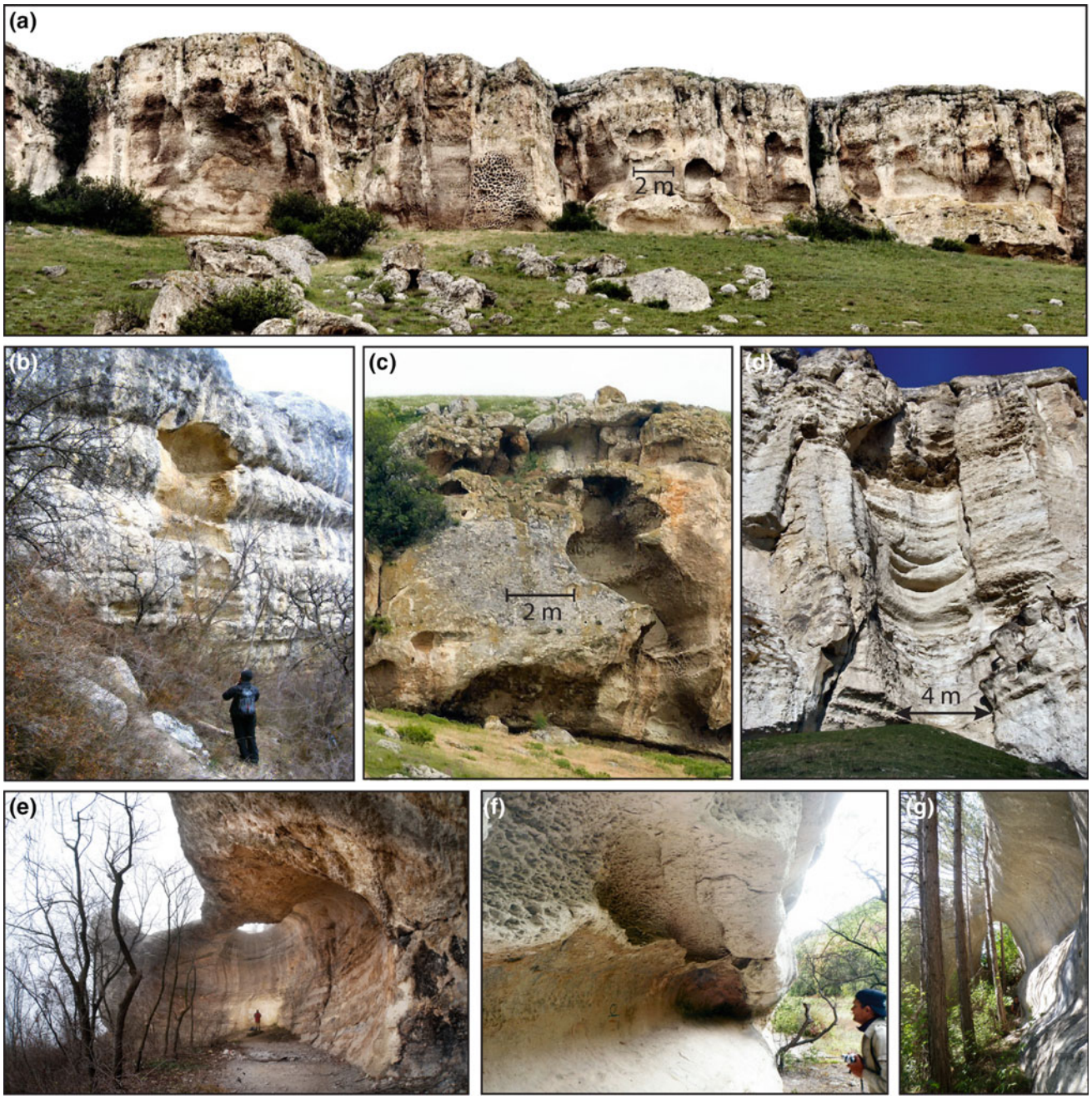

Fig. 11 Examples of half-conduits and other concave features in cuesta cliffs: **a**, **c**, **e**, **f** and **g** in the Eocene limestones; **b** and **d** in the Paleocene limestones. **a**, **c** and **e** in the central sector; **d** in the eastern sector; other photographs are from the southwestern sector

of "full" conduits (Fig. 11g) or are associated with caves, chambers or rock shelters.

These morphologies, as well as the presence on the footslopes of large fallen rock boulders that retain fragments of similarly sculptured walls, unambiguously suggest that cliffs form mainly by block toppling which opens karst rifts and other elements of void-conduit systems. The peculiar sculptured morphology of cliffs is caused mainly by speleogenetic processes rather than by weathering.

5 Cave Sediments and Formations

Karst rifts are devoid of speleothems and commonly have debris fill in the bottom. Those rifts which are opened to the cuesta dip slope receive weathering shatter material from the surface, sometimes forming weakly cemented breccia at the bottom.

Sediments in "common" caves are represented mainly by various clays filling lower parts of passages, breakdown

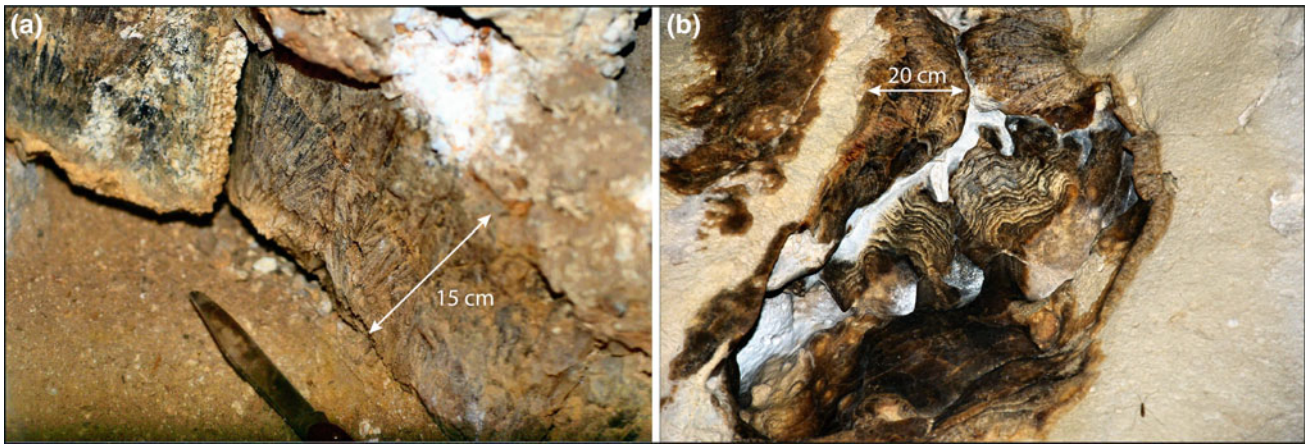

Fig. 12 Subaqueous calcite crust in Tavrskaya Cave

slabs of the host rock, and in places by bat guano accumulations 1–5 cm in thickness. Stream and flood sediments are entirely absent. Many caves have thin mineral coatings in lower parts of the walls, ranging in thickness from a few mm to 1–2 cm, which mineralogy is still to be studied. Subaerial speleothems are rare, with a notable exception of Tavrskaya Cave where stalactites, stalagmites, flowstone and moonmilk are quite abundant in the North gallery.

In two places in Tavrskaya Cave, in a small rift-like cave nearby (Podarochnaya Cave), and in Besh-Kosh-4 Cave located 10 km to the northwest, a phreatic dark-brown palisade calcite has been found that forms 7–15-cm-thick complexly zoned crust (Fig. 12). In Tavrskaya Cave, near the junction of the Koziy passage rift with the North gallery, this calcite occurs as partly re-dissolved patches in a rising chimney (Fig. 12b). The subaqueous origin of this calcite is confirmed by petrographic and fluid inclusion studies. Fluid inclusions are all-liquid (indicating the deposition temperature lower than ca. 50 °C), contain over 99 mol% of water and are characterized by ratios of dissolved gasses typical of the carbonates, deposited in phreatic conditions (Newman et al. 1996). This calcite was precipitated when the caves were a part of the karst plumbing systems of rising springs, likely lukewarm, pouring in bottoms of valleys incising into the overlying clay thickness (Fig. 13a).

6 Dating of Speleothems and the Landscape Evolution

U/Th dating from the base parts of four stalagmites Tavrskaya Cave yielded ages ranging within 125–130 ka, and four U/Th dates obtained from samples of phreatic calcite taken in Tavrskaya and Podarochnaya caves range from 417 (+44/−31) to 263 (+3/−3) ka (Klimchouk et al. 2011). These dating results provide constraints on the timing of important speleogenetic and geomorphological events. The dates from the subaqueous calcite suggest that phreatic conditions in the caves in the Paleocene limestones lasted through the Middle Pleistocene till at least 263 ka (Fig. 13a). In fact, the phreatic conditions lasted somewhat longer, as the phreatic calcite in a rising chimney of Tavrskaya Cave was partially re-dissolved, likely in response to a change in hydrochemistry induced by intensification of the lateral groundwater circulation in the homocline aquifer during latest phases of the disclosure of the confined system. The dates from the base of stalagmites indicate that by 130 ka vadose conditions have already been established in the caves of the Paleocene cuesta (Fig. 13b).

These data reveal that the Paleocene cuesta escarpment had formed during the end of the Middle Pleistocene (between 263 and 130 ka). Previously, based on geomorphological and geodynamic speculations, most of researchers placed the timing of the Paleocene cuesta formation to the Late Pliocene and believed that this cuesta had have been already well expressed in the landscape by the Early Pleistocene (e.g., Nikishin et al. 2006; Vakhrushev 2010). Thus, our new data show that the erosional dismembering of the homocline of the northern slope of the Main Range of the Crimean Mountains and the expression of the Inner Range in the southwestern sector of the Piedmont occurred significantly later in time than it was thought before.

7 Conduit Wallrock Alteration

A systematic study of carbon and oxygen isotope composition of bedrock in the walls of caves and presumed remnants of karst conduits in cliffs in the Paleocene cuesta has revealed alterations induced by fluid–rock interactions

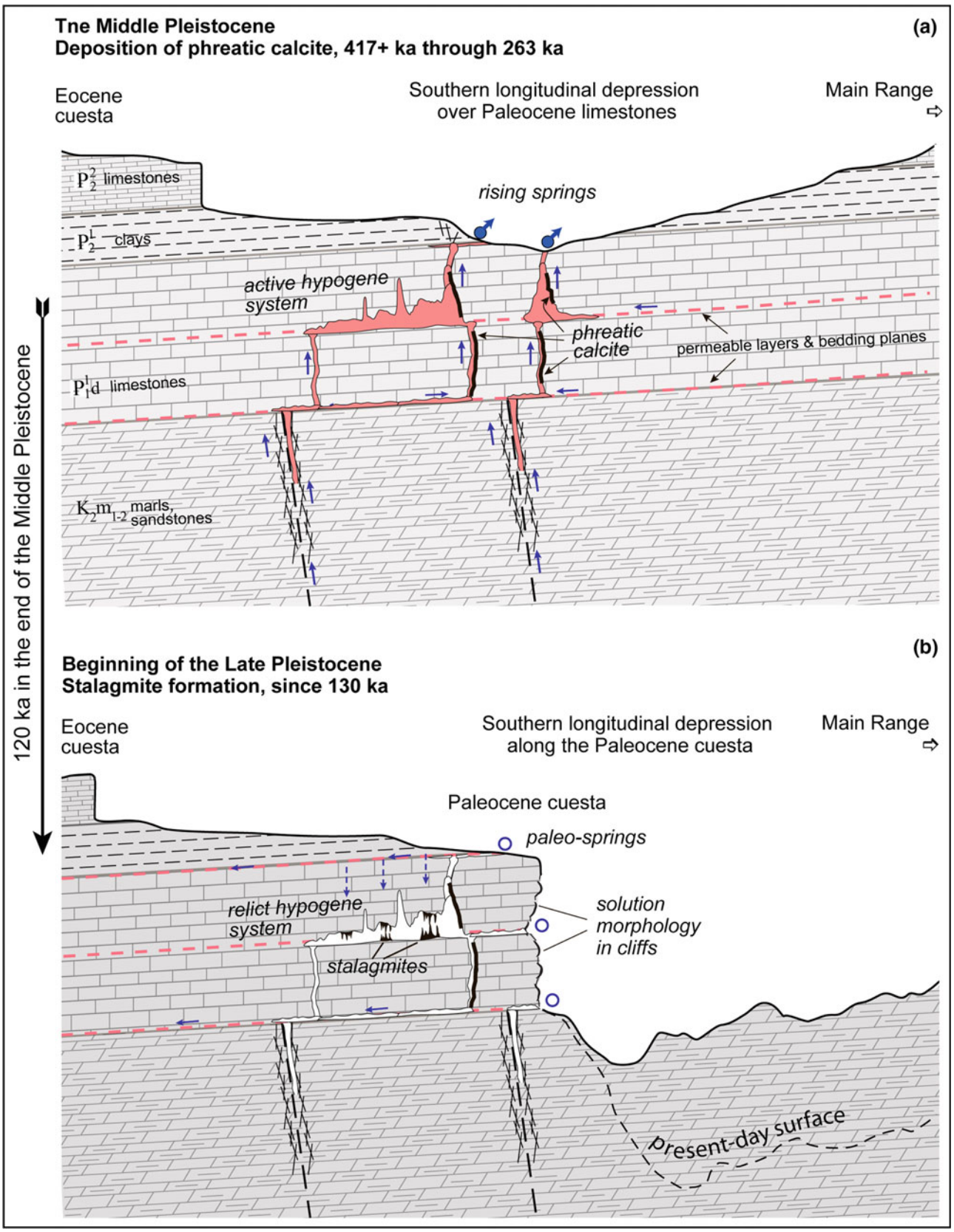

Fig. 13 Conditions of speleogenesis and the landscape evolution in the southwestern sector of the Crimean Piedmont in the Middle–Early Pleistocene. A schematic representation of geomorphological and hydrogeological conditions for the late hypogene (**a**) and vadose (**b**) phases of speleogenesis in the Paleocene limestones (modified from Klimchouk et al. 2011)

associated with hypogene karstification (Dublyansky et al. 2014). Several events of the fluid history, each resulting in isotopic alteration of the bedrock, are recognized.

(1) Early development of hypogene karst conduits shifted $\delta^{18}O$ and $\delta^{13}C$ toward lower values by 1–2‰ and 1–3‰, respectively, relative to the unchanged rock. This alteration, documented both in caves and in cliffs, encompasses a zone ranging in width from several tens of centimeters to a few meters.
(2) Ribs and protrusions of honeycomb structures in the cuesta cliffs are characterized by the $\delta^{18}O$ and $\delta^{13}C$ values shifted toward slightly more positive values (by up to 3 and 1‰, respectively). This character of isotopic alteration strongly suggests a link to deep-seated fluids enriched in both ^{18}O and ^{13}C isotopes. Such waters of deep origin are known in Crimea in association with mud volcanoes on the Kerch Peninsula, east of the Piedmont (see Fig. 1a for their location). It was suggested (Klimchouk et al. 2013; Dublyansky et al. 2014) that similar deeply derived water affected the Crimean Piedmont during the Middle Miocene, the time of the peak activity of the mud volcanoes (Shniukov et al. 1992).
(3) Late-stage hypogene karstification resulted in a high-magnitude shift of the $\delta^{18}O$ toward lower values (by 5–6‰) within a thin (5–15 mm) alteration halo. In most cases, $\delta^{13}C$ was also significantly shifted toward lower values (by 6–9‰), but in one case a shift toward higher values (by ca. 2‰) was observed. In cores from Podarochnaya and Besh-Kosh caves, which transected both the phreatic calcite crust and bedrock, the most-altered values of limestone are similar to the isotopic composition of the speleothem calcite, suggesting the action of same waters.

These results support not only the hypogene origin of caves but also the same origin of conspicuous features in the cuesta cliffs, thus corroborating a conclusion based on field observations that the formation of cliffs was largely controlled by hypogene karst structures.

8 Speleogenesis

We presented multiple lines of evidence strongly supporting the hypogene origin of all categories of cavities and conduits described above: karst rifts, “common” caves, rock shelters and tafoni, and isolated chambers. Speleogenesis occurred in confined conditions by flow that rose along cross-formational tectonic discontinuities (major fractures, fracture zones and faults) across the clay–carbonate strata of the upper tectonostratigraphic story (Upper Cretaceous, Paleogene and Neogene formations), interacting with lateral flow in stratabound aquifers in this story.

The reconstruction of the regional geological, geomorphological and hydrogeological evolution of the region (Klimchouk et al. 2013) provides another line of evidence supporting hypogene speleogenesis as it demonstrates favorable conditions for its development. The Crimean Piedmont extends along the junction between the fold-thrust structure of the Mountainous Crimea and the Scythian Plate, above the regional suture (Fig. 14)—a zone that was geodynamically active since the Jurassic. To the east of the Piedmont along this zone, in the Kerch Peninsula (Fig. 1a), a focused rise of deep fluids, evidenced by numerous mud volcanoes, continues through the Neogene and Pleistocene till present, with a peak intensity in the Middle Miocene (Shniukov et al. 1992). Isotopic fingerprints of similar fluids, associated with hypogene karst features, are found in the Piedmont (see Sect. 7; Dublyansky et al. 2014).

The regional uplift in the Sarmatian (Late Miocene) interrupted a period of marine sedimentation (Oligocene–Miocene), caused the removal of the Cretaceous–Paleogene cover in the most uplifted area of the present-day Main Range, and formed the homocline in its northwestern and northern slope. The Main Range and the upper parts of the homocline became the marginal recharge area of the North Crimean artesian basin. The groundwater flow in aquifers of the Cretaceous–Paleogene cover was intercepted by fracture corridors in the suture zone (the present-day Piedmont belt), where it mixed with rising deep fluids and partially discharged to the surface. This situation favored hypogene karstification along the Piedmont during the Late Miocene–Pliocene. Proportions of deep rising flow and stratabound aquifer flow components in the Piedmont varied through time depending on pulses of geodynamic activity in the suture zone and variations in the lateral aquifer flux induced by changes in geomorphological and climatic conditions. The continued uplift of the Main Range and erosion in its northwest slope caused progressive removal and dismembering of the Cretaceous–Paleogene cover during the Late Pliocene–Early Pleistocene. As suggested by the dating of phreatic speleothems (Sect. 6), by the end of the Middle Pleistocene the development of the hypogene void-conduit systems in the Inner Range has ceased due to the erosional incision into the Paleocene limestones.

All types of cavities described in this chapter represent integral, complexly structured, but functionally united void-conduit systems (Fig. 15a). The basic elements of hypogene void-conduit systems, which form their spatial framework, are karst rifts developed in the limestone sequences. They form along major sub-vertical fractures dissecting certain lithostratigraphic units, arranged in fracture zones (corridors). Flow rising through fracture zones locally followed stratiform high-permeability features (such

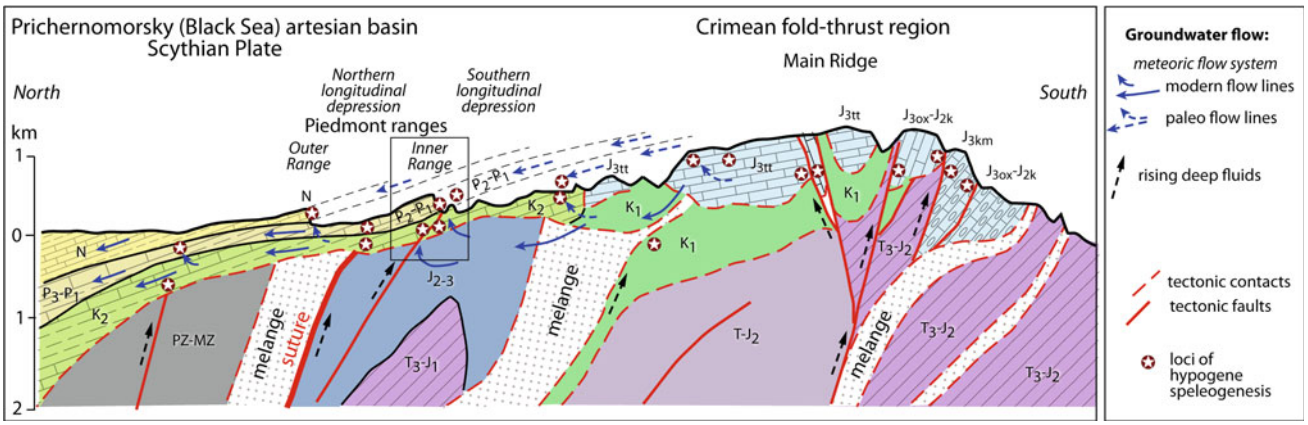

Fig. 14 Schematic geological cross section across the Crimean fold-thrust region and its junction with the Scythian Plate (simplification based on Yudin 2011), showing modern and paleo-flow systems and localization of hypogene speleogenesis. The black rectangle encompasses a domain further detailed in Fig. 15

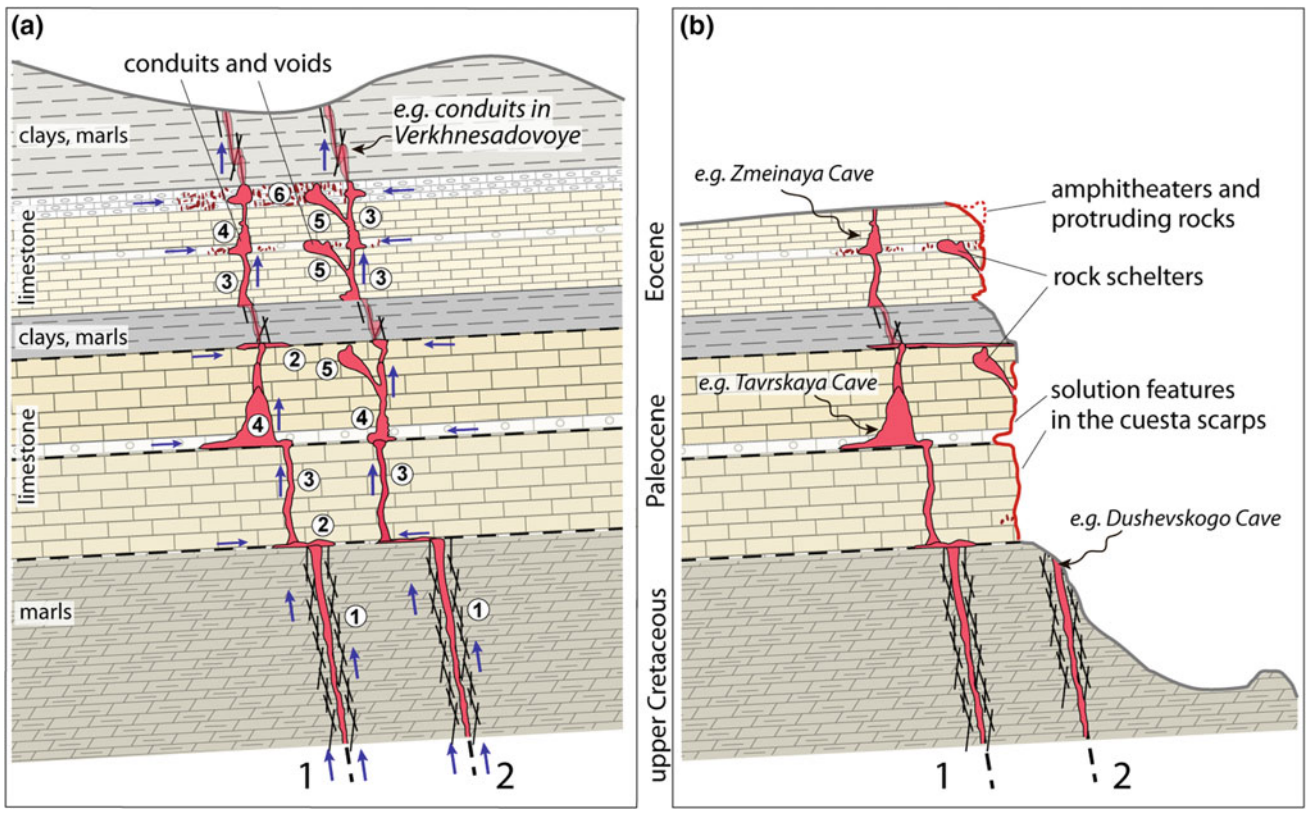

Fig. 15 Conceptual model of hypogene speleogenesis in the Crimean Piedmont. **a** Structure and functioning of void-conduit systems during main stages of hypogene speleogenesis. Numbers in circles indicate morphogenetic components: *1* rift-type conduits along faults and damage zones in the Maastrichtian marls; *2* solutionally enlarged bedding partings; *3* rift-type conduits along sub-vertical fractures in limestones; *4* large passages with abundant convection dissolution speleomorphs, formed along intersections of sub-vertical fracture conduits with bedding-parallel high permeability elements or through merging of closely spaced rifts; *5* «blind» chambers formed along inclined pinnate fractures; *6* zones of touching-vug porosity rimming major conduits and voids. **b** Exposure of hypogene solution morphology at cuesta cliffs in the present-day geomorphic situation. Modified from Klimchouk et al. (2013)

as bedding planes and porous or densely fractured beds), developing conduits or zones of touching-vug porosity that connected laterally offset fractures in different units. "Blind" side chambers formed along inclined pinnate fractures, and widened intervals of the rifts formed along intersections with stratiform high-permeability elements. The main

speleogenetic process, clearly discerned from hydrostratigraphic/structural relations and morphology of caves and features at cliffs, is the renewal of the aggressiveness due to mixing of deep flow rising along rifts with stratabound flow in the layered aquifer system. Dissolution by rising thermal waters and by sulfuric acid (due to oxidation of H_2S) could locally to play a role but evidence for these mechanisms is lacking so far.

When surface denudation/erosion reached the limestone sequence, the presence of hypogenically karstified rift-dominated zones in the Piedmont obviously guided erosional incision and the formation of the cuesta cliffs (Fig. 15b). The exposure of conduits and voids in the cliffs, as well as weathering of the alterite in the walls of hypogenic karst features, accounts for the rich variety of the conspicuous morphologies in the cuesta escarpments (rock shelters, notches, sub-vertical half-conduits, tafoni and honeycomb structures).

9 Summary and Outlook

Despite long history of karst and cave studies in Crimea, hypogene speleogenesis has been recognized in the Piedmont Crimea only recently. The major pre-requisites for hypogene karst development in the region are its position at the margin of the Prichernomorsky artesian basin, and in a geodynamically active regional suture zone, which separates the fold-thrust structure of the Crimea Mountains and the Scythian plate. Speleogenesis occurred in confined conditions by flow that rose across the Upper Cretaceous–Paleogene–Neogene clay–carbonate succession along cross-formational tectonic discontinuities and interacted with lateral flow in stratabound aquifers.

The Crimean Piedmont is an outstanding example of a region where the recognition of hypogene speleogenesis entails a fundamentally new interpretation of the regional geomorphological evolution and the origin of remarkable landscape features, previously attributed to weathering processes.

Acknowledgements The authors are grateful to colleagues at the Ukrainian Institute of Speleology and Karstology, particularly to V. Naumenko, S. Tokarev and B. Vakhrushev, for their assistance in field studies. This study was partially supported by a grant 0110U002248 of the Ministry of Education and Science of Ukraine to AK.

References

Amelichev GN, Klimchouk AB, Timokhina EI (2011) Speleogenesis in Cretaceous and Eocene deposits of the valleys of Zuya and Burulcha rivers (eastern part of the Crimean Piedmont). Speleol Karstol (Simferopol) 7:52–64 (in Russian)

Blaga NN, Popov AV (2009) Some aspects of morphogenesis of rock shelters of the Inner Range of the Crimean Mountains. Cultura Narodov Prichernomorya (Simferopol) 155:7–9 (In Russian)

Bush I (2010) An integrated approach to fracture characterization. Oil Rev Middle East 2:88–91

Dublyansky VN, Lomaev AA (1980) Karst caves of Ukraine. Naukova Dumka, Kiev (in Russian)

Dublyansky YV, Klimchouk AB, Spötl C et al (2014) Isotope wallrock alteration associated with hypogene karst of the Crimean Piedmont, Ukraine. Chem Geol 377:31–44

Dubois C, Quinif Y, Baele JM et al (2014) The process of ghost-rock karstification and its role in the formation of cave systems. Earth Sci Rev 131:116–148

Dushevsky VP (1987) Speleological knowledge on the Piedmont Crimea karst area. In: Abstracts of the conference "Problems of studies, ecology and protection of caves". Institute of Geological Sciences, Academy of Sciences of the UkrSSR, Kiev (in Russian)

Dushevsky VP, Kuznetsov AG (1991) Singularities of development of karst in low-mountain areas of the cuesta relief. In: Proceedings of the conference "Studies and Utilization of Karst in Western Caucasus". Sochi (in Russian)

Gorbach LP (1972) Stratigraphy and mollusk fauna of the early Paleocene of the Crimea. Nedra, Moscow (in Russian)

Klimchouk AB (2007) Hypogene speleogenesis: hydrogeological and morphogenetic perspective. National Cave and Karst Research Institute, Special Paper No. 1, Carlsbad, New Mexico

Klimchouk AB (2009) Morphogenesis of hypogenic caves. Geomorphology 106:100–117

Klimchouk AB, Tymokhina EI (2011) Morphogenetic analysis of Tavrskaya cave (Inner Range of the Crimean Piedmont). Speleol Karstol (Simferopol) 6:36–52 (in Russian)

Klimchouk AB, Tymokhina EI, Amelichev GN (2009) Hypogene speleogenesis in the Piedmont Crimea range. In: Klimchouk A, Ford D (eds) Hypogene speleogenesis and karst hydrogeology of artesian basins. Ukrainian Institute of Speleology and Karstology Special Paper 1, Simferopol, pp 159–171

Klimchouk AB, Tymokhina EI, Amelichev GN et al (2011) U/Th dating of speleothems of karst caves in the southwest part of the Inner Range of the Mountainous Crimea and determination of relief age and its development dynamics. Speleol Karstol (Simferopol) 7:29–39 (in Russian)

Klimchouk AB, Tymokhina EI, Amelichev GN (2012) Speleogenetic effects of interaction between deeply derived fracture-conduit flow and intrastratal matrix flow in hypogene karst settings. Int J Speleol 2:37–55

Klimchouk AB, Timokhina EI, Amelichev GN et al (2013) Hypogene karst of Crimean Piedmont and its geomorphological role. DIP, Simferopol (in Russian)

Lushchik AV, Morozov VI, Meleshin VP et al (1981) Groundwaters of karst platform regions in the south of Ukraine. Naukova Dumka, Kiev (in Russian)

Lushchik AV, Lisichenko GV, Yakovlev EO (1988) Formation of the groundwater regime in areas of active geodynamic processes. Naukova Dumka, Kiev (in Russian)

Lygina EA (2010) Danian and Eocene Platforms of the Crimea: build-up and conditions of formation (PhD thesis). Moscow University, Moscow (in Russian)

Monroe WH (1970) A glossary of karst terminology. Geological survey water-supply paper 1899-K. U.S. Geological Survey. U.S. Government Printing Office, Washington, DC

Newman BD, Norman DI, Gundimeda N et al (1996) Understanding the genesis of nonmarine calcite deposits through quadrupole mass

spectrometric analysis of fluid inclusion gases. Chem Geol 132:205–213

Nikishin AM, Alekseev AS, Baraboshkin EY et al (2006) Geological history of the Bakhchisaray region of Crimea. Moscow State University, Moscow (in Russian)

Ogata K, Senger K, Braathen A et al (2014) Fracture corridors as seal-bypass systems in siliciclastic reservoir-cap rock successions: field-based insights from the Jurassic Entrada Formation (SE Utah, USA). J Struct Geol 66:162–187

Questiaux J-M, Couples GD, Nicolas R (2010) Fractured reservoirs with fracture corridors. Geophys Prospect 58:279–295

Shestopalov VM, Blinov PV, Lyutyi GG et al (2010) Modern principles of hydrogeological regionalization. Zbirnik naukovyh prac UkrDGRI 3–4:147–157 (in Russian)

Shniukov EF, Gnatenko GI, Nesterovsky VA et al (1992) Mud volcanism of the Kerch-Taman region. Naukova Dumka, Kiev (in Russian)

Singh SK, Abu-Habbiel H, Khan B et al (2008) Mapping fracture corridors in naturally fractured reservoirs: an example from Middle East carbonates. First Break 26(5):109–113

Timokhina EI, Klimchouk AB, Amelichev GN (2011) Geomorphology and speleogenesis of the marginal southwestern part of the Eocene cuesta of the Inner Range of the Crimea Mountains. Speleol Karstol (Simferopol) 7:40–51 (in Russian)

Timokhina EI, Klimchouk AB, Amelichev GN (2012) Role of hypogene karst in the geomorphogenesis of the Inner Range of the Crimean Mountains. Speleol Karstol (Simferopol) 9:38–51 (in Russian)

Vakhrushev BO (2010) Crimean Mountains. In: Vakhrushev BO, Kovalchuk IP, Komlev OO et al (eds) Relief of Ukraine. Slovo, Kiev, pp 432–485 (in Russian)

Yudin VV (2011) Geodynamics of the Crimea. DIP, Simferopol (in Russian)

The Role of Hypogene Speleogenesis in the Formation of the Ordinskaya Cave, Fore-Urals, Russia

26

O.I. Kadebskaya and N.G. Maksimovich

Abstract

This chapter describes the Ordinskaya Cave in the Fore-Urals region, Russia, which is the largest underwater cave of sulfate rocks in the world. The explored length of the cave is about 4900 m. The regional distribution of karst features indicated that a large amount of recharge entered the lower passages during all stages of development. The groundwater in the cave is aggressive with respect to sulfate. Discharge of water with higher mineralization was documented during the spring floods. During summer low-flow periods, subaqueous springs discharge waters under artesian conditions with a lower solute content. In the cave, the degree of saturation of water increases from the bottom to the top in the spring season and is the reverse in the summer. Seasonal variations in the groundwater chemical composition reflect the contribution from the artesian system. The geological data indicate a strong relationship between the karst features and the regional fault network. The characteristic features of the Ordinskaya Cave make it a model object of artesian hypogene speleogenesis.

Keywords

Speleogenesis in gypsum • Hypogene speleogenesis • Ordinskaya cave • Russia

1 Introduction

In the Perm krai (Fig. 1), gypsum karst is intensely developed in the Lower Permian formations in the southern part of region. This chapter is devoted to the Ordinskaya Cave, the largest underwater cave in sulfate rocks in the world, located in a karstified massif of the Kazakovskaya Gora.

The distribution of karst features throughout the watershed area revealed that powerful, concentrated recharge into the sulfate rocks occurred from the underlying formations during all stages of the cave development process (Kadebskaya and Maksimovich 2009; Sivinskih 2009). Today, recharge also occurs from the river through fractures in the valley slope and forms surface infiltration. The groundwater in the cave is aggressive with respect to sulfate.

Studies of the karstified massif of the Kazakovskaya Gora reveal successive stages of karst evolution. The characteristic features of the Ordinskaya Cave make it a model of artesian hypogene speleogenesis. Studies revealed seasonal variations in the chemical composition of cave waters and of cave microclimate parameters.

2 Geologic and Geomorphic Setting

Ordinskaya Cave is located in the western flank of the Ufimsky Swell of the East European Platform. The crest of the swell dips moderately to the north. Kazakovskaya Gora (Kazakovskaya Mount) is part of the plateau highland and is up to 60 m high relative to the bed of the adjacent Kungur River. The elevation of the massif above sea level varies from 137 m (water surface at the pond in the Kungur River)

O.I. Kadebskaya (✉)
Mining Institute of the Ural Branch of the RAS, Perm, Russia
e-mail: icecave@bk.ru

N.G. Maksimovich
Institute of Natural Science of Perm State University, Perm, Russia

© Springer International Publishing AG 2017

A. Klimchouk et al. (eds.), *Hypogene Karst Regions and Caves of the World*,
Cave and Karst Systems of the World, DOI 10.1007/978-3-319-53348-3_26

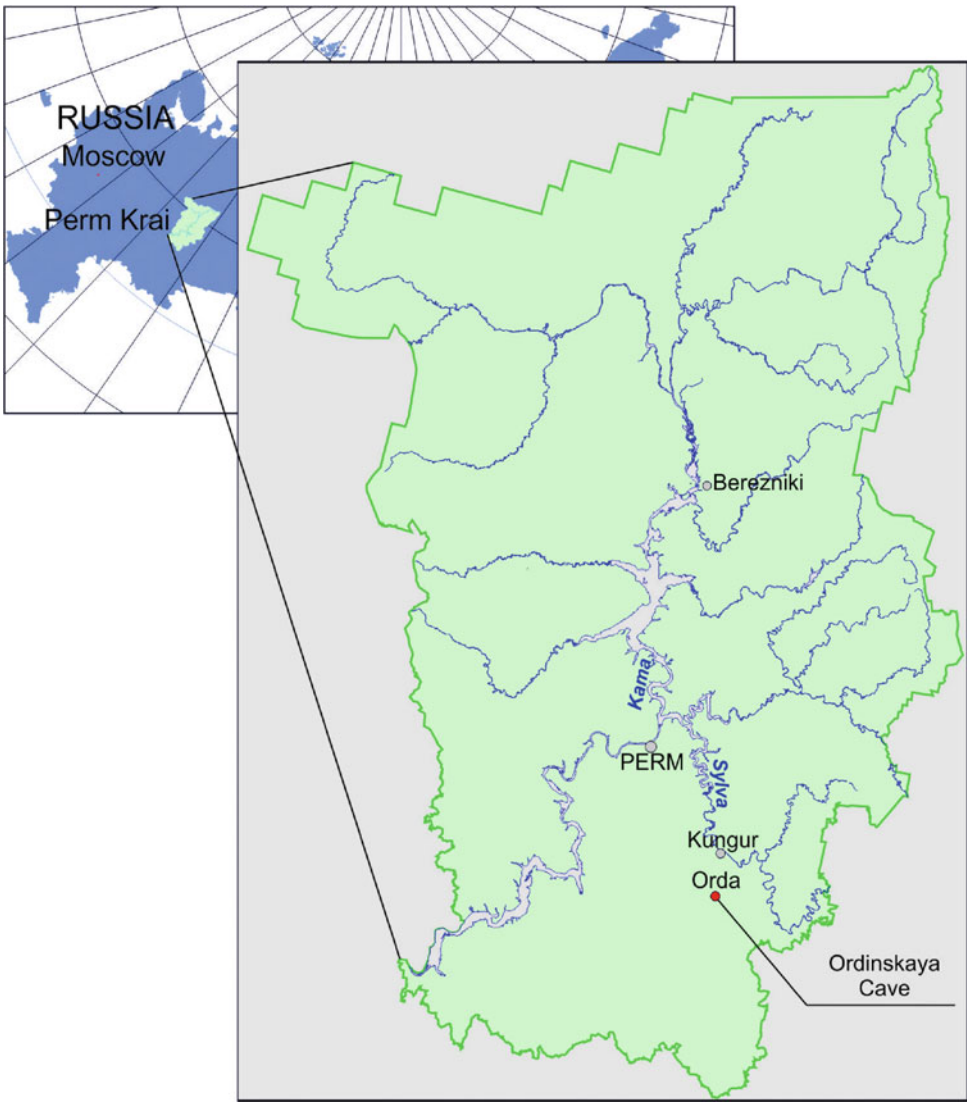

Fig. 1 Location map of the Ordinskaya cave

to 196 m. According to Gorbunova et al. (1992), this area belongs to the Irenskaya zone of intense karst in gypsum and anhydrites. It is bounded to the east by a carbonate karst area of the Ufimskoye Plateau.

According to the classification of evolutionary types of karst of Klimchouk (1996), different types of karst are distinguished in the area. Denuded karst develops in areas where soluble rock is exposed at the surface. Mantled karst occurs in areas where eluvial and alluvial sediments cover the karstified rocks. Intrastratal karst develops locally, where sulfates lie beneath insoluble sediments of the Solikamskian horizon. Sinking streams are typical for such areas (e.g., Turaevka, Yakovka, Sudinka, and Kungur Rivers). The area hosts 77 known caves, the longest of which is Ordinskaya Cave with 4.9 km of passages, explored mainly underwater. The Ordinskaya Cave entrance is located on the southeastern slope of the Kazakovskaya Gora near the Orda village of the Permskiy krai (Fig. 1).

The first record of the cave appeared in 1969 (Maksimovich 1969). In the beginning of 1990s, speleologists from Perm led by A. Smolnikov and I. Lavrov surveyed the dry part of the cave. In March 1994, V. Komarov explored the first 100 meters of underwater passages (Lavrov et al. 2005). Today, the explored length of the cave is 4900 m. The dry part of the cave in the entrance area is approximately 300 m long, and the rest of cave extends underwater, which makes Ordinskaya Cave the world's longest underwater cave in gypsum.

Continuous observations of groundwater flow, hydrochemical sampling, and petrographic and mineralogical studies have been conducted in the cave since 1998. The authors together with cave divers (Maksimovich et al. 2006) explored the underwater part of cave. Standard technical diving equipment was used for underwater explorations. Surveying of karst features at the surface was performed using a Nikon DTM-352 Total Station (Kadebskaya and Maksimovich 2009).

At the foot of Kazakovskaya Gora, the Kungur River bends sharply to the north. In the 1970s, two dam ponds (the upper pond Arsenovsky and the lower pond Ordinskiy) were constructed here. Near the cave, the river valley is narrow and deep, and the average valley width is approximately 230 m, but the ponds width is 180–210 m (Fig. 2). Downstream of the north Kungur River bend, the valley broadens and terraces appear (Kadebskaya et al. 2009).

The western part of the Orda village is located on the first and second terraces at elevations ranging from 140 to 160 m. Small abandoned channels and boggy areas occur on these terraces. A dry valley lies between the second and third terraces at the northern part of the hill, along the Kungur River. The valley terminates at the silted depression and dammed Bannoye Lake, whose water is used for household purposes. Total dissolved solids in the lake is 150 mg/L, which is a characteristic value for reservoirs recharged by rainfall and snowmelt. The third terrace, visible on the southwestern and northeastern parts of Kazakovskaya Gora, has elevations ranging from 160 to 180 m. Karst features are

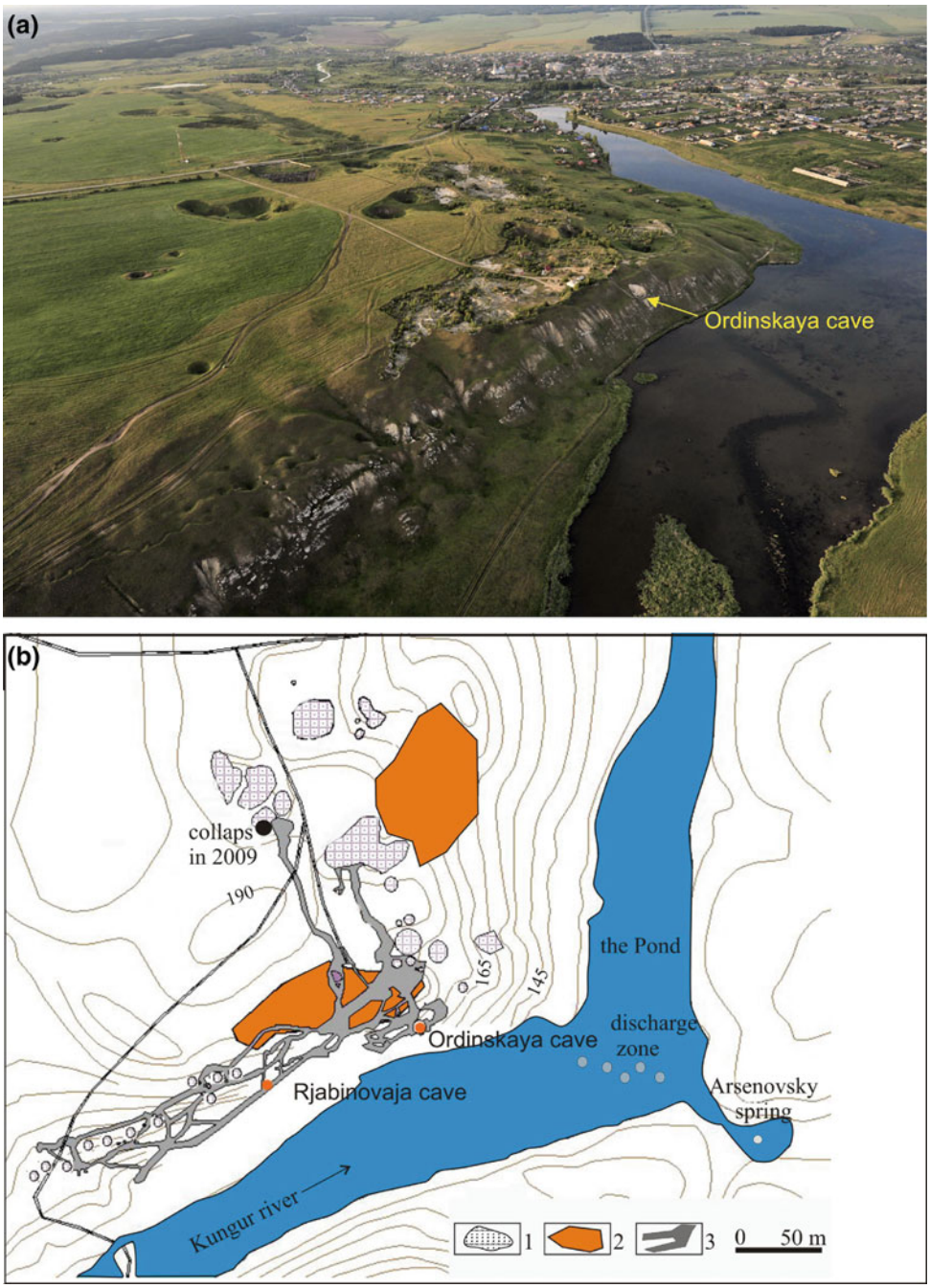

Fig. 2 Karstic features of Kazakovskaya Gora (**a** photograph by A. Filimonov; **b** topographic map): *1* karst sinkholes; *2* quarries; *3* outline of Ordinskaya cave

unevenly distributed. Sinkholes are located mostly to the east of Ordinskaya Cave, where they were partially leveled during the operation of construction stone quarries.

Elevations of the fourth terrace are 180–196 m above sea level. Small dry valleys with sinkholes on their sides and bottoms cut the slope of the fourth terrace. Small sinkholes are saucer shaped with grass-covered slopes (1–5 m in diameter and up to 3 m deep). Large sinkholes, which are 5–10 m in diameter and up to 10 m deep are conical and have rocky, steep walls. During snowmelt, they partially or entirely swallow temporary streams from the hill slopes.

The largest sinkholes on Kazakovskaya Gora are located on the fourth terrace, north of the main cave's galleries. They range from 80 to 94 m in diameter and are about 30 m deep. They often occur close to each other and have dry bottoms and complex shapes. Some sinkholes have fresh collapse features on their slopes. The largest sinkhole (35 × 40 m by 17 m deep) occurred in the fall of 2008 at an elevation of 185 m (the southern ledge). A gypsum outcrop with an apparent thickness of 7 m is exposed at the south wall of the sinkhole at a depth of 10 m (Fig. 3). This is the biggest collapse sinkhole that has formed in the Irenskaya karst zone during the last 15 years.

The density of karst landforms within the studied area is approximately 42 features per square km. Four new collapse sinkholes have been documented during the last 15 years.

Geological mapping in the 1950s in the Permskiy krai region identified two zones of the Upper Devonian reef structures located to the west and east of the Ufimsky Swall. Mikhaylov and Buldakov reported that the large hydrogeological zones of increased water abundance are related to those structures (Fig. 4). The Kishertsko-Irginskaya zone lies to the east, and the Kungurskaya zone lies to the west of the Ufimsky Swell (Mikhaylov and Oborin 2006). Springs with high discharges occur within these zones along active tectonic faults.

Previously, it was found that the Kungurskaya reef zone was offset several tens of meters by diagonal normal faults (Fig. 5). One of the faults stretches north of Kazakovskaya Gora, and another one passes along the southeastern slope. The vertical displacement at the second fault is about

Fig. 3 This collapse sinkhole on Kazakovskaya Gora appeared in July 2009

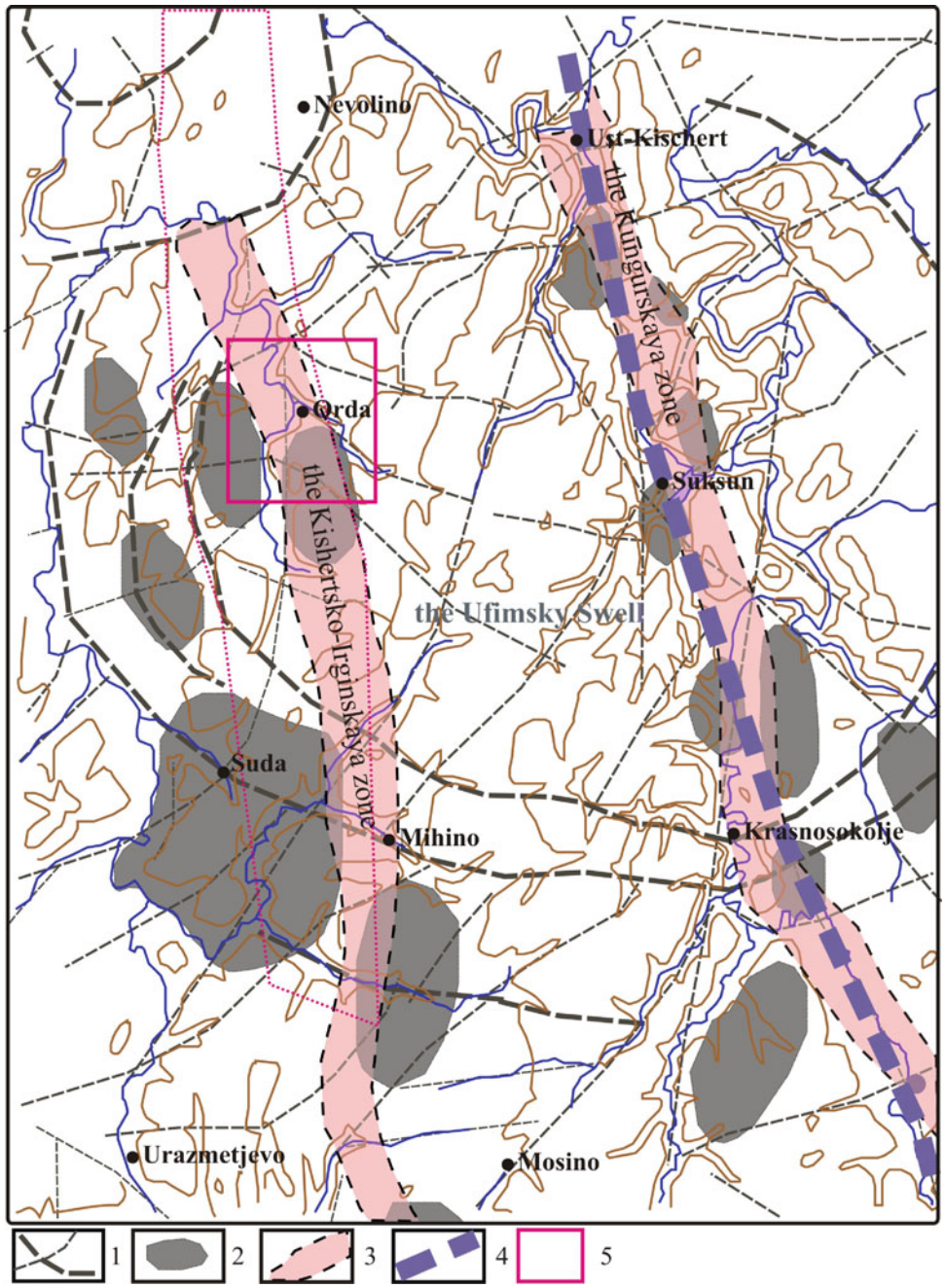

Fig. 4 Structural tectonic scheme of the Sylva-Iren interfluve: *1* neotectonic lineaments related to the Earth's rotation; *2*, *3* positive structures and linear fracture zones; *4* the border between the East European Platform and Urals Foredeep; *5* the study area

17–22 m. The cave, the Arsenovsky Spring, and subaqueous springs in the bed of the Kungur River are all aligned along this fault. An analysis of the neotectonic lineaments (Figs. 4 and 5) allows us to assume that these faults are subjugated to concentric shear dislocations.

3 Stratigraphy

The sulfate rocks are underlain by the Filippovian horizon (P_1k^{fh}) comprised of thin-bedded, locally recrystallized, dolomite. In the cave, the following carbonate and sulfate

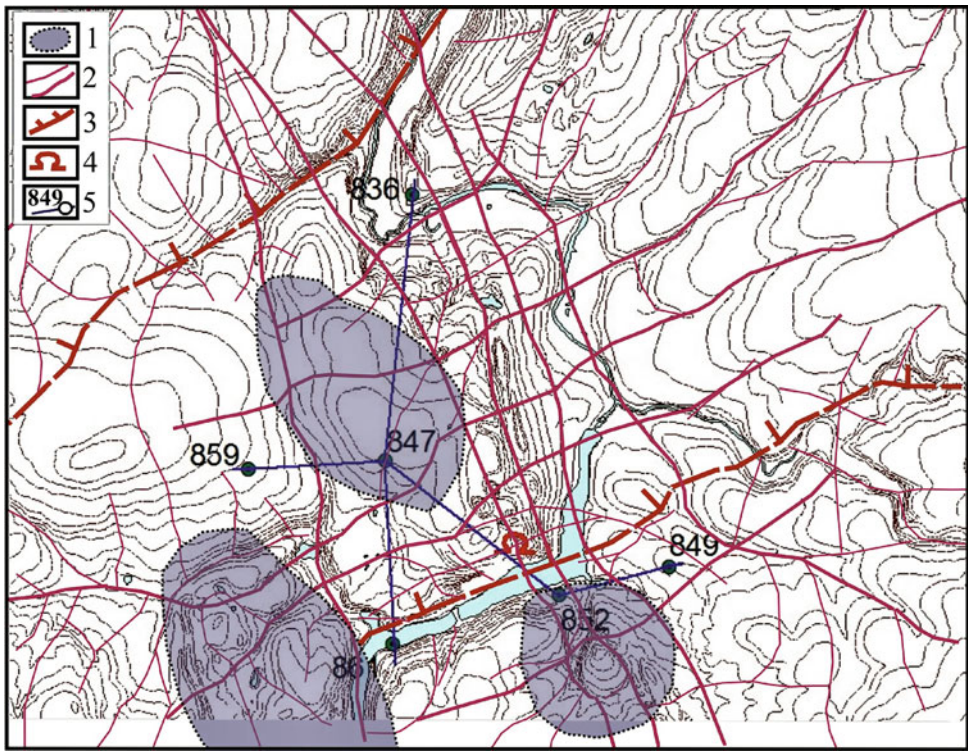

Fig. 5 Tectonic map of the Ordinskaya Cave area: *1* reefs; *2* lineaments of different order affecting the modern relief; *3* faults; *4* cave entrance; *5* boreholes and relevant cross sections

members are identified from bottom to top (Fig. 6). They are members of the Irenskaya Group.

1. Ledyanopeshcherskaya member (P_1ir^1lp), 20–25 m thick, is composed of gypsum and anhydrite. It is located entirely below the water table. The deepest parts of the cave (e.g., the Krasnoyarskiy passage and Podval (Basement Chamber) are located very close to the underlying Philippovian dolomites.
2. Nevolinskaya member (P_1ir^2nv), 4–8 m thick, is comprised of pelitomorphic and oolitic dolomite with a thin gypsum interlayer. The bottom of the member is exposed above Glavnoye (Main) Lake, just about the entrance in the underwater part of cave. The Ledyanoy Dvorets (Ice Palace) occurs in the upper part of the member, in the dry part of cave.
3. Shalashninskaya member (P_1ir^3sh) is 12–15 m thick and composed of the massive and nodular gypsum-anhydrite and anhydrite rock. The bottom of the member is exposed in the Ledyanoy Dvorets (Ice Palace).
4. Elkinskaya member (P_1ir^4el), 3–4 m thick, consists of light-gray and gray, fine-grained dolomite.
5. Demidkovskaya member (P_1ir^5dm), 12–18 m thick, is exposed at the cave entrance and in the collapse sinkhole on Kazakovskaya Gora and consists of massive and nodular gypsum.
6. Tyuyskaya member (P_1ir^6ts), total thickness 5–10 m, is exposed on the grass-covered slope of the Kazakovskaya Gora and in small quarries. In the lower part, the member consists of white and light-gray, fine-grained, locally silicified dolomite and is characterized by the occurrence of palygorskite. The upper part of the member consists of rubbly, cavernous dolomite and calcitic dolomite with boxwork patterns (Fig. 7).

The distribution of residual carbonates in the area suggests widespread hypergene alteration with secondary dolomites forming part of the weathering crust. Hypergene alteration consisted in dolomite leaching and recrystallization. Disintegration of the residual carbonates into boulder-, cobble-, to gravel-sized fragments only in the upper part of the section suggests that physical weathering occurred in the rock, which was already subjected to the chemical weathering.

Ordinskaya Cave has a vertical range of 50 m and occurs within the Tyuyskaya, Demidkovskaya, Elkinskaya, Shalashninskaya, Nevolinskaya, and Ledyanopeshcherskaya members of the Irenskaya Group.

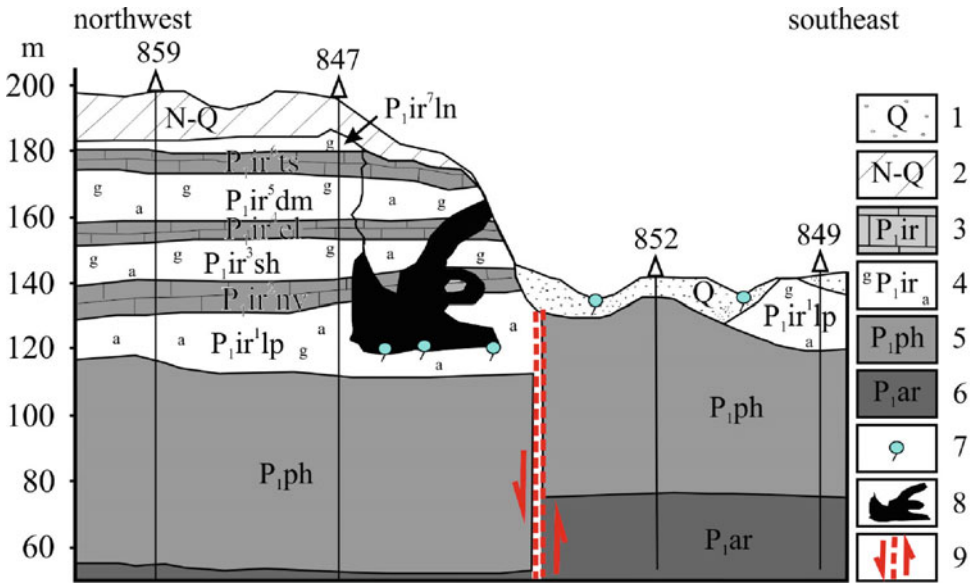

Fig. 6 Geologic section across Ordinskaya Cave: *1*, *2* Quaternary alluvial and Neogene-Quaternary eluvial sediments; *3* carbonate members of the Irenskaya Suite (Tyuyskaya, Elkinskaya, and Nevolinskaya); *4* sulfate members of the Irenskaya Suite (Lunezhskaya, Demidkovskaya, Shalashninskaya, and Ledyanopeshcherskaya); *5* limestones and dolomites of the Philippovian horizon; *6* limestones of the Artinskian horizon; *7* points of discharge of sulfate-hydrocarbonate-calcium waters; *8* Ordinskaya Cave; *9* fault and direction of blocks displacement

Fig. 7 *Left* fragment of outcrop of the Tyuyskaya member in Ordinskaya Cave area; *right* boxwork pattern on recrystallized and leached residual carbonate rock (the width of the scene is ~0.5 m)

Presently, Ordinskaya Cave is designated as a geological natural landmark of regional significance (Maksimovich et al. 2006). In 2009, it was suggested the area be included as a key part of the proposed "Natural Park of the Permian Period."

4 Cave Morphology

The entrance to the Ordinskaya Cave (Fig. 8) is situated on the steep south slope of Kazakovskaya Gora at 163 m a.s.l., 40 m above the river. It opened by collapse, forming a

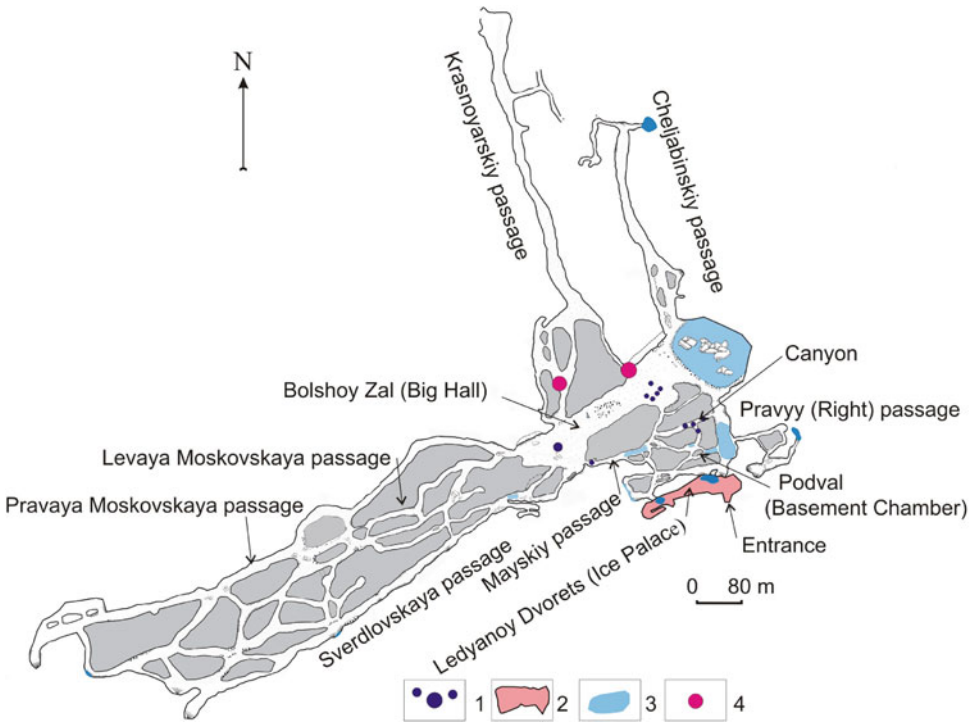

Fig. 8 Map of Ordinskaya cave (compiled by Osipov D.V. in January 2010 and updated by Zhigalov A. in 2016, with permission): *1* subaqueous springs (feeders), *2* dry part of the cave with lakes, *3* air cupolas in the underwater part of cave, *4* vertical pipes

sinkhole 40 m in diameter. During winter, the dry part of the cave cools, forming ice stalagmites, stalactites, and sublimation crystals (Fig. 9a, b).

In the dry part of the cave and the underwater galleries located along the Kungur River (Sverdlovskaya and Levaya Moskovskaya galleries), blocks of sulfate and carbonate rocks have been disrupted by tectonic faults and tilted toward the river valley.

Seasonal changes of the groundwater and surface water levels have caused deformation of the lower part of the Ledyanopeshcherskaya member due to anhydrite hydration. Thin bedrock walls separating major passages were tilted toward the river valley opening fresh vertical fractures where river water entered the cave. Generally, such major passages are high (up to 15 m) and relatively narrow (1.5–5 m), and are 25–50 m long. In places, the width of the walls between the adjacent parallel passages is only 1.0–3.5 m (Fig. 9c, d). Thin pillars failed with time and narrow passages coalesced. Remnants of almost destroyed pillars are observed in Bolshoy Zal (Big Hall) and Mayskiy passage (Fig. 9e, f).

Widening occurs locally at the contact of the rocks of different structure in the Ledyanopeshcherskaya member that results in two-story passages, as observed in the passages such as Levaya Moskovskaya, Sverdlovskaya, and Krasnoyarskiy. Widening in the lower story occurs along the dolomite bed in the bottom of the Ledyanopeshcherskaya member. Passages in this story are commonly wide but low and display the fractured dolomite layer in their walls (Fig. 10a). The upper story of parallel passages occurs in the nodular gypsum-anhydrite bed, separated from the underlying bed of massive fine-grained anhydrite by thin layers of clay-carbonate material (Fig. 10b). In places, rock blocks between passages at different levels fall down and obstruct the entrance to lower passages. In large passages, flat ceilings formed where breakdown occurred (Fig. 10c). In some cases, the flat ceilings of the major cave passages have formed along the present water level at the contact of the Ledyanopeshcherskaya and Nevolinskaya members.

Underwater video recorded by cave divers, Filimonov A., Bizyukin A., and Gorbunov A., showed clusters of rounded hollows about 1 m deep in the cave floor. These hollows (Fig. 10d, e) are identified as the rising subaqueous springs, referred to as feeders (following Klimchouk 2007, 2009). The feeders mostly occur in Bolshoy Zal and Podval, in Osnovnaya Gallery, and in Canyon, Krasnoyarskiy, and Chelyabinskiy passages. The number of feeders in these areas is greater than it shown on the cave map (Fig. 8). As reported by divers, the size of feeders has significantly increased during the last 3–4 years. The pulsating water currents rise out of the feeders during high water.

Analysis of the distribution of karst features in the watershed area suggests powerful upward inflow of water through the lower channels along a linear elongated zone occurred in all stages of cave development. The gypsum-anhydrite formation has been dissolved not only from the top and the sides, but also (perhaps dominantly) from the bottom forming the void-conduit system in the northeastern part of Kazakovskaya Gora. Based on locations

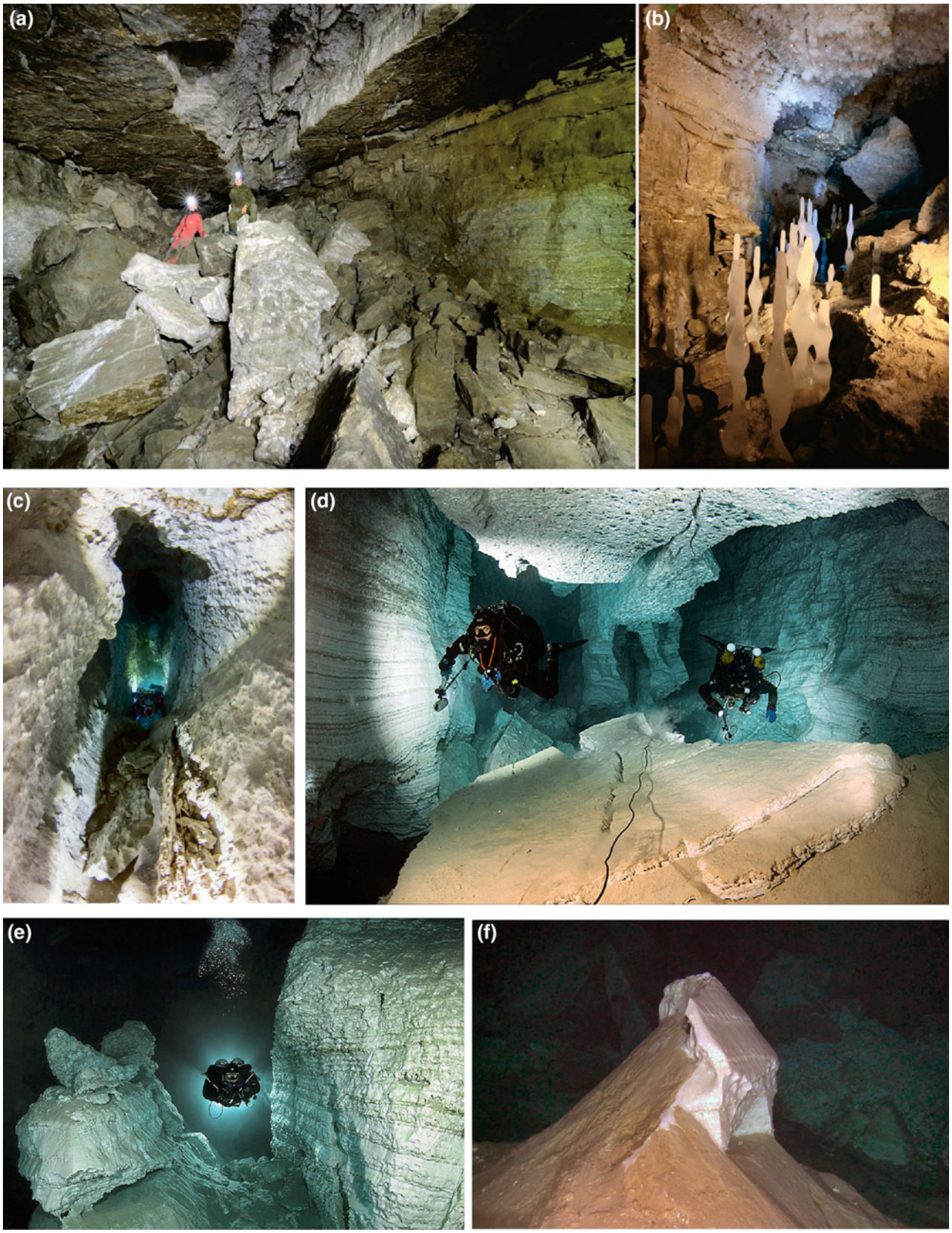

Fig. 9 Morphologic features of Ordinskaya Cave: **a** Dry part of the cave (photograph by Ya. Zanda); **b** Stalagmites in dry part of cave (photograph by A. Filimonov); **c** one of the narrow parallel galleries in Levaya (*Left*) Moskovskaya passage that often merged laterally due to wall collapse (photograph by A. Gorbunov); **d** blocks of collapsed pillars between the parallel galleries (photograph by V. Lyagushckin); **e** large passage formed by coalescence of adjacent passages (photograph by V. Lyagushckin); **f** remnant of an almost destroyed pillar in Bolshoy Zal (Big Hall; photograph by A. Gorbunov)

Fig. 10 Morphologic features of Ordinskaya Cave: **a** Krasnoyarskiy passage (photograph by A. Gorbunov); **b** Upper and lower parallel galleries (photograph by A. Bizyukin); **c** The settling down of rock blocks (photograph by A. Bizyukin); **d** and **e** subaqueous springs (feeders) in the lower part of Ordinskaya Cave, governing the rising inflow of hydrocarbonate-calcium water in the gypsum-anhydrite formation (photograph by A. Gorbunov)

of ravines and large karst sinkholes (up to 100 m), it can be assumed that most of the underground passages of Ordinskaya Cave have already been destroyed by collapse.

Hydrogeological observations pointed out the direction of groundwater flow. Gorbunov A.A. (pers.comm.) reported vertical flow occurred during spring flooding in 2009. Water carrying suspended clay particles flowed from the lower horizontal Podval passage through a subvertical channel of the Canyon passage into the overlying horizontal Glavnyy passage. Upward water flow is also confirmed by the cave morphology. A feature referred to as Bolshoy Puzyr (Big Bubble) is a dome about 12 m in diameter, located at the intersection of the Canyon and Osnovnaya passages. A number of smaller domes can be seen on the ceiling of the Glavnyy passage and toward the Bolshoy Zal (Fig. 11a).

Different flow directions were observed in the Moskovskiy and Sverdlovskiy passages, which are likely related to lithostatic unloading along the valley. Groundwater flow in these passages coincides with the Kungur River flow direction. Intense fracturing of the karst massif contributes to the influx of muddy river water into distant sections of these passages during flooding.

Flood waters reach the dry part of the cave in approximately 5–7 days. Wood debris carried into the cave probably by flood water has been found in some sections of the Moskovskiy and Sverdlovskiy passages. The muddy water was not observed in the Krasnoyarskiy and Chelyabinskiy passages. The suspended material that rises from the bottom of the Moskovskiy passage moves toward the dry part of the cave even during low flow, suggesting a continuous northeastern flow direction.

Measurements of the water levels in the cave and in the pond in the Kungur River, conducted by Pyatunin M.C. during the summer low-water season (July 23, 2009), indicated that the water table in the cave is 27 cm higher than the water level in the pond. Such a difference in water levels confirms artesian water provides recharge to the cave. The water influx from the underlying beds, the hydrological regime of wells in the southern part of Kazakovskaya Gora, and invariant water level in the cave lakes during pond dewatering in 2005 are direct evidence for subartesian recharge to the cave.

The oldest part of cave occupies the area from the entrance to the end of the Chelyabinskiy and Krasnoyarskiy passages. This is confirmed by the following lines of evidence: occurrence of feeders mainly in chambers of Bolshoy Zal and Podval, in the Osnovnaya Gallery, and in the Canyon, Krasnoyarskiy, and Chelyabinskiy passages; lower elevation of the bottom; the proximity of the underlying Philippian dolomites; documented upward water inflow through feeders; dissolution of the pillars between parallel passages, and coalescence of the passages into larger features of up to 60 m in width and up to 150 m in length. Hypogene speleogenesis in this part of cave is confirmed also by the lack of karst landforms on the surface.

Moskovskaya and Sverdlovskaya galleries are younger features related to rock dissolution along the fractures caused by entrenchment of the Kungur River valley. There are no feeders in this part of cave, the galleries are mostly narrow (2–3 m wide), the pillars/walls between parallel galleries are preserved, and the bottom of galleries is located at higher elevations. The depth of these galleries from the surface is less than 25 m because they are close to the edge of the valley. Sinkholes on the slope connect to the cave galleries by the vertical channels formed by infiltration water. The river waters enter the karst massif during the spring high water season, which causes water turbidity. The bedding planes in this part of the cave are inclined toward the river which is not true away from the edge of the valley.

5 Hydrochemical Characteristics of the Cave Water

Local groundwater is characterized by SO_4-HCO_3-Ca and TDS up to 2.4 g/L, which is typical for areas of sulfate karst development (Gorbunova et al. 1992; Dublyanskiy 2005). Water samples in the cave were collected mostly from the surface of pools. Sampling conducted by cave divers (Gorbunov A.A., Mikhalev D.A., and Shchukin A.V.) in the main underwater cave passages and subaqueous feeders of the Arsenovsky Spring (Fig. 11d, e) made it possible to determine water composition at different levels of the cave during periods of high and low water (Table 1).

The highest HCO_3 content (up to 317 mg/L) was documented in water from subaqueous outlets of the Arsenovsky Spring (Fig. 11d) and in the Bolshoy Zal in the cave. The same or slightly lower values (to 280 mg/L) are obtained for samples from Chelyabinsliy, Krasnoyarskiy, Moskovskiy passages, Osnovnaya Gallery, and Podval. The lowest HCO_3 content (195 mg/L) was observed in the sample from the Kungur River taken upstream from the cave.

High HCO_3 could be interpreted as an evidence of water inflow from the underlying limestones and dolomites of the Philippian and Artinskian horizons, while high TDS might be a result of mixing of water rising from the Philippian horizon and highly mineralized water in the Irenskaya Suite.

The saturation index SIgyp (Ford and Williams 2007) was used to assess the water's capability to dissolve gypsum. Methodology is based on the determination of the

Fig. 11 Morphologic features of Ordinskaya Cave (**a** through **c**) and subaqueous feeders in the Arsenovsky Spring (**d** and **e**): **a** Tall parallel passages, coalesced in the lower part into a single Glavnyy passage due to partial destruction of pillars. Note a number of smaller cupolas and channels in the ceiling (photograph by A. Bizyukin); **b** and **c** ellipsoidal and spherical cupolas in the ceiling of the Glavnyy passage (photograph of A. Gorbunov); **d** subaqueous springs (feeders) in the Arsenovsky Spring (photograph by V. Lyagushckin); **e** discharge of hydrocarbonate-calcium waters on the bottom of Arsenovsky Spring (photograph by A. Gorbunov)

Table 1 Chemical composition of waters in Ordinskaya Cave area. Equilibrium concentration of gypsum and its comparison with an equilibrium equivalent concentration of calcium sulfate in water (study of 2009)

No.	Sampling locality	Sampling date in 2009	TDS (g/dm^3)	SO_4 (g/dm^3)	Ca (g/dm^3)	N_{SO4}	n_{Ca}	C_{SO4}	C_{Ca}	Ion activity	Saturation Index, mol/L	Solubility, g/L	Solubility coeff.
1	Cave, Bolshoy Zal, feeder	Apr 24	2.436	1.413	0.589	0.015	0.01473	0.006043	0.006046	0.000037	−0.077	2.0	0.94
2	Cave, Bolshoy Zal, feeder	May 25	2.265	1.315	0.581	0.014	0.01453	0.00605	0.006416	0.000039	−0.050	1.92	0.97
3	Cave, Bolshoy Zal, ceiling	May 25	2.253	1.296	0.581	0.014	0.01453	0.005991	0.006448	0.000039	−0.053	1.90	0.97
4	Levaya (Left) Moskovskaya passage, entrance	May 25	2.344	1.356	0.581	0.014	0.01453	0.006027	0.006199	0.000037	−0.067	1.95	0.95
5	Levaya (Left) Moskovskaya passage, end	May 25	2.344	1.356	0.581	0.014	0.01453	0.006027	0.006199	0.000037	−0.067	1.95	0.95
6	Moskovskiy passage, bottom	May 22	2.175	1.248	0.5611	0.013	0.014028	0.005975	0.006449	0.000039	−0.054	1.84	0.97
7	Moskovskiy passage, top	May 22	2.349	1.365	0.557	0.014	0.013928	0.00605	0.005928	0.000036	−0.085	1.91	0.93
8	Osnovnaya Gallery, bottom	May 22	2.377	1.384	0.561	0.014	0.01403	0.006065	0.005901	0.000036	−0.086	1.93	0.93
9	Osnovnaya Gallery, top	May 22	2.443	1.423	0.557	0.014	0.013928	0.006068	0.005701	0.000035	−0.100	1.95	0.92
10	Podval, bottom	May 22	2.257	1.306	0.565	0.014	0.014128	0.006028	0.00626	0.000038	−0.063	1.89	0.96
11	Krasnoyarskiy passage, bottom	May 22	2.290	1.335	0.569	0.014	0.014229	0.006075	0.006214	0.000038	−0.062	1.91	0.96
12	Bolshoy Zal, top	Aug 14	2.215	1.287	0.561	0.013	0.014028	0.006051	0.006333	0.000038	−0.056	1.86	0.97
13	Bolshoy Zal, bottom	Aug 14	2.214	1.287	0.569	0.013	0.014229	0.006053	0.006426	0.000039	−0.050	1.88	0.97
14	Bolshoy Zal, feeder	Aug 14	2.296	1.345	0.569	0.014	0.014229	0.006104	0.006198	0.000038	−0.062	1.92	0.96
15	Podval, feeder	Aug 14	2.266	1.326	0.585	0.014	0.014629	0.006093	0.006455	0.000039	−0.048	1.93	0.98
16	Arsenovsky Spring	Apr 24	2.444	1.443	0.585	0.015	0.014629	0.006147	0.005985	0.000037	−0.074	2.02	0.95
17	Podzuevskiy Spring	Aug 14	2.233	1.287	0.565	0.013	0.014128	0.006003	0.006328	0.000038	−0.060	1.87	0.96
18	Glavnoye Lake, top	Aug 14	2.283	1.326	0.557	0.014	0.013928	0.006048	0.006100	0.000037	−0.073	1.89	0.95
19	Kungur River, upstream	Aug 14	1.946	1.179	0.497	0.012	0.012425	0.006314	0.006386	0.000040	−0.034	1.68	0.99
20	Kungur River, downstream	Aug 14	2.054	1.238	0.513	0.013	0.012826	0.006279	0.006246	0.000039	−0.046	1.75	0.98

Samples 2–5 were collected by U.V. Nazarova and analyzed in the Laboratory of hydrochemical analysis of the Perm state University by Naumov D.Yu. Samples 1, 6–20 were analyzed in the Laboratory of geology of technogenic processes of the Perm State University by Melnikova E.A

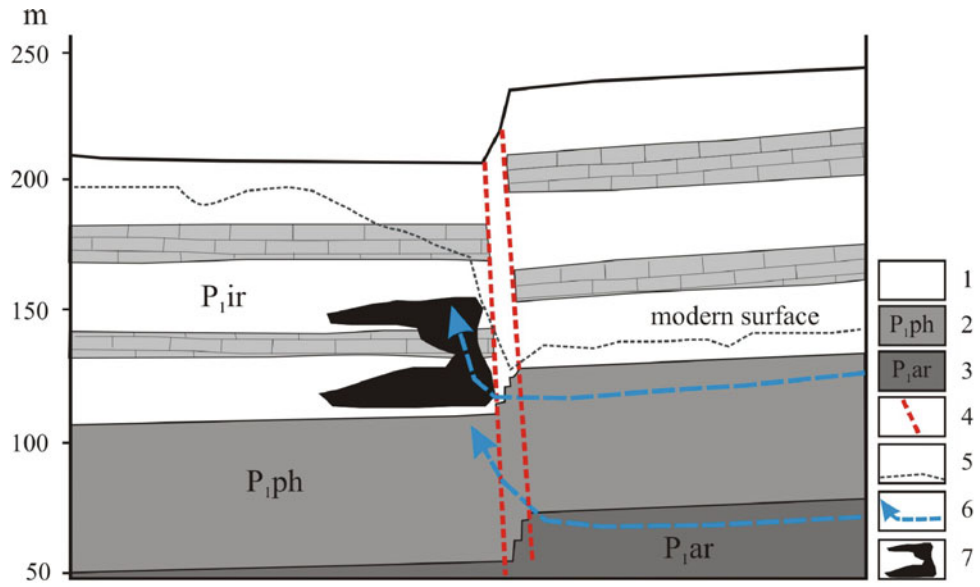

Fig. 12 Conceptual model of the Ordinskaya Cave formation in the fault zone (Chaykovskiy and Kadebskaya 2009): *1* sulfate and carbonate rocks of the Irenskaya Suite; *2* limestones and dolomites of the Philippian horizon, *3* Artinskian limestones; *4* fault; *5* modern surface; *6* direction of artesian water flow; *7* Ordinsakaya cave

equilibrium concentration of calcium sulfate and its comparison to measured concentration in water. A comparison of water chemical composition in the Bolshoy Zal during periods of high and low water at different levels shows no significant difference in TDS. Cave waters are aggressive to sulfates (solubility coefficient is less than 1). The degree of saturation of water in the spring season increases upward from feeders at the bottom to the top of the cave. In summer, the concentration increases in the opposite direction (downward), this may be the evidence of a seasonal evolution in the chemical composition of the discharging water.

We suppose that during high water, local meteoric water does not mix rapidly with water from feeders and concentrates in the upper part of the cave. The water, recharged to the artesian system in the Ufimskoye Plateau during spring flooding, discharges into the cave during low flow.

6 Discussion: Speleogenetic Model

During the first stage of speleogenesis of Ordinskaya Cave, groundwater discharged upward along the linear, northeastern strike of the fault zone. The subartesian waters from the underlying Philippian and Artinskian horizons formed the Canyon Chamber and Osnovnaya, Krasnoyarskaya, and Chelyabinskaya passages (Fig. 12). Later on, the Moskovskaya and Sverdlovskaya passages were formed, following neotectonic formation of stress release fractures along the Kungur River and hydration processes.

With time, the southeastern block rose and the Kungur River valley shifted northeast. Uplift of the southern left-bank block relative to the present location of Kazakovskaya Gora lowered the groundwater level at the northern end causing intense leaching of the sulfate-carbonate rock. Fluorine-enriched waters infiltrated into the

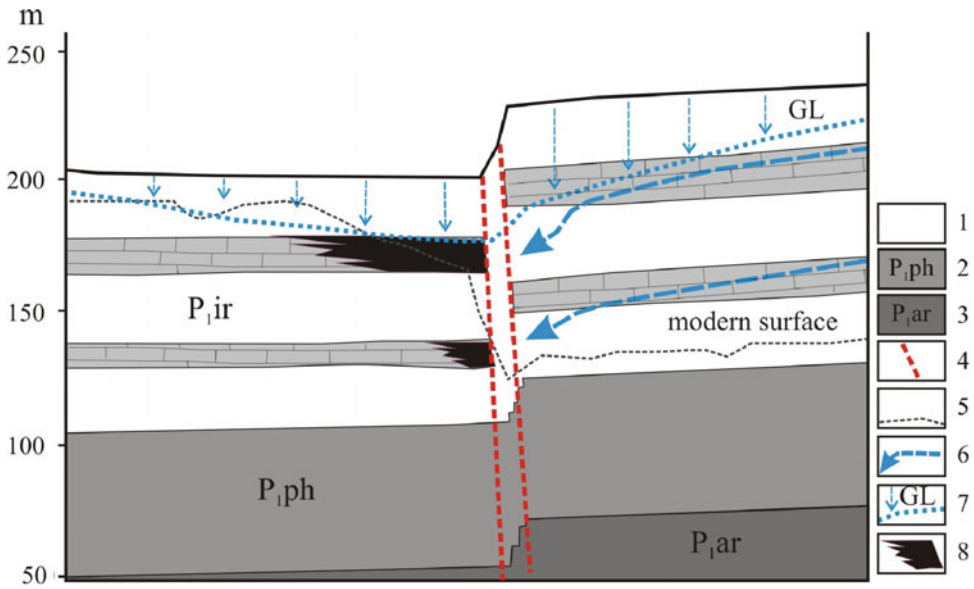

Fig. 13 Model of the formation of fluorite mineralization in the fault zone: *1* sulfate and carbonate rocks of the Irenskaya Suite (P_1ir); *2* limestones and dolomites of the Philippian horizon; *3* Artinskian limestones; *4* fault; *5* modern surface; *6* direction of streams enriched in fluorine; *7* groundwater level and water infiltration in the vadose zone; *8* location of fluorite deposits in carbonate members

Kazakovskiy block and precipitated fluorite along the fault in carbonates of the Irenskaya Group (Fig. 13).

7 Conclusions

Kazakovskaya Gora and Ordinskaya Cave represent unique natural features of great scientific, aesthetic, and recreational importance. The cave, which was traditionally considered the result of downward infiltration and lateral groundwater flow, is actually formed by upward flow of artesian water along faults. The location and configuration of the cave were controlled by a diagonal fault system along with northeast trending normal faults.

Finding upward-flowing feeder inlets in Ordinskaya Cave that discharge groundwater with high HCO_3 content provides direct evidence that inflow of artesian waters from the Philippian limestones and dolomites continues today. Recharge to this confined aquifer system occurs in the Ufimskoye Plateau. Neotectonic activation induced vertical displacement of blocks and opened passageways for these waters to rise across the sulfate formation and to form caves there. Ordinskaya Cave is an outstanding example of artesian hypogene speleogenesis in the sense of Klimchouk (2016).

References

Chaykovskiy II, Kadebskaya OI (2009) The role of tectonics in formation of mineralization and karst of the Kazakovskaya Gora. In: Proceedings of the conference Geologiya i poleznye iskopaemye Zapadnogo Urala, Perm State University, Perm, pp 18–24 (in Russian)

Dublyanskiy VN (ed) (2005) Kungur ice cave: results of the regime observation. UB RAS, Yekaterinburg (in Russian)

Ford D, Williams PD (2007) Karst hydrogeology and geomorphology. Wiley

Gorbunova KA, Andreychuk VN et al (1992) Karst and caves of the Perm region. Perm State University, Perm (in Russian)

Kadebskaya OI, Maksimovich NG (2009) Geological, hydrogeological and hydrogeochemical pre-requisites of the Ordinskaya Cave formation. In: Peshchery, v 32. Perm State University, Perm, pp 11–22 (in Russian)

Kadebskaya OI, Maksimovich NG, Zhakova UV (2009) Karst features at the area of Ordinskaya Cave (Perm krai, Russia). Speleologiya i karstologiya 3:60–65 (in Russian)

Klimchouk AB (1996) The typology of gypsum karst according to its geological and geomorphological evolution. In: Klimchouk AB, Lowe D et al (eds) Gypsum Karst of the World. Int J Speleol, Theme issue 25(3–4):49–60

Klimchouk AB (2007) Hypogene speleogenesis: hydrogeological and morphogenetic perspective. Special paper no. 1, National Cave and Karst Research Institute, Carlsbad, NM

Klimchouk A (2009) Morphogenesis of hypogenic caves. Geomorphology 106(1):100–117

Klimchouk AB (2016) Types of hypogene speleogenesis. In: Chavez T, Reehling P (eds) Proceedings of deep karst: origins, resources, and management of hypogene karst, NCKRI symposium 6, National Cave and Karst Research Institute, Carlsbad, New Mexico

Lavrov I, Maximovich E, Maximovich N (2005) Ordinskaya cave—the longest underwater cave in Russia. In: Proceedings of conference water resources and environmental problems in karst, Serbia, Montenegro, 13–19 Sept 2005, Belgrade, pp 771–776

Maksimovich GA (1969) Caves of gypsum karst. In: Peshchery. v 8. Perm State University, Perm, pp 5–29 (in Russian)

Maksimovich NG, Maksimovich EG, Lavrov IA (2006) Ordinskaya Cave. The longest underwater cave of Russia. Knizhnyy mir, Perm (in Russian)

Mikhaylov GK, Oborin AA (2006) Underground fresh waters resources of Sylvenskiy ridge. UB RAS, PSU, Perm (in Russian)

Sivinskih P (2009) Features of geological conditions of the Ordinskaya underwater cave, fore-Urals, Russia. In: Klimchouk AB, Ford DC (eds) Hypogene speleogenesis and karst hydrogeology of Artesian basins. Special Paper, Ukrainian Institute of Speleology and Karstology, Kiev, vol 1, pp 267–271

Part II

The Middle East and Central Asia

Geodynamic Control of Hypogene Karst Development in Central Anatolia, Turkey

27

C. Serdar Bayarı, N. Nur Özyurt, A. Koray Törk, Pınar Avcı, İ. Noyan Güner, and Emrah Pekkan

Abstract

Hypogene karst development in central Anatolia, Turkey is represented by unique collapse dolines (obruks) developed mainly in Neogene lacustrine limestone formations. Many of these obruks are located in two separate rectilinear zones, one of which appears to mark the suture zone between Tauride-Anatolian and Sakarya Zone tectonic blocks of the Anatolian plate. The other zone coincides with the alignment of three dormant volcanoes. Formation of obruks seems to be associated with upwelling of carbon dioxide released from deep-rooted igneous activity sources along these zones since Late Miocene. Formation of obruks still continues today, whereas the size of recent collapses is much smaller than ancient examples probably due to weakening volcanism. Recent obruk formations are observed in an area where the youngest volcanic activity seems to have occurred. Frequency of obruk formation increased in recent years because of the groundwater's accelerating piezometric head decline. The stable carbon and noble gas isotope data previously obtained from regional groundwater samples suggested both crustal and mantle sources for the carbon dioxide required for obruk formation. It seems likely that many of the large-scale karst cavity-collapse structures in the world are linked with excessive carbon dioxide release from mantle in orogenic plateaus like central Anatolia.

Keywords

Obruk • Hypogene karst • Volcanogenic carbon dioxide • Konya Basin • Turkey

C.S. Bayarı (✉)
Department of Geological Engineering, Hacettepe University, 06800 Ankara, Turkey
e-mail: serdar@hacettepe.edu.tr

N.N. Özyurt · P. Avcı
Department of Geological Engineering, Hydrogeological Engineering Section, Hacettepe University, 06800 Ankara, Turkey
e-mail: nozyurt@hacettepe.edu.tr

P. Avcı
e-mail: pavci@hacettepe.edu.tr

A.K. Törk
Cave and Karst Research Unit, General Directorate of Mineral Research and Exploration, Dumlupınar Bulvarı No:139, 06800 Ankara, Turkey
e-mail: cave@mta.gov.tr

İ.N. Güner
Hydrogeological Research Unit, General Directorate of Mineral Research and Exploration, Dumlupınar Bulvarı No:139, 06800 Ankara, Turkey
e-mail: n.guner@mta.gov.tr

E. Pekkan
Research Institute of Satellite and Space Sciences, Anadolu University, 26470 Eskisehir, Turkey
e-mail: epekkan@anadolu.edu.tr

© Springer International Publishing AG 2017
A. Klimchouk et al. (eds.), *Hypogene Karst Regions and Caves of the World*, Cave and Karst Systems of the World, DOI 10.1007/978-3-319-53348-3_27

1 Introduction

Recent observations and reassessment of data available at global scale indicate that hypogenic karst development by upwelling fluids is much more widespread than previously thought (e.g., Klimchouk 2000, 2007). Both H_2S and CO_2—originating from deep crustal and mantle sources—lead to karst development in buried and exhumed carbonate rock environment. Evidences suggest that development of secondary porosity in carbonate rocks by hypogene processes may exceed the size of those of epigene processes by several orders of magnitude. Many of the world's largest karst cavities have been formed by hypogene processes. Geological formations with such an extreme porosity and hydraulic conductivity constitute an important medium for storage and transmission of groundwater, natural gas, and oil reserves.

Until recently, the processes leading to hypogene karst development and the properties of hypogene karst features have not yet been well understood because of the limited number of direct observations. However, an increasing number of new evidences and reassessments of existing data provides new insights on the development of hypogene karst. It seems that, in a considerable number of cases, the hypogene karst development is a product of an accompanying intrusive and/or extrusive magmatic activity. In this context, the obruks developed in Konya Closed Basin (KCB) of central Anatolia constitute a sound example of hypogene karst landforms developed by carbonic acid dissolution sustained by extreme flux of CO_2 from mantle and crustal sources. Obruk is a Turkish geomorphic term describing the collapse dolines located commonly in the KCB (e.g., UNESCO 1972). Obruks are cylindrical, upside-down truncated cone, or bowl shaped collapse dolines with surface diameters and depths up to several hundred meters and more than hundred meters, respectively. The rate of obruk formation in KCB has increased exponentially since the late 1970s and reached a life and property-threatening level at the present time.

The processes that result in obruk formation have been debated for a long time. Examples of hypotheses include, (a) an explosive volcanogenic origin as in the case of maar volcanism (e.g., Frech 1916 in Erinç 2001), (b) enhanced carbonate rock dissolution driven under a wetter paleoclimate during the "pluvial" periods of the Pleistocene (e.g., Erol 1986), (c) locally enhanced subsurface dissolution driven by volcanogenic carbon dioxide discharges (e.g., Canik and Çörekçioğlu 1986), and (d) dissolution by a combination of hypogene karstification and mixing corrosion between surface recharge and groundwater (Pekkan 2004). Bayarı et al. (2009a, b, c) provide a detailed evaluation of the geological, hydrogeological, hydrogeochemical, and isotopic data and propose an endogenous hypogenic origin (e.g., Klimchouk 2016; Klimchouk Chap. 1) driven by the extensive release of carbon dioxide due to the magmatic/volcanic activity since Late Miocene. Recent data obtained during the last decade provide additional information on factors that control spatio-temporal obruk formation. It appears that the spatial distribution of obruks has been determined by tectonics, whereas the increasing groundwater abstraction determines the higher rate of formation during the last decades. In the following, we present the fundamental properties of KCB with regards to obruk formation, describe basic morphological characteristics of obruks, summarize the data proving their hypogene origin, and evaluate the geology and tectonics that lead to obruk formation. Finally, a conceptual model of hypogenic obruk formation is presented.

2 Study Area

2.1 Location and Climate

The obruks are located in the endorheic Konya Closed Basin of central Anatolia, Turkey (Fig. 1). The basin occupies an area slightly greater than 50,000 km^2 and is separated into northern and southern closed subbasins by an east-west trending intermediate rise, called "Obruk Plateau". The northern and southern basins hosted large paleolakes that have expanded and contracted many times since Pliocene. The Salt Lake located in the northern basin is a remnant of the former paleolake. The elevations of the plains at the bottom of northern and southern subbasins are 905 and 1000 m (all elevations are above sea level), respectively. The elevation of the KCB water divide increases from about 950 m at the northern tip to around 2500 m in the Taurus Mountains in the south. Obruk Plateau has a mean elevation of about 1050 m.

A semi-arid continental climate is prevalent in the KCB. Mean annual precipitation and potential evapotranspiration are around 400 and 1400 mm, respectively. However, annual precipitation varies from around 800 mm in the Taurus Mountains to less than 200 mm around Karapınar town. Most of the precipitation falls between November and May. Mean annual air temperature at the lower part of the subbasins is about 11.5 °C. Groundwater is abundant in almost every part of the subbasins so that extensive irrigated agriculture is engaged. Animal grazing is common in elevated parts of the basin, where access to groundwater is costly.

An alternation of cool-humid and cool-dry climatic conditions is inferred for the KCB during the Pleistocene glacial periods. (e.g., Kuzucuoğlu 2004; Roberts 1983), whereas a wetter climate is proposed during the Pliocene (e.g., Erol 1986). Between Late Pliocene and mid-Holocene, two large freshwater paleolakes formed in the northern and southern

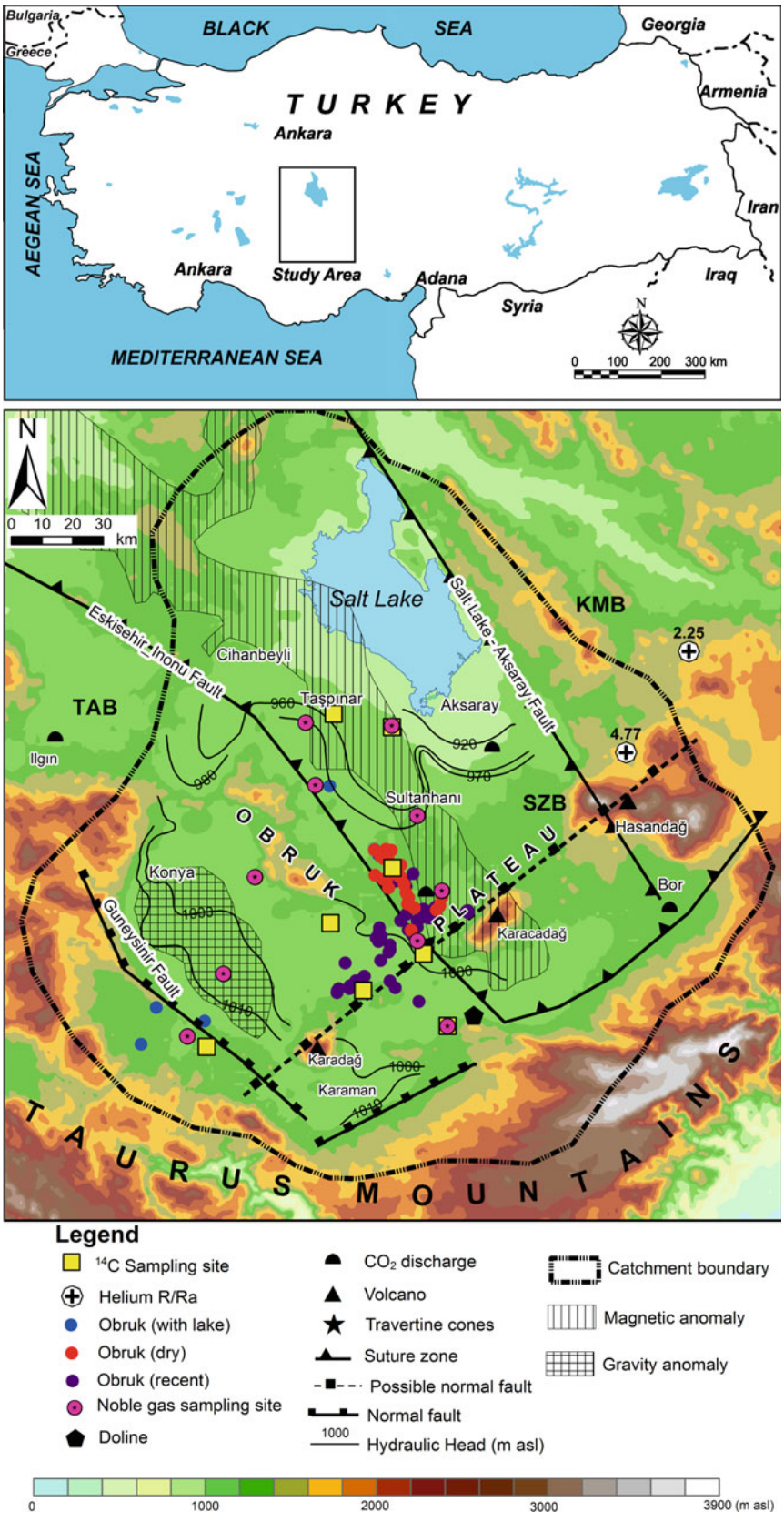

Fig. 1 Location and morphological maps of KCB, showing obruks and associated features

subbasins mainly because of the reduced evapotranspiration favored by low temperature and likely by the widespread cloudiness. The southern paleolake—where most of the recent obruks are formed—reached its maximum extent of 4000 km^2 during the Last Glacial Maximum (ca. 20,000 years BP) (Erinç 2001; Dirik and Erol 2000).

2.2 Regional Geology and Hydrogeology

Formation and spatio-temporal distribution of the obruks in KCB seems to be controlled by the geology and tectonics, whereas increasing groundwater use also increased the rate of formation during the last decades. According to a simplified assessment by Bayarı et al. (2009a), the geology of the basement rock associations in KCB is determined by three lithospheric plates (see Figs. 1 and 2), namely, Tauride-Anatolide Block (TAB), Sakarya Zone Block (SZB), and Kırşehir Massive Block (KMB) (e.g., Okay and Tüysüz 1999). These blocks came together upon the closure of the Neo-Tethys Ocean and are overlain by Paleogene and younger rock units. Obruks are formed mainly in Neogene-aged lacustrine carbonates that may or may not be overlain by Plio-Quaternary-aged, mostly lacustrine, sediments.

The TAB comprises mainly rocks of detritic (i.e., conglomerate, sandstone, and shale), metamorphic, ophiolitic, and marine carbonate origin (i.e., dolomite, dolomitic limestone, and limestone) formed between Early Paleozoic and Late Mesozoic. According to Okay and Tüysüz (1999),

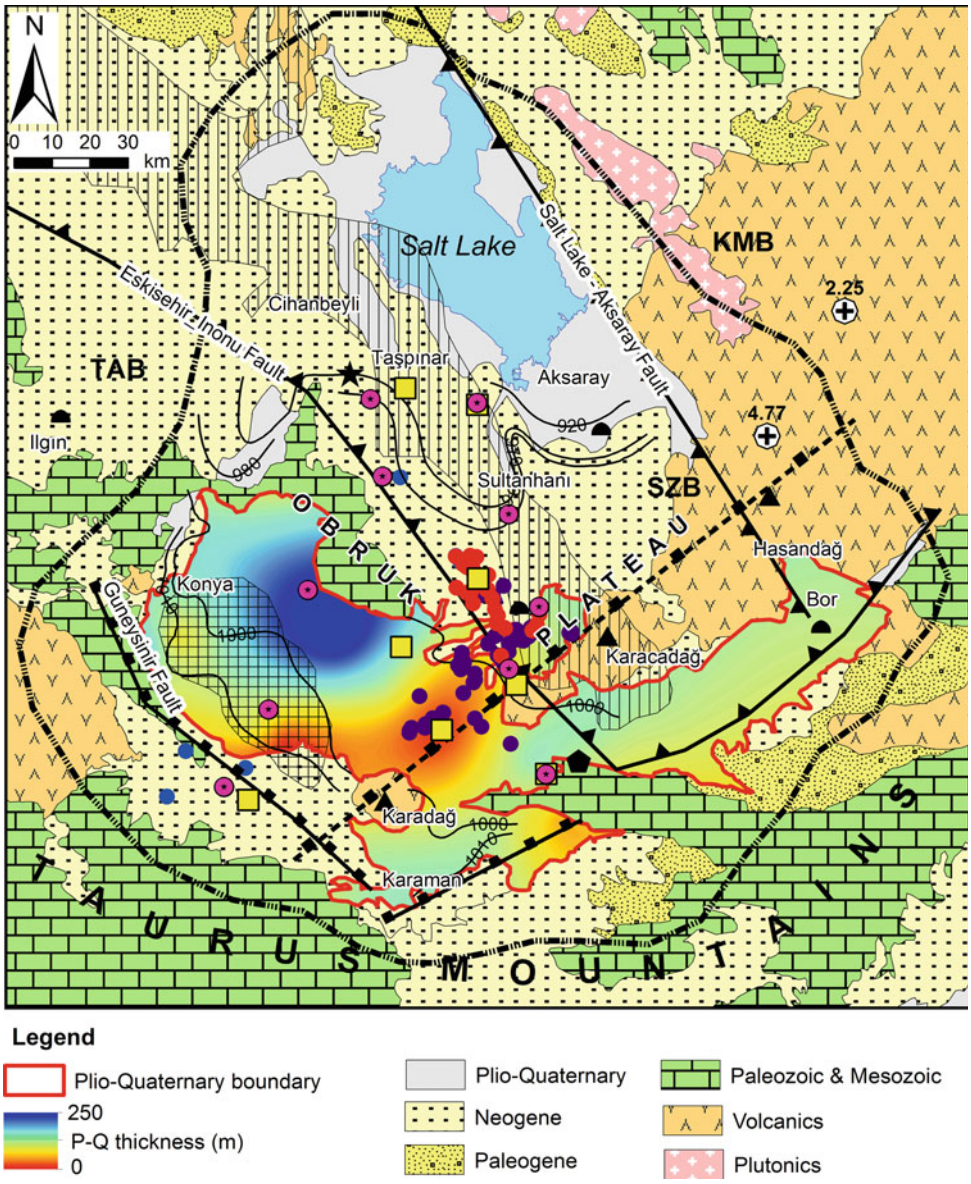

Fig. 2 Simplified geological map of KCB (Modified after MTA 2016. See Fig. 1 for the legend items not shown here)

the TAB is characterized by its south to southeast vergent thrust pile structure that includes a massive body of ophiolite and an accretionary complex, known as ophiolitic mélange. The SZB starts at the bottom with a Triassic subduction-accretion complex. This unit is overlain by Jurassic clastics, Jurassic to Cretaceous carbonates, Middle-Late Cretaceous clastics, and volcanics. The Paleogene carbonates and clastics constitute the top of the SZB. Moreover, salt diapirs and pillows have drilled through the Cretaceous to Oligocene sequence of the SZB between 1000 and 4000 m depths from the surface (Arıkan 1985). The third component (KMB) is made up of metamorphic and granitic rocks of Cretaceous age. The Paleogene rocks of TAB and SZB are similar and include clastics (conglomerate, shale, sandstone, and siltstone) and marine carbonates. From bottom to top, turbiditic sandstone and shale alternation overlain by marine limestone and volcanoclastics and laterally discontinuous evaporitic rocks constitute the Eocene sequence. The Oligo-Miocene sequence starts with continental clastics, tuffs, limestones. and evaporites at the bottom and terminates with a gypsum-shale alternation at the top. The Neogene (Late Miocene to Late Pliocene) sequence from bottom to top includes a basal conglomerate and the alternation of lacustrine limestone and weakly cemented marl and limestone. Paleolake deposits and alluvial fans characterize the detrital nature of the Plio-Quaternary deposits.

The boundary between the KMB and SZB (i.e., the suture zone) is marked by the currently right-lateral Salt Lake—Aksaray Fault, whereas the Eskişehir-Sultanhanı Fault (e.g., Dirik and Erol 2000) marks the boundary between TAB and SZB. Furthermore, the extensional tectonics regime which started after the amalgamation of TAB, SZB, and KMB lithospheric plates during the Late Miocene resulted in the formation of the normal faults like Güneysınır Fault and others located along the northern flank of the Taurus Mountains (see Figs. 1 and 2).

Except for the three obruks located around the Güneysınır Fault, the rest of the old obruks developed along a northwest trending rectilinear zone over the Obruk Plateau. This zone seems to extend parallel to the Eskişehir-Sultanhanı Fault zone (i.e., the buried suture zone between TAB and SZB). A magnetic anomaly, located between 5 and 15 km depth below the surface, extends also along this zone. Cores obtained from exploratory oil drillings indicate an association between the anomaly and magmatic rocks like diabase and splitic basalt (Aydemir and Ateş 2006). Likewise, a gravity anomaly exists near to the Güneysınır Fault. On the other hand, the recent obruks have developed along a northeast trending zone parallel to the line of the Plio-Quaternary volcanoes of Karadağ, Karacadağ, and Hasandağ.

Extensive epigenic karst development is observed in the carbonate rocks belonging to TAB particularly at the higher parts of the Taurus Mountains, where more maritime air masses can access from the Mediterranean Sea at south. The top part of the Neogene sequence, comprising weakly cemented marl and limestone, does not expose remarkable dissolution features. However, the sponge-looking cores of lacustrine limestone obtained in some drillings from the bottom of the Neogene expose an extensive dissolution at depths (Fig. 3). Unlike travertines with similar view, all the cavities in these cores are extremely well connected. Pressurized air applied to any cavity from outside discharges through a number of cavities without any resistance. Almost all of the cavities in such cores include a silica lining that may be indicative of the temporal changes in the chemistry of the hypogene fluids. It is not clear whether these sponge-like cavities are synsedimentary, formed later, or both. Another observation indicating extreme karst development in the unexhumed, deep part of the Neogene is the large dissolution cavities cut during the drillings. These cavities are commonly in the order of a meter in height but may reach up to 10 m.

According to Bayarı et al. (2009a), the simplified regional hydrogeological framework of the KCB involves two aquifer systems comprising of a shallow and productive freshwater aquifer at the top and a confined, poor, and deep thermal aquifer with saline groundwater. The Taurus Mountains at the south of KCB are the main recharge area of these aquifers (see Figs. 1 and 2). The Paleogene rocks located between the TAB and SZB at the bottom and Neogene and younger units at the top form an effective aquitard between these aquifers. However, the regional groundwater flow both in the shallow and freshwater (i.e., Neogene) and deep and thermal water (i.e., TAB) aquifers is from the Taurus Mountains that make up the main recharge area at the south toward the Salt Lake that constitutes the main discharge area at the north. The hydraulic head measurements carried out in the Neogene aquifer in the early 1970s, when the aquifer was almost in a pristine state, point to a head decline from 1100 m at the foot of Taurus Mountains to 905 m, the bottom elevation of the Salt Lake. Despite the hydraulic head lowering that occurred due to extensive groundwater abstraction during the last 45 years, the hydraulic gradient is still able to sustain a flow toward the Salt Lake.

The Plio-Quaternary sediments behave as an aquitard, as they are made mainly of clay, silt, and marl (Fig. 4). Therefore, the initially unconfined groundwater flow system in the Taurus Mountains at the south becomes confined northward, where the Plio-Quaternary aquitard covers the bottom of the plain in the southern subbasin. Further downstream, the flow system becomes unconfined again in

Fig. 3 Sponge-like dissolution cavities developed in the Neogene limestone

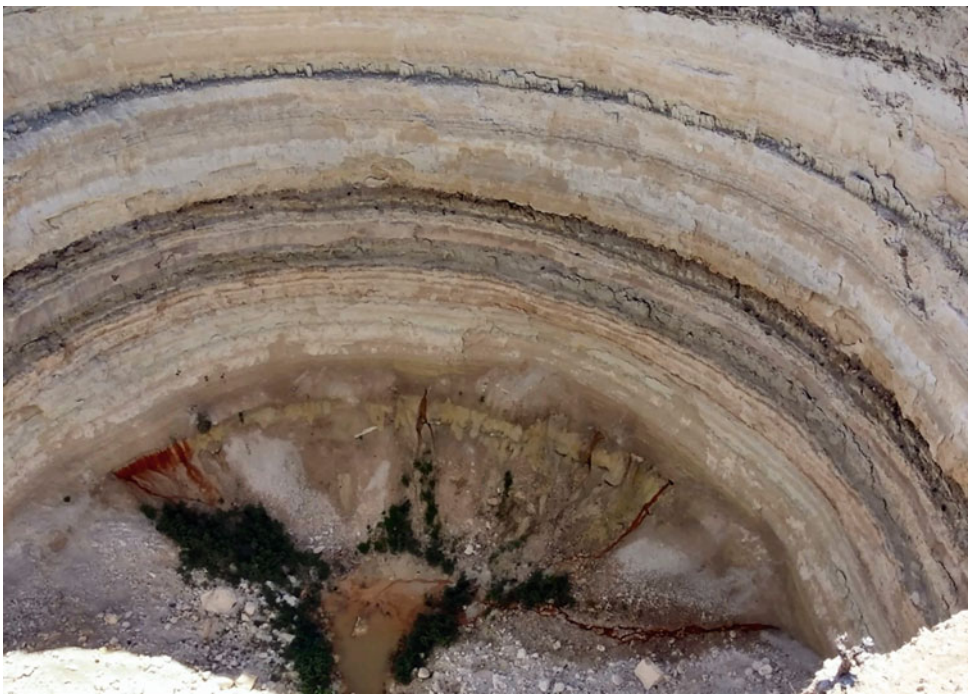

Fig. 4 View of the Plio-Quaternary deposits inside a recently formed obruk. Total depth in view is about 10 m. Some of the *dark horizons* are tephra layers. Note the groundwater exposed at the *bottom center*

the intermediate rise of the "Obruk Plateau" which is made up of TAB, SZB, and Neogene units. The Plio-Quaternary aquitard confines the flow system again between the Obruk Plateau and Salt Lake subbasin in the north. During the pristine state of the Neogene aquifer, that is, before the significant groundwater abstraction started in the early 1970s, part of the recharge from the Taurus Mountains has been overflowing from springs at the mountain foot and in the northern rim of the Obruk Plateau creating lakes and wetlands. However, such discharges have ceased in time because the extreme groundwater abstraction has lowered the piezometric level in the Neogene aquifer. In some places, the total head decline reached 45 m as of 2015. The head drop leads to an inevitable land subsidence in the Plio-Quaternary aquitard (e.g., Üstün et al. 2015).

Many of the recent obruks appear to form above the places where the thickness of Plio-Quaternary sediments, ranging between 0 and 250 m, is low (see Fig. 2). Therefore, it seems that the development of new obruks is linked to the ceiling collapse of large cavities due to decreasing buoyancy

by groundwater, which is also manifested as subsidence in the above lying Plio-Quaternary sediments and in the aquitard beds within the Neogene aquifer.

According to observations obtained from drillings, the thermal groundwater in TAB and SZB is encountered only at sites close to Quaternary volcanic activity sources (i.e., volcanoes, cinder cones, maars, CO_2 discharges), whereas the TAB and SZB contains fresh groundwater in other places. While presence of volcanogenic ions (i.e., Li, Br) indicates that part of the deep thermal groundwater leaks into the Neogene aquifer, the main discharge occurs in the travertine springs near Taşpınar, in the sodium sulfate lakes near Cihanbeyli and in the thermal springs distributed around the KCB. It appears that some of the deep thermal groundwater feeds the Salt Lake as well. Bayarı et al. (2009b) argue that a saline groundwater seepage into the Salt Lake through the Paleogene aquitard is needed to sustain the centuries-long salt production, because only 2.5% of annual salt production can be supplied by precipitation.

3 Morphological Properties

In a recent study by the Geological Survey of Turkey (Törk et al. 2013), the total number of obruks in the KCB was 262. This number includes both old (148 cases) and recent (114 cases) obruks. The "recent" obruks are defined as those witnessed by local people since the 1970s. Among all old obruks, 41 of them have been spotted and measured in the field and 107 of them have been spotted on 1/25,000 scale topographic maps. According to the measured dimensions of the old obruks, the N–S and E–W axes lengths range from 5 to 735 m and from 7.5 to 730 m, respectively. These values indicate most obruks to have a circular shape (Figs. 5 and 6). From a geometrical viewpoint, the obruks may have cylindrical, conical, or upside-down truncated or bowl shapes depending on the geological framework they have developed and on the degree of erosion they have been exposed to. Some of the old obruks developed in the deep part of Neogene limestone have upside-down truncated conical shapes as seen in some of the volcanogenic collapse dolines (e.g., Sistema Zacaton, Gary and Sharp 2006; Gary Chap. 52). It appears that the obruks with loose walls gain a bowl shape in time. The depth of old obruks ranges from 0.2 to 118 m. On the other hand, it is clear that these dimensions are time variable because of the failure of obruk walls in time.

The recent obruks have the N–S and E–W axes lengths ranging from 1 to 61 m and from 1 to 70 m, respectively. Likewise, these younger obruks have a circular shape at the surface as well. They have a depth ranging between 1 and 80 m. Both old and recent obruks have been developed between altitudes of 990 and 1090 m asl. A few of the old and recent obruks intercept the piezometric surface, hosting a groundwater body on their bottom. As of 2013, the ranges of piezometric levels intersected by old and recent obruks are ~945–965 and 980–970 m, respectively.

Typically, majority of the old obruks are located in the Obruk Plateau along a NW trending zone where the Neogene carbonates can be seen at the surface. However, many of the recent obruks developed along a NE trending zone near Karapınar town (see Figs. 1 and 2) where the Neogene carbonates cannot be seen because of the overlying Plio-Quaternary sediment cover.

A characteristic property of old obruks is that they are always bigger than the recent obruks in view of surface dimension and depth. Perhaps, this is because the magmatism and the accompanying carbon dioxide flux have been more intense during the time of their formation. Another characteristic of the old obruks is the linear increase of the obruks' depth as their position moves from the Taurus Mountains (Bayarı et al. 2009a). The depth of old obruks

Fig. 5 A recent obruk with a circular hole at the surface (person for scale in the *upper left*)

Fig. 6 An old obruk with cone-in-cone collapse rims (the water surface measures 170 m across, on May 2013)

increases from about 30 m at the south (e.g., Timraş Obruk) to 225 m at the north (e.g., Kızören Obruk). Along the same route, groundwater-dissolved carbon dioxide content increases linearly as well, from a CO_2aq/CO_2atm ratio of 20 in the south to 375 in the north. In other words, the size of the old obruks seems to be correlated to the present carbon dioxide flux into Neogene groundwater. The varying CO_2 content is probably associated with the volume of the buried magmatic body. Linear variation of the depths of old obruks does not seem to be associated with the thickness of the overlying Plio-Quaternary sediment cover. All of the old obruks are observed in places where the Plio-Quaternary cover does not exist. However, the pits of old obruks developed within the Plio-Quaternary cover might have been filled completely by the lake bottom sediments during the Quaternary glacial periods when large lakes formed in the southern and northern subbasins of the KCB.

Some of the old obruks (e.g., Kızören and Meyil) possess a cone-in-cone geometry (see Fig. 6) which is expressed by a concave surface at top then, a vertical wall which is followed by another concave surface and another vertical wall (see Bayarı et al. 2009a for details). This geometry indicates that the initial collapse has been followed by another one probably because of a secondary dissolution phase triggered by a rejuvenated volcanism. There is a number of travertine cones located at 40 km NW of the rectilinear zone of old obruks (Figs. 1 and 2). Some of these travertine deposits have a "younger cone on top of an older cone", a shape indicating a two-stage development (Erinç 2001; Bayarı et al. 2009a). The cone-in-cone geometry does not seem to be associated with the vertical variation of the strength of material, as it has a uniform structure. It is known that the Plio-Quaternary volcanism in the KCB intensified and weakened several times. Details of multiphase volcanism in the central Anatolia since Paleogene are given by Ercan (1986). Thus, a two (or more)-stage development both for obruks and travertine cones sounds possible.

4 Evidences of Hypogenic Obruk Formation

The processes leading to obruk formation have been debated for a long time (e.g., Frech 1916 in Erinç 2001; Erol 1986; Canik and Çörekçioğlu 1986; Pekkan 2004). Bayarı et al. (2009a, b, c) recently provided a wide range of evidences of a hypogenic origin. In an attempt to determine the radiocarbon age of groundwater in the KCB, Bayarı et al. (2009b) noticed that concentrations of chloride, fluoride, and lithium in groundwater samples (see Figs. 1 and 2 for sampling sites) increase along the regional flow path extending from the Taurus Mountains to the Salt Lake. Normally, these elements are associated with volcanic minerals and are preserved in groundwater. Moreover, the dissolved CO_2 concentration (i.e., logPCO_2 in atm) in groundwater increases from an air–water equilibrium value of −2.2 at the foot of Taurus Mountains to about −1.0 in the rest of the flow path (Fig. 7). The radiocarbon age of groundwater increases from recent at the mountain flank to about 43,000 years at the south of the Salt Lake. It is clear that a continuous supply is needed in order to keep such a high-dissolved CO_2 content along such a long flow path for a period of thousands of years.

Bayarı et al. (2009b) consider various likely CO_2 sources such as the soil zone, the atmosphere, organic matter oxidation, and geogenic production. Because of the extent of the Plio-Quaternary aquitard, the CO_2 input from the soil zone to the groundwater along the regional flow path is possible only at the Taurus Mountains and at the Obruk Plateau. However, except during Holocene, when the climate became favorable for greater biological activity,

the Late Pleistocene climate in KCB was cold and dry (e.g., Roberts 1983). Thus, considerable CO_2 input to groundwater either from the Taurus Mountains or from the Obruk Plateau is not plausible for recharge older than 10,000 years. CO_2 production due to organic matter oxidation cannot be an accountable source for carbon dioxide either, because the Neogene aquifer is poor in organic matter and the groundwater along the entire flow path is rich in sulfate but does not have H_2S. These observations prove that the redox processes in the regional groundwater system do not extent beyond the post-oxic zone, and only the dissolved oxygen is used for oxidation (e.g., Appelo and Postma 1993). Therefore, a considerable CO_2 production via organic matter oxidation is not possible. Eventually, a geogenic (i.e., mantle and crustal) input is left as the only option for the source of high CO_2 dissolved in groundwater.

A firm evidence of carbon dioxide input into the groundwater system from geogenic sources comes from the stable carbon isotope signal of the total dissolved inorganic carbon (TDIC) (see Fig. 7). The $\delta^{13}C$_TDIC values of groundwater at two sampling sites located at the beginning of the regional flow path are around −7 to −5.5‰ (Vienna-PDB). The main recharge area is located on the lee side of the Taurus Mountains where the vegetation changes from woody trees at high elevations and steppe-type plants at the mountain foot. Therefore, a $\delta^{13}C$ signal around −12/−14 (‰ V-PDB) may be assumed for the root zone hosting both C3 and C4 type plants. Likewise, a $\delta^{13}C$ signal of 0 (‰ V-PDB) may be assumed for the carbonate rocks in the recharge area. Thus, the $\delta^{13}C$_TDIC signals at the beginning of the flow path indicate a 50/50 mixing between soil carbon dioxide and carbonate minerals, which is an expected situation. In the rest of the flow path, $\delta^{13}C$_TDIC signal becomes stable around −1.5‰ (Vienna-PDB). If a $\delta^{13}C$ signal of +3 or +4 (‰ V-PDB) is attributed to lacustrine Neogene carbonates (e.g., Bayarı et al. 2009b; Horton and Chamberlain 2016), then CO_2 with a $\delta^{13}C$ signal of 0‰ (Vienna-PDB) would be required in order to attain a $\delta^{13}C$ signal observed in TDIC. Such an enriched $\delta^{13}C$ signal is typical of CO_2 originating from mantle and crustal sources.

Artesian groundwater discharges with abundant dissolved CO_2 (>95%) and low values in H_2S (<10 ppm, by volume) and is frequently encountered in drillings in many parts of the KCB (see Figs. 1 and 2). In areas close to Aksaray, Karapınar, Bor, and Ilgın settlements, liquid CO_2 has been extracted from the groundwater abstracted from well fields drilled in the Neogene aquifer (Fig. 8). In some facilities, production rates may exceed 10 tons per day (Bayarı et al. 2009b). The $\delta^{13}C$ of carbon dioxide extracted from the cool and thermal groundwater samples collected at various sites in the KCB has values of around 0‰ (Vienna-PDB) (e.g., Afşin and Elhatip 1999; Ercan et al. 1995).

Presence of strong CO_2 degassing is also encountered in some of the recent obruks just after they formed and pose a risk for the birds and explorers. This phenomenon is more apparent in obruks which are deep enough so that the wind at the surface cannot penetrate into the bottom area where carbon dioxide (which diffuses very slowly in air) accumulates until being assimilated by diffusive and/or advective processes.

Another evidence for the hypogenic origin of obruks comes from the dissolved helium isotopes. Studies conducted by Ercan et al. (1995) and Güleç et al. (2002) on helium isotopes dissolved in thermal water springs located next to the eastern water divide of KCB revealed remarkably high R/Ra values that indicate a strong gas contribution from the crust and mantle (see Figs. 1 and 2). In this notion, R and Ra indicate the $^3He/^4He$ ratios of the sample and the water to be in equilibrium with the atmosphere. The main source of ^3He is the mantle, whereas most of the ^4He is produced by U–Th series decay in the crust. Presence of crustal and mantle gas flux into the cool groundwater of the Neogene aquifer has been demonstrated by Özyurt and Bayarı (2014) from the helium isotope signals of groundwater samples collected along two transects extending from the Taurus Mountains to the Salt Lake. Measured ^3He and ^4He concentrations have been found to vary between 10^{-13} and 10^{-12} cm^3 STP/g H_2O and 10^{-7} and 10^{-6} cm^3 STP/g H_2O, respectively. The R/Ra value of a water which is in equilibrium with atmosphere is about 1 and the R/Ra ratios of the samples collected along the transects range from 0.88 to 2.13, suggesting the presence of crustal/mantle gas flux in groundwater. Reinterpretation of Özyurt and Bayarı (2014) data reveals that there is more crustal gas flux than from mantle gas flux (Fig. 9). Moreover, it was also found that the amount of gas from crustal and mantle sources increases along with the increasing radiocarbon age of groundwater in the southern subbasin. This shows that time is an important factor in the amount of accumulated crustal/mantle gas in the confined aquifer systems. However, the helium isotope concentrations along the transects investigated by the authors differ considerably suggesting a spatially variable gas flux. The systematically increasing helium concentrations decline sharply in the Obruk Plateau partly because of the release of this gas into the atmosphere and partly because of the dilution by intermediate recharge that occurs in this unconfined section of the Neogene aquifer.

5 Conceptual Model of Hypogene Karst Development in the KCB

A revised and extended version of the conceptual model of hypogene karst development in the KCB, previously developed by Bayarı et al. (2009a), is presented below.

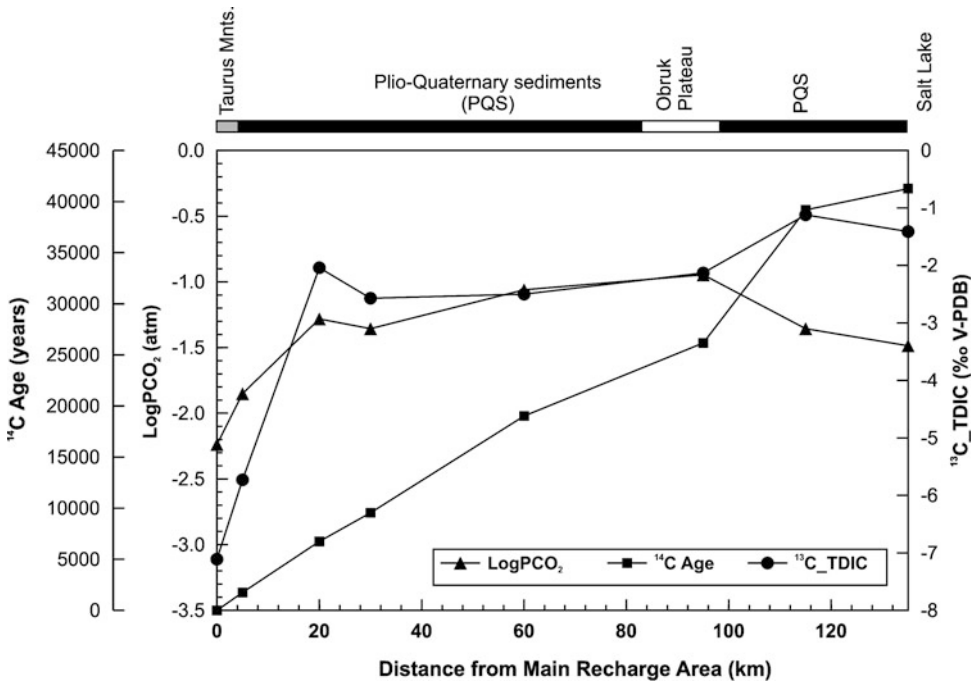

Fig. 7 Variation of log P_{CO2}, $\delta^{13}C$_TDIC and radiocarbon age along the regional flow path of the Neogene aquifer in the KCB (modified after Bayarı et al. 2009a)

Fig. 8 An artesian well in the KCB, sprinkling groundwater rich in geogenic CO_2

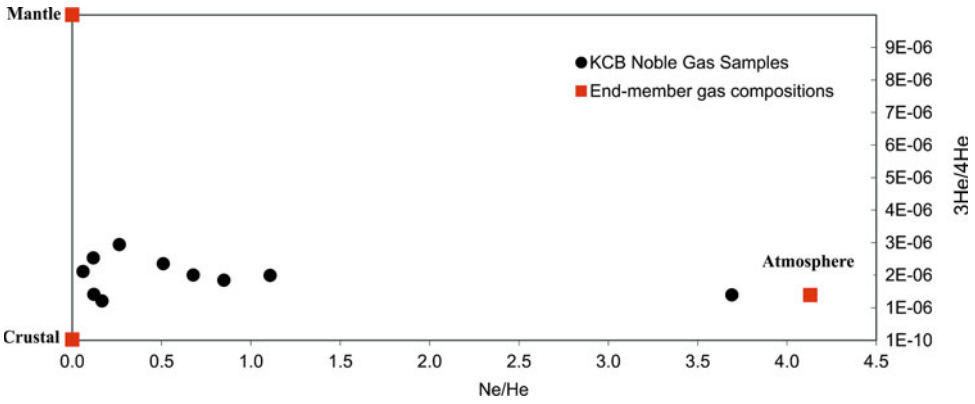

Fig. 9 Source end-members of the dissolved noble gases in the groundwater of the Neogene aquifer

An extensive evaluation of the available information indicates that the formation of obruks is a consequence of the complex interaction between geological, geochemical, and hydrogeological players governed by the tectonics of the KCB. Figure 10 outlines the conceptual model.

First of all, it is clear that the main driver of dissolution is the spatially vast and voluminous geogenic CO_2 flux supplied from the crustal and mantle sources. Secondly, the production of geogenic CO_2 appears to be associated with the magmatism that has been rejuvenated from time to time since Late Miocene which marks the beginning of the neotectonic period in Turkey (e.g., Bozkurt 2001; Şengör and Yılmaz 1981). According to Okay (2008), the new tectonic era, which is still active today, started in Anatolia in the Oligo-Miocene after the final amalgamation of the various continental fragments. The neotectonic phase is characterized by continental sedimentation, widespread calc-alkaline magmatism, and extension and strike-slip faulting, all of which have occurred in the KCB. The neotectonics of Turkey include both compressional and extensional regimes. The Taurus Mountains belt is the product of a compressional tectonics, whereas part of the KCB to the north of the mountain sector has been shaped by the extensional tectonics that followed the uplifting. The extensional thinning of the lithospheric plate under the KCB since Late Tertiary caused an asthenospheric rise accompanied by the formation of spatially widespread magmatism in and around the KCB until Late Holocene. Numerous dormant volcanoes, cinder cones, maars, CO_2 discharges, and hydrothermal springs scattered in and around the KCB are the products of this magmatism (e.g., Keller 1974; Ercan 1986) (see Figs. 1, 2 and 10). The Ar/Ar ages obtained from different parts of Late Miocene-Quaternary-aged volcanic successions in central Anatolia provided volcanic activity episodes around 0.096, 1.85, 2.52, 5.19, 6.14, 6.34, 7.20, 8.17, 8.26, 8.44, 9.12, 9.19, and 9.20 ka (kilo annum) before present (Aydar et al. 2013). A mural, found in the Çatalhöyük Neolithic proto-city dated 9000 years before present (UNESCO 2016) depicts a landscape with explosive summit eruption of the Hasan Dağı twin-peaks volcano. Schmitt et al. (2014) showed that the (U–Th)/He zircon eruption age of 8.97 ± 0.64 ka overlaps closely with ^{14}C ages of cultural strata containing the mural. Therefore, an Early Holocene volcanism in the KCB is also evident.

The heat flux emanating from the magmatic intrusion causes the metamorphism of carbonate rocks belonging to TAB and SZB, and this process (e.g., Heat + $CaCO_3$ + $SiO_2 \rightarrow CO_2 + CaSiO_3$) produces substantial amounts of carbon dioxide. Moreover, the mantle itself is another major source of carbon dioxide. The deep-seated geogenic carbon dioxide, other gasses such as He and solutes (like volcanogenic elements, Li and F) are transported toward the surface by the upwelling fluids driven by thermal convection (see Fig. 10). The asthenospheric intrusion is expected to create at least a moderate geothermal gradient of 2.5 °C/100 m (Çoşkun 2004). As the thermal fluid loses its initial heat capacity in the near-surface environment, it sinks again toward the heat source to complete the convective circulation. During this process, the part of groundwater that is lost from the system is substituted by the recharge from the Taurus Mountains. On the other hand, the CO_2 flux from mantle may also be a sudden event like the earthquakes that occur in the overpressurized upper crust. Such gas releases are expected to upwell along the fault lines/zones. Therefore, the linear obruk development zones in the KCB may also be associated with the local seismicity which may be linked to the synchronous volcanism.

The groundwater in the Neogene aquifer is rich in deep-seated volatile components but poor in volcanogenic elements. Bayarı et al. (2009b) argue that despite the low concentration of volcanogenic elements (i.e., Li and F) in the Neogene aquifer, abundance of geogenic CO_2 implies that the Paleogene aquitard behaves like a selective membrane that favors migration of volatile components of deep groundwater while nongaseous components are retarded effectively. The migration of CO_2 through the Paleogene aquitard may have been eased by the supercritical state of this gas ($scCO_2$). The supercritical state of CO_2 is reached at

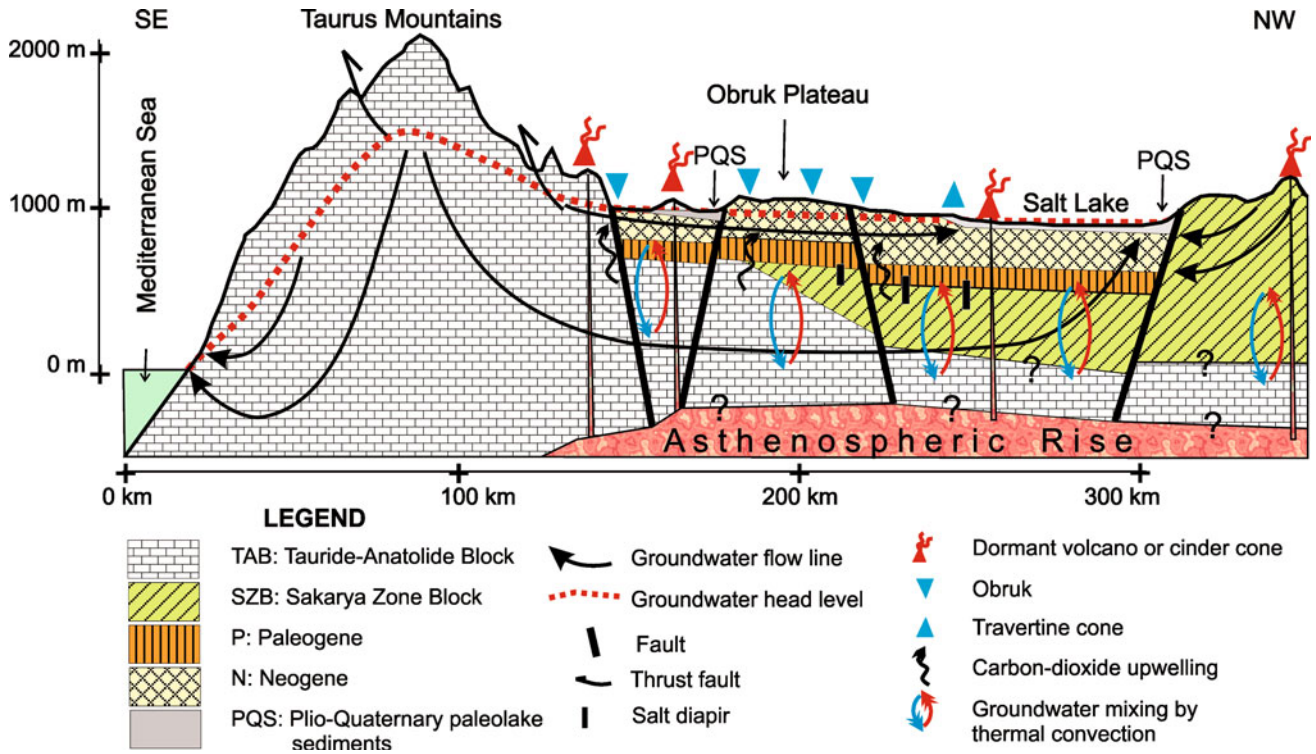

Fig. 10 Conceptual model of the regional hydrogeologic system leading to hypogenic karst development in the KCB. Modified after Bayarı et al. (2009a). Depth of asthenospheric rise is not to scale

31 °C and 7.4 MPa, corresponding to a depth range of about 350–750 m. A supercritical fluid can diffuse through solids like a gas, and dissolve materials like a liquid. Therefore, the $scCO_2$ travels easily from the parent magma through low-permeability rock and make the groundwater very aggressive to carbonate minerals upon mixing (e.g., Decker et al. 2015 and references therein).

The thermal groundwater seeping into the Neogene aquifer is mixed with the fresh groundwater moving from the Taurus Mountains toward the Salt Lake. Thus, there are two vectors affecting mass transport of deep-seated components in the Neogene aquifer: (a) the upward migration of thermal fluid due to the density gradient and/or sudden release of fluids from the upper crust due to earthquakes and, (b) the lateral regional flow of groundwater toward the Salt Lake. Bayarı et al. (2009b) argue that the volatile components physically dissolved in groundwater (i.e., CO_2 gas) degas during the upwelling because of the decreasing hydrostatic pressure acting upon the water mass. Thus, the release of gas bubbles creates a larger gas–liquid interface along which more CO_2_aq is formed. This enhances the dissolution in the near-surface environments like the base of obruks and pathways of karstic/thermal water springs fed by CO_2 rich groundwater.

The large-sized old and small-sized recent obruks are clustered in the Neogene limestone over the Obruk Plateau and in the Plio-Quaternary sediments around Karapinar, respectively. As it turns out, the Obruk Plateau where the Neogene aquifer is unconfined should have functioned as an escape route for the release of excessive dissolved gas from the groundwater into the atmosphere during the peak of magmatic activity. Hence, most of the carbonate mineral dissolution and the eventually large-sized obruk formation have occurred on the plateau. Unlike old obruks, the recent ones have been developed along a northeast trending zone that is parallel to Karadağ, Karacacadağ, and Hasandağ volcanoes (see Figs. 1, 2 and 10). Here, the Neogene aquifer is confined by the overlying Plio-Quaternary sediments so that as "escape route" similar to the one on the Obruk Plateau seems unlikely. The reason of the change of direction of obruk development zones from a northwest trend of old obruks to a northeast trend of recent obruks is not clear and may be related to the varying age of volcanism in different directions.

6 Conclusions and Outlook

Recent observations and reassessment of available data show that the collapse doline (obruk) formation in the KCB of central Anatolia is a consequence of hypogenic karst development driven by the geogenic (i.e., crustal and mantle) CO_2 flux from a magmatic source. This

hypogene karst system includes a complex interaction among geological, geochemical, and hydrogeological players governed by the neotectonics of the KCB.

The extensional tectonics since Late Miocene resulted in a lithospheric thinning and accompanying asthenospheric rise under the KCB. The consequent volcanism, which is currently in a dormant phase, continued episodically until Early Holocene. A number of independent evidences support a geogenic source for the source of CO_2. These include, (i) high dissolved CO_2 in groundwater, (ii) a $\delta^{13}C$_TDIC signal of around −1.5‰ (V-PDB), (iii) artesian groundwater discharges with abundant dissolved CO_2, (iv) remarkably high R/Ra values observed in hydrothermal springs and wells, and (v) relatively high dissolved He isotopes in cool groundwater, indicating crustal and mantle gas sources.

Many of the obruks are formed mainly in Neogene-aged lacustrine carbonates along two separate zones that seem to have been defined by tectonic discontinuities. The old obruks whose time of formation is unknown are scattered along a northwest trending rectilinear zone over the Obruk Plateau, where the Neogene aquifer is unconfined. This alignment seems to follow the suture zone between two continental lithospheric fragments. The recent obruks started to develop mainly along a northeast trending zone located to the south of Obruk Plateau, where the Neogene aquifer is confined by the overlying Plio-Quaternary aquitard since the 1970s (with an increasing frequency since 2005). The extent of this zone coincides with the alignment of three dormant volcanoes.

An important issue regarding the obruk development is the geometry and potential location of the cavities in which the collapse occurs. Systematic underwater exploration studies by scuba diving and remotely operated submersible vehicle surveys should be conducted to determine the underwater geometry and associated conduit features of the obruks. Recent exploratory drilling studies guided by the geophysical anomalies of resistivity and microgravity observations are expected to be helpful to better understand the processes leading to obruk formation.

Obviously, the presented conceptual model of hypogene karst development in the KCB is an oversimplification of a complex natural system and may be improved by additional observations. However, the outlines of the model are believed to be representative of many orogenic plateaus affected by magmatic activity elsewhere in the world. Therefore, many karst systems previously associated with epigenic development models should be re-evaluated for a possible hypogene development component if their geological evolution includes an orogenic plateau formation. Such examinations may provide a new viewpoint for oil and gas exploration and help to better assess the existing karst aquifer as water resources.

Acknowledgements The ideas expressed in this paper have evolved in years through discussions with many colleagues. We particularly appreciate the discussions with Dr A. Klimchouk (Natl. Academy of Science of Ukraine, on hypogenesis), Dr N. Plummer (USGS, on groundwater radiocarbon age modeling), and Dr K. Solomon (University of Utah, on evaluating noble gas data). Some of the presented data have been collected with the in-kind and financial support of the following institutions: The Scientific and Technological Research Council of Turkey (TUBITAK grant no 108Y004), International Atomic Energy Agency (IAEA grant no TUR-16283), and Isotope Hydrology Laboratory of the Water Authority of Jordan. Comments of anonymous reviewers helped to improve the manuscript. The authors declare no conflicting interests.

References

Afşin M, Elhatip H (1999) Hydrogeochemical and isotopic evaluation of travertine depositing Tuzlusu thermal springs in Aksaray. In: Fendekova M, Fendek M (eds) Proceedings of IAH XXIX congress, Cape Town, Nov 2000, pp 647–653

Appelo CAJ, Postma D (1993) Geochemistry, groundwater and pollution. A.A. Balkema, Leiden, Rotterdam, The Netherlands

Arıkan Y (1985) Geology and petroleum potential of the Tuz Gölü Basin. J MTA 85(2):17–38 (in Turkish)

Aydar E, Çubukçu HE, Şen E, Akın L (2013) Central Anatolian Plateau, Turkey: incision and paleoaltimetry recorded from volcanic rocks. Turkish J Earth Sci 22:739–746

Aydemir A, Ateş A (2006) Interpretation of Sülüklü-Cihanbeyli-Gölören magnetic anomaly, Central Anatolia, Turkey: an integration of geophysical data. Phys Earth Planet Inter 159:167–182

Bayarı CS, Pekkan E, Özyurt NN (2009a) Obruks, as giant collapse dolines caused by hypogenic karstification in central Anatolia, Turkey: analysis of likely formation processes. Hydrogeol J 17 (2):327–345

Bayarı CS, Özyurt NN, Kilani S (2009b) Radiocarbon age distribution of groundwater in the Konya closed basin, central Anatolia, Turkey. Hydrogeol J 17(2):347–365

Bayarı CS, Özyurt NN, Pekkan E (2009c) Giant collapse structures formed by hypogenic karstification: the obruks of the Central Anatolia, Turkey. In: Klimchouk AB, Ford DC (eds) Hypogene speleogenesis and karst hydrogeology of Artesian basins. Ukraine Institute of Speleology and Karstology, Special Paper 1, Simferopol, pp 83–90. ISBN 978–966-2178-38-8

Bozkurt E (2001) Neotectonics of Turkey—a synthesis. Geodin Acta 14(1–3):3–30

Canik B, Çörekçioğlu I (1986) The formation of sinkholes (Obruk) between Karapinar and Kizoren-Konya. In Proceedings of symposium on karst water resources, Ankara-Antalya, July 1985, IAHS Publ no. 161, IAHS, Wallingford, UK, pp 193–205

Çoşkun B (2004) Aksaray and Ecemis faults-diapiric salt relationships: relevance to the hydrocarbon exploration in the Tuz Gölü (Salt Lake) Basin, Central Anatolia, Turkey. Energ Sour 26: 1005–1022

Decker DD, Polyak VJ, Asmerom Y (2015) Depth and timing of calcite spar and "spar cave" genesis: implications for landscape evolution studies, In: Feinberg J, Gao Y, Alexander EC Jr (eds) Caves and Karst across time. Geol Soc Am Spec Pap: 516, pp 103–110

Dirik K, Erol O (2000) Tectonomorphological evolution of Tuz Gölü and surrounding area, Central Anatolia-Turkey. In: Workshop of Haymana-Tuzgolu-Ulukisla Basins, Publ. of the Turkish Association of Petroleum Geologists, Ankara, pp 27–46 (in Turkish)

Ercan T (1986) Cenozoic volcanism in central Anatolia. MTA Bull 107:119–140

Ercan T, Matsuda J, Nagao K, Kita I (1995) Noble gas isotopic composition in gas and water samples from Anatolia. In: Proceedings of geology of the Black sea region, 7–11 Sept 1992, Ankara, MTA General Directorate, Ankara, pp 197–206

Erinç S (2001) Geomorphology II, 3rd edn. Der Publ. House, Istanbul (in Turkish)

Erol O (1986) The relationships between the phases of the development of the Konya-Karapinar obruks and the Pleistocene Tuz Gölü and Konya pluvial lakes. In: Günay G, Johnson IE (eds) Karst water resources Proceedings of the Ankara-Antalya symposium, July 1985, IAHS Publ. No. 161, IAHS, Wallingford, UK, pp 207–213

Frech F (1916) Geologie Kleinasiens in Bereich der Bagdadbahn [Geology of Asia Minor as regards the Baghdad Railway]. Z Deut Ges Geowiss 68:1–326

Gary MO, Sharp JM (2006) Volcanogenic karstification of Systema Zacaton, Mexico. Geol Soc Am Spec Pap 404:79–89

Güleç N, Hilton DR, Mutlu H (2002) Helium isotope variations in Turkey: relationship to tectonics, volcanism and recent seismic activities. Chem Geol 187:129–142

Horton TW, Chamberlain CP (2016) Stable isotopic evidence for Neogene surface downdrop in the central Basin and Range Province. Geol Soc Am Bull 118(3–4):475–490

Keller J (1974) Quaternary maar volcanism near Karapinar in Central Anatolia. Bull Volcanol 38:378–396

Klimchouk A (2000) Speleogenesis under deep-seated and confined settings. In: Klimchouk AB, Ford DC, Palmer AN, Dreybrodt W (eds) Speleogenesis: evolution of karst aquifers. National Speleological Society, Huntsville, pp 244–260

Klimchouk A (2007) Hypogene speleogenesis: hydrogeological and morphogenetic perspective. Special Paper no. 1, National Cave and Karst Research Institute, Carlsbad, NM, USA

Klimchouk A (2016) Types of hypogene speleogenesis. In: Chavez T, Reehling P (eds) Proceedings of DeepKarst 2016: origins, resources, and management of hypogene Karst, April 11–14, NCKRI symposium 6. National Cave and Karst Research Institute: Carlsbad, New Mexico, pp 47–49

Kuzucuoğlu C (2004) Upper and late Pleistocene environmental changes in Anatolia, reconstructed from sediment sequences and landforms studies. In: Proceedings of the international symposium on earth system sciences. Istanbul, pp 19–27

MTA (2016) Geological maps of Turkey. http://www.mta.gov.tr/v2.0/daire-baskanliklari/jed/index.php?id=500bas. Accessed 7 June 2016

Okay AI (2008) Geology of Turkey: a synopsis. Anschnitt 21:19–42

Okay A, Tüysüz O (1999) Tethyan sutures of northern Turkey. In: Durand B, Jolivet L, Horvath F, Seranne M (eds) The Mediterranean basins: tertiary extensions within the Alpine Orogen. Geol Soc Lond Spec Pub 156, pp 475–515

Özyurt NN, Bayarı CS (2014) Helium isotopes as indicator of current hypogenic karst development in Taurids karst region, Turkey. In: Klimchouk A, Sasowsky I, Mylroie J, Engel SA, Engel AS (eds) Hypogene cave morphologies: selected papers and abstracts of the symposium held February 2 through 7, 2014, San Salvador Island, Bahamas. Karst Waters Institute Special Publication 18, Karst Waters Institute, Leesburg, Virginia, pp 77–81

Pekkan E (2004) Investigation of the hydrogeochemical processes that affects the formation of obruks as karstic depressions located in the Konya closed basin. M.Sc. thesis, Institute of Science, Hacettepe University Ankara, Turkey (in Turkish)

Roberts N (1983) Age, paleoenvironments, and climatic significance of late Pleistocene Konya lake, Turkey. Quat Res 19:154–171

Schmitt AK, Danışık M, Aydar E, Şen E, Ulusoy İ, Lovera OM (2014) Identifying the volcanic eruption depicted in a neolithic painting at Çatalhöyük, Central Anatolia, Turkey. PLOS ONE 9(1):e84711. doi:10.1371/journal.pone.0084711

Şengör AMC, Yılmaz Y (1981) Tethyan evolution of Turkey: a plate tectonic approach. Tectonophysics 75(3–4):199–241

Törk K, Erduran B, Yılmaz P, Sülükçü S, Güner İN, Ateş S, Mutlu G, Keleş S, Çınar A, Demirbaş Ş, Sertel N, Özerk C, Bulut A, Yeleser L, Avcı K, Ayva A, Toksoy AT (2013) Determination of the karstic collapse areas in the Konya Basin and hazard assessments. General Directorate of Mineral Research & Exploration. Ankara. Report No: 11605, Ankara (in Turkish)

UNESCO (1972) Glossary and multilingual equivalents of 227 Karst terms. UNESCO, Paris

UNESCO (2016) Neolithic Site of Çatalhöyük. http://whc.unesco.org/en/list/1405. Accessed 26 Sept 2016

Üstün A, Tuşat E, Yalvaç S, Özkan İ, Eren Y, Özdemir A, Bildirici İÖ, Üstüntaş T, Kırtıloğlu OS, Mesutoğlu M, Doğanalp S, Canaslan F, Abbak RA, Avşar NB, Şimşek FF (2015) Land subsidence in Konya Closed Basin and its spatio-temporal detection by GPS and DInSAR. Environ Earth Sci 73:6691–6703

The Judean Desert—The Major Hypogene Cave Region of the Southern Levant

28

Amos Frumkin, Boaz Langford, and Roi Porat

Abstract

The Judean Desert in eastern Israel consists of a Late Cretaceous epicontinental carbonate terrain formed at the interface between the Neotethys Ocean and the Gondwanian African-Arabian plate. Various rock types were deposited through fluctuations between marine and continental environments due to ingressions and regressions. Orogenic folding of the Syrian Arc fold system occurred between the Late Cretaceous and the Neogene. The folds formed a barrier for deep flowing groundwater, which upwelled along the SE flank of the folds. Possibly mixing with local confined circulation, the hypogene flow created maze caves at the top of the Late Cretaceous limestone, under the confinement of thick chalk, and marl successions. The larger caves are up to 3.5-km-long 2D mazes, less commonly with some additional tiers. Speleogenesis occurred most likely during the Oligocene, when far-field recharge could reach the Judean Desert. During the Neogene, the Dead Sea transform has dissected the region, forming a deep endorheic depression at the eastern border of the Judean Desert. This was followed by the lowering of the water table and related dewatering of the caves. Fault escarpments and downcutting canyons have dissected the caves, forming the present entrances. The caves are mostly dry, with rare speleothems. Gypsum rinds indicate that hydrogen sulfide and sulfuric acid took part in speleogenesis.

Keywords

Maze caves • Desert karst • Sulfuric acid • Syrian Arc • Confined caves

1 Introduction

Hypogene caves may allow reconstruction of landscape evolution and paleo-hydrogeology over long periods. To achieve this, knowledge of regional hydrogeology and hypogene cave systems is needed (e.g., Audra and Palmer 2015; Klimchouk 2013, 2015).

Following a major cave survey effort (e.g., Langford and Frumkin 2013), the Judean Desert, eastern Israel (Fig. 1), stands out as the most important hypogene cave province in the southern Levant (Israel, Jordan, Syria, Lebanon). Few other similar caves are known in nearby regions (e.g., Frumkin and Gvirtzman 2006; Kempe et al. 2006).

The Judean Desert is one of the driest regions in the southern Levant, so the conditions giving rise to the abundance of hypogene caves should be understood. The long-term aridity of the region has prevented the formation of epigenic caves, which helps in identifying and understanding the hypogene caves and their features.

The Judean Desert borders for this study were selected on a hydrogeological basis: from the narrowest Mt. Scopus confinement in the south-western Jordan valley in the north to the Hemar-Be'er Sheva paleovalley in the south (Bar and Zilberman 2016), and from the Dead Sea depression in the east to the border between rain-shadow semi-arid zone and the Judean Mountains in the west (Fig. 1).

A. Frumkin (✉) · B. Langford · R. Porat
Cave Research Center, Institute of Earth Sciences, The Hebrew University of Jerusalem, 91904 Jerusalem, Israel
e-mail: amos.frumkin@mail.huji.ac.il

© Springer International Publishing AG 2017

A. Klimchouk et al. (eds.), *Hypogene Karst Regions and Caves of the World*,
Cave and Karst Systems of the World, DOI 10.1007/978-3-319-53348-3_28

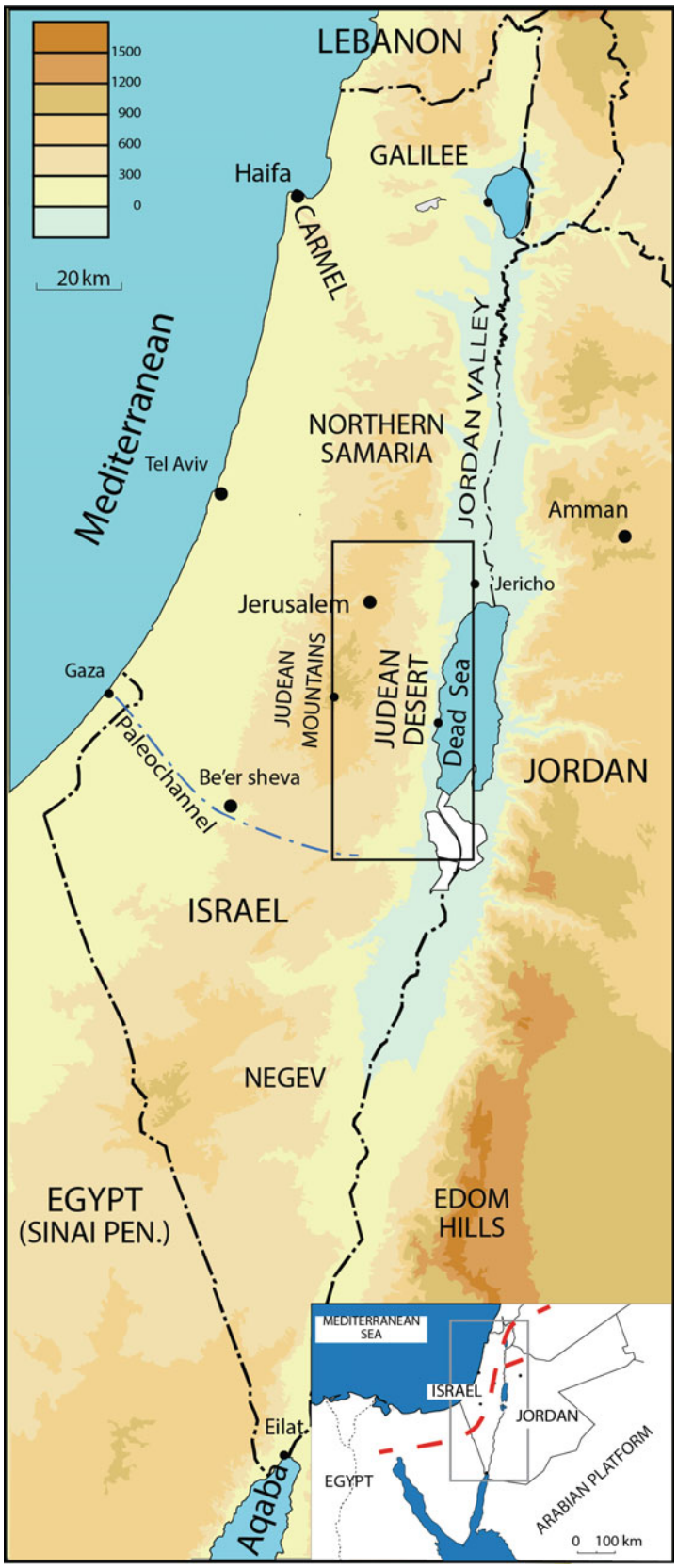

Fig. 1 Judean Desert on a topographic map of Israel. The rectangle is enlarged in Fig. 2. Paleochannel separating the Judean and Negev deserts was active during Oligocene–Miocene times. *Dashed red line* in the inset shows the rough trace of the Syrian Arc fold system

2 Geology and Hydrogeology of the Judean Desert

Located on the leeward flank of the Judea Mountains (Fig. 1), the region is a rain-shadow desert, experiencing dry Mediterranean to hyper-arid climate, with cool rainy winters and hot dry summers. Mean annual precipitation varies from 500 mm on the western semi-arid zone to 60 mm on the Dead Sea shore to the east. Annual potential evapotranspiration varies from 1600 mm in the west to 2100 mm in the east. Over 70% of the annual precipitation is lost by evapotranspiration. Surficial runoff is rare, limited to intense precipitation events, or downstream of a few springs that support intermittent or perennial flow.

Present karst denudation rates of flat-lying bedrock outcrop along interfluves decrease by an order of magnitude from $\sim$20 mm ka^{-1} in the Mediterranean/semi-arid border zone on the west to 1–3 mm ka^{-1} in the hyper-arid zone at the Dead Sea escarpment (Ryb et al. 2014).

The development of the present hydrogeological configuration of the Judean Desert can be traced to the updoming of the Late Paleozoic Helez Swell and erosional removal of most Paleozoic sedimentary cover during the Late Carboniferous–Early Permian. Permian marine inundation followed by Mesozoic marine and continental deposition formed the sedimentary sequence underlying the Judean Desert.

A tilting of the whole area toward the present Mediterranean coast was associated with the onset of rifting during the Early Triassic.

Three major Mesozoic tectonic stages are observed as follows:

(1) Local differential movements mark the Early Triassic to Early Jurassic extensional stage, characterized by synsedimentary, generally rapid subsidence of local troughs due to differential movements and block tilting along NE-SW to NNE-SSW directed listric normal faults (Garfunkel and Derin 1984). This caused small-scale variations in facies and thickness of overlying sediments. Intensive magmatic and volcanic activity marks the end of the initial rifting phase in the area, ending the first stage.

(2) Subsequently, a passive margin was formed, contrasting the previous stage of local differential movements by the development of a dominating wedge of uniform marine sequences, thickening toward the subsiding area of the present eastern Mediterranean, and occasionally interfingering with continental clastics. A carbonate platform is formed along this downwarping shelf of the Neotethys Ocean. This stage was associated with the opening and extension of the Neotethys Ocean that decelerated during Late Cretaceous.

In the Judean Desert region, sedimentation of epeiric platform carbonates prevailed until Senonian time, with a general transgressive trend interfingering occasionally with the clastic sediments originating from the Arabo-Nubian craton in the southeast (Flexer et al. 1989). The majority of the accumulated sediments of the second stage belong to the Judea Group, a sequence mainly comprising massive limestone and dolostone, sometimes intercalated with limestone, marl, and chalk. The common deposition environment was a wide shallow platform lagoon with barrier reefs isolating the lagoon from the open sea (Sass and Bein 1978). Reef patches produced several massive permeable limestone bodies that later attracted groundwater flow and speleogenesis. The Judea Group, therefore, serves today as the major regional karstic aquifer of Israel (Weinberger and Rosenthal 1998), draining naturally to large springs along both sides of the mountain range, with steep gradients to the east, in the Judean Desert (Kafri and Arad 1978).

Marine inundation of the shallow platform was occasionally interrupted by regressions and subaerial exposure events. Following each regression, eogenetic karstification developed to varying degrees, as well as shallow braided rivers and pedogenesis (e.g., Sandler 1996). These are currently observed as paleokarst features within the bedrock sequence, which in some occasions have been reactivated by later telogenetic karstification.

(3) In the Late Cretaceous, at the onset of the closure of the Neotethyan Ocean, the Syrian Arc structure was formed, extending from northern Egypt in the southwest to Syria in the northeast (e.g., Freund et al. 1975; Shahar 1994). The compressional stress field reactivated the Early Mesozoic normal faults, this time acting as reverse faults, and leading to the establishment of the NNE directed, double plunging Hebron and Ramallah monocline structures, at the ESE side of larger box anticlines (Fig. 2b). In addition to the major ESE-facing monoclines, the Syrian Arc structure appears within the Judean Desert as undulations and subfolds.

The stress field responsible for the Syrian Arc folding lasted from the Turonian to Paleocene (Reches et al. 1981), during which the Mount Scopus Group was deposited in deeper (few hundred m) sea water. Comprising mainly chalk and marl, as well as some chert, limestone, and phosphorites, Mount Scopus Group serves as impervious caprock, hydraulically confining the Judea Group aquifer. Today Mount Scopus Group crops out and is preserved across most of the Judean Desert plateau, particularly in synclines and partly on the anticlinal flanks (Fig. 2). Following the subsidence of the Dead Sea rift, the regional water table has fallen below the Mt. Scopus Group confinement.

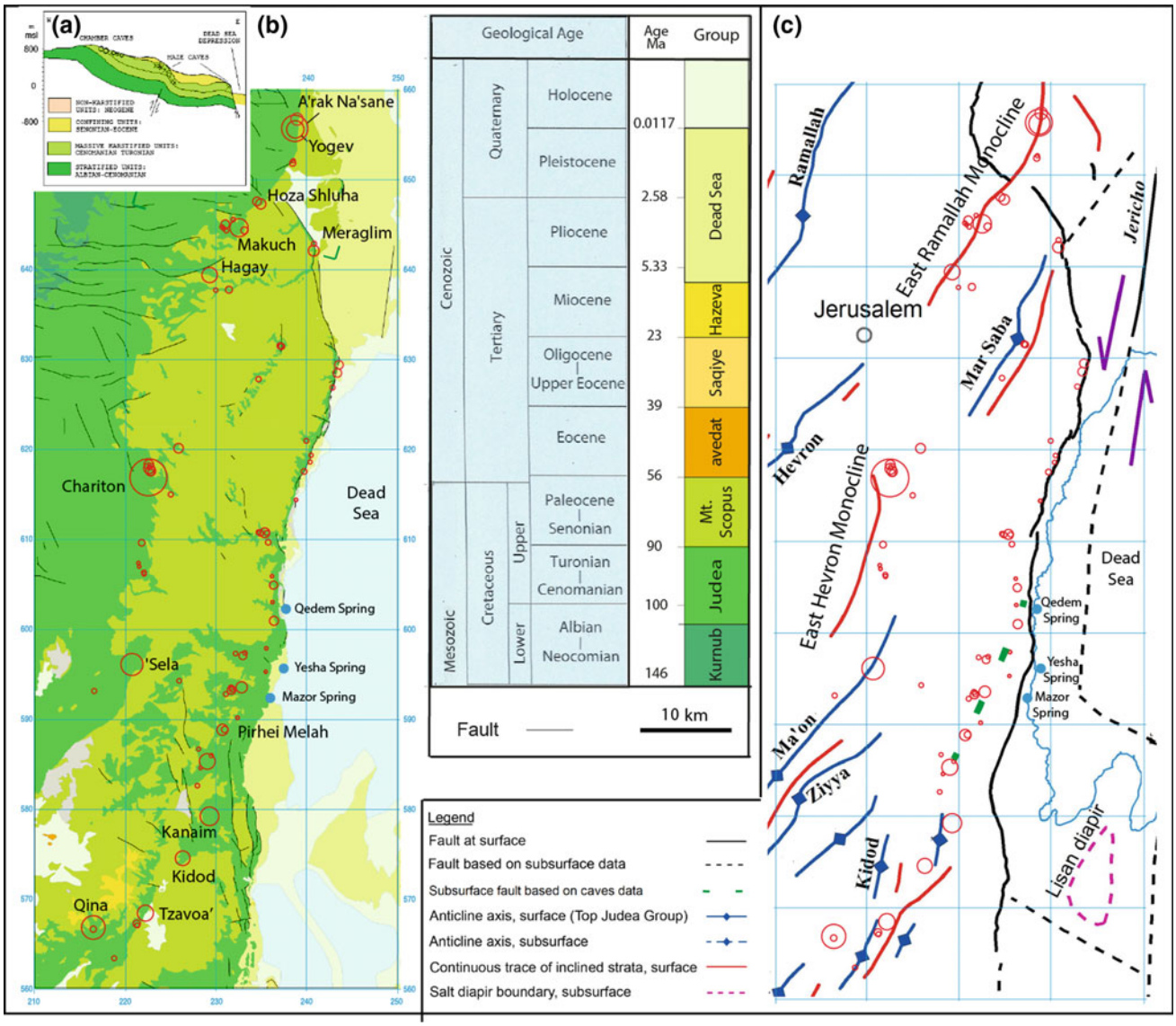

Fig. 2 Distribution of Judean Desert caves and springs associated with hypogene water. **a** Geological cross-section of northern Judean Desert from Meraglim Cave (east) to Ramallah anticline (west). *X* indicates maze cave and *O* indicates chamber cave. **b** Geological map. Cave systems are indicated by *circles* whose area is proportional to the cave length. A cave system is regarded here as caves whose entrances are within 100 m from each other. Caves and springs mentioned in this chapter are shown by name. **c** Map of major geological structures, structure after Sneh and Weinberger, Geological Survey of Istael. Cave systems are shown as in **b**

During the Late Eocene and Oligocene periods, regional upwarping brought about the uplift of southern and central Israel (Avni et al. 2012; Segev et al. 2011), as well as a vast region to the south, toward the Afar Dome. Since, then the ridge has been sculptured by subaerial karst denudation (Frumkin 1992; Ryb et al. 2014), fluvial erosion, as well as subsurface dissolution and cave formation (Frumkin and Fischhendler 2005). Late Eocene to Neogene sediments are restricted to structural lows, sometimes onlapping at the flanks of the major monoclines. In the Judean Desert, these sediments appear mainly as remnants in caves and depressions, as well as in the Dead Sea basin (Frumkin 2001; Lisker et al. 2010a; Matmon et al. 2014).

Israel was part of the African-Arabian plate until the end of the Oligocene, when the Dead Sea transform, later becoming the Dead Sea rift and its basins, separated Israel from the Arabian plate.

The Dead Sea transform, a major regional structure, forms the eastern border of the Judean Desert. The Dead Sea transform links the Red Sea divergent plate boundary to the orogenic belt in the Turkey plate convergence zone where it meets the East Anatolian Fault Zone. The overall amount of left-lateral motion along the Dead Sea transform since the Early Miocene (~20 Ma) is estimated ~105 km (Freund et al. 1970). Two phases of sinistral strike-slip motion were reported. Sixty-five km is assigned to the Miocene and the

rest to the Pliocene until Holocene (Garfunkel 1997). The first phase is characterized by a more or less straight fault line with insignificant morphotectonic features. Due to the stronger compressional character, the Judean Desert–Dead Sea transform border became dominated by step faults resulting in transpression and pressure release by strain releasing bands and pull-apart basins (Garfunkel 1997; Quennel 1984), such as the Dead Sea depression.

The Dead Sea morphotectonic depression has developed as an endorheic basin since the Mid-Late Miocene, when tectonic subsidence started to prevail over the filling of the basin. This was associated with an arching uplift of the Judean Mountains range along a north-south axis. The Dead Sea, currently (2016) 430 m below MSL, is the lowest subaerial surface on earth, with a catchment area of ~43,000 km^2. Late Miocene transgressions reached the downfaulted Jordan—Dead Sea depression, depositing evaporites (Zak 1967). Throughout the Pliocene-Quarternary, additional marine incursions and lakes deposited thick evaporites and clastics of the Dead Sea Group within the Dead Sea depression (Stein 2001; Lisker et al. 2009). Of these, the most widely exposed is the Late Pleistocene Lisan Formation observed along the Jordan Valley, the Dead Sea, and the lower Judean Desert canyons and caves (Lisker et al. 2009). The occurrence of speleothems in the Judean Desert caves, as well as high levels of Lake Lisan and other indications shows that the last glacial period has been the wettest period in the southern Levant, including the Judean Desert, during the Mid-Late Quaternary (Enzel et al. 2008; Frumkin et al. 2000; Lisker et al. 2010b; Vaks et al. 2006; Torfstein et al. 2013). The transition to the Holocene brought about increasing aridity and low levels of the Dead Sea (Frumkin et al. 2001; Bookman et al. 2004).

The Cenozoic erosional history of the region may be divided into two main stages as follows:

(1) Regional denudation stage, lasting from the Late Eocene retreat of the sea through the Miocene, creating the 'Judean erosion surface' across the entire southern Levant (Picard 1943). The denudation truncated the tops of the Syrian Arc anticlines, where the denudation still persists today (Ryb et al. 2014). The Judean erosion surface cuts through limestone and dolostone, as well as chalk and marl formations of the Late Cretaceous to Eocene age. The major denudation agent in the mountain range has been karstic dissolution, as indicated by morphological evidence and the spatially uniform removal of the rock (Frumkin 1992).

(2) The second stage lasted since the Late Miocene until today. During this period, the Dead Sea depression has subsided in the east, and the mountain range has uplifted as an arch-like, NS trending ridge. The combined processes introduced considerable relief to the eastern flank of the Judean Mountains, reaching today ~1400 m, from ~1000 m a.s.l. at the water divide to −430 m at the Dead Sea. The modern divide, which does not always match the structural axis, was established during this phase close to the new uplift axis. The Judean Desert plateau has tilted eastward. The enhanced relief favors well-developed subaerial drainage and deep incision of ephemeral streams in most of the area, cutting through the Judean Desert plateau and exposing hypogene, isolated caves (Frumkin and Fischhendler 2005).

The [up to] 700 m high fault escarpment bounding the Dead Sea basin, and the deep canyons dissecting the escarpment, is the most conspicuous morphologic features of the area. Further to the west, the Judean Desert plateau is dissected by the upper reaches of these canyons, where they are less entrenched. These canyons, where they cut through the Judea Group, mainly at the Syrian Arc flexures, serve as the best window to the hypogene caves of the region (Fig. 3a). The Judean Desert interfluves and synclines are dominated by outcrops of the Mount Scopus Group, forming undulating chalk hills. Judea Group outcrops are more common at the southern and northern parts of the Judean Desert plateau, in addition to the fault escarpment and canyons.

Two main aquifers exist in the Judean Desert:

The upper aquifer is within the Judea Group carbonates. Today, it is mostly phreatic or perched on impervious layers and locally confined. The phreatic parts utilize today the structurally determined perched pathways in a river-like underground flow pattern (Ben-Itzhak and Gvirtzman 2005). Prior to the Dead Sea depression development, the upper aquifer was predominantly confined under the Mt. Scopus Group.

The deep aquifer consists mostly of siliclastic rocks of Paleozoic to Lower Cretaceous age, divided into several sub-aquifers. Isolation from the upper aquifer and low carbonate contents results in sub-neutral pH values of 6.3–6.7, and anoxic conditions associated with H_2S content. These features are observed in Mazor-Yesha-Qedem springs (Fig. 2) and associated wells along the Dead Sea shore (Guttman and Simon 1984; Gavrieli et al. 2001; Stern 2010).

Along the Dead Sea depression, both aquifers contribute water to an aquifer within Quaternary loose sediments, which also gets water from the Dead Sea.

Fig. 3 Cave entrances in relation to their setting: **a** Hoza Shluha Cave in tilted bedrock at the monocline; **b** Chariton Cave in horizontal bedrock. *Note* elliptical cross-sections of the passages that were truncated by erosion

3 Cave Morphology

Almost all Judean Desert caves are relict, without modern dissolution processes. Their length varies between a few meters to 3.5 km. 'Phreatic morphology' is common, such as elliptical cross-sectional of passages (Fig. 3b), smooth walls, cupola, solution pockets, and 'boneyard'-like tubes (Fig. 4). These are encountered in the entire region, although in some places, particularly near the fault escarpment, and it is obscured due to tectonic deformation and physical weathering, decomposition of cave walls, and mechanical breakdown of the bedrock ceilings (Fig. 4a). Some of these are similar to (and sometimes confused with) condensation corrosion features such as cupola.

In plan view, the longer caves are mazes (Fig. 5), with elongated intersecting passages and few chambers, located

Fig. 4 Morphology of Judean Desert hypogene caves: **a** *double tiers* of passages converge at a chamber, Pirhei Melah Cave. Walls are partly crumbled by physical erosion. **b** Solution pockets, Yogev Cave. Note shepherds graffiti. **c** Remaining bedrock protrusions between solution pockets, Qina Cave. **d** 'Boneyard' passages and pockets, Qina Cave

mainly at intersections of passages (Fig. 4a). Small caves usually have the form of rudimentary passage segments or small isolated chambers. West of the Judean Desert, chamber caves are the common type, while mazes become rare (Frumkin and Fischhendler 2005). Most Judean Desert cave passages developed along junction lines between fractures and bedding planes, mainly within hard Turonian limestone at the uppermost part of the Judea Group, mostly within Shivta, and occasionally Nezer formations.

The maze caves commonly have small areal coverage and large passage density. The longest and most developed maze cave in the Judean Desert is Chariton Cave, whose length is 3450 m and areal coverage of 4600 m^2 (Frumkin 2015). The maze cave with the largest volume is A'raq Na'sane. Most cave passages reach up to 3 m and rarely 10 m in width (Figs. 5 and 6). Mean length/width ratio is >100 in the longer maze caves, while in the shorter ones 20< length/width <100 (Frumkin and Fischhendler 2005). Passages of large caves are often interconnected in networks comprising several sets of parallel passages, developed along sets of parallel fissures. Several tiers (up to three) appear in some of the larger caves, forming three-dimensional networks (Figs. 4, 6b, 7 and 8). Each tier commonly follows a single bedding plane, with passages developed along its intersection with fractures. Fractures and bedding planes are initially of submillimeter to sub-centimeter width. Caves are commonly sub-concordant with bedrock stratification: In horizontal beds the caves are horizontal, and in inclined beds they are inclined in the direction of the local dip. However, although bedding plane

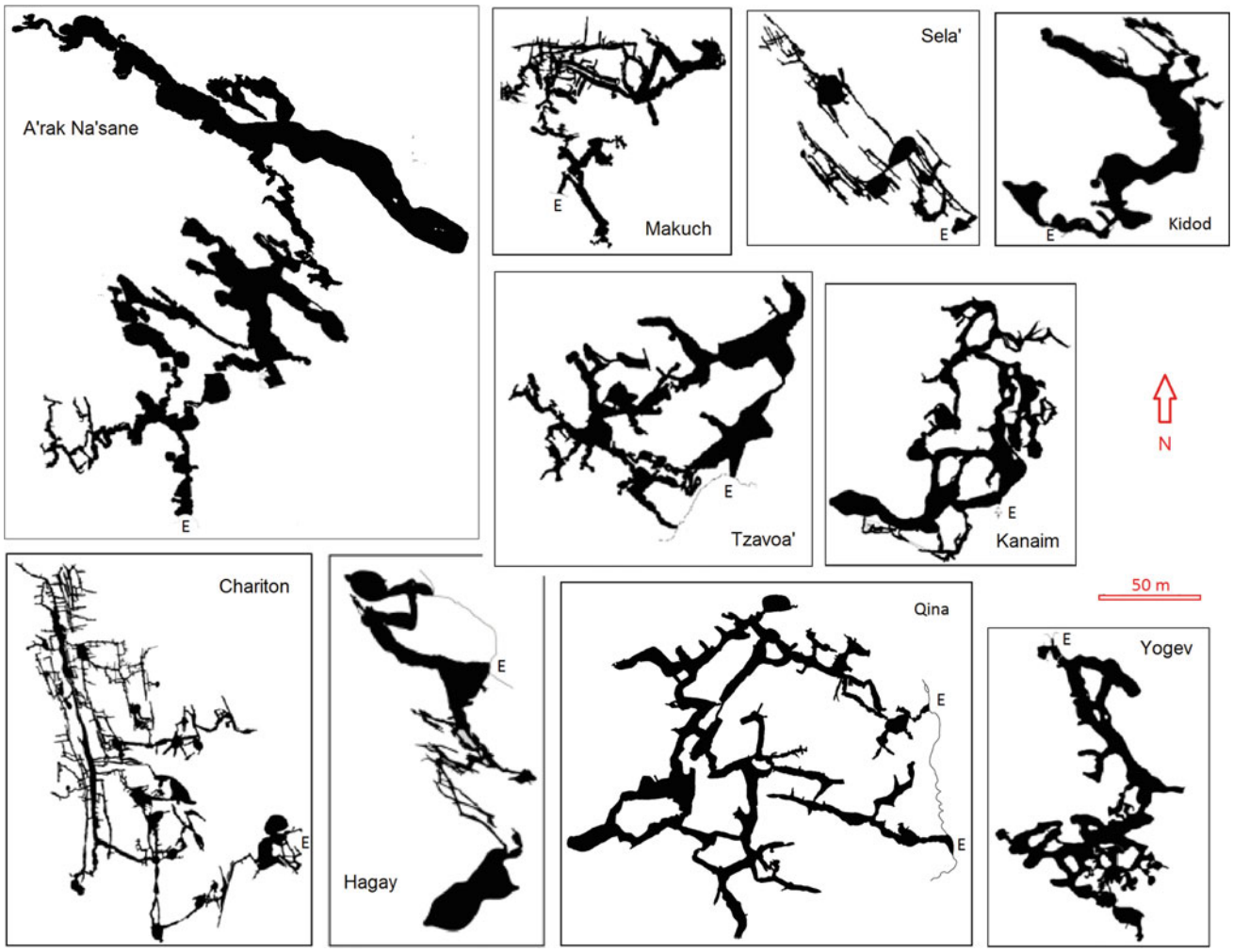

Fig. 5 Plans of the ten largest hypogene caves in the Judean Desert. *E* indicates the cave entrances

control on cave initiation is evident, the final passage gradient commonly alternates within a single passage, indicating that passages were not formed by vadose flow.

Some cave segments with key-like cross-sectional have a blocked rift-like fissure at the bottom (Fig. 6c). Original water inlet and outlet tubes can be observed at the side or the bottom of passages (Fig. 6d). These have the form of small holes, individual shafts, or elongated fissures. Horizontal passages of the studied maze caves terminate abruptly or gradually. Ceiling pockets and cupola usually have clear fissure control or indications of water input or output. Rising shafts extend in and out of passages (Fig. 7). Those that extend upward commonly end abruptly in smooth ceiling cupola. In some caves, passages are clustered around a central rising shaft. Some rising shafts are vertically dendritic (e.g., Chariton and Tzavoa caves, Fig. 7). Sediments indicative of fast-flowing water, such as pebbles are not observed deep within the caves, except some rare intrusions of fluvial clastics into some entrance passages via the breached opening. Bubble trails and ceiling channels are rare. Scallops of fast-flowing water were not observed, but rarely the walls present some systematic large (m scale) solution pockets, which may be interpreted as sluggish water scallops.

The most important speleogenetic deposits are gypsum rinds, common in the southern Judean Desert (Fig. 8). These are mm to tens of cm thick, covering in some places the entire walls of passages. Water table-related deposits, such as folia and rafts, are rarely observed.

The maze caves in the eastern Judean Desert are commonly dry today, and mostly devoid of vadose speleothems, while the ones in the west are usually wetter, sometimes with water drips, as expected from the precipitation gradient. In some rare cases, water accumulates in a natural basin within the cave, following rain events, which last commonly for few hours. In some cases, rim deposits and condensation corrosion features appear, associated with humid air flow (Fig. 5b). Collapse features are rare along narrow passages,

Fig. 6 Morphology of Judean Desert hypogene caves: **a** tube connecting parallel passages, Chariton Cave; **b** multilevel tubes along a single fracture; **c** passage with rift-like bottom, Sela' Cave; **d** tube entering chamber with possible overhanging bubble trail, Sela' Cave (Width of photo ~1 m)

Fig. 7 Rising shafts in Judean Desert hypogene caves: **a** entrance shaft of Kanaim Cave, looking upward; **b** *vertical* connection between two cave tiers, looking downward, Sela' Cave

but more common in wider sections and chambers, especially near the Dead Sea escarpment, where bedrock is often shattered by tectonic stress.

4 Cave Setting and Speleogenesis

At present, Judean Desert caves generally hang high and dry, up to 500 m above the base of the fault escarpment (e.g., Caves of the Spear; Porat et al. 2009), and up to few hundred m above the bottom of the deep canyons (e.g., Cave of the Letters; Frumkin 2001).

Thus, both setting and morphology of the vast majority of the caves indicate that they formed under the water table, prior to the fault escarpment formation and canyon incision. The wider scale distribution of caves does not indicate water table control. Rather, the caves follow the uppermost, Turonian, rock formations of Judea Group, at any level they occur.

Caves within inclined strata of monoclines are in some cases slightly less inclined than the bedrock layers, possibly

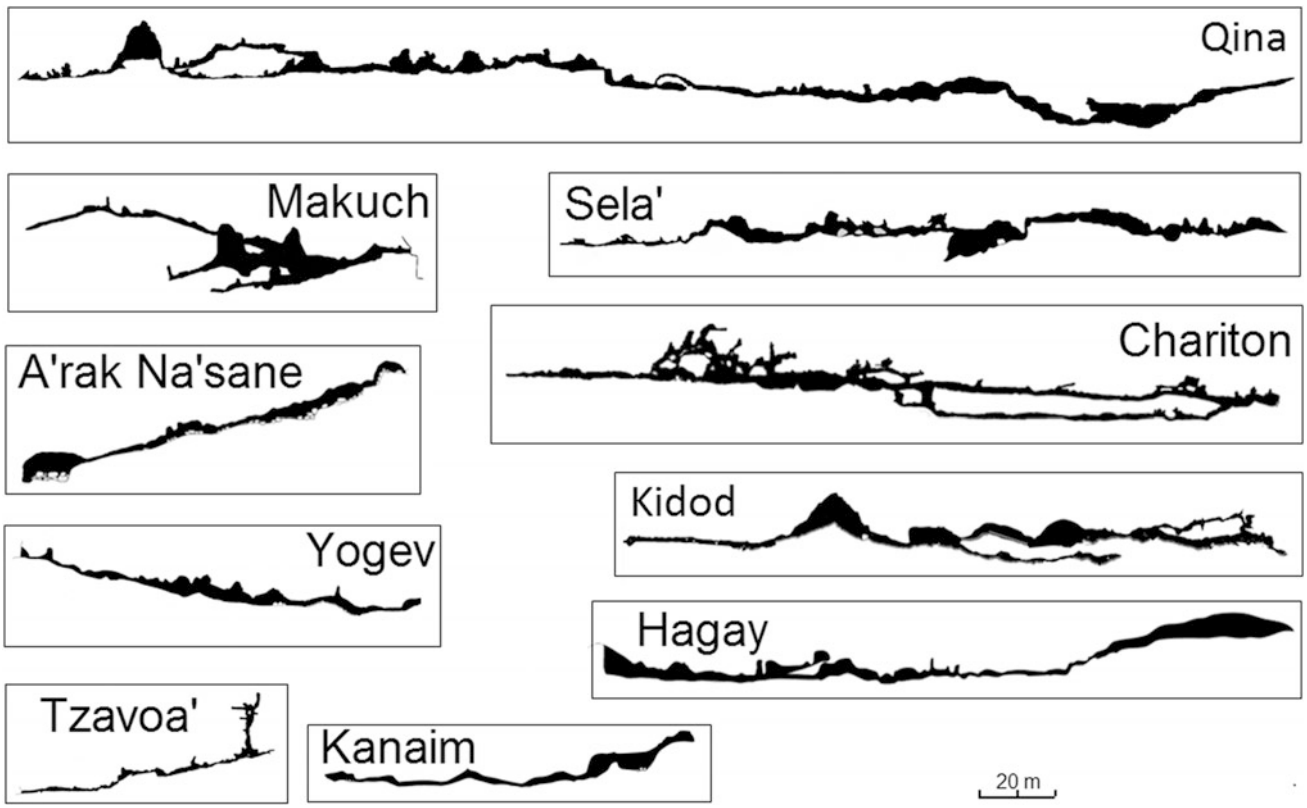

Fig. 8 Typical profiles of the ten largest hypogene caves in the Judean Desert

indicating local water table control during speleogenesis within inclined strata, followed by additional tilting.

The development of the Dead Sea depression since the Late Miocene dewatered the upper Judea Group, promoting subaerial stream incision. Caves were dissected either by the Dead Sea fault escarpment (Fig. 9) or by streams and canyons (Fig. 3).

The caves appear to have no genetic relationship to the present topography: There are no sinks which drain concentrated subaerial runoff into them, and no conduit outlets which could have served as springs draining the cave water to the surface. Rather, the caves were isolated from the surface, with diffuse flow routes into and out of the caves, through tiny (<1 mm wide) fissures. The present access into the studied caves is gained by entrances of relatively recent origin—intersection of the blind underground voids by erosion or fault escarpments. The shape and number of entrances depend on the breaching location with respect to the cave (Fig. 9).

It is assumed that the known caves are only a sample of a larger population of isolated caves, most of which are still concealed underground, while some others have been totally removed by subaerial erosion. Large outcrops of the studied formations allow good representation of the whole population. Epigenic branchwork caves (sensu Palmer 2007), with genetic relationship with the present surface, are hardly observed. This is attributed to: (1) the present low precipitation/evapotranspiration ratio of this dry environment; (2) the most diffuse infiltration over limestone and dolostone outcrops, often associated with dense fracturing of rift-associated tectonic stress origin.

Spatial distribution of maze caves is not homogenous across the Judean Desert. They are found usually within few hundred meters distance from the edge of the remaining cover of Mt. Scopus Group. Cave distribution under undissected parts of the Judean Desert plateau, where Mt. Scopus Group cover is intact, is not well known. Most known maze caves are located along marginal zones, where Mt. Scopus Group has been breached by fluvial erosion and Dead Sea escarpment faults. The associated distribution of the caves and the Mt. Scopus Group caprock indicates that during speleogenesis the caprock had been continuous, confining the Judea Group aquifer.

The caves are mostly aligned along two SSW-NNE trending lines. These lines follow the main monoclines of the region and their continuation. This indicates that the caves are associated with the deep underlying, reactivated SSW-NNE faults, which are partly draped by the monoclines

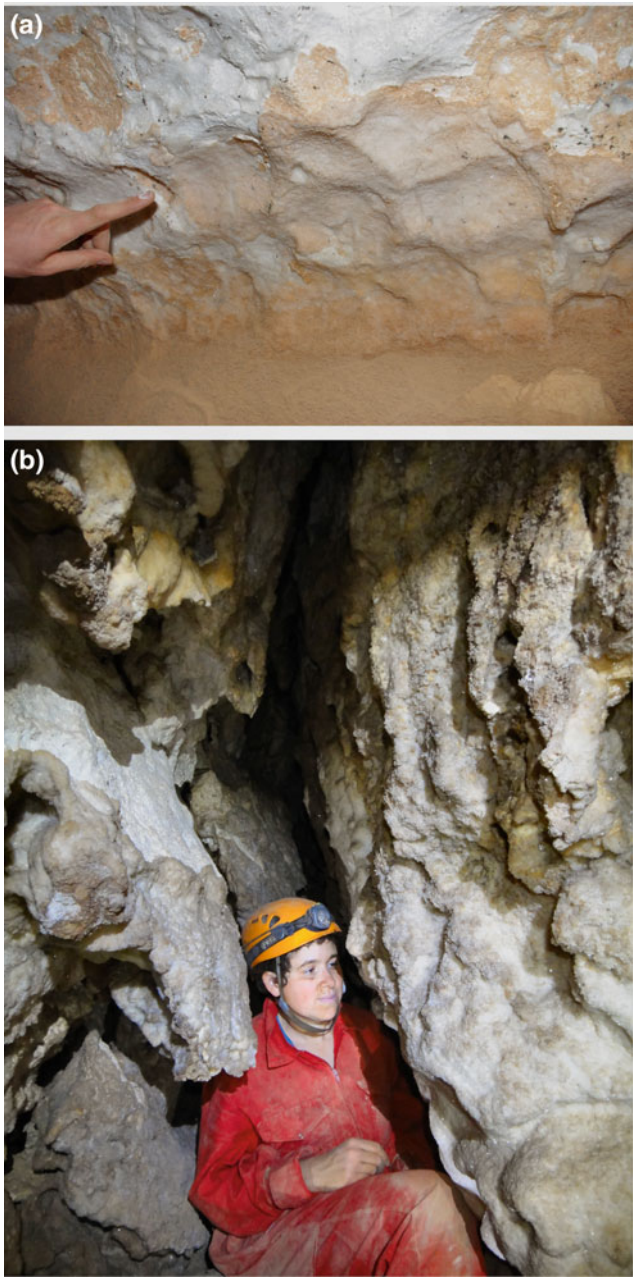

Fig. 9 Gypsum crusts in Judean Desert hypogene caves: **a** *thin crust* covering corrosion grooves, Kanaim Cave; **b** *thick crust* covering vertical fracture and cavity walls, Qina Cave

(above). These faults may have acted as conduits, supplying hypogene water to the Judea Group aquifer, followed by hypogene speleogenesis under the confinement.

5 Age of the Caves

Tens of U-Th dates of vadose speleothems in Judean Desert maze caves show that the caves are older than few hundred thousand years (Vaks et al. 2006; Lisker et al. 2010b).

Burial age dating of fluvial deposits trapped in cave entrances using Al–Be cosmogenic isotopes was performed in two Judean Desert caves (Matmon et al. 2014). In the Cave of the Letters, fluvial deposition by the early canyon occurred until ~3.1–2.8 Ma. These dates indicate that during that time the early Nahal Hever already started entrenching toward the young Dead Sea depression, and during its entrenchment it has cut the cave and deposited sand and silt inside the entrance. The fluvial deposits cover aquatic laminar sediments within the cave entrance, which were probably deposited in a lake that occupied the depression (Frumkin 2001). At the upper eastern side of Masada cliff, 'Cave 2008' shoreline/fluvial deposits are dated by cosmogenic isotopes to ~3.6 ± 0.4 Ma. These ages show that the caves were already developed and breached during the Pliocene.

The above-mentioned dated deposition occurred above the water table, indicating a Pliocene (or earlier) dewatering of the caves, probably associated with tectonics. Thus, these ages constrain a minimal age limit for speleogenesis of the dated caves. The age of speleogenesis can only be estimated indirectly, using the relation of caves to tectonic, erosional, and sedimentary features, inside and outside the caves.

A large portion of the Judean Desert caves appears in the higher parts of erosional or tectonic escarpments (above). The water-filled conditions under which the caves had developed indicate that during cave formation, the relief was much lower than today and the escarpments hardly existed. More specifically, caves along the Jordan valley–Dead Sea fault escarpment must have predated the Late Neogene faulting phase associated with the present topographic low of the Jordan–Dead Sea depression (Fig. 9). Initial aquatic sediments of marine origin within the rift indicate that it already existed during the Late Miocene (Belmaker et al. 2013; Matmon et al. 2014), constraining speleogenesis to the mid-Miocene or earlier. On the other hand, the Judean Desert emerged above sea level during the Late Eocene period, which constrains the maximal speleogenetic age. Assuming that some relief was needed for speleogenesis to occur, and Oligocene seems to be the oldest possible age of the caves.

An interesting viewpoint can be obtained from regional cave surveys. After tens of years of cave studies in Israel, the northernmost major maze cave is Araq Na'asane, at the northern edge of the Judean Desert cave province. Notably, large (>500 m) maze caves were not found in the northern Samaria-Galilee-southern Lebanon regions (Fig. 1), i.e., the northern part of the southern Levant. These regions generally share the same lithological sequence (with some older outcrops) as the Judean Desert, with more Mesozoic carbonates and less clastics as one moves northward, toward the realm of the Tethys Ocean. Water availability also increases as one leaves the Judean Desert northward, toward the

Mediterranean climate zone. Thus, the regional distribution of maze caves does not conform to lithology and present precipitation.

A possible solution to this hypogene cave distribution could be that during speleogenesis the northern regions of the southern Levant were still submerged by the sea. During Early-Middle Eocene times, the entire southern Levant was submerged, as evidenced by marine deposits (Sneh 1988; Lewy et al. 1995). During the middle Miocene, the Judean–Galilee mountain range was already exposed. In between, mainly during the Oligocene, the Judean Mountains and Judean Desert already emerged, experiencing denudation, while northern Samaria, Carmel, and lower Galilee were apparently still submerged (Gvirtzman et al. 2011).

The overall evidence suggests that the main speleogenetic period was the Oligocene, when the Judean erosion surface was formed. At this period, a huge recharge area was supplying groundwater to deep aquifers along the Syrian Arc.

6 Speleogenesis and Groundwater Flow

6.1 Stratabound Flow

The following features suggest that speleogenesis occurred under confined stratabound conditions: (1) the macro- and micromorphology of the maze caves; (2) their spatial proximity to the Mt. Scopus Group caprock confinement; (3) their association with the uppermost karstic formation of the Judea Group; and (4) the relative rarity of vadose speleothems, indicating that even today the caves are poorly connected to epikarst seepage.

On a geological time scale, groundwater circulation at the top of an aquifer must be more stable under confined conditions than under phreatic unconfined conditions (Freeze and Cherry 1979). This is the case because the unconfined phreatic water table falls in response to any small tectonic uplift (or base level lowering), which forces the flow to occur along a lower bed or to be channeled in perched conditions. On the other hand, a small tectonic uplift would not significantly affects a confined flow, and it would consistently occurs along a single bed until the uplift is large enough for the potentiometric level to fall below the entire confined system.

In the Judean Desert, confined flow took place prior to the Neogene tectonic–erosional cycle, which breached the Mt. Scopus Group along canyons and fault escarpments. When the Dead Sea depression and associated canyons developed, the groundwater level fell dramatically, bringing the higher caves into vadose conditions. Fluvial erosion cuts the caves open, but much of the confining cover still exists on the Judean Desert plateau, as well as along synclines and hill crests.

Maze caves have been widely discussed in the speleological literature, and attributed to confined hypogene circulation (Klimchouk 2007, 2013), to high-discharge floodwater or infiltration from a sandstone caprock (Palmer 2007), to turbulent flow under high hydraulic gradient (Howard and Groves 1995), and to sustained high gradients and mixing zones (Palmer 2007). The maze caves discussed here can be assigned to a combination of some of these effects: sustained high hydraulic gradients under confined artesian circulation, and hypogene, rising water flow, and possibly mixing with lateral flow.

The physical cause for maze morphology probably lies in the high pressure of aggressive groundwater injected into soluble beds under confined conditions. This water spreads into every possible fissure, so the renewed aggressiveness is consumed along the two- or three-dimensional network of fissures. This results in caves whose passage network distribution is a replica of the prevailing fissure distribution around the site of renewed aggressiveness. The relatively flat, lateral development of the maze caves was favored (Fig. 5), indicating that the zone of water aggressiveness was close to the confinement, and bedding planes were more important than fractures for cave inception.

6.2 Rising Flow from Deep Aquifers

Several features indicate that upwelling hypogene flow from deeper aquifers played a major role in Judean Desert speleogenesis:

(1) The morpho-hydraulic features, including the good connection to underlying strata relative to no connection to overlying strata.
(2) Gypsum rinds in some southern caves indicate rising of deep water, loaded with hydrogen sulfide, a by-product of microbially mediated redox reactions. These rinds indicate dissolution of limestone by sulfuric acid, with co-precipitation of gypsum.
(3) The lineaments-like spatial distribution of caves along the monoclines indicate that the caves formed along the trace of the deep, ancient faults which probably served as routes for rising water through low-permeability rock layers.
(4) The main southern line of caves cuts the Dead Sea shore where its main hydrothermal, sulfidic springs flow today: the Mazor-Yesha-Qedem springs (Fig. 2). This suggests that rising hydrothermal water along this line is an ongoing process.

The overall picture is a rising flow from deep, hypogene aquifers, along major deep faults, becoming aggressive upon reaching the uppermost karstic beds of the Judea

Group. Conduit enlargement could take place also just above the water table, where hydrogen sulfide and evaporating water could condense on cave walls and dissolve limestone by sulfuric acid.

The aggressiveness of groundwater can be achieved by several ways, such as hydrogen sulfide—sulfuric acid related processes; mixing corrosion at the confluence of rising and lateral flows; cooling of hydrothermal water, as it equilibrates with cooler rock (Dublyansky 2013); and mixing with cool epigenic water close to the confinement.

Recharge of water which flowed laterally in the confined Turonian limestone probably occurred at the nearby anticlinal outcrops of these rocks, west of the Judean Desert, at the Judean erosion surface (Fig. 2a). The recharge of hypogene water could occur along outcrops of older strata not only across the Judean erosion surface, but also in far-field 'Nubian' sandstone outcrops. This issue will be discussed further elsewhere. The recharge of hypogenic water was also possible via downward leakages across overlying aquifer systems, as well as from internal sources, but these sources are less likely to contribute large amounts of water.

7 Conclusions

The Judean Desert is the major province of maze caves in the southern Levant. The cave morphology, setting, and sediments all indicate speleogenesis under prolonged confined, hypogene conditions. Caves were predominantly formed in Turonian limestone by water rising from deep aquifers, under the confinement of Senonian chalks and marls. The hypogene water seems to have risen along deep, reactivated faults. The water contained hydrogen sulfide that contributed to speleogenesis by sulfuric acid. This is indicated by the presence of gypsum rinds in some of the caves.

The main speleogenetic period was most likely the Oligocene, before the development of the Dead Sea depression. The major Neogene tectonic stage of the Dead Sea transform, associated with canyon incision, dewatered the caves, rendering them relict, and hanging high above the falling base level.

The recharge of the deep aquifers could take place at far-field 'Nubian' sandstone outcrops. The Syrian Arc acted as a barrier for groundwater flow toward the sea, which stabilized along the western side of the Judean Mountains. The truncated Judean Desert plateau, at the SE side of the Syrian Arc, was a major site for hypogene speleogenesis by the upwelling deep waters.

References

Audra PH, Palmer AN (2015) Research frontiers in speleogenesis, dominant processes, hydrogeological conditions and resulting cave patterns. Acta Carsologica 44(3):315–348

Avni Y, Segev A, Ginat H (2012) Oligocene regional denudation of the northern Afar dome: pre-and syn-breakup stages of the Afro-Arabian plate. Geol Soc Am Bull 124:1871–1897

Bar O, Zilberman E (2016) Subsidence and conversion of the Dead Sea basin to an inland erosion base level in the early middle Miocene as inferred from geomorphological analysis of its ancient western fluvial outlet. Geomorphology 261:147–161

Belmaker R, Lazar B, Beer J, Christl M, Tepelyakov N, Stein M (2013) ^{10}Be dating of neogene halite. Geochim et Cosmochim Acta 122:418–429

Ben-Itzhak LL, Gvirtzman H (2005) Groundwater flow along and across structural folding: an example from the Judean Desert, Israel. J Hydrol 312:51–69

Bookman R, Enzel Y, Agnon A, Stein M (2004) Late Holocene lake levels of the Dead Sea. Geol Soc Am Bull 116:555–571

Dublyansky YV (2013) Karstification by geothermal waters. In: Frumkin A (ed), Treatise on geomorphology, vol 6. Academic Press, San Diego, CA, pp 57–71

Enzel Y, Amit R, Dayan U, Crouvi O, Kahana R, Ziv B, Sharon D (2008) The climatic and physiographic controls of the eastern Mediterranean over the late Pleistocene climates in the southern Levant and its neighboring deserts. Glob Planetary Change 60 (3):165–192

Flexer A, Gilat A, Hirsch F, Honigstein A, Rosenfeld A, Reuffer T (1989) Late Cretaceous evolution of the Judean Mountains as indicated by ostracodes. Terra Nova 1:349–358

Freeze RA, Cherry JA (1979) Groundwater Prentice-Hall Inc. Englewood Cliffs, New Jersey

Freund R, Garfunkel Z, Zak I, Goldberg M, Weissbrod T, Derin B (1970) The shear along the Dead Sea rift. Philos Trans R Soc Lond Ser A 267:107–130

Freund R, Goldberg M, Weissbrod T, Druckman Y, Derin B (1975) The Triassic-Jurassic structure of Israel and its relation to the origin of the eastern Mediterranean. Geological Survey of Israel, Jerusalem

Frumkin A (1992) Karst origin of the upper erosion surface in the Northern Judean Mountains, Israel. Israel J Earth Sci 41:169–176

Frumkin A (2001) The cave of the letters sediments—indication of an early phase of the Dead Sea depression? J Geol 109:79–90

Frumkin A (2015) Chariton cave. In: Frumkin A (ed) Atlas of the Holey Land Magnes, Jerusalem, p 90–95 (Hebrew)

Frumkin A, Fischhendler I (2005) Morphometry and distribution of isolated caves as a guide for phreatic and confined paleohydrological conditions. Geomorphology 67(3):457–471

Frumkin A, Ford DC Schwarcz HP (2000) Paleoclimate and vegetation of the last glacial cycles in Jerusalem from a speleothem record. Global Biogeochemical Cycles 14:863–870

Frumkin A, Gvirtzman H (2006) Cross-formational rising groundwater at an artesian karstic basin: the Ayalon Saline Anomaly, Israel. J Hydrol 318:316–333

Frumkin A, Kadan G, Enzel Y, Eyal Y (2001) Radiocarbon chronology of the Holocene Dead Sea: attempting a regional correlation. Radiocarbon 43(2C):1179–1190

Garfunkel Z (1997) The history and formation of the Dead Sea Basin. In: Niemi TM, Ben-Avraham Z, Gat Y (eds) The Dead Sea—the lake and its setting. Oxford University Press, Oxford, pp 36–55

Garfunkel Z, Derin (1984) Permian—early Mesozoic tectonism and continental margin formation in Israel and its implications for the history of the Eastern Mediterranean. In: Dixon JE, Robertson AHF (eds) The Geological evolution of the Eastern Mediterranean, vol 17. Geological Society Special Publications, pp 87–201

Gavrieli I, Yechieli Y, Halicz L, Spiro B, Bein A, Efron, D (2001) The sulfur system in anoxic subsurface brines and its implication in brine evolutionary pathways: the Ca-chloride brines in the Dead Sea area. Earth Planetary Sci Lett 186(2):199–213

Guttman J, Simon E (1984) Hydrological study of the western Dead Sea shore, stage 1 (Hebrew). TAHAL Consulting Engineers Ltd., Tel Aviv

Gvirtzman Z, Steinberg J, Bar O, Buchbinder B, Zilberman E, Siman-Tov R, Rosensaft, M (2011) Retreating Late Tertiary shorelines in Israel: implications for the exposure of north Arabia and Levant during Neotethys closure. Lithosphere 3(2):95–109

Howard AD, Groves CG (1995) Early development of karst systems 2, Turbulent flow. Water Resour Res 31:19–26

Kafri U, Arad A (1978) Paleohydrology and migration of the ground-water divide in regions of tectonic instability in Israel. Geol Soc Am Bull 89:1723–1732

Kempe S, Al-Malabeh A, Al-Shreideh A, Henschel HV (2006) Al-Daher Cave (Bergish), Jordan, the first extensive Jordanian limestone cave: a convective Carlsbad-type cave. J Cave Karst Stud 68(3):107–114

Klimchouk AB (2007) Hypogene speleogenesis: hydrogeological and morphogenetic perspective. National Cave and Karst Research Institute, Carlsbad

Klimchouk AB (2013) Hypogene speleogenesis. In: Frumkin A(ed) Treatise on geomorphology, vol 6. Academic Press, San Diego, pp 220–240

Klimchouk AB (2015) The karst paradigm: changes, trends and perspectives. Acta Carsologica 44(3):289–313

Langford B, Frumkin A (2013) The longest limestone caves of Israel. In: Filippi M, Bosak P (eds) Proceedings of the 16th international congress of speleology, vol 2. UIS, Brno p, pp 105–109

Lewy Z, Almogi-Labin A, Siman-tov R (1995) The paleoecologic and paleogeographic significance of upper Maastrichtian and lower Eocene rocks recently discovered in Jerusalem, Israel. Israel J Earth Sci 44:25–32

Lisker S, Vaks A, Bar-Matthews M, Porat R, Frumkin A (2009) Stromatolites in caves of the Dead Sea fault escarpment: implications to latest Pleistocene lake levels and tectonic subsidence. Quatern Sci Rev 28:80–92

Lisker S, Porat R, Frumkin A (2010a) Late Neogene rift valley fill sediments preserved in caves of the Dead Sea Fault Escarpment (Israel): palaeogeographic and morphotectonic implications. Sedimentology 57:429–445

Lisker S, Vaks A, Bar-Matthews M, Porat R, Frumkin A (2010b) Late Pleistocene palaeoclimatic and palaeoenvironmental reconstruction of the Dead Sea area (Israel) based on speleothems and cave stromatolites. Quatern Sci Rev 29:1201–1211

Matmon A, Fink D, Davis M, Niedermann S, Rood D, Frumkin A (2014) Unraveling rift margin evolution and escarpment development ages along the Dead Sea fault using cosmogenic burial ages. Quatern Res 82:281–295

Palmer AN (2007) Cave geology. Cave Books, Dayton, Ohio

Picard L (1943) Structure and evolution of Palestine. Hebrew University, Jerusalem

Porat R, Eshel H, Frumkin A (2009) The 'caves of the spear': refuge caves from the Bar-Kokhba revolt north of En-Gedi. Israel Explor J 59:21–46

Quennel A (1984) The Western Arabia rift system. In: Dixon J, Robertson A (eds) The geological evolution of the Eastern Mediterrean, vol 17. The Geological Society of London Spec. Pub., pp 775–788

Reches Z, Hoexter D, Hirsch F (1981) The structure of a monocline in the Syrian Arc system, Middle East - surface and subsurface analysis. J Pet Geol 3:413–425

Ryb U, Matmon A, Erel Y, Haviv I, Benedetti L, Hidy, AJ (2014) Styles and rates of long-term denudation in carbonate terrains under a Mediterranean to hyper-arid climatic gradient. Earth Planetary Sci Lett 406:142–152

Sandler A (1996) A Turonian Subarial Event in Israel: Karst, sandstone and pedogenesis. Geol Surv Israel Bull 85:1–52

Sass E, Bein A (1978) Platform carbonates and reefs in the Judean Hills, Carmel and Galilee. Tenth international congress on sedimentology, vol 2. International Association of sedimentologists, Jerusalem, pp 239–274

Segev A, Schattner U, Lyakhovsky V (2011) Middle-Late Eocene structure of the southern Levant continental margin—tectonic motion versus global sea-level change. Tectonophysics 499 (1):165–177

Shahar J (1994) The Syrian arc system: an overview. Palaeogeogr Palaeoclimatol Palaeoecol 112(1):125–142

Sneh A (1988) Regional lithostratigraphy of the Eocene Avedat Group, Israel. Geological Survey of Israel, Jerusalem

Stein M (2001) The sedimentary and geochemical record of neogene-quaternary water bodies in the Dead Sea Basin—inferences for the regional paleoclimatic history. J Paleolimnol 26 (3):271–282

Stern O (2010) Geochemistry, hydrology and paleo-hydrology of Ein Qedem spring Geologocal Survey of Israel Report GSI/17/2010, Jerusalem

Torfstein A, Goldstein SL, Kaga, EJ, Stein M (2013) Integrated multi-site U–Th chronology of the last glacial Lake Lisan. Geochim et Cosmochim Acta 104:210–231

Vaks A, Bar-Matthews M, Ayalon A, Matthews A, Frumkin A, Dayan U, Halicz L, Almogi-Labin A, Schilman B (2006) Paleoclimate and location of the border between Mediterranean climate region and the Saharo-Arabian Desert as revealed by speleothems from the northern Negev Desert, Israel. Earth Planetary Sci Lett 249:384–399

Weinberger G, Rosenthal E (1998) Reconstruction of natural groundwater flow paths in the multiple aquifer system of the northern Negev (Israel), based on lithological and structural evidence. Hydrogeol J 6:421–440

Weissbrod T (2005) The paleozoic of Israel and environs. In: Hall JK, Krasheninnikov VA, Hirsch F, Benjamini C, Flexer A (eds) Geological framework of the Levant, vol II. Historical Productions-Hall, London, pp 283–316

Zak I (1967) The geology of Mount Sedom PhD dissertation (in Hebrew, English abstract), The Hebrew University of Jerusalem

An Introduction to Hypogene Karst Regions and Caves of Iran

29

Hossein Karimi Vardanjani, Shirin Bahadorinia, and Derek C. Ford

Abstract

Iran is divided into five major geologic zones—the Zagros, Sanandaj-Sirjan, Central Iran, the East and Southeast, and the Alborz. About 10.5% of the country is underlain by carbonate rock formations, chiefly in a broad western strip, in the northeast, and central parts. Geomorphologic investigations have found clear differences between the extent and intensity of karst surface landform development, karst being more abundant in wetter regions such as the Zagros and very limited in arid Central Iran. Iran is within a very active tectonic region, with some sporadically active volcanoes, strong and widespread seismic activity, numerous active faults, and thermal springs. The hypogene caves that have been studied to date are found chiefly in just three areas: the North West and the Central and Eastern zone where they are associated with the igneous activity, and the Zagros Mountains. Although there is no modern volcanic or other igneous activity in the Zagros, the occurrence of oil fluids is considered to be a potential cause for hypogene cave development. The development of the two largest karst caves in Iran, Katalekhor and Alisadr, is attributed to ascending CO_2 due to volcanic activity. Other large caves such Karaftoo and Kangohar were created by magmatic fluids. Excavations for dams and water transmission tunnels in the non-volcanic Zagros zone have discovered some remarkable, active hypogene systems. Oil brines are considered to be the most important contributor to their development.

Keywords

Iran • Hypogene caves • Alisadr cave • Katalekhor cave • Oil brines

1 Introduction

About 10.5% of Iran is underlain by carbonate rock formations (Karimi Vardanjani 2015). These formations are mostly spread in the western strip of the country (Zagros Mountains), in the northeast and central parts (Fig. 1). Although due to the limitation of financial resources there have been few advanced studies of the karst formations in Iran, the severe shortage of water for drinking and industry has led to much well digging and exploration. Many excavations for dam construction have also provided significant information about karst in Iran. Investigation of caves is in an early stage, and only a few caves have been studied scientifically. Organized amateur caving began in 1945 (Javanshad 1995). British cavers discovered and explored the deepest cave, Ghar Parau, in the 1960s. Czech cavers and the Geological Survey of Iran organized more systematic surveying campaigns in the 1990s and in the early years of the present century, focusing on the Hormoz region where they discovered remarkably long caves in salt; one of them,

H. Karimi Vardanjani (✉)
AbAtiPazhouh Consulting Engineers, Ahwaz, Iran
e-mail: hkarimi@abati.ir

S. Bahadorinia
Karst Research Institute ZRC SAZU, Postojna, Slovenia
e-mail: sbahadorinia@gmail.com

D.C. Ford
Geography and Earth Sciences, McMaster University, Hamilton, ON L8S 4K1, Canada
e-mail: dford@mcmaster.ca

© Springer International Publishing AG 2017

A. Klimchouk et al. (eds.), *Hypogene Karst Regions and Caves of the World*,
Cave and Karst Systems of the World, DOI 10.1007/978-3-319-53348-3_29

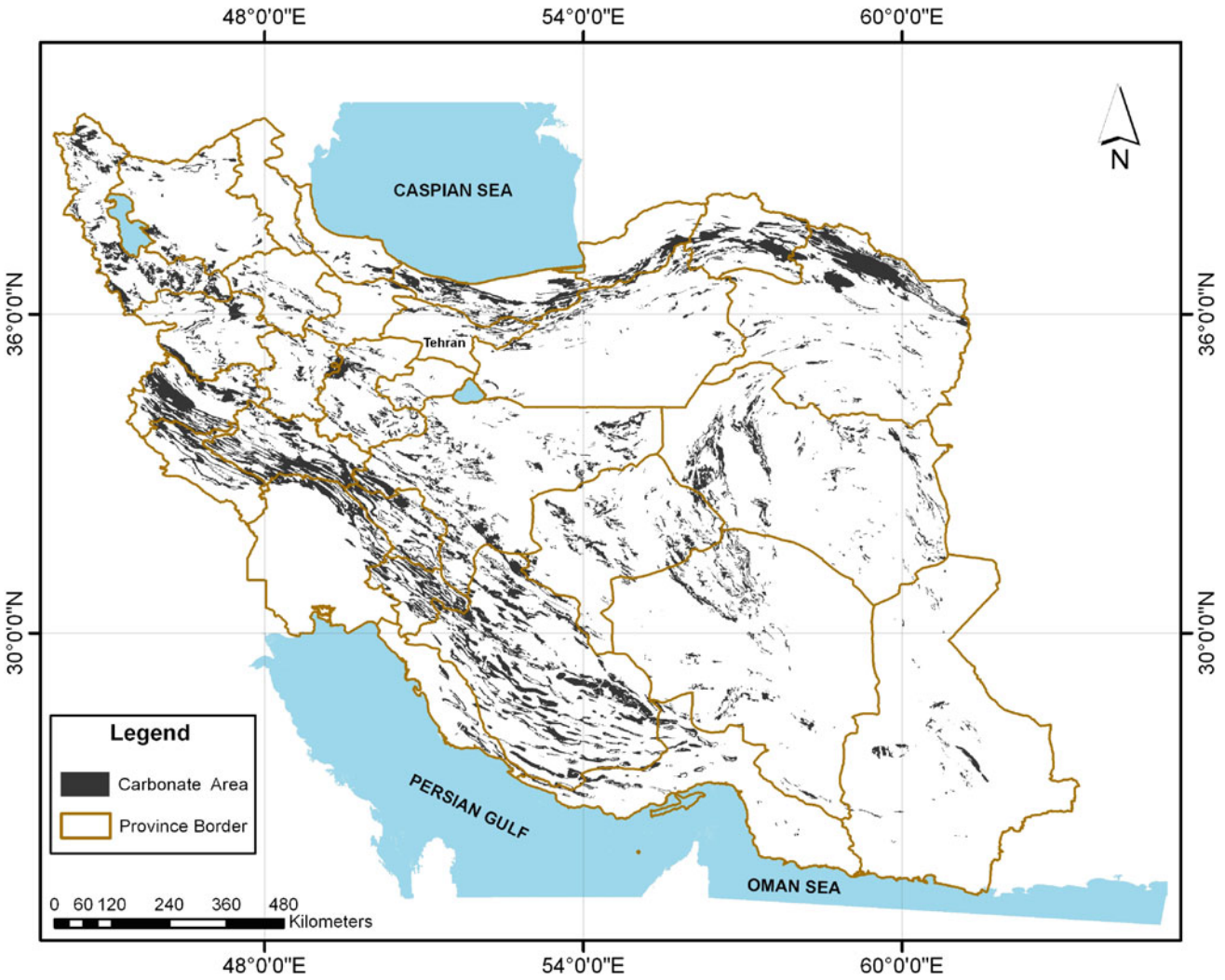

Fig. 1 Distribution of carbonate formations of Iran (adapted from Geological Survey & Mineral Exploration Organization of Iran)

Tri Nahacu, is currently the longest known salt cave of the world at 6580 m (Bosák 2002; Bosák et al. 1999, 2006). Subsequently, there have been speleological training expeditions organized by some of the leading Iranian mountaineering clubs, and the Union Internationale de Spéléologie (UIS) has helped to overcome the lack of international contacts for the Iranian caving community. The first "Iran Cave Directory" in English, published by Raeisi and Laumanns (2003), provided details on some 550 caves. A second edition (Raeisi and Laumanns 2009) increased this to more than 850 caves. In 2011, an Iranian Cavers and Speleologists Association (ICSA) was founded and currently has more than one hundred members from all over the nation.

Although there are now more than 850 known caves in Iran, the explored length of most of them is less than 1000 m. The short length of these caves has been attributed to the active and developing nature of the orogenic belts in the country and the continuous shifts in the erosional base levels. However there are some longer limestone caves in Iran, the most popular being Alisadr and Katalekhor. Although in terms of tourism these caves are very striking and successful, from the geological perspective there has been little investigation of cave genesis, and the role of hypogene processes in their formation has rarely been considered. In recent years, efforts have begun to identify the extent of hypogene development and a few caves such as Kalahroud, Yeke chah, Mirza, and Monj., have been attributed largely or entirely to hypogene processes. However, most of these efforts have been limited by lack of funding. In this chapter, an overview of the geology of Iran will first be presented, and then we will attempt to interpret the available information, introduce the established hypogene caves in Iran, and discuss the general causes of their formation. It is emphasized that this chapter can be no more

than just an introduction to the nature and extent of hypogene cave development in Iran.

2 Overview of the Geology of Iran

Iran is located in the middle of the Alpine-Himalaya fold belt that extends from the European Alps, through the circum-Black Sea region and Iran into the Himalayas and onward to the shores of the Pacific Ocean. Geologically, Iran is divided into five major zones—the Zagros, Sanandaj-Sirjan, Central Iran, the East and Southeast, and the Alborz (Fig. 2). Each zone contains smaller distinct structural sub-zones. The Central Iran zone is a triangular area in the center of the country that has a particularly complicated geology; the strata range from old metamorphic rocks (Precambrian) to recent semi-active volcanoes. The Alborz Mountains, lying between the Central zone and the south side of the Caspian Sea, are a central section of the Alpine-Himalaya orogeny, with a west-to-east extension. Within this zone, Kopet-Dagh is one of the important regions since it is located at the intersection of two Eurasia and Gondwana super continents. Kopet-Dagh Basin was formed after the continental rifting linked to the spreading of the South Caspian Basin in the late Early Jurassic and the spreading stage in the Late Bajocian (Taheri et al. 2009). An approximately east–west trending extensional basin developed in this region during Middle Jurassic time (Thomas et al. 1999; Kavoosi et al. 2009), which was inverted during the Cenozoic to create the present day folded belt (Robert et al. 2014). These extensional basement faults were reactivated as reversals of the dextral strike–slip faults to sinistral strike–slip faults in the central and the western parts of the Kopet-Dagh Basin (Hollingsworth et al. 2006). As noted, western Iran is comprised of a major mountain chain, the Zagros Fold, and Thrust Belts, formed by the collision of the Arabian Plate with the Iranian Plate. This structural zone has three sub-zones and is separated from the Central zone by the narrower Sanandaj-Sirjan metamorphic zone. The majority of the oil resources of Iran are found in the sedimentary rocks of the Zagros zone, especially in the Asmari carbonate formation. Lack of igneous activity differentiates this zone from the Sanandaj-Sirjan and Central Iran zones. The Urumieh-Dokhtar sub-zone, the most important volcanic zone in Iran, is a narrow strip about 10 km wide and 1500 km long in the north of Sanandaj-Sirjan zone. The eastern mountains of Iran are mostly oriented north-to-south and were formed by the closure of the ocean between Central Iran and Afghanistan-Pakistan in the Late Cretaceous (Fig. 3).

3 The Development of Surface Karst Features in Iran

In addition to the structural complications, there are important climatic differences between the various carbonate regions of Iran. The annual precipitation in the Central zone is mostly less than 100 mm, while in some areas of Zagros, it is more than 1300 mm. Areas to the south of the Caspian Sea (Alborz zone) are the rainiest ones, with annual precipitation of more than 1500 mm. Geomorphological investigations have found clear differences between the extent and size of karst landforms in arid Central Iran in comparison with the more abundant karst in wetter regions such as the Zagros. The larger karstic features such as poljes and sinkholes are not observed in the central arid regions. Rillenkarren, runnelkarren, etc., are also rarely observed, being replaced by honeycomb forms, pit-and-tunnel karren, micro spitzkarren, and other similar features associated with arid conditions. Valleys and other depressions in carbonate formations in the desert areas are of tectonic origin, primarily a function of faulting. Therefore, they cannot be considered to be true karst features. However, the physical and chemical (dissolution) roles of water in exploiting the catchment basins that they form are obvious.

In the Zagros Mountains, the Kopet-Dagh zone, and the Alborz area among others, surface karst features include abundant outcrops with small karren such as rillen, rinnen, and rundkarren. Stream sinks and solution and collapse dolines are found but are not common. There are a few poljes of predominantly solutional origin (e.g., Temi Lake, Zagros; see Karimi Vardanjani 2015). However, the majority of the well-known and important caves in Iran such as Alisadr and Katalekhor among others have developed in areas where surface karst landforms are rare and cave genesis by meteoric sinking streams appears to be unlikely.

Based on these observations, the principal causes of cave formation in Iran are discussed below.

4 Factors Contributing to the Formation of Hypogene Caves in Iran

As stressed before, Iran lies in a very active tectonic region. This has led to the presence of sporadically active volcanoes, high seismic activity, numerous active faults, thermal springs, etc., in many areas. However, hypogene caves that have been studied are found chiefly in just three areas—the North West, the Central and Eastern zone where they are related to igneous activity, and the Zagros zone. Although there is no modern volcanic or other igneous activity in the

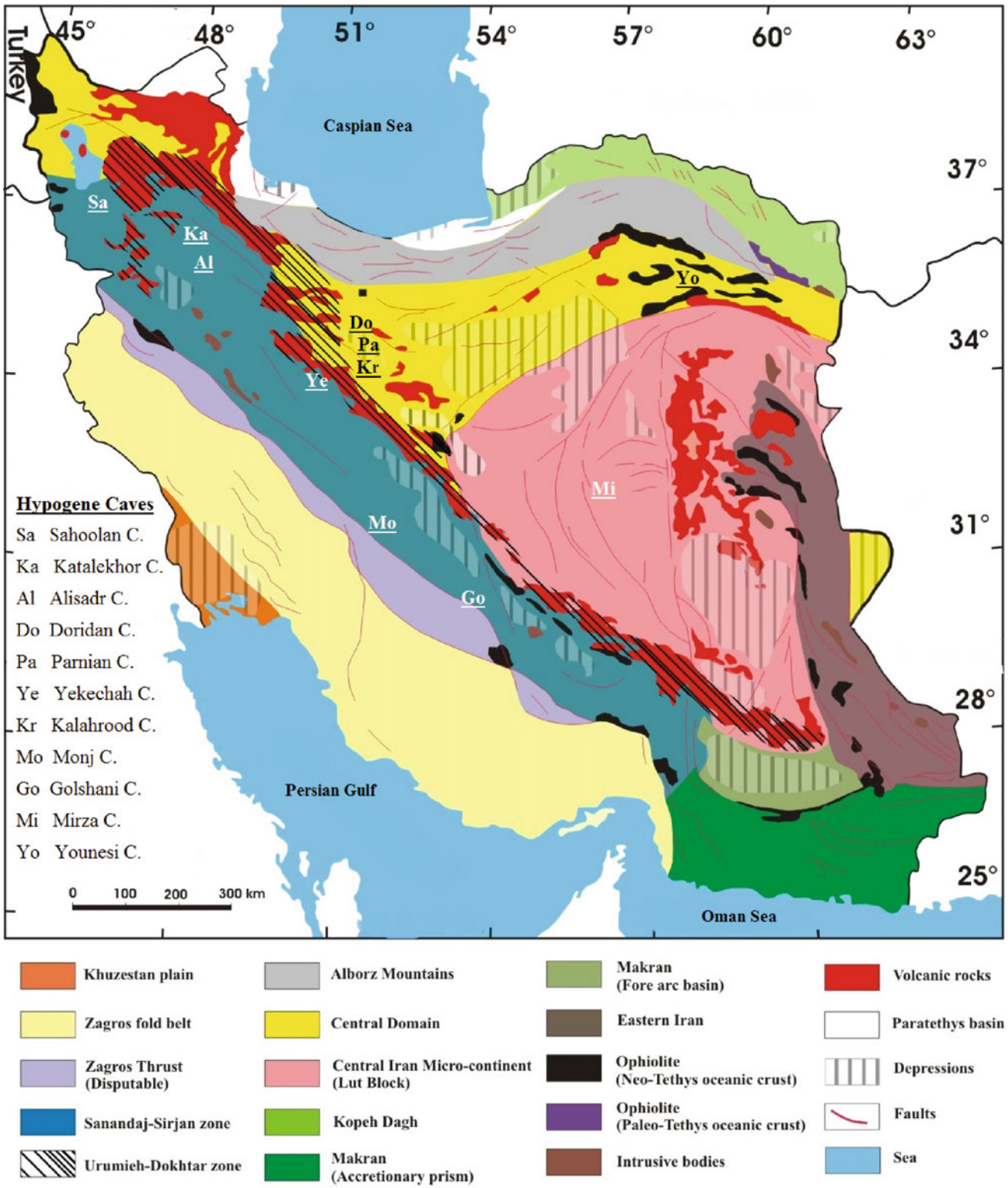

Fig. 2 Location of some of the studied hypogene caves on the structural geology map of Iran (adapted from Nezafati 2006)

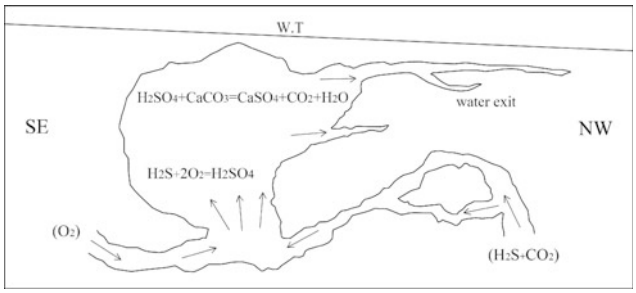

Fig. 3 Conceptual model for the formation of Monj Cave (Yoosefi Naghani 2008)

Zagros, the presence of oil fluids is considered to be a potential cause for the formation of hypogene caves.

5 Caves Associated with Hydrothermal Waters in Non-igneous Areas

By definition, hydrothermal waters are spring waters of deep origin with mean temperatures at least 4 °C above the ambient temperature of the meteoric springs in the local environment (Schoeller 1962; Dubljansky 2013). These waters may also contain greater quantities of gases and minerals in solution. The main causes of their upward flow are tectonic forces, gas pressure in oil reservoirs, overpressure related to fluid expulsion due to compaction under lithostatic loads, and thermal decay of rocks, among others (see Klimchouk Chap. 1). The occurrence of numerous thermal or sulfur springs in some regions of Iran where their formation cannot be related to igneous activities may be attributed to the following:

(a) Oil brines: in extensive areas in south and southwest Iran, major carbonate formations, such as the Asmari (Oligo-Miocene) and Sarvak (Albian to Cenomanian), are important oil reservoirs. The discharge of their natural gas to the surface through fractures (e.g., along the Abolfares to Ramhormoz City highway) and also the existence of springs with bitumen and many others with high sulfate content emerging from limestone indicate the channeling role of the limestone beds even where the oil brines are at shallow depths. For instance, by investigating ionic and isotopic ratios, admixture of underground water with oil brines has been confirmed at Garab Spring in the Khaeiz Anticline (Azhdari et al. 2014). Rezaei and Moore (2000) also attributed the composition of sulfur springs in Mamasani City to oil brines.

(b) Bacterial sulfate reduction: the existence of organic matter-bearing shales in some carbonate formations, such as the Asmari, and neighboring formations (e.g., Garou Formation) have led to the finding that H_2S gas may be generated by bacterial sulfate reduction. For example, after reaching a specific shale layer, drilled wells in the carbonate Asmari Formation become sulfurous. Other examples are gas emissions during Nosood Tunnel excavation (Rezaei et al. 2011) and Aspar Tunnel excavation (Mir Mehrabi et al. 2010).

(c) Faults: The penetration of meteoric precipitation into the earth down fault paths and its subsequent upward return create thermal springs at some places. Such cases are observed especially around active faults in Iran. Morteza Ali Spring in Tabas City is one of the springs where hydrochemical and isotopic studies have indicated their meteoric origin (Chitsazan et al. 2015).

As sulfur waters can be chemically aggressive with respect to limestone, hypogene caves are to be expected in areas with sulfur springs. Although there has been no surficial evidence of their existence, at least two hypogene caves have been discovered by accident during excavations for economic development.

5.1 Monj Cave

Monj Cave, with a volume of about 2500 m^3, is a single room that was found during excavation of the detour tunnel for the Karoon 4 Dam in Chaharmahal and Bakhtiari Province in 2003. The tunnel is located in the Asmari Formation, and the cave was found where it intercepted the Monj Fault. The interior of the cave does not have a regular geometric shape, being in the form of a dome with variably curving walls. It was formed at the contact of white chalk with a marl limestone. There are numerous large faults in the vicinity of the cave, but they do not appear to affect its form or characteristics. There are two separate springs in the cave, one of thermal (sulfur) water and the other with freshwater. At the time of excavation, flow of the sulfur spring was 70 L/s, which reduced to 50 L/s after the excavation and after the level of underground water had fallen by 20 m. The source of this water lies in oil reservoirs in the Asmari Formation, with flow upward on the Monj Fault. The standard deposits of karst cavities are not observed in this cave, but its walls are covered by a thin layer of gypsum that was attributed to hypogene H_2S reacting with the limestone (Yoosefi Naghani2008), as in Carlsbad Caverns, New Mexico (Hill 1990).

5.2 Golshani Cave

Hypogene karst was reported by Koleini et al. (2013) in exploratory drillings for the Salman Farsi Dam on the

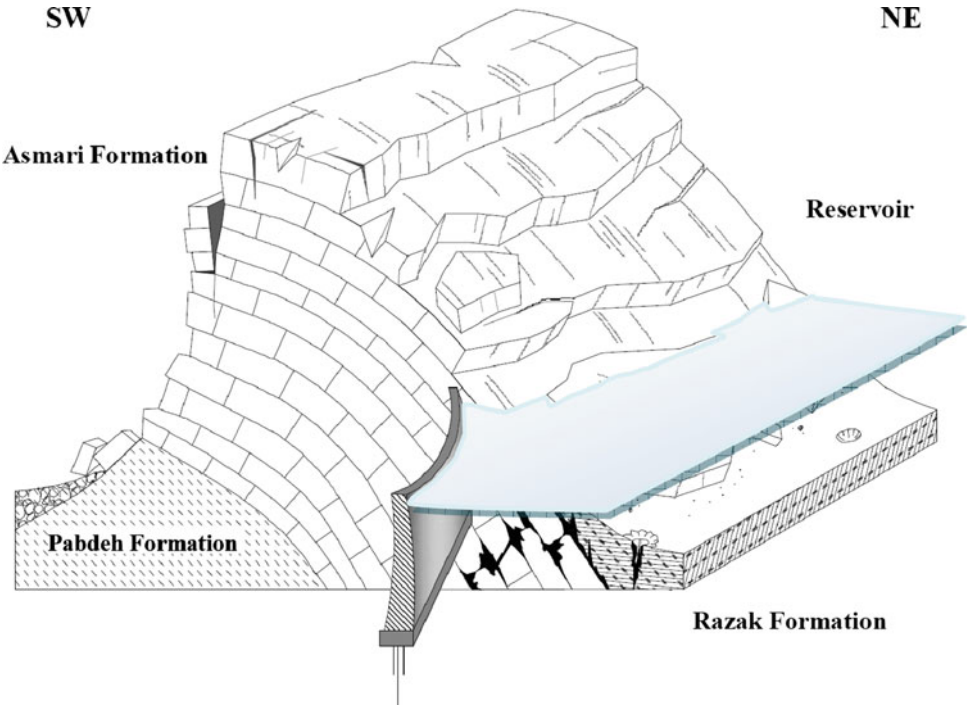

Fig. 4 Block diagram of the Salman Farsi dam foundation rocks on the northern flank of the Changal Anticline, showing the dam body/cutoff curtain, reservoir area, and location of the Pabdeh (marl), Asmari (karstic limestone), and Razak (gypsum) formations (Koleini et al. 2013)

Ghareh Agahaj River. The site is on the northern flank of the Changal Anticline in the Zagros Mountains, about 140 km south of Shiraz and 12 km northeast of city of Ghir. The foundation rock for the dam is the Asmari Formation (Oligo-Miocene), with underlying shale of the Pabdeh Formation in the core of the anticline to create a watertight underground barrier. The hydrogeological features of the Salman Farsi dam site are the results of the regional geological setting. The impervious and compressed anticline core is a barrier prohibiting groundwater flow from an upper valley (local base level of erosion) to the Ghir Plain, the regional base level (Fig. 4). A number of springs (thermal as well as meteoric water) discharge along a limestone gorge section upstream of the barrier. A well-developed sub-vertical fracture system intersecting frequent, steep, and penetrable bedding planes created an initial network for preferential groundwater flow, i.e., the limestone rock mass was fully exposed to karstification processes, and turbulent water flow was able to produce large channels and caverns.

A total of 40 springs were found at river level at the dam site, 30 on the left flank and 10 on the right, all discharging from the middle parts of the Asmari Formation. The springs can be divided into two groups: cold meteoric water springs with average annual temperatures of 23–26 °C; artesian hot springs from deeper, karstified limestone in the central unit, with temperatures ranging from 38 to 40 °C. The water issuing from the hot springs plays a key role in dissolution of the limestone through joints, bedding planes, faults, and their intersections. Numerous karst features have been detected by speleological investigations, with the largest one being Golshani Cave (150,000 m^3) in the right flank (Fig. 5).

Due to the occurrence of marl and marly limestone, such karst features are rarely found in the lower and upper parts of the Asmari sequence. The middle Asmari Formation acts as a preferential permeable zone for aggressive hot water rising through the connected discontinuities. The mechanical strength of the rock mass has permitted the development of interconnected and relatively clean pathways for movement of chemically aggressive water originating at depth.

6 Caves Associated with Igneous Activity

Volcanic activity throughout the center of Iran (the Urumieh-Dokhtar Volcanic Belt) formed mountain chains that extend from the northwest limits of the country (Sahand and Sabalan Mountains) almost to its southeast border with Pakistan (Bazman and Taftan Mountains). This belt is parallel to the Zagros zone, 1700 km in length and about 150 km wide. The volcanism is mostly Tertiary in age (Darvishzadeh 1992). So strong and widespread was volcanic activity in Iran that this period has been named "The Era of Magmatism" (Aghanabati 2004). During it, all regions except the Zagros experienced greater or lesser amounts of magmatic activity. It is to be expected that caves associated with igneous activity will be found in these areas. Studies are confirming that the majority of caves known in the central and northwestern areas of Iran are of hypogene origin.

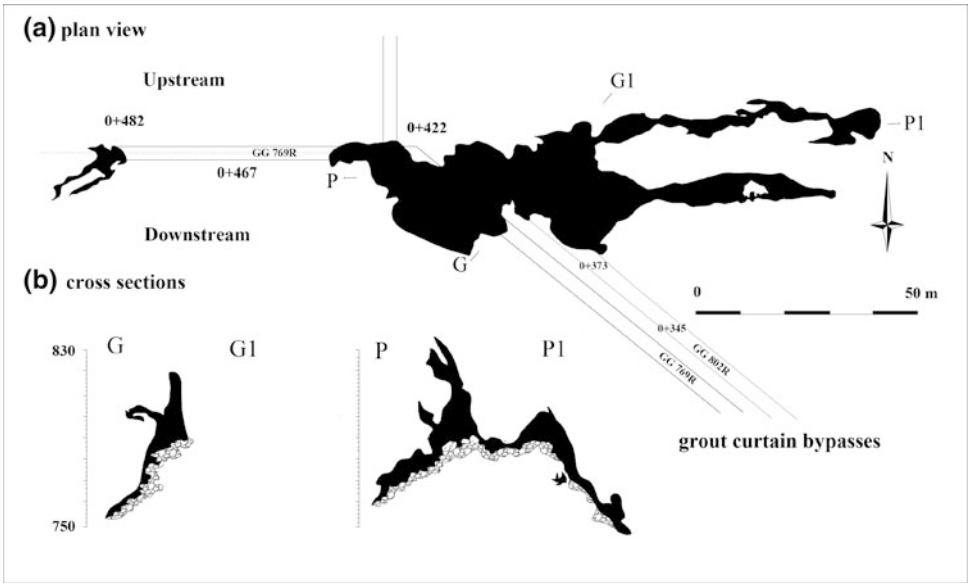

Fig. 5 **a** Plan of Golshani Cave in the right flank of the Salman Farsi Dam; *ruled lines* show location of exploration and grouting tunnels. **b** Two cross sections to show the size of the rooms (adapted from Koleini et al. 2013)

The existence of two extinct volcanoes in Northwestern Iran, Sahand and Sabalan, together with several thermal springs, has made the northwest a likely region for hypogene caves. Among the several caves known in this area (e.g., Hampoeil, Gharaiji, etc.), the most comprehensive studies have been at Sahoolan Cave.

Sahoolan Water Cave, with a length of 350 m, is located near the city of Mahabad and is one of the major tourist caves in Iran. From the structural geology perspective, this cave is in the Khoy-Mahabad sub-zone (the intersection of Alborz and Sanandaj-Sirjan zones). It develops in limestone and dolomite of the Rooteh Formation (Permian). This is one of the most active areas of crustal tectonics in Iran (Asghari Moghadam et al. 2006). There are extensive outcrops of Quaternary basalts and travertine layers within two kilometers of the cave. The limestones are mostly without any karst surface features. The deposits in Sahoolan Cave are mostly stalactites and stalagmites, rimstone dams, anthodite, etc.

Although more comprehensive studies must be conducted in order to determine the exact development model for this cave, provisional studies performed by Asghari Moghadam et al. (2006) confirm the concurrent role of epigene and hypogene sources (including CO_2 and SO_4 from recent volcanic activities) in its formation.

7 Central and Eastern Iran

7.1 Western Central Iran

The largest known and mapped caves in Iran are Katalekhor Cave and Alisadr Cave, which are 60 km apart in Zanjan and Hamadan provinces, respectively. These two caves are among the most visited caves in the world, and Alisadr Cave averaging 800,000 tourist visits each year.

7.1.1 Alisadr Cave (Ghar Alisadr)

Alisadr Cave is the second longest cave of Iran at 11,440 m (Fig. 6). It is currently one of the ten most important show caves of the world (Laumanns et al. 2001). It is located 60 km NNW of Hamadan City. Alisadr Range stands out as an isolated, steep-sided ridge surrounded by alluvial fans and plains. It is part of the western structural units of the Central Iran zone. The host rock, the Sanandaj-Sirjan Formation (Dumas et al. 1993) is of Jurassic origin, composed of alternating bands of schists and sandstones along the base, a blackish-gray band of clay-like limestone interspersed with thin layers of schist in the center, and lighter, crystalline limestone on top. It is a result of high-temperature, high-pressure metamorphism related to volcanic activity west of the Alisadr Ridge. The limestones are impure with many insoluble constituents, which possibly intensify the acidity of the percolating water (Kaufmann 2002). The annual rainfall is approximately 300 mm.

The most comprehensive studies of Alisadr Cave were carried out by Laumanns et al. (2001). According to them, Alisadr Cave is developed under and along a stagnant karst water table. More than 4 km of the cave passages are presently developed at the water table, with large lakes of crystal clear water reaching depths of around 15 m. The temperature of the water is ~12 °C, and with a pH value of seven, the water is nearly saturated with calcite. The water table fluctuates annually by around 0.5–1 m, with a maximum in late spring to early summer. At this time, some

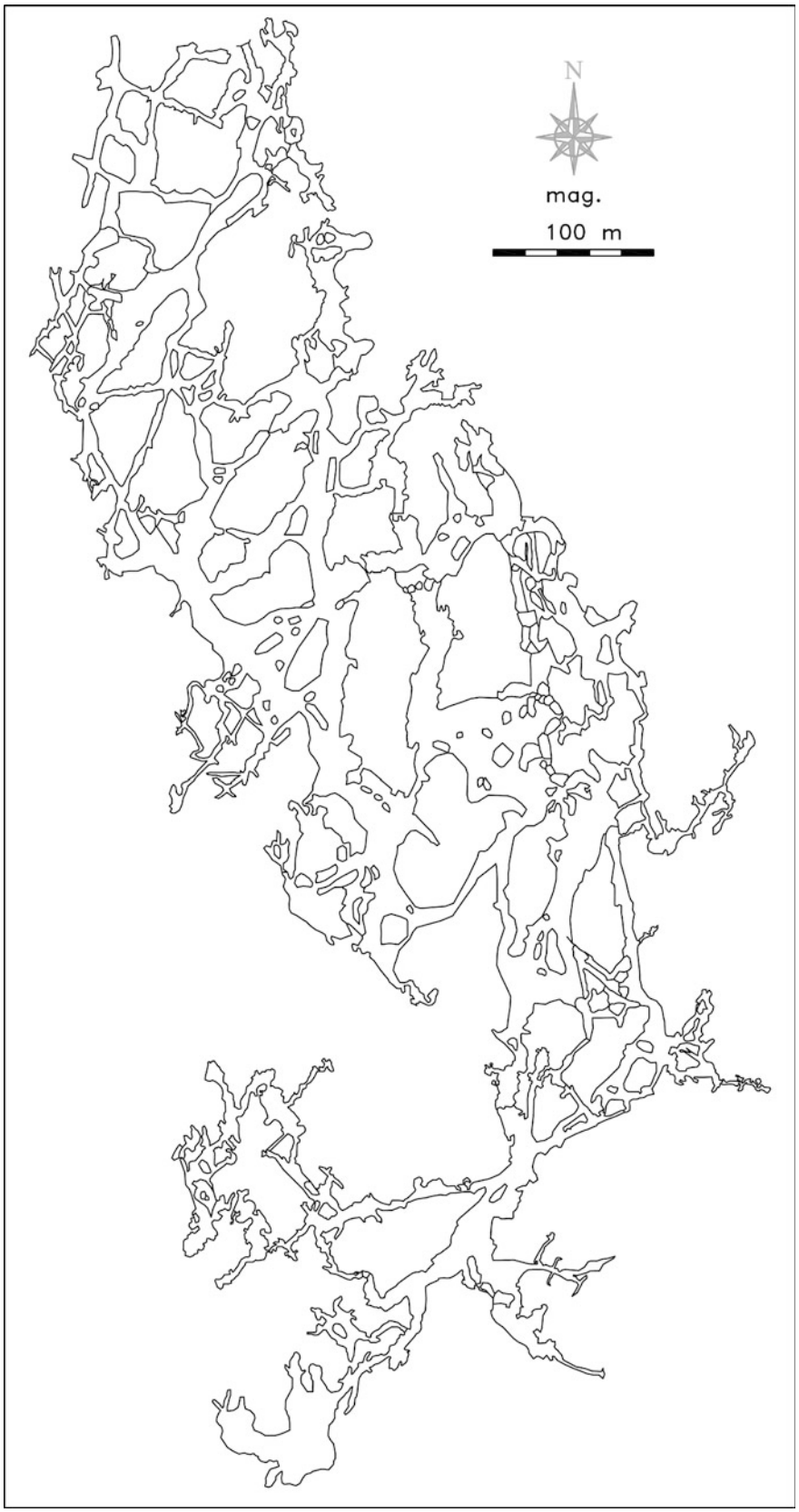

Fig. 6 General plan of Alisadr Cave, based on two topographic survey expeditions (adapted from Laumanns et al. 2001)

water may spill to a spring (Kaufmann 2002). This cave was described by Ford and Williams (2007) as containing an outstanding and very extensive example of notch.

Speleogenetic model. After deposition of the Jurassic limestone on top of an impermeable schist sequence, tectonic forces folded and uplifted the strata. The folded Jurassic limestones and schists are unconformably overlain by horizontally bedded limestones and marls of Eocene to Oligocene age. Therefore, the folding must have taken place at some point during the Cretaceous to Early Tertiary. The region has been affected by later periods of volcanism, beginning in the Late Tertiary and continuing throughout the Pleistocene.

The uplift of the limestone sequences created the main fracture directions, determining that the pattern of cave passages in Alisadr Cave predominantly follows the strike of the very steeply dipping beds. The bedding planes and joints were enlarged by phreatic solution, but became drained because of the continuous uplift and so remained small in size (Fig. 7).

Gorgoloh is a major spring approximately 20 km south of Alisadr Cave. Its water emerges from a small pond in the middle of an alluvial plain, discharging about 30 L/s. A peculiarity is the large amount of CO_2 that emerges mixed with the water from the several meters deep rock fissure. The cold water appears to "boil" above the fissure, being agitated and broken by the constant stream of gas.

Classic karstification does not seem to play an important role in this cave area as no epigene caves or karst features can be found above the groundwater level. One reason might be that the semiarid climate has not allowed for substantial vegetation growth and the formation of a thick soil—generally the prime source of CO_2 for rainwaters that seep into the ground. This limitation makes Alisadr Cave a highly interesting scientific object because cave development under the influence of ascending CO_2 can easily be studied in it. The occurrence of thick aragonite deposits around the water table level supports an hypothesis of volcanic influence, as this mineral has been classically associated with a relatively warm environment (>12 °C; Schoeller 1962). Ascending CO_2 mixed with water filling the bedding plane fractures created a comparatively strong carbonic acid that rapidly dissolved the limestone, generating wide lens-shaped passages along the fractures. The Alisadr Cave aquifer appears

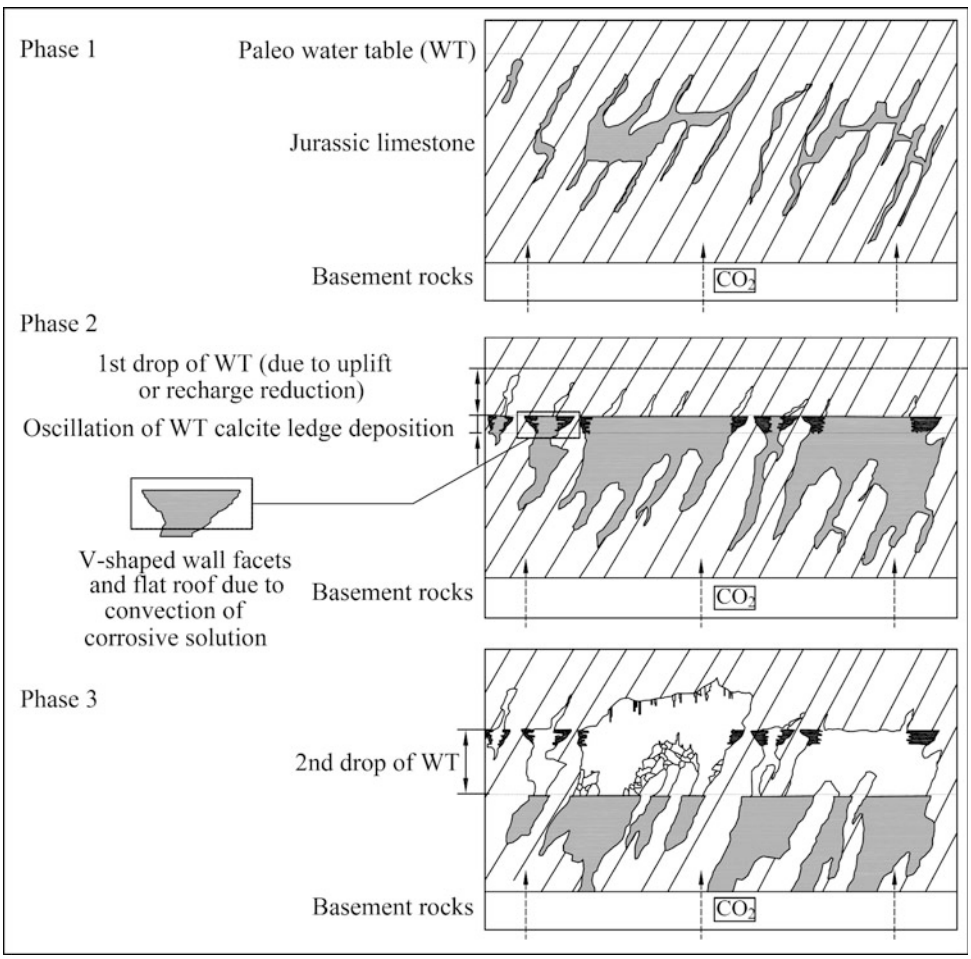

Fig. 7 Speleogenetic model for caves in the Alisadr area, for details on the speleogenetic phases see text (adapted from Laumanns et al. 2001)

to have been characterized by slow to nearly stagnant groundwater circulation during the development of the cave. The cave lacks all of the features associated with vigorous vadose or shallow phreatic water flow (e.g., passages with canyon-like or tube-shaped cross sections). Corrosion notches and lesser, inclined facets are present in nearly all of the passages, indicating slow convectional overturn of the water. No evidence was found for regular stream sink recharge of the aquifer. Thus, the wide passages of Alisadr Cave developed under slow-flowing phreatic conditions that resulted in the maze of galleries.

There are now extensive and thick calcite and aragonite shelfstones at the water table surface. Oscillation of the water line, possibly due to climatic changes, has created up to nine of these calcite ledges within a height of less than two meters, indicating nine former water levels.

At places in Alisadr Cave, widening of passages by the notches made the overlying rocks unstable and breakdown occurred that created high rift passages and chambers above the water-filled galleries. This process is responsible for the biggest room in Alisadr Cave, known as "Freedom Hall" (100 × 60 × 15–40 m).

With the last phase of uplift, the upper passages of Alisadr Cave became dry and then accessible. Very unusually, a situation developed in which the current water table inside the cave was slightly higher than the surrounding plains, being impounded by enclosing schists. Consequently, the water finds its way out of the aquifer, resulting in two small karst springs, one near the cave entrance in the north and the other at the southern extremity of the Alisadr ridge.

Less than 30 km SW of Alisadr, there are extensive outcrops of Late Tertiary to Early Pleistocene volcanic rocks. The vigorous production of CO_2 can be interpreted as a post-volcanic phenomenon. The large amounts of autogenic CO_2 provide subterranean waters with major potential to dissolve carbonate rocks. It can be seen in the stream that flows from the Gorgoloh spring that this process continues today. For several kilometers from the spring itself, the stream precipitates travertine, encrusting moss, cyanobacteria, and other organic material. This demonstrates that the acidic waters forming new cave systems at the present time are dissolving carbonate. On the Gorveh quadrangle of the regional geological map, there are large occurrences of travertines that were precipitated from cold and hydrothermal springs, many of which are highly enriched in sulfuric acid and CO_2—both potential solvents for the carbonates. These travertines are associated with the Quaternary volcanism (Laumanns et al. 2001).

7.1.2 Katalekhor Cave

Katalekhor Cave is located 165 km southwest of Zanjan city, about 410 km from Tehran and about 60 km north of Alisadr Cave. The surveyed length of the cave is about 20,318 m, currently by far the longest cave of Iran and the Middle East (Edalatian Arasteh 2015).

Katalekhor Cave is developed in the Oligocene–Miocene Qom Formation. The main entrance to this cave is situated about 1719 m a.s.l. in the northern flank of a W–E oriented anticline SW of Garmab village in the Central Iranian tectonic zone. The cave has a 1250-m long visitor path. The passages of Katalehkhor Cave form a maze with an anastomotic pattern that has three levels (Sivand 2001). Most studies (Rezaei and Nakhaei 2008; Arshadi and Laumanns 2004; Sivand and Bagherinejad 2008) have suggested an epigene source for the cave, with lowering of the water-level successively forming three clearly distinct levels of cave passages. The first level even has a small but distinct sub-level that may be regarded as independent, thus creating four levels in total. Based on the elevations of the levels in relation to the cave entrance, the drop of the water-level took place in two rapid steps of approximately 25 m each (Laumanns et al. 2001). During long periods before and between the drops, flat-roofed passages, with V-shaped cross sections typical of convection along the ceiling and the walls of galleries submerged in CO_2-enriched solutions, were developed. The suggested source of the CO_2 was meteoric water that recharged the water table from the top of the anticline range (Arshadi and Laumanns 2004). However, Ahmadzadeh and Elmizadeh (2014) propose that, before any meteoric waters, the penetration and ascent of deep waters of magmatic origin due to fault pressures may have played the principal role in the cave development. Eventually, recharge from the magmatic source was gradually reduced and the succeeding, epigene processes create the present form.

7.2 Central Iran (Esfahan and Markazi Provinces)

In recent years, several studies have been conducted on caves of this region. Identification and geological investigation indicate the primary role of hypogene processes in their formation (Bahadorinia and Hejazi 2016). The most important caves are Kalahroud, Doridan, and Yeke chah.

7.2.1 Kalahroud Cave

Kalahroud Cave, with a mapped length of 4503 m, is located approximately 300 km south of Tehran and 50 km north of Esfahan. The local elevations range 2100–2900 m a.s.l. The region is semiarid to arid, with ~165 mm average annual precipitation and a mean temperature of ~22 °C The regional landscape is typical of warm to hot desert mountain morphology, being dominated by steep ravines and gorges created by stream dissection of the massifs, with detrital fans and alluvial flats around their margins, and all are created during rare (a-periodic) flood events (Fig. 8).

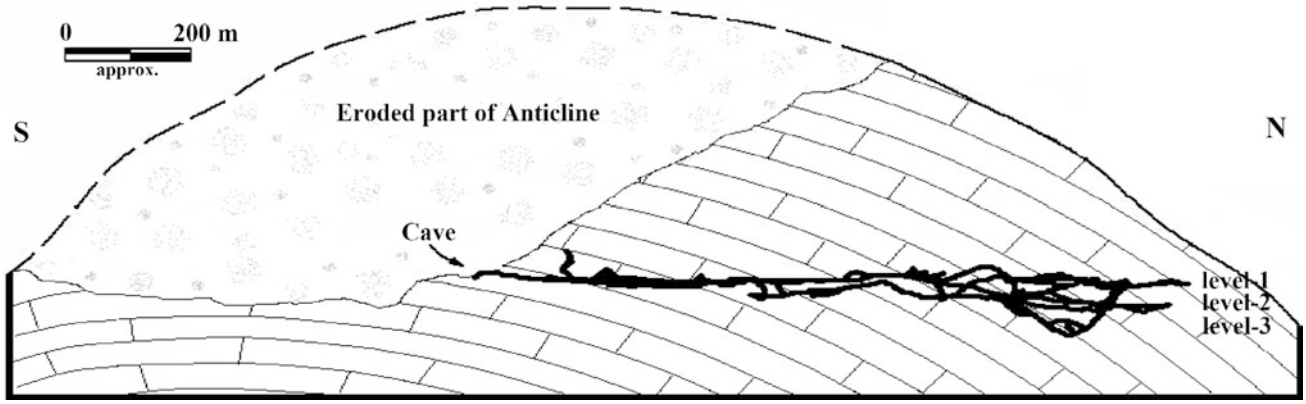

Fig. 8 Schematic section of Katalekhor Cave and Saghizloo Anticline (adapted from Ahmadzadeh and Elmizadeh 2014)

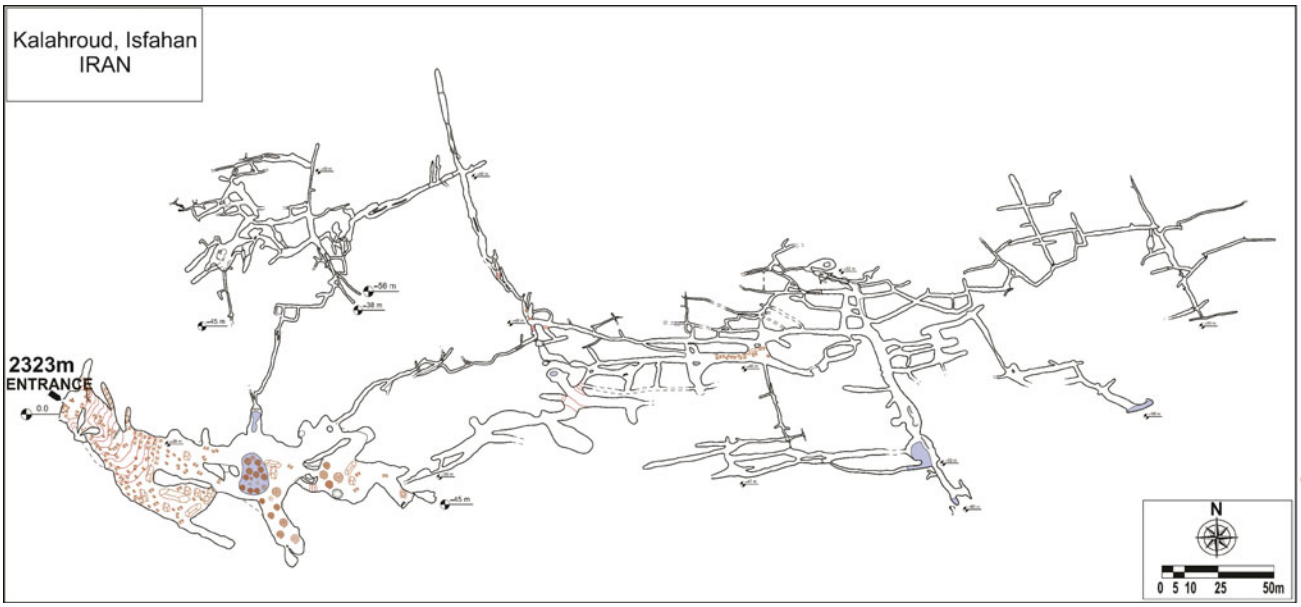

Fig. 9 Plan of Kalahroud Cave, showing the location of corrosion notches and phreatic shafts

The cave has developed in a cuesta that has been entrenched by a shallow gorge. The host formation is a thick to massively bedded *Orbitolina* limestone with lesser, thinner beds of arenaceous limestone and silty shale (Taft Formation—Cretaceous) totaling 40 m in thickness. It is underlain by 80+ m of conglomerate and sandstone with limestone intercalations, and overlain by 50 m of thin-bedded marly limestones that function as a weakly permeable caprock. The strata dip southeasterly at ~15° and are intersected by strong joint sets oriented north and east (Fig. 9).

The cave passages developed up the dip and along the strike to discharge hypogene water to the gorge. As Fig. 9 illustrates, the cave is predominantly a rectilinear joint maze of tall, narrow passages with irregular ceiling heights. There are many solutional pockets and partitions (Fig. 10a). Paragenetic enlargement above deep deposits of silt and clay is common, the sediments being the insoluble residues of the host limestone. The inflowing source waters rise up through rounded solutional shafts that become impenetrably small at depths of a few meters. The maze has a height range of only ~30 m. As the gorge to which it drained was deepened over time, the passages were progressively drained. There was a major collapse at the downstream end in the west part, probably induced by a surficial invading torrent during the rare floods. The hypogene source waters were impounded behind the breakdown barrier, allowing two large corrosion notch enlargements of the maze to form immediately upstream of it. Notching is at the level of the bedrock floor of the gorge. Thick shelfstones and subaqueous nodular precipitate then accumulated one–two meters below the corrosion notch (Fig. 10c, d), indicating that the source

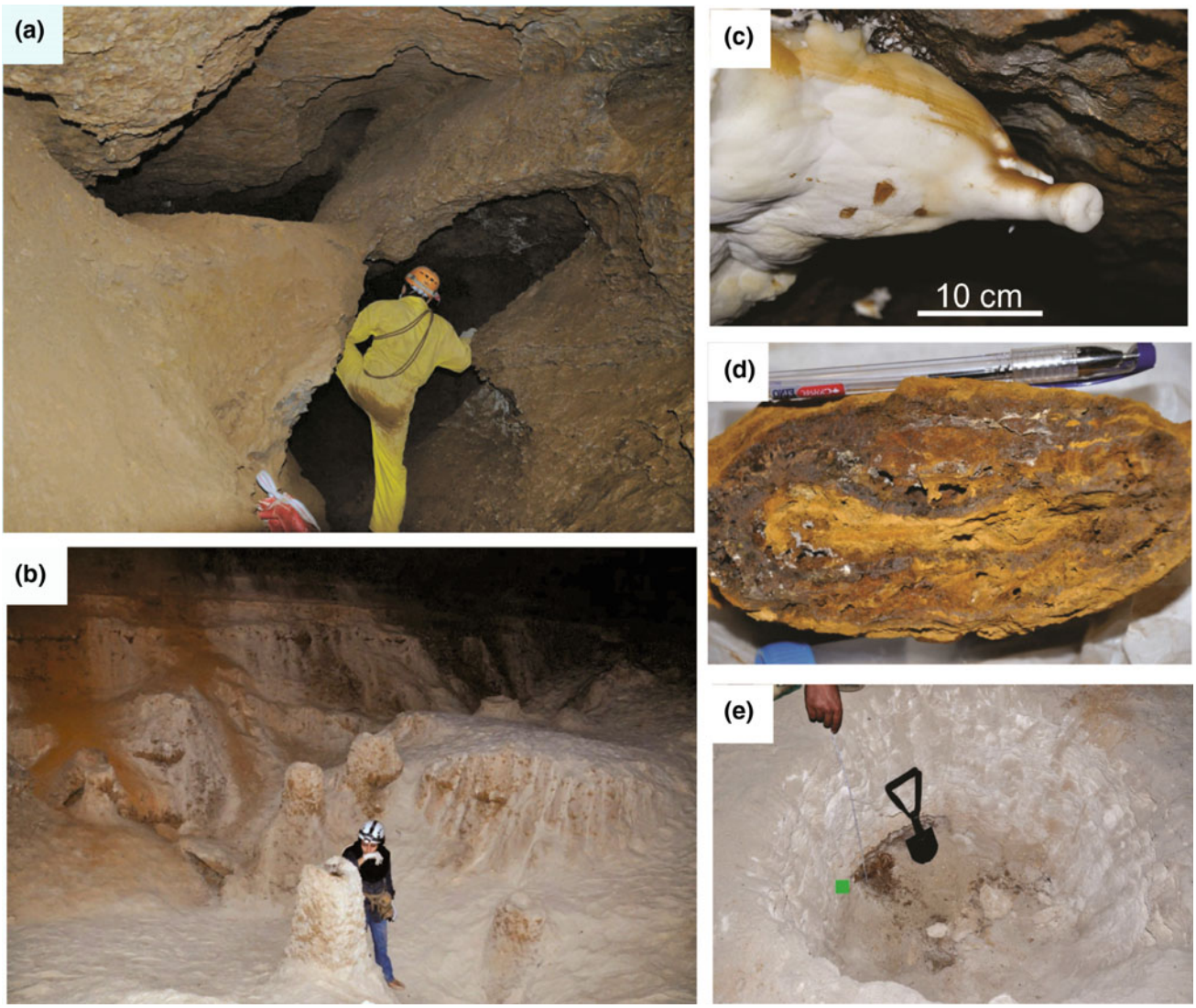

Fig. 10 Kalahroud Cave. **a** An example of the solutional partitions seen in the maze. **b** Holocene calcite raft deposits in the first (*downstream*) corrosion notch chamber. **c** A calcite shelfstone nodule in the maze. **d** A subaqueous nodule of calcite, silt, manganese, etc., in the first chamber. **e** 70 cm of calcite rafts burying silt deposits in the first chamber. The U-series age of 8950 ± 630 years came from the bottom of this excavation. Photographs by S. Bahadorinia

water flooding was so infrequent that evaporation was able to lower the ponding level. Today water ponding appears to be even more infrequent and is dominated by the formation and deposition of calcite rafts (Fig. 10b). One U-series measurement of a sample from the base of the thickest raft deposit (Fig. 10e) yielded an age of 8950 ± 630 years, i.e., Early Holocene (Bahadorinia et al. 2015, 2016).

As noted, the hypogene source waters are being discharged from constricted phreatic shafts close to the base of the Taft limestone. This suggests that much of the water rises from below, passing through the underlying conglomerates and sandstones via fractures, i.e., Kalahroud Cave is an example of an inter-formational hypogene groundwater flow system.

7.2.2 Sangriz Cave

Near Kalahroud Cave in the village of Alavijeh, there is a much smaller cave, Sangriz, that displays other characteristic evidences of upward moving fluids, including phreatic lifting shafts with bubble tracks and gypsum precipitates (Fig. 10). This cave has not been subjected to detailed studies.

7.2.3 Yeke chah Cave

This cave, located in the Golpaygan area of Esfahan province, has been investigated by Hejazi et al. (2015). Strong evidences for a hypogene origin were found. Yeke chah is a solution cave that has been raised above the former water table by vigorous tectonic events. In some parts of the cave,

Fig. 11 Sangriz Cave. **a** Bubble tracks from rising flow. **b** The exit shaft, with typical phreatic form and gypsum precipitates. Photographs by S. Bahadorinia

there are very large deposits of cave clouds (Fig. 11), besides gypsum sediments and the traces of bubble trails. Some inlet and outlet shafts are also observed in the cave and in exposures of the host rock on the surface. Uplift and the existence of many faults in Golpaygan area have played a substantial role in the formation of this cave.

7.2.4 Doridan Cave

Doridan Cave is formed in limestone on Arsh Mountain, in the Delijan area in the north of the Central Iran zone. Like the other studied caves, there are the distinctive morphological features of hypogene flow and solution, such as partitions, cupolas, rising shafts, and suites of characteristic minerals, plus weathered sediments on the floor of the cave and rounded gypsum precipitates on its walls (Derakhshan et al. 2015). Arsh Mountain is located close to a granite massif and evidences of thermal fluid discharges such as thermal springs and evaporative sediments have been reported in the region (Fig. 12).

7.3 Eastern Iran (Khorasan Razavi Province), Younesi Cave

The Younesi area lies to the south of Khorasan Razavi province. Like other areas in the vicinity of the Tabas Desert, it has a hot and dry climate. It is a desert area with scattered low mountains. Caves of the Younesi area are formed chiefly in Cretaceous limestone, metamorphosed into reddish marble limestone in some places. There are abundant evidences that the carbonate rocks were penetrated by thermal fluids, including quartz crystal deposits around the cave and in nearby dissolution cavities (Fig. 13). The morphologic characteristics and types of the minerals are suggestive of a hypogene origin. For example, Tak Sara Cave is a single fluid pathway with an upward-developing pattern of passages that has spiral branches in the higher levels. Walls of the cave are covered with very coarse dogtooth spar crystals 10–20 cm in length. Thick gypsum crusts that then formed on the walls have since been substantially corroded or

Fig. 12 Phreatic speleothems of Yeke chah Cave. Cave cloud calcites have been deposited in most cave passage. Photograph by S. Bahadorinia)

Fig. 13 View looking up a solutional conduit in Younesi Cave. The uniform wall cover of calcite is seen to be corroded in many places, possibly an effect of condensation corrosion in the more recent past. Photograph by S. Bahadorinia

Fig. 14 Younesi Cave: Scalenohedral calcite developed under hydrothermal conditions. *Photograph* with permission of A. Eshqi

eroded in many places. Younesi is few kilometers away from thermal water outlets at Ferdos and volcanic rocks in the Bejestan area. Vigorous active tectonics together with thermal fluids are the determining factors for hypogene cave formation in this area. Blour and Aghol sookhteh are other local caves with similar characteristics (Fig. 14).

7.4 Southeastern Iran (Kerman Province), Mirza Cave

The village of Davaran is located in southeastern Iran, north of the city of Rafsanjan. The climate is semiarid. Mirza Cave is located in a mountain range north of the village. The host rocks are limestones of Late Triassic age. Folding of Pliocene sedimentary rocks in this area indicates that there was significant Late Neogene deformation. Evidence of tectonic activity includes displacement of solution pockets and tubes in the ceiling of Mirza Cave. It shows that, after formation of the cave, structural forces shifted some parts of it. This cave is formed in a fault and consists of smaller branches above a main chamber. A massive cupola formed by convectional circulation by upward flowing fluids precipitated subaqueous deposits including very large mammillaries in all parts of the cave. These and several inlets and outlet rising shafts are the main morphologic evidences of hypogene origin (Yusefipuor and Bahadorinia 2015). At present, this cave is dry and decaying.

8 Conclusions

The investigation of caves in Iran, especially in the Central Iran zone, shows the predominant role of hypogene processes in the formation of many of them. According to these investigations, some of the largest caves in Iran, including Karaftoo and Kangohar, were developed by magmatic fluids. Excavations for dams and water transmission tunnels in the non-volcanic Zagros zone have discovered some remarkable, active hypogene systems that have created many problems for the construction engineers. However, many of the studies reported here must be regarded as representative of the initial stages of speleological research in Iran, and further research by isotopic methods is needed.

References

Aghanabati A (2004) Geology of Iran. Geological survey of Iran, Tehran

Ahmadzade M, Elmizadeh H (2014) Geomorphological evolution of Karst Cave in Katalekhor. In: 32nd national and the 1st international geosciences congress, Geological Survey of Iran, Tehran, Iran, 15–18 Feb 2014

Arshadi S, Laumanns M (2004) Speleological project Ghar Kataleh-khor. ISSN19, pp 1617–8572

Asghari Moghadam A, Moayed M, Nadiri A (2006) Geological and geomorphological studies of Sahoolan Cave, north west of Iran. Journal of Tabriz University (in Persian)

Azhdari A, Mohammadi Z, Zarei H (2014) Identification of salinity sources in Garab Spring, Behbahan, using ionic ratio and isotopic

content. In: 32nd national and the 1st international geosciences congress, Geological Survey of Iran, Tehran, Iran, 15–18 Feb 2014
Bahadorinia S, Hejazi SH (2016) Hypogen speleogenesis system in Central Iran. In: 34th national and 2nd international geoscience congress, 22–24 Feb, Tehran, Iran
Bahadorinia S, Hejazi SH, Nadimi A (2015) Paleo environment reconstruction based on sedimentology investigations and dating analysis: case study in Kalahroud cave, North of Esfahan, Iran. In: Hajna NZ, Mihevc A, Gostinčar P (eds) Proceedings of 23rd international karstological school "Classical Karst". Postojna, Slovenia
Bahadorinia S, Hejazi SH, Nadimi A, Ford DC, Wainer K (2016) The morphology and development of Kalahroud Cave, Iran. Int J Speleol 45(3):243–257
Bosák P (2002) Karst processes from the beginning to the end: how can they be dated? In: Gabrovsek F (ed) Evolution of Karst: from Prekarst to Cessation. Institut za raziskovanje krasa, ZRC SAZU, Postojna-Ljubljana, pp 191–223
Bosák P, Bruthans J, Filippi M et al (1999) Karst and Caves in the Salt Diapirs, SE Zagros Mts, Iran. Acta Carsol 28:41–75
Bruthans J, Šmíd J, Filippi M, Zeman O (2000) Thickness of cap rock and other important factors affecting morphogenesis of salt karst. Acta Carsol 29(2):51–64
Bruthans J, Filippi M, Šmíd J, Palatinus L (2002) Tří Naháčů and Ghar-e Daneshyu Caves—the world's second and fifth longest salt caves. Int Caver 2002:27–36
Bruthans J, Filippi M, Zare M, Asadi N, Vilhelm Z (2006) 3 N Cave (6580 m): longest salt cave in the world. NSS News 64(9):10–18
Chitsazan M, Karimi Vardanjani H, Karimi H, Charchi A (2015) A comparison between karst development in two main zones of Iran: case study—Keyno anticline (Zagros Range) and Shotori anticline (Central Iran). Arab J Geosci 8:10833–10844. doi:10.1007/s12517-015-1961-x
Darvishzadeh A (1992) Geology of Iran. Amirkabir Publication, Tehran
Derakhshan E, Hejazi SH, Bahadorinia S (2015) Geological investigation on Doridan Cave (South east of Delijan). In: Hajna NZ, Mihevc A, Gostinčar P (eds) Proceedings of 23rd international karstological school "Classical Karst". Postojna, Slovenia
Dubljansky YV (2013) Karstification by geothermal waters. In: Frumkin A (ed) Treatise on geomorphology, vol 6. Academic Press, San Diego, pp 57–71
Dumas D, Mietton M, Maire R (1993) La grotte touristique d'Aiisadre (region d'Hamadan, Iran). Karstologia 23:54–55
Edalatian Arasteh S (2015) The map of Katalekhor Cave, I. R. Iran Mountaineering & Sport Climbing Federation and Iranian Cave and Speleology Association (ICSA)
Ford DC, Williams PW (2007) Karst hydrogeology and geomorphology. Wiley, Chichester
Hejazi SH, Jamali H, Molaei M (2015) Yekke cha Cave speleogenesis, East of Golpaygan, Iran. In: Hajna NZ, Mihevc A, Gostinčar P (eds) Proceedings of 23rd international karstological school "Classical Karst". Postojna, Slovenia
Hill CA (1990) Sulfuric acid speleogenesis of Carlsbad Cavern and its relationship to hydrocarbons, Delaware Basin, New Mexico and Texas. AAPG Bull 74:1685–1694
Hollingsworth J, Jackson J, Walker R, Gheitanchi MR, Bolourchi MJ (2006) Strike-slip faulting, rotation and along-strike elongation in the KopehDagh Mountains, NE Iran. Geophys J Int 166:1161–1177
Javanshad A (1995) Caves and cavers (in persian). Tehran
Karimi Vardanjani H (2015) Karst hydrogeology and geomorphology (in persian). Eram publication, Shiraz
Karimi Vardanjani H (2016) Hydrogeological study of Keyno Anticline using hydrochemical and isotope investigations. PhD thesis, Shahid Chamran University
Kaufmann G (2002) Ghar Alisadr, Hamadan, Iran, first results on dating calcite shelfstones. Cave Karst Sci 29:129–133
Kavoosi M, Lasemi Y, Sherkati S, Moussavi-Harami R (2009) Facies analysis and depositional sequences of the Upper Jurassic Mozduran Formation, a reservoir in the Kopet Dagh Basin, NE Iran. J Pet Geol 32:235–260
Koleini M, Van Rooy JL, Bumby A (2013) Hypogenic karstification and conduit system controlling by tectonic pattern in foundation rocks of the Salman Farsi Dam in South-Western Iran. Int J Environ Chem Ecol Geol Geophy Eng 7:258–265
Laumanns M, Brooks S, Dorsten I, Kaufmann G, Lopez-Correa M, Koppen B (2001) Speleological project Ghar Alisadr (Hamadan, Iran). Tech. Rep. 4, Berliner Hohlenkundliche Berichte
Mir Mehrabi H, Ghfouri M, Lashkari Pour Gh, Hasan Pour J (2010) Tunnel drilling hazards in the H2S bearing areas, a case study: Aspar tunnel. Eniviron Sci Technol 16:93 (in Persian)
Nezafati N (2006) Au–Sn–W–Cu–Mineralization in the Astaneh-Sarband Area, West Central Iran including a comparison of the ores with ancient bronze artifacts from Western Asia. PhD Thesis, Eberhard-Karls-Universität Tübingen
Raeisi E, Laumanns M (2003) Cave directory of Iran. Berliner Hohlenkundliche vol 10, p 101
Raeisi E, Laumanns M (2009) Iran cave directory, 2nd edn. Berliner Höhlenkundliche Berichte vol 37, Speläoclub Berlin
Rezaei M, Moore F (2000) The hydrogeology and geochemistry of Mamasani hot spring. In: 4th symposium of the geological society of Iran
Rezaei M, Nakhaei M (2008) Genesis of Katalekhor karstic cave, Zanjan Province. Iranian Journal of Geology 6:11–19
Rezaei S, Sahabi F, Memariani M (2011) The geochemical investigation of the source of H_2S in the nossod tunnel (Kermanshah Province, Iran). In: 15th symposium of the geological society of Iran
Robert A, Letouzey RJ, Kavoosi M, Sherkati Sh, Mueller C (2014) Structural evolution of the Kopeh Dagh fold-and-thrust belt (NE Iran) and interactions with the South Caspian Sea Basin and Amu Darya Basin. Mar Pet Geol 57:68–87
Schoeller H (1962) Les Eaux Souterraines. Masson et Cie, Paris
Sivand SM (2001) Hydrogeological study of the Kataleh-Khor Cave (Iran, Zanjan). Abstract International Karstological School, Postojna
Sivand S, Bagherinejad R (2008) Kataleh-khor karstic Cave in Zanjan Province (Iran), hydrogeology and mapping. In: International conference on water resources: emphasis on regional development
Taheri J, Fursich F, Wilmsen M (2009) Stratigraphy, depositional environments and geodynamic significance of the Upper Bajocian Bathonian Kashafrud Formation, NE Iran. Geol Soc Lond Spec Publ 312:205–218
Thomas J, Cobbold P, Shein V, Douaran SL (1999) Sedimentary record of Late Paleozoic to recent tectonism in Central Asia–analysis of subsurface data from the Turan and South Kazakh domains. Tectonophysics 313:243–263
Yoosefi Naghani B (2008) Origin and development of Monj Cave. Karoon IV reports (in Persian), IWPCO
Yusefipuor Z, Bahadorinia S (2015) First speleological and biological investigation on Mirza Cave. Kerman, Iran, ICSA report

Hypogene Karst in the Tyuya-Muyun and the Kara-Tash Massifs (Kyrgyzstan)

30

Yuri Dublyansky, Wasili Michajljow, Katalin Bolner-Takács, Jaroslav Hromas, Kinga Székely, Attila Hevesi, and Sandor Kraus

Abstract

Two small limestone ridges, Tyuya-Muyun and Kara-Tash, located in the southern fringe of the intermontane Fergana Valley in SW Kyrgyzstan, host a suite of caves, some of which previously contained Ra, U, and Cu ores that were emptied by mining in the first half of the twentieth century. In early 1920's, mining geologists used the concept of "classical" karst to predict the morphology of ore lodes. These predictions proved largely unsuccessful, because the origin of karst was more complex than first predicted. Speleogenetic history of the massifs comprises of early epigene, hypogene (thermal, ore bearing), and late epigene karst stages. Some caves bear traces of all three stages, whereas others are monogenetic (hypogene).

Keywords

Tyuya-Muyun • Hypogene karst • Fersmana cave • Speleogenesis

1 Study Area: Climate, Geology, and Hydrogeology

The study area is located in SW Kyrgyzstan, in Osh Province at the foothills of northwestern Alai range of the southern Tian Shan Mountains (40,356° N, 72,600° E). Climate in the area is continental with dry and hot summers (Dsa, according to Köppen–Geiger classification). The mean annual temperature is 10.4 °C and the mean annual rainfall is 360 mm.

The study area includes a plateau which gently inclines to the north, with mean altitude of 1400 m. The northward flowing Aravan River dissects the plateau, forming a relatively narrow 5-km-long and 200-m-deep valley. To the south, the plateau is bordered by the Nookat basin—a 10-km-wide latitudally extended (>30 km) depression with

Y. Dublyansky (✉)
Institute of Geology, Innsbruck University, Innrain 52, 6020 Innsbruck, Austria
e-mail: juri.dublyansky@uibk.ac.at

W. Michajljow
Foundation for Preservation and Studies of Caves, Bishkek, Kyrgyzstan
e-mail: michajljow@mail.de

K. Bolner-Takács · S. Kraus
Hungarian Speleological Society, Pusztaszeri út 35, 1025 Budapest, Hungary
e-mail: mkbt@t-online.hu

S. Kraus
e-mail: mkbt@t-online.hu

J. Hromas
Cave Administration of the Czech Republic, Květnové Náměstí 3, 252 43 Průhonice, Czech Republic
e-mail: spravajeskynicr@caves.cz

K. Székely
Institute for Nature Conservation, Füst Milán u. 12, 1039 Budapest, Hungary
e-mail: b.szekelykinga@gmail.com

A. Hevesi
Institute of Geography and Geoinformatics, University of Miskolc, 3515 Miskolc-Egyetemváros, Hungary
e-mail: ecoheves@uni-miskolc.hu

© Springer International Publishing AG 2017
A. Klimchouk et al. (eds.), *Hypogene Karst Regions and Caves of the World*, Cave and Karst Systems of the World, DOI 10.1007/978-3-319-53348-3_30

mean altitude of 1400 m. The Alay range (altitudes up to 5000 m) lies further to the south.

The area is built up of four suites of rocks, each having distinct lithology, separated by tectonic and stratigraphic discontinuities (Fig. 1): (1) Paleozoic sedimentary suites interstratified with effusive volcanic rocks. Sedimentary rocks represent deep sea facies (intercalation of coal bearing and clayey shales, fine-grained sandstone, black shales and quartzose schists, and finely laminated, sometimes bituminous limestones), Cambrian to Early Devonian in age. The strata have an overall E–W strike and near vertical dip. (2) Two slabs of massive Lower Carboniferous (Visean) and Upper Devonian limestone, 650 and 350 m thick, respectively, sandwiched between the above-described Paleozoic suites and separated from them by steep normal faults. These limestones build up the Tyuya-Muyun and the Kara-Tash massifs. (3) Mesozoic rocks comprised of Jurassic continental lacustrine deposits (sandstone, conglomerate, brown coal) as well as Cretaceous marine and lagoon facies (red conglomerate, clays with layers of aleurolite and sandstone, limestone, dolomite, sandstone). The dislocated Cretaceous variegated sediments overlay the eroded surface of the Paleozoic rocks. (4) A suite of Paleogene-Neogene deposits that comprise of conglomerate, sandstone, loess, etc. The suite overlies eroded and dislocated Mesozoic and Paleozoic rocks. The Paleogene-Quaternary rocks form the surface of the plateau and mantle the floor of the Nookat basin.

The Tyuya-Muyun massif is a slab of Lower Carboniferous limestone, ca. 650 m-wide, stretching in east-west direction for ca. 6 km. The NNE-SSW trending faults dissect the slab into smaller blocks. These blocks "plunge" stepwise under the Paleogene-Quaternary deposits toward east and west. The Visean limestone of the Tyuya-Muyun ridge is recrystallized, in places brecciated, and hosts numerous veins of white calcite.

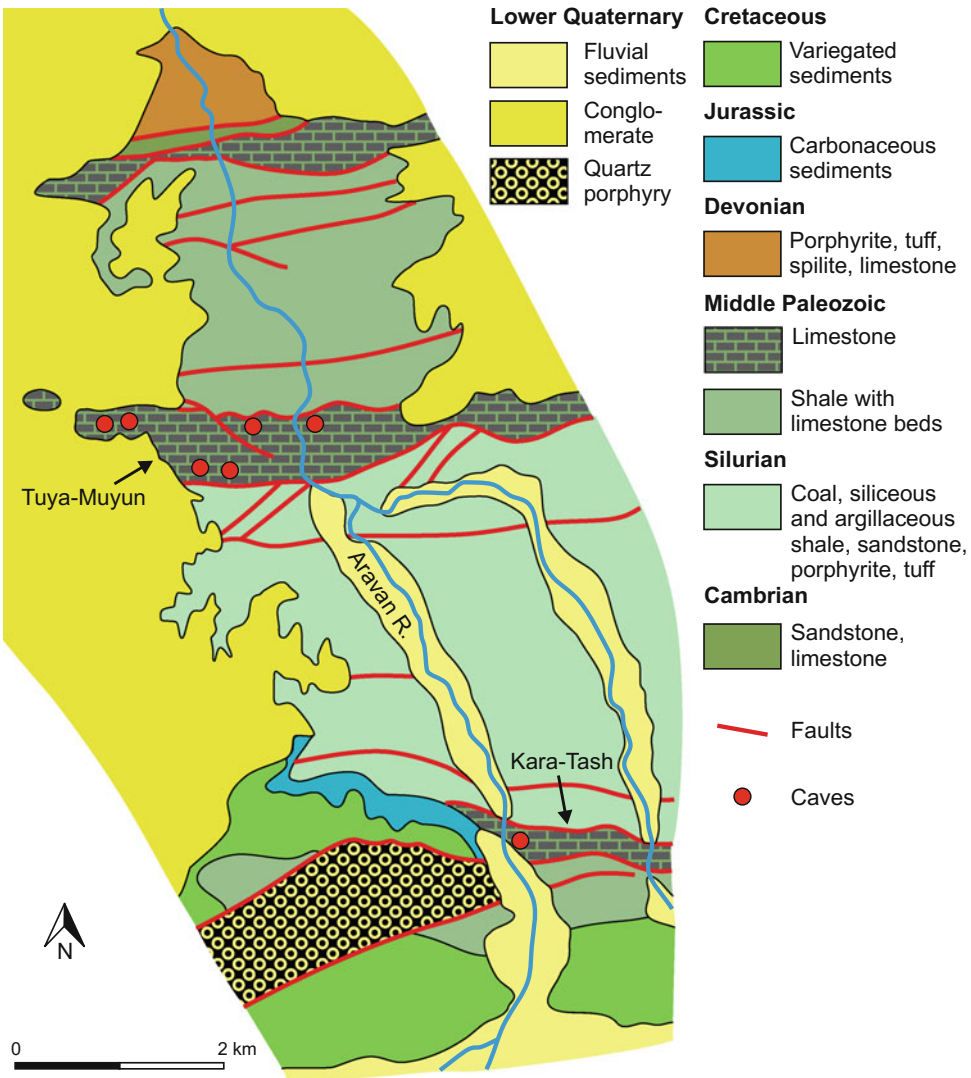

Fig. 1 Generalized geological map of the Tyuya-Muyun mining district in the Aravan River area (after Kazansky 1970)

The hydrogeological district of the Tyuya-Muyun ridge has an area of ca. 200 km^2. The Aravan River (high flow in summer is 20–30 m^3/s) transits the district, flowing in a NNW direction. It is fed by snowmelt and, to a lesser extent, by rainfall in the recharge area of the Alai Ridge. The river cuts both the Kara-Tash and the Tyuya-Muyun ranges, forming deeply incised gorges. The gorge in the Tyuya-Muyun massif is called Dangi (*var.* Tange).

Deeply incised ravines forming a convoluted network and dissecting the plateau remain dry in summer. Natural springs are scarce in the study area, which is due to: (1) the pronounced continental character of climate; (2) poor transmissivity and storativity of Paleozoic rocks (with notable exception of the Tyuya-Muyun carbonates, which will be discussed later); and (3) the orthogonal relationships of the topographic/hydraulic gradient (northward) and strike of major geological structures (east-west), making groundwater flow in direction of the hydraulic gradient largely impossible (Butov and Zaitsev 1935).

Carbonate rocks of the Tyuya-Muyun massif are recharged by infiltration from the Paleogene-Quaternary aquifer, as well as by capture of surface runoff in ravines, which intersect the massif in its western-most part. Fractures and karst transmit the water eastward in the Tyuya-Muyun massif. Previously, the waters of the massif discharged through three natural, lukewarm springs (Fig. 2). The largest of them, *Kok-Bulak* spring was located on the southern slope of the massif, ca. 200 m westward of the mouth of the Dangi gorge and ca. 50 m above the level of the Aravan River. Its mean annual discharge was 6.4 L/s and T = 20–23 °C (which is ca. 10 °C greater than the mean annual air temperature in the area). In 1932, the spring orifice was artificially lowered. Hydrogeologists reported that the spring channel extends downward, forming several spirals closely adjacent to each other and located along the line of tectonic fault. The *Southern Tange* spring was located at the southern mouth of the Dangi gorge, ca. 10 m above the Aravan River. The discharge rate was 0.14 L/s, T = 18–22 °C. The *Northern Tange* spring was located closer to the northern end of the Dangi gorge, 30–40 m above the Aravan River. The discharge rate was 2.4 L/s, T = 18–22 °C. Cumulatively, the three springs discharged 150,000–300,000 m^3 of water per year. Historical data on chemical composition of the springs is shown in Table 1.

The three springs described above no longer exist. In 1947–1950, during revision work at the Tyuya-Muyun mine, a 2200-m-long drainage adit was driven from the southern entrance of the Dangi gorge (Fig. 2). Thus, a new, artificial water conduit was created, which intercepted the flow of all three natural springs. The adit entered the Main Lode at a depth of −220 m, which lowered the water table in the massif by 45.5 m. Only part of the adit is currently accessible due to rock collapses in ca. 1 km from entrance and in the vicinity the Main Lode.

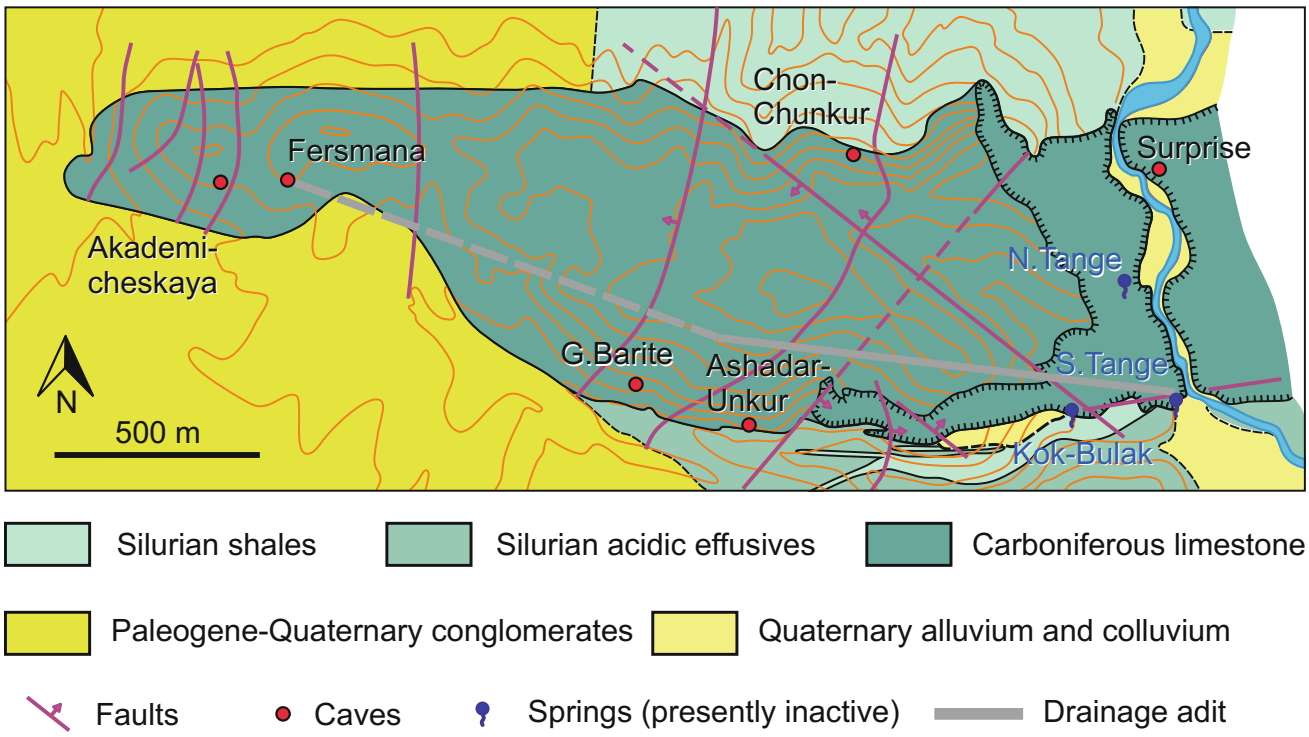

Fig. 2 Geological map of the Tyuya-Muyun massif (after Kazansky 1970) showing caves, springs, and the drainage adit driven into the Main Lode (Fersmana cave). The contour line interval is 25 m

Table 1 Chemical composition of springs of the Tyuya-Muyun massif in June 1925 (mg/L; by Uklonsky 1927)

Spring	HCO_3	SO_4	Cl	Ca	Mg	Na	K
Kok-Bulak	204.3	297.5	140.4	102.1	39.5	112.5	10.9
S. Tange	201.3	293.8	140.4	99.6	39.5	111.0	9.6
N. Tange	263.2	295.4	145.5	No data			

Note Colloidal SiO_2 (0.0130 and 0.0176 mg/L) and Fe (0.0017 and 0.00084 mg/L) were determined in waters from Kok-Bulak and S. Tange springs

The water flow system in the Tyuya-Muyun massif comprises two major components: upwelling slightly thermal waters and downward- to laterally flowing waters recharged at the surface. The deep-seated component can be inferred from constant (through the year) discharge rate, chemical composition, and lukewarm temperature of the Kok-Bulak spring (Uklonsky 1927; Zaitsev 1940). Input of the surface-fed infiltration was observed in the Main Lode: Pavlenko (1933) reported that the free water level in the mine began to rise in April–May and started to decline in June (annual amplitude of 3–4 m), coinciding with active snowmelt on the plateau adjacent to the Tyuya-Muyun massif from south and west. Rains did not affect the water table.

Chemical analysis of water along the drainage adit provided further insights into the hydrogeology of the massif (Fig. 3). All waters analyzed from the interior of the massif were warmer than the mean annual temperature in the area. A major inflow of thermal water between the two collapses blocking the adit can be inferred. Thermal water also emerges in an upwelling spring 880 m from entrance into the adit (point 3 in Fig. 3; 22.4 °C). Thermal waters are enriched in Na and SO_4 and depleted in Ca. Water discharging from some fractures in the walls and the roof of the adit also has temperatures higher than the main stream of the adit. This suggests that the rock above the water table is heated due to continuous influx of thermal waters from beneath.

2 Caves and Mineralization

Tyuya-Muyun is known in ore literature as an unusual type of U–V–Cu deposit hosted by karst cavities (Dahlkamp 2010). The site was subject to Cu mining, possibly as early as the second century BC to the second century AC (Scherbakov 1924). Uranium was discovered at Tyuya-Muyun in 1899 and mining begun in 1908, primarily aimed at recovering Ra. Operations were interrupted by World War I in 1914, the Russian Revolution of 1917, and the ensuing period of turmoil. Mining and exploration resumed at Tyuya-Muyun in 1926; which resulted in the first radium produced by the Soviet Union. In 1928, water inflow into the mine disrupted mining activities. The final exploitation period lasted from 1947 until 1954. It included construction of a drainage adit from the Aravan River to the Main Lode. Another purpose of the adit was to verify the hypothesis of Fersman (1927), according to which additional mineralized solution pipes or karst caverns may occur at this level (none of either was found).

The Tyuya-Muyun massif hosts about 50 mineralized and non-mineralized tube-like, solutional cavities, including six "real" caves: Fersmana (Main Lode), Akademicheskaya, Great Barite, Chon-Chunkur, Ashadar-Unkur, and Surprise. All caves have characteristic hypogene morphology and some of them host spectacular mineral deposits featuring large euhedral crystals of calcite (up to 50 cm in size) and tabular barite (up to 15 cm). The massif Kara-Tash hosts only one cave, Pobednaya, also featuring a prominently hypogene morphology. Caves of the massifs were studied during an international karst expedition Tyuya-Muyun-1989 (Dublyansky et al. 1989).

Fersmana Cave. The largest cave in the Tyuya-Muyun massif, Fersmana, also known as the Main Lode in ore literature, is a vertically extensive (>220 m) complex cave channel (Fig. 4). Drilling efforts demonstrated that mineral-filled solutional cavity continues some 100 m below the bottom of the mine. The cavity was originally filled with a suite of epigenic cave sediments and flowstone as well as a suite of hypogene gangue (calcite, barite) and ore (U-, V-, and Cu) minerals. Four new minerals: tangeite $CaCu(VO_4)(OH)$, turanite $Cu_5(VO_4)_2(OH)_2$, tyuyamunite $Ca(UO_2)_2V_2O_8{\cdot}6H_2O$, and alaite $V_2O_5{\cdot}H_2O$, were discovered here in 1909-1926. Ores contained various amounts of descloizite, vanadinite, carnotite, and uraninite. Most of the U minerals are the result of oxidation of the "primary ore" composed of colloidal pitchblende (UO_2). The Main Lode was mined for Ra in 1904–1914 and 1922–1928, and for U in 1948. As its mineral content was removed, this complex karstic ore body became a cave again. During mining, large shaft, as well as numerous exploratory drifts and winzes were excavated at different levels, so that the now abandoned Tyuya-Muyun mine is presently a complex three-dimensional arrangement of (modified) natural and artificial underground passages with total length of ca. 4580 m.

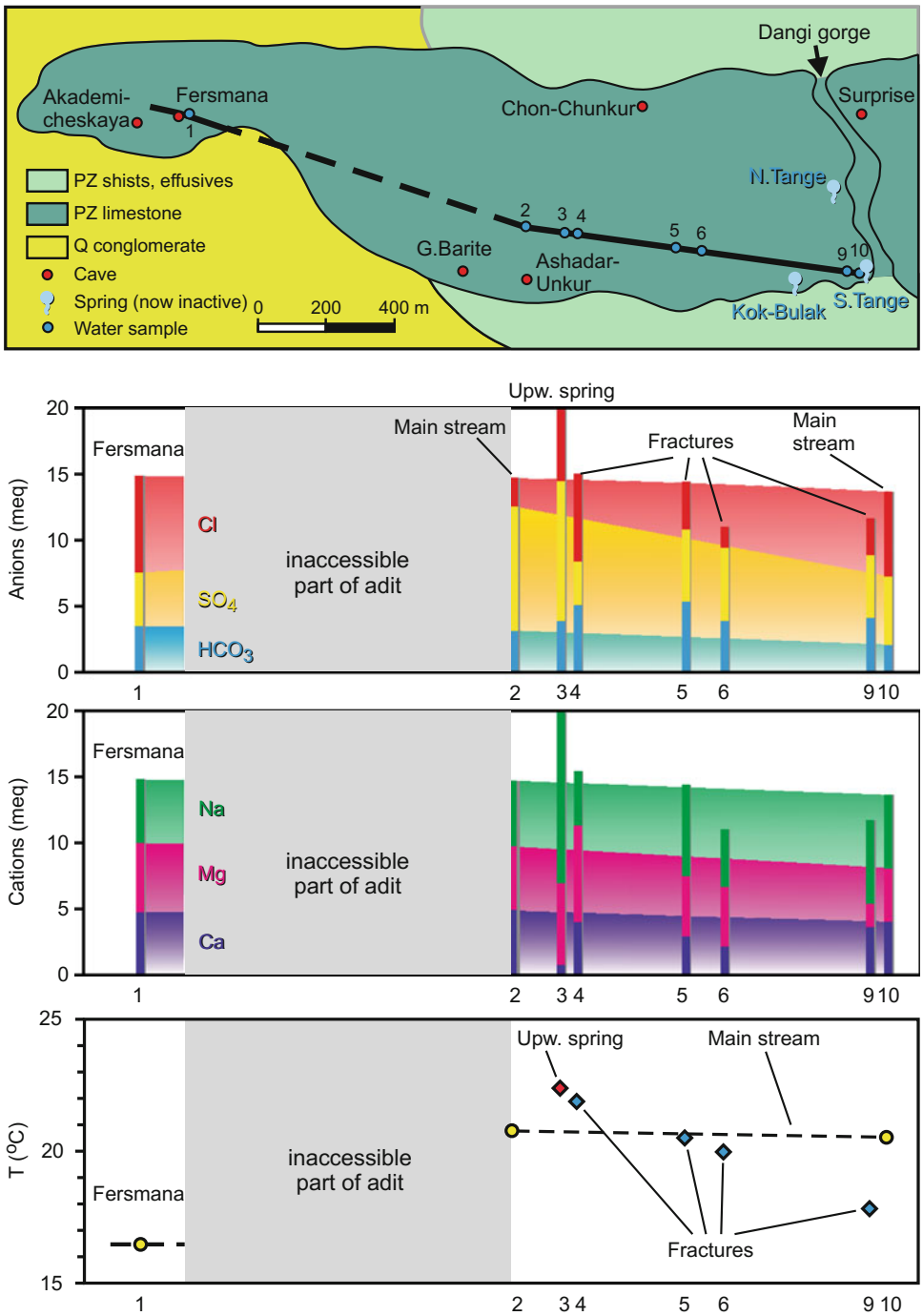

Fig. 3 Water chemistry and temperature in the Tyuya-Muyun massif

Akademicheskaya Cave. The cave filled with ore minerals was discovered to the west of the Main Lode. As its upper part was comparable in size to the Main Lode, the mining engineers hoped that Akademicheskaya would significantly boost the reserves of the mine. The lode, however, terminated abruptly at a depth of ca. 60 m, being truncated by a fault. Patches of columnar calcite overgrown by barite can be observed in some places in the cave. Mining operations significantly altered the morphology of the cave, and detailed descriptions of features of its filing are not available. Speleogenetic characteristics of this cave are, therefore, unknown.

Great Barite Cave. The cave represents a natural "super-geode". It is a single chamber inclined at ca. 45°, measuring ca. 114 m in length and having vertical extension of 56 m (Fig. 5). Initially, the cave was accessed through a vertical shaft, coinciding with the central part of a solution pipe, 3–4 m in diameter, lined with large crystalline calcite.

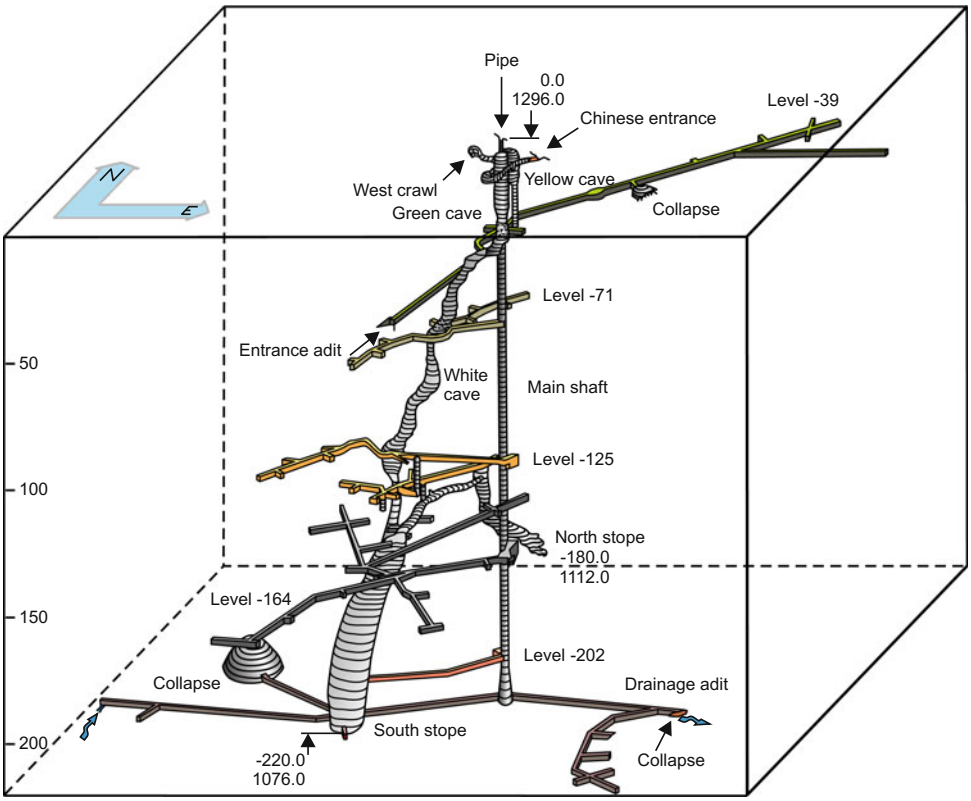

Fig. 4 Fersmana Cave or Main Lode of Tyuya-Muyun. The cave was entirely filled (except for a few widenings) by U–V–Cu ore and calcite-barite gangue mineralization. This 3D rendering shows historic names of cave parts, as well as a complex of drifts at different levels (*Topo* Hromas J, Dublyansky Y, Chapligin I, Bolner K, Kraus S. *Rendering* Jančarik A, Nosek P)

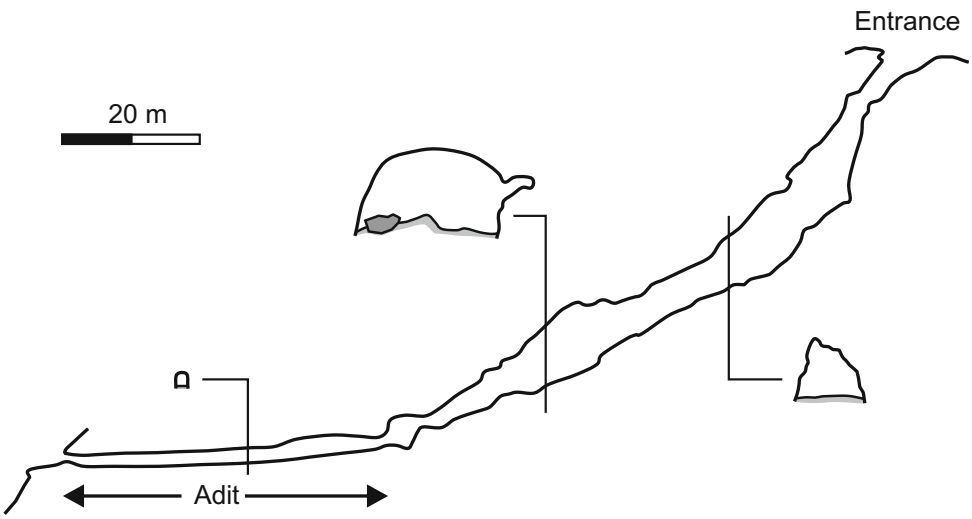

Fig. 5 Great Barite Cave (*Topo* Hromas J, Kučera B, Székely K)

An adit was subsequently driven into the basal part of the cave; the latter was severely vandalized and much of its mineral infill was removed. The walls of the initial cave chamber were coated with an up to 1-m-thick layer of hydrothermal calcite, producing sometimes large (up to 50 cm) scalenohedral crystal terminations (Fig. 6). This calcite was precipitated from waters with temperature not exceeding 60 °C (fluid inclusion data; Dublyansky 1990). A layer of columnar calcite with scalenohedral terminations but of much smaller size followed, forming at similar temperatures. On this calcite, an up to 1-m-thick layer composed of large (up to 10 cm) tabular crystals of yellow–green barite was deposited. Barite was formed at lower temperatures (evidenced by all-liquid inclusions). Massive cave sediments, such as thick red clays with intercalating layers of calcite flowstone ("marble onyx") are present in the lower parts of the cave.

It is important to note that, aside from the first stage of cave development when the main volume of the "geode" was formed, subsequent dissolution and deposition stages are

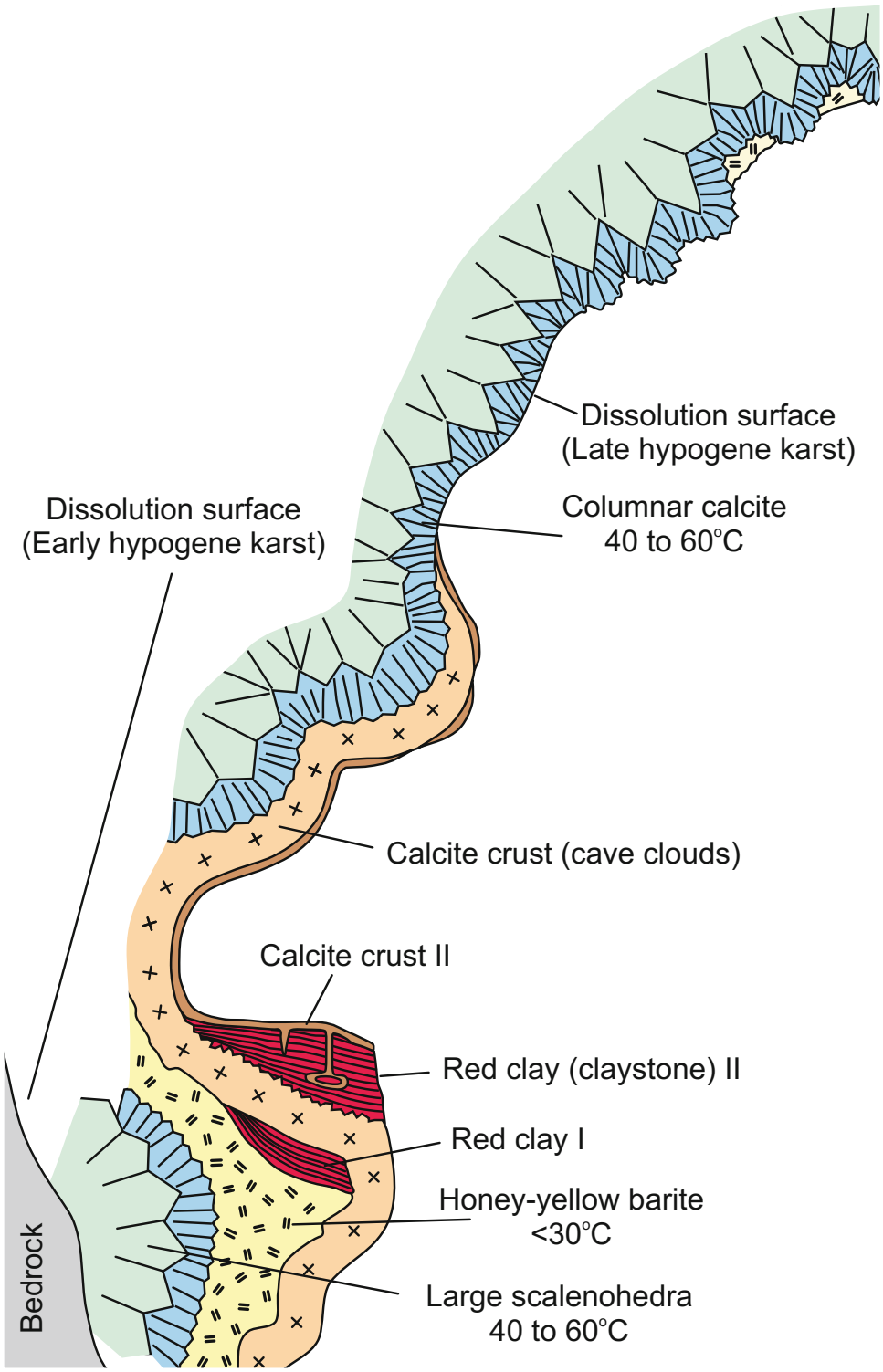

Fig. 6 Mineralization and dissolution in Great Barite Cave

recognizable. In places, the thick layer of hydrothermal calcite, as well as limestone bedrock is cut by solution surfaces, forming meter-sized near-spherical rounded pockets. At lower levels, white calcite crust ("cave clouds") coats the walls of the cave represented by earlier mineral deposits (Fig. 6).

Ashadar-Unkur Cave (Dragon Cave). The cave (length is 80 m, vertical extent is 26 m) consists of two chambers with somewhat irregular shape (Fig. 7). The cave opens through a portal on the steep southern slope of the Tyuya-Muyun massif and has a second entrance on the massif surface. The

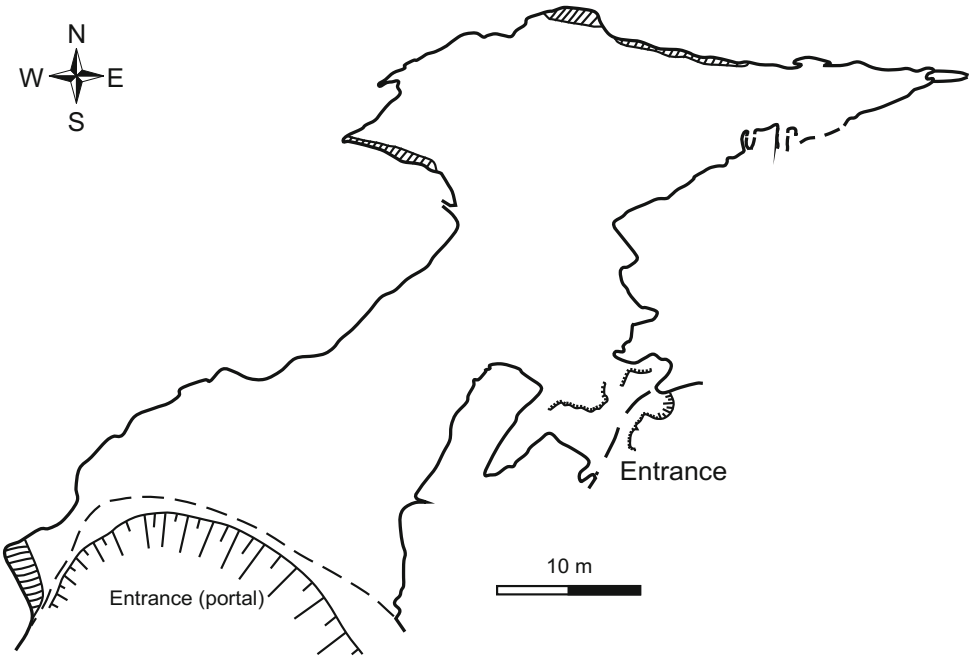

Fig. 7 Ground plan of Ashadar-Unkur Cave (*Topo* Kučera B, Hromas J)

cave floor consists of collapsed blocks of limestone. The cave contains little mineralization, represented by small amounts of barite crystals (subaqueous deposits) and calcite deposits reflecting the ponded water (rafts and platelets) as well as subaerial conditions (popcorn, small dripstone formations). It is most likely that the cave formed at the latest stages of hypogene karstification (deposition of barite) and at some point in time, it functioned as a spring discharging upwelling water. Accumulations of platelets record the state, when the spring almost ceased to exist and the water table level was receding. In the near-entrance part of the cave, there is a 2-m-thick deposit of loess. Due to cave's large open entrances, its inner surface was subsequently affected by frost shattering and in many places lost its smoothness; mineral deposits have been largely destroyed.

Chon-Chunkur Cave. It is the only cave known on the northern slope of the Tyuya-Muyun massif. Its length is 60 m, vertical extent is 35 m (Fig. 8). In the lower part of the cave, the walls are coated with a layer of barite crystals (up to 5 cm thick) followed by a ca. 12-cm-thick layer of columnar calcite with rhombohedral terminations ("cave clouds"). Walls in the upper part of the cave are barren, smooth, and shaped by dissolution. Locally, popcorn, flowstone, drapery, small stalactites, and helicities, as well as one stalagmite were found in the cave. Near the entrance, there are remnants of loess deposits.

Surprise Cave. The cave opens in the eastern wall of the Dangi gorge some 49 m above the floor of the canyon. The canyon wall below the entrance hosts numerous solution pockets and even a chamber (informally known as Petrova Cave), some of which are coated with scalenohedral calcite crystals. The cave represents a three-dimensional

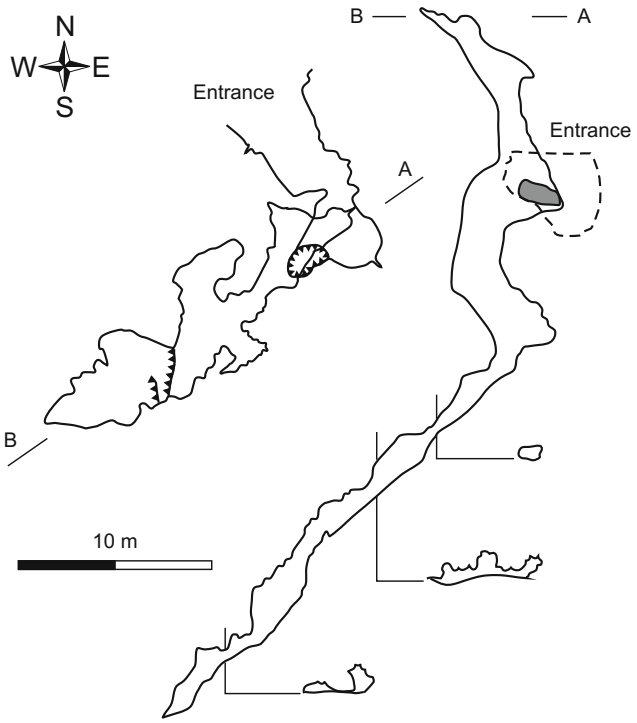

Fig. 8 Plan and vertical projection of Chon-Chunkur Cave (*Topo* Bolner K, Kraus S)

arrangement of narrow anastomosing crawlways, chambers, rising tubes (Fig. 9), as well as series of spherical chambers and niches of different sizes, developing upward and terminating blindly. The total length of passages is 220 m, vertical extent 80 m. The interior part of the cave is coated with a layer of calcite crystals reaching 5–8 cm in size

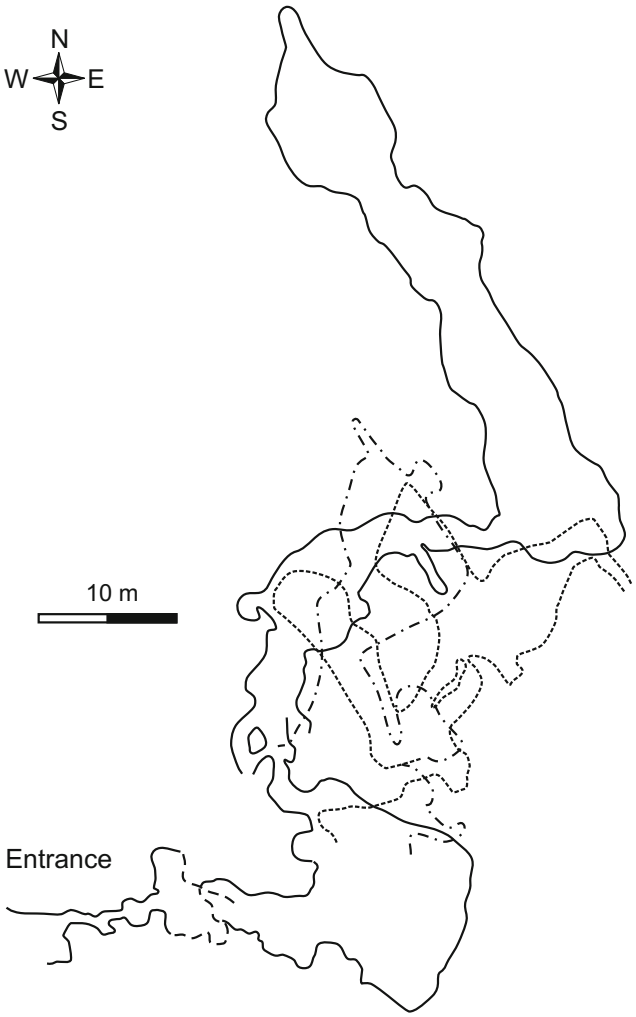

Fig. 9 Surprise Cave, plan (*Topo* Kučera B, Dublyansky Y, Székely K)

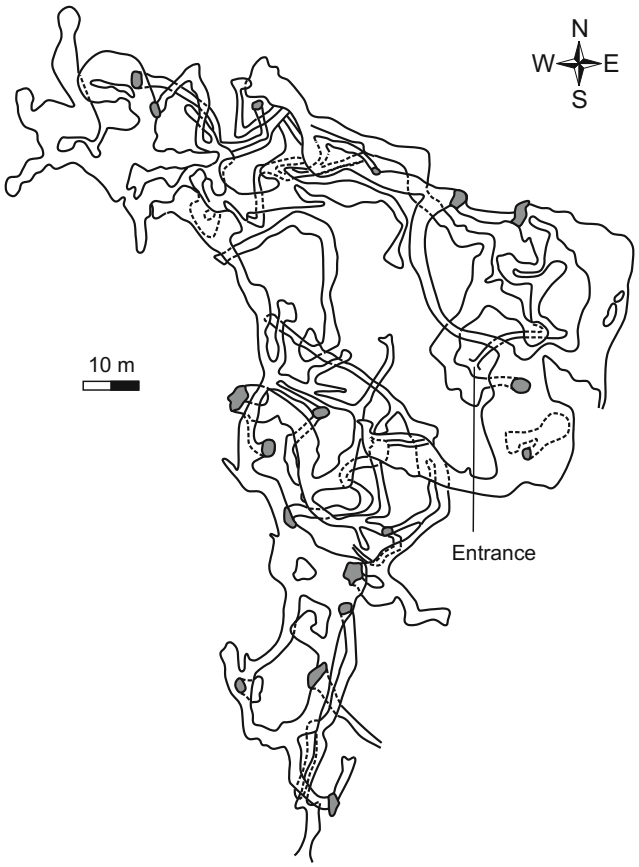

Fig. 10 Pobednaya Cave, plan (*Topo* Speleoclub "Nadezhda", Bishkek)

(largest crystals were 40 cm in length) with scalenohedral shape. Rafts and platelets (markings of the near-water table conditions) were found in four locations in the cave, and subaerial speleothems (popcorn and flowstone) occur locally. The cave formed before the incision of Aravan River and formation of the Dangi gorge; it was opened, and partly destroyed by this incision.

Pobednaya Cave. This is the only known cave in the Kara-Tash massif, located in 3.5 km south of the Tyuya-Muyun. The cave is a three-dimensional maze with total length of ca. 1200 m and vertical extent of ca. 80 m. It is a combination of narrow anastomotic tubular channels and rounded chambers (Fig. 10). The cave hosts sporadic occurrences of pinkish aggregates of barite crystals (up to 4 cm in size), as well as gypsum.

The distribution of mineralization in the Tyuya-Muyun massif exhibits a degree of symmetry. To the east and west of the Main Lode (Fersmana Cave), the number of mineralized bodies and the abundance of minerals decreases, while mineralogy becomes simpler. In Fersmana Cave and some smaller cavities nearby the mineral infilling comprise several generations of calcite (both speleothemic and hydrothermal), U-, V-, and Cu-ore minerals, quartz–hematite, and two generations of barite. Toward the periphery of the massif ore minerals, quartz, hematite, and one variety of barite disappear, so that more distal caves contain primarily calcite and diminishing amounts of barite. The gray, coarsely crystalline "ore marble" in Fersmana Cave and large (up to 30–50 cm-long) scalenohedral crystals of calcite in the Great Barite and the Surprise caves was deposited at temperatures not exceeding 60°C from saline (15–19 mas.% NaCl-equiv.) water (Dublyansky 1990).

3 Speleogenesis

As the focus of mining and exploratory activities, and viewed as the solution to the "radium problem" of Russia early in the twentieth century, Tyuyua-Muyun attracted attention of leading researchers of the time. Opinion that the Tyuya-Muyun deposit may have karst origin was first voiced

by Vernadsky (1914). Ten years later, it was reported that "*…in most parts of the ore body, the ore marble is underlain by simple karstic deposits … not unlike common mineral deposits in caves and other karstic cavities*" (Fersman 1928). By the time when Tyuya-Muyun was studied, the karst origin was established for several ore deposits of the world, such as Reibl (Austria), Iglesias (Sardinia), Tsumeb (Africa), and deposits of MVT type in the USA (Missouri) and UK (Devonshire). However, as Fersman (1928) noted: *"… no deposits have preserved the karst cavity in such a pure form as Tyuya-Muyun, because the latter did not, or almost did not, carry chemical solutions capable of actively replacing the compact carbonaceous rocks; solutions of vanadium and uranium turned out to be much less active in this regard as compared to zinc and lead salts*" (p. 28).

The main points of the model put forth by Fersman and Scherbakov (1925) can be summarized as follows:

1. The primary cavity has a karstic origin (Karst 1).
2. The karst process was interrupted by a thermal process. Upwelling, slightly thermal waters (<60 °C) filled the Karst 1 cavities. Thermal ore process occurred in two stages: (1) introducing Cu, U, V, and Fe along with metasomatic replacement of carbonate karst deposits, and (2) deposition of barite crusts.
3. The thermal process grades into normal karst process (Karst 2). The deposited ores were partly reworked.

The work of Fersman and Scherbakov relied heavily upon insights of the most prominent karstologists of the time, such as František Pošepny, Eduard Martel, Alfred Grund, and Jovan Cvijic. Based on this knowledge, they interpreted the Main Lode as a mature karst system, which formed in response to lowering of the Aravan River after the Eocene. Fersman gave the following prediction of the morphology of the Main Lode: "*… we should expect that the Main Lode with its −140 m depth must morphologically change, possibly through a series of other bell-shaped cavities … into horizontal karst passages, which either terminate blindly, or connect into the common channel, located between −170 and −190 m-depth from the shaft entrance. This new element may connect the Main Lode with other karst elements of the ore field, as well as establish connection with water-bearing network of the limestone*" (Fersman 1928, p. 26-27).

The hypothesis of Fersman-Scherbakov coherently explained virtually all observations available in 1925–1928, when the mine did not reach the –150 m depth. Further advancement of the mine, however, disproved this forecast. Between −140 and −150 m the ore body, indeed, temporarily become horizontal (cf. Figure 4), but then plunged again. At −174.5 m, the so far dry mine started to experience the inflow of karst water. Using water pumping, the mine was deepened to −195 m, after which exploitation stopped in 1928. The problem of mine flooding prompted the first systematic study of the area by hydrogeologists. Butov and Zaitsev (1935) established that the old karst of Tyuya-Muyun is decoupled from the modern-day relief and, respectively, from the modern base level of the Aravan River. It was realized that the karst, therefore, could have been very old and the ore body could extend to a greater depth. According to Butov and Zaitsev (1935) history of karst at Tyua-Muyun comprised the following stages:

1. From the Late Carboniferous until the Mesozoic, the Tyuya-Muyun massif was an elevated mountain terrain, along with the adjacent from north and south Paleozoic rocks. During this time pre-Cenozoic Karst 1 developed.
2. In the Cenozoic, the massif became separated from areas of subsidence to the north and to the south of it, which in Jurassic, Cretaceous, and Paleogene times accumulated sediments.
3. By end of the Paleogene orogenic processes reactivated, and the previously formed suite of Meso- and Cenozoic deposits was folded; after this a peneplain was formed. By end of the Neogene, a river network developed on the surface of peneplain and a new stage of karstification (Karst 2) occurred.
4. The Quaternary Karst 2 evolved during the stepwise uplift of the Tyuya-Muyun massif and associated erosion cycle.

Crucial observations leading to revision of the previous models were reported by mining engineer Alexander Kirikov, who carefully documented the ore body after each 4-6 m advancement of the mine face (Kirikov 1929). He found that besides the pre-ore karst channel, there is also the so-called ore channel. In contrast to the karst channel, which has a vertically elongated cross-sectional, the ore channel has a horizontally elongated elliptical cross-sectional. The axis of the ore channel is displaced upward relative to the earlier karst channel, so that deposits of the karst channel often serve as a footwall in the ore body. Ores fill the karst channel only where it is intersected or overlapped by ore channel. The ore channel following the precursor karst channel was only found in caves hosting the U-V mineralization; it was not present in caves hosting barite and barite-copper mineralization.

Summarizing, the history of karst at Tyuya-Muyun includes the following stages (Fig. 11).

Pre-ore epigene Karst 1 developed in conditions of high-energy relief. The karst-forming water flowed freely downward, forming large, near vertical caves (e.g., Fersmana and Akademicheskaya caves). Caves formed at this

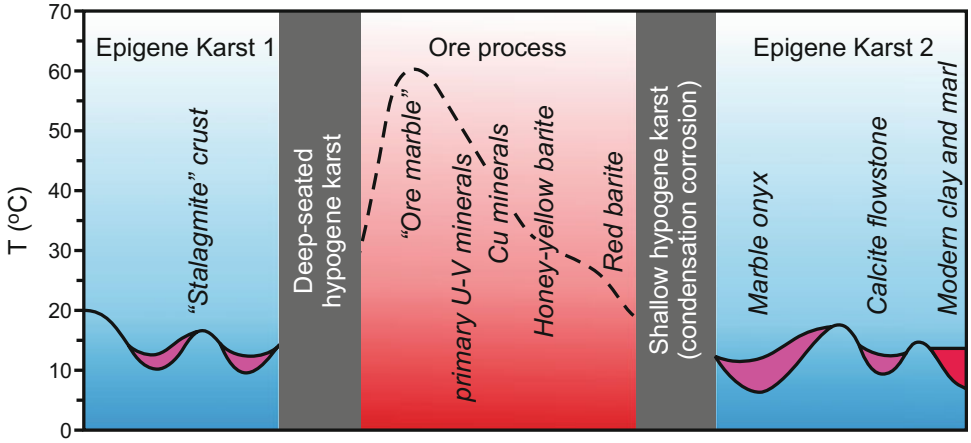

Fig. 11 Generalized solutional and depositional stages during formation of the Tyuya-Muyun caves. The sequence is best represented in the Main Lode (Fersmana Cave). In other caves, only parts of the sequence can be present. Modified from Fersman (1928)

stage commonly host indurated water-transported sediments in their less steep parts. The eastern wall of the Dangi gorge truncates a paleocave passage (the Upper Dangi paleokarst channel) ca. 5 m in diameter, which is entirely filled with indurated clay and sand deposits that recorded multiple episodes of cave infilling by sediments. This may be an extreme case demonstrating eventual choking of cavity and its exclusion from circulation. According to P. Bosak (personal communication), composition of pre-ore karst clastic sediments corresponds to the Lower Cretaceous (Barremian-Aptian) deposits on the plateau surface. This indicates the pre-Lower Cretaceous age of the pre-ore epigene Karst 1.

One of the unanswered questions is: What was the base level for the pre-ore epigene karst at Tyuya-Muyun? There is no doubt that it was developing, when the tectonic slab of the massif was already placed in its current, near vertical position. It is also certain that the basis of erosion was located lower than the current level of Aravan River. The overall westward trend of passages in Fersmana and Akademicheskaya caves and in the Upper Dangi paleo-channel, as well as stepwise sinking of the Paleozoic limestones in this direction, suggests that waters at the time of pre-ore karst discharged to the west of the massif.

Deep-seated hypogene (hydrothermal) karst developed after the pre-ore epigene Karst 1. The ore channel of the Main Lode, most other caves of the Tyuya-Muyun massif, and Pobednaya Cave in the Kara-Tash massif formed at this stage. Depending on their position relative to the "core" of hydrothermal system and the initial permeability structure of the bedrock, the caves acquired various morphologies. For example, Fersmana Cave, whose ore channel developed along its epigenic precursor, acquired gross morphology, which is generally not typical of the hypogene karst. Poorly soluble sediments that accumulated in the pre-ore epigene karst channel "armored" the footwall of the developing hypogene ore channel, and forced it to cut upward relative to its precursor. Other caves have morphologies typical of the hypogene speleogenesis.

Caves that formed in different parts of the Tyuya-Muyun massif host different mineral deposits. For example, the dissolutional stage was followed by deposition of low-temperature hydrothermal (ca. 60 °C) calcite ("ore marble") on the walls of Fersmana and Akademicheskaya caves. Subsequently, red (due to presence of disperse hematite) barite, and then honey-yellow large-crystalline barite were deposited. The temperatures of fluids later decreased, so that the latter barite formed at ca. <30 °C. Large scalenohedral calcite crystals and palisade calcite aggregates form instead of the "ore marble" in Great Barite Cave. They, too, form from <60 °C solutions and are followed by lower temperature barite. Walls of Surprise Cave are lined with scalenohedral calcite (temperature of formation <60 °C) but contain only traces of barite.

The fabrics of mineralization indicate that deposition occurred when cavities were entirely filled with mineral-forming solutions. This requires subsidence, and possibly burial, of the Tyuya-Muyun massif at this stage. Similar to the epigene precursor, the hypogene caves formed prior to the incision of the Dangi gorge. This can be concluded from the observation that both early epigene and hypogene caves are dissected by the canyon. Because of this, their age must be pre-Oligocene.

Shallow hypogene (hydrothermal) karst followed the deposition of minerals in previously formed caves. Indications of dissolution that followed the main mineralization stage can be observed in Great Barite and Chon-Chunkur caves, where solutional surfaces are apparent above the upper limit of the "cave cloud" calcite (cf. Figure 6). The latter indicates conditions of a stagnant water pool, which is commonly observed in hypogene caves. Close spatial association of depositional and dissolutional environment sug-

gests that dissolution could have been due to a condensation corrosion mechanism. If this is the case, then the second dissolutional stage could have occurred over the course of general uplift of the area, when hypogene caves formed at depth moved upward and intersected the (possibly still slightly thermal) water table. At this stage, condensation corrosion could have affected some of the caves, and specific near-water table types of speleothems (cave clouds in Great Barite Cave, rafts and platelets in Ashadar-Unkur and Surprise caves) formed.

Post-ore epigene Karst 2 has a much smaller extent than the two early karst stages. The morphology of small solutional forms (primarily, karstified fractures) suggests vadose conditions and a dominantly descending flow, but their small extent suggests that the conditions were not favorable for karst. Findings of alluvial gravels at the top of the massif (at 1400 m) suggest that it could have been covered by alluvial fans in Oligocene. On the other hand, proximity of study area to the major Alay mountain range suggests that climatological conditions in Pleistocene may also be unfavorable for karstification (cold and dry during glacials, while hot and arid during interglacials). Deposition of loess on the surface of the massif (remnants of these deposits were preserved in Ashadar-Unkur and Chon-Chunkur caves) may also have played a role by consuming carbonate aggressiveness of infiltrating waters.

Although formation of new caves was very limited in the late stages of the geological history of the area, some of the previously formed caves served as hosts for newly forming cave deposits. Massive karst sediments and chemical deposits ("marble onyx", flowstone) were described in the axial part of the Tyuya-Muyun Main Lode (Fersman 1928; Smolyaninova 1970). Unfortunately, these deposits were completely destroyed by mining activities and are not available for examination. Massive layers of similar deposits were found at the bottom part of Great Barite Cave.

4 Conclusions

Karst caves in the Tyuya-Muyun massif in southern Kyrgyzstan have a complex speleogenetic history. The first stage was one of epigene karst; during this stage deep, steeply plunging vadose caves have formed. The second stage was that of hypogene karst. Solution cavities forming at depth by rising thermal waters exploited the precursor early epigene karst cavities but also formed monogenetic caves. General tectonic uplift moved the previously formed caves closer to water table; at late stages, dissolution continued above the water table, likely by a condensation corrosion mechanism. At the end of the hypogene stage, some caves could have functioned as springs. The final epigene karst stage produced few solutional features; it is primarily recognized by young karst sediments deposited in caves that formed at the first two stages.

The early part of the hypogene karst was associated with ore processes, over the course of which minerals of uranium, vanadium, and copper were deposited in preformed caves. The ore system acted locally in the western part of the Tyuya-Muyun massif; caves distal to the core of this system (including Pobednaya Cave in Kara-Tash massif south of Tyuya-Muyun) were not mineralized. Karst of Tyuya-Muyun represents a complex sequence of hypogene and epigene karst, as well as the ore process, overlapping in spatial and temporal senses.

References

Butov PI, Zaitsev IK (1935) O gidrogeologii i karste Tyuya-Muyuna (On hydrogeology and karst of Tyuya-Muyun). Notes of All-Union Mineralogical Society, 2, 64, 1, Leningrad, pp 145–131

Dahlkamp FJ (2010) Uranium deposits of the world. Asia. Springer

Dublyansky YV (1990) Zakonomernosti formirovaniya i modelirovaniye gidrotermokarsta (Particularities of formations and modelling of hydrothermal karst). Nauka, Novosibirsk

Dublyansky Y, Hevesi A, Hromas J, Kraus S, Mahanykova V, Mikhailov V, Mucke D, Sanykova V, Szekely K, Takacs-Bolner K (1989) Tyuya-Muyun (USSR, Kirghizia—preliminary results of the speleological researches carried out by the International Expedition in 1989). In: Abstracts of the 10-th international congress of speleology, Budapest, 1989

Fersman AE (1927) K morfologii i geokhimii Tyuya-Muyuna (On morphology and geochemistry of Tyuya-Muyun). Works on studies of radium and radioactive ores. Academy of Sciences of the USSR, Leningrad, pp 1–90

Fersman AE, Scherbakov DI (1925) Tyuya-Muyunskoye mestorozhdeniye radievikh rud v Fergane (The Tyuya-Muyun deposit of radium ores in Fergana). Works of NTO, p 74

Fersman AE (1928) Uran-vanadieviy rudnik Tyuya-Muyun v Turkestane (Uranium-vanadium mine Tyuya-Muyun in Turkestan). Reports of the Geological Committee

Kazansky VI (1970) Geologo-strukturniye osobennosti mestorozhdeniya Tyuya-Muyun (Geological and structural particularities of the Tyuya-Muyun deposit). Notes on geology and geochemistry of ore deposits. Nauka, Moscow, pp 34–57

Kirikov AP (1929) Tyuya-Muyunskoje mestorozhdeniye ragiya (The Tyuya-Muyun deposit of radium). Reports of the Geological Committee, New Series

Pavlenko DM (1933) Noviye danniye o geologii i genezise mestorozhdeniya Tyuya-Muyun v Uzbekistane (New data on geology and origin of the Tyuya-Muyun deposit in Uzbekistan). Probl Sov Geol 10:123–142

Scherbakov DI (1924) Mestorozhdeniya radioaktivnikh rud i mineralov Fergany i zadachi ikh dalneyshego issledovaniya (Deposits of radioactive ores and minerals in Fergana and problems of their further studies). Materials of studies of natural productive forces of Russia. Academy of Sciences of the USSR, Leningrad

Smolyaninova NN (1970) Nekotoriye danniye po mineralogii i genezisu mestorozhdeniya Tyuya-Muyun (Some data on mineralogy and origin of the Tyuya-Muyun deposit). Articles on geology and geochemistry of ore deposits. Nauka, Moscow, pp 58–90

Uklonsky AS (1927) Geokhimicheskaya kharakteristika vod Tyuya-Muyuna (Geochemical characteristic of waters of the Tyuya-Muyun). Works on studies of radium and radioactive ores. Academy of Sciences of the USSR, Leningrad. pp 111–126

Vernadsky VI (1914) O neobkhodimosti issledovaniya radioaktivnikh mineralov v Rossiyskoy Imperii (On the need to study radioactive minerals of the Russian Empire). Works of Radium expedition of the Russian Academy of Sciences. Imperial Academy of Sciences, Petrograd

Zaitsev IK (1940) Voprosy izucheniya karsta v SSSR (Issues of karst studies in the USSR). Gosgeolizdat, Leningrad-Moscow

Part III
North America

Hypogene Speleogenesis in the Guadalupe Mountains, New Mexico and Texas, USA

31

Harvey R. DuChene, Arthur N. Palmer, Margaret V. Palmer, J. Michael Queen, Victor J. Polyak, David D. Decker, Carol A. Hill, Michael Spilde, Paul A. Burger, Douglas W. Kirkland, and Penelope Boston

Abstract

The Guadalupe Mountains consist of an uplift of Permian carbonate shelf deposits in a semiarid landscape. A variety of speleogenetic processes, mostly hypogene, have made them one of the world's best-known cave regions. The most notable caves are Carlsbad Cavern, which contains the largest known cave room in the USA, and Lechuguilla Cave, now the world's 7th longest. Because the caves are no longer active, there was early confusion about their origin. This was resolved when long-dormant sulfuric acid processes were recognized, with H_2S supplied by nearby oil fields. Potassium-argon dating of the by-product mineral alunite in the Guadalupes indicates speleogenetic ages from 12 to 4 million years, decreasing with lower elevation. Caves show abundant evidence for subaerial corrosion, both by sulfuric acid and carbonic acid in water films. Many seemingly phreatic features have resulted from this subaerial process. Microbial alteration of bedrock has contributed to weathering. There is evidence that isolated caves of greater age, lined by large scalenohedral calcite, were formed by supercritical CO_2 in deep thermal water.

Keywords

Sulfuric acid speleogenesis • Structural control • Alunite dating • Supercritical CO_2 • Microbial effects

1 Introduction

The semiarid Guadalupe Mountains are located in southeastern New Mexico and western Texas, where tensional stress has fragmented the region into isolated mountains separated by broad sediment-floored basins. This area is part of the semiarid Chihuahuan Desert. Annual precipitation is less than 35 cm, and most falls in summer when evapotranspiration is high, so groundwater recharge is slight. Surface karst in the limestones is limited mainly to superficial karren. Caves of the Guadalupes are known for their size, beauty, and scientific value. They serve as one of the

H.R. DuChene
P.O. Box 362 Lake City, CO 81235, USA
e-mail: hrduchene@gmail.com

A.N. Palmer (✉) · M.V. Palmer
Department of Earth and Atmospheric Sciences, State University of New York, Oneonta, NY 13820-4015, USA
e-mail: arthur.palmer@oneonta.edu

J. Michael Queen
814 North Canal St., Carlsbad, NM 88220, USA
e-mail: jmofguads@gmail.com

V.J. Polyak · D.D. Decker · C.A. Hill · M. Spilde
Department of Earth and Planetary Sciences, University of New Mexico, Albuquerque, NM 87131, USA
e-mail: polyak@unm.edu

D.D. Decker
e-mail: dave.decker@caves.org

C.A. Hill
e-mail: Carolannhill@aol.com

M. Spilde
e-mail: mspilde@unm.edu

© Springer International Publishing AG 2017
A. Klimchouk et al. (eds.), *Hypogene Karst Regions and Caves of the World*,
Cave and Karst Systems of the World, DOI 10.1007/978-3-319-53348-3_31

world's clearest models of sulfuric acid speleogenesis, although this process has almost completely ceased. Inevitably, there are several contrasting interpretations.

2 Geologic Setting

The Guadalupe Mountains are the global-type area for strata of the Guadalupian Epoch, dating from 272 to 260 Ma (million years ago). The mountains form a massive shelf-margin limestone block (Capitan Limestone), with bedded, gently dipping shelf carbonates extending northwestward, and coarse carbonate talus dipping steeply southeastward into the adjacent Delaware Basin (Fig. 1). The massive block is usually called a "reef," but it shows few characteristics of a true reef (Dunham 1972). Near the Guadalupe Escarpment, the uppermost part of the Delaware Basin is filled with gypsum-rich evaporates of the Permian Castile Formation. The Delaware Basin is floored by younger gypsum-rich evaporites of the Permian Castile Formation. To the west, the Guadalupes stand high and isolated along the eastern flank of the Rio Grande Rift, a tectonic feature of continental scale, the easternmost fault system in the Basin and Range Province.

The largest Guadalupe caves are located in the central parts of the mountains in Carlsbad Caverns National Park and neighboring federal lands. Currently, the largest are Lechuguilla Cave (223 km long, 489 m deep) and Carlsbad Cavern (52 km long, 316 m deep); see Figs. 2, 3, and 4. Carlsbad and several smaller caves are open to the public via National Park Service tours. All three major limestone types (massive, stratified deposits, and talus) are displayed in the caves (Hill 1987; DuChene 2000; Queen and Hose 2006). Hypogene karst of the Delaware Basin is described by Stafford in Chap. 32.

P.A. Burger
National Park Service, 240 West 5th Avenue, Anchorage, AK 99501, USA
e-mail: paul_burger@nps.gov

D.W. Kirkland
2819 North Surrey Drive, Carrollton, TX 75006, USA
e-mail: dwkirkland@verizon.net

P. Boston
NASA Astrobiology Institute, Ames Research Ctr., Moffett Field, Mountain View, CA 94035, USA
e-mail: penelope.j.boston@nasa.gov

3 Character of Guadalupe Caves

Guadalupe caves typically consist of irregular rooms and passages in several overlapping tiers, with a combination of steeply ascending and semi-horizontal passages. Some caves, or parts of caves, have network or spongework patterns, or consist of simple widening of one or more fractures. Many passages and rooms have narrow fissures in their floors that descend several tens of meters along fractures that terminate downward in narrow constrictions or plugs of weathered rock (Fig. 3a). The caves show no clear relationship to the present topography or to points of surface recharge, and the water table is accessible in only a few places today. In addition to Carlsbad Cavern, two other caves are described in this chapter: Spider Cave and Lechuguilla Cave, respectively 1.8 and 5.8 km WNW of the Carlsbad Entrance.

Caves include some very large vaulted rooms, including the Big Room of Carlsbad. Passages and rooms in the Capitan are guided mainly by nearly vertical fractures. Shelf carbonates to the northwest are prominently bedded and impose some tendency toward tiers of passage development. The Yates Formation, near the top of the shelf sequence, contains much dolomite and siltstone, and caves in this unit (e.g., Spider Cave and upper levels of Lechuguilla and Carlsbad) display deep colorful weathering.

The structural characteristics of the local rock units have a great effect on the pattern and appearance of the cave passages (see Sect. 6). The massive Capitan has virtually no bedding, and passages and rooms are guided mainly by prominent, nearly vertical fractures, although many rooms have been enlarged so much by dissolution that the initial guiding fractures are barely visible (e.g., Fig. 3b). Passages in the stratified shelf carbonates tend to be wider and less clearly guided by fractures. Much of Lechuguilla Cave is located in backreef strata.

4 Development of Speleogenetic Concepts

The first technical study of Carlsbad Cavern and neighboring caves was by Bretz (1949), who saw many clues to support a phreatic origin—apparent lack of water-table control, random solution pockets, great variation in passage size, and poor relation to present topography.

In the early 1970s, Queen (1973, 1981) noticed that much of the gypsum had replaced the local limestone. Fossils and rock textures can be traced directly from one to the other. He concluded that the gypsum had replaced limestone in saline brine and that later freshwater dissolution of the gypsum had produced the present caves. Jagnow (1977) noted evidence for pyrite oxidation in several Guadalupe caves accompanied

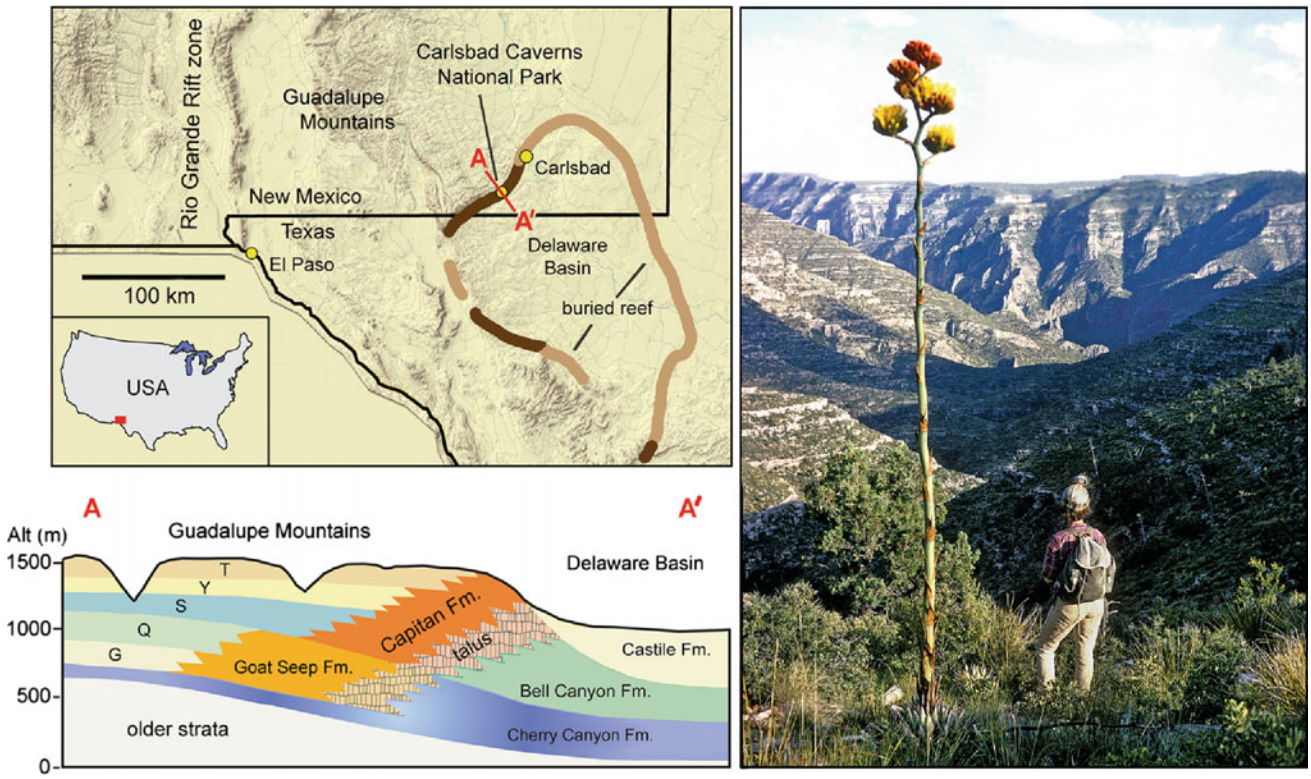

Fig. 1 Location of the Capitan reef and Delaware Basin, with Rio Grande Rift to the west (modified from Harris et al. 1997). Limestone strata: *G* goat seep, *Q* queen, *S* seven rivers, *Y* Yates, *T* Tansill. Digital elevation map by Paul Burger. Cross section from Palmer and Palmer (2012). The photograph shows the gently dipping limestones and typical dissected plateau topography of the Guadalupes (Photograph by A. N. Palmer)

by corrosion from the resulting sulfuric acid. He attributed most of the caves to this process.

Unknown to the others, Egemeier (1973, 1981, 1987 posthumous) had made a doctoral study of speleogenesis in the Bighorn Basin of Wyoming (M. Palmer et al. Chap. 32), where caves were actively forming by H_2S rising from oil fields to the water table and oxidizing to sulfuric acid, thus enlarging the caves with secondary gypsum as a by-product. Egemeier visited Carlsbad briefly in 1971 and left a note in the National Park Service files suggesting this origin for the cave.

That note spurred Donald Davis, then a guide at the Park, to document related evidence, such as deposits of elemental sulfur (Davis 1973; see Fig. 5). Later, Davis (1980) proposed that mixing of H_2S-rich brine with oxygen-rich water accounted for speleogenesis at and below the water table. This process was validated by Carol Hill (1981, 1987) and corroborated by Kirkland (1982) by measuring isotopically "light" sulfur ($\delta^{34}S \sim -13.9‰$) in the cave gypsum versus an average of +10.3‰ for gypsum in the Delaware Basin. Thus, the cave gypsum was not derived directly from basin deposits, but was apparently produced by H_2S oxidation.

5 Models of Guadalupe Speleogenesis

Because the main speleogenetic events in the Guadalupes have ceased, some aspects of their origin are speculative—particularly the H_2S source and water flow patterns. Several contrasting models have appeared over the past few decades, and studies of active H_2S caves have clarified what must have occurred in the Guadalupes. No two models completely agree, but the general picture is clear.

5.1 Hill Model—H_2S Rising from the Delaware Basin

Hill (1987, 1990, 1996, 2000) interprets Guadalupe speleogenesis in four major steps:

1. Late Permian caves formed by brecciation and dissolution along fissures.
2. Mesozoic freshwater phreatic dissolution formed spongework, interconnected cavities in three-dimensional mazes (Fig. 3c). K–Ar dating of montmorillonite clay yielded 188 ± 7 Ma. The Guadalupe Mountains region

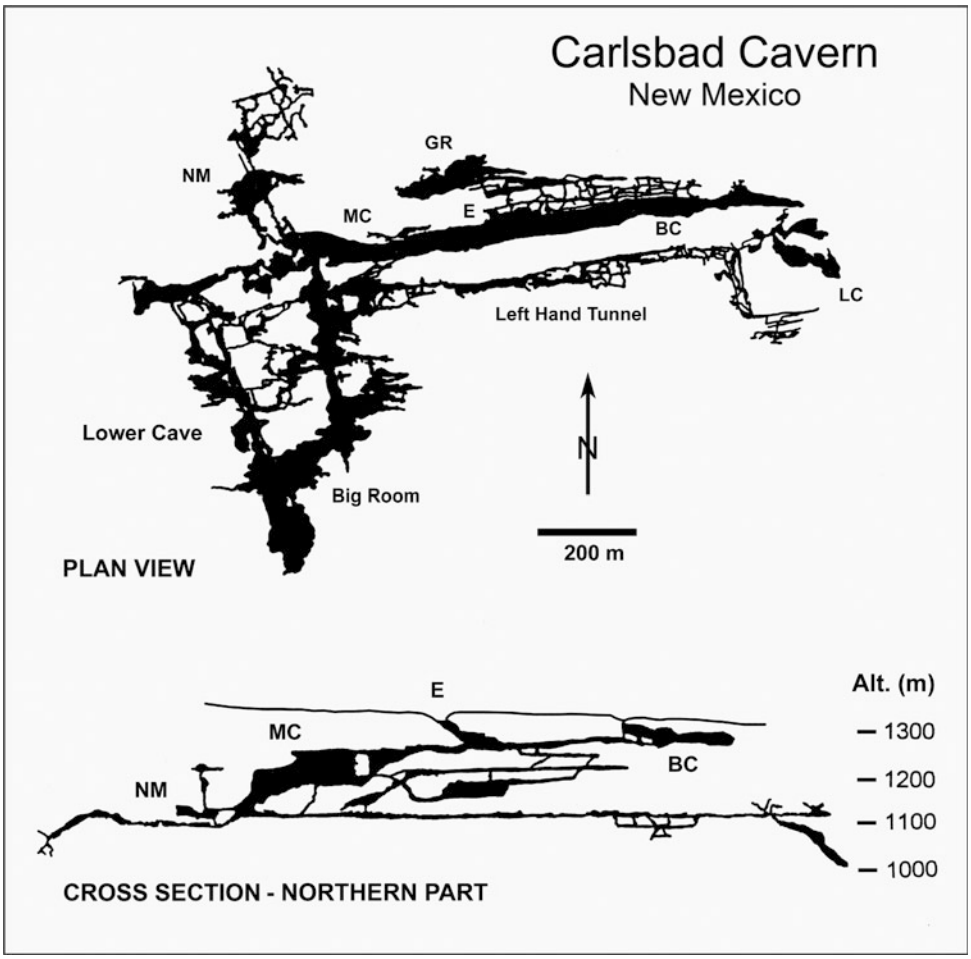

Fig. 2 Map and profile of Carlsbad Cavern, showing its ramifying pattern and distinct tiers of development along former positions of the water table. Most of the major passages and rooms are open to the public via National Park Service tours. From map by Cave Research Foundation

rose during the Laramide orogeny (latest Cretaceous to early Cenozoic), reactivating groundwater flow and dissolution.

3. Oligocene volcanism (30–40 Ma) formed intrusive dikes and Mississippi Valley-type (MVT) ores as late as 20 Ma. Ascending H_2S formed sulfide deposits in reducing zones. Later sulfuric acid caves formed along the same structures and strata. Tensional stress from late Oligocene through early Miocene (~30–20 Ma) tilted the Guadalupes eastward and formed block-faulted structures, accompanied by the origin of small thermal caves lined by large calcite crystals (see Sect. 9.2). Fluid inclusions and oxygen isotopes suggest temperatures of ~30–65 °C (Hill 1996).
4. Major sulfuric acid cave enlargement occurred (Miocene), intersecting all older voids, by H_2S generated from hydrocarbons and ascending into the Capitan. The timing was established at 12–4 Ma, when alunite dating was developed (Sect. 9; Polyak et al. 1998). Oil-gas fields of the Delaware Basin (or farther north, or at depth beneath the Guadalupes) were considered the source. Most caves are located <12 km northwest of the edge of the basin. Various levels of cave development presumably match phases of uplift. As rates of uplift and tilting decreased, mammillary calcite and related forms were deposited in standing water, representing the last stages of water-table drop. Dissolution by sulfuric acid is shown by the presence of massive gypsum blocks, endellite (a mineral derived from clay at low pH), and the presence of uranium minerals deposited along redox boundaries.

The Delaware Basin is rich in petroleum and is capped with halite and gypsum deposits. H_2S is present in many wells. Rather than escaping upward to the surface, H_2S migrated beneath low-permeability salt layers into the forereef beds and ultimately up into the Guadalupe Mountains. There are several ways in which sulfide-rich water could have entered the Guadalupes: water might have been expelled upward by compaction of low-permeability beds; or it may have been driven laterally into the carbonate mountain block by a high water table in the Delaware Basin, before the basin sediments had been eroded to their present position.

Fig. 3 Solution features in Carlsbad Cavern, typical of those in most Guadalupe caves. **a** Rift in the floor of the main level in *Left Hand* Tunnel (~15 m deep). **b** A narrow part of the Big Room at the same level. **c** Spongework along the perimeter of the Big Room, known as the Boneyard (see Sect. 6.2) (Photographs by A. Palmer)

5.2 Kirkland Model—H_2S Migration Patterns

Kirkland (2014) also favors migration of H_2S solutions from the Delaware Basin into the Guadalupe Mountains (Fig. 6a). Before Cenozoic dissolution, the Late Permian Castile extended throughout the basin. It consisted of a thick (~0.5 km) sequence of alternating beds of halite and anhydrite that once reached the top of the Capitan front. Mainly in the late Miocene, the paleo-Guadalupe tectonic block (including the mountains and much of the basin) was tilted 1–2° eastward, allowing fresh artesian groundwater to move down-dip into permeable strata beneath the Castile. From there, under hydraulic pressure, the groundwater rose along fractures, dissolving Castile halite at many local sites up to ~30 km east of the shelf edge. Long cavernous voids formed by convective dissolution in halite beds directly beneath bedded anhydrite (both units being persistent and thick), while water was forced by hydraulic pressure back to the northwest toward the reef front. Many voids developed up-dip until the process terminated at the face of the Permian Capitan and foreslope beds.

High heat flow in the Delaware Basin (Oligocene–late Miocene) generated methane at depth just before and during cave development along the mountain front. Methane ascended into the Castile evaporites by the same pathways along which the groundwater rose and sank by convection. Dissolved gaseous methane reacted with SO_4^{2-} derived from dissolution of Castile anhydrite. Anaerobic sulfate reduction catalyzed by microbes generated many millions of metric tons of both H_2S and CO_2 in aqueous solution. Dissolution of $CaSO_4$ released Ca^{2+}, which reacted with the CO_2 to replace anhydrite with calcite, forming large knobs ("castiles") of resistant limestone, each extending roughly a few thousand square meters (Kirkland and Evans 1976).

Brine moving back up-dip carried much H_2S in solution and was forced by hydraulic pressure through pores and

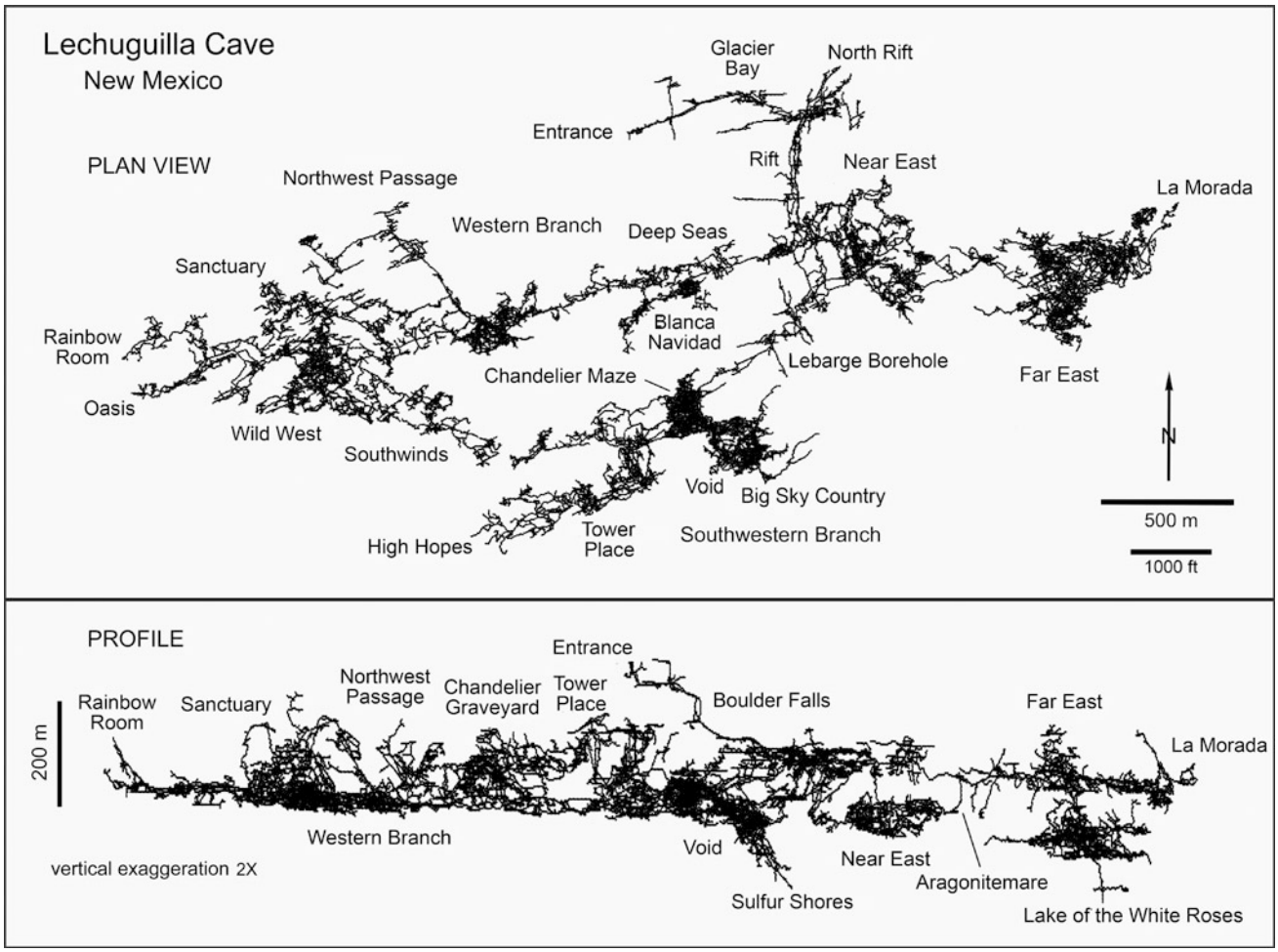

Fig. 4 Map and profile of Lechuguilla Cave (courtesy of National Park Service). Note deep rifts and several levels of development

fractures (mainly within the foreslope strata) into the Capitan aquifer, where it accumulated in low areas because of the high brine density. As erosion removed Late Permian and younger cover progressively from southwest to northeast, the reef was partly exposed to vadose conditions, where oxygen was available. The H_2S outgassed from ponded brine and reacted with aqueous O_2 to form H_2SO_4, which rapidly formed large caves that cut across and integrated many of the voids formed during prior speleogenetic events and masked them with a sulfuric acid overprint.

5.3 DuChene-Cunningham Model—Relation to Regional Tectonics

Dating of Guadalupe caves shows a decrease in age from high to low elevation within the mountains (Sect. 9.1; Polyak et al. 1998). This is often attributed to gradual uplift of the mountains while the water table remained at approximately the same elevation. However, DuChene and Cunningham (2006) attribute this age distribution to a declining water table caused by the loss of the original upland recharge area (Fig. 6b). In the past, uplands of the late Laramide (~38–35 Ma) Alvarado Ridge provided an immense recharge area that supplied water to aquifers draining eastward into the Delaware Basin (Lindsay 1998). The Alvarado Ridge is the predecessor of the extensional Rio Grande Rift, which extends from southern Wyoming to western Texas (Eaton 1986). The Guadalupes occupy part of the eastern flank of the Alvarado Ridge and Rio Grande Rift. Opening of the Rift fragmented the recharge area and reduced groundwater flow. Rifting began about 29–27 Ma, with maximum extension at 17–14 Ma, culminating at 7–4 Ma (Seager and Morgan 1979; Eaton 1987, Chapin and Cather 1994).

When recharge was active, during the mid-Cenozoic, oil was displaced from large accumulations on the northwest shelf and Central Basin Platform of the Delaware Basin by groundwater moving downslope from the crest of the Alvarado Ridge. This implies that groundwater flow was

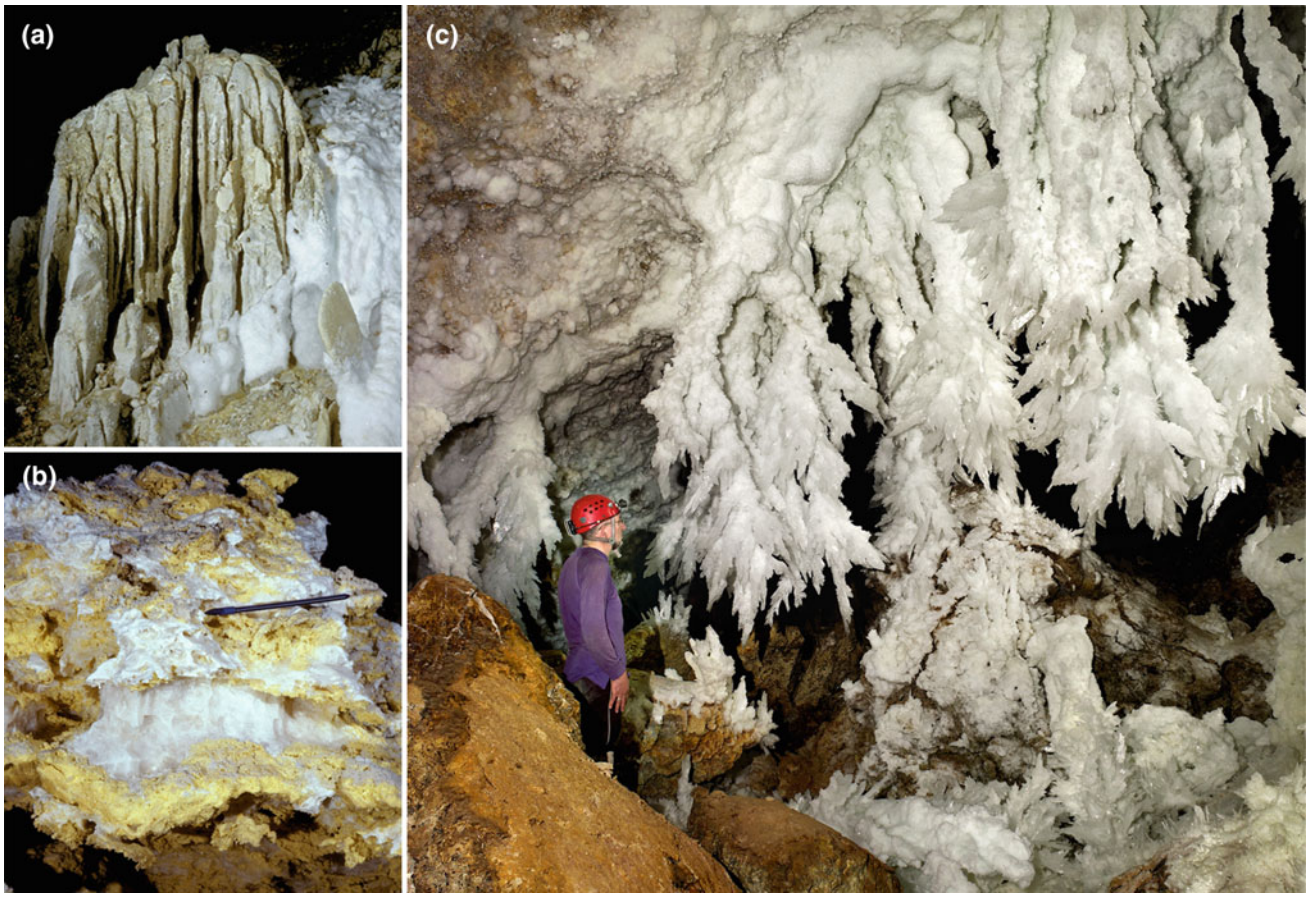

Fig. 5 Gypsum and related features, such as these in Lechuguilla Cave, provide clues to past environmental conditions. **a** Rills in limestone formed by water dripping from blocks of gypsum. This gypsum is a secondary precipitate from evaporation of the dripwater. Vertical scale ~1 m. **b** Sulfur (*yellow*) interbedded with gypsum (pen for scale). These are primary deposits formed during sulfuric acid speleogenesis. Sulfur deposition requires a low pH out of contact with typical karst water. It formed above the water table on surfaces of gypsum, which could sustain a low pH. **c** Gypsum is easily remobilized by dripping vadose water, which recrystallizes as "chandeliers" and similar deposits (Photographs by A. Palmer)

much greater than it is today. The recharge area supporting this strong flow must have extended much farther west at that time. Since 29 Ma, extensional faulting of blocks along the western border of the uplift (King 1948) reduced the upland recharge area, reducing hydrostatic head and allowing the water table to drop. Freshwater influx also introduced microbes into oil reservoirs in Guadalupian strata, causing biodegradation of petroleum and generating large amounts of H_2S. The water table in the Guadalupe Mountains began to fall ~14–12 Ma in response to erosion and tectonism. Meanwhile, oxygen-rich meteoric water mixed with H_2S-rich water to form sulfuric acid, which enlarged caves at the water table. Further faulting along the Rio Grande Rift caused abrupt drops in the water table, which shifted the zone of sulfuric acid dissolution eastward and downward. Cave levels formed by sulfuric acid record water-table position versus time. Elevation differences between cave levels may correlate with episodes of Rio Grande Rift tectonism since ~12 Ma. Speleogenesis ceased when the water table fell to the level of the Pecos River.

DuChene and Cunningham (2006) suggested that petroleum in Permian reservoirs may have been located west of the Pecos River in the northwestern shelf of the Delaware Basin, as well as farther east, as suggested by Hill (1981) and Kirkland (1982). Many of the existing hydrocarbon traps contain >1.5% H_2S. Today, the northwesterly H_2S sources have been breached by erosion, but they retain much oil. Twenty times more oil has been produced from northwestern shelf reservoirs than conventional reservoirs in the central part of the basin, and it would have supplied enormous amounts of H_2S.

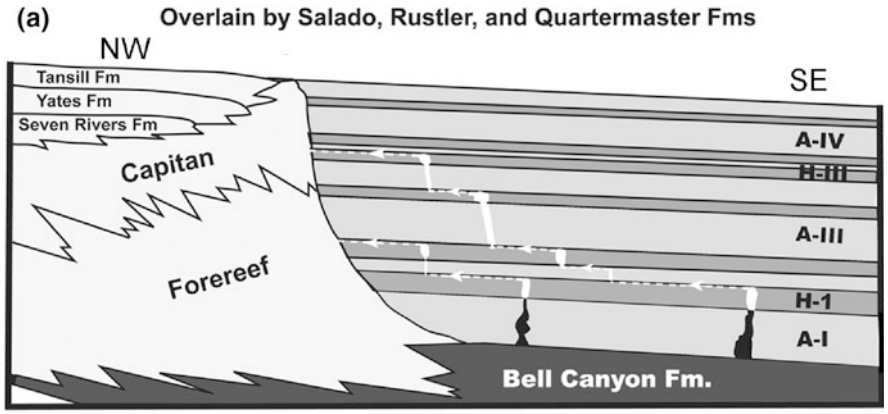
(a)
Overlain by Salado, Rustler, and Quartermaster Fms
NW
SE
Tansill Fm
Yates Fm
Seven Rivers Fm
Capitan
Forereef
A-IV
H-III
A-III
H-1
A-I
Bell Canyon Fm.

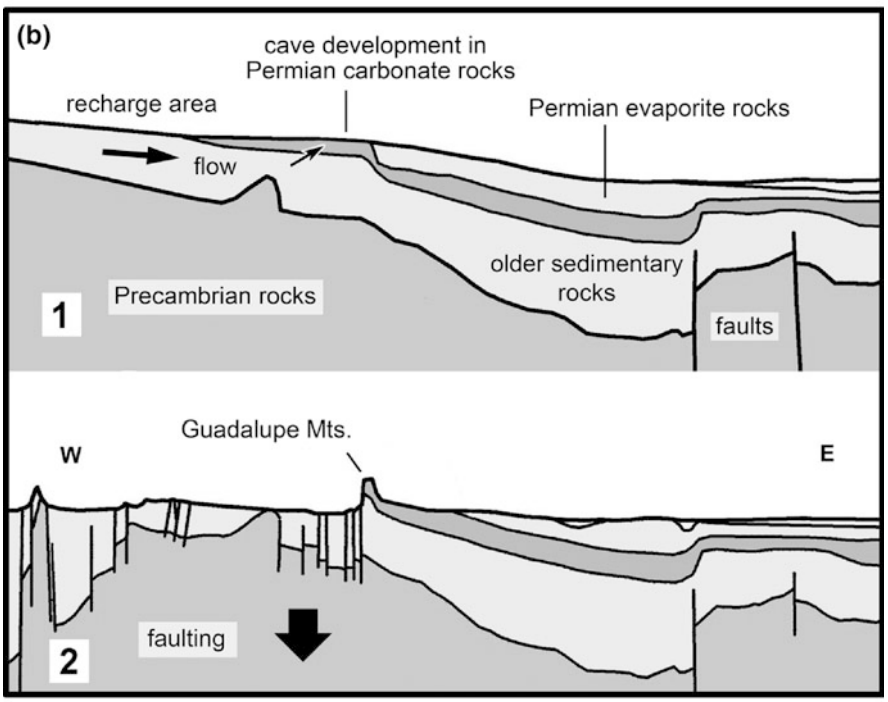
(b)
cave development in
Permian carbonate rocks
recharge area
Permian evaporite rocks
flow
older sedimentary
rocks
Precambrian rocks
1
faults
Guadalupe Mts.
W
E
faulting
2

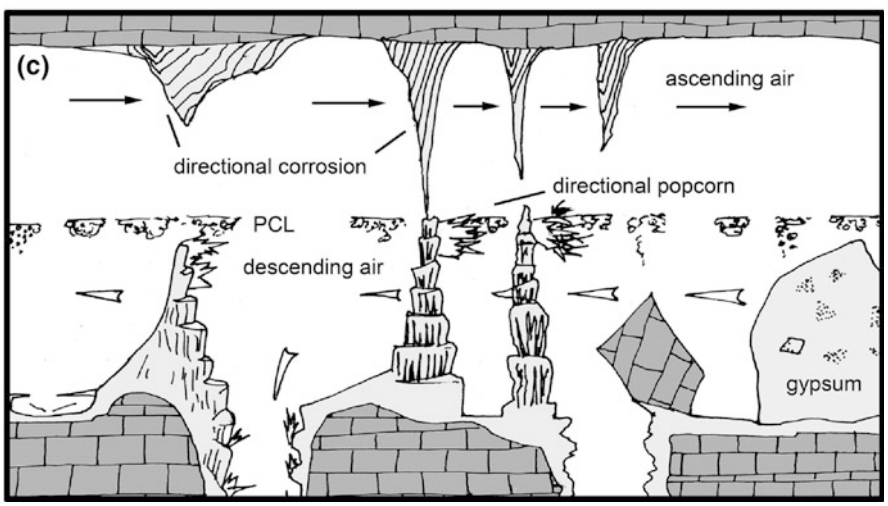
(c)
ascending air
directional corrosion
directional popcorn
PCL
descending air
gypsum

◀ **Fig. 6** Varied developmental models of Guadalupe speleogenesis (see Sects. 5.1–5.4). **a** Hill (1987) and Kirkland (2014) consider that H_2S entered the Guadalupe Mountains from the Delaware Basin. This idealized diagram by Kirkland shows his interpretation of H_2S rising across the strata during the late Miocene, after uniform tilting of the mountains by ~1°. A-1—A-IV (*light gray*) and H-1—H-III (*dark gray*) = anhydrite and halite members of Castile; *lightest gray* carbonates; *black* porous biogenic limestone; *white lines* and *dashes* conduits across anhydrite and along tops of halite members. **b** DuChene and Cunningham (2006) interpret the main H_2S source to be from the northwest, in an extension of the Guadalupe upland that has since been downfaulted by tectonic rifting, thus terminating active sulfuric acid speleogenesis in the remaining Guadalupe block. **c** Queen (1994a, b, 2009c) acknowledges early phreatic dissolution by sulfuric acid, as well as by earlier mixing of freshwater and saline water, but stresses enlargement of the caves by circulating moist air, shown by arrows. *PCL* "popcorn line," the upper limit of subaerial evaporitic speleothem deposition, with condensation corrosion above. Gypsum blocks are generally confined to evaporative areas. The popcorn line is discontinuous over open pits in the floor and is absent on surfaces with no source of saturated seepage

5.4 Queen Model—Importance of Subaerial Processes

Queen (1994a, b, 2009a, b, c) describes several difficulties with the sulfuric acid interpretation: The isotopic signatures of sulfur measured by Hill (1981) could not be maintained in solution as H_2S migrated from hydrocarbon sources in the Delaware Basin to the Guadalupe shelf edge because of interaction with dissolved components in adjacent solutions. Nearly all H_2S must have been transported in dissolved form and susceptible to isotopic exchange. Its high solubility in water would prevent it from outgassing at water depths more than roughly a meter below the water table (Palmer and Palmer 2000). Also, to oxidize a given volume of H_2S in basinal brine to H_2SO_4 would require at least 100 times as much freshwater. Instead, Queen invokes subaerial processes to form most speleogenetic features, including gypsum blocks and crusts, corrosion residues, spongework, cupolas. Furthermore, studies of subaerial corrosion residue in Spider Cave suggest that subaerial passage enlargement exceeds subaqueous enlargement by about 50 times. Section 7 gives some geochemical support.

Queen also recognizes at least six karst episodes, which include dissolution, collapse, sediment fill, and mineral precipitates. He attributes that phase of speleogenesis to mixing between brine and freshwater similar to that in oceanic carbonate islands (e.g., Queen 1994c). In the first stages, he envisions freshwater occurring in lenses along the Guadalupe shelf edge, with underlying brines related to those in the Delaware Basin, analogous to seacoast settings. The last stages followed the waning of Laramide orogeny (latest Cretaceous to Oligocene) and subsequent Basin and Range extensional tectonics. During this time, the freshwater was localized beneath carbonate exposures surrounded by evaporites, like islands in a sea. Flow patterns were adjusted to the regional tectonics and geomorphology. The brines were probably in equilibrium with evaporite deposits nearby. The principal chemical and hydrologic drives are related to brine–freshwater mixing in unconfined freshwater lenses, as observed in seacoast carbonates (e.g., Mylroie and Mylroie Chap. 32).

Although Queen agrees that sulfide oxidation played a role in phreatic speleogenesis, he sees no indication that it was very important, mainly because of the limited availability of dissolved oxygen. He interprets much of what others consider phreatic speleogenesis to be instead vadose (Fig. 6c). Massive gypsum deposits all form in the evaporative part of the air circulation cycle; clays such as endellite show distributions inconsistent with subaqueous origin and require low pH incompatible with carbonate-rich phreatic water. Various speleogens can be attributed to atmospheric circulation, even though they are typically viewed as phreatic (Thrailkill 1971). These include rims, vents, cupolas, and certain ceiling channels. By this model, most accessible Guadalupe caves are today relatively mature (atmospheres <100% humidity, low in CO_2 and H_2S) with diminished condensation and evaporation. In their immature state, such caves would contain high levels of H_2S, which can be unhealthy to cavers.

6 Structural Control of Caves

The following section is based mainly on the work of Burger (2009, 2016).

6.1 Regional Tectonics

Four major tectonic events influenced Guadalupe cave development. The first three established the structural framework for water movement and cave development, and the last disrupted the flow by removing most of the recharge area. The first period of fracturing was syndepositional and parallel to the Capitan escarpment, caused by differential compaction as the Capitan grew over earlier deposits (Mruk 1985). Only the fractures oriented parallel to the escarpment contain significant early dolomitization (Melim and Scholle 1989), which supports their early age. Early stratigraphers observed steep basin-dipping stratification and outcrops with shelfward-dipping beds on the opposite side of the Capitan front (Newell et al. 1953; Smith 1973; Pray and Esteban

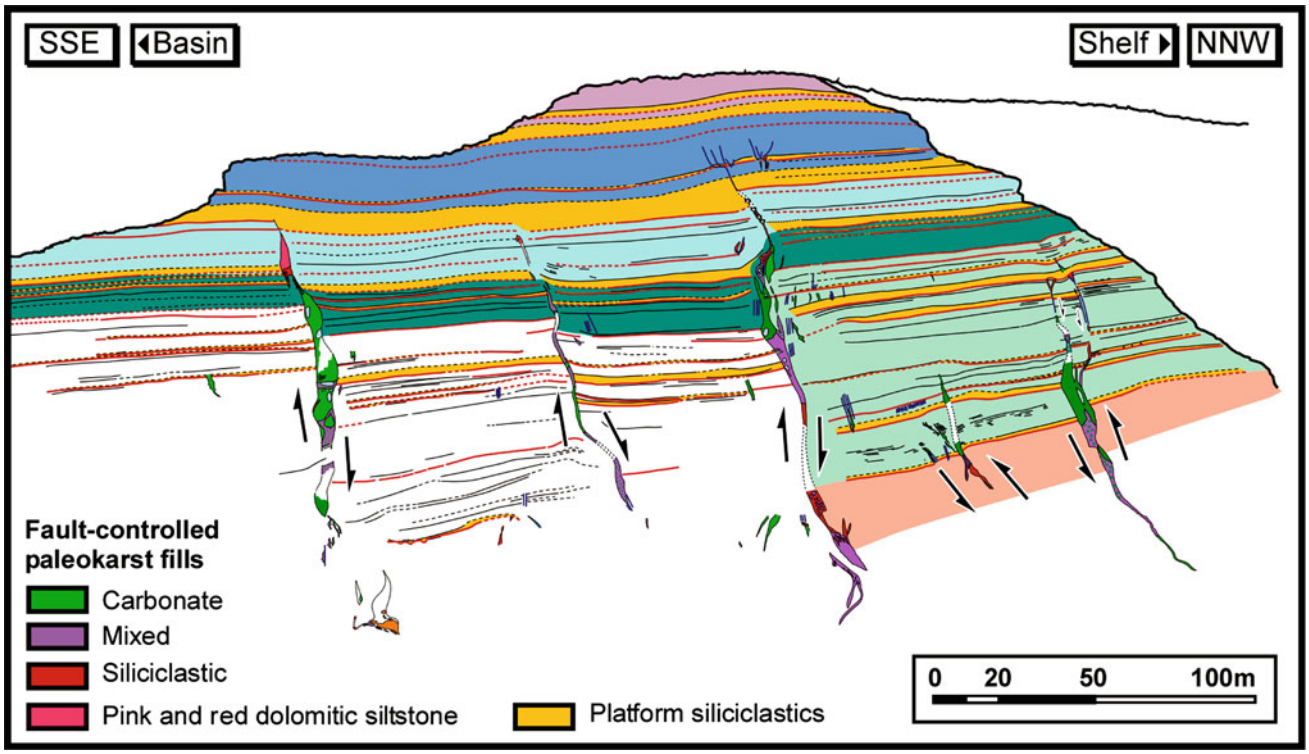

Fig. 7 Profile of a Slaughter Canyon outcrop showing variable fill types in solution-modified syndepositional faults (From Koša and Hunt 2006). Also note the way bedding appears to drape over fault tips resembling shallow antiforms

1977; Hurley 1989). The majority were syndepositional faults, as shown by variations in unit thickness (Hunt et al. 2002; Koša 2003; Koša and Hunt 2006; Fig. 7). They characterized them as dip-slip faults parallel to the shelf margin that are segmented vertically and laterally, with displacements up to 30 m. They dip steeply shelfward and basinward and grew incrementally during deposition of the Yates and Tansill formations.

These features were open, repeatedly dissolved, and filled with breccia and local sediment (Koša and Hunt 2006). Open fractures filled with contemporary shelf sediment were called "Neptunian dikes." They formed extensive, semi-vertical sheet-like chimneys. Interpreted as paleocave systems (the "Phase 1 fissure karst" of Hill 1986), they can have more than 270 m of vertical relief, extend at least 1.2 km along strike, and can be typically less than 10 m wide, but also up to 90 m wide.

Structural deformation during the Laramide occurred in two episodes: (1) **Laramide compression:** Deposition of the Capitan and infilling of the Delaware Basin was complete by around 230 Ma, and the area was tectonically quiescent until the Laramide orogeny (80–40 Ma), which resulted in as much as 1.2 km of uplift and broad tilting of the region to the NNW (Hill 1996). Topographic effects are subdued in the Guadalupe Mountains compared to the Rocky Mountains farther north. However, orthogonal fractures oriented NW–SE and NE–SW are attributed to compression during this orogeny. (2) **Alvarado Ridge, uplift and fracturing**: The Alvarado Ridge, part of which is shown in Fig. 1 as the Rio Grande Rift, is a regional uplift (38–35 Ma) extending from southern Wyoming to westernmost Texas (Eaton 1986, 1987), and into Mexico. The geometry of the uplift and distribution of Miocene–Pliocene sediments on its eastern limb suggest that it is an east-facing monocline on the eastern margin of the Colorado Plateau. The Guadalupe Mountains are part of this structure. It established the catchment area for the deep-circulating hydrologic system that initiated cave development in the Guadalupes (DuChene and Cunningham 2006).

The final tectonic phase that influenced cave development was the initiation of Basin and Range tectonics and the opening of the Rio Grande Rift, beginning around 30 Ma (Hill 1996). Opening of the Rio Grande Rift fragmented the east limb of the Alvarado Ridge and significantly reduced the size of the catchment area, thus reducing the hydraulic head and rate of groundwater flow in the Guadalupes.

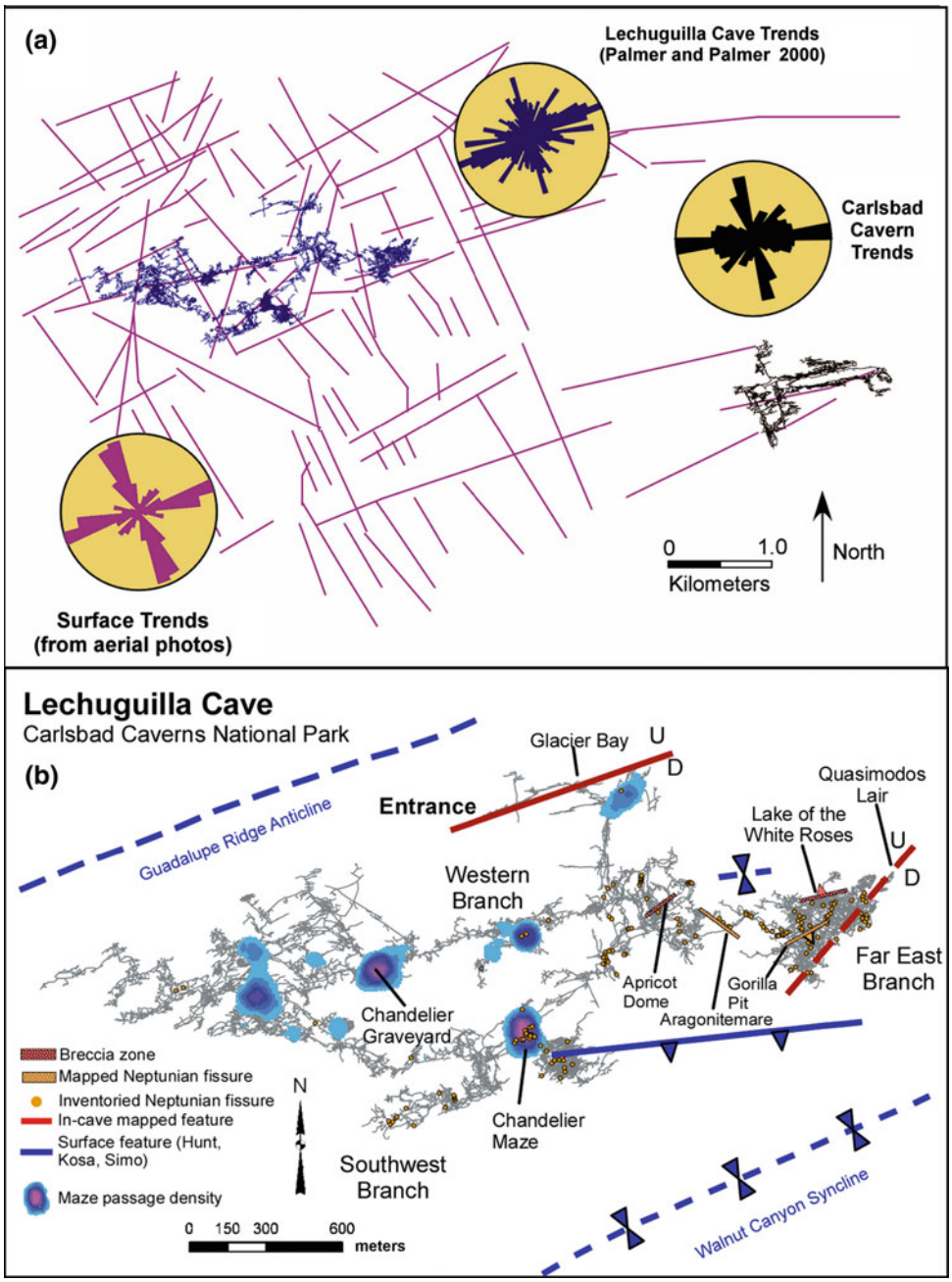

Fig. 8 **a** Comparison between fracture trends mapped at the surface over Lechuguilla Cave and Carlsbad Cavern, and trends of passages in the caves. **b** Plan map of Lechuguilla Cave showing structural control. Increasing density of mazes is shown by concentric colors (Structural mapping by P. Burger)

6.2 Structural Features in Caves

Bedrock features are difficult to identify in the caves because they are typically obscured by secondary deposits. Queen (1981) observed faults and related features (e.g., chaotic breccias) in Carlsbad Cavern and noted evidence for early karst along those trends. Burger (2009, 2016) showed a correlation between syndepositional faults and vertical fissure trends in cave features that intersected strata and linked multiple levels of cave development. These features apparently directed upward flow paths during speleogenesis. Both Carlsbad and Lechuguilla offer extensive three-dimensional geologic views of structures that have influenced their development (Fig. 8).

The entrance of Lechuguilla Cave appears to be located along the crest of a small anticline (Jagnow 1989), but the structure is more likely sediment draped over an active syndepositional fault, as described by Koša (2003; Fig. 7). Breccia in the entrance series of the cave and an obvious fault in the wall of Glacier Bay are aligned on the same

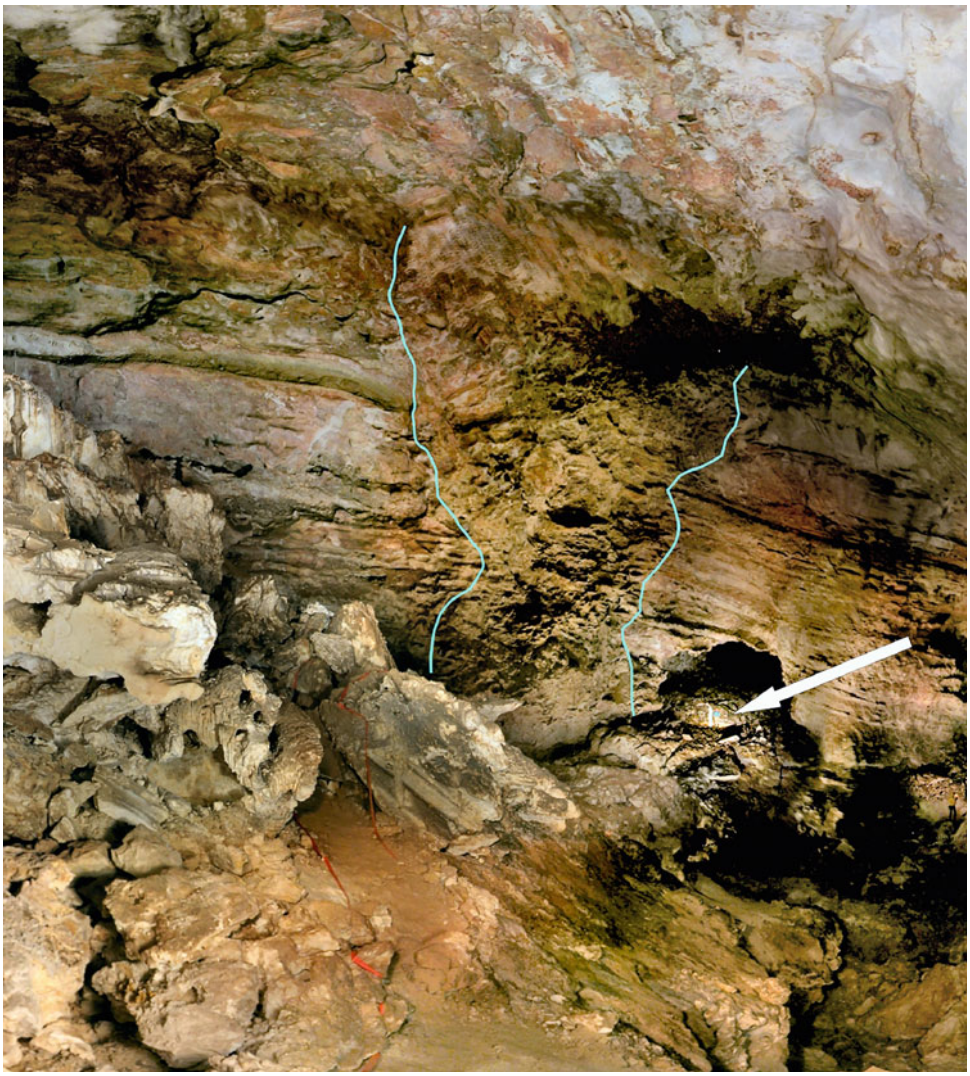

Fig. 9 Probable syndepositional fault zone exposed in Glacier Bay, Lechuguilla Cave. Person for scale (at *arrow*); *vertical line* shows person's height (Photograph by Stan Allison, courtesy of Gene Cooper, Four Chambers Studio)

trend (Fig. 9), suggesting they are related to a fault that can be traced from the Entrance to Glacier Bay, a horizontal distance of more than 470 m. This is the only place where distinct, offset bedding has been observed inside Lechuguilla Cave, but that is likely due to limited exposures as well as secondary mineral deposition and weathering at other sites. Early karstification along these faults has resulted in large breccia zones across which it is impossible to trace bedding.

The Far East section of Lechuguilla Cave, from Firefall Hall to Quasimodos Lair (Fig. 10) is a major passage that cuts 122 m vertically across formation boundaries from the Capitan upward into the backreef beds. At its upper end, the passage follows a significant fault. The boundary between the fault and the adjoining calcite-cemented breccia is sharp with no evidence of transitional crackle breccia. This fault has no expression on the surface above the cave but has clearly influenced passage development. It shows both the difficulty in using surface mapping to predict cave development and the usefulness of the underground exposures accessible in Guadalupe Mountain caves. Other examples of syndepositional faults include many of the well-traveled vertical routes connecting major cave levels.

Mapping of Lechuguilla Cave included inventories to gather geologic data at each survey station. DuChene (2000) developed a mineral inventory and classified breccia bodies in the cave. Data at more than 14,730 points show a strong correlation between breccia zones and dense mazes (Fig. 8b). One of the most distinct areas of this development is in the Chandelier Maze. The Lebarge Borehole (Fig. 4), a tunnel $\sim$15 m in diameter, ends abruptly at the edge of a dense, three-dimensional maze extending east–west for more than 300 m. This maze area ends where breccia borders intact bedrock. To the south, the maze terminates at a steeply inclined passage leading to one of the deepest points in the cave. Other less well-defined spongework mazes occupy

Fig. 10 Fault Breccia in Quasimodos Lair, Far East, Lechuguilla Cave (Photograph by P. Burger)

distinct calcite-matrix breccias in the foreslope facies (Jagnow 1989; DuChene 2000).

6.2.1 Post-Depositional Faults and Fractures

Jagnow (1979) generated radial histograms for more than 50 Guadalupe caves and found a strong correlation between passage trends and linear features mapped on the surface by King (1948) and Hayes (1964). All researchers have noticed prominent trends roughly parallel to the Guadalupe front (even following the trends where the orientation changes), and a second set roughly orthogonal to the first.

7 Late Stages of H_2SO_4 Speleogenesis in Guadalupe Caves

Late in the development of Guadalupe caves, the H_2S input diminished and finally ceased (see Sect. 5.3). Until that time, the H_2SO_4 process was still intense, at least in the lowest cave levels. The caves had acquired their main patterns by that time, and entrances were providing abundant oxygen transfer. Air circulation became the dominant control of dissolution and precipitation patterns, as suggested in Sect. 5.4 (Queen 2009c), and many definitive features of the Guadalupe caves are subaerial in origin. These include spongework (Fig. 3c), ascending ceiling channels, domes, etc. Although formed by H_2SO_4 from the absorption of $H_2S + O_2$ in condensation moisture, these features are hypogenic, at least by the definition of Palmer (1991), in which the aggressive agents are generated by deep-seated processes. Corrosion by the absorption of CO_2 by moisture films does not qualify if the gas is supplied from the surface.

Exposed bedrock and secondary minerals give clues to the environmental conditions at the end of H_2S influx. Alteration of clays to alunite—$KAl_3(SO_4)_2(OH)_6$—is a useful indicator of environmental conditions. The stability field for alunite is almost always constrained to pH < 4 (Palmer 2007), conditions achieved by a sulfuric acid environment isolated from normal karst water. The pH of karst groundwater is almost never below 6.5 because of HCO_3^- buffering. Lower pH is available only where the reactive surface consists of non-carbonate minerals. In limestone, alunite production must take place above the water table. Dating of alunite by measuring its ($^{40}K/^{40}Ar$) ratio can determine the age of the mineral and can also constrain the timing of water-table decline (Polyak et al. 1998 and Sect. 9.1).

Another widespread phenomenon in late-stage cave modification was dolomitization of the bedrock surfaces and carbonate speleothems (Polyak and Provencio 2001; Palmer and Palmer 2012). It is recognized as a whitish rind, although not all white rinds are dolomitic. X-ray diffraction shows that many of these are close to, or even at, perfect dolomite composition (see also Thrailkill 1971). It provides evidence for post-drainage geochemical environments. The dolomite rind can also be dated (Polyak et al. 2016; see Sect. 9.1).

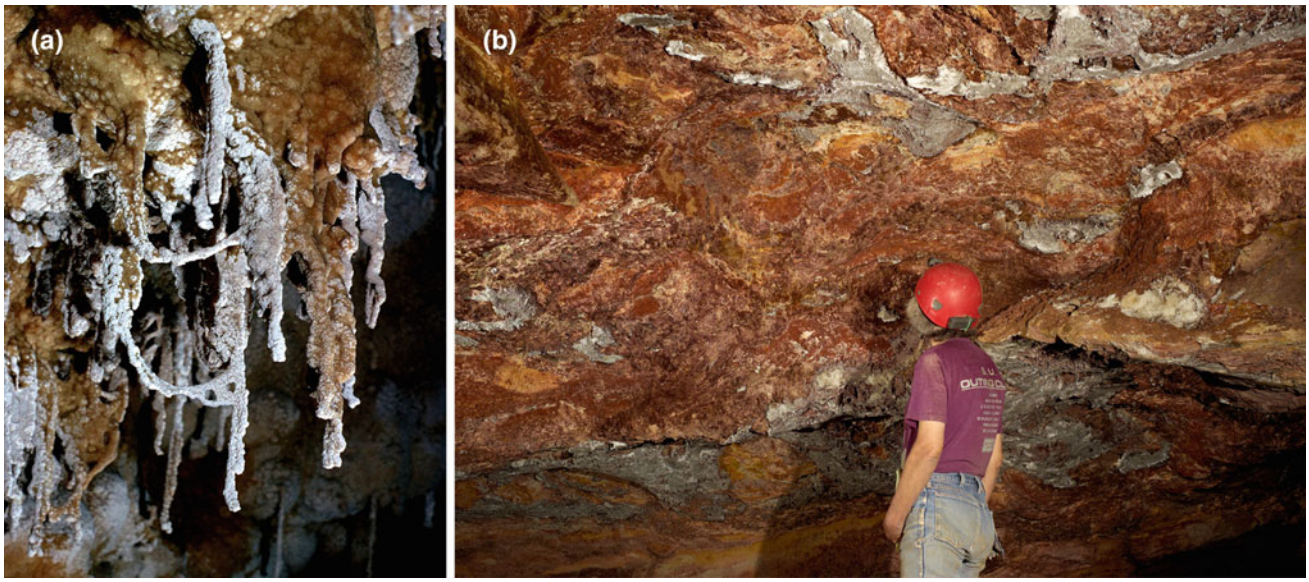

Fig. 11 Aspects of microbial activity in the Guadalupe caves include both fossilized and active forms. **a** Microbial filaments coated with calcite (forming "U-loops") in Lechuguilla Cave. Compare with active examples in Hose and Rosales, Chap. 32. **b** Weathering zones of oxidized Fe–Mn minerals in the silty Yates Formation exposed in Spider Cave are the examples of "speleosols" as defined by Spilde et al. (2009) (Photographs by A. Palmer)

8 Geomicrobiology

Most Guadalupe caves contain abundant evidence for microbial activity, both as living and fossil forms and geochemical products. The discovery of Lechuguilla Cave focused attention on this topic and triggered a burst of interest in the field (Sasowsky and Palmer 1994). Many research papers followed (e.g., Cunningham et al. 1995; Northup et al. 2000; Melim et al. 2001; Northup et al. 2003). Aspects of microbial mediation even include cave origin by the production of hydrogen sulfide and sulfuric acid. Common internal features include colorful speleosols, a combination of weathered bedrock material and microbial organics (Spilde et al. 2009), and diverse "biothems" produced by mineral coating of microbial filaments, such as pool fingers, U-loops (Fig. 11a), and web-like features (Davis et al. 1990; Davis 2000; Queen and Melim 2006). Observations in active sulfide-rich caves elsewhere include actively growing filaments and textures similar to the petrified examples in Guadalupe caves. Many, perhaps most, of these features are not strictly hypogenic by themselves, but they are most abundant in hypogenic caves where energy has been released by oxidation–reduction reactions.

8.1 Ferromanganese Deposits

Ferromanganese deposits (FMD) are known throughout the rock record. Most are subaqueous, but in a few caves, they were deposited subaerially. They have been reported from many caves around the world (Spilde et al. 2003; Maltsev 1997). Lechuguilla and Spider Caves in the Guadalupes contain some of the largest known deposits of unconsolidated FMD (Fig. 11b). These are oxide-rich fluffy coatings on cave walls and ceilings variously colored pink, red, brown, purplish-black, black, and gray (Spilde et al. 2005). These were once considered insoluble residue from corrosion of carbonate rock by air circulation in caves (Queen 1994b), but recent investigations show that they result from microbial oxidation of reduced Mn and Fe extracted from the limestone (Spilde et al. 2005, 2009).

With scanning electron microscopy of these deposits from Lechguilla Cave, Cunningham et al. (1995) observed microbial structures that they considered biogenic. Further studies by Northup et al. (2003) revealed a diverse microbial community. Sequence analysis revealed organisms related to known Fe- and Mn-oxidizing/reducing bacteria.

8.2 Speleosols

FMD in Guadalupe caves have three layers: a foundation of unaltered bedrock grading outward to a leached layer of poorly consolidated rock ("punk rock") overlain at the surface by an oxide-rich ferromanganese layer. Punk rock was described by Hill (1987) as bedrock corroded to a soft flaky texture. It forms subaerially and tends to flake off and accumulate as piles of dark silt (Hill 1987). It is commonly white, but also light pink or yellow, depending on the Al and Si content of the original rock. Weathering can extend many

centimeters into cave walls (Spilde et al. 2005). Spilde, Boston, and colleagues found that FMD are enriched in Fe and Mn as much as three orders of magnitude above the bedrock and differ in mineralogy and chemistry from insoluble residue tests of the bedrock. Simple dissolution of the carbonate rock produces abundant SiO_2 and Al_2O_3 with low concentrations of MnO and average Mn/Fe ~ 0.07. However, FMD contain relatively low silica and alumina and higher Mn/Fe ratio (0.8) in the darkest samples, suggesting microbial Mn enrichment (Spilde et al. 2005). Mass balance analysis of bedrock, punk rock, and FMD, with Ti as an insoluble element, indicates that up to 75% of the soluble material is removed from the punk rock with a 2X increase in dolomite porosity, but as much as 99.9% is removed from the limestone with up to 5.5X increase in porosity (Spilde et al. 2009). They propose that cave FMD be called speleosols, because the chemical and microbial processes resemble those of pedogenesis. These features are not necessarily hypogenic, or limited to hypogene caves; but they are most abundant in these caves because of the energy supplied by redox processes, and evidence for them is best preserved in the protected hypogene environment.

9 Dating of Guadalupe Caves

Dating of speleothems provides estimates that clearly postdate cave origin. However, the reaction of sulfuric acid with certain clays during active speleogenesis can produce potassium-bearing minerals that reveal the true speleogenetic age, or at least the most recent phase of H_2SO_4 cave enlargement. This technique was developed in the Guadalupe caves, as described below.

9.1 Alunite Dating of Sulfuric Acid Cave Origin

The mineral alunite ($KAl_3(SO_4)_2(OH)_6$) is produced by the alteration of potassium-rich clays in low-pH, high-sulfate environments. This provides support for sulfuric acid speleogenesis in the Guadalupes. Dating these deposits by the argon method ($^{40}Ar/^{39}Ar$ from potassium), Polyak et al. (1998) obtained dates for a variety of Guadalupe caves at different altitudes. The results showed a consistent decline in age with altitude, as well as a good correlation between caves at similar altitudes. The oldest dates (~12 Ma) were from caves in the high western parts of the Guadalupes and the youngest (~4 Ma) in the Big Room and Lower Cave of Carlsbad Cavern, near the base of the Guadalupe escarpment (Fig. 12).

Polyak et al. (2016) used U–Pb dating to estimate the age of the speleogenic dolomite crust in the lower levels of Carlsbad Cavern to be 4.1 Ma (see Sects. 5.3 and 6.1). This crust is a by-product of bedrock alteration and gives another independent method of dating the caves.

Integrating cave development into the regional tectonic history gives perspective to these dates. The Alvarado Ridge (see Sects. 5.3 and 6.1) began to rise in early Tertiary time, and by 38–35 Ma (Gregory and Chase 1992), it was an immense upland recharge area for aquifers where groundwater flowed to the east (see Sect. 5.3; DuChene and Cunningham 2006). Evidence for early rift tectonism that cut off this recharge area is not apparent in the caves, but subsidence of the graben on the western margin of the Guadalupes began during the interval 14–4 Ma, which fits well with the 12–4 Ma cave ages reported by Polyak et al. (1998). During this time, the water table in the Capitan aquifer fell at least 1100 m between the highest

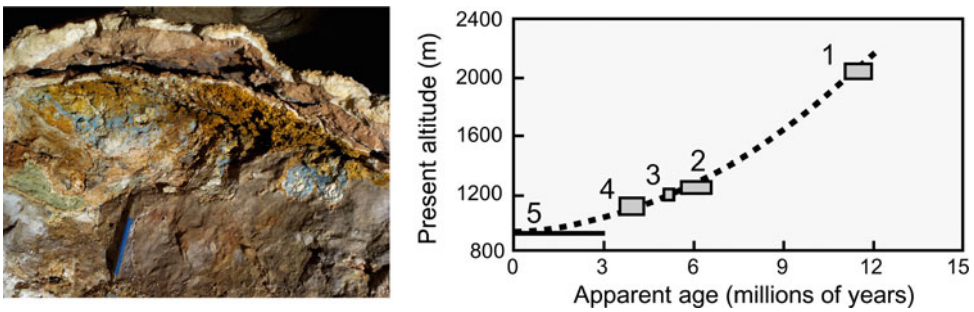

Fig. 12 Dating of the speleogenetic mineral alunite by Polyak et al. (1998) has shown the decline of the water table with time in Guadalupe caves. **a** The colorful minerals are speleogenetic, formed only at acidic pH. Those in the photograph are mainly halloysite (endellite), both *blue* and *green* varieties; but alunite (*white*) is a potassium-rich mineral of similar origin that can be dated with K/Ar methods. The composition of the *white* mineral surrounded by *blue* in the photograph has not been tested (Photograph by A. Palmer). **b** Alunite dating of the latest phases of sulfuric acid cave origin shows a drop in water-table elevation with time. Age versus elevation for several cave levels in the Guadalupes, with distance and direction measured from the Carlsbad entrance: *1* Cottonwood Cave and Virgin Cave (30–35 km SW); *2* endless Cave (22 km N) and Glacier Bay (Lechuguilla Cave); *3* Lake Lebarge (Lechuguilla Cave); *4* New Mexico Room, Big Room, and Green Clay Room (Carlsbad Cavern); *5* present water table below the cavern

(westernmost) caves in the Guadalupes and the deepest points in Lechuguilla Cave (Polyak and Provencio 2000). The present locations of sample sites mark the position of the water table at each pulse of sulfuric acid speleogenesis. Alunite dates at major levels in the caves provide a record of periods when the water table was relatively stable. Intervals between levels reflect the times when either there was no speleogenetic activity, or the water table was dropping too rapidly to provide datable by-products.

9.2 Dating of Early Spar-Lined Caves

Isolated solution pockets in the Guadalupes range up to several tens of meters in diameter and are lined by large scalenohedral calcite crystals up to 30 cm long (Fig. 13). Many have been intersected by the presently accessible caves of H_2SO_4 origin. For one of these crystals, Lundberg et al. (2000) obtained U/Pb dates of 91.3 ± 2.8 Ma (Late Cretaceous, correlating with early Laramide orogeny in the Rocky Mountains). This date was considered preliminary because only one of many stages of crystal growth was investigated. Fluid inclusions showed a thermal origin (~30–85 °C), which suggests a magmatic heat source.

Recent investigations of similar caves by Decker et al. (2015, 2016) provide evidence for spar events that predate H_2SO_4 speleogenesis. They applied the concept of supercritical carbon dioxide ($scCO_2$) to explain hypogene dissolution and calcite precipitation. CO_2 forms a supercritical fluid when the fluid temperature and pressure simultaneously exceed 31 °C and 73 atm pressure (Fig. 13). In its supercritical state, CO_2 behaves as both a gas and a liquid.

This model explains the dissolution of deep, typically single-chambered caves and their calcite precipitates by use of the equilibrium solubility of CO_2 in solution, which varies with temperature and pressure (André and Rajaram 2005; Dublyansky 2000). In its supercritical state, groundwater cools as it rises toward shallow depths. Limestone and dolomite solubilities increase as temperature drops, allowing cave formation; but at shallow depths (~500 m) the pressure reduction causes CO_2 to begin degassing, which results in calcite precipitation. This model can account for both the dissolution of the caves and the precipitation of spar soon afterward without requiring a drop in the water table. However, it does not explain the CO_2 origin, flow paths, or its fate in the warmer, deeper brines.

Decker et al. (2015, 2016) determined the depths of spar formation from two samples, corroborated by one from the Grand Canyon (Arizona). The Grand Canyon sample, from a cave in the Redwall Limestone, was dated at 232 Ma at an estimated depth of 750 m below the water table (vertical distance from spar to overlying sedimentary deposits of the same age). The depths of origin of the two spar crystals from different levels in Carlsbad Cavern were calculated from the position of alunite samples with similar dates (Polyak et al. 1998), which represent conditions at or slightly above the water table. Interpolating the position of the water table from the alunite ages and comparing it to the age and depth of

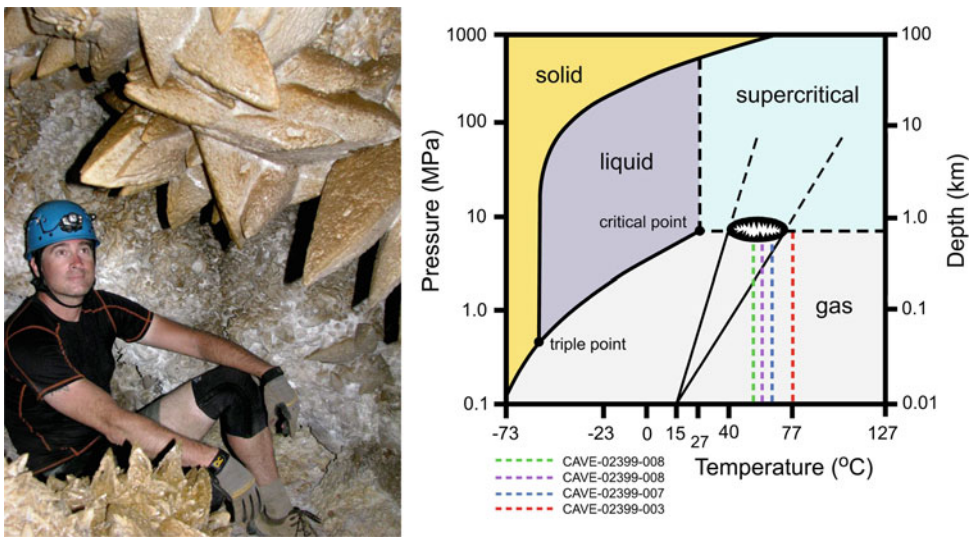

Fig. 13 Analysis of dogtooth spar in the early solution pockets in the Guadalupes shows evidence for dissolution and later precipitation related to supercritical CO_2 (Decker et al. 2015, 2016). The *spar-lined* pocket shown here is intersected by the Western Branch of Lechuguilla Cave (Photograph by Ben Schwartz). The phase diagram for CO_2 versus temperature and water pressure (*depth*) shows the stability range of supercritical CO_2 ($scCO_2$) in *blue*, and the approximate positions of analyzed spar samples. One megapascal = 9.87 atmospheres. Graph modified from Finney and Jacobs (2010)

nearby spar show that these crystals grew at depths of 700 and 360 m below the contemporary water table (see Fig. 13).

These three depths, 750, 700, and 360 m, are within the transition zone from supercritical to subcritical CO_2 at 500 ± 250 m below the water table, depending on the geothermal gradient and hydrostatic pressure (Decker et al. 2015). This transition occurs at 31.1 °C and 7.4 MPa (André et al. 2007; Domingo et al. 2004; Kharaka et al. 2006), and this region can move up or down as temperature and pressure change with new or waning magmatism, basin filling, or denudation. In areas of crustal tension, decompression melting can easily occur. Melting at these depths causes the magma to degas CO_2 (interpreted here to be in the supercritical state; Lowenstern 2001). $ScCO_2$ is much less dense and less viscous than water and moves rapidly through pores until it encounters basinal brines, where it is dissolved into pore fluids (Heinrich et al. 2003). If enough $scCO_2$ is generated, it can displace the brine, and, at the brine-$scCO_2$ interface, dissolution of carbonate rock is intense enough to form caves (André et al. 2010).

This model, based on our depths of origin of spar crystals and their correspondence to the depth of $scCO_2$–$subCO_2$ transformation, explains the origin of the spar caves (Decker et al. 2015). With many samples having spar ages that coincide roughly with the ignimbrite episode, the model also suggests that $scCO_2$ speleogenesis is related to magmatic activity and is therefore rather short-lived (~1–2 My). This speleogenetic model involves the retreating brine (and dissolved carbonate) leaving void spaces, which are then filled with $scCO_2$. As magmatic activity wanes, the generation of $scCO_2$ declines and eventually the brines return to fill the new voids. These brines are still supersaturated with $scCO_2$, but as the temperature decreases the $scCO_2$/$subCO_2$ transition zone moves downward, causing an increase in $subCO_2$ partial pressure and a corresponding degassing of the brines. This lowers the CO_2 content and the capacity of the brines to hold dissolved $CaCO_3$ (Moore et al. 2005; Spycher et al. 2003). At this point, calcite begins to precipitate slowly; and at these temperatures and pressures, scalenohedral spar is the most likely crystal form (Domingo et al. 2004). The model explains the origin and timing of both the spar caves and the spar itself.

Decker et al. (2015) studied 18 of these voids, and 27 previously broken spar samples were studied for U/Pb geochronology and Sr isotope geochemistry. The two older ages match the timing of ignimbrite volcanic activity at 32–28 Ma (Chamberlin et al. 2002). One spar sample gave an age of 29.28 ± 0.45 Ma and two others from Carlsbad Cavern, used to determine depths of spar formation, gave dates of 13.5 ± 0.52 and 9.45 ± 0.14 Ma (Decker et al. 2015). Sr isotope values for spar in the range of 0.709–0.716 are consistent with fluid that mixed with brines in equilibrium with deep basement rock, in contrast to the Permian limestone (0.707); see Burke et al. (1982).

A plot of elevations and locations of sample sites, versus those of springs in the city of Carlsbad, showed that a downward rotation of 1.3° to the southwest (to restore the Guadalupe tectonic block to a horizontal datum) brings all sample elevations to within 250 m of each other. This is half the thickness of the cavernous strata that include the Capitan and adjacent backreef and forereef carbonates (Zimmerman 1962; Harris and Grover 1989; Hill 1996).

This new model describes the origin and movement of CO_2 as well as the process of dissolving the voids and precipitating the spar crystals. It improves the understanding of this highly complicated regime without having to invoke multiple stages of water-table movement over several 100 m and tens of millions of years.

10 Conclusions

Our understanding of H_2S-H_2SO_4 speleogenesis relies strongly on the study of Guadalupe caves. This chapter has described only a small fraction of the work done in this region. Many of the early concepts and techniques in the field were developed here, but new insight is continually being gained from independent advances in other countries (see, e.g., Galdenzi and Jones Chap. 8; Onac and Drăguşin Chap. 16, and Hose and Rosales Chap. 54). While studies in active sulfuric acid caves provide invaluable data, inactive caves such as those in the Guadalupes have allowed deep exploration in areas that would otherwise be nearly impossible.

References

André BJ, Rajaram H (2005) Dissolution of limestone fractures by cooling waters: early development of hypogene karst systems. Water Resour Res 41(1)

André L, Audigane P, Azaroual M, Menjoz A (2007) Numerical modeling of fluid–rock chemical interactions at the supercritical CO_2–liquid interface during CO_2 injection into a carbonate reservoir, the Dogger aquifer (Paris Basin, France). Energy Convers Manag 48(6):1782–1797

André L, Azaroual M, Menjoz A (2010) Numerical simulations of the thermal impact of supercritical CO_2 Injection on chemical reactivity in a carbonate saline reservoir. Transp Porous Med 82:247–274

Bretz JH (1949) Carlsbad Caverns and other caves of the Guadalupe block, New Mexico. J Geol 57(5):447–463

Burger PA (2009) Structural and facies control of hypogenic karst development in the Guadalupe Mountains, New Mexico, USA. In: NCKRI symposium 1 advances in hypogene karst studies. National Cave and Karst Institute, Carlsbad, New Mexico, pp 60–70

Burger PA (2016) The influence of syndepositional faulting and breccia zones on hypogene cave development in the Guadalupe Mountains, New Mexico. National Cave and Karst Institute (In Press)

Burke WH, Denison RE, Hethreington EA, Koepnick RB, Nelson HF, Otto JB (1982) Variations of seawater $^{87}Sr/^{86}Sr$ throughout phanerozoic time. Geology 10:516–519

Chamberlin RM, Chapin CE, McIntosh WC (2002) Westward migrating ignimbrite calderas and a large radiating mafic dike swarm of Oligocene age, central Rio Grande Rift, New Mexico: Surface expression of an upper mantle diapir?. Geological Society of America Annual Meeting, Denver CO

Chapin CE, Cather SM (1994) Tectonic setting of the axial basins of the northern and central Rio Grande Rift. In: Keller GR, Cather SM (eds) Basins of the rio grande Rift: structure, stratigraphy, and tectonic setting. Geological Society of America Special Paper, vol 291, pp 5–25

Cunningham KI, Northup DE, Pollastro RM, Wright WG, LaRock EJ (1995) Bacteria, fungi, and biokarst in Lechuguilla Cave, Carlsbad Caverns National Park, New Mexico. Environ Geol 25(1):2–8

Davis DB (1973) Sulfur in Cottonwood Cave, Eddy County, New Mexico. National Speleol Soc Bull 35(3):89–95

Davis DG (1980) Cave development in the Guadalupe Mountains: a critical review of recent hypotheses. National Speleol Soc Bull 42 (3):42–48

Davis DG (2000) Extraordinary features of Lechuguilla Cave, Guadalupe Mountains, New Mexico. J Cave Karst Stud 62 (2):147–157

Davis DG, Palmer MV, Palmer AN (1990) Extraordinary subaqueous speleothems in Lechuguilla Cave, New Mexico. National Speleol Soc Bull 52:70–86

Decker DD, Polyak VJ, Asmerom Y (2015) Depth and timing of calcite spar and 'spar cave' genesis: Implications for landscape evolution studies. Geological Society of America, GSA Special Publication 516—Caves and Karst Across Time

Decker DD, Polyak VJ, Asmerom Y (2016) A supercritical CO_2 hypogene speleogenesis model: the origin of spar caves and cave spar in the Guadalupe Mountains, USA. National Cave and Karst Research Institute Deep Karst Symposium proceedings, Carlsbad, New Mexico USA

Domingo C, García-Carmona J, Loste E, Fanovich A, Fraile J, GómezMorales J (2004) Control of calcium carbonate morphology by precipitation in compressed and supercritical carbon dioxide media. J Cryst Growth 271(1):268–273

DuChene HR (2000) Bedrock features of Lechuguilla Cave, Guadalupe Mountains, New Mexico. J Cave Karst Stud 62(2):109–119

DuChene HR, Cunningham KI (2006) Tectonic influences on speleogenesis in the Guadalupe Mountains, New Mexico and Texas. In: Land L, Lueth VW, Raatz W, Boston P, Love DL (eds) Caves and karst of southeastern New Mexico: Socorro, New Mexico, New Mexico Geological Society 57th annual field conference, pp 211–218

Dunham RJ (1972) Capitan reef, New Mexico and Texas—facts and questions to aid interpretation and group discussion. Permian Basin Section-SEPM Publication, vol 72–14, p 297

Dublyansky YV (2000) Dissolution of carbonates by geothermal waters. In: Klimchouk AB, Ford DC, Palmer AN, Dreybrodt W (eds) Speleogenesis—evolution of Karst Aquifers. National Speleological Society, Huntsville, pp 158–159

Eaton GP (1986) A tectonic redefinition of the Southern Rocky Mountains. Tectonophysics 132:163–193

Eaton GP (1987) Topography and origin of the southern Rocky Mountains and Alvarado Ridge. In: Coward M, Dewey JF, Hancock L (eds) Continental extension tectonics, vol 28. Geological Society Special Publication, pp 355–369

Egemeier SJ (1973) Cavern development by thermal waters with a possible bearing on ore deposition. Ph.D. dissertation, Stanford University, California

Egemeier SJ (1981) Cavern development by thermal waters. National Speleol Soc Bull 43(2):31–51

Egemeier SJ (1987) A theory for the origin of Carlsbad Caverns. National Speleol Soc Bull 49(2):73–76

Finney B, Jacobs M (2010) Carbon dioxide pressure-temperature phase diagram, Wikimedia Commons

Gregory KM, Chase CG (1992) Tectonic significance of paleobotanically estimated climate and altitude of the late Eocene erosion surface, Colorado. Geology 20:81–85

Harris PM, Grover GA (1989) Subsurface and outcrop examination of the Capitan Shelf Margin, Northern Delaware Basin, San Antonio, TX, Society of Economic Paleontologists and Mineralogists core workshop vol 13, p 481

Harris AG, Tuttle E, Tuttle SD (eds) (1997) Geology of national parks, 5th edn. Kendall/Hunt Publishing Company, Dubuque 758 p

Hayes PT (1964) Geology of the Guadalupe Mountains, New Mexico. US Geological Survey Professional vol 446, p 69

Heinrich JJ, Herzog HJ, Reiner D M (2003) Environmental assessment of geologic storage of CO_2. In: Second national conference on carbon sequestration, Washington, Massachusetts Institute of Technology

Hill CA (1981) Speleogenesis of Carlsbad Caverns and other caves of the Guadalupe Mountains. Proceedings of 8th International Congress of Speleology, Bowling Green, KY, pp 143–144

Hill CA (1987) Geology of Carlsbad Cavern and other caves in the Guadalupe Mountains, New Mexico and Texas. New Mexico Bureau of mines and mineral resources, Socorro, NM. Bulletin 117:150

Hill CA (1990) Sulfuric acid speleogenesis of Carlsbad Cavern and its relationship to hydrocarbons, Delaware Basin, New Mexico and Texas. Am Assoc Pet Geol Bull 74(11):1685–1694

Hill CA (1996) Geology of the Delaware Basin—Guadalupe, Apache, and Glass Mountains, New Mexico and Texas. Society of Economic Paleontologists and Mineralogists, Permian Basin Section, Publication, pp 96–39

Hill CA (2000) Overview of the geologic history of cave development in the Guadalupe Mountains, New Mexico. National Speleol Soc Bull 62:60–71

Hunt DW, Fitchen WM, Koša E (2002) Syndepositional deformation of the Permian Capitan reef carbonate platform, Guadalupe Mountains, New Mexico, USA. Sediment Geol 154:89–126

Hurley NF (1989) Facies mosaic of the lower seven rivers formation, McKittrick Canyon, New Mexico. In: Harris PM, GA Grover (eds) Subsurface and outcrop examination of the Capitan Shelf Margin, northern Delaware Basin, vol 13. Society of Economic Paleontologists and Mineralogists, Core Workshop, pp 325–346

Jagnow DH (1977) Geologic factors influencing speleogenesis in the Capitan Reef complex, New Mexico and Texas. M.S. Thesis, Albuquerque, University of New Mexico, p 197

Jagnow DH (1979) Cavern development in the Guadalupe Mountains. Columbus, Ohio, Cave Research Foundation, p 55

Jagnow DH (1989) The geology of Lechuguilla Cave, New Mexico. In: Harris PM, Grover GA (eds) Subsurface and outcrop examination of the Capitan shelf margin, northern Delaware Basin, vol 13. Society of Economic Paleontologists and Mineralogists Core Workshop, pp 459–466

Kharaka Y, Cole D, Hovorka S, Gunter W, Knauss K, Freifeld B (2006) Gaswater-rock interactions in Frio Formation following CO_2 injection: implications for the storage of greenhouse gases in sedimentary basins. Geology 34(7):577–580

King PB (1948) Geology of the southern Guadalupe Mountains, Texas. US Geological Survey Professional Paper, vol 215, p 183

Kirkland DW (1982) Origin of gypsum deposits in Carlsbad Caverns, New Mexico. New Mex Geol 4:20–21

Kirkland DW (2014) Role of hydrogen sulfide in the formation of cave and karst phenomena in the Guadalupe Mountains and western Delaware basin, New Mexico and Texas. NCKRI Special Pulication, vol 2, p 77

Kirkland DW, Evans R (1976) Origin of limestone buttes, gypsum plain, Culberson County, Texas. Am Asso Petrol Geol Bull 60:2005–2018

Koša E (2003) Heterogeneity in the structure, diagenesis and fill of syndepositional faults in carbonate strata. Upper Permian Capitan Platform, Guadalupe Mountains, New Mexico, USA, Ph.D. thesis, University of Manchester, England

Koša E, Hunt DW (2006) Heterogeneity in fill and properties of karst-modified syndepositional faults and fractures: upper Permian Capitan platform, New Mexico, USA. J Sediment Res 76:131–151

Lindsay RF (1998) Meteoric recharge, displacement of oil columns and the development of residual oil intervals in the Permian basin. In: DeMis WD, Nelis MK (eds) The search continues into the 21st century, vol 98–105. West Texas Geological Society Publication, pp 271–273

Lowenstern JB (2001) Carbon dioxide in magmas and implications for hydrothermal systems. Miner Deposita 36(6):490–502

Lundberg JL, Ford DC, Hill CA (2000) Preliminary U-Pb Date on Cave Spar, Big Canyon, Guadalupe Mountains, New Mexico, USA. J Cave Karst Stud 62(2):144–148

Maltsev V (1997) Cupp-Coutunn Cave, Turkmenistan. In: Hill, Forti (eds) Cave minerals of the world. National Speleological Society, Huntsville, Alabama

Melim LA, Shinglman KM, Boston PJ, Northup DE, Spilde MN, Queen JM (2001) Evidence of microbial involvement in pool finger precipitation, Hidden Cave, New Mexico. Geomicrobiol J 18:311–330

Melim LA, Scholle PA (1989) Dolomitization model for the forereef facies of the Permian Capitan Formation, Guadalupe Mountains, Texas-New Mexico. In: Harris PM, Grover GA (eds) Subsurface and outcrop examination of the Capitan shelf margin, Northern Delaware Basin, Tulsa, OK, SEPM Core Workshop No. 13, pp 407–413

Moore J, Adams M, Allis R, Lutz S, Rauzi S (2005) Mineralogical and geological consequences of the long-term presence of CO_2 in natural reservoirs: an example from the Springerville-St. Johns Field, Arizona, and New Mexico, USA. Chem Geol 217:365–385

Mruk DH (1985) Cementation and dolomitization of the Capitan Limestone (Permian), McKittrick Canyon, West Texas. Unpublished MS thesis. University of Colorado, p 155

Newell KJ, Fischer AG, Whiteman AJ, Hickox JE, Bradley JE (1953) The Permian reef complex of the Guadalupe Mountains region. Texas and New Mexico. W. H. Freeman and Co., San Francisco

Northup DE, Dahm CN, Melim LA, Spilde MN, Crossey LJ, Lavoie KH, Mallory LM, Boston PJ, Cunningham KI, Barns SM (2000) Evidence for geomicrobiological interactions in Guadalupe caves. J Cave Karst Stud 62(2):80–90

Northup DE, Barns SM, Yu LE, Spilde MN, Schelble RT, Dano KE, Crossey LJ, Connolly CA, Boston PJ, Natvig DO, Dahm CN (2003) Diverse microbial communities inhabiting ferromanganese deposits in Lechuguilla and Spider Caves. Environ Microbiol 5(11):1071–1086

Palmer AN (2007) Cave geology. Cave Books, Dayton Ohio, p 454

Palmer AN, Palmer MV (2000) Hydrochemical interpretation of cave patterns in the Guadalupe Mountains, New Mexico. J Cave Karst Stud 62(2):91–108

Palmer MV, Palmer AN (2012) Petrographic and isotopic evidence for late-stage processes in sulfuric acid caves of the Guadalupe Mountains, New Mexico, USA. Int J Speleol 41(2):231–250

Polyak VJ, McIntosh WC, Güven N, Provencio P (1998) Age and origin of Carlsbad Cavern and related caves from $^{40}Ar/^{39}Ar$ of alunite. Science 279:1919–1922

Polyak VJ, Provencio P (2000) Summary of the timing of sulfuric-acid speleogenesis for Guadalupe Caves based on ages of alunite. J Cave Karst Stud 62(2):72–74

Polyak VJ, Provencio PP (2001) By-product materials related to H_2S-H_2SO_4 influenced speleogenesis of Carlsbad, Lechuguilla, and other caves of the Guadalupe Mountains, New Mexico. J Cave Karst Stud 63:23–32

Polyak VJ, Provencio PP, Asmerom Y (2016) U–Pb dating of speleogenetic dolomite: a new sulfuric acid speleogenesis chronometer. Int J Speleol 45(2):103–109

Pray LC, Esteban M (eds) (1977) Upper Guadalupian Facies, Permian Reef Complex, Guadalupe Mountains, New Mexico and West Texas, vol 2—Road logs and locality guides (1977 Field Conference Guidebook). Midland, TX, Permian Basin Section-SEPM Publication, vol 77–16, p 194

Queen JM (1973) Large-scale replacement of carbonate by gypsum in some New Mexico caves (abs.). National Speleological Society Convention, Bloomington, Indiana, Abstracts, p 12

Queen JM (1981) Discussion and field guide to the geology of Carlsbad Cavern. In: Preliminary report to the national park service for the 7th international congress of speleology, p 64

Queen JM (1994a) Influence of thermal atmospheric convection on the nature and distribution of microbiota in cave enevironments. In: Sasowsky ID, Palmer MV (eds) Breakthroughs in Karst Geomicrobiology and Redox Geochemistry, Special Pub 1. Karst Waters Institute, Charles Town, WV, pp 62–64

Queen JM (1994b) Speleogenesis in the Guadalupes: the unsettled question of the role of mixing, phreatic or vadose sulfide oxidation. In: Sasowsky ID, Palmer MV (eds) Breakthroughs in Karst geomicrobiology and redox geochemistry, special pub 1. Karst Waters Institute, Charles Town, WV, pp 64–65

Queen JM (1994c) A conceptual model for mixing zone diagenesis based on the hydrogeology of Bermuda. In: Sasowsky ID, Palmer MV (eds) Breakthroughs in Karst geomicrobiology and redox geochemistry, special pub 1. Charles Town, WV, Karst Waters Institute, pp 65–66

Queen JM (2009a) Geologic setting, structure, tectonic history and paleokarst as factors in speleogenesis in the Guadalupe Mountains, New Mexico and Texas, USA. In: Proceedings of 15th international congress of speleology, Kerrville, Texas, pp 952–957

Queen JM (2009b) Pre-drainage development of the caves of the Guadalupe Mountains, New Mexico and Texas, USA. In: Proceedings of 15th international congress of speleology, Kerrville, Texas, pp 958–963

Queen JM (2009c) Post-drainage evolution of the caves of the Guadalupe Mountains, southeastern New Mexico and west Texas, USA. In: Proceedings of 15th international congress of speleology, Kerrville, Texas, pp 964–970

Queen JM, Hose L (2006) Trail guide to, and discussion of, the geology of Carlsbad Cavern: Main Corridor and Big Room. In: Land L, Lueth VW, Raatz W, Boston P, Love DL (eds) Caves and karst of southeastern New Mexico. In: Socorro, New Mexico, New Mexico geological society 57th annual field conference, pp 151–160

Queen JM, Melim LA (2006) Biothems: biologically influenced speleothems in caves of the Guadalupe Mountains, New Mexico, USA. In: Land L, Lueth VW, Raatz W, Boston P, Love DL (eds) Caves and karst of southeastern New Mexico. Socorro, New Mexico, New Mexico geological society 57th annual field conference, pp 167–174

Sasowsky ID, Palmer MV (eds) (1994) Breakthroughs in karst geomicrobiology and redox geochemistry. Karst Waters Institute Special Publication, Charles Town, West Virginia 1

Seager WR, Morgan P (1979) Rio grande Rift in southern New Mexico, west Texas and northern Chihuahua. In: Riecker RE (ed) Rio grande Rift: tectonics and magmatism. American Geophysical Union, pp 87–106

Smith DB (1973) Geometry and correlation along Permian Capitan Escarpment, New Mexico and Texas: discussion. Am Asso Petrol Geol Bull 57:940–945

Spilde MN, Boston PJ, Northup DE (2003) Subterranean soil development. J Cave Karst Stud 65(3):188

Spilde MN, Northup DE, Boston PJ, Schelble RT, Dano KE, Crossey LJ, Dahn CN (2005) Geomicrobiology of cave ferromanganese deposits: a field and laboratory investigation. Geomicrobiol J 22:99–116. doi:10.1080/01490450590945889

Spilde MN, Kooser A, Boston PJ, Northup DE (2009) Speleosol: a subterranean soil. In: Proceedings of the 15th international congress of speleology, Kerrville, Texas, pp 338–344

Spycher N, Pruess K, Ennis-King J (2003) CO_2–H_2O mixtures in the geological sequestration of CO_2. I. Assessment and calculation of mutual solubilities from 12 to 100 °C and up to 600 bar. Geochem et Cosmochim Acta 67(16):3015–3031

Thrailkill JV (1971) Carbonate deposition in Carlsbad Caverns. J Geol 79:683–695

Zimmerman JB (1962) Permian of the Central Guadalupe Mountains, Eddy County, New Mexico, West Texas, Roswell and Hobbs Geological Societies, p 115

Hypogene Evaporite Karst of the Greater Delaware Basin

32

Kevin W. Stafford

Abstract

The Permian Basin of west Texas and southeastern New Mexico is host to extensive karst development in carbonate and evaporite strata. The Delaware Basin and associated Northwestern Shelf include both Guadalupian and Ochoan evaporites with diverse hypogene karst features of four general types: fluvial-induced; pressure gradient-dominated; density convection-dominated; and hydrocarbon-enhanced. Although many classic definitions of hypogene speleogenesis emphasize confined or semi-confined hydrogeologic conditions, analyses of Permian evaporites of this region show that hypogene karst can develop in near-unconfined conditions as long as local meteoric influences are minimal. Since the early Paleogene, eastern migration of the Pecos River in New Mexico has created a persistent potentiometric low as a target for upward migration of fluids, producing multi-story rectilinear maze caves as well as large cenote-like collapse structures in the Seven Rivers Formation, with less dramatic examples also common throughout the back-reef facies. Within the Castile Formation, evidence of hypogene speleogenesis is common, ranging from isolated rise structures nearly 100 m deep to multi-story maze caves and intrastratal brecciation. Evaporite calcitization and associated sulfur ores are common as the result of sulfate reduction in the presence of ascending hydrocarbon-rich fluids. Overlying strata of Salado and Rustler formations also host hypogene karst, but to a much lower documented degree and largely associated only with cross-formational breccia pipes and intrastratal brecciation.

Keywords

Evaporites • Permian • Delaware Basin • Gypsum Plain • Hypogene caves

1 Introduction

Extending eastward from the well-known hypogene karst of the Guadalupe Mountains in Permian carbonates, strata in the neighboring Permian Basin are host to complex and morphologically diverse hypogene karst in evaporite units. This complexity is driven by variations in groundwater flow, interaction with ascending hydrocarbons and mineralogical variations arising from both facies interfingering and geochemical processes, which have produced significant local diagenetic alterations of the host strata. Additionally, the high solution kinetics of halite and gypsum promote rapid dissolution, not only enhancing hypogene karst development but also promoting more rapid surface denudation by epigene processes that increase surficial breaching of hypogene features.

The most extensive evaporite karst documented in the region is contained in the Delaware Basin and extends northward onto the Northwestern Shelf of the Permian Basin (Fig. 1). In the eastern portion of the Delaware Basin, much

K.W. Stafford (✉)
Department of Geology, Stephen F. Austin State University, Nacogdoches, TX 75962, USA
e-mail: staffordk@sfasu.edu

© Springer International Publishing AG 2017
A. Klimchouk et al. (eds.), *Hypogene Karst Regions and Caves of the World*, Cave and Karst Systems of the World, DOI 10.1007/978-3-319-53348-3_32

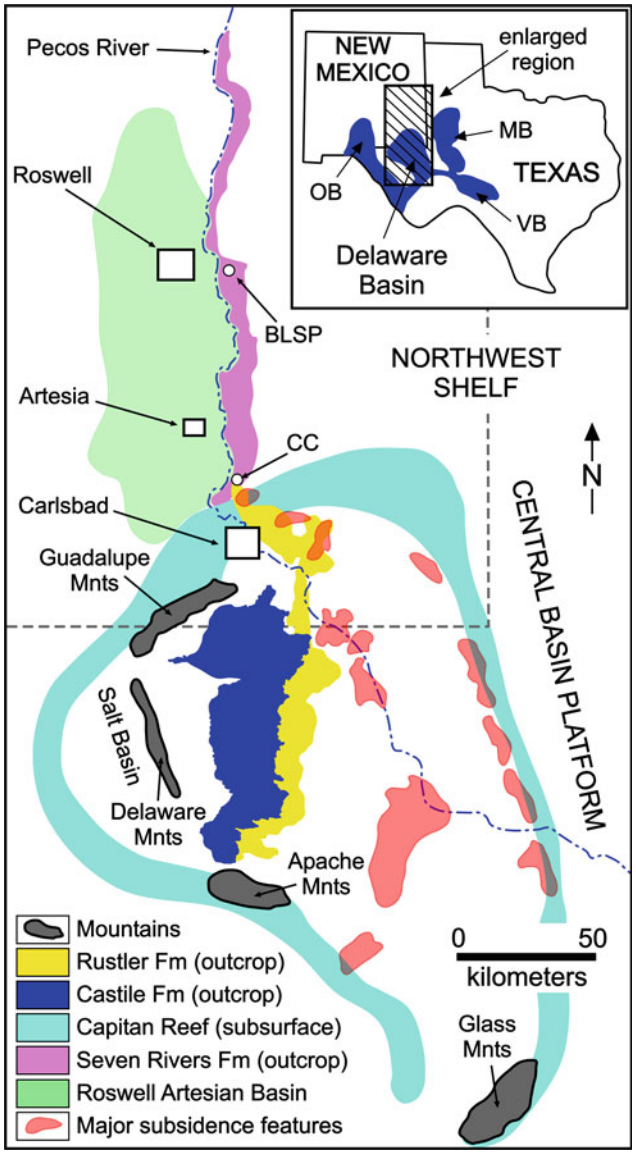

Fig. 1 Location map of greater Delaware Basin and Gypsum Plain of west Texas and eastern New Mexico, including outcrops of lithologic units discussed in this report and major geologic and hydrologic structures (adapted from Stafford et al. 2008a). Features abbreviated above include: *BLSP* Bottomless Lakes State Park; *CC* Coffee Cave; *OB* Orogrande Basin; *MB* Midland Basin; *VB* Val Verde Basin

of the soluble rock is buried in the subsurface. In the western and central portions of the basin, outcrops of Ochoan strata (Castile and Rustler formations) extend from the Apache Mountains of Texas to the Carlsbad region of New Mexico. Guadalupian evaporite karst development is common from Carlsbad northward along the Pecos River, where interbedded carbonates and evaporites are hosts to hypogene karst in the Artesia Group, the back-reef equivalent of the Capitan Reef. The region of surficial exposure of evaporite strata throughout this region is traditionally referred to as the Gypsum Plain (Hill 1996), because surface exposures are dominated by gypsum, although other evaporites, mainly halite, are present in the subsurface and anhydrite dominates deeper basin deposits. Intrastratal dissolution has effectively eliminated halite outcropping within the region.

Today the region is characterized as part of the semiarid southwest of the USA on the northern edge of the Chihuahuan Desert, although the climate was significantly wetter in the past (e.g., Pleistocene). Ephemeral streams and arroyos that commonly exhibit flash flooding dominate the landscape, with the only perennial stream in the region being the Pecos River, which bisects the area from north to south. Base flow of the Pecos River is generally maintained by artesian discharge. Throughout the Cenozoic, the Pecos has persisted as a potentiometric low throughout eastern New Mexico and west Texas, with a gradual migration toward the east, and has had a significant effect on hypogene speleogenesis in the region (Stafford et al. 2009).

2 Geology

Evaporite karst of southeastern New Mexico and west Texas is mainly associated with late Permian Guadalupian and Ochoan strata. During deposition of the interbedded shelf carbonates and evaporites of the Artesia Group, specifically the Seven Rivers Formation, conditions on the Northwestern Shelf were increasingly hypersaline inland from the Capitan Reef complex (Fig. 2; Scholle et al. 2004). During episodic Guadalupian sea-level lowstands, the Northwestern Shelf was subaerially exposed and eolian sands migrated across the region to deposit siliciclastics of the Cherry Canyon and Bell Canyon Formations in the Delaware Basin (Scholle et al. 2004). By the end of the Guadalupian, continued growth of the Capitan Reef restricted open-marine circulation into the Delaware Basin, turning the basin into a restricted inland sea during the Ochoan, causing a shift from carbonate-dominated to evaporite-dominated deposits.

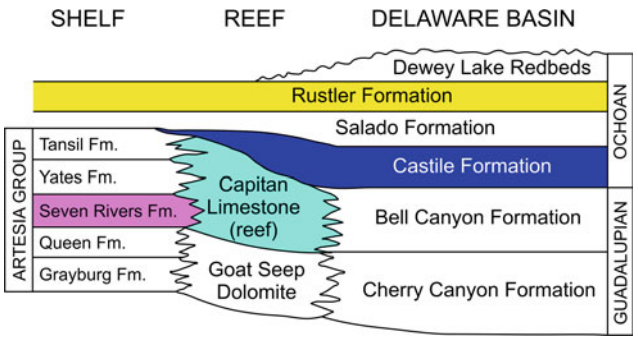

Fig. 2 Stratigraphic diagram of formations of the Delaware Basin region, including basin, reef and shelf facies. Note *color shading* of select units correlate with Fig. 1 (adapted from Scholle et al. 2004)

Early Ochoan basin evaporites of the Castile Formation in the Delaware Basin were laminated sulfates (Kelley 1971). Mid-Ochoan deposits were halide-dominated (Salado Formation) that capped the basin and extended across the surrounding region, including the Capitan Reef and Central Basin Platform. Episodic sea-level advances in the late Ochoan produced cyclic carbonate-sulfate deposits across the region (Rustler Formation). By the end of the Permian, transgression had capped the region with siliciclastic Dewey Lake redbeds (Hill 1996).

Tectonism affected the region throughout the Mesozoic and Cenozoic. Regional uplift during the Laramide induced stratal tilting of 3–5° toward the east/northeast (Hentz and Henry 1989). Basin and Range extension produced block faulting on the far western margin of the Delaware Basin and produced conjugate joint sets throughout the region oriented ~N75°E and ~N15°W (Nance 1993). Associated igneous activity, with emplacement of dike structures within the northern Delaware Basin, elevated regional thermal gradients throughout the remainder of the Cenozoic (Hentz and Henry 1989).

Significant evaporite karst development within the region occurs mainly in the Guadalupian Seven Rivers Formation within the Northwestern Shelf region, and within Ochoan deposits that fill and cap the Delaware Basin (Stafford and Nance 2009). Of these strata, Ochoan Castile evaporites appear to host the most extensive and diverse hypogene karst features, although there may be sampling bias.

3 Evaporite Karst

Evaporite karst development is highly varied throughout the Gypsum Plain, including caves developed primarily by either epigene or hypogene processes. Evaporite cave exploration and mapping has been conducted throughout the region, primarily by the Gypsum Karst Project (GYPKAP) of the National Speleological Society (e.g., Eaton 1987; Belski 1992; Lee 1996) and by the Texas Speleological Survey (TSS) (e.g., Redell and Fiesler 1977). However, detailed studies of lithologic, hydrogeologic and geochemical controls on speleogenesis have been limited (i.e., Anderson et al. 1978; Kirkland and Evans 1976; Land 2003; Stafford et al. 2008a, b, c).

Because of near-linear solution kinetics of evaporites, dramatic landscapes have developed throughout the Gypsum Plain including development of large sinks, incised arroyos and caves. Purely epigene cave development within the region is common but is easily distinguishable from hypogene-dominated cave development. Epigene caves tend to be associated with large solutional sinkhole development coupled with caves that are laterally limited, exhibit rapid decreases in average cave aperture away from insurgences, and are strongly controlled by joints and faults, forming shallow groundwater recharge systems (Fig. 3; Stafford et al. 2008b). Most epigene caves do not extend more than a few tens of meters into the subsurface, likely because they are near saturation resulting from overland flow as fluid is channeled into the subsurface; thus they are unable to dissolve significant additional bedrock to form extensive caves. In contrast, hypogene caves can form large, complex evaporite karst features across the greater Delaware Basin as fluid is delivered to soluble zones laterally or from below, with saturated fluids often armoring the margins of solutional porosity to enable undersaturated fluids to be delivered to a progressing solution front. Confined to semi-confined conditions promote more complex hypogene karst forms in the region.

Evaporite hypogene caves within the study area vary significantly in morphology, including, but not limited to: (1) isolated vugs, (2) multi-story maze caves, (3) isolated riser tubes; (4) extensive brecciation; (5) large-scale collapse structures; and (6) diagenetically altered bedrock. While hypogene karst is traditionally defined as formed in confined to semi-confined conditions with components of free and forced convection flow (Klimchouk 2007), hypogene evaporite karst across the Gypsum Plain exhibits varying degrees of dominance in physical and chemical drivers that promote karst development. Therefore, hypogene karst described in the following sections is grouped based on the apparent

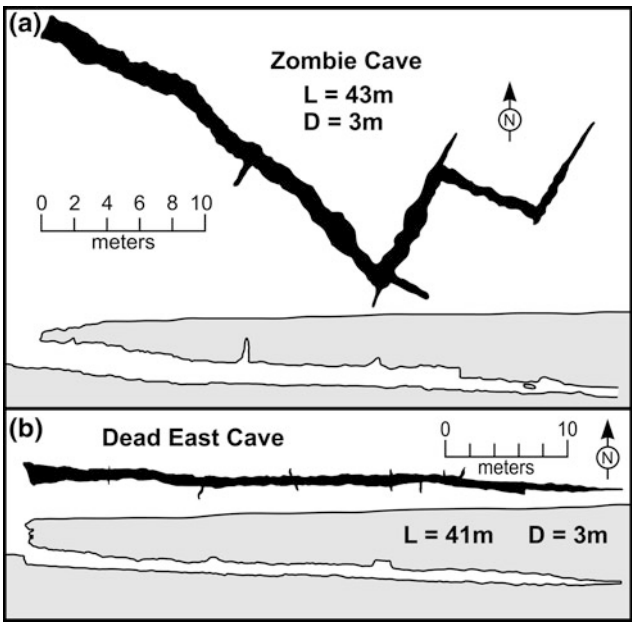

Fig. 3 Archetypal epigene caves of the Gypsum Plain, Zombie Cave (**a**) and Dead East Cave (**b**), developed in the Castile Formation (adapted from Stafford et al. 2008b). Note the strong control fractures exhibit on cave development, the rapid decrease in passage aperture away from insurgence and the limited vertical and horizontal extents that typify epigene evaporite karst throughout the Gypsum Plain

dominant control on speleogenesis although there is some overlap.

3.1 Fluvial-Induced Hypogene Karst

The Pecos River has been a major potentiometric low within west Texas and eastern New Mexico since early Cenozoic time and has had a significant effect on the speleogenetic evolution of the area. This fluvial system has been a major potentiometric driver for upward migration of groundwater associated with hypogene karst development both on the Northwestern Shelf and the Delaware Basin interior (Stafford et al. 2009). These fluvial-induced, hypogene, evaporite karst phenomena include cenote-like structures at Bottomless Lakes National Park and Coffee Cave on the Northwestern Shelf as well as large-scale subsidence troughs within the Delaware Basin.

Bottomless Lakes State Park is located near Roswell, New Mexico (Fig. 1) on the eastern margin of the Pecos River and consists of a series of eight, cenote-like features with artesian discharge. The features are developed in interbedded carbonate mudstone and gypsum of the Seven Rivers Formation along the Seven Rivers Escarpment (Land 2003). Ascending waters from the underlying San Andres limestone are directed upward toward the Pecos River potentiometric low resulting in intrastratal dissolution and upward stoping to create steep-walled cenotes associated with artesian discharge to the Pecos River (Fig. 4). Because water being delivered from the San Andres limestone is saturated with respect to calcite but undersaturated with respect to gypsum, it exhibits significant solutional aggressivity as it passes through Seven Rivers evaporite strata (Land 2003). Artesian discharge has decreased significantly in recent decades as intensive pumping for agricultural purposes has induced declines in hydraulic head (Land and Newton 2008), likely diminishing the extent of active hypogene karst development throughout the region. While discharge does not occur at historic volumes any more, karst features of Bottomless Lakes State Park provide clear evidence of large-scale, collapse structures dominantly formed by forced convection flow in a breached hypogene system.

Coffee Cave is located north of Carlsbad, New Mexico, along the eastern margin of the Pecos River (Fig. 1) and formed in a similar hydrogeologic setting as Bottomless Lakes State Park; it is located on the southern margin of the Roswell Artesian Basin and in interbedded Seven Rivers dolomite and gypsum of the Artesia Group. However, Coffee Cave (Fig. 5), along with several smaller caves in the immediate area, is a multi-story, rectilinear maze cave formed largely in confined conditions (Stafford et al. 2008a). The cave consists of at least four horizons of cave development with average passage size increasing with depth and distance from the erosional scarp, suggesting that solutionally aggressive fluids were delivered from below based on solution kinetics of gypsum; fluids being derived from surficial sources (i.e., Pecos River) should exhibit greatest solutional development near entrance regions adjacent to the erosional scarps. Throughout Coffee Cave, hypogene morphometric features are abundant, including well-developed cupolas, risers, half-tubes and ceiling channels (Stafford et al. 2008a); but more importantly, many of these features show connectivity that is indicative of the classic morphometric suite of rising fluids which has been associated with hypogene speleogenesis (Klimchouk 2007). The Pecos River was the primary driver for upward migration of fluids associated with dissolution of Coffee Cave; however, unlike Bottomless Lakes, Coffee Cave shows significant evidence

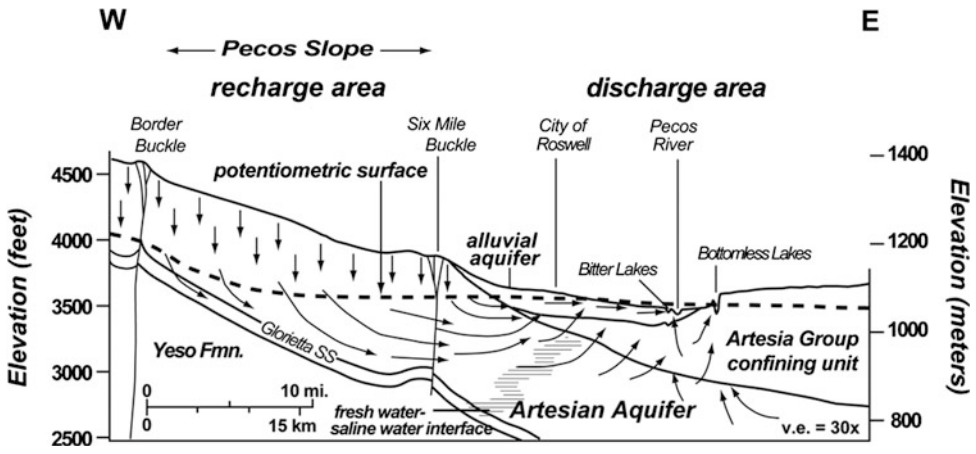

Fig. 4 Conceptual cross section model of hydrogeology associated with the Roswell Artesian Basin and formation of cenote-like structures at Bottomless Lakes State Park near Roswell, New Mexico (from Land 2006). Note that the hydrogeology associated with Coffee Cave, which is formed in the Seven Rivers Formation of the Artesia Group, is nearly identical to this model by Land (2006)

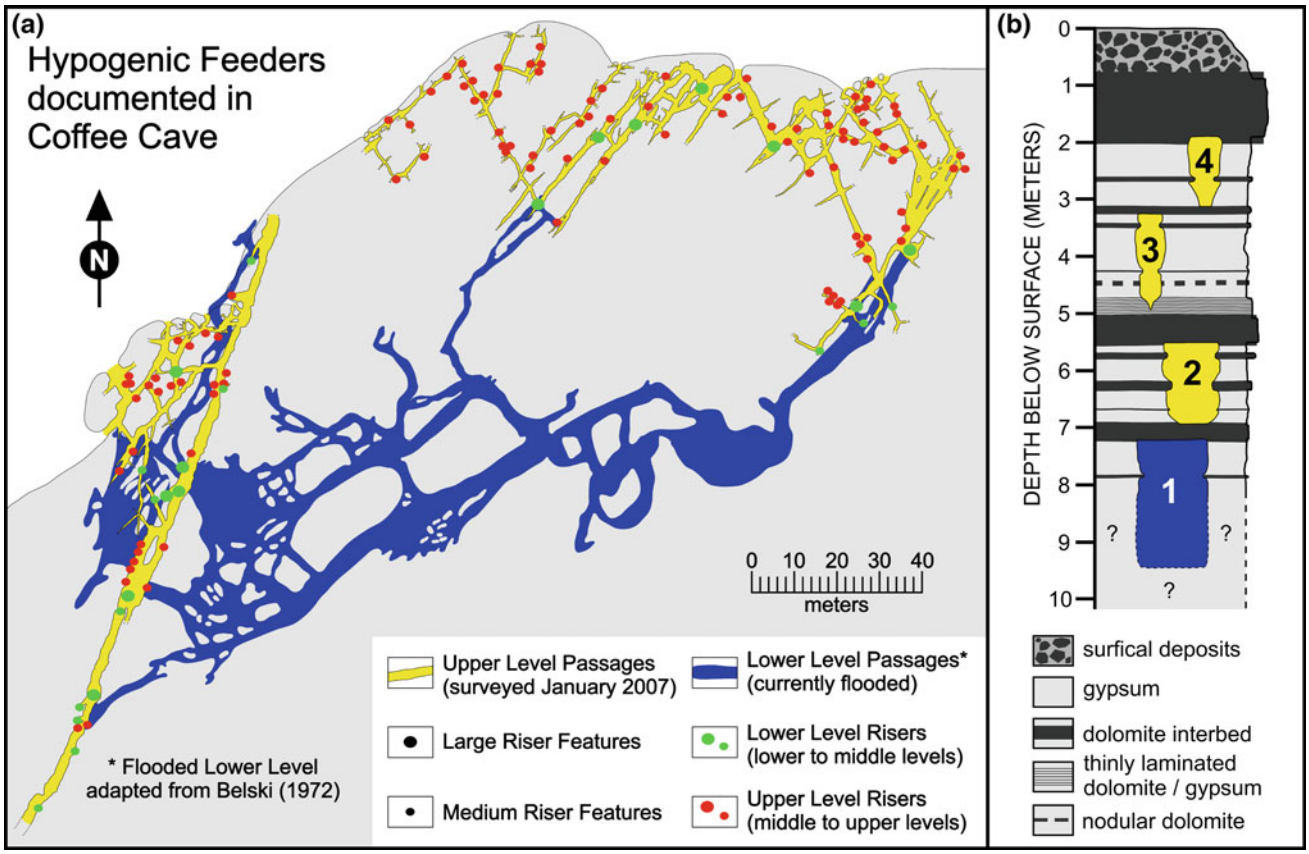

Fig. 5 Simplified plan view map (**a**) and stratigraphic section (**b**) of Coffee Cave. Note the rectilinear maze-like morphology of the cave (**a**), with cave development horizons in *yellow* indicating regions above the current water table and horizons in *blue* below the current water table which were explored decades ago when regional groundwater extraction was greater and water tables were lower. Locations of significant riser features are marked as *red* and *green*. Simplified stratigraphic section (**b**) depicts relationship of the four primary soluble gypsum horizons and associated dolomite layers that separate these horizons (adapted from Stafford et al. 2008a)

of density convection associated with sluggish fluid migration in a semi-confined system prior to Pecos River breaching. Coffee Cave is an excellent example of multi-story, hypogene speleogenesis with dissolution focused within gypsum horizons, while horizons of less-soluble, residual dolomite provide separations for multi-story cave development. Coffee Cave exhibits characteristics similar to classically defined hypogene, evaporite, maze caves of western Ukraine (Klimchouk 2007).

Within the Delaware Basin interior, several large subsidence features filled with Quaternary sediments occur along or in close proximity to the Pecos River (Fig. 1; Malley and Huggington 1953). As the Pecos River, and ancestral Rio Grande, migrated within the Delaware Basin, it created a potentiometric low throughout the Cenozoic that continuously induced upward migration of confined fluids through underlying evaporite strata of Castile, Salado and Rustler formations. This upward fluid migration has resulted in intense, localized intrastratal dissolution of evaporites and many of these large-scale, subsidence features are the result of intrastratal dissolution at depth that have created sag structures in overlying strata (Malley and Huggington 1953). While these large features are likely the result of a system where dissolution is dominated by density convection that has created void space at depth, ultimately the location and spatial distribution is tied directly to the approximate current location of the Pecos River and ancestral Rio Grande (Stafford et al. 2009).

3.2 Pressure Gradient-Dominated Hypogene Karst

The most extensive evaporite karst development documented in the Gypsum Plain occurs within the Castile Formation outcrop area in the Delaware Basin interior. Here, numerous caves show clear evidence of hypogene origins that exhibit classic morphological suites of rising fluids and form cave patterns ranging from complex maze caves in highly folded/fractured strata to single isolated rising tubes in strata that do not exhibit significant brittle or ductile deformation (Stafford et al. 2008b, c). Castile evaporites are

underlain by Bell Canyon siliciclastics and all strata dip approximately 3–5° to the east/northeast within the Delaware Basin (Horak 1985). Meteoric precipitation in the western portion of the Delaware Basin, including allogenic waters from the Delaware Mountains, enters the Bell Canyon aquifer system east of the dissolution edge of the Castile outcrop area. These waters descend beneath the Castile Formation and into confined conditions where they subsequently exploit leaky confining conditions of the Castile evaporites and rise upwards, creating hypogene void structures.

Distribution of karst features is highly clustered with greatest concentrations of development along the western and northern regions where total thickness of the Castile evaporites is reduced as a result of intrastratal dissolution and surface denudation (Stafford et al. 2008c). This spatial pattern suggests two things: (1) hypogene karst development is most intense proximal to aquifer recharge into underlying Bell Canyon strata to the west, and (2) hypogene karst development is more intense in the lower portion of the Castile Formation, near the underlying contact with Bell Canyon siliciclastics. These two associations provide strong evidence for hydrostatic pressure-driven fluid migration from underlying Bell Canyon strata through soluble zones of overlying leaky Castile evaporites. It is probable that significantly more hypogene karst features are forming by the same process in the Castile Formation further to the east, but have yet to be breached by surface denudation as thickness of Castile strata increases significantly as it dips into the subsurface. Two specific caves exhibit the morphological variability within this region: Dead Bunny Hole and Crystal Cave (Fig. 6).

Dead Bunny Hole is located near the far eastern margin of the central region of the Castile outcrop area and is a complex maze cave with a current surveyed length and depth of 439 and 14 m, respectively. The cave is formed along a series of northwest/southeast trending anticlinal structures with secondary passage development primarily associated with roughly east/west joint sets. The cave consists of three offset levels of development that correlate to lithologic variability and the cave increases in average passage diameter with depth away from the sinkhole entrance that drains an approximately one square kilometer area that is too small to have formed a cave of this size in gypsum by epigene processes (Stafford et al. 2008b). Throughout the cave, morphological features that have been associated with hypogene development are common, including abundant risers, cupolas, half-tubes and regions of highly porous, "boneyard" morphology (Fig. 7). The lower portions of the known cave are close to the contact with underlying Bell Canyon strata, placing it in an optimum location for upward migration from confined waters of the siliciclastic aquifer.

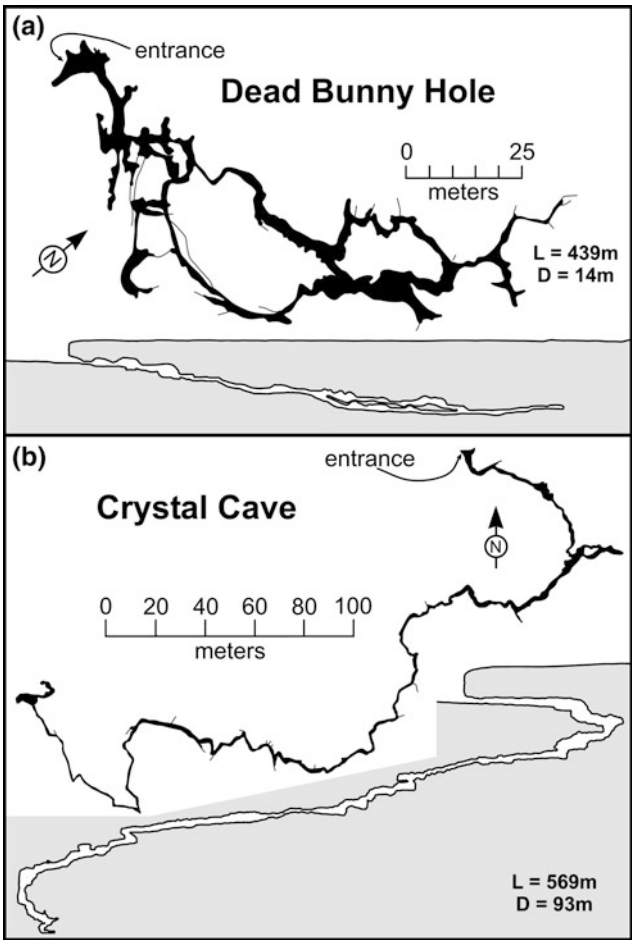

Fig. 6 Simplified plan and profile maps of Dead Bunny Hole (**a**) and Crystal Cave (**b**) (adapted from Stafford et al. 2008b). Dead Bunny Hole exhibits northeast/southwest trending cave passages which are developed along the axes of anticlines, while other passages in this hypogene maze cave are developed along fractures. Crystal Cave (**b**) is developed along the dip of local strata as an isolated riser feature. *L* surveyed length; *D* surveyed depth

In contrast to Dead Bunny Hole, Crystal Cave (Fig. 6) is a single rising tube that has formed the deepest known cave in the Castile outcrop area with a surveyed length and depth of 569 and 93 m, respectively (Stafford et al. 2008b). The cave descends fairly steeply with intermittent small drops and larger dome pits as the cave alternates between elliptical passages and tall domal passages; the lowermost portion of the known cave is developed in a selenite mass with the end of the known cave consisting of a sump within a riser-like feature. Gypsum texture and lithologic variability are significant throughout the cave but appears to have little control on speleogenetic development, as is often observed in hypogene caves. While upper portions of the cave have a well-developed floor channel with scalloping and incised notches at the tops of pits, the upper portions of these passages and lower portions of the cave show little evidence of

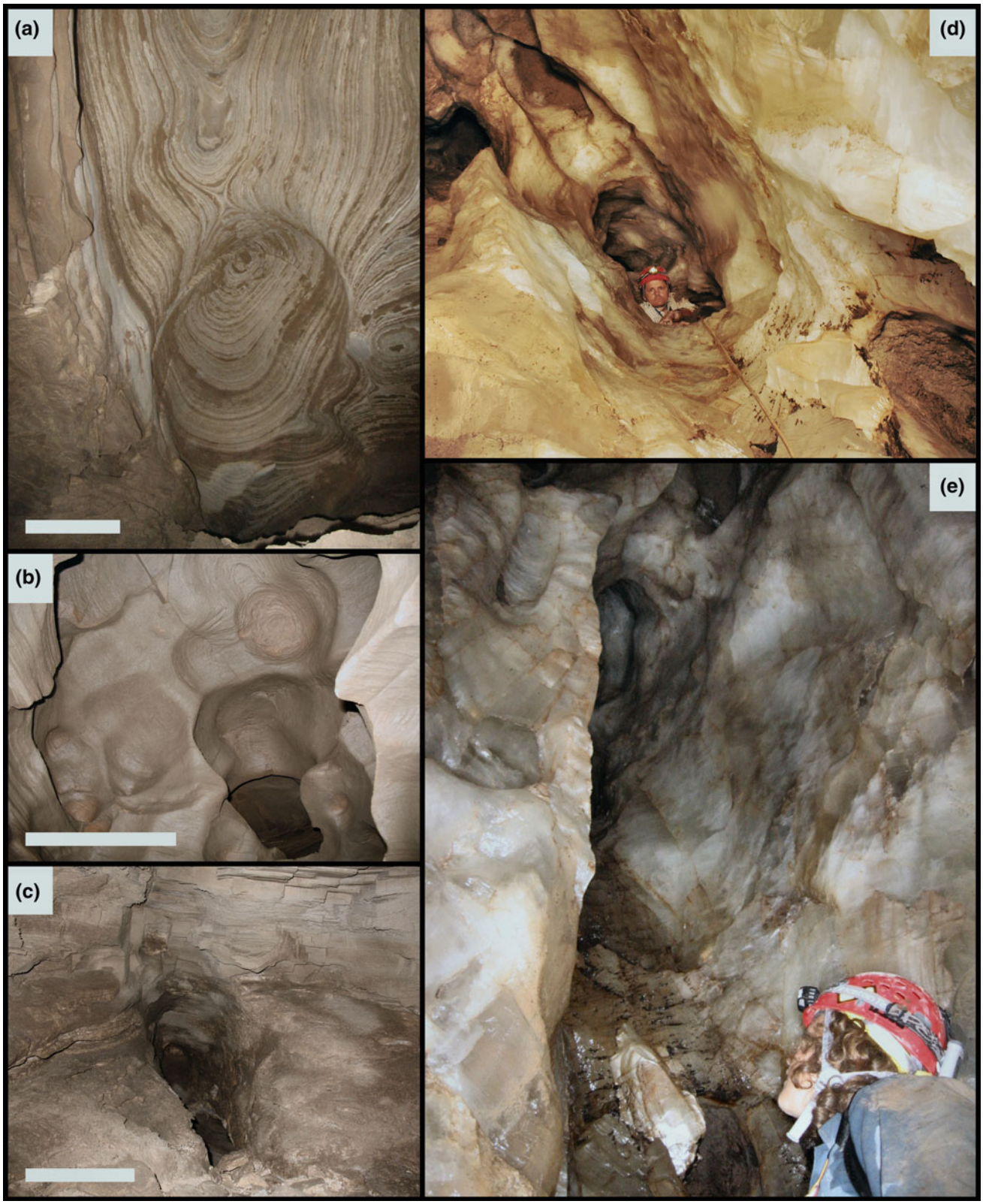

Fig. 7 Photographs of typical morphologies indicative of hypogene speleogenesis in Dead Bunny Hole (**a**, **b**, **c**) and Crystal Cave (**d**, **e**), including cupolas (**a**), cuspate ceilings (**b**), risers (**c**), complex riser pits (**d**) and wall channels (**e**). *Scale bars* are approximately 50 cm in length. **a**, **b**, **d** and **e** are ceiling and wall features viewed upward; **c** is a floor/wall feature viewed downward

epigene overprinting. The ceiling undulates throughout in a series of small domal structures occasionally interrupted by larger domed regions with a ceiling half-tube connecting morphological features (Fig. 7). While passage development does not appear to be significantly correlated with fractures or other planar failures, the general dip of the cave is roughly aligned with the local bedrock dip, indicating that in the absence of highly fractured bedrock, single, ascending riser caves form in association with dip of local strata.

3.3 Density Convection-Dominated Hypogene Karst

Hypogene karst development that is dominantly driven by density (free) convection within the Gypsum Plain region is widespread and extensive, generally in the form of intrastratal dissolution (Stafford et al. 2008b). As solutionally aggressive fluids ascend, they dissolve surrounding evaporite strata and become denser, saline brines that subsequently sink to lower horizons. As this phenomenon progresses, void space created at depth can no longer support overlying strata, and collapse with upward stoping occurs. In time, upward stoping can progress to breach land surfaces, as solutionally aggressive fluids are continuously supplied to the base of the collapse structure. In the fluvial-induced and pressure gradient-dominated hypogene karst examples above, density convection is a component of the dissolution process, but appears to be secondary to the forced convection/hydrostatic pressure-driven portion. In contrast, intrastratal dissolution appears to exhibit a less significant and poorly defined component of forced convection during porosity development. Therefore, density convection associated with variations in total dissolved solids (and likely thermal gradients) is the dominant driving mechanism for intrastratal dissolution.

Examples of density convection-dominated hypogene karst have been documented in outcrops of Castile evaporites (Stafford et al. 2008b, c), but manifestations of intrastratal dissolution indicate that it is widespread throughout the region, most notably in the Salado and Rustler formations (Anderson and Kirkland 1980; Bachman 1980). These karst phenomena can be grouped into two basic categories, breccia pipes and blanket breccias, where breccia pipes are vertical collapse structures and blanket breccias are laterally extensive horizons of collapse. If these breccia features breach the land surface during their formation, they exhibit a distinct shift from density convection-driven dissolution to forced convection-dominated dissolution, as an outlet is established for fluids to leave the previously confined system.

Anderson and Kirkland (1980) proposed a model of brine density convection for formation of breccia pipes within the Delaware Basin, where waters undersaturated with respect to evaporite minerals would rise from underlying siliciclastic/carbonate units as low density fluids into overlying evaporite strata (Fig. 8). Intrastratal dissolution within evaporites results in breccia pipes (Fig. 8a) and blanket breccias (Fig. 8b). Undersaturated waters are delivered to solution fronts as the result of lower densities. As dissolution continues, saturated waters transport dissolved solids away from the dissolution front. As density convection proceeds

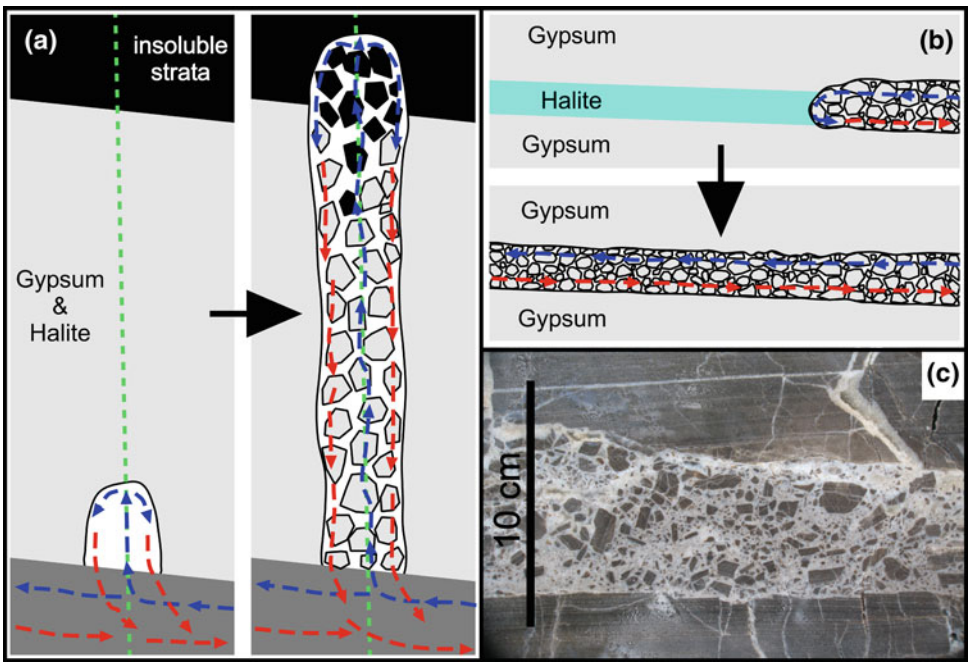

Fig. 8 Intrastratal dissolution within evaporites results in breccia pipes (**a**) and blanket breccias (**b**). Undersaturated waters (*blue dashed arrow lines*) are delivered to solution fronts as the result of lower densities; as dissolution continues, saturated waters (*red dashed arrow lines*) transport dissolved solids away from the dissolution front. As density convection proceeds and sufficient soluble rock has been removed from the system, stratal support is lost and collapse occurs, producing brecciation as seen in the slabbed hand sample (**c**)

and sufficient soluble rock has been removed from the system, stratal support is lost and collapse occurs, producing brecciation (Fig. 8c).

The vertical nature of these structures is attributed to processes where low density, solutionally aggressive fluids rise through the center of collapsing structure while high density, saturated fluids descend along margins of the collapse structure. Thus maximum dissolution is focused along the central axis of the breccia pipe while margins are armored from further dissolution by saturated fluids. Breccia pipes have been documented as relatively small scale features, less than 100 m in diameter, throughout the Castile outcrop area where ascending fluids were delivered from the underlying Bell Canyon aquifer (Lee and Williams 2000). However, a series of large collapse structures have also been documented in the eastern portion of the Delaware Basin that created subsidence regions (Fig. 1), each extending over tens of square kilometers and are associated with ascending fluids from the underlying Capitan Reef aquifer system (Bachman 1980).

Most blanket breccia appears to have formed by lateral migration of fluids that were undersaturated with respect to chloride which promoted dissolution of halite interbeds but did not significantly affect adjacent sulfate minerals (Anderson et al. 1972). As a result of intrastratal halite dissolution, loss of support of overlying strata induced localized collapse and widespread subsidence. Blanket breccias are widespread throughout the Castile outcrop area but are generally less than a meter in vertical thickness. Blanket breccias are known to be much more extensive in the subsurface where intrastratal dissolution has effectively removed all halite horizons from the Castile Formation in the western Delaware Basin as well as all Salado evaporites in this region (Anderson et al. 1972). An unconformable contact between the Castile Formation and Rustler Formation exists in the central Delaware Basin where the Salado Formation has been completely removed by intrastratal dissolution. This has resulted in a generally thinning of evaporite sequences from east to west across the Delaware Basin, with maximum intrastratal dissolution occurring in the west that has been overprinted by extensive surface denudation in outcrop. Large subsidence valleys form narrow linear topographic lows within the western Castile outcrop area. Here graben boundary faults up to 75 m deep occur which are coincident with upper limits of halite dissolution (Hentz and Henry 1989). Similarly, dissolution troughs along the Pecos River described above in the fluvial-induced hypogene karst section likely exhibit a significant component of this type of subsidence collapse.

3.4 Hydrocarbon-Enhanced Hypogene Karst

The Permian Basin is one the world's largest petroleum producing regions, which has had an effect on regional speleogenetic evolution. Evaporite calcitization is common within the Castile outcrop area where ascending light hydrocarbons have risen through evaporite strata and fueled sulfate reduction either through bacterial sulfate reduction (BSR) or thermochemical sulfate reduction (TSR) (Stafford et al. 2008d). As a result of sulfate reduction, hydrogen sulfide and calcite saturated fluids formed which precipitate penecontemporaneously as native sulfur and secondary calcite (Machel 1987). BSR occurs over a wide range of low-temperature (0 to ~80 °C) sedimentary environments in the presence of light organic compounds; TSR generally occurs at higher temperatures (~100 to 180 °C) as an inorganic process. TSR, like BSR, will occur as long as sulfate and organic compounds are present, but TSR does not require active involvement of microbial organisms and thus can proceed in confined environments without complete removal of hydrogen sulfide by-products that can be toxic to sulfate-reducing bacteria (Machel 1992).

Kirkland and Evans (1976) first reported on evaporite calcitization related to the occurrence of "castiles" for which the Castile Formation is named. These "castiles" form positive-relief structures across the Castile outcrop, which are resistant, residual highs resulting from differential erosion between calcitized and uncalcitized evaporites. Stafford et al. (2008d) reinvestigated more than 1000 individual calcitized masses within the region and found they exhibit distinct clustering as is expected in hypogene speleogenetic processes. Individual calcitized buttes reach more than 40 m in elevation above the surrounding terrain, although they are generally less than 10 m in height (Fig. 9). Calcitized masses occur along linear trends of ~N70°E, ~N55°E and

Fig. 9 Cluster of "Castile Buttes" approximately 20 m tall. Note brighter white regions on calcitized masses, indicated by *black arrows*, which are secondary gypsum actively forming around degassing, hydrogen sulfide vents

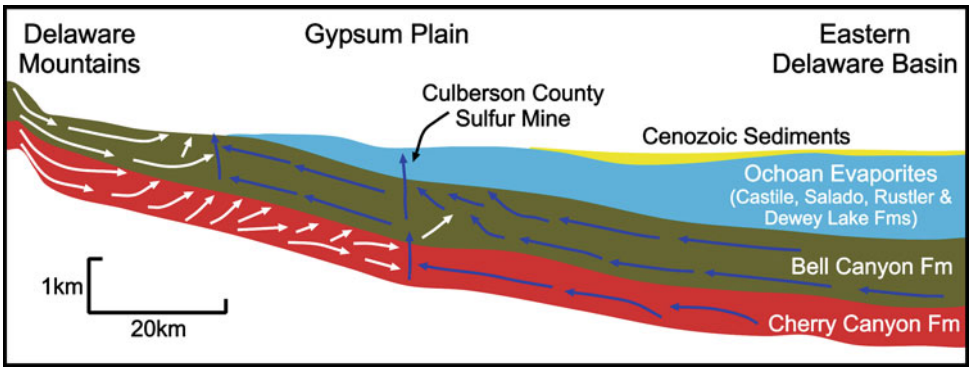

Fig. 10 Conceptual paleo-hydrogeologic model of hypogene fluid migration coupled with ascending hydrocarbons that promoted sulfate reduction to form calcitized masses and associated native sulfur ore deposits (adapted from Lee and Williams 2000)

~N40°W, which is comparable to reported fracture orientations within the region attributed to Basin and Range extension (Stafford et al. 2008d). Most calcitized buttes contain a core of highly brecciated material, indicating a diagenetic connection to breccia pipe development but the periphery of masses generally exhibit minimal alteration; some calcitized masses still exhibit active degassing of hydrogen sulfide based on discernable odor and the presence of secondary gypsum around vent areas (Fig. 9). Similarly, blanket breccias and strata proximal to the Bell Canyon contact commonly exhibit varying degrees of evaporite calcitization that may extend laterally for several kilometers and interfinger with non-calcitized regions.

Sulfur deposits are commonly associated with calcitized evaporites. Sulfur deposits have been documented in both the Castile and Rustler formations (Wessel and Wimberly 1992) and some have been economically mined, including the Culberson Ore Body, the Pokorny Sulfur Deposit and the Phillips Ranch Sulfur Deposit (Lee and Williams 2000). These sulfur deposits occur as vug to cavernous ore bodies as well as fracture and breccia infillings, all largely associated with calicitized zones (Wallace and Crawford 1992). Modeling by Lee and Williams (2000) indicated basinal fluids migrating updip from the Bell Canyon Formation and meteoric fluids migrating downdip through the Cherry Canyon induced calcitization and penecontemporaneous sulfur emplacement (Fig. 10). While surface exposures of calcitization of Salado evaporites have not been documented, subsurface occurrences associated with sulfur ore deposits confirm that this process is not limited to the Castile Formation.

Kirkland and Evans (1976) report that light carbon isotopes ($\delta^{13}C$) in calcitized masses are indicative of hydrocarbon migration into sulfate rocks that was likely sourced from upward migration of methane from the Bell Canyon and other formations of the Delaware Mountain Group. Sulfur isotope ($\delta^{34}S$) analyses of associated sulfur ore deposits fell within a wide range that could not be attributed to definitively BSR or TSR, but Kirkland and Evans (1976) suggested that BSR was the most probable mechanism for evaporite calcitization. However, elevated geothermal gradients within the region since the Neogene and associated emplacement of igneous dikes during Basin and Range extension could have provided the thermal regime for TSR calcitization (Hentz and Henry 1989; Stafford et al. 2008d). The common occurrence of native sulfur within the region suggests that BSR may have been limited by inability to remove microbial waste by-products from the system.

Further supporting hypogene speleogenesis, secondary tabular gypsum (selenite) deposits are common next to many calcitized masses, which are often in close proximity to known hypogene caves (Stafford et al. 2008c, d). Individual selenite crystals often exceed several meters in length and entire selenitic masses may outcrop over several hundred square meters; rarely, isolated sulfur crystals are found within selenite masses. These selenite masses appear to have filled large voids or as masses associated with brecciated zones. Hill (1996) postulated that these selenite bodies formed by oxidation of sulfur deposits. While large selenite masses do not unequivocally indicate hypogene speleogenetic processes in the region, they appear to provide strong evidence of an evolving speleogenetic system where sulfur ore deposits have been oxidized.

4 Conclusions

Confined to semi-confined conditions are not a prerequisite for hypogene karst in evaporites of the greater Delaware Basin, although semi-confined conditions promote more extensive cave and solutional porosity development. Unique fluid chemistries are not required for hypogene evaporite dissolution within this region, although unique chemistries can promote increased dissolution and mineral alteration (i.e., calcitization, sulfur ore emplacement), while elevated

thermal regimes can accentuate these processes. Ultimately, the common characteristic of hypogene karst within evaporite strata of the Gypsum Plain is that solutionally aggressive fluids are delivered from beneath the soluble horizon and that these ascending fluids outcompete surficial, meteoric processes. Once surface denudation and arroyo/sinkhole development are significant enough to focus water into the subsurface, these systems transition from hypogene-dominated to epigene-dominated.

Hypogene karst development within the greater Delaware Basin region is consistent with traditionally defined hypogene karst, but variations in the dominance of controlling mechanisms occur throughout the region creating a complex and diverse speleogenetic history for the Gypsum Plain. Fluvial-induced hypogene karst is clearly dominated by the presence of a persistent potentiometric low created by incising river basins which promote development of larger, more extensive karst phenomena that tend to cluster, but remain as isolated features within these clusters. Similarly, pressure gradient-dominated hypogene karst appears to be predominant in regions where dipping strata place evaporites in close proximity to recharge zones of underlying high permeability aquifer systems. In contrast to fluvial-induced and pressure gradient-dominated hypogene karst where variations in hydrostatic pressure dominate the speleogenetic process, density convection-dominated hypogene karst appears to be largely controlled by flow driven by variations in fluid saturation.

The continuously evolving, evaporite karst system of the greater Delaware Basin continues to pose unique challenges both to academic investigations and land management practices. The extensive nature of evaporite karst throughout the region is far more complicated than previously recognized and will require numerous detailed investigations in the future. Although we know that hypogene speleogenesis is widespread throughout these evaporite strata, unbreached hypogene caves remain an unpredictable geohazard risk throughout the region.

References

Anderson RY, Kirkland DW (1980) Dissolution of salt deposits by brine density flow. Geology 8:66–69

Anderson RY, Dean WE, Kirkland DW, Snider HI (1972) Permian Castile varved evaporite sequence, West Texas and New Mexico. Geol Soc Am Bull 83:59–85

Anderson RY, Kietzke KK, Rhodes DJ (1978) Development of dissolution breccias, northern Delaware Basin and adjacent areas. New Mexico Bureau Mines Min Resour Bull 159:47–52

Bachman GO (1980) Regional geology and Cenozoic history of the Pecos Region, Southeastern New Mexico. U.S. Geological Survey Open File Report 80-1099

Belski D (ed) (1992) GYPKAP report volume #2. Southwestern Region of the National Speleological Society, Albuquerque, NM

Eaton J (ed) (1987) GYPKAP 1987 annual report. Southwestern Region of the National Speleological Society, Alamogordo, NM

Hentz TF, Henry CD (1989) Evaporite-hosted native sulfur in Trans-Pecos Texas: relation to late-phase Basin and Range deformation. Geology 17:400–403

Hill CA (1996) Geology of the Delaware Basin, Guadalupe, Apache and Glass Mountains: New Mexico and West Texas. Permian Basin Section—SEPM, Midland, TX

Horak RL (1985) Trans-Pecos tectonism and its affects on the Permian Basin. In: Dickerson PW, Muelberger WR (eds) Structure and tectonics of Trans-Pecos Texas, West Texas Geological Society, Midland, TX

Kelley VC (1971) Geology of the Pecos Country, Southeastern New Mexico. New Mexico Bureau of Mines and Mineral Resources, Socorro, NM

Kirkland DW, Evans R (1976) Origin of limestone buttes, Gypsum Plain, Culberson County, Texas. Am Asso Petrol Geol Bull 60:2005–2018

Klimchouk A (2007) Hypogene speleogenesis: hydrogeological and morphometric perspective. National Cave and Karst Research Institute, Special paper no. 1, Carlsbad, NM

Land L (2003) Evaporite karst and regional ground water circulation in the lower Pecos Valley. In: Johnson KS, Neal JT (eds) Evaporite karst and engineering and environmental problems in the United States, Oklahoma Geological Survey Circular 109, Norman, OK

Land L (2006) Hydrogeology of Bottomless Lakes State Park. In: Land L, Lueth V, Raatz B, Boston P, Love D (eds) Caves and Karst of Southeastern New Mexico: New Mexico Geological Society, Guidebook 57. Albuquerque, NM, pp 95–96

Land L, Newton BT (2008) Seasonal and long-term variations in hydraulic head in a karstic aquifer: Roswell Artesian Basin, New Mexico. J Am Water Resour Assoc 44(1):175–191

Lee J (ed) (1996) GYPKAP report volume 3. Southwestern Region of the National Speleological Society, Alamogordo, NM

Lee MK, Williams DD (2000) Paleohydrology of the Delaware Basin, western Texas: overpressure development, hydrocarbon migration, and ore genesis. Am Asso Petrol Geol Bull 84(7):961–974

Machel HG (1987) Saddle dolomite as a by-product of chemical compaction and thermochemical reduction. Geology 15:936–940

Machel HG (1992) Low-temperature and high-temperature origins of elemental sulfur in diagenetic environments. In: Wessel GR, Wimberly BH (eds) Native sulfur: developments in geology and exploration. Society of Mining, Metallurgy, and Exploration Inc., Littleton, CO, pp 3–22

Malley VC, Huffington RM (1953) Cenozoic fill and evaporite solution in the Delaware Basin, Texas and New Mexico. Geol Soc Am Bull 64:539–546

Nance R (1993) Application of the standard tablet method to a study of denudation in gypsum karst, Chosa Draw, southeastern New Mexico. University of Northern Colorado, Thesis

Redell JR, Fiesler RG (1977) The caves of far west Texas. Texas Speleological Survey, Austin, TX

Scholle PA, Goldstein RH, Ulmer-Scholle DS (2004) Classic upper Paleozoic reefs and bioherms of west Texas and New Mexico. New Mexico Institute of Mining and Technology, Socorro, NM

Stafford KW, Nance R (2009) The gypsum plain of southeastern New Mexico and far west Texas. In: Palmer A, Palmer M (eds) Caves and karst of the USA. National Speleological Society, Huntsville, AL, pp 267–272

Stafford KW, Land L, Klimchouk A (2008a) Hypogenic speleogenesis within Seven Rivers evaporites: Coffee Cave, Eddy County, New Mexico. J Cave Karst Stud 70(1):47–61

Stafford KW, Nance R, Rosales-Lagarde L, Boston P (2008b) Epigene and hypogene karst manifestations of the Castile Formation: Eddy

County, New Mexico and Culberson County, Texas. Int J Speleol 37(2):83–98

Stafford KW, Rosales-Lagarde L, Boston PJ (2008c) Castile evaporite karst potential map of the Gypsum Plain, Eddy County, New Mexico and Culberson County, Texas: a GIS methodological comparison. J Cave Karst Stud 70(1):35–46

Stafford KW, Ulmer-Scholle D, Rosales-Lagarde L (2008d) Hypogene calcitization: evaporite diagenesis in the western Delaware Basin. Carbonates Evaporites 23(2):89–103

Stafford KW, Klimchouck AB, Land L, Gary MO (2009) The Pecos River hypogene speleogenetic province: a basin-scale karst paradigm for eastern New Mexico and west Texas, USA. In: Stafford KW, Land L, Veni G (eds) NCKRI symposium 1: advances in hypogene karst studies. National Cave and Karst Research Institute, Carlsbad, NM, pp 121–135

Wallace CSA, Crawford JE (1992) Geology of the Culberson ore body. In: Wessel GR, Wimberly BH (eds) Native sulfur: developments in geology and exploration. Society of Mining, Metallurgy, and Exploration Inc., Littleton, CO, pp 91–105

Wessel GR, Wimberly BH (eds) (1992) Native sulfur: developments in geology and exploration. Society of Mining, Metallurgy, and Exploration, Inc., Littleton, CO

Geology of Quartz-Lined Hypogene Caves of Southeastern Arizona

33

Nicole K. Davis and Brian A. McMillan

Abstract

Chiricahua Crystal Cave may be the only known limestone cave in the world that intersects room-sized quartz geodes (up to 16 m across). The cave is a relatively deep, laterally confined network maze, with zones of breakdown and vertical shafts. Large euhedral quartz crystals are found at all levels of the cave, lining vugs that range in size from centimeters to tens of meters. These geodes are crosscut by a network of phreatic tubes and abruptly terminating fissures that show little evidence of top-down flow or connection with surface hydrology. All surfaces of the cave below a certain elevation are covered with a thick coating of calcite mammillaries. The cave reflects a series of distinct geochemical environments. We propose that deep-seated hydrothermal silicic acid initiated the formation of the vugs and deposited a quartz rind as it cooled. Hypogenic (and likely hydrothermal) carbonic acid dissolved the subsequent passages and then vacated the cave. Subaerial conditions prevailed for a time before fluid once again entered the cave. A cooler, calcite-rich pool filled the lower reaches of the cave, depositing mammillaries in a stable environment with slow, steady atmospheric and hydrological mixing. Additional features, such as cupolas, solution pockets, phreatic tubes, corroded and altered surfaces, and vertical pits at the bottom of the cave (possible feeders), are also compatible with bottom-up thermal processes.

Keywords

Quartz crystals • Mammillaries • Geodes • Volcanics • Network maze

1 Introduction

Chiricahua Crystal Cave and adjacent Little Crystal and Baby Crystal caves are geologically unique: 20–50% of their mainly limestone surfaces are coated with a thick layer of well-developed quartz crystals (Fig. 1). These crystals, contained in giant geodes up to 16 m across, were mined in the late nineteenth-century (Zimmerman 2016) but are now protected by the Federal Cave Resources Protection Act (U.S. Congress 1988). The main cave is a network of vertical and horizontal passages along fractures or veins that contain highly altered rock. The maze of tubes and fissures overprints and interconnects preexisting quartz-lined vugs (geodes), which are distributed throughout the cave except in the most remote areas. There is also a "bathtub ring" of calcite mammillaries at a consistent depth throughout the entire cave.

The vugs, geodes, network maze, and mammillaries were each produced by a geochemically distinct fluid, but it is not clear whether the responsible fluids were from related or separate sources. The presence of exotic quartz crystals indicates that at least one of the fluid sources was hydrothermal. Our interpretation of the other speleogenetic

N.K. Davis (✉) · B.A. McMillan
2568 E. Copper St. #5, Tucson, AZ 85716, USA
e-mail: nicolekristinadavis@gmail.com

B.A. McMillan
e-mail: brianmcmillan@mac.com

© Springer International Publishing AG 2017

A. Klimchouk et al. (eds.), *Hypogene Karst Regions and Caves of the World*,
Cave and Karst Systems of the World, DOI 10.1007/978-3-319-53348-3_33

Fig. 1 Quartz crystals up to 8 cm wide decorate the walls, floors, and ceilings in many parts of Chiricahua Crystal Cave (photograph by Adam Zipkin)

phases is speculative but can serve as a guide to further study.

The cave appears to be primarily or exclusively hypogenic, with little evidence of epigenic flow. There are no coarse-grained sediments to indicate past floodwater activity. Gypsum deposits and other evidence for sulfuric acid dissolution were not identified in the cave, and no other evidence was found to link it with the sulfuric acid regime in the nearby Guadalupe Mountains of New Mexico (DuChene et al. Chap. 31).

2 Regional Setting

Crystal Cave is located in the Chiricahua Mountains of southeastern Arizona which is part of the basin and range extensional province, a series of parallel mountain ranges separated by broad basins. Remnants of ancient calderas give evidence that large silica-rich volcanoes were prevalent in the region 25–170 Ma (Jurassic to Early Neogene Period; Dickinson 2003).

The Chiricahuas include fault-controlled mountains and a caldera complex. The rim of the 26.9-Ma Turkey Creek Caldera is approximately 1.5 km from the cave (Fig. 2). The slightly older Portal Caldera (27.6 Ma; McIntosh and Bryan 2000) and remnants of 29.6-Ma volcanics (Pallister et al. 1994) have also been mapped nearby. Silica-rich volcanics overlie Paleozoic and Mesozoic sedimentary sequences that were highly deformed by Laramide crustal shortening. Crystal Cave is located in an anticline of Permian Concha Limestone, the uppermost Paleozoic unit in the area (Drewes et al. 1995; Lawton and Olmstead 1995).

3 Methods

Chiricahua Crystal Cave was mapped using standard cave-surveying techniques (Zimmerman 2016). This chapter is a brief introduction to an ongoing project initiated in conjunction with the mapping effort. We conducted a geologic inventory throughout the cave, including the presence, mineralogy, size, and stratigraphic position of quartz crystals; presence and identity of other minerals; lithology and structure of exposed bedrock; and morphology and relationships of cave passages. We also analyzed the composition of 18 rock, mineral, and sediment samples using spectral analysis. These and other details related to the project are included in Davis and others (2016, available through the authors).

4 Cave Description

Chiricahua Crystal Cave contains 3.8 km of mapped passages that occupy a relatively small plan view (<0.2 km^2) but a large vertical extent (82 m; Fig. 3; Zimmerman 2016). Many of the passages overlie each other. Most of the cave is composed of a ~10,000-m^3 breakdown chamber and ~6 levels of passages that fall in the same vertical plane. Cave passages cross or terminate 40–60 m below nearby valley floors, apparently with no hydrological connection. The cave appears to be constrained within structural and/or lithologic boundaries, which apparently have also guided the location of small local valleys.

The cave is dominated by a network maze of tubes and fissures that generally follow fractures with four main orientations, probably two pairs of joint sets. It is likely that the dominant NW–SE and NE–SW joints are related to basin and range extension, and the secondary E–W and N–S joints were active during Laramide compression and reactivated by postcaldera cooling and contraction. Some joint-controlled

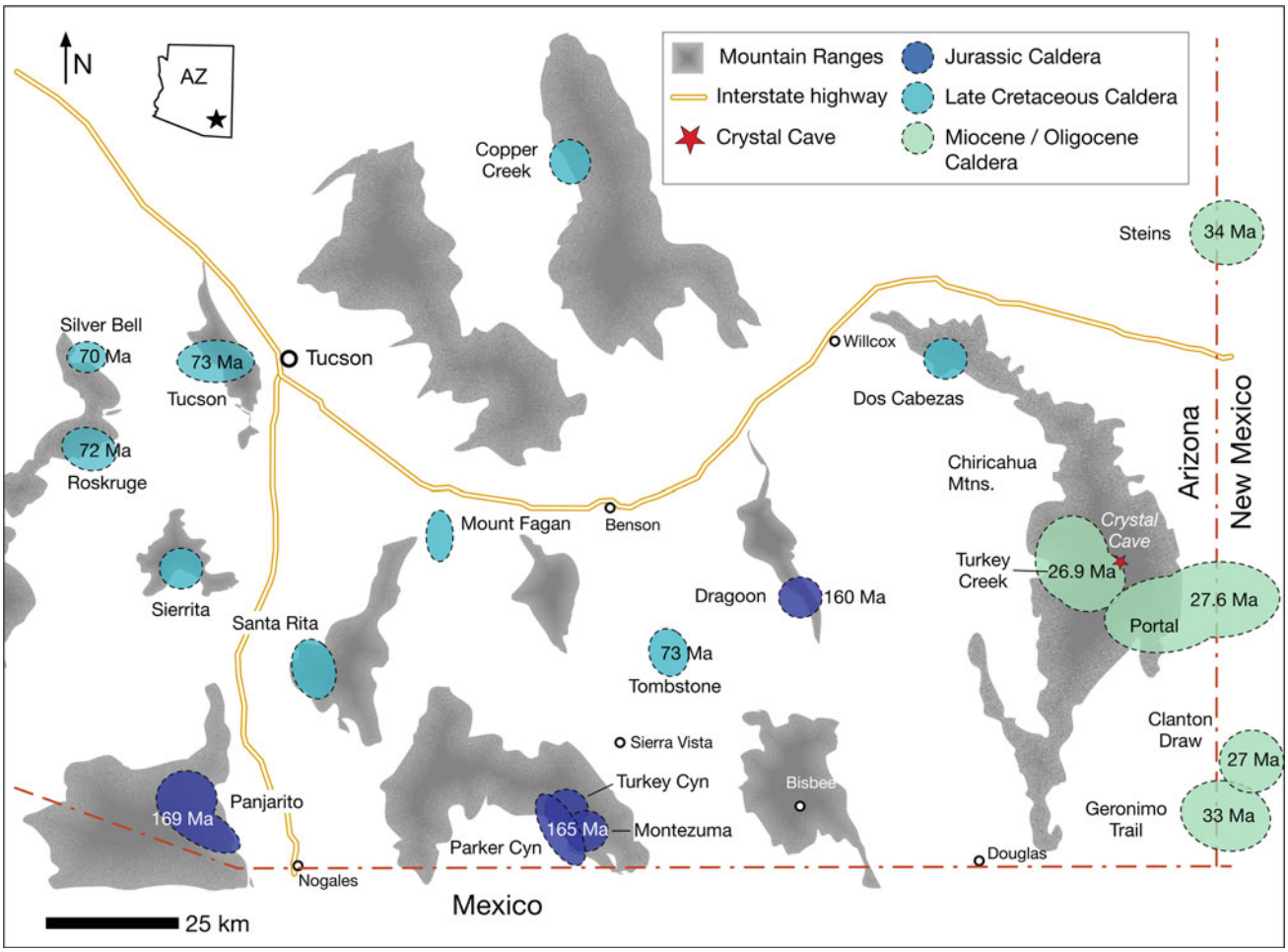

Fig. 2 Calderas and fault-bounded mountain ranges of southeastern Arizona (after Dickinson 2003; Pallister et al. 1994; Marjaniemi 1969; Anderson et al. 2005; Lipman and Sawyer 1985; McIntosh and Bryan 2000)

passages are partly filled with mineral deposits, perhaps veins of altered igneous rock and/or mineralization caused by hydrothermal fluids. The maze passages intersect quartz-lined geodes.

Six former entrances (now sealed) were probably either opened by miners or exposed by surface erosion after the cave formed. There is no indication that any of them formed hydrologically or contemporaneously with the cave. The modern cave entrance is an enlarged joint at the base of a 6-m cliff of silicified Concha Limestone (Drewes et al. 1995; Lawton 2017, personal communication). This outcrop contains small quartz geodes and other minerals indicative of hydrothermal alteration. It was silicified by the same metasomatism that accompanied the emplacement of quartz crystals in the cave (Brod 1994). Drewes and others (1995) suggested that siliceous pods locally replaced Paleozoic limestone during Cretaceous to Paleocene igneous activity in this region. Outside the cave entrance, a fault separates the silicified limestone from Late Jurassic rift basin deposits (Lawton and Olmstead 1995; Olmstead and Young 2000).

4.1 Geodes

The quartz crystals coat the interior of irregular (roughly round) vugs in the limestone. These cavities vary in diameter from a few centimeters to more than 10 m. The long axis of the largest observed geode measures approximately 16 m. Geodes are fairly evenly distributed throughout the cave with the exception of the dead-end spur passages (Fig. 4). In these farthest lateral reaches of the cave, isolated small geodes (~30–50 cm diameter) are sometimes found, but extensive exposures of quartz are absent.

The original geode configuration is difficult to reconstruct because the processes that exposed them also altered and sometimes damaged them beyond recognition. Also, some crystals are obscured by later deposits such as calcite mammillaries. A few intact quartz-lined passages are clearly tubes that seem to have formed along enlarged fractures or veins, while others are large spherical rooms with no other visible geodes nearby. Most appear to be medium-sized spheroids (1–3 m diameter) that form clusters.

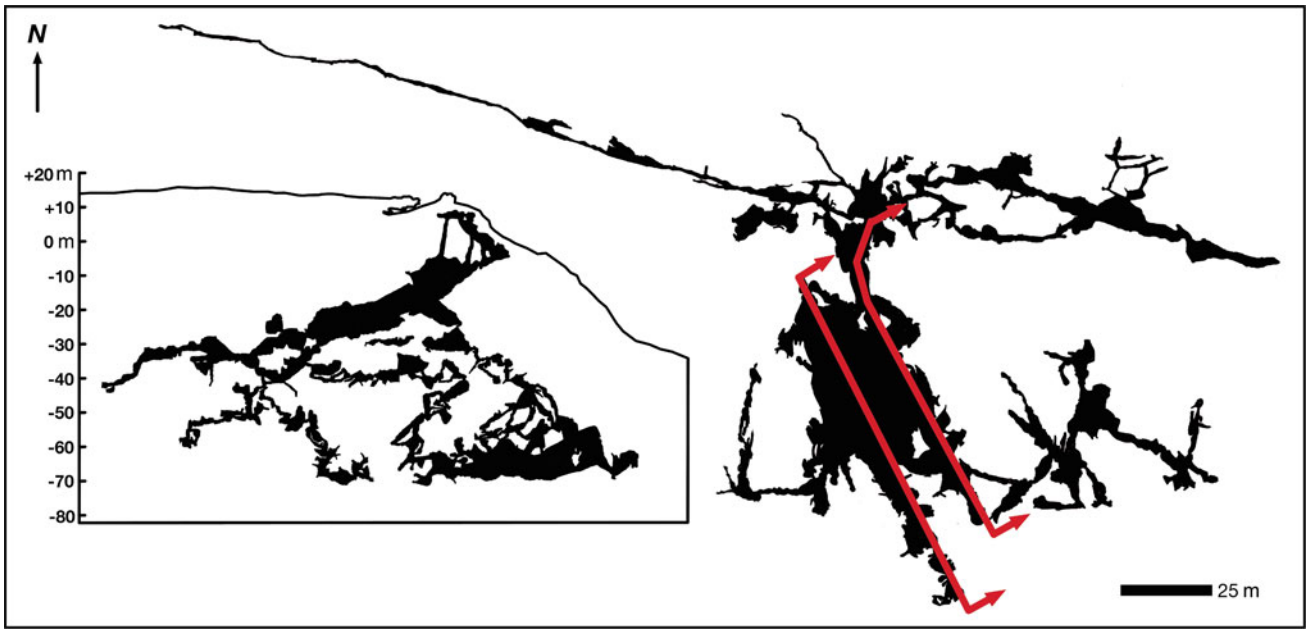

Fig. 3 Crystal Cave in plan and profile view (from Zimmerman 2016). Profile view is a composite of the two parallel slices of the cave shown on the plan view and does not show all of the cave passages

Fig. 4 Distribution of quartz crystals in Chiricahua Crystal Cave. Quartz is basically absent from the spur passages that make up the northeast, southeast, and northwest reaches of the cave

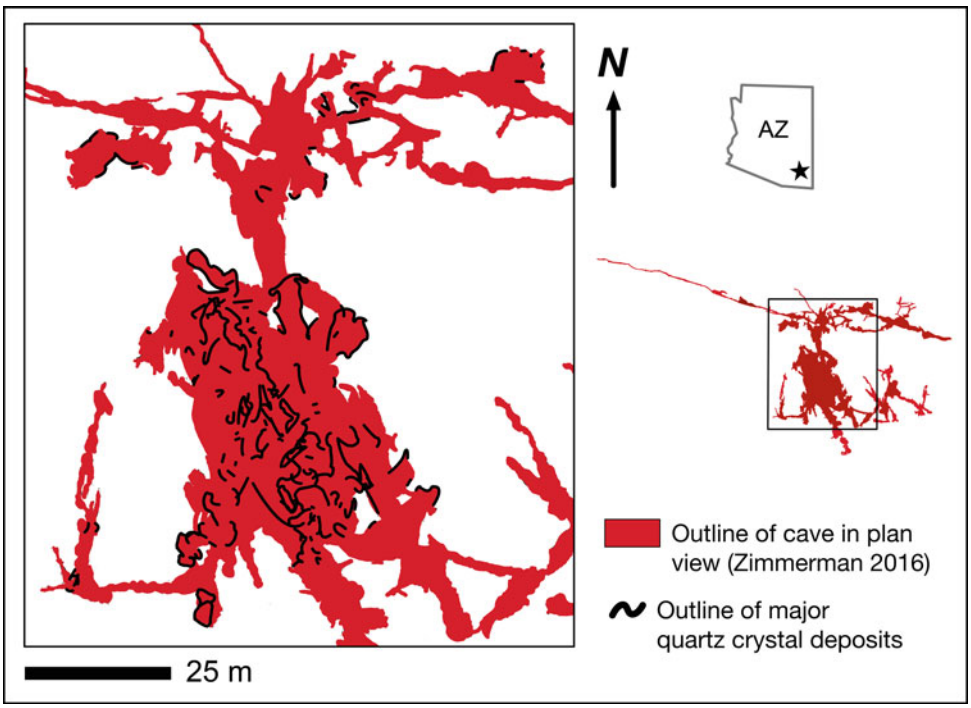

The presence of quartz provides evidence for hydrothermal activity and suggests that it played an important role in cave development. The most likely source for the quartz is cooling of a supersaturated aqueous solution (Brod 1991; Ford and Williams 2007) that started out in the range of 50 to 300 °C (Dublyansky 1997), and most probably between 100 and 200 °C (Hill and Forti 1997; Onac and Forti 2011). In the Alban Hills of Italy, Turi (1969) found that limestone vugs and the crystals that fill them are formed by the same thermal fluids. This is also likely in Crystal Cave.

The hot waters were most likely associated with the Turkey Creek Caldera (Hill 1978), putting the age of the quartz at approximately 25–30 Ma. The quartz could also be associated with a younger volcanic event. For example, the

basalt-rich San Bernardino volcanic field (0.2–3.3 Ma) is ~25 km from the cave (Lynch 1978).

4.2 Quartz Crystals

The most distinctive features of Crystal Cave are euhedral hexagonal quartz pyramids that cover all surfaces in many areas of the cave. Quartz crystals are present at 52% of stations inventoried. The crystals are generally uniform in size on any given surface, but range in size from place to place throughout the cave. Surfaces coated with very small crystals (1–3 mm diameter) are most abundant, but 1, 2–3, and 6 cm are also common, with a maximum of ~8 cm. Large crystals such as these indicate slow deposition under uniform conditions. The quartz coatings display 1–3 layers which may represent multiple depositional events (see Hill 1978). The total thickness of the coatings, including the length of projecting crystals, is equal to or greater than the diameter of the individual crystals at that location and varies from 1 mm to 12 cm. The crystals are clear, although many are stained or coated with various minerals, cave formations, or clay.

Where the underlying surface has been exposed, e.g., by mining, the quartz is typically deposited on banded chert, chert nodules, limestone bedrock (highly altered in places), or limestone nodules. Some crystals also overlie hydrothermally altered, silicified, or laminated rock. In a few locations, quartz is deposited on what appears to be calcite veinlets (boxwork) that form fin-like projections and "windows" (see Sect. 4.3). As Hill (1978) pointed out no quartz was found overlying speleothems or calcite crystals, despite reports by other investigators (Yang and Kowalewsky 1999; Strong 2009). Often the quartz forms mammillaries, because crystals tend to grow in radial patterns (Fig. 5). Broken exposures show that some of these "crystal balls" nucleated around chert or limestone, but in some cases, the crystals grew outward from a central point with no visible nucleus.

Nearby Little and Baby Crystal caves are geologically related to Chiricahua Crystal Cave. There are no other known caves in southern Arizona that contain quartz geodes of this size and abundance, and we are not aware of any others in the world. However, quartz geodes of comparable size are frequently intersected in limestone during mining operations. Ore bodies and hydrothermal minerals are often associated with carbonate rocks and are contemporaneous with hypogene speleogenesis (Lowe 2000; Klimchouk 2007, 2009).

We have observed 2-cm euhedral quartz pyramids ~100 m below the surface in the silver mines of Tombstone, AZ, in limestone that correlates with the Permian Concha Limestone of Chiricahua Crystal Cave. The Tombstone ores are associated with a 73-Ma caldera (Fig. 2). Quartz geodes exposed by mining are also described by Bella and others (2016) in small hypogenic caves in metasomatic silicic rocks related to hydrothermal limestone caves in the Carpathian Mountains of Slovakia. The quartz was estimated to have formed at temperatures above 200 °C during the evolution of a Miocene caldera (10.7–15 Ma).

4.3 Veins and Altered Surfaces

A variety of veins and altered materials are common in Crystal Cave, in addition to the silicified rock mentioned in Sect. 4. It is likely that the same hydrothermal activity that formed the cave also created these altered surfaces. Many of the cave passages form along intrusions or fractures displaying alteration products. These include (1) shiny black to brown calcite veinlets; (2) veinlets and vugs lined with very small (1–3 mm) quartz crystals; (3) possible igneous dikes; (4) soft white siliceous chalk; and (5) spongy, porous, crumbly rock weathered to sand/clay of various colors including brown, red, and yellow.

These features are interpreted as older than or contemporaneous with the tubes and fissures because they are most abundant in fractures that have been enlarged into network maze passages. No offsets were observed along these fractures, though alteration and weathering make this distinction difficult. Although some large quartz geodes appear to have formed along fractures, it is unclear whether the geodes are older or younger than the alteration products in the fractures. It is possible that alteration occurred repeatedly along the same fractures during multiple hydrothermal events.

There are places in the cave where more resistant, typically vertical features in the limestone have been exposed in relief as the cave formed. Many of these are perpendicular to the passages and therefore project from the cave walls as matching fins or a thin wall with a window. Some of the windows are man-made, presumably to allow exploration beyond. Most of these features are preserved by coatings of quartz or calcite mammillaries, so the composition of the underlying material is hidden. Some broken edges exhibit shiny black-brown calcite veinlets in the core, often coated with a thin layer of 1–3-mm quartz crystals (Fig. 6). These tiny crystals are seen in many locations throughout the cave, mainly in small veinlets and vugs along fractures, and may represent a second hydrothermal event that postdates the large geodes.

In several locations, a contact is visible between the limestone and a darker rock that may be an igneous intrusion

Fig. 5 Quartz "crystal balls." The distance across both orbs is ~45 cm. Individual crystals are ~3 cm wide (photograph by Todd Martin)

Fig. 6 At the core of a broken exposure is a thin layer of black/brown calcite, coated with tiny quartz crystals, mud, and calcite mammillaries. Tape measure for scale, in inches

(Fig. 7). This rock is commonly weathered to an orange-brown color and is difficult to evaluate given the lack of a fresh surface. It appears to have a light-colored matrix and dark-colored 1–2-mm phenocrysts. Vugs filled with 1–3-mm quartz crystals are often associated with this rock. Dacite and rhyolite dikes related to the Turkey Creek Caldera are mapped along regional and local faults on the land surface (Drewes et al. 1995). These could also be exposed in the cave. It is likely that fractures provided conduits for both hydrothermal fluids and igneous intrusions.

Fig. 7 Fissure passage with possible igneous dike exposed in the right wall

Many exposures that look like chalk and colorful sand/clay represent altered Concha Limestone, as shown by visible in situ fossils. Their composition is mainly silica, indicating metasomatism or another type of replacement. The colors may represent hydrothermal clays, mineral staining, or alteration products.

Certain surfaces in the cave appear to have been chemically corroded. There seems to be no mechanical action involved, which suggests a chemical process such as condensation-corrosion (e.g., Dublyansky and Dublyansky 2000). The corrosion was powerful: In some places, even the highly resistant quartz crystals are affected. Quartz dissolution would require a different process than limestone dissolution.

4.4 The Network Maze

Tubes and fissures of various sizes crosscut the geodes and carve out around and behind them, representing a later stage of cave formation. Cupolas and solution pockets found throughout the cave probably formed during this phase as well. The morphology and hydrological configuration of the tubes and fissures, coupled with a lack of evidence of flowing water entering from above, imply that the fluids that formed these passages were hypogenic.

Interconnected fissures (and, to a lesser extent, tubes) follow regional fractures and comprise the network maze. The fissure passages show little evidence of flowing water and in plan view many of them end abruptly in formation chokes. They are well-distributed throughout the cave laterally, but are concentrated in two elevation zones. These may represent two water table or mixing zone equilibrium lines.

A number of tubes throughout the cave dip upward in a downstream direction, which shows they formed in a phreatic environment (Palmer 2007, p. 142). Many tubes alternate between horizontal and vertical segments. These "staircases" may be rising water shafts (Ford and Williams 2007, p. 241), dissolved by hypogenic water traveling upward in search of a hydrological outlet. Some vertical segments have been enlarged into fissures. An abundance of vertical shafts, choked with fine-grained sediment and/or breakdown, are found at the bottom of the cave. These may be feeder tubes that delivered fluid from a deep-seated source.

4.5 Breakdown

Following the formation of the network maze, a massive breakdown event occurred. The bedrock was highly deformed by tectonic and caldera-related processes resulting in faults, folds, joints, igneous intrusions, and hydrothermal alteration zones. The least resistant parts of the limestone had been eaten away to form geodes and maze cave passages. Phreatic tubes had deflected around the quartz crusts of many geodes, dissolving away the limestone behind them and leaving them unsupported. As the hypogenic fluid source petered out, the water level in the cave would have dropped, triggering the collapse of any unstable rock. Due to this failure, many previously-isolated geodes probably became connected with the rest of the cave. The heart of Crystal Cave is a large chamber with breakdown boulders up to 12 m across and remnants of collapsed geodes in its ceiling and walls (Fig. 8). The central room and the area

Fig. 8 Large central room of Crystal Cave showing two gigantic breakdown boulders that fell from joint-controlled ceiling fractures. One boulder is in the *left* foreground. The other, with stalagmites, is visible in the *center* background. On the ceiling (on right) are remnants of two quartz geodes. These are among the many vugs that probably contributed to weakening the ceiling for collapse (photograph by Adam Zipkin)

directly underneath are a complex, multi-story breakdown maze that makes up a significant part of the cave.

5 Calcite Speleothems

5.1 Mammillaries

Calcite mammillaries (Fig. 9) completely coat the passages below a certain depth. There are at least seven separate areas at the bottom of Crystal Cave that converge toward the main breakdown chamber above, but do not connect to each other at depth. The mammillaries begin at the same altitude in each of these areas. Therefore, a perched pool seems unlikely. These ~1–10-cm-thick phreatic deposits begin 60 m below the cave entrance and are continuous over a vertical range of 20 m. Mammillaries do not appear to thin toward the bottom, indicating a prolonged period of sustained immersion under rather constant geochemical conditions. Perhaps this is due to slow and consistent input from a hypogenic water source and restricted atmospheric mixing. Mammillaries have been described in many other caves in the western USA, many of which are hypogenic and some of which are also hydrothermal.

A variety of interesting formations below the mammillary line appear to be soda straws and/or stalactites, draperies, rimstone dams, stalagmites, and raft cones coated with mammillaries. These speleothems demonstrate that there was a significant vadose period before the deposition of the mammillary coating. This in turn implies that perhaps the cave also had contact with epigenic waters before and/or after this vadose phase. This is supported by the presence of scallops at various locations in the cave. Though they have no discernable flow direction, the scallops indicate the presence of flowing water. Thus, the tubes and fissures and/or mammillaries may be epigenic or partially epigenic.

5.2 Raft Cones and Condensation Drip Cones

More than 50 formations with flat tops, hollow centers, or both are found between 60 and 70 m below the entrance in Crystal Cave (Fig. 10). They are probably calcite raft and condensation drip cones coated with mammillaries. The size of these formations is impressive: They are anywhere from 2 cm to 1.8 m tall and 10–60 cm in diameter. Some consist of well-cemented irregular plates (rafts). Others are flat-topped indicating drips splashed, evaporated, and spread out to form the flat top. The flat tops are not at a consistent elevation and therefore did not form at the surface of a single pool. Many have drip holes, supporting their origin by high-CO_2 condensation water (Dublyansky and Dublyansky 2000). Isotopic studies (e.g., Palmer and Palmer 2012) could shed more light on the source water. The mammillary

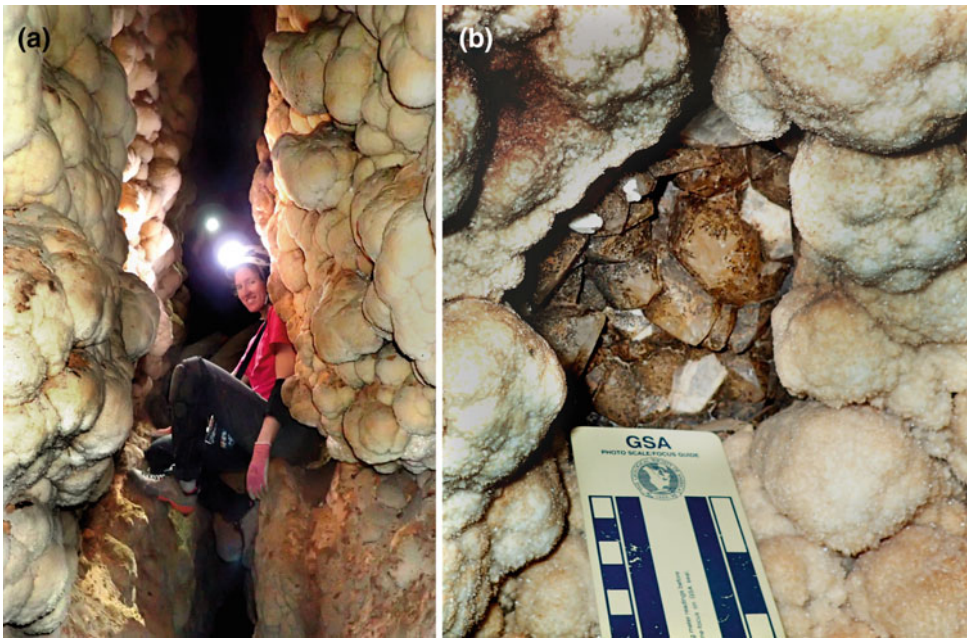

Fig. 9 **a** Mammillary crust in lower part of cave. **b** Quartz crystals covered with mammillary crust. *Left* side of ruler is in centimeters

Fig. 10 Eight flat-topped formations are visible in this photograph. Each of the tops is at a different elevation. *Yellow* tape used for survey station marker (photograph by Adam Zipkin)

coating shows that they predate or are contemporaneous with the mammillary stage.

5.3 Subaerial Speleothems

A wide array of well-developed vadose cave formations are found throughout Crystal Cave at all levels. These include stalactites, stalagmites, flowstone, helictites, popcorn, and other coralloids. Some are actively growing under present climate conditions and are the youngest features in the cave. They are found overlying quartz, phreatic surfaces, breakdown, and mammillaries.

6 Cave Evolution

We propose nine phases for the formation of Chiricahua Crystal Cave in Fig. 11. Based on the current understanding of regional and local geologic events, we can suggest a few

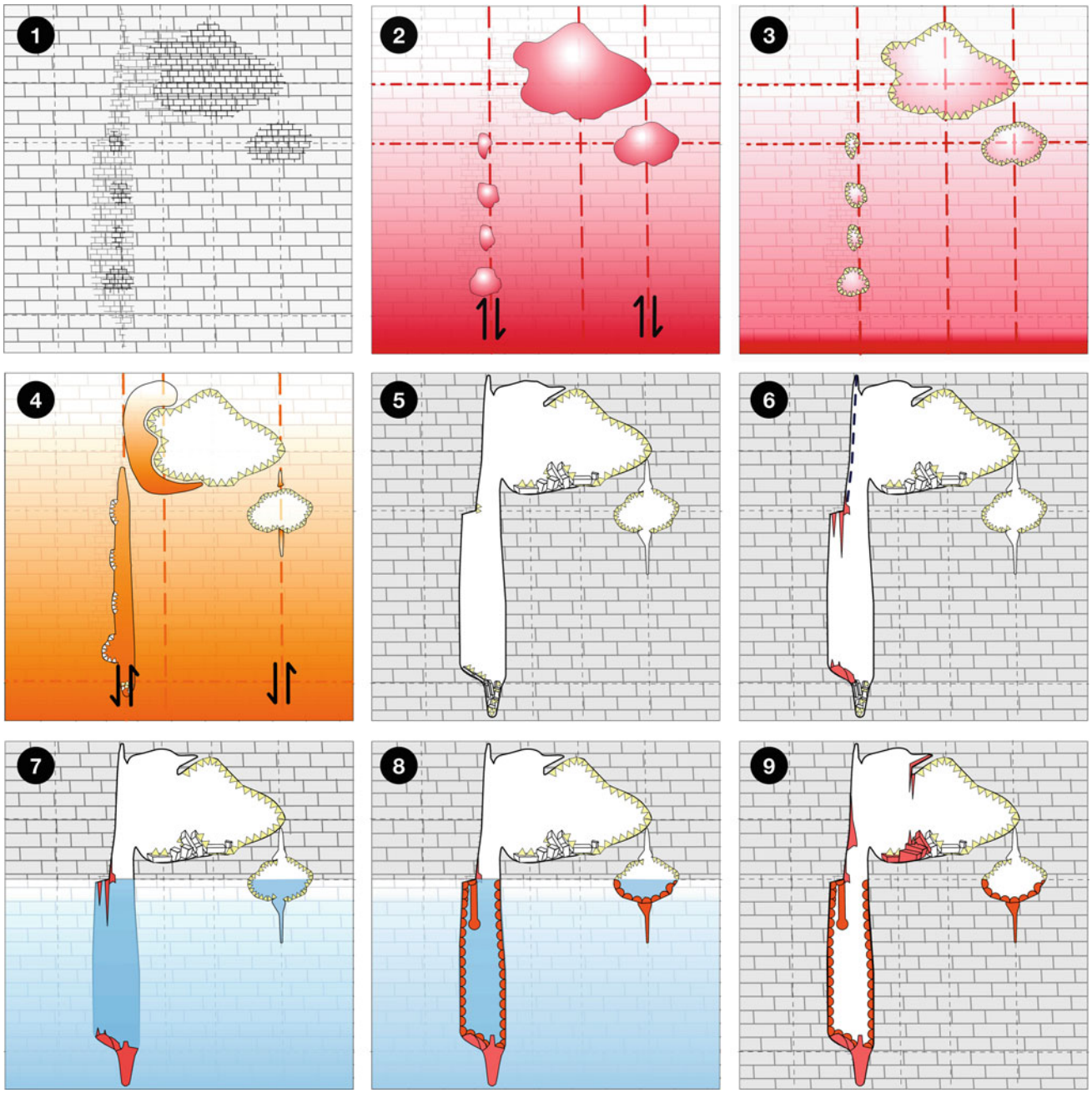

Fig. 11 Proposed sequence of events for the development of Chiricahua Crystal Cave: *1* the Concha Limestone formed, with zones of varying mineralogy and porosity that would be more susceptible to dissolution in the future. *2* Regional compression caused folding and faulting that increased the permeability of the limestone. Deep-seated hydrothermal silicic acid initiated vug formation and caused silicification of the overlying bedrock and hydrothermal alteration along joints in the limestone. *3* The solution began to cool and precipitated quartz. *4* Regional extension triggered joint formation and again increased the permeability of the limestone. Hypogenic, hydrothermal carbonic acid traveled along these conduits, dissolving phreatic tubes and fissures that crosscut the quartz geodes. Hydrothermal fluids chemically altered surfaces in the cave and along joints in the limestone. A more in-depth examination of the possible chemical reactions is required to determine which is more likely, but we propose the following processes or a combination thereof: (a) The remaining solution from Steps 2 and 3 had the capacity to dissolve more limestone than the initial silicic acid-rich fluid because it became enriched in calcite as it dissolved the vugs and became more aggressive as it cooled. (b) A second pulse of hydrothermal fluid, this time carbonic acid, entered the cave from below. (c) A mixing zone developed as meteoric water or another hypogenic water source combined with the hypogenic fluid in Step 4a or 4b. *5* The water drained out, triggering a massive collapse of the quartz geodes and other passages. At this point, the cave structure likely resembled the current cave. *6* Subaerial speleothems were deposited by meteoric waters. *7* Water again entered the cave, from above and/or below, and filled the lower passages to a uniform and stable level. This water was probably much cooler than that in Steps 2 and 4. *8* Calcite crust (mammillaries) precipitated in the lowermost parts of the cave. *9* As surface processes continued to remove Oligocene overburden, the cave became less confined, and meteoric waters percolated down through cracks, depositing subaerial speleothems of many varieties in all levels of the cave

general ages to accompany the proposed chronology. Quantitative geochronological data—for example, fluid inclusion studies of the quartz crystals and U–Th dating or isotopic studies of the mammillaries—might help to further constrain the timing and conditions.

During the Laramide Orogeny, regional compression triggered uplift in the area where the Chiricahua Mountains are today, perhaps reactivating ancient fault lines. Extensive folding and faulting occurred, including the anticline in which Crystal Cave later developed. One joint system (two perpendicular joint sets) probably formed at this time.

Igneous activity was prevalent in southern Arizona from the Jurassic to Early Neogene due to tectonic forces on the western margin of the craton. Catastrophic volcanism from shallow magma chambers left the landscape peppered with silica-rich calderas (Fig. 2), including two in the Chiricahua Mountains (27.6 and 26.9 Ma). At or before the time of the Turkey Creek volcanism (26.9 Ma), igneous intrusions and hot silicic acid may have risen from the magma body into the Permian Concha Limestone along reactivated Laramide joints and faults, dissolving out large cavities in the more susceptible areas. Perhaps the thermal water traveled to the top of the limestone and was hindered when it hit a confining layer above. This same fluid may have then lined the cavities with large subaqueous quartz crystals as it cooled. The fluid was trapped in the core of the anticline for a prolonged period of time while the quartz precipitated. The dense quartz coating hydrologically sealed off the individual geodes from the rest of the limestone.

After its final eruption, the Turkey Creek Caldera began a long process of cooling. Joints may have formed and/or reactivated as the bedrock contracted and regional basin and range extension began. These new fractures may have opened up the quartz geodes and made new pathways for hot water to travel toward the surface. Perhaps hydrothermal fluids reached the surface in the form of geysers and hot springs, causing hydrothermal alteration in subsurface fractures along the way. The fluids were rich in carbonic acid from dissolution of the limestone, and though still hydrothermal, they were probably cooler than the previous silicic acid because they formed later in the evolution of the caldera. The carbonic acid-rich water enlarged the fractures, forming an extensive network of tubes and fissures in a phreatic, hypogenic environment, perhaps in conjunction with meteoric water.

As the caldera continued to cool and the hydrothermal water source began to peter out, the water drained from the cave, initiating a phase of massive breakdown of unstable ceilings and walls. Meteoric water entering the cave from above deposited subaerial speleothems.

Water then filled the bottom of the cave again to the level of the bathtub ring, depositing mammillaries on all surfaces including vadose speleothems. After a prolonged period of deposition under stable conditions in a relatively closed phreatic environment, this water also exited the cave, leaving only perched pools. Much of the overburden (Oligocene volcanic deposits) was removed by surface erosion, increasing hydrological and atmospheric input from the surface. Subaerial speleothems began to coat the various surfaces of the cave, a process which continues to a limited extent today.

7 Conclusions

Chiricahua Crystal Cave and neighboring Little and Baby Crystal caves reflect the extraordinary geologic history of the fault-controlled mountains and caldera fields of southeastern Arizona. Room-sized quartz geodes with large, well-developed, pyramid-shaped crystals are evidence of local and regional hypogenic and hydrothermal activity. The quartz was probably deposited by superheated water from an ancient caldera 25–30 million years ago. If so, the cave, or at least part of it, is also that old.

Quartz geodes of this magnitude and abundance have not been reported in any other naturally accessible limestone cave. It seems the conditions that create such geodes rarely converge with those that form limestone caves in proximity to the land surface. However, similar geodes are often intersected by mining and other subsurface operations. In these cases, the geodes are often removed by the mining or other process that revealed them, so it is not possible to examine their relative stratigraphy and relationship to other cave phases. Crystal Cave provides a rare opportunity to study the geochemistry of vug and geode formation, for example, the potential role of silicic acid in limestone dissolution and the relationship of deep-seated or pre-lithification vug formation to later cave development.

Crystal Cave is the product of tectonic, igneous, and geomorphological forces, perhaps on a timescale of millions of years. All that remains are traces of the powerful forces that shaped this cave. From these, we have begun to assemble its fascinating story, but there are still more questions than answers. Ample opportunity remains to contest or constrain the timing and nature of the evolution of this remarkable cave.

Acknowledgements Survey work was done by Western Mappers under the leadership of Cartographer Robert Zimmerman. Our deep appreciation goes to him for coordinating this project and inviting us to study the geology, and to the US Forest Service for permission to conduct this work. Many cavers and friends helped collect data and discuss ideas and shared our enthusiasm for this project. Art and Peggy Palmer, Carol Hill, Sarah Truebe, Benjamin Tobin, Robert Zimmerman, Rodney Tennyson, Jessica Garcia, Phill Oltmann, Shana Wolff, Jennifer Foote, Liz Heness, and Robert Reuss freely shared their knowledge and helped point us in the right direction. Timothy Lawton provided his expertise and maps of the surface geology. Tom Kaye

opened his laboratory to us and guided the spectral analysis (Davis et al. 2016). Adam Zipkin provided essential photographs and patiently accompanied us on many geology trips. Thanks also to Tombstone's Good Enough Mine, for granting us special access, and Carey Granger who led our expeditions there.

References

Anderson TH, Nourse JA, McKee JW, Steiner MB (eds) (2005) The Mojave-Sonora megashear hypothesis: development, assessment and alternatives. Geological Society of America Special Paper 393

Bella P, Gaál L, Šucha V, Koděra P, Milovský R (2016) Hydrothermal speleogenesis in carbonates and metasomatic silicites induced by subvolcanic intrusions: a case study from the Štiavnické vrchy Mountains, Slovakia. Int J Speleol 45(1):11–25

Brod L (1991) A work trip to Cochise County. Desert Caver 21(3):23–25

Brod L (1994) Chiricahua Crystal Cave—report. Survey Trip No. 7. Desert Caver 24(1):10–14

Davis NK, McMillan BA, Kaye TG, Truebe SA (2016) Geologic guidebook for Chiricahua Crystal Cave, in Zimmerman, Chiricahua Crystal Cave, Monograph 1: The Underground Conservancy, Tucson, AZ

Dickinson, WR (2003) Excursion to Gardner Canyon: sedimentology and tectonic context of Mesozoic Strata in the Santa Rita Mountains, southeastern Arizona. Arizona Geological Survey Contributed Report CR-03-A. Arizona Geological Survey, Tucson, AZ, 29 p

Drewes H, du Bray EA, Pallister JS (1995) Geologic map of the Portal Quadrangle and vicinity, Cochise County, Southeast Arizona. U.S. Geological Survey Miscellaneous Investigations Series Map I-2450, scale 1:24,000

Dublyansky VN, Dublyansky YV (2000) The role of condensation in karst hydrogeology and speleogenesis. In: Klimchouk AB, Ford DC, Palmer AN, Dreybrodt W (eds) Speleogenesis: evolution of karst aquifers. National Speleological Society, Huntsville, Alabama, pp 100–112

Dublyansky YV (1997) Hydrothermal cave minerals. In: Hill CA, Forti P (eds) Cave minerals of the world, 2nd edn. National Speleological Society, Huntsville, Alabama, pp 252–255

Ford D, Williams PD (2007) Karst hydrogeology and geomorphology. Wiley, New York

Hill CA (1978) Chiricahua Crystal Cave, Arizona. Cave Research Foundation, Annual report, p 19

Hill CA, Forti P (1997) Cave minerals of the world, 2nd edn. National Speleological Society, Huntsville, Alabama

Klimchouk AB (2007) Hypogene speleogenesis: hydrogeological and morphogenetic perspective. Special Paper 1, National Cave and Karst Research Institute, Carlsbad, New Mexico

Klimchouk AB (2009) Principal characteristics of hypogene speleogenesis. In: Land L, Veni G, Stafford KW (eds) Advances in hypogene karst studies: NCKRI symposium 1, National Cave and Karst Research Institute, Carlsbad, New Mexico, pp 1–11

Lawton TF, Olmstead G A (1995) Stratigraphy and structure of the lower part of the Bisbee Group, northeastern Chiricahua Mountains, Arizona. In: Jacques-Ayala C, González-León C M, Roldán-Quintana J (eds) Studies on the Mesozoic of Sonora and adjacent areas. Boulder, Colorado, Geological Society of America Special Paper 301

Lipman PW, Sawyer DA (1985) Mesozoic ash-flow caldera fragments in southeastern Arizona and their relation to porphyry copper deposits. Geology 13:652–656

Lowe DJ (2000) Role of speleogenesis in the development of hydrocarbon and mineral deposits. In: Klimchouk AB, Ford DC, Palmer AN, Dreybrodt W (eds) Speleogenesis: evolution of Karst Aquifers. National Speleological Society, Huntsville, Alabama, pp 473–480

Lynch DJ (1978) The San Bernardino Volcanic Field of southeastern Arizona. In: New Mexico geological society guidebook, 29th field conference, land of Cochise, pp 261–268

Marjaniemi DK (1969) Geologic history of an ash-flow sequence and its source area in the Basin and Range province of southeastern Arizona. PhD Dissertation, The University of Arizona, Tucson, AZ

McIntosh WC, Bryan C (2000) Chronology and geochemistry of the Boot Heel volcanic field, New Mexico: New Mexico geologic society guidebook, 51st Field Conference, Southwest passage—a trip through the Phanerozoic, pp 157–174

Olmstead GA, Young K (2000) Late Jurassic ammonites from the northeastern Chiricahua Mountains, southeast Arizona. New Mex Geol 22(1):1–7

Onac BP, Forti P (2011) Minerogenetic mechanisms occurring in the cave environment: an overview. Int J Speleol 40:79–98

Pallister JS, du Bray E.A, Latta JS (1994) Geologic map of the Rustler Park Quadrangle, Cochise County, Arizona. U.S. Geological Survey Geologic Quadrangle Map GQ-1696, scale 1:24,000

Palmer AN (2007) Cave geology. Cave Books, Dayton, OH

Palmer MV, Palmer AN (2012) Petrographic and isotopic evidence for late-stage processes in sulfuric acid caves of the Guadalupe Mountains, New Mexico, USA. Int J Speleol 41(2):231–250

Strong TR (2009) Basin and range province of Southern Arizona In: Palmer AN, Palmer MV (eds) Caves and Karst of the USA, pp 260–262

Turi B (1969) Carbon and oxygen isotopic composition of carbonates in limestone blocks and related geodes from the "Black Pozzolans" Formation of the Alban Hills. Chem Geol 5:195–205

US Congress (1988) Federal Cave Resources Protection Act, Public law 100–691 100th Congress

Yang R, Kowalewsky D (1999) Chiricahua Crystal Cave, Cochise County, Arizona. The Desert Caver, Escabrosa Grotto 29(3):8–15

Zimmerman R (ed) (2016) Chiricahua Crystal Cave, Monograph 1: the underground conservancy, Tucson, AZ, 88 p

A Conceptual Model for Hypogene Speleogenesis in Grand Canyon, Arizona

34

Victor J. Polyak, Carol A. Hill, Yemane Asmerom, and David D. Decker

Abstract

Although Grand Canyon hosts exceptionally well-formed vadose caves and exemplary paleokarst, it also contains hypogene caves that provide important information on the canyon's age and evolution. These caves exhibit speleogenetic materials, passage morphologies, and locations near the top of the Mississippian Redwall Limestone that represent major hypogene dissolution phases. Cave origin resulted from CO_2 and H_2S in solutions that upwelled from depth and mixed with Redwall–Muav aquifer water. Lack of abundant speleogenetic gypsum suggests that CO_2 was the primary solutional agent, while upwelling H_2S likely played only a minor role. Each phase of hypogene speleogenesis in our model encompasses the following sub-events, from deep to shallow: (1) dissolution of cave passages 500 ± 250 m below the water table or potentiometric surface, sometimes with Fe- and Mn-oxide by-products; (2) deposition of calcite spar linings (~50–100 m below the water table); (3) deposition of calcite mammillary coatings (1–20 m below the water table); (4) deposition of calcite folia at the water table; and (5) deposition of gypsum rinds a few meters above the water table. Controls on the amount of cave dissolution and speleogenetic by-products probably include regional water table fluctuations during the Miocene and Pliocene, in combination with magmatic/tectonic pulses that pumped CO_2 and H_2S from below. The complete cycle of Grand Canyon hypogene speleogenesis includes a largely dissolutional phase under confined conditions and a later (mostly by-product) phase taking place under unconfined conditions. The process terminates when the water table descends below the cave.

Keywords

Grand Canyon • Hypogene caves • Calcite spar • Confinement • Supercritical CO_2

1 Introduction

Grand Canyon is one of the most remarkable landscapes on Earth, exposing almost two billion years of geologic history (Fig. 1). Within these strata, which are wonderfully exhibited in the canyon walls, is a thick sequence of limestones and dolostones of the Mississippian Redwall Limestone and underlying Cambrian Muav Formation (Fig. 2), referred to here as the strata that define the Redwall–Muav aquifer. Hundreds of caves are hosted by this thick carbonate sequence, most of them being accessible only by foot and/or boat.

V.J. Polyak (✉) · C.A. Hill · Y. Asmerom · D.D. Decker
Department of Earth and Planetary Sciences, University of New Mexico, Albuquerque, NM 87131, USA
e-mail: polyak@unm.edu

1.1 Geologic Setting of Caves

Until about 20 years ago, karst features in Grand Canyon were classified into two main categories (1) Mississippian paleokarst features near the top of the Redwall Limestone, and (2) vadose caves of the Kaibab Plateau, eastern Grand Canyon, and of Marble Canyon, exposed either at the base

© Springer International Publishing AG 2017

A. Klimchouk et al. (eds.), *Hypogene Karst Regions and Caves of the World*,
Cave and Karst Systems of the World, DOI 10.1007/978-3-319-53348-3_34

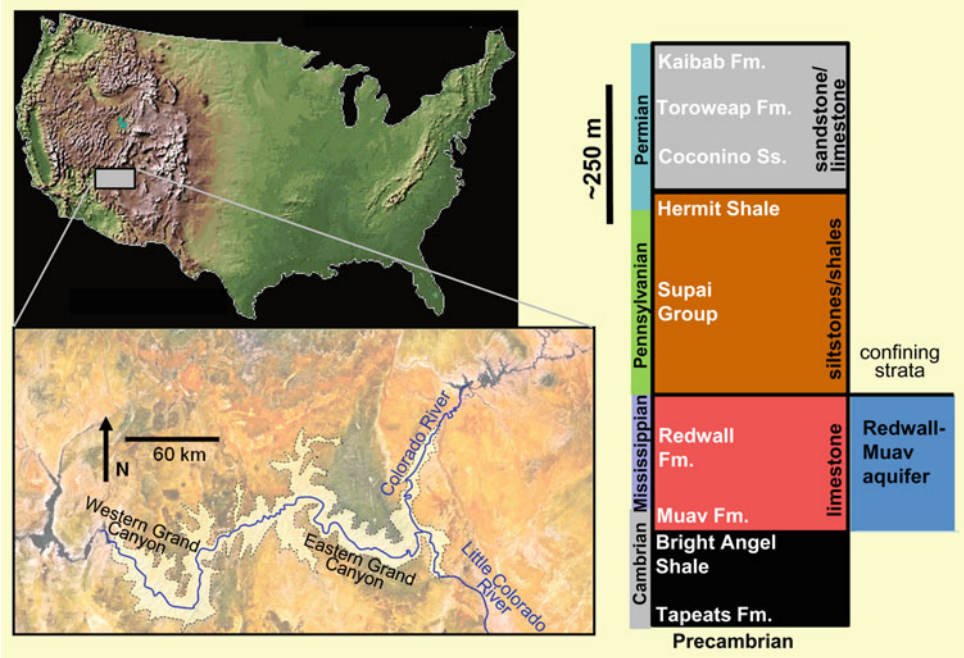

Fig. 1 *Top* location of Grand Canyon on an elevation map of the USA (elevation map courtesy of www.Theodora.com/maps). *Bottom* satellite image of Grand Canyon (from NASA World Wind) showing eastern and western segments. *Right* generalized stratigraphy of Grand Canyon showing the Redwall-Muav aquifer limestones that are capped by less permeable sandstones, siltstones, and mudstones of the Supai Group and Hermit Shale. See Beus and Morales (1990) and Blakey and Ranney (2008) for detailed discussions of the stratigraphy

of the carbonate sequence or at river level. (3) Huntoon (2000) was the first to identify a third category: phreatic caves, which he proposed were independent of the development of paleokarst and vadose karst. In addition to these three karst types, Hill and Polyak (2014) proposed a karst-piracy mechanism for integrating the Colorado River *under* the Kaibab uplift to connect the eastern side of the Grand Canyon with the western side ~6 Ma (million years ago). This karst-connection stream cave remains hypothetical, because widening and erosion of the canyon has apparently obliterated all evidence for it.

Overlying the Redwall Limestone is a ~300 m sequence of less permeable siliciclastic rocks of the Hermit Formation and Supai Group (Fig. 2). Hydrologically, this series forms (or once formed) a confining unit for the underlying Redwall and Muav carbonate units when the potentiometric surface is within or above the Supai Group of rocks, consistent with the phreatic speleogenetic model of Huntoon (2000). More recently, these phreatically developed caves have also been attributed to hypogene speleogenesis (Hill et al. 2001; Polyak et al. 2008; Hill and Polyak 2010), largely consistent with confined hypogene speleogenesis as defined by Klimchouk (2007). Some of the recently discovered examples are of significant size (e.g., Leandra's Cave, with >12 km of surveyed length; Rice 2012).

1.2 Hypogene Caves in Grand Canyon

The definition and types of hypogene speleogenesis are still being discussed. Two types are now recognized: caves in which the solutional potential is generated below the land surface (Palmer 1991) and caves in which the solutionally aggressive water rises from depth (Klimchouk 2007). We demonstrate both, with the geochemical approach yielding absolute evidence, and the hydrogeologic approach allowing for geomorphic interpretations related to the age and origin of Grand Canyon.

Hypogene caves of Grand Canyon are generally horizontal and characterized by ramiform or maze-type passage patterns typical of phreatic caves (Palmer 1991). They are located in the Mooney Falls Member of the Redwall Formation in eastern Grand Canyon, and within the Muav and undivided Cambrian limestones, Redwall Limestone, and Supai-equivalent limestones in western Grand Canyon. All of these hypogene caves have in common certain speleogenetic by-products, which include Fe- and Mn-oxides, calcite spar (large euhedral crystals lining cave walls), mammillary calcite, folia, cave rafts, and gypsum rinds (Figs. 3 and 4). These deposits and their chemical and isotopic signatures have been previously described by Hill et al. (2001), Polyak et al. (2008), Hill and Polyak (2010), and Polyak et al. (2014). The karst hydrology of Grand Canyon has been covered by Hill and Polyak (2010). However, Grand Canyon hypogene speleogenesis has not yet been well defined as an exemplary event. Here we discuss the conceptual model of hypogene speleogenesis in more detail and its relationship to the evolution of Grand Canyon, with emphasis on how caves formed during magmatic/tectonic episodes over at least the last 17 My and their dependence on the position of the potentiometric surface (or water table) with time.

Fig. 2 The Redwall formation on the south rim of eastern Grand Canyon. Most hypogene caves are located near the top of this formation

2 Evidence for Hypogene Speleogenesis

Early on, Hill et al. (2001) recognized that the gypsum rinds coating the spar, mammillaries, and bedrock in Grand Canyon caves are evidence for sulfuric acid speleogenesis; the light $\delta^{34}S$ values of the gypsum show that the sulfur source was deep below the caves. The sequence of by-products deposited during speleogenesis was reported to be (from early to late): cave spar, mammillaries, folia, and gypsum rinds (Polyak et al. 2008; Hill and Polyak 2010). This evidence, in combination with cave patterns, passage morphology (domes, etc.; Fig. 4), and positions of entrances, is a strong indicator that these phreatically developed caves are entirely hypogene. In the remainder of this chapter, we will present a more detailed discussion of the evidence mentioned in the Introduction.

2.1 Cave Spar: Evidence for Deep Phreatic Dissolution

The bedrock walls of many Grand Canyon caves are coated with calcite cave spar (large >1 cm euhedral scalenohedral and rhombohedral crystals) (Fig. 5), which we suggest is a

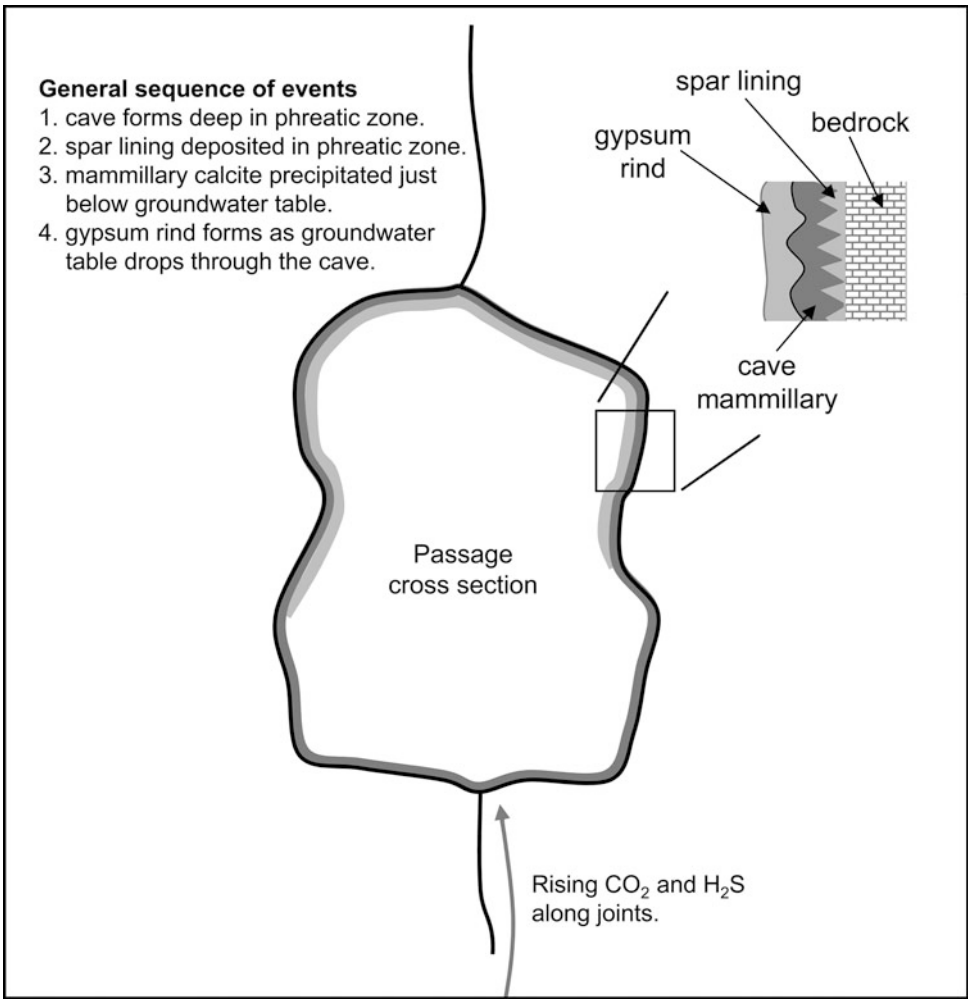

Fig. 3 Sequence and timing of by-product deposition during hypogene speleogenesis

good indicator of the depth of speleogenesis. Some phreatic Grand Canyon caves are entirely coated with spar linings (Polyak et al. 2008), which are characterized by columnar structure, uniform coverage of walls, and commonly by rhombohedral crystal terminations. There is at least one exception in Moria Cave on the Kaibab arch where crystals are larger and not columnar. In Bida Cave, eastern Grand Canyon, where the spar linings are coated with mammillary calcite, the contact between these two speleothems appears conformable. Both have the same strontium isotope values (Fig. 5), which supports the proposition that both types of 'speleogenetic' speleothems formed from the *same* rising solutions mixing with aquifer water, with spar deposition somewhat continuous with mammillary deposition as the water table dropped. Cave spar has been measured to form at depths of 500 ± 250 m below the water table in relatively unconfined conditions in the Guadalupe Mountains of New Mexico (DuChene, Chap. 31). These Guadalupe spar caves and their crystal linings have recently been interpreted to have formed at the depth where supercritical CO_2 transforms to aqueous CO_2 (Decker et al. 2015). Until more specific modeling can account for confined aquifer conditions, we propose a similar depth of origin for the hypogene caves of Grand Canyon. If the potentiometric surface was 500 ± 250 m above the Redwall–Muav aquifer when most of the cave dissolution took place, then the caves would have formed in a mainly confined system.

3 A Proposed Definition of Grand Canyon Hypogene Speleogenesis: Not Strictly Confined

Grand Canyon hypogene speleogenesis is dependent on upwelling aggressive components (H_2S, CO_2) mixing with the water of the Muav–Redwall aquifer (Hill and Polyak 2010). Whenever the water table is positioned above these limestones, the speleogenetic conditions are *confined* by the overlying low-permeability Supai Group. This stratigraphic relationship leads to an interpretation that regional hypogene speleogenesis is driven by the below-lying source of CO_2 and H_2S, where major dissolution occurs primarily in a

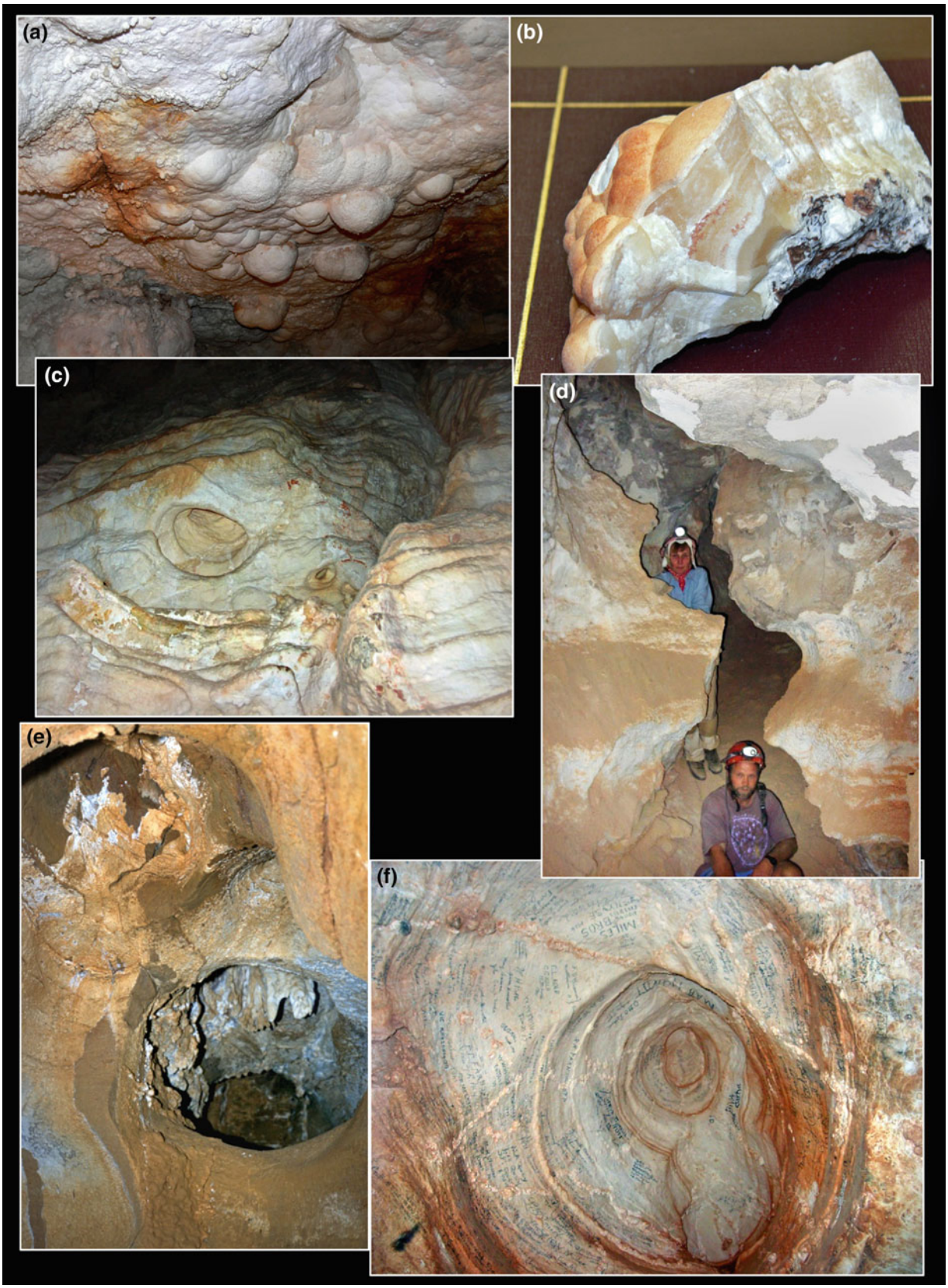

Fig. 4 Passage features characteristic of hypogene speleogenesis: **a** mammillary coating, Grand Canyon Caverns, **b** typical sample of eastern Grand Canyon mammillary calcite, **c** Cupolas in cave wall, **d** passage profile in an eastern Grand Canyon cave and **e, f** small domes in ceiling of Cave of the Domes, eastern Grand Canyon

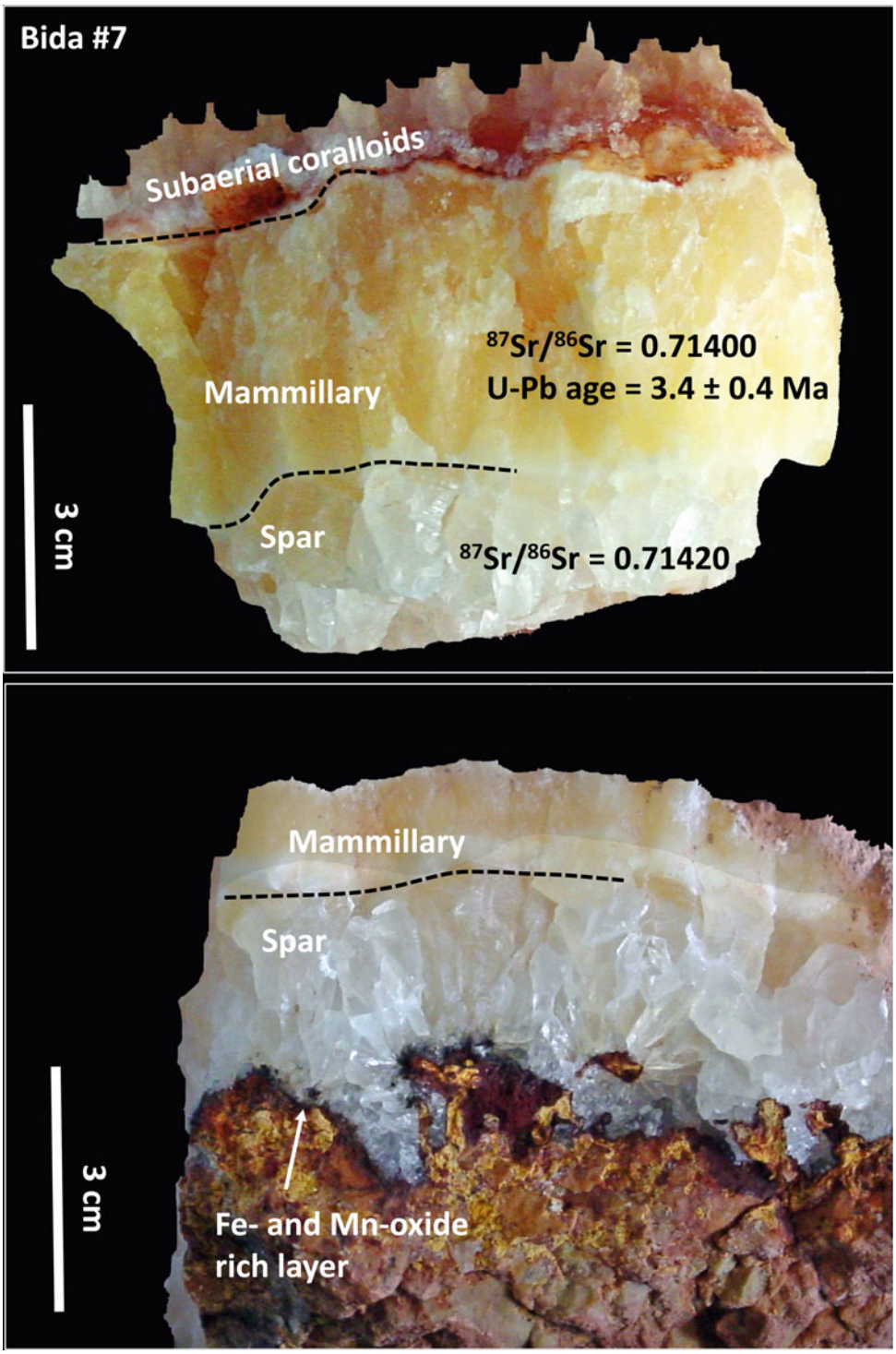

Fig. 5 Spar lining and mammillary coating of cave surfaces. *Top* mammillary calcite coating deposited directly on spar lining, Bida Cave, eastern Grand Canyon. In this example, the $^{87}Sr/^{86}Sr$ ratio value of the mammillary calcite is the same as that measured in the calcite spar. Note that the calcite spar has no color, whereas the mammillary calcite is yellowish orange, characteristic of most mammillary calcite in the Grand Canyon. Mammillaries are the most useful speleogenetic by-products because they can be readily dated by U–Pb methods. *Bottom* note the Fe- and Mn-rich layer underlying the spar

confined aquifer. However, because the water table had been descending relative to stratigraphic position during the last 4 million years as the Colorado River incised much of eastern Grand Canyon for example, the upwelling H_2S and/or CO_2 would have stopped dissolving cave passages when the water table fell below them. That period of speleogenesis, from the time the potentiometric surface dropped into the Redwall–Muav aquifer to the time when the water table dropped below the cave, would have taken place in *unconfined* conditions and is largely a by-product phase of hypogene speleogenesis with evidence of only minor dissolution. Therefore, we define Grand Canyon hypogene speleogenesis as including a (1) major dissolution phase that occurs in the deep phreatic zone under confined conditions, followed by a

(2) deposition phase at shallower depth, which may also involve only minor dissolution. All of these products of speleogenesis result from upwelling hypogene water mixing with ambient aquifer water. The dropping water table in our speleogenetic model ties the speleogenesis intimately to the evolution and incision of Grand Canyon (Hill and Polyak 2010).

4 The Volcanic–Tectonic Speleogenesis Pump

Did these caves form from the continuous upward migration of CO_2 and H_2S along joints, or was this process episodic due to periodic magmatic and/or tectonic events? Decker et al. (2015) demonstrated that most cave spar in Guadalupe Mountains spar caves was precipitated simultaneously with the ignimbrite event of 36–28 Ma, the volcanic phase of spar-cave genesis proposed by Hill (1996). That regional flare-up in New Mexico and West Texas likely caused an increase in groundwater temperatures, but also an increased rate of CO_2 rise. We suggest that the same magmatic associations took place in the Grand Canyon region. Measured U–Pb ages for cave mammillaries in Grand Canyon range from 17 to 0.9 Ma (Polyak et al. 2008), which equates roughly with the period of Basin and Range magmatic and tectonic activity in that region (McQuarrie and Wernicke 2005). We also suggest that these events served as 'pumps' to provide the necessary ingredients for speleogenesis in the Redwall–Muav aquifer via joints that were opened by increased pressures and/or tectonic movement. Our proposition suggests that hypogene speleogenesis was episodic and that complete speleogenesis may have required more than one volcanic–tectonic episode.

5 Application of the Grand Canyon Hypogene Speleogenesis Model

5.1 Cave Size Versus Position of the Potentiometric Surface

According to the model of Decker et al. (2015), the major dissolution phase for Grand Canyon hypogene caves is likely to have occurred at depths of 500 ± 250 m below the potentiometric surface. This model considers the action of supercritical CO_2, where the pressure–temperature relationship is ideal for dissolution followed by deposition of large spar crystals (see DuChene et al. Chap. 31). However, the depth of spar formation was possibly shallower in Grand Canyon than the spar that lined geode-like spar caves in the Guadalupe Mountains, because of the more clearly confined conditions that prevailed during the major dissolution phase in the Grand Canyon. Under confined conditions at these depths, assuming aquifer flow rates sufficient to carry away dissolved carbonate, we may consider that most dissolution occurred primarily during magmatic/tectonic pulses. The ideal zone for CO_2-generated dissolution under confined conditions in Grand Canyon was near the top of the Redwall–Muav aquifer in the Mooney Falls Member, where Mississippian paleokarst porosity was the most abundant, and this is where most hypogene caves are located (Hill and Polyak 2010). For larger hypogene caves to form in Grand Canyon, it would have been necessary for the potentiometric surface to remain stationary in the overlying Supai strata for a long time. The greater the duration of a stable potentiometric surface, the better the chance for multiple magmatic/tectonic pulses to dissolve large caves. According to this model, smaller caves would be predicted to date from periods of descending potentiometric surface, resulting in a shorter time for speleogenesis. Larger caves in Grand Canyon may therefore correlate with a longer stability of the potentiometric surface, ~500 m above the top of the optimal cave-forming zones of the upper Redwall Formation. This likely took place in eastern Grand Canyon before 4 Ma, because the results from Polyak et al. (2008) show that the water table in the Grand Canyon region has dropped over the past 4 My at rates of 100–300 m/My. This model suggests that the potentiometric surface was static at 250–750 m above the cave-forming zone of the Redwall for a long period of time prior to 4 Ma, which would allow the larger caves of eastern Grand Canyon to form in the Redwall.

5.2 Hypogene Deposits in Non-carbonate Rocks

Hypogene deposits in the Grand Canyon region are not restricted to the Muav–Redwall carbonates, but can also occur to a lesser degree in non-carbonate rocks. For instance, Polyak et al. (2008) reported mammillaries from a small remnant cave formed in the Supai sandstones in Marble Canyon, and a zone of mammillary-like calcite was observed in a sequence of basalts on the Hualapai Plateau. These small caves and deposits are probably widespread throughout Grand Canyon. In the case of mammillary-like calcite in basalt, only the unconfined phase of hypogene processes could have accounted for deposition of calcite in fractures and voids within the basalt.

5.3 Restricted Distribution of Hypogene Events in Grand Canyon

Although the details of hypogene speleogenesis in Grand Canyon are still open to discussion, we propose that the dissolution of carbonate rocks, and the deposition of Fe and

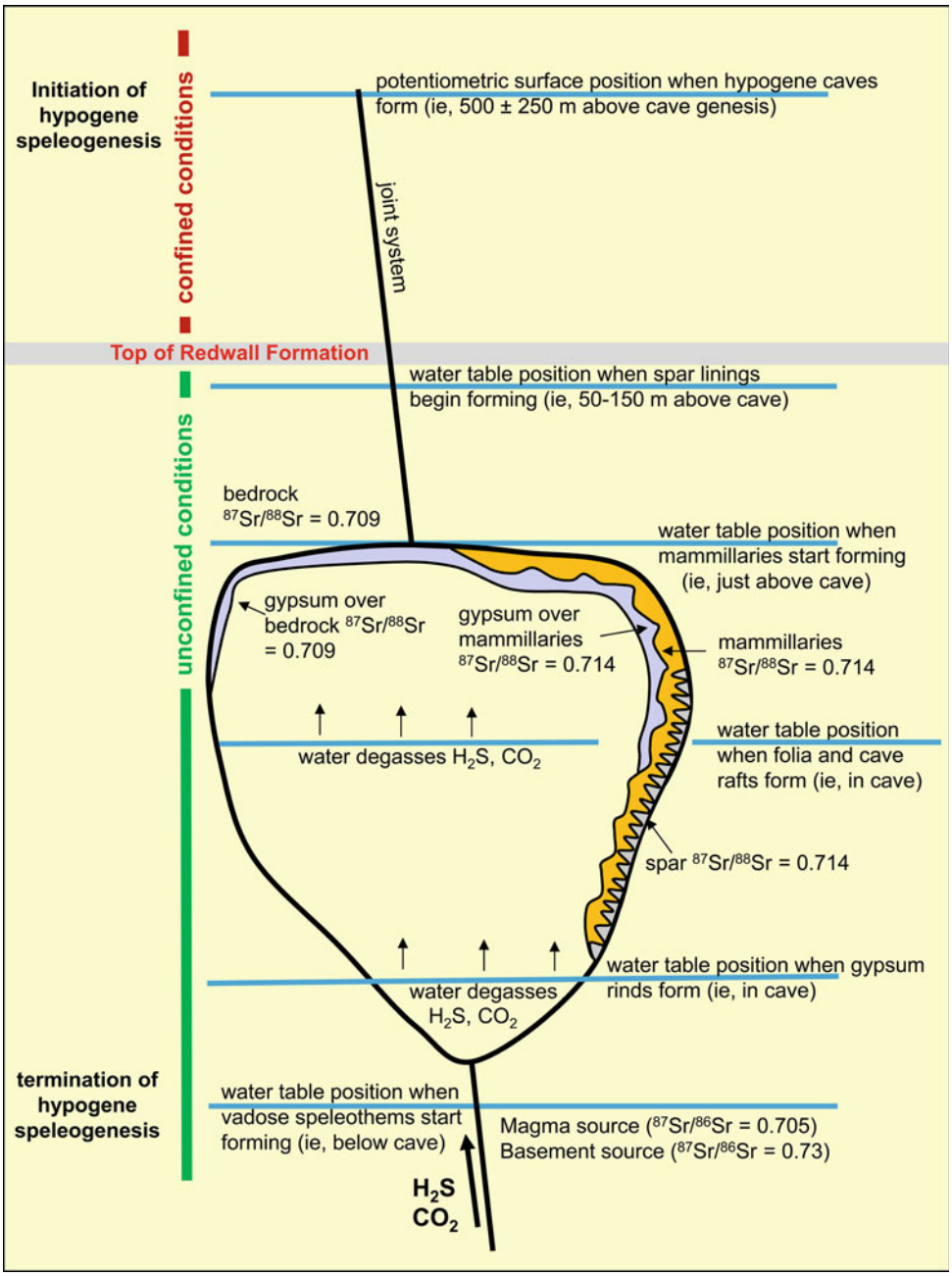

Fig. 6 Model of the complete cycle of hypogene cave origin during a falling water-table scenario typical of the eastern Grand Canyon

Mn oxides, cave spar, mammillary calcite, folia, cave rafts, and gypsum rind, constitute an *entire* hypogene speleogenetic event (Fig. 6). The various sub-events all involve the mixing of upwelling components with ambient aquifer water. Therefore, the cycle of Grand Canyon hypogene speleogenesis ceases only when the water table descends below the cave, after which normal epigenic-subaerial processes take place. However, some caves that formed during these events did not experience every stage in the sequence and may be devoid of the expected by-products except for the Fe and Mn oxide by-products of the very early speleogenesis stage. Therefore, where the water table descended slowly or remained stable for a long time, larger caves may contain evidence for *all* sub-events. An example is Bida Cave, a medium-sized cave containing evidence for the entire speleogenetic sequence. Most hypogene caves in Grand Canyon contain evidence for only one, or a few, of the sub-events.

6 Conclusions

Most of the Grand Canyon hypogene caves and their spar linings formed well below the water table or potentiometric surface, with major dissolution occurring at depths

of 250–750 m, whereas spar linings were likely deposited at depths of 50–100 m. By our model, as the potentiometric surface descended through the non-permeable Supai siltstones and mudstones, and into the karstic Redwall and Muav carbonates, it evolved into a relatively flat water table. The mammillaries probably formed a few meters to a few tens of meters below the water table, the folia and cave rafts at the water table, and gypsum rinds within a few meters above the water table. In eastern Grand Canyon, the ~3.5–3.8 My age of the mammillaries represents the time when the water had already descended into the Redwall Formation (Polyak et al. 2008). At that time, the water table in the upper Redwall Limestone was relatively flat and remained at the same level as the Colorado River as the river was carving eastern Grand Canyon. Therefore, hypogene speleogenesis is intimately associated with canyon evolution, because its timing and duration were determined by the rate of water-table descent. The western Grand Canyon and its speleogenetic history are more complicated, as shown by the presence of paleocanyons and older mammillaries (17 and 7.5 Ma; Polyak et al. 2008). However, evidence for hypogene speleogenesis has great potential to further contribute important information on the evolution of the western Grand Canyon and how it differs from that of the eastern Grand Canyon.

Phreatic caves in eastern Grand Canyon were largely dissolved in a confined hydrologic system at depths of 500 ± 250 m by the mixing of upwelling CO_2 and H_2S and horizontally moving Redwall–Muav aquifer water, in accordance with the supercritical CO_2 model of Decker et al. (2015). Fe- and Mn-oxides formed during confined conditions and are considered the earliest by-products of this type of speleogenesis. Because hypogene speleogenesis is intimately associated with rising CO_2 and H_2S, all events related to hypogene speleogenesis during unconfined conditions are present until the water table descends below the caves. Therefore, we include both the dissolution phase and related deposition phase as a complete cycle of hypogene speleogenesis. This contrasts with the better known model of H_2SO_4 speleogenesis of Guadalupe Mountains caves presented by Egmeier (1973), Hill (1996), and others, where most of the major cave dissolution occurred at the water table and the H_2SO_4 speleogenesis cuts across much older spar-lined spar caves. The early stage of cave development was much more important in the Grand Canyon, and modifications related to hypogene speleogenesis that might be related to the latter stage continued to occur in the same voids created in this early stage.

Given that the water table was stationary at 500 ± 250 m above the upper Redwall Limestone for millions of years, our model predicts that extensive cave systems should form throughout multiple magmatic/tectonic events (each event triggers a hypogene speleogenesis event), whereas small caves should form during times when the water table was descending. The flow rate in the aquifer should also play an important role.

Completion of an entire sequence of hypogene speleogenesis would take place only if magmatic/tectonic activity that triggers these events occurs continuously or frequently from the time the potentiometric surface is positioned 500 ± 250 m above the upper Redwall Limestone to the time that the water table in the Redwall–Muav aquifer descends below the caves. Bida Cave in eastern Grand Canyon preserves evidence for all of these sub-events and represents an entire sequence of Grand Canyon hypogene speleogenesis. However, most hypogene caves in Grand Canyon contain evidence for only some of these sub-events—for example, some caves contain only mammillary calcite or only gypsum rinds. Given that magmatism/tectonism supplies the CO_2 and H_2S for speleogenesis, caves that contain only gypsum rinds must have formed during episodes that would have acquired rinds only during a second magmatic/tectonic pulse, when the water table was located at the base of the cave. In this example, two separate magmatic/tectonic pulses probably occurred (two speleogenesis sub-events): one to dissolve the void, and the other to form the rinds. Our model also allows speleogenetic materials to form in voids in non-carbonate rocks (e.g., mammillaries in fissures and voids within Supai Group siltstones or Miocene basalts) because the solutions that rose through the Redwall–Muav Limestone were able to precipitate calcite whenever CO_2 was released in fissures and voids, regardless of local lithology.

Acknowledgements We thank Paula Provencio for materials research and analyses that helped advance our understanding of speleogenetic by-product materials. We are grateful to Art and Peggy Palmer for discussions of hypogene speleogenesis in the Black Hills of South Dakota, Guadalupe Mountains, New Mexico, and Grand Canyon, which helped shape our ideas; and to Bogdan Onac for discussions of sulfur isotope geochemistry of Grand Canyon caves.

References

Beus SS, Morales M (1990) Grand Canyon geology. Museum of Northern Arizona Press, Flagstaff, AZ

Blakey R, Ranney W (2008) Ancient landscapes. Grand Canyon Association, Grand Canyon, AZ

Decker DD, Polyak VJ, Asmerom Y (2015) Depth and timing of calcite spar and 'spar cave' genesis: implications for landscape evolution studies. In: Feinberg J, Gao Y, Alexander EC Jr (eds) Caves and Karst across time, vol 516. Geological Society of America, Special Paper, pp 103–111. doi:10.1130/2015.2516(08)

Egmeier SJ (1973) Cavern development by thermal waters with a possible bearing on ore deposition. Unpublished Ph.D. dissertation, Standford University

Hill CA (1996) Geology of the Delaware basin, Guadalupe, Apache, and Glass Mountains, New Mexico and West Texas. Permian Basin Section-SEPM Publication, pp 96–39

Hill CA, Polyak VJ (2010) Karst hydrology of Grand Canyon, Arizona, USA. J Hydrol 390:169–267

Hill CA, Polyak VJ (2014) Karst piracy: a mechanism for integrating the Colorado River across the Kaibab uplift, Grand Canyon, Arizona. USA Geosphere 10(4):627–640. doi:10.1130/Geos00940.1

Hill CA, Polyak VJ, McIntosh WC, Provencio PP (2001) Preliminary evidence from Grand Canyon caves and mines for the evolution of Grand Canyon and the Colorado River system. In: Young RA, Spamer EE (eds) Proceedings of symposium at Grand Canyon National Park, June 2000, vol 12. Grand Canyon Association Monograph, pp 141–147

Huntoon PW (2000) Variability of karstic permeability between unconfined and confined aquifers, Grand Canyon region, Arizona. Environ Eng Geosci VI(2):155–170

Klimchouk AB (2007) Hypogene speleogenesis: hydrogeological and morphogenetic perspective. National Cave and Karst Research Institute, Carlsbad, NM

McQuarrie N, Wernicke BP (2005) An animated tectonic reconstruction of southwestern North America since 36 Ma. Geosphere 1 (3):147–172. doi:10.1130/GES00016.1

Palmer AN (1991) Origin and morphology of limestone caves. Geol Soc Am Bull 103:1–21

Polyak VJ et al (2014) Isotopic studies of byproducts of hypogene speleogenesis and their contribution to the geologic evolution of the western United States. In: Kimchouk A, Sasowsky ID, Mylroie J, Engel SA, Engel AS (eds) Hypogene cave morphologies, vol 18. Karst Waters Institute Special Publication, pp 88–94

Polyak V, Hill C, Asmerom Y (2008) Age and evolution of the Grand Canyon revealed by U–Pb dating of water table-type speleothems. Sci 319(5868):1377–1380

Rice SE (2012) Surveying Leandras Cave, longest in Arizona. Cave and Karst Programs, National Park Service, Inside Earth 15(1):4–5

Condensation Corrosion Speleogenesis in the Amargosa Desert and the Tecopa Basin

35

Yuri Dublyansky, John Klenke, and Christoph Spötl

Abstract

We summarize observations on condensation corrosion caves above a regional, moderately thermal aquifer in the Devils Hole Ridge near Ash Meadows (Nevada) as well as at a site near Shoshone (California). At Devils Hole, water of the regional aquifer has been saturated with respect to calcite (i.e., non-aggressive) for the last 2–3 million years. Caves at both sites have been initially formed by extensional tectonics and further enlarged by condensation corrosion.

Keywords

Condensation corrosion • Devils Hole • Tecopa • Hypogene speleogenesis

1 Introduction

The term "condensation corrosion" refers to the development of cavities in soluble rock, above the water table, through the action of water, which originates from condensation of water vapor on the rock walls. Aggressiveness with respect to carbonate rock is caused by the uptake of gases (CO_2 or H_2S) from the cave air into the condensate giving rise to acidic solutions. Advective air movement typically produces small-scale cave wall morphologies, which can be observed in both hypogene and epigene caves (particularly near entrances). Characteristic solution mesomorphologies, such as spherical and hemispherical niches and bell holes, develop where free convection of cave air is involved. The highest potential for condensation corrosion is expected in hypogene settings, where the water is commonly thermal (temperature gradient promoting free convection, enhanced evaporation and condensation) and contains elevated amounts of CO_2 and/or H_2SO_4 (enhanced aggressiveness of condensate with respect to the carbonate rock).

In most cases studied so far, condensation corrosion developed during the latest stages of hypogene (thermal) speleogenesis, when caves, initially formed under phreatic conditions, emerged into the vadose zone. This created a situation characterized by (a) a significant free water surface available for evaporation and (b) open air-filled space in which convective air movement can develop. With the exception of several caves in Hungary (e.g., Sátorkö-puszta and Bátori Caves) for which condensation corrosion could be the leading if not the only speleogenetic mechanism, condensation corrosion in most caves does not affect the cave gross morphology, but is only responsible for modifications of the meso- and micromorphology.

Importantly, the two types of speleogenesis occurring at radically different environments—phreatic dissolution and condensation corrosion under vadose conditions—produce similar solutional forms.

Y. Dublyansky (✉) · C. Spötl
Institute of Geology, Innsbruck University,
Innrain 52, 6020 Innsbruck, Austria
e-mail: juri.dublyansky@uibk.ac.at

C. Spötl
e-mail: christoph.spoetl@uibk.ac.at

J. Klenke
Nye County Nuclear Waste Repository Project Office,
2101 E. Calvada Blvd, Ste 100, Pahrump,
NV 89048, USA
e-mail: jklenke@co.nye.nv.us

© Springer International Publishing AG 2017

A. Klimchouk et al. (eds.), *Hypogene Karst Regions and Caves of the World*,
Cave and Karst Systems of the World, DOI 10.1007/978-3-319-53348-3_35

2 Geology and Hydrogeology

The area of interest belongs to the northern Great Basin region, which has experienced large-scale extension during the last 20 million years. The extension was not uniform throughout the region; the study area lies within the greatly extended domain (Wernicke 1992). Hydrologically, the study area belongs to the Death Valley Regional Groundwater Flow System (DVRFS), a deep, fracture-controlled aquifer that encompasses ca. 100,000 km^2 of mountain ranges and low-elevation intermontane basins. Overall, groundwater in DVRFS moves through permeable zones down hydraulic gradients from areas of recharge to regional areas of discharge. The topography produces numerous interconnected local subsystems within the major flow system. Water that enters the system in a recharge area may discharge in the nearest topographic low, or it may be transmitted to a regional discharge area.

Devils Hole Ridge is a small elongate mountain, ca. 3.0 × 0.7 km, built of middle to upper Cambrian limestone (Bonanza King Formation), jutting out some 250 m above the floor of the southern Amargosa Desert. Immediately south of the Devils Hole Ridge lies the Ash Meadows oasis, the discharge area of the regional-scale (>12,000 km^2) Ash Meadows Groundwater Flow System. The latter is recharged by infiltration at the upper elevations of the Spring Mountains (ca. 3600 m a.s.l., annual precipitation ~1000 mm; Winograd et al. 1998). The water flows northwest toward Frenchman Flat, merging with additional flow from the White River groundwater flow system along the way (Fig. 1). From Frenchman Flat, the water follows a high-transmissivity zone southward and ultimately discharges at the springs in Ash Meadows oasis (Winograd and Thordarson 1975). The curved flow path reflects the presence of an aquitard block at the northwestern end of the Spring Mountains (Fig. 1).

The **Shoshone site** is located at the northern fringe of the Tecopa Basin. It represents a small hill, ca. 1.0 × 0.7 km, built of Cambrian limestone (undifferentiated Nopah, Bonanza King and Carara Formations), rising ca. 80 m above the valley floor of the Amargosa River. The flow path bringing water to the basin is less certain. Current hydrogeological models of the DVRFS (e.g., Belcher 2004; USGS 2010) envisage a southwestward interbasin flow sourced from the Spring Mountains (Fig. 1, SM). An alternative interpretation calls for a southward flow from the Ash Meadows–Amargosa Valley area (Fig. 1, AM) along the Ash Meadows fault zone (e.g., Miner et al. 2007).

In both regions, caves are associated with steeply dipping extensional fractures. Aquifers tapped by the caves host moderately thermal (34 °C at Devils Hole and 30 °C at Shoshone) water. This water is part of a regional groundwater flow system and has attained temperatures in excess of the mean annual air temperature that prevailed at the time and place of recharge (Miner et al. 2007). The carbonate aquifer tapped at both sites is not a simple artesian (confined) aquifer; due to the complex geologic structure of the area, it is confined by young and partly indurated sediments beneath valleys and unconfined beneath ridges.

3 Caves of the Devils Hole Ridge

Four caves are known in the Devils Hole Ridge. The famous **Devils Hole** represents a nearly rectangular 23 × 7 m surface collapse into a steeply dipping fault-controlled fissure, which intersects the water table at 15 m below the land surface forming a 1.8 × 5.5 m pool. The water-filled part of this tectonic cave extends more than 140 m deep. The surface collapse represents a remnant of the subaerial chamber, which probably collapsed 50–60 ka (Riggs 1991). Another subterranean air-filled chamber, Browns Room, lies about 50 m northeast of Devils Hole; it is only accessible by SCUBA diving.

Devils Hole #2 Cave (a.k.a. Devils Hole Cave) is located 200 m north of Devils Hole proper. It represents a NE-striking extensional fissure which intersects the water table at a depth of 43 m. The fissure was concealed at the surface by a ca. 1.5-m-thick layer of carbonate-cemented alluvium/colluvium of Pliocene–Pleistocene age associated with a small WNW-trending wash on the eastern slope of the Devils Hole Ridge. The entrance to the cave opened when this indurated layer was breached from below by condensation corrosion. The cave consists of two chambers separated by a "plug" of collapsed blocks. The upper chamber is near-vertical, 5–15 m wide and 25 m high. The floor of the chamber is largely horizontal and consists of the collapsed rocks. The lower chamber represents a tectonic fissure dipping ~60°, which intersects the thermal water table and continues underwater to unknown depth (more than 100 m).

Devils Hole Prospect is a cave located 50 m north of and ca. 12 m higher than Devils Hole proper. The entrance to the cave was opened during mineral prospecting, in the course of which indurated alluvium/colluvium material filling a ca. 1.5-m-wide near-vertical fissure in the limestone was removed. Unlike other caves in the Devils Hole Ridge, whose internal volume was created primarily by extensional tectonics, the Devils Hole Prospect Cave owes its enlargement almost exclusively to dissolution. The cave is carved in both Paleozoic limestone and indurated fault filling. Parts of the cave hosted by carbonate rocks show a characteristic solution-related morphology with abundant spherical niches, cusps, pendants, partitions and cupolas. The same morphologies can be seen in the calcite-cemented fault-fill material.

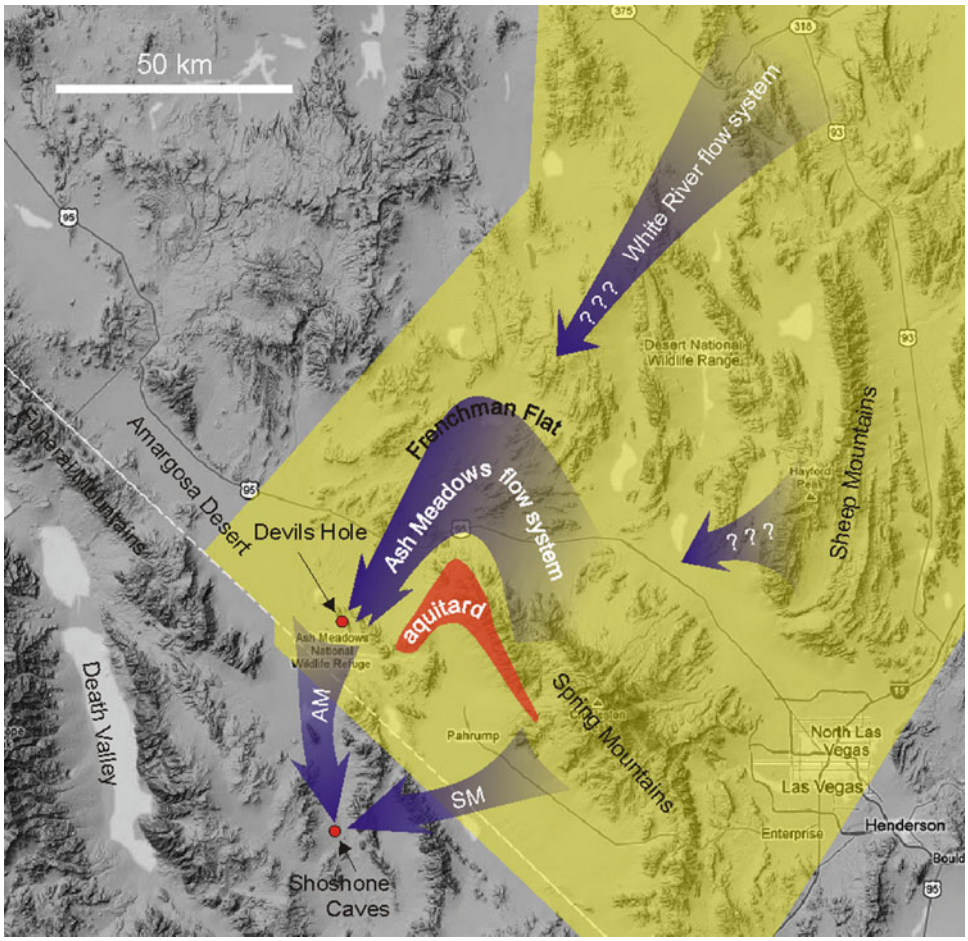

Fig. 1 Regional flow in the study area. The main flow path of the Ash Meadows Flow System is simplified from Winograd and Thordarson (1975). AM (Ash Meadow) and SM (Spring Mountain) are alternative flow paths proposed for the Tecopa Basin by Miner et al. (2007). The location of the carbonate corridor (*yellow-colored*) is from Dettinger (1989), who did not map its extent beyond the Nevada–California border. Study sites are marked by *red dots*

Unnamed Cave is a collapse in alluvium, related to an extension fissure underneath, located ~1.1 km north of Devils Hole by Carr (1988). In 2014, the entrance was 2.5 × 1.5 m (Fig. 2). Under a ~3-m layer of moderately indurated alluvium, a ~1-m-wide near-vertical extension fissure opens in Cambrian limestone. The surface of the fissure is smoothed by dissolution. The fissure narrows and becomes impassable at a depth of ca. 10 m. Air in the cave is dry, indicating that there is presently no direct connection to the thermal water table beneath.

4 Caves Near Shoshone

Shoshone Cave was first described by Emerson (1951). Two caves, Upper and Lower Shoshone, were later reported as a habitat of the endemic whip-scorpion *Trithyreus shoshonensis* (Briggs and Hom 1972). The authors noted that the survival of these scorpions would not be possible in the Californian desert with its freezing winters if not for the heating of the cave by thermal groundwater.

Examining the site in February of 2014, we found three caves, all opened or modified by mining operations. Similar to Devils Hole Ridge, caves at Shoshone have characteristic "extension fissure" morphologies, modified by condensation-related dissolution.

Lower Shoshone Cave was affected by mining operations (purportedly, prospecting for hematite). At the bottom, the cave intersects the slightly thermal (30 °C) aquifer in a small, 1 × 1.5 m pond. The steep fissure continues below the water surface to unknown depth. A ~1-cm-thick mammillary calcite crust is present on some of the rock under water. Because of the large opening at the entrance, the outside cool air flows freely into the cave, lowering the temperature inside to 22–23 °C and lowering the humidity (i.e., non-condensing). The upper part of the cave, where the fissure is up to 5 m wide, features abundant solutional forms, including cupolas and pendants. In places, cave walls show patches of white popcorn-like botryoidal calcite, deposited under subaerial conditions.

Upper Shoshone Cave does not provide direct access to the water table, although it is clearly connected to it by impassable passages. The air temperature in the cave

Fig. 2 Unnamed cave in alluvium north of Devils Hole. The layer of alluvium penetrated by collapse (**a**) is ca 3 m thick. The solution-widened fissure in Cambrian limestone underneath (**b**) is ca. 1 m wide; it narrows and becomes impassable ca. 10 m deeper

exceeds 26 °C (Fig. 3) and the humidity at the time of visit was close to or exceeding 100%, resulting in condensation. Near the entrance, condensation of humid air resulted in the growth of patches of green moss. The walls of the caves are smooth, affected by solution and commonly feature pendants, side wall cupolas, partitions and rock bridges. Patches of subaerial popcorn calcite are present as well (Fig. 4).

Middle Shoshone Cave can be accessed through an artificially widened pit in the limestone and is equipped with a wooden ladder. The pit leads to a natural part of the cave which shows morphologies and deposits very similar to other two Shoshone caves.

5 Monogenetic Solution Cavities

All caves described from Devils Hole Ridge and Shoshone site in preceding sections are associated with extensional fissures. In fact, in all but one of them (Devils Hole Prospect Cave), most of the cave volume can be attributed to tectonic extension, while dissolution can be held responsible for the meso- and micromorphological features.

This does not hold true for smaller cavities found at both sites. Such cavities commonly develop in massive rock, lacking any guiding cracks or fissures. Cavities are exposed on bedrock slopes and are truncated by slope retreat to different degrees: some of them open as small-diameter (7–10 cm) holes which widen inward, whereas others are truncated or even almost completely destroyed. The common morphological feature of these cavities is their near-circular cross section in plan view. In vertical cross section, they show spherical, spheroidal (vertically elongated) and tubular shapes. The diameter of the cavities ranges between 10 and 130 cm. Many of them are filled with loose detrital deposits (silt, sand and gravel) introduced after the truncation of cavities. Most of the cavities have barren walls, but some host speleothems formed under subaerial conditions (corallites, popcorn; Fig. 5).

The largest solution cavity formed without obvious relation to extension tectonics was observed at the Shoshone site (Fig. 6). It is a fragment of a vertical cave channel several meters in diameter, with a complex cross section (combination of circular and flattened tubes). At some point in time, the cave was truncated by denudation and filled by detrital material.

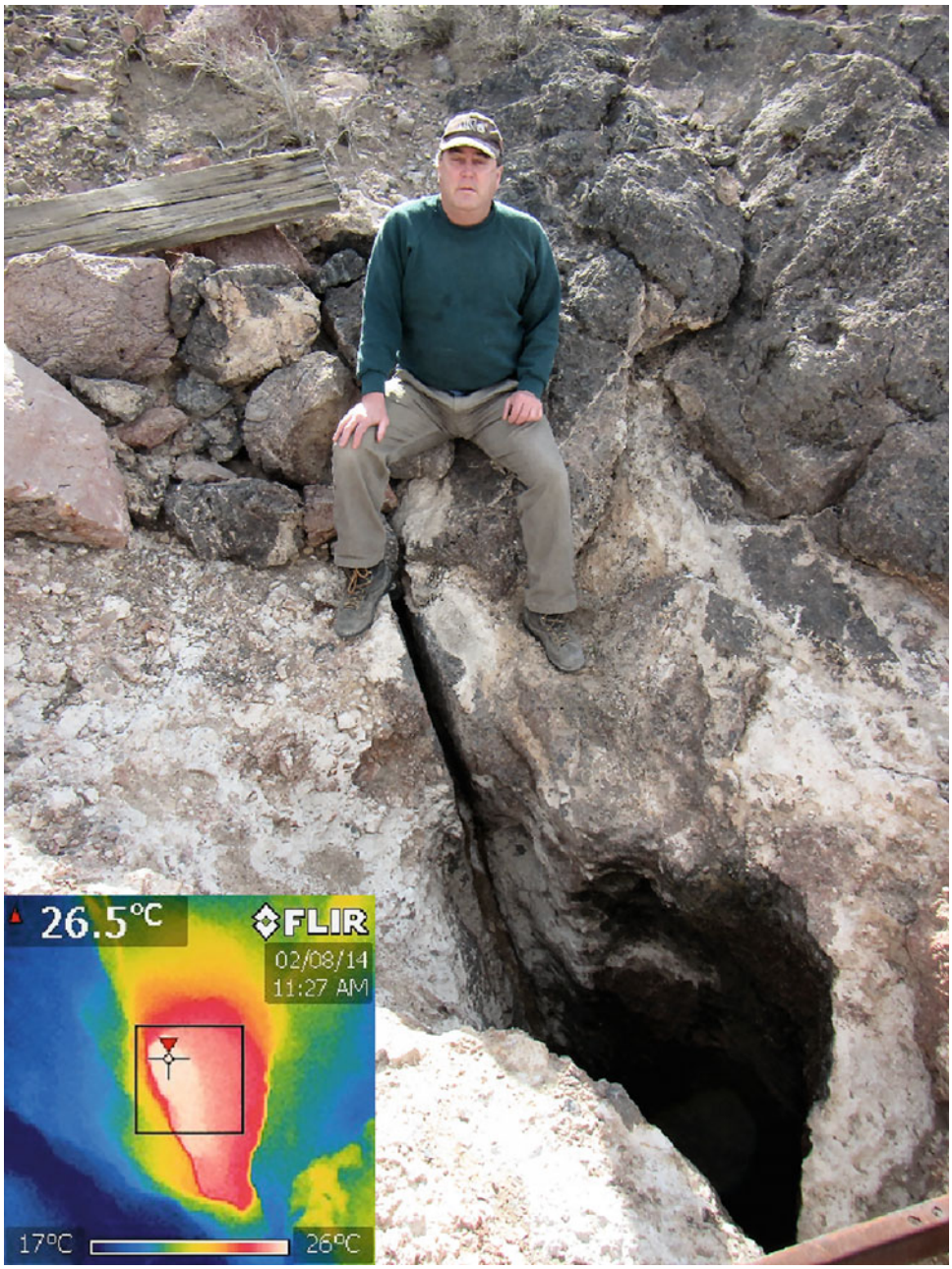

Fig. 3 Entrance to Upper Shoshone Cave. *Insert* thermal image of the entrance taken with a FLIR i7 infrared camera

6 Mesomorphological Features Produced by Condensation Corrosion Speleogenesis

Initially, the origin of Devils Hole was attributed to solution enlargement of tectonic fractures (Winograd and Thordarson 1975; Dudley and Larson 1976). Subsequently, Riggs et al. (1994) posited a purely tectonic, i.e., extensional origin of the Devils Hole passages, a process they dubbed "tectonic speleogenesis." Condensation corrosion was identified as an agent responsible for partial destruction of calcite deposits in Browns Room, a subaerial chamber in Devils Hole (Riggs and Deacon 2002). Subsequently, Dublyansky and Spötl (2015) described a wide spectrum of condensation corrosion-related morphological features in the Devils Hole Ridge. Our observations indicate that similar morphologies are also observed in the Shoshone caves.

Solution-smoothed walls were observed in the upper chamber of Devils Hole #2, in Devils Hole Prospect and in all three Shoshone caves. The walls parallel to the strike of the fissures are uniformly affected by solution, creating smooth slightly undulating surfaces.

Flat (slot-shaped) channels along fractures and calcite veins: Small channels with characteristic solution morphology, precluding any involvement of gravity-driven water

Fig. 4 Upper Shoshone Cave. Solution forms and a patch of subaerial popcorn (*lower right corner*). Picture looking down into the narrowing (impassable) continuation of the cave

flow, cut through both the bedrock limestone and the calcite veins on the eastern and western walls of the upper chamber of Devils Hole#2. The orientation of the channels coincides with the orientation of the chamber, which suggests that they developed along preexisting extensional fractures (and associated calcite veins).

Cupolas in indurated alluvium/colluvium: The ceilings of the upper chamber of Devils Hole #2 and in Devils Hole Prospect caves are composed of carbonate-cemented colluvium/alluvium. Dissolutional cupola-like forms are present in the ceilings with the solution surfaces cutting uniformly across massive limestone bedrock as well as alluvium/colluvium consisting of cobbles, finer-grained material and carbonate cement. Small cupola-shaped cavities (10–50 cm in diameter) in this heterogeneous material are locally separated by millimeter-thin partitions.

Horizontal tubes: Two horizontal solution channels 3–7 m long with a roughly isometric cross section of 30–50 cm diameter were found in the vertical walls of the Devils Hole 2 and the Devils Hole Prospect caves. Although the development of horizontal channels is difficult to rationalize in the context of the condensation corrosion, we suggest that it is another morphological form related to this speleogenetic mechanism.

Fig. 5 Solution cavity in the Devils Hole Ridge. Note the absence of a guiding fissure and calcite corallites coating the walls. Coralloid from an adjacent cavity was dated to 413 ± 12 and 318 ± 8 ka (Dublyansky and Spötl 2015)

Fig. 6 Solution cave exposed by retreat of the rock surface, Shoshone. Detrital material was removed from the cavity

Punk rock: The southern wall of the upper chamber of Devils Hole #2 Cave shows a layer of soft, powdery material, extending into the wall up to 2 cm and eventually passing into hard, unaltered limestone. Despite its softness, the layer preserves the original structure and coloration of the bedrock. We propose that the punk rock alteration is a manifestation of condensation corrosion.

Pendants, partitions and undulating tubular channels: These smaller and more elaborate solution morphologies

were observed in Devils Hole Prospect Cave and in the Upper and Lower Shoshone Caves (Fig. 4).

7 Discussion

7.1 Condensation Corrosion: Dead or Alive?

Due to the very small potential of vadose recharge on the Devils Hole Ridge (surface area ca. 2 km^2, vadose zone less than 250 m thick), epigenic speleogenesis was deemed to be largely impossible there, even under less arid climate conditions in the past. The Shoshone site seems to be equally or even less suitable for epigenic karst development. Its surface area is only ca. 0.7 km^2, and the elevation above the valley floor does not exceed 80 m.

Condensation corrosion appears to be the only mechanism capable of producing solutional cavities in such locations. In Devils Hole Ridge, dissolution took place above a marginally thermal (34 °C) aquifer, which has been slightly supersaturated with respect to calcite (i.e., incapable of bedrock dissolution) for the last several million years. The Shoshone caves are located above an aquifer with a temperature of 30 °C.

On the basis of a microclimatic study, Dublyansky and Spötl (2015) concluded that condensation corrosion is not presently operational in any of the studied caves of Devils Hole Ridge. All these caves are presently open to the dry desert atmosphere, which drastically reduced the potential of condensation. Yet, active development of the process elsewhere in the subsurface of the Devils Hole Ridge is entirely possible and even likely. At Shoshone, the Lower Cave is presently well ventilated due to past mining activities and condensation corrosion is no longer operational. In contrast, the Upper Shoshone Cave has a tight entrance, restricting ventilation. Condensation is still active there and can be observed on the walls near the entrance.

7.2 Conditions Promoting Condensation Corrosion

Structural conditions: One of the parameters controlling the amount of evaporation from a thermal water table (and, therefore, the amount of water available for condensation corrosion), is the surface area of the subterranean thermal lake. The potential of condensation corrosion increases with increasing evaporation surface. In many hypogene caves, condensation corrosion occurred during late stages of hypogene karstification above thermal lakes. As discussed above, at Devils Hole Ridge, subaqueous karstification can be ruled out, because the water has been saturated with respect to calcium carbonate for perhaps as long as three million years. At both sites, Devils Hole Ridge and Shoshone, the cavities occupied by the subterranean thermal lakes were created by extensional tectonics. Such lakes occur whenever open fractures intersect the thermal water table. Because the region has remained in an extensional regime since the mid-Tertiary, such subterranean thermal water bodies are likely to be widespread and, by inference, condensation corrosion may have occurred (and likely still occurs) in many as yet unidentified locations.

In addition to creating evaporation surfaces, extensional fractures provide an open space above the thermal water table in which free air convection can develop. Extensional tectonics, collapse and condensation corrosion operate in concert creating and enlarging the open space underground. As none of the processes has a direct relationship to the Earth's surface, the result of this concerted action will remain unnoticed at the surface above these cavities, until the upward-propagating cavities intersect the downward-moving (due to denudation) land surface.

Thermal conditions: A temperature gradient exists between the body of thermal water and the land surface. The aquifer underneath Devils Hole Ridge has maintained a nearly constant temperature of ~34 °C for hundreds of thousands of years (Kluge et al. 2014; Tripati et al. 2015), meaning that the thermal conditions for condensation corrosion may have persisted for an equally long period of time. Extensional tectonic conditions could also create fractures which are open to the surface but do not intersect the thermal water table. Movement of cool air in such fractures provides additional cooling of the rock mass and leads to the development of a complex thermal field in the vadose zone of the rock including local thermal gradients in the bedrock, which are not vertical.

Microclimatic conditions: The potential for and the intensity of condensation change with distance from the heat source (thermal lake). Condensation corrosion is least intensive near the thermal water table, where the difference in temperature between the thermal water pool and the surrounding rock is small. As the warm and moist air buoyantly moves upward along an open fracture, it cools, and at a certain distance, its temperature may reach thermal equilibrium with the surrounding rock. Both buoyant movement and condensation will then no longer be possible. Additionally, the heat released due to condensation warms the rock surface, decreasing the local thermal air-rock gradient. For condensation to proceed, this heat must be removed through solid-state thermal conduction (Dreybrodt et al. 2005) and/or by downward flow of the condensate. It can be inferred, therefore, that there is a certain combination of parameters at which condensation corrosion is most intense, and this combination is specific to each given cave configuration.

Condensation corrosion stops as soon as the conditions necessary for its operation cease to exist. One of the most

efficient ways to stop condensation corrosion is to drastically change the microclimate inside the cave, for example, by enabling ventilation. In desert climatic conditions, such as at Devils Hole Ridge and Shoshone, condensation corrosion will slow down when a channel or cupola, carving its way up through the rock, intersects with the land surface. Cool and dry air flowing into the cave then mixes with ascending warm and moist air, decreasing its temperature and relative humidity. Condensation may terminate entirely if enough dry air enters the cave. In non-desert conditions, the downward flow of cool and moist air after the opening of the cave to the surface will not necessarily terminate condensation corrosion.

Acknowledgements The authors acknowledge the Death Valley National Park Service for permission to conduct research at Devils Hole and the park personnel (K. Wilson and R. Freeze) for field assistance. Partial support for this research was provided by FWF grant P263050.

References

Belcher WR (ed) (2004) Death Valley regional ground-water flow system, Nevada and California; Hydrogeologic framework and transient ground-water flow model. US Geol Surv Sci Invest Rep 2004–5205

Briggs TS, Hom K (1972) A cavernicolous whip-scorpion from the northern Mojave Desert, California (Schizomida: Schizomidae). Occasional papers of the California Academy of Sciences 98

Carr WJ (1988) Geology of the Devils Hole area, Nevada. US Geol Surv Open-File Rep 87–560

Dettinger MD (1989) Distribution of carbonate-rock aquifers in Southern Nevada and the potential for their development: summary of findings, 1985–88. Program for the study and testing of carbonate-rock aquifers in eastern and southern Nevada. Summary Report No. 1, Carson City, Nevada

Dreybrodt W, Gabrovšek F, Perne M (2005) Condensation corrosion: a theoretical approach. Acta Carsol 34(2):317–348

Dublyansky YV, Spötl C (2015) Condensation-corrosion speleogenesis above a carbonate-saturated aquifer: Devils Hole Ridge, Nevada. Geomorphology 229:17–29

Dudley WW, Larson JD (1976) Effect of irrigation pumping on desert pupfish habitats in Ash Meadows, Nye County, Nevada. US Geol Surv Prof Paper 927

Emerson D (1951) Shoshone Cave. Calif Caver 3(3):2

Kluge T, Affek HP, Dublyansky Y, Spötl C (2014) Devils Hole paleotemperatures and implications for oxygen isotope equilibrium fractionation. Earth Planet Sci Lett 400:251–260

Miner RE, Nelson ST, Tingey DG, Murrell MT (2007) Using fossil spring deposits in the Death Valley region, USA to evaluate palaeoflowpaths. J Quat Sci 22:373–386

Riggs AC (1991) Geohydrologic evidence for the development of Devils Hole, southern Nevada as an aquatic environment. In: Pister EP (ed) Proceedings of the desert fishes council 20 and 21, pp 47–48

Riggs AC, Deacon JE (2002) Connectivity in desert aquatic ecosystems: The Devils Hole Story. In: Sada DW, Sharpe SE (eds) Spring-fed wetlands: important scientific and cultural resources of the intermountain region, Las Vegas, NV. DHS Publication No. 41210, 7–9 May, 2002

Riggs AC, Carr WJ, Kolesar PT, Hoffman RJ (1994) Tectonic speleogenesis of Devils Hole, Nevada, and implications for hydrogeology and the development of long, continuous paleoenvironmental records. Quat Res 42:241–254

Tripati AK, Hill PS, Eagle RA, Mosenfelder JL, Tang J, Schauble EA, Eiler JM, Zeebe RE, Uchikawa J, Coplen TB, Ries JB, Henry D (2015) Beyond temperature: clumped isotope signatures in dissolved inorganic carbon species and the influence of solution chemistry on carbonate mineral composition. Geochim Cosmochim Acta 166:344–371

USGS (US Geological Survey) (2010) Death Valley regional groundwater flow system, Nevada and California—Hydrogeologic framework and transient groundwater flow model. Belcher WR, Sweetkind DS (series eds) US Geol Surv Prof Paper 1711, p 398

Wernicke BP (1992) Cenozoic extensional tectonics of the U.S. Cordillera. In: Burchfiel BC, Lipman PW, Zoback ML (eds) The Cordilleran orogen—conterminous US. Geological Society of America, Geology of North America G–3:553–581

Winograd IJ, Thordarson W (1975) Hydrogeologic and hydrochemical framework, south-central Great Basin, Nevada-California, with special reference to the Nevada test site. US Geol Surv Prof Paper 712-C

Winograd IJ, Riggs AC, Coplen TB (1998) The relative contributions of summer and cool-season precipitation to groundwater recharge, Spring Mountains, Nevada, USA. Hydrogeol J 6:77–93

Structural Settings and Hypogenic Flow Paths for Three Colorado Caves

36

R. Mark Maslyn, Harvey R. DuChene, and Frederick G. Luiszer

Abstract

Colorado, a state with diverse geology and high topographic relief, contains several significant hypogene cave systems. Three are described here: the Orient Mine Cave System, Cave of the Winds, and Glenwood Caverns. All are located near present thermal springs, which help to determine the chemistry of the cave-forming water. The Orient Mine Caves were encountered during mining operations to extract limonite ore for the manufacture of steel. The ore follows the bedding, but hypogene cave galleries also cut across bedding and extend upward as domes. The galleries were formed by warm water rising along the San Luis fault and mixing with cool recharge from nearby mountains. Cave of the Winds follows the plunge of an anticline and probably formed when water with high CO_2 rose along faults and mixed with shallow meteoric water. At Glenwood Caverns, carbonic acid in rising thermal water is responsible for most speleogenetic dissolution, but some dry parts of the cave have a sulfuric acid overprint.

Keywords

Geologic structure • Thermal springs • CO_2 • Limonite • H_2S

1 Introduction

This paper concerns three of the many hypogenic caves of Colorado, which illustrate the influence of structure and stratigraphy on cave development: the Orient Mine Caves, Cave of the Winds, and Glenwood Caverns (Fig. 1). These show contrasting examples of deep flow, each located no more than 1.6 km (1 mile) from currently active thermal spring systems that are possible analogs for the water that formed the caves. The Orient Mine Caves are located on the west side of the Sangre de Cristo Range of the Rocky Mountains, adjacent to the San Luis Valley. Cave of the Winds is located near the Pikes Pike massif near the eastern margin of the Front Range. Glenwood Caverns is located on Colorado's Western Slope, near the border between the Rocky Mountains and the Colorado Plateau. They are all located in Mississippian (lower Carboniferous) and older carbonates (Fig. 2).

R.M. Maslyn (✉)
10268 Dusk Way, Littleton, CO 80125, USA
e-mail: mmaslyn@msn.com

H.R. DuChene
PO Box 362, Lake City, CO 81235, USA
e-mail: hrduchene@gmail.com

F.G. Luiszer
Department of Geological Sciences, University of Colorado, Boulder, CO 80303, USA
e-mail: luiszer@colorado.edu

2 Caves of the Orient Mine

The Orient Mine and associated caves are located 15 km southeast of the town of Villa Grove in Saguache County. The mine is on the western edge of the Sangre de Cristo Mountains, in Mississippian Leadville Limestone, near the San Luis fault, which is the interface between the Sangre de Cristo Mountains and the San Luis Valley graben (Fig. 3). The limestone dips steeply to the east. Geologists first noted

© Springer International Publishing AG 2017

A. Klimchouk et al. (eds.), *Hypogene Karst Regions and Caves of the World*,
Cave and Karst Systems of the World, DOI 10.1007/978-3-319-53348-3_36

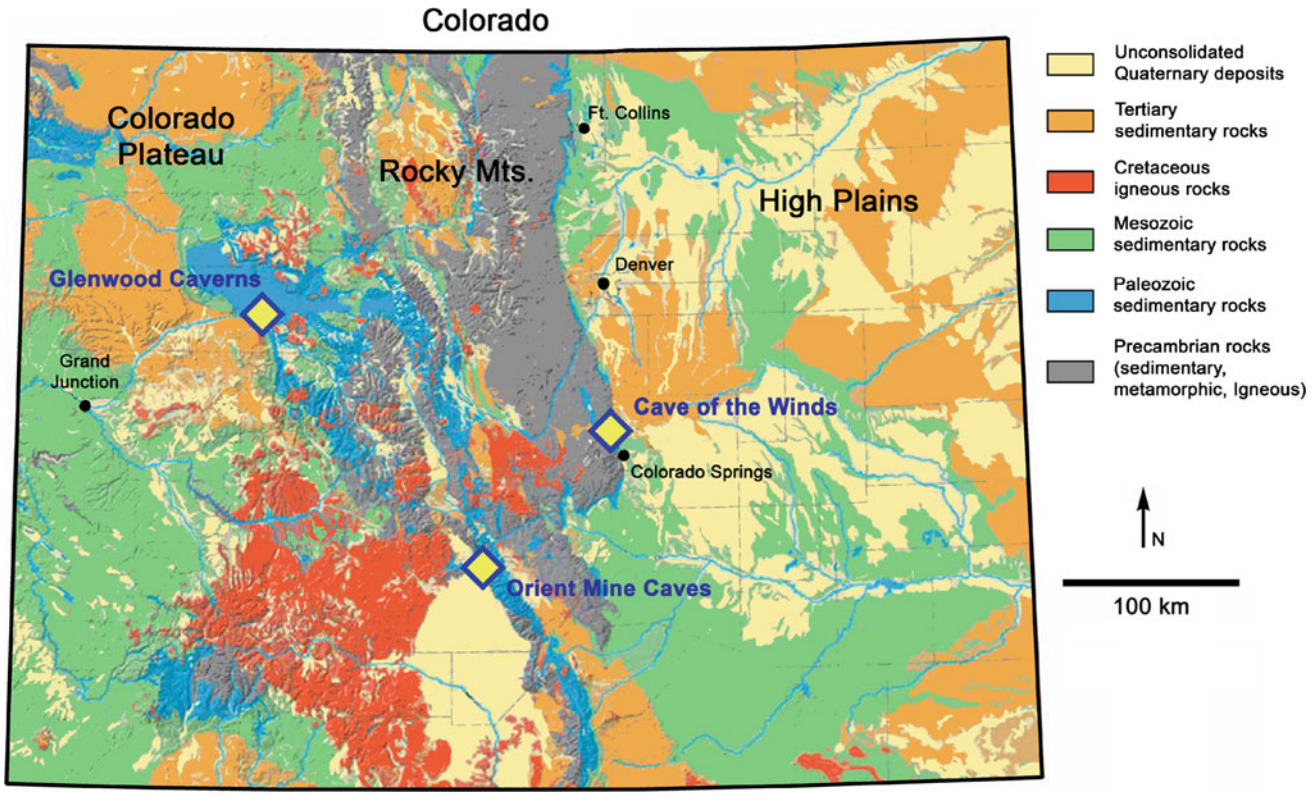

Fig. 1 Map of Colorado showing locations of caves discussed in this paper and their relationship to geologic provinces. Geologic map from the Colorado Geological Survey

limonite deposits in the area after the Hayden expedition of 1873. Mining began in 1880 and continued through 1932, supplying approximately 1,540,000 metric ton of limonite ore (Balleweg 1990) used for steel manufacturing. The caves were encountered during the mining operations.

There are three periods of solutional development represented, the first being Paleozoic. Unconformities in the Devonian Dyer Dolomite and the overlying Mississippian Leadville Limestone contain prominent paleokarst features including solution breccias and filled caves (Fig. 4). Maslyn (1976) documented similar features at the same stratigraphic levels in the Leadville in the area of Aspen, where they host base metal silver deposits. Paleozoic dissolution near the present Orient Mine produced a series of separate chambers up to 365 m long and 23 m wide that were later filled with sediment and breccia from the overlying Pennsylvanian Molas formation. Post-depositional thermal events altered the cave sediments to limonite, the principal ore in the Orient Mine. These ore bodies are generally parallel to the bedding and in places extend upward as domes (Fig. 4). The steep dip of the rock is apparent in the figure as well as the great width (55 m) of the excavated cave passage.

Open solution caves encountered during mining operations were described by Stone (1934), Dover (1981), Davis (1986), Fish (1986), and Balleweg (1990). Stone (1934) noted numerous solutional cavities in the Chaffee and Leadville formations that range in size up to caves 18–20 m wide that can be followed for "hundreds of feet." Some caves terminate in the limonite-mineralized paleokarst fill (Fig. 5). Aardvark Caverns is the largest single cave within the mine, with an estimated passage length of 370–460 m and passage heights up to 30 m (Balleweg 1990; Dover 1981). Svetz (1984) further described the cave, noting "In one portion of the cave, there was a large amount of gypsum crystals covering the walls. Most of them were brown, having been covered by the dust from the mining operation. We finished taking pictures and went through the rest of the cave which consisted mostly of one long, large passageway with small offshoots." Miners used the caves as access routes between mine levels and paleokarst-hosted limonite ore bodies.

Unlike the limonite-filled chambers, these caves are horizontal and crosscut the bedding. They, therefore, post-date Paleozoic anticlinal arching and the Miocene San

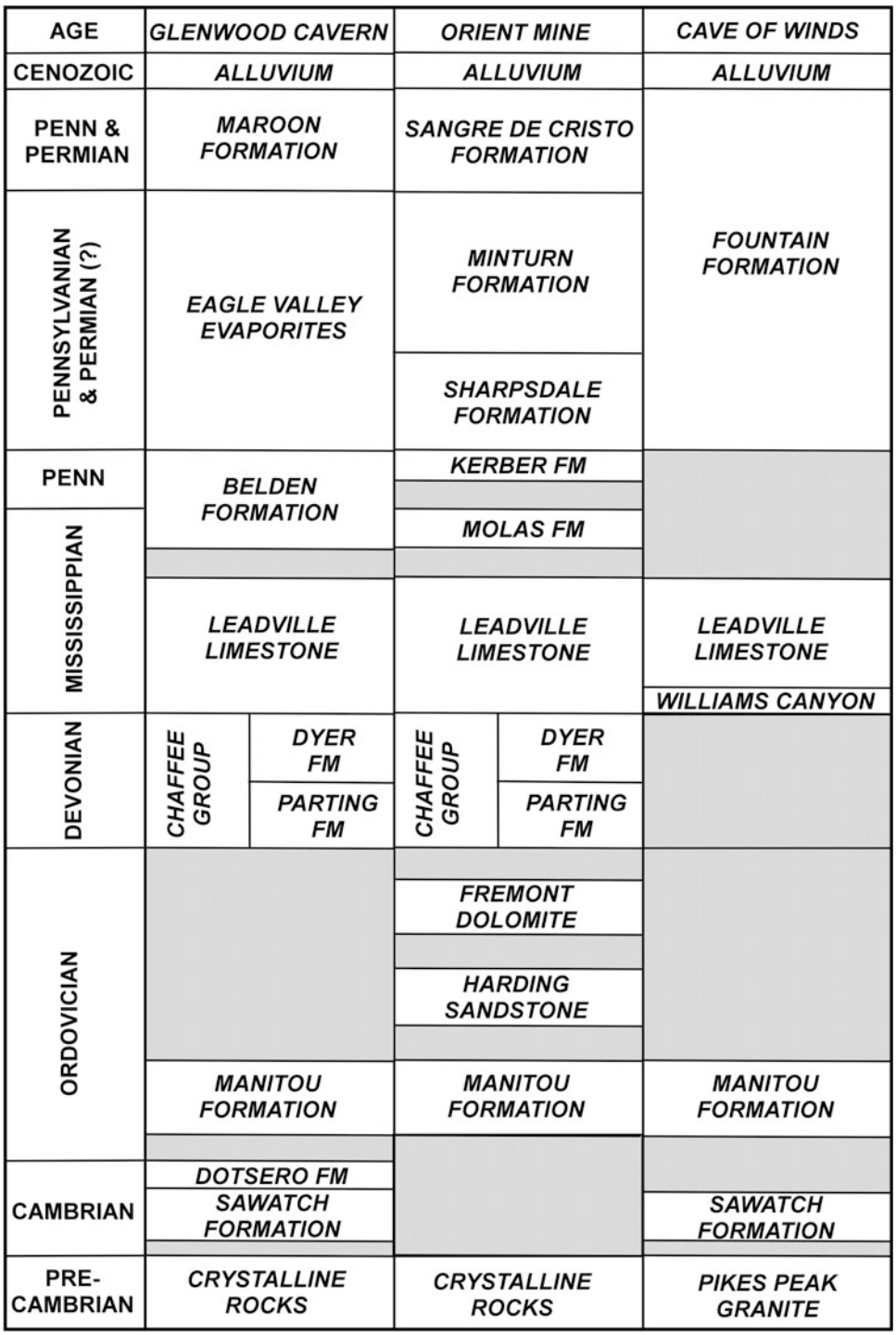

Fig. 2 Correlation of Paleozoic strata of Colorado. See text for the stratigraphic position of the caves. Ordovician, Devonian, and Mississippian strata are mainly carbonates and contain most of the caves in Colorado. Many unconformities along carbonate strata contain paleokarst features. The top of the Mississippian section is a pronounced unconformity in Colorado, as well as throughout much of the western United States. Strata overlying the unconformity are mostly arkoses, except in western Colorado where a thick section of Pennsylvanian evaporites and shales lies between the carbonates and the younger Pennsylvanian and Permian strata. (See Palmer, Chap. 38 for an example in South Dakota.)

Luis Valley rifting. They apparently formed in the late Neogene when thermal water was forced upward from the San Luis Basin along the San Luis fault, converging with cool surface waters flowing down-gradient from the adjacent Sangre de Cristo Mountains. Dissolution took place where the two waters mixed, as suggested by present evidence for groundwater mixing at the Valley View Hot Springs ~1.5 km south of the mine (see Table 1). The springs yield thermal water of 35–36 °C in a structural setting similar to the Orient Mine Caves and are considered to be a modern

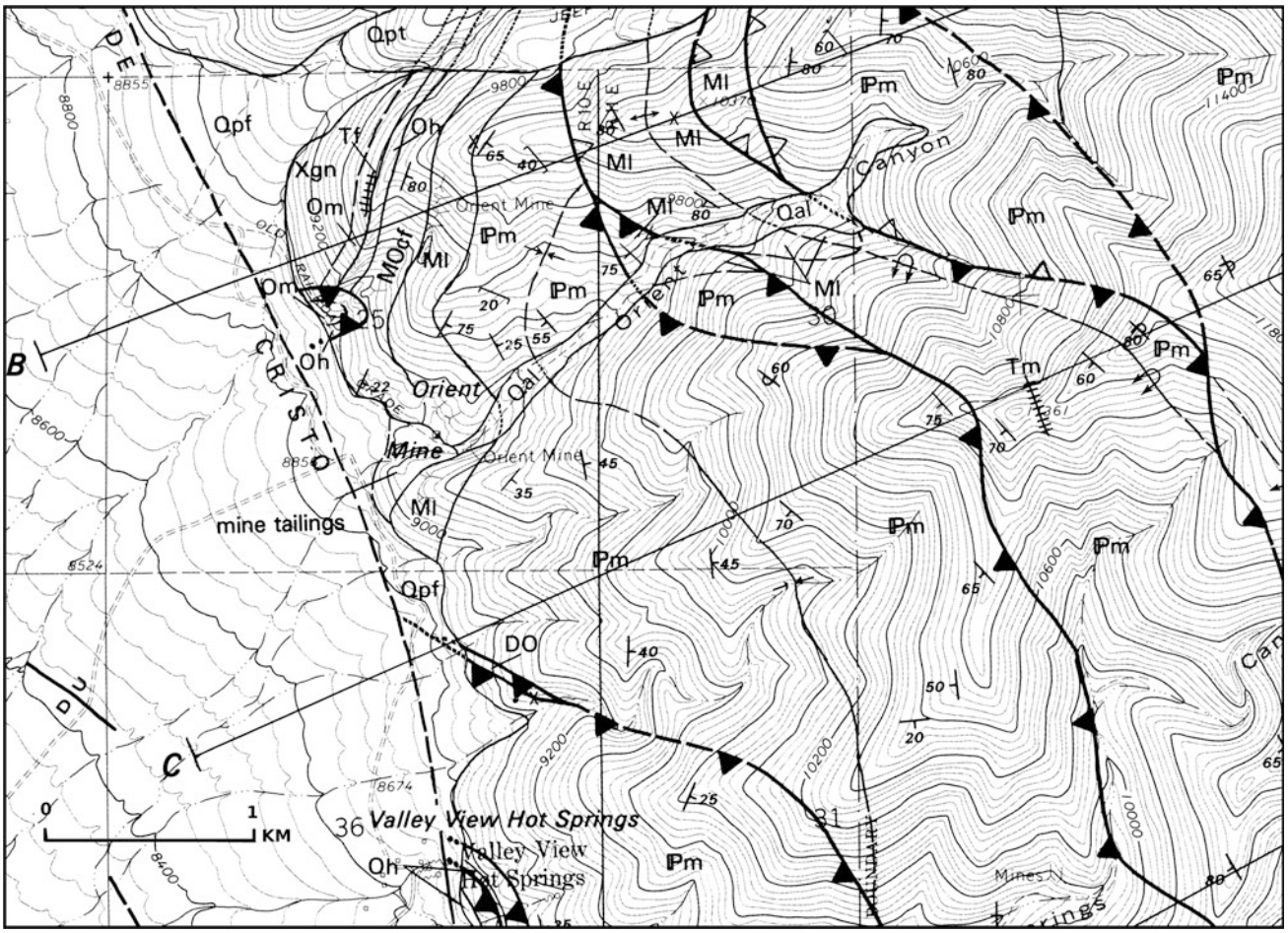

Fig. 3 Geologic map of the Orient Mine area from Lindsey and Soulliere (1987) showing its relation to the San Luis fault zone. The mine is located near the center of the map. Valley View Hot Springs is located at the bottom-center of the map. *Map legend* Precambrian Gneiss; *Om* Ordovician Manitou; *DO* Devonian-Ordovician undifferentiated; *Ml* Mississippian Leadville; *Pm* Pennsylvanian Minturn (including Sharpsdale); *Tm, Tf* Tertiary Intrusives; *Qaf* Quaternary Alluvial Fan; *Qal* Quaternary Alluvium

analog of the hydrologic conditions that were active during cave origin. More recently, vadose processes have modified the hypogene caves.

2.1 Stratigraphy

The oldest rock in the Sangre de Cristo Mountains is Precambrian gneiss cut by pegmatitic and mafic intrusions of Precambrian age. These rocks were exposed in the Ordovician during a major erosional event. Overlying the unconformity is a sequence of carbonate and clastic formations composed of Ordovician Manitou Dolomite, Harding Sandstone, and Fremont Dolomite. The Devonian Chaffee Group rests on the Fremont Dolomite and comprises the Parting Sandstone and the overlying Dyer Formation. Unconformably, overlying the Dyer is the Mississippian Leadville Limestone, one of the most important cave-bearing units in Colorado. Major erosion followed deposition of the Leadville and resulted in regional karstification of the Mississippian carbonate strata. Overlying the Leadville Limestone are Pennsylvanian arkoses more than 3 km thick. Arkosic strata include the Minturn Formation and the overlying Sangre de Cristo formation, which are exposed above the Orient Mine in the adjacent Sangre de Cristo Mountains (Fig. 2).

Paleokarst breccias and cave fills are present in the Dyer Formation and Leadville Limestone (Fig. 6). Limonite deposits are restricted to paleokarst in the Leadville, but hypogenic caves are present in both the Dyer and Leadville formations. The Leadville Limestone varies greatly in total thickness as a result of the karst unconformities at the top of each of the three members. The stratigraphic column of Balleweg (1990, Fig. 6) shows a total formation thickness of 73–102 m. Some of the caves filled with paleokarst sediment can be relatively large. For example, Fig. 4 shows the

Fig. 4 Downward view into a Mississippian-age paleokarst cave conduit after removal of the limonite ore filling the passage. Distance from the near cave wall to the encircled adit on the far wall is 55 m. Photo by K.J. Balleweg

Fig. 5 Paleokarst fill intersected by a hypogenic cave passage in the orient mine. Note the rounded solutional bedrock surfaces of the cave walls. Photo by K.J. Balleweg

outline of a formerly filled paleokarst cave after removal of the limonite ore. The cave is concordant with the bedding and slopes steeply downward.

Tertiary intrusive events in the area are generally minor, with the exception of the Oligocene Rio Alto Stock, 6.4 km northeast of the Orient Mine. Balleweg (1990) speculated that alteration of the paleokarst cave fill breccias to limonite ore was related to Tertiary intrusive events.

2.2 Geologic Structure

One of the major factors contributing to the occurrence of mineral springs at Valley View Hot Springs and the Orient Mine caves is the complex geologic structure of the area. During the Paleogene Laramide orogeny, Paleozoic sediments in the Sangre de Cristo Range were strongly deformed, resulting in a broad north–south trending, doubly plunging anticline with steeply dipping limbs. Remnants of this fold are present in a band that crosses the Sangre de Cristo Range and on the west side of the San Luis Valley. Thrust faults that accompanied development of the dome are present at the Orient Mine, at Valley View Hot Springs, and as north-trending features in the Pennsylvanian–Permian sedimentary section in the nearby mountains. At the Orient Mine, cavernous strata dip an average of 75° east (Fig. 4).

In the Oligocene to early Miocene, extensional faulting related to the opening of the Rio Grande rift caused the San Luis Valley to subside along large-scale normal faults. The dome that formed during Laramide compression was broken and the western part down-faulted into the San Luis Valley where it was covered with synorogenic sediments derived from the uplifts on the margins of the rift. (See Fig. 7, and Tweto 1979).

2.3 Hypogenic Flow Paths

Davis (1986) and Balleweg (1990) speculated on the origin of the Orient Mine caves. Both suggest that the water originated in the Sangre de Cristo Mountains. Although there are

Table 1 Chemistry of Mineral Hot Springs and Valley View Hot Springs (Barrett and Pearl 1976; discussion in Hinkle and Erdman 1995)

Chemical variable	Mineral Hot Springs	Valley View Hot Springs
As (µg/L)	30	1
B (µg/L)	372	30
Cd (µg/L)	0.5	1
Ca (mg/L)	58	48
Cl (mg/L)	40	1.8
F (mg/L)	4	0.4
Fe (µg/L)	60	20
Li (µg/L)	322	8
Mg (mg/L)	13	14
Mn (µg/L)	20	7
Hg (µg/L)	Not detected	Not detected
N (mg/L)	2.1	0.21
Phosphate as P (mg/L) (mg/L)	0.03	0.01
Phosphate as ortho-PO_4 (mg/L)	0.08	0.03
K (mg/L)	14	2.4
Se (µg/L)	Not detected	Not detected
SiO_2 (mg/L)	48	19
Na (mg/L)	140	3.6
So_4 (mg/L)	180	85
Zn (µg/L)	7	5
Alkalinity as $CaCO_3$ (mg/L)	283	103
Alkalinity as HCO_3 (mg/L)	345	125
Non-CO_3 hardness (mg/L)	not detected	76
Total hardness (mg/L)	200	176
Specific conductance	1014	366
Total dissolved solids (mg/L)	680	237
pH field	6.7	6.8
Discharge (L/s)	6.8	4.7
Temperature (°C)	60	34

Note Dilution of concentrations at Valley View Hot Springs as the result of mixing with water from the Sangre de Cristo Mountains

vadose features such as slot canyons, allogenic sediment, stream channels, and waterfall undercuts in the uppermost caves (Davis 1986), we believe that these are overprints resulting from recent influx of surface water, and that most of the cave passages and galleries resulted from dissolution by hypogene waters. Balleweg (1990) noted that several of the caves adjacent to the limonite zones exhibit "rounded surfaces, solution corrosion, and local caves," that appear more characteristic of phreatic dissolution (Fig. 5).

McCalpin (2013) observed that thermal water at Valley View Hot Springs likely originated in the adjacent San Luis basin and is forced to the surface by hydrostatic pressure. He also noted that at least part of the water issuing from the springs is cool, with its most likely source in the Sangre de Cristo uplands to the east. The warm and cool waters mix near Valley View Hot Springs, resulting in cooling of the hot spring water. The spring temperatures fluctuate from year to year. In dry years, when there is less runoff from the mountains, there is less cool water available to dilute the upwelling basinal hot water, and the spring water is warmer. During years of high precipitation, when more runoff is available, the temperature of the springs is cooler. This suggests a mixing zone located at or near the springs (McCalpin 2013; see Fig. 7).

Another indication of the mixing of two waters is provided by the chemical analysis at Valley View Hot Springs at the eastern edge of the San Luis Valley near the Orient Mine Caves, compared to that of the Mineral Hot Springs waters near the center of the San Luis Valley (Table 1). It is clear that ionic concentrations at Valley View Hot Springs

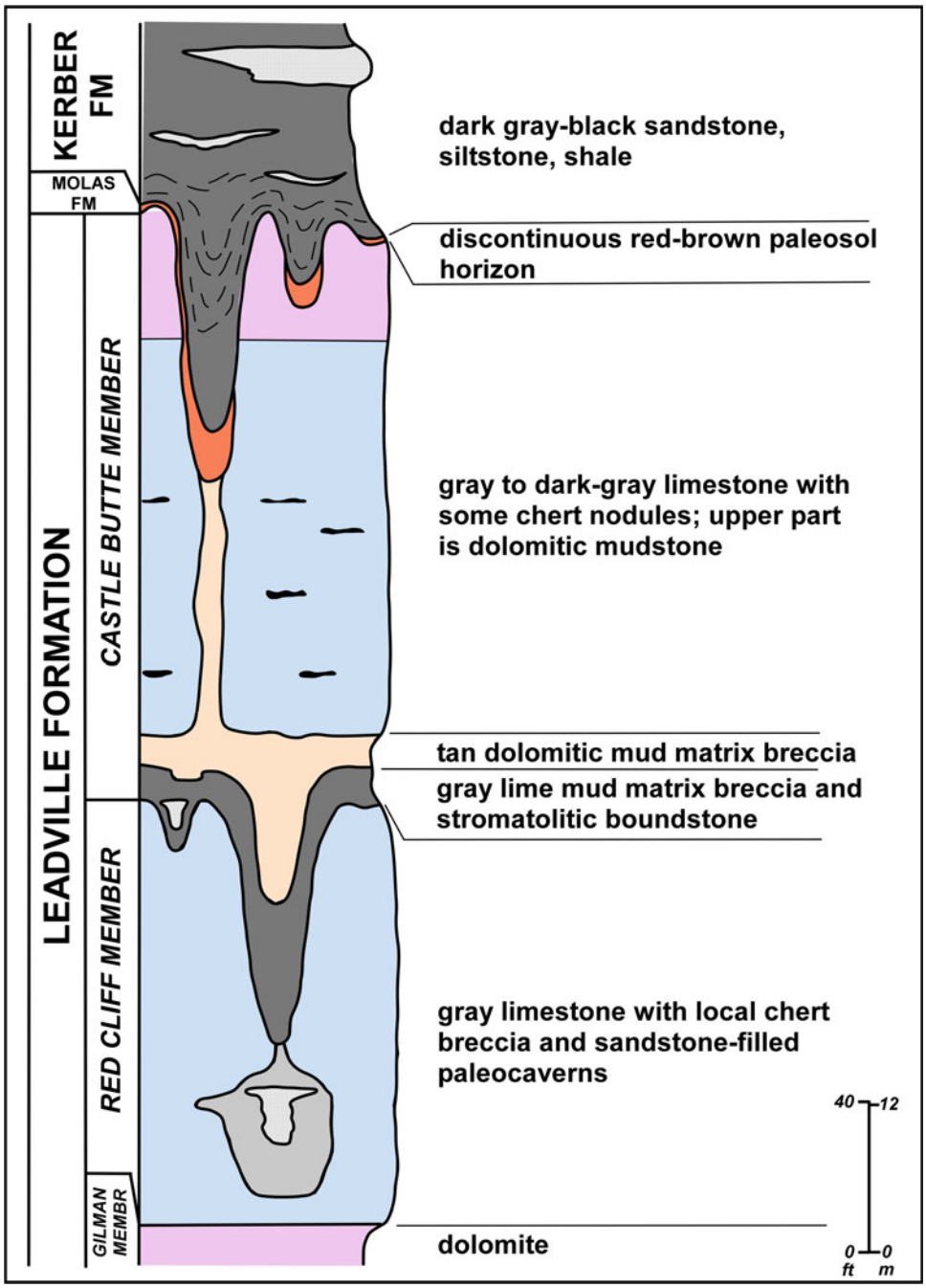

Fig. 6 Composite stratigraphic column for the Leadville Formation in the orient mine area. From Balleweg (1990)

are generally diluted in comparison to those of the Mineral Hot Springs.

Figure 7 is a cross section through the Orient Mine area showing the various faults that directed both the downward and upward water flows. Note that the sedimentary section near the Orient Mine is steeply dipping, and that thrust faults cut Pennsylvanian and Permian strata topographically above and east of the mine. These faults and associated fractures are believed to collect and channel water downward from the Sangre de Cristo Range. According to the favored speleogenetic model, water travels from the crest of the Sangre de Cristo Range through fractures and along thrust-fault surfaces and rises to the surface within the more permeable carbonate rocks of the Leadville and Dyer Formations. Simultaneously, warm water is forced from Tertiary-age basin aquifers into the fractured rocks along the San Luis fault. The fault zone acts as a conduit, channeling water upward where it mixes with cool, mountain-derived water.

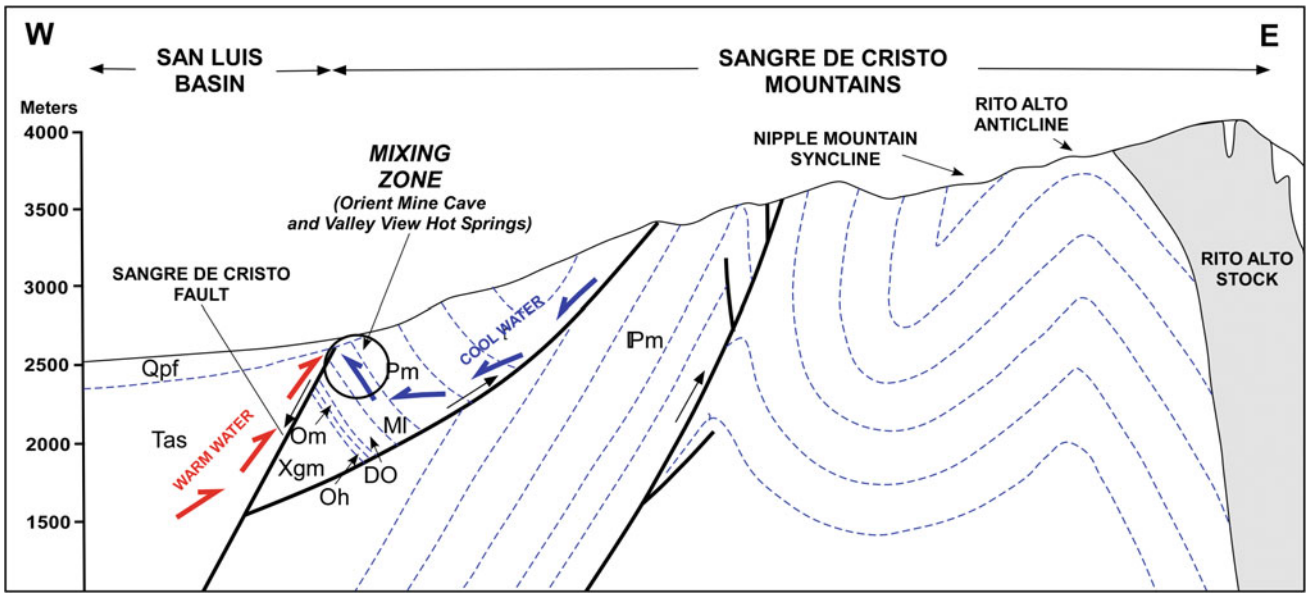

Fig. 7 Geologic cross section showing hypothetical flow paths for warm and cool water. The diagram represents the paleo-flow at the time of the formation of the Orient Mine Caves and the present-day flow at Valley View Hot Springs, which are located in the mixing zone. Base cross section adapted from Lindsey and Soulliere (1987) and corresponds to Section C on Fig. 3. *Formation symbols Xgm* Precambrian Gneiss; *Om* Ordovician Manitou; *DO* Devonian-Ordovician undifferentiated; *Ml* Mississippian Leadville; *Pm* Pennsylvanian Minturn (including Sharpsdale); *Tm, Tf* Tertiary Intrusives; *Qaf* Quaternary Alluvial Fan; *Qal* Quaternary Alluvium

At depth, the thrust faults are cut by the basin-bounding Sangre de Cristo normal fault at the edge of the San Luis Valley. Sufficient hydraulic head is generated by the 1220 m elevation difference between the crest of the range and the caves to force underlying meteoric water to rise to the present surface elevation of the Orient Mine. Thus, in the past, it is likely that water flowed upward through porous and fractured Paleozoic carbonates to the elevation of the Orient Mine, where it mixed with hypogenic water from the San Luis valley and formed open cave galleries. The Valley View Hot Springs, 1.6 km south of the Orient Mine Caves, is a present-day analog to the hydrologic flow paths and conditions that existed during the formation of the Orient Mine Caves.

3 Cave of the Winds

Cave of the Winds is a show cave with 3.2 km of surveyed passages located 1.5 km north of the resort community of Manitou Springs, Colorado (Figs. 1, 8, 9). Manitou Springs is known for its mineral water from natural springs and wells. The temperature of spring and well water is slightly warmer than that of shallow groundwater, putting them in the category of warm springs (Luiszer 1997).

3.1 Geologic Setting

Principal cave development is in the Ordovician Manitou Limestone, with lesser development in the overlying Williams Canyon formation and Leadville Limestone, both of Mississippian (early Carboniferous) age. The cave is developed in a south-plunging anticline composed of Cambrian through Pennsylvanian (late Carboniferous) strata (Fig. 9). Overlying the carbonates are the Pennsylvanian arkosic Glen Eyrie Formation and the Fountain Formation. Both of these units are aquicludes that prevent water from flowing upward from the carbonates and are treated hydrologically as a single unit. Paleozoic strata extend northwest–southeast in the footwall of the Ute Pass high-angle reverse fault. Water enters fractures in the granite, travels downward to the fault, then rises where the fault overlies south-dipping Paleozoic strata (Fig. 10).

The cave is located near the crest of a northwest–southeast-trending anticline (Fig. 8) and is one of several similar ones in the area. The anticline parallels a northwest–southeast-trending syncline to the south. The east limb of the syncline is truncated and partly overlain by Pikes Peak Granite along the Ute Pass high-angle reverse fault. The faults formed as a result of the regional compressional event that caused the Ute Pass fault. Figure 8 shows the structural

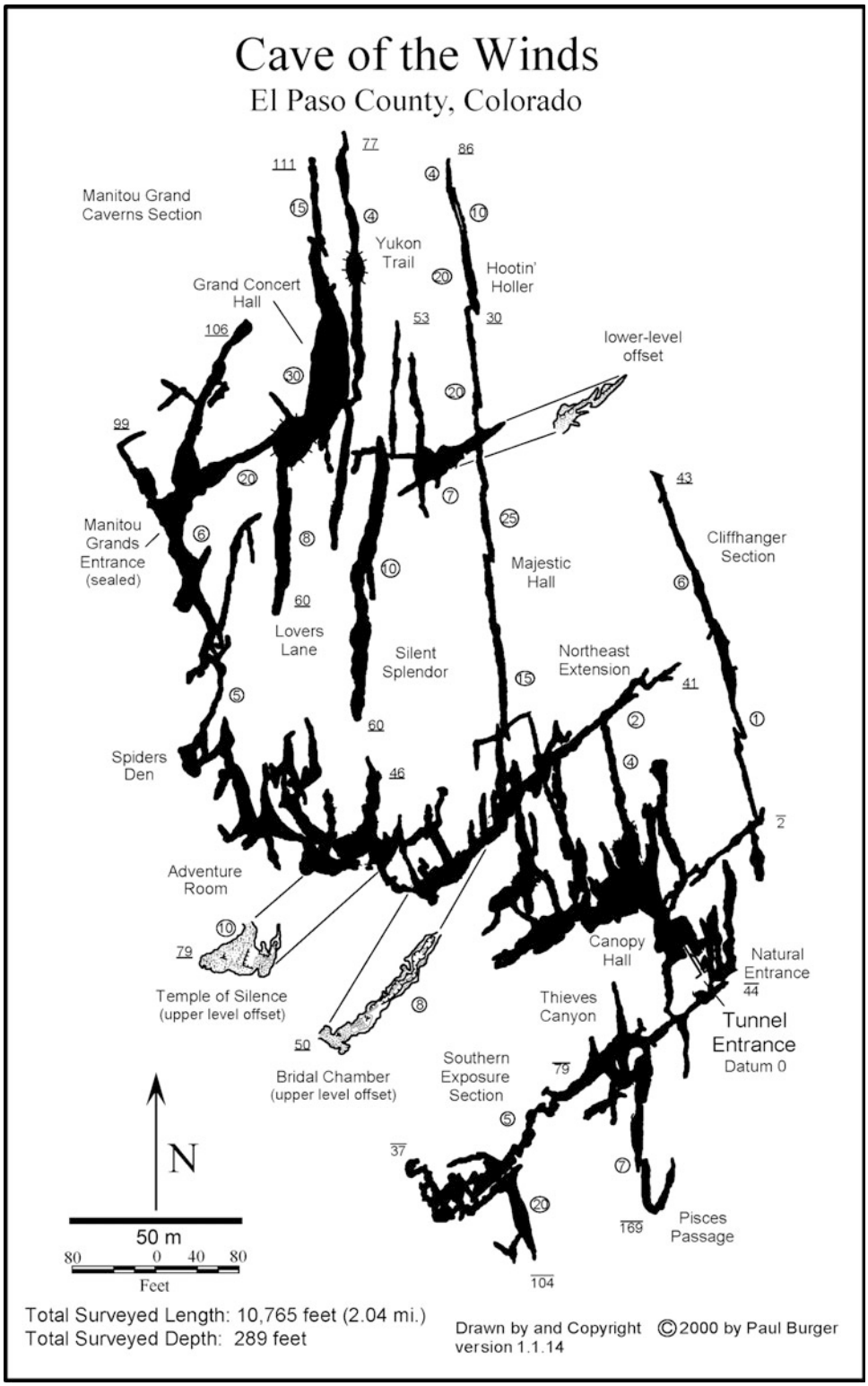

Fig. 8 Map of Cave of the Winds, courtesy of Paul Burger, National Park Service

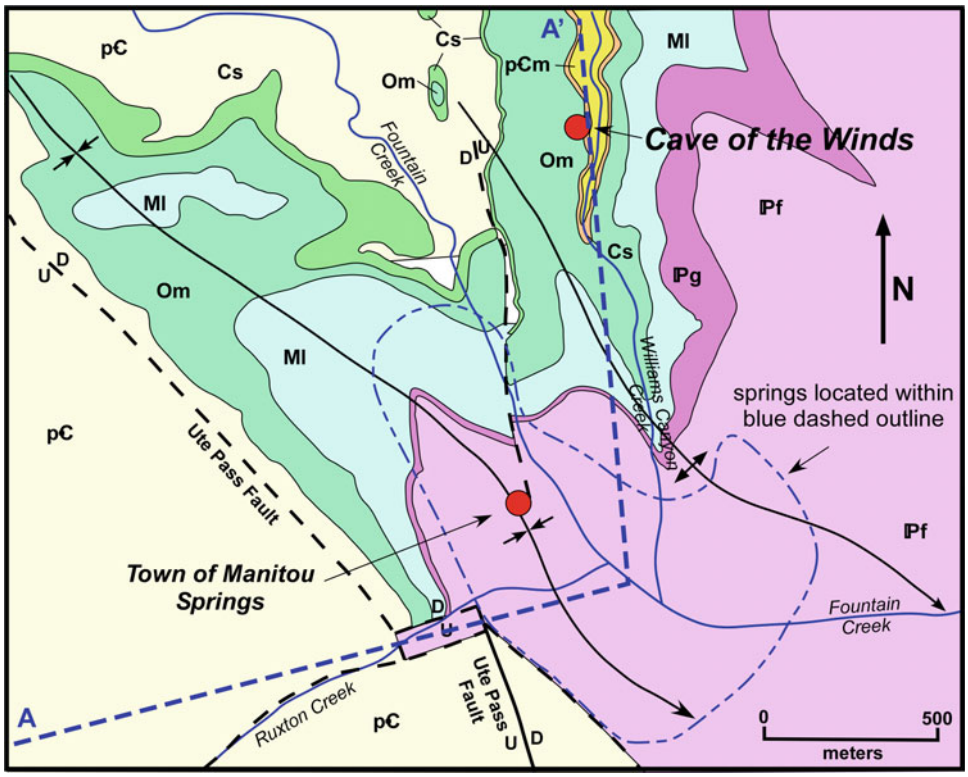

Fig. 9 Geologic Map and section of the Manitou Springs area from Luiszer (1997) after Bianchi (1967). Cave of the Winds is indicated in the upper center of the map. Note the northwest–southeast-trending Williams Canyon Anticline and adjoining syncline through Manitou Springs parallel with the northwest–southeast-trending Ute Pass Thrust Fault in the southwestern portion of the area. *Formation symbols IPf* Fountain Formation; *IPg* Glen Eyrie Formation; *Ml* Leadville Limestone Formation and Williams Canyon formation; *Om* Manitou Limestone; *Cs* Sawatch Sandstone; *pC* Pikes Peak Granite; *pCm* biotite migmatite

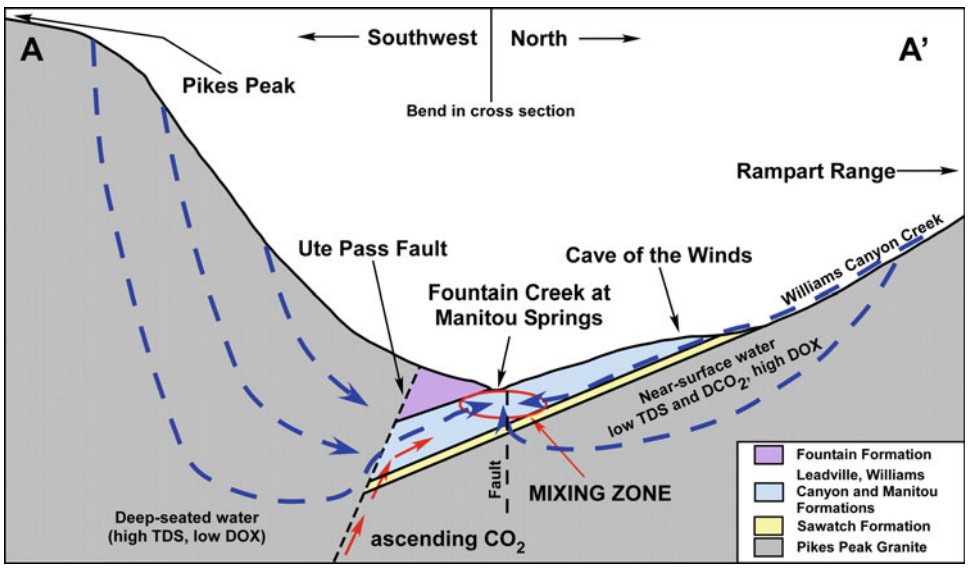

Fig. 10 Hypogenic water flow paths that are interpreted to have formed Cave of the Winds. Water descends along fractures in the Pikes Peak Massif to intersect the Ute Pass Fault and then traverses the fault to enter the Paleozoic cave-forming carbonates (after Luiszer 1997)

features as well as the outcrops of Paleozoic strata and Pikes Peak Granite (Luiszer 1997).

3.2 Speleogenesis

Cave of the Winds was formed where ancestral Fountain Creek crossed Paleozoic carbonate strata near the axis of the Williams Canyon anticline, allowing oxygenated surface water to mix with deep-seated anoxic water. Cave development began ~4.5 mA, as determined by aminostratigraphy, magnetostratigraphy, and interpretation of geomorphic features (Luiszer 1997). At that time, springs similar to those in Manitou Springs today emerged from sediments in the paleo-valley north and up-slope from Cave of the Winds. Mineral water high in CO_2 from these springs mixed with

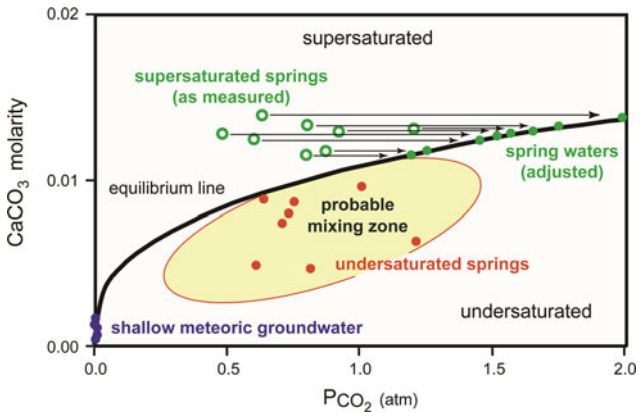

Fig. 11 Water chemistry at Manitou Springs. PCO_2 of supersaturated springs has been adjusted to what they must have been at depth, before degassing. Undersaturated springs fall in the probable mixing zone between shallow and deep groundwater. From Luiszer (1994)

dilute surface water from ancestral Fountain Creek to form a chemically aggressive solution that dissolved the carbonate rocks.

Present-day hydrologic processes in the town of Manitou Springs reflect the ancient cave-forming processes. The hydrologic system responsible for the Cave of the Winds is long-lived and still active. Evidence includes several terrace levels that record the positions and elevations of ancestral Fountain Creek descending from the north and above Cave of the Winds, in steps down to the town of Manitou Springs. Many of these terrace levels are marked with iron-stained alteration associated with hypogene water flow in the cave. Evidence that speleogenesis continues today is found in water-well drilling logs where bit drops into caverns beneath the city are reported. This is evidence that in the past a similar hydrologic system was located above the present-day Cave of the Winds.

Waters in the present Manitou—Williams Canyon—Leadville aquifer below the town of Manitou Springs can be divided into four groups on the basis of water chemistry, reflecting the sources and amount of surface water mixing with the ascending mineral water (Fig. 11). Water chemistry and precipitates from the mixing of surface and hypogenic waters support the hypogenic mixing hypothesis (Luiszer 1997). Precipitates in the cave include iron and manganese oxides. Luiszer (1994) documented that the iron oxide deposits were bacterially produced.

Speleogenetic sediments from two episodes of paleokarst development are found at and near Cave of the Winds. These episodes karstified the Lower Ordovician Manitou and along the interface between the Manitou and the overlying Mississippian Williams Canyon (Forster 1977), and at the contact of the Williams Canyon with the overlying Mississippian Leadville Limestone. Preserved features include filled caves and bedding-plane fissure fills, which provided some of the earliest and most permeable routes for local water flow. However, the majority of cave development took place along fractures developed during the Laramide orogeny (Blanton 1973).

Ascending hypogenic waters were confined in the Manitou—Williams Canyon—Leadville aquifer by the overlying Fountain Formation aquiclude. Confinement concentrated the dissolution of carbonates of the aquifer and illustrates the classic interbedded aquifer/aquiclude hypogenic flow model. In the town of Manitou Springs, a thin remnant of the Fountain Formation is breached in three places, allowing mineral water to emerge from the surface adjacent to Fountain Creek.

3.3 Interpretation of Groundwater Flow Paths

The water that formed Cave of the Winds initially entered fractures in the granite of the Pikes Peak massif south of Manitou Springs (Luiszer 1997). This granite mass (which includes the 4302 m Pikes Peak itself) towers almost 2130 m above the elevation of Cave of the Winds. After descending through fractures in the granite, this water was diverted northward and upward along the Ute Pass Fault toward the town of Manitou Springs. Where the fault intersected the Paleozoic carbonates, water entered the fractured and soluble strata and moved northward until it reached the Fountain Creek paleo-valley (Luiszer 1997). Mixing of the hypogene water with the surface water in the paleo-valley produced chemically aggressive waters in the mixing zone and can account for the origin of Cave of the Winds (Fig. 11).

4 Glenwood Caverns

Glenwood Caverns contains 4.8 km of mapped passages in southwest-dipping Mississippian Leadville Limestone (Fig. 12). It is a show cave under its present name, but originally was known as Fairy Cave. It is located in Iron Mountain above the town of Glenwood Springs, where the southwest-flowing Colorado River crosses the Grand Hogback Monocline on the southwest side of the White River Uplift (Fig. 13; Kirkham et al. 1996). The area lies at the western end of Glenwood Canyon, which has been incised through Paleozoic Precambrian rocks at the boundary between the Rocky Mountain orogenic province and the Colorado Plateau.

4.1 Geologic Setting

The Colorado River cuts across the regional structural grain east of Glenwood Springs, but it flows subparallel to the

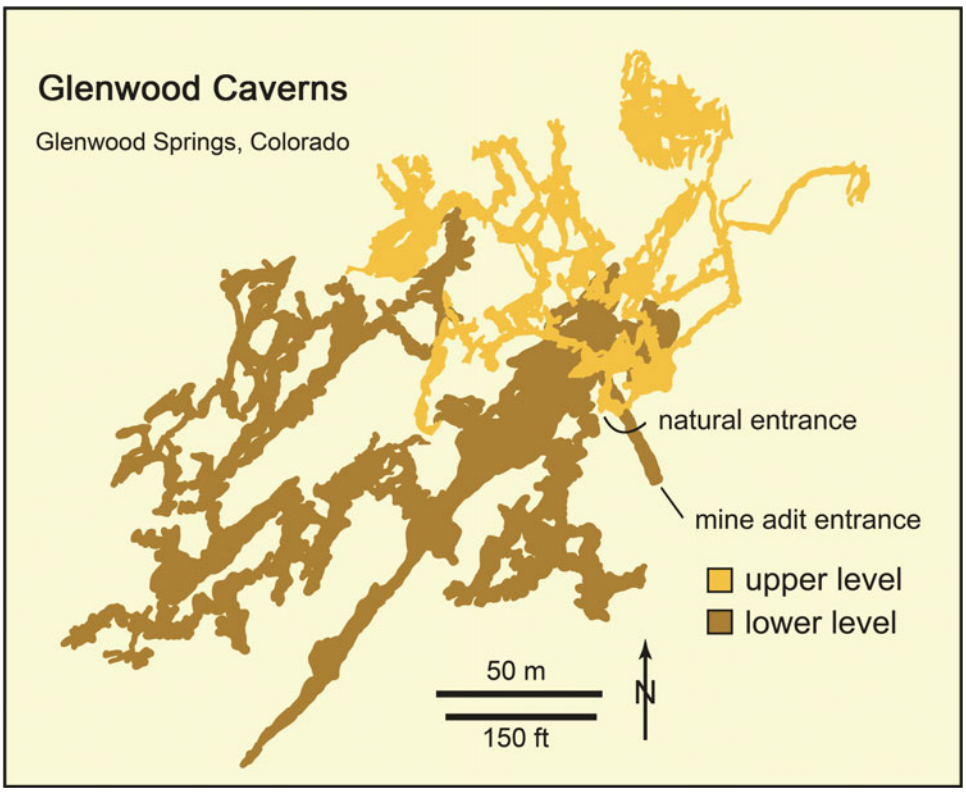

Fig. 12 Map of Glenwood Caverns, Glenwood Springs, Colorado (after Anderson and Barton 2002)

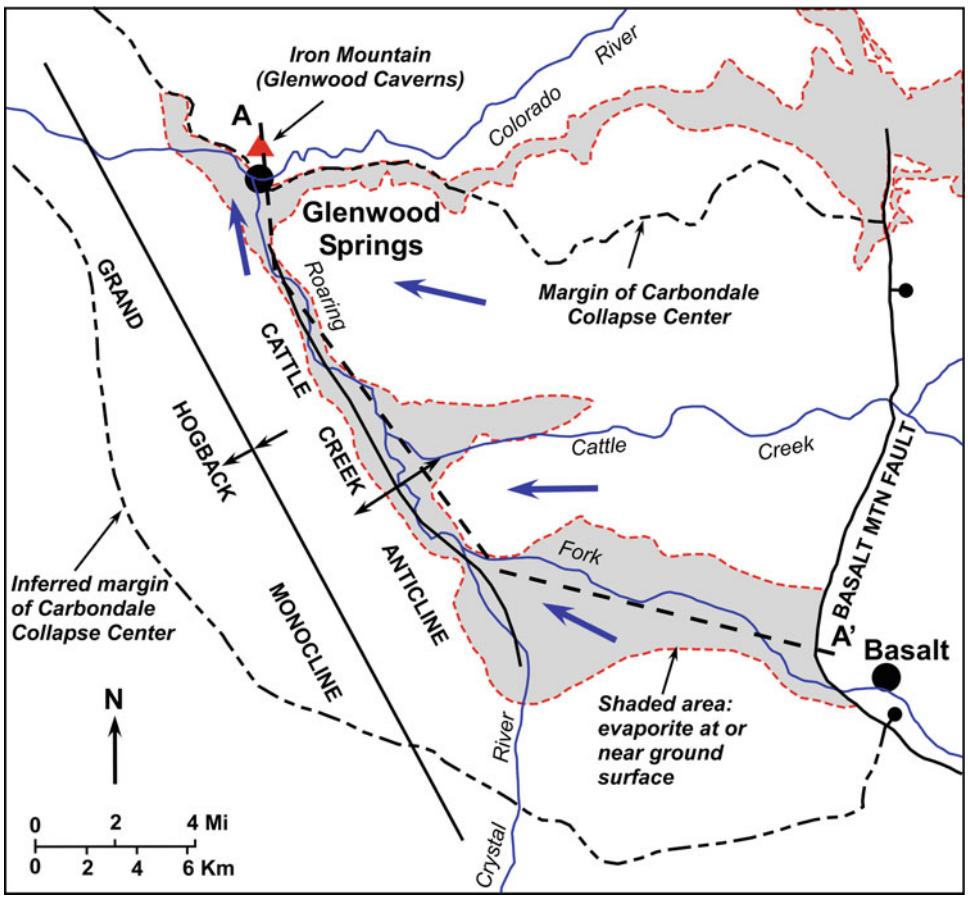

Fig. 13 Generalized geologic map of the Glenwood Caverns area showing water flow within Pennsylvanian evaporites in the Carbondale Collapse center. The dashed line *A*–*A*′ indicates the trace of the cross section shown in Fig. 14. The White River Uplift lies north and east of Glenwood Springs. Modified from Kirkham et al. (2001)

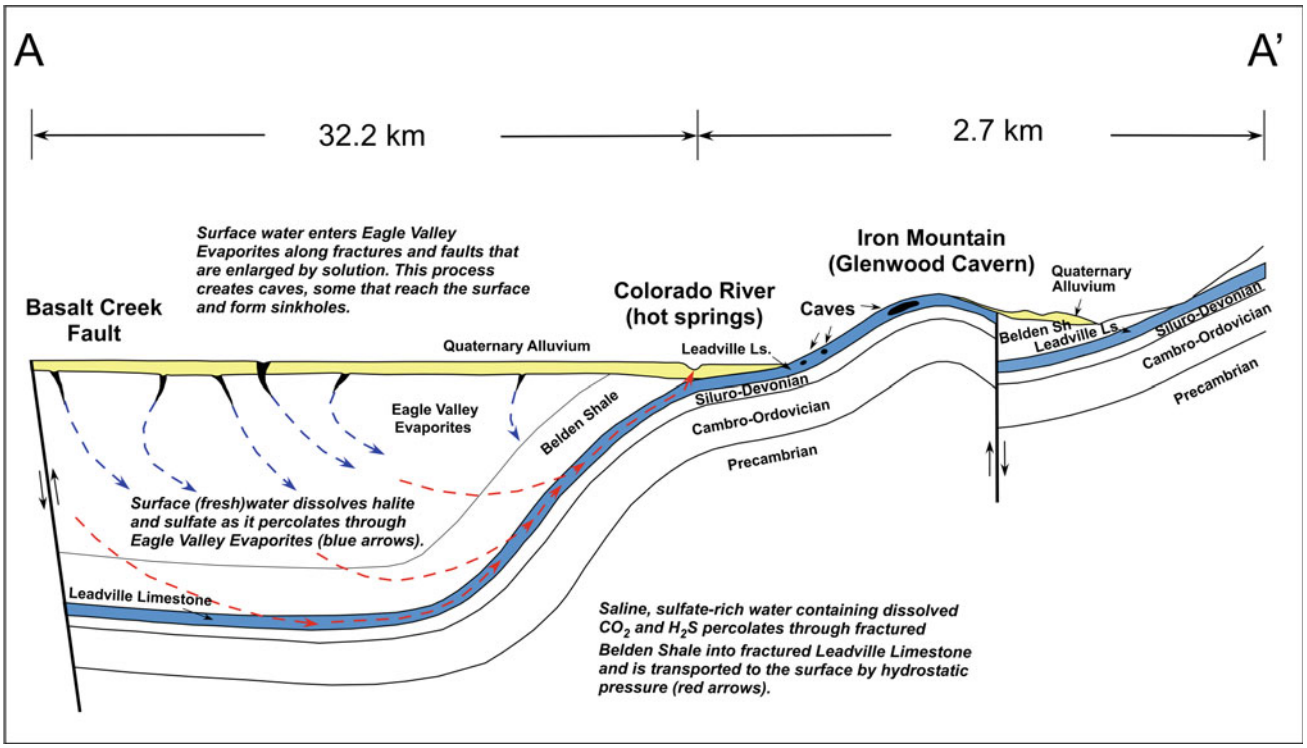

Fig. 14 Diagrammatic cross section of hypogenic water flow paths from the Carbondale Collapse Center into the Mississippian Leadville Limestone, and upwards into the Glenwood Caverns area. Derived from Kirkham et al. (1997)

structural strike where it crosses the Grand Hogback Monocline. Roaring Fork, a tributary, flows northward along the strike of the monocline to form part of a topographic low known as the Carbondale Collapse Center (Kirkham and Scott 2002). The floor of the Collapse Center is composed of Tertiary and Quaternary gravels covering remnants of Pennsylvanian evaporites and Tertiary basalt flows. The gravel and basalt partly overlie an elongate diapir composed of Eagle Valley formation evaporites in the core of the anticlinal bend of the Grand Hogback Monocline.

The Carbondale Collapse Center collects runoff from surrounding mountains, which drains to the Colorado River via the Roaring Fork River and its tributaries. In the subsurface, water moves through permeable zones within Eagle Valley evaporites, dissolving halite and sulfates. Over time, water carrying large amounts of dissolved sulfate and halite enters older Paleozoic sediments, in particular the Leadville Limestone, on its way to springs. In the subsurface, water warms with increasing depth as it moves from south to north (Figs. 13 and 14).

4.2 Speleogenesis

Thermal water containing CO_2 and H_2S reaches the surface at twelve springs and at least six seeps at or near the Colorado River at Glenwood Springs. These springs provide a modern analog for the water that formed the cave. Carbonic acid in rising thermal water was responsible for most speleogenetic dissolution in Iron Mountain, although some dry passages in Glenwood Caverns have a sulfuric acid overprint.

The hot springs and seepage areas along the Colorado River in Glenwood Springs have a cumulative discharge is 15–19 m^3/s migrating up through fractures and faults from the Leadville Limestone (Barrett and Pearl 1976; Gelden 1989). Water temperatures range from 44 to 47 °C (111–117 °F) (Gelden 1989). Water from two test wells on the north side of Glenwood Springs, near the Colorado River, contains dissolved H_2S ranging from 1.2 to 2.1 mg/L. A CO_2 concentration of 110 mg/L was reported in water from one of these wells (Gelden 1989).

Mississippian Leadville Limestone and older formations overlie Precambrian crystalline rocks (Figs. 2 and 14). The Leadville Limestone at Glenwood Caverns is 61 m thick and is composed of gray, coarse to finely crystalline, fossiliferous limestone in the upper part, and dolomite with chert nodules in the lower part (Kirkham et al. 1997). Glenwood Caverns is developed in the Leadville near the top of Iron Mountain (Fig. 13). The historic Fairy Cave entrance is near the top of the mountain, 399 m above Glenwood Springs and the Colorado River. The cavern has a vertical relief of 84.7 m (Anderson and Barton 2002; Fig. 12).

Base level gradually fell in response to downcutting by the Colorado River. As this occurred, the zone of active cave enlargement migrated downward as well, while progressively deeper phreatic cave passages became air filled. At the water table, H_2S escaped into the cave atmosphere, to be reabsorbed into films of oxygenated meteoric and condensation water on gallery walls and other surfaces. Here, H_2S was oxidized to sulfuric acid, which immediately reacted with the limestone and the calcite speleothems, partially altering them to gypsum. Most of this gypsum was dissolved and removed from the cave, but gypsum crust is preserved in areas protected from water (DuChene et al. 2003).

Late in the developmental history of the cave, while the cave was enlarging at depth by calcite dissolution, carbon dioxide was simultaneously lost to the atmosphere near the water table. This caused the remaining water to become supersaturated with respect to calcite, resulting in subaqueous deposition of calcite in mammillary layers that range up to 10 cm thick. Calcite mammillaries from Glenwood Caverns have been age-dated using Uranium series analysis. Dates of 1.36 ± 0.25 Ma and 1.72 ± 0.25 Ma were determined for two samples (Polyak et al. 2013). These dates show the time of calcite mammillary deposition and establish a minimum age for the cave.

4.3 Biogenic Deposits

Both Cave of the Winds and Glenwood Caverns have biogenic features and/or deposits. Biogenic processes are suggested by the authors for the enrichment of the limonite ore bodies at the Orient Mine Caves but have not been studied there. Luiszer (1994, 1997) included scanning electron microscope photos of one of these deposits at Cave of the Winds showing that it is composed of *Leptothrix* bacteria (Fig. 15). Luiszer (1994) included a similar photo from Glenwood Caverns stating "The filaments are indicative of the bacteria *Leptothrix*. The mammillary growths coating the filaments are probably the result of inorganic precipitation of Fe-oxide."

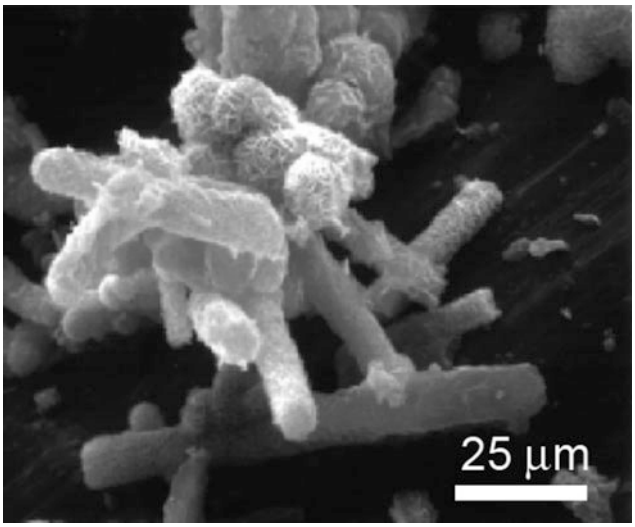

Fig. 15 Scanning electron microscope image of *Leptothrix* bacteria in an iron deposit in Cave of the Winds. From Luiszer (1997)

Limonite deposits are contained in the Barn, the largest room in Glenwood Caverns, and in nearby Discovery Glenn. In one area, large cavities between early-stage breccia blocks are filled with iron oxide and calcite. Luiszer (unpublished) states that "All of the iron oxide deposits … contain elevated concentrations of arsenic … and lead. The uniform small size (1–2 µm) and the globular morphology of the grains … suggest biologically mediated precipitation by bacteria such as *Siderocapsa* or *Pediomicrobium*" (see Fig. 16, an iron deposit in the Discovery Glenn section of the cave).

Pool fingers and U-Loops are also present in Glenwood Caverns. Fossilized DNA was not found in the pool fingers, so no relationship could be made between them and similar present-day features in nearby Glenwood Hot Spring. However, more than 50 new candidate Bacterial, and three new Archaeal species were identified (H. Barton *in* DuChene et al. 2003).

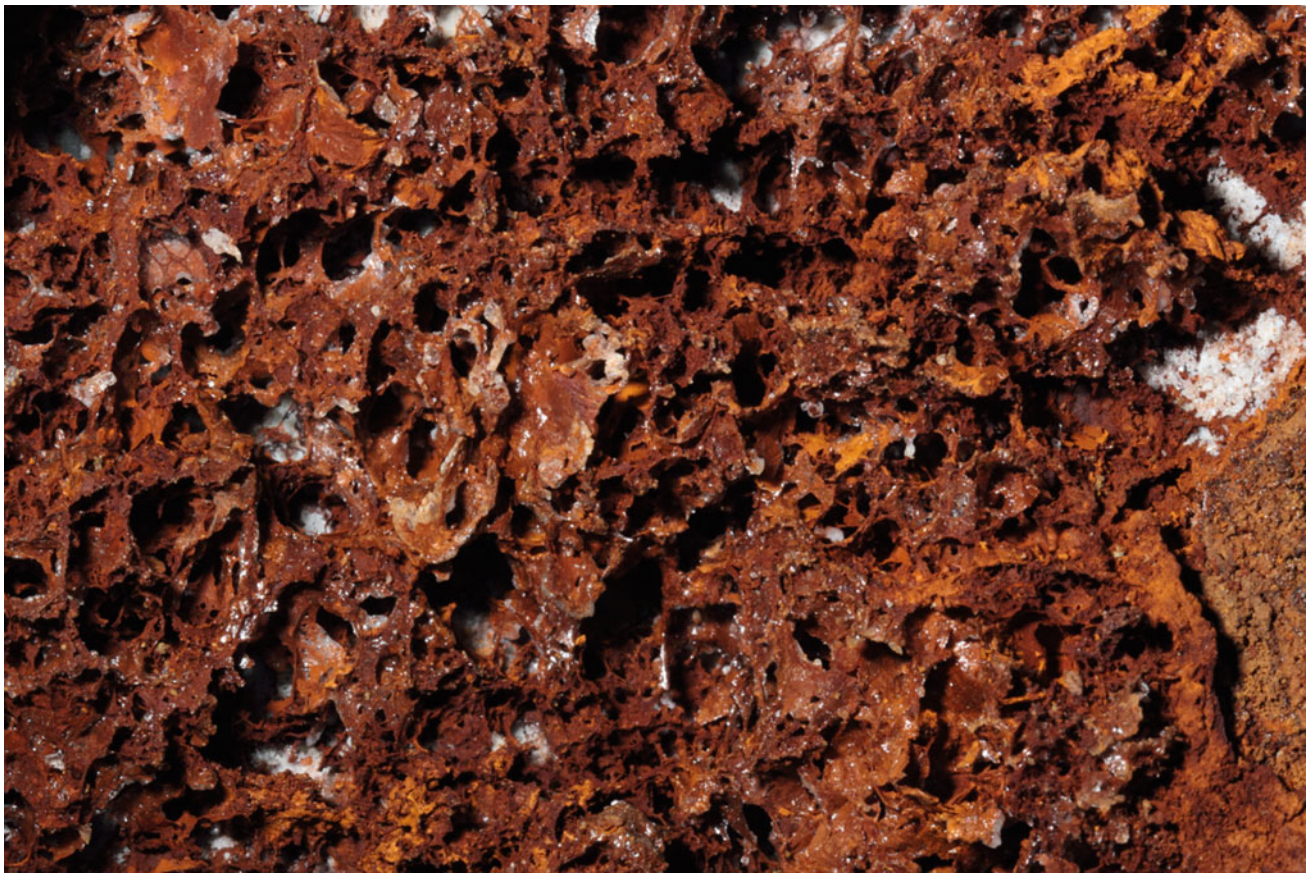

Fig. 16 Bacterially produced iron deposit in Discovery Glenn at Glenwood Caverns. Photo by Norm Thompson

5 Conclusions

Western Colorado contains Paleozoic limestone formations exposed in uplifts within the Colorado Rocky Mountain province, where they have been subjected to both epigenic and hypogenic cave origin. Where those processes are hypogenic, cave and karst development is associated with rising thermal water containing dissolved CO_2, and, at Glenwood Caverns, H_2S. Cave of the Winds and Glenwood Caverns resulted from dissolution caused by mixing of ascending warm or hot water with oxygenated surface water. The Orient Mine caves are partly the result of paleokarst development that may (or may not) have been hypogenic. However, mixing-zone processes associated with rising water during the Neogene caused hypogenic cave development at the Orient Mine. It is likely that caves in similar geologic settings in Colorado owe at least part of their origin to hypogenic processes. In Cave of the Winds and Glenwood Caverns, microbiological studies of iron and manganese deposits indicate that microbes were active during speleogenesis.

Acknowledgements Several individuals and organizations contributed to the preparation of this chapter. All caves described here are privately owned, and their owners graciously provided access and information. Norm Thompson provided copies of the survey notes and maps of the Orient Mine caves, and Paul Burger contributed a version of his Cave of the Winds survey map specifically formatted for this article. Donald Davis provided information on the Orient Mine caves from his explorations in 1961 and 1986. He and Richard Rhinehart provided references to articles published in Rocky Mountain Caving, as well as helpful comments on early drafts of this chapter. Arthur and Margaret Palmer contributed valuable feedback and suggestions.

References

Anderson TE, Barton HA (2002) Fairy Cave. Garfield County, Colorado. Unpublished map

Balleweg KJ (1990) Geology of the orient limonite deposit. Saguache County, Colorado. Unpublished MS thesis T-3605, Colorado School of Mines, Golden, CO

Barrett JK, Pearl RH (1976) Hydrogeological data of thermal springs and wells in Colorado. Colorado Geological Survey, Department of Natural Resources, Information Series 6

Bianchi L (1967) Geology of the Manitou-Cascade Area, El Paso County, Colorado with a study of the permeability of its crystalline rocks. Unpublished MS thesis, Golden, Colorado School of Mines, Colorado

Blanton TL (1973) The Cavern gulch faults and fountain creek flexure, Manitou Spur, Colorado. Unpublished MS thesis, Syracuse University, Syracuse, New York

Davis DG (1986) Frost and iron: return to the Orient Mine Caves. Rocky Mountain Caving, Colorado Grotto, Denver, Colorado 3(3):32–34

Dover G (1981) Aardvark Caverns Trip Report. Pueblo Underground Bulletin, Southern Colorado Mountain Grotto, Pueblo, Colorado 5(2):5–8

DuChene HR et al. (2003) Geological and biological features of Glenwood Cavern, Glenwood Springs. In: Abbot DM Jr, Wray LL (eds) Geology in the next decade. American Institute for professional geologists guidebook, Field Trip D, pp 37–41

Fish L (1986) The disoriented mine. Rocky Mountain Caving Colorado Grotto, Denver, Colorado, 3(3):35–37

Forster JR (1977) Middle-ordovician sub-aerial exposure and deep weathering of the lower ordovician manitou formation along the ute pass fault. Geol Soc Am Abstr Progr 9:722

Gelden AL (1989) Hydrogeology of the Leadville Limestone and other Paleozoic rocks in northwestern Colorado, with results of aquifer tests at Glenwood Springs. U.S. geological survey water-resources investigations report 87–4195

Hinkle ME, Erdman JA (1995) Geochemical and biochemical surveys near the Mineral Valley view hot springs known geothermal resource areas, northern San Luis Valley, Colorado. U.S. Geological Survey, Open-File Report OF-95-569, scale 1:100,000

Kirkham RM et al (1996) Field trip guidebook on the geology and geologic hazards of the Glenwood Springs area, Colorado. In: Thompson RA, Hudson MR, Pillmore CL (eds) Geologic excursions to the Rocky Mountains and beyond. Colorado Geological Survey Special Publication 44: CD-ROM

Kirkham RM et al (1997) Geologic map of the Glenwood Springs Quadrangle, Garfield County, Colorado. Colorado Geological Survey Map MS 31, 1:24,000

Kirkham RM et al (2001) Late Cenozoic regional collapse due to evaporite flow and dissolution in the Carbondale Collapse Center, West-Central Colorado. Mt Geol 38(4):193–210

Kirkham RM, Scott RB (2002) Introduction to late Cenozoic evaporite tectonism and volcanism in west-central Colorado. In Kirkham RM et al (eds) Late Cenozoic evaporite tectonism and volcanism in west-central Colorado. Geol Society America Special Paper 366:1-14

Lindsey DA, Soulliere SJ (1987) Geologic map and sections of the Valley View Hot Springs quadrangle, Custer and Saguache Counties, Colorado. U.S. Geological Survey, Miscellaneous Field Studies Map MF-1942, scale 1:24,000

Luiszer FG (1997) Genesis of the cave of the winds, Manitou Springs, Colorado. PhD thesis, University of Colorado, Boulder, Colorado

Luiszer FG (1994) Speleogenesis of cave of the winds, Manitou Springs, Colorado. In Sasowsky ID and Palmer MV (eds) Breakthroughs in karst geomicrobiology and redox geochemistry. Karst Waters Institute, Special Publication 1: 91–109

Maslyn RM (1976) Late-Mississippian paleokarst in the Aspen, Colorado area. Unpublished master's thesis, Colorado School of Mines, Golden, Colorado

McCalpin JP (2013) Hot Springs Geology 101: where the water comes from. Orient Land Trust website. http://www.olt.org/nature/geology

Polyak VJ et al (2013) Incision history of Glenwood Canyon, Colorado, USA, from the uranium-series analyses of water-table speleothems. Int J Speleol 42(3):193–202

Stone JB (1934) Limonite deposits at the orient mine. Colo Econ Geol 29:317–329

Svetz D (1984) Return to Aardvark Cavern. Rocky Mountain Caving, Colorado Grotto, Denver, Colorado 1(2):27–29

Tweto O (1979) The Rio grande rift system in colorado. In: Riecker RE (ed) Rio Grande Rift: tectonics and magmatism. American Geophysical Union, Washington, pp 33–56

Sulfuric Acid Caves of the Bighorn Basin, Wyoming

37

Margaret V. Palmer, Arthur N. Palmer, and Donald G. Davis

Abstract

The Bighorn Basin of Wyoming is a region of thermal springs and caves, some with lethal levels of H_2S and CO_2. It also contains many productive oil wells. In one of these caves, "sulfuric acid speleogenesis" was first recognized and documented in North America by Egemeier in 1973. He proposed that most of the cave dissolution was subaerial and the result of H_2S oxidation to H_2SO_4. Later studies by microbiologists have refined his measurements and show that much of the H_2SO_4 is generated in the stream by sulfur-oxidizing bacteria, by the process of "microbial sulfuric acid speleogenesis." Other caves with similar chemistry are known in the region, but they have only been partly explored because of the locally high sulfide concentrations in their atmospheres.

Keywords

Sulfuric acid speleogenesis • Petroleum reservoirs • Sulfur • Sulfur-oxidizing bacteria

1 Introduction

The flanks of the Rocky Mountain uplifts in the state of Wyoming contain several examples of active and inactive hypogenic caves formed by sulfuric acid (Hill et al. 1976; Fig. 1). Excellent examples are found in the synclinal Bighorn Basin in the northern part of the state. Many of these caves have fluctuating levels of H_2S and CO_2 that can be dangerously high. Water from the surrounding mountain ranges enters the permeable Madison Limestone of Mississippian (lower Carboniferous) age, which is confined by shale beds and is heated at depths as much as 2000 m below the surface before rising under artesian pressure along anticlines (Fig. 2). Caves and springs are common around the edges of the basin along small anticlines and faults (Fig. 2). Active caves smell of hydrogen sulfide, are variably warm, and contain discontinuous gypsum crusts. Best known are the Kane Caves, which were studied by Egemeier (1973, 1981), the first in North America to propose a sulfuric acid origin for caves such as these. Although an igneous source cannot be ruled out, the source of H_2S in the springs is most probably from extensive oil fields in the Bighorn Basin (Love and Good 1982). Scattered tar-like deposits are found in the Kane Caves.

In 1937, excavation of a tunnel to tap irrigation water from the Buffalo Bill Reservoir, west of Cody, Wyoming, intersected several caves in the Madison Limestone, the largest being ~50-m wide. This cave was reported to contain sulfur deposits and strange speleothems, but until recently it remained inaccessible to organized speleologists because of limited access to the entrance tunnel (Rhinehart 2009).

M.V. Palmer · A.N. Palmer (✉)
Department of Earth and Atmospheric Sciences, State University of New York, Oneonta, NY 13820-4015, USA
e-mail: arthur.palmer@oneonta.edu

M.V. Palmer
e-mail: palmeran@oneonta.edu

D.G. Davis
441 Kearney Street, Denver, CO 80224-1237, USA
e-mail: dgdavis@nyx.net

© Springer International Publishing AG 2017
A. Klimchouk et al. (eds.), *Hypogene Karst Regions and Caves of the World*,
Cave and Karst Systems of the World, DOI 10.1007/978-3-319-53348-3_37

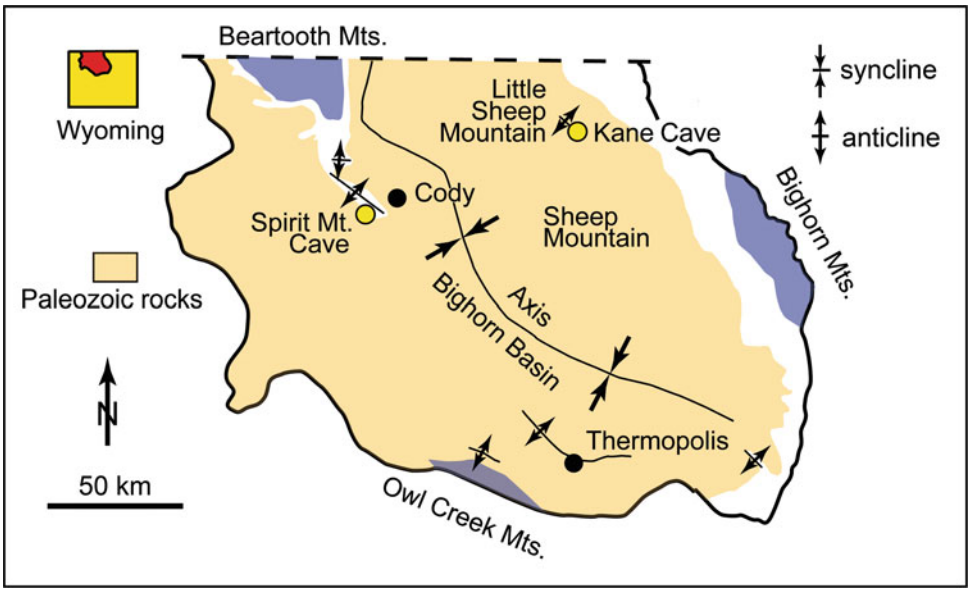

Fig. 1 Location map of hypogenic karst features in the Bighorn structural Basin, Wyoming

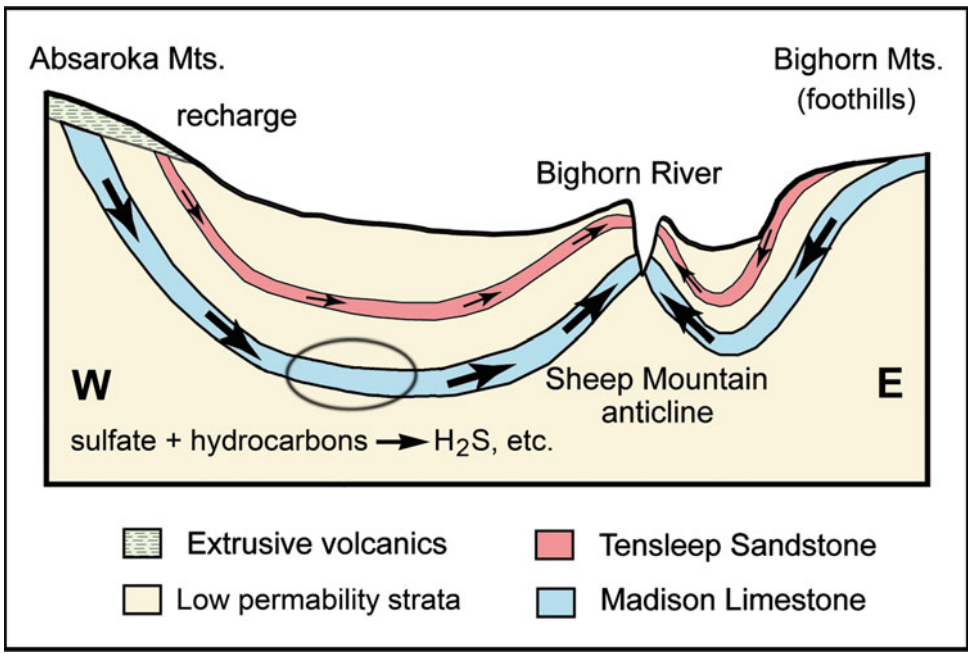

Fig. 2 Generalized geologic cross section through the Bighorn Basin

2 The Kane Caves

Margaret V. Palmer, Arthur N. Palmer

2.1 Advances in Sulfuric Acid Speleogenesis

In the early 1970s, Stephen Egemeier, a PhD candidate at Stanford University, chose the Kane Caves along the banks of the Bighorn River as the site for his dissertation studies. These caves occupy two levels, the upper inactive one 25 m directly above the lower. Both caves are single linear passages about 300-m long that end abruptly. They were apparently fed by the same water source but at different times. They are similar in character, but the upper level has a larger average passage size and its morphology is disrupted by breakdown. There is no traversable connection between the two caves.

The map in Fig. 3 shows only the lower (active) cave. It discharges directly into the Bighorn River at exactly the same level. Upstream in the cave, water enters at three places through narrow slots 15–30-cm wide in the bedrock floor (Fig. 4). The stream has a perennial cumulative flow of ~7.5 L/s. The ceilings above and a short distance

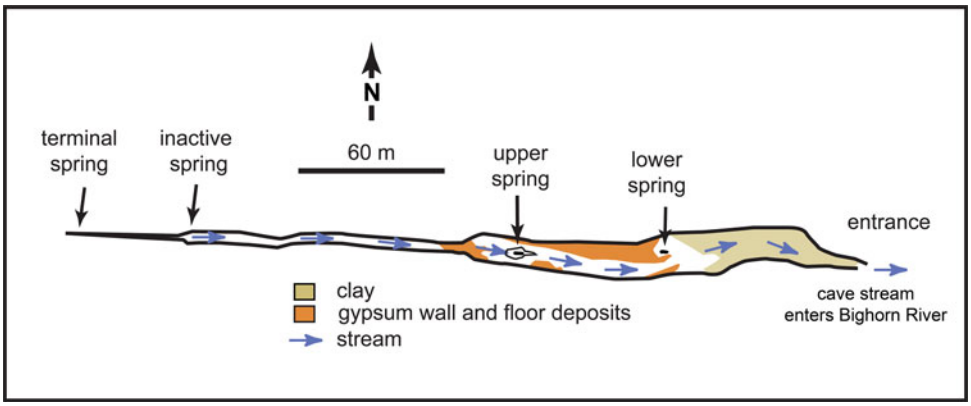

Fig. 3 Plan view of Lower Kane Cave

Fig. 4 View into a rising spring vent along a narrow fissure (~20 cm wide). Note microbial filaments immersed in the water. Photograph by A.N. Palmer

downstream are higher than elsewhere, about 10 m at the two largest springs (Fig. 5). The springs are surrounded by vivid red, yellow, and black deposits composed mainly of bacterial filaments. Many of the walls are coated with a soft wet gypsum crust, in places sparsely capped with sulfur, and mounds of gypsum have accumulated on the cave floor next to the stream. Some of the gypsum is removed by dissolution during periods of flood. The cave springs have rather steady discharge, so back-flooding from the river is probably responsible for most gypsum dissolution. All of the springs contain deposits of black sulfide minerals and radioactive, uranium- and vanadium-rich mud in which sulfate-reducing bacteria have been identified. When disturbed, the mud emits H_2S and possibly methane. On removal from the cave, the sulfides readily oxidize. Other metals in the mud include silver, copper, iron, lead, and zinc. The internal cave springs appear to be traps for these metals and radioactive materials. The petroleum-related source of H_2S is supported by seeps and balls of hydrocarbons in the upper cave and in various places in the lower cave.

Egemeier (1973, 1981) found that H_2S in aqueous solution was highest at the springs and decreased downstream from the springs. He measured a decrease from 6 to 1 ppm within 100 m downstream from the upper spring. Over the same distance, he measured a rapid rise in dissolved oxygen from 0.1 to 5 ppm. He concluded that most of the decrease in H_2S was due to loss to the cave air. H_2S in the air was high enough for cavers to experience nausea and headache within a few hours. The stream water was not saturated with respect to sulfate, although it rose rapidly where the stream encountered gypsum mounds. Bicarbonate in the cave stream was relatively constant, so he concluded that carbonic acid did not play a significant role in cave development. CO_2 increased upstream from the cave entrance, which suggested that it had been produced in the cave by sulfuric acid dissolution.

On the basis of these observations, Egemeier's hypothesis was that dissolution was mainly subaerial. As H_2S rises in the springs, oxygen from the cave air is dissolved into the spring water to form sulfuric acid, which dissolves the limestone. Much of the H_2S escapes into the air, where it is absorbed by water droplets on the cave walls and oxidizes to H_2SO_4, causing limestone dissolution and leaving a replacement crust of gypsum (Fig. 6). Acidic water droplets suspended from the gypsum achieve very low pH because the gypsum shields them from being neutralized by reaction

Fig. 5 Lower Kane Cave, facing upstream toward the H_2S springs. The *red material* in the water is composed of iron hydroxide, which locally coats sulfur-oxidizing bacteria. Note the *white mounds* of gypsum that have fallen from the wall in zones of intense sulfuric acid corrosion of limestone. The gypsum is being removed in solution by the cave stream. Photograph by Kevin Downey

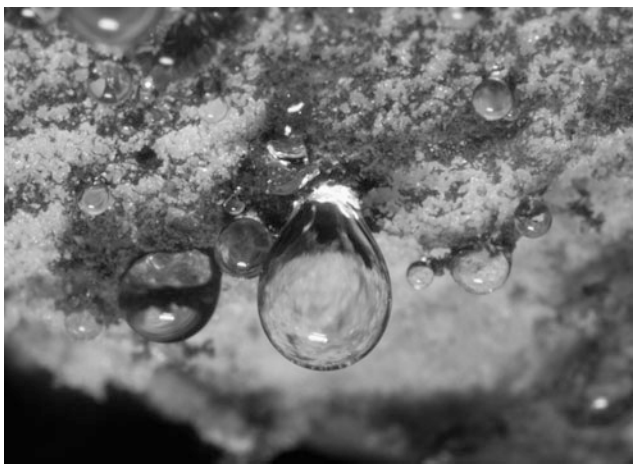

Fig. 6 Water droplets on gypsum-coated ceiling of Lower Kane Cave, which have absorbed H_2S and O_2 to produce sulfuric acid. The pH of typical drops is <1.0. Photograph by Kevin Downey

with the underlying carbonate rock. Diffusion of sulfuric acid through the gypsum rind to the carbonate surface sustains the solutional retreat of the bedrock walls.

This reaction produces CO_2, which helps to explain its high level in the cave air. Relict bedrock patterns were found in some of the gypsum crusts, confirming their replacement origin. Trace elements in the gypsum crust are also consistently related to the carbonate bedrock, with higher concentrations in the gypsum. Gypsum was observed to grow rapidly and spall off, dissolving into the stream. The gypsum crust has an irregular thickness but is thickest (2–5 cm) at the springs. Upward passage enlargement greatly increasing at the springs offered further confirmation of the hypothesis.

2.2 Microbiology of the Kane Caves

Lower Kane Cave has also been the focus of microbiological studies of sulfur-related bacteria (Stern et al. 2002; Engel et al. 2004). The bacteria are concentrated around the points where H_2S-rich water enters the cave and oxidizes. They identified filamentous sulfur-oxidizing "*Epsilonproteobacteria*" and *Gammaproteobacteria* (*Thiothrix*) that generate sulfuric acid as a metabolic by-product (Fig. 7).

The team conducted chemical measurements that provide a fresh view of the chemical processes in the cave, as well as an indication of variations in the cave chemistry with time since Egemeier's work. They concluded that microbial corrosion is concentrated at floor level beneath the microbial mats around the springs. Microscopic grooves in the carbonate bedrock were found beneath microbial filaments, further supporting the presence of microbially enhanced dissolution. They found that only a small percentage (8%) of the dissolved H_2S in the stream volatilizes into the cave air to dissolve the cave walls. This seems to contrast with Egemeier's hypothesis, although the H_2S that does escape into the air is quickly consumed by absorption into moisture on the cave walls and ceiling, where H_2SO_4 generation causes carbonate dissolution. This subaerial dissolution is widespread, as shown by the great passage enlargement above the water inlets, and the gradual decrease in cross-sectional area downstream from those points.

The Engel et al. team also found that microbes can oxidize sulfur at low oxygen levels at which auto-oxidation is impossible. Thus bacterial activity may allow dissolution to take place deeper in the phreatic zone than expected. The team concluded that abiotic oxidation of H_2S alone could not account for the origin of the cave, and that bacteria locally depress the pH relative to surrounding cave water. They proposed that this activity could potentially account for cave enlargement far below the water table.

The decrease in H_2S oxidation with depth below the water table can be observed in inactive inlets to sulfuric acid

Fig. 7 Sulfide-rich stream in Lower Kane Cave, showing white filamentous microbial mats ("*Epsilonproteobacteria*") with air-breathing freshwater gastropods (*Physella*). These are endemic to Lower Kane Cave. Photograph by Horton H. Hobbs III

caves. For example, in the Guadalupe Mountains of New Mexico (DuChene, Chap. 31), many areas with nearly flat floors contain fissures in their floors that typically extend downward 10–30 m (rarely more), narrowing downward to inaccessible inlets. This pattern appears to reflect diminished H_2S oxidation with distance from subaerial conditions. It is likely that microbial activity plays a significant role in subaqueous dissolution, but that it diminishes rapidly with depth where water is rising.

2.3 Summary: Kane Caves

Because of their easy access, simple morphology, and well-displayed hypogenic features, the Kane Caves have served as the type example of sulfuric acid speleogenesis in the USA. Observations in Lower Kane Cave were used in developing the model of cave origin in the far more complex caves of the Guadalupe Mountains.

Stephen Egemeier was a New York caver with experience only in cold epigenic caves. His ability to grasp the essence of sulfuric acid speleogenesis was aided by the clarity of the relationships in Lower Kane Cave. Also, because of its stark contrast with the caves familiar to him, he was led to think in new directions. Steve died prematurely in 1985 without expanding on his work, but he left a solid legacy.

The work of Engel et al. (2004) is representative of the explosion of microbiological studies in karst and their relation to geology. Note also the contribution of microbiologists to the study of sulfuric acid caves, as described in other chapters. They have not only opened a new avenue of cave research, but the resulting insight is being extended to other unusual environments on Earth as well as to other planets (Boston 2000).

3 Caves of the Shoshone River Basin

Donald G. Davis

On the west side of the Bighorn Basin, west of the town of Cody, Wyoming, the east-flowing Shoshone River has cut a canyon through more than 100 m of faulted Mississippian Madison Limestone, which crops out at both ends of the canyon and near the canyon rim. Where the eastward-dipping limestone extends below river level, there are large travertine terraces with several hot springs degassing CO_2 and H_2S ("Geysers" were reported here in the late nineteenth century, though we have seen no explicit reports of periodic eruptive behavior.). Similar reported hydrothermal features were inundated by construction of the Buffalo Bill irrigation-storage dam, completed in 1910 (Love and Good 1982). This is an area of many hypogenic caves.

3.1 Spirit Mountain Caverns

Spirit Mountain Caverns, which contains more than 1000 m of surveyed passage, is situated in Heart Mountain along the

Shoshone River, up-dip from the Cody thermal springs and more than 300 m higher. This cave was designated a National Monument in 1909. It was never developed successfully, and the Monument was de-listed in 1954. Containing considerable gypsum deposits and (reportedly) elemental sulfur, it was suspected to be of hydrothermal sulfuric acid origin (Aley and Aley 1979) and to have been developed when the river and hot spring outlets were at the cave level. There are two primarily linear passages, one below the other, with pits connecting the two levels. There may be additional lower levels that have been blocked by the commercialization efforts. The cave has extensive gypsum crusts, and at times H_2S is reported to have been present in the cave air.

3.2 Shoshone Canyon Conduit Cave

In 1937, a conduit was constructed to tap irrigation water from the Buffalo Bill Reservoir, west of Cody, Wyoming, along the Shoshone River below Spirit Mountain Caverns. Reports circulated that the conduit intersected several cave passages (Hill et al. 1976). According to Dr. J.D. Love (US Geological Survey, Laramie, Wyoming), the intersected chamber was surveyed, and some sulfur stalactites and stalagmites were collected. A letter found in the National Archives in Denver, Colorado (Rhinehart 2008) from the general project manager stated that "the miners encountered many small and several large natural caverns…. At times the material [being mined] is almost pure sulfur and other times just small streaks with limestone the predominating material…. Some of these caverns are very large; in fact, the boys have been unable to determine their extent because of sulfide gases which come from lower depths. The volume of gas varies with weather conditions. When the barometer is low, more gas evidently generates and when the barometer is high, the volume is considerably reduced. This gas is so extensive that it requires more than ordinary ventilation and at times comes so strong that there is a layer of at least two feet, which forms in the bottom of the tunnel and one can stand some distance away looking down along the tunnel line when the lights are burning and distinctly see this gas layer. It has the appearance of a white smoke. These conditions are certainly giving us a difficult situation to handle."

The danger was confirmed when, on April 1, 1937, three men on the mucking crew were overcome by gas; while unconscious on the mine-car tracks, two of them were killed, and one injured, when struck by the muck train. On two occasions, sulfur deposits were ignited—"the fumes from the burning sulfur caused a four day shut down until the fumes were put out."

The project history continued to describe the most extensive cave they encountered (Fig. 8), which occupied the entire width of the tunnel: "In order to cross this, cave muck was hauled in and a fill, which in places had a depth of forty feet [~12 m], was constructed across the cave. The original height of the cave was some ninety feet [~27 m]. The cave contains heavy gases, mostly carbon dioxide and sulfur dioxide, which fluctuate in amount and elevation to which they raise in large cave and it has not been possible to explore, except for only brief periods, the openings to right and left of tunnel line which probably extend for some considerable distance. Numerous gypsum and sulfur stalactites hung from the ceilings when the cave was encountered, but most of these have been removed by souvenier [sic] hunters." (The reference to "sulfur dioxide" presumably should have been hydrogen sulfide.)

3.2.1 Exploring the Shoshone Canyon Conduit Cave: 2009

Inspired by these historical materials, a group of Colorado cavers determined to seek access to examine the cave. The Bureau of Reclamation had gated and closed the tunnel because of the danger to the public, but the water was distributed by the local Heart Mountain Irrigation District, which conducted annual inspections of the condition of the tunnel. We were allowed to accompany one of these visits

Fig. 8 Cross section of the Shoshone Canyon Conduit Cave. Photograph by L.S. Corey from National Archives, Denver, Colorado. *Scale* unknown, but probably 1–2 m from floor to ceiling

on April 6, 2009. No water was in the tunnel because it is generally shut off when irrigation was not needed. Walking from the downstream entrance about 200 m into the horseshoe-shaped concrete-lined tunnel, we came to the cavern chamber and the open-topped, 3-m tall concrete flume crossing it for some 40 m.

At that time, the temperature outside was much colder than in the tunnel, and a ventilation portal farther upstream was open, so that cold air was flowing strongly through the flume in the upstream direction and spilling over its sides into the cave. Mindful of the historical gas hazard, a gas meter was carried. Near the flume, the smell of hydrogen sulfide was noticeable, but the oxygen content was normal, and the H_2S level was too slight to register on the meter. Air temperatures ranged from 5.5 °C near the flume to 11.1 °C in more distant places.

The group spent only about two hours in the cave and had to leave because of time constraints. The trip was documented by Rhinehart (2009).

3.2.2 Exploring the Shoshone Canyon Conduit Cave: 2010

A second visit to the cave was arranged in 2010 (Rhinehart 2010). The group intended to explore the passages farther from the flume, and to survey as much as possible (Fig. 9). Unfortunately, the tunnel's ventilation ports were not open this time, and little air was moving along the flume. The H_2S odor was perceptible but, as during the previous trip, it was too low to register on the meter. The oxygen level inside the flume was approximately normal atmospheric at 21%. However, within a few meters below, it declined to 18%. The survey was continued, though not comfortably, at that oxygen level. However, a few meters lower, O_2 dropped to 14%, presumably accompanied by a corresponding CO_2 increase (the meter did not measure CO_2), which induced rapid feelings of panic and the need for immediate return to better oxygenated air. Two survey shots were made into the large southeast passages, but it was not possible to go as far as the preceding year.

The group was more successful in the northwestern passage, descending to a low point ~12 m below the rim of the flume, then back up to a "pass" on the other side of which was a vertical drop equipped with an old, but well-preserved, wooden ladder descending into a room not visible on the previous reconnaissance. Beyond this chamber was a passage leading to a pit ~2 m across, where the O_2 level again dropped to 14%, preventing further survey downward. A total of 164 m of passage was surveyed, and much of it was large. A complete survey would probably double the passage length. Everyone's eyes smarted for several hours after exiting the cave.

3.2.3 Cave Features: Speleogenesis

The Shoshone Canyon Conduit Cave lies about 50 m higher than the present elevation of the Shoshone River several hundred meters to the north. Except for one place where aggressive dripping water was attacking the outside of the south wall of the concrete flume (its pH was zero on a measuring strip!), there was no visible water anywhere in the cave, or any evidence of former ponding or stream flow. The highly variable and irregular passage cross sections, with the cave axis aligned approximately along strike of the eastward-dipping Madison Limestone, could be consistent with the cave having developed phreatically slightly below base level when the river was near the cave level.

However, except for mined surfaces, virtually every limestone surface in the cave is encrusted with sheets, nodular deposits, loose sugary-textured floor deposits, and stalactiform growths of mixed gypsum and elemental sulfur, suggesting that substantial enlargement could have taken place via condensation-corrosion and gypsum replacement of limestone, in the zone of aeration above the water table. Although the tunnel workers did not report warm or hot temperatures when they first struck the caves, the voids must have developed in a warmer and less well-ventilated regime, probably with a significantly higher H_2S concentration than the trace amount observed today. While there is no apparent reason to exclude hypogene carbonic acid as a major- or dominant-agent of limestone dissolution here, the ubiquity and abundance of sulfur leave no doubt that H_2S oxidation to sulfuric acid has been significant.

3.2.4 Cave Features: Chemical Deposits and Speleothems

Water-borne, mechanically deposited sediment is absent in the cave thus far explored, but the floors in many areas are buried beneath loose, granular whitish material which has apparently sifted down from wall and ceiling coatings. A sample of this taken during the 2009 trip could be ignited with a match, melting and burning with a blue flame and giving off SO_2, confirming the reports of sulfur fires in the cave during tunnel construction. Analysis by Dr. Fred Luiszer (University of Colorado, Denver) found that the material was roughly 50% elemental S and 50% gypsum.

Carbonate speleothems are entirely absent in the Shoshone Conduit Cave, presumably because the atmospheric CO_2 and H_2S and the thermally-driven air currents promote development of corrosive acidic condensation on exposed surfaces. During the 2009 trip, we observed local clusters of rough-surfaced, sharp-pointed stalactites presumably composed of mixed gypsum and sulfur, but failed to find any of the enigmatic stalactiform "elephant-foot" speleothems that are so interesting in the 1937 photographs. Apparently all of

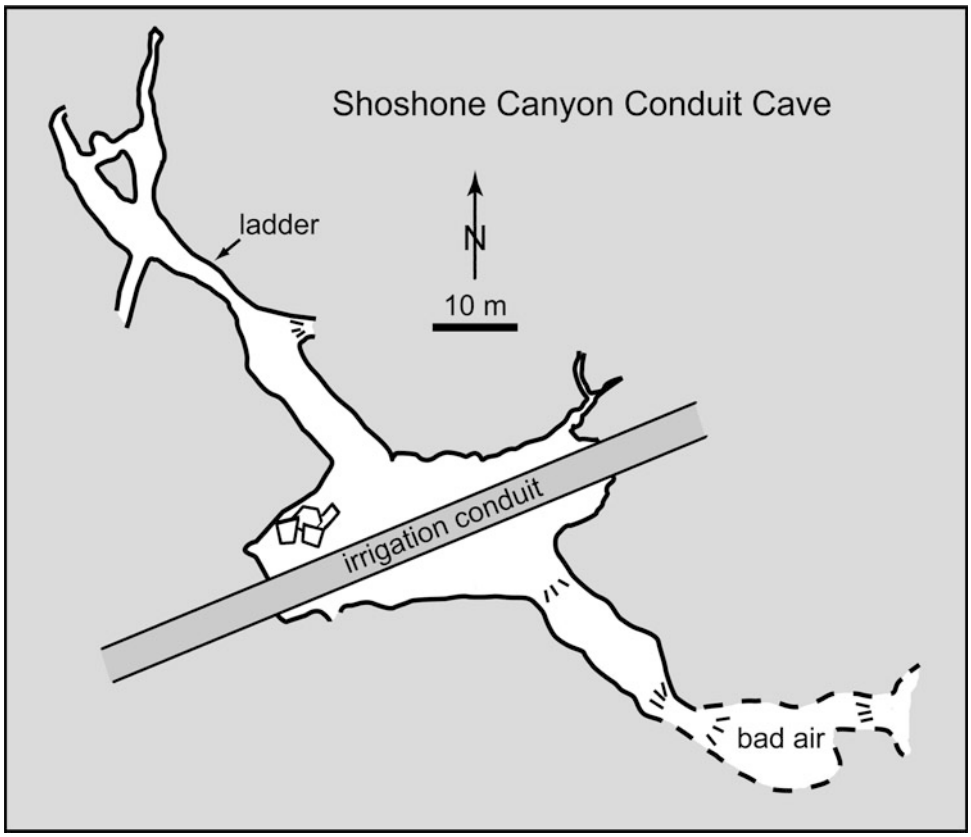

Fig. 9 Partial map of Shoshone Canyon Conduit Cave. From map by Mike Frazier et al. Openings lead to large passages, as yet unexplored

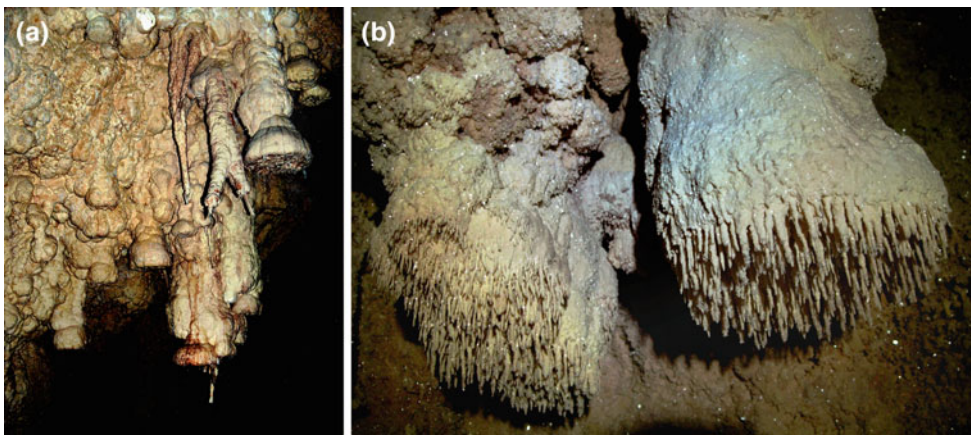

Fig. 10 *Flat-bottomed* speleothems in Shoshone Canyon Conduit Cave. Photographs by Rick Rhinehart (**a**) and Dr. John Spear (**b**) vertical dimensions of *photographs* approximately 2 m in photograph (**a**), <1 m in photograph (**b**)

those that were visible from the flume had been collected in the past, and leaving stubs with fibrous structure and concentric rings, their structure becoming more amorphous toward the outside. In 2010, however, we were relieved to find a sizable room farther from the flume, in which a number of these speleothems remained intact (Fig. 10). Some were up to at least 60-cm long and 25-cm wide, with flared, flat-bottomed ends. A few are terminated in bristling clusters of crystalline points up to several cm long.

The Shoshone Canyon Conduit "elephant feet" are clearly not shelfstone rings where stalactites have dipped into standing water, because no two terminate at the same level. I propose that the "elephant feet" are not ordinary dripstone stalactites, but are evaporative structures most closely related to the flat-bottomed speleothems known as "trays," of which examples composed of gypsum are known (Calaforra and Forti 1994; Doran and Hill 1998). Probably they have developed where slight seepage or condensation moisture collects at protuberances on the ceiling, dissolves gypsum from the surrounding crust, and then slowly seeps downward while evaporating, depositing an evaporite-based stalactite of the usual elongated-cone shape. At a certain distance from

the ceiling, the moisture becomes gradually exhausted by evaporation. The result is to raise its solute concentration and increase outward growth until the remaining moisture evaporates entirely, thus ending preferential growth at the tip while sideways growth continues and creating the flared bottom which may be flat, or slightly indented. Some of these speleothems have smaller "donut rings" or short stalactites extending below the original bottoms; these are probably produced by rejuvenated flow. Similar, though less symmetrical, tiered gypsum trays were noted by Doran and Hill (1998) in Torgac Cave, New Mexico, which is developed in gypsum, and which were explained in much the same way.

Evaporite speleothems of other forms also occur in the cave. Beneath some stalactite clusters are mounds resembling stalagmites and flowstone. One place in the ladder room has bright yellow, slender stalactites up to ~20-cm long, probably colored by a higher-than-average sulfur content. A passage above contains green crystals and slender greenish-tinted stalactites and was named Emerald City.

A short crawl adjacent to the flume contained several transparent, bright blue-green, curved extrusive "flowers" up to two- or three-cm long. Preliminary analysis indicates that the flowers may be composed of melanterite ($FeSO_4 \cdot 7H_2O$; Carl Bern, US Geological Survey, Denver, 2011 e-mail). Unlike the greenish stalactites mentioned above, these growths may be anthropogenic: the floor in this passage appears to be construction-waste earth and rubble discarded to the side of the flume fill, and the flowers may have grown from embedded bits of iron attacked by sulfuric acid condensate.

3.3 Summary—Shoshone Canyon Conduit Cave

Our brief investigations confirm that the Shoshone Canyon Conduit Cave is an active hypogene cave with highly variable levels of lethal H_2S and CO_2—a younger analog of Spirit Mountain Caverns, and similar in many respects to other notable hypogenic caves of the western USA such as Lower Kane Cave, Wyoming; Sulfur Cave, Colorado; and the Glenwood Canyon caves in Colorado. It differs from these others in being relatively dry and having no known standing or flowing water, although such water could exist at base level. The dryness and sulfidic atmosphere have fostered more profuse and varied sulfur/evaporite speleothems than is usual in wetter sulfidic caves.

Our observations did not indicate obvious micro- or macrobiota in the cave, nor did we observe visible microbial deposits such as mats, filaments, streamers, or mucolites. However, the possibility of such biota merits laboratory examination of cave materials. Unfortunately, permission has not been forthcoming for further visits to the cave.

References

Aley T, Aley C (1979) Cave assessment, monitoring and management recommendations for Spirit Mountain Caverns. Bureau of Land Management, Worland District, Wyoming. Ozark Underground Laboratory, Missouri

Boston P (2000) Life below and life 'out there'. Geotimes 45(8):14–17

Calaforra JM, Forti P (1994) Two new types of gypsum speleothems from New Mexico: gypsum trays and gypsum dust. Natl Speleol Soc Bull 56(1):32–37

Doran LM, Hill CA (1998) Gypsum trays in Torgac Cave, New Mexico. J cave Karst Stud 60(1):39–43

Egemeier SJ (1973) Cavern development by thermal waters with a possible bearing on ore deposition. Ph.D. Dissertation, Stanford University, California

Egemeier SJ (1981) Cavern development by thermal waters. Natl Speleol Soc Bull 43(2):31–51

Engel AS, Stern LA, Bennett PC (2004) Microbial contributions to cave formation: new insights into sulfuric acid speleogenesis. Geol 32:369–372

Hill C, Sutherland W, Tierney L (1976) Caves of Wyoming. Geol Surv Wyoming Bull 59:1976

Love JD, Good JM (1982) Hydrocarbons in thermal areas, northwestern Wyoming. In: 33rd Annual field conference guidebook. Wyoming Geological Association, Geology of Yellowstone Park Area, pp 265–288

Rhinehart R (2008) Sulfur galleries: the caves of Wyoming's Shoshone Canyon. Rocky Mt Caving 25(1):29–39

Rhinehart R (2009) Caverns of the moon: a visit to Wyoming's Shoshone Canyon conduit cave. Rocky Mt Caving 26(2):21–27

Rhinehart R (2010) Crystal labyrinth: new explorations in Wyoming's Shoshone Canyon conduit cave. Rocky Mt Caving 27(3):20–27

Stern LA, Engel AS, Bennett PC (2002) In-situ microbial calcite dissolution by sulfur-oxidizing bacteria in a limestone cave. In: Abstract to the 2002 international symposium of subsurface microbiology, Copenhagen, Denmark

Hypogenic Versus Epigenic Aspects of the Black Hills Caves, South Dakota

38

Arthur N. Palmer

Abstract

The Black Hills contain several extensive maze caves in the early Carboniferous Madison Limestone. They include Wind Cave and Jewel Cave, which are among the world's longest and most complex. Their origin is debated, with diverse hypotheses ranging from artesian conditions to rising thermal water. Recent evidence indicates a polygenetic origin including early Carboniferous diagenesis and paleokarst; deep burial by Carboniferous–Cretaceous strata; re-exposure of the limestone by the Laramide Orogeny (early Paleogene); and major cave enlargement in the late Paleogene along old paleokarst zones. Cave enlargement depended mainly on diffuse recharge through overlying sandstone, mixing with lateral inflow through carbonate outcrops. Only a few of these processes were hypogenic, but recognizing them all helps to clarify the limits of that process.

Keywords

Polygenetic caves • Confined aquifer • Paleokarst • Diagenesis • Mixing dissolution

1 Introduction

Nearly all Black Hills caves are network mazes in the Madison Limestone of Mississippian (early Carboniferous) age. The largest are Jewel Cave and Wind Cave, which are administered by the National Park Service (www.nps.gov/jeca; www.nps.gov.wica). Surveyed lengths in 2016 are 294 km (Jewel) and 230 km (Wind)—presently the world's third and sixth longest known caves. They underwent several stages of paleokarst and deposition of calcite crusts and may represent the most complex of any documented caves. Most Black Hills caves now lie almost entirely above the water table, and significant growth has ceased. Their origin has been interpreted in many ways, mostly involving deep-seated processes. Clarifying their genesis is the main goal of this chapter.

2 Regional Setting

The Black Hills are the eroded remnants of a structural dome formed during the Laramide Orogeny (ca. 65–55 Ma); see Figs. 1 and 2. They rise to 2207 m above sea level, with a relief of ~1200 m above the surrounding plains. Precambrian metamorphic and igneous rocks are exposed in the center, and sedimentary strata of Cambrian through Cretaceous age dip away in all directions. Surrounding plains are composed of mostly Cretaceous and Cenozoic strata. The two major caves are located in the southern Black Hills, where the Madison consists of 100–180 m of limestone and dolomite. The Madison is overlain by the Minnelusa Formation, consisting of 100–200 m of Pennsylvanian–Permian quartz sandstones interbedded with shales, carbonates, and sulfates. The Minnelusa forms a semipermeable cap over the Madison, and together they serve as an extensive artesian aquifer. Much of their groundwater recharge feeds springs around the perimeter of the Black Hills.

A.N. Palmer (✉)
Department of Earth and Atmospheric Sciences, State University of New York, Oneonta, NY 13820-4015, USA
e-mail: arthur.palmer@oneonta.edu

© Springer International Publishing AG 2017
A. Klimchouk et al. (eds.), *Hypogene Karst Regions and Caves of the World*, Cave and Karst Systems of the World, DOI 10.1007/978-3-319-53348-3_38

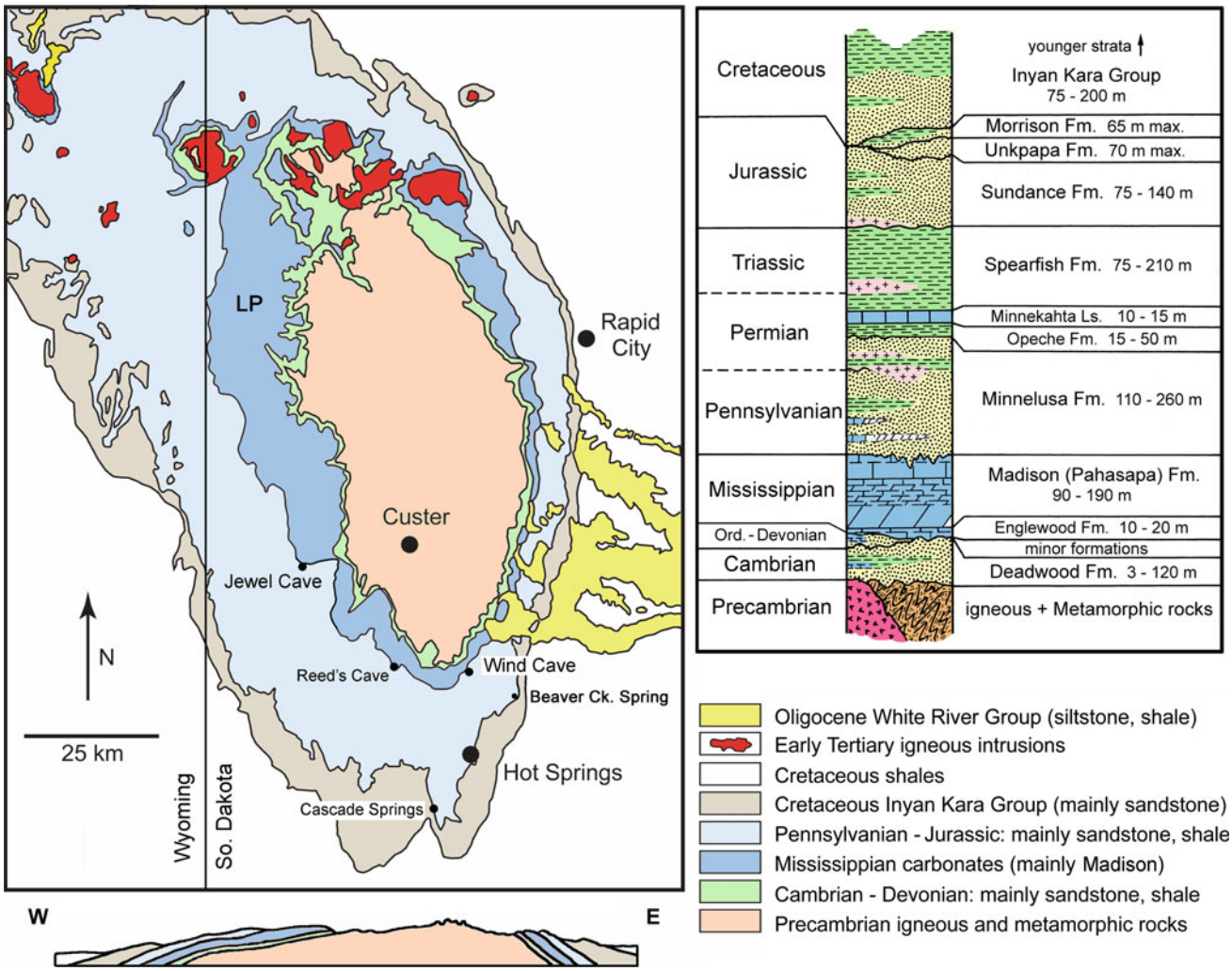

Fig. 1 Geology of the Black Hills (after Carter et al. 2002). Mississippian + Pennsylvanian = Carboniferous. Major caves are limited to the southeastern half, along the boundary between *light and dark blue*. *LP* Limestone Plateau (see Sect. 5.5)

3 Cave Descriptions

Jewel and Wind caves consist of angular network mazes with several intersecting fracture-controlled trends (Fig. 3). Wind Cave is ~300 m lower in altitude than Jewel. Most other caves in the Black Hills have similar characteristics but all are much smaller. Strong winds in the caves reveal much undiscovered void space. Reeds Cave, midway between Jewel and Wind, is smaller (6.9 km) with features intermediate between the other two. All three contain several tiers determined by strata and genetic history. They intersect relict Paleozoic caves and breccias from an extensive mid-Carboniferous paleokarst. The partitioning of Carboniferous into Mississippian and Pennsylvanian Periods in North America illustrates the widespread significance of this paleokarst interval.

The local Madison Limestone is composed of three units, each 30–50 m thick. The lowest is thick-bedded dolomite with prominent vertical fractures. Its cave passages are sparse and consist mainly of tall, narrow fissures. The middle unit consists of interbedded limestone and dolomite in which caves follow fractures and bedding-plane partings to form complex networks on several levels. In places, chert beds form barriers between cave levels that are penetrated only by a few small holes. Most middle-level passages are highly irregular in pattern and cross section. The uppermost unit is massive limestone. Its caves are rambling and smooth-walled, with many upward-terminating domes.

Most passages in Jewel Cave are lined by a 15-cm-thick calcite crust, except in the uppermost levels where most has been removed by later dissolution (Fig. 4a). In Wind Cave, calcite covers only the lower-level walls and is rarely more

Fig. 2 Land surface over Wind Cave, where the Minnelusa formation overlies the Madison Limestone. Much of the surface is covered by thin Neogene sediment

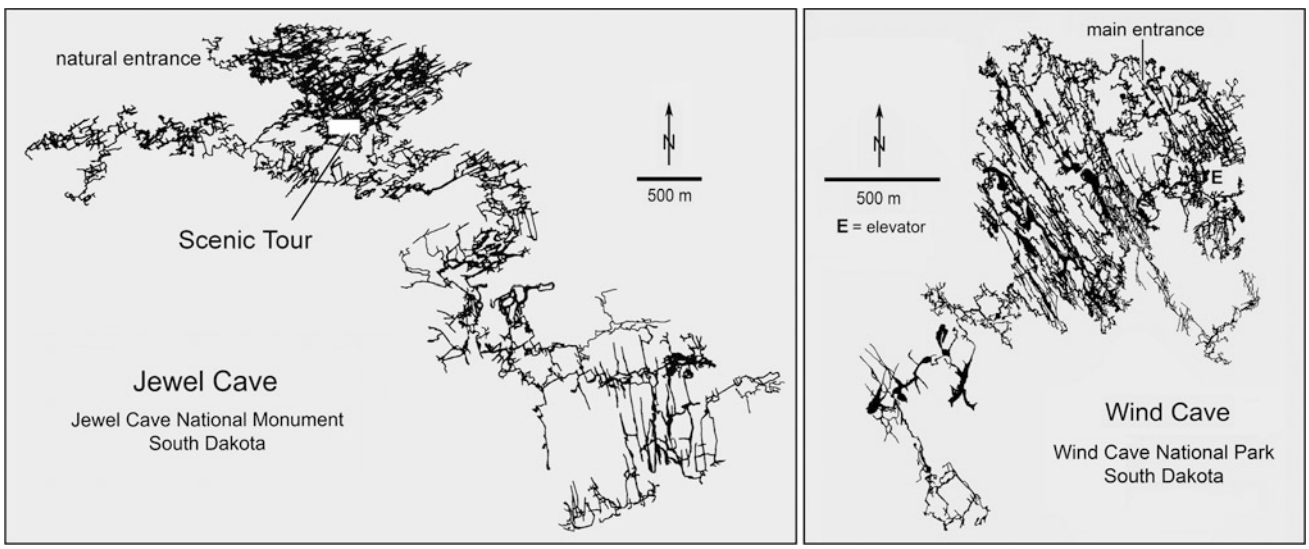

Fig. 3 Maps of Jewel Cave and Wind Cave (courtesy of Jewel Cave National Monument and Wind Cave National Park). Recent discoveries are not shown, but they do not significantly alter these basic patterns

than 2 cm thick. Boxwork is abundant in Wind Cave (Fig. 4b), especially in the middle-level dolomites. It consists of thin calcite fins that project from weathered rock surfaces. Jewel Cave contains little boxwork, but paleokarst breccias are abundant in the same strata. The deepest parts of Wind and Jewel contain small water table lakes. Allogenic sediment is rare in the caves, except for small deposits of sand, gravel, and boulders delivered by rare floodwaters.

4 Interpretations of Cave Origin

For more than a century, several conflicting genetic models have been developed for these caves, but none has received exclusive approval. They are described here, with points of support and conflict. The most likely explanation is proposed in Sect. 6, following a detailed account of the local geologic history. It involves a combination of processes that

Fig. 4 Typical scenes in Jewel Cave (**a**) and Wind Cave (**b**). *Note* the calcite crusts in Jewel and the boxwork in Wind

defy simple classification. The final goal of this chapter is to determine which, if any, of them are hypogenic (Sect.8).

4.1 Artesian Model

The major Black Hills Caves are located in an extensive artesian aquifer, so speleogenesis by artesian flow seems appropriate. This model was proposed by Tullis and Gries (1938), Deal (1962) and Howard (1964), all with strong karst backgrounds. Evidence includes the clear pattern of recharge from up-dip regions and discharge through overlying less permeable strata to springs around the perimeter of the hills. Wells in the Madison and Minnelusa show a systematic decrease in hydraulic head between recharge areas and springs.

4.2 Thermal Model

Other researchers favored speleogenesis by hot water rising from depth. Owen (1898) noted the similarity of cave entrances to the orifices of geysers at Yellowstone National Park. Unaware of the inverse relationship between calcite solubility and temperature, she also attributed the calcite crusts to cooling of thermal water. White and Deike (1962) supported a thermal origin by noting crystalline quartz and hematite in Wind Cave, although recent evidence shows that they were deposited prior to the Black Hills uplift (see Sect. 5.3).

Investigations by Bakalowicz et al. (1987) showed thermal signatures for oxygen isotopes in calcite wall crusts. They concluded that hot water rose from depth, cooled, and became more aggressive, to form caves at shallow depth. As

the water table dropped, CO_2 escaped from solution, allowing the shallowest water to precipitate calcite. This view is widely accepted. Weaknesses are (1) the caves do not reach the bottom of the limestone, nor the top except in a few places; and (2) the major wall crusts were deposited on subaerially weathered surfaces. See Sect. 7 for a discussion of isotopes in the calcite deposits.

4.3 Diffuse Recharge Through the Minnelusa

Palmer (1975) noted that the major caves were located beneath a thin sandstone of basal Minnelusa and that diffuse infiltration into the limestone could potentially form maze caves, as in many humid regions. But it seemed unlikely because the caves rarely reach the sandstone contact.

Wiles (2013) also preferred diffuse infiltration, but with flow through the Minnelusa between entrenched stream valleys, descending into the underlying limestone and back upward in multiple loops along its course. This model has the same limitations noted above, and also an improbable flow pattern.

4.4 Dissolution by Mixing of Waters

Palmer and Palmer (1989, 2008) and Palmer et al. (2015) present another variant of diffuse recharge. Water infiltrating through the basal Minnelusa sandstone, mixing with lateral inflow from the Madison outcrop, can produce an unsaturated solution. Production of aggressiveness requires a strong CO_2 contrast between the two water sources. Although infiltration is limited in today's dry climate, this model fits the available chemical and hydrologic data and explains the cave patterns. Unlike other models, this one relies on zones of high permeability provided by the Carboniferous paleokarst. Supporting evidence is given in Sect. 6. First, a summary of the geologic history is needed.

5 Geologic History of the Black Hills Karst

The regional geology has been studied for more than a century, but with little attention to cave origin. The following interpretation of cave events is based mainly on mapping and laboratory studies since 1978 at the invitation of the National Park Service (Palmer and Palmer 2008).

5.1 Early Chemical Reactions (Carboniferous)

The Madison carbonates are shallow-marine deposits that extend throughout much of the Northern Rocky Mountain region. They originally contained interbedded anhydrite and gypsum. Soon after deposition, sulfate-related processes took place that had a great impact on later karst. In the Black Hills, most of the sulfates were removed by dissolution or replaced by other minerals when they were exposed to fresh groundwater. Some of these features were noted farther west by Sando (1988) and others. Their effects on later caves and karst are described here.

Soon after burial, several early diagenetic processes took place. Sulfate reduction produced hydrogen sulfide, some of which reacted with dissolved iron to form pyrite. Secondary dolomite crystals grew along the walls of pores (typical in sulfate-reducing environments). Reduction probably involved organic compounds from marine sediments or nearby hydrocarbon sources.

Mid-Carboniferous emergence of the carbonate strata above sea level took place caused by the Antler orogeny, which produced mountain uplifts farther west (Sando 1988). Infiltrating water removed many of the sulfates by dissolution, and oxidation of pyrite and hydrogen sulfide to sulfuric acid produced local porosity in the carbonates. Hydration of anhydrite and the structural instability of gypsum caused chaotic fracturing and brecciation, with cementing of fragments by calcite (Figs. 4 and 5).

Some sulfates were converted to calcite by the common-ion effect, where dissolution of gypsum and anhydrite forced calcite to precipitate, while dolomite continued to dissolve. Gypsum veins in the carbonate rock were converted to calcite with a yellow-brown color imparted by iron oxides from pyrite oxidation (Fig. 5a, c). Replacive bodies of calcite still contain relict anhydrite crystals and pseudomorphs, and also fossil microbial filaments (Fig. 5d). Carbonate breccias are abundant in Jewel Cave (Fig. 5a, b), but at Wind Cave the disruption was limited mainly to fractures. Calcite veins along the fractures are preserved as boxwork (Figs. 4b and 5c). Brown scalenohedral ("dog-tooth") calcite lined the interiors of remaining voids (Fig. 5a).

These features can still be seen in paleokarst bodies exposed within the present caves. In Wind Cave, many boxwork zones can be traced along favorable beds for hundreds of meters. Initial fractures in the carbonate bedrock were apparently filled with gypsum, and when the bedrock was later corroded by sulfuric acid, the gypsum veins were virtually unaffected. The veins were later replaced by calcite through the common-ion effect during the influx of meteoric water. In the present caves, boxwork has been accentuated by later dissolution of surrounding porous bedrock and reinforcement of veins by mineral accretion. By contrast, most boxwork in other cave regions consists of resistant quartz veins that project outward simply because of their great contrast in solubility with the surrounding bedrock.

These diagenetic features have similarities with certain hydrothermal deposits but show no evidence for rising water

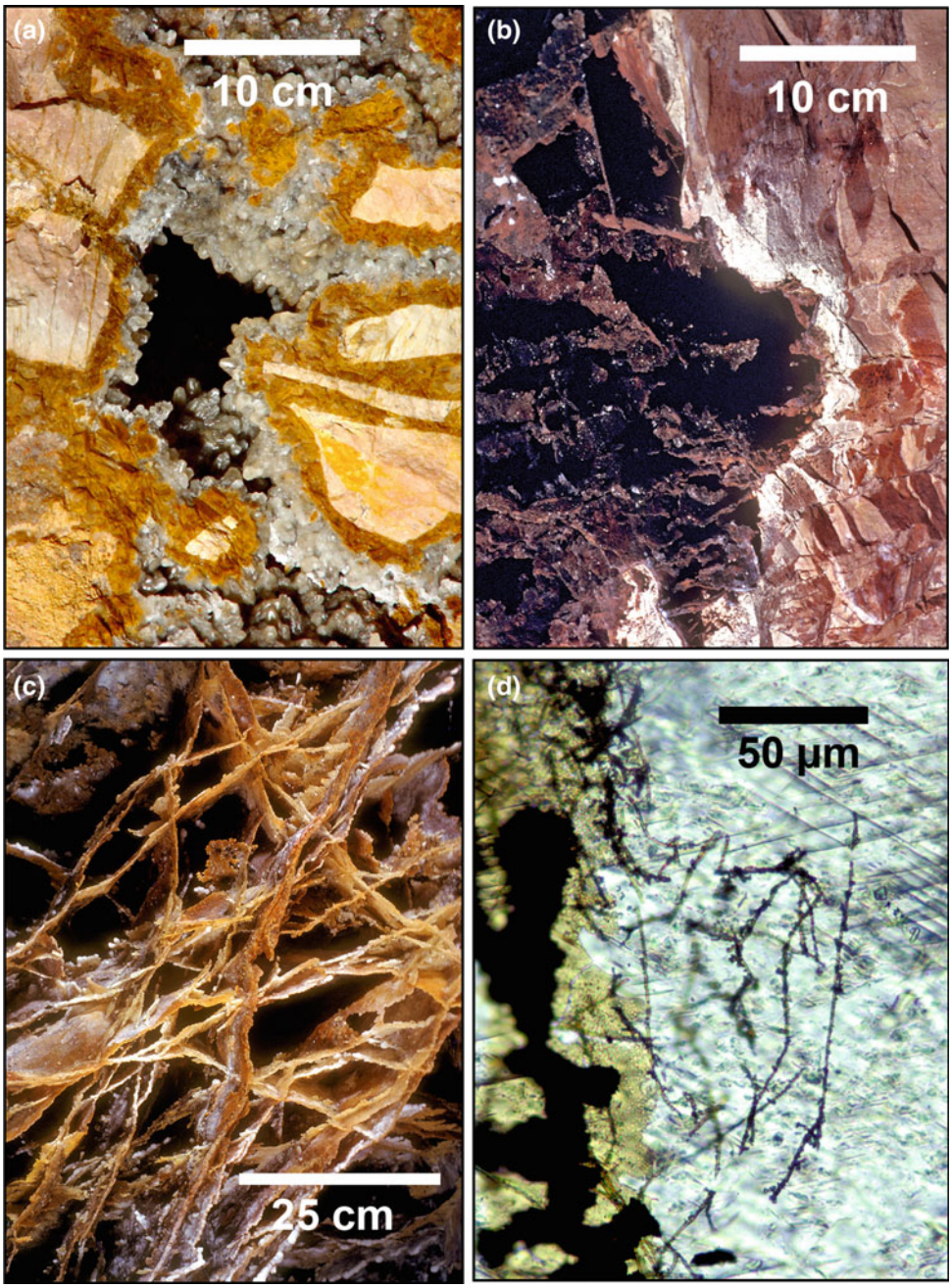

Fig. 5 Early diagenetic features in cave walls. **a** Carbonate breccia in Jewel Cave, with solution porosity and brown matrix of secondary calcite after gypsum. **b** Sulfuric acid corrosion of carbonate bedrock, Wind Cave (*white reaction rind*). **c** Calcite boxwork veins in Wind Cave, equivalent to *brown matrix* in limestone breccia. **d** Microbial filaments of iron-oxidizing microbes in diagenetic calcite

or thermal conditions. However, they represent processes with only minor relation to surface water.

5.2 Early Stage of Meteoric Karst

In the future location of the Black Hills, the Antler uplift merely produced a low-relief surface that developed sparse dolines and fissures extending 30–50 m into the Madison. This karst episode accounts for the widespread paleokarst throughout the region (Fig. 6). The uppermost levels of the Black Hills caves apparently date from that time, although many were further enlarged during the Cenozoic. Today, they consist of irregular rooms with narrow connections through the chert zone to underlying passages. It is likely that mixing between fresh infiltrating water and deeper saline water contributed to their origin. Their rambling patterns and irregular cross sections suggest slow water movement. Some contain chimneys or collapse rooms that extend upward to the base of the Minnelusa, where they terminate in unconsolidated red or yellow sands. These karst features are marginally hypogenic, because some of their dissolution

Fig. 6 Mississippian–Pennsylvanian paleokarst features include sinkholes, fissures, and caves in the upper unit of the Madison Limestone. **a** Paleo-sinkhole filled with basal Minnelusa sand near Jewel Cave, exposed by faulting. **b** Paleokarst collapse breccias and later calcite cements in an upper level of Jewel Cave. The uppermost levels are thought to be paleokarst voids that were either not filled with sediment or lost their sediment by sapping into lower passages

involved mixing of chemically contrasting groundwater types, for example, with salinity contrasts (Plummer 1975; see Chap. XX-Bahamas). These cave features were enlarged and modified by later processes (see Sect. 5.5).

5.3 Burial of Carboniferous Karst

This early karst was deeply buried by the transgressive Minnelusa Formation (late Carboniferous). In the Black Hills, the Minnelusa is 110–260 m thick and consists mainly of quartz sandstones and shales with interbedded dolomite and gypsum. Most upper-level voids in the Mississippian karst were filled with the basal sandy sediment, but at greater depth many were only partly filled or remained empty.

For 250 million years, through the end of the Cretaceous, the paleokarst was buried by mainly detrital sediments to a maximum of ~2 km thick. During burial, all unfilled paleokarst voids were lined by clear to white scalenohedral calcite, which covered bedrock, earlier minerals, and surfaces of Pennsylvanian cave fill (Figs. 6b and 7a). This calcite is an easily identified time marker and distinguishes Paleozoic karst features from those of later age. U/Pb dating of this calcite (Victor Polyak, in Palmer et al. 2009) was inconclusive because of low uranium content. However, the brown calcite lining of Mississippian voids (Fig. 5a) gave a wide scattering of possible dates, the youngest and clearest being 109 ± 0.13 million years (Polyak, personal communication 2015). This date is puzzling because the brown calcite is overlain in many places by Pennsylvanian sediments (~320 Ma). Isotopic exchange during long exposure to deep groundwater may have skewed the U/Pb signature toward younger dates.

5.4 Laramide Orogeny

From near the end of the Cretaceous through approximately mid-Eocene, the Black Hills were uplifted by the Laramide Orogeny, which included the Rocky Mountains farther west. A radial pattern of fractures was produced in the Black Hills that guided many of the later cave passages. Late in the burial history, probably during the earliest stages of uplift, many deep-seated voids and crystals were lined by ~1-mm quartz crystals (Fig. 7b) and thin stalactites of hematite. They coat some of the deep-burial scalenohedral calcite crystals and are clearly hypogenic.

5.5 Main Phase of Speleogenesis

During Laramide uplift, erosion removed the Mesozoic and late Paleozoic strata, exposing the Madison Limestone. Caves began to form as groundwater flow was established in the limestone, but the earliest were long ago destroyed as

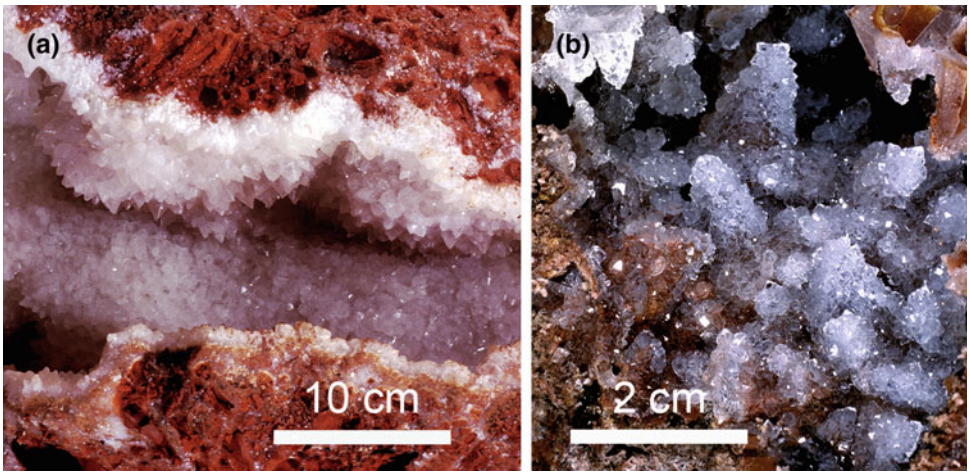

Fig. 7 Post-paleokarst, deep-burial features: **a** scalenohedral calcite crystals up to 1 cm long covered the surfaces of all openings in the early caves and paleokarst, **b** small quartz crystals overlying all surfaces, including scalenohedral calcite, late in the Mesozoic burial history—possibly related to the earliest stages of the Laramide Orogeny. They are local in extent and are typically related to fault zones

limestone was eroded from the highest elevations. It was not until the Black Hills evolved almost to their present form that the present caves developed, as shown by the close relationship between caves and the present exposures of Madison and Minnelusa.

From approximately late Eocene to late Oligocene (~40–30 Ma), the last major enlargement of the caves took place. There is much debate about the exact process (see Sect. 4). However, most of the present cave features are the result of enlargement of much older diagenetic and paleokarst voids. The older openings provided the most permeable zones, and it was along them that the latest cave enlargement was concentrated. Most caves in the region are clustered around the southern, eastern, and northeastern flanks of the Black Hills, where early diagenetic and paleokarst features are abundant. In contrast, paleokarst is rare on the western and northwestern flanks of the hills (Limestone Plateau in Fig. 1), and known caves are almost non-existent there despite much searching.

5.6 Late-Stage Weathering and Deposits

The newly enlarged caves gradually drained as the climate became drier in the early Oligocene. Bedrock surfaces in caves were exposed to condensation corrosion. They developed smooth but irregular surfaces with soft weathering rinds, many of them colored red or yellow from oxidation.

The caves were later flooded by stagnant water, and their weathered surfaces were coated with multiple layers of calcite (Fig. 8a, b), typically 15 cm thick in Jewel Cave and thinner in Wind and Reeds caves. A representative sample from Jewel Cave was U/Pb dated (V. Polyak in Palmer et al. 2009) to 25 Ma at the base and 14.7 Ma at the outer surface. This lengthy flooding was apparently caused by blockage of springs around the southeastern perimeter of the Black Hills as thick sediment accumulated over the area. Cascade Spring and Beaver Creek Spring in Fig. 1 are the outlets for water in Jewel and Wind caves. The sediment included material eroded from mountain ranges to the west (including the Black Hills), augmented by volcanic ash (Evanoff 1990). In Badlands National Park, east of the Black Hills, these deposits are exposed as dissected plateaus of colorful siltstone of the White River Group (Eocene-Oligocene) and younger strata (Fig. 9). The calcite deposits in the caves preserve a record of this history.

Similar deposits in Wind Cave are sparse and dating has been unsuccessful because of low uranium content. It is also likely that while the Jewel crusts were being deposited ~300 m higher, Wind Cave remained deeply phreatic and not susceptible to calcite deposition.

Mid-Miocene erosion removed much of the sediment around the Black Hills (Harksen 1969), including the material that blocked the springs, and the caves gradually drained. Remnants of these sedimentary beds are still present over much of the surface around the lower flanks of the Black Hills (Figs. 1 and 2).

Thinner calcite crusts up to 2 cm thick were deposited in the lower half of Wind Cave during the past 300,000 years, about 2 cm thick at the lowest point and diminishing irregularly upward to zero thickness 80 m above (dated by Ford et al. 1993; Paces et al. 2013). Between layers in the crust are weathered zones and evaporative minerals such as aragonite, which indicate alternate flooding and draining, probably related to glacial advances and retreats farther east.

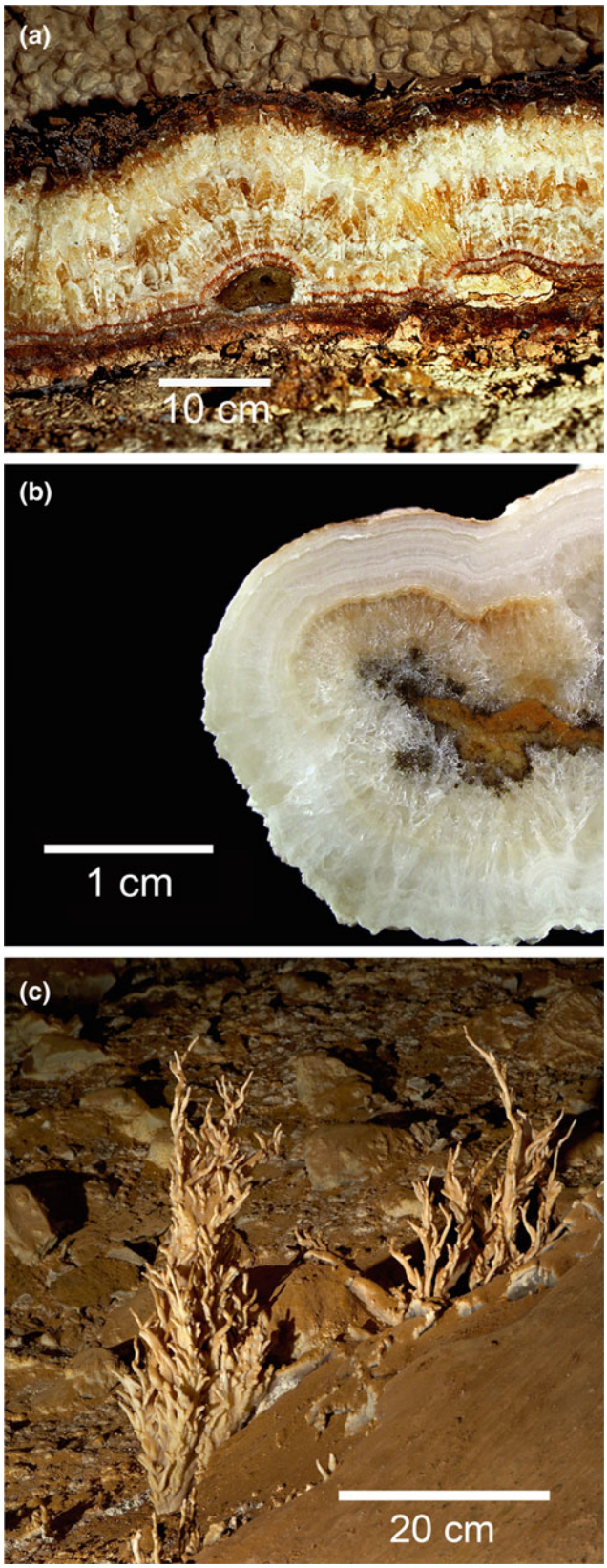

Fig. 8 Post-speleogenetic features: **a** calcite crust in Jewel Cave overlying a weathered zone. **b** Sawed slab of Pleistocene calcite crust, Wind Cave. *Note* recrystallization of lower edge during periodic inundation. **c** Helictite bushes formed by water rising along a fault zone in Wind Cave. They correlate with the crusts in (**b**)

Laminations and clusters of dark Mn–Fe oxides and hydroxides, containing microscopic filaments of Fe- and Mn-oxidizing microbes, show evidence for upward seepage (Fig. 8b). These represent intermittent inputs of anoxic water, with oxidation taking place in the cave. The calcite crust is not the final stages of thermal cave origin, as originally thought.

Along fault zones in Wind Cave, the initial rising water deposited subaqueous calcite helictites in upward-branching patterns (Fig. 8c; Davis 1989), Most have an initial or intermediate Mn–Fe oxide layer containing microbial filaments resembling those in the wall crusts. Sampling has been sparse and limited to already-broken fragments. Thermal $\delta^{18}O$ signatures in the calcite were originally interpreted as thermal deposits following the cave origin (Bakalowicz et al. 1987; Ford et al. 1993). They grew in an area of weathered carbonate sediment up to 2 m thick, much of which has since been removed by periodic flooding-draining cycles. From δ18O data, LaRock and Cunningham (1995) estimated depositional temperatures of ~28–36 °C. These are mildly thermal, but they do not relate to the cave origin. The static water that deposited the calcite was apparently warmed by convection/conduction from a mild thermal anomaly at Hot Springs (see Fig. 1). This relationship is also valid for the Oligocene–Miocene calcite in Jewel Cave, but involved lower temperatures, perhaps because of the greater distance from the thermal anomaly.

The effect of these many gentle but sustained processes is evident in the smooth but irregular contours of the bedrock surfaces in the caves (e.g., Fig. 10). Most of these features show no systematic orientation, as would be the case in aggressive rapidly moving water. In a few places, mostly in Jewel Cave, vent-like passages are formed or modified by sustained local condensation corrosion in subterranean winds.

6 Speleogenesis by Mixing of Water Sources

Despite enthusiasm for Cenozoic cave origin by rising thermal water or artesian flow, neither fits the geologic setting: (1) Nowhere do the caves reach the bottom of the Madison Limestone, and they reach its top in only a few places. Discordant flow across the strata by rising aggressive water is therefore not feasible. (2) The caves terminate rather abruptly both up-dip and down-dip, which contradicts an origin by thermal water rising up the dip, or by solutionally aggressive down-dip artesian water. Instead, the main stage of cave enlargement is best explained by mixing between two water types: high-CO_2 water entering up-dip limestone exposures, and low-CO_2 water produced by infiltration into the Madison through the basal Minnelusa sandstone (see Sect.4.3). The small size and sparse distribution of caves in the recharge areas suggest that lateral recharge from the

Fig. 9 Oligocene siltstones of the White River group in Badlands National Park, 50 km east of Wind Cave. These sediments correlate in age with the calcite crust in Jewel Cave. They apparently blocked springs in the southeastern Black Hills, causing deposition of calcite crusts in the caves (see Fig. 1)

surface was near calcite saturation. Although most cave origin took place in semiconfined conditions, it was not caused by the confinement (i.e., artesian conditions).

6.1 Geochemical Model

As infiltrating water enters narrow fractures and pores in the sandstone, it quickly loses direct contact with soil CO_2. When it reaches the limestone it remains in this nearly closed environment, while carbonate dissolution greatly depletes the CO_2. Where the descending water mixes with the laterally flowing high-CO_2 water from the Madison outcrops, mixing between the two water types produces an undersaturated solution capable of dissolving more limestone (Palmer and Palmer 1989, 2013). The concept of mixing corrosion was first developed by Laptev (1939) and Bögli (1964).

Mixing of small amounts of low-CO_2 water with larger amounts of high-CO_2 water can account for slow but persistent cave enlargement mainly along the high-permeability zones of Carboniferous paleokarst. Today, the infiltrating

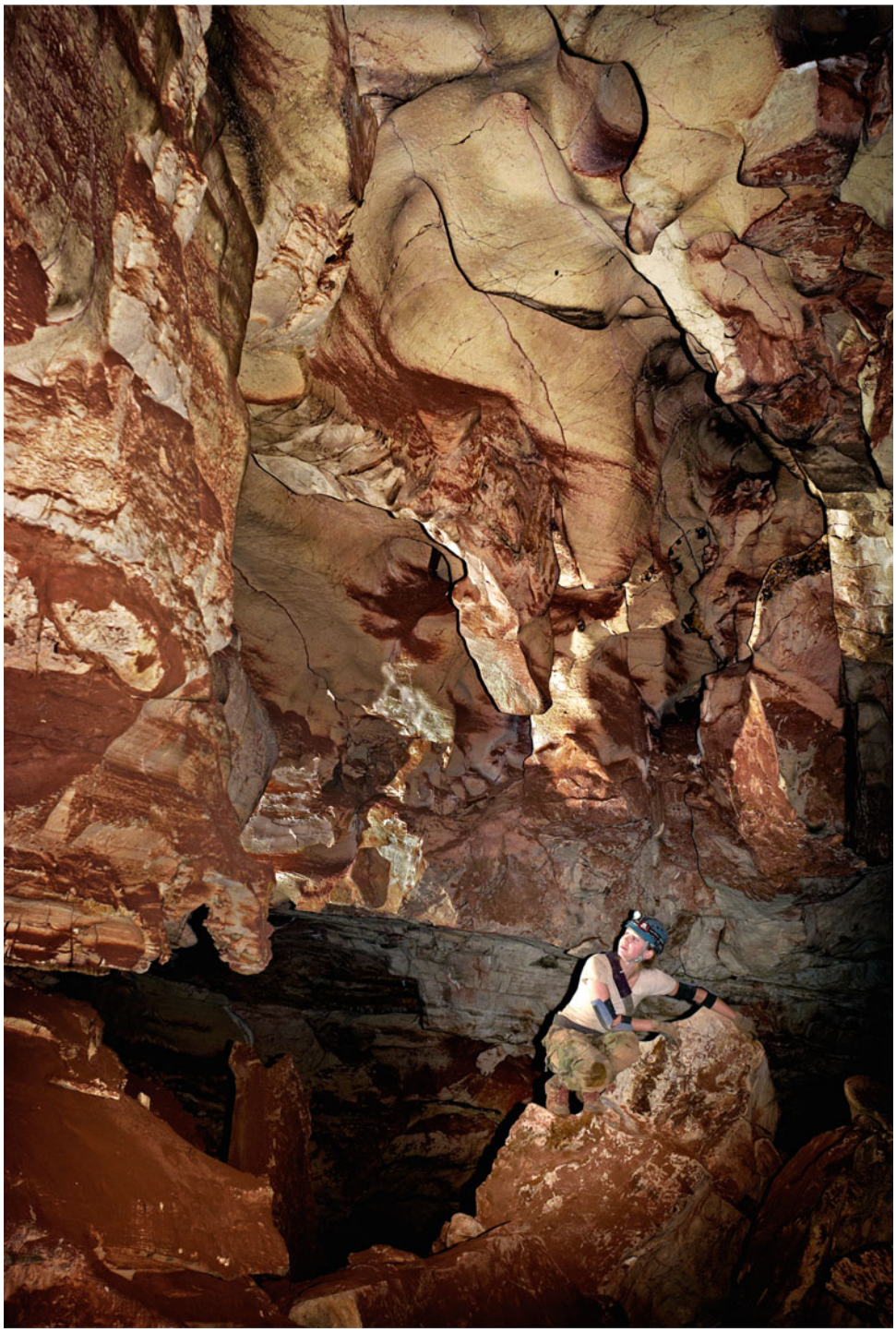

Fig. 10 Typical scene in the upper levels of Wind Cave, where irregular bedrock sculpturing and remnants of paleofill give the impression of hypogenic origin. That impression is only partly justified (see Sect. 8)

water is exposed to the cave air and quickly gains CO_2. But when the caves were water filled and still actively forming, the two sources could mix to form a solution undersaturated with calcite and capable of enlarging the caves. As a result, most of the cave volume appears to have resulted from two entirely different styles of dissolution separated by ~300 million years (compare with Sect. 5.2).

6.2 Field Data and Interpretation

There is much support for this mixing model: (1) Nearly all cave passages occupy limestone that is overlain by thin Minnelusa sandstone. (2) Caves extend great distances along the strike of the beds, following local trends of the thin Minnelusa cover. (3) Passages terminate, or become very

narrow, where the sandstone is either absent or is overlain by thicker Minnelusa with carbonate beds exposed at the surface.

This model also requires a concentrated source of water entering the exposed limestone up-dip from the Minnelusa cap. Up-dip from Jewel Cave is Hell Canyon, with the largest catchment area in the southwestern Black Hills. Up-dip from Wind Cave is a broad valley extending at least 10 km, but today only its lower end contains sustained water flow. A similar relict valley lies up-gradient from Reeds Cave. These features give evidence that when the caves formed, tens of millions of years ago, their topographic setting was similar to that of today. It is unlikely that the entire stream flow sank underground at the caves. More likely, dispersed leakage through the stream bed was responsible. Evidence includes the scarcity of coarse detrital sediment in the caves.

Was there enough infiltration through the sandstone to form the caves? Measurement of present infiltration rates into Jewel and Wind Caves through the Minnelusa Formation (Wiles 1992) suggests roughly 30 L/year per square meter of cave passage. Only ~1% of the cave area receives recharge today, and not all of it solutionally aggressive toward carbonates; but it is probable that infiltration was more intense and widespread in past wetter climates. Even at the present low rates, mixing between infiltration water and lateral inflow from the Madison outcrops could dissolve the entire cave volume in roughly 4 million years (volume of pre-existing paleovoids excluded). This time span should have been easily available in the early- to mid-Oligocene when the caves achieved their present size, and with the infiltration rate probably much greater than it is today. This setting provided maximum dissolution exactly where the caves are located today; and it was also compatible with the stratigraphic position of the caves. No other known mechanism seems to explain these relationships.

Almost all major Black Hills caves underlie the thin up-dip edge of the Minnelusa Formation, where it contains much sandstone overlying the Madison Limestone. This relationship is valid for at least 90% of the known cave passages. In the down-dip direction, where the Minnelusa cover is more than ~50 m thick, underlying caves diminish in size and terminate rather abruptly (at least the exploration does).

Figure 11 shows a cross section through Jewel Cave from the regional geologic map of Fagnon (2009), which includes a projected profile of the cave supplied by Michael Wiles (NPS). The cave is limited almost entirely to a narrow stratal section roughly 40–80% from the base to the top of the Madison Limestone and overlain by thin basal Minnelusa sandstone. Where Minnelusa carbonates lie at or near the surface, underlying cave passages are few or absent. The model of vertical infiltration through insoluble sandstone, combined with lateral recharge through Madison outcrops, seems feasible. Note that some passages extend beyond the zones of aggressive infiltration, because undersaturation does not cease abruptly; it continues in the downflow

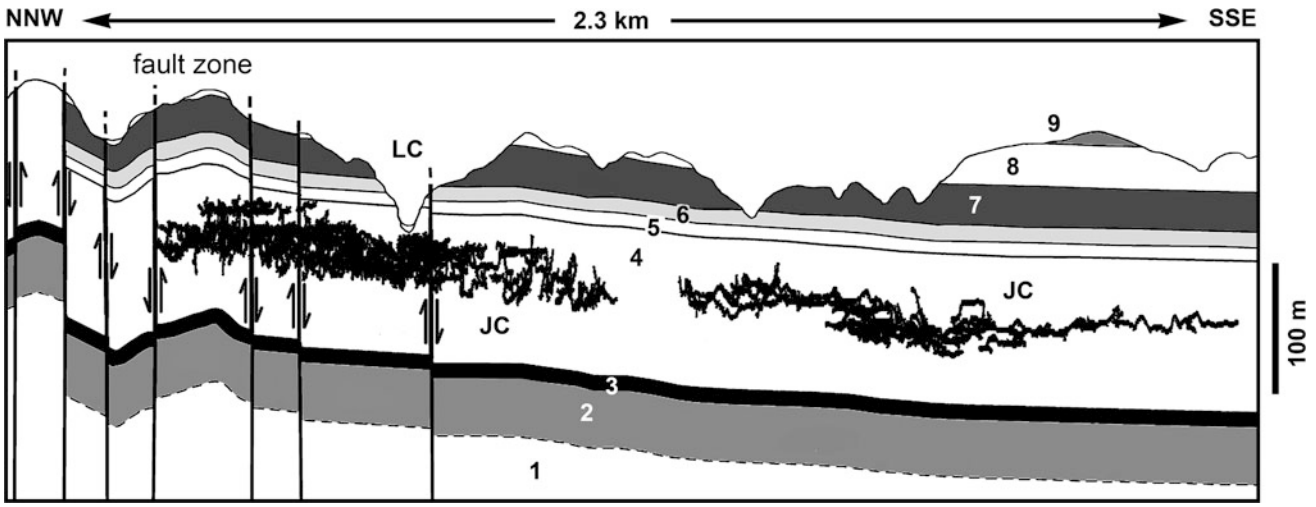

Fig. 11 Stratigraphic position of the known parts of Jewel Cave, shown in profile on the geologic map of the Jewel Cave quadrangle (Fagnon 2009; cave profile by M. Wiles). *JC* a narrow strip of the Jewel Cave profile, projected onto the plane of the figure (gap in cave is where it extends beyond range of profile; Jewel Cave fault zone; *LC* lithograph canyon; *1* Precambrian; *2* Cambrian–Ordovician conglomerate and sandstone; *3* Ordovician–Devonian Englewood limestone; *4* Mississippian Madison limestone. Lower units of Pennsylvanian Minnelusa formation: *5* basal sandstone; *6* limestone; *7* sandstone and shale; *8* sandstone and carbonates; *9* sandstone and limestone. Section is greatly exaggerated vertically. Passage density is greatest below exposures of thick sandstone (*7*) at or near the surface. Passages are sparse beneath thick Minnelusa cover, especially where limestone is exposed at the surface (*8*). Flow of aggressive water from recharge areas makes it possible for caves to persist beyond the zones favorable to speleogenesis

direction for some distance with diminishing solutional effect.

Geochemical modeling of the mixing zone (Palmer and Palmer 2013) shows that in a perfectly closed system, the CO_2 content of infiltrating water (partial pressure, PCO_2) would decrease to less than 0.0001 atm, with calcite saturation at only ~15 mg/L. From drip-water chemistry measured in Wind Cave by Long et al. (2012), we calculated PCO_2 values as low as ~0.0006 atm. This is extremely low for cave water, even though it has already absorbed some CO_2 from the cave air after emerging into the cave. This value agrees with low CO_2 measurements of Wind Cave air by Miller (1989), where absorption of CO_2 by infiltrating water has apparently lowered the ambient CO_2 in the upper cave levels.

Cave streams fed by water from the Madison outcrop have a mean $PCO_2 > 0.004$ atm. Because infiltration through the Minnelusa is usually less than the flow of streams from the limestone outcrops, the PCO_2 of infiltrating water would quickly rise nearly to that of the main flow when the two water mix. The amount of dissolution can be calculated with geochemical software (e.g., PHRE-EQC: http://wwwbrr.cr.usgs.gov/projects/GWC_coupled/phreeqc.v1/). Each liter of water infiltrating through the sandstone would gain ~0.02 cm^3/L of calcite. The total cave growth would be the sum of these small increments over time. Where the limestone is not covered by Minnelusa, the small size of solution conduits suggests that inflow to the caves through the limestone outcrops has always been close to saturation. This agrees with the chemistry of the streams in and around the caves today.

Also, where paleokarst is absent, the modern caves are small or entirely inaccessible. In this region, at least, this indicates the importance of the older openings in the development of newer caves. The boundaries of the original paleokarst probably account for the many sharp terminations in the present cave passages (e.g., the northeastern limit of Wind Cave, Fig. 3b). These boundaries have been carefully explored, only to reveal tiny holes in bedrock that are too narrow for humans.

In the up-dip direction, where the limestone is not capped by sandstone, the lack of large caves suggests that the lateral inflow of water from streams was limited in discharge and close to saturation. Recharge into the limestone was probably limited to leakage through stream beds, rather than entire sinking streams (ponors). Figure 12 shows the approximate relationship of the water sources. The exact ratio between lateral and vertical recharge was apparently not critical.

7 Isotopic Interpretations

Strongly negative $\delta^{18}O$ values in the cave calcite deposits have been used as indicators of thermal water (Bakalowicz et al. 1987). A standard of reference is post-drainage dripstone, with $\delta^{18}O$ VPDB = −8 to −12.5‰, which was apparently deposited at current temperatures of 10–14 °C. At these temperature ranges, a one-unit decrease in $\delta^{18}O$ is proportional to ~4 °C increase, if other variables are constant (calculated from Faure and Mensing 2005). Other calcite deposits fall into four categories:

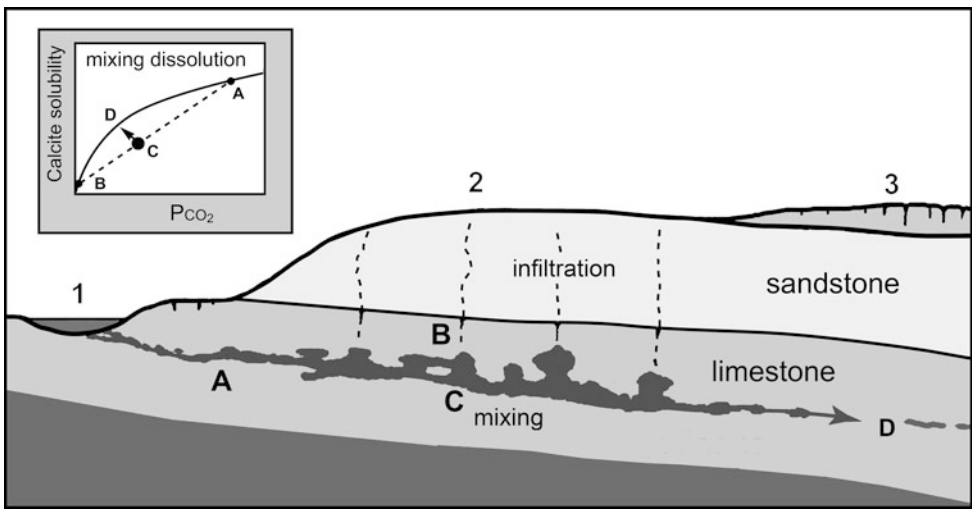

Fig. 12 Effect of mixing corrosion between two waters similar to those entering Wind Cave today: *1* infiltration and leakage from surface streams entering the Madison outcrop; *2* infiltration through the basal Minnelusa sandstone. Both waters are at or near saturation at their respective PCO_2 values, high at *A* but very low at *B* because of closed-system dissolution of limestone. The mixture *C* is highly undersaturated. Equilibrium is reached by a continuous migration toward *D* (closed system with CO_2 consumed as calcite dissolves). Note the optimum mixing effect caused by the low CO_2 in the closed system at *B*. Diagram is greatly simplified to clarify the relationships

1. Brown calcite matrix in Mississippian breccias ($\delta^{18}O = -8$ to $-11‰$); see Sect. 5.1. This appears to represent temperatures similar to those of today, but the isotopic composition of water at that time is uncertain. The latitude was near today's equator.
2. White calcite, deep-burial, Mesozoic ($\delta^{18}O = -16$ to $-19.5‰$). Light isotopes are compatible with high temperatures at burial depths up to 2 km (see Sect. 5.3).
3. Boxwork veins ($\delta^{18}O = -14.5$ to $-21‰$). Petrographic analysis indicates a Mississippian age, with pre-Pennsylvanian weathering in paleokarst pockets. Later, when they were exposed to warm water ~2 km below the surface, their large ratio of surface area to volume made them susceptible to isotopic exchange. If so, their highly negative isotopic signatures do not represent their original environment closer to the surface (see Sect. 5.3).
4. Post-speleogenic crusts on cave walls: Jewel Cave (Oligocene–Miocene, $\delta^{18}O = -11$ to $-16‰$); Wind Cave (late Pleistocene, $\delta^{18}O = -13$ to $-18‰$; see Sect. 5.6). Lighter isotopes in Wind Cave could be due to the known positive thermal anomaly in the southeastern Black Hills, which could have driven thermal conduction and convection, with the calcite at Wind influenced more than at Jewel. The anomaly apparently had no significant effect on the shallow-water cave origin (see Sect.6). The subaqueous calcite also had no relation to the water that formed the caves.

8 Conclusion: Hypogenic Aspects of the Black Hills Caves

There is no simple answer to the question of whether the Black Hills caves are hypogenic. Carboniferous diagenesis took place below the surface, first with no surface water input, and later by the mixing of meteoric water with deep saline water (Fig. 5). Because aggressive solutions were generated below the surface, this process was hypogenic by the criterion of Palmer (1991), but it is uncertain whether rising water was involved, as required by the standard of Klimchouk (2007). The later Carboniferous paleokarst event was dominated by surface infiltration and does not qualify (Fig. 6). The lengthy period of deep burial (Carboniferous through Cretaceous) produced thermal calcite and quartz, but apparently no porosity (Fig. 7).

The main Eocene–Oligocene cave enlargement qualifies as hypogenic only because dissolution required the mixing of chemically contrasting waters below the surface (Fig. 12). The late Oligocene–Miocene and late Pleistocene calcite crusts do not represent speleogenesis, although small amounts of solutionally aggressive fluids were periodically produced by oxidation of reduced Fe–Mn species in rising groundwater that re-flooded the caves (Fig. 8).

Almost any view inside these caves (e.g., Fig. 10) seems to demand a hypogenic explanation. But the caves are clearly polygenetic and cannot be classified in any simple way. They demonstrate multiple phases of dissolution, sedimentary fill, and mineralization over more than 300 million years, with clear evidence for each phase. The search for a full understanding of these caves will last far into the future.

Acknowledgements Thanks to the following people: My wife Peggy Palmer, collaboration on all field mapping and petrography; Victor Polyak (University of New Mexico), U/Pb dating; Jim Paces (US Geological Survey, Denver), U/Th dating and isotopic analysis; Dan Legnini (Argonne National Laboratory), X-ray fluorescence. Discussions of concepts: Dwight Deal, Mike Wiles, Derek Ford, Andy Long. Field assistance: Rod Horrocks, Marc Ohms, Jeri Frederick, Steve Baldwin, Herb and Jan Conn, Nathan Farrar, Rick Olson, Richard Zopf, Paula Provencio, Carl Bern, Jeff Hughes, Jennifer Back. Partial support was provided by the National Park Service, and the Research Foundation of State University of New York.

References

Bakalowicz MJ, Ford DC, Miller TE, Palmer AN, Palmer MV (1987) Thermal genesis of dissolution caves in the Black Hills, South Dakota. Geol Soc Am Bull 99:729–738

Bögli A (1964) Mischungskorrosion, ein Beitrag zum Varkarstungsproblem. Erdkunde 18(2):83–92

Carter JM, Driscoll DG, Williamson JE (2002) Atlas of water resources in the Black Hills area, South Dakota. US Geological Survey Hydrologic Investigations Atlas HA-747

Davis DG (1989) Helictite bushes: a subaqueous speleothem? Natl Speleological Soc Bull 22(1):5–18

Deal DE (1962) Geology of Jewel Cave National Monument, Custer County, South Dakota. MA thesis, University of Wyoming

Evanoff E (1990) Early Oligocene paleovalleys in southern and central Wyoming: evidence of high local relief on the late Eocene unconformity. Geology 18(5):443–446

Fagnon B (2009) Geologic map of the Jewel Cave Quadrangle South Dakota South Dakota Geological Survey, Geologic Quadrangle map 9

Faure G, Mensing TM (2005) Isotopes: principles and applications. Wiley, Hoboken NJ

Ford DC, Lundberg J, Palmer AN, Palmer MV, Schwarcz HP, Dreybrodt W (1993) Uranium-series dating of the draining of an aqui-fer: the example of Wind Cave, Black Hills, South Dakota. Geol Soc Am Bull 105:241–250

Harksen JC (1969) The Cenozoic history of southwestern South Dakota. In: Harksen JC, Macdonald JR (eds) Guidebook to the major Cenozoic deposits of southwestern South Dakota. South Dakota geological survey guidebook, vol 2, pp 11–28

Howard AD (1964) Model for cavern development under artesian ground water flow, with special reference to the Black Hills. Natl Speleological Soc Bull 26(1):7–16

Klimchouk AB (2007) Hypogene speleogenesis: hydrogeological and morphogenetic perspective. National Cave and Karst Research Institute special paper no 1

Laptev FF (1939) Aggressive action of water on carbonate rocks, gypsum, and concrete. In: Trudy Spetsgeo, vol 1. State Science Technical Publishing, Moscow-Leningrad (in Russian)

LaRock EJ, Cunningham KI (1995) Helictite bush formation and aquifer cooling in Wind Cave, Wind Cave National Park, South Dakota. Natl Speleological Soc Bull 57(1):43–51

Long AJ, Ohms MJ, McKaskey DRG (2012) Groundwater flow, quality (2007–10), and mixing in the Wind Cave National Park area, South Dakota. US geological survey scientific investigations report 2011–5235

Miller TE (1989) Evidence of quaternary tectonic activity, and for regional aquifer flow at Wind Cave, South Dakota. Natl Speleological Soc Bull 51:111–119

Owen LA (1898) Cave regions of the Ozarks and Black Hills. Johnson Reprint Corp., New York (1970 reprint)

Paces JB, Palmer MV, Palmer AN, Emmons M (2013) Pleistocene water-table fluctuations and shifts in aquifer contributions in Wind Cave National Park, Black Hills, South Dakota, USA [abs.]. Geol Soc Am Abstr Programs 45:7, 640

Palmer A (1975) Origin of maze caves. Natl Speleological Soc Bull 37 (3):56–76

Palmer A (1991) Origin and morphology of limestone caves. Geol Soc Am Bulletin 103(1):1–21

Palmer A, Palmer M (1989) Geologic history of the Black Hills caves, South Dakota. Natl Speleological Soc Bull 51(2):72–99

Palmer A, Palmer M (2008) Field guide to the paleokarst of the Black Hills. In: Sasowsky I, Feazel C, Mylroie J, Palmer A, Palmer M (eds) Karst from recent to reservoirs, vol 14. Karst Waters Institute Special Pub-l, pp 189–230

Palmer A, Palmer M (2013) Effects of CO_2-depleted vadose seepage in karst. In: Filippi M, Bosák P (eds) Proceedings of 16th international congress of speleology, vol 2, Brno, Czech Republic, pp 393–398

Palmer A, Palmer M, Polyak V, Asmerom Y (2009) Genetic evolution of the Black Hills caves, South Dakota, USA. In: White W (ed) Proceedings of 15th international congress of speleology, vol 2, Kerrville, Texas, pp 946–951

Palmer A, Palmer M, Paces J (2015) Geologic history of the Black Hills caves, South Dakota. In: Feinberg J, Gao Y, Alexander E (eds) Caves and Karst across time: Geol Soc Am Special Paper, vol 516, pp 87–101

Plummer LN (1975), Mixing of sea water with calcium carbonate ground water. In: Whitten EHT (ed) Quantitative studies in the geological sciences. Geol Soc Am Memoir 142:219–236

Sando WJ (1988) Madison Limestone (Mississippian) paleokarst: a geologic synthesis. In: James NP, Choquette PW (eds) paleokarst. Springer, New York, pp 256–277

Tullis EL, Gries JP (1938) Black Hills caves. Black Hills Eng 24 (4):233–271

White WB, Deike GH (1962) Secondary mineralization in Wind Cave, South Dakota. Natl Speleological Soc Bull 24:74–87

Wiles M (1992) Infiltration at Wind and Jewel Caves, Black Hills, South Dakota, MS thesis, South Dakota School of Mines and Technology

Wiles M (2013) Paleohydrology and the origin of Jewel Cave. In: Land L, Joop M (eds) Proceedings of 20th National Cave and Karst management symposium Carlsbad, NM National Cave and Karst Research Institute, p 3340

Hypogene Karst Collapse of the Devonian Prairie Evaporite Basin in Western Canada

39

Paul L. Broughton

Abstract

Regional dissolution trends configured the Middle Devonian Prairie Evaporite basin across Western Canada, resulting in the largest known collapse of a hypogene evaporite karst dominated by halite beds. Dissolution-collapse subsidence resulted from aquifer flows to the north-east within the Alberta and Williston basins, up-structure towards the eastern margin of the salt basin. A 1000-km-long and 150-km-wide salt dissolution trend developed along the eastern evaporite basin margin. The flows occurred as the Western Canada foreland basin deepened in response to the Columbian (Middle Jurassic-Early Cretaceous) tectonism. A second dissolution pattern developed across the southern Saskatchewan area of the Williston basin. Dissolution trends removed up to 250-m-thick beds across south-central Saskatchewan and 100–150-m-thick beds in north-eastern Alberta. These salt dissolution patterns advanced along sets of fault-fracture lineaments that widened and coalesced into larger salt removal areas. The dissolution trends configured the overlying strata as subsidence-collapse troughs tens of km long. In northern Alberta, troughs up to 50 km long configured the Upper Devonian limestone karst palaeotopography, subsequently covered by Lower Cretaceous Athabasca Oil Sands. This bitumen deposit, the largest known, overlies a 300-km-long segment of the dissolution trend that extends along the eastern margin of the Middle Devonian evaporite basin. Syndepositional sand trends up to 25 km long accumulated over collapsed chains of Devonian fault blocks that responded to salt dissolution patterns in the substrate. These sand reservoirs trapped Late Cretaceous-Early Palaeogene oil migrations into the area.

Keywords

Prairie Evaporite Formation • Western Canada • Athabasca Oil Sands • Roncott Platform-Hummingbird Trough • Foreland Alberta basin

1 Introduction

The Prairie Evaporite basin of the Elk Point Group (Middle Devonian) accumulated halite beds up to 250 m thick in southern Saskatchewan and north-central Alberta (Fig. 1). The evaporite basin extends across most of Western Canada, southwards into eastern Montana and western North Dakota, and northwards into the Northwest Territories. The evaporite basin resulted from a restricted arm of the Boreal Sea along the northern margin of Laurasia. The Presqu'ile reef barrier at the northern seaward end of this basin ensured sustained evaporation, resulting in accumulation of thick halite beds. The deposits consist mostly of halite (40–80%), variously mixed with anhydrite and calcareous mudstone. Potash accumulated in south-central Saskatchewan resulted in one of the most important potash mining districts in the world.

P.L. Broughton (✉)
P.O. Box 6976, Station D, Calgary, AB T2P 2G2, Canada
e-mail: broughton@shawcable.com

© Springer International Publishing AG 2017
A. Klimchouk et al. (eds.), *Hypogene Karst Regions and Caves of the World*,
Cave and Karst Systems of the World, DOI 10.1007/978-3-319-53348-3_39

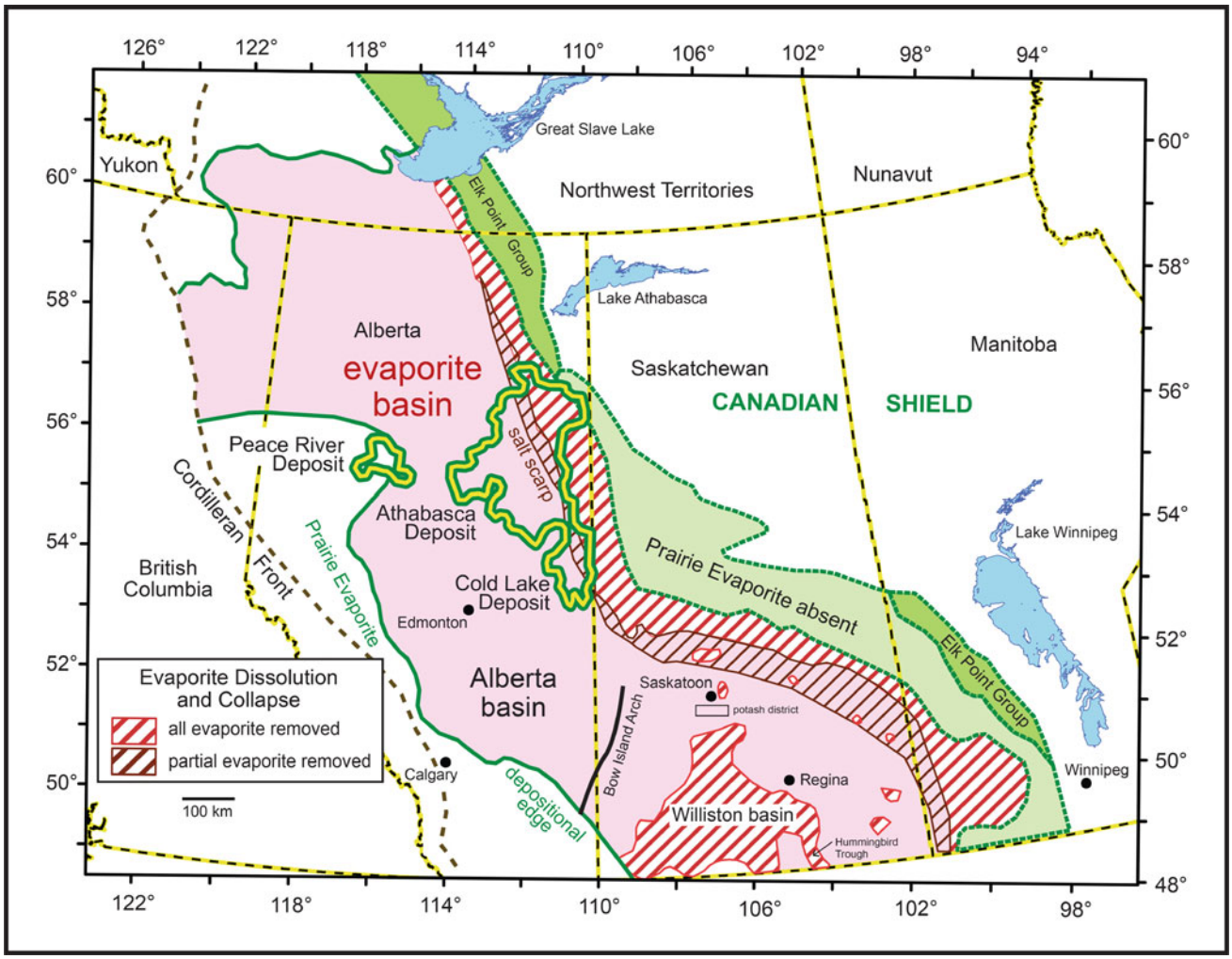

Fig. 1 The middle Devonian Prarie Evaporite basin across Western Canada Sedimentary Basin accumulated halite-dominated salt beds up to 250 m thick. Overlying Palaeozoic strata consisting mostly of carbonate beds accumulated in the Alberta and Williston basins, were separated by the Bow Island Arch, and covered by Jurassic and Cretaceous strata. Deep basin aquifer flows to the north-east in the Cordilleran foreland Alberta basin responded to the Middle Jurassic-Early Cretaceous Columbian orogeny as the underlying Craton buckled. Aquifer flows across southern Saskatchewan were to the north and north-east as the intra-cratonic Williston basin subsided, resulting in extensive salt removal areas. A 1000-km-long and 150-km-wide dissolution trend developed along the eastern margin of the Prairie Evaporite basin, extending from NE Alberta to SE Saskatchewan and SW Manitoba. The northern Athabasca and the eastern Cold Lake oil sands were emplaced a segment of this regional dissolution trend. Modified from Meijer Drees (1994) and Broughton (2013, 2015)

Multi-stage salt dissolution patterns resulted from aquifer flows directed along cross-cutting fracture and fault lineaments that dissected these Middle Devonian evaporite beds, resulting in 10s–100s of km long collapse-subsidence structures that configured the overlying strata (Anderson and Knapp 1993). As a result, this area of Western Canada developed the largest known hypogene interstratal halite salt karst. Unusual structural features developed because halite is 130–150 times more soluble than gypsum and 1000s times more soluble than limestone. Dissolution patterns in 100–250-m-thick halite beds extend for 100s–1000s of km^2, resulting in overlying collapse-subsidence structures that provided regional accommodation spaces for hydrocarbon reservoirs in northern Alberta and southern Saskatchewan. The impacts by salt dissolution trends on the structural and stratigraphic framework of southern Saskatchewan have been documented by numerous researchers of the Saskatchewan Geological Survey since the 1960s and 1970s (DeMille et al. 1964; Holter 1969; Gendzwill 1978; Broughton 1977, 1985; Irvine et al. 1978; McTavish and Vigrass 1987), and across northern Alberta since the 1970s by the Alberta Geological Survey and the oil exploration industry (Hein et al. 2013).

Multiple regional and local flow systems impacted the salt removal patterns, such as a basin loading and compaction-driven flow system to the north-east and a more localized shallower topography-driven flow system towards surface lows. Interpretations differ on the origin and timing of these salt removal patterns, but it is generally accepted that the dissolution resulted from subsurface water flows upwards into the Prairie Evaporite salt beds. Uncertainty remains regarding the relative impact on the dissolution patterns by: (1) influxes of meteoric water flows into the subsurface along permeable beds coming in contact with shallowly buried salt beds; (2) regional aquifer water flows responding to basin deepening, resulting flows up-structure to the north-east towards the basin margin; (3) formation water flows vertically up-section resulting from sediment compaction, mostly from Keg River strata into the overlying salt beds. It is uncertain if aquifer flows up-structure to the north-east were for 10s–100s of km, or were incremental without flushing the entire flow system. All of these hypogene processes may have contributed to the widespread dissolution patterns in the halite salt basin, but the relative impact by each remains uncertain. This chapter interprets the impact on these dissolution processes by continental-scale tectonism, which exerted major regional controls on the development of the foreland Alberta and intra-cratonic Williston basins as constituents of the Western Canada Sedimentary Basin. The hydraulic head, charged in the mountainous terrains to the west and south-west, provided the drive for the water flows north-eastwards (Garven and Freeze 1984; Garven 1989) and variously mixed with influxes of surface charged ground water flows. Alternative models suggest that most salt dissolution patterns resulted only from localized vertical water movements within the Devonian strata as a result of sediment loading and compaction (Bachu and Underschultz 1993; Bachu et al. 1993; Bachu 1995, 1999).

2 Geologic Setting

This chapter reviews the origin and distribution of the hypogene salt karst dissolution patterns that configured the Prairie Evaporite basin and impacted overlying strata across southern Saskatchewan and northern Alberta. Examples are documented for several of the most important salt dissolution trends: (1) Roncott Platform-Hummingbird Trough complex in southern Saskatchewan, (2) potash district of central Saskatchewan and (3) the Athabasca Oil Sands and substrate in north-eastern Alberta.

Multi-stage salt dissolution patterns resulted from aquifer flows directed along cross-cutting fracture and fault lineaments that dissected these Middle Devonian evaporite beds, resulting in 10–100s of km long collapse-subsidence structures that configured the overlying strata (Anderson and Knapp 1993). As a result, this area of Western Canada developed the largest known hypogene interstratal halite salt karst. Unusual structural features developed because halite is 130–150 times more soluble than gypsum and 1000s times more soluble than limestone. Dissolution patterns in 100–250-m-thick halite beds extend for 100s–1000s of km^2, resulting in overlying collapse-subsidence structures that provided regional accommodation spaces for hydrocarbon reservoirs in northern Alberta and southern Saskatchewan. The impacts by salt dissolution trends on the structural and stratigraphic framework of southern Saskatchewan have been documented by numerous researchers of the Saskatchewan Geological Survey since the 1960s and 1970s (DeMille et al. 1964; Holter 1969; Gendzwill 1978; Broughton 1977, 1985; Irvine et al. 1978; McTavish and Vigrass 1987), and across northern Alberta since the 1970s by the Alberta Geological Survey and the oil exploration industry (Hein et al. 2013).

The Middle Devonian Prairie Evaporite basin was covered by a 1.5–2.5-km-thick interval of Palaeozoic and Mesozoic strata across southern Saskatchewan, in contrast to only 200–300 m preserved across north-eastern Alberta. Most of the stratigraphically equivalent strata did not accumulate or were subsequently eroded during the Jurassic uplift of the north-eastern Alberta basin (Meijer Drees 1994; Grobe 2000). The pre-Cretaceous interval is only 200–400 m thick and mostly represented by Devonian strata. As a result, the Lower Cretaceous Athabasca sands accumulated on a Devonian karstic palaeotopography.

The post-burial structure of the Prairie Evaporite basin was largely controlled by the Jurassic deformation of the Western Canada foreland basin, resulting from early Cordilleran tectonism associated with the eventual rise of the Rocky Mountain chain (Fig. 2). The Cordilleran fold and thrust fault belt developed as the deformation front advanced eastwards. North-eastern Alberta was uplifted during the Middle-Late Jurassic to Early Cretaceous Columbian orogeny, as the Craton buckled below foreland basin. The tectonism broadly configured the Prairie Evaporite salt basin into regional sub-basins eastwards of the Rocky Mountain foothills: (1) the Alberta basin with uplifted areas across north-eastern Alberta, and (2) the Williston basin with the northern rim across southern Saskatchewan, northwards of the central Montana Uplift and the Black Hills (Parker 1967; LeFever and LeFever 2005). The Alberta and Williston basins were separated by the Bow Island Arch (Fig. 1) and covered by thick Cretaceous strata resulting in the Western Canada Sedimentary Basin (WCSB).

Tectono-stratigraphic and palaeogeography models formulated during the last several decades suggest that the regional controls on development of hypogene aquifers in western North America responded to continental-scale

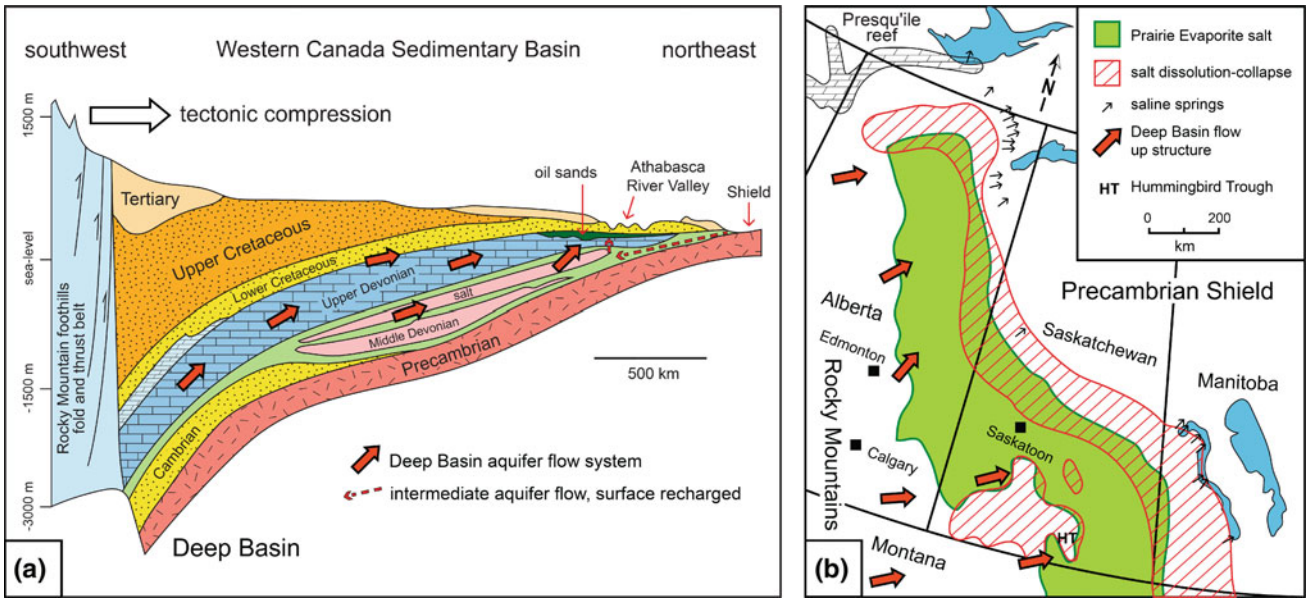

Fig. 2 Subsidence of the foreland Alberta basin during the Columbian orogeny, followed by Laramide tectonism resulting in the Rocky Mountain terrain, resulted in sedimentary loading as deep basin formation waters migrated up-structure to the north-east. Aquifer flows resulting in extensive areas of salt removal configured the Middle Devonian Prairie Evaporite basin as the largest known hypogene halite karst collapse: **a** Alberta basin aquifer flows up-structure to the north-east resulted from the hydraulic head charged in uplifted terrains responding to the Middle Jurassic to Early Cretaceous Columbian orogeny, and subsequent Laramide tectonism resulting in the Rocky Mountain foothills. Flows to the north-east up-structure were towards lower topographic discharge areas, such as the Athabasca River Valley. Salt removal trends configured the overlying Devonian strata, and the palaeotopography was subsequently covered by Cretaceous deposits accumulated as the Athabasca Oil Sands; **b** aquifer flows in the Alberta and Williston basins resulted in a 1000-km-long and 150-km-wide dissolution trend along the eastern margin of the Prairie Evaporite basin, and the northern Williston basin area across southern Saskatchewan

tectonism (Garven 1989). Burial-uplift cycles during Devonian-Carboniferous (Antler) extensional and compressional tectonism resulted in a mixture of shallow hypogene and meteoric epigene aquifer flows into the Prairie Evaporite salt beds. In contrast, deep-seated hypogene aquifer flows significantly impacted the buried salt basin in the Cordilleran foreland as a result of Middle Jurassic-Early Cretaceous (Columbian), and to a lesser extent Late Cretaceous-Palaeogene (Laramide) tectonism resulting in the Rocky Mountains. These orogenic events were linked to the creation of the Palaeozoic Pangaea supercontinent and subsequent Mesozoic fragmentation that separated North and Central America from Europe and Western Africa.

The Columbian-Laramide tectonism resulted in deep basin aquifer flows along permeable strata up-dip to the north-east towards the eastern margin of the Prairie Evaporite basin (Figs. 1 and 2). The hydraulic head, charged in the mountainous terrains, provided the drive for the deep-seated aquifer flows northwards and eastwards into topographically low terrains as they mixed with expelled connate waters resulting from compaction of deeply buried sediments during sedimentary loading (Garven and Freeze 1984; Garven 1989). Dissolution trends occurred earlier in southern Saskatchewan, across the area of the Roncott Platform-Hummingbird Trough complex, during the Late Devonian-Carboniferous, followed by Middle Jurassic-Early Cretaceous dissolution stages across both southern Saskatchewan and northern Alberta. Other significant dissolution stages were related to Pleistocene loading and unloading with the invasion of subglacial meltwaters interfering with the regional aquifer flows.

3 Regional Salt Dissolution Patterns

The Middle Devonian Keg River Formation, consisting of platform carbonates with overlying bioherm mound trends, provided aquifer pathways into the overlying Prairie Evaporite aquitards, as well as the overlying Upper Devonian strata, resulting in a well-developed regional aquifer system. Late Palaeozoic carbonates, consisting mostly of Mississippian-Permian beds, accumulated across southern Saskatchewan (Fig. 3) but were regionally poor aquifers having only limited extent. In contrast, the Lower Cretaceous Mannville Group accumulated in southern Saskatchewan and stratigraphic equivalents in Alberta, including the McMurray Formation (Aptian), formed highly permeable sandstone aquifers if not bitumen cemented.

The Prairie Evaporite hypogene karst and configured overlying strata extend along three regional trends: (1) the

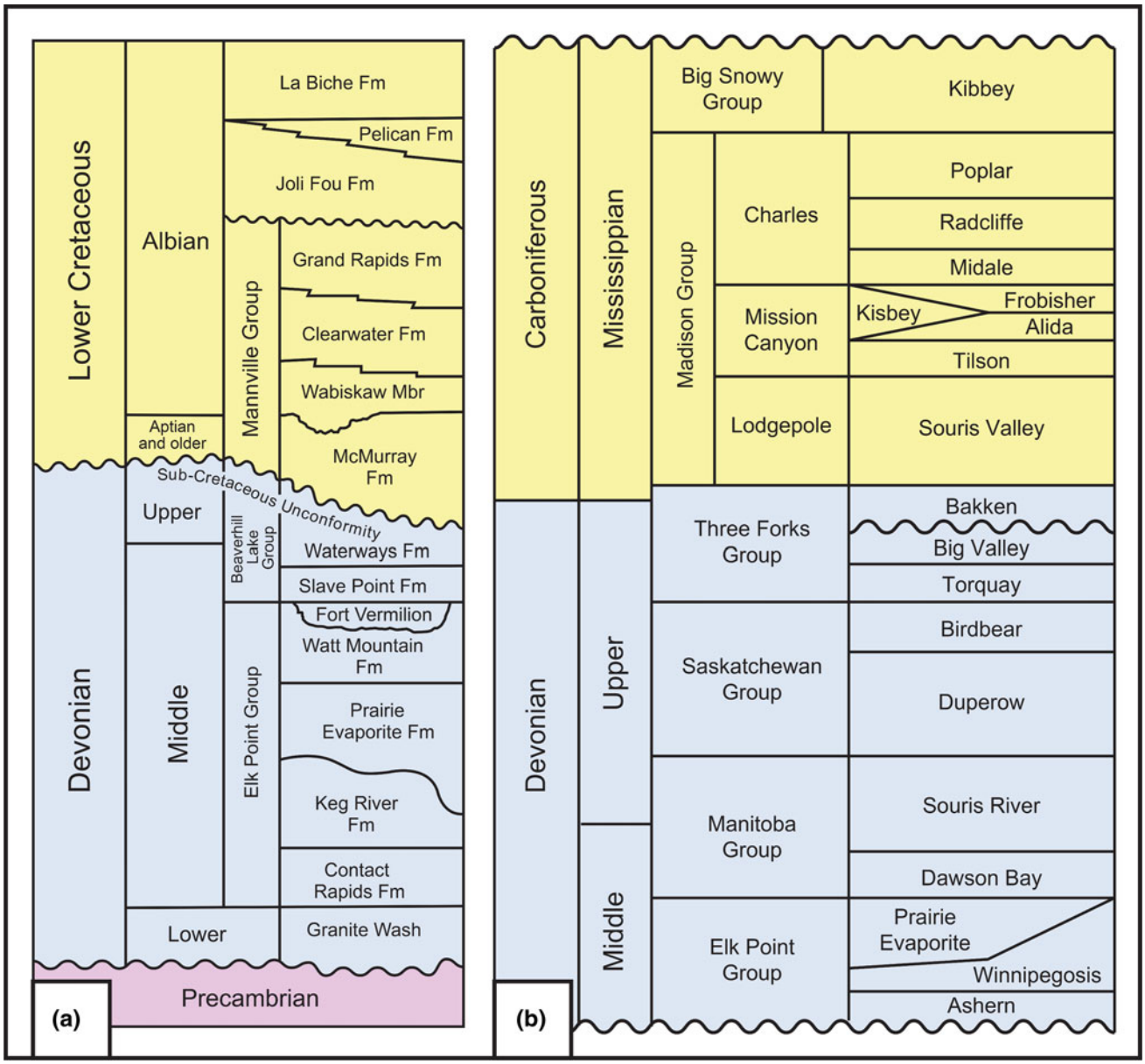

Fig. 3 Stratigraphic chart of the Western Canada Sedimentary Basin: **a** Devonian and Cretaceous formations in the Athabasca Oil Sands deposit area of the northern Alberta basin; **b** Devonian and Carboniferous formations in the southern Saskatchewan area of the northern Williston basin

1000-km-long and 150-km-wide dissolution trend along the eastern evaporite basin margin, extending from NE Alberta to SE Saskatchewan and SW Manitoba; (2) the Roncott Platform-Hummingbird Trough structural complex in the southern Saskatchewan area of the Williston basin; and (3) the halite-potash sub-basin in south-central Saskatchewan.

3.1 Area 1: Eastern Basin Margin

Regional deep basin aquifer flows up-structure to the north-east were mostly along Devonian strata in north-eastern Alberta, resulting from subsidence of the foreland Alberta basin responding to buckling of the underlying Craton during Middle-Late Jurassic to Early

Cretaceous Columbian tectonism, and intra-cratonic Williston basin subsidence across southern Saskatchewan. These regional aquifer flows resulted in a 1000-km-long and 100–150-km-wide dissolution trend along eastern margin of the Prairie Evaporite basin (Fig. 1). A 300-km-long segment of this dissolution front, known as the salt scarp, underlies the Lower Cretaceous Athabasca Deposit in north-eastern Alberta (Figs. 1 and 4).

Dissolution trends within the Middle Devonian halite-anhydrite beds below the Cretaceous Athabasca Deposit were multi-stage events from Late Devonian to Cretaceous (pre-Aptian), but mostly Middle Jurassic to Early Cretaceous events that dissected the salt scarp and segmented the overlying Upper Devonian limestone karstic surface terrain. These dissolution trends expanded during the Aptian, concurrent with deposition of McMurray Formation sand deposits (Bachu 1995, 1999; Anfort et al. 2001; Hein et al. 2013; Schneider and Grobe 2013; Broughton 2013, 2015).

The basin-scale flow system drive to the north-east was along the Middle and Upper Devonian beds for the entire

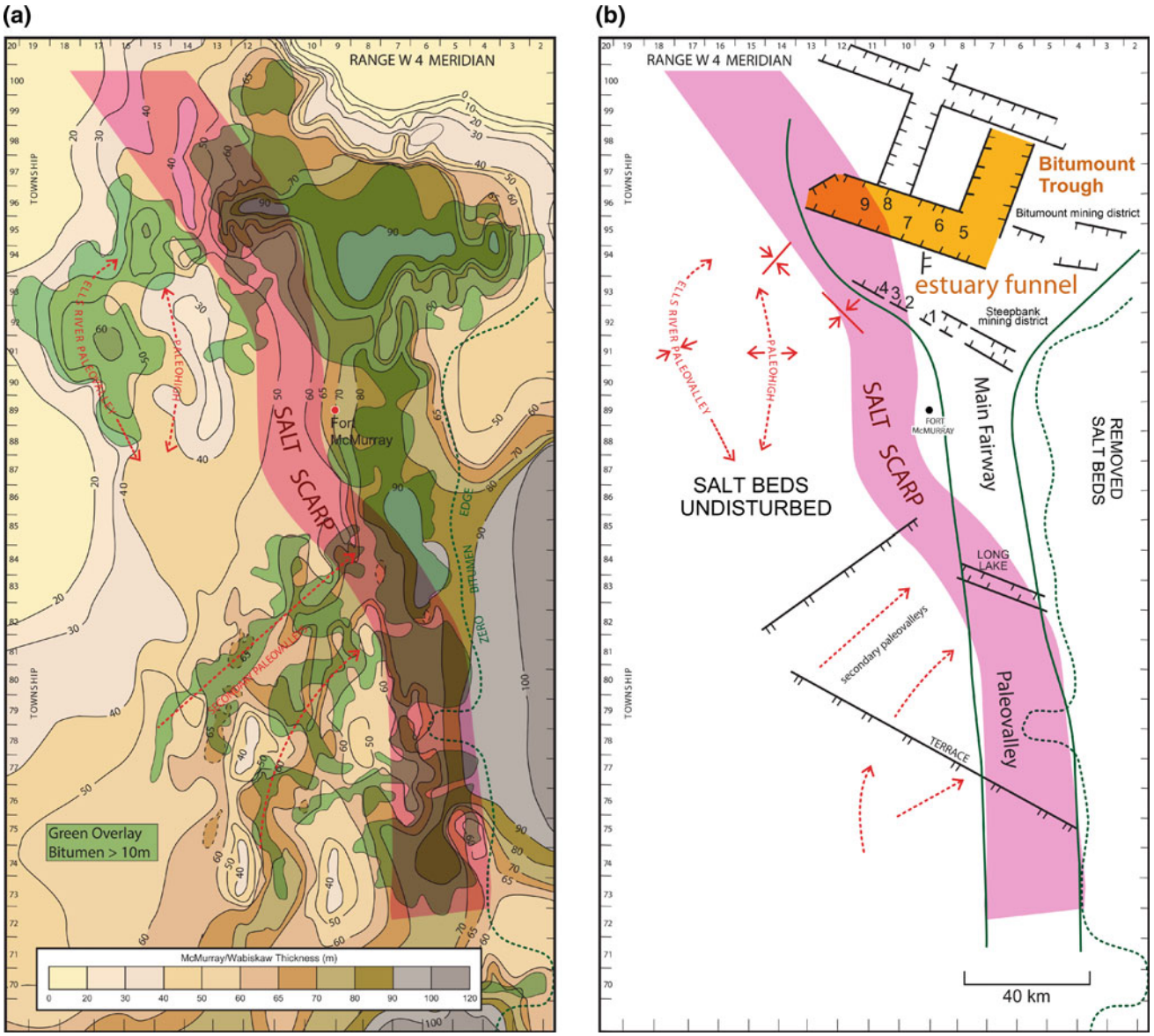

Fig. 4 Geology of the Lower Cretaceous Athabasca Oil Sands in north-eastern Alberta: **a** thickness of McMurray Formation (Aptian) and overlying Wabiskaw Member, Clearwater Formation (Albian) strata with distribution of bitumen sands >10 m. The underlying 300-km-long salt scarp in the Prairie Evaporite (Middle Devonian), 200 m below, separated undisturbed salt beds from dissolution areas to the east; **b** structural configuration of the Devonian karstic palaeotopography covered by Lower Cretaceous strata accumulated as the Athabasca Oil Sands. Open pit bitumen sand mines are distributed along bitumen sand trends filling 10s of km-long troughs on the sub-Cretaceous unconformity

length of Alberta (Bachu and Underschultz 1993; Bachu et al. 1993). However, other researchers suggest that deep basin flows did not move as far to the north-east as the area of the Athabasca Deposit but incrementally pushed formation waters into the area without completely flushing the regional flow system (Connolly et al. 1990). Nevertheless, hydrogeological studies by Mahood et al. (2012) of the Devonian limestone karst below the Athabasca sand deposit documented the extent of a vast karst aquifer flow system for tens of kilometres.

Geochemical studies on stable isotope ratios and composition of dissolved solids indicate that the regional aquifer flows to the north-east mixed with invading glacial meltwater counter-flows to the south-west along most of the 1000-km-long eastern margin of the evaporite basin. The influxes of subglacial meltwaters, driven by the hydraulic head created by a 1.5–2-km-thick Laurentide ice sheet, were sufficiently pressured to reverse the regional aquifer flow along north-eastern margins of the Alberta and Williston basins (Anderson and Hinds 1997; Grasby and Chen 2005). Subsequent to this flow reversal by glacial meltwaters, the regional aquifer to the north-east was re-established after withdrawal of the ice sheet. As a result, the salt dissolution sourced brine springs and saline lakes were distributed along topographic lows near the eastern evaporite basin margin from north-eastern Alberta to south-western Manitoba (Figs. 1 and 2), such as along the Athabasca River Valley (Gibson et al. 2013).

3.2 Area 2: Roncott Platform-Hummingbird Trough

Multi-stage salt dissolutions in the Prairie Evaporite impacted overlying strata across south-central Saskatchewan as a result of aquifer flows northward up-structure across the northern Williston basin in north-eastern Montana and western North Dakota, which were charged across upland terrains such as the Montana Uplift and the Black Hills areas and related ancestral structures. Multi-stage dissolution-collapse structures developed along the northern rim of the Williston basin across most of southern Saskatchewan (Smith and Pullen 1967; Holter 1969). The Roncott Platform, a salient of salt beds largely unaffected by dissolution trends, was bounded on the east by the 150-km-long Hummingbird Trough (Fig. 2b). Salt dissolution trends were initiated during the Late Devonian along the eastern and western margins of an area of undisturbed salt beds, resulting in the proto-Roncott Platform. More extensive stages of Mississippian to Jurassic salt bed removals along the Hummingbird Trough further configured the eastern margin of the Roncott Platform. Post-Jurassic salt removal patterns across most of southern Saskatchewan finalized the structural configuration of the Roncott Platform-Hummingbird Trough complex. The Hummingbird and Lake Alma oil pools, which produce 40 degree API light oil, are located within salt dissolution-collapse features in the southern reaches of the Hummingbird Trough (Smith and Pullen 1967).

3.3 Area 3: Potash Sub-basin

South-central Saskatchewan area developed as a sub-basin area of the Prairie Evaporite, resulting in the concentration of commercially attractive potash deposits near the city of Saskatoon. The sylvite and carnallite beds accumulated with halite deposits in a sub-basin, separated from the halite-anhydrite accumulations elsewhere (Fuzesy 1982). This potash district is characterized by 100-m-high brine-filled dissolution chimneys, often collapsed, that cross-cut beds consisting of halite-gypsum-anhydrite and potash minerals.

Seismic surveys, often 3D arrays, have been extensively used across the potash mining district to avoid the mine tunnels coming into contact with these brine-filled chimneys or collapsed structures leached of ore. Figure 5a illustrates a depth-migrated 3D seismic profile imaging one of these collapsed 100-m-high salt dissolution chimneys (Nemeth et al. 2002). The overlying 500-m-thick strata, consisting of Upper Devonian carbonates and Cretaceous clastic beds, were faulted and fragmented as they sagged over collapsed chimney roofs. The chimneys of the potash mining district provide a collapse structure analogue useful for interpreting collapse patterns in the fragmented Upper Devonian-Lower Cretaceous strata of the northern Athabasca Deposit (Fig. 5b).

Also, influxes of subglacial and pro-glacial meltwaters into the regional aquifer during the Pleistocene resulted in regional-scale collapse subsidence and structures across south-central Saskatchewan. Examples across the potash district and beyond are the Saskatoon, Rosetown and Regina structural lows (Christiansen 1967; Christiansen and Sauer 2002).

4 Impact of Salt Removal on Overlying Athabasca Oil Sands

The Athabasca Oil Sands are the largest and commercially the most important of the three Lower Cretaceous bitumen-saturated sand deposits in northern Alberta (Figs. 1 and 4). The 45,000-km^2 Athabasca Oil Sands Deposit accumulated as a 200 billion m^3 or a trillion barrel resource (Berbesi et al. 2012; Adams et al. 2013; Hein et al. 2013). Late Cretaceous-Early Palaeogene Laramide tectonism

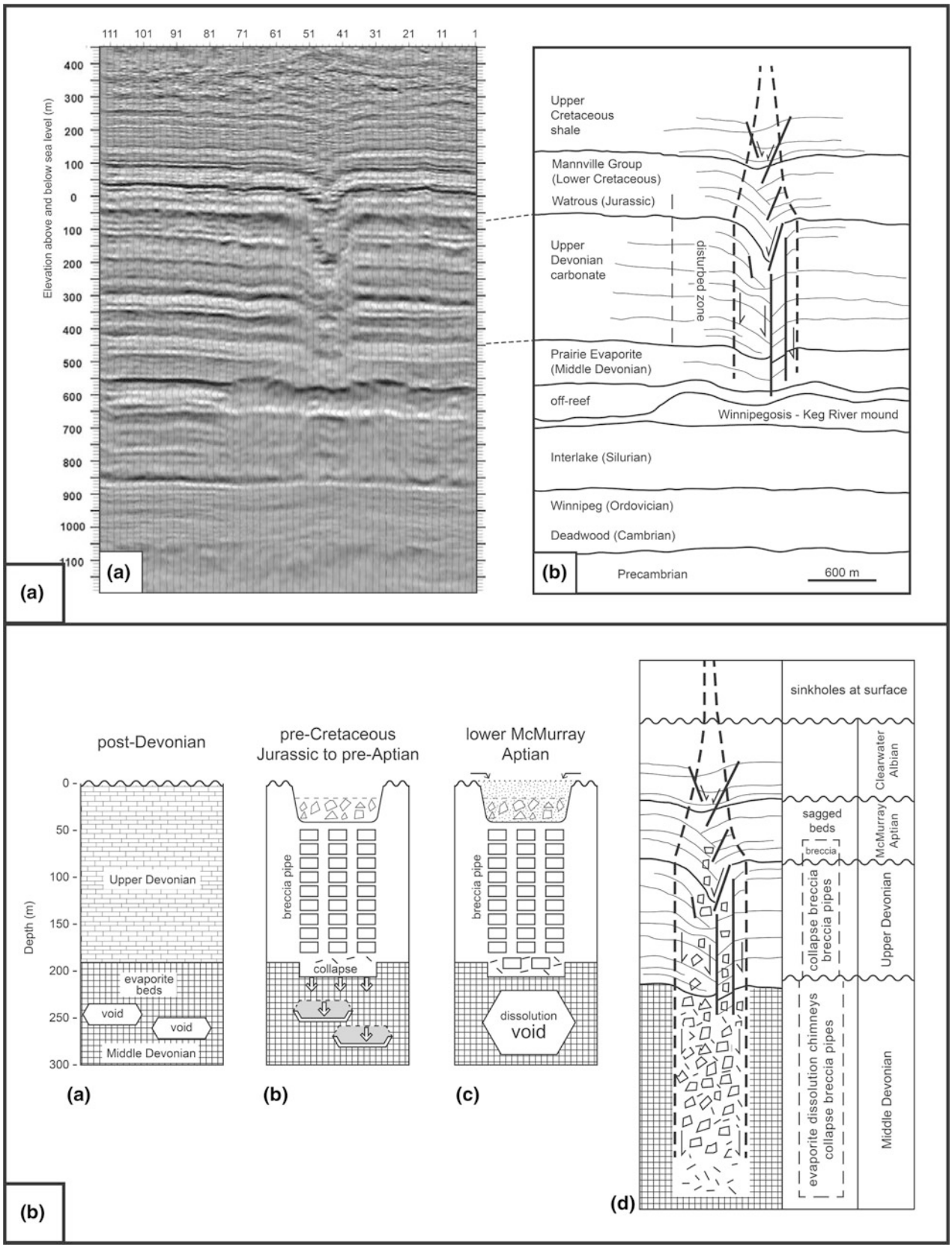

Fig. 5 Structural impact of a collapsed dissolution chimney on overlying strata: **a** 3D seismic imaging of a 100-m-high chimney collapse within Prairie Evaporite halite and potash beds, central Saskatchewan (modified from Nemeth et al. 2002). The salt removal differentially subsided and rotated fault blocks, consisting of overlying Devonian and Cretaceous strata. This resulted in concave collapse patterns that are an analogue for interpreting fault block patterns in the Athabasca Oil Sands; **b** interpretation of the fault block patterns in the Athabasca Oil Sands

resulted in oil sourced from mostly Devonian to Mississippian shale beds accumulated in the deep basin of west-central Alberta, to migrate eastward up-structure into unconsolidated sand reservoirs of the Athabasca Deposit, mostly represented by strata of the McMurray Formation (Aptian) and to a lesser extent by the overlying sands of the Wabiskaw Member, Clearwater Formation (Albian) (Fig. 3). Oil flows trapped by these sand reservoirs were subsequently biodegraded into highly viscous bitumen (Head et al. 2003; Higley et al. 2009; Berbesi et al. 2012; Adams et al. 2013). The low-permeability Clearwater shale (Albian) top-sealed these McMurray Formation sand reservoirs, resulting in the Athabasca Oil Sands (Fig. 4).

The Athabasca Oil Sands in north-eastern Alberta is a reference case for a hypogene karst impacted by a very low 1:2 thickness ratio of salt removal to overlying strata. This hypogene halite-dominated karst is unlike other halite karsts consisting of relatively thin halite beds, such as the near-surface sinkhole-prone margins of the Dead Sea (Frumkin and Raz 2001; Closson 2005; Closson and Abou Karaki 2009; Ezersky and Frumkin 2013). Significant salt removal stages occurred during the Columbian orogeny lasting from the Middle-Late Jurassic into Early Cretaceous, resulting in structural impacts that configured both the pre-Cretaceous strata and concurrent deposition patterns by the McMurray Formation. These dissolution fronts in the salt beds rapidly advanced along the regional sets of cross-cutting lineaments, oriented SW–NE and NW–SE, which probably followed fault patterns between underlying Precambrian blocks.

The dissolution of 100–150 m of Prairie Evaporite salt beds configured a mosaic of differentially subsided fault blocks consisting of 200–250-m-thick Middle-Upper Devonian strata. The dissolution patterns resulted in a reticulated limestone karst palaeotopography characterized by valleys and ridges, onto which braided river and floodplain deposits of the lower McMurray Formation accumulated along the topographic lows. These lower McMurray deposits and Devonian palaeohighs were subsequently covered by fluvial-estuarine deposits of the middle McMurray Formation. The Devonian fault blocks above the removal salt areas continued to differentially subside during accumulation of McMurray deposits, resulting in syndepositional trends up to 25 km long following underlying salt dissolution trends only 200 m below (Broughton 2015, 2016).

Regional salt dissolution subsidence and collapse structures resulted in a tectono-stratigraphic framework that partially to significantly controlled deposition patterns in the overlying Athabasca sand deposits.

4.1 Salt Scarp and Palaeovalley Trunk

The N–NW-oriented Middle Devonian salt scarp is a 300-km-long segment of the 1000-km-long dissolution trend along the eastern margin of the Prairie Evaporite basin (Figs. 1 and 4). It demarcates the westernmost advance by the dissolution front below the length of the Athabasca Deposit and separates the 100–150-km-wide salt removal areas to the east from mostly undisturbed salt beds to the west. A 175–250-m-thick interval of fragmented and block-faulted Middle-Upper Devonian strata overlies the 10–20-km-wide salt scarp and salt removal areas to the east. The salt scarp has been strongly dissected by cross-cutting SW–NE- and SE–NW-oriented fracture-fault lineaments that lengthened and widened by advancing dissolution fronts. The northward trending main palaeovalley on the overlying sub-Cretaceous unconformity surface parallels the eastern edge of the scarp and represents the structural offset fronting the 100-m relief along the eastern margin of the underlying salt scarp.

4.2 Bitumount Trough and Dissection of the Salt Scarp

The 50-km-long V-shaped Bitumount Trough is the largest collapse structure on the sub-Cretaceous unconformity surface (Flach and Mossop 1985; Hein et al. 2000, 2001; Hein and Cotterill 2006; Broughton 2013, 2015). It resulted from collapse of Middle-Upper Devonian strata above the salt removal trends between cross-cutting pairs of parallel lineaments, responding to chains of chimney dissolution sites that coalesced into liner dissolution trends (Fig. 5b). The trough was filled with sand and mud beds of the McMurray Formation but continued differential subsidence by fault blocks resulted in syndepositional trends following sag lows up to 120 m deep.

Many examples of these differentially subsided Devonian-McMurray fault blocks have been exposed along bench cuts in the mines located above the salt scarp and to the east overlying salt removal areas (Broughton 2015, 2016) (Fig. 6). A major stage of collapse subsidence occurred during and at the end of the lower McMurray interval. This impacted the Bitumount Trough but not most areas to the south (Fig. 4). Figure 6a illustrates an example of an 800-m-long fault block of Devonian-lower McMurray strata exposed in the Muskeg River Mine, located along the west-central Bitumount Trough (Fig. 4b). Dissection along the length of salt scarp was more extensive during deposition of the middle-upper McMurray, resulting in fault blocks tilts

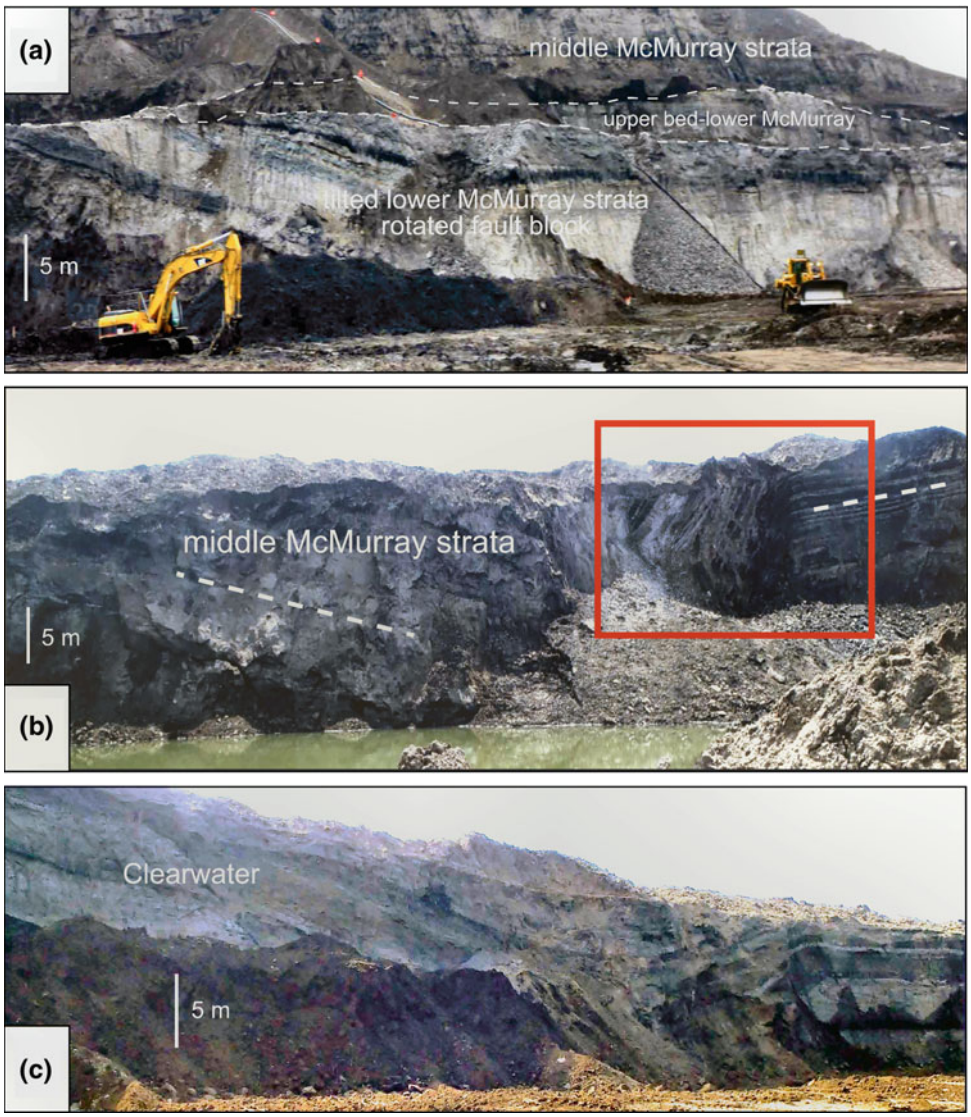

Fig. 6 Differentially subsided and rotated fault blocks, consisting of strata of the McMurray and Clearwater formations, overlying dissolution trends that dissected the salt scarp: **a** example of multiple rotations and tilts by an 800-m-long lower McMurray fault block exposed in the Muskeg River Mine, Bitumount Trough district; **b** example of a km-long middle McMurray fault block that broke into colliding segments during the collapse, uncovered along a bench cut in the Steepbank mining district. The smaller middle splinter block (frame) rotated to a near-vertical position as it was crushed between the larger blocks, resulting in a vertical breccia pipe; **c** example of diminished collapse-subsidence dissipated upwards into the Clearwater Formation, resulting in 100 m across bed sags

and collapses throughout all of the mining areas (Fig. 6b). Most McMurray breccia pipes and sinkholes occurred towards the close of lower interval deposition (Broughton 2013), but some sites were reactivated during the middle-upper intervals, and others extend upwards to the subglacial topography as a result of glacial loading and invasion of fresh glacial meltwaters that rejuvenated dissolution along the salt scarp.

An analogue provided by the structural pattern resulting from the collapse of strata overlying giant dissolution chimneys in the potash mining district of south-central Saskatchewan (Fig. 5a) is used to interpret the concave collapse-rotated structural patterns by the Athabasca fault blocks. Overlying fault blocks tilted and cratered inwards, resulting in elongated concave patterns with cross-cutting vertical faults extending upwards from the collapsed chimney roofs. These fault block collapse patterns are similar to the rotated fault block patterns and associated breccia pipes exposed in mine cuts of the Athabasca Oil Sands. There, the inwardly tilted Devonian-McMurray block structures dissipate upwards, forming smaller-scale grabens (Fig. 6c). These step-down fault blocks were often draped by larger-scale bed sags, often 100–150 m across in the overlying Clearwater shale (Fig. 6c). Fracture zones with minimal vertical offsets may extend further upwards to the subglacial surface and result in aligned sinkholes that responded to glacial loading and unloading (Anderson and Hinds 1997).

4.3 Central Collapse

A 200-km^2 central collapse area on the sub-Cretaceous structure developed northwards of the Bitumount Trough

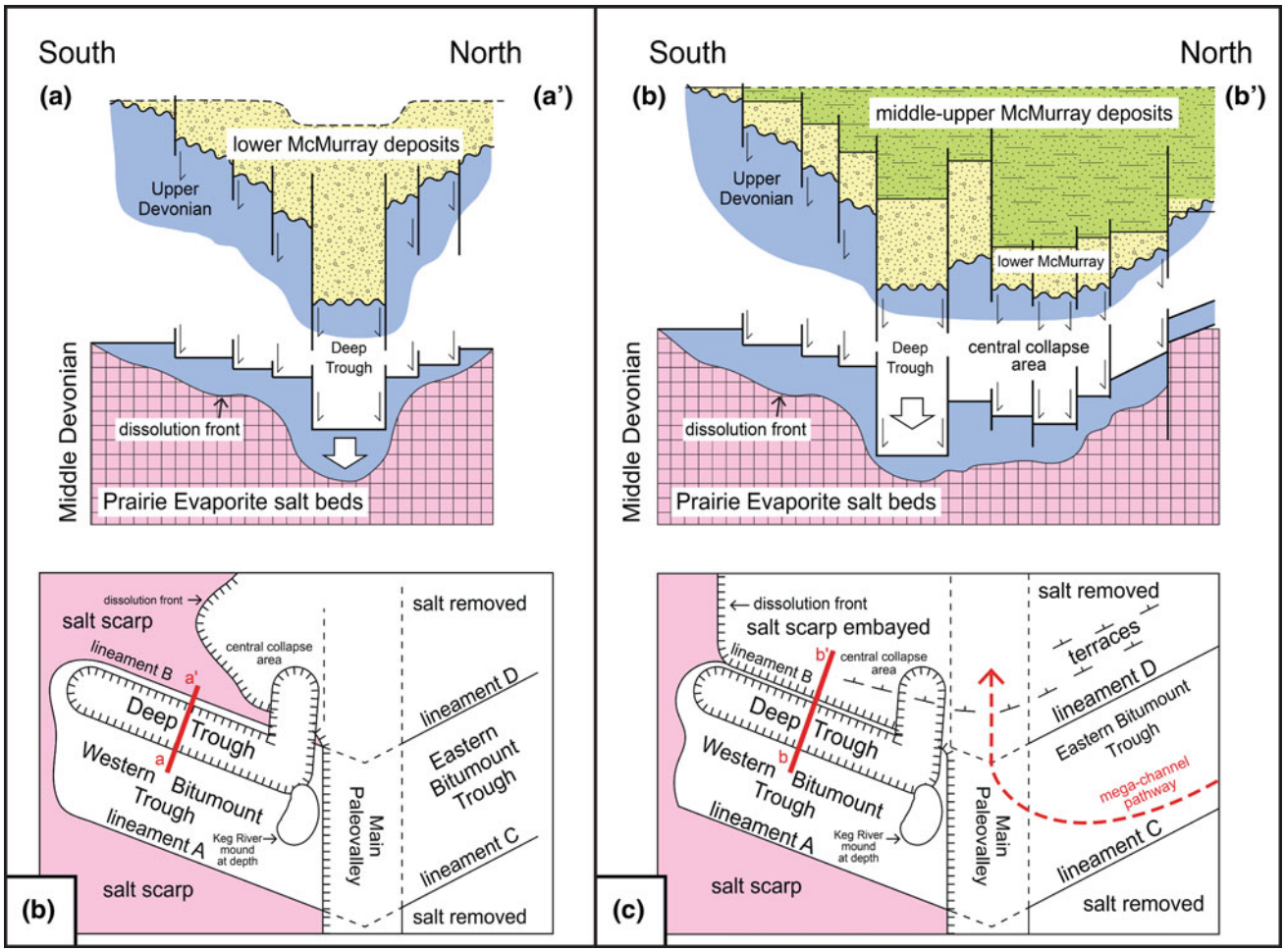

Fig. 7 Schematic illustration of lower and middle-upper McMurray Formation sand deposits accumulated above the salt dissolution trends in the Middle Devonian substrate: **a** 20–25-km-long syndepositional trend consisting of lower McMurray sand beds follows the collapsed northern margin of the Bitumount Trough; **b** northward migration of the dissolution trend during the middle-upper McMurray into the central collapse area resulted in a second 20-km-long syndepositional sand trend parallel to the lower McMurray trend

(Figs. 7 and 8). This extensive salt removal area resulted in discontinuous terraces, consisting of aligned fault blocks, on the sub-Cretaceous and overlying lower McMurray structural surfaces that stair step-down into the central collapse. This regional depression developed mostly during middle-upper McMurray deposition, consistent with advances of the underlying dissolution fronts northward of the older Bitumount Trough (Broughton 2016). Sinuous rivers of the McMurray channel belt, constrained along stable substrate of the main palaeovalley, flowed northward onto the unstable floor of this funnel-form lower estuary (Fig. 4 b). The main palaeovalley fairway branched into multiple 10s of km-long sub-parallel fluvial-estuarine tidal channels aligned parallel to the NW-oriented structural grain induced by underlying salt collapse trends. Sand transport fairways cascaded over these step-down terraces, permitting collinearly aligned aggradations of fluvial-tidal point bar complexes as multi-km-long sand reservoirs (Fig. 8). The internal architectures of these 10s of metre-thick sand deposits responded to deposit-wide erosion surfaces resulting from cycles of collapse–subsidence, stabilized substrate and erosion, and renewed subsidence and aggradation. These McMurray sand reservoirs trapped Late Cretaceous-Early Palaeogene oil migrations in the area. Subsequent biodegradation resulted in giant commercially attractive bitumen sand deposits.

4.4 Fault Block Collisions and Breccia Pipe-Sinkhole Complexes

Pre-Cretaceous sinkholes were distributed on the karstic Middle-Upper Devonian palaeotopography with limestone wall that permitted stable pits up to 100 m deep and 20 m across. They were subsequently filled and covered over by Cretaceous sands of the McMurray Formation (Broughton

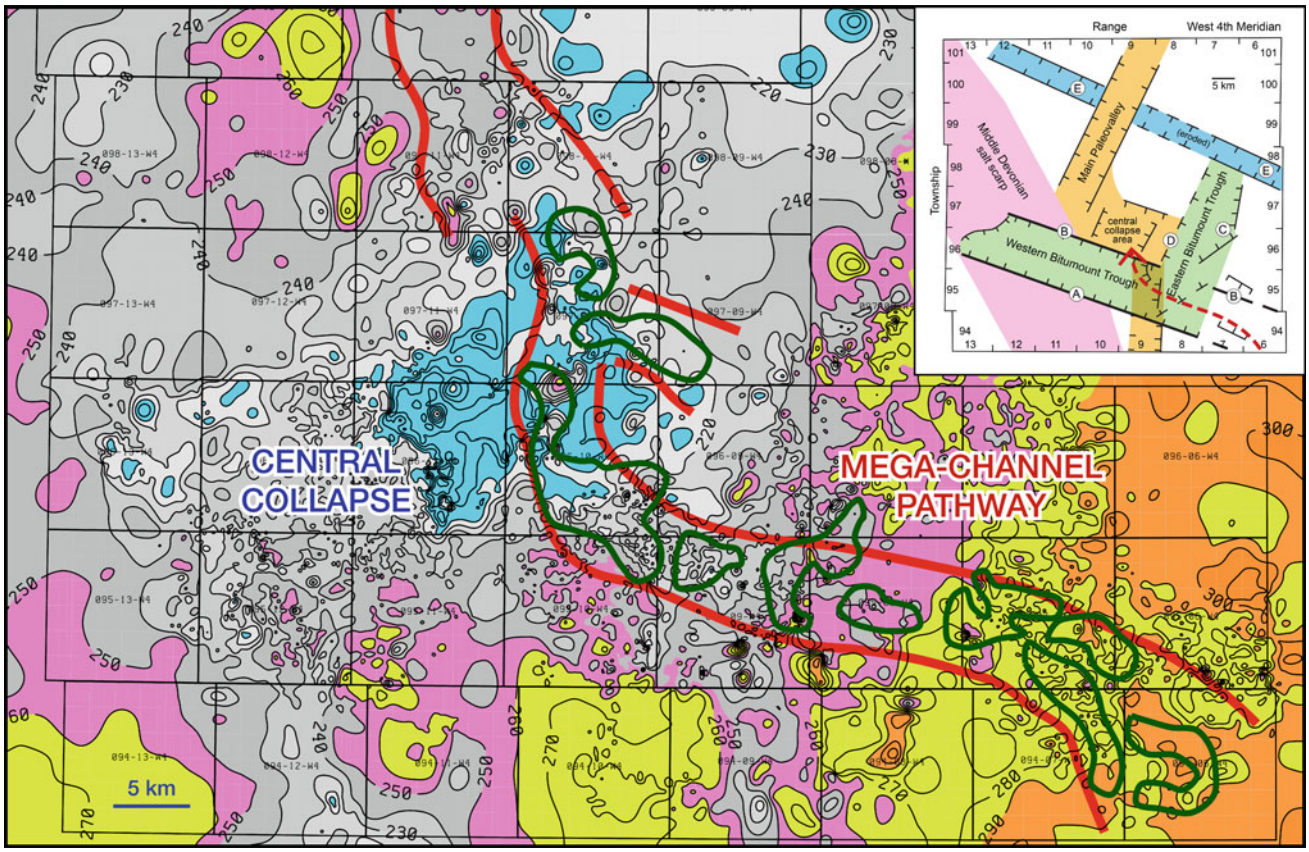

Fig. 8 Example of a middle McMurray fairway transporting sand northwards towards the Boreal Sea. The fairway cascaded over structural terraces, consisting of aligned Devonian-lower McMurray fault blocks that stepped down into the central collapse, responding to the north-westward migration of underlying salt dissolution trends. These step-downs provided aggradation sites for stacked point bars, resulting in collinearly aligned giant middle McMurray sand reservoirs that subsequently trapped oil migrations into the area

2013). The lower reaches of the pits were usually filled by chaotic breccia of collapsed blocks of limestone wall rock, mixed with erratically oriented discontinuous lenticular fragments of lower McMurray sand and silt beds. The uppermost 10–30-m-thick fill intervals of the deeper sinkholes often accumulated stratified sand, mud and peat (lignite) beds. These sinkholes developed as the upper reaches of breccia pipes that extended downwards into salt removal zones within the Middle Devonian Prairie Evaporite substrate.

Multiple aligned sinkholes formed NW–SE- and NE–SW-oriented trends and often amalgamated into 3–4-km-long sinkhole valleys on the Devonian palaeotopography (Broughton 2013). Sinkholes also formed within the overlying McMurray sand beds but were subject to almost immediate collapse because of unstable walls consisting of unconsolidated sand. Post-burial sinkholes deformed the McMurray beds as gravity-driven sags over subsiding or rotating fault blocks, and were often further deformed by compressional block-to-block collisions (Fig. 9). Trends consisting of multiple sinkholes developed on the subglacial and Holocene surficial topography (Fig. 10). These aligned sinkholes are distributed along multi-km-long NW–SE- and SW–NE-oriented lineaments on the surface but rooted in underlying salt removal patterns (Haug et al. 2009, 2014; Broughton 2013).

Nearly all McMurray sinkholes exposed by mine cuts were positioned against near-vertical normal fault planes between adjacent fault blocks. Various styles of open and closed sinkholes formed along the upper reaches of the block-to-block collision zones, resulting in discordant tilted beds on opposite sides of each sinkhole. Most McMurray sinkholes emplaced along the block-to-block fault plane display a range of U- and V-shaped sagged bed styles up to 20–25 m across, but some exceed 100 m in diameter. Sinkholes are observed to be positioned within the upper reaches of the block-to-block collision zones, emplaced above breccia pipes although the separations may be 10s of metre-long intervals. Sag-type sinkholes often splintered into faulted compartments, resulting from sustained compression along the collision zone. Sinkholes may include wedge-thickened mud beds that record sag-slippage along

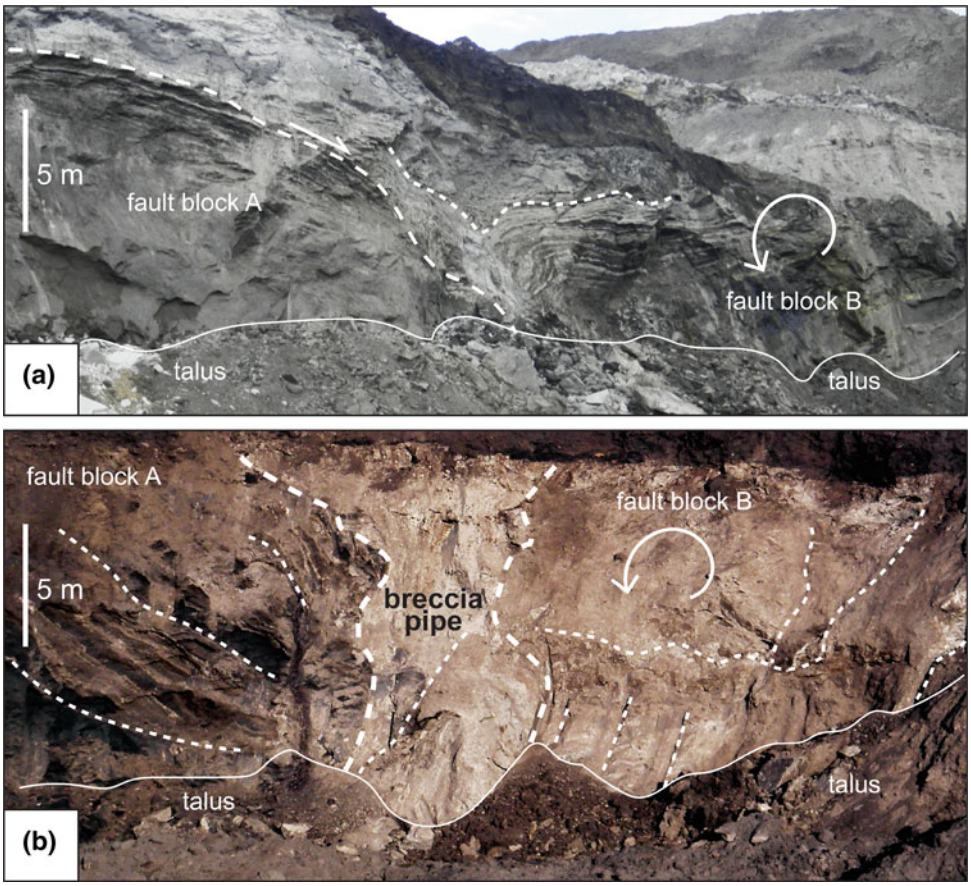

Fig. 9 Bed deformations along the lower and middle collision zone between adjacent differentially subsided fault blocks: **a** twisted beds in block-to-block mid-collision zone resulted from rotational trajectories at impact; **b** lower collision zone resulting in breccia pipes consisting of chaotic blocks, often with vertically oriented bed fragments. Examples from the Muskeg River Mine

the fault plane between adjacent blocks (Fig. 10a), in contrast to compression-fragmented sinkholes that splintered and compartmentalized. Breccia pipes have never been observed overlying sinkholes but often formed within fragmented sinkholes.

Breccia pipes are widely distributed in southern Saskatchewan above salt removal areas, peripheral to the Roncott Platform, and across the northern Athabasca Deposit in north-eastern Alberta (Ford 1997; Broughton 2013). The morphogenesis of breccia pipes within the Cretaceous beds of the Athabasca Deposit, cross-cutting underlying Middle-Upper Devonian limestone beds, differs from the salt removal areas across southern Saskatchewan because of the unusually low 1:2 thickness ratio between removed salt beds and the overlying strata. This low ratio resulted in unusual styles of breccia pipe-sinkhole complexes associated with the Athabasca Deposit (Fig. 9). The collision structures observed at the Athabasca Deposit resulted in unusual compressional and extensional bed deformations along the collision zone that modified the breccia pipe-sinkhole complexes created along the fault plane between adjacent blocks. Characteristically well-defined breccia pipes, consisting of chaotic blocks mixed with 1–5-m-long vertically aligned bed fragments, were often overlain by vertically twisted beds imposed by oblique shearing between the fault blocks (Fig. 9a). In contrast, some block-to-block collision zones lack breccia fragmentation and developed zigzag fault contact planes with suture-like welds between adjacent blocks (Broughton 2015).

The potash district chimney analogue suggests that cataclysmic collapses by dissolution chimneys up to 100 m high occurred between fault blocks that cratered inwards over the collapsing chimney roofs. Mining operations across the northern and eastern Athabasca Deposit exposed numerous examples of these rotated fault block collisions. Figure 6a illustrates an exhumed 800-m-long lower McMurray fault block that collapse-rotated during the mid-lower interval and collapsed again towards the close of the lower interval. Similar middle McMurray fault block collapse-rotations occurred along the length of the underlying salt scarp. Smaller splinter blocks were crushed into breccia zones between larger fault blocks as the blocks pulled apart, rotated and further collided with oblique trajectories, fragmenting into smaller splinter blocks 10s of metres across. Trajectory wobbles resulted in fault blocks that converged, collided and diverged from each other during their vertical collapse (Fig. 9). These movements resulted in block-to-block collision zones with deformed and

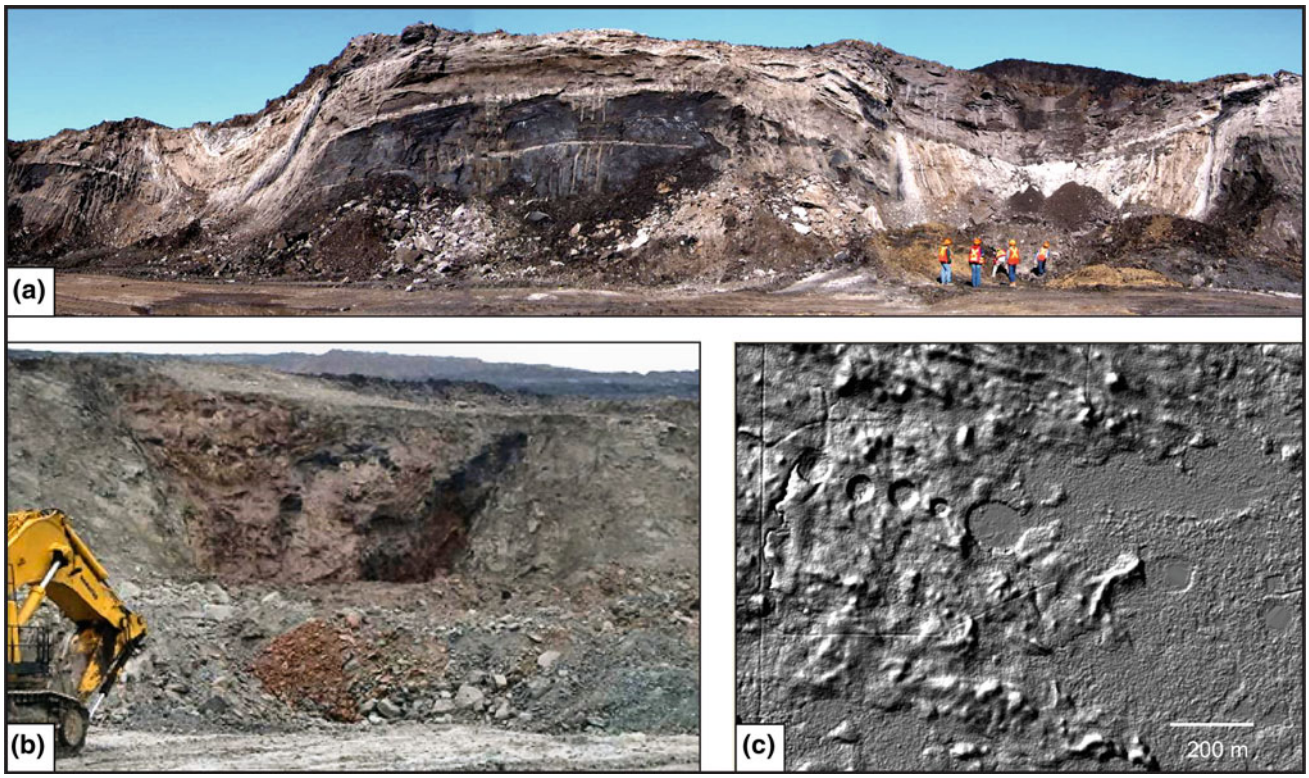

Fig. 10 Sinkholes developed along the upper collision zone between colliding fault blocks, usually overlying breccia pipes: **a** two of a series of aligned lower McMurray sinkholes, each fault bound, exposed in the Aurora North Mine, west-central Bitumount Trough; **b** sinkhole on the sub-Cretaceous unconformity surface with collapsed lower McMurray beds, exposed along a bench cut in a Steepbank district mine; **c** LiDAR imaging of aligned sinkholes, 10–130 m in diameter, distributed along a SE-oriented subglacial lineament, north-western Bitumount Trough

fragmented beds that transitioned into breccia pipes and irregular brecciated zones (Fig. 9).

5 Conclusions

Aquifer flows up-structure to the north-east resulted in dissolution trends in the Middle Devonian Prairie Evaporite beds accumulated across Western Canada, resulting in the largest known hypogene halite karst. Earliest stage dissolution trends, coinciding with the Antler orogeny, developed as early as the Late Devonian but were more prevalent during the Carboniferous across southern Saskatchewan and only to a lesser extend across northern Alberta. In contrast, widespread dissolution patterns developed during the Cretaceous subsidence of the Williston basin and its ancestral structures. Extensive salt removal area developed as the foreland Alberta basin subsided as the Craton below deformed during the Middle-Late Jurassic to Early Cretaceous Columbian orogeny. Two regional sub-basins, the Alberta basin and the Williston basin to the south-east, separated by the Bow Island Arch, were covered by thick Jurassic and Cretaceous sediments shed from the Rock Mountain terrains, resulting in the overarching Western Canada Sedimentary Basin. The sub-basins underpinning the WCSB controlled flow regimes up-structure to the north-east towards the eastern margin of the Devonian evaporite basin, resulting in a 1000-km-long and 150-km-wide salt removal trend extending from NE Alberta to SE Saskatchewan and into SW Manitoba. Extensive dissolution trends also developed across the southern Saskatchewan area of the northern Williston basin.

A final stage of these multiple dissolution events resulted from Pleistocene glacial loading and unloading when pressured subglacial meltwaters invaded the north-east flowing regional aquifers. The hydraulic head resulting from a 2-km-thick Laurentide ice sheet was sufficient to have reversed the flow direction, as well as rejuvenate dissolution along the salt scarp by the invading under-saturated waters. The regional flows to the north-east towards the basin margin were reinstated following withdrawal of the ice sheet. Dissolution of the salt beds in the subsurface continues into the present day, resulting in saline water seeps to surface along topographic lows.

The regional aquifer flows dissected the Middle Devonian salt beds along NW–SE- and NE–SW-oriented dissolution trends that probably relate to structural trends emanating from adjustments between Precambrian fault blocks in the basement only a few hundred metres below, responding to Columbian and Laramide orogenic events that warped the underlying basement. The 10s of km-long collapse troughs, oriented to the NW and to the NE, followed dissolution trends in the evaporite beds below that removed halite-anhydrite beds up to 250 m thick across southern Saskatchewan and 100–150 m thick across north-eastern Alberta.

The Athabasca Deposit in northern Alberta is an archetypal example of a dynamic, often cataclysmic, hypogene karst collapse that responded to regionally low 1:2 thickness ratio of removed salt to overlying strata. The impacts of halite bed dissolution-collapse karst processes have aspects of breccia pipe-sinkhole dynamics unique to the Athabasca Oil Sands. Unusual bed deformation structures resulted from oblique collision trajectories by adjacent collapsing fault blocks. The collision zones between adjacent fault block collapses resulted from rotational trajectories that formed breccia pipes overlain by obliquely twisted and sheared beds having funnel-form structures. Alternatively, some block-to-block collision zones lacked these structures and were welded together by zigzag-shaped interlocking fault planes. The lower and middle contact areas between colliding fault blocks, dominated by breccia pipes and shear-twisted bed deformations, pass upwards into the sinkhole-dominated zones. Upper reaches of these gravity-driven collapsed fault blocks were characterized by colliding rotations that resulted in sag-type sinkholes emplaced along the fault planes. Continued collisional compressions of many sag-style sinkholes resulted in fragmentation into brecciated compartments.

Salt dissolution fronts advanced along the sets of parallel and cross-cutting lineament patterns oriented to the NW and to the NE. Dissolution fronts advanced rapidly along these lineament trends, dissecting the salt scarp, as linear arrays of chimney dissolution sites that subsequently coalesced and collapsed the overlying strata. Lengthening and widening of these cross-cutting dissolution trends resulted in larger salt removal areas, enhancing the westward migration of the salt scarp dissolution front. Collapse of the overlying Devonian strata resulted in 10s of km-long structural trends on the Devonian unconformity surface, consisting of mosaics of differentially subsided fault blocks.

The largest of these developed on the Upper Devonian karstic palaeotopography is the 50-km-long V-shaped Bitumount Trough, subsequently filled and covered over by Lower Cretaceous McMurray Formation deposits. These karst collapse-induced structural trends partially to extensively controlled distribution of giant fluvial and fluvial-estuarine point bars, each covering 10s of km^2. These Mississippi River-scale fluvial bars, 1–5 km long and 20–60 m thick, accumulated as sand reservoirs that trapped Laramide oil migrations into the area. Subsequent biodegradation resulted in commercially attractive bitumen deposits. Such a single sand bar deposit can sustain a bitumen mine operating at 200,000 barrels per day for 100 years, a voluminous operational-scale unique to the Athabasca Deposit.

References

Adams J, Larter S, Bennett B, Huang H, Westrich J, Van Kruisdijk C (2013) Dynamic interplay of oil mining, charge timing, and biodegradation in forming the Alberta oil sands: insights from geologic modeling and biogeochemistry. In: Hein F, Leckie D, Larter S, Suter J (eds) Heavy-oil and oil-sand petroleum systems in Alberta and beyond, vol 64. American Association of Petroleum Geologists, Studies in Geology, p 23–102

Anderson N, Hinds R (1997) Glacial loading and unloading: a possible cause of rock salt dissolution in the Western Canada Basin. Carbonates Evaporites 12:43–52

Anderson N, Knapp R (1993) An overview of some of the large scale mechanisms of salt dissolution in western Canada. Geophysics 58:1375–1387

Anfort S, Bachu S, Bentley L (2001) Regional-scale hydrogeology of the upper devonian sedimentary succession, south-central Alberta basin, Canada. Am Asso Petrol Geol Bull 85:637–660

Bachu S (1995) Synthesis and model of formation-water flow, Alberta basin, Canada. Am Asso Petrol Geol Bull 79:1159–1178

Bachu S (1999) Flow systems in the Alberta basin: patterns, types and driving mechanisms. Bull Can Pet Geol 47:455–474

Bachu S, Underschultz J (1993) Hydrogeology of formation waters, northeastern Alberta. Am Asso Petrol Geol Bull 77:1745–1768

Bachu S, Underschultz J, Hitchon B, Cotterill D (1993) Regional-scale subsurface hydrogeology in northeast Alberta. Alberta Research Council, Alberta Geological Survey, Bulletin, p 61

Berbesi L, De Primio R, Anka Z, Horsfield B, Higley D (2012) Source rock contributions to the lower cretaceous heavy oil accumulations in Alberta: a basin modelling study. Am Asso Pet Geol Bull 96:1211–1234

Broughton PL (1977) Origin of coal basins by salt solution. Nat 270:420–423

Broughton PL (1985) Geology and resources of the Saskatchewan coalfields. In: Patching T (ed) Coal in Canada. Canadian Institute of Mining and Metallurgy, Special vol, pp 87–99

Broughton PL (2013) Devonian salt dissolution-collapse breccia flooring the Cretaceous Athabasca oil sands deposit and development of lower McMurray Formation sinkholes, northern Alberta basin, Western Canada. Sed Geol 283:57–82

Broughton PL (2015) Syndepositional architecture of the northern Athabasca oil sands deposit, northeastern Alberta. Can J Earth Sci 52:21–50

Broughton PL (2016) Alignment of fluvio-tidal bars in the middle McMurray Formation: implications for structural architecture of the Lower Cretaceous Athabasca oil sands deposit, northern Alberta. Can J Earth Sci 52:896–930. doi:10.1139/cjes-2015-0137

Christiansen E (1967) Collapse structures near Saskatoon, Saskatchewan. Can J Earth Sci 4:757–767
Christiansen E, Sauer E (2002) Stratigraphy and structure of Pleistocene collapse in the Regina Low, Saskatchewan, Canada. Can J Earth Sci 39:1411–1423
Closson D (2005) Structural control of sinkholes and subsurface hazards along the Jordanian Dead Sea coast. Environ Geol 270:290–301
Closson D, Abou Karaki N (2009) Salt karst and tectonics: sinkholes development along tension cracks between parallel strike-slip faults, Dead Sea, Jordon. Earth Surf Proc Land 34:1408–1421
Connolly C, Walter L, Baadsgaard H, Longstaffe F (1990) Origin and evolution of formation waters, Alberta Basin, Western Canada Sedimentary Basin: II, Isotope systematic and water mixing. Appl Geochem 5:397–413
DeMille G, Shouldice JR, Nelson H (1964) Collapse structures related to evaporites of the Prairie Formation, Saskatchewan. Geol Soc Am Bull 75:307–316
Ezersky M, Frumkin A (2013) Fault-dissolution front relations and the Dead Sea sinkhole problem. Geomorphology 201:35–44
Flach P, Mossop G (1985) Depositional environments of Lower Cretaceous McMurray Formation, Athabasca oil sands, Alberta. Am Asso Petrol Geol Bull 69:1195–1207
Ford D (1997) Principal features of evaporite karst in Canada. Carbonates Evaporites 12:15–23
Frumkin A, Raz E (2001) Collapse and subsidence associated with salt karstification along the Dead Sea. Carbonates Evaporites 16:117–130
Fuzesy A (1982) Potash in Saskatchewan. Saskatchewan Energy and Mines Report 181
Garven G (1989) A hydrogeological model for the formation of the giant oil sands deposits of the Western Canada Sedimentary Basin. Am J Sci 289:105–166
Garven G, Freeze RA (1984) Theoretical analysis of the role of groundwater flow in the genesis of stratabound ore deposits, 2, quantitative results. Am J Sci 284:1125–1174
Gendzwill D (1978) Winnipegosis mounds and Prairie Evaporite Formation of Saskatchewan—seismic study. In: Estelle D, Miller R (eds) 1978 Williston Basin symposium—economic geology of the Williston Basin. 24th annual conference, Montana Geological Society, pp 121–130
Gibson J, Fennell J, Birks S, Yi Y, Moncur M, Hansen B, Jasechko S (2013) Evidence of discharging saline formation water to the Athabasca River in the oil sands mining region, northern Alberta. Can J Earth Sci 50:1244–1257
Grasby S, Chen Z (2005) Subglacial recharge in the Western Canada Sedimentary Basin—impact of Pleistocene glaciations on basin hydrodynamics. Geol Soc Am Bull 117:500–514
Grobe M (2000) Distribution and thickness of salt within the Devonian Elk point group, Western Canadian Sedimentary Basin. Alberta Energy and Utilities Board, Alberta Geological Survey, Earth Sciences Report 2000–02
Haug K, Chao D, Hein F, Greene P (2009) Mapping surficial features in the Athabasca oil sands area using airborne LIDAR. Abstracts, 2009 Gussow Geoscience Conference Canadian Society of Petroleum Geologists Banff
Haug K, Greene P, Mei S (2014) Geological characterization of the Lower Cretaceous shale in the Athabasca oil sands area, Townships 87–99, Ranges 1–13, West of the Fourth Meridian. Alberta Geological Survey, Open File Report 2014-04
Head I, Jones D, Larter S (2003) Biological activity in the deep subsurface and the origin of heavy oil. Nature 426:344–352
Hein F, Cotterill D, Berhane H (2000) Atlas of lithofacies of the McMurray Formation, Athabasca oil sands deposit, northeastern Alberta: surface and subsurface. Alberta Geological Survey, Earth Science Report 200–07
Hein F, Langenberg C, Kidston C, Berhane H, Berezniuk T (2001) A comprehensive field guide for facies characterization of the Athabasca oil sands, northeast Alberta. Alberta Energy Utilities Board, Special Report, p 13
Hein F, Cotterill D (2006) The Athabasca oil sands—a regional geological perspective, Fort McMurray area, Alberta, Canada. Nat Resour Res 15:85–102
Hein F, Dolby G, Fairgrieve B (2013) A regional geologic framework for the Athabasca oil sands, northeastern Alberta, Canada. In: Hein F, Leckie D, Larter S, Suter J (eds) Heavy-oil and oil-sand petroleum systems in Alberta and Beyond, vol 64. American Association of Petroleum Geologists, Studies in Geology, pp 207–250
Higley D, Lewan M, Roberts L, Henry M (2009) Timing and petroleum sources for the Lower Cretaceous Mannville Group oil sands of northern Alberta based on 4-D modelling. Am Asso Petrol Geol Bull 93:203–230
Holter M (1969) Middle devonian prairie evaporite of Saskatchewan. Saskatchewan Department of Mineral Resources, Report, p 123
Irvine J, Broughton P, Whitaker S (1978) Coal resources of southern Saskatchewan: a model for evaluation methodology. Geological Survey of Canada Economic Geology Report 30, Saskatchewan Department of Mineral Resources Report 209, Saskatchewan Research Council Report 20, vol 1, p 150, microfiche, vol 2, p 78, Atlas, 56 plates
LeFever J, LeFever R (2005) Salts in the Williston Basin North Dakota. North Dakota Geological Survey, Report of Investigations 103
McTavish G, Vigrass L (1987) Salt dissolution and tectonics, south-central Saskatchewan. In: Carlson CG, Christopher JE (eds) Fifth international Williston Basin symposium, vol 9. Saskatchewan Geological Society, Special Publication, pp 157–168
Mahood R, Verhoef M, Stokes F (2012) Paleozoic stratigraphic framework beneath the Muskeg River Mine (Twp 95, Rge 9–10): controls and constraints on present day hydrogeology. Abstracts, Canadian Society of Petroleum Geologists, 2012 GeoConvention, Calgary, Alberta
Meijer Drees N (1994) Devonian Elk point group of the Western Canada Sedimentary Basin. In: Mossop G, Shetsen I (eds) Geological Atlas of the Western Canada Sedimentary Basin. Canadian Society of Petroleum Geologists Alberta Research Council, pp 129–147
Nemeth B, Danyluk T, Prugger A (2002) Benefits of 3D poststack depth migration: case study from the Potash belt of Saskatchewan. Abstracts, 2002 CSEG Geophysics Convention
Parker J (1967) Salt solution and subsidence structures, Wyoming, North Dakota and Montana. Am Asso Petrol Geol Bull 51: 1929–1947
Schneider C, Grobe M (2013) Regional cross-sections of devonian stratigraphy in northeastern Alberta (NTS 74D, E). Alberta Geologic Survey, Open File Report 2013–05
Smith D, Pullen J (1967) Hummingbird structure of southeast Saskatchewan. Bull Can Pet Geol 15:468–482

Orogeny and Hydrothermal Karst: Stratabound Pb–Zn Sulphide Deposition at Pine Point, Northern Canada

40

Paul L. Broughton

Abstract

A large lead–zinc ore body formed along the Presqu'ile barrier reef at the northern margin of the Prairie Evaporite (Middle Devonian) salt basin in northern Canada. An early stage of finely crystalline dolomitization of the Pine Point Formation limestone was patchy. A second dolomitization stage resulted in the coarsely crystalline massive Presqu'ile dolomite. Deep-seated hydrothermal brines flowed eastward up-structure, across a segment of the McDonald basement fault, into the eastern end of the barrier reef complex along earlier multi-km-long karst dissolution trends. These metalliferous hydrothermal brines resulted in 30–50-km-long and 2–3-km-wide Mississippi Valley-type Pb–Zn sulphide trends along the base of the Presqu'ile dolomite. The sulphide mineralization was distributed as tabular stratabound ore pods, 100–250 m-long and 10–20 m-thick, and ovoid vertical bodies up to 60 m, cross-cutting the Presqu'ile dolomite and extending into the overlying beds. Mineralizing thermal fluids directed along earlier karstic dissolution trends filled available porosity, including sediment filled cave sites, or hydrothermal brines extensively expanded the pre-existing dissolution trends by solution-replacement of the surrounding host dolomite, resulting in sulphide deposition where chemical conditions were favourable. Spatiotemporal relationships are uncertain between karstification stages, depths of burial, and distribution of these sulphide ore pods. Early stage near-surface karstification may have occurred as early as Devonian, followed by deeper burial during the late Carboniferous Antler Orogeny. Alternatively, the near-surface karstification was Antler, followed by hydrothermal karstification with deep burial during Middle Jurassic-Early Cretaceous (Columbian) to Late Cretaceous (Laramide) tectonism.

Keywords

Pine Point • Northern Canada • Mississippi Valley-type Pb–Zn sulphide mineralization • Presqu'ile reef • Hydrothermal karstification

1 Introduction

The Pb–Zn sulphide deposit at Pine Point is located at the eastern end of the Middle Devonian Presqu'ile barrier reef, along the south shore of Great Slave Lake in the Northwest Territories, northern Canada (Fig. 1). The 400-km-long barrier reef accumulated along the seaward northern margin of the Prairie Evaporite Formation salt basin of the Elk Point Group. During the Middle Devonian, the barrier reef complex restricted flow into a shallow arm of the Panthallassic Ocean that extended into the Laurentia continental land mass from present day northern Alberta to eastern Montana and western North Dakota. The reef separates Muskeg River Formation anhydrite beds accumulated along the northern Prairie Evaporite salt basin from more seaward carbonate deposits to the north, such as accumulations by the Buffalo River and Windy Point formations (Fig. 2).

P.L. Broughton (✉)
P.O. Box 6976, Station D, Calgary, AB T2P 2G2, Canada
e-mail: broughton@shawcable.com

© Springer International Publishing AG 2017

A. Klimchouk et al. (eds.), *Hypogene Karst Regions and Caves of the World*,
Cave and Karst Systems of the World, DOI 10.1007/978-3-319-53348-3_40

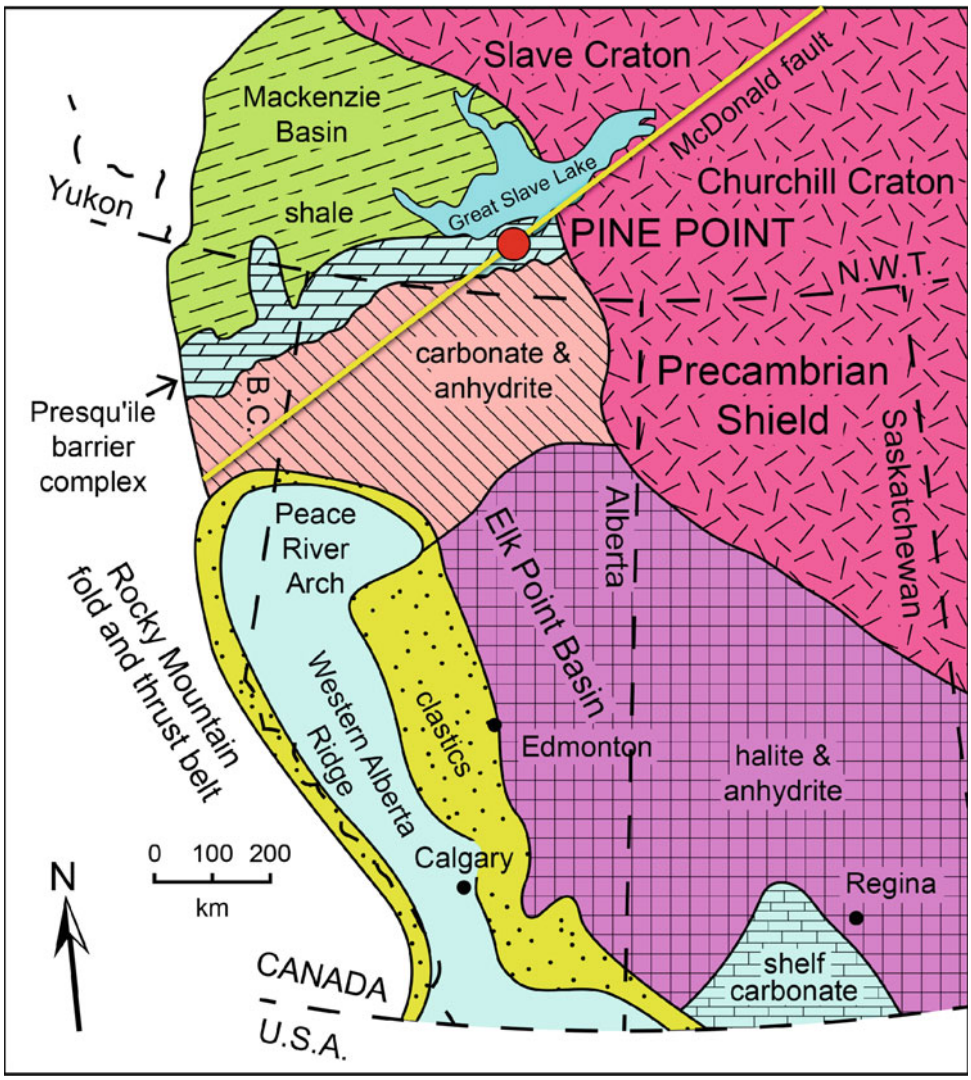

Fig. 1 Location of the Pine Point deposit at the eastern end of the Middle Devonian Presqu'ile barrier reef along the seaward northern margin of the Prairie Evaporite salt basin of the Elk Point Group. The Pb–Zn sulphide deposit overlies a segment of the McDonald fault array and shear zone separating the Churchill and Slave Cratons of the Canadian Shield

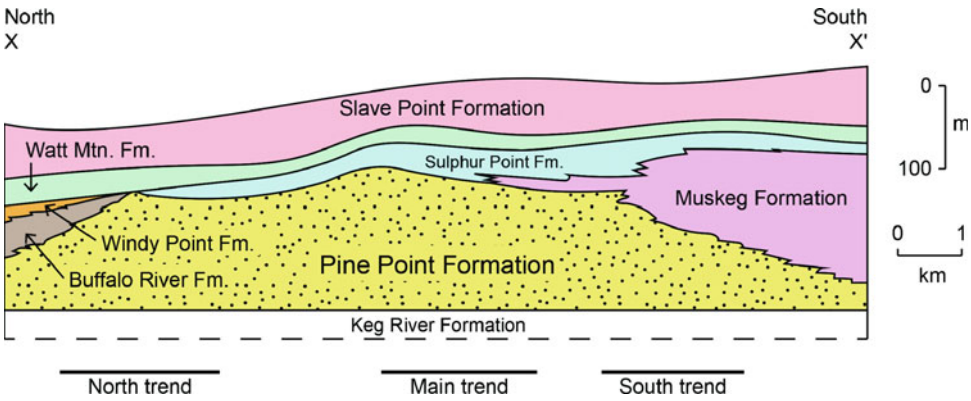

Fig. 2 Middle Devonian stratigraphy of the Presqu'ile barrier reef. Trace located on Fig. 4. Modified after Rhodes et al. (1984) and Giroux and McCartney (2001)

The sulphide deposit was discovered by fur traders in 1898, but because of its remote location, there was no mining activity until the 1960s. From 1964 to 1988, Cominco Ltd. mined 64 million tons of ore averaging 3% lead and 7% Zn. More than 10 million tons of Pb and Zn metal were recovered from nearly 100 ore pods distributed along a 70-km-long and 20-km-wide sulphide mineralized trend (Qing and Mountjoy 1994a, b, c; Giroux and McCartney 2001; Hannigan 2007; Paradis et al. 2007). Most ore bodies contained 100,000 to as much as 18 million tons of sulphide

ore. These ore pods were distributed as sub-horizontal tabular and vertically inclined ovoid bodies, typically 100–200 m-long and 20–40 m to as much as 80 m-thick. The Pine Point deposit with 95 mm tons of ore is larger than other significant Canadian deposits having Mississippi Valley-type emplacements, such as the Nanisivik (6 mm tons of ore) and Polaris (23 mm tons of ore) sites located further to the north.

The source of the lead and zinc at Pine Point resulted from its location at the eastern end of the Presqu'ile barrier reef, overlying a segment of the regional McDonald basement fault array. This fault trend follows the shear zone that separates the Churchill and Slave Cratons of the Precambrian Shield (Fig. 1). The Pb and Zn compounds at Pine Point and other Mississippi Valley-type deposits were probably sourced from geothermal sites within the Precambrian basement. A known thermal anomaly site, located along this shear zone between the Churchill and Slave Cratons, is 300 km down-structure from the Pine Point deposit (Campbell 1966; Hitchon 1993). Hydrothermal brines in contact with such geothermal anomalies in the Precambrian basement became metalliferous, and subsequently flowed along permeable beds into the eastern Presqu'ile barrier reef (Fritz 1969; Fritz and Frape 1982; Krebs and Macqueen 1984).

Mississippi Valley-type Pb–Zn sulphide deposits are stratiform and typically lack evidence of cross-cutting igneous intrusions as sources for metalliferous fluids. Prior to about 1990, these type of ore deposits were interpreted as having a low temperature origin resulting from shallow aquifer flows into buried karsts. However, it has been since observed in several major deposits, including Pine Point that the sulphide mineralized zones cross-cut palaeokarst surfaces. The ore deposits were associated with late stage thermal dolomitization formed at a higher range of temperatures, resulting in mineralization trends unlike the constrained geometrics associated with meteoric karst. It is now accepted that sulphide mineralization at Pine Point and other large scale Mississippi Valley-type deposits followed deep burials of previously formed near-surface karstic terrains. Furthermore, these deposits are now interpreted as having resulted from continental scale tectonism, such as orogenic events impacting North America and Europe during the Late Devonian-Permian and Cretaceous-Paleogene periods (Leach et al. 2001). Over 70% of the commercially attractive Mississippi Valley-type ore deposits worldwide formed during the Late Palaeozoic continental collisions that culminated in Pangea. The other deposits having this type of mineralization resulted from the breakup of this supercontinent during Late Cretaceous-Paleogene Laramide orogeny in North America, Alpine tectonism in Europe and elsewhere in Africa and Asia.

Karstification of the barrier reef carbonate trend resulted in stratabound dissolution trends at the level of the sub-horizontal contact between the limestone and dolostone beds of the Pine Point Formation with the overlying massive Presqu'ile dolomite. The dissolution trends may have resulted in connectivity to some extent between more cavernous areas, the origin of which has been suggested by the apparent distribution of tabular ore pods interpreted as dolomitized and mineralized cave filling sediment. Early researchers, including the Pine Point mine geologists, interpreted pervasive laminated textures of the sulphide mineralization as evidence for hydrothermally altered stratified cave sediment (Rhodes et al. 1984). Although the ore zones have cave-like pod shapes collinearly aligned as having been formed along karstic dissolution trends, they are not interconnected. Some mineralized zones have vertical orientations, often associated with collapse breccia. An alternative interpretation suggests that metalliferous thermal brines followed the earlier formed karstic dissolution trends, but largely replaced the surrounding dolomite host rock by hydrothermal solution-replacement processes. This hydrothermal karstification resulted in detached ore pods having a distribution pattern with similarity to the older karstic dissolution trends, subsequently deeply buried. This alternative model suggests that stratiform deposits, such as saddle dolomite layers interbedded with sheet-like layers of sulphide minerals, do not represent replacements of stratified cave filling sediment. These laminated and banded deposits resulted from solution-replacement backfilling precipitations as the hydrothermal alteration front advanced into the micro-fractured wall rock, beyond the earlier formed but narrower dissolution trends (Qing and Mountjoy 1990, 1992, 1994a, b; Qing 1998).

2 Stratigraphic and Structural Setting

The Presqu'ile barrier reef accumulated as a Middle Devonian (Givetian) bioclastic carbonate shoal along the seaward northern margin of the Prairie Evaporite, Elk Point Group, salt basin (Figs. 1 and 2). The Pine Point deposit is located at the eastern end of this reef trend (Figs. 2 and 3). The lower interval, represented by the Pine Point Formation strata (>175 m), consists of reef and non-reef sub-tidal packstone and floatstone facies. The Pine Point limestone passes southward into anhydrite dominated beds of the Muskeg Formation, accumulated along the northern margin of the evaporite basin. The overlying Sulphur Point limestone beds (>65 m) were altered by disseminated finely crystalline dolomite spar. A more pervasive coarsely crystalline massive dolomite replaced most of the Sulphur Point beds along the upper reaches of the barrier reef, including some of the uppermost Pine Point Formation beds (Qing 1998). This massive dolomite trend is recognized as the Presqu'ile dolomite. The northern margin of the barrier reef was

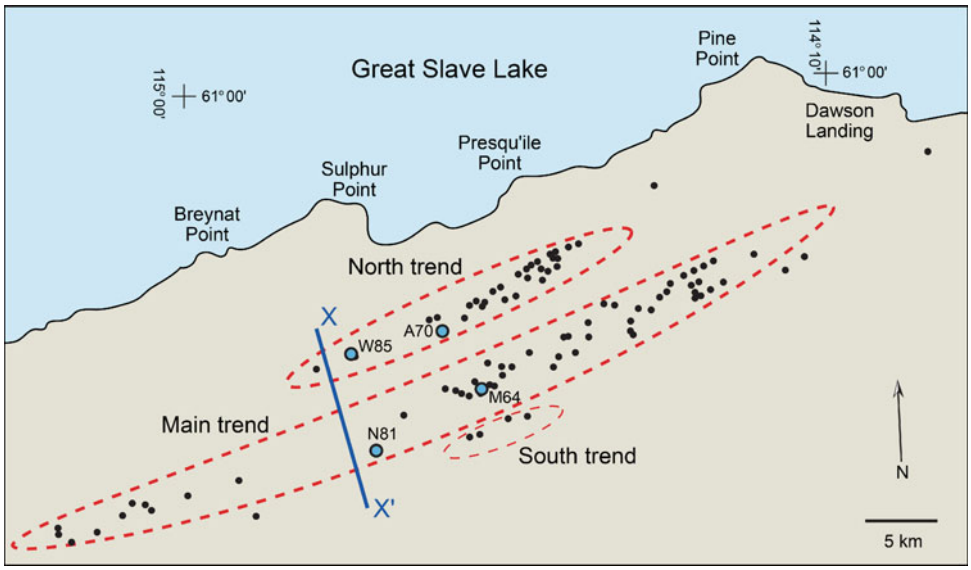

Fig. 3 Distribution of the Pine Point Pb–Zn sulphide ore bodies along the Main and North trends at the eastern end of the Presqu'ile barrier reef, located along the south shore of the Great Slave Lake. The trace of the section X–X′, illustrated by Fig. 2, is located. Locations are provided for ore bodies designated as W85, N81, A70 and M64, illustrated by Figs. 3 and 7. Modified after Weyer (1983) and Giroux and McCartney (2001)

onlapped by strata of the Buffalo River and Windy Point Formations (Fig. 2). The Sulphur Point strata were partially eroded, resulting from a sea-level drop. This unconformity separates the barrier complex from the overlying 10–30-m-thick Watt Mountain strata (Meijer Drees 1988).

The eastern end of the Presqu'ile dolomite overlies a segment of the McDonald basement fault system, which extends along the eastern Great Slave Lake shear zone and separates the Churchill and Slave Cratons of the Canadian Shield (Fig. 1). Geothermal sites along this basement fault array probably sourced Pb and Zn compounds into the hydrothermal brines that flowed eastward into the Presqu'ile dolomite trend, resulting in sulphide mineralization (Skall 1975; Krebs and Macqueen 1984; Gromek et al. 2012). The hydrothermal brines flowed along structural pathways at the eastern end of the reef trend, resulting from aligned fault block patterns responding to incremental movements along the McDonald fault array. These structural adjustments, concurrent with carbonate deposition and during shallow burial, also impacted the karstic dissolution patterns resulting in paralleling near-linear trends within the reef complex. As a result, two major and several minor sulphide mineralization trends developed at Pine Point (Fig. 3).

3 Dolomitization Along the Presqu'ile Barrier Reef

The underlying Pine Point limestone beds were only partially dolomitized in contrast to the overlying Sulphur Point strata, which resulted in the massive Presqu'ile dolomite. Early stage partial dolomitization of the limestone beds accompanied by dissemination of pyrite and marcasite partially filled available porosity. Second stage dolomitization followed deep burial. A stage of coarsely crystalline dolomite replaced the upper interval of the reef trend consisting of the Sulphur Point Formation beds, resulting in the massive Presqu'ile dolomite. This late stage dolomitization occurred during sulphide mineralization at sites in the previously formed massive dolomite, resulting in thermal saddle dolomite (Fig. 4). It is uncertain as to why the underlying Pine Point beds remained unaltered or hosted only finely disseminated dolomite spar. Skall (1975) and Krebs and Macqueen (1984) suggest that early flows of warm ascending deep-seated hypogene brines altered the carbonates of the barrier complex below the more or less impermeable beds of the overlying Watt Mountain Formation. This constrained the thickness of the altered interval, resulting in a stratabound coarsely crystalline dolomite. It also explains why zones of coarsely crystalline dolomitization extend locally downward into uppermost intervals of the underlying Pine Point beds (Fig. 5).

It is uncertain as to when sufficient burial depths were achieved resulting in formation of the massive Presqu'ile dolomite, and deep-seated hydrothermal processes resulting in saddle dolomite. Saddle dolomite, a crystal habit form characterized by curved crystal faces, is a geothermometer used to indicate the temperature range of hydrothermal brines at the time of mineral precipitation. Saddle dolomite at Pine Point occurred within the temperature range of 92–178 °C in brines having salinities of 11–29% NaCl (Qing and Mountjoy 1994a, b, c). Similarly, fluid inclusion studies in sphalerite crystals suggest brine temperatures in a range of 50–100 °C (Roedder 1967, 1968). These elevated temperatures, necessary for Pb–Zn sulphide mineralization, cannot be achieved by geothermal gradients resulting from deep basin burial of formation fluids without the exposure to hydrothermal flows. For example, a maximum burial depth

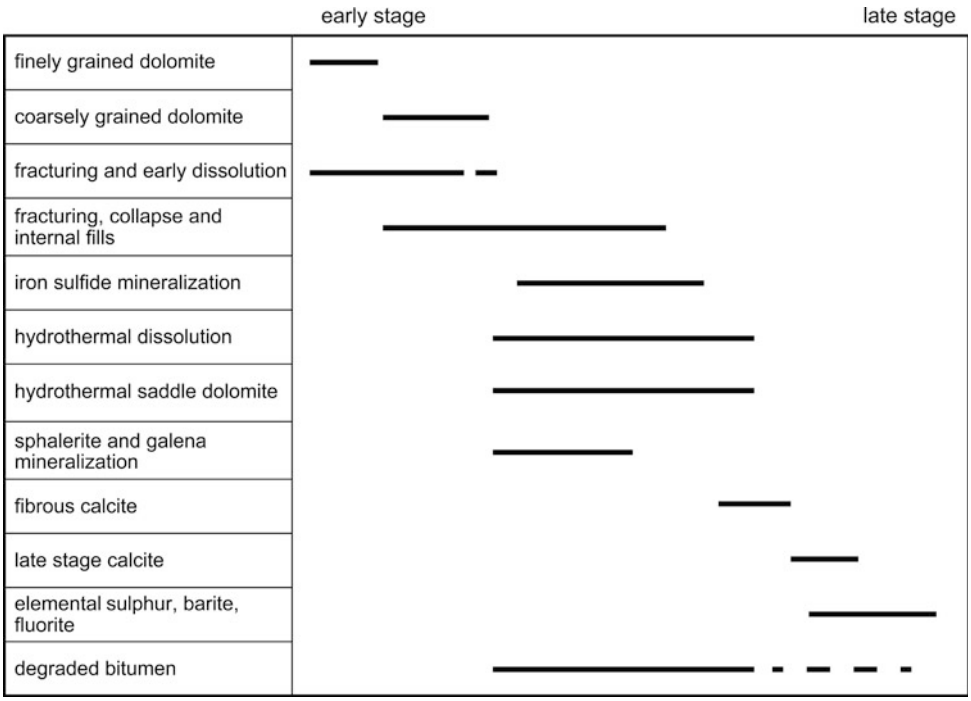

Fig. 4 Paragenesis model for mineralization at Pine Point. Generalized after Krebs and Macqueen (1984) and Qing and Mountjoy (1994a, b, c)

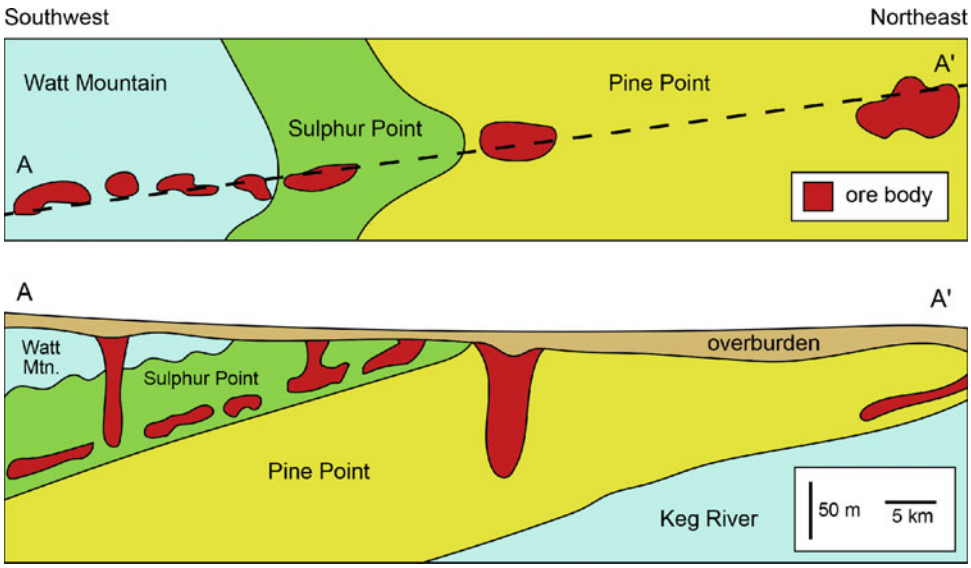

Fig. 5 Schematic distribution of tabular stratabound and vertically oriented ovoid Pb–Zn sulphide ore bodies. Modified after Rhodes et al. (1984) and Giroux and McCartney (2001)

of 1500 m has been calculated for Mississippian-age strata at Pine Point by Krebs and Macqueen (1984). A geothermal gradient of 30º/km of burial by the Presqu'ile barrier reef would result in the brine having a temperature of 60 °C, insufficient for precipitation of saddle dolomite and sphalerite. Formation of saddle dolomite necessitates temperature and salinity conditions to be in the range of 90–100 °C or higher, possible with hydrothermal fluids sourced along the McDonald fault.

Early stage dolomitization, resulting in widely disseminated finely crystalline spar, may have occurred during relatively shallow burial. In contrast, the massive coarsely crystalline dolomitization was probably during a later stage of the same burial cycle associated with the Antler orogeny, which extended from the Late Devonian into the Early Carboniferous. Alternatively, the early stage finely disseminated spar responded to shallow burial during the Antler orogeny, but the massive coarsely crystalline Presqu'ile dolomite occurred considerably later, during deep burial associated with Jurassic-Cretaceous Columbian orogeny, prior to late stage invasion by metalliferous hydrothermal flows during Laramide tectonism (Qing and Mountjoy 1990, 1994a, b, c).

4 Stratabound Mineralization

Massive sulphide mineralization followed coarsely crystalline dolomitization upon deep burial of the earlier formed karstic dissolution trends resulting from near-surface aquifer flows into the reef complex. Pathways for metalliferous hydrothermal fluids were directed along the underside of the Presqu'ile dolomite at the level approximated by the contact between the Pine Point and overlying Sulphur Point formations (Qing and Mountjoy 1994a, b, c). These stratabound ore pods are mapped as the 50 km-long Main trend and the parallel 30-km-long North trend (Fig. 3). The 3-km-wide Main trend has 3 sinuous channel-like trends, in contrast to the 2-km-wide North trend with 4 channel-like trends. A cluster of ore bodies was also uncovered south of the Main trend (Fig. 3). Larger ore bodies distributed along the Main trend often have higher grade zones with up to 12% combined lead and zinc. Only a few similarly rich ore bodies were discovered along the North trend.

The ore bodies are shape classified as either sub-horizontal tabular stratabound deposits or vertically oriented ovoid pods (Fig. 5). The distribution of the numerous, but detached, ore pods consists of mostly sub-horizontal stratabound tabular ore bodies up to 250 m-long and 10–20 m-high (Lajoie and Klein 1979; Rhodes et al. 1984). An example of a tabular stratabound mineralized zone is the N81 ore pod (Fig. 6a). The distribution of stratabound tabular ore pods is interspersed with vertically oriented ovoid- or lenticular-shaped ore bodies that extend upward, or downward, from the same level at the base of the Presqu'ile dolomite (Kyle 1981; Krebs and Macqueen 1984; Rhodes et al. 1984). Vertical mineralized zones are up to 250 m-long, 20–30 m-wide and up to 50–60 m-high. The vertical ore pods extend upward from the level of the tabular stratabound deposits, but are not necessarily connected to any (Figs. 5 and 6). They cross-cut the overlying Presqu'ile dolomite and often extend into the overlying Watt Mountain and Sulphur Point strata. Also, a few vertical deposits extend downward into underlying Pine Point Formation. Examples of vertically oriented sulphide mineralized deposits are illustrated by the W85 and A70 ore pods (Fig. 6b). The M64 ore pod is a stratabound tabular deposit with some vertical emplacement attributes (Fig. 7). It is a 43–48 m-high and 27-m-wide-lenticular-shaped zone of massive sulphide mineralization.

The vertically oriented ovoid-shaped mineralized zones resulted from metalliferous thermal brines following permeable pathways within high domed zones of fractured rock or collapses resulting in breccia pipes (Rhodes et al. 1984). These high domed ore pods often have a well-developed breccia, resulting in a concave-upward generalized structure characterized by bed sags and radially dispersed fractures in the surrounding wall rock (Fig. 3b). A meshwork of crackle breccia often extended upward and outward from vertically oriented ore pods. Some collapse breccia includes clasts derived from the overlying Watt Mountain and Slave Point formations, suggesting 10s of metre collapses. The uppermost levels in some breccia pipes include clasts of Pleistocene till incorporated into the mineralized breccia fabrics (Weyer 1983). This suggests an extended interval, perhaps intermittent, of mineralizing fluid circulation lasting into the Quaternary (Rhodes et al. 1984).

Karstification of the Middle Devonian barrier reef resulted in dissolution trends and collapse breccia that provided pathways for dolomitizing and subsequently metalliferous thermal brines (Haynes and Kesler 1987; Sangster 1988; Hannigan 2007; Paradis et al. 2007). The extent to which interconnectivity along these near-linear dissolution channels, and formation of cavernous voids if any, impacted the distribution of mineralized zones is controversial. Earlier interpretations, mostly by geologists associated with the mining activity, suggested that the distribution of ore pods coincided with the stratabound dissolution channels, particularly cavernous chambers plugged by sediment, and breccia pipes. This model interprets the shapes of sulphide ore pods as replications of earlier formed porous zones distributed along these karstic dissolution features.

The lack of continuity between the ore pods may have resulted from sulphide mineralization concentrated at zones having relict porosity following dolomitization along the earlier formed karstic dissolution trends, such as within sediment fills of caves. Evidence for the development of large 10s of metre across cave-like dissolution sites has been suggested by shapes of the ore pods, and by the apparently pervasive cave fill sediment, subsequently mineralized. The M64 ore body was interpreted by Rhodes et al. (1984) as an important example of sulphide mineralization of stratified cave fill sediment that plugged a cavernous site (Fig. 7), formed within uppermost Pine Point beds and the overlying Presqu'ile dolomite. The central zone of this sulphide mineralized cave fill was impacted by a collapse breccia, subsequently mineralized. Rhodes et al. (1984), Giroux and McCartney (2001) and others have also interpreted the apparently extensive distribution of early karstification stage cave fills, mostly consisting of green shale. The now-altered green shale accumulations were interpreted as surface detritus transported into the shallow karstic cave system, probably during the Devonian (Rhodes et al. 1984). However, these green shales have been sufficiently altered by dolomitization and hydrothermal processes that their origin as cave fill cannot be confirmed. Any direct evidence for the existence of caves such as walls with speleothems has been obliterated by the dolomitization and thermal alteration during sulphide mineralization.

Alternatively, hydrothermal processes resulted in solution replacement of the host dolomite. The sulphide

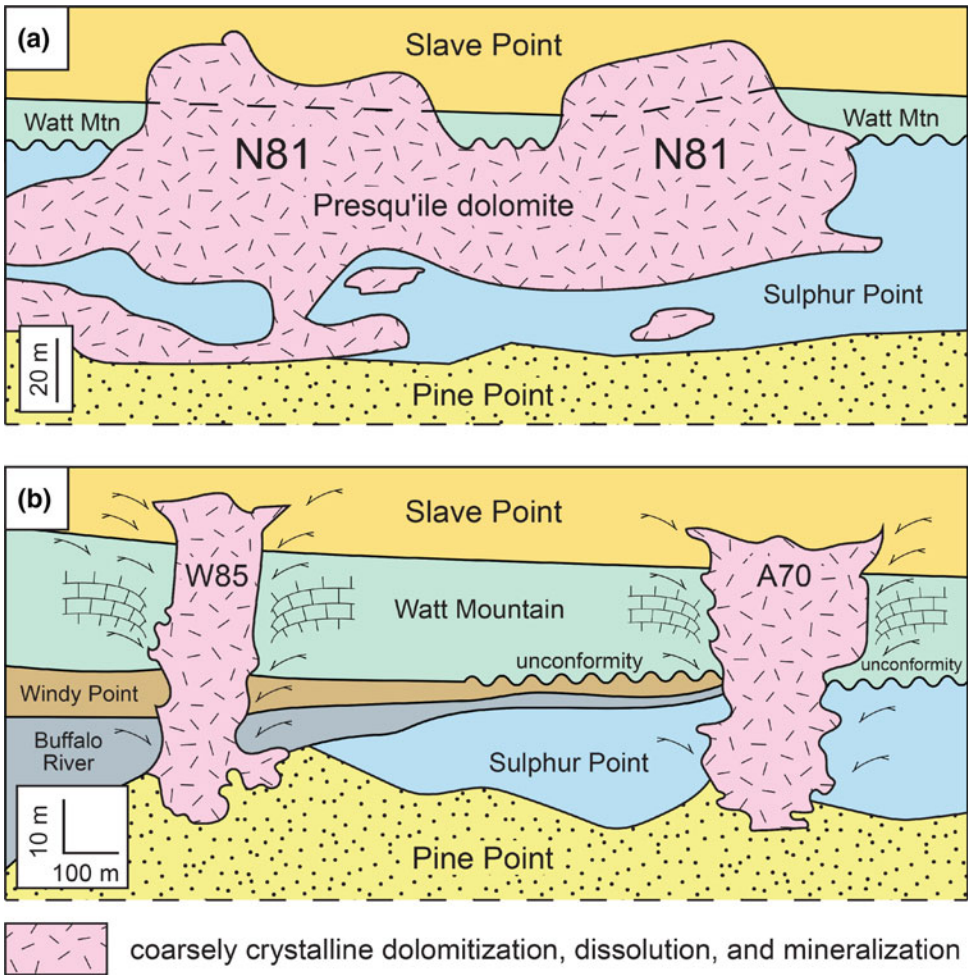

Fig. 6 Coarsely crystalline dolomitization that altered the Presqu'ile reef includes tabular sub-horizontal stratabound and ovoid vertical zones that host massive sulphide ore bodies: **a** example of the N81 ore pod illustrating stratabound sulphide mineralization along the base of the massive Presqu'ile dolomite interval of the Sulphur Point Formation. The massive dolomite host rock with Pb–Zn sulphide mineralization also cross-cuts the overlying Watt Mountain and Slave Point beds; **b** illustration of the W85 and A70 ore pods consisting of vertically oriented Presqu'ile dolomite zones with sulphide mineralization extending upward from the Sulphur Point stratigraphic level into the overlying Watt Mountain and Slave Point strata. Dissolution along the base of the massive dolomite often triggered breccia pipes, resulting in adjacent sagged beds and fracture patterns. Breccia collapses and associated fracture patterns provided pathways for sulphide mineralizing thermal brines to ascend into the overlying Watt Mountain and Slave Point beds. These ore bodies are located on Fig. 4. Modified after Rhodes et al. (1984) and Qing and Mountjoy (1994c)

mineralization resulted at sites where the chemical conditions for precipitation were favourable. The hydrothermal karstification process followed the earlier formed dissolution trends, but was not confined to these pathways. The early stage karstic dissolution network was not as well developed as otherwise interpreted, and may have lacked any voluminous tabular shaped cavernous chambers that supposedly were plugged by stratified cave sediment and subsequently permeated by sulphide mineralizing thermal brines. Nevertheless, the karst dissolution network was sufficiently developed that upon deep burial, the metalliferous thermal fluids were channelled along the more constrained dimensionality of earlier karstic conduits, but greatly enlarged these dissolution trends by hydrothermal solution replacement of the encasing dolomite host rock. This alternative model suggests that the pervasive laminated textures associated with the sulphide deposits were not mineralized thermal alterations of stratified cave sediment. The apparent stratification resulted from waves of solution-replacement backfilling precipitations by sulphide layers as the hydrothermal fluids progressed into the host dolomite rock at sites permeated by fracture networks. Dżulyński and

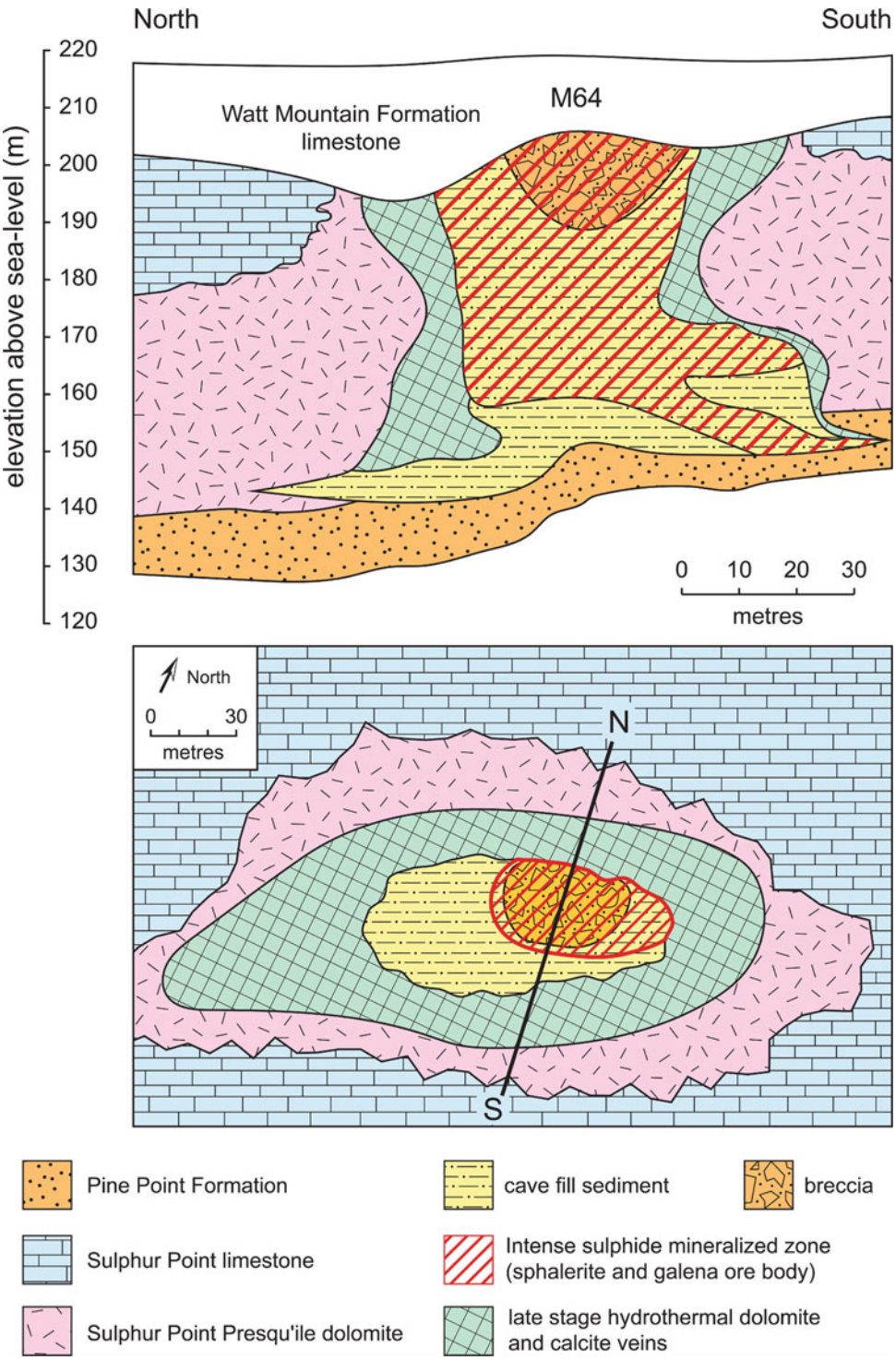

Fig. 7 M64 Pb–Zn ore pod within the Presqu'ile dolomite, 43–48 m-high and 27 m-wide, combines tabular stratabound and vertically oriented breccia pipe attributes: **a** profile of the sulphide ore pod, interpreted by Rhodes et al. (1984) as mineralized stratified cave-fill sediment, and mineralization along fractures resulting from breccia collapse; **b** subcrop map illustrating concentric mineralized zones consisting of an inner core of sulphide permeated collapse breccia derived from fragmented Sulphur Point and lesser amounts of Watt Mountain beds. The sphalerite-galena mineralized zone passes outward into massive coarsely crystalline dolomite altered by thermal saddle dolomite and late stage calcite. Site of the M64 ore body is located on Fig. 4. Modified after Rhodes et al. (1984)

Sass-Gustkiewicz (1989) interpretation of Pb–Zn deposits in Silesia recognized similar types of dissolution concurrent with Pb–Zn sulphide precipitations as hydrothermal karst.

5 Sulphide Mineralization and Paragenetic Sequencing

The sulphide mineral assemblage at Pine Point is similar to other Mississippi Valley-type deposits, consisting mostly of galena (PbS), sphalerite (ZnS), and marcasite and pyrite (FeS_2). The Pine Point mineral assemblage almost entirely consists of very finely crystalline deposits with a distinct paragenetic sequencing. The Pine Point deposit has a generally recognized sequencing initiated with iron sulphide, mostly pyrite and marcasite, followed by lead and zinc sulphides with concurrent to late stage thermal dolomite (saddle dolomite) and calcite spar (Figs. 5 and 8). This is consistent with other major Mississippi Valley-type deposits worldwide.

These Mississippi Valley-type sulphide deposits resulted from thermal brines that migrated from deeper areas of sedimentary basins toward and onto adjacent carbonate platforms (Anderson 1975; Arne 1991; Carrière and Sangster 1999). However, the chemistries of these fluids and the role of sulphate reduction resulting in precipitations of lead and zinc sulphides are uncertain. Some models suggest that these base metal ions or compounds were transported in metal-rich hydrothermal fluids with low sulphate content that mixed with hydrogen sulphide at deposition sites to trigger precipitations with shifts in the brine pH (Sverjensky 1984, 1986). A variation on this model suggests that the Pb

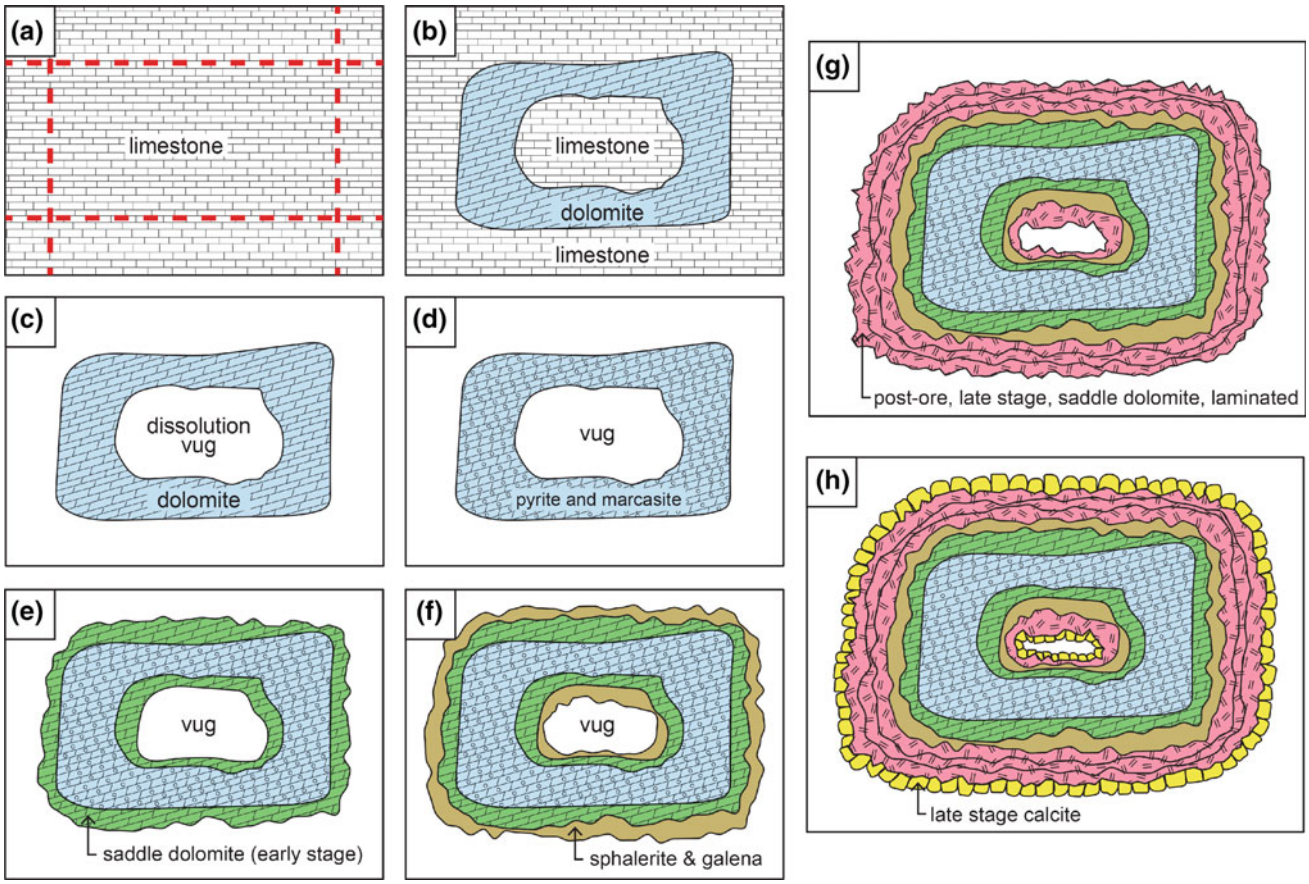

Fig. 8 Paragenesis along the Presqu'ile barrier reef at Pine Point: **a** and **b** limestone and finely crystalline dolostone beds were fragmented by cross-hatch fracture patterns, providing pathways for fluids that altered the host rock into a coarsely crystalline dolomite. Envelopes of coarsely crystalline dolomite formed along the margins of the limestone fragments, retaining unaltered central areas of limestone; **c** and **d** dissolution of the limestone cores resulted in dolomite crust lined voids with pyrite and marcasite intergrowths; **e** invading hydrothermal fluids resulted in layers of saddle dolomite that encased the previously formed dolomite layers. The resulting crusts further lined remaining voids, concurrent with early stage sphalerite precipitation; **f** hydrothermal sulphide deposits dominated by sphalerite and galena; **g** laminated deposits of dolomite and saddle dolomite; **h** late stage calcite filled most of the remaining porosity and covered layers of saddle dolomite and earlier sulphide mineralized zones. Modified after Krebs and Macqueen (1984)

and Zn were transported together with reduced sulphur in the brine, and precipitation resulted upon cooling. Alternatively, precipitations may have occurred when sulphate in solution was reduced upon contact with organic matter or hydrocarbons. The presence of organic fracture fills, mostly tar-like bitumen, supports this interpretation. The collinear distribution of individual mineralized sites at Pine Point, trending along karstic dissolution patterns, may have resulted from chemical sensitivity at favourable precipitation sites.

The finely crystalline dolomitization stage was followed by coarsely crystalline replacement resulting from fluid flows along fracture networks in the carbonate beds (Fig. 8 a). Incipient dolomitization occurred along the margins of limestone fragments, forming a dolomitic envelope with an unaltered limestone core (Fig. 8b). Early dissolution of the limestone core resulted in vug porosity lined by dolomite with pyrite and marcasite intergrowths (Fig. 8c, d). Kyle (1981) observed that the early stage marcasite and pyrite mineralization resulted in halo-like zones that were subsequently filled by massive aggregates of Pb and Zn sulphides. Layers of coarsely crystalline thermal saddle dolomite precipitated as crusts that further lined the voids (Fig. 8e), often concurrent with early precipitation of sphalerite and galena. Widespread sphalerite and galena mineralization followed (Fig. 8f). The sphalerite deposits often had botryoidal or banded textures layered over finely crystalline dolomite and iron sulphide deposits (Fig. 8f, g). Galena co-precipitated with the sphalerite at Pine Point, but larger galena crystals formed after deposition of banded sphalerite (Kyle 1981). Alternating precipitations of dolomite and saddle dolomite partially filled most of the remaining fracture and vug porosities (Fig. 8g). Late stage calcite veins encased laminated deposits consisting of saddle dolomite and sphalerite-galena. The calcite filled most remaining porosity within the Pb–Zn sulphide deposit and outward into the nearby host wall rock (Fig. 8h). Thermal degradation of oil seeps into the reef trend resulted in tar-like bitumen residues (Fig. 5), and pyro-bitumen flakes along fractures (Macqueen and Powell 1983). The contact between the sulphide body and the dolomite host rock is invariably abrupt, although late stage calcite often extends outward into the host rock without any sulphide mineralization.

6 Tectonic Controls on Hydrothermal Karstification and Sulphide Mineralization

The origin of the Mississippi Valley-type massive sulphide deposit at Pine Point, and elsewhere, has been widely accepted as an emplacement superimposed on a previously formed karstic dissolution network. These sulphide zones often cross-cut palaeokarst features, resulting in conflicting interpretations regarding the relative contributions on their distribution between the earlier near-surface karst resulting from shallow aquifers charged by meteoric waters, and subsequent deep burial resulting in deep-seated mineralizing hydrothermal brines that reconfigured the earlier karst system. Current karstification models suggest that continental scale tectonism controlled how these shallow meteoric and hypogene processes combined to alter the previously formed karstic dissolution patterns and controlled the distribution of massive lead and zinc sulphide deposits (Garven and Freeze 1984; Garven 1986; Adams et al. 2000; Leach et al. 2001).

The Presqu'ile barrier reef was an effective permeability pathway at a regional scale positioned along anhydrite beds accumulated at the northern end of the Prairie Evaporite salt basin. This permitted dolomitizing fluids followed by metalliferous hydrothermal brines to flow eastward from deeper areas of the Alberta foreland basin into the reef along the previously formed karstic dissolution trends. These karstification stages were tectono-stratigraphic responses to Late Devonian-Carboniferous (Antler) or alternatively Middle Jurassic-Late Cretaceous (Columbian and Laramide) orogenies.

The Antler orogeny model proposes that cycles of shallow burial and near-surface emergence of the Middle Devonian barrier reef during Late Devonian resulted in parallel dissolution trends by circulation of meteoric groundwaters as shallow aquifers (Kyle 1981; Krebs and Macqueen 1984). A major stage of karstification occurred when the barrier reef was partially emergent near the end of Sulphur Point deposition, prior to the erosional surface topography being covered over by Watt Mountain beds. Deeper burial by the Late Carboniferous resulted in metalliferous hydrothermal brine flows along these previously formed dissolution trends aligned along the base of the Presqu'ile dolomite. Techniques used to determine the age of the sulphide mineralization at Pine Point, such lead isotope studies and Rb–Sr isochron of sphalerite data, have yielded Antler related ages (Cumming et al. 1990; Nakai et al. 1993). The resulting stratabound sulphide ore bodies resulted from increased regional tectonism during the early Pennsylvanian to Permian periods (Krebs and Macqueen 1984).

The alternative Laramide orogeny model interprets the sulphide deposits as resulting from hydrothermal solution-replacement karstification processes that were only partially related to mineralization along pre-existing karstic dissolution trends. Accordingly, the near-surface dissolution channels formed during Antler tectonism were markedly less developed prior to deep burial than previously interpreted. Deep-seated aquifers of the Alberta foreland basin, including metalliferous hydrothermal brines, flowed into the Presqu'ile reef trend along these pre-existing dissolution trends after deep burial (Fig. 9). The hydrothermal drive provided by the hydraulic head induced by the Laramide mountainous terrains to the west permitted saline formation fluids and

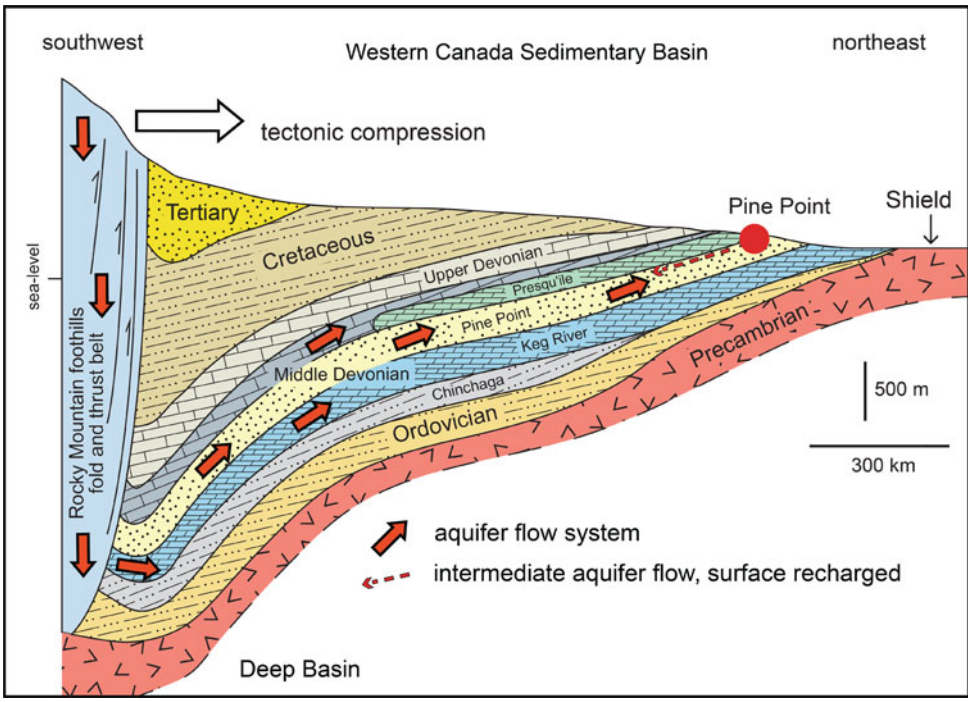

Fig. 9 Laramide tectonism resulting in the elevated terrains of the Alberta foreland basin to the west of the Pine Point deposit. The resulting hydraulic head enhanced the deep-seated aquifer water flows, including metalliferous hydrothermal flows across the McDonald basement fault and into the Pine Point area and along the Middle Devonian Presqu'ile barrier reef. Modified from Garven and Freeze (1984) and Garven (1985)

hydrothermal brines to flow 100s of kilometres to the east, across the McDonald basement fault and into lower topographic areas such as the barrier reef (Garven 1985). Sedimentary loading in the deepening basin also enhanced the flow of these brines laterally and up-structure into the Presqu'ile dolomite trend (Nesbitt and Muehlenbachs 1994; Nelson et al. 2002). Late Cretaceous mineralization is suggested by palaeomagnetism data (Symons et al. 1993), ratios of Sr isotopes (Qing and Mountjoy 1992) and apatite fission-track analysis (Arne 1991). This hypogene hydrothermal karst model, proposed by Garven and Freeze (1984) and Garven (1985), for the Pine Point deposit has been applied to the mid-continent of the USA by Bethke and Marshak (1990).

7 Conclusions

The Mississippi Valley-type sulphide deposit at Pine Point resulted in the largest and most commercially attractive lead–zinc ore accumulation in Canada having this style of stratabound mineralization. A two-stage karstification controlled the distribution pattern of the sulphide ore zones. The earlier karstification occurred during cycles of shallow burial and emergence by the barrier reef during the early phases of the Antler orogeny. Following deep burial during the Carboniferous period of the late Antler orogeny, brine flows along these pre-existing dissolution trends resulted in the coarsely crystalline Presqu'ile dolomite. The dolomitization replaced the Sulphur Point limestone beds and extended upward into areas of the overlying Watt Mountain and Slave Point beds. Metalliferous hydrothermal brine flows into the eastern end of the Presqu'ile dolomite, accumulated at the seaward northern end of the Middle Devonian Prairie Evaporite salt basin, were partially controlled by these previously formed dissolution trends along the base of the massive dolomite.

The emplacement of these Mississippi Valley-type sulphide deposits may have occurred towards the end of the Antler orogeny, or alternatively during deep burial resulting from Cretaceous Laramide tectonism. The distribution of sulphide ore bodies were collinearly aligned along several karstic dissolution trends, stratabound along the base of the massive coarsely crystalline dolomite. The mineralization pattern was not continuous and the sulphide mineralization sites were detached from each other. This may have resulted from the distribution pattern of sediment filled caves developed within the massive dolomite, providing permeable pathways for the metalliferous hydrothermal brines. Bed sags and collapses into underlying cavernous sites resulted in breccia pipes in the dolomitized Sulphur Point that often extended upward into the overlying Watt Mountain and Slave Point beds. These karstic dissolution trends and dolomitization patterns resulted in tabular stratabound and vertical shaped ore pods that may have replicated the shapes of earlier, but now obliterated, cavernous dissolution features. Alternatively, sulphide mineralization patterns were controlled by hydrothermal karst processes resulting in laminated sulphide deposits during solution replacement of the wall rock, and not necessarily replacements of stratified cave fill.

References

Adams JJ, Rostron BJ, Mendoza CA (2000) Evidence for two-fluid mixing at Pine Point, NW Territories. J Geochem Explor 69:103–108

Anderson GM (1975) Precipitation of Mississippi Valley–type ores. Econ Geol 70:937–942

Arne DC (1991) Regional thermal history of the Pine Point area, Northwest Territories, Canada, from apatite fission-track analysis. Econ Geol 86:428–435

Bethke CM, Marshak S (1990) Brine migration across North America —the plate tectonics of groundwater. Annu Rev Earth Planet Sci Lett 18:287–315

Campbell N (1966) The lead-zinc deposits of Pine Point. Canadian Mining and Metallurgical Bulletin 59:953–960

Carrière JJ, Sangster DF (1999) A multidisciplinary study of carbonate-hosted zinc-lead mineralization in the MacKenzie Platform (a.k.a. Blackwater and Lac de Bois platforms) Yukon and Northwest Territories, Canada. Geological Survey of Canada, Open File Report 3700, p 145

Cumming G, Kyle J, Sangster D (1990) Pine Point: a case history of lead isotope homogeneity in a mississippi valley-type district. Econ Geol 85:133–144

Dżulyński S, Sass-Gustkiewicz M (1989) Pb–Zn ores. In: Bosák P (ed) Paleokarst a systematic and regional review. Academia, Praha, pp 377–397

Fritz P (1969) Oxygen and carbon isotopic composition of carbonates from the Pine Point lead-zinc ore deposits. Econ Geol 64:733–742

Fritz P, Frape SK (1982) Saline waters in the Canadian Shield—a first overview. Chem Geol 36:179–190

Garven G (1985) The role of regional fluid flow in the genesis of the Pine Pont deposit, Western Canada sedimentary basin. Econ Geol 80:307–324

Garven G (1986) The role of regional fluid flow in the genesis of the Pine Point deposit—a reply. Econ Geol 81:1015–1020

Garven G, Freeze RA (1984) Theoretical analysis of the role of groundwater flow in the genesis of stratabound ore deposits, 2, Quantitative results. Am J Sci 284:1125–1174

Giroux GH, McCartney I (2001) Report on the Great Slave reef lead-zinc deposits, Pine Point, N.W.T., for Tamerlane Ventures, Inc. Giroux Consultants Ltd., p 39

Gromek P, Gleeson SA, Simonetti A (2012) A basement-interacted fluid in the N81 deposit, Pine Point Pb–Zn District, Canada: Sr isotopic analyses of single dolomite crystals. Miner Deposita 47:749–754

Hannigan P (2007) Metallogeny of the Pine Point Mississippi Valley-Types zinc-lead district, Southern Northwest Territories. In: Goodfellow WD (ed) Mineral deposits of Canada: a synthesis of major deposit-types, district Metallogeny, the Evolution of Geological Provinces, and Exploration Methods. Special Publication 5, Geological Association of Canada, Mineral Deposits Division, pp 609–632

Haynes FM, Kesler SE (1987) Chemical evolution of brines during Mississippi Valley-type mineralization: evidence from East Tennessee and Pine Point. Econ Geol 82:53–71

Hitchon B (1993) Geochemistry of formation water, northern Alberta, Canada: their relation to the Pine Point ore deposit. Alberta Geological Survey, Open File Report 1993–14, p 93

Krebs W, Macqueen R (1984) Sequence of diagenetic and mineralization events, Pine Point lead-zinc property, Northwest Territories, Canada. Bull Can Pet Geol 32:434–644

Kyle JR (1981) Geology of the Pine Point lead-zinc district. In: Wolf KH (ed) Handbook of strata-bound and stratiform ore deposits, vol 9. Elsevier, New York, pp 643–741

Lajoie JJ, Klein J (1979) Geophysical exploration at the Pine Point Mines Ltd., zinc-lead property, Northwest Territories, Canada. In: Hood PJ (ed) Geophysics and geochemistry in the search for metallic ores, vol 31. Geological Survey of Canada, Report, pp 653–664

Leach DL, Bradley D, Lewchuk MT, Symons DTA, de Marsily G, Brannon J (2001) Mississippi Valley-type lead-zinc deposits through geological time: implications from recent age dating. Miner Deposita 36:711–740

Macqueen RW, Powell TG (1983) Organic geochemistry of the Pine Point lead-zinc ore field and region, Northwest Territories, Canada. Econ Geol 78:1–25

Meijer Drees NC (1988) The Middle Devonian sub-Watt Mountain unconformity across the Tathlina uplift, District of Mackenzie and northern Alberta, Canada. In: International symposium on the devonian system, vol 2. Canadian Society of Petroleum Geologists, pp 477–494, 2 Aug 1987

Nakai S, Halliday AN, Kesler SE, Jones HD, Kyle JR, Lane TE (1993) Rb-Sr dating of sphalerites from Mississippi Valley-type (MVT) ore deposits. Geochim Cosmochim Acta 57:417–427

Nelson J, Paradis S, Christensen J, Gabites J (2002) Canadian Cordilleran Mississippi Valley-type deposits: a case for Devonian-Mississippian back-arc hydrothermal origin. Econ Geol 97:1013–1036

Nesbitt BE, Muehlenbachs K (1994) Paleohydrology of the Canadian Rockies and origins of brines, Pb–Zn deposits and dolomitization in the Western Canada Sedimentary Basin. Geology 22:243–246

Paradis S, Hannigan P, Dewing K (2007) Mississippi Valley-type lead-zinc deposits. In: Goodfellow W (ed) Mineral deposits of Canada: a synthesis of major deposit-types, district metallogeny, the evolution of geological provinces, and exploration methods. Geological Association of Canada, Mineral Deposits Division, Special Publication 5, pp 185–203

Qing H (1998) Petrography and geochemistry of early-stage, fine- and medium-crystalline dolomites in Middle Devonian Presqu'ile barrier at Pine Point. Sedimentology 45:433–446

Qing H, Mountjoy EW (1990) Petrology and diagenesis of Middle Devonian Presqu'ile barrier—implications on formation of dissolution vugs and breccias at Pine Point and adjacent subsurface, district of Mackenzie. Geological Survey of Canada, Current Research, Paper 1990-D, pp 37–45

Qing H, Mountjoy EW (1992) Large-scale fluid flow in the Middle Devonian Presqu'ile barrier, Western Canada Sedimentary Basin. Geol 20:903–906

Qing H, Mountjoy EW (1994a) Rare-earth element geochemistry of dolomites in the Presqu'ile barrier and implications for water/rock ratio during dolomitization. Sedimentology 41:787–804

Qing H, Mountjoy EW (1994b) Origin of dissolution vugs, caverns, and breccias in the Middle Devonian Presqu'ile barrier, host of Pine Point Mississippi Valley-type deposits. Econ Geol 89:858–876

Qing H, Mountjoy EW (1994c) Formation of coarsely crystalline, hydrothermal dolomite reservoirs in the Presqu'ile barrier, Western Canada Sedimentary Basin. Bull Am Assoc Petrol Geol 78:55–77

Rhodes D, Lantos EA, Lantos JA, Webb RJ, Owens DC (1984) Pine Point orebodies and their relationship to the stratigraphy, structure, dolomitization, and karstification of the Middle Devonian barrier complex. Econ Geol 79:991–1055

Roedder E (1967) Environment of deposition of stratiform (Mississippi Valley-type) ore deposits, from studies of fluid inclusions. Econ Geol, Monogr 3:349–361

Roedder E (1968) Temperature, salinity, and origin of the ore-forming fluids at Pine Point, Northwest Territories, Canada. Econ Geol 63:439–450

Sangster DF (1988) Breccia-hosted lead-zinc deposits in carbonate rocks. In: James NP, Choquette PW (eds) Paleokarst. Springer, New York, pp 102–116

Skall H (1975) The paleoenvironment of the Pine Point lead-zinc district. Econ Geol 70:22–45

Sverjensky DA (1984) Oil field brines as ore-forming solutions. Econ Geol 79:23–27

Sverjensky DA (1986) Genesis of Mississippi Valley-type lead-zinc deposits. Annu Rev Earth Planet Sci 14:177–199

Symons DT, Pan H, Sangster DF, Jowett EC (1993) Paleomagnetism of the Pine Point Zn–Pb deposits. Can J Earth Sci 30:1028–1036

Weyer KU (1983) Salt dissolution, karst geology, glacial events and ground water flow in the Pine Point region, N.W.T. research report on joint project between Cominco Ltd., and National Hydrology Research Institute, p 461

Hypogene Processes in the Balcones Fault Zone Segment of the Edwards Aquifer of South-Central Texas

41

Geary M. Schindel and Marcus Gary

Abstract

The Balcones Fault Zone segment of the Edwards Aquifer of south-central Texas is one of the most important and prolific karst aquifers in the United States. It is formed within the lower Cretaceous Edwards Group Limestone. Since deposition, it has undergone subaerial exposure, burial in the upper Cretaceous, faulting, igneous intrusion, uplift in the Miocene, and weathering processes. The Balcones Fault Zone consists of mostly normal en-echelon faults with as much as 300 m of displacement striking northeast–southwest and dipping down toward the Gulf of Mexico. It forms the Contributing, Recharge, and Artesian zones of the aquifer. Karst characteristics of the Edwards Aquifer are the result of both epigene and hypogene processes, which continue today. The subaerial exposure of the Edwards Limestone (Recharge Zone) contains epigene karst features typical of a karst landscape that contains remnants of relict hypogene processes. Many relict caves in the Edwards Limestone outcrop show evidence of being formed by ascending water. Some appear to be associated with paleo-springs that were abandoned as water levels in the aquifer declined. Evidence of current hypogene processes is found in the saline water zone, which is part of the Artesian Zone. Extremely high permeabilities have been developed by dissolution at depth and driven by a number of processes including artesian hydraulic heads, mixing corrosion, and biogenic acids. As a result, well production in the Artesian Zone is commonly limited only by the size of the pump.

Keywords

Edwards Aquifer • Artesian karst • Groundwater • Epigene speleogenesis • Hypogene speleogenesis

1 Introduction

The Balcones Fault Zone segment of the Edwards Aquifer, south-central Texas, is one of the most important and prolific karst aquifers in the United States (Fig. 1). From the Rio Grande River along the Mexican border in the west, it extends east to San Antonio, then northeast through the cities of San Marcos and Austin for a distance of approximately 450 km. The Edwards Aquifer ranges from 10 to 60 km wide and can contain fresh water (total dissolved solids < 1000 mg/L) at depths as great as 1200 m below the surface. The aquifer is the source of water for more than 2 million people in the greater San Antonio area. It is used for agricultural, industrial, and municipal purposes; creates a critical habitat for endangered species that depend on continuous spring flows; provides water for ecosystem maintenance and municipal, agricultural, and industrial users along the San Marcos and Guadalupe rivers, which flow to the Gulf of Mexico.

G.M. Schindel (✉) · M. Gary
Edwards Aquifer Authority, 900 E. Quincy Street,
San Antonio, TX 78215, USA
e-mail: gschindel@edwardsaquifer.org

M. Gary
e-mail: mgary@edwardsaquifer.org

© Springer International Publishing AG 2017

A. Klimchouk et al. (eds.), *Hypogene Karst Regions and Caves of the World*,
Cave and Karst Systems of the World, DOI 10.1007/978-3-319-53348-3_41

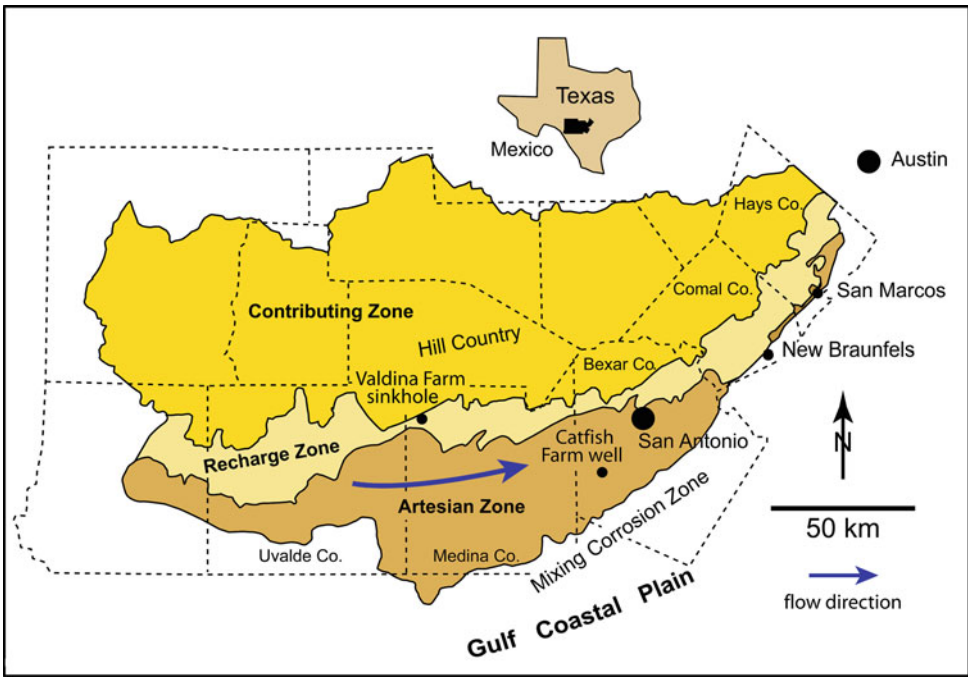

Fig. 1 Location map Edwards Aquifer region, Texas

2 Aquifer Characteristics

The Edwards Aquifer system has been divided into three major components: the Contributing Zone, the Recharge Zone, and the Artesian Zone, which operate as a massive water collection, storage, and delivery system (Fig. 2). The Contributing Zone is the largest area and is composed of outcrops of the Edwards Limestone and underlying Glen Rose Limestone, which were juxtaposed by the Balcones Fault Zone. The Contributing Zone makes up part of the Edwards Plateau, and the dissected edge of the Plateau forms the Texas Hill Country. The Contributing Zone collects rainwater and spring flow and forms the headwaters of the major surface streams in the region. The streams flow southward and lose most of their flow as they cross the Recharge Zone, the area where the Edwards Limestone is exposed at the surface. Groundwater also flows between the Glen Rose Limestone and the Edwards Limestone at depth through fault planes and dissolutional features. Finally, water flows from the Recharge Zone into the Artesian Zone, where the Edwards Limestone has been down-faulted by the Balcones Fault Zone to as much as 1200 m below the surface. The Artesian Zone delivers extremely large quantities of water to production wells and to Comal and San Marcos springs—the largest springs in the southwestern USA. The overall groundwater flow is from southwest to northeast (Fig. 1).

The Edwards Aquifer is formed within the 150–300 m thick Edwards Group Limestone and associated units, which were deposited in early Cretaceous time. The Edwards Limestone was initially deposited as a biochemical precipitate in both shallow and deep marine environments, and it has been modified over time by numerous geologic processes including lithification, fracturing and faulting, igneous intrusions, subaqueous and subaerial dissolution, and physical weathering. The Edwards Limestone has been highly karstified, resulting in a triple permeability aquifer with matrix, fracture, and conduit permeability (Hovorka et al. 1995, 2004). It consists of shallow-marine sedimentary rocks dipping gently toward the Gulf of Mexico and offset by a series of normal en-echelon, down-to-the-coast, northeast-striking faults that comprise the Balcones Fault Zone. Some faults have as much as 300 m of displacement, but most have much less. The fault zone is no longer active (Ferrill et al. 2003). In the fault zone, the limestone is downthrown so that younger, less permeable rocks cover it, where water becomes artesian, driven downdip by hydrostatic pressure. This is the Artesian Zone, where freshwater circulates to depths of more than 1200 m, and 800 m below sea level.

The highly interconnected openings in the Edwards Limestone result in some of the highest yielding wells in the world (Fig. 3). Numerous wells pump more than 40,000 L/min with no measurable draw down. Many wells flow at several thousand liters per minute because of the vertically upward gradient in the Artesian Zone. The Catfish Farm well, located in southern Bexar County, was estimated to yield more than 120,000 L/min and discharged water under artesian pressure more than 10 m above ground. It produced an amount of water approximately equal to one-quarter of

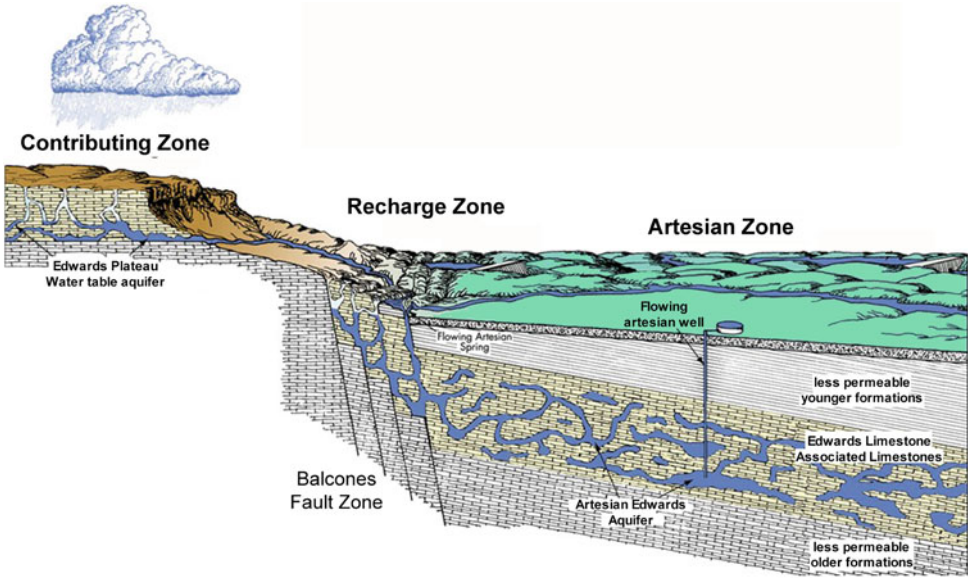

Fig. 2 Cross section of the Edwards Aquifer in Bexar County, Texas

Fig. 3 Example of porosity in the Edwards Limestone. Pen for scale. Photo by A.N. Palmer

the total use by the city of San Antonio (population ~1.4 million). Modeling by Lindgren et al. (2004) indicated groundwater flowpaths in the aquifer to have permeabilities ranging from 300 to 48,000 m/day. The residence time for water in the aquifer ranges from a few hours to many years.

The distribution of highly adapted biota in the aquifer system also reflects on the continuous nature of large conduits in the Artesian Zone. The Edwards Aquifer has one of the most diverse fauna of any groundwater system, which also attests to the cavernous porosity of the aquifer. More than 40 endemic species utilize the aquifer and include both vertebrate and invertebrate species. Some are found across wide areas of the aquifer and provide insight into the interconnected nature of the conduits. Much of the fauna, including two species of catfish, are found along the saline water/fresh water interface. These areas do not experience a rapid influx of storm water during rain events, and the ecological communities do not depend on detritus entering the aquifer. Rather, they appear to be based on bacteria that

utilize the chemical gradient along the downdip saline water/fresh water interface (Rye et al. 1981).

3 Karst Processes

Regional flow systems in the Edwards Aquifer reflect a combination of processes that occurred over time, including epigene speleogenesis near the surface and hypogene processes in the artesian portions of the aquifer. Karstification has occurred since the aquifer was first subaerially exposed, soon after deposition. After burial by younger deposits, the paleokarst features may have been inception horizons for later karstification. Some researchers have proposed substantial secondary permeability prior to downfaulting and creation of the Artesian Zone. Early researchers proposed epigene karst processes for formation of the Edwards Aquifer driven by circulating meteoric waters along structural and paleokarst features. The epigene karst theory assumes karst features are produced from downward or horizontal groundwater movement, but Klimchouk (2007) concludes that waters rising from depth (hypogene) are also important agents of karst development. Worthington (2001) has shown that deep circulation systems are more efficient in regional aquifer systems owing to the lower viscosity of water at the higher temperatures at depth. Hypogene processes in the Edwards Aquifer were little known or understood until recently. Epigene processes are now overprinting relict hypogene features in the recharge and shallow artesian portions of the aquifer.

3.1 Epigene Karstification

Epigene karstification in surface exposures of the Edwards Limestone has created sinkholes, sinking (losing) streams, caves, springs, and a well-integrated subsurface drainage system. Epigene processes enhance permeability as solutionally aggressive surface water moves downward or horizontally through the carbonate rocks. Caves and sinkholes in the Recharge and Contributing zones provide insight into the formation of active and relict portions of the Edwards Aquifer. Caves and enlarged fractures and faults actively recharge water to the Edwards Aquifer, augmenting the input from surface streams and direct recharge. Worthington (2003) concluded that south-flowing groundwater dissolved conduits parallel to losing streams in the Recharge Zone, which is consistent with maps of the few caves that are fed by sinking streams (Fig. 4).

Some caves located along the southeastern edge of the Edwards Plateau, within the Contributing Zone, are actively draining a portion of the plateau. Perry Water Cave is an example of an active stream cave in Real County. This cave has more than 9 km of mapped stream passage. Other caves have been isolated and abandoned from active groundwater circulation by lowering of the land surface of the Recharge Zone and/or retreat of the edge of the Edwards Plateau. Most of these caves are found in the Edwards Limestone near the tops of hillsides. There are also active epigene caves formed in the Recharge Zone. Indian Creek Cave, located in Uvalde County, has a flowing stream along much of its length (Fig. 4). The cave entrance is a vertical shaft located in a dry creek bed which was discovered by excavation. The cave is more than 5 km in length and passages also traverse an igneous dike. Entrance into caves associated with active recharge features of the Edwards Aquifer are relatively rare, and most entrances in active streamways appear to be filled with cobbles and boulders derived from the edge of the Edwards Plateau. Ruhe Sink in Medina County is an insurgence cave located in a stream channel that opens and closes depending upon the state of floodwater and bedload in the stream.

Several caves located in the Recharge Zone have morphologies that are characteristic of caves formed by ascending water. Some of the best examples are Valdina Farm (Seco Creek) Sinkhole, in Medina County, which includes a 50 m deep entrance pit. The entrance area contains a number of large cupolas that indicate they were formed by ascending water. Valdina Farm is located just upgradient of the Woodward Cave Fault. Kneaper Ranch Cave also appears to have formed by ascending water and is located just upgradient from a large fault displacing the Edwards Limestone against the younger Buda Limestone. These faults may have acted as barriers to groundwater flow and forced water upward. These caves also appear to preserve a record of upward-flowing water as a result of much higher aquifer levels in the geologic past.

3.2 Hypogene Karstification

Recent data and new interpretations suggest an additional process that contributed to the formation and structure of the Edwards Aquifer (Klimchouk 2007). Epigene processes occur near the ground surface and advance downward, although water becomes saturated with respect to calcite and loses its ability to continue to dissolve at depth. Consequently, Klimchouk (2007) concluded that rising waters from depth are important agents of karst development. Palmer (2000) argued that hypogene karst is formed by water in which the solutional aggressiveness has been produced at depth independent of surface or soil CO_2 or other near-surface acid sources. Klimchouk (2007) suggested that hypogene speleogenesis should instead refer to ascending groundwater as a medium of transport of aqueous and non-aqueous matter and energy, and that the main attribute

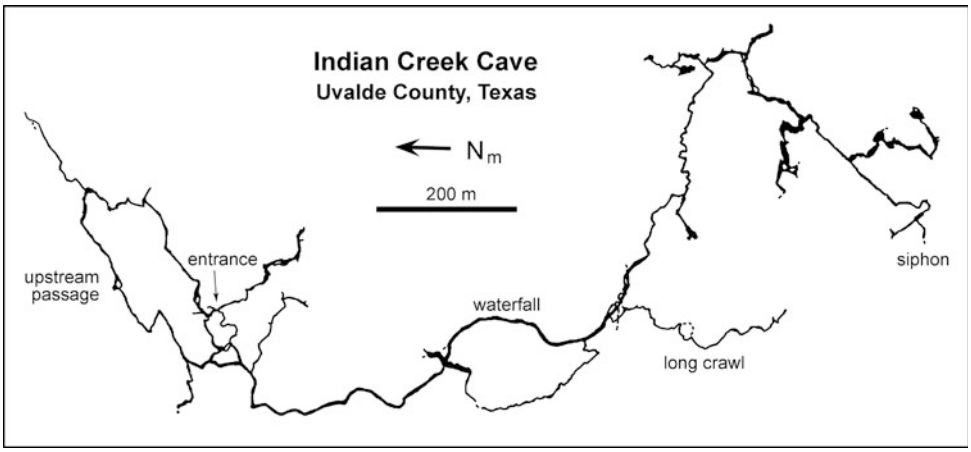

Fig. 4 Map of Indian Creek Cave, Uvalde County, Texas. Courtesy University of Texas Grotto 1962 survey. This is an active epigene cave in the Recharge Zone

of hypogene karst is its "lack of genetic relationship with groundwater recharge from the overlying surface" (Dublyansky 2014). Regardless of which definition is utilized, dissolution at depth in the Edwards Aquifer has occurred both in the past and at present.

One of the principal lines of evidence for current hypogene processes in the Edwards Aquifer is saline groundwater, which is adjacent to fresh water near the downdip limit of the Artesian Zone. The boundary between fresh and saline groundwater is called the saline water/fresh water interface, or Bad Water Line, where total dissolved solids (TDS) reach 1000 mg/L (recommended drinking water standard). Generally, TDS increases rapidly south of the Bad Water Line (toward the Gulf of Mexico) to values equal to or exceeding sea water. The saline water zone is enriched with chloride and sulfate, which indicates water trapped in the formation during lithification (connate water), as well as dissolution of gypsum, as identified in geophysical logs of wells in the saline water zone. In addition, saline water may be migrating up-dip from deeper zones in the south. Mixing of waters of contrasting chemistry has resulted in mixing corrosion, as defined by Bögli (1964). The saline water portion of the aquifer is noted for its high concentrations of hydrogen sulfide (H_2S). The production of H_2S by bacterially mediated processes such as sulfate reduction also increases the aggressiveness of the water along the Bad Water Line. Sulfate-reducing bacteria use the sulfate and trace amounts of organic material as energy/food sources. The reduction of sulfate produces hydrogen sulfide, which forms sulfuric acid (H_2SO_4) when mixed with oxygenated water.

In addition, water in the deeper portions of the Artesian Zone is warmed because of the depth of circulation, where temperatures commonly exceed 30 °C. The increase in temperature decreases the viscosity of water and creates a preference for deeper flow paths for regional aquifer systems. As the water rises and cools, its ability to dissolve calcium carbonate increases (Worthington 2001).

Mixing corrosion plays an important role in dissolution along the saline water/fresh water interface. This has allowed the creation of large horizontal flow paths from major recharge features in the western portion of the aquifer to discharge at Comal and San Marcos springs to the northeast —a distance of more than 200 km. Migration of the Bad Water Line downdip over geologic time certainly accounts for some of the high permeability throughout the Artesian Zone. Klimchouk (2007) describes a suite of characteristic karst geomorphologic features that develop in such hypogene zones (areas of rising transverse flow zones), although active examples in the Edwards Aquifer are currently located in the artesian zone, including the area beneath karst springs, and therefore it is difficult to examine their features.

Relict caves located in the recharge zone appear to be formed by ascending water rather than descending water characteristic of epigene processes. In addition, many caves in the Recharge Zone contain high concentrations of CO_2, some above safe working levels. It is clear that CO_2 did not originate from organic material washed into cave entrances during rainfall events. However, the source and role of CO_2 in caves in the Recharge Zone is unclear. The source may be the off-gassing from biologic processes in groundwater. Another source may be from bacteria feeding on petroleum and degassing CO_2 from the Edwards Limestone rock mass above the water table. Absorption by condensing water could result in condensation corrosion, which has been observed on the walls of some caves in the Recharge Zone.

4 Evolution of the Edwards Aquifer

The evolution of the Edwards Aquifer has occurred from areas of higher elevation to lower elevations, which is generally from west to east. The western portion of the Edwards Aquifer region, including parts of Kinney, Uvalde, and Medina Counties, appears to have been the first areas

exposed to epigene karst processes. Many relict caves that are no longer part of the active hydrologic system exhibit structures that indicate that they were formed by upward-flowing water. These paleo-springs were abandoned as water levels in the aquifer decreased, most likely as a result of springs opening at lower elevations (in eastern Medina County and Bexar County). San Antonio Spring (203 m msl = above mean sea level) and San Pedro Spring (200 m msl), both located in San Antonio, are currently overflow springs that discharge water when aquifer levels are above average. These springs most likely had a larger discharge when aquifer levels were higher during the early evolution of the aquifer. Comal Springs (188 m msl), the largest spring in the southwestern USA, is located in New Braunfels, approximately 45 km northeast and at a lower elevation than the San Antonio spring complex. Comal Springs emerges along the Comal Springs fault, and with time, it has become more efficient, increasing its flow while dropping the water levels in Bexar and eastern Medina Counties. This resulted in San Antonio and San Pedro springs becoming overflow springs and only flowing when aquifer conditions were above average. San Marcos Springs (175 m msl), in San Marcos, is at a lower elevation than Comal Springs and averages approximately two thirds the flow of Comal Springs. As dissolution continues and water levels decline over the next few hundred thousand years, San Marcos Springs will probably become more efficient and become the dominant spring in the Edwards Aquifer, and Comal Springs will be relegated to an overflow spring. Ultimately, Barton Springs (133 m msl), located in Austin near the Colorado River, at a lower elevation than Comal or San Marcos Springs, may become the primary spring for the San Antonio segment of the Edwards Aquifer.

5 Conclusion

The Edwards Aquifer is one of the largest and most productive aquifer systems in the United States. Water is concentrated by the Contributing Zone and is added to the aquifer through the Recharge Zone, and delivered to wells and springs by the Artesian Zone. Although epigene processes have contributed to the hydraulic characteristics of the aquifer, several features reflect the impact of hypogene processes. Mixing corrosion in the saline water zone has created extremely large flowpaths in the aquifer more than 200 km long that yield water at thousands of liters per minute to wells and springs. The depth of circulation in the artesian portions of the aquifer exceeds 1000 m where water temperatures approach 30 °C. The result is a highly productive aquifer system that meets the water needs of most of the people in south-central Texas.

Acknowledgements The authors would like to acknowledge the contributions of Steve Johnson, Dr. E. Calvin Alexander, Dr. Stephen Worthington, and Dr. Alexander Klimchouk in their development of a conceptual understanding of the Edwards Aquifer.

References

Bögli A (1964) Erosion par mélange des eaux. Int J Speleol 1:61–70

Dublyansky YV (2014) Hypogene speleogenesis—discussion of definitions. In: Klimchouk A, Sasowsky I, Mylroie J, Engel SA, Engel AS (eds) Hypogene cave morphologies. Selected papers and abstracts of the symposium held February 2 through 7, 2014, San Salvador Island, Bahamas. Karst Waters Institute Special Publication 18. Karst Waters Institute, Leesburg, Virginia, 111 p

Ferrill DA, Sims DW, Morris AP, Waiting, DJ, Franklin N (2003) Structural controls on the Edwards Aquifer/Trinity Aquifer interface in the Camp Bullis Quadrangle, Texas, CNWRA, Southwest Research Institute®, San Antonio, TX, 126 p

Hovorka SD, Mace RE, Collins EW (1995) Regional distribution of permeability in the Edwards Aquifer. Prepared for Edwards Underground Water District, Bureau of Economic Geology, The University of Texas at Austin, 128 p

Hovorka S, Phu T, Nicot JP, Lindley A (2004) Refining the conceptual model for flow in the Edwards Aquifer—characterizing the role of fractures and conduits in the Balcones Fault Zone Segment. Bureau of Economic Geology, Jackson School of Geosciences, The University of Texas at Austin, 53 p

Klimchouk AB (2007) Hypogene speleogenesis: hydrogeological and morphogenetic perspective. Special paper no. 1, National Cave and Karst Research Institute, Carlsbad, NM, 106 p

Lindgren RJ, Dutton AR, Hovorka SD, Worthington SRH, Painter S (2004) Conceptualization and simulation of the Edwards Aquifer, San Antonio region, Texas. U.S. Geological survey scientific investigations report 2004–5277, 143 p

Palmer AN (2000) Hydrogeologic control of cave patterns. In: Klimchouk A, Ford D, Palmer A, Dreybrodt W (eds) Speleogenesis: evolution of karst aquifers, National Speleological Society, Huntsville (AL), pp 77–90

Rye RO, Back W, Hansaw BB, Rightmire CT, Pearson FJ (1981) The origin and isotopic composition of dissolved sulfide in groundwater from carbonate aquifers, Florida and Texas. Geochim Cosmochim Acta 45(10):1941–1950

Worthington SRH (2001) Depth of conduit flow in unconfined carbonate aquifers. Geol Soc Am 29(4):335–338

Worthington SRH (2003) Conduits and turbulent flow in the Edwards Aquifer. Worthington groundwater, contract report for Edwards Aquifer Authority, 42 p

Hypogenic Caves and Paleokarst of the Arbuckle Mountains, Oklahoma

42

Kevin William Blackwood

Abstract

The Arbuckle Mountains form a small but complex geologic province characterized by thick sequences of intensely folded and faulted carbonates, sandstones, and shales of the Late Cambrian through Pennsylvanian (Late Carboniferous). Caves, karst, and paleokarst features are abundant in several limestone and dolomite formations. The region hosts a diverse range of settings and mechanisms capable of forming both epigenic and hypogenic caves. Hypogenic features are found in caves throughout the Arbuckles, but most commonly where deformation has been severe. Carbonate dissolution in these areas is aided by the mixing of fresh and saline waters, and by microbial interaction with hydrocarbons. It is probable that more than one process has been involved in forming hypogenic caves and paleokarst.

Keywords

Arbuckle Mountains • Deep karst • Hypogenic caves • Paleokarst • Faults

1 Introduction

The Arbuckle Mountains are a southwestern extension of the Appalachian Mountains that has been greatly eroded and mostly overlain by younger strata, so that the connection with the main mountain chain is no longer visible at the surface. This little-known karst area provides a narrow window into a great thickness of carbonate rocks. There is very little literature on the karst of this region, and only the beginning phase of its study is described here.

2 Caves and Karst of the Arbuckles

The Arbuckles form a large inlier of folded and faulted Paleozoic and Precambrian rocks in southern Oklahoma. The inlier encompasses an area of roughly 2600 km^2 (Fig. 1) and contains 3350 m of Late Cambrian through Devonian strata, composed almost entirely of carbonate rocks. Sandstones and thin interbedded shales occupy only a small fraction of the stratigraphic column (Ham 1973). The carbonates of the Cambrian–Ordovician Arbuckle Group, exposed in road cuts along Interstate 35, have been measured to more than 2040 m thick (Fay 1989).

The mountains show evidence for several structural and geochemical environments that favor hypogene speleogenesis. Several caves with hypogenic features are known on the north flank of the Arbuckle anticline north of the Chapman Ranch Fault (Fig. 1, Blackwood et al. 2015), and their genetic processes are currently being investigated.

The Arbuckle Mountains constitute an eroded anticline. The rocks at the anticlinal crest were once capped by confining and semi-confining units that have since been gradually eroded away. The hypogene caves and paleokarst features on the north flank of the Arbuckle Mountains developed in chaotic settings, within rocks that are heavily folded and faulted. Outcrops of the upper Arbuckle Group, previously overlain by semi-confining units of the Simpson Group, contain vast networks of solutionally widened joints,

K.W. Blackwood (✉)
East Central University, 1100 E 14th Street,
Ada, OK 74820, USA
e-mail: karstgeoscience@gmail.com; kevwbla@ecok.edu

© Springer International Publishing AG 2017

A. Klimchouk et al. (eds.), *Hypogene Karst Regions and Caves of the World*,
Cave and Karst Systems of the World, DOI 10.1007/978-3-319-53348-3_42

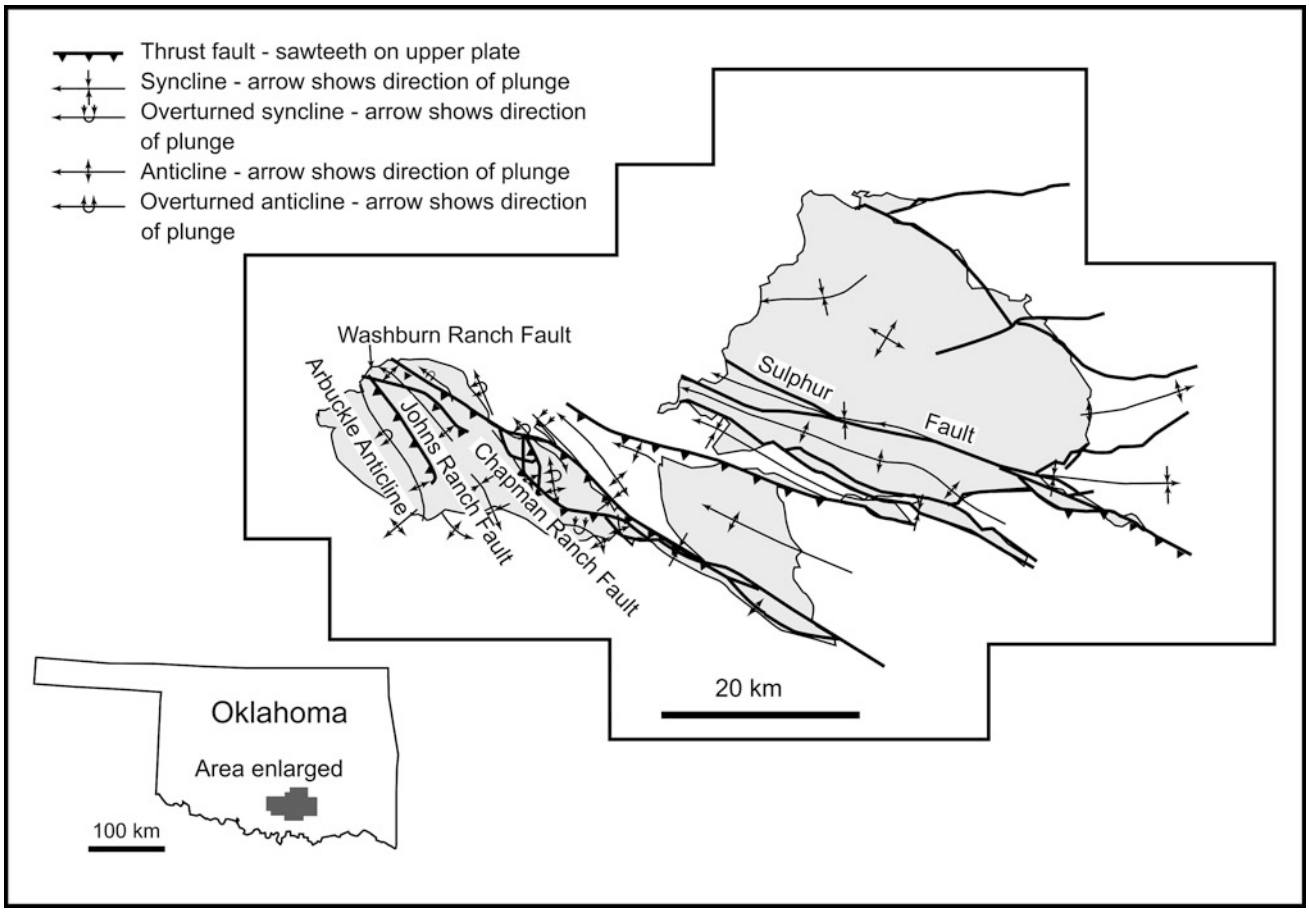

Fig. 1 Location of the Arbuckle Mountains (*bottom*), with geologic structure (*top*) showing the trend of the chapman ranch fault (modified from Christensen et al. 2011)

some of which are wide enough to allow human entry. These resemble network mazes, which are commonly associated with hypogenic cave origin (Klimchouk 2007; Palmer 2007). Morphological investigations within these caves have not yet confirmed whether these features are hypogenic, because overprinting by descending vadose water has modified them. For example, Stribbling Cave (Fig. 2a), located in steeply dipping rock beneath a confining shale bed, is a possible example of a hypogenic cave not formed along a fault. Epigenic processes now dominate on the southern flank of the Arbuckle anticline, where semi-confining beds overlie the upper Arbuckle Group. However, there is also evidence for limited hypogenic cave origin in the southern flank. Hypogenic karst development appears to continue today where the soluble carbonates are overlain by confining strata along the flanks of the anticline.

3 Hypogenic Caves and Paleokarst

Paleokarst in the Arbuckle Mountains first generated interest in 1987 when a well in the Cottonwood Creek oil field encountered a solutionally enlarged fissure or cavern in an upper Arbuckle unit at a depth of approximately 2600 m, when the bit dropped nearly 6 m (Johnson 1991; Puckett et al. 2009). The discovery of oil in this zone led to further studies of the karst and paleokarst features. Becker (1988) considered them to have formed by submarine processes. Later, Wilson (1993), in studies of correlative paleokarst in road cuts, attributed their origin and alteration to Pennsylvanian–Permian hydrothermal activity on the basis of thermal signatures of oxygen isotopes in veins and surrounding halos. The ascending thermal fluids were thought to be episodic and possibly related to hydrocarbon migration (Lynch and Al-Shaieb 1991).

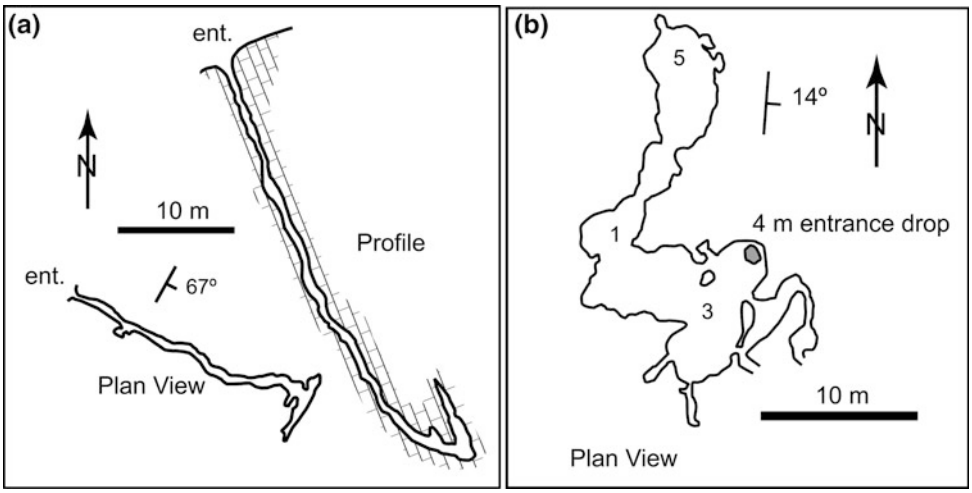

Fig. 2 **a** Map and profile of Stribbling Cave. Located in Limestone that dips about 65°, this is one of the few hypogenic caves that did not form along a prominent fault. The cave origin is considered to be related to ascending fluids and confinement by the Woodford Shale. Map by (Curtis 1959). **b** Map of White Woman Cave (Curtis 1959). Numbers refer to ceiling height in meters

Along the Arbuckle anticline, paleokarst features are found only north of the Chapman Ranch Fault (Fig. 1) where folding and faulting has been most severe. This may indicate that they were related to orogenic processes rather than eogenetic karst. Chemical paleomagnetic studies by Elmore (2001) suggested that basinal or orogenic fluids migrated laterally through paleo-aquifers, with local vertical flow along fractures, during multiple events that spanned approximately 60 My during the late Paleozoic. Six episodes of karstification have been identified from paleokarst features in the uppermost limestone sequence (Viola Formation), with horizontally stratified fill indicating post-orogenic burial (Sykes 1997). This burial and preservation of fossil caves took place during the Permian (Chaplin 1999, 2008).

The presence of hypogenic caves in the Arbuckle Mountains was suggested by Christensen et al. (2011) and was confirmed in part through morphological investigations by Blackwood (2014) using criteria discussed by Klimchouk (2007)—irregular rooms, wall and ceiling features that indicate rising flow, and lack of genetic relationship with the surface (Figs. 3 and 4). The first scientific publication on caves of the Arbuckle Mountains (Curtis 1959) described 11 examples and noted four of them were the "dry type," i.e., playing no apparent role in the present storage or transport of groundwater. It is thought that the hypogenic caves formed at the same time as the paleokarst, but were either never buried or have since been exhumed (Blackwood et al. 2015). Interpretation is complicated by the fact that hypogene caves may involve several different mechanisms that operate simultaneously or in sequence (Klimchouk 2014). In certain caves, especially those on the south flank, stratal confinement may have played a greater role than tectonics, while also hosting corrosive fluids produced by mixing of chemically contrasting waters and biodegradation of hydrocarbons.

Known hypogenic caves in the Arbuckle Mountains share many similarities. Most are close to large faults near the crests of hills where surface recharge is typically negligible. Known caves are not extensive, typically consisting of several irregular rooms of complex geometry, or isolated chambers. Cupolas and wall features are common (Figs. 2b and 5). Several of the caves contain deep pits, which have been interpreted as rising shafts on the basis of cupolas directly overlying them. The pits remain largely unexplored because of high levels of carbon dioxide that do not have the seasonal variation seen in other Arbuckle caves (Gantt 2012). Hydrogen sulfide and strong hydrocarbon odors have also been documented in unpublished field reports by the Arbuckle Mountains Grotto (National Speleological Society). The caves are almost always dry, even after strong storms such as a tropical storm in June of 2015 that dumped 30 cm of rain in a 24-h period (Blackwood 2015). Speleothems are also abundant, some of which consist of iron precipitates.

In the Devil's Garden Cave System, near Falls Creek (Fig. 6), a passage terminates in carbonate-cemented terra rossa clays, which are commonly associated with the paleokarst. This cave system contains many characteristics typical of hypogenic caves with ascending fluids or internally corrosive fluid geochemistry, such as wall and ceiling features, and irregular rooms. The presence of paleokarst fills is rather common in several other hypogenic caves in the Arbuckle Mountains. The presence of paleokarst sediments in the hypogenic caves suggests that the caves and paleokarst are contemporaneous.

Fig. 3 Upward view into a rising shaft in Birds Eye Cave

4 Speleogenetic Settings

The following settings have been documented in the Arbuckle Mountains and apparently favored the development of hypogenic cave and karst features, both past and present.

4.1 Basinal and Orogenic Fluid Flow Through Deep Fractures

The Arbuckle Mountains are intensely folded and faulted, and many of the faults extend to the Precambrian basement. Vertical fault displacements of more than 2300 m have been measured from well logs and cuttings (Allen and Newman 2012), while major strike-slip faults have lateral displacements of more than 60 km (Scheirer and Hosford Scheirer 2006). Evaluations of vertical fracturing from geophysical and thermal data by Halihan et al. (2009) indicate that many of the faults and other fractures that extend to the aquifer bottoms may be acting as conduits for the rapid vertical circulation of groundwater throughout the geologic units, which would suppress or eliminate any geothermal gradients within the Arbuckle aquifers.

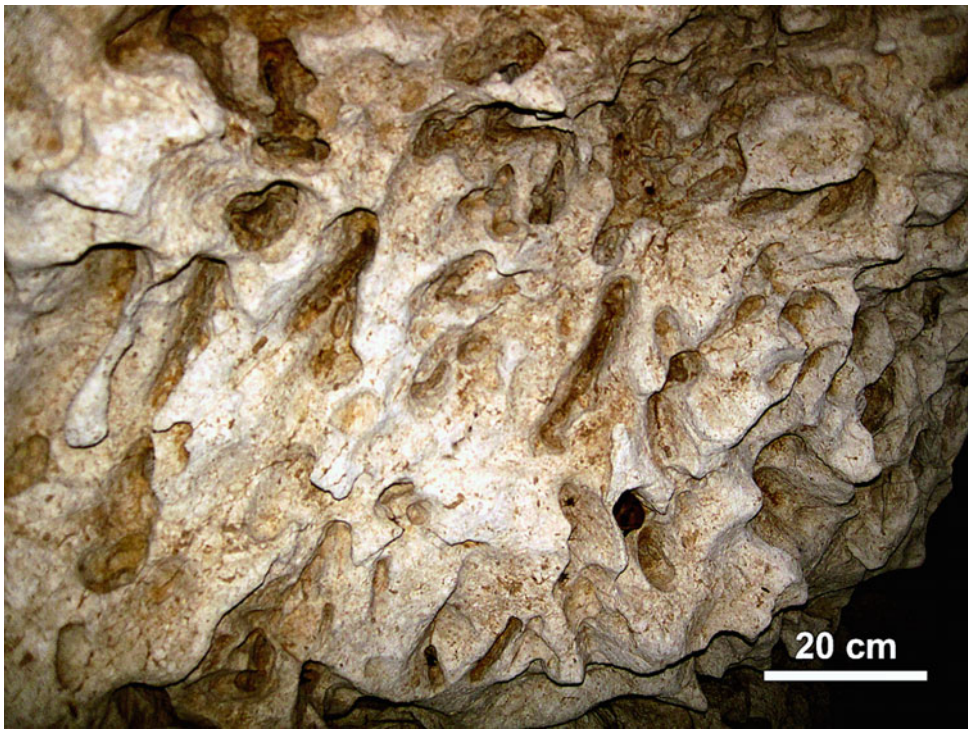

Fig. 4 Dissolution features in Birds Eye Cave. These channels terminate upward in solution pockets

Observation of vertical fracturing and drilling data suggests that the permeability of the aquifers increases with depth. Borehole temperature data show that the groundwater is 0.5 °C colder at depth than at the water table. For groundwater to cool the rocks and fluid samples to temperatures 10–15 °C below those expected, and also to maintain a nearly zero temperature gradient, vertical circulation of fluids through the aquifers must be rapid. Therefore, if hydrothermal processes were involved in the area, they are no longer active.

It is expected that this zone of vertical flow extends to the Precambrian basement at a depth of approximately 1 km. It is possible that the vertical flow paths are more permeable than the lateral paths between springs and wells (Halihan et al. 2009). During the Arbuckle-Simpson Hydrology Study (Christensen et al. 2011), the best MODFLOW groundwater modeling results were obtained when the vertical hydraulic conductivity was increased substantially, to 1000 times greater than the horizontal conductivities. The improved results appear to be compatible with vertical flow along the Sulphur Fault, which may be locally masked beneath the confining Pennsylvanian strata.

Brown iron ores are common throughout the Arbuckle Mountains, typically as mounds, and are usually associated with faults. Their appearance resembles the mound springs of the Great Artesian Basin in southern Australia (Decker and Williams 1986). The source of these iron ores is likely from the Reagan Sandstone, an iron-rich formation overlying rhyolite and granite basement rocks. Merritt (1940) suggests that the structure of the Arbuckle Mountains may have induced artesian circulation, which would have caused iron-bearing solutions to rise to the surface along faults under pressure.

4.2 Mixing of Fresh Water with Brine and Petroleum Beneath Confining Units

The Arbuckle Mountains once contained brines and petroleum that have since been largely flushed from the aquifers (Puckett et al. 2009), although traces of hydrocarbons can still be detected in some freshly broken rock samples. Petroleum is found in economic quantities, along with brines, only where the Arbuckle rocks are located hundreds of meters beneath the Pennsylvanian strata.

Wells drilled through the confining units along the flanks of the Arbuckle Mountains often exhibit artesian flow and sulfide odors. Freshwater springs are typically located farther up-gradient near the base of the Arbuckle Mountains where there are no confining units. The area defined by these springs and wells is thought to indicate the location of the freshwater/brine transition zone. Their contrast with the water chemistry beneath confining units may be sufficient to drive disequilibrium and dissolution mechanisms (Klimchouk 2007). Unpublished isopach maps constructed from well data by Robert Allen (Ardmore Sample Cut and

Fig. 5 Cupola in Dead Man Cave. Freshly broken rocks contain strong hydrocarbon odors

Library) indicate the presence of aquifers with sulfur-rich water extending several kilometers beyond the flanks of the freshwater aquifers.

The development of paleokarst within the Viola Limestone is most likely the result of petroleum and brine flushing beneath a confining unit. The Viola Limestone underlies the Sylvan Shale, an organic-rich oil-producing shale and effective aquitard. Almost all caves surveyed in the Viola Limestone contain features that are compatible with a hypogenic origin.

4.3 Aggressive Agents

Caves of the Arbuckle Mountains are well known for their seasonally high levels of atmospheric carbon dioxide (Veni and Palmer 2009). High CO_2 levels in caves are often the result of decaying organic matter where passage geometries inhibit air circulation (Badino 2009). However, it is likely that some of the carbon dioxide in the Arbuckle caves could be released from depth. Generation of CO_2 and organic acids at high temperatures by the conversion of organic matter to

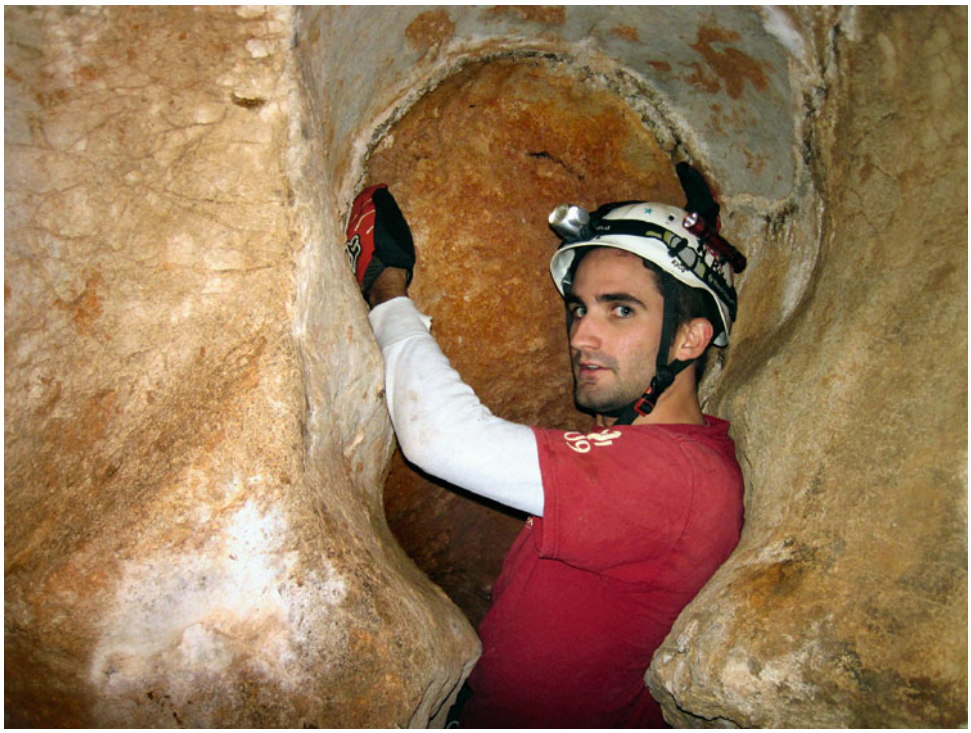

Fig. 6 Paleokarst fill terminating a passage in the Devil's Garden Cave System (photograph by Stacy Gantt-Blackwood)

petroleum can increase the porosity of carbonate rocks in oilfields (Kharaka et al. 1986). Field investigations in Arbuckle caves by Gantt (2012) showed preliminary results of high CO_2 levels in pits that we now recognize as the rising shafts of hypogenic caves. However, the CO_2 source in these caves remains unknown.

The role of sulfuric acid in the Arbuckle Mountains is unclear, although hydrogen sulfide is common near the flanks of the Arbuckle Mountains. Small concentrations of dissolved sulfate have been detected in water wells and springs along the flanks of the Arbuckle Mountains (Christensen 2009). At least one of the hypogenic caves appears to have gypsum crystals in its walls near a rising shaft where a hydrogen sulfide odor is currently being investigated. Pyrite is also present in many of the formations in the Arbuckle Mountains, and its oxidation may contribute to the groundwater aggressiveness.

5 Evidence for Modern Upwelling Fluids

Artesian springs are being modeled as part of the Arbuckle-Simpson Hydrology Study (Beard 2014). This includes the investigation of possible upwelling in a cave in the eastern Arbuckle Mountains. Although there is little present evidence for upwelling, perhaps as the result of overprinting by epigenic processes, geophysical studies show a deep vertical conductive feature extending well beneath the cave.

The caves described by Curtis (1959) as "dry caves," thought to no longer play a role in groundwater flow and storage, were exposed in December 2014 to a flooding event apparently unrelated to local surface recharge. Water welled upward from the drain of White Woman Cave (Fig. 2b) to flood the cave one meter deep (Blackwood 2014). The flood removed sediment from the walls and left an obvious water line throughout the cave. Photograph comparisons show that the cave had flooded to the same level in the past. But such events are apparently rare, as shown by an inscription dating from 1952, written on a wall in carbide smoke, which was partially removed when the carbon-coated sediment was washed away. This indicates that the cave has probably not flooded to that level since then. It is possible that this cave was formed by fluids rising through faults as a result of reactivation of the Washburn Fault, which underlies the cave.

It is also possible that upwelling of water in White Woman Cave was related to the recent spike in Oklahoma earthquakes due to wastewater injection. Water could also have been ejected upward through the nearby Washburn Ranch Thrust Fault during earthquakes that occurred in the area at approximately the same time.

6 Conclusions

Evidence of infilling in certain hypogenic caves suggests that the caves and paleokarst are more or less contemporaneous in the Arbuckle Mountains. Many paleokarst features are thought to have been formed by hydrothermal fluids ascending through fractures and are perhaps orogenic. Although various aggressive agents may play a role, carbonic acid is probably the dominant one at present. Some caves contain elevated levels of CO_2, perhaps because of degassing from groundwater. Mixing of freshwater and saline water may be the dominant solutional agent near the base of the anticline, at the boundary of the two fluids where artesian springs discharge water with elevated levels of sodium chloride. Biodegradation of hydrocarbons trapped in the rocks, as well as oxidation of pyrite, may also contribute, but their effect has not yet been quantitatively determined. Sulfide-rich artesian waters discharging along the anticlinal flanks, at the edge of the oil fields, suggest an active hypogene setting.

Any of these processes, combined with mixing of waters of contrasting chemistry, could serve as mechanisms for the development of paleokarst and caves during earlier geologic periods. These processes were possibly episodic, and several developmental processes may have operated simultaneously.

Acknowledgements Thanks to the following for their help on this project: Stacy Gantt-Blackwood, John Brooks, Corky Corcoran, Todd Halihan, Kaitlyn Beard, Pride Abongwa, Kyle Spears, John Richins, Britney Temple, Bob Allen, John Wilson, Jona Tucker, Lainee Sanders, Tom Thompson, Jon Fields, the various landowners, Arbuckle Karst Conservancy & Research Institute, and members of the Arbuckle Mountains Grotto of the National Speleological Society.

References

Allen RW, Newman RL (2012) The Arbuckles below your feet. Oklahoma Geological Survey presentation

Badino G (2009) The legend of carbon dioxide heaviness. J Cave Karst Stud 71(1):100–107

Beard KS (2014) Investigation of upwelling along the eastern boundary fault of the Arbuckle-Simpson aquifer. Geological Society of America South-Central Section—48th annual meeting. Abstract and presentation

Becker RD (1988) Stratigraphy and depositional characteristics of the bromide dense unit and viola limestone, subsurface Central Oklahoma, unpublished M.S. thesis. University of Tulsa, Oklahoma

Blackwood KW (2014) Hypogenic karst in the Arbuckle Mountains. Proc Okla Acad Sci 93(2013):70

Blackwood KW (2015) Arbuckle Karst Conservancy and Research Institute 2015 Annual Report. p 21

Blackwood KW, Beard KS, Halihan T (2015) Development and distribution of hypogenic caves and paleokarst features in the Arbuckle Mountains of South Central Oklahoma, USA. American Association of Petroleum Geologists, Annual convention and exhibition, Denver, Colorado, 3 June 2015

Chaplin JR (1999) Generalized geologic time scale of Oklahoma (Permian). Oklahoma Geological Survey educational publication 6

Chaplin JR (2008) Outcrop analogs in the Arbuckle Mountains, Oklahoma of selected reservoir rocks, source beds, and seals—application to petroleum exploration. Oklahoma Geological Survey field trip guide to the Arbuckle Mountains for British Petroleum Inc., pp 27–31

Christensen SC (2009) Geochemical investigation of the Arbuckle-Simpson aquifer, south-central Oklahoma. U.S. Geological Survey Scientific Investigations Report 2009–5036, p 26

Christensen S, Osborn NI, Neel CR, Faith JR, Blome CD, Puckett J, Pantea MP (2011) Hydrogeology and simulation of groundwater flow in the Arbuckle-Simpson aquifer, south-central Oklahoma. U. S. Geological Survey Scientific Investigations Report 2011–5029, pp 10, 11, 18–98

Curtis NM (1959) Caves in the Arbuckle Mountains area, Oklahoma: Oklahoma Geological Survey. Okla Geol Notes 19(2):20–31

Decker P, Williams WD (1986) Limnology in Australia, mound springs of the Great Artesian Basin, pp 403–420

Elmore RD (2001) A review of paleomagnetic data on the timing and origin of multiple fluid-flow events in the Arbuckle Mountains, Southern Oklahoma. Pet Geosci 7(3):223–229

Fay RO (1989) Geology of the Arbuckle Mountains along Interstate 35, Carter and Murray counties, Oklahoma (Guidebook 26/Oklahoma Geological Survey), p 2

Gantt SI (2012) Analysis of hypoxic caves in the Arbuckle Mountains of south central Oklahoma. 101st annual technical meeting of the Oklahoma Academy of Science (abstract)

Halihan T, Mouri S, Puckett J (2009) Evaluation of fracture properties of the Arbuckle-Simpson aquifer. Final report for the Arbuckle-Simpson Hydrology Study, pp 1–60

Ham WE (1973) Regional geology of the Arbuckle Mountains, Oklahoma. Oklahoma Geological Survey Special Publication 1

Johnson KS (1991) Geologic overview and economic importance of late Cambrian and Ordovician rocks in Oklahoma. Late Cambrian-Ordovician Geology of the Southern Midcontinent, 1989 symposium: Oklahoma Geological Survey Circular 92: 1–14

Kharaka Y, Law L, Carothers W, Goerlitz D (1986) Role of organic species dissolved in formation water from sedimentary basins in mineral diagenesis. In: Gautier DL (ed) Roles of organic matter in sediment diagenesis. Society of Economic Paleontologists and Mineralogists, Special Publication 38: 111–122

Klimchouk AB (2007) Hypogene speleogenesis: hydrogeological and morphogenetic perspective. National Cave and Karst Research Institute, Carlsbad, New Mexico, pp 5–97

Klimchouk AB (2014) The methodological strength of the hydrogeological approach to distinguishing hypogene speleogenesis. Hypogene Cave Morphologies Special Publication. National Cave and Karst Research Institute, Carlsbad, New Mexico

Lynch M, Al-Shaieb Z (1991) Paleokarstic features and thermal overprints observed in some of the Arbuckle cores in Oklahoma. Arbuckle Group workshop and field trip, Oklahoma Geological Survey, Special Publication 91–3

Merritt CA (1940) Mineral report no. 4: iron ores. Oklahoma Geological Survey Report

Palmer AN (2007) Cave geology. Cave Books, Dayton, Ohio
Puckett J, Halihan T, Faith J (2009) Characterization of the Arbuckle-Simpson aquifer. Final report submitted to the Oklahoma Water Resources Board, Stillwater, Oklahoma State University School of Geology
Scheirer DS, Hosford Scheirer A (2006) Gravity investigations of the Chickasaw National Recreation Area, south-central Oklahoma. U.S. Geological Survey Open-File Report 2006–1083
Sykes M (1997) Paleokarst characteristics of the surface and subsurface in the Viola Limestone (Ordovician) Arbuckle Mountains, Oklahoma. Shale Shaker J (Oklahoma City Geological Society March–April 1997)
Veni G, Palmer A (2009) Eastern Kansas and Oklahoma. In: Palmer A, Palmer M (eds) Caves and karst of the USA. National Speleological Society, Huntsville, Alabama, p 180
Wilson JL (1993) The Lower Ordovician Great American Bank of the Southwestern United States. In: Keller DR, Reed CL (eds) Paleokarst, karst-related diagenesis, reservoir development, and exploration concepts: examples from the Paleozoic section of the southern mid-continent: 1993 annual field trip guidebook. Permian Basin Section-SEPM, Arbuckle Mountains, Oklahoma, p 41

Hypogene Speleogenesis in the Southern Ozark Uplands, Mid-Continental United States

43

Rodney Tennyson, Van Brahana, Victor J. Polyak, Adriana Potra, Matt Covington, Yemane Asmerom, Jim Terry, Erik Pollock, and David D. Decker

Abstract

Giant spar crystals were discovered in Chilly Bowl Cave in northern Arkansas in an area of deep faults between the Ouachita orogenic province and the Ozark uplands. The crystals provide data that support hypogene speleogenesis, including fluid inclusion paleotemperatures, ^{13}C and ^{18}O, and U–Pb dates that are inconsistent with an epigenetic water source. During the Ouachita orogeny, thermal brines entered the Paleozoic carbonates of the Ozarks to form spar-lined caves (U/Pb spar dates = 52 ± 2 million years). This age significantly extends the range of cave ages in the region. The chemistry of the early waters was derived from the deeply buried Ouachita foreland basin. The spar crystals are intersected by more recent caves related to the present topography which experience upward flow below confining units and by definition are also hypogenic.

Keywords

Hypogene karst • Rising groundwater • Eocene calcite • Fault control • MVT deposits

1 Introduction

The Ozark Plateaus (Fig. 1) of south-central USA contain more than 8500 reported caves, tens of thousands of springs, and a diverse suite of other karst landforms (Imes and Emmett 1994; Brahana et al. 2005; Hays et al. 2016). They occupy an early- to mid-Paleozoic carbonate platform, with hydraulic confinement provided by late Carboniferous terrigenous rocks around its margins (Figs. 2 and 3). Precambrian basement rocks are exposed in the core of the St. François Mountains ~230 km northeast of the study area (Fig. 1).

R. Tennyson
1303 CR 919, Alpena, AR 72611, USA
e-mail: arcavermom@aim.net

V. Brahana (✉)
University of Arkansas, 20 Gearhart Hall, Fayetteville, AR 72701-1201, USA
e-mail: brahana@uark.edu

V.J. Polyak · Y. Asmerom · D.D. Decker
Department of Earth and Planetary Sciences, University of New Mexico, 221 Yale Blvd, Northrop Hall, 87131 Albuquerque, NM, Mexico
e-mail: polyak@unm.edu

Y. Asmerom
e-mail: asmerom@unm.edu

D.D. Decker
e-mail: dave.decker@caves.org

A. Potra
University of Arkansas, 22 Gearhart Hall, Fayetteville, AR 72701-1201, USA
e-mail: potra@uark.edu

M. Covington
University of Arkansas, 28 Gearhart Hall, Fayetteville, AR 72701-1201, USA
e-mail: mcoving@uark.edu

J. Terry
1103 W. Olive, Rogers, Toronto, AR 72756, Canada
e-mail: chillycaver@cox.net

E. Pollock
Stable Isotope Lab, University of Arkansas, Fayetteville, AR 72701, USA
e-mail: epolloc@uark.edu

© Springer International Publishing AG 2017
A. Klimchouk et al. (eds.), *Hypogene Karst Regions and Caves of the World*, Cave and Karst Systems of the World, DOI 10.1007/978-3-319-53348-3_43

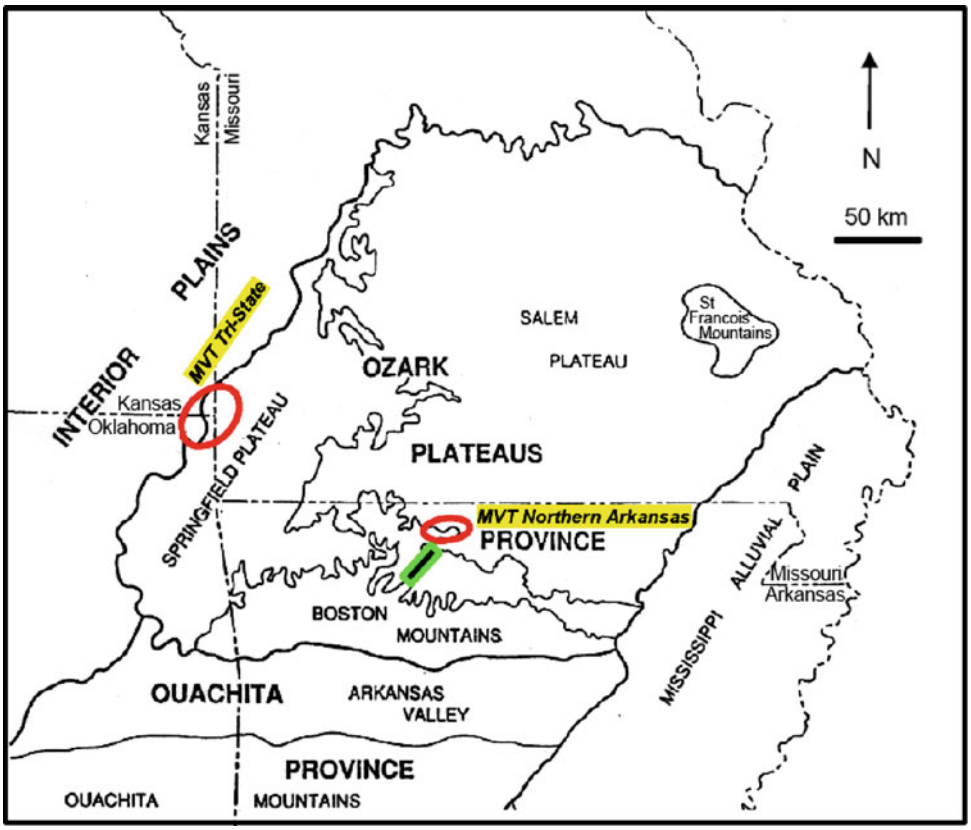

Fig. 1 Major physiographic provinces of the Ozark Plateaus. MVT deposits nearest the study area are shown as *red ellipses* and are identified by highlighting. The Flatrock Creek fault is shown by a green highlighted northeast-trending *black line*. Physiographic boundaries modified from Imes and Emmett (1994)

Much of the Ozark karst is epigenic (Bretz 1956). Hypogenic karst features are also present, but they have seldom been recognized because of overprinting by younger epigenic processes (Tennyson et al. 2008; Brahana et al. 2009). Understanding the distinction between these two karst types has evolved rapidly over the past several decades (Klimchouk et al. 2000; Klimchouk 2007).

This chapter concentrates on hypogene features observed in three caves along the Flatrock Creek fault in Newton County, northern Arkansas (Fig. 4). The caves (Chilly Bowl, Big Hole, and Endless Cave) are entered through surface pits along the fault (Fig. 5). Much of the data introduced here are from Chilly Bowl, but all three caves contain related hypogene features.

2 Field Geology

The Ozarks have been exposed to erosion since the Mesozoic, but are overlain in places with more recent sedimentary strata that are nearly flat-lying. The caves are in the Mississippian Boone Formation and are overlain by confining beds of the Batesville Sandstone and Fayetteville Shale (Fig. 3). The area has been disrupted by faults, joints, and slight tilting from various stages of uplift. The geology of the field area has been shown by structural mapping (Hudson and Murray 2004), a Bouguer gravity map of Arkansas (Hendricks 1988), and by drilling records and field observations.

Geophysical surveys (Hendricks 1988) show basement faults in northwest Arkansas have a dominant northeast-southwest pattern. During the Ouachita orogeny (late Paleozoic, ~318–271 Ma), these faults were reactivated, and new ones were developed, both extending from basement to land surface in overlying Paleozoic rocks (Haley et al. 1993; Hudson 2001; Johnson 2008). Soft sediment deformation along a major northeast-trending basement fault about 120 km west of the study area shows that movement along the fault was active as early as Osagean time (about 360 Ma), when St. Joe sediments were not yet indurated (Chandler 2001). Gravity anomalies suggest that reactivation of basement faults has been a major control of fracturing in this part of the Ozarks (Hendricks et al. 1981; Hendricks 1988).

3 Cave Descriptions

Mapping of the caves has been conducted since 1980 by the Middle Ordovician Lower Earth Society (MOLES) using standard cave-mapping techniques. Geologic data are also recorded (Figs. 6 and 7). Big Hole Cave and Chilly Bowl Cave have received the most intensive study of any caves in the area, and they are briefly described here.

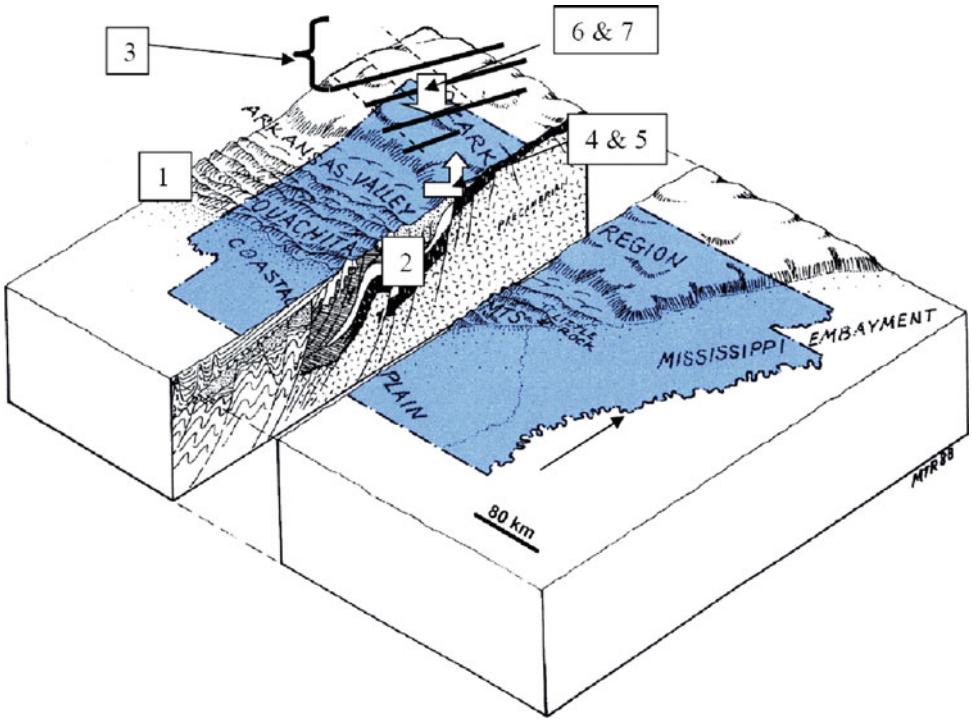

Fig. 2 Generalized conceptual model of hypogene speleogenesis of the southern Ozarks of northern Arkansas. Block diagram modified from Guccione (1993). *1* Compression caused by oblique closure (from east to west) of Ouachita orogeny. *2* Reactivation of deep basement faults, resulting in differential uplift that accommodates shortening from compression. *3* Faulting and tilting of relatively thin sedimentary-rock cover into orthogonally jointed and faulted blocks. *4* Expulsion of deep, hot (90–130 °C), aggressive water from the south by tectonic forcing along faults, creating dissolution (hypogene) and MVT deposits in tri-state and northern Arkansas regions. *5* Pulses of warm water deposited calcite spar and drusy quartz in fractures and voids in pores in carbonate rocks and previously created hypogene caves. *6* Very long history of weathering (on the order of tens of millions of years) lowered base level of main streams and drains, with continued pulses of warm water. *7* Multiple stages of overprinting of early hypogene karst by later hypogene karst processes from captured surface water and meteoric recharge; ephemeral and partial plugging of preexisting voids with speleothems and insoluble debris washed into caves from land surface and from reworked cave debris

3.1 Big Hole Cave

Big Hole Cave contains a series of large phreatic canyons and tubes at essentially a single level, which suggests a fairly simple epigenetic evolution. However, this part of the cave simply follows the top of a more complex phreatic series. A deeper part of the cave reveals that most of the upper passages are nearly filled with clay, and that the true depth of the system is much greater than originally thought. The present cave stream is fed by infiltration through domes and flows southeast on top of the clay fill. In the northern part of the cave, other domes drain into a deeper inaccessible part of the cave in which the clay has been partly removed. This latter drainage flows south-southwest, along the trend of the Flatrock Creek fault. This stream is at least 61 m below the entrance level of the cave and cannot resurge anywhere to the north or east. Groundwater appears to be dammed along the fault in the area between Big Hole and Chilly Bowl. The survey shows little gradient through the caves, so a dammed zone along the fault seems likely. The lower levels of Big Hole commonly back-flood to depths of more than 15 m, sometimes for months or years, with imperceptibly slow drainage. After discovery of this feature in 1980–81, it was nearly 13 years before the lowest portions of Big Hole were drained enough to complete the survey. Many faults are visible in Big Hole, as are large calcite deposits of suspected thermal origin.

3.2 Chilly Bowl Cave

Chilly Bowl Cave is probably the most intensively studied cave in the southern Ozarks (Tennyson et al. 2008; Brahana et al. 2009). It intersects features that are clearly much older and has spawned a whole new concept in Arkansas cave development. Faults are common and clearly visible in the cave, but only a few are large enough to be shown on published geologic maps—at the typical American scale of 1:24,000 = 2000 ft/in. (Hudson and Murray 2004). Most of them appear to have been important in controlling groundwater flow at the scale of individual caves.

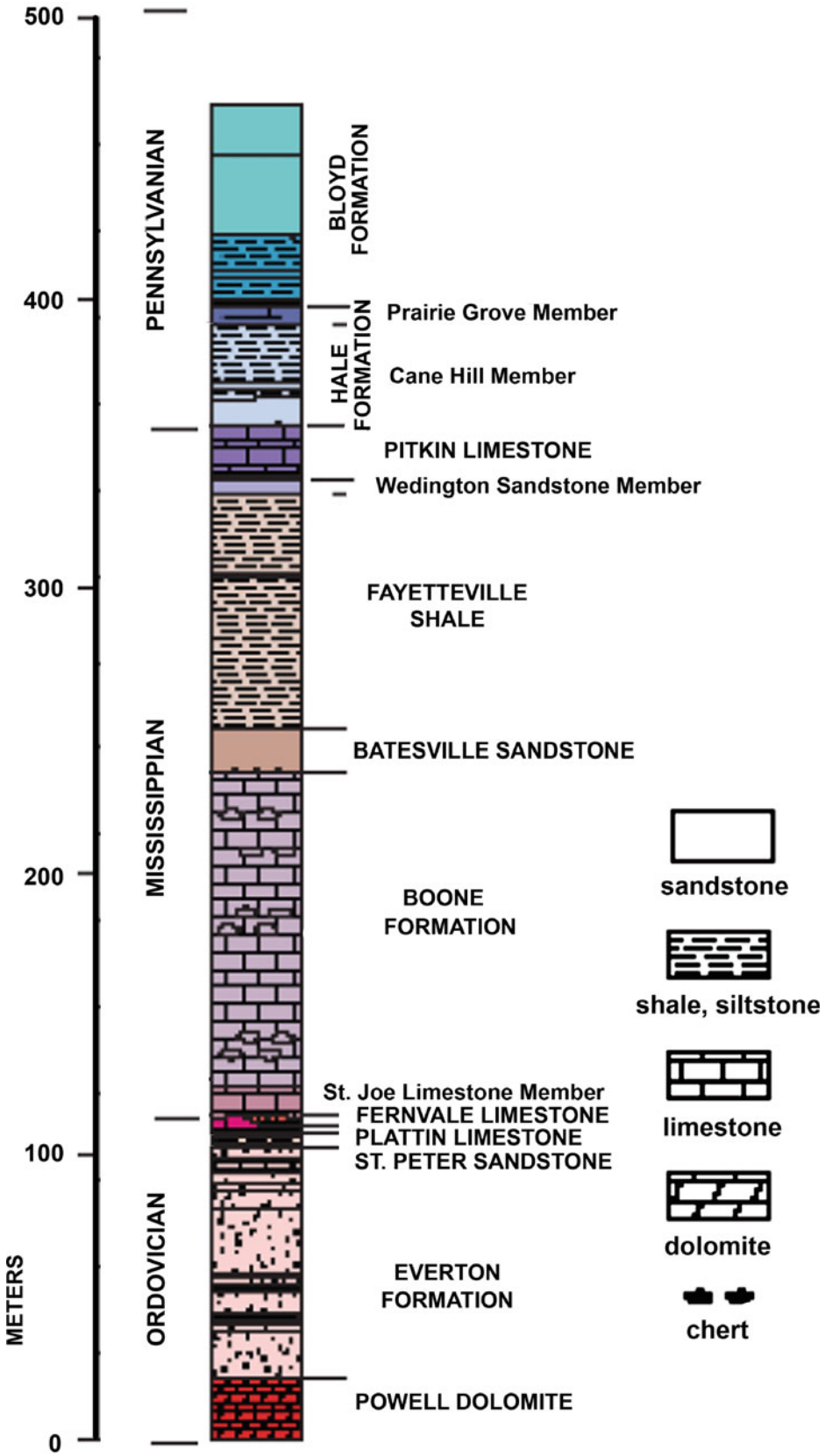

Fig. 3 Partial stratigraphic column in the study area (from Hudson and Murray 2004)

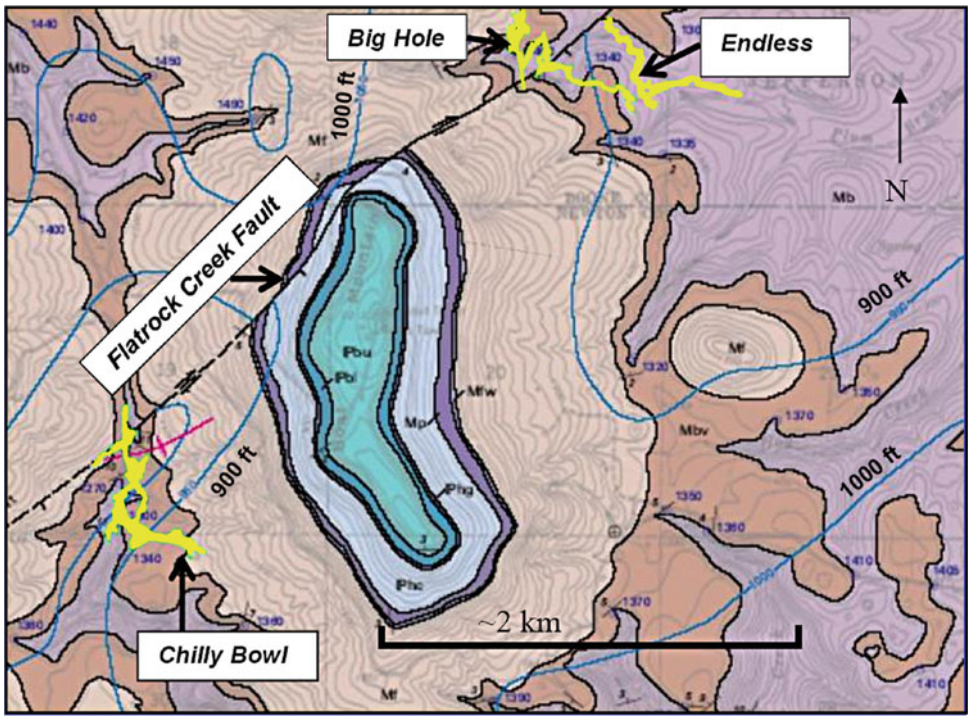

Fig. 4 Geologic map and cave locations in the main study area. Structural contours on top of the Boone Formation are shown in *blue*, and cave locations are in *yellow*. Geology from Hudson and Murray (2004) and cave locations from Tennyson et al. (2008). Note the relationship of the caves to the Flatrock Creek fault. For key to *map colors*, see Fig. 3. Structural contour interval = 100 ft (~30 m)

The most unusual aspect of Chilly Bowl Cave is its clearly hypogenic room, the Fortress of Solitude. This occurs in the uppermost reaches of Chilly Bowl Cave, and is about 10 m in diameter and is lined by large scalenohedral calcite crystals (Fig. 8). The crystals reach lengths as much as two meters. Sometime after the crystals were deposited, the spar was intersected by the main cave. Flooding coated the rooms and crystals with mud, typically at least a centimeter thick. The walls and crystals that underlie the mud are deeply etched by dissolution. In addition, many joints and faults in the cave contain veins of calcite and probably other minerals that project from the solutional walls.

4 Laboratory Data

Laboratory tests were run on the calcite spar from Chilly Bowl Cave to determine stable-isotope data and U-Pb ages at the University of New Mexico, Department of Earth and Planetary Sciences Radiogenic Isotopes Laboratory.

4.1 Sample Preparation and Analysis

For $\delta^{13}C$ and $\delta^{18}O$ analysis, powdered samples of approximately 3 mg each were obtained with a rotary tool and were reacted with H_3PO_4 in a common acid bath. Liberated CO_2 was cryogenically separated using a series of dry ice–ethanol–liquid nitrogen traps. Purified CO_2 was trapped in a glass cold finger, and isotopic analysis was carried out with a Delta Plus IRMS (Thermo Finnigan, Bremen, Germany) equipped with a multi-port dual inlet. Samples were normalized with standard reference gases from Oztech and NBS-19, and a standard (standard deviation <0.1 per mil) was prepared in the same manner as the samples.

A spar sample was etched with 3% nitric acid and broken in a clean napkin. Five pieces were analyzed. Each was dissolved in 15 N nitric acid, and a ^{205}Pb–^{233}U–^{236}U spike was added for isotope dilution analysis. U and Pb were cleaned and separated using anion resin chemistry. Separates were analyzed on a Thermo Neptune MC-ICPMS. Standard Pb and U solutions NBS-981 and CRM-112 were used to correct for mass discrimination. Four-point isochron ages were measured with the MC-ICPMS. Data were reduced with PBDAT (Ludwig 1994) and ISOPLOT (Ludwig 2001), using decay constants for ^{235}U and ^{238}U from Schoene et al. (2006).

Fluid inclusion temperature analysis was run on the Chilly Bowl calcite with a Leica Leitz Laborlux S microscope equipped with a USGS-modified fluid inclusion heating/cooling stage. A subsample was prepared by using a mortar and pestle to gently crush and cleave thin (100–500 μm) pieces of crystal. The subsample was then surveyed for two-phase inclusions. Standard #1 synthetic fluid inclusion from Syn Flinc was used for the low-temperature calibration, and standard #4 Syn Flinc was used for high-temperature calibration. A zero calibration using iced pure water was checked before and after calibration.

Fig. 5 Entrance shaft of Big Hole Cave (~38 m)

4.2 Analytical Results

Stable-isotopic analyses were derived for subsamples of a scalenohedral calcite crystal from the Fortress of Solitude (Fig. 9 and Table 1). Most values cluster in the center of the isotope graph and apparently represent typical cave conditions. The "heavier" $\delta^{13}C$ values (higher on the graph) are consistent with minor amounts of CO_2 degassing. The "lighter" $\delta^{18}O$ values (farthest left) verge on thermal conditions, but apparently do not represent significantly high temperatures. As expected for massive spar, none of the $\delta^{13}C$ values indicate significant degassing or evaporation

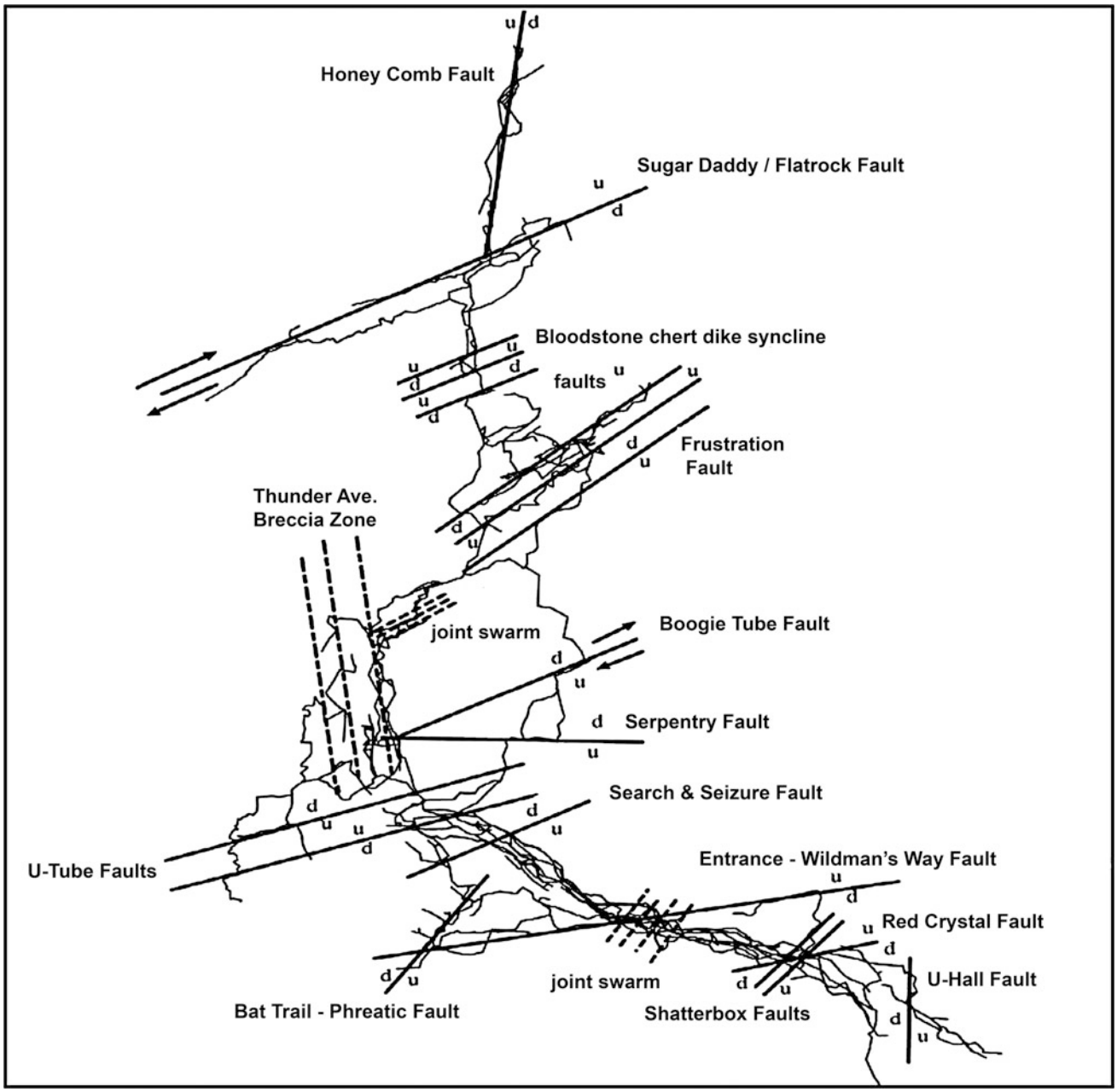

Fig. 6 Plan view of Chilly Bowl Cave illustrating the influence of faulting on the cave pattern. Relative motion along faults: *u* upthrown, *d* downthrown (after Tennyson et al. 2008). For scale and orientation, see Fig. 4

(zones of dripstone and coralloids on graph). However, some of the samples (A-6, A-7, A-8) show significantly "light" $\delta^{13}C$ values (low on the graph), which typically indicate a CO_2 source generated by oxidation of hydrocarbons (e.g., methane) from depth.

Uranium-lead 2-D isochron analysis of the calcite provided an age of 52 ± 2 Ma, which places its origin in the early Eocene. All five subsamples show secular equilibrium with respect to $^{230}Th/^{238}U$ and $^{234}U/^{238}U$, and U concentrations of 1.5–2.7 ppm. A temperature of formation of 52 ± 2 °C was also calculated. Fluid inclusion temperatures on three separate subsamples of cave spar yielded temperatures of 52.0 ± 0.5, 51.0 ± 0.5, and 57.5 ± 0.5 °C, which are compatible with the marginally thermal interpretation of the data shown in Fig. 9. (Note: the coincidence of "52" for both age and temperature is coincidental, and not a transcription error.)

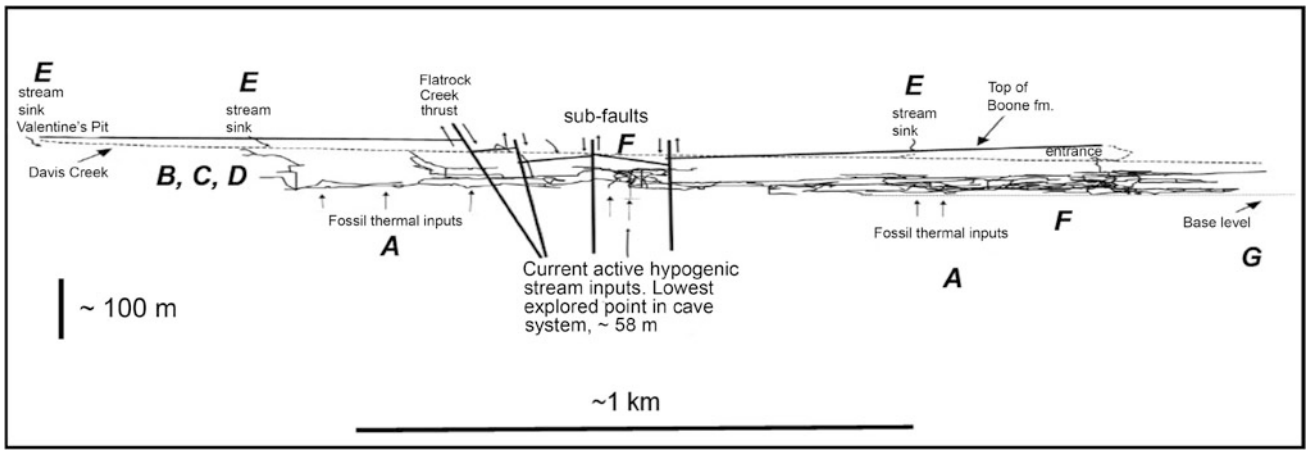

Fig. 7 Profile of Chilly Bowl Cave illustrating tectonic control (after Tennyson et al. 2008). See Table 1 for key to alphabetic labels

Fig. 8 Fortress of Solitude, an *upper-level* passage in Chilly Bowl Cave uniquely preserved with large calcite spar crystals precipitated from hydrothermal water. *Inset photograph* a backlit crystal showing incipient cleavage planes, and approximate area of anomalous $\delta^{13}C$ described in Table 2. A broken sample from an in situ crystal was used for stable-isotope analysis

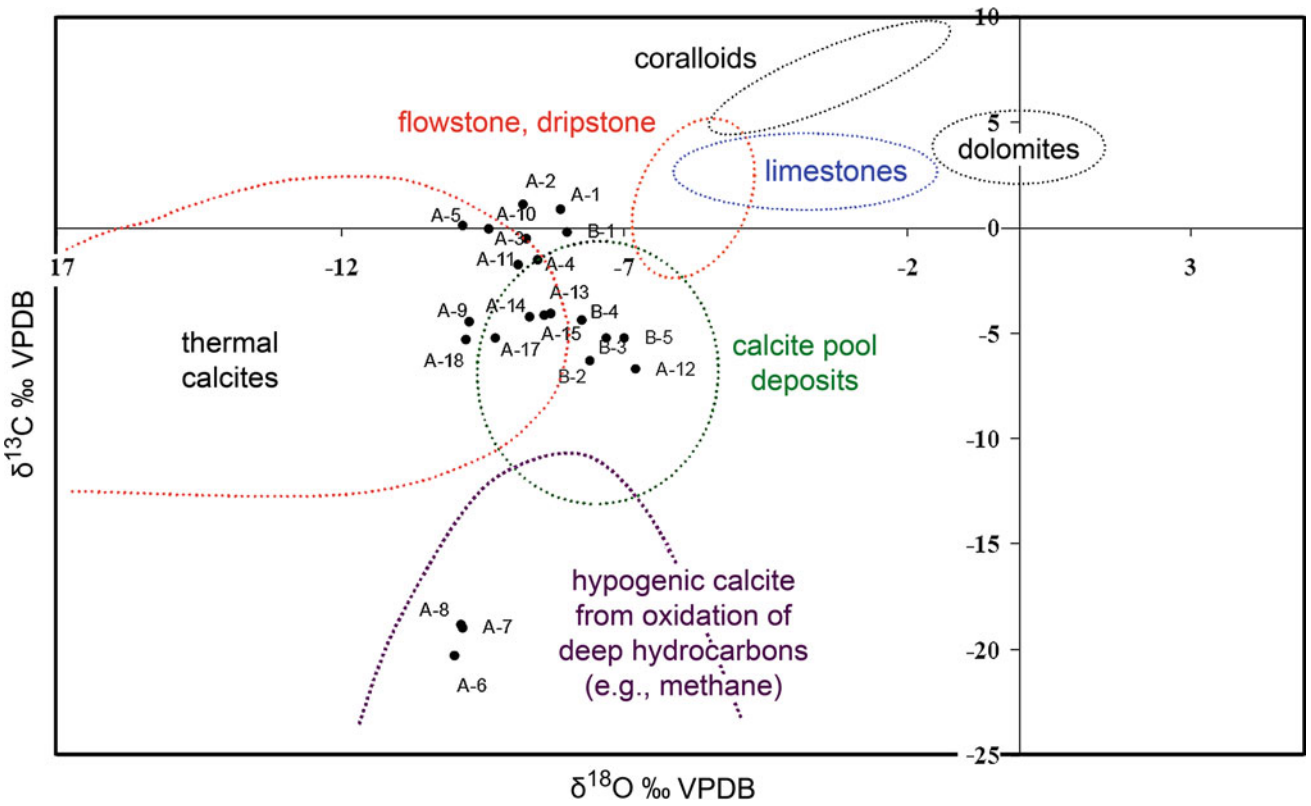

Fig. 9 $\delta^{13}C$ versus $\delta^{18}O$ for samples in this project (per mil, VPDB) superposed on typical ranges of values expected in various genetic environments (modified from Palmer 2007). Boundaries are approximate and vary with geographic location and environmental conditions. Samples A-6 through A-8 are anomalously light in $\delta^{13}C$, consistent with hypogenic calcite derived from the oxidation of hydrocarbons to CO_2. Most other samples fall in a zone of typical cave calcites near the margins of thermal deposits

5 Interpretation of Cave Development

Two periods of cave development are recognized in the study area: early semi-isolated chambers lined by giant calcite crystals (spar dates ~52 Ma), and later multi-level cave passages that intersected these earlier openings. These are compared to other contemporaneous events in the region.

5.1 Relation of Caves and Cave Deposits to the Ouachita Orogeny

The spar deposits and related cave development overlapped in time with the multi-pulse groundwater expulsion from the Ouachita orogeny, which emplaced ore deposits at the distal end of the groundwater flow system, primarily in Missouri, with lesser occurrences in Kansas, Oklahoma, and Arkansas. These are known as "MVT" deposits—Mississippi Valley type. The ores were emplaced in pulses by high-temperature fluids over the period from 251 to 39 million years ago (Coveney et al. 2000)—i.e., from earliest Triassic to late Eocene.

The MVT minerals sphalerite, galena, and chalcopyrite are disseminated throughout much of the study area in non-commercial quantities. These indicate deep regional flow, mainly along basement faults. Under confined conditions, geothermal water was expelled from the foreland basin along the southern flank of the orogenic belt and was driven northward toward the Ozark Dome. Farther south, in our field area, mineralizing fluids were injected into the overlying carbonate rocks via integrated faults and joints. Although the relationship of these episodes to the present karst is still uncertain, the general process is compatible with development of the early spar-lined karst voids along the Flatrock Creek Fault. The dates of the large Chilly Bowl calcite crystals coincide with the post-orogenic phases of the Ouachita orogeny. Expulsion of solutionally aggressive water by the tectonic stresses would have favored the origin of caves and solution pockets along faults, and a later slow increase in temperature was a likely environment for the growth of large calcite crystals. A comparison with the early spar-lined caves of the Guadalupe Mountains of New Mexico (DuChene et al., Chap. 31) may be revealing.

On the basis of homogenization temperatures for fluid inclusions in sphalerite, Leach (1979) and Leach and Rowan (1986) showed that MVT sphalerite was deposited during a northward cooling of deep basinal brines. The temperature is

Table 1 Stable isotopes ($\delta^{13}C$, $\delta^{18}O$) for each data point measured on the cleavage face (labeled A) and outside of the spar crystal (labeled B) from chilly bowl cave

Sample ID	$\delta^{13}C$ (VPDB)	$\delta^{18}O$ (VPDB)
A-1	0.83	−8.09
A-2	1.03	−8.76
A-3	−0.53	−8.71
A-4	−1.59	−8.50
A-4 (rerun)	−1.75	−8.51
A-4 (duplicate)	−1.22	−8.39
A-5	0.03	−9.83
A-6	−20.28	−9.97
A-7	−19.02	−9.84
A-8	−18.83	−9.86
A-8 (duplicate)	−18.74	−9.59
A-9	−4.48	−9.71
A-10	−0.09	−9.38
A-11	−1.79	−8.84
A-12 (duplicate)	−6.71	−6.79
A-12 (rerun)	−6.88	−6.70
A-13	−4.07	−8.27
A-14	−4.28	−8.65
A-15	−4.19	−8.40
A-15 (duplicate)	−4.03	−8.16
A-16	NS	NS
A-15 (rerun)	−4.16	−8.32
A-17	−5.29	−9.25
A-18	−5.37	−9.76
B-1	−0.29	−7.98
B-2	−6.35	−7.59
B-2 (rerun)	−6.27	−7.40
B-2 (duplicate)	−6.18	−7.29
B-3	−5.29	−7.31
B-4	−4.39	−7.72
B-5	−5.24	−6.99
B-5 (duplicate)	−5.25	−6.97

Anomalous sampling locations A-6 through A-8 on the spar are approximately located on the inset photograph in Fig. 5. Anomalous samples are shaded. "Duplicate" indicates separate duplicate samples from the same location in the crystal. Rerun indicates laboratory analyses rerun on a single sample. *NS* no sample

interpreted to have been above 100 °C in the general location of our study area. The temperature of formation of 52 °C for the cave spar is compatible with a low MVT brine temperature.

Isotopes from the core of the amber-colored calcite spar of Chilly Bowl Cave (Tennyson et al. 2008; Brahana et al. 2009; Fig. 9 and Table 1) reveal anomalous $\delta^{13}C$ of about 20‰ VPDB, which is compatible with CO_2 derived from organic compounds associated with deep flow through the organic-rich shales of the Arkoma hydrocarbon basin, which lies between the Ouachita and Ozark Mountains. These isotopic measurements validate the hypogenic nature of the spar crystals, at least of their earliest stages. They contrast with the generally "heavier" $\delta^{13}C$ values for typical calcite from the region (PD Hays 2008, Fayetteville, Arkansas, personal communication).

5.2 A Multi-level Cave System

The early spar-lined voids in the Fortress of Solitude in Chilly Bowl Cave are intersected by the main stream that formed the more recent parts of the cave. This water etched and partially removed the crystals, and covered them with

Fig. 10 Scallops in wall of Fortress of Solitude have truncated large calcite crystals. *Note* striations along cleavage planes in the calcite. *Width* of image ~1 m. Photograph by A. Palmer

varied thicknesses of mud (Fig. 10). Scalloped solutional surfaces on the spar give evidence for rapid flow, and the mud coating was apparently the legacy of periodic slow-moving floodwaters ponded by downstream constrictions.

Today, shallow groundwater flow that enters the caves generally follows the dip of the strata below the Fayetteville Shale and chert beds in the Boone Formation, except where the insoluble beds are absent or breached by fractures. Therefore, caves in the Boone Formation are somewhat isolated from surface flow. The water follows discordant faults and major joints in most areas, except where local mineralization has sealed them with low-solubility minerals. Water flow in these areas is forced up or around the barriers.

Caves along the Flatrock Creek fault appear to have been formed and enlarged by flow moving upward from ~30 m below the land surface along the same faults that were presumably used by deep-seated fluids in the past (Figs. 6 and 11). The asymmetry of scallops in conduits shows evidence for upward flow. Deposits of cobbles in some of the tubes show that the cave currently receives much recharge from the surface, with deep loops extending well below the water table. A vertical shaft filled with standing water in Chilly Bowl during normal flow conditions was explored by divers to a depth of about 10 m to a water-filled passage leading both upstream and downstream (Fig. 11).

According to the Klimchouk (2009) definition that hypogene cave origin is caused by rising water, much of the origin of these caves, even the most recent, can be considered hypogene. This would be especially valid during times of high recharge, when water flows toward the surface along faults.

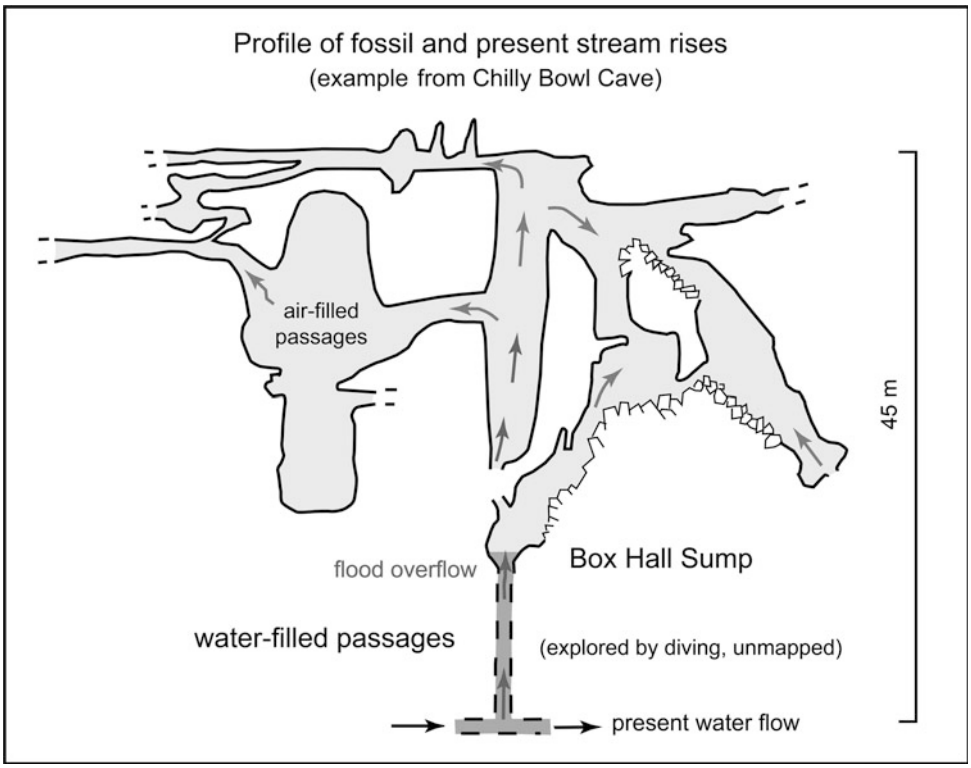

Fig. 11 Detail of rising-water input, Chilly Bowl Cave. The source of the water is obscure. *Arrows* indicate direction of water flow

Flow that is highly discordant to the strata is typical in this highly faulted area. Similar deep loops in phreatic cave passages are common to the north, in Missouri (Criss and Osburn 2009). Deep-seated faulting is considered to have been an influence. Dye traces in Missouri have revealed that the catchment areas of certain large artesian springs extend upstream as much as 64 km. Some conduits in Missouri extend more than 100 m below present stream valleys, in places penetrating below sea level.

6 Summary

This brief report documents two different episodes of hypogene speleogenesis in caves of the study area. Early semi-isolated rooms formed and were later lined with giant crystals of Eocene age during low-temperature thermal conditions. A post-orogenic stage of the Ouachita orogeny was probably responsible for the migration of thermal fluid from the south that was driven up by reactivation of basement faults in the cave area. The heat was geothermal; faults offered preferred paths for deep fluid flow; and the shale and sandstone cover of terrigenous sedimentary rocks supplied the insulation and confinement to allow the hot water to retain an anomalously high temperature far north into the Ozarks. The overlying carbonate cover was karstified by multiple pulses of hot water, especially in areas overlying the deep faults (Table 2).

Later meteoric recharge extensively modified the original hypogenic karst features as local flow captured surface streams and meteoric runoff. Extensive local faulting and a confining caprock caused artesian flow conditions especially during high flow. Evidence for ascending flow is common, making this a recent hypogene karst event.

There is a gradation between epigenic and hypogene conditions, and simple phreatic loops are generally not considered hypogene. However, deep water sources, clearly hypogene, have played an important part in the early origin and mineralization of the caves. This cave region provides a good case history of their interaction through time.

Table 2 Interpretation, relevance, and timing of key events that affected speleogenesis of chilly bowl cave

Episode	Feature/evidence	Interpretation	Relative timing	Comments
A	Near-vertical shafts cutting across bedding and chert layers; scallops indicate upward flow	Upward, cross formational flow, along sections of fractures	Likely old, formed by vertically upward flow in confined conduits	Strong evidence of hypogenic flow; scallops indicate flow direction from below
B	Amber dogtooth spar crystals	Precipitated from hot water expelled from Ouachita Basin during multiple pulses along major basement faults	Old, although younger than attribute A	Likely part of paragenetic sequence after MVT lead and zinc deposits
C	Stable isotopes—particularly carbon-13	Carbon-13 data in core of measured crystal consistent with methane source	Multiple pulses of water producing MVT and spar, bound by earliest olistoliths related to basement faulting (Chandler 2001)	Carbon-13 data and methane source are consistent with flow from an organic-rich environment, such as Arkoma Basin
D	Radionuclide dating of spar	Uranium-lead dating of calcite spar crystals indicates 52 ± 2 million years old. Sphalerite from tri-state region has been dated at 150 MYO	These analyses provide strong absolute age date for spar. Samples do not appear to have not been contaminated with lead	Radionuclide dating of uranium-lead yields a date of 52 ± 2 million years ago
E	Surface erosion, land-surface lowering, and capture of meteoric surface water	Karst drainage of surface water was opportunistic, and followed flow paths of least resistance	Stable isotopes are consistent with mixing of hypogenic and meteoric waters; this mixing was present in the outer margins of the spar crystal; this represents a significant time interval	Multiple periods of stream capture appear to have overprinted earlier zones of focused flow from hypogenic sources
F	Cavern morphology (Figs. 6 and 7) and erosional features	Typical morphology in plan and section for hypogenic cave (Klimchouk 2007)	Developed over long period of time; overprinting of old hypogenic features by younger epigenic features dominates cave, but is far from complete	Strongly influenced by initial hypogenic development
G	Fluid inclusions	Homogenization temperatures of nearby sphalerite deposits indicate $T > 100$ °C (Leach 1979); areal distribution shows cooling northward	Radionuclides indicate multiple stages of fluid expulsion from the south starting with Ouachita orogeny	Thermal water from a non-meteoric source is supported by these data and is consistent with flow and geochemical signatures

Attribute locations within cave are approximated on Fig. 2

Acknowledgements The authors gratefully acknowledge significant contributions made by Emily Frank and Jeanna Tennyson in exploring and mapping Chilly Bowl Cave, by Dawn Cannon in communicating attributes of the cave to the karst community, and by the members of the Middle Ozark Lower Earth Society (MOLES), who helped with numerous excursions into challenging caves along the Flatrock Creek fault. We also thank Art and Peggy Palmer for helpful suggestions.

References

Brahana JV, Hays PD, Al-Qinna M, Murdoch JF, Davis RK, Killingbeck JJ, Szilvagyi E, Doheny-Skubic M, Chaubey I, Ting TE, Thoma G (2005) Quantification of hydrologic budget parameters for the vadose zone and epikarst in mantled karst. In: Kuniansky EL (ed) U.S. Geological Survey Karst Interest Group proceedings, Rapid City, South Dakota, US Geological Survey Scientific Investigations Report 2005–5160, pp 44–152

Brahana JV, Tennyson R, Terry J, Hays PD, Pollock E (2009) Reactivated basement faulting as a hydrogeologic control of hypogene speleogenesis in the southern Ozarks of Arkansas, USA. In: Stafford KW, Land L, Veni G (eds) Advances in hypogene karst studies. In: NCKRI Symposium 1. Carlsbad, NM. National Cave and Karst Research Institute, pp 99–110

Bretz JH (1956) Caves of Missouri. Mo Geol Surv Water Resour, 39

Chandler SL (2001) Carbonate olistoliths, St. Joe and Boone limestones (Lower Mississippian), Northwestern Arkansas. MS thesis, University of Arkansas, Fayetteville

Coveney RM, Ragan VM, Brannon JC (2000) Temporal benchmarks for modeling phanerozoic flow of basinal brines and hydrocarbons in the southern midcontinent based on radiometrically dated calcite. Geology 28(9):795–798

Criss RE, Osburn GR (2009) Geologic character of Missouri caves and karst. In: Palmer AN, Palmer MV (eds) Caves and karst of the USA. National Speleological Society, Huntsville Alabama, pp 158–162

Guccione MJ (1993) Geologic history of Arkansas through time and space: National Science Foundation unnumbered publication, Grant No. ESI-8855588, University of Arkansas, Fayetteville

Haley BR, Glick EE, Bush WV, Clardy BF, Stone CG, Woodward MB, Zachry DL (1993) Geologic map of Arkansas. Arkansas Geological Commission and U.S. Geological Survey, scale 1:500,000

Hays PD, Knierim KJ, Breaker B, Westerman DA, Clark BR (2016) Hydrogeology and hydrologic conditions of the Ozark plateaus aquifer system. U.S. Geological Survey Scientific Investigation Report 2016–5137. http://dx.doi.org/10.3133/sir20165137

Hendricks JD, Keller GR, Hildenbrand TG (1981) Bouguer gravity map of Arkansas. U.S. Geological survey geophysical investigations map GP-944, scale 1:500,000

Hendricks JD (1988) Bouguer gravity map of Arkansas. U.S. Geological Survey Professional Paper 1474

Hudson MR (2001) Coordinated strike-slip and normal faulting in the southern Ozark dome of northern Arkansas—deformation in a late paleozoic foreland. Geology 28:511–514

Hudson MR, Murray KE (2004) Geologic map of the Hasty quadrangle, Boone and Newton counties, Arkansas. U.S. Geological Survey Scientific Investigations Map 2847, Version 1.0, scale 1:24,000

Imes JL, Emmett LF (1994) Geohydrology of the Ozark plateaus aquifer system in parts of Missouri, Arkansas, Oklahoma, and Kansas U.S. Geological Survey Professional Paper 1414–F

Johnson T (2008) Geologic map of the Forum Quadrangle with a karst inventory, Madison County, Arkansas. MS thesis, University of Arkansas, Fayetteville

Klimchouk A (2007) Hypogene speleogenesis: hydrogeological and morphogenetic perspective. National Cave and Karst Research Institute Special paper No. 1

Klimchouk A (2009) Principal characteristics of hypogene speleogenesis. In: Stafford KW, Land L, Veni G (eds) Advances in hypogene karst studies. NCKRI Symposium 1. NM. National Cave and Karst Research Institute, Carlsbad, pp 1–11

Klimchouk A, Ford DC, Palmer AN, Dreybrodt W (eds) (2000) Speleogenesis—evolution of karst aquifers. National Speleological Society, Huntsville Alabama

Leach DL (1979) Temperature and salinity of the fluids responsible for minor occurrences of sphalerite in the Ozark region of Missouri. Econ Geol 74:931–937

Leach DL, Rowan EL (1986) Genetic link between Ouachita foldbelt tectonism and the Mississippi valley-type lead-zinc deposits of the Ozarks. Geology 14:931–935

Ludwig KR (1994) PBDAT, A computer program for processing Pb–U–Th isotope data, version 1.24. U.S. Geological Survey Open File Report 88–542

Ludwig KR (2001) ISOPLOT 3.60. Spec. Publ. 4, Berkeley Geochronol Cent, Berkeley, California

Palmer AN (2007) Cave Geology. Cave Books, Dayton Ohio

Schoene B, Crowley JL, Condon DJ, Schmitz MD, Bowring SA (2006) Reassessing the uranium decay constants for geochronology using ID-TIMS U–Pb data. Geochim Cosmochim Acta 70:426–445

Tennyson R, Terry J, Brahana V, Hays P, Pollock E (2008) Tectonic control of hypogene speleogenesis in the southern Ozarks—implications for NAWQA and beyond. In: Kuniansky EL (ed) U.S. Geological Survey Karst Interest Group proceedings, Bowling Green, Kentucky. U.S. Geological Survey Scientific Investigations report 2008-5023

Sulfides in the Mammoth Cave Area, Kentucky

44

Rickard A. Olson

Abstract

The Mammoth Cave area is best known for its epigenic caves. However, the area also contains examples formed or modified by sulfide-rich brines, some associated with petroleum. These include hydrogen sulfide in shallow aquifers generated by reduction in gypsum and anhydrite beds and nodules a few tens of meters beneath the lowest cave passages in Mammoth Cave; sulfides generated in oil reservoirs located in structural traps; and rare sulfide seeps intruding into the cave system that cause local dissolution and a proliferation of cave biota. A highly acidic stream enters at least one cave in the region, and although its effect is subdued by nearby sources of meteoric water, it demonstrates the potential for significant hypogene cave development in the region. Oxidation of iron sulfide inclusions in the host limestones has produced weathering rinds and minor solutional effects on cave passages.

Keywords

Mammoth Cave • Hydrogen sulfide • Hydrocarbons • Hypogenic seeps • Biota

1 Introduction

Mammoth Cave is located in the Central Kentucky Karst region (White et al. 1970; Palmer 1981). The climate is temperate, with an annual mean precipitation of 132 cm. Meteoric water is largely responsible for the development of carbonate caves in the region, and this process continues today. Gently dipping limestones of Mississippian age (early Carboniferous) are covered in many areas by a non-carbonate caprock that protects upper-level passages from surface erosion and allows extensive caves to form, such as Mammoth Cave, the world's longest known cave. Up the structural dip to the southeast, the caprock has been removed by erosion, exposing a broad plain (Pennyroyal Plateau), noted for its many dolines and river caves. Speleogenesis in the region is dominated by the action of CO_2-rich meteoric groundwater. However, this short chapter concerns the little-known effects of hypogene processes on local cave development, particularly by oxidation of hydrogen sulfide.

2 Sulfur-Rich Brine Without Hydrocarbons

Crossing much of the Central Kentucky Karst is a structural monocline where the local bedrock dips more steeply to the north (Fig. 1). Along this monocline are three known places where sulfur-rich brine has risen under artesian conditions in the past, and in places continues to do so. A colorful description from 1845 is given at Sulphur Well (SW in Fig. 1)—with dimensions converted to the metric system: From observing nearby brine seeps, Ezekiel Neal drilled for salt water near the Little Barren River. At a depth of 55 m, the 45-kg auger and 55-m drill pipe were suddenly ejected from the well and flew over the top of a large sycamore tree. Water shot from the 15-cm-diameter well to a height of 6–9 m for an extended period (Sulphur Well Homemakers 2000). Today, the water continues to rise slowly from a

R.A. Olson (✉)
1950 Roy Hunter Road, Cave City, KY 42127, USA
e-mail: rickardolson16@gmail.com

© Springer International Publishing AG 2017

A. Klimchouk et al. (eds.), *Hypogene Karst Regions and Caves of the World*,
Cave and Karst Systems of the World, DOI 10.1007/978-3-319-53348-3_44

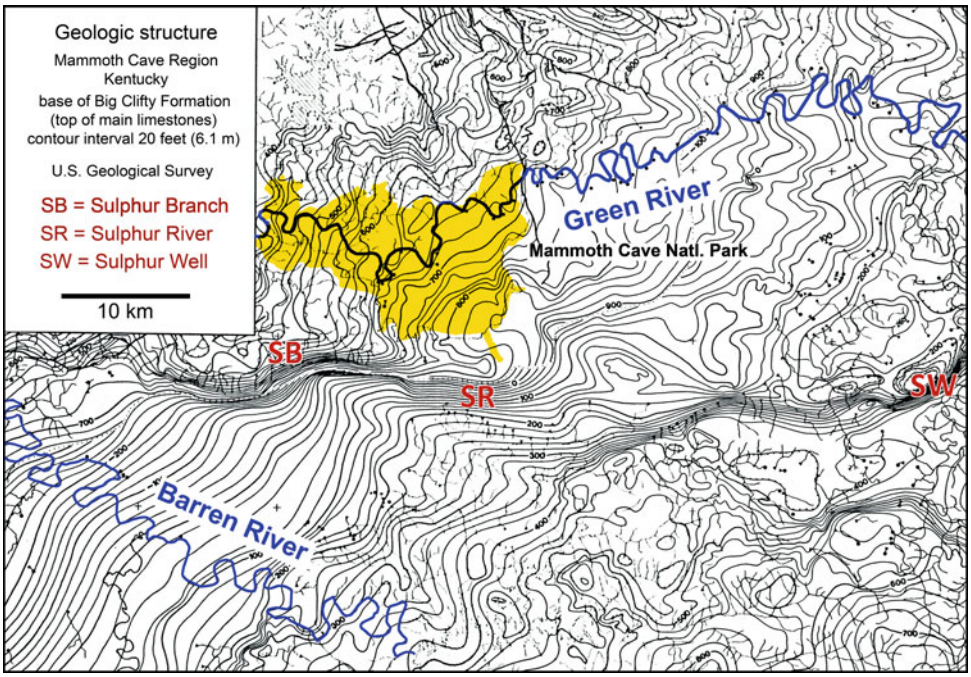

Fig. 1 Structural contour map of the south-central Kentucky Karst. The east–west band where the contour lines are clustered is a monocline where the bedrock dips more sharply to the north. Known modern or historic sites of rising sulfurous brine are indicated by SW (Sulphur Well), SR (Sulphur River), and SB (Sulphur Branch of Alexander Creek). Modified from Quinlan and Rowe (1978). Note that "sulphur" (traditional English spelling) is still used occasionally in the USA in preference to the American "sulfur" to add an old-time flavor

concrete structure built around the well casing at a roadside park (Fig. 2).

3 Sulfur-Rich Brine with Hydrocarbons

Near the center of Fig. 1 is privately owned Parker Cave. Sulphur River (SR), one of five stream passages in the cave, contains a concentrated H_2S brine. It has been interpreted as leakage from a nearby oil well (Quinlan and Rowe 1978). However, Olson (1992) raised the question of whether the sulfide source was instead a naturally rising brine. This interpretation was later supported by the discovery of other natural brine seeps along the monocline in Fig. 1. The brine is a type associated with oil fields, although there is no indication of hydrocarbons in Parker Cave.

Of these sites, Sulphur River is the only one extensively studied (Thompson and Olson 1988; Roy 1988; Olson and Thompson 1988; Angert et al. 1998). The brine enters at ceiling level through a narrow passage in an otherwise epigenic stream canyon. It feeds a small waterfall that has deposited a feature called The Phantom, a soft, porous flowstone mass. In the small room at this site, H_2S in the air is absorbed by water droplets on the ceiling to produce sulfuric acid measured at an average pH of 0.13. The sulfuric acid appears to have been responsible for enlarging the passage to room size (Fig. 3). It is questionable whether this could have occurred since the oil exploration of the 1920s. Roy (1988) characterized the Phantom waterfall waters as similar to oil-field brines in Mississippian strata elsewhere in the region.

At the canyon floor, this brine joins an otherwise normal carbonate-rich, aerated cave stream. From the field data of Roy (1988), Palmer (2007) summarized its effect on dissolution potential. Where the waterfall entered, the stream pH dropped from 7.98 to 6.40, calcite saturation index changed from +0.67 (supersaturated) to distinctly undersaturated (−0.21), and the dolomite saturation index changed from +0.43 to −0.53 (again from supersaturated to highly undersaturated). Saturation index = log (ion activity product/equilibrium constant), so in a saturated solution SI = 0. The value for dolomite is divided by 2 to adjust for dolomite producing twice as many ions as calcite. The addition of the sulfide-rich water to a normal surface-fed cave stream can enhance the rate of speleogenesis in a passage like Sulphur River without significantly changing the overall passage morphology. One might expect the passage to be more typical of hypogean caves, but much of the special character of a hypogenic cave depends on a rising flow pattern. Enhanced carbonate dissolution from hypogean sources in the Mammoth Cave area may not be visibly different from dissolution by epigean water.

Despite the high levels of atmospheric hydrogen sulfide (or indirectly because of it), the diversity and abundance of cave life in the Sulphur River passage are also high. The related oxidation reactions are strongly exothermic, providing energy sources. Two types of annelids, a cave snail, five species of collembolans, a psocopteran, two types of beetles, one type of spider, and several species of mites were collected here (Lisowski et al. 1985). Pearson and Jones (1998) found 9 cave crayfish (*Oroconectes pellucidus*) and one surface crayfish (*Cambarus tenebrosus)* upstream from the

Fig. 2 The well drilled at the town of Sulphur Well in 1845 is shown in the center of the photo. Note the close proximity of the well to the Little Barren River. Sulfide-rich brine still flows under artesian conditions. Photo by R. A. Olson

Phantom waterfall. Immediately downstream from the waterfall, they found 3 cave crayfish plus one surface crayfish, but all were soft shelled, apparently because of the low pH. It is amazing that they could survive here at all, and they would likely do better farther downstream where the acid is buffered by meteoric carbonate-rich waters.

Fig. 1, at SB, is Sulphur Branch of Alexander Creek, a small surface stream. In the past, it received water from Chameleon Spring, located a short distance west of Chalybeate, Kentucky (Peale 1886). There was even a hotel in Sulphur Hollow, where people came to "take the waters" (Norman Warnell, Brownsville, Ky., personal communication (2012)). As people in the region drilled water wells for domestic use, the aquifer was modified to the extent that sulfurous water no longer flowed from the springs, and the hotel is now gone. It is remarkable that this deep water was able to rise through the sandstone caprock that overlies the main limestones, and into the thin overlying Haney Limestone.

Water rich in hydrogen sulfide can rise high enough to enter the headwaters of drainage basins that feed the Mammoth Cave system. Besides the three known locations along the monocline where brine has been documented, there may be many more that remain undiscovered, similar to the underground Sulphur River. Energy inputs from photosynthetic sources are seasonal, but energy inputs from chemosynthetic sources are not, and so biomass from this latter source could raise the minimum level of food supply coming into the Mammoth Cave System. Other known sulfur springs in the region are not associated with the monocline, but each must have a geologic story to tell about groundwater flow patterns.

4 A Sulfide Seep in Mammoth Cave

Bullitt (1845) reported a "sulphur spring" in Marianne's Pass in Mammoth Cave which was rediscovered in 2007 by National Park Service Guide Bruce Hatcher, who reported unusual organic-rich seeps not far from a tour trail in the central part of the tourist area (Fig. 4). He was concerned that there might be a leaky sewer line. However, he also noted a slight hydrocarbon odor that is not consistent with sewage. Thousands of springtails are located on the moist

Fig. 3 The enlarged room where sulfide-rich brine enters Sulphur River in Parker Cave. Condensate droplets in this room are rich in sulfuric acid with a pH of ~0.13. The speleothem is a soft porous flowstone mass rich in microbial filaments. Photo by Norm Pace

organic-rich surfaces of the seeps (Rick Toomey, NPS, personal communication, 2010). Crickets and cave beetles are also common near the seeps. Marianne's Pass is located in a structural syncline (Palmer 1981) with small faults visible in the vicinity.

The hydrocarbon seeps were tested for both E. coli and fecal coliform, and the results for both were <1 cfu/100 ml (cfu = colony forming units)—i.e., below the detection limit. Sewage yields results of thousands of cfu, so a sewer-line leak is highly improbable.

The main seep is lined with microbial mats containing black and white precipitates resembling those where hydrogen sulfide is being oxidized (Fig. 4). Although no H_2S odor is apparent, 0.15 mg/L of H_2S was detected (A. Palmer, personal communication 2010). These seeps appear to be fed by water rising from below, but not up a drill hole. The seeps are weathered into the limestone walls, probably by a weak solution of sulfuric acid, and this would take a lot of time.

Subsurface hydrocarbons in the area can be under considerable pressure. For example, an oil strike at Arthur, Kentucky, produced a gusher in recent times (Kentucky New Era 1995). Oil and gas are abundant in the Mammoth Cave area, and there are asphalt mines just west and north of the park (Fig. 5). These tar sands resulted from hydrocarbons moving up through faults where the lighter fractions evaporated, leaving behind the tar.

5 Sulfides from Reduction of Gypsum and Anhydrite

In Mammoth Cave, biological communities are generally thought to be primarily supported by organic matter produced by photosynthesis. However, almost anywhere in the region, water with hydrogen sulfide can be reached by drilling 150 m or less, as is common for water wells. Near the middle of the St. Louis limestone are beds of gypsum (Palmer 1981), and even some anhydrite (Freeman 1951). Anaerobic microbial reduction in these sulfates is the most likely source of hydrogen sulfide in the freshwater aquifer. H_2S-bearing water may be rising under artesian conditions via fractures to the aerobic zone (Krothe and Libra 1983; Palmer 2007). In contact with oxygen, hydrogen sulfide can be used by sulfur-oxidizing bacteria as an energy source to convert carbon dioxide into organic carbon compounds via chemosynthesis, and H_2S can be oxidized to sulfuric acid.

6 Pyrite Oxidation in Exposed Carbonate Bedrock

In passages protected by the overlying Fraileys Shale, only minor amounts of water penetrate the underlying carbonate bedrock at Mammoth Cave. In anoxic zones, pyrite (FeS_2) was deposited along with the carbonates during the Mississippian Period and has been oxidizing for a long time near the land surface. This produces a small amount of sulfuric acid, which immediately reacts with the carbonate bedrock, yielding a calcium sulfate solution. This water can be drawn through primary pores in the rock to cave passages where the water evaporates and deposits gypsum in the form of wall crusts, flowers, needles, etc. Isotopic signatures of sulfur in the gypsum do not indicate a microbial role in the oxidation of pyrite (Metzger et al. 2015), so these sulfur reactions probably have no significance to Mammoth Cave ecosystems. Also, little effect on speleogenesis is expected or observed. Sulfate wedging enhances breakdown but does not increase passage volume.

Fig. 4 Dr. Horton Hobbs observing seeps in Marianne's Pass Photo by R.A. Olson

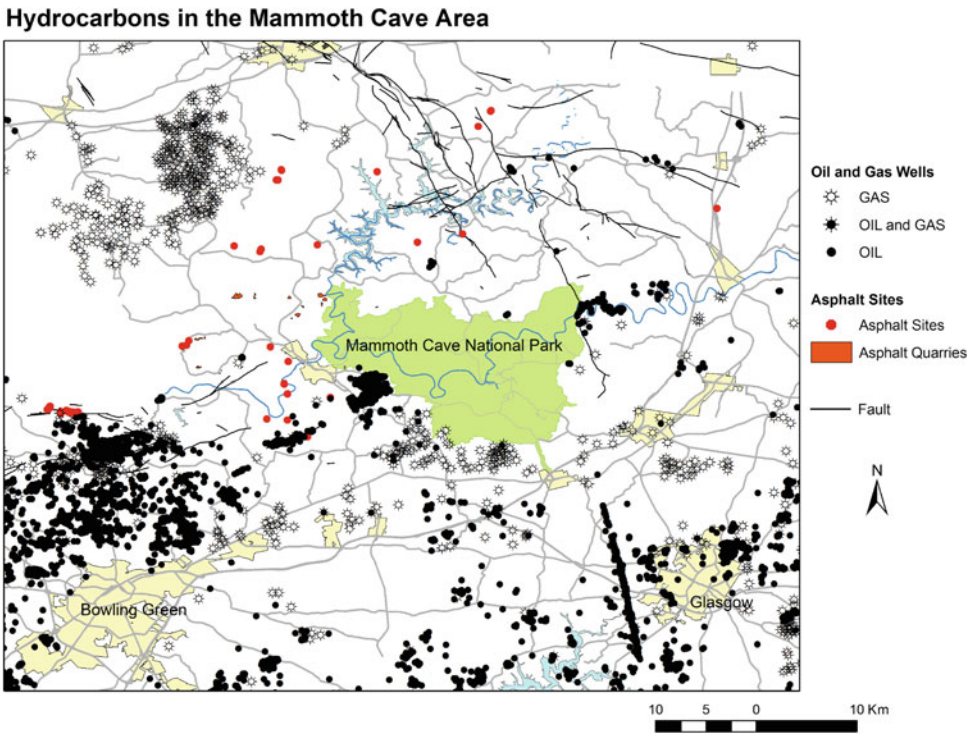

Fig. 5 Map of the Mammoth Cave area showing oil and gas wells plus historic asphalt mines. Map courtesy of Rick Toomey

7 Biodiversity as an Indicator of H_2S Speleogenesis

Mammoth Cave is known not only for length, but also for significant diversity of cave life. This can be a useful indicator of environmental conditions related to speleogenesis. Culver and Sket (2000) attribute high biodiversity in karst to its areal extent, high productivity such as chemoautotrophy, inclusion of phreatic habitat within caves, and length of caves. Groundwater rich in hydrogen sulfide is ubiquitous in the region at depths just below modern stream levels. In addition to the sulfur input at Parker Cave, there are likely to be many more examples that are cryptic. I have observed many times that the water at the confluence of the largest

streams in Mammoth Cave (Hawkins River and Logsdon River) has a milky turbidity consistent with colloidal sulfur. This location would be ideal for investigating the impact of H_2S on the energetics of the aquatic ecosystem of the cave, and also an opportunity to estimate the possible contribution of sulfuric acid to the development of Mammoth Cave. The Edwards Aquifer (Schindel et al. Chap. 41) is an example of chemoautotrophic energy inputs to subterranean aquatic life which helps protect against extinction and therefore contributes to increased biodiversity (Hutchins et al. 2016).

Hydrocarbon inputs should be considered as well, because even though this energy source is easily consumed by heterotrophic bacteria, it represents a source distinct from organic matter produced by recent photosynthesis. Methane concentrations below that of surface air were detected in three Kentucky caves, including Mammoth Cave, during the summer of 2012. The largest methane concentrations in the cave atmosphere were observed at cave entrances, and decreasing methane concentrations were noted farther inside (Webster et al. 2012). It is thought that methane-oxidizing bacteria on cave walls may be responsible for the lower concentrations deep in the cave. Oxidation of methane yields carbon dioxide and water, so it may provide a small-scale contribution to subaerial limestone corrosion. Chemoautotrophy has not been specifically considered as a factor in the high biodiversity of Mammoth Cave; but given the examples in this chapter, perhaps it should be (Olson 2013).

8 Conclusions

Even well-accepted models of epigenic cave origin, such as Mammoth Cave, can be affected by deep-seated processes. H_2S-rich water inputs to cave passages in the Mammoth Cave area indicate that sulfuric acid speleogenesis is occurring on a small scale. Considering the enormous length of cave passages in the region, there are probably many more examples yet to be found.

Acknowledgements Many thanks to Art and Peg Palmer, Horton Hobbs III, and Rickard Toomey III for help with the fieldwork, and to Kurt Helf for reviewing this paper.

References

Angert E, Northup D, Reysenbach A, Peek A, Goebel B, Pace N (1998) Molecular phylogenentic analysis of a bacterial community in Sulphur River in Parker Cave, Kentucky. Am Miner 83:1583–1592

Bullitt A (1845) Rambles in the Mammoth Cave during the year 1844 by a visiter. Morton and Griswold, Louisville, Kentucky

Culver D, Sket B (2000) Hot spots of subterranean biodiversity in caves and wells. J cave karst stud 62(1):16

Freeman L (1951) Regional aspects of Silurian and Devonian stratigraphy in Kentucky. Issue 6 of Bulletin Series IX, Kentucky Geological Survey: 347, 349, 408, 415, 434,512, 527, 528

Hutchins B, Engel A, Nowlin W, Schwartz B (2016) Chemolithoautotrophy supports macroinvertebrate food webs and affects diversity and stability in groundwater communities. Ecol 97(6):1530–1542

Kentucky New Era (1995) Oil boom boosting hopes of community. Kentucky New Era Newspaper, Hopkinsville, Kentucky, 19 Apr 1995

Krothe N, Libra R (1983) Sulfur isotopes and hydrochemical variations in spring waters of Southern Indiana, USA. J Hydrol 61:267–283

Lisowski E, Olson R, Roy W, Thompson B (1985) Geochemistry and biology of Sulphur River, Parker Cave, Kentucky. Cave Research Foundation 1985 annual report, pp 26–27

Metzger G, Fike D, Osburn R, Guo C, Addison A (2015) The source of gypsum in Mammoth Cave. Ky Geol 43(2):187–190

Olson R (1992) The source of Sulphur River in Parker Cave, Kentucky, a case of oil well pollution or a natural rise of brine? Natl Speleol Soc Bull 54(2):85–86

Olson R (2013) Potential effects of hydrogen sulfide and hydrocarbon seeps on Mammoth Cave Ecosystems. In: Mammoth Cave National Park's 10th research symposium, pp 25–30, 14–15 Feb 2013

Olson R, Thompson B (1988) Scanning electron microscopy and energy dispersive X-ray analysis of artificial and natural substrates from the phantom flowstone of sulphur river in Parker Cave. Ky Natl Speleol Soc Bull 50:47

Palmer A (1981) A geological guide to Mammoth Cave National Park. Zephyrus press, Teaneck, NJ, p 64, 102

Palmer A (2007) Cave geology. Cave Books, Dayton, OH, pp 224–225

Peale A (1886) Lists and analyses of the mineral springs of the United States. U.S. Geological Survey Bulletin 32. Washington Government Printing Office, p 235

Pearson W and Jones T (1998) A final report based on a faunal inventory of subterranean streams and development of a cave aquatic biological monitoring program using a modified index of biotic integrity. Report on file at Mammoth Cave National Park, Division of Science and Resources Management, p 139

Quinlan J, Rowe D (1978) Hydrology and water quality in the Central Kentucky Karst: phase II, part A: preliminary summary of the hydrogeology of the Mill Hole sub-basin of the Turnhole Spring Groundwater Basin. University of Kentucky Water Resources Research Institute, Lexington, Kentucky

Roy W (1988) Preliminary assessment of the solution equilibria of Sulphur River in Parker Cave, Kentucky. NSS Bull 50:37–41

Sulphur Well Homemakers (2000) Sulphur well history. Reprinted April 2000. The Printing Press, Edmonton, Kentucky

Thompson B, Olson R (1988) A preliminary survey of the protozoa and bacteria from Sulphur River in Parker Cave, Kentucky. Natl Speleol Soc Bull 50:42

Webster KD, Etiope G, Drobniak A, Schimmelmann A, Pratt L (2012) Measurement of terrestrial methane concentrations comparable to proposed methane concentrations on Mars. International Workshop on Instrumentation for Planetary Missions, Abstract #1009, Greenbelt, Maryland, 10–12 Oct 2, http://www.lpi.usra.edu/meetings/ipm2012/pdf/1009.pdf

White W, Watson R, Pohl E, Brucker R (1970) The central Kentucky karst. Geogr Rev 60:88–115

Sulfur-Based Speleogenesis in the Cumberland Plateau, USA

45

Lee J. Florea

Abstract

By any measure, both in the classical (Crawford in groundwater as a geomorphic agent. Allen and Unwin, Boston, pp 294–338, 1984; White in geomorphology and hydrology of karst terrains. Oxford University Press, New York, 1988; Sasowsky and White in Water Resour Res 30(12):3523–3530, 1994) and the present framework (Anthony and Granger in J Cave Karst Stud 66(2):46–55, 2004; Simpson and Florea in Caves and karst of America. National Speleological Society, Huntsville, pp 70–79, 2009), the karst landscapes of the Cumberland Plateau (western margin of the Appalachian Basin, eastern USA) are epigenic in nature. Discrete meteoric recharge is conveyed through sinking streams, sinkholes, and an epikarst reservoir into an integrated conduit system and toward topographically lower springs (Florea in J Hydrol 489:201–213, 2013a). The purpose of this brief manuscript is not to redefine that context, but to summarize a suite of data (Florea in investigations into the potential for hypogene speleogenesis in the Cumberland Plateau of southeast Kentucky, U.S.A. Brno, Czeck Republic, pp 356–361, 2013b; Florea in Acta Carsologica 42(2): 277–289, 2013c; Florea in Earth Surf Proc Land, 2015) that suggest that geochemical reactions involving sulfur associated with shallow petroleum reservoirs may have played a role in a polygenetic evolution of some Cumberland Plateau caves.

Keywords

South Central Kentucky • Sulfur isotopes • Carbon isotopes • Hypogenic karst • Principal component analysis

1 Hydrogeologic Setting

The focus of this paper is cave development in the Cumberland Plateau in carbonates of the middle-Mississippian Slade Formation (Ettensohn et al. 1984; Fig. 1) concentrating on the area of the deeply dissected topography of the Cumberland Escarpment, where the carbonates are exposed beneath a cap of early Pennsylvanian sandstones and conglomerates of the Lee Formation. Relief along the escarpment varies from less than 100 m in northeastern Kentucky and southwestern Ohio to more than 600 m in southern Tennessee and northeastern Alabama. East of the escarpment, down the stratigraphic dip, the limestones of the Slade Formation (equivalent to the 'Big Lime' or Newman Limestone in Kentucky, and the Greenbrier Limestone in the eastern Appalachians) are located below the surface in the Appalachian Basin and form a historically important target for petroleum exploration (McFarlan 1943). West of the escarpment, the Slade Formation has been removed by erosion along the axis of the Cincinnati Arch.

The middle-Mississippian carbonates extend through much of North America. Where they are exposed at the surface, they host world-class karst in Appalachia (White and White 2009) and along the margin of the Illinois Basin (including Mammoth Cave, Palmer 2009). Hypogenic

L.J. Florea (✉)
Indiana Geological Survey, Indiana University,
611 Walnut Grove, Bloomington, IN 47405, USA
e-mail: lflorea@indiana.edu

© Springer International Publishing AG 2017

A. Klimchouk et al. (eds.), *Hypogene Karst Regions and Caves of the World*,
Cave and Karst Systems of the World, DOI 10.1007/978-3-319-53348-3_45

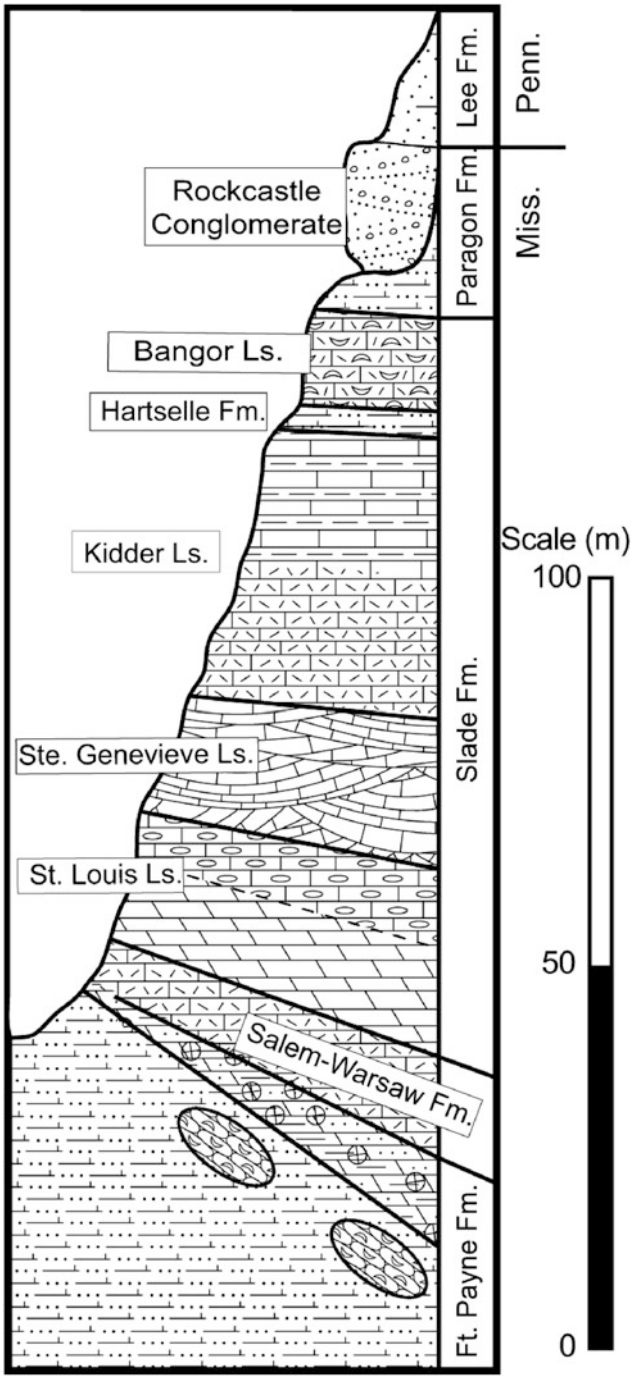

Fig. 1 Stratigraphy of the Cumberland Escarpment of South Central Kentucky

cave origin is a well-established process in many parts of the time-equivalent Madison Limestone of the western USA.

In southeastern Kentucky, the focus of this chapter, the Slade Formation is divided (in decreasing age) into the St. Louis, Ste. Genevieve, Kidder, and Bangor Limestone members (Fig. 1). In Tennessee, the Ste. Genevieve and Kidder are combined as the Monteagle Limestone. Toward northeastern Kentucky, these carbonate units thin dramatically and include significant clastic layers, yet they still host the significant karst of Carter Caves State Park (Engel and Engel 2009). In Tennessee and Alabama, these strata are thicker with few clastic beds, except for the Hartselle Formation, which separates the Monteagle and Bangor Limestones (Hoffelt 2009). Underlying, less soluble, cross-bedded siltstones of the Salem–Warsaw Formation locally acts as a base for conduit development (Simpson and Florea 2009). In the classic epigenic model applied to Cumberland-style karst, allogenic recharge from the plateau surface descends as vadose drainage in a stair-step pattern through the carbonate strata of the plateau margin (Crawford 1984) and coalesces into sinuous base-level conduits that generally parallel the surface valleys and topographic contours (Sasowsky and White 1994). Springs emerge at the base of the escarpment and the carbonate sequence. Levels of relict conduits were formed in response to episodic stream incision controlled in part by the advance and retreat of Pleistocene glaciers (Anthony and Granger 2004; Florea 2015).

2 Petroleum Geology

Commercial petroleum ventures along the Cumberland Escarpment began in the 1880s where natural sulfur seeps in base-level streams indicated a shallow reserve. Production peaked in the 1920s from reservoirs in the mixed carbonate-clastic margin of the Mississippian-age Borden Delta (McFarlan 1943) with most wells experiencing intense but short-term production (as much as 3×10^5 liters per day). Current exploration focuses on deeper and more productive Ordovician strata.

Fieldwork summarized by Florea (2013b, c) describes a concentration of natural petroleum seeps in the watershed of the Upper Cumberland River, in particular, the sub-watersheds of Beaver and Otter Creeks in Wayne County, Kentucky, and the Wolfe and Obey River watersheds of Pickett/Fentress Counties, Tennessee (Fig. 2). These seeps emerge from the Salem–Warsaw Formation through fractures in the streambed and largely consist of brines with dissolved sulfate and sulfide concentrations of >2 and >0.1 mmol/L, respectively (Florea 2013c). They emerge in the streams because buoyant convection conveys the brine to the points of lowest hydraulic head.

Petroleum seeps and associated reservoirs are concentrated in South-Central Kentucky and North-Central Tennessee, where meteoric flushing of basin fluids in the Cumberland Saddle has been less than in the Jessamine and Nashville Domes to the north and south (Parris et al. 2009). The seeps are also concentrated along the axes of anticlinal structures, where brine discharge noticeably reduces stream pH.

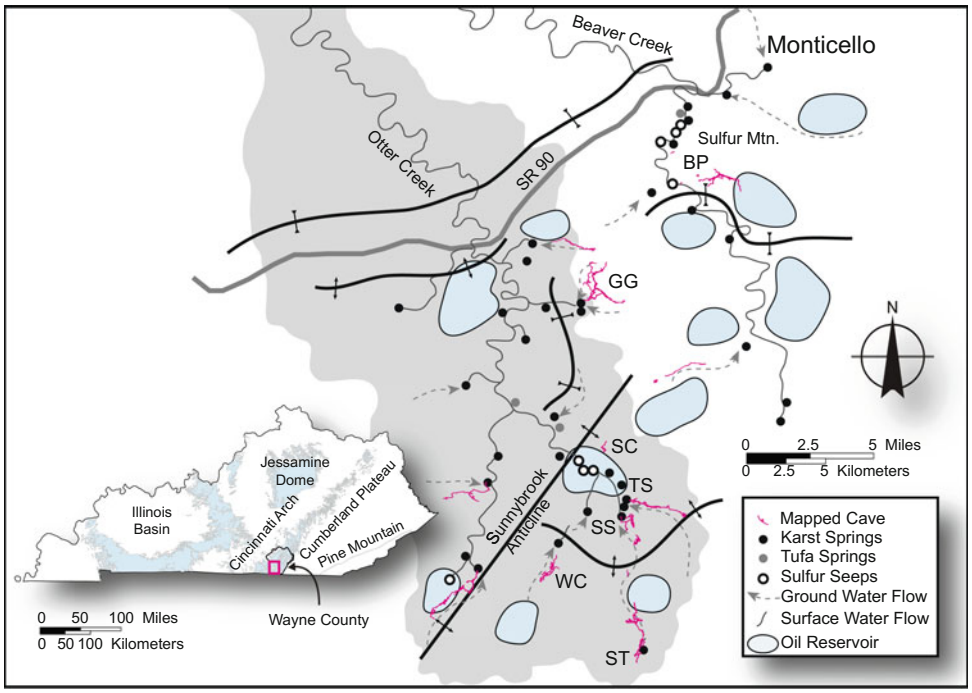

Fig. 2 Otter Creek watershed (*light gray shaded region*) and surroundings in South Central Kentucky. Principal mapped caves, karst springs, Tufa springs, sulfur seeps, groundwater flow paths, and structural features are shown. Areas of historic petroleum production from shallow reservoirs indicated by *light blue* areas. *BP* Bowman's Pit Cave, *GG* Grayson Gunnar Cave, *SC* Spelunger Cave, *SS* Sandy Spring, *ST* Stream Cave, *TS* Triple-S Cave, *WC* Wind Cave. Adapted from Fig. 1 of Florea (2013b). Index map of Kentucky includes principal karst regions in *cyan* with structural features labeled. The location of Wayne County is shown with a *magenta box* for the location of the Otter Creek watershed

3 Cave Exploration

Since 1997, cavers have surveyed more than 60 km of cave passage along the Cumberland Escarpment in Wayne County, Kentucky. This builds upon decades of exploration that resulted in more than 470 km of cave survey in the Kentucky segment of the Cumberland Escarpment (Simpson and Florea 2009) and more than 660 km of mapped passage along the Cumberland Plateau of Tennessee. Significant examples include Sloans Valley (40 km) and Coral Cave (36 km) in Pulaski County, Kentucky, and Blue Spring Cave (61 km) and Xanadu Cave (39 km) in White and Fentress Counties, Tennessee.

Deep caves along the escarpment commonly span the entire vertical range of the Mississippian carbonates, 104 m in southeastern Kentucky (Coral Cave) and 192 m in southern Tennessee (Rawhide Horror Hole). Vertical shafts tend to form in hillsides near the contact with overlying clastic rocks and capture allogenic recharge from the plateau surface (Brucker et al. 1972). Where the carbonates are free of clastic layers, these shafts are appreciably deeper, although limited by the regionally extensive Hartselle Formation.

In general, Cumberland Escarpment caves are aligned with five distinct geomorphic levels. The oldest level dates to the late Miocene (4–5.7 My) and 80+ m above base level at the elevation of the Highland Rim Peneplain (Anthony and Grainger 2007; Florea 2015). The most recent and lowest levels are separated by 20–30 m and apparently reflect the upstream migration of a nickpoint on the upper Cumberland River (Anthony and Granger 2007; Simpson and Florea 2009). Features of epigenic cave origin are widespread throughout these caves and include passage morphologies consistent with dendritic networks of shafts, canyons, drains formed in the vadose zone, and influenced by the stratigraphic dip. Phreatic and water table passages are meandering and anastomosing tubes of elliptical cross section, typically aligned along the stratigraphic strike (Palmer 1991). Dissolution scallops on passage walls indicate the direction and speed of flow (Curl 1974), and sediment on passage floors reflects the competence of cave streams to transport allogenic clastics during storm events (White 2007). Secondary cave deposits comprise a range of carbonate and evaporate speleothems (primarily calcite and gypsum) with morphologies that mainly indicate a vadose origin (Hill and Forti 1997).

4 The Role of Sulfur in Speleogenesis

Despite the dominance of decisive epigenic processes, some caves in South-Central Kentucky include passage geometries that differ from those of typical epigenic caves. They include diagnostic features such as rising half-tubes and blind cupolas, which fit a hypogenic interpretation (Klimchouk 2007). These features are often of minor extent, and it is difficult to distinguish them from epigenic features overprinted during epiphreatic conditions (Jeannin 2001; Florea and Vacher 2011) or paragenesis (Renault 1958; Ford and Ewers 1978), where rising waters during floods are guided by insoluble confining beds or sediments. Interestingly, however, survey notes from the caves with hypogenic features include references to petroleum or sulfide-rich brine. Furthermore, these caves are near active petroleum seeps in surface streams.

An example of a cave of potentially mixed origin is Spelunger Cave in the Otter Creek watershed of Wayne County, Kentucky. Its entrance is a fracture in the Bangor Limestone located on the crest of the Sunnybrook Anticline, in the saddle between two clastic-capped knobs. A 10-m slope leads to a ledge in the Hartselle Formation and a 49 m shaft into a large room. Passages that lead from this chamber are largely free of breakdown and have inconsistent geometries, variable ceiling heights, and a 'looping' character. Their wall morphology includes depositional features resembling mammillaries, associated with a phreatic origin (Hill and Forti 1997). In adjacent Otter Creek, a series of petroleum seeps is concentrated along the crest of the Sunnybrook Anticline (Fig. 2).

Another set of examples are the Wind Cave, Triple-S, and Redmond Creek cave systems, both in the headwaters of Otter Creek (Fig. 2)—all three systems include visible petroleum or brine leaking into cave streams from bedding planes or fractures. Wind Cave, or 'Oil Cave', includes 5 km of mapped passage with a lower active level known for an oily sheen and globs of oil that coat some rocks. Triple-S includes more than 7 km of mapped passage in two primary levels. The relict, now segmented upper level of Triple-S is connected to a base-level active conduit. A major tributary to that base level is termed 'Gasoline Alley', a reference to the odor of hydrocarbons found in that section of cave. The Redmond Creek System comprises 40 caves and 15 km of mapped passage enclosed within a 1900 ha watershed and alluviated sinkhole (Florea 2015). Several caves, such as Stream Cave, emerge at the contact between the Bangor Limestone and Hartselle Formation, only to sink into the underlying Kidder Limestone. From Stream Cave, groundwater travels some 6.6 km through cave passage and alluvium to rise within Natural Bridge Caverns and emerge at Sandy Springs. Passages within Natural Bridge Caverns can exceed 0.2 ha. Smaller active passages include known petroleum seeps.

The examples of Spelunger, Wind Cave, Triple-S, Redmond Creek, and other similar caves along the Cumberland Escarpment suggests that sulfur may have some role in the local speleogenesis. If so, what geochemical evidence might support this claim? Investigations over the past eight years have included the thick gypsum present in many caves, carbon isotopes in karst groundwater, and the flux of dissolved ions in karst springs.

4.1 Sulfur Isotopes in Gypsum

Deposits of sulfur-based minerals are common in many caves throughout the world. Recent attention to these minerals in karst settings has concentrated mainly on caves known to be hypogenic, such as those in the Guadalupe Mountains of New Mexico (DuChene et al., Chapter 31). In caves of South-Central Kentucky, such as Spelunger Cave, gypsum forms thick white crusts, bladed crystals, and fibrous extrusions attached to the walls of cave passages and floor sediments. Similar gypsum deposits throughout Appalachia have long been attributed to downward seepage of sulfate-enriched vadose waters (Pohl and White 1965; White and White 2003) in areas overlain by sulfide-rich clastic caprock. More recent data suggest that gypsum deposits coincide with pyrite-rich zones in the limestone stratigraphy (Palmer and Palmer 1995; Palmer 2007). In secondary gypsum, the range of values for the stable isotopes of sulfur ($\delta^{34}S$) is coincident with that of pyrite in strata immediately surrounding the cave, as shown by Metzger et al. (2015) in Mammoth Cave, Kentucky, with a mean value of −8.9‰.

Similar results are observed in a group of 15 gypsum samples from three caves in South-Central Kentucky, including Spelunger (Fig. 3). $\delta^{34}S$ values of these samples range between −6.9 and +10.6‰ (Florea et al. 2011). These values lie within the range of $\delta^{34}S$ values from authigenic pyrite in the Pennsylvanian caprock and are bounded by the $\delta^{34}S$ values of microbially mediated sulfate and sulfide from nearby petroleum seeps, which are +21.3 and −11.3‰, respectively. Values of $\delta^{18}O$ in these same gypsum samples indicate a mixed source between the atmosphere (+23.8‰), meteoric recharge (−6.6 to −8.1‰), and sulfur-rich brine (+13.8‰) (Onac et al. 2011). Two samples from deeper passages in Spelunger are curiously depleted with respect to ^{34}S and suggest a potential interaction with sulfide in brine.

4.2 Carbon Isotopes in Karst Groundwater

In karst groundwater, soil-derived dissolved inorganic carbon (DIC) reacts with limestone and produces groundwater DIC that is a theoretical 50% blend of soil and bedrock carbon, as

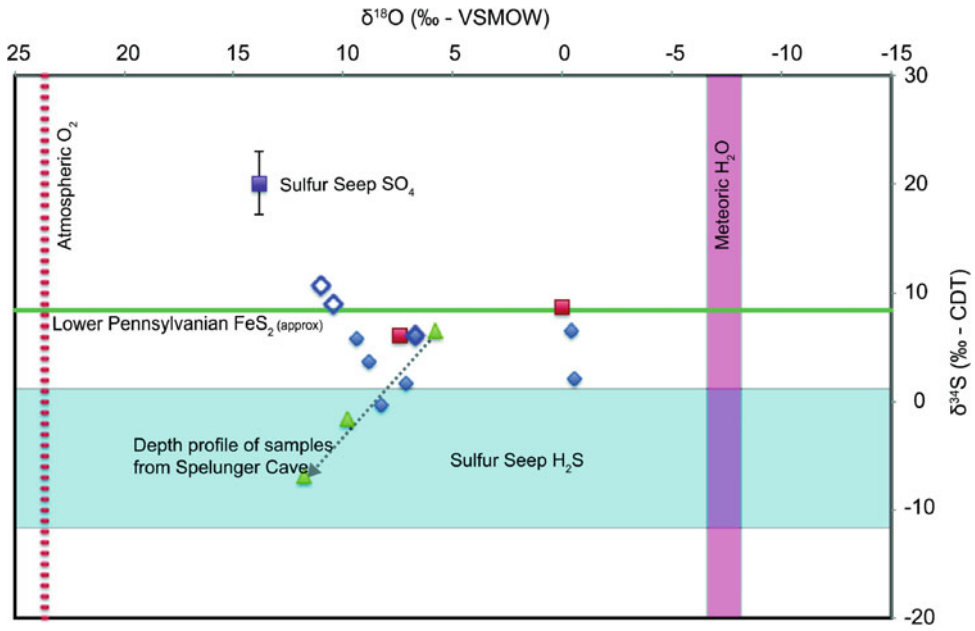

Fig. 3 Sulfur ($\delta^{34}S$) and oxygen ($\delta^{18}O$) isotope composition for secondary gypsum deposits in Bowman's Pit Cave (*open and filled blue diamonds* for the upper and lower levels, respectively), Grayson Gunnar Cave (*filled red squares*), and Spelunger Cave (*filled green triangles*). Isotopic composition of sulfate from sulfur seeps is shown as a *filled purple square* (from Onac et al. 2011)

controlled by the carbonate equilibrium reactions. Stable isotopes of this inorganic carbon, $\delta^{13}C_{DIC}$, theoretically reflect a similar blend of sources. Thus, spatial variations in bedrock carbon, climate, and land use have a first-order influence on the $\delta^{13}C_{DIC}$ in emerging spring water. However, $\delta^{13}C_{DIC}$ in karst groundwater can be significantly more complex than simple source mixing and may include changes induced by CO_2 enrichment or degassing along the flow path (Marlier and O'Leary 1984), by CO_2 sequestration owing to silicate weathering (Berner et al. 1983), or through microbial decomposition of organic carbon.

In the dynamic flow conditions of epigenic karst, variations in spring discharge from droughts or storm events may result in changes of DIC and $\delta^{13}C_{DIC}$. At Sandy Springs, for example, the flux of DIC (0.1–110 g/s) is directly proportional to discharge; 48% of the flux occurs during the time when the discharge is elevated above mean values (Florea 2015). Modeled DIC concentrations <3 mmol/L and values of $\delta^{13}C_{DIC}$ are inversely proportional to discharge, reflecting dilution and greater contributions of soil CO_2 during storm events. They are also directly proportional to the calcite saturation of the water (C/Cs), reflecting greater contributions of bedrock carbon (Florea 2013c; Fig. 4). At base-flow conditions, when spring waters are saturated with calcite, values of $\delta^{13}C_{DIC}$ (−8.1‰) are more enriched in ^{13}C than would be anticipated by simple carbonate equilibrium reactions (Florea 2013c). This indicates an additional contribution of bedrock carbon without corresponding carbon from soil CO_2. The oxidation of dissolved sulfides from brines is one process by which pH can decrease, which drives additional bedrock carbonate into solution. Measurements of brines from petroleum seeps reveal $\delta^{13}C_{DIC}$ values enriched in ^{13}C (−4.5 to −5.5‰).

4.3 Dissolved Ions in Karst Water

In the classic geochemical model of epigenic karst (see Sect. 4.2), the molar concentrations of total dissolved solids in solution will vary primarily according to the rate of reaction with the bedrock and the flux of water moving through the aquifer (Ford and Williams 2007). Thus, changes in the concentration of Mg^{2+}, Ca^{2+}, and HCO_3^- should account for most of the variation with time in geochemical data from a karst spring, such as at Sandy Springs (Florea 2013b). However, principal component analyses, a form of factor analysis, of these data reveal a more nuanced picture (Fig. 5). Concentrations of dissolved Mg^{2+}, Ca^{2+}, K^+, NO_3^-, and HCO_3^- covary and comprise parameters inversely proportional to discharge, so they decrease when discharge increases. In contrast, concentrations of Na^+, Cl^-, SO_4^{2-}, and total organic carbon (TOC) vary independently of discharge, are directly related to pH, and demonstrate the likely entrainment of organic-depleted brines into the karst aquifer. In these same analyses, the variation in $\delta^{13}C_{DIC}$ is potentially related to geochemical processes associated with both meteoric recharge and the entrainment of brines (Florea 2015).

In a closed epigenic system driven solely by the carbonate equilibrium reactions, the molar ratio of cations to bicarbonate in solution, $(Ca^{2+} + Mg^{2+})/HCO_3^-$, should be approximately 0.5; one cation will be produced for every two bicarbonates in solution, one each from the bedrock and from soil CO_2. The addition of sulfate reactions with bedrock will add cations to the system without bicarbonate and will therefore increase the ratio. In the geochemical model for data at Sandy Springs (Florea 2015), the ratio was 0.64, signifying that 28% of carbonate dissolution in the

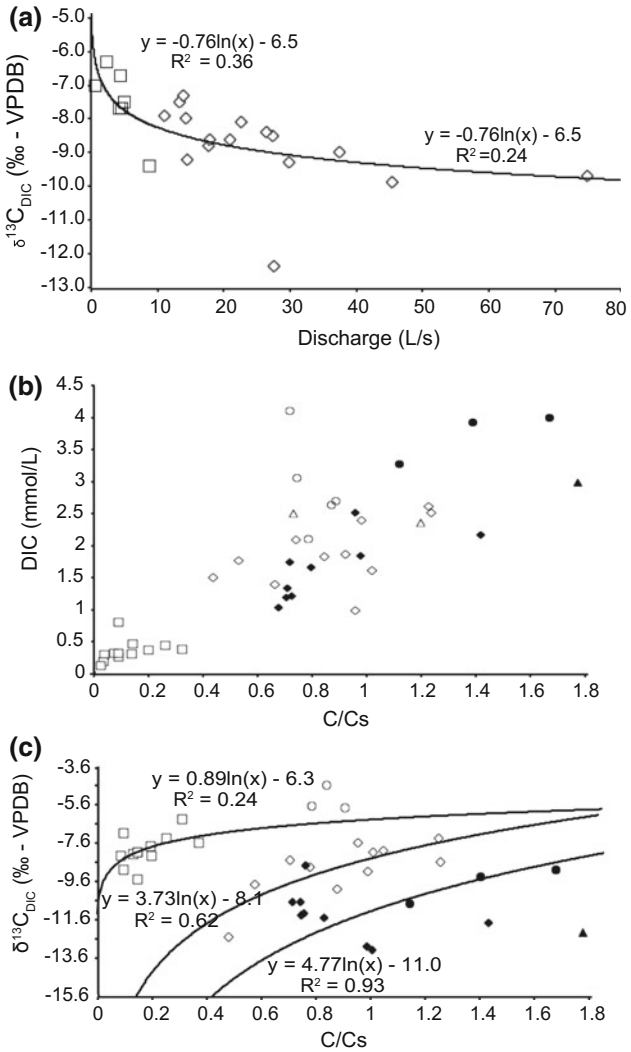

Fig. 4 Measurements of dissolved inorganic carbon (DIC) at Stream Cave (*open squares*), Sandy Springs (SS *open diamonds*), and sulfur seeps (*open circles*) from 2010–2011. Also shown are DIC measurements from 2012 samples including those from karst springs (*filled diamonds*), the Tufa spring (*filled triangle*), and the sulfur seeps (*filled circles*). From top to bottom: **a** $\delta^{13}C_{DIC}$ versus measured discharge; Stream Cave *open squares*, Sandy Springs *open diamonds*. **b** $\delta^{13}C_{DIC}$ versus C/Cs (saturation ratio, where 1.0 = saturation); logarithmic regressions shown for data from SC and SS. DIC concentration in the form of HCO_3^- is compared to calcite saturation ratio (C/Cs). **c** Values of $\delta^{13}C_{DIC}$ compared to calcite saturation index; logarithmic regressions for data from Stream Cave and Sandy Springs. Adapted from Figs. 3 and 5 of Florea (2013b)

watershed is potentially derived from sulfur-based reactions and is likely to come from brines entrained into the active flow system. Although this number must be tempered by the open-system nature of the aquifer—which may drive degassing, potential biogeochemical reactions with organic carbon, and sources from atmospheric deposition and sedimentary gypsum—the data, combined with the other lines of evidence in this manuscript, provide a robust indication that sulfur does play a role in karst processes. Most importantly, the flux of inorganic carbon, modeled at Sandy Springs, comprises soil- and bedrock-derived carbon, accounts for meteoric recharge and entrained brines, and contributes to a landscape evolution model that consistently and correctly positions cave levels above base level with known ages established by cosmogenic isotopes (Anthony and Grainger 2007; Florea 2015).

5 Summary

The caves and karst associated with the Cumberland Plateau in Kentucky and Tennessee serve as examples of epigenic speleogenesis with direct meteoric recharge and soil-sourced CO_2 driving the bulk of cave development, passage morphology, secondary mineralization, and geochemistry. Selected data presented in this paper do not change the overall framework, but they do provide an interesting foundation for a discussion of the role that hypogenic processes play in the formation of Cumberland-style caves. Curious but uncommon passage morphologies include speleogens of unclear origin and are found in watersheds that include petroleum seeps of sulfide-rich brines in base-level streams. Pervasive gypsum in these caves can largely be explained by the oxidation of sulfide minerals in the bedrock. Values of $\delta^{18}O$ in these same gypsum samples indicate a source that is mixed between the atmosphere (+23.8‰), meteoric recharge (−6.6 to −8.1‰), and sulfur-rich brine (+13.8‰) (Onac et al. 2011). Two samples from deeper passages in Spelunger are curiously depleted with respect to ^{34}S and suggest a potential interaction with sulfide in brine. Carbon isotopes of DIC from karst springs follow expected trends, but in some cases are interestingly shifted in the direction of bedrock carbon more than can be explained through the carbonate equilibrium reactions in a closed system. Dissolved ions offer a more persuasive argument for the influence of sulfur; those associated with brines covary with pH and are independent of ions linked with changes in discharge. Geochemical models based on time series data at karst springs are more enriched in bedrock cations than predicted by simple carbonate equilibrium reactions. This suggests that entrained sulfur-rich brines have a consequential role in the carbon flux from karst springs and resulting landscape evolution.

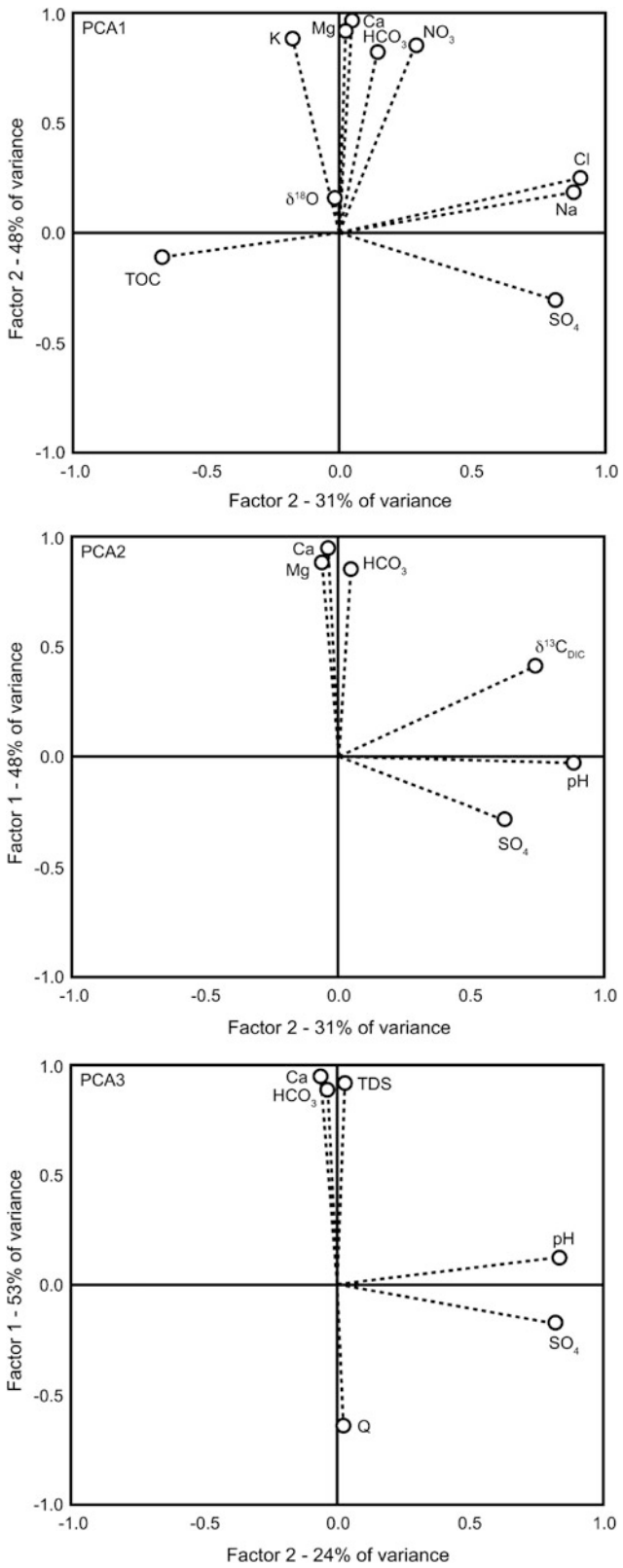

Fig. 5 Principal component analysis plots for data from Sandy Springs showing the eigenvalue weighting of each variable for PCA1, PCA2, and PCA3. The percent of variance accounted for by each eigenvalue is given on the axis. Components of sample TDS associated with shallow groundwater are heavily weighted on eigenvalue 1 and are anti-correlated to discharge. Components of sample TDS associated with shallow brines are heavily weighted on eigenvalue 2 and are anti-correlated to TOC. The pH covaries with shallow brines. The isotopes of DIC have complex loading. Figure originally published in Florea (2013b) and (2015)

References

Anthony DM, Granger DE (2004) A late tertiary origin for multilevel caves along the western escarpment of the Cumberland Plateau, Tennessee and Kentucky, established by cosmogenic ^{26}Al and ^{10}Be. J Cave Karst Stud 66(2):46–55

Anthony DM, Granger DE (2007) A new chronology for the age of Appalachian erosional surfaces determined by cosmogenic nuclides in cave sediments. Earth Surf Proc Land 32:874–887

Berner RA, Lasaga AC, Garrels RM (1983) The carbonate–silicate cycle and its effect on atmospheric carbon dioxide over the past 100 million years. Am J Sci 284:641–683

Brucker RW, Hess J, White WB (1972) Role of vertical shafts in the movement of ground water in carbonate aquifers. Ground Water 10(6):5–13

Crawford NC (1984) Karst landform development along the Cumberland Plateau Escarpment of Tennessee. In: LeFleur RG (ed) Groundwater as a geomorphic agent. Allen and Unwin, Boston, MA, pp 294–338

Curl RL (1974) Deducing flow velocity in cave conduits from scallops. Natl Speleol Soc Bull 36(2):1–5

Engel AS, Engel SA (2009) A field guide for the karst of Carter Caves State Resort Park and the surrounding area, Northeastern Kentucky. In: Engel AS, Engel SA (eds) Field guide to cave and karst lands of the United States, Karst Waters Institute Special Publication 15, pp 154–171

Ettensohn FR, Rice CR, Dever GR Jr, Chesnut DR (1984) Slade and paragon formations; New stratigraphic nomenclature for Mississippian rocks along the Cumberland Escarpment in Kentucky. US Geological Survey Bulletin 1605-B. US Geological Survey, Reston, VA

Florea LJ (2013a) Selective recharge and isotopic composition of shallow groundwater within temperate, epigenic carbonate aquifers. J Hydrol 489:201–213. doi:10.1016/j.jhydrol.2013.03.008

Florea LJ (2013b) Investigations into the potential for hypogene speleogenesis in the Cumberland Plateau of southeast Kentucky, U.S.A. In: Proceedings of the 16th international congress of speleology, Brno, Czeck Republic, pp 356–361

Florea LJ (2013c) Isotopes of carbon in a karst aquifer of the Cumberland Plateau of Kentucky, USA. Acta Carsologica 42(2): 277–289

Florea LJ (2015) Carbon flux and landscape evolution in epigenic karst aquifers modeled from geochemical mass balance. Earth Surf Proc Land. doi:10.1002/esp.3709

Florea LJ, Vacher HL (2011) Communication and forestructures at the geological intersection of caves and subsurface water flow—hermeneutics and parochialism. Earth Sci Hist 30(1):85–105

Florea LJ, Stinson CL, Weaver E, Lawhon N, Wynn JG (2011) Finding holes in a theory or finding a theory in holes—the potential role of hypogene speleogenesis for caves of the Cumberland Plateau in southeastern Kentucky. Geol Soc Am Abstr Programs 43(2):19

Ford DC, Ewers RO (1978) The development of limestone cave systems in the dimensions of length and depth. Int J Speleol 10(3–4): 213–244

Ford DC, Williams P (2007) Karst hydrogeology and geomorphology. Wiley, Chichester

Hill CA, Forti P (1997) cave minerals of the world, 2nd edn. National Speleological Society, Huntsville, AL

Hoffelt J (2009) The Cumberland Plateau of Tennessee. In: Palmer AN, Palmer MV (eds) Caves and Karst of America. National Speleological Society, Huntsville, AL, pp 85–91

Jeannin P-Y (2001) Modeling flow in phreatic and epiphreatic karst conduits in the Holloch Cave (Muotatal, Switzerland). Water Resour Res 37(2):191–200

Klimchouk AB (2007) Hypogene speleogenesis: hydrogeological and morphogenetic perspective. National Cave and Karst Research Institute Special Paper 1, 106 pp

Marlier JF, O'Leary MH (1984) Carbon kinetic isotope effects on the hydration of carbon dioxide and the dehydration of bicarbonate ion. J Am Chem Soc 106:5054–5057

McFarlan AC (1943) Geology of Kentucky. University of Kentucky Press, Lexington, KY

Metzger JG, Fike DA, Osburn GR, Guo CJ, Aadison AN (2015) The source of gypsum in Mammoth Cave, Kentucky. GSA Bull 43(2): 187–190. doi:10.1130/G36131.1

Onac BP, Wynn JG, Sumrall JB (2011) Tracing the sources of cave sulfates: a unique case from Cerna Valley, Romania. Chem Geol 288:105–114

Palmer AN (1991) Origin and morphology of limestone caves. Geol Soc Am Bull 103:1–21

Palmer AN (2007) Cave geology. Cave Books, Dayton, OH

Palmer AN (2009) The Mammoth Cave Region, Kentucky. In: Palmer AN, Palmer MV (eds) Caves and karst of America. National Speleological Society, Huntsville, AL, pp 108–113

Palmer AN, Palmer MV (1995) Geochemistry of capillary seepage in Mammoth Cave: Mammoth Cave National Park. In: 4th science conference, pp 119–133

Parris TM, Webb DJ, Fedorchuk N, Daugherty S, Takacs K, Schumacher A (2009) Brine chemistry in the Illinois and Appalachian Basins of Kentucky—implications for geologic carbon sequestration. American Association of Petroleum Geologists Eastern Section Meeting, Evansville, Indiana

Pohl ER, White WB (1965) Sulfate minerals—their origin in the central Kentucky Karst. Am Miner 50:1461–1465

Renault P (1958) Eléments de spéléomorphologie karstique. Annales de. Spéléologie 13(1–4):23–48

Sasowsky ID, White WB (1994) The role of stress release fracturing in the development of cavernous porosity in carbonate aquifers. Water Resour Res 30(12):3523–3530

Simpson LC, Florea LJ (2009) The Cumberland Plateau of Eastern Kentucky. In: Palmer AN, Palmer MV (eds). Caves and karst of America. National Speleological Society, Huntsville, AL, pp 70–79

White WB (1988) Geomorphology and hydrology of karst terrains. Oxford University Press, New York

White WB (2007) Cave sediments and paleoclimate. J Cave Karst Stud 69(1):76–93

White WB, White EL (2003) Gypsum wedging and cavern breakdown: Studies in the Mammoth Cave system, Kentucky. J Cave Karst Stud 65(1):43–52

White WB, White EL (2009) The Appalachian Mountains. In: Palmer AN, Palmer MV (eds) Caves and karst of America. National Speleological Society, Huntsville, AL, pp 17–23

Hypogene Caves of the Central Appalachian Shenandoah Valley in Virginia

46

Daniel H. Doctor and Wil Orndorff

Abstract

Several caves in the Shenandoah Valley in Virginia show evidence for early hypogenic conduit development with later-enhanced solution under partly confined phreatic conditions guided by geologic structures. Many (but not all) of these caves have been subsequently invaded by surface waters as a result of erosion and exhumation. Those not so affected are relict phreatic caves, bearing no relation to modern drainage patterns. Field and petrographic evidence shows that carbonate rocks hosting certain relict phreatic caves were dolomitized and/or silicified by early hydrothermal fluid migration in zones that served to locally enhance rock porosity, thus providing preferential pathways for later solution by groundwater flow, and making the surrounding bedrock more resistant to surficial weathering to result in caves that reside within isolated hills on the land surface. Features suggesting that deep phreatic processes dominated the development of these relict caves include (1) cave passage morphologies indicative of ascending fluids, (2) cave plans of irregular pattern, reflecting early maze or anastomosing development, (3) a general lack of cave breakdown and cave streams or cave stream deposits, and (4) calcite wall and pool coatings within isolated caves intersecting the local water table, and within unroofed caves at topographic locations elevated well above the local base level. Episodes of deep karstification were likely separated by long periods of geologic time, encompassing multiple phases of sedimentary fill and excavation within caves, and reflect a complex history of deep fluid migration that set the stage for later shallow speleogenesis that continues today.

Keywords

Shenandoah Valley • Maze caves • Episodic speleogenesis • Silicification • Dolomitization • Mississippi Valley Type ores • Virginia

1 Introduction

The purpose of this chapter is to illustrate the geologic and hydrologic framework within which the processes of speleogenesis and karstification in the central Appalachian Shenandoah Valley may be interpreted, and to provide observations and interpretations of several caves within that context. The information presented here on specific caves complements previously published field guides (Doctor et al. 2014, 2015), and a contribution to the Proceedings of the NCKRI Deep-Karst 2016 symposium (Doctor and Orndorff 2016).

D.H. Doctor (✉)
U.S. Geological Survey, 12201 Sunrise Valley Drive, Mail Stop 926A, Reston, VA 20192, USA
e-mail: dhdoctor@usgs.gov

W. Orndorff
Virginia Natural Heritage Program, 8 Radford Street, Christiansburg, VA 24073, USA
e-mail: Wil.Orndorff@dcr.virginia.gov

© Springer International Publishing AG 2017
A. Klimchouk et al. (eds.), *Hypogene Karst Regions and Caves of the World*, Cave and Karst Systems of the World, DOI 10.1007/978-3-319-53348-3_46

2 Background

2.1 Geologic Setting

The Shenandoah Valley is a smaller region within the greater Valley and Ridge physiographic province. In the state of Virginia, the central portion of the Shenandoah Valley is roughly 30 km wide at its greatest extent between mountains of the Blue Ridge province to the east and the ridges and valleys of the Appalachians to the west (Fig. 1). The general geologic structure of the Shenandoah Valley is a northeast–southwest-trending synclinorium that is bounded by the Blue Ridge thrust zone to the east and the North Mountain thrust zone to the west (Fig. 2). The valley is underlain by carbonate and siliciclastic sedimentary rocks; to a large extent, the carbonate rocks flank the valley on both sides, with siliciclastic rocks forming the central portion of the valley.

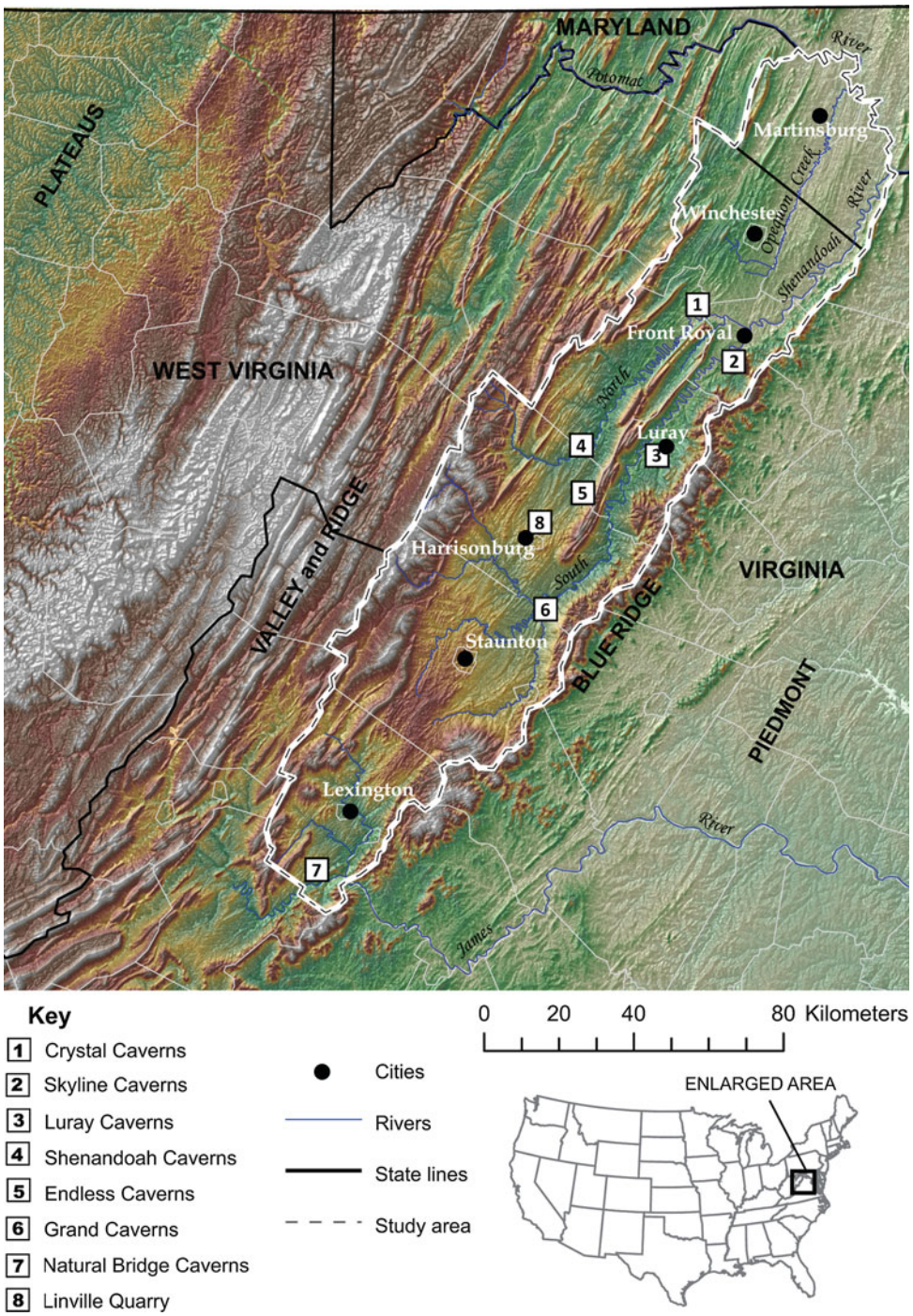

Fig. 1 Map of the central Appalachian region with the study area outlined

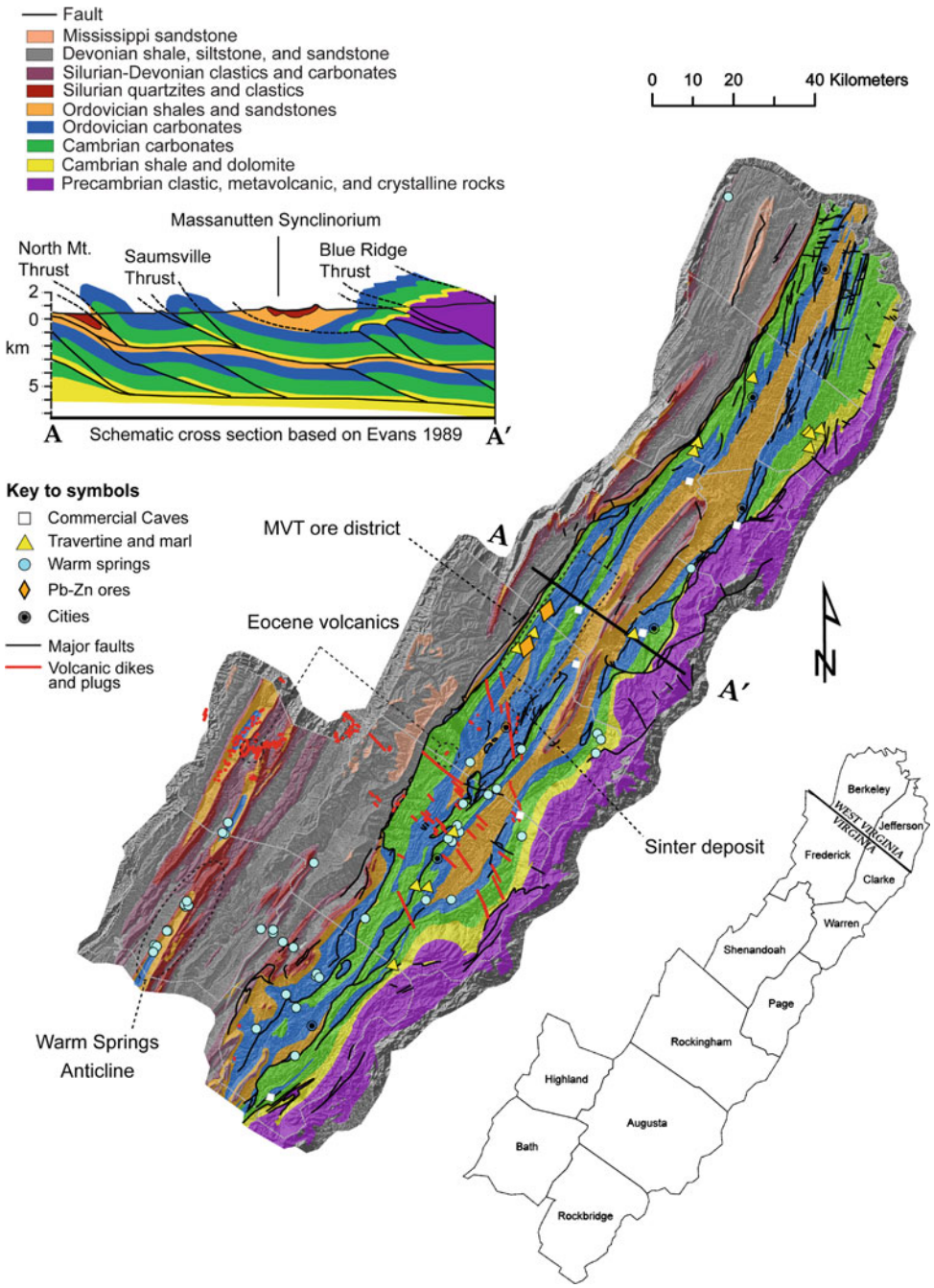

Fig. 2 Generalized geologic map and cross section of the study area from Virginia Division of Mineral Resources (2003)

The rocks are composed of Paleozoic marine sediments, and the carbonates comprise a thick package (>3000 m total thickness) of Cambrian and Ordovician carbonate platform deposits. These rocks have experienced multiple histories of deformation; however, the majority of the present structure is a consequence of the late Paleozoic to early Mesozoic (~320–220 Ma) Alleghanian orogeny. Karst features are present in all carbonate units in the Shenandoah Valley. These rocks include the Lower Cambrian Tomstown Dolomite, the Lower to Middle Cambrian Waynesboro Formation, the Middle Cambrian Elbrook Formation, the Upper Cambrian to lowest Ordovician Conococheague Limestone, the Lower Ordovician Beekmantown Group (limestone and dolomite), and the Middle Ordovician New Market Limestone, Lincolnshire Limestone, and Edinburg Formation.

Paleokarst features are present within the upper Beekmantown Group and the overlying New Market Limestone. This contact correlates with the Knox/Beekmantown unconformity, a regional paleokarst surface (Palmer and Palmer 2011). However, there is no observed correlation between this paleokarst horizon in the regional stratigraphy and the location of caves and other karst features in our

study area. Caves and solution features occur in all carbonate units, regardless of age, and appear to be primarily controlled by local structural conditions (Doctor et al. 2008).

Igneous intrusive dikes, sills, plugs, and diatremes are found scattered within the central Appalachian Valley and Ridge province (Southworth et al. 1993; Tso et al. 2004) (Fig. 2). These intrusive igneous rocks show two main age distributions: Late Jurassic (144–157 Ma) and Middle to Late Eocene (35–48 Ma) (Southworth et al. 1993). The Late Jurassic intrusive activity is attributed to Mesozoic extension that occurred during the separation of the African and North American continents and the opening of the Atlantic Ocean. The Middle to Late Eocene igneous rocks are the youngest igneous rocks in the Eastern USA, and their close proximity with the Jurassic rocks is thought to be related to reactivation of pre-existing structural weaknesses during a period of Cenozoic continental extension (Southworth et al. 1993). The close association of igneous intrusive rocks with certain cave and karst features suggests an association between the tectonic extension enabling the emplacement of igneous intrusions and the deep circulation of meteoric waters capable of karstification.

2.2 Evidence of Early Hydrothermal Fluid Circulation

Multiple episodes of fluid migration have affected the rocks of the Shenandoah Valley during orogenesis that likely set the stage for deep solution to occur later in geologic time. Growth of carbonate crystals in large vugs, recrystallization of carbonates, and replacement of carbonate minerals by silica are commonly observed in fault zones, and in areas of intensive folding of the rock strata. In addition, deposition of metal sulfide minerals within the carbonate rocks is common, and several economic deposits have been found within the Shenandoah Valley (Herbert and Young 1956). The primary economic deposits are located on the western side of the Shenandoah Valley in the Timberville region (Shenandoah and Rockingham Counties, Virginia—Fig. 2). The deposits occur in association with dolomitization in breccias along a 16 km zone following the regional strike of the valley (Herbert and Young 1956). Lead and zinc sulfide Mississippi Valley-Type (MVT) ore deposition either accompanied or post-dated late Alleghanian regional hydrothermal fluid migration (Hearn et al. 1987). Fluid inclusion analyses of rocks from the Timberville district indicate that fluid temperatures were in the range of 100–170 °C, and sulfur isotope analyses suggest that the source of the sulfur was from connate brines (Appold et al. 1995). Ordovician carbonates of the Beekmantown Group are generally the host rocks for mineral deposits of sphalerite, galena, pyrite, chalcopyrite, and greenockite.

Where MVT ores fill solutional cavities or display geometries resembling maps of cave networks, such deposits may be considered an aspect of hydrothermal karst (Palmer 2009) or reactivation of paleokarst (Palmer and Palmer 2011). Maps of the geometries of MVT deposits in the Shenandoah Valley are rare; however, the geometry of the Bowers-Campbell ore deposit located near the town of Broadway is a noteworthy example. At this locality, the ore mineralization occurs at the top of a large breccia body that extends horizontally along strike of the bedrock and vertically across the dip (Fig. 3).

Although the breccia is not thought to have formed from the collapse of a large solutional cavity prior to sulfide mineralization, marker beds traced into the breccia from the surrounding rock show distinct evidence of having dropped downward into the breccia (Herbert and Young 1956). Herbert and Young (1956) state that a local zone of tension permitted the lens-shaped breccias to form as chatter breccias, and that the "only place for solution in the formation of these breccias is in the possibility of hydrothermal solutions enlarging a pre-existing chatter breccia pattern" (Herbert and Young 1956, p. 45). Regardless of the cause of the brecciation, solutional porosity must have developed in order to permit infilling of the breccia with sulfide-bearing ores.

Such a setting for metal sulfide deposition may have been similar to that of the large calcite crystals observed within voids intersected during quarry operations at the Belmont Quarry in Staunton. A sample obtained from this quarry on display at the Virginia Department of Mines, Minerals and Energy shows large (up to 10 cm) euhedral crystals of scalenohedral calcite (Fig. 4). Some of these calcite crystals contain inclusions of pyrite (Penick 1987), indicating co-occurrence of sulfide-bearing solutions with the growth of the calcite.

2.3 Modern Hydrology of the Shenandoah Valley Karst

The modern carbonate aquifer of the Shenandoah Valley in Virginia is perhaps best characterized as a phreatic karst system developed within an artesian basin that has been overprinted by late fluviokarst evolution (Fig. 5). The more recent fluviokarst evolution is generally manifested in the upper few tens of meters of exposed carbonate bedrock, especially in proximity to incised surface drainages and where ancient alluvial sediments have mantled the bedrock (Doctor et al. 2014).

The karstic aquifer discharges to numerous springs that range in flow rate across 3 orders of magnitude. Spring discharge accounts for 60–90% of stream flow (Harlow et al. 2005), thus most streams in the karst areas of the Valley are gaining rather than losing. Some larger springs exhibit a

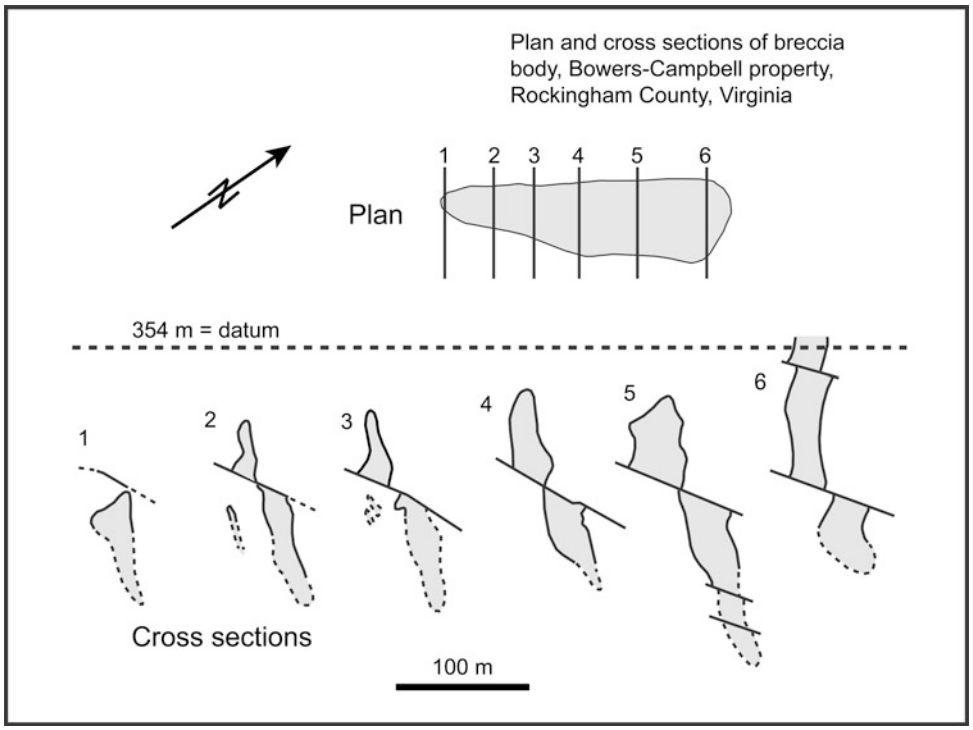

Fig. 3 Plan and cross section of the Bowers-Campbell Pb–Zn sulfide ore deposit. The breccia body is elongated along strike and crosses the rock strata at a high angle. Ore mineralization was concentrated at the top of the deposit, and faulting deformed the deposit post-deposition (from Herbert and Young, 1956)

Fig. 4 Large (5–10 cm) crystals of rhombohedral and scalenohedral calcite, some containing pyrite inclusions. This specimen was obtained from a quarry at Staunton, Virginia and is on display at the Virginia Department of Mines, Minerals and Energy in Charlottesville, Virginia

delayed response to rainfall events, with long hydrograph recession periods and muted chemical variability (Vesper et al. 2008; Doctor et al. 2011). Circulation of ground water through conduits exceeds depths of 300 m as evidenced by a small number of high-yield deep wells; most wells are finished less than 100 m below land surface and yield between 3.6 and 600 L/min (Cady 1936).

Constraints on the maximum depth of karst ground water circulation are provided by geologic structure and water temperatures of springs. Reeves (1932) defined thermal

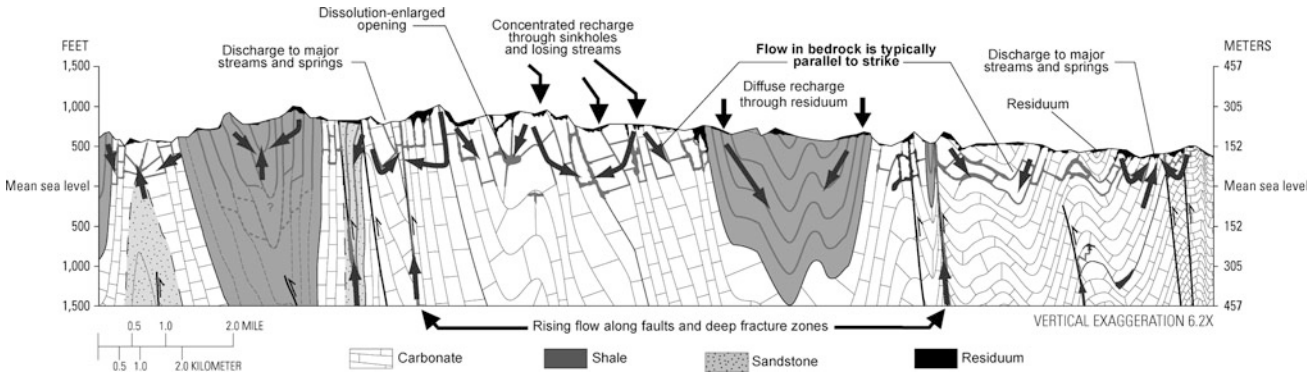

Fig. 5 Conceptual illustration of groundwater circulation within the Shenandoah Valley karst. Note the greater degree of bedrock solution at depths less than about 152 m (500 ft.) below ground surface, and enhanced solution along faults and fold axes at greater depths (modified after Nelms and Moberg 2010)

springs in the Shenandoah Valley as those with water temperature above mean ambient temperature of 12.6 °C that maintain such temperatures across seasonal cycles; however, true hot springs have temperatures that are a minimum of 5 °C above ambient. At least 15 mildly thermal springs have been identified within the Shenandoah Valley (Reeves 1932) (Fig. 2). One of these, Dices Spring, exhibits constant groundwater temperature at 17.9 ± 0.04 °C, which is approximately 5 °C above ambient temperature (Doctor et al. 2014). The spring is located adjacent to a cross-strike fault that cuts a major regional thrust fault (Gathright et al. 1978), and flow to the spring is likely generated from depths where these faults intersect.

Other warm and truly hot springs exist in the wider Valley and Ridge province (Reeves 1932). For example, a zone of hot (>30 °C) carbonate waters exists within the Warm Springs Anticline structure in Bath County, Virginia, south and west of the Shenandoah Valley (Fig. 2). These hot springs have been interpreted to gain their heat from deep circulation (>3 km) of meteoric water along fractures and faults (Perry et al. 1979). Siliceous sinter deposits are found in the vicinity of these hot springs, indicating former deposition of silica at the surface in the geologic past. Similar siliceous sinter deposits are found at the surface in the Shenandoah Valley near Harrisonburg in Rockingham County (Nolde and Giannini 1997). Primary precipitates of banded silica mixed with iron oxides have also been observed to have replaced carbonates adjacent to igneous intrusive rocks, such as on Mole Hill, a plug of mantle-derived basalt that intruded the carbonate rock of the Beekmantown Formation near Harrisonburg, Virginia (Doctor et al. 2014). Given the presence of ancient warm spring deposits and modern warm springs, hydrothermal activity appears to have played at least a local role in ancient karst development in the Shenandoah Valley.

Geologic controls on ground water flow strongly influence discharge and geochemistry of springs in the Shenandoah Valley (Vesper et al. 2008; Yager et al. 2013). Geochemical characteristics between different springs vary widely, although temporal geochemical variability of a single spring may be small. Larger perennial springs often occur along faults, and many lie above base-level streams (Doctor and Orndorff 2016). Upward flow gradients in wells occur particularly where cross-strike faults and joints intersect either bedding planes or strike-parallel faults (McCoy and Kozar 2008).

In areas where cross-strike faults, joints, and lineaments intersect thrusts or fold axes, the waters may emerge as tufa and travertine-depositing springs and seeps. The total depth of circulation of the modern system may be only several hundred meters, such as in the case of the mildly warm springs in the Shenandoah Valley; however, true hot springs in the Warm Springs region indicate depths of circulation up to a few kilometers. Continued landscape erosion causes cavern drainage and collapse, especially near base-level streams where downcutting permits subsurface piracy of surface tributary streams that flow toward base level through the exposed caverns. As surface karstification continues, the intersection of the hypogenic and epigenic flow systems results in the integration of ground water flow within a structurally compartmentalized carbonate aquifer.

Recharge to the deeper portion of the aquifer system occurs primarily at higher elevations on the ridges that flank the valley, and from focused recharge via sinking streams into carbonate units lying beneath colluvial and alluvial fan deposits that blanket the carbonates at the base of the ridges (Doctor et al. 2014). Flow may migrate across the Shenandoah Valley along faults and lineaments, and along bedding planes within the broader fold structures (Reeves 1932; Cady 1936; Hobba et al. 1979). Anticlinal crests and limbs provide the most efficient pathways for rising fluids, due in large part to sub-vertical fracturing parallel to the fold axis. Thrust faults may also provide the pathways for deep recharge and discharge.

Estimated ground water ages of certain large springs in the carbonate units are on the order of one to two decades (Plummer et al. 2000; Yager et al. 2013). This is not to say that the spring waters do not have a component of very recent water. All of the ground water ages represent a mixture of ground water components of multiple residence times, and as such great disparity between ages of the components is expected. However, the fraction of very young water decreases in cases where ground water ages of more than several years are obtained, as is evidenced in the gas chemistry of the springs (Yager et al. 2013). It is noteworthy that many of the spring waters even yield to age-dating methods using gas equilibration techniques in a karst setting, thus indicating that closed-system chemical evolution of ground water along deep flowpaths is occurring.

3 Caves

More than 450 caves are known in the Cambrian and Ordovician strata of Virginia. Certainly, not all of these caves are of deep phreatic origin. In the following discussion, we present some general descriptions of several caves we suspect were influenced by hypogenic processes through at least part of their formational history, with subsequent overprinting to various degrees by later phreatic and surficial karstification. At present, our ideas concerning the origins of these caves are somewhat speculative; however, we describe them here in order to stimulate future study of these noteworthy Appalachian caves.

3.1 Luray Caverns

Luray Caverns is located in Page County, Virginia, and is formed within the lower part of the Rockdale Run Formation of the Beekmantown Group. The cave passages are structurally controlled by bedding and fractures associated with low amplitude folds (Hack and Durloo 1977) (Fig. 6a). The eastern portion of the cave is formed within a shallow syncline, and the western portion (containing the greatest volume of cave) is located within a northeast plunging anticline. Bedrock dip is generally low; the steepest dips have been measured in the anticline nose up to 25°. The cave exists in a zone of bedrock that has been extensively recrystallized, such that sucrosic, euhedral dolomite is the dominant mineralogy (Fig. 6b). Hydrothermal dolomitization is often localized in the vicinity of faults, where fluids may migrate upward along steep gradients and dolomitization fronts can move rapidly through rocks (Davies and Smith 2006). Large euhedral grains of dolomite often result, enhancing the overall porosity and permeability of the rock. This appears to be the case at Luray Caverns, where the initial limestone and dolomite has been extensively altered to secondary sugary dolomite in a restricted zone of the bedrock that coincides with the cave (Fig. 6b).

Conspicuous features of Luray Caverns include ubiquitous calcite flowstone, stalactites, stalagmites, and draperies that cover nearly all parts of the cave (Fig. 7a). Where exposed in the cave walls, the bedrock is smoothly sculpted, and passage cross sections change dimension rapidly. Large bedrock pendants hang from the ceilings and may be breached by windows (Fig. 7a). Smooth-walled tubular passages and anastomoses along bedding planes are common, and small channels emanating from fissures with ceilings sloping upward that widen toward larger passages are seen near floor level (Fig. 7b). In some places, calcite coats all parts of the walls, including beneath overhangs, indicating precipitation of calcite under flooded conditions (Fig. 7c). In other places, a rind of corroded bedrock to a depth of several millimeters is evident and has peeled away from less altered rock.

Within the dolomite are areas of silica boxwork and chert that protrude from the cave walls and ceilings as large spongy masses (Fig. 7d). These spongy chert masses appear to have replaced the fossil structure within biohermal thrombolites, and "in thin sections form a rectilinear network in the dolomite" (Hack and Durloo 1977). In outcrops on the surface overlying the cave, euhedral quartz crystals are observed along fractures within biohermal zones. These zones of dolomitization and silicification indicate focused pathways of early hydrothermal fluids that altered the bedrock, enhanced porosity, and likely provided areas for enhanced solution with later groundwater flow.

Luray Caverns exhibits many examples of domes, cupolas, and ceiling channels, collectively referred to as "niches" by Hack and Durloo (1977). The niches are most prevalent within the marker horizon of sucrosic dolomite, and in some places, the niches are filled with laminated mud as much as 1 m thick. The cave contains no significant deposits to indicate floodwater formation by large, fast-flowing streams. A brecciated marker horizon of low dip is present throughout the cave (Fig. 7e) and may have also acted as an inception horizon (Lowe 2000) for cavern development.

The deepest part of Luray Caverns is along a single, large fissure that transects the length of the cave trending approximately north–south. It is possible that this fissure provided a pathway for rising fluids, which when intersecting the more permeable rock strata composed of sucrosic dolomite spread out laterally to form the cave. Other smaller "feeder" passages also lead to lower levels of the cave, some of which lie along this fissure (Fig. 6a).

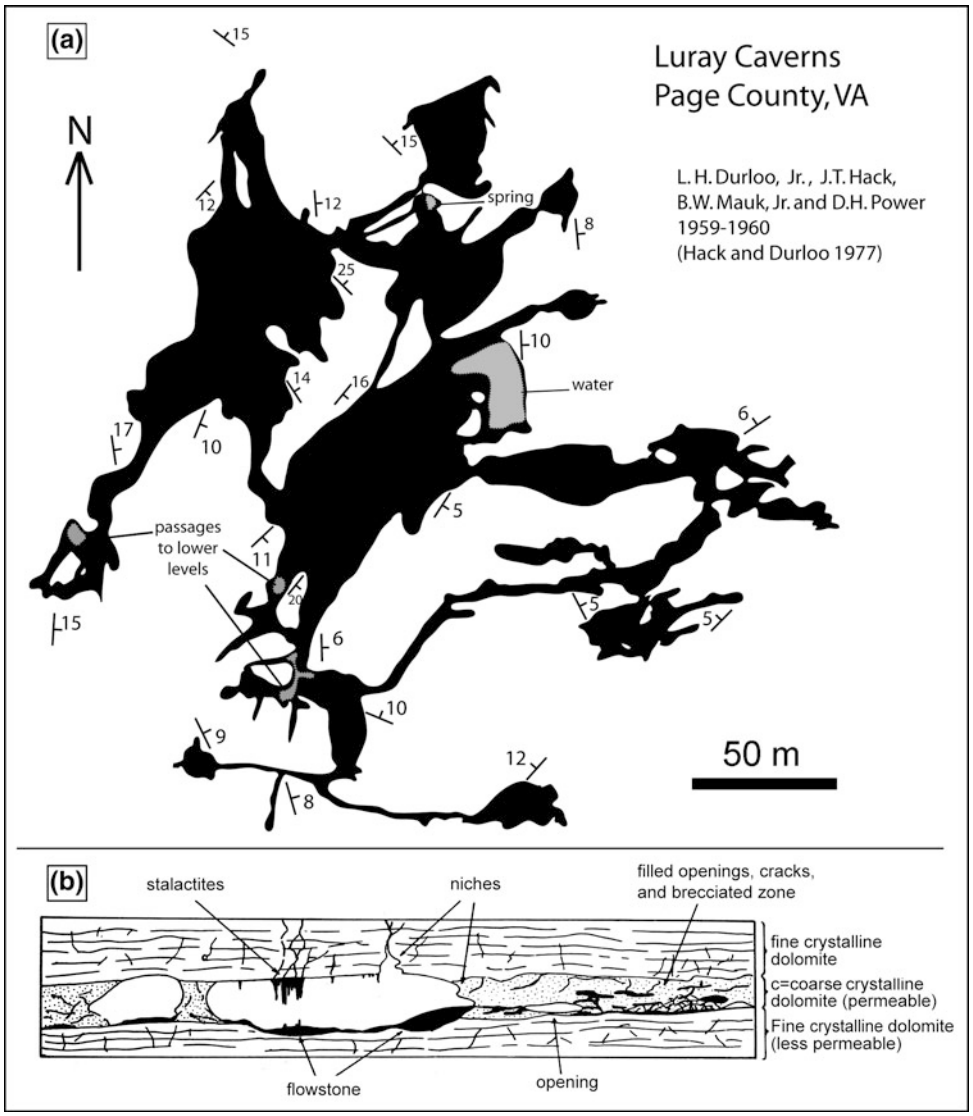

Fig. 6 **a** Map of Luray Caverns. **b** Schematic cross section illustrating coarse-grained dolomite horizon for cave development at Luray Caverns (from Hack and Durloo 1977)

3.2 Grand Caverns and Madison Saltpetre Cave

Grand Caverns is located in Augusta County, Virginia, and is formed within the Conococheague Limestone in an overturned anticlinal fold that forms a hill (Cave Hill) adjacent to South River, a tributary of the Shenandoah River (Fig. 8). The total surveyed length of the cave is 6.14 km and the total surveyed depth is 35.4 m. The cave entrance lies about 20 m above the river. Bedding is sub-vertical throughout much of the main cave, and passages form a network maze along bedding planes and joints when seen in plan view; however, in profile, the vertical development is greater than 20 m. In places where the dip of the rock flattens out near the hinge of the fold, the passages widen as a result of ceiling collapse along bedding, and passage orientations are again controlled by joints.

Jurassic volcanic dikes have been mapped in the immediate vicinity of Cave Hill (Fig. 8). The northwesterly trend of these dikes parallels that of several passages in Grand Caverns that cut across the strike of the bedrock. In addition, a linear feature approximately 10 km south of Grand Caverns was identified by LiDAR (Light Detection And Ranging) imagery, and subsequently named the Harriston Fault (Wieczorek et al. 2004). The trend of this feature is also sub-parallel to the trend of one set of cave passages, and the lineament itself extends directly toward Grand Caverns. This linear feature is young in comparison with the dikes, evidenced by its expression within the Neogene (or younger) colluvium blanketing the foot of the Blue Ridge (Doctor et al. 2014).

Several passages parallel the orientation of the nearby igneous dikes. Two caves within Cave Hill immediately

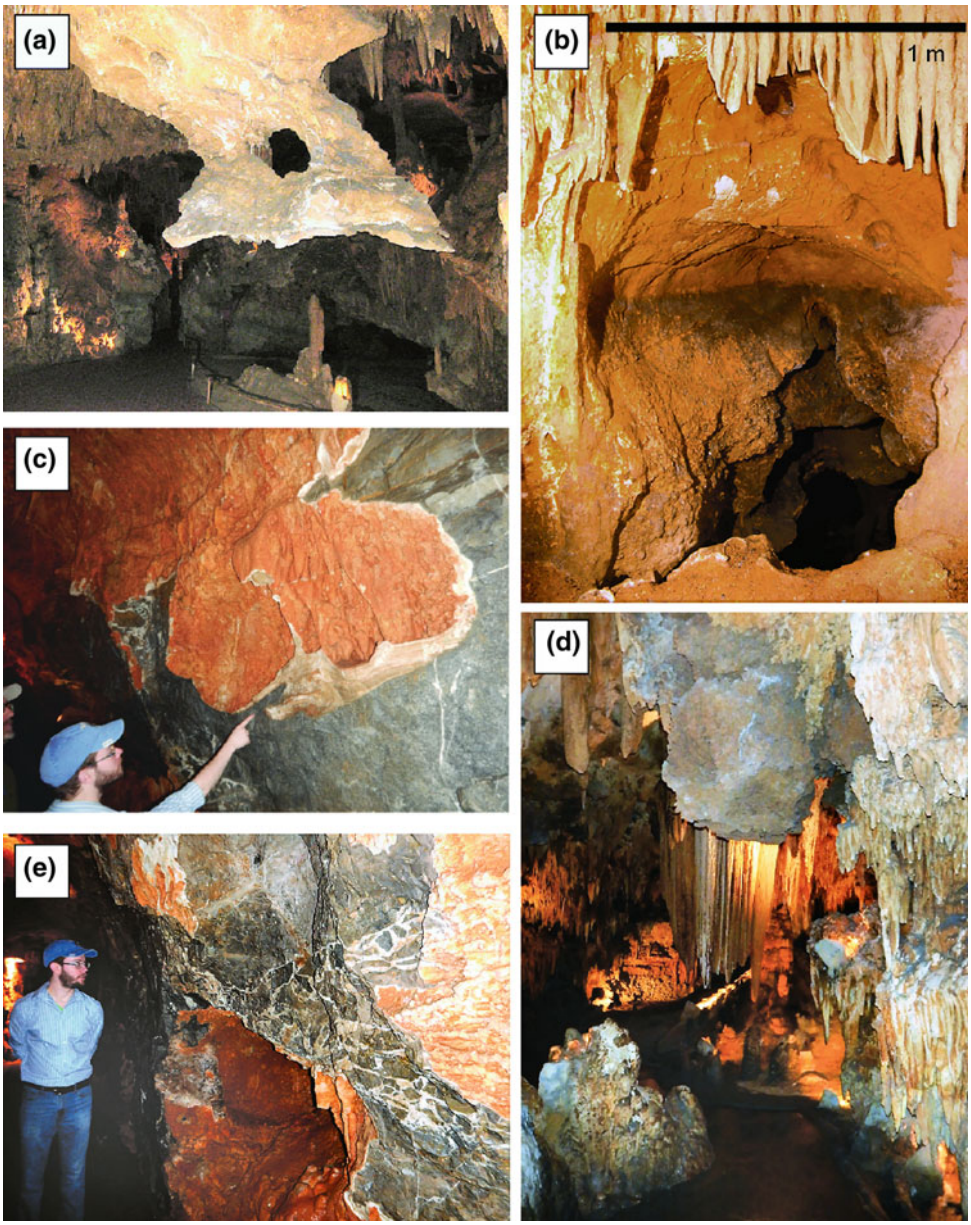

Fig. 7 Photographs of Luray Caverns. **a** Bedrock pendant breached by a solutional window within a highly decorated portion of the cave along the tour path; **b** a typical "feeder" passage, indicating solution due to rising flow; **c** a coating of calcite lining the bedrock wall beneath an overhang that was broken during tour path construction to reveal the internal layering parallel to the wall, indicating precipitation under flooded conditions; **d** a large, gray, spongy mass of chert hangs over the tour path, indicating early silicification of dolomite within the horizon of cave formation. **e** a zone of brecciation evident where the bedrock walls are exposed along the tour route in the cave, and a possible inception horizon for cave formation

adjacent to Grand Caverns are Steger's Fissure and Madison Saltpetre Cave. These smaller caves contain steeply dipping passages that extend at least 13 m and 30 m below river level, respectively (Kastning 1995; Fig. 8).

Grand Caverns shows evidence of long-term fluctuations in static water level throughout the cave, manifested as calcite wall coatings (Fig. 9a) and flowstone interlayered with laminated fine sediments (Fig. 9b). Formerly subaqueous coatings of calcite occur on the walls in several portions of the cave, representing past stable water levels within the cave (Fig. 9a, c). Cave morphology includes passages formed along bedding planes and joints (Fig. 9a, f), abrupt changes in passage dimensions, thin partitions of less-soluble beds breached by collapse, dead-end passages terminating in bedrock walls, ceiling cupolas, and fills composed mainly of fine sediments. Grand Caverns famously has a number of large shield formations that hang from the ceiling, some at odd angles (Fig. 9d, e).

The sediments filling the cave are predominantly of clay or silt-size fraction composed of mostly quartz, and lesser amounts of kaolinite, hematite, and goethite with minor expandable smectite and/or chlorite. Some minerals in the sediment fills had their source in the insoluble fraction of the impure host carbonate bedrock. Such preferential solution is evident in the thin fins of silty, dolomitic "ribbons" that jut out from the walls of the cave due to differential weathering (Fig. 9c, f). These ribbons are a common feature resulting from the intertidal depositional environment of the

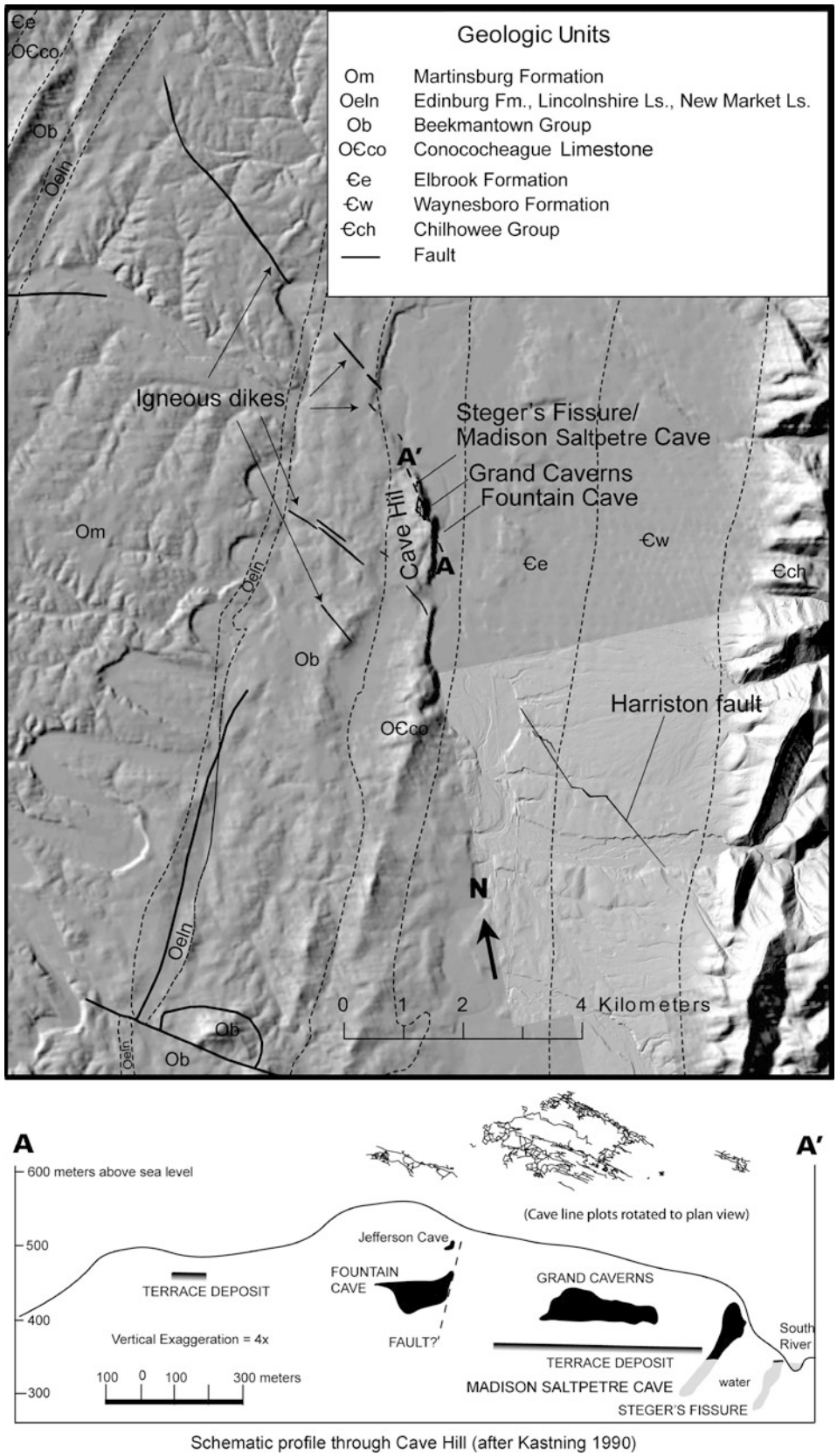

Fig. 8 Geologic setting and profile of Grand Caverns. Note jurassic igneous dikes and Harriston fault parallel NE-SW trend of cave passages along joints. In profile, cave passages extend tens of meters below river level

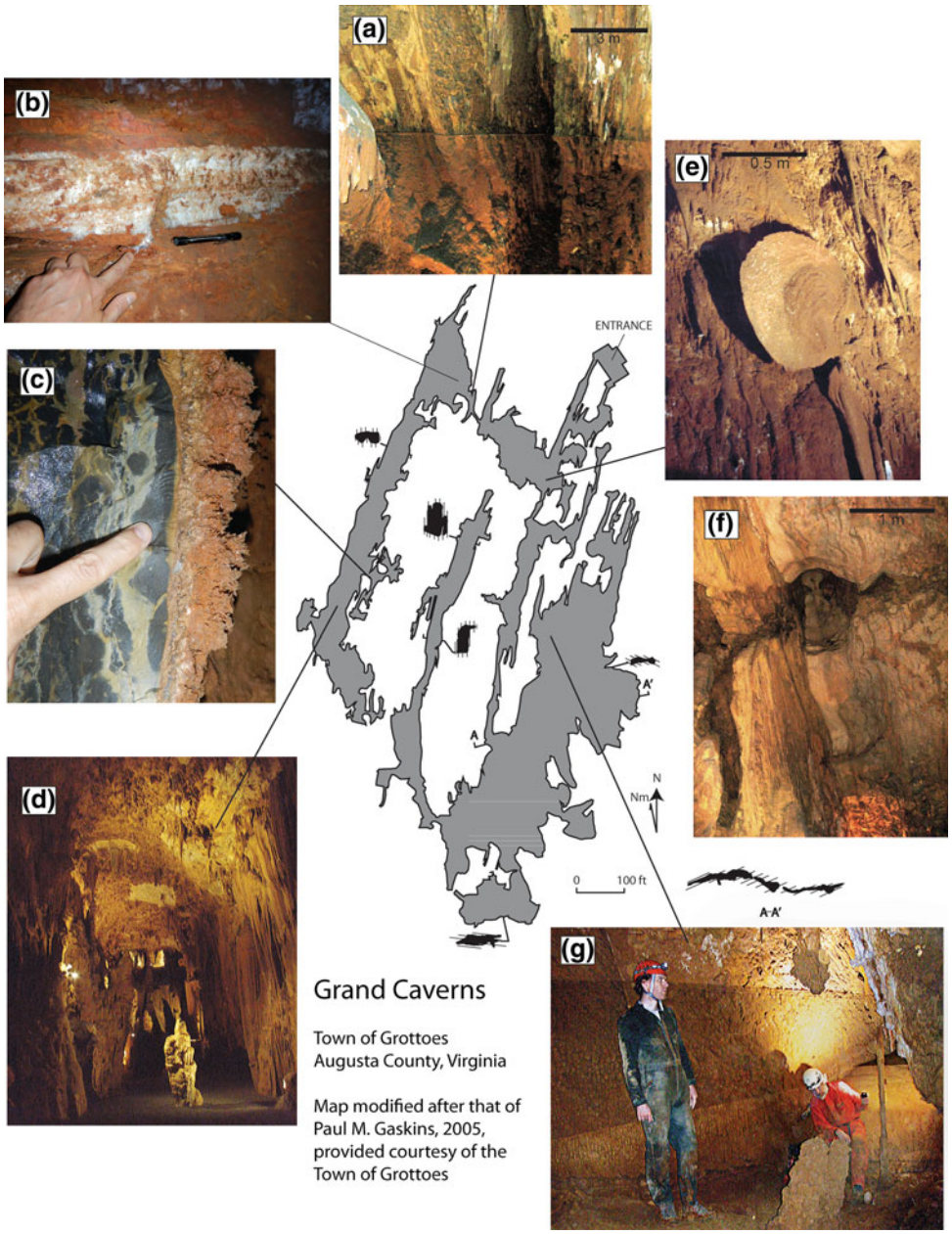

Fig. 9 Photographs of Grand Caverns. **a** Calcite coating on the walls of a former pool in the still water room; **b** interlayered clay-sized quartz and iron-oxide sediment with calcite flowstone; **c** calcite spar lining a passageway is evident where the fresh broken bedrock surface was exposed during construction of the tour path; **d** the Great Hall passage is approximately 20 m in height, the stalagmite in the center of the passage is 2.4 m tall, and shield formations hang from the ceiling; **e** Ajax's Shield is a centerpiece formation within the cave, jutting like the fin of a fish from the wall of the cave; **f** cupolas such as this one formed along joint that cuts across the near-vertical bedding are common within the cave; **g** multiple water levels recorded by overlapping calcite coatings on the walls and hanging bedrock pendants in the new discovery section of the cave

Conococheague Limestone. When the insoluble mineral fractions of the ribbons are weathered out from the walls, they occasionally fall free under their own weight and become encased in the finely laminated iron-oxide rich clay fills as "dropstones" (Doctor et al. 2014).

In places, calcite flowstone formed atop sediment banks is buried with overlying clay-sized laminated deposits (Fig. 9b). There are no significant deposits of sand, gravel, or cobbles derived from outside the cave, except perhaps where small vadose streams enter the cave from above. Pool coatings of calcite on the walls with dogtooth spar crystals up to a few centimeters in length are evident in at least two portions of the cave, representing former stable water levels with calcite-saturated water having persisted for long periods of time. Research is ongoing to determine if these water levels show coincident timing and elevations.

Kastning (1995) reported two paleomagnetic reversals within the sediments of Grand Caverns and suggested an age range for the sedimentation to be 0.7–1.1 million years. This information provides some constraint on the lower limit of the age of the cave, which Kastning (1995) used to estimate a denudation rate in the vicinity of Cave Hill of 23–41 m/Ma.

Madison Saltpetre Cave is one of the first caves known to have been surveyed and documented in Virginia, and was described by Thomas Jefferson in his *Notes on the State of*

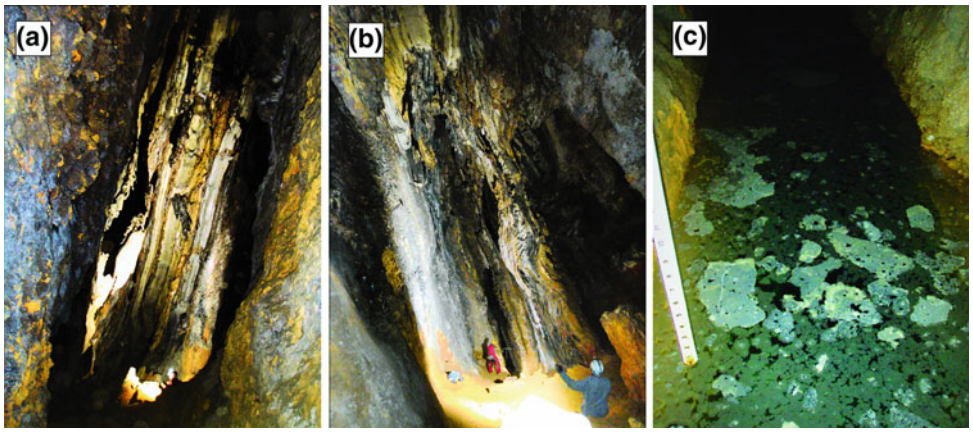

Fig. 10 Photographs of Madison Saltpetre Cave. **a** View toward ceiling within the main shaft of the cave; **b** view down to the pool within the main shaft of the cave; **c** calcite rafts forming on the pool in the cave

Virginia. Madison Saltpetre Cave is composed of a series of large rooms that trend along strike of the bedding and are much longer and taller than they are wide (Fig. 10a, b). The cave has a vertical extent of over 20 m. The bottom of the cave ends at a water-filled fissure; during low water levels, calcite rafts form on the surface of the pool (Fig. 10c). This pool hosts a rare species of a phreatobytic stygobiont crustacean *Antrolana lira* (Madison Cave isopod), which is endemic and restricted to the Shenandoah Valley (Bowman 1964; Holsinger et al. 1994; Hutchins 2007).

Recent monitoring of Madison Cave isopod habitat by the Virginia Department of Conservation and Recreation provides further evidence consistent with a hypogene origin (Fig. 11). The Madison Cave isopod is restricted to phreatic habitats, and its type locality is Madison Saltpetre Cave, where there is extensive morphological evidence of hypogene speleogenesis, such as ceiling cupolas, blind passage terminations, and windows within bedrock partitions between adjacent rooms. The cave exposes two "lakes," each at the bottom of passages trending along the strike of sub-vertical bedding with ceilings plunging at about 45°. The East Lake is reported in Holsinger (1975) to be 21 m deep before ending in submerged collapse. Marked isopods have been observed moving between the two lakes, as well as to nearby Steger's Fissure. In Steger's Fissure, divers reached a depth of 26 m within a chamber 30 m long by 16 m wide (M. Futrell, Virginia Speleological Survey, pers. comm. 2016). Calcite rafts accumulate on the surface of the lakes, nearly blocking the view into the clear blue water below (Fig. 10c). Fragments of calcite rafts are perched on the passage walls above the lakes, presumably stranded when water levels were higher. The monitoring apparatus is set up at the East Lake, which lies between the other two phreatic windows. The monitoring scheme consists of Hobo U24 conductivity loggers, Hobo U20 Level loggers and barologgers, and Aquatec 210TY Turbidity loggers (any use of trade, firm, or product names is for descriptive purposes only and does not imply endorsement by the U.S. Government). Temperature measurements are recorded as well by the two Hobo loggers. There are several remarkable things about the data from Madison Saltpetre Cave. During 4 years of nearly continuous monitoring, specific conductance varies only about 2% from the mean value of 461 microsiemens/cm on an annual cycle, and shows no response to precipitation events. Temperature (12.16 ± 0.08°C) and turbidity (essentially undetectable) remained constant and showed no response to precipitation events. In addition, water level response to precipitation events is very gradual, suggesting no close connection to surface waters. Instead, the waters of Madison Saltpetre Cave appear to still be connected to a deeper phreatic system with no close connection to the numerous nearby surface karst features. This is consistent with a genetic history of hypogene origins, currently exposed as an air-filled cave due to uplift and erosion.

We hypothesize a relation between the Harriston fault, local sub-parallel igneous dikes, and the cave development within Cave Hill. A nearby landowner whose property lies immediately adjacent to the Harriston fault reported iron oxide deposits fouling her plumbing and discoloring toilets and sinks, with the occasional scent of "rotten eggs" (hydrogen sulfide) coming from her well water, and at least one small (unexplored) cave shaft on the property (T. Mongold, pers. comm. 2013). A possible sequence of events for the formation of the caves on Cave Hill is as follows: (1) Alleghanian deformation resulting in the folds that comprise Cave Hill, (2) extensional fracturing and emplacement of Mesozoic igneous dikes created fracture permeability through the rocks underlying Cave Hill, (3) fractures in the rock were exploited by groundwater upwelling from the phreatic aquifer, and (4) ponding within the axial zones of the folds dissolved out the cave passages, with some base-level control on sub-horizontal enlargement of the cave. The chemical aggressiveness needed to create the cave passages was likely the result of mixing corrosion between deep and shallow sources of

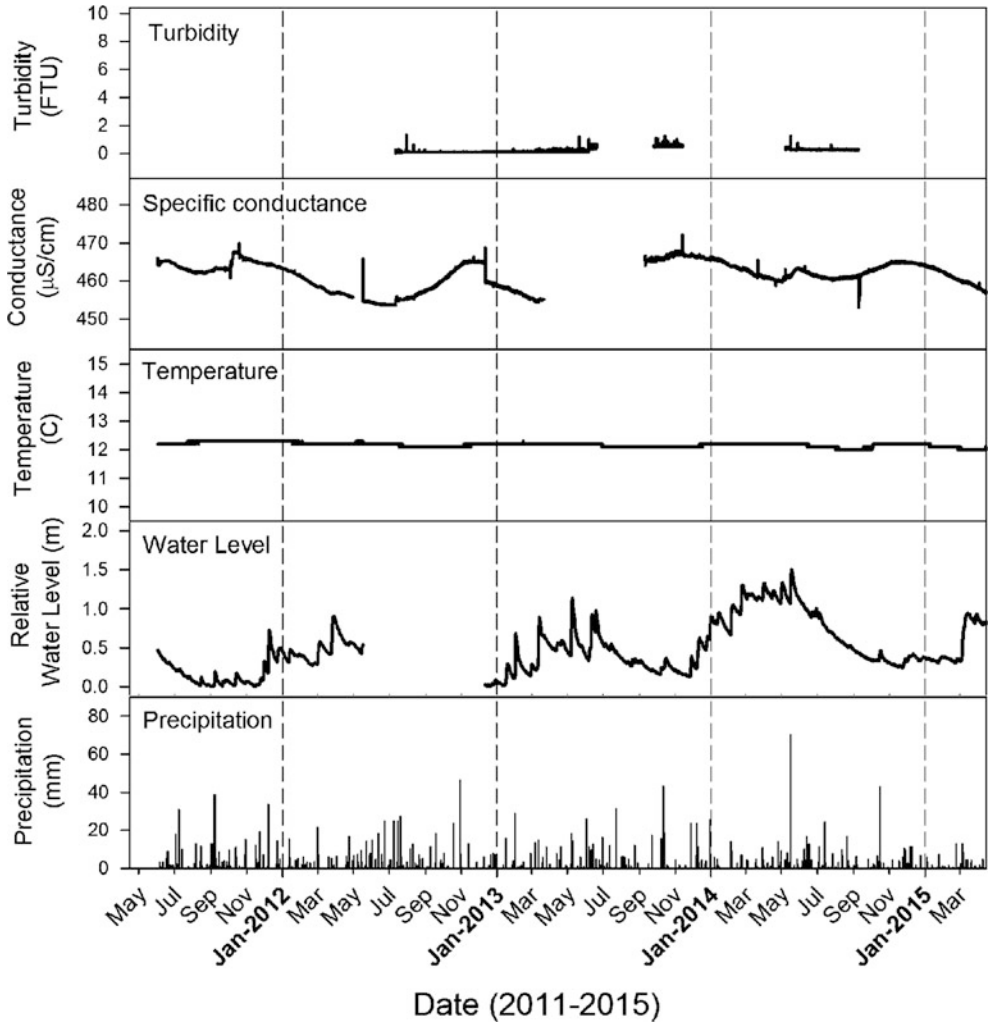

Fig. 11 Continuous monitoring within the lower pool of Madison Saltpetre Cave for over 4 years illustrates very stable water temperature, specific conductance, and turbidity in spite of fluctuations in pool water level. Note the subtle seasonal shifts in specific conductance vary within a range of only 19 microsiemens, and the water temperature is extremely stable at 12.16 ± 0.08 °C (n = 34,267)

water, although these depths are unknown. Water migrating from depth along vertical fractures may have encountered igneous dikes, incorporating a significant load of dissolved, reduced iron. Upon mixing with more oxygen-rich waters in the zone of solutional void development, this iron would have become oxidized. Ferric iron and silica in solution are most soluble at low pH, so upon reaction with the carbonate rock, the iron and silica in solution would have precipitated into the water-filled voids, and settled out to occlude the cave passages with a fine size fraction of iron oxides and quartz.

In spite of the fact that South River flows immediately below the entrance of Grand Caverns and Madison Saltpetre Cave, there is no evidence that the river ever flowed within either cave, as there is a notable absence of fluvial sand or gravels in the cave sediments. In Grand Caverns, a general absence of breakdown blocks along the main tour route of the cave, except in a few places. Breakdown is much more evident in the newly discovered section, and there it is clear that a catastrophic ceiling collapse occurred without being accompanied by fluvial reworking of the collapsed cave sediments. However, Kastning (1995) reported solutional scallops in the ceiling of the cave at the southern end of the tour route that would indicate flow velocities of 35–70 cm/s. These velocities are high enough to have transported gravel-size sediments, yet such deposits are not observed. Kastning (1995) also reported solutional scallops that indicate upwelling of water from below through a passage now blocked with sediment. It is possible that the high flow velocities indicated by the solutional scallops resulted from rising flow of phreatic groundwater under artesian pressure, rather than from invasion of a surface stream into the cave.

3.3 Mole Hill, Onyx Hill, and Round Hill Cave

Just west of Harrisonburg are several conical shaped hills within the Shenandoah Valley that represent anomalous features of high relief relative to the valley floor. One of these is Mole Hill, which is a plug of mantle-derived basalt that intruded carbonate rocks of the Beekmantown Group. The age of the basalt is 48.5 Ma (Southworth et al. 1993). The intrusive igneous activity evidently caused localized explosive hydrothermal circulation that silicified the host carbonate rocks. Brecciation accompanied silicification, and abundant silicified carbonate breccia is found on the flanks of the hill. No caves are known on Mole Hill; however, solutional conduits are seen in outcrops of carbonate rock; a sample of this rock was obtained for further analysis. Thin section analysis by electron microprobe reveals that progressive silicification of the rock occurred by replacement of non-euhedral dolomite grains by microcrystalline chert (Fig. 12). Other rocks observed as float on the hill were replaced with iron oxi-hydroxides and silica; primary carbonate sedimentary textures and fossils were preserved in the altered iron and silica-rich rock (Doctor et al. 2014).

Onyx Hill is another hill immediately west of Mole Hill that contains an unroofed cave. Evidence of the former cave is a large broken stalagmite or column formation that lies on the ground within a single joint-controlled passage that cuts across bedding of the host rock (Doctor et al. 2014). The walls of the unroofed cave are lined with finely laminated deposits of snowy white calcite interlayered with iron oxides, colloquially called "onyx." Onyx is a misnomer for this deposit, as true onyx is composed of chalcedony, not carbonate; however, because local geographic features are named for this type of deposit, we will use the term here. The unroofed cave is 460 m above sea level. This is nearly 90 m above the floodplain of North River, which flows at the base of the hill and is the nearest base-level stream. The onyx that was mined lined the walls of portions of the unroofed cave to a thickness of more than 15 cm. The onyx-like calcite coating the walls of the depression is evidently a phreatic deposit. Another unroofed cave in the vicinity, located on an unnamed hill, was mined for onyx. The onyx is also evidently a phreatic mammillary calcite lining the walls of an unroofed cave to a thickness of more than 15 cm. The unroofed cave is at an elevation of 465 m above sea level, at least 100 m above North River, which flows at the base of the hill and is the nearest base-level stream.

Round Hill is a third conical hill formed within the Beekmantown Group carbonates located approximately 1.5 km west of Bridgewater, Virginia. The hill contains a rather large cave for the Shenandoah Valley, Round Hill Cave. The hill lies within the hanging wall of a reverse fault dipping approximately 12° to the southeast and is likely intersected by steeper, later formed faults. Passages are formed along bedding planes and joint fractures, and the dip of the bedding is rather shallow, approximately 15° to the southeast. The entrance to the cave is formed along a bedding plane and joint intersection on the northwest side of the hill, thus the passage descends at an angle into the hillside (Fig. 13). The ceiling of the entrance room is lined with layered secondary calcite. Smaller cave entrances observed along a railroad grade approximately 3 m above river level also show coatings of dogtooth spar

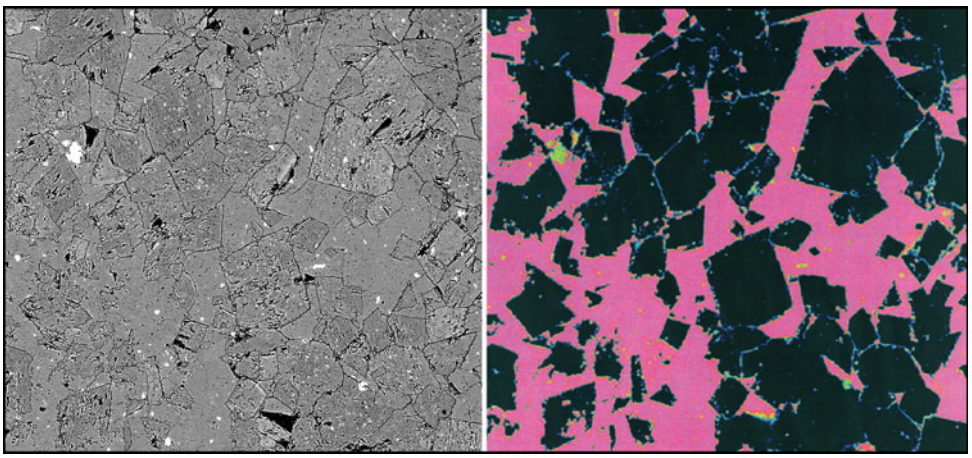

Fig. 12 (*left*) Backscatter electron image of a thin section of altered dolomitic bedrock from Mole Hill, showing euhedral grain boundaries along dolomite rhombs; (*right*) an electron microprobe silica map of the same view. The width of each image is 2 mm. *Pink areas* are microcrystalline quartz, *green areas* are authigenic K-feldspars, and black areas are dolomite. Note progression of silica alteration at grain boundaries (*blue*)

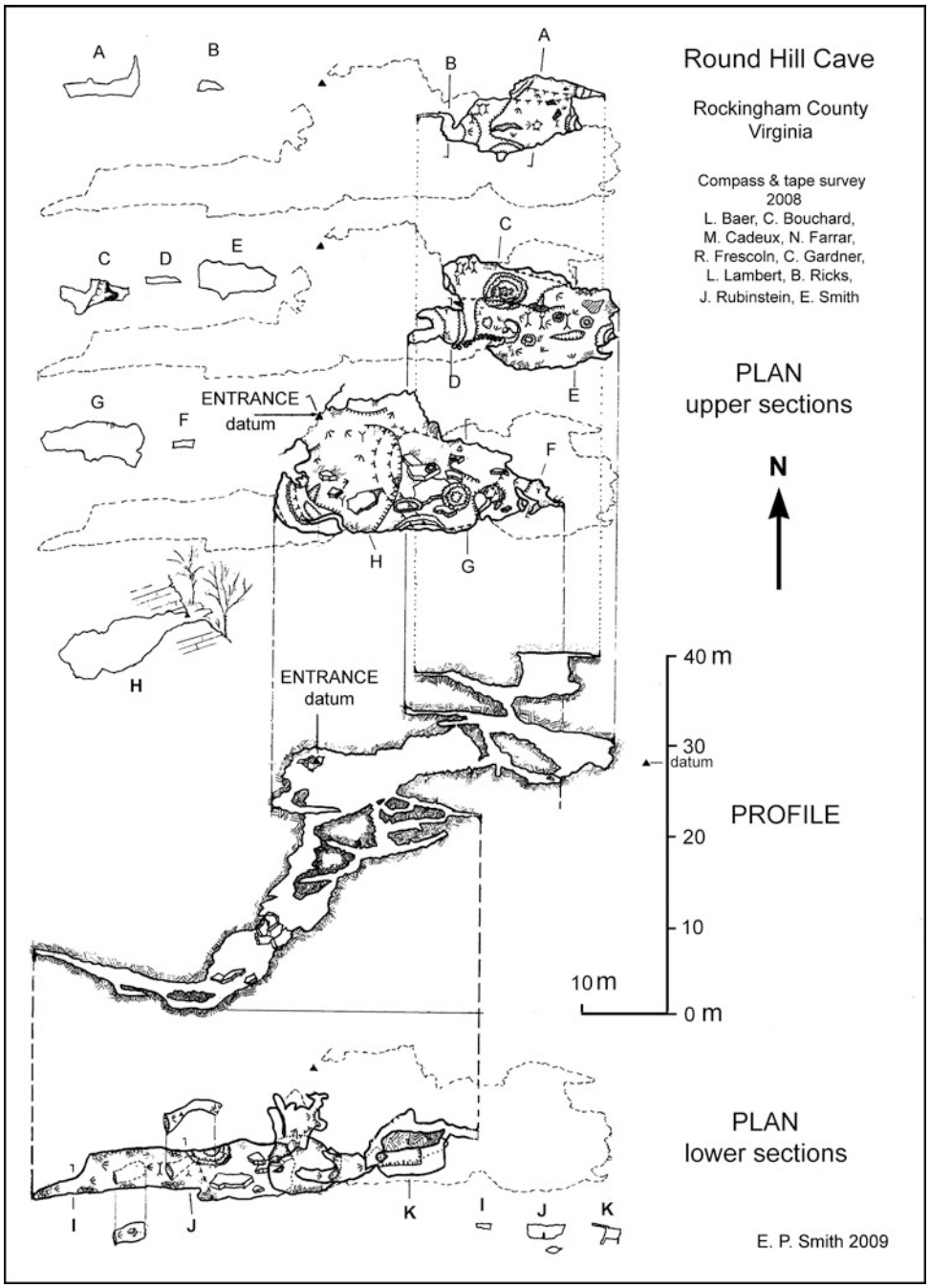

Fig. 13 Map and profile of Round Hill cave (courtesy of Edward P. Smith)

calcite. The bedrock immediately underneath the sparry calcite is corroded, vuggy, partially silicified to chert. Cupolas, ceiling channels, and dead-end passages characterize the cave morphology. The bedrock exposures around the entrance show evidence of fracturing with thick, layered calcite veins filling openings (2–5 cm thick). Brecciation and silicification to chert is evident in float of bedrock pieces scattered near the entrance. The map and profile of the cave (Fig. 13) illustrates that the cave is more extensive in its vertical dimension than in its horizontal dimension. Passages at different levels are connected by narrow, sinuous tubes, as opposed to vadose canyons. There are no active streams in the cave or any deposits indicative of former stream flow.

North River flows at the base of the hill, approximately 20 m immediately below the entrance of the cave. Near river level, smaller solutional conduits can be observed in bedrock outcrops, but are blocked with sediment. Some of these conduits are lined with sparry calcite coatings, indicating former phreatic flooding of the conduits.

4 Summary

Several large caves in the Shenandoah Valley exhibit morphologic features that can be interpreted as resulting from ascending phreatic fluids. The locations of the caves are determined by local geologic structures such as lineaments, faults, and folds. Sub-water table stream flow evidently overprints the maze character of certain cave passages, yet no indication of a modern free surface stream exists.

Recognition of hypogenic karst systems formed in association with hydrothermal fluid migration through folded and faulted rocks in active tectonic regions is globally widespread. Less common are hypogenic caves described in passive tectonic margins, such as within the ancient fold-thrust belt of the Appalachians. The caves described here host inner coatings and pool deposits of sparry calcite that suggest hydrothermal development and are hosted within bedrock that has undergone early hydrothermal alteration to dolomite and silica. Such deposits suggest that the formational history of these caves may extend further back into geologic time than previously considered.

Enhancement of cavernous porosity formed at depth is likely the result of mixing between rising and infiltrating waters, as well as surface lowering through erosion and cavern modification by invading surface streams. This process has resulted in caves both atop ridges and in the valleys, and an unusually deep karst aquifer in the Shenandoah Valley.

Acknowledgements The authors are most grateful to all of the cavers who mapped the caves discussed in this chapter. Randall Orndorff, David Weary, Christopher Swezey, John Repetski, Robert Denton, Anna Balog-Szabo, and David Nelms provided valuable field assistance and discussion about the geology, hydrology, and features of the study area. We also thank the editors and reviewers for their helpful suggestions that improved the manuscript.

References

Appold MS, Kesler SE, Alt JC (1995) Sulfur isotope and fluid inclusion constraints on the genesis of Mississippi valley-type mineralization in the Central Appalachians. Econ Geol 90(4)

Bowman TE (1964) *Antrolana lira*, a new genus and species of troglobitic cirolanid isopod from Madison Cave, Virginia. Int J Speleol 1:229–236

Cady RC (1936) Ground-water resources of the Shenandoah Valley, Virginia. Va Geol Surv Bull 45:137 (2 plates)

Davies GR, Smith LB Jr (2006) Structurally controlled hydrothermal dolomite reservoir facies: an overview. AAPG Bull 90:1641–1690

Doctor DH, Orndorff W (2016) Deep phreatic influence on caves and karst in the central Appalachian Great Valley. In: Chavez T, Reehling P (eds) NCKRI symposium 6, proceedings of DeepKarst 2016: origins, resources, and management of Hypogene Karst. National Cave and Karst Research Institute, Carlsbad, New Mexico, pp 89–104

Doctor DH, Weary DJ, Brezinski DK, Orndorff RC, Spangler LE (2015) Karst of the Mid-Atlantic region in Maryland, West Virginia, and Virginia. In: Brezinski DK, Halka JP, Ortt RA Jr (eds) Tripping from the fall line: field excursions for the GSA annual meeting. Baltimore, Maryland, 2015, Geol Soc Am Field Guide 40:425–484. doi:10.1130/9780813700403

Doctor DH, Weary DJ, Orndorff RC, Harlow GE Jr, Kozar MD, Nelms DL (2008) Bedrock structural controls on the occurrence of sinkholes and springs in the northern Great Valley karst, Virginia and West Virginia. In: Proceedings of the 11th multidisciplinary conference on sinkholes and engineering and environmental impacts of karst. Tallahassee, Florida, 23–26 Sept, pp 12–22

Doctor DH, Farrar NC, Herman JS (2011) Interaction between shallow and deep groundwater components at fay spring in the Northern Shenandoah Valley Karst. USGS Karst interest group proceedings. Fayetteville, Arkansas, 26–29 Apr, U.S. Geological Survey Scientific Investigations Report 2011-5031, pp 25–34

Doctor DH, Orndorff W, Maynard J, Heller MJ, Casile GC (2014) Karst geomorphology and hydrology of the Shenandoah Valley near Harrisonburg, Virginia. In: Bailey CM, Coiner LV (eds) Elevating geoscience in the Southeastern United States: NEW ideas about old terranes—field guides for the GSA southeastern section meeting. Blacksburg, Virginia, 2014, Geol Soc Am Field Guide 35:161–213. doi:10.1130/2014.0035(06)

Gathright TM, Henika WS, Sullivan JL (1978) Geology of the Mount Sidney quadrangle, Virginia. Virginia division of mineral resources publication 11, scale 1:24,000, 1 sheet

Hack JT, Durloo LH (1977) Geology of Luray Caverns Virginia. Virginia division of mineral resources report of investigations 3, 43 p, 1 plate

Harlow GH Jr, Orndorff RC, Nelms DL, Weary DJ, Moberg RM (2005) Hydrogeology and ground-water availability in the carbonate aquifer system of Frederick County, Virginia. U.S. Geological Survey Scientific Investigations Report 2005-5161, 30 p

Hearn PP Jr, Sutter JF, Belkin HE (1987) Evidence for late-paleozoic brine migration in Cambrian carbonate rocks of the central and southern Appalachians: implications for Mississippi Valley-type sulfide mineralization. Geochim Cosmochim Acta 51:1323–1334

Herbert P Jr, Young RS (1956) Sulfide mineralization in the Shenandoah Valley of Virginia. Va Div Geol Bull, vol 70

Hobba WA Jr, Fisher DW, Pearson FJ Jr, Chemerys JC (1979) Hydrology and geochemistry of thermal springs of the Appalachians. U.S. Geological Survey Professional Paper 1044-E

Holsinger JR (1975) Descriptions of Virginia caves. Va Div Mineral Resour Bull 85:450

Holsinger JR, Hubbard DA Jr, Bowman TE (1994) Biogeographic and ecological implications of newly discovered populations of the stygobiont isopod crustacean *Antrolana lira* Bowman (Cirolanidae). J Nat Hist 28:1047–1058

Hutchins B (2007) Genetic divergence among populations of the Madison Cave Isopod, *Antrolana lira.* 2007 Natl Speleol Soc Conven Program Abs, p 77

Kastning EH III (1995) Evolution of a karstic groundwater system, Cave Hill, Augusta County, Virginia: a multi-disciplinary study. In: Beck BF (ed) Karst Geo Hazards. Balkema, Rotterdam, pp 141–148

Lowe DJ (2000) The speleo-inception concept. In: Klimchouk AV, Ford DC, Palmer AN, Dreybrodt W (eds) Speleogenesis: evolution of karst aquifers. National Speleological Society of America, Huntsville, pp 65–75

McCoy KJ, Kozar MD (2008) Use of sinkholes and specific capacity distributions to assess vertical gradients in a karst aquifer. Environ Geol 54:921–935

Nelms DL, Moberg RM Jr (2010) Hydrogeology and groundwater availability in Clarke County, Virginia. U.S. Geol Surv Sci Invest Rep 2010-5112, 119 p. (http://pubs.usgs.gov/sir/2010/5112/)

Nolde JE, Giannini WF (1997) Ancient warm springs deposits in Bath and Rockingham Counties, Virginia. Va Miner 43(2):9–16

Palmer MV (2009) Mississippi-valley-type (MVT) ores in carbonate rocks of the USA. In: Palmer AN, Palmer MV (eds) Caves and karst of the USA. National Speleological Society, Huntsville, Alabama, pp 424–425

Palmer AN, Palmer MV (2011) Paleokarst of the USA: a brief review. In: Kuniansky EL (ed) U.S. geological survey karst interest group proceedings. Fayetteville, Arkansas, 26–29 Apr 2011. U.S. Geological Survey Scientific Investigations Report 2011–5031

Penick DA Jr (1987) Virginia mineral locality index. Va Miner 33 (1):1–10

Perry LD, Costain JK, Geiser PA (1979) Heat flow in western Virginia and a model for the origin of thermal springs in the folded Appalachians. J Geophys Res 84(B12):6875–6883

Plummer LN, Busenberg E, Böhlke JK, Carmody RW, Casile GC, Coplen TB, Doughten MW, Hannon JE, Kirkland W, Michel RL, Nelms DL, Norton BC, Plummer KE, Qi H, Revesz K, Schlosser P, Spitzer S, Wayland JE, Widman PK (2000) Chemical and isotopic composition of water from springs, wells, and streams in parts of Shenandoah National Park, Virginia, and vicinity, 1995–1999. U.S. geological survey open file report 00-373

Reeves F (1932) Thermal springs of Virginia. Va Geol Surv Bull 36:56 (2 plates)

Southworth CS, Gray KJ, Sutter JF (1993) Middle Eocene intrusive igneous rocks of the central Appalachian Valley and Ridge Province —setting, chemistry, and implications for crustal structure. In: Evolution of sedimentary basins—appalachian basin, U.S. Geol Surv Bull 1839 (Chapter J)

Tso JL, McDowell RR, Avary KL, Matchen DL, Wilkes GP (2004) Middle eocene igneous rocks in the valley and ridge of Virginia and West Virginia. USGS Circular 1264 Trip 4:137–161

Vesper DJ, Grand RV, Ward K, Donovan JJ (2008) Geochemistry of a spring-dense karst watershed located in a complex structural setting, Appalachian Great Valley, West Virginia, USA. Environ Geol. doi:10.1007/s00254-008-1541-4

Virginia Division of Mineral Resources (2003) Digital representation of the 1993 geologic map of Virginia, publication 174, scale 1:500,000, CD ROM (ISO-9660)

Wieczorek G, Harrison RW, Morgan BA, Weems RE, Obermeier SF (2004) Detection of faults and fault traces in the Shenandoah Valley, Virginia using LIDAR imagery. Geol Soc Am Abs Programs 36 (2):120

Yager RM, Plummer LN, Kauffman LJ, Doctor DH, Nelms DL, and Schlosser P (2013) Comparison of age distributions estimated from environmental tracers by using binary-dilution and numerical models of fractured and folded karst. Shenandoah Valley of Virginia and West Virginia, USA. Hydrol J. doi:10.1007/s10040-013-0997-9

Hypogene Karst Springs Along the Northeastern Border of the Appalachian Plateau, New York State

47

Arthur N. Palmer, Penny M. Taylor, and Levia A. Terrell

Abstract

The northern border of the Appalachian Plateaus in New York State is a limestone–dolomite escarpment with sulfate rocks at depth and hypogene karst springs at its base. All springs contain dissolved carbonates, but many are also exceptionally rich in sulfate, sulfide, or CO_2. None connect to traversable caves, but their chemistry provides clues to their internal character, flow depth, and underground processes. Many show evidence for dedolomitization driven by sulfate dissolution, which forces calcite travertine to precipitate at the surface. Isotopic variation and radium content reveal groundwater flow patterns. Chemical contrasts with nearby epigenic caves highlight the nature of the hypogene springs. A nearby but separate spring area, fed by deep flow along faults, illustrates the effects of high-pressure CO_2 on carbonate groundwater. Despite the lack of underground access, these karst areas give much insight into hypogene processes.

Keywords

Hypogene springs • Sulfate • Common-ion effect • Travertine • Isotopes

1 Introduction

The northern edge of the Appalachian Plateau is an escarpment that extends east–west across the width of New York State west of Albany (Fig. 1). It is formed by relatively resistant Silurian and Devonian carbonate rocks that stand 100–300 m above the Mohawk–Hudson River lowlands. Infiltration in the upland feeds many karst springs at its base, many of them hypogene. The hypogene springs have no known accessible entrances, but several geochemical methods are described here that help to determine flow patterns and processes within the carbonate aquifers.

The main study area is located 40–100 km WNW of Albany, between the towns of Sharon Springs and Richfield Springs. Groundwater recharge takes place mainly into mixed carbonate and detrital rocks of the Devonian age and discharges through Silurian strata that are covered in places by continental glacial till (Fig. 2). The deepest flow extends into the Salina Group, which contains interbeds of anhydrite and gypsum, and rises to springs along the base of the plateau where the land surface lies above the base of the soluble rocks. Artesian springs cluster in areas where the glacial cover is thin or absent. Discharge from any single spring is generally less than 10 L/sec.

Nearby Saratoga Springs is a high-CO_2 hypogenic system in which water rises along faults in Ordovician limestone to many outlets. It is included in this study to illustrate the variety of karst springs in the region.

A.N. Palmer (✉)
Department of Earth and Atmospheric Sciences, State University of New York, Oneonta, NY 13820-4015, USA
e-mail: arthur.palmer@oneonta.edu

P.M. Taylor
Department of Geology, Mt. Holyoke College, South Hadley, MA, 01075 USA
e-mail: pmtaylor@mtholyoke.edu

L.A. Terrell
Arcadis Engineering, 6723 Towpath Road, East Syracuse, NY 13057, USA
e-mail: levia.terrell@arcadis.com

© Springer International Publishing AG 2017

A. Klimchouk et al. (eds.), *Hypogene Karst Regions and Caves of the World*, Cave and Karst Systems of the World, DOI 10.1007/978-3-319-53348-3_47

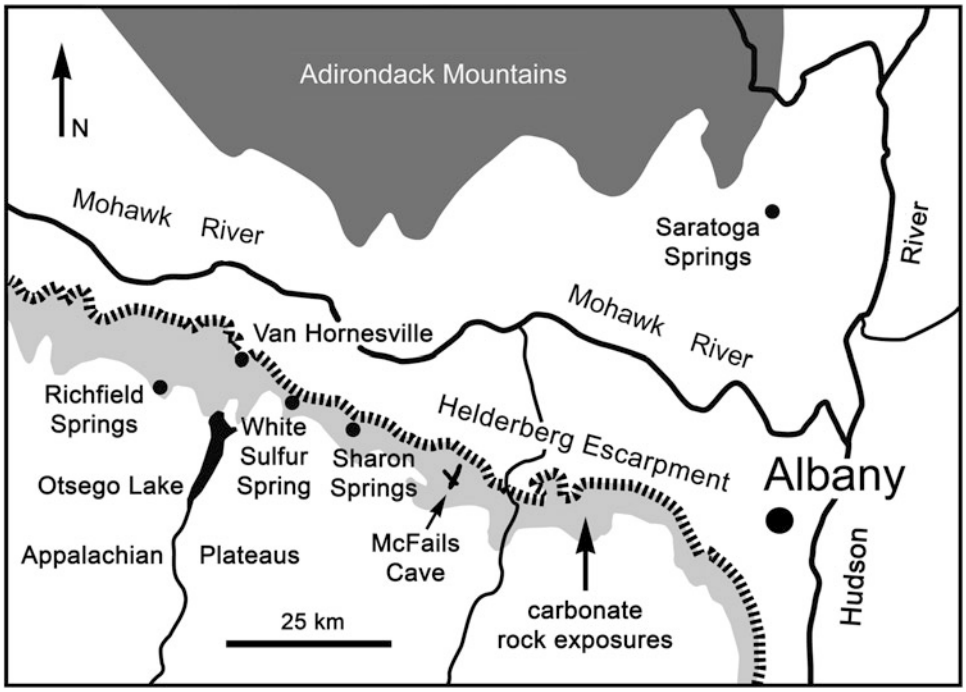

Fig. 1 Map of the study area. The Van Hornesville field site, Richfield Springs, and Saratoga Springs are located on public land. Others are privately owned

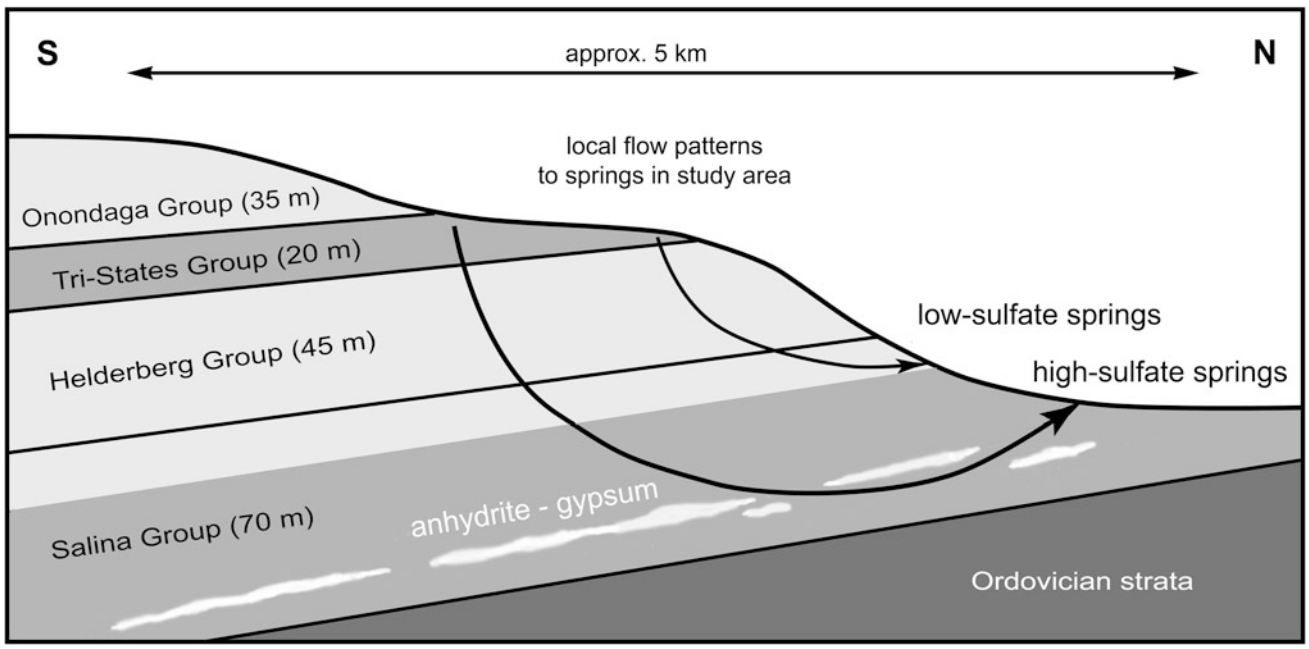

Fig. 2 Generalized geologic cross section through the main study area. *Light gray,* carbonate rocks; *medium gray,* interbedded carbonates, sandstones, and shales; *dark gray,* sandstones and shales. Stratal thickness and lithologies are variable (after Rickard and Zenger 1964; Fisher 1979). The Silurian–Devonian boundary is roughly in the middle of the Helderberg Group. Where stream valleys have exposed the strata in the down-dip direction, drainage is mainly toward the south. The northerly cross-stratal flow shown here is rather local

2 Hypogene Versus Epigene Karst Systems

Hypogene springs in the study area are highly mineralized, with rather stable discharge, temperature, and chemistry (Table 1). Most of the deep flow acquires large concentrations of sulfate, and locally sulfide, and some of its springs feed streams that deposit calcite travertine. Several of the sulfide springs were once the sites of popular resorts where visitors could bathe in "healing" waters, some of which border on toxic. Much of the chemistry is related to hypogene cave origin, and our goal was to examine the spring chemistry to clarify the nature of their groundwater flow and processes. Local springs include four chemical types: (1) oxygen-rich with high carbonate but low sulfate and Mg; (2) oxygen-rich with high carbonate, sulfate, and Mg; (3) nearly anoxic with high H_2S, sulfate, and Mg; and (4) high CO_2, carbonate, and salinity. Springs of type (1) may not qualify as hypogene because there is no specific evidence for rising water or deep-seated reactions. Nearby epigene caves and karst springs also have water of type 1. McFails Cave, 15 km SE of Sharon Springs, contains several long vadose stream passages and is used here as the epigene standard (Palmer 2007). A separate group of artesian springs 75 km ENE of Sharon Springs (water type 4) is included here for comparison—the famous Saratoga Springs, which rise along faults.

2.1 Influence of Sulfates on Travertine Deposition

Our initial goal was to determine why certain springs deposited calcite travertine (tufa) at the surface and others did not (Taylor 2000). The town of Van Hornesville was the primary study area because of its abundant spring-fed travertine (Fig. 3). Thirty sites were analyzed, each at least twice (summer vs. winter). Most of the springs are minor seeps with no visible indication of their chemical character. Most travertine is located at least several tens of meters downstream from the springs, at local rapids and waterfalls where degassing of CO_2 is enhanced.

Table 1 Summary of spring and cave data in the main study area, plus epigenic McFails Cave for contrast

Location	Q (L/min)	T (° C)	pH	PCO_2 (atm)	H_2S (mg/L)	Ca^{2+} (ppm)	Mg^{2+} (ppm)	SI calcite	SI dolomite	SI gypsum	Source
Richfield Sp.	12.8	8.9	7.35	0.0074	19.15–48.12	562.74–593.75	80.32–96.40	+0.47 to +0.50	+0.10 to +0.16	+0.02 to +0.23	LT
White Sulfur Sp.	15.8	8.6	7.35	0.0062	8.74–13.7	565.41–638.00	55.48–30.69	+0.38 to +0.42	−0.14 to −0.07	+0.09 to +0.12	LT
Pavilion Sp.	388	8.5	7.1	0.015	20.06–26.45	550.19–562.81	73.46–86.04	+0.16 to +0.25	−0.19 to −0.13	+0.05 to +0.07	LT
Gardner Sp.	55.3	8.5	7.1–7.9	0.002–0.014	0.083–4.54	568.79–587.36	65.37–34.00	+0.20 to +1.00	−0.21 to +0.43	+0.04 to +0.26	LT
Guilfoyle well	–	8.3	7.20	0.055	0.2	544	102	+0.128	−0.18	+0.20	PT
Stocking well	Limited access	9.8	6.72	0.075	High, no data	326.4	151.5	+.001	−0.10	−0.32	AF
McFail's Cave (epigene)	~50 to ~10^5	7.9	7.9	0.0027	<DL	2.14	0.392	+0.64	+0.44	−1.76	AP
Van Hornesville (<500 ppm SO_4)	Many	13.1	7.85	0.0037	<DL	132	25.5	+0.53	−0.23	−1.19	PT
Van Hornesville (>500 ppm SO_4)	Many	12.4	7.95	0.0028	<DL	323.6	45.48	+0.86	+0.47	−0.28	PT
Saratoga Hathorn Sp.	–	10	6.37	0.977	–	936	453	+0.69	+0.59	–	AP

Single figures are mean values. *DL* below detection limit. *SI* saturation index. SI is defined here as $(2/n)\log(IAP/Ksp)$, where n number of ions released per molecule (2 for calcite, 4 for dolomite), to adjust for greater sensitivity of SI to minerals with $n > 2$. *IAP* ion activity product. *Zero SI* saturated; *negative SI* undersaturated; *positive SI* supersaturated. *Ksp* solubility product, calculated from data recommended by Langmuir (1971) for dolomite, and Busenberg and Plummer (1982) for other carbonate equilibria. Hypogenic springs have little variation compared to nearby epigenic caves. *Sources* Taylor (2000), Terrell (2008), Fetterman (2001), Palmer (2007)

Fig. 3 Main travertine mound at Van Hornesville, formed by several spring-fed streams supersaturated with calcite (photographs by A.N. Palmer)

All spring waters in the area contain much Ca^{2+} and HCO_3^-, as expected in a karst area. However, travertine is deposited only by water high in sulfate (>400 mg/L) and Mg (>20 mg/L). Springs with no travertine are low in all three. The sulfate is apparently derived from beds of anhydrite and/or gypsum located an average of 50–100 m below the surface in the lower Salina Group (Fig. 2). The Mg is apparently from dolomite, which is most abundant in the upper Salina.

We simulated the chemical evolution of the spring water with a personalized version of the computer model WATEQ (http://wwwbrr.cr.usgs.gov/projects/GWC_coupled/). Simply adding increments of dissolved carbonate and sulfate minerals to water failed to produce the observed field chemistry. Instead, it was necessary to include incongruent dissolution, in which the dissolving of anhydrite or gypsum is accompanied by precipitation of calcite driven to supersaturation by dissolution of the Ca sulfates. This is the process of dedolomitization.

In the study area, the process operates as follows: (1) dissolution of limestone at and near the surface by infiltrating water; (2) slower dissolution of dolomite; (3) rapid dissolution of anhydrite and/or gypsum at greater depth, within the Salina beds, which forces calcite to precipitate; (4) by removing much Ca^{2+} and HCO_3^- from solution, calcite precipitation decreases the saturation level of dolomite; dolomite cannot precipitate but instead continues to dissolve slowly. The process is diagrammed in Fig. 4.

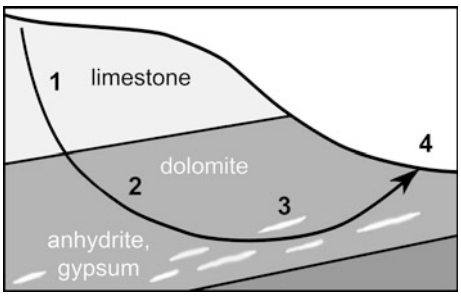

Fig. 4 Incongruent dissolution between carbonates and sulfates: In the Van Hornesville field area, infiltrating water first encounters limestone (**1**) and slowly approaches calcite saturation. Dolomite also dissolves (**2**), but more slowly than calcite. Calcite saturation is enhanced, but dolomite remains unsaturated. (**3**) When the water comes in contact with gypsum or anhydrite, they dissolve rapidly. The resulting influx of Ca^{2+} forces calcite to precipitate. This prevents Ca^{2+} and HCO_3^- from rising in the solution, so dolomite remains unsaturated and continues to dissolve slowly. The spring water (**4**) is rich in Mg^{2+} and SO_4^{2-}. It is also supersaturated with calcite, which allows travertine to be deposited at the surface

Supersaturation of calcite persists to the springs and beyond. In contact with surface air, the streams rapidly release CO_2, especially at highly turbulent rapids and waterfalls, which boosts calcite supersaturation and accelerates travertine deposition. The relatively high Mg concentration of the spring water is a by-product of slow but persistent dolomite dissolution within the aquifer while calcite precipitates. Geochemical modeling shows that lengthy dedolomitization can ideally increase dolomite solubility up to 7 times, and gypsum

about 1.5 times, while the combination is able to precipitate more calcite than was originally dissolved (Palmer and Palmer 2004). The Ca and carbonate required for the excess calcite are supplied mainly by dissolution of anhydrite/gypsum and dolomite. Much secondary porosity is produced along the flow routes because the volume of precipitated calcite is less than that of the dissolved gypsum and dolomite. This process had been recognized before in the Madison aquifer of South Dakota (Back et al. 1983), in Spain by Bischoff et al. (1994), and in Oklahoma by Raines and Dewars (1997). It appears to be more widespread than is generally realized.

In our study area, as groundwater rises toward the springs it first exits the zone of sulfate beds. The water remains supersaturated with calcite, but (without the contribution of Ca from sulfates) calcite precipitation slows and dolomite drifts toward saturation. At and beyond the springs, degassing of CO_2 can drive both calcite and dolomite to supersaturation. This is observed in many of the water samples. Mg remains high as a by-product of dedolomitization. Water at former spas in Sharon Springs was advertised as "magnesian" to inspire thoughts of great medicinal virtue.

Travertine has accumulated only in streams with calcite supersaturation more than about 12 times the equilibrium value, i.e., with saturation index >+1.1 (Table 1). To determine rates of calcite deposition from the sulfate springs, artificial substrates of glass (frosted and unfrosted, 50 cm^2) and of copper were installed for up to 8 months in several Van Hornesville springs, housed in through-flow containers tethered to the stream beds (Taylor 2000). Detrital material was intercepted by filters. Calcite precipitation was measured by the increase in mass. Copper is mildly toxic to certain biota and may inhibit deposition.

Twenty slides were placed in a small spring-fed stream with SIcalcite = +1.3, which contained many travertine dams. Two were placed in the main Otsquago Creek (SI also = +1.3), which contained no visible travertine. They remained in place for up to 8 months, with some removed periodically for analysis. Calcite accumulated on all exposed surfaces, including those in the stream with no visible travertine. Frosted slides had the greatest accumulation. Measured precipitation rates were between 11.2 and 40.2 mg/cm^2/yr. The differences are not easy to explain because of variations in water chemistry, frosting texture, flow details, etc.

In contrast, most deposition of travertine in caves and in surface streams is the result of simple degassing of CO_2, which does not involve the elevated sulfate and magnesium observed in this study.

2.2 Validation of Sulfate Source

Claypool et al. (1980) have provided data on the variation of $\delta^{34}S$ in sulfate rocks of various geologic ages. The relationship should be valid for sulfate dissolved from these materials, if isotopic fractionation has not interfered. Dissolved sulfate in spring water in our main field area has a $\delta^{34}S$ range of +26.08 to +27.13‰ (Terrell 2008), which exactly matches the range of Silurian marine sulfates (these include the lower strata in our study area; Fig. 5). The agreement validates the sulfur source and shows that no significant isotopic fractionation has taken place or that the sulfate has not been derived from oxidation of H_2S. Knowing the strata also provides information on the depth of groundwater circulation and the processes described in 2.1. Dedolomitization and porosity development are therefore related to those specific beds.

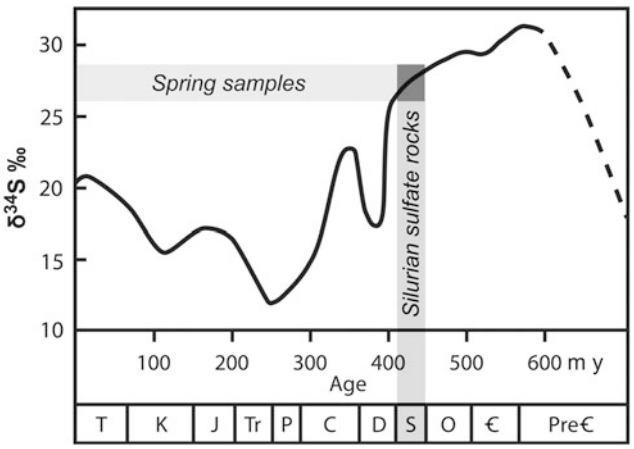

Fig. 5 Correlation between $\delta^{34}S$ in sulfates of the sulfide spring water of the study area and $\delta^{34}S$ of sulfates in Silurian seawater (see Claypool et al. 1980). *Note* the close match between the two, which identifies the sulfate source as the Silurian Salina beds, rather than oxidation of H_2S from other sources

3 Sulfide Springs

Several springs in the main study area are enriched in hydrogen sulfide up to 48 mg/L (Terrell 2008). They are easily detected by nose. PCO_2 values range from 0.0062 to 0.075 atm, above the range of typical sulfate springs in the region. This wide spread indicates considerable variation in flow paths, reducing conditions, and distribution of solid sulfates. Negative $\delta^{34}S$ (−2.77 to −21.21‰) indicates, as expected, that the H_2S is produced by bacterial reduction of sulfates in anoxic environments (Clark and Fritz 1997).

Despite the high solubility of anhydrite and gypsum, all of the measured sulfide springs are supersaturated with those minerals. In solution, they behave identically, and their saturation levels are best expressed as SI of gypsum, because that is the stable species at the surface where the chemistry is measured. Gypsum supersaturation is driven by oxidation of H_2S to H_2SO_4 at and near the surface. The sulfuric acid is

quickly neutralized by reaction with the local limestone, which also inhibits travertine deposition in the spring-fed streams. Surfaces around the springs tend to accumulate white powdery material, a combination of sulfur from incomplete H_2S oxidation, gypsum, and bacterial filaments (Fig. 6). Highly negative $\delta^{34}S$ in the spring water (−29 to −30‰) suggests microbial reduction of sulfate (Terrell 2008). Although these systems may never evolve into accessible caves, they represent processes that are common in hypogene speleogenesis.

Fetterman (2001) provides other nearby examples of sulfide-rich springs, including Stocking well, an artificial drill hole midway between Richfield Springs and Sharon Springs (Fig. 1). SIcalcite = −0.23 and SIgypsum = −2.35 to +0.31. A few nearby surface streams have sulfate concentrations up to 1000 mg/L and high PCO_2 (>0.01 atm). Degassing of H_2S and no measurable O_2 at the artesian well indicate deep groundwater circulation in a reducing environment.

Fig. 6 Access hole to stream from Pavilion Spring. Note mineralized crust on walls composed of gypsum, calcite, minor sulfur, and filaments of sulfide-oxidizing microbes. As is typical of sulfide springs, H_2S is abundant and oxidizes to sulfur on non-carbonate surfaces. In open conditions such as this, oxidation potential is higher and sulfuric acid forms, which is quickly neutralized in contact with carbonates

4 Travertine Deposition: Sulfate Springs Versus Epigenic Caves

McFails Cave is located 15 km ESE of Sharon Springs, in the Coeymans–Manlius–Rondout formations. Water enters through several sinkholes and small sinking streams. The main passage consists of a long canyon joined by several tributaries and ends in a passage filled with water as the result of partial blockage of the spring by glacial sediment (Cooper and Mylroie 2015). Most of the cave is well aerated, and it provides a good epigenic standard.

The stream in the main passage varies greatly in calcite saturation level (Palmer 2007). During the wet season, it is unsaturated, but in the dry season, it is usually supersaturated because of loss of CO_2 through entrances. The calcite saturation index varies from roughly −1.10 to +1.25. The main cave streams are undersaturated only during the highest 20–30% of flow.

During the unusually dry summer of 1995, the entire main stream bed became coated with calcite to an average thickness of 0.3 mm, at mean SIcalcite = +1.25 (Fig. 7). The following wet season included a major flood (50-year return period), when the main stream entering the cave had SIcalcite = −1.9. In the following May, when the cave was again accessible, the calcite coating had been removed, except in sheltered areas, and was completely gone by the end of the next wet season. Undersaturation alternating with supersaturation is typical of epigenic caves in the region, but this sequence of travertine deposition and dissolution occurs only rarely. These deposits contrast with the long-lasting travertine dams in sulfate-rich streams fed by deep groundwater at Van Hornesville.

The surface travertine (tufa) at Van Hornesville is highly porous and irregular and usually contains trapped vegetal material. Much of its porosity is produced by decay of the organic material. In contrast, the travertine observed in McFails Cave was smooth, non-porous, and more uniformly distributed. Similar to the travertine at hypogene springs, the greatest deposition rate in the cave was at waterfalls, where turbulence enhanced the rate of CO_2 loss to the air.

5 Isotopic Interpretation of Groundwater

Analysis of oxygen and hydrogen isotopes in the spring water and that of radium isotopes released from uranium in bedrock are helpful in tracking the timing and flow paths of groundwater.

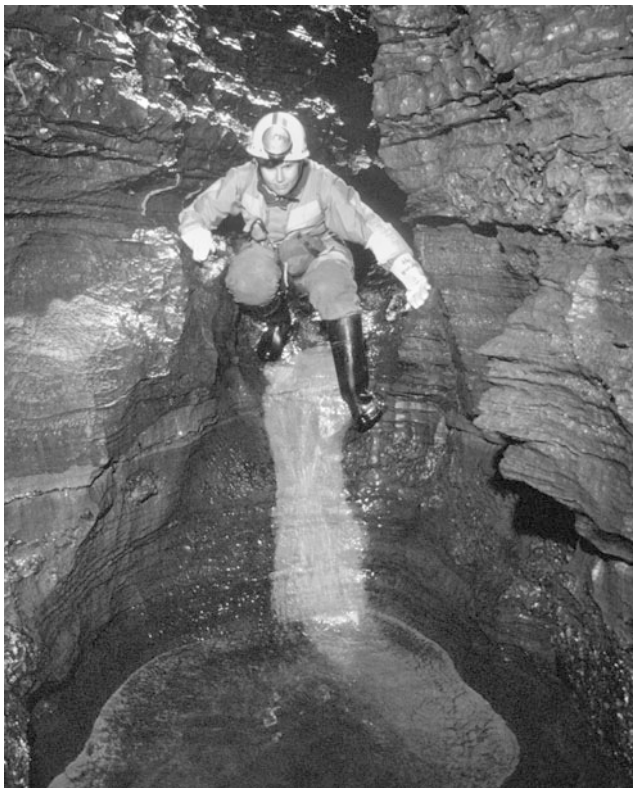

Fig. 7 Upstream portion of the main passage in McFails Cave during the summer of 1995, showing calcite coating on the canyon floor

5.1 Tracking of Groundwater Sources and Residence Times

Isotopic values for δ^2H versus $\delta^{18}O$ in the study area show a very limited range for the suspected hypogene springs (Fig. 8, E). Combined with the small seasonal variation in discharge, this isotopic clustering suggests that the sources of hypogene spring water have remained underground and mixed for several seasons before emerging.

Analysis of tritium (radioactive ^3O) also helps to determine the maximum time that spring water has remained below ground by indicating roughly the elapsed time since it fell as precipitation. Tritium values of 11 tritium units were detected in the year 2004 at all sulfide-rich springs in the study area. This value is compatible with a mean groundwater residence time of less than 10 years (Kehew 2001). This is a reasonable value for these local flow systems.

Bedrock contains trace amounts of uranium and thorium (^{238}U, ^{235}U, ^{232}Th). Decay of ^{238}U produces ^{226}Ra (half-life = 1601 yr), and ^{235}U produces ^{223}Ra (half-life = 11.4 days). Decay of ^{232}Th produces both ^{228}Ra (half-life = 5.75 yr) and ^{224}Ra (half-life = 3.64 days). These isotopes are released by rock dissolution and gradually decay to radon (Rn) and finally to lead (Pb). To sample dissolved radium isotopes, 200–400 L of water are pumped through a 2 μm filter to remove sediment, followed by a Mn oxide filter to which the radium adsorbs. Our radon isotopes were analyzed at the US Geological Survey Radium Isotope Laboratory in Reston, Virginia.

The ratio $^{228}Ra/^{226}Ra$ is near 1.0 in the sulfide springs, and the activity of each isotope is high, which suggests lengthy contact with bedrock (Kraemer and Genereux 1998). Seasonal variation in discharge is minor, with a maximum range of 0.7–7 L/min. These measurements are compatible with the <10-year estimate of groundwater age from the tritium data.

Radium isotopes can be used to date groundwater residence times, as well as rates of groundwater flow from small pores or narrow fissures into bodies of surface water (Kraemer and Genereux 1998) or into karst conduits. Carbonate rocks generally have higher U/Th ratios than clastic rocks. The ratio therefore is an indicator of the lithology in which the groundwater source has been in longest or most intimate contact.

All radium isotopes in the hypogene spring water of the study area have high activities: ^{226}Ra = +7.9 to +70 dpm/100 L and ^{228}Ra = +49 to +68 dpm/100 L (dpm = disintegrations per minute). Ratios of $^{228}Ra/^{226}Ra$ are close to 1.0, the stable value in detrital sedimentary rocks, so the water has been in contact with these rocks for a relatively long time (Kraemer and Genereux 1998).

5.2 Identifying and Dating Hypogenic Water Plumes

As water travels through narrow rock fissures with large areas of contact and long residence times, it equilibrates with the isotopes of the local bedrock ($^{235}U/^{238}U \sim 0.0466$). That is also the equilibrium ratio for the decay products $^{223}Ra/^{226}Ra$. Because ^{224}Ra and ^{228}Ra come from the same parent (^{232}Th), the $^{224}Ra/^{228}Ra$ activity ratio is ideally ~ 1.0. High activities of the long-lived ^{226}Ra and ^{228}Ra indicate lengthy and intimate contact with bedrock. Because marine carbonates typically have low Th/U ratios, the ratios of their by-products ($^{228}Ra/^{226}Ra$) tend to be low.

High activities of the short-lived ^{224}Ra and ^{223}Ra indicate water that has recently emerged from pores and narrow fissures. In large water bodies, they decay faster than they can be replaced from the rock. The elapsed time since seepage from the limestone has entered the water body can be estimated by the amount of disequilibrium. With time, the $^{224}Ra/^{228}Ra$ ratio decreases, usually by mixing between incoming seepage and the main water body, but if the seepage retains its identity as a plume without substantial mixing (as in a lake fed by springs), the ratio decreases along an exponential decay curve instead of linearly. The identity of the plume can be recognized for about 30 days.

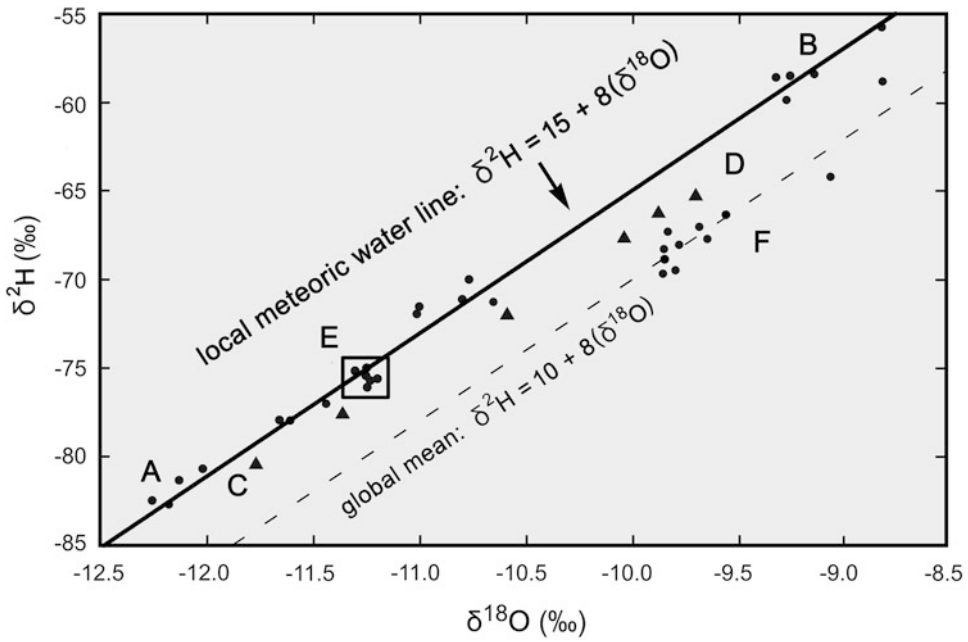

Fig. 8 Plot of δ^2H versus $\delta^{18}O$ for the study area (VSMOW units) in the Richfield Springs–Sharon Springs area. *A*–*B* seasonal trend of meteoric water (rainfall, surface streams): varies from cool and wet at *lower left* to warm and dry at *upper right*; *C*–*D* seasonal trend of cave water (drips, vadose streams), *E* clustering of hypogene spring water; *F* evaporative water from swamps and lakes. From Terrell (2008), Siemion (2006), Moskal (2009). Local meteoric waterline based on rainfall data from T Kraemer (USGS) and A & M Palmer. δ^2H and $\delta^{18}O$ represent deviations from standard mean ocean water (SMOW, Vienna standard)

In Otsego Lake, water rises in several places from the underlying Onondaga Limestone aquifer. Relatively high PCO_2 up to ~0.005 atm can identify local groundwater inputs (vs. values averaging ~0.001 atm elsewhere in the lake). There can also be temperature contrasts with the relatively warm surficial lake water in the summer. The limestone directly underlies the northern end of the lake and extends ~200 m below the lake bottom at the southern end, estimated from the 1–2 C stratal dip. The bedrock is overlain by a varied thickness of glacial and lacustrine deposits. Rising plumes can be released from the limestone through intervening high-permeability gravel. The mean residence time for water in the lake (volume ÷ discharge rate) is roughly 980 days, so it is possible for influent water plumes to retain their identity for long times.

The location and evolution of the rising plumes can be interpreted from radon isotopes. The most conspicuous example was detected roughly 0.3 km from the southern end of the lake at a depth of 25–30 m (Moskal 2009). The water rises rapidly enough that the short-lived ^{223}Ra and ^{224}Ra retain their identity (with half-lives of only 11.1 and 3.54 days). Because of their differences in decay rate, the time since the water was released from the bedrock can be estimated from the isotope ratio, up to a limit of about 30 days (see Kraemer 2005 for details). Full equilibrium requires approximately 200 days.

Figure 9 shows the plot of ^{223}Ra versus ^{224}Ra in the lake samples. The "youngest" sample is located at point X, farthest from the 0, 0 point. As long as the plume retains its identity without mixing, the decay history plots along the curved line, which is calculated from the two contrasting decay rates. Eight other samples from elsewhere in the lake show anomalously high ^{223}Ra and ^{226}Ra, and their ratios fall close to the same decay curve. Their position on the curve shows their ages since their release into the lake. Most other lake samples are relatively "old," as shown by their clustering close to the (0, 0) point.

6 Saratoga Springs: A High-CO_2 Artesian System

This cluster of springs is located 75 km east–northeast of Sharon Springs (Fig. 1). It has no genetic relation with springs in the main study area, but the Saratoga Springs represent an additional type of hypogene karst system with no direct access to the subsurface. These are noted for extremely high CO_2 content and artesian pressure (Fig. 10). They are clearly hypogenic karst features, because their water is rising and slightly warm and performs much carbonate dissolution at depth. At the surface, they cease to be aggressive toward carbonates because of rapid CO_2 loss.

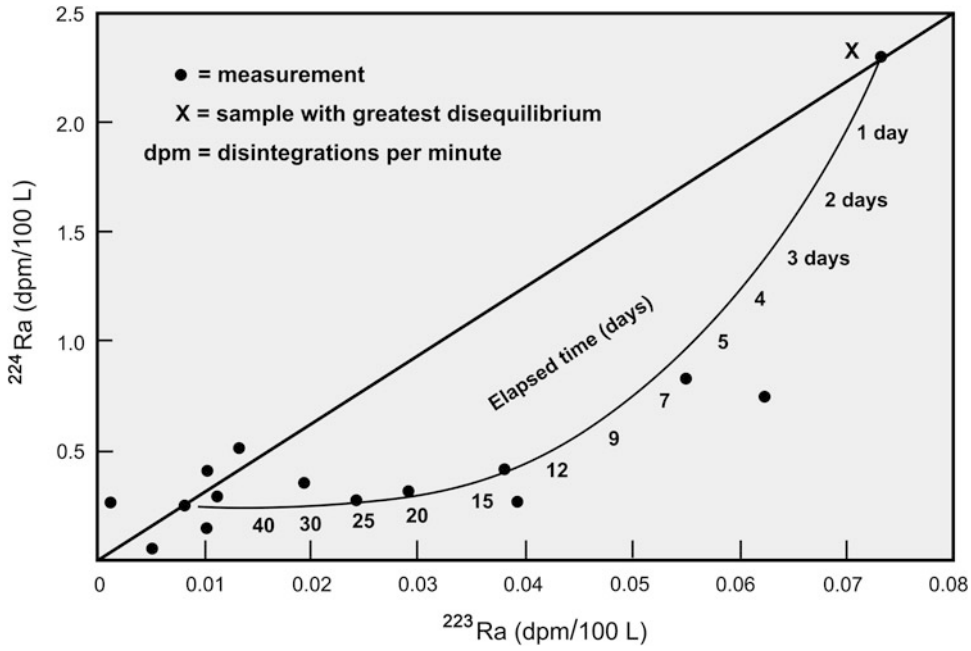

Fig. 9 Ra isotope evolution for deep spring waters entering Otsego Lake (after Moskal 2009). See Kraemer (2005) for conceptual details

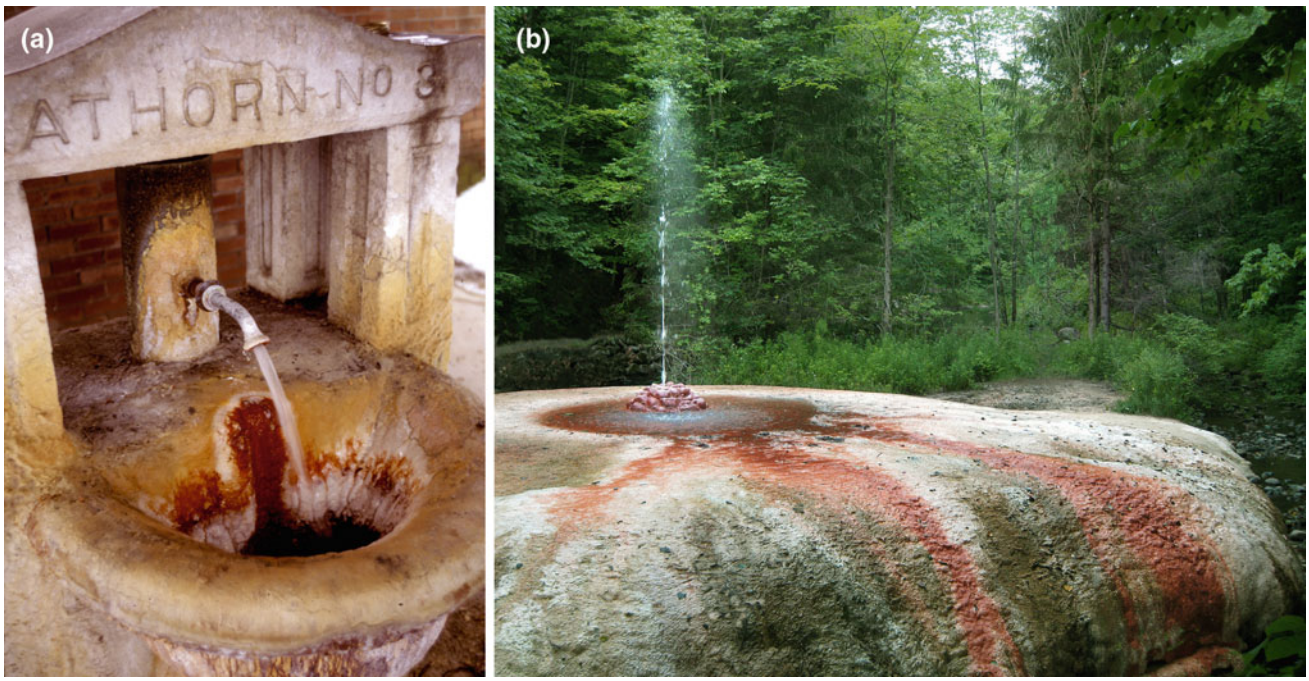

Fig. 10 Representative springs in the Saratoga Springs system. **a** Hathorn #3; **b** Geyser Island Spouter, which emerges from an artificial drillhole. Its carbonate travertine has built up during the past century

The springs lie in lowlands near the Hudson River valley, southeast of the Adirondack Mountains. Most of the springs rise through faulted Precambrian rocks overlain by Cambrian–Ordovician sandstones and carbonates. Although not generally considered karst springs, most are bubbly with unusually high carbon dioxide derived from depth and contain much dissolved carbonate. They are slightly thermal, 9–13 °C, about 1–4 °C above the regional average. Some have a faint H_2S odor. This is the best-known group of springs in New York State. In the nineteenth century, the waters were advertised as "refreshing" and able to cure many ills, including malaria! In the early 1900s, there were more than 200 private wells tapping into the springs.

The sources of the spring water and its dissolved load are still uncertain, but recently developed analytical techniques are providing evidence (Hollocher et al. 2002; Siegel et al. 2004; Rao et al. 2005). Suggested sources of the high CO_2 include mantle degassing and expulsion from deep sedimentary basins. The high salinity is considered to be from deep connate brines.

Our analysis at Hathorn Spring #3 showed very high calcite supersaturation. Computing the PCO_2 required to hold the calcite at equilibrium, we calculated a value of more than 6 atm. This could be achieved at a depth of about 200 m. However, the temperature of the water at that depth should be higher than the measured value of 9–11 °C, so it is likely that there is mixing between deep and shallow groundwater.

With advances in analytical methods, the spectrum of water analyses is growing. For example, studies at the Saratoga springs by Siegel et al. (2004) showed that the $\delta^{13}C$ (−5.8‰ to +0.8‰ VPDB) in dissolved inorganic carbon, and elevated $^3He/^4He$ ratios, suggests that the CO_2 source is the mantle or an ancient deep crystallized igneous melt. Stable isotopes define a mixing line between modern local meteoric waters ($\delta^2H \sim 70‰$) and a component with heavier δ^2H but similar $\delta^{18}O$ values. This trend and the trend of $^{87}Sr/^{86}Sr$ versus 1/Sr support the possibility that brines typical of the Precambrian basement rocks contribute salinity to the Saratoga Springs. These observations provide evidence for migration of water from the Adirondack Mountains southward to the topographically low McGregor fault system in the Hudson River lowlands.

Rao et al. (2005) measured chloride concentrations and the ratios $^{36}Cl/Cl$ and Cl^-/Br^- to determine the salinity source, mixing patterns, and evolutionary history of the groundwater. Chloride concentrations of 300–6500 mg/L are far greater than that of local fresh water. Typical Cl^-/Br^- ratios are 100–140. $^{36}Cl/Cl$ ratios range from (3 to 22) $\times 10^{-15}$, much lower than in present rainwater. $^{36}Cl/Cl$ ratios greater than 1500×10^{-15}, compared to pre-bomb rainwater ratio of 400×10^{-15} in rainwater, indicate that Cl^- and ^{36}Cl in these springs are derived mainly from subsurface non-meteoric sources. ^{36}Cl concentrations and Cl^-/Br^- ratios eliminate the possibility of magmatic, ancient marine, pore fluid, and evaporite contributions to the springs. A comparison of $^{36}Cl/Cl$ and Cl/Br ratios in the Saratoga Springs with secular equilibrium $^{36}Cl/Cl$ ratios and with Cl/Br ratios in potential host formations indicates that subsurface water–rock interactions are the main source of ^{36}Cl to the springs, especially those involving the Ordovician carbonates that compose the aquifer, and the underlying Cambrian clastic rocks. The more dilute springs appear to be a mixture of saline water and a meteoric component, probably resulting from the addition of meteoric water as the groundwater rose to the surface along the fault zone.

7 Summary

The ascending karst springs described here do not provide direct access to caves, but their chemical and physical attributes reveal much information about subsurface processes. Steep topographic and hydraulic gradients, as well as the presence of faults and deep sulfate beds, provide the ingredients for deep karst processes, flow patterns, and sulfate–carbonate interactions. As new techniques are developed, a clearer understanding of groundwater characteristics should become available from the analysis of spring water.

Acknowledgements Thanks to Thomas Kraemer of the U S Geological Survey, Reston, Virginia, for providing field equipment and for isotopic measurements. Graduate students Andrew Fetterman, Elias Moskal, and Jason Siemion at State University of New York, Oneonta, offered insight into nearby springs and caves. Thanks also to Margaret Palmer for field and laboratory assistance.

References

Back W, Hanshaw BB, Plummer LN, Rahn PH, Rightmire CT, Rubin M (1983) Process and rate of dedolomitization: mass transfer and 14C dating in a regional carbonate aquifer. Geol Surv Abstr Bull 94:1414–1429

Bischoff JL, Juliá R, Shanks WC, Rosenbauer RJ (1994) Karstification without carbonic acid: bedrock dissolution by gypsum-driven dedolomitization. Geology 22:995–998

Busenberg E, Plummer LN (1982) The kinetics of calcite solution and precipitation in geologically relevant situations of karst areas. I: open system. Chem Geol 48:189–211

Clark ID, Fritz P (1997) Environmental isotopes in hydrogeology. Lewis Publishers, CRC Press, Boca Raton

Claypool GE, Holser WT, Kaplan IR, Sakai H, Zak I (1980) The age curves of sulfur and oxygen isotopes, in marine sulfate and their mutual interpretation. Chem Geol 28:199–260

Cooper MP, Mylroie JE (2015) Glaciation and speleogenesis. Springer, Cham

Fetterman AR (2001) Geochemistry of surface and subsurface water flow in the Otsego Lake basin, Otsego County, NY. MA thesis, State University of New York, Oneonta

Fisher DW (1979) Devonian stratigraphy and paleoecology in the Cherry Valley, New York Region. NY State Geol Assoc Guidebook 51:20–46

Hollocher K, Quintin L, Ruscitto D (2002) Geochemistry and source of the saratoga springs. In: McClelland J and Karabinos P (eds.) New York State Geological Association, Field Trip Guidebook, Lake George, New York, Trip C-11, 1–15

Kehew AE (2001) Applied chemical hydrogeology. Prentice Hall, Upper Saddle River, NJ

Kraemer TF (2005) Radium isotopes in Cayuga Lake, New York: indicators of inflow and mixing processes. Limnol Oceanogr 50:158–168

Kraemer TF, Genereux DP (1998) Applications of uranium- and thorium-series radionuclides in catchment hydrology studies. In: Kendall C, McDonnell J (eds) Isotope tracers in catchment hydrology. Elsevier, Amsterdam, pp 679–722

Langmuir D (1971) The geochemistry of some carbonate ground waters in central Pennsylvania. Geochimica et Cosmochimica Acta 35(10): 1023–1045

Moskal EJ (2009) The use of radium isotopes and water chemistry to determine patterns of groundwater recharge to Otsego Lake, Otsego County, New York. MA thesis, State University of New York, Oneonta

Palmer AN (2007) Variation in rates of karst processes. Acta Carsologica 36(1):15–24

Palmer AN, Palmer MV (2004) Sulfate-carbonate interactions in the development of karst. Northeast Geol Environ Sci 26(1–2): 93–106

Raines MA, Dewers TA (1997) Dedolomitization as a driving mechanism for karst generation in Permian Blaine Formation, Southwestern Oklahoma, USA. Carbonates Evaporites 12(1):24–31

Rao U, Hollocher K, Sherman J, Eisele I, Frunzi M, Swatkoski S, Hammons A (2005) The use of 36Cl and chloride/bromide ratios in discerning salinity sources and fluid mixing patterns: a case study at Saratoga Springs. Chem Geol 222(1–2):94–111

Rickard LV, Zenger DH (1964) Stratigraphy and paleontology of the Richfield Springs and Cooperstown Quadrangles. State University of New York, Albany, New York

Siegel DI, Lesniak KA, Stute M, Frape S (2004) Isotopic geochemistry of the Saratoga Springs: implications for the origin of solutes and source of carbon dioxide. Geology 32(3):257–260

Siemion J (2006) Use of isotopes, tracer tests, and dissolved solids to characterize a karst aquifer. MA thesis, State University of New York, Oneonta

Taylor PM (2000) Calcite deposition from high-sulfate springs, Van Hornesville, New York. MA thesis, State University of New York, Oneonta

Terrell L (2008) Chemistry of sulfide-rich karst springs in Otsego and Schoharie Counties, New York. MA thesis, State University of New York, Oneonta

Carbonate-Hosted Massive Sulfide Deposits and Hypogene Speleogenesis: A Case Study from Nanisivik Zinc/Lead Mine Baffin Island, Canada

48

Derek C. Ford

Abstract

Nanisivik zinc/lead mine is located at Lat. 73°N in northwestern Baffin Island. The host rock is a pervasively dolomitized Proterozoic platform carbonate overlain by a shale aquitard. The principal deposit, the Main Ore, is of zinc, lead, and iron sulfide plus gangue minerals, chiefly secondary dolomite. It extends for 3 km along a horst and is terminated at both ends by modern valley entrenchments. The Main Ore body is consistently ~100 m wide and five to seven m thick. The ceiling is a wide, horizontal corrosion bevel. Within the Main Ore are two or more generations of tapered fins of dolomite that extend into the cavity. The fin edges are sinuous, some meandering. Sharp, horizontal corrosion notches 20–30 cm high extend into the dolomite walls. They are filled with layered pyrites which continue into the ore body, truncating earlier, dipping mineral bodies. Sedimentary textures suggest that the ore cavity formed by paragenesis in a channel-flow mode, with ore and gangue deposition on the floor taking place in tandem with dissolutional cavity creation upward. Fluid inclusions indicate derivation of the metals from exchange reactions with metalliferous sediments (the underlying shales), indicating low water/rock ratios and moderate temperatures. The ore fluids were similar to oilfield brines. Sulfur isotope fractionations indicate temperatures of 90–150 ± 40 °C, suggesting that the Main Ore formed along a gas/brine interface at a depth of at least 1600 m. Latest studies suggest a Grenville age (~1.1 Ga) for the Main Ore.

Keywords

Hypogene paragenesis • Sulfides and gangue minerals • Metasomatism

1 Introduction

Carbonate rocks, chiefly dolomites, host a large proportion of the world's economic deposits of zinc, lead, and associated elements, in the form of massive accumulations of sulfide minerals that are intermingled with penecontemporaneous ('secondary') precipitates of dolomite. Historically, there have been two principal views on the origin of these deposits: first, that they are 'epigene,' implying that the ores are fillings of preexisting karst voids and were deposited by mechanical in wash or chemical precipitation from surface waters passing underground, much like the accumulation of bauxite ore in sinkholes or similar traps; alternatively, that they are 'hypogene,' precipitated from solutions flowing upward or laterally into the carbonate formations, often having derived from (or passed through) other types of rocks such as shales that supplied the metals, and arriving via fractures. Although a few deposits may be genuinely epigene, today it is widely recognized that some form of hypogene origin applies to most of those that have ores in economic concentrations (Dzulynski and Sass-Gutkiewicz 1989).

There remains controversy on several important questions concerning the hypogene creation and morphology of the ore

D.C. Ford (✉)
Geography and Earth Sciences, McMaster University, Hamilton, ON L8S 4K1, Canada
e-mail: dford@mcmaster.ca

© Springer International Publishing AG 2017

A. Klimchouk et al. (eds.), *Hypogene Karst Regions and Caves of the World*,
Cave and Karst Systems of the World, DOI 10.1007/978-3-319-53348-3_48

bodies—do the precipitating fluids (1) invade and infill preexisting, open karst features, perhaps modifying their form a little by minor solution and collapse of bedrock? Or (2) is the morphology largely or entirely created by the dissolution and precipitation activities of the ore-bearing fluids themselves ('syngenetic development')? If the latter is true, is the process (at one extreme) one of progressive molecule by molecule replacement of dolomite by sulfide as the fluid permeates the rock widely (metasomatism)?—or, at the other extreme, does the fluid first open a cave by dissolution and then infill it with the ore and secondary (gangue) minerals?

Most of the hypogene ore bodies in carbonate rocks display one or two of three basic morphologies. In the West, the more common of these were first described in detail in the Tri-State mining region west of the Mississippi River and so are known as 'Mississippi Valley type' deposits (MVT). The first morphologic type is a domelike ('beehive-shaped'—Sass-Gutkiewicz 1974) breakdown chamber, commonly tens to a few hundred meters in diameter. The ore fills interstices in the breakdown and may exhibit a variety of sedimentary and crystalline forms (e.g., Sass-Gutkiewicz op. cit; Sangster 1988). The second morphology is a reticulate pattern of long, narrow, and quite high corridors of breakdown that are filled with the ore and gangue: This is very similar to the patterns seen in many open maze caves, and in a very few instances, there are some truly open passages mingled with the ore galleries (e.g., Devil's Hole Mine, England; Ryder 1975). The third, less common morphology is described by Sangster (op. cit.) as 'columnar,' being curvilinear or irregular breakdown bodies that can vary considerably in width and are usually discontinuous. Sometimes, they occur in arcuate groupings. The principal example of this morphology is to be found in the Pine Point zinc/lead mines along the south shore of Great Slave Lake, Canada (Rhodes et al. 1984): Today, I would interpret much of the form there as a product of ore fluid invasion and enlargement of the reefal flank margin type of caves described by Mylroie and Carew (1990) in the modern Bahamas. To conclude this brief review, it is important to stress that in all three morphologies the ores occur chiefly as interstitial fillings in bedrock breakdown. Sangster (op. cit.) emphasizes the additional point that there is usually very little alteration of this bedrock by metasomatic processes, merely narrow rims in a few places.

The author had the opportunity to investigate the Nanisivik zinc/lead mine in detail in 1981 and 1982, shortly after it had opened, and later co-supervised a PhD study there (Ghazban 1988). The morphology of the 'Main Ore' (principal ore body) differed quite markedly from the MVT types summarized above because it displays sinuous, meandering channel-flow forms such as are common in meteoric water caves, especially those in the most soluble rocks, gypsum, and salt. There was little breakdown. It is presented and interpreted here as an example of hypogene speleogenesis with syngenetic ore deposition, in a setting that is paragenetic and hyperacidic.

2 Nanisivik Geography and Geology

Nanisivik (Inuit—'the place where they find things') zinc/lead mine is located at Lat. 73°N in northwestern Baffin Island. The mine operated between 1976 and 2002, producing 120,000–140,000 tonnes of concentrate for shipping. Pertinent geographical and geological features are shown in Figs. 1 and 2. The local horst and graben topography has been much scoured by glaciers of the island ice caps. The Main Ore and other economic deposits are contained within a horst block that rises to a little more than 400 m above sea level today. Two valleys have been eroded across the horst, truncating the Main Ore at its west end and separating it from a pair of smaller deposits in the east, the Ocean View and Kuhulu Trends. There is an arctic climate, with permafrost present to depths greater than 100 m today and a temperature of −12 °C in the mine.

The basement rocks are granites and gneisses of Archean age, now exposed to the south by the block faulting (Fig. 2). They were unconformably overlain by thick sequences of clastic and carbonate sediments of middle Proterozoic age (1200–1000 Ma). The host rock is the Society Cliffs Formation (HSC), a subtidal to tidal algal platform carbonate containing some gypsum and organic interbeds. It displays evidence of occasional marine emergent epikarstification during its accumulation (Ghazban et al. 1993). The formation is ∼460 m thick in this region, medium to massively bedded, and pervasively dolomitized. It rests on >900 m of mixed shales, siltstones, sandstones, and impure dolomites (HAB—the Arctic Bay Fm) and is overlain by the Victor Bay Fm (HVB), 150+ m of shales and minor limestones that function as an aquitard or aquiclude. These formations were buried by >1000 m of later Proterozoic strata and then uplifted with some local folding and block faulting as shown in Fig. 2. Considerable erosion followed before re-burial and the unconformable deposition of >500 m of Cambrian sedimentary rocks. In an early geological report, Clayton and Thorpe (1982) asserted that all of the formations were then cut by gabbro dykes which they dated at 476 Ma and which also intersect and displace the ore bodies, indicating that the latter must be older: Both the age of the dyke and its displacing effects are now disputed (Sherlock et al. 2004—see below)

In the Main Ore horst block, the Society Cliffs dolomites dip consistently to the northwest at an angle of 15°, across the trend of the ore bodies. Graben to the north and south are roofed in the Victor Bay shales (Fig. 2).

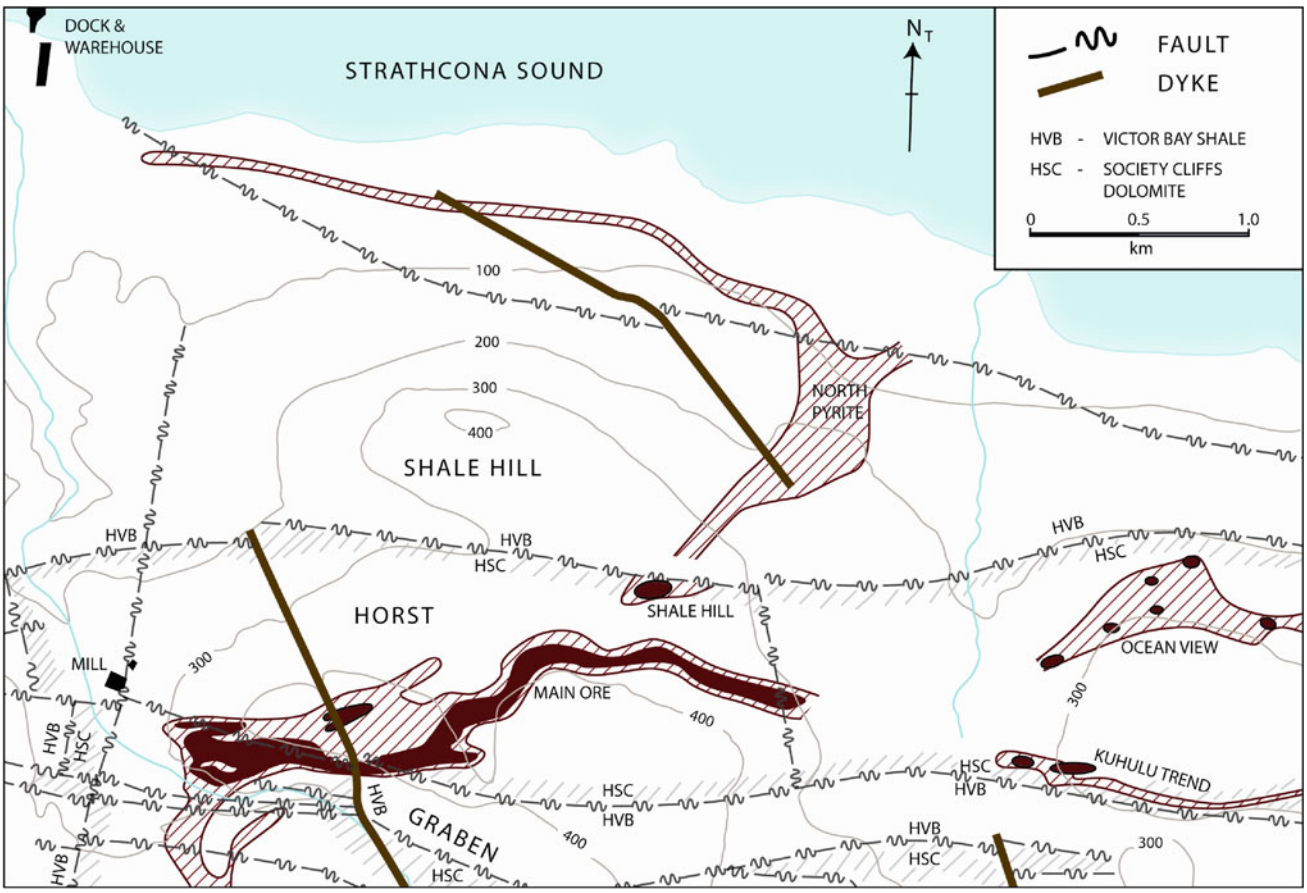

Fig. 1 Plan view of the pyrite and zinc–lead deposits at Nanisivik, Baffin Island, Canada. Sulfide bodies are indicated by *cross-hatching*, with ore-grade deposits shown in *deeper red*. HVB, HSC delineate outcrop of the principal geological formations. *Contour interval* meters above sea level

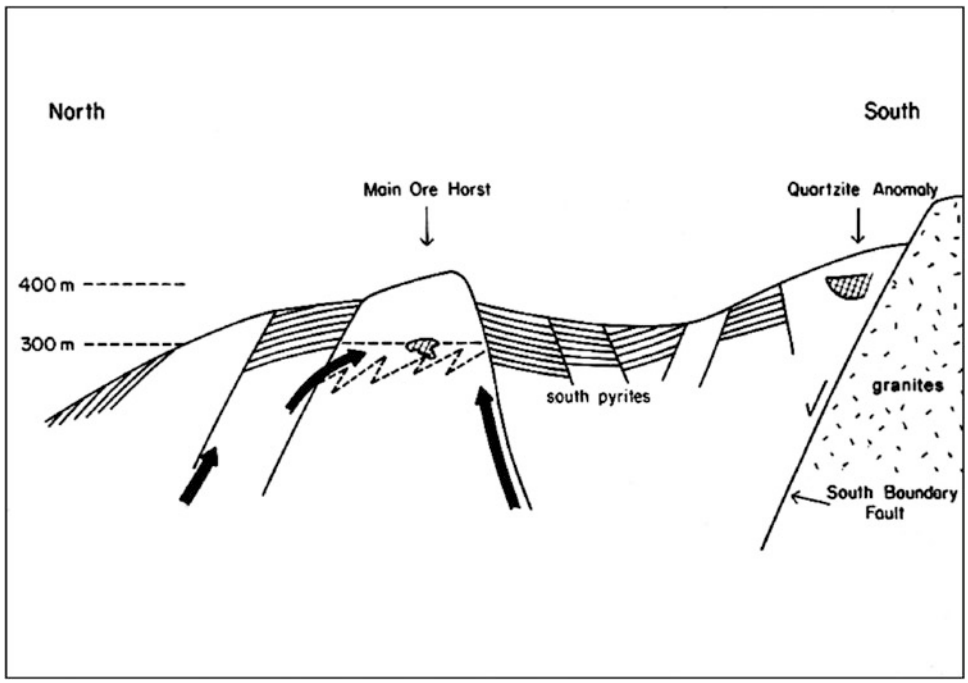

Fig. 2 Sketch cross section of the geological structure along a N–S transect at Nanisivik (Baffin Island, Canada), showing location of the principal sulfide bodies. *Arrows* indicate possible fluid flows

3 Morphologic Features of the Main Ore Mine

The Main Ore extends for three km E–W along the horst (Fig. 1). It is horizontal, oriented close to the strike of the steeply dipping dolomites but sinuous so that it meanders discordantly across any strictly strike-oriented path. It is ~300 m above sea level and terminated at both ends by the modern valleys entrenched across it. Ocean View and the Kuhulu Trend, the two lesser bodies to the east, are preserved at the same elevation on the further side of the valley. To the north, a narrow, elongated ore body, the North Pyrite, has been mapped by exploration drilling as ascending at the Society Cliffs–Victor Bay contact through a series of graben until it enters the horst at the same elevation as the Main Ore; only at that elevation do its concentrations of sphalerite and galena attain the ore grade. To the south of the horst further, minor and below-grade, pyrite bodies extend to higher elevations (Fig. 2).

The Main Ore body is a quite remarkable piece of underground morphology. Figure 3 attempts to display this with a series of cross sections. The body is consistently ~100 m in width and five to seven m in height from ceiling to floor. The ceiling is a nearly planar, horizontal bevel that does not differ in its elevation of ~300 m above sea level by as much as two meters except where it is displaced a little by the gabbro dykes (Clayton and Thorpe 1982). This ceiling has not collapsed despite being a great, flat span crosscutting dolomite beds that were dipping in cantilever array with respect to it. The sulfides scarcely extend above it anywhere. When inspected by the author in 1981 and 1982, a few small (half meter-sized) solution pockets could be seen in one small area of the mine ceiling; they followed dip or strike joints and did not appear to contain any large amounts of pyrite or exhalative precipitates. They may be recent features, but below one example mining operations had left a sloping fragment of corrosional surface (the root of a fin—see below) with a section of layered clay resting upon it that looked very much like flood clay on any ledge in a meteoric water cave: The clay appeared altered (blanched and hardened) but was not accessible for sampling to confirm this. A particularly striking feature was the apparent absence of any substantial quantities of breakdown anywhere in or under the sulfide ore masses, with one exception—for 200 m along the southwest side of the mine, both bedrock and ore had collapsed in large blocks that were now firmly cemented by large masses of ground ice; this collapse is attributed to Quaternary subglacial dissolution, long after the ore was deposited (Ford 1987).

Irregularly along its length, the Main Ore mass is underlain by a 'keel' or 'manto' (mine geologists' expressions) of below-grade ore that is up to ten meters or more in depth (Fig. 3). However, this keel is discontinuous, as are other quasi-horizontal bodies detected by drilling that, where they are encountered, are rather consistently centered at depths of 40–50 m below the Main Ore. Olson (1984) interpreted the keel as a later stage vadose entrenchment beneath a Main Ore phreatic cavity and likened the pair to the morphology of some of the major passages in the Mammoth Cave System, Kentucky. However, there is nothing like the Main Ore cavity (if such it was) in Mammoth Cave, and the discontinuous nature of the keel appears to rule out continuous vadose entrenchment. An alternative explanation is offered below.

3.1 Fins and Corrosion Notches in the Main Ore

Two striking features in the Main Ore are the fins and the mineral-filled corrosion notches found there. The fins are considered first and illustrated in Figs. 4, 5, 6, and 7. Fins of bedrock projecting into a passage are common features in meteoric water caves. Figure 4a shows the typical relationship between rock and channel that may be expected there—the fins are concordant to the bedding, it is the slightly less soluble beds that project, and projection is rarely greater than 1 or 2 m. In contrast, within the Main Ore, fins of dolomite in situ extend from both south (updip) and north (downdip) walls into the cavity (Fig. 4b; Ford 1986). Their form varies in detail, but all are tapered. Some extend more than 20 m in from the boundary walls of dolomite. Note that fin surfaces truncate the bedding. In plan view, the edges of the fins are sinuous or meandering, with a meander wavelength of approximately 50 m (Fig. 5). At several places in the mine in 1981 and 1982, it could be seen that there were (or had been before the mining) at least two generations of fins one above the other and with the meanders out of phase with each other, as can sometimes be seen in salt mine cavities that have been subjected to occasional flooding (Fig. 6).

The meandering, tapered form of the fins leaves little doubt that they were fluid dynamic flow forms. Their large size and discordant relationships with the dolomite bedding imply that they should be very fragile, requiring mechanical support from either the continuous buoyant presence of dense fluid, or solid underpinning with co-precipitated ore and gangue minerals, or both. Figure 7 shows the author's proposed explanation of their formation. They appear to be the remains of intersecting 'paragenetic' cavities. Standard models of paragenesis in meteoric water caves are shown in Fig. 7a: The depositional environment is one that permits net accumulation of insoluble sediments on the floor, causing the cave roof to be dissolved upward to maintain the channel

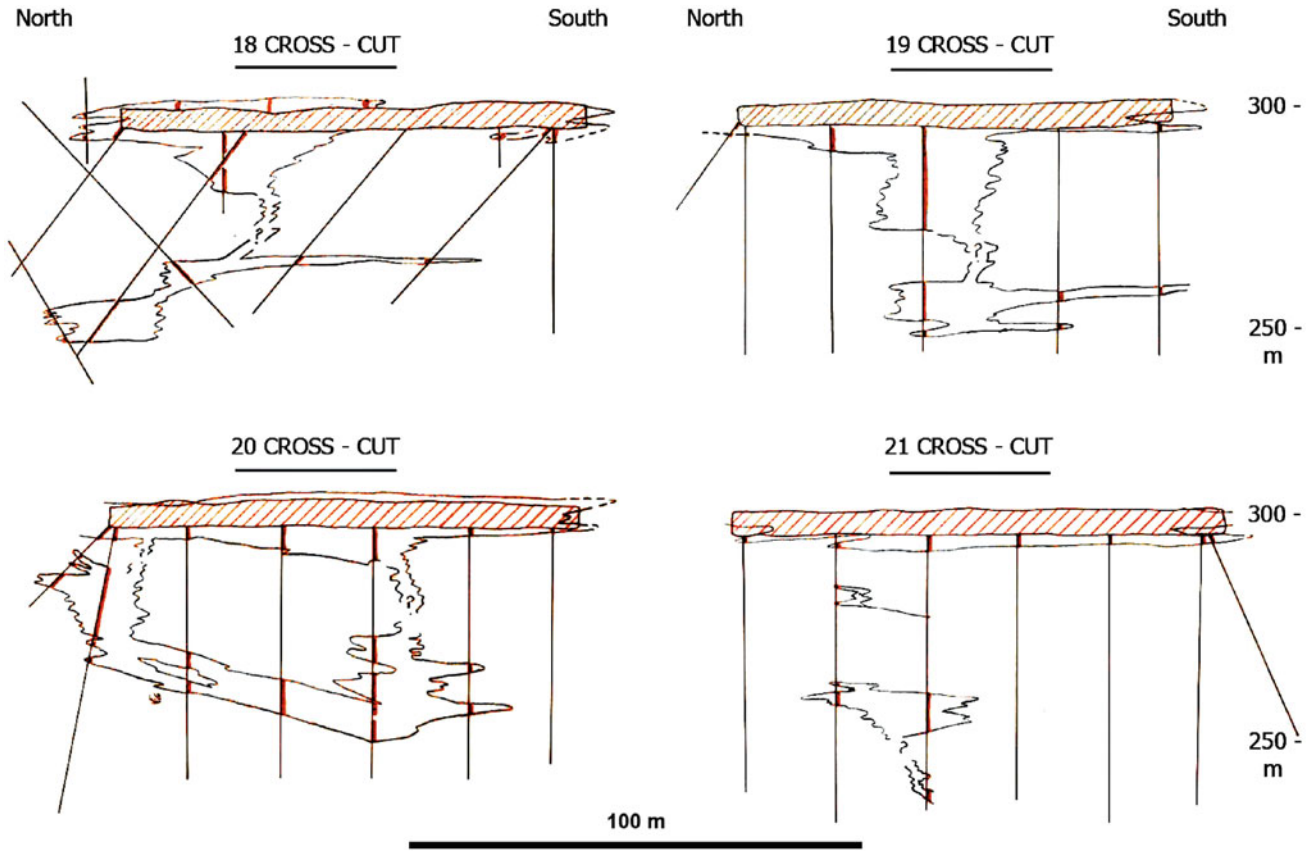

Fig. 3 The form of the Nanisivik Main Ore body and underlying manto pyrite deposits at a sample of mined adits (crosscuts, shown in *red hatching*) across the East–West trend of the ore body that, in each case, extended to or very close to the limits of the ore. Location of exploratory, six-inch drill core holes below the Main Ore is shown in *black*, with the presence of ore and gangue minerals marked in *red*; the morphology of the manto deposits that is shown is the mine geologists' interpretations of these drill core interceptions

cross-sectional area, until a water table is intersected (Ford and Williams 2007; page 232). In Fig. 7a, steady dissolution upward to one fixed water table is shown on the left and, on the right, the more complex case where the water table itself shifts upward from time to time, as it might do, for example, in the flanks of a river valley that is being aggraded. The meandering fin morphology in the Main Ore walls was created by the overlap of two successive paragenetic channels in an upward shifting interface scenario (Fig. 7b). Contemporary precipitation of ore and gangue minerals may have helped to support portions of the roof spans. The nature of the fluid interface itself at Nanisivik (whether a water table or other) will be considered later.

Corrosion notching at a water line is a common feature in meteoric water caves. Typical examples are illustrated in Fig. 8. At its most simple, a notch may form at the water line where there is a slow drip into a pool that introduces fresh carbonic acid (H_2CO_3) to its surface (Fig. 8a). In limestone caves, the author has seen corrosion notches of this kind that are as much as 2 m deep (Fig. 8b). Where the water is ponded behind some natural dam, entire sections of submerged cave roof may be dissolved up to the water line, creating a ceiling bevel (Fig. 8c). More extreme notching is known to be created where H_2S from hypogene sources is released at or just below a water table, the Big Room at Carlsbad Caverns (one of the world's largest known open cave chambers) being an example (Ford and Williams 2007; Palmer 2007).

At Nanisivik, very sharp corrosion notches that are horizontal and 20–30 cm high extend into the dolomite walls for at least 20 m (the limit of deep crosscuts in the mine). They are filled with layered pyrites which continue out into the ore body as regular sheets truncating earlier, dipping mineral layers until they themselves are truncated by later fillings (Fig. 9a–c). Note that they often have a discordant relationship with the fins, suggesting that they are later features in most examples (Fig. 9b). If the mine geologists' interpretation of their frequent drill cores was correct, in the western half of the cavity is one exceptional corrosion notch that is filled with layered pyrite. This feature is horizontal,

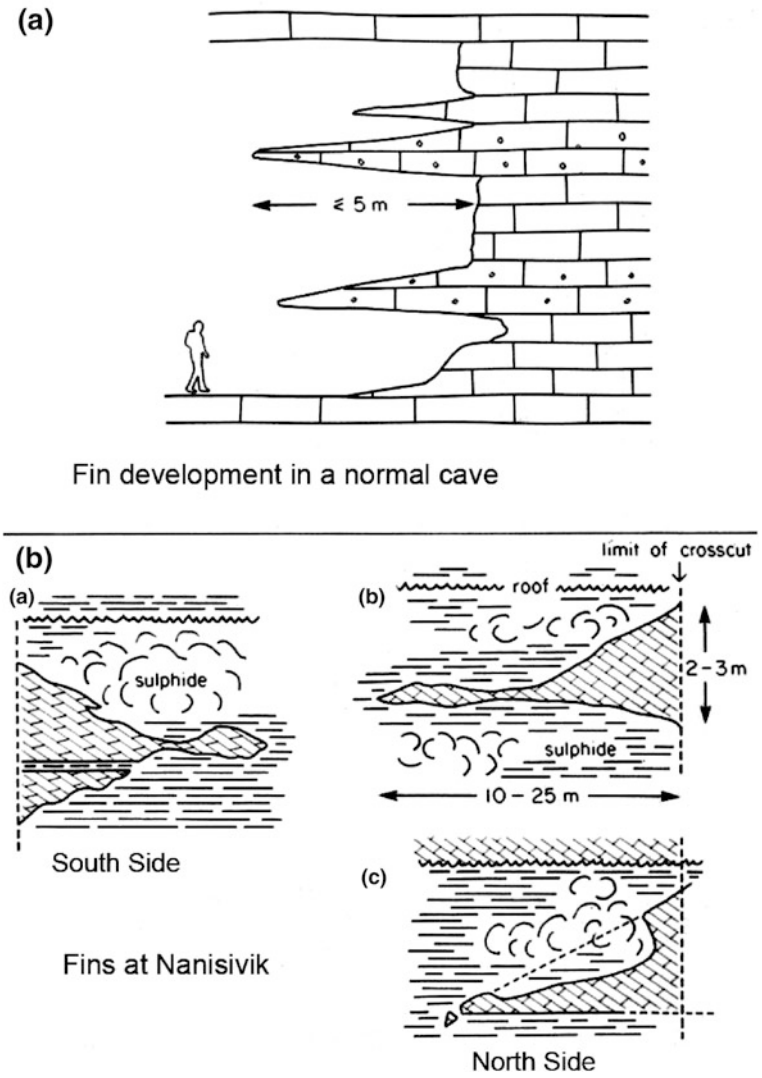

Fig. 4 The morphology of bedrock fins in typical meteoric water caves (**a**) compared to examples of dolomite fins in the Nanisivik Main Ore that were measured by the author in 1981 and 1982 (**b**)

1 m deep, and extends across the dipping dolomites for a distance of 350 m toward Shale Hill north of the main cavity (Fig. 1; Fig. 9, lower right); it is the greatest example of corrosion notching that I am aware of anywhere. The roof of the Main Ore cavity itself can be considered to be a ceiling bevel formed at the close of a single stage; its modern extent is 300,000 m^2 ($\sim$3000 $\times$ 100 m), having been reduced by surface erosion at both ends.

3.2 Sedimentology and Geochemistry of the Ore Fillings

The fillings are pyrite (FeS_2), galena (PbS), sphalerite ZnS), minor accessory minerals, and the gangue minerals—secondary dolomite ($CaMg(CO_3)_2$), which is volumetrically predominant, chiefly as white sparry dolomite, calcite ($CaCO_3$), and quartz (SiO_2). The bulk porosity is quite high, but most pores today are filled with ice because, as noted, the mine is entirely within permafrost and has a temperature of −12 °C. Generalizing, the ore displays four sedimentary modes (Fig. 10): (1) as regular layers settled or precipitated on the floor, or lapping onto the upper faces of fins where they lie subparallel to the sloping fin surfaces; (2) as chaotic polymict breccias; these were chiefly in the center of the body, strongly suggestive of channel cut-and-fill episodes of erosion and deposition, including avalanching of earlier deposits off of the lateral fins into an abruptly emptied center; (3) as the horizontal, thin but layered, pyrite sheets noted above (Fig. 9), that crosscut earlier type 1 and 2 sediments and fill corrosional slashes into the dolomite walls; and (4) as metasomatic replacements of dolomite.

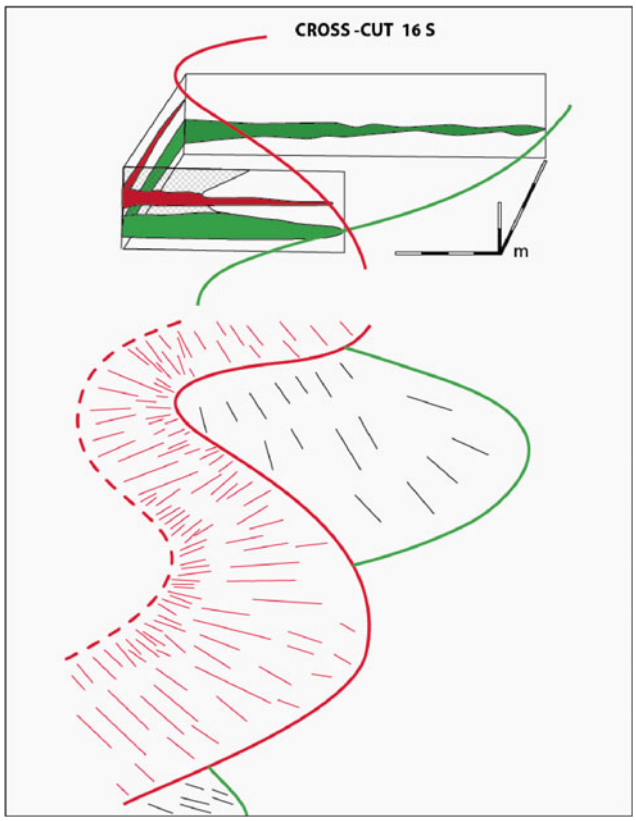

Fig. 5 Schematic drawing to illustrate the meandering forms of a pair of bedrock fins (lower in *green*, upper in *red*) measured in 1981 at crosscut 16 and east of it, Nanisivik Main Ore. *Scale bar* at the crosscut is marked at 1-m intervals. The true wavelengths of the pair of meanders in the lower sketch were about 50 m

Ghazban (1988) found metasomatism to be more widespread than the author observed in exposures laid bare in the earlier mining (1981 and 1982), but ore-bedrock contacts remain generally sharp (as seen in the example in Fig. 6) and the depth of isotopic alteration of bedrock where we have examined it is trivial (Fig. 11).

The isotopic compositions of the dolomite gangue suggest that they were partly a by-product of dissolution replacement of the host rock, and partly due to sulfate reduction by hydrocarbons and related organic matter derived from the large volumes of shaly rocks above and below the Society Cliffs dolomite in the region (Ghazban et al. 1992). Throughout the mine, freshly blasted rock stank of bitumen. The stable isotopic compositions of fluid inclusions from more than 400 published analyses of gangue dolomite (principally), plus sphalerite, galena, calcite, and quartz (Olson, 1984; McNaughton and Smith, 1986; Ghazban et al. 1991), are consistent with derivation of the metals primarily from exchange reactions with large volumes of metalliferous sediments, indicating low water/rock ratios and generally moderate temperatures in the system. The ore fluids were similar to many modern oilfield brines (Fig. 12). Based on fluid inclusion homogenization temperatures and isotope fractionations between co-precipitating minerals, the various authors estimated temperatures to be in the range 90–170 ± 40 °C in most samples, but rising as high as 250 ± 50 °C in some of the late-stage precipitates. These findings point firmly to the conclusion that the Nanisivik ore deposits are of hydrothermal origin, in waters with high concentrations of dissolved solids (brines); $CaCl_2$ was the most abundant solute in the fluid inclusions, suggesting that the waters originated as seawater trapped in interstices in the regional shales and siltstones.

4 Modeling the Genesis of the Main Ore Cavity and Its Deposits

There are two schools of thought among the scientists who consider that economic massive sulfide deposits are of hypogene origin. One school advocates the infilling of pre-existing karst, with relatively little modification of the karst morphology. Sangster (1988) writes that '… the other school, advocated chiefly for the Polish deposits, proposes that "the emplacement of ores and formation of underground karst were parts of the same formative processes and essentially simultaneous" (Sass-Gutkiewicz et al. 1982)'.

4.1 Syngenesis and Paragenesis

At the Main Ore, the field evidence is overwhelmingly in favor of the Polish syngenetic model, as indicated by its horizontality, width, ceiling beveling, and general lack of bedrock breakdown. In addition, the presence of two or more levels of sharp fins exhibiting meandering channel-flow form, and the sedimentological evidence of onlapping sulfides covering those fins before avalanching into channels to form the polymict breccias there strongly support the notion of a paragenetic mode of dissolution and deposition as hypothesized in Fig. 7. The dolomite was dissolved upward (and laterally outward where the corrosion interface was stable in its elevation for substantial periods of time) with more or less simultaneous precipitation of sulfides and gangue minerals underneath.

Lebedev (1974) and others have shown that many modern hydrothermal systems are strongly episodic in their behavior, with long periods of comparatively low and stable discharge being interrupted by brief spells of abundant flow (surges): In some instances, the surges are correlated with regional earthquakes. In the Main Ore, the contrast between

Fig. 6 *Upper left* The tip of a small dolomite fin overlain and underlain by Type 1 ore deposits, Main Ore, Nanisivik. Note the very sharp upper contact between dolomite and ore. There is some Type IV metasomatic alteration dolomite (*bright white*) on the underside. Patches of ground ice are seen in the ore above the fin. The *scale bar* is graduated in decimeters. *Lower left* A display of Type 2 chaotic ore in the central flow channel of the Main Ore, overlain by *white* sparry dolomite at the *top*. *Right* Waterline corrosion notches, fins, and ceiling bevels in the Cardona Salt Mine, Spain. Notching and beveling are completely discordant with tight concertina folding in the diapiric salt. (Photograph courtesy of J. Cardona)

the dynamic nature of the channel cut-and-fill sulfide breccia events, on the one hand, and the long periods of stability suggested by the astonishing pyrite-filled corrosion notches slashed horizontally for tens to hundreds of meters laterally into the bedrock, on the other hand, are clear evidence of a sequence of many, dynamically very contrasted episodes in the history of development.

4.2 Age and Depth of Formation of the Main Ore

The question of age remains controversial. Symons et al. (2000) accepted Clayton and Thorpe's (1982) contention that the gabbroic dykes displace the Main Ore, which thus must be older. Using paleomagnetic measurements of the ores and gabbros and correlating the results with polar wander curves, they placed the age of the dykes at ~720 Ma and the ore as early as 1095 ± 10 Ma, which is soon after deposition of the end of the Arctic Bay shales that cover the host dolomites. In good agreement, Hnatyshin et al. (2011) cite ten Re–Os analyses of Nanisivik pyrite yielding an age of 1114 ± 120 Ma (Grenvillian). In flat contradiction, however, Sherlock et al. (2004) contend that the dykes do not displace the ore, which thus is younger. They discovered small quantities of altered siliciclastic deposits scattered throughout the ores and interpreted them as insoluble residues of dolomite solution plus, perhaps, other clay colloids from nearby shales. The ^{40}Ar:^{39}Ar dating method was applied to samples of orthoclase derived from

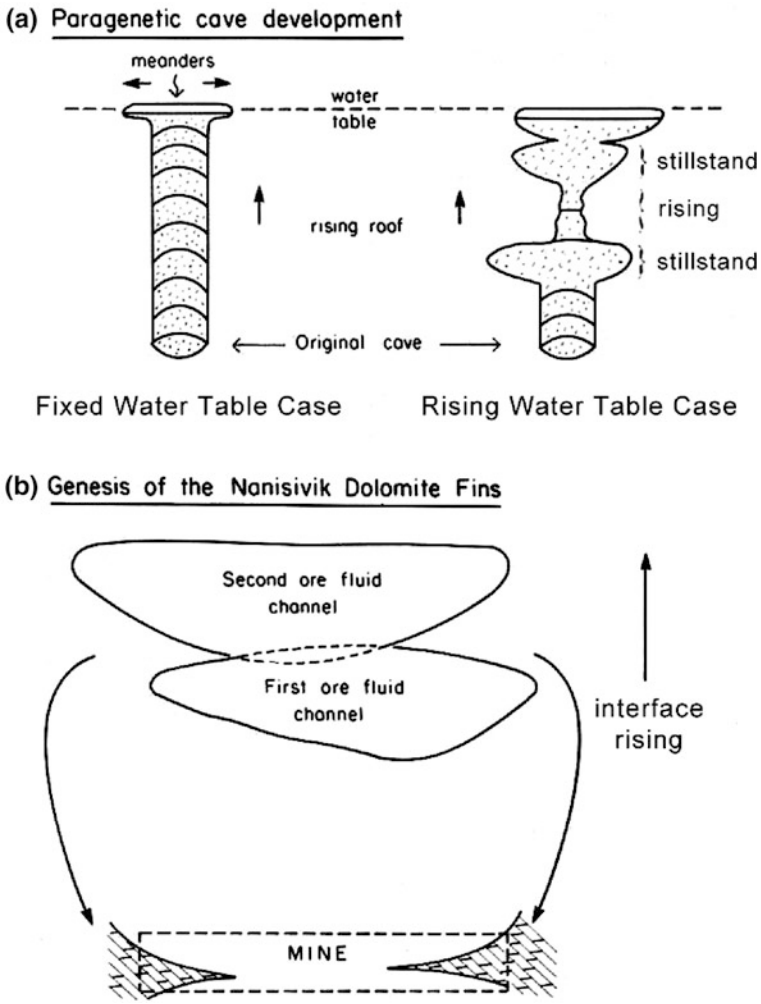

Fig. 7 **a** Development of paragenetic cave morphology toward water table in meteoric water caves: *on left*, where the water table is fixed throughout evolution; *on right*, where it is shifted upward episodically. **b** The author's interpretation of the genesis of the fins seen at Nanisivik Mine

the altered material, giving ages around 461 Ma (Middle Ordovician). It is possible that the altered clays the author observed resting on a fragment of fin near the roof in the Main Ore in 1981 (see above) belonged to this category of deposits.

Based on their thermal water temperature findings, McNaughton and Smith (1986) estimated that the Main Ore emplacement took place at a depth of at least 1600 m underground. Certainly, by the Middle Ordovician, the host dolomites at Nanisivik had been deeply buried and then deformed, uplifted, and eroded, followed by a second burial beneath 500+ m of Cambrian sedimentary rocks. This history accords well with a 1600+ m depth for the ore emplacement.

McNaughton and Smith (1986) also derived a vertical thermal gradient as great as 60 °C/100 m from the fluid inclusion measurements at the Ore; this is probably an overestimate, but it does underscore the very dynamic nature of the flow system that is also indicated by the morphologic and sedimentary evidence outlined above.

4.3 A Model for the Main Ore Emplacement

Figure 13 presents the author's model for the syngenetic dissolution of host dolomite and emplacement of the Main Ore at Nanisivik. Figure 13a shows the regional picture. Readers must imagine the entire structure to be sinking beneath a load of many hundreds of meters of later Proterozoic and possibly Cambrian sediments that are not shown. Basin waters are being expelled through the more permeable formations and the major fractures.

Figure 13b is a close-up of the Main Ore horst. It is known that there were minor episodes of karstification during deposition of the dolomite. After it was folded and faulted, further karstification may have occurred during the

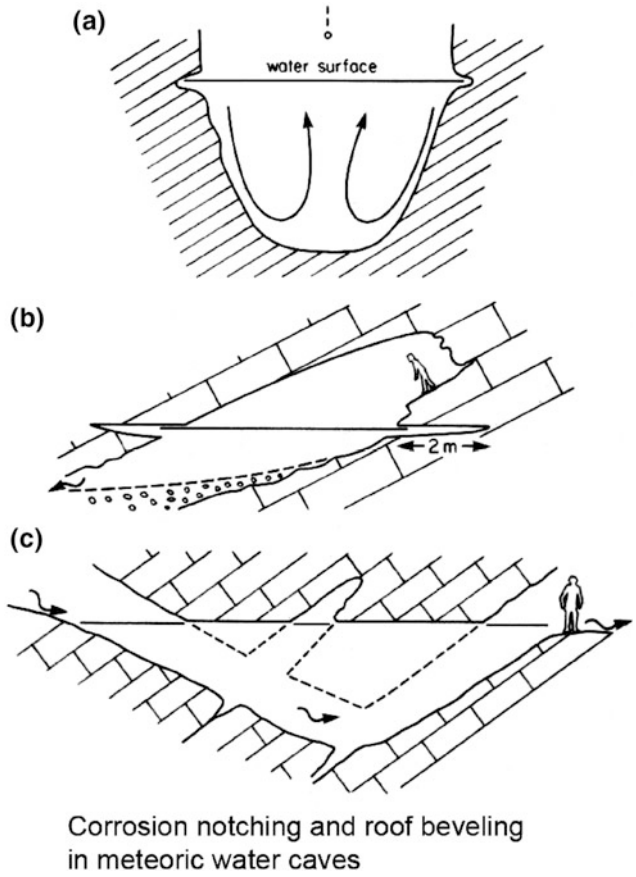

Fig. 8 Corrosion notching and roof beveling in meteoric water caves; see the text for details

long erosional time interval before Cambrian deposition began. This is suggested by two pieces of circumstantial evidence. The first is the sharp northward jog in the middle of the Main Ore, which shifts the channel from a southside strike-oriented position in the horst to a similar central position (Fig. 1); this kind of behaviour often indicates that the hypogene flow was ascending toward an open target (a cave) in the rock and became diverted along it (Ford 1996). Second, and associated with the first, is the very irregular spatial distribution and size of the sulfide deposits detected in the manto below the Main Ore body (Fig. 3). It suggests the presence of scattered, small dip tubes (proto-caves; Ford and Williams 2007; 214–7) in the north-dipping strata underneath the Main Ore level. Ore fluids rising up the northern boundary fractures were able to migrate out into the body of the dolomite horst block via these tubes and begin sulfide deposition as the pressure dropped.

Figure 13c completes the story. The graben is sinking, with episodic stillstands of the kind illustrated in Fig. 7a. One such (Number 2 in the figure) is a little longer in duration and gives rise to the larger concentrations of sulfides seen from place to place at ~250 m asl in the manto zone. Then, the fluid interface is stable but oscillating for a long period in a 7 m high zone that is now centered at 300 m asl. At least two successive paragenetic channels were created within this narrow range, forming the bulk of the Main Ore body. Flow discharge was markedly episodic during its formation, including periods of steady paragenetic excavation/deposition, stronger surges that temporarily emptied portions of the central channel, and long periods of quiescence when very deep corrosion notches of little height could be cut into the host rock at precisely fixed levels of the fluid interface.

Further sinking eventually uncoupled the Main Ore body from its fluid sources, some of which were evidently redirected upwards to the south, where the final surviving pyrite body in the local area was deposited at 350–380 m asl in the Quartzite Anomaly (Fig. 13a).

4.4 Dissolution and the Fluid Interface

Ghazban (1988) showed that degradation of the local shale bodies (Arctic Bay and Victor Bay formations) to produce the kerogen predecessors of oil would release more than sufficient CO_2 to supply the carbonic acid necessary for the volumes of dissolution of the Society Cliffs dolomite that occurred during emplacement of the ore bodies. However, the exceptionally deep corrosion notches suggest that there was some contribution from stronger acids: H_2S from the reduction of gypsum, interacting with the metal chloride solutions to precipitate the sulfides, probably yielded the extra H^+ in abundance.

What was the nature of the fluid interface? This question is not within the author's area of competence, but the combination of high temperatures with stability over time suggests that it must have been either an oil/brine interface or possibly a gas/brine interface. The geographical area covered by the Main Ore horst, including the Ocean View and Kuhulu Trend extensions, is similar to that of many small oil or gas fields, and the horst and graben geometry with shale aquitards would have offered opportunities for structural trapping.

4.5 The Regional Tectonic Setting

The Nanisivik massive sulfide deposits are strikingly atypical of worldwide MVT deposits (see Bradley and Leach 2003) in that they appear to have accumulated in an extending (sinking) tectonic setting rather than one of the variety of collisional settings (orogenic forelands) which

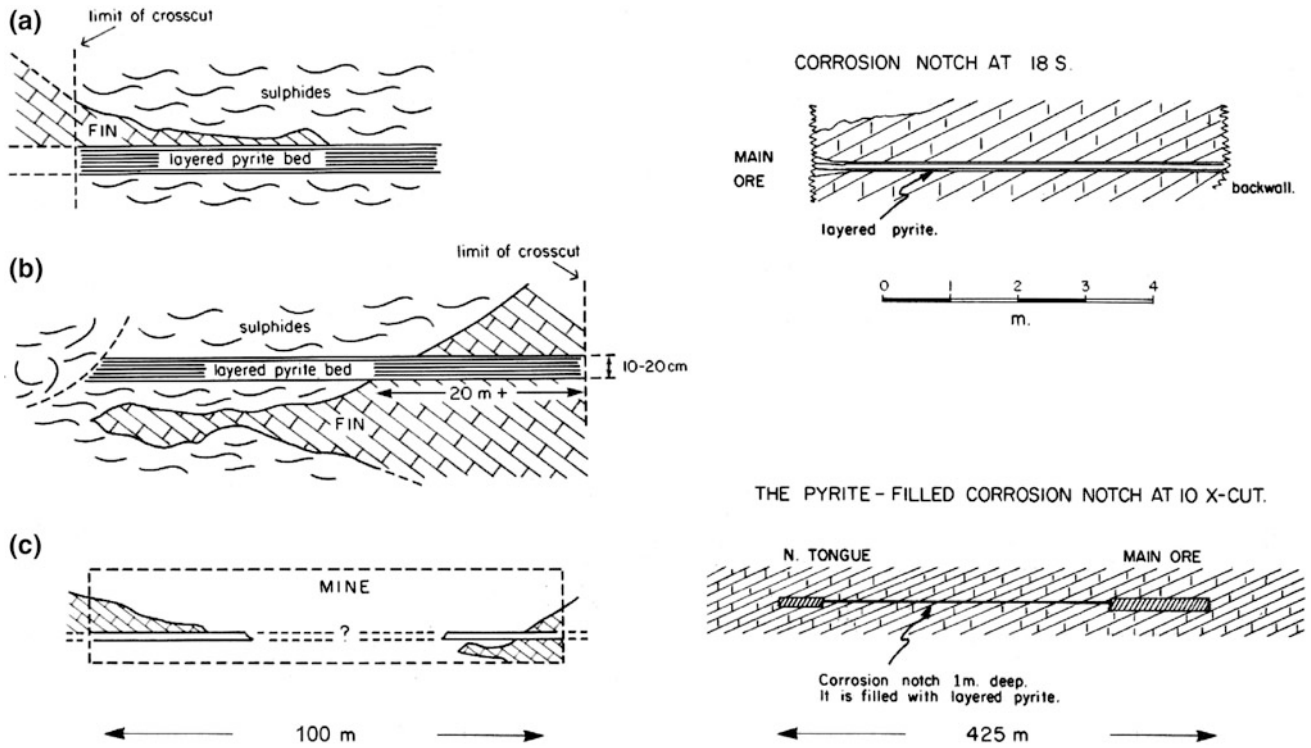

Fig. 9 Examples of pyrite-filled corrosion notches in the Nanisivik Main Ore body, based on field sketches by the author in 1981, and mine drilling records at No. 10 crosscut

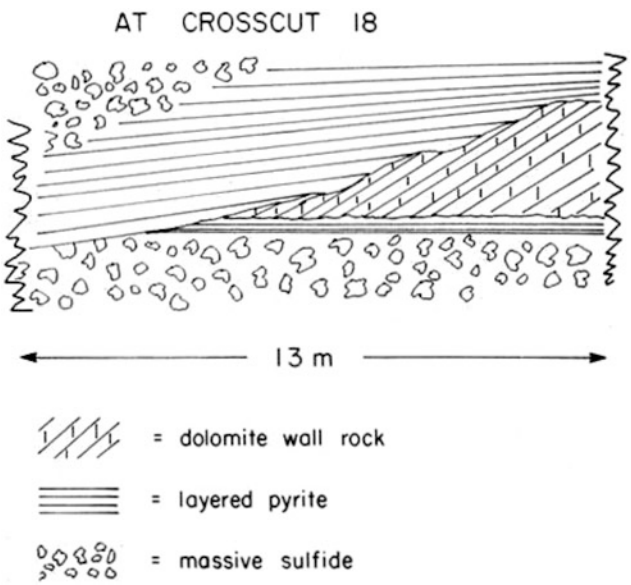

Fig. 10 Illustrating four modes of ore and gangue mineral deposition in the Nanisivik Main Ore body. Type 1 as relatively thick beds onlapping a fin of dolomite; type 2, chaotic polymict breccias **a** early stage, beneath the fin, and **b** later stage, occupying a channel cut into type 1 deposits: type 3, layered pyrite corrosion notch filling, with thin beds. Type 4, metasomatic replacements of dolomite. From the author's field measurements at crosscut 18 in 1981

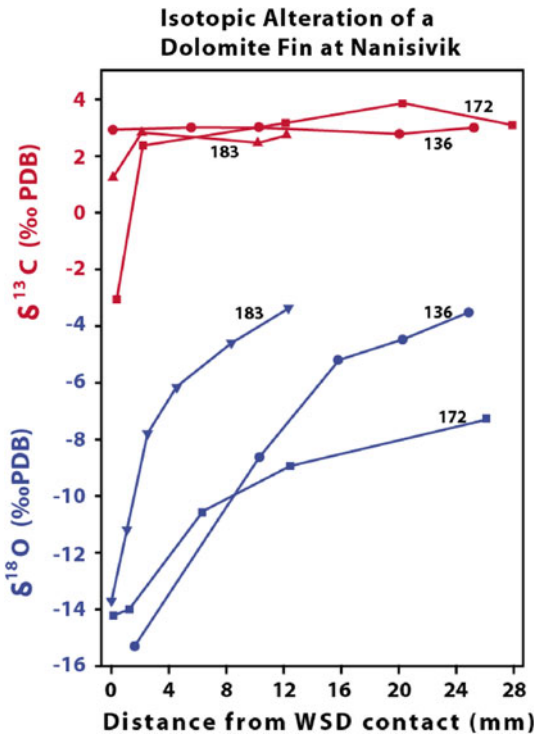

Fig. 11 Illustrating the depth of isotopic alteration beneath the surface of a fin of dolomite bedrock that was overlain by white sparry dolomite (*WSD*). The scale is in mm (From Ghazban 1988)

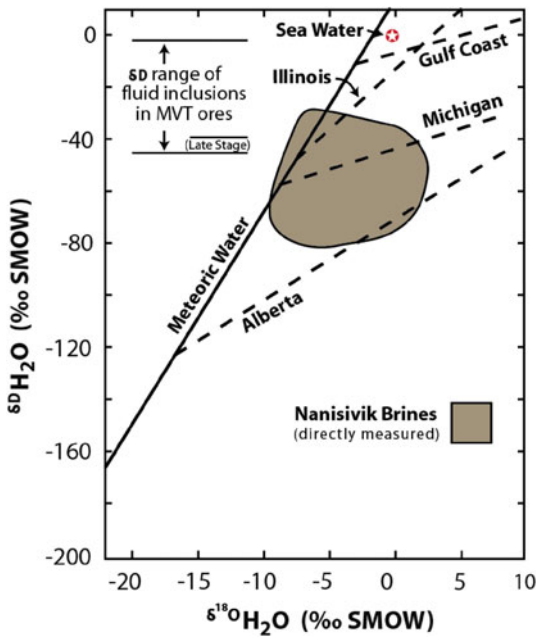

Fig. 12 Range of the oxygen and hydrogen isotopic composition of fluid inclusions extracted from ore and gangue minerals samples of the Nanisivik Main Ore compared to modern seawater, worldwide rain and snow (the Global Meteoric Water Line), and brine samples from selected oilfields (From Ghazban 1988)

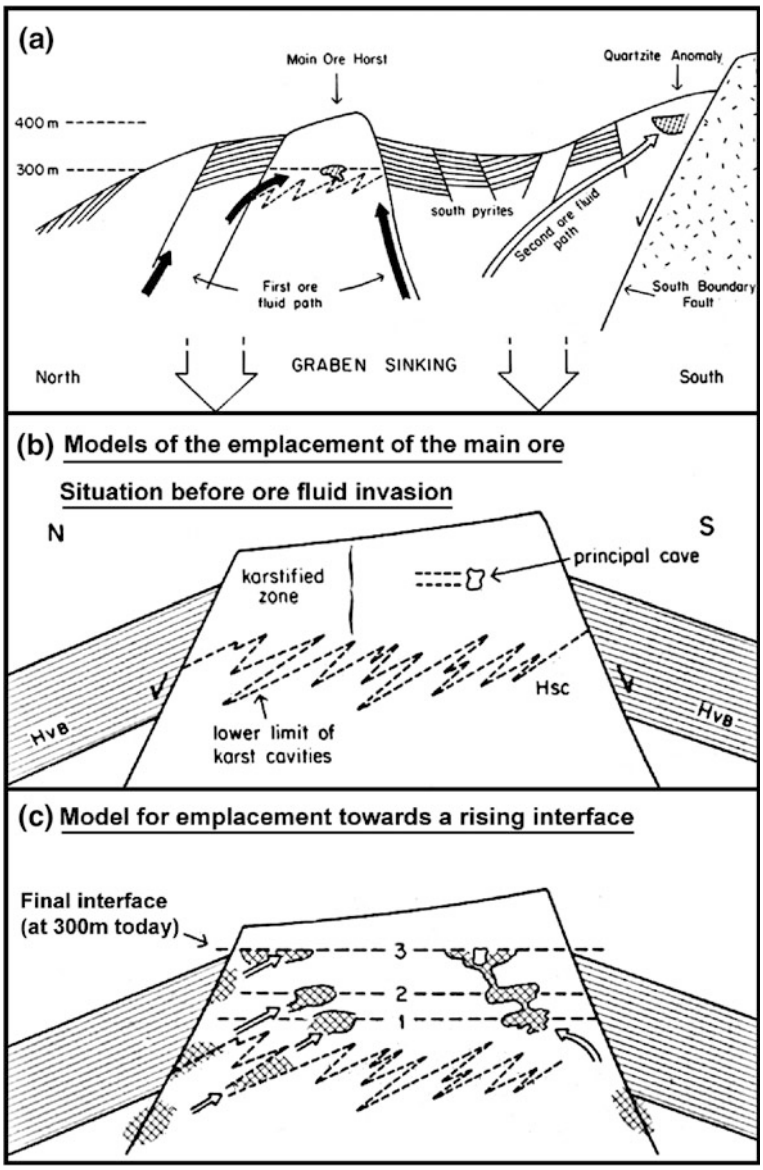

Fig. 13 Model for the emplacement of the Main Ore and manto massive sulfide deposits at Nanisivik zinc–lead mine. See the text for details

predominate. Turner et al. (2016) argue that the strata accumulated in an 'impactogen,' '… a type of intracontinental rift basin that form during continent-continent collisions…'. The Nanisivik deposit is a seemingly rare example of a zinc deposit that formed during supercontinent assembly and highlights a previously unrecognized environment in which sediment-hosted zinc deposits can form. This may help to explain the very unusual and spectacular speleomorphic features (both dissolutional and depositional) that have been described here in the Main Ore.

5 Conclusions

The massive sulfides at the Nanisivik Mine were emplaced in a syngenetic mode by thermal waters (brines) of hypogene origin. Host dolomite was dissolved, and the sulfide and gangue minerals were precipitated essentially simultaneously at a given site. The principal mode of cavity excavation and mineral deposition was paragenesis, wherein a corrosional ceiling is dissolved upward in balance with the rising elevation (increasing thickness) of deposits on the floor below. Most dissolution took place at or close to an interface between brine and oil or brine and gas. Rates of discharge of the brine ranged widely, sometimes surging to carve channels through previously deposited ore, at other times being semi-static and creating deep corrosion notches precisely at the interface. Deposition took place in an extensional (sinking) basin setting in which metal-rich formation fluids from clastic rocks could be expelled through the host dolomites.

Acknowledgements The author is indebted to Michel Bakalowicz, Fereydoun Ghazban, Donald Sangster, and Henry Schwarcz for discussion of the many intriguing problems of the Nanisivik MVT deposits. Part of the costs of this work was supported by research grants to Ford and Schwarcz from the National Science and Engineering Research Council of Canada.

References

Bradley DC, Leach DL (2003) Tectonic controls of Mississippi Valley-type mineralization in orogenic forelands. Miner Deposita 38:652–667

Clayton RH, Thorpe L (1982) Geology of the Nanisivik zinc-lead deposit. Geol Assoc Can Spec Pap 25:739–758

Dżulynski S, Sass-Gutkiewicz M (1989) Pb-Zn ores. In: Bosák P, Ford DC, Głazek J, Horáček I (eds) Paleokarst—a systematic and regional review. Academia Praha/Elsevier, Prague/Amsterdam, pp 377–397

Ford DC (1986) Genesis of paleokarst and strata-bound zinc/lead sulfide deposits in a Proterozoic dolostone, Northern Baffin Island—a discussion. Econ Geol 81(6):1562–1563

Ford DC (1987) Effects of glaciations and permafrost upon the development of Karst in Canada. Earth Surf Proc Land 12(5): 507–522

Ford DC (1996) Paleokarst phenomena as "targets" for modern karst groundwaters: the contrasts between thermal water and meteoric water behaviour. Carbonate Evaporites 10(2):138

Ford D, Williams P (2007) Karst hydrogeology and geomorphology. Wiley, Chichester

Ghazban F (1988) Stable isotope studies of sulphides, gangue minerals, wall rocks and their fluid inclusions at Nanisivik, Baffin Is, Canada. PhD thesis, Dept Geol, McMaster University

Ghazban F, Schwarcz HP, Ford DC (1991) Stable isotopic composition of the hydrothermal fluids responsible for the Nanisivik Zn–Pb deposits, Northwest Territories, Canada. Appl Geochem 6:257–266

Ghazban F, Schwarcz HP, Ford DC (1992) Correlated strontium, carbon and oxygen isotopes in carbonate gangue at the Nanisivik zinc-lead deposits, northern Baffin Island, Canada. Chem Geol (Isot Geosci Sect) 87:137–146

Ghazban F, Ford DC, Schwarcz HP (1993) Multistage dolomitization in the Society Cliffs Formation, northern Baffin Island, NWT, Canada. Can J Earth Sci 29(7):1459–1473

Hnatyshin D, Morden R, Turner E, Kontak D, Creaser RA (2011) Re-Os and fluid inclusion constraints on the timing and nature of sulphide mineralization at Nanisivik and Hawker Creek, Baffin Island, Nunavut. Geol Soc Am 43(5):633 (Abstracts with Programs)

Lebedev LM (1974) Recent ore-forming hydrothermal systems. Nedra, Moscow (in Russian)

McNaughton K, Smith TE (1986) A fluid inclusion study of sphalerite and dolomite from the Nanisivik lead-zinc deposit, Baffin Island, Northwest Territories, Canada. Econ Geol 81:713–720

Mylroie JE, Carew JL (1990) The flank margin model for dissolution cave development in carbonate platforms. Earth Surf Proc Land 15:413–424

Olson RA (1984) Genesis of paleokarst and strata-bound zinc-lead sulphide deposits in a Proterozoic dolostone, northern Baffin Island, Canada. Econ Geol 79:1056–1103

Palmer AN (2007) Cave geology. Cave Books, Dayton

Rhodes D, Lantos EA, Lantos JA, Webb RJ, Owens DC (1984) Pine Point orebodies and their relationship to structure, dolomitization and karstification of the Middle Devonian barrier complex. Econ Geol 70:91–1055

Ryder PF (1975) Phreatic network caves in the Swaledale area, Yorkshire. Trans Brit Cave Res Assoc 2(4):177–192

Sangster DF (1988) Breccia-hosted lead-zinc deposits in carbonate rocks. In: James NP, Choquette PW (eds) Paleokarst. Proceedings of a society of economic paleontologists and mineralogists' symposium. Springer, pp 102–116

Sass-Gutkiewicz M (1974) Collapse breccia in the ore-bearing dolomite of the Olkusz mine (Cracow-Silesian region). Rocz Pol Towarz Geol 44:217–226

Sass-Gutkiewicz M, Dzulynski S, Ridge JD (1982) The emplacement of zinc-lead sulfide ores in the Upper Silesian district—a contribution to the understanding of Miisissippi Valley-type deposits. Econ Geol 77:392–412

Sherlock RL, Lee JKW, Cousens BL (2004) Geologic and Geochronologic Constraints on the Timing of Mineralization at the Nanisivik Mississippi Valley-type Deposit, Northern Baffin Island, Nunavut, Canada. Econ Geol 99:279–293

Symons DTA, Symons TB, Sangster DF (2000) Paleomagnetism of the Society Cliffs dolostone and the age of the Nanisivik zinc deposits, Baffin Island, Canada. Miner Deposita 35:672–682

Turner E, Long DGF, Rainbird RH, Petrus JA, Rayner NM (2016) Late Mesoproterozoic rifting in Arctic Canada during Rodinia assembly: impactogens, trans-continental far-field stress and zinc mineralisation. Terra Nova 28(3):188–194

Hypogene Speleogenesis on the Florida Platform

49

Sam B. Upchurch

Abstract

The Florida Platform includes many examples of suspected hypogene karst, on- and offshore. These features occur in carbonate strata of Early Cretaceous to Late Pleistocene age. Transition zones between fresh and saline groundwater systems can be shown thermodynamically to be developing hypogene karst by groundwater mixing. Although the resulting flank-margin caves have not been confirmed on the basis of cave morphology, several probable examples exist. Carbonate rocks in deeper horizons of Paleocene/Eocene and Cretaceous age are bounded by gypsum/anhydrite and contain strata with unusual porosity development and high hydraulic conductivities. These strata appear to contain hypogene porosity created either along a deep or ancient saline water/freshwater transition zone or by interaction with H_2SO_4. There is evidence that collapse zones from these deeper strata have migrated upward to the modern land surface. The even deeper, Cretaceous system appears to contain H_2SO_4-driven hypogene porosity.

Keywords

Floridan aquifer • Sunniland Formation • Hypogene speleogenesis • Mixing-zone speleogenesis

1 Introduction

This paper discusses (1) the development of porosity by dissolution of carbonate rocks by groundwater mixing along freshwater/saline water transition zones (transition zones) and (2) the development of cavernous porosity by rock interactions with H_2SO_4 created by oxidation of H_2S in systems influenced by evaporite strata. Because of the extensive groundwater geochemical data developed by studies in the 1970s and 1980s (i.e., Back and Hanshaw 1970; Herman et al. 1985), the groundwater systems of the Florida Platform (Fig. 1) have long been used to demonstrate how groundwater mixing at transition zones can cause dissolution of limestone (i.e., Plummer 1975). However, it was only recently that researchers have suggested that hypogene speleogenesis may have affected Florida karst systems (i.e., Randazzo 1997; Cunningham and Walker 2009; Garman 2010; Herbert and Upchurch 2016). This paper presents a summary of the known or suspected hypogene karst systems on the Florida Platform.

2 Stratigraphy and Hydrostratigraphy of the Florida Platform

Systems that have karst known or inferred to have resulted from hypogene processes include the (1) limestone aquifers of south Florida (freshwater/saltwater mixing in Pleistocene and Pliocene strata of the surficial aquifer system (SAS)), (2) upper Floridan aquifer (UFA) of peninsular Florida (coastal freshwater/saline water mixing in Eocene to Miocene strata), (3) lower Floridan aquifer (LFA) (saltwater mixing and/or H_2S oxidation in Paleocene to Eocene strata),

S.B. Upchurch (✉)
SDII Global Corporation, 4509 George Road,
Tampa, FL 33634, USA
e-mail: flwaterdoc@gmail.com

© Springer International Publishing AG 2017

A. Klimchouk et al. (eds.), *Hypogene Karst Regions and Caves of the World*,
Cave and Karst Systems of the World, DOI 10.1007/978-3-319-53348-3_49

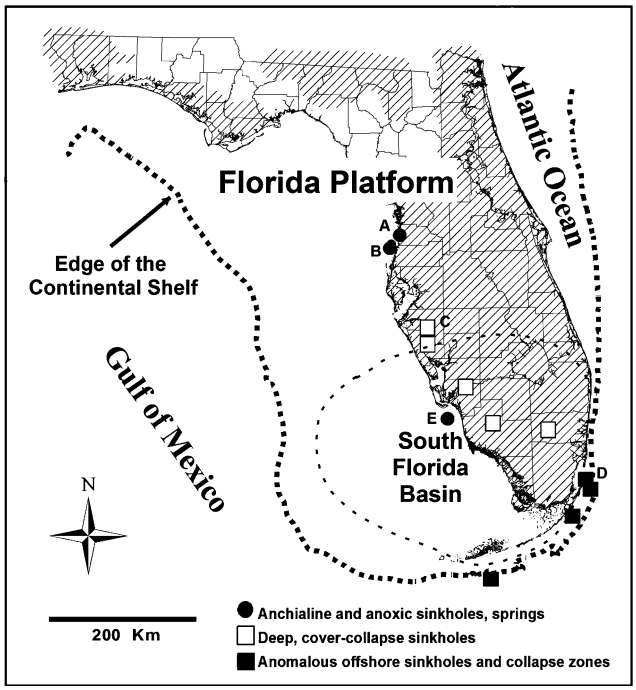

Fig. 1 The Florida Platform and South Florida Basin. Areas are *shaded* where middle confining units of the Floridan aquifer system were mapped by Miller (1986, 1990). *Symbols* are sites discussed in text

and (4) deep strata of the South Florida Basin (H_2S oxidation in Cretaceous, oil-bearing strata) (Table 1).

Identification of hypogenic karst in Florida is complicated because (1) sea levels and groundwater potentials have fluctuated vertically over hundreds of meters, vertically "smearing" the record of speleogenesis; (2) fluctuating transition zones exist in a long and active marine coastline; (3) the broad and hydrogeologically active continental shelf and margin appear to be involved in karst processes; (4) high modern water tables render detailed examination of caves difficult with access limited to cave divers; and (5) a deeply subsiding basin of Cretaceous and younger strata apparently has deeply buried hypogene karst that formed at shallow depths in south Florida.

2.1 Surficial Aquifer System

With the exception of south Florida, the SAS (Table 1) primarily consists of sand and clayey shell deposits. In extreme south Florida, the Pleistocene Miami and Key Largo limestones and the Pliocene Tamiami Formation contain significant limestone strata, which are karstic. The modern freshwater–seawater transition zone is present within these strata in coastal areas, and mixing-zone speleogenesis is probable.

2.2 Intermediate Aquifer System and Confining Beds

The SAS is separated from the underlying Floridan aquifer system (FAS) by the clay- and silt-rich Miocene strata of the Hawthorn Group (Table 1). Pyrite (Price and Pichler 2002) and rarely gypsum (Upchurch 1992) serve as sources of H_2S within local aquifers of the Hawthorn Group and in the underlying UFA.

2.3 Floridan Aquifer System

The FAS is subdivided into the two aquifers throughout much of the state. The UFA occurs within Eocene to Early Miocene strata and is composed of locally karstic limestone and dolostone (Table 1). The UFA is separated from the LFA by a series of confining beds known as the middle confining unit (MCU). The MCU consists of one or more widespread aquitards (Fig. 1) composed of low-permeability gypsum/anhydrite beds and dolostone.

Transition zones are well developed in the UFA near the modern coastline. Fresh and brackish water springs a few kilometers offshore suggest the transition zone extends offshore in many areas (Scott et al. 2004).

Deep, UFA groundwater skims along the gypsum-/anhydrite-rich strata of the underlying MCU. Dissolution results in a SO_4-enriched hydrochemical facies in lower UFA groundwater (Copeland et al. 2011). Where the UFA is unconfined, this facies may be diluted by local recharge; however, it is likely to be well developed as a hydrochemical facies in confined conditions where dilution from above is minimal. If organic carbon is available, this SO_4-rich water undergoes reduction to H_2S (Rightmire et al. 1974; Rye et al. 1981; Sacks and Tihansky 1996). Important and possibly karstic features of the LFA are the highly permeable "boulder zones." The term was coined for a high-permeability zone encountered in deep petroleum test wells in south Florida. The south Florida boulder zones range from −610 to −1040 m NGVD (Miller 1990).

Based on chloride and total dissolved solid content, LFA groundwater in south Florida is seawater (i.e., Sproul 1977). Analyses of SO_4 and Cl contents suggest that SO_4 content is elevated by a factor of approximately 1.5 relative to seawater (Haberfeld 1991).

Table 1 Hydrostratigraphic relationships of the lower Floridan aquifer system and Sunniland Formation in south Florida.

Epoch	Formation		Lithology	Hydrostratigraphic unit	Unit thickness (m)
Holocene	Undifferentiated		Quartz sand, silt, clay, shell	Surficial Aquifer System (SAS)	0–100
Pleistocene	Miami and Key Largo limestones, undifferentiated strata		Limestone, quartz sand, clay, and shell		0–55
Pliocene	Tamiami Formation		Silt, sandy clay, shell, limestone		0–30
Miocene to Late Oligocene	Hawthorn Group	Peace River Formation	Interbedded sand, silt, gravel, clay, limestone, dolostone, phosphatic sand	Intermediate Aquifer and Confining Unit (ICU)	180–275
		Arcadia Formation	Sandy limestone, shell beds, dolostone, phosphatic sand, silt, clay		
Early Oligocene	Suwannee Limestone		Limestone	Upper Floridan Aquifer (UFA)	210–370
Late Eocene	Ocala Limestone		Limestone		
Middle Eocene	Avon Park Formation		Limestone, dolostone		150–240
			Dolostone, gypsum/anhydrite	Middle Confining Unit (MCU)	
Early Eocene	Oldsmar Formation		Dolostone, gypsum/anhydrite	Lower Floridan Aquifer (LFA)	430–550 Incl. Boulde Zone (120±)
Paleocene	Cedar Keys Formation		Dolostone, dolomitic limestone		
			Massive anhydrite	Sub-Floridan Confining Unit	370±
Albian–Maastrichtian	Pine Key Formation		Limestone and dolostone	Possible hypogenic karst systems	835±
	Naples Bay Group		Alternating layers of limestone, dolostone, anhydrite		760±
	Big Cypress Group				
Aptian	Ocean Reef Group	Rattlesnake Hammock Fm.			
		Lake Trafford Fm.	Upper: Limestone, dolostone; lower: anhydrite	Upper confining beds	45±
		Sunniland Fm.	Limestone, anhydrite	Proposed hypogene karst system	75–85
	Glades Group	Punta Gorda Anhydrite	Anhydrite	Lower confining beds	245±
		Lehigh Acres Formation	Dolostone, shale	Possible hypogene karst systems	195±

Data sources Miller (1986), Huddlestun et al. (1988), and others
Additional Cretaceous and Jurassic strata underlie the Glades Group sediments

2.4 Cretaceous Strata

The Cretaceous strata that underlie the FAS include several sequences that consist of carbonate rocks bounded above and below by anhydrite. These strata meet the criteria of Klimchouk (2009, 2013, 2014) for hypogene speleogenesis. Of these strata, the Aptian Sunniland Formation is a likely candidate owing to its high hydraulic conductivities, association with petroleum, and the spatial distribution and performance of petroleum-producing zones (Applegate and Pontigo 1984; Mitchell-Tapping and Mitchell-Tapping 2003; Herbert and Upchurch 2016).

3 Speleogenesis at Freshwater/Saline Water Transition Zone Systems

3.1 Upper Floridan Aquifer

Water-quality data from shallow (<200 m) UFA groundwater systems in Florida have long been used to demonstrate the mechanisms of mixing-zone speleogenesis at transition zones. These water masses mix, resulting in waters that may be chemically undersaturated with respect to calcite (Plummer 1975). Where coastal UFA water is stratified with a lower SO_4-rich facies and, below that, a Na–Cl facies, there

may be two mixing-zone contacts along which speleogenesis may occur.

A limited number of vadose and phreatic caverns have been attributed to groundwater mixing in Florida (Polk and Brinkman 2013). Where cavern origin has been discussed, most caves are considered epigenetic (i.e., Florea and Vacher 2006; Florea et al. 2003, 2007). Mixing-zone origins have been suggested as a result of (1) proximity to modern or ancient coastlines, (2) modern water-quality conditions, and/or (3) rare erosional patterns (i.e., maze-work caves and cupolas) in vadose caverns (Polk and Brinkman 2013). Given the many Plio–Pleistocene sea-level oscillations, it is likely that epigenetic caves have been modified by hypogene processes.

There are several unusually deep coastal cave systems that are currently being explored by deep diving. The best known of these deep caverns are Diepolder II and Weeki Wachee Springs (A, Fig. 1). These cave systems have been touted as the deepest phreatic caves in the USA. The Weeki Wachee Springs cavern has been explored to a depth of at least 124 m in a cavern that has been explored to 1400 m in length (Neill and Anderson 2009). The Diepolder II cavern has been explored to a depth of 110 m at 470 m from the base of the entrance sinkhole (Clesi and King 1991). These coastal cavern systems are unique because of their depth and the large rooms that exist at depth (Figs. 2 and 3). The profiles of the caves are approximately parallel to the groundwater mixing zone. Little else is known about their architecture. These coastal cavern systems appear to be the best candidates for hypogenic speleogenesis by groundwater mixing in Florida at the present time.

3.2 Lower Floridan Aquifer

There is confusion about the importance of karst processes in the boulder zones of the LFA. This confusion appears to be related to differences in the interpretation of such words as "cavernous" as used by early investigators. In some cases, contexts of early reports on the boulder zones appear to suggest that the authors were communicating size of the cavities in the boulder zones, not origin. Whatever the intent, words such as karst, dissolution, and cavern are contained in discussions of high-permeability boulder zones in the literature.

Vernon (1970) attributed "cavernous" porosity in the boulder zones to calcite dissolution with concomitant dolomitization in a transition zone. Puri and Winston (1974) described the boulder zones as intricate networks of vugs and large cavities. Miller (1990) thought that the boulder zones represent caverns that are interconnected by pipes or solution tubes. Winston (1995) argued that boulder zone(s) contain cavities and wall-collapse zones. Safko and Hickey (1992) and Duerr (1994) examined LFA borehole video logs and geophysical logs and concluded that the porosity of the boulder zone is from fracturing, not dissolution. Missimser and Maliva (2004) argued that the porosity is a result of fracturing associated with tectonic movement within the South Florida Basin (Fig. 1). Visual inspection of borehole videos of the boulder zone by the author suggests that dissolution is at least a contributing cause of the porosity. Dissolution fluting and cupola-like indentations can occasionally be observed on cavity walls.

It is possible that mixing-zone hypogene speleogenesis is occurring in the LFA. For example, high hydraulic conductivity zones in the LFA may be a result of mixing on a transition zone powered by geothermally driven groundwater circulation. Kohout (1975) and Kohout et al. (1977) proposed that intrusion of cool seawater along the coast was a result of convective flow driven by the geothermal gradient within the FAS. This hypothesis has been confirmed by numerous investigations (i.e., Meyer 1989; Clark et al. 2004; Hughes et al. 2010). In the Kohout groundwater circulation model, seawater enters the LFA on the Atlantic continental margin, migrates inland where it is geothermally heated, and rises to return to the east coast continental margin by convective flow. Meyer (1989) estimated that groundwater movement in the boulder zone was about 17 m/year.

Sproul (1977) identified anomalous areas of high and low heat flow in the LFA. The high geothermal anomalies were thought to reflect upwelling of warmer than normal saline groundwater. Warm-water springs are found in an upwelling area in southwest Florida (i.e., cenotes Warm Mineral and Little Salt springs; Cockrell 1975; Clausen et al. 1979; C, Fig. 1) and submarine Mud Spring (Fanning et al. 1981; E, Fig. 1). These springs discharge deep, saline water, possibly from the LFA. The cenotes are examples of deep (open avens are <50 m deep) collapse sinkholes. Similar deep collapse features exist elsewhere in south Florida (Fig. 1).

This circulation system presents opportunities for mixing-zone speleogenesis associated with seawater and native Ca–HCO_3 water. Given the gypsum/anhydrite strata that confine the LFA, the Kohout circulation model also suggests opportunities for hypogene speleogenesis by carbonate rock dissolution by sulfate-rich water.

3.3 Anchialine Sinkhole Systems

Anchialine caves consist of caverns wherein the freshwater lens is in contact with seawater within the cavern (Bishop et al. 2015). Anchialine sinkholes are common near the Gulf of Mexico coastline (B, Fig. 1). Anchialine sinkholes have a well-developed chemocline/pycnocline at the transition zone. The zone of density change traps particulate organics, microbes, pyrite framboids, and clay minerals (Garman 2010; Garman et al. 2011) resulting in a turbid, low visibility

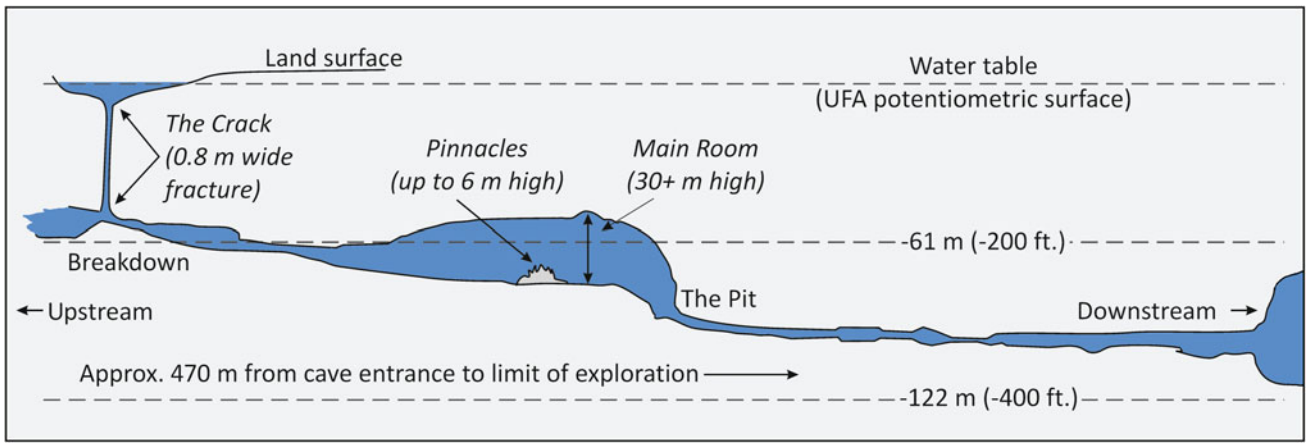

Fig. 2 Diepolder II cavern profile. *Vertical* datum is the phreatic surface. Modified from Clesi and King (1991)

Fig. 3 Divers explore the Ballroom in Diepolder II. *Photograph courtesy* of Mark Long

layer upon which cave divers often comment. Microbial activity chemically reduces SO_4 obtained from the underlying saline water forming H_2S and colloidal to clay-sized FeS_2 framboids. Garman (2010) suggested that pH lowering by H_2SO_4 from oxidation of sulfide within or just above the turbid zone may cause speleogenesis.

There is a probability that localized development of biologically mediated, sulfide/sulfate transitions can result in hypogene modifications of epigene conduits. Given the excursions of sea level during the Pliocene and Pleistocene, such modifications could result in local features common to hypogene systems.

4 Evaporite-Bound Systems

There are several evaporite-bound sequences of strata with breccias and large void spaces that likely include hypogene karst. The uppermost example is the LFA. Early to Middle Cretaceous sediments in the South Florida Basin (Fig. 1) may also include hypogene karst within a basin that has subsided as much as 3500 m.

4.1 Lower Floridan Aquifer

The stratigraphy of the LFA compares favorably with Klimchouk's (2007, 2009) criteria for hypogene speleogenesis. The upper and lower confining strata include gypsum or anhydrite, and there is a well-developed groundwater circulation system associated with breccias and fractures (boulder zones) that may have been enlarged by dissolution.

There is minimal direct evidence at this time to suggest that ongoing or former hypogenesis has enhanced the porosity of the LFA. However, others have suggested its existence based on geophysical or geochemical studies that reveal evidence of deep-seated dissolution features. Randazzo (1997) speculated that hypogene speleogenesis had enhanced porosity in the LFA based on sulfate mineralization in aquifer water. Cunningham and Walker (2009), and Cunningham (2013, 2015) utilized seismic methods to identify deep-seated collapse zones, some of which are associated with sinkhole-like depressions offshore of the Miami area of southern Florida (D, Fig. 1). They attributed these collapse features to hypogenic processes within the deep FAS.

The deep cenotes and collapse sinks in southern Florida may have a similar origin. Little Salt Spring (C, Fig. 1) discharges anoxic, H_2S-rich groundwater from a vent at 73 m depth (Yang et al. 2008). This water is mixing with shallow, oxic water resulting in H_2SO_4. While the cenote is 75 m deep, the bottom is a debris cone and no one knows how deep the collapse-filled aven extends. The presence of the vent opens the possibility that the cenote is a deep-seated collapse rather than a feature limited to the UFA, within which the cenote's known extent lies. Similar cenotes in the Yucatan Peninsula of Mexico have been attributed to sulfur reduction–oxidation origins (Stoessell et al. 1993; Schmitter-Soto et al. 2002; Socki et al. 2002).

There are numerous offshore sinkholes that are currently at elevations too deep to have formed on a saline water transition zone. For example, the 200+ km long Pourtales and Miami terraces (D, Fig. 1) offshore of southeastern Florida have sinkholes at water depths of 180–450 m (Jordan 1954; Mullins and Neumann 1979; Land and Paull 2000), which are well below the projected Plio–Pleistocene low sea stands. The terraces appear to be associated with passive continental margin normal faulting. The sinkholes, which are reported to be up to 800 m in diameter and 250 + m deep, are developed either in the Eocene Avon Park or in Oldsmar Formation (Land and Paull 2000) (Table 1). The terraces appear to have subsided to these depths after karstification and probably hypogene speleogenesis in the LFA.

4.2 The Lower Cretaceous Sunniland Formation

The Aptian Sunniland Formation (Table 1) is an important petroleum-production horizon in southwest Florida (Fig. 4). Eleven individual fields occur in a northwest–southeast linear trend that corresponds with a series of rudistid knolls (Mitchell-Tapping and Mitchell-Tapping 2003; Herbert and Upchurch 2016) that developed along a hinge line in the South Florida Basin (Fig. 1). Southwest of the trend, Lower Cretaceous strata dip to the southwest and extend offshore in the Gulf of Mexico. Oil production has been sustained since the 1940s, and many of the small fields have produced over a million barrels.

Near the location of the Sunniland Trend, the Sunniland Formation is at about 3500 m below sea level. It is underlain by the Lower Cretaceous Punta Gorda Formation (Table 1), a massive limestone and anhydrite formation that serves as a lower confining unit. The reservoir seal is the Lake Trafford Formation, a similar, massive sequence of anhydrite and dense limestone.

The Sunniland Formation is up to 75 m in thickness (Huddlestun et al. 1988). The basal unit consists of a lower "rubble zone" of brecciated, petroliferous limestone. "Black shale," which overlies the "rubble zone," is a dense, argillaceous limestone with abundant organics that are thought to be the source of the oil, from either within or adjacent to the trend (Palacas 1978; Palacas et al. 1981, 1984a, b; Applegate and Pontigo 1984). Overlying the organic facies is a low porosity limestone to dolomitic limestone which may serve as a semi-confining unit for fluid migration (Herbert and Upchurch 2016). Next is a shallow-water, intertidal limestone. Mitchell-Tapping and Mitchell-Tapping (2003) reported evidence of hypersaline solutions associated with "phreatic" conditions in this facies. Herbert and Upchurch (2016) interpreted the "phreatic conditions" to represent evidence of dissolution and brecciation. Above the intertidal limestone is a fragmental, intertidal limestone with abundant rudistid "debris mounds". Mitchell-Tapping and Mitchell-Tapping (2003) also reported evidence of phreatic conditions in this facies. This facies is a major oil-production zone. Finally, the primary oil producer in the Sunniland Trend is a fossiliferous limestone deposited under marine regression conditions (Mitchell-Tapping and Mitchell-Tapping 2003). The facies shows evidence of bioturbation and deposition of secondary anhydrite.

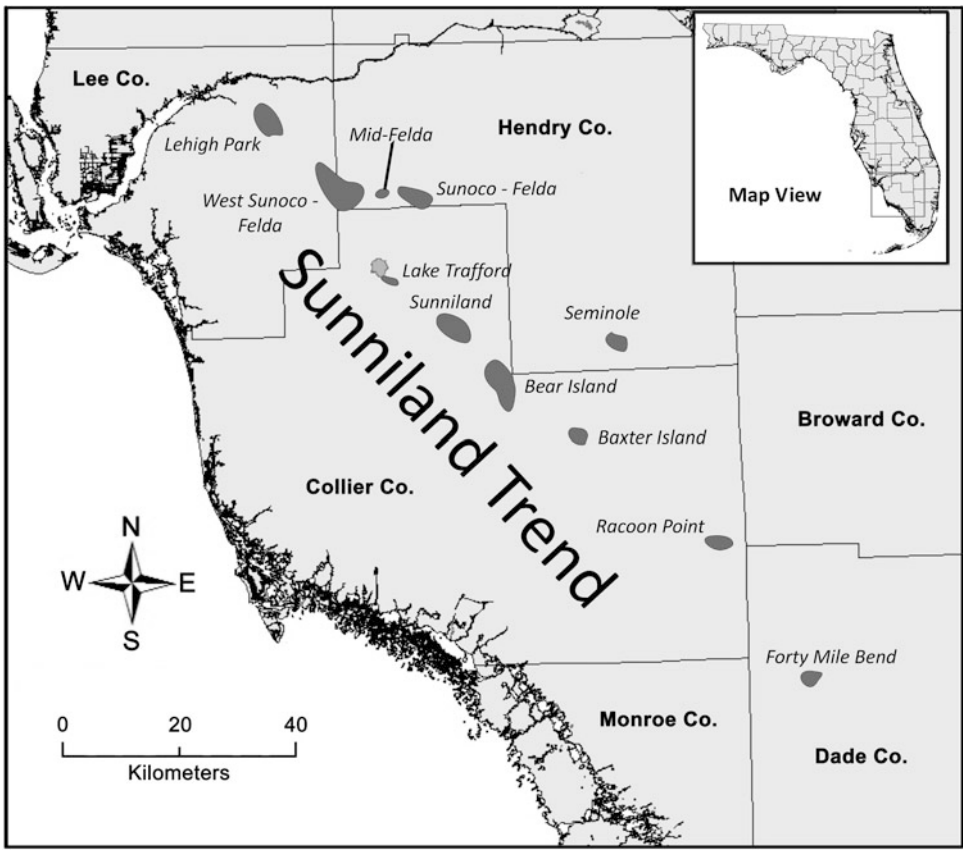

Fig. 4 Oil fields within the Sunniland Trend in southwest Florida (Herbert and Upchurch 2016)

Palacas et al. (1984a, b) noted that Lower Cretaceous limestone in the eastern Gulf of Mexico had staining and residual asphalt that appeared to represent a "post-migration alteration product of a mature oil that has migrated from source rocks deeper in the section, or from stratigraphically equivalent … [strata] … down-dip …." The petroleum was found to be compositionally similar to Sunniland petroleum. If the maturity and organic carbon content constraints are valid, there appears to be an unaccounted for petroleum-migration path operative in the Sunniland Trend oil fields.

Production figures suggest that the amount of recoverable oil and ease of extraction are high relative to the size and distribution of the low-relief fields. Production data and distribution of wells within the fields suggest that some form of conduit flow and secondary stratigraphic-trap development exists. Within fields, closely spaced wells show a pattern of variable production with wells that have produced 10^8 L of oil in close proximity to dry or low-recovery wells. Intervals of no core recovery or weight-of-drill string gaps are commonly described in drilling logs (Herbert and Upchurch 2016). This information combined with the concerns about source strata and petroleum maturity suggests a more complicated system than has previously been described.

The stratigraphy associated with the Sunniland Formation is consistent with the conditions proposed by Klimchouk (2007, 2009) for hypogene speleogenesis. The formation is confined above and below by anhydrite, and there is evidence of fluid movement within the formation with the petroleum categorized as "sour crude." Produced formation water releases an odor of H_2S upon degassing in the oil–water separator. The reports of widespread breccias and "phreatic conditions" suggest the possibility of H_2SO_4-related speleogenesis. The current depth of the Sunniland Formation suggests that speleogenesis, if it occurred, developed prior to subsidence.

Finally, Paull and Dillon (1980), Paull and Neumann (1987), Commeau et al. (1987), and Chanton et al. (1993) discuss brine seeps near the base of the continental slope off Florida in both the Atlantic Ocean and Gulf of Mexico. The seeps offshore of southwestern Florida are about −3270 m MSL and are in Cretaceous limestone approximately at the same stratigraphic position as the Sunniland. According to these authors, the seeps appear to be locations of developing karst as a result of dissolution, causing sapping at the base of the continental margin.

Chanton et al. (1993) characterized limestone dissolution at the seeps as being a result of mixing of seawater and sulfate-depleted brine derived from the Cretaceous

sediments. Two sulfide sources were suggested to explain the isotopic compositions of sedimentary pyrite at the seeps. These are (1) a ^{34}S-enriched source derived from the Florida Platform and (2) a ^{34}S-depleted component derived from microbial reduction of seawater sulfate.

In summary, there is evidence of sulfur-driven geochemical reactions in pore or conduit waters within the Cretaceous sediments in the vicinity of the Sunniland Trend. This, combined with stratigraphic sequencing of anhydrite and fractured limestone strata consistent with Klimchouk's model, evidence of collapse and brecciation, and a distribution of oil production suggestive of large conduits, suggests that hypogene speleogenesis may be responsible for development of the "plumbing" system that has resulted in migration of oil into the structures forming the Sunniland fields.

5 Conclusions

Karst on the Florida Platform includes examples of probable mixing-zone and H_2SO_4-related hypogene speleogenesis. Evidence of mixing-zone speleogenesis at transition zones includes chemical data indicating chemical undersaturation with respect to calcite and unusually deep and large, coastal cavern systems. Coastal anchialine caverns may be undergoing conduit modifications as a result of sulfide–sulfate reduction–oxidation reactions and H_2SO_4-related dissolution. Within the deep LFA and Cretaceous strata, there is evidence of H_2SO_4-related dissolution in the sense of Klimchouk (2007, 2009).

References

Applegate AV, Pontigo FA (1984) Stratigraphy and oil potential of the Lower Cretaceous Sunniland Formation on south Florida. Florida Geological Survey Report of Investigation No 89, Tallahassee (FL)

Back W, Hanshaw BB (1970) Comparison of chemical hydrogeology of the carbonate peninsulas of Florida and Yucatan. J Hydrol 10:330–368

Bishop RE, Humphreys WF, Cukov N, Žic V, Boxshall GA, Cukov M, Iliffe TM, Kršinić F, Moore WS, Pohlman JW, Sket B (2015) "Anchialine' redefined as a subterranean estuary in a crevicular or cavernous geological setting. J Crustac Biol 35(4):511–514

Chanton JP, Martens CS, Paull CK, Coston JA (1993) Sulfur isotope and porewater geochemistry of Florida escarpment seep sediments. Geochim Cosmochim Acta 57(6):1253–1266

Clark JE, Bennett MW, Murrell MT, Stute M, Rademacher LK (2004) Time scale of seawater circulation and dolomitization within the lower Floridan aquifer. Geol Soc Am Abstr Programs 36:327

Clausen CJ, Cohen AD, Emiliani C, Holman JA, Stipp JJ (1979) Little Salt Spring, Florida; a unique underwater site. Science 203:609–614

Clesi D, King J (1991) Team Diepolder '91: our story. Underw Speleology 18(3):7–12

Cockrell WA (1975) Warm mineral springs: a multi-disciplinary approach to a 10,000 BP archeological site (Abs.). Florida Scientist 38, Supplement 1, p 19

Commeau RF, Paull JA, Commeau JA, Poppe LJ (1987) Chemistry and mineralogy of pyrite-enriched sediments at a passive margin sulfide brine seep: abyssal Gulf of Mexico. Earth Planet Lett 82(1–2):62–74

Copeland R, Dorian NA, White AJ, Upchurch SB (2011) Regional and statewide trends in Florida's spring and well groundwater quality (1991–2003). Florida Geological Survey, Bulletin No. 69 (Revised)

Cunningham KJ (2013) Marine seismic-reflection data from the southeastern Florida platform: a case for hypogenic karst (Abs.). International Association of Hydrogeologists, Proceedings, International Symposium on Hierarchical Flow Fystems in Karst Regions, p 59

Cunningham KJ (2015) Seismic-sequence stratigraphy and geologic structure of the Floridan aquifer system near "boulder zone" deep wells in Miami-Dade County, Florida. US Geological Survey Scientific Investigations Report 2015–5013

Cunningham KJ, Walker C (2009) Seismic-sag structural systems in Tertiary carbonate rocks beneath southeastern Florida, USA: evidence for hypogenic speleogenesis? In: Klimchouk A, Ford D (eds) Hypogene speleogenesis and karst hydrogeology of artesian basins. Ukrainian Institute of Speleology and Karstology Special Paper 1, pp 151–158

Duerr AD (1994) Types of secondary porosity of carbonate rocks in injection and test wells in southern peninsular Florida. US Geological Survey Water-Resources Investigations Report 94–4013

Fanning KA, Byrne RH, Breland JA, Betzer PR, Moore WS, Elsinger RJ, Pyle TE (1981) Geothermal springs of the west Florida continental shelf: evidence for dolomitization and radionuclide enrichment. Earth Planet Lett 52:345–354

Florea LJ, Vacher HL (2006) Cave levels, marine terraces, paleoshorelines, and the water table in peninsular Florida. In: Onac BP, Tamas T, Constantin S, Persoiu A (eds), Archives of climate change, Karst Waters Institute, Special Publication 10, pp 188–192, accessed 8/20/2013 at http://works.bepress.com/lee_florea/34

Florea LJ, Kelley K, Hashimoto T, Miller D, Mrykalo R (2003) Karst geomorphology and relation to the phreatic surface: Briar Cave, Marion County, Florida. In: LJ Florea, HL Vacher, EA Oches (eds). Karst studies in west-central Florida: USF seminar in karst environments 2003, Proceedings of the University of South Florida seminar in karst environments, pp 7–19

Florea LJ, Vacher HL, Donahue B, Naar D (2007) Quaternary cave levels in peninsular Florida. Quat Sci Rev 26:1344–1363

Garman KM (2010) The biogeochemistry of submerged coastal karst features in West Central Florida. Ph.D. dissertation, University of South Florida, p 191

Garman KM, Rubelmann H, Karlen DJ, Wu T, Garey JR (2011) Comparison of an inactive submarine spring with an active nearshore anchialine spring in Florida. Hydrobiologia 677:67–87

Haberfeld JL (1991) Hydrogeology of effluent disposal zones, Floridan aquifer, south Florida. Ground Water 29(2):186–190

Herbert TA, Upchurch SB (2016) The potential role of hypogene speleogenesis in the lower Floridan aquifer and Sunniland Oil Trend, south Florida, U.S.A. In: Chavez T, Reehling P (eds) Proceedings of Deep Karst 2016: origins, resources, and management of hypogene karst, Carlsbad, New Mexico. April 11–14, 2016. National Cave and Karst Research Institute, Symposium 6, pp 119–129

Herman JS, Back W, Pomar L (1985) Geochemistry of groundwater in the mixing zone along the east coast of Mallorca, Spain. Karst water resources (Proceedings of the Ankara—Antalya Symposium, July 1985) IAHS publication no.161, pp 467–479

Huddlestun PF, Hunter ME, Scott T, Chowns TM, Lloyd JM (1988) Southern Florida, CSD 140, Col. 31. In: Lindberg FA (ed) Gulf Coast Region, Correlation of stratigraphic units of North America (COSUNA) project. American Association of Petroleum Geologists, Tulsa (OK)

Hughes JD, Vacher HL, Sanford WE (2010) Three-dimensional flow in the Florida Platform: Theoretical analysis of Kohout convection at its type locality. Bull, Am Assoc Petrol Geol 94:889–917
Jordan GF (1954) Large sinkholes in Straits of Florida. Am Asso Petrol Geol Bull 38:1810–1817
Klimchouk AB (2007) Hypogene speleogenesis: hydrogeological and morphogenetic perspectives. National Cave and Karst Research Institute, Carlsbad (NM)
Klimchouk AB (2009) Principal characteristics of hypogene speleogenesis. In: Stafford KW, Land L, Veni G (eds) NCKRI Symposium 1 Advances in Hypogene Karst Studies, p 1–11
Klimchouk A (2013) Hypogene speleogenesis, its hydrogeological significance and the role in evolution of karst. DIP, Simferopol (in Russian)
Klimchouk A (2014) The methodological strength of the hydrogeological approach to distinguishing hypogene speleogenesis. In: Klimchouk A, Sasowsky ID, Mylroie J, Engel SA, Engel AS (eds) Hypogene cave morphologies. Leesburg VA, Karst Waters Institute, Special Publication 18, pp 4–12
Klimchouk A, Tymokhina E, Amelichev G (2012) Speleogenic effects of interaction between deeply derived fracture-conduit flow and interstratal matrix flow in hypogene karst settings. Int J Speleology 41(2):161–179
Kohout FA (1975) A hypothesis concerning cyclic flow of salt water related to geothermal heating in the Floridan aquifer. Trans NY Acad Sci 28:249–271
Kohout FA, Henry HR, Banks JE (1977) Hydrogeology related to geothermal conditions of the Floridan Plateau. In: Smith DL, Griffin GM (eds) The geothermal nature of the Floridan Plateau. Florida Bureau of Geology, Special Publication 21
Land LA, Paull CK (2000) Submarine karst belt rimming the continental slope in the Straits of Florida. Geo Mar Lett 20:123–132
Meyer FW (1989) Hydrogeology, ground-water movement, and subsurface storage in the Floridan aquifer system is southern Florida. U.S. Geological Survey Professional Paper 1403-G
Miller JA (1986) Hydrogeologic framework of the Floridan aquifer system in Florida, and in parts of Georgia, Alabama and South Carolina. US Geological Survey Professional Paper 1403-B
Miller JA (1990) Ground water atlas of the United States: segment 6, Alabama, Florida, Georgia, South Carolina. US Geological Survey Hydrologic Atlas 730-G
Missimser TM, Maliva RG (2004) Tectonically induced fracturing, folding and groundwater flow in south Florida. Gulf Coast Assoc Geol Soc Trans 54:443–459
Mitchell-Tapping HJ, Mitchell-Tapping AM (2003) Exploration of the Sunniland Formation of southern Florida. Trans Gulf Coast Assoc Geol Soc 53:599–609
Mullins HT, Neumann AC (1979) Geology of the Miami Terrace and its paleo-oceanographic implications. Marine Geology 30:205–232
Neill L, Anderson J (2009) Cave divers explore deepest parts of Weeki Wachee Springs. Tampa Bay Times, 19 April 2009 (http://www.tampabay.com/news/humaninterest/cave-divers-explore-deepest-parts-of-weeki-wachee springs)
Palacas JG (1978) Distribution of organic carbon and petroleum source rock potential of Cretaceous and lower Tertiary carbonates, South Florida Basin. US Geological Survey Open-File Report 78–140
Palacas JG, Daws TA, Applegate AV (1981) Preliminary petroleum source rock assessment of Pre-Punta Gorda rocks (lowermost Cretaceous—Jurassic?) in south Florida. Trans Gulf Coast Assoc Geol Soc 31:369–376
Palacas JG, Anders DE, King JD (1984a) South Florida Basin—prime example of carbonate source rocks of petroleum. In: Palacas JG (ed) Petroleum geochemistry and source rock potential of carbonate rocks. Tulsa (OK): American Association of Petroleum Geologists Studies in Geology 18: 71–96
Palacas JG, King JD, Claypool GE (1984b) Origin of asphalt and adjacent oil stains in lower cretaceous fractured limestones, Deep Sea Drilling Project Leg 77. In: Buffler RT, Schlager W et al. (eds) Initial reports of the Washington (DC): Deep Sea Drilling Project 77: 477–488
Paull CK, Dillon WP (1980) Erosional origin of the Blake Escarpment: an alternative hypothesis. Geology 8:538–542
Paull CK, Neumann AC (1987) Continental margin brine seeps: their geological consequences. Geology 15:545–548
Plummer LN (1975) Mixing of sea water with calcium carbonate ground water. In: Whitten EHT (ed) Quantitative studies in geological sciences, Geological Society of America Memoir 142, pp 219–236
Polk J, Brinkman R (2013) Climatic influences on coastal cave and karst development in Florida. In: Lace MJ, Mylroie JE (eds) Coastal Karst Landforms, Dordrecht, Springer Science, Coastal Research Library, Book 5, Chapter 15, pp 317–345
Price RE, Pichler T (2002) Naturally occurring arsenic in the upper Floridan aquifer, southwest Florida: Implications for aquifer storage recovery. American Water Resources Association, Proceedings of the AWRA Summer Specialty Conference, Ground Water/Surface Water Interactions, pp. 387–392
Puri HS, Winston GO (1974) Geologic framework of the high transmissivity zones in south Florida. Florida Bureau of Geology Special Publication 20
Randazzo AF (1997) The sedimentary platform of Florida: Mesozoic to Cenozoic. In: Randazzo AF, Jones DS (eds) The geology of Florida. Gainesville (FL): University Press of Florida. Chapter 4, pp 39–56
Rightmire CT, Pearson FJ, Back W Jr, Rye RO, Hanshaw BB (1974) Distribution of sulfur isotopes in ground waters from the principal artesian aquifer of Florida and the Edwards aquifer of Texas United States of America. Vienna, International Atomic Energy Agency, Isotope techniques in groundwater hydrology, pp 191–207
Rye RO, Back W, Hanshaw BB, Rightmire CT, Pearson FJ Jr (1981) The origin and isotopic composition of dissolved sulfide in groundwater from carbonate aquifers in Florida and Texas. Geochim Cosmochim Acta 45(10):1941–1950
Sacks LA, Tihansky AB (1996) Geochemical and isotopic composition of ground water, with emphasis on sources of sulfate, in the upper Floridan aquifer and intermediate aquifer system in southwest Florida. US Geological Survey Water-Resources Investigations Report 96–4146
Safko PS, Hickey JJ (1992) A preliminary approach to the use of borehole data, including television surveys, for characterizing secondary porosity of carbonate rocks in the Floridan aquifer system. US Geological Survey Water-Resources Investigations Report 91–4168
Schmitter-Soto JJ, Comin FA, Escobar-Briones E, Herrera-Silveira J, Alcocer J, Suárez-Morales E, Elías-Gutíerrez M, Díaz-Arce V, Marín LE, Steinich B (2002) Hydrogeochemical and biological characteristics of cenotes in the Yucatan Peninsula (SE Mexico). Hydrobiologica 467:215–228
Scott TM, Means GH, Meegan RP, Means RC, Upchurch SB, Copeland RE, Jones J, Roberts T, Willet A (2004) Springs of Florida. Florida Geological Survey, Bulletin 66
Socki RA, Perry EC Jr, Romanek CS (2002) Stable isotope systematics of two cenotes from the northern Yucatan Peninsula. Mex Limnol Oceanogr 47(6):1808–1818
Sproul CR (1977) Spatial distribution of ground water temperature in south Florida. In: Smith DL, Griffin GM (eds) The geothermal nature of the Floridan Plateau. Florida Bureau of geology, Special Publication No. 21, pp 65–89
Stoessell RK, Moore YH, Coke JG (1993) The occurrence and effect of sulfate reduction and sulfide oxidation on coastal limestone dissolution in Yucatan cenotes. Groundwater 31(4):566–575

Upchurch SB (1992) Quality of waters in Florida's aquifers. In: Maddox GL, Lloyd JM, Scott TM, Upchurch SB, Copeland R (eds) Florida ground water quality monitoring program—Volume 2, Background Hydrogeochemistry, Florida Geological Survey, Special Publication No. 34, Ch. IV, pp 12–52, 64–84, 90–347

Vernon RO (1970) The beneficial uses of zones of high transmissivities in the Florida subsurface for waste storage and waste disposal. Florida Bureau of Geology Information Circular No. 70

Winston GO (1995) The boulder zone dolomites of Florida, Volume 2, Paleogene zones of the southwestern peninsula. Miami (FL): Miami Geological Society

Yang Y, Schaperdoth I, Albrecht H, Freeman KH, Macalady JL (2008) Geomicrobiology and hopanoid content of a sulfidic subsurface vent biofilm, Little Salt Spring, Florida. Am Geophys Union Abs 1:0517

Hypogene Karst Influences in the Upper Floridan Aquifer

50

Jason D. Gulley and Jason S. Polk

Abstract

Dissolution of eogenetic carbonates in the Upper Floridan aquifer has produced the world's densest assemblage of first-magnitude cave springs. Conceptual and numerical models of cave origin in the aquifer have emphasized epigenic and mixing-dissolution processes. We draw upon recent research concerning phreatic caves in the Suwannee River Basin, and dry caves in the west and central Florida, to suggest instead that many caves in the aquifer formed by hypogenic processes. Formerly, undersaturation generated in the subsurface has usually been ascribed to the mixing of, or temperature changes in, subsurface fluids. Here, we describe an alternate process. Cave formation at modern water tables in the aquifer has been linked to respiration of CO_2 in the deep vadose zone and at water tables. Respired CO_2 generates carbonate mineral undersaturation when it hydrates to carbonic acid at water tables. Because undersaturated waters are created at the water table, caves form as isolated macropores. Caves at modern water tables in the aquifer lack initial connections to the surface (e.g., entrances) and have morphologies that are unrelated to surface drainage, making them similar in many respects to flank margin caves (see Mylroie and Mylroie, Chap. 51). Since many caves that are below the modern water table have similar morphologies to caves that are at the modern water table, it is likely that they formed by similar processes operating at water tables associated with lower sea levels. These caves became sources of springs and flooded sinkholes when Holocene sea-level rise elevated water tables close to, and above, the land surface.

Keywords

Florida karst • Carbonate undersaturation • Eogenetic aquifer • Carbon dioxide

1 Introduction

The eogenetic limestones of the Upper Floridan aquifer include, from youngest to oldest, the Suwanee and Ocala Limestones, and the Avon Park Formation of Eocene–Oligocene age and are underlain by carbonate evaporites of the Oldsmar, and Cedar Key Formations of Paleocene–Eocene age (see Table 1 of Upchurch Chap. 49). They are capped in places by the siliciclastic Oligocene–Miocene Hawthorn Group. The limestones contain the world's densest assemblage of first-magnitude karst springs (flow >100 cubic feet per second, i.e., >2.83 m^3/sec). The Florida Geological Survey (2002) lists more than 700 springs in the aquifer (Fig. 1), at least 30 of which are rated as first magnitude. Completely phreatic caves that feed many of these springs are some of the most visited cave-diving sites in the world. They include the Devil's cave system at Ginnie Springs, Little River Spring, Peacock Springs, Madison Blue

J.D. Gulley (✉)
School of Geosciences, University of South Florida, Tampa, FL 33620, USA
e-mail: jdgulley@usf.edu

J.S. Polk
Department of Geography and Geology, Western Kentucky University, Bowling Green, KY 42101, USA
e-mail: jason.polk@wku.edu

© Springer International Publishing AG 2017

A. Klimchouk et al. (eds.), *Hypogene Karst Regions and Caves of the World*,
Cave and Karst Systems of the World, DOI 10.1007/978-3-319-53348-3_50

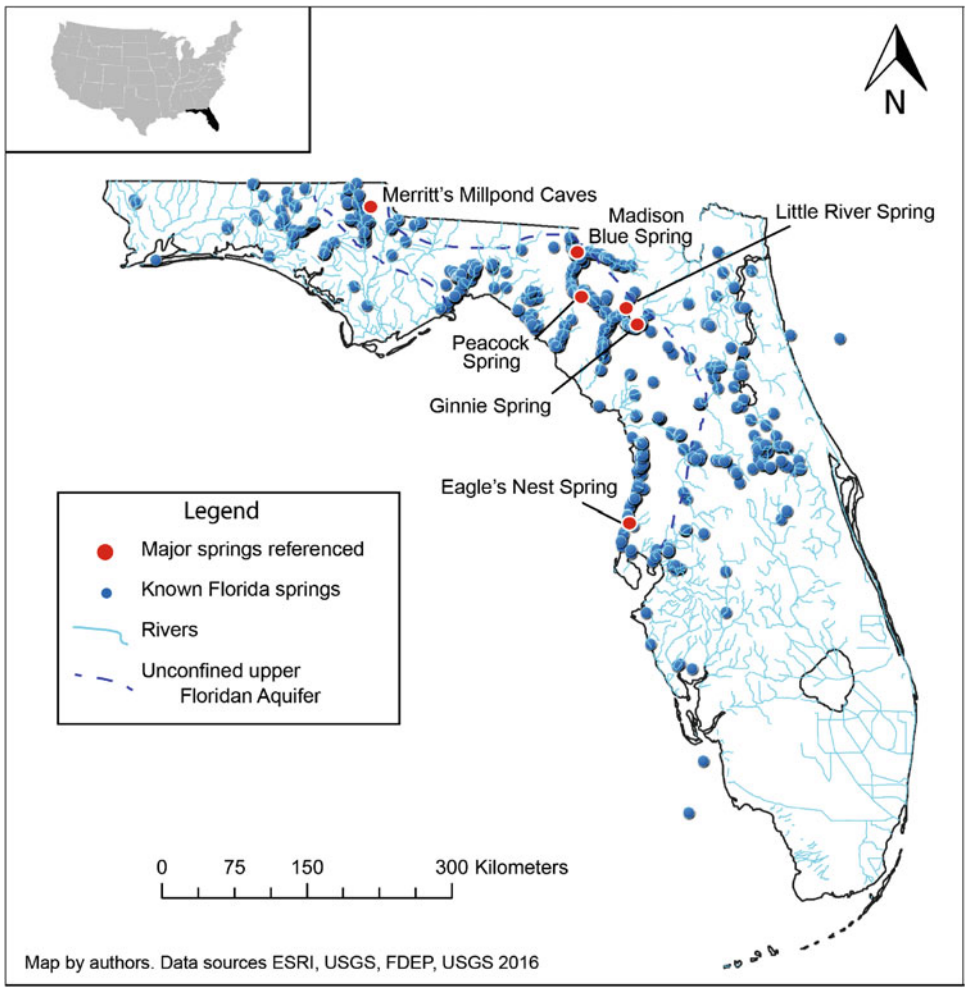

Fig. 1 Map of Florida showing spring locations, confining unit extent, major rivers, and the locations of the springs and cave features mentioned in text (created by authors)

Springs, Eagle's Nest, and the Millpond caves (Fig. 1). These and other caves in the Upper Florida aquifer extend to depths of tens of meters, and in some places more than 100 m, below the modern water table. This chapter describes a model for the origin of certain shallow-phreatic caves by the generation of CO_2 between the soil zone and water table. This is an example of cave origin that operates at the outer limits of hypogene processes.

2 Origin of Caves in the Upper Floridan Aquifer

Until recently, there were two prominent groups of hypotheses for cave formation in the Upper Floridan aquifer. One group emphasized the importance of groundwater, postulating that caves formed by groundwater flow paths converging on springs (Fig. 2b, e.g., Rhoades and Sinacori 1941). Dissolution was considered to be driven by mixing of water from various flow paths at the spring (Kincaid 1999). Caves were therefore thought to nucleate at the river and

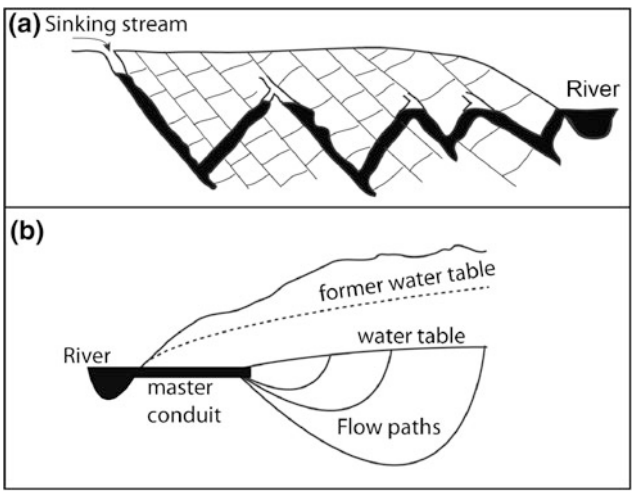

Fig. 2 Historically popular conceptual models for cave formation in Florida, adapted from Gulley et al. (2013b). **a** Caves formed as a result of flow path convergence at rivers and conduits grew up gradient from springs (i.e., headward sapping of Rhoades and Sinacori 1941); **b** Caves formed by sinking streams that emerged as springs downstream

conduits grew upgradient through headward sapping. A second group emphasized the importance of surface water, postulating that caves formed from sinking streams (Beck 1986) or where surface water and groundwater mixed at the water table (Fig. 2a; Dreybrodt et al. 2009).

Both hypotheses considered that cave formation occurs in a hydrogeological setting similar to modern conditions, consistent with some (though not necessarily all) observations of both air-filled and phreatic cave systems. The headward-sapping hypothesis was apparently inspired by the observation that some springs discharging from the Upper Floridan aquifer did not appear to be connected to sinking streams. Similarly, the hypothesis of sinking-stream origin for caves was based on observations that many of the streams that flow off adjacent siliciclastic sediments (Hawthorne Group) sink at the contact with the Upper Floridan aquifer (see Upchurch, Chap. 49, and Upchurch and Lawrence 1984; Martin and Dean 2001; Moore et al. 2010).

Both hypotheses, however, are inconsistent with certain morphological observations and geochemical considerations. The headward-sapping hypothesis was a popular explanation for conduit formation in all karst aquifers prior to the 1960s, but it was developed before there was a full understanding of calcite dissolution kinetics and the hydrogeology of carbonate aquifers (White and Culver 2007). It has largely been replaced by hypotheses of cave formation that emphasize the interaction between flow rate and dissolution capacity (e.g., Palmer 1991). While the headward-sapping hypothesis has persisted as an explanation for springs in Florida, it can be discounted as a plausible genetic mechanism on the basis of morphological inconsistencies between cave passages in the Upper Floridan aquifer and those expected from headward sapping (Gulley et al. 2013b). Flow path convergence and headward sapping should form a dendritic cave system that discharges to a single spring and extends upstream away from its outlet river. Many caves in the Upper Floridan aquifer, however, have conduits that extend beneath rivers and discharge via multiple springs, which are commonly located on both sides of a river (Fig. 3). In one extreme example, the Suwanachoochee cave system, it is possible for a cave diver to enter a spring on the Withlacoochee River, swim under both the Withlacoochee and Suwannee rivers, and exit via another spring on the Suwannee River (Gulley et al. 2013b). Geochemical data from the Upper Floridan aquifer also suggest that the headward-sapping hypothesis is unlikely because the waters in the Upper Floridan aquifer have too little chemical variability to generate significant calcite undersaturation when mixed (Gulley et al. 2013b, 2014a).

Cave origin by modern sinking streams is also unlikely because many springs in the Upper Floridan aquifer are not only located far from sinking streams (Gulley et al. 2011, 2013b), but also lack geochemical evidence that they discharge water from sinking streams, even during large storm events (Martin and Gordon 2000). The characteristics of bedrock in the Upper Floridan aquifer do not appear to favor the origin of phreatic loops.

In many areas, Hawthorn siliciclastic sediments cover the carbonate rocks and act as a partial confining layer (Moore et al. 2010). The Cody Scarp, formed by the eroded edge of the Hawthorn northeast of the study area, provides a steep hydraulic gradient that influences rivers flowing north and south along the Ocala Uplift, where the carbonates have little or no regional dip. The carbonates have high matrix permeability, as well as prominent fractures that trend NE–SW and NW–SE. Although deep phreatic passages commonly form from sinking streams in more indurated karst aquifers, their origin is aided by limestone beds that dip steeply below the water table in the direction of regional hydraulic gradient (Ford and Ewers 1978). However, the Upper Floridan aquifer lacks steeply dipping beds that enhance flow deep beneath the water table. Also, because high matrix permeability allows water to freely flow through unfractured bedrock, the ability of fractures to focus flow is diminished relative to telogenetic karst aquifers (Budd and Vacher 2004). Thus, it seems likely that the Upper Florida aquifer in our study area would not be a favorable host for sinking streams to form caves extending tens of meters below the water table.

3 Models of Cave Origin

Morphological studies suggest that caves in the Upper Floridan aquifer are similar to flank margin caves in eogenetic carbonate islands (Fig. 6; Florea 2006; Moore 2009; Gulley et al. 2013b; Polk and Brinkmann 2013; see Mylroie and Mylroie Chap. 51), which may suggest a shared hypogene origin. Elevations of prominent cave passages in the Upper Floridan aquifer are coincident with modern and paleo-water table elevations, which are ultimately controlled by sea-level still-stands (Florea et al. 2007). Cave entrances are located at higher elevations than main passages and appear to have formed by collapse or accidents of erosion. Many cave passages terminate laterally in solid bedrock, suggesting that they were not formed by conducting water from discrete inputs to springs (Florea 2006; Moore 2009; Gulley et al. 2013b).

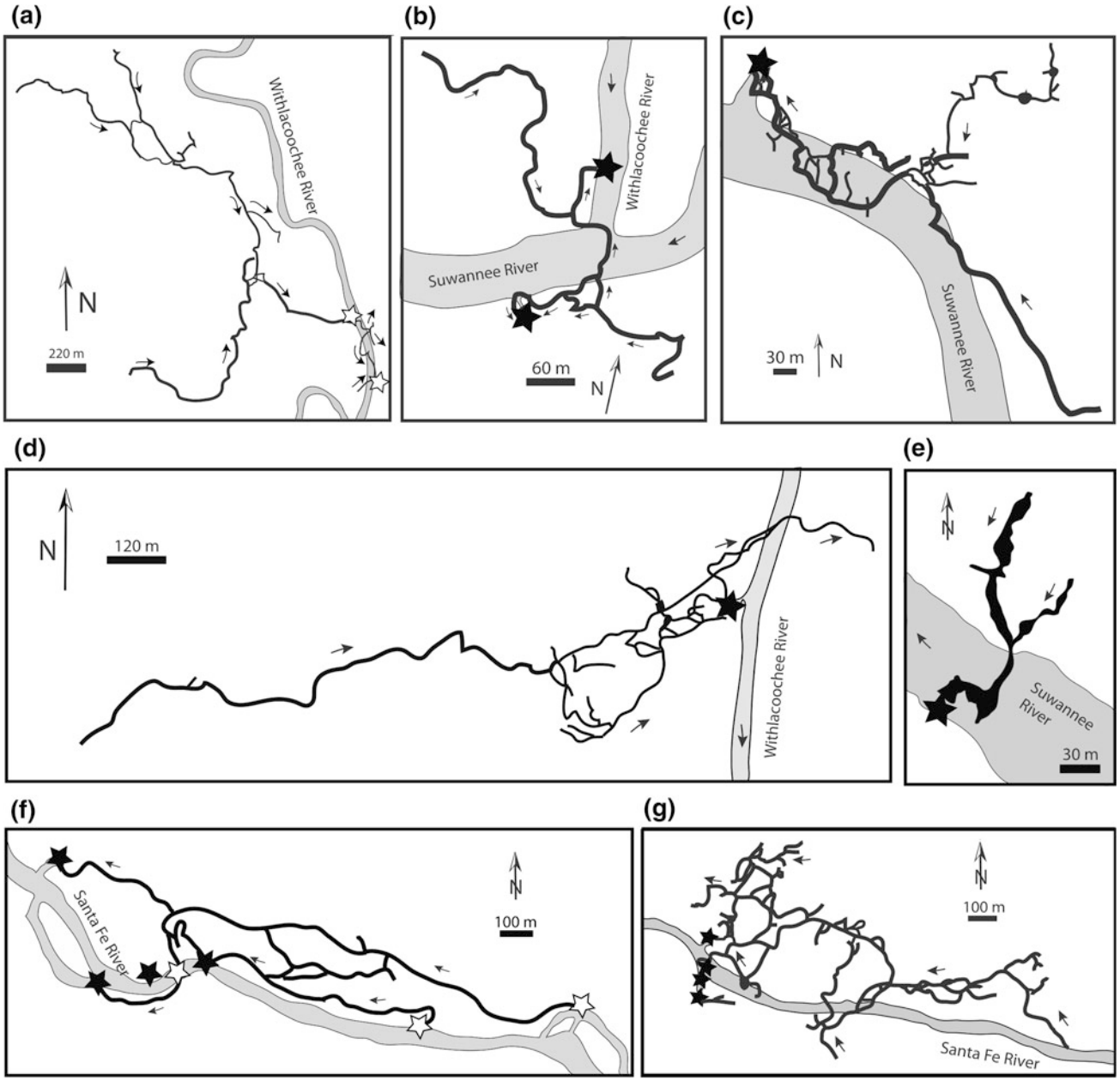

Fig. 3 Adapted from Gulley et al. (2013b): Many entirely phreatic cave systems in Florida have conduits that are 10s of meters below the water table and have passages that extend beneath rivers and discharge via multiple springs that are located on opposite sides of a river, including: **a** M2 Blue-Fennel's Funnel (courtesy of Michael Poucher); **b** Suwannacoochee cave system (courtesy of Michael Poucher); **c** Little River Spring (courtesy of the National Speleological Society Cave Diving Section); **d** Madison Blue Spring (courtesy of Michael Poucher); **e** Anderson Spring; **f** Siphon Creek cave system (courtesy of Wes Skiles); **g** Devil's cave system (courtesy of Bob Schulte)

Recent speleogenetic models in the Upper Floridan aquifer suggest that caves are forming at water tables from CO_2 that is respired in the deep vadose zone or at water tables (Gulley et al. 2013b, 2014a, b; Kaufmann 2016). CO_2 concentrations increase below the soil zone to concentrations that can exceed 5% by volume (e.g., Wood and Petraitis 1984; Wood 1985; Benavente et al. 2010; Breecker et al. 2012), indicating a subsurface CO_2 source. The CO_2 hydrates to carbonic acid at the water table, where it contributes to calcite undersaturation that drives cave formation

Fig. 4 Plan view of Briar Cave. *Dark gray areas* indicate passages that are partially water filled (i.e., extend partially below the water table)

(Gulley et al. 2013b, 2014a, b). For example, production of subsoil CO_2 generates seasonal calcite undersaturation at the water table in Briar Cave, in central Florida (Fig. 4; Gulley et al. 2014a). Briar Cave has no association with sinking streams, and only one small entrance at the highest point in the cave, about 12 m above the average water table position. As in similar caves with entrances at their high points, ventilation is seasonal, with air flowing into the cave when outside temperatures decrease below cave temperature. In contrast, in late summer, outside air temperatures rarely decrease below cave air temperature and, consequently, ventilation no longer occurs (Fig. 5a). During these periods of no ventilation, CO_2 concentrations in the cave increase, resulting in the cancelation of many cave trips due to "bad air." Geochemical analysis of water collected during these "bad air" periods demonstrates that the pCO_2 of water at the water table is increasing with time, generating calcite undersaturation in the local water (Fig. 5b). These observations highlight the fact that water tables in eogenetic karst aquifers are not only sites of CO_2 degassing, as is commonly assumed, but may also be subject to CO_2 "ingassing." This production of subsurface CO_2 and associated ingassing at water tables has been proposed to drive cave enlargement at the modern water table within the Upper Floridan aquifer, as at Briar Cave, and at lower paleo-water tables associated with low sea levels (e.g., Florea et al. 2007) (Fig. 6).

Fractures play an important role in the development of caves in the upper Florida aquifer. Fracture traces are visible throughout the Florida peninsula trending NE–SW and NW–SE, with other minor fracture sets distributed throughout the region (Florea 2006). Microbial oxidation of organic matter in fractures (Holden and Fierer 2005) allows the pCO_2 in them to exceed that of the water in surrounding unfractured bedrock, creating geochemical gradients (Gulley et al. 2014a). Fractures also provide linear flow paths that are more efficient than those in adjacent bedrock, causing water to flow from the surrounding matrix into the fractures. Consequently, fractures allow water to flow from areas of relatively low pCO_2 into areas of higher pCO_2 (where CO_2 production occurs primarily in the vadose zone). Alternatively, CO_2 can move from areas of low concentrations of organic matter to areas of higher concentration. CO_2 production is driven primarily by oxidation of organic matter, which is most effective at the water table. Along fractures, dissolution along the water table results in a characteristic "plus-sign" morphology (Fig. 7b and c; Florea 2006). Connectivity between fractures and other areas of high permeability allows the formation of extensive cave systems. Larger passages tend to be centered on joints, with low-wide crawlways connecting adjacent joints (Fig. 7c; Gulley et al. 2014a).

Florida's phreatic cave systems draw divers from around the world. These systems also probably originated by dissolution at water tables, though at elevations lower than those today. Although the scarcity of speleothems in many of Florida's phreatic caves has been assumed to indicate that the caves were never subaerially exposed (Gulley and Polk 2014), evidence shows that many caves were dry during the Last Glacial Maximum (Polk 2009) and that surface rivers are relatively recent. Sediment cores from phreatic caves indicate that, prior to 11 ka BP, air-filled conditions prevailed at depths that are now >70 m below the modern water table (Alvarez-Zarikian et al. 2005; Winkler et al. 2016). The Okefenokee Swamp, headwaters of the Suwannee River, was dry until 7.5 ka BP (Cohen et al. 1984). Archeological sites prior to 5 ka BP cluster around sinkholes, rather than river sites, suggesting that karst windows provided the only access to water (Clausen et al. 1975; Faught and Carter 1998). Speleothem dating identifies speleothems that were deposited during the Last Glacial Maximum and throughout

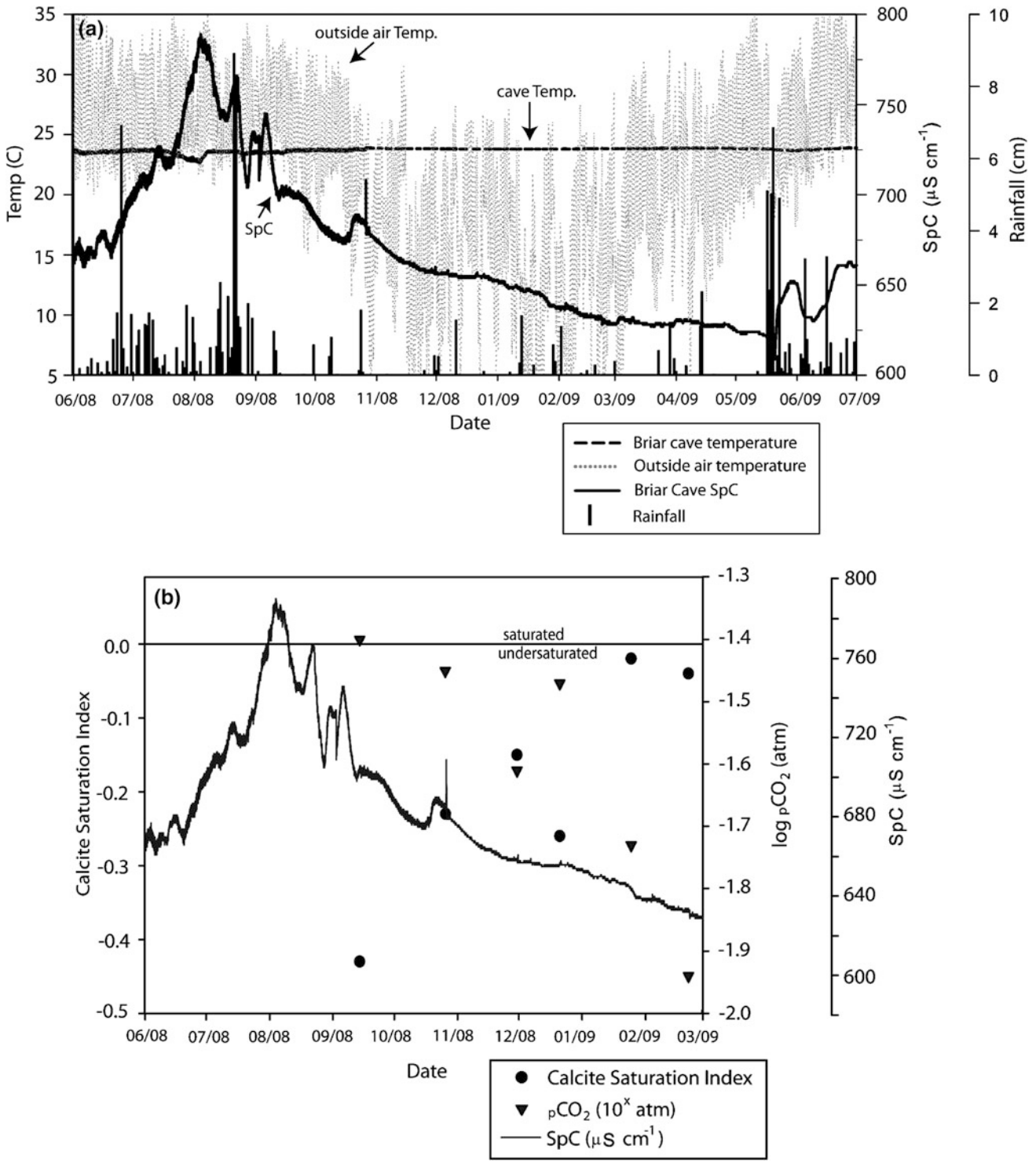

Fig. 5 **a** Time series of Specific Conductivity (SpC), temperature, and rainfall data collected at Briar Cave. Meteorological data were derived from the Florida Automated Weather Network station (FAWN; www.fawn.ifas.ufl.edu) at Oklawaha. **b** Discrete measurements of pCO_2 and SI_{CAL} of water at the water table in Briar Cave are superimposed on time series SpC data. SpC data depicted in both panels were measured using a conductivity logger installed at the water table inside Briar Cave

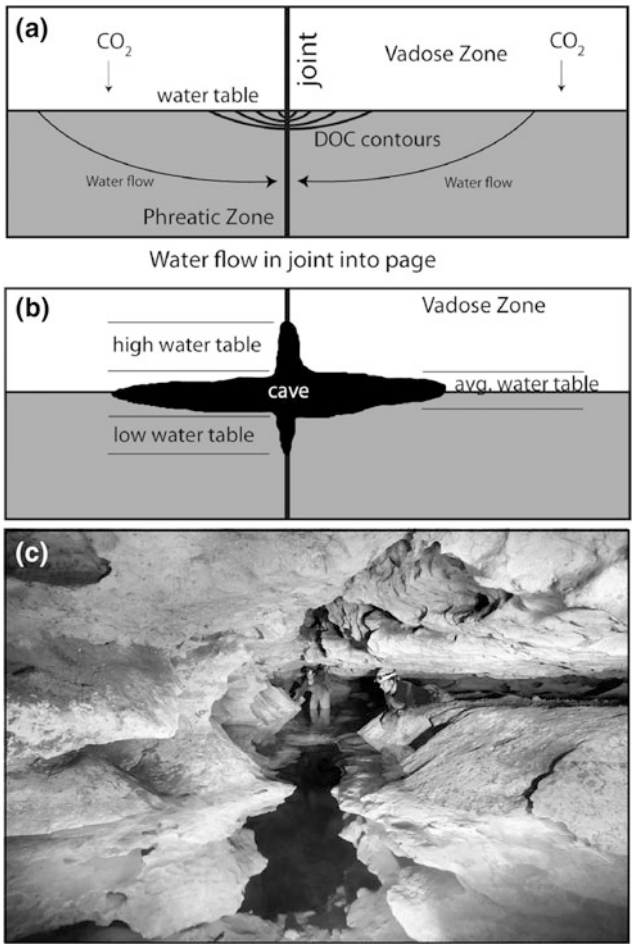

Fig. 6 Cross-sectional view of cave formation in eogenetic limestone at the intersection of joints and the water table. **a** The distribution of pCO_2 in the vadose zone is heterogeneous, with higher pCO_2 occurring in joints relative to matrix porosity. As water flows from the matrix (low pCO_2) into joints (high pCO_2), the increase in pCO_2 causes more CO_2 to dissolve into water, where it hydrates to form carbonic acid. High fluxes of water along joints maintain a fresh supply of solvent and remove the by-products of dissolution. **b** Over time, cave passages dissolve from limestone bedrock. Enlargement at the average elevation of the water table forms low, wide passages, with the vertical extensions along the joint reflecting dissolution during extreme high and low water table episodes. **c** Photograph from Roosevelt Cave, near Ocala, showing the plus-sign morphology at the modern water table (photo by Sean Roberts)

the Holocene in areas that would have been influenced, if not inundated, by freshwater during sea-level highstands during that time interval (Polk 2009).

Finally, the deepest points of the bedrock-lined Suwannee River channel extend only about 10 m below modern sea level (Mossa and Konwinski 1998), indicating that the cycles of river incision, cave formation, and channel aggradation that occurred in continental river basins in response to sea-level fluctuations (Granger et al. 1997, 2001; Anthony and Granger 2007) did not occur in Florida. The preponderance of evidence suggests that surface drainage features in Florida disappeared as water tables declined far below the land surface during low sea levels (Gulley et al. 2013b).

Because surface drainage was absent and could not have formed the caves that now lie below the water table in the Upper Floridan aquifer (Gulley et al. 2014b), and because the chemical compositions of water in the Upper Florida aquifer do not have sufficient chemical contrast to generate significant undersaturation with respect to calcite (Gulley et al. 2014a), we suggest that many of the phreatic caves were formed by the same processes that are operating at modern water tables. Because water table elevations have fluctuated with sea level, caves that are now below the water table formed at water table elevations associated with lower sea levels (e.g., Florea et al. 2007). While these caves formed by hypogene processes, they became connected to the modern river systems by a combination of sea-level rise, river incision, and surface erosion (Fig. 8). The rise of the water table where the Upper Floridan aquifer is unconfined has flooded isolated karst features that are not connected to any surface drainage features (e.g., Eagle's Nest). Springs, such as those in the Suwannee River Basin, formed when these hypogene caves became integrated into more recently developed cave systems fed by surface drainage (Gulley et al. 2014b). Near-surface water tables allowed floodwaters from adjacent watersheds that are underlain by siliciclastic materials to propagate across carbonate bedrock. These floodwaters are highly undersaturated with respect to calcite, and cycles of flooding have allowed rivers and stream channels to incise into cave voids that formed during previous lower sea levels (Gulley et al. 2011, 2013a; Brown et al. 2014).

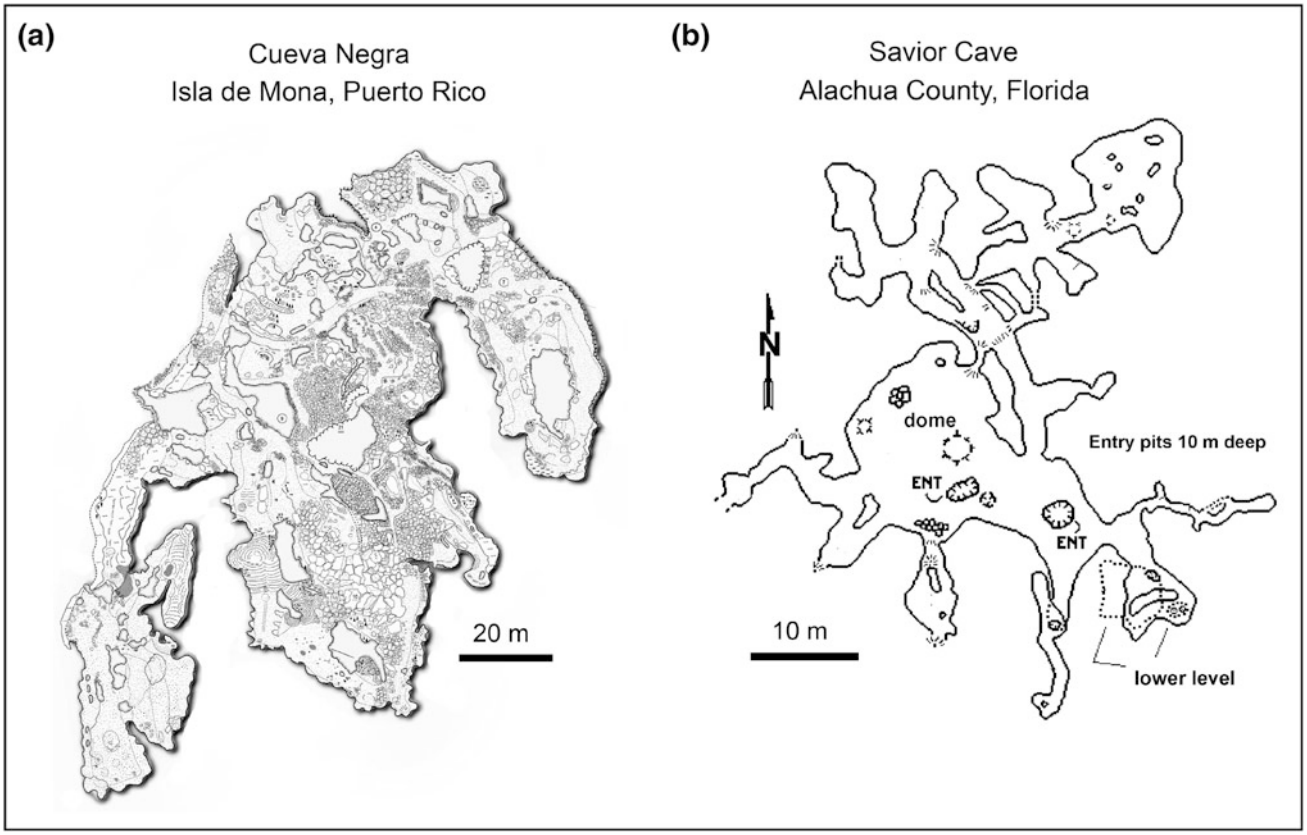

Fig. 7 Maps of a Florida "water table" cave and flank margin cave. **a** Cueva Negra in Puerto Rico (courtesy Pat Kambesis). **b** Savior Cave in Alachua County, Florida (courtesy of Florida Cave Survey, cartography by Albert A. Krause). Visual comparison of the two maps indicates the scale of the two caves is not that different, suggesting similarities in their morphology, though the caves are inferred to have formed from differing mechanisms

This genetic model, in which Florida's phreatic caves were originally hypogene and later integrated into surface drainage, provides a simple explanation for some of the more perplexing observations of Florida's phreatic caves. The presence of conduits extending under rivers and springs, with water discharging from the same cave on both sides of a river (Fig. 3), can easily be explained as the recent of rivers recently incising into hypogene caves (Fig. 8) (Gulley et al. 2013b). Spring outlets can therefore be viewed as accidents of erosion that post-date speleogenesis. Although these caves may have been hypogene in origin, they are now subject to epigene overprinting. Rapid increases in river stage during floods cause many of these springs to reverse flow, allowing highly undersaturated river water to flow into the conduits and enlarge them (Gulley et al. 2013a; Polk and Brinkmann 2013).

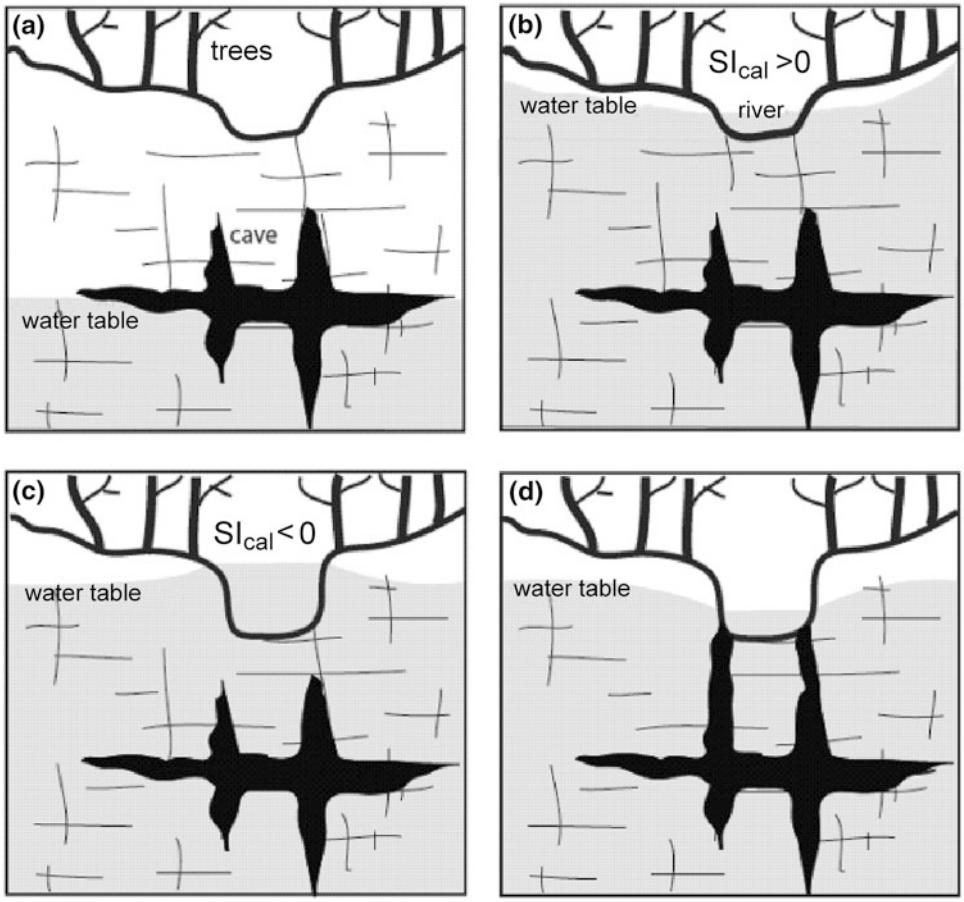

Fig. 8 Modified from Gulley et al. (2011). Springs that discharge water from the Upper Floridan aquifer to river channels originated when isolated caves that formed at lower water tables became connected to river channels that formed during higher sea levels. **a** Caves formed at lower water tables during low sea-level stands. **b** Cave voids ended up below the water table when sea-level rise elevated water tables above low points in the surface topography. During base flow conditions, water in the rivers was groundwater that was saturated with respect to calcite. **c** Floods that were initiated by runoff from adjacent siliciclastic rocks raised river stage faster than groundwater heads, causing water from the river to flow into the aquifer. Because runoff from siliciclastics was highly undersaturated with respect to calcite, dissolution enlarged the river channel and dissolved connections between the river and underlying cave along joints. **d** After repeated cycles of flooding and enlargement, caves became connected to the river to form springs. Because springs formed wherever the river incised into the underlying cave systems, cave passages can extend under rivers and even discharge via multiple spring vents that are located on opposite sides of the river. Similar caves that formed as isolated cavities but did not become integrated into river systems to form springs also exist. These caves are accessed via water-filled collapse features or solution pipes

4 Conclusions

Evidence for potential hypogene influences in the Upper Floridan aquifer suggests that dissolution is driven by conditions that fit the current hydrological criteria for evaluating hypogene karst (see Klimchouk 2014). In addition, it is suggested here that dissolution in eogenetic carbonates driven by CO_2 gradients can also be included in the model. The speleogenetic model described here is based on field measurements in the area of study and does not necessarily apply to all caves in the aquifer, e.g., those generated by runoff from the Cody escarpment.

While this chapter focuses mainly on the Upper Floridan aquifer, other current research on the lower Floridan and Biscayne aquifers suggests that more typical processes of hypogene speleogenesis may occur at depth (Cunningham and Walker 2009; Herbert and Upchurch 2016). Future work is likely to help understand the complex speleogenesis taking place in Florida's carbonate platform.

The caves described here have formed by the generation of carbonate mineral undersaturation in subsurface waters, which is considered a valid criterion for hypogenic cave origin (Palmer 1991), as distinguished from those that are formed by rising groundwater (Klimchouk 2014); however, the genesis of the caves described here apparently happens at the outer limits of the hypogenic regime.

References

Alvarez-Zarikian CA, Swart PK, Gifford JA, Blackwelder PL (2005) Holocene paleohydrology of little salt spring, Florida, based on ostracod assemblages and stable isotopes. Palaeogeogr Palaeoclimatol Palaeoecol 225(1–4):134–156. doi:10.1016/j.palaeo.2004.01.023

Anthony DM, Granger DE (2007) A new chronology for the age of Appalachian erosional surfaces determined by cosmogenic nuclides in cave sediments. Earth Surf Process Land 32(6):874–887. doi:10.1002/esp.1446

Beck B (1986) A generalized genetic framework for the development of sinkholes and Karst in Florida, U.S.A. Environ Geol 8(1):5–18. doi:10.1007/BF02525554

Benavente J, Vadillo I, Carrasco F, Soler A, Liñán C, Moral F (2010) Air carbon dioxide contents in the Vadose Zone of a mediterranean Karst. Vadose Zone J. 9:126–136. doi:10.2136/vzj2009.0027

Breecker DO, Payne AE, Quade J, Banner JL, Ball CE, Meyer KW, Cowan B (2012) The sources and sinks of CO_2 in caves under mixed woodland and grassland vegetation. Geochim Cosmochim Acta 96:230–246

Brown AL, Martin JB, Screaton EJ, Ezell JE, Spellman P, Gulley J (2014) Bank storage in karst aquifers: the impact of temporary intrusion of river water on carbonate dissolution and trace metal mobility. Chem Geol 385:56–69

Budd DA, Vacher HL (2004) Matrix permeability of the confined Floridan Aquifer, Florida. USA Hydrogeol J 12(5):531–549

Clausen CJ, Brooks HK, Wesolowsky AB (1975) The early man site at warm mineral springs, Florida. J Field Archaeol 2(3):191–213. doi:10.1179/009346975791491006

Cohen AD, Spackman W, Dolsen P (1984) Occurrence and distribution of sulfur in peat-forming environments of Southern Florida. Int J Coal Geol 4(1):73–96. doi:10.1016/0166-5162(84)90008-9

Cunningham K, Walker C (2009) Seismic-sag structural systems in tertiary carbonate rocks beneath Southeastern Florida, USA: Evidence for Hypogenic Speleogenesis? In: Klimchouk A, Ford D (eds) Hypogene speleogenesis and karst hydrogeology of Artesian Basins. pp 151–158

Dreybrodt W, Romanov D, Kaufmann G (2009) Evolution of isolated caves in porous limestone by mixing of phreatic water and surface water at the water table of unconfined aquifers: a model approach. J Hydrol 376:200–208

Faught M, Carter B (1998) Early human occupation and environmental change in northwestern Florida. Quat Int 49–50:167–176. doi:10.1016/S1040-6182(97)00061-X

Florea L (2006) Architecture of air-filled caves within the Karst of the Brooksville Ridge, West-Central Florida. J Caves Karst 68(2):64–75

Florea LJ, Vacher HL, Donahue B, Naar D (2007) Quaternary cave levels in peninsular Florida. Quat Sci Rev 26(9–10):1344–1361. doi:10.1016/j.quascirev.2007.02.011

Florida Geological Survey (2002) First magnitude springs of Florida. Florida Geological Survey Open Report No. 85. Tallahassee, Florida, p 151

Ford D, Ewers R (1978) The development of limestone cave systems in the dimensions of length and depth. Can J Earth Sci 15(11):1783–1798

Granger DE, Kirchner JW, Finkel RC (1997) Quaternary downcutting rate of the New River, Virginia, measured from differential decay of cosmogenic 26Al and 10Be in cave-deposited alluvium. Geology 25(2):107–110

Granger DE, Fabel D, Palmer AN (2001) Pliocene—Pleistocene incision of the Green River, Kentucky, determined from radioactive decay of cosmogenic 26Al and 10Be in Mammoth Cave sediments. Geol Soc Am Bull 113(7):825–836. doi:10.1130/0016-7606(2001)113<0825:PPIOTG>2.0.CO;2

Gulley JD, Polk JS (2014) Possible explanations for the lack of formations in underwater caves in Florida. Und Spel 41(1):6–7

Gulley J, Martin JB, Screaton EJ, Moore PJ (2011) River reversals into karst springs: a model for cave enlargement in eogenetic karst aquifers. Geol Soc Am Bull 123(3–4):457–467

Gulley J, Martin J Spellman P, Moore P, Screaton E (2013a) Dissolution in a variably confined carbonate platform: effects of allogenic runoff, hydraulic damming of groundwater inputs, and surface–groundwater exchange at the basin scale. Earth Surf Process Land 38(14):1700–1713, doi:10.1002/esp.3411

Gulley JD, Martin JB, Moore PJ, Murphy J (2013b) Formation of phreatic caves in an eogenetic karst aquifer by CO2 enrichment at lower water tables and subsequent flooding by sea level rise. Earth Surf Process Land 38(11):1210–1224. doi:10.1002/esp.3358

Gulley J, Martin J, Moore P (2014a) Vadose CO_2 gas drives dissolution at water tables in eogenetic karst aquifers more than mixing dissolution. Earth Surf Process Land 39(13):1833–1846

Gulley JD, Martin JB, Spellman P, Moore PJ, Screaton EJ (2014b) Influence of partial confinement and Holocene river formation on groundwater flow and dissolution in the Florida carbonate platform. Hydrol Process 28(3):705–717. doi:10.1002/hyp.9601

Herbert TA, Upchurch SB (2016) The potential role of hypogene speleogenesis in the lower Floridan aquifer and Sunniland Oil Trend, South Florida, U.S.A. In: Chavez T, Reehling P (eds) Proceedings of DeepKarst 2016: origins, resources, and management of hypogene karst, symposium 6, National Cave and Karst Research Institute, Carlsbad, New Mexico, pp 119–129, 11–14 Apr 2016

Holden PA, Fierer N (2005) Microbial processes in the Vadose Zone. Vadose Zone J 4(1):1–21. doi:10.2113/4.1.1

Kaufmann G (2016) Modeling karst aquifer evolution in fractured, porous rocks. J Hydrol. doi:10.1016/j.jhydrol.2016.10.049

Kincaid T (1999) Morphologic and fractal characterization of saturated Karstic Caves. Ph.D. dissertation, University of Wyoming

Klimchouk A (2014) The methodological strength of the hydrogeological approach to distinguishing hypogene speleogenesis. In: Klimchouk A, SasowskyI, Mylroie J, Engel S, and Engel AS (eds) Hypogene Cave Morphologies. Special publication 18 of the Karst Waters Institute pp 4–13

Martin J, Gordon S (2000) Surface and groundwater mixing, flow paths, and temporal variations in chemical compositions of karst springs. In: Sasoswky I, Wicks CM (eds) Groundwater flow and contaminant transport in carbonate aquifers. A.A. Balkema, pp 65–92

Martin JB, Dean RW (2001) Exchange of water between conduits and matrix in the Floridan aquifer. Chem Geol 179(1–4):145–165

Moore PJ (2009) Effects of continental overprinting on cave development in eogenetic karst: an example from the Florida-Bahamas platform. In: White W (ed) Proceedings of the 15th international congress of speleology, vol 1. International Union of Speleology, Kerrville, TX, pp 528–532

Moore PJ, Martin JB, Screaton EJ, Neuhoff P (2010) Conduit enlargement in an eogenetic karst aquifer. J Hydrol 393:143–155

Mossa J, Konwinski J (1998) Thalweg variability at bridges along a large karst river: the Suwannee River, Florida. Eng Geol 49(1):15–30

Palmer A (1991) Origin and morphology of limestone caves. Geol Soc Am Bull 103(1):1–21. doi:10.1130/0016-7606(1991)103<0001:OAMOLC>2.3.CO;2

Polk JS (2009) Proxy records of climate change in tropical and subtropical Karst environments. Dissertation, Department of Geography and Environmental Science and Policy, University of South Florida

Polk JS, Brinkmann R (2013) Climatic influences on coastal cave and Karst development in Florida. In: Lace M, Mylroie J (eds) Coastal karst landforms. Springer, pp 317–345

Rhoades R, Sinacori MN (1941) Pattern of ground-water flow and solution. J Geol 49(8):785–794

Upchurch S, Lawrence F (1984) Impact of ground-water chemistry on sinkhole development along a retreating scarp. In: Beck B (ed) Sinkholes: their geology, engineering and environmental impact. A.A. Balkema, Rotterdam, pp 23–28

White WB, Culver DC (2007) Benchmark papers in karst science. Karst Waters Institute, Leesburg VA

Winkler TS, van Hengstum PJ, Horgan MC, Donnelly JP, Reibenspies JH (2016) Detrital cave sediments record Late Quaternary hydrologic and climatic variability in northwestern Florida, USA. Sediment Geol 335:51–65

Wood WW (1985) Origin of caves and other solution openings in the unsaturated (vadose) zone of carbonate rocks: a model for CO_2 generation. Geology 13(11):822–824. doi:10.1130/0091-7613(1985)13<822:OOCAOS>2.0.CO;2

Wood WW, Petraitis MJ (1984) Origin and distribution of carbon dioxide in the unsaturated zone of the southern high plains of Texas. Water Resour Res 20(9):1193–1208. doi:10.1029/WR020i009p01193

Bahamian Flank Margin Caves as Hypogene Caves

51

John Mylroie and Joan Mylroie

Abstract

Fieldwork in the Bahamian Archipelago in the 1970s and 1980s identified a new cave type, the *flank margin cave*, as macroscopic dissolutional voids developed in the *margin* of a freshwater lens, under the *flank* of the enclosing landmass. These voids are produced by three conditions that exist at the lens margin: mixing dissolution, organic decay horizons, and the increase in freshwater flow rate. The water flow enters flank margin caves as diffuse flow and exits as diffuse flow, a flow regime that produces dissolutional sculpture lacking turbulent flow features, such as asymmetric scallops. The caves are tied to sea level, which controls the freshwater lens position, and as such are excellent indicators of past sea-level position. The caves form without entrances and become accessible only after subaerial erosion has breached their ceilings or walls. Flank margin caves initiate as individual globular dissolutional voids that then intersect as the voids enlarge, increasing cave size in a sudden stepwise manner. As cave development is restricted to the lens margin, the largest flank margin caves acquire a linear shape as voids interconnect parallel to the lens margin. Flank margin caves are hypogene caves based on their diffuse, slow-flow regimes, because the dissolutional aggressiveness is generated below the surface by mixing, and the ascending marine water following the base of the lens to the site of dissolution at the lens margin. Because these caves form rapidly at shallow depths, there is a debate as to their hypogene classification, but they meet all criteria for hypogene speleogenesis.

Keywords

Bahamas • Flank margin caves • Hypogene caves • Diffuse flow • Rapid speleogenesis

1 Introduction

The goal of this paper was to determine whether the flank margin caves in the Bahamas are hypogenic or not. The definition of hypogene caves is an open debate, as reviewed by Dublyansky (2014) and elsewhere in this book. Many definitions are quite lengthy (Klimchouk 2007), and others are tied to a specific method of generating aggressivity in the groundwater (e.g., Worthington and Ford 1995). Palmer (2000), p. 82, proposed a general definition that most workers can agree on: "Hypogene caves are formed by water in which aggressiveness has been produced at depth, independent of acid sources at or near the surface." This definition, however, by focusing on acidity, does not include hypogene caves formed in evaporate rocks. Palmer (2007) explicitly includes flank margin caves as hypogene, as does Klimchouk (2014). In February 2014, a conference was held at the Gerace Research Centre on San Salvador Island, Bahamas, "Hypogene Cave Morphologies," to specifically address issues involving hypogene caves and, in addition, how flank margin caves fit (or do not fit) into that classification (Klimchouk et al. 2014).

J. Mylroie (✉) · J. Mylroie
Department of Geosciences, Mississippi State University, Mississippi State, MS 39762, USA
e-mail: mylroie@geosci.msstate.edu

© Springer International Publishing AG 2017

A. Klimchouk et al. (eds.), *Hypogene Karst Regions and Caves of the World*,
Cave and Karst Systems of the World, DOI 10.1007/978-3-319-53348-3_51

1.1 Regional Setting

The Bahama Islands, or Bahamian Archipelago, comprise a 1400-km-long portion of a NW–SE-trending archipelago that extends from Little Bahama Bank off the coast of Florida to Great Inagua Island, just off the coast of Cuba (Fig. 1) as the country of The Bahamas. The archipelago extends farther southeast as the Turks and Caicos Islands, a separate political entity (overseas territory of the UK), and terminates with Silver Bank and Navidad Bank. The northwestern Bahama Islands are isolated landmasses that project above sea level from two large carbonate platforms, Little Bahama Bank and Great Bahama Bank. To the southeast, beginning in the area of San Salvador Island, the Bahamas comprise small isolated platforms capped by islands that commonly cover a significant portion of the available platform area. The Bahamian platforms have been sites of carbonate deposition since at least Cretaceous time, resulting in a minimum carbonate sedimentary cover thickness of 5.4 km (Meyerhoff and Hatten 1974) and perhaps as much as 10 km (Uchupi et al. 1971). The large platforms to the northwest are dissected by deep channels and troughs (Fig. 1), whereas the isolated platforms of the southeastern Bahamas mostly are surrounded by deep water. Water depths on the shallow platforms are generally less than 10 m. The Bahamas are tectonically stable (Mayaguana Island may be an exception to this rule, see Kindler et al. 2010), with slow isostatic subsidence of 1–2 m per 100,000 years occurring (Carew and Mylroie 1995a). The geologic literature on the Bahamas is extensive, but the bulk of the early literature deals with the flooded carbonate banks and related deepwater environments. A thorough overview of Bahamian island geology can be found in Curran and White (1995), Vacher and Quinn (Chap. 3, 1997), and Kindler et al. (2010). In summary, the rocks are all Mid to Late Quaternary carbonates dominated by eolian calcarenites or eolianites and subtidal facies. All rocks above 8-m elevation are eolian. The carbonate sequences of the Bahamas

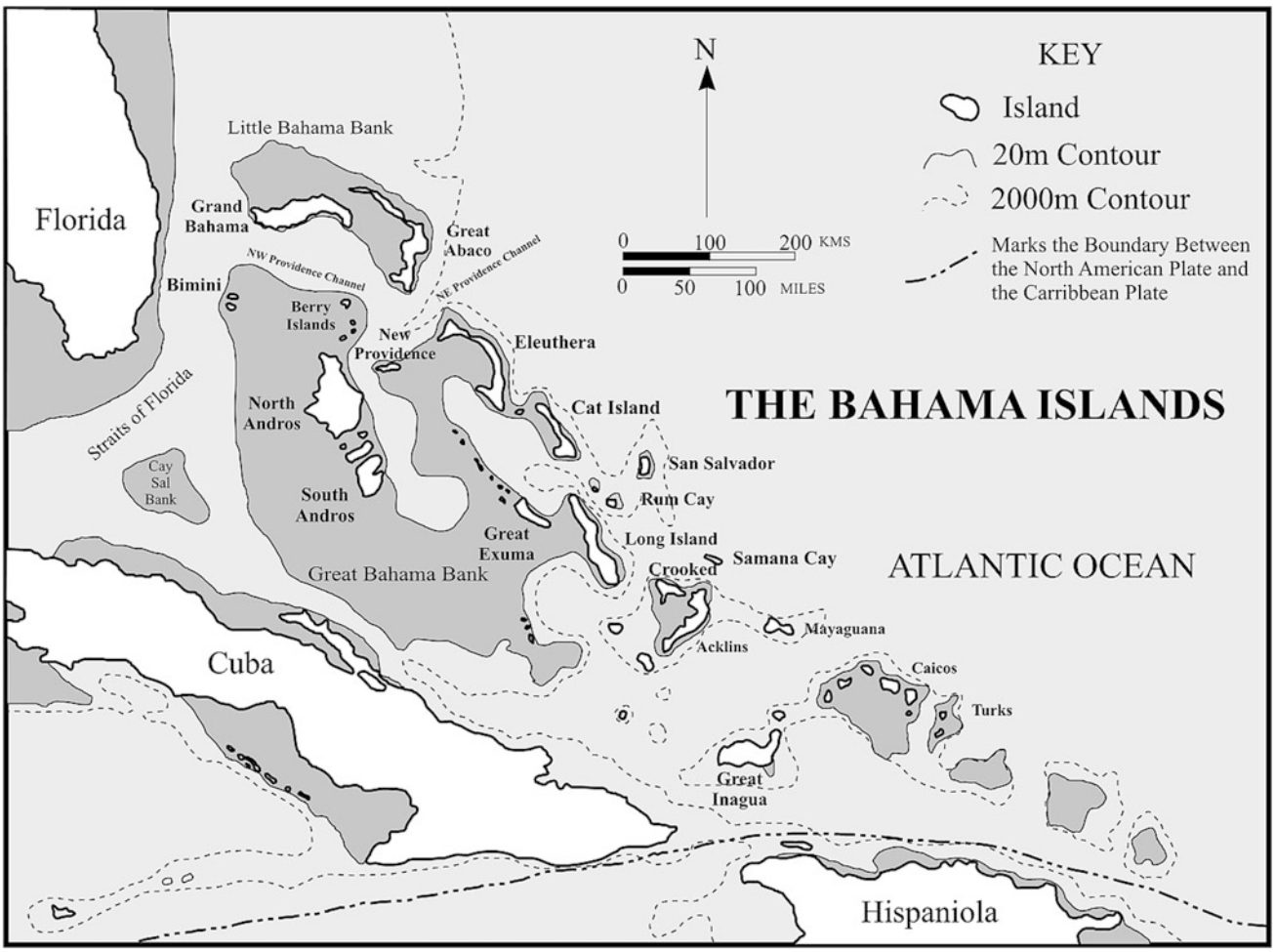

Fig. 1 Map of the Bahamian Archipelago, including the separate political entities The Bahamas (Center and Northwest) and the Turks and Caicos Islands (Southeast)

can be viewed as individual packages deposited on each sea-level highstand, separated by erosional unconformities (usually marked by paleosols) produced by each sea-level lowstand (Carew and Mylroie 1995b). Because of their young age, these rocks are often poorly lithified.

1.2 Freshwater Lens Hydrology and Karst Processes

In any essentially homogeneous body of rock like that of the carbonates forming the Bahamian islands, the freshwater lens floats on underlying, denser seawater that permeates the subsurface (Fig. 2). The model for the ideal behavior of such water masses is the Ghyben–Herzberg–Dupuit model. In reality, variations in rock permeability and other factors result in distortion of the ideal lens shape in the Bahamas (e.g. Vacher and Mylroie 2002). Nonetheless, the Ghyben–Herzberg–Dupuit model serves as a useful first approximation of the relationship between the freshwater and underlying marine groundwater in an island.

The youthfulness of Bahamian carbonate rocks creates different water flow dynamics than are found in the dense, diagenetically mature carbonates of continental interiors. The Bahamas exemplify what has been described as *eogenetic karst*, defined by Vacher and Mylroie (2002), p. 183, as "the land surface evolving on, and the pore system developing in, rocks undergoing eogenetic, meteoric diagenesis." The term "eogenetic" is from Choquette and Pray (1970), p. 215, and they defined the three time-porosity stages of carbonate rock evolution: "the time of early burial as *eogenetic*, the time of deeper burial as *mesogenetic*, and the late stage associated with long-buried carbonates as *telogenetic*." Eogenetic carbonate rocks have not undergone extensive compaction or cementation and retain much of their primary depositional porosity. Most carbonate islands, and almost all carbonate islands found in tropical or subtropical locations, are made up of eogenetic limestones (Late Cenozoic) that were deposited at the setting in which they presently occur.

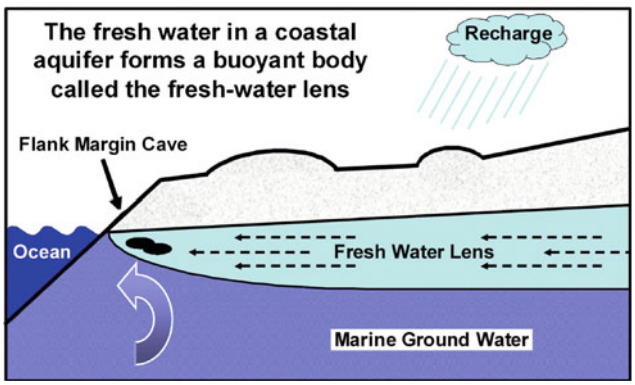

Fig. 2 Simplified diagrammatic representation of the freshwater lens in a carbonate island. *Dashed arrows* indicate flow within the lens; *larger curved arrow* indicates marine water entrained by the freshwater lens flow, ascending from depth. This image, as with most seen in the scientific literature, is vertically exaggerated, making the lens seem to have a steeper curvature than actually exists

2 Flank Margin Caves

Caves develop by mixing dissolution at the margin of the freshwater lens, under the flank of the enclosing landmass, so they are called *flank margin caves* (Mylroie and Carew 1990; Mylroie 2013). Within the freshwater lens, dissolution is favored at specific sites. The top of the lens is where descending vadose water mixes with the phreatic water of the lens. These waters are both commonly saturated with $CaCO_3$, but at different initial conditions. This mixing of waters results in enhanced dissolution of $CaCO_3$. Similar mixing dissolution occurs at the base of the freshwater lens, where freshwater and marine water mix (called a *halocline* if the boundary is sharp, a *mixing zone* if the boundary is gradational in salinity). Of these two mixing zones, the freshwater mixing with marine water at the bottom of the lens appears more important, perhaps because the top of the lens is vulnerable to CO_2 degassing, which may counteract the mixing dissolution environment there.

Both the top and bottom of the freshwater lens are density boundaries. Organics that collect at these two boundaries can oxidize to produce excess CO_2 to drive dissolution. If organic loading is significant, the system may become anoxic, allowing a variety of unusual biogeochemical environments that can promote $CaCO_3$ dissolution. In blue holes, the large surface openings accept major amounts of organic debris, including macroscopic vegetative remains as well as particulate matter, which collect at the halocline. In those cases, anoxia at the halocline produces H_2S which drives dissolution (Bottrell et al. 1991). For regular vadose flow in these eogenetic carbonate aquifers, large organic material is filtered out, and only dissolved organic carbon (DOC) and small particulate matter can reach the freshwater lens, although vadose fast-flow routes called pit caves can transport large organic particles downward at specific sites. In continental settings, it has been shown that DOC and fine particulate organics can percolate downward through the vadose zone and promote dissolution within the aquifer (Wood and Petraitis 1984). In the Bahamas, it has been shown that organics can migrate to the freshwater lens and, through bioremediation of sulfur under anoxic conditions, enhance dissolution in flank margin caves (Bottrell et al. 1993).

The freshwater lens integrates all the catchment it receives and discharges it to the ocean. The lens also thins as it approaches the coast. These two factors result in the fastest

flow velocities in the lens being found at the distal margin of the lens. Chemical reactions that occur here will have the advantage in that reactants are brought in, and products removed, faster than elsewhere in the lens. The lens margin also brings the top and bottom of the lens into the same area, such that the mixing impact of each environment is added together, as is the biogeochemical activity of any included organics at those boundaries. As a result, the greatest amount of $CaCO_3$ dissolution should occur at the lens margin. Decades of fieldwork in the Bahamas and in other localities (Mylroie and Mylroie 2007) has shown that the largest caves found on small, simple carbonate islands are in this location. As noted earlier, these caves are named *flank margin caves* because of the location in what would have been the margin of the lens, under the flank of the enclosing landmass. The term was developed in the late 1980s (Mylroie and Carew 1990) based on work in the Bahamas and has since been expanded to a variety of island types around the world, including throughout the Bahamas (Mylroie and Mylroie 2007), Isla de Mona (Frank et al. 1998), the Mariana Islands (Jenson et al. 2006), Puerto Rico (Lace 2008), Barbados (Machel et al. 2011), the Adriatic coast (Otonicar et al. 2010), Australia (Mylroie and Mylroie 2009a), Mallorca (Mylroie et al. 2015a), Curacao (Kambesis et al. 2015), and New Zealand (Mylroie et al. 2008). The dissolutional mechanism is extremely powerful and cuts across a variety of primary and secondary features in caves, as shown in Fig. 3.

Flank margin caves develop as dissolutional voids within a diffuse, slow-flow regime. They form without entrances, and human access can only be later gained after other erosional processes, such as hillslope retreat or ceiling collapse, open them to the outside environment. They have a consistent passage pattern in part controlled by their size. Their

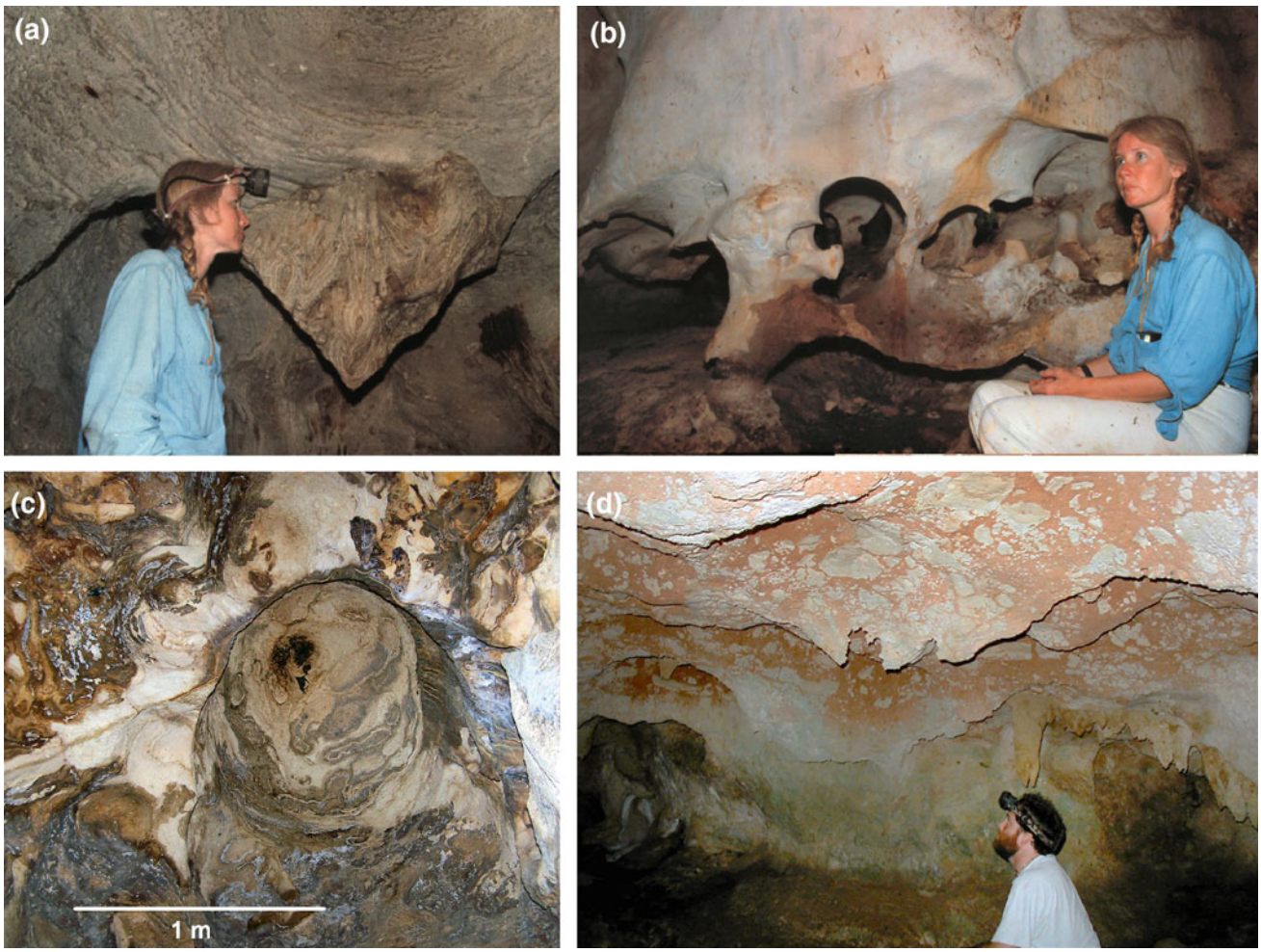

Fig. 3 Examples of dissolutional morphology in flank margin caves. **a** Smooth surface cut across both bedrock and flowstone, Hunts Cave, New Providence Island, Bahamas (indicating a phreatic–vadose–phreatic series of events). **b** Complex dissolutional structure, Harry Oakes Cave, New Providence, Bahamas. **c** Dissolutional surface cut smoothly through *Acropora palmata* fossils and matrix, looking upward at the roof of Suicide Cow Cave, Barbados. The central cylindrical dissolution feature is a bell hole (see text for a full explanation). **d** Paleosol cut smoothly by dissolution, Red Roof Cave, Long Island, Bahamas

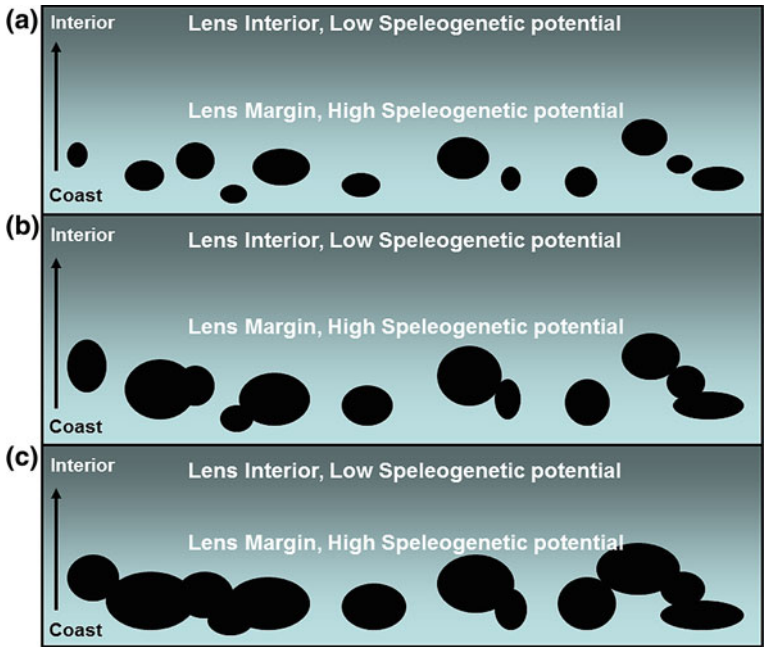

Fig. 4 Diagrammatic model of how flank margin caves grow in size: lens interior to the *top* of each panel and lens margin to the *bottom* of each panel. **a** Initial development is as single voids of simple shape. **b** As each voids enlarges, it connects with adjacent voids and undergoes a sudden jump in cave size as the connection occurs. **c** Collections of chambers can enlarge and intersect other chamber collections, creating another sudden jump in cave size. Flank margin caves can only get big by connecting parallel to the lens margin, as the lens interior is low in speleogenetic potential

size is in turn controlled by how long the freshwater lens was stable at a single position. Small flank margin caves are commonly single chambers with a few short side passages. Larger caves are a collection of chambers, and the largest caves are amalgamations of chamber collections (Fig. 4). The caves fit the *ramiform* and *spongework* classifications of Palmer (1991), but with specific asymmetries related to their position at the lens margin. First, the chambers nearest the lens margin are usually the largest (Fig. 5). To the rear of these chambers are smaller passages that head inward to what was once the lens interior. Cave configuration is of phreatic surfaces developed in a diffuse, slow-flow regime (Fig. 6). As the original chamber enlarged, marine water invaded the chamber and the mixing front moved to the back, inland wall of the chamber as a series of individual freshwater discharge points and hence mixing locations (Labourdette et al. 2007). These passages grew headward into the lens as the lens margin retreated inland. The passages may have cross-connected to create a maze-like set of passages, but they all end in blank bedrock walls (Fig. 6c). These passage terminations are the position of the mixing front when sea-level fell and the caves became senescent. If the lens was stable for a sufficient time, a second set of chambers may develop, parallel to the original set of chambers and to the lens margin, but interior to the initial row of chambers. Because the geochemically active portion of the lens margin does not penetrate deep into the island interior, flank margin caves can continue to grow in size only by amalgamating in a shore-parallel manner with other collections of chambers forming in the same way. Therefore, the initially globular caves elongate along the lens margin by these connections (Fig. 4). Caves with linear surveys of over 1 km are found on many islands: Hole in the Wall Cave (Abaco), Fig. 7a; Hamilton's Cave (Long Island), Fig. 7b; Hatchet Bay Cave and Ten Bay Cave (Eleuthera), Fig. 8 being examples; Conch Bar Cave (Middle Caicos) is currently being resurveyed.

2.1 Flank Margin Cave Metrics

The use of areal footprint to quantify cave size can be justified by comparing the 1207 m survey length of Hole in the Wall Cave to the 1200 m survey length of Hatchet Bay Cave to the 1030 m survey length of Hamilton's Cave, very similar values. The areal footprint of those three caves, in the same order, is 3422, 5934, and 8931 m^2, respectively. Cave size for these flank margin caves is best quantified by measuring their areal footprint. Given that the caves are vertically restricted because of their development in the thin distal margin of the freshwater lens, areal footprint is a proxy for cave volume. This footprint is then a measure of how much carbonate rock has been removed by dissolutional processes.

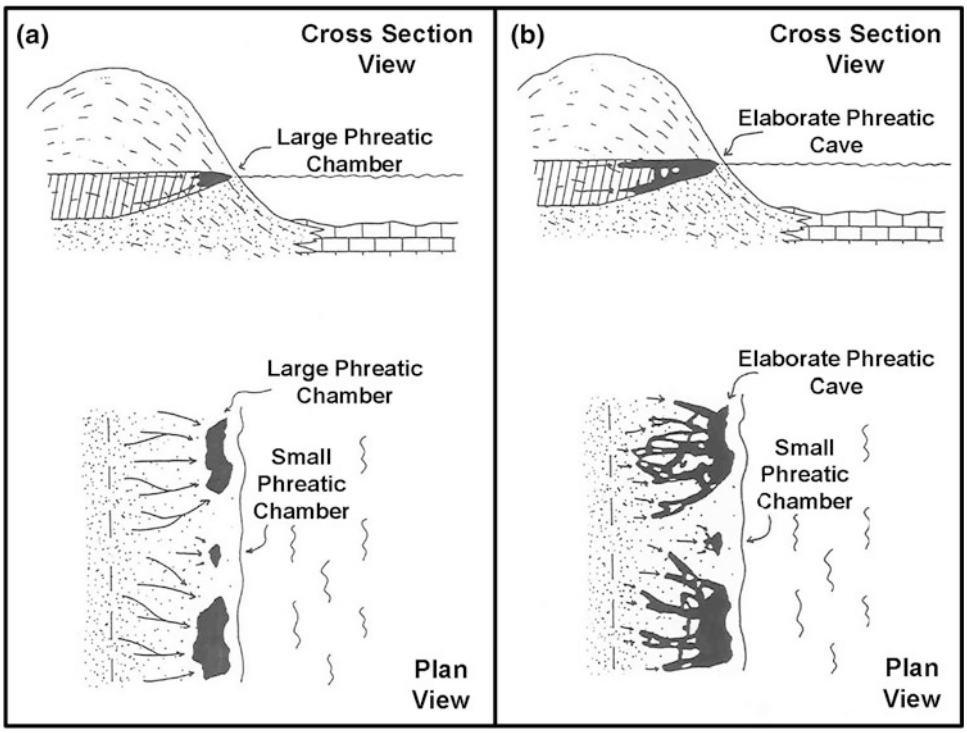

Fig. 5 Bahamian model for flank margin cave formation. **a** Sea-level rise places a freshwater lens into an eolianite ridge and dissolution of simple cave chambers begins at the lens margin. **b** Through time, the chambers enlarge and sea water invades, displacing the lens margin to the rear of the chambers, where continuing dissolution produces cave complexity in a ramiform pattern (from Mylroie and Carew 1990)

The stepwise growth of flank margin caves in the Bahamas has been demonstrated by empirical data and by computer modeling. Analysis of Bahamian flank margin cave size, as given by the aerial footprint of mapped caves, produces a rank-order plot that displays discrete cave size categories 100 m^2 or less, between 100 and 1000 m^2, and over 1000 m^2 (Roth 2004). When modeled on a computer, using the idea of chamber enlargement and connection, the results exactly match the empirical data (Labourdette et al. 2007). In addition, the computer predicts a fourth cave size category of 18 m^2 or less, not recorded on the empirical data as caves of that small size were not mapped as being too little for the effort involved (an explorational bias), but are recognized to actually exist. Comparison of flank margin cave area to perimeter plots demonstrates that small flank margin caves approximate a rectangle with an aspect ratio of 1/2 to 1/10, whereas stream (epigenic) caves approximate a rectangle with a 1/100 aspect ratio. However, because flank margin caves can only get big (>1000 m^2) by extending parallel to the lens margin, as these caves enlarge their aspect ratio becomes closer to a rectangle at 1/100, similar to a stream cave.

Flank margin caves contain a suite of phreatic dissolutional forms which all are consistent with slow flow. The features associated with turbulent stream flow, such as wall scallops or sediment bars and deposits, are absent in flank margin caves. The cave interiors are characterized by cuspate, curvilinear walls, isolated bedrock pillars, globular rooms, maze-like areas, and dead-end passages (Fig. 6). Another common feature are bell holes, vertical cylindrical holes in ceilings that can be meters high and up to a meter wide (Fig. 3c). Their origin has been ascribed to three main options: condensation corrosion, bat activity, and convective phreatic flow. The debate has been significant, and the entire topic is discussed in Birmingham et al. (2010). We support the convective phreatic flow hypothesis and consider bell holes diagnostic indicators of a diffuse flow regime that would not shear vertical convection cells in phreatic water (Mylroie and Mylroie 2009b).

2.2 Banana Holes

Abundant, but smaller caves called *banana holes* (Fig. 9) were originally hypothesized to have developed by mixing dissolution at the top of the lens, away from the lens margin (Harris et al. 1995). In the Bahamas, banana holes commonly develop in the broad, low-elevation regions that make up significant parts of these islands. As a result, their roofs are prone to collapse, and they are common surface features. Once collapsed, they collect soil and vegetative debris, as well as water, and are favored for the growing of specialty crops, such as bananas, which is how their name, *banana hole*, was derived (Harris et al. 1995). The model proposed by Harris et al. (1995) attempted to explain how numerous shallow dissolution voids could develop over wide areas (up to 3000/km^2), as a result of vadose and phreatic mixing at the top of the freshwater lens. Concerns about CO_2

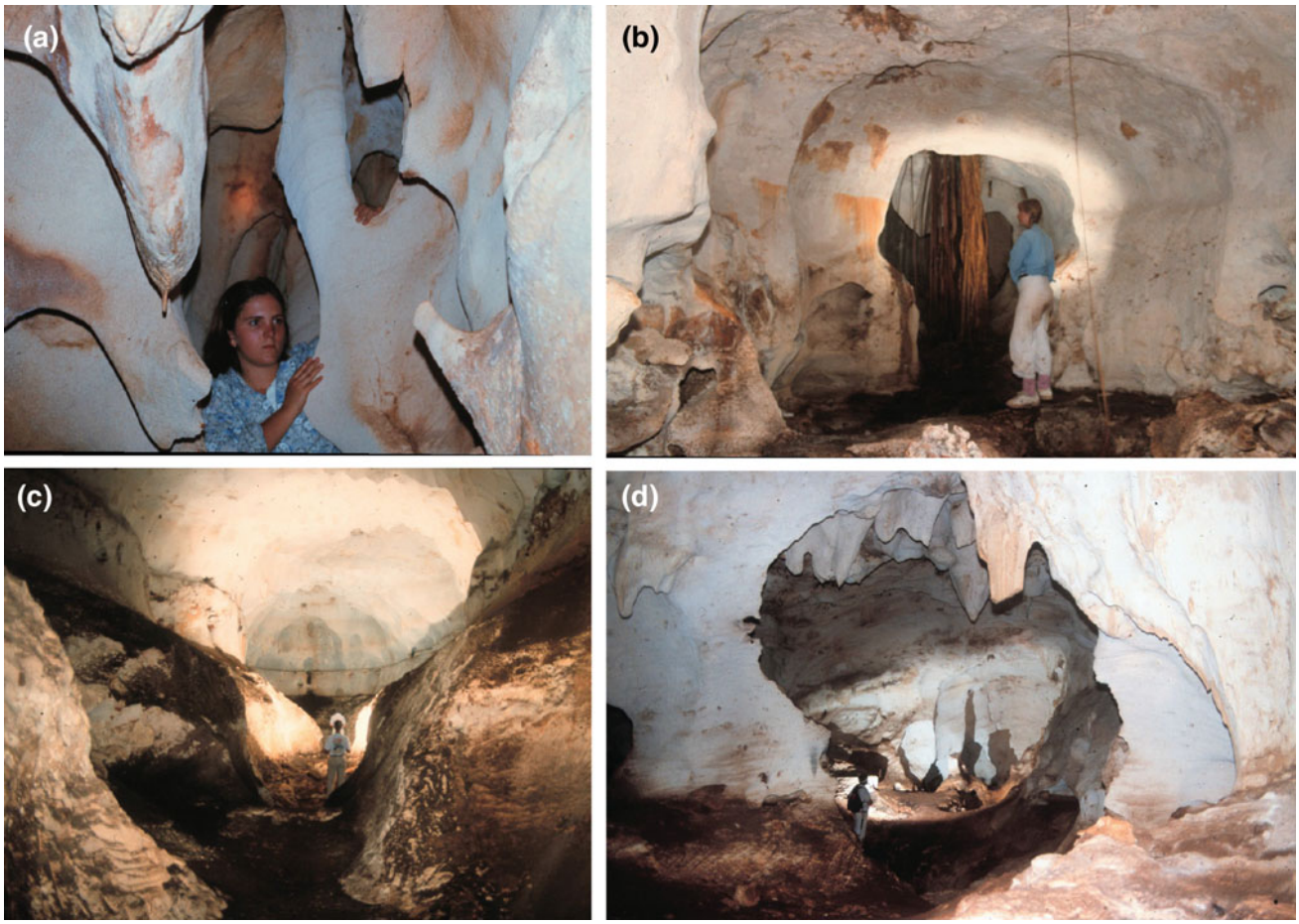

Fig. 6 Flank margin cave phreatic morphologies from the Bahamas. **a** Dissolutional sculpture cutting dipping eolianite beds, Lighthouse Cave, San Salvador. **b** Cuspate passage formed by linking globular chambers, Harry Oakes Cave, New Providence. **c** Large phreatic tube ending in a blank bedrock wall, Salt Pond Cave, Long Island. *The blank wall* indicates the position of the mixing front when sea level fell and the cave was abandoned by the freshwater lens. **d** Large chamber, Hamilton's Cave, Long Island. The cave formed during the last interglacial (MIS 5e), a time span of 9000 years

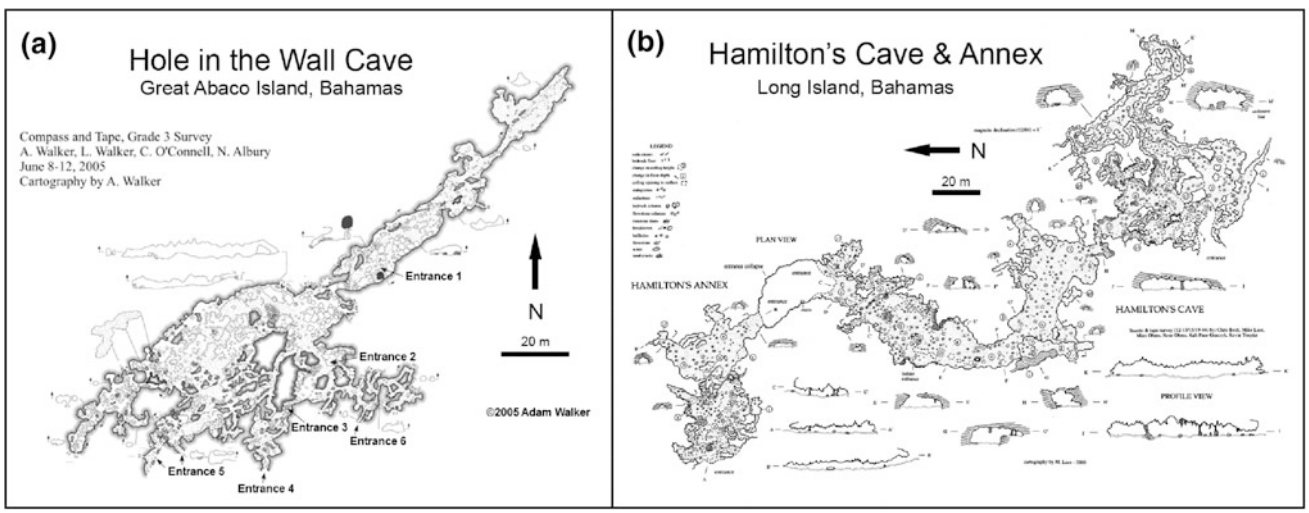

Fig. 7 Maps of large-size Bahamian caves. **a** Hole in the Wall Cave, Abaco. The lens margin was to the *bottom right* of the image. **b** Hamilton's Cave, Long Island. North is to the *left*, and the lens margin was to the *bottom* and *bottom right* of the image

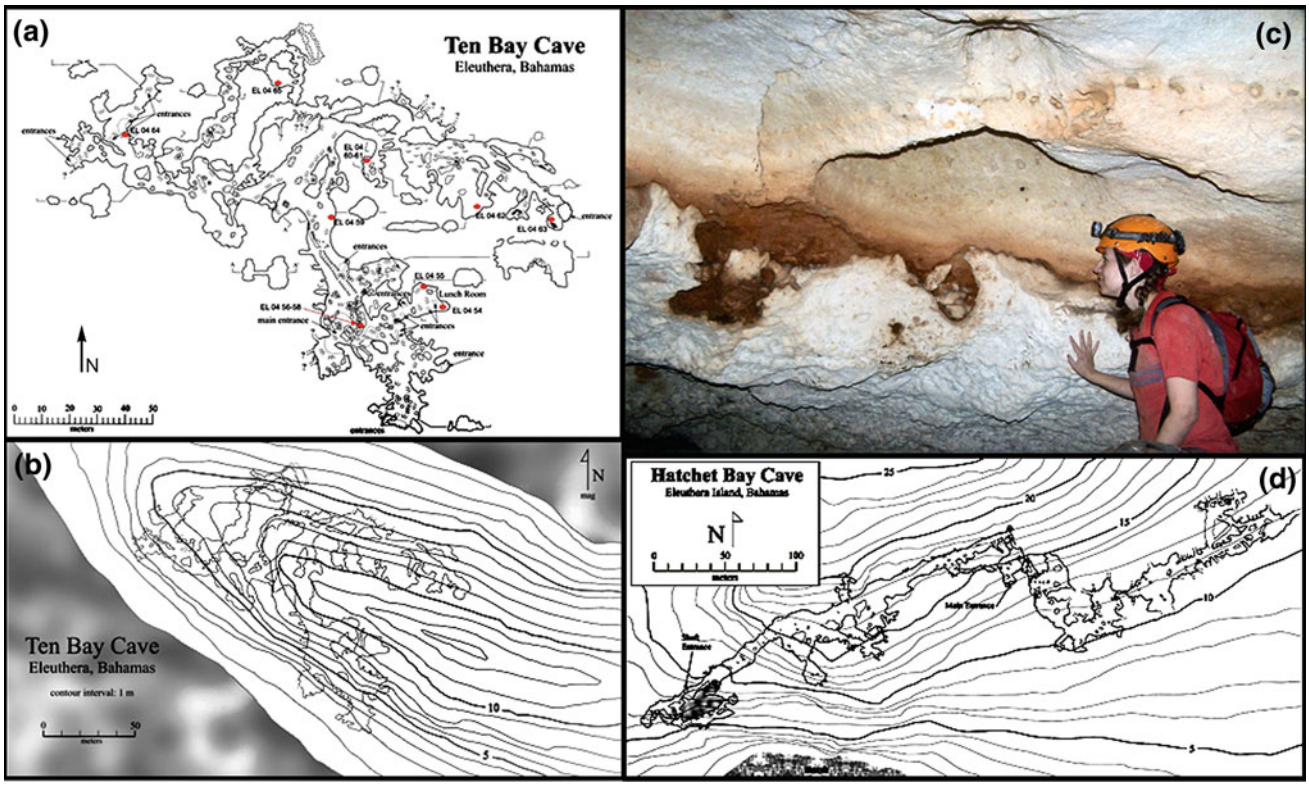

Fig. 8 Maps of large-size Bahamian caves with special circumstances. **a** Map of Ten Bay Cave, which appears to not have the preferred linear orientation typical of large Bahamian caves. **b** Topographic overlay for Ten Bay Cave, demonstrating that the cave wraps around the terminus, or "nose" of the dune, and is linear on each side. This type of flank margin cave is unofficially called a "nose cave." **c** Paleosol between two separate eolianites along the north side of Hatchet Bay Cave. **d** Map of Hatchet Bay Cave, the linear nature of the *left* (west) part of the cave is the result of the paleosol retarding cave development to the north; note all major side passages are to the south

degassing at the top of the lens called this model into question. Further work in a number of Bahamian Islands (Mylroie et al. 2015b) demonstrated that banana holes were always found in fossil prograding strandplains from the last interglacial (MIS 5e), in that the facies at the dry base of the banana holes were subtidal, commonly displaying herringbone crossbedding (Fig. 9d), which graded upward into beach and then back-beach facies, as seen in Holocene strandplains today. Strandplains form by excess sediment accumulation leading to infilling of the shallow subtidal environment. In the Bahamas, carbonate sediment progrades across shallow lagoons (Fig. 10a). This process is episodic, producing a series of low coast-parallel beach ridges. The freshwater lens follows the land as it progrades seaward; after each depositional episode, the freshwater lens, and its speleogenetic margin, advances seaward. This process creates a series of small flank margin caves, with each band of caves abandoned as the strandplain progrades, and the lens margin follows (Fig. 10b). Banana holes are an excellent example of syndepositional caves, as each cave forms while carbonate deposition is still occurring slightly seaward of the cave's position at that time. The strandplain environment means that these caves will have thin roofs, prone to collapse. These observations indicate that flank margin cave formation is extremely rapid, in the order of hundreds to a few thousand years time.

2.3 The Carbonate Island Karst Model

The Bahamas were the starting point for the development of what has become the Carbonate Island Karst Model (Jenson et al. 2006; Mylroie and Mylroie 2007; Mylroie 2013) or CIKM. The salient points of this model are shown in Table 1. The key aspects are that cave and karst development in carbonate islands is very different from that found in carbonate rocks of continental interiors, where most karst research has been done. Basically, karst development under the CIKM is controlled by the youthful age of the rock involved (almost always Cenozoic, commonly Quaternary), the dissolutional aggressivity provided by mixing of freshwater and seawater, and the change in sea level created by glacioeustasy and tectonics. Island configuration, especially as regards carbonate and non-carbonate rocks, is also crucial. This last item has little meaning in the Bahamian Archipelago, as these islands are 100% carbonates. "Island karst"

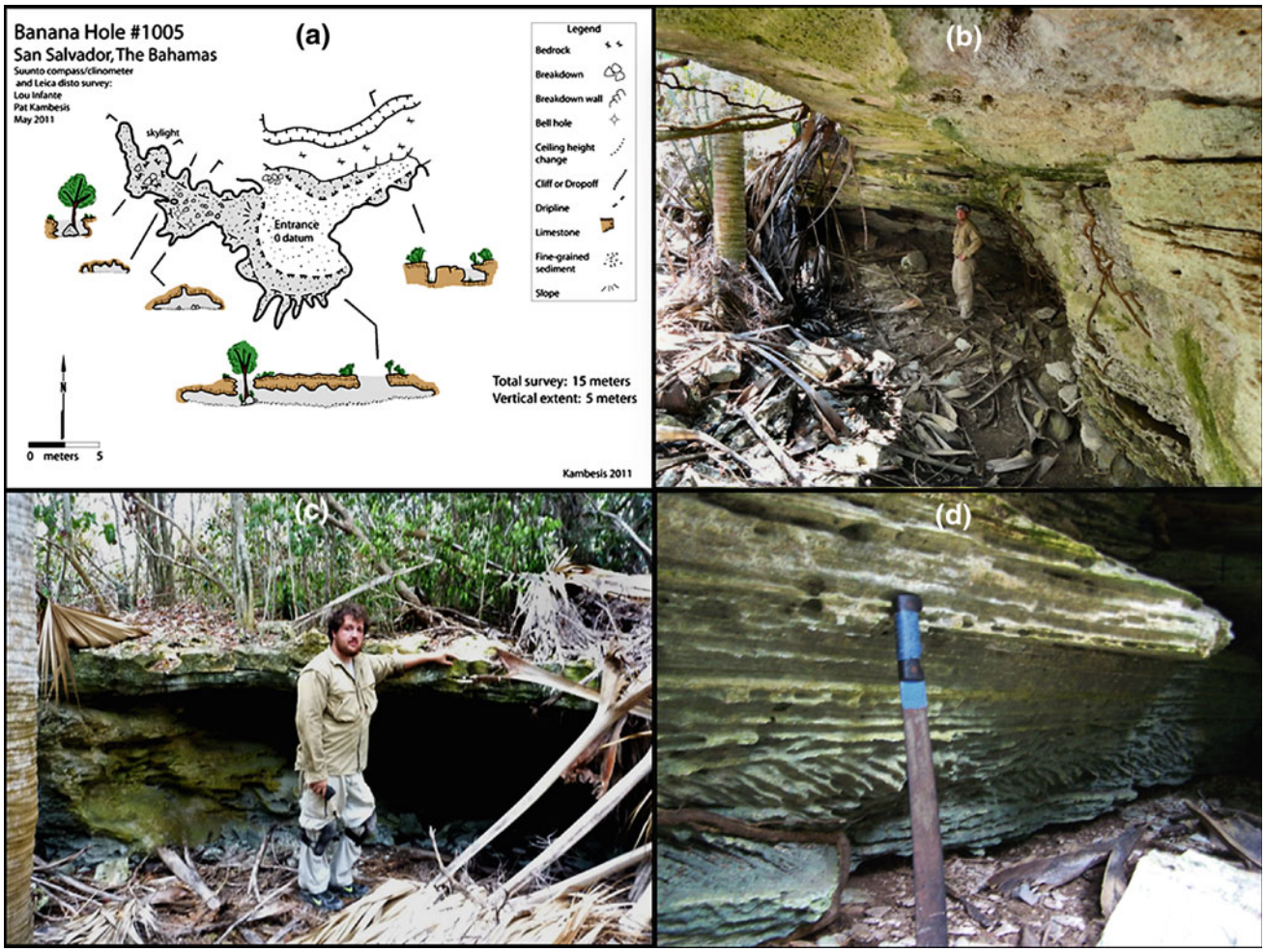

Fig. 9 Bahamian banana holes. **a** Map of a typical Bahamian banana hole, showing both roofed and unroofed sections. **b** Uncollapsed portion of a banana hole, demonstrating large size, and tree growth in the collapsed portion. **c** Partially collapsed banana hole, demonstrating the thin roof which makes the void roofs prone to failure by collapse. **d** Herringbone crossbedding in a banana hole wall, indicating development in subtidal facies

has been defined as that which forms under the constraints of the CIKM, whereas karst that develops in the interior of islands, removed from CIKM controls, is "karst on islands" (Vacher and Mylroie 2002). For example, the caves and karst found in the Bahamas is island karst, but the cockpit karst of Jamaica, or the Mogote karst of Cuba and Puerto Rico, is karst on islands, as it is isolated from coastal conditions and differs little from what would be found in a tropical, continental interior karst.

3 Are Flank Margin Caves Hypogene Caves?

The debate regarding flank margin caves and hypogene origin has two issues. First, are flank margin caves truly isolated from surface conditions? Second, are ascending waters (*per ascensum*) truly involved with flank margin cave genesis? The answer to both questions may hinge on the matter of scale. Flank margin caves, especially in the Bahamas, formed only a few meters to tens of meters below the land surface. Is this distance sufficient to indicate separation of the cave genesis from surface influences? Flank margin cave genesis occurs in the freshwater lens, which is the result of integration of diffuse flow recharge from the land surface to the lens. That recharge can take months to reach the lens (Jocson et al. 2002), and the freshwater lens shows no spikes (sudden changes) associated with specific recharge events, as epigene caves do. The fact that the lens is a product of surface recharge is of no importance, as all water involved in hypogene cave development initially has a surface origin (unless magmatic juvenile water, and even some of that water may have been ocean water subducted down a trench). Even connate water in sediments was originally derived from ocean water, which itself mixes

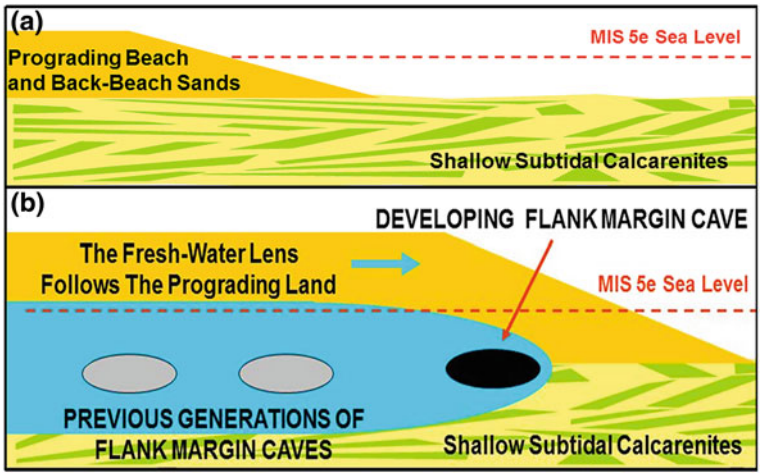

Fig. 10 Diagram displaying banana hole formation in a prograding strandplain. **a** Initial condition during the last interglacial (MIS 5e), with subtidal facies in a lagoon, and a prograding beach. **b** The beach continues to prograde, creating a strandplain, and the freshwater lens follows. Flank margin cave development occurs, but as the strandplain grows episodically, flank margin cave development is initiated, then abandoned as the lens moves seaward and new flank margin caves initiate

Table 1 Components of the Carbonate Island Karst Model, or CIKM (Jenson et al. 2006)

Carbonate Island Karst Model	
Common attributes that distinguish island karst from karst of interior settings	Distinct geomorphic types that distinguish carbonate islands from one another
The karst is eogenetic	Simple Carbonate Island: Non-carbonate rocks remain below the zone of freshwater influence, and recharge is exclusively autogenic (Fig. 1)
Dissolution is enhanced at the surface, bottom, and margin of the freshwater lens by mixing of waters and trapping of organic materials at these boundaries	Carbonate Cover Islands: Non-carbonate basement rocks deflect percolating water and partition the freshwater lens (Fig. 1)
Glacioeustatic sea-level fluctuations impose dissolutional and diagenetic imprints reflecting the vertical migration of the lens	Composite Islands: Non-carbonate basement exposed at the surface, and allogenic recharge is delivered to insurgences on the contacts
Tectonic uplift and subsidence overprint the glacioeustatic imprints with additional dissolutional and diagenetic imprints as well as structural modifications	Complex Islands: Interfingering of carbonate/non-carbonate facies and faulting combine to produce complex aquifer features (Fig. 1)

entirely every 1600 years (Garrison 2013). The Guadalupe Mountains caves of New Mexico require a water table in contact with an oxygen-rich vadose zone to oxidize H_2S–HSO_4 (Palmer 2007, Fig. 8.55). That shallow water table has as much dependence on surface conditions as the freshwater lens of an island. In continental conditions, significant water age seems to be the unstated assumption, when in reality all that matters is that the water body, in this case a freshwater lens, is unresponsive to transitory surface conditions, such as meteoric events, and the CO_2 level of that vadose water.

The second issue in the Bahamian example is the ascending water (*per ascensum*) requirement. The flow dynamics of the freshwater lens, from the interior to the coast, creates a drag on the underlying marine water, such that marine flow is dragged seaward and upward to the lens margin (Fig. 2). The mixing of marine and freshwater is thought to be the single largest driver of dissolution in flank margin cave genesis; that dissolutional potential is produced at the lens base and margin, meeting the requirement that the dissolution potential be produced at depth separately from surface CO_2 sources and ascends to the site of dissolution and speleogenesis.

Organic loading, to create anoxic conditions, was presented earlier as a driver of dissolution to help produce flank margin caves. That organic material comes from surface sources, and it could be argued to violate the isolation of the freshwater lens necessary to meet the hypogene cave definition. Again, the difference between H_2S derived from a deep oil reservoir and organic carbon reaching the freshwater lens by diffuse recharge is only a matter of scale in time and space. Most petroleum found in reservoirs originated in a shallow marine environment where the organics were first created by photosynthesis and subsequent food chain

modification. The fact that anoxic conditions can exist at the top and bottom of a freshwater lens argues for isolation from the oxygenated conditions of the earth's surface.

The scale issue involves both time and distance. Most hypogene caves in continental settings are modeled as having formed over a long period of time from water with a substantial residence time and at some significant depth beneath the earth's surface. Flank margin caves have formed at shallow depths in rapid amounts of time. Are the deep and old water assumptions the actual issue? It is clear from examining continental hypogene and coastal flank margin caves that they both originated in a slow-flow regime. Water input and output from these cave systems was by diffuse, and not conduit, flow. They have the very similar dissolutional morphologies and speleogens (Mylroie and Mylroie 2009c; Klimchouk 2014). Simply put, *hypogene caves result from slow diffuse flow decoupled from surface hydrology*. Decoupled does not mean isolated, which means in this case that the diffuse, slow-flow regime that produces hypogene caves creates a buffer between surface hydrology and surface geochemistry, which allows the subsurface flow regime and geochemistry to dominate and express itself. Hypogene caves are part of the surface hydrologic cycle. Without flow eventually back to the surface, reactants and products could not continue to move in the flow system. The mere word *flow* implies both a source and a destination. That flow is decoupled, but not truly isolated, from surface conditions.

Flank margin caves have been problematical because while they are produced by diffuse flow, isolated from surface conditions, they are shallow and do not require ascent of water from great depths. The relatively short diffuse flow pathway of the freshwater lens, and the very high dissolutional potential produced by fresh and marine water mixing, allows these caves to form very rapidly, perhaps the most rapid development known for caves in carbonate rocks. The longer time window for continental hypogene cave development reflects the longer diffuse flow paths involved and the more limited rate at which dissolution can occur.

4 Summary

The Bahamas are a 100% carbonate environment. These carbonates are eogenetic—youthful, diagenetically immature, with high primary porosity. They do not behave like limestones from continental interiors. The groundwater environment is dominated by the freshwater lens. As a result, cave and karst development proceeds differently than that experienced by most cavers and cave scientists, to produce flank margin caves. The Carbonate Island Karst Model, or CIKM, takes into account these factors, as well as the control of sea level, and hence the freshwater lens, by glacioeustasy and tectonics. The Bahamas are the simplest possible aspect of the CIKM. There are no tectonic influences and no non-carbonate rock to produce allogenic recharge or to partition the lens. Despite these simplifications, and the short time intervals of sea-level highstands in which speleogenetic processes could act, the Bahamas have a wide variety of caves of significant complexity. That these caves formed in a 9000-year time window makes them even more impressive.

Flank margin caves are hypogenic, decoupled from surface hydrology, and created by marine water ascending along the freshwater lens base to create voids at the lens margin. Despite the shallow depth at which they form, and the rapid time window in which they form, the key factor is development in a diffuse, slow-flow system with dissolutional potential developed in situ in the freshwater lens, decoupled from surface conditions. Continental hypogenic caves form deeper, and more slowly than flank margin caves, but contain remarkably similar slow-flow speleogens. Whether or not flank margin caves fit the hypogene cave condition is not the critical factor. It is clear that both develop under slow-flow conditions, which by definition require the caves to be decoupled from surface flow conditions. Decoupled does not mean entirely independent, as any flow system, be it turbulent or diffuse, requires water input and output, and in the final analysis, surface conditions play a role in that flow system. The true separation of dissolutional cave types is between coupled, turbulent flow systems, essentially epigenic, and decoupled, diffuse, slow-flow systems, essentially hypogenic.

References

Birmingham AN, Lace MJ, Mylroie JR, Mylroie JE (2010) Bell hole origin: constraints on developmental mechanisms, Crooked Island, Bahamas. In: Martin JB, Siewers FD (eds) Proceedings of 14th symposium on the geology of the Bahamas and other carbonate regions, pp 18–30

Bottrell SH, Smart PL, Whitaker F (1991) Geochemistry and isotope systematics of sulphur in the mixing zone of Bahamian blue holes. Appl Geochem 6:99–103

Bottrell SH, Carew JL, Mylroie JE (1993) Bacterial sulphate reduction in flank margin environments: evidence from sulphur isotopes. In: White B (ed) Proceedings of the 6th symposium on the geology of the Bahamas: Port Charlotte, Florida, Bahamian Field Station, pp 17–21

Carew JL, Mylroie JE (1995a) Quaternary tectonic stability of the Bahamian Archipelago: evidence from fossil coral reefs and flank margin caves. Quatern Sci Rev 14:144–153

Carew JL, Mylroie JE (1995b) A stratigraphic and depositional model for the Bahama Islands. In: Curran HA, White B (eds) Geological Society of America Special Paper 300, Terrestrial and shallow marine geology of the Bahamas and Bermuda

Choquette PW, Pray LC (1970) Geologic nomenclature and classification of porosity in sedimentary carbonates. Am Assoc Pet Geol Bull 54(2):207–250

Curran HA, White B (eds) (1995) Geological Society of America Special Paper 300, Terrestrial and shallow marine geology of the Bahamas and Bermuda

Dublyansky YV (2014) Hypogene speleogenesis—discussion of definitions. In: Klimchouk A, Sasowsky ID, Mylroie JE, Engel SA, Engel AS (eds) Hypogene karst morphologies, Karst Waters Institute Special Publication, vol 18. pp 1–3

Frank EF, Mylroie J, Troester J, Alexander EC, Carew JL (1998) Karst development and speleogenesis, Isla de Mona, Puerto Rico. J Cave Karst Stud 60(20):73–83

Garrison T (2013) Oceanography, an invitation to marine science. Brooks/Cole, Belmont

Harris JG, Mylroie JE, Carew JL (1995) Banana holes: unique karst features of the Bahamas. Carbonates Evaporites 10(2):215–224

Jenson JW, Keel TM, Mylroie JR, Mylroie JE, Stafford KW, Taborosi D, Wexel C (2006) Karst of the Mariana Islands: the interaction of tectonics, glacioeustasy and fresh-water/sea-water mixing in island carbonates. Geological Society of America Special Paper 404, pp 129–138

Jocson JMU, Jenson JW, Contractor DN (2002) Recharge and aquifer responses: Northern Guam Lens Aquifer, Guam, Mariana Islands. J Hydrol 260:231–254

Kambesis PN, Mylroie JR, Mylroie JE, Larson EB, Owen-Nagel AM, Sumrall JB (2015) Influence of karst denudation on the Northwest Coast of Curaçao. In: Glumac B, Savarese M (eds) Proceedings of the 16th symposium on the geology of the Bahamas and other carbonate regions, pp 200–212

Kindler P, Mylroie JE, Curran HA, Carew JL, Gamble DW, Rothfus TA, Savarese M, Sealey NE (2010) Geology of Central Eleuthera, Bahamas: a field trip guide. Gerace Research Centre, San Salvador Bahamas

Klimchouk A (2007) Hypogene speleogenesis: hydrogeological and morphogenetic perspective. National Cave and Karst Research Institute Special Paper 1

Klimchouk A (2014) The methodological strength of the hydrological approach to distinguishing hypogene speleogenesis, In: Klimchouk A, Sasowsky ID, Mylroie JE, Engel SA., Engel AS (eds) Hypogene karst morphologies. Karst Waters Institute Special Publication 18, pp 4–12

Klimchouk A, Sasowsky ID, Mylroie JE, Engel SA, Engel AS (2014) Hypogene karst morphologies. Karst Waters Institute Special Publication 18

Labourdette R, Lascu I, Mylroie J, Roth M (2007) Process-like modeling of flank margin caves: from genesis to burial evolution. J Sediment Res 77:965–979

Lace MJ (2008) Coastal cave development in Puerto Rico. J Coastal Res 24:508–518

Machel HG, Sumrall JB, Kambesis PN, Mylroie JR, Mylroie JE, Lace MJ (2011) Multiple cave types in Miocene and Pleistocene carbonates of Barbados, West Indies. In: Engel AS, Engel SA, Moore PJ, Duchene H (eds) Carbonate geochemistry: reactions and processes in aquifers and reservoirs. Special Publication 16, Karst Waters Institute, Leesburg, Virginia, pp 43–46

Meyerhoff AA, Hatten CW (1974) Bahamas salient of North America: tectonic framework, stratigraphy, and petroleum potential. Am Assoc Pet Geol Bull 58:1201–1239

Mylroie JE (2013) Coastal karst development in carbonate rocks. In: Lace MJ, Mylroie JE (eds) Coastal karst landforms. Coastal Research Library 5, Springer, Dordrecht, pp 77–109

Mylroie JE, Carew JL (1990) The flank margin model for dissolution cave development in carbonate platforms. Earth Surf Proc Land 15:413–424

Mylroie JE, Mylroie JR (2007) Development of the carbonate island karst model. J Cave Karst Stud 69:59–75

Mylroie JE, Mylroie JR (2009a) Caves as geologic indicators, Kangaroo Island. Aust J Cave Karst Stud 71(1):32–47

Mylroie JE, Mylroie JR (2009b) Unique dissolutional morphologies in caves: a result of convective flow regimes? In: White WB (ed) Proceedings of 15th international congress of speleology, National Speleological Society, Huntsville, Alabama, vol 2. pp 916–922

Mylroie JE, Mylroie JR (2009c) Diagnostic features of hypogenic karst: is confined flow necessary? In: Stafford KW, Land L, Veni G (eds) Advances in hypogene karst studies: NCKRI symposium 1. National Cave and Karst Research Institute, Carlsbad, New Mexico, pp 12–26

Mylroie JE, Mylroie JR, Nelson CN (2008) Flank margin cave development in telogenetic limestones of New Zealand. Acta Carsologica 37(1):15–40

Mylroie JE, Kambesis PN, Owen-Nagel AM, Sumrall JB, Larson EB, Mylroie JR, Lace MJ (2015a) Flank margin cave development at Cala Pi and Cala Figuera, Mallorca Island, Spain. In: Glumac B, Savarese M (eds) Proceedings of 16th symposium on the geology of the Bahamas and other carbonate regions, pp 213–221

Mylroie JE, Ho HC, Infante LR, Kambesis PK, Leist JW (2015b) Banana holes as syndepositional flank margin caves within an advancing strandplain and their prediction using fuzzy-based modeling. In: Glumac B, Savarese M (eds) Proceedings of 16th symposium on the geology of the Bahamas and other carbonate regions, pp 222–236

Otonicar B, Buzijak N, Mylroie JE, Mylroie JR (2010) Flank margin cave development in carbonate talus breccia facies: an example from Cres Island Croatia. Acta Carsologica 39(1):79–91

Palmer AN (1991) Origin and morphology of limestone caves. Geol Soc Am Bull 103:1–21

Palmer AN (2000) Hydrogeologic control of cave patterns. In: Klimchouk AB, Ford DC, Palmer AN, Dreybrodt W (eds) Speleogenesis: evolution of karst aquifers. National Speleological Society, Huntsville, pp 77–90

Palmer AN (2007) Cave geology. Cave Books, Dayton

Roth MJ (2004) Inventory and geometric analysis of flank margin caves of the Bahamas. M.Sc. thesis, Mississippi State University

Uchupi E, Milliman JD, Luyendyk BP, Brown CO, Emery KO (1971) Structure and origin of the Southeastern Bahamas. Am Assoc Pet Geol Bull 55:687–704

Vacher HL, Quinn TM (eds) (1997) Geology and hydrogeology of carbonate islands, Elsevier Science Publishers

Vacher HL, Mylroie JE (2002) Eogenetic karst from the perspective of an equivalent porous medium. Carbonates Evaporites 17(2):182–196

Wood WW, Petraitis MJ (1984) Origin and distribution of carbon dioxide in the unsaturated zone of the Southern High Plains. Water Resour Res 20:1193–1208

Worthington S, Ford DC (1995) High sulfate concentrations in springs: an important factor in conduit initiation? Environ Geol 25:9–15

Sistema Zacatón: Volcanically Controlled Hypogenic Karst, Tamaulipas, Mexico

52

Marcus Gary

Abstract

Sistema Zacatón includes the second deepest underwater cave in the world. It is hypothesized to have formed by volcanogenic karstification, a process that relies on four components to initiate and develop deep subsurface voids: a carbonate matrix, a system of preferential flow paths (e.g., fractures), volcanic activity that increases groundwater acidity, and groundwater flux through the system. Results are compiled into a multiphase speleogenetic model, most phases of which are of Late Pleistocene age. Surface rocks consist of carbonate travertine with Pleistocene mammoth fossils found within the rock matrix. The rocks are interpreted as a hydrothermal travertine terrace formed as nearby volcanic activity peaked, and thus representing the end member of a carbonate mass transfer system originating deep in the subsurface. The modern karst system includes a dynamic array of deep, phreatic sinkholes (also called cenotes) propagated upward through the travertine and exposing hydrothermal water supersaturated with carbon dioxide to the atmosphere. In some cenotes, seals of a second stage of travertine formed as CO_2 degassed, capping the sinkholes with hydrologic barriers. Volcanogenic karstification worldwide is not limited to Sistema Zacatón, although the localized nature, coupled with the extreme degree of karstification, makes it an ideal modern analog for classifying certain other karst systems as volcanogenic.

Keywords

Volcanic hypokarst • Cenotes • Travertine • Geophysical mapping • Robotic surveying

1 Introduction

This chapter documents a unique category of hypogene karst that results from a combination of geological factors, including volcanism. It focuses on the karst area of Sistema Zacatón in northeastern Mexico (Fig. 1) and includes several extremely deep water-filled mega-sinkholes. El Zacatón, the primary feature, is the largest cenote (phreatic sinkhole) in the system and may be the deepest such feature on earth (Gary et al. 2003). Prior to this study, no previous scientific studies had documented the geology, hydrology, biology, or other environmental details of this karst system.

2 Site Description

This research is based on underwater cave exploration during the late 1980s and 1990s that revealed many unique characteristics of the area, including the extreme depth of El Zacatón (Kristovich 1994). The influence of volcanic activity is inferred from several observations. Thick Cretaceous carbonates were uplifted and fractured during Late Laramide deformation (80–55 Ma; English and Johnson 2004), and later igneous events (Pliocene intrusive and Pleistocene extrusive activity) dramatically altered the local

M. Gary (✉)
Edwards Aquifer Authority, 900 E. Quincy,
San Antonio, TX 78215, USA
e-mail: mgary@edwardsaquifer.org

© Springer International Publishing AG 2017
A. Klimchouk et al. (eds.), *Hypogene Karst Regions and Caves of the World*,
Cave and Karst Systems of the World, DOI 10.1007/978-3-319-53348-3_52

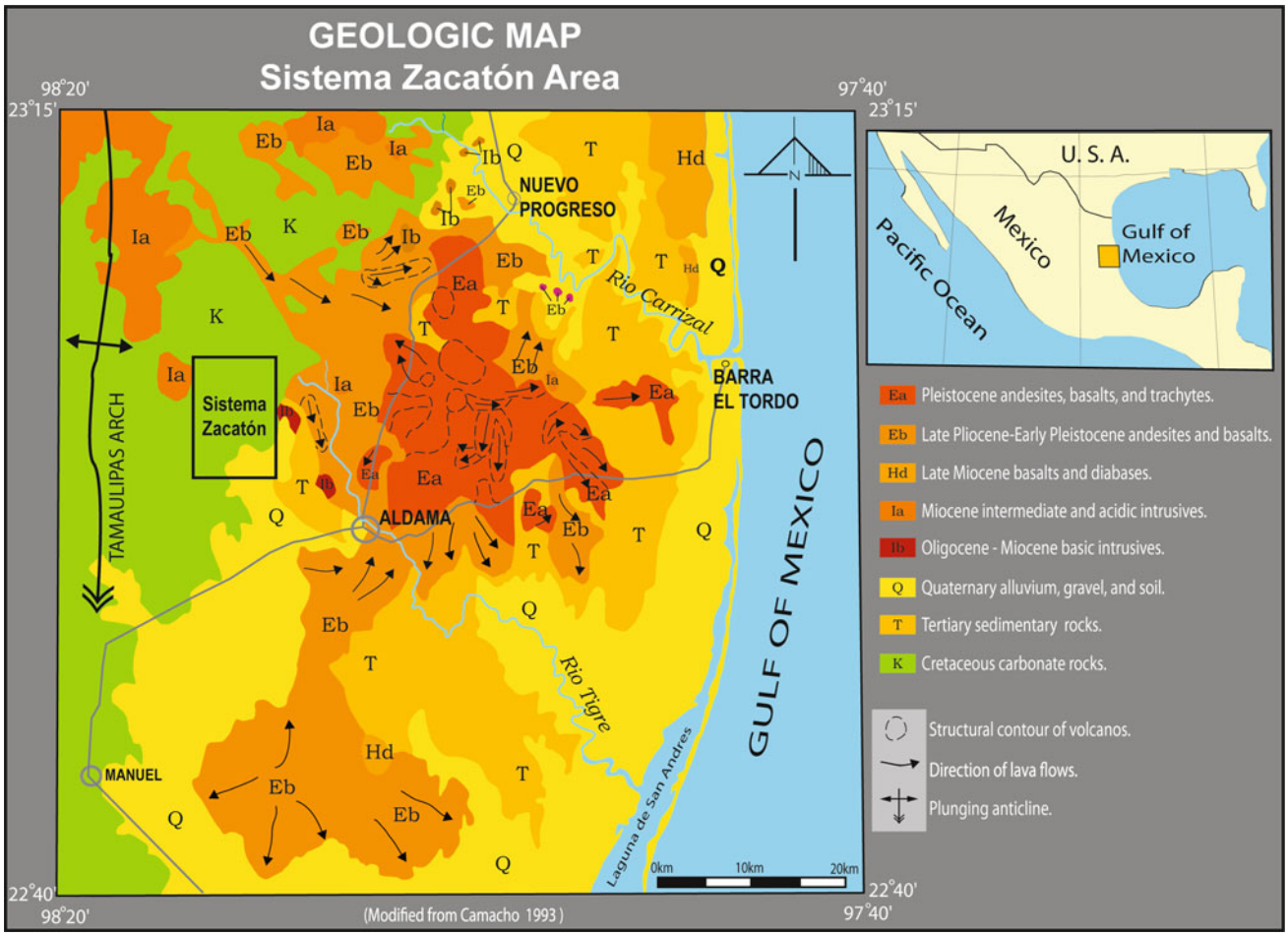

Fig. 1 Map of the Sistema Zacatón karst area, showing its proximity to Cretaceous limestone, Oligocene-Miocene intrusive rocks, and Pliocene-Pleistocene extrusive volcanic rocks

landscape (Camacho 1993; Ramirez Fernandez et al. 2007). The hypothesis is also supported by water chemistry and isotopic data, and travertine terrace deposits typical of thermal springs. Sistema Zacatón includes a variety of karst features (Fig. 2): ramiform vadose cave passages (>2 km surveyed to date), deep phreatic shafts, horizontal phreatic conduits, collapse dolines, broad overland travertine deposits, travertine-capped sinkholes, relict spring travertine, and many minor karst features throughout (e.g., rillenkarren).

3 Geologic Setting

Major karst features in northeastern Mexico are located in Cretaceous carbonate rocks containing a wide variety of carbonate facies (Fig. 1). Lower Cretaceous rocks in the region form a thick accumulation (>2000 m) of forereef, reef margin, and backreef deposits (Goldhammer 1999). These units include the El Abra and Tamabra formations, which extend from the eastern edge of the Sierra Madre Oriental near Ciudad Valles (including the Sierra de El Abra) to areas 200 km west. No significant reef deposits have been identified in this region (Goldhammer 1999; Camacho 1993; Enos 1983; Enos and Stephens 1993). Upper Cretaceous deposits dominated by argillaceous limestone and shales cover much of northeastern Mexico (Camacho 1993).

By the end of the Cretaceous, an advancing Laramide fold and thrust belt from the southwest caused major uplift and exhumation of younger more easily eroded strata. Large thrust faults, overturned folds, and normal faults typify the Sierra Madre Oriental, as thin-skinned deformation shaped the landscape (Suter 1987). The Sierra de Tamaulipas is the expression of the Tamaulipas Arch, a 200-km-long domal anticline in the Gulf of Mexico coastal plain east of the fold and thrust belt of the Sierra Madre Oriental (Fig. 1). The Sierra de Tamaulipas resulted from basement-involved deformation and is structurally separate from the larger mountains of the Sierra Madre Oriental 100 km to the west. Major uplift ceased in both the Sierra Madre Oriental and Sierra de Tamaulipas by mid-Eocene, and in many places,

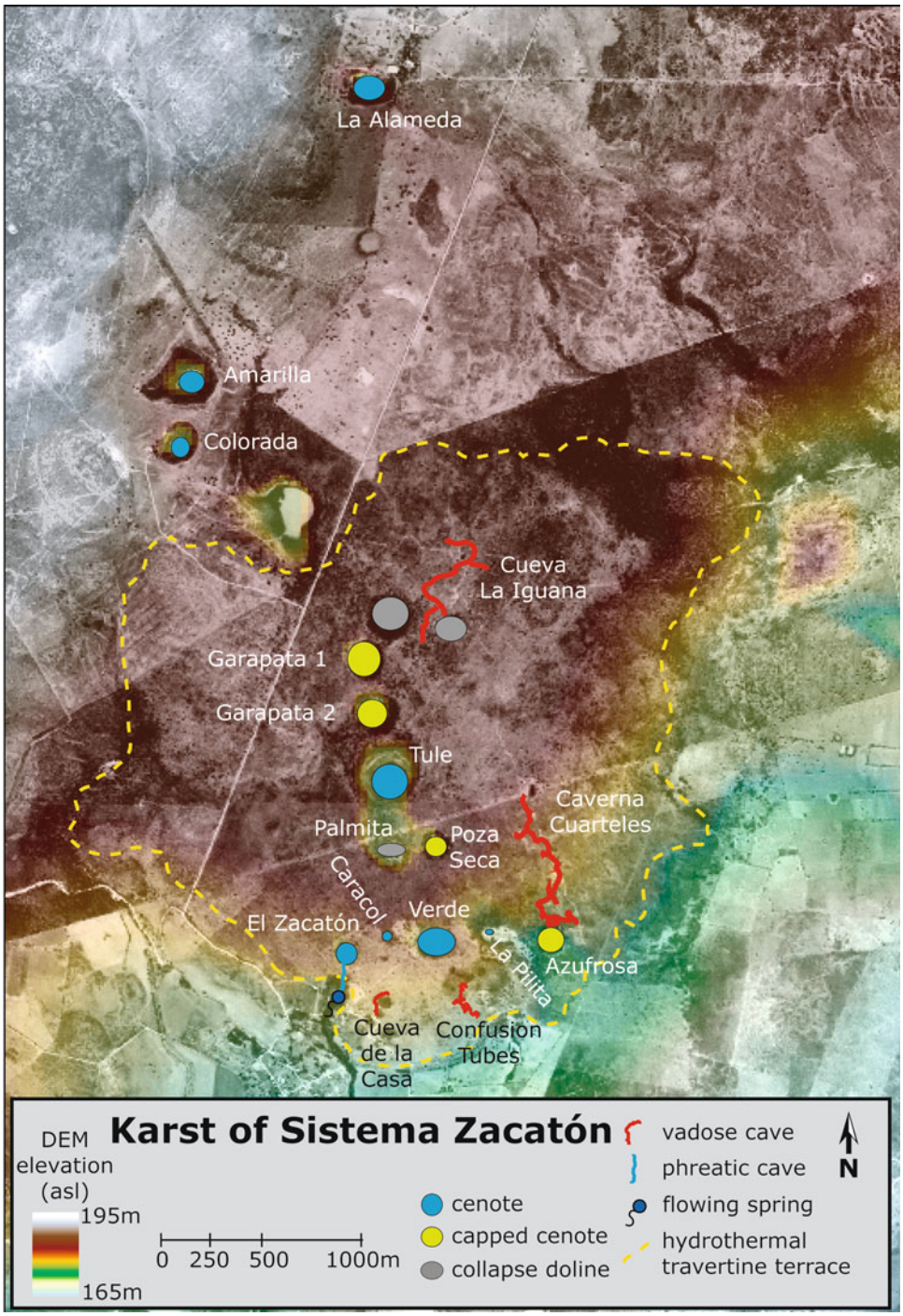

Fig. 2 Site map of Sistema Zacatón showing the diverse nature of karst features and Pleistocene hydrothermal travertine

lower Cretaceous carbonates have since been above sea level (Ford 2000).

Tertiary igneous activity had a significant impact on the regional geomorphology. Intrusive rocks of Oligocene through Pliocene age intruded into parts of the Sierra de Tamaulipas, causing basaltic lava to erupt along frontal sections of the Sierra Madre Oriental. The most recent and largest area of extrusive rocks is located along the southeastern flanks of the Sierra de Tamaulipas. This is the Villa Aldama volcanic complex, which consists of Pliocene-Pleistocene lava flows and shield volcanoes. Its most recent igneous rocks are dated at 250 ka (Camacho 1993; Vasconcelos and Ramírez Fernández 2004). Sistema Zacatón is located 5 km from these rocks (Fig. 1), and hydrothermal activity associated with Sistema Zacatón is inferred to have resulted from this magmatic activity.

3.1 Structural Trends

The most striking expressions of Sistema Zacatón are the large circular sinkholes (cenotes) that dominate the study area (Fig. 3). El Zacatón is the deepest of the sinkholes. The primary trend of the cenotes is roughly linear, north–south, which coincides with the trend of observed fractures. This trend parallels the axis of the Sierra de Tamaulipas anticline (Fig. 1) and implies structural control of speleogenesis related to Laramide uplift. A secondary east–west fracture trend is evident in the southern cenotes. Superficially, all the cenotes appear similar; but substantial variations in water chemistry, rock type, and aqueous biological habitats indicate significant differences. Their wide distribution raises questions about the subsurface conduit system(s) that connect or isolate each cenote, and which provide the basis for hypotheses of travertine deposition.

3.2 Travertine Deposition

Hydrothermal karst systems contain distinct types of calcite precipitates that provide insight regarding hydrogeologic conditions that prevailed during mineral formation (Dublyansky 2000a). There are several types of precipitated calcite in the study area: (1) hydrothermal hot spring travertine mound (Azufrosa Formation); (2) thick travertine lids that formed along water table boundary zones in open sinkholes; (3) subaqueous "dogtooth spar" in some of the anoxic water; (4) broad overland travertine flows; (5) subaerial speleothems in dry caves (Fig. 4); and (6) Paleo-spring travertine crusts. The varied travertine morphologies can be used to interpret the evolution of the system.

4 Microbial Biomats

Observations from years of exploratory diving at Sistema Zacatón have identified unique biological coatings in three of the cenotes: El Zacatón, Caracól, and La Pilita (Gary et al. 2003; Gary 2004; Sahl et al. 2011). These biomats are thin purple–red blankets with some white filamentous areas (Fig. 5). They are commonly underlain by solid $CaCO_3$ (limestone or travertine) that is expressed as either spar calcite fingers or unconsolidated $CaCO_3$ soup as much as 1 m deep. Biomats in Caracol and El Zacatón have a white powdery coating inferred to be elemental sulfur produced by bacteria in the mats. The biomats in these three cenotes have thin cohesive membranes, and in places gas bubbles collect beneath the biomats. The microbial communities in these cenotes change with increasing depth. Shallow communities are typically green (algae and bacteria), and purple biomats are present at depths of approximately 3 m. Below the photic zone ($>\sim 100$ m depth) or within dark phreatic tunnels, the walls are devoid of the thick mats, indicating that these are phototrophic communities. The bacteria on the walls of the cenotes may be a type of autotrophic, photosynthetic purple bacteria (Gary 2004). Microbial communities of Sistema Zacatón are complex and diverse and may be similar to those developed in such settings as the Yellowstone hydrothermal spring system of Wyoming (Barger 1978; Fouke et al. 2000).

5 Mapping and Geologic Interpretation

Underwater exploration at Sistema Zacatón reached human limits when Jim Bowden descended to a depth of 289 m on April 6, 1994 (Gilliam 1995). Unmanned robotic exploration is required to document the immense geometry of the underwater caves. The DEPTHX (DEep Phreatic THermal eXplorer) vehicle was developed with support from NASA to approach this problem, with the additional impetus of developing robotic means for space exploration. During the winter and spring of 2007, DEPTHX conducted three-dimensional (3-D) underwater mapping missions of four cenotes in Sistema Zacatón: El Zacatón, Caracol, Poza Verde, and La Pilita (Gary et al. 2008). The detailed maps discovered no lateral tunnels connecting the cenotes, which are only 100–200 m apart. The deepest cenote, El Zacatón, was explored to a depth of 319 m (339 m including the above water cliff), making it the deepest underwater vertical shaft and second deepest underwater cave in the world (Fig. 6). No side tunnels were discovered. The 3-D data revealed geomorphic features of the cenotes that document how the karst system may have evolved through time. Geochemical data collected during mapping missions indicate that water in the three warmest cenotes is homogeneous, and that the coolest cenote displays chemoclines similar to those in lacustrine settings. Data collected by DEPTHX are used with other geologic information to investigate the specific processes of hypogenic karstification that formed the cave system.

5.1 Geophysical Mapping of Travertine Caps

Sistema Zacatón displays some of the most distinctive travertine morphologies yet documented. Some sinkholes are dry or contain shallow lakes with flat travertine (tufa) floors. Other deeper water-filled sinkholes have flat floors that lack the cone of collapse material commonly observed in these types of shafts. The hypothesis that these floors have large water-filled voids beneath them was tested with electrical resistivity imaging (ERI) to determine the shapes of both open cenotes and travertine-covered sinkholes. Three separate flat travertine caps were imaged with this method:

Fig. 3 Primary cenotes and springs at Sistema Zacatón. The cloudy *white* of El Nacimiento, Él Zacatón, and Azufrosa is from phototrophic sulfur-reducing bacteria synthesizing H_2S to elemental sulfur

Fig. 4 Phreatic and vadose caves of Sistema Zacatón show various types of cave development in the shallow subsurface in the Pleistocene travertine of the Azufrosa Formation. The rock matrix shown in these photos is composed entirely of travertine. No marine limestone is present at this level (Dry Cave photographs by Art Palmer; underwater photogragh by Robin Havens)

(1) La Pilita, which is partially open, exposing the structure of the cap over a deep water-filled shaft; (2) Poza Seca, which is dry and vegetated; and (3) Tule, which contains a shallow (<1 m) lake. A fourth ERI survey was conducted adjacent to the open cenote Verde. At La Pilita, the presence of water-filled void spaces detected by ERI was verified by SCUBA exploration, and new voids are inferred. ERI data at Poza Seca demonstrate a thin (<2 to 4+ m) layer interpreted as the travertine cap underlain by a conductive region (consistent with the resistivity of water) extending at least 25 m below the cap. No lower boundary of the void was evident in the ERI data (Fig. 7, left). ERI measurements at Tule show evidence for a large water-filled void beneath a thin (<2 to 4+ m) cap. A deep, higher resistivity layer indicates a flat lower boundary 45 m deep that may be a second cap, similar to that at Verde. ERI measurements adjacent to Verde hints at a deep water-filled cavity below this 45 m deep layer (Fig. 7, right). These findings support the hypothesis of capped water-filled voids and may have implications for paleo-climate models of the Late Pleistocene. The capped voids may provide habitats for anoxic microbial communities to evolve in isolated isothermal environments.

6 Geochemistry

Hydrogeologic characteristics of karst groundwater systems reflect the integrated result of local speleogenesis. At Sistema Zacatón, the geologic history of the karst includes hydrothermal karstification associated with a local Pleistocene magmatic event. Physical and geochemical

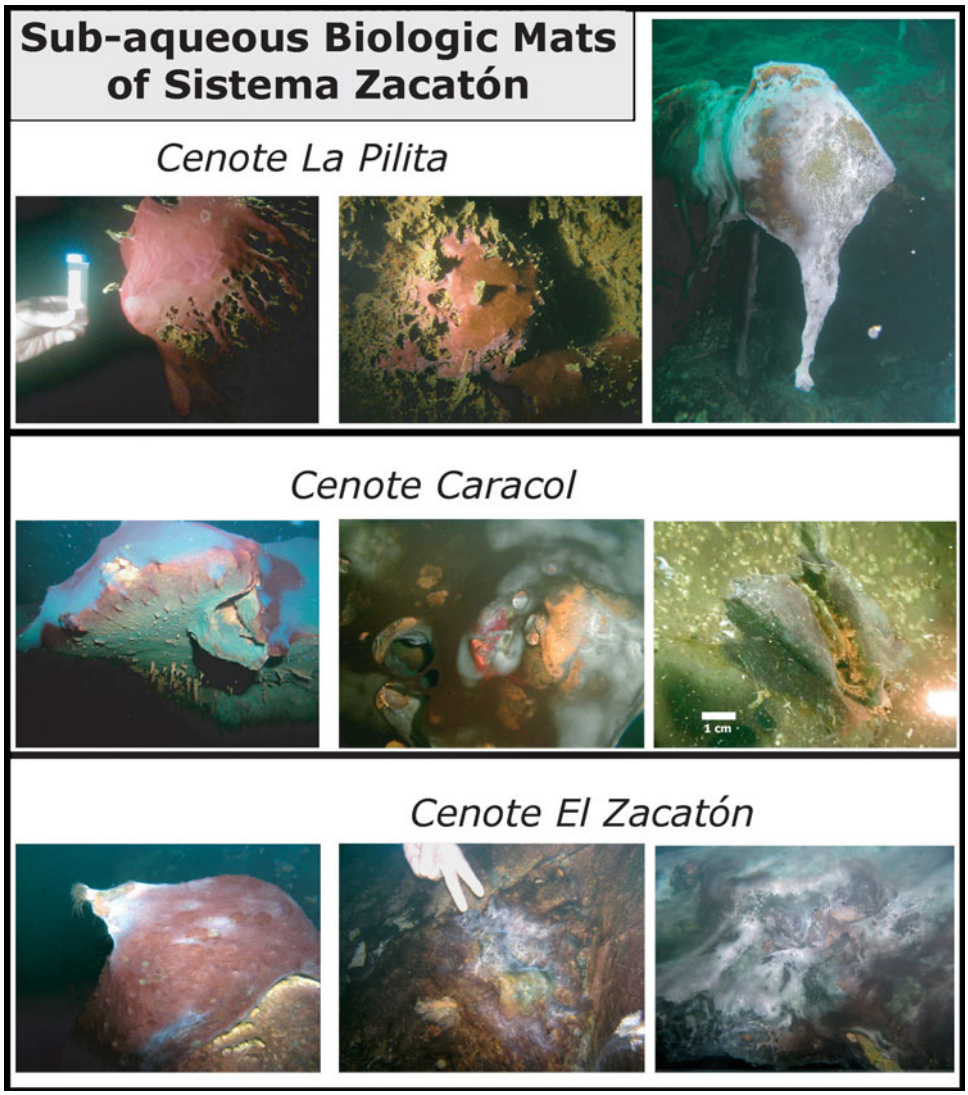

Fig. 5 Subaqueous biomats in Sistema Zacatón are composed of a broad array of bacteria and archaea. These biomats are present only in strongly reducing thermal waters, where oxygen is almost completely absent, and H_2S is detectable in the water

hydrogeologic data were collected at Sistema Zacatón from 2000 to 2007, and include spring discharge, water levels, temperature (spatial and temporal), geochemical profiles, ion geochemistry, stable and radiogenic isotopes, and microbial interactions. These data reveal three major findings: (1) There is some degree of rock–water interaction between the groundwater and the matrix limestone and nearby volcanic rocks. Evidence includes $^{87/86}$Sr isotope ratios (mean 0.707187) lower than those of nearby Cretaceous limestone (0.7073–0.70745), sulfur isotope values in deep water of −1.8‰, and DIC carbon isotopes. (2) Discrete hydrologic barriers developed in response to sinkhole formation, travertine precipitation, and shifts in the local water table, which created relatively isolated water bodies with significant contrasts in water chemistry. These characteristics are seen most clearly in cenote Verde, where there is a steep hydraulic gradient (0.046), as well as seasonal variations in water temperature, thermoclines, chemoclines, and oxic water. The surrounding cenotes of El Zacatón, Caracol, and La Pilita have constant water temperatures both in profile and temporally, similar water levels, and almost completely anoxic conditions. (3) The anoxic, hydrothermal cenotes contain unique microbial communities that are involved in observed sulfur cycles and probably influence mineralization along the cenote walls.

Several types of hydrogeologic data collected at Sistema Zacatón characterize the karst groundwater system. Patterns in physical and chemical hydrogeologic conditions support the hypotheses formulated from the previously described methods, which interpreted the geomorphic expression of

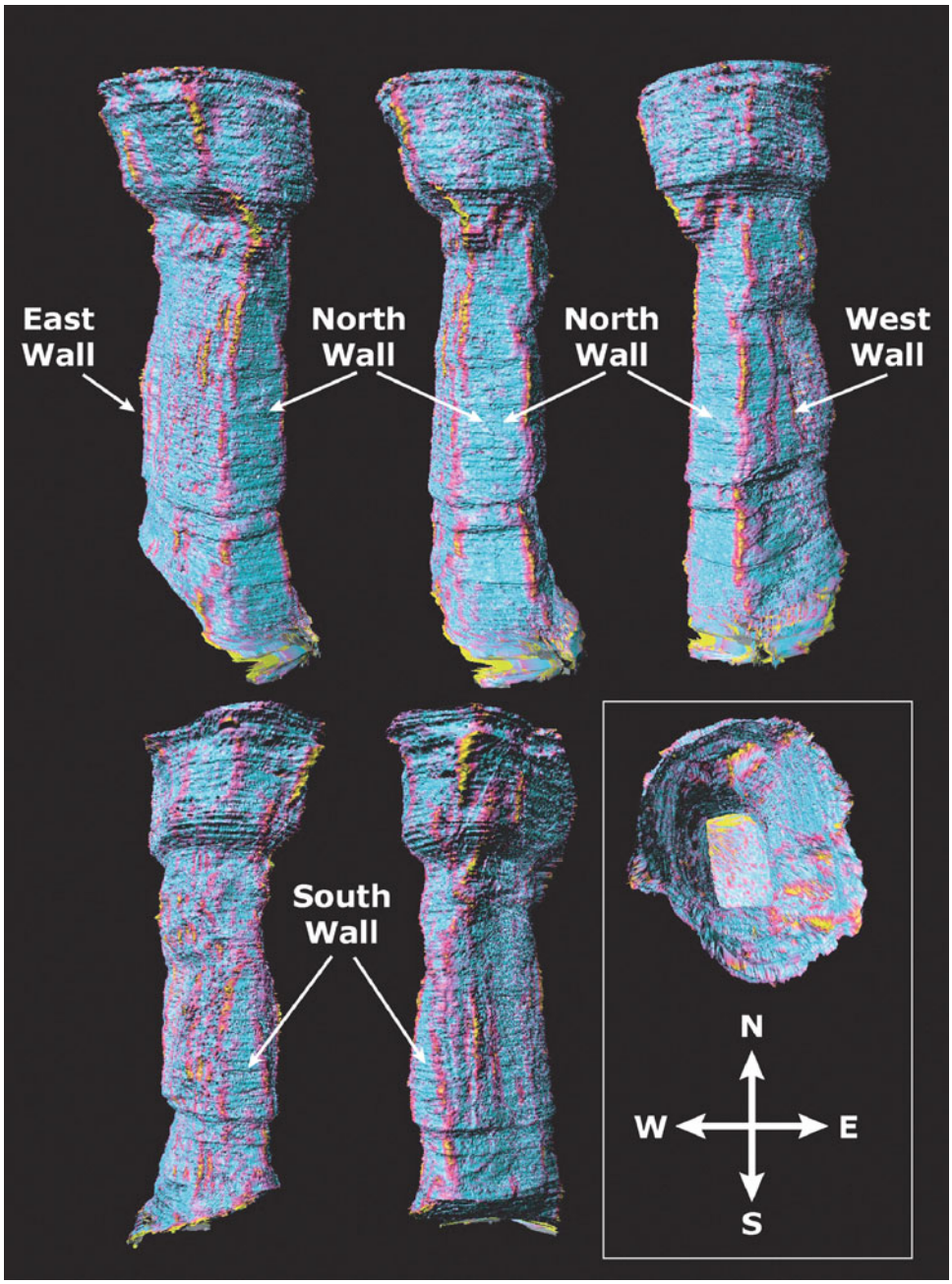

Fig. 6 Three-dimensional underwater model map of the cenote El Zacatón, showing the round surface expression, which changes to an almost perfect *rectangle* below 80 m depth at the contact between Cretaceous limestone and overlying Pleistocene hot spring travertine

features. Discrete hydraulic barriers formed in response to sinkhole development, travertine precipitation, and local water table shifts. The relatively isolated water bodies have significantly different water chemistry, not only because of limited connections to deep groundwater, but also from the evolution of unique sulfur (and likely carbon) metabolizing microbial communities that influence the geochemical conditions and rock–water interaction in non-isolated cenotes. An integrated model of the aqueous geochemical system is shown in Fig. 8, which summarizes many of the local hydrogeologic conditions. The main findings are that (1) groundwater has been influenced by interactions with magmatic rocks, producing hydrothermal conditions; (2) stage 2 travertine seals of some cenotes effectively isolate surface water bodies from the deep aquifer; and (3) microbial processes influence some of the geochemical cycles that are present in Zacaton, Caracol, Pilita, and Azufrosa, where H_2S is commonly detected.

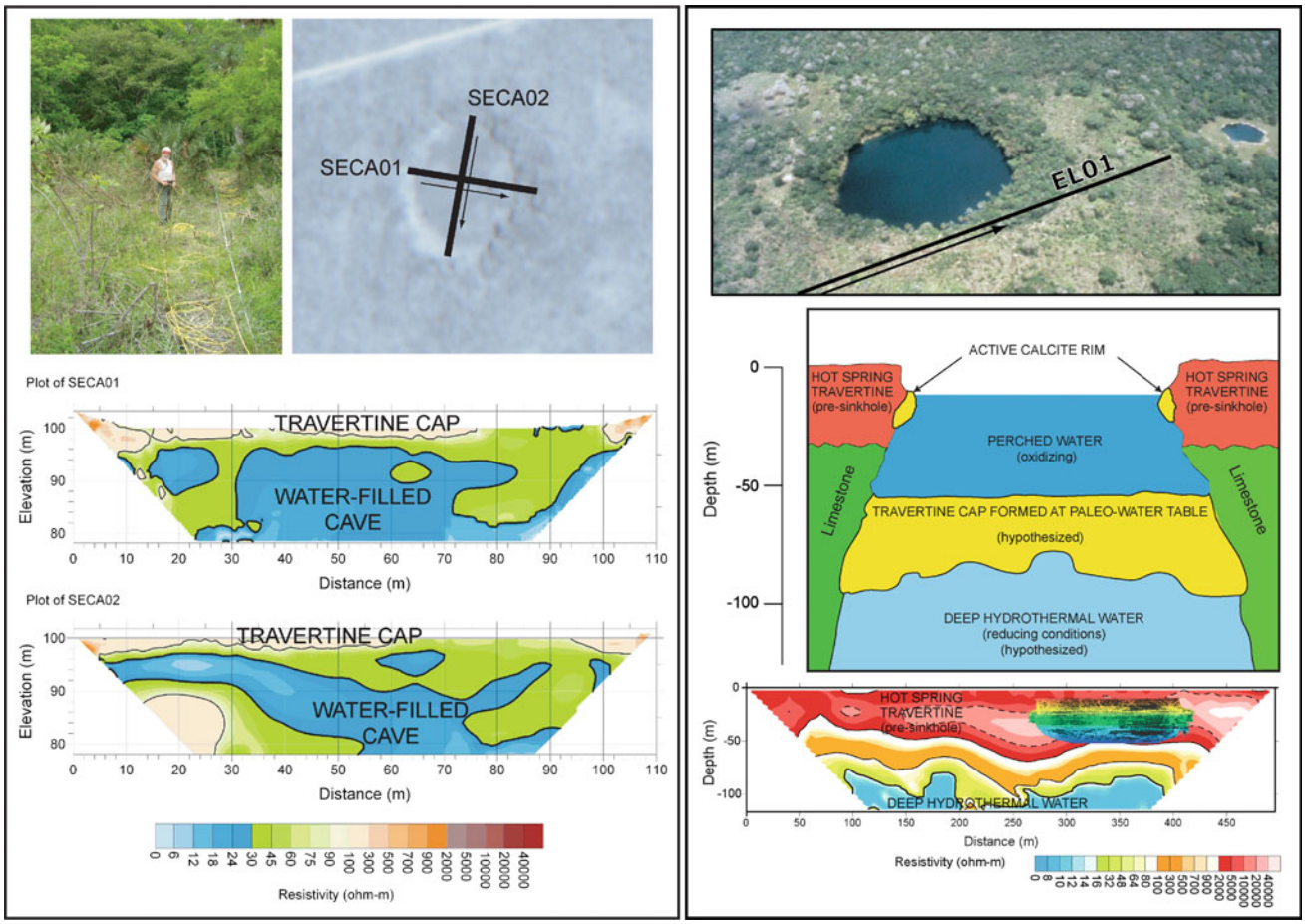

Fig. 7 ERI geophysical surveys document the nature of cenotes capped with travertine. *Left* Poza Seca; *right* Poza Verde

7 Volcanogenic Karst

Hypogene speleogenesis has been defined several ways in the karst literature. Palmer (1991, 2007) distinguishes it as the product of deep-seated sources of solutional aggressiveness, whereas Klimchouk (2007) defines it as the product of rising waters, independent of the source of aggressiveness. By either definition, caves formed by the volcanic gases of CO_2 and H_2S, sulfidic, and carbonic acids from petroleum-laden rocks qualify as hypogenic.

Most of the karst systems attributed to hypogene speleogenesis are currently located in the vadose zone (e.g., Lower Kane Cave, Chap. 10), whereas in most cases, the processes that formed the caves described here took place in phreatic conditions. The two deepest explored phreatic caves in the world, Pozzo del Merro, Italy, and El Zacatón, Mexico, (Gary et al. 2003; Knab 2009) are both hypothesized to have developed in hypogene settings, specifically in the subset defined as a *volcanogenic karst system* (VKS) (Gary and Sharp 2006, 2009).

Volcanogenic karst systems (VKS) are formed when a groundwater system in soluble rock interacts with volcanic activity in the subsurface. This interaction can produce conditions favorable for intensive karstification in local geographical areas and at considerable depth. Although the karst may have surface expression, it is possible that no recognizable karst development is present at the overlying surface. This makes identification and investigation of volcanogenic karst difficult, and the literature on VKS is limited.

However, the geologic processes involved in development of VKS are well documented and include fundamental components common to all karst systems. These include (1) sufficient thickness of carbonate strata; (2) preferential groundwater flow paths (e.g., fractures); (3) groundwater flux (required for mass transfer of dissolved rock), aided by convection (e.g., driven by heat); and (4) volcanic activity to provide the source of CO_2 and/or H_2S and to accelerate kinetics.

Components 1–3 are common to all active karst systems, and some form of solutional aggressiveness must also be

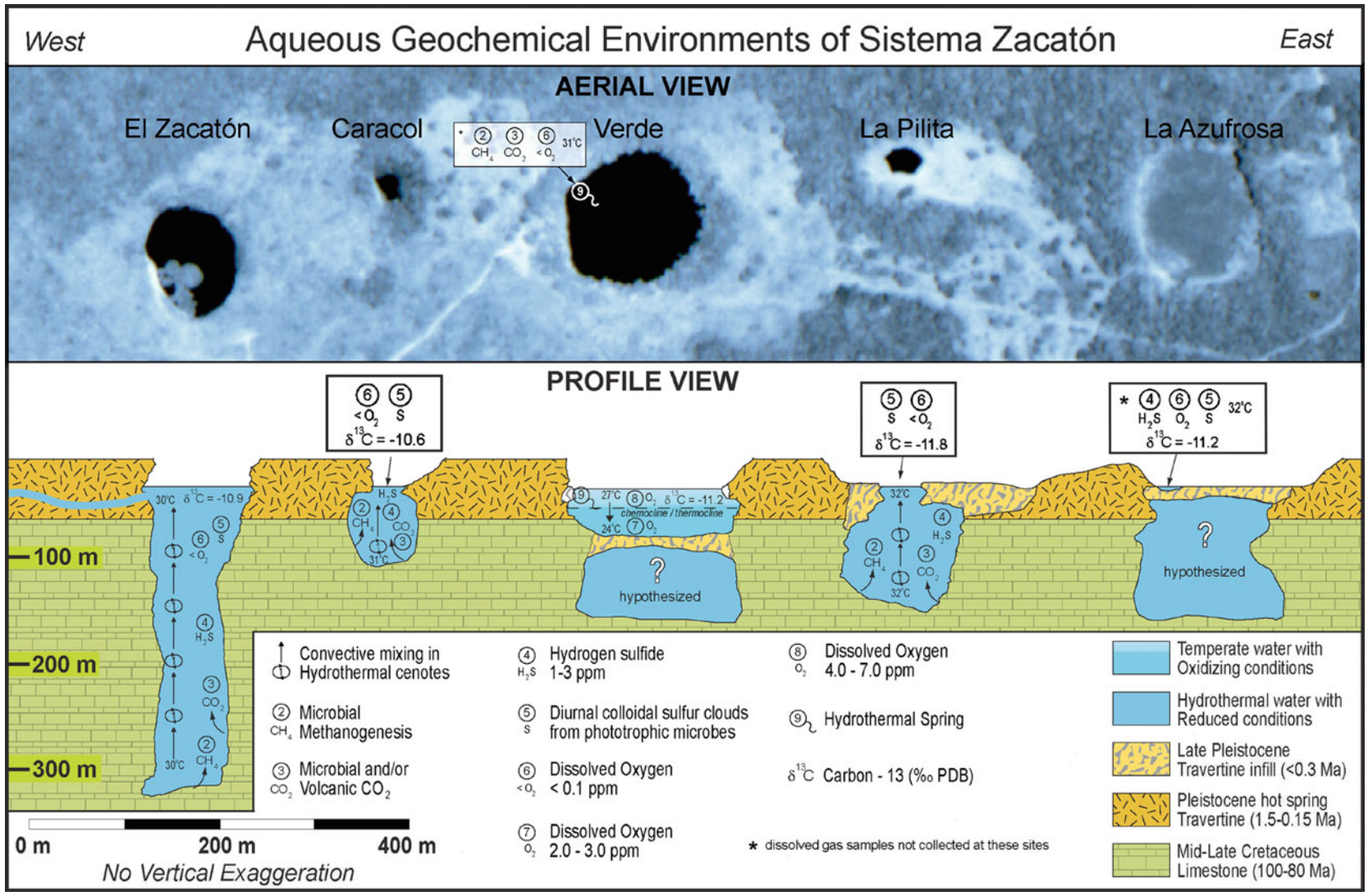

Fig. 8 Schematic cross-sectional of major cenotes of Sistema Zacatón, showing the dynamic nature of the karst

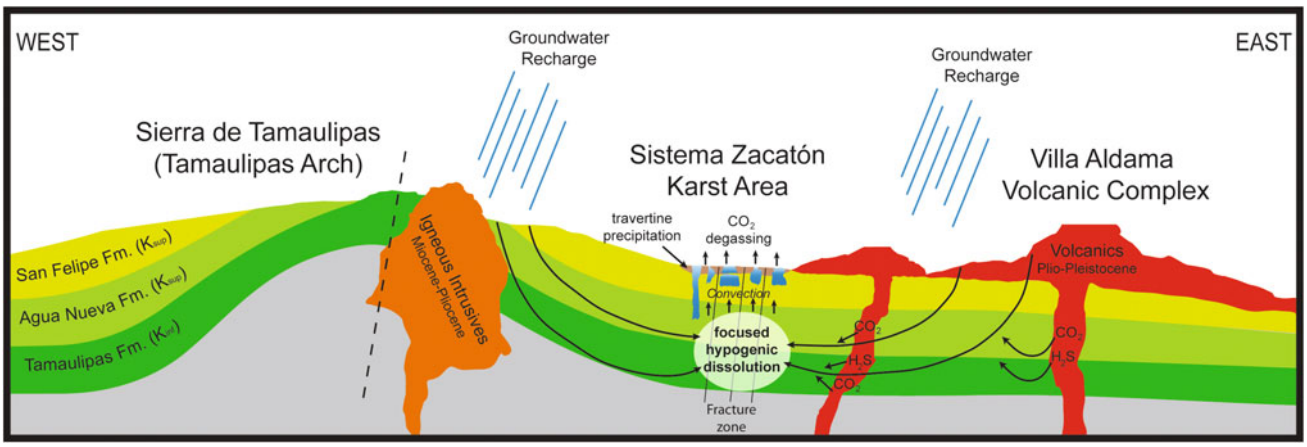

Fig. 9 Regional hydrogeologic model shows hypothesized flow paths and rock–water interactions that provide the key components to form a volcanogenic karst system

present. Component 4 is unique to VKS, because the major sources of acid are derived from the interaction of groundwater with volcanic rocks at depth. Klimchouk (2007) modified a conceptual model of groundwater flow from Tóth (1999) to show regional settings of hypogenic and epigenic karst systems and included interaction of a magmatic zone, adding CO_2 and heat to the groundwater system. The addition of heat is inherent to VKS; it creates hydrothermal conditions that can provide upward convection of fluids through preexisting fractures and increase the flux of groundwater. Dublyansky (2000b) discusses karst development by geothermal waters, with the effects of rising thermal water, H_2S and mixing with H_2S and CO_2 to accelerate dissolution. A general review of the interaction of volcanic activity and karst is given by Salomon (2003). Figure 9 shows the conceptual model of Sistema Zacatón's hydrogeology related to its volcanogenic origin.

Recognition of volcanogenic karstification as a specific type of hypogene speleogenesis is useful when characterizing karst systems on a global scale. Several karst systems have been directly identified with volcanic activity in modern settings, but others may have been influenced by volcanism during earlier time periods. Such relict systems may have features and characteristics that are difficult to relate directly to volcanogenic processes, but recognizing the VKS model in these settings may improve interpretation of the geologic framework and secondary porosity development when modeling the modern hydrogeologic system.

8 The Speleogenetic Model

The conceptual model of the speleogenesis and timing of karstification for Sistema Zacatón is based on the following data: Field geologic mapping, three-dimensional imaging, and geophysical methods characterize the unique morphology and mineralization of this karst system. Associating the geomorphology with the geochronology provides the basis for defining important phases of karstification, in some cases by applying the basic rules of superposition. An important aspect of the karst development is the extent, type, and morphology of the various stages of travertine deposition. The sequence of precipitation is correlated directly with the development of karst features.

8.1 Integration of Geomorphic Features

The morphology of karst features and rock formations directly and indirectly observable from the surface was analyzed to develop a speleogenetic model. Detailed underwater mapping by state-of-the-art technology created detailed 3-D models of the cenotes. ERI geophysical studies document travertine lids covering several cenotes and lid morphology that may provide insight into Late Pleistocene water-level fluctuations. Travertine-capped sinkholes (stage 2 travertine) developed at levels of prolonged water-level stability. Additional geophysical evidence at cenote Verde indicates the presence of one of these structures 40–50 m below modern water levels. The presence of this feature is applied to the interpretation of water level, water temperature, and geochemical profiles pictured in Fig. 10.

8.2 Multiphase Speleogenesis

The multiphase karstification model for Sistema Zacatón is based on interpretations of the travertine types and morphologies, locations of caves, presence of important fossils (mammoths), and observed hydrogeologic conditions.

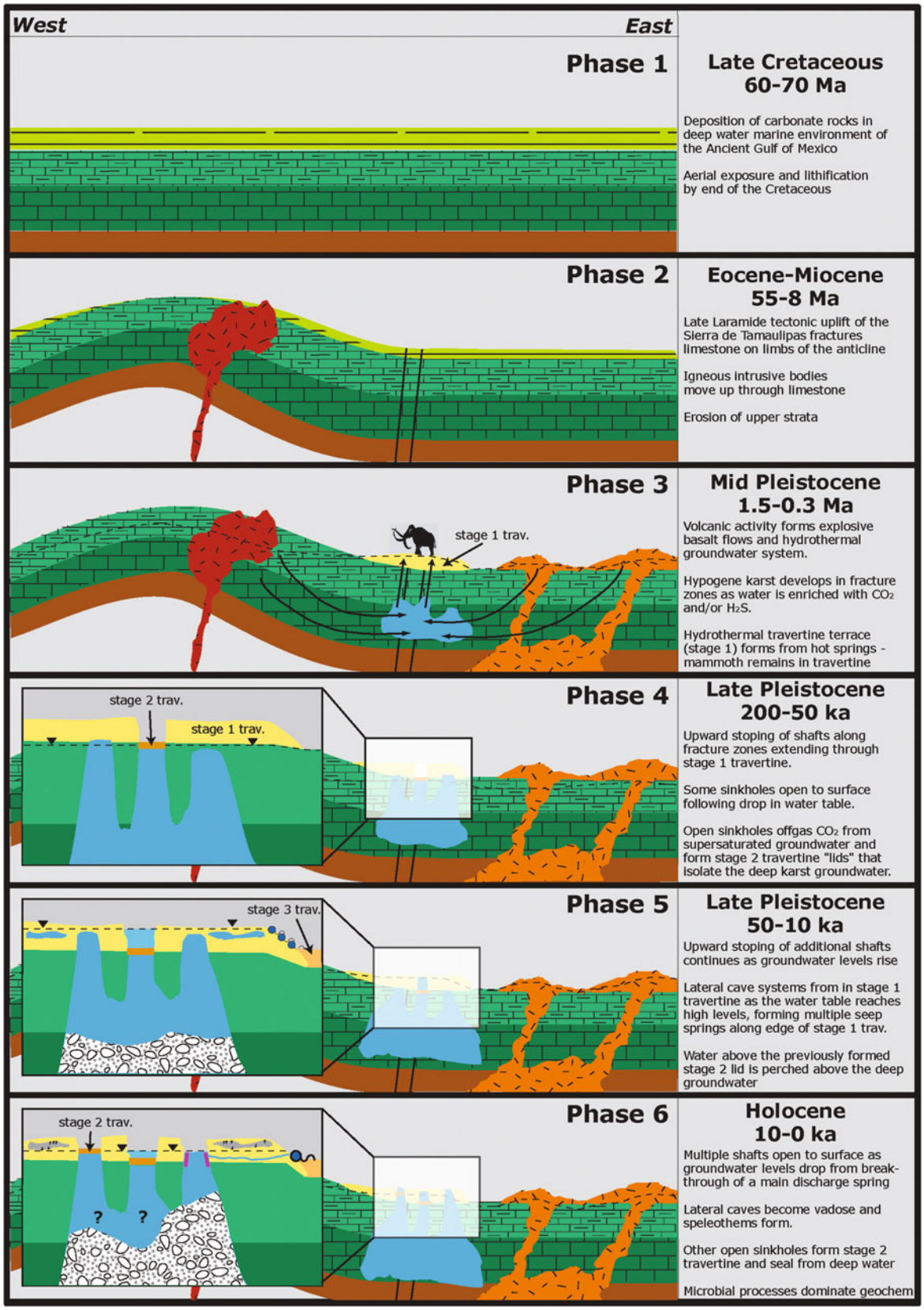

Fig. 10 Schematic diagram showing the karst evolution of Sistema Zacatón

The result is a six-phase karst evolution model (Fig. 8). Initial hypothesized phases were presented by Gary and Sharp (2006), but modifications of the initial hypotheses from additional information have provided a revised model. The most important modification is the integration of the Azufrosa Travertine as a major event related to the sequence of karstification. The six phases of karstification are as follows:

1. Deposition of marine limestone (Late Cretaceous).
2. Laramide uplift and fracturing of the limestone; igneous intrusions in Sierra de Tamaulipas (Eocene-Miocene).
3. Volcanic activity; hypogenic karstification along fracture zone; hot spring travertine terrace (stage 1) formed during high water table; and mammoths in fossil record (Pleistocene).
4. Continued hypogenic karstification; upward stoping of shafts to the surface through stage 1 travertine as water levels drop; and open shafts form stage 2 travertine as CO_2 outgasses from thermal water (Late Pleistocene).
5. Continued hypogenic karstification; additional shafts open to the surface; lateral phreatic caves form in stage 1 travertine; and seepage springs discharge hydrothermal water along margin of stage 1 travertine under high water table conditions (Late Pleistocene).
6. Continued hypogenic karstification; breakthrough of spring at El Nacimiento lowered the water table to its modern level; stage 3 travertine deposited by water flowing from El Nacimiento; shallow lateral caves became vadose, allowing subaerial speleothems to form; and additional stage 2 travertine forms caps over some open cenotes (Holocene).

Phases 3–6 took place in the Pleistocene, possibly within the last 200,000 years. The presence of mammoth fossils in the Azufrosa Travertine (Stage 1) indicates that sinkholes opened after these large mammals migrated into the region. This constraint restricts the hypothesized timing of the system to the Mid-Late Pleistocene, which coincides with active volcanism in the Villa Aldama volcanic complex, dated at 250 ka (Camacho 1993). This phase of karstification is interpreted to have occurred in a wet climate. Later, drops in the water table initiated collapse of many of the sinkholes. The lower water table is recorded in the travertine cap of Verde, 45 m below the modern water level. Another water table rise as much as 65 m formed lateral cave systems near diffuse discharge points in the system. All of the shallow karst development took place in the Azufrosa Travertine, and therefore must be of Late Pleistocene age. The present vadose caves from the final two phases of speleogenesis show features and passage patterns that indicate a phreatic origin, which shows that water levels late in the karst evolution were significantly higher than those of today.

The final major karst event was a local drop in water levels, likely due to the breakthrough of a lateral cave passage draining the cenote of El Zacatón through El Pasaje de la Tortuga Muerta, which discharges through El Nacimiento. Formation of this single discrete discharge point focuses on advective dispersion of dissolved carbonate minerals and is currently depositing travertine downstream of the karst area. This process has been dated to the Late Holocene. The later drops in water levels are related to the final opening of additional sinkholes as the decrease in buoyancy caused structural failure of the rock. As the later caves became aerially exposed, speleothems began to form throughout the caves (Fig. 10).

The geomorphic aspects of the karst are revealed by the modern physical and chemical hydrogeologic data observed at Sistema Zacatón, particularly by the identification of isolated but effective flow barriers interpreted as a result of the travertine caps in sinkholes. Evolving stages of this phenomenon are observed at the cenotes of Caracol, Verde, La Pilita, Azufrosa, Poza Seca, and Tule. Analysis of water levels from the cenotes surrounding Verde indicates effective hydrologic isolation of the surface water body. Geochemical and temperature data reinforce the hypothesis that it has limited connection to the deep groundwater of Zacatón, Caracol, and La Pilita. Direct access to the deep hydrothermal karst system in these cenotes makes it possible to observe the evolution of microbial communities and their substantial influence on the modern geochemistry, particularly reduction–oxidation processes and sulfur cycling.

9 Conclusion

Deep cenotes and travertine deposits at Sistema Zacatón are considered to be global models of volcanogenic karst based on geologic observations, geochemistry, and proximity to volcanic deposits. Geochemically, CO_2 (and/or) H_2S-rich warm water dissolve voids at depth which propagate upward. At the water table, CO_2 and H_2S degas causing large amounts of carbonate precipitation and microbial growth. As the water table falls, the cenotes become covered with a carbonate cap rock. This type of activity is primarily observed in carbonate regions near volcanos or other igneous activity.

References

Barger KE (1978) Geology and thermal history of Mammoth Hot Springs, Yellowstone National Park, Wyoming. US Geol Surv Bull 1444:49–50

Camacho AF (1993) Compilación geologica de la vertiente del golfo de Mexico, area 1. Comision federal de electridad, subdirecion tecnica,

gerencia de estudios de ingenieria civil, subgerencia de estudios geologicos, departamento de geologia. G-43:123–130
Dublyansky YV (2000a) Hydrothermal speleogenesis—its settings and peculiar features. Speleogenesis evolution of karst aquifers, National Speleological Society, pp 292–297
Dublyansky YV (2000b) Dissolution of carbonates by geothermal waters. In: Klimchouk A, Ford D, Palmer A, Dreybrodt W (eds.) Speleogenesis: evolution of karst aquifers. Huntsville, Ala., National Speleological Society, pp 158–159
English JM, Johnson ST (2004) The Laramide orogeny: what were the driving forces? Int Geol Rev 46(9):833–838
Enos P (1983) Sedimentation and diagenesis of mid-cretaceous platform margin—East Central Mexico. Dallas Geol Soc: 5–20
Enos P, Stephens BP (1993) Mid-cretaceous basin margin carbonates, east-central Mexico. Sedimentology 40:539–556
Ford DC (2000) Deep phreatic caves and groundwater systems of the Sierra de El Abra, Mexico. Speleogenesis evolution of karst aquifers, National Speleological Society, pp 325–331
Fouke BW, Farmer JD, Des Marias DJ, Pratt L, Sturchio NC, Burns PC, Discipulo MK (2000) Depositional facies and aqueous-solid phase geochemistry of travertine-depositing hot springs (Angel Terrace, Mammoth Hot Springs, Yellowstone National Park, U.S.A.). J Sediment Res 70(3):565–585
Gary MO (2004) Preliminary analysis of microbial habitats and geochemical environments of Sistema Zacatón, Mexico. Geological Society of America Abstracts with Programs. 36(5) session 106–13:259
Gary MO, Sharp JM Jr (2006), Volcanogenic karstification of Sistema Zacatón. In: Harmon RS, Wicks CM (eds) Perspectives on karst geomorphology, hydrology, and geochemistry; a tribute volume to Derek C. Ford and William B. White. Geological society of America special paper 404:79–89
Gary MO, Sharp JM Jr (2009) Volcanogenic karstification: implications of this hypogene process. National cave and Karst research institute symposium 1, Advances in hypogene karst studies, pp 27–39
Gary MO, Sharp JM Jr, Caramana G, Havens RH (2003) Volcanically influenced speleogenesis: forming El Sistema Zacatón, Mexico, and Pozzo Merro, Italy, the deepest phreatic sinkholes in the world. Geological Society of America Abstracts with programs 34(7) session 19–4:52
Gary MO, Fairfield N, Stone WC, Wettergreen D, Kantor G and Sharp JM Jr (2008) 3-D mapping and characterization of Sistema Zacatón from DEPTHX (Deep Phreatic Thermal Explorer). In: Proceedings of the 11th multidisciplinary conference on sinkholes and the engineering and environmental impacts of karst. American Society of Civil Engineers Geotechnical Special Publication 183, pp 202–212
Gilliam B (1995) Deep Diving—an Advanced Guide to Physiology. Procedures and systems. Watersport Books, San Diego, pp 37–47
Goldhammer RK (1999) Mesozoic sequence stratigraphy and paleogeographic evolution of Northeast Mexico. Geol Soc Am Spec Pap 340:3–14
Klimchouk A (2007) Hypogene speleogenesis: hydrologeological and morphogenetic perspective. National Cave and Karst Research Institute, special paper no. 1, p 106
Knab O (2009) Die tiefsten Unterwasserhöhlen der Welt. Im Tiergarten, Zürich
Kristovich AK (1994) Zacatón. A history. Int Assoc Nitrox Tech Divers J 94 (4):6
Palmer AN (1991) Origin and morphology of limestone caves. Geol Soc Am Bull 103:1–21
Palmer AN (2007) Cave geology. Cave Books, Dayton
Ramírez Fernández JA, Velasco Tapia F, Viera Decida F, Vasconcelos Fernandez JM and Gary MO (2007), Tertiary interplate mafic magmatism in the Eastern Mexican alkaline province: Villa Aldama volcanic complex geological society of America abstracts with programs, 2007 annual meeting, Denver, p 390
Sahl JW, Gary MO, Harris JK, Spear JR (2011) A comparative molecular analysis of water-filled sinkholes in North-Eastern Mexico. Environ Microbiol 13(1):226–240
Salomon JN (2003) Karst system response in volcanically and tectonically active regions. Annals of geomorphology. Karst Changing World supplement 131:89–112
Suter M (1987) Structural traverse across the Sierra Madre Oriental fold—thrust belt in East-Central Mexico. Geol Soc Am Bull 98:249–264
Tóth J (1999) Groundwater as a geologic agent: an overview of the causes, processes, and manifestations. Hydrogeol J 7:1–14
Vasconcelos JM, Ramírez Fernández JA (2004) Geología y petrología del complejo volcánico de Villa Aldama. Tamaulipas Ciencia UANL 7(1):40–44

The Naica Caves, Chihuahua, Mexico

53

Paolo Forti

Abstract

The caves of Naica (Chihuahua, Mexico) have been known since the beginning of the nineteenth century, when they were intersected by mines. They became world famous in 2000 when the mining activities intersected three small caves, which hosted gigantic gypsum crystals. Their genesis and evolution is strictly related to rising thermal fluids induced by Tertiary intrusive magmatic activity, giving rise to polysulfide deposits. Speleogenesis began about 1.5 Myr BP, induced by rising thermal water. This process lasted for a relatively short time. Later evolutionary stages varied from cave to cave, reflecting alternately deep-seated phreatic, epiphreatic, and vadose environments. Deposition of the giant gypsum crystals began ~400–350 Kyr BP, when the water temperature dropped below 58 °C. Their growth suddenly ceased in 1985, when mine dewatering dried up the caves. Besides the giant gypsum crystals, Naica caves contain a wide variety of other cave minerals (over 40), ten of which are new for the cavern environment. In addition, they include fossil pollen trapped in the gypsum lattice, which allow reconstruction of the external climate of 350 Kyr BP, and microorganisms new to science, which were preserved in the fluid inclusions of the gypsum crystals for tens or even hundreds of thousands of years. In 2015, mining intercepted a major thermal water source, which flooded the mine, and the Cueva de los Cristales and other caves at −290 m were flooded by more than 160 m of hot water.

Keywords

Giant crystals • Speleogenesis • Exploration • Multidisciplinary research • Mexico

1 Introduction

The mine caves of Naica (Chihuahua, Mexico) became world renowned a century ago, when gypsum crystals up to 2 m in length were revealed in the Cueva de las Espadas (Degoutin 1912; Foshag 1927). In 2000, mining activities at the −290 m level intercepted three smaller caves (Cueva de los Cristales, Ojo de la Reina, and Cueva de las Velas) hosting the largest known gypsum crystals in the world. The largest of them, more than 12-m long, was found in Crystal Cave (Fig. 1; London 2003).

In 2006–2010, the Naica caves were part of a general research project, which the mine owner, the Peñoles Company, committed to the La Venta Exploring Team from Italy and Speleoresearch and Films from Mexico City (Bernabei et al. 2009). Multidisciplinary studies (Forti and Sanna 2010) showed the Naica caves to be perhaps the most interesting hypogenic caves of the world (Badino and Forti 2013), not only because of their giant crystals, but also for many other aspects in different scientific fields, including geochemistry, mineralogy, microclimate, physiology, palynology, and even astrobiology.

P. Forti (✉)
Italian Institute of Speleology, Department of Biological, Geological and Environmental Sciences, University of Bologna, Via Zamboni, 67, 40126 Bologna, Italy
e-mail: paolo.forti@unibo.it

© Springer International Publishing AG 2017

A. Klimchouk et al. (eds.), *Hypogene Karst Regions and Caves of the World*, Cave and Karst Systems of the World, DOI 10.1007/978-3-319-53348-3_53

Fig. 1 Giant gypsum crystals in Cueva de los Cristales. Explorers are equipped with refrigerated suits and breathing equipment. *Photograph* Peter Carstens, La Venta and S/F Archives

2 Geologic Setting

Naica mine is located in a semidesert region 100 km southeast of Chihuahua (Mexico). The mine entrance is 1385 m asl in the northern flank of the Sierra de Naica, a 12-km long, 7-km wide anticlinal structure of carbonate rocks, oriented NW-SE, which outcrops from an extensive alluvial plain. At the regional scale, the Naica carbonate sequence consists of limestone, dolomitic limestone, and calcitic dolostone with micritic interbeds overlying an Aptian evaporitic sequence. Carbonate deposition began in the Albian (Cretaceous), and sedimentation continued for several tens of millions of years. In the mine, the entire ore body is within the carbonate sequence. No trace of the Aptian evaporites has been found in cores, even those more than 1-km deep.

Tertiary intrusive magmatic activity 26.2–25.9 My ago produced SiO_2-rich dikes within the carbonate sequence (Megaw et al. 1988). In 2007, a drill hole close to the mine shaft encountered an igneous body about 1140 m below the surface (unpublished Naica Mine report; see Fig. 2).

The polysulfide (Pb, Zn, Ag) ore bodies are related to hydrothermal flows (Erwood et al. 1979) induced by the Tertiary dikes. The mineral deposit, which consists mainly of pyrite, pyrrhotite, sphalerite, galena, and chalcopyrite,) occurs as chimneys and mantos (strata-bound deposits) developed within dikes and carbonate bedrock. The latter are strongly altered and partly transformed to calc-silicates. During a later stage, when the thermal fluids cooled, veins of calcite, anhydrite, and quartz formed within the ore bodies (Stone 1959).

Hydrothermal circulation was controlled mainly by two different fault sets, and, therefore, so were the locations of the mineral deposits. Most important are the Gibraltar, Naica, and Montaña faults (Fig. 2), which still guide the thermal water flow within the Naica anticline. Almost all the water entering the deep mine galleries comes through fractures related to these faults, and all the main caves are strictly related to them (Fig. 2). Mine activities have reached −750 m below the mine entrance (level 0 = 1385 m above sea level), and some are 620 m below the original groundwater level, which was at −130 m (1255 m above sea level).

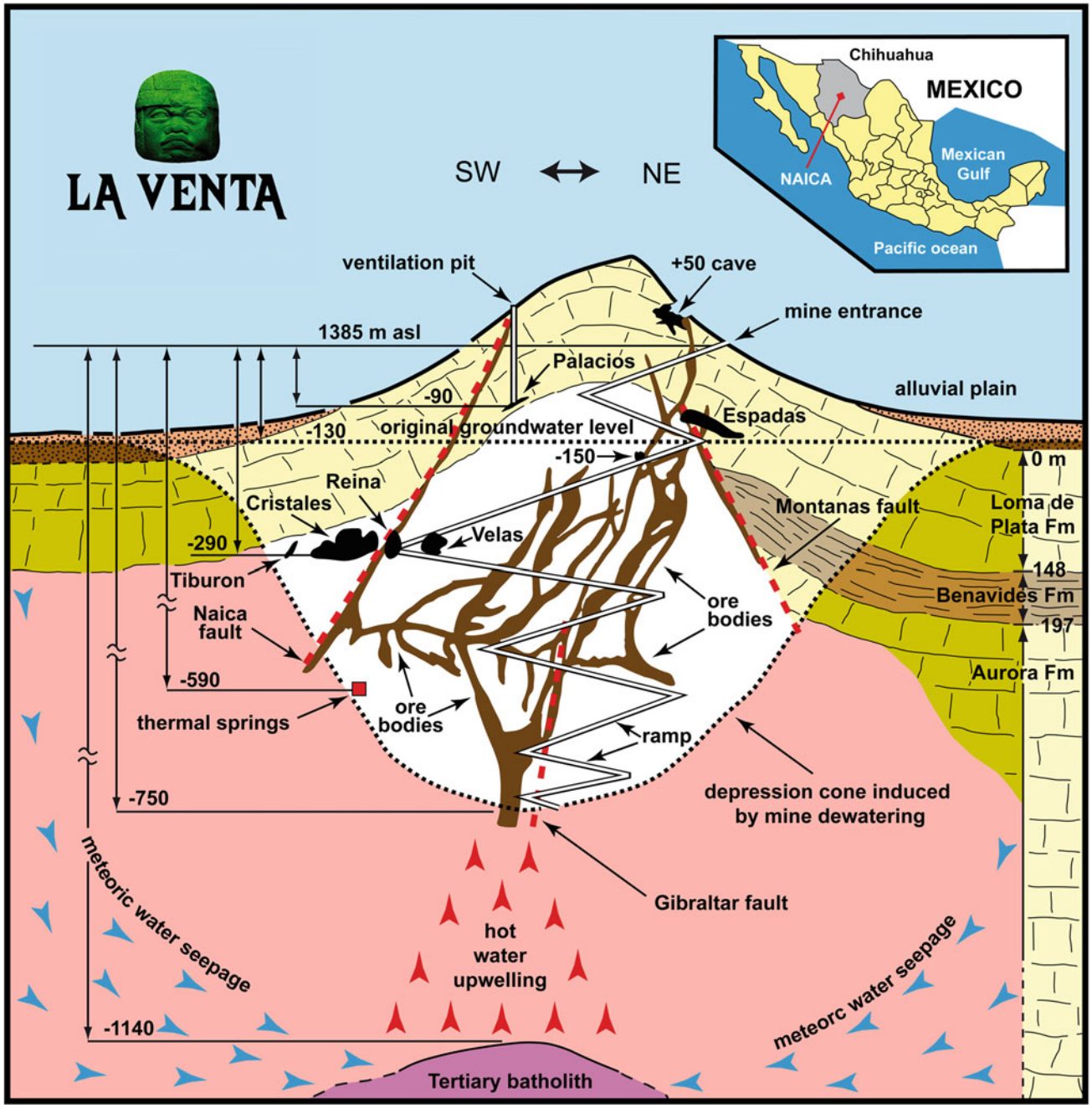

Fig. 2 Index map and sketch of the Naica mine. The natural cavities, closely connected to the main faults, are related to the groundwater level just before dewatering caused by mining. On the *right* is the carbonate sequence observed in several cores drilled in the Naica ridge (modified from Forti 2010)

Dewatering of more than 1 m^3/sec was required to keep the mines dry. The entire Naica area is still a thermal anomaly. Water entering the mine galleries has a temperature close to 53 °C. The origin of these waters is meteoric, even though the average residence time in the thermal aquifer is more than 50 years (García-Ruiz et al. 2007).

3 Exploring and Mapping the Caves

Before starting the project, it was necessary to solve the problem of survival in such a hostile environment (Badino and Forti 2007). It was impossible to enter the caves without special equipment and suitable training, to avoid death

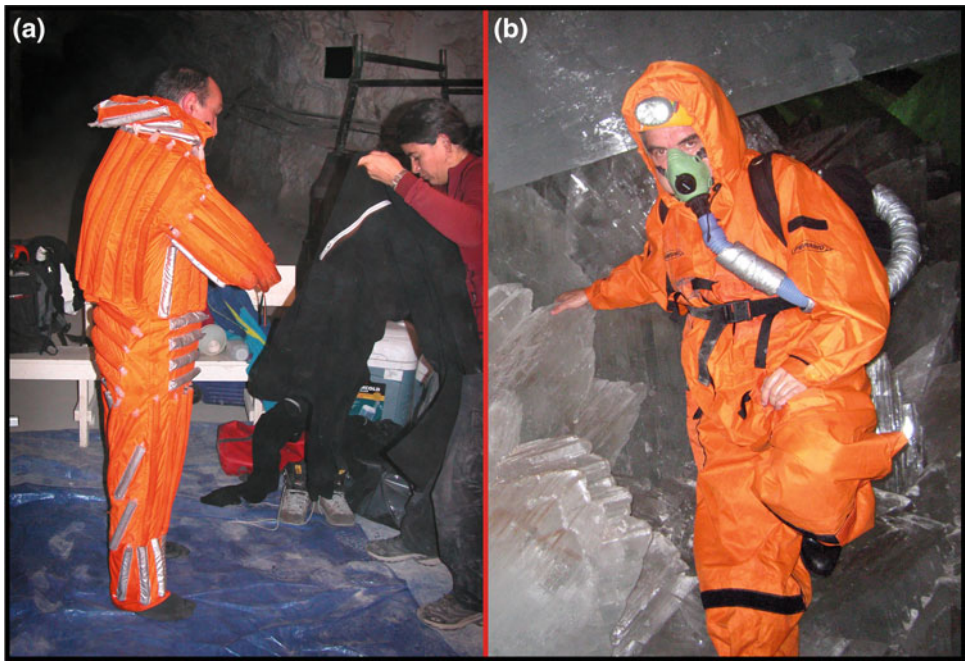

Fig. 3 **a** Special suit with pockets for ice to create a heat barrier. **b** The cold-breather device (*Photographs* Tullio Bernabei, La Venta and S/F Archives)

within a few minutes. The cave temperature (45–48 °C) and relative humidity (100%) induce condensation over the colder surfaces (human bodies) and consequently a fast heating of them (hyperthermia). Not only do human cells degenerate above 42°, they begin to cook. Survival techniques for longer periods had also to consider the risk of burns to the eyes and, even more dangerous, to the lungs. For this reason, the first expeditions were devoted entirely to protection—in particular, refrigerated suits and breathers (Fig. 3). Later, by using these devices, and following specific protocols, it was possible to stay inside the caves for more than 1.5 h. But sometimes these prolonged stays caused unexpected and dangerous physiological stress (Giovine et al. 2009). After solving the survival problems, a detailed survey of the Cueva de los Cristales was made using a laser scanner (Canevese et al. 2009), while the other caves were mapped with traditional methods (Figs. 4 and 5). Only the cave at +50 m was not surveyed because it had been almost destroyed by mining activities.

4 Cave Morphology

Despite the thick carbonate sequence, karst voids are extremely rare inside the Naica mine. In more than 100 years of mining and 100 km of excavated galleries, only seven true caves were intersected (Fig. 2) and all are rather small. However, there are many small relict karst voids filled with gypsum in the carbonates below the −200 level (Forti 2010).

Cave morphologies are different from what is expected for hypogenic voids. They take the shape of the discontinuities that transmit the thermal water, and it was slightly aggressive for only a short time. Cueva de las Espadas, Cueva del Tiburon, and Ojo de la Reina are fractures related to the main faults, whereas Cueva de los Cristales, Cueva de las Velas, and Cueva Palacios represent widened bedding planes. There is no information about the nearly destroyed cave at +50 m.

Purely solutional features are restricted to the mine roof near the entrance of Cueva de los Cristales (Fig. 6a) and a small part of the roof of Cueva de las Velas. Widespread corrosion in the upper part of Cueva de las Espadas (Fig. 6b) is clearly related to a later stage, when lowering of the thermal waters exposed the cave to air and accelerated condensation-corrosion (Gázquez et al. 2012).

5 Gypsum and Related Deposits

The main characteristic of the Naica caves is the presence of thick chemical deposits (Fig. 7), mainly giant gypsum crystals, even though phreatic gypsum deposition never occurred in the highest two caves. Cueva Palacios at −90 m hosts only thin gypsum helictites developed by aerosol (Beverly and Forti 2010) when the thermal groundwater was a few meters below. There is no gypsum at all in the +50 m cave. Other minerals—mainly metallic oxides resulting from oxidation of the polysulfide ore—were deposited before and/or during development of the gypsum crystals, and

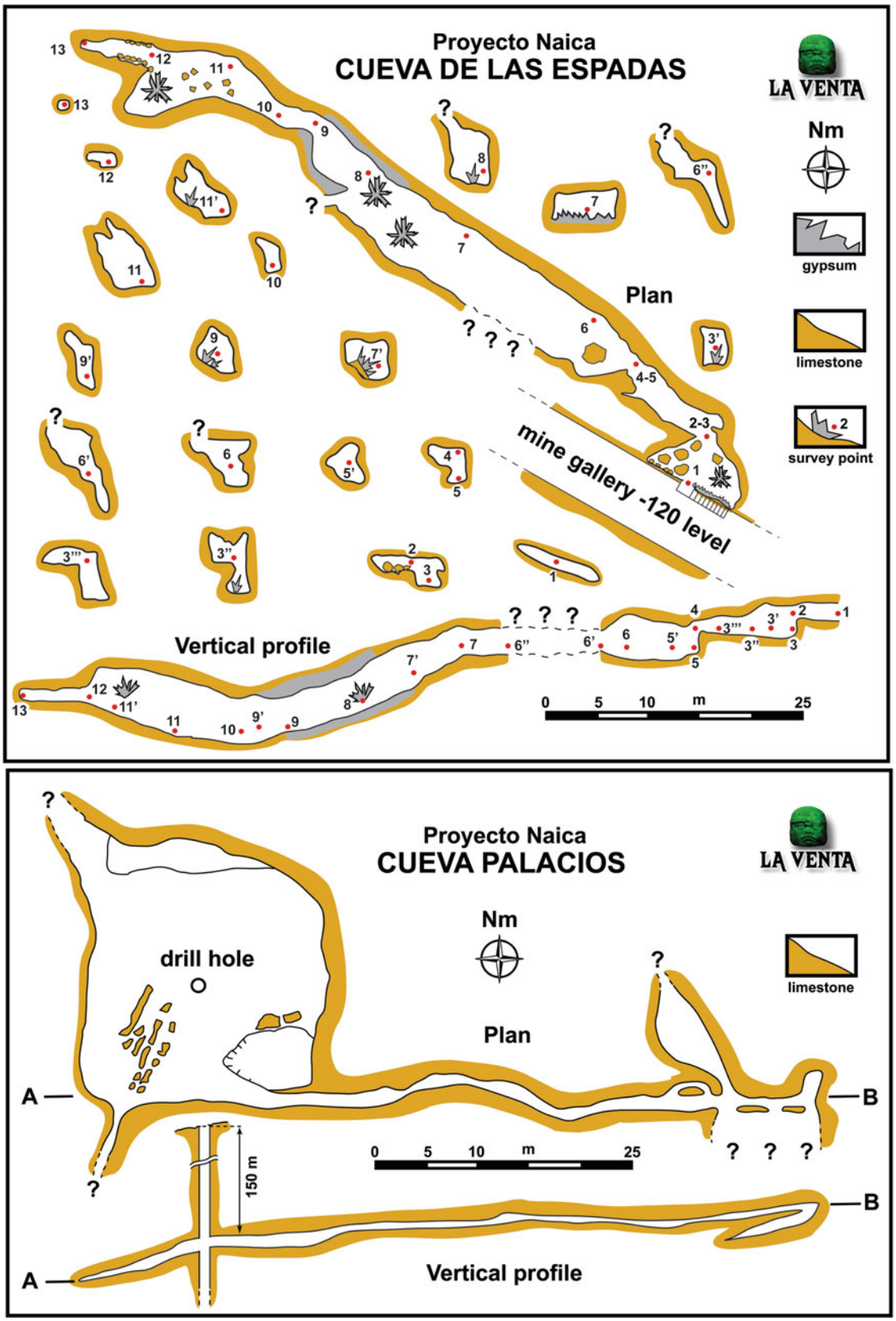

Fig. 4 Maps of Cueva de las Espadas (−120 m level) and Cueva Palacios (−90 m)

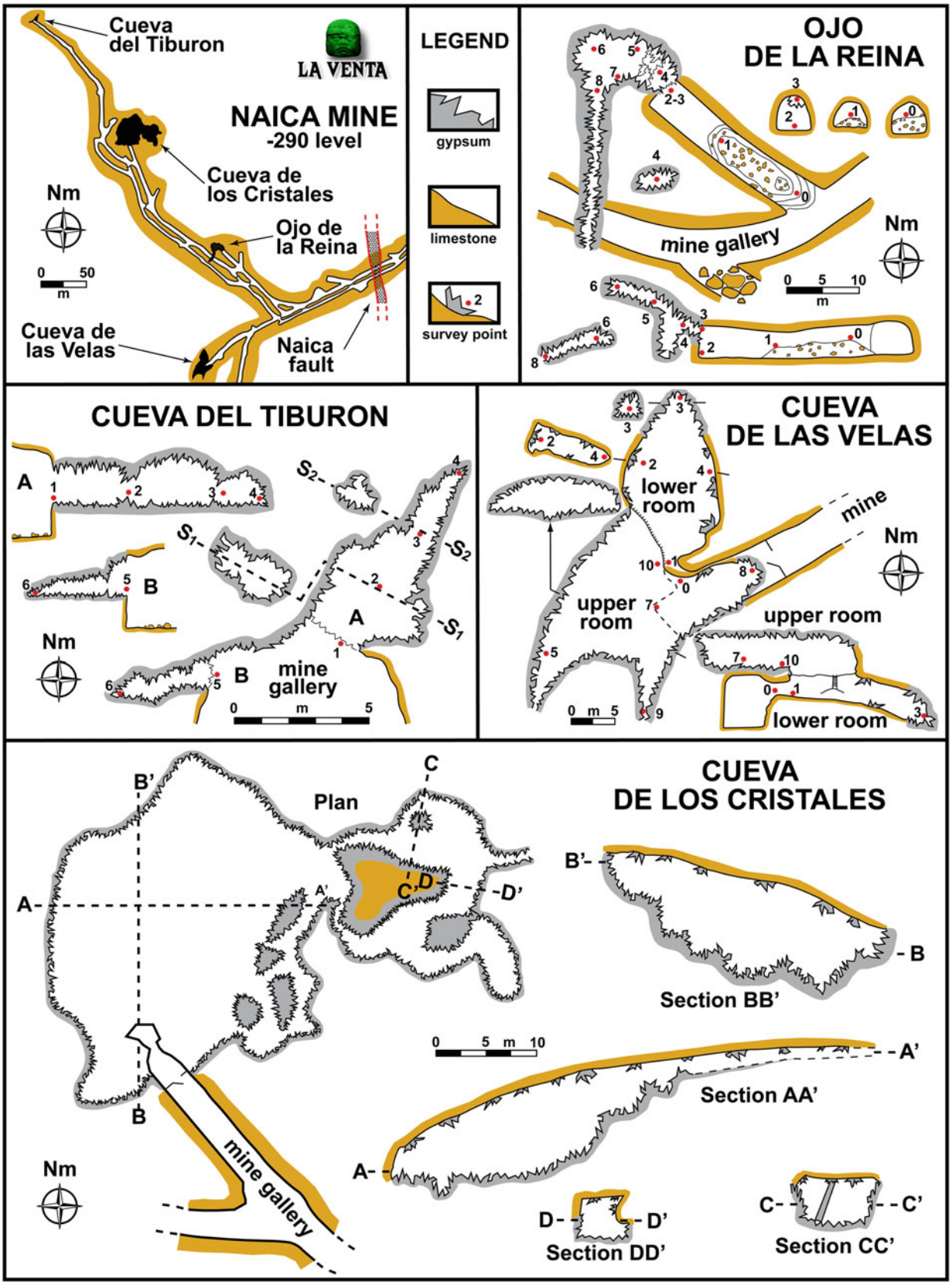

Fig. 5 Maps of caves at the −290 m level

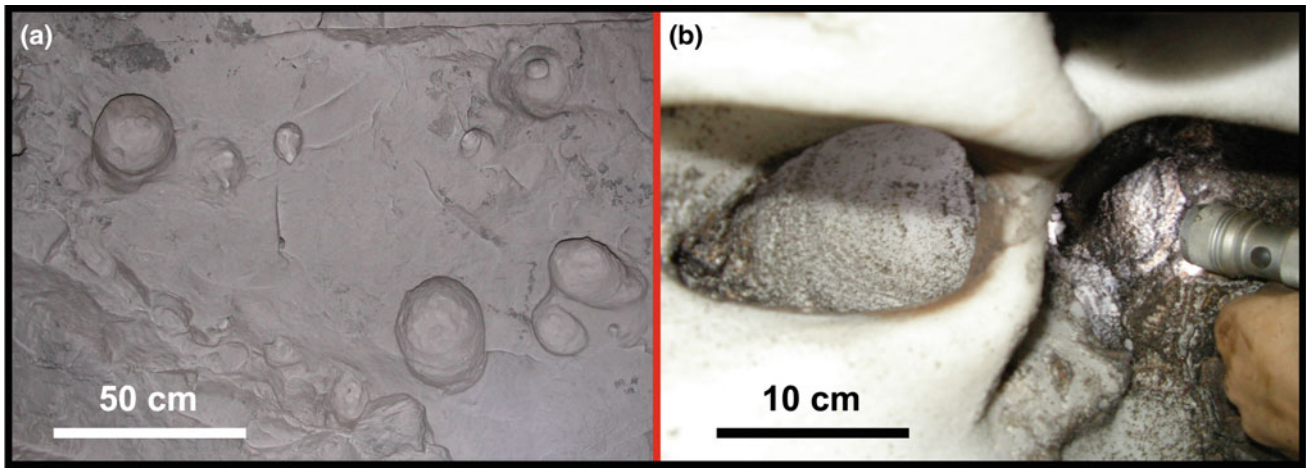

Fig. 6 **a** Small corrosion domes exposed in the roof of the access gallery to Cueva de los Cristales. **b** Enhanced condensation-corrosion of the limestone wall in the upper part of the Cueva de las Espadas (*Photograph* Laura Sanna)

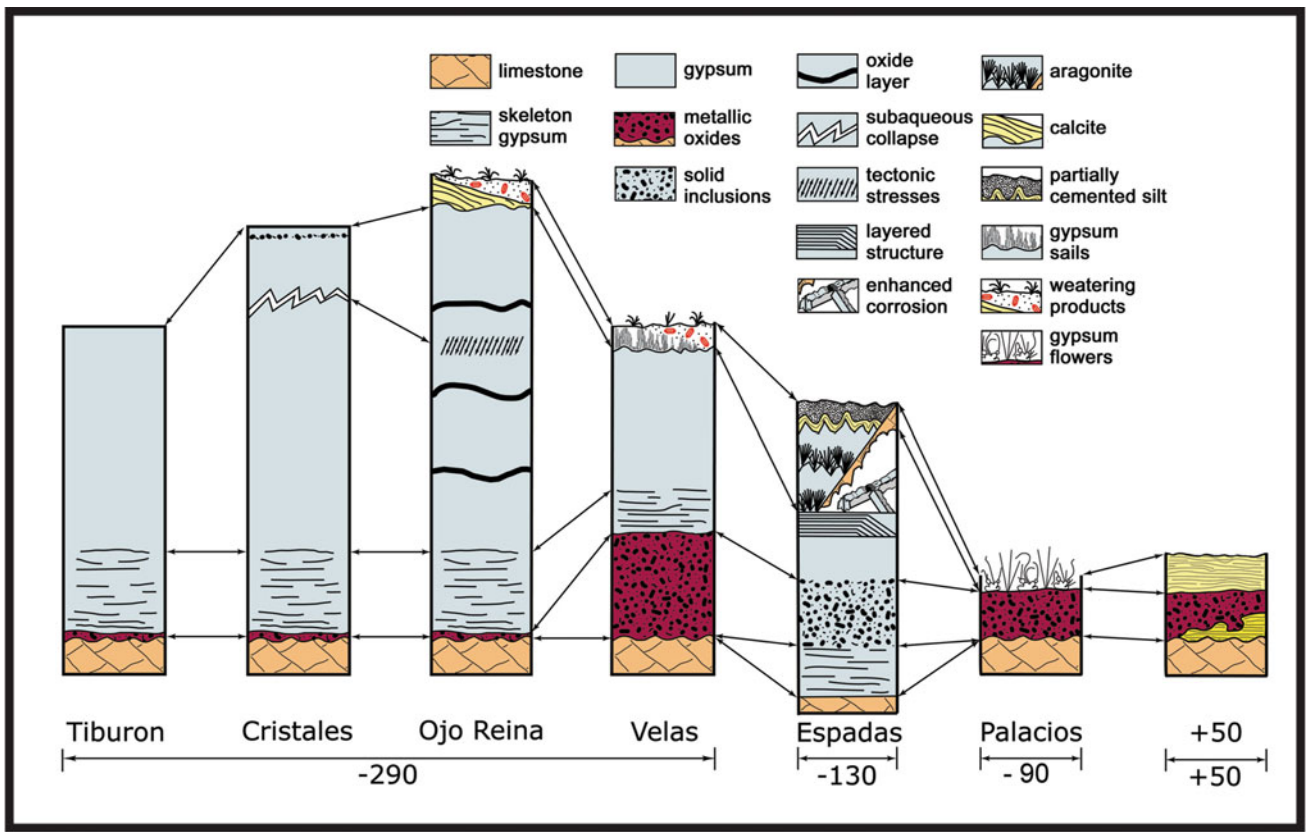

Fig. 7 Stratigraphy of the chemical deposits the Naica caves. Depositional sequences vary from cave to cave, but many of the processes are similar, so it was possible to correlate most of them (Modified from Forti 2010)

many others are still forming (Forti et al. 2009), the genesis of which is related to recent aeration.

The five caves containing giant gypsum crystals show a depositional sequence that differs slightly from cave to cave. In those at −290 m (Cristales, Ojo, Velas, and Tiburon), metallic oxides-hydroxides were deposited before gypsum deposition began, whereas in Cueva de las Espadas this process began when the gypsum crystals were already forming, which resulted in the development of a thick interval of solid inclusions inside these crystals (Fig. 7).

Deposition of the giant crystals was induced by the gypsum-anhydrite solubility disequilibrium (García-Ruiz et al. 2007). Anhydrite is less soluble than gypsum above 58 °C and more soluble at lower temperatures (Fig. 8), so below 58 °C, gypsum is deposited while anhydrite lenses, dispersed throughout the carbonate sequence, are dissolved. This mechanism explains why in Cueva de las Espadas, located 160 m higher and close to the water table, the temperature drop was faster than in caves at −290 m, and deposition started earlier. The anhydrite-gypsum solubility relationship is indirectly corroborated by the presence of small celestite crystals just below or even inside the gypsum, because the anhydrite structure is able to host more strontium than that of gypsum. Inside Cueva Palacios, no phreatic gypsum was deposited, except for thin clearly vadose helictites, because the groundwater level was evidently below Palacios but above Espadas when gypsum deposition was favored.

A seismo-tectonic shock hit the Naica area while the large gypsum crystals were being deposited (Sanna et al. 2011). It was registered in both Cueva de los Cristales, where some of the largest crystals broke and were later covered by 12–15 cm of gypsum overgrowth; and in the Ojo de la Reina, where plastic deformation of some crystals occurred. No evidence of such stresses has been observed in the two other caves at −290 m, even though the caves probably underwent the same events, being very close to each other and related to the same fault (Fig. 2). Cueva de las Espadas, linked to a different fault (Montañas fault), may have been unaffected by this event.

The last stage in the evolution of gypsum in the upper part of Espadas was marked by several clearly visible growth layers in the final 5–6 mm of their development. Up to 17 different layers are present in some of the crystals. These layers may be related to fluctuations of the boundary between thermal and fresh water in this part of the cave (Panieri et al. 2008). During these fluctuations, the lower part of Espadas was permanently underwater, but the presence of air caused a gradation in gypsum crystals from very large on the lake bottom to progressively smaller toward the water surface, where crystal growth ceased (Calaforra et al. 2013). The controlling factor was strong evaporation, which caused the greatest supersaturation at the water–air interface and decreasing toward the bottom of the cave. Therefore, the largest crystals were developed on the lake bottom, where nucleation was less frequent, while the size of the crystals progressively decreased toward the ceiling because of the increased nucleation rate.

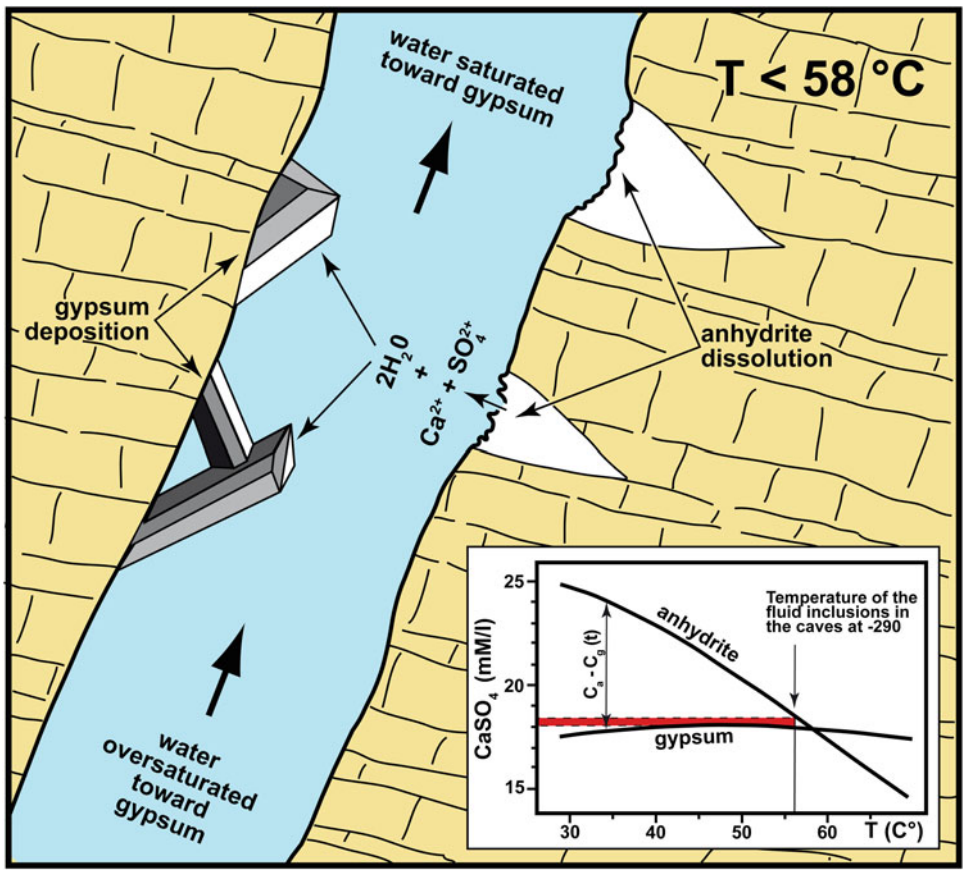

Fig. 8 Development of gypsum crystals induced by the gypsum-anhydrite solubility disequilibrium and (*insert*) gypsum-anhydrite solubility diagram with the temperature range in the caves of Naica at the time in which gypsum crystals were growing, indicated by shading. Below 59 °C, the solubility of gypsum is lower than that of anhydrite; therefore, it is forced to precipitate from an anhydrite saturated solution. Consequently, water becomes undersaturated with respect to anhydrite which must dissolve. The combination of these two opposite processes maintains a very slight supersaturation with respect to gypsum. (After Forti et al. 2009; insert modified from García-Ruiz et al. 2007)

At the beginning of the nineteenth century, before dewatering due to mining, the groundwater level was just a few meters below Cueva de las Espadas (Fig. 2), and, therefore, the deposition of phreatic gypsum had already ceased. In the deeper Cristales, Reina, Velas, and Tiburon Caves, gypsum deposition continued unperturbed until 30 years ago, when the mine dewatering stopped the process. All gypsum crystals in these caves contain a very thin solid inclusion layer about 1 mm below the crystal surface. This layer is thicker and more evident in upward-facing crystal faces, and absent in those facing downward, suggesting gravitational deposition. This may relate to the beginning of the mining activities, which enhanced the water mixing within the thermal aquifer even at great depths.

Finally, the rapid dewatering induced by mining did not represent the end of gypsum deposition at the −290 level. In Cueva de las Velas, gypsum crystals of a completely new form were developed in the few tens of days of its dewatering, which we called "sails" (Bernabei et al. 2007). This speleothem consists of extremely thin and elongated skeletal crystals that grew epitaxially only on the tips of the upward-facing gypsum crystals (Fig. 9). Their origin was controlled by capillary rise along the crystal faces with strongest evaporation at the crystal apices. This mechanism provided a high supersaturation for a few days, until the distance from the falling water level to the crystal tips exceeded the capillary fringe.

5.1 Fluid Inclusions

One of the main characteristics of the gypsum crystals is the presence of thousands of huge (>200 μm in diameter) and often gigantic (Fig. 10a) fluid inclusions (Garofalo et al. 2009). They are typically located along crystallographic planes (primary fluid inclusions), and in almost all the occurrences the trapped fluid is mostly one-phase (liquid), only occasionally being two-phase (liquid–vapor). Two aqueous fluids with distinct bulk salinity were observed: one in the range 3–6 $w_{\text{NaCl equiv.}}$ (most of the fluid inclusions of the −290 m caves) and the other between 7 and 8 $w_{\text{NaCl equiv}}$ (the highest values mainly in the dark portions of the crystals from Cueva de las Espadas, which are rich in oxide-hydroxide solid inclusions). Finally, samples of gypsum crystals developing close to the thermal springs in the mine galleries at the −590 m level (Fig. 2) have fluid inclusions with an even lower bulk salinity of 1.8–2.0 $w_{\text{NaCl equiv.}}$ Analyses of single-fluid inclusions showed that, in addition to Ca and S, the major components were Mg, Na, and K (in order of abundance), whereas Mn and Pb were minor and commonly below the detection limit. Only the fluid inclusions within the dark rims (rich in solid inclusion of oxides-hydroxides) of crystals from Cueva de las Espadas, with high Na and Mg concentrations (10,000–70,000 μg/g), have a relatively high Pb content (up to about 10,000 μg/g).

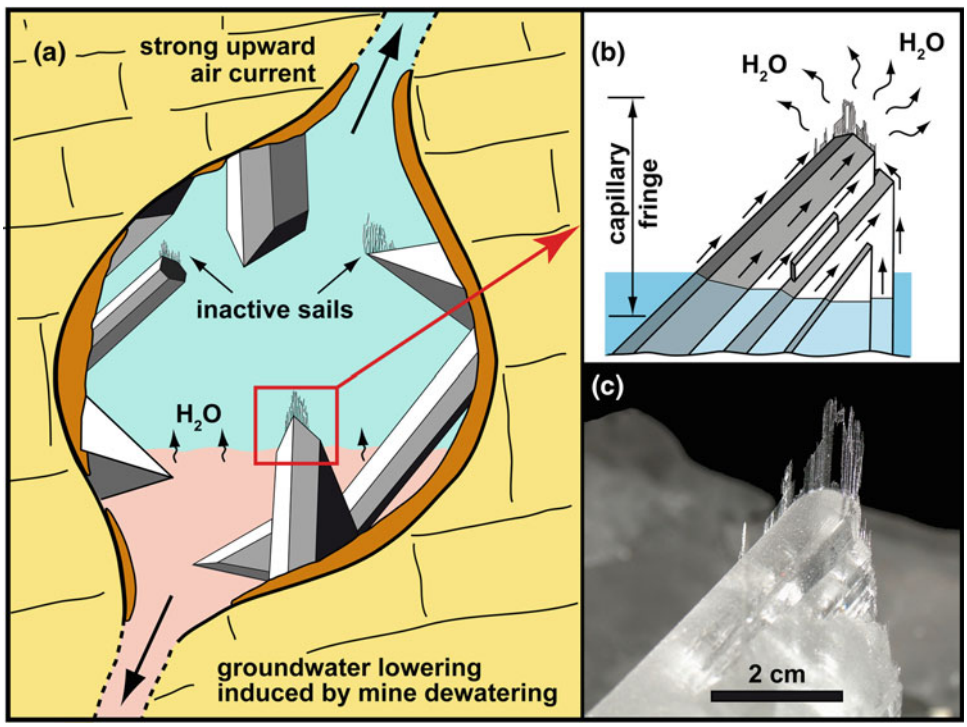

Fig. 9 **a** Evolution of "sails" induced by artificial lowering of groundwater. **b** When large crystals were partially exposed to atmospheric capillary rise and evaporation, it caused supersaturation at the crystal apices and consequent evolution of "sails" whose shape is controlled by strong upward airflow (modified from Bernabei et al. 2007). **c** Cueva de las Velas: "sail" growing epitaxially upon a pre-existing gypsum crystal (*Photograph* Tullio Bernabei, Archivio La Venta and S/F)

The distribution of total homogenization temperatures in Cueva de los Cristales is between 49 and 57 °C, which is much the same as that of Espadas, while in Ojo de la Reina this interval is narrowed to 56–57 °C. Hence, in contrast with the distribution of bulk salinity and Mg–Na concentration values, total homogenization occurs in a narrow range within the entire Naica karst system.

It was possible to demonstrate (Garofalo et al. 2010) that the partial mixing of the hypersaline upper solution with the deeper less-concentrated water constantly induces a slight supersaturation with respect to gypsum, thus enhancing the growth of the giant gypsum crystals within the −290 m caves. Exceptional crystal growth was not possible in Cueva de las Espadas because of periods of high supersaturation induced by evaporation, which caused rapid nucleation.

Finally, isotopic analyses of gypsum hydration water (Gázquez et al. 2012, 2013) revealed that $\delta^{18}O$ of the Naica aquifer water ranged between −8.62 and −7.23‰, while δD was between −63.04 and −52.48‰ over the past 200 Kyr. These data are described by a line ($\delta D = 7.97\ \delta^{18}O + 5.81$) that is close to the current meteoric water line at Naica.

The chemical and isotopic differences in fluid inclusions at the −290 and 120 m levels indicate and change in the main moisture source of precipitation (Pacific Ocean/Gulf of Mexico) (Garofalo et al. 2010; Gázquez et al. 2012, 2013).

5.2 Microorganisms Trapped in Gypsum Crystals

A study of the solid and fluid inclusions trapped inside the crystals, started during the "Projecto Naica," is still underway. Some of the solid inclusions contain a rich assortment of organisms (Fig. 10b) fossilized by newly formed minerals during the first oxidation stage (Fig. 7). This discovery suggested the possibility that these microorganisms might still viable for DNA genetic studies. Water extracted from fluid inclusions and solid inclusions in the gypsum crystals from Cueva de los Cristales indicate that they formed in oxygen-rich and oxygen-depleted environments for a long time (Boston et al. 2012). Biomats slowly developed, making DNA studies possible, as well as research into their closest representatives (where possible). The microorganisms revealed interesting genetic relationships to living organisms identified from various unusual and extreme chemical environments (Boston et al. 2012, 2013), which were able to precipitate minerals when cultured in the laboratory.

It has been demonstrated that living organisms were trapped inside the gypsum crystals at the time of their development (approximately 35 Kyr BP, according to the positions of the inclusions inside the crystals and U–Th ages calculated by Sanna et al. 2011), and that they maintained some of their viable activities up to the present. Moreover, it can be supposed that inclusions in the inner central parts of the largest crystals could contain information about microorganisms living up to 400 Kyr BP in the hydrothermal aquifer of Naica. This is an extraordinary example of the dramatic geochemical and biological influences that mantle-derived materials can ultimately have on microbiology and a perfect opportunity to study hyperthermophile (extremely heat-tolerant) microorganisms and their potential for long-term viability within crystals. NASA was directly involved in this research, and it has successfully tested a new miniaturized Raman spectrometer inside the Cueva de los Cristales. This apparatus will be sent in the near future to Mars to look for evidence of living microorganisms on the surface of that planet.

Among the solid inclusions in Naica, one of the most intriguing findings was the presence of well-preserved pollen grains (Holden 2008) trapped inside the giant gypsum crystals (Fig. 10e). Their presence within the crystal lattice can only be explained by assuming that meteoric water seepage brought them deep into the thermal aquifer where the pollen was introduced into the caves by the hot water forming the crystals, which consequently trapped them inside their structure. Pollen and/or sporomorphs (Garofalo et al. 2010) have been found in all analyzed samples from the Naica caves, but detailed investigation has taken place only in Cueva de los Cristales. These cave pollens were extracted from the same crystal and the same area from which the absolute age of 34.544 ± 0.819 Kyr was obtained (Table 1, Sample N1). A total of over 40 pollen grains have been detected, and some of them are perfectly preserved. Among these are *Quercus* cf. *garryana*, *Lithocarpus densiflora* cf., *Cupressus*, *Taxus*, *Plantago*, and *Lycopodium* spores have been detected. The identified pollen is compatible with a humid broadleaf forest, presently extant in the southwestern areas of the USA, suggesting that about 35 Kyr BP the Naica area had a much more humid climate than today.

5.3 Gypsum Growth Rate

The great size of the selenite crystals in the Naica caves is attributable to the extremely low rates of nucleation and growth. To evaluate the current rate of hydrothermal gypsum precipitation in the mine, a vessel was placed at the −590 m level in a hot location where thermal water with a temperature of about 51 °C was still dripping from the mine wall rock. Inside the vessel, a closed system was maintained to prevent CO_2 exchange between the cave air and the sample into the solution (Forti and Lo Mastro 2008). Then tablets of prismatic polycrystalline gypsum were placed inside the vessel to support crystallization in saturated conditions

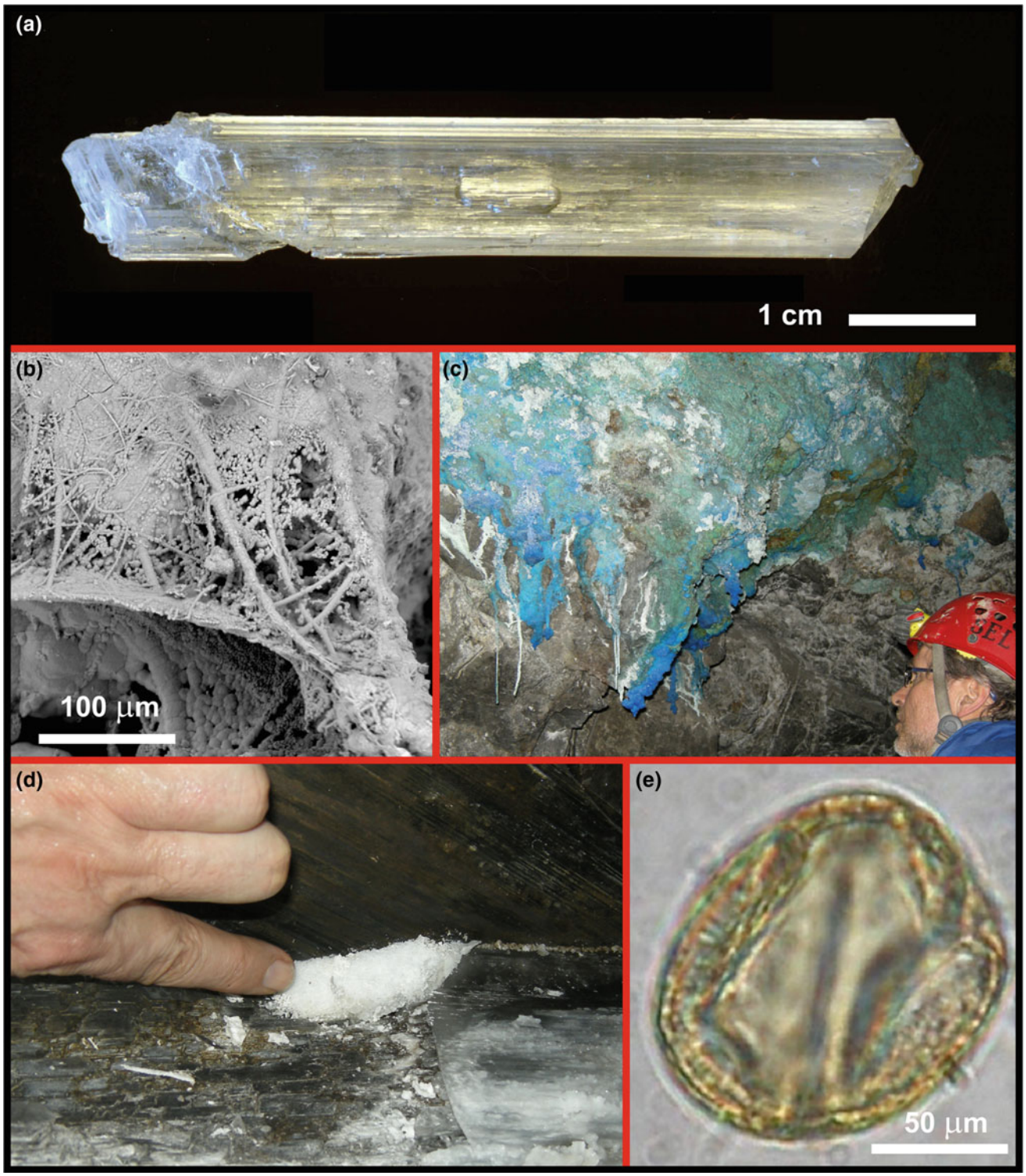

Fig. 10 **a** Cueva de las Espadas: gypsum crystal hosting a large two-phase fluid inclusion. **b** SEM image of fossilized biogenic structures in the oxide-hydroxide deposits below the gypsum crystals of Cueva de las Espadas (*Photograph* Ermanno Galli, University of Modena and Reggio Emilia). **c** Cave at the −150 m level: poly-mineral speleothems (composed of antlerite, azurite, calcantite, Cu-pentahydrite, gypsum, malachite, and melanterite) developed after the mine dewatering in 1985 (*Photograph* Paolo Forti, La Venta and S/F Archives.). **d** Ojo de la Reina: powder composed of an admixture of very soluble Mg–Na compounds (blödite, epsomite, hexahydrite, kieserite, pentahydrite) together with minor gypsum and halite, derived from the evaporation of water formerly trapped in a huge fluid inclusion (*Photograph* Paolo Forti, La Venta and S/F Archives). **e** First pollen extracted from a gypsum crystal of Cueva de los Cristales (*Photograph* Anna Maria Mercuri, University of Modena e Reggio Emilia)

Table 1 Ages of Naica crystals (modified from Sanna et al. 2011)

ID	Mineral	Cave	Age (Kyr)	2σ+	2σ−
N01-1	Gypsum	Ojo	191.018	13.75	12.5
N1	Gypsum	Cristales	34.544	0.82	0.81
N07-10	Gypsum	Cristales	158.526	101.64	51.96
ESP1-1	Gypsum	Espadas	57.01	1.77	1.77
ESP1-2	Aragonite	Espadas	14.491	4.15	4.03
ESP-surf	Calcite	Espadas	7.863	0.04	0.04

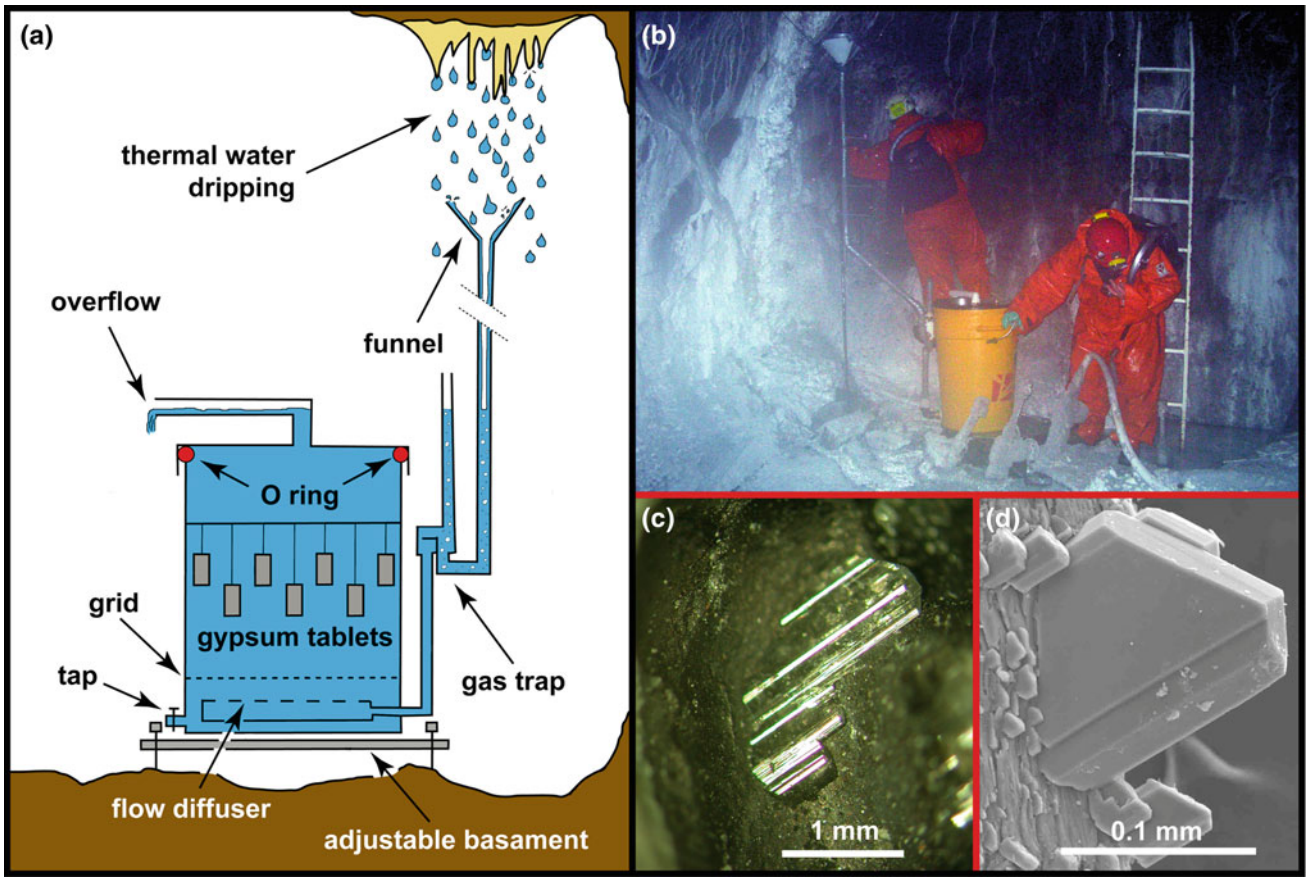

Fig. 11 **a** Sketch of the sampling device developed by La Venta to reproduce conditions for the development of gypsum crystals from the thermal water in the Naica mine (see Fig. 2). **b** The device in use just below the thermal spring at the −590 m level (*Photograph* Laura Sanna, La Venta and S/F Archives.) **c** SEM image of tiny gypsum crystals grown in about one year (*Photograph* Ermanno Galli, University of Modena e Reggio Emilia)

(Fig. 11). After two years, the current gypsum precipitation rate was ∼42 mm/Kyr at 50 °C, corresponding to ∼4–5 mm/Kyr at 58 °C. Later similar growth rates were estimated from U–Th dating of a giant crystal from Cueva de los Cristales (0.35–1.12 mm/Kyr, over the past 200 Kyr; Sanna et al. 2010, 2011). All these data agree with those obtained by Van Driessche et al. (2011) (0.5 mm/Kyr at 55 °C) for the deposition of gypsum from the current water of the Naica aquifer. On the basis of these experiments, it appears that the giant crystals of Naica experienced the slowest growth rates yet measured for a mineral (Van Driessche et al. 2011).

5.4 Age of Crystals

Data from fluid inclusions show that deposition temperatures in the latest 50,000 years were 1–2 °C lower in Cueva de las Espadas (56–54 °C) than in caves at the −290 m level

(55–58 °C) (Garofalo et al. 2009). It seems reasonable that the temperature stayed rather constant during the entire period of crystal development, so that when the first crystals began to develop in Espadas, the temperature at the −290 level would still be above 60 °C, thus avoiding gypsum precipitation in those caves. The elapsed time before the beginning of the depositional process at the −290 m level may be roughly estimated from the temperature drop that occurred at the groundwater level, and from the ages of the crystals. The present temperature at the top of the thermal aquifer (−590 m level) is 53–54 °C (unpublished data, Naica Mine). So, since the beginning of gypsum deposition in Espadas, the temperature drop at the water table has been about 5–6 °C.

Data from fluid inclusions (Garofalo et al. 2009) demonstrate that the giant crystals of Cueva de los Crystales developed between 55 and 58 °C in about 250,000 years, according to the available $^{230}Th/^{234}U$ dates (Table 2 sample N01-1 and N07-10, Sanna et al. 2011), and from artificial growth experiments (Forti and Lo Mastro 2008; Van Driessche et al. 2011).

Starting from these data, a time lapse of about 100,000 years corresponds to a decrease of about 2 °C. Consequently, the beginning of gypsum deposition in Cueva de las Espadas can be placed at about 400–350 Kyr BP. The broken crystals in Cueva de los Cristales were covered by 12–15 cm of gypsum overgrowth. The available U/Th dates (Sanna et al. 2011) give 35 Kyr BP for a location 5 cm below the outer surface of the crystal (N1 of Table 1), and the experimental growth data (4–5 mm/Kyr) allow a rough estimate of the period in which the seismo-tectonic stresses occurred: from 80 to 40 Kyr BP. Finally, the development of the sails in Cueva de las Velas occurred in 1985, during the fast dewatering of that cave.

Because there are no U/Th measurements for the gypsum in Palacios cave, it is difficult to estimate the age of its vadose helictites. It is evident that they developed in an aerated environment when the water table was below that level (−90 m). Even with no absolute data, it is possible to state they began to form 350,000 years ago (e.g., they grew contemporaneously with the earliest phreatic gypsum crystals of Cueva de las Espadas). This is because a partially corroded calcite flowstone is present just below the deposits of metallic oxides-hydroxides, which is also present inside the gypsum crystals of Cueva de las Espadas.

6 Other Chemical Deposits

Even if 99% of the chemical deposits in the Naica caves are gypsum, scientific interest in the other deposits is very high. Mineralogical analyses identified the presence of over 40 different cave minerals (Forti et al. 2007, 2008, 2009), 10 of which (antlerite, hectorite, orientite, pentahydrite-Cu, plumojarosite, starkeyite, szmikite, szmolnokite, woodruffite, and an unidentified Al, Mg, Cu, Zn silicate) are new for the cave environment. Most are oxides-hydroxides, developed in two distinct periods of oxidation of the ore bodies. In the first stage, which occurred deep inside the thermal aquifer before and/or during the deposition of the giant gypsum crystals, a large quantity of material was deposited but only a few minerals developed. This process was clearly controlled by microorganisms, as testified by widespread biogenic structures preserved within these deposits (Fig. 10 b) (Forti et al. 2009).

The second oxidation stage, started less than 50 years ago when mine dewatering progressively caused aerated conditions (Forti et al. 2007, 2009). In this case, the process was abiotic as proved by the total absence of any biogenic forms and it induced the deposition of small amounts of material but with an extremely high chemical variability (Fig. 10c, d) due to the high number of active minerogenetic mechanisms (Table 2).

In addition to these two stages of ore body oxidation, an important minerogenetic period was restricted to Cueva de las Espadas, where some small "pseudo-stalagmites"

Table 2 Environmental control over the active minerogenetic processes within the Naica caves and related temperature variations (after Forti et al. 2009, modified)

Environment	Processes	Chemical deposits	T decrease
Vadose	Organic matter mineralization	Organic mineral and phosphate deposition	Very fast
	CO_2 diffusion	Calcite speleothem evolution	
	Acid aggression	Gypsum, metallic sulfates and silicates deposition	
	Inorganic oxidation	Oxide-hydroxides deposition	
	Evaporation	Gypsum "sails" development, sulfates and halides deposition	
Epiphreatic	CO_2 diffusion	Aragonite deposition	Slow
Deep phreatic	Organic oxidation	Oxide-hydroxide deposition and limestone corrosion	Extremely slow
	Gypsum/anhydrite disequilibrium	Giant gypsum crystals and celestite development	

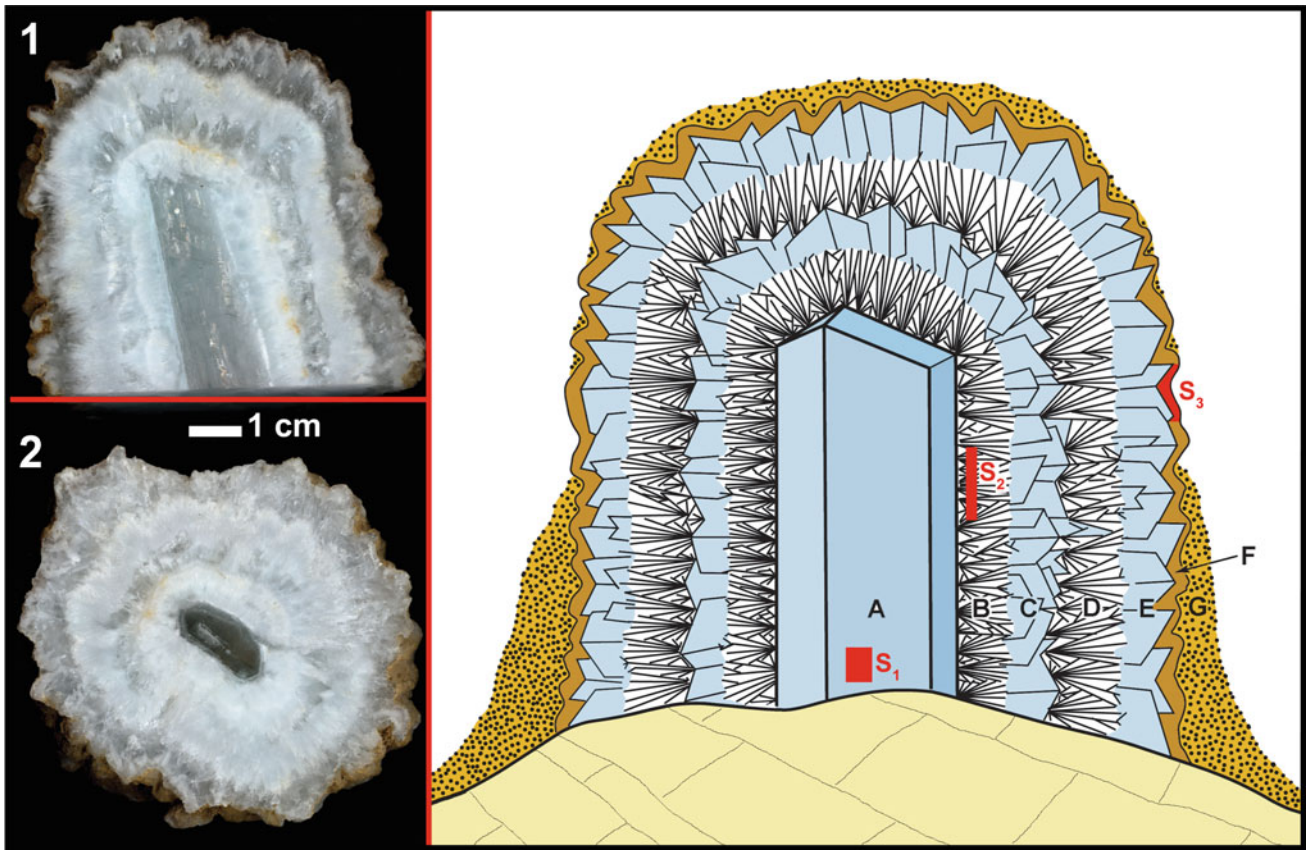

Fig. 12 Vertical (*1*), horizontal (*2*) sections, and a graphical representation of a pseudo-stalagmites grown inside the terminal lake of Cueva de las Espadas: *A* gypsum, *B* aragonite, *C* gypsum, *D* aragonite, *E* gypsum, *F* calcite, *G* clay and silt. S_1, S_2, and S_3 are the sampling points for U/Th dating (modified from Forti and Sanna 2010)

(Gázquez et al. 2012) developed in its deepest part (Fig. 12). They have an inner nucleus consisting of a euhedral prismatic gypsum crystal, over which two white layers of acicular aragonite (0.5 cm each) developed with alternating layers of gypsum macro-crystals (each 0.5 cm). Then, the speleothem was covered with a thin layer (1–2 mm) of hazel-brown calcite. The thickness of these five overgrowth layers suggests a rather constant time span, not exceeding 2–3 thousand years for each. Finally, the speleothems were partly covered by poorly cemented, thin silty-clay deposits, which represent the latest stage in the depositional sequence in this cave (Forti et al. 2009).

The development of these pseudo-stalagmites started just after a long period of low groundwater, which completely drained Cueva de las Espadas. The resulting strong condensation caused dissolution of most, if not all, of the previously deposited gypsum and also induced enhanced corrosion of the limestone walls and ceilings in the upper levels of the cave (Fig. 6b). About 60 Kyr BP (Table 1, ESP1-1; Sanna et al. 2011), thermal water refilled Cueva de las Espadas. Immediately gypsum deposition began again, and the inner gypsum core of the pseudo-stalagmites was formed. At 14 Kyr BP (Table 1, ESP 1-2), the groundwater level fell again, allowing air to enter, but only in the upper part of the cave. This allowed growth of aragonite by diffusion of CO_2 into the thermal water (Forti et al. 2008). A following high groundwater level reestablished saturated conditions, which allowed gypsum to be deposited. The cave experienced yet another episode of low and high stands, with the growth of a new gypsum layer that was later covered by aragonite. About 8 Kyr BP (Table 1, ESP-surf), thermal water drained from Cueva de las Espadas and meteoric seepage water developed an upper layer of thin brown calcite. The difference in age between the first aragonite layer and the last calcite layer confirms that each of the five layers developed in less than 2000 years. Finally, during the last century, mining activities initially caused deposition of silt and clay over the pseudo-stalagmites (a layer that correlates with the solid inclusion layer ~1 mm below the upper surfaces of the crystals at the −290 m level), and the seepage of meteoric water into the caves ended.

The dewatering processes, active after 1985, exposed the thermal inlets at −590 m to the mine atmosphere. This caused the rapid development of speleothems composed of

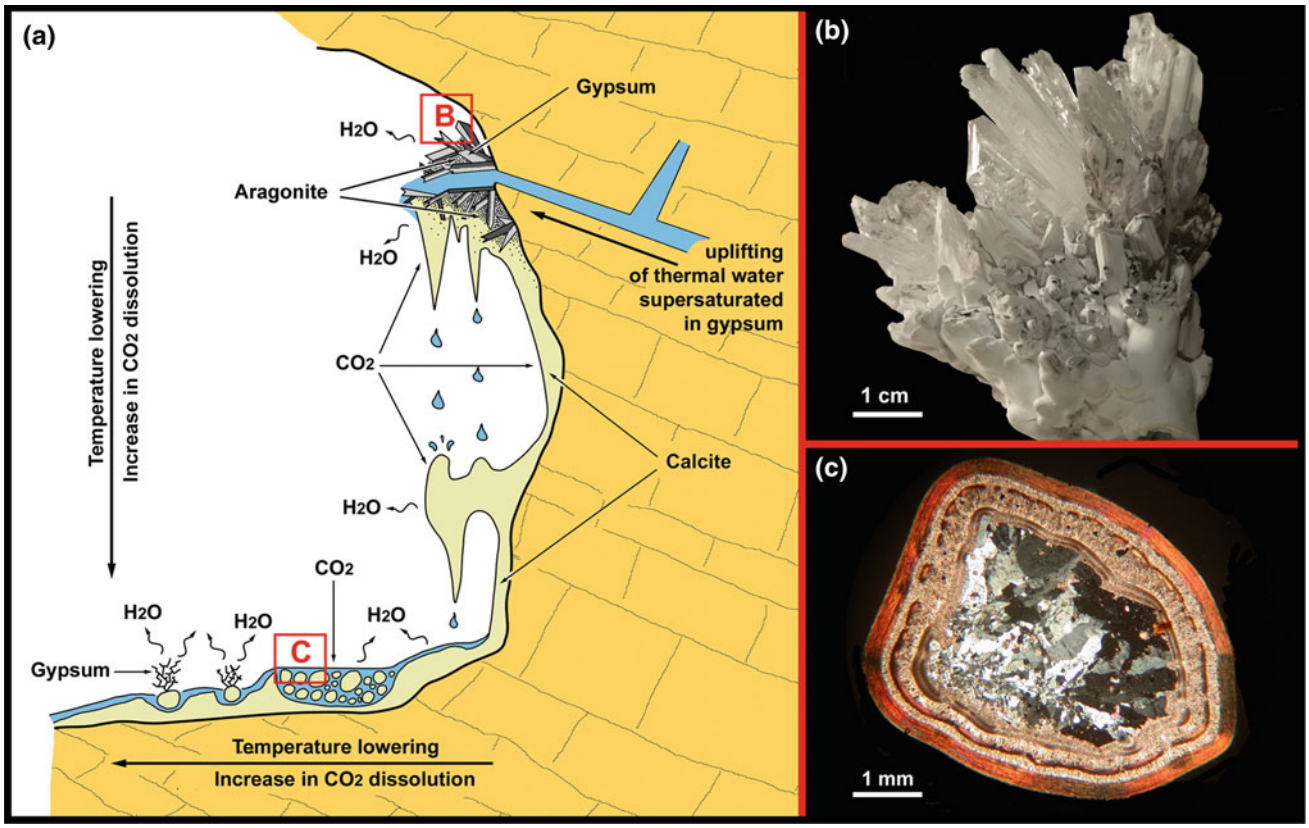

Fig. 13 **a** Genetic sketch for the speleothems growing in the thermal springs at the −590 m level (modified from Forti et al. 2008). **b** Fragment of speleothem growing in contact with the rising thermal water: It consists of gypsum crystals partially covered by aragonite flowstone (*photograph* Paolo Ferrieri, University of Bologna). **c** Polarized photomicrograph of a polished section of cave pearl with a partly re-dissolved gypsum nucleus. The external layers consist of micritic calcite (*white grains*) partially replacing the original thin aragonite layers (*red laminated structures*) (*Photograph* Antonio Rossi, University of Modena e Reggio Emilia)

calcium carbonate (aragonite and/or calcite) instead of gypsum. These deposits were formed because CO_2 quickly migrated from air into the dripping water (Fig. 13) thus turning the previous slight gypsum supersaturation into a strong calcium carbonate supersaturation. The local environmental conditions (51 °C and rapid evaporation) initially caused the formation of aragonite, which quickly transformed to calcite, thanks in part to the relatively fast temperature drop from the spring location toward the mine galleries.

Several years later, cooling of the cavern environment, induced by mine dewatering and ventilation, produced a third minerogenetic oxidation period within Ojo de la Reina, Cueva de las Velas, and later Cueva de los Cristales (Fig. 14). Metallic sulfides dispersed within the cave walls gradually oxidized, giving rise to several new diagenetic compounds, some of which are rare or even new for the cave environment (Forti et al. 2007, 2009).

Finally, within Ojo de la Reina, since 2005, increased condensation around the gypsum crystals led to their fast dissolution and transformation to calcite speleothems (Fig. 13), following the same mechanism just outlined for the speleothems that developed near the thermal springs in the −590 m level. Dissolution of gypsum in Ojo de la Reina was particularly rapid along major exfoliation planes and at times reached the giant fluid inclusions, which caused these solutions to drain (Badino et al. 2011). As these fluids evaporated, they formed several types of secondary cave minerals (Fig. 10d).

7 Main Stages in Development of the Naica Karst

The initial stage was about 25 Myr BP, when regional intrusive magmatic activity formed a batholith about 1140 m below the Naica ridge. During the entire first stage, thermal fluids responsible of the evolution of the Naica ore bodies were characterized by net deposition and, therefore, no karst voids could develop.

A second stage started about 1.5 Myr BP, when tectonic stresses partially displaced the ore bodies, giving rise to open

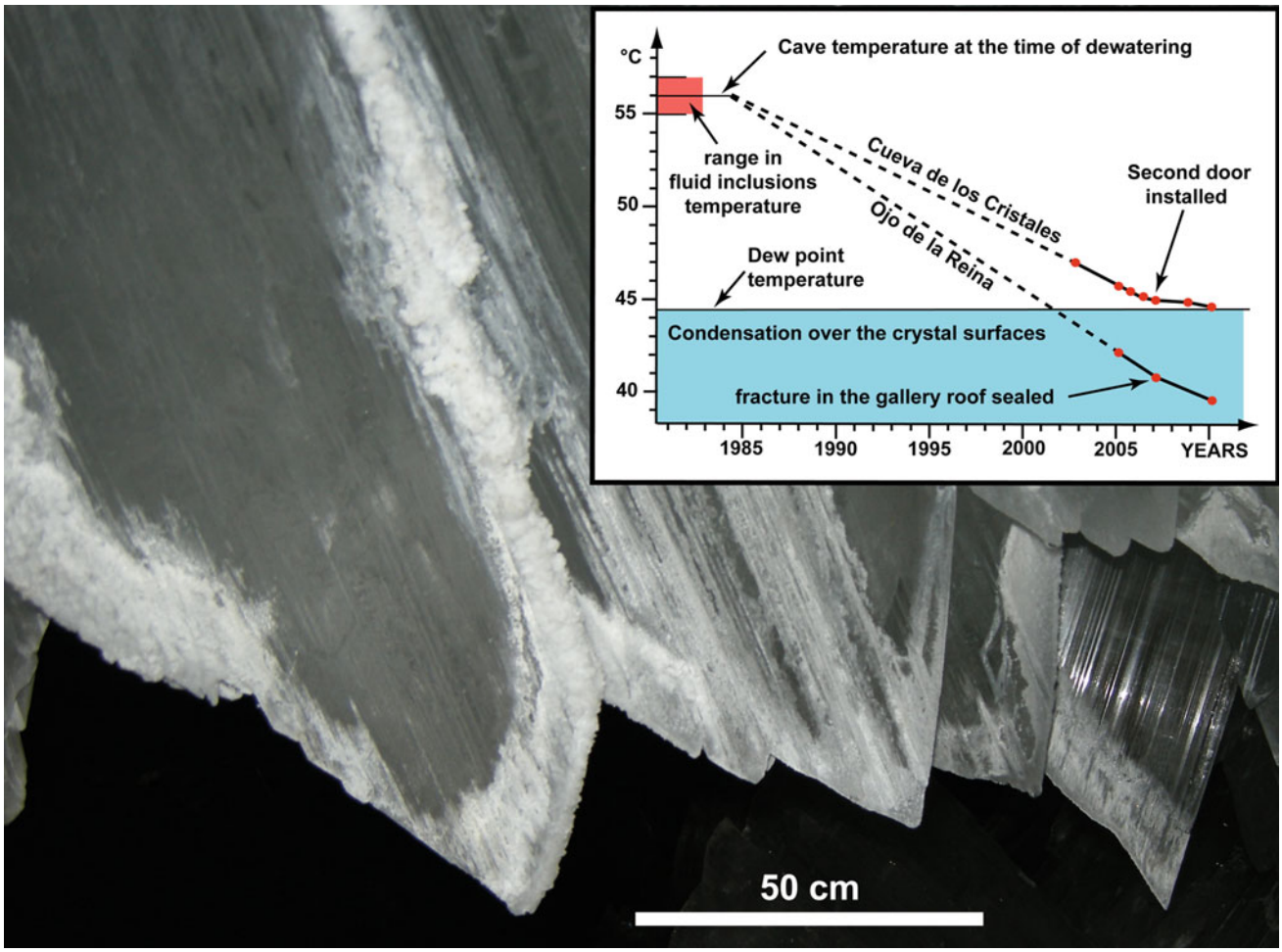

Fig. 14 Ojo de la Reina: view of the giant selenite crystals partially covered by secondary calcite deposits (*Photograph* Paolo Forti, La Venta and S/F Archives) The evolution of the temperature inside Cueva de los Cristales and Ojo de la Reina caves after their dewatering (after Badino et al. 2011)

joints and fractures related to three faults (Naica, Gibraltar, and Montañas), which controlled the rise of thermal fluids. Meanwhile, the thermal water cooled below 100–120 °C and became aggressive. Thus, small cavities could develop at different levels within the aquifer (Fig. 15b). This stage was short—only a few thousand, or tens of thousands, of years.

Shortly after development of the caves, the groundwater level declined and the resulting evolution differed from cave to cave. The groundwater dropped below the +50 m cave very early; in fact, it has no evidence of phreatic gypsum deposit. This cave is about 220 m above Cueva de las Espadas (Badino and Forti 2013) (Fig. 2), and, therefore, if the temperature decrease was constant or slightly faster than that observed between Espadas and caves at −290 m, deposition of gypsum in the +50 m cave should have started 150 My earlier than in Espadas. Therefore, the +50 m cave was already dry at 550–400 Kyr BP. This fact is corroborated by the presence of partially eroded calcite speleothems below the first deposits of oxides-hydroxides (Fig. 7).

About 160 m below the +50 m Cave, Cueva Palacios hosts only small vadose gypsum helictites (Fig. 7). Therefore, this cave also stood above the groundwater level when conditions for deposition of phreatic gypsum

Fig. 15 Chronology of the main evolutionary stages within the Naica ridge from 25 to 60 Kyr BP. **a** High-level thermal fluids deposited polysulfide ore within the Naica ridge. **b** Aggressive thermal fluids at 100–120 °C rose along the three main regional faults, to form caves at different levels. **c** After a drop in the water table, which dewatered the +50 m and Palacios caves, thermal water became supersaturated with respect to gypsum and its nucleation took place at the −120 m level. **d** Huge selenite speleothems began to grow at the −290 m level, while water table fluctuations in epiphreatic conditions produced gypsum corrosion in Cueva de las Espadas. **e** A new period of phreatic gypsum precipitation occurred in all caves at the −120 and −290 levels (modified from Sanna et al. 2011) ▶

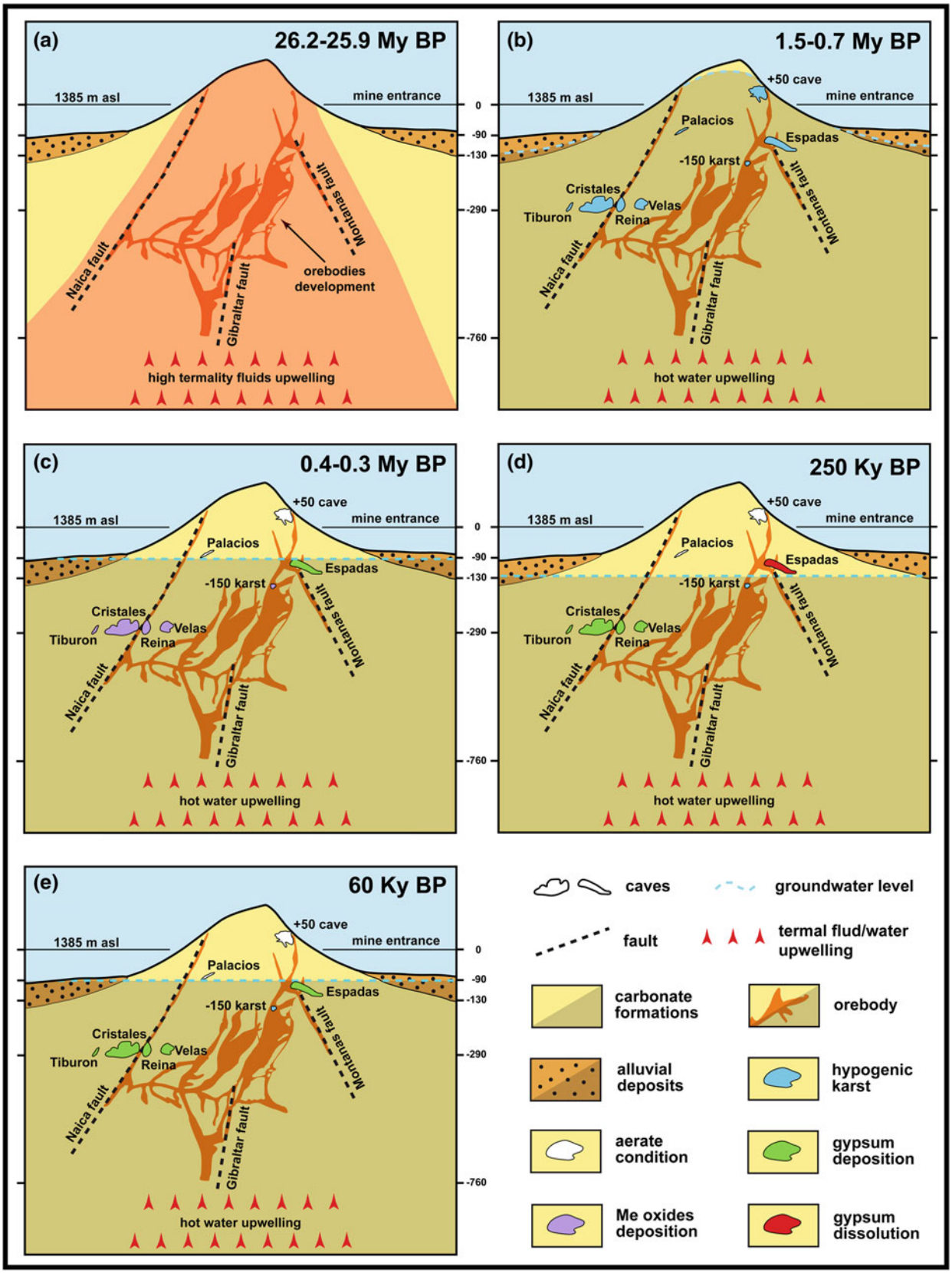
(a)
26.2-25.9 My BP
1385 m asl
mine entrance
Naica fault
Gibraltar fault
Montanas fault
orebodies development
high termality fluids upwelling
(b)
1.5-0.7 My BP
+50 cave
Palacios
Espadas
-150 karst
Cristales
Tiburon
Velas
Reina
hot water upwelling
(c)
0.4-0.3 My BP
(d)
250 Ky BP
(e)
60 Ky BP
0
-90
-130
-290
-760
caves
groundwater level
fault
termal flud/water upwelling
carbonate formations
orebody
alluvial deposits
hypogenic karst
aerate condition
gypsum deposition
Me oxides deposition
gypsum dissolution

were achieved. Thus, about 400–300 Kyr BP, the groundwater level must have been between Cueva Palacios and Cueva de las Espadas (Fig. 15c). The groundwater level remained rather static for a long time, during which gypsum crystals developed only in Espadas, and trapping within their lattice, the oxides-hydroxides generated by the first strong oxidation period. These were in turn deposited directly on the floor and walls of the −290 m caves. Shortly after the oxidation event, deposition of gypsum also started at the −290 m level (250 Kyr BP). In the same period, the groundwater level dropped below Espadas, where strong condensation caused dissolution of almost all the gypsum crystals (Fig. 15d).

At this time, Espadas was the only cave which experienced different stages in its development, while all the other cavities were inactive (the upper ones) or maintained deposition of gypsum until they were dried up by mining dewatering. In Espadas, all the evolutionary steps were strictly controlled by the migration of the groundwater level.

At 70–60 Kyr BP, saturated conditions were restored and a new generation of gypsum crystals developed (Fig. 15e). In a rather short time, the thermal–fresh water boundary fluctuated around the level of the cave, as testified by the layered structures on the outer surfaces of the previous generation of gypsum crystals (Panieri et al. 2008). At 15 Kyr BP, the cave became partially aerated, allowing deposition of the first aragonite layer over the pseudo-stalagmites in the bottom of the cave (Fig. 16f). Later, up to 8 Kyr BP, the groundwater level fluctuated with a frequency of roughly 2000 years, and thus Cueva de las Espadas moved from aerated to saturated conditions twice, as shown by the two gypsum and aragonite layers (Figs. 12 and 16g). Finally, at 6–5 Kyr BP, the cave was exposed to meteoric water seepage with the development of a layer of calcite on top of the pseudo-stalagmites (Fig. 16h). This process was suddenly interrupted by the mining thirty years ago (Fig. 16h). At that time, the deeper caves (Cristales, Ojo de la Reina, and Velas) suddenly changed from deep phreatic to vadose conditions and deposition of phreatic gypsum immediately stopped.

But this did not represent the end of cave development: The cone of depression had significant consequences on cave development, giving rise to the evolution of several new diagenetic minerals owing to active oxidation of polysulfides. A few years after dewatering, cooling of the caves caused hot moist condensation in the area of the giant gypsum crystals, causing parts of them to be converted to calcite.

The very last stage in the evolution of the Naica cave occurred at the end of 2015 AD because the mining activities ended (Fig. 16l). The consequent rise of the thermal waters restored the original groundwater level a few tens of meters below Cueva de la Espadas, so the gypsum crystals of the caves below that level began to grow again.

8 Final Loss

As soon the caves at the −290 m level were discovered, it was clear that they would remain accessible for only a short time. The owner of the mine explained that it would be economically impossible for them to continue dewatering the mine after the ore bodies were totally exploited. In 2002, they predicted that this event would occur in less than 10 years (Naica Mine private communication).

During development of the "Naica Project," La Venta explored all possible ways (local, national, and international) to keep these caves accessible after the mining ended, and they prepared projects to reach this goal. The suggested solutions would also have had a social function: The existence of the village of Naica (with about 4000 inhabitants) depends entirely on the mine. It might have had a touristic future if the caves had remained accessible. Unfortunately, La Venta's effort received much theoretical acceptance but no practical solution.

In early 2015, the mining intersected a completely unexpected major thermal vein that flooded the lower levels of the mine. Dewatering procedures were unsuccessful, and so the mine was abandoned in October. In about one year, the caves were submerged in more than 160 m of hot water. The remaining air-filled caves are Espadas, Palacios, and the one at +50 m, but they are inaccessible because the mine is closed.

This is a shame for cavers and scientists throughout the world, who have lost the possibility of visiting such an astonishing world. But for the giant crystals, it is the best possible solution. During the 15 years of aeration, they not only stopped growing but also degraded as a result of the cave visitation and, even worse, they started to dissolve and to transform into calcite speleothems as their surface temperatures decreased below that of the surrounding

Fig. 16 Chronology of the main evolutionary stages within the Naica ridge from 15 Kyr BP to 2015 AD. At the −120 m level, further oscillations in the water table produced two epiphreatic cycles with aragonite deposition on submerged gypsum crystals at 15 Kyr (**f**) and 7.9 Kyr BP (**g**) while inside the caves at the −290 m level, gypsum continued to precipitate. **h** The thermal water left definitively Espadas cave, and a short period of meteoric seepage was active in a quickly ▶ cooling, vadose environment with deposition of a thin calcite cover. **i** The cone of depression induced by mine dewatering suddenly interrupted gypsum deposition at the −290 m level. **l** After mining activities ended, the groundwater level was restored just below Espadas (modified after Sanna et al. 2011)

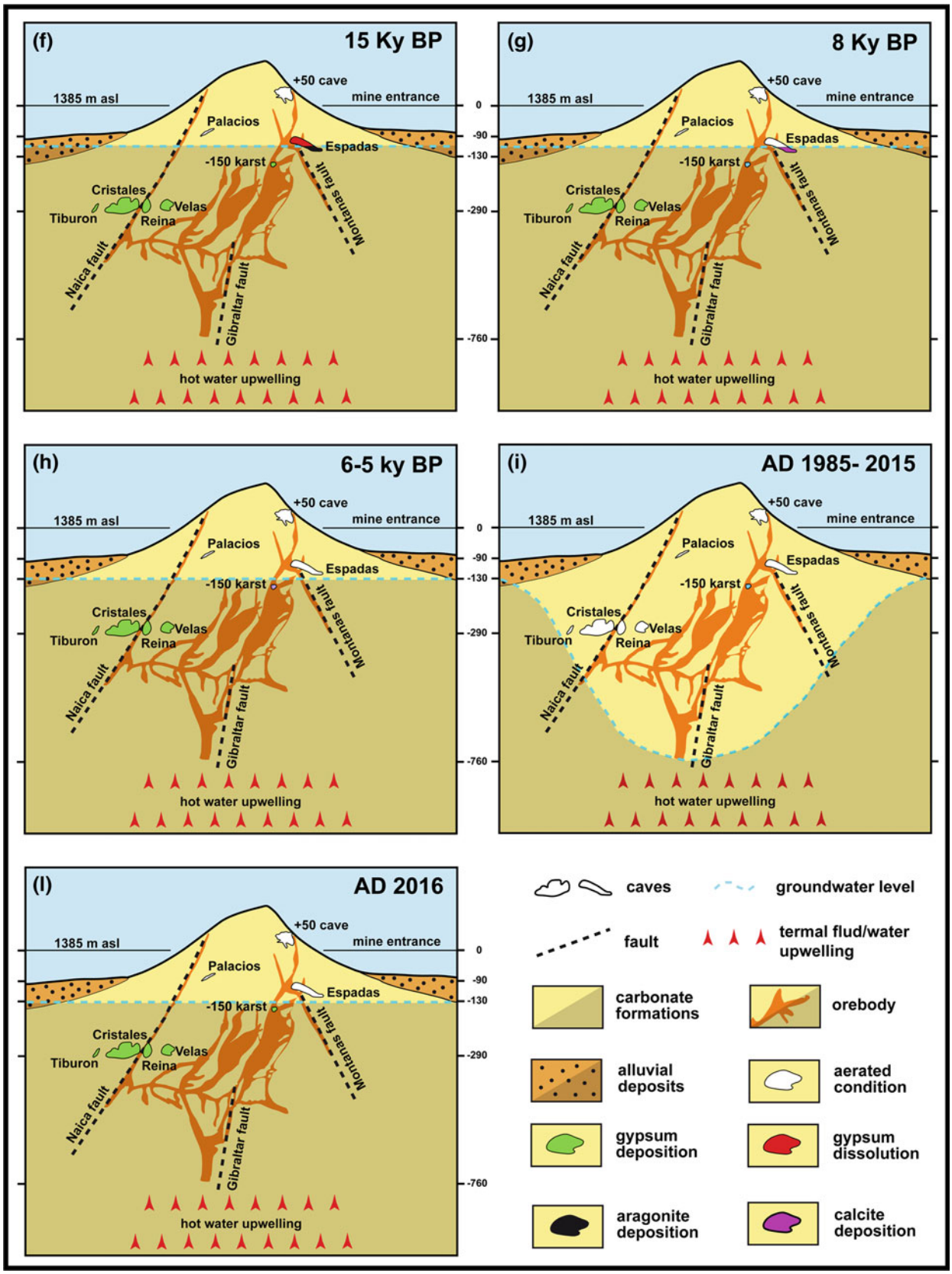
(f)
15 Ky BP
(g)
8 Ky BP
(h)
6-5 ky BP
(i)
AD 1985- 2015
(l)
AD 2016
1385 m asl
+50 cave
mine entrance
Palacios
Espadas
-150 karst
Cristales
Tiburon
Velas
Reina
Naica fault
Gibraltar fault
Montanas fault
hot water upwelling
0
-90
-130
-290
-760
caves
groundwater level
fault
termal flud/water upwelling
carbonate formations
orebody
alluvial deposits
aerated condition
gypsum deposition
gypsum dissolution
aragonite deposition
calcite deposition

atmosphere. Now, in the depth of the thermal aquifer, the crystals will grow again and maybe, in unknown future time, someone will again have the chance to see them shining, bigger, and better looking than ever. In any case, the next generations will keep alive the memory of the Naica caves thanks to the photographs, studies, and publications made during and just after the "Naica Project."

Acknowledgements The author thanks Peñoles Company for allowing access to the Naica Mine and La Venta Esplorazioni Geografiche and C/Producciones for leading the "Naica Project" (2006–2009).

References

Badino G, Forti P (2007) The exploration of the caves of the giant crystals (Naica, Mexico). Nat Speleol Soc News 65(2):12–18

Badino G, Forti P (2013) Naica caves: perhaps the most important mine caves of the world. Memore Istituto Italiano di Speleologia 2(28): 29–40

Badino G, Calaforra Chordi JM, Forti P, Garofalo P, Sanna L (2011) The present day genesis and evolution of cave minerals inside the Ojo de la Reina cave (Naica Mine, Mexico). Int J Speleol 40(2):125–131

Bernabei T, Forti P, Villasuso R (2007) Sails: a new gypsum speleothem from Naica (Chihuahua, Mexico). Int J Speleol 36(1): 23–30

Bernabei T, Casagrande G, Davila A, De Vivo A, Ferreira A, Giovine G, Infante G, Lo Mastro F (2009) The naica project. In: White WB (ed) Proceedings 15th international congress of speleology, Kerrville Texas (USA), 1, p 283–288

Beverly M, Forti P (2010) L'esplorazione della Grotta Palacios nella miniera di Naica. Speleologia 63:46–49

Boston PJ, Spilde MN, Northup DE, McMillan C (2012) Long-term persistence of microorganism in geological materials: lazarus, rip van winkle, and the walking dead. Life detection in extraterrestrial samples conference

Boston PJ, Spilde MN, Northup DE, McMillan C (2013) Crunchy on the outside, tender on the inside: the persistence of microorganisms in geological materials. In: De Waele J, Forti P, Naseddu A (eds) Mine caves. Memore Istituto Italiano di Speleologia 27:27–28

Calaforra, JM, Forti P, Gázquez F, Sanna L (2013) La gradazione dei cristalli di gesso nella Cueva de las Espadas (Naica, Messico): Un classico esempio del controllo della sovrasaturazione sui processi di nucleazione. 20° Congresso Italiano di Speleologia. Trieste, 2011. pp 325–332

Canevese EP, Tedeschi R, Forti P (2009) Laser scanner in extreme environments: the caves of Naica. The American Surveyor February 2009, pp 3–10

Degoutin N (1912) Les grottes à cristaux de gypse de Naica. Revista de la Societad Cientifica Antonio Alzate 32:35–38

Erwood RJ, Kesler SE, Cloke PL (1979) Compositionally distinct, saline hydrothermal solutions, Naica Mine, Cihuahua, Mexico. Econ Geol 74:95–108

Forti P (2010) Genesis and evolution of the caves in the Naica Mine (Chihuahua, Mexico). Zeitschrift für Geomorphologie 54(supplement 2):285–306

Forti P, Lo Mastro F (2008) Il laboratorio sperimentale di -590 nella Miniera di Naica (Chihuahua, Mexico). Mondo Sotterraneo 21(1–2): 11–26

Forti P, Sanna L (2010) The Naica project. A multidisciplinary study of the largest gypsum crystal of the world. Episodes 33(1):23–32

Forti P, Galli E, Rossi A (2007) The mineralogical study on the Cueva de las Velas (Naica, Mexico). Acta Carsologica 36(2):75–85

Forti P, Galli E, Rossi A (2008) Il sistema Gesso-Anidrite-Calcite: nuovi dati dalle concrezioni della miniera di Naica (Messico). Memorie Istituto Italiano di Speleologia 21:139–149

Forti P, Galli E, Rossi A (2009) Minerogenesis in the Naica caves (Chihuahua, Messico). In: White WB (ed) Proceedings 15th international congress of speleology, Kerrville Texas (USA), 1, p 300–305

Foshag W (1927) The selenite caves of Naica, Mexico. Am Miner 12:232–252

García-Ruiz JM, Villasuso R, Ayora C, Canals A, Otálora F (2007) The formation of gypsum megacrystals. Geology 35(4):327–330

Garofalo PS, Fricker M, Günther D, Forti P, Mercuri AM, Loreti M, Capaccioni B (2010) Climatic control on the formation of the gigantic gypsum crystals of the Naica caves (Mexico)? Earth Planet Sci Lett 289(3/4):560–569

Gázquez F, Calaforra JM, Forti P, Rull F, Martínez-Frías J (2012) Gypsum-carbonate speleothems from Cueva de las Espadas (Naica mine, Mexico): mineralogy and paleoenvironmental implications. Int J Speleol 41(2):210–220

Gázquez F, Calaforra JM, Stöll H, Sanna L, Forti P, Lauritzen S-E, Delgado-Huertas A, Rull F, Martínez-Frías J (2013) Isotope and trace element evolution of the Naica aquifer (Chihuahua, Mexico) over the past 60,000 yr revealed by speleothems. Quat Res 80: 510–521

Giovine G, Badino G, De Vivo A, Lo Mastro F, Casagrande G, Davila A, Hidalgo G (2009) The Naica caves and physiology. In: White WB (ed) Proceedings 15th international congress of speleology, Kerrville, Texas (USA), 3, p 1980–1984

Holden C (2008) Life in crystal. Science 319:391

London D (2003) New "cave of the crystals" at Naica, Chihuahua, Mexico. Earth Scientist, Magazine of school of geology and geophysics, University of Oklahoma 704:24–27

Megaw PKM, Ruiz J, Titley SR (1988) High-temperature, carbonate-hosted Pb–Zn–Ag (Cu) deposits of Northern Mexico. Econ Geol 83:1856–1885

Panieri G, Forti P, Gasparotto G, Soliani L (2008) Studio delle inclusioni solide presenti nei cristalli di gesso della Grotta delle Spade (Naica, Messico). Memorie dell'Istituto Italiano di Speleologia s. II (19): 335–343

Sanna L, Saez F, Simonsen S, Constantin S, Calaforra JM, Forti P, Lauritzen SE (2010) Uranium-series dating of gypsum speleothems: methodology and examples. Int J Speleol 39(1):35–46

Sanna L, Forti P, Lauritzen SE (2011) Preliminary U/Th dating and the evolution of gypsum crystals from Naica Caves (Mexico). Acta Carsologica 40(1):17–28

Stone JG (1959) Ore genesis in the Naica District, Chihuahua, Mexico. Econ Geol 54:1002–1034

Van Driessche AES, García-Ruiz JM, Tsukamoto K, Patiño-López LD, Satoh H (2011) Ultraslow growth rates of giant gypsum crystals. Proc Nat Acad Sci 108:15721

Sulfur-Rich Caves of Southern Tabasco, Mexico

54

Louise D. Hose and Laura Rosales-Lagarde

Abstract

Sulfur-rich karst springs that drain middle to Late Cretaceous carbonates in southern Tabasco, Mexico, contain elevated total dissolved solids with high chloride and either high sulfide or sulfate. The mostly meteoric waters circulate along intermediate-depth flow paths, interacting with Jurassic evaporites and then mixing with shallow-circulating rainwater to produce brackish, sulfur- and NaCl-rich spring waters. Several caves, notably Cueva de Villa Luz and Cueva de Luna Azufre near Tapijulapa, are developing from these waters. Both are fed by small, warm subterranean springs that release hydrogen sulfide and carbon dioxide at the water–air interface. These gases combine with water vapor in the air and moisture on cave walls to form acidic solutions, which enlarge the cave passages. Speleogenesis is aided by abundant chemoautotrophic microbes that facilitate oxidation and the production of acid solutions. Cave walls and ceilings display several distinctive colonies of these microbes, notably filamentous bundles (snottites) and biovermiculations. The organisms also reside in unusual mineral deposits, including sulfur folia, sulfur crusts, and gypsum paste. Pore fluids in these deposits and growths have very low pH despite their proximity to limestone walls. Speleogenesis appears to follow a three-step process: (1) an early sulfide-rich phreatic phase; (2) a sulfide-rich, vadose–phreatic phase of chemical alteration and mechanical stoping; and (3) a tertiary sulfide-depleted phase of epigenic speleogenesis. The second phase of development dominates speleogenesis in Cuevas de Villa Luz and Luna Azufre.

Keywords

Sulfur • Chemoautotrophic microbes • H_2S • Petroleum

1 Introduction

The state of Tabasco, Mexico, is widely recognized as rich in productive petroleum fields associated with elemental sulfur and sulfides, and sulfur-rich springs, and its actively developing sulfur-rich caves (Gold 1999; Hose and Pisarowicz 1999; Rosales-Lagarde et al. 2014). These sulfidic caves inform us about the breadth of life in the subsurface (Northup et al. 2005), the potential for chemoautotrophic ecosystems on other planets (Boston et al. 2001, 2006), the genesis of certain notable caves worldwide (Hose and Macalady 2006), the development of porosity and evolution of petroleum basins (Hill 2000; DuChene 2009), and the development of Mississippi Valley-type ore deposits (Hill 2000).

Most notable in Tabasco are the sulfur-rich caves in the southern part of the state, particularly in Villa Luz Park near the town of Tapijulapa (Fig. 1). The 2-km-long Cueva de

L.D. Hose (✉)
Department of Geological Sciences and Engineering, University of Nevada, Reno, NV 89557, USA
e-mail: hose@drkarst.net

L. Rosales-Lagarde
Department of Physical and Life Sciences, Nevada State College, Henderson, NV 89002, USA
e-mail: laura.rosales@nsc.edu

© Springer International Publishing AG 2017

A. Klimchouk et al. (eds.), *Hypogene Karst Regions and Caves of the World*,
Cave and Karst Systems of the World, DOI 10.1007/978-3-319-53348-3_54

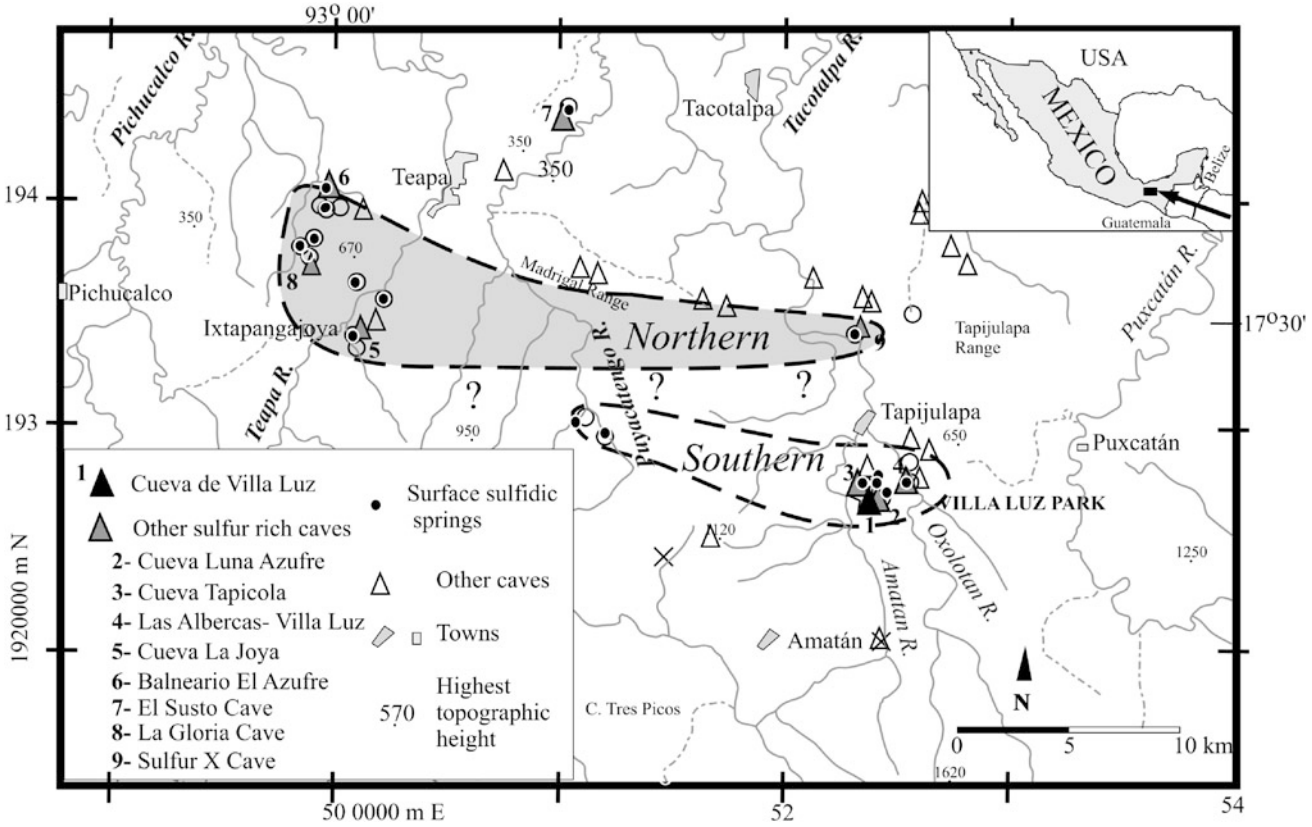

Fig. 1 Location map showing sulfur-rich caves and sulfidic surface springs in the southern part of Tabasco. Caves and springs south of Tapijulapa and east of Ixtapangajoya are part of the Southern Zone of Rosales-Lagarde et al. (2014). The other caves and springs are part of their Northern Zone

Villa Luz has been widely publicized largely because of its robust, mostly chemoautotrophic ecosystem, and its abundant and charismatic form of microfauna, the "snottite" (Fig. 2; Pain 1998; Eliot 2001; Hose 2001).

2 Regional Setting

2.1 Location

The state of Tabasco extends south from the southernmost shores of the Gulf of Mexico to the foothills of the Sierra de Chiapas (Fig. 1). The topography of the region drops sharply from about 2800 m asl in the Sierra de Chiapas (south of the Tabasco border) to approximately 20 m asl on the Tabasco fluvial plain (INEGI 1983a, 1985). Known Tabasco caves developed between 17 m asl and 102 m asl (Rosales-Lagarde 2013). The mean annual atmospheric temperature is ~27 °C, the mean precipitation varies from 3400 to 4500 mm/year, and the dominant vegetation consists of tropical rain forest partially replaced in the lowlands by grassland due to fires and land use changes (Salazar-Conde et al. 2004; INEGI 1983b; Ramos-López 2003).

2.2 Regional Geology

2.2.1 Stratigraphy

Figure 3 shows the pertinent regional stratigraphy. Subsurface rocks consist, from oldest to youngest, of (a) a probable plutonic basement; (b) Paleozoic schist and quartzite; (c) Middle to Upper Jurassic halite and clastic deposits, with minor carbonates and anhydrite. Overlying strata exposed at the surface consist of discontinuous outcrops of (a) Cretaceous dolostone interbedded with anhydrite, transitioning upward to limestones with chert, to limestones with marl; (b) Paleogene to Neogene marls, shales and other clastic rocks, and sparse carbonates; (c) Pliocene granodiorite; (d) Pliocene to Recent andesitic to basaltic lava flows and

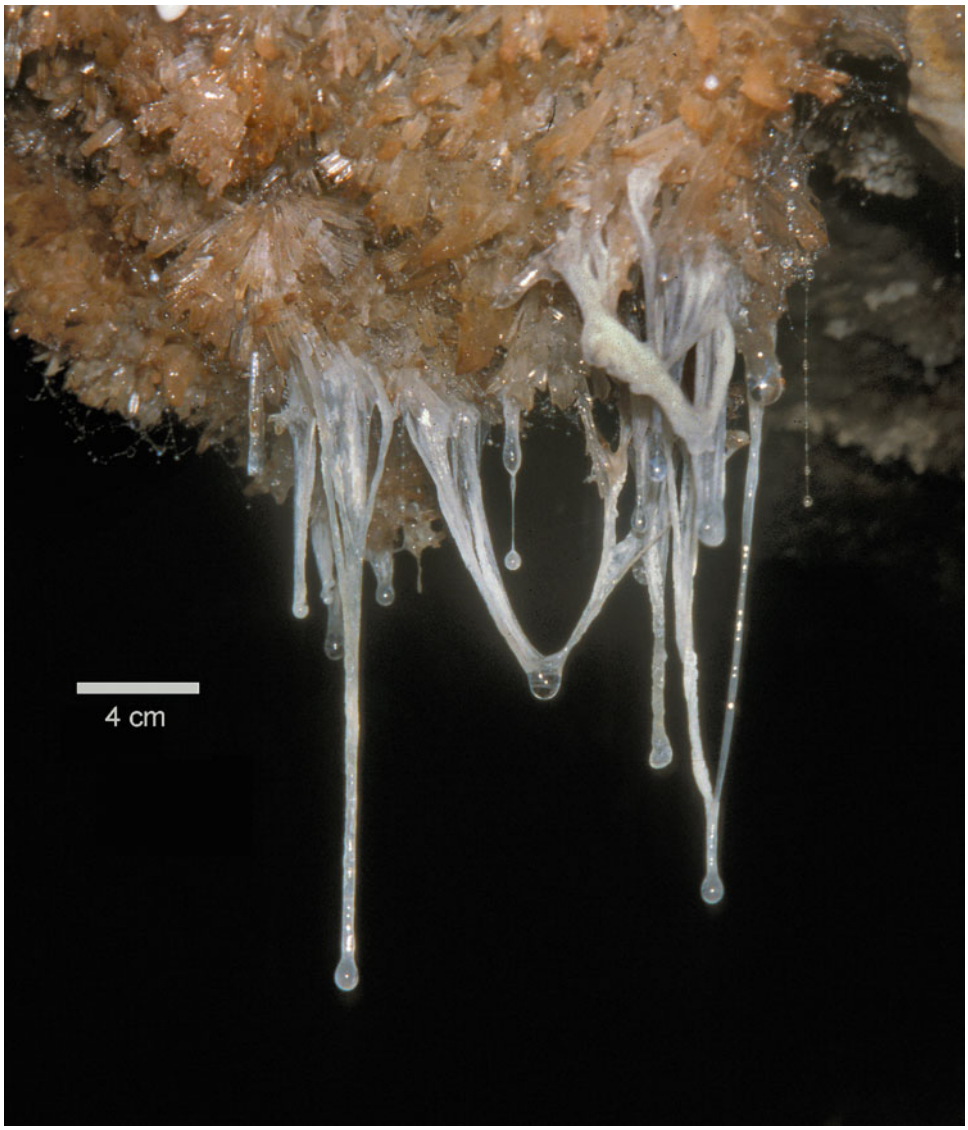

Fig. 2 Biofilms ("snottites") hanging from gypsum crystals on ceiling, Cueva de Villa Luz. Photo by A.N. Palmer

pyroclastic volcanics; and (e) Quaternary fluvial and tufa deposits.

Adding to the geologic diversity of the region is El Chichón Volcano which erupted last in 1982. This volcano is located 50 km southwest from Cueva de Villa Luz (Fig. 1).

2.2.2 Lithologies with Karst Features

Many dissolution features have been reported in outcrops and in the subsurface. Alcántara-García et al. (2004) identified karst features through petrographic analysis of carbonate core samples from the Lower to Upper Cretaceous. Additionally, conspicuous moderate to mature karst occurs in Cretaceous dolomite and limestone, carbonate conglomerate, and Quaternary tufa outcrops (Rosales-Lagarde 2013). More than 60 caves associated with these karst features have been surveyed by the Caves of Tabasco Project, the Sociedad Espeleológica de Tabasco, A.C., and Grupo Jaguar Extremo. Among those surveyed, only nine caves drain to H_2S-rich springs. The bedrock in these nine caves consists of middle to Late Cretaceous dolostone, dolomitized limestone, and limestone with some shale (Rosales-Lagarde 2013).

2.2.3 Middle Cretaceous Limestone

Most observed Tabasco caves have developed in middle Cretaceous carbonates (Albian to Cenomanian; 113-91 Ma). Limestone of this age also contains most of the great Mexican caves of the Sierra Madre Oriental and Sierra Madre del Sur. Throughout their range, these strata are typically thick

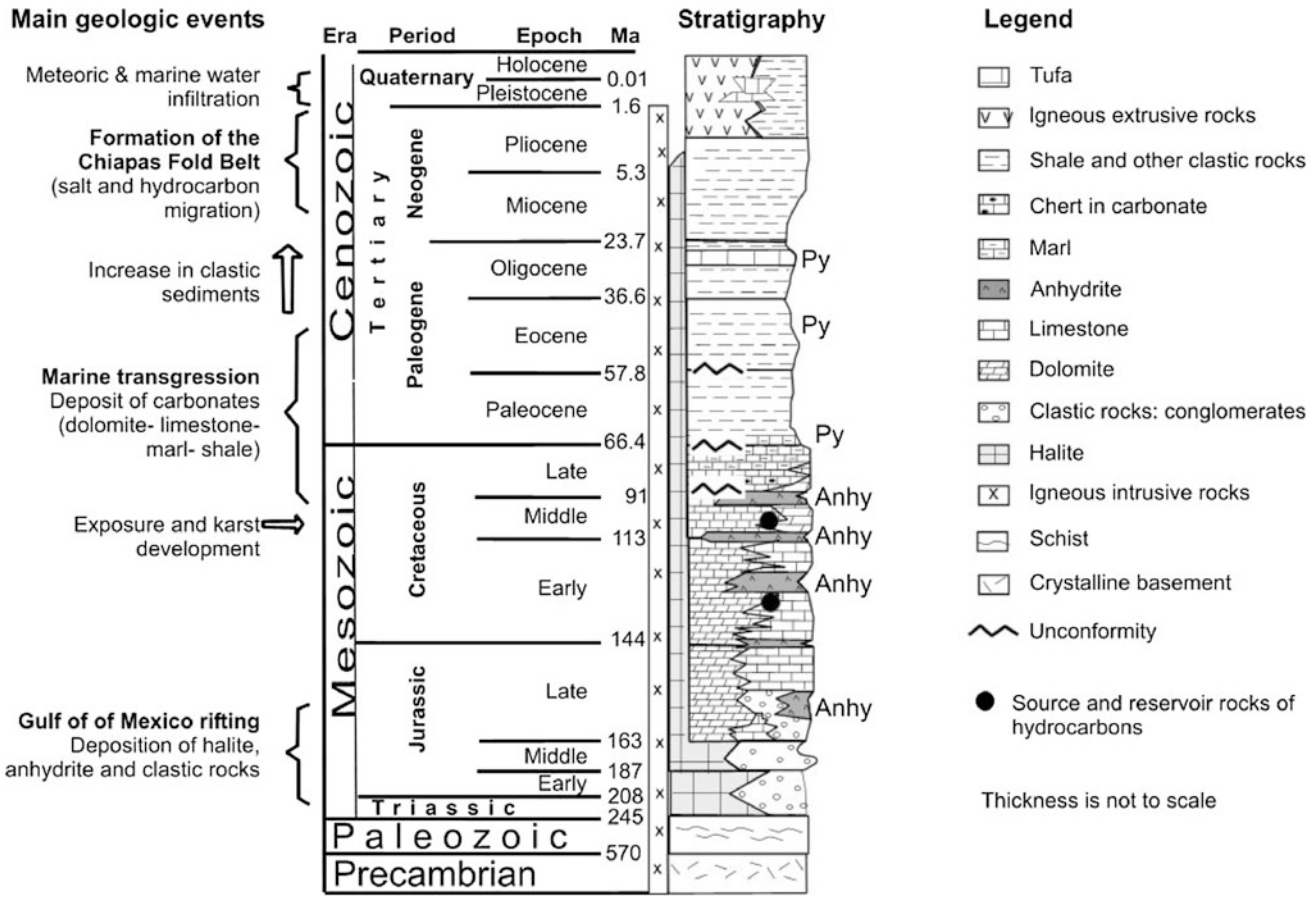

Fig. 3 Simplified regional stratigraphic column showing the main units and geologic events that affected the region, modified from unpublished PEMEX data (Modified after Rosales-Lagarde et al. 2014)

to massive. This is also the case for the old carbonates of Tabasco, which also tend to be dolomitized (Rosales-Lagarde 2013). However, bedding of Middle and Late Cretaceous units has greater variation, including thin beds of limestone, dolomite, marl, and massive to thick beds with unaltered rudist fossils. Lenses of anhydrite form "active" confining beds throughout the Cretaceous—i.e., they act as impermeable barriers to groundwater flow but also dissolve and contribute to increased groundwater salinity (Rosales-Lagarde 2013).

2.2.4 Regional Structure

Several tectonic events have affected the area (Aquino-López 2004; Meneses-Rocha 2001; Garcia-Palomo et al. 2004). Northwest-trending horst-and-graben structures are formed in the Late Triassic and Jurassic during the opening of the Gulf of Mexico. Development of a passive continental margin, accompanied by evaporite accumulation during the Jurassic, was followed by deposition of Cretaceous limestone with some anhydrite. Minor uplift and erosion began in the Late Cretaceous, and by mid-Tertiary, northeast-directed compression and transpression resulted in folding and left-lateral strike-slip and thrust faults. Shallow detachment faults over the Jurassic evaporites facilitated the formation of the northwest-trending Neogene fold belt (Meneses-Rocha 2001; Aquino-López 2004).

2.3 Hydrology

The major rivers of the area drain from south to north (INEGI 1983b). Some of their water is supplemented by various springs in Cretaceous carbonates, either seeping through fractures or caves or as alluviated springs, some associated with faults. Rosales-Lagarde et al. (2014) characterized them as fresh or brackish on the basis of their total

dissolved solids, which varied from ~300 to more than 12,000 mg/L (see Drever 1982). Water temperatures are typically a few degrees warmer than the average atmospheric temperature for the area. Chloride ranges from 6 to 4700 mg/L, and sulfate from 70 to 2900 mg/L. Some springs contain no free oxygen and abundant sulfide, whereas others are rich in oxygen and lack sulfide. Carbon dioxide, both dissolved and as bubbles, is unusually high in these waters.

Although sulfur-rich, cave- and conduit-spring waters in Tabasco show significant variation in chloride and other chemical and physical parameters, all studied Tabascan springs and cave streams are apparently derived from meteoric water, on the basis of their isotopic composition (Rosales-Lagarde et al. 2014). They also concluded that the variation in karst spring characteristics depends partly on elevation of recharge sources, depth of flow, and nature of water–rock interaction. Brackish waters tend to be derived from higher elevation recharge and follow longer, deeper flow paths with greater water–rock interaction. Freshwater karst springs have shorter residence times and shallower flow paths, with source areas only slightly higher than their discharge points. The two water types appear to mix and result in a variety of intermediate combinations (Rosales-Lagarde et al. 2014). Others (Birkle et al. 2002, 2009; Birkle and Angula 2005) proposed that older (possibly Pleistocene) rainfall recharged the region and circulated among the nearby petroleum fields before rising to the surface. However, Spilde et al. (2004) note that tritium values in the region's most significant karst spring indicate modern water. The brackish springs flow from two main subsurface environments or aquifers, subdivided into Northern and Southern (Fig. 1, caption).

High TDS, chloride, sulfate, and carbon dioxide, along with elevated temperature, characterize the brackish cave streams and karst springs of the region. Many potential sources have been identified, including evaporite beds lower in the stratigraphic column (Fig. 3), El Chichón volcano (~50 km to the west), and the petroleum fields ~15 km to the northwest of the spring area (Hose and Pisarowicz 1999; Hose et al. 2000). Spilde et al. (2004) found that helium isotopic ratios in one karst spring indicated a volcanic or upper mantle origin of some gases (CO_2, H_2S, N_2, He, and CH_4). Rosales-Lagarde et al. (2014) determined that brackish spring water in the northernmost springs may have followed flow paths to a maximum depth of 2000 m, on the basis of similarity of chemical attributes to those of a nearby oil well. According to Rosales-Lagarde et al. (2014), the high chloride and TDS resulted from dissolution of evaporite layers enhanced at fault detachment surfaces in the underlying Jurassic and lower Cretaceous units (Fig. 3). The source of the sulfate is attributed to dissolution of underlying anhydrite. The brackish, thermal waters then rise along fractures and faults. At depth, bacterial reduction of sulfates, probably augmented by the presence of organic matter, provides the sulfide-rich water that feeds certain karst springs.

3 Sulfur-Rich Caves

Nine active sulfur-rich caves have been explored in Tabasco. Most are concentrated in the southern part of the state, near the town of Tapijulapa (Fig. 1).

3.1 Sulfur-Rich Caves in the Southern Zone

The longest and largest of the sulfur-rich caves in the southernmost part of Tabasco are in Villa Luz Park. Cueva de Villa Luz has about 2 km of mapped passages, with a total relief of ~40 m. It consists of anastomosing passages with more than 30 sulfur-rich subterranean springs feeding the vadose stream that flows through most of its passages (Fig. 4). Nearby Cueva Luna Azufre is a little over 500 m long with five identified sulfur-rich springs rising into the air-filled passages. Approximately half a dozen sulfur-rich springs rise along a fault adjacent to the carbonate outcrops in the area of the Villa Luz Alberca (swimming pool). Just east of the park boundary, a phreatic karst conduit, locally called Tapicola spring, flows moderately sulfur-rich water out of a tufa mass (Rosales-Lagarde 2013).

3.1.1 Cueva de Villa Luz (CVL)

Cueva de Villa Luz (CVL) is the most studied and notorious cave in Tabasco (Fig. 4). Its toxic, sulfide-rich atmosphere, robust chemoautotrophic-based ecosystem, and unique geological and biological deposits have drawn the attention of the world's popular science media (Petit 1998; Hose 1999; Eliot 2001) in addition to an international cadre of scientists. Indigenous people recognized the unique character of the cave and considered it sacred long before scientists and cavers became aware of it (Tobler et al. 2010). The cave is also known as (and occasionally reported in the literature as) Cueva de las Sardinas, Cueva del Azufre, and Cueva de las Sardinas Ciegas. After much consideration, Mexican researcher Rosales-Lagarde (2013) concluded that Cueva de Villa Luz should be the preferred name for the cave in publications.

Located about 79 m asl near the town of Tapijulapa (Fig. 1), the cave is developing in a pod of middle Cretaceous limestone along a northwest-plunging anticline (Fig. 5). A fault truncates the carbonate outcrop to the south. The large Oxolotán River, about one kilometer to the east, serves as the regional base level (Fig. 1). Numerous sulfur-rich springs rise from the cave floor under and adjacent to the anastomosing subterranean stream. The water has

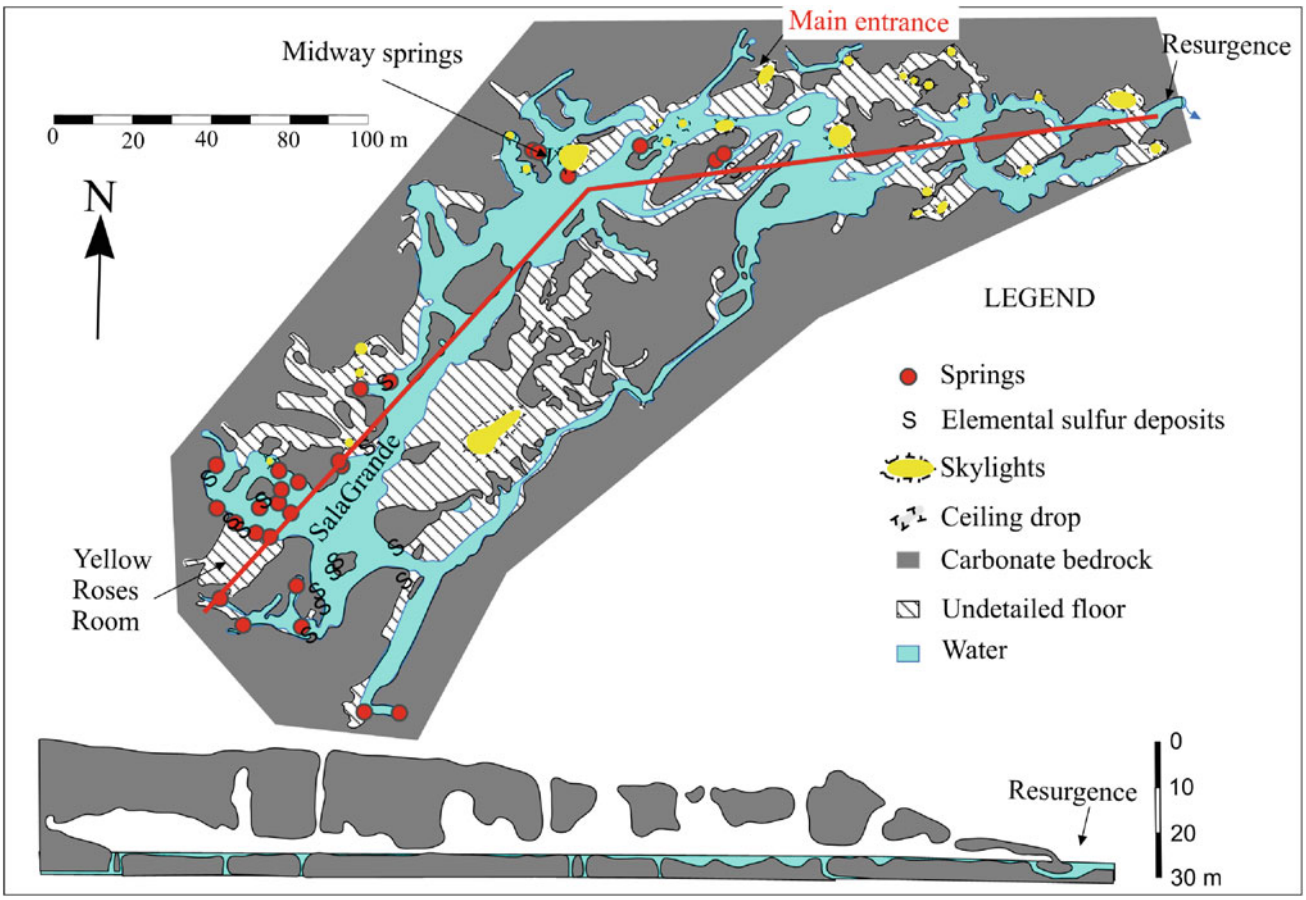

Fig. 4 Map of Cueva de Villa Luz. Modified from Hose and Pisarowicz (1999) by Rosales-Lagarde

a distinctive white color throughout most of the cave and well beyond the spring at the surface. Colloidal sulfur and abundant suspended white microbial filaments cause the unusual coloration (Hose et al. 2000; Rosales-Lagarde 2013). Cave passages generally follow the strike of the east limb of the anticline. Most of the sulfur-rich inlets are in the upstream portion of the cave, and most of the skylights are located in the downstream section of the cave.

The upstream cave atmosphere is consistently high in hydrogen sulfide (commonly 10–30 ppm) and seems related to the proximity of highly sulfidic cave-floor springs (where H_2S gas is typically high and moisture in contact with the atmosphere has a pH of around 3). The gas concentration is countered by the proximity of skylight entrances, where the circulation of fresh air lowers the H_2S concentration. Levels of nitrogen, oxygen, and CO_2 are usually distributed in ratios consistent with those at the surface, but occasional "bursts" have rapidly lowered the oxygen content to less than 9%. On other occasions, the CO_2 concentration has rocketed up to more than 3%. In the Yellow Roses room, measured H_2S levels in the cave atmosphere have exceeded 210 ppm—the limit of the monitoring meter. These "burst" events have always been observed in the upstream part of the cave, usually near the most sulfidic, anoxic springs. Bursts of extremely high atmospheric CO_2 and H_2S have been observed about a half a dozen times each, but not simultaneously. One hypothesis for this behavior suggests that the springs suddenly release gases that have been trapped within the upstream parts of the feeder conduit (Rosales-Lagarde 2013). However, these events have always been observed when researchers were moving through the stream, and they have never been recorded when instruments were left in place for several days to monitor atmospheric gases and water chemistry. Thus, these events may represent disturbance and release of trapped gases in the sediments of accessible streams.

The subterranean springs dispersed throughout CVL all have a consistent 28 °C temperature, but they vary significantly from one another in chemical composition and, to a minor degree, with time. Inlet waters fall into two categories: (1) Those with high discharge have high H_2S content (300–500 mg/L), mean PCO_2 = 0.03–0.1 atm, no measureable O_2, pH ranging from 6.3 to 6.9, and (at the most sulfidic spring, Yellow Roses) varying amounts of

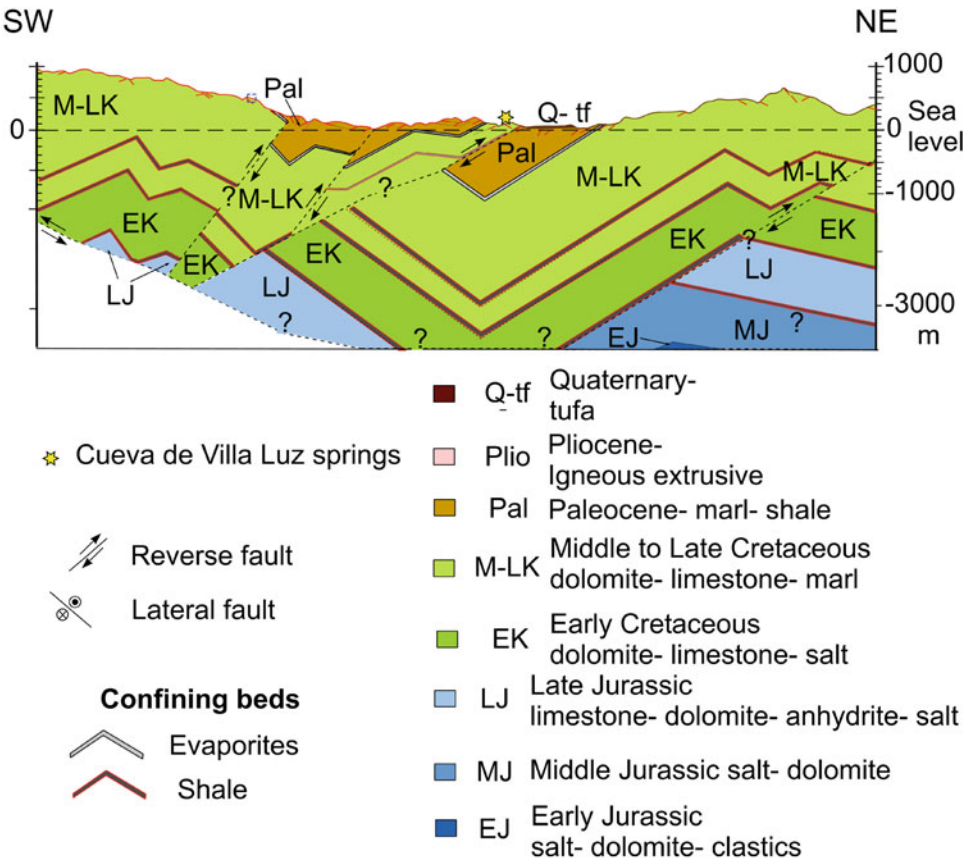

Fig. 5 Regional southwest–northeast cross section through the Villa Luz Park (Modified from Rosales-Lagarde 2013)

formaldehyde (Hose et al. 2000); (2) smaller inlets typically have less than 0.1 mg/L H_2S, mean $PCO_2 = 0.02$ atm, modest O_2 content (up to 4.3 mg/L), and pH typically 7.0–7.7 (Hose et al. 2000, and unpublished data). Total dissolved solids average around 3000 ppm for all inlets, mainly because of high concentrations of Na^+ and Cl^- (~440 and ~740 mg/L respectively). Ca^{2+}, Mg^{2+}, HCO_3^-, and SO_4^{2-} concentrations are also high in comparison with freshwater springs (Rosales-Lagarde et al. 2014). All of these parameters remain generally consistent throughout the seasons and years. However, following a very large storm event, there was a dramatic two-day drop in TDS accompanied by elevated pH and O_2, and by lowered H_2S and water temperature, in the Yellow Roses spring. This demonstrates that some local meteoric water joins the conduit waters before they emerge into the cave. Researchers have interpreted the differences and similarities of the various cave inlets to represent the same anoxic, sulfide-rich, artesian waters that follow inaccessible conduits to the surface. The oxygenated waters are exposed to aerating conditions upflow from the inlets so that original H_2S has been largely lost due to outgassing and oxidation to sulfate, accompanied by an increase in sulfate concentration of about 4%. Alternatively, sulfide production may not have occurred in some inlets (Hose et al. 2000; Rosales-Lagarde et al. 2014).

The walls and ceilings of the cave display distinctive colonies of microbes, most notably "snottites" (Fig. 2) and biovermiculations (microbially dense clay vermiculations). Organisms also reside within unusual mineral deposits, including sulfur folia, elemental sulfur crusts, and gypsum paste (fine-grained gypsum resulting from corrosion of the limestone walls) (Hose 2009). The pore fluids in all of these deposits and growths have very low pH, commonly recorded near zero despite their immediate proximity to the cave's limestone walls.

Interstitial water in cave deposits on the walls and floor of the cave demonstrate a broad spectrum of pH values: 0.0 for guano intermixed with gypsum paste and moistened with sulfuric acid water drops; 0.0–0.7 for gypsum paste and guano-gypsum paste; 2.0–2.4 for deposits containing red clay; negative values to +3.0 for snottite bacteria colonies; and 3.1–3.8 for brown biovermiculations. Circumneutral values of 6.4–7.2 were measured in various stream-bottom mucks and in water samples containing filamentous bacteria (Hose and Pisarowicz 1999; Hose et al. 2000).

The robust ecosystem in CVL has drawn the most attention. The cave contains a startlingly high subterranean

biomass (Hose et al. 2000; Tobler et al. 2006; Palacios-Vargas 2009). Two primary energy sources drive the ecosystem: a chemoautotrophic line of energy and surface-derived sources with organic material brought into the cave by debris falling into skylight entrances; and the energy provided by bats and others vertebrates visiting the cave. The terrestrial source dominates local areas of the cave, such as the immediate area under skylights and in the two rooms where bats tend to rest (Estrada-Bárcenas 2005; Palacios-Vargas 2009). However, most life in the cave appears to thrive on autotrophic bacteria (Hose et al. 2000). Abundant bacterial colonies line the walls and hang from the ceilings of the cave (Fig. 2), living off energy-rich sulfide oxidation reactions along with carbon and water in the air and on walls, which facilitate growth of autotrophic bacteria and production of sulfuric acid and sulfate ions. Other microbes, invertebrates (especially midges), and fish consume the autotrophic bacteria and each other (Gorden and Rosen 1962; Hose and Pisarowicz 1999). The abundant, small, cave-adapted fish (*Poecila Mexicana*; Fig. 6) are consumed by invertebrates and by local humans in an annual ceremonial harvest called *La Pesca de la Sardina*, which reenacts a historical (and possibly pre-historic) Zoque tradition (Tobler et al. 2010).

3.1.2 Cueva de Luna Azufre

The 560-m-long Cueva de Luna Azufre (CLA) is developing in a slightly older, partially dolomitized part of the Villa Luz Park limestone block along the southern boundary fault (Rosales-Lagarde 2009). The cave has a total relief of ~19 m. Its passages display a ramiform pattern (Palmer 1991) mostly developed along a fault of undetermined offset and related fractures (Fig. 7). One of the notable differences between Luna Azufre and Villa Luz is the relative abundance of exposed carbonate bedrock in CLA. The ubiquitous gypsum paste and microbial deposits in CVL are less abundant in CLA (Hose 2005).

Five small (<1 L/s) subterranean springs have been identified as rising from the floor of the cave containing about 15–20% higher total dissolved solids than the springs in CVL. Atmospheric and aquatic H_2S are present in CLA, but markedly lower and dissolved oxygen is higher than in CVL, although the latter is far more extensively studied. Atmospheric CO_2 was recorded as 3 ppm, an order of

Fig. 6 *Poecila mexicana* in Cueva de Villa Luz stream. Photo by Roberto Porter. Width of foreground ~1 m

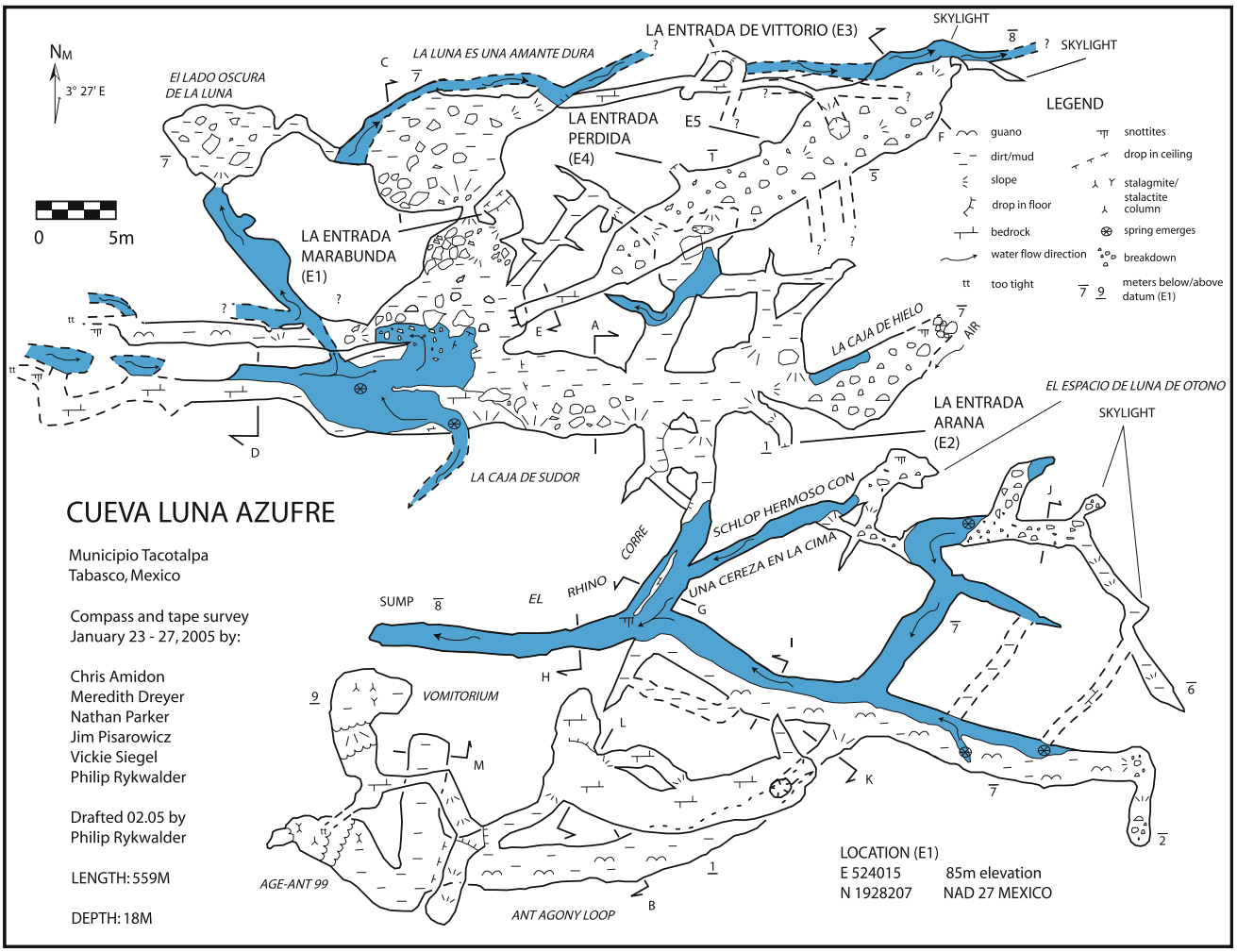

Fig. 7 Map of Cueva Luna Azufre in Villa Luz Park (from Pisarowicz 2005)

magnitude higher than ambient surface conditions (Hose 2005). Measured spring temperatures in CLA are about 30 °C, 2° warmer than CVL, and pH has been recorded as 7.2–7.5 (Rosales-Lagarde 2013). No "bursts" of elevated atmospheric H_2S or CO_2, or dramatic drops in O_2, have been observed in CLA.

The cave's biology is much less dense than CVL, but the CLA streams have fish, eel, and invertebrates. Abundant biovermiculation accumulations and a few snottites grow on the cave's walls and ceilings, causing localized areas of very low (<3.5) pH. Its largest subterranean spring regularly produces small biomat clumps. Bats reside in the cave, and their guano provides another source of energy to the subterranean life.

3.1.3 Caves of the Phreatic Zone

A short distance to the west of CLA, along the same fault, several small- to moderate-flow, surface springs rise out of apparent conduits too small to enter. The largest feeds the park's swimming pool, called Villa Luz Albercas. Its water is sulfide-rich, oxygen-depleted, and chemically indistinguishable from the sulfide-rich springs within Cueva de Villa Luz.

Just northeast of the park, a moderate-size spring rises from a tufa conduit. The water's high CO_2 content provided naturally carbonated water to a short-lived soda pop production business in the nearby town of Tapijulapa. The spring is named for the soda pop, *Tapicola*. While large enough to allow entry by a human, the subaqueous cave has not been explored. As the waters emerge from the ground, the chemistry is consistent with the other sulfur-rich springs in the area. However, the total dissolved solid level is around 2500 ppm (~17% lower than CVL), temperature is about a half degree lower than CVL, and pH is about 7.3 (Rosales-Lagarde 2013).

3.1.4 Other Caves

Most other caves explored in the Southern Zone of Tabasco's karst region demonstrate classic epigenetic development. If hypogenic sulfidic processes contributed to their formation, the evidence has been overwhelmed by

epigenetic processes and freshwater flooding. Notable paleocaves in the area with ceiling alcoves and blind passages that hint a hypogenic origin include Las Grutas de Cuesta Chica on the east side of the Oxolotán River. These caves are currently high enough above the river to avoid flooding.

3.2 Sulfur-Rich Caves of the Northern Zone

There are four caves with sulfur-rich waters identified in the Northern Zone, El Azufre spa, La Joya Cave El Susto Cave, and Sulfur X Cave. These caves are located nearby the major rivers at small outcrops of highly weathered limestone to dolostone of middle to Late Cretaceous age (Meneses-Rocha 2001). Active sulfur-rich caves in this Zone are small and less studied than those in the Southern Zone. However, all of these caves contain different concentrations of sulfur brackish-rich water, gypsum, and selenite in the walls, biovermiculations, and extensive, well-developed, rillenkarren, and sometimes small snottites.

4 Speleogenesis of Sulfur-Rich Caves in Tabasco

Galdenzi (1990) summarized the speleogenesis in the Frasassi Caves in Italy as a three-step process: (1) an early sulfide-rich phreatic phase forming incipient karst conduits; (2) a secondary sulfide-rich vadose–phreatic phase of chemical stoping; and (3) a tertiary sulfide-depleted vadose phase of epigenic speleogenesis. Examining the caves in Villa Luz Park and other active sulfidic caves around the world, Hose and Macalady (2006) expanded this model as a general process of sulfidic speleogenesis, and all three phases appear to be active in the caves of Tabasco. The early phreatic phase develops incipient conduits near the top of the sulfur-rich aquifer. Artesian, sulfur-rich waters gain corrosive strength as they mix with descending, shallow, meteoric water.

Just above the phreatic–vadose interface, Phase 2 processes accelerate conduit enlargement as (1) a combination of sulfide- and CO_2-rich spring waters degas; (2) convection drives the relatively dense but warmer than ambient temperature gases upward through the cave atmosphere where it combines with O_2, water vapor, and condensed water on the cave walls and ceiling; (3) microbes facilitate oxidation of H_2S to H_2SO_4; (4) sulfuric acid alters the limestone walls and ceilings to gypsum (both microcrystalline "paste" and selenite); (5) chunks of the limestone-cum-gypsum walls and ceilings stope onto the floor and into the stream; (6) the spoils (gypsum sediments) are removed as solute and suspended load in cave streams. Stream passages, paleophreatic rifts, and ceiling alcoves rapidly enlarge during this phase (early Phase 2 illustrated in Fig. 8). Epigenic processes may also impact the cave development, but the aggressive, sulfidic speleogenesis overwhelms their impact at this stage.

As the water table drops, surface downcutting continues, and sulfidic waters and gases abandon the original passages (Late Phase 3). Epigenetic processes now have the opportunity to obscure the earlier, sulfidic activity.

Research here also supports and expands on Galdenzi's (1990) three-stage process for the development of sulfur-rich caves: (1) an early sulfide-rich phreatic phase forming incipient karst conduits; (2) a secondary, sulfide-rich, vadose–phreatic phase of chemical alteration and mechanical stoping; and (3) a tertiary sulfide-depleted vadose phase of epigenic speleogenesis. The second phase of development dominates speleogenesis in actively developing, sulfur-rich caves in Tabasco, like Cueva de Villa Luz. Phase 1 processes continue in the submerged tubes that feed subterranean and Tapicola springs, and Phase 3 processes take place in the upper levels of some of these caves and in paleocaves that are now abandoned by artesian, sulfur-rich waters.

While researchers have focused on the actions of sulfuric acid dissolution, greatly facilitated by microbial activities, as the primary agent of speleogenesis in Tabasco's sulfur caves (Hose and Pisarowicz 1999; Hose et al. 2000; Boston et al. 2012), several other processes are also active. During Phase 1, the accompanying high levels of CO_2 suggest that mixing zone dissolution, as originally proposed by Bögli (1964), takes place both at depth and at the surface. The presence of interbedded anhydrite, dolomite, and limestone in the middle Cretaceous unit that hosts the caves suggests that the common-ion effect described by Palmer (2007, p. 121–122) may also contribute to Phase 1 speleogenesis. During Phase 2, CO_2 and condensed moisture on the walls and in the cave atmosphere combine with CO_2 to form H_2CO_3. This carbonic acid undoubtedly participates in dissolving the limestone. In addition, thermal gradients drive undersaturated air currents and facilitate condensation corrosion (limestone dissolution of the walls and ceilings) in air-filled passages (Queen 1994; Hose and Macalady 2006; Audra et al. 2007). In Phase 3, epigenetic processes caused by infiltrating, surface-derived waters play a final role in development of the caves.

5 Summary

Studies of the sulfur-rich caves in Tabasco have significantly increased our understanding of sulfidic dissolution processes in carbonate bedrock, the range of subsurface life (particularly chemoautotrophic-based ecosystems), and the behavior of

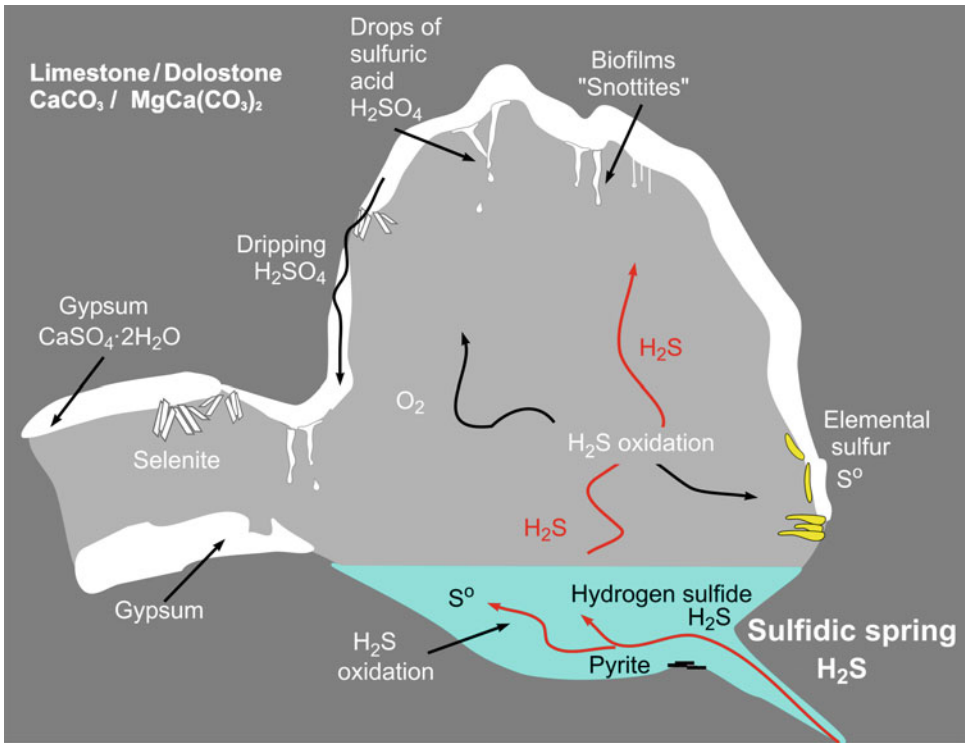

Fig. 8 Sulfidic processes during Phase 2 of speleogenesis. Modified from Hose et al. (2000) and Palmer and Palmer (1998)

petroleum basin fluid migration. Since the study of Cueva de Villa Luz, many other examples of sulfuric acid speleogenesis have been recognized and studied throughout the world.

Acknowledgements The authors wish to thank the people and officials of the Tapijulapa community, the authorities from the Municipio de Tacotalpa, Teapa, and Ixtapangajovya for their generous support and kindness. LDH's research was financially supported by grants from the National Speleological Foundation, Richmond Area Speleological Society, and National Geographic Society grants 6541-99, and 6634-9. LR-L's research was supported by Consejo Nacional de Ciencia y Tecnología, the National Cave and Karst Research Institute, the Matuszeski Grant, the Anita and Anton Budding Research Grant, and the Graduate Student Association Travel Grant from New Mexico Institute of Mining and Technology. The authors benefitted from assistance from members of the National Speleological Society's Caves of Tabasco Project, especially from Jim Pisarowicz and Vickie Siegel. The personnel from PEMEX Exploración y Producción Zona Sur, especially Dr. Javier Meneses-Rocha, granted access to geologic information and oil wells. Consejo Nacional del Agua Villahermosa, Instituto Nacional de Estadística y Geografía, and the Secretaría de Agua Potable y Alcantarillado del Estado de Tabasco also provided useful information.

References

Alcántara-García JM, Ham-Wong JM, Medina-Flores U, Hernandez-Penaloza JJ, de la Cruz-Rivera VM, Pena-Ramirez H, Namson J, Spaw JM (2004) Identification and evaluation of plays in the Simojovel Project, southeastern Mexico. American Association of Petroleum Geologists, International Conference Oct 24–27, Cancun, Mexico

Alquino-López JA (2004) Sureste basin, Mexico, and associated sub-basins: an update and future potential. AAPG International Conference, Oct 24–27, Cancun, Mexico

Audra P, Hobléa F, Bigot J-Y, Nobécourt J-C (2007) The role of condensation-corrosion in thermal speleogenesis: study of a hypogenic sulfidic cave in Aix-les-Bains, France. Acta Carsologica 36(2):185–194

Birkle P, Angulo M (2005) Conceptual hydrochemical model of late Pleistocene aquifers at the Samario-Sitio Grande petroleum reservoir, Gulf of Mexico, Mexico. Appl Geochem 20:1077–1098

Birkle P, Martínez-García B, Milland-Padron CM, Eglington BM (2009) Origin and evolution of formation water at the Jujo-Tecominoacán oil reservoir, Gulf of Mexico. Part 2: Isotopic and field-production evidence for fluid connectivity. Appl Geochem 24:555–573

Birkle P, Portugal E, Rosillo-Aragón JJ, Fong JL (2002) Evolution and origin of deep reservoir water at the Activo Luna oil field, Gulf of Mexico, Mexico. AAPG Bull 86:457–484

Bögli A (1964) Mischungskorrosion, ein Beitrag zur Verkarstungs-problem. Erdkunde 18:83–92

Boston PJ, Hose LD, Northup DE, Spilde MN (2006) The microbial communities of sulfur caves: A newly appreciated geologically driven system on Earth and potential model for Mars. In: Harmon RS, Wicks C (eds) Perspectives on Karst Geomorphology, Hydrology, and Geochemistry—a Tribute Volume to Derek C. Ford and William B. White. Geological Society of America Special Paper 404, pp 331–344

Boston PJ, Spilde MN, Northup DE, Melim LA, Soroka DS, Kleina LG, Lavoie KH, Hose LD, Mallory LM, Dahm CN, Crossey LJ, Schelble RT (2001) Cave biosignature suites: microbes, minerals and Mars. Astrobiol J 1(1):25–55

Boston PJ, Spilde MN, Northup DE, Melim LA, Rosales-Lagarde L (2012) Speleogenetic effects of microbial communities in carbonate systems. Geol Soc Am Abs Programs 44(6):32

Drever J (1982) The Geochemistry of Natural Waters. Prentice-Hall, New Jersey

DuChene HR (2009) The relationship of oil-field-derived hydrogen sulfide in the Permian (Guadalupian) Artesia Group to sulfuric acid speleogenesis in the Guadalupe Mountains, New Mexico and Texas. In: Stafford KW, Land LL, Veni G (eds), Advances in Hypogene Karst Studies. NCKRI symposium 1, National Cave and Karst Research Institute, Carlsbad, NM, pp 111–120

Eliot J (2001) Deadly haven: Mexico's poisonous cave. National Geographic, May issue

Estrada-Bárcenas D (2005) Biodiversidad de microartrópodeos en una cueva multienergetica en Tabasco, México. M.Sc. thesis, UNAM, Mexico

Galdenzi S (1990) Un modello genetico per la Grotta Grande del Vento. In: Galdenzi S, Menichetti M (eds) Il carsismo della Gola di Frasassi: Memoire Istituto Italiano di Speleologia, II-4:123–142

García-Palomo AA, Macías JL, Espindola JM (2004) Strike-slip faults and K-alkaline volcanism at El Chichón volcano, southeastern Mexico. J Volcanol Geoth Res 136(3):247–268

Gold T (1999) The Deep Hot Biosphere. Copernicus, New York

Gorden MS, Rosen DE (1962) A cavernicolous form of the Poeciliid fish *Poecilia sphenops* from Tabasco, Mexico. Copeia 2:360–368

Hill CA (2000) Overview of the geologic history of cave development in the Guadalupe Mountains, New Mexico: J Caves Karst Stud 62 (2):60–71

Hose LD (1999) Cave of the sulfur eaters. Natl Hist Mag, 54–61

Hose LD (2001) Hydrochemical characteristics of a unique sulfur-rich karst system in southern Mexico. Geol Soc Am Abs Programs 33(6)

Hose LD (2005) A scientist looks at Cueva Luna Azufre. AMCS Activities News 28:54–55

Hose LD (2009) Recent observations in a remarkably dynamic, sulfide-rich, hypogenic cave in southern Mexico. Proceedings of fifteenth international congress of speleology, pp 1525–1530

Hose LD, Macalady JL (2006) Observations from active sulfidic karst systems: is the present the key to understanding past sulfuric acid speleogenesis? 57th annual fall field conference guidebook, Caves and Karst of SE New Mexico. New Mexico Geological Society, Socorro NM, pp 185–194

Hose LD, Palmer AN, Palmer MV, Northup DE, Boston PJ, DuChene HR (2000) Effects of geomicrobiological processes in a hydrogen sulfide-rich, karst environment. Chem Geol: Spec Geomicrobiol Issue 169:399–423

Hose LD, Pisarowicz JA (1999) Cueva de Villa Luz, Tabasco, México: Reconnaissance study of an active sulfur spring cave. J Cave Karst Stud 61(1):13–21

INEGI (1983a) Carta Geológica escala 1:250,000 Villahermosa E15–8, 1st edn, México

INEGI (1983b) Carta Hidrológica de Aguas Superficiales 1:250,000 Villahermosa E15–8, scale 1:250,000, 1st edn, Mexico

INEGI (1985) Carta Geológica escala 1:250,000 Tuxtla Gutierrez E15–11. 1st edn, México

Meneses-Rocha JJ (2001) Tectonic evolution of the Ixtapa graben, an example of a strike-slip basin in southeastern Mexico: Implications for regional petroleum systems. In: Bartolini C, Buffler RT, Cantú-Chapa A (eds) Memoir 75, 183–216

Northup DE, Turner AL, Spilde MN, Boston PJ, Alvarado A, Hose LD (2005) Sulfur-based microbial communities from Cueva de Villa Luz, an extreme sulfide-rich cave. Abs Gen Meet, Am Soc Microbiol 105(N-065)

Pain S (1998) Acid house. New Scientist 6 June, 42–46

Palacios-Vargas JG (2009) Los Estudios Bioespeleológicos de la Cueva de Villa Luz y sus perspectivas. Mundos Subterrán 20:22–26

Palmer AN (1991) Origin and morphology of limestone caves. Geol Soc Am Bull 103:1–21

Palmer AN (2007) Cave Geology. Cave Books, Dayton, OH

Palmer AN, Palmer MV (1998) Geochemistry of Cueva de Villa Luz, Mexico, an active H_2S cave (abstract). J Cave Karst Stud 60:188

Petit C (1998) The walls are alive: U.S. News and World Report, February 9 issue, pp 59–60

Pisarowicz J (2005) Return to Tabasco. AMCS Activities Newsl 28:27–57

Queen JM (1994) Influence of thermal atmospheric convection upon the nature and distribution of microbiota in cave environments. In: Sasowsky ID, Palmer MV (eds) Breakthroughs in Karst Geomicrobiology and Redox Geochemistry. Charles Town, WV, Karst Waters Institute Special Publication 1, pp 62–63

Ramos-López AE (2003) Aplicación de un índice de calidad para cuerpos de agua del Estado de Tabasco, México. Bachelors thesis in Environmental Engineering, Universidad Juárez Autónoma de Tabasco, Villahermosa, Tabasco

Rosales-Lagarde L (2009) Mexico news: Tabasco. AMCS Activities Newsl 32:32

Rosales-Lagarde L (2013) Sulfidic karst springs and speleogenesis in the Sierra de Chiapas. Assoc Mex Cave Stud Bull 24

Rosales-Lagarde L, Boston P, Campbell A, Hose L, Axen G, Stafford KW (2014) Hydrogeology of northern Sierra de Chiapas, Mexico: a conceptual model based on a geochemical characterization of sulfide-rich karst brackish springs. Hydrogeol J 22(6):1447–1467

Salazar-Conde E, Zavala-Cruz J, Castillo-Acosta O, Cámara-Artigas R (2004) Evaluación espacial y temporal de la vegetación de la Sierra Madrigal, Tabasco, México (1973–2003). Investigaciones Geográficas: Boletín del Instituto de Geografía, Universidad Nacional Autónoma de México. 54:7–23

Spilde MN, Fischer PR, Northup DE, Turin HJ, Boston PJ (2004) Water, gases, and phylogenetic analyses from sulfur springs in Cueva de Villa Luz, Tabasco, México (abstract). Geol Soc Am Abs Programs 36(5):258

Tobler M, Culumber ZW, Plath M, Winemiller KO, Rosenthal GG (2010) An indigenous religious ritual selects for resistance to a toxicant in a livebearing fish. Biol Lett. doi: 10.1098/rsbl.2010.0663

Tobler M, Shlupp I, Heubel KU, Riesch R, de León FDG, Giere O, Plath M (2006) Life on the edge: hydrogen sulfide and the fish communities of a Mexican cave and surrounding waters. Extremophiles 10:577–585

Part IV

South America, Africa, and Australia

Hypogene Caves and Karst of South America

55

Augusto S. Auler

Abstract

Knowledge about karst in South America is still limited due to the paucity of cave exploration and the lack of scientific assessment of most cave regions. However, the South American continent presents favorable conditions for the development of hypogene cave systems, especially ancient ones, now decoupled from routes of cave-forming fluids. The majority of recognized hypogene caves occur near the borders of cratonic areas, in Precambrian carbonates. The best-known example comprises the large maze caves (TBV-TBR) near the village of Laje dos Negros, northeastern Brazil, and the hypogene karst of the Vazante area, south-central Brazil. Although other areas have not been subjected to detailed speleogenetic studies, several other sites present caves with hypogene characteristics, such as in the Iron Quadrangle area (state of Minas Gerais), northern state of Bahia, and western states of Mato Grosso and Mato Grosso do Sul, in Brazil. In the Argentinian Patagonia, associated with the Andes Mountain chain, the Las Brujas Cave has been interpreted as a hypogene system. An isolated occurrence of possible quartzite hypogene cave is also described.

Keywords

Hypogene karst • Hypogene caves • South America

1 Introduction

South America is not particularly endowed with carbonate karst, which is estimated to correspond to less than 2% of the total area (Auler 2004). Quartzites and sandstones are more widespread and in tropical conditions are also subject to dissolutional processes, generating significant caves and karst (Wray 1997; Auler 2012; Fabri et al. 2015). Hypogene caves have, so far, been recognized both in carbonate and quartzite, besides a possible earlier role of hypogene processes in caves in iron formations.

Cave exploration and karst research in South America are still limited and significant areas remain to be properly explored. Brazil, Venezuela, and Argentina have had organized national speleological federations for many decades and are the three better-researched countries, but Peru, Colombia, and Bolivia also show incipient organized caving and growing karst research. The recognition of hypogene caves and karst is very sketchy at present. And even when recognized, detailed studies have not yet been performed. The first scientific report of a hypogene cave in South America was produced by Forti et al. (1993) in the Las Brujas Cave in Argentina, followed by the first published account on the speleogenesis of Toca da Boa Vista system in northeastern Brazil (Auler 1995). Toca da Boa Vista (TBV) and the neighboring Toca da Barriguda (TBR) are the only caves so far subjected to comprehensive speleogenetic studies (Auler and Smart 2003; Klimchouk et al. 2016; Ennes-Silva et al. 2016; see Auler et al., Chap. 56) although

A.S. Auler (✉)
Instituto do Carste, Rua Barcelona 240/302,
Belo Horizonte, MG 30360-260, Brazil
e-mail: aauler@gmail.com

© Springer International Publishing AG 2017

A. Klimchouk et al. (eds.), *Hypogene Karst Regions and Caves of the World*,
Cave and Karst Systems of the World, DOI 10.1007/978-3-319-53348-3_55

the hypogene caves in the vicinity of the zinc mine of Vazante have also been the focus of important work (Bittencourt 2008; Bittencourt et al. 2009; Bittencourt and Reis Neto 2012; see Auler and Souza, Chap. 57). In this review, caves that display hypogene features will be briefly described, even if no further speleogenetic study has been performed. A previous review on the Brazilian examples (Auler 2009) will be expanded, including new sites from Argentina and Brazil.

2 Hypogene Caves and Karst in South America

The present configuration of the South American continent comprises ancient cratonic areas and mobile belts mostly in the eastern portion, the extensive Andean Belt on the western limit and several Phanerozoic foreland basins (Fig. 1). Karst occurs mostly in the first two domains, associated with Precambrian carbonates and quartzites in the now stable cratonic settings or in areas subjected to the influence of the orogenetically active Andean Mountain Chain. The hypogene karst areas described in this review (Fig. 1) are mostly associated with tectonically stable (since 600 Ma) sequences in cratonic settings or linked to the complex and active (since 500 Ma) Andean Belt (Cordani et al. 2000).

2.1 Las Brujas Cave, Argentina

Las Brujas Cave is located in central-western Argentina, at the foothills of the Andes Chain, close to the city of Malargue, Mendoza Province (35° 48′ 02″S; 69° 49′ 13″W). The cave is located in a syncline developed in Upper Jurassic dolomitic limestone of the La Manga Formation, subjected to intense faulting resulting in two sets of joint systems oriented 005-090° and 070-150° (Sancho et al. 2004). Cave morphology displays rectilinear passages along vertical faults (Sancho et al. 2004) in a ramiform/network pattern (Fig. 2). Cupolas and subcircular passages occur (Sancho et al. 2004). The cave shows noteworthy gypsum precipitation in the deeper sections, comprising thick microcrystalline crusts (up to 50 cm thick) sometimes filling entire passages (Forti et al. 1993).

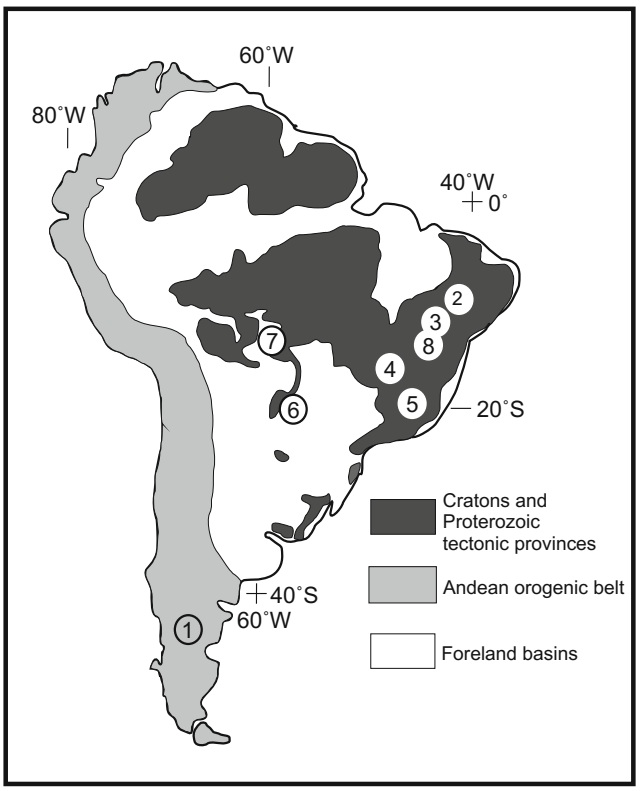

Fig. 1 Simplified tectonic framework of South America (based on Cordani et al. 2000) and location of hypogene sites described in this chapter. *1* Las Brujas Cave; *2* TBV-TBR system; *3* Calixto Cave; *4* Vazante area; *5* Iron Quadrangle; *6* Bodoquena Range; *7* Western Mato Grosso; *8* Espinhaço Range

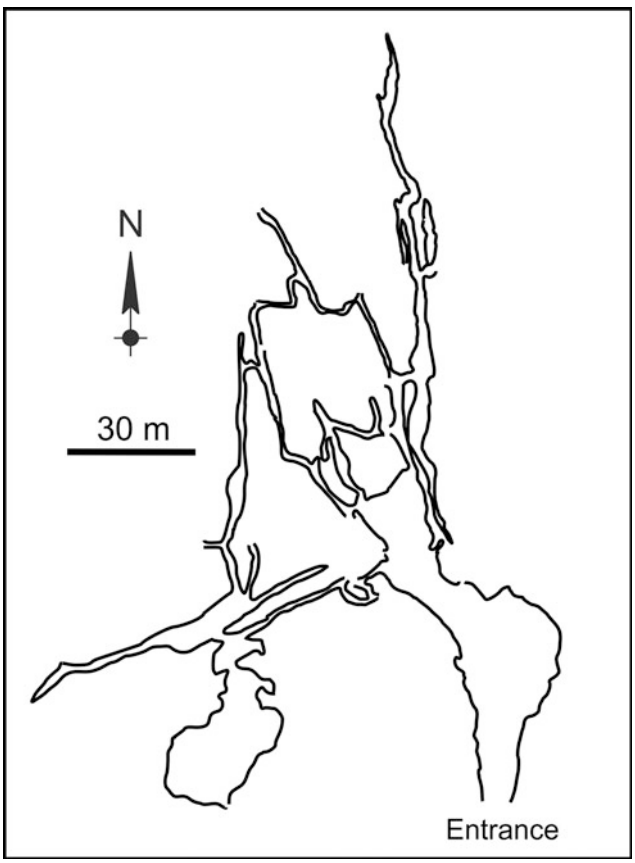

Fig. 2 Plan map of Las Brujas Cave. From Forti et al. (1993)

The presence of gypsum which could not be related to any of the overlying formations led Forti et al. (1993) and Mikkan (1995) to suggest genesis through oxidation of rising H_2S, generating sulfuric acid that would promote carbonate dissolution and gypsum precipitation. The origin of H_2S was assigned to oil fields detected in the surroundings of the area (Forti et al. 1993). Sancho et al. (2004), however, proposed an epigenic origin for Las Brujas Cave, followed by fast water table drawdown due to high rates of denudation and fluvial incision.

2.2 Toca da Boa Vista and Toca da Barriguda Cave System, Brazil

Toca da Boa Vista (TBV) and Toca da Barriguda (TBR) (coordinates TBV 10° 09′ 45″S, 40° 51′ 35″W; TBR 10° 08′ 26″S, 40° 51′ 08″W) are the two best-studied hypogene caves in South America and are described in detail in Auler et al. (Chap. 56). They are hosted in Proterozoic carbonates within the São Francisco Craton, in the vicinity of the contact with the Riacho do Pontal mobile belt, in northeastern Brazil. The two caves are separated by only 700 m and are developed in five units of the Salitre Formation, Una Group. The caves develop as an elongated N45E-oriented swarm of cave passages displaying hypogene features, such as network/ramiform pattern (Fig. 3), feeders, cupolas, rift passages, pendants, and wall projections. They show master passages associated with anticline hinges with mean orientation of 15° along NNE-oriented passages and 30°–90° in NE–SW- to E–W-oriented passages (Ennes-Silva et al. 2016).

Cave genesis was initially interpreted by Auler and Smart (2003) as due to sulfuric acid dissolution through metallic sulfide oxidation within the bedrock. Klimchouk et al. (2016) proposed a classic hypogene mechanism in which rising flow would migrate upwards through the basal units and then laterally upon reaching less permeable sealing units.

Timing of speleogenesis cannot be constrained with certainty due to the absence of chronological markers associated with the initial carbonate dissolution, but a correlation with ancient Proterozoic tectonic events or the breakup of Pangea has been suggested (Klimchouk et al. 2016).

2.3 Hypogene Caves of Chapada Diamantina, Brazil

Carbonates of the Salitre Formation, Una Group also outcrop to the south of the TBV-TBR area, forming the vast Irecê and Una basins which are separated from each other by quartzite ridges. Due to increased rainfall, epigenic karst forms tend to overwrite possible hypogene features. A few caves display hypogene patterns such as the ramiform Calixto Cave (Fig. 4) (coordinates 13° 17′ 35″S, 41° 03′ 48″W). This cave contains very irregular chambers, some vertical rifts, cupolas, in a pattern reminiscent of the TBV-TBR system, although at a much smaller scale.

Auler (1999) recognized possible hypogene characteristics in other caves in the area and assigned the genesis as due to oxidation of metallic sulfide within the bedrock.

2.4 Hypogene Karst of Vazante, Brazil

The Vazante Group hosts South America's most important zinc mineralization. Associated with the fault-controlled zinc body in the surroundings of the town of Vazante, there are several hypogene caves, described in detail in Auler and Souza (Chap. 57). The Vazante Hypogene Karst develops in Proterozoic dolostones of the Morro do Calcário and Serra do Poço Verde formations. The longest and better-known cave is Lapa Nova (coordinates 17° 59′ 00″S, 46° 53′ 27″W) which is located only a few hundred meters offset from the mineralized shear zone (Bittencourt et al. 2009) (Fig. 5). Besides accessible caves presently in the vadose zone, tunnels in the underground zinc mine allow the observation of numerous vertical fragments of hypogene caves (Bittencourt et al. 2009). Borehole data show the presence of voids at depths in excess of 600 m below the surface (Bittencourt and Reis Neto 2012). Caves display a dominant network pattern, although ramiform caves can also be recognized. Feeders, cupolas, and outlets occur in most caves.

Hypogene speleogenesis exploited the mineralized zone. The zinc body behaves as a seal, creating a significant hydraulic head difference between both sides of the zinc-rich zone (Bittencourt et al. 2009). Rising groundwater is able to bypass the fault zone at depth, where the mineralized zone pinches out. Ascending water flows along the fault zone and diverts laterally through inclined bedding planes overlaid by impermeable beds, creating both relict (such as Lapa Nova) and active hypogene caves represented by Vauclusian springs (Bittencourt and Reis Neto 2012).

2.5 Karst of the Iron Quadrangle, Brazil

The Quadrilátero Ferrífero (Iron Quadrangle) area in southeastern Brazil has a complex geological history with several Mid-Proterozoic formations subjected to multiple

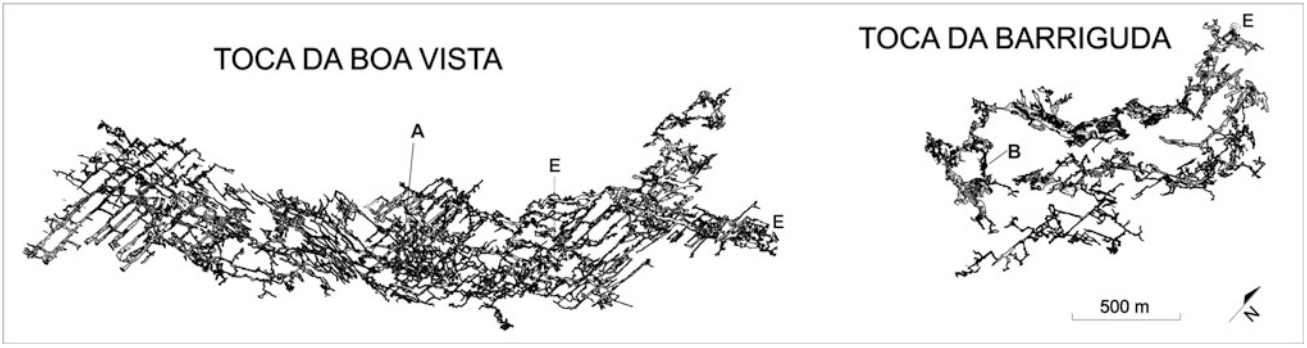

Fig. 3 Plan map of Toca da Boa Vista and Toca da Barriguda. Cave map courtesy of Grupo Bambuí de Pesquisas Espeleológicas

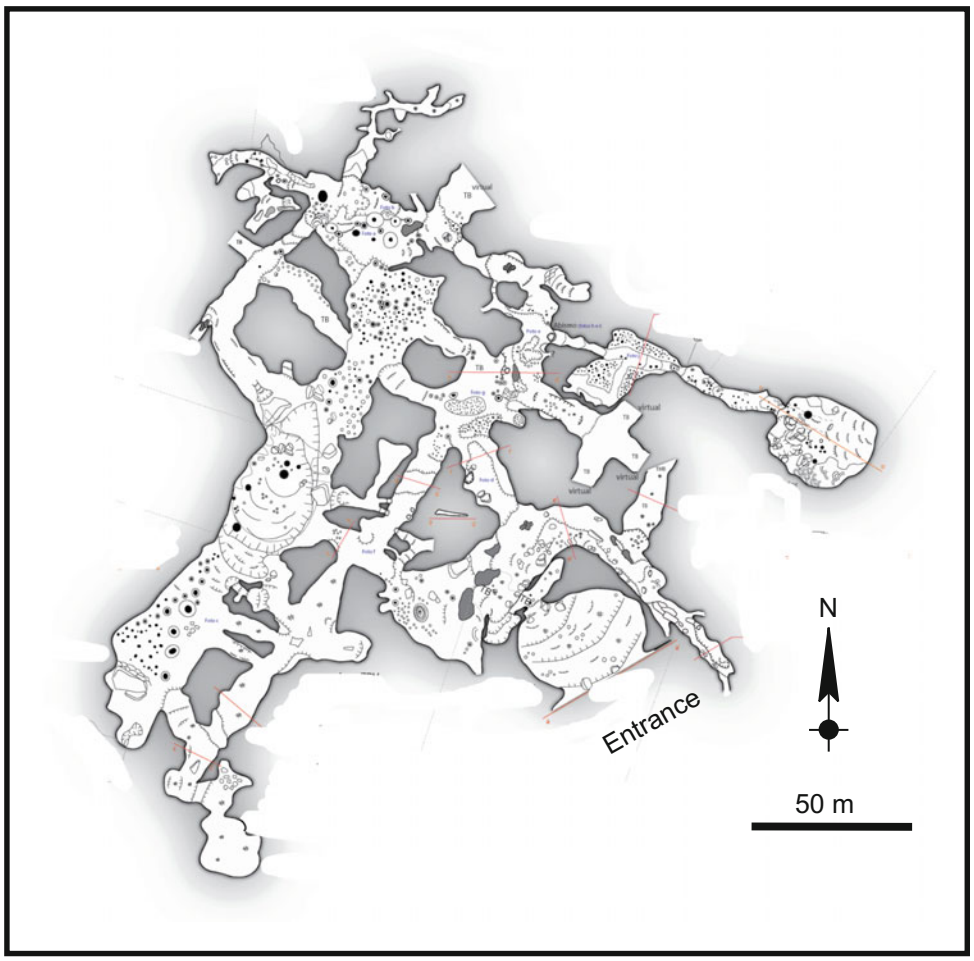

Fig. 4 Plan of Calixto Cave. Reproduced from Barreto (2016)

tectonic events. Metamorphosed and deformed carbonates occur mostly in the Gandarela and Fecho do Funil formations, sandwiched between quartzite and banded iron formation. The area contains few caves, most fragmentary in nature, the longest one being the 900-m-long Igrejinha Cave (coordinates 20° 27′ 01″S, 43° 42′ 16″W). This cave shows a ramiform pattern, large chambers, and rift-like side passages. Other caves such as the 400-m-long Antonio Pereira Cave display cupolas, pendants, and ascending passages.

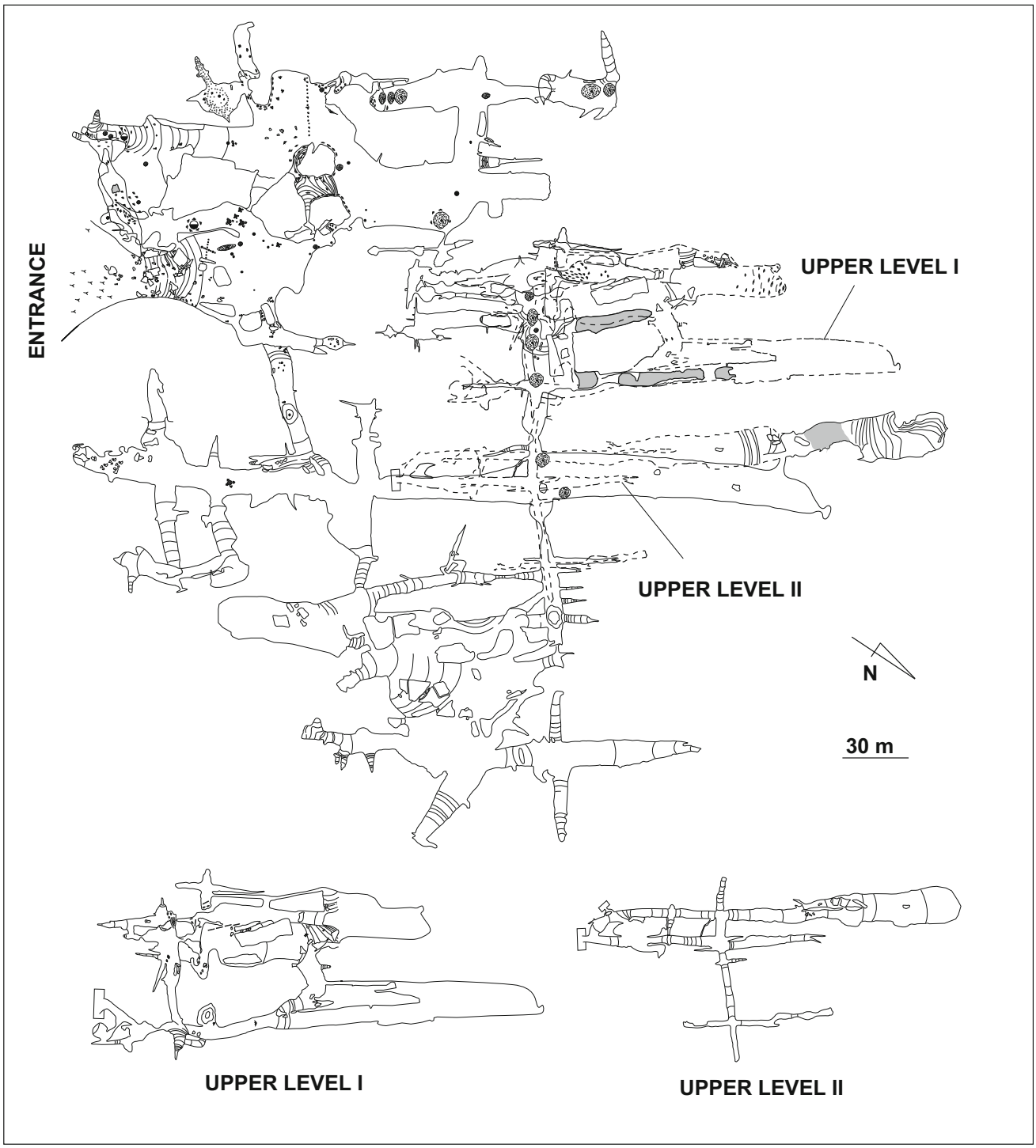

Fig. 5 Plan map of Lapa Nova (courtesy of Sociedade Excursionista e Espeleológica)

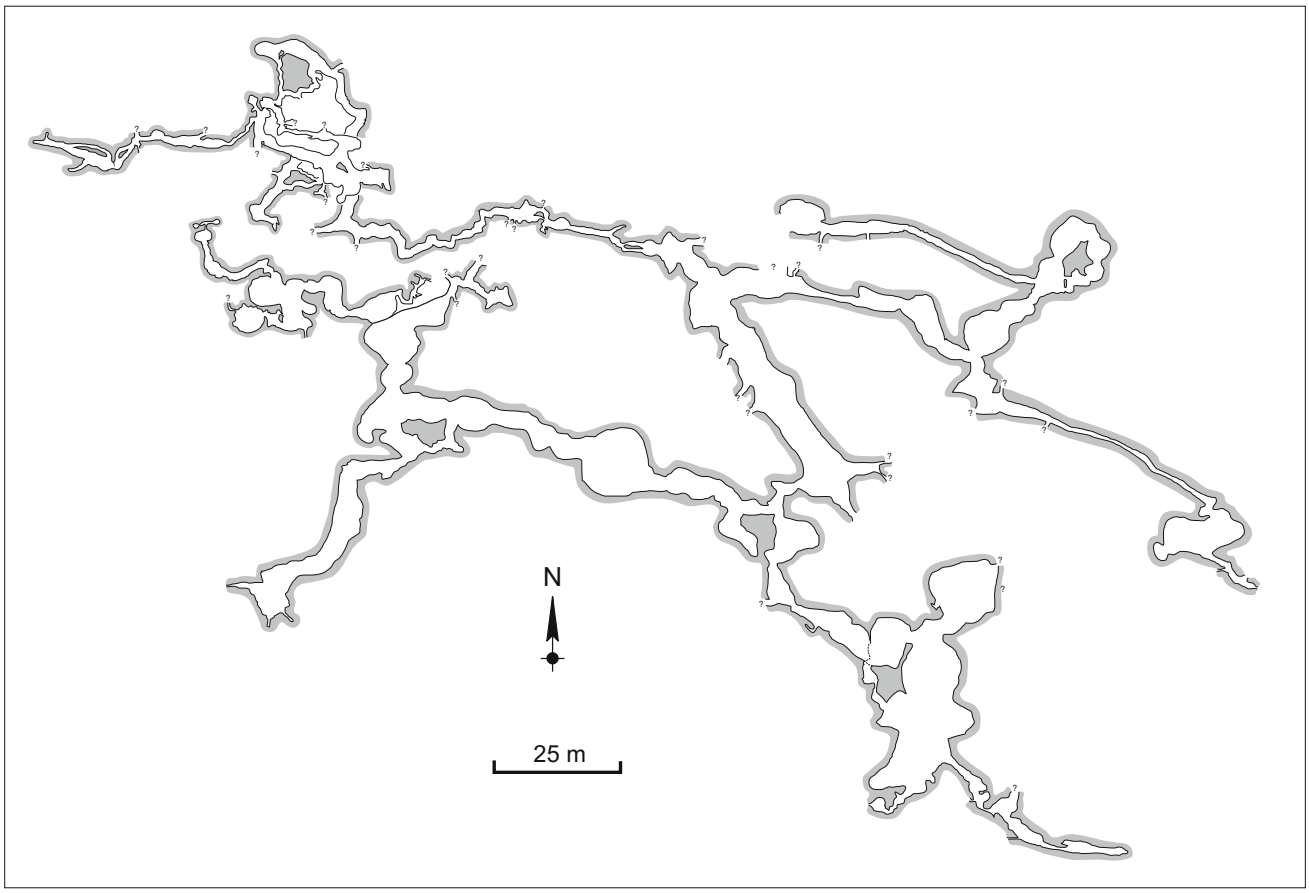

Fig. 6 Plan map of Dente de Cão Cave. Map courtesy of Grupo Espeleológico Serra da Bodoquena

The complex tectonic structure of the area and the several layers of differing formations result in a favorable setting for rising water flow through units of distinct permeability. However, apart from a local study by Scholz et al. (1998) that associated short caves to pyrite oxidation, no further speleogenetic work has been performed.

Several iron ore caves occur in the iron-rich rocks of the Cauê Formation and their alteration products. The morphology of some of these caves is suggestive of deep-seated processes, with later modification by vadose groundwater flow linked to slope processes (Auler et al. 2014).

2.6 Hypogene Caves of the Bodoquena Range

The late Proterozoic Corumbá Group contains significant karst, associated with the high relief Bodoquena Ridge and the surrounding low plains dotted with residual hills. The area is subjected to the Andean tectonics and contains over 100 registered caves, many representing active hydrological systems. Dente de Cão Cave (coordinates 20° 44′ 48″S, 56° 47′ 04″W) (Fig. 6) is a 3-km-long cave that displays a full suite of hypogene features, such as an anastomotic/ramiform pattern, a sequence of circular chambers linked by smaller passages, cupolas, feeders, outlets, absence of fluvial sediments, and no relationship to surface geomorphology (Auler 2009).

In the lower plains, some of the flooded caves and springs are suggestive of rising hypogene outlet morphology, such as 220-m-deep Lagoa Misteriosa (coordinates 21° 27′ 31″S, 56° 27′ 10″W) (Fig. 7). Divers have reported hydrothermal water coming from side passages (Gilberto Menezes pers. comm.). Another possible hypogene cave is the deep Ceita Curé Spring.

2.7 Hypogene Caves of the Western State of Mato Grosso

Karst in this poorly studied area of western Brazil contains some caves that may be related to hypogene processes. The

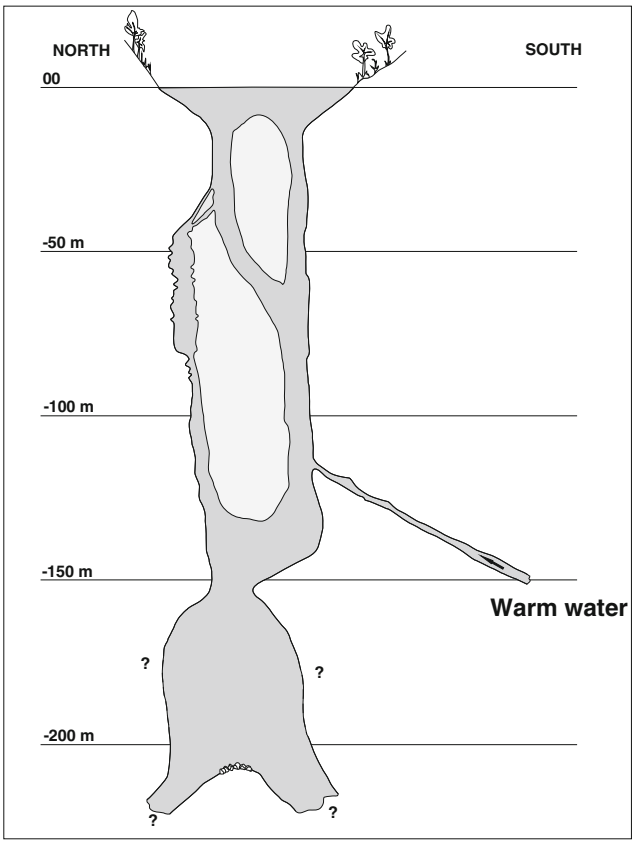

Fig. 7 Profile of Lagoa Misteriosa. Sketch map courtesy of Gilberto Menezes

deep water-filled sinkhole of Água Milagrosa (coordinates 16° 02′ 38″S, 57° 31′ 43″W) develops in the Late Proterozoic Araras limestone and has been explored to depths in excess of 180 m. The longest cave in the area is Jabuti Cave (coordinates 15° 33′ 56″S, 57° 59′ 19″W) (Fig. 8), a 3.8-km-long ramiform horizontal cave characterized by large vaulted irregular rooms separated by pillars and narrower passages. Abundant condensation corrosion and thick sediment fill mask the floor morphology (Auler 2009).

2.8 Quartzite Hypogene Cave in the Espinhaço Range

Hundreds of quartzite caves have been identified in the Mid-Proterozoic quartzites of the Espinhaço Supergroup. One cave, PF-59 (coordinates 14° 31′ 56″S, 42° 32′ 04″W), was intersected by a small amethyst quarry and originally had no opening to the surface. PF-59 cave contains a single rounded chamber (Fig. 9) with walls and ceiling partially covered by quartz crystals. Morphology and precipitates are not compatible with normal quartzite speleogenesis as seen elsewhere in the Espinhaço Range, suggesting the possibility of hypogene processes, although no further studies have so far been performed. If confirmed, this would be the second known hypogene quartzite cave in the world (Sauro et al. 2014).

3 Final Remarks

Karst studies in South America are still incipient; the few hypogene caves identified so far suggest that considerable potential exists for further findings. In particular, carbonates

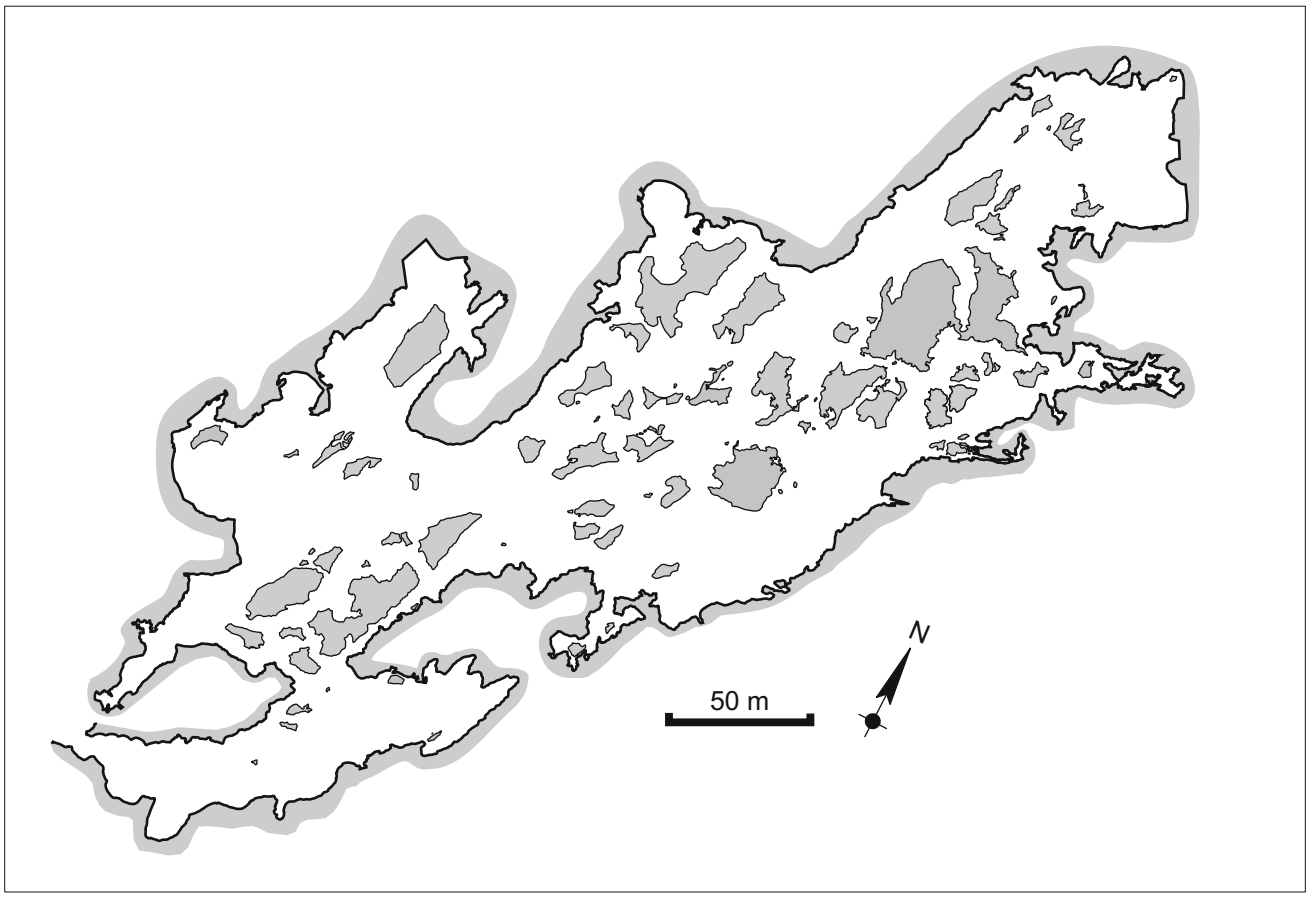

Fig. 8 Plan map of Jabuti Cave. Map courtesy of Fabiana Bezerra

in the tectonically active zone of the Andes Mountain Chain may contain yet unrecognized hypogene systems. Much of eastern South America (mostly Brazil) was last subject to tectonic movements during the Brasiliano orogeny at c. 600 Ma, and most hypogene caves, such as TBV-TBR system, are now relict.

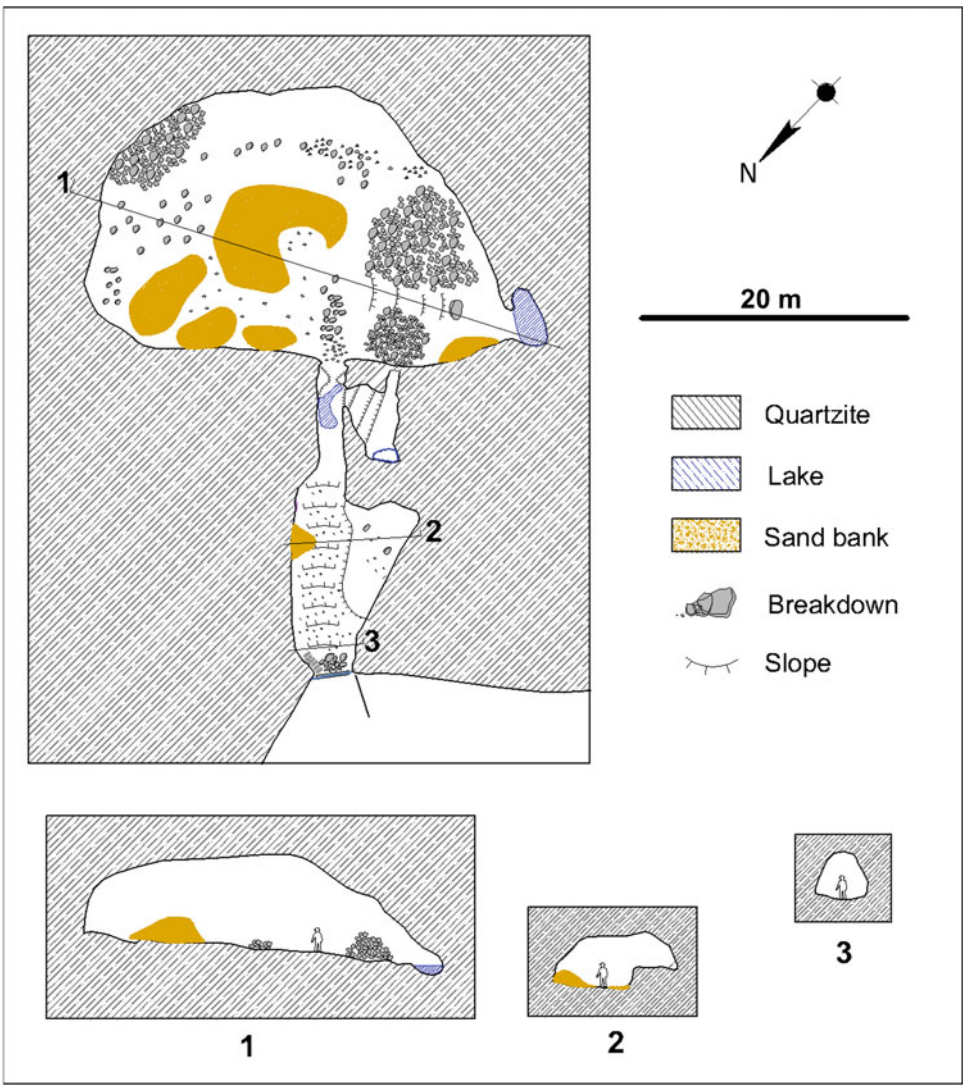

Fig. 9 Plan map of PF-59. Map courtesy of Bahia Mineração

Acknowledgements Grupo Bambuí de Pesquisas Espeleológicas and Carste Ciência e Meio Ambiente were helpful during cave exploration and data generation. We acknowledge various caving clubs for providing cave maps.

References

Auler AS (1995) Evidências de dissolução por ácido sulfúrico na espeleogênese do Grupo Una, Bahia. In: Abstracts of the VIII Simpósio de Geologia de Minas Gerais, Sociedade Brasileira de Geologia, Diamantina, 11–17 Sept 1995

Auler AS (1999) Karst evolution and palaeoclimate in eastern Brazil. PhD thesis, University of Bristol

Auler AS (2004) South America. In: Gunn J (ed) Encyclopedia of Cave and Karst Science. Taylor and Francis, New York, pp 53–57

Auler AS (2009) Styles of hypogene cave development in ancient carbonate areas overlying non-permeable rocks in Brazil and the influence of competing mechanisms and later modifying processes. In: Klimchouk A, Ford DC (eds) Hypogene Speleogenesis and Karst hydrogeology of Artesian Basins, Simferopol

Auler AS (2012) Quartzite caves of South America. In: White WB. Culver DC (eds) Encyclopedia of caves. Academic Press, Chennai

Auler AS, Smart PL (2003) The influence of bedrock-derived acidity in the development of surface and underground karst: evidence from the Precambrian carbonates of semi-arid Northeastern Brazil. Earth Surf Proc Land 28:157–168

Auler AS, Piló LB, Parker CW, Senko JM, Sasowsky ID, Barton HA (2014) Hypogene cave patterns in iron ore caves: convergence of forms or processes? In: Klimchouk A, Sasowsky ID, Mylroie J, Engel SA, Engel AS (eds) Hypogene cave morphologies. Karst Waters Institute Special Publication vol 18, pp 15–19

Barreto EAS (2016) Reconstituição da paleoprecipitação no sul do nordeste brasileiro durante os dois últimos ciclos glaciais a partir da aplicação de registros isotópicos de oxigênio de estalagmites da Chapada Diamantina (Bahia). Universidade de São Paulo, Thesis

Bittencourt C (2008) Carstificações hipogênica e epigênica—Influências sobre a exploração de minério de zinco da mina de Vazante—MG. Dissertation, Universidade Federal do Paraná

Bittencourt C, Reis Neto JM (2012) O sistema cárstico de Vazante—carste em profundidade em metadolomitos do Grupo Vazante—MG. Rev Bras Geociências 42:1–10

Bittencourt C, Auler AS, Reis Neto JM, Bessa V, Silva MVA (2009) The influence of hypogene and epigene speleogenesis in the

evolution of the Vazante Karst, Minas Gerais state, Brazil. In: Ford DC (ed) Klimchouk A. Simferopol, Hypogene Speleogenesis and Karst Hydrogeology of Artesian Basins

Cordani UG, Sato K, Teixeira W, Tassinari CCG, Basei MAS (2000) Crustal evolution of the South American Platform. In: Cordani UG, Milani EJ, Thomaz Filho A, Campos DA (eds) Tectonic evolution of South America. CPRM, Brasilia, pp 19–40

Ennes-Silva RA, Bezerra FHR, Nogueira FCC, Balsamo F, Klimchouk A, Cazarin CA, Auler AS (2016) Superposed folding and associated fracturing influence hypogene karst development in Neoproterozoic carbonates, São Francisco Craton, Brazil. Tectonophysics 666:244–259

Fabri FP, Auler AS, Calux AS, Cassimiro R, Augustin CHRR (2015) Cave morphology and controls on speleogenesis in quartzite: the example of the Itambé do Mato Dentro area in southeastern Brazil. Acta Carsologica 44:23–35

Forti P, Benedetto C, Costa G (1993) Las Brujas cave (Malargue, Argentina): an example of oil pools control on the speleogenesis. Theor Appl Karstology 6:87–93

Klimchouk A, Auler AS, Bezerra FHR, Cazarin CL, Balsamo F, Dublyansky Y (2016) Hypogenic origin geologic controls and functional organization of a giant cave system in Precambrian carbonates Brazil. Geomorphology 253:385–405

Mikkan RA (1995) Observations sur le karst de Bardas Blancas—Malargue (Andes de Mendoza, Argentina). Karstologia 26:39–46

Sancho C, Peña JL, Mikkan R, Osácar C, Quinif Y (2004) Morphological and speleothemic development in Brujas Cave (South Andean Range, Argentina): palaeoenvironmental significance. Geomorphology 57:367–384

Sauro F, De Waele J, Onac BP, Galli E, Dublyansky Y, Baldoni E, Sanna L (2014) Hypogenic speleogenesis in quartzite: the case of Corona'e Sa Craba Cave (SW Sardinia, Italy). Geomorphology 211:77–88

Scholz R, Barata R, Mayrink P, Corteletti R, Addad JE (1998) Gênese de cavernas em dolomite na região do Córrego do Eixo, Quadrilátero Ferrífero, Minas Gerais. In: Abstracts of the XL Congresso Brasileiro de Geologia, Sociedade Brasileira de Geologia, Belo Horizonte, 11–16 Oct 1998

Wray RAL (1997) A global review of solutional weathering forms on quartz sandstone. Earth-Sci Rev 42:137–160

Origin and Evolution of Toca da Boa Vista and Toca da Barriguda Cave System in North-eastern Brazil

56

Augusto S. Auler, Alexander Klimchouk, Francisco Hilário R. Bezerra, Caroline L. Cazarin, Renata Ennes-Silva, and Fabrizio Balsamo

Abstract

Toca da Boa Vista and Toca da Barriguda (TBV-TBR) are two of the longest caves in South America and, although not physically connected, share a common origin and evolution. Together, they comprise over 145 km of passages that are mostly developed in five lithological units in a Precambrian dolomite host rock. The now relict caves display a mixed ramiform/spongework/network pattern that shows clear hypogene morphology. The inception of speleogenesis cannot be precisely determined but likely occurred several tens (if not hundreds) of millions of years ago, placing this system among the oldest caves in the world. The TBV-TBR system is controlled by a NE–SW-oriented fracture corridor; passages follow anticlines and troughs, showing morphological variations depending on the vertical position in relation to the carbonate units. The cave system is represented by a laterally extensive maze controlled by a highly fractured unit in which ascending flow was restricted by an upper less fractured unit (hydraulic seal). The long evolutionary history of the cave left numerous imprints, including widespread and remarkable condensation-corrosion processes that dissolved the bedrock and speleothems, abundant chemical and clastic sedimentation phases and flooded lower passages. Following the interception of the cave by surface denudation, a remarkably rich late Quaternary vertebrate fossil assemblage accumulated.

Keywords

Hypogene • Toca da Boa Vista • Toca da Barriguda • Speleogenesis

A.S. Auler (✉)
Instituto do Carste, Rua Barcelona 240/302, Belo Horizonte, MG 30360-260, Brazil
e-mail: aauler@gmail.com

A. Klimchouk
Institute of Geological Sciences, National Academy of Sciences, 55-B Gonchara Street, Kiev, 01054, Ukraine
e-mail: klim@speleogenesis.info

F.H.R. Bezerra · R. Ennes-Silva
Geodynamics and Geophysics, Federal University of Rio Grande do Norte, Natal, 59072-970, Brazil
e-mail: bezerrafh@geologia.ufrn.br

R. Ennes-Silva
e-mail: renata.aesilva@gmail.com

C.L. Cazarin
Centro de Pesquisa e Desenvolvimento Leopoldo Américo Miguez de Mello (Cenpes), Petrobras, Rio de Janeiro, 21941-915, Brazil
e-mail: cazarin@petrobras.com.br

F. Balsamo
NEXT—Natural and Experimental Tectonic Research Group, Department of Physics and Earth Sciences, University of Parma, 43124 Parma, Italy
e-mail: fabrizio.balsamo@unipr.it

© Springer International Publishing AG 2017
A. Klimchouk et al. (eds.), *Hypogene Karst Regions and Caves of the World*, Cave and Karst Systems of the World, DOI 10.1007/978-3-319-53348-3_56

1 Introduction

The semi-arid zone of north-eastern Brazil contains large caves that display typical hypogene morphology. These caves were first visited by cavers in the late 1980s, and intensive exploration and mapping revealed a major cave system with a total combined length exceeding 145 km as of July 2016. Approximately 20 hypogene caves have been recorded in the area, the most important ones being clustered in the vicinity of the village of Laje dos Negros in the northern state of Bahia (Fig. 1). Toca da Boa Vista (TBV—10°09′45″S, 40°51′35″W) and Toca da Barriguda (TBR—10°08′26″S, 40°51′08″W) are the most extensive caves, with individual lengths of 111 and 34 km, respectively, as of July 2016. The distance between the closest passages in each cave is approximately 700 m, but no physical connection has been discovered to date. Because these caves display similar features and share a common evolutionary history, they are referred to as the TBV-TBR cave system.

The climate in the area is semi-arid, with an annual precipitation mean of 483 mm, concentrated mostly in the austral summer months (November–March). The mean annual monthly temperature is 26.9 °C, with a monthly average maximum of 32.4 °C and an average minimum of 22.0 °C (1962–2015 series from the Petrolina station, 100 km to the NE) (INMET 2016). The vegetation comprises dry deciduous xerophytic low arboreal species known as caatinga, one of the recognized biomes of Brazil. This vegetation occupies a dry belt between the wetter Atlantic (east) and the Amazon (west) rainforests.

Karst surface landforms in the area are conspicuously absent, with the exception of isolated collapse dolines. Thin soil, capped by residual chert, overlies the carbonate, which is exposed only in discrete outcrops associated with scarps along gentle limestone hills. In stark contrast to the subdued karst landscape, the spectacular underground karst is represented by several caves. Most of them are fragments of once longer caves interrupted by breakdown, sediment blockage or surface removal. Two of these caves, however, TBV and TBR, are now the longest caves in South America and are prime examples of hypogene speleogenesis in an ancient cratonic setting (Auler and Smart 2003; Klimchouk et al. 2016).

These caves have been the subject of several studies focusing on the remarkably rich Quaternary deposits (Czaplewski and Cartelle 1998; Cartelle and Hartwig 1996; Hartwig and Cartelle 1996; Wang et al. 2004; Auler et al. 2004, 2006, 2009). In addition to the pioneering work by Auler and Smart (2003), two recent publications provide details on the speleogenesis (Klimchouk et al. 2016) and structural geology (Ennes-Silva et al. 2016) of the cave system. This work reviews the existing literature and summarizes the mechanisms and controls involved in the generation of these important caves. Furthermore, it adds new geochemical data that provide additional information on the post-speleogenetic evolution of the system.

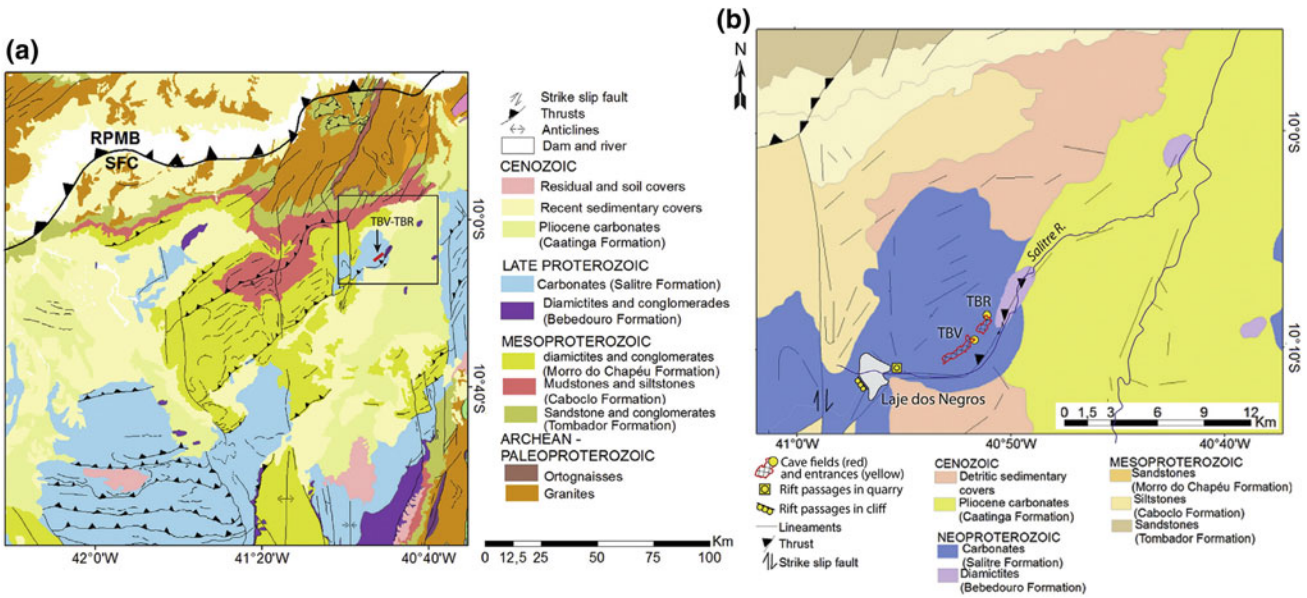

Fig. 1 Regional (**a**) and local (**b**) geology of the study area. TBV-TBR cave system is depicted in **a** as a *red rectangle* marked by an *arrow*. Geology simplified from Bizzi et al. (2003)

2 Geology of the Area

The TBV-TBR cave system is developed in Precambrian carbonate rocks of the Salitre Formation, Una Group. These carbonates, dated to 600–670 Ma (Misi and Veizer 1998), comprise mostly marine limestones and dolomites that cover, in separate basins, much of the northern portion of the state of Bahia. The stratigraphy of the Salitre Formation was established in the Irecê basin, some 150 km to the SW of the study area. The lack of representative outcrops in the separate carbonate basin that contains the TBV-TBR system hinders correlation with the established sequences described by Misi and Kyle (1994) in the Irecê basin, prompting the development of a stratigraphic study inside the caves. The base and top of the carbonate sequence cannot be established because no contacts have been identified in the study area. Field observations suggest that basal formations comprise either Archean schists of the Rio Salitre Belt or Precambrian diamictites of the Bebedouro Formation. The upper sequences of the Una Group have been denuded in the study area, and the carbonates are now overlain by much younger palustrine carbonates of the Caatinga Formation (Penha 1994; Auler 1999).

The TBV-TBR system is located on the northern border of the São Francisco Craton, close to the limit with the Riacho do Pontal Fold Belt (Fig. 1). The carbonates were subjected to tectonic forces during the collision between these structural units in the Brasiliano orogeny c. 620–580 Ma (van Schmus et al. 2008). Two phases of deformation were recognized in the area: folds and thrusts that strike NNE–SSW and folds and thrusts that strike E–W, both associated with the later stages of the Brasiliano event (Caxito and Uhlein 2013; Lagoeiro 1990).

Analyses of the cave-bearing stratigraphic units were performed in the TBV-TBR system to not only overcome the lack of geological studies at the local scale but also understand the relationship between rock types, fracture pattern and cave morphology. Five main units were identified (Cazarin 2015) (Fig. 2), and a total of 26 X-ray fluorescence analyses were performed on the carbonate bedrock, avoiding chert intercalations (Table 1). Unit 1, the lowermost unit, presents massive oolitic grainstone with cross-bedding and shows a near total absence of chert layers and disseminated silica. This unit is at least 15 m thick, and its base has not been observed. Unit 2 comprises peloidal grainstone with intraclasts with plane-parallel stratification and chert nodules. Its chemistry is essentially similar to that of Unit 1 but with slightly higher silica content. This unit is 1.5–2 m thick. Unit 3, up to 1 m thick, contains microbial carbonates with laminites, stromatolites and thrombolites. It presents higher contents of Al, Fe and P. Unit 4 is represented by a thin (<1 m) siliciclastic layer containing siltstone, fine-grained sandstones, clays and marls. Si, Ca and Mg are the main constituents. Unit 5, the uppermost cave-bearing unit, is composed of grainstone containing abundant chert layers and is over 10 m thick. This unit has a geochemical signature similar to that of the lower carbonate units but with a somewhat higher silica content. Other upper units are exposed due to breakdown in restricted areas in the caves. Breccia units occur in a few sections in TBR and display similar geochemical contents but are silica-poor. The geochemical similarity between the dolostones that comprise the cave bedrock units suggests that joint characteristics, chert content and hydrodynamic factors are the main factors in the resulting differences in cave morphology. Each of these units exhibit their own pattern of fracture systems and responded in distinct ways during speleogenesis (Klimchouk et al. 2016): Unit 1 contains major fractures often occurring in swarms of fractures, rarely extending into the upper units; fractures in Units 3–4 are less conspicuous but more densely packed; Unit 5 contains fewer fractures, restricting upward flow and acting as a hydraulic seal (Klimchouk et al. 2016), except in few places where its integrity is disrupted by large vertical fractures.

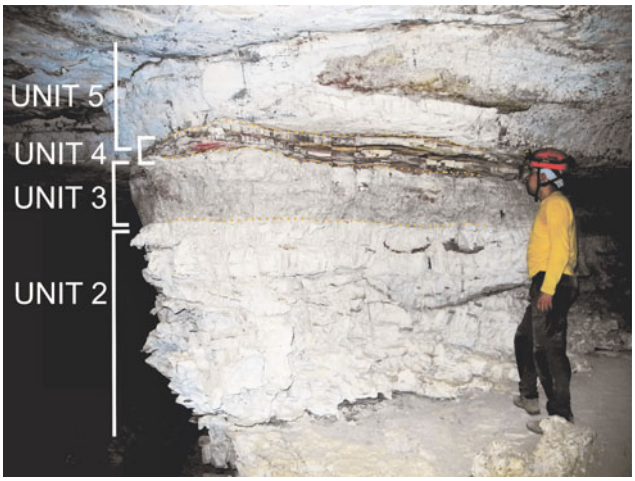

Fig. 2 Passage in TBV showing Units 2–5. Unit 1 occurs beneath the passage floor

3 Cave Hypogene Morphology

The TBV-TBR cave system comprises a complex elongated swarm of passages with a general N45E direction (Fig. 3) that has developed at the north-western edge of a NE–SW-striking thrust fault (Ennes-Silva et al. 2016) (Fig. 1). These authors recognized variations in passage orientation depending on the cave sector, with passages along either ~NNE (0°–20°) or ~E–W (70°–100°) directions, which is not in general coincident with the main trend of the cave passages. The plan view of the caves (Fig. 3), although

Table 1 Whole rock X-ray fluorescence analyses of the cave-bearing stratigraphic units of the TBV-TBR cave system

	CaO	MgO	SiO_2	Fe_2O_3	Al_2O_3	P_2O_5	K_2O	LOI
Unit 1 (n = 5)	31.96	20.02	2.11	0.15	0.20	0.10	0.08	45.24
Unit 2 (n = 4)	31.23	19.83	3.77	0.21	0.28	0.18	0.12	44.25
Unit 3 (n = 5)	31.16	19.02	3.83	0.46	0.51	0.94	0.17	43.68
Unit 4 (n = 4)	17.35	14.40	24.20	3.42	8.47	0.30	3.47	27.55
Unit 5 (n = 4)	29.48	19.10	5.58	0.55	1.35	0.32	0.45	42.95
Breccia (n = 2)	31.85	20.10	0.71	0.16	0.20	0.73	0.07	46.00

Units 2 and 5 contain intercalations of chert which were not sampled. Oxide values are in %. Only major oxides (>0.1%) are shown

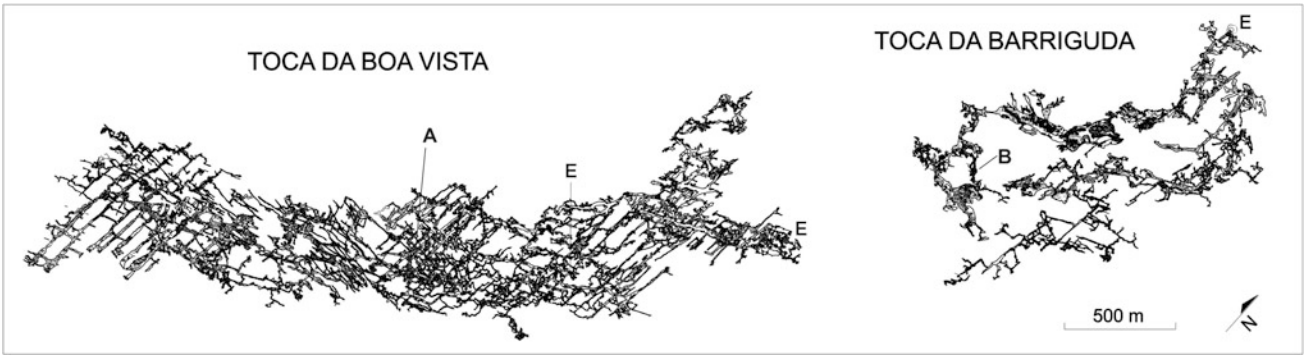

Fig. 3 Plan view of Toca da Boa Vista and Toca da Barriguda. Map courtesy of Grupo Bambuí de Pesquisas Espeleológicas. *E* Entrance. *Letters A* and *B* denote sectors detailed in Fig. 4

exhibiting a clear structural control on the passage directions, does not allow for a complete assessment of cave patterns because many smaller passages have not yet been mapped. The basic morphological features of these caves were described by Auler and Smart (2003), such as a mixed network/ramiform pattern (Fig. 4), abrupt variations in cross section, lack of vadose speleogens and fluvial sediments, presence of cupolas and wall projections and extensive evidence of condensation-corrosion processes (dolomitic sand, friable walls and speleothems).

When passage morphology is coupled with the previously described lithostratigraphic units, it becomes clear that the lithostratigraphic units, with their specific patterns of fractures and chert abundance, play an important role in passage configuration. Passages in Unit 1 constitute the lower storey in the cave system, although their distribution is not necessarily horizontal. They are generally wider, usually displaying ramiform pattern and comprising some of the larger chambers in the system, such as in the northern boundary of both TBV and TBR (Fig. 4c). The absence of chert allows for a full expression of dissolutional features related to the morphological suite of rising flow as defined by Klimchouk (2007, 2009). Cupolas are widespread, especially in TBR (Fig. 5), with some being over 10 m high and sometimes developed over speleothem. Rock pendants, pillars, irregular rock projections and smaller vertical rifts are common throughout the caves but are more prominent in the lower storey. Widespread dissolution along well-marked joints results in wall retreat at the joint level, creating highly irregular ceilings and walls. Blind passages and alcoves are common, and many side passages end abruptly. The lower storey passages occur throughout most of TBR (except the NE section close to the entrance) and form the northern limit of TBV. They connect to clusters of galleries developed in upper units (the middle storey) through rifts, domepits or inclined ramps. Passage configuration in the middle storey contrasts with the lower storey, being in general smaller, with rectangular cross sections controlled by chert bands, and presenting a higher density of passages than the ones in the lower storey (Fig. 6). In plan view, these passages sometimes show a spongework pattern, consisting of low passages separated by pillars (Fig. 4a). Network sectors occur in select areas of TBV and TBR (Fig. 4b) and are usually associated with high rift passages regardless of lithostratigraphic unit. Master passages in the middle storey are associated with anticline hinges with limbs that dip gently between 10° and 30° (Fig. 7). These anticline hinges have a mean orientation of 15° along NNE-oriented passages and 30°–90° in NE–SW- to E–W-oriented passages (Ennes-Silva et al. 2016). Passages in Unit 5 constitute the upper storey in the system. They have a rift morphology, often heavily modified by breakdown. Figure 6 shows a passage formed by breakdown (collapse) of a rock partition between two parallel rifts into a cavity that should have

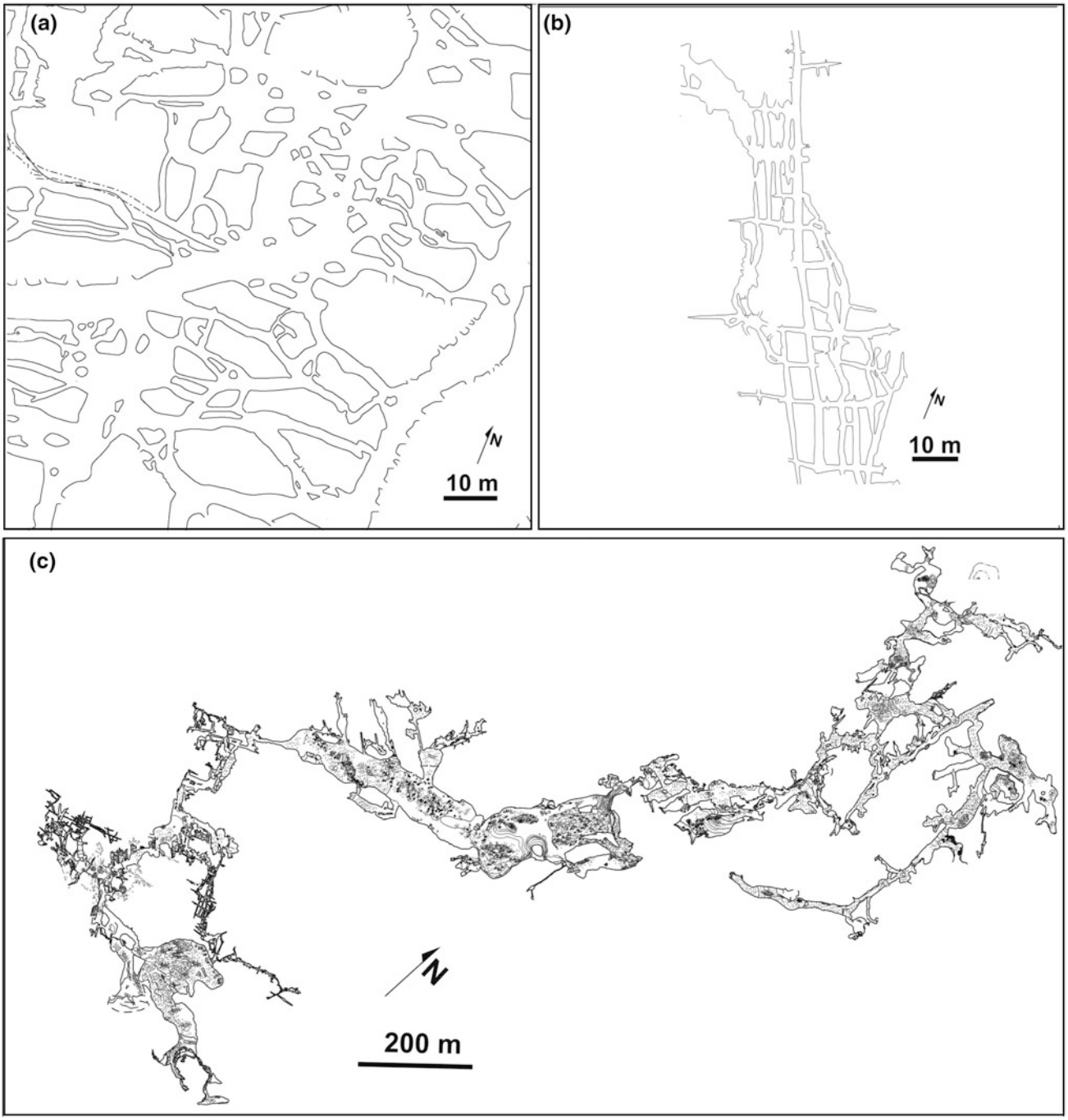

Fig. 4 Cave patterns in selected portions of the TBV-TBR system. **a** Spongework-like passage in TBV developed in Units 2–5. Pillars between laterally extensive passages result in a complex pattern that is similar to spongework but differs in terms of genesis. **b** Network passage in TBR. **c** Northern passages in TBR. These large passages are developed in Unit 1 and display a general ramiform pattern with some network sectors. Locations of sectors **a** and **b** can be found in Fig. 3

existed below (in the middle or lower storey). Breakdown has altered the ceiling profiles in the middle storey in many areas of the system.

Examination of the full section of passages is difficult because the floor is invariably masked by breakdown, fine-grained sedimentation or speleothems. Small vertical or cylindrical channels are frequent in walls and are interpreted as indications of former side feeders. Larger features are less frequent and consist mostly of vertical rift passages, some of which are approximately cylindrical and a few reach the water table. Outlet features, showing rift morphology or cylindrical "cupola" shapes, are much less frequent, being

Fig. 5 Chamber in TBR developed in Unit 1 showing abundant hypogene features such as cupolas and wall projections. The *whitish colour* is due to condensation-corrosion residue the original dolostone colour being usually *grey*. Photograph by Luciana Alt and Vitor Moura

restricted to very few areas, such as the vertical entrances of TBV. In the context of the group of features defined as the morphological suite of rising flow (Klimchouk 2007, 2009), the extensive lateral development of the cave allows for an impressive display of intermediate features, while basal forms (feeders) are mostly masked by later events, and rising features (outlets) tend to be rare. For a more detailed review of cave morphology in the TBV-TBR system, refer to Klimchouk et al. (2016).

4 Origin and Timing of Speleogenesis

The hypogene character of the TBV-TBR system was recognized by Auler (1999) and Auler and Smart (2003). Studies by Misi and Kyle (1994) have identified large bodies of sulphide within the B1 Unit of the Una Group, the same unit interpreted by Auler (1999) as hosting the TBV-TBR system. Furthermore, the Archean schists of the Rio Salitre Belt, possibly the basal rock below the carbonates, contain sulphide-rich layers (Ribeiro et al. 1993), which may have provided additional acidity. Auler and Smart (2003) proposed a mode of speleogenesis in which oxidation of metallic sulphides (both disseminated and massive) within the bedrock generated sulphuric acid and promoted dissolution of the carbonate. This "shallow" hypogene model of speleogenesis is especially attractive in stable cratonic areas, in which recent hydrothermal or tectonic activity is often absent.

The recent work by Klimchouk et al. (2016) and Ennes-Silva et al. (2016), combining detailed morphological, stratigraphical and structural analysis, has shed new light on the timing and controls on speleogenesis in the area. Klimchouk et al. (2016) have proposed a classical hypogene model in which acidic fluids rising from feeders promoted carbonate dissolution and cave development. The rising fluids exploited the numerous vertical fractures arranged in a superposed deformation pattern (Ennes-Silva et al. 2016).

Fig. 6 Passage in TBV developed in Unit 5 (the upper storey). Abundant chert layers and rift-like or rectangular shapes are typical of cave passages in this lithostratigraphic unit. The original passage morphology in the area shown in the photograph was rifts. This passage was formed by breakdown (collapse) of a rock partition between two parallel rifts into a cavity that should have existed below. Photograph by Luciana Alt and Vitor Moura

These fractures formed a "fracture corridor", a swarm of joints and faults that guided the general development of the cave system (Klimchouk et al. 2016). Joint patterns and the more massive character of Unit 1 focused the vertical dissolution. Although lateral development of passages in this unit is restricted, the high fracture density in local swarms favoured the coalescence of adjacent passages, resulting in larger volumes in the system (Klimchouk et al. 2016). Vertical migration of water was hampered by differences in joint density, limiting the growth of the cave system above Unit 5. Favourable joints in the upper units allowed the generation of outlets in only a few select places, mostly in TBV (Fig. 8).

The initial depth of cave formation cannot be established with precision but was probably on the order of several hundred metres. The preserved beds of the Salitre Formation in the area are likely no more than 200 m thick, but its original thickness could have been significantly greater (Misi et al. 2007). Additionally, the abundant presence of stylolites may suggest a considerable initial burial depth for the cave-bearing carbonate horizon, in the range of 600–900 m (Van Golf-Racht 1982). Furthermore, deposition of younger sequences could have been responsible for additional burial episodes, as suggested by Japsen et al. (2012).

The origin of the acidic water could have involved more than one source. Avenues of ascending water could have been related to the many ancient faults associated with the nearby contact between the São Francisco Craton and the Riacho do Pontal Fold Belt. The chemistry of the cave-forming water cannot be established with certainty, but the general lack of poorly soluble sulphur-derived minerals, such as halloysite or alunite (Hill 1990; Polyak et al. 1998), suggests that H_2S was not the main source of acidity. Furthermore, gypsum occurs only as restricted, isolated

Fig. 7 Master passages in the middle storey trending E–W are usually controlled by gentle anticlines as shown in this TBV passage. Originally developed in Units 2–4 these passages can be heavily modified by breakdown with the ceiling stoping upward into Unit 5 as shown in this photograph taken near the main entrance. Photograph by Luciana Alt and Vitor Moura

specimens and not as massive deposits, as would be expected from the reaction between sulphuric acid and the carbonate as reported from sulphuric acid caves in other semi-arid areas (Hill 1987). This reinforces the suggestion that a massive input of SO_4 was not involved in the speleogenesis.

Events that could promote the rise of acid water have been tentatively outlined by Klimchouk et al. (2016). Two main possibilities were discussed by these authors: (i) hydrothermal activity along faults could have promoted the migration of hypogene fluids towards the carbonates during the later events related to the Brasiliano orogeny (c. 550 Ma) or (ii) during rift generation associated with the break-up of Pangea (Triassic–Cretaceous). Either of these two possibilities would place the TBV-TBR caves among the oldest on Earth.

5 Cave Evolution and Later Modification Processes

Hypogene caves, being dependent on acid sources from below and not being related to meteoric water, are usually formed at considerable depths. In stable cratonic areas, uplift and denudation progresses slowly, and low values for the latter (2.5–40 m/Ma) have been obtained for the São Francisco Craton (Amaral et al. 1997; Auler et al. 2002; Braucher et al. 1998; Harman et al. 1998). In such contexts, caves will remain in the subsurface for a prolonged period before surface bisecting and unroofing take place. The possible scenarios for speleogenesis discussed previously hint at extremely long timescales for cave evolution. Furthermore, it is possible that earlier phases of speleogenesis were overprinted by the main cave-forming episode. Throughout

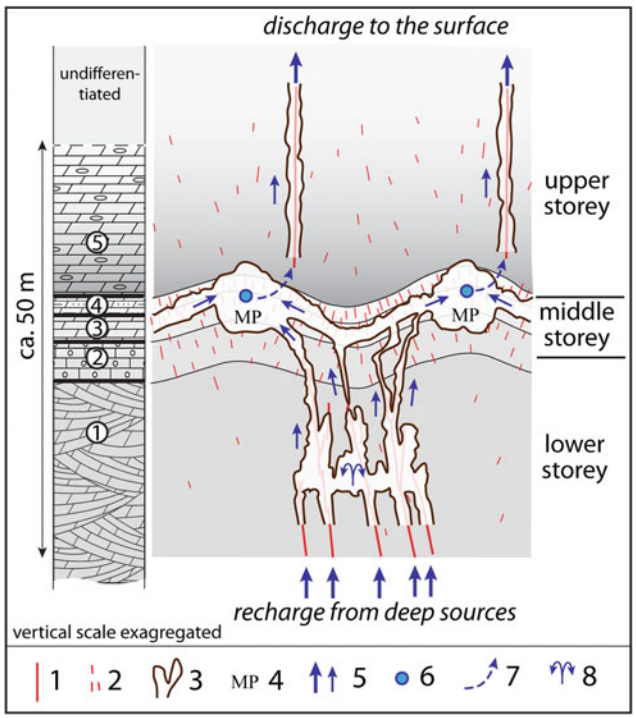

Fig. 8 Schematic diagram of the vertical structure and functional organization of the TBV-TBR cave system (modified from Klimchouk et al. 2016): *1* major fractures intersecting the bed interfaces; *2* minor fractures (predominantly strata-bound joints); *3* solution cavities; *4* master passages in the middle storey (shown in cross sections); *5* flow directions; *6* lateral flow in the direction normal to the profile plane; *7* convergence of lateral flow in remote outlet conduits in Unit 1; and *8* natural convective circulation

the evolutionary history of a cave system, more recent processes tend to mask or obliterate older ones, making the establishment of a complete and well-integrated history of cave evolution difficult.

The presence of breccia bodies intersected by existing passages (Fig. 9a) and isolated cavities in heavily altered bedrock lined by calcite spars that were beyond U-series dating limits (>650 ka) (Fig. 9c) suggests early dissolutional processes in the phreatic environment that could have predated the main speleogenetic phase. Furthermore, at Morrinho Cave, an isolated segment of hypogene cave approximately 9 km south-west from TBV, a large breccia wall cemented by calcite shows dissolutional passages. This calcite cement was also beyond U-series dating limits (>650 ka) (Fig. 9b).

The lower levels of the caves were subject to intense sedimentation. This is particularly conspicuous in the SW portion of Toca da Boa Vista, where massive fine sedimentation occurred. These sediments are generally highly indurated and contain quartz, haematite, muscovite and kaolinite, with some pyrolusite-rich layers (Fig. 10). Palaeomagnetic dating in two sequences of indurated sediment coupled with fluvial incision rates of nearby valleys suggests correlation with the two major reversal episodes of the Matuyama Epoch at 1.19–1.77 or 1.95–2.6 Ma (Auler 1999).

Throughout the TBV-TBR system, the disintegration of both bedrock and speleothems results in significant accumulations of whitish dolomitic powder that shares the same mineralogical characteristics as the bedrock (Auler 1999). This subaerial process is related to condensation corrosion and affects both the bedrock and speleothems (Auler and Smart 2004). Cupolas in speleothems well above the present phreatic zone attest to the efficiency of this mechanism. The rates of condensation corrosion were obtained by Auler and Smart (2004) (Table 2), demonstrating that, given enough time, it can be a powerful dissolutional process, capable of considerably expanding already existing cave passages.

Another ubiquitous process that weathers the dolomitic cave walls is represented by reactions between bat guano and the bedrock (Onac and Forti 2011). In the TBV-TBR system, the guano-derived phosphate minerals, whitlockite, hydroxyapatite and fluorapatite, are extremely common in areas with present or past bat populations. They develop as alteration crusts that can be over 1 cm thick (Fig. 11). The disintegration of these crusts result in a fine-grained beige sediment common in areas close to existing or former entrances.

The TBV-TBR cave system is a valuable repository of palaeoenvironmental information. The abundant speleothem deposition has allowed for the precise determination of past periods of increased rainfall in the area (Auler et al. 2004; Wang et al. 2004), during which the area was covered (at least partially) by rainforest, thereby providing a faunistic connection between the adjacent rainforests (Auler et al. 2004). Past markers of water table rise are represented by calcite rafts and shelfstone. Those are especially conspicuous at the northern limit of TBV. U-series dating by Auler and Smart (2001) has pinpointed episodes of water table rise (associated with past wetter periods) at 17.3–20.1 ka and c. 145 ka, the later one associated with a 13 m rise compared to present levels. Remarkably, well-preserved fossil remains (Cartelle and Hartwig 1996; Hartwig and Cartelle 1996) have reinforced the former existence of a forested environment in addition to providing unique insights into the skeletal morphology of previously little known or entirely new fossil species, such as large monkeys (Cartelle and Hartwig 1996; Halenar and Rosenberger 2013). The earliest date of these fossils, c. 300 ka (Auler

Fig. 9 **a** Dolostone breccia in TBR. **b** Breccia cemented by calcite dated to >650 ka in Morrinho Cave (see pencil for scale). **c** Heavily altered cave wall containing a geode with ancient (>650 ka) calcite in TBV (scale bar = 10 cm)

et al. 2006), also represents a minimum age of surface interception, when the exposure of cave passages made the cave accessible to ancient surface fauna.

The long and still poorly known evolutionary history of this remarkable cave system is only outlined at present due to the lack of further dateable evidence. Because of the natural preservation potential of its environment, it represents a valuable asset in providing critical palaeoenvironmental information on presently semi-arid north-eastern Brazil.

Fig. 10 Sedimentary sequence in the south-western sector of TBV showing pyrolusite-rich layers

Table 2 Rates of condensation corrosion derived from U-series dating of outer rims of speleothems (from Auler and Smart 2004)

Sample	U (ppm)	$^{234}U/^{238}U$	$^{230}Th/^{234}U$	$^{230}Th/^{232}Th$	$^{234}U/^{238}U$ initial	Age (ka)
TBV1-95	0.171 ± 0.002	1.46 ± 0.02	0.869 ± 0.016	57	1.76	182.9 ± 10.5
TBV-17T	0.420 ± 0.006	1.73 ± 0.02	0.744 ± 0.014	754	2.06	129.8 ± 5.5
TBV-32	0.050 ± 0.001	1.18 ± 0.02	0.962 ± 0.022	24	1.39	275.2 (+41 − 38)
TBV-41	0.103 ± 0.004	1.50 ± 0.07	0.801 ± 0.030	206	1.76	152.7 (+21 − 19)
TBV-46	0.043 ± 0.003	1.40 ± 0.10	0.707 ± 0.039	33	1.56	123.2 (+25 − 21)

Sample	Age (ka)	Weathering rind thickness (mm)	Rate (mm/ka)
		Range	Range
TBV1-95	182.9 ± 10.5	5.0–71.0	0.027–0.39
TBV-17T	129.8 ± 5.5	0.1–1.0	0.00077–0.0077
TBV-32	275.2 (+41 − 38)	3.0–16.0	0.011–0.058
TBV-41	152.7 (+21 − 19)	1.5–7.0	0.0098–0.046
TBV-46	123.2 (+25 − 21)	0.1–1.0	0.00077–0.0077

Fig. 11 Phosphate crust overlying Unit 1 bedrock in TBR. These crusts are commonly composed of whitlockite and hydroxyapatite but also less commonly of the mineral fluorapatite

6 Conclusions

The TBV-TBR cave system is presently the longest cave system in South America, with a combined length of 145 km. The cave system is a swarm of passages located in the vicinity of a major NE–SW-trending thrust fault. The passages follow a superimposed folding system that is controlled by gently dipping anticline hinges with average strikes of ~NNE (0°–20°) or ~E–W (70°–100°). The passages have developed in five distinct stratigraphical units in the Salitre Formation of the Una Group carbonates. The lower one, Unit 1, contains the largest passages and presents abundant signs of hypogene morphology. The passages in the upper levels are smaller and more densely packed, with the vertical growth limited by variations in joint density as well as less soluble horizons in the Unit 4 siltstone. The TBV-TBR cave system presents abundant evidence of hypogene morphology in the form of cupolas, wall projections, pendants and partitions and shows very irregular cave walls and ceilings at the metre scale. Features related to water input (feeders) occur at various levels, although only a few major ones have been identified throughout the cave system. Outlet features in Unit 5 occur in very few areas, being restricted due to the massive character and presence of chert layers in the bedrock above the cave-bearing units.

Tectonic control of the cave is provided by joints and folds related to the nearby contact zone between the São Francisco Craton and the Riacho do Pontal Fold Belt. The latest orogeny in the area (and the only one to affect the carbonates), the Brasiliano orogeny at c. 580 Ma, could have provided conditions for ascending fluids. Another possibility involves hydrothermal fluids associated with the break-up of Pangea at approximately 130 Ma.

The relationships among great depth, low uplift rates and long timescales allow for a prolonged interaction between the TBV-TBR cave system and the surrounding environment. The system presents abundant evidence of

post-speleogenetic modification processes. Condensation corrosion has significantly altered cave walls and speleothems, resulting in the expansion of existing passages and deposition of massive deposits of dolomitic sand. Clastic sedimentation is responsible for partially filling the cave passages, and at least three major events can be recognized. Speleothem deposition is abundant, and speleothems have provided valuable information regarding past periods of water table rise and past pluvial phases in this now semi-arid zone. The opening of the present and former entrances allowed the penetration of a varied fauna assemblage that left complete skeletons and internationally important and remarkably complete faunal remains. The massive presence of bat guano and bones has led to chemical weathering of the cave walls, generating abundant phosphate deposits. The TBV-TBR cave system has witnessed a long and complex history since cave inception and contains important evidence of the geological and palaeoenvironmental evolution of the area during this period.

Acknowledgements The exploration of the TBV-TBR system started in 1987 and has been carried out by Grupo Bambuí de Pesquisas Espeleológicas, who produced the cave maps and provided support for many scientific projects. We thank the Brazilian Agency of Petroleum (ANP) for support in the Porocarste Project (UFRN-Petrobras). CECAV/ICMBIO staff helped with fieldwork and provided the required permits. We acknowledge the help of local people, especially the welcoming friends of Laje dos Negros and surrounding villages. Luciana Alt and Vitor Moura provided some of the photographs; Ezio Rubbioli helped with figures. Xianfeng Wang provided the U/Th dates.

References

Amaral G, Born H, Hadler JC, Iunes PJ, Kawashita K, Machado DL Jr, Oliveira EP, Paulo SR, Tello CA (1997) Fission track analysis of apatites from São Francisco Craton and Mesozoic-alcaline-carbonatite complexes from central and southeastern Brazil. J S Am Earth Sci 10:285–294

Auler AS (1999) Karst evolution and paleoclimate in Eastern Brazil. PhD Thesis, University of Bristol

Auler AS, Smart PL (2001) Late Quaternary paleoclimate in semiarid northeastern Brazil from U-series dating of travertine and water-table speleothems. Quatern Res 55:159–167

Auler AS, Smart PL (2003) The influence of bedrock-derived acidity in the development of surface and underground karst: evidence from the Precambrian carbonates of semi-arid Northeastern Brazil. Earth Surf Proc Land 28:157–168

Auler AS, Smart PL (2004) Rates of condensation corrosion in speleothems of semi-arid northeastern Brazil. Speleogenesis Evol Karst Aquifers 2:2

Auler AS, Smart PL, Tarling DH, Farrant AR (2002) Fluvial incision rates derived from magnetostratigraphy of cave sediments in the cratonic area of eastern Brazil. Z fur Geomorphol 46:391–403

Auler AS, Wang XF, Edwards RL, Cheng H, Cristalli OS, Smart PL, Richards DA (2004) Quaternary ecological and geomorphic changes associated with rainfall events in presently semi-arid northeastern Brazil. J Quat Sci 19:693–701

Auler AS, Piló LB, Smart PL, Wang X, Hoffmann D, Richards DA, Edwards RL, Neves WA, Cheng H (2006) U-series dating and taphonomy of quaternary vertebrates from Brazilian caves. Palaeogeogr Palaeoclimatol Palaeoecol 240:508–522

Auler AS, Smart PL, Wang XF, Piló LB, Edwards RL, Cheng H (2009) Cyclic sedimentation in Brazilian caves: mechanisms and palaeoenvironmental significance. Geomorphology 106:142–153

Bizzi LA, Schobbenhaus C, Vidotti RM, Gonçalves JH (2003) Geologia tectônica e recursos minerais do Brasil. Texto mapas e SIG. CPRM, Brasília

Braucher R, Bourlès DL, Colin F, Brown ET, Boulangè B (1998) Brazilian laterite dynamics using in situ-produced ^{10}Be. Earth Planet Sci Lett 163:197–205

Cartelle C, Hartwig WC (1996) A new extinct primate among the pleistocene megafauna of Bahia Brazil. Proc Natl Acad Sci USA 93:6405–6409

Caxito FDA, Uhlein A (2013) Arcabouço tectônico e estratigráfico da faixa Riacho do Pontal. Geonomos 21:19–37

Cazarin CL (2015) Controle faciológico do sistema cárstico hipogênico de Campo Formoso BA: sistema conduto-barreira. MSc dissertation, Universidade Federal do Rio de Janeiro

Czaplewski NJ, Cartelle C (1998) Pleistocene bats from cave deposits in Bahia Brazil. J Mammal 79:784–803

Ennes-Silva RA, Bezerra FHR, Nogueira FCC, Balsamo F, Klimchouk A, Cazarin CA, Auler AS (2016) Superposed folding and associated fracturing influence hypogene karst development in Neoproterozoic carbonates, São Francisco Craton, Brazil. Tectonophysics 666:244–259

Halenar LB, Rosenberger AL (2013) A closer look at the "*Protopithecus*" fossil assemblages: new genus and species from the Pleistocene of Minas Gerais Brazil. J Hum Evol 65:374–390

Harman R, Gallagher K, Brown R, Raza A, Bizzi L (1998) Accelerated denudation and tectonic/geomorphic reactivation of the cratons of northeastern Brazil during the late Cretaceous. J Geophys Res 103:27091–27105

Hartwig WC, Cartelle C (1996) A complete skeleton of the giant South American primate *Protopithecus*. Nature 381:307–311

Hill CA (1987) Geology of Carlsbad Caverns and other caves in the Guadalupe Mountains New Mexico and Texas. New Mex Bur Min Mineral Resour Bull 117:1–150

Hill CA (1990) Sulfuric acid speleogenesis of Carlsbad Caverns and its relationship to hydrocarbons Delaware Basin New Mexico and Texas. Am Assoc Petrol Geol Bull 74:1685–1694

INMET (2016) Banco de dados meteorológicos para ensino e pesquisa. Estação meteorologia Petrolina-PE (OMM: 82983). http://www.inmet.gov.br/portal/index.php?r=bdmep/bdmep. Accessed 15 July 2016

Japsen P, Bonow JM, Grenn PF, Cobbold PR, Chiossi D, Magnavita L, Pedreira A (2012) Episodic burial and exhumation in NE Brazil after opening of the South Atlantic. Geol Soc Am Bull 124:800–816

Klimchouk AB (2007) Hypogene Speleogenesis: hydrogeological and morphogenetic perspective. National Cave and Karst Research Institute, Carlsbad

Klimchouk AB (2009) Morphogenesis of hypogenic caves. Geomorphology 106:385–405

Klimchouk A, Auler AS, Bezerra FHR, Cazarin CL, Balsamo F, Dublyansky Y (2016) Hypogenic origin geologic controls and functional organization of a giant cave system in Precambrian carbonates Brazil. Geomorphology 253:385–405

Lagoeiro LE (1990) Estudo da deformação nas sequências carbonáticas do Grupo Una na região de Irecê Bahia. MSc dissertation, Universidade Federal de Ouro Preto

Misi A, Kyle JR (1994) Upper Proterozoic carbonate stratigraphy diagenesis and stromatolitic phosphorite formation, Irecê Basin, Bahia, Brazil. J Sediment Res A64:299–310

Misi A, Veizer J (1998) Neoproterozoic carbonate sequences of the Una Group Irecê Basin Brazil: chemostratigraphy age and correlations. Precambr Res 89:87–100

Misi A, Kaufman AJ, Veizer J, Powis K, Azmy K, Boggiani PC, Gaucher C, Teixeira JBG, Sanches AL, Iyer SS (2007) Chemostratigraphic correlation of Neoproterozoic successions in South America. Chem Geol 237:22–45

Onac BP, Forti P (2011) Minerogenetic mechanisms occurring in the cave environment: an overview. Int J Speleol 40:79–98

Penha AEPP (1994) O calcário Caatinga de Ourolândia Bahia: feições diagnósticas gênese e evolução de um perfil calcrete. MSc dissertation, Universidade Federal da Bahia

Polyak VJ, McIntosh WC, Güven N, Provencio P (1998) Age and origin of Carlsbad Cavern and related caves from $^{40}Ar/^{39}Ar$ of alunite. Science 279:1919–1922

Ribeiro AF, Garrido IA, Brito RSC, Nonato IF (1993) Geologia e potencialidade para mineralizações de ouro e sulfetos da Faixa Rio Salitre Juazeiro—Bahia. Companhia Baiana Pesquisas Minerais Salvador Série Arq Abertos 3:1–9

van Golf-Racht TD (1982) Fundamentals of fractured reservoir engineering. Elsevier, Amsterdam

van Schmus WR, Oliveira EP, Silva Filho AF, Toteu SF, Penaye J, Guimarães IP (2008) Proterozoic links between the Borborema Province NE Brazil and the Central African Fold Belt. In: Pankhurst RJ, Trouw RAJ, Brito-Neves BB, DeWit MJ (eds) West Gondwana: pre Cenozoic correlations across the South Atlantic Region, vol 294. Geological Society of London Special Publication, pp 69–99

Wang X, Auler AS, Edwards RL, Cheng H, Cristalli PS, Smart PL, Richards DA, Shen CC (2004) Wet periods in northeastern Brazil over the past 210 ka linked to distant climate anomalies. Nature 432:740–743

Hypogene Speleogenesis in the Vazante Group, Minas Gerais, Brazil

57

Augusto S. Auler and Tatiana A.R. Souza

Abstract

The Proterozoic carbonates of the Vazante Group, located in southeastern Brazil, host important zinc deposits related to emplacement of hydrothermal metal-rich solutions along a fault zone. Karst landscape comprises a series of elongated residual carbonate hills containing both epigene and hypogene caves. In the vicinity of the mineralized zone, several caves display hypogene morphology, especially in the surrounding areas of the town of Vazante. The caves predominantly have a network pattern controlled by N60W- and N45E-oriented joints and display cupolas, feeders, rising channels, and outlets. Some of the major caves occur close to the Vazante Fault zone. The intercalation of layers of distinct permeability, due to both the stratigraphic sequence and by the fault-oriented mineralized zone, creates aquifer compartments with differing hydraulic heads. Breaching of the aquitard represented by the zinc-rich lens allows rising flow along the fault zone, leading to lateral flow in favorable bedding plane horizons overlaid by impermeable beds. This flow results in both active and now relict hypogene caves. Fragments of hypogene caves have been recorded at depth (in excess of 600 m below the surface) both through tunnels in the underground mine and in deep boreholes.

Keywords

Hypogene • Vazante group • Speleogenesis • Zinc mineralization

1 Introduction

Carbonates of the Neoproteorozoic Vazante Group of southeastern Brazil host economically important zinc mineralization (Cunha et al. 2007; Misi et al. 2014; Slezak et al. 2014). Four major deposits (Vazante, Morro Agudo, Ambrósia, and Fagundes) have been subject to studies in which the mode and timing of the mineralization have been assessed (Babinski et al. 2005; Monteiro et al. 2007). The southern portion of the Vazante Group harbors 102 known caves, with both epigenic and hypogenic characteristics, mostly comprising now fragmentary drained caves affected by surface epigenic processes.

The most important zinc deposit occurs in association with the Vazante shear zone, in the surrounding areas of the town of Vazante, located at the southern limit of the Vazante Group. This area presents several caves displaying network patterns and hypogene mesoforms, such as cupolas and feeders. The location of some of the major caves close to the zinc body suggests a link between cave genesis and mineralization.

The study area is located in the northeastern Brazilian state of Minas Gerais and comprises a SW–NE elongated carbonate basin dotted with residual hills surrounded by topographically higher metapelitic rocks (Fig. 1). The average annual temperature is 21.6 °C, and the rainfall reaches an average annual 1470 mm (Bittencourt et al. 2008) in a

A.S. Auler (✉) · T.A.R. Souza
Instituto do Carste, Rua Barcelona 240/302,
Belo Horizonte, MG 30360-260, Brazil
e-mail: aauler@gmail.com

T.A.R. Souza
e-mail: tatiana.souza@carste.com.br

© Springer International Publishing AG 2017

A. Klimchouk et al. (eds.), *Hypogene Karst Regions and Caves of the World*,
Cave and Karst Systems of the World, DOI 10.1007/978-3-319-53348-3_57

highly seasonal climate with precipitation concentrated in the summer austral months between October and March.

The Vazante area has witnessed many studies dealing with the depositional context and age of the carbonates (Azmy et al. 2001, 2006, 2008, 2009; Rodrigues et al. 2012; Geboy et al. 2013; Misi et al. 2014) and the genesis of mineralization (Misi et al. 1999; Cunha et al. 2007; Monteiro et al. 2007; Appold and Monteiro 2009; Slezak et al. 2014; Misi et al. 2014), but comparatively few studies relate to speleogenesis (Bittencourt 2008; Bittencourt et al. 2008; Bittencourt et al. 2009; Bittencourt and Reis Neto 2012). In this review, we describe the underground karst in the area, the hypogene speleogenetic model, and its relationship to the regional hydrogeology and the mineralized body.

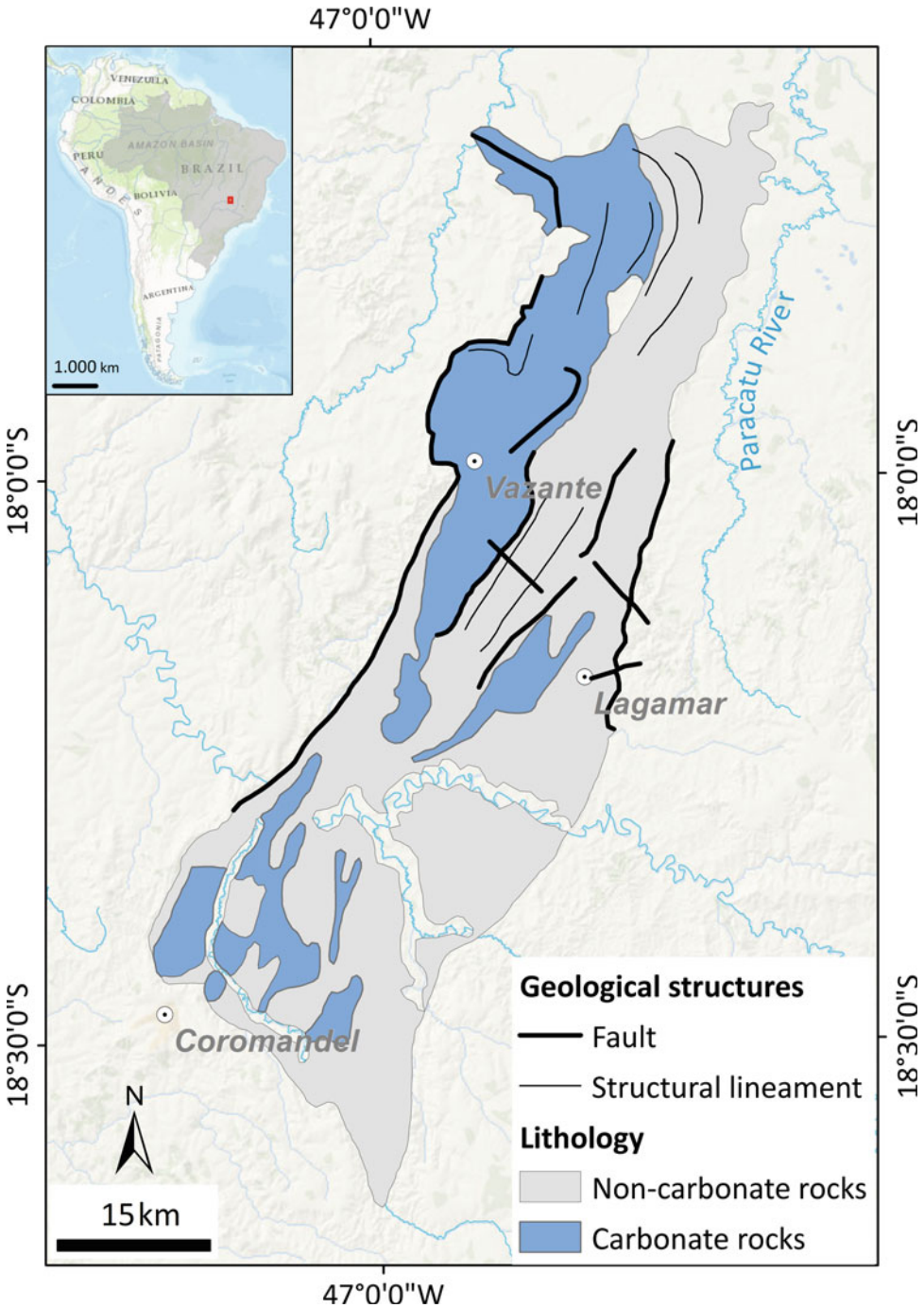

Fig. 1 Location of the Vazante hypogene karst and local geology

2 Geology and Hydrogeology

The Vazante Group is a carbonate-dominated marine platform sequence (Azmy et al. 2009) that extends approx. 300 km in the N–S direction in the external zone of the Brasilia fold belt (Cunha et al. 2007). Its thickness has been estimated to be at least 2.5 km (Cunha et al. 2007). The seven formations, according to Cunha et al. (2007), initially comprise the basal Santo Antonio do Bonito Formation, which presents quartzite, conglomerate, diamictite, and slate that have been interpreted as a glaciogenic unit (Geboy et al. 2013). This formation grades into pelites and siltstone of the Rocinha Formation. The Lagamar Formation comprises dark gray limestone with columnar stromatolites (Dardenne et al. 2009) and a basal conglomerate, quartzite, and slate (Cunha et al. 2007). The Serra do Garrote Formation is a thick succession of dark gray to greenish-gray slate (Cunha et al. 2007). The Serra do Poço Verde Formation is dominated by dolomites and is divided into three members. According to Monteiro et al. (2007), from the base to the top, the Lower Morro do Pinheiro Member is composed of dolostone with cyanobacteria mats, oncolithic doloarenite, intraformational breccias, and lenses of dolostone with columnar stromatolites; the Lower Pamplona Member, host of the Vazante mineralization, is made of gray to pink micritic cyanobacteria-laminated dolostone, gray to green slates, and sericite phyllite; the Middle Pamplona Member comprises gray to pink dolostone, doloarenite, lamellar breccia, dolostone with columnar stromatolites, and shale lenses. The Morro do Calcário Formation is also predominantly dolomitic and contains stromatolithic bioherm and biostrome facies, breccias, oolithic and oncolithic doloarenite, and dolorudite (Monteiro et al. 2007). The topmost formation contains rhythmic carbonaceous phyllite, sericite-chlorite phyllite, and carbonate-bearing metasiltstone assigned to the Serra da Lapa Formation (Cunha et al. 2007) (Fig. 2).

The age of the Vazante Group is controversial, but Re–Os and U–Pb ages of the Serra da Lapa Formation indicate deposition at 1.0–1.1 Ga (Azmy et al. 2008), while Re–Os ages for the Serra do Garrote Formation suggest ages of 1.3 Ga (Geboy et al. 2013). The entire sequence was metamorphosed to low greenschist facies (Rodrigues et al. 2012) during the Pan-African/Brasiliano orogeny (ca. 600 Ma). The sequence displays pervasive cleavage related to regional folding and tectonic contacts with the Canastra Group to the west and the Bambui Group to the east (Rodrigues et al. 2012).

The Vazante Group hosts the largest Zn–Pb deposits in South America (Cunha et al. 2007). The major deposits are Vazante (including its northern extension), Morro Agudo, Ambrósia, and Fagundes. Although caves with hypogene characteristics have been described in the northern portions of the Vazante Group (Souza et al. 2016), detailed studies have been performed only in the surrounding areas of the Vazante mineralized zone. The Vazante mineralization represents a major example of a non-sulfide Zn deposit and is related to a N50/60NW-oriented shear zone (Babinski et al. 2005). In addition to being fault controlled, there is a marked stratigraphic control—the deposit is hosted by gray- to pink-colored dolostone, slate, and phyllite of the Lower Pamplona Member, close to the contact with the dark gray dolostone of the Upper Morro do Pinheiro Member (Monteiro et al. 2007).

The Vazante ore is interpreted as being the result of mixing between a hydrothermal, metal-rich fluid and cooler meteoric water. It is hypothesized that deep-seated metalliferous brines associated with the Brasiliano deformation of the Vazante Group ascended along the shear zone (Babinski et al. 2005). This fluid was probably acidic, and reducing, and it came into contact with basic, oxidizing meteoric water in a shallower environment (Appold and Monteiro 2009), resulting in zinc deposits associated with willemite, minor sulfides (sphalerite and galena), and oxidized ore (hemimorphite, hydrozincite, smithsonite, fanklinite, and pyromorphite) (Babinski et al. 2005). The Vazante mineralization is hosted within two generations of tectonic-hydrothermal breccia formed during the Brasiliano orogeny (Slezak et al. 2014).

The complex geological setting surrounding the mineralized zone resulted in multiple aquifer systems with distinct hydrogeological behavior, due not only to rock composition, but also to the degree of dolomitization, intercalation of less permeable lenses, fracturing, and karstification (Bittencourt et al. 2008). A schematic view of the aquifer systems in the Morro do Calcário Formation is summarized in Fig. 3.

3 Karst Landforms

Karst landforms develop over dolomitic sequences of the Lagamar, Serra do Poço Verde, and Morro do Calcário Formations. However, hypogene features in the study area have been recognized only over the latter two formations. Surface karst is marked by dolomite residual hills, usually NE–SW elongated, developed over an essentially soil-filled flat surface, and bordered by topographically higher phyllite hills of the Serra do Garrote Formation (Fig. 4). These phyllite hills have shallow soil layers allowing surface runoff to generate allogenic recharge that sinks upon reaching the carbonates in the southern portion of the area. The alluvial and colluvial soil overlying carbonates can reach a thickness of over 100 m (Bittencourt 2008), inhibiting the manifestation of surface karst features. However, geophysics and borehole data have revealed a highly irregular epikarst displaying buried pinnacles (Bittencourt and Reis Neto 2012).

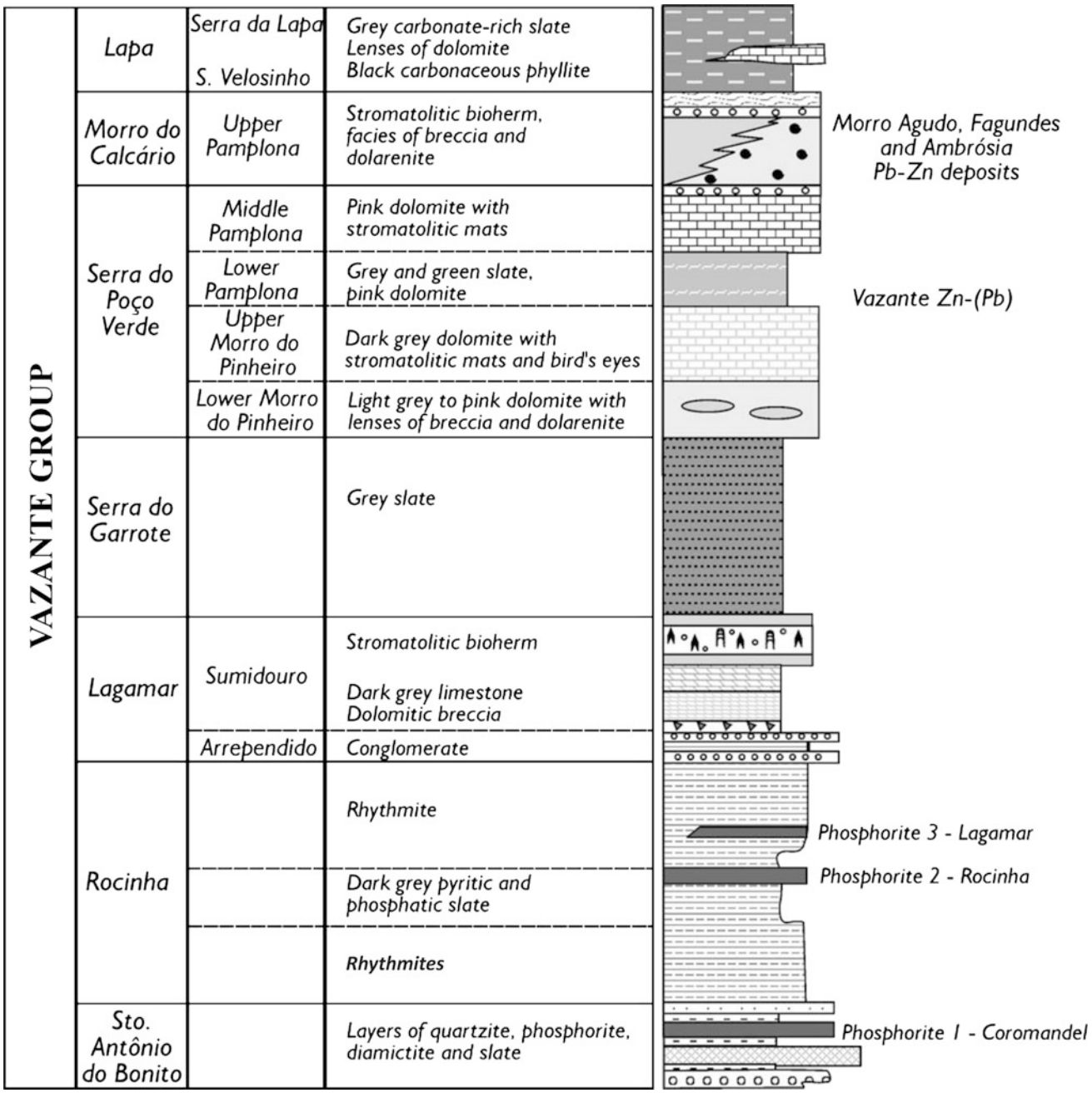

Fig. 2 Stratigraphic column of the Vazante Group. From Babinski et al. (2005)

The residual hills develop over dolomite outcrops occupying 0.26% of the karst landscape (Souza et al. 2016) covered by semi-deciduous forest that stands in stark contrast to the presently agricultural use of the lower flat surrounding surface (Fig. 4). Limited karrens were observed over dolomite outcrops. Smaller residual knobs of carbonate occur, marking the gradual disaggregation of the dolomite hills. Solution dolines are subdued due to the thick soil cover. However, near the Vazante zinc mine, groundwater pumping at rates in excess of 6300 m^3/h resulted in induced sinkholes (Bittencourt et al. 2008). A few karst springs occurs in the area, and some are presently dry due to mine dewatering.

3.1 Morphology of Hypogene Caves

At present, 102 caves have been identified in the southern portion of the Vazante Group carbonates, of which 43 display hypogene morphology. The largest concentration

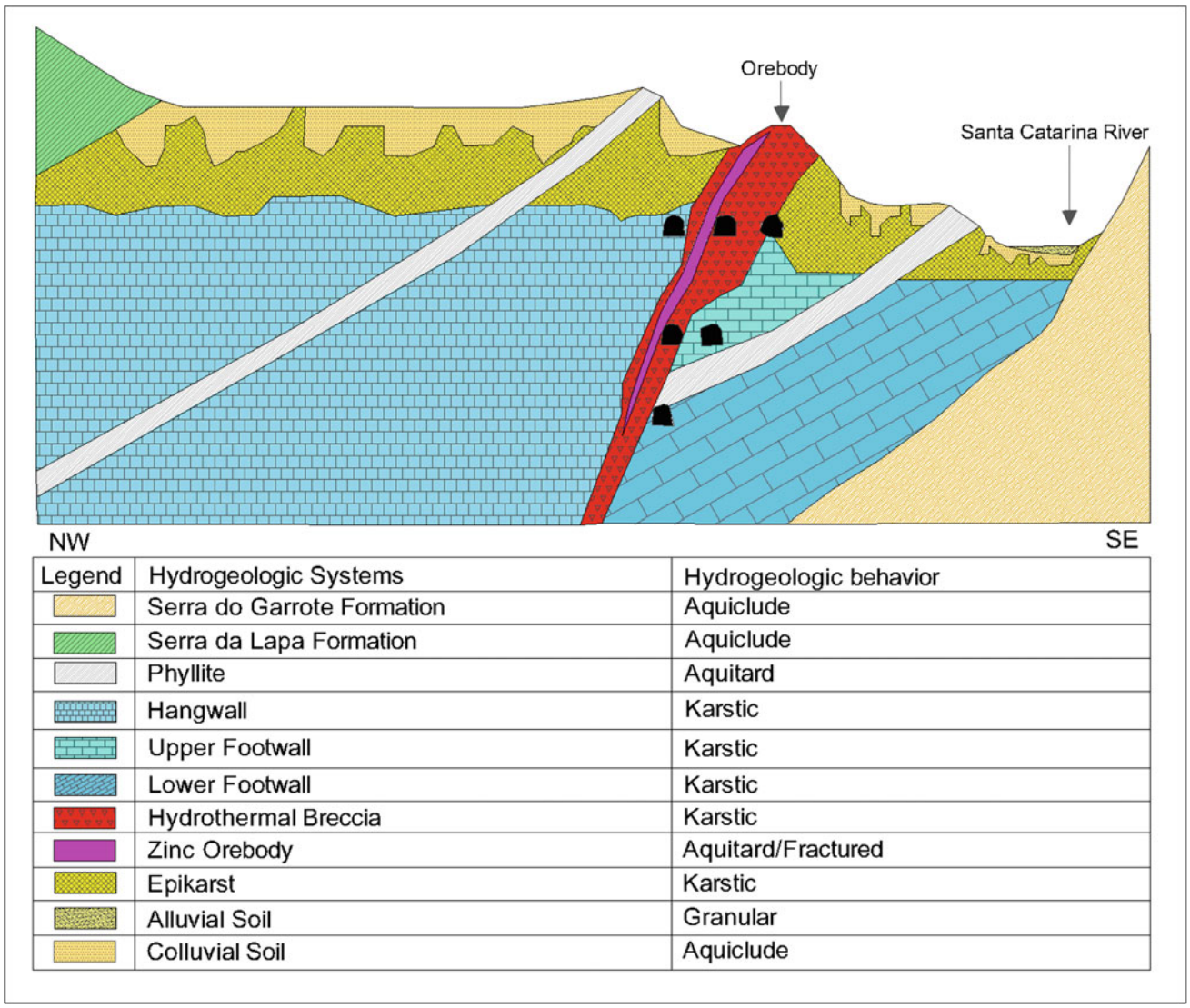

Legend	Hydrogeologic Systems	Hydrogeologic behavior
	Serra do Garrote Formation	Aquiclude
	Serra da Lapa Formation	Aquiclude
	Phyllite	Aquitard
	Hangwall	Karstic
	Upper Footwall	Karstic
	Lower Footwall	Karstic
	Hydrothermal Breccia	Karstic
	Zinc Orebody	Aquitard/Fractured
	Epikarst	Karstic
	Alluvial Soil	Granular
	Colluvial Soil	Aquiclude

Fig. 3 Aquifers associated with the Vazante zinc mineralization. Position of underground mine tunnels is marked as *black arches*. From Bittencourt (2008)

Fig. 4 Residual elongated dolomite hills over a soil-covered plain. Photograph by Marcelo Andrê

occurs associated with the mineralized zone (Fig. 5). Most cave entrances are located at the base or at the lower slope of the dolomite hills, but cave passages usually lie below the surface plain. Many hypogene caves are marked by single small descending openings, suggesting that they were originally entranceless caves. In fact, observations in over 300,000 m of boreholes show several voids at depths in excess of 800 m below the surface (Fig. 6), a clear evidence of deep karstification. Overall, 53% of the voids develop in association with breccia related to the mineralization, 30% develop over pink dolomite of the footwall and 7% develop in gray dolomite of the upper hangwall (Bittencourt and Reis Neto 2012), and the remaining 10% are distributed in siltstone, doloarenite, dolorudites, and undifferentiated dolomites. Caves are frequently truncated by sediment infilling, suggesting that presently accessible caves are fragments of once larger systems. Only two caves surpass 1 km in length, both close to the mineralized zone: Lapa Nova and Gruta da

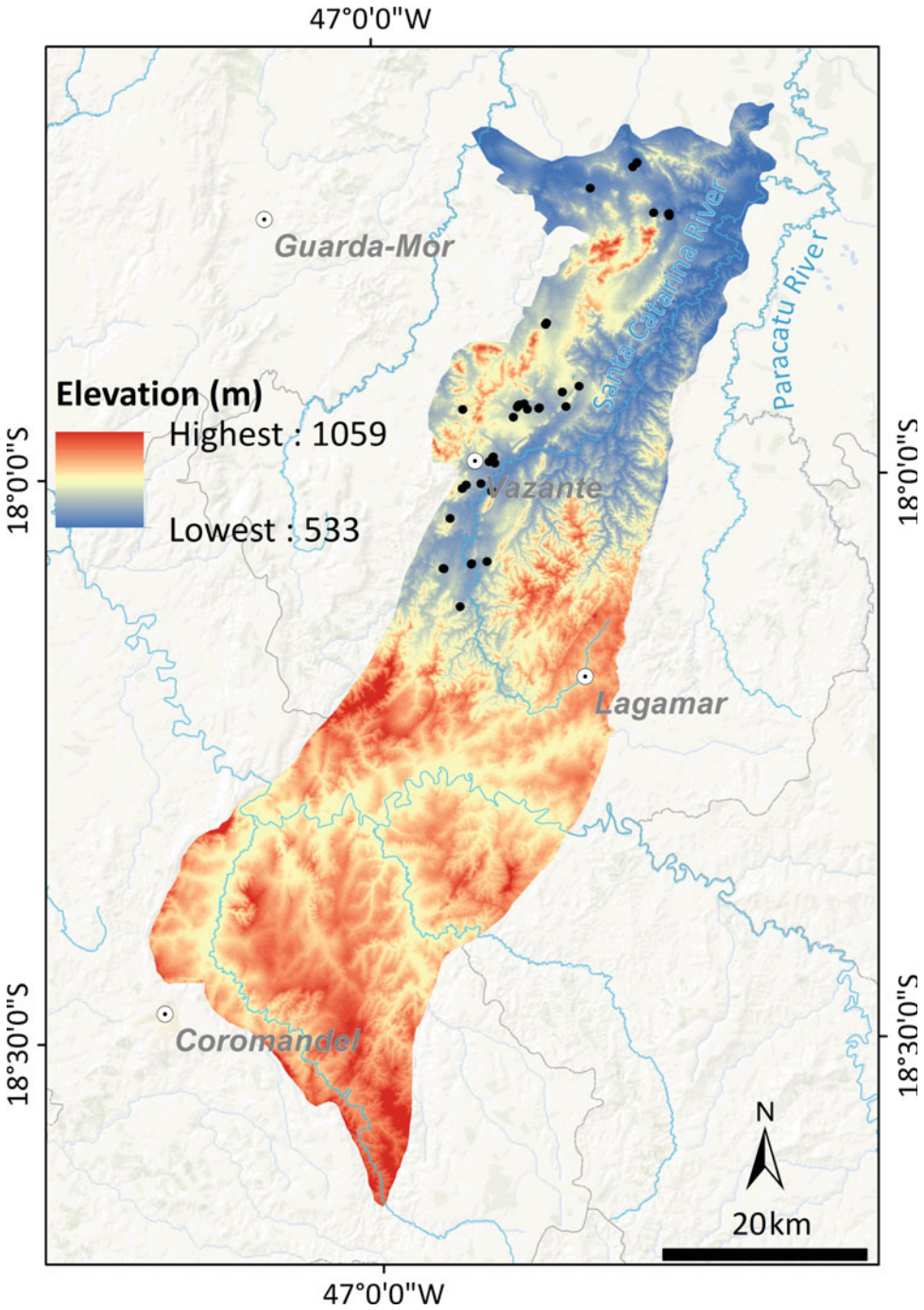

Fig. 5 Relief and location of caves (*black dots*) displaying hypogene morphology

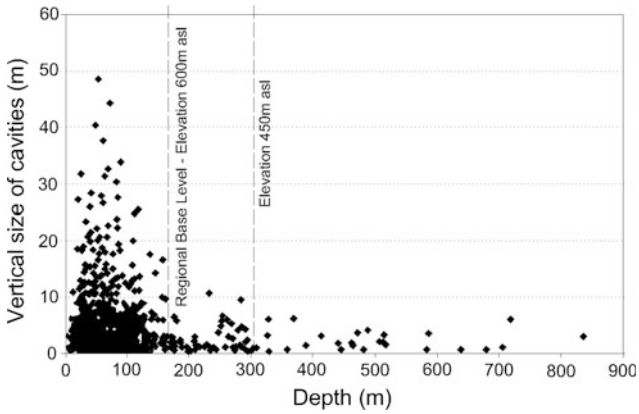

Fig. 6 Depth and vertical size of cavities detected in boreholes. From Bittencourt (2008)

Delza, respectively, with 4.5 and 1.6 km passage length. There is a marked association between cave location and the zinc mineralization (Bittencourt and Reis Neto 2012), although there is an offset of a few hundred meters between them.

Caves display a predominantly network pattern characterized by an orthogonal set of joints oriented N60W and N45E. A ramiform pattern can also be recognized in a few smaller caves. Most rectilinear passages show rift-like morphology (Fig. 7), but in some sections, flat ceilings are marked by less permeable units. A typical network cave passage is approximately 5-m wide and 8-m high, although there is much dimensional variation. Lapa Nova and Lapa da Delza caves are among the few that display larger chambers. A thick sedimentary cover resulting in horizontal cave passages invariably masks the floor. In a few caves, however, vertical passages that are probably related to former ascending routes can be observed. Figure 8 shows some representative hypogene cave plans in the Vazante area.

The underground mining operation allows for observation of hypogene cave fragments at depth. These entranceless cavities are mainly elongated and predominantly vertical, controlled by structures oriented to the NW and by the banding of the rock (Bittencourt et al. 2009). Prior to mine dewatering, they probably functioned as vertical ascending routes for groundwater.

At mesoscale, hypogene forms comprise cupolas, vertical tubes, rising wall tubes, rising chains of cupolas, and outlets (Bittencourt et al. 2009) (Fig. 9). In a few caves in stromatolithic dolomite, peculiar and outstanding cupolas develop

Fig. 7 Rift passage at Lapa da Delza cave. Photograph by Marcelo Andrê

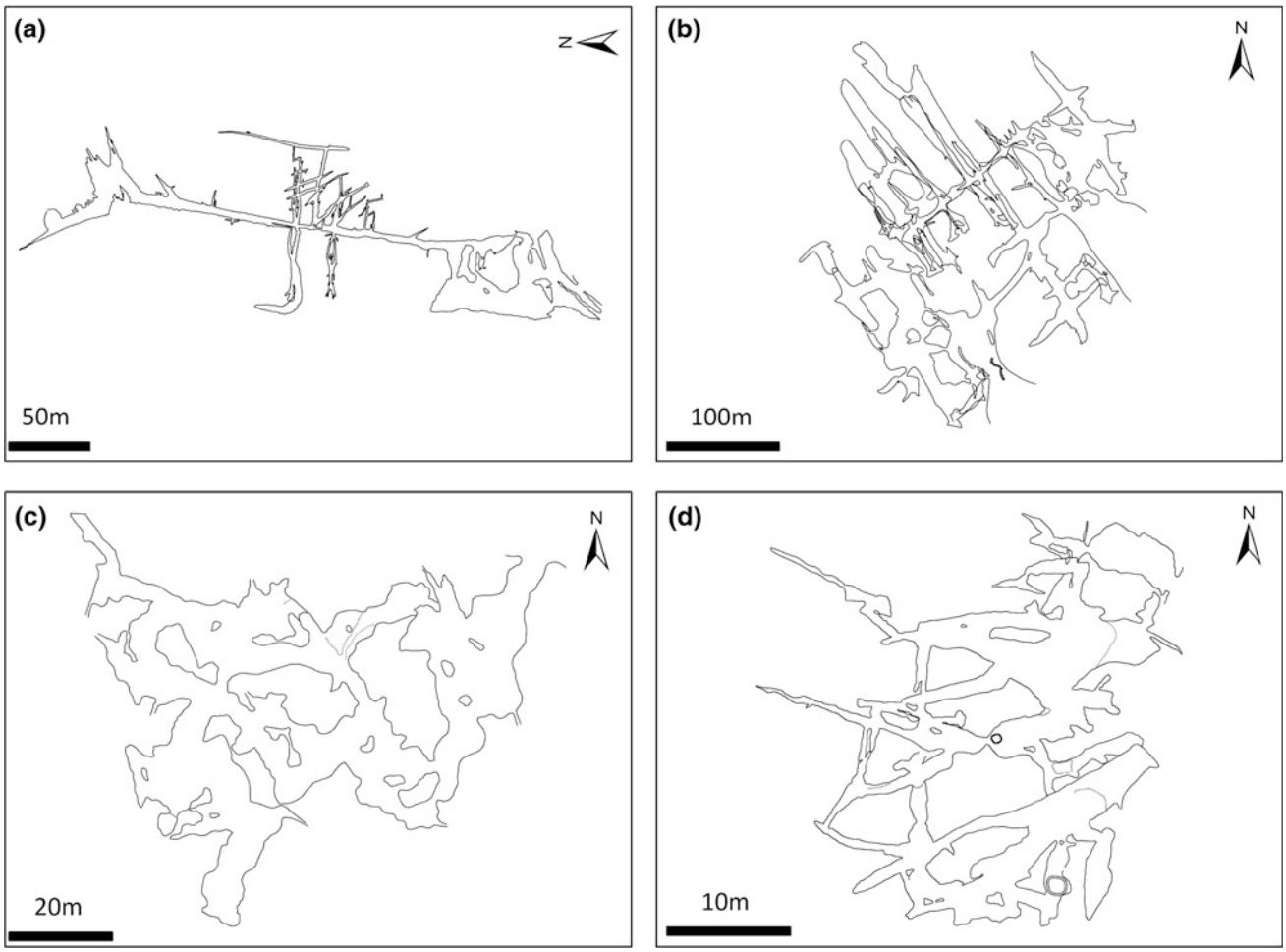

Fig. 8 Selected hypogene cave patterns in the Vazante area. (**a**) Lapa da Delza; (**b**) Lapa Nova; (**c**) VT-04; (**d**) VT-288

over columnar stromatolites described by Moeri (1972) and Dardenne (2009). This is especially prominent in the VT-04 cave (Fig. 10). At Lapa Nova and Lapa Nova II caves, feeders are mostly concentrated close to the mineralized zone.

Epigenic processes are now affecting the caves in the Vazante area (Bittencourt et al. 2009). Abundant clastic sedimentation, probably associated with cyclic climate-controlled sedimentary influx events (Auler et al. 2009), filled considerable portions of the caves, and later hydrological/sedimentary processes, such as paragenesis, have partially overprinted prior hypogenic forms.

4 Hypogene Speleogenesis

The close association between hypogene cave location (and cave feeders) and the mineralized zone hints at the possibility of a genetic relationship between speleogenesis and mineralization. Although the mineralization was created by deep-seated hydrothermal processes during the Brasiliano orogeny (Monteiro et al. 2007), there is no evidence that the present karstification is chronologically associated with the metalliferous rising fluids and associated zinc emplacement. Bittencourt and Reis Neto (2012) observed that the voids and caves observed at depth in the mine tunnels occur associated with the carbonate breccia, but their genesis is not related. However, the brecciated horizons associated with hydrothermal alteration and mineral precipitation were interpreted by Bittencourt (2008) as an early event of karstification, presently manifested as paleokarst unrelated to the later hypogene speleogenesis.

There is a marked difference in permeability between the hydrogeological compartments of the aquifer, resulting in distinct degrees of confinement. Water table levels prior to mine drawdown showed an elevation difference of approximately 40 m between the hangwall and footwall of the mineralized zone (Fig. 11). Although cavities were identified in the breccia and associated carbonate lenses, the zinc mineralized body is essentially impermeable, behaving as an

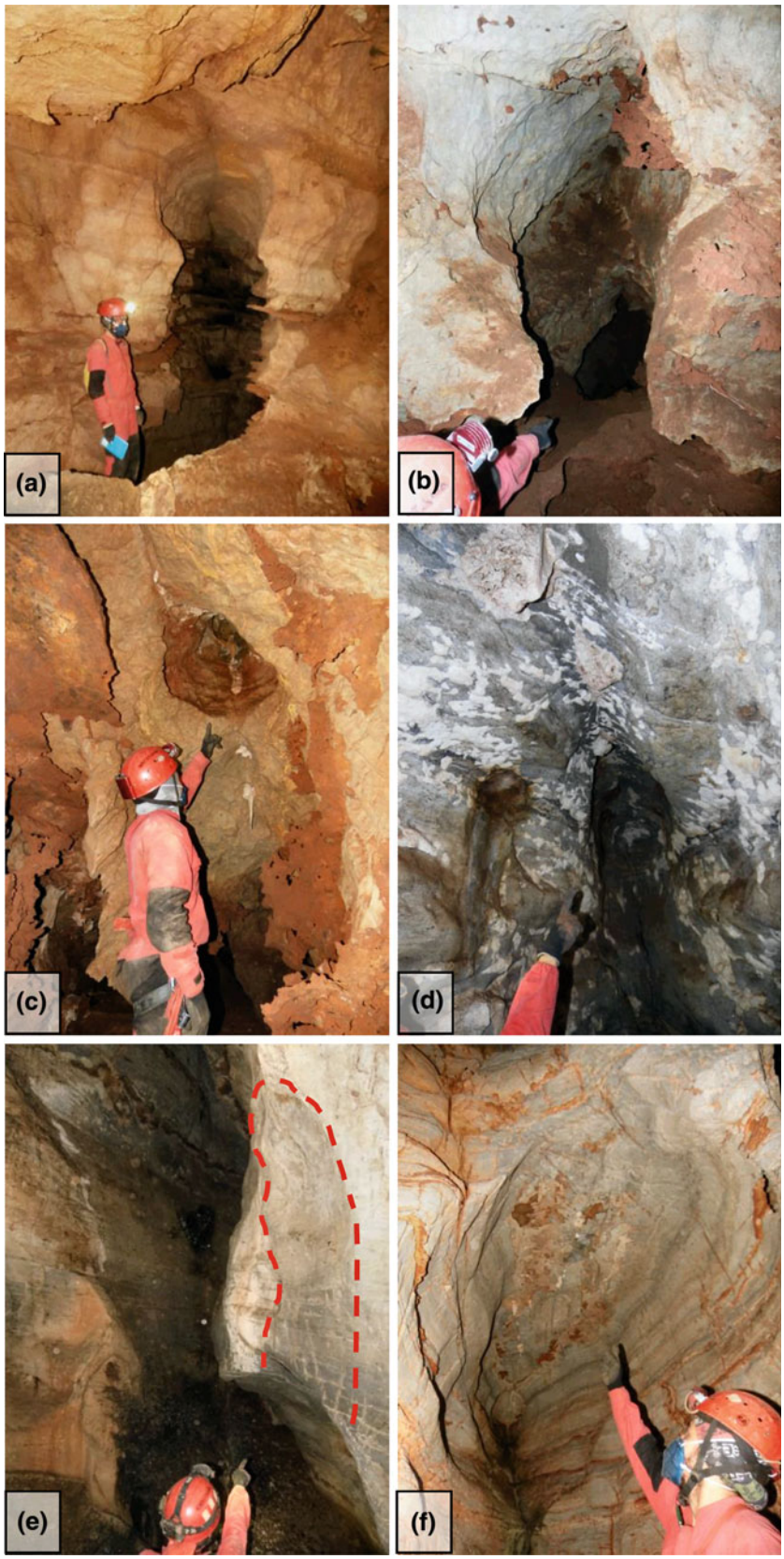

Fig. 9 Hypogene mesoforms in the Vazante area. Side feeders with rising wall channels in caves VT-188 (**a**), Guariroba (**b**), Sr. Antônio Andrade (**d** and **e**). Cupola at the ceiling of Guariroba cave (**c**) and Sr. Antônio Andrade cave (**f**)

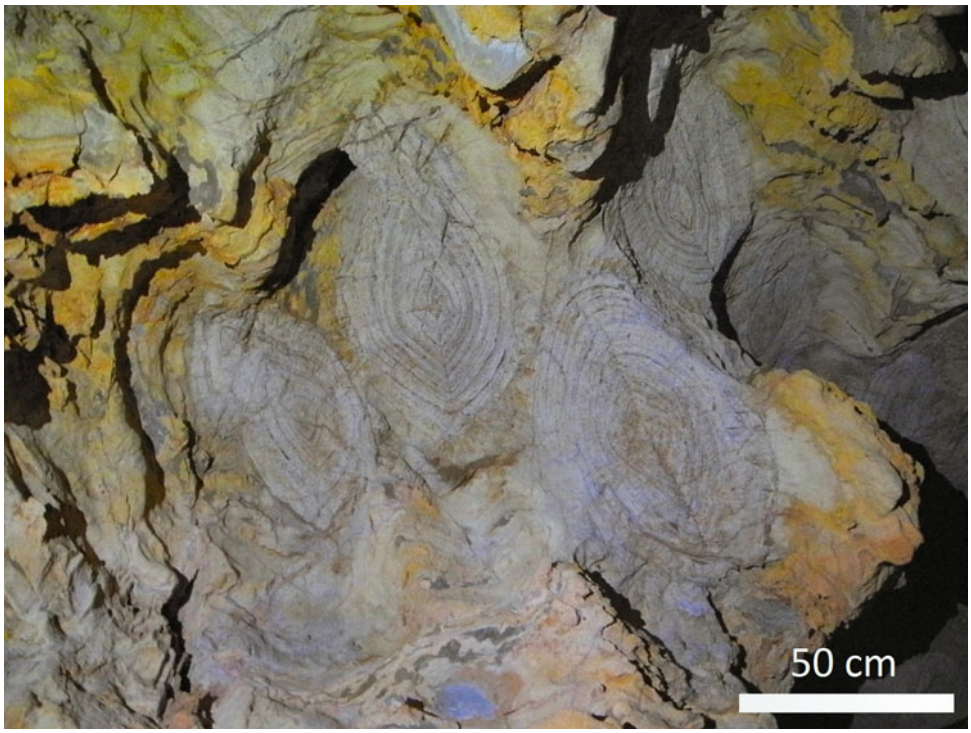

Fig. 10 Columnar stromatolites are more susceptible to dissolution than the surrounding dolostone, resulting in preferential development of cupolas over stromatolites. View of the ceiling of VT-04 cave

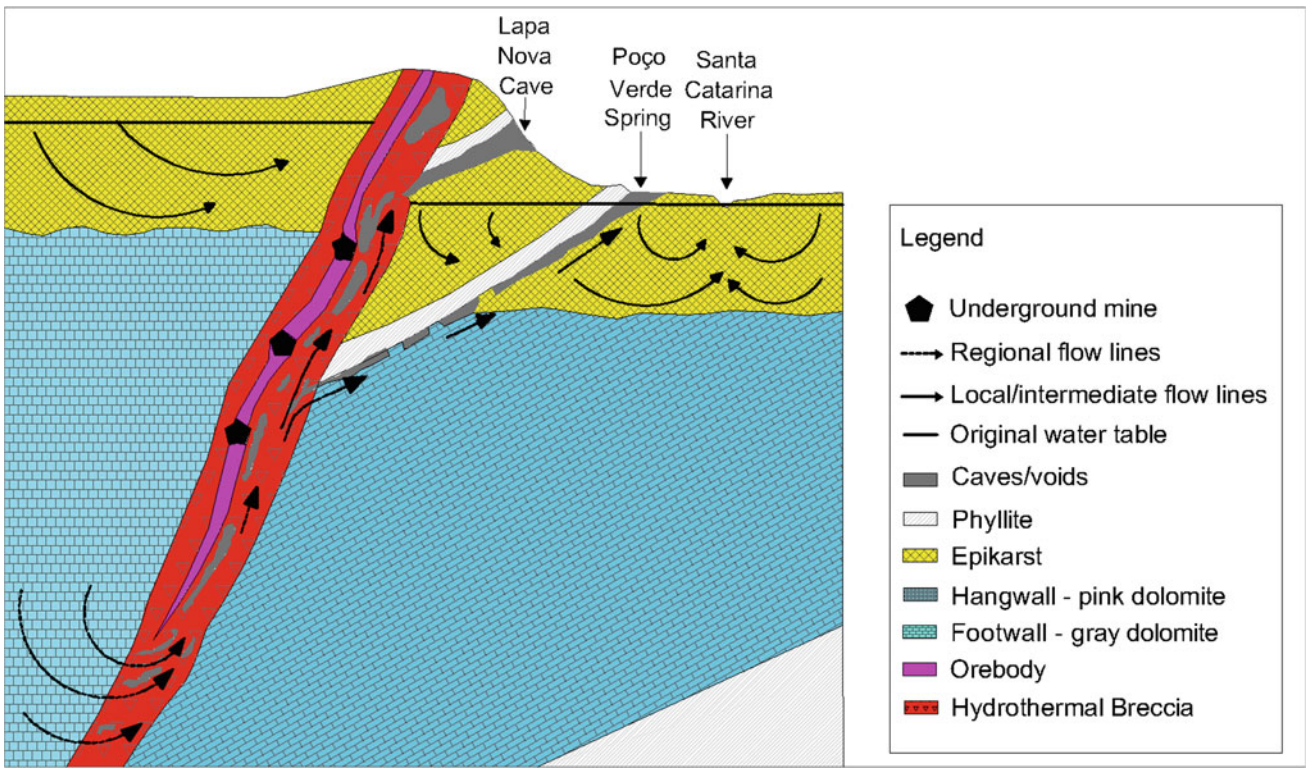

Fig. 11 Hypogene speleogenesis model for the Vazante Karst. From Bittencourt et al. (2009)

aquitard and representing a hydraulic seal that results in a semi-confined situation controlled by the position of the mineralized body (Bittencourt 2008).

In places at depth where the zinc mineralization forms continuous lenses, ascending flow will dissolve the carbonate breccia, creating the caves observed in mine tunnels

(Bittencourt 2008). However, since the zinc body is not continuous, it allows interconnection between the hangwall and footwall aquifers. The rising groundwater is able to cross the brecciated zone and flow along the inclined shear zone. The presence of impermeable phyllite layers diverts groundwater flow toward the inclined bedding plane, where hypogene caves are generated (Fig. 11). Lapa Nova cave, now in the vadose zone, represents a former phase of hypogene speleogenesis. Some active springs (now dry due to mine pumping), such as Poço Verde, comprise vauclusian conduits belonging to the present speleogenetic phase (Bittencourt 2008).

5 Conclusions

The Vazante Karst develops in Proterozoic dolostones and hosts important Pb–Zn deposits. Hydrothermal metalliferous fluids migrated upward along the Vazante shear zone during the Brasiliano orogenetic event at ca. 600 Ma and generated a complex assemblage of brecciated carbonates associated with discontinuous lenses of zinc-rich minerals. Close to the mineralized zone, several hypogene caves have been identified, suggesting a correlation between the mineralized body and the hypogene cave-forming processes.

Caves display a dominant network pattern and develop usually at the base of residual dolostone hills. Sediment infilling usually truncates cave passages, which present feeders, cupolas, rising channels, and outlets. Smaller fragments of hypogene caves can also be observed at depth at the Vazante mine tunnels and are conspicuous in boreholes up to depths in excess of 600 m below the present surface.

The complex stratigraphic setting surrounding the mineralized body results in several aquifers displaying different hydrogeological properties. In particular, the impermeable nature of the zinc body results in a hydraulic seal that is breached in places where the metal-rich lens is discontinuous. Thus, groundwater confinement promotes rising flow along the Vazante shear zone. In places where the carbonate presents less permeable phyllite layers, flow diverts toward bedding-controlled carbonate layers, resulting in the generation of both relict and active karst features such as caves and springs. Epigenic processes have fragmented caves and overprinted some hypogene features.

Acknowledgements The study of the hypogene karst of Vazante was primarily performed by Cristian Bittencourt, with the continuous support from Votorantim Metais. We acknowledge the help of Carste Ciência e Meio Ambiente and, in particular, Rafael Cruz for collaborating with the drawing of figures.

References

Appold MS, Monteiro LVS (2009) Numerical modelling of hydrothermal zinc silicate and sulfide mineralization in the Vazante deposit Brazil. Geofluids 9:96–115

Auler AS, Smart PL, Wang X, Piló LB, Edwards RL, Cheng H (2009) Cyclic sedimentation in Brazilian caves: mechanisms and palaeoenvironmental significance. Geomorphology 106:142–153

Azmy K, Veizer J, Misi A, Oliveira TF, Sanchez AL, Dardenne MA (2001) Dolomitization and isotope stratigraphy of the Vazante Formation São Francisco Basin Brazil. Precambr Res 112:303–329

Azmy K, Kaufman AJ, Misi A, Oliveira TF (2006) Isotope stratigraphy of the Lapa Formation São Francisco Basin Brazil: implications for late Neoproterozoic glacial events in South America. Precambr Res 149:231–248

Azmy K, Kendall B, Creaser RA, Heaman L, Oliveira TF (2008) Global correlation of the Vazante Group São Francisco Basin Brasil: Re–Os and U–Pb radiometric age constraints. Precambr Res 164:160–172

Azmy K, Sylvester P, Oliveira TF (2009) Oceanic redox conditions in the late Mesoproterozoic recorded in the upper Vazante Group carbonates of São Francisco Basin Brazil: evidence from stable isotopes and REEs. Precambr Res 168:259–270

Babinski M, Monteiro LVS, Fetter AH, Bettencourt JS, Oliveira TF (2005) Isotope geochemistry of the mafic dikes from the Vazante nonsulfide zinc deposit Brazil. J S Am Earth Sci 18:293–304

Bittencourt C (2008) Carstificações hipogênica e epigênica—Influências sobre a exploração de minério de zinco da mina de Vazante—MG. Dissertation, Universidade Federal do Paraná

Bittencourt C, Reis Neto JM (2012) O sistema cárstico de Vazante—carste em profundidade em metadolomitos do Grupo Vazante—MG. Revista Brasileira de Geociências 42:1–10

Bittencourt C, Bessa V, Araújo EA (2008) The Vazante underground mine—An example of controlled water table drawdown in karstic areas. In: Yuhr LB, Alexander Jr EC, Beck BF (eds) Sinkholes and the engineering and environmental impacts of karst. Geotechnical Special Publication No. 183. ASCE, Reston, p 732

Bittencourt C, Auler AS, Reis Neto JM, Bessa V, Silva MVA (2009) The influence of hypogene and epigene speleogenesis in the evolution of the Vazante Karst, Minas Gerais state, Brazil. In: Klimchouk A, Ford DC (eds) Hypogene speleogenesis and karst hydrogeology of Artesian Basins, Simferopol

Cunha IA, Misi A, Babinski M, Iyer SSS (2007) Lead isotope constraints on the genesis of Pb–Zn deposits in the Neoproterozoic Vazante Group Minas Gerais Brazil. Gondwana Res 11:82–395

Dardenne MA (2009) *Conophyton* de Cabeludo, Grupo Vazante. In: Winge M, Schobbenhaus C, Souza CRG, Fernandes ACS, Berbert-Born M, Queiroz ET, Campos DA (eds) Sítios geológicos e paleontológicos do Brasil, vol II. CPRM, Brasília, p 303

Dardenne MA, Campos JEG, Campos Neto MC (2009) Estromatólitos colunares no sumidouro do Córrego Carrapato, Lagamar, MG. In: Winge M, Schobbenhaus C, Souza CRG, Fernandes ACS, Berbert-Born M, Queiroz ET, Campos DA (eds) Sítios geológicos e paleontológicos do Brasil, vol II. CPRM, Brasília, p 311

Geboy NJ, Kaufman AJ, Walker RJ, Misi A, Oliveira TF, Miller KE, Azmy K, Kendall B, Poulton SW (2013) Re–Os age constraints and new observations of proterozoic glacial deposits in the Vazante Group, Brazil. Precambr Res 238:199–213

Misi A, Iyer SS, Tassinari CCG, Kyle JR, Coelho CES, Franca-Rocha WJS, Gomes ASR, Cunha IA, Carvalho IG (1999) Geological and isotopic constraints on the metallogenic evolution of the proterozoic sediment-hosted Pb–Zn (Ag) deposits of Brazil. Gondwana Res 2:47–55

Misi A, Azmy K, Kaufman AJ, Oliveira TF, Sanchez AL, Oliveira GD (2014) Review of the geological and geochronological framework of the Vazante sequence, Minas Gerais, Brazil: implications to metallogenic and phosphogenic models. Ore Geol Rev 63:76–90

Moeri E (1972) On a columnar stromatolite in the Precambrian Bambui Group of Central Brazil. Eclogae Geol Helv 65:185–195

Monteiro LVS, Bettencourt JS, Juliani C, Oliveira TF (2007) Nonsulfide and sulfide-rich zinc mineralizations in the Vazante Ambrósia and Fagundes deposits Minas Gerais Brazil: mass balance and stable isotope characteristics of the hydrothermal alterations. Gondwana Res 11:362–381

Rodrigues JB, Pimentel MM, Buhn B, Matteini M, Dardenne M, Alvarenga CJS, Armstrong RA (2012) Provenance of the Vazante Group: new U–Pb, Sm–Nd, Lu–Hf isotopic data and implications for the tectonic evolution of the Neoproterozoic Brasília Belt. Gondwana Res 21:439–450

Slezak PR, Olivo GR, Oliveira GD, Dardenne MA (2014) Geology, mineralogy, and geochemistry of the Vazante Northern Extension zinc silicate deposit, Minas Gerais, Brazil. Ore Geol Rev 56:234–257

Souza TAR, Auler AS, Perroni G, França LG, Piló H, Gomide A, Alt L, Moura V (2016) Distrito cárstico Vazante-Paracatu. Patrimônio espeleológico, arqueológico e paleontológico. Carste Ciência e Meio Ambiente, Belo Horizonte, p 1600

Hypogene Caves in North Africa (Morocco, Algeria, Tunisia, Libya, and Egypt)

58

Philippe Audra

Abstract

This chapter aims to describe the hypogene caves of North Africa. A few hypogene caves are known in Morocco, Tunisia, Libya, and Egypt. Algeria hosts most of hypogene caves known in this region. This includes hydrothermal cave springs (Aïn Ouarka, Hassi Dermam, Aïdour), mazes related to CO_2 degassing (Kef el Kaous), iron-ore related caves (Rouïna) and sulfuric acid speleogenesis (SAS) caves especially in the Azerou massif. This last area displays numerous caves recording the geomorphic evolution that follows the gradual exhumation of the thermal aquifer. Preliminary analytical data (geomorphology, mineralogy, isotopes, and U/Th dating) are presented.

Keywords

Hypogene caves • North Africa • Azerou • Biban • Sulfuric acid speleogenesis

1 Introduction

Karst in North Africa occurs in two zones: the wet mountainous Atlas range stretching along the coast of Morocco, Algeria, and Tunisia, and the arid Sahara covering the inner part of the last mentioned country which also extends toward Libya and Egypt. In the Atlasic range, hypogene caves mainly derive from the still very active tectonics allowing fast flow uplift along deep faults. In the Saharan area, there is no active epigene karstification due to the lack of rainfall and also of biogenic CO_2 from vegetation (Webb and White 2013). Consequently, if not inherited from past wetter periods, caves are mostly hypogene. They concentrate in the discharge area of the aquifers where groundwater flows up and fed the oases.

Hypogene karst and caves were hardly the main focus of study, except for Collignon (1983a, 1989 and references herein). Otherwise, and generally without being mentioned explicitly as hypogene, they were often encountered by geologists of the past colonial time, by mining geologists studying "hydrothermal mineralization," or by hydrogeologists working for the development of the water resources. Many publications deal with hydrothermal mineralization in karst, either related to the ore genesis (e.g., Gutzmer et al. 2006; Melki and Zargouni 1991) or to the aquifer dynamic (e.g., Djidi et al. 2008). However, they pay little attention to karst voids structure (i.e., caves) and on their role on the considered topics. All in all, there were neither continuous researches due to frequent political changes or instabilities, nor regular speleological explorations and cave inventories, and recent research outcomes are mainly focused on mine geology or groundwater. As a consequence, the very few published occurrences can be fully presented in this chapter. Moreover, due to the absence of effective environmental protection and to the fast economic development of these countries, many caves and karsts are endangered and have disappeared due to construction work or through quarrying.

In this chapter, hypogene caves are described by countries (Table 1), from Morocco in the West to Egypt in the East, passing through Algeria, Tunisia, and Libya, based on bibliographic references and on personal field experience from the Biban area.

P. Audra (✉)
University of Nice Sophia Antipolis, Sophia Antipolis Cedex, France
e-mail: audra@unice.fr

© Springer International Publishing AG 2017

A. Klimchouk et al. (eds.), *Hypogene Karst Regions and Caves of the World*,
Cave and Karst Systems of the World, DOI 10.1007/978-3-319-53348-3_58

Table 1 Hypogene caves and related hydrothermal karst springs from North Africa

Cave	Lat. (°)	Long. (°)	Alt. (m)	Length (m)	Depth (m)	Country	Region, massif	Observation	Reference
Kef Aziza	32° 1'47.04″N	3° 47'17.24″O	1100	3500	?	Morocco	Atlas	Dry hydrothermal cave	Audra, unp., Buzio et al. (2003)
Chameau cave	34° 50′ 17.72″N	2°21′ 21.89″W	485	1150	Approx. 50	Morocco	Beni Snassen	Low thermal spring (26 °C)	Audra, unp.
Aïdour cave	35°42′ 49.84″N	0°39′ 48.06″W	34		−32	Algeria	Oran	Thermal cave, 78 °C. *Destroyed*	Arambourg(1912)
Rhar Es Skhoun	36° 9′ 41.11″N	4°21′ 35.01″E	630	1750	132 (+10/ −122)	Algeria	Biban	Inactive SAS $T = 33$ °C. *Not accessible*	Collignon (1983a)
Rhar Sidi Bakou	36° 9′ 48.95″N	4°21′ 44.39″E	700	90	+35	Algeria	Biban	Inactive SAS	Collignon (1983a)
Rhar Amalou/Rhar Kab Srhir	36° 8′ 33.64″N	4°19′ 58.55″E	680	2000	68 (+9/ −59)	Algeria	Biban	Inactive SAS. *Destroyed*	Collignon (1983a)
Rhar Zenedia	36° 8′ 19.91″N	4°19′ 38.60″E	640	180	15 (+10/ −5)	Algeria	Biban	Inactive SAS. *Destroyed*	Collignon (1983a)
Rhar Medjraba (Gde gr. de l'Azrou)	36°10′ 41.67″N	4°22′ 58.51″E	665	1500	83 (+28/ −55)	Algeria	Biban	Inactive SAS	Collignon (1983a)
Azerou Caves no. 1 to 8	36°10′ N	4°22′E	688–728	<30	<20	Algeria	Biban	Inactive SAS	Audra and Cailhol, unp
Hammam El Biban	36°11′ 48.85″N	4°23′ 23.52″E	470	0	0	Algeria	Biban	7 L/s 85 °C	Collignon (1983a)
Hassi Dermam	137.4	159.8	1 005		−52	Algeria	Tlemcen	Thermal spring, 26 °C	Collignon (1989)
Aïn Ouarka	32°43′ 50''N	0°9′W	1 040	50	−5	Algeria	Mts Ksour	Carbonic spring	Collignon (1989)
Kef el Kaous	35°12′N	1°38′W	30	4100	−10/+30	Algeria	Traras	Inactive maze	Collignon (1984)
Rouina Caves	36°12′ 23.15″N	1°48′ 57.14″E	340			Algeria	Abids	Mined Fe ore	Saint-Ours (1959)
Mgharet PK4+396.50	approx. 36.4°N	approx. 6.3°E	approx. 400		−46	Algeria	Djebel Al Akhal	Inactive SAS. *Filled with concrete*	Gédéon-Jabbour and Tabet (2009)
Hammam Trozza	35.55°N	9.58°E				Tunisia	Djbel Trozza	Vapor shaft close to Pb–Zn mine	Hamed et al. (2014)
El-Balayza caves	26°59′ 45.73″N	31°14′ 51.06″E	80			Egypt	Assiut	Presumed hypogene	Mostafa (2012)

2 Morocco

Morocco harbors numerous extensive caves. However, no hypogene or hydrothermal cave is recognized in published accounts. Bini (2007) mentions Kef Aziza (Buzio et al. 2003), which is located at the contact between Atlas and Sahara, where dense cupolas showing neighboring vertical convection cells could match with air convection above thermal flow along a horizontal passage. A recent visit (author) shown that the convective features must be attributed to condensation-corrosion related to bat guano. However, crystallization temperatures were calculated using $\delta^{18}O$ thermometer equation, assuming that $\delta^{18}O$ was constant and similar to the modern average $\delta^{18}O$ of groundwater and rain in this area, resulting in values of 25–30 °C for calcite speleothems (F. Gazquez, unpubl.). The Chameau Cave is located in Eastern Province close to the Mediterranean Sea. It drains part of the large aquifer of the Beni Snassen Mountain. The spring shows a classical karstic behavior with large amplitude of discharge, temperature, turbidity, and conductivity (Tayebi 2011). However, during the long dry season, low water is under influence of a low thermal component (25.5 °C). Carbonic degassing of supersaturated water produces in the cave subaqueous calcite deposits with clouds carved by bubble trails, and thick travertine deposits down to the spring.

3 Algeria

3.1 Mgharet PK4 + 396.50 (Gédéon-Jabbour and Tabet 2009)

This cave is located beneath the Djebel al Akhal in the wilaya ("province") of Mila. It was intersected during a tunnel excavation made for the water transfer from the reservoir of Beni Haroun toward the city of Constantine. The cave is an upward developing dendritic cave (Audra Chap. 3), made of stacked spheres and cupolas connected by narrow vertical fissures. It was explored in 2006 during tunnel excavation down to 46 m, and soon after it was filled with concrete. The lowest part of the cave is covered by gypsum, and at the bottom, "punched black blocks" were found that could correspond to Fe/Mn ore deposits. The morphology of cupola and the abundant gypsum deposits point toward sulfuric acid speleogenesis (SAS) with air convection and condensation–corrosion in a thermal context. Several hammam (spas) are present in the close vicinity, using sulfate hot waters (~50 °C).

3.2 Rouïna Caves (Saint-Ours 1959)

The Rouïna iron lode is located in the wilaya of Aïn Defla, about 100 km to the SW of Algiers. The mining activity encountered small natural caves without connection to the surface. This area is built of several hundreds of meters of thick Mesozoic limestones resting on shales. The hydrothermal mineralization is of Pliocene age, with successively precipitated hematite, oligiste, and siderose, which was used in the construction of the Eiffel Tower. Caves are generally made of high passages with very irregular surface, numerous dead ends, and cupolas on the ceiling. Ceiling cupolas are weathered as boxwork to a depth of about 6 cm; the weathering layer is made of the siliceous remnants of the limestone with thin hematite partitions. About 1.5 m below the top of cupolas, walls are entirely covered with a 30–50-cm-thick transparent calcite and dolomite popcorn crust. Meteoric flowstones and seepage are absent. Saint-Ours (1959) concludes to an epithermal speleogenesis in phreatic environment with low upflow velocity.

3.3 Kef el Kaous (Collignon 1984)

Kef el Kaous cave is located along the sea side in the Traras massif, near Honaine city in the wilaya of Tlemcen, about 150 km to the southwest of Oran. The Traras range displays very complex and still active tectonics. The cave develops in a Liassic limestone slice, deeply weathered by thermalism. The limestone is of minor extension (<1 km^2) and only crops out along the marine cliff. The limestone is entirely covered by diverse rocks (including marls, evaporites, and ophites) which prevent surface recharge. Part of the cave was already known and mined for its phosphates.

The cave develops as an extremely dense maze (>4 km below a surface of 0.07 km^2; Fig. 1). Passages are partly guided by fractures. However, the maze extension is independent of the main geological structure as it extends horizontally. Only some cupolas and tubes rise from some chambers above the main basal plan. The floor is covered by calcite, guano, and sand from wall weathering, fluvial sediments such as sand, silts, and clay, and by numerous rock debris. Some collapses are aligned along extensional fractures associated to gravity movements parallel to the marine cliff. Where visible, walls are covered by thick calcite crusts forming laminated clouds, with a clear shelf at mid-height recording an intermediate stage of water level, which is associated to tower cones built of calcite raft accumulation (Fig. 2). Seepage through the marly and evaporite covers is saturated in sulfates and chlorides. Since humidity levels do not reach saturation, gypsum precipitates as stalactites and even as crystals in oversaturated pools after evaporation. Phosphates are encountered as dykes cut by the cave, made of dark, soft, and porous material, and as accumulations in sediments. These phosphate dykes are interpreted as paleokarst fills, older than the overthrusting marls. Those associated to fluvial fine-grained sediments must have been reworked from the phosphate dykes.

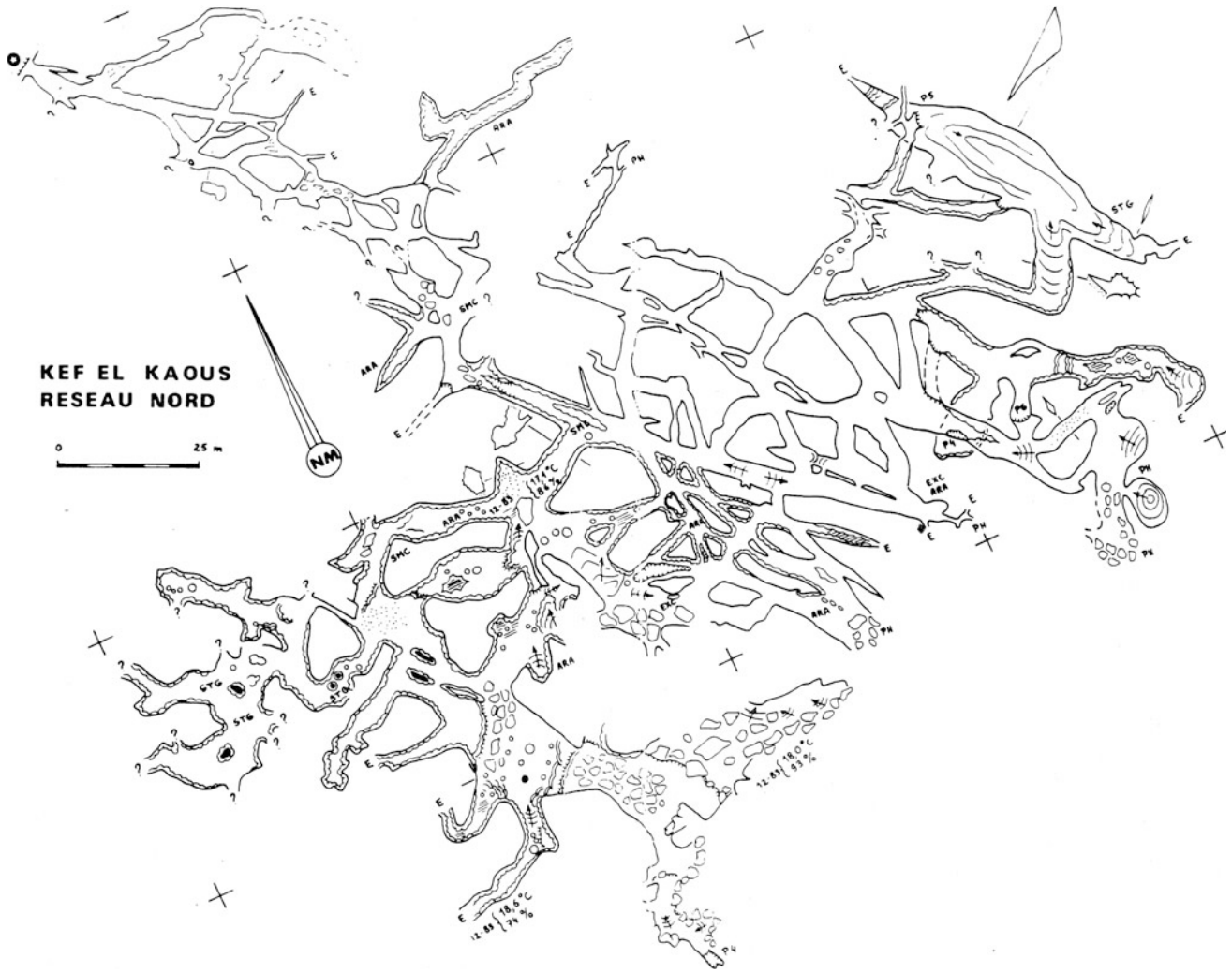

Fig. 1 Plan view of the northern part of Kef el Kaous maze, Algeria (after Collignon 1984)

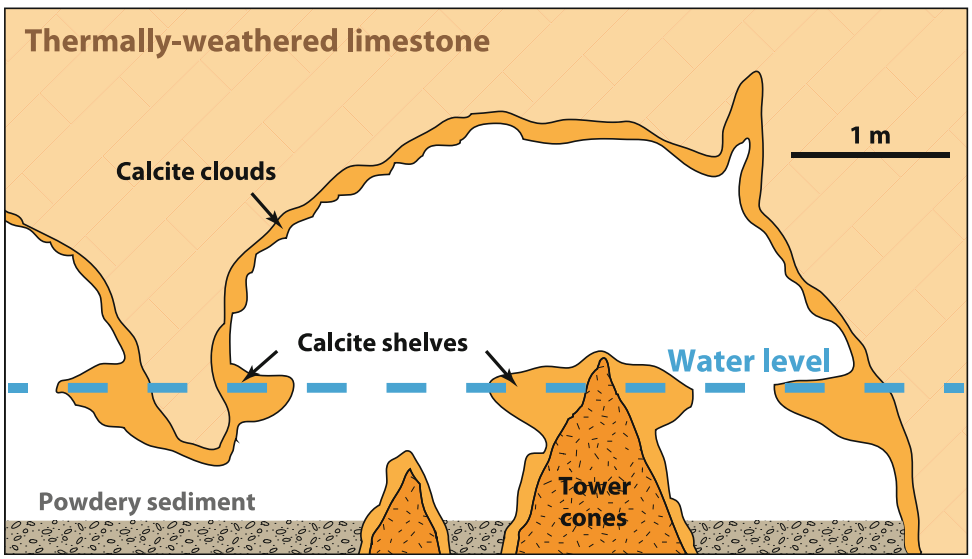

Fig. 2 Kef el Kaous Cave, Algeria. Underwater cave clouds are coating walls and ceiling. Tower cones built of calcite rafts accumulation and pool shelves record an intermediate stage of the draining of the cave (after Collignon 1984)

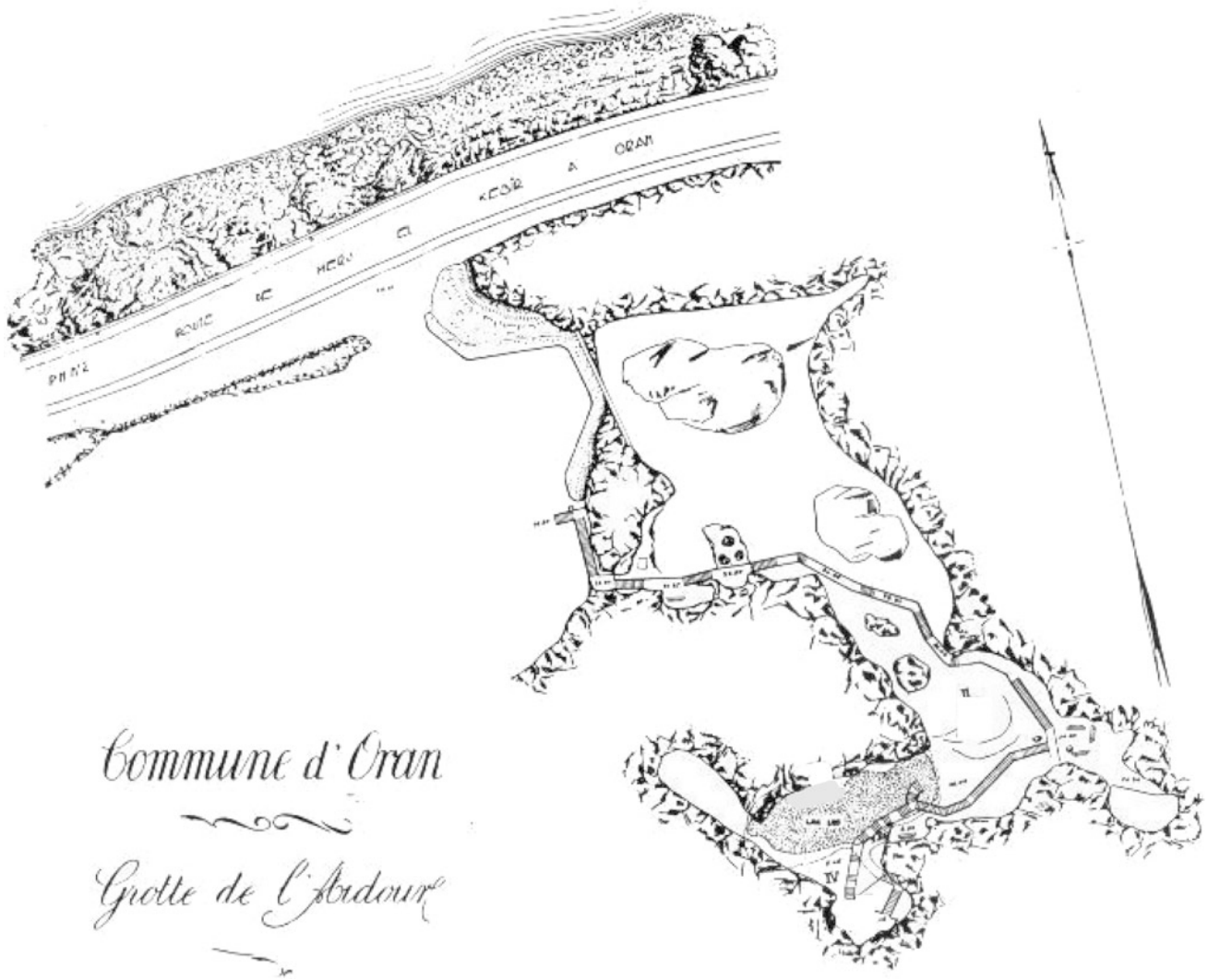

Fig. 3 Plan view of Aïdour cave, which was located along the sea (no scale provided). A gallery with large chambers led at 30 m depth to a warm lake (78 °C) at the sea level (from A. Levraux, in Pillon 2007)

The hypogene origin of the cave is shown by the absence of relationship with the surface covered by impervious rocks, by the restricted size of the local extension of the limestone, by the horizontal extension of the maze, and by the thick underwater calcite deposits associated to oversaturated water. Such active deposition might be related to CO_2 degassing of deep upwelling groundwater, possibly also to the mixing with the nearby seawater. The relationship with the strong hydrothermal weathering of the rock is still obscure, and the cave might have witnessed a late hydrothermal stage.

3.4 Aïn Ouarka (Collignon 1989)

Aïn Ouarka (the "Leaf Spring"), is located in the Ksour Mountains, in the wilaya of Naâma, 60 km east to Aïn-Sefra, and belongs to the South-Atlasic range. It opens in a scenery cirque, in the center of an eroded anticline, where cold (21 °C) and warm (46 °C/3 L/s) springs are mixing. Both springs are salty, due to the Triassic halite and gypsum, which are present at depth and are also cropping out as diapir. Cave walls are covered with calcite crusts.

3.5 Hassi Dermam Spring (Collignon 1989)

The spring is located in the Tlemcen karst plateau. The temperature is 26 °C. It has been explored by scuba diving down to −52 m, and the flooded passage continues further down. The conduit is lined by subaqueous calcite crust, suggesting a probable CO_2 degassing and supersaturation of the rising water. Up to now, it seems to be the only case of thermal spring where the rising conduit is accessible.

3.6 Aïdour Cave

Aïdour Cave is located to the west of Oran city, along the rocky shoreline. It owes its name from the local limestone summit. The cave was discovered in 1911 during road construction and named from an Arabian tale transcribed in the beginning of nineteenth century, related to a spirit living in a cave (Arambourg 1912). After large chambers (30 × 50 m) decorated with massive flowstones, the remote part goes down at 30° with a lower ceiling, until it reaches a 10 × 20 m lake, 6.5 m deep (Levraux A., in Pillon 2007, Fig. 3). The lake is located at about 30 m depth, i.e., 1.55 m above sea level. Calcite clouds are present (Arambourg 1912). Vapors were rising from the lake, which had a temperature of 78 °C. The cave is related to the nearby spa of "Bains de la Reine," named after the visit in sixteenth century of Joan the Mad, the daughter of the Spanish queen Isabel the Catholic. The chemical facies of the thermal spring was of chloride–sodium type (6–7 g/L) with minor calcium and magnesium, with a discharge of 6 L/s, and a temperature of 46 °C (Nicati 1870). The cave was opened for visitors in 1935, but unfortunately was later destroyed during the building of the Mers el Kebir harbor for French submarines.

3.7 The SAS of the Azerou Massif and Hamman el Biban

The Azerou massif belongs to the external Maghrebides range, where overthrusting occurred in the Lower Miocene (Collignon 1983b). An erosional window in the Tellian nappes allows outcropping of the "autochthonous" South-Tellian Biban nappe (Durand-Delga 1969). The Biban nappe is mainly built of marls and marly limestone. The Azerou series punches out through the Biban nappes as a

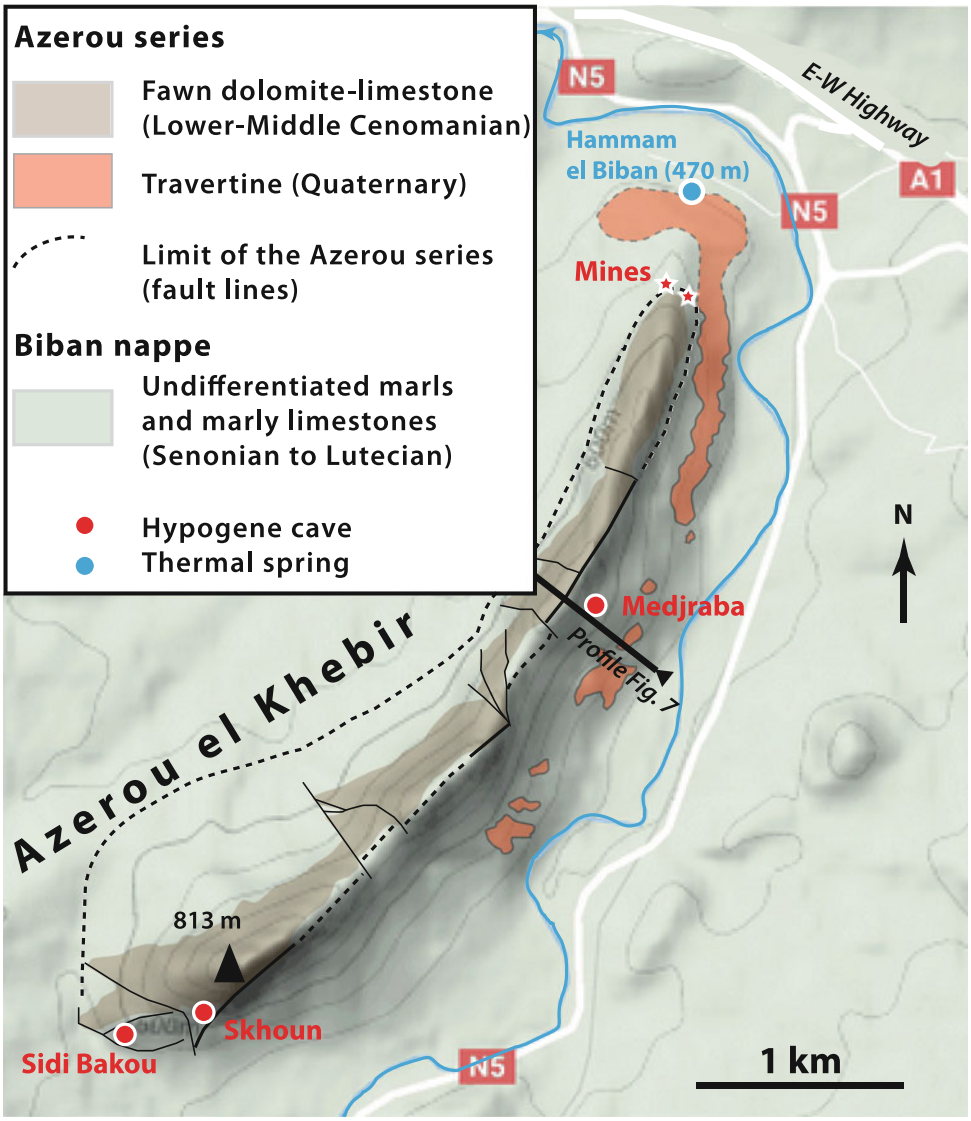

Fig. 4 Simplified geological map of the Azerou massif and the Hamman el Biban area (geology after Coiffait and Vila 1976, modified)

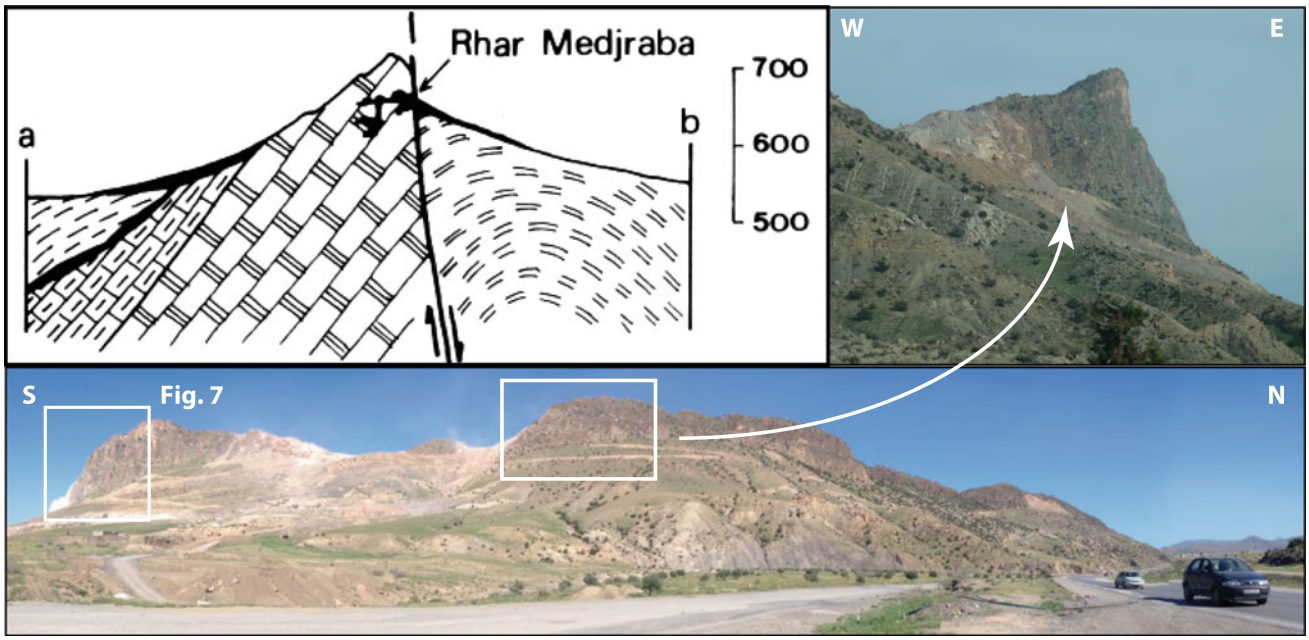

Fig. 5 *Left* Geological profile of the Azerou el Kebir showing its half-horst structure punching out through the marly Biban nappe (Coiffait and Quinif 1976). *Right* View of the same area showing the eastern cliff, up to 150 m high and made of fawn dolomite and limestone; to the *left* of the picture, the western side displays a gentler slope. The foreground shows marls of the Biban nappe. *Bottom* general view of the eastern face of the Azerou el Khebir where quarrying activity is intense. Rhar es Skhoun Cave locates to the *left side* of the picture, Hammam el Biban to the *right*. The Azerou es Srhir is not visible and locates further to the *left*

half-horst marked out by faults and abnormal contacts (Figs. 4 and 5). The Azerou relief is built of Cenomanian fawn dolomite and limestone overlooking the surrounding lowlands mainly made of marls, the Soummam depression to the north and the Setif "high plains" to the south. Triassic evaporites are present along the overthrust planes. Due to the NW dip, the western side of Azerou has gentle slopes, whereas the eastern side corresponds to the fault line and displays steep slopes or cliffs up to 150 m high. The Azerou peaks at 813 m a.s.l. The Azerou oued ("river") follows northward the eastern slope then turns to the west across the Biban (Iron Door) water gap. Hammam el Biban, the thermal spring, pours out at 470 m a.s.l. at the northern end of the Azerou. The Azerou massif is split in two parts, to the north the Azerou el Khebir (the "Large Azerou") and to the south the Azerou es Srhir (the "Small Azerou"). Unfortunately, this southern part almost entirely disappeared after recent quarrying. Several travertine terraces are present along the valley, the lowermost level being about 10 m above the river. It occurs only around the Biban thermal spring, with the largest extensions and with massive travertine mounds corresponding to presently inactive outflow points (Fig. 6). Two terraces of stratified travertine are present along the eastern slope at +40 and +70 m above the river level, some fossilizing old pebble terraces. The highest and southernmost travertine occurrence is located at the foot of Azerou es Shrir and is perched on a residual hill. These travertines are connected to a past thermal activity and clearly show a gradual shift of the outflow from the highest altitude to the south, toward the current thermal spring of Hamman el Biban to the north.

In the southern part of Azerou el Khebir, the cliff is carved by huge half-tubes about 100 m high and 10–20 m wide (Fig. 7). These tubes correspond to hydrothermal chimneys developed along the fault line. Hydrothermal flow was rising along the contact of the carbonate rocks, which were eroded. Later erosion of the marly compartment exhumed the chimneys. Cave entrances are located at different altitudes along these chimneys. Part of the walls of the chimneys and of the caves are covered with a thick (>1 m) lining of calcite spar that sometimes completely fills the voids (Fig. 8).

Several major caves are known in this area (Coiffait and Quinif 1976; Collignon 1983a, b, 1989). Rhar Es Skhoun, Rhar Amalou, and Rhar Medjraba are the largest, with lengths of 1.5–2 km and depth of about 100 m (Table 1). They are made of passages up to 20 m wide, of rift-like galleries, and of succession of chambers and narrows. They show mostly a horizontal development with sometimes significant slope or irregularities. Rhar Sidi Bakou is a unique, large, and steeply rising gallery. Mazes are developing from bedding planes and extend independently of structure as "swiss-cheese" mazes with round circumvolutions and blind passages (Rhar Amalou), or following joints

Fig. 6 *Left* Travertine mounds +10 m above base level close to Hammam el Biban springs. *Center* Travertine terraces along the Azerou el Khebir. *Right* Residual hills covered with travertine at the foot of Azerou es Srhir

Fig. 7 *Left* The northern part of Azerou el Khebir displays 100-m-high hydrothermal chimeys where numerous cave entrances are located. The chimneys have been exhumed following erosion of the marls along the fault line. *Right* Detail of a hydrothermal chimney, where large caves occur; see person for scale

in a network pattern (Rhar Medjraba; Fig. 9). Vertical shafts, up to 50 m deep, developed along faults, connect the horizontal levels in both Rhar es Skhoun and Rhar Medjraba. The host rock lithology (limestone or dolomite) seems to be not decisive regarding the morphology of the caves (Collignon 1983a).

The areas opened to the surface contain guano deposits, ash, and soot from the traditional users of caves, and at shallow depth calcite speleothems associated to meteoric seepage. However, all cave features clearly indicate the absence of fast-flowing water and of surface-related deposits such as clay or fluvial material. On the contrary, the profiles of the passages points toward an initial slow rising flow and a later aerial stage with active condensation–corrosion evidenced by large cupolas and niches filled with gypsum. In places, walls are deeply weathered and cupola is the most frequent feature with almost perfect hemispherical shapes mostly independent of fissures or bedding planes (Collignon 1983b). In Rhar Medjraba entrance zone, the largest cupolas reach up to 20 m in diameter. Subaqueous calcite clouds carved by bubble trails are diagnostic of degassing thermal pools, whereas calcite vents and large popcorns were developing above these thermal pools from air convection making local evaporation and precipitation.

The mineralogy of cave deposits is related to the successive speleogenetic phases. The calcite spars are associated to the early phase of deep phreatic flow. Rhar Sidi Bakou and Rhar Amalou are covered with large spar crystals (Collignon 1983b). Spar also occurs as dykes, as lining with centripetal growth, or as complete fills (Fig. 8). They are often smoothed by subsequent condensation–corrosion as evidenced by the presence of massive gypsum deposits. Green calcite occurs in the southern part of Azerou el Kebir. To the north, in the vicinity of the Biban spring, a Pb–Zn mine is associated to an early hydrothermal phase. Bouragba and Chabou (2015) distinguish early sulfidic epigenetic mineralizations of thermal origin (pyrite, sphalerite, galena) included in vein of calcite, dolomite, and quartz. Secondary oxidized minerals are represented by smithsonite, cerussite, azurite, hematite, and gypsum. Iron oxides are present in Rhar Medjraba (Coiffait and Quinif 1978) displaying typical spongy texture associated with microbial mats. Some

Fig. 8 Entrance of Azerou 4 cave is entirely covered with large calcite spar

bipyramidal quartz crystals are found in Rhar Amalou and Rhar Zenadia. However, their origin, detrital or hydrothermal, is still questionable (Collignon 1983a). The second aerial phase of sulfuric acid speleogenesis (SAS) is characterized by massive saccharoid gypsum especially present in the lower series of Rhar es Skhoun and of Rhar Medjraba. Gypsum classically occurs as wall crusts or as massive deposits on the floor pierced by drip holes. In Rhar es Skhoun, secondary large crystals are growing downward from the ceiling (Collignon 1983b).

Cave microclimate is under direct influence of the geothermal heat. In the lower part of Rhar es Skhoun, the temperature reaches up to 32.6 °C, i.e., 16 °C above the mean local temperature (Collignon 1983b). However, no significant concentration of H_2S or CO_2 (<0.5%) has been measured (Collignon 1983b). This demonstrates that currently, there is probably no direct connection between the caves and the thermal water body, which has only an indirect effect on the geothermal gradient that heats the rock. Active hydrothermalism is present in Hamman el Biban spring. With a discharge of about 7 L/s, the temperature reaches 80 °C, one of the highest in Algeria. The salinity content is 16 g/L, with a carbonate–chloride–sulfate profile (Collignon 1983a), which is consistent with the mineral deposits around the springs (calcite, aragonite, gypsum, halite, sylvite, and sulfur). In addition, H_2S and CO_2 degassing is visible with a strong bubbling and a characteristic smell. A well reaching the water table at 120 m depth in Azerou es Srhir quarry, several kilometers away, shows a hydraulic gradient of only 1.5%, characteristic of a well-developed karstification.

Preliminary isotopic composition of spring water, of gypsum hydration water, and of travertine deposits allows understanding of past and current dynamics (Gazquez F., unpubl.). Isotopic values of SAS gypsum hydration water and spring water show a good agreement with the local meteoric water (around −7‰ for $\delta^{18}O$ and −48‰ for $\delta^{2}H$). Crystallization temperatures were calculated using the $\delta^{18}O$ thermometer equation, assuming that $\delta^{18}O$ was constant and similar to the modern average $\delta^{18}O$ of groundwater and rain in North Algeria, resulting in values of 25–30 °C for calcite spars, and 12–19 °C for the meteoric flowstones. $\delta^{34}S$ of SAS gypsum in Rhar Medjraba is −12.3‰ and in the sulfur deposits of the Biban spring is −24.3‰. Such depleted values are consistent with precipitation from H_2S oxidation and bacterial reduction, respectively.

Finally, U/Th dating has been performed on calcite spars, popcorn, and travertines (H. Cheng, unpubl., Fig. 10). They clearly show clustered ages: spars are older than 0.5 Ma, subaqueous clouds are 7 ka, calcite popcorns of Rhar Medjraba are 254 ka, and travertines are 378 ka for the +40 m above base-level middle terrace and 27 ka for the lower +10 m above base-level terrace.

Field and analytical data allow characterizing the hypogene evolution of the Biban hydrothermal spring and the Azerou karst. Following the recent Pliocene–Quaternary tectonic uplift, the marls of the Biban nappes were gradually eroded, opening a hydrogeological window in the Cenomanian carbonates of the Azerou series. In an early phase, older than 0.5 Ma, thermomineral water of meteoric origin was rising along the fault line and outflowed above the current 800 m altitude. It opened large hypogene chimneys by dissolving the carbonate compartment and partly filled them with calcite spar due to CO_2 degassing at shallow depth. Taking into account timescales and base-level lowering, a trend can be recognized, with initial deposition of green calcite spar to the south gradually shifting to the deposition of white calcite and sulfur ore deposits to the north, associated to a possible cooling and

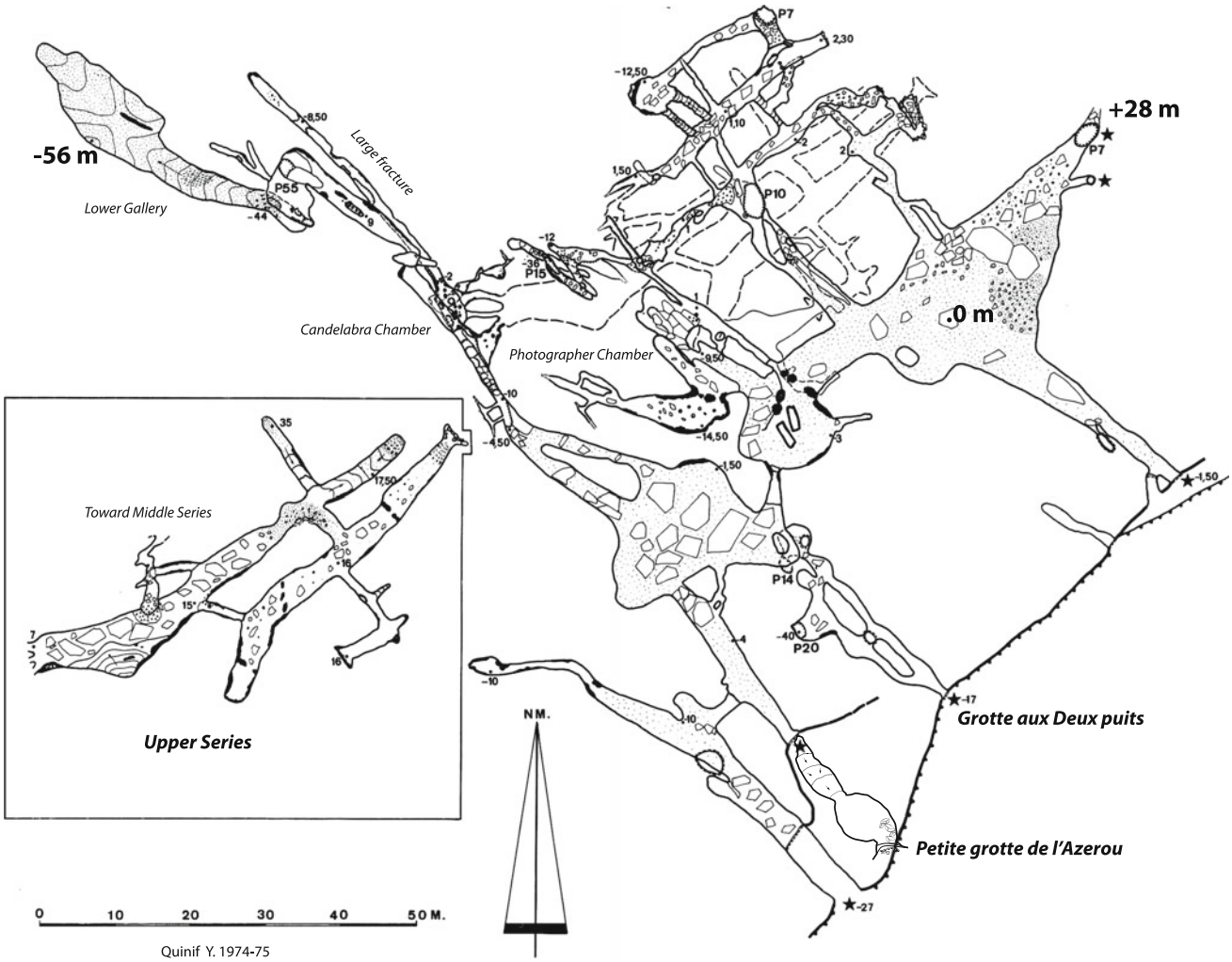

Fig. 9 Plan of Rhar Medjraba cave (after Coiffait and Quinif 1976)

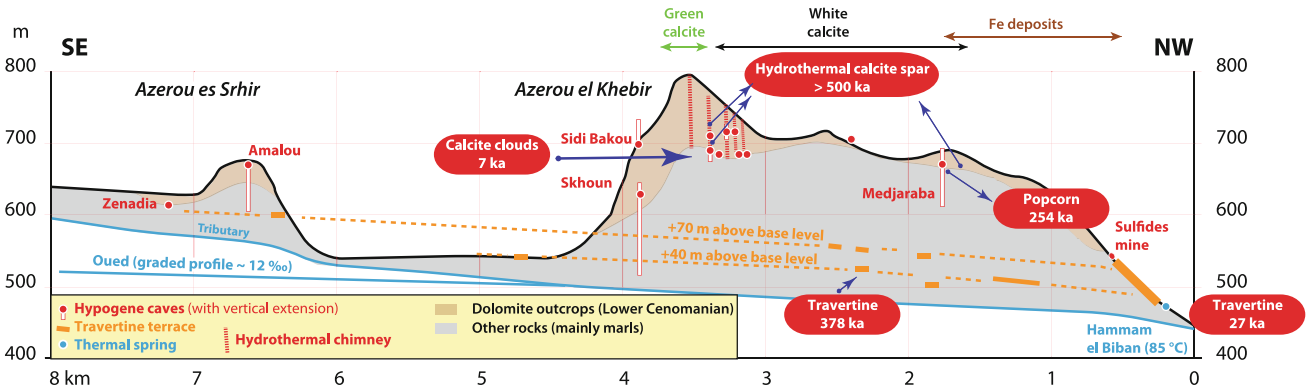

Fig. 10 Synthetic evolution of the Azerou hydrothermal and sulfuric karst. For further details see text

to some mixing with shallow water. This initial phase seems to have occurred within a low thermal environment at about 25–30 °C.

At 378 ka, the valley was already entrenched down to the current +40 m above base-level terrace, together with the correlative exhumation of the carbonate massif. SAS

speleogenesis in aerial conditions was very active, developing extensive cave systems with massive gypsum deposits above the water table. Condensation–corrosion processes were extremely active because of thermal gradient and sulfuric acid corrosion, producing dense cupola morphologies. Correlative travertine terraces were deposited due to the sulfate content of the water allowing strong calcite oversaturation by the common-ion effect. The geomorphic evolution, evidenced by both caves and travertines, followed the entrenchment trend and the gradual northward shift of the speleogenesis and the thermal discharge.

Currently, accessible caves have no direct connection with the thermal body and are indirectly heated by thermal conduction through the rock massif. The Biban spring is still depositing various carbonates and evaporites, whereas its temperature seems to have recently risen up to 80 °C.

The Azerou massif is currently one of the most interesting and best studied sites regarding hypogene speleogenesis, especially SAS, in North Africa. However, the whole massif and their caves are seriously endangered by intense quarrying activity. The southern part of Azerou es Shrir already disappeared, including the caves Rhar Amalou and Rhar Zenedia (Table 1). In Azerou el Khebir, Rhar es Skoun Cave, which is the most interesting site, is now inaccessible and already partly destroyed (Figs. 5 and 7).

4 Tunisia

Hammam Trozza is located 30 km to the SW of Kairouan. It is a well-known cave opened in a cliff and accessible by steps carved in the rock. Vapors with sulfur content are coming from fissures at the bottom of the shaft. Local people use the entrance room as "vaporium" for therapy. This thermal activity is connected to the nearby Pb–Zn ore (Hamed et al. 2014). However, we could not obtain confirmation whether the cave was artificially excavated or simply arranged from a natural (karstic?) cave or fissure.

5 Libya

Libya is known for large karst areas in Cyrenaica and for the extensive use of fossil water pumped in the deep aquifers of the desert, mainly in sandstone. These artesian aquifers generally discharge in low structural areas (synclines), which are also topographic depressions covered by sand deposits called "erg." Such discharge areas are at the origin of oases. The Awbari erg is located to the SW of Libya, in the Murzuq Basin. Some artesian lakes are found in the middle of the sand desert (26° 54′N, 13° 28′E). The presence of Paleozoic carbonates at shallow depth suggests focused upflows within the limestone, discharging in discrete spots (Burdon and Gonfiantini 1991). Such hydrogeological setting would be favorable to hypogene speleogenesis.

6 Egypt

6.1 El-Balayza Caves (Mostafa 2012)

El-Balayza city is located in Middle Egypt in Assiut governorate. Small caves open along the scarp defining the limit between the Nile Valley and the Western Plateau. Caves follow horizontal bedding planes and joints of the well-bedded Oligocene limestone. They are devoid of fluvial sediment. Rift-like feeders together with cupolas, wall and ceiling channels, suggest rising flow. Some conduits are sealed by calcite spar. Manganese and iron oxides deposits are closely related to the feeders. The author suggests an origin associated to the rifting period from Oligocene to Pliocene.

6.2 Western Desert Unroofed Caves (Pickford 2011; Wanas et al. 2009)

In the Western White desert, cave features have been identified in Crystal Mountain (Gebel Bellorat). Extensive degraded karst features are mainly composed of unroofed caves, which remnants are actually mainly their filling made of hardened fauna-rich deposits (breccia, speleothems). These karst features are visible in Maastrichtian chalk anticlines. The development of these caves has been attributed to Late Miocene wetter periods, where karst processes would have been more effective. Considering their close association to anticlines, these authors question the relationships with erosional processes that firstly truncated the positive structures then opened hydrogeological windows that focused groundwater upflow. Providing that tectonic conditions were only a structural pre-request and that aeolian processes only later modified these areas, they consider that oases location and development might be actually closely related to karst processes. Even if this term is not explicitly mentioned by these authors, such karst development falls in the hypogene speleogenesis type, providing it would be related to focused upflows of aquifers discharging in low topographic areas (the oases) while using the positive structures (the anticlines).

6.3 Western Desert Presumed Sag Structures (Tewksbury et al. 2016)

In the same desert, Tewksbury et al. (2016) studied by remote-sensing extensive areas of closed syncline

depressions. They are developed in otherwise flat-lying white limestones of early Eocene age. Since these synclines are not associated to anticlines and domes and since there is no report of evaporite at depth, the authors suggest that these synclines could be sag structures, instead of folds associated to fault propagation or to deep evaporite dissolution. Their age is quite well constrained since they are cut by the fracture system associated with the Red Sea rifting. In that case, hypogene speleogenesis in limestone, possibly associated to post-eocene magmatic activity, would be a credible candidate for the development of such deep-seated collapses or sag structures.

Acknowledgements Part of this work was carried out in the frame of the French–Algerian bilateral project PHC Tassili no. 13MDU884. Djamel Boubaya (Univ. of Tebessa) collected the water samples at Hammam el Biban. Mohammed Belaoud and Said Ramdam are thanked for their collaboration during cave survey. The Benouerkhou family is acknowledged for its nice welcoming in the village during our field work. Thanks are due to Bernard Collignon for scientific discussions and for providing determinant information for the logistic and for the access to the area. Alfredo Buzio provided documentation about Kef Aziza Cave. Hai Cheng (Xi'an Jiaotong University, China) is warmly thanked for U/Th dating of the calcite samples of Azerou massif. Fernando Gazquez (Univ. of Cambridge, UK) provided isotopic analyses of Azerou massif and Kef Aziza.

References

Arambourg C (1912) La caverne de l'Aïdour (Oran). Bulletin de la Société de géographie et d'archéologie de la province d'Oran 32:403–409

Bini A (2007) Morphologie et genèse de quelques types de coupoles. 17e Rencontre d'octobre, Orgnac 37–44

Bouragba N, Chabou MC (2015) Contribution à l'étude des minéralisations de la chaîne des Azerou (Biban, Bordj Bou Arreridj). 3ème Colloque International sur la Géologie du Sahara. Ouargla 1:25–28

Burdon DJ, Gonfiantini R (1991) Lakes in the Awbārī sand sea of Fazzan, Libya. In: Salem MJ, Busrewil MT, Ben Ashour AM (eds) The geology of Libya. Elsevier, vol 5, pp 2027–2041

Buzio A, Cantaluppi G, De Blasi M, Guffanti M, Repetto G (2003) Kef Aziza, la lunga storia di una grotta pre-sahariana. Speleologia 49:74–78

Coiffait PE, Quinif Y (1976) La grande grotte de l'Azérou el Kébir. Spelunca 3:97–112

Coiffait PE, Quinif Y (1978) Fracturation et karstification d'un massif: l'exemple de l'Azerou el Kebir (Algérie du nord). Int J Speleol 10:245–252

Coiffait PE, Vila JM (1976) La série renversée des Azérous. C R Soc Géol Fr 6:269–271

Collignon B (1983a) Spéléogenèse hydrothermale dans les Bibans (Atlas tellien, Nord de l'Algérie). Karstologia 2:45–54

Collignon B (1983b) Rhar Es Skhoun: étude d'une grotte thermale des Bibans. Spelunca 12:19–24

Collignon B (1984) Étude morphologique et structurale de la grotte de Kef el Kaous (Algérie). Spelunca Mémoires 13:88–92

Collignon B (1989) Les karsts hydrothermaux d'Algérie. 10th International Congress of Speleology. Budapest 3:758–776

Djidi K, Bakalowicz M, Benali A (2008) Mixed, classical and hydrothermal karstification in a carbonate aquifer: Hydrogeological consequences. The case of the Saida aquifer system, Algeria. Comptes Rendus. Geosciences 340(7):462–473

Durand-Delga M (1969) Mise au point sur la structure du nord-est de la Berbérie. Publ Serv Géol Algérie 39:89–131

Gédéon-Jabbour B, Tabet J (2009) Mgharet PK4+396.50. Grotte hydrothermale de Djebel Akhal. Spéléorient 5:94–98

Gutzmer J, Beukes NJ, Rhalmi M, Mukhopadhyay J (2006) Cretaceous karstic cave-fill. Manganese-lead-barium deposits of Imini, Morocco. Econ Geol 101(2):385–405

Hamed Y, Redhaounia B, Ben Sâad A, Hadji R, Demdoum A (2014) Hydrothermal waters from the Trozza basin: case of karst aquifer (Central Tunisia). Colloque international sur l'hydrogéologie et la géothermie, Guelma, Algérie (abstract)

Melki F, Zargouni F (1991) Post Jurassic brittle tectonics of the Hammam Zriba mine (Northeastern Tunisia) and related karst and fluorine, barytine and celestine occurrences in carbonate environments. Bulletin de la Société géologique de France 162(5): 851–858

Mostafa AA (2012) Caves of the Nile valley (Governorate of Assiut, Middle Egypt): a long-term interaction between human societies and their environment. Géomorphologie 18(1):37–44

Nicati C (1870) Notice sur le Bains de la Reine, près d'Oran en Afrique. Bulletin de la Société Vaudoise des Sciences Naturelles 10 (64):611–616. doi:10.5169/seals-256584

Pickford M (2011) Diagenèse des spéléothèmes du Miocène supérieur (Désert libyque, Égypte) Karstologia 57:13–18

Pillon JC (2007) La grotte de l'Aïdour. http://home.nordnet.fr/jcpillon/piedgris/clotilde4.html. Accessed 30 July 2016

Saint-Ours J (1959) Les grottes de Rouina (Algérie). Annales de Spéléologie 5(4):149–150

Tayebi A (2011) Vulnérabilite des ressources en eau karstiques en milieu méditerranéen semi-aride: le massif des Beni Snassen (Maroc oriental). Approche pluridisciplinaire et utilisation des méthodes 'SIG'. Thesis, University of Grenoble, France, 388 p

Tewksbury BJ, Tarabees EA, Mehrtens CJ (2016) Is hypogene karst a plausible model for formation of extensively developed non-tectonic synclines in Eocene limestones of the Western desert, Egypt? In: Chavez T, Reehling P, editors. Proceedings of DeepKarst (eds) Origins, resources, and management of hypogene Karst, April 11–14, Carlsbad, New Mexico: NCKRI Symposium 6. Carlsbad, New Mexico: National Cave and Karst Research Institute, pp 201–203

Wanas HA, Pickford M, Mein P, Soliman H, Segalen L (2009) Late Miocene karst system at Sheikh Abdallah, between Bahariya and Farafra, Western Desert, Egypt: Implications for palaeoclimate and geomorphology. Geologica Acta 7(4):475–487

Webb JA, White S (2013) Karst in deserts. Treatise on. Geomorphology 6:397–406

Hypogene Karst in Southern Africa

59

J. Martini

Abstract

In this region, the most typical hypogene caves are located in the arid (10–300 mm/year) NW of Namibia, developed in relatively pure dolostone and calcitic marble. Their origin is mainly evidenced by past hydrothermal activity, which formed chimneys terminating upward into bell-shaped ceilings and alveolar niches, as well as regular and extensive dogtooth calcite coatings on the walls. Barite occurs in one cave. They seem to have formed by low salinity solutions at temperatures not exceeding 70 °C. These caves are widely dispersed in the carbonate-rock areas, and surficial karst morphology is absent or very poorly developed. In this dry area, caves not displaying typical hydrothermal characteristics are also known. The passage morphology is phreatic, forming complex networks, but encompassing only very small areas. They are often reduced to single voluminous chambers. This limited lateral extension might possibly suggest localized upwelling from deep aquifers. Further East in Namibia, in the Otavi Mountains and in the northern part of the Kalahari region, under a higher rainfall regime (500–600 mm/year), the karst is better developed, but less evidences of hydrothermal activity have been observed. Only in one cave unusual chemical composition of groundwater is suggesting deep leaching of silicate rocks. Although the caves are more frequent and better developed, forming complex phreatic mazes and voluminous chambers, they still do not extend widely. Thus, it is possible that hydrothermal activity did occur more commonly, but is less obvious and obscured by surficial water dilution. In NW South Africa, the karst is developed in thick, very cherty dolostone, and due to a wetter climate, the intensity of dissolution is fairly intense. Probably in part due to this impure nature, however, groundwater flow is sluggish, but caves are frequent, mainly forming phreatic mazes of restricted extension and no long interconnected systems. No direct hydrothermal evidences have been reported. Nevertheless, a fair permeability has been proved to be present down to great depth, a condition favorable for the formation of upwelling plumes of moderately warm water in the aquifer. This suggests hypogene processes to be responsible for the caves developed under thick shale cover.

Keywords

Hypogene • Hydrothermal • Desert • Namibia • South Africa

J. Martini (✉)
Rue du Perbet, 07700 Saint Remèze, France
e-mail: jacquesmartini07@orange.fr

© Springer International Publishing AG 2017

A. Klimchouk et al. (eds.), *Hypogene Karst Regions and Caves of the World*,
Cave and Karst Systems of the World, DOI 10.1007/978-3-319-53348-3_59

1 Introduction

Compared to other regions of the world, hypogene karst is not well developed in Southern Africa. Consequently, only little attention has been paid to this subject, and the publications are few. However, in Namibia, small caves, typically of hydrothermal origin, have been identified and will be considered first. Then Botswana and South Africa will be reviewed, where hypogene karst is less certain, but nevertheless possible.

2 Namibia

2.1 Caves in the Namib Desert

In this dry area, forming a narrow, but extensive band, along the Atlantic coast, the rainfall is particularly low (10–20 mm/year). Epikarst morphology is completely lacking. In this desert, however, four small caves have been reported, which are hosted in highly deformed marble lenses of the Damara metamorphic belt (Upper Proterozoic). The largest and most interesting of them is Rössing West Cave (Martini and Marais 1996; Irish et al. 2000), exhibiting alveolar ceilings, cupolas, and blind chimneys developed from a sub-horizontal phreatic-type passage (Figs. 1 and 2). This morphology is diagnostic of hydrothermal speleogenesis. A narrow crack in the apex of one of these globular cavities accidentally provided an entrance to the cave. Apart from the morphology, relicts of calcite crusts on the walls are also informative about the evolution of the cave. A first phase deposited coarse radiating crystals, with liquid inclusions without gas bubbles, thus indicating depositional temperatures below 50–70 °C. This was followed by a dissolution period and then by a second phase of finer botryoidal crystallization. A second corrosive event followed, then a deposition of flowstone after the final dewatering of the cavity. The formation of flowstone is surprising and is certainly quite ancient, considering the extremely dry conditions prevailing in this region since a long time. U/Th dating gave an age in excess of 300 ka for the oldest flowstone and of 27–37 ka from ^{14}C for the most recent one (Heine and Geyh 1984).

2.2 Temple of Doom Cave

The most informative of the hydrothermal caves in Southern Africa is the Temple of Doom (Martini and Marais 1996). It is still situated in an arid environment, but under higher rainfall conditions (100 mm/year), and is developed in the very top of the Otavi dolostone (Upper Proterozoic), on the apex of an anticline at the point where the latter dips under an impervious cover of Mulden phyllite (Figs. 1 and 3). The entrance appears as a narrow crack opened by the collapse of a part of the ceiling of a chamber (Fig. 4). From there, the cave extends as a simple phreatic tube ending in a water table pool at −84 m. In the highest part of the cave, large alveoli, domes, and blind chimneys occur. The winter temperature was 26–27 °C in the entrance chamber and rose to 32 °C at the terminal pool.

Mainly in the deepest part, the walls and blocks fallen from the ceiling are covered by crusts of barite crystals (Martini and Marais 1996). Originally, these crusts must have widely coated the walls (Fig. 5), but due to a posterior dissolution phase, they are presently reduced to relicts preserved mainly at the base of the walls. Microprobe analysis showed that the barite is very pure, without Sr. It contains fluid inclusions, which are filled with a very low salinity solution with no gas phase, therefore indicating a deposition temperature inferior to 50–70 °C. On the cave floor, the barite deposition was preceded by sedimentation of friable, crystalline secondary dolomite, which also forms botryoidal crusts on the walls. An analysis of this mineral revealed a high Ba content (886 ppm).

Apart from the Temple of Doom, other caves seem very rare in the surroundings. Only a large sinkhole has been located 3.5 km to the E of the Temple of Doom, in a very similar stratigraphic and structural context (Fig. 3). Its bottom is filled by scree, but in places, the walls are coated with radiating calcite containing fluid inclusions with small bubbles indicating a relatively high temperature (70–100 °C). At 37.5 km to the NNE of the Temple of Doom, barite has been reported filling small cavities, again at the very point where a dolostone anticline dips under Mulden cover (Rabie 1949). The fact that these 3 sites are situated at the southernmost outcrops of the carbonate rock and that the water table is reached in the Temple of Doom suggests that the systems were still active not a very long time ago, relatively, as only a limited denudation could have taken place since this time. The hydrothermal activity could even be sub-actual, as such a low-temperature hydrothermal activity is observed 35–50 km to the N and to the NW of Temple of Doom. There are a number of small springs arising from dolostone around the localities of Sesfontein and Warmquelle, with temperatures varying from 27 to 35 °C (Guj 1969). This temperature range is hardly higher than the maximum values measured in the poorly ventilated sections of the local epigenetic caves.

2.3 Nooitgedag Caves

In an area of higher rainfall (250 mm/year), four caves are located in a steeply dipping band of marble of the Damara belt (Figs. 1 and 6). They are comparable to the caves of the

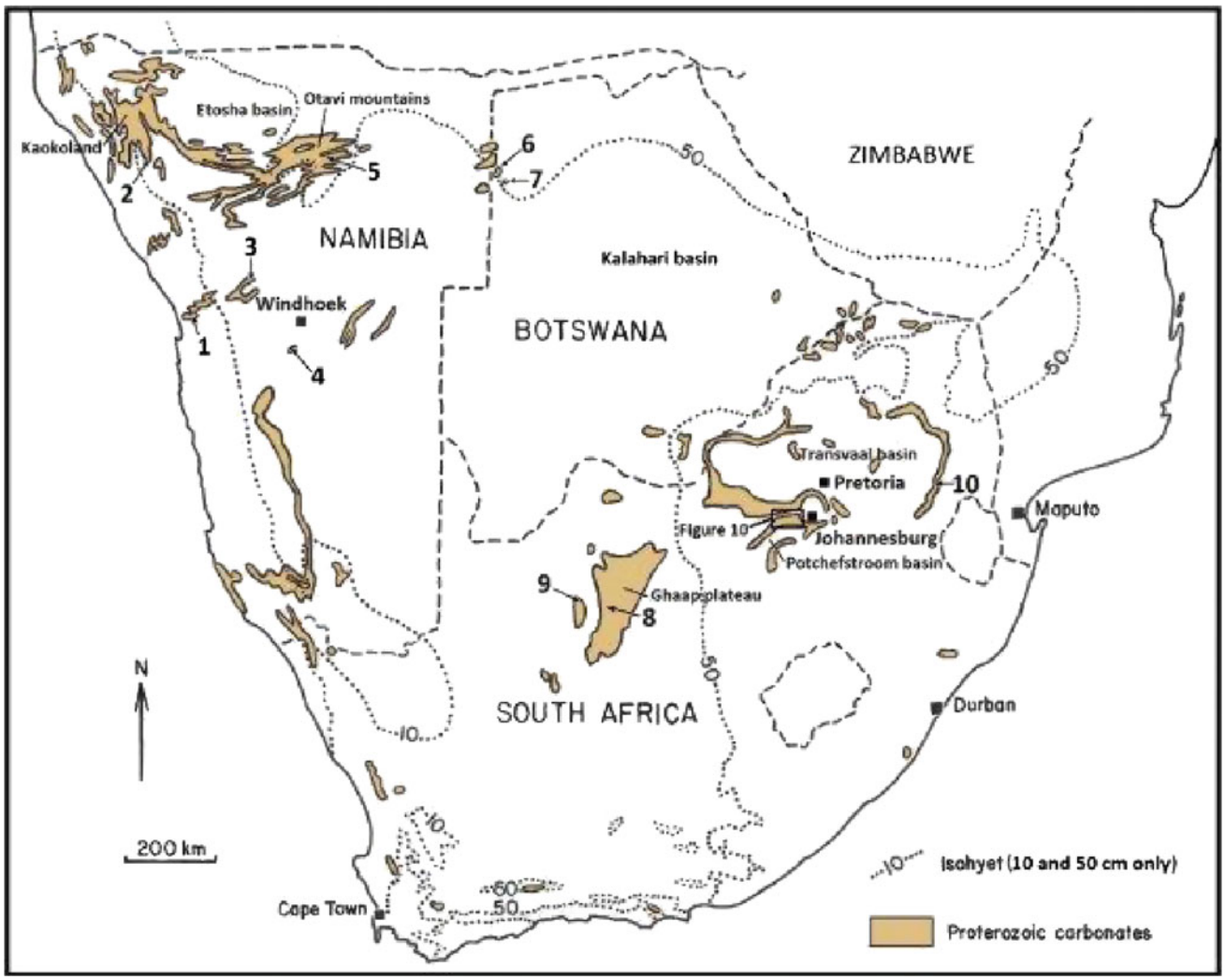

Fig. 1 Distribution of Proterozoic carbonates and of described localities: *1* Rössing W cave; *2* Temple of Doom Cave; *3* Nooigedag caves; *4* Naos cave; *5* Pofadder cave; *6* Gcwihaba Hills; *7* Koanaka Hills; *8* Bushmansgat; *9* Sishen Fe Mine; *10* Mbobo Mkulu cave

Namib Desert, but are more extensive, reaching 755 m of combined passage lengths in cave I (Irish et al. 1992; Marais et al. 1996). These caves do not reach the water table. They are developed very close to each other on about a same horizontal level, at shallow depth, forming densely packed mazes. Hydrothermal morphology is suggested by alveolar domes and blind chimneys. The most remarkable of them has been observed in cave III, in the form of a narrow crack ending at 7 m from the bottom, where it widens into a globular chamber with an alveolar ceiling (Fig. 6). In caves I, II, and III, tower (raft) cones grew in pools, now dry (Figs. 6 and 7). This type of "pseudo stalagmites" typically, although not exclusively, forms in pools under hydrothermal conditions (Hill and Forti 1997; Gázquez and Calaforra 2013). The fact that caves I and II are very close to each other, but poorly or not interconnected, is perhaps also related to localized upwelling sites.

2.4 Naos Cave

This cave (Fig. 1) is situated in comparable geological and climatic conditions of Nooitgedag caves. It consists essentially of a wide, 165-m-long, inclined passage ending in a lake marking the water table at the depth of 57 m (Irish and Marais 1990). No hydrothermal morphology has been observed, but the cave walls have been coated by layers of coarsely crystallized calcite at least twice. These two deposition phases seem to have been separated by a dissolution period. The second phase is constantly 2–3 cm thick from the entrance to the lake. Here too, the fluid inclusions contain only liquid, indicating low temperature. Nevertheless, as the water was obviously oversaturated in calcite down to a relatively great depth, a rather unusual situation in non-hydrothermal systems, a deep origin seems probable.

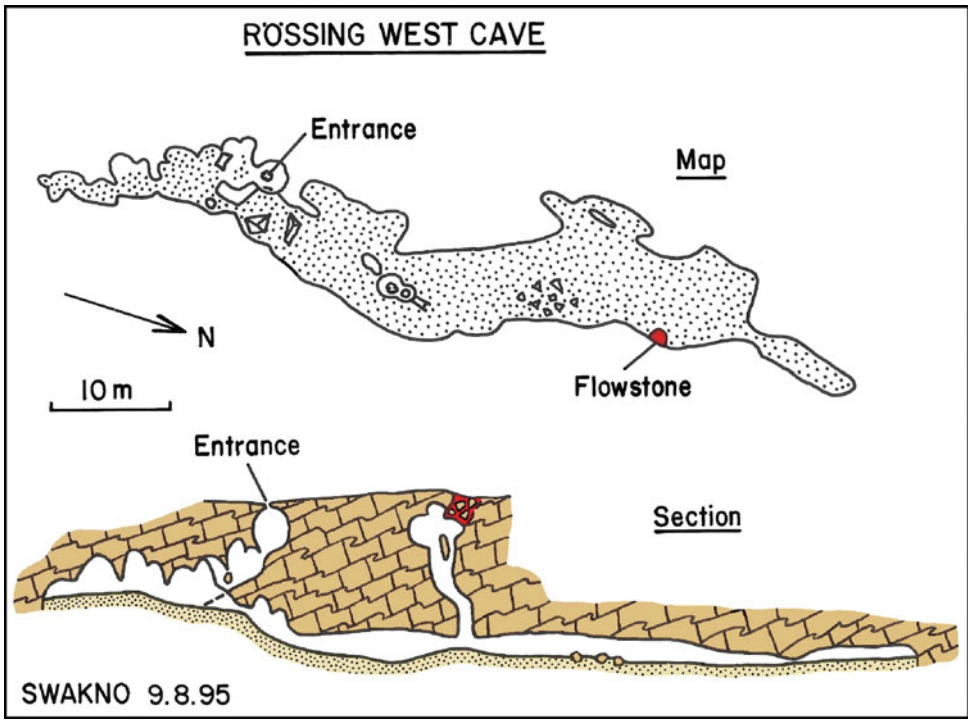

Fig. 2 Rössing W cave

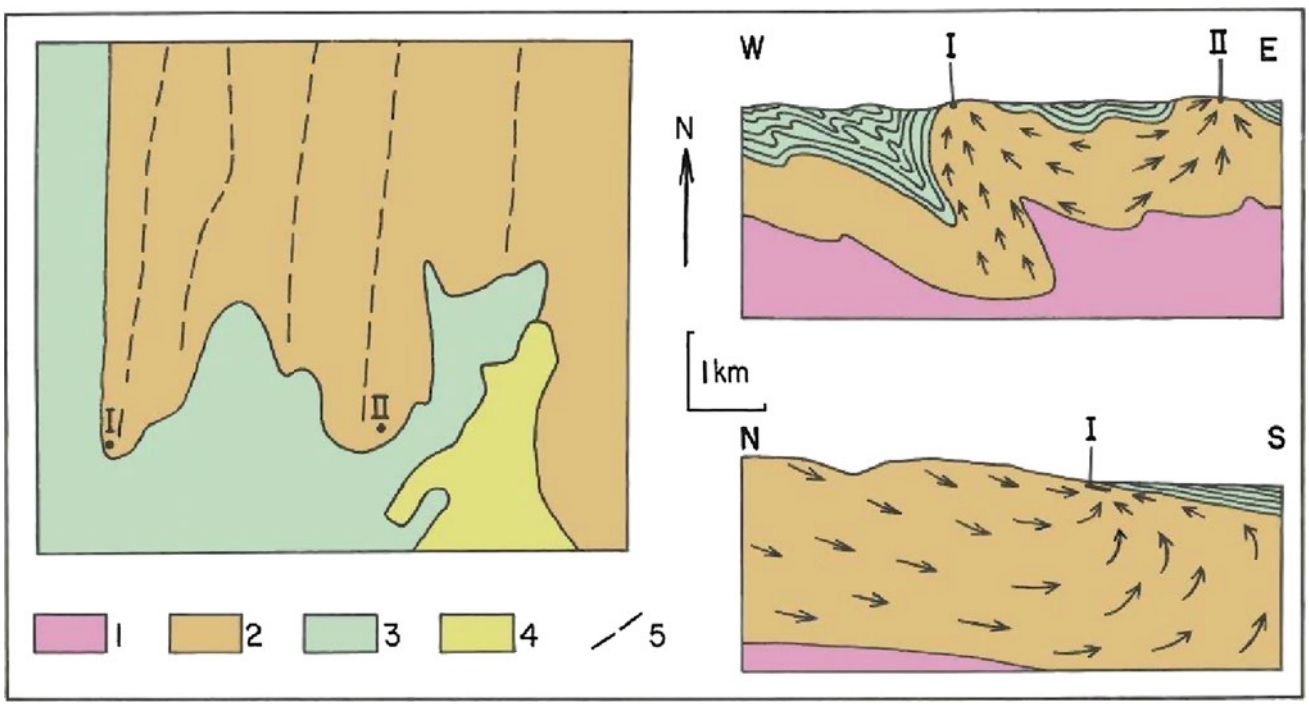

Fig. 3 Detail geological map in the vicinity of Temple of Doom Cave: I Temple of Doom Cave; II sinkhole. Legend: *1* Nosib Group (siliciclastics); *2* Otavi Group (dominantly dolostone); *3* Mulden Group (phyllite, conglomerate); *4* Jurassic–Cretaceous (siliciclastics, basalt); *5* anticline axis. *Arrows* indicate groundflow direction

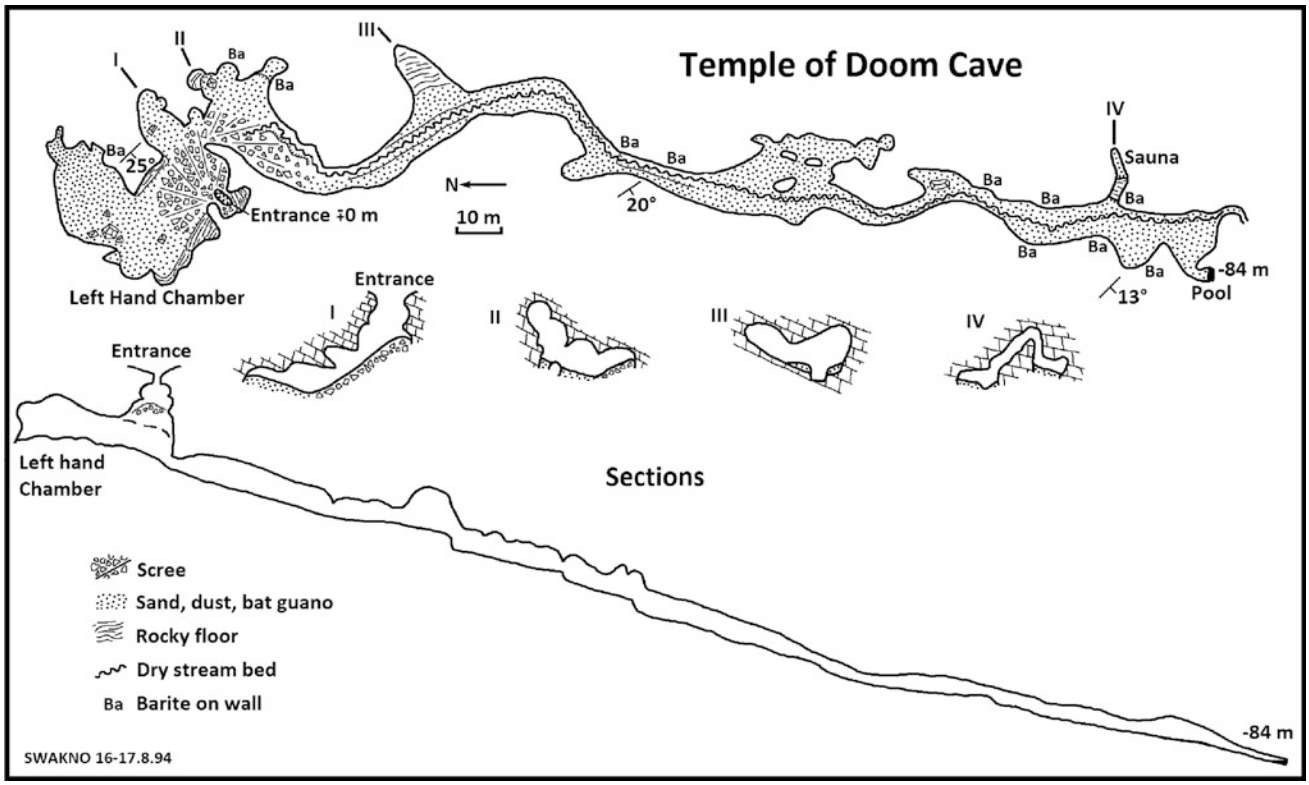

Fig. 4 Temple of Doom Cave

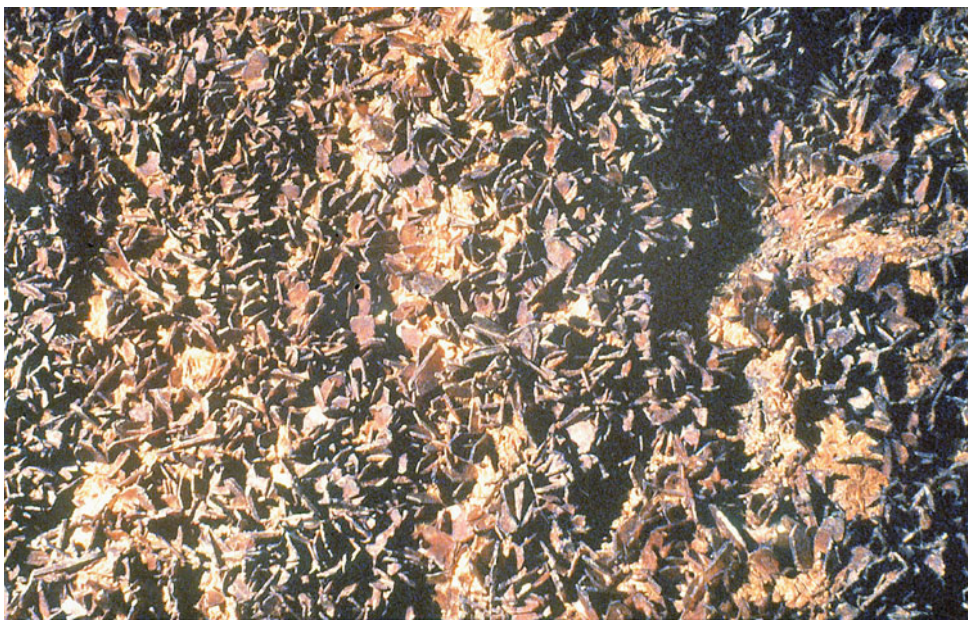

Fig. 5 Barite on wall in Temple of Doom Cave. Crystal blades size: 1–2 cm. Picture by E. Marais

2.5 Other Caves of Possible Hypogene Origin

In the Kaokoland (Fig. 1), seven potholes and sinkholes have been investigated in the dolostone of the Upper Otavi Group (Martini et al. 1999). This region is included in a 100–300 mm/year rainfall area and remains poor in caves, which are almost always reduced to single large chambers that later developed into large sinkholes by roof collapse. In half of them, it is only indirectly possible to assess the size of the original chambers. In other ones, phreatic morphology

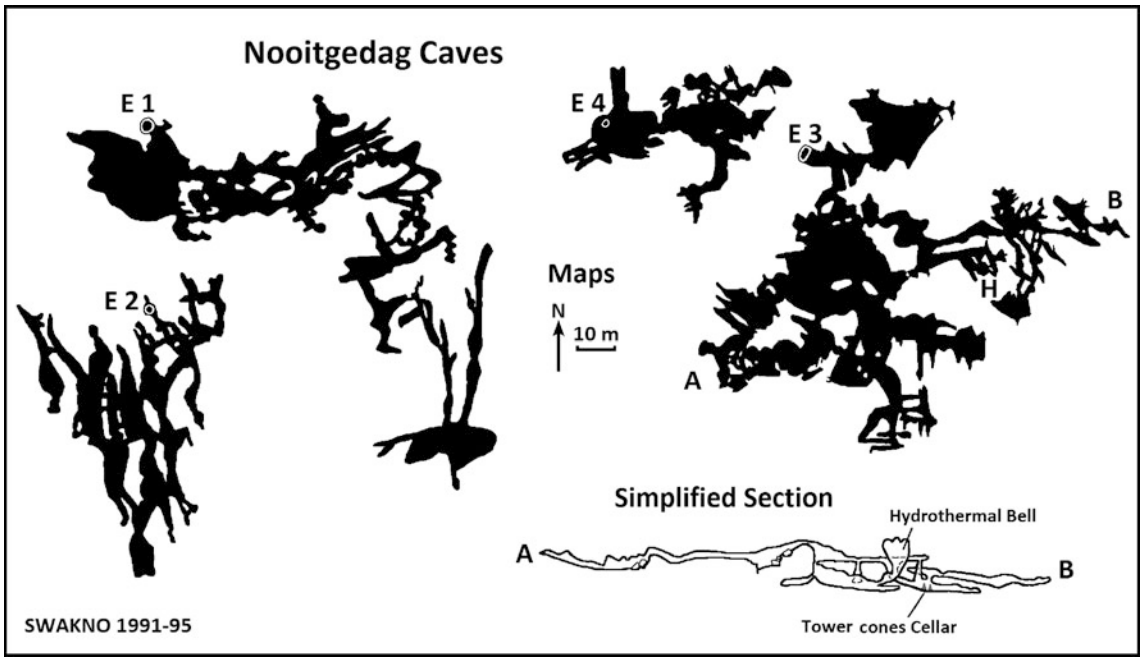

Fig. 6 Nooitgedag caves

relicts were observed on the walls, but no lateral passages were radiating from them. The water table has never been reached.

2.6 Caves in the Otavi Mountains

This region represents the most important and best-investigated karst of Namibia (Fig. 1). It is still controlled by a relatively dry climate, although with a higher rainfall, varying from 400 to 500 mm/year. The karst is developed in the carbonate rocks of the Otavi Group and accessorily in the calcareous Cenozoic sediments of the continental endorheic Kalahari and Etosha basins. Although no large-scale surface karst morphology developed, karren are quite common, especially on limestone. Caves can form voluminous caverns, large underground lakes in the mountain land, and deep cenotes in the pediplain. For instance, the Guinas cenote measures 140 × 70 m at the surface and has been dived down to 132 m (Penney et al. 1988). The surface of the underground lake in Dragon's Breath Cave covers 2 ha. Complex phreatic mazes of restricted lateral extension have also been explored. Great but sluggish variations in the water table elevation have been well monitored by the Namibian department of water affairs. For instance, the water table may rapidly rise up to more than 10 m during a rainy year and then slowly level off during 10 years. This suggests that these voluminous pockets of water are not interconnected by large channels. Therefore, in these cases, it is not impossible to argue that they result from localized upwelling.

Among the regional caves, Pofaddergat is worthy of detailed description since it is more informative as far as hypogene origin is concerned. It consists of a horizontal phreatic system (Fig. 8), in which 2.8 km of passages have been explored (Martini et al. 1990; Marais et al. 1996). In its southern part, the cave is developed in steeply dipping limestone of the Abenab Subgroup and in its northern one in horizontal calcareous sediments of the Kalahari basin. The latter forms here an indentation penetrating a valley in the mountain land. Several pools have been encountered in 1987, but during wet episodes, flooding must affect the entire system, as evidenced by watermarks on the walls a few meters above the observed water table. The largest pool has been dived in 1987 down to the depth of 40 m, where the bottom was not yet in sight. The water was slightly aerated, and the divers observed gas bubbles generated by agitation. Analyses revealed that it contains nearly 1 g of dry residue (Martini 1991) and is distinct from the other regional karst waters. In particular, Na^+ is high (28.5 mg/l) and not equilibrated by Cl^-, producing a very low mCl/mNa (0.12). SO_4^{2-} is also unusually high, 90.3 mg/l as compared to 1–9 mg/l in the other regional karst waters (Marchant 1980).

Fig. 7 Tower cones in Nooitgedag cave I. *Note* acute apical angle and secondary raft calcification

3 Botswana

To the East of the Otavi Mountains, the carbonate rocks of the Damara orogeny form a small cluster of hills protruding through the sand of the Kalahari basin. The climatic conditions are comparable with those prevailing in the Otavi Mountains (400–500 mm/year). These hills are situated on both sides of the Namibia–Botswana border, but the caves occur mainly in the latter country (Fig. 1). The Aha hills represent the most important outcrops, but the informative caves, however, are developed immediately south of the latter, in the modest Gcwihaba Hills, which harbor four fair-sized caves: the well-known Gcwihaba Cave, already reported in 1932 (Cooke and Baillieul 1974); Wa Doum discovered in 1991 (Ritter et al. 1994); Diviner and Dimopo Caves found in 2013 by boring on gravimetric anomalies (Ellis et al. 2014). These caves are typically phreatic and form irregular large chambers interconnected by short constrictions. For instance, the largest chamber in Diviner Cave reaches 180 × 75 m in horizontal dimensions. Both passages and chambers display variable widths and short recesses imparting them irregular outlines. These systems are roughly developed on a level close to the Kalahari plain, or slightly below it. The large connections to the surface are through roof collapses and narrow pits, or perhaps lacking completely in the case of the caves found by boreholes. Narrow passages seem to extend down to a hypothetic water table, which has not been reached because of prohibitively high CO_2.

Caves have also been discovered 20 km further to the SE, in the Koanaka Hills, which consist of 3 isolated small dolostone protrusions (Fig. 1). Bone Cave is situated in the second hill and Blue Cave in the third one (Ritter et al. 1994). Here too these caves develop at, or slightly below the level of the Kalahari plain, and their access is through sub-vertical passages, possibly of vadose origin. Bone Cave consists of one single large, amoeboid-shaped chamber. The most interesting one is Blue Cave in the third hill. Its morphology differs from the other regional caves, as it consists of a particularly dense assemblage of numerous parallel fissure-type passages, which are all getting thinner and petering out before reaching the basal outline of the hill. This maze is encompassed in an oval 150 × 75 m in size, but nevertheless the measured passage lengths totaled 1.8 km (Ritter et al. 1994). It must be stressed that this lateral limit is not due to lithological constraints. Both caves are positioned in their hill centers, under their summits, and the passages do not extend to the outline of the rocky outcrops (Fig. 9).

4 South Africa

In South Africa, the only important stratigraphic unit to be affected by karst activity and that might exhibit some hypogene evidences is the Malmani Subgroup, mainly developed in the NE of the country (Fig. 1). This unit is 200–1800 m thick and 2.5 Ga old. It consists of dolostone and minor limestone, with a dolomite component unusually rich in Fe and Mn (0.5–2.0%). This carbonate rock is stromatolitic and rich in silica-forming thin beds and nodules of chert, which may constitute up to 50% of the rock. In this part of the country, one may distinguish two karst areas.

4.1 SW Region

In this zone, the climate is relatively dry, less than 500 mm/year (Fig. 1), and no karst morphology and caves have been reported in dolostone. Only a few caves and karst springs are localized along a limestone belt in the W of the Ghaap plateau. The Bushmansgat represents the only

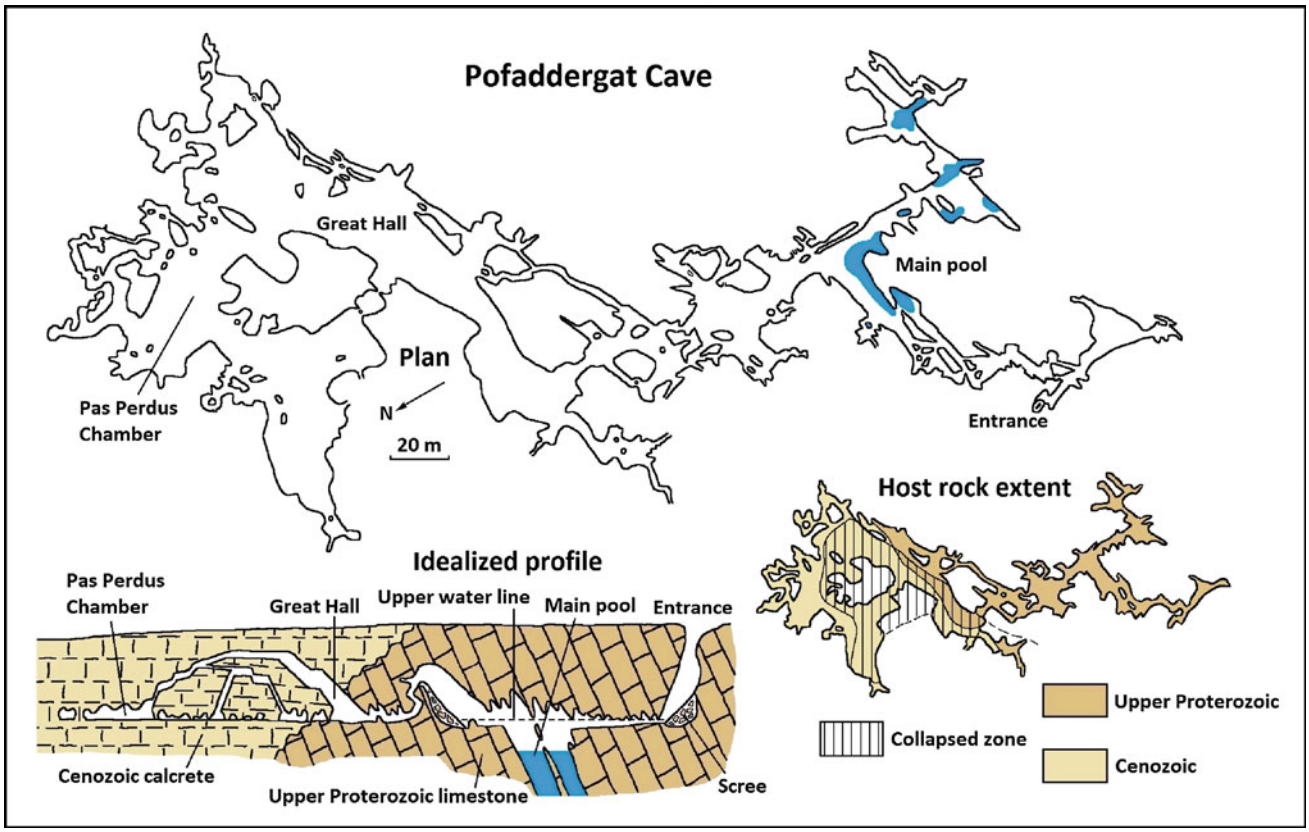

Fig. 8 Pofadder cave

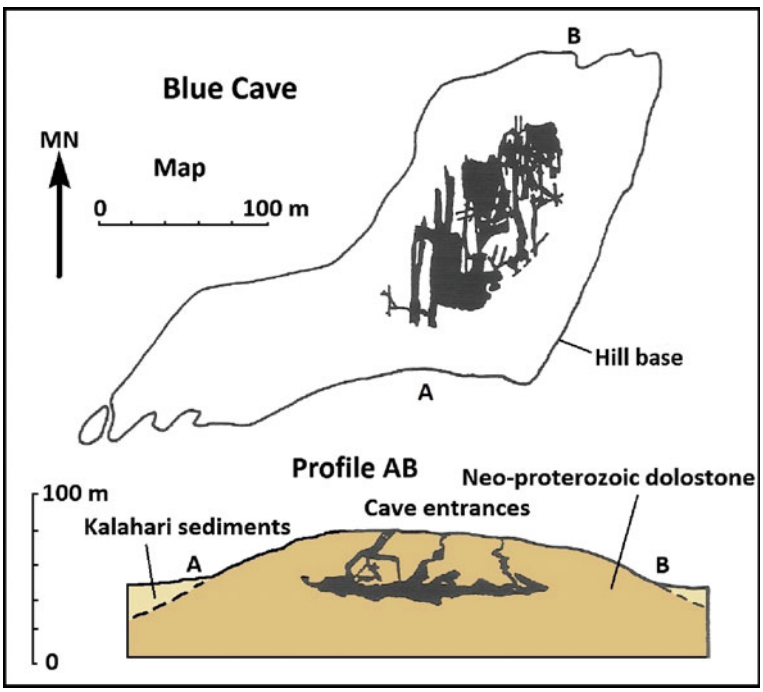

Fig. 9 Blue cave. Survey after Ritter et al

outstanding cavity worth to be mentioned, as potential for a hypogene origin. It consists of a cenote appearing as a small pond at the depth of 30 m in a funnel-shaped doline. Below the water surface, the cavity widens progressively into a huge, elongated chamber 76 × 240 m in size at −100 m. It has been dived down to the bottom at −262 m, but there the chamber dimensions have not been measured (Penney 1994).

From the opencast workings of Sishen Fe Mine, to the W of the Ghaap plateau (Fig. 1), another large cavity has been discovered in 1989, which could also be a candidate for hypogene cave. The geological context consists of a flat, thick hematite body resting on dolostone. The cavity was explored by drilling, shaft sinking, and echo sounding (ISCOR 1990). This revealed a chamber two-thirds under water measuring 260 m in length, 70 m in width, and 45 m in height. It mainly formed by progressive roof collapse in the ore, a process that started from an initial karstic cavity in the dolostone.

4.2 NE Region

This zone extends beyond the 500 mm/year limit. The karst is relatively well developed in the dolostone cropping out around the Transvaal and Potchefstroom basins (Fig. 1). On account to the rock impurity, surficial weathering often leaves a thick residual mantle of chert fragments and Fe–Mn oxides. The underground dissolution is well developed, with numerous phreatic caves displaying complex labyrinths (Martini and Kavalieris 1976). Even if their combined passage lengths often amount to several kilometers, they do not extend more than a few hundred meters from the centers of the mazes. This suggests that these cave systems are poorly interconnected, a characteristic that is also deductible from the regular discharge rate of the karst springs. Indeed, they react very slowly to important rainfall events, with a delay of the peak in flow rate, which may vary from 6 months to two years (Enslin 1968).

The far West Rand region, 50 km to the West of Johannesburg, is situated on the northern limb of the Potchefstroom basin (Figs. 1 and 10). It is of particular interest for studies, as it hosts the most important caves in the country and has been particularly well investigated because of the devastating effect resulting from artificial dewatering of aquifers in connection with deep gold mining (i.e., Brink and Partridge 1965). This dewatering was decided in the early 1960s after a dramatic flooding at more than 1000 m deep in a mine, when the workings approached the dolostone too closely. This resulted in dramatically accelerating the normal rate of sinkholes development by roof collapse through thick residual cover, and in drying up most of the springs controlled by syenite and dolerite dykes compartmenting the aquifer (Fig. 10).

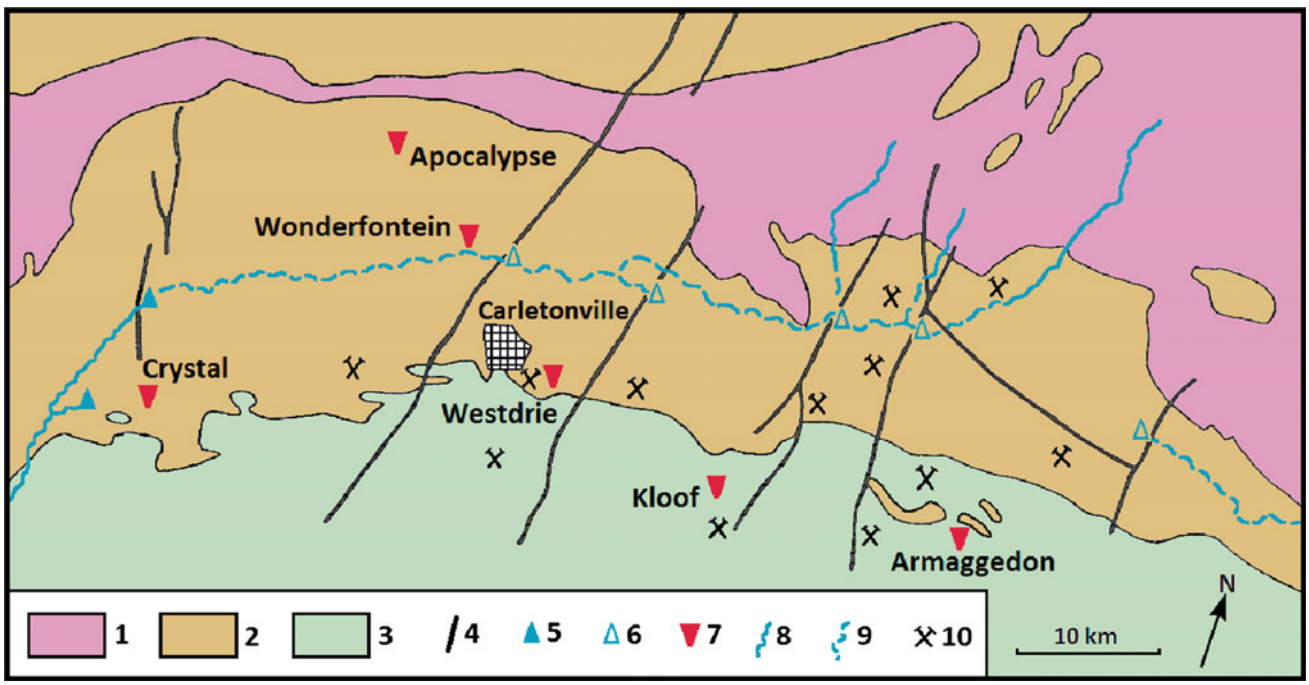

Fig. 10 Far West Rand karst: *1* pre-Malmani dolostone terrains; *2* Malmani dolostone; *3* post-dolostone terrains (Pretoria Group); *4* syenite or dolerite dyke; *5* active spring; *6* dried spring; *7* major cave or karst feature; *8* active stream; *9* dried stream; *10* gold mine below dolostone. Location of Fig. 10 can be seen in the insert in Fig. 1

Monitoring the water table lowering allowed to calculate the aquifer porosity in function of depth, which varies from as high as 14% at the water table to less than 2% 150 m below it. Further down, karst dissolution remains active at much greater depths, as crevasses filled with wad (soft complex assemblage of Mn and Fe oxides), that is the residuals left after incongruent dolomite dissolution, have been encountered 500 m below the former water table during shaft sinking (pers. info. from Westdriefontein mining engineers). This indicates that water was still oxygenated at that depth, suggesting a relatively rapid downward flow rate. The mine flooding mentioned above, which was difficult to control, also indicates good permeability at great depth. In the local caves, it was possible to measure the width of the initial joints controlling the cave passages, since the chert bands have not been affected by karst dissolution (Martini 2007). Widths of 1–2 mm were observed commonly, but reaching up to 30 mm. The widths measured in quartzite at the depth of 1500 m in the gold mines are in the order of 0.4–0.8 mm, but reaching a maximum of 25 mm (De Kock 1964).

Following this dewatering, from these man-induced sinkholes, it was easy to explore a number of caves previously below the water table. Nevertheless, it was not possible to penetrate deeper than 80 m below the level of the previous water table, it even seemed that the passages level off at about this depth (Martini 1990; Moen and Martini 1996). A recently discovered cave, partly of the same nature, deserves a more detailed description, as it could be informative for a possible hypogene genesis. In early 1999, a new sinkhole burst up to the surface and shortly after was inspected by mine geologists and by the author. They plumbed it down to 50 m with laser and observed that it was entirely open in the shales of the Pretoria Group (the stratigraphic unit resting unconformably on the dolostone). They did not negotiate the pit. In early 2013, the sinkhole was independently rediscovered by the cavers of the Potchefstroom Potholing Club, who explored a voluminous, deep, and particularly extensive cave they named Armageddon (Tucker 2015). The entrance pit provided access to an exceptionally long canyon-like passage opened by dissolution in very cherty dolostone (Fig. 11). Over a length of 2 km, the canyon follows a single sub-linear fracture, displaying widths varying from a few meters to 50 m and heights averaging 20–30 m, reaching 50 m in places. The Malmani–Pretoria Groups contact observed at the base of the entrance pit seems to follow the canyon ceiling and smoothly levels off at the depth of 200 m. This close proximity of the canyon ceiling to the base of the shale is suggested by the presence of goethite speleothems in the entrance chamber at −70 to 80 m and close to the end of the cave at −200 m (Tucker et al. 2015). On Google imagery, it also appears clearly that the layering of the shale cover is regularly thickening from the entrance to the surface projection of the canyon end.

In the Far West Rand, such deep karst development under thick overburden was already suspected for a long time (Enslin 1974), as 14 km to the W of Armageddon the major Kloof sinkhole (Fig. 10) punctured the first quartzite bed of the Pretoria Group, which forms a prominent widely developed regional cuesta. When first observed by the author, it presented a shallow flat bottom, but deepened itself

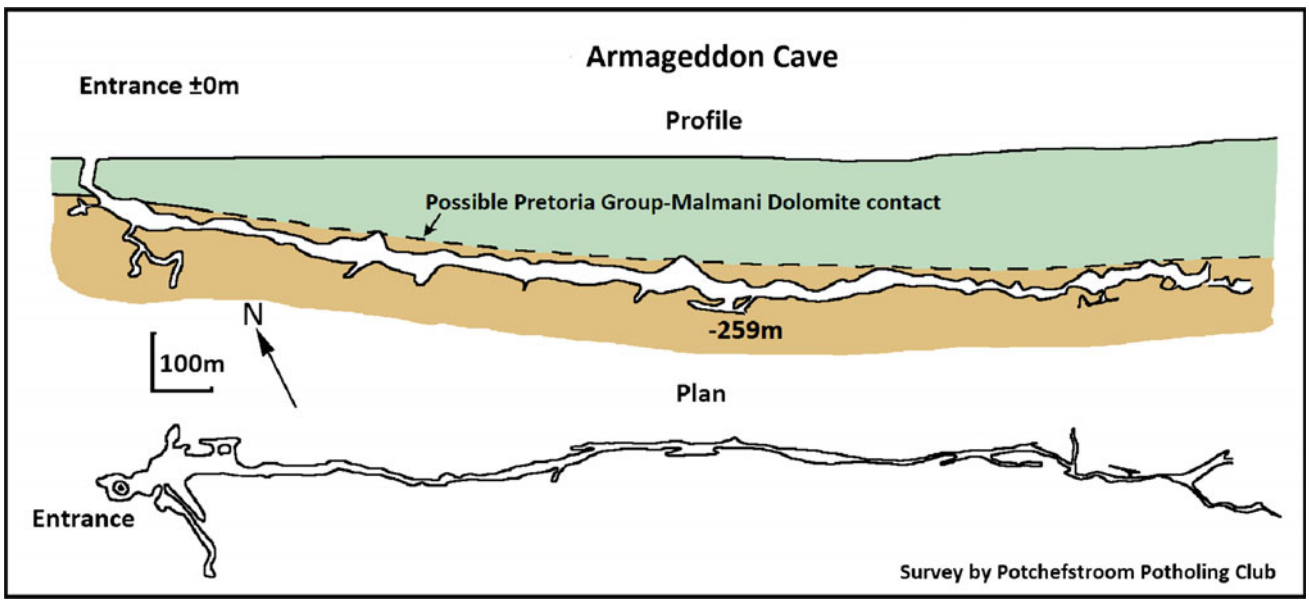

Fig. 11 Armageddon cave

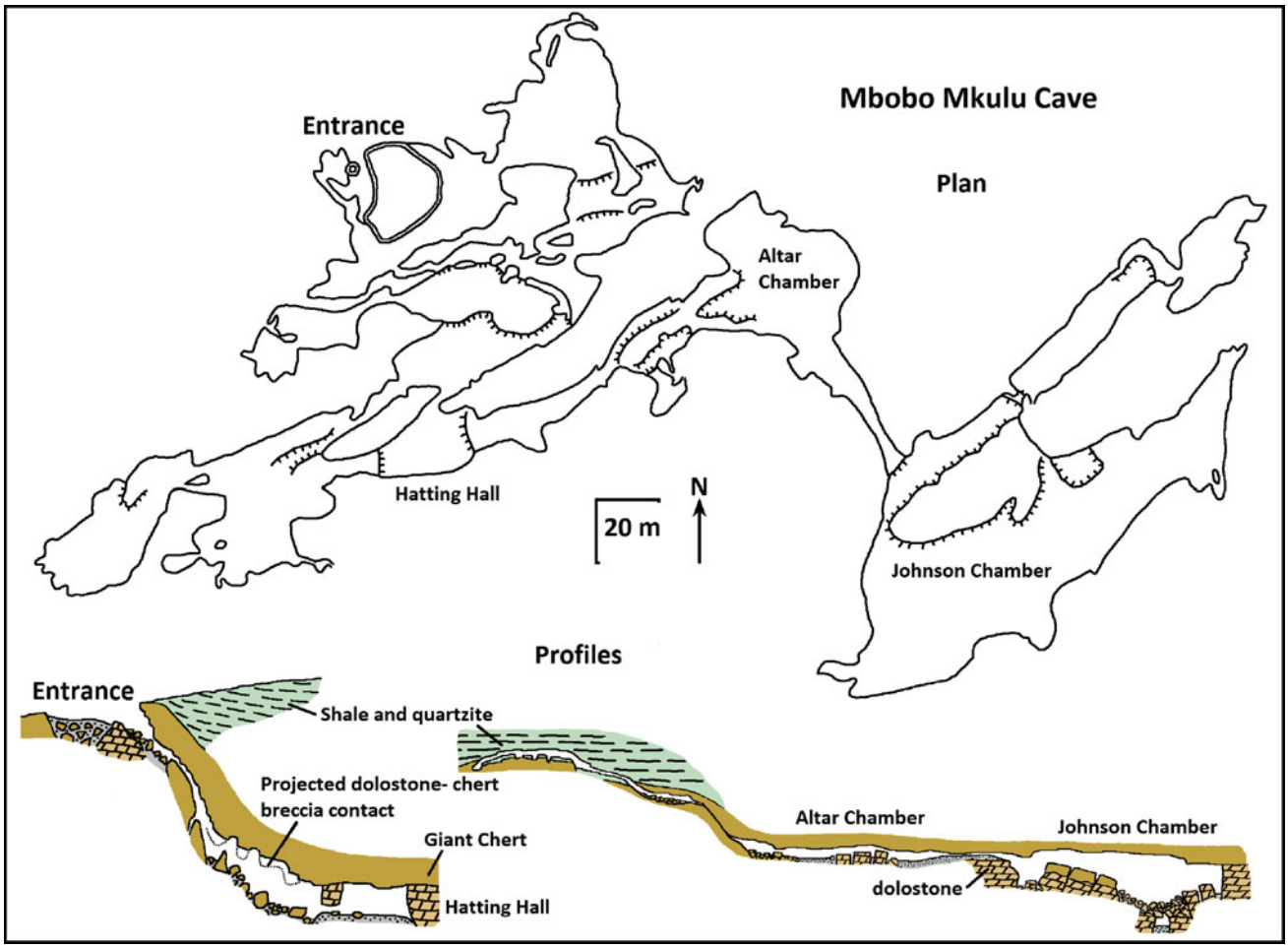

Fig. 12 Mbobo Mkulu cave

after subsidence was renewed several years later. This sinkhole suggests the roof collapse of a large chamber at an even greater depth than for the deepest reaches of Armageddon. Indeed, in the latter cave, the canyon does not extend to under this quartzite cuesta. It seems, however, that this deep karstification is not widely distributed and is rather localized, since shaft sinking through the dolostone under shale cover did not encounter the serious technical problems like in the workings sited directly on dolostone (pers. info. from mining engineers). Thus, it seems likely that under shale cover, only the major, well-opened joints were enlarged by karst dissolution. The best example is Armageddon cave, where most of the dissolution was concentrated in a single over a 2-km-long joint.

This type of cave development immediately below a Pretoria Group overburden is more common in the eastern limits of the Transvaal basin (Fig. 1). In this part of the country, the Malmani dolostone crops out in a deeply incised and rugged escarpment. The caves of this type display a phreatic morphology, and the Giant Chert Member forms the ceiling. This member is a chert breccia of pre-Pretoria paleokarstic origin. The caves tend to develop voluminous chambers, and like in the case of Armageddon, the phreatic passages are not grouped in dense, complex phreatic mazes. The most important of these "chert roof caves" is Mbobo Mkulu (Figs. 12 and 13). It is outstanding by the abundance of goethite and allophane speleothems, which are deposited from dripping water oozing through the ceiling after having dissolved minerals in the Pretoria shale, which contains disseminated sulfides, mainly pyrite and pyrrhotite (Martini et al. 1997). This very low-grade mineralization extends widely in the same stratigraphic horizon. Sulfide oxidation produces very acidic solutions dissolving phyllosilicates in the shale, explaining the presence of Fe–Al–Si speleothems. Measurements of pH in the solutions actively depositing goethite varied from 1.5 to 6.5. These speleothems have also been observed in the other chert roof caves of the escarpment (Fig. 14). The actual thickness of the shale above Mbobo Mkulu does not exceed 50 m, but by visualizing the environment when speleogenesis could have been active

Fig. 13 Chert ceiling in Mbobo Mkulu Cave. *Note* undulating surface marking stratigraphic unconformity

Fig. 14 Goethite–hematite flowstone supporting chert ceiling, in Christmas cave

below the water table, it is necessary to greatly increase the thickness of this overburden. Indeed, the cave is actually perched on top of a ridge 380 m above a major stream. This means that when this river was flowing at the same elevation as the cave, the overburden should have been proportionally thicker.

5 Discussion About Speleogenesis

In Southern Africa, the most obvious hypogene imprinting has been observed in the arid NW Namibia, especially in the Temple of Doom Cave, where it is evidenced by deposition of barite and a structural setting favorable for hydrothermal

activity: Its localization at the point where a dolostone anticline dips under an impervious cover suggests the cell model of Fig. 3. Following rainfall onto dolostone, water sinks and after warming raises under cover and is collected against the impervious cover, where it is channeled by the inversed gutter formed by the axial top of the anticline. A comparable circulation cell has been proposed for the hydrothermal springs in Budapest (see Mádl-Szönyi et al., Chap. 17). Caves formed by mixing with surficial water and by cooling. During the waning stage of speleogenesis, barite and calcite precipitated, alternating with recurrences of dissolution.

In the arid zone receiving less than 300 mm/year, other caves presenting evidences of hydrothermal activity have been observed, but in a less informative geological context than in the case of the Temple of Doom. In the extremely arid Namib Desert, the source of groundwater was probably infiltration from the casual streams, which originate from the more rainy regions in the East. It seems that the very minor karst activity observed is exclusively hydrothermal, but the structural context is poorly informative. In the Kaokoland, under a slightly higher rainfall, caves are sparsely distributed, not extensive and mostly reduced to single large chambers. No hydrothermal evidences have been observed up to now. Only the voluminous size of the cavities and their probable enclosed nature might suggest speleogenesis by localized upwelling flow from the depth.

Further to the W, in the Otavi Mountains, the rainfall rises to 400–500 mm/year, and the karst is better developed. Numerous caves have been explored, which are all confined phreatic mazes and large chambers, but no hydrothermal morphological evidences have been observed. Only an unusual chemical composition has been identified in the water of Pofaddergat Cave, suggesting a hypogene origin. It was proposed that the sodium and sulfate could have originated from leaching of arkose in the subjacent Nosib Group and in pyritiferous black shale in the basal part of the Otavi Group (Martini 1991). The leaching could have taken place only at moderate depths, since the water temperature (25 °C) is normal for the region. Furthermore, as no typical morphology and mineral have been observed, it was proposed that Pofaddergat was a "cold hydrothermal cave".

In the hills protruding from the Kalahari sand in western Botswana, the caves belong also to the phreatic type, with restricted lateral extensions and therefore are possibly hypogene. Bone and Blue Caves are informative about their origin. In both cases, the cave extensions are co-centered with the hills outlines, suggesting that the actual hill morphology controls their genesis. If this association of hill relief with cave is not fortuitous, it would be possible to argue that the caves could have developed at a contact of fresher water with the more saline solutions of the Kalahari aquifer, which surrounds and penetrates the hill at depth. This fresher water could have formed a thin lens, directly fed by summer rain, restricted to the hill perimeter and resting on the more concentrated solution of the Kalahari aquifer. By extension, all the caves in these hills could then belong to the halocline type, rather than to the hypogene one. Alternatively, it is possible to argue that the hills trigger artesian upwelling from the Kalahari aquifer.

In South Africa, the great majority of the important cave systems, whether active or fossil, are phreatic and display restricted extensions. No conventional evidences for hydrothermal origin have been observed. Their limited extension and the sluggish reaction of the aquifer to rainy episodes have been attributed to impurities in the dolostone (Martini and Kavalieris 1976). But in several of these maze systems, it is obvious that the passages reduce their size at the periphery. Consequently, a speleogenesis by upwelling fluids remains one of the possible hypotheses.

It has been established elsewhere that the setting of a carbonate bed exposed to epikarstic dissolution and also dipping under impervious strata represents a favorable condition for the formation of hydrothermal cells. Therefore, it seems logic that in South Africa, cells could have developed in similar structural situations. In the case of the "chert roof caves", such a process appears likely. A circulation comparable to that proposed for Temple of Doom Cave could be applied: Rain water infiltrates the dolostone from the epikarst, cools the rock by downward circulation, then warms up and rises under shale cover, where it follows the impervious roof in order to close the cycle. This model is in agreement with the common knowledge that the thermal gradient in karstic rock is low due to cooling by downward water circulation and with the observation of unusually high temperatures in caves developed under thick shale cover (i.e., Bitterli et al. 1991). The good joint permeability observed in the Far West Rand should have facilitated this process. The considerably slower rate of dolomite dissolution, compared to calcite (Busenberg and Plummer 1982), would also contribute to deep karstification. Moreover, Fe^{2+} and Mn^{2+}, present in the dolomite lattice might facilitate this process.

Moreover, cavity development against the roof would initially have been facilitated by water infiltrating the shale, becoming very acidic after oxidizing sulfides on the way and then attacking the dolostone when reaching it (i.e., Tisato et al. 2012). This process, however, would presumably not be responsible for the excavation of large chambers, as the volume of sulfides is proportionally too small and the permeability of the shale too limited. It would only have opened small channels concentrating the flow against the ceiling and thus have increased the circulation rate. The efficiency of the heat source would have been proportional to the geothermal gradient, which is about 1°/100 m in the Far West Rand, what means that the temperature warming could not have

exceeded 15 °C if the circulation cell remained confined in a 1500 m dolostone thickness. Here too this hypogene genesis could be classified as "cold hydrothermal".

By considering Southern Africa as a whole, it appears that genuine hypogene caves are not widespread due to their situation in a relatively stable cratonic region and that they are preferentially localized in the arid areas of Namibia. This distribution pattern is also reflected in the temperature of the hot springs in Southern Africa (Kent 1949). The warmer spring are localized in Namibia, with a maximum of 80 °C, whereas in South Africa, they are not much higher than the normal temperatures of groundwater. This does not mean, however, that hydrothermal activity is absent in more humid regions, like NE South Africa is, but may be present and overwritten by surficial groundwater circulation. In these wetter regions, however, convections cell due to heat from the Earth may be produced, but at lower temperatures, generally not leaving a hydrothermal print.

References

Bitterli T, Funken L, Jeannin P-Y (1991) Der Bärenschacht-der alte Traum von −950 m Tiefe. Stalactite 2(91):71–92

Brink A, Partridge T (1965) Transvaal Karst: some consideration of development and morphology, with special reference to sinkholes and subsidences on the Far West Rand. South African Geogr J 47:11–34

Busenberg E, Plummer LN (1982) The kinetics of dissolution of dolomite in CO_2-H_2O systems at 1.5–65 °C and 0–1 atm pCO_2. Am J Sc 282:45–78

Cooke H, Baillieul T (1974) The caves of Ngamiland and interim report on explorations and fieldwork 1972–74. Botswana Notes Rec 6:147–153

De Kock W (1964) The geology and economic significance of the West Wits Line, 323–386. In: Haughton S (ed) The geology of some ore deposits in Southern Africa. Geology Society, South Africa, p 626

Gázquez F, Calaforra JM (2013) Origin of double tower raft cones in hypogenic caves. Earth Surf Proc Land 38(4):1655–1661

Guj P (1969) The springs of Sesfontein and Warmquelle, Kaokofeld, South West Africa. Geology Survey of South Africa p 16

Ellis R (2014) Gcwihaba training and cave expedition (unpublished report)

Enslin J (1968) Dolomitic water supplies in the Transvaal, Republic of South Africa. International Association of Hydrogeologists Memorie Congress. Istanbul 1967, pp 426–433

Enslin J (1974) personal information about Kloof sinkhole

Heine K, Geyh MA (1984) Radiocarbon dating of speleothems from Rössing cave, Namib Desert, and palaeoclimatic implications (pp 465–470). In: Vogel J-C (ed) Late Cenozoic Palaeoclimates of the southern hemisphere. A A Balkerma, Rotterdam, 520 pp

Hill C, Forti P (1997) Cave Minerals of the World, 2nd ed Nat Speleol Soc Huntsville (Ala.), pp 1–464

Irish J, Marais JEJ, Martini J (1992) Cave investigations in Namibia III, some 1991 SWAKNO results. Bull S Afr Speleo Assoc 32:48–71

Irish J, Martini J, Marais E (2000) Cave investigation in Namibia VI; The desert caves in and around the Namib-Naukluft Park. Cimbebasia 16:177–193

ISCOR (1990) South African Iron and Steel Industrial Corporation (unpublished report)

Kent LE (1949) The thermal water of the Union of South Africa and South West Africa. Trans Geol Soc South Africa 52:231–264

Marais E, Irish J, Martini J (1996) Cave Investigations in Namibia V; 1993 SWAKNO results. Bull S Afr Speleol Assoc 36:58–78

Marchant JW (1980) Hydrogeochemical exploration at Tsumeb. PhD thesis, University of Cape Town

Martini J (1990) Grottes naturelles mises au jour par l'influence de l'homme sur l'environment: exemple des "sinkholes" du Far West Rand, Transvaal, Afrique du Sud. Spelunca 39:33–36

Martini J (1991) Some data on the chemistry of karst water from the Otavi Mountainland, Namibia and interpretation. Bull S Afr Spelaeol Assoc 32:74–78

Martini J (2007) Le problème de l'ouverture des vides initiaux pré-karstiques: cas de la dolomie siliceuse du Sous-Groupe de Malmani, Afrique du Sud. Karstologia 50:31–38

Martini J, Irish J, Marais E (1990) Les grottes du Sud-Ouest African Namibie. Spelunca 38:24–29

Martini J, Kavalieris I (1976) The karst of the Transvaal (South Africa). Int J Speleol 8:229–251

Martini J, Marais E, Irish J (1999) Contribution à l'étude du karst et des grottes du Kaokoland (Namibie). Karstologia 34:1–8

Martini J, Marais J (1996) Grottes hydrothermales dans the Nord-Ouest de la Namibie. Karstologia 28:13–18

Martini J, Wipplinger P, Moen H (1997) Mbobo Mkulu Cave, South Africa. In: Hill C, Forti P (eds) Cave minerals of the world, 2nd edn. National Speleological Society, Huntsville, pp 336–339

Moen H, Martini J (1996) The exploration of Swartgat Sinkhole. Bull S Afr Spelaeol Assoc 36:45–49

Penney A (1994) The surveying of Bushmansgat, Northern Cape. Bull S Afr Spelaeol Assoc 33:16–20

Penney A, Maxwell C, Roux D (1988) Guinas Lake. Bull S Afr Spelaeol Assoc 29:6–10

Rabie LP (1949) The Geology of the Sesfontein-Puros area. Private Report Kaokofeld Expl Co, unpublished

Ritter RC, Mann PM, Doepel J et al (1994) Gcwihaba Cave Project: final report, p 72

Tisato N, Sauro F, Bernasconi S et al (2012) Hypogenic contribution to speleogenesis in a predominant epigenetic karst system: a case study from the Venetian Alps, Italy. Geomorphology 151:156–163

Tucker S (2015) Armageddon Cave. S Afr Spelaeol Assoc Bull 41:28–47

A Review of the Geomorphological Context and Stratigraphy of the Sterkfontein Caves, South Africa

60

Dominic Stratford

Abstract

The Sterkfontein Caves, located in the southwest of the Cradle of Humankind, Gauteng, is the world's richest *Australopithecus*-bearing locality and has yielded iconic fossils like Mrs Ples (StS 5) and Little Foot (StW 573), as well as *Paranthropus robustus*, *Homo ergaster* and *Homo habilis* fossils and large Earlier Stone Age lithic assemblages. The cave deposits have also yielded enormous assemblages of associated fossil fauna and document over three and a half million years of landscape, environmental, faunal and hominid evolution. These fossiliferous cave deposits represent a more recent episode of a geological history spanning 2.6 Ga years, beginning with the deposition of the dolomites, to the commercial exploitation of the caves by lime miners in the early twentieth century. The location and morphology of the karst caves is a result of a combination of factors including lithological variation within the two host dolomite formations, an early karstification and infilling of the dolomites over two billion years ago and local dolomite fracturing. Vadose zone collapse in densely fractured areas has enlarged chambers and passages, and played a major role in the location and nature of the openings to the landscape. When open to the landscape, a broad range of geomorphological processes, including re-dissolution of interred deposits, creates dynamic sedimentary environments with complex stratigraphic histories. This article reviews the geomorphological history of the Sterkfontein Caves in an effort to consolidate this information as we press forward with new stratigraphic and geomorphological work at the site.

Keywords

Sterkfontein • Dolomites • Karst geomorphology • Paleocave deposits • *Australopithecus*

1 Introduction

The Cradle of Humankind World Heritage Site covers an area of approximately 800 km^2 in the northwest of Gauteng Province, South Africa (Fig. 1). The boundaries of the Cradle of Humankind (hereafter Cradle) partially enclose the exposed and karstified dolomite, which hosts the prolific hominid-bearing caves. The densest group of excavated fossil-bearing sites, including Sterkfontein, is located in the south-western area of the Cradle near the Blaauwbank river valley (Fig. 1). The Blaauwbank River, which is now an ephemeral stream, wanders through gravel and floodplain deposits, relics of its more energetic past.

The site of the Sterkfontein Caves occupies the top of a low hill about 300 m south of, and rising 50 m above (1491 m asl), the Blaauwbank River. Paleoanthropological attention was brought to Sterkfontein, while speleothem mining was displacing large quantities of fossil-bearing

D. Stratford (✉)
Department of Archaeology, School of Geography, Archaeology and Environmental Studies, University of the Witwatersrand, Johannesburg, South Africa
e-mail: Dominic.Stratford@wits.ac.za

© Springer International Publishing AG 2017

A. Klimchouk et al. (eds.), *Hypogene Karst Regions and Caves of the World*,
Cave and Karst Systems of the World, DOI 10.1007/978-3-319-53348-3_60

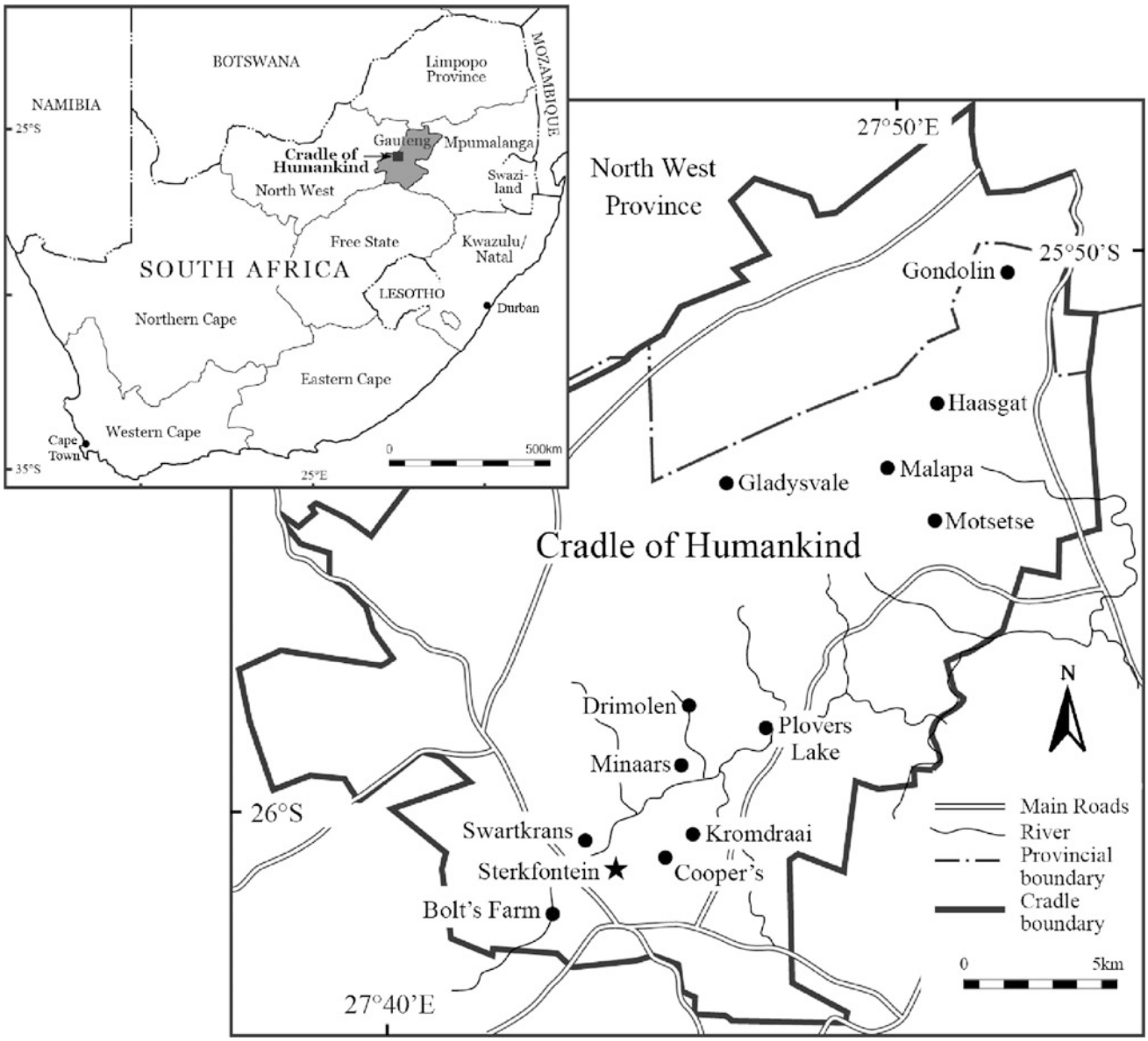

Fig. 1 Sterkfontein and other key fossil sites within the Cradle of Humankind, Gauteng, South Africa

sediments associated with large stalagmites, stalactites and flowstones that were exposed on the landscape surface after the erosion of the cave roof. The by-product of the mining was the creation of large fossil-bearing dumps. It was in one of these dumps (Dump 18) that the first hominid fossil was found in 1936 (Broom 1936). The Sterkfontein site remains one of the most prolific and long-studied fossil hominid localities in the world, yielding over 800 hominid specimens. Key finds include the first adult cranium of an *Australopithecus* found in 1936 (TM1511), the first complete adult *Australopithecus* cranium (StS 5) (Broom 1947), affectionately known as Mrs Ples, three partial *Australopithecus* skeletons (Sts 14; StW 431; StW 573) (Broom et al. 1950; Tobias 1987; Clarke 1998), and the most complete skeleton of an *Australopithecus* yet discovered (StW 573) (Clarke 1998, 2013). This article reviews the geomorphological history of the Sterkfontein Caves in an effort to consolidate this information as we press forward with new stratigraphic and geomorphological work at the site (e.g. Bruxelles et al. 2014; Stratford et al. 2014, 2016).

2 Geological Setting

The dolomites that host the caves of the Cradle of Humankind, and Sterkfontein, have an extensive geological history that has influenced the formation and geomorphology of the caves as well as the deposits accumulated within them.

The karst caves of the Cradle of Humankind formed within the dolomites of the Malmani Subgroup which were deposited under epeiric conditions (Eriksson et al. 1995) between 2550 and 2423 Ma, and reach a thickness of 1450 m close to Sterkfontein (Truswell and Eriksson 1975). A range of tidal, deep water and chemical depositional environments accumulated the dolomite and chert beds within a general carbonate ramp model (Truswell and Eriksson 1975; Sumner and Grotzinger 2004). The Sterkfontein Caves have formed within and across the boundary of the two lower formations of the Malmani Subgroup (Eriksson et al. 1995; Martini et al. 2003) (Fig. 2). The basal member, the Oaktree Formation, is poor in chert bed density and is overlain by the Monte Christo Formation, comparatively rich in chert beds (Martini et al. 2003). The difference in chert bed density between these two formations has played an important role in the formation and geomorphology of the current cave system. At Sterkfontein, the dolomite dips between 25° and 30° northwest, a result of the uplift of the Johannesburg Dome to the southeast (Eriksson 1988), and intracratonic basin sag caused by thermal subsidence within the Transvaal Basin to the north (Eriksson et al. 2001).

The depositional history of the Transvaal Basin since the deposition of the Malmani dolomites is complex and ends with the 2050 Ma deposition of the Bushveld Igneous Complex (Eriksson et al. 1995). In this 400 Ma post-Malmani period, processes include basinal tectonic extensional subsidence and thermal subsidence with cycles of epeiric drowning. It is these kinds of basin development and rifting processes that may have provided ideal circumstances for rising hydrothermal solutions to penetrate the dolomites and develop hypogene caves. The dominant basinal processes are punctuated by pre-rift uplift and base-level falls which resulted in subaerial exposure, erosion and accumulation of associated deposits into the early karst (Ryan 1986; Eriksson et al. 1993). It is likely that over the long period between the formation of the dolomites and their burial beneath the Bushveld Complex, several phases of karstification took place through either epigenic or hypogenic processes. The subaerial exposure, karstification and

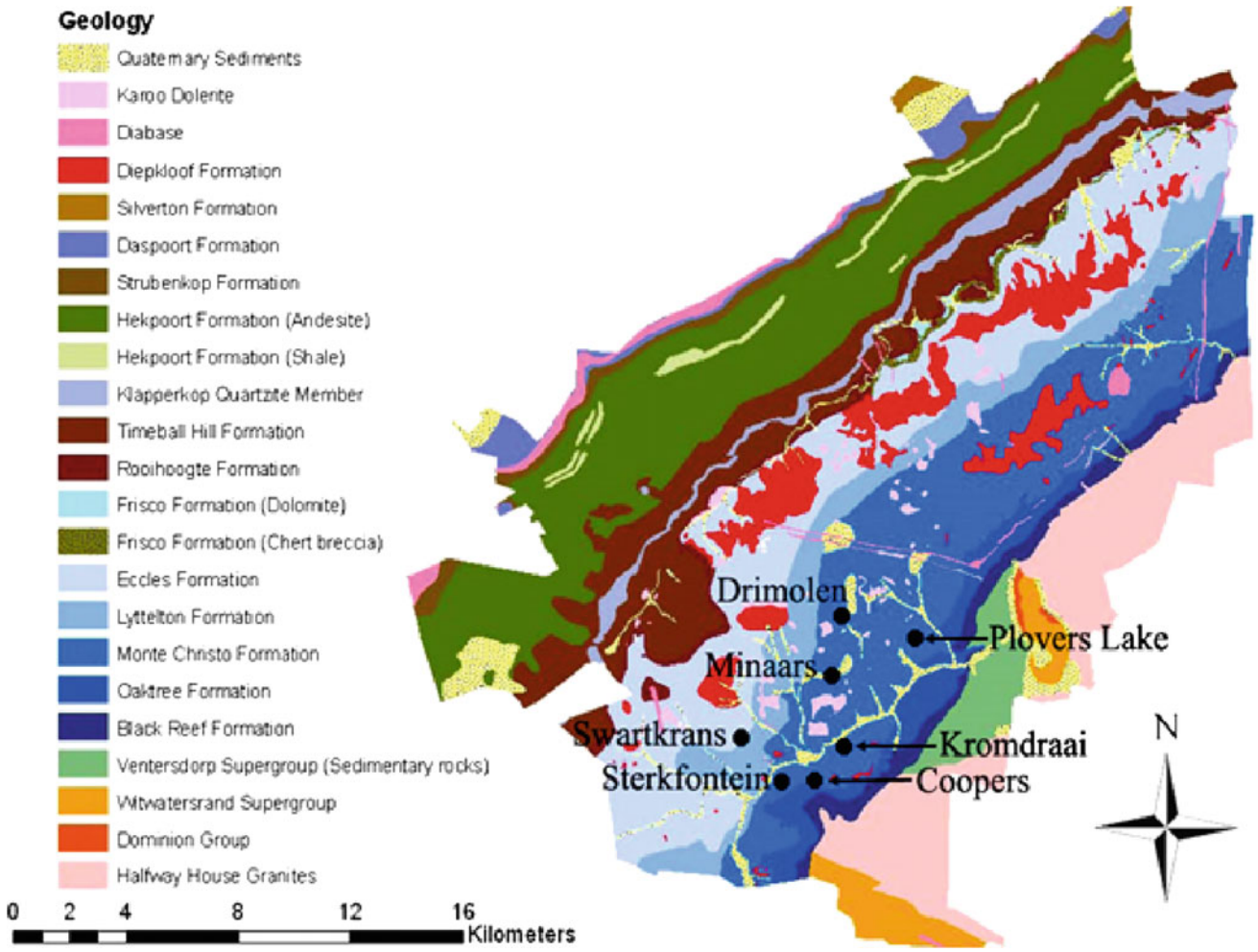

Fig. 2 Geological map of the Cradle of Humankind (adjusted from Obbes 2000)

denudation of the dolomites between 2423 and 2200 Ma (Button 1973) removed the upper beds of the Malmani Subgroup leaving just the Oaktree and Monte Christo formations around the south-western Cradle and Sterkfontein.

In the Sterkfontein area, some of the early karst forms and open faults and fractures in the Monte Christo Formation were filled by the chert breccias of the Rooihoogte Formation (Eriksson 1988; Dirks and Berger 2013). This formation represents the proximal and medial portions of extensive alluvial fans formed from the weathering of the uplifted dolomite landscape (Catuneanu and Eriksson 2002). It must be noted, however, that there may be other genetic processes contributing to the development of the Rooighoogte Formation. The silicious cement that binds the chert breccia may have formed through hydrothermal activity. Remnants of this chert breccia paleokarst fill are found in close association with the cave sites of Coopers Cave, Gladysvale, Kromdraai, Malapa, Sterkfontein and Swartkrans. Where this association is found, it is clear that the unconformities formed by the chert breccia-filled paleokarst and dolomite provided the focus for the next generation of karstification, as the dolomites were again exposed and weathered.

The age of the formation of the Sterkfontein Caves is difficult to estimate. Erosion of the African land surface during the Cretaceous contributed significantly to the removal of Karoo Supergroup sediments that had buried the Malmani dolomites (Partridge 1973; Martini 2006). The following uplift and south-westward tilting associated with the onset of the Post-African I erosion cycle, starting in the Miocene (Partridge 2010), facilitated further river incision, and perhaps started to expose the dolomites on the landscape, thereby renewing karstification (Partridge 1973; Beukes et al. 1999). Martini et al. (2003) suggest a date of between 5 and 18 Ma for the start of the formation of the Sterkfontein Caves, based on the Miocene uplift, erosion and exposure, and the oldest deposits yet found in the caves. Alternatively, it has been proposed that the caves formed below covering Karoo sediments only to be opened when those deposits were eroded and the dolomites exposed at about 2 Ma (Dirks and Berger 2013). This has recently been revised by Dirks et al. (2016) who propose that the dolomites were exposed in the Miocene but caves were not forming until a rapid karstification and opening in the Pleistocene—as judged by the absence of Miocene or Early Pliocene deposits (Dirks et al. 2016). This is an odd assumption to make given that the extensive and multilevel caves have to form underground before they can open to the surface and accumulate sediments, two processes that may take significant amounts of time. Martini et al. (2003) proposed a more parsimonious model with the caves starting to form underground, as the dolomites were exposed in the Miocene, and then only starting to open in the Late Pliocene. The rolling hills of the Blaauwbank river valley are characteristic of landscapes produced by the rivers of the Post-African I erosion cycle draining to the southwest (Martini et al. 2003) and suggest an earlier exposure than the Plio-Pleistocene.

3 Karstification and Cave Geomorphology

3.1 Karstification

There have been several works that have focused on the specific karstification process that formed the Sterkfontein Caves (e.g. Partridge 1978; Wilkinson 1983; Martini et al. 2003). The hyperphreatic model of cave formation has received greater support over the history of geological research at the site (Partridge 1978; Pickering and Kramers 2010). The classic hyperphreatic model proposes that lowering piezometric surface will form successively deeper parts of the cave network as water moves through deeper parts of the system (Palmer 2007), creating progressively deeper and younger karst galleries. This model is supportive of the lowering water table levels relating to uplift and erosion cycles as proposed by Partridge (1973). Accordingly, Partridge (1978) and Partridge and Watt (1991) placed the base of their allogenic deposit sequence, named ‘Member 2’ of the ‘Sterkfontein Formation’, within the mid-level Silberberg Grotto. Following the hyperphreatic model, the 4.5 km of passages beneath the Silberberg Grotto formed more recently and necessarily contain younger or reworked sediments. The relatively rapid downcutting of the rivers, and associated surface erosion rates, found in the northern part of the Cradle (Dirks et al. 2010—erosion rates have been recently reassessed in Dirks et al. 2016) may provide the hydrological scenario for such a formation process, but the same geomorphological situation is not found in the southern area of the Cradle where landscape erosion rates and river incision are significantly slower (Granger et al. 2015).

Contrastingly, Wilkinson (1973, 1983, 1985) proposed a ‘deep phreatic’ karstification process, suggesting the entire vertical extent of the cave system was developed by the time the caves opened to the surface through a period of vadose zone collapse. This is based on detailed geomorphological mapping of the cave network and tracking autogenic and allogenic colluvial deposits to the base of the system.

A further alternative could be hypogenic karstification—i.e. cave formation through rising water flow (Martini et al. 2003; Klimchouk 2007). This may have contributed to the earliest karstification of the dolomites (2423–2200 Ma), when hot water may have risen close to the landscape surface during periods of thermal subsidence of the Transvaal Basin (Eriksson et al. 2001). Large quartz nodes have been found near chert breccia deposits (Rooihoogte Formation) associated with the early phases karstification found across

the Cradle and may be related to rising thermal water (Pers. Obs). In more recently formed carbonate basins in Namibia, large quartz formations can be found at the base of some complex, deep cave systems suggesting a definite relationship between recent karst formation and rising thermal water. The role of hypogenic process in the development of the most recent (Miocene) karst in the Cradle is difficult to assess for two main reasons, first—extensive infilling of sediments and associated localized erosion has obscured many informative karstification features, and second—extensive mining of speleothem has damaged the walls and ceilings of the cave and removed informative mineral deposits that documented the early formational stages. We have to be conscious of the potential for the contribution of multiple karstification processes represented on the Cradle landscape and in single cave networks over the very long geological history of these dolomites.

Recent geological studies have identified another possible karstification process involving the in situ chemical alteration of the dolomite into 'ghost rock' (Bruxelles et al. 2009; Dubois et al. 2014). This process creates pseudophreatic karst morphologies but differs in the process of dissolution and final removal of the dolomite. Residual dolomitic alterite is removed as base levels (piezometric surface) drop, leaving vertically fully developed karst networks as the caves open to the surface through vadose zone collapse. Low penetration of meteoric recharge, near-static groundwater (Martini et al. 2003) and observed in situ remnant dolomitic alterite in fine powder or boxwork structures preserved at all levels of the caves support this formation model, and work is ongoing to test this theory.

Identification of the specific development model and the stages and timings of base-level lowering in the Sterkfontein Caves has important implications for the maximum age of the interred fossil and artefact-bearing deposits, a subject that remains a source of significant and continued debate (e.g. Berger et al. 2002; Clarke 2002; Walker et al. 2006; Pickering and Kramers 2010; Herries and Shaw 2011; Granger et al. 2015; Dirks et al. 2016). The hyperphreatic model suggests that fossiliferous deposits found in the deepest areas must be younger than, or reworked from, older upper chambers following several significant base-level lowering stages, even while the caves where open to the surface. In contrast, both the ghost rock model and Wilkinson's (1985) model propose that some of the deepest deposits may be the oldest and could date to well in excess of three million years. This requires the base level to have lowered to near its current elevation prior to the caves opening to the surface. The maximum proposed date by Wilkinson for the lower deposits has been supported by some work (Partridge et al. 2003; Granger et al. 2015), but challenged by others (Berger et al. 2002; Pickering and Kramers 2010; Herries et al. 2013). Recent renewed geomorphological and stratigraphic work at Sterkfontein supports Wilkinson's (1983, 1985) observations of early allogenic sediments being deposited at the base of the system, with remnants of preserved taluses found in some deep chambers (Stratford et al. 2014), but has not yet succeeded in providing new absolute dates for these early sediments.

There are several clues in the hydrology of the system that support the latter scenario of karstification. First, there is an absence of hierarchical convergent 'branchwork' passages (Palmer 2007), suggesting that slow groundwater flow is likely to have prevailed throughout the formation of the current generation of caves. Second, there is a dominance of fissure flow through secondary porosity features as the main regime for recharge. Diffuse flow is minimal and restricted to the deepest chambers, and flow through conduits is generally restricted to vertical passages and fractures. The dominance of tall and narrow passages suggests fracture control on groundwater flow and speleogenesis. The dominance of the fissure flow also accounts for the slight variation seen in the water table level in different areas of the caves (Gillieson 1996). Conduit enlargement through mechanical removal is minimal but was likely to have contributed slightly more significantly during the removal of the alterite and early opening of the caves, as evidenced by fine gravels, rounded sands and shallow channel erosion features found in deep deposits.

3.2 Cave Geomorphology

The vertical amplitude of the karst network at Sterkfontein is difficult to estimate as passages descend below the piezometric surface. Martini et al. (2003) propose an amplitude of around 50 m. Lateral karst development is guided by dominant and subordinate fracture systems within the heavily fractured dolomites. Figure 3 shows Wilkinson's reconstruction of major fracture systems at Sterkfontein in relation to the passages and chambers of the Sterkfontein network. Figure 4 shows the same fracture zones in relation to the surface-exposed deposits and several major hominid fossil finds. The insert in Fig. 4 shows an infrared image of the southern surface-exposed deposits. Warm air rising from the cave shows openings and permeable sediments filling openings. The infrared image illustrates the continued influence of the fracture zones in the distribution of fissure flow processes (further described later). High-resolution mapping of the lower cave system is ongoing (Stratford et al. 2016) and will allow more detailed modelling of upper and lower karst levels in relation to the fracture systems and hydrological processes. The high density and orientation of fracturing is a result of the long history of uplift in the southeast and subsidence to the north and northwest forming a dominant fracture system orientated roughly southwest–northeast and a subordinate system orientated north–south.

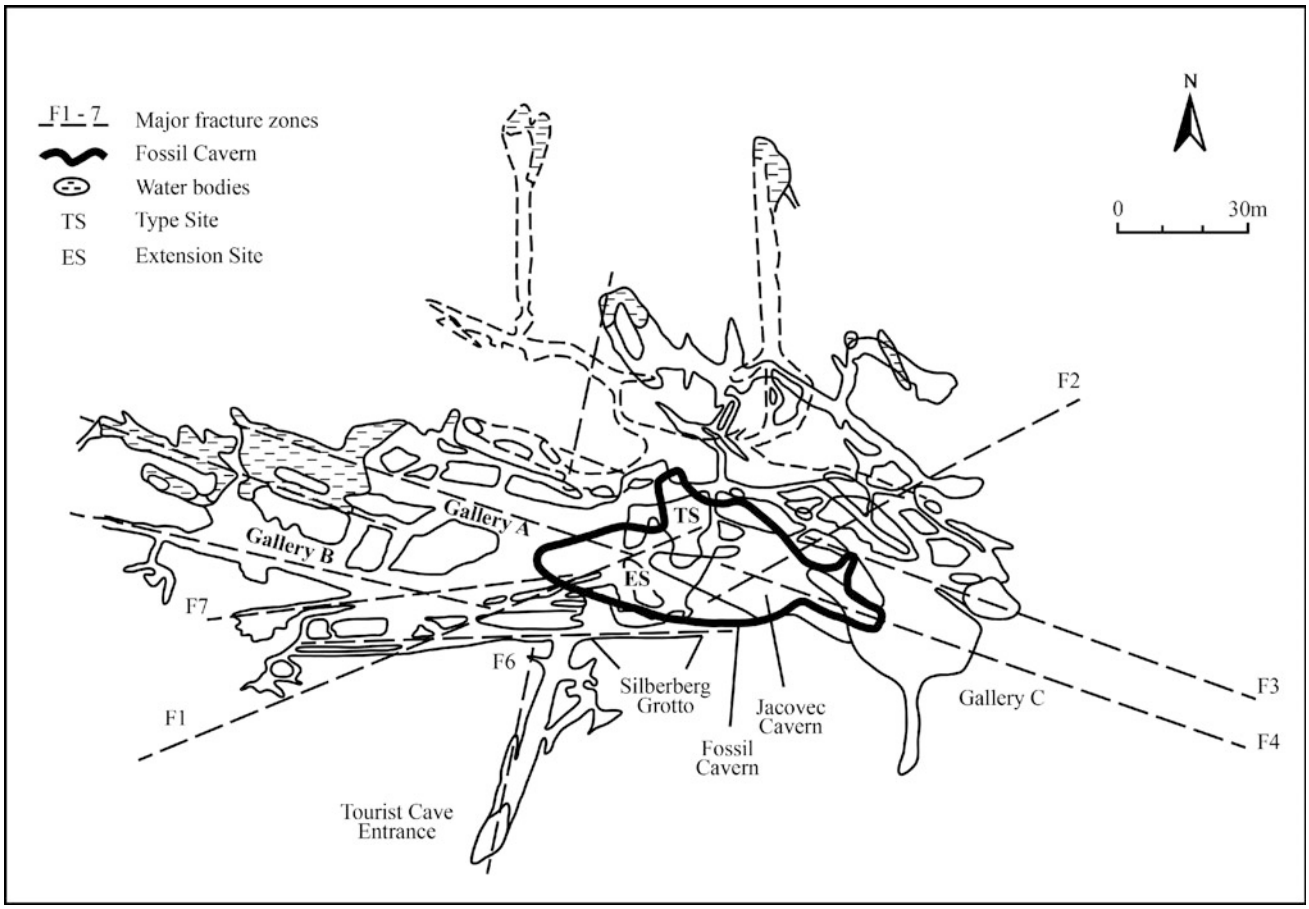

Fig. 3 Geomorphological plan of the Sterkfontein Cave system. Major controlling fracture zones are shown in relation to the upper form (Fossil Cavern *bold line*), and the lower form (subterranean area *thin lines*). From Wilkinson (1983)

The influence of these fracture zones can be seen in the roughly perpendicular intersections of the major passages and galleries. The cave network is limited to an area roughly 350 m east–west and 250 m north–south. The development of dolerite sills and dykes, and a large silicified fault to the east (Wilkinson 1973) provide weak constraints to the east–west karst development. North–south constraints are more firmly controlled by the southwest–northeast and southeast–northwest-orientated fracture zones, with few underground passages forming extensively past them.

In the phreatic zone, deep, narrow vertical fractures enable water penetration and dissolution of tall, narrow passages in chert-poor areas. In chert-rich areas, superimposed passages form between chert beds but in the same plane as the fracturing. In the vadose zone, the fractures have several influences: First, they are the focus of collapse, increasing passage height, and in some cases facilitating articulation with the landscape. Second, they provide fissure flow pathways for meteoric recharge, facilitating localized speleothem formation and localized dissolution of host rock and infills which may enlarge openings and facilitate further collapse. Allogenic sediment accumulation, erosion and speleothem growth are generally focused around these fractures, and as Wilkinson comments, '*entry points increase in number and size with proximity to the centre of the system, namely the intersection area of fracture zones* (1983, p. 519)'. The activity of these fracture systems and associated fissure flow can be seen in the spatial organization of openings, re-karstification of sediments and multiple generations of intrusive speleothem growth throughout the network.

The combination of fracture systems and different chert densities has formed two main karst morphologies at Sterkfontein, an upper and lower. An upper level is represented by a single large, deep chamber formed partly in the chert-rich Monte Christo dolomite. The contents of the upper parts of the chamber were exposed on the landscape surface after the erosion of the cave roof and contain the hominid-and stone tool-bearing localities named the 'Type Site' (TS in Figs. 3 and 4) and 'Extension Site' (ES in Figs. 3 and 4) (excavation area outlined in Fig. 3 and dark blue in Fig. 4) and were the focus of early excavations by

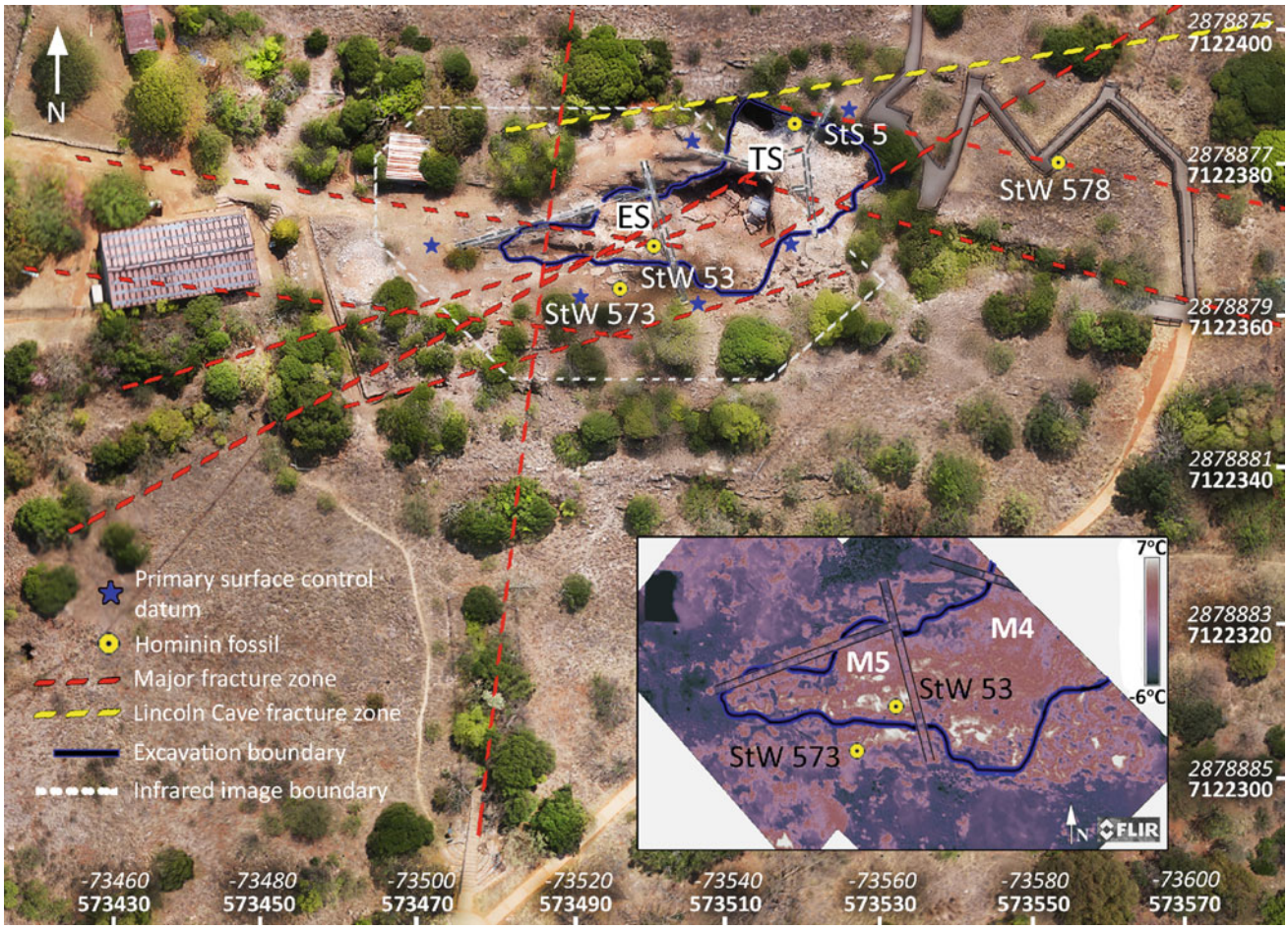

Fig. 4 Fracture zones in relation to the Sterkfontein surface excavation site and four major hominid finds—StS 5, StW 53, StW 573 and StW 578. Major zones are indicated in *red dashed lines*, and the excavation outline is marked in a *thick blue line*. Figure *inset* represents an aerial infrared photograph of an area of the southern part of the surface site which is demarcated by the same *thick blue line*. Ambient temperatures during the flight were about −6 °C. *Red* areas are warmer (3–6 °C) and *white* areas represent temperatures of greater than +7°C. The areas of Member 4 and Member 5 are indicated by 'M4' and 'M5' in the figure *inset*. 'TS' indicates the area of the type site, and 'ES' indicates the area of the extension site as seen in Fig. 3. UTM coordinates (*bold*) and local Lo27 coordinates (*italic*) are given on the *bottom* and *right* axes (aerial photograph DJ Stratford; *Inset* courtesy of L Bruxelles)

Broom (1936) (Broom et al. 1950) and later more intensive excavations by Tobias and Hughes (Tobias and Hughes 1969). Lateral dimensions of this chamber are controlled by the convergence of five fracture zones (Figs. 3 and 4). Enormous collapsed blocks in the lower areas of the surface excavations in this chamber suggest that large roof pendants (perhaps remnants of early walls) collapsed at various stages while the chamber was filling with allogenic sediments. The early morphology of this chamber, prior to any opening to the surface and under phreatic conditions, may have been characterised by short, broad passages developed between chert beds. The Silberberg Grotto, a mid-level chamber in the network, represents one of perhaps several basal portions of this large chamber and was developed within the upper Oaktree dolomite. These basal areas are now separated by, or completely filled with, a combination of authigenic and allogenic infill and speleothem. Small passages allowing the distribution of sediments and fluids into deeper areas directly from the upper (now landscape-exposed) level are abundant. The southern wall of the Silberberg Grotto represents the southern limit of the chamber and the Sterkfontein network (Wilkinson 1973; Pickering and Kramers 2010). The small perpendicular passage which extends south past this boundary (Fig. 3) and is currently used as the main tourist entrance to the caves, is not a natural passage but was created as an access for the lime miners through heavy blasting along a poorly developed north–south fracture zone.

The lower level is more extensive than the upper, with passage length in excess of 4.5 km (Martini et al. 2003). Here, passage development is influenced by fracture system direction, density and chert-poor dolomite, creating very tall,

narrow, passages. Passages can generally be described as labyrinthine in the east of the lower levels where fracturing is denser but collapse in the vadose zone is less extensive. In the west, passages are more parallel, or forming parallelogram-like polygons, developing closely along dense and active compound fracture systems that are slightly more distant from one another (Gallery A and B in Fig. 3). Density of fracture system plays an important role here in the lateral dimensions of the chambers and passages, with vadose zone collapse joining spaces between tall, narrow, closely parallel passages, forming galleries, e.g. 'Gallery B' in the Milner Hall (Fig. 5). Inter-gallery passages are generally smaller and perpendicularly orientated, developing along the subordinate north–south trending fracture zones.

Fig. 5 Sterkfontein Milner Hall. Note the sloping dolomite and interbedded chert (A) and evidence of the vadose zone collapse on the cave floor (B). View looking west along 'Gallery B' in Fig. 3. Railing in background is 1 m high and roof is 13 m high (*Photograph* DJ Stratford)

4 Paleocave Deposits and Their Geomorphology

Opening of the caves to the landscape surface occurs through a combination of vadose zone collapse and localized meteoric dissolution along vertical fractures. Openings are often very deep, and in some cases connect the landscape directly to the base of the network 30 m below (Fig. 6). Generally at Sterkfontein, openings to the caves form along the southern boundaries of the network (Figs. 3, 4; Wilkinson 1973; Clarke 2006). This is evident across the system and may be in part a contribution of opening enlargement developing along 'dip tubes' (Ford 1971; Palmer 2007). The concentration of openings along the southern fracture systems has caused dynamic erosion and depositional processes. The continued focus of fissure flow near the southern fracture systems can be seen in the re-karstification of parts of the surface-exposed breccia (see Fig. 7) and in the frequency of openings and blocked openings more densely concentrated in the south of the site (see 'hot spots' across the southern area of the site in the infrared image inset in Fig. 4). Where deposits are evidently associated with a northern opening, it is most likely that they have entered via an opening on the southern boundary of another chamber. For example, the large talus deposit associated with the northern wall of the Milner Hall is likely to have developed from a southern entrance to a chamber associated with the Lincoln Cave (Fault Cave) which lies directly over the northern area of the Milner Hall (Reynolds et al. 2003; Stratford 2011).

When surface erosion has intersected with the uppermost passages, long deep gullies are opened. Typically, openings are very steep sided and represent a serious natural trap danger to animals. As a result, 'death trap' assemblages represent a common bone accumulation agent (e.g. Pickering 1999; Pickering et al. 2004; Kibii 2004). Concentration of vegetation around the cave openings, particularly the wild olive (*Olea oleaster*), is thought to have provided shelter for primates, carnivores and sometimes hominids, accounting for the high proportions of these taxa represented in the fossil assemblages.

Passages between system levels are also often characterized by narrow, steep, and sometimes vertical conduits. Oldowan-bearing deposits found in the western Fossil Cavern are joined to the underlying Name Chamber via 12 m vertical shaft. This passage provides a distributive conduit, redistributing sediments, fossils and artifacts and spreading them through a maze of connected passages in the lower level (Avery et al. 2010; Stratford et al. 2012, 2014).

Fig. 6 A typical cave opening at Sterkfontein. This particular opening articulates directly to the base of the system, some 25 m below. Notice the established vegetation around the opening (*Photograph* D. J. Stratford)

Fig. 7 Re-karstification within the stony Member 4 breccia at the western end of the surface-exposed Sterkfontein breccias. The deep vertical cavities within the eroded surface of the Member 4 deposit have been subsequently filled with stone tool-bearing Member 5 sediments. Breccia to the *left and right of the red* sandy breccia is *Australopithecus*-bearing Member 4 (*Photograph* L. Bruxelles with permission)

Once open, the caves started to accumulate allogenic sediments, animal bones, stone tools and occasionally the bones of our hominid ancestors. Sediments generally accumulate through colluvial processes with varying degrees of water interaction, developing a range of sedimentary facies related to gravity flows. Within the cave, sediments can be calcified, decalcified, eroded and reworked through multiple phases by meteoric and percolating water. In areas of high fracture density, fluid and solute introduction through fissure flow is increased, thereby intensifying localized chemical and mechanical modification. Combinations of processes can distribute sediments (and their interred bones), artefacts and chemical components vertically and laterally en masse or as separate components through the caves. This can stratigraphically isolate assemblages (Farrand 2001; Bosch and White 2004; Goldberg and Sherwood 2006; White 2007; Ford and Williams 2007) or create sorted assemblages with biased faunal, chemical and particle representations (Adams et al. 2007; Stratford et al. 2014; Val and Stratford 2015). The complex multiscale implications of these processes on sediments, fossils and artefacts create long and convoluted stratigraphic histories, a condition that is aptly demonstrated by the number of stratigraphic investigations of the Sterkfontein deposits since the first hominid discovery in 1936 (e.g. Cooke 1938; Brain 1958; Robinson 1962; Wilkinson 1983; Partridge and Watt 1991; Pickering and Kramers 2010; Herries and Shaw 2011; Stratford et al. 2014). Table 1 lists the major stratigraphic works together with the sources of data for these contributions and the associated interpretations.

The current lithostratigraphic sequence used at Sterkfontein was proposed by Partridge (1978) and comprises five major members organized in broad chronostratigraphic order. Member 1 is an autogenic deposit formed during the early vadose zone collapse of the cave. Member 2 is an extensive deposit (Stratford et al. 2014) in which the famous

Table 1 Major stratigraphic works conducted at Sterkfontein

Author	Year	Interpretations
Cooke	1938	Recognized the deposits as a single breccia body exposed at the surface and 'lower cave'
Brain	1958	Recognized the deposits as a single breccia exposed in two underground areas
Robinson	1962	Divided the breccias into 'Lower', 'Middle' and 'Upper'. Underground sediments were a single breccia except for a collapse of 'middle' breccia into the Name Chamber
Wilkinson	1973	Proposed a 'deep phreatic' karstification model from the continuous exposures of breccias through all depths of the caves
Partridge	1978	Described the five major members of the 'Sterkfontein Formation' from breccia exposures in the Silberberg Grotto and surface excavations Silberberg Grotto is considered the base of the sequence
Wilkinson	1983, 1985	Reinterpretation of the full depth of deposits in relation to the formation of the caves. Proposes the deepest deposits may be the oldest
Partridge and Watt	1991	Supports Partridge's initial interpretation that the Silberberg Grotto contains the oldest sediments from descriptions of sediment cores
Clarke	1994	Proposed three phases of formation in the M5 deposit and clarifies Robinson's (1962) hypothesis of collapsed M4 sediments in the Name Chamber
Kuman and Clarke	2000	Refined M4 and M5 stratigraphy and proposed distribution of hominid specimens in relation to the M4/M5 boundary
Clarke	2006	Proposed the erosion and collapse of the StW 573 torso and subsequent intrusion of speleothem in the resultant void
Reynolds et al.	2007	Proposed the erosion and movement of fossils and artefacts from the western Member 5 areas through an articulating tunnel into the Lincoln Cave
Ogola	2009	Proposed the continuation of M4 below the Member 5 west deposit
Pickering and Kramers	2010	Proposed a reassignment of Member 3 as distal Member 4, suggest deepest deposits in the Milner Hall and Jacovec Cavern are younger than M2 in the Silberberg
Herries and Shaw	2011	Generally proposed younger dates for the deposits and an intermediate age for the StW 53 infill between M4 and M5.
Stratford et al.	2012	Suggested a rapid and gradual reworking of the Oldowan-bearing M5 sediments into the Name Chamber and Milner Hall
Stratford et al.	2014	Suggested M2 accumulated to a depth close to the current base level thereby implying the current depth of the caves was formed when the caves opened to the surface
Bruxelles et al.	2014	Proposed a refined sequence of depositional and erosional processes active in the taphonomy of StW 573 and identified intrusive flowstone characters in speleothems around the skeleton

Author	Year	Major data resources
Cooke	1938	Faunal representation; sediment description
Brain	1958	Faunal representation; sediment description
Robinson	1962	Faunal and stone tool representation; sediment description
Wilkinson	1973	Cave geomorphology; deposit distribution
Partridge	1978	Sedimentological analysis of exposed breccias
Wilkinson	1983, 1985	Cave geomorphology; deposit distribution
Partridge and Watt	1991	Sedimentological analysis of sediment core samples

(continued)

Table 1 (continued)

Author	Year	Major data resources
Clarke	1994	Sediment description and stone tool; hominid representation
Kuman and Clarke	2000	Hominid and stone tool representation and spatial distribution; sediment description
Clarke	2006	Faunal representation; taphonomy; deposit and sediment feature description
Reynolds et al.	2007	Artefact, hominid, faunal representation; U-Pb speleothem dates
Ogola	2009	Artefact, hominid and faunal representation; taphonomy
Pickering and Kramers	2010	U-Pb dating of speleothem, longitudinal facies identification from exposed breccias and Partridge's 1989 sediment cores
Herries and Shaw	2011	Paleomagnetic seriation of siltstones and associated speleothems; faunal and artefact representation and ESR dates
Stratford et al.	2012	Deposit and sediment description, macro- and microfauna and artefact representation
Stratford et al.	2014	Sedimentological and geochemical analysis; artefact and fauna representation; taphonomy; spatial analysis of deposits
Bruxelles et al.	2014	Micromorphology, geochemistry, sedimentology

StW 573 'Little Foot' skeleton was found (Clarke 1998). Member 3 lies largely conformably on the capping flowstone of Member 2 in the Silberberg Grotto, but has not yet been systematically sampled for fossils. Member 4 was exposed on the landscape surface through speleothem mining and has yielded more *Australopithecus* specimens than any other hominid locality in the world. Member 5 contains the earliest stone tool assemblages in Southern Africa (Kuman and Clarke 2000) and examples of the earliest member of the *Homo* genus. Vertical and lateral boundaries continue to be debated across all the deposits and are generally proposed from a range of variables such as faunal taxonomic representation, core sample facies correlation and artefact presence or absence. Very little is known about the internal stratigraphy and formation processes of these deposits, although current work is focusing on increasing stratigraphic resolution. As an example, Member 4, containing the vast majority of *Australopithecus* fossils, may have taken up to 500,000 years to accumulate (dating to between about 2.6–2.1 Ma) (Cooke 1974; Herries and Shaw 2011) and documents a significant landscape, environmental and faunal evolutionary window. Geomorphological understanding of this deposit is, however, lacking, with basic boundaries, geometry and formation history still being debated. What is clear is that only residual primary depositional forms remain within a framework of diagenesis.

As the landscape surface is eroded, new openings to some of the deepest chambers have been formed and old openings have been opened again depositing new sediments across the system and at all levels. Where water has been channelled, old deposits have been undercut and locally collapsed, resulting in voids filled by later sediments or flowstones. It is exactly this process that has caused a great deal of confusion over the dating of the StW 573 *Australopithecus* skeleton in the Silberberg Grotto (Bruxelles et al. 2014; Granger et al. 2015). In some cases, re-karstification of autogenic and allogenic cave deposits has formed irregular and occasionally vertical unconformities between sediment bodies. Such a situation can be seen in surface-exposed deposits in the western area of the excavation where deep vertical cavities have been eroded into the irregular surface morphology of the stony Member 4 (Fig. 7). In this case, the cavities have been filled by stone tool-bearing Member 5 sediments, and only through dedicated stratigraphic work has this situation been recognized (Kuman and Clarke 2000). New studies suggest that highly irregular and vertical deposit contacts are frequent at Sterkfontein. These processes create dynamic depositional environments with complex intra- and inter-deposit stratigraphic histories and deposit boundaries which are difficult to predict during excavation and very difficult to reconstruct retrospectively.

5 Summary

The Cradle of Humankind World Heritage Site preserves a long and complex history of geological, landscape and environmental processes spanning over two billion years. This is highlighted with a flash of hominid evolution preserved in the cave infills of the Sterkfontein Caves over approximately the last three and a half million years. We would, however, have no information regarding the evolution of local hominid species during the Late Pliocene and Pleistocene if it were not for the timeous opening of the caves

during a period of our evolution that is so intriguing. Ancient geological processes provided the lithologies, fracture zones and fluid flow patterns that have influenced the morphology of the cave network, the distribution of fauna on the landscape, when and how the cave will open, and how sediments, bones and artefacts will be deposited and distributed through the cave system. The result is a dynamic karst environment with a long and complicated infilling history.

What is clear from the continuing debate about basic stratigraphy and karst evolution at Sterkfontein is that dedicated research is needed to clarify the fundamental mechanisms and relative (followed by absolute) timings of the evolution of the karst, the landscape, and the fossiliferous deposits at Sterkfontein and throughout the Cradle of Humankind.

Acknowledgements I would like to thank Alexander Klimchouk for inviting me to contribute to this book and Alexander Klimchouk and Augusto Auler for their constructive reviews of this work. I would also like to thank Panagiotis Karkanas for his useful comments during the draft stages of the manuscript and Laurent Bruxelles for his help in studying the site. None of this work would have been possible without the invaluable financial support of PAST, NRF, CoE for Palaeosciences and the Leakey Foundation.

References

Adams JW, Herries AIR, Kuykendall KL, Conroy GC (2007) Taphonomy of a South African cave: geological and hydrological influences on the GD 1 fossil assemblage at Gondolin, a Plio-Pleistocene paleocave system in the Northwest Province, South Africa. Quat Sci Rev 26(19):2526–2543

Avery DM, Stratford DJ, Sénégas F (2010) Micromammals and the formation of the Name Chamber at Sterkfontein, South Africa. Geobios 43:379–387

Berger LR, Lacruz R, de Ruiter DJ (2002) Brief communication: revised age estimates of *Australopithecus*-bearing deposits at Sterkfontein, South Africa. Am J Phys Anthropol 119:192–197

Beukes NJ, van Niekerk HS, Gutzmer J (1999) Post Gondwana African land surfaces and pedogenetic ferromanganese deposits on the Witwatersrand at the West Wits Gold Mine, South Africa. S Afr J Geol 102:65–83

Bosch RF, White WB (2004) Lithofacies and transport of clastic sediments in karstic aquifers. In: Sasowsky ID, Mylroie J (eds) Studies of cave sediments: physical and chemical records of palaeoclimate. Kluwer Academic/Plenum Publishers, New York, pp 1–23

Brain CK (1958) The transvaal ape-man-bearing cave deposits. Transvaal Museum Memoir No. 11. Pretoria

Broom R (1936) A new fossil anthropoid skull from South Africa. Nature 138:486–488

Broom R (1947) Discovery of a new skull of the South African ape-man, Plesianthropus. Nature 159:672

Broom R, Robinson JT, Schepers GWH (1950) Sterkfontein Ape-Man Plesianthropus. Mem Transvaal Mus 4:1–117

Bruxelles L, Quinif Y, Wienin M (2009) How can ghost rocks help in karst development? In: 15th International congress of speleology proceedings, speleogenesis, pp 814–818

Bruxelles L, Clarke RJ, Maire R, Ortega R, Stratford D (2014) Stratigraphic analysis of the Sterkfontein StW 573 *Australopithecus* skeleton and implications for its age. J Hum Evol 70:36–48

Button A (1973) A regional study of the stratigraphy and development of the Transvaal Basin in the eastern and northeastern Transvaal. PhD Thesis. University of the Witwatersrand, South Africa

Catuneanu O, Eriksson PG (2002) Sequence stratigraphy of the Precambrian Rooihoogte—Timeball Hill rift succession, Transvaal Basin, South Africa. Sed Geol 147:71–99

Clarke RJ (1994) On some new interpretations of Sterkfontein stratigraphy. S Afr J Sci 90:211–214

Clarke RJ (1998) First ever discovery of a well-preserved skull and associated skeleton of Australopithecus. S Afr J Sci 94:460–463

Clarke RJ (2002) On the unrealistic 'revised age estimates' for Sterkfontein. S Afr J Sci 98:415–419

Clarke RJ (2006) A deeper understanding of the stratigraphy of Sterkfontein fossil hominid site. Trans R Soc S Afr 61(2):111–120

Clarke RJ (2013) Australopithecus from Sterkfontein Caves, South Africa. In: Reed KE, Fleagle JG, Leakey RE (eds) The palaeobiology of australopithecus, vertebrate palaeobiology and palaeoanthropology. Springer, Dordrecht, pp 105–123

Cooke HBS (1938) The Sterkfontein bone breccia: a geological note. S Afr J Sci 35:204–208

Cooke HBS (1974) Plio-Pleistocene deposits and mammalian faunas of eastern and southern Africa. In: Proceedings of 5th Congress on the Neogene of the Mediterranean BRGM, Paris 78(1):99–108

Dirks PHGM, Berger LR (2013) Hominin-bearing caves and landscape dynamics in the Cradle of Humankind, South Africa. J Afr Earth Sci 78:109–131

Dirks PHGM, Kibii JM, Kuhn BF, Steininger C, Churchill SE, Kramers JD, Pickering R, Farber DL, Meriaux A, Herries AIR, King GCP, Berger LR (2010) Geological setting and age of *Australopithecus sediba* from Southern Africa. Science 328:205–207

Dirks PHGM, Placzek CJ, Fink D, Dosseto A, Roberts E (2016) Using 10Be cosmogenic isotopes to estimate erosion rates and landscape changes during the Plio-Pleistocene in the Cradle of Humankind, South Africa. J Hum Evol 96:19–34

Dubois C, Quinif Y, Baele J-M, Barriquand L, Bini A, Bruxelles L, Dandurand G, Havron C, Kauffmann O, Lans B, Maire R, Martin J, Rodet J, Rowberry MD, Tognini P, Vergari A (2014) The process of ghost-rock karstification and its role in the formation of cave systems. Earth-Sci Rev 131:116–148

Eriksson PG (1988) Sedimentology of the Rooihoogte formation, Transvaal sequence. S Afr J Geol 91:477–489

Eriksson PG, Schweitzer JK, Bosch PJA, Schereiber UM, Van Deventer JL, Hatton CJ (1993) The Transvaal sequence: an overview. J Afr Earth Sci 16:25–51

Eriksson PG, Hattingh PJ, Altermann W (1995) An overview of the geology of the Transvaal sequence and Bushveld complex, South Africa. Miner Deposita 30:98–111

Eriksson PG, Altermann W, Catuneanu O, van der Merwe R, Bumby AJ (2001) Major influences on the evolution of the 2.67–2.1 Ga Transvaal basin, Kaapvaal craton. Sed Geol 141–142:205–231

Farrand WR (2001) Sediments and stratigraphy in rockshelters and caves: A personal perspective on principles and pragmatics. Geoarchaeol Int J 16(5):537–557

Ford DC (1971) Geologic structure and a new explanation of limestone cavern genesis. Trans Cave Res Group G B 13:81–94

Ford DC, Williams PW (2007) Karst geomorphology and hydrology. Chapman and Hall, London

Gillieson D (1996) Caves: processes, development, and management. Blackwell, Oxford

Goldberg P, Sherwood SC (2006) Deciphering human prehistory through the geoarchaeological study of cave sediments. Evol Anthropol 15:20–36

Granger DE, Gibbon RJ, Kuman K, Clarke RJ, Bruxelles L, Caffee MW (2015) New cosmogenic burial ages for Sterkfontein Member 2 *Australopithecus* and Member 5 Oldowan. Nature 522:85–88

Herries AIR, Shaw J (2011) Palaeomagnetic analysis of the Sterkfontein palaeocave deposits: Implications for the age of the hominin fossils and stone tool industries. J Hum Evol 60:523–539

Herries AIR, Pickering R, Adams JW, Curnoe D, Warr G, Latham AG, Shaw J (2013) A multi-disciplinary perspective on the age of Australopithecus in Southern Africa. In: Reed K, Fleagle JG, Leakey R (eds) The Paleobiology of *Australopithecus*. Springer, Dordrecht, pp 21–40

Kibii J (2004) Comparative taxonomic, taphonomic and palaeoenvironmental analysis of 4–2.3 million year old Australopithecine cave infills at Sterkfontein. Unpublished doctoral dissertation, University of Witwatersrand, Johannesburg

Klimchouk AB (2007) Hypogene Speleogenesis: hydrogeological and morphogenetic perspective. Special Paper no. 1, National Cave and Karst Research Institute, Carlsbad, NM, p 106

Kuman K, Clark RJ (2000) Stratigraphy, artefact industries and hominid associations, member 5. J Hum Evol 38:827–847

Martini JEJ (2006) Karst and Caves. In: Johnson MR, Anhaeusser CR, Thomas RJ (eds) The geology of South Africa. Geological Society of South Africa and Council for Geoscience Publication, Pretoria, pp 261–668

Martini JEJ, Wilinger PE, Moen HFG, Keyser A (2003) Contribution to the speleology of Sterkfontein cave, Gauteng province, South Africa. Int J Speleol 32:43–49

Obbes AM (2000) The structure, stratigraphy and sedimentology of the Black Reef-Malmani-Rooihoogte succession of the Transvaal Supergroup southwest of Pretoria. Council of Geoscience Bulletin 127, Pretoria

Ogola C (2009) The Sterkfontein western breccias: stratigraphy, fauna and artefacts. Ph.D. Dissertation. University of the Witwatersrand. Johannesburg

Palmer AN (2007) Cave geology. Cave Research Foundation, Ohio, USA

Partridge TC (1973) Geomorphological dating of the cave opening at Makapansgat, Sterkfontein, Swartkrans and Taung. Nature 246: 75–79

Partridge TC (1978) Re-appraisal of lithostratigraphy of Sterkfontein hominid site. Nature 275:282–286

Partridge TC (2010) Tectonics and geomorphology of Africa during the Phanerozoic. In: Werdelin L, Sanders WJ (eds) Cenozoic Mammals of Africa. Published to California Scholarship Online, pp 3–17

Partridge TC, Watt IB (1991) The stratigraphy of the Sterkfontein hominid deposit and its relationship to the underground cave system. Palaeont Afr 28:35–40

Partridge TC, Granger DE, Caffee MW, Clarke RJ (2003) Lower Pliocene hominid remains from Sterkfontein. Science 300:607–612

Pickering TR (1999) Taphonomic Interpretations of the Sterkfontein Early Hominid site (Gauteng, South Africa) reconsidered in the light of recent evidence. Unpublished doctoral dissertation. University of Wisconsin

Pickering R, Kramers JD (2010) Re-appraisal of the stratigraphy and determination of new U-Pb dates for the Sterkfontein hominin site, South Africa. J Hum Evol 59:70–86

Pickering TR, Clarke RJ, Moggi-Cecchi J (2004) Role of carnivores in the accumulation of the Sterkfontein Member 4 hominid assemblage: a taphonomic reassessment of the complete hominid fossil sample (1936–1999). Am J Phys Anthropol 125:1–15

Reynolds SC, Vogel JC, Clarke RJ, Kuman K (2003) Preliminary results of excavation at Lincoln Cave, Sterkfontein, South Africa. S Afr J Sci 99:286–288

Reynolds SC, Clarke RJ, Kuman K (2007) The view from the Lincoln Cave: mid to late Pleistocene fossil deposits from Sterkfontein hominid site, South Africa. J Hum Evol 53(3):260–271

Robinson JT (1962) Sterkfontein stratigraphy and the significance of the extension site. S Afr Arch Bull 17:87–107

Ryan PJ (1986) The Witkop fluorspar mine near Zeerust, western Transvaal. In: Anhaeusser CR, Maske S (eds) Mineral deposits of Southern Africa, vol 1. Geological Society of South Africa Publication, pp 843–849

Stratford DJ (2011) The underground central deposits of the Sterkfontein Caves, South Africa. Unpublished PhD dissertation, University of the Witwatersrand, Johannesburg

Stratford DJ, Bruxelles L, Clarke RJ, Kuman K (2012) New stratigraphic interpretations of the fossil and artefact-bearing deposits of the Name Chamber, Sterkfontein. S Afr Arch Bull 67:159–167

Stratford DJ, Grab S, Pickering TR (2014) The stratigraphy and formation history of fossil- and artefact-bearing sediments in the Milner Hall of Sterkfontein Cave, South Africa: new interpretations and implications for palaeoanthropology and archaeology. J Afr Earth Sci 96:155–167

Stratford DJ, Merlo S, Brown S (2016) The development of a new geospatial framework for the palaeoanthropological site of the Sterkfontein Caves, Cradle of Humankind, Gauteng, South Africa. J Field Arch 41(2):211–221

Sumner DY, Grotzinger JP (2004) Implications for Neoarchaean ocean chemistry from primary carbonate minerology of the Camberland-Malmani Platform, South Africa. Sedimentology 51:1273–1299

Tobias PV (1987) 21st Annual Report of PARU and its Presursors. Department of Anatomy, University of the Witwatersrand, Johannesburg

Tobias PV, Hughes AR (1969) The New Witwatersrand University Excavation at Sterkfontein: progress report, some problems and first results. S Afr Arch Bull 24:158–169

Truswell JF, Eriksson KA (1975) A palaeoenvironmental interpretation of the early Proterozoic Malmani Dolomite from Zwartkops, South Africa. Precambr Res 2:277–303

Val A, Stratford DJ (2015) The macrovertebrate fossil assemblage from the Name Chamber, Sterkfontein: taxonomy, taphonomy and implications for site formation processes. Palaeontol Afr 50:1–17

Walker J, Cliff RA, Latham AG (2006) U-Pb isotopic age of the StW573 hominid from Sterkfontein, South Africa. Science 314:1592–1594

White WB (2007) Cave sediments and palaeoclimate. J Cave Karst Stud 69(1):76–93

Wilkinson MJ (1973) Sterkfontein cave system: evolution of a karst form. M.A. thesis, University of the Witwatersrand, Johannesburg

Wilkinson MJ (1983) Geomorphic perspectives on the Sterkfontein Australopithecine breccias. J Arch Sci 10:515–529

Wilkinson MJ (1985) Lower-lying and possibly older fossilferous deposits at Sterkfontein. In: Tobias PV (ed) Hominid evolution: past, present and future. Alan R. Liss, New York, pp 165–170

Hypogene Caves of the Tasmanic Karsts of Eastern Mainland Australia

61

R.A.L. Osborne

Abstract

The Tasmanic karsts of eastern Australia extend from the south-eastern tip of Tasmania to the far north of Queensland. The mainland section incorporating the eastern parts of Victoria, New South Wales and Queensland contains more than one hundred and twenty bodies of cavernous Palaeozoic limestone, most of which form impounded karsts. Many of these karst areas are small, difficult to access, contain a small number of caves and have received little attention from cavers and even less attention from scientists. Some 21 karst areas stand out for their number of caves and their diversity of underground features. Almost all of the Tasmanic caves in mainland Australia show a high degree of structural guidance and are developed in massive high-purity limestone. Solution dolines are rare or absent in the surrounding karst. Some caves appear to have been formed entirely by a single hypogenic event while others have been modified by several hypogenic events (multiphase caves). In other caves, hypogene forms have been overprinted by later epiphreatic, paragenetic, fluvial and breakdown events (multiphase/multiprocess caves). Where there are active rivers in the caves, the rivers are often much smaller than the cavities they flow through, take complex paths through the rock and are captured into pre-existing cavities. The evidence for a hypogene origin of these caves is largely morphological, but is supported by circumstantial evidence such as intersection of palaeokarst, proximity to regional faults and tenuous relationships with the surrounding geomorphology and hydrology.

Keywords

Hypogene caves • Australia • Morphology • Speleogens • Speleogenesis

1 Introduction

Scientific study of the caves of eastern mainland Australia has been quite limited. J.N. Jennings published a great deal about the caves of eastern Australia from a traditional fluvial viewpoint, Jennings (1963, 1964, 1965, 1968, 1982, 1985), James et al. (1978). The first late twentieth century review was Osborne and Branagan (1988), which focussed on the likely age of the caves and their relationship to topography. Osborne (1996) first raised the possibility of a hypogene or other non-fluvial origin for the eastern mainland Australian caves. The more recent review by Osborne (2010) focussed on changes in ideas about the caves, rather than the characteristics of the caves. While there are good databases giving the length and depth of these caves, there is little else recorded about many of the caves.

Rather than reviewing the 21 better-known cavernous karsts, this chapter uses examples from them to illustrate the

This chapter is dedicated to the memory of the recently deceased Ken Grimes (1944–2016) a pioneer and major contributor to the geological study of Australian caves.

R.A.L. Osborne (✉)
Sydney School of Education and Social Work, A35,
The University of Sydney, Sydney, NSW 2006, Australia
e-mail: armstrong.osborne@sydney.edu.au

© Springer International Publishing AG 2017

A. Klimchouk et al. (eds.), *Hypogene Karst Regions and Caves of the World*,
Cave and Karst Systems of the World, DOI 10.1007/978-3-319-53348-3_61

key types and characteristics of hypogene caves in eastern mainland Australia. Most of the information given is based on the author's observations except in the cases of Texas Caves in Queensland, which were flooded in 1976 where data collected by the late Grimes (1978) prior to their flooding is used and Chillagoe Caves where data has been supplied by the Chillagoe Caving Club.

1.1 Geological Setting

The dominant geological provinces in eastern mainland Australia are the Palaeozoic Tasman Orogen and the Permo-Triassic Sydney-Bowen Basin (Fig. 1).

The Tasman Orogen is divided into two distinct sections, the Lachlan-Thompson Orogen to the west and the New England Orogen to the east. Multiple folding episodes in the Tasman Orogen mean that most caves in eastern mainland Australia are developed in dipping and often steeply dipping limestones. Deformation in the Lachlan-Thompson Orogen concluded with the Early Carboniferous Kanimblan Orogeny and deformation in the New England Orogen concluded with the Permo-Triassic Hunter-Bowen Orogeny. The New England Orogen is divided into two zones, the western Tamworth Trough and an eastern zone comprised of several distinct blocks. From the Late Carboniferous to the Middle Triassic the Sydney-Bowen Basin, composed of marine and terrestrial siliciclastics with significant deposits of freshwater coal, formed an elongate trench between the eroding mountain chains of the two deformed orogens.

The Lachlan-Thompson Orogen contains Ordovician to Devonian limestones deposited in tropical shelf environments with caves preferentially developed in high-purity lime-mudstones. In the New England Orogen, limestones in the western Tamworth Trough are Devonian olistoliths, similar in lithology to the limestones of the Lachlan-Thompson Orogen. The Carboniferous to Permian limestones of the blocks in the eastern New England Orogen are cool water shelf deposits and include oolitic, crinoidal and crinoidal-bryozoan facies. There is little karstification in the oolites, with caves and surface karst principally developed in the crinoidal and crinoidal-bryozoan facies. Unlike the situation in the Northern Hemisphere, there are no Mesozoic carbonates in eastern Australia.

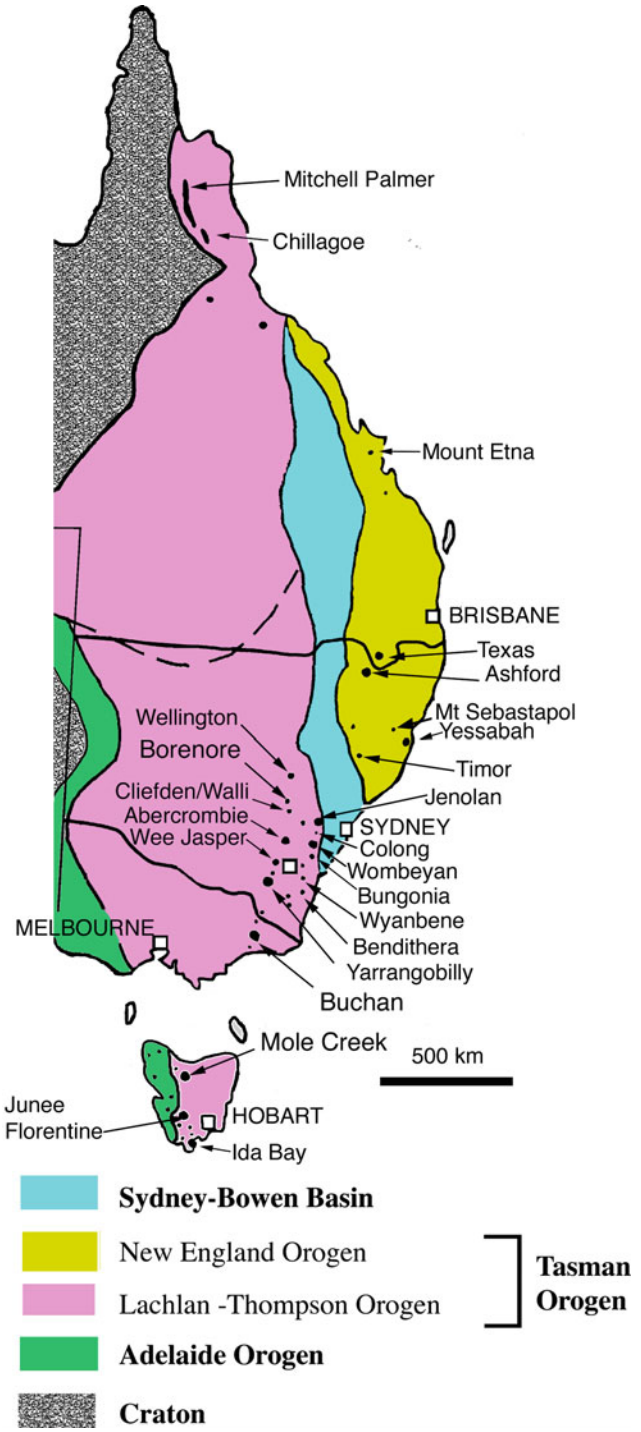

Fig. 1 Eastern Australia showing geological provinces, twenty-one significant cavernous karsts in eastern mainland Australia and three significant cavernous karsts in Tasmania

1.2 Geomorphic Setting

The dissected plateaux of the Eastern Highlands and their dramatic eastern boundary, the Great Escarpment (Ollier 1982), dominate the landscape of eastern Australia. To the east of the Great Escarpment there is a narrow coastal plain, while the incised western edge of the Highlands slopes more gently, forming the Western Slopes and Plains (Fig. 2).

In the south, the drainage divide runs roughly along the centre of the Eastern Highlands, but between Brisbane and

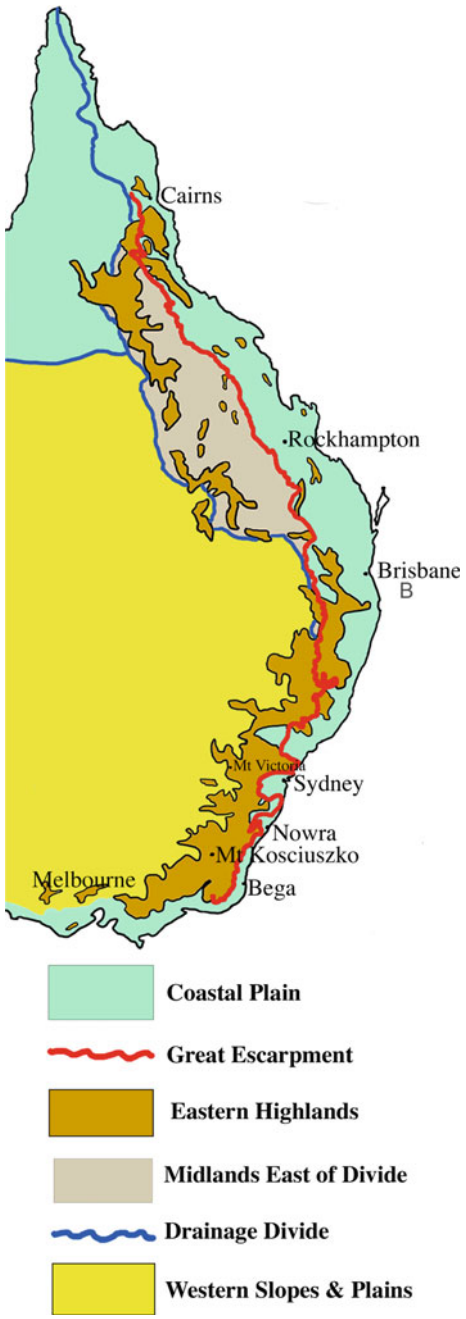

Fig. 2 Eastern mainland Australia showing major landscape features. Great Escarpment simplified after Ollier (1982)

Cairns the drainage divide (blue line in Fig. 2) is significantly west of the Escarpment.

Uplift of the Eastern Highlands is related to the opening of the Tasman Sea, beginning about 90 Ma. While many of the plateau surfaces making up the Eastern Highlands have an elevation of approximately 1000 m, some sections of the Highlands have been uplifted higher later, notably the Snowy Mountains in the south, reaching an elevation of 2228 m at Mount Kosciuszko and the western edge of the Blue Mountains Plateau with an elevation of 1043 m at Mount Victoria.

Many of the significant cavernous karsts in eastern mainland Australia are located in the incised eastern edge of the Eastern Highlands west of the escarpment but east of the drainage divide. These include Bendithera, Bungonia, Colong, Jenolan, Timor, Sebastapol and Wombeyan. Yessabah and Mt Etna are located east of the Escarpment, while Cooleman Plain is located in the centre of the Highlands, just west of the drainage divide. Three significant karsts, Abercrombie, Wee Jasper and Yarrangobilly are located in the incised zone on the western side of the Highlands. The most significant karsts in the Western Slopes and Plains are Borenore, Cliefden, Walli and Wellington.

1.3 Outcrop Pattern and Surface Karst

Most of the cavernous limestone in eastern mainland Australia crops out as narrow, elongate impounded karsts with a general north–south orientation following the strike of the bedrock (Fig. 3). While rocky bluffs of limestone are common, dolines are relatively uncommon and polje unknown. Karren are well developed except where the limestone is covered by canopy forest. There are few dry valleys and limestone gorges. Dry valleys are usually not perched, as underground drainage is inefficient and erosion by strong water flows during floods allows valley floor incision to keep up with cave development.

Karst areas in eastern mainland Australia differ from those in Tasmania in having specific vegetation growing on the limestone. A good example of this is seen in Fig. 4, showing vegetation growing on the limestone outcrop at Bendithera Caves, NSW. In this case, the calciphile plant is an endemic species of *Acacia*, commonly called the Bendithera Wattle.

2 Cave Types

Caves in eastern mainland Australia are small and shallow by international standards. Most caves are less than 50 m deep with only eight exceeding 100 m in depth and nine exceeding three kilometres in plan length. Open ponors are rare with most of the few perennial streams that do sink into caves sinking through sand and gravel in streambeds.

Six distinct types of hypogene caves can be recognised in eastern mainland Australia: Hall and Narrows Caves, Maze caves, Cupola dominated caves, Caves with deep shafts, Multiphase/Multiprocess Caves and Single chamber caves.

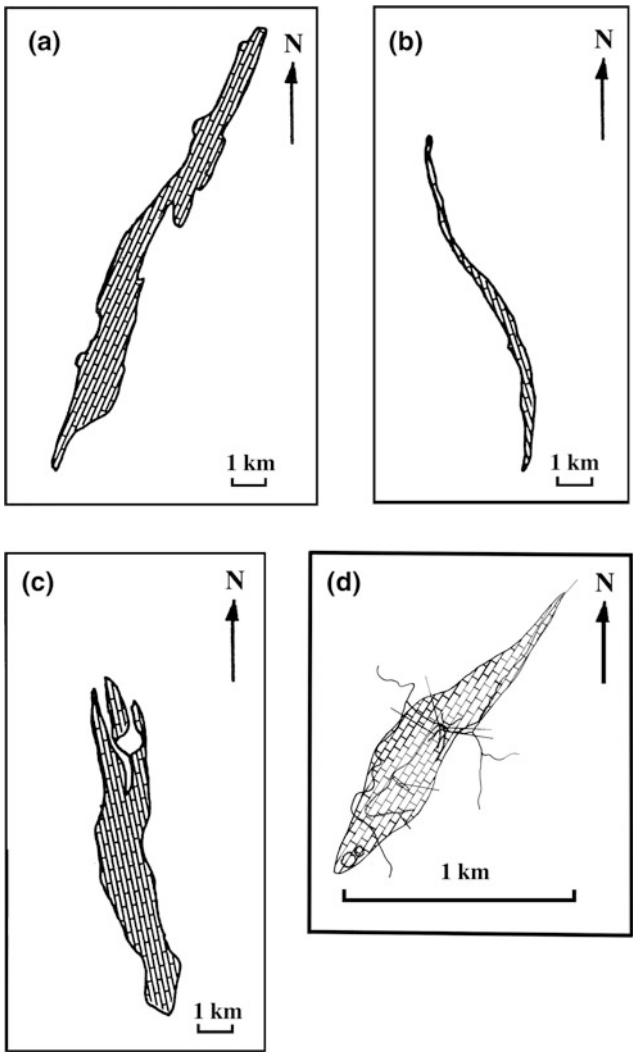

Fig. 3 Impounded karsts, modified after Osborne (1999): **a** Bungonia, **b** Jenolan, **c** Yarrangobilly, **d** Colong. Note small size and elongate N–S trending outcrop pattern

2.1 Hall and Narrows Caves

Osborne (2001) described caves with strong structural guidance in which the main cavities (Halls) terminate blindly along strike and are joined by small cavities (Narrows) generally guided by cross-joints as Hall and Narrows caves (Fig. 5a). Osborne (2001) was greatly influenced by the inception horizon concept and gave considerable emphasis to the role of bedding with the idea that "halls" were guided by bedding while the "narrows" were guided by cross-joints.

The key idea about Hall and Narrows caves was that there had never been a lateral flow of water in the elongate cavities because they terminated blindly at both ends except where later surface processes had intersected them. Thus, Hall and Narrows caves could not have had a conventional fluvial origin. Halls and Narrows style of development is common both in individual caves and as segments of caves in both the Lachlan-Thompson and New England Orogens. Key features of these caves are the presence of blind terminations (Fig. 5b), general isolation from the local hydrology, entrances produced by breakdown, surface lowering or cliff retreat, a lack of scallops and other fluvial speleogens and a lack of fluvial sediments even when the cave entrance is close to a large stream.

2.1.1 Highs and Lows and "String of Sausages" Development

In describing Cathedral Cave at Wellington, Osborne (2007) noted that the cave was characterised by distinct zones with high ceilings he called "highs" and separated by zones with low ceilings he called "lows". This style of development has been found to be quite common in eastern Australian caves and in caves elsewhere considered to have a hypogene origin. In describing the morphology of eastern Australian caves, it has proved useful to introduce a new descriptive term "string of sausages" to describe a style of cave development often found in Hall and Narrows caves, where sets of joint-guided elongate solution cavities are separated by narrow squeezes in bedrock. An excellent example of this type of development can be seen in Belfry Cave at Timor (see Fig. 6).

2.2 Maze Caves

Three of the longest caves in eastern mainland Australia, Queenslander Cave at Chillagoe in Queensland (10 km) (Fig. 7a), Colong Cave (6 km) and Taplow Maze Cave (3 km) in NSW (Fig. 7b), are mazes or in the case of Colong Cave much of its plan length forms a maze. New mapping by Phil Maynard of the Sydney University Speleological Society of Mammoth Cave, an 8.4-km-long section of the more than 36-km-long Jenolan Caves system in NSW, has shown that in plan, the cave has an underlying rectilinear structure. Smaller maze-like caves include Dip Cave at Wee Jasper and Moparabah Cave near Kempsey, NSW.

Eastern Australian maze caves have similar patterns of development and speleogens to those of Hall and Narrows caves and can be considered to be large and/or multi-story versions of Hall and Narrows caves.

There has been little detailed study of maze caves in eastern mainland Australia, but this is changing due to Taplow Maze Cave at Cliefden being threatened by flooding from a proposed dam, the surveying of new, detailed maps of maze caves, and the growing international interest in the origin and evolution of maze caves.

Fig. 4 Vegetation at Bendithera, where the limestone outcrop in the middle ground has distinctly lower vegetation than the forest higher up the hill

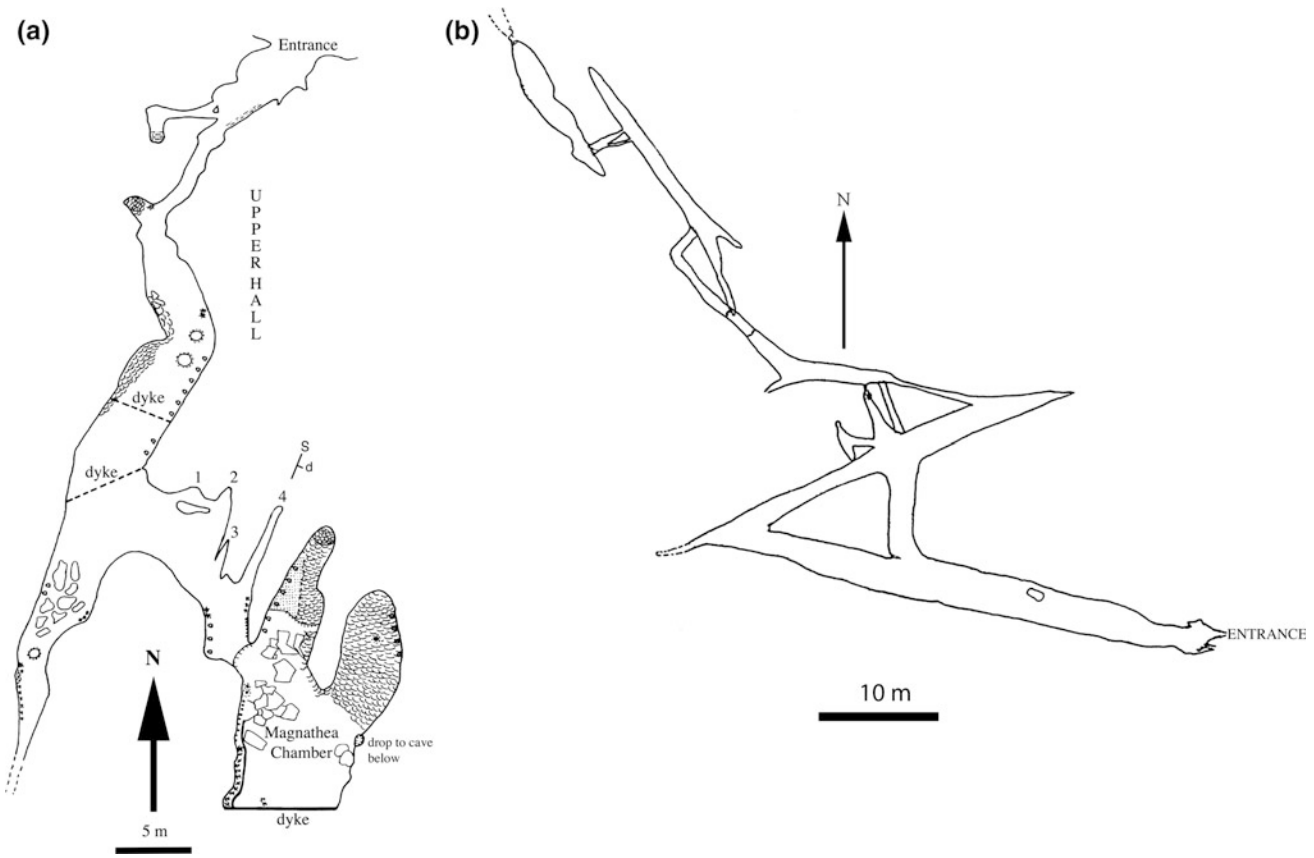

Fig. 5 **a** Flying Fortress Cave, Bungonia after (Osborne 2001). The cave follows joints dipping down to the east, while bedding dips to the west. Note also blind halls and termination of Magnathea Chamber by a dyke. **b** Fig Tree Cave, Sebastapol, NSW. Simplified map courtesy of Kempsey Speleological Society, Note blind halls and structural guidance

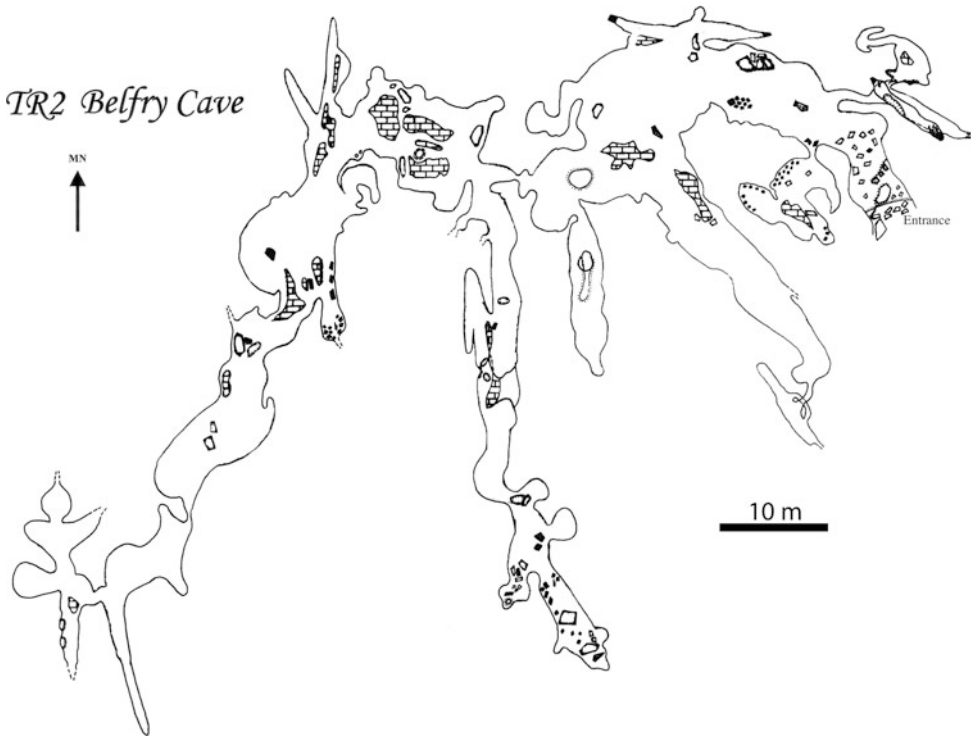

Fig. 6 Simplified outline map of Belfry Cave, Timor, NSW, courtesy of Newcastle and Hunter Valley Speleological Society. Note "string of sausages" development in southerly tending halls

2.3 Cupola Dominated Caves

Cupolas and related forms such as cathedrals dominate some caves in eastern Australia (Osborne 2004). Cupola dominated caves include the well-documented Cathedral Cave at Wellington (Osborne 2007) Ashford Cave in northern NSW, Swansong Cave at Cliefden Caves and Bevan's Pot at Texas Caves (Grimes 1978).

Unfortunately, detailed documentation and measurement of cupolas has only been undertaken in Cathedral Cave at Wellington and in the southern show caves at Jenolan.

Cathedral Cave at Wellington has more than 17 cupolas, with ten conical and elliptical cupolas (Fig. 8a, b) and seven hemispherical cupolas (Fig. 8c) recorded in the cave inventory. Cathedral Cave also contains three elliptical chambers, "cathedrals" of Osborne (2004). The ceiling vault of one of the cathedrals, the Well Chamber is shown in Fig. 8d. Ashford Cave contains large hemispherical cupolas, but these are not recorded on existing maps of the cave nor have they been properly documented. Swansong Cave at Cliefden contains high shaft-like cupolas and complex elliptical cupolas with curved pendants at their base (Fig. 8e).

The map of Bevan's Pot at Texas Caves in Grimes (1978) (Fig. 8f) shows eight cupola-like features in the ceiling. The sections show two elliptical cupolas (1 and 2 in Fig. 8f) the largest, with a long axis of 3 m, a short axis of 1.5 m, rising 3.5 m above the floor and penetrating at least 1 m above the general ceiling line.

Two hemispherical cupolas (4 and 5 in Fig. 8f) can also be seen in Section B-B′.

2.4 Caves with Deep Shafts

Caves with depths greater than 50 m are quite uncommon in mainland Australia. The greatest concentration of deep caves occurs at Bungonia, NSW, adjacent to a 360-m deep gorge and canyon. Key features of the caves at Bungonia are relatively horizontal sections of cave close to the surface, which connect to deep vertical shafts. Many of the shafts narrow with depth. The traditional explanation of these shafts has been that they are vadose in origin. Osborne (2001) interpreted the shallow caves close to the surface as Hall and Narrows caves, implying a hypogene origin. It is possible that these shafts are small-scale versions of the "giant ascending shafts" described by Audra and Palmer (2015). The similarity can be seen by comparing the section of Argyle Hole at Bungonia (Fig. 9) with the section of the very much larger Hranica Propast in Figure 38 of Audra and Palmer (2015).

2.5 Multiphase/Multiprocess Caves

Caves at five of the best-known cavernous karsts in eastern mainland Australia, Colong, Jenolan, Wee Jasper, Wombeyan and Yarrangobilly, show evidence of overprinting by

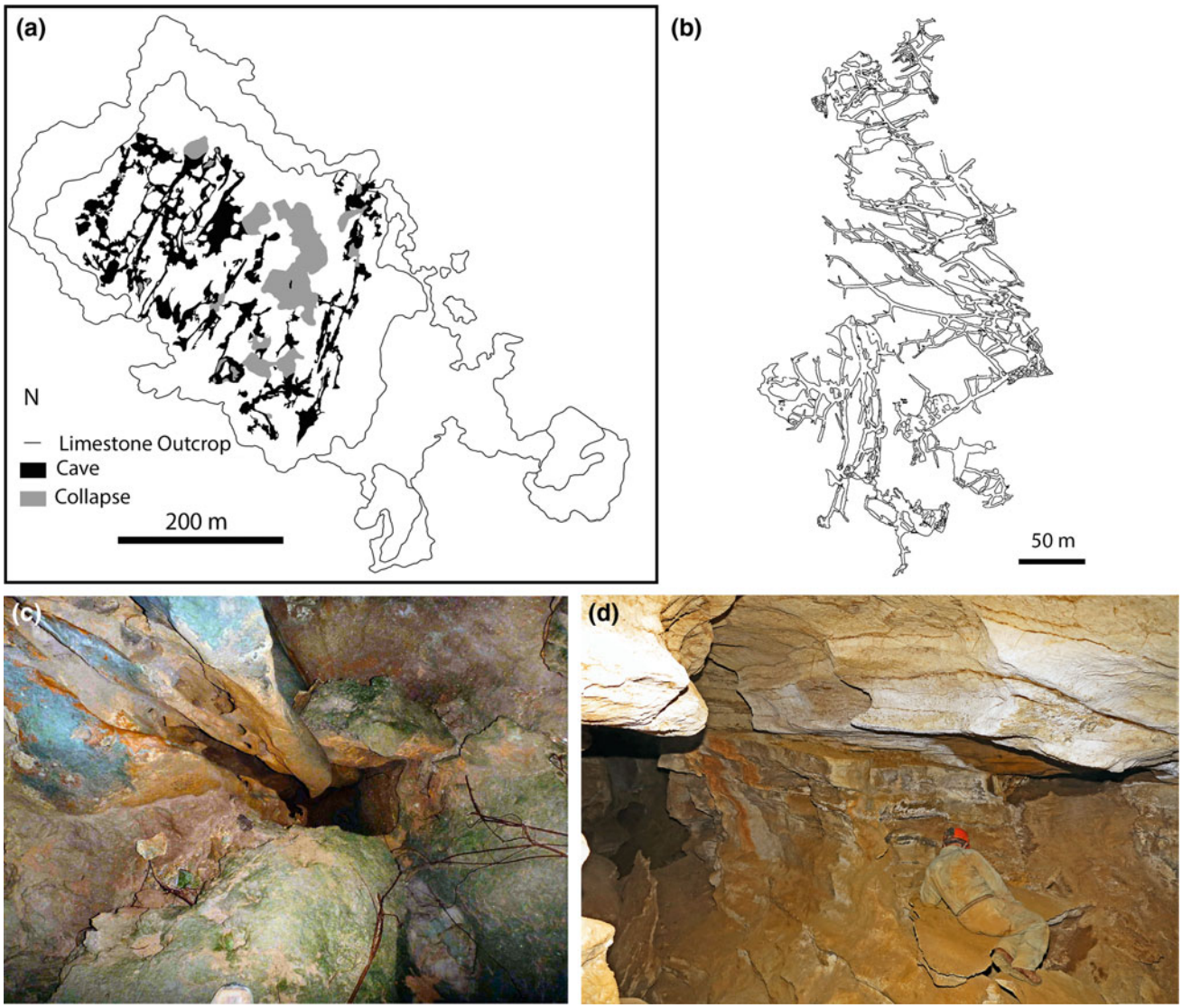

Fig. 7 Maze Caves: **a** map showing Queenslander and related caves at Chillagoe. Note dominant NE–SW orientation. Map courtesy of Chillagoe Caving Club. **b** Map of Taplow Maze Cave at Cliefden. Note morpho-structural domains with changes in the orientation of halls. Map courtesy of Phil Maynard and Sydney University Speleological Society. **c** Floor feeder in Queenslander Cave, Chillagoe. Shaft approx. 600 mm in diameter. Image Peter Bannink. **d** "Y" junction in Taplow Maze Cave, note person with red helmet for scale

multiple phases of speleogenesis caused by different processes. Overprinting processes include hypogene speleogenesis, paragenesis, epigenesis, invasive fluvial speleogenesis, contemporary fluvial speleogenesis and breakdown (Fig. 10).

In these caves, the processes currently active, such as vadose fluvial processes and breakdown, are not those responsible for most of the earlier development of the caves. At Jenolan, Osborne (2014) noted the striking difference between the morphology of the younger active stream passage and the morphology of the older large paragenetic conduits located at higher levels in the cave. He commented that in the case of Jenolan Caves, the present was not the key to the past.

2.6 Single Chamber Caves

Single chamber caves occur not only in karsts with many caves, such as Bendithera (Main Cave), Cliefden (Tetanus Cave), Mt Sebastapol (Daylight Cave), Timor (Main Cave) and Wombeyan (Durrin's Tower Cave), but also as the only cave in tiny isolated limestone outcrops east of Wellington, NSW such as Douglas Cave at Stuart Town and the nearby

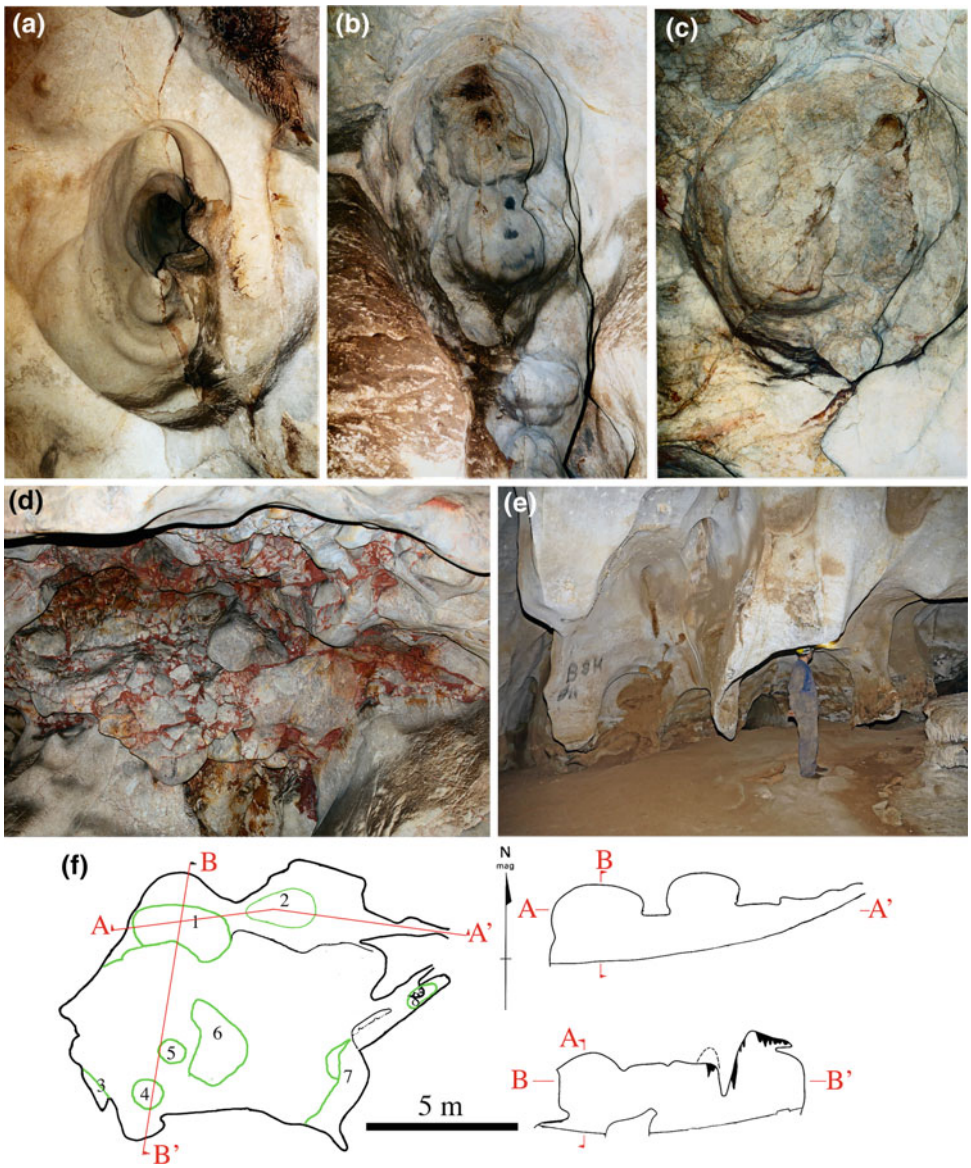

Fig. 8 Cupola Dominated Caves: **a** The politician's ear, a conical cupola in Cathedral Cave, Wellington. Long outer axis 2.5 m, short outer axis 1 m, penetration above ceiling level 3.5 m. **b** Kissing Cave, an elliptical cupola in Cathedral Cave looking up at an angle of 20°. Cupola is 5 m long by 2 m wide and 6 m high. **c** Hemispherical cupola in Dino Room, Cathedral Cave 1.5 m in diameter. **d** Looking up into vault of the Well Chamber, Cathedral Cave. Vault is 10.4 m high by 1 m wide north–south. **e** Elliptical cupola with curved pendants at its base, Swanson Cave, Cliefden. **f** Simplified map and sections of Bevan's Pot at Texas Caves after Grimes (1978). *Green lines* outline cupolas

Finches Cave, an isolated cenote-like cave in a fault sliver of limestone surrounded by insoluble rock.

While the caves in the isolated blocks are clearly not part of a larger system, most of the single chamber caves in karsts with many caves are spatially and/or hydrologically isolated from the other caves.

Daylight Cave at Sebastapol shown in Fig. 11 below is a rectangular cavity with a breakdown entrance at its south-west end and a blind termination at its north-east end, Solution notches (b in Fig. 11) are well developed in the north-west wall, and there are no scallops. The notches may relate to still-stands in the incision of the adjacent valley into the margin of the Great Escarpment.

Single chamber caves may be the lower sections of caves that have been largely eroded away. Single chamber caves, particularly those developed in small isolated bodies of limestone, cannot have formed by any process that involved the lateral movement of water, making them important elements of the case for hypogene speleogenesis. These caves have some similarity to the chamber caves described by Frumkin and Fischhendler (2005), which they attributed to mixing corrosion between infiltrating vadose water and static groundwater.

3 Features of Caves in Eastern Mainland Australia

3.1 Strong Structural Guidance

Strong structural guidance is a characteristic of most caves in eastern mainland Australia, including those with significant

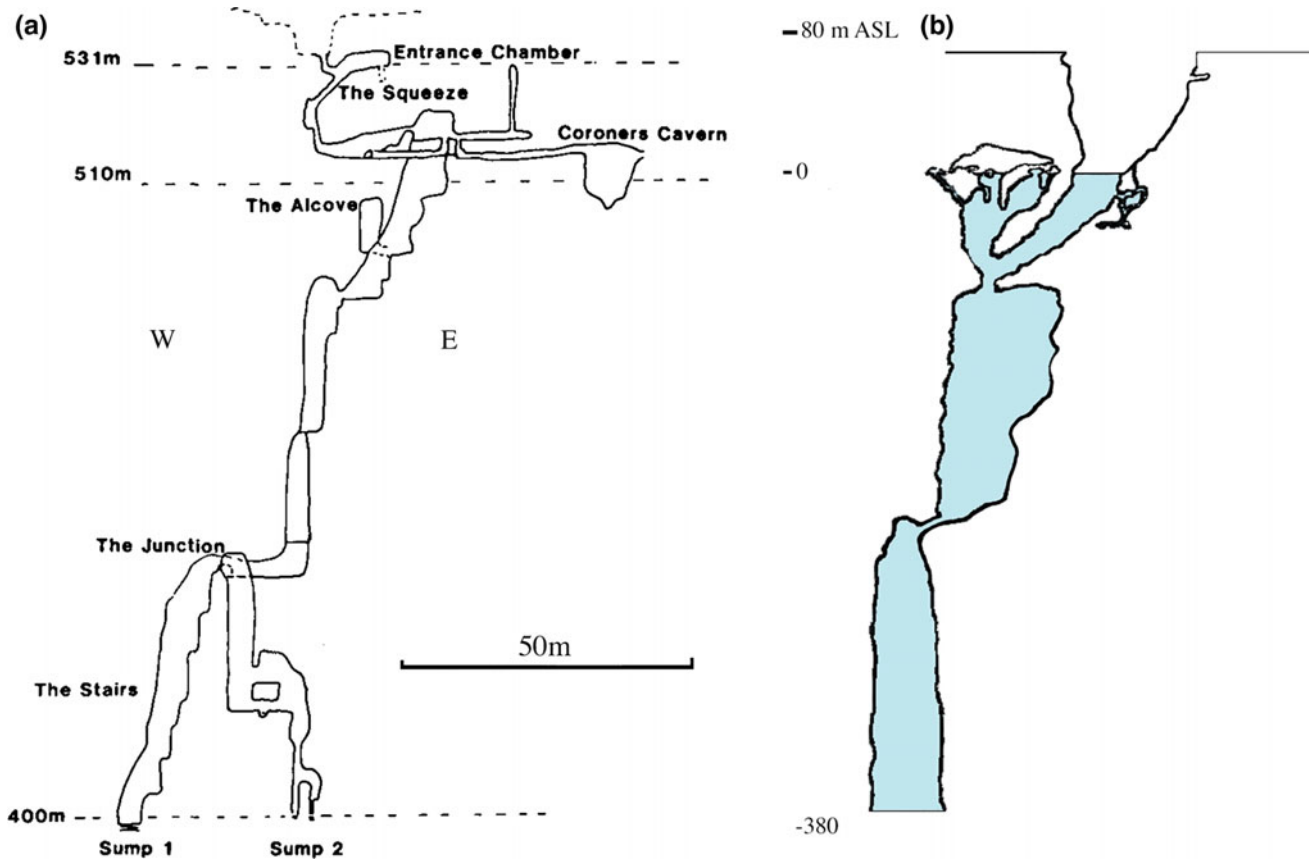

Fig. 9 **a** Argyle Hole, Bungonia, projected long section after A. Pavey, from Ellis et al. (1972). Reproduced courtesy of the Sydney Speleological Society. **b** Hranica Propast, Czech Republic simplified after Audra and Palmer (2015)

Fig. 10 Looking up into the ceiling of Castle Cave, Yarrangobilly. Note epiphreatic ceiling planning off old speleothem (vadose) and intersecting an older elliptical cupola (hypogene). Cupola axis is approx. 1 m long

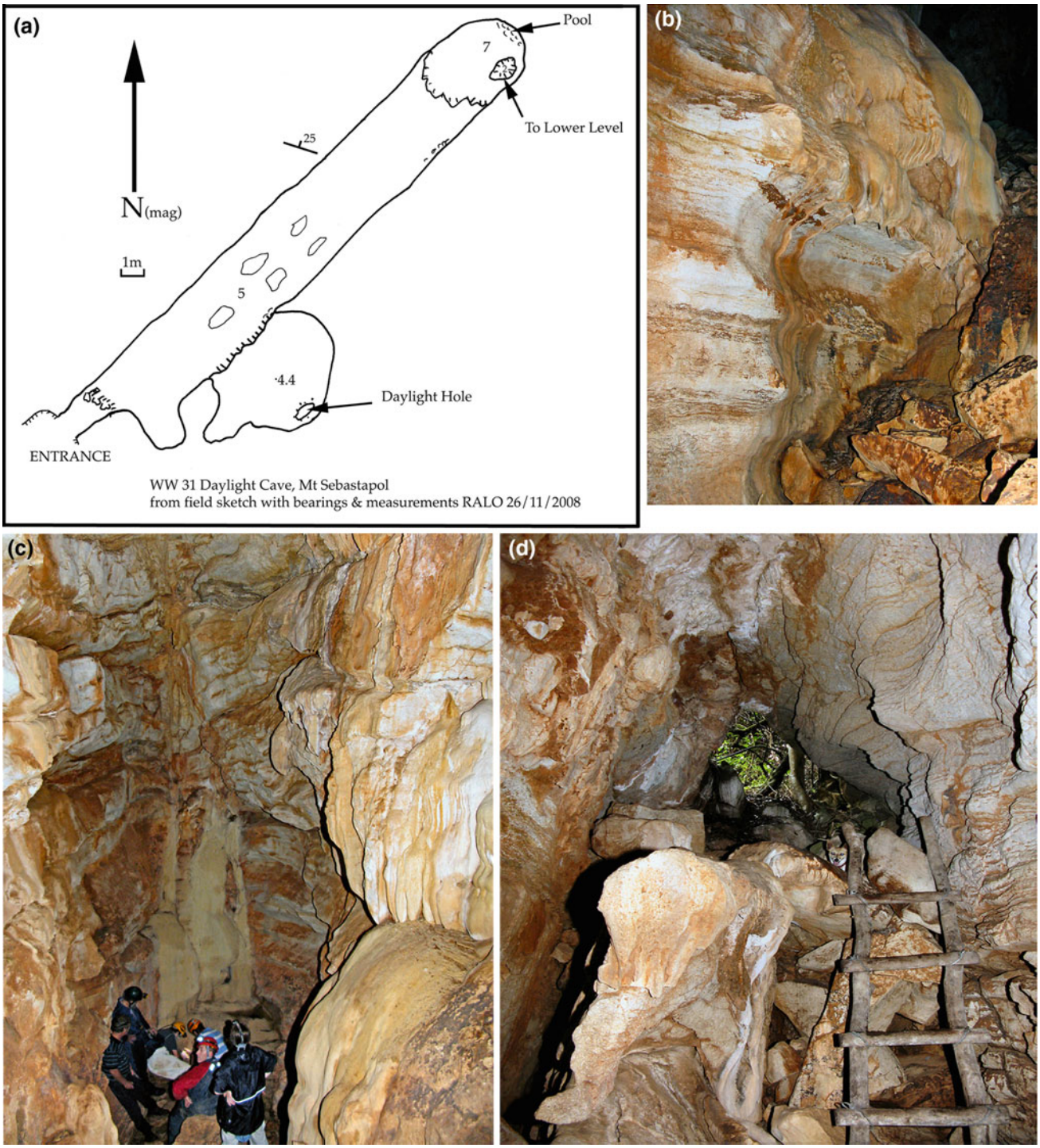

Fig. 11 Daylight Cave, Mt Sebastapol: **a** map, note blind termination at NE end of cave. **b** wall notches approximately 300 mm high. **c** Blind termination. **d** Breakdown entrance looking out

streams. Observations made since 2001 have shown that the major structural influence on cave development in eastern mainland Australia is neither bedding nor geological boundaries but jointing.

The cause of structural guidance was revised for the Cathedral Chamber at Wellington Caves, traditionally thought to have formed along the obvious boundary between massive and thinly bedded limestone, but shown by Osborne (2007) to be guided by a vertical joint in the thinly bedded limestone. Similarly, cave passages with sloping walls at Bungonia, traditionally regarded as "bedding plane flatteners", are now found to be guided by joints dipping perpendicular to the bedding, rather than bedding (Osborne 2013).

In addition to vertical and strongly dipping structural guidance, low dipping to horizontal joints also guide cave development in some locations. This can be very confusing, and it can be difficult to distinguish between the influence of horizontal jointing and that of paragenesis and epiphreatic solution.

Strong structural guidance is not restricted to eastern mainland Australian caves lacking significant streams. It is found in caves with perennial streams such as Murray Cave at Cooleman Plain, NSW. Strong structural guidance is also a feature of surface topography in eastern mainland Australia, with major surface streams following the north–south structural grain for tens and in one case hundreds of kilometres before flowing either east to the sea or west to the inland drainage basins.

3.2 Intersection of Palaeokarst

Caves at 18 localities in eastern mainland Australia are known to intersect palaeokarst. This includes most of the better-known karst areas in the Lachlan-Thompson Orogen. Palaeokarst deposits also occur in quarries and surface outcrop in three other karst localities, but have yet to be found in the adjacent caves. In the Permian limestone karsts of the eastern New England Orogen, palaeokarst is found in caves at Yessabah and Mt Sebastapol.

A range of palaeokarst deposits is intersected by caves. These include filled tubes, clastic and pyroclastic dykes, lava flows, pipes, veins, breccias and large masses that can be misinterpreted as bedrock. Palaeokarst materials found in the caves include basalt, megabreccia (Fig. 12a), crackle breccia, crystal vughs (Fig. 12b), volcaniclastics (Fig. 12c), caymanites (marine carbonate turbidites) (Fig. 12d), sandstones (wackes and arenites), conglomerates (Fig. 12e) and speleothem (Fig. 12f). Palaeokarst deposits in the caves are intersected by both hypogene and fluvial cavities and occur at all vertical levels within the caves.

Caves in some karsts intersect a variety of palaeokarst deposits and materials. Caves at Jenolan intersect conglomerates, sandstones, caymanites, crackle breccias, and crystal vughs. At Bungonia, caves intersect clastic dykes, caymanite filled joints and large masses of caymanite, while at Wombeyan, caves intersect crackle breccias, crystal vughs, ferruginous sandstone dykes, volcaniclastic dykes and tube fills.

3.3 Cupolas

Except for the two large domes in the Jenolan Show Caves interpreted as "symmetrically scoured potholes", (Dunlop 1979) cupolas and related hypogene cavities and speleogens seem to have been unrecognised in eastern Australian caves before the very late 1990s. The term cupola first appeared in the literature on Australian caves in Osborne (1999). Some of the best examples of cupolas occur at Jenolan Caves (Fig. 13).

Cupolas are known to occur in caves at 24 cavernous karsts in eastern mainland Australia, and hypogene speleogens are known to occur at 38. These numbers illustrate the lack of good data about the caves rather than the likely abundance of these features.

3.4 Dykes, Partitions and Portals

Caves at Bungonia, Colong, Jenolan, Wombeyan and Mt Etna intersect or are terminated by clastic, pyroclastic and dolerite dykes. Most dykes follow joints roughly perpendicular to bedding. At Bungonia, thick dolerite dykes terminate solution chambers in Grill and Flying Fortress caves (Fig. 5a). Thin dykes of dolerite exposed in the walls of Flying Fortress Cave have been replaced by carbonate consisting of calcite pseudomorphs after plagioclase in a dark calcite groundmass.

Colong Cave the third longest cave in eastern mainland Australia with a plan length of 6 km intersects many dolerite dykes with both vertical and shallow-dipping orientation. Osborne (1985, 2003) proposed that the cave began as separate per-ascensum cavities formed in compartments between the dykes and that fluvial and paragenetic cave development was only possible after the dykes had been breached.

Some of the east–west trending cavities in Colong Cave have been formed by the weathering and complete removal of dykes, leaving behind open joints.

At Jenolan, Walli and Wombeyan Caves openings in dykes and insoluble beds, called portals by Osborne (2003),

Fig. 12 Palaeokarst: **a** Megabreccia exposed in wall of Castle Cave, Yarrangobilly, note head for scale. **b** Crystal vugh intersected by passage in Sigma Cave, Wombeyan. Lens cap 50 mm. **c** Volcaniclastic dyke in wall of Bullio Cave, Wombeyan. Lens cap 50 mm. **d** Mass of caymanite palaeokarst, dipping to left, intersected by cave, River Cave, Jenolan. **e** Conglomerate, brown filling crystal-lined vugh, Lucas Cave, Jenolan. White rule 250 mm. **f** Palaeokarst flowstone interested by wall of Main Cave, Timor

have formed by weathering under vadose conditions, creating connections between originally unconnected cavities.

3.5 Triangular Profiles

Elongate cavities with triangular profiles are common in eastern Australian caves. Good examples are found in Imperial Cave at Jenolan, Fig Tree Cave at Mt Sebastapol and Queenslander Cave at Chillagoe (Fig. 14). Triangular cavities narrow upwards into tight joints, suggesting solution from below, rather than a mixing corrosion origin by seepage from above.

It is important to recognise that the flat floors of these cavities are composed of sediment so the shape of the lower parts of these cavities remains unknown.

Fig. 13 Cupolas at Jenolan: **a** Sequence of rising cupolas at western end of the Temple of Baal, Image Bojan Otoničar. **b** Complex cupola in the Temple of Baal, Image Bojan Otoničar. Note cupolas within cupolas. **c** 45 m high double cupola in the Temple of Baal. Originally, this was two separate cupolas but the separating wall failed in the distant past. Shaft is 4 m in diameter. **d** Complex cupolas guided by a dipping structure in the Mud Tunnels. Large cupola in centre of image is 3 m in diameter. **e** Ceiling with many cupolas in the mud tunnels. **f** Looking up into the 4-m-diameter Commonwealth Dome which is the top of the 26-m-high cupola forming the Persian Chamber in the Orient Cave. **g** 3-m-diameter conical cupola in the Pool of Cerberus. **h** Looking up into the complex high ceiling of the Cathedral in Lucas Cave

3.6 Speleogens

Osborne (2004) described a suite of speleogens that occur in caves containing cupolas: "ceiling half-tubes, rising half-tubes, wall notches, symmetrical wall and ceiling pockets, very large scallops, rock bridges, cave walls with circular sections in plan view, curved wall, ceiling and floor projections (i.e. curved pendants, juts and blades), bellholes, symmetrical pits (approx. 40 mm diameter pits and approx. 10 mm diameter pits) and pseudonotches".

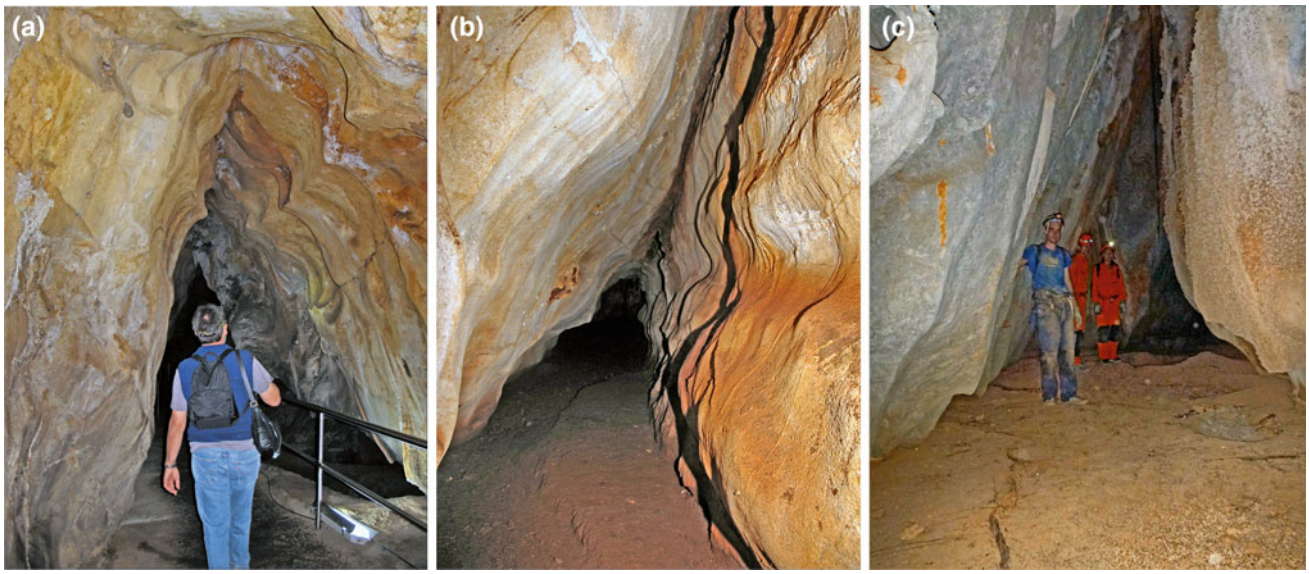

Fig. 14 Triangular profiles: **a** Imperial Cave, Jenolan, Image Bojan Otoničar. **b** Fig Tree Cave, Mt Sebastapol, passage is approximately 2 m wide by 4 m high. **c** September Cave, Chillagoe. Image Peter Bannink

If we add a few more features to this list such as, spongework (Fig. 15a), straight wall, floor and ceiling projections (vertical and horizontal blades) (Fig. 15b), elaborate ceiling pendants, similar to the "Elephant feet" of Audra et al. (2002) (Fig. 15c), mega scallops and cusps (Fig. 15d), projecting corners (Fig. 15e) and double-blind tubes (Fig. 15f), this makes a list of the types of speleogens found in many eastern mainland Australian caves.

3.7 Warm Springs and Degassing Deposits

Warm springs are reported to occur at three cavernous karsts in eastern mainland Australia: Cliefden (Warm Spring 29 °C, cave temperature 19 °C), Wee Jasper (Warm Spring 30 °C, cave temperature 16 °C) and Yarrangobilly (Warm Spring 27 °C, cave temperature 10 °C). Only at Wee Jasper is the spring directly associated with a cave and degassing deposits.

Similarly degassing deposits such as calcite rafts, raft breccias, raft cones and clouds are also found at only a few localities in eastern mainland Australia (Fig. 16). It is difficult to know if warm spring and degassing deposits are genuinely rare or if the apparent rarity is an artefact of reporting.

Calcite rafts forming on the surface of ponds or sitting on groundwater in the caves are known to occur at seven localities and are likely to occur in more. Cemented raft breccias are less common, reported from only four localities, Cliefden, Jenolan, Timor and Wellington, while raft cones are only known from Gaden Cave at Wellington. Cave clouds are found at Chillagoe, Cliefden, Timor, Wee Jasper and Wellington. In Gaden Cave at Wellington, raft breccias, raft cones, clouds and spar crystals occur together in an assemblage similar to that found in the thermal caves of Budapest (Leél-Őssy et al. 2011). While most of these deposits are relatively small, the clouds at Chillagoe are quite large.

3.8 Paragenesis

While not hypogene features, paragenetic conduits and paragenetic enlargement of chambers are important features of caves in karsts located near the edge of the Sydney Basin. At Jenolan, paragenetic conduits provide the connections between otherwise isolated cupola swarms, contributing to the integration of the cave system.

Paragenetic conduits are well developed at both Jenolan and Colong Caves while large breakdown chambers at Wombeyan show evidence of paragenesis. Paragenesis is also likely to be an important process in the development of karst bridges at Jenolan and Borenore.

In River Cave at Jenolan, paragenetic conduits have rising and falling notches ("a" in Fig. 17). The apices of the rises in the notches are often located at junctions with side channels, where sediments entering the caves in the past have raised the flow path of the water. River Cave also contains a paragenetic loop ("b" in Fig. 17) with a ceiling composed of flowstone and bedrock and a deep mass of sediment forming its aggregated floor.

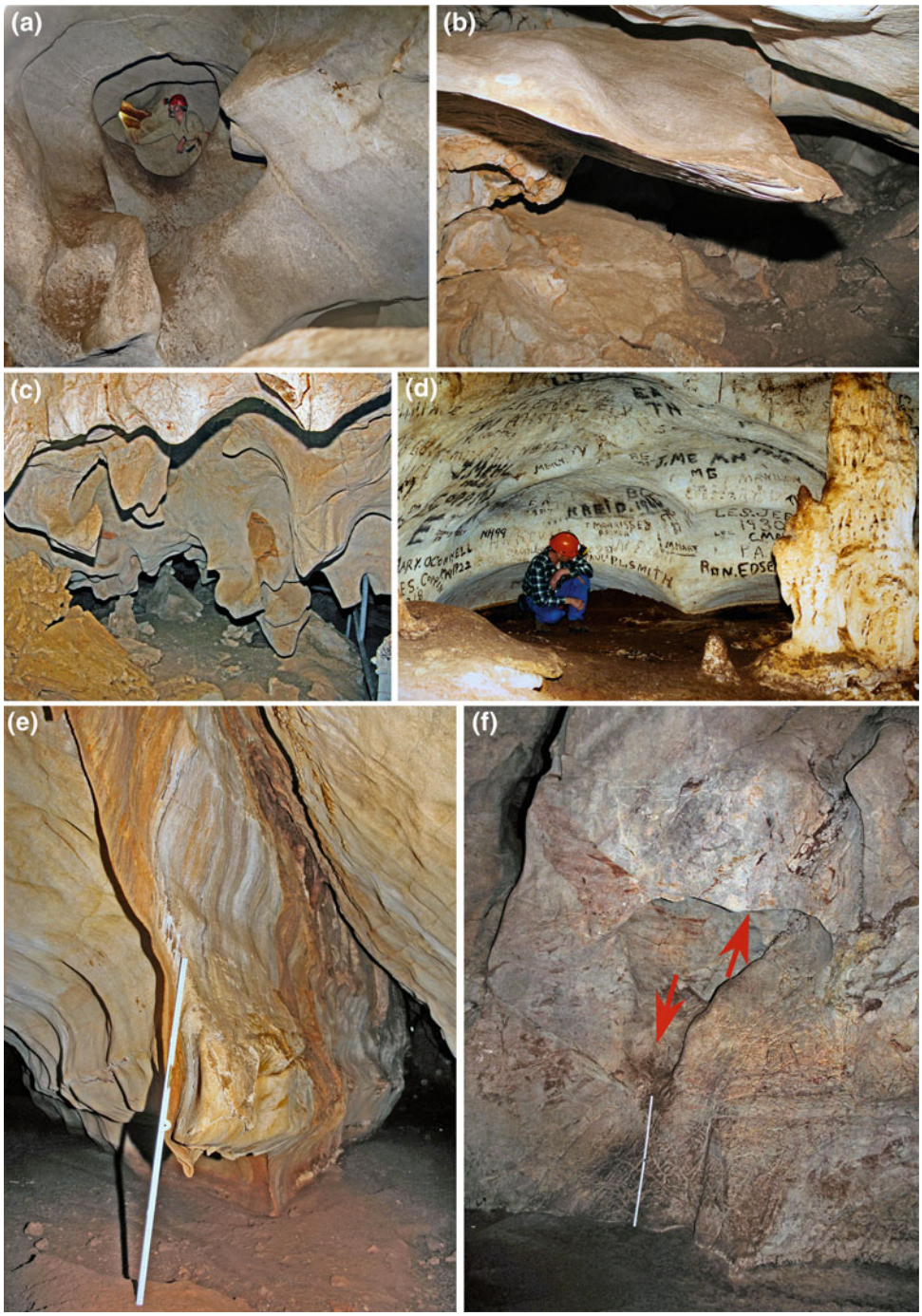

Fig. 15 Speleogens: **a** Spongework, Transmission Cave, Cliefden. Note person in red helmet for scale. **b** Sub-horizontal blade, Moparabah Cave, NSW. Blade projects approximately 1.5 m. **c** Elaborate ceiling pendants, Chandelier Cave, Mt Etna. **d** Mega scallops/cusps, Bendithera Main Cave. Note person in red helmet for scale. **e** Projecting corner, Fig Cave, Mt Sebastapol. *White rule* is 1 m. **f** Double-blind tube, Cathedral Cave, Wellington. *Red arrows* point to blind ends of the tube. *White rule* is 1 m long

3.9 Breakdown

Breakdown chambers are late-stage features of the caves and are known to occur at twelve localities including Cliefden, Colong, Jenolan, Wombeyan, Wyanbene and Yarrangobilly. In some caves, there is a clear relationship between breakdown and the weathering of pyrite in veins in the limestone or in palaeokarst deposits as described by Osborne (2002). At Wombeyan Caves, breakdown chambers have been modified by paragenesis. More recent partial removal of the sediment

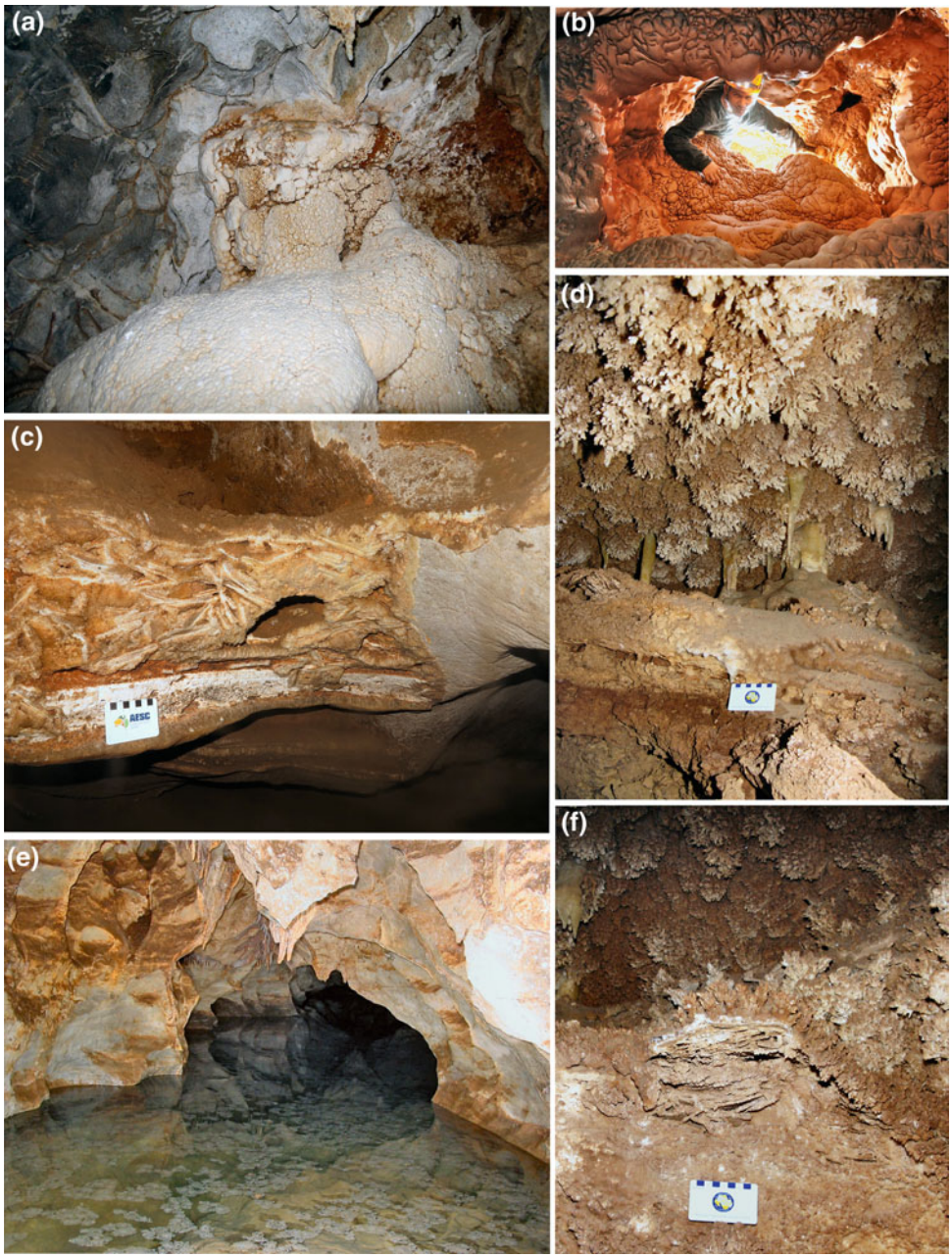

Fig. 16 Degassing deposits: **a** clouds, thermal Paddock Cave, Wee Jasper. Field of view is approximately 3 m high. **b** Clouds, Queenslander Cave, Chillagoe Image by Winifred Weiss. **c** Raft Breccia, Transmission Cave, Cliefden. **d** Spar, Gaden Cave, Wellington. **e** Degassing lake with rafts, Moore's Lake Cave, Timor. Lake is approximately 4 m wide. **f** Raft Cone, Gaden Cave, Wellington

has revealed large angular breakdown blocks in a clay matrix in sediment below paragenetic ceilings (c in Fig. 17).

3.10 Sediments and Sediment Removal

Because eastern mainland Australian caves are located in impounded karsts, there is a ready source of insoluble sediment available to fill these caves. The most widespread sediment in these caves is red silt, historically referred to as *red earth*. Red earth is generally considered to be desert dust from Central Australia, blown east by ice age dust storms (Osborne 1991, 1992; a in Fig. 18). Red earth is often associated with Pleistocene vertebrate fossils.

The oldest cave sediment, more correctly palaeokarst, dated by fossils is the Pliocene osseous sandstone forming the second lowest strata exposed in the Wellington Caves Phosphate Mine (b in Fig. 18). These unusual sediments consist of lithified excrement from large extinct carnivorous bats (Osborne 2008). There is a significant gap in the cave sediment and palaeokarst stratigraphy between this Pliocene deposit and the older palaeokarst deposits considered to be Permian on stratigraphic grounds. While karst areas such as Bungonia, Colong and Jenolan were buried under the

Fig. 17 Paragenesis: **a** rising and falling paragenetic notches, Pool of reflections, River Cave, Jenolan. **b** Paragenetic sediment remnants in rising tube at upstream end of paragenetic loop, River Cave, Jenolan. **c** Flat ceiling with channel in ceiling of Fig Tree Cave, Wombeyan. Note large angular breakdown blocks in sediment below false floor

Sydney Basin for most of the Mesozoic, the apparent lack of Tertiary sediments older than Pliocene in the cave sediment/palaeokarst sequence is a puzzle.

Unlithified mass flow deposits containing boulders, cobbles, gravel and mud, but no sand, occur at Jenolan and Colong (c in Fig. 18). Dating by Osborne et al. (2006) of mass flow sediment at Jenolan indicates a Late Carboniferous, age suggesting an association with Permo-Carboniferous glaciation.

The oldest dated unlithified sediments in eastern Australian caves are the yellow clay deposits in Jenolan Caves dated at 340 Ma by Osborne et al. (2006) (d in Fig. 18). These appear to have a volcanic ash origin. Laminated mud occur in caves with little or no fluvial influence (e in Fig. 18) while paragenetic processes at Jenolan and Wombeyan are associated with both fine mud and coarse gravels (f in Fig. 18). Contemporary streams in caves transport sand as a base load (g in Fig. 18) and coarser sediments in rare flood conditions.

False flowstone floors and sediment remnants are abundant in most caves in eastern mainland Australia. This suggests that the caves are currently undergoing a phase of sediment removal.

3.11 Relationships Between Caves and Ore Bodies

The Tasman Orogen is a significant province for metalliferous ores and many cavernous karsts occur in close

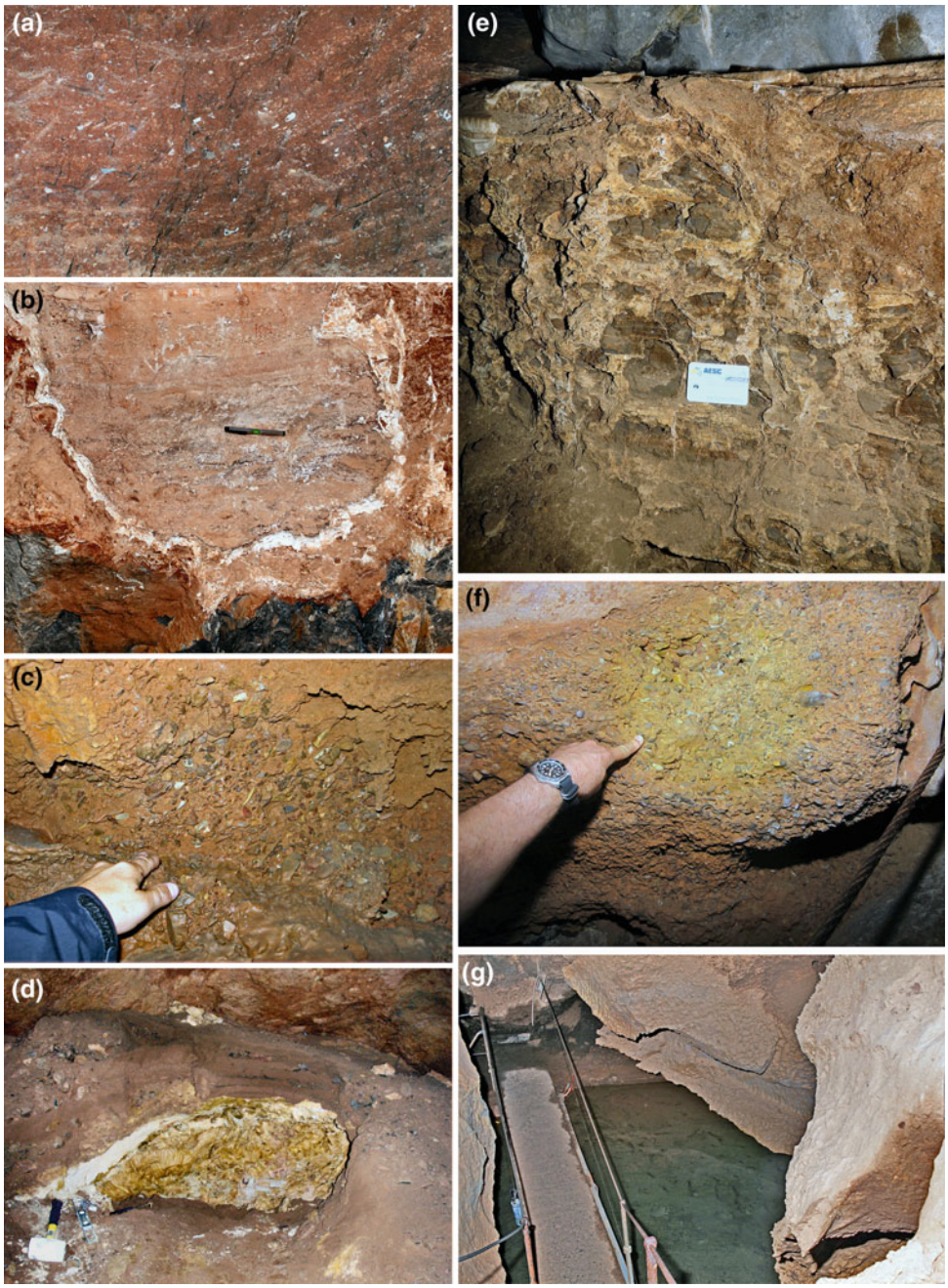

Fig. 18 Cave sediments: **a** Pleistocene Red Earth, Phosphate Mine, Wellington Caves. **b** Pliocene osseous sandstone, Phosphate Mine, Wellington Caves. Scale in centre of image is 90 mm long. **c** Late Carboniferous mass flow deposit of gravel in a mud matrix, Temple of Baal, Jenolan, Image Bojan Otoničar. **d** Yellow Carboniferous clay, Temple of Baal, Jenolan. White mallet head at bottom left of image is 70 mm long. **e** Laminated mud with calcite veins filling mud cracks, Gable Cave, Cliefden. White card is 85 mm long. **f** Paragenetic fluvial gravel, River Cave, Jenolan. **g** Contemporary fluvial sand with ripples in the Jenolan underground river

proximity to ore bodies, mines and prospective areas. The Red Dome copper deposit is located at the southern end of the Chillagoe karst, Cliefden Caves are right next door to old Barite mines, the region around Wellington, Borenore and Cliefden caves is prospective for porphyry copper/gold deposits.

Mt Sebastapol is adjacent to the Mt Jacob gold prospect and to the west at Willi Willi, copper and gold have been mined from the limestone.

Osborne (1996) recognised a relationship between caves and sulphide-bearing materials at Abercrombie, Bungonia, Buchan, Cooleman Plain, Jenolan, Mt Etna, Wombeyan, Wyanbene and Yarrangobilly. The most striking example is at Wyanbene where much of the cave has formed by the weathering and erosion of a joint-guided ore body.

Much more work needs to be done to explore the relationships between ore mineralisation and cave development in eastern mainland Australia.

4 Discussion

Most of the caves in eastern mainland Australia appear to have been initially excavated by a non-fluvial, hypogene process. Speleogens in the caves suggest that this process involved convecting or slowly rising water. There is little evidence available about the chemistry, temperature or source of this water, but the proximity of many caves to regional faults suggests that they may be involved. Warm springs occur in three cavernous karsts, but only one cave has a direct relationship with warm spring water and the water there only has a temperature between twenty and thirty degrees and is not particularly aggressive or mineralised. More work is required on the relationship between caves and ore bodies, and research now underway has a focus on identifying possible remnants of ancient cave linings and examining their isotopic composition. It is hoped that this work will shed new light on the origin of non-fluvial caves in eastern mainland Australia.

Acknowledgements The author would like to thank P.J. Osborne for proofreading and many colleagues, friends, cave managers and cavers who have assisted in his study of caves over the last forty years.Except where otherwise indicated, images in this chapter are by the author. Phil Maynard and Sydney University Speleological Society are thanked for the use of their maps. Sydney Speleological Society has always assisted by allowing the use of figures from their publications. Bojan Otoničar is thanked for the use of his photographs from Jenolan Caves.Newcastle and Hunter Speleological Society provided maps of caves at Timor, and Kempsey Speleological Society provided maps of caves at Sebastapol. Chillagoe Caving Club provided the map of Queenslander Cave, and club members Peter Bannink and Winifred Weiss provided photos and helped with information about the Chillagoe karst. George Bradford, Geoff Kell and Andy Spate assisted with cave and spring temperature data. The text has been significantly improved by suggestions from Alexander Klimchouk and Jo DeWaele.

References

Audra P, Palmer AN (2015) Research frontiers in speleogenesis: dominant processes, hydrological conditions and resulting cave patterns. Acta Cars 44(3):315–348

Audra P, Bigot J-Y, Mocochain L (2002) Hypogenic caves in Provence (France). Specif Featur Sediment Acta Cars 31(3):33–50

Dunlop BT (1979) Jenolan Caves, 11th edn. New South Wales Department of Tourism, Sydney, 96 p

Ellis RA, Hawkins L, Hawkins R, James J, Middleton G, Nurse B, Wellings G (eds) (1972) Bungonia Caves, Sydney Speleological Society Occasional Paper, vol 4, p 230

Frumkin A, Fischhendler I (2005) Morphometry and distribution of isolated caves as a guide for phreatic and confined paleohydrological conditions. Geomorphology 67(3):457–471

Grimes KG (1978) The geology and geomorphology of the Texas Caves, Southeastern Queensland. Mem Queensl Mus 19(1):17–59

James JM, Francis G, Jennings JN (1978) Bungonia Caves and Gorge; a new view of their geology and geomorphology. Helictite 16 (2):53–63

Jennings JN (1963) Geomorphology of Dip Cave Wee Jasper, New South Wales. Helictite 1(3):43–58

Jennings JN (1964) Geomorphology of punchbowl and signature Caves, Wee Jasper, New South Wales. Helictite 2(2):57–71

Jennings JN (1965) Bungonia Caves and rejuvenation. Helictite 3 (4):79–84

Jennings JN (1968) Geomorphology of Barber Cave, Cooleman Plain, New South Wales. Helictite 6(2):23–29

Jennings JN (1982) Principles and problems in reconstructing karst history. Helictite 20(2):37–82

Jennings JN (1985) Karst geomorphology. Blackwell, Oxford, p 293

Leél Őssy S, Szanyi G, Surányi G (2011) Minerals and speleothems of the Józef-hegy Cave (Budapest, Hungary). Int J Speleol 40(2): 191–203

Ollier CD (1982) The Great Escarpment of eastern Australia: tectonic and geomorphic significance. J Geol Soc Austr 29(1–2):13–22

Osborne RAL (1985) Letter, dykes and cave development at Colong Caves, New South Wales. Helictite 23(1):33–35

Osborne RAL (1991) Red earth and bones: the history of cave sediment studies in New South Wales, Australia. J Earth Sci Hist 10(1):13–28

Osborne RAL (1992) Australian red earth and bones. J Proc R Soc NSW 125(3/4):111

Osborne RAL (1996) Vadose weathering of sulfides and limestone cave development-Evidence from eastern Australia. Helictite 34(1):5–15

Osborne RAL (1999) The origin of Jenolan Caves: elements of a new synthesis and framework chronology. Proc Linn Soc NSW 121:1–26

Osborne RAL (2001) Halls and narrows: network caves in dipping limestone, examples from eastern Australia. Cave and Karst Sci 28 (1):3–14

Osborne RAL (2002) Cave breakdown by vadose weathering. Int J Spel 31(1/4):37–53

Osborne RAL (2003) Partitions, compartments and portals: cave development internally impounded karst masses. Speleogenesis Evol Karst Aquifers: Virtual Sci J 1(4):1–12. www.speleogenesis.info

Osborne RAL (2004) The troubles with cupolas. Acta Cars 33(2):9–36

Osborne RAL (2007) Cathedral Cave, Wellington Caves, New South Wales, Australia. A multiphase, non-fluvial cave. Earth Surf Proc Landf 32:2075–2103

Osborne RAL (2008) Cave turbidites. Acta Cars 37(1):41–50

Osborne RAL (2010) Rethinking eastern Australian caves. In: Bishop P, Pilans B (eds) Australian landscapes. Geological Society of London Special Publications 346, pp 298–308

Osborne RAL (2013) Exhumation of palaeokarst by vadose weathering: a telling example from eastern Australia. In: Filippi M, Bosák P (eds), Proceedings of the 16th international congress of speleology, July 21–28, Brno. Volume 3: 275–279

Osborne RAL (2014) Understanding the origin and evolution of Jenolan Caves: the next steps. Proc Linn Soc NSW 136:77–97

Osborne RAL, Branagan DF (1988) Karst landscapes in New South Wales. Earth Sci Rev 25:467–480

Osborne RAL, Zwingmann H, Pogson RE, Colchester DM (2006) Carboniferous clay deposits from Jenolan Caves, New South Wales, Australia. Austral J Earth Sci 53(3):377–405